

# REVIEWS

## Peptide Nucleic Acid (PNA). A DNA Mimic with a Peptide Backbone

Peter E. Nielsen,\* Michael Egholm,<sup>†</sup> and Ole Buchardt<sup>†</sup>

Research Center for Medical Biotechnology, Department of Biochemistry B, The Panum Institute, Blegdamsvej 3c, DK-2200 Copenhagen N, Denmark, and Department of Organic Chemistry, The H. C. Ørsted Institute, Universitetsparken 5, DK-2100 Copenhagen Ø, Denmark. Received July 29, 1993

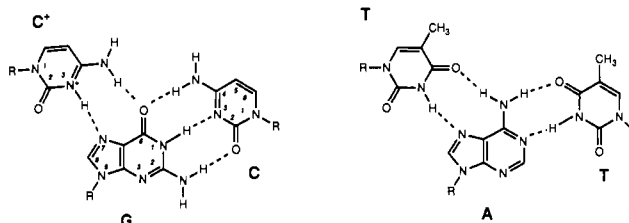
### INTRODUCTION

During the last decade major efforts have been made to develop synthetic reagents that bind sequence specifically (or selectively) to double stranded DNA thereby in principle being mimics of DNA recognizing proteins such as gene repressors or transcription factors. Apart from the scientific importance of such reagents for understanding the molecular chemistry of DNA recognition, sequence specific DNA-recognizing ligands have obvious potentials for the development of gene-targeted drugs and molecular biology tools (1).

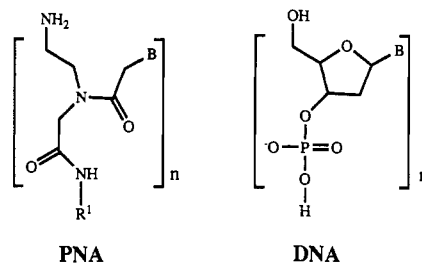
Most success in this area has been obtained using oligonucleotides that bind to double-stranded DNA by triple helix formation (Figure 1) (2-7), and although a general solution for the problem of recognizing mixed purine-pyrimidine sequences is yet to come, major progress has been made in recent years (8-13).

We decided to try exploiting the "triple helix principle" for constructing a fully synthetic DNA-recognizing ligand which would rely on hydrogen bonding/recognition by heterocycles like the natural nucleobases. Especially, we wished to construct an oligomeric type of reagent in which the heterocycles were connected *via* a backbone not being composed of deoxy ribose phosphate esters. Thus, in essence we aimed at making a "DNA analogue" in which the backbone had been replaced by one which from a synthetic point of view (ease of synthesis and synthetic flexibility) would be more amicable.

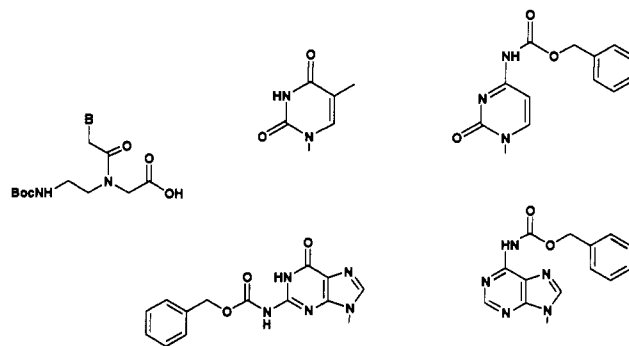
The new backbone was designed using computer model building combined with chemical "common sense" (14-15) to be structurally homomorphous to the deoxyribose phosphate backbone, synthetically accessible, and amenable to automated assembly synthesis. We decided to rely on the Merrifield solid-phase synthesis of peptides using the *tert*-butoxycarbonyl (Boc) protection strategy. The resulting target molecule is composed of a backbone containing *N*-(2-aminoethyl)glycine units in which the nucleobase is attached to the glycine nitrogen *via* a methylene carbonyl linker (Figure 2) (14-19). Since we consider these molecules as chimera between nucleic acids (the nucleobases) and (pseudo)peptides (the backbone) we termed them peptide nucleic acid (PNA). We acknowledge that this is not strictly a chemically correct name, since PNA molecules are neither acids nor natural peptides. However, with the name we wished to emphasize that peptide chemistry is used for the oligomerization and that PNA is a very close analogue of nucleic acids. Some colleagues have suggested the name "polyamide nucleic acid analogue" be more appropriate. However, we still



**Figure 1.** Nucleobase triplets for oligonucleotide triple helix formation in the pyrimidine-purine-pyrimidine motif. Recognition of adenine and guanine by thymine and protonated cytosine, respectively.



**Figure 2.** Chemical structures of DNA and PNA.



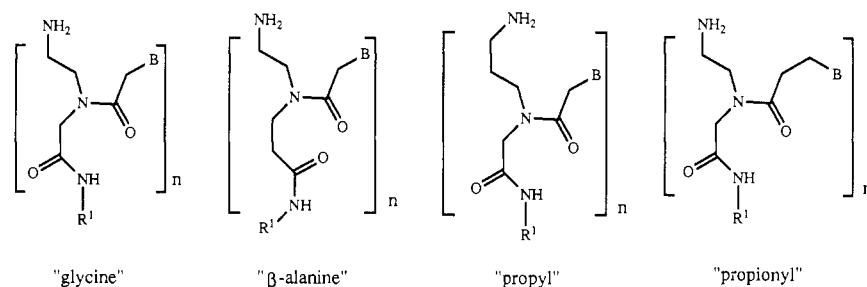
**Figure 3.** Monomers used for the solid phase synthesis of PNA oligomers.

prefer "peptide nucleic acid" at least for the type of compounds prepared so far.

### CHEMISTRY

PNA oligomers are assembled from the protected monomers shown in Figure 3 (16-18). The primary amino group is protected with the *tert*-butoxycarbonyl (Boc) group, and the exocyclic amino groups of the nucleobases are protected with the benzyloxycarbonyl (Z) group. The oligomer synthesis essentially follows the Merrifield solid-phase synthesis approach, and the Z groups used for protection of the exocyclic amino groups are removed during the cleavage from the support with hydrogen fluoride.

\*Author to whom correspondence should be addressed.



**Figure 4.** Examples of PNA backbone modifications.

In our laboratories 10–20 mers containing all the four nucleobases are routinely synthesized from the now commercially available monomers. The coupling reaction yields are somewhat dependent on the sequence of the oligomer, but no definite pattern has been identified yet. The crude PNA-oligomers are purified by reversed-phase HPLC, and after freeze drying of the collected pure fractions the PNA-oligomer is ready for use in most cases.

#### HYBRIDIZATION

Although PNA was designed as a DNA major groove binding ligand it can also be regarded as a DNA analogue with the potential of sequence specific hybridization to Watson–Crick complementary oligonucleotides.

In the field of antisense technology numerous DNA analogues with modified backbone have been prepared and examined in order to obtain medicinally useful antisense drugs. These modifications include among others analogues with backbones containing phosphorothioates, methylphosphonates, phosphorodithioates, formacetal, or thioformacetal bridges (5, 20, 21). These are all structurally isomorphous, and their backbones have a high degree of chemical resemblance to the deoxyribose phosphate backbone. All these analogues have retained DNA-like hybridization properties, although the stability of the resulting duplexes varies significantly among the analogues. “Peptide nucleic acids” consisting of pseudopeptides based on aminopentanoic or aminohexanoic acid (22) or serine (23) have been described, but their hybridization properties have not been studied in any detail.

PNA's based on the *N*-(2-aminoethyl)glycine backbone proved to be very potent DNA mimics in terms of hybridization to complementary oligonucleotides. Thus, it was found that the  $T_m$  of an all thymine PNA (H-T<sub>10</sub>-Lys-NH<sub>2</sub><sup>1</sup>) complexed with (dA)<sub>10</sub> was 72 °C (16) compared to 23 °C for the corresponding (dT<sub>10</sub>)/(dA<sub>10</sub>) complex, and similar results were obtained for PNA containing both thymine and cytosine (17). The cause of the unprecedented high thermal stability of these homopyrimidine PNA/DNA complexes turned out to be formation of (PNA)<sub>2</sub>/DNA triplexes (16–18, 24) (quite logically in retrospect), where the DNA strand presumably binds two PNA strands, one by Watson–Crick and the other by Hoogsteen base pairing (Figure 1). These (PNA)<sub>2</sub>/DNA triplexes are indicated by circular dichroism analyses to have a helical structure not drastically different from (poly d(T))<sub>2</sub>/poly d(A) (24).

In accordance with these results, further experiments showed that pyrimidine–purine mixed PNAs bind to Watson–Crick complementary oligonucleotides (DNA or RNA) forming duplexes of higher thermal stability than the corresponding DNA/DNA or DNA/RNA duplexes (19). The results so far indicate a thermal stabilization of ~1

°C per base pair at physiological ionic strength (19 and unpublished results).

Since the PNA backbone is achiral there is *a priori* no reason why PNA should only bind to complementary oligonucleotides in one orientation as is the case for DNA or RNA. Accordingly, experiments show that both with complementary DNA and RNA binding in the antiparallel (amino-terminal of the PNA facing the 3'-end of the oligonucleotide) as well in the parallel orientation is possible although the antiparallel complex is approximately 1 °C per base pair thermally more stable than the parallel one for PNA/DNA (RNA) duplexes (19 and unpublished results). However, triplex complexes between PNA and DNA in the parallel orientation were found to be the more stable (17 and unpublished results). (Thus, it may be that the most stable (PNA)<sub>2</sub>/DNA complexes are formed with one PNA in the antiparallel (the Watson–Crick) and another with reverse polarity in the parallel (the Hoogsteen) orientation.) Finally, circular dichroism studies have indicated that PNA/DNA (or RNA) duplexes are helical with a geometry not drastically different from that of DNA/DNA or DNA/RNA duplexes. On the basis of the thermal hyperchromicity of PNA and on measurements of PNA–DNA hybridization kinetics it may even be inferred that single-stranded PNA is as structured as single-stranded DNA in terms of base stacking. Thus, PNA appears to be a very close structural mimic of DNA (19). These results also imply that the nucleobases play a significant role in determining the helical structure of DNA (and RNA).

#### STRUCTURE/ACTIVITY STUDIES

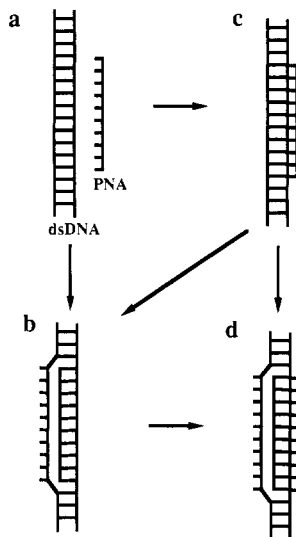
A few chemical modifications of the PNA backbone have been made so far to define the “structural window” that results in PNA's being good DNA mimics. For instance, extension of the backbone with a methylene group at any of the three linkers (Figure 4) results in PNA molecules with dramatically decreased binding affinity for complementary DNA (25 and manuscript in preparation). However, single units with such an extended backbone may be incorporated into PNA oligomers with the (aminoethyl-glycine) backbone, thereby providing a means of “fine tuning” the binding affinity (25 and manuscript in preparation). These results show that keeping the proper distances within the backbone and between the backbone and the nucleobases is critical. The effects of other changes of backbone which influence its rigidity/flexibility, hydrophilicity, electric charge, etc., remain to be seen.

#### STRAND DISPLACEMENT BINDING TO DSDNA

Experiments designed to test the binding of PNA H-T<sub>10</sub>-Lys-NH<sub>2</sub> to a double-stranded d(A)<sub>10</sub>/d(T)<sub>10</sub> target contained within a DNA restriction fragment showed unexpectedly that the PNA did not bind by PNA/(DNA)<sub>2</sub> triplex formation but rather by strand displacement in

<sup>1</sup> The PNAs are written from the amino to the carboxyl terminal using conventional peptide nomenclature.





**Figure 5.** Schematic models for the formation of a PNA-dsDNA strand-displacement complex.

which the PNA binds to the complementary (A)-strand and thereby displaces the noncomplementary (T)-strand (14). This conclusion was initially based on enzymatic and chemical probing experiments showing that the T-strand became extremely susceptible to digestion by the single strand specific nuclease S1 and also to oxidation by  $\text{KMnO}_4$  (14). The strand displacement mode of binding has subsequently been supported by electron microscopy and DNA unwinding studies (26).

Recent results with cytosine- and thymine-containing PNA's have revealed that the strand displacement binding of such PNA's is pH dependent in the pH 5–7 range and that N7 of guanines in the target DNA strand is protected from reaction with dimethyl sulfate (27). Both of these observations are fully consistent with a binding mode in which two PNA's are required for the formation of a stable strand displacement complex involving both Watson-Crick and Hoogsteen base pairing. Three different mechanisms can be envisaged for the formation of this complex (Figure 5). It may be formed either *via* an initial PNA/(DNA)<sub>2</sub> triplex (routes a–c–d or a–c–b–d) or *via* a strand displacement complex with a single PNA (route a–b–d), but kinetic data are required to distinguish between these. We imagine that the displacement binding takes place *via* the dynamic breathing motion (base pair opening) of the DNA double helix. This mechanism is consistent with the observation that concentrations higher than 50 mM  $\text{Na}^+$  severely inhibit the binding of at least some PNA's to dsDNA, presumably by stabilizing the double helix, which could reduce the probability for base pair opening. The triplex mechanism is also supported by the observation that so far strand displacement binding has only been observed with pyrimidine rich PNA's, *i.e.*, those that form (PNA)<sub>2</sub>/DNA triplexes, and not with those PNA's that only form PNA/DNA duplexes.

#### MOLECULAR BIOLOGY

Analogously to the triple helix forming oligonucleotides (28–30), binding of PNA to a dsDNA target interferes with the binding of proteins which also recognize this target. For instance, cleavage of DNA by restriction enzymes is inhibited if an occupied PNA binding site is present proximal to (31) or overlapping (32) the restriction enzyme recognition sequence.

Due to the high stability of the (PNA)<sub>2</sub>/DNA complexes transcription elongation by phage (33), *E. coli* (unpub-

lished), or human (32 and Vickers et al., manuscript in preparation) RNA polymerases is arrested at an occupied PNA binding site provided that the PNA is binding to the template strand. This is in contrast to oligonucleotide triple helix sites at which transcription elongation arrest is only efficient if the oligonucleotide is covalently bound (*e.g.* by psoralen photocrosslinking) to the DNA template (34–36). Alternatively, the triple helix may be targeted to the promoter (37,38).

The sensitivity of the displaced strand toward nuclease S1 can be exploited to target the S1 cleavage to double stranded DNA using PNA. In particular, when two neighboring PNA sites are present either on the same strand or even better on opposite strands, a PNA directed double strand DNA cleavage by S1 takes place and PNA may thus be used to target DNA restriction cleavage (39).

It should be emphasized that in all of the above cases, the PNA-dsDNA complexes were formed prior to the enzyme experiments since the ionic strength of the buffers required for enzyme action is not compatible with the low salt conditions necessary for the formation of the PNA strand displacement complexes. However, once formed in low salt, the salt concentration can be raised to at least 500 mM without disrupting the complexes studied so far (26, 31, 33 and unpublished results), *i.e.* the complexes are kinetically trapped.

#### ANTISENSE ACTIVITY

Although only very few results concerning the antisense action of PNA have been published, PNA appears to be a promising candidate for antisense drugs. Binding of PNA to ssRNA seems to parallel the binding to ssDNA except that the stability of PNA/RNA complexes is higher than that of PNA/DNA complexes (19).

*In vitro* translation experiments have shown that a truncated protein product corresponding to translational elongation arrest at the PNA binding site is produced with a 20-mer PNA (32). This is interesting since targeting by phosphodiester or phosphorothioate oligonucleotides to sites within the mRNA does not cause translational elongation arrest. Therefore, the target has to be positioned in a control region such as the ribosome binding site or the oligonucleotide/mRNA complex must be a substrate for RNase H. However, since the PNA used in this case contained 90% pyrimidines, it has the propensity of forming (PNA)<sub>2</sub>/RNA triplexes and this was not assayed. Thus, the PNA translational arrest may be a special property of triplex forming PNA's.

The same authors also performed cell-microinjection experiments showing that a PNA targeted to the mRNA for the large T-antigen in cells transformed with an SV40 vector could suppress the expression of this gene as measured by immunofluorescence microscopy (32). The necessity of employing microinjection is due to the apparent inability of the PNA's tested so far to efficiently enter cells.

#### ANTIGENE ACTIVITY

The ability of PNA to cause transcription elongation arrest imply a very interesting potential for PNA as gene targeted drugs at the dsDNA level, especially since oligonucleotide triplex formation is not able to arrest RNA polymerase unless the oligonucleotide is modified in a way that allows a covalent crosslink to the target to be formed (34–36). However, another aspect apart from the cell-uptake issue has to be considered before this may be reality. As mentioned earlier, strand displacement binding of PNA's T<sub>10</sub>, T<sub>4</sub>CT<sub>5</sub>, or T<sub>4</sub>CT<sub>2</sub>CT<sub>2</sub> to dsDNA is inhibited at

Na<sup>+</sup> concentrations above 50 mM (26, 31) and thus presumably also at physiological conditions in the cell nucleus (although this has not been investigated). Therefore, PNAs with the propensity of binding to dsDNA under *in vivo* conditions should be investigated.

## EVOLUTION

Fundamental questions concerning the evolution of the genetic material remain unanswered. For instance, was there a primordial genetic material different from DNA (or RNA), and if so, what was the structure, and why did nature settle on DNA as the universal genetic material? Studies on PNA may shed light on these questions (40).

The finding that at least in principle it is possible to store genetic information in molecules that do not have a phosphate sugar backbone (like DNA or RNA) but for instance a peptide backbone (like PNA) is a conceptual leap since the number of possible structures one may suggest for primordial genetic material has increased dramatically. Thus, novel avenues for exploration have been opened (40).

## PROSPECTS

It should be clear from the above presentation that the development of PNA and the investigation of its physicochemical and biological properties is only in its infancy and that much work is still required to assess if it will be able to bear fruit in terms of new gene targeted drugs and reagents and give new insight into the physical and biological properties of DNA and maybe even evolution.

## LITERATURE CITED

- Nielsen, P. E. (1991) Sequence selective DNA recognition by synthetic ligands. *Bioconjugate Chem.* 2, 1–12.
- Moser, H. E., and Dervan, P. B. (1987) Sequence-specific cleavage of double helical DNA by triple helix formation. *Science* 238, 645–650.
- Doan Le, T., Perrouault, L., Praseuth, D., Habhou, N., Decout, J. L., Thuong, N. T., Lhomme, J., and Helene, C. (1987) Sequence-specific recognition, photocrosslinking and cleavage of the DNA double helix by an oligo-[ $\alpha$ ]-thymidylate covalently linked to an azidoproflavine derivative. *Nucl. Acids Res.* 15, 7749–7760.
- Helène, C., and Toulmé, J.-J. (1990) Specific regulation of gene expression by antisense, sense, and antigene nucleic acids. *Biochim. Biophys. Acta*, 1049, 99–125.
- Crook, S. T. (1992) Oligonucleotide therapy. *Curr. Opin. Biotechnol.* 3, 656–661.
- Maher, L. J., Wold, B., and Dervan, P. B. (1991) Oligonucleotide-directed DNA triple-helix formation: an approach to artificial repressors? *Antisense Res. Dev.* 1, 277–81.
- Helene, C. (1993) Sequence-selective recognition and cleavage of double-helical DNA. *Curr. Opin. Biotechnol.* 4, 29–36.
- Beal, P. A., and Dervan, P. B. (1991) Second structural motif for recognition of DNA by oligonucleotide-directed triple-helix formation. *Science* 251, 1360–3.
- Griffin, L. C., and Dervan, P. B. (1989) Recognition of thymine adenine base pairs by guanine in a pyrimidine triple helix motif. *Science* 245, 967–71.
- Kiessling, L. L., Griffin, L. C., and Dervan, P. B. (1992) Flanking sequence effects within the pyrimidine triple-helix motif characterized by affinity cleaving. *Biochemistry* 31, 2829–34.
- Milligan, J. F., Krawczyk, S. H., Wadwani, S., and Matteucci, M. D. (1993) An anti-parallel triple helix motif with oligodeoxynucleotides containing 2'-deoxyguanosine and 7-deaza-2'-deoxyxanthosine. *Nucl. Acids Res.* 21, 327–33.
- Stilz, H. U., and Dervan, P. B. (1993) Specific recognition of CG base pairs by 2-deoxynucleoside within the purine-pyrimidine triple-helix motif. *Biochemistry* 32, 2177–85.
- Jayasena, S. D., and Johnston, B. H. (1992) Intramolecular triple-helix formation at (PunPyn).(PunPyn) tracts: recognition of alternate strands via Pu.PuPy and Py.PuPy base triplets. *Biochemistry* 31, 320–7.
- Nielsen, P. E., Egholm, M., Berg, R. H., and Buchardt, O. (1991) Sequence selective recognition of DNA by strand displacement with a thymine-substituted polyamide. *Science* 254, 1497–1500.
- Nielsen, P. E., Egholm, M., Berg, R. H., and Buchardt, O. (1993) Peptide Nucleic Acids (PNA). DNA analogues with a polyamide backbone. in "Antisense Research and Application" (Crook, S. and Lebleu, B. Eds.) pp 363–373, CRC Press, Boca Raton.
- Egholm, M., Buchardt, O., Nielsen, P. E., and Berg, R. H. (1992) Peptide nucleic acids (PNA). Oligonucleotide analogues with an achiral peptide backbone. *J. Am. Chem. Soc.* 114, 1895–1897.
- Egholm, M., Buchardt, O., Nielsen, P. E., and Berg, R. H. (1992). Recognition of guanine and adenine in DNA by cytosine and thymine containing peptide nucleic acids (PNA). *J. Am. Chem. Soc.* 114, 9677–9678.
- Egholm, M., Behrens, C., Christensen, L., Berg, R. H., Nielsen, P. E., and Buchardt, O. (1993) Peptide nucleic acids containing adenine or guanine recognize thymine and cytosine in complementary DNA sequences. *J. Chem. Soc., Chem. Commun.* 800–801.
- Egholm, M., Buchardt, O., Christensen, L., Behrens, C., Freier, S. M., Driver, D. A., Berg, R. H., Kim, S. K., Norden, B., and Nielsen, P. E. (1993) PNA Hybridizes to Complementary Oligonucleotides Obeying the Watson-Crick Hydrogen Bonding Rules. *Nature* 365, 566–568.
- Uhlmann, E., and Peyman, A. (1990) Antisense oligonucleotides: A new therapeutic principle. *Chem. Rev.* 90, 544–584.
- Jones, R. J., Lin, K.-Y., Milligan, J. F., Wadwani, S., and Matteucci, M. D. (1993) Synthesis and binding properties of pyrimidine oligonucleoside analogs containing neutral phosphodiester replacement: The formacetal and 3'-thioformacetal internucleoside linkages. *J. Org. Chem.* 58, 2983–2991.
- Huang, S.-B., Nelson, J. S., and Weller, D. D. (1991) Acyclic nucleic acid analogues: Synthesis and oligomerization of  $\gamma$ ,4-diamino-2-oxo-(2H)-pyrimidinepentanoic acid and  $\gamma$ ,4-diamino-2-oxo-(2H)-pyrimidinehexanoic acid. *J. Org. Chem.* 56, 6007–6018.
- Wada, T., Masumi, N., Mochizuki, E., Inaki, Y., and Takemoto, K. (1992) Synthesis and interaction studies of water-soluble nucleic acid analogs containing serine as a spacer. *Nucleic Acids Symp. Ser.* 27, 115–6.
- Kim, S. K., Nielsen, P. E., Egholm, M., Buchardt, O., Berg, R. H., and Norden, B. (1993) Right-handed triplex formed between peptide nucleic acid PNA-T<sub>3</sub> and poly(dA) shown by linear and circular dichroism spectroscopy. *J. Am. Chem. Soc.* (in press).
- Hyrup, B., Egholm, M., Rolland, M., Nielsen, P. E., Berg, R. H., and Buchardt, O. (1993) Modification of The Binding Affinity of Peptide Nucleic Acids (PNA). PNA with Extended Backbones Consisting of 2-Aminoethyl- $\beta$ -Alanine or 3-Aminopropylglycine Units. *J. Chem. Soc., Chem. Commun.* 518–519.
- Cherny, D. Y., Belotserkovskii, B. P., Frank-Kamenetskii, M. D., Egholm, M., Buchardt, O., Berg, R. H., and Nielsen, P. E. (1993) DNA unwinding upon strand displacement of binding of PNA to double stranded DNA. *Proc. Natl. Acad. Sci. U.S.A.* 90, 1667–1670.
- Nielsen, P. E., Egholm, M., and Buchardt, O. (1993) Evidence for (PNA)<sub>2</sub>/DNA Triplex Structure Upon Binding of PNA to dsDNA by Strand Displacement. *J. Mol. Recognit.* (in press).
- Francois, J. C., Saison-Beahouras, T., Thuong, N. T., and Helene, C. (1989) Inhibition of restriction endonuclease cleavage via triple helix formation by homopyrimidine oligonucleotides. *Biochemistry* 28, 9617–9.
- Hanvey, J. C., Shimizu, M., and Wells, R. D. (1990) Site-specific inhibition of EcoRI restriction/modification enzymes by a DNA triple helix. *Nucleic Acids Research* 18, 157–61.

- (30) Maher, L. J., Wold, B., and Dervan, P. B. (1989) Inhibition of DNA binding proteins by oligonucleotide-directed triple helix formation. *Science* 245, 725-30.
- (31) Nielsen, P. E., Egholm, M., Berg, R. H., and Buchardt, O. (1993) Sequence specific inhibition of restriction enzyme cleavage by PNA. *Nucleic Acids Res.* 21, 197-200.
- (32) Hanvey, J. C., Peffer, N. C., Bisi, J. E., Thomson, S. A., Cadilla, R., Josey, J. A., Ricca, D. J., Hassman, C. F., Bonham, M. A., Au, K. G., Carter, S. G., Bruckenstein D. A., Boyd, A. L., Noble S. A., and Babiss, L. E. (1992) Antisense and antigene properties of peptide nucleic acids. *Science* 258 1481-1485.
- (33) Nielsen, P. E., Egholm, M., Berg, R. H., and Buchardt, O. (1993) Peptide Nucleic Acids (PNA). Potential Antisense and Anti-gene Agents. *Anti Cancer Drug Design* 8, 53-63.
- (34) Duval-Valentin, G., Thuong, N., and Helene, C. (1992) Specific inhibition of transcription by triple helix-forming oligonucleotides. *Proc. Natl. Acad. Sci. U.S.A.* 89, 504-508.
- (35) Young, S. L., Krawczyk, S. H., Matteucci, M. D., and Toole, J. J. (1991) Triple helix formation inhibits transcription elongation in vitro. *Proc. Nat. Acad. Sci. U.S.A.* 88, 10023-6.
- (36) Grigoriev, M., Praseuth, D., Guieysse, A. L., Robin, P., Thuong, N. T., Helene, C., and Harel-Bellan, A. (1993) Inhibition of gene expression by triple helix-directed DNA cross-linking at specific sites. *Proc. Natl. Acad. Sci. U.S.A.* 90, 3501-5.
- (37) Grigoriev, M., Praseuth, D., Robin, P., Hemar, A., Saison-Behmoaras, T., Dautry-Varsat, A., Thuong, N. T., Helene, C., and Harel-Bellan, A. (1992) A triple helix-forming oligonucleotide-intercalator conjugate acts as a transcriptional repressor via inhibition of NF kappa B binding to interleukin-2 receptor alpha-regulatory sequence. *J. Biol. Chem.* 267, 3389-95.
- (38) Durland, R. H., Kessler, D. J., Gunnell, S., Duvic, M., Pettitt, B. M., and Hogan, M. E. (1991) Binding of triple helix forming oligonucleotides to sites in gene promoters. *Biochemistry* 30, 9246-55.
- (39) Demidov, V., Frank-Kamenetskii, M. D., Egholm, M., Buchardt, O., and Nielsen, P. E. (1993) Sequence selective double strand DNA cleavage by PNA targeting using nuclease S1. *Nucleic Acids Res.* 21 2103-2107.
- (40) Nielsen, P. E. (1993) Peptide Nucleic Acid (PNA): A model structure for the primordial genetic material. *Origins Life* (in press).

# ARTICLES

## Oligonucleotide-Poly(L-lysine)-Heparin Complexes: Potent Sequence-Specific Inhibitors of HIV-1 Infection

Geneviève Degols,\* Christian Devaux,<sup>†</sup> and Bernard Lebleu

Institut de Génétique Moléculaire Montpellier, CNRS-Université de Montpellier, 1919 route de Mende, BP 5051, 34033 Montpellier Cedex 01, France, and CRBM du CNRS, Centre de tri des molécules anti-HIV, Institut de Biologie, Université de Montpellier, Bd Henri IV, 34060 Montpellier Cedex, France. Received July 29, 1993\*

Poly(L-lysine)-conjugated oligonucleotides complementary to the translation initiation region of the tat protein were tested for their capacity to inhibit HIV-1 replication in *de novo* infected cells. Sequence-specific antiviral effects were observed with these conjugates at 0.5  $\mu$ M; their activity was transient, and the viral production was only delayed for a few days. Interestingly, their efficiency was significantly increased by the addition of heparin, a sulfated polyanion that also presents antiviral properties against HIV-1. A single addition, at the time of virus exposure, of the ternary complex formed between oligonucleotide-poly(L-lysine) (75 nM) and heparin (50  $\mu$ g/mL) totally protects cells from HIV-1 infection. Primary interference with virus adsorption is essential for the strong antiviral effect. However, this protection remains strictly sequence specific as demonstrated in experiments performed with different HIV-1 isolates. As comparison, treatments that combine AZT and heparin at the same concentrations did not promote such a complete protection.

### INTRODUCTION

The urgent need for chemotherapy of AIDS has directed considerable research interest toward effective anti-HIV agents.<sup>1</sup> A rational approach to inhibiting HIV-1 replication involves the use of antisense oligomers that can selectively bind to complementary sequences of viral RNA (Uhlmann and Peyman, 1990). Oligomers with various targets and backbone modifications inhibit HIV infection although with little sequence specificity in *de novo* infected cells (for review: Matsukura (1993)). Indeed, the most efficient is a (dC)<sub>28</sub> homopolymer with phosphorothioate internucleotidic linkages ( $EC_{50}$  = 0.5  $\mu$ M) (Matsukura et al., 1987). Letsinger et al. (1989) have modified the 3' end of oligomers complementary to the splice acceptor site of HIV-1 with a cholesteryl group. This modification increased the antiviral properties of oligomers ( $EC_{50}$  = 0.2  $\mu$ M for a 20-mer phosphorothioate derivative) but did not improve their sequence specificity. Recently, we have observed that PLL-conjugated oligomers complementary to the translation initiation region of the tat protein protect cells from the cytopathic effect of HIV-1 (Degols et al., 1992). The  $EC_{50}$  of these conjugates was around 0.15  $\mu$ M, which represents a significant improvement as compared to nonconjugated oligomers with a natural phosphodiester backbone ( $EC_{50}$  ranging from 20 to 50  $\mu$ M for various targets) (Goodchild et al., 1988). Interestingly, these PLL conjugates exhibit a sequence-specific antiviral effect in *de novo* infection assays. Unfortunately, a major drawback

of these PLL conjugates resides in their notable cytotoxicity against lymphoid cells. Previous work of Ryser and Shen (1978) has revealed that the cell growth inhibitory effect of methotrexate linked to PLL was markedly increased in the presence of heparin. This polyanion is known to form a very stable  $\alpha$  helix with PLL (Gelman and Blackwell, 1973). Enhanced biological effects of poly-(rI)-poly(rC) were also observed in ternary complexes with PLL and (carboxymethyl)cellulose (Levy and Quinn, 1985). Rettenmayer et al. (1986) even reported clinical trials of these complexes in the treatment of advanced ovarian cancer. Likewise, we have observed that the efficiency of PLL-conjugated oligomers was significantly increased when administered to cells in ternary complexes with polyanions such as heparin (Degols et al., 1991) and that this procedure reduced the toxicity of PLL (Morgan et al., 1988).

Sulfated polyanions like heparin are of great interest since they are also potential chemotherapeutic agents against AIDS (Baba et al., 1988a). The antiviral activity of these compounds primarily results from the inhibition of virus adsorption to the cell membrane ( $ED_{50}$  of heparin = 0.6  $\mu$ g/mL) (Baba et al., 1988b). In the same concentration range, effects on viral RNase H activity have also been observed (Moelling et al., 1989). Sulfated polyanions, but not heparin, have also been shown to prevent syncytia formation in infected cells (Baba et al., 1990).

In this paper, we have explored the potential of ternary oligomer-PLL-heparin complexes as inhibitors of HIV-1 replication. Strong cooperative effects between heparin and antisense oligomers were observed since the treated cells appeared to be completely protected from infection. Particular attention has been made to ascertain the sequence specificity of the antisense oligomer in the overall effect of these complexes.

\* To whom correspondence should be addressed. Telephone: 33-67-61-36-61; Fax: 33-67-04-02-45.

<sup>†</sup> Centre de tri des molécules anti-HIV.

\* Abstract published in *Advance ACS Abstracts*, December 15, 1993.

<sup>1</sup> Abbreviations: PLL, poly(L-lysine); RT, reverse transcriptase; AZT, azidothymidine; HIV-1, human immunodeficiency virus type 1;  $ED_{50}$ , 50% inhibition concentration;  $CD_{50}$ , % cytotoxic concentration.

## EXPERIMENTAL PROCEDURES

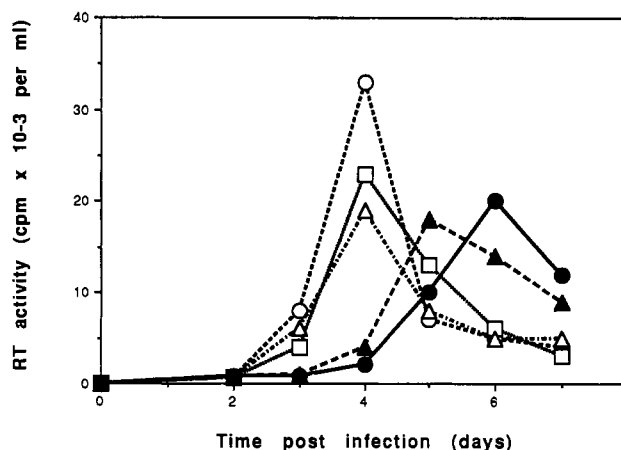
**Oligomer Synthesis and Covalent Linkage to PLL.** Tat BRU (5'-CTAGGATCTACTGGCTrA<sup>3'</sup>), tat random (5'-CATCGGAGTCTCGATCrA<sup>3'</sup>), and tat ELI (5'-TTAGGATCTACTGGATrA<sup>3'</sup>) oligomers were synthesized on a riboadenosine-derivatized support using a Biosearch Cyclone automatic DNA synthesizer and purified by reversed-phase chromatography. Covalent linkage to PLL through a *N*-morpholine ring was achieved by periodic acid oxidation and borocyanohydride reduction of the 3' end ribose, as previously described (Leonetti et al., 1988).

**Cell Culture and Virus Isolates.** MT4 cells (human T cell leukaemia virus type 1, transformed human leukaemic CD4<sup>+</sup> cell line) (Harada et al., 1985) were maintained at 37 °C/5% CO<sub>2</sub> in RPMI medium supplemented with 10% (v/v) fetal calf serum, 2 mM glutamine, 100 µg/mL of penicillin, and 100 µg/mL of streptomycin. HIV-1 BRU (Barré-Sinoussi et al., 1983) and HIV-1 ELI (Alizon et al., 1986) isolates (provided by Dr. L. Montagnier, Institut Pasteur) were propagated on CEM cells.

**Assay for HIV Inhibition.** MT4 cells were harvested in the exponential growth phase (3 × 10<sup>6</sup> cells/mL) and infected with an equal volume of virus containing medium (0.01 moi). Polyanions were already added at this time of the assay. After 30 min incubation at 4 °C, cells were washed three times with RPMI medium, diluted to 3 × 10<sup>5</sup> cells/mL, and incubated at 37 °C with PLL conjugates or oligomer-PLL-polyanion complexes. Samples were removed from the cultures at various time intervals to determine cell count, cell viability (trypan blue exclusion), syncytia formation, and reverse transcriptase (RT) activity (Rey et al., 1984). Each experiment was made in duplicate and repeated at least three times. A typical experiment is reported in Figures 1 and 2.

**Enzyme-Linked Immunosorbent Assay.** ELISA plates were coated overnight with 10 µg/mL of inactivated virus in sodium carbonate buffer, pH 9.6. Plates were washed and saturated with phosphate buffer saline (PBS) containing 1% (w/v) bovine serum albumin. One hundred µL of monoclonal antibody at the appropriate dilution (as defined by lack of reactivity with uninfected CEM cells) was added, and the plates were incubated for 1 h at room temperature. Bound immunoglobulins were detected as previously described (Robert-Hebmann et al., 1992b) by adding 100 µL of goat-anti-mouse IgG H+L peroxidase conjugate (Immunotech) at a 10<sup>3</sup>-fold dilution and *o*-phenylenediamine as a substrate. The anti-HIV core-protein-specific monoclonal antibodies (mAb) RL4-72-1, RL16-24-5, MO1-34-1, and MO9-42-2 used for these experiments have been described previously (Robert-Hebmann et al., 1992a). Briefly, mAb RL4-72-1 and RL16-24-5 were obtained from mice immunized with HIV-1 NDK; mAb MO1-34-1 and MO9-42-2 were produced from mice immunized with HIV-2 ROD. mAb RL16-24-5 reacts with an HIV-1 NDK p17 gag-strain specific epitope. mAb RL4-72-1 and MO1-34-1 react with different HIV subtype-specific markers. Finally, MO9-42-2 reacts with both HIV-1 and HIV-2 p25 gag epitopes.

**PCR Analysis of HIV-1 DNA in Infected Cells.** Total HIV-1 DNA production was evaluated by PCR, according to the following procedure. A total of 5 × 10<sup>5</sup> cells was washed four times in PBS. After centrifugation the pellet was resuspended in 50 µL of H<sub>2</sub>O and heated for 5 min at 95 °C. To this suspension was added an equal volume of the amplification mixture: 20 mM Tris-HCl, pH 8.3, containing 120 mM dNTPs, 1.5 mM MgCl<sub>2</sub>, 50 mM KCl, 0.005% Tween 20, 0.005% NP40, 0.001% gelatin, 20 ng of each of the oligomer primers (5'-CGTTTCAGAC-



**Figure 1.** Time course of HIV production in cells treated with oligomer-PLL conjugates. Oligomer-PLL conjugates or free PLL were inoculated at 0.5 µM and tat BRU oligomer at 40 µM. HIV-1 BRU expression was followed by measuring RT activity at indicated times after infection: untreated cells, ○; cells treated with PLL, □; cells treated with tat BRU oligomer, ▲; cells treated with tat random oligomer-PLL conjugate, △; cells treated with tat BRU oligomer-PLL conjugate, ●.

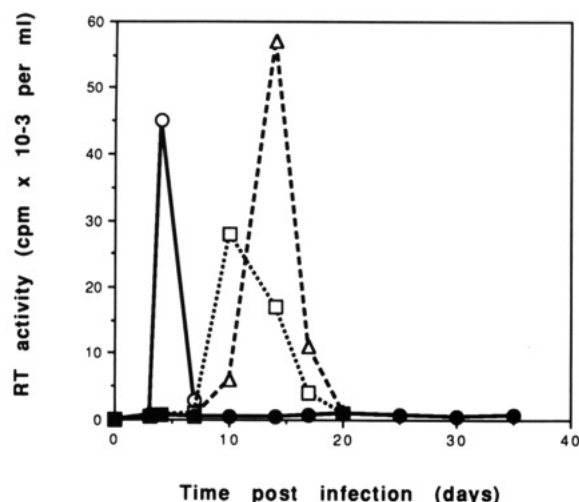
CCACCTCCCAATCCC3', nucleotides 7947-7981 sense and 5'-GGGTTTTCTTTTAAAAAGTGGCTAAGATC3', nucleotides 8628-8656 antisense), and 2 units of Taq DNA polymerase. The mixture was submitted to a first denaturation cycle for 5 min (92 °C) followed by primer hybridization for 3 min (53 °C) and polymerization for 3 min (72 °C) in a thermal cycler. Thirty additional cycles were performed in the following conditions: 7 s/92 °C denaturation, 30 s/53 °C hybridization, 3 min/72 °C polymerization (15 min for the last cycle). To control the reaction, a *c-myc* fragment was amplified in the same reaction mixture with primer oligomers 5'-CGAGTTA-GATAAAGCCCCGAAAACC3' (417-436) and 5'-TCCCTG-GTCCCCCTCCTGC3' (513-537). The amplified products (the 709 base pairs HIV fragment and the 120 base pairs *c-myc* fragment) were analyzed by electrophoresis through a 1.5% (w/v) agarose gel.

## RESULTS

**Transient Inhibition of HIV Multiplication with Oligomer-PLL Conjugates.** Several studies have demonstrated that oligomers complementary to the translation initiation region of tat protein mRNA are good inhibitors of HIV in *de novo* infection systems (Zamecnik et al., 1986). Accordingly, the 16-mer tat BRU oligomer (see Experimental Procedures for sequence) conjugated to PLL promotes a strong sequence-specific antiviral effect: more than 90% inhibition of RT activity was observed 4 days after infection with a single addition of oligomer-PLL at 0.5 µM (Degols et al., 1992).

Despite a strong initial reduction in virus production, tat BRU oligomer-PLL conjugates only delay virus multiplication by a few days (Figure 1). Likewise, protection against the viral cytopathic effect in the oligomer-PLL-treated cells was only transient (data not shown). Temporary antiviral effects were also observed with single additions of nonconjugated tat BRU oligomer (Figure 1). In this case, however, the antiviral activity required much larger concentrations of antisense oligomers; moreover, no sequence-specific effect is observed in these conditions (Degols et al., 1992).

The transient activity of PLL conjugates was not due to the emergence of a variant virus population escaping recognition by antisense oligomers. Indeed, the viral

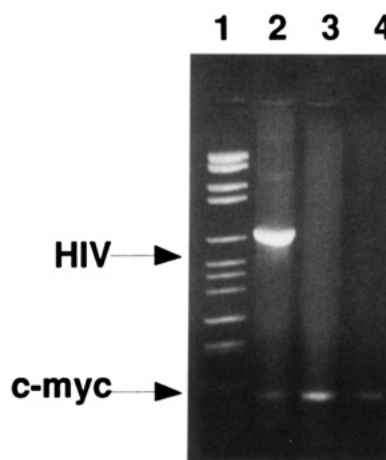


**Figure 2.** Protection of MT4 cells against HIV-1 multiplication by oligomer-PLL-heparin ternary complexes. Cells were incubated with heparin (50  $\mu\text{g/mL}$ ) and 0.5  $\mu\text{M}$  oligomer-PLL during virus adsorption. A second addition of ternary complex was made after cells were washed and transferred to 37  $^{\circ}\text{C}$ . RT activity was measured in the supernatant of the cultures at the indicated times: untreated cells,  $\circ$ ; cells treated with heparin,  $\square$ ; cells treated with heparin and random oligomer-PLL conjugate,  $\Delta$ ; cells treated with heparin and tat BRU oligomer-PLL conjugate,  $\bullet$ .

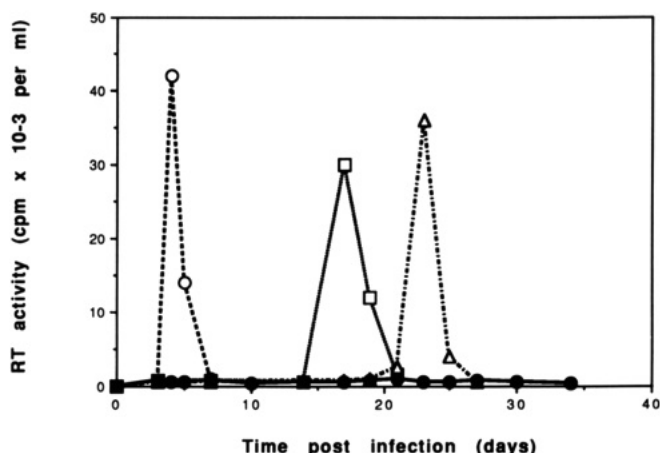
population isolated from cells treated with oligomer-PLL conjugates after 6 days was found to be as sensitive as the initial viral population when MT4 cells were reinfected with these viruses in the presence of oligomer-PLL conjugates (data not shown). We have observed the same phenomenon with nonconjugated phosphodiester oligomers and phosphorothioate analogs (data not shown).

**Antiviral Activity of Oligomer-PLL Conjugates Is Enhanced by Sulfated Polyanions.** The short life of the antiviral effects of PLL-conjugated or nonconjugated oligomers might be a major drawback to their use. Recently, we have observed that the efficiency of oligomer-PLL conjugates as antisense inhibitors of gene expression was significantly increased by the addition of polyanionic substances such as heparin (Degols et al., 1991). Since this sulfated polyanion also presents antiviral properties against HIV-1 (Baba et al., 1988a), we evaluated the efficiency of ternary complexes between oligomer-PLL conjugates and heparin on HIV-1 infected cells. Dose-dependent studies have demonstrated that the final concentration of heparin has to be higher than 20  $\mu\text{g/mL}$  to improve the efficiency of oligomer-PLL conjugates in infected cells (data not shown). This concentration is much higher than its  $\text{ED}_{50}$  against HIV-1 ( $\text{ED}_{50} = 0.6 \mu\text{g/mL}$ ) (Baba et al., 1988b).

For the antiviral assays, ternary complexes were added to the cells during virus adsorption at 4  $^{\circ}\text{C}$ ; a second addition was made immediately after cell transfer to 37  $^{\circ}\text{C}$  (see Experimental Procedures for infection protocol). The cells were then diluted every 4 days without any further addition of ternary complexes. Under these conditions, a very strong antiviral effect was observed. No RT activity could be detected in the supernatants of infected cells treated with the tat BRU oligomer ternary complex for as long as 2 months while heparin alone or tat BRU oligomer-PLL conjugate only delayed HIV production (Figure 2). A ternary complex composed of heparin and an unrelated random oligomer-PLL conjugate behaved like heparin alone in keeping with a sequence-specific effect of these complexes (Figure 2). The HIV infection of cells treated with ternary complexes was also



**Figure 3.** PCR amplification of HIV DNA in cells treated with ternary complexes. A 709 bp fragment of HIV DNA and a 120 bp fragment of *c-myc* oncogene were coamplified by PCR (see Experimental Procedures) in cell lysates: 1, DNA molecular weight marker VI; 2, lysate of control cells 4 days after infection; 3, lysate of uninfected cells; 4, lysate of cells treated with tat BRU oligomer-PLL (0.5  $\mu\text{M}$ ) and heparin (50  $\mu\text{g/mL}$ ) 30 days after infection.



**Figure 4.** Comparison of the antiviral activity of ternary complexes with AZT or with AZT and heparin. Cells were incubated with heparin (50  $\mu\text{g/mL}$ ) and oligomer-PLL conjugates (0.5  $\mu\text{M}$ ) or with AZT (0.5  $\mu\text{M}$ ) and heparin during virus adsorption; a second addition was made after transferring cells to 37  $^{\circ}\text{C}$ . Reverse transcriptase activities were measured at the indicated times: untreated cells,  $\circ$ ; cells treated with heparin and tat BRU oligomer-PLL conjugate,  $\bullet$ ; cells treated with AZT,  $\square$ ; cells treated with AZT and heparin,  $\Delta$ .

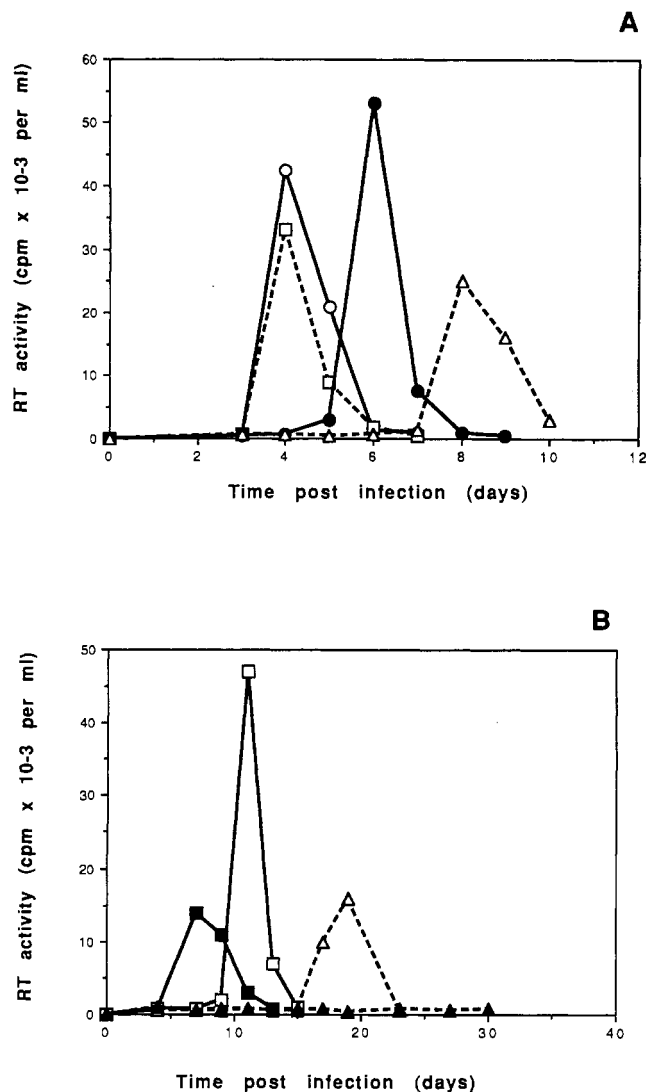
followed by PCR. This analysis revealed the absence of HIV DNA even 1 month after infection (Figure 3). A complete suppression of virus production by these ternary complexes was observed at concentrations at tat BRU oligomer as low as 75 nM (data not shown).

As a comparison, these tat BRU oligomer-PLL-heparin complexes inhibited HIV-1 multiplication more strongly than AZT (0.5  $\mu\text{M}$ ) or a combination of AZT (0.5  $\mu\text{M}$ ) and heparin (50  $\mu\text{g/mL}$ ) (Figure 4).

As expected, the toxicity of PLL on lymphoid cells is reduced in these complexes. The cytotoxic dose of PLL is increased 20-fold in the presence of 50  $\mu\text{g/mL}$  of heparin ( $\text{CD}_{50} = 15 \mu\text{M}$ ) (data not shown), so that ternary complexes exhibit a therapeutic index higher than 200.

**Approaches to the Mechanism of Action of Oligomer-PLL-Heparin Ternary Complexes.** We tried to evaluate which part of the strong antiviral effect observed with these ternary complexes could be attributed to the oligomer-PLL conjugate or to the sulfated polyanion. We





**Figure 5.** Mechanisms of the antiviral activity of ternary complexes. A. Sequence-specific antisense activity: cells were incubated with poly(L-glutamine) (50  $\mu$ g/mL) and PLL conjugates (0.5  $\mu$ M) as described in Figure 4. Reverse transcriptase activities were measured at the indicated times: untreated cells, O; cells treated with tat BRU oligomer-PLL conjugate, ●; cells treated with poly(L-glutamine), □; cells treated with poly(L-glutamine) and tat BRU oligomer-PLL conjugate, Δ. B. Antiviral activity of heparin: cells were incubated with heparin (50  $\mu$ g/mL) and oligomer-PLL conjugates (0.5  $\mu$ M) either throughout the infection procedure (heparin, □; tat BRU oligomer-PLL conjugate + heparin, Δ) or only after cell transfer at 37 °C (heparin, ■; tat BRU oligomer-PLL conjugate and heparin, ▲). Reverse transcriptase activities were measured at the indicated times.

have previously observed that nonsulfated polyanions, such as poly(L-glutamine), also enhanced the antisense-mediated biological activity of oligomer-PLL-conjugates in experiments targeting the *c-myc* oncogene (Degols et al., 1991). Poly(L-glutamine) did not have any intrinsic antiviral effect as verified in Figure 5a. Only a slight increase in the efficiency of the PLL conjugate was observed with poly(L-glutamine) at 50  $\mu$ g/mL: it delayed the appearance of RT activity for only 2 days more than oligomer-PLL conjugate alone (Figure 5a).

Heparin has been shown to inhibit viral infection at the stage of HIV-1 adsorption to cells (Baba et al., 1988b). However, in the concentration range we used, sulfated polyanions also inhibit RNase H activity (Moelling et al., 1989). We observed that a single addition of ternary complexes after the cells were transferred to 37 °C strongly

**Table 1.** Characterization of the Virions Produced in Dually Infected Cells Treated with Ternary Complexes<sup>a</sup>

HIV-1 isolates used for cell infection	oligomer <sup>b</sup>	antibody			
		MO1.34	RL4.72	MO9.42	RL16.24
BRU	—	—	+	+	—
ELI	—	+	—	+	—
BRU + ELI	—	+	+	+	—
BRU + ELI	tat BRU + tat ELI	—	—	—	—
BRU + ELI	tat BRU	+	+	+	—
BRU + ELI	tat ELI	+	+	+	—

<sup>a</sup> The nature of the virions produced was determined at the day of maximal RT activity by ELISA assay as described in the Experimental Procedures. The results are expressed with respect to the mean value of absorbance intensity at 492 nm for three independent experiments: + refers to an ELISA positive reaction (absorbance higher than 0.5) and — refers to an ELISA negative reaction (absorbance lower than 0.5). MO1.34 reacts with ELI isolate, RL4.72 reacts with BRU isolate, MO9.42 reacts with both isolates, and RL16.24 presents no reactivity with BRU or ELI isolates. <sup>b</sup> Oligomer in the ternary complex formed with PLL and heparin.

delayed HIV multiplication but did not allow complete protection against HIV infection (Figure 5b), in keeping with a heparin-mediated effect on viral adsorption.

**Sequence Specificity of the Activity of the Oligomer-PLL-Heparin Ternary Complexes.** Although the antiviral effect of ternary complexes can be attributed in part to heparin, protection against HIV infection also depends on the sequence of the oligomer (see Figure 2). We have previously used HIV-1 isolates differing in their sequence at the oligomer target site to evaluate the sequence specificity of oligomer-PLL conjugates (Degols et al., 1992). For instance, HIV-1 BRU and HIV-1 ELI differ by only two nucleotides at the tat mRNA translation initiation target site. Ternary complexes directed to the HIV-1 BRU or to the HIV-1 ELI were tested in cells infected with each of these isolates. Complete inhibition of virus multiplication was only observed with the oligomer that perfectly hybridized the targeted sequence (data not shown), an observation that agrees with our previously reported data using oligomer-PLL conjugates (Degols et al., 1992).

Antiviral assays were performed with cells infected simultaneously with the two HIV-1 isolates. Anti-HIV core protein-specific monoclonal antibodies that discriminate between HIV-1 BRU and HIV-1 ELI were used for this study. Cells infected with both isolates were totally protected from infection if they were treated with ternary complexes containing both tat ELI and tat BRU oligomer-PLL conjugates at 0.5  $\mu$ M (Table 1). We then investigated the behavior of cells infected with both isolates and treated with ternary complexes containing only one of the two antisense oligomers. If oligomers act specifically on tat mRNA expression it is expected that the tat protein produced by one isolate would rescue transcription from the other isolate. On the contrary, if oligomers act nonspecifically on HIV genome expression or inhibit the first stages of infection (e.g., reverse transcription or virus adsorption), no complementation is expected. Experimental data (Table 1) demonstrated that in cells treated with tat BRU or with tat ELI oligomers the progeny virions had characteristics of both HIV-1 BRU and ELI, whereas cells treated with both oligomers did not produce any virus.

## DISCUSSION

We have attempted here to enhance the antiviral properties of antisense oligomers and to improve their specificity in *de novo* infected cells. Indeed, phospho-

diester oligomers, oligomer analogs, or PLL-conjugated oligomers only promote transient antiviral effects on HIV infection. The transience of these effects has rarely been discussed in the literature, since the antiviral effects of oligomers were generally measured at a single time point post infection. This point has been documented recently by Lisiewicz et al. (1992). They observed that *de novo* infected cells treated every 3 or 4 days with phosphorothioate oligomers directed against the gag gene or rev regulatory protein were totally protected from HIV multiplication for several weeks. However, HIV-1 production would resume rapidly after cessation of the treatment. As documented here, cells treated with oligomer-PLL conjugates specific to the tat protein mRNA were only protected from HIV cytopathic effects for 2 days. The appearance of RT activity in the supernatant of treated cells was delayed for the same time and decreased rapidly as infected cells died. This is reminiscent of previous work by Rhodes and James (1990) who observed a transient inhibition of HIV infection in transfected cells constitutively expressing antisense RNAs. As it was also demonstrated in our case, transience did not result from mutations of the input virus. As suggested by the authors, a complete extinction of virus production might be difficult to achieve since HIV tat mRNA escaping from antisense inhibition will further stimulate regulatory protein synthesis. Alternative strategies attempting to target more than a single event in virus multiplication were therefore worth considering.

In this respect, we have described in this study that the addition of heparin with oligomer-PLL conjugates considerably enhanced their antiviral activity. Cells were totally protected from infection using oligomer concentrations in the complex as low as 75 nM. Interestingly, treatments that combined AZT and heparin at the same concentration did not promote such a strong protection. A part of this antiviral activity results from an enhancement of the antisense effect as previously described for polyanion ternary complexes directed to the *c-myc* mRNA (Degols et al., 1991). However, attempts to inhibit HIV infection with nonsulfated polyanions revealed only a slight increment in the antisense activity of oligomer-PLL conjugates. The anti HIV-1 activity of these ternary complex thus results to an appreciable extent from the antiviral properties of heparin itself. Indeed, as it was already shown for ternary complexes directed to the *c-myc* mRNA (Degols et al., 1991), high amounts of heparin (50  $\mu$ g/mL) are needed to improve the antisense properties of oligomer-PLL conjugates. At this concentration, heparin interferes with virus adsorption and can also inhibit RNase H activity (Baba et al., 1988b; Moelling et al., 1989). Our experiments demonstrate that primary interference with virus adsorption is essential for the strong antiviral effect of the ternary complexes to be achieved. Indeed, a single addition of ternary complexes before HIV-exposed cells were transferred to 37 °C strongly delayed virus multiplication but did not fully protect cells against infection. Most likely, cooperative effects between heparin and oligomer-PLL conjugates do occur.

In the overall antiviral effect of these complexes, the part due to the antisense oligomer remains sequence specific. Experiments performed with HIV isolates presenting sequence variability demonstrated that only two mismatches in the target site were responsible for a significant reduction of the antisense contribution to the antiviral effect of the complexes.

An interesting observation came from experiments in which cells were infected simultaneously with two HIV-1

isolates. These cells were totally protected from infection when treated with complexes containing oligomers specific of each isolate. However, if these cells were treated with oligomer complexes targeted only at one of these isolates, pseudotype virions presenting characteristics of the two isolates were recovered in the cell culture supernatant, as demonstrated by ELISA assays. The isolate which is not sensitive to the antisense oligomers treatment apparently complemented transcriptional defects of the other isolate by an unknown mechanism. Indeed, HIV-1 isolates cross interfere with each other so that HIV-1 producing cells cannot be superinfected by other HIV-1 isolates (Hard & Cloyd, 1990). However, Haseltine and co-workers (Helland et al., 1991) observed that the tat protein produced in one cell could activate HIV-1 promoter-directed gene expression in adjacent cells. This indirectly provides information on the mechanism of action of the tat oligomers in this model. It is in line with a primary action of anti tat oligomer on the expression of this regulatory protein.

Major advances have been made in cancer chemotherapy by combining agents that are active on cell proliferation through different mechanisms. Similar strategies have already been attempted to protect cells against HIV infections. For instance, treatments combining  $\alpha$ -interferon and zidovudine have been tested both in vitro against HIV infected cells (Hartshorn et al., 1987) and in AIDS patients (Edlin et al., 1992). The potential of combined therapies is confirmed by our results. However, a major problem related to the anticoagulant activity of heparin remains if they are to be used in AIDS patients. Other sulfated polyanions with weaker anticoagulant activity should be tested in ternary complexes with oligomers in order to design complexes suitable for patient treatment. As the persistence of viral reservoirs is implicated in the progression of HIV infection, we also intend to further evaluate the potential of ternary complexes in chronically infected cells.

#### ACKNOWLEDGMENT

We wish to thank Prof. L. Montagnier (Institut Pasteur, Paris, France) for his kind gift of HIV-1 isolates. We are grateful to Claudine David and Véronique Robert-Hebmann (CRBM, Montpellier, France) for maintenance of viral stocks and monoclonal antibodies production, respectively. This work has been supported by research grants of the Centre National de la Recherche Scientifique, the Agence Nationale pour la Recherche contre le Sida, and GENSET to B.L.

#### LITERATURE CITED

- Alizon, M., Wain-Hobson, S., Montagnier, L., and Sonigo, P. (1986) Genetic variability of the AIDS virus: Nucleotide sequence analysis of two isolates from African Patients. *Cell* 46, 63-74.
- Baba, M., Nakajima, M., Schols, D., Pauwels, R., Balzarini, J., and De Clercq, E. (1988a) Pentosan polysulfate, a sulfated oligosaccharide, is a potent and selective anti-HIV agent in vitro. *Antiviral Res.* 9, 335-343.
- Baba, M., Pauwels, R., Balzarini, J., Arnout, J., Desmyter, J., and De Clercq, E. (1988b) Mechanism of inhibitory effect of dextran sulfate and heparin on replication of human immunodeficiency virus. *Proc. Natl. Acad. Sci. U.S.A.* 85, 6132-6136.
- Baba, M., Schols, D., Pauwels, R., Nakashima, N., and De Clercq, E. (1990) Sulfated Polysaccharides as Potent Inhibitors of HIV-Induced Syncytium Formation: A new Strategy Towards AIDS Chemotherapy. *J. Acq. Immun. Def. Synd.* 3, 493-499.
- Barré-Sinoussi, F., Chermann, J. C., Rey, F., Ngyere, M. T., Chamaret, S., Gruest, J., Dauguet, C., Axler-Blin, C., Brun-



- Vezinet, F., Rouzioux, C., Rosenbaum, W., and Montagnier, L. (1983) Isolation of a T-lymphotropic retrovirus from a patient at risk for acquired immunodeficiency syndrome (AIDS). *Science* 220, 868-871.
- Degols, G., Leonetti, J. P., Mechti, N., and Lebleu, B. (1991) Antiproliferative effects of antisense oligonucleotides directed to the RNA of c-myc oncogene. *Nucleic Acids Res.* 19, 945-948.
- Degols, G., Leonetti, J. P., Benkirane, M., Devaux, C., and Lebleu, B. (1992) Poly(L-Lysine)-conjugated oligonucleotides promote sequence-specific inhibition of acute HIV-1 infection. *Antisense Res. Dev.* 2, 293-301.
- Edlin, B. R., Weinstein, R. A., Whaling, S. M., Ou, C. Y., Connolly, P. J., Moore, J. L., and Bitran, J. D. (1992) Zidovudine-Interferon- $\alpha$  combination therapy in patients with advanced human immunodeficiency virus type 1 infection: biphasic response of p24 antigen and quantitative polymerase chain reaction. *J. Infect. Dis.* 165, 793-798.
- Gelman, R. A., and Blackwell, J. (1973) Heparin-polypeptide interactions in aqueous solution. *Arch. Biochem. Biophys.* 159, 427-433.
- Goodchild, J., Agrawal, S., Civeira, M. P., Sarin, P. S., Sun, D., and Zamecnik, P. C. (1988) Inhibition of human immunodeficiency virus replication by antisense oligodeoxynucleotides. *Proc. Natl. Acad. Sci. U.S.A.* 85, 5507-5511.
- Harada, S., Koyanagi, Y., and Yamamoto, N. (1985) Infection of HTLVIII/LAV in HTLVI carrying cells MT2 and MT4 and application in a plaque assay. *Science* 229, 563-566.
- Hart, A. R., and Cloyd, M. W. (1990) Interference patterns of human immunodeficiency viruses HIV-1 and HIV-2. *Virology* 177, 1-10.
- Hartshorn, K. L., Vogt, M. W., and Chou, T. C. (1987) Synergistic inhibition of human immunodeficiency virus in vitro by azidothymidine and recombinant alpha A interferon. *Antimicrob. Agents Chemother.* 31, 168-172.
- Helland, D. E., Welles, J. L., Caputo, A., and Haseltine, W. A. (1991) Transcellular transactivation by the human immunodeficiency virus type 1 tat protein. *J. Virol.* 65, 4547-4549.
- Leonetti, J. P., Rayner, B., Lemaitre, M., Gagnor, C., Milhaud, P., Imbach, J. L., and Lebleu, B. (1988) Antiviral activity of conjugates between poly(L-lysine) and synthetic oligodeoxyribonucleotides. *Gene* 72, 323-332.
- Letsinger, R. L., Zhang, G., Sun, D. K., Ikeuchi, T. and Sarin, P. S. (1989) Cholesteryl-conjugated oligonucleotides: synthesis, properties, and activity as inhibitors of replication of human immunodeficiency virus in cell culture. *Proc. Natl. Acad. Sci. U.S.A.* 86, 6553-6556.
- Levy, H. B., and Quinn, T. (1985) in *Bioactive Polymeric Systems* (C.G. Gebelin, and C.E. Caraher, Jr., Eds.) pp 387-415, Plenum Press: New York.
- Liszewicz, J., Sun, D., Klotman, M., Agrawal, S., Zamecnik, P., and Gallo, R. (1992) Specific inhibition of human immunodeficiency virus type 1 replication by antisense oligonucleotides: an in vitro model for treatment. *Proc. Natl. Acad. Sci. U.S.A.* 89, 11209-11213.
- Matsukura, M., Shinozuka, K., Zon, G., Mitsuya, H., Reitz, M., Cohen, S., and Broder, S. (1987) Phosphorothioate analogs of oligodeoxynucleotides: inhibitors of replication and cytopathic effects of human immunodeficiency virus. *Proc. Natl. Acad. Sci. U.S.A.* 84, 7706-7710.
- Matsukura, M. (1993) Antiviral activity of antisense oligonucleotides against human immunodeficiency virus (HIV). In *Antisense Research and Application* (S. T. Crooke, and B. Lebleu, Eds.) pp 505-520, CRC Press, Boca Raton.
- Moelling, K., Schulze, T., and Diringer, H. (1989) Inhibition of human immunodeficiency virus type 1 RNase H by sulfated polyanions. *J. Virol.* 63, 5489-5491.
- Morgan, D. M. L., Clover, J., and Pearson, J. D. (1988) Effects of synthetic polycations on leucine incorporation, lactate dehydrogenase release and morphology of human umbilical vein endothelial cells. *J. Cell. Sci.* 91, 231-238.
- Rettenmayer, M. A., Berman, M. L., and Di Saia, P. J. (1986) Treatment of advanced ovarian cancer with polyinosinic-polycytidilic lysine carboxymethylcellulose (poly(ICLC)). *Gynecol. Oncol.* 24, 359-361.
- Rey, M. A., Spire, B., Dormont, D., Barré-Sinoussi, F., Montagnier, L., and Chermann, J. C. (1984) Characterization of the RNA dependent DNA polymerase of a new human T-lymphotropic retrovirus (LAV). *Bioch. Biophys. Res. Commun.* 121, 126-133.
- Rhodes, A., and James, W. (1990) Inhibition of human immunodeficiency virus replication in cell culture by endogenously synthesized antisense RNA. *J. Gen. Virol.* 71, 1964-1974.
- Robert-Hebmann, V., Emiliani, S., Jean, F., Resnicoff, M., Traincard, F., and Devaux, C. (1992a) Clonal analysis of murine B-cell response to the human immunodeficiency virus type 1 (HIV1)-gag p17 and p25 antigens. *Mol. Immunol.* 29, 729-738.
- Robert-Hebmann, V., Emiliani, S., Resnicoff, M., Jean, F., and Devaux, C. (1992b) Subtyping of human immunodeficiency virus isolates with a panel of monoclonal antibodies: identification of conserved and divergent epitopes on p17 and p25 core proteins. *Mol. Immunol.* 29, 1175-1183.
- Ryser, J. P., and Shen, W. S. (1978) Conjugation of methotrexate to poly(L-lysine) increases drug transport and overcomes drug resistance in cultured cells. *Proc. Natl. Acad. Sci. U.S.A.* 75, 3867-3870.
- Uhlmann, E., and Peyman, A. (1990) Antisense oligonucleotides: A new therapeutic principle. *Chem. Rev.* 90, 544-584.
- Zamecnik, P. C., Goodchild, J., Taguchi, Y. and Sarin, P. S. (1986) Inhibition of replication and expression of human T-cell lymphotropic virus type III in cultured cells by exogenous synthetic oligonucleotides complementary to viral RNA. *Proc. Natl. Acad. Sci. U.S.A.* 83, 4143-4146.

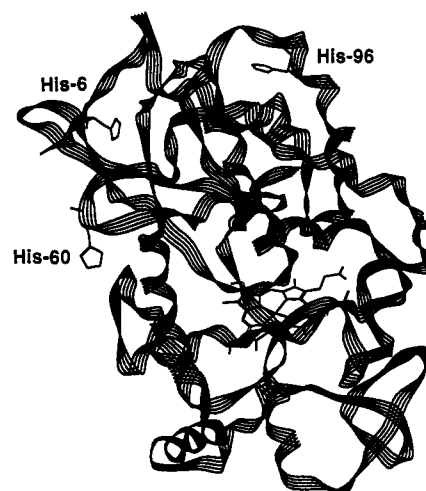
## Derivatization of Yeast Cytochrome c Peroxidase with Pentaammineruthenium(III)<sup>†</sup>

Ted Fox,<sup>‡</sup> Ann M. English,\* and Bernard F. Gibbs<sup>§</sup>

Department of Chemistry and Biochemistry, Concordia University, 1455 de Maisonneuve Boulevard West, Montreal, Québec, Canada H3G 1M8. Received April 27, 1993<sup>¶</sup>

Cytochrome c peroxidase (CCP) was derivatized using aquopentaammineruthenium(II) [ $a_5Ru^{II}H_2O$ ] resulting in stable, covalently-linked derivatives that were purified by cation-exchange FPLC. Spectrophotometric determination of  $a_5RuHis$ :heme ratios allowed identification of two derivatives containing one  $a_5RuHis$  per CCP molecule. The histidine-specific reagent, diethyl pyrocarbonate (DEPC), which reacted with three histidine residues in native CCP (6, 60, 96) at pH 7, reacted with only two histidines in both  $a_5RuHis$ CCP species. X-ray crystallography showed that  $a_5Ru$  is coordinated to His60 in one derivative [Fox et al. (1990) *J. Am. Chem. Soc.* 112, 7426]; HPLC and mass spectral analysis of the tryptic peptides of the other derivative identified a peptide (MW = 1469 Da) corresponding to residues 1-12 of CCP plus  $a_5Ru$ , indicating His6 as the site of modification. Mass spectral analysis of native CCP,  $a_5RuHis60$ CCP, and the  $a_5RuHis6$  derivative yielded MWs of 33 536, 33 717, and 33 901 Da, respectively, revealing that a second site is ruthenated in the His6 derivative. Mass spectral analysis of a shoulder separated from the  $a_5RuHis60$ CCP FPLC peak also indicated the presence of CCP with bound  $a_5Ru$  (MW = 33 718 Da). Differential pulse voltammetry of this shoulder, which has negligible  $a_5RuHis$  absorption, gave a peak at -68 mV (vs NHE) which is in the range expected for reduction of  $a_5Ru^{III}(\text{carboxylato})$  complexes, as well as a peak at 42 mV due to the presence of ~20%  $a_5RuHis60$ CCP. The extent of ruthenation at sites other than histidine was unexpected and illustrates that  $a_5Ru^{II}H_2O$  is less specific for histidine than previously thought. Activity measurements and stability of enzyme intermediates were measured to further characterize the  $a_5Ru$ CCP species and showed that the derivatives have similar properties to native CCP.

Cytochrome c peroxidase (CCP),<sup>1</sup> which catalyzes the oxidation of ferrocyanochrome c by hydrogen peroxide, has a single protoporphyrin IX heme noncovalently-bound to a polypeptide of 294 residues (Bosshard et al., 1991). Figure 1 shows a computer graphics display of the  $C_\alpha$  backbone of CCP indicating the location of the heme and the surface-exposed histidines (6, 60, 96) that are the most likely candidates for modification by histidine-specific reagents. Of the three remaining histidines, His181 has a raised  $pK_a$  of ~8 due to hydrogen bonding with both heme propionate-7 and Asp37; His175 coordinates the heme  $Fe^{III}$ , and His52 is buried in the distal pocket (Poulos & Finzel, 1984). Diethyl pyrocarbonate (DEPC) reacts specifically with histidine residues and has proven to be a useful probe of protein structure and function (Miles, 1977) and of the number of modifiable histidines (Jackman et al., 1988a). A previous study of DEPC modification of CCP (Bosshard



**Figure 1.** Surface histidine residues and the heme of CCP superimposed on the  $C_\alpha$  backbone generated from the X-ray structure of CCP (Finzel et al., 1984) using Sybyl software version 5.5 (Tripos Associates, Inc., St Louis, MI).

et al., 1984) showed that His6, -60, and -96 are readily modified at pH 7, as expected. At pH 8, His52 and -181 also react with DEPC, presumably because the hydrogen-bonding network involving His181 is broken and access to the heme cavity is increased. Only His175 remains unmodified since its N(3) atom is coordinated to the heme  $Fe^{III}$  (Bosshard et al., 1984).

The *N*-carbethoxyhistidine derivatives formed upon reaction with DEPC are unstable to hydrolysis and cannot be isolated. Aquopentaammineruthenium(II) ( $a_5Ru^{II}H_2O$ ) is another reagent used extensively for histidine derivatization. Following oxidation of  $Ru^{II}$  to  $Ru^{III}$ , the resultant  $a_5RuHis$ -protein complexes are stable, and such complexes

<sup>†</sup> This research was supported by a grant from NSERC (Canada) to A.M.E.

\* Author to whom correspondence should be addressed.

<sup>‡</sup> Present address: Vertex Pharmaceuticals Inc., 40 Allston Street, Cambridge, MA 02139.

<sup>§</sup> Address: Biotechnology Research Institute, 6100 Royalmount, Montreal, Canada H4P 2R2.

<sup>¶</sup> Abstract published in *Advance ACS Abstracts*, November 15, 1993.

<sup>1</sup> Abbreviations: AP-ESI MS, atmospheric pressure electrospray ionization mass spectrometry;  $a_5Ru$ , pentaammineruthenium(III) with  $a = NH_3$ ;  $a_5Ru^{II}$ , pentaammineruthenium(II); CCP, cytochrome c peroxidase (EC 1.11.1.5); CCP-CN, cyanide complex of CCP; CAPS, 3-(cyclohexylamino)-1-propanesulfonic acid; compound I, the two-electron-oxidized intermediate of CCP containing an oxyferryl iron; DEPC, diethyl pyrocarbonate; DPV, differential pulse voltammetry;  $Fe^{IV}=O$ , oxyferryl iron; FPLC, fast protein liquid chromatography; HPLC, high-performance liquid chromatography.

have been isolated and characterized for a large number of proteins including ribonuclease A (Matthews et al., 1978, 1980), lysozyme (Recchia et al., 1982),  $\alpha$ -lytic protease (Recchia et al., 1982), cytochromes c (Yocom et al., 1982, 1983; Bowler et al., 1989), cytochrome  $c_{551}$  (Osvath et al., 1988), cytochrome  $b_5$  (Jacobs et al., 1991), myoglobins (Crutchley et al., 1985; Casimiro et al., 1993), HIPIP (Jackman et al., 1988b, 1988c, Sola et al., 1989), azurin (Margalit et al., 1984), plastocyanin (Jackman et al., 1988d), and glucose oxidase (Degani & Heller, 1988). Several properties of  $a_5\text{RuHis}$ -derivatized proteins have been investigated including catalytic activity, ligand binding, protein fluorescence, tertiary structure, reduction potentials of metal centers, and NMR spectra. Also, electron-transfer kinetics between the native redox and ruthenium centers have been examined in detail for the heme, blue copper, and iron-sulfur proteins listed above (Bowler et al., 1990).

His6, -60, and -96 of CCP are expected to show relatively high reactivity with  $a_5\text{Ru}^{\text{II}}\text{H}_2\text{O}$  because of their accessibility. Computer graphic analysis indicates that the imidazole ring of His60 is highly solvent-exposed, and the N(3) atom is not within hydrogen-bonding distance of neighboring residues. His6 and -96 are less exposed and their N(3) atoms are within hydrogen-bonding distance of peptide oxygens, so these residues should be less reactive toward  $a_5\text{Ru}^{\text{II}}\text{H}_2\text{O}$  than His60. Modification of His181 and His52 should only occur at pH 8, and the resultant derivatives should exhibit properties very different from native CCP (Bosshard et al., 1984).

This paper reports the results of an investigation of the reactivity of CCP toward  $a_5\text{Ru}^{\text{II}}\text{H}_2\text{O}$  under various reaction conditions. Derivatives were isolated by cation-exchange FPLC and characterized using absorption spectroscopy, AP-ESI mass spectrometry, DPV, and HPLC analysis of tryptic peptides. DEPC reactivity was used to confirm  $a_5\text{Ru}$  coordination to histidine (Jackman et al., 1988a); enzyme activities and stabilities of enzyme intermediates probed the effects of  $a_5\text{Ru}$ -coordination on CCP function. Mass spectral analysis revealed extensive derivatization of CCP with  $a_5\text{Ru}$  at sites other than histidine, and DPV confirmed this for one FPLC fraction.

## EXPERIMENTAL SECTION

**Materials.** CCP was isolated from bakers' yeast (English et al., 1986; Smulevich et al., 1989), cytochrome c (Type III), horse heart myoglobin (95–100%), lysozyme (chicken egg white, grade I), and trypsin (TPCK-treated) were obtained from Sigma, and horse skeletal muscle myoglobin (>98%) was purchased from Calbiochem; all proteins were used without further purification. Reagent-grade chemicals were obtained from the following sources: diethyl pyrocarbonate (DEPC); imidazole, L-histidine, potassium cyanide (Sigma); sodium dithionite, mercuric oxide, mossy zinc metal (Fisher); chloropentaammineruthenium(III) chloride [ $a_5\text{RuCl}(\text{Cl})_3$ ] (Strem); ammonium hexafluorophosphate (99%), 4,4'-bipyridine (Aldrich). Protein and buffer solutions were prepared using nanopure water (Barnstead) and filtered using 0.2- and 1.2- $\mu\text{m}$  Acrodisc filters (Gelman Sciences). Pharmacia was the supplier of the FPLC system and all chromatographic resins. Absorption spectra were obtained on a Hewlett-Packard 8451A diode-array spectrophotometer, and electrochemical measurements were performed on a BAS 100A electrochemical analyzer.

**Methods.** Preparation of Small Ruthenium Complexes. Zn/Hg amalgam was prepared by slowly adding mercuric oxide to pieces of mossy zinc in 0.1 M  $\text{H}_2\text{SO}_4$

followed by vigorous stirring. *Note:* this should be performed under a fume hood. The amalgam was rinsed with nanopure water, air dried, and stored at room temperature. [ $a_5\text{RuH}_2\text{O}(\text{PF}_6)_2$ ] was prepared by the published procedure (Callahan et al., 1985) involving [ $a_5\text{RuCl}(\text{Cl})_3$ ] reduction over the amalgam and was stored at 4 °C in a vacuum desiccator. Histidinepentaammineruthenium(III) chloride ( $a_5\text{RuHis}$ ) was also prepared by the published procedure (Sundberg & Gupta, 1973).

**CCP Enzymatic Activity and Compound I Stability.** A spectrophotometric CCP assay using ferrocyclochrome c as reducing substrate (Yonetani & Ray, 1965) was used to determine the enzymatic activity of native CCP and its derivatives. Compound I forms upon the reaction of ferric CCP with peroxides (Bosshard et al., 1991) and possesses an oxyferryl heme ( $\text{Fe}^{\text{IV}}=\text{O}$ ) which spontaneously decays to ferric heme. The rate of compound I decay was monitored spectrophotometrically at 424 nm which is a maximum in the difference spectrum of ferric and oxyferryl CCP.

**Reactions of CCP with  $a_5\text{Ru}^{\text{II}}\text{H}_2\text{O}$ .** CCP was exposed to 20-fold molar excess  $a_5\text{Ru}^{\text{II}}\text{H}_2\text{O}$  under argon at room temperature in 0.1 M phosphate (pH 7.0) for 3 h. In a typical preparation, 5–10 mg of CCP (0.2–0.4 mM) were deaerated by bubbling argon over the protein solution for 1 h, and  $a_5\text{Ru}^{\text{II}}\text{H}_2\text{O}$  in degassed buffer was transferred by gas-tight syringe to the vessel containing the protein. The reaction was terminated by loading the product mixture onto a G-25 gel filtration column (2.5  $\times$  20 cm) equilibrated with reaction buffer. The products (0.1–1 mg in 25–500  $\mu\text{L}$  of 50 mM acetate buffer, pH 5.1) were separated on a FPLC HR 5/5 Mono-S column.

**Spectrophotometric Determination of  $a_5\text{RuHis}$ :Heme Ratios.** The absorption maximum of  $a_5\text{RuHis}$  ( $\epsilon_{303} = 2.1 \text{ mM}^{-1} \text{ cm}^{-1}$ ) (Sundberg & Gupta, 1973) at pH 5 increases and red-shifts at pH 10 ( $\epsilon_{370} = 3.4 \text{ mM}^{-1} \text{ cm}^{-1}$ ) (Recchia et al., 1982), making spectrophotometric determination of the complex more sensitive at high pH. CCP is unstable above pH 8 (Dowe & Erman, 1985) but was stabilized by forming the cyanide complex (Erman, 1974) in 0.1 M CAPS buffer (pH 11) containing 10 mM KCN. Protein concentrations were determined spectrophotometrically assuming  $\epsilon_{422} = 103 \text{ mM}^{-1} \text{ cm}^{-1}$  (Erman, 1974) for the cyanide adducts of both native CCP and its derivatives. The absorption spectrum of CCP-CN was subtracted from those of cyanide adducts of the major FPLC fractions. If a resultant difference spectrum had a broad band with  $\lambda_{\text{max}} = 370 \text{ nm}$ , the CCP species present was assumed to be modified at a histidine residue, and  $a_5\text{RuHis}$ :heme ratios were estimated using the extinction coefficients given above.

**DEPC Reactions.** Concentrations ( $\sim 0.1 \text{ M}$ ) of freshly prepared DEPC stock solutions in anhydrous ethanol were determined by adding known volumes to 1.0 mM histidine or imidazole solutions and measuring the absorbance increase at 240 nm ( $\epsilon = 3.2 \text{ mM}^{-1} \text{ cm}^{-1}$ ) for the histidine and 230 nm ( $\epsilon = 3.3 \text{ mM}^{-1} \text{ cm}^{-1}$ ) for the imidazole derivatives, respectively (Miles, 1977). DEPC is rapidly hydrolyzed in aqueous solution, having a half-life of 9 min in phosphate buffer at pH 7 (Miles, 1977), so following general practice >10-fold excess was used. The concentrations of native CCP and the  $a_5\text{RuHis}$  derivatives were determined spectrophotometrically assuming  $\epsilon_{408} = 98 \text{ mM}^{-1} \text{ cm}^{-1}$  (Yonetani & Anni, 1987). Since  $\epsilon_{408} = 0.25 \text{ mM}^{-1} \text{ cm}^{-1}$  for the free  $a_5\text{RuHis}$  complex (Sundberg & Gupta, 1973), its contribution to the absorbance at 408 nm was not considered. Reactions of DEPC with histidine,

$a_5\text{RuHis}$ , CCP, and  $a_5\text{RuHisCCP}$  in 0.1 M phosphate buffer (pH 7.0) were monitored spectrophotometrically at 240 nm, and the number of histidines modified was determined from the final absorbance at this wavelength.

**HPLC Analysis of Tryptic Digests.** To identify sites of  $a_5\text{Ru}$  attachment, 0.5–0.8 mg of the CCP samples in 0.1 M  $\text{NH}_4\text{HCO}_3$ , pH 8.0, were digested at 37 °C for 16 h at 50:1 (w/w) CCP:trypsin. Samples were applied to a reversed-phase Vydak C18 column (0.46 × 25 cm) equilibrated with 0.1% TFA in water, and the peptides were eluted using a linear 0–60% acetonitrile gradient (0.5%/min) at a flow rate of 1 mL/min and collected for amino acid and mass spectral analysis. Absorbances at 210, 280, 303, and 400 nm were monitored to detect peptide backbone, aromatic residues,  $a_5\text{RuHis}$ , and heme, respectively.

**Desalting of Protein Samples Prior to Amino Acid and Mass Spectral Analyses.** Native CCP was dialyzed using Spectrapor dialysis tubing (6000–8000 MW cutoff) against water for 6 h. Due to the smaller amounts of material available, all derivatized CCP species were passed over the C18 column equilibrated with 0.1% TFA and were eluted using a linear 10–70% acetonitrile gradient (1%/min) at a flow rate of 1 mL/min.

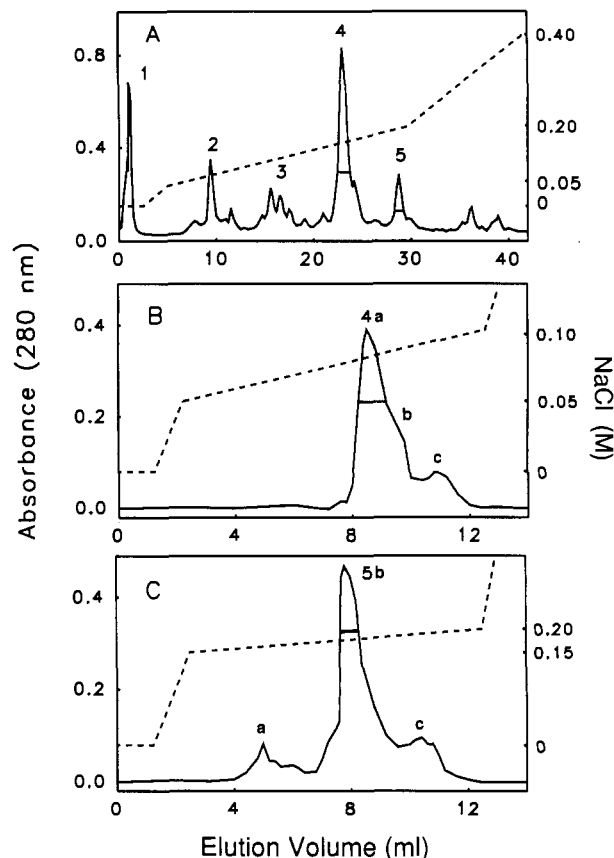
**Amino Acid Analysis.** HPLC-purified peptide and protein samples were dried by speed vacuum centrifugation in acid hydrolysis tubes. Samples were hydrolyzed (150 °C for 1 h) and analyzed on a Beckman System 6300 high-performance analyzer according to the general procedure of Spackman et al. (1958) with modifications (Veeraragavan, et al., 1990).

**AP-ESI Mass Spectra of Protein and Peptide Samples.** To confirm the presence of the  $a_5\text{Ru}$  group, derivatized protein and peptides were subjected to mass spectrometry on a SCIEX API III spectrometer operated in the positive ion mode for detection of protonated species (Covey et al., 1988). The lyophilized samples were dissolved in 10% acetic acid (pH 2.2) prior to injection into the mass spectrometer. Egg white lysozyme and horse skeletal muscle myoglobin were used as molecular weight standards.

**DPV of Fractions 4a and 4b.** DPV was carried out on these fractions since sufficient sample was available. The electrochemical cell consisted of a 1-mm glassy carbon working electrode (Cypress Systems), a Ag/AgCl reference electrode, and a Pt counter electrode. Protein samples were deoxygenated and blanketed with  $\text{N}_2$  during measurements. Addition of 4,4'-bipyridine, which was used as an electron-transfer promoter at gold electrodes for ruthenated heme proteins (Yocom et al., 1982; Crutchly et al., 1985), did not alter the voltammograms obtained at the glassy carbon electrode.

## RESULTS

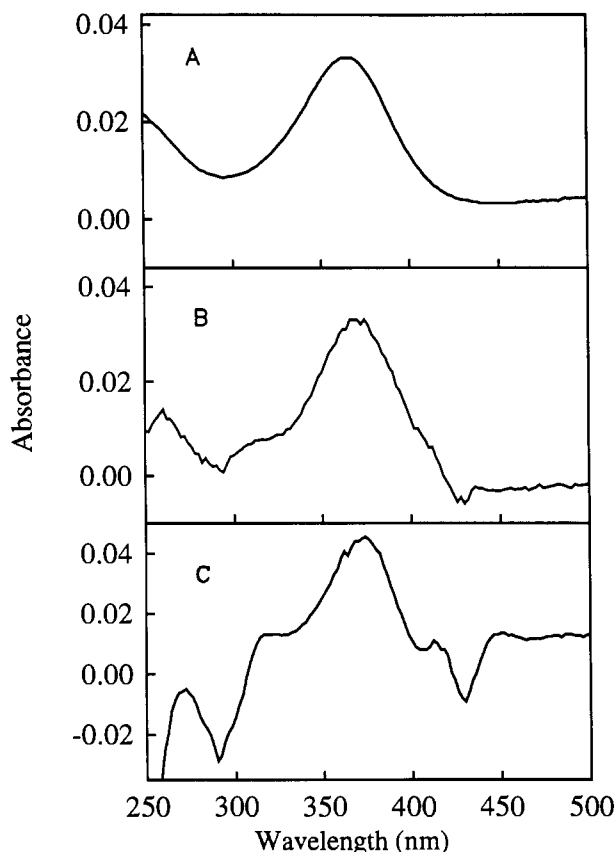
**CCP Reaction with  $a_5\text{Ru}^{\text{II}}\text{H}_2\text{O}$ .** The modification of CCP by  $a_5\text{Ru}^{\text{II}}\text{H}_2\text{O}$  was attempted under a number of different reaction conditions. Reactions carried out at pH 5 and 8 resulted in the precipitation of large amounts of protein. Furthermore, the products of the pH 8 reaction were highly cationic and required a salt concentration of  $\geq 1$  M to be eluted from the cation-exchange column. The instability of the pH 5 and 8 reaction products is not surprising considering that native CCP is only stable between pH 4 and 8 (Erman, 1974; Dowe & Erman, 1985; Yonetani & Anni, 1987). Modification of CCP by 20-fold excess  $a_5\text{Ru}^{\text{II}}\text{H}_2\text{O}$  at pH 7.0 did not result in protein precipitation, and ~95% protein was recovered from the reaction mixture.



**Figure 2.** Cation-exchange FPLC (Mono S, HR 5/5 equilibrated with 50 mM acetate, pH 5.1) of 1 mg of (A) the CCP ruthenation reaction mixture, (B) band 4 from A, and (C) band 5 from A. Samples were eluted using the NaCl gradients in 50 mM acetate (pH 5.1) indicated by the dashed lines. Flow rate = 0.5 mL/min, fraction size (A) 0.5 mL, (B) and (C) 0.25 mL.

**Cation-Exchange FPLC.** Native CCP has a pI of 5.28 (Bosshard et al., 1991) and binds strongly to anion-exchange resins such as DEAE at neutral pH. Following removal of excess small reagents, the  $a_5\text{Ru}^{\text{II}}\text{H}_2\text{O}$  reaction products also bound to DEAE at pH 7 but were eluted as a single broad band (not shown). However, good separation was obtained by cation-exchange chromatography at pH 5, and the FPLC Mono-S elution profile at  $\text{NaCl} \leq 0.2$  M of the products was composed of at least five bands (Figure 2A). Band 1 was eluted in the void volume like native CCP; rechromatography revealed that bands 2–5 could be further resolved. Band 4 separated into fractions 4a, 4b, and 4c under a shallower NaCl gradient (Figure 2B); when rechromatographed isocratically at the salt concentration corresponding to its peak position (70 mM NaCl), fraction 4a was separated from its shoulder, fraction 4b. Similarly, band 5 was resolved in 3 fractions (Figure 2C), and fraction 5b, the major component, was rechromatographed at 170 mM NaCl without further separation. The percent yields of fractions 4a and 5b from the ruthenation reaction were estimated to be 7.0 and 0.5%, respectively. As described below, fraction 4a was found to be a singly-derivatized CCP species with  $a_5\text{Ru}$  coordinated to His60 whereas fraction 4b is thought to consist mainly of CCP derivatized at a carboxylate side chain. Fraction 5b is doubly-derivatized CCP with  $a_5\text{Ru}$  bound to His6 and to a nonhistidine residue.

**Spectrophotometric Determination of  $a_5\text{RuHis}$ :Heme Ratios.** The difference spectra (Figure 3), obtained on subtraction of the CCP–CN spectrum from those of the cyanide complexes of fractions 4a and 5b, show a positive



**Figure 3.** Difference spectra obtained by subtracting the spectrum of 10 μM CCP-CN from that of (A) a 1:1 noncovalent mixture of 10 μM CCP-CN and a<sub>5</sub>RuHis, (B) the cyanide complex of 10 μM fraction 4a, (C) the cyanide complex of 10 μM fraction 5b. Spectra were recorded in 0.1 M CAPS buffer (pH 11.0) with 10 mM KCN.

**Table 1. Characterization of CCP and a<sub>5</sub>Ru<sup>III</sup>H<sub>2</sub>O Reaction Products**

species <sup>a</sup>	a <sub>5</sub> RuHis:Heme <sup>b</sup>	% activity <sup>c</sup>	t <sub>1/2</sub> for decay of compd I <sup>d</sup> (h)
CCP <sup>e</sup>	0	100 ± 6	5.5 ± 0.8 (10) <sup>f</sup>
band 1	0	101 ± 9	ND <sup>g</sup>
band 2	0	99 ± 7	ND
band 3 <sup>h</sup>	0.80 ± 0.12	88 ± 9	ND
fraction 4a	0.92 ± 0.16	100 ± 5	3.0 ± 0.6 (8)
fraction 5b	0.97 ± 0.30	93 ± 5	2.9 ± 0.8 (5)

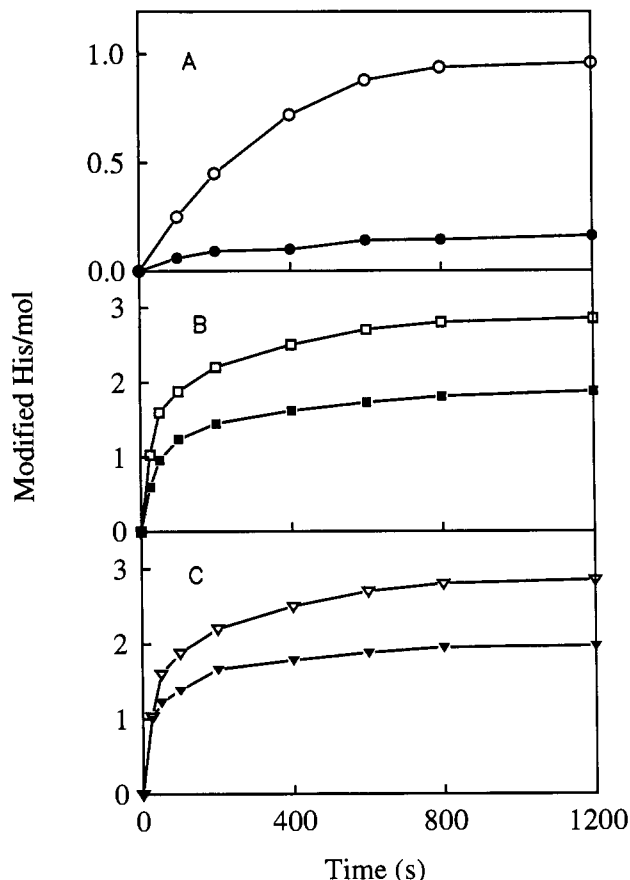
<sup>a</sup> Fractions purified by cation-exchange FPLC (see Figure 2).

<sup>b</sup> Estimated from a<sub>5</sub>RuHis and heme absorbances at 370 and 422 nm, respectively (see text). <sup>c</sup> Enzyme activity relative to native CCP.

<sup>d</sup> Half-life obtained from semilog plot of the absorbance decrease at 424 nm. <sup>e</sup> Native CCP that had not been exposed to the ruthenation procedure. <sup>f</sup> Number of measurements of t<sub>1/2</sub>. <sup>g</sup> ND = not determined.

<sup>h</sup> Band 3 is a heterogeneous mixture (see Figure 2A).

peak at 370 nm consistent with a<sub>5</sub>Ru-derivatization at histidine. Table 1 lists the a<sub>5</sub>RuHis:heme ratios of the FPLC bands in Figure 2 estimated from their relative absorbances at 370 and 422 nm. Band 1 in the void volume is assumed to be native CCP since it has no 370-nm absorption. Band 2 bound to the cation-exchange column but does not exhibit a<sub>5</sub>RuHis absorption. Band 3 appears to be a mixture of at least four species of low abundance with an average a<sub>5</sub>RuHis:heme ratio of 0.8. Fraction 4a, and the less abundant 5b, exhibited average a<sub>5</sub>RuHis:heme ratios of >0.9, which strongly suggests that each of these derivative contains a<sub>5</sub>Ru bound to a single histidine residue. Fractions 4b and 5c, the shoulders separated from fractions 4a and 5b (Figure 2B and C), have insignificant 370-nm absorption.



**Figure 4.** Reaction in 0.1 M phosphate buffer (pH 7.0) of 50-fold excess DEPC with (A) 100 μM histidine (○) and free a<sub>5</sub>RuHis (●); (B) 10 μM native CCP (□) and fraction 4a (■); and (C) 10 μM CCP (▽) and fraction 5b (▼). The absorbance increase at 240 nm is expressed as the number of histidines modified per mole using Δε = 3.3 mM<sup>-1</sup> cm<sup>-1</sup>. Fractions 4a and 5b are from the ruthenation reaction (Figure 2) and have a<sub>5</sub>Ru bound at His60 and His6, respectively.

**Enzymatic Activity and Compound I Stability.** The major species isolated by FPLC retained the activity of native CCP (Table 1). Compound I spontaneously decays to ferric CCP with a half-life of 5 h for the native enzyme (Erman & Yonetani, 1975). Following addition of H<sub>2</sub>O<sub>2</sub> to fractions 4a and 5b, the absorbance decrease at 424 nm due to compound I decay was exponential over 6–9 h (correlation coefficients >0.99) with slightly shorter half-lives (3 h) than native CCP.

**DEPC Reactions.** As can be seen from Figure 4A, addition of 50-fold excess DEPC to free a<sub>5</sub>RuHis gives rise to negligible absorbance increase at 240 nm compared to that observed for histidine. Thus, a<sub>5</sub>Ru coordination effectively blocks DEPC modification of free histidine as was observed previously for histidine residues in proteins (Jackman et al., 1988a). The reaction of 50-fold excess DEPC with native CCP resulted in the rapid modification of three histidines at pH 7.0 but modification of only two histidines in fractions 4a and 5b (Figure 4B and 4C). Also, the absorbance increase at 240 nm was reversed on addition of hydroxylamine (Miles, 1977) which removed the carbethoxy group from the CCP species. These results confirm that a<sub>5</sub>Ru is coordinated to a reactive, surface histidine in fractions 4a and 5b.

**Identification of the a<sub>5</sub>Ru-Modified Histidines in Fractions 4a and 5b.** X-ray structure determination showed that a<sub>5</sub>Ru is coordinated to His60 in fraction 4a (Fox et al., 1990). The crystal structure of fraction 5b could not be determined (S. Edwards, personal commu-

**Table 2. Molecular Weights of  $a_5Ru^{III}H_2O$  Reaction Products**

species	obsd MW <sup>a</sup> (Da)	calcd MW <sup>b</sup> (Da)	$a_5RuHis:heme^c$	total $a_5Ru:CCP^d$
lysozyme	14 305 ± 1	14 305		
myoglobin <sup>e,f</sup>	16 952 ± 1	16 952		
CCP <sup>e</sup>	33 536 ± 1	33 533	0	0
heme <sup>g</sup>	616	616		
fraction 4a <sup>e</sup>	33 717 ± 3	33 719 <sup>h</sup>	1	1
fraction 4b <sup>e</sup>	33 718 ± 3	33 719 <sup>h</sup>	0	1
fraction 5b <sup>e</sup>	33 901 ± 3	33 905	1	2
fraction 5c <sup>e</sup>	33 800 ± 4 <sup>i</sup>		0	

<sup>a</sup> Determined by AP-ESI mass spectrometry. <sup>b</sup> Calculated from sequence data or the chemical formula for protoporphyrin IX heme. <sup>c</sup> Determined spectrophotometrically (see Table 1). <sup>d</sup> Determined from the MW difference between apoCCP and each fraction. <sup>e</sup> MW of apoprotein is observed due to heme dissociation at low pH (see text). <sup>f</sup> Horse skeletal muscle myoglobin. <sup>g</sup> Protoporphyrin IX heme isolated by HPLC during desalting of CCP samples prior to mass spectral analysis. <sup>h</sup> MW of apoCCP plus  $RuN_5H_{15}$  (186 Da). <sup>i</sup> Mass difference (264 Da) between fraction 5c and native CCP has not been assigned to a chemical species.

nication) so it was necessary to carry out HPLC analysis of the tryptic peptides of this sample. The tryptic peptide map of CCP is complex yielding >60 peaks. A diode-array detector was used to identify peaks with no protein absorbance at 280 nm (since the tryptic peptides containing His6 and His96 contain no Tyr or Trp residues), but which possess the 303-nm absorbance expected for  $a_5RuHis$  at low pH. Mass spectral analysis identified a peptide with a molecular weight of 1469 Da corresponding to residues 1–12 plus  $a_5Ru$  (TTPLVHVASVEK +  $RuN_5H_{15}$ , MW = 1281 + 186 Da). In addition, a much less intense peak with MW = 1285 Da was assigned to peptide 1–12 that has lost  $a_5Ru$  on ionization. Since no peak corresponding to residues 91–97 (FLEPIHK, MW = 884 Da) was observed in the mass spectrum, fraction 5b is assumed to contain a derivative with  $a_5Ru$  bound to His6, and not His96, the other surface-exposed histidine in CCP (Figure 1).

**Mass Spectral Analysis of Ruthenated Protein and Peptide Samples.** Table 2 summarizes the mass spectral data. Using lysozyme (MW = 14 305 Da) as a molecular weight standard, the mass spectrum of apoCCP (Figure 5) yielded a MW of 33 536 Da compared to the value of 33 533 Da calculated from the sequence. The heme removed during desalting by HPLC has a MW of 616 Da, as expected for protoporphyrin IX heme ( $FeC_{34}N_4O_4H_{32}$ ). The mass spectrum of CCP desalted by dialysis was identical to that shown in Figure 5 except for an additional peak at 616 due to heme which dissociated from the polypeptide at the low pH (2.2) used to record the spectra. Horse skeletal muscle myoglobin, which also possesses a noncovalently-bound protoporphyrin IX heme, was found to have a molecular weight of 16 952 Da identical to that calculated for the polypeptide (16 952 Da) alone (Zaia et al., 1992).

Until this point it was assumed that fractions 4a and 5b contained CCP derivatized only at His60 and His6, respectively. This was confirmed for  $a_5RuHis60CCP$  (MW = 33 717 ± 3 ≈ 33 536 + 186 Da), consistent with the X-ray analysis. However, a MW of 33 901 ± 3 (~33 536 + 2(186) Da) indicated that fraction 5b possesses two  $a_5Ru$  groups per apoCCP. Since DEPC reacted with two of its three surface histidines (Figure 4C), the second  $a_5Ru$  must be attached at a site other than histidine.

Mass spectra were also obtained for the fractions labeled 4b and 5c in Figure 2B and C, respectively. Fraction 4b possesses one  $a_5Ru$  group (MW = 33 718 ± 3 Da) but has negligible  $a_5RuHis$  absorption at 370 nm. Fraction 5c has

MW of 33 800 ± 4 Da which is 264 Da higher than native CCP making it difficult to speculate as to the identity of this species of low abundance.

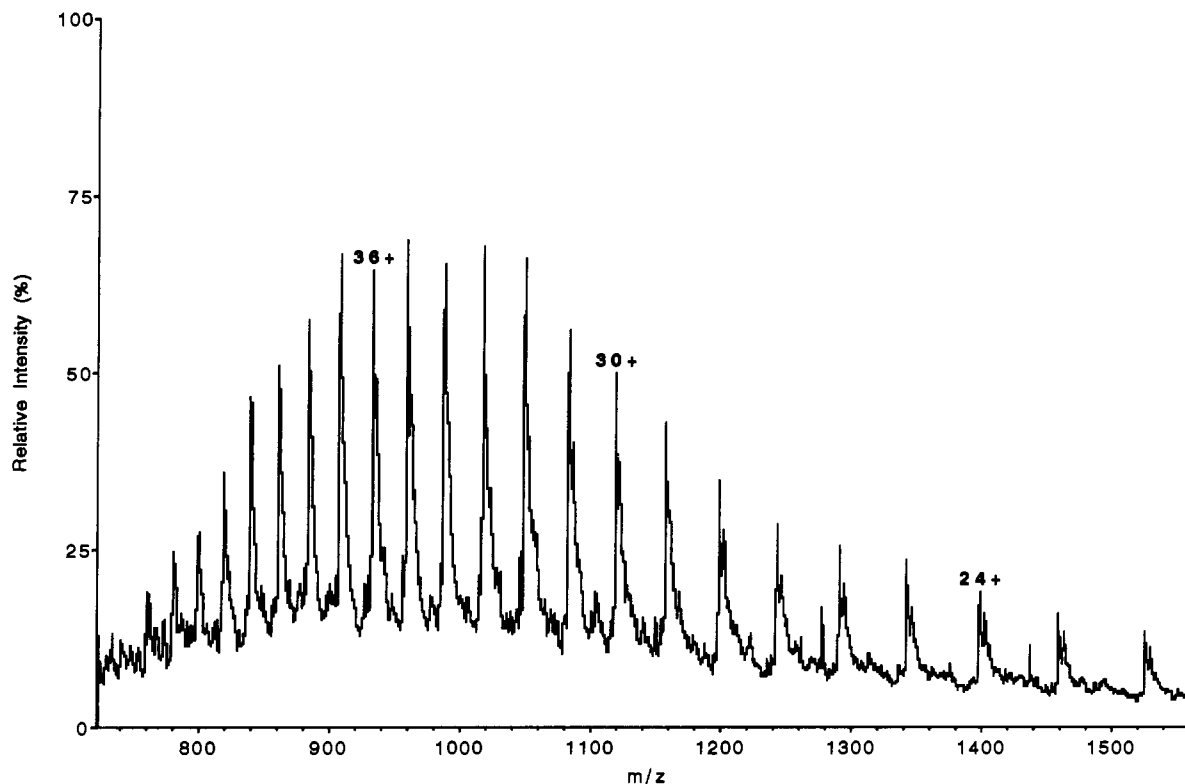
**DPV of Fractions 4a and 4b.** Two peaks at +42 and -68 mV (vs NHE) appear in the DPV of fraction 4b (Figure 6). The peak at 42 mV is assigned to the reduction of  $a_5Ru^{III}$  coordinated to His60 since the single peak observed in the DPV of fraction 4a has the same potential within experimental error. From the observed peak currents, fraction 4b is estimated to contain ~20%  $a_5Ru(His60)-CCP$  consistent with negligible  $a_5RuHis$  absorption at the protein concentration (10  $\mu M$ ) used to obtain difference spectra like those shown in Figure 3. The appearance of a second peak at negative potential in the voltammogram of fraction 4b suggests binding of  $a_5Ru$  to an anionic ligand such as  $-COO^-$  since this would stabilize the  $Ru^{III}$  form of the complex (Lim et al., 1972).

## DISCUSSION

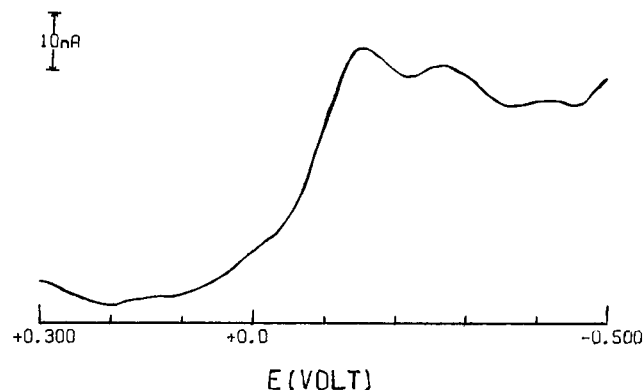
Extensive derivatization of CCP occurred when the protein was incubated with 20-fold excess  $a_5Ru^{III}H_2O$  at room temperature for 3 h in phosphate buffer (pH 7.0). This reaction time is short compared to the 1–3 days required for ruthenation of horse heart cytochrome c (Yocom et al., 1982, 1983) but longer than the 60 min for horse heart myoglobin (S. Marmor, unpublished results) or the 30 min for sperm whale myoglobin (Crutchley et al., 1985). These reaction times mirror the accessibility of the histidine residues; both myoglobin and CCP have surface histidines, but in cytochrome c the histidines are buried within the protein matrix.

Table 1 summarizes the properties of the various species isolated by cation-exchange chromatography from the reaction of  $a_5Ru^{III}H_2O$  and CCP. Two  $a_5RuHis$ -containing derivatives of CCP were purified to homogeneity; fraction 4a has been identified by X-ray crystallography as  $a_5RuHis60CCP$  (Fox et al., 1990), and fraction 5b has been shown by peptide mapping to be CCP with  $a_5Ru$  bound at His6. However, the mass spectral results revealed that fraction 5b and also fraction 4b possess coordinated  $a_5Ru$  that was not detected by difference spectroscopy. Binding of  $a_5Ru$  to cysteine, methionine (Kuehn & Taube, 1976), or carboxylate (Stritar & Taube, 1969) side groups of CCP is also possible. Since the single cysteine and five methionines in CCP are less solvent-exposed than the surface histidines, they are unlikely ruthenation sites. On the other hand, CCP carboxylates demonstrated high reactivity in crosslinking reactions with cytochrome c (Moench et al., 1987). Carboxylate complexes of  $a_5Ru$  exhibit UV-vis spectra with  $\lambda_{max}$  at ~290 nm ( $\epsilon = 1.5 \text{ mM}^{-1} \text{ cm}^{-1}$ ) (Stritar & Taube, 1969). Weak absorption at this wavelength would be difficult to detect under the intense absorption of CCP centered at 278 nm ( $\epsilon = 75 \text{ mM}^{-1} \text{ cm}^{-1}$ ) (Bosshard et al., 1991). However, the presence of a peak at -68 mV (vs NHE) in the DPV of fraction 4b is consistent with  $a_5Ru$  coordination to a carboxylate side chain of CCP since anionic ligands shift  $a_5Ru^{III/II}$  potentials to negative values (Lim et al., 1972). Nevertheless, it should be noted that the redox properties of protein-bound  $Ru$  appear to be highly sensitive to the protein environment since the reported  $a_5Ru^{III/II}His$  potentials vary by ~70 mV (Bowler et al., 1990). Similar variation may be anticipated for the redox properties of  $a_5Ru$  bound at nonhistidine sites.

As shown here (Figure 4) and previously (Jackman et al., 1988a), DEPC is an excellent probe of histidine modification by  $a_5Ru$ . However, it is not a reliable indicator of the number of histidines that will react readily



**Figure 5.** AP-ESI mass spectrum of native CCP (25  $\mu$ g) dissolved in 50  $\mu$ L of 10% acetic acid (pH 2.2) infused at a flow rate of 2  $\mu$ L/min.



**Figure 6.** Reduction of fraction 4b by differential pulse voltammetry: volts vs Ag/AgCl; 1-mm glassy carbon electrode; pulse amplitude = 25 mV; scan rate = 5 mV/s; 0.16 mM ruthenated CCP in deoxygenated 70 mM NaCl, 10 mM 4,4'-bipyridine, 50 mM acetate buffer pH 5.1.

with  $a_5\text{Ru}^{\text{II}}\text{H}_2\text{O}$ . For example, in horse heart myoglobin eight histidines are modified by DEPC in 20–30 min whereas only three surface histidines are ruthenated in 60 min (S. Marmor, unpublished results). Konopka and Waskell (1988) obtained similar results and showed in addition that at DEPC:histidine ratios  $>55$ , all eleven histidines could be modified resulting in complete dissociation of the heme from the globin. The higher reactivity of DEPC with proteins is probably due to its hydrophobic nature which should allow it greater access to buried histidines than  $a_5\text{Ru}^{\text{II}}\text{H}_2\text{O}$ .

The crystal structure of the 1:1 complex between CCP and cytochrome c (Pelletier & Kraut, 1992) reveals that the cytochrome binding domain is below the heme as the enzyme is depicted in Figure 1. Therefore, it is not surprising that  $a_5\text{RuHis60CCP}$  possesses enzyme activity comparable to native CCP or that DEPC modification of the surface histidines does not result in activity loss

(Bosshard et al., 1984). Since  $a_5\text{RuHis6a}_5\text{RuCCP}$  (fraction 5b) also exhibits full activity, the nonhistidine site modified in this derivative must not fall within the cytochrome c binding region. The half-life for compound I decay in the absence of exogenous reductants is  $\sim 5$  h for native CCP and  $\sim 3$  h for fractions 4a and 5b. Recombinant CCP from *E. coli*, which possesses a 3-D structure almost identical to yeast CCP (Wang et al., 1990), also has a half-life for compound I of  $\sim 3$  h (Erman & Vitello, 1992); hence, minor structural changes can alter the stability of compound I.

The reported activities of other ruthenated enzymes vary considerably. For example, lysozyme retains 70% activity on binding a single  $a_5\text{Ru}$  whereas  $\alpha$ -lytic protease is completely inactive when its single histidine, which plays a key role in catalysis, is ruthenated (Recchia et al., 1982). Ribonuclease A retains 65% activity when one  $a_5\text{Ru}$  center is attached but only 22% activity when two are present (Matthews et al., 1978, 1980). Glucose oxidase was ruthenated to promote electrochemical communication between its two FAD redox centers and electrode surfaces. The modification was carried out in 3 M urea and resulted in an average attachment of 14 ruthenium centers per enzyme molecule. Remarkably, this heterogeneous mixture of  $a_5\text{Ru}$ -derivatized species retains 70% (Degani & Heller, 1988).

In this study, mass spectral analysis identified two species (fractions 4b and 5b) with  $a_5\text{Ru}$  attached to sites other than histidine. Thus, it appears that  $a_5\text{Ru}^{\text{II}}\text{H}_2\text{O}$  is less specific for histidine residues than previously thought. Consequently, determination of histidine-bound  $a_5\text{Ru}$  only may lead to incomplete characterization of Ru-derivatized proteins. Without atomic absorption or mass spectral analysis other ruthenation sites may remain undetected which could pose problems in further studies. Atomic absorption has been commonly used to determine the extent of protein ruthenation (Yocom et al., 1983; Osvath



et al., 1988) but this technique is orders of magnitude less sensitive than AP-ESI mass spectrometry and often suffers from interferences due to the protein matrix.

The preparation of  $a_5\text{RuHis}$  derivatives has provided a useful probe for studying long-range electron transfer in CCP (Fox et al., 1990) and in a large number of metalloproteins as reviewed by Bowler et al. (1990). Also, ruthenation has aided in assigning histidine signals in NMR (Yocom et al., 1983) and in estimating the contribution of individual tryptophans to protein steady-state fluorescence (Recchia et al., 1982; Fox et al., 1993). However, it is important to consider the reactivity of  $a_5\text{Ru}^{II}\text{H}_2\text{O}$  with sites other than histidine, and the present study highlights the value of mass spectrometry in product characterization.

#### ACKNOWLEDGMENT

We wish to thank Fernando Battaglini for carrying out the DPV measurements and George Tsaprailis for preparing a number of tryptic digests of CCP and for helpful discussions. Carlos Faerman is also thanked for assistance in preparing Figure 1.

#### LITERATURE CITED

- Bosshard, H. R., Anni, H., and Yonetani, T. (1991) in *Peroxidases in Chemistry and Biology* (Everse, J., Everse, K. E., and Grisham, M. B., Eds.) Vol. II, p 51, CRC Press, Boca Raton.
- Bosshard, H. R., Banziger, J., Hasler, T., and Poulos, T. L. (1984) *J. Biol. Chem.* 259, 5683.
- Bowler, B. E., Meade, T. J., Mayo, S. L., Richards, J. H., and Gray, H. B. (1989) *J. Am. Chem. Soc.* 111, 8757.
- Bowler, B. L., Raphael, A. L., and Gray, H. B. (1990) *Prog. Inorg. Chem.* 38, 259.
- Callahan, R. W., Brown, G. M., and Meyer, T. J. (1985) *Inorg. Chem.* 24, 1443.
- Casimiro, D. R., Wong, L.-L., Colón, J. L., Zewert, T. E., Richards, J. H., Chang, I.-J., Winkler, J. R., and Gray, H. B. (1993) *J. Am. Chem. Soc.* 115, 1485.
- Covey, T. R., Bonner, R. F., Shushan, B. I., and Henion, J. (1988) *Rapid Commun. Mass Spec.* 2, 249.
- Crutchley, R. J., Ellis, W. R., and Gray, H. B. (1985) *J. Am. Chem. Soc.* 107, 5002.
- Degani, Y., and Heller, A. (1988) *J. Am. Chem. Soc.* 110, 2615.
- Dowe, R. J., and Erman, J. E. (1985) *Biochim. Biophys. Acta* 827, 183.
- English, A. M., Laberge, M., and Walsh, M. (1986) *Inorg. Chim. Acta* 123, 113.
- Erman, J. E. (1974) *Biochemistry* 13, 39.
- Erman, J. E., and Vitello, L. B. (1992) *J. Am. Chem. Soc.* 114, 6592.
- Erman, J. E., and Yonetani, T. (1975) *Biochim. Biophys. Acta* 393, 350.
- Finzel, B. C., Poulos, T. L., and Kraut, J. (1984) *J. Biol. Chem.* 259, 13027.
- Fox, T., Hazzard, J. T., Edwards, S. L., English, A. M., Poulos, T. L., and Tollin, G. (1990) *J. Am. Chem. Soc.* 112, 7426.
- Fox, T., Ferreira-Rajabi, L., Hill, B. C., and English, A. M. (1993) *Biochemistry* 32, 6938.
- Jackman, M. P., Lim, M. C., Osvath, P., Harshani de Silva, D. G. A., and Sykes, A. G. (1988a) *Inorg. Chim. Acta* 153, 205.
- Jackman, M. P., McGinnis, J., Powls, R., Salmon, G. A., and Sykes, A. G. (1988b) *J. Am. Chem. Soc.* 110, 5880.
- Jackman, M. P., Lim, M.-C., Salmon, G. A., and Sykes, A. G. (1988c) *J. Chem. Soc., Chem. Commun.* 179.
- Jackman, M. P., Lim, M.-C., Sykes, A. G., and Salmon, G. A. (1988d) *J. Chem. Soc., Dalton Trans.* 2843.
- Jacobs, B. A., Mauk, M. R., Funk, W. D., MacGillivray, R. T. A., Mauk, A. G., and Gray, H. B. (1991) *J. Am. Chem. Soc.* 113, 4390.
- Konopka, K., and Waskell, L. (1988) *Biochim. Biophys. Acta* 954, 189.
- Kuehn, C. G., and Taube, H. (1976) *J. Am. Chem. Soc.* 98, 689.
- Lim, H. S., Barclay, D. J., and Anson, F. C. (1972) *Inorg. Chem.* 11, 1460.
- Margalit, R., Kostic, N. M., Che, C.-M., Blair, D. F., Chaing, H.-J., Pecht, I., Shelton, J. B., Shelton, J. R., and Gray, H. B. (1984) *Proc. Natl. Acad. Sci. U.S.A.* 81, 6554.
- Matthews, C. R., Erickson, P. M., Van Vliet, D. L., and Petersheim, M. (1978) *J. Am. Chem. Soc.* 100, 2260.
- Matthews, C. R., Erickson, P. M., and Froebe, C. L. (1980) *Biochim. Biophys. Acta* 624, 499.
- Miles, E. W. (1977) *Methods Enzymol.* 47, 431.
- Moench, S. J., Satterlee, J. D., and Erman, J. E. (1987) *Biochemistry* 26, 3821.
- Osvath, P., Salmon, G. A., and Sykes, A. G. (1988) *J. Am. Chem. Soc.* 110, 7114.
- Pelletier, H., and Kraut, J. (1992) *Science* 258, 1748.
- Poulos, T. L., and Finzel, B. C. (1984) *Pept. Protein Rev.* 4, 115.
- Recchia, J., Matthews, C. R., Rhee, M., and Horrocks, W. D. (1982) *Biochim. Biophys. Acta* 702, 105.
- Smulevich, G., Mantini, A. R., English, A. M., and Mauro, J. M. (1989) *Biochemistry* 28, 5058.
- Sola, M., Cowan, J. A., and Gray, H. B. (1989) *Biochemistry* 28, 5261.
- Spackman, D. H., Stein, W. H., and Moore, S. (1958) *Anal. Chem.* 30, 1190.
- Stritar, J. A., and Taube, H. (1969) *Inorg. Chem.* 8, 2281.
- Sundberg, R. J., and Gupta, G. (1973) *Bioinorg. Chem.* 3, 39.
- Veeraragavan, K., Colpitts, T., and Gibbs, B. F. (1990) *Biochim. Biophys. Acta* 1044, 26.
- Wang, J., Mauro, J. M., Edwards, S. L., Oatley, S. J., Fishel, L. A., Ashford, V. A., Xuong, N.-H., and Kraut, J. (1990) *Biochemistry* 29, 7160.
- Yocom, K. M., Shelton, J. B., Shelton, J. R., Schroeder, W. A., Worosila, G., Isied, S. S., Bordignon, E., and Gray, H. B. (1982) *Proc. Natl. Acad. Sci. U.S.A.* 79, 7052.
- Yocom, K. M., Winkler, J. R., Nocera, D. G., and Gray, H. B. (1983) *Chim. Scripta* 21, 29.
- Yonetani, T., and Anni, H. (1987) *J. Biol. Chem.* 262, 9547.
- Yonetani, T., and Ray, G. S. (1965) *J. Biol. Chem.* 240, 4503.
- Zaia, J., Annan, R. S., and Biemann, K. (1992) *Rapid Commun. Mass Spectrom.* 6, 32.



# Molecular Modeling of Phytochrome Using Constitutive C-Phycocyanin from *Fremyella diplosiphon* as a Putative Structural Template

William Parker,<sup>†</sup> Peter Goebel,<sup>‡</sup> Charles R. Ross, II,<sup>‡</sup> Pill-Soon Song,<sup>†</sup> and John J. Stezowski<sup>\*‡</sup>

Department of Chemistry and Institute for Cellular & Molecular Photobiology, University of Nebraska, Lincoln, Nebraska 68508. Received January 28, 1993\*

Phytochrome, the ubiquitous photosensor in green plants, is similar to C-phycocyanin in a number of ways. We have produced a model of the phytochrome chromophore binding pocket based on the X-ray crystal structure of C-phycocyanin from *Fremyella diplosiphon* [Duerring *et al.* (1991) *J. Mol. Biol.* 217, 577-592]. Twenty residues around the chromophore binding site of C-phycocyanin were changed to the corresponding residues of *Avena* phytochrome A for the modeling. In the minimized model, Arg-318, Ala-319, the methylene of Ser-322, Leu-325, Gln-326, and Tyr-327 (using the numbering of the *Avena* sequence; Cys-323 is chromophore bound) form a pocket on one side of the chromophore. The other side of the chromophore lacks hydrogen-bond donors and is involved only in van der Waals contact with the chromophore. The overall structure of the model may be described as one peptide segment "anchoring" the chromophore hydrophobically, covalently, and electrostatically from several directions, while the other key peptide segment simply provides a hydrophobic surface for the chromophore to rest against. The red light absorbing (Pr) chromophore of the model is buried more deeply in the binding pocket than the far red light absorbing (Pfr) chromophore. This apparently reflects reduced compatibility of the chromophore with the pocket upon photoisomerization, which requires the insertion of hydrophilic parts of ring D into the hydrophobic core of the protein. This concept is consistent with the experimental evidence that photoisomerization of the Pr chromophore is followed by movement of the chromophore from its binding pocket. In the proposed model, increased exposure of hydrophobic portions of the Pfr chromophore compared to the Pr chromophore is consistent with the red shift observed in the first intermediate of the Pr to Pfr photoconversion. The proposed model may be tested by mutation experiments, thus providing a viable model to foster the current rapid progress of molecular biology in this field.

## 1. INTRODUCTION

Phytochrome is the ubiquitous red-light sensor found in photosynthetic plants. The roughly 120 kDa protein adopts two distinct forms, a red-light-absorbing form (Pr) and the physiologically active far-red-light-absorbing form (Pfr). Phytochrome has been the subject of a large number of studies (Thomas and Johnson, 1991, for review). The protein is encoded by several genes which are expressed at different times during plant development. Phytochrome can be obtained from dark-grown plants (so-called type I phytochrome, the *phyA* gene product) and from light-grown plants (so called type II phytochrome, for which at least two different genes are expressed, *phyB* and *phyC*). The biochemical characteristics of type I phytochrome have been well-studied in *Avena* (oat) and to a lesser extent in *Pisum* (pea); the sequence of several phytochromes are known (for sequences and references see, Quail *et al.*, 1991). Numerous spectral studies including UV-vis, fluorescence, fluorescence anisotropy, various types of Raman, circular dichroism, NMR, and infrared spectroscopy have revealed a great deal of detail about both the chromophore conformation/configuration and the peptide conformation (Thomas and Johnson, 1991, for review). Small-angle X-ray scattering (Tokutomi *et al.*, 1989), as well as electron microscopy (Jones and Erickson, 1989), have yielded a low-resolution model of

phytochrome which entails a chromophore-containing domain of approximately 70 kDa connected by a linker region to a nonchromophore domain of about 50-55 kDa. Recently, transgenic phytochrome has been expressed in yeast (Deforce *et al.*, 1991; Wahleithner *et al.*, 1991) and products of mutated gene sequences are being characterized (Deforce *et al.*, 1991; Cherry *et al.*, 1992; Stockhaus *et al.*, 1992; Edgerton and Jones, 1992). In spite of this progress, the tertiary structure of the phytochrome polypeptide and how it specifically interacts with its noncyclic tetrapyrrole chromophore is not known.

The three-dimensional structure of the phytochrome chromophore and a segment of protein immediately surrounding the chromophore (the chromophore pocket) have recently been modeled using Chou-Fasman (Chou & Fasman, 1974) and GOR (Garnier *et al.*, 1978) predictions as the starting point for calculating the protein conformation (Gabriel and Hooper, 1991). Although such modeling without a structural template having sequence homology is very unreliable, no other phytochrome model has been published. A more conventional approach to modeling would involve the use of homologous proteins as a starting point for protein conformation. There are, unfortunately, no proteins with high sequence homology to phytochrome for which the three-dimensional structure is known. It has been observed, however, that there are similarities between phytochrome and C-phycocyanin, a protein for which crystal structures of examples from several different sources have been determined at high resolution (Schirmer *et al.*, 1985, 1986; Duerring *et al.*, 1991).

C-phycocyanin, found in cyanobacteria (blue-green algae), cryptomonads, and eukaryotic red algae, is also a

\* Author to whom correspondence should be addressed.

<sup>†</sup> Department of Chemistry and Institute for Cellular & Molecular Photobiology.

<sup>‡</sup> Department of Chemistry.

\* Abstract published in *Advance ACS Abstracts*, December 15, 1993.

light-harvesting pigment-protein adduct. The protein is found in water-soluble antenna complexes on the surface of thylakoid membranes. The functional unit of the light-harvesting complex, called a phycobilisome, is composed of  $\alpha$  and  $\beta$  C-phycocyanins [an  $(\alpha\beta)_6$  dodecamer] (for review, see Huber, 1989). The  $\alpha$  and  $\beta$  subunits have the same basic fold, which is related to the globin fold (Schirmer *et al.*, 1985). There are nine helices, labeled X, Y, A, B, E, F', F, G, and H (no  $\beta$ -sheet), involved in the C-phycocyanin fold (Schirmer *et al.*, 1985). There are two chromophores covalently bound to the  $\beta$  subunit (at residues  $\beta$ -84 and  $\beta$ -155) and one chromophore bound to the  $\alpha$  subunit (at residue  $\alpha$ -84). The  $\alpha$ -84 and  $\beta$ -84 chromophores are topologically equivalent and are covalently bound to Cys-84, which is seven residues from the N-terminus of helix E. These chromophores are very nearly structurally identical to the phytochrome chromophore, the exception being an ethyl group in C-phycocyanin on ring D compared with a vinyl group in phytochrome (Lagarias and Rapoport, 1980; Figure 1). Apophytochrome is capable of binding the C-phycocyanin chromophore (Elich *et al.*, 1988; Elich and Lagarias, 1989).

There are several additional similarities between phytochrome and C-phycocyanin. The red-light-absorbing Pr form of phytochrome and C-phycocyanin have very similar absorption spectra (Parker *et al.*, 1950; Siegelman *et al.*, 1966). C-phycocyanin (the  $\alpha$ -84 and  $\beta$ -84 chromophores only; Arciero *et al.*, 1988a-c) and apparently phytochrome (Elich & Lagarias, 1989; Deforce *et al.*, 1991; Wahleithner *et al.*, 1991) are able to incorporate chromophores without the aid of an enzyme. Also, the CD spectrum of phytochrome is consistent with a predominantly  $\alpha$ -helical protein (Sommer and Song, 1990; L. Deforce and P.-S. Song, unpublished results).

The most striking sequence similarity between phytochrome and C-phycocyanin lies in a conserved arginine five residues N-terminal to the chromophore binding site. This corresponds to the second residue of helix E in C-phycocyanin (Partis & Grimm, 1990; Quail *et al.*, 1991). This arginine, when present, is involved in interactions with the chromophore ring B propionate side chain (Schirmer *et al.*, 1986; Duerring *et al.*, 1991) of the  $\alpha$ -84 and/or  $\beta$ -84 chromophores, depending on the organism. In addition, phytochrome contains a conserved glutamine three residues C-terminal to the chromophore-bound cysteine. The corresponding position near the  $\beta$ -84 chromophore in C-phycocyanin is occupied by an aspartate, which takes part in an important interaction with the ring B and ring C nitrogen atoms of the  $\beta$ -84 chromophore. A similar structural role has been proposed for the glutamine three residues C-terminal to the phytochrome chromophore (Partis and Grimm, 1990).

In light of the above similarities, several investigators in the phytochrome field have postulated that the protein structure of phytochrome may be structurally similar to that of C-phycocyanin (W. Rüdiger, quoted by Quail *et al.*, 1992; Quail *et al.*, 1992; Partis and Grimm, 1990). Although there is clearly no strong sequence homology between phytochrome and C-phycocyanin, C-phycocyanin is currently the only protein with proposed structural similarity to phytochrome. Thus, a phytochrome model based on the phycocyanin structure is perhaps the best starting point for mutagenic work. In fact, such studies are now being pursued, although no model has yet been published (Deforce *et al.*, 1994).

We describe initial results of modeling studies on the chromophore and chromophore pocket of phytochrome based on the structure of the  $\beta$ -84 chromophore (and the

surrounding pocket) of constitutive C-phycocyanin from *Fremyella diplosiphon* (Duerring *et al.*, 1991). The suitability of the starting model was tested by constructing correlation diagrams (Argos *et al.*, 1983) between the phytochrome chromophore-binding region and constitutive  $\alpha$  and  $\beta$  C-phycocyanins. Our goal was to derive a viable model as close as possible to experimental observation. Consequently, we limited refinement of the model to energy-minimization techniques. The viability of the resultant model is discussed with respect to known physical properties of the phytochromes.

## 2. METHODS

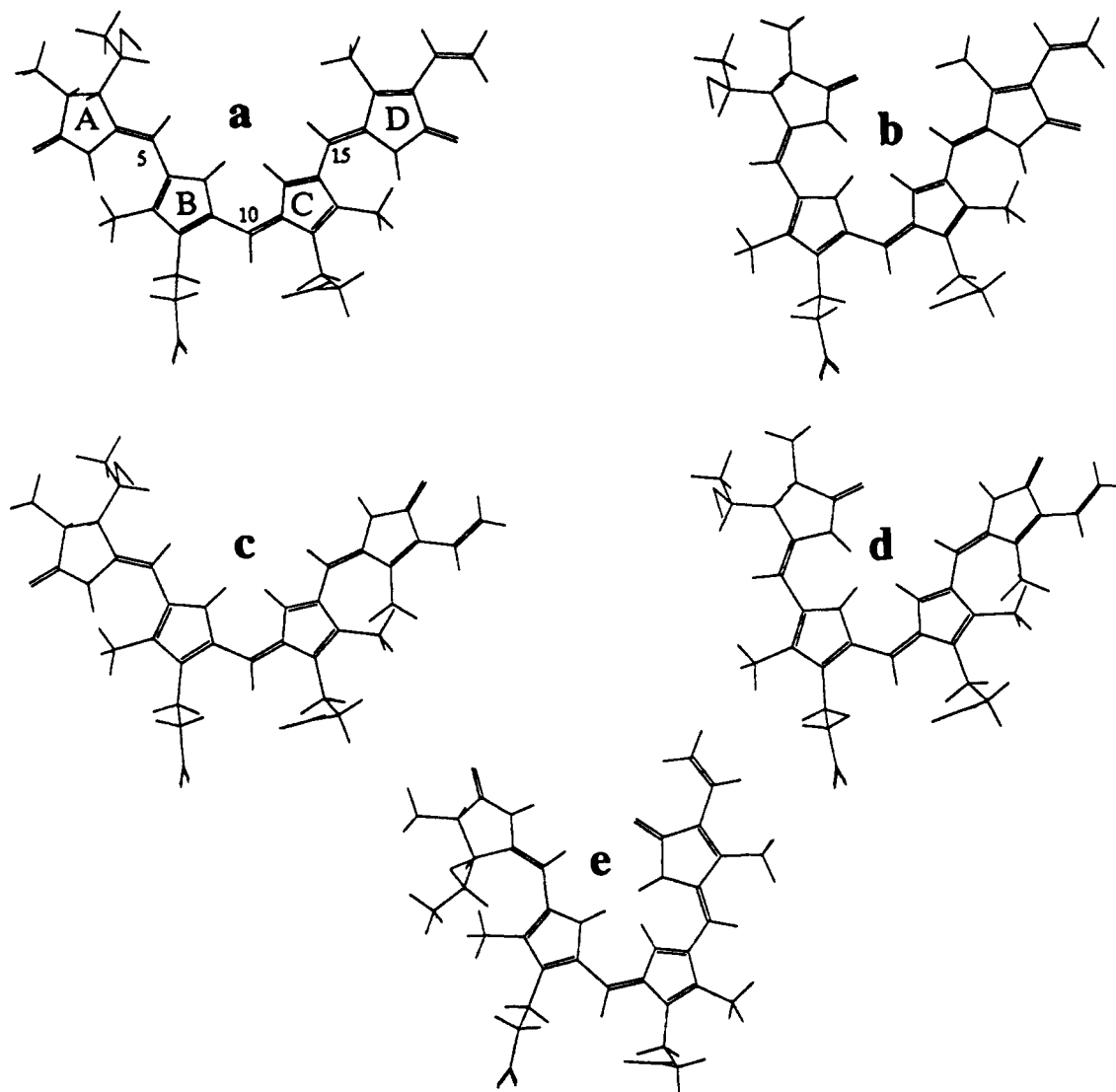
**(a) Correlation of Amino Acid Sequences.** Sequences were correlated using the method of Argos *et al.* (1983), which is designed to reveal and align structural and/or functional homology in amino acid sequences for which there is no direct sequence homology. Sequences were correlated by first representing amino acids with six selected physical parameters: the tendency to form  $\alpha$ -helix,  $\beta$ -sheet, and turn, hydration potential, hydrophobicity, and polarity (Argos *et al.*, 1983). Type I *Avena* phytochrome residues (Hershey *et al.*, 1985) around the chromophore binding residue (Cys-323) were compared with both  $\alpha$  and  $\beta$  C-phycocyanin sequences. Sequences (Mazel *et al.*, 1988; Fuglistaller *et al.*, 1983) of both constitutive C-phycocyanins for which three-dimensional structures are known were used. The shorter phytochrome sequence fragment was moved along the phycocyanin sequences using a moving algorithm (Rose, 1978). A correlation value ( $C_p(i)$ ) was obtained at each window position ( $i$ ) for each physical parameter ( $p$ ), using the following cross-correlation function:

$$C_p(i) = \frac{\sum_{j \in [i, w]} X_p(j) \cdot Y_p(j)}{\left[ \sum_{j \in [i, w]} S_p^2(j) \cdot \sum_{j \in [i, w]} Y_p^2(j) \right]^{1/2}}$$

where  $w$  is the size of the window (equal to the size of the phytochrome sequence),  $j$  is the position of a residue in window  $w$ ,  $X_p(j) = x_p(j) - x_p$  and  $Y_p = y_p(j) - y_p$ . These values  $x_p(j)$  and  $y_p(j)$  correspond to physical parameter values for sequences  $x$  and  $y$  at residue position  $j$ . The values  $x_p$  and  $y_p$  are the mean parameter values for sequences  $x$  and  $y$  at residue position  $j$ . The values  $x_p$  and  $y_p$  are the mean parameter values for all residues in sequences  $x$  and  $y$ , respectively. A window of five residues was used to smooth both the physical parameter profiles and the final correlation values. The correlations for all physical parameters were averaged for an overall correlation between sequences at a given window position (Argos *et al.*, 1983).

In addition, the more recent method of Argos (Argos, 1987) was also used. This method is an extension of the method described above. In addition to physical parameters, a Dayhoff mutation matrix is used for the comparison. Also, sequences are aligned using a multiple windowing approach, where all parts of a given sequence are compared to all parts of another sequence. Window lengths from 5 to 35 were used in the comparison.

**(b) Oscillator Strength Ratio Determination.** Highly purified phytochrome (the purity index or SAR > 1.1) was isolated by a modification of the Vierstra & Quail (1983) and Chai *et al.* (1987b) methods as previously described (Sommer and Song, 1990). Spectra were recorded with a Hewlett-Packard 8452 diode-array spec-



**Figure 1.** Pr (a,b and e) and Pfr (c and d) chromophores are shown in both the extended (a and c) and the semicyclic (b and d) conformations. The pyrrole rings and the C-5, C-10, and C-15 positions are labeled in a. All chromophores have a formal positive charge on the ring C pyrrole nitrogen atom. The propionate side chains on the rings B and C are not protonated. Chromophore conformations and configurations are as follows: (a) C<sub>5</sub>-Z,anti, C<sub>10</sub>-Z,syn, C<sub>15</sub>-Z,anti, (b) C<sub>5</sub>-Z,syn, C<sub>10</sub>-Z,syn, C<sub>15</sub>-Z,anti, (c) C<sub>5</sub>-Z,anti, C<sub>10</sub>-Z,syn, C<sub>15</sub>-E,anti, (d) C<sub>5</sub>-Z,syn, C<sub>10</sub>-Z,syn, C<sub>15</sub>-E,anti, and (e) C<sub>5</sub>-Z,anti, C<sub>10</sub>-Z,syn, C<sub>15</sub>-Z,syn.

trophotometer. Photoconversion was carried out using a Fiber-Lite Model 190 fiber optic illuminator from Dolan-Jenner Industries, Inc. (Woburn, MA). Irradiation was continued until no further photoconversion was observed. Red (660 nm) and far-red (730 nm) interference filters (halfband width =  $10 \pm 2$  nm) from The Optometrics Corporation (Ayer, MA) were used for wavelength selection.

The fitting of phytochrome spectra to Gaussian curves was performed on a SUN Spark Station 1 + GX using the spectral analysis program provided by General Electric NMR Instruments Corp. A baseline of  $Y = 0$  was used for the curve fitting. Fits obtained for spectra in wavelength (nm) were converted to wavenumber ( $\text{cm}^{-1}$ ) before integration to yield oscillator strengths. The oscillator strength ratio ( $f_{\text{vis}}/f_{\text{uv}}$ ) of the visible region divided by the near-UV or Soret region was determined from these Gaussian integrals.

**(c) Production of the Initial Phytochrome Model: The Chromophore.** All modeling calculations were performed on a Silicon Graphics workstation IRIS 4D/320 VGX using MOPAC 6<sup>1</sup> for the semiempirical and

Discover<sup>2</sup> for the force field algorithms. The program Insight II was used for graphics display and model building.

We selected two representative conformations for the noncyclic tetrapyrrole phytochrome chromophore to insert into a model derived from the  $\beta$  subunit extracted from the crystal structure of constitutive C-phycocyanin from *Fremyella diplosiphon*. The two chromophore conformations (Song *et al.*, 1991 for review) chosen were extended (*anti-syn-anti*; Figure 1a,c) and semicyclic (*syn-syn-anti*; Figure 1b,d). Oscillator-strength ratios of the phytochrome spectra are consistent with a semicyclic conformation of the chromophore (Song *et al.*, 1979; Song and Chae, 1979; see discussion below). However, the extended form of the chromophore (Figure 1a,c) is considered to be a viable option because of the similarities between phytochrome and C-phycocyanin. A third possible chromophore conformation, the semicyclic *anti-syn-syn* (Figure 1e), was considered unlikely, since it would require the conjugated chromophore rings B, C, and D to be

<sup>1</sup> Available from QCPE (Bloomington, IN).

<sup>2</sup> Discover and Insight II are distributed by Biosym Technologies Inc., San Diego, CA.

extensively nonplanar, and is not consistent with oscillator-strength ratios or transition dipole angles (Song & Chae, 1979).

It appears that a *Z* to *E* photoisomerization at C-15 (ring D is turned; Figure 1) is the primary structural change in the chromophore upon photoisomerization (Rüdiger *et al.*, 1983; Rüdiger, 1987; Farrens *et al.*, 1989; Fodor *et al.*, 1990). We have examined both *Z* (Pr chromophore; Figure 1a, 1b) and *E* (Pfr chromophore; Figure 1c, 1d) configurations at C-15 of the semicyclic and extended conformations.

The chromophore structure present in  $\beta$  C-phycocyanin from the three-dimensional structure was used as the starting point for modeling the extended conformation (Pr form); the ethyl group of the C-phycocyanin was replaced by a vinyl group in the model. The starting geometries of the semicyclic chromophores and extended Pfr chromophore were derived from force field calculations using the Newton-Raphson algorithm starting from a planar geometry. This minimization routine was selected because it yielded excellent results on the extended conformation. For example, the root mean square (rms) deviation between the backbone of the minimized chromophore (extended) and the C-phycocyanin chromophore was 0.37 Å using the Newton-Raphson algorithm. By contrast, force field calculations using steepest decent, conjugate gradients (Fletcher & Reeves, 1964; Fletcher, 1980, for review), and quasi-Newton-Raphson (Fletcher, 1980, for reviews) algorithms, as well as MOPAC 6 (Stewart, 1990) with AM1 parameterization (Dewar *et al.*, 1985), all yielded structures which were considerably out of plane compared with that observed in the C-phycocyanin chromophore structure.

**(d) Production of the Initial Phytochrome Model: The Protein.** We selected the  $\beta$  subunit of C-phycocyanin to model phytochrome. The  $\beta$  subunit was chosen over the  $\alpha$  subunit because the  $\beta$ -84 chromophore contacts, unlike those for the  $\alpha$ -84 chromophore, are confined to the monomer (Duerring *et al.*, 1991). In addition, Arg-79 is present in the  $\beta$  subunit but not in the  $\alpha$  subunit in the *Fremyella* structure. Residues Arg-79 to Val-95 to the C-phycocyanin sequence were replaced by Arg-318 to Ile-334 of the *Avena* phytochrome sequence (Hershey *et al.*, 1985). (This sequence is identical to the *Oryza* and *Cucurbita* type I phytochrome sequences.)

In native C-phycocyanin there is a tyrosine (Tyr-119) on the helix F side of the chromophore that is in hydrogen-bonding distance to Asp-87. This allows room for the Asp-87 in the C-phycocyanin to coordinate with the nitrogens of rings B and C of the chromophore. In the model structure, however, this tyrosine precludes interaction of the more bulky glutamine residue with the ring nitrogens. Further, since Asp-87 of C-phycocyanin is replaced by a Gln residue in the model, any hydrogen bonding at position 87 must be different in the model compared to C-phycocyanin. Rather than substantially reorient the tyrosine and possibly helix F, we developed our model using a phenylalanine in place of the tyrosine at position 119.

The replacement procedure used held backbone atoms constant. In addition, all torsion angles that the new residue had in common with the previous residue were maintained. After amino acid replacement, the semicyclic chromophore was superimposed on the C-phycocyanin tetrapyrrole using the ring B and ring C heavy atoms. After some minor readjustment of the linker group (both Cys-84 and the chromophore side chain) and modest adjustment of the model in the binding pocket, the chromophore was attached to the peptide backbone. All

calculations were performed with a 5.0-Å solvent shell around the protein monomer except at regions where contact with other subunits took place. Since calculations were performed on a single monomer, these subunit contact areas were constrained throughout the calculations.

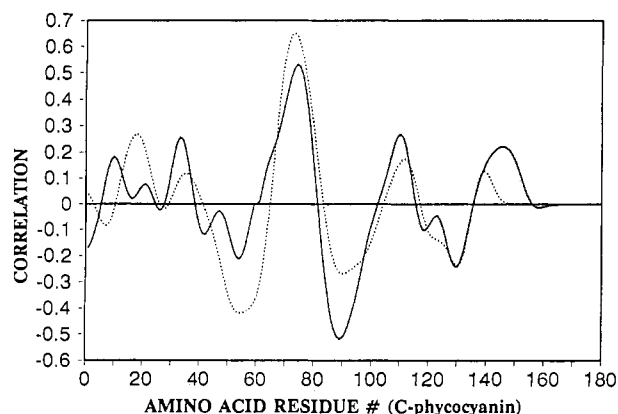
Myoglobin has a very similar fold around its heme group to that which C-phycocyanin has around its chromophore (Schirmer *et al.*, 1985). The similar folding pattern between C-phycocyanin and myoglobin exists even though there is essentially no sequence homology. That is, the degree of homology between C-phycocyanin and myoglobin is not dramatically different than that between phytochrome and C-phycocyanin, even though considerable structural similarities have been demonstrated. Thus, we also examined myoglobin as a potential model for phytochrome.

**(e) Minimization.** A conjugate gradient minimization (Fletcher and Reeves, 1964) was used for all models. A standard approach was adopted for the minimization process (Greer, 1991). All heavy atoms were initially constrained to their original position. Constraints on side chain atom movement were released after a few iterations (once the rms derivative dropped below 10 kcal mol<sup>-1</sup> Å<sup>-1</sup>). After initial chromophore minimization within the pocket, its coordinates were fixed and the surrounding residues were released for refinement. This approach was developed after initial unrestrained minimization of the entire pocket had yielded chromophore conformations that were considerably more out of plane than expected. Once a rms derivative of approximately 0.2 kcal mol<sup>-1</sup> Å<sup>-1</sup> was reached, all restraints were removed from the chromophore and surrounding residues. Force constants between 100 and 500 kcal mol<sup>-1</sup> Å<sup>-1</sup> were used to constrain atoms to their original positions. Convergence was set at 0.1–0.15 kcal mol<sup>-1</sup> Å<sup>-1</sup> rms derivative for all minimizations of phytochrome models. After minimization of the model, residues present in other phytochrome sequences not identical to the *Avena* sequence were introduced into the model using the replacement procedure described above (for sequences and references, see Quail *et al.*, 1991) to assess the validity of the model.

### 3. RESULTS

**(a) Correlation.** The correlations (Argos *et al.*, 1983) between the fragment of phytochrome (–RAPHSC\*HLQYMENMNSIASLVMA–; C\* is chromophore bound) and the  $\alpha$  and  $\beta$  subunits of C-phycocyanin are shown in Figure 2. There is a distinct maximum in the correlation near the chromophore binding pocket of C-phycocyanin. This alignment of the phytochrome fragment with C-phycocyanin is shown in Scheme 1. In contrast, the correlation achieved in the rest of the sequence is maximally 50% of that achieved at the chromophore binding pocket (Figure 2). The maximum correlation of the phytochrome fragment occurs at C-phycocyanin residue 74 of the  $\beta$  subunit and at residue 73 of the  $\alpha$  subunit (corresponding to the peaks in Figure 2). Perfect alignment of the chromophore binding cysteines would occur at a sequence alignment at residue 79 (Scheme 1).

Although the correlation using phytochrome residues Arg-318 to Ala-340 (Figure 2; numbering according to the *Avena* type I sequence is used throughout) is reasonably clear, there is no distinct correlation in the region immediately surrounding this area. This was demonstrated using the window approach of Argos (Argos, 1987). In the  $\beta$ -subunit, the alignment extended from phycocy-

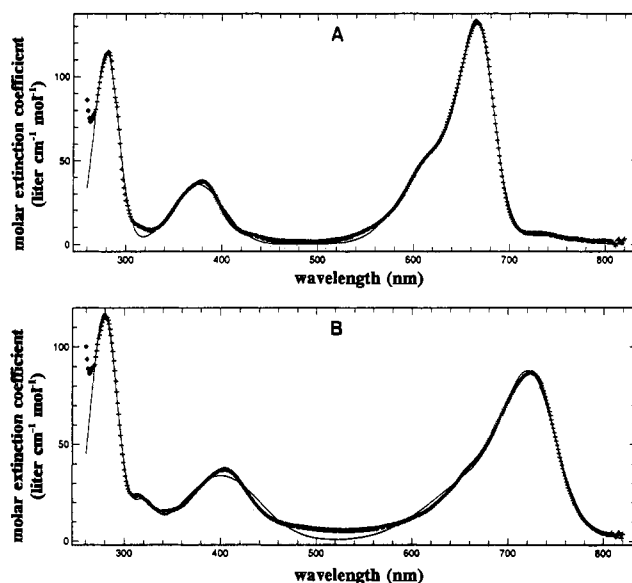


**Figure 2.** Correlation diagram using the method of Argos *et al.* (1983) is displayed. The phytochrome sequence fragment RAPHSCHLQYMNMSIASLVMA was correlated with both  $\alpha$  C-phycoerythrin (---) and  $\beta$  C-phycoerythrin (—) sequences using different window positions (x axis) of the smaller phytochrome fragment. The best alignment occurred when the phytochrome fragment was within five or six residues of the chromophore binding site of both C-phycoerythrins (maxima in figure).

anin residue 81 to residue 103, but not beyond. In the aligned region, the alignment was 3.1 standard deviations above the mean alignment score. This lack of extended alignment is evident at helix F of C-phycoerythrin, where there is close interaction with the chromophore. If an extended alignment of the two sequences is made starting from the chromophore binding pocket, the corresponding region of phytochrome (a) contains a proline in the center, (b) is very poorly conserved, and (c) contains deletions or additions in several of the known phytochrome sequences. For these reasons, we elected to model only the helix E region near the chromophore (residues 79–95).

**(b) Oscillator Strength Ratios.** The spectra of the Pr and Pfr forms of phytochrome are shown in Figure 3. The sum of Gaussian distributions which produced the best fit is also displayed. The visible and Soret bands of the Pr spectra were fit using three Gaussian distributions [1,  $A = 35.7$ ,  $W = 61.5$ ,  $S = 375.1$ ; 2,  $A = 58.4$ ,  $W = 86.6$ ,  $S = 630.3$ ; 3,  $A = 97.5$ ,  $W = 37.5$ ,  $S = 667.1$ , where  $A$  = amplitude in molar extinction,  $W$  = width (in nm), and  $S$  = shift (in nm)]. The visible and Soret bands of the Pfr spectra were also fit using three Gaussian distributions (1,  $A = 34.0$ ,  $W = 92.6$ ,  $S = 400.7$ ; 2,  $A = 36.7$ ,  $W = 36.7$ ,  $W = 129.8$ ,  $4S = 680.0$ ; 3,  $A = 60.4$ ,  $W = 59.3$ ,  $S = 723.9$ ). Integration of the Gaussian curves and division of the integral or oscillator strength of the visible region by the integral of the near-UV region or Soret band (ratio =  $f_{\text{vis}}/f_{\text{uv}}$ ) yielded results similar to previous work which did not utilize curve-fitting methods (Song *et al.*, 1979; Song and Chae, 1979). A value of 0.88 was obtained for Pfr and 1.36 was obtained for Pr. These values lie between ratios calculated for extended and cyclic chromophores (Table 1) and are consistent with a semicyclic conformation for the phytochrome tetrapyrrole.

**(c) Phytochrome Models.** Replacement of C-phycoerythrin (Arg-79 to Val-95) with phytochrome residues (Arg-318 to Ile-334; numbering according to the *Avena* type I sequence; Hershey *et al.*, 1985) produced no bad contacts in the protein. Figure 4 illustrates the minimized structure of the C-phycoerythrin ( $\beta$  subunit) based model with the residues that were changed to the phytochrome sequence shown as CPK structures. The modified region of the C-phycoerythrin comprises 10% of the  $\beta$  subunit (Figure 4). The modified region interacts with the majority of the rest of the structure, with the exception of the X and Y helices (bottom of Figure 4). These helices are involved



**Figure 3.** Spectra of (A) Pr and (B) Pfr phytochrome are shown (+++). The sum of the Gaussian curves used to fit the phytochrome spectra is also included (—). Data points in the UV region not used for the curve fitting are circled. The Pfr spectrum was obtained by subtraction of a 12% contribution of the Pr form to the photoequilibrated Pfr spectrum (Lagarias *et al.*, 1987).

**Table 1. Oscillator Strength Ratios (Visible over Soret or Near-UV;  $f_{\text{vis}}/f_{\text{uv}}$ ) of Several Chromoproteins and Free Chromophores**

chromophore or protein	chromophore conformation	$f_{\text{vis}}/f_{\text{uv}}$
isophorobilin	extended	6.4 <sup>a</sup>
C-phycoerythrin	extended	4.1 <sup>b</sup>
Pr phytochrome	semicyclic? <sup>c</sup>	1.36 <sup>d</sup>
Pfr phytochrome	semicyclic? <sup>c</sup>	0.88 <sup>d</sup>
denatured C-phycoerythrin	cyclic or cyclohelical	0.43 <sup>b</sup>
21,24-methanobilindione	cyclic	0.15 <sup>c</sup>

<sup>a</sup> Determined by Glazer and Hixon (1971). <sup>b</sup> Determined by Scheer and Kufer (1977). <sup>c</sup> Unknown conformation. <sup>d</sup> Determined by integration of Gaussian curves obtained from the spectra in Figure 3. <sup>e</sup> Determined by Falk and Thirring (1981).

in interaction with other subunits in the C-phycoerythrin complex and not in monomer chromophore interaction.

Most amino acid replacements filled the same space and were involved in the same interactions as were the corresponding original amino acids in the initial C-phycoerythrin template. Two exceptions to this were the replacement of Ala-83 with serine, and the replacement of Asp-87 with glutamine. In the case of Asp-87 substitution, the model glutamine was initially placed so that the carbonyl of the side chain hydrogen bonded with the chromophore in a similar fashion as did the aspartate in the original C-phycoerythrin structure. This was done in order to satisfy hydrogen-bonding requirements of the chromophore. An alternative and unexplored approach may be the inclusion of a water molecule in the chromophore pocket. It was also possible to initially position the Ala-83 replacement (serine) in one of two positions. The first, with the hydroxyl group exposed to solvent, seemed to be the less stable, as the serine in this position minimized to a second position, hydrogen bonded to the E-helic backbone at Arg-79.

The myoglobin-based modeling attempt, unlike the C-phycoerythrin-based system, did not give satisfactory results. Initial replacement of the heme group with the minimized phytochrome chromophore was accomplished



## Scheme 1

MLDAFAKVVVSQADARGEYLSGSQIDALSALVADGNKRMDVVNRITGNSSTIVANAARS

LFAEQPGLIAPGGNAYTSRRMAA $\text{CLRDMEILRYVTYAIFAGDASVLDDRCLNGLKET}$   
RAPHS $\text{CHLQYMNMNNSIASLVMA}$ 

YLALGTPGSSVAVGVQKMKDAALAIAGDTNGITRGDCASLMAEVASYFDKAASAVA

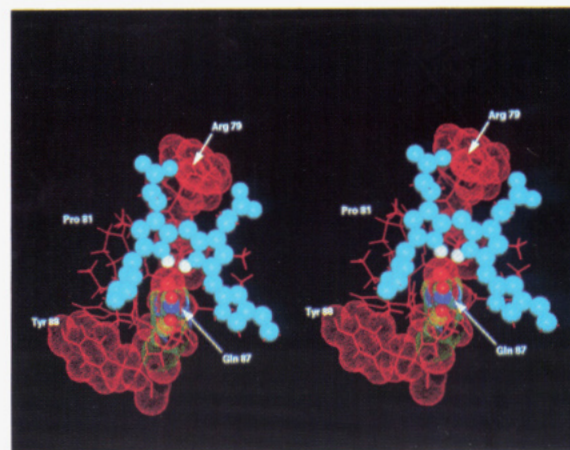


**Figure 4.** Phytochrome model developed from the  $\beta$  subunit of C-phycoerythrin is shown with all atoms of residues Arg-79 to Ile-95 shown as  $1.0 \times$  van der Waals radii CPK models. The chromophore is also displayed as a  $1.0 \times$  van der Waals radii CPK model.

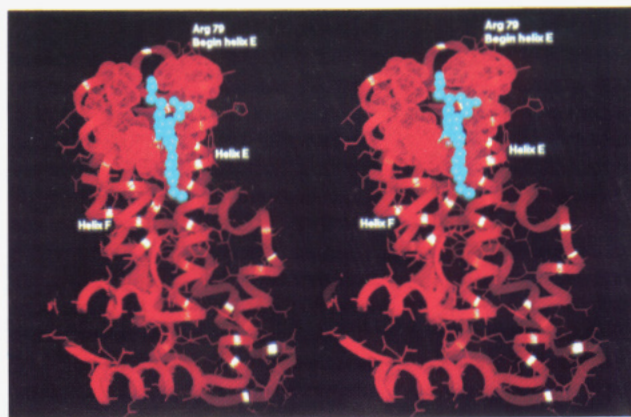
using superposition of rings B and C of the heme and phytochrome chromophore. Readjustment of the chromophore to allow for covalent attachment to helix E required a dramatic movement of ring A (7 Å), but little movement of rings C and D. This resulted in a large hole in the center of the protein (several angstroms wide) that could not readily be filled by neighboring protein side chain atoms. Thus, a modeling approach based on myoglobin was not pursued.

The rms deviation (in the final stages of minimization) between unconstrained backbone atoms of the model and the initial C-phycoerythrin structure was 1.45 Å for the extended chromophore conformation and 1.53 Å for the semicyclic chromophore. The primary difference in backbone position occurred in the loop between helix F' and helix G. A similar difference was also noted upon minimization of the monomeric  $\beta$ -subunit of C-phycoerythrin. The rms deviation between the minimized and unminimized C-phycoerythrin was 1.31 Å (using all backbone atoms which were not constrained in the final stages of minimization). The structural difference after minimization is probably, at least in part, a result from minimization of the  $\beta$  monomer in the absence of the rest of the  $(\alpha\beta)_6$  complex. In addition, the F helix is not well-resolved in the crystal structure, and may therefore have some flexibility. Regardless of the cause, similar conformational changes in the peptide backbone seen after minimization of the model occur during minimization of the native C-phycoerythrin structure.

The chromophore region of the phytochrome model developed using a semicyclic conformation of the chromophore is shown in Figure 5. The interactions of Gln-87 with the ring B and ring C nitrogen atoms and the interactions between Arg-79 and the ring B propionic acid side chain are evident in the figure. Rings B and C are both within hydrogen-bonding distance to the Gln-87 side chain. The van der Waals contact between Tyr-88 of the model with ring A and the moiety linking the protein to the chromophore can also be seen in Figure 5 (bottom left



**Figure 5.** Stereo pair of part of the phytochrome model using the semicyclic chromophore. The Pfr chromophore configuration (*E* at C-15) is shown in this model. Residues Arg-79 to Tyr-88 are displayed with the chromophore in the foreground. The heavy atoms of the chromophore tetrapyrrole, heavy atoms of the vinyl and propionic acid side chains of the chromophore, heavy atoms of the Gln-87 side chain, and the hydrogens on the ring B and ring C nitrogens are shown as CPK structures with surfaces at  $0.5 \times$  van der Waals radii. Arg-79, Ser-83, and Tyr-88 are represented with a dotted surface at  $1.0 \times$  van der Waals radii.

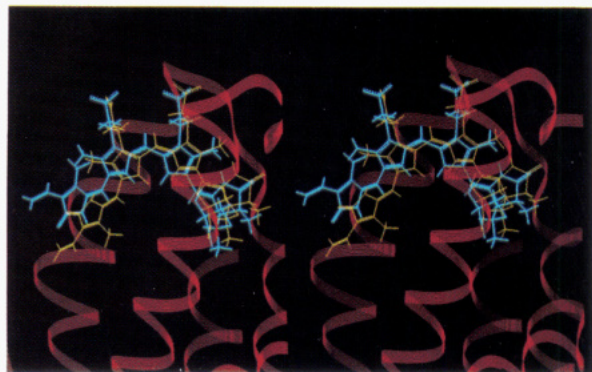


**Figure 6.** Stereo pair photograph of the phytochrome model taken using the semicyclic Pr (*Z* at C-15) chromophore conformation. Ring D is in the bottom front while ring A is in the background. Helix F is to the left of the chromophore and helix E is to the right of the chromophore. The surface of residues immediately surrounding the chromophore are represented with a dotted surface at  $1.0 \times$  van der Waals radii. Heavy atoms of the tetrapyrrole and heavy atoms of the vinyl and propionic acid chromophore side chains are shown as CPK models at  $0.5 \times$  van der Waals radii.

of figure). The out of plane geometry of ring A with respect to the rest of the chromophore in the semicyclic conformation is apparent in the figure.

Figure 6 illustrates the semicycle chromophore in the binding pocket of the phytochrome model. The residues immediately surrounding the chromophore are highlighted at the van der Waals surface. In this stereoscopic





**Figure 7.** Superimposed extended Pfr and extended Pr models. The Pr chromophore is shown in yellow and the Pfr chromophore in blue. The ribbon of the Pr model is displayed.

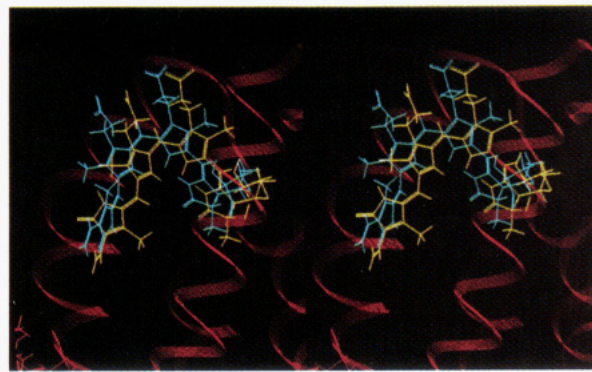
projection, helix E is on the right-hand side of the chromophore and helix F is on the left. Interaction of Arg-79 with the propionic acid side chain of ring B can be seen at the top right of the figure. This model contains two hydrogen bonds between this propionic acid and Arg-79. Arg-79 does not approach the ring C propionic acid side chain as closely. The apparent anchoring of the chromophore by helix E is also evident in Figures 6 and 7. Both Gln-87 (from below) and Arg-79 (from above) appear to hold the chromophore in place. The side chain of Ser-83, between Arg-79 and Gln-87 in Figure 6, forms a hydrogen bond to the backbone of helix E in the model. Helix F (left side of the figure) appears to provide a hydrophobic surface for the chromophore to rest against (Figure 6).

The chromophore pocket modeled using an extended chromophore conformation yielded a similar result as described above for the semicyclic chromophore. In both the semicyclic and extended models, the tetrapyrrole backbone of the chromophore is largely buried in the protein. However, the outside edge of rings C and D and the ring D vinyl group are relatively exposed to solvent. The ring B and ring C propionic acid side chains are also quite exposed and hydrogen bonded to solvent molecules in the model structure.

It is interesting that ring D, which is significantly rotated during photoisomerization (*Z* to *E* configurational change at C-15), is the most exposed to solvent. In this respect, the model is similar to the native C-phycocyanin structure, where ring D is not well anchored in the protein monomer and is often not resolved well in the crystal structure (Schirmer *et al.*, 1985, 1986). The ring D exposure does allow for rotation during photoisomerization, and there are no hydrogen-bonding interactions of this ring with the surrounding protein.

Figure 7 shows the extended Pr and Pfr chromophores superimposed on each other. All atoms were used for the superimposition calculation. It is evident that the Pfr chromophore (blue) is shifted out for the chromophore pocket relative to the Pr chromophore (yellow). The Pr chromophore has the hydrophobic side of ring D relatively deeply buried in the hydrophobic interior of the protein compared to the Pfr chromophore (blue). Ring D of the Pfr chromophore, on the other hand, is positioned such that the hydrophobic side that the hydrophobic side is exposed to solvent, while the hydrophilic side faces the hydrophobic interior of the protein. This repositioning of the hydrophobic and hydrophilic sides of ring D likely results in the shift of the Pfr chromophore out of the chromophore pocket.

Figure 8 illustrates the semicyclic Pr (yellow) and Pfr (blue) chromophores. As was the case in the extended



**Figure 8.** Superimposed semicyclic Pfr and Pr models. The Pfr chromophore is illustrated in blue and the Pr chromophore in yellow. The Pr ribbon is shown.

models, the semicyclic Pr chromophore is more deeply buried in the protein pocket than the Pfr chromophore (Figure 8). The Pfr chromophore (blue) is positioned toward the top and further away from helix E compared to the semicyclic Pr chromophore (a viewed in Figure 8). On the other hand, the extended Pfr chromophore (Figure 7, blue chromophore) is shifted to the left compared to the extended Pr chromophore (Figure 7, the same viewpoint is used as in Figure 8).

#### 4. DISCUSSION

When Parker *et al.* (1950) first noted the spectral similarity between C-phycocyanin and phytochrome, they pointed out the possibility that phytochrome may also be an open chain tetrapyrrole, similar to C-phycocyanin. Given this and the similarities between the two proteins discussed by a number of authors, it is not surprising that the correlation of the phytochrome chromophore pocket with the C-phycocyanin sequence would yield some similarity near the chromophore pocket of C-phycocyanin. The correlation is shifted five or six residues to the N-terminus of the phycocyanin sequence (Scheme 1). This is the width of the smoothing window used and may have little significance. On the other hand, minimization of the phytochrome model has indicated that helix E of phytochrome may be several residues shorter than helix E of C-phycocyanin, thus accounting for the difference. This putative shortening of helix E may be caused by hydrogen bonding of Ser-83 to the peptide backbone, as indicated by force field calculations.

The oscillator strength ratio of the visible over the Soret bands ( $f_{\text{vis}}/f_{\text{uv}}$ ) is considered to be a clear indicator of the conformation of a tetrapyrrole (Song *et al.*, 1979; Scheer, 1981, for review). Linear tetrapyrroles have a relatively large  $f_{\text{vis}}/f_{\text{uv}}$ , as the spectra resemble that of a linear polyene. Cyclic tetrapyrroles, on the other hand, possess a much smaller  $f_{\text{vis}}/f_{\text{uv}}$ , as illustrated in Table 1. The Gaussian fitting of the phytochrome spectra (Figure 3) followed by determination of the  $f_{\text{vis}}/f_{\text{uv}}$  for both forms of phytochrome (Table 1) demonstrates that the  $f_{\text{vis}}/f_{\text{uv}}$ , and presumably the chromophore conformation of phytochrome, lie between the extended and cyclic forms. MO calculations have been performed on a number of chromophore conformations in the past (Chae, 1977). These calculations on almost 30 chromophores yielded an average  $f_{\text{vis}}/f_{\text{uv}}$  of 17.3 for extended chromophores, 1.29 for semicyclic chromophores, and 0.21 for cyclic ones. These numbers are qualitatively consistent with phytochrome containing a semicyclic chromophore; experimental evidence has not yet been obtained. Also, the modeling results do not provide any clear indication as to whether the extended or semicyclic chromophore is more suitable.



Helix E in the chromophore pocket of C-phycocyanin is involved in anchoring the chromophore, similar to the model. In addition, helix F or C-phycocyanin, like the model, is acting much like a hydrophobic surface for the chromophore to rest against. Helix F is structurally critical for chromophore-protein interactions. There is, however, virtually no sequence conservation between the  $\alpha$  and  $\beta$  subunits of C-phycocyanin in the helix F region. It appears that this structure (a hydrophobic surface) may be formed by a variety of sequences in C-phycocyanin and is therefore not conserved. If a predominantly structural rather than functional role of helix F is present in phytochrome, the possible implications are quite interesting. First, the exact sequence of helix F may not be critical to the chromophore conformation or the function of the chromophore and thus may not be highly conserved. A predominantly structural role of helix F would indicate that helix E has an important functional role during phototransformation. This must be the case if the model is valid, since the chromophore undergoes a 31° (or 149°) movement during phototransformation (Sundqvist and Bjorn, 1983; Ekelund *et al.*, 1985). This chromophore movement would require considerable involvement of helix E in the model, since this helix is anchoring the chromophore (Figures 6 and 7).

With this in mind, it is interesting to note that the semicyclic Pfr chromophore is shifted away from helix E compared to the Pr chromophore (Figure 8). This is not the case for the extended chromophore-containing model (Figure 7). Both Pfr chromophores (semicyclic and extended) are considerably shifted out of the chromophore pocket compared to the Pr chromophores (figures not shown). This results in a more solvent exposed Pfr chromophore. It is not likely that models using the same chromophore pocket can be viable for both the Pr and Pfr chromophores since the chromophore undergoes a substantial movement upon photoconversion (31° or 149°; Sundqvist and Bjorn, 1983; Ekelund *et al.*, 1985). The chromophore is inserted *in vivo* in the Pr form. In addition, the Pr spectrum, not the Pfr spectrum, is similar to the C-phycocyanin spectrum. Thus, the present model based on the Pr chromophore is more likely viable than the Pfr model. However, the initial photoisomerization from Pr to Pfr does not entail the *Z* to *E* isomerization at C-15. This is presumably followed by reorientation and exposure of the chromophore (movement from the Pr pocket; Hahn *et al.*, 1984). The present model suggests a mechanism for this. The removal/exposure of the hydrophobic side of ring D toward the exterior and insertion of the hydrophilic side of ring D into the hydrophobic core of the protein may force the chromophore to move out of the pocket. This is consistent with the shifting of both extended (Figure 7) and semicyclic (Figure 8) model Pfr chromophores out of the chromophore pocket compared to the model Pr chromophores. Our model also suggests an explanation for the red shift of the first intermediate upon conversion of Pr to Pfr. This spectral shift from 666 to 700 nm involves 34 nm (Eifeld and Rüdiger, 1985). The model accounts for this initial shift, since exposure of the conjugated ring system (around ring D in the model) will cause a red shift of any absorbance band. The apparent compatibility of our model with both (a) a photoisomerization mechanism and (b) spectral qualities of the first Pr to Pfr intermediate adds credibility to the model as a basis for future experimental design.

We take the fact that the initial replacement of C-phycocyanin residues with phytochrome residues produced no bad contacts (even without torsion angle adjustment; data not shown) as a good indication that the

model is a viable one. This is especially true given the large volume of protein modified and the extensive interaction of that region with the rest of the protein (Figure 4). A further indication that the model is viable is the observation that other phytochromes, including type II phytochrome, contain differences in their sequences which still accommodate the backbone conformation and side chain positions of the model. All amino acid differences which have been published (see Quail *et al.*, 1991 for sequences and references) were inserted into the minimized phytochrome model. No bad contacts were found (data not shown). This is to be expected for a valid model, since the conformations of different phytochromes should be highly conserved near the chromophore given the fairly high degree of primary sequence conservation in the molecule near that region.

The sequence of *Solanum* (potato) type I phytochrome was reported recently by Heyer and Gatz (1992) and serves to strengthen the viability of the models developed here. This sequence has a tyrosine residue at position 322 which is immediately N-terminal to the chromophore attachment site. All other type I phytochromes have a serine at this position. Starting with the model developed from the C-phycocyanin structure and the *Avena* sequence (Figures 4 and 6–8), we replaced the relevant serine (Ser-83) with a tyrosine. The resultant structure, after minimization, showed virtually no change in backbone conformation or chromophore position from the *Avena* model (rms deviation of all unconstrained residues = 0.012 Å). In the potato model, the tyrosine residue is parallel to the chromophore at a van der Waals contact distance. In addition, there is a possible hydrogen bond between the tyrosine hydroxyl and the ring C propionate.

There are a number of difficulties that must be hurdled before phytochrome can be crystallized. Not only is purification of native phytochrome difficult, but solubility is often poor, partially unfolded molecules as well as copurifying contaminants are generally present in preparations, multiple phytochrome genes are expressed *in vivo*, and purification of transgenic phytochrome has not been achieved. Although a crystal structure may seem out of reach at this time, transgenic studies on the phytochrome protein are proceeding at a rapid pace (Deforce *et al.*, 1991; Wahleithner *et al.*, 1991; Cherry *et al.*, 1992; Stockhaus *et al.*, 1992). These developments necessitate a viable model on which to base intelligent decisions for mutant generation and analysis. We have used the known structure of C-phycocyanin to produce a reasonable model of the phytochrome chromophore and surrounding pocket. This model has already been used to design mutagenesis experiments (Deforce *et al.*, 1993). In particular, Arg-318, Ser-322, and Gln-326 (numbering according to the type I *Avena* sequence) interact closely with the chromophore of the model. Modification of one or more of these residues should produce considerable spectral and/or photochemical differences between the wild type and the modified protein in at least one form (Pr or Pfr). Other mutations, while perhaps less straight forward to interpret, may also serve to test the model. For example, the E helix, and therefore the chromophore pocket, should be disrupted by insertion of prolines between Ser-322 and Gln-332. The same effect is not expected in the region N-terminal to Ser-322. Modification of Tyr-327 to a smaller residue will generate a void in the center of the protein. This should destabilize the chromophore binding region without direct interaction with the chromophore. The use of multiple replacements at these positions would be an excellent test of the model.



The replacement of the entire region in phytochrome with C-phycoyanin residues would serve as the acid test. This would likely generate a stable Pr molecule, but without photoreversibility to another state. Specifically, Arg-86 and Asp-87 bind the C-phycoyanin chromophore much more strongly than do their corresponding amino acids (Leu and Gln, respectively) in the phytochrome model.

Experimental testing of the model, perhaps as described above, is necessary to verify its viability. The modeling we report is based on much less sequence homology than is necessary to yield a readily accepted model in the absence of supporting experimental evidence. Future experimental data may also result in improvement of the model by movement of side chains and/or by chromophore reorientation. In addition, it is probable that "inverse folding" algorithms such as the one proposed by Jones *et al.* (1992) may also serve as a validity check of the model. Such a three-dimensional test may require the inclusion of multiple subunits in the analysis, since subunit contacts effect solvent accessibility in the phycocyanin structure. It is anticipated that the current work will catalyze further development of three-dimensional phytochrome models, using newly developed folding algorithms (Jones *et al.*, 1992, for example) and/or experimental results.

#### ACKNOWLEDGMENT

We thank Prof. Dr. Robert Huber for X-ray coordinates of C-phycoyanin from *Fremyella diplosiphon* and Drs. Jenny P. Glusker and Mick Partis for helpful discussion. Also, we thank Todd Wells for the spectra of highly purified phytochrome, Drs. Rich Shoemaker and Kurt Wulser for curve fitting of spectra, and Susanne Meza-Keuthen for help with preparation of the manuscript. This work was supported in part by USPHS NIH Grant RO1-GM36956 and NSF Grant CHE-9214428. P.G. also wishes to thank the UNL Center of Biotechnology for a graduate fellowship.

#### LITERATURE CITED

- Arciero, D. M., Bryant, D. A., and Glazer, A. N. (1988a) *In Vitro* Attachment of Bilins to Apophycocyanin I. Specific Covalent Adduct Formation at Cysteinyln Residues Involved in Phycocyanobilin Binding in C-phycoyanin. *J. Biol. Chem.* **263**, 18343-18349.
- Arciero, D. M., Dallas, J. L. and Glazer, A. N. (1988b) *In Vitro* Attachment of Bilins to Apophycocyanin II. Determination of the Structures of Tryptic Bilin Peptides Derived from the Phycocyanobilin Adduct. *J. Biol. Chem.* **263**, 18350-18357.
- Arciero, D. M., Dallas, J. L. and Glazer, A. N. (1988c) *In Vitro* Attachment of Bilins to Apophycocyanin III. Properties of the Phycoerythrobilin Adduct. *J. Biol. Chem.* **263**, 18358-18363.
- Argos, P. (1987) A Sensitive Procedure to Compare Amino Acid Sequences. *J. Mol. Biol.* **193**, 385-396.
- Argos, P., Henei, M., Wilson, J. M. and Kelly, W. N. (1983) A Possible Nucleotide-Binding Domain in the Tertiary Fold of Phosphoribosyl Transferases. *J. Biol. Chem.* **258**, 6450-6457.
- Bowie, J. U., Luthy, R. and Eisenberg, D. (1991) A Method to Identify Protein Sequences That Fold into a Known Three-Dimensional Structure. *Science* **253**, 164-170.
- Chae, Q. (1977) Excited States of Photomorphogenic and Visual Receptors. Ph.D. Dissertation, pp 31-42, Texas Tech University, Lubbock, TX.
- Chai, Y.-G., Song, P.-S., Cordonnier, M.-M., and Pratt, L. H. (1987a) A Photoreversible Circular Dichroism Spectral Change in Oat Phytochrome Is Suppressed by a Monoclonal Antibody that Binds Near Its N-terminus and by Chromophore Modification. *Biochemistry* **26**, 4947-4952.
- Chai, Y.-G., Singh, B. R., Song, P.-S., Lee, J., and Robinson, G. W. (1987b) Purification and Spectral Properties of 124 kDa Oat Phytochrome. *Anal. Biochem.* **163**, 322-330.
- Cherry, J. R., Hondred, D., Walker, J. M. and Vierstra, R. D. (1992) Phytochrome Requires the 6-kDa N-terminal Domain for Full Biological Activity. *Proc. Natl. Acad. Sci. U.S.A.* **89**, 5039-5043.
- Chou, P. Y. and Fasman, G. D. (1974) Prediction of Protein Conformation. *Biochemistry* **13**, 222-244.
- Deforce, L., Furuya, M., and Song, P.-S. (1993) Mutational Analysis of the Pea Phytochrome A Chromophore Pocket: Chromophore Assembly with Apophytochrome A and Photoreversibility. *Biochemistry* **32**, 14165-14172.
- Deforce, L., Tomizawa, K.-I., Ito, N., Farrens, D., Song, P.-S. and Furuya, M. (1991) *In Vitro* Assembly of Apophytochrome and Apophytochrome Deletion Mutants Expressed in Yeast with Phycocyanobilin. *Proc. Natl. Acad. Sci. USA* **88**, 10392-10396.
- Dewar, M. J. S., Zebisch, E. G., Healy, E. F. and Stewart, J. J. P. (1985) AM1: A New General Purpose Quantum Mechanical Molecular Model. *J. Am. Chem. Soc.* **107**, 3902-3909.
- Duerring, M., Huber, R., Bode, W., Ruembeli, R. and Zuber, H. (1990) Refined Three-Dimensional Structure of Phycoerythrocyanin from the Cyanobacterium *Mastigodladus laminosus* at 2.7 Å. *J. Mol. Biol.* **211**, 633-644.
- Duerring, M., Schmidt, G. B. and Huber, R. (1991) Isolation, Crystallization, Crystal Structure Analysis and Refinement of Constitutive C-phycoyanin from the Chromatically Adapting Cyanobacterium *Fremyella Diplosiphon* at 1.66 Å Resolution. *J. Mol. Biol.* **217**, 577-592.
- Edgerton, M. D. and Jones, A. M. (1992) Localization of Protein-Protein Interactions Between Subunits of Phytochrome. *Plant Cell* **4**, 161-171.
- Eifeld, P. and Rüdiger, W. (1985) Absorption Spectra of Phytochrome Intermediates. *Z. Naturforsch.* **40c**, 109-114.
- Ekelund, N. G. A., Sundqvist, C., Quail, P. H. and Vierstra, R. D. (1985) Chromophore Rotation in 124-kDalton *Avena Sativa* Phytochrome as Measured by Light-Induced Changes in Linear Dichroism. *Photochem. Photobiol.* **41**, 221-223.
- Elich, T. D. and Lagarias, J. C. (1989) Formation of a Photo-reversible Phycocyanobilin-Apophytochrome Adduct *In Vitro*. *J. Biol. Chem.* **264**, 12902-12908.
- Elich, T. D., McDonagh, A. F., Palma, L. A. and Lagarias, J. C. (1988) Phytochrome Chromophore Biosynthesis. *J. Biol. Chem.* **264**, 183-189.
- Falk, H. and Thirring, K. (1981) *Tetrahedron* **37**, 761-766.
- Farrens, D. L., Holt, R. E., Rospendowski, B. N., Song, P.-S. and Cotton, T. M. (1989) Surface Enhanced Resonance Raman Scattering Spectroscopy Applied to Phytochrome and Its Model Compounds 2. Phytochrome and Phycocyanin Chromophores. *J. Am. Chem. Soc.* **111**, 9162-9169.
- Fletcher, R. (1980) *Practical Methods of Optimization*, Vol. 1, John Wiley and Sons, New York.
- Fletcher, R. and Reeves, C. M. (1964) Function Minimization by Conjugate Gradients. *Comput. J.* **7**, 149-154.
- Fodor, S. P. A., Lagarias, J. C. and Mathies, R. A. (1990) Resonance Raman Analysis of the Pr and Pfr Forms of Phytochrome. *Biochemistry* **29**, 11141-11146.
- Fuglistaller, P., Suter, F. and Zuber, H. (1983) The Complete Amino-Acid Sequence of Both Subunits of Phycoerythrocyanin from the Thermophilic Cyanobacterium *Mastigocladus laminosus*. *Hoppe-Seyler's Z. Physiol. Chem.* **364**, 691-712.
- Gabriel, J. L. and Hooper, J. K. (1991) Molecular Modelling of Phytochrome. *J. Theor. Biol.* **151**, 541-556.
- Garnier, J., Osguthorpe, D. J. and Robson, B. (1978) Analysis of the Accuracy and Implications of Simple Methods for Predicting the Secondary Structure of Globular Proteins. *J. Mol. Biol.* **120**, 97-120.
- Glazer, A. N. and Hixon, C. S. (1977) Subunit Structure and Chromophore Composition of *Phodophytan* Phycoerythrins. *J. Biol. Chem.* **252**, 32-41.
- Greer, J. (1991) Comparative Modeling of Homologous Proteins. *Methods in Enzymol.* **202**, 239-252.
- Hahn, T. R., Song, P.-S., Quail, P. H. and Vierstra, R. D. (1984) Tetranitromethane Oxidation of Phytochrome Chromophore

- as a Function of Spectral Form and Molecular Weight. *Plant Physiol.* **74**, 755-758.
- Hershey, H. P., Barker, R. F., Idler, K. B., Lissemore, J. L. and Quail, P. H. (1985) Analysis of Cloned cDNA and Genomic Sequences for Phytochrome: Complete Amino Acid Sequences for Two Gene Products Expressed in Etiolated *Avena*. *Nucleic Acids Res.* **13**, 8543-8559.
- Heyer, A. and Gatz, C. (1992) Isolation and Characterization of a cDNA-clone Coding for Potato type A Phytochrome. *Plant Mol. Biol.* **18**, 535-544.
- Huber, R. (1989) A Structural Basis of Light Energy and Electron Transfer in Biology. *EMBO J.* **8**, 2125-2147.
- Jones, A. M. and Erickson, H. P. (1989) Domain Structure of Phytochrome from *Avena sativa* Visualized by Electron Microscopy. *Photochem. Photobiol.* **49**, 479-483.
- Jones, D. T., Taylor, W. R. and Thornton, J. M. (1992) A New Approach to Protein Fold Recognition. *Nature* **358**, 86-89.
- Lagarias, J. C. Kelly, J. M., Cyr, K. L. and Smith, W. O., Jr. (1987) Comparative Photochemical Analysis of Highly Purified 124 Kilodalton Oat and Rye Phytochromes *In Vitro*. *Photochem. Photobiol.* **46**, 5-13.
- Lagarias, J. C. and Rapoport, H. (1980) Chromopeptides from Phytochrome. The Structure and Linkage of the Pr Form of the Phytochrome Chromophore. *J. Am. Chem. Soc.* **102**, 4821-4828.
- Mazel, D., Houmard, J. and Tandeau de Marsac, N. (1988) A Multigene Family in *Calothrix* sp. PCL 7601 Encodes Phycocyanin, the Major Component of the cyanobacterial Light-Harvesting Antenna. *Mol. Gen. Genet.* **211**, 296-304.
- Parker, M. W., Hendricks, S. B. and Borthwick, H. A. (1950) Action Spectrum for the Photoperiodic Control of Floral Initiation of the Long-Day Plant *Hyoscyamus niger*. *Bot. Gaz.* **111**, 242-252.
- Partis, M. D. and Grimm, R. (1990) Computer Analysis of Phytochrome Sequences from Five Species: Implications for the Mechanism of Action. *Z. Naturforsch.* **45c**, 987-998.
- Phillips, S. E. V. (1980) Structure and Refinement of Oxymyoglobin at 1.6 Å Resolution. *J. Mol. Biol.* **142**, 531-554.
- Quail, P. H., Hershey, H. P., Idler, K. B., Sharrock, R. A., Christensen, A. H., Parks, B. M., Somers, D., Tepperman, J., Bruce, W. B. and Dehesh, K. (1991) Phy-Gene Structure, Evolution, and Expression. In *Phytochrome Properties and Biological Action* (B. Thomas and C. B. Johnson, Eds.) NATO ASI Series, Vol. H 50, pp 13-38, Springer-Verlag, Berlin.
- Rose, G. D. (1978) Prediction of Chain Turns in Globular Proteins on a Hydrophobic Basis. *Nature* **272**, 586-590.
- Rüdiger, W. (1987) Phytochrome: the Chromophore and Photoconversion. *Photobiophys. Photobiophys. (suppl.)* **217-227**.
- Rüdiger, W., Thummler, F., Cmiel, E. and Schneider, S. (1983) Chromophore Structure of the Physiologically Active Form (Pfr) of Phytochrome. *Proc. Natl. Acad. Sci. U.S.A.* **80**, 6244-6248.
- Scheer, H. (1981) Biliproteins. *Angew. Chem. Int. Ed. Engl.* **20**, 241-261.
- Scheer, H. and Kufer, W. (1977) Conformational Studies on C-phycocyanin from *Spirulina platensis*. *Z. Naturforsch. C* **32**, 513-519.
- Schirmer, T., Bode, W., Huber, R., Sidler, W. and Zuber, H. (1985) X-ray Crystallographic Structure of the Light-Harvesting Biliprotein C-phycocyanin from the Thermophilic Cyanobacterium *Mastigodladus laminosus* and its Resemblance to Globin Structures. *J. Mol. Biol.* **184**, 257-277.
- Schirmer, T., Huber, R., Schneider, M., Bode, W., Miller, M. and Hackert, M. L. (1986) Crystal structure Analysis and Refinement at 2.5 Å of Hexameric C-phycocyanin from the Cyanobacterium *Agmenellum quadruplicatum*. *J. Mol. Biol.* **188**, 651-676.
- Siegelman, H. W., Turner, B. C., and Hendricks, S. B. (1966) The Chromophore of Phytochrome. *Plant Physiol.* **41**, 1289-1292.
- Song, P.-S. and Chae, Q. (1979) The Transformation of Phytochrome to its Physiologically Active Form. *Photochem. Photobiol.* **30**, 117-123.
- Song, P.-S., Chae, Q. and Gardner, J. G. (1979) Spectroscopic Properties and Chromophore Conformations of the Photomorphogenic Receptor: Phytochrome. *Biochim. Biophys. Acta* **576**, 479-495.
- Song, P.-S., Suzuki, S., Kim, I.-D. and Kim, J. H. (1991) Properties and Evolution of Photoreceptors. In *Photoreceptor Evolution and Function* (M. G. Holmes, Ed.) pp 21-63, Academic Press, San Diego, CA.
- Stewart, J. J. P. (1990) *MOPAC-A General Molecular Orbital Package Version 6.0*, Frank J. Seiler Research Laboratory, United States Air Force Academy, Colorado Springs, CO.
- Stockhaus, J., Nagatani, A., Halfter, U., Kay, S., Furuya, M. and Chua, N.-H. (1992) Serine to Alanine Substitutions at the Amino-Terminal region of Phytochrome A Result in an Increase in Biological Activity. *Genes Develop.* **6**, 2364-2372.
- Sundqvist, C. and Bjorn, L. O. (1983) Light-Induced Linear Dichroism in Photoreversibly Photochromic Sensor Pigments II. Chromophore Rotation in Immobilized Phytochrome. *Photochem. Photobiol.* **37**, 69-75.
- Thomas, B. and Johnson, C. B. (eds) (1991) *Phytochrome Properties and Biological Action*, NATO ASI Series, Vol. H 50, Springer-Verlag, Berlin.
- Tokutomi, S., Nakasako, M., Sakai, J., Kataoka, M., Yamamoto, K. T., Wada, M., Tokunaga, F., and Furuya, M. (1989) A Model for the Dimeric Molecular Structure of Phytochrome Based on Small Angle X-ray Scattering. *FEBS Lett.* **247**, 139-142.
- Vierstra, R. D., and Quail, P. H. (1983) Purification and Initial Characterization of 124-kilodalton Phytochrome from *Avena*. *Biochemistry* **22**, 2498-2505.
- Vierstra, R. D., Quail, P. H., Hahn, T.-R., and Song, P.-S. (1987) Comparison of the Protein conformations between Different Forms (Pr and Pfr) of Native (124 kDa) and degraded (118/114 kDa) Phytochromes from *Avena sativa*. *Photochem. Photobiol.* **45**, 429-432.
- Wahleithner, J. A., Li, L. and Lagarias, J. C. (1991) Expression and Assembly of Spectrally Active Recombinant Holophytochrome. *Proc. Natl. Acad. Sci. U.S.A.* **88**, 10387-10391.

# Thiolate and Phosphorothioate Functionalized Fluoresceins and Their Use as Fluorescent Labels

Christopher Bieniarz,\* Douglas F. Young, and Michael J. Cornwell

Abbott Laboratories, Diagnostics Division, Department of Immunochemistry, Abbott Park, North Chicago, Illinois 60064-3500. Received May 26, 1993\*

We report the syntheses of two new fluorescein derivatives, 3',6'-dihydroxy-3-oxo-2-[(phosphonothio)acetyl]spiro[isobenzofuran-1(3*H*),9'-9*H*-xanthene]-6-carboxylic acid hydrazide, disodium salt, a phosphorothioate fluorescein, and 3',6'-dihydroxy-3-oxo-2-(mercaptoacetyl)spiro[isobenzofuran-1(3*H*),9'-9*H*-xanthene]-6-carboxylic acid hydrazide, a mercaptoacetyl fluorescein. The latter is derived from the first compound by hydrolysis of the phosphate. Direct nonenzymatic labeling of the maleimide-derivatized IgG molecule by the novel mercaptoacetyl fluorescein is discussed. We also present a new method of bioconjugating phosphorothioate-functionalized fluorophores to a maleimide-derivatized protein, based on the alkaline phosphatase-catalyzed hydrolysis of the S-P bond of the phosphorothioate and the concomitant liberation of the fluorophore thiolate. This last species reacts *in situ* with the maleimide on the protein. A high degree of conjugation control is achieved in that modulation of the stoichiometry of the label and enzyme results in incorporation from seven to eight fluorophores per protein, depending on the ratio of the phosphorothioate fluorescein to alkaline phosphatase. The quantum yield of the mercaptoacetyl fluorescein relative to 6-carboxyfluorescein is 0.22 and  $\lambda_{\text{exc}} = 494 \text{ nm}$  and  $\lambda_{\text{em}} = 517 \text{ nm}$ .

## INTRODUCTION

The reaction of thiolate anion with a suitable electrophile is one of the most important methods of bioconjugation chemistry (1). In general, excellent results are obtained by functionalizing the first entity with an electrophilic reagent (*i.e.*, maleimide or haloacetyl) and a subsequent reaction with a thiolate functionality on the second entity. The three reagents considered below are introduced through a nucleophilic attack by the amine of the protein or hapten on the carbonyl of the active ester of the thiolating reagent. The generation of thiolates on proteins is frequently achieved through a reduction of the intrinsic disulfide bonds (2). However, cleaving the cystine bonds has the drawback of affecting the tertiary and quaternary structure of some proteins. Lately, the use of 2-iminothiolane (3) has seen increased use, mainly because of the efficiency and high yield of the thiolations. While 2-iminothiolane generates thiol functionality directly as a consequence of the ring opening of the 4-mercaptobutyr-imidate, SPDP<sup>1</sup> (3) and SATA (4) introduce thiols in a protected form as 2-pyridyl disulfide and thioacetyl moieties, respectively. Consequently, it is necessary to deprotect the thiols prior to the reaction with the thiol-reactive group. In the case of SPDP, this is accomplished by reductive cleavage of the 2-pyridyl disulfide group using DTT as a reducing agent. After reduction, DTT and pyridine-2-thione have to be removed from the reaction medium by chromatography or dialysis. Deprotection of the thiol of the SATA reagent calls for even harsher conditions of 0.2 N NaOH, aqueous NH<sub>3</sub> (5), or hydroxylamine (4) which may be incompatible with base-sensitive haptens or proteins. While the coupling reagents men-

tioned above are most frequently used in the modification of proteins, they also may be applied for the modification of small molecules, *i.e.*, haptens, fluorophores, chromophores, chemiluminophores, and drugs for the purpose of conjugating these entities to proteins.

We have recently reported an efficient, high-yielding method of converting halides to mercaptans (6). The method consists of reacting an aliphatic or activated aromatic halide with 1 or 2 equiv of the sodium thiophosphate tribasic dodecahydrate (Sigma) in methanol or aqueous DMF. The intermediate alkyl or aryl phosphorothioate is hydrolyzed *in situ* over a broad pH range, 4-7, yielding thiolate ion and phosphate. The latter is an innocuous byproduct which in most bioconjugations need not be removed, since it does not interfere in the reaction process or in the next step of conjugation.

In this paper we describe the adaptation of this method to the synthesis of a novel thiolated fluorescein derivative and the use of this fluorophore in labeling of an immunoglobulin, goat anti-hCG IgG. We also describe a new method of self-catalyzed conjugation of a novel fluorescein phosphorothioate to alkaline phosphatase, consisting of exposing in a buffered aqueous solution the fluorescein phosphorothioate to the action of bovine intestinal alkaline phosphatase suitably modified with maleimides. The principle is shown in Scheme 1.

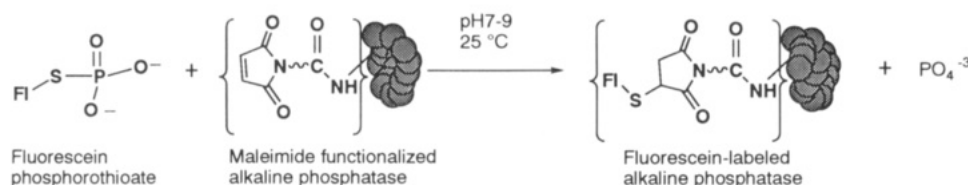
Alkaline phosphatase is first chemically modified by introduction of maleimide groups. This modification has minimal effect on the enzymatic activity. Alkaline phosphatase catalyzes the hydrolytic cleavage of the sulfur-phosphorus bond of the phosphorothioate (7). The deprotected nucleophilic thiolate of the label molecule (in this work, a fluorescein derivative) reacts with the maleimides on the enzyme completing the conjugation.

While most fluorescein labels are functionalized with electrophilic groups which may react with nucleophiles on the protein, very few fluorescein derivatives functionalized with nucleophilic groups have been reported. The most important examples are 4'-(aminomethyl)fluorescein (8) and 5- and 6-(aminomethyl)fluorescein (9). In this work we extend the repertoire of the nucleophilic fluorescein

\* Abstract published in *Advance ACS Abstracts*, December 15, 1993.

<sup>1</sup> Abbreviations (in order of appearance in the text): SPDP, *N*-succinimidyl 3-(2-pyridyldithio)propionate; SATA, *N*-succinimidyl *S*-acetylthioacetate; DTT, dithiothreitol; DMF, dimethylformamide; hCG, human chorionic gonadotropin; TNBS, 2,4,6-trinitrobenzenesulfonic acid; SEC, size exclusion chromatography; 6-CF, 6-carboxyfluorescein.

Scheme 1



derivatives by disclosing thiolated and phosphate-protected thiolated fluoresceins and describe methods of conjugating these new fluorophores to biologically important molecules. The alternative methods relying on the reaction of iminothiolane nucleophile and iodoacetyl fluoresceins have the disadvantage of the required pre-functionalization of the protein with a thiolate which under many experimental conditions undergoes oxidative dimerization to disulfides and possibly undesirable crosslinking of the protein to be labeled with the fluorophore. The new nucleophilic fluorophores described in this paper avoid the above complications. A very useful feature of this chemistry is that it allows the quantitation of the maleimide functionalities introduced into a protein at an intermediate stage of a bioconjugation. Since the fluorescein derivatives are highly chromogenic, the measurement of absorbance of the maleimide linker-functionalized protein after the reaction with the mercaptoacetyl fluorescein allows the quantitation of the introduced maleimides.

#### EXPERIMENTAL PROCEDURES

**Materials.** Except as noted, reagents were obtained commercially and used without further purification. All solvents were HPLC grade. Anhydrous DMF, Sephadex G-25 gel filtration packing, hydrazine hydrate, and silica gel 60 Merck 70-230 mesh were purchased from Aldrich Chemical Co. 6-Carboxyfluorescein *N*-hydroxysuccinimide ester was obtained from Research Organics, Inc. Bromoacetic acid *N*-hydroxysuccinimide ester, sodium thiophosphate dodecahydrate, 2,4,6-trinitrobenzenesulfonic acid (TNBS), 5,5'-dithiobis(2-nitrobenzoic acid) (Ellman's reagent), *p*-nitrophenyl phosphate, and all buffer components were from Sigma Chemical Co. The extended heterobifunctional maleimide active ester, succinimidyl 4-[(*N*-maleimidomethyl)tricaproamido]cyclohexane-1-carboxylate (30 atom linker), was prepared as previously described (10). Bovine intestinal alkaline phosphatase, purchased from Boehringer Mannheim Co. as a 10 mg/mL solution in triethanolamine, NaCl, MgCl<sub>2</sub>, and ZnCl<sub>2</sub>, was dialyzed against 0.1 M phosphate buffer pH 7.0 containing 0.1 M NaCl, 0.1 M MgCl<sub>2</sub>, and 0.1 M ZnCl<sub>2</sub> and used as a 1 mg/mL solution. Anti-hCG IgG was from Abbott Laboratories. Determination of protein concentrations was accomplished with Bio-Rad Protein Assay Kit, from Bio-Rad Laboratories.

**General Procedures.** Electronic spectra were recorded on a Hewlett-Packard 8452A diode array spectrophotometer. Nuclear magnetic resonance spectra were obtained on a Varian Gemini-300 instrument. Fluorescence spectra were recorded on a Hitachi F-3010 fluorescence spectrophotometer. HPLC analyses were performed on a Spectra-Physics instrument equipped with an SP8490 dual-wavelength detector. Elemental analyses were by Oneida Research Services Inc., Whitesboro, NY.

**3',6'-Dihydroxy-3-oxospiro[isobenzofuran-1(3*H*),9'-9*H*-xanthene]-6-carboxylic Acid Hydrazide (2).** To a stirred solution of 6-carboxyfluorescein *N*-hydroxysuccinimide ester (1) (2.500 g, 5.29 mmol) in methanol (25 mL) was added slowly dropwise a solution of hydrazine

hydrate (0.270 g, 5.29 mmol) in methanol (5 mL). The solution was stirred for 1 h at room temperature and stored overnight at 2 °C. The precipitated product was filtered and dried at reduced pressure: yield 1.50 g, 73%; <sup>1</sup>H NMR (300 MHz, DMSO-*d*<sub>6</sub>) δ 4.59 (br, 2H), 6.57 (dd, 4 H, *J* = 12 Hz), 6.70 (s, 2H), 7.64 (s, 1 H), 8.06 (d, 1 H, *J* = 8 Hz), 8.13 (d, 1 H, *J* = 8 Hz), 10.02 (br, 2 H); MS (FAB) *m/z* 391 (*M* + *H*)<sup>+</sup>.

**3',6'-Dihydroxy-3-oxospiro[isobenzofuran-1(3*H*),9'-9*H*-xanthene]-6-carboxylic Acid (Bromoacetyl)hydrazide (3).** To a solution of bromoacetic acid *N*-hydroxysuccinimide ester (0.582 g, 2.46 mmol) in dry DMF (20 mL) was added dropwise over 2.5 h a solution of hydrazide fluorescein 2 (1.000 g, 2.46 mmol) in DMF (50 mL). The reaction mixture was stirred for a further 4 h and evaporated on the rotary evaporator. The product was chromatographed on silica gel using a 5–20% gradient of methanol in methylene chloride as the eluant to yield 0.500 g (40%) of 3. Silica TLC showed a single spot, *R*<sub>f</sub> 0.37 CH<sub>2</sub>Cl<sub>2</sub>/CH<sub>3</sub>OH (4/1): <sup>1</sup>H NMR (300 MHz, DMSO-*d*<sub>6</sub>) δ 3.95 (s, 2H), 6.59 (dd, 4 H, *J* = 8 Hz), 6.70 (s, 2 H), 7.72 (s, 1 H), 8.12 (d, 1 H, *J* = 8 Hz), 8.18 (d, 1 H, *J* = 8 Hz), 10.16 (s, 2 H); MS (FAB) *m/z* 513 (*M* + *H*)<sup>+</sup>.

**3',6'-Dihydroxy-3-oxospiro[isobenzofuran-1(3*H*),9'-9*H*-xanthene]-6-carboxylic Acid 2-(Mercaptoacetyl)hydrazide (5).** To a solution of 3 (0.250 g, 0.490 mmol) in DMF (0.75 mL) was added a solution of sodium thiophosphate (0.182 g, 0.490 mmol) in water (3 mL). The mixture was stirred for 20 h after which the solvents were removed under reduced pressure. The residue was dissolved in water (2 mL), diluted to 150 mL with ethanol, and cooled in the refrigerator. The precipitated solid was removed by filtration, and the filtrate was concentrated to 5 mL. Product was precipitated out by addition of 200 mL of diethyl ether to yield 0.220 g (89%) of 5. TLC analysis revealed a single, fluorescent spot, *R*<sub>f</sub> 0.40, CH<sub>2</sub>Cl<sub>2</sub>/CH<sub>3</sub>OH (4/1), 1% CH<sub>3</sub>COOH v/v: <sup>1</sup>H NMR (300 MHz, CD<sub>3</sub>OD) δ 3.61 (s, 2H), 6.62 (d, 4H, *J* = 12 Hz), 6.92 (d, 2H, *J* = 9 Hz), 7.75 (s, 1H), 8.08 (s, 2H); MS (FAB) *m/z* 463 (*M* - *H*)<sup>+</sup>. Anal. Calcd for C<sub>23</sub>H<sub>16</sub>N<sub>2</sub>O<sub>7</sub>S·2H<sub>2</sub>O: C, 55.20; H, 4.02; N, 5.60. Found: C, 55.39; H, 4.02; N, 5.84.

**3',6'-Dihydroxy-3-oxospiro[isobenzofuran-1(3*H*),9'-9*H*-xanthene]-6-carboxylic Acid 2-[(Phosphonothio)acetyl]hydrazide, Disodium Salt (4).** This compound was prepared like 5 except the mixture of 3 (0.100 g, 0.195 mmol) and sodium thiophosphate dodecahydrate (0.0772 g, 0.195 mmol) was stirred in aqueous DMF for only 20 min. The solvents were removed under reduced pressure, and the residual solid was dissolved in 4 mL of MeOH, diluted to 200 mL with acetone, and cooled in an ice bath. The product was filtered out and dried under vacuum to yield 68 mg (0.063 mmol, 33%) of 4. Repeated recrystallization from a minimal volume of MeOH yielded sample used for elemental microanalysis. Silica TLC done in solvents of increasing polarity revealed a fluorescent spot at the origin, without any higher *R*<sub>f</sub> components: <sup>1</sup>H NMR (300 MHz, CD<sub>3</sub>OD) δ 3.44 (d, 2H, *J* = 15.4 Hz), 6.54 (d, 4H, *J* = 12 Hz), 7.03 (d, 2H, *J* = 9 Hz), 7.75 (s, 1H), 8.06 (s, 2H); <sup>31</sup>P NMR (CD<sub>3</sub>OD) δ 18.12 (s), H<sub>3</sub>PO<sub>4</sub> as external standard; MS (FAB) *m/z* 465 (*M* - PO<sub>3</sub>)<sup>+</sup>; IR (KBr) 3240,

1570, 1460, 1385, 1120, 1090, 962  $\text{cm}^{-1}$ . Anal. Calcd for  $\text{C}_{23}\text{H}_{15}\text{N}_2\text{O}_{10}\text{SPNa}_2\cdot 4\text{H}_2\text{O}\cdot 4\text{NaBr}$ : C, 25.85; H, 2.17; N, 2.62. Found: C, 25.74; H, 2.20; N, 2.95.

**Labeling of Anti-hCG IgG with Mercaptoacetyl Fluorescein 5.** (a) *Functionalization of Anti-hCG IgG with 30-Atom Linker Maleimide.* Anti-hCG IgG (1.3 mL of 6.6 mg/mL stock solution) was diluted to 2.0 mL with 0.1 M phosphate buffer, pH 7.0. This solution was concentrated to 200  $\mu\text{L}$  using an Amicon Centricon concentrator equipped with a 30 000 MW cutoff membrane and diluted with 2.0 mL of the buffer, and the procedure was repeated three more times to purify the protein. Protein concentration was 7.05 mg/mL as determined by the Warburg-Christian method (11). To that buffered pH 7.0 solution of IgG (1.13 mL) was added 0.720 mg (20 equiv/protein) of the 30-atom maleimide linker in DMF (150  $\mu\text{L}$ ). The solution was incubated for 1 h at room temperature while rotating at 100 rpm, after which the conjugate was chromatographed on a G-25 column using 0.1 M phosphate buffer, pH 7.0. The fractions containing the protein were collected and pooled.

(b) *Conjugation of Mercaptoacetyl Fluorescein 5.* To 0.90 mL of pH 7.0 buffered 2.23 mg/mL solutions of the 30-atom linker derivatized IgG were added 20, 40, or 100  $\mu\text{L}$  of 2.0 mg/mL (5, 10, or 25 equiv/IgG) solutions of 5. The solutions were incubated overnight at 5  $^{\circ}\text{C}$  while rotating at 100 rpm. The conjugates were chromatographed on a G-25 column using pH 7.0 phosphate buffer as eluant. Collected 25-drop fractions were examined at  $A_{280}$  and  $A_{490}$  for the presence of protein and fluorescein derivative, respectively. The appropriate fractions were pooled and examined by HPLC using a Bio-Rad Bio-Sil SEC-125 column.

(c) *Determination of the Number of Fluorophore Labels/IgG by UV/vis Spectroscopy.* IgG concentrations in the pooled fractions above were determined by Bio-Rad Protein Assay, based on the Bradford dye-binding procedure (12). From the standard curve of protein concentration vs absorbance, the value of IgG concentration of the pooled fractions was 0.43 mg/mL ( $2.9 \times 10^{-6}$  M) for the 25 equiv of 5/IgG prep. From the plot of fluorophore concentration vs absorbance at  $\lambda = 490$  nm and the measurement of absorbance at that wavelength of the pooled labeled protein fractions, the number of fluorophores/IgG was determined.

(d) *Determination of the Number of Fluorophore Labels/IgG by Fluorescence Spectroscopy.* Fluorescence measurements were made at submicromolar concentrations of the fluorophore in order to avoid inner filter effect (13). The spectra were acquired at  $\lambda_{\text{exc}} = 490$  nm and  $\lambda_{\text{em}} = 517$  nm. From the standard plot of the fluorescence vs concentration of mercaptoacetyl fluorescein 5 and the measurements of the fluorescence of the pooled antibody fractions, the number of fluorophores/IgG was measured.

**Labeling of Calf-Intestinal Alkaline Phosphatase with Phosphorothioate Fluorescein 4.** (a) *Functionalization of Calf-Intestinal Alkaline Phosphatase with 30-Atom Maleimide Linker.* Calf-intestinal alkaline phosphatase (1.5 mL of 10 mg/mL solution) was diluted to 2.0 mL with pH 7.0 phosphate buffer containing 0.1 M NaCl,  $\text{MgCl}_2$ , and  $\text{ZnCl}_2$  and concentrated down to 200  $\mu\text{L}$  using an Amicon Centricon concentrator equipped with a 30 000 MW cutoff membrane, and rediluted to 2.0 mL with phosphate buffer, and the procedure was repeated two more times to purify the protein. Protein concentration was 9.00 mg/mL by the Warburg-Christian method (11). To 1.33 mL of the buffered solution of that protein, 2.70 mg (50 equiv/enzyme) of the 30-atom maleimide linker

in 300  $\mu\text{L}$  of DMF was added, and the solution was incubated for 1 h at room temperature while rotating at 100 rpm. The conjugate was then chromatographed on a G-25 column, and fractions containing protein were collected and pooled. Quantitation of TNBS reactive amines revealed that only seven amines were titratable in the linker-functionalized enzyme while 20 could be titrated in the native enzyme.

(b) *Conjugation of Phosphorothioate Fluorescein 4.* To three aliquots of 30-atom maleimide linker functionalized alkaline phosphatase (1.40 mL of 2.5 mg/mL solutions) was added 0.686, 1.37, or 2.06 mg of 4 in 900  $\mu\text{L}$  of pH 7.0 phosphate buffer (27, 55, or 82 equiv/protein). The solutions were incubated at 5  $^{\circ}\text{C}$  while rotating at 100 rpm. After 48 h the material was fractionated on a G-25 column. The fractions which showed absorbance at both 280 and 490 nm were collected, pooled, and examined on a size exclusion Bio-Rad Bio-Sil SEC 400 HPLC column.

(c) *Determination of the Number of Fluorophore Labels/Alkaline Phosphatase by UV/vis Spectroscopy.* Protein concentrations of the pooled fractions above were determined as for the case of IgG. From the standard curve of protein concentration vs absorbance, the values of alkaline phosphatase concentrations of the pooled fractions were  $7.73 \times 10^{-6}$ ,  $8.20 \times 10^{-6}$ , and  $6.93 \times 10^{-6}$  M for preps run with 27, 55, and 82 equiv of 4/alkaline phosphatase, respectively. From a standard plot of fluorophore concentration vs absorbance at  $\lambda_{\text{max}} = 490$  nm and the determination of the absorbance of the pooled labeled protein fractions at that wavelength, the number of fluorophores/alkaline phosphatase was determined.

(d) *Determination of the Number of Fluorophore Labels/Alkaline Phosphatase by Fluorescence Spectroscopy.* This was done following the same technique as described above for IgG labeling.

**Measurement of the Relative Quantum Yield of 5.** The quantum yield of this fluorophore relative to 6-carboxyfluorescein (6-CF) was determined by the quotient of the integrated emission intensities over all wavelengths of mercaptoacetyl fluorescein 5 and 6-CF (14)

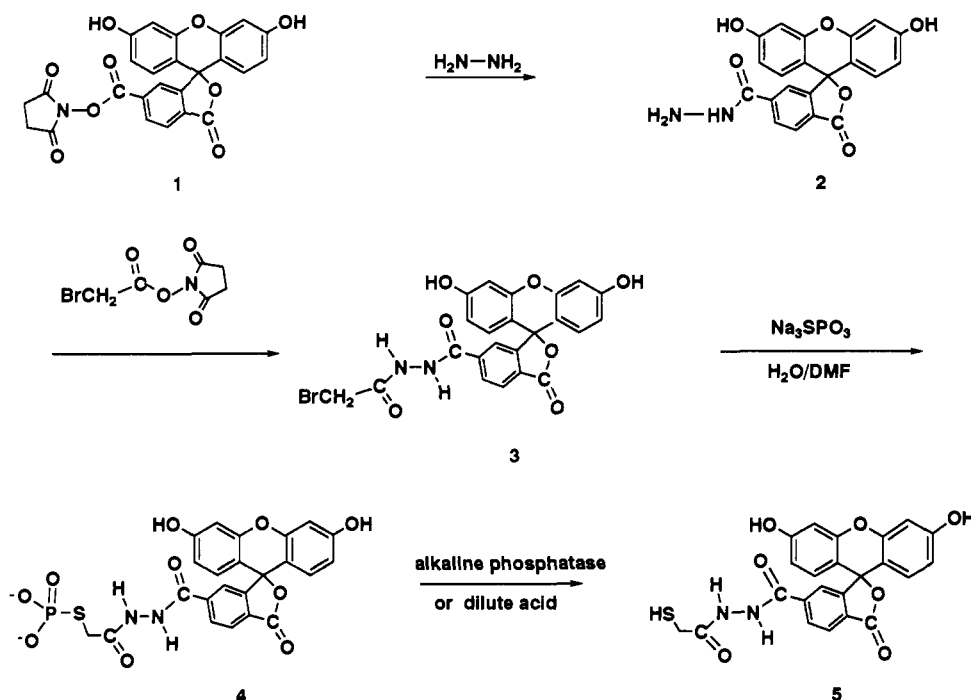
$$Q_{\text{F5}}/Q_{\text{F6-CF}} = I_5/I_{6\text{-CF}}(\text{OD}_{6\text{-CF}}/\text{OD}_5)$$

where  $I_5$  and  $I_{6\text{-CF}}$  refer to the integrated emission intensities of the sample and standard, respectively. All solutions were 0.10 M phosphate buffer, pH 7.0.

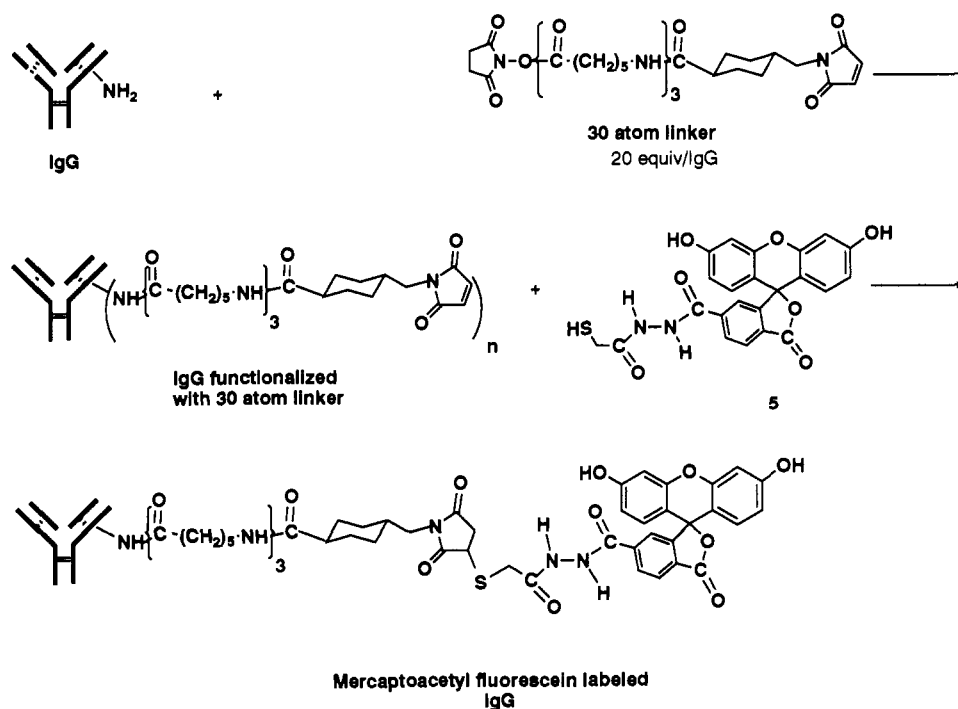
## RESULTS

The synthesis of the novel fluorophores 4 and 5 is depicted in Scheme 2. Hydrazinolysis of 6-carboxyfluorescein *N*-hydroxysuccinimide ester 1 in methanol yielded hydrazide fluorescein 2, which was subsequently reacted with bromoacetic acid *N*-hydroxysuccinimide ester in dry DMF. The resulting (bromoacetyl)hydrazide fluorescein 3 was reacted with 1 equiv of sodium thiophosphate in aqueous DMF yielding phosphorothioate fluorescein 4. The cleavage of the phosphate was done by aqueous dilute acid at pH 4–5 (6, 15, 16), by prolonged stirring in a neutral aqueous solution, or enzymatically by alkaline phosphatase-catalyzed hydrolysis at pH 7.0. The resulting mercaptoacetyl fluorescein 5 was completely free of the difluorescein disulfide as demonstrated by the following experiments. When a 1:1 aqueous methanolic solution of an aliquot of 5 was incubated with a 20-fold excess of *N*-ethylmaleimide for 1 h at room temperature, TLC of the reaction solution revealed complete disappearance of the original single spot at  $R_f$  0.40,  $\text{CH}_2\text{Cl}_2/\text{CH}_3\text{OH}$  (4/1), 1%  $\text{CH}_3\text{COOH}$  v/v, and concomitant appearance of a new fluorescent spot at  $R_f$  0.72. In a second experiment,

Scheme 2



Scheme 3



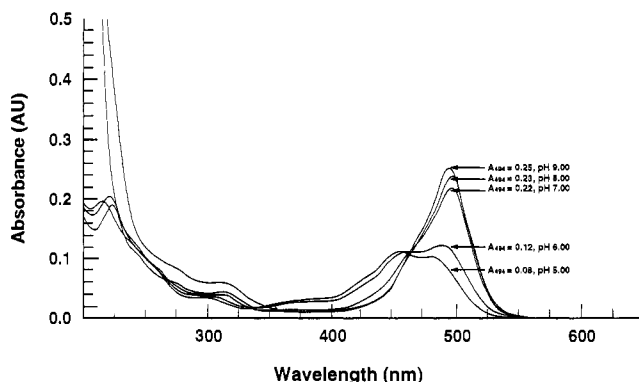
aqueous solution of 5 was oxygenated by bubbling air into the solution through a micropipette. After 24 h the starting material was almost completely oxidized; the new spot,  $R_f$  0.00 showed greatly diminished fluorescence.

The compounds 4 and 5 were stored lyophilized at room temperature for periods of several months without any decomposition. We have first exploited the nucleophilicity of the novel mercaptoacetyl fluorescein derivative 5 for labeling of a model IgG molecule, anti-hCG, prefunctionalized with extended length heterobifunctional maleimide active esters (30-atom linkers). In an earlier work we demonstrated that this extended length coupling agent, succinimidyl 4-[(*N*-maleimidomethyl)tricaproylamido]cyclohexane-1-carboxylate, offers several advantages as a

coupling agent over the shorter, more hydrophobic heterobifunctional reagents used in the past (10). Scheme 3 shows the construction of the conjugate.

IgG was first derivatized with a 20-fold molar excess of the 30-atom heterobifunctional maleimide succinimide active ester. The maleimide ring is known to be unstable at neutral or higher pH (17). Consequently, the maleimide-functionalized protein was never stored in buffered solution for longer than 24 h. Instead, it was chromatographed on a size-exclusion column in order to remove the unreacted heterobifunctional reagent and was used immediately in the thiolation step. In preliminary experiments (data not shown), we determined that a 25-fold molar excess of 5 over IgG resulted in optimal labeling.





**Figure 1.** Dependence of the absorption spectra of  $1.0 \times 10^{-5}$  M mercaptoacetyl fluorescein 5 upon the pH. The sigmoidal fit of the absorbances vs pH yielded a  $pK_a$  value of 6.4 for the formation of the dianion of 5.

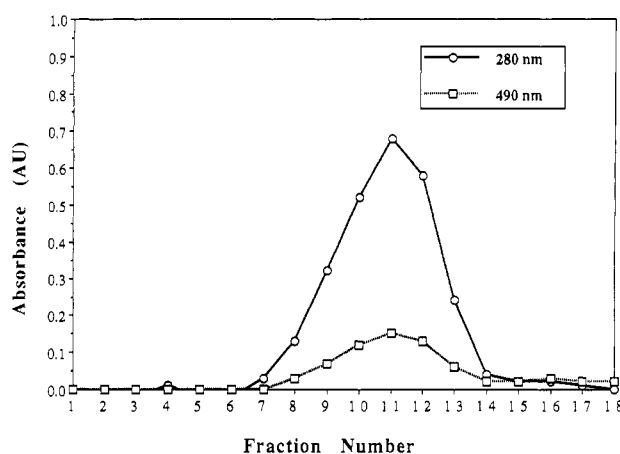
This stoichiometry allowed a controlled labeling of protein by the fluorophores at the optimal 2:1 ratio of the label per IgG, thus avoiding ambiguities associated with fluorophore self-quenching and impairment of the antibody-binding capacity observed with overmodification. Size-exclusion HPLC chromatogram of unlabeled and fluorophore-labeled anti-hCG IgG revealed two peaks, at 7.74 and 6.76 min, respectively. Integration of the peak areas at  $A_{280}$  showed 71% fluoresceinated IgG and 29% unmodified IgG.

In a 0.1 M phosphate buffer at pH 7.0 and at  $\lambda$  490 nm, 5 has an apparent extinction coefficient  $\epsilon_{490} = 23\,064\text{ M}^{-1}\text{ cm}^{-1}$ . The dependence of the absorbance spectra of  $1 \times 10^{-5}$  M 5 upon the pH is shown in Figure 1.

These spectral changes reflect the equilibria between the dianion and monoanion of the fluorescein derivative 5 and are consistent with the data reported in the literature for other fluorescein derivatives (18,19). From the above data we determined the  $pK_a$  for the formation of the most intensely chromophoric dianionic species of 5 to be 6.4, as compared to 6.5 of the carboxyfluorescein (19).

This reagent is a strong fluorophore, with  $\lambda_{exc} = 494\text{ nm}$  and  $\lambda_{em} = 517\text{ nm}$ . The quantum yield of fluorescence of 5 relative to 6-CF measured as described in the Experimental Procedures is  $Q_5/Q_{6-CF} = 0.22$ . In order to study the effect of the mercaptan substituent of 5 on its fluorescence and extinction coefficient,  $5 \times 10^{-5}$  M pH 7.0 solution of 5 was incubated with  $5 \times 10^{-3}$  M *N*-ethylmaleimide. The solution was examined by periodic absorbance and fluorescence scans over a period of 24 h. There was no change in fluorescence or absorbance profiles of 5. Figure 2 depicts the plot of absorbances at  $A_{280}$  and  $A_{490}$  of G-25 eluted fractions. Since the molar absorptivity of this fluorophore at 490 nm is four times larger than at 280 nm, only 6% of the absorbance at 280 nm should be due to the conjugated fluorophore, the remaining 94% being attributable to the IgG in the fraction. The unconjugated fluorophore elutes at fraction number above 20 (data not shown).

Since our interest centers around the use of these novel mercaptofluoresceins as protein labels, we required a controlled conjugation of these fluorophores to the protein. In order to ascertain the fluorophore/IgG ratio, the quantitation based on absorbance measurements was compared with fluorescence determination. The measurements of the IgG concentrations using Bio-Rad Protein Assay were done by constructing a standard curve of  $A_{594}$  vs anti-hCG IgG which gave a linear fit ( $R^2 = 0.996$ ) over a 10-fold range of IgG concentrations and reading the unknown concentrations off the curve. On the basis of



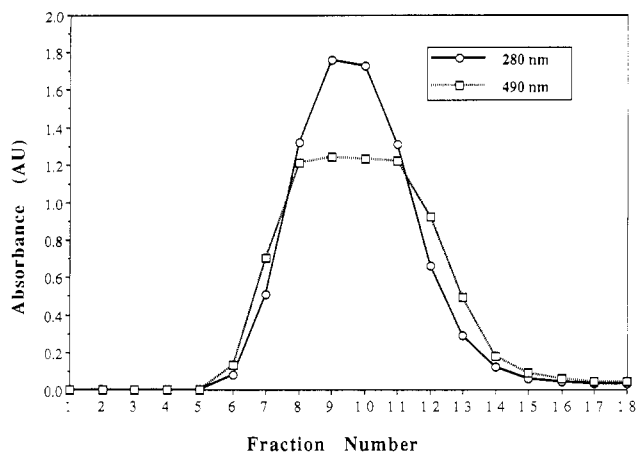
**Figure 2.** Plots of absorbances at 280 and 490 nm of G-25-eluted fractions of 5/anti-hCG conjugates. IgG was prefuc-tionalized with 20 equiv of the 30-atom maleimide heterobi-functional linker and incubated at 5 °C with  $4.0 \times 10^{-7}$  M (25 equiv) of 5. Fractions 10–12 were collected, pooled, and examined by HPLC. Integration for the peak areas at  $A_{280}$  determined 71% fluoresceinated IgG and 29% unmodified IgG.

**Table 1.** Number of Fluorophore Labels Introduced into Two Different Proteins, Anti-hCG (Experiment 1) and Bovine Calf Intestinal Alkaline Phosphatase (Experiment 2) as a Function of the Stoichiometry of 5 and 4 with Respect to Anti-hCG and Alkaline Phosphatase, Respectively, As Determined by Absorbance (A) and Fluorescence (F) Measurements

experiment 1			experiment 2		
equiv of 5/IgG used	no. of 5/IgG by A	by F	equiv of 4/alk phos used	no. of 4/alk phos by A	by F
5	0	1	27	7	4
10	1	2	55	7	4
25	2	3	82	8	5

our determined value of the apparent extinction coefficient of 5 and the IgG concentrations, the number of fluorophores introduced per mole of IgG was calculated at three different stoichiometries of 5/IgG. Similarly, a fluorescence standard curve of 5 allowed the determination of the number of fluorophores per IgG. The results of the labeling of IgG by thiolated fluorophore are shown in Table 1. Clearly, the level of the fluorescein incorporation into the protein increases as the number of equivalents of the fluorophore per mole of IgG is increases. When 5 equiv of 5 per IgG is used, only very low levels of fluoresceination is achieved. Increasing the ratio of 5/IgG to 10 or 25 results in introduction of one to three fluorescein labels per IgG.

In the following text we show that the precursor of 5, 3',6'-dihydroxy-3-oxo-2-[(phosphonothio)acetyl]-spiro[isobenzofuran-1(3*H*),9'-9*H*-xanthene]-6-carboxylic acid hydrazide, disodium salt, the phosphorothioate fluorescein 4, is also a very useful fluorophore marker of proteins. Scheme 1 summarizes the process of self-catalyzed labeling of a maleimide prefuc-tionalized alkaline phosphatase by 4. We derivatized bovine alkaline phosphatase with extended length heterobifunctional maleimide active ester (30-atom linker) as described in the Experimental Procedures. The residual activity of the derivatized enzyme was 81% of the native alkaline phosphatase activity. When an aqueous solution of 4 is exposed at pH 7–9 to the action of the maleimide-derivatized alkaline phosphatase, the latter catalyzes very efficiently the hydrolysis of the sulfur-phosphorus bond of the phosphorothioate, generating mercaptoacetyl fluorescein 5 described above. In preliminary experiments with several alkyl phosphorothioates we determined that



**Figure 3.** Plots of absorbances at 280 and 490 nm of G-25 eluted fractions of the fluorophore-labeled alkaline phosphatase. Alkaline phosphatase was prefunctionalized with 50 equiv of the 30-atom maleimide heterobifunctional linker and incubated at 5 °C for 48 h with  $1.9 \times 10^{-6}$  mol (82 equiv) of 4 according to the method depicted in Scheme 1. Since the molar absorptivity of this fluorophore at 490 nm is four times larger than at 280 nm, 17% of the absorbance at 280 nm should be due to the conjugated fluorophore, the remaining 83% being attributable to the alkaline phosphatase in the fraction. The unconjugated fluorophore elutes at fraction number above 20. Fractions 8–11 were collected, pooled, and analyzed by HPLC.

at pH 7.0 the half-life of the alkaline phosphatase-catalyzed release of thiolate is approximately 15 min while the controls in absence of enzyme revealed virtually no free thiols even after 1–2-h incubation. The resulting mercaptoacetyl fluorescein nucleophile reacts with the maleimide electrophile on the alkaline phosphatase, completing the conjugation. We were interested in ascertaining the number of fluorophores which may be conjugated to alkaline phosphatase by this method without significantly compromising the catalytic activity of the enzyme, while simultaneously eliciting the highest possible fluorescent signal from the labels. We show in Table 1 that increasing the stoichiometric ratio of 4 to alkaline phosphatase resulted in higher levels of incorporation of the fluorophores. Interestingly, the conjugation of the fluorophore to the maleimide-derivatized enzyme caused more pronounced loss of enzymatic activity than the loss resulting from the derivatization of the enzyme with the 30-atom linker alone. Approximately 70% of the native enzyme activity was lost after 27, 55, or 82 equiv of 4 per alkaline phosphatase was used as compared to only 20% loss upon derivatization with 30-atom linker. The extinction coefficient of 4 in 0.1 M phosphate buffer at pH 7.0 is  $\epsilon_{490} = 53\,636 \text{ M}^{-1} \text{ cm}^{-1}$ , 2.3 times higher than the value of the apparent extinction coefficient of 5. Under these conditions,  $\lambda_{\text{exc}} = 496 \text{ nm}$  and  $\lambda_{\text{em}} = 517 \text{ nm}$ . Figure 3 shows the plot of absorbances at  $A_{280}$  and  $A_{490}$  of G-25-eluted fractions of the labeled alkaline phosphatase.

Since the molar absorptivity of this fluorophore at 490 nm is four times larger than at 280 nm, comparison of the values of the maxima in the plots of Figure 3 shows that 17% of the absorbance at 280 nm should be due to the conjugated fluorophore, the remaining 83% being attributable to the alkaline phosphatase in the fraction. The unconjugated fluorophore elutes at fraction number above 20 (data not shown).

Fluorescence spectra of the compounds 4 and 5 at pH 7.0 are shown in Figure 4. The relative fluorescence intensity  $I_4/I_5$  is 5.0. We interpret this markedly lower fluorescence of the mercaptoacetyl fluorescein 5 as compared to its phosphorothioate precursor 4 as well as the

comparatively low apparent extinction coefficient of 5 in the Discussion below.

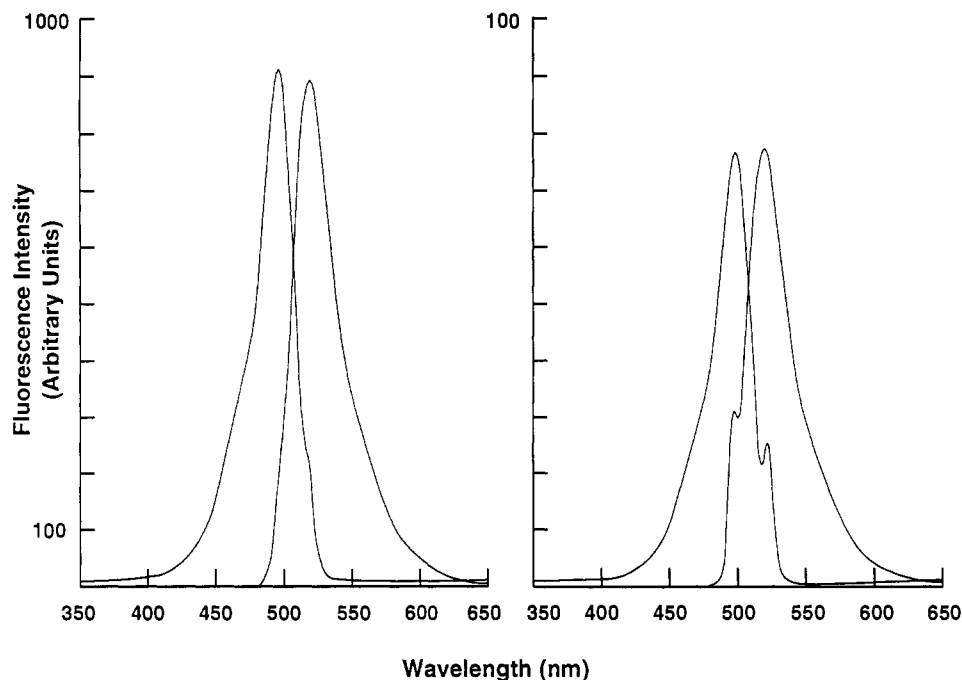
Table 1 shows that the self-catalyzed functionalization of alkaline phosphatase (experiment 2) is a very efficient process. Between seven and eight fluorophores were introduced into the alkaline phosphatase, as determined by absorbance measurements. TNBS titration of the accessible amines of the native alkaline phosphatase evidenced 20 amines, while after the derivatization of the enzyme with the 30-atom heterobifunctional maleimide linker, only seven amines could be titrated. This implies that an average of 13 maleimide linkers were incorporated into alkaline phosphatase and up to 60% of these were labeled with the fluorophore 4. Fluorescence-based measurements were consistently lower than the absorbance readings, as opposed to experiment 1, where the absorbance readings were consistently lower than the fluorescence readings. This seeming discrepancy is explainable and will be addressed in the Discussion.

## DISCUSSION

The two new fluorescein derivatives, phosphorothioate fluorescein 4 and mercaptoacetyl fluorescein 5, allow nucleophilic attachment of the fluorescein molecules to the electrophile-functionalized proteins, thus enriching the repertoire of methods available to the chemist for fluorescence labeling of biologically relevant molecules. The labeling of proteins by thiolation of their lysines with iminothiolane followed by the reaction with iodoacetylated fluorescein has been used frequently in the past (20, 21). However, that method does not allow spacial separation between the iminothiolane-derivatized protein and the fluorophore label. By functionalizing the protein with the extended arm 30-atom maleimide linker and building phosphate-protected thiolate into the fluorophore we achieved greater control of the distance between the label and the protein as well as improved control of the bioconjugation process. Often it is desirable to detect and quantitate the number of maleimide or haloacetyl linkers introduced into a protein in the first stage of the conjugation process. In the concluding paragraph of the Results we have demonstrated the utility of these fluorescein derivatives for that purpose. The derivative 4, a phosphate-protected mercapto fluorescein, is particularly useful in alkaline phosphatase-catalyzed deprotection and labeling, depicted in Scheme 1. We have been inspired in the design of this methodology by the reported excellence of alkyl and aryl phosphorothioates as substrates for alkaline phosphatase (7). Although thiols are classically protected as *S*-acetyl, *S*-benzoyl (22), unsymmetrical disulfides (23), or thiosulfates (24), these methods, which originate from organic synthesis, require harsh deprotection conditions and yield byproducts which have to be removed before reaction with the protein. In contrast, the phosphorothioates treated by buffered solutions of alkaline phosphatase yield thiolates very efficiently, as demonstrated by experiments summarized in Table 1. Moreover, the byproduct is an innocuous phosphate ion which need not be removed since it does not affect the conjugation process.

We were interested in establishing the limits of conjugation stoichiometry for the two fluorophores. Table 1 summarizes the results of the direct labeling of the maleimide derivatized anti-hCG IgG with 5 (experiment 1) and self-catalyzed labeling of alkaline phosphatase with 4 (experiment 2). In experiment 1 we aimed at labeling the IgG molecule with very few fluorophores so as not to impair the antibody binding capabilities. We found that





**Figure 4.** Excitation and emission spectra of  $2.8 \times 10^{-6}$  M phosphorothioate fluorescein 4 (left) and  $1 \times 10^{-6}$  M mercaptoacetyl fluorescein 5 (right). Both spectra were acquired in a 0.1 M phosphate buffer at pH 7.00. Relative fluorescence intensity  $I_4/I_5$  is 5.0.

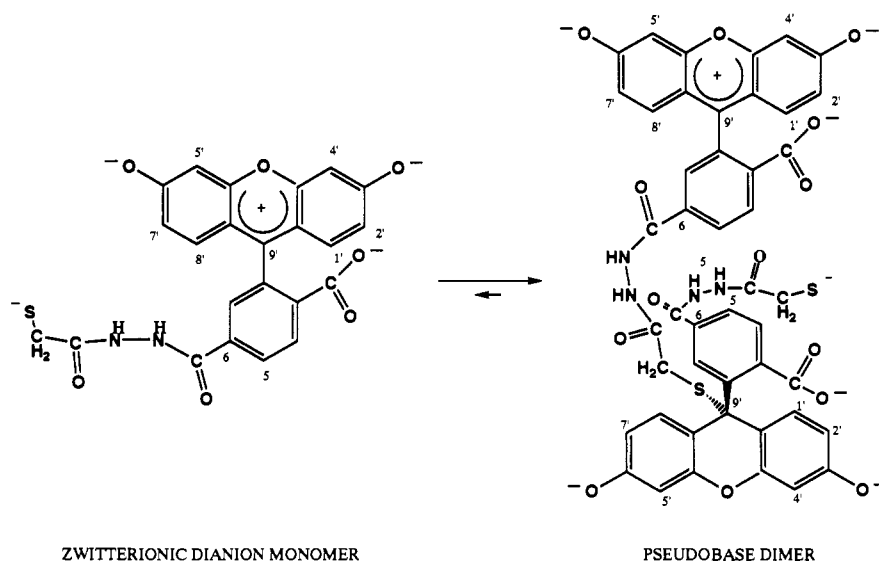
functionalization of IgG with 20 equiv of the 30-atom heterobifunctional maleimide active ester followed by conjugation with fluorophore 5 allows incorporation of one to three fluorophores per IgG depending on the ratio of fluorophore to IgG employed in each conjugation. Under the conditions of our experiments, absorbance-based determinations of the number of fluorophores per IgG yielded lower values than the fluorimetric determination. This most likely is due to the error in the Bradford dye-binding procedure (12) because of reading very low absorbance values of the fluoresceinated antibody at 490 nm and also possibly to the overestimate of the IgG concentration after its derivatization with the 30-atom heterobifunctional linker reagent. We showed that mercaptoacetyl fluorescein 5 was completely free from dimeric disulfide oxidation impurities as demonstrated by spot to spot TLC conversion of the compound 5 to its *N*-ethylmaleimide adduct of higher  $R_f$ , the oxidation of the compound 5 to a new compound of  $R_f$  0.00, and very low fluorescence. Indeed, dimers of fluorescein linked through coupling arms possessing disulfides have been reported to have very low quantum yields, 0.11 and 0.17, for difluorescein disulfide and *N,N'*-difluorescein thiocarbamylcystamine, respectively, presumably due to internal quenching through aromatic stacking interactions (25). Micromolar concentrations of fluorophores may be reliably determined fluorimetrically provided no inner filter effect or other forms of fluorescence quenching are present (26).

Thus, we believe that in case of low levels of fluorophore functionalization the fluorimetric determination is more reliable. In experiment 2, summarized in Table 1, we aimed at maximal functionalization of the protein calf intestinal alkaline phosphatase with phosphorothioate fluorescein 4. We found that the self-catalyzed labeling of alkaline phosphatase is an efficient process, seven to eight fluorophores being incorporated into the protein. We have previously determined that derivatization of this enzyme with 50 equiv of 30-atom maleimide heterobifunctional reagent causes only about 20% loss of the enzymatic activity. Since 30% of the native unlabeled alkaline phosphatase activity remained regardless of whether 27, 55, or 82 equiv of 4 was employed, this invariance of the

residual enzymatic activity on the stoichiometry of 4 used in the labeling suggests that the additional loss of the enzymatic activity most likely occurred as the result of covalent attachment of fluorophore to the enzyme. Unlike in experiment 1, in experiment 2 the fluorimetric determination of the number of incorporated fluorophores yielded about 40% lower values as compared to the determinations done by absorbance. The number of incorporated fluorophores as measured fluorimetrically stays approximately constant yielding values between four and five fluorophores per protein. However, the determinations performed by absorbance reading yielded values of seven to eight fluorophores per protein. We attribute the discrepancy between the fluorescence and absorbance measurements to the concentration quenching of the fluorescein labels on the surface of the enzyme (26). Since the molecular radius of the alkaline phosphatase is approximately 30 Å (27), eight molecules of 4 on the surface of the enzyme correspond to an effective molarity of the fluorophore of approximately  $1.3 \times 10^{-4}$  M, a concentration at which the inner filter effect indeed should be expected to introduce significant errors in the measurements (28). Thus, at higher concentrations of the fluorophores, we believe that the values determined by absorbance readings are more reliable.

An intriguing feature of mercaptoacetyl fluorescein 5 is its markedly lower extinction coefficient as compared to the parent carboxyfluorescein at pH 7.00. Thus, we measured the extinction coefficient of mercaptoacetyl fluorescein 5 to be 35% and 44% of the extinction coefficients of 6-CF and phosphorothioate fluorescein 4, respectively, at pH 7.00. Since our measurement of the  $pK_a = 6.4$  for the dianionic 5 is so close to the reported value of  $pK_a = 6.5$  for 6-CF, the differences in the values of the extinction coefficients cannot be explained in terms of differences in ionization of the xanthene phenols. It is also unlikely that this discrepancy is due to the formation of the spiro lactone of the phthalate carboxylate at C9' in the compound 5 because the extinction coefficient of 4 at 53 636 M<sup>-1</sup> cm<sup>-1</sup> is 2.3 times higher than the value of the apparent extinction coefficient of 5. We explain these

Scheme 4



discrepancies in terms of the intermolecular dimerization of the compound **5** as depicted in the Scheme 4.

The intermolecular nucleophilic attack of the side chain thiolate on C9' tertiary carbonium ion is likely in view of the known and analogous reactivity of the nucleophiles at C9' in the acridinium series and the equilibrium between acridinium esters and their colorless, non-chemiluminescent pseudobases (29, 30). The extent to which the equilibrium is shifted to the dimer pseudobase form should manifest itself in the correspondingly lower apparent extinction coefficient at 490 nm and also proportional diminution of the fluorescence quantum yield of this fluorophore. The intramolecular thiolate addition to C9' position can be discounted on steric and thermodynamic grounds. We obtained support for this interpretation by reexamining the MS FAB(−) spectrum of **5** in nitrobenzyl alcohol matrix, which showed weak ions at  $m/z$  925 and 947 corresponding to MW of 926 and 948 for the dimer of **5** and its sodium salt. That these did not originate from the difluorescein disulfide was demonstrated in our TLC experiments which clearly indicated presence of free thiol. It is likely that during the isolation of the compound **5** from methanolic ether the less soluble dimeric or even trimeric form of **5** crystallized out. On silica gel or in MS FAB only the monomeric **5** would be observed. The incubation of pH 7.0 solution of **5** with 100-fold molar excess of *N*-ethylmaleimide led to no change in the fluorescence intensity of **5**. This suggests multimeric structure of **5** in which the inner filter effect quenching of the fluorescence would be responsible for the markedly depressed fluorescence of **5**. Although several sulfur-containing fluorescein derivatives have been shown to have strongly reduced fluorescence due to collisional intramolecular quenching between the xanthene moiety and thiolate ion on the substituent chain—apparent quantum yields between 0.01 and 0.11 (25, 26)—this last factor probably plays a much smaller role in the reduced fluorescence of **5** as compared to the proximity effects of the fluorophores in the dimeric or trimeric form of **5**.

Since our structural data of this compound could not discern between monomeric, dimeric, or higher aggregates, we report our results in terms of the apparent extinction coefficient of **5**. Thus, if the real structure of **5** is dimeric, the values in experiment 1 of Scheme 1 would be half of those reported. Although the present work describes a self-catalytic conjugation of a phosphorothioate derivative

of a fluorophore to alkaline phosphatase, we have exploited the use of alkaline phosphatase as catalyst in unmasking thiolate for subsequent conjugation of the thiolate to suitably derivatized biological compounds, i.e., antibodies, haptens, and other enzymes. This work is in progress and will be reported in due course.

#### ACKNOWLEDGMENT

We are grateful to Dr. Susan J. Tomazic-Allen for critical reading of the manuscript. We also thank Dr. Jeffrey Huff of the Department of Immunochemistry, Abbott Diagnostics Division, and Professor Richard G. Lawton of the University of Michigan Department of Chemistry for stimulating discussions.

**Supplementary Material Available:** Absorbance at 490 nm vs concentration plots of 6-carboxyfluorescein, mercaptoacetyl fluorescein **5**, and phosphorothioate fluorescein **4** in 0.1 M phosphate buffer pH 7.0 (1 page). Ordering information is given on any current masthead page.

#### LITERATURE CITED

- (1) (a) Means, G. E., and Feeney, R. E. (1990) Chemical modification of proteins: history and applications. *Bioconjugate Chem.* 1, 2–12. (b) Kitagawa, T., Shimozono, T., Aikawa, T., Yoshida, T., and Nishimura, H. (1981) Preparation and characterization of heterobifunctional crosslinking reagents for protein modification. *Chem. Pharm. Bull.* 29, 1130–1135. (c) Ishikawa, E., Imagawa, M., Hashida, S., Yoshitake, S., Hamaguchi, Y., and Ueno, T. (1983) Enzyme-labeling of antibodies and their fragments for enzyme immunoassays and immunohistochemical staining. *J. Immunoass.* 4, 209–327.
- (2) Cleland, W. W. (1964) *Biochemistry* 3, 480–482.
- (3) (a) Jue, R., Lambert, J. M., Pierce, L. R., and Traut, R. R. (1978) Addition of sulfhydryl groups to *Escherichia coli* ribosomes by protein modification with 2-iminothiolane (methyl 4-mercaptobutyrimidate). *Biochemistry* 17, 5399–5406. (b) Hillel, S. and Wu, C. W. (1977) Subunit topography of RNA polymerase from *Escherichia coli*. A cross-linking study with bifunctional reagents. *Biochemistry* 16, 3334–3342. (c) Carlsson, J., Drevin, H., and Axen, R. (1978) Protein thiolation and reversible protein-protein conjugation N-succinimidyl 3-(2-pyridylthio)propionate, a new heterobifunctional reagent. *Biochem. J.* 173, 723–737.
- (4) Duncan, R. J. S., Weston, P. D., and Wrigglesworth, R. (1983) A new reagent which may be used to introduce sulfhydryl groups into proteins, and its use in the preparation of conjugates for immunoassay. *Anal. Biochem.* 132, 68–73.

- (5) Greene, T. W., and Wuts, P. G. M. (1991) *Protective Groups in Organic Synthesis*, p 298, John Wiley & Sons, Inc., New York.
- (6) Bieniarz, C., Cornwell, M. J., (1993) A facile, high-yielding method for the conversion of halides to mercaptans. *Tetrahedron Lett.* 34, 939-942.
- (7) Alkyl and aryl phosphorothioates are excellent substrates of alkaline phosphatase; see: (a) Neumann, H., Boross, L., and Katchalski, E. (1967) Hydrolysis of *S*-substituted monoesters of phosphorothioic acid by alkaline phosphatase from *Escherichia coli*. *J. Biol. Chem.* 242, 3142-3147. (b) Neumann, H. (1968) Substrate selectivity in the action of alkaline and acid phosphatases. *J. Biol. Chem.* 243, 4671-4676.
- (8) Shipchandler, M. T., Fino, J. R., Klein, L. D., and Kirkemo, C. L. (1987) 4'-(Aminomethyl) fluorescein and its *N*-alkyl derivatives: useful reagents in immunodiagnostic techniques. *Anal. Biochem.* 162, 89-101.
- (9) Mattingly, P. G. (1992) Preparation of 5- and 6-(aminomethyl)fluorescein. *Bioconjugate Chem.* 3, 430-431.
- (10) (a) Bieniarz, C., Welch, C. J., and Barnes, G. (1991) Heterobifunctional Coupling Agents. U.S. Patent No. 4,994,385. (b) Bieniarz, C., Welch, C. J., Barnes, G., and Schlesinger, C. A. (1991) Covalent Attachment of Antibodies and Antigens to Solid Phases Using Extended Length Heterobifunctional Coupling Agents. U.S. Patent No. 5,002,883. (c) Bieniarz, C., Welch, C. J., and Barnes, G. (1991) Heterobifunctional Maleimide Containing Coupling Agents. U.S. Patent No. 5,053,520. (d) Bieniarz, C., Welch, C. J., Barnes, G., and Schlesinger, C. A. (1991) Covalent Attachment of Antibodies and Antigens to Solid Phases Using Extended Length Heterobifunctional Coupling Agents. U.S. Patent No. 5,063,109.
- (11) Layne, E. (1957) Spectrophotometric and Turbidimetric Method for Measuring Proteins. In *Methods in Enzymology* (S. P. Colowick, and N. O. Kaplan, Eds.) Vol. 3, p 447, Academic Press, New York.
- (12) Bradford, M. (1976) A Rapid and sensitive method for the quantitation of microgram quantities of protein utilizing the principle of protein-dye binding. *Anal. Biochem.* 72, 248-254.
- (13) Lakowicz, J. R. (1983) *Principles of Fluorescence Spectroscopy*, pp 44-45, Plenum Press, New York.
- (14) Jameson, D. M. (1984) *Fluorescein Hapten: An Immunological Probe* (E. W. Voss, Ed.) p 35, CRC Press, Inc., Boca Raton, FL.
- (15) Milstien, S., and Fife, T. H. (1967) The hydrolysis of *S*-aryl phosphorothioates. *J. Am. Chem. Soc.* 89, 5820-5826.
- (16) Fife, T. H., and Milstien, S. (1969) Carboxyl-group participation in phosphorothioate hydrolysis. The hydrolysis of *S*-(2-carboxyphenyl)phosphorothioate. *J. Org. Chem.* 34, 4007-4012.
- (17) (a) Gregory, J. D. (1955) The stability of *N*-ethylmaleimide and its reaction with sulfhydryl groups. *J. Am. Chem. Soc.* 77, 3922-3923. (b) Kitagawa, T., Shimozono, T., Aikawa, T., Yoshida, T., and Nishimura, H. (1981) Preparation and characterization of heterobifunctional crosslinking reagents for protein modification. *Chem. Pharm. Bull.* 29, 1130-1135.
- (18) Gharfeh, S. G. (1978) Preparation and Identification of the Sulfonic Acids of Fluorescein and the Metallofluorochromic Indicator Calcein. Iowa State University, Ph.D. Dissertation, University Microfilms International, Ann Arbor, MI.
- (19) Babcock, D. F., and Kramp, D. C. (1983) Spectral properties of fluorescein and carboxyfluorescein. *J. Biol. Chem.* 258, 6389.
- (20) Ando, T. (1984) Fluorescence of fluorescein attached to myosin SH1 distinguishes the rigor state from the actin-myosin-nucleotide state. *Biochemistry* 23, 375.
- (21) Steinberg, M., and Kapakos, J. G. (1984) Ligand binding to Na/K-ATPase fluorescently labeled with 5-iodoacetamido-fluorescein. *Ann. N. Y. Acad. Sci.* 435, 1544.
- (22) Greene, T. W., and Wuts, P. G. M. (1991) *Protective Groups in Organic Synthesis*, p 298 John Wiley & Sons, Inc., New York.
- (23) Greene, T. W., and Wuts, P. G. M. *Ibid.* p 302.
- (24) March, J. (1992) *Advanced Organic Chemistry*, p 410, John Wiley & Sons, Inc., New York.
- (25) Wingender, E., and Arellano, A. (1982) Synthesis and properties of the new thiol-specific reagent difluorescein disulfide: its application on histone-histone and histone-DNA interactions. *Anal. Biochem.* 127, 351-360.
- (26) Lakowicz, J. R. (1983) *Principles of Fluorescence Spectroscopy*, pp 257-295, Plenum Press, New York.
- (27) McComb, R. B., Bowers, G. N., and Posen, S. (1979) *Alkaline Phosphatase*, pp 219-221, Plenum Press, New York.
- (28) Jameson, D. M. (1984) *Fluorescein Hapten: An Immunological Probe* (E. W. Voss, Ed.) pp 52-53, CRC Press, Inc., Boca Raton, FL.
- (29) Weeks, I., Beheshti, I., McCapra, F., Campbell, A. K., and Woodhead, J. S. (1983) Acridinium esters as high-specific-activity labels in immunoassay. *Clin. Chem.* 29, 1474-1479.
- (30) McCapra, F. (1976) Chemical mechanisms in bioluminescence. *Acc. Chem. Res.* 9, 201-208.

# An Immunotoxin with Increased Activity and Homogeneity Produced by Reducing the Number of Lysine Residues in Recombinant *Pseudomonas* Exotoxin<sup>†</sup>

Waldemar Debinski<sup>‡</sup> and Ira Pastan\*

Laboratory of Molecular Biology, Division of Cancer Biology and Diagnosis Centers, National Cancer Institute, National Institutes of Health, 37/4E16, 9000 Rockville Pike, Bethesda, Maryland 20892. Received June 7, 1993\*

*Pseudomonas* exotoxin A (PE) is a protein composed of 613 amino acids arranged into three major, and one minor, domains. Immunotoxins (ITs) containing PE38, a mutant form of PE which lacks the cell binding domain (Ia, amino acids 1-252) and 16 amino acids from domain Ib (amino acids 365-380), are extremely potent cytotoxic agents which can cause a complete regression of various human carcinomas grown in nude mice. However, these ITs are a mixture of several different chemical forms since the coupling between the antibody and the toxin may occur between either the light or heavy chain of the antibody and one of the four primary amino groups present on the truncated toxin. To modify the toxin with heterobifunctional crosslinking reagents only at specific sites, we replaced lysines 590 and 606 with glutamines and lysine 613 with arginine (PE38QQR). We also added two different peptide sequences, each containing a lysine residue, at the N-terminus of PE38. In one of these the sequence is ANLAEEAFK ("Lys" peptide), and in the other, the sequence is LQGTKLMAEE ("NLys" peptide). The mutant toxins were coupled using a thioether linkage to monoclonal antibody B3 which recognizes an antigen present in large amounts on many human cancers. PE38QQR-containing recombinant toxins can only be linked to an antibody through the N-terminal methionine or the lysine within the peptide. B3-LysPE38QQR and B3-NLysPE38QQR were four times more cytotoxic to target cells than the corresponding B3-LysPE38 and B3-NLysPE38 ITs. Furthermore, the antitumor effect of B3-NLysPE38QQR was significantly greater than that of B3-NLysPE38. We conclude that B3-LysPE38QQR and B3-NLysPE38QQR are more active because they are more homogenous components with all the antibody coupled to the N-terminus of the toxin and not some to the C-terminus, producing ITs with very low cytotoxic activity.

## INTRODUCTION

Targeted toxins have been shown to be effective antitumor agents in animal models of solid human cancer (1). The usefulness of targeted toxins in clinical practice is in the initial phase of evaluation (reviewed in ref 1). As a prerequisite for clinical studies in humans, it is important to produce highly specific immunotoxins (ITs) that show antitumor activities in animal models. Furthermore, dose-limiting side effects of ITs administration are often due to the nonspecific toxicity of the toxin component (1). One way to minimize the nonspecific toxicity is to decrease the amount of IT required to produce an antitumor effect. It is also important that ITs can be produced in high yields to supply the necessary amount of drug needed for treatment at a reasonable cost.

Various toxins have been utilized to construct ITs (2). These toxins are either the purified natural products from plants and bacteria or they are made as recombinant proteins and produced in *E. coli*. Our laboratory uses *Pseudomonas* exotoxin A (PE) for chemical coupling to monoclonal antibodies (MAbs) or to make recombinant

immunotoxins with single-chain antibodies (3). PE has a complex three-domain structure which reflects the multistep pathway by which PE kills eukaryotic cells (Figure 1). Domain Ia contains the receptor binding sequence (5-7), domain II is the site of a proteolytic cleavage and it is necessary for toxin translocation through an intracellular membrane into the cytosol (8,9), and domain III is the enzymatic domain which ADP-ribosylates elongation factor-2 (EF-2) leading to the irreversible arrest of protein synthesis and cell death (6,10). To kill a cell, PE must be cleaved by an intracellular protease between arginine 279 and glycine 280 to produce a 37-kDa C-terminal fragment (8). This 37-kDa protein, composed of all of domain III and a portion of domain II, is capable of penetrating into the cytosol (Figure 1). The amino acids at the C-terminus of PE, REDLK, are absolutely necessary for the cytotoxic activity, and this sequence resembles the endoplasmic reticulum retention signal, KDEL (11). Chimeric toxins and ITs containing KDEL were constructed and found to be more cytotoxic than molecules ending in REDLK (12; unpublished data). The REDLK and KDEL sequences are not necessary for the ADP-ribosylating activity of PE.

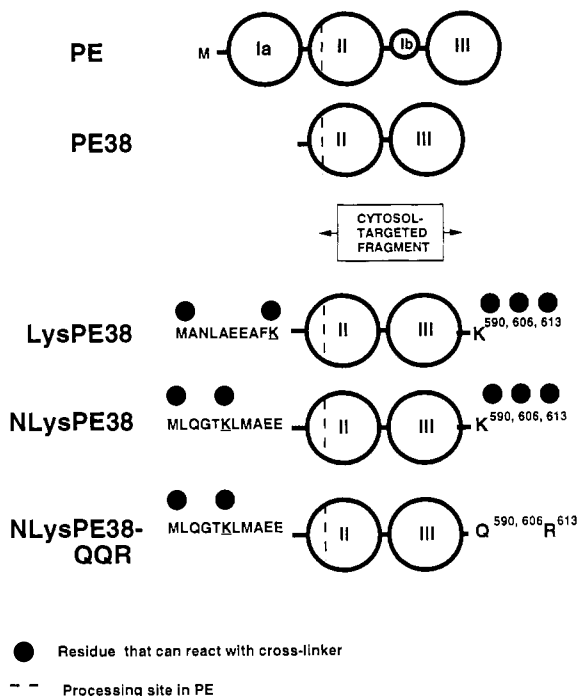
To make conventional immunotoxins, we now use recombinant truncated forms of PE, such as PE40, which has domain Ia deleted, or PE38 which has domain Ia and 16 amino acids from domain Ib (365 to 380 of PE) deleted (13,14). The ITs containing truncated PE are made using heterobifunctional cross-linking reagents which attach to amino groups on the N-terminal methionine of the toxin or on lysine residues. PE40 and PE38 have three lysine residues which are located in domain III at positions 590,

<sup>†</sup> Part of this work has been presented at the 3rd International Symposium on Immunotoxins, Orlando, FL, June 19-21, 1992.

\* To whom correspondence should be addressed. Phone: (301) 496-4797; Facsimile: (301) 402-1344.

<sup>‡</sup> W. Debinski received a postdoctoral fellowship from the Medical Research Council of Canada. Present address: Laboratory of Molecular Targeting, Research Center, Hotel-Dieu Hospital of Montreal, 3850 St. Urbain Street, Pavillon Marie de la Ferre, Montreal, Quebec, Canada H2W-1T8.

\* Abstract published in *Advance ACS Abstracts*, November 15, 1993.



**Figure 1.** Schematic drawing of *Pseudomonas* exotoxin A (PE) and its truncated forms. Circles correspond to the structural domains of PE: domain Ia is a binding domain (aa 1–252), domain II contains the site of proteolytic cleavage (aa 253–404), and domain III is an ADP-ribosylating enzyme (aa 405–613). The dashed line indicates the cleavage site after arginine 279 in PE. N-terminal sequences, given in a single letter code, correspond to the amino acids added to the PE38 sequences. Also listed are the positions of the three lysine residues in domain III at positions 590, 606, and 613; amino acid 613 is the last residue in PE.

606, and 613 (4). An additional lysine residue has been introduced within a nine amino acid peptide ("Lys" peptide) added to PE40 at its N-terminus to form LysPE40 (13). LysPE40 is conjugated to antibodies more easily than PE40, and the resulting ITs are more active (13). Another version of the toxin has been recently made which has one lysine residue in a 10 amino acid peptide preceding PE40 ("NLys" peptide); it has been termed NLysPE40 (15).

To avoid chemical modification of domain III with cross-linking reagents, which should produce inactive or less active ITs by interfering with the ability of the 37-kDa fragment to be translocated to the cytosol, we changed the lysines at positions 590, 606, and 613 to other amino acids using site-directed mutagenesis. In studies with an antibody directed against the human transferrin receptor (HB21), PE40 with mutations in the lysines in the carboxyl terminal portion of the toxin was conjugated through a disulfide bond to HB21 and produced a more cytotoxic IT and at higher yields (16). In addition, we noticed that some forms of the mutant PE40 molecules were produced in better yields in *E. coli* than others with lysine residues untouched. In the present work, we tested the following: (i) if the action of the ITs containing selectively modified forms of PE38 had a better antitumor activity in mice, (ii) whether the peptides added at the amino terminus of PE40 and NLysPE40 (or PE38) and elimination of lysine residues in truncated toxins are responsible for their better expression in *E. coli*, and (iii) whether it is possible to use a thioether rather than a disulfide bond to combine the toxin with the antibody and to retain the higher cytotoxicity of conjugates.

## MATERIALS AND METHODS

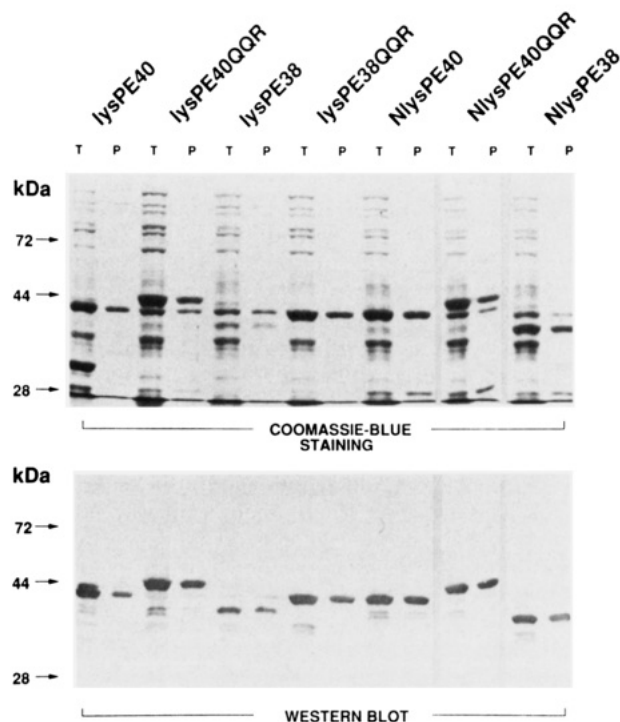
**Bacterial Strains and Plasmids.** Plasmids encoding various forms of recombinant truncated PE are indicated in Table 1. Plasmid pJB1PE38 encodes LysPE38, and it has been previously described (13). Plasmid pMS8-38 encodes NLysPE38; it was prepared by subcloning a 1013 bp fragment cut with SalI, EcoRI restriction enzymes from plasmid pJB1PE38 into a plasmid pWD402 (16) cut with the same enzymes. Plasmid pWD402-38, encoding LysPE38QQR, was formed by ligating a 460 bp DNA excised with BamHI and EcoRI from plasmid pWD402 to plasmid pJB1PE38 digested accordingly. Finally, plasmid pMS8-38-402, encoding NLysPE38QQR, was produced as plasmid pWD402-38 with a difference that the vector to which the BamHI, EcoRI 460 bp fragment was ligated derived from the plasmid pMS8-38. The cloning procedures for other plasmids encoding proteins listed in this work are available from the authors on request. The plasmids were propagated in the HB101 strain of *E. coli* and expressed in strain BL21 ( $\lambda$ DE3) as described (18).

**Expression and Purification of Recombinant PE38s.** Bacteria of the BL21 ( $\lambda$ DE3) which carry a T7 DNA-polymerase gene in a lysogenic and inducible form were transformed with plasmids encoding various forms of truncated PE. Transformed BL21 were grown in LB broth in small-scale cultures (5 mL) or in super-broth in cultures from 1 to 10 L. Cells were allowed to grow to absorbances of 0.5 (5-mL cultures) to 10.0 (fermentor runs) at 650 nm when 1-thio- $\beta$ -D-galactopyranoside was added to a final concentration of 1 mM. Cells were harvested 90–120 min later and centrifuged to give a bacterial pellet. Then, the bacteria were osmotically shocked in order to prepare the periplasm in which all forms of PE38 were predominantly found. PE38s were purified using a Pharmacia fast protein liquid chromatography (FPLC) system as previously described (15). The toxins were purified to homogeneity and analyzed by sodium dodecyl sulfate/polyacrylamide gel electrophoresis (SDS-PAGE). The proteins were detected by staining with Coomassie-Blue or by immunoblot analysis which was performed using polyclonal antisera to PE.

**Construction of Immunoconjugates.** To make ITs, we used essentially the same protocol as previously described (15). Briefly, monoclonal antibody B3 was modified with a 6-fold excess of 2-iminothiolane (2-IT) to provide sulfhydryl groups (19). The toxins were derived with a 10-fold excess of succinimidyl 4-(*N*-maleimido-methyl)cyclohexane-1-carboxylate (SMCC) to provide maleimides ready to react with thiols present on the derivatized antibody (20). The ITs were purified by two-step liquid chromatography (13).

**Protein Synthesis Inhibition Assay.** ITs were tested on the epidermoid carcinoma A431, breast carcinoma MCF-7, and several other carcinoma cell lines. Their activities were determined by measuring inhibition of [ $^3$ H]-leucine incorporation into cells (6). ID<sub>50</sub> indicates the concentration of IT at which the isotope incorporation fell by 50% when compared to nontreated cells.

**ADP Ribosylation Assay.** ADP ribosylation activity was assayed by the method of Collier and Kandel (21). Briefly, wheat germ extract was used as a source of EF-2. Samples of recombinant toxins were diluted 1:20 in PBS/0.02% BSA directly before the assay. [ $^{14}$ C]NAD provided labeled ADP ribose for transfer to EF-2. After 15 min of incubation, the samples were treated with trichloroacetic acid, and the precipitates were counted in a liquid scintillation counter.



**Figure 2.** SDS-PAGE and immunoblot analysis of the truncated recombinant forms of PE performed under nonreducing conditions: T, total cell pellet; P, periplasm. An equivalent amount of proteins was added on each lane: 2.4  $\mu$ g for T and 1.4  $\mu$ g for P.

**Treatment of Nude Mice Bearing Human Epidermoid Carcinoma Tumors.** A431 cells were injected subcutaneously on day 0 into female nude mice (four to five mice per group). Tumors developed in all injected animals, and the tumor size reached about 5  $\times$  5 mm on day 4. The mice started to receive ITs intraperitoneally (ip) on day 4, and the treatment continued on days 6–9 or the treatment started on day 5 and continued on days 6–8. Tumors were measured with a caliper, and the formula for tumor volume calculation was as previously reported (13). LD<sub>50</sub>s were established in FVB/NR and Balb/c female mice that received a single ip injection of ITs and were observed for 3 days afterwards.

## RESULTS

**Expression of Various Truncated Forms of PE in *E. coli*.** We attempted to engineer recombinant forms of PE that would be expressed at high levels, exported predominantly into the periplasm, and suitable for modification with heterobifunctional cross-linking reagents at specific sites in the process of conjugation with antibodies. The first form of PE40 we investigated, LysPE40, has a nine amino acid extension containing an additional lysine added at its amino end to facilitate its chemical modification (13). It was expressed in *E. coli* together with a protein of molecular weight around 30 kDa which was not recognized by polyclonal antisera against PE and was probably  $\beta$ -lactamase (Figure 2). The same toxin but with amino acids 365–380 deleted, LysPE38 was expressed at lower levels than LysPE40. In both cases most of the toxin was exported into the periplasm. Interestingly, when the three C-terminal lysines were changed so that there were glutamines at positions 590 and 606 and arginine at position 613, the expression of these toxins and the amount in the periplasm visibly improved (Figure 2). The QQR substitutions did change the mobility of the toxins on SDS-PAGE gel. Very little LysPE40QQR or LysPE38QQR

appears in the medium (not shown). NLysPE40 and NLysPE38 which contain a different sequence at the amino terminus than LysPE40 or LysPE38 (Figure 1) are expressed at high levels, and most of the protein is exported into the periplasm. Thus, the addition of the N-terminal peptide preceding domain II and III in NLys-toxin (MLQGTKLMAEE; Figure 1) preserves its export into the periplasm.

**Growth of *E. coli* with PE38 Toxins and a Yield of Toxin.** The differences in behavior in *E. coli* producing various PE38 toxins is summarized in Table 1. BL21 cells transformed with plasmids encoding LysPE38 and LysPE38QQR have doubling times of around 1 h. On the contrary, cells containing plasmids encoding NLysPE38 and NLysPE38QQR have a doubling time of 34 and 30 min, respectively. More importantly, we obtained much more purified NLysPE38QQR than LysPE38 from a typical fermentor run performed under identical conditions (Table 1).

**Preparation of B3-PE38s ITs.** It has been previously found that ITs made with PE38 are more active than those made with PE40 (unpublished data). Therefore, B3 was coupled to LysPE38, LysPE38QQR, NLysPE38, and NLysPE38QQR as described in the Materials and Methods. All possible care was taken to maintain identical coupling and purification conditions to make all four ITs. The Mono-Q and TSK chromatography profiles of all four ITs were indistinguishable (data not shown). However, the final yield of IT tended to be higher for NLysPE38- and NLysPE38QQR-containing conjugates than that for the Lys-toxin counterparts (33 and 25% vs 20 and 18% of starting materials, respectively; Table 1). More experiments are needed to establish statistically meaningful differences between the yields of various ITs. It is noteworthy that we could further improve the yield of IT up to 60% of the original material using NLysPE38QQR. The SDS-PAGE profiles of purified ITs were very similar for all the B3 ITs under both nonreducing and reducing conditions (data not shown).

**Cytotoxic Activities of B3 ITs.** We compared the cytotoxic activities of B3 conjugates on A431 epidermoid carcinoma cells. As shown in Figure 3, B3-LysPE38 and B3-NLysPE38 were very active with an ID<sub>50</sub> of 4 ng/mL (21 pM). However, the two conjugates containing PE38QQR were even more active ( $p < 0.02$ ;  $n = 5-7$ ; Student's *t*-test); the ID<sub>50</sub>s averaged 1 ng/mL (5.2 pM). These results show that eliminating lysine residues at the C-terminus of the toxin increases significantly the cytotoxicity of resulting ITs. Furthermore, this increased activity is not due to the precise sequence of amino acids at the amino terminus of PE38.

**Toxicity of B3-PE38s in Mice.** We determined the LD<sub>50</sub>s for the B3 ITs in mice (Table 1). We found that LD<sub>50</sub>s for B3-LysPE38 and B3-NLysPE38 were 112.5  $\mu$ g/mouse and were not distinguishable from each other when given as a single ip injection. B3-NLysPE38QQR was more toxic to mice with an LD<sub>50</sub> of 87.5  $\mu$ g/mouse (30% increase).

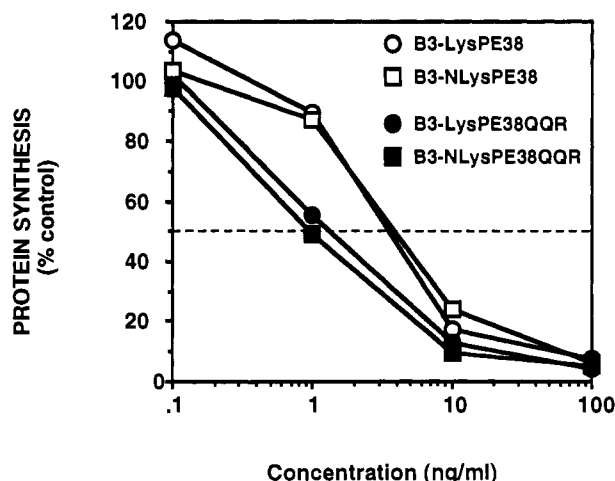
**Antitumor Activities of B3-PE38 Immunotoxins.** Since our goal was to prepare more active antitumor agents, we tested B3 coupled to two forms of NLysPE38 on A431 solid tumor xenografts in nude mice. The mice were injected with A431 cells on day 0 and received treatment of five injections of 5, 7.5, and 10  $\mu$ g per day of either B3-NLysPE38 or B3-NLysPE38QQR, starting on day 4 when tumors reached 40–50 mm<sup>3</sup> (Figure 4A). B3-NLysPE38 caused a significant antitumor effect at all doses used, but it did not produce a complete regression of the tumors at up to 10  $\mu$ g per day (50  $\mu$ g total dose). In contrast,



Table 1. Various Forms of PE38 and Their Chemical Conjugates with MAb B3

toxin (plasmid)	doubling time of <i>E. coli</i> (min)	efficiency of expression, (mg protein/OD × vol) <sup>b</sup>	B3 immunotoxins		
			final yield, (% starting material)	ID <sub>50</sub> on A431 cells (ng/mL)	LD <sub>50</sub> <sup>a</sup> (μg/mouse)
LysPE38 (pJBIPE38)	60	2.6	20	4	112.5
LysPE38QQR (pWD402-38)	60		18	1	
NLysPE38 (pMS8-38)	34		33	4	112.5
NLysPE38QQR (pMS8-38-402)	30	14.8	25	1	87.5

<sup>a</sup> FVB/NCR female mice; average from two experiments. <sup>b</sup> OD: optical density. Vol: volume of culture.

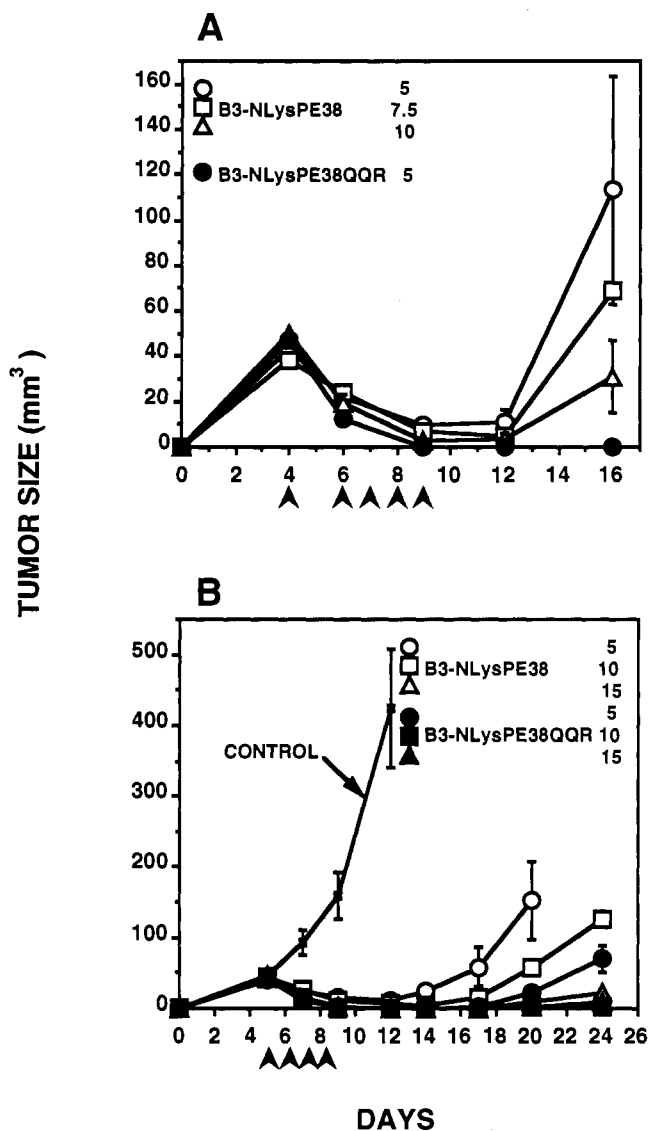


**Figure 3.** Inhibition of protein synthesis in A431 cells by B3 ITs purified on a TSK size-exclusion column. The interrupted line shows 50% of [<sup>3</sup>H]leucine incorporation. Isotope incorporation was measured as described in the Materials and Methods. The points correspond to the average of determinations performed in triplicates.

B3-NLysPE38QQR eliminated the tumors at a dose as low as 5 μg per day for 5 days (25 μg total dose). Injections of 7.5 and 10 μg per day also completely eliminated the tumors (not shown). This experiment demonstrated that B3-NLysPE38QQR had a greater antitumor potency than B3-NLysPE38.

Since the conjugates with NLysPE38QQR exhibited higher toxicity in mice than those containing NLysPE38, we performed another experiment on A431 xenografts in which the doses of the ITs were established on the basis of their LD<sub>50</sub> values. The mice bearing the A431 tumors were injected with doses corresponding to 5, 10, and 15% of their LD<sub>50</sub>s (Figure 4B). When B3-NLysPE38QQR was injected for 4 days at 5% of the LD<sub>50</sub> dose (4.4 μg/mouse/day; total dose 17.6 μg) complete tumor regression occurred in all animals. As expected, the higher doses of this IT produced the same effect. B3-NLysPE38 was a less potent antitumor agent. Even at a dose of 15% of the LD<sub>50</sub> complete tumor regression occurred in only 80% of the treated mice (16.8 μg/mouse/day; 67.2 μg total dose).

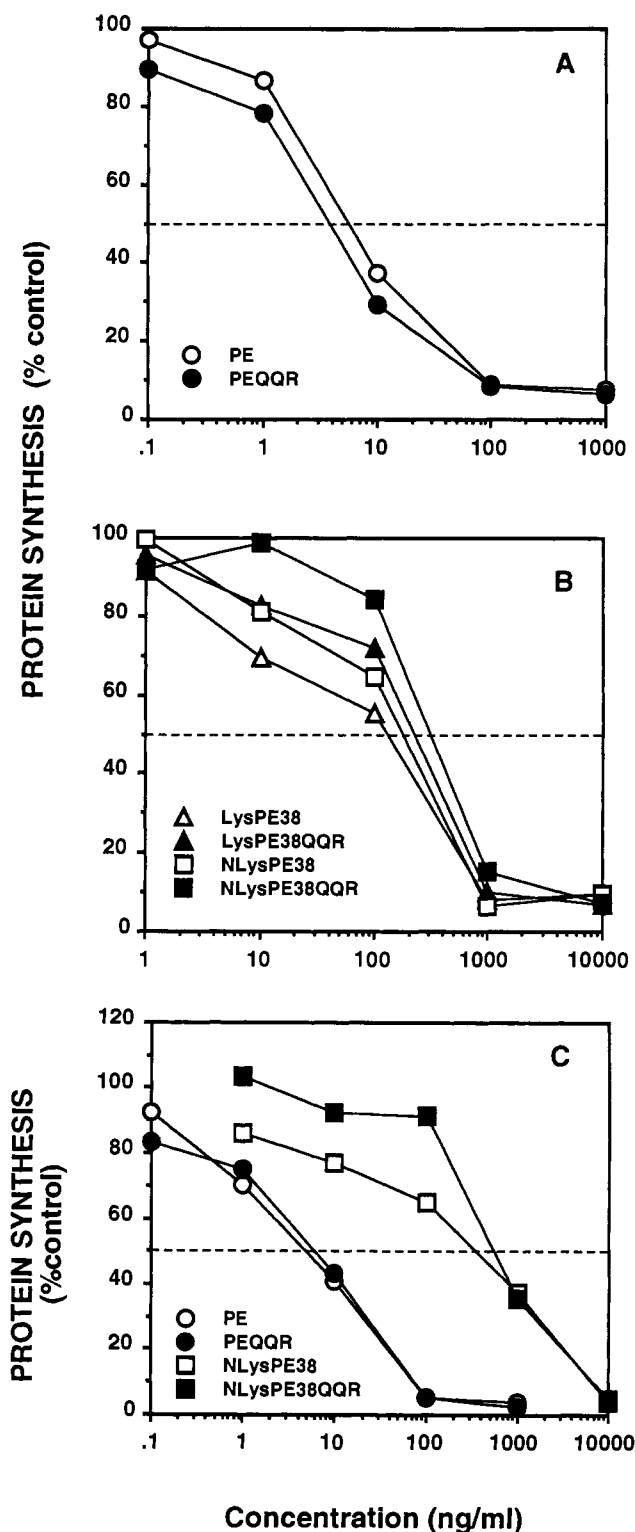
**Toxicities of the Toxins Containing "QQR" Mutations.** To rule out the possibility that the amino acid changes at the C-terminus of the PE38 toxins increased toxin activity directly instead of preventing coupling to the carboxyl terminal we performed several control studies. We tested the cytotoxicity of PE/PE38 and their QQR derivatives on different cancer cell lines (Figure 5). PE and PEQQR had the same toxic activity on MCF-7 cells (Figure 5A). Similar results were obtained on CRL-1739 gastric carcinoma and LNCaP prostate carcinoma cell lines (data not shown). Furthermore, LysPE38QQR and



**Figure 4.** Antitumor effect of B3-NLysPE38 (open symbols) and B3-NLysPE38QQR (full symbols) on A431 xenografts in nude mice. A431 cells were inoculated subcutaneously on day 0 ( $3 \times 10^6$  cells/mouse), and the mice were treated ip on the days indicated by the arrowheads. In A, equal amounts of B3-NLysPE38 and B3-NLysPE38 QQR were injected into animals, and the numbers (5, 7.5, 10) correspond to μg/mouse/day. SEs are shown as vertical bars for all data points with the exception of animals receiving 7.5 μg/day of B3 IT. In B, the mice received equivalent doses (5, 10, 15%/mouse/day) according to the LD<sub>50</sub> values of both ITs. SEs are shown for the control animals and for 5% LD<sub>50</sub>/mouse/day of both B3-NLysPE38 and B3-NLysPE38QQR treated mice.

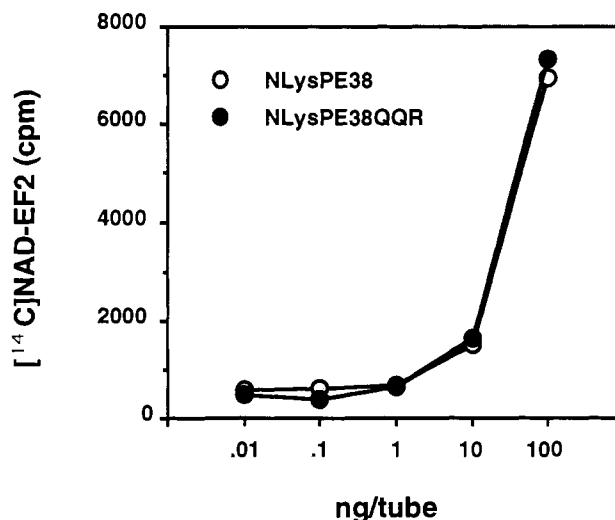
NLysPE38QQR did not appear to show any greater nonspecific toxicity than that exhibited by LysPE38 and





**Figure 5.** Cytotoxicity and nonspecific toxicity in MCF-7 (A and B) and in A431 (C) cells of PE and various forms of PE38, respectively. The interrupted line shows 50% [ $^3$ H]leucine incorporation.

NLysPE38 on MCF-7 cells (Figure 5B). If anything, the QQR derivatives were slightly less cytotoxic. We evaluated the effects of the various toxins on the A431 cells which had been used in the antitumor experiment and found that PE had the same activity as PEQQR and that NLysPE38 had the same activity as NLysPE38QQR (Figure 5C). We also found that in mice PE and PEQQR had the same LD<sub>50</sub> and that NLysPE38 and NLysPE38QQR also had the same LD<sub>50</sub> (17.5  $\mu$ g/mouse).



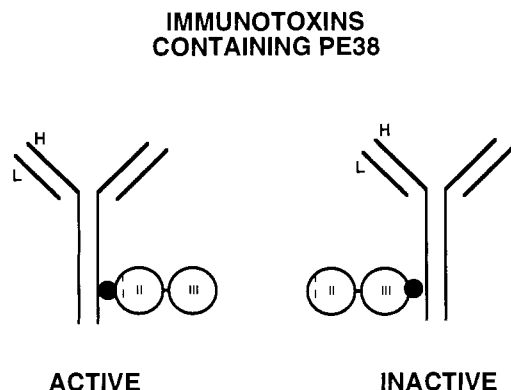
**Figure 6.** ADP ribosylating activities of NLysPE38 and NLysPE38QQR. Each result is the mean of three determinations.

**ADP Ribosylating Activities of Toxins and ITs.** Since the changes at the C-terminus of PE38 might influence the ADP ribosylating activity of domain III we measured the ADP ribosylating activity of NLysPE38 and NLysPE38QQR. The toxins were used at various amounts per reaction. We did not observe any appreciable difference between the enzymatic activity of NLysPE38 and NLysPE38QQR (Figure 6). Since the coupling of NLysPE38QQR to MAb B3 may result in a different ADP ribosylating activity than that of NLysPE38 conjugated to B3, both B3 conjugates were tested for their ADP ribosylating activities and no differences were observed.

## DISCUSSION

We have made ITs composed of MAb B3 coupled to various forms of recombinant PE38 with different N- and C-terminal ends. ITs containing forms of PE38 with lysine residues substituted with Gln at positions 590 and 606 and Arg at position 613 at the C-terminus (QQR) were more cytotoxic to cancer cell lines than ITs containing a wild-type carboxyl terminus. On the other hand, changes in the extension peptide at the amino end of the toxin did not have any impact on the activity of the ITs. Moreover, the higher cytotoxicity of B3-NLysPE38QQR was translated into a better antitumor effect in nude mice bearing human xenografts.

**Coupling of the N-Terminus of the Toxin to MAb Increases the Cytotoxic Activity of IT.** When B3 was coupled to NLysPE38QQR through a noncleavable linker, the IT was more active than B3-NLysPE38 prepared in the same way. The same phenomenon was observed with a LysPE38 version of the toxin and found for other monoclonals, such as C242, directed against colorectal cancer and mono- and divalent versions of HB21 (15, 22; unpublished observation). We have demonstrated that the QQR mutation at the C-terminal end does not increase the cytotoxicity of PE, as has been observed with changes in the last five amino acids in PE (11). The most plausible explanation for higher cytotoxicity of ITs with QQR is that Lys- or NLysPE38QQR is chemically derived at one site at the amino terminus prior to the processing site of PE which lies between amino acids 279 and 280 (Figure 1). The proteolytic cleavage inside the cells produces a 37-kDa (or 35-kDa in case of PE38) fragment which must be translocated into the cytosol. If the toxin is coupled to the light or heavy chain of the antibody by its carboxyl end, a large protein would be produced that would be



**Figure 7.** Schematic drawing of the structure of ITs composed of a MAb and either PE38 or PE38QQR: MAb, Y letter; H, heavy chain; L, light chain. All other symbols are as in Figure 1. Note that the toxin can also be linked to the light chain.

difficult to translocate (Figure 7) even if larger, e.g., 62-kDa, proteins have been shown to translocate to the cytosol (23). In addition, coupling to the C-terminus may prevent the REDLK sequence from bringing the toxin to the endoplasmic reticulum. The 35-kDa fragment derived from NLysPE38QQR would be neither chemically changed nor attached to a chain of the antibody thus leaving the fragment free to reach the endoplasmic reticulum and translocate into the cytosol. Thus, because of the increased homogeneity, B3-NLysPE38QQR would be more active. On the contrary, B3-PE38s are a mixture of conjugates between the N- and C-terminal ends of the toxin and the antibody chains (Figure 7).

**"QQR" Mutations Increase the Cytotoxicity of ITs by a Mechanism Different from KDEL Mutations or Mutations that Eliminate the Need for Toxin Proteolysis.** The increase in the potency of PE resulting from introducing the KDEL sequence at its C-terminus makes PE-containing ITs more active *in vitro* but also more toxic in animals (R. Kreitman, L. Pai, and I. Pastan, unpublished results). Even though B3-NLysPE38QQR was somewhat more toxic to animals than B3-NLysPE38, its therapeutic efficacy was improved. One reason is that B3-NLysPE38QQR does not compete for B3 binding sites with inactive molecules of IT, as in the case of B3-LysPE38. B3-LysPE38 molecules that are inactive on tumor cells still may be toxic to the liver.

PE38s need to be proteolytically processed inside cells (Figures 1 and 7). One may argue that by eliminating the need for the proteolysis step it would be possible to increase the supply and subsequent cytotoxicity of the cytosol-targeted fragment of the toxin. Our laboratory has recently engineered a PE35 molecule which like the Ricin A chain does not require proteolysis for activation and initiation of translocation (24). However, the cytotoxicities and antitumor activities of ITs containing PE35 or NLysPE38QQR are similar (W. Debinski and I. Pastan, unpublished results). Thus, the processing of PE38 attached to B3 is not a rate-limiting step in its cytotoxicity on several cancer cell lines tested.

**Export of Truncated PE Toxins into the Periplasm of *E. coli* May Be Related to a Negatively Charged N-Terminus.** NLysPE38 and NLysPE38QQR are produced in large amounts in *E. coli* and easily purified to near-homogeneity. It has been previously noted that PE40 is almost completely exported into the periplasm (18). The N-terminal sequence of PE40 does not, however, resemble classic signal sequences that enable bacterial proteins to be exported out of the cytoplasm (25). Introduction of "Lys" and "NLys" peptides does make the

N-terminus of the toxin more similar to the classic pattern of signal sequences. The N-terminal amino acids in PE38, LysPE38, and NLysPE38, with the charged residues in bold type, are as follows:

NH<sub>2</sub> MAEGGSLAALTAHQACHLPL... - PE38

NH<sub>2</sub> MANLAEEAFKGGSLAALTAH... - LysPE38

NH<sub>2</sub> MLQGTKLMAEEGGSLAALTA... - NLysPE38

Thus, these PE38s have a negatively charged N-terminus, and the charge is confined to the amino end or to the middle of the first 20–25 N-terminal amino acids. Recent reports suggest that a single net negative charge present in leader sequences of venoms may play a role in their export (26). All our PE38 versions of PE also have a single net negative charge within their 25 amino-terminal amino acids, as did the first form of PE40 produced in this laboratory (18). All of them have glutamic acids present near the amino end. It has also been found that a glutamic acid neutralizing the positive charge of either arginine or lysine had a strongly beneficial effect on protein export in prokaryotes (27). This negative charge provided by the glutamic acid could represent a favorable feature for some proteins to be transported through the membranes.

## SUMMARY

ITs containing selectively modified PE38, such as LysPE38QQR or NLysPE38QQR, are more active agents than their counterparts with a wild type c-terminus due to an increase in the specific potency of the IT. NLysPE38 or NLysPE38QQR can be produced in large amounts so that material for clinical trials can be readily obtained.

## ACKNOWLEDGMENT

We thank E. Lovelace and A. Harris for assistance with tissue cell culture and A. Jackson and J. Evans for secretarial help.

## LITERATURE CITED

- (1) Pastan, I., and FitzGerald, D. (1991) Recombinant toxins for cancer treatment. *Science* 254, 1173–1177.
- (2) Frankel, A. E., Ed. (1988) *Immunotoxins*, Kluwer Academic Publishers, Dordrecht, Netherlands.
- (3) Pastan, I., Chaudhary, V., and FitzGerald, D. (1992) Recombinant toxins as novel therapeutic agents. *Ann. Rev. Biochem.* 61, 331–354.
- (4) Gray, B. L., Smith, D. H., Baldrige, J. S., Harkins, R. N., Vasil, M. L., Chen, E. Y., and Heyneker, H. L. (1984) Cloning, nucleotide sequence and expression in *Escherichia coli* of the exotoxin A structural gene of *Pseudomonas aeruginosa*. *Proc. Natl. Acad. Sci. U.S.A.* 81, 2645–2649.
- (5) Allured, V. S., Collier, R. J., Carroll, S. F., and McKay, D. B. (1986) Structure of exotoxin A of *Pseudomonas aeruginosa* at 3.0-Ångstrom resolution. *Proc. Natl. Acad. Sci. U.S.A.* 83, 1320–1324.
- (6) Hwang, J. D., FitzGerald, D. J., Adhya, S., and Pastan, I. (1987) Functional domains of *Pseudomonas* exotoxin identified by deletion analysis of the gene expressed in *E. coli*. *Cell* 48, 129–136.
- (7) Jinno, Y., Chaudhary, V. K., Kondo, T., Adhya, S., FitzGerald, D. J., and Pastan, I. (1988) Mutational analysis of domain I of *Pseudomonas* exotoxin: Mutations in domain I of *Pseudomonas* exotoxin that reduce cell binding and animal toxicity. *J. Biol. Chem.* 263, 13203–13207.

- (8) Ogata, M., Chaudhary, V. K., Pastan, I., and FitzGerald, D. J. (1990) Processing of *Pseudomonas* exotoxin by a cellular protease results in the generation of a 37,000 kDa toxin fragment that is translocated to the cytosol. *J. Biol. Chem.* 265, 20678-20685.
- (9) Siegall, C. B., Ogata, M., Pastan, I., and FitzGerald, D. J. (1991) Analysis of sequences in domain II of *Pseudomonas* exotoxin A which mediate translocation. *Biochemistry* 23, 7154-7159.
- (10) Iglewski, B. H., and Kabat, D. (1975) NAD-dependent inhibition of protein synthesis by *Pseudomonas aeruginosa* toxin. *Proc. Natl. Acad. Sci. U.S.A.* 72, 2284-2288.
- (11) Chaudhary, V. K., Jinno, Y., FitzGerald, D., and Pastan, I. (1990) *Pseudomonas* exotoxin contains a specific sequence at the carboxyl terminus that is required for cytotoxicity. *Proc. Natl. Acad. Sci. U.S.A.* 87, 308-312.
- (12) Seetharam, S., Chaudhary, V. K., FitzGerald, D., and Pastan, I. (1991) Increased cytotoxic activity of *Pseudomonas* exotoxin and two chimeric toxins ending in KDEL. *J. Biol. Chem.* 266, 17376-17381.
- (13) Batra, J. K., Jinno, Y., Chaudhary, V. K., Kondo, T., Willingham, M. C., FitzGerald, D. J., and Pastan, I. (1989) Antitumor activity in mice of an immunotoxin made with anti-transferrin receptor and a recombinant form of *Pseudomonas* exotoxin. *Proc. Natl. Acad. Sci. U.S.A.* 86, 8545-8549.
- (14) Siegall, C. B., Chaudhary, V. K., FitzGerald, D. J., and Pastan, I. (1989) Functional analysis of domains II, Ib and III of *Pseudomonas* exotoxin. *J. Biol. Chem.* 264, 14256-14261.
- (15) Debinski, W., Karlsson, B., Lindholm, L., Siegall, C. B., Willingham, M. C., FitzGerald, D., and Pastan, I. (1992) Monoclonal antibody C242-*Pseudomonas* exotoxin A: A specific and potent immunotoxin with antitumor activity on a human colon cancer xenograft in nude mice. *J. Clin. Invest.* 90, 405-411.
- (16) Debinski, W., Jinno, Y., Siegall, C. B., FitzGerald, D. J., and Pastan, I. (1992) Genetic modifications in a primary structure of PE40 that enable its selective chemical derivatization. Monoclonal antibodies: Applications in Clinical Oncology in Epenetos, E. E., Ed. pp 503-511, Chapman and Hall Medical, London.
- (17) Pastan, I., Lovelace, E. T., Gallo, M. G., Rutherford, A. V., Magnani, J. L., and Willingham, M. C. (1991) Characterization of monoclonal antibodies B1 and B3 that react with mucinous adenocarcinomas. *Cancer Res.* 51, 3781-3787.
- (18) Chaudhary, V. K., Xu, Y.-H., FitzGerald, D., Adhya, S., and Pastan, I. (1988) Role of domain II of *Pseudomonas* exotoxin in the secretion of proteins into the periplasm and medium by *Escherichia coli*. *Proc. Natl. Acad. Sci. U.S.A.* 85, 2939-2943.
- (19) Traut, R. R., Bollen, A., and Sun, T.-T. (1973) Methyl-4-mercaptobutyrimidate as a cleavable cross-linking reagent and its application to the *Escherichia coli* 30S ribosome. *Biochemistry* 12, 3266-3273.
- (20) Yoshitake, S., Yamada, Y., Ishikawa, E., and Masseyoff, R. (1979) Conjugation of glucose oxidase from *Aspergillus niger* and rabbit antibodies using *N*-hydroxysuccinimide ester of *N*-(4-carboxycyclohexylmethyl)-maleimide. *Eur. J. Biochem.* 101, 395-399.
- (21) Collier, R. J., and Kandel, J. (1971) Structure and activity of diphtheria toxin. I. Thiol-dependent dissociation of a fraction of toxin into enzymatically active and inactive fragments. *J. Biol. Chem.* 246, 1496-1503.
- (22) Debinski, W., and Pastan, I. (1992) Monovalent immunotoxin containing truncated form of *Pseudomonas* exotoxin as potent antitumor agent. *Cancer Res.* 52, 5379-5385.
- (23) Debinski, W., Siegall, C. B., FitzGerald, D., and Pastan, I. (1991) Substitution of foreign protein sequences into a chimeric toxin composed of transforming growth factor  $\alpha$  and *Pseudomonas* exotoxin. *Mol. Cell Biol.* 11, 1751-1753.
- (24) Theuer, C. P., FitzGerald, D., and Pastan, I. (1992) A recombinant form of *Pseudomonas* exotoxin not requiring proteolytic processing for cytotoxicity. *J. Biol. Chem.* 267, 16872-16877.
- (25) von Heijne, G. (1986) Net N-C charge imbalance may be important for signal sequence function in bacteria. *J. Mol. Biol.* 192, 287-290.
- (26) Jones, D., Sawicki, G., and Wozniak, M. (1992) Sequence, structure and expression of a wasp venom protein with a negatively charged signal peptide and a novel repeating internal structure. *J. Biol. Chem.* 267, 14871-14878.
- (27) Li, P., Beckwith, J., and Inouye, H. (1988) Alteration of the amino terminus of the mature sequence of a periplasmic protein can severely affect protein export in *Escherichia coli*. *Proc. Natl. Acad. Sci. U.S.A.* 85, 7685-7689.

# (Aminomethyl)phosphonate Derivatives of Oligonucleotides

Reza Fathi,\* Qing Huang, Jia-Lin Syi, William Delaney, and Alan F. Cook

PharmaGenics, Inc., 4 Pearl Court, Allendale, New Jersey 07401. Received July 7, 1993\*

Oligothymidylate (aminomethyl)phosphonates have been prepared, and their enzymatic and physicochemical properties have been studied. The individual isomers of the protected dimers have been separated, characterized, and incorporated into oligonucleotides in which the backbone consists of alternating (aminomethyl)phosphonate and phosphodiester linkages. One of these net neutral, single isomer oligonucleotides forms a duplex with its complementary sequence which is more stable than the corresponding natural counterpart, whereas the other isomer is considerably less stable. Specificity of hybridization is maintained, as determined by the reduction in melting temperature observed upon the introduction of mismatches into the complementary strand of the duplex. The (aminomethyl)-phosphonate linkage is stable toward enzymatic degradation but can be hydrolyzed in aqueous solution at elevated temperature.

## INTRODUCTION

Oligonucleotides offer the promise of an important new approach to the design of therapeutic agents, in which the biological target is RNA or DNA rather than conventional *in vivo* targets such as enzymes, proteins, or receptors. Natural oligonucleotides, however, suffer from a number of disadvantages, such as their relatively poor uptake into cells and lack of resistance to degradation by cellular enzymes. These disadvantages have stimulated efforts to prepare backbone-modified derivatives which are not subject to these limitations. Several reports have described backbone modifications in which one of the nonbridging oxygen atoms attached to phosphorus has been replaced by another atom while retaining the negative charge. Substitution of one oxygen atom by sulfur produces phosphorothioates, a class of compounds which has been widely studied and found to offer increased resistance to degradation as compared with natural oligonucleotides (Stein et al., 1988) while retaining the ability to stimulate endogenous cellular ribonuclease-H activity (Dagle et al., 1990). This latter enzyme has been shown to degrade the RNA strand of a DNA/RNA duplex. Although phosphorothioates are more stable than phosphodiester, they are somewhat susceptible to degradation by nucleases and suffer from the further disadvantage that they are normally produced as complex mixtures of stereoisomers due to the chirality of the phosphorus atom and the lack of a convenient stereospecific synthetic procedure. Replacement of both nonbridging oxygen atoms attached to phosphorus produces phosphorodithioates (Marshall and Caruthers, 1993) which offer the advantage of being achiral at phosphorus, resistant to nuclease degradation, and capable of directing RNase-H-mediated cleavage of RNA in hybrid duplexes.

A second approach to modification of the phosphodiester backbone is the replacement of the negatively charged oxygen by an uncharged group to produce a neutral species. This type of modification is best exemplified by methylphosphonates, which have been shown to be transported into cells by endocytosis and are more resistant to degradation (Shoji et al., 1991). Methylphosphonates, however, suffer from the disadvantage of being relatively

insoluble in water and aqueous buffers. A variety of other neutral analogs, such as triesters and phosphoramidates, have also been previously described (Barrett et al., 1974; Dagle et al., 1991).

A third approach is to replace the negatively charged oxygen with a cationic group. Cationic molecules have previously been used to enhance the delivery of conjugates into cells. The iron-transport protein transferrin, for example, has been conjugated to cationic molecules such as protamine or polylysine in order to transport nucleic acids (Wagner et al., 1990), and cationic lipids have been used in a liposome-mediated transfection protocol for the introduction of DNA into the nuclei of animal cells. The delivery of proteins and peptides such as albumin (Kumagai et al., 1987) and enkephalin (Pardridge et al., 1987) across the blood-brain barrier has been enhanced by conjugation to cationic molecules such as hexamethylenediamine, and a variety of drugs, including methotrexate and daunomycin, have been conjugated to polylysine in attempts to improve their uptake and efficacy (Arnold, 1985). Cationic molecules have also been attached to oligonucleotides in attempts to improve their activity *in vivo*. Conjugation of polylysine to oligonucleotides directed against VSV (Lemaitre et al., 1987) and HIV (Stevenson & Iverson, 1989) sequences has been shown to produce enhanced effects as compared with their unmodified counterparts. Polylysine is efficiently transported into mammalian cultured cells by nonspecific adsorptive endocytosis preceded by nonspecific interactions with negatively charged molecules on the surface of the cell (Leonetti et al., 1990), but it has also been shown to produce toxic effects at higher concentrations.

A few oligonucleotides with cationic groups attached to the backbone via phosphoramidate linkages have been described (Letsinger et al., 1988). Under appropriate conditions these modified oligonucleotides bound more effectively than their natural counterparts to complementary sequences and in addition showed unusual salt-dependent effects. Other examples of cationic oligonucleotides have not yet been reported. In view of the potential for enhancement of uptake by cationic moieties, we have developed methods for the synthesis of a series of backbone-modified oligonucleotides in which the negatively charged oxygen has been partially replaced by a positively charged aminomethyl group, and the enzymatic

\* Corresponding author. Tel: 201-818-1000; Fax: 201-818-9044.

• Abstract published in *Advance ACS Abstracts*, December 1, 1993.

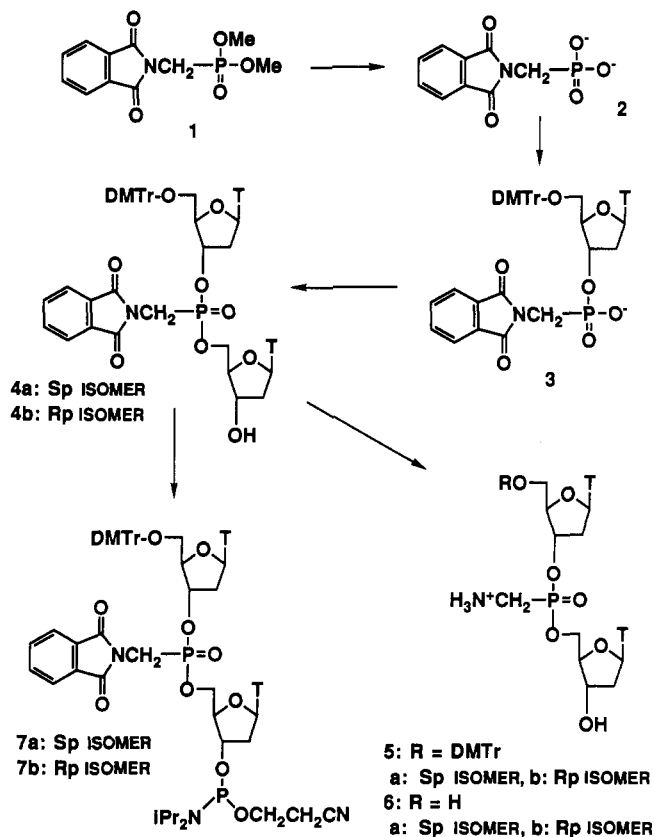
and physicochemical properties of these compounds have been studied. The initial results are described below.

## EXPERIMENTAL PROCEDURES

**Materials and Methods.** Oligonucleotides were synthesized using an Applied Biosystems Model 394 DNA synthesizer. 5'-*O*-(dimethoxytrityl)thymidine, 1-(2,4,6-trimethylbenzenesulfonyl)nitrotriazolide (MSNT), and  $\beta$ -(cyanoethyl) chloro *N*-diisopropylamino phosphite were purchased from Peninsula Laboratories, Inc. (Belmont, CA). Dimethyl (phthalimidomethyl)phosphonate was purchased from Lancaster Synthesis Inc. (Windham, NH). Silica gel for column chromatography (130–270 mesh) was obtained from Aldrich Chemical Co. Ultraviolet spectra were obtained with a Shimadzu UV 160U spectrophotometer using 1-mL quartz cuvettes. Extinction coefficients of oligonucleotides were determined using a published procedure (Rychlik and Rhoads, 1989). HPLC purifications were performed using a Waters 600E system controller equipped with a multisolvent delivery system and a Model 991 photodiode array detector. Reversed-phase HPLC was performed using a Waters RCM (8 mm  $\times$  10 cm) C<sub>4</sub> column for analytical purposes and a C<sub>4</sub> RCM (25 mm  $\times$  10 cm) column for preparative use. A gradient of 0.1 M triethylammonium acetate buffer pH 7.0 (TEAA)/acetonitrile was generally employed. Anion-exchange chromatography was performed on a Dionex NucleoPac column (Dionex Corporation, Sunnyvale, CA) using a linear gradient of 25 mM Tris-HCl, pH 8.0, containing 5% CH<sub>3</sub>CN, increasing to 25 mM Tris-HCl/1 M NH<sub>4</sub>Cl, pH 8.0. NMR spectra were recorded using a Varian VXR-400-MHz spectrometer. Unless otherwise stated, <sup>31</sup>P NMR were run in DMSO-*d*<sub>6</sub>, broad band decoupled, and referenced to H<sub>3</sub>PO<sub>4</sub> as an external standard, and <sup>1</sup>H NMR spectra were referenced to external tetramethylsilane as standard. Polyacrylamide gel electrophoresis was performed using a 15% acrylamide gel containing 7 M urea with 0.09 M trisborate/EDTA (1  $\times$  TBE) buffer, pH 8; bands were detected by UV shadowing. Molecular modeling simulations were performed on a Silicon Graphics Crimson system (Silicon Graphics, Inc., Mountain View, CA), using Biograf molecular modeling software from Molecular Simulations Inc., (Burlington, MA). The AMBER force field (Weiner et al., 1986) was used for molecular mechanics simulations.

**Preparation of the Triethylammonium Salt of (Phthalimidomethyl)phosphonic Acid (2).** Dimethyl (phthalimidomethyl)phosphonate (1, Figure 1, 2.0 g, 7.4 mmol) was dissolved in chloroform (15 mL), and bromotrimethylsilane (2 mL, 15 mmol) was added dropwise to the solution. After 2 h the reaction mixture was concentrated under reduced pressure, and the residue was redissolved in chloroform (8 mL) followed by dropwise addition of triethylamine (20 mL) with cooling in an ice bath. After being stirred at room temperature for 2 h, the mixture was filtered and concentrated to dryness. The residue was dissolved in methanol (10 mL) and added dropwise to anhydrous diethyl ether (600 mL). The precipitate was filtered, washed with ether, and dried over P<sub>2</sub>O<sub>5</sub> to yield 2.1 g (65%) of pure 2 as the triethylammonium salt. UV (H<sub>2</sub>O) max: 298 nm. <sup>1</sup>H NMR (DMSO-*d*<sub>6</sub>):  $\delta$  (ppm) 8.0 (m, 4H, aromatics), 3.8 (d, 2H, *J* = 11.0 Hz, CH<sub>2</sub>), 2.96 (q, 2H, *J* = 7.4, C<sub>2</sub>H<sub>5</sub>), 1.16 (t, 3H, *J* = 7.3 Hz, C<sub>2</sub>H<sub>5</sub>). <sup>31</sup>P NMR:  $\delta$  11.0 (s).

**5'-*O*-(Dimethoxytrityl)thymidine 3'-(Phthalimidomethyl)phosphonate (3).** The triethylammonium salt of 2 (1.7 g, 5 mmol) was dried by coevaporation with pyridine (3  $\times$  10 mL), dissolved in dry pyridine (40 mL),



**Figure 1.** Synthesis of dinucleotide (aminomethyl)phosphonates.

and treated with triisopropylbenzenesulfonyl chloride (TPS-Cl, 3.0 g, 9.9 mmol) followed by a solution of 5'-*O*-(dimethoxytrityl)thymidine (2.0 g, 3.67 mmol) in dry pyridine (40 mL) which had also been previously dried by coevaporation with pyridine. The resulting mixture was stirred at room temperature overnight under a dry nitrogen atmosphere, diluted with aqueous sodium bicarbonate (3%, 350 mL), and extracted with ethyl acetate (3  $\times$  150 mL). The combined organic layers were dried over anhydrous magnesium sulfate and filtered, and the solvent was removed under reduced pressure. The residue was purified by silica gel column chromatography (100 g) using CH<sub>2</sub>Cl<sub>2</sub>/MeOH/Et<sub>3</sub>N (30:1:0.3, 2.8 L followed by 30:2:0.3, 1.1 L) as solvent. The appropriate fractions were collected and combined to yield 1.8 g (57%) of pure 3 as a white foam. UV max (H<sub>2</sub>O): 270 nm. <sup>1</sup>H NMR (DMSO-*d*<sub>6</sub>):  $\delta$  (ppm) 7.8 (m, 4H, aromatic), 7.5 (d, 1H, H<sub>6</sub>), 7.3–6.8 (m, 13H, DMTr), 6.2 (t, 1H, H<sub>1'</sub>), 4.8 (m, 1H, H<sub>3'</sub>), 4.1 (m, 1H, H<sub>4'</sub>), 3.7 (s, 6H, OMe), 3.5 (d, 2H, *J* = 11.0 Hz, CH<sub>2</sub>), 3.1–3.3 (m, 2H, H<sub>5'</sub>), 2.6 (q, 2H, C<sub>2</sub>H<sub>5</sub>), 2.4–2.2 (m, 2H, H<sub>2'</sub>), 1.3 (d, 3H, CH<sub>3</sub>), 1.0 (t, 3H, C<sub>2</sub>H<sub>5</sub>). <sup>31</sup>P NMR:  $\delta$  (ppm): 11.0 (s).

**Preparation of 5'-[[5'-*O*-(Dimethoxytrityl)thymid-3'-yl](phthalimidomethyl)phosphonyl]thymidine (4).** Compound 3 (2.0 g, 2.3 mmol) was dried by coevaporation with pyridine (3  $\times$  15 mL), redissolved in dry pyridine (80 mL), and treated with MSNT (0.75 g, 2.5 mmol) for 15 min at room temperature. Thymidine (0.6 g, 2.3 mmol) was dried by pyridine coevaporation in the same way, dissolved in pyridine (15 mL), and added to the solution of 3. The reaction mixture was stirred at room temperature under a dry nitrogen atmosphere for 2.5 h and then diluted with aqueous sodium bicarbonate (5%, 300 mL) and extracted with ethyl acetate (3  $\times$  200 mL). The organic layers were combined, dried over anhydrous magnesium sulfate, and concentrated under reduced pressure. The

residue was purified by column chromatography on silica gel (100 g) using  $\text{CH}_2\text{Cl}_2/\text{MeOH}/\text{Et}_3\text{N}$  (30:1:0.3) as solvent. Ten-mL fractions were collected. Fractions 120–126 contained the faster eluting Sp isomer **4a**, fractions 127–157 contained a mixture of both isomers, and fractions 158–170 contained the slower eluting Rp isomer **4b**. The appropriate fractions were collected, evaporated to dryness, and dried *in vacuo* over  $\text{P}_2\text{O}_5$  to give 0.17 g of **4a**, 0.2 g of **4b**, and 0.7 g of a mixture of isomers. TLC (silica gel 60F-254, 10 × 10 cm, 0.2-mm thickness)  $\text{CH}_2\text{Cl}_2/\text{EtOH}$  (15:1)  $R_f$  0.41 (faster, Sp isomer) and  $R_f$  0.34 (slower, Rp isomer).

**Separation of Isomers of 4 by HPLC.** The mixture of isomers of **4** (2.64 g) was dissolved in 0.1 M TEAA/ acetonitrile (1:1, 36 mL) and injected in four separate aliquots onto a reversed-phase  $\text{C}_4$  Vydac column (5 × 25 cm). The column was eluted with a linear gradient from 35 to 80% acetonitrile in 0.1 M TEAA, and the Sp and Rp isomers were eluted at 37–43 and 45–48 min, respectively. The appropriate fractions were pooled, extracted with ethyl acetate (3 × 50 mL), evaporated to dryness, and dried *in vacuo* over  $\text{P}_2\text{O}_5$ . This procedure yielded 500 mg of the faster, Sp isomer **4a** and 350 mg of the slower, Rp isomer **4b**, total yield 57%. Analytical HPLC of the pooled fractions using a reversed-phase  $\text{C}_4$  column indicated that pure isomers were obtained in each case.

$^{31}\text{P}$  NMR (DMSO- $d_6$ ): **4a**  $\delta$  (ppm) 20.8 (s); **4b**  $\delta$  19.94 (s).  $^1\text{H}$  NMR (DMSO- $d_6$ ): **4a**  $\delta$  (ppm) 7.73 (m, 4H, phthalimido), 6.8–7.37 (m, 15H, trityl, 2 ×  $\text{H}_6$ ), 6.22 (t, 1H,  $\text{H}_{1'}$ ), 5.90 (t, 1H,  $\text{H}_{1'}$ ), 5.21 (m, 1H,  $\text{H}_{3'}$ ), 3.71 (s, 6H,  $-\text{OCH}_3$ ), 1.69 (s, 3H,  $\text{CH}_3$ ), 1.42 (s, 3H,  $\text{CH}_3$ ); **4b**  $\delta$  (ppm) 7.76 (m, 4H, phthalimido), 6.79–7.73 (m, 15H, trityl group; 2 ×  $\text{H}_6$ ), 6.07 (t, 1H,  $\text{H}_{1'}$ ), 6.2 (t, 1H,  $\text{H}_{1'}$ ), 5.23 (m, 1H,  $\text{H}_{3'}$ ), 4.06 (d, 2H,  $J = 10$  Hz,  $\text{CH}_2\text{P}$ ), 3.72 (s, 6H,  $-\text{OCH}_3$ ), 1.65 (s, 3H,  $\text{CH}_3$ ), 1.37 (s, 3H,  $\text{CH}_3$ ).

**5'-[[5'-O-(Dimethoxytrityl)thymid-3'-yl](aminomethyl)phosphonyl]thymidine (5a and 5b).** A sample of **4a** (52 mg, 0.05 mmol) was dissolved in acetonitrile (800  $\mu\text{L}$ ) and treated with ethylenediamine (400  $\mu\text{L}$ ). After 6 h at room temperature the reaction mixture was dried under vacuum and coevaporated with toluene (3 × 500  $\mu\text{L}$ ) followed by absolute ethanol (3 × 500  $\mu\text{L}$ ). The residue was purified on a  $\text{C}_4$  semipreparative HPLC column (Waters RCM, 25 mm × 10 cm) with a gradient of 35–80% acetonitrile in 0.1 M TEAA. The desired material eluting at 7.13 min was collected and evaporated to dryness to give **5a** as a white solid, 39.4 mg (90.6%).

$^1\text{H}$  NMR (DMSO- $d_6$ ):  $\delta$  (ppm) 7.44 (s, 1H,  $\text{H}_6$ ), 7.42 (s, 1H,  $\text{H}_6$ ), 7.19–7.34 (m, 9H, trityl), 6.84 (d, 4H,  $J = 8.12$  Hz, trityl), 6.18 (t, 1H,  $\text{H}_{1'}$ ), 6.12 (t, 1H,  $J = 7.0$  Hz,  $\text{H}_{1'}$ ), 5.1 (m, 1H,  $\text{H}_{3'}$ ), 3.8–4.3 (m, 5H, CH), 3.1–3.38 (m, 2H,  $\text{H}_5$ ), 2.94 (d, 2H,  $J = 9.4$  Hz,  $\text{CH}_2\text{P}$ ), 2.0–2.5 (m, 4H,  $\text{H}_2$ ), 1.7 (s, 3H,  $\text{CH}_3$ ), 1.34 (s, 3H,  $\text{CH}_3$ ).  $^{31}\text{P}$  NMR: (DMSO- $d_6$ )  $\delta$  (ppm) 31.25 (s).

An identical procedure was used to prepare **5b**, 40.3 mg (92.6%).  $^1\text{H}$  NMR (DMSO- $d_6$ ):  $\delta$  (ppm) 7.5 (s, 1H,  $\text{H}_6$ ), 7.44 (s, 1H,  $\text{H}_6$ ), 7.19–7.32 (m, 9H, trityl), 6.85 (d, 4H,  $J = 8.5$  Hz, trityl), 6.2 (t, 1H,  $\text{H}_{1'}$ ), 6.12 (t, 1H,  $J = 7.2$  Hz,  $\text{H}_{1'}$ ), 5.11 (m, 1H,  $\text{H}_{3'}$ ), 3.86–4.22 (m, 5H, CH), 3.1–3.3 (m, 2H,  $\text{H}_5$ ), 2.9 (d, 2H,  $J = 9.8$  Hz,  $\text{CH}_2\text{P}$ ), 2.0–2.5 (m, 4H,  $\text{H}_2$ ), 1.71 (s, 3H,  $\text{CH}_3$ ), 1.34 (s, 3H,  $\text{CH}_3$ ).  $^{31}\text{P}$  NMR:  $\delta$  (ppm) 30.73 (s).

**5'-Thymid-3'-yl(aminomethyl)phosphonyl]-5'-thymidine (6a, 6b).** Compound **5a** or **5b** (25 mg, 0.025 mmol) was detritylated using 2 mL of 1% (v/v) dichloroacetic acid in  $\text{CH}_2\text{Cl}_2$ , and after 0.5 h the reaction mixture was dried *in vacuo*. The residue was diluted with 1 mL of water and extracted with ethyl acetate (4 × 1 mL). The

aqueous layer was lyophilized to give a white solid which was dissolved in 0.1 M TEAA (1.5 mL) and purified on an analytical reversed-phase column. The column was eluted with a linear gradient of 5–25% acetonitrile in 0.1 M TEAA.

The Rp isomer **6b** (11.3 mg) was obtained by collection of the peak which eluted after 10.85 min.  $^1\text{H}$  NMR (DMSO- $d_6$ )  $\delta$  (ppm) 7.66 (s, 1H,  $\text{H}_6$ ), 7.47 (s, 1H,  $\text{H}_6$ ), 6.16 (t, 2H, 2 ×  $\text{H}_{1'}$ ,  $J = 7.0$  Hz), 4.98 (m, 1H,  $\text{H}_{3'}$ ), 4.23 (m, 1H, CH), 4.12 (m, 2H, 2 ×  $\text{H}_5$ ), 4.00 (m, 1H, CH), 3.89 (m, 1H, CH), 3.56 (m, 2H, 2 ×  $\text{H}_5$ ), 2.96 (d, 2H,  $\text{CH}_2$ ,  $J = 9.8$  Hz), 2.0–2.5 (m, 4H, 4 ×  $\text{H}_2$ ), 1.75 (s, 3H,  $\text{CH}_3$ ), 1.73 (s, 3H,  $\text{CH}_3$ ).  $^{31}\text{P}$  NMR:  $\delta$  (ppm) 30.7 (s).

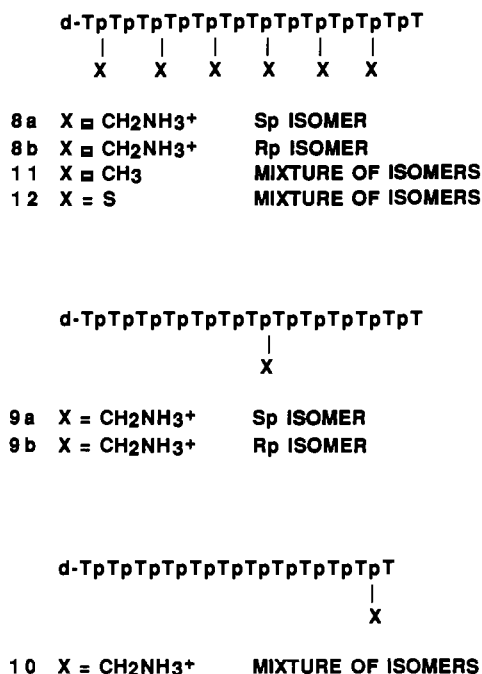
The Sp isomer **6a** (11.1 mg) was obtained by collection of the peak which eluted after 13.62 min.  $^1\text{H}$  NMR (DMSO- $d_6$ ):  $\delta$  (ppm) 7.66 (s, 1H,  $\text{H}_6$ ), 7.51 (s, 1H,  $\text{H}_6$ ), 6.16 (t, 2H, 2 ×  $\text{H}_{1'}$ ,  $J = 6.8$  Hz), 4.98 (m, 1H,  $\text{H}_{3'}$ ), 4.0–4.23 (m, 4H, 2 × CH, 2 ×  $\text{H}_5$ ), 3.89 (m, 1H, CH), 3.56 (m, 2H, 2 ×  $\text{H}_5$ ), 2.95 (d, 2H,  $\text{CH}_2$ ,  $J = 10.25$  Hz), 2.0–2.5 (m, 4H, 4 ×  $\text{H}_2$ ), 1.76 (s, 3H,  $\text{CH}_3$ ), 1.73 (s, 3H,  $\text{CH}_3$ ).  $^{31}\text{P}$  NMR:  $\delta$  (ppm) 31.3 (s).

**Synthesis of 5'-[[5'-O-(Dimethoxytrityl)thymid-3'-yl](phthalimidomethyl)phosphonyl]thymidine 3'-[cyanoethyl (N,N-diisopropylamino)phosphoramidite] (7a).** A sample of **4a** (470 mg, 0.47 mmol) was dried by coevaporation with pyridine, dissolved in dry acetonitrile (100 mL) under nitrogen, and treated with stirring with (2-cyanoethoxy)bis(N,N'-diisopropylamino)phosphine (0.37 mL, 1.18 mmol), diisopropylamine (0.09 mL, 0.66 mmol), and tetrazole (33 mg, 0.47 mmol). After 1 h at room temperature, the mixture was partitioned between 5% aqueous sodium bicarbonate and ethyl acetate (50 mL of each). The aqueous layer was extracted with ethyl acetate (3 × 20 mL), and the combined organic layers were washed with water (2 × 50 mL) and dried over magnesium sulfate. The solids were removed by filtration, and the filtrate was concentrated to a gum which was purified by column chromatography on silica gel (45 g). The column was eluted with  $\text{CH}_2\text{Cl}_2/\text{MeOH}/\text{Et}_3\text{N}$  (100:1.67:1, 616 mL), and the appropriate fractions were combined and evaporated to yield 300 mg (53%) of **7a** as a white foam. An identical procedure was used to prepare **7b** from **4b**.

**General Procedure for Oligonucleotide Synthesis and Deprotection.** Oligonucleotides were prepared on a DNA synthesizer using the 1  $\mu\text{mol}$  cycle. The alternating 13-mers **8a** and **8b** (Figure 2) were synthesized using a standard phosphoramidite cycle with the dimer phosphoramidites **7a** and **7b**, respectively (0.1 M in acetonitrile), and coupling times of 2 min per cycle. The oligonucleotide **10**, having one aminomethyl group at the 3'-terminus, was synthesized by a combination of phosphoramidite and phosphotriester methods. The cycle for the first addition was modified to deliver TPS-Cl (0.3 M) in pyridine followed by **3** in a solution of N-methylimidazole (0.15 M) in pyridine, and the coupling time was increased to 9 min per cycle. After addition of the protected (aminomethyl)-phosphonate, the synthesis was completed using standard phosphoramidites, cycles, and reagents. Cleavage from the support and removal of the phthalyl group was accomplished by treatment of the solid support with ethylenediamine (500  $\mu\text{L}$ ) for 1 h at 55 °C. The supernatant was removed and evaporated to dryness *in vacuo*, and the support was washed with anhydrous ethanol (4 × 200  $\mu\text{L}$ ) followed by 0.1 M TEAA (2 × 200  $\mu\text{L}$ ). The washings were combined with the residue from the supernatant and evaporated to dryness for purification.

**Oligonucleotide Purification.** The tritylated oligonucleotide was loaded onto an analytical reversed-phase





**Figure 2.** Structures of oligonucleotide (aminomethyl)phosphonates.

HPLC column in 5% acetonitrile/0.1 M TEAA, washed with 50 mL of the same solvent, and eluted from the column with a linear gradient of 5–70% acetonitrile in 0.1 M TEAA over 45 min with a flow rate of 10 mL/min. The fractions containing the product were diluted with water and lyophilized, and the residue was dissolved in water and assayed by UV absorbance at 260 nm. Detritylation was accomplished by treatment with 0.1 M acetic acid (2 mL) for 2.5 h at room temperature. After lyophilization, the residue was taken up in water (1 mL) and purified by reversed-phase HPLC. The fractions containing the product were lyophilized, redissolved in water, and assayed. Desalting, if required, was carried out on a C<sub>4</sub> HPLC column which was eluted with a gradient from 5 to 70% acetonitrile in water.

**Characterization of Oligonucleotides.** NMR spectroscopy was used for the characterization of modified oligonucleotides. The <sup>31</sup>P NMR spectrum of the alternating (aminomethyl)phosphonate-phosphodiester oligonucleotide 8a, (Sp isomer) is shown in Figure 3. The spectrum consists of two peaks in a 1:1 ratio, one due to the PO resonances and the other, downfield peak, due to the (aminomethyl)phosphonates as expected for an alternating oligonucleotide with six P–O bonds and six P–CH<sub>2</sub>NH<sub>3</sub><sup>+</sup> bonds. The spectrum provides additional evidence that the P–C bonds survived deprotection of the phthalimido group.

Oligonucleotides were also examined by gel electrophoresis (Figure 4). The electrophoretic mobilities of the alternating (aminomethyl)phosphonate/phosphodiester oligonucleotides show an expected correspondence between the degree of backbone substitution and electrophoretic mobility. Thus, the alternating oligomer 8a (lane 2) migrates only a small fraction of the distance traveled by the unmodified (phosphodiester) oligomer of the same size (lane 1). Presumably, the amino groups are partially ionized under the relatively high pH conditions of the gel so that the net charge of the modified oligonucleotide is slightly negative rather than zero. The purities of the oligonucleotides were also established by HPLC and quantified by UV absorbance at 260 nm after deprotection and detritylation.

**Thermal Denaturation Experiments.** These experiments were carried out using a Gilford Response II temperature-controlled spectrophotometer by monitoring the changes in absorbance at 260 nm versus temperature, with a heating rate of 1 °C/min from 0 to 60 °C. Extinction coefficients needed to calculate the molar ratios of oligonucleotides were obtained by the method of Rychlik and Rhoads (1989). Melting curves were obtained in both low salt (150 mM NaCl, 10 mM Na<sub>2</sub>HPO<sub>4</sub>) and high salt (1 M NaCl, 10 mM Na<sub>2</sub>HPO<sub>4</sub>) conditions at pH 7. Samples were not heated prior to denaturation measurements in order to minimize hydrolysis of the (aminomethyl)phosphonate linkages. Transition temperatures were obtained from the first-order derivative plot of absorbance versus temperature. For experiments involving dissociation of triplex structures, 50 mM Tris, 20 mM MgCl<sub>2</sub>, 0.1 M NaCl, pH 7, was used as the buffer.

**Hydrolytic Stability of 6a and 6b.** The dinucleotides 6a and 6b were incubated at pH 7.1 in TEAA buffer at 37 °C over 50 h. Aliquots were removed at intervals and injected onto a C<sub>4</sub> reversed-phase HPLC column, and the rate of degradation was determined by measurement of the area remaining under the peak corresponding to starting material.

**Incubation of 6a and 6b with Mung Bean and S<sub>1</sub> Nucleases.** (a) *Mung Bean Nuclease.* Solutions of the natural dimer d-TpT and aminomethyl-modified dimers 6a and 6b (1 OD<sub>260</sub>) in 50 μL of buffer (30 mM sodium acetate, 50 mM sodium chloride, 1 mM zinc chloride, pH 5, 5% (v/v) glycerol) were equilibrated at 0 °C for 30 min and treated with mung bean nuclease (U.S. Biochemicals, 50 units/μL, 5 μL), and the solutions were stored at 0 °C. Aliquots (5 μL) of the reaction mixture were injected onto an analytical reversed-phase HPLC column and eluted with a gradient of 5–70% acetonitrile in 0.1 M TEAA buffer (pH 7.1). The area under the peak corresponding to starting material was plotted vs time to determine *t*<sub>1/2</sub> values.

(b) *S<sub>1</sub> Nuclease.* Solutions of the natural dimer d-TpT and aminomethyl-modified dimers 6a and 6b (1 OD<sub>260</sub>) in 50 μL of buffer (50 mM sodium acetate, 250 mM sodium chloride, 1 mM zinc chloride, pH 4.6, containing 50 μg/mL of bovine serum albumin) were equilibrated at 0 °C for 30 min and treated with 2 μL of S<sub>1</sub> nuclease (U.S. Biochemicals, 263 units/μL), and the solutions were stored at 0 °C. Aliquots (5 μL) of the reaction mixture were injected onto an analytical reversed-phase HPLC column and eluted with a gradient of 5–70% acetonitrile in 0.1 M TEAA buffer (pH 7.1), and the area under the peak corresponding to starting material was plotted versus time to determine *t*<sub>1/2</sub> values.

## RESULTS AND DISCUSSION

**Synthetic Strategy.** Two general strategies can be envisaged for the synthesis of (aminomethyl)phosphonate derivatives of oligonucleotides, (a) the triester approach involving a pentavalent phosphorus intermediate and (b) the phosphoramidite approach which uses trivalent phosphorus chemistry. For the synthesis of dinucleotides or oligonucleotides with relatively few aminomethyl substituents, the triester approach appeared to be the most convenient since suitable derivatives of (aminomethyl)phosphonic acid are commercially available. For protection of the amino group of (aminomethyl)phosphonic acid during oligonucleotide synthesis, an alkali-labile group was envisaged so that concomitant deprotection of the aminomethyl and the base-protecting groups could be accomplished using ammonia. Protecting groups which are

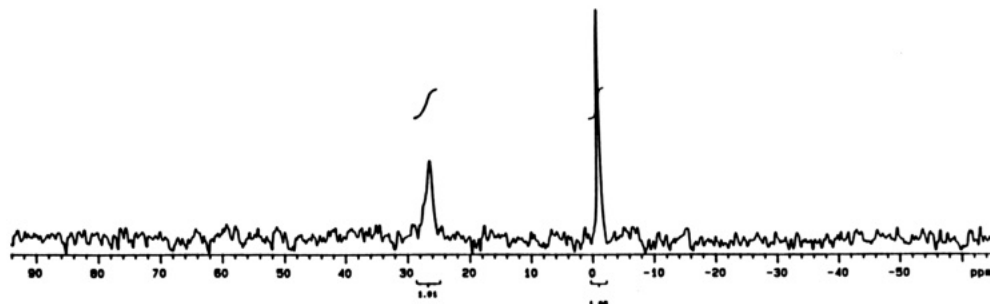


Figure 3.  $^{31}\text{P}$  NMR spectrum of the alternating 13-mer 8a.

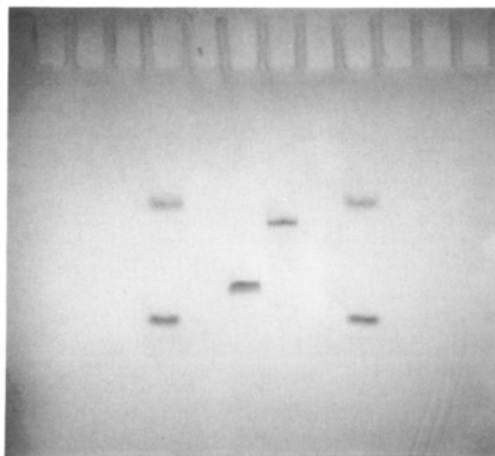


Figure 4. Polyacrylamide gel electrophoresis of 8a (lane 2, second from right) versus d-T(pT)<sub>12</sub> (lane 1, second from left). Outside lanes are bromophenol blue and xylene cyanol markers.

potentially suitable for this purpose include trifluoroacetyl, (fluorenyloxy)carbonyl, and phthalimido, as well as a few other commonly used groups. Of these, the phthalimido group was selected since (a) it can be removed by either ammonia or ethylenediamine and (b) its lipophilicity might be of value in chromatographic purification by reversed-phase HPLC. The benzyloxycarbonyl group has been used previously during the preparation of aminomethyl derivatives of mononucleotides (Gulyaev & Holy, 1972; Holy & Gulyaev, 1974) but since removal of this group required 36% hydrogen bromide in acetic acid, it would not be suitable for use with purine deoxynucleotides.

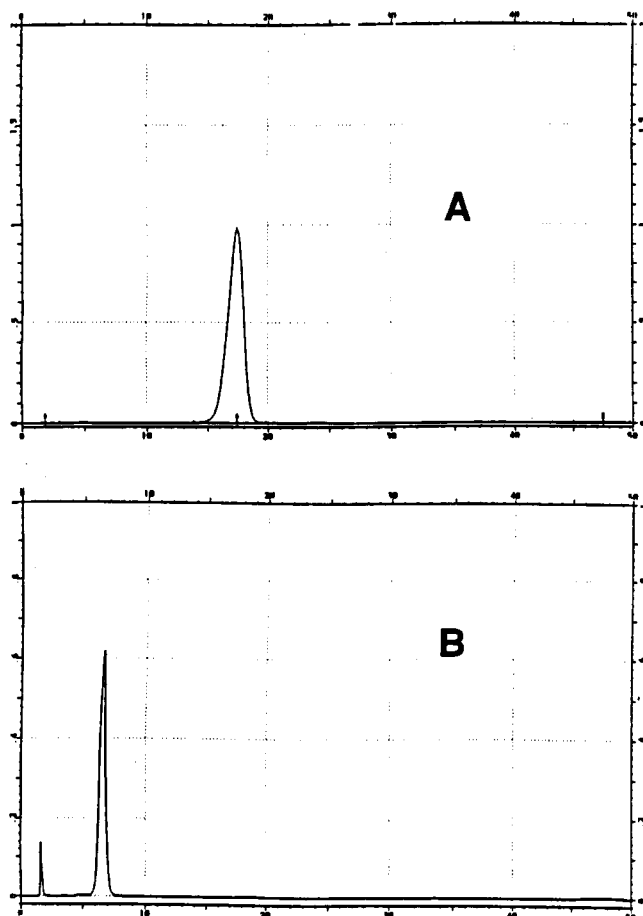
**Dinucleotide Synthesis.** Reaction of commercially available dimethyl (phthalimidomethyl)phosphonate (1) (Figure 1) with trimethylsilyl bromide cleaved the methyl ester groups to give (phthalimidomethyl)phosphonate (2) which was isolated as its pyridinium or triethylammonium salt. Reaction of 2 with 5'-(dimethoxytrityl)thymidine using TPS-Cl as the condensing agent produced the monomer 3, which was purified by silica column chromatography and isolated as its triethylammonium salt. The NMR spectrum of 3 indicated the presence of aromatic protons corresponding to the phthalimido group, and the phosphorus NMR indicated the presence of a singlet at  $\delta$  11.0 due to the phosphonate phosphorus atom.

Compound 3 was used to prepare the dinucleotide (phthalimidomethyl)phosphonate 4 by reaction with thymidine using TPNT or TPS-Cl as the coupling agent. Examination of the reaction products by TLC indicated the presence of two isomers which were poorly resolved in all solvent systems employed. A partial resolution of the mixture could be achieved by silica column chromatography, although the bulk of the material was eluted as a mixture of isomers which required rechromatography. A more complete separation of the mixture could be achieved by reversed-phase HPLC, and using this pro-

cedure several hundred milligrams of pure, single-isomer dinucleotides 4a and 4b could be obtained. The  $^1\text{H}$  NMR of 4a showed two clearly resolved triplets corresponding to the anomeric protons of the sugar moieties as well as aromatic protons corresponding to the trityl and phthalimido groups. The  $\text{CH}_2\text{P}$  protons were partially obscured by the sugar proton resonances at around 4.1 ppm, but the methyl protons from the thymine residues were observed as sharp singlets at approximately 1.4 and 1.7 ppm. A similar spectrum was obtained for the Rp isomer 4b, except that the  $\text{CH}_2\text{P}$  protons were clearly distinguishable as a doublet at 4.0 ppm. In both isomers one  $\text{C}_3\text{-H}$  resonance was observed considerably downfield from the other, presumably due to the fact that one 3'-carbon is substituted with a phosphonate group whereas the other is unsubstituted. In spectra of dried samples of 4a, a doublet at 5.4 ppm, which could be exchanged with  $\text{D}_2\text{O}$ , indicated the presence of a secondary 3'-hydroxyl group. No impurities, such as 3',3'-isomers, were detected. Presumably, the difference in reactivity between the 5'- and 3'-hydroxyl groups is sufficient to ensure the regioselectivity of the reaction to form the 3',5'-dimer. The  $^{31}\text{P}$  NMR spectra of both 4a and 4b showed singlet resonances downfield from those previously reported for the methylphosphonate analogs (Seela and Kretschmer, 1991) due to the deshielding effect of the protonated aminomethyl group, a result consistent with the downfield shift observed for (difluoromethyl)phosphonate analogs (Bergstrom and Shum, 1988).

Cleavage from the support and removal of the phthalyl group were accomplished with ethylenediamine, since this reagent was previously found to be suitable for the deprotection of oligonucleotide methylphosphonates (Ebright et al., 1988) which have been shown to be unstable to strongly alkaline conditions. Treatment of 4a with ethylenediamine gave the 5'-tritylated aminomethyl dimer 5a (90% yield) as shown in Figure 5. Panel A shows an HPLC trace of the tritylated phthalimidomethyl dinucleotide 4a, and panel B is the reaction mixture after treatment with ethylenediamine for 6 h at room temperature, in which the deprotected dimer 5a elutes at 6.5 min. The unprotected monomer has been shown to elute at 2 min in this system, and the small peak at 1.5 min is probably material derived from the cleaved phthalimido group. This figure demonstrates the efficiency of the deprotection step and shows that cleavage of the backbone during deprotection is minimal. Similar results were obtained with 5b, which was obtained in 92.6% yield from 4b using the same procedure.

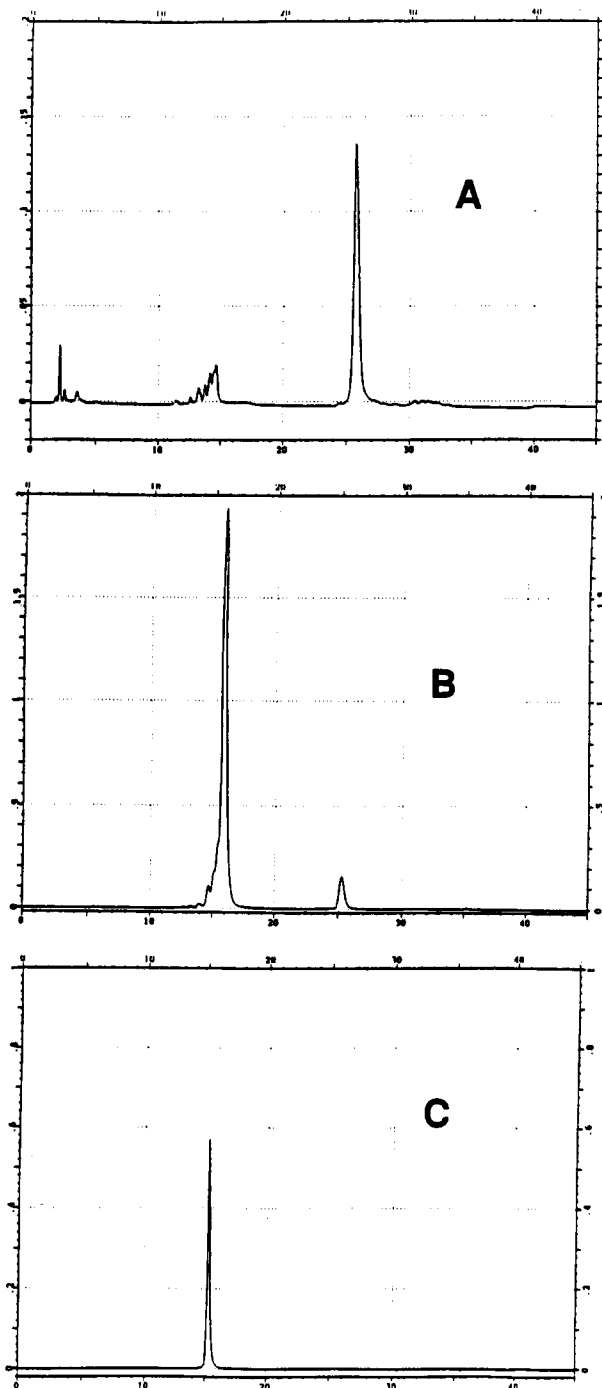
These dinucleotides were isolated by HPLC and characterized by NMR. In contrast to those of 4a and 4b, the  $^1\text{H}$  NMR spectra of 5a and 5b were very similar, both showing two clearly resolved triplets corresponding to the anomeric protons as well as sharp singlets for the thymine methyl groups. For both isomers the  $\text{CH}_2\text{P}$  resonances were clearly distinguishable at 2.9 ppm. Detritylation was



**Figure 5.** Deprotection of the 5'-trityl phthalimidomethyl dinucleotide **4a**. Panel A: **4a**. Panel B: reaction mixture after treatment with ethylenediamine for 6 h at room temperature.

accomplished using dichloroacetic acid to give the completely unprotected dimers **6a** and **6b** which were used for enzymatic studies as described below. Samples of both isomers of **4–6** were spotted onto a thin-layer silica plate, sprayed with ninhydrin, and heated to determine the presence or absence of amino groups. As expected, both isomers of **5** and **6** produced a purple coloration, indicative of the presence of amino groups, whereas the protected compounds **4a** and **4b** did not give a positive reaction.

**Oligonucleotide Synthesis.** The protected dimers **4a** or **4b** could be converted into their corresponding 3'-(cyanoethyl (*N,N*-diisopropylamino)phosphoramidite) **7a** or **7b** and used to prepare oligonucleotide sequences **8a** and **8b** (Figure 2) in which the (aminomethyl)phosphonate moieties alternate with natural phosphodiester linkages. For coupling the dinucleotide phosphoramidite **7a** or **7b** was used at a concentration of 0.15 M and the coupling time was increased to 120 s; under these conditions a coupling yield of approximately 99% was normally obtained as determined by trityl assay. After cleavage of the tritylated oligonucleotides from the support, **8a** and **8b** were partially purified by reversed-phase HPLC to remove failure sequences followed by detritylation using aqueous acetic acid and a second HPLC purification. This is exemplified by the synthesis and purification of **8a**, which is shown in Figure 6. Panel A shows the quality of the crude tritylated oligonucleotide after synthesis, cleavage from the support, and removal of the phthalyl group by treatment with ethylenediamine; the main peak corresponding to tritylated oligonucleotide is eluted at approximately 25 min, with the untritylated failure sequences



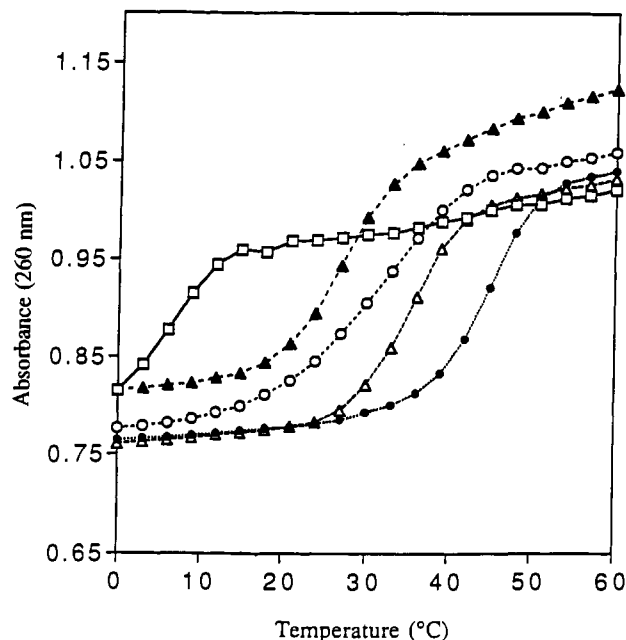
**Figure 6.** Synthesis and purification of the alternating 13-mer **8a**. Panel A: crude, tritylated (aminomethyl)-13-mer from the DNA synthesizer. Panel B: detritylation reaction mixture. Panel C: purified, deprotected oligomer **8a**.

being eluted at 13–15 min. Approximately 45 OD<sub>260</sub> units of crude material were obtained from a 1 μmol scale synthesis. The crude material was purified by preparative HPLC, and the tritylated oligonucleotide was isolated and treated with aqueous acetic acid. Panel B shows the material obtained after detritylation, the detritylated oligonucleotide being eluted at 16 min with a residual amount of tritylated material eluting at approximately 25 min. The detritylated material was again purified by HPLC, and the pure product **8a** is shown in panel C. Using this procedure, 33 OD<sub>260</sub> units of pure **8a** were obtained from a 1 μmol synthesis, which demonstrates the efficiency of the deprotection and isolation procedures. Similar results were obtained for **8b**.

The monomer **3** was also used to introduce aminomethyl groups into specific sites of thymine-containing oligonucleotides by employing reactions similar to those employed for phosphotriester chemistry with 1-(triisopropylbenzenesulfonyl)-3-nitro-1,2,4-triazole or TPS-Cl as the coupling agent. Compound **3** was reacted with support-bound thymidine using a modified cycle on a DNA synthesizer, and after evaluation of various conditions the most effective coupling procedure employed a 0.15–0.18 M solution of **3** in pyridine containing *N*-methylimidazole, TPS-Cl (0.3 M), and a coupling time of 9 min. After this initial cycle, the oligonucleotide chain was extended using standard phosphoramidite chemistry to produce the 3'-end-capped thymine-containing dodecamer **10** (Figure 2) which was purified by HPLC as previously described for **8**. Although not studied in this work, this type of 3'-end-capped oligonucleotide could be of value in preventing *in vivo* degradation by 3'-exonucleases. The aminomethyl functionality could also be used for attachment of non-radioactive reporter groups such as biotin or fluorescein. A preliminary experiment indicated that biotin could be attached by reaction of **10** with biotin *N*-hydroxysuccinimide ester.

**Assignment of Stereochemistry at Phosphorus.** The stereochemical assignments for the isomers of the protected dinucleotides **4a** and **4b** were tentatively made based on phosphorus NMR data. A recent report (Loschner and Engels, 1990) described the determination of configuration of diastereomeric, protected dinucleoside methylphosphonates using a 2-D NMR ROESY technique. These authors observed that the Rp isomers always exhibited <sup>31</sup>P NMR signals upfield from those of the Sp isomers. Other workers (Seela and Kretschmer, 1991) described data on <sup>31</sup>P NMR chemical shifts of an extensive series of protected dinucleotide methyl phosphonates and H-phosphonates and also noted that in all cases the signals for the Rp isomers were upfield from the Sp isomers. It was also postulated by these authors that this correlation is a general phenomenon. By extrapolation to the protected (aminomethyl)phosphonates **4a** and **4b**, the compound having the upfield resonance (**4b**) is considered to be the Rp isomer and the compound with the downfield resonance (**4a**) is assigned as the Sp isomer. 2-D NMR experiments are needed to provide a more conclusive determination of these stereochemical assignments.

**Hybridization Properties.** The single isomer oligonucleotides **8a** and **8b**, having alternating (aminomethyl)-phosphonate/phosphodiester backbone moieties, were hybridized to complementary DNA or RNA sequences to study their ability to form duplexes and compared to the corresponding natural, all-phosphodiester sequence which was used as a control. Two other backbone-modified oligonucleotides of the same length were also prepared and examined: (a) an alternating methylphosphonate/phosphodiester oligonucleotide **11** and (b) an alternating phosphorothioate/phosphodiester oligonucleotide **12**, these latter two oligonucleotides being mixtures of isomers, since the individual isomers could not be readily separated. For hybridization studies the modified oligonucleotide and its complementary sequence were mixed in an equimolar ratio, and the absorbance of the mixture at 260 nm versus temperature was measured from 0 to 60 °C. The rate of heating was maintained at 1 °C/min, and the samples were not heat denatured prior to measurement in order to minimize hydrolysis at elevated temperatures (see below). At the end of the experiment a sample was examined by HPLC to confirm that the extent of degradation was



**Figure 7.** Thermal denaturation of equimolar mixtures of **8a** (—□—), **8b** (—●—), **11** (—○—), **12** (—▲—), and d-T(pT)<sub>12</sub> (—△—) with d-A(pA)<sub>12</sub> in 150 mM NaCl, 10 mM Na<sub>2</sub>HPO<sub>4</sub>, pH 7.

negligible. The results of these experiments are shown in Figure 7. When the individual isomers of the alternating aminomethyl oligonucleotides were hybridized to d-A(pA)<sub>12</sub> they showed markedly different properties. The Sp isomer **8a** was destabilized compared to the natural duplex whereas the Rp isomer **8b** formed a duplex which was more stable than its natural counterpart. In comparison, both the methyl phosphonate **11** and the phosphorothioate **12**, both of which were mixtures of isomers, were somewhat destabilized as compared with the natural duplex. A previous report (Lesnikowski et al., 1990) in which isomeric pairs of methyl phosphonate octamers were hybridized to d-pA<sub>15</sub> also showed that the duplex with the Sp isomer was relatively unstable, whereas the duplex with the Rp isomer was much more stable than its natural counterpart. These findings emphasize the importance of using single isomers in physicochemical and biological experiments wherever possible, since hybridization to target is strongly dependent upon the isomer employed.

When the salt conditions were varied in the above hybridization experiments, the alternating (aminomethyl)-phosphonate/phosphodiester **8b** and the methylphosphonate/phosphodiester **11** showed less salt dependence than the fully anionic phosphodiester or the alternating phosphorothioate/phosphodiester **12**. This may be due to the fact that the negative charges are reduced in both **8b** and **11**. A previous report of hybridization of another type of cationic oligonucleotide with more bulky phosphoramidate linkages (Letsinger et al., 1988) reported that the stability of a duplex of an alternating cationic/phosphodiester oligonucleotide with poly-dA was essentially independent of the salt concentration. These workers also investigated the effect of pH on the hybridization of an oligonucleotide with weakly basic morpholino groups attached to the phosphorus atoms and observed that the hybrid was stabilized by protonation. Although the pK's of the aminomethyl oligonucleotides in the present study were not measured, it is anticipated that the aminomethyl groups will be fully protonated at pH 7 based on previously reported pK measurements of (aminomethyl)phosphonate

**Table 1. Hybridization of Modified Oligonucleotides to Complementary Sequence d-A(pA)<sub>12</sub>**

oligonucleotide	modification at phosphorus	isomer	melting temp (°C)	
			low salt <sup>a</sup>	high salt <sup>b</sup>
d-T(pT) <sub>12</sub>	none	n/a	35	46
8a	aminomethyl	Sp	<10	15
8b	aminomethyl	Rp	45	50
11	methyl	mixed	32	38
12	thioate	mixed	27	38

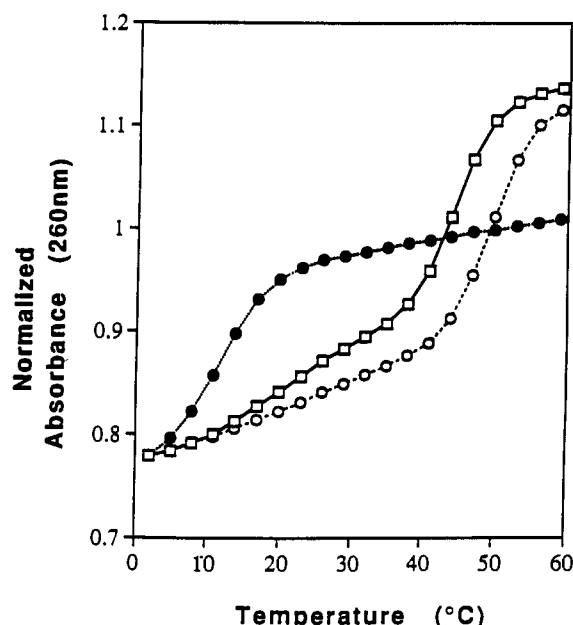
<sup>a</sup> 150 mM NaCl, 10 mM Na<sub>2</sub>HPO<sub>4</sub>. <sup>b</sup> 1 M NaCl, 10 mM Na<sub>2</sub>HPO<sub>4</sub>.

and its derivatives (Robitaille et al., 1991). A summary of these thermal denaturation experiments is shown in Table 1.

Hybridization of the alternating sequences 8a and 8b to the oligoribonucleotide r-A(pA)<sub>12</sub> revealed similar patterns, with the duplex of the Rp isomer being slightly more stable than the natural duplex and the Sp isomer being considerably less stable. In both cases the RNA-DNA duplex was slightly less stable than the corresponding DNA-DNA duplex as has previously been observed for poly-rA:poly-dT versus poly-dA:poly-dT (Chamberlin, 1965; Riley et al., 1966).

The alternating sequences 8a and 8b were each hybridized with d-A(pA)<sub>12</sub> in a 2:1 ratio in order to examine the possibility of triplex formation. For these experiments a pH 7 buffer containing magnesium chloride was employed, since this has previously been shown to stabilize triplexes of short oligonucleotides (Pilch et al., 1990). Hybridization of the Sp isomer 8a with d-A(pA)<sub>12</sub> in a 2:1 ratio showed only one transition at low temperature, presumably due to dissociation of the duplex. For the Rp isomer 8b a very broad transition was observed with a midpoint at approximately 21 °C, suggestive of dissociation of a triplex structure, followed by a sharp transition at 49 °C corresponding to dissociation of the duplex. The melting profile of d-T(pT)<sub>12</sub> with d-A(pA)<sub>12</sub> in a ratio of 2:1 under the same conditions showed a similar profile to that of 8b, with a broad transition centered at 21 °C corresponding to dissociation of the third strand followed by a sharper transition at 44 °C due to dissociation of the duplex. For the natural oligonucleotide, the triplex transition was determined from a first derivative plot, whereas with 8b an exact measurement could not be obtained. These thermal denaturation curves are shown in Figure 8. The results obtained with the natural triplex are similar to those previously reported for the natural decanucleotides d-T(pT)<sub>10</sub> and d-A(pA)<sub>10</sub> (Pilch et al., 1990). These authors also observed a broad transition for the dissociation of the triplex strand.

The melting profile of 8a with d-A(pA)<sub>12</sub> and d-T(pT)<sub>12</sub> in a 1:1:1 ratio was also examined. In this case the first transition was detected at 12 °C followed by a second transition at 44 °C. Presumably, the first transition is due to dissociation of 8a as the third strand, followed by dissociation of the natural duplex at higher temperature. Melting of 8b with d-A(pA)<sub>12</sub> and d-T(pT)<sub>12</sub> in a 1:1:1 ratio showed well-defined transitions at 20 and 47 °C. In this case assignments for the transitions are not obvious since both d-T(pT)<sub>12</sub> and 8b are capable of forming triplex structures. The transitions observed may well be due to melting of a mixture of structures in which both 8b and d-T(pT)<sub>12</sub> are to some extent aligned in antiparallel fashion to form the duplex and in parallel to form the triplex. Further experiments are needed to more fully understand the structures involved in this process. A summary of the results of triplex formation is shown in Table 2.

**Figure 8.** Thermal denaturation of a 2:1 mixture of 8a (...●...), 8b (- - -○- - -), or d-T(pT)<sub>12</sub> (-□-) vs d-A(pA)<sub>12</sub> in 50 mM Tris, 20 mM MgCl<sub>2</sub>, 0.1 M NaCl, pH 7.**Table 2. Triplex Formation of Oligonucleotide (Aminomethyl)phosphonates<sup>a</sup>**

oligonucleotides	ratio	melting temp (°C)	
		first transition	second transition
d-T(pT) <sub>12</sub> /d-A(pA) <sub>12</sub>	2:1	21	44
8a/d-A(pA) <sub>12</sub>	2:1	12	
8b/d-A(pA) <sub>12</sub>	2:1	~21	49
8a/d-A(pA) <sub>12</sub> /d-T(pT) <sub>12</sub>	1:1:1	12	44
8b/d-A(pA) <sub>12</sub> /d-T(pT) <sub>12</sub>	1:1:1	20	47

<sup>a</sup> In 50 mM Tris, 20 mM MgCl<sub>2</sub>, 0.1 M NaCl, pH 7 buffer.

**Table 3. Hybridization of 9a and 9b to Complementary Sequences d-A(pA)<sub>5</sub>pX(pA)<sub>6</sub> Possessing a Mismatch Opposite to the Aminomethyl Group**

oligonucleotide	melting temp (°C)				ΔT <sub>m</sub> (°C) vs matched sequence
	X = A	X = T	X = G	X = C	
d-T(pT) <sub>12</sub>	35.5	23	23	23	12.5
9a	30	16.5	16.5	16.5	13.5
9b	37	25	25	25	12

**Specificity of Hybridization.** Since positively charged oligonucleotides such as (aminomethyl)phosphonates might potentially be able to bind in a nonspecific manner to the negatively charged phosphodiester backbone of a complementary DNA or RNA strand, we have investigated the specificity of binding of these compounds. For these experiments tridecanucleotides 9a and 9b, each with one aminomethyl group in the middle of the sequence, were synthesized and hybridized to a series of partially complementary sequences d-A(pA)<sub>5</sub>pG(pA)<sub>6</sub>, d-A(pA)<sub>5</sub>pT(pA)<sub>6</sub>, and d-A(pA)<sub>5</sub>pC(pA)<sub>6</sub> each having a mismatched base opposite to the aminomethyl group. The natural tridecanucleotide d-T(pT)<sub>12</sub> was also used as a control. 9a and 9b were prepared by the phosphoramidite approach, with the dimer phosphoramidites 7a or 7b being used in the DNA synthesizer at the appropriate cycle of the synthesis. The melting temperatures of these pairs of oligomers are displayed in Table 3. For the natural duplex, introduction of a mismatch into the complementary strand (X = T, C or G) results in a 12.5 °C lowering of melting temperature as compared with the fully complementary



sequence. For the Rp isomer, which forms a more stable duplex as compared to the natural sequence, a reduction in  $T_m$  of 12 °C was observed for the mismatched hybrids, whereas for the less stable Sp isomer a corresponding reduction of 13.5 °C was observed. The similarities between the mismatch destabilization of the natural phosphodiester and that observed for the backbone-modified oligonucleotide indicates that the aminomethyl oligonucleotides retain their specificity of duplex formation to a degree comparable to their natural counterparts.

**Molecular Modeling.** In order to gain further insight into the results of the hybridization experiments, duplexes of single isomer alternating (aminomethyl)phosphonate/phosphodiester oligomers **8a** or **8b** with the natural phosphodiester oligonucleotide d-A(pA)<sub>12</sub> as the complementary strand were examined by molecular mechanics. The B' form duplex was used as the starting point, since previous workers have shown that this form is preferred over the B form for the d-pT<sub>13</sub>:d-pA<sub>13</sub> duplex (Saenger, 1984). The B' form is slightly different from the B form, the rise and turn per unit base being 3.46 Å and 37° versus 3.38 Å and 36° for the latter. An STO-3G basis set *ab initio* calculation was carried out prior to the minimization experiments to determine the atomic point charges of the aminomethyl groups; the Gaussian 90 program (Gauss, Inc., 4415 Fifth Ave., Pittsburgh, PA 15123) was used for this calculation. These point charges were required for the electrostatic term in the potential energy function and were imported into the Biograf program. Dihedral angle space searches were then carried out to find the lowest energy starting conformation of the aminomethyl group. This was done by simultaneously rotating the C-P and N-C bonds of the aminomethyl phosphonate group in increments of 30° from 0 to 360° and identifying the conformation with the lowest energy. This lowest energy conformation was used as the initial conformation of the aminomethyl group.

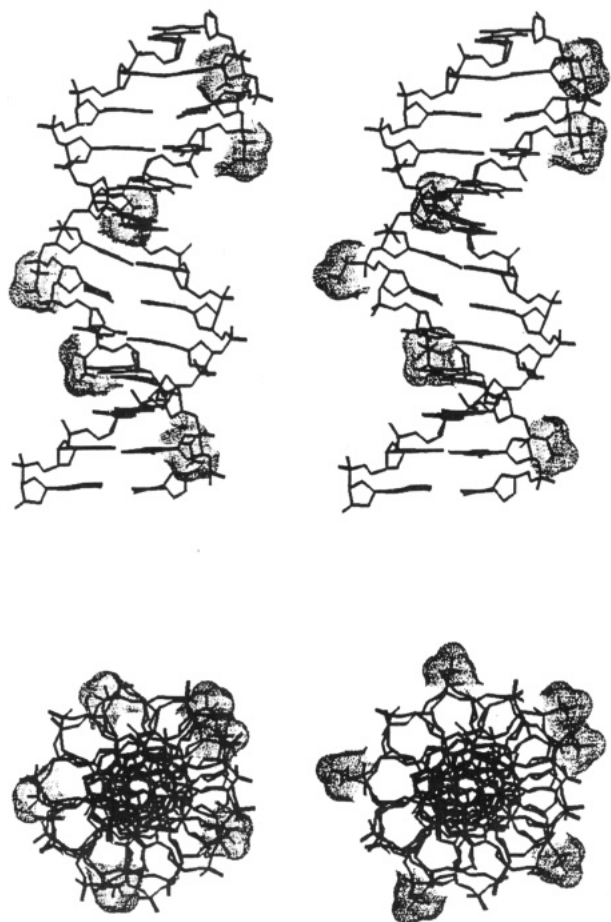
Since previous workers (Kollman et al., 1981; Van Gunsteren et al., 1986; Singh et al., 1985; Miaskiewicz et al., 1993; Seibel et al., 1985; Kollman et al., 1982) have demonstrated that simulation of environmental effects such as water, sodium ions, and boundary conditions can significantly affect the results obtained from the modeling of DNA duplexes, sodium ions were added to neutralize the excess of negative charges due to the phosphate groups, the initial distance between the sodium ions, and the phosphate groups being 3.5 Å. Two layers of water (5.6 Å thickness) were then introduced to solvate the duplex, and the water molecules were initially placed 2.8 Å from the duplex. Since the water molecules introduced via the Biograf program were initially in a lattice arrangement, these water positions were minimized for 500 steps (250 steps using the steepest descent method and then 250 steps using the conjugated gradient method) while keeping the B' form duplex geometry fixed. After this procedure, the duplex, water, and ions were allowed to move together in the second stage of the minimization (500 steps), which was used to remove all the unfavorable contacts between atoms. Adaptation of a previously reported method (Kollman et al., 1981) was used to calculate the strand-strand binding energy (SSBE) which is defined as the total energies of all the bases in the duplex minus the energies of the bases in the individual strands. Sugar and phosphate groups were not included in these calculations. The strand-strand binding energies were calculated for duplexes of **8a** and **8b** with their natural complements as well as for the natural oligonucleotide duplex. The results are as follows:

duplex	SSBE (kcal/mol)
<b>8b</b> /d-A(pA) <sub>12</sub>	-495
<b>8a</b> /d-A(pA) <sub>12</sub>	-486
d-T(pT) <sub>12</sub> /d-A(pA) <sub>12</sub>	-492

These results indicate that if the SSBE is the main determinant for the thermal stability of the duplex, the Rp isomer **8b** would be expected to have the highest melting temperature, the Sp isomer **8a** should have the lowest melting temperature, and the natural duplex would be expected to be intermediate between the two isomers. The predicted stabilities are thus consistent with the observed data obtained by optical absorption experiments. Examination of the minimized structures reveals several features which may account for the predicted and observed stabilities. Duplexes of **8a** and **8b** with d-A(pA)<sub>12</sub>, in which the aminomethyl groups are highlighted using a dot matrix surface, are illustrated in Figure 9. The model of the duplex with **8a** (left panel) shows that the aminomethyl groups are turned towards the interior of the duplex, resulting in unfavorable steric interactions with the base and sugar moieties. The duplex with **8b**, on the other hand (right panel), shows that the aminomethyl groups are projecting toward the exterior, thus reducing steric interactions with the base and sugar moieties and enhancing favorable interactions with solvent. This difference is more clearly visible in the end views of the duplexes (bottom panels). A detailed examination of the structures generated by molecular modeling indicates that the aminomethyl groups of the Sp isomer are likely to be relatively close (3.6 Å) to the methyl groups of the thymine bases, whereas for the Rp isomer these groups are predicted to be much further apart (7.5 Å). Similar conclusions were reached for duplexes of isomers of oligonucleotide methylphosphonates (Lesnikowski et al., 1990). The close contacts between the aminomethyl groups of the Sp isomer **8a** and the thymine methyl groups result in a significant propeller twist between the thymine-adenine base pairs, and this would be expected to significantly decrease the strength of the hydrogen bonding. This propeller twist also would be expected to produce some distortion of the backbone of the duplex.

An analysis of the proximities of the aminomethyl and phosphodiester functional groups was also performed. The formation of weak intrastrand ionic bonds between the aminomethyl groups and the adjacent phosphate oxygen atoms is possible, since for both Rp and Sp isomers these groups were approximately 4.7–5.0 Å apart. The presence of intrastrand interactions between aminomethyl and phosphodiester groups might reduce interstrand repulsion due to the negative charges on the phosphate groups, and such a reduction in repulsion might contribute to the higher melting temperature of the **8b**/d-A(pA)<sub>12</sub> duplex versus the natural duplex. The corresponding distances between the aminomethyl groups and the phosphodiester groups of the opposite strand were too far apart to be able to interact, so that interstrand duplex-stabilizing interactions of this kind would not be anticipated.

**Stability in Aqueous Solution.** In order to study the stability of (aminomethyl)phosphonates in aqueous solution, the dinucleotides **6a** and **6b** were incubated in pH 7.0 aqueous buffer at 37 °C with thymidyl-3'-(methylphosphonyl)-5'-thymidine being used as a control. Aliquots were removed at various time intervals and injected onto a C<sub>4</sub> reversed-phase column for quantification of the amount of starting material remaining. Under these conditions degradation of both **6a** and **6b** was detected; half lives of 42 h for the Sp isomer and 45 h for the Rp isomer were calculated from the plot of percent of



**Figure 9.** Conformations of duplexes between **8a** (left panels) or **8b** (right panels) and d-A(pA)<sub>12</sub>. The aminomethyl substituents are highlighted using dot surface matrices.

remaining starting material versus time. No degradation of the corresponding methylphosphonate was detected under the same conditions. Hydrolysis of the (aminomethyl)phosphonates **6a** and **6b** proceeded almost exclusively by P–O bond cleavage to yield a mixture of thymidine-3'- and 5'-(aminomethyl)phosphonates and thymidine. One possible explanation for the greater lability of the (aminomethyl)phosphonate could be due to the greater inductive effect of the protonated aminomethyl group as compared to the methyl group, which would result in the phosphorus atom being more susceptible to attack by water or other nucleophiles. Alternatively, intramolecular attack on phosphorus by the amino group to give a three-membered cyclic intermediate followed by cleavage of the phosphorus–oxygen bond could be considered as an alternate possibility. Three membered ring compounds containing phosphorus, nitrogen, and carbon have previously been isolated by Niecke et al. (1983). Hydrolysis of the alternating sequences **8a** and **8b** was also examined under the same conditions, and a similar pattern of degradation was observed, the half lives of the Rp and Sp isomers both being 13 h. These results are summarized in Table 4.

**Enzymatic Studies.** The enzymatic digestion of the dinucleotide (aminomethyl)phosphonates **6a** and **6b** was studied in an attempt to determine whether the (aminomethyl)phosphonate analogs are likely to be substrates for diesterases. At the mononucleotide level Gulyaev and Holy (1972) have previously shown that both uridine and adenosine 5'-(aminomethyl)phosphonates were resistant to the action of bacterial alkaline phosphatase but that snake venom 5'-nucleotidase produced substantial cleavage

**Table 4.** Stability of Oligonucleotide (Aminomethyl)phosphonates in Aqueous Solution

oligonucleotide	length	$t_{1/2}$ (h)	
		37 °C	25 °C
<b>6a</b>	dinucleotide	42	nd
<b>6b</b>	dinucleotide	42	nd
<b>Tp(Me)T</b>	dinucleotide	stable	nd
<b>8a</b>	13-mer	13	70
<b>8b</b>	13-mer	13	70

to give the nucleoside and (aminomethyl)phosphonic acid. The enzymatic incubations of **6a** and **6b** were performed at 0 °C to minimize the hydrolysis which was observed at higher temperatures, and under these conditions neither isomer was degraded by mung bean or S1 nuclease under conditions which cleaved the natural dimer in 30 min. The residual activity of the enzyme in the incubation mixture after 24 h was assessed by adding 5  $\mu$ L of the mixture to a sample of the natural dimer d-TpT followed by incubation and reinjection onto an HPLC column. Rapid cleavage of d-TpT demonstrated that the enzyme had lost only a few percent of its activity during the course of the original incubation with the dinucleotide (aminomethyl)phosphonate.

## CONCLUSIONS

(Aminomethyl)phosphonates represent the simplest example of an interesting new class of cationic, backbone-modified oligonucleotides. Molecules with a net charge of zero can be prepared by alternating the (aminomethyl)phosphonate and phosphodiester groups in the oligonucleotide backbone, and in contrast to other neutral, backbone-modified analogs such as methylphosphonates, (aminomethyl)phosphonates are very soluble in water. The individual isomers vary widely in their ability to form duplexes, with the Rp isomer being more stable than its natural counterpart and the Sp isomer being much less stable. Specificity of hybridization was retained as determined by Tm experiments with oligonucleotides possessing a mismatch opposite to the aminomethyl group. Evidence for triplex formation was observed for the Rp isomer although a sharp transition was not observed. (Aminomethyl)phosphonates are resistant to enzymatic degradation but can be hydrolyzed in aqueous solution at elevated temperature. Introduction of aminomethyl groups into oligonucleotides provides an opportunity for the attachment of nonradioactive reporter groups for diagnostic purposes. Studies on other examples of novel cationic oligonucleotides are in progress and will be described in the near future.

## LITERATURE CITED

- Arnold, L. J. (1985) Polylysine-drug Conjugates. *Methods Enzymol.* 112, 270–285.
- Barrett, J. C., Miller, P. S., and Ts'o, P. O. P. (1974) Inhibitory Effect of Complex Formation with Oligodeoxyribonucleotide Ethyl Phosphotriesters on Transfer Ribonucleic Acid Aminoalkylation. *Biochemistry* 13, 4897–4906.
- Bergstrom, D. E., and Shum, P. W. (1988) Synthesis and Characterization of a new Fluorine Substituted Nonionic Dinucleoside Phosphonate Analogue, P-Deoxy-P-(difluoromethyl)thymidyl(3'-5')thymidine. *J. Org. Chem.* 53, 3953–3958.
- Chamberlin, M. J. (1965) Comparative Properties of DNA, RNA, and Hybrid Homopolymer Pairs. *Fed. Proc.* 24, 1446–1457.
- Dagle, J. M., Andracki, M. E., DeVine, R. J., and Walder, J. A. (1991) Physical Properties of Oligonucleotides containing Phosphoramidate-modified Internucleoside Linkages. *Nucleic Acids Res.* 19, 1805–1810.

- Dagle, J. M., Walder, J. A., and Weeks, D. L. (1992) Targeted Degradation of mRNA in Xenopus Oocytes and Embryos Directed by Modified Oligonucleotides: studies of An2 and Cyclin in Embryogenesis. *Nucleic Acids Res.* 18, 4751-4757.
- Ebright, Y., Tous, G. I., Tsao, J., Fausnaugh, J., and Stein, S. (1992) Chromatographic Purification of Non-ionic Methylphosphonate Oligodeoxynucleotides. *J. Liquid Chromatog.* 11, 2005-2017.
- Gulyaev, N. N., and Holy, A. (1972) Ribonucleoside 5'-Aminomethanephosphonates: Synthesis and Affinity towards some Phosphomonoesterases. *FEBS Lett.* 22, 294-296.
- Holy, A., and Gulyaev, N. N. (1974) Uridine 2'(3')-Aminomethanephosphonate and Related Compounds: Unusual Degradation by Ribonucleases. *J. Carbohydr. Nucleosides, Nucleotides*, 1, 85-96.
- Kollman, P. A., Weiner, P. K., and Dearing, A. (1981) Studies of Nucleotide Conformations and Interactions. The Relative Stabilities of Double-Helical B-DNA Sequence Isomers. *Biopolymers* 20, 2583-2621.
- Kollman, P., Keeper, J. W., and Weiner, P. (1982) Molecular-Mechanics Studies on d(CGCGAATTCGCG)<sub>2</sub> and dA<sub>12</sub>.dT<sub>12</sub>: An Illustration of the Coupling Between Sugar Repuckering and DNA Twisting. *Biopolymers* 21, 2345-2376.
- Kumagai, A. K., Eisenberg, J. B., and Pardridge, W. M. (1987) Absorptive-mediated Endocytosis of Cationized Albumin and a  $\beta$ -Endorphin-cationized Albumin Chimeric Peptide by Isolated Brain Capillaries. *J. Biol. Chem.* 262, 15214-15219.
- Lemaitre, M., Bayard, B., and LeBleu, B. (1987) Specific Antiviral Activity of a Poly(L-lysine)-conjugated Oligodeoxyribonucleotide Sequence Complementary to Vesicular Stomatitis Virus N-Protein mRNA Initiation Site. *Proc. Natl. Acad. Sci. U.S.A.* 84, 648-652.
- Leonetti, J.-P., Degols, G., and LeBleu, B. (1990) Biological Activity of Oligonucleotide-Poly(L-lysine) Conjugates: Mechanism of Cell Uptake. *Bioconjugate Chem.* 1, 149-153.
- Lesnikowski, Z. J., Jaworska, M., and Stec, W. J. (1990) Octa-(thymidine methanephosphonates) of Partially Defined Stereochemistry: Synthesis and Effect of Chirality at Phosphorus on Binding to Pentadecadeoxyriboadenylic Acid. *Nucleic Acids Res.* 18, 2109-2115.
- Letsinger, R. L., Singman, C. N., Histand, G., and Salunkhe, M. (1988) Cationic Oligonucleotides. *J. Am. Chem. Soc.* 110, 4470-4471.
- Loschner, T., and Engels, J. W. (1990) Diastereomeric Dinucleoside-methylphosphonates: Determination of Configuration with the 2-D NMR ROESY Technique. *Nucleic Acids Res.* 18, 5083-5088.
- Marshall, W. S. and Caruthers, M. H. (1993) Phosphorodithioate DNA as a potential drug. *Science* 259, 1564-1570.
- Miaskiewicz, K., Osman, R., and Weinstein, H. (1993) Molecular Dynamics Simulation of the Hydrated d(CGCGAATTCGCG)<sub>2</sub> Dodecamer. *J. Am. Chem. Soc.* 115, 1526-1537.
- Niecke, E., Ruger, R., Lysek, M., and Schoeller, W. W. (1983) Aminophosphinidene Derivatives. *Phosphorus Sulfur* 18, 35-38.
- Pardridge, W. M., Kumagai, A. K., and Eisenberg, J. B. (1987) Chimeric Peptides as a Vehicle for Peptide Pharmaceutical Delivery Through the Blood-brain Barrier. *Biochem. Biophys. Res. Commun.* 146, 307-313.
- Pilch, D. S., Levenson, C., and Shafer, R. H. (1990) Structural Analysis of the (dA)<sub>10</sub>.2(dT)<sub>10</sub> Triple Helix. *Proc. Natl. Acad. Sci. U.S.A.*, 87, 1942-1946.
- Riley, M., Maling, B., and Chamberlin, M. J. (1966) Physical and Chemical Characterization of Two- and Three-stranded Adenine-Thymine and Adenine-Uracil Homopolymer Complexes. *J. Mol. Biol.* 20, 359-389.
- Robitaille, P.-M. L., Robitaille, P. A., Brown, G. G., and Brown, G. B. (1992) An analysis of the pH-dependent Chemical-Shift Behaviour of Phosphorus-Containing Metabolites. *J. Magn. Reson.* 92, 73-84.
- Rychlik, W., and Rhoads, R. E. (1989) A Computer Program for Choosing Optimal Oligonucleotides for Filter Hybridization, Sequencing and in vitro Amplification of DNA. *Nucleic Acids Res.* 17, 8543-8551.
- Saenger, W. (1984) *Principles of Nucleic Acid Structure*, Chapter 9, p 223, Springer-Verlag, New York.
- Seela, F., and Kretschmer, U. (1991) Diastereomerically Pure Rp and Sp Dinucleoside H-Phosphonates: The Stereochemical Course of their Conversion into Methylphosphonates, Phosphorothioates, and <sup>18</sup>O Chiral Phosphates. *J. Org. Chem.* 56, 3861-3869.
- Seibel, G. L., Singh, U. C., and Kollman, P. (1985) A Molecular Dynamics Simulation of Double-helical B-DNA including Counterions and Water. *Proc. Natl. Acad. Sci. U.S.A.* 82, 6537-6540.
- Shoji, Y., Akhtar, S., Periasamy, A., Herman, B., and Juliano, R. L. (1991) Mechanism of Cellular Uptake of Modified Oligodeoxynucleotides containing Methylphosphonate Linkages. *Nucleic Acids Res.* 19, 5543-5550.
- Singh, U. C., Weiner, S. J., Kollman, P. (1985) Molecular Dynamics Simulation of d(C-G-C-G-A).d(T-C-G-C-G) with and without "hydrated" counterions. *Proc. Natl. Acad. Sci. U.S.A.* 82, 755-759.
- Stein, C. A., Subasinghe, C., Shinozuka, K., and Cohen, J. S. (1988) Physicochemical Properties of Phosphorothioate Oligonucleotides. *Nucleic Acids Res.* 16 3209-3221.
- Stevenson, M., and Iverson P. L. (1989). Inhibition of Human Immunodeficiency Virus Type 1-Mediated Cytopathic Effects of Poly(L-lysine)-conjugated Synthetic Antisense Oligodeoxynucleotides. *J. Gen. Virol.* 70, 2673-2682.
- Van Gunsteren, W. F., Berendsen, H. J. C., Geurtsen, R. G., and Zwinderman, H. R. J. (1986) A Molecular Dynamics Computer Simulation of an Eight Base Pair DNA Fragment in Aqueous Solution: Comparison with Experimental Two-Dimensional NMR Data. *Ann. N. Y. Acad. Sci.* 482, 287-303.
- Wagner, E., Zenke, M., Cotten, M., Beug, H., and Birnstiel, M. L. (1990) Transferrin-polycation Conjugates as Carriers for DNA Uptake into Cells. *Proc. Natl. Acad. Sci. U.S.A.* 87, 3410-3414.

# Boronated Starburst Dendrimer-Monoclonal Antibody Immunoconjugates: Evaluation as a Potential Delivery System for Neutron Capture Therapy<sup>1,2</sup>

Rolf F. Barth,<sup>\*,†</sup> Dianne M. Adams,<sup>†</sup> Albert H. Soloway,<sup>‡</sup> Fazlul Alam,<sup>‡,§</sup> and Michael V. Darby<sup>‡</sup>

Department of Pathology and College of Pharmacy, The Ohio State University, Columbus, Ohio 43210.  
Received May 10, 1993<sup>®</sup>

Boron neutron capture therapy (BNCT) is based on the nuclear capture reaction that occurs when boron-10, a stable isotope, is irradiated with low-energy or thermal neutrons ( $\leq 0.025$  eV) to yield high LET  $\alpha$  particles and recoiling  ${}^7\text{Li}$  nuclei [ ${}^{10}\text{B} + n_{\text{th}} \rightarrow [{}^{11}\text{B}] \rightarrow {}^4\text{He}(\alpha) + {}^7\text{Li} + 2.39$  MeV]. Approximately  $10^9$  boron-10 atoms must be delivered to each target cell in order to sustain a lethal  ${}^{10}\text{B}(n,\alpha){}^7\text{Li}$  reaction. If MoAbs are to be used for targeting boron-10, then it is essential that they recognize a surface membrane epitope that is highly expressed on tumor cells and that a large number of boron-10 atoms be attached to each antibody molecule. In order to heavily boronate MoAbs, we have utilized starburst dendrimers (SD), which are precise, spherical macromolecules composed of repetitive poly(amidoamino) groups. Second- and fourth-generation dendrimers, having 12 and 48 reactive terminal amino groups and molecular weights of 2414 and 10 632 Da, respectively, were boronated using an isocyanato polyhedral borane,  $\text{Na}(\text{CH}_3)_3\text{NB}_{10}\text{H}_8\text{NCO}$ . The boronated starburst dendrimers (BSD), in turn, were derivatized with *m*-maleimidobenzoyl *N*-hydroxysulfosuccinimide ester (sulfo-MBS). The MoAb IB16-6, which is directed against the murine B16 melanoma, was derivatized with *N*-succinimidyl 3-(2-pyridyldithio)propionate (SPDP). The MBS-derivatized BSD and SPDP-derivatized MoAb were reacted to yield stable immunoconjugates. The *in vivo* distribution patterns of  ${}^{125}\text{I}$ -labeled native and boronated MoAb IB16-6 and SD were studied in normal and tumor-bearing C57Bl/6 mice carrying sc implants of the B16 melanoma. The data obtained demonstrated that SD have a propensity to localize in the liver and spleen and that the absolute amount appeared to be directly related to the molecular weight and number of reactive terminal amino groups. Further studies are required to determine whether the properties of the boronated dendrimers can be modified so as to reduce their hepatic and splenic localization.

## INTRODUCTION

Boron neutron capture theory, which recently has been reviewed by us (1, 2), is based on the nuclear reaction that occurs when a stable isotope, boron-10 ( ${}^{10}\text{B}$ ), is irradiated with low-energy ( $\leq 0.025$  eV) neutrons to yield high LET radiation consisting of  $\alpha$  particles and recoiling  ${}^7\text{Li}$  nuclei [ ${}^{10}\text{B} + n_{\text{th}} \rightarrow [{}^{11}\text{B}] \rightarrow {}^4\text{He}(\alpha) + {}^7\text{Li} + 2.39$  MeV]. It has been estimated that  $\sim 35$ – $50$   $\mu\text{g}$  of  ${}^{10}\text{B}$  must be delivered per gram of tumor in order to sustain a lethal  ${}^{10}\text{B}(n,\alpha){}^7\text{Li}$

reaction (3) and, if this is extrapolated to the cellular level, that  $\sim 10^9$  boron-10 atoms must be delivered to each tumor cell (4). The use of MoAbs for the delivery of radionuclides, drugs, and toxins for therapeutic purposes has been the subject of intensive investigation over the past decade (5). A few investigators, including ourselves, have focused on the possible use of MoAbs directed against tumor-associated antigens for targeting boron-10 to tumors (6–21). If boronated antibodies directed against tumor-associated antigens are to be used for targeting, then it is essential that they react with a surface antigen that is expressed with very high density (i.e.,  $> 10^5$  antigenic sites per cell) and that a large number of  ${}^{10}\text{B}$  atoms ( $\sim 2$ – $5 \times 10^3$ ) be attached to each antibody molecule (4, 10). Using a high molecular weight macromolecule, poly-DL-lysine, and an isocyanatopolyhedral borane,  $\text{Na}(\text{CH}_3)_3\text{NB}_{10}\text{H}_8\text{NCO}$ , we have prepared a boronated polylysine containing 23% boron by weight and having  $> 1700$  boron atoms per polymeric unit (13). This boronated macromolecule was then attached to MoAbs utilizing two heterobifunctional reagents, *N*-succinimidyl 3-(2-pyridyldithio)propionate (SPDP), which was used to introduce latent sulfhydryl groups into the boronated polylysine, and *m*-maleimidobenzoyl *N*-hydroxysulfosuccinimide ester (sulfo-MBS), which was used to introduce sulfhydryl-reacting maleimido groups into MoAbs (12, 13). The resulting immunoconjugates retained a high degree of *in vitro* immunoreactivity but had lost their *in vivo* tumor-localizing properties (14). There are several possible explanations for these results. The poly-DL-lysine used in these studies was not a uniform

\* Author to whom correspondence should be addressed at The Ohio State University, Department of Pathology, 165 Hamilton Hall, 1645 Neil Ave., Columbus, OH 43210.

<sup>†</sup> Department of Pathology.

<sup>‡</sup> College of Pharmacy.

<sup>§</sup> Present address: U.S. Borax Inc., Valencia, CA 91380.

<sup>®</sup> Abstract published in *Advance ACS Abstracts*, January 1, 1994.

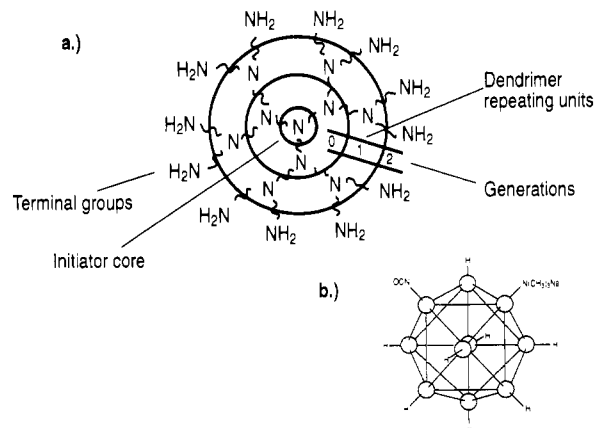
<sup>1</sup> Abbreviations used: MoAb, monoclonal antibody; sc, subcutaneous; ip, intraperitoneal; sulfo-MBS, *m*-maleimidobenzoyl *N*-hydroxysulfosuccinimide ester; DCP-AES, direct current plasma-atomic emission spectroscopy; SD, starburst dendrimer; 0°, 1°, 2°, 3°, and 4°, zero, first, second, third, and fourth generation; BSD, boronated starburst dendrimer; SPDP, *N*-succinimidyl 3-(2-pyridyldithio)propionate; ELISA, enzyme-linked immunoabsorbent assay; iodogen, 1,3,4,6-tetrachloro-3 $\alpha$ ,6 $\alpha$ -diphenylglycoluril; BPL, boronated poly-DL-lysine; RES, reticuloendothelial system; sulfo NHS, *N*-hydroxysulfosuccinimide; PBS, phosphate-buffered saline; MMI, Michigan Molecular Institute; LET, linear energy transfer.

<sup>2</sup> Parts of this work have been presented at the Fourth and Fifth International Symposia on Neutron Capture Therapy held in Sydney, Australia, Dec 4–7, 1990, and Columbus, OH, Sept 14–17, 1992, respectively.

macromolecular species, but rather a mixture of molecules whose weights averaged 35 kD. Following boronation, these differences in molecular weights were further increased, which raised the following questions. Was the decrease *in vivo* tumor localization and higher hepatic uptake attributable at least in part to the inhomogeneity of the boron-containing polymeric species that had been conjugated to the MoAbs? Or could these results be attributed to the high molecular weight of the polymer, its conformation and shape, and the chemical nature of the functional groups attached to it? In order to answer these questions, it became apparent that an alternative approach was required to produce boron-containing immunoconjugates that would retain both their immunoreactivity and *in vivo* tumor-localizing properties.

In contrast with our research, which has focused on boronating polymers prior to their incorporation into MoAbs, Varadarajan and Hawthorne have concentrated on the Merrifield solid-phase peptide synthesis as a means for generating precision macromolecules containing a predetermined number of boron atoms per oligomer (19). They have described a group of carboranyl compounds that can be linked to MoAbs (18–20), the first of which was a phenyl isothiocyanate derivative that could be directly reacted with antibody molecules (18). Although immunoreactivity and immunolocalization of the native MoAbs were retained, the number of boron atoms that could be attached per molecule of antibody was small. For this reason, they turned their attention to a carboranyl amino acid, 5-(2-methyl-1,2-dicarba-*closo*-dodecaboran-(12)-1-yl)-2-aminopentanoic acid, which was then employed for the synthesis of a carboranyl peptide using solid-phase Merrifield methods (19). Conjugations of a dipeptide and undecapeptide were carried out by means of carboxyl activation with *N*-hydroxysulfosuccinimide and *N,N*-diisopropylcarbodiimide with antibody directed against carcinoembryonic antigen (19). As many as 9.4 molecules of the carboranyl peptide could be linked to each molecule of antibody, thereby meeting the requirement of attaching a large number of boron atoms per antibody molecule. Hydrophobic binding of the oligomers to the MoAbs was observed, although these could be removed by means of HPLC with nonionic detergents. This elegant work obviated the problem of heterogeneity of the boronating species. An alternative approach would be to boronate a uniform macromolecular species, and although there might be variations in the number of boron atoms attached to each macromole, the small size of the boronating species would reduce variations in molecular weight of the boronated polymer to a very narrow range.

In the present report, we describe our efforts to prepare boron-containing immunoconjugates using a precision macromolecule consisting of repetitive poly(amidoamino) groups arranged in a starburst pattern (22–24). The dendrimers are composed of an initiative core, interior layers of repetitive monomeric units, and outer functional groups that can be reacted with a variety of chemicals and ligands (24). They are referred to as “starburst dendrimers” because of their branching, treelike pattern (Figure 1), and their synthesis has been described in detail by Tomalia et al. (22). Briefly, a primary amine is used for the initiative core, and following alkylation, monomeric amines were added on in a repetitive, stepwise fashion (23). Zero-generation dendrimers have a molecular weight of 360 Da and three reactive terminal amino groups. The dendrimers are doubled geometrically as they are increased in size from zero to fourth generation (22), the latter having a molecular weight of 10 632 Da and 48 terminal amino



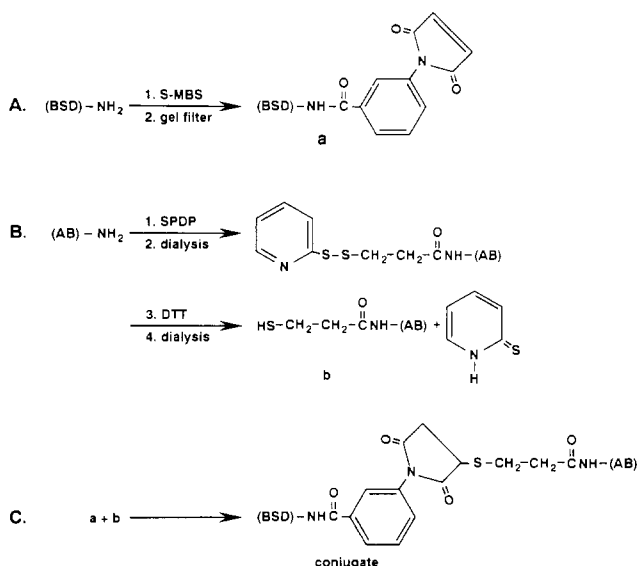
**Figure 1.** (a) Schematic diagram of a starburst dendrimer. The example shown here is a second-generation dendrimer having 12 reactive terminal amino groups and a molecular weight of 2414 Da. (b) Structure of the methyl isocyanato polyhedral borane  $\text{Na}(\text{CH}_3)_3\text{NB}_{10}\text{H}_5\text{NCO}$ .

groups. The dendrimers differ from other oligomeric macromolecules in their maximized telechelic functional density, high branching, and uniformity in size. For these reasons, we have chosen them as the macromolecular carrier for boron-10 in order to achieve the high levels of boronation of antibody molecules that are required to sustain a lethal  $^{10}\text{B}(n,\alpha)^7\text{Li}$  reaction at the cellular level. Following boronation and linkage of the starburst dendrimers to a MoAb, we have studied its *in vivo* pharmacokinetics and compared this to native antibody and radiolabeled zero- through fourth-generation starburst dendrimers.

## EXPERIMENTAL PROCEDURES

**Reagents.** Zero- (SD-0), first- (SD-1), second- (SD-2), third- (SD-3), and fourth-generation (SD-4) starburst dendrimers were generously provided by Polysciences, Inc., Warrington, PA, and the Michigan Molecular Institute, Midland, MI. The molecular homogeneity of the dendrimers was characterized by means of capillary electrophoresis. Those obtained from the Michigan Molecular Institute were highly uniform and corresponded to a single molecular species for each generation (H. Brothers, personal communication). Electropherograms of dendrimers obtained from Polysciences, on the other hand, revealed some molecular heterogeneity, and for this reason, the distribution studies of radiolabeled dendrimers were carried out with those obtained from the Michigan Molecular Institute. Immunoconjugates were prepared using dendrimer preparations from both sources. The isocyanato polyhedral borane  $\text{Na}(\text{CH}_3)_3\text{NB}_{10}\text{H}_5\text{NCO}$  (Figure 1) was prepared in our laboratory, as previously described (13). Other reagents were purchased from commercial sources as indicated: sulfo-MBS, Pierce Chemical Co., Rockford, IL; SPDP, Sigma Chemical Co., St. Louis, MO; ABC vectastain kit, Vector Laboratories, Inc., Burlingame, CA; Bolton-Hunter reagent, ICN Biochemicals Inc., Costa Mesa, CA; and iodogen, Pierce Chemical Co. The MoAb IB16-6 has been described in detail elsewhere (26, 27). Briefly, it was produced against the murine B16-BL6 melanoma and reacts specifically with parental B16 cells, as well as with the B16-F1, B16-F10, B16-BL6, and B16-F10FLR sublines (26). It is of the IgG<sub>2a</sub> subclass, has an affinity constant ( $K_A$ ) that ranged from  $(5.6 \text{ to } 9.4) \times 10^8 \text{ M}^{-1}$ , and recognizes an epitope expressed with a density of  $4.8 \times 10^4$  to  $2.5 \times 10^5$  antigenic sites per tumor cell (27).





**Figure 2.** Conjugation of a boronated starburst dendrimer (BSD) to a MoAb utilizing the heterobifunctional reagents *m*-maleimobenzoyl *N*-hydroxysulfosuccinimide ester (sulfo-MBS) and *N*-succinimidyl 3-(2-pyridyldithio)propionate (SPDP).

**Boronation of Starburst Dendrimer and Derivatization.** One mL of either 2°- or 4°-generation starburst dendrimer suspension was adjusted to pH 9.0 with 1 M  $\text{Na}_2\text{CO}_3/\text{NaHCO}_3$  buffer, and to this was added 20 mg of solid  $\text{Na}(\text{CH}_3)_3\text{NB}_{10}\text{H}_8\text{NCO}$ , following which the mixture was stirred for 1–3 days at ambient temperature. At this point, derivatization of the BSD was carried out as follows. One mg (2 mmol) of sulfo-MBS was added to the boronated dendrimer suspension, and the mixture was allowed to stand for 30 min at ambient temperature and then passed through a Sephadex-G25 column ( $0.9 \times 50$  cm) and eluted with 0.1 M Tris-HCl buffer, pH 8.6, containing 0.2 M NaCl. One-mL fractions were collected, optical density was measured at 280 nm using a Beckman DU-6, spectrophotometer (Beckman Instruments Inc., Irvine, CA), and boron content was determined by means of DCP-AES, using an ARL Spectrospan VB spectrometer (Applied Research Laboratories, Brea, CA), as described in detail elsewhere (28). Boron-containing macromolecule fractions were pooled and used for the preparation of immunoconjugates, as described below. Nonboronated dendrimers were derivatized using the same method.

**Preparation of Immunoconjugates.** The synthetic scheme for preparation of the immunoconjugates is summarized in Figure 2. To a stirred solution containing 5 mg (30  $\mu\text{mol}$ ) of IB16-6 MoAb in PBS, pH 7.4, was added 2.5 mg (8 mmol) of solid SPDP in aliquots over 2 h at ambient temperature. The mixture was dialyzed at 4 °C against 4 L of PBS, pH 7.4, with three changes of PBS, and the sample was treated with 20 mmol of dithiothreitol at 37 °C for 30 min. The absorbance at 343 nm, due to pyridine-2-thione released in deprotecting the thiol group ( $E = 8080$ ), was measured with a Beckman DU-6 spectrophotometer. The results indicated that an average of two thiol groups were introduced per antibody molecule. The derivatized MoAb was dialyzed at 4 °C against 4 L of PBS, pH 7.4, with two changes of PBS. It was then dialyzed against 2 L of 0.1 M Tris-HCl buffer, pH 8.6. The derivatized starburst dendrimer or boronated starburst dendrimer was combined with the derivatized MoAb and allowed to stand for 24 h at ambient temperature. The volumes of the reaction mixtures ranged from 5 to 10 mL, so that MoAb concentrations were  $\sim 1$  mg per mL during the reaction.

The reaction mixtures were then concentrated on Centricon-3 concentrators (Amicon, Inc., Beverly, MA 01915) and then loaded onto a Sephacryl S-300 column ( $1.2 \times 19$  cm) and eluted with 0.1 M Tris-HCl buffer, pH 8.6, containing 0.2 M NaCl. Occasionally, unconcentrated reaction mixtures were aliquoted and chromatographed on the Sephacryl S-300 column. Fractions of approximately 1 mL were collected. Protein concentrations were determined by the Lowry method (29) and by radial immunodiffusion, and boron concentrations were determined by DCP-AES (28). In order to determine whether aggregates were present in the immunoconjugate preparations, apoferritin (MW 443 000 Da) was chromatographed on a Sephacryl S-300 column, and its elution pattern was compared to that of the immunoconjugates. The apoferritin was eluted five to six fractions earlier than the MoAb-BSD, thereby indicating that the immunoconjugates consisted of nonaggregated MoAbs.

**Determination of Immunoactivity of Boronated IB6-6.** B16 melanoma cells were added in 100- $\mu\text{L}$  aliquots containing  $1.25 \times 10^5$  cells to each well of a 96-well microtest plate and incubated for 24 h at 37 °C. Medium was removed, and 100  $\mu\text{L}$  of formalin was added to fix the cells. After 10 min at ambient temperature, formalin was removed, and the wells were washed three times with PBS. Each well was then filled with 100  $\mu\text{L}$  of PBS containing 1–75  $\mu\text{g}$  of IB16-6 or known amounts of boronated IB16-6 with duplicates of each sample. The plates were incubated at 37 °C for 2 h, following which the samples were removed from the wells, and the plates were then washed three times with PBS. The ELISA was carried out using a Vectastain ABC kit. Biotinylated rabbit anti-rat IgG, 15 mg/mL in 80  $\mu\text{L}$  of PBS containing 1% rabbit serum, was added to each well, and plates were incubated for 20 min at 37 °C. The biotinylated antibody was then removed, and the wells washed three times with PBS. Forty  $\mu\text{L}$  of avidin-biotin-horseradish peroxidase complex in 0.1% Tween 20 in PBS were then added to each well, and plates were incubated at 37 °C for 20 min. Supernatants were removed, the wells were washed five times with PBS, 100  $\mu\text{L}$  of 3 mg/mL of *o*-phenylenediamine in 0.02% hydrogen peroxide, 0.1 M citrate, and 0.2 M  $\text{NaH}_2\text{PO}_4$ , pH 5.5, were added to each well, and the color was allowed to develop. The reaction was terminated by the addition of 40  $\mu\text{L}$ /well of 6 M HCl, and the absorbance was read at 492 nm with an ELISA microreader (Model 2550 EIA, Bio-Rad Laboratories; Hercules, CA).

**Iodination of Starburst Dendrimers.** Zero-, 1°-, 2°-, 3°-, and 4°-generation dendrimers having 3, 6, 12, 24, and 48 reactive terminal amino groups, respectively, and molecular weights ranging from 360 to 10 633 Da were radiolabeled using  $^{125}\text{I}$ -labeled Bolton-Hunter reagent (31). The specific activity was  $\sim 4000$  Ci/mmol, and 250  $\mu\text{Ci}$  were used for each dendrimer preparation. The Bolton-Hunter reagent was removed from the shipping vial with either a 10- or 25- $\mu\text{L}$  Hamilton syringe and placed into a 500- $\mu\text{L}$  or 1-mL reaction flask depending upon the volume of dendrimer solution to be added. A gentle stream of nitrogen was then used to evaporate the residual benzene in the reaction flask, after which dendrimer solutions were added. For labeling, the amounts of dendrimer used were as follows: 0° generation, 8 mg; 1°, 4 mg; 2°, 2 mg; 3°, 1 mg; and 4°, 500  $\mu\text{g}$  in PBS, pH 7.4. Reaction flasks were stirred overnight at ambient temperature. Alternatively, with dendrimers obtained from the Michigan Molecular Institute, dendrimers were added directly to the vials containing the Bolton-Hunter reagent and the reactions carried out in these vials. Mixtures were passed through

PD-10 disposable columns (Pharmacia-LKB Technology, Piscataway, NJ), and  $^{125}\text{I}$  dendrimers were eluted with PBS. Fractions of approximately 1 mL were collected and assayed for  $^{125}\text{I}$  radioactivity in a Tracor Analytic  $\gamma$  scintillation counter, Model 1185 (TM Analytic, Elk Grove, IL). Approximately 10% labeling efficiency was achieved.

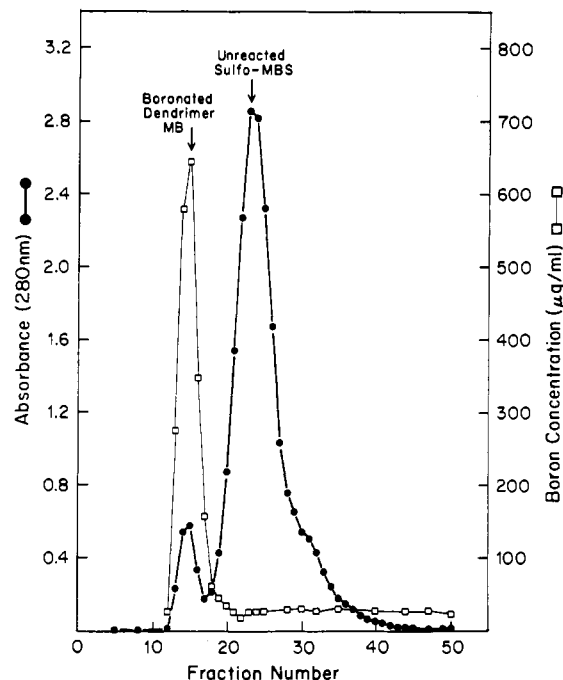
**Iodination of MoAbs and Boronated Starburst Dendrimers.** Although  $\text{B}_{10}\text{H}_{10}^{2-}$  can be directly iodinated (31), we have chosen an alternative approach to iodinate BSD, MoAbIB16-6, and boronated IB16-6 using the iodogen oxidation method (32). Twenty  $\mu\text{g}$  of iodogen in chloroform was evaporated to dryness in 10- $\times$ -75-mm soda lime glass tubes. One mg of BSD, MoAb, or conjugate was dissolved in 200  $\mu\text{L}$  of sodium phosphate buffer, pH 7.2, and added to the reaction tube. This was followed by the addition of 1 mCi of  $^{125}\text{I}$  sodium iodide (specific activity, 100 mCi/mL Dupont-NEN Boston, MA). The reaction was allowed to proceed for 10 min, after which unbound  $^{125}\text{I}$  was removed from the radiolabeled substrate by Sephadex G-25 column chromatography using PD-10 disposable columns. Labeling efficiency was  $\sim 10\%$  for BSD and  $\sim 30\text{--}40\%$  for boronated IB16-6. The percentage of  $^{125}\text{I}$  bound to the protein was determined by instant thin-layer chromatography and trichloroacetic acid precipitation. If the level of binding was  $<85\%$ , the sample was further purified using a Centricon 10 microconcentrator (Amicon, Danvers, MA) in order to eliminate the remaining unbound  $^{125}\text{I}$ .

**Biodistribution of  $^{125}\text{I}$ -Labeled SD, BSD, and Immunoconjugates.** C57Bl/6 mice were purchased from Animal Production Unit, National Cancer Institute, Frederick, MD. They were placed on drinking water, supplemented with 0.1% Lugol's iodine solution, 48 h prior to the initiation of and then for the duration of the distribution studies. Groups of four mice were used for each time point, and animals were injected ip with 10  $\mu\text{g}$  of  $^{125}\text{I}$ -labeled test agents, as indicated in Figures 6–8. Animals were bled via the retroorbital sinus at varying time intervals, ranging from 1 to 72 h postinjection, and then were killed by cervical dislocation. Liver, spleen, and muscle samples were obtained, and radioactivity was determined by counting in a Tracor Analytic  $\gamma$  scintillation counter. Distribution of the test agents was determined as percent of the total dose of radioactivity administered, which varied from agent to agent, and expressed as percent uptake per gram of tissue. For tumor localization studies, animals were implanted sc with B16 melanoma cells into the right flank, and the tumor was allowed to grow  $\approx 4$  mm in diameter at which time animals were injected ip with the test agents.

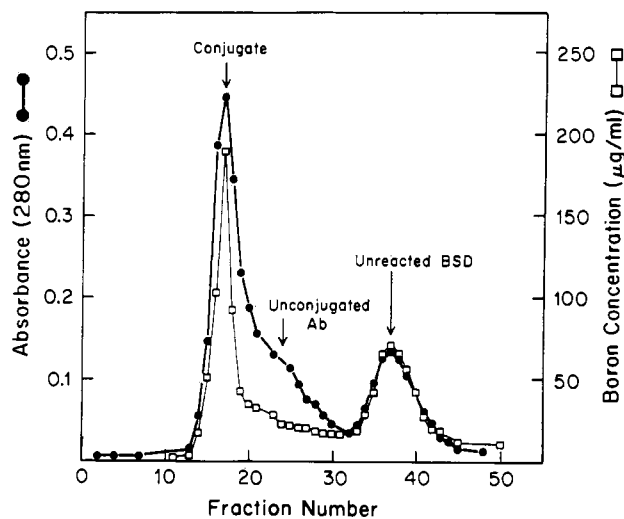
Standard errors of mean uptake showed considerable variability and ranged from 5% to 37% and generally were smaller when larger amounts of radioactivity (i.e.,  $>10\%$  of injected dose) were detected in a particular organ site.

## RESULTS

**Boronation and Iodination of Dendrimers and Antibody.** Chromatographic separation of the reaction mixture containing 4<sup>th</sup>-generation dendrimer (SD-4),  $\text{Na}(\text{CH}_3)_3\text{NB}_{10}\text{H}_6\text{HCO}$ , and sulfo-MBS on Sephadex G-25 revealed that both the maximum amount of dendrimer and boron content were present in fractions 13–16 (Figure 3). It was concluded that this fraction contained the derivatized BSD. Boronation of SD-4 yielded boron levels in the range of 250 to 1000 atoms of boron per molecule of dendrimer. This range in the degree of boronation was due to variation in the molar ratios of BSD to MoAb, as well as to the degree of boronation of the dendrimers.

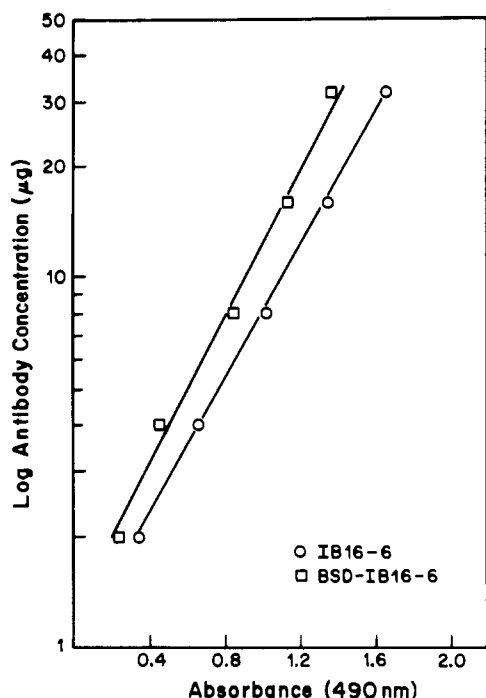


**Figure 3.** Sephadex G-25 column chromatographic profile of BSD. Fourth-generation starburst dendrimer was studied for 1–3 days with  $\text{Na}(\text{CH}_3)_3\text{NB}_{10}\text{H}_6\text{HCO}$  at ambient temperature. Sulfo-MBS was added, and the mixture was incubated for 30 min at ambient temperature. The BSD-sulfo-MBS mixture was passed through a Sephadex G-25 column (0.9  $\times$  50 cm) and eluted with 0.1 M Tris-HCl buffer, pH 8.6, containing 0.2 M NaCl. Fractions of  $\sim 1$  mL each were collected, absorbance was measured at 280 nm, and boron values were determined by means of DCP-AES.



**Figure 4.** Sephacryl S-300 column chromatographic profile of BSD-MoAb conjugate. Sulfo-MBS-treated BSD was combined with the SPDP-derivatized IB16-6 antibody, allowed to incubate for 24 h, loaded onto a Sephacryl S-300 column (1.2  $\times$  19 cm), and eluted with 0.1 M Tris-HCl buffer, pH 8.6, containing 0.2 M NaCl. Fractions of  $\sim 1$  mL each were collected, absorbance was measured at 280 nm, and boron values were determined by DCP-AES.

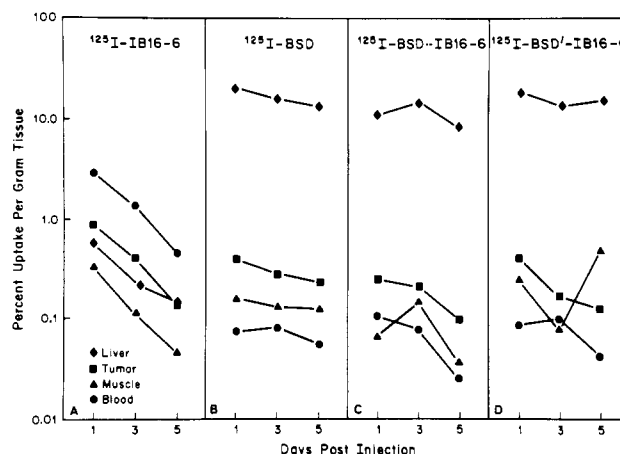
Following conjugation of the BSD and MoAb IB16-6, chromatographic separation on Sephacryl S-300 yielded two boron peaks, fraction 15–18 and 35–40 (Figure 4). Protein content was associated with fractions 15–18, indicating that it contained the BSD conjugated to the MoAb. The ratio of MoAb determined the number of boron atoms per antibody molecule, and for BSD-IB16-6, which was used in localization experiments, there were



**Figure 5.** Determination of immunoreactivity of boronated IB16-6. B16 melanoma cells were added to each well of a 96-well microtest plate and incubated for 24 h at 37 °C. Media was then decanted, cells were fixed with formalin, and then 1–75  $\mu\text{g}/\mu\text{L}$  of either of IB16-6 or boronated IB16-6 was added, with duplicates of each sample. ELISA was carried out using a Vectastain ABC kit with biotinylated anti-rat IgG and avidin–biotin horseradish peroxidase complex. BSD-IB16-6 retained 82% of the immunoreactivity of the native antibody.

1690 atoms per molecule of IB16-6. BSD'-IB16-6, which was produced by increasing the ratio of BSD to MoAb, had 8150 atoms of boron per molecule of antibody. Since the conjugation reaction was carried out at pH 8.6, there may have been covalent binding of the amino groups in the dendrimer to the MoAb in addition to linkage of MoAb and BSD via maleimide–sulfhydryl bridges. This would explain the higher than expected numbers of boron atoms that were detected, based on thiol groups per antibody molecule. As determined by ELISA, immunoreactivity of BSD-IB16-6 conjugate, which contained 2200 boron atoms per molecule of antibody, and native MoAb were compared at concentrations ranging from 1 to 75  $\mu\text{g}$  of protein per sample (Figure 5). With 5  $\mu\text{g}$  of each sample IB16-6 had an absorbance reading of 0.79 compared to 0.65 for BSD-IB16-6, indicating that the conjugate retained 82% (0.65/0.79) of the immunoreactivity of the native antibody. When boron atoms per molecule of antibody were increased to 5000, immunoreactivity of conjugate was 46% of the immunoreactivity of the native antibody.

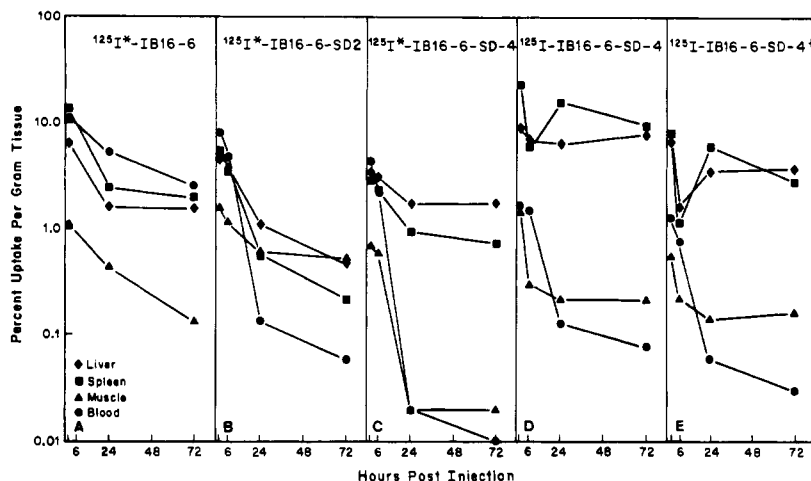
**Biodistribution Studies.** The distribution profiles for  $^{125}\text{I}$ -IB16-6 and  $^{125}\text{I}$ -BSD-IB16-6 immunoconjugates following ip administration to C57Bl/6 mice carrying the B16 melanoma are shown in Figure 6. Less than 0.6% of the radiolabeled native antibody localized in the liver at 1 day (Figure 6A), and this rapidly decreased to <0.2% by 5 days. In contrast, 20% of the injected dose of BSD (Figure 6B) and 11% of the  $^{125}\text{I}$ -BSD-IB16-6 (Figure 6C) were present in the liver at 1 day, and this decreased to 13% (Figure 6B) and 8% (Figure 6C), respectively, at 3 days. The amount  $^{125}\text{I}$ -IB16-6 localized in the tumor was 0.4% at 1 day (Figure 6A) and 0.2% at 5 days, indicating that although this MoAb was highly specific *in vitro*, it had poor *in vivo* tumor localizing activity. A 4-fold increase in the number of boron atoms to 8150 per molecule of



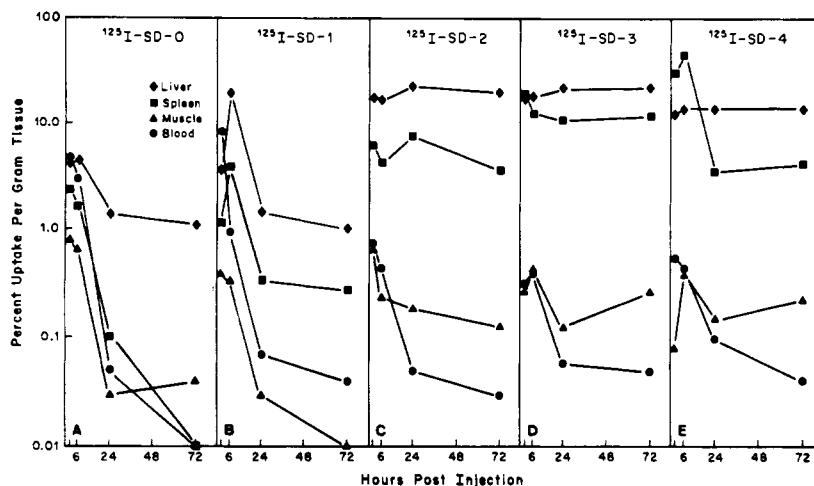
**Figure 6.** Distribution of  $^{125}\text{I}$ -labeled MoAb immunoconjugates and dendrimer in B16 melanoma-bearing C57Bl/6 mice ( $n = 4$ ) (reprinted from *Advances in Neutron Capture Therapy*; copyright Plenum Press, 1993). All test agents were iodinated using iodogen  $\text{Na}[^{125}\text{I}]\text{I}$ . Boronated starburst dendrimer BSD (B) was prepared using  $\text{Na}(\text{CH}_3)_3\text{NB}_{10}\text{H}_8\text{NCO}$  as the boronating species and 4°-generation dendrimer. BSD was conjugated to MoAb IB16-6 using sufo-MBS and SPDP as the linkers (C). BSD'-IB16-6 (D) had 4× more boron per molecule of antibody than BSD-IB16-6 (C). Test agents were injected ip into C57Bl/6 mice carrying sc implants of the B16 melanoma.

dendrimer (Figure 6D) did not produce any biologically significant alterations in distribution compared to that seen with a conjugate containing 1690 atoms of boron per molecule (Figure 6C). Native IB16-6, radiolabeled with iodogen (Figure 7A), showed 6% uptake in the liver at 1 h, and this was reduced to 1.5% at 72 h. Splenic uptake was 12% at 1 h and 2% at 72 h. When 2°- (SD-2) and 4°-generation (SD-4) dendrimers were linked to IB16-6 MoAb and iodinated using the iodogen method (Figure 7B and C), hepatic uptake at 1 h was ~5% for both conjugates, but at 72 h, IB16-6-SD-2 values were 0.6% whereas IB16-6-SD-4 were 2%. Splenic values at 1 h were 5.5% for IB16-6-SD-2 and 3.7% for IB16-6-SD-4, and at 72 h these values had declined to 0.2% and 0.7%, respectively. When IB16-6-SD-4 was iodinated using the Bolton-Hunter reagent (Figure 7D, E), both hepatic and splenic values were increased over those obtained with conjugates iodinated using iodogen (7A–C). The distribution profiles of immunoconjugates prepared from 4°-generation dendrimers obtained from Polysciences Inc. (Figure 7D) and those obtained from the Michigan Molecular Institute (Figure 7E) showed some differences. Hepatic and splenic localization of the former (7D) were greater than those observed with the latter (7E), although blood and muscle levels were identical for both immunoconjugates.

These observations led to the next series of experiments summarized in Figure 8. The distributions of  $^{125}\text{I}$  labeled 0°, 1°, 2°, 3°, and 4°-generation, nonboronated starburst dendrimers (SD-0, SD-1, SD-2, SD-3 and SD-4), obtained from MMI, were studied in non-tumor-bearing C57Bl/6 mice. Animals were killed at 1, 6, 24, and 72 h following ip administration of the iodinated dendrimers. Six hours following injection, hepatic localization was 4.5% for SD-0 and ranged from 14.3 to 19.3% for SD-1, SD-2, SD-3, and SD-4. By 72 h, this had decreased to 1.2% for SD-0 and SD-1 and ranged from 14.1 to 23.3% for SD-2, SD-3, and SD-4. The amounts of SD-0 detected in the spleen ranged from 1.7% at 6 h to 0.01% at 72 h. SD-2 had a splenic value of 3.9% at 6 h. Splenic values for SD-2, SD-3, and SD-4 were 4.4, 12.8, and 46%, respectively, at 6 h and at 72 h were 3.7, 12.1, and 4.3%, respectively.



**Figure 7.** Distribution of  $^{125}\text{I}$ -labeled MoAb and immunoconjugates in nontumor-bearing C57Bl/6 mice ( $n = 4$ ). Test agents with an asterisk after the  $^{125}\text{I}$  were iodinated using iodogen, (A–C) and other test agents (D and E) were iodinated using the Bolton–Hunter reagent. SD-2 (B) and SD-4 (C, D) were obtained from Polysciences, Inc., and SD-4\* was obtained from MMI. Test agents were injected ip into non-tumor-bearing C57Bl/6 mice.



**Figure 8.** Distribution of  $^{125}\text{I}$ -labeled  $\text{O}^0$ -,  $1^0$ -,  $2^0$ -,  $3^0$ -, and  $4^0$ -generation starburst dendrimers obtained from MMI. All dendrimers were iodinated using the Bolton–Hunter reagent. Test agents were injected ip into non-tumor-bearing C57Bl/6 mice ( $n = 4$ ).

## DISCUSSION

In the present study, we have described a method for boronating SD with an isocyanato polyhedral borane,  $\text{Na}(\text{CH}_3)_3\text{NB}_{10}\text{H}_8\text{NCO}$ , the isothiocyanato group of which is hydrolytically stable and reacts with free amino groups. This compound originally had been synthesized by us for the boronation of poly-DL-lysine (13), and using a method originally described by Tsukada et al. (33), it is directed to a derivatized site on the antibody molecule, rather than randomly attached. This method had been employed successfully by us for the boronation of MoAbs (12–14), and despite the possibility of complicating cross-linking reactions, it appeared to work quite well, as evidenced by the presence of a single homogeneous species following Sephacryl S-300 column chromatography. SD recently has been employed by Roberts et al. (34) to attach a large number of molecules of the chelating agent  $N$ -(4-nitrobenzyl)-5-(4-carboxyphenyl)-10,15,20-tris(4-sulfo-phenyl)porphine to MoAbs. Copper-67 subsequently was incorporated into the immunoconjugates by reacting them with  $^{67}\text{CuCl}_2$ . The dendrimer–MoAb conjugates demonstrated high radiolabeling efficiency, but no mention was made of their *in vitro* immunoreactivity or *in vivo* tumor localizing properties. We report for the first time that BSD–MoAb immunoconjugates retained a high level of

immunoreactivity *in vitro* but had a strong propensity to localize in the liver and spleen, the two major organs of the RES. Studies with nonboronated dendrimers revealed that this was directly related to the molecular weight and number of terminal amino groups of the macromolecule. SD-0, which has a MW of 360 Da and three terminal amino groups, had the lowest hepatic and splenic uptake, although this still was 1% and 0.01% respectively, of the injected dose of radioactivity at 72 h. The hepatic uptake of SD-2, SD-3, and SD-4 was  $\sim 5\times$  greater than SD-0 and persisted at these high levels for at least 72 h. These findings provide an explanation for the high hepatic uptake of the conjugate BSD–IB16-6, which was observed in our immunolocalization studies (Figure 5).

Although the MoAb IB16-6 has high *in vitro* affinity and specificity for the B16 melanoma, we previously had observed that this MoAb does not have high *in vivo* tumor uptake (35). This, however, is more representative of the distribution of mouse MoAbs administered to humans (5), where the percent injected dose localizing in a tumor may be even less than that which we observed with IB16-6. Discordance between *in vitro* reactivity and *in vivo* tumor uptake has been observed by others (36) and in part is probably related to the screening method that was used to select these hybridomas, i.e., *in vitro* immunoreactivity rather than *in vivo* tumor localization. It is noteworthy

that BSD-IB16-6 retained 82% of the immunoreactivity of the native IB16-6, and this establishes that the methodology that we have employed to produce the immunoconjugates does not interfere with the combining site of the antibody molecule. Higher molecular weight SD may not be suitable for the preparation of immunoconjugates that are to be used *in vivo*, unless the conjugate can be administered by a route that initially does not lead to the liver, such as sc or intracerebral. It is unlikely that the high hepatic and splenic uptake of the immunoconjugates and 2<sup>o</sup>-, 3<sup>o</sup>-, and 4<sup>o</sup>-generation dendrimers were due to the ip route of administration. Several investigators, including ourselves, have shown that the distribution profiles and tumor uptake of ip-administered MoAbs are similar to those observed following iv administration, although there may be some initial delay in reaching the target site (37-39). The distribution profiles of dendrimers obtained from the MMI (Figure 8) and those obtained from Polysciences, Inc., which have been reported by us elsewhere (40), were remarkably similar despite the molecular heterogeneity of the latter. This suggests that the RES of mice injected with these dendrimers was incapable of detecting the molecular heterogeneity that was seen by capillary electrophoresis.

MoAbs still remain an attractive system for delivering radionuclides, drugs, toxins, and <sup>10</sup>B to tumors, but the chemical linkage of these agents to the antibody molecule significantly alters its *in vivo* localizing properties. IB16-6-BSD-4, which had been iodinated using the Bolton-Hunter reagent, showed 2-3× greater hepatic uptake than that which had been labeled using iodogen and persisted at higher levels. Splenic uptake of IB16-6-BSD-4, labeled with Bolton-Hunter reagent, was even greater than hepatic uptake and was almost identical to that of <sup>125</sup>I-labeled BSD-4. Since radiolabeled with the Bolton-Hunter reagent covalently links an iodinated phenyl ring similar to tyrosine to amino side chains of lysine residues or to N-terminal amino groups of the protein (41), it is unlikely that the differences *in vivo* distribution of Bolton-Hunter-labeled IB16-6-BSD-4 versus iodogen-labeled IB16-6-BSD-4 were due to differences in the rate of dehalogenation. Hydrolysis or enzymatic degradation of the aromatic ring of tyrosine labeled by iodogen would be similar to that of the iodinated phenyl group of antibody labeled with the Bolton-Hunter reagent. However, since the Bolton-Hunter reagent would have radiolabeled the boronated starburst dendrimer attached to the antibody, in addition to the antibody itself, it is possible that the increased splenic and hepatic uptake of the immunoconjugate labeled with it was due to the iodinated dendrimer alone, following enzymatic cleavage of the MoAb-BSD conjugate within the liver or spleen. At pHs below 8-9 the dendrimers would become protonated but this would not occur if all of the other terminal amino groups were derivatized (D. A. Tomalia, personal communication). If there were anionic sites on Kupffer cells of the liver, and cationic sites on the <sup>125</sup>I-labeled dendrimers, this might provide a possible explanation for the hepatic and splenic accumulation that was observed. Clegg et al. have carefully studied the biodistribution patterns of branched polypeptides having a poly-L-lysine backbone, but which differed in ionic charge, side-chain structure, and molecular size (42). Irrespective of their size or primary structures at branch sites, polycationic peptides were rapidly cleared from the circulation and accumulated in the liver and spleen. Although this may be useful for certain very specific reasons, i.e., targeting enzymes to the liver (43) or delivering antigens to the RES system in order to stimulate

an immune response, it clearly is a major limitation if the goal is to target a tumor.

Most recently, Hawthorne's group has produced immunoconjugates using carboranyl peptides and peptide active ester reagents HHS and *N,N*-diisopropylcarbodiimide (20). The resulting conjugates had as many as 490 B atoms per molecule and retained their immunoreactivity, but there was a significant loss in tumor-localizing properties (23% for native antibody compared to 4.4-5% for the conjugates). It was concluded that random conjugation of large boron trailer reagents to MoAbs would be excessively cumbersome and that greater simplicity and structural certainty would be required in order to produce immunoconjugates that would meet all of the necessary requirements necessary for successful immunotargeting. For these reasons, we (44) and others (45) have focused our interest on the development of bispecific MoAbs, one combining site of which would recognize a tumor-associated antigen and the other agent that is to be delivered to the tumor (45). Since these antibodies are unmodified, they presumably would behave in a manner similar to the native MoAbs and have longer blood half-lives and better tumor-localizing properties. At this point in time, we have succeeded in producing a MoAb directed against BSD (44) and now are in the process of identifying a suitable fusion partner that can be used to target gliomas. It remains to be determined whether this approach will be any more successful than the chemical methods that have been employed to link <sup>10</sup>B macromolecules to MoAbs.

#### ACKNOWLEDGMENT

We thank Michigan Molecular Institute and Polysciences, Inc., for generously providing us with dendrimers and Dr. Herbert Brothers for carrying out capillary electrophoresis on them, Ms. Stephanie Walters for secretarial assistance, and Dr. Scott Wilbur for his helpful suggestions in the preparation of this manuscript. This work has been supported by United States Department of Energy Grant DE-AC02-76CH000016.

#### LITERATURE CITED

- (1) Barth, R. F., Soloway, A. H., and Fairchild, R. G. (1990) Boron neutron capture therapy of cancer. *Cancer Res.* 50, 1061-1070.
- (2) Barth, R. F., Soloway, A. H., Fairchild, R. G., and Brugger, R. M. (1992) Boron neutron capture therapy for cancer. Realities and prospects. *Cancer* 70, 2955-3007.
- (3) Javid, M., Brownell, G. L., and Sweet, W. H. (1952) The possible use of neutron capture isotopes such as boron-10 in the treatment of neoplasms: II. Computation of the radiation energy and estimates of effects in normal and neoplastic brain. *J. Clin. Invest.* 31, 603-610.
- (4) Tolpin, E. L., Wellum, G. R., Dohan, F. C., Jr., Kornblith, P. L., and Zamenhof, R. G. (1975) Boron neutron capture therapy of cerebral gliomas: II. Utilization of the blood-brain barrier and tumor-specific antigens for the selective concentration of boron in gliomas. *Oncology* 32, 223-246.
- (5) Waldmann, T. A. (1991) Monoclonal antibodies in diagnosis and therapy. *Science* 252, 1657-1662.
- (6) Barth, R. F., Johnson, C. W., Wei, W.-Z., Carey, W. E., Soloway, A. H., and McGuire, J. E. (1982) Neutron capture using boronated monoclonal antibody directed against tumor-associated antigens. *Cancer Detect. Prev.* 5, 315-323.
- (7) Mizusawa, E., Dahlman, H. L., Bennett, S. J., Goldenberg, D. M., and Hawthorne, M. F. (1982) Neutron capture therapy of human cancer; *in vivo* results on tumor preparation of boron-



- labeled antibodies to carcinoembryonic antigens. *Proc. Natl. Acad. Sci. U.S.A.* 79, 3011-3014.
- (8) Goldenberg, D. M., Sharkey, R. M., Primus, F. J., Mizusawa, E., and Hawthorne, M. F. (1984) Neutron capture therapy of human cancer: *in vivo* results on tumor localization of boron-10-labeled antibodies to carcinoembryonic antigen in the GW-39 tumor model system. *Proc. Natl. Acad. Sci. U.S.A.* 81, 560-563.
- (9) Soloway, A. F., McGuire, A. H., Barth, R. F., Carey, W. E., and Adams, D. (1986). Dicesium N-succinimidyl 3-(undecahydro-closo-dodecarboranyl-dithio)propionate, a novel heterobifunctional boronating agent. *J. Med. Chem.* 28, 522-525.
- (10) Barth, R. F., Soloway, A. H., and Adams, D. M. (1986) Delivery of boron-10 for neutron capture therapy by means of polyclonal and monoclonal antibodies: progress and problems. *Neutron Capture Therapy*. (H. Hatanaka, Ed.) pp 346-352, Nishimura Co. Ltd., Niigata, Japan.
- (11) Barth, R. F., Alan, F., Soloway, A. H., Adams, D. M., and Steplewski, Z. (1986). Boronated monoclonal antibody 17-1A for potential neutron capture therapy of colorectal cancer. *Hybridoma* 5, Suppl. 1, s43-s50.
- (12) Alam, F., Barth, R. F., and Soloway, A. H. (1989) Boron containing immunoconjugates for neutron capture therapy of cancer and for immunocytochemistry. *Antibody, Immunoconjugates, Radiopharm.* 2, 145-163.
- (13) Alam, F., Soloway, A. H., Barth, R. F., Mafune, N. Adams, D. M., and Knoth, W. H. (1989) Boron neutron capture therapy; linkage of a boronated macromolecule to monoclonal antibodies directed against tumor associated antigens. *J. Med. Chem.* 32, 2326-2330.
- (14) Barth, R. F., Mafune, N., Alam, F., Adams, D. M., Soloway, A. H., Makroglou, G. E., Oredipe, D. A., Blue, E., and Steplewski, Z. (1989) Conjugation, purification and characterization of boronated monoclonal antibodies for use in neutron capture therapy. *Strahlenther. Onkol.* 165, 142-145.
- (15) Abraham, R., Muller, R., and Gabel, D. (1989). Boronated antibodies for neutron capture therapy. *Strahlenther. Onkol.* 165, 148-151.
- (16) Pettersson, M. L., Courel, M. N., Girard, N., Gabel, D., and Delpech, B. (1989) *In Vitro* immunological activity of a dextran-boronated monoclonal antibody. *Strahlenther. Onkol.* 165, 151-152.
- (17) Tamat, S. R., Patwardhan, A., Moore, D. E., Kabral, A., Bradstock, K., Hersey, P., and Allen, B. J. (1989) Boronated monoclonal antibodies for potential neutron capture therapy of malignant melanoma and leukaemia. *Strahlenther. Onkol.* 165, 145-147.
- (18) Vardarajan, A., Sharkey, R. M., Goldenberg, D. M., and Hawthorne, M. F. (1991) Conjugation of phenylisothiocyanate derivatives of carborane to antitumor antibody and *in vivo* localization of conjugates in nude mice. *Bioconjugate Chem.* 2, 102-110.
- (19) Vardarajan, A., and Hawthorne, M. F. (1991) Novel carboranyl amino acids and peptides: reagents for antibody modification and subsequent neutron-capture studies. *Bioconjugate Chem.* 2, 242-253.
- (20) Paxton, R. J., Beatty, B. G., Vardarajan, A., and Hawthorne, M. F. (1992) Carboranyl peptide-antibody conjugates for neutron-capture therapy: preparation, characterization, and *in vivo* evaluation. *Bioconjugate Chem.* 3, 241-247.
- (21) Barth, R. F., Soloway, A. H., and Adams, D. M. (1992) Delivery of boron-10 for neutron capture therapy by means of monoclonal-antibody-starburst dendrimer immunoconjugates *Progress in Neutron Capture Therapy for Cancer* (B. J. Allen, D. E. Moore, and B. V. Harrington, Eds.) pp 265-268, Plenum Press, New York.
- (22) Tomalia, D. A., Baker, H., Dewald, J., Hall, M., Kallos, G., Martin, S., Roeck, S., Ryder, J., and Smith, P. (1985) A new class of polymers: Starburst-dendritic macromolecules. *Polymer J. (Tokyo)* 17, 117-132.
- (23) Tomalia, D. A., Baker, H., Dewald, S., Hall, M., Kallos, G., Martin, S., Roeck, S., Ryder, J., and Smith, P. (1986) Dendritic macromolecules: synthesis of starburst dendrimers. *Macromolecules* 19, 2466-2468.
- (24) Tomalia, D. A., Berry, V., Hall, M., and Hedstrand, D. M. (1987) Starburst dendrimers 4. Covalently fixed unimolecular assemblages reminiscent of spheroidal micelles. *Macromolecules* 20, 1164-1167.
- (25) Tomalia, D. A., Kaplan, D. A., Kruger, W. J., Cheng, R. C., Tomlinson, I. A., Fazio, M. J., and Hedstrand, D. M. (1988) Starburst conjugates with pharmaceuticals and antibodies and metals. Eur. Pat. Appl. no. 873072664.
- (26) Johnson, C. W., Barth, R. F., Adams, D. M., Holman, B., Price, J. E. and Sautins, I. (1987) Phenotypic diversity of murine B16 melanoma detected by anti-B16 monoclonal antibodies. *Cancer Res.* 47, 1111-1117.
- (27) Tzeng, J. J., Barth, R. F., Johnson, C. W. and Adams, D. M. (1989) Distinct and non-cross reactive epitopes are recognized on B16 melanoma by LAK cells and anti-B16 monoclonal antibodies. *Proc. Soc. Exp. Biol. Med.* 193, 285-292.
- (28) Barth, R. F., Adams, D. M., Soloway, A. H., Mechetner, E. B., Alam, F., and Anisuzzam, A. B. K. M. (1991) Determination of boron in tissues and cells using direct-current plasma atomic emission spectroscopy. *Anal. Chem.* 63, 890-893.
- (29) Lowry, O. H., Rosebrough, N. J., Farr, A. L., and Randall, R. J. (1951) Protein measurement with the Folin phenol reagent. *J. Biol. Chem.* 193, 265-275.
- (30) Bolton, A. E., and Hunter, W. M. (1973) The labeling of proteins to high specific radioactivities by conjugation to a <sup>125</sup>I-containing acylating agent. *Biochem. J.* 133, 529-539.
- (31) Muetterties, E. L., and Knoth, W. H. (1968) *Polyhedral Boranes*, pp 108-110, Marcel Dekker, Inc., New York.
- (32) Fraker, P. J., and Speck, J. C. (1978) Protein and cell membrane iodinations with a sparingly soluble chloranide, 1,3,4,6-tetrachloro-3 $\alpha$ ,6 $\alpha$ -diphenylglycoluril. *Biochem. Biophys. Res. Commun.* 80, 849-857.
- (33) Tsukada, Y., Kato, Y., Umamoto, N., Takeda, Y., Hara, T., and Hirai, H. (1984). An antifetoprotein antibody-daunorubicin conjugate with a novel poly-L-glutamic acid derivative as an intermediate drug carrier. *J. Natl. Cancer Inst.* 73, 721-729.
- (34) Roberts, J. C., Adams, Y. E., Tomalia, D., Mercer-Smith, J. A., and Lavalley, D. K. (1990). Using subunit dendrimers as linker molecules to radiolabel antibodies. *Bioconjugate Chem.* 1, 305-308.
- (35) Price, J. E., Barth, R. F., Johnson, C. W., and Staubus, A. E. (1984) Injection of cells and monoclonal antibodies into mice. Comparison of tail vein and retroorbital routes. *Proc. Soc. Exp. Biol. Med.* 177, 347-353.
- (36) McCready, D. R., Balch, C. M., Fidler, I. J., and Murray, J. L. (1989) Lack of comparability between binding of monoclonal antibodies to melanoma cells *in vivo*. *J. Natl. Cancer Inst.* 81, 682-687.
- (37) Ward, B. G., and Wallace, K. (1987) Localization of the monoclonal antibody HMFG2 after intravenous and intraperitoneal injection into nude mice bearing subcutaneous and intraperitoneal human ovarian cancer xenografts. *Cancer Res.* 47, 4714-4718.
- (38) Wahl, R. L., Barrett, J., Geatti, O., Liebert, M., Wilson, B. S., Fisher, S., and Wagner, J. G. (1988) The intraperitoneal delivery of radiolabeled monoclonal antibodies: studies on the regional delivery advantage. *Cancer Immunol. Immunother.* 26, 187-201.
- (39) Wahl, R. L. (1990) Intraperitoneal delivery of monoclonal antibodies in cancer imaging with radiolabeled antibodies. *Cancer Imaging with Radiolabeled Antibodies* (D. M. Goldenberg, Ed.) pp 123-149, Kluwer Academic Publishers, Norwell, MA.
- (40) Barth, R. F., Adams, D. M., Soloway, A. H., and Darby, M. V. (1993) *In vivo* distribution of boronated monoclonal antibodies and starburst dendrimers in *Advances in Neutron Capture Therapy* (A. H. Soloway, R. F. Barth, and D. E. Carpenter, Eds.) Plenum Press, pp 351-356, New York.
- (41) Wilbur, D. S. (1992) Radiohalogenation of proteins: an overview of radionuclides, labeling methods, and reagents for conjugate labeling. *Bioconjugate Chem.* 3, 433-470.
- (42) Clegg, J. A., Hudecz, F., Mezo, G., Pimm, M. V., Szekerke, M., and Baldwin, R. W. (1990) Carrier design: biodistribution

- of branched polypeptides with a poly(L-lysine) backbone. *Bioconjugate Chem.* 1, 425-430.
- (43) Poznansky, M. J., and Bhardwaj, D. (1980) Antibody-mediated targeting of  $\alpha$ -1,4-glucosidase-albumin polymers to rat hepatocytes. *Biochemical J.* 196, 89-93.
- (44) Liu, L., Adams, D. M., Barth, R. F., and Soloway, A. H. (1993) Production of monoclonal antibodies (MoAbs) reactive with boronated isocyanate for BNCT. *Proc. Am. Assoc. Cancer Res.* 34, 474.
- (45) Hawthorne, M. F. (1991) Biochemical applications of boron cluster chemistry. *Pure Appl. Chem.* 63, 327-334.
- (46) Norlan, O., O'Kennedy, R. O. (1990) Bifunctional antibodies: concept, production and applications. *Biochim. Biophys. Acta* 1040, 1-11.

# Poly(pyrrolicarboxamides) Linked to Photoactivable Chromophore Isoalloxazine. Synthesis, Selective Binding, and DNA Cleaving Properties

Philippe Herfeld, Philippe Helissey, and Sylviane Giorgi-Renault\*

Laboratoire de Chimie Thérapeutique, CNRS URA 1310, Faculté des Sciences Pharmaceutiques et Biologiques, 4, Avenue de l' Observatoire, 75270 Paris Cédex 06, France

Hélène Goulaouic, Jeanne Pager, and Christian Auclair

Laboratoire de Pharmacologie moléculaire, CNRS URA 147, INSERM U140, Institut Gustave Roussy, 94800 Villejuif, France. Received July 13, 1993\*

In an attempt to obtain DNA sequence-specific cleaving molecules, we have synthesized two types of hybrid groove binders composed of an isoalloxazine (flavin) chromophore linked through a polymethylenic chain to either a bis- or a tris(pyrrolicarboxamide) moiety related to netropsin and distamycin, respectively. In both types of molecules, the polymethylenic chain is linked to the alloxazine ring either in the N<sub>10</sub> position or in the N<sub>3</sub> position. As netropsin and distamycin, the hybrid derivatives preferentially bind to A + T-rich sequences and recognize sequences such as 5'-ATTT. Upon visible light irradiation the flavin moiety undergoes a redox cycling process generating superoxide anion and hydroxyl radical. Generation of oxy radicals appears to be more efficient with the hybrids in which the polymethylenic chain is linked at the N<sub>10</sub> position. The generation of oxy radicals results in the occurrence of single strand break in supercoiled DNA. Breaks preferentially occur in the vicinity of A + T-rich sequences. The advantage of flavin relative to other oxy radicals generating compounds such as ferrous-EDTA is that it does not require chemical reduction but can be reduced either by visible light or by cellular enzymes, both conditions being compatible with pharmacological constraints.

The design of sequence-specific cleaving molecules for double-helical DNA requires the linkage of a DNA-cleaving moiety to a sequence-specific DNA-binding molecule. Targeted cleavage of double-helical polynucleotides by either complementary oligonucleotides (Moser and Dervan, 1987; François et al., 1988) or poly(pyrrolicarboxamide) derivatives coupled to metal-chelating agents generating oxy radicals (Schultz et al., 1982; Youngquist and Dervan, 1985) has been attempted by several groups. It was found that these functionalized hybrid molecules may act as artificial nucleases and can serve as models for the design of molecules of pharmacological interest (Dervan, 1986). From this point of view, relevant investigations should include the identification of suitable functionalizing moieties. Along this line, we have synthesized various molecules composed of either a bis- or a tris(pyrrolicarboxamide) moiety related to netropsin and distamycin, respectively, linked to an isoalloxazine (flavin) chromophore. The rationale supporting the synthesis of such molecules is as follows: on one hand, netropsin and distamycin are natural antibiotics that recognize and specifically bind to A + T-rich nucleotide sequences in the minor groove of double-helical DNA (B-form) (Hahn, 1975; Kopka et al., 1985; Zimmer, 1975). On the other hand, upon two-electron reduction, the flavin chromophore reoxidizes in the presence of molecular oxygen through a one-electron transfer process generating oxy radicals (Ballou et al., 1969; Misra and Fridovich, 1972; Michelson, 1977) capable of DNA breaks (Korycka-Dahl and Richardson, 1980). In view of the potential pharmacological

relevance of such compounds and compared to other oxy-generating systems such as ferrous-EDTA, the major interest of the flavin chromophore is that this compound does not require chemical reduction but can be reduced either by visible light or by reduced nicotinamide adenine dinucleotides and intracellular reductase enzymes such as DT diaphorase. In the hybrid molecules, we chose to preserve the amidinium function of netropsin and distamycin that seems to be necessary for the efficient recognition of A + T-containing sequences (Debard et al., 1989; Subra et al., 1991). Consequently, either the guanidinium function of the netropsin or the formamide group of the distamycin has been replaced by a polymethylenic chain linked to an isoalloxazine nucleus either in the N<sub>3</sub> position or in the N<sub>10</sub> position. The present paper describes the synthesis and the main properties of bis- and tris(pyrrolicarboxamide)-flavin hybrid molecules in terms of selective DNA binding and cleaving properties.

## EXPERIMENTAL PROCEDURES

Melting points were determined on a Maquenne apparatus and are uncorrected. The IR spectra were recorded on a Perkin-Elmer 157G spectrophotometer, and only the principal sharply defined peaks are reported. The <sup>1</sup>H NMR spectra were recorded on a Bruker 250-MHz spectrometer. Mass spectra were determined either by FAB (fast atom bombardment) on a VG 70-SEQ (VG Analytical Ltd, G.B.) apparatus, source FAB (positive ions) with direct introduction using glycerol-thioglycerol (1:1) as a matrix, or by DCI/NH<sub>3</sub> (desorption chemical ionization, ammonia as vector gas) on a Nermag R 10-10C instrument. Thin-layer chromatography was carried out on Merck GF 254 silica gel plates. Flash chromatography was performed on silica gel (Lichroprep Si 60, Merck).

\* To whom all correspondence should be addressed. Phone: (33) 1 43 26 52 75. Fax: (33) 1 43 29 14 03.

\* Abstract published in *Advance ACS Abstracts*, December 15, 1993.

**Ethyl 5-(7,8,10-Trimethylisoalloxazin-3-yl)pentanoate (2).** To a suspension of lumiflavin (1) (Kuhn and Weygand, 1934a) (10 g, 39 mmol) in dry DMF (800 mL) were added dry  $K_2CO_3$  (27 g, 195 mmol) and ethyl 5-bromopentanoate (31 mL, 195 mmol), and the resulting mixture was stirred at 40 °C for 48 h. After DMF was distilled off,  $H_2O$  (600 mL) was added. The residue was partitioned between  $H_2O$  and  $CH_2Cl_2$ . The organic layer was evaporated in vacuo to give a solid that was triturated with ligroin, collected by filtration, washed with ligroin, and then purified by flash chromatography using  $CH_2Cl_2$ -AcOEt (9.0:1.0) as an eluent to give 6.33 g (42%) of compound 2: mp 187 °C (EtOH); IR (KBr) 1695, 1730 [ $\nu(CO)$ ]  $cm^{-1}$ ; NMR ( $CDCl_3$ )  $\delta$  1.19 (t, 3,  $CH_2CH_3$ ), 1.68 (m, 4,  $CH_2(CH_2)_2CH_2$ ), 2.30 (t, 2,  $CH_2CO$ ), 2.40 (s, 3, 7- $CH_3$ ), 2.50 (s, 3, 8- $CH_3$ ), 4.04 (m, 7,  $NCH_2$ ,  $NCH_3$ ,  $OCH_2$ ), 7.35 (s, 1, 9-H), 8.0 (s, 1, 6-H); attributions of 6-H, 9-H, 7- $CH_3$ , and 8- $CH_3$  were given according to Förty (1970); MS  $m/z$  385 [(M + H)<sup>+</sup>]. Anal. ( $C_{20}H_{24}N_4O_4$ ) C, H, N.

**5-(7,8,10-Trimethylisoalloxazin-3-yl)pentanoic Acid (3).** The ester 2 (1 g, 2.6 mmol) in 2 N HCl (10 mL) was stirred under reflux for 2.5 h. After cooling, the precipitate was collected by filtration and washed with  $H_2O$ . It was purified by dissolution in a saturated  $NaHCO_3$  solution and then by reprecipitation by the addition of 6 N HCl until a pH of 1 was reached to afford 0.853 g (92%) of compound 3: mp 250 °C; IR (KBr) 1710, 1720 [ $\nu(CO)$ ], 3500 [ $\nu(OH)$ ]  $cm^{-1}$ ; NMR ( $Me_2SO-d_6$ )  $\delta$  1.52 (m, 4,  $CH_2(CH_2)_2CH_2$ ), 2.18 (t, 2,  $CH_2CO$ ), 2.35 (s, 3, 7- $CH_3$ ), 2.47 (m, 8- $CH_3$  and  $Me_2SO$ ), 3.81 (t, 2,  $NCH_2$ ), 3.93 (s, 3,  $NCH_3$ ), 7.72 (s, 1, 9-H), 7.88 (s, 1, 6-H), 11.92 (s, 1,  $COOH$ ); MS  $m/z$  357 [(M + H)<sup>+</sup>]. Anal. ( $C_{18}H_{20}N_4O_4$ ) C, H, N.

**3-[1-Methyl-4-[1-methyl-4-[[4-(7,8,10-trimethylisoalloxazin-3-yl)butyl]carboxamido]pyrrole-2-carboxamido]pyrrole-2-carboxamido]propionamidinium Chloride (5a) and 1,3-Dicyclohexyl-1-[5-(7,8,10-trimethylisoalloxazin-3-yl)pentanoyl]urea (6).** Acid 3 (0.4 g, 1.12 mmol) was dissolved in DMF (15 mL), and to this were added DCC (0.46 g, 2.24 mmol) and amine 4a (Lown and Krowicki, 1985) (0.445 g, 1.12 mmol). After 4 days at 20 °C, the solvent was removed under reduced pressure, and the residue was triturated with dry  $Et_2O$ . The resulting solid was dissolved into the minimum of MeOH and was precipitated by adding dry  $Et_2O$ . After filtration the compound was purified by flash chromatography (solvent: MeOH) to give 0.122 g (15%) of compound 5a. The washing layers and first fractions of flash chromatography contained many impurities and a secondary compound that was identified as 6 after purification of a small amount by flash chromatography [solvent: AcOEt- $CH_2Cl_2$  (8.0:2.0)].

**5a:** mp 210–211 °C; IR (KBr) 1580, 1640 [ $\nu(CO)$ ], 2950, 3300 [ $\nu(NH)$ ]  $cm^{-1}$ ; NMR ( $Me_2SO-d_6$ )  $\delta$  1.47 (m, 4,  $CH_2(CH_2)_2CH_2$ ), 2.20 (t, 2,  $CH_2CO$ ), 2.34 (s, 3, 7- $CH_3$ ), 2.47 (m, 8- $CH_3$ ,  $CH_2C(=NH_2)NH_2$  and  $Me_2SO$ ), 3.42 (quint, 2,  $NHCH_2$ ), 3.73 (s, 6, 2  $NCH_3$ ), 3.87 (t, 2,  $NCH_2$ ), 3.93 (s, 3, 10- $CH_3$ ), 6.80, 6.83, 7.07, 7.13 (4s, 4  $\times$  1, pyrrolic H), 7.77 (s, 1, 9-H), 7.90 (s, 1, 6-H), 8.16 (t, 1,  $NHCH_2$ ), 8.80 (broad s, 4,  $C(=NH_2)NH_2$ ), 9.73 (s, 1, NH), 9.81 (s, 1, NH); MS (FAB) 670.42 [(M - Cl)<sup>+</sup>].

**6:** mp 231 °C; IR (KBr) 1585 [ $\nu(CO)$  amide], 1655, 1700 [ $\nu(CO)$ ], 2930, 3300 [ $\nu(NH)$ ]  $cm^{-1}$ ; NMR ( $CDCl_3$ )  $\delta$  1.21 (m, 8H,  $CH_2$ ), 1.72 (m, 14H,  $CH_2$ ), 1.91 (m, 2H,  $CH_2$ ), 2.40 (s, 3, 7- $CH_3$ ), 2.45 (t, 2,  $CH_2CO$ ), 2.51 (s, 3, 8- $CH_3$ ), 3.62 (m, 1,  $CH$ ), 3.93 (m, 1,  $CH$ ), 4.02 (t, 2,  $NCH_2$ ), 4.07 (s, 3,  $NCH_3$ ), 7.36 (m, 1, NH), 7.39 (s, 1, 9-H), 8.0 (s, 1, 6-H); MS  $m/z$  563 [(M + H)<sup>+</sup>], 438 [(M + 2H -  $CONHC_6H_{11}$ )<sup>+</sup>].

**3-[1-Methyl-4-[1-methyl-4-[1-methyl-4-[[4-(7,8,10-**

**trimethylisoalloxazin-3-yl)butyl]carboxamido]pyrrole-2-carboxamido]pyrrole-2-carboxamido]propionamidinium Chloride (5b).** Acid 3 (0.4 g, 1.12 mmol) was dissolved in DMF (28 mL), and to this were added DCC (0.46 g, 2.24 mmol), amine 4b (Lown and Krowicki, 1985) (0.55 g, 1.12 mmol) successively. After the solution was stirred at 20 °C for 90 h, amine 4b (0.05 g, 0.1 mmol) was again added. Twenty-four h later, after filtration, the mixture was evaporated to dryness under reduced pressure. The residue was dissolved in dry MeOH (20 mL) and precipitated by the addition of dry  $Et_2O$ . The resulting solid was purified by flash chromatography using MeOH as an eluant to give 0.156 g (17%) of compound 5b. As in the synthesis of 5a, 6 was isolated as a secondary compound.

**5b:** mp 262–264 °C dec; IR (KBr) 1585, 1640 [ $\nu(CO)$ ], 3320 [ $\nu(NH)$ ]  $cm^{-1}$ ; NMR ( $Me_2SO-d_6$ )  $\delta$  1.57 (m, 4,  $CH_2(CH_2)_2CH_2$ ), 2.23 (m, 4,  $CH_2CO$ ;  $CH_2C(=NH_2)NH_2$ ), 2.35 (s, 3, 7- $CH_3$ ), 2.45 (m, 8- $CH_3$  and  $Me_2SO$ ), 3.36 (m, 2,  $NHCH_2$ ), 3.77 (s, 6, 2  $NCH_3$ ), 3.80 (s, 3,  $NCH_3$ ), 3.86 (t, 2,  $NCH_2$ ), 3.93 (s, 3, 10- $CH_3$ ), 6.80 (s, 2, pyrrolic H), 6.97, 7.07, 7.13, 7.16 (4s, 4  $\times$  1, pyrrolic H), 7.75 (s, 1, 9-H), 7.88 (4s, 1, 6-H), 8.10 (m, 2, 2NH), 9.73 (m, 1, NH), 9.83 (m, 1, NH); MS (FAB) 793.2 [(M - Cl + H)<sup>+</sup>], 792 [(M - Cl)<sup>+</sup>].

**6-(7,8-Dimethylisoalloxazin-10-yl)hexanoic Acid (8).** 6-(7,8-Dimethylisoalloxazin-10-yl)hexanol (7) (Förty et al., 1968) (2 g, 5.85 mmol) was added gradually at 0 °C to a mixture of  $HNO_3$ ,  $d = 1.38$  (50 mL), and sodium nitrite (100 mg, 1.45 mmol). The temperature of the reaction was allowed to rise to obtain a clear solution. The solution was then immediately poured over ice, and the resulting precipitate was collected by filtration and washed with ice-water. It was then dissolved in a 5% solution of sodium hydrogen carbonate and filtered, and the crude acid was precipitated from the filtrate by the addition of hydrochloric acid and purified by dry flash chromatography [solvents:  $CH_2Cl_2$ -MeOH (9.8:0.2) to (9.6:0.4)] to give 1.48 g (71%) of 8 (lit. (Förty et al., 1968) 67%): mp 276–277 °C dec; IR (KBr) 1640, 1715 [ $\nu(CO)$ ], 3160 [ $\nu(NH)$ ], 3500 [ $\nu(OH)$ ]  $cm^{-1}$ ; NMR ( $Me_2SO-d_6$ )  $\delta$  1.42 (m, 2,  $CH_2$ ), 1.52 (m, 2,  $CH_2$ ), 1.68 (m, 2,  $NCH_2CH_2$ ), 2.18 (t, 2,  $CH_2CO$ ), 2.35 (s, 3, 7- $CH_3$ ), 2.45 (m, 8- $CH_3$  and  $Me_2SO$ ), 4.52 (m, 2,  $NCH_2$ ), 7.72 (s, 1, 9-H), 7.84 (s, 1, 6-H), 11.27 (s, 1, NH), 11.96 (s, 1,  $COOH$ ); MS  $m/z$  357 [(M + H)<sup>+</sup>].

**3-[1-Methyl-4-[1-methyl-4-[[5-(7,8-dimethylisoalloxazin-10-yl)pentyl]carboxamido]pyrrole-2-carboxamido]pyrrole-2-carboxamido]propionamidinium Chloride (9a).** Compound 9a was prepared in the same manner as used for 5a from 6-(7,8-dimethylisoalloxazin-10-yl) hexanoic acid (8) (0.356 g, 1 mmol), DCC (0.406 g, 2 mmol), and amine 4a (Lown and Krowicki, 1985) (0.397 g, 1 mmol). After being stirred at 20 °C for 2 days, the reaction mixture was treated in the same manner as used for 5a and then purified by flash chromatography (solvent: MeOH) to give 0.24 g (34%) of 9a. The first fractions contained some impurities and compound 10, identified by comparison with the compound isolated in the reaction of 8 with *p*-nitrophenol and DCC.

**9a:** mp 225–227 °C dec; IR (KBr) 1580, 1640 [ $\nu(CO)$ ], 3290 [ $\nu(NH)$ ]  $cm^{-1}$ ; NMR ( $Me_2SO-d_6$ )  $\delta$  1.45 (m, 2,  $(CH_2)_2CH_2CH_2(CH_2)_2$ ), 1.80 (m, 4,  $CH_2CH_2CH_2CH_2CH_2$ ), 2.28 (m, 4,  $CH_2C(=NH_2)NH_2$  and  $CH_2CO$ ), 2.33 (s, 3, 7- $CH_3$ ), 2.45 (m, 8- $CH_3$  and  $Me_2SO$ ), 3.36 ( $NHCH_2$  and  $H_2O$ ), 3.75 (s, 6, 2  $NCH_3$ ), 4.51 (t, 2,  $NCH_2$ ), 6.77, 6.84, 7.09, 7.15 (4s, 4  $\times$  1, pyrrolic H), 7.71 (s, 1, 9-H), 7.84 (s, 1, 6-H), 8.08 (s, 2, 2NH), 9.78 (m, 2, 2NH); MS (FAB) 670.43 [(M - Cl)<sup>+</sup>].

**3-[1-Methyl-4-[1-methyl-4-[1-methyl-4-[[5-(7,8-di-**

**2-carboxamido]pyrrole-2-carboxamido]pyrrole-2-carboxamido]propionamidinium Chloride (9b).** Acid 8 (0.4 g, 1.12 mmol), DCC (0.46 g, 2.24 mmol), and amine 4b (Lown and Krowicki, 1985) (0.55 g, 1.12 mmol) were stirred in DMF (30 mL) for 3 days. DCC (0.055 g, 0.22 mmol) and amine 4b (0.054 g, 0.11 mmol) were again added, and stirring was continued for 3 more days. Treatment was the same as used for 5b, and purification was achieved by flash chromatography (solvent: MeOH) to give 0.138 g (15%) of 9b: mp 264–268 °C dec; IR (KBr) 1580, 1640 [ $\nu(\text{CO})$ ], 3290 [ $\nu(\text{NH})$ ]  $\text{cm}^{-1}$ ; NMR ( $\text{Me}_2\text{SO}-d_6$ )  $\delta$  1.42 (m, 2,  $(\text{CH}_2)_2\text{CH}_2(\text{CH}_2)_2$ ), 1.60 (m, 4,  $\text{CH}_2\text{CH}_2\text{CH}_2\text{CH}_2\text{CH}_2$ ), 2.22 (m, 4,  $\text{CH}_2\text{CO}$  and  $\text{CH}_2\text{C}(=\text{NH}_2)\text{NH}_2$ ), 2.31 (s, 3, 7- $\text{CH}_3$ ), 2.45 (8- $\text{CH}_3$  and  $\text{Me}_2\text{SO}$ ), 3.36 ( $\text{NHCH}_2$  and  $\text{H}_2\text{O}$ ), 3.69 (m, 9, 3  $\text{NCH}_3$ ), 4.44 (t, 2,  $\text{NCH}_2$ ), 6.69, 6.75, 6.89, 6.98, 7.04, 7.09 (6s, 6  $\times$  1, pyrrolic H), 7.62 (s, 1, 9-H), 7.72 (s, 1, 6-H), 8.01 (m, 2, 2 NH), 9.69 (m, 2, 2 NH); MS (FAB) 793.2 [(M – Cl + H) $^+$ ].

**1,3-Dicyclohexyl-1-[6-(7,8-dimethylisoalloxazin-10-yl)hexanoyl]urea (10).** A mixture of acid 8 (0.2 g, 0.56 mmol), *p*-nitrophenol (0.094 g, 0.674 mmol), and DCC (0.14 g, 0.674 mmol) in DMF (10 mL) was stirred for 24 h at 40 °C.  $\text{H}_2\text{O}$  was added, and the resulting precipitate was filtered, washed with  $\text{H}_2\text{O}$ , and then purified by flash chromatography using  $\text{CH}_2\text{Cl}_2$ –MeOH (9.8:0.2) as an eluent to give 0.192 g (61%) of 10 without traces of *p*-nitrophenyl ester.

10: mp 204–208 °C; IR (KBr) 1580 [ $\nu(\text{CO})$  amide], 1660, 1700 [ $\nu(\text{CO})$ ], 3040, 3160, 3300 [ $\nu(\text{NH})$ ]  $\text{cm}^{-1}$ ; NMR ( $\text{CDCl}_3$ )  $\delta$  1.18 (m, 8,  $\text{CH}_2$ ), 1.62 (m, 14,  $\text{CH}_2$ ), 1.89 (m, 2,  $\text{CH}_2$ ), 2.41 (s, 3, 7- $\text{CH}_3$ ), 2.46 (t, 2,  $\text{CH}_2\text{CO}$ ), 2.53 (s, 3, 8- $\text{CH}_3$ ), 3.62 (q, 1,  $\text{CHNH}$ ), 3.92 (t, 1, CH), 4.64 (t, 2,  $\text{NCH}_2$ ), 6.83 (m, 1, CONH), 7.38 (s, 1, 9-H), 8.02 (s, 1, 6-H), 8.48 (s, 1, NH); MS  $m/z$  563 [(M + H) $^+$ ], 438 [(M + 2H –  $\text{CONHC}_6\text{H}_{11}$ ) $^+$ ].

**DNAs and Polynucleotides. Preparation of pBR322 DNA.** *E. coli* HB101 transformed with the monomeric form of the plasmid pBR322 were grown to late log phase in LB media with ampicilline (100  $\mu\text{g}/\text{mL}$ ) before addition of chloramphenicol (150  $\mu\text{g}/\text{mL}$ ). After continued growth at 37 °C overnight, cells were harvested by centrifugation, and the covalently closed form of the plasmid was purified by centrifugation to equilibrium in cesium chloride–ethidium bromide with 1-butanol saturated with water, and the DNA was precipitated. Concentration of DNA was evaluated from UV absorption at 260 nm.

**Oligonucleotide Synthesis.** The 25-base-pair oligonucleotide was synthesized on an oligonucleotide Applied synthesizer, purified by gel electrophoresis, and 5'-end-labeled by using polynucleotide kinase and  $^{32}\text{P}$  ATP (Amersham) according to an established procedure (Maniatis et al., 1989).

**Oxy Radical Production. ESR Spectroscopy.** ESR spectroscopy was performed using a Bruker ER 100 D apparatus. Under the standard operating conditions, the microwave frequency was in the 9.670-GHz range, modulation 1.25 G, and microwave power 100 mW. The production of oxy radicals upon visible light irradiation was assessed using the spin trap 5,5-dimethylpyrroline 1-oxide (DMPO) as probe.

**Superoxide Dismutase (SOD)–Inhibitable Cytochrome *c* Reduction.** Superoxide anion production was quantitated using the measurement of the reduction of cytochrome *c* FeIII to cytochrome *c* FeII at 550 nm in the presence and in the absence of SOD according to the standard procedure (McCord et al., 1977).

**Circular Dichroism.** CD spectra were recorded on a Roussel-Jouan dichrograph Mark IV. Samples were placed

in a quartz cell (3 mL, 1-cm path length) thermostated at 25 °C. In typical experiments, DNA concentrations were 70  $\mu\text{M}$ , and concentrations of the ligands were in the range from 1 to 7  $\mu\text{M}$ . Data were stored in a Minc 11/23 computer and corrected for the dichroism of the buffer. CD signal intensities were recorded at 315 nm for netropsin and derivatives and at 330 nm for distamycin and derivatives. At the equilibrium, the amount of ligand bound to DNA was estimated using the equation

$$\text{Cb} = \text{Ct}(1 - H_b/H_{\text{max}}) \quad (1)$$

where Ct is the ligand concentration (free plus bound),  $H_b$  the intensity of the induced CD signal at the equilibrium, and  $H_{\text{max}}$  the intensity of the CD signal when all ligand is bound to DNA. For every ligand concentration,  $H_{\text{max}}$  is obtained from the nonlinear regression fitting of the curve (rectangular hyperbola) which describes the variation of the CD signal as a function of DNA concentration. In the experimental conditions used,  $H_{\text{max}}$  is a linear function of Ct. The association constant values were estimated from the Scatchard equation

$$\text{Cb}/\text{Cf} = K(n - \text{Cb}) \quad (2)$$

where Cb is expressed as ligand bound per nucleotide, Cf is the free ligand concentration,  $K$  the association constant, and  $n$  the Cb value obtained in the presence of saturating concentration of ligand.

**Viscometric Experiments.** Viscometric measurements were performed at 25 °C in a semimicrodilution capillary viscometer linked to an IBM XT computer. The capacity of tested compounds to increase the length of sonicated calf thymus DNA was measured using standard operating conditions (Saucier et al., 1971).

**Footprinting Experiments. DNase I Footprinting.** DNase I was obtained from Boehringer and prepared as a 3125 units/mL stock solution in 0.15 M NaCl containing 1 mM  $\text{MgCl}_2$ . It was stored at –20 °C and diluted to working concentration immediately before use.

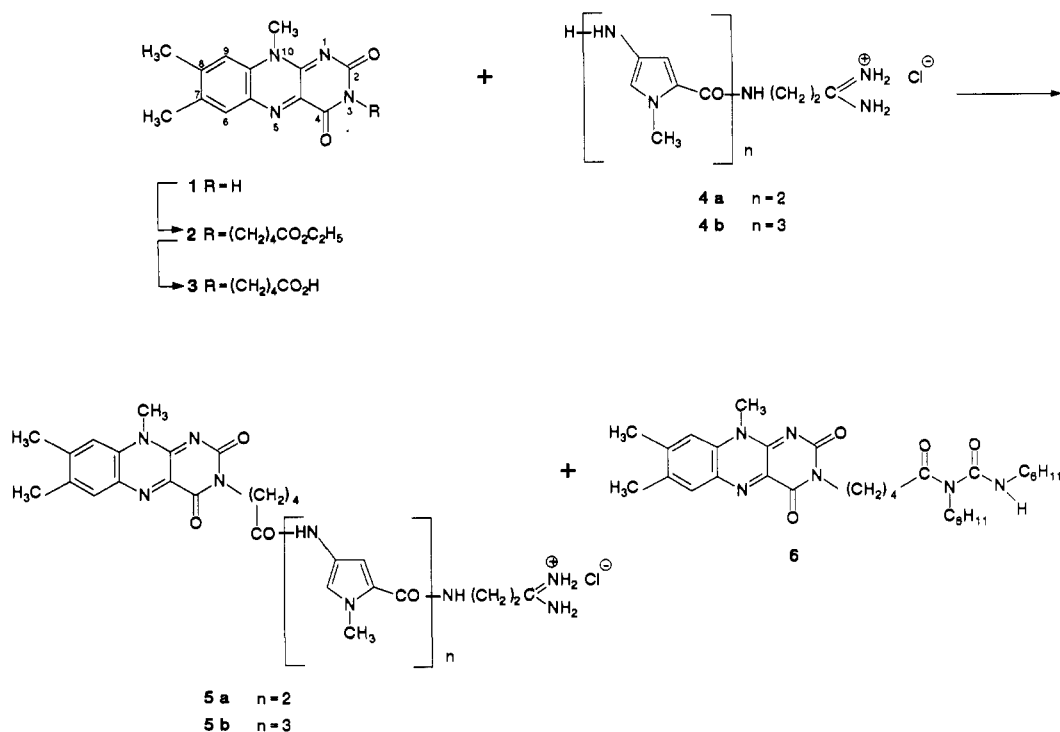
We prepared end-labeled 25-bp labeling the 5' end with radioactive phosphorus and purifying the labeled 25-bp fragment by electrophoresis on 5% acrylamide gel and electroelution. Samples (3.7  $\mu\text{L}$ ) of the labeled oligonucleotide (500 000 cpm), mixed with 28 ng of psP 65 DNA as carrier, were incubated with 5  $\mu\text{L}$  of drug solution at 4 °C for 1 h and then digested with 2  $\mu\text{L}$  of DNase I (final concentration 0.3 units/ $\mu\text{L}$ ). The reaction was allowed to run for 3 min and then quenched by adding 2.3  $\mu\text{L}$  of  $\text{AcONH}_4$  (3 M) and EDTA (0.25 M). DNA samples were then ethanol precipitated at –20 °C, isolated by centrifugation, washed with cold 75% ethanol, dried using a speed-vac concentrator, and dissolved in formamide containing 0.1% bromophenol blue.

**Gel Electrophoresis.** DNA fragments were separated by electrophoresis in gels composed of 15% polyacrylamide containing 8 M urea and Tris/borate/EDTA buffer. After 3 h of electrophoresis at 1500 V, the gels were directly subjected to autoradiography at –70 °C with an intensifying screen.

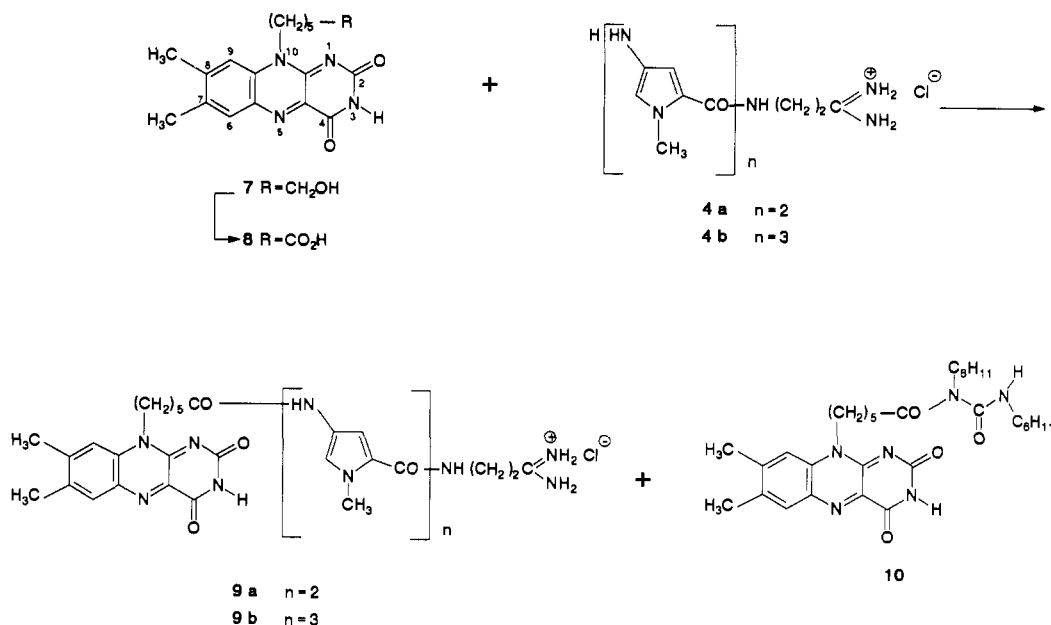
**Densitometry.** Autoradiographs from the footprinting experiments were analyzed using a Joyce scanning microdensitometer to produce profiles from which the relative intensity of each band was measured. These intensities were calculated in terms of fractional cleavage ( $f$ ) =  $A_i/A_t$ , where  $A_i$  is the area under band *i* and  $A_t$  the mean of the sum of the areas under all bands in the corresponding gel lane. Protection or enhancement in the presence of drug were expressed in percent of fractional cleavage compared to control.



Scheme 1



Scheme 2



**DNA Strand Breakage.** Strand breakage was monitored in phosphate buffer 0.05 M (pH 8.0) containing 1 mM EDTA, plasmid pBR322 DNA, and compound to be tested. The mixtures were irradiated using a polychromatic lamp with a energy of the incident light close to 1.5 W·m<sup>-2</sup>·A). The cleavage products were separated on 7% agarose gel in a flat bed electrophoresis apparatus (15 × 20 cm, gel thickness 4–5 mm) at a field strength of 6–8 V/cm. The electrophoresis buffer used was Tris-acetate 0.04 M, EDTA 2 μM, pH 7.4. The gels were then stained under gentle shaking for 30 min with ethidium bromide and photographed for 1 min under 354-nm UV light on Polaroid 665 positive/negative film. For quantitative evaluation, the negatives were scanned with a gel scanner. The mapping procedure was performed essentially as described by Barton and Raphael (1985). DNA samples

were electrophoresed in either 7% (DNA degradation) or 1% agarose gel (mapping procedure). Gels were stained with ethidium bromide and scanned. When required, band sizes were quantitated by using markers of known molecular weight.

## RESULTS AND DISCUSSION

**Chemicals.** The synthesis of the hybrid compounds **5a**, **5b**, **9a**, and **9b** required first the preparation of flavins with a polymethylenic carboxylic acid linker **3** and **8** and of the aminoallopyrroles bearing an amidinium function **4a** and **4b** (Schemes 1 and 2). Compounds **4a** and **4b** were prepared from 1-methyl-4-nitropyrrole-2-carboxylic acid (Bialer et al., 1978) following the reported multistep synthesis (Lown and Krowicki, 1985; Penco et al., 1967). In general, Lown's synthesis (1985) was applied with some

minor modifications except for the condensation of amines with 1-methyl-4-nitropyrrole-2-carboxylic acid *via* its acyl chloride. According to Lown (1985), the acid was converted into its acyl chloride by heating with a slight excess of thionyl chloride in THF for 5 min, avoiding longer heating which leads to side products. But in our hands, the reaction remained incomplete under these conditions and it went to completion after 75 min of heating (monitored by TLC). Interestingly, refluxing the acid for 1–2 h in an excess of thionyl chloride afforded a purer acyl chloride. Condensations of amines with acyl chloride according to Penco (1967) replacing benzene by dichloromethane (20 °C, aqueous solution of sodium bicarbonate, organic solvent) afforded purer compounds in better yields than condensations according to Lown (1985) (Hünig's base, –20 °C, THF).

The acid **3** was prepared from lumiflavin (7,8,10-trimethylisoalloxazine) (**1**) (Scheme 1). The simplest of the previously described syntheses of lumiflavin involves reduction of 4,5-dimethyl-2-nitro-*N*-methylaniline and subsequent reaction of the amine thus obtained with alloxan. Reduction was done either by stannous chloride (Kuhn et al., 1934b; Kuhn and Reinemund, 1934c) or by catalytic hydrogenation either on charcoaled palladium using acetic acid as solvent (Grande et al., 1977) or on Raney nickel in ethanol (Hemmerich, 1958). We chose to reduce the nitro compound over palladium in ethanol to give the free base which was then condensed with alloxan in the presence of hydrochloric acid according to Kuhn (1934a). When condensation was carried out in acetic acid, reduction took place in this solvent and as a result a mixture of lumiflavin (60%) and lumichrome (7,8-dimethylalloxazine) (40%) was obtained (NMR titration). Such a demethylation was observed by Hemmerich when sodium 3-amino-4-(methylamino)benzene sulfonate was taken as starting material (Hemmerich et al., 1960). We used the crude compound **1** for the subsequent step because of the tedious and unsuccessful purification of lumiflavin (Kuhn et al., 1934b; Kuhn and Reinemund, 1934c; Grande et al., 1977). Reaction with ethyl 5-bromopentanoate in DMF in the presence of potassium carbonate gave **2** that was hydrolyzed to give the acid **3**.

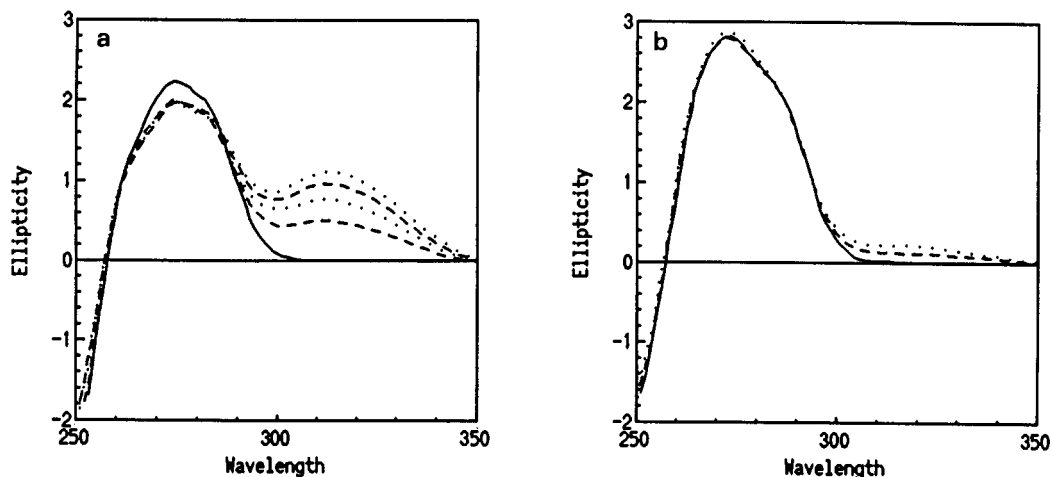
The acid **8** was obtained by Föry (1968) in 65–75% yields by the oxidation of the corresponding alcohol **7** with nitric acid at 20 °C. But in our hands, this method gave a mixture of products. We found that addition of sodium nitrite to the reaction mixture at 0 °C afforded 71% of **8** after purification.

Several methods were examined to obtain the flavin-oligopyrrole-linked structure. Formation of peptide linkage by condensation of the amine, **4a**, or **4b** with the acyl chloride of **3** or **8** was unsuccessful because the acids did not react with either thionyl chloride or oxalyl chloride. Whereas such a reaction was claimed by Takeda (1987) in the case of other isoalloxazines with one to three methylene chains, condensation was achieved by using DCC in DMF. Hybrid compounds **5a**, **5b**, **9a**, and **9b** were formed along with additional byproducts which were identified as the products of reaction of the acid **3** or **8** with DCC and subsequent transposition to give acylureas **6** and **10**, respectively. Formation of acylureas is known to be suppressed by carrying out the reaction in less polar solvents, e.g., dichloromethane (Ljunquist and Folkers, 1988). In our case, we had to use DMF because of the insolubility of the acids in other suitable solvents. The reaction was also tried in DMF–dichloromethane (1:1) but the yields of desired compounds could not be improved. Contrary to Bialer (1980) product of condensation of DCC

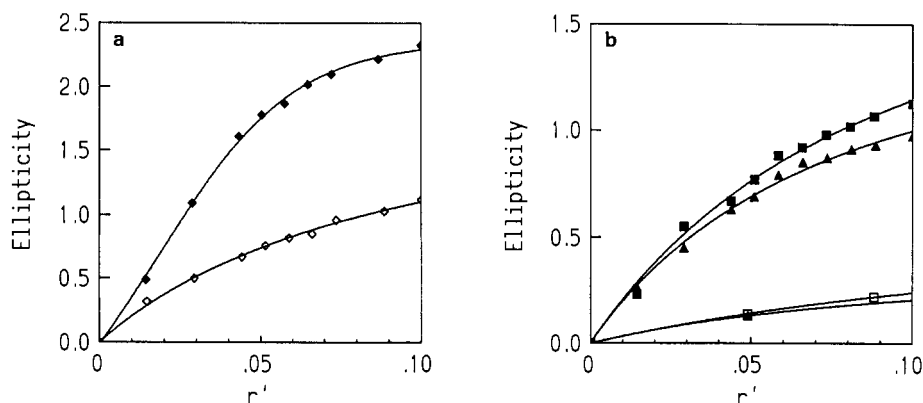
with 4-aminopyrrole derivatives was not obtained. Other classical methods usually used in peptidic synthesis were unsuccessful. No reaction occurred in the presence of coupling reagents alone: HOBt, BOP (Castro et al., 1976), *N,N'*-carbonyldiimidazole (Föry et al., 1968), *p*-nitrophenol trifluoroacetate (Castro et al., 1976). Presumably, difficulties to create these amide linkages are due, on one hand, to the poor reactivity of the acid functions of **3** and **8** because of the chain folding back on the ring system (Föry et al., 1970) and, on the other hand, to the poor nucleophilicity of the aromatic amines **4**. We tried to prepare **5a** by another way: the condensation of the flavin **3** with the amino-oligopyrrole bearing a nitrile chain and subsequent Pinner's reaction. This way was not pursued because condensation of the acid **3** with this amine gave poor yields.

The polar hybrid derivatives containing amidinium functions were readily analyzed for purity by TLC on silica gel with methanol as eluent, and acetic acid was necessary as a cosolvent. Also, for such polar compounds FAB-MS proved satisfactory for determining the molecular composition.

**Binding to Natural DNAs. Circular Dichroism.** The question arises whether the structural modification of netropsin or distamycin resulting from the removal of either the guanidine moiety or the formyl function, respectively, and the linkage of the isoalloxazine chromophore could result in a significant change in the selective binding to A + T-rich sequences. In order to estimate the binding preference of the hybrid molecules to A + T-rich containing DNA sequences, we have performed a circular dichroism (CD) study of the binding of netropsin, distamycin, and the synthesized compounds to natural DNAs extracted from *clostridium perfringens* (containing 68% A + T) and from *micrococcus lysodeikticus* (containing 72% G + C). We first recorded the CD spectra of these natural DNAs in the presence of increasing concentrations of netropsin and distamycin taken as control ligands. We obtained typical CD spectra as previously described in the literature (spectra not shown). It can be observed that the addition of netropsin in a solution containing *clostridium* DNA results in the appearance of an induced dichroic signal in the 315-nm range. In contrast and in agreement with the binding preference to A + T-rich sequences, similar amounts of netropsin produce a markedly weaker signal when added to the solution containing DNA purified from *micrococcus*. In both spectra, the presence of an isoelliptic point suggests a single mode of binding between the ligand and the DNAs within the limits of concentrations used. Figure 1a and b shows the CD spectra of DNA from *clostridium* (a) and *micrococcus* (b) recorded in the presence of increasing concentrations of compound **5a**. As in the case of netropsin, a new CD band is observed for the **5a**–*clostridium* DNA complex in the vicinity of 315 nm whereas a very weak induced signal appears in the presence of *micrococcus* DNA. Figure 2 shows, as an example, typical curves describing the variation of the ellipticity at 315 nm as a function of the concentration of netropsin (a) and compound **5a** (b). The same experiments have been further performed (spectra not shown) using the netropsin hybrid **9a**, distamycin, and the distamycin hybrids **5b** and **9b**. In all cases, and for every tested compound, similar behavior as in Figure 1 was observed except that in the presence of distamycin or distamycin derivatives the CD signal of the ligand–DNA complexes occurs in the 330-nm range. When the variation of CD-induced signal intensity upon the ligand binding is sufficiently high as it is in the presence of DNA from *clostridium* (see Figure 2), the variation of the signal



**Figure 1.** Circular dichroism spectra of (a) *clostridium perfringens* and (b) *micrococcus lysodeikticus* DNAs in the presence of increasing concentrations of compound 5a. Assay medium was composed of 10 mM cacodylate buffer (pH 7.0), 0.1 M NaCl, and 70  $\mu$ M DNA.  $r'$  (ligand to nucleotide ratio) was from 0 to 0.1.



**Figure 2.** Ellipticity at 315 nm of ligand-DNA complexes as function of ligand concentration. (a) Netropsin-induced ellipticity in the presence of *clostridium* DNA (♦) and *micrococcus* DNA (◇). (b) Netropsin derivative-induced ellipticity in the presence of *clostridium* DNA (5a (■), 5b (▲)) and *micrococcus* DNA (5a (□), 5b (Δ)). The operating conditions were as indicated in the legend of Figure 1.  $r'$  indicates ligand to nucleotide ratio.

**Table 1. Comparative DNA Binding Parameters of Netropsin, Distamycin, and the Related Hybrid Molecules**

compd	$K_{app}^a$ ( $M^{-1}$ )	slope <sup>b</sup>
netropsin	$1.0 \times 10^6$	-0.03
5a	$4.6 \times 10^5$	0.10
9a	$4.4 \times 10^5$	0.00
distamycin	$1.0 \times 10^7$	0.00
5b	$1.6 \times 10^6$	0.15
9b	$1.2 \times 10^6$	0.05

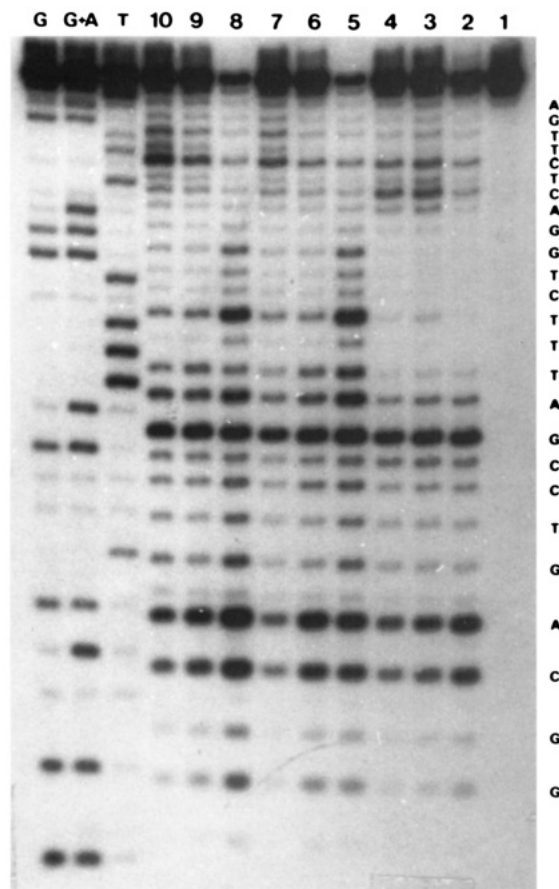
<sup>a</sup> The association constants of the hybrid ligands for DNAs were estimated from CD spectra and Scatchard analysis as described in the Experimental Section. <sup>b</sup> Slope of the straight line given by the equation  $\log \nu/\nu_0 = k \log(1 + 2r)$  which account for the increase in the viscosity of sonicated DNA as function of the amount of ligand bound ( $r$ ). In standard operating conditions, the experiments were performed in acetate buffer pH 5.0 containing 100 mM NaCl.

intensity as a function of the concentration of compound present in the medium can be treated as a binding curve from which the amount of compound bound to the DNA can be calculated (see Experimental Section). Scatchard plots of these data allow one to estimate the association constant value  $K_{app}$ . The values so obtained are indicated in Table 1 and show that the  $K_{app}$  values of the respective hybrid molecules to *clostridium* remain in the same order of magnitude compared to netropsin and distamycin.

**Viscometric Data.** Information on the nature of the binding to DNA (intercalation versus external binding) can be provided by the viscometric determination of the length increase of sonicated DNA (Saucier et al., 1971).

In this technique, the theoretical treatment of viscosimetric data have shown that if  $\log \rho/\rho_0$  is plotted vs  $\log(1 + 2r)$  where  $\rho$  and  $\rho_0$  are the intrinsic viscosity of sonicated DNA in the presence and in the absence of the tested drug and  $r$  the number of molecules bound per nucleotides, the slope value of the straight line so obtained is expected to be near 2.2 for intercalating agents (Saucier et al., 1971). It was found that the slope values obtained upon binding of the tested compounds to DNA isolated from *Clostridium* are in the range of 0.10 to 0.20 (Table 1). These results indicate that for all tested molecules the isoalloxazine chromophore is not able to intercalate between DNA base pairs.

**Footprinting Experiments.** According to quantitative footprinting data (Ward et al., 1988), it appears that netropsin preferentially protects the 5'ATTT sequence. We have therefore synthesized a 25-mer containing this target sequence included within a random sequence. Typical DNaseI-induced cleavage patterns for the 25-mer of the synthetic oligonucleotide fragment are presented in Figure 3. Experiments performed in the presence of netropsin or distamycin (from  $10^{-6}$  to  $10^{-5}$ M) show a very strong protection against cleavage located at the target site 5'ATTT. It should be noticed that the adjacent 5'CTGG sequence appears to be efficiently protected as well. This fragment corresponds to the binding site of the enzyme whose 3'  $\rightarrow$  5' processing is blocked by the presence of the ligand bound to the target site ATTT. In the presence of identical concentrations of tested compounds,



**Figure 3.** Autoradiogram of a DNase I footprinting experiment of 25 base-pair oligonucleotide in the absence and in the presence of netropsin, **9a**, and **5a**. Lane 1: oligonucleotide alone. Lanes 5 and 8: DNase digest (3 and 5 min, respectively) of the oligonucleotide alone. Lanes 2–4: DNase I digests (3 min) in the presence of 1, 5, and 10  $\mu$ M netropsin. Lanes 6 and 7: digests (3 min) in the presence of 5 and 10  $\mu$ M compound **9a**. Lanes 9 and 10: digests (3 min) in the presence of 5 and 10  $\mu$ M **5a**. In all experiments, DNA digestion was performed at 4 °C in working buffer (pH 7.0).

**Table 2.** Protection against DNase I Digest (%)<sup>a</sup>

sequence	netropsin	distamycin	<b>5a</b>	<b>5b</b>	<b>9a</b>	<b>9b</b>
A	82	95	60	82	80	56
T	100	100	70	100	100	72
T	100	100	100	100	100	100
T	94	100	85	100	89	100

<sup>a</sup> Protection against the DNase I digest of the ATTT sequence in the presence of 10<sup>-6</sup> M ligands. The extent of DNase I digestion was estimated by scanning the PAGE autoradiogram of the 5'-labeled 25-mer digest as described in the Experimental Section. For each nucleotide, the percent of protection was calculated compared to the extent of DNase I digestion obtained in the absence of ligand.

the target site appears to be markedly protected as well but to a lower extent. Table 2 summarizes the efficiency of protection of the target site against DNase I expressed in percent. The values obtained show that all hybrid compounds display a similar pattern of protection, the adenine being the less protected base and the central thymine the most protected one. From these results it can be concluded and in agreement with CD data that despite the modification of the netropsin or distamycin moiety, the hybrid compounds have preserved the ability to selectively recognize A + T-containing sequences.

**Generation of Oxy Radicals upon Visible Light Irradiation.** The generation of oxy radicals (superoxide anion and OH<sup>•</sup> radical) upon illumination of solutions containing flavin is known to occur through a redox cycling

**Table 3.** Production of Oxy Radicals upon Illumination by Visible Light

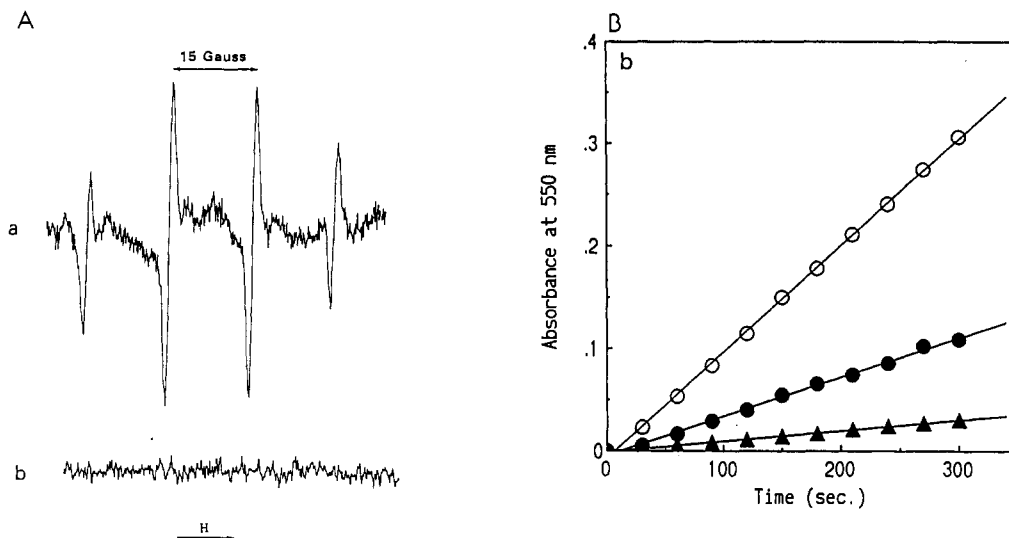
compd	detection of DMPO-OH <sup>a</sup>	production of O <sub>2</sub> <sup>•-</sup> <sup>b</sup> (nmol/min/nmol)
<b>5a</b>	+	0.73
<b>9a</b>	+	1.67
<b>5b</b>	+	0.88
<b>9b</b>	+	4.10

<sup>a</sup> Occurrence of the ESR quartet signal of the DMPO spin adduct DMPO-OH. Operating conditions were as described in the Experimental Section. Assay medium was composed of phosphate buffer 0.05 M, pH 8.0 containing 1 mM EDTA, 10  $\mu$ M drug, and 50 mM DMPO. Irradiation time was 5 min. In all cases, no signal can be detected in the presence of 10  $\mu$ g of SOD. <sup>b</sup> O<sub>2</sub><sup>•-</sup> production was measured using SOD-inhibitable cytochrome c reduction. The assay medium was described as in the legend of Figure 4. O<sub>2</sub><sup>•-</sup> production was calculated assuming that 1 mol of O<sub>2</sub><sup>•-</sup> reduces 1 mol of cytochrome c. The molecular extinction of cytochrome c FII at 550 nm was taken as 22 000 M<sup>-1</sup> cm<sup>-1</sup>.

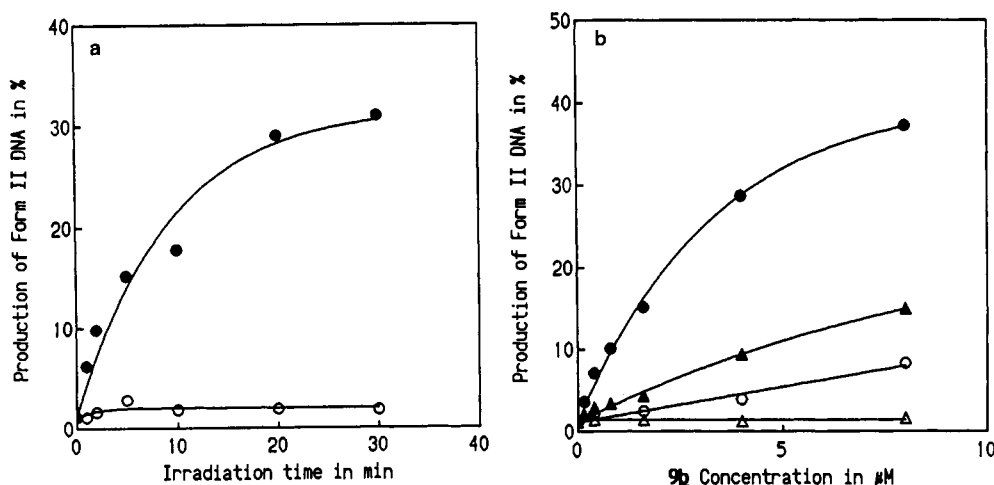
process involving as an initial step the photoreduction of the flavin triplet state. This reaction is followed by the reoxidation of the reduced form of the flavin chromophore through one-electron transfer process to molecular oxygen (Ballou et al., 1969). The photoreduction of flavin requires the presence of additional electron donor such as EDTA- or thiol-containing compounds. DNA and to a lesser extent RNA, have been suggested as well to act as electron donor in this reaction (Korycka-Dahl and Richardson, 1980). We have measured the flux of O<sub>2</sub><sup>•-</sup> production using as a probe the superoxide dismutase-inhibitable cytochrome c reduction (McCord et al., 1977), assuming that one molecule of O<sub>2</sub><sup>•-</sup> is required to reduce one molecule of cytochrome c.

Results in Figure 4b and Table 3 show that in our experimental conditions the irradiation of 5  $\mu$ M of any tested compounds results in the production of O<sub>2</sub><sup>•-</sup>. Clearly, the flux of O<sub>2</sub><sup>•-</sup> is significantly higher using compounds **9a** and **9b** in which the side chain is attached in the N<sub>10</sub> position of the flavin chromophore as in the natural compound riboflavin. In order to test the further occurrence of hydroxyl-radical production we have performed a spin trapping experiment using DMPO as probe (Buettner and Oberley, 1978). As indicated in Figure 4a, the DMPO-OH spin adduct (1:2:2:1 quartet, *g* = 2.007, *a<sub>N</sub>* = 14.8 G) resulting from the reaction between OH<sup>•</sup> and the DMPO is generated upon light irradiation of compound **9b** taken as an example. The signal intensity is strongly decreased by the addition of SOD or catalase indicating that both O<sub>2</sub><sup>•-</sup> and H<sub>2</sub>O<sub>2</sub> are involved in the production of OH<sup>•</sup>.

**DNA Breaks.** In the presence of molecular oxygen, the irradiation by visible light of a solution containing 5  $\mu$ mol of the most efficient oxy radical generator, compound **9b**, 1 mM EDTA, and supercoiled DNA, yields nicked circular form II DNA. The kinetics of the appearance of single-strand break occurs according to a pseudo-first-order reaction with an apparent rate constant of 0.11 min<sup>-1</sup> (Figure 5a). For a given irradiation time, the extent of DNA cleavage increases as a function of ligand concentration as shown in Figure 5b. The generation of form II is strongly inhibited by the addition of catalytic amounts of superoxide dismutase (SOD), whereas the addition of catalase or the OH radical scavenger mannitol result as well in a marked inhibition of the DNA strand breakage (data not shown). These observations are in agreement with the involvement of OH<sup>•</sup> radical as the main DNA breaking agent. Because of the marked inhibitory action of SOD, it is likely, as suggested by the spin-trapping experiments, that the production of OH<sup>•</sup> occurred through



**Figure 4.** Oxy radicals production upon irradiation of **9b** by visible light. (A) ESR spectra of the spin trap DMPO. The assay medium was composed of 0.05 M phosphate buffer (pH 8.0) containing 1 mM EDTA, 50 mM DMPO, and 10  $\mu$ M **9b**. The spectra were recorded after a 5-min irradiation performed either in the absence (a) or in the presence (b) of 10  $\mu$ g SOD. (B) Kinetics of **9b**-mediated cytochrome c reduction. The assay medium was composed of phosphate buffer 0.05 M (pH 8.0) containing 1 mM EDTA, 0.1 mM cytochrome c, and 10  $\mu$ M **9b**.  $\circ$  indicates with irradiation alone,  $\bullet$  with irradiation and in the presence of 0.5  $\mu$ g/mL SOD, and  $\blacktriangle$  with irradiation and in the presence of 1  $\mu$ g/mL SOD.



**Figure 5.** **9b**-mediated single strand break of pBR322 plasmid upon visible light irradiation. Strand breakage was monitored in phosphate buffer 0.05 M (pH 8.0) containing 1 mM EDTA, 30  $\mu$ M plasmid DNA, and various concentrations of **9b**. The mixtures were irradiated using a polychromatic lamp yielding an energy of the incident light close 1.5 W·cm<sup>-2</sup>. (a) Kinetics of form II production upon irradiation of a mixture as indicated above, in the absence  $\circ$  or in the presence of 5  $\mu$ M compound **9b**  $\bullet$ . (b) DNA form II production obtained after 30-min irradiation and in the presence of increasing concentrations of **9b**.  $\bullet$  indicates the standard conditions,  $\blacktriangle$  the presence of 0.5  $\mu$ g SOD,  $\circ$  the presence of 1  $\mu$ g SOD, and  $\triangle$  standard conditions without light.

**Table 4.** Extent of pBR322 Form II Generation upon Light Irradiation<sup>a</sup>

compd	production of form II DNA (%)
<b>5a</b>	4.3
<b>9a</b>	7.9
<b>5b</b>	4.8
<b>9b</b>	27.6

<sup>a</sup> Form II DNA was estimated from the fluorescent corresponding band intensity detected on gels stained with ethidium bromide as shown in Figure 5a. Form II production was estimated after 20-min light irradiation of solutions containing 5  $\mu$ M of each tested compound.

a classical Fenton reaction (Fee and Valentine, 1977). Similar behavior is obtained using compounds **5a**, **9a**, and **5b**. However, the extent of DNA breakage as measured in standard operating conditions appears to be related to the oxy radicals generating efficiency as shown in Table 4.

**Mapping of the Strand Cleavage of pBR322 DNA.** The experimental procedure used to map the single-strand

cleavage sites of oxy radicals involves the following steps (Barton and Raphael, 1985): the remaining form I and nicked circles were linearized with restriction enzymes known to cleave the plasmid at only one site. Subsequent treatment of the linearized DNAs with nuclease S1 which is specific for single-stranded regions cleaved the DNA at sites only opposite to the nick, producing a pair of linear fragments. This procedure yields distinct fragments only if single strand cleavage occurs at specific sites. Non-specific cleavage produces fragments of all sizes and hence a smear on the gel.

The treatment of the mixture containing supercoiled and form II DNA by the restriction enzyme EcoRI yields complete linear digests as evidenced by the appearance of a single band of 4.4 kbp. The subsequent treatment of the linearized fragments from untreated DNA by nuclease S1 results, as expected, in no detectable change in the size and intensity of the single band of linear DNA. Similar treatment of the linearized DNA fragment from single-



**Table 5. Mapping of the Strand Cleavage of the pBR322 DNA Promoted by Compound 5a**

sequence <sup>a</sup>	position <sup>b</sup>	approx size of the discrete bands <sup>c</sup>
AAAAAA	4113	4100
AAAAAA	3697	3700
TATTAATT	3536	3500
AAAAAA	3107	3100
AAAAA	2571	
		2430 <sup>d</sup>
AAAAA	2514	
AAAAAA	1929	1900 <sup>d</sup>

<sup>a</sup> Main AT-rich sequences identified on pBR322. <sup>b</sup> Position of the AT-containing sequences on the plasmid starting from Eco RI site.

<sup>c</sup> Sizes of the discrete bands separated on agarose gel following linearization of the plasmid by Eco RI and subsequent treatment with nuclease S1 as described in the Experimental Section. <sup>d</sup> Possible complementary bands resulting from breaks at either 1900 or 2500 bp.

strand breaks containing DNA results in a strong decrease in the intensity of the 4.4 kbp band with the appearance of discrete bands indicating that the breaks occurred preferentially at the level of defined sequences. In contrast, the irradiation of mixtures containing DNA and concentrations of riboflavin leading to identical oxy radicals flux results in the appearance of smear on the gel as expected for randomly distributed DNA breakages (data not shown). The sizes of the bands obtained with the conjugates allow a rough estimation of the position of the cleavage. Table 5 summarizes the results obtained in the presence of 5a.

Five fragments of approximate size of 4100, 3700, 3500, 3100, and 1900 bp were clearly detected and correspond to breaks occurring in regions composed of at least five AT bp tracks (Table 5). This is in agreement with the selective binding of the hybrid ligands to these sequences and the occurrence of breakages in the vicinity of the binding sites. A very similar pattern of breakages was observed in the presence of the distamycin derivative 9b.

In conclusion, the present work demonstrates the suitability of isoalloxazine chromophore in view of functionalization of selective DNA-binding ligands such as polypyrrrolecarboxamide derivatives. The conjugates so obtained remain able to bind to double-stranded DNA preferentially to A + T-rich regions. The isoalloxazine chromophore remains able to produce oxy radicals leading to single-strand breakage in the vicinity of DNA-binding sites in operating conditions compatible with pharmacological constraints. This approach can be extended to the functionalization of various DNA-binding ligands including to antisens and triplex-forming oligonucleotides.

#### ACKNOWLEDGMENT

This work was supported by grant (to S.G.-R.) from the Association pour la Recherche sur le Cancer (ARC) and by grant from the Agence Nationale pour la Recherche sur le SIDA (ANRS) (to C.A.). The authors express their gratitude to Dr. A. Deroussent for mass spectra recording.

#### LITERATURE CITED

- Ballou, D., Palmer, G., and Massey, V. (1969) Direct demonstration of superoxide anion production during the oxidation of reduced flavin and of its catalytic decomposition by erythrocuprein. *Biochem. Biophys. Res. Commun.* 36, 898–904.
- Barton, J. K., and Raphael, A. L. (1985) Site specific cleavage of left-handed DNA in pBR322 by tris-(diphenylphenantrolin)-Co(III). *Proc. Natl. Acad. Sci. U.S.A.* 82, 6460–6464.

- Bialer, M., Yagen, B., and Mechoulam, R. A. (1978) Total synthesis of distamycin A, an antiviral antibiotic. *Tetrahedron* 34, 2389–2391.
- Bialer, M., Yagen, B., and Mechoulam, R. A. (1980) Elucidation of a condensation product of 4-aminopyrrole derivatives and dicyclohexylcarbodiimide. *J. Heterocycl. Chem.* 17, 1797–1798.
- Buettner, G. R., and Oberley, L. W. (1978) Consideration in the spin trapping of superoxide and hydroxyl radical in aqueous system using DMPO. *Biochem. Biophys. Res. Commun.* 83, 69–73.
- Castro, B., Dormoy, J. R., Dourtoglov, B., Evin, E., Selve, C., and Ziegler, J. C. (1976) Peptide coupling reagents VI. A novel cheaper preparation of benzotriazoloxyltris (dimethylamino)-phosphonium hexafluorophosphate (BOP reagent). *Synthesis* 751–752.
- Debard, F., Perigaud, C., Gosselin, G., Mrani, D., Rayner, B., Le Ber, P., Auclair, C., Balzarini, J., De Clercq, E., Paoletti, C., and Imbach, J. L. (1989). Minor groove binding agents: synthesis and studies of bithiazole-linked netropsin derivatives. *J. Med. Chem.* 32, 1074–1083.
- Dervan, P. B. (1986) Design of sequence specific DNA-binding molecules. *Science* 232, 464–471.
- Fee, J. A., and Valentine, J. S. (1977) Chemistry of O<sub>2</sub><sup>•-</sup>. In *Superoxide and Superoxide dismutase* (Michelson, A. M., McCord, J. M., and Fridovich, I., Eds.) p 19, Academic Press, New York.
- François, J. C., Saison-Behmoaras, T., Barbier, C., Chassignol, M., Thuong, N. T., and Hélène, C. (1988) Sequence-specific recognition and cleavage of duplex DNA via triple helix formation by oligonucleotides covalently linked to phenanthroline-copper chelate. *Proc. Natl. Acad. Sci. U.S.A.* 86, 9702–9706.
- Föry, W., Mac Kenzie, R. E., and McCormick, D. B. (1968) Flavinyll peptides; I. Synthesis of flavinyll-aromatic amino acids. *J. Heterocycl. Chem.* 5, 625–630.
- Föry, W., Mac Kenzie, R. E., Ying-Hsiueh Wu, F., and McCormick, D. B. (1970) Flavinyll peptides. III. Studies of intramolecular interactions in flavinyll aromatic amino-acids by proton magnetic resonance. *Biochem. J.* 99, 515–525.
- Grande, H. J., van Schagen, C. G., Jarbandhan, T., and Müller, F. (1977) An <sup>1</sup>H-NMR spectroscopic study of alloxazines and isoalloxazines. *Helv. Chim. Acta* 60, 348–366.
- Hahn, F. E. (1975) *Antibiotics III. Mechanism of Action of Antimicrobial and Antitumoral Agents* (Corcoran, J. W., and Hahn, F. E., Eds.) p 79, Springer-Verlag, New York.
- Hemmerich, P. (1958) Syntheses in the Lumiflavin Series III. *Helv. Chim. Acta* 41, 514–520.
- Hemmerich, P., Prijs, B., and Erlenmeyer, H. (1960) Studies in the Lumiflavin Series VI. Alkylation and Disalkylation Reactions of (Iso)alloxazines: 1,3,10-Trimethylflavosemiquinone. *Helv. Chim. Acta* 43, 372–394.
- Kopka, M. L., Yoon, C., Goodsell, D., Pjura, P., and Dickerson, R. E. (1985) Binding of an antitumoral drug to DNA: Netropsin and C-G-C-G-A-A-T-T-B<sup>+</sup>C-G-C-G. *J. Mol. Biol.* 183, 553–563.
- Korycka-Dahl, M., and Richardson, T. (1980) Photodegradation of DNA with fluorescent light in the presence of riboflavin and photoprotection by flavin triplet state quenchers. *Biochim. Biophys. Acta* 610, 229–234.
- Kuhn, R., and Weygand, F. (1934a) Synthesis of 9-Methylisoalloxazines. *Ber.* 67, 1409–1413.
- Kuhn, R., Reinemund, K., and Weygand, F. (1934b) Synthesis of Lumilactoflavins. *Ber.* 67, 1460–1463.
- Kuhn, R., and Reinemund, K. (1934c) Upon the Synthesis of 6,7,9-Trimethylflavins (Lumilactoflavins). *Ber.* 67, 1932–1936.
- Ljungquist, A., and Folkers, K. (1988) The reaction of pyridinecarboxylic acids with dicyclohexylcarbodiimide and *p*-nitrophenol. *Acta Chem. Scand. B* 42, 408–410.
- Lown, J. W., and Krowicki, K. (1985) Efficient total syntheses of the oligopeptide antibiotics netropsin and distamycin. *J. Org. Chem.* 50, 3774–3779.
- Maniatis, T., Fritsch, E. F., and Sambrook, J. *Molecular Cloning: A Laboratory Manual*, Vol. 1, Cold Spring Harbor Laboratory, Cold Spring Harbor, NY.

- McCord, J. M., Crapo, J. D., and Fridovich, I. (1977) Superoxide dismutase assay. *Superoxide and Superoxide dismutase* (Michelson, A. M., McCord, J. M., and Fridovich, I. Eds.) p 11, Academic Press, New York.
- Michelson, A. M. (1977) Chemical production of superoxide anions by reaction between riboflavin, oxygen and reduced nicotinamid adenin dinucleotide. *Superoxide and Superoxide dismutase* (Michelson, A. M., McCord, J. M., and Fridovich, I., Eds.) p 87, Academic Press, New York.
- Misra, H. P., and Fridovich, I. (1972) The univalent reduction of oxygen by reduced flavins and quinones. *J. Biol. Chem.* 247, 188-192.
- Moser, H. E., and Dervan, P. B. (1987) Sequence specific cleavage of double helical DNA by triple helix formation. *Science* 238, 645-650.
- Penco, S., Redaelli, S. and Arcamone, F. (1967) Distamicine A-Nota II. sintesi totale. (Distamycin A. II. Total synthesis). *Gazz. Chim. Ital.* 97, 1110-1115.
- Saucier, J. M., Festy, B. and Le Pecq, J. B. (1971) The change of the torsion of the DNA helix caused by intercalation. *Biochimie* 53, 973-976.
- Schultz, P. G., Taylor, J. S., and Dervan, P. B. (1982) Design and synthesis of sequence specific DNA cleaving molecules: (Distamycin-EDTA) iron(II). *J. Am. Chem. Soc.* 104, 6861-6863.
- Subra, F., Carteau, S., Pager, J., Paoletti, J., Paoletti, C., Auclair, C., Mrani, D., Gosselin, G., and Imbach, J. L. (1991) Bis (pyrrolocarboxamide) linked to intercalating chromophore oxazolopyridocarbazole (OPC): selective binding to DNA and polynucleotides. *Biochemistry* 30, 1642-1650.
- Takeda, J., Ohta, S., and Hirobe, M. (1987) Synthesis and characterization of novel flavin-linked porphyrins. Mechanism for flavin-catalyzed inter- and intramolecular 2e/1e electron-transfer reactions. *J. Am. Chem. Soc.* 109, 7677-7688.
- Ward, B., Rehfuess, R., and Dabrowiak, J. C. (1988). Determination of netropsin-DNA binding constants from footprinting data. *Biochemistry* 27, 1198-1205.
- Youngquist, R. S., and Dervan, P. B. (1985) Sequence specific recognition of DNA by oligo(N-methylpyrrolocarboxamide). *Proc. Natl. Acad. Sci. U.S.A.* 82, 2565-2569.
- Zimmer, C. (1975) Effects of the antibiotics netropsin and distamycin A on the structure and function of nucleic acids. *Prog. Nucl. Ac. Res. Mol. Biol.* 15, 285-318.

## In Vivo Activities of Acidic Fibroblast Growth Factor-*Pseudomonas* Exotoxin Fusion Proteins

Clay B. Siegall,\* Susan L. Gawlak, Dana F. Chace, June R. Merwin,<sup>†</sup> and Ira Pastan<sup>‡</sup>

Bristol-Myers Squibb, Pharmaceutical Research Institute, Molecular Immunology Department, 3005 First Avenue, Seattle, Washington 98121, and Laboratory of Molecular Biology, National Cancer Institute, National Institutes of Health, Bethesda, Maryland 20892. Received June 18, 1993\*

Fibroblast growth factor receptors are highly expressed in a variety of cancer cells and activated vasculature. Using chimeric toxins targeted to cell-surface aFGF receptors, we have demonstrated specific cytotoxic activity to these cell types. These molecules, aFGF-PE40 and aFGF-PE4E KDEL, are fusion proteins containing acidic FGF and either a 40- or a 66-kDa binding defective form of *Pseudomonas* exotoxin, respectively. Both aFGF-toxin fusion proteins were able to inhibit protein synthesis *in vitro* in a variety of carcinoma cell lines. The half-life of aFGF-PE40 in serum was found to be 41 min when coadministered with heparin. Administration of aFGF-PE40 or aFGF-PE4E KDEL with heparin inhibits the growth of established KB and preestablished A431 epidermoid carcinoma xenografts in athymic mice. The antitumor activities of the two aFGF-toxin fusion proteins were equivalent against the KB tumor xenografts. While we were able to slow the growth of the KB tumor xenografts, we were unable to cause tumor regressions. Histochemical analysis of treated versus untreated tumor tissue revealed a difference in tumor size but not of vascularity. We conclude that aFGF-PE40 and aFGF-PE4E KDEL have *in vivo* antitumor activity that targets the tumor cell mass rather than vascular structures in mice xenografted with human epidermoid carcinoma.

### INTRODUCTION

*Pseudomonas* exotoxin (PE) is a single polypeptide made up of three structurally and functionally distinct domains (1, 2). Domain I contains the cell-binding activity, domain II the translocation activity, and domain III the ADP-ribosylation activity. PE kills cells by ADP-ribosylating elongation factor 2, resulting in inhibition of cellular protein synthesis. Alteration in the binding domain of PE results in a loss of cytotoxic activity against cells displaying PE receptors (3-5). Replacing the lost binding activity with a growth factor through fusion with the mutant PE molecule restores its cytotoxic activity but redirects the toxin to a specific growth factor receptor (6-8).

We have recently reported on the cytotoxic activity of fusion proteins composed of acidic fibroblast growth factor (aFGF) and two mutant forms of *Pseudomonas* exotoxin A (PE) against a variety of cancer cell lines (9). FGF-toxin fusion proteins were produced to target FGF receptors that have been found in high numbers on cancer cells (10, 11). The specific aFGF-PE chimeric molecules were termed aFGF-PE40 and aFGF-PE4E KDEL. PE40 is a truncated form of PE that is missing the binding domain (domain I) but retains domains II and III (3, 12). PE4E is a mutated form of PE in which four glutamates in domain I have been substituted in place of four positively charged residues. This form of PE is the functional equivalent of PE40 (13). The KDEL sequence, which encodes the endoplasmic reticulum retention sequence, is substituted at the carboxyl end of aFGF-PE4E KDEL in place of the native REDLK residues to increase the cytotoxicity of the molecule (14, 15). Chimeric toxins of

this type include TGF $\alpha$ -PE40, IGF TYPE I-PE40, and aFGF-PE40 (9, 16-18), all employing *Pseudomonas* toxin, and EGF-DAB, utilizing a mutated form of Diphtheria toxin (19).

Growth factor-toxins have been shown to be effective antitumor reagents against human tumor xenografts implanted in mice (20-22). In this report, we have explored the effects of the two aFGF-PE forms in the treatment of established and preestablished tumor xenografts in athymic mice. Our findings indicate that it is possible to target tumor cells for elimination using toxins directed at the aFGF receptor.

### EXPERIMENTAL PROCEDURES

**Animals and Cell Lines.** For all experiments performed in animals, 6-week-old athymic mice weighing 16-20 g were used (strain BALB/c, Harlan Sprague-Dawley, Indianapolis, IN). MCF-7 (breast carcinoma cells) and A431 and KB (epidermoid carcinoma cells) were purchased from American Type Culture Collection (Rockville, MD). L2987 (lung carcinoma cells), A2780 (ovarian carcinoma cells), and RCA (colon carcinoma cells) were from I. Hellström (Bristol-Myers Squibb, Pharmaceutical Research Institute, Seattle, WA).

**Plasmids and Constructions.** The plasmids pCSF40 F(+)/T and pCS F4K F(+)/T were previously described (9). The plasmid pCS F4KD<sup>553</sup> encodes a mutant form of aFGF-PE4E KDEL that has no ADP-ribosylation activity due to its single amino acid deletion at residue 553 (glutamate) in the PE sequence (23, 24). Plasmid pCS F4KD<sup>553</sup> was prepared by digesting pCSF4K at its BamHI and EcoRI sites, removal of the resulting 0.45-kb fragment, and replacement with a similar 0.45-kb fragment from pCSF40D<sup>553</sup> (9).

**Expression and Purification of aFGF-Toxins.** Plasmids were transformed with bacterial strain BL21 ( $\lambda$ DE3) and cultured as previously described (9). The fusion toxins were induced at OD<sub>650</sub> = 2.0 with 1 mM isopropyl 1-thio- $\beta$ -D-galactopyranoside (IPTG) and har-

\* To whom correspondence should be addressed.

<sup>†</sup> Present address: TargeTech Inc., 290 Pratt St., Meriden, CT 06450.

<sup>‡</sup> National Cancer Institute.

\* Abstract published in *Advance ACS Abstracts*, December 1, 1993.

vested 90 min later. The protein was purified from inclusion bodies by denaturation in guanidine-HCl and renaturation by rapid dissolution in phosphate-buffered saline supplemented with 0.4 M L-arginine. The renatured proteins were purified by a two-step chromatography procedure involving anion-exchange followed by heparin-affinity, as previously described (9).

**Protein Synthesis Inhibition Assay.** The tumor cells were cultured in RPMI 1640 supplemented with 10% fetal bovine serum, 2 mM L-glutamate, and 50 units/mL of penicillin/streptomycin. The cell monolayers were plated into 96-well tissue culture plates at  $1 \times 10^4$ /well and allowed to adhere and grow for 16 h at 37 °C. Chimeric aFGF-toxins were diluted in growth media and 0.1 mL added to each well for 20 h at 37 °C. The cells (assay done in triplicate or quadruplicate) were pulsed with [ $^3$ H]leucine (1  $\mu$ Ci/well) for an additional 4 h at 37 °C. The cells were harvested using a 96-well automated system (Tomtec, Orange, CT) after freeze-thawing of the plate. Protein synthesis was determined by counting the incorporation of [ $^3$ H]leucine into cellular protein using an LKB-Beta-Plate liquid scintillation counter.

**Serum Level of aFGF-PE40 (+ Heparin).** Five pairs of athymic mice were injected intravenously with a single dose of aFGF-PE40 (0.5 mg/kg, 100 units/mL of heparin). At indicated time points, each pair of injected animals was bled (200  $\mu$ L each bleeding). The blood was kept on ice for 15 min and centrifuged at 2000 rpm in a 4 °C microfuge. The serum was retained and tested in an inhibition of protein synthesis assay with MCF-7 breast carcinoma cells to determine the amount of aFGF-PE40 protein present in each sample. The amount of protein synthesis inhibition found in the serum samples at various time points was compared to a standard curve of aFGF-PE40 (+ heparin) against the same MCF-7 cells. The protein synthesis assay was performed essentially the same as above.  $T_{1/2\alpha}$  was calculated using the MKModel Version 4 software package (Biosoft, Milltown, N. J.).

**Lethality of aFGF-Toxins in Athymic Mice.** Groups of five mice were injected intravenously with either aFGF-PE40 or aFGF-PE4E KDEL. The aFGF-toxin protein was injected in PBS supplemented with 100 units/mL of heparin. The animals were observed for 21 days.

**Necropsy Analysis.** Tissues from major organs, including lungs, kidney, liver, stomach, duodenum, ileum, cecum, and spleen were removed from sacrificed animals 48 h after injection of 1.5 mg/kg of aFGF-PE40 in PBS supplemented with 100 units/mL of heparin. The tissues were fixed in 10% formalin, blocked in paraffin, sectioned at 5  $\mu$ m, and stained with hematoxylin and eosin.

**Antitumor Activity of aFGF-PE40 and aFGF-PE4E KDEL.** KB and L2987 tumor fragments were implanted into female athymic mice (nu/nu) at 4–6 weeks of age with tumor fragments maintained from serial *in vivo* passage of established xenografts. Approximately 2 weeks following subcutaneous implantation of the tumor fragments onto the back of the mice, the mice were randomized for those with tumor sizes ranging from 75 to 100 mm<sup>3</sup>. The tumor-bearing animals were intravenously injected with the chimeric aFGF-toxins (with 100 units/mL of heparin) as per specific administration schedule via the tail vein. There were five animals in each treatment group, and tumors were measured on a 3–4-day regular schedule with calipers. A431 cells ( $1 \times 10^6$ ) were subcutaneously injected into groups of athymic mice. For treatment at day 1 post implant, animals could not be randomized due to tumor size. At day 5 post implant, animals were randomized

**Table 1. Cytotoxic Activities of aFGF-PE40 and aFGF-PE4E KDEL Chimeric Proteins on Various Cell Lines**

cell line (type)	EC <sub>50</sub> , <sup>a</sup> ng/mL			PE
	aFGF-PE40	aFGF-PE4EK <sup>b</sup>	aFGF-PE4EK <sup>b</sup> D <sup>563</sup>	
A2780 (ovarian Ca)	60	40	>500	90
L2987 (lung Ca)	200	150	>500	20
KB (epidermoid Ca)	60	50	>500	35
A431 (epidermoid Ca)	8	9	>500	6
RCA (colon Ca)	15	10	>500	32
MCF-7 (breast Ca)	40	10	>500	25

<sup>a</sup> EC<sub>50</sub> is the amount of aFGF-toxin needed to inhibit 50% of protein synthesis. <sup>b</sup> K = KDEL.

into groups of five based on the appearance of small A431 tumor nodules.

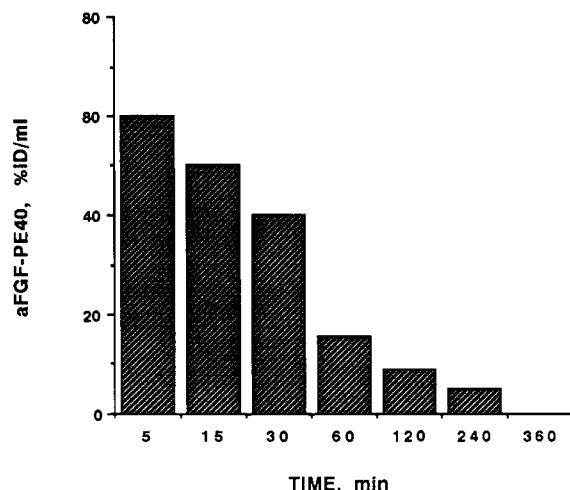
**Histologic Examination of Treated and Untreated Tumor Tissue.** Athymic mice were implanted with KB tumor sections as described above. Mice ( $\pm$  treatment with aFGF-PE40 (+heparin), 0.3785 mg/kg, 1 d  $\times$  3) were sacrificed 24 days post-tumor implant, and the tumors were removed. The tumor tissue was rinsed with PBS and cut into three longitudinal sections which were then fixed in 10% formalin. The samples were blocked in paraffin, sectioned at 8  $\mu$ m, and stained with hematoxylin and eosin prior to being mounted onto slides and inspected with light microscopy at (13X and 100X).

## RESULTS

**In Vitro Protein Synthesis Inhibition Activity.** The sensitivity of a variety of cancer cells to aFGF-PE40 and aFGF-PE4E KDEL was assessed. The two forms of aFGF-PE were active in inhibiting protein synthesis in A431, L2987, RCA, A2780, MCF-7, and KB carcinoma cell lines (Table 1). A431 cells were the most sensitive of the cell lines to both aFGF-toxin forms. A mutant form of aFGF-PE4E KDEL, termed aFGF-PE4E KDEL D<sup>563</sup>, in which there is no ADP-ribosylation activity, did not inhibit protein synthesis (EC<sub>50</sub> > 500 ng/mL) in any of the cell lines tested (Table 1).

**Serum Level Analysis of aFGF-PE40.** Since heparin has been shown to potentiate the biological effects of aFGF (25–28) and potentiate the cytotoxic activity of aFGF-toxins (29), heparin was coinjected with aFGF-PE40 in a serum level assay. Acidic FGF-PE40, with 100 units/mL of heparin, was injected via the tail vein into athymic mice. Blood was obtained at various times following injection, and the serum was isolated as described in the Experimental Procedures. The serum was diluted in growth media and compared to known amounts of aFGF-PE40 (and heparin) in a cytotoxicity assay against MCF-7 breast carcinoma cells. By comparing the protein synthesis inhibition activity of the serum samples with known amounts of aFGF-PE40, the amount of functional aFGF-PE40 present in the serum at different time points was determined. The data show that aFGF-PE40 can be recovered from blood when coadministered with heparin (Figure 1). The  $T_{1/2\alpha}$  of aFGF-PE40, with heparin coadministration, is 41 min. At 6 h post administration, there was no aFGF-PE40 detectable in the serum.

**Lethality in Athymic Mice.** Before assessing the ability of aFGF-PE to inhibit tumor growth *in vivo*, the maximum tolerated dose of the chimeric toxin was estimated by injecting the two different molecules intravenously in groups of five athymic mice. Different administration schedules and dose regimens were tested, and the results are listed in Table 2. Acidic FGF-PE4E KDEL was approximately 2–3-fold more lethal to mice



**Figure 1.** Serum levels and  $T_{1/2\alpha}$  of aFGF-PE40 in mice. Acidic FGF-PE40 levels were determined by measuring inhibition of protein synthesis with serum samples taken at various time points following injection of 0.5 mg/kg of aFGF-PE40 against MCF-7 breast carcinoma cells. These data were compared to an inhibition of protein synthesis assay using known amounts of aFGF-PE40 against the same cell line. Heparin was added to the injected aFGF-PE40 fusion protein at 100 units/mL. The  $T_{1/2\alpha}$  for aFGF-PE40 was 41 min.

**Table 2.** Maximum Tolerated Doses of aFGF-Toxin Fusion Proteins (Intravenous Injections) in Athymic Mice

dose (mg/kg)	adminstrn schedule	total dose (mg/kg)	lethality (%) (dead/total)
<b>aFGF-PE4E KDEL</b>			
0.25	single dose	0.25	0
0.375	single dose	0.375	0
0.5	single dose	0.5	40
0.625	single dose	0.625	100
0.25	q1d × 3	0.75	0
0.375	q1d × 3	1.125	40
0.375	q4d × 3	1.125	0
0.5	q4d × 3	1.5	80
<b>aFGF-PE40</b>			
0.5	single dose	0.5	0
1.0	single dose	1.0	0
1.5	single dose	1.5	20
2.0	single dose	2.0	80
0.5	q1d × 3	1.5	20
1.0	q1d × 3	3.0	80
0.5	q4d × 3	1.5	0
1.0	q4d × 3	3.0	60

than was aFGF-PE40. No lethality was observed at single-dose amounts of 0.375 mg/kg for aFGF-PE4E KDEL and 1.0 mg/kg for aFGF-PE40. Administration of larger total doses without lethality was possible using multiple injections of the aFGF-toxin fusion proteins (Table 2). Higher total doses of the fusion proteins could be given if an administration schedule of q4d × 3 was utilized rather than a schedule of q1d × 3.

**Toxicity of aFGF-PE40 toward Mouse Tissue.** The effects of aFGF-PE40 on normal cells was determined in mice since FGF receptors are widespread (30–32). Mice were injected with a single dose of a sublethal amount of aFGF-PE40 (1.5 mg/kg) and the mice sacrificed 48 h later so that necropsies could be performed. Histological analyses indicated significant organ damage in both the liver and spleen (data not shown). The liver cells showed marked polyploidy characterized by a wide variation in nuclear size and chromatin content. There were numerous mitotic figures, and many hepatocytes were binucleate. Additionally, there was a substantial number of nuclear and cytoplasmic remnants in a generalized distribution

within the liver sections analyzed. The spleen was enlarged, and there was excessive hematopoiesis. The red pulp was mildly congested, and the lymphoid follicles were enlarged as compared to nontreated mice. No toxicity was found in any of the other tissues analyzed.

**Antitumor Activity of aFGF-PE40.** To assess the *in vivo* antitumor activity of aFGF-toxins, KB cells were xenografted into athymic mice. While KB cells were not the most sensitive cell line tested in this study, aFGF-toxin fusion proteins were still quite cytotoxic to the cells, with  $EC_{50}$  values of 50–60 ng/mL (Table 1). Additionally, when passaged into animals using trocar-implanted tumor tissue, KB tumor xenografts grew into highly vascularized tumors in a very tight size range making for extremely reproducible experiments.

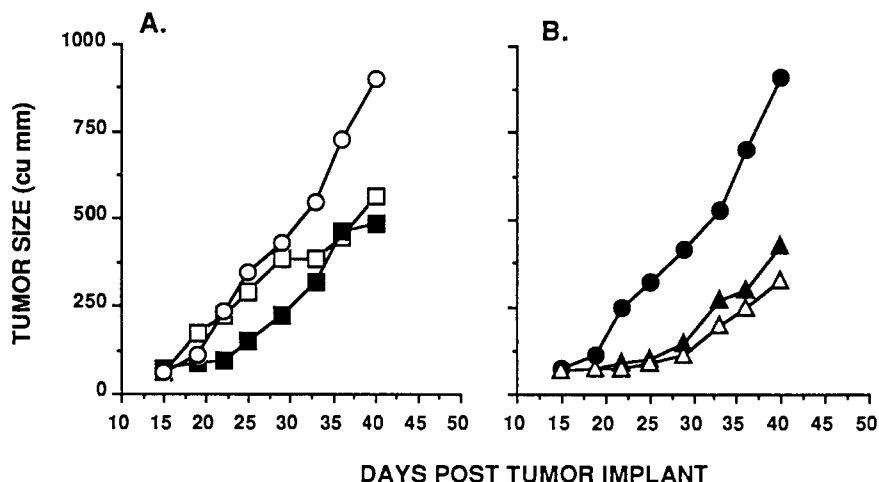
KB tumor cells were implanted into nude mice and allowed to grow until the tumor size was between 200 and 400 mm<sup>3</sup>. The tumor xenografts were serially sectioned and passaged into additional mice using a trocar. When the tumor xenografts were established and vascularized (approximately 75–100 mm<sup>3</sup>, 15–17 days following implantation), the mice were randomized and set into groups of five per cage. Mice were treated with intravenous injections of chimeric toxin supplemented with 100 units/mL of heparin, using a variety of administration schedules.

Acidic FGF-PE4E KDEL or aFGF-PE40 was administered using a treatment schedule of q1d × 3 (Figure 2A and B), respectively. Higher doses of aFGF-PE40 were used, as it was less toxic to the mice (Table 2). In Figure 2A, the experimental control was treatment with aFGF-PE4E KDEL D<sup>553</sup>, a noncytotoxic mutant form of aFGF-PE4E KDEL. In Figure 2B, untreated animals were the control. Tumor xenografts from these two control groups grew at essentially the same rate, indicating that the noncytotoxic aFGF-toxin form did not inhibit tumor growth. Administration of aFGF-PE4E KDEL at 0.25 mg/kg was able to inhibit tumor growth while a dose of 0.125 mg/kg had very little antitumor effect (Figure 2A). Surprisingly, at the lower dose of aFGF-PE4E KDEL, there was a slight inhibition of tumor growth, matching that of the higher dose from days 33–40. Administration of aFGF-PE40 was able to generate a stronger antitumor response as compared to aFGF-PE4E KDEL (Figure 2B). Mice with the KB xenografts were injected with both 0.375 and 0.25 mg/kg of aFGF-PE40, using the same q1d × 3 schedule. The antitumor effect was approximately the same for both doses.

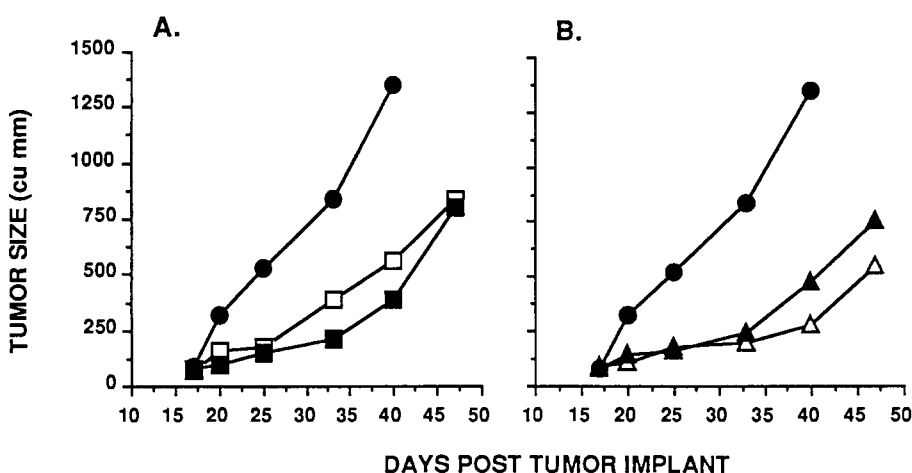
Higher doses of chimeric toxin could be administered to mice without toxicity by prolonging the time between doses. Figure 3 shows the effects of the fusion proteins using a q4d × 3 schedule. The antitumor activity of both aFGF-PE4E KDEL and aFGF-PE40 against the KB tumor xenografts was similar. With aFGF-PE4E KDEL at doses of 0.375 and 0.25 mg/kg, the antitumor activity was nearly identical (Figure 3A). The same was found for aFGF-PE40 (0.5 and 0.375 mg/kg) (Figure 3B).

As shown in both Figures 2 and 3, the KB tumor xenograft growth was significantly retarded by the administration of aFGF-PE40 or aFGF-PE4E KDEL. The effect on the tumor was most profound during the course of administration and for a short period following the treatment. This usually was found between days 15 and 30 post tumor implant. Following this period, the tumors grew back and had the appearance of a normal growing tumor. The most significant antitumor response came from the q4d × 3 administration of both aFGF-toxin forms,





**Figure 2.** Effect of aFGF-PE4E KDEL and aFGF-PE40 on human tumor xenografts in athymic mice, schedule 1. BALB/c athymic mice were subcutaneously implanted with KB tumor xenografts. When the tumors reached approximately 75 mm<sup>3</sup>, day 15, treatment was initiated. Intravenous administration, on a schedule of q1d  $\times$  3, was used. There were five mice per treatment group: (A) aFGF-PE4E KDEL (D<sup>553</sup> mutant) 0.375 mg/kg (○), aFGF-PE4E KDEL 0.125 mg/kg (□), aFGF-PE4E KDEL 0.25 mg/kg (■); (B) aFGF-PE40 0.25 mg/kg (▲), aFGF-PE40 0.375 mg/kg (Δ), nontreated controls (●). Heparin was added in all administrations at 100 units/mL.



**Figure 3.** Effect of aFGF-PE4E KDEL and aFGF-PE40 on human tumor xenografts in athymic mice, schedule 2. KB tumor xenografts were implanted as in Figure 2. Treatment was initiated day 17 post tumor implant. Intravenous administration of aFGF-toxin (+ heparin, 100 units/mL), on a schedule of q4d  $\times$  3, was used. There were five mice per treatment group: (A) aFGF-PE4E KDEL 0.375 mg/kg (□), aFGF-PE4E KDEL 0.25 mg/kg (■), nontreated controls (●); (B) aFGF-PE40 0.375 mg/kg (▲), aFGF-PE40 0.5 mg/kg (Δ), nontreated controls (●).

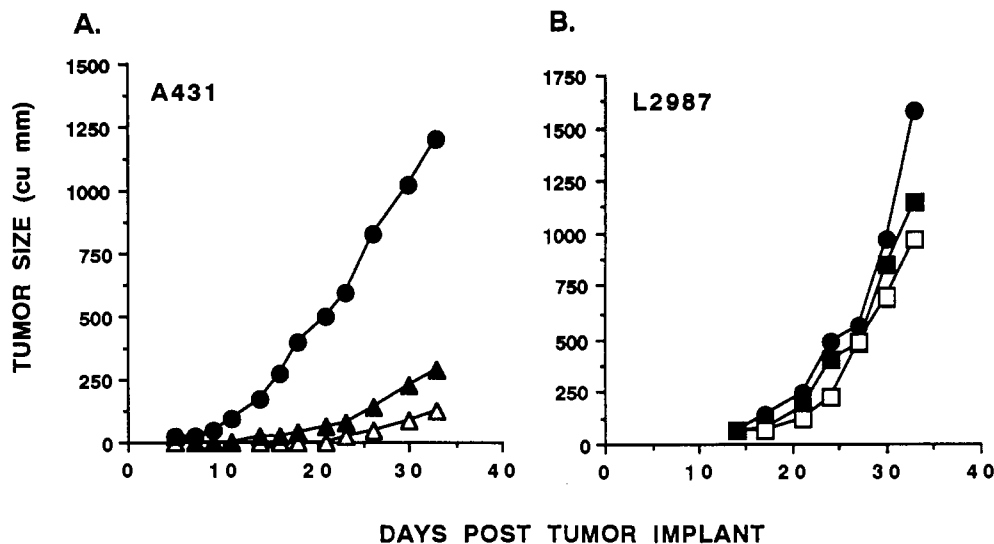
although by day 40, tumors treated with either q4d  $\times$  3 or q1d  $\times$  3 were found to be approximately the same size (500 mm<sup>3</sup>).

**Antitumor Activity of aFGF-Toxin Forms against A431 and L2987 Tumor Xenografts.** The antitumor activity of aFGF-PE40 was also evaluated using mice carrying A431 xenografts. A431 cells were the most sensitive line tested to aFGF-PE40, with an EC<sub>50</sub> value of 8 ng/mL (Table 1). A431 tumor cells were injected into nude mice and either treated with 0.5 mg/kg of aFGF-PE40 supplemented with 100 units/mL of heparin on days 1, 3, and 5 following injection of tumor cells or treated on days 5, 7, and 9 postimplant. Untreated animals similarly implanted with A431 tumor cells were used as controls. Both administration schedules were able to inhibit tumor growth (Figure 4A). Tumors were blocked from growing for 23 and 11 days post implant if treatment was initiated 1 and 5 days after implant, respectively.

The *in vivo* antitumor activity of aFGF-PE4E KDEL was also assessed against mice xenografted with the least sensitive line tested in this study, L2987 lung carcinoma cells (EC<sub>50</sub> value = 150 ng/mL, Table 1). L2987 cells were passaged into animals exactly as done for KB tumor

xenografts. Acidic FGF-PE4E KDEL was administered to two groups of mice using a treatment schedule of q4d  $\times$  3 and doses of 0.25 and 0.375 mg/kg. At both doses, there was minimal antitumor activity compared to untreated animals (Figure 4B).

**Histochemistry of Treated Tumor Sections.** To determine how aFGF-PE40 inhibited the growth of the KB tumor xenografts, tumors were excised from treated and control animals and compared histochemically. Since aFGF is a known vascular growth factor, we wanted to determine whether a cytotoxic form of the growth factor would inhibit vascularization associated with proliferating tumors. Acidic FGF-PE40 did not preferentially eliminate vessels in the treated tumors versus the nontreated tumor tissue, as shown in Figure 5. There were very few differences between the treated and control tumors other than size. A section made through the middle of the untreated tumor mass measured approximately 1.7  $\times$  1.1 cm (Figure 5, panel A), while a similar section of the aFGF-PE40 treated tumor measured 0.5  $\times$  0.7 cm (Figure 5, panel F). At the edge of the tumors there were large vessels feeding the tumor which appeared to be encapsulated (Figure 5, panels B and D). There was solid tumor mass



**Figure 4.** Antitumor activity of aFGF-toxin fusion proteins in mice xenografted with (A) A431 epidermoid carcinoma cells and (B) L2987 lung carcinoma cells. In both models, aFGF-toxin fusion protein was administered intravenously with 100 units/mL of heparin: (A) aFGF-PE40 treatment (0.5 mg/kg, q2d  $\times$  3) was initiated day 5 post implant ( $\blacktriangle$ ), day 1 post implant ( $\triangle$ ), nontreated controls ( $\bullet$ ); (B) aFGF-PE4E KDEL treatment was initiated day 14 post tumor implant using a schedule of q4d  $\times$  3, 0.375 mg/kg ( $\square$ ), 0.25 mg/kg ( $\blacksquare$ ), nontreated controls ( $\bullet$ ).

underneath the highly vascularized edge. The central sections of the treated and untreated tumor mass had areas of necrosis (N), fibrosis (F), and a large infiltrate of polymorphonuclear cells (Figure 5, panels C and E). There appeared to be less microvasculature in the treated tumor samples; however, this was not quantitated. The untreated tumor contained more hemorrhagic areas.

## DISCUSSION

We have prepared many growth factor-toxins using a variety of forms of *Pseudomonas* exotoxin. In this report, we compare two forms, aFGF-PE40 and aFGF-PE4E KDEL, and demonstrate that they both have antitumor activity against established human KB tumor xenografts and preestablished A431 tumor cells in athymic mice. The antitumor activity resulted in an inhibition of continued KB tumor growth during and for a short time following administration of the chimeric toxin. The treatment did not result in regression of the tumor xenografts (Figures 2 and 3). While a more dramatic antitumor effect was found using A431 tumor cells *in vivo*, these experiments used tumors that were not fully established (Figure 4A). Against established L2987 tumor xenografts that were weakly sensitive to the protein synthesis inhibitory effects of aFGF-toxin fusion protein *in vitro* there was no or minimal antitumor activity (Figure 4B).

Heparin was coadministered (100 units/mL) with aFGF-toxins since it potentiates the effects of FGF on the growth of cells by prolonging its biological lifetime (25–28) as well as potentiating the cytotoxic effects of aFGF-toxin fusion protein (29). The serum half-life of aFGF-toxin fusion protein coinjected with heparin was 41 min (Figure 1).

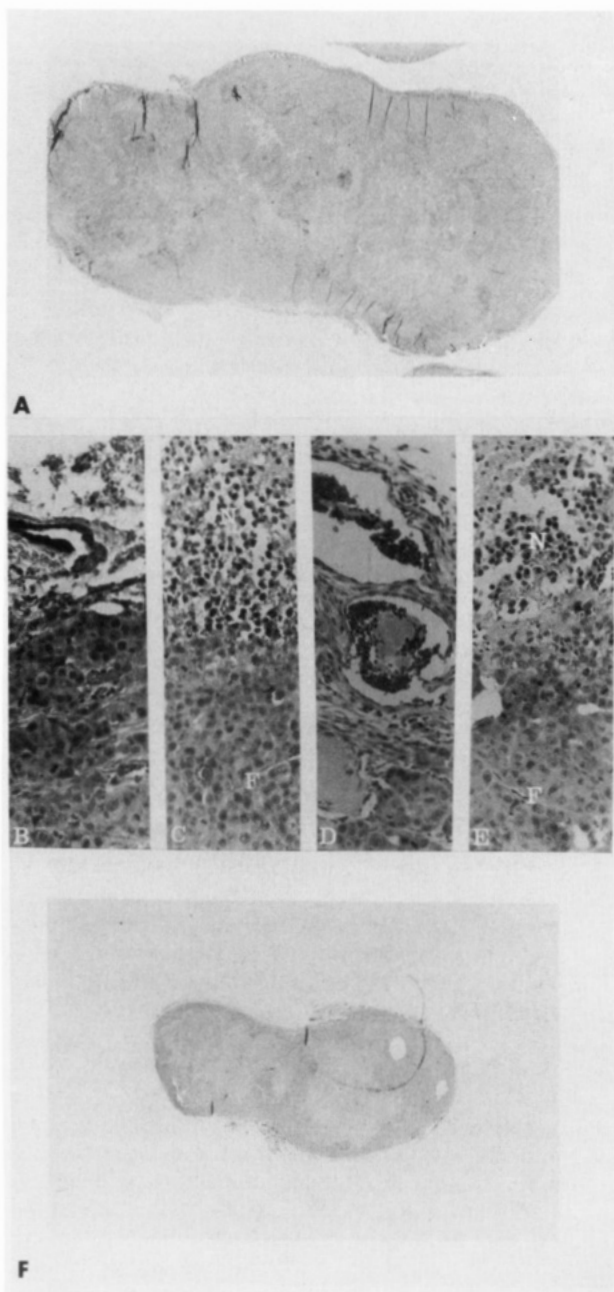
Acidic FGF-PE4E KDEL was devised to increase the cell-specific cytotoxic activity (14, 15), and as shown in Table 1, it is more cytotoxic on certain cell lines than aFGF-PE40 (Table 1). However, it also is more toxic to athymic mice (Table 2). In fact, it would appear that the therapeutic window with aFGF-PE40 is larger than the window with aFGF-PE4E KDEL against most carcinoma cell lines due to the increased toxicity of aFGF-PE4E KDEL. This type of difference was also found for another chimeric toxin which was composed of interleukin 6 and various forms of PE (33). In the IL6 study, IL6-PE4E

KDEL was at least 2-fold more toxic to animals than both IL6-PE40 and IL6-PE4E (C. B. Siegall, unpublished observation). Thus, it may not be advantageous to construct chimeric toxins in which KDEL is included at the carboxyl end since although there is a slight increase in its cytotoxic effects against some cell lines the increase in the nonspecific *in vivo* toxicity may be greater.

Acidic FGF-toxin molecules are not only cytotoxic to tumor cells but they also are cytotoxic to rapidly proliferating vasculature-bearing aFGF receptors (9). We have also found that aFGF-PE4E KDEL is cytotoxic to endothelial cells using an *in vitro* model of angiogenesis (34). In addition, aFGF-PE4E KDEL was cytotoxic to cardiac smooth muscle and endothelial cells isolated as primary culture from rats (35).

In the current study, analysis of treated and nontreated KB tumor xenografts with histochemical techniques revealed that the tumor cells were affected by the aFGF-toxin treatment while the vascular tissue was not (Figure 5). The vascular cells that supply the xenograft are of mouse origin, while the tumor tissue is of human origin. Acidic FGF binds to both human and mouse aFGF receptor and therefore should be able to target the actively proliferating vasculature that is supplying the tumor with blood. In contrast to antibody-toxin chimeric molecules in which the antibody binds to the human tumor xenograft and not to mouse tissue (36), growth factor-toxins such as aFGF-toxin fusion proteins are valid for use in mouse models, since aFGF-PE40 binds to both mouse and human aFGF receptor.

We do not know whether *in vivo* vasculature displays enough cell surface aFGF receptors to be sensitive to aFGF-toxin. Our previous results studying proliferating endothelial cells have shown that the endothelial cells are sensitive to the protein synthesis inhibition activity of aFGF-toxin chimeric molecules (35). However, the levels that are needed to reach 50% of protein synthesis is 100 ng/mL for endothelial cells *in vitro*. This level is slightly higher than the level of aFGF-toxin needed to affect KB tumor cells in culture (Table 1). It is possible that at the administered dose the endothelial cells of the vascular tissue supplying the blood to the tumor xenografts were not sensitive to the aFGF-toxin. Alternatively, it is



**Figure 5.** Histologic examination of aFGF-PE40-treated and -untreated KB tumor tissue. Mice carrying KB tumor xenografts were either treated with aFGF-PE40 (0.375 mg/kg, 1d  $\times$  3) or untreated and sacrificed 24 days post tumor implant. The tumors were removed, fixed in 10% formalin, blocked in paraffin, and sectioned at 8  $\mu$ m. The tissue was stained with hematoxylin and eosin, mounted onto slides, and inspected under light microscopy. Nontreated tumors (A–C) measured 1.7  $\times$  1.1 cm while treated tumors (D–F) measured 5  $\times$  7 mm. Whole mounts (A, F), edge of tumor mass (B, D), center of mass (C, E). N = necrosis; F = fibrosis. Magnification: A, F = 13X, B–E = 100X.

possible that reduced vascular development due to aFGF-toxin treatment could have resulted in reduced tumor growth.

A similar type of growth factor–toxin molecule that is active against cells with FGF receptors is bFGF-SAP, a chemical conjugate composed of basic FGF and the plant toxin, saporin (37). This molecule is valuable in culturing pancreatic islet cells since bFGF-SAP can eliminate the fibroblast cells that frequently block initiation of islet cells in culture (38). Basic FGF-SAP is specifically cytotoxic to cells displaying bFGF-receptors (39) and can inhibit the growth of human tumor xenografts in nude mice (22).

Treatment of metastatic tumors is one of the most important areas in cancer chemotherapy. There is a direct correlation between metastasis and tumor angiogenesis (40). Thus, we attempted to target both the tumor tissue and the vasculature with these aFGF–toxin molecules. Although we could not definitively show that aFGF–toxins were able to target the tumor vasculature in this model system (Figure 5), this type of investigation may lead to the discovery of new and powerful proteins and/or drugs that will be potent inhibitors of human tumor growth.

#### ACKNOWLEDGMENT

We thank Drs. P. Senter, P. Friedman, and E. Wolff for critical reading of the manuscript, and Drs. P. Trail, P. Fell, and K. E. Hellström for helpful suggestions.

#### LITERATURE CITED

- (1) Gray, G. L., Smith, D. H., Baldrige, J. S., Harkins, R. N., Vasil, M. L., Chen, E. Y., and Heyneker, H. L. (1984) Cloning, nucleotide sequence, and expression in *Escherichia coli* of the exotoxin A structural gene of *Pseudomonas aeruginosa*. *Proc. Natl. Acad. Sci. U.S.A.* 81, 2645–2649.
- (2) Allured, V. S., Collier, R. J., Carroll, S. F., and McKay, D. B. (1986) Structure of exotoxin A of *Pseudomonas aeruginosa* at 3.0-Å resolution. *Proc. Natl. Acad. Sci. U.S.A.* 83, 1320–1324.
- (3) Hwang, J., FitzGerald, D. J. P., Adhya, S., and Pastan, I. (1987) Functional domains of *Pseudomonas* exotoxin identified by deletion analysis of the gene expressed in *E. coli*. *Cell* 48, 129–136.
- (4) Jinno, Y., Chaudhary, V. K., Kondo, T., Adhya, S., FitzGerald, D. J., and Pastan, I. (1988) Mutational analysis of domain I of *Pseudomonas* exotoxin. *J. Biol. Chem.* 263, 13202–13207.
- (5) Chaudry, G. J., Wilson, R. B., Draper, R. K., and Clowes, R. C. (1989) A dipeptide insertion in domain I of exotoxin A that impairs receptor binding. *J. Biol. Chem.* 264, 15151–15156.
- (6) Pastan, I., and FitzGerald, D. (1989) *Pseudomonas* exotoxin: chimeric toxins. *J. Biol. Chem.* 264, 15157–15160.
- (7) FitzGerald, D., and Pastan, I. (1989) Targeted toxin therapy for the treatment of cancer. *J. Natl. Cancer Inst.* 81, 1455–1463.
- (8) FitzGerald, D., Chaudhary, V. K., Kreitman, R. J., Siegall, C. B., and Pastan, I. (1992) in *Genetically Engineered Toxins* (A. E. Frankel, Ed.) pp 447–462, New York, Marcel Dekker.
- (9) Siegall, C. B., Epstein, S. E., Speir, E., Hla, T., Forough, R., Maciag, T., FitzGerald, D., and Pastan, I. (1991) Cytotoxic activity of chimeric proteins composed of acidic fibroblast growth factor and *Pseudomonas* exotoxin on a variety of cell types. *FASEB J.* 5, 2843–2849.
- (10) Armstrong, E., Vainikka, S., Patanen, J., Korhonen, J., and Alitalo, R. (1992). Expression of fibroblast growth factor receptors in human leukemia cells. *Cancer Res.* 52, 2004–2007.
- (11) Luqmani, Y. A., Graham, M., and Coombes, R. C. (1992) Expression of basic fibroblast growth factor, FGFR1 and FGFR2 in normal and malignant human breast, and comparison with other normal tissues. *Br. J. Cancer* 66, 273–280.
- (12) Kondo, T., FitzGerald, D., Chaudhary, V. K., Adhya, S., and Pastan, I. (1988) Activity of immunotoxins constructed with modified *Pseudomonas* exotoxin lacking the cell recognition domain. *J. Biol. Chem.* 263, 9470–9475.
- (13) Chaudhary, V. K., Jinno, Y., Gallo, M. G., FitzGerald, D., and Pastan, I. (1990) Mutagenesis of *Pseudomonas* exotoxin in identification of sequences responsible for the animal toxicity. *J. Biol. Chem.* 265, 16306–16310.
- (14) Chaudhary, V. K., Jinno, Y., FitzGerald, D., and Pastan, I. (1990) *Pseudomonas* exotoxin contains a specific sequence at the carboxyl terminus that is required for cytotoxicity. *Proc. Natl. Acad. Sci. U.S.A.* 87, 308–312.
- (15) Seetharam, S., Chaudhary, V. K., FitzGerald, D., and Pastan, I. (1991) Increased cytotoxic activity of *Pseudomonas* exotoxin

- and two chimeric toxins ending in KDEL. *J. Biol. Chem.* 266, 17376-17381.
- (16) Strom, T. B., Anderson, P. L., Rubin-Kelley, V. E., Williams, D. P., Kiyokawa, T., and Murphy, J. R. (1991) Immunotoxins and cytokine toxin fusion proteins. *Ann. N. Y. Acad. Sci.* 636, 233-250.
- (17) Siegall, C. B., Xu, Y. H., Chaudhary, V. K., Adhya, S., FitzGerald, D., and Pastan, I. (1989) Cytotoxic activities of a fusion protein comprised of TGF $\alpha$  and *Pseudomonas* exotoxin. *FASEB J.* 3, 2647-2652.
- (18) Prior, T. I., Helman, L. J., FitzGerald, D. J., and Pastan, I. (1991) Cytotoxic activity of a recombinant fusion protein between insulin-like growth factor I and *Pseudomonas* exotoxin. *Cancer Res.* 51, 174-180.
- (19) Shaw, J. P., Akiyoshi, D. E., Arrigo, D. A., Rhoad, A. E., Sullivan, B., Thomas, J., Genbauffe, F. S., Bacha, P., and Nichols, J. C. (1991) Cytotoxic properties of DAB486EGF and DAB389EGF, epidermal growth factor (EGF) receptor-targeted fusion toxins. *J. Biol. Chem.* 266, 21118-21124.
- (20) Heimbrook, D. C., Stirdivant, S. M., Ahern, J. D., Balishin, N. L., Patrick, D. R., Edwards, G. M., Defeo, J. D., FitzGerald, D. J., Pastan, I., and Oliff, A. (1990) Transforming growth factor alpha-*Pseudomonas* exotoxin fusion protein prolongs survival of nude mice bearing tumor xenografts. *Proc. Natl. Acad. Sci. U.S.A.* 87, 4697-4701.
- (21) Pai, L. H., Gallo, M. G., FitzGerald, D. J., and Pastan, I. (1991) Anti-tumor activity of a transforming growth factor alpha-*Pseudomonas* exotoxin fusion protein (TGF $\alpha$ -PE40). *Cancer Res.* 51, 2808-2812.
- (22) Beitz, J. G., Davol, P., Clark, J. W., Kato, J., Medina, M., Frackelton, A. R. Jr., Lappi, D. A., Baird, A., and Calabresi, P. (1992) Antitumor activity of basic fibroblast growth factor-saporin mitotoxin *in vitro* and *in vivo*. *Cancer Res.* 52, 227-230.
- (23) Douglas, C. M., and Collier, R. J. (1987) Exotoxin A of *Pseudomonas aeruginosa*: substitution of glutamic acid 553 with aspartic acid drastically reduces toxicity and enzymatic activity. *J. Bacteriol.* 169, 4967-4971.
- (24) Carroll, S. F., and Collier, R. J. (1987) Active site of *Pseudomonas aeruginosa* exotoxin A glutamic acid 553 is photolabeled by NAD and shows functional homology with glutamic acid 148 of *Diphtheria* toxin. *J. Biol. Chem.* 262, 8707-8711.
- (25) Schreiber, A. B., Kenney, J., Kowalski, W. J., Friesel, R., Mehlman, T., and Maciag, T. (1985) Interaction of endothelial cell growth factor with heparin: Characterization by receptor and antibody recognition. *Proc. Natl. Acad. Sci. U.S.A.* 82, 6138-6143.
- (26) Gospodarowicz, D., and Cheng, J. (1986) Heparin protects basic and acidic FGF from inactivation. *J. Cell. Physiol.* 128, 475-484.
- (27) Rosengart, T. K., Kupferschmid, J. P., Ferrans, V. J., Casscells, W., Maciag, T., and Clark, R. E. (1988) Heparin-binding growth factor I (endothelial cell growth factor) binds to endothelium *in vivo*. *J. Vasc. Surg.* 7, 311-317.
- (28) Damon, D. H., Lobb, R. R., D'Amore, P. A., Wagner, J. A. (1989) Heparin potentiates the action of acidic fibroblast growth factor by prolonging its biological half-life. *J. Cell. Physiol.* 138, 221-226.
- (29) Gawlak, S. L., Pastan, I., and Siegall, C. B. (1993) Basic FGF-*Pseudomonas* exotoxin chimeric proteins; Comparison with acidic FGF-*Pseudomonas* exotoxin. *Bioconjugate Chem.* (in press).
- (30) Burgess, W. H., and Maciag, T. (1989) The heparin-binding (fibroblast) growth factor family of proteins. *Annu. Rev. Biochem.* 58, 575-606.
- (31) Basilico, C., and Moscatelli, D. (1992) The FGF family of growth factors and oncogenes. *Adv. Cancer Res.* 59, 115-165.
- (32) Gospodarowicz, D. (1989) Fibroblast growth factor. *Crit. Rev. Oncogen.* 1, 1-26.
- (33) Siegall, C. B., Kreitman, R. J., FitzGerald, D. J., and Pastan, I. (1991) Antitumor effects of interleukin 6-*Pseudomonas* exotoxin chimeric molecules against the human hepatocellular carcinoma, PLC/PRF/5 in mice. *Cancer Res.* 51, 2831-2836.
- (34) Merwin, J. R., Lynch, M. J., Madri, J. A., Pastan, I., and Siegall, C. B. (1992) Acidic fibroblast growth factor-*Pseudomonas* exotoxin chimeric protein elicits antiangiogenic effects on endothelial cells. *Cancer Res.* 52, 4995-5001.
- (35) Biro, S., Siegall, C. B., Fu, Y.-M., Speir, E., Pastan, I., and Epstein, S. E. (1992) *In vitro* effects of a recombinant toxin targeted to the fibroblast growth factor receptor on rat vascular smooth muscle and endothelial cells. *Circulation Res.* 71, 640-645.
- (36) Friedman, P. N., Chace, D. F., Trail, P. A., and Siegall, C. B. (1993) Anti-tumor activity of the single-chain immunotoxin BR96 sFv-PE40 against established breast and lung tumor xenografts. *J. Immunol.* 150, 3054-3061.
- (37) Lappi, D. A., Martineau, D., and Baird, A. (1989) Biological and chemical characterization of basic FGF-saporin mitotoxin. *Biochem. Biophys. Res. Commun.* 160, 917-923.
- (38) Beattie, G. M., Lappi, D. A., Baird, A., and Hayek, A. (1990) Selective elimination of fibroblasts from pancreatic islet monolayers by basic fibroblast growth factor-saporin mitotoxin. *Diabetes.* 39, 1002-1005.
- (39) Lappi, D. A., Maher, P. A., Martineau, D., and Baird, A. (1991) The basic fibroblast growth factor-saporin mitotoxin acts through the basic fibroblast growth factor receptor. *J. Cell. Physiol.* 147, 17-26.
- (40) Weidner, N., Semple, J. P., Welch, W. R., and Folkman, J. (1991) Tumor angiogenesis and metastasis: correlation in invasive breast carcinoma. *N. Engl. J. Med.* 324, 1-8.

# Design and Synthesis of a Protein Device That Releases Insulin in Response to Glucose Concentration

Yoshihiro Ito,\* Dong-June Chung, and Yukio Imanishi

Department of Polymer Chemistry, Faculty of Engineering, Kyoto University, Yoshida Honmachi, Sakyo-ku, Kyoto, Japan 606-01. Received June 3, 1993\*

To synthesize a glucose-sensitive insulin-releasing protein device, insulin was esterified with methanol and connected to glucose oxidase with intervention of a disulfide compound, 5,5'-dithiobis(2-nitrobenzoic acid). On adding glucose to an aqueous solution containing the hybrid enzyme, the modified insulin was released. The amount of insulin released increased with increasing concentration of added glucose. The insulin release from the hybrid enzyme was specific to glucose. The activity of released insulin was about 80% of the unmodified insulin.

## INTRODUCTION

The control of drug release in response to external signals, e.g., pH change, temperature change, solubility change, antigen/antibody reaction, or electric potential, has been investigated (1-4). We have been interested in the synthesis of an insulin-releasing device in response to glucose concentration as one of the drug-delivery systems that are responsive to physiological substances. Toward this goal, we have synthesized a membrane device to which insulin was connected with an intervening disulfide linkage together with glucose dehydrogenase (GDH),<sup>1</sup> nicotinamide adenine dinucleotide (NAD), and flavin adenine dinucleotide (FAD) (5). In the presence of glucose, electrons generated in the oxidation reaction of glucose catalyzed by GDH are transferred to the disulfide linkage via immobilized NAD and FAD and undergo a reductive cleavage of the disulfide bond to release insulin.

In the present investigation, the improvement of the efficiency of insulin release from the membrane device was aimed at, and a protein device was synthesized, in which insulin was connected to an enzyme, glucose oxidase (GOD), with an intervening disulfide linkage as shown in Figure 1. In contrast to GDH, GOD possesses a coenzyme FAD and functions without demanding the addition of FAD. Therefore, a more efficient use of electrons in the reductive cleavage of a disulfide linkage in the protein device than in the membrane device was expected.

## MATERIALS AND METHODS

**Reagents.** The enzyme GOD (EC 1.1.3.4) from *Aspergillus niger* (G-8135, type X, 128 IU/mg protein), insulin from bovine pancreas (I-5500, 24.4 IU/mg protein), and albumin of bovine origin (A-6003) were purchased from Sigma Chemical Co. (St. Louis, MO). 5,5'-Dithiobis(2-nitrobenzoic acid) (DTNB), 1-ethyl-3-(3-(dimethylamino)propyl)carbodiimide hydrochloride, which is a water-soluble carbodiimide (WSC),  $\beta$ -D(+)-glucose, galactose, maltose, urea, acrylamide, and a toluene solution of liquid scintillation were purchased from Nacalai Tesque Inc.

\* Abstract published in *Advance ACS Abstracts*, December 15, 1993.

<sup>1</sup> Abbreviations: GDH, glucose dehydrogenase; NAD, nicotinamide adenine dinucleotide; FAD, flavin adenine dinucleotide; GOD, glucose oxidase; DTNB, 5,5'-dithiobis(2-nitrobenzoic acid); WSC, water-soluble carbodiimide; PBS, phosphate-buffered saline; GPC, gel permeation chromatography.

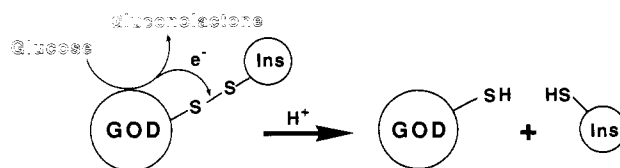


Figure 1. Insulin-releasing mechanism of the protein device in response to glucose addition, Ins representing insulin.

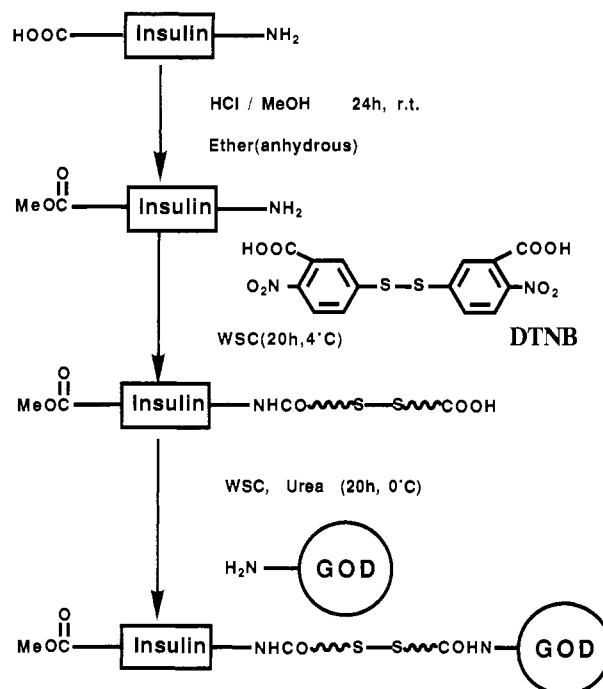


Figure 2. Synthetic scheme of the protein device.

(Kyoto, Japan). <sup>14</sup>C-Glucose (1-5 mCi/mmol) was purchased from DuPont (Wilmington, DE) and used for the measurement of biological activity of insulin.

Phosphate-buffered saline (pH 7.0) was prepared by dissolving NaCl (8 g), KCl (0.2 g), KH<sub>2</sub>PO<sub>4</sub> (0.2 g), Na<sub>2</sub>HPO<sub>4</sub> (1.15 g), MgCl<sub>2</sub> (0.1 g), and CaCl<sub>2</sub> (0.1 g) into 1 L of distilled water.

**Synthesis of Insulin/GOD Hybrid.** The insulin/GOD hybrid was synthesized according to the scheme shown in Figure 2. First, in order to prevent inter- and intramolecular cross-linking reactions of proteins in the

WSC-activated reaction between insulin and DTNB or between DTNB-insulin and GOD, the carboxyl groups of insulin (500 mg) were esterified in 10% HCl-methanol (40 mL) at room temperature for 24 h (6). The insulin methyl ester was precipitated from the reaction solution by adding anhydrous ether. The precipitate was dissolved in PBS and purified by using a gel permeation chromatography (GPC) column packed with Sephadex G-15 (eluent, PBS). The elution pattern was monitored with an absorbance at 280 nm. The fractions of product, insulin methyl ester, were collected, desalted by dialysis, and finally freeze-dried. The product was a white powder (the yield was 99%).

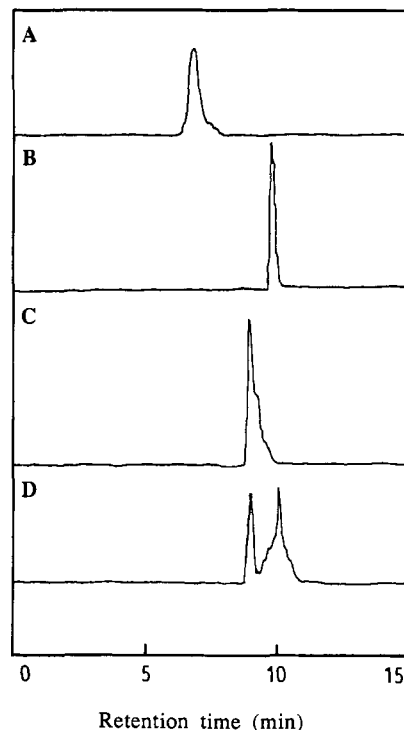
The amount of carboxyl groups esterified with methanol was determined using 9-anthryldiazomethane (Funakoshi Co. Ltd., Tokyo). The dye (1 mg) was dissolved in 50  $\mu$ L of acetone and diluted with 450  $\mu$ L of methanol. The dye solution was added into a sample solution, and the mixture was allowed to stand at room temperature for 1 h. After the sample was purified with a G-10 GPC column, the amount of dye coupled to the sample was measured by fluorescence. The relative emission intensity at 412 nm was recorded when the excitation wavelength was 365 nm.

DTNB (1 g) was dissolved in water (50 mL) containing  $\text{Na}_2\text{HPO}_4$  (0.827 g), and the solution was mixed with WSC (1 g). To the resulting solution was added insulin methyl ester (150 mg) dissolved in 50 mL of water, and the mixture was stirred at 4 °C for 20 h. The reaction product was precipitated in methanol and purified by the same method using the G-15 GPC column (eluent, PBS). After the product was desalted and freeze-dried, a white powder was obtained (the yield was 69%).

The insulin methyl ester modified with DTNB (DTNB-insulin) (20 mg), WSC (34.8 mg), GOD (16.15 mg), and urea (2 M) was dissolved in 10 mL (pH 5.5) of 0.1 M borate-buffered solution, and the resulting solution was stirred at 4 °C for 20 h. The presence of urea was based on the fact that ferrocene derivatives were efficiently coupled into the GOD to be electron mediators in the presence of urea as reported by Degani and Heller (7). After the urea was removed by ultrafiltration (Milipore membrane), the reaction product was purified by a G-50 GPC column (eluent, PBS) to collect the insulin/GOD hybrid. After the product was desalted and freeze-dried, a white powder was obtained (the yield was 61%).

**Release of Insulin from the Insulin/GOD Hybrid.** An aqueous sugar (glucose, galactose, or maltose) solution was added to a PBS (5 mL) containing the insulin/GOD hybrid (10 mg) at 37 °C. A portion of the solution was taken out after 1 min, and the time-dependent amount of released insulin was determined on the basis of a 276-nm absorption intensity of the solution eluted through a reversed-phase column packed with a Biofine RPC-PO (JASCO, Tokyo, Japan). The determination was done with a calibration curve which was made by using known amounts of insulin.

**Biological Activity of Released Insulin.** The biological activity of insulin was assayed by the determination of the amount of glucose taken up by adipocytes (8). An albumin-containing Krebs-Ringer bicarbonate buffer solution (1 mL) was added to adipocytes (mouse origin), and the mixture was incubated for 2 h in the presence of glucose/ $^{14}\text{C}$ -glucose (100/1 mol/mol, total concentration, 8.3  $\mu\text{M}$ , 100  $\mu\text{L}$ ) and an insulin derivative (12.5 mU/mL, 20  $\mu\text{L}$ ). The culture was terminated by adding 8 N  $\text{H}_2\text{SO}_4$  (200  $\mu\text{L}$ ). Fat containing  $^{14}\text{C}$ -glucose, which was taken up by the cells, was extracted with a toluene liquid scintillation solution. The amount of  $^{14}\text{C}$  was determined by using an



**Figure 3.** HPLC diagrams of unmodified GOD (A), untreated insulin (B), insulin/GOD hybrid (C), and insulin/GOD hybrid + glucose (D): eluent, PBS (pH 7.0); column, Biofine RPC-PO (JASCO, Tokyo, Japan); flow rate, 0.5 mL/min; operating pressure, 30 kgf/cm<sup>2</sup>; detection, UV absorption at 276 nm.

Aloka LSC 1000 scintillator (Tokyo, Japan) and compared with that in the incubation with native insulin to assess the relative biological activity of the insulin derivative.

## RESULTS AND DISCUSSION

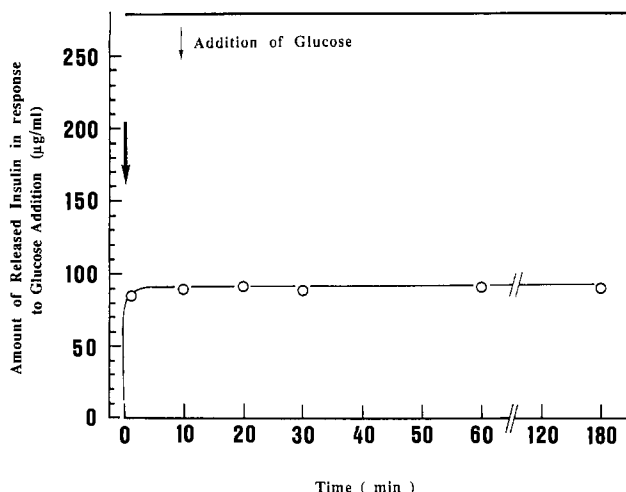
**Synthesis of the Insulin/GOD Hybrid.** By the esterification reaction 55% of the carboxyl groups in insulin were esterified with methanol. This was less than the value reported previously (6).

When the DTNB was coupled to insulin, the elemental analysis of the reaction product of insulin and DTNB in a molar ratio of 1/5 gave the S content of 3.36%, indicating that two of the three amino groups in a molecule of insulin were used for the reaction with DTNB.

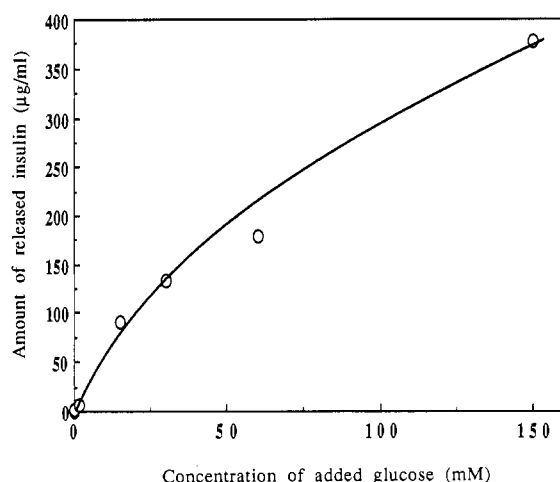
When the DTNB-insulin was coupled to GOD, the elemental analysis of the reaction product of DTNB-insulin and GOD in a molar ratio of 1/1 showed the S content of 2.27%, indicating that 20 mol % of GOD amino groups was used for coupling with DTNB-insulin and 5.8 insulin molecules were included in the hybrid. On the other hand, by cleaving with 0.5 vol % of mercaptoethanol 6.3 insulin molecules were released. The molecular weight of the hybrid was estimated to be 193 kDa by GPC (Cosmosil/Cosmogel made by Nacalai Tesque, Inc., Kyoto, Japan). This result indicates that 6.6 insulin molecules were linked to a GOD molecule. These results demonstrated that about six insulin molecules were linked to GOD through each disulfide bond of DTNB.

**Insulin Release upon Glucose Addition.** High-performance liquid chromatography diagrams of aqueous solutions containing the insulin/GOD hybrid or unmodified insulin before and after glucose addition are shown in Figure 3. A new peak appeared on adding glucose in the solution containing the insulin/GOD hybrid. The retention time of the new peak almost agreed with that





**Figure 4.** Time-dependent insulin release from the insulin/GOD hybrid in response to glucose addition (15 mM).



**Figure 5.** Release of insulin from the insulin/GOD hybrid in response to different concentrations of glucose added (0.15, 1.5, 15, 30, 60, and 150 mM).

for the unmodified insulin, although the new peak was not completely the same as that of the native insulin since the released insulin was methyl esterified and carried 2-nitro-5-mercaptobenzonic acid. The retention times of both A and B chains of insulin, which were obtained by the degradation method reported previously (9), were markedly longer than that of the native insulin. These observations imply that the insulin/GOD hybrid released insulin upon addition of glucose without side reactions, e.g., a cleavage of disulfide linkages of insulin itself. This conclusion was also deduced from the biological activity described below.

The time-dependent release of modified insulin from the insulin/GOD hybrid was measured, and the result is shown in Figure 4. The insulin was immediately released from the hybrid on adding an aqueous glucose solution.

The amount of insulin released 30 min after the addition of glucose solution of varying concentrations was measured, and the data are summarized in Figure 5. The amount of released insulin increased with increasing concentration of glucose solution. However, the rate of insulin release was not controlled by the concentration of glucose added. It was considered that the insulin would have a maximal rate as long as the glucose concentration was higher than its  $K_m$  with glucose oxidase.

The number of modified insulin molecules released on oxidation of a glucose molecule was calculated to be 1.3

**Table 1. Biological Activities of Insulin Derivatives**

insulin deriv	rel biological activity <sup>a</sup> (%)	insulin deriv	rel biological activity <sup>a</sup> (%)
native insulin	100 ± 16	DTNB-Ins	73 ± 20
Me-Ins	95 ± 9	released insulin	81 ± 9

<sup>a</sup> The relative biological activity is normalized by the activity of native insulin as a standard, 100%.

$\times 10^{-3}$ . This value is nearly 40-fold of  $3.4 \times 10^{-5}$ , which was the number of insulin molecules released per a molecule of glucose oxidized in the previously reported membrane device (5). The comparison shows that the protein device is more efficient in releasing insulin than the membrane device.

Sugars other than glucose did not induce insulin release from the insulin/GOD hybrid. This result indicates a glucose specificity of the insulin/GOD hybrid. In addition to the experiment with 2-mercaptoethanol, in order to confirm that the modified insulin was released after reductive cleavage of disulfide bond, NADH and FADH<sub>2</sub> instead of glucose were added to the solution containing the protein device. The modified insulin was also released by the addition of reducing agents. These observations were also previously reported with the membrane system using glucose dehydrogenase (5).

**Biological Activity of Released Insulin.** Biological activities of insulin methyl ester, DTNB-insulin, and insulin/GOD hybrid were determined by the <sup>14</sup>C-glucose uptake method and are shown in Table 1 relative to that of unmodified insulin. The biological activity of insulin decreased slightly by the esterification with methanol and to 73% by the connection of DTNB. The biological activity of the released insulin was 81% of that of unmodified insulin. The relative biological activities are comparable to those of insulins modified with sugars (10). The different activities between the released insulin and the DTNB-insulin could be explained in terms of different bulkiness of substituents connected to amino groups of insulin.

This hybrid is a prototype of a protein device working like a molecular machine. For practical use, this protein device will be encapsulated by a semipermeable membrane through which the released insulin can permeate, or will be modified with polyethylene glycol, thus being immunisolated from biocomponents such as immunoglobulin in the body.

#### LITERATURE CITED

- (1) Ito, Y. (1992) Enzyme modification for drug delivery molecular devices. In *Synthesis of Biocomposite Materials* (Y. Imanishi, Ed.) pp 137-180, CRC Press, Boca Raton.
- (2) Ito, Y., Casolaro, M., Kono, K., and Imanishi, Y. (1989) Design and synthesis of insulin-releasing system in response to glucose. *J. Controlled Release* 10, 195-202.
- (3) Ito, Y., Kotera, S., Inaba, M., Kono, K., and Imanishi, Y. (1990) Control of poly(acrylic acid) grafts of pore size of polycarbonate membrane with straight pores. *Polymer* 31, 2157-2161.
- (4) Ito, Y., Inaba, M., Chung, D. J., and Imanishi, Y. (1992) Control of water permeability by pH and ionic strength through a porous membrane having poly(carboxylic acid) surface-grafted. *Macromolecules* 25, 7313-7316.
- (5) Chung, D. J., Ito, Y., and Imanishi, Y. (1992) Glucose-sensitive insulin-releasing system using redox reaction. *J. Controlled Release* 18, 45-54.
- (6) Levy, D., and Carpenter, F. H. (1970) Insulin methyl ester. Specific cleavage of a peptide chain resulting from a nitrogen to oxygen acyl shift at a threonine residue. *Biochemistry* 9, 3215-3222.

- (7) Degani, Y. and Heller, A. (1988) Direct electrical communication between chemically modified enzymes and metal electrodes. 2. Methods for bonding electron-transfer relays to glucose oxidase and D-amino-acid oxidase. *J. Am. Chem. Soc.* 110, 2615-2620.
- (8) Moody, A. J., Stan, M. A., Stan, M., and Glieman, J. (1974) A simple free fat cell bioassay for insulin. *Horm. Metab. Res.* 6, 12-16.
- (9) Florence, T. M. (1980) Degradation of protein disulfide bonds in dilute alkali. *Biochem. J.* 189, 507-520.
- (10) Seminoff, L. A., Gleeson, J. M., Zheng, J., Olsen, G. B., Holmberg, D. L., Mohammad, S. F., Wilson, D., and Kim, S. W. (1989) A self-regulating insulin delivery system. II. In vivo characteristics of a synthetic glycosylated insulin. *Int. J. Pharm.* 54, 251-257.

# Preparation and Characterization of Interleukin-2-Gelonin Conjugates Made Using Different Cross-Linking Reagents<sup>1</sup>

Gordon D. McIntyre,<sup>†</sup> Charles F. Scott, Jr.,<sup>‡</sup> Jerome Ritz, Walter A. Blättler,<sup>§</sup> and John M. Lambert<sup>\*§</sup>

Division of Tumor Immunology, Dana-Farber Cancer Institute, Boston, Massachusetts 02115. Received August 9, 1993\*

Conjugates of IL-2 with the ribosome-inactivating protein gelonin were prepared using heterobifunctional reagents to link the proteins *via* disulfide, acid-labile, and noncleavable linkers. In each case, one protein was modified using 2-iminothiolane. The sulfhydryl groups so introduced were then reacted either with 2-nitro-5-dithiobenzoate groups or with iodoacetamido groups which had been introduced into the second protein. In the case of the acid-labile linkage, a reagent which forms a labile bond upon reaction with amino groups, 4-(iodoacetamido)-1-cyclohexene-1,2-dicarboxylic acid anhydride (its synthesis is described in this paper) was used to modify the toxin. The conjugates were separated from nonconjugated proteins by gel filtration on Sephadex G100 (SF). Each was analyzed with respect to its ribosome-inactivating activity, its ability to bind to the IL-2 receptor, and its *in vitro* cytotoxicity. The ribosome-inactivating activity of gelonin was unaffected by modification with 2-iminothiolane and was retained in conjugates prepared using this reagent. Modification of the toxin with 4-(iodoacetamido)-1-cyclohexene-1,2-dicarboxylic acid anhydride to form the acid-labile link drastically reduced the activity of the toxin. However, the activity of the toxin was recovered following acid treatment to release the native protein. Conjugates containing each type of linkage exhibited both specific binding and selective cytotoxicity toward cells expressing the IL-2 receptor. The most potent of these toxins, that containing the disulfide linkage, exhibited a cytotoxicity which was 2 orders of magnitude greater than that of unconjugated gelonin.

## INTRODUCTION

A specific cytotoxic agent for selective killing of activated T cells would be of major therapeutic value in the treatment of T cell leukemia (Krönke *et al.*, 1985, 1986) and autoimmune diseases such as rheumatoid arthritis (Paliard *et al.*, 1991) and for the prophylaxis and treatment of graft-versus-host disease in tissue transplantation (Derocq *et al.*, 1987; Vitetta and Uhr, 1984; Kupiec-Weglinski *et al.*, 1988). Natural toxins from plants and bacteria, when conjugated to specific monoclonal antibodies, provide a powerful tool for selective elimination of particular populations of cells by allowing target-specific delivery of cytotoxins (Blättler *et al.*, 1989; Vitetta *et al.*, 1987). The ribosome-inactivating proteins (Olsnes and Pihl, 1982; Stirpe and Barbieri, 1986; Lambert *et al.*, 1988) seem to be ideal toxic agents for this purpose. Most effort has been directed toward using the plant protein ricin (Olsnes and Pihl, 1982; Frankel *et al.*, 1986; Vitetta *et al.*, 1987). This protein consists of two nonidentical subunits (A and B chains) that are joined by a disulfide bond (Olsnes and Pihl, 1982). The B chain has the property of binding to cell surface carbohydrates and promotes the uptake of the A chain into cells. Entry of the A chain into the cytoplasm results in the death of the cell by catalytic inactivation of its ribosomes (Endo *et al.*, 1987).

The single-chain ribosome-inactivating proteins have properties and characteristics similar to those of the ricin A chain alone (Stirpe and Barbieri, 1986; Endo *et al.*, 1988). They are highly effective at inactivating ribosomes in cell-free systems but are relatively nontoxic to intact cells because of lack of a B chain activity. These proteins are good candidates for the preparation of cytotoxic conjugates and have several advantages over ricin A chain: they are extremely stable proteins, resistant to proteolysis, and safe to purify without the extreme safety precautions necessary for work with ricin (Stirpe and Barbieri, 1986). They have been widely used in recent years for the preparation of immunotoxins (Thorpe *et al.*, 1981; Lambert *et al.*, 1985; Lambert *et al.*, 1988; Vitetta *et al.*, 1987).

Ligands other than antibodies can be used in order to deliver toxins to defined cell populations. Indeed, cytotoxic conjugates prepared using ligands such as thyrotropin-releasing factor (Bacha *et al.*, 1983), insulin (Miskimins and Shimizu, 1979), chorionic gonadotropin (Oeltman, 1985; Oeltman and Heath, 1979), leutenizing hormone (Singh *et al.*, 1989), epidermal growth factor (Cawley *et al.*, 1980; Shimizu *et al.*, 1980; Simpson *et al.*, 1982), transferrin (Raso and Basala, 1984), and  $\alpha_2$ -macroglobulin (Martin and Houston, 1983) exhibit specific cytotoxicity toward cells expressing the relevant receptors. The availability of recombinant lymphokines has prompted us to consider the usefulness of one of these ligands as an agent for targeting ribosome-inactivating proteins to T cells. We describe here the preparation of conjugates consisting of the T-cell growth factor, interleukin-2 (Smith, 1980), and the single chain ribosome-inactivating protein, gelonin (Stirpe *et al.*, 1980). Conjugates were prepared using disulfide, acid-labile, and noncleavable linkages. Each conjugate was analyzed for its ribosome-inactivating activity, its ability to bind to the IL-2<sup>2</sup>-receptor, and its *in vitro* cytotoxicity.

\* To whom correspondence should be addressed at ImmunoGen, Inc., 148 Sidney St., Cambridge, MA 02139. Telephone: (617) 497-1113. Fax: 617-497-5406.

<sup>†</sup> Present address: Department of Cell Biology, Glaxo, Inc., Five Moore Dr., Research Triangle Park, NC 27709.

<sup>‡</sup> Deceased.

<sup>§</sup> Present address: ImmunoGen, Inc., 148 Sidney St., Cambridge, MA 02139.

\* Abstract published in *Advance ACS Abstracts*, December 1, 1993.

<sup>1</sup> This work was supported by a grant from ImmunoGen, Inc.

## EXPERIMENTAL PROCEDURES

**Materials.** With the exception of the materials listed below, all reagents were obtained either from the sources described in the appropriate references or from Sigma Chemical Co., St. Louis, MO.

Recombinant IL-2 (human) was generously supplied by Biogen, Inc., Cambridge, MA. 2-Iminothiolane was purchased from Pierce Chemical Co., Rockford, IL. Gelatin (EIA grade) was from Bio-Rad Laboratories, Richmond, CA. L-[U-<sup>14</sup>C]Cysteine-HCl (32.5 mCi/mol) was from Amersham Corp., Arlington Heights, IL, and was diluted to a specific radioactivity of 0.5 mCi/mmol with nonradiolabeled cysteine-HCl before use. Labeled Bolton-Hunter reagent (*N*-succinimidyl 3-(4-hydroxy-5-[<sup>125</sup>I]-iodophenyl)propionate; 2000 Ci/mmol) was also purchased from Amersham. [Methyl-<sup>3</sup>H]thymidine (4 Ci/mmol) was obtained from ICN Biomedicals, Inc., Costa Mesa, CA. A rabbit reticulocyte lysate system for cell-free protein synthesis, which included L-[3,4,5-<sup>3</sup>H]leucine (specific radioactivity 146.5 Ci/mmol), was obtained from New England Nuclear, Boston, MA, as was Biofluor scintillation cocktail. Betafluor scintillation cocktail was from National Diagnostics, Somerville, NJ. *N*-Succinimidyl iodoacetate (which is available from Sigma Chemical Co.) was synthesized by Mr. B. Kuenzi in our laboratories.

Seeds from *Gelonium multiflorum* were from United Chemical and Allied Products, 10 Clive Row, Calcutta-1, India, and were obtained through the Meer Corp., North Bergen, NJ.

C57 BL/6 female mice and Lewis rats were purchased from Jackson Laboratories, Bar Harbor, ME. The animals were maintained in accordance with the guidelines of the Committee of Animal Care of the Dana-Farber Cancer Institute and those prepared by the Committee on Care and Use of Laboratory Animals of the Institute of Laboratory Animal Resources, National Research Council (DHEW publication No. [NIH] 78-23, revised 1978). Rat and murine splenocytes were prepared as described by Kleiman *et al.* (1984).

The CTLL-2 cell line (Baker *et al.*, 1979) was a generous gift of Dr. Kendall Smith, Dartmouth Medical School, Dartmouth, NH.

**Synthesis of 4-(Iodoacetamido)-1-cyclohexene-1,2-dicarboxylic Acid.**<sup>3</sup> 1,4-Cyclohexadiene-1,2-dicarboxylic acid di-*tert*-butyl ester was prepared from butadiene and acetylenedicarboxylic acid di-*tert*-butyl ester as described by Weber *et al.* (1980) and was then subjected to a standard hydroboration reaction with diborane in tetrahydrofuran to give 4-hydroxy-1-cyclohexene-1,2-dicarboxylic acid di-*tert*-butyl ester: <sup>1</sup>H NMR (CDCl<sub>3</sub>) δ 1.50 (s, 18H), 1.66–2.62 (m, 7H), 3.95 (m, 1H); IR (neat) ν<sub>max</sub> 3430, 1710, 1645.

4-Amino-1-cyclohexene-1,2-dicarboxylic acid di-*tert*-butyl ester could be prepared from this alcohol in three steps: The alcohol (7.14 g, 23.9 mmol) and *p*-toluenesulfonyl chloride (6.49 g, 33.5 mmol) were dissolved in dry pyridine (43 mL), and the solution was stirred at ambient temperature overnight. Water was then added (0.66 mL), and stirring was continued for another 0.5 h. The solution was then concentrated in the cold under reduced pressure and the residue taken up into ether and washed succes-

sively with cold 1 M H<sub>2</sub>SO<sub>4</sub>, 1 M NaHCO<sub>3</sub>, and water. After drying and removal of the ether, the crude tosylate was dried under high vacuum for 4 h and then dissolved in dry acetonitrile (90 mL). Sodium azide (1.94 g, 200 mmol) and 15-crown-5 (0.95 g, 4.3 mmol) were added, and the solution was refluxed overnight under N<sub>2</sub>(g). The cooled solution was then filtered and concentrated to an oil which was redissolved in dry ether (100 mL) and subjected to a second filtration. Removal of the ether afforded a yellowish oil which was dissolved in dry methanol (75 mL) for the reduction of the azido group. 1,3-Propanedithiol (6.49 g, 60 mmol) and triethylamine (6.07 g, 60 mmol, distilled from 1-naphthyl isocyanate) were added, and the mixture was stirred at room temperature under N<sub>2</sub>(g) for 40 h. The reaction mixture was then filtered and the filtrate concentrated on an aspirator with gentle heating, yielding an orange oil which was purified by flash chromatography on silica gel. The column (200 mL) was first washed with CHCl<sub>3</sub> (500 mL) and CHCl<sub>3</sub>-MeOH (95:5 v/v, 300 mL) and then eluted with CHCl<sub>3</sub>-MeOH (80:20 v/v). The pure amine was recovered as a colorless oil in 56% yield (3.96 g, 13.3 mmol): <sup>1</sup>H NMR (CDCl<sub>3</sub>) δ 1.50 (s, 18H), 1.6–2.6 (m, 8H), 2.97 (m, 1H); IR (neat) ν<sub>max</sub> 3360, 1710, 1650.

The amine (297 mg, 1 mmol), iodoacetic acid (186 mg, 1 mmol), and *N*-(ethoxycarbonyl)-2-ethoxy-1,2-dihydroquinoline (250 mg, 1 mmol) were dissolved in dry dichloromethane (5 mL), and the solution was stirred under N<sub>2</sub>(g) at room temperature overnight. The reaction mixture was then poured into cold 0.1 M HCl, and the product was extracted with ethyl acetate. The combined extracts were washed with water, dried, and concentrated yielding pure 4-(iodoacetamido)-1-cyclohexene-1,2-dicarboxylic acid di-*tert*-butyl ester as an oil, which solidified to a brittle foam upon drying under high vacuum (452 mg, 0.97 mmol): <sup>1</sup>H NMR (CDCl<sub>3</sub>) δ 1.50 (s, 18H), 1.6–2.7 (m, 7H), 3.66 (s, 2H), 6.26 (d, *J* = 8 Hz, 1H). The di-*tert*-butyl ester (0.412 mg, 0.88 mmol) was converted with trifluoroacetic acid (4 mL) quantitatively into the diacid 4-(iodoacetamido)-1-cyclohexene-1,2-dicarboxylic acid: <sup>1</sup>H NMR (Me<sub>2</sub>SO-*d*<sub>6</sub>) δ 1.2–2.8 (m, 7H), 3.6 (s, 2H), 8.3 (d, *J* = 8 Hz, 1H), 9.7 (broad s, 2H).

**Preparation of Conjugates.** IL-2 was supplied by Biogen, Inc., as a solution (0.91 mg/mL) in 50 mM sodium acetate buffer, pH 3.5. Prior to conjugation, this material was dialyzed exhaustively at 4 °C against distilled water and was then buffered by the addition of triethanolamine base, HCl, and disodium EDTA from stock solutions so that the final concentration of buffer was 20 mM at pH 8.0 containing 1 mM EDTA. Gelonin was purified from the seeds of *Gelonium multiflorum* as described by Stirpe *et al.* (1980) and was stored frozen at -70 °C at a concentration of 5–6 mg/mL in 10 mM potassium phosphate buffer, pH 7.2, containing NaCl (145 mM). Stock solutions of 2-iminothiolane were prepared as described previously (Lambert *et al.*, 1978).

Conjugates of IL-2 with gelonin (Figure 1) were prepared using the synthetic routes described below. With the exception of the reactions used to introduce the functional groups into the proteins, the procedure for conjugation of IL-2 with gelonin, and for the purification of the conjugate, was the same in each case and is described in detail only for conjugate A.

**Conjugate A (Disulfide Link).** A solution of IL-2 (0.8 mg/mL) in 20 mM triethanolamine-HCl, pH 8.0, containing EDTA (1 mM) was degassed and then treated with 2-iminothiolane (2 mM) at 0 °C for 45 min under nitrogen. The excess reagent was removed by gel filtration

<sup>2</sup> Abbreviations used: IL-2, interleukin-2; bicine, *N,N*-bis(2-hydroxyethyl)glycine; bis-Tris, 2-[bis(2-hydroxyethyl)amino]-2-(hydroxyethyl)propane-1,3-diol; CTLL, cytolytic T lymphocyte line; DMEM, Dulbecco's modified Eagles medium; HEPES, *N*-(2-hydroxyethyl)piperazine-*N*-2-ethanesulfonic acid; MES, 2-(*N*-morpholino)ethanesulfonic acid; SDS, sodium dodecyl sulfate.

<sup>3</sup> Blättler, W. A., and Lambert, J. M. (1988) U.S. Patent No. 4,764,368. Acid-cleavable compound.

at 4 °C on Sephadex G25 (fine) equilibrated with 50 mM triethanolamine-HCl, pH 8.0, containing EDTA (1 mM). The conditions described here result in the addition of 0.7–0.9 sulfhydryl groups per IL-2 molecule. Gelonin (5–6 mg/mL) was diluted to 4 mg/mL with distilled water, 0.5 M triethanolamine-HCl, pH 8.0, and 0.1 M disodium EDTA, pH 8.0, so that the final concentrations of triethanolamine and EDTA were 60 and 1 mM, respectively. The solution was degassed and then treated with 2-iminothiolane (1 mM) at 0 °C for 45 min under nitrogen. The excess reagent was removed by gel filtration at 4 °C on Sephadex G25 (fine) equilibrated with 5 mM bis-Tris-acetate, pH 5.8, containing NaCl (50 mM) and EDTA (1 mM). Under these conditions, 0.6–0.8 sulfhydryl groups were introduced per gelonin molecule. The modified gelonin was treated with 5,5'-dithiobis(2-nitrobenzoic acid) (10 mM) at 4 °C for 30 min in order to form the mixed disulfide of the modified gelonin and 2-nitro-5-thiobenzoate. This material was purified by gel filtration at 4 °C on Sephadex G25 (fine) equilibrated with 50 mM triethanolamine-HCl, pH 8.0, containing EDTA (1 mM). Conjugate A was prepared by incubating the mixed disulfide (0.3 mg/mL final concentration) with a slight molar excess of the modified IL-2 at 4 °C for 16 h under nitrogen, after which the reaction mixture was treated with iodoacetamide (1 mM) at 4 °C for 1 h in order to block any remaining free sulfhydryl groups. The conjugate was purified by gel filtration at 4 °C on Sephadex G100 (superfine) equilibrated with 20 mM bicine-NaOH, pH 8.5, containing betaine (250 mM). Fractions containing pure conjugate were pooled and dialyzed against bicine-NaOH, pH 8.5, containing NaCl (150 mM). The conjugate was then concentrated to 0.12 mg/mL using a Millipore CX10 microconcentrator, frozen in small aliquots (250  $\mu$ L) using liquid nitrogen, and stored at -70 °C.

**Conjugate B (Acid-Labile Link).** Sulfhydryl groups were introduced into IL-2 using 2-iminothiolane as described above. Gelonin was modified using 4-(iodoacetamido)-1-cyclohexene-1,2-dicarboxylic acid anhydride. The reagent was prepared immediately before use by treating 4-(iodoacetamido)-1-cyclohexene-1,2-dicarboxylic acid (0.125 M) in dimethyl sulfoxide with dicyclohexylcarbodiimide (0.15 M) at 25 °C for 1 h, and following filtration the solution was used without further purification. Gelonin (5–6 mg/mL), diluted to 4 mg/mL with 100 mM sodium phosphate buffer, pH 7.0, containing EDTA (1 mM), was treated with the anhydride (312.5  $\mu$ M, assuming complete reaction of the dicarboxylic acid) at 25 °C for 15 min. Excess reagent was removed by gel filtration at 4 °C on Sephadex G25 (fine) equilibrated with 50 mM triethanolamine-HCl, pH 8.0, containing EDTA (1 mM). Under these conditions, approximately 0.8 iodoacetamido groups were introduced per gelonin molecule.

**Conjugate C (Noncleavable Link).** Iodoacetamido groups were introduced into IL-2 using *N*-succinimidyl iodoacetate. A solution of IL-2 (0.8 mg/mL) in 50 mM triethanolamine-HCl, pH 8.0, containing EDTA (1 mM) was treated with *N*-succinimidyl iodoacetate (208  $\mu$ M), added from a 40 mM solution in dioxane, at 30 °C for 15 min. The reaction was terminated by gel filtration at 4 °C on Sephadex G25 (fine) equilibrated with 50 mM triethanolamine-HCl, pH 8.0, containing EDTA (1 mM). About 0.9 iodoacetamido groups were introduced per IL-2 molecule. Sulfhydryl groups were introduced into gelonin using 2-iminothiolane as described above.

**Conjugate D (Noncleavable Link: Toxin Inactive).** Sulfhydryl groups were introduced into IL-2 using 2-iminothiolane as described above. Gelonin (5–6 mg/mL) was

diluted to 4 mg/mL with 100 mM sodium phosphate buffer, pH 7.0, containing EDTA (1 mM) and was then treated with *N*-succinimidyl iodoacetate (200  $\mu$ M) at 30 °C for 15 min. Excess reagent was removed by gel filtration at 4 °C on Sephadex G25 (fine) equilibrated with 50 mM triethanolamine-HCl, pH 8.0, containing EDTA (1 mM). The conditions described here result in the introduction of about 0.7 iodoacetamido groups per gelonin molecule.

**Measurement of Extent of Protein Modification.** Sulfhydryl groups introduced into the proteins were quantified spectrophotometrically by the method of Ellman (1959). The incorporation of iodoacetamido groups into the proteins was measured by incubating samples of the modified proteins (0.2–1.2 mg/mL) with excess [ $^{14}$ C]-cysteine (1.7 mM; 0.5 mCi/mmol) in 50 mM triethanolamine-HCl buffer, pH 8.0, containing EDTA (1 mM) for 1 h at 25 °C. The labeled proteins were separated from [ $^{14}$ C]cysteine by gel filtration at 4 °C on columns (4 mL) of Sephadex G25 (fine) equilibrated with 50 mM triethanolamine-HCl, pH 8.0, containing EDTA (1 mM). Fractions (0.2 mL) were counted in 4 mL of Biofluor scintillation cocktail using a Packard Tri-Carb Model 2000 CA scintillation counter (efficiency for  $^{14}$ C was 90 %).

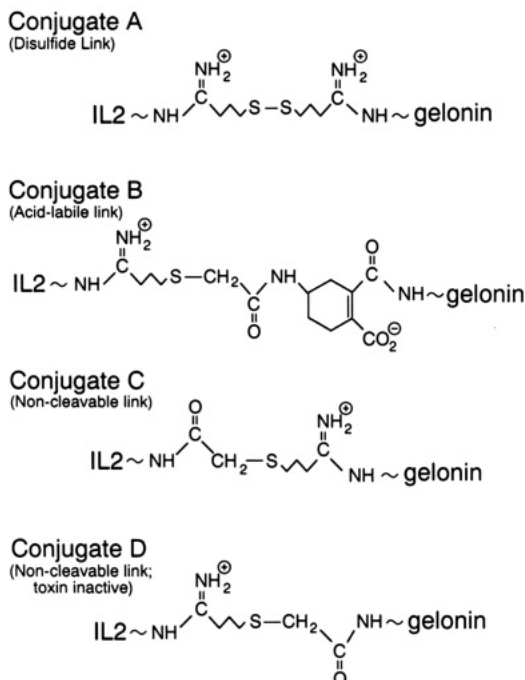
**Polyacrylamide Gel Electrophoresis.** Electrophoresis in the presence of 0.1 % (w/v) SDS was carried out in acrylamide gel slabs (145 mm  $\times$  90 mm  $\times$  0.75 mm) prepared according to Laemmli (1970). Samples of protein in 25  $\mu$ L of buffer, pH 8.5, were prepared for electrophoresis by mixing with urea (28 mg) and 3  $\mu$ L of a solution of SDS (20 % w/v) containing iodoacetamide (100 mg/mL) and incubating at room temperature for 1 h. The urea was necessary to ensure complete denaturation of proteins in the absence of heating, and iodoacetamide was added to react with any free sulfhydryl groups (Lambert *et al.*, 1978). Proteins were stained with Coomassie Brilliant Blue R250.

**Measurement of Protein Concentration.** Concentrations of purified proteins were determined from their  $A_{280\text{nm}}$ , using  $E^{1\%}_{1\text{cm}}$  values of 6.7 for gelonin (Stirpe *et al.*, 1980) and 7.0 for IL-2 [the latter value was measured in a solution of IL-2 whose concentration was determined by two different methods using bovine serum albumin as a standard (Lowry *et al.*, 1951; Bradford, 1976)]. The protein concentrations of the purified conjugates were also estimated from their  $A_{280\text{nm}}$ , using an  $E^{1\%}_{1\text{cm}}$  value of 6.8.

**Ribosome-Inactivating Activity of the Conjugates.** The inhibitory activity of gelonin toward protein synthesis was measured in a rabbit reticulocyte lysate system. The assay was based on that of Pelham and Jackson (1976), using materials provided by New England Nuclear supplemented with additional reagents as described in detail previously (Lambert *et al.*, 1985; Lambert and Blättler, 1988).

**Binding Studies.** IL-2 was labeled using the method of Bolton and Hunter (1973). IL-2 (5  $\mu$ g) was reacted with 250 pmol of *N*-succinimidyl 3-(4-hydroxy-5-[ $^{125}$ I]iodophenyl)propionate in 10  $\mu$ L of 0.1 M sodium borate buffer, pH 8.5, at 0 °C for 15 min. In order to prevent the subsequent labeling of carrier proteins, the reaction solution was then treated at 0 °C for 15 min with 200  $\mu$ L of 0.5 M glycine in 0.1 M sodium borate, pH 8.5. Labeled IL-2 was purified by gel filtration at 4 °C on Sephadex G25 (fine) equilibrated with 50 mM sodium phosphate buffer, pH 7.5, containing 0.25 % (w/v) gelatin. The pure sample had a specific radioactivity of 18.8  $\mu$ Ci/ $\mu$ g.

CTLL-2 cells were maintained in exponential growth in DMEM supplemented with 40 % (v/v) conditioned medium (prepared using rat splenocytes as described by Gillis



**Figure 1.** IL-2-gelonin conjugates using different types of linkers.

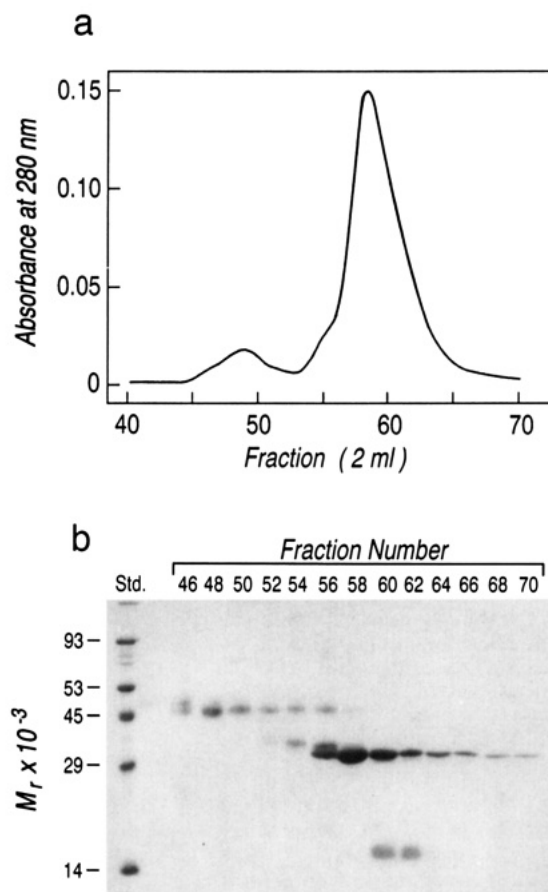
*et al.* (1978)), fetal calf serum (10% (v/v)), penicillin (100 U/mL), streptomycin (100 µg/mL), and fungizone (0.25 µg/mL).

Binding assays were carried out in RPMI 1640 medium containing 25 mM HEPES buffer, pH 7.2, and 10 mg/mL of bovine serum albumin (assay buffer). CTLL-2 cells ( $70 \times 10^6$  cells) were washed three times with 50 mL of assay buffer at room temperature, incubated with 50 mL of the buffer for 1 h at 37 °C, and then washed a further three times at room temperature (Robb *et al.*, 1981). Dilutions of IL-2 or of conjugate were prepared in final volumes of 100 µL of assay buffer containing  $5 \times 10^5$  CTLL-2 cells and 7.0 fmol of  $^{125}\text{I}$ -labeled IL-2. The level of nonspecific binding was determined by including mixtures which contained an excess of unlabeled IL-2 (500 pmol). The mixtures were incubated for 1 h at 4 °C in 0.7 mL Eppendorf tubes after which 0.4 mL of assay buffer was added, and the cells were pelleted at 13 000 rpm for 2 min at 4 °C. The cells were washed twice with 0.5 mL of ice-cold assay buffer, and bound label was then measured using an LKB Model 1272  $\gamma$  counter.

**Proliferation Assays.** Proliferation assays were carried out in 96-well flat-bottom microtiter plates in RPMI 1640 medium supplemented with fetal calf serum (10% (v/v)), penicillin (100 U/mL), streptomycin (100 µg/mL), and fungizone (0.25 µg/mL). Dilutions of IL-2 or of the conjugates were prepared in triplicate in 200 µL of the above medium containing  $0.5 \times 10^6$  murine splenocytes and either concanavalin A (1 µg/mL) or lipopolysaccharide (1 µg/mL). Mixtures containing no added IL-2 or conjugate were also prepared. The plates were incubated for 48 h at 37 °C, and each well was pulsed with 1 µCi of [*methyl*- $^3\text{H}$ ]thymidine for the final 4 h of the incubation. The cells were harvested on glass fiber filters using a PHD harvester (Cambridge Biotechnology, Inc., Cambridge, MA), and the incorporated label was counted in 4 mL of Betafluor scintillation cocktail.

## RESULTS

**Preparation and Purification of Conjugates.** Four conjugates of IL-2 with gelonin (Figure 1) were prepared



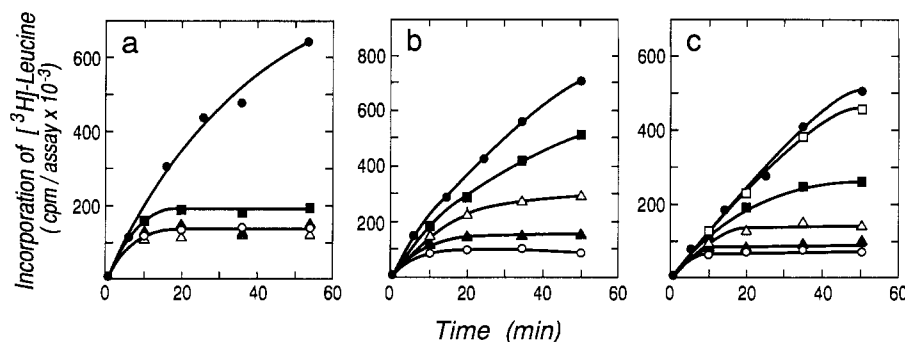
**Figure 2.** Gel filtration of an IL-2-gelonin conjugation reaction mixture and analysis of the elution profile by SDS-polyacrylamide gel electrophoresis. IL-2 and gelonin were conjugated as described in the Experimental Procedures for the preparation of conjugate D. Panel a: elution profile of the conjugation mixture (2.2 mg of protein in 2 mL) submitted to gel filtration through a column (99 cm  $\times$  1.6 cm) of Sephadex G100 (superfine) equilibrated with 20 mM bicine-NaOH buffer, pH 8.5, containing 250 mM betaine. Panel b: 12.5% (w/v) SDS-polyacrylamide gel of samples taken from fractions of the elution profile shown in panel a. The gel was run under nonreducing conditions as described in the Experimental Procedures, and the calibration of  $M_r$  was from the mobility of proteins of known subunit  $M_r$  (Std): phosphorylase b (93 000), glutamate dehydrogenase (53 000), ovalbumin (45 000), carbonic anhydrase (29 000), and lysozyme (14 300).

using the synthetic routes described in the Experimental Procedures. In each case, the two proteins were modified to introduce complementary reactive groups and were then cross-linked in a reaction which gave only the heterodimer in high yield.

In order to minimize the formation of high molecular weight polymeric conjugates, the proteins were modified to introduce on average only 0.6 to 0.9 reactive groups per molecule. The conditions required for the introduction of mercaptobutyrimidoyl groups into gelonin using 2-iminothiolane have already been described (Lambert *et al.*, 1985). For each of the other modification reactions, preliminary experiments were carried out to determine the conditions required to introduce the appropriate number of reactive groups into either IL-2 or gelonin.

Examination of the conjugation reaction mixtures by SDS-polyacrylamide gel electrophoresis (not shown) demonstrated that a major product of each reaction was a heteroconjugate ( $M_r \sim 46$  000) consisting of one IL-2 molecule ( $M_r$  15 000; Liang *et al.*, 1985) linked to one gelonin molecule ( $M_r$  30 500; Thorpe *et al.*, 1981; Lambert *et al.*, 1988) as inferred from the mobility of the stained protein bands. Bands corresponding in apparent molec-





**Figure 3.** Effect of the modification of gelonin on its inhibitory activity toward protein synthesis in a cell-free system from rabbit reticulocyte lysates. Protein synthesis was measured by the incorporation of [ $^3$ H]leucine into protein precipitable with trichloroacetic acid as described in the Experimental Procedures. The incorporation of radioactivity in the controls within 50 min was in the range of 500 000–700 000 cpm per assay (volume 27  $\mu$ L) and was counted with an efficiency of 20–25% (Packard Tri-Carb Model 2000 CA scintillation counter). Samples of gelonin modified to introduce iodoacetamido groups and the corresponding control samples of nonmodified gelonin were treated with 2-mercaptoethanol (1 mM) for 1 h at 25  $^{\circ}$ C before assay. All samples were maintained under reducing conditions prior to the assay by the inclusion of dithioerythritol (2 mM) in the sample buffer. Panel a: inhibition of protein synthesis by gelonin modified using 2-mercaptoethanol: (●) control assay; (○) assay that contained 20 pg of gelonin; (▲, △, ■) assays that contained 20 pg of gelonin modified with 2-mercaptoethanol to introduce 0.5 sulfhydryl groups per molecule of gelonin (▲), 1.14 groups per gelonin (△), or 2.93 groups per gelonin (■). Panel b: inhibition of protein synthesis by gelonin modified using 4-(iodoacetamido)-1-cyclohexene-1,2-dicarboxylic acid anhydride: (●) control assay; (○) assay that contained 20 pg gelonin; (▲, △, ■) assays that contained 20 pg of gelonin modified with 0.49 iodoacetamido groups per molecule of gelonin (▲), 0.66 groups per gelonin (△), or 1.90 groups per gelonin (■). Panel c: inhibition of protein synthesis by gelonin modified using *N*-succinimidyl iodoacetate: (●) control assay; (○) assay that contained 20 pg of gelonin; (▲, △, ■, □) assays that contained 20 pg of gelonin modified with *N*-hydroxysuccinimidyl iodoacetate to introduce 0.56 iodoacetamido groups per molecule of gelonin (▲), 0.9 groups per gelonin (△), 1.38 groups per gelonin (■), or 2.69 groups per gelonin (□).

ular weight to small amounts of IL-2–gelonin conjugates with IL-2 to gelonin stoichiometries of 1:2 and 2:1 could also be seen in the gels. Other products of the conjugation reaction included small quantities of cross-linked gelonin and cross-linked IL-2 which likely result from the formation of protein–protein disulfide bonds following the modification of either IL-2 or gelonin using 2-mercaptoethanol. In addition, IL-2 contains a nonbonded sulfhydryl group (Liang *et al.*, 1985) which, although not sufficiently reactive to be of use in the preparation of conjugates (J.M. Lambert, unpublished results), may participate in the formation of disulfide cross-linked IL-2.

The most effective way to obtain samples of pure IL-2–gelonin was found to be a single step of gel filtration on Sephadex G100 (superfine). Under conditions of low ionic strength, there was a significant interaction between IL-2 and gelonin which resulted in some contamination of the purified conjugate with unconjugated gelonin. This was minimized by the inclusion of 250 mM betaine in the buffer used for gel filtration. Figure 2a shows the elution profile obtained when the reaction mixture obtained in the preparation of conjugate D was purified in this manner. Similar profiles were obtained for each of the other conjugation reaction mixtures. Two incompletely separated peaks of protein were obtained. Analysis of the peaks by SDS–polyacrylamide gel electrophoresis (Figure 2b) showed that the first peak (fractions 45–53) consisted primarily of the IL-2–gelonin conjugate ( $M_r$  ~46 000), although bands that may correspond to small amounts of IL-2 dimer and trimer contaminated the trailing and leading edges of the peak. The second peak consisted of unconjugated gelonin (peak fraction 58) and IL-2 (peak fraction, 61).

The yields of conjugate, based on densitometric analysis of samples analyzed by SDS–polyacrylamide gel electrophoresis, were in the order of 15–20% with respect to IL-2. Purified material for biological testing was obtained by pooling only those fractions which contained no contaminating proteins. This material, which represented less than 60% of the total conjugate formed, was at least 95% pure as judged by SDS–polyacrylamide gel electrophoresis.

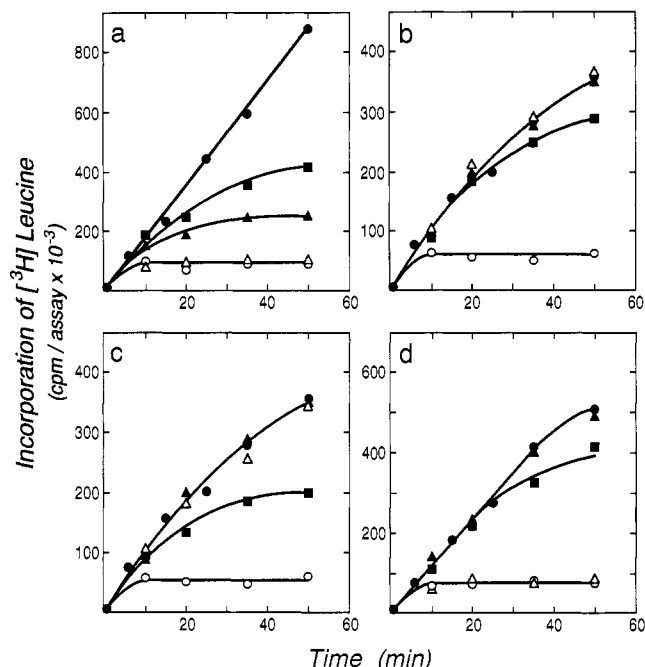
#### Effect of Modification of Gelonin on Its Ribosome-Inactivating Activity.

The ability of gelonin to inactivate ribosomes was measured by dilution of samples into an assay of cell-free protein synthesis using the rabbit reticulocyte system. Figure 3 shows the effects of chemical modification on the ribosome-inactivating activity of gelonin. Under the conditions used, 20 pg of native gelonin completely inhibited protein synthesis within 10–20 min. Modification of gelonin using 2-mercaptoethanol had little effect on the catalytic activity of the toxin (Figure 3a); even the introduction of 2.9 groups caused only a minimal reduction in the ribosome-inactivating activity of the protein. In contrast, modification with either 4-(iodoacetamido)-1-cyclohexene-1,2-dicarboxylic acid anhydride (Figure 3b) or with *N*-succinimidyl iodoacetate (Figure 3c) resulted in a significant decrease in the enzymatic activity of the protein. Comparison of these results with assays carried out with further dilutions of native gelonin indicated that the modification of an average of 1 residue per gelonin molecule using these reagents resulted in a 50–70% reduction in the activity of the toxin (this result indicated to us that it was possible that the modified molecules of gelonin were completely inactivated).

#### Ribosome-Inactivating Activity of the Conjugates.

The ribosome-inactivating activity of the purified conjugates was also measured using the cell-free assay system. Both conjugates which had been prepared using gelonin modified with 2-mercaptoethanol (conjugates A and C) exhibited significant ribosome-inactivating activity, although the activity was reduced relative to that of native gelonin by about 60–80% as estimated by comparison with assays carried out with serial dilutions of native gelonin (Lambert and Blättler, 1988). However, preincubation of the conjugate formed with a disulfide linkage (conjugate A) with dithioerythritol released fully active gelonin that was indistinguishable from native gelonin in its ability to inhibit protein synthesis in these assays (Figure 4a). As expected, the activity of conjugate C was unaffected by preincubation with dithioerythritol (result not shown).

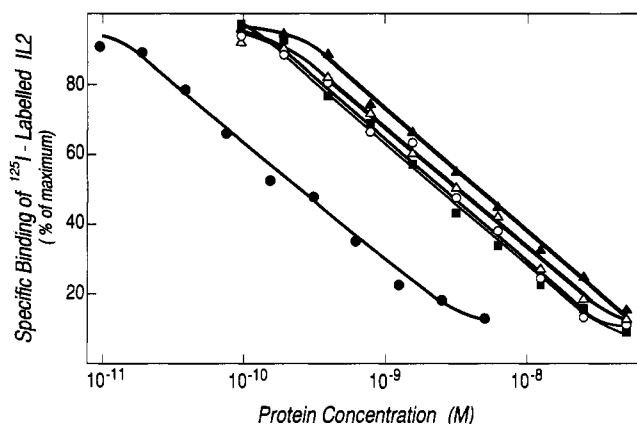
The ability of gelonin to inhibit protein synthesis was drastically reduced in purified preparations of both conjugate D and conjugate B. Whereas protein synthesis



**Figure 4.** Inhibition of protein synthesis in a cell-free system from rabbit reticulocyte lysates by gelonin or by conjugates of IL-2 with gelonin. Protein synthesis was measured by the incorporation of [<sup>3</sup>H]leucine into protein precipitable with trichloroacetic acid as described in the Experimental Procedures. The incorporation of radioactivity in the controls within 50 min was in the range of 350 000–900 000 cpm per assay (27  $\mu$ L) and was counted with an efficiency of 20–25% (Packard Tri-Carb Model 2000 CA scintillation counter). Panel a: (●) control assay; (○) assay that contained 20 pg of gelonin; (▲, △) assays that contained an amount of conjugate A (disulfide link) that contained 20 pg of gelonin without (▲) and with (△) pretreatment of the conjugate with dithioerythritol (20 mM) for 30 min at 30 °C; (■) assay that contained an amount of conjugate C (noncleavable link) equivalent to 20 pg of gelonin. Panel b: (●) control assay; (○) assay that contained 20 pg of gelonin; (▲, △, ■) assays that contained an amount of conjugate D (noncleavable link) equivalent to 20 pg (▲), 200 pg (△), or 2 ng (■) of gelonin. Panel c: (●) control assay; (○) assay that contained 20 pg of gelonin; (▲, △, ■) assays that contained an amount of conjugate B (acid-labile link) equivalent to 20 pg (▲), 200 pg (△), or 2 ng (■) of gelonin. Panel d: (●) control assay; (○) assay that contained 20 pg of gelonin; (▲, △, ■) assays that contained an amount of conjugate B equivalent to 20 pg of gelonin after incubation of the conjugate (23  $\mu$ g/mL) for 48 h at 37 °C, either in 100 mM MES-HCl buffer, pH 5.5, containing 0.1 mg/mL of bovine serum albumin (△) or in 100 mM sodium phosphate buffer, pH 7.2, containing 0.1 mg/mL of bovine serum albumin (■).

was completely abolished in 10–15 min by 20 pg of native gelonin, an amount of conjugate D equivalent to 2 ng of gelonin failed to completely inhibit protein synthesis, even after 50 min (Figure 4b). Similarly, amounts of conjugate B (acid-labile link) corresponding to 2 ng of gelonin were required for complete inhibition of protein synthesis which was achieved only after about 40 min, while 200 pg of conjugated gelonin failed to cause any inhibition of protein synthesis in these assays (Figure 4c). In the case of the acid-labile conjugate B, however, the release of gelonin by incubation of the conjugate in MES-HCl buffer, pH 5.5, at 37 °C for 48 h completely restored the ability of the gelonin to inhibit protein synthesis (Figure 4d). A control treatment of the conjugate at pH 7.2 and 37 °C for 48 h yielded less than 20% of the ribosome-inactivating activity of native gelonin.

**Binding of the Conjugates to CTLL-2 Cells.** The ability of the conjugates to bind to the IL-2 receptor was

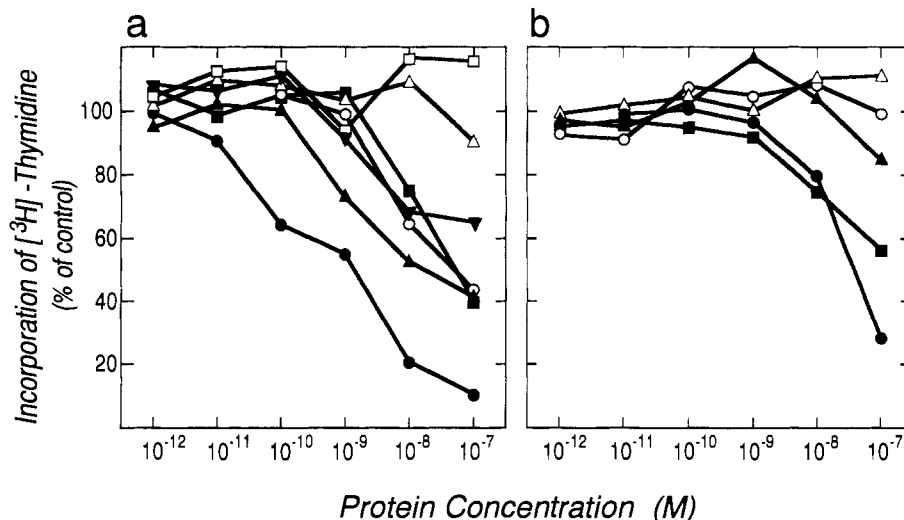


**Figure 5.** Competitive inhibition of the binding of <sup>125</sup>I-labeled IL-2 to CTLL-2 cells by IL-2 or by conjugates of IL-2 with gelonin. Binding experiments were carried out at 4 °C as described in the Experimental Procedures. Under the conditions of the assay, 50% of the labelled IL-2 (3.5 fmol; 2200 cpm) bound to the cells in the absence of competing ligand. Nonspecific binding represented 7% of the total binding capacity of the cells. The curves show the inhibition of the binding of label to CTLL-2 cells by IL-2 (●), conjugate A (○), conjugate B (▲), conjugate C (△), and conjugate D (■).

measured by competitive displacement of <sup>125</sup>I-labeled IL-2 from CTLL-2 cells. Figure 5 shows a series of binding curves comparing the binding of the four conjugates with that of nonconjugated IL-2. Under the conditions used (see Experimental Procedures), 50% of the label specifically bound by the cells was displaced by 400 pM IL-2. The displacement curves for the conjugates indicate that the attachment of gelonin to IL-2 has reduced the binding affinity by about 1 order of magnitude, concentrations of conjugate of between 3 and 7 nM being required to displace 50% of the label bound to the IL-2 receptor.

**Inhibition of T-Cell and B-Cell Responses.** The inhibition of lymphocyte proliferative responses, as measured by the inhibition of incorporation of [<sup>3</sup>H]thymidine relative to controls, was used as a measure of cytotoxicity. Concanavalin A was used as a T-cell mitogen. Conjugate A, in which IL-2 was linked to gelonin through a disulfide bond, clearly inhibited the proliferative response of murine splenocytes to concanavalin A (Figure 6a). The IC<sub>50</sub> of the conjugate, ~500 pM, is 2 orders of magnitude lower than the IC<sub>50</sub> for native gelonin (50 nM). An admixture of IL-2 and gelonin showed only the same cytotoxicity as gelonin alone. The acid-labile and noncleavable conjugates were less effective than conjugate A. The IC<sub>50</sub> of the noncleavable conjugate C was only 10-fold lower than the IC<sub>50</sub> of native gelonin, and the effect of the acid-labile conjugate B on the T-cell response was indistinguishable from that of the unconjugated toxin.

Concanavalin A induces expression of IL-2 receptors and production of IL-2 by mouse lymphocytes (Robb *et al.*, 1981). Growth of the activated lymphocytes is maintained by stimulation of the cells by autocrine and paracrine IL-2. Under these conditions, it is possible that the IL-2-gelonin conjugates might inhibit the proliferative response of lymphocytes to concanavalin A by direct competition for binding to the IL-2 receptor rather than by the inhibition of protein synthesis. This possibility was examined using conjugate D in which the ability of gelonin to inhibit protein synthesis was reduced by several orders of magnitude. This conjugate showed no effect on the proliferative response of the lymphocytes at any concentration tested (Figure 6a), indicating that the effects of the other conjugates were dependent on the presence



**Figure 6.** Cytotoxicity of conjugates of IL-2 with gelonin. The inhibition of proliferative responses in lymphocytes as measured by the inhibition of the incorporation of  $[^3\text{H}]$ thymidine relative to controls was used as a measure of cytotoxicity as described in Methods. Panel a: inhibition of T-cell response; murine splenocytes were stimulated with concanavalin A and incubated for 48 h in the presence of conjugate A (●), conjugate B (○), conjugate C (▲), conjugate D (△), gelonin (■), IL-2 (□), or an admixture of IL-2 and gelonin (▼). Panel b: inhibition of B cell response; murine splenocytes stimulated with lipopolysaccharide and incubated for 48 h in the presence of conjugate A (●), conjugate B (○), conjugate C (▲), conjugate D (△), or gelonin (■).

of the active toxin and were not simply due to competition of binding at the level of the IL-2 receptor.

In order to confirm the selectivity of the conjugates for cells expressing the IL-2 receptor, their effect on the proliferative response of lymphocytes to the B-cell mitogen lipopolysaccharide was examined. Figure 6b shows that the proliferative response of murine splenocytes to lipopolysaccharide was not affected by the acid-labile conjugate or by the two non-cleavable conjugates. The conjugate of IL-2 linked to gelonin through a disulfide bond did exhibit some toxicity in this assay system, but only over the range of concentrations at which native gelonin itself was toxic.

## DISCUSSION

Studies with immunotoxins have established that the nature of the linkage used in the preparation of such conjugates, the amount of binding to the cell surface, and the extent of internalization of the conjugates are important factors influencing their cytotoxicity toward target cells (Lambert *et al.*, 1985; Goldmacher *et al.*, 1989). Single-chain ribosome-inactivating proteins, such as gelonin, do not bind to the cell surface and rely on fluid-phase pinocytosis as their only mode for internalization (Goldmacher *et al.*, 1986). When gelonin is conjugated to monoclonal antibodies that recognize antigens which are present in high numbers on the cell surface, and which are internalized efficiently, the cytotoxicity of the conjugates may be 2–4 orders of magnitude greater than that of the unconjugated toxin (Thorpe *et al.*, 1981; Lambert *et al.*, 1985; Lambert *et al.*, 1988; Goldmacher *et al.*, 1989).

In this paper, we describe conjugates between IL-2 and gelonin prepared with disulfide, acid-labile, and non-cleavable linkers. The most potent of these conjugates, that containing a disulfide bond, exhibited a cytotoxicity which was 2 orders of magnitude greater than that seen with unconjugated gelonin, as judged by the effect of the conjugate on the proliferative response of murine splenocytes to concanavalin A. *In vitro* assays showed that cleavage of the disulfide bond restored the full catalytic activity of the toxin which may account, in part, for the observation that the conjugate containing the disulfide bond (conjugate A) was more effective in inhibiting T cell

function than that prepared using a noncleavable link (conjugate C). The cleavable disulfide linkage may also allow the toxin to escape more readily into the cytoplasm from the membrane-bound IL-2/IL-2 receptor complex.

As previously reported (Lambert *et al.*, 1985), gelonin was not affected by modification with 2-iminothiolane in its ability to inhibit protein synthesis. In contrast, modification of the toxin with either *N*-succinimidyl iodoacetate or with 4-(iodoacetamido)-1-cyclohexenyl-1,2-dicarboxylic acid anhydride resulted in a drastic reduction in its ability to inactivate ribosomes. The reason for the striking difference in the effects of modifying gelonin using these cross-linking reagents is not clear. One could speculate that these reagents react preferentially with different amino groups on gelonin, one of which is important for catalytic activity. Another factor is the preservation of the positive charge of amino groups upon reaction with 2-iminothiolane. If this were important for maintaining full catalytic activity, then modification with *N*-succinimidyl iodoacetate or with 4-(iodoacetamido)-1-cyclohexenyl-1,2-dicarboxylic acid anhydride, each of which react with amino groups to form neutral amides, might be expected to inactivate the toxin. In this respect, it is interesting to note that modification of gelonin with other cross-linking reagents which form uncharged amide bonds, for example, *N*-hydroxysuccinimide esters such as *N*-succinimidyl 3-(2-pyridyldithio)propionate, also reduce its ability to inactivate ribosomes (Thorpe *et al.*, 1981; Blättler *et al.*, 1985; Senter *et al.*, 1985).

The conjugate of gelonin coupled to IL-2 through a noncleavable thioether linkage (conjugate D) showed no cytotoxicity, as expected, since the catalytic activity of the toxin was almost completely abolished. When gelonin was linked to IL-2 through the acid-labile linkage (conjugate B) the ribosome-inactivating activity of the gelonin in this conjugate was also almost completely abolished. However, the catalytic activity of the toxin from conjugate B was fully restored following release of the native toxin by incubation under mildly acidic conditions (pH 5.5), as expected from previous work with analogous reagents (Kirby and Lancaster, 1970; Blättler *et al.*, 1985). In spite of this, the cytotoxicity observed for conjugate B was no more than that seen with unconjugated gelonin, although

it is generally assumed that many ligands bound to cell-surface receptors are internalized into acidified vesicles (endosomes) (Mellman *et al.*, 1986). However, the fact that *any* cytotoxicity is seen at all (comparison of conjugate B with conjugate D) indicates that *some* active (native) gelonin was indeed released from the conjugate, most likely in an acidic intracellular compartment. Whatever the explanation for the poor efficacy of this conjugate, these results with IL-2 conjugates suggested that gelonin is more readily released to the cytoplasm from a disulfide-linked conjugate than from a conjugate with an acid-labile linker.

In the present study, at least three factors may have affected the efficiency with which the IL-2-gelonin conjugates are internalized. Firstly, it is clear from binding studies that the attachment of gelonin to IL-2 decreases the affinity of the lymphokine for its receptor by about 1 order of magnitude. Such a decrease in binding affinity has been reported for a number of hormone-toxin constructs (Chang *et al.*, 1977; Bacha *et al.*, 1983) and may reflect the steric effects of attaching a protein toxin to a relatively small targeting vehicle, although we cannot rule out from these experiments an effect on binding due to the chemical modification itself. Secondly, although T lymphocytes express as many as 60 000 IL-2 receptors per cell, the efficient internalization of IL-2 occurs via a small population of high-affinity IL-2 receptors which are present on activated T-cells at a density of only 2000-4000 receptors per cell (Robb *et al.*, 1981; Weissman *et al.*, 1986). Thirdly, in the test system used, stimulation of lymphocytes by concanavalin A is known to result in the autocrine production of IL-2 (Robb *et al.*, 1981), and the endogenous IL-2 produced may reduce the cytotoxicity of IL-2-gelonin conjugates by direct competition at the level of the receptor. Clearly, these factors may limit the potential cytotoxicity of the IL-2-gelonin conjugates.

The cytotoxicity of the IL-2-gelonin made with a disulfide linker for cells expressing the IL-2 receptor was similar to that of an immunotoxin prepared using the A chain of ricin and an anti-IL-2 receptor antibody (anti-Tac) which binds to an epitope found in the p55 subunit of both the high- and low-affinity IL-2 receptors (Krönke *et al.*, 1986). However, these conjugates of single-chain ribosome-inactivating proteins targeting the IL-2 receptor, and other similar conjugates targeting other antigens, are far less potent than intact ricin (Goldmacher *et al.*, 1989; Blättler *et al.*, 1989). These observations have led to the suggestion that the B chain of ricin is not only responsible for binding to the cell surface but may also participate in the transport of the A chain across the membrane (Vitetta *et al.*, 1983; Blättler *et al.*, 1989) or may direct the A chain to a particular intracellular compartment from which the A chain can gain access to the cytoplasm (Goldmacher *et al.*, 1992; Newton *et al.*, 1992). Similar cell surface binding and transport functions have been ascribed to distinct portions of the bacterial toxins diphtheria toxin (Greenfield *et al.*, 1987) and pseudomonas exotoxin A (Hwang *et al.*, 1987). The selective removal or modification of the binding domains of these proteins by protein engineering has resulted in the generation of toxins (Greenfield *et al.*, 1987; Hwang *et al.*, 1987) which may be more potent than proteins such as gelonin or ricin A-chain if they retain all the elements important for translocation or correct intracellular routing (Pastan *et al.*, 1992). A number of genetic constructs have been reported in which such engineered proteins have been linked to hormones, and in particular, to IL-2 (Murphy *et al.*, 1988; Pastan *et al.*, 1992). These constructs appear to show selective toxicity both *in vitro* (Lorberboum-Galski *et al.*, 1988; Ogata *et al.*,

1988) and *in vivo* (Kelley *et al.*, 1988; Case *et al.*, 1989; Lorberboum-Galski *et al.*, 1989; Pastan *et al.*, 1992). Unfortunately, comparison of the potencies of conjugates of pseudomonas exotoxin A or diphtheria toxin with that of the IL-2-gelonin conjugate (disulfide link) is not possible owing to the wide variation in the biological test systems used in different laboratories.

An alternative approach to the production of a more potent toxin for specific targeting has been to chemically modify the cell-surface binding sites of ricin in order to block the ability of the toxin to bind to cells, while retaining the B-chain functions that promote efficient A-chain translocation into the cytoplasm (Lambert *et al.*, 1991a,b). It is likely that such modified toxins would also be highly effective reagents for the production of toxic conjugates using lymphokines such as IL-2.

#### LITERATURE CITED

- Bacha, P., Murphy, J. R., and Reichlin, S. (1983) Thyrotropin-releasing Hormone-Diphtheria Toxin-related Polypeptide Conjugates: Potential Role of the Hydrophobic Domain in Toxin Entry. *J. Biol. Chem.* 258, 1565-1570.
- Baker, P. E., Gillis, S., and Smith, K. A. (1979) Monoclonal Cytolytic T-cell Lines. *J. Exp. Med.* 149, 273-278.
- Blättler, W. A., Kuenzi, B. S., Lambert, J. M., and Senter, P. D. (1985) New Heterobifunctional Protein Cross-Linking Reagent That Forms an Acid-Labile Link. *Biochemistry* 24, 1517-1525.
- Blättler, W. A., Lambert, J. M., and Goldmacher, V. S. (1989) Realizing the Full Potential of Immunotoxins. *Cancer Cells* 1, 50-55.
- Bolton, A. E., and Hunter, W. M. (1973) The Labelling of Proteins to High Specific Radioactivities by Conjugation to a <sup>125</sup>I-Containing Acylating Agent: Application to the Radioimmunoassay. *Biochem. J.* 133, 529-539.
- Bradford, M. M. (1976) A Rapid and Sensitive Method for the Quantitation of Microgram Quantities of Protein Utilizing the Principle of Protein Dye Binding. *Anal. Biochem.* 72, 248-254.
- Case, J. P., Lorberboum-Galski, H., Lafyatis, R., FitzGerald, D., Wilder, R. L., and Pastan, I. (1989) Chimeric cytotoxin IL2-PE40 delays and mitigates adjuvant-induced arthritis in rats. *Proc. Natl. Acad. Sci. U.S.A.* 86, 287-291.
- Cawley, D. B., Herschman, H. R., Gilliland, D. G., and Collier, R. J. (1980) Epidermal Growth Factor-Toxin A Chain Conjugates: EGF-Ricin A Is a Potent Toxin While EGF-Diphtheria Fragment A Is Nontoxic. *Cell* 22, 563-570.
- Change, T.-M., Dazord, A., and Neville, D. M. (1977) Artificial Hybrid Protein Containing a Toxic Protein Fragment and a Cell Membrane Receptor-binding Moiety in a Disulfide Conjugate. *J. Biol. Chem.* 252, 1515-1522.
- Derocq, J.-M., Laurent, G., Casellas, P., Vidal, H., Poncelet, P., Fauser, A., Demur, C., and Jansen, F. (1987) Rationale For the Selection of Ricin A-chain Anti-T Immunotoxins For Mature T Cell Depletion. *Transplantation* 44, 763-769.
- Ellman, G. L. (1959) Tissue Sulfhydryl Groups. *Arch. Biochem. Biophys.* 82, 70-77.
- Endo, Y., Mitsui, K., Motizuki, M., and Tsurugi, K. (1987) The Mechanism of Action of Ricin and Related Toxic Lectins on Eukaryotic Ribosomes: The Site and the Characteristics of the Modification in 28S Ribosomal RNA Caused by the Toxins. *J. Biol. Chem.* 262, 5908-5912.
- Endo, Y., Tsurugi, K., and Lambert, J. M. (1988) The Site of Action of Six Different Ribosome-Inactivating Proteins From Plants on Eukaryotic Ribosomes: The RNA N-Glycosidase Activity of the Proteins. *Biochem. Biophys. Res. Commun.* 150, 1032-1036.
- Frankel, A. E., Houston, L. L., and Issell, B. F. (1986) Prospects for Immunotoxin Therapy in Cancer. *Annu. Rev. Med.* 37, 125-142.
- Gillis, S., Baker, P. E., Ruscetti, F. W., and Smith, K. A. (1978) Long-Term Culture of Human Antigen-Specific Cytotoxic T Cell Lines. *J. Exp. Med.* 148, 1093-1098.

- Goldmacher, V. S., Tinnel, N. L., and Nelson, B. C. (1986) Evidence That Pinocytosis in Lymphoid Cells Has a Low Capacity. *J. Cell. Biol.* 102, 1312-1319.
- Goldmacher, V. S., Scott, C. F., Lambert, J. M., McIntyre, G. D., Blättler, W. A., Collinson, A. R., Stewart, J. K., Chong, L. D., Cook, S., Slayter, H. S., Beaumont, E., and Watkins, S. (1989) Cytotoxicity of Gelonin and Its Conjugates With Antibodies Is Determined by the Extent of Their Endocytosis. *J. Cellular Physiol.* 14, 222-234.
- Goldmacher, V. S., Lambert, J. M., and Blättler, W. A. (1992) The Specific Cytotoxicity of Immunoconjugates Containing Blocked Ricin is Dependent on the Residual Binding Capacity of Blocked Ricin: Evidence That the Membrane Binding and A-chain Translocation Activities of Ricin Cannot be Separated. *Biochem. Biophys. Res. Commun.* 183, 758-766.
- Greenfield, L., Johnson, V. G., and Youle, R. J. (1987) Mutations in Diphtheria Toxin Separate Binding from Entry and Amplify Immunotoxin Selectivity. *Science* 238, 536-539.
- Hwang, J., Fitzgerald, D. J. P., Adhya, S., and Pastan, I. (1987) Functional Domains of Pseudomonas Exotoxin Identified by Deletion Analysis of the Gene Expressed in E. Coli. *Cell* 48, 129-136.
- Kelley, V. E., Bacha, P., Pankewycz, O., Nichols, J. C., Murphy, J. R., and Strom, T. B. (1988) Interleukin 2-diphtheria Toxin Fusion Protein Can Abolish Cell-mediated Immunity *In Vivo*. *Proc. Natl. Acad. Sci. U.S.A.* 85, 3980-3984.
- Kirby, A. J., and Lancaster, P. W. (1970). Steric Assistance for Intramolecular Catalysis. *Proc. Biochem. Soc. Symp.* 31, 99-103.
- Kleiman, N. J., Freidman, D. L., and Di Sabato, G. (1984) Preparation of Single-Cell Suspensions from Lymphoid Organs. *Methods Enzymol.* 108, 43-49.
- Krönke, M., Depper, J. M., Leonard, W. J., Vitetta, E. S., Waldmann, T. A., and Greene, W. C. (1985) Adult T Cell Leukemia: A Potential Target for Ricin A Chain Immunotoxins. *Blood* 65, 1416-1421.
- Krönke, M., Schlick, E., Waldmann, T. A., Vitetta, E. S., and Green, W. C. (1986) Selective Killing of Human T-Lymphotropic Virus-I Infected Leukemia T-Cells by Monoclonal Anti-Interleukin 2 Receptor Antibody-Ricin A Chain Conjugates: Potentiation by Ammonium Chloride and Monensin. *Cancer Res.* 46, 3295-3298.
- Kupiec-Weglinski, J. W., Diamantstein, T., and Tilney, N. L. (1988) Interleukin 2 Receptor-Targeted Therapy—Rationale and Applications in Organ Transplantation. *Transplantation* 46, 785-792.
- Laemmli, U. K. (1970) Cleavage of Structural Proteins During the Assembly of the Head of Bacteriophage T<sub>4</sub>. *Nature* 227, 680-685.
- Lambert, J. M., Jue, R., and Traut, R. R. (1978) Disulfide Cross-Linking of *Escherichia coli* Ribosomal Proteins with 2-Iminothiolane (Methyl 4-Mercaptobutyrimidate): Evidence that the Cross-Linked Protein Pairs Are Formed in the Intact Ribosomal Subunit. *Biochemistry* 17, 5406-5416.
- Lambert, J. M., Senter, P. D., Yau-Young, A., Blättler, W. A., and Goldmacher, V. S. (1985) Purified Immunotoxins That Are Reactive with Human Lymphoid Cells: Monoclonal Antibodies Conjugated to the Ribosome-Inactivating proteins Gelonin and the Pokeweed Antiviral Proteins. *J. Biol. Chem.* 260, 12035-12041.
- Lambert, J. M., and Blättler, W. A. (1988a) Purification and Biochemical Characterization of Immunotoxins. *Immunotoxins* (A. E. Frankel, Ed.) pp 323-348, Kluwer Academic Publishers, Boston, MA.
- Lambert, J. M., Blättler, W. A., McIntyre, G. D., Goldmacher, V. S., and Scott, C. F. (1988b) Immunotoxins Containing Single Chain Ribosome-inactivating Proteins. *Immunotoxins* (A. E. Frankel, Ed.) pp 175-209, Kluwer Academic Publishers, Boston, MA.
- Lambert, J. M., Goldmacher, V. S., Collinson, A. R., Nadler, L. M., and Blättler, W. A. (1991a) An Immunotoxin Prepared with Blocked Ricin: A Natural Plant Toxin Adapted for Therapeutic Use. *Cancer Res.* 51, 6236-6242.
- Lambert, J. M., McIntyre, G., Gauthier, M. N., Zullo, D., Rao, V., Steeves, R. M., Goldmacher, V. S., and Blättler, W. A. (1991b) The Galactose-Binding Sites of the Cytotoxic Lectin Ricin can be Chemically Blocked in High Yield with Reactive Ligands Prepared by Chemical Modification of Glycopeptides Containing Triantennary N-Linked Oligosaccharides. *Biochemistry* 30, 3234-3247.
- Liang, S.-M., Allet, B., Rose, K., Hirschi, M., Liang, C.-M., and Thatcher, D. R. (1985) Characterization of Human Interleukin 2 Derived from *Escherichia coli*. *Biochem. J.* 229, 429-439.
- Lorberboum-Galski, H., Kozak, R. W., Waldmann, T. A., Bailon, P., FitzGerald, D. J. P., and Pastan, I. (1988) Interleukin 2 (IL2) PE40 Is Cytotoxic to Cells Displaying Either the p55 or p70 subunit of the IL2 Receptor. *J. Biol. Chem.* 263, 18650-18656.
- Lorberboum-Galski, H., Barret, L. V., Kirkman, R. L., Ogata, M., Willingham, M. C., FitzGerald, D. J., and Pastan, I. (1989) Cardiac Allograft Survival in Mice Treated With IL-2-PE40. *Proc. Natl. Acad. Sci. U.S.A.* 86, 1008-1012.
- Lowry, O. H., Rosebrough, N. J., Farr, A. L., and Randall, R. J. (1951) Protein Measurement with the Folin Phenol Reagent. *J. Biol. Chem.* 193, 265-275.
- Martin, H. B., and Houston, L. L. (1983) Arming  $\alpha_2$ -Macroglobulin with Ricin A Chain Forms a Cytotoxic Conjugate That Inhibits Protein Synthesis and Kills Human Fibroblasts. *Biochim. Biophys. Acta* 762, 128-134.
- Mellman, I., Fuchs, R., and Helenius, A. (1986) Acidification of the Endocytic and Exocytic Pathways. *Annu. Rev. Biochem.* 55, 663-700.
- Miskimins, W. K., and Shimizu, N. (1979) Synthesis of a Cytotoxic Insulin Cross-Linked to Diphtheria Toxin Fragment A Capable of Recognizing Insulin Receptors. *Biochem. Biophys. Res. Commun.* 91, 143-151.
- Murphy, J. R., Williams, D. P., Bacha, P., Bishai, W., Waters, C., and Strom, T. B. (1988) Cell Receptor Specific Targeted Toxins: Genetic Construction and Characterization of an Interleukin 2 Diphtheria Toxin-Related Fusion Protein. *J. Receptor Res.* 8, 467-480.
- Newton, D. L., Wales, R., Richardson, P. T., Walbridge, S., Saxena, S. K., Ackerman, E. J., Roberts, L. M., Lord, J. M., and Youle, R. J. (1992). Cell Surface and Intracellular Functions for Ricin Galactose Binding. *J. Biol. Chem.* 267, 11917-11922.
- Oeltman, T. N. (1985) Synthesis And *In Vitro* Activity of a Hormone-Diphtheria Toxin Fragment A Hybrid. *Biochem. Biophys. Res. Commun.* 133, 430-435.
- Oeltman, T. N., and Heath, E. C. (1979) A Hybrid Protein Containing the Toxic Subunit of Ricin and the Cell-specific Subunit of Human Chorionic Gonadotropin. *J. Biol. Chem.* 254, 1028-1032.
- Ogata, M., Lorberboum-Galski, H., FitzGerald, D., and Pastan, I. (1988) IL-2-PE40 is Cytotoxic For Activated T Lymphocytes Expressing IL-2 Receptors. *J. Immunol.* 141, 4224-4228.
- Olsnes, S., and Pihl, A. (1982) Toxic lectins and related proteins. *Molecular Actions of Toxins and Viruses* (P. Cohen, and S. van Heynigen, Eds.) pp 51-105, Elsevier, Amsterdam.
- Paliard, X., West, S. G., Lafferty, J. A., Clements, J. R., Kappler, J. W., Marrack, P., and Kotzky, B. L. (1991) Evidence for the Effects of a Superantigen in Rheumatoid Arthritis. *Science* 253, 325-329.
- Pastan, I., Chaudhay, V., and FitzGerald, D. (1992) Recombinant Toxins As Novel Therapeutic Agents. *Annu. Rev. Biochem.* 61, 331-354.
- Pelham, H. R. B., and Jackson, R. L. (1976) An Efficient mRNA-Dependent Translation System from Reticulocyte Lysates. *Eur. J. Biochem.* 67, 247-256.
- Raso, V., and Basala, M. (1984) A Highly Cytotoxic Transferrin-Ricin A Chain Conjugate Used to Select Receptor-modified Cells. *J. Biol. Chem.* 259, 1143-1149.
- Robb, R. J., Munck, A., and Smith, K. A. (1981) T Cell Growth Factor Receptors. *J. Exp. Med.* 154, 1455-1474.
- Senter, P. D., Tansey, M. J., Lambert, J. M., and Blättler, W. A. (1985) Novel Photocleavable Protein Crosslinking Reagents and Their Use in the Preparation of Antibody-Toxin Conjugates. *Photochem. Photobiol.* 42, 231-237.
- Shimizu, N., Miskimins, W. K., and Shimizu, Y. (1980) A Cytotoxic Epidermal Growth Factor Cross-Linked To Diphtheria Toxin A-Fragment. *FEBS Lett.* 118, 274-278.

- Simpson, D. L., Cawley, D. B., and Herschman, H. R. (1982) Killing of Cultured Hepatocytes by Conjugates of Asialofetuin and EGF Linked to the A Chains of Ricin or Diphtheria Toxin. *Cell* 29, 469-473.
- Singh, V., Sairam, M. R., Bhargavi, G. N., and Akhras, R. G. (1989) Hormonotoxins. *J. Biol. Chem.* 264, 3089-3095.
- Smith, K. A. (1980) T-Cell Growth Factor. *Immunol. Rev.* 51, 337-357.
- Stirpe, F., Olsnes, S., and Pihl, A. (1980) Gelonin, a New Inhibitor of Protein Synthesis, Nontoxic to Intact Cells; Isolation, Characterization, and Preparation of Cytotoxic Complexes with Concanavalin A. *J. Biol. Chem.* 255, 6947-6953.
- Stirpe, F., and Barbieri, L. (1986) Ribosome-inactivating Proteins up to Date. *FEBS Lett.* 195, 1-8.
- Thorpe, P. E., Brown, A. N. F., Ross, W. C. J., Cumber, A. J., Detre, S. I., Edwards, D. C., Davies, A. J. S., and Stirpe, F. (1981) Cytotoxicity Acquired by Conjugation of an Anti-Thy1.1 Monoclonal Antibody and the Ribosome-Inactivating Protein, Gelonin. *Eur. J. Biochem.* 116, 447-454.
- Vitetta, E. S., Cushley, W., and Uhr, J. W. (1983) Synergy of Ricin A Chain-containing Immunotoxins and Ricin B Chain-containing Immunotoxins in *In Vitro* Killing of Neoplastic Human B Cells. *Proc. Natl. Acad. Sci. U.S.A.* 80, 6332-6335.
- Vitetta, E. S., Fulton, R. J., May, R. D., Till, M., and Uhr, J. W. (1987) Redesigning Nature's Poisons to Create Anti-Tumor Reagents. *Science* 238, 1098-1104.
- Vitetta, E. S., and Uhr, J. W. (1984) The Potential Use of Immunotoxins in Transplantation, Cancer Therapy, And Immunoregulation. *Transplantation* 37, 535-538.
- Weber, G., Menke, K., and Hopf, H. (1980) Alkynes and Cumulenes XII. The Use of Di-*tert*-butyl Acetylenedicarboxylate in Diels-Alder Additions. *Chem. Ber.* 113, 531-541.
- Weissman, A. M., Harford, J. B., Svetlik, P. B., Leonard, W. L., Depper, J. M., Waldmann, T. A., Greene, W. C., and Klausner, R. D. (1986) Only high-affinity receptors for interleukin 2 mediate internalization of ligand. *Proc. Natl. Acad. Sci. U.S.A.* 83, 1463-1466.



# TECHNICAL NOTES

## Carboxymethyldextran Lactone: A Preactivated Polymer for Amine Conjugations

Ned D. Heindel,\* Michael A. Kauffman, Eric K. Akyea, Stephanie A. Engel, Michael F. Frey, C. Jeffrey Lacey, and Roger A. Egolf

Department of Chemistry & Institute for Health Sciences, Lehigh University, Bethlehem, Pennsylvania 18015.  
Received September 8, 1993\*

The linking of amino haptens to carboxymethyldextran (CMD) requires carboxyl activation, for example, via carbodiimides. We have discovered that substantial *N*-acylurea, derived from these carbodiimides, can be trapped on the CMD backbone. As an alternative, CMD can be conveniently lactonized by heating in inert solvents, and this carboxymethyldextran lactone (CDL) can be employed directly for amine conjugation.

Conjugates of various dextran derivatives (carboxymethyldextran, polyaldehyde dextran, aminopropyl dextran, dextran hydrazide) have proven very useful for drug targeting, controlled release, and immunoconjugate spacer applications (1-4). In most cases the dextran derivative must be prepared *de novo* just prior to conjugation, requires the use of an activating catalyst (frequently a mixed anhydride or carbodiimide), or requires a post-conjugation reduction to stabilize a hydrolytically-labile imine bond.

In particular, couplings to carboxymethyldextran (CMD) which frequently use a carbodiimide activation are especially problematic because of the short half-life of the activating reagent in water, a necessary solvent for most such conjugates (5). Also, an equally serious problem during coupling is the established tendency of carbodiimides to undergo *O*- to *N*-acyl shifts to form the more stable *N*-acylureas thereby leading to nonproductive couplings (6).

Interest of our group in tumor delivery of radiotherapeutic levels of  $^{125}\text{I}$  on biologically-stable carriers (7) prompted the synthesis of a dextran framework to which would be attached a highly reactive aromatic amine for electrophilic radioiodination. Using established carbodiimide coupling techniques we coupled 4-methoxybenzylamine to carboxymethyldextran (8). We were amazed, however, to observe that the degree of substitution determined by UV quantification (4) of our methoxybenzylamine chromophore was in substantial disagreement with the degree of substitution determined by another commonly-employed technique which uses the % nitrogen analysis to determine drug load (9), in our case 4-methoxybenzylamine content. High resolution  $^1\text{H}$ -NMR studies soon demonstrated that our carboxymethyldextran conjugate contained an appreciable amount of bound *N*-acylurea derived from the carbodiimide.

To address this problem we developed a readily-prepared, shelf-stable, preactivated dextran derivative which permits facile drug coupling without the use of small molecule promoters. This derivative, carboxymethyldex-

tran lactone (CDL), is obtained in high yield from the thermal cyclodehydration of carboxymethyldextran (Scheme 1). We have shown that CDL can be loaded with 4-methoxybenzylamine, without activating catalysts (Scheme 2), in conversions superior to those obtained by conjugating the parent carboxymethyldextran to small molecules in more traditional fashions.

### EXPERIMENTAL PROCEDURES

**Materials and Methods.** The dextran used in these studies was high-purity, clinical-grade 40-kD dextran produced by Pharmachem Corp., Bethlehem, PA. The carboxymethyldextran (CMD) employed herein was prepared by carboxymethylation of 40-kD dextran as described by Novak and analyzed for degree of substitution by the titration procedure described therein (10). The degree of substitution was 1.02  $\text{CH}_2\text{COOH}$  groups per repeating glucose. Ho's  $^1\text{H}$ -NMR method for determination of carboxymethyl groups per glucose residue (by integration ratios of the grouping of multiple  $-\text{OCH}_2-\text{COOH}$ 's to the  $\text{C}_1\text{-H}$ ) gave a degree of substitution of 1.06 on this sample (11). Infrared spectra were obtained as 1% disks in potassium bromide on a Mattson Polaris high-resolution FTIR. Ultraviolet spectra were obtained in water on a Perkin-Elmer Lambda 5 UV-vis spectrophotometer. Differential scanning calorimetry (DSC) was performed on a Perkin-Elmer 1020 Series DSC7 thermal analysis system. Combustion analyses were performed on a Perkin-Elmer Model 2400 combustion analyzer by QTI Corporation, Bound Brook, NJ, with pre- and post-run calibration for % N (using high purity acetamide standard) and a standard deviation from the calculated value of  $\pm 0.02\%$  on the calibration standard.

Loading levels of agents onto the dextran were determined by published techniques in which spectrophotometric quantification (by reference to a curve obtained from preprepared standard solutions) and combustion analyses for % nitrogen were employed (9, 12, 13). For the UV measurements, conjugates of 4-methoxybenzylamine were read at  $272.6 \lambda_{\text{max}}$ .

**Preparation of Carboxymethyldextran Lactone (CDL).** Lactonization was effected by heating the CMD in a well-stirred suspension at reflux in four different

\* Abstract published in *Advance ACS Abstracts*, November 15, 1993.

solvent systems, toluene (bp 109–110 °C), mixed xylenes (bp 138–144 °C), diglyme (bp 162 °C), and acetonitrile (bp 82 °C). A typical procedure involved suspending 0.65–0.75 g of dried carboxymethyl dextran in 15–30 mL of the anhydrous solvent in a round-bottomed flask. The contents were magnetically stirred at reflux for 5 h, cooled to ambient temperature, and filtered. The white solid thus obtained possessed diminished water solubility and was vacuum dried to constant weight. DSC analysis showed no distinct phase transitions between 30 and 290 °C but evidenced a marked exothermic sample decomposition between 292 and 335 °C. Infrared analysis of the product showed a barely detectable absorption from the original carboxymethyl dextran carboxylic acid C=O stretch at 1734 cm<sup>-1</sup> constituting less than 10% of the integrated intensity of the entire C=O envelope. The major absorption, the lactone carbonyl, appears at 1755 cm<sup>-1</sup> in CDL.

**Condensation with 4-Methoxybenzylamine.** Standard conditions for lactone-opening (Scheme 2) with 4-methoxybenzylamine in toluene, xylene, diglyme, and acetonitrile were 6- to 10-fold mole excess of the amine per mole of available lactone residues in the dextran. Reactants were stirred at reflux in a volume of solvent 10–15 times the mass of the reactants for 5–20 h. This technique gave polyamides whose maximum degrees of substitutions (UV and %N analysis) fell between 60 and 90% of the originally available carboxyl concentrations.

Specifically, when 0.62 g of CDL, 4.2 g (31 mmol) of 4-methoxybenzylamine, and 50 mL of xylene were heated and stirred at 90 °C for 20 h, the resulting yellow conjugate precipitate could be isolated by filtration, taken up in distilled water, and subjected to exhaustive dialysis to remove unbound drug (Spectrapor membrane dialysis bag, MW cutoff 12 000–14 000, dialyzed against distilled water for 5 days, two changes/day). The contents of the bag were evaporated *in vacuo* to 20 mL and lyophilized to produce a fluffy white solid. By the ultraviolet measurement method, the degree of substitution of the methoxybenzylamine on the dextran obtained on a sample which had been lyophilized and vacuum-dried to constant weight was 0.78 mol/mol of glucose units for the toluene-derived product, 0.62 mol/mol of glucose for the xylene-derived material, and 0.60 mol/mol for the diglyme-derived substance. The values for degree of substitution obtained by %N (combustion) analysis were within  $\pm 8\%$  of the ultraviolet-quantification results. These conjugates decomposed above 250 °C and displayed characteristic infrared spectra: the amide I band at 1652 cm<sup>-1</sup>, the amide II band at 1562 cm<sup>-1</sup>, and the residual carboxyl absorptions at 1734 cm<sup>-1</sup>. There was a complete absence of the lactone absorption.

**Direct in Situ Lactonization-Conjugation.** A 25-mL round-bottom flask was charged with 0.279 g of CMD (1.28 mmol of carboxyl residues), 1.00 g (8.02 mmol) of 4-methoxybenzylamine, and 10 mL of anhydrous xylene. The reaction mixture was stirred and heated to 90 °C and maintained at that temperature for 20 h. Cooling the reaction mixture to room temperature was followed by the addition of 20 mL of distilled water which partitioned the product-conjugate into the aqueous layer. That layer was dialyzed as noted and lyophilized and a sample dried to constant weight. The degree of substitution was determined to be 0.56 amines/glucose residue by ultraviolet quantification.

**Carbodiimide-Activated Conjugation of CMD with *p*-Methoxybenzylamine.** To a solution of CMD (0.125 g) dissolved in 50 mL of distilled water was added a single

portion of 4-methoxybenzylamine (0.60 g, 4.37 mmol). These reactant quantities represent a 6.2/1 molar ratio of amine to dextran-pendant carboxyls in the CMD. The same ratio of amine to lactone was employed in the standard coupling to CDL. The pH in the well-stirred solution was adjusted and maintained at  $4.5 \pm 0.5$  with 6 N HCl or saturated aqueous sodium bicarbonate while a total of 206 mg (1.07 mmol) of *N*-[3-(dimethylamino)propyl]-*N'*-ethylcarbodiimide hydrochloride (EDC) was added in five equal portions over a 3.5-h period. When the addition of the carbodiimide was complete the reaction mixture was stirred for 18 hours at ambient temperature, transferred to a Spectrapor membrane dialysis bag (MW cutoff 12 000–14 000), and dialyzed against distilled water (5 days, two changes/day). The contents of the bag were evaporated *in vacuo* to 20 mL and lyophilized to produce a fluffy white solid whose degree of amide substitution was 0.24 by UV measurement at 272.6 nm. Three duplicate nitrogen combustion analyses gave values of  $3.60 \pm 0.05\%$ . A <sup>1</sup>H-NMR obtained in D<sub>2</sub>O on a 360-MHz Bruker spectrometer revealed unexpected resonances at 0.95 ppm consistent with pendant methyl moieties.

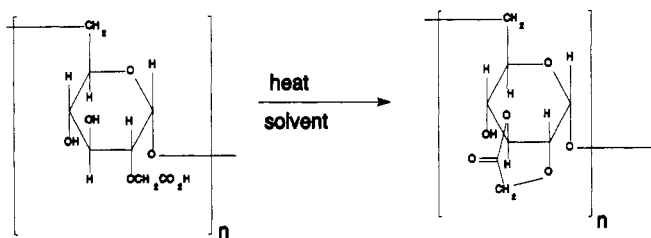
## RESULTS AND DISCUSSION

The carboxymethyl dextran lactone synthesized herein is structurally related to the previously reported so-called Sephadex lactone prepared by carbodiimide-induced dehydration of the highly cross-linked carboxymethyl dextran (Sephadex) beads (14). Akanuma reports an absorption of 1735 cm<sup>-1</sup> for C=O in carboxymethyl Sephadex and 1760 cm<sup>-1</sup> for the C=O in carboxymethyl Sephadex lactone (14). A structurally similar  $\delta$ -lactone was generated on ganglioside GM3 by acid-catalyzed internal cyclization of the sialic acid carboxyl with a C-2 hydroxyl in the galactosyl residue; its carbonyl was assigned at 1750 cm<sup>-1</sup> (15). While the main lactone absorption in CDL is at 1755 cm<sup>-1</sup>, expansion of the C=O spectral envelope reveals at least eight distinct IR bands between 1760 and 1744 cm<sup>-1</sup>. The parent carboxymethyl dextran displays at least three carboxyl bands between 1730 and 1734 cm<sup>-1</sup>.

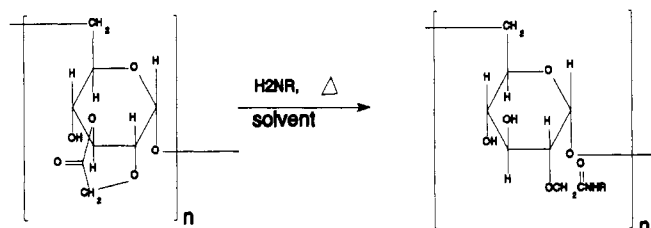
Carboxymethyl dextran with a degree of substitution of 1.06 carboxymethyls/glucose would, of course, be expected to be a mixture of O-substituted CH<sub>2</sub>COOH isomers. By careful <sup>1</sup>H-NMR peak assignments to the methylene resonances at 4.0–4.5 ppm in carboxymethylcellulose, Ho was able to distinguish substitution occurring at the C-2 OH from the C-3 OH and from the C-6 OH (11). He observed a slight kinetic bias to carboxymethylation at the C-2 hydroxyl but with all possible isomers being formed, and he further reported that the ratio of the integrated methyleneoxy region to the C-1 H provided a reliable technique to determine degree of substitution. The carboxymethyl dextran employed in our studies (which had a degree of substitution of 1.02 by titration) did display at least three resolvable methyleneoxy resonances between 4.0 and 4.5 ppm and a degree of substitution (by NMR) of 1.06. With multiple sites of carboxymethylation many possible internal lactones can result and the structure given in Scheme 1 is simply one illustration. Likewise, the ring-opening amide structure in Scheme 2 is just one of several alternative representations.

While infrared spectra of lactonized product always showed a trace of carboxylic acid absorption, titration proved an unreliable way of determining the degree of lactonization since both lactone functions and nonlactonized carboxyl groups responded. The water-insoluble CDL reacted and dissolved upon mixing with standardized

## Scheme I



## Scheme II



aqueous base. Inference of the number of accessible lactones could be deduced from the ring-opening experiments for which the maximum observed degrees of substitution reflected the maximum lactone concentration on the CDL. With 4-methoxybenzylamine and CDL by the conjugation method employed herein one could obtain up to 90% incorporation of amine with respect to original carboxylic content. Furthermore, while CMD and amine do not form amide in aqueous media without an activation promoter, we have found that they do couple in boiling xylene, presumably via *in situ* generation of lactone.

Comparison of two methods for conjugating methoxybenzylamine to carboxymethylated dextrans, direct coupling to CDL versus EDC mediated coupling to CMD, shows EDC to be inferior both in maximum load and in ease of quantification. Unproductive linking on the part of EDC led to the well-known, unreactive, *N*-acyl-rearranged products (5,6) which gave disparate analytical results for UV and %N analysis. UV analysis of the chromophore of the EDC product revealed a degree of substitution of 0.24 and predicts nitrogen content to be 1.34% of the total mass, while combustion analysis shows %N to be 3.60%. These data can be reconciled only if a second, nonchromaphoric source of nitrogen was coupled to the dextran. <sup>1</sup>H-NMR analysis of the conjugate evidenced the presence of the urea at levels high enough to account for the increased nitrogen content.

We believe that this novel reactive dextran lactone can be a useful polymeric drug carrier for clean, facile conjugations without the need for carbodiimide promoters which may subsequently leave *N*-acylurea residues. Applications to couplings in aqueous media and to the conjugation of pharmaceutical entities are under study.

## ACKNOWLEDGMENT

This research was supported by NIH grant ES 03647, the Brady Cancer Research Institute, and the W. W. Smith Charitable Trust. M.A.K. and S.A.E. were supported by an NSF-REU Program Grant.

## LITERATURE CITED

- (1) Schechter, B., Pauzner, R., Wilchek, M., and Arnon, R. (1986) Cis-Platinum (II) Complexes of Carboxymethyldextran as Potential Antitumor Agents. *Cancer Biochem. Biophys.* 8, 289-298.
- (2) Heindel, N. D., Van Dongen, J. M. A. M., Fitzpatrick, D. A., Mease, B. A., and Schray, K. J. (1987) Macromolecular Attachment as a Metabolic Stabilizer for a Labile Radiosensitizer. *J. Pharm. Sci.* 76, 384-386.
- (3) Heindel, N. D., Zhao, H., Leiby, J., VanDongen, J., Lacey, C. J., Lima, D. A., Shabsoug, B., and Buzby, J. H. (1990) Hydrazide Pharmaceuticals as Conjugates to Polyaldehyde Dextran. *Bioconjugate Chem.* 1, 77-81.
- (4) Shih, L. B., Xuan, H., Sharkey, R. M., and Goldenberg, D. M. (1990) A Fluorouridine-Anti-CEA Immunoconjugate is Therapeutically Effective in a Human Colonic Cancer Xenograft Model. *Int. J. Cancer* 46, 1101-1106.
- (5) Gilles, M. A., Hudson, A. Q., and Borders, C. L., Jr. (1990) Stability of Water-Soluble Carbodiimides in Aqueous Solution. *Anal. Biochem.* 184, 244-248.
- (6) Wong, S. S. (1991) *Chemistry of Protein Conjugation and Cross-Linking*, pp 122-123, CRC Press, Boca Raton.
- (7) Heindel, N. D., Frey, M. F., Emrich, J. G., and Bender, H. (1992) Synthesis and Use of Tyraminyl-Cellobiose for Glioma Cell <sup>125</sup>I-Radioimmunotherapy. *Pharm. Res.* 9, 101S.
- (8) Rosemeyer, H., and Seela, F. (1984) Polymer-linked Acycloguanosine. *Makromol. Chem.* 185, 687-695.
- (9) Hurwitz, E., Kashi, R., Arnon, R., Wilchek, M. and Sela, M. (1985) The Covalent Linking of Two Nucleotide Analogues to Antibodies. *J. Med. Chem.* 28, 137-140.
- (10) Berger, C., and Novak, L. J. (1958) Ferrous Carboxymethyl Dextran. U. S. Patent 2,862,920.
- (11) Ho, F. F.-L., and Klosiewicz, D. W. (1980) Proton Nuclear Magnetic Resonance Spectrometry for Determination of Substituents and their Distribution in Carboxymethylcellulose. *Anal. Chem.* 52, 913-916.
- (12) Wilchek, M., and Bayer, E. A. (1987) Labeling Glycoconjugates with Hydrazine. *Methods Enzymol.* 138, 429-442 and references cited therein.
- (13) Zhao, H. and Heindel, N. D. (1991) Determination of Degree of Substitution of Formyl Groups in Polyaldehyde Dextran. *Pharm. Res.* 8, 400-402.
- (14) Akanuma, H. and Yamasaki, M. (1978) Simple Hydrazidation Method for Carboxymethyl Groups on Cross-Linked Dextran. *J. Biochem.* 84, 1357-1362.
- (15) Yu, R. K., Koerner, T. A. W., Ando, S., Yohe, H. C., and Prestegard, J. H. (1985) High-Resolution Proton NMR Studies of Gangliosides. III. Elucidation of the Structure of Ganglioside GM3 Lactone. *J. Biochem.* 98, 1367-1373.

# Bioconjugate Chemistry

MARCH/APRIL 1994  
Volume 5, Number 2

© Copyright 1994 by the American Chemical Society

## LETTERS

---

### Labeling Monoclonal Antibodies with $^{90}\text{Y}$ trium- and $^{111}\text{In}$ dium-DOTA Chelates: A Simple and Efficient Method

Min Li,<sup>†</sup> Claude F. Meares,<sup>\*,†</sup> Gao-Ren Zhong,<sup>‡</sup> Laird Miers,<sup>‡</sup> Cheng-Yi Xiong,<sup>‡</sup> and Sally J. DeNardo<sup>‡</sup>

Department of Chemistry, University of California, Davis, California 95616, and Department of Internal Medicine, University of California Davis Medical Center, Sacramento, California 95817. Received October 17, 1993\*

---

Yttrium-90 and indium-111 have been attached to a monoclonal antibody with a bifunctional chelating agent (DOTA-peptide). Using the unique features of this DOTA-peptide and its complexes with trivalent yttrium and indium, the bifunctional chelating agent was prelabeled with either radiometal and then conjugated to chimeric monoclonal antibody L6. Both radiolabeling procedures and yield are suitable for the practical preparation of radiopharmaceuticals. Biodistribution studies in tumor-bearing mice showed that, e.g., on day 3 after intravenous injection of a  $^{90}\text{Y}$  immunoconjugate, liver uptake was  $5.4 \pm 1.5\%$  ID/g, bone uptake  $2.0 \pm 0.5\%$  ID/g, and tumor uptake  $18.0 \pm 8.0\%$  ID/g.

---

Macrocyclic bifunctional chelating agents have been developed to tag monoclonal antibodies with radiometals for *in vivo* diagnosis and therapy (1-7); in particular, mAbs labeled with DOTA<sup>1</sup> derivatives incorporating yttrium-90 and indium-111 have shown excellent kinetic stability under physiological conditions (2, 5, 7, 8). However, the slow formation of yttrium-DOTA complexes (9-11) presents a technical problem that can lead to low radiolabeling yields unless conditions are carefully controlled.

The conventional labeling process involves conjugation

of the bifunctional chelating agent to the antibody, followed by labeling with the radiometal. An alternative method is *prelabeling*, in which the bifunctional chelating agent is first radiolabeled and then conjugated to the mAb. Prelabeling has been used to eliminate the nonspecific binding of  $^{99\text{m}}\text{Tc}$  to mAbs (12-14). Moi *et al.* initially used prelabeling to attach  $^{67}\text{Cu}$  to a mAb with the first macrocyclic bifunctional chelating agent, a TETA derivative (1), and recently Schlom *et al.* (15) employed such a procedure to label a mAb with a  $^{177}\text{Lu}$ -DOTA derivative.

Prelabeling involves three steps: (1) radioactive chelate formation (in the absence of antibody), (2) chelate purification, and (3) antibody conjugation. It has several potential advantages: in step 1, metal chelate formation is easier to control because there is no competition from metal-binding sites on the protein, and the chelation conditions are not limited by the need to avoid denaturing the antibody; in step 2, excess chelating agent can be removed before the radioactive chelate is attached to the

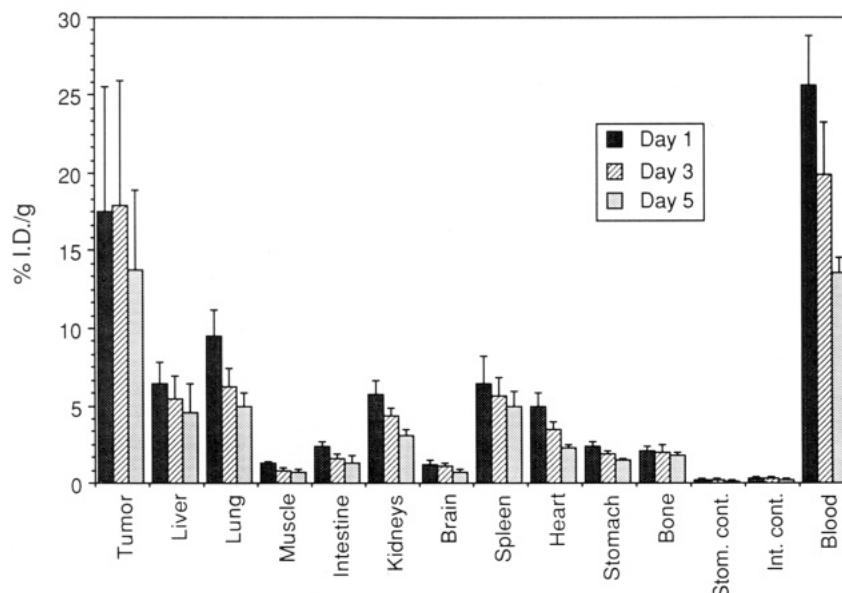
---

<sup>†</sup> University of California.

<sup>‡</sup> University of California Davis Medical Center.

\* Abstract published in *Advance ACS Abstracts*, February 1, 1994.

<sup>1</sup> Abbreviations used: DOTA, 1,4,7,10-tetraazacyclododecane-*N,N',N'',N'''*-tetraacetic acid; DTPA, diethylenetriaminepentaacetic acid; mAbs, monoclonal antibodies; TETA, 1,4,8,11-tetraazacyclotetradecane-*N,N',N'',N'''*-tetraacetic acid; % ID/g, percent of injected dose per gram of tissue.



**Figure 1.** Biodistribution of  $^{90}\text{Y}$ -DOTA-Gly<sub>3</sub>-L-Phe-amide-thiourea-chimeric mAb L6 (3) in HBT tumor-bearing nude mice at days 1, 3, and 5. For each time point, data were acquired from seven animals. The values are given as average percent of injected dose per gram of tissue. Error bars represent 1 standard deviation.

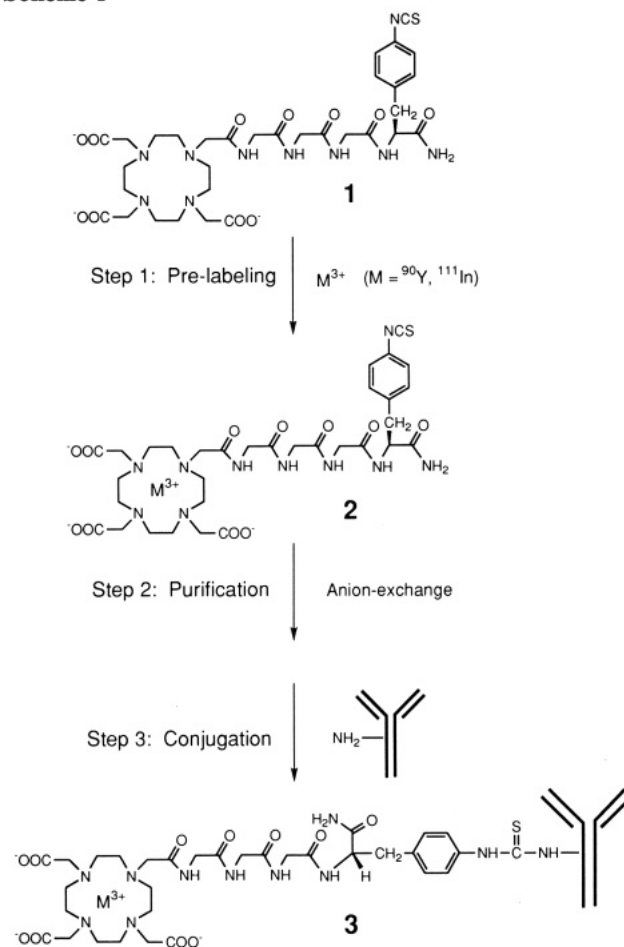
protein, thus avoiding the production of multiply labeled immunoconjugates with unfavorable biological properties (16); in step 3, the antibody is chemically modified and radiolabeled in one step, minimizing chemical manipulation of the antibody and reducing losses.

The medically useful radiometals have short half-lives (17); high efficiencies of both labeling and conjugation are important for practical applications. The prelabeling approach permits use of a large excess of bifunctional chelating agent to achieve a high chelation yield quickly in step 1, but requires a rapid purification method to remove unlabeled reagent in step 2. Here, we report an easy and efficient method for prelabeling a peptide-linked DOTA derivative with  $^{90}\text{Y}$  or  $^{111}\text{In}$  and conjugating it to a mAb.

The labeling procedure is outlined in Scheme 1. The bifunctional chelating agent DOTA-Gly<sub>3</sub>-L-(*p*-isothiocyanato)-Phe-amide (1) was prepared by the method described recently (7). Carrier-free  $^{90}\text{Y}$  (DuPont NEN) in 0.05 M HCl was dried in a heating block under  $\text{N}_2(\text{g})$ , and 100  $\mu\text{L}$  of 20 mM 1 in 0.2 M  $(\text{CH}_3)_4\text{N}^+$  acetate, pH 5.0, was added. The mixture was incubated at 37  $^\circ\text{C}$  for 30 min, followed by addition of 25  $\mu\text{L}$  of 50 mM DTPA in 0.1 M  $(\text{CH}_3)_4\text{N}^+$  acetate, pH 6.0, for 15 min at room temperature (to complex any remaining free yttrium). The solution was loaded onto an anion-exchange column,<sup>2</sup> and the column was spun for 2 min at  $\sim 2000$  g, followed by elution with four 125- $\mu\text{L}$  aliquots of  $\text{H}_2\text{O}$  by centrifugation at  $\sim 2000$  g for 2 min each. Most of the radioactive 2 was recovered in the first four fractions (see Table 1). One-step elution with 0.5 mL of  $\text{H}_2\text{O}$  was performed for comparison, but it gave 18% lower recovery than stepwise elution.

All the eluted fractions were collected and concentrated to  $\sim 15$   $\mu\text{L}$  with a speed-vac concentrator (Savant Instruments) without heating. (It should be possible to avoid this step when larger amounts of radioactivity are used, e.g., for clinical-scale preparations.) The concentrated

**Scheme 1**



solution was mixed with 1 mg of chimeric mAb L6 (18  $\mu\text{L}$ , 56 mg/mL, Oncogen/Bristol-Myers) (18) in 0.1 M  $(\text{CH}_3)_4\text{N}^+$  phosphate, pH 9.0. The pH was adjusted to 9.5 using aqueous 2.0 M triethylamine. The mixture was incubated at 37  $^\circ\text{C}$  for 1 h, and 3 was isolated using a centrifuged gel-filtration column (19, 20). Yields are listed in Table 1.

$^{111}\text{In}$  labeling was carried out similarly.

<sup>2</sup> The column had been prepared by filling a 1-mL disposable tuberculin syringe with 500  $\mu\text{L}$  of DEAE cellulose anion-exchange resin (1 mequiv/dry g, Sigma Chemical Co.) and prespun for 3 min at  $\sim 2000$  g. The resin had been converted to the acetate form prior to use.

**Table 1. Results for DOTA-Peptide Radiolabeling and Conjugation**

radionuclide	starting radioactivity, mCi (vol, $\mu$ L)	recovery for step 2, <sup>a</sup> %	recovery for step 3, <sup>a</sup> %	overall recovery, <sup>a</sup> %
yttrium-90	2.1–3.9 (2–5)	80 $\pm$ 5	40 $\pm$ 2	30 $\pm$ 4
indium-111	4.9–6.2 (12–30)	70 $\pm$ 9	73 $\pm$ 3	42 $\pm$ 4

<sup>a</sup> Average recovered radioactivity  $\pm$  standard deviation, for  $\geq 3$  runs.

The radiochemical purity of both <sup>90</sup>Y- and <sup>111</sup>In-labeled immunoconjugates **3** was determined to be  $>95\%$  by gel filtration HPLC, cellulose acetate electrophoresis, and silica gel TLC (20). A solid-phase radioimmunoassay (21) was performed using <sup>125</sup>I-labeled chimeric L6 as a standard. The immunoreactivity of <sup>90</sup>Y-DOTA-Gly<sub>3</sub>-L-Phe-amide-thiourea-chimeric L6 was  $107 \pm 5\%$  relative to <sup>125</sup>I-labeled antibody.

Compound **1** forms *neutral* complexes **2** with trivalent metals. The other important species in the chelation reaction mixture, such as excess chelating agents, complexes containing *divalent* metals, and DTPA complexes, are negatively charged. Thus, the DOTA-peptide complexes with trivalent metals can be filtered quickly through an appropriately designed anion-exchange column in H<sub>2</sub>O to separate them from anionic species. The neutral chelate avoids the need for more complex processes in step 2, such as HPLC with mixed organic/aqueous solvents (15).

In the chelation step, the yield after anion exchange was typically  $>70\%$  of the starting radioactivity. Particularly for <sup>90</sup>Y solutions, the levels of metal impurities appear to vary with each batch of carrier-free radiometal. The identity of these impurities is difficult to determine, but most common metal contaminants are divalent ions. Prelabeling deals with the impurity problem by using a large excess of chelating agent and then removing the excess. This is preferable to using a large excess of chelate-tagged mAb conjugate, which cannot be fractionated later to remove unwanted contaminants. (Obviously, prelabeling does not eliminate trivalent metal complexes from the product.)

In the conjugation step, a high concentration of mAb is desired, so that each chelate isothiocyanate will frequently encounter amino groups with which to react. For the small amounts of radioactivity used here, the radiolabeled bifunctional chelating agent was concentrated before adding it to the mAb to avoid dilution of the conjugation mixture. At the chosen conjugation conditions (1 h incubation at 37 °C, pH 9.5, [mAb]  $\geq 20$  mg/mL), the conjugation yield was over 40%. Longer incubation times would lead to higher conjugation yields, but we expect that for radioactivity levels appropriate for clinical use ( $\sim 100$  mCi) radiolysis will become important at longer times. The isothiocyanate group on the bifunctional chelating agent is potentially subject to hydrolysis during labeling and conjugation, but control experiments showed loss of  $<5\%$  of the isothiocyanate.

In the conventional labeling method, the ratio of attached chelates to mAb is usually  $>1$  in order to provide enough chelating groups for a good radiolabeling yield. However, the chelates that are actually used for labeling comprise less than 5% of the total attached chelates on the mAb. The excess chelating groups may affect the biological properties of mAbs, e.g., by inducing an immune response (16), and impure metal solutions may require large amounts of immunoconjugate. With prelabeling, a far smaller number of chelates becomes attached to the

mAb, but practically all are radiolabeled; thus, the number of modified mAbs is significantly reduced, and the number of multiply-modified mAbs is essentially zero. The radiolabeled mAbs are fully immunoreactive and are expected to have more favorable biological properties, including less immunogenicity. Another reason for using DOTA-peptide is to reduce the accumulation of radioactivity in the liver by introducing a cleavable linker between the chelate and the mAb (7).

To examine the properties of the conjugate *in vivo*, <sup>90</sup>Y-labeled **3** was injected into HBT tumor-bearing nude mice (22) for organ distribution and tumor uptake studies. The results of these animal studies (Figure 1) showed that the radioactivity level in the liver varied from  $6.4 \pm 1.5\%$  ID/g on the first day to  $5.4 \pm 1.5\%$  ID/g on the third day to  $4.6 \pm 1.9\%$  ID/g on the fifth day. The tumor uptake was  $17.5 \pm 8.0\%$  ID/g on day 1,  $18.0 \pm 8.0\%$  ID/g on day 3, and  $13.8 \pm 5.2\%$  ID/g on day 5. The bone uptake was  $2.1 \pm 0.3\%$  ID/g,  $2.0 \pm 0.5\%$  ID/g, and  $1.8 \pm 0.2\%$  ID/g on days 1, 3, and 5. The levels of radioactivity in liver and bone are satisfactorily low (8), and the tumor uptake is good. Coupled with its other expected advantages, these results indicate that prelabeling mAbs with metal complexes of **1** has considerable promise.

#### ACKNOWLEDGMENT

We thank Justin K. Moran and Douglas P. Greiner for helpful discussions and Xu-Bao Shi for immunoreactivity assays. This work was supported by Research Grants CA16861 and CA47829 from the National Cancer Institute, NIH.

#### NOTE ADDED IN PROOF

Since submission of this paper, more yttrium-90 labeling experiments have been performed, and the labeling yield has been improved. For a total of nine experiments, the recovery for step 2 is now  $75 \pm 8\%$ , the recovery for step 3 is  $58 \pm 15\%$ , and the overall recovery is  $40 \pm 11\%$ .

#### LITERATURE CITED

- Moi, M. K., Meares, C. F., McCall, M. J., Cole, W. C., and DeNardo, S. J. (1985) Copper Chelates as Probes of Biological Systems: Stable Copper Complexes with a Macrocyclic Bifunctional Chelating Agent. *Anal. Biochem.* **148**, 249–253.
- Moi, M. K., Meares, C. F., and DeNardo, S. J. (1988) The Peptide Way to Macrocyclic Bifunctional Chelating Agents: Synthesis of 2-(p-Nitrobenzyl)-1,4,7,10-tetraazacyclododecane-*N,N',N'',N'''*-tetraacetic Acid and Study of Its Yttrium(III) Complex. *J. Am. Chem. Soc.* **110**, 6266–6267.
- Cox, J. P. L., Craig, Andrew, S., Helps, L. M., Jandowski, K. J., Parker, D., Eaton, M. A. W., Millican, A. T., Millar, K., Beeley, N. R. A., and Boyce, B. A. (1990) Synthesis of C- and N-Functionalised Derivatives of 1,4,7-Triazacyclononane-1,4,7-triyltriacetic acid (NOTA), 1,4,7,10-Tetra-azacyclododecane-1,4,7,10-tetrayltetra-acetic Acid (DOTA), and Diethylenetriaminepenta-acetic Acid (DTPA): Bifunctional Complexing Agents for the Derivatisation of Antibodies. *J. Chem. Soc., Perkin Trans. 1* 2567–2576.
- Parker, D. (1990) Tumor Targeting with Radiolabeled Macrocyclic-Antibody Conjugates. *Chem. Soc. Rev.* **19**, 271–291.
- Meares, C. F., Moi, M. K., Diril, H., Kukis, D. L., McCall, M. J., Deshpande, S. V., DeNardo, S. J., Snook, D., and Epenetos, A. A. (1990) Macrocyclic Chelates of Radiometals for Diagnosis and Therapy. *Br. J. Cancer, Suppl.* **10**, 21–26.
- Gansow, O. A. (1991) Newer Approaches to the Radiolabeling of Monoclonal Antibodies by Use of Metal Chelates. *Nucl. Med. Biol.* **18**, 369–381.
- Li, M., and Meares, C. F. (1993) Synthesis, Metal Chelate Stability Studies, and Enzyme Digestion of a Peptide-Linked



- DOTA Derivative and Its Corresponding Radiolabeled Immunoconjugates. *Bioconjugate Chem.* 4, 275–283.
- (8) Deshpande, S. V., DeNardo, S. J., Kukis, D. L., Moi, M. K., McCall, M. J., DeNardo, G. L., and Meares, C. F. (1990) Yttrium-90-Labeled Monoclonal Antibody for Therapy: Labeling by a New Macrocyclic Bifunctional Chelating Agent. *J. Nucl. Med.* 31, 473–479.
- (9) Kasprzyk, S. P., and Wilkins, R. G. (1982) Kinetics of Interaction of Metal Ions with Two Tetraaza Tetraacetate Macrocycles. *Inorg. Chem.* 21, 3349–3352.
- (10) Kodama, M., Koike, T., Mahatma, A. B., and Kimura, E. (1991) Thermodynamic and Kinetic Studies of Lanthanide Complexes of 1,4,7,10,13-Pentaaazacyclopentadecane-*N,N',N'',N'''*-Pentaacetic Acid and 1,4,7,10,13, 16-Hexaazacyclopentadecane-*N,N',N'',N'''*,*N''''*,*N'''''*-hexaacetic Acid. *Inorg. Chem.* 30, 1270–1273.
- (11) Wang, X., Jin, T., Comblin, V., Lopez-Mut, A., Merciny, E., and Desreux, J. F. (1992) A Kinetic Investigation of the Lanthanide DOTA Chelates. Stability and Rates of Formation and of Dissociation of a Macrocyclic Gadolinium(III) Polyaza Polycarboxylic MRI Contrast Agent. *Inorg. Chem.* 31, 1095–1099.
- (12) Fritzberg, A. R., Abrams, P. G., Beaumier, P. L., Kasina, S., Morgan, A. C., Reno, J. M., Sanderson, J. A., Srinivasan, A., Wilbur, D. S., and Vanderheyden, J. (1987) Specific and Stable Labeling of Antibodies with Technetium-99m with a Diamide Dithiolate Chelating Agent. *Proc. Natl. Acad. Sci. U.S.A.* 85, 4025–4029.
- (13) Franz, J., Volkert, W. A., Barefield, E., K., and Holmes, R. A. (1987) The Production of <sup>99m</sup>Tc-Labeled Conjugated Antibodies Using a Cyclam-Based Bifunctional Chelating Agent. *Nucl. Med. Biol.* 14, 569–572.
- (14) Linder, K. E., Wen, M. D., Nowotnik, D., P., Malley, M. F., Gougoutas, J. Z., Nunn, A. D., and Eckelman, W. C. (1991) Technetium Labeling of Monoclonal Antibodies with Functionalized BATOs. 1. TcCl(DMG)<sub>3</sub>PITC. *Bioconjugate Chem.* 2, 160–170.
- (15) Schlom, J., Siler, K., Milenic, D. E., Eggenesperger, D., Colcher, D., Miller, L. S., Houchens, D., Cheng, R., Kaplan, D., and Goeckler, W. (1991) Monoclonal Antibody-based Therapy of a Human Tumor Xenograft with a <sup>177</sup>Lutetium-labeled Immunoconjugate. *Cancer Res.* 51, 2889–2896.
- (16) Kosmas, C., Snook, D., Gooden, C. S., Courtenay-Luck, N. S., McCall, M. J., Meares, C. F., and Epenetos, A. A. (1992) Development of Humoral Immune Responses Against a Macrocyclic Chelating Agent (DOTA) in Cancer Patients Receiving Radioimmunoconjugates for Imaging and Therapy. *Cancer Res.* 52, 904–911.
- (17) Wessels, B. W., and Rogus, R. D. (1984) Radionuclide Selection and Model Absorbed Dose Calculations for Radiolabeled Tumor Associated Antibodies. *Med. Phys.* 11, 638–645.
- (18) Fell, H. P., Gayle, M. A., Yelton, D., Lipsich, L., Schieven, G. L., Marken, J. S., Aruffo, A., Hellström, K. E., Hellström, I., and Bajorath, J. (1992) Chimeric L6 Anti-tumor antibody. Genomic Construction, Expression, and Characterization of the Antigen Binding Site. *J. Biol. Chem.* 267, 15552–15558.
- (19) Penefsky, H. S. (1979) A Centrifuged-Column Procedure for the Measurement of Ligand Binding by Beef Heart F<sub>1</sub>. *Methods Enzymol.* 56, Part G, 527–530.
- (20) Meares, C. F., McCall, M. J., Reardan, D. T., Goodwin, D. A., Diamanti, C. I., and McTigue, M. (1984) Conjugation of Antibodies with Bifunctional Chelating Agents: Isothiocyanate and Bromoacetamide Reagents, Methods of Analysis, and Subsequent Addition of Metal Ions. *Anal. Biochem.* 142, 68–78.
- (21) DeNardo, S. J., Peng, J.-S., DeNardo, G. L., Mills, S. L., and Epstein, A. L. (1986) Immunochemical Aspects of Monoclonal Antibodies Important for Radiopharmaceutical Development. *Nucl. Med. Biol.* 13, 303–310.
- (22) Hellström, I., Horn, D., Linsley, P., Brown, J. P., Brankovan, V., and Hellström, K. E. (1986) Monoclonal Mouse Antibodies Raised against Human Lung Carcinoma. *Cancer Res.* 46, 3917–3923.

# REVIEWS

## Low-Density Lipoprotein as a Vehicle for Targeting Antitumor Compounds to Cancer Cells

Raymond A. Firestone

Bristol-Myers Squibb Pharmaceutical Research Institute, P.O. Box 5100, Wallingford, Connecticut 06492-7660.  
Received October 4, 1993

### INTRODUCTION

It is difficult to eradicate cancer cells *in vivo* because they share with normal cells, for the most part, the same biochemical machinery. There is no cytotoxic substance that is completely selective for malignant cells, and all those presently in use cause dose-limiting toxic side effects. For this reason there is a growing emphasis on targeting, i.e., selective delivery of drugs to tumors in ways that bypass normal body tissues.

Among the vehicles that can be used for this purpose is low-density lipoprotein (LDL), a normal blood constituent that is the body's principal means for delivery of cholesterol to tissues. Cholesterol, a major constituent of mammalian cell membranes, is obtained by cells either by making it themselves or by picking it up from LDL or both. Cancer cells, like all dividing ones, need large amounts of cholesterol because they are making new membrane. There is ample evidence that many types of cancer cells indeed have unusually great LDL requirements. The evidence is 2-fold: measurements of LDL uptake by tumor cells and depletion of LDL in the blood of cancer patients resulting from high uptake by the tumor (*vide infra*). Thus, if LDL could be made to carry antitumor drugs, it would serve as a targeting vehicle. This concept was proposed in 1981-2 (1,2) and has been reviewed several times since then (3-7).

LDL consists of spherical particles 220 Å in diameter containing a nonpolar core of approximately 1500 molecules of cholesterol esterified with long-chain fatty acids such as oleate or linoleate. Around the core is a phospholipid oriented, like a micelle, with the polar ends outward and the lipophilic fatty acid chains inward. Mixed with the phospholipid is unesterified cholesterol, presumably as a stabilizer, and also a single molecule per LDL particle of apoprotein B which binds to specific cell surface receptors. After binding, the receptors, which are grouped together in coated pits, are internalized by endocytosis and taken to lysosomes, where the cholesteryl esters are hydrolyzed, making free cholesterol available to the cell. The LDL receptors are then recycled to the cell surface. The half-life of LDL in the blood is measured in days, but after binding to fibroblasts,  $t_{1/2}$  for internalization is only 10 min. The mechanism of the LDL system was elucidated by Brown, Goldstein, and co-workers (8-10).

### LDL UPTAKE BY CANCER CELLS

It is not surprising that malignant cells have high LDL requirements because rapidly dividing cells do. Indeed, there is a tendency for growing cells to acquire cholesterol from without and for differentiated cells from within (11). The first report regarding cancer and LDL in 1978 was that human acute myeloid leukemia (AML) cells take up 3-100× more LDL than normal cells (12). Human AML

take up 4-25× more LDL than normal white blood cells (13), and the high *in vitro* uptake of AML correlates with high *in vivo* uptake (14). Human monocytic (FAB-M5) and myelomonocytic (FAB-M4) leukemias and chronic myeloid leukemia in blast crisis (but not acute lymphoblastic leukemia [ALL]) take up much more LDL than normal mononuclear cells, peripheral granulocytes, or nucleated bone marrow cells (15).

Some human solid tumors are also avid for LDL. Epidermoid cervical cancer EC-50 absorbs 15× more LDL than fetal adrenal tissue (which has exceptionally high uptake) and 50× more than normal gynecologic tissue. Endometrial adenocarcinoma AC-258 absorbs 10× more than normal (1). EC-50 and four other gynecologic cancers have greater LDL uptake than normal cervical tissues (16). Gastric carcinoma and parotid adenoma exceed every normal cell type (17). Many brain tumors bind 2-3× more LDL than normal brain, especially medulloblastoma, oligodendroglioma, and malignant meningioma (18). In most of a group of nine patients, lung tumor tissue's uptake exceeded that of neighboring normal lung by 1.5-3× (19). Other tumors, for which quantitative comparisons are lacking, have high LDL uptake: glioma V-251MG (20), G2 hepatoma (21, 22), squamous lung tumor (23), and choriocarcinoma (24). Most human tumors have not yet been surveyed, so it is reasonable to suppose that many more will be found to have exceptionally high LDL requirements. This expectation is foreshadowed by the frequent finding of depletion of LDL in the blood of cancer patients, to be discussed subsequently.

Mouse tumors have also been studied. Fibrosarcoma MS-2 takes up several times more LDL than normal tissue (liver, spleen, muscle, fat, heart) (25), and similarly for MAC 13 tumors as well as four others (26).

The most sinister aspect of cancer is its tendency to spread, or metastasize, throughout the body. This is most often the cause of death, even after resection of the primary tumor, because mets are not only difficult to find but also to kill with standard chemotherapy. Therefore, particularly noteworthy is the small but growing body of evidence that tumor cells that are exceptionally metastatic (27, 28), aggressive (29-31), or undifferentiated (11, 32, 33) are also exceptional in their LDL requirements. If this is borne out in future studies, LDL-based therapy will be even more valuable than it presently appears.

Some tumors, however, do not internalize great amounts of LDL, e.g., ALL (mentioned above) (15), chronic lymphocytic leukemia (CLL) (34), several colon adenocarcinomas (35), Lewis rat renal carcinoma (36), cervical cancer EC-168 (37), epitheloid carcinoma A-431 (38), and guinea pig leukemic lymphocytes (39). The latter three have plenty of LDL receptors, but internalization is deficient. Thus, it is important to show not only binding

but also internalization of LDL before concluding that a given cell type is ripe for LDL targeting.

Some noncancerous pathogens have also been found to have high LDL requirements and therefore are candidates for LDL-based therapy. These will be discussed at the end of this paper.

#### DEPLETION OF LDL IN THE BLOOD OF CANCER PATIENTS

If tumor cells sequester abnormally large amounts of LDL, one would expect to see reduced levels of plasma cholesterol in cancer patients. This is indeed a well-documented phenomenon, first reported in 1939 when it was observed that leukemia patients had unusually low blood cholesterol (40).

There was then a hiatus before the recent spate of papers, which was prompted by the question of what overall effects would ensue if people were to lower their cholesterol to improve cardiovascular health. As expected, comparison of blood cholesterol with mortality in large cohorts revealed a positive association, i.e., high cholesterol correlates with high mortality, but a frequent and unexpected observation was a *negative* association, i.e., rise in mortality at the lowest cholesterol levels. Thus, there is an overall U-shaped relationship between cholesterol and mortality. The excess deaths at very low cholesterol turned out to be due to previously undiagnosed cancer. Cause and effect were not immediately obvious, but it is now abundantly clear that it is cancer that brings about a reduction in cholesterol, and not low cholesterol that causes cancer.

In the 1980 Whitehall study of 17 718 men followed 7.5 years, a U-shaped curve was observed whose anomaly (the upward shift in mortality at lowest cholesterol levels) disappeared after subtraction of cancer cases (lung, stomach, colon) diagnosed within 2 years after the study began, suggesting that these men had undiagnosed early cancer which caused a drop in cholesterol level (41). In a similar study of 7603 French men followed for 6.6 years, cancer patients undiagnosed at entry had reduced cholesterol (170 mg/dL), lowest with fastest-growing tumors, especially pancreas, larynx, esophagus, leukemia, stomach, and colon (42). A 10-year study of a 39 000 patient cohort in Finland found an inverse cancer-cholesterol correlation, especially stomach and lung, during the first years of followup (43). The lowest quintile of serum cholesterol among 160 000 men and women corresponded to elevated cancer of the lung, prostate, and colon for men and breast, uterus, colon, and lung for women during the first two years after cholesterol measurement (44). Among 3805 hyperlipidemic men there was a drop in serum cholesterol between 8 months and 2 years prior to diagnosis (45). Among 10 295 men and women followed for 14 years, there was a sharp rise in cancer mortality at the lowest cholesterol level, greatest at <5 years followup and for older people (46). A similar observation was made in a cohort of 7478 men followed 17–20 years in which the inverse cancer-cholesterol correlation was diminished but not completely eliminated when deaths during the first five, and even more so 10, years were excluded (47). An inverse association was observed between serum cholesterol and colon, but not rectal, cancer in 7926 Japanese-American men over a 20-year span, more pronounced <10 years than >10 years before diagnosis, in the order  $Dukes\ B > C > A, D$ . The risk doubled for cholesterol <180 vs >200 mg/dL (48). In the MRFIT trial, 350 977 men were followed 12 years after cholesterol determination. Low cholesterol was associated with cancer of the liver, pancreas, lung, lymphatic, and hemopoietic systems, the association fading

with time (49). Among 3091 Dutch men and women followed 28 years, the risk factor for gastrointestinal cancer (men only), years 3–15, was 4.2 for the lowest vis-à-vis the highest cholesterol quintile, falling to *ca.* 1.0 after that. For lung cancer in men and GI cancer in women there was no association (50). In other cohorts of 7716 (colon, pharyngeal, oral, esophageal, liver) (51) and 1910 (52) patients, as well as several smaller studies, lowering of cholesterol close to diagnosis was observed for cervical (53), colon (54), prostate (55), stomach, bladder, CNS, and colorectal cancers (56).

A more direct connection between cholesterol depletion in the patient and high LDL uptake by the cancer was made in a few studies. Lowered serum cholesterol in AML patients was closely correlated with high uptake by the AML cells of  $^{14}C$ -sucrose-loaded LDL in vivo and of  $^{125}I$ -LDL in vitro (14). In 59 leukemia patients, blood cholesterol was inversely correlated with the rate of high affinity degradation of LDL by the leukemia cells (57).

Inverse cancer-cholesterol correlations can be reversed. In the study just cited (57), when the leukemia cell burden was reduced by chemotherapy, blood cholesterol rose. Similarly, only in AML patients with high leukemia cell counts was low cholesterol observed (47/85), which rose during remission (58). Patients with a variety of leukemias and lymphomas had reduced cholesterol levels which rose to that of normal controls after chemotherapy-induced response, but not if the therapy failed (59). In cancer patients who responded to chemotherapy, LDL increased as follows (no. of patients, % LDL increase): malignant lymphoma (17, 32%); small cell lung cancer (11, 7%); transitional cell carcinoma (7, 7%); breast (16, no change) (60).

Of special importance is the fact that the effect of cancer in lowering blood cholesterol is greatest with the most aggressive, metastasizing tumors, in accord with their greater LDL requirements (*vide supra*). In the cited study of hyperlipidemic men, the drop in serum cholesterol was seen especially with nonlocalized rather than localized cancer (45). In another study, 83% of cancer patients presented with hypocholesterolemia, which was most severe with the most undifferentiated morphology (61). An inverse colon cancer-cholesterol correlation was most marked with the most advanced cases, particularly for women (62). Plasma LDL was lowered with acute leukemia, bladder, and breast carcinoma, especially the most aggressively metastasizing cases (30). LDL receptor activity in breast (29) and other (11, 34) cancers is higher the greater the degree of malignancy. Tumors of low but not high differentiation have high LDL uptake (11, 34) and reduce plasma cholesterol the most (32, 61). Survival time, a measure of tumor aggressiveness, is lowest with highest LDL uptake in breast cancer (29, 30) and with lowest serum LDL in AML, chronic myeloid leukemia (CML) (31), and other types (42). Metastatic prostate cancer is associated with lower cholesterol levels than nonmetastatic (55).

There are many additional studies in which were seen an inverse relationship between plasma cholesterol and cancer of many types (63–69), as well as a few reporting no relationship (71–73). Diet is not responsible (74). The great preponderance of the evidence therefore favors the theory that the reduced cholesterol often observed in cancer patients is the result of uptake of LDL by the tumor and not the cause of the cancer (75).

## RECONSTITUTION OF LDL WITH CYTOTOXIC DRUGS

In order to kill tumors with drugs that are targeted in LDL, the drugs must somehow be bound to the LDL in such a way that (1) they cannot escape from it while traveling in the blood enroute to the tumor, (2) their cytotoxicity is chemically or physically masked while LDL-bound, and then restored after entering the target cells, (3) in quantity  $\times$  killing power there is enough drug to kill cancer cells contained in the reconstituted LDL (r-LDL), whose uptake is limited by the number of LDL receptors on the tumor cells and their rate of internalization, and (4) the presence of Apo B and its binding power to LDL receptors are retained. The ability of the drug, once released from its carrier, to escape from lysosomes must also be taken into account (76).

Association of a drug with LDL may be stable or unstable. Any or several of the following experiments must therefore be done to ensure that the drug enters cells only via LDL receptors. (1) Receptor-positive but not receptor-negative cells should be killed. (2) r-Me-LDL should be taken up by scavenger receptors (e.g., on macrophages) but not normal ones. Scavenger receptors take up damaged (methylated or acetylated) rather than normal LDL. Macrophages have many more scavenger than normal LDL receptors. (3) Saturability of uptake can be demonstrated by blocking LDL receptors with native LDL. It should reduce r-LDL uptake and cytotoxicity, while Me-LDL should not. (4) Cytotoxicity *in vitro* may be stronger with r-LDL than with free drug, although this is not necessarily the case. *In vivo* results must be interpreted with care, since even leaky r-LDL might be superior to free drug given as a bolus, if leakage is slow and steady (depot effect). (5) Benzyl alcohol inhibits LDL uptake and is therefore a possible test for the mechanism of killing (77).

The first published procedure was that of Krieger, in which LDL is isolated, lyophilized on potato starch, stripped of its core by heptane extraction, and reconstituted by adding the drug in a nonpolar solvent which is then evaporated and replaced with aqueous buffer (78). Lipophilic groups ("LDL anchors") on the drug, such as oleyl, linoleyl, retinyl, or cholesteryl, are required for successful, stable reconstitution (79). Since the entire core (which stabilizes the particle) is replaced, there is little tolerance for nonoptimal (i.e., poorly anchored) structures, but the carrying power of the r-LDL is high. The principal problems are imperfect anchoring, which leads to leakage of the drug from the r-LDL or failure to reconstitute altogether, and the creation of aggregated r-LDL, which is rapidly cleared by the reticuloendothelial system (RES). Contamination by aggregate therefore requires an extra step to remove it and lowers the yield (80).

The Masquelier procedure (81) differs in that sucrose is substituted for starch, and the core is not discarded. This makes for easier reconstitution without aggregation, and the r-LDL's pharmacokinetics are close to that of native LDL, but its carrying power for drug is lower.

In a more drastic process, LDL is taken apart with detergent (sodium deoxycholate, SDOC) and the Apo B reconstituted with drug and EPC (egg phosphatidyl choline) into a microemulsion. Yields and carrying power are high (82-86). In a comparison of these three procedures by another group, the first was favored (87).

A modified microemulsion technique has been described by Samadi-Boboli and co-workers (88). 9-Methoxyellipticine-cholesteryl oleate-DMPC (dimyristoyl phosphatidyl choline) microemulsion is incubated with LDL, a simple

procedure which, however, gives lower carrying power (5-10 molecules drug/LDL particle) and drug yield (2.5%). There is greater carrying power (70 molecules/LDL) with the oleyl *N*-methylellipticinium 9-ester (89) and still greater (400 molecules) with improvements in reconstitution technique (90).

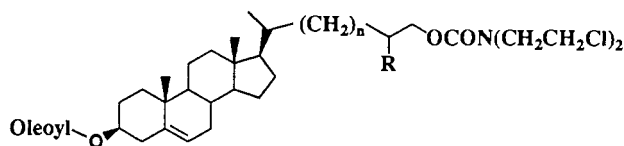
Drugs can be chemically linked to LDL (81, 91). This has the advantage that leakage will not occur. However, the carrying power is limited, and increasing the load reduces binding to the LDL receptor, presumably because derivatization of Apo B alters it. Also, unless the drug is released efficiently after endocytosis, its cytotoxic power may be lowered (91). Boronated LDL has been made, carrying enough boron for boron neutron capture therapy (92), but there are no data on receptor-negative cells or competition with native LDL.

Finally, drugs can be associated with LDL by mixing them together in various ways. The advantage is that these procedures are very simple. The disadvantages can be low drug loading and leakage of drug from the complex, probably because some of it remains in the surface layer of the LDL and does not reach the core. LDL can be mixed directly with the drug (23, 93-95), with the drug as a dry film (96) (40 drug molecules/LDL can be incorporated but 78% is easily released in serum) (97), or with a drug-cholesteryl ester microemulsion (88, 89, 98). Facilitated transfer (99) using natural transfer proteins has been tried (5, 100), giving 18 molecules/LDL (87).

## CYTOTOXICITY OF LDL-DRUG CONJUGATES

The first cytotoxic compound incorporated into LDL was 25-hydroxycholesteryl oleate, in 1978 (101). This was followed by pyrene-cholesteryl oleate, a photosensitizer (102).

We reported in 1984 a series of antitumor compounds reconstituted with LDL by the original method (103). Some compounds failed to reconstitute, others leaked out of the r-LDL, and still others reconstituted stably but had insufficient killing power. Two LDL anchors were required to prevent leakage. One drug, known as "compound 25", met all criteria in that it afforded stable r-LDL that killed all the target cells at reasonable r-LDL concentrations, while r-Me-LDL was not cytotoxic. Excess native LDL abolished cytotoxicity. The results were the same in other hands using reconstitution by the microemulsion (104), but not the modified sucrose technique (105), presumably because less drug is carried when not all the core is removed. An increase in cytotoxicity was needed, and this has now been achieved in compounds 1 and 2 (106), which have twice the number of warheads and twice the killing power. Apparently, in compound 25 the limit of enzymic carbamate-hydrolyzing power had been reached.



"Cpd 25":  $n=1$ ,  $R=H$

1 :  $n=1$ ,  $R=CH_2OCON(CH_2CH_2Cl)_2$

2 :  $n=3$ ,  $R=CH_2OCON(CH_2CH_2Cl)_2$

In addition to compound 25, Lundberg has also reconstituted prednimustine in a microemulsion, achieving 338 molecules/Apo B in particles  $2.5\times$  the diameter of native LDL that were stable for months (86). Activity was *ca.*

1.5× free drug, with the difference greatest at low concentration. Receptor-negative cells were not used.

Using their own modified method (Masquelier's) (81), Vitols et al. reconstituted LDL with the water-insoluble drug WB 4291 (1-[bis(2-chloroethyl)amino]-3-methylnaphthalene), incorporating 1500 molecules/LDL (107). This r-LDL showed receptor-mediated cytotoxicity in vitro in that native but not methylated LDL abolished cytotoxicity. Normal (receptor-positive) more than mutant (receptor-negative) cells were killed, but since the ID<sub>50</sub> ratio was only 1:3, some leakage of drug out of the r-LDL was indicated. Clearance time in rabbits was longer for this r-LDL than that made by the Krieger (78) method. Median survival time (MST) of leukemic mice was prolonged 2.5× ip-ip with 40% survivors, but MST was increased only 1.42× iv-iv. LDL reconstituted with AD-32 (400–500 molecules/LDL) by Krieger's method was taken up via LDL receptors, but leaky (108). Stability of the r-LDL was improved with combined linoleyl and retinyl anchors (100–200 molecules/LDL), giving rise to selectivity and cytotoxicity (109).

Soula's group reported binding and degradation of r-LDL bearing *N*-methyllellipticinium-9-oleate to be normal, saturable, and blocked by native but not Me-LDL (89). Macrophages absorbed r-LDL and LDL equally, and much less than acetyl-LDL, indicating normal behavior for the r-LDL. Drug uptake in r-LDL exceeded that of free drug. Cytotoxicity to L1210 was dose-dependent, greater than that of free drug, and blocked by native but not Me-LDL. Receptor-negative cells were not used. Loss of free drug in human serum plateaued at 10%. These results show uptake of r-LDL via LDL receptors, but do not rule out some leakage.

Uptake, cytotoxicity, and intracellular distribution of an LDL–daunomycin (DNM) complex (made by simple mixing) by lung cancer cells was equal to that of free DNM, although intracellular metabolism of DNM from the complex was slower, possibly because the presence of LDL upset lysosomal digestion of DNM; comparison with free DNM + LDL was not made (23). Receptor-mediated uptake of LDL–DNM was not demonstrated, either by suppression with free LDL or by lack of uptake by receptor-negative cells, so that leakage of DNM from the complex before uptake is possible.

An estramustine–LDL complex (110) made by Masquelier's procedure (81) (modified), containing 143 drug molecules/LDL, was 100× less active than free drug against two cell lines, with no effect of native LDL (110). Dose-response persisted above LDL receptor saturation. Thus, nonspecific uptake of the complex or free drug played a major role. Similarly, prednimustine–LDL (163 molecules/LDL) had 10× less cytotoxicity than free drug, not affected by native LDL (111). Conclusions are similar.

Dioleoyl floxuridine, incorporated into r-LDL by Krieger's method (50–70 molecules/LDL), was taken up by Hep G2 cells via LDL receptors (although leakage was not ruled out) and had a serum half-life shorter than native but >6–9× longer than free drug (87).

Vincristine–LDL (VC/LDL), prepared by Masquelier's method, has been given to nine patients with ovarian or endometrial carcinoma (112). Uptake of r-LDL by the liver and adrenals was suppressed with chenodeoxycholic acid and prednisolone, respectively (*vide infra*). Side effects were peripheral neuropathy/paraesthesia (mild to severe, said to be less than with VCSO<sub>4</sub> alone), abdominal pain, and significant alopecia, showing that some if not most of the VC probably leaked out of the r-LDL. This is not surprising since VC has no good LDL anchors.

LDL can also be used to target photosensitizing drugs (113, 114). Cytotoxicity then ensues only after irradiation. This has two potential advantages: toxicity can be postponed until after non-tumor-bound drug has been cleared from the body, and if the sensitizer operates catalytically, less drug is needed. In the first example, pyrene-cholesteryl oleate was targeted in r-LDL, exclusively via LDL receptors since receptor-negative cells were not harmed, inducing cell death after irradiation at 300–400 nm (115). Porphyrins can be associated with LDL (130–250 molecules/LDL) without inhibiting LDL receptor binding (116) or processing (117), and uptake can be enhanced 1.5–1.8× by lovastatin, which upregulates LDL receptors by inhibiting cholesterol biosynthesis (118). A porphyrin derivative (BPD), associated with LDL by simple mixing, catalyzed photodynamic killing of cells 7× better than BPD alone at 37 °C, and 6× better than at 4 °C showing the importance of internalization (119). However, porphyrins can exchange between LDL, other phospholipids, and cell membranes, reducing the targeting specificity. This might lead to long-lasting photosensitivity in patients (113). In vivo, hematoporphyrin is carried to a mouse tumor by LDL (120). Mixing LDL with BPD before injection improves the antitumor effect of light (121).

#### UP- AND DOWNREGULATION OF LDL RECEPTORS

It is desirable to deliver the drug only to the tumor and to exclude it from nontumor sites. However, competing with the tumor for r-LDL are normal tissues and organs, particularly the liver because of its size and LDL receptor content, and the adrenals whose uptake/g is particularly high. Since the drugs to be targeted have some selectivity toward cancer cells, normal organs can take some hits, but protection of the liver and adrenals is nevertheless desirable. Bile acid feeding suppresses hepatic LDL receptor activity in dogs (122), and a key paper reports that feeding of sodium taurocholate and hydrocortisone sodium succinate to tumor-bearing mice reduces LDL uptake in the liver by 36% and in the adrenals by 59%, with insignificant reduction in uptake by the tumor (123). Also reported to downregulate the liver's uptake of LDL are feeding saturated fats (124), cholesterol with hydrogenated coconut oil (124), and fasting (125) which is said to downregulate LDL receptors on healthy but not tumor cells (5).

Another strategy for protecting the liver is based on the fact that normal LDL receptors do not bind to Ac-LDL, Me-LDL, or oxidized LDL (Ox-LDL), which instead are avidly taken up via scavenger LDL receptors, e.g., by macrophages (*vide supra*). Cholesterol liberated from Ac-LDL after endocytosis via scavenger receptors enters the metabolically active pool (126) and thus presumably functions normally in downregulating LDL receptor expression. Therefore, I propose that the liver, which is rich in scavenger (on sinusoidal epithelial and Kupffer cells) (127) as well as normal LDL receptors, might be downregulated by cholesterol-loaded Ac-LDL, Me-LDL, or Ox-LDL which would not downregulate LDL receptor expression on tumor cells. Sinusoidal epithelial cells of the spleen, bone marrow, adrenals, and ovaries also take up Ac-LDL (127) and might be downregulated at the same time.

Another way of protecting the adrenals arises from the fact that angiotensin II increases their LDL uptake and receptor number (128). I suggest that ACE inhibitors, which prevent angiotensin II formation, might then reduce LDL uptake by the adrenals.

Increasing the activity of LDL-mediated endocytosis in tumor cells would also be beneficial, provided normal cells were not concomitantly upregulated. LDL receptor activity is indeed stimulated in normal cells by HMGCoA-reductase inhibitors (129, 130) or bile acid sequestrants (129–131), verapamil (132), cachectin, and some growth factors (133), TGF- $\beta$  (134), TNF- $\alpha$ , and IL-1 (135). There is one report that HMGCoA reductase inhibitors upregulate normal rat hepatocytes more than Hep-G2 cells (136) (bad news if confirmed). On the other hand, compactin is reported to upregulate LDL receptors on Hep-G2 cells with little effect on normal human fibroblasts (137). Oncostatin M potentially upregulates LDL uptake by Hep-G2 cells, more than normal cells (138). The upshot is that we cannot yet tell whether upregulation of tumor LDL receptor activity by the above methods would or would not be therapeutically beneficial.

#### REMOVAL OF LDL FROM THE PATIENT BEFORE TREATMENT

During treatment, drug-bearing r-LDL must compete with native LDL for access to LDL receptors on the tumor cells, requiring elevated doses of r-LDL. This can be countered by removing LDL from the patients' blood (delipidation) prior to treatment (139–141). Although restoration of normal LDL levels takes days (141), it might be best to delipidate immediately prior to treatment because it induces upregulation of LDL receptors throughout the body (142), and it is unknown whether upregulation in this way would be greater for tumor or normal cells.

However, in hepatocytes, unlike fibroblasts, cholesterol derived from LDL only weakly downregulates LDL receptor activity (143), so that one might expect that LDL depletion will upregulate liver uptake in only a small way. In low-LDL media, ACAT inhibitors block time-dependent upregulation in normal hepatocytes more than in Hep-G2 cells (144). I suggest, then, that this is a way to prevent liver upregulation during delipidation.

Numerous methods have been developed for extracorporeal removal (145) of LDL for the sake of hypercholesterolemic patients. Macroporous bead cellulose removes LDL but not HDL (146). The following methods remove the indicated amounts of LDL: plasmapheresis 73% (147), apheresis with dextran sulfate cellulose 62–64% (139), continuous adsorption on Apo B-antibody column 82% (140), anti-LDL antibody/Sepharose 80% (141), and apheresis 76% (148). Intravenous infusion of liposomes removes >90% of plasma cholesterol from both normal and Watanabe rabbits (149). Continuous intraoperative separation of red blood cells by machine in 3–4 min for autologous transfusion has been reported to be safe and efficient (150), opening the possibility that LDL could be extracted from the patient's own blood, returning his delipidated plasma and blood cells, and making the drug-bearing r-LDL from his own LDL. LDL obtained via apheresis is also suitable for reconstitution with drugs (151).

#### LDL UPTAKE BY PARASITES

Although this topic is not cancer-related, it is worthwhile noting that diseases other than cancer might possibly be treated with drugs carried in r-LDL. *Trypanosoma brucei* has LDL receptors that are stable despite surface antigen variation (152) and requires LDL, having 800 high- and 52 000 low-affinity LDL receptors (153) which carry the LDL to intracellular acidic vacuoles for proteolysis and then recycle (154). *Schistosoma mansoni* parasites take up LDL via specific and saturable binding, breaking it

down in the lumen or gut rather than lysosomes (155). *Trichomonas vaginalis*, a common human parasite, has high LDL requirements (156). *Leishmania amastigotes* residing in macrophages are killed 3 $\times$  more efficiently by methotrexate (MTX)-maleyl BSA, via the Ac-LDL receptor, than by free MTX (157).

#### CONCLUSION

In order to successfully treat cancer by means of LDL-mediated drug targeting, it is necessary to develop a method of securely associating drugs with LDL in such a way that they are released inside, and only inside, the target cells, find drugs potent enough to kill tumor cells when delivered in this way, and work out reliable and convenient ways to delipidate patients. All these things separately have been accomplished, if not to perfection at least in a practical way. Therefore, the path is now open to human trials. Although numerous potential tumor targets have already been identified, and presumably others yet unidentified will be uncovered, it seems to me that the best opportunity for the first strike is against a hematological malignancy such as AML because cure is presently very difficult, access of r-LDL to the target cells is unimpeded, and LDL uptake by this particular tumor is especially high.

#### LITERATURE CITED

- (1) Gal, D., Ohashi, M., MacDonald, P. C., Buchsbaum, H. J., and Simpson, E. R. (1981) Low-density lipoprotein as a potential vehicle for chemotherapeutic agents and radionuclides in the management of gynecologic neoplasms. *Am. J. Obstet. Gynecol.* 139, 877.
- (2) Counsell, R. E., and Pohland, R. C. (1982) Lipoproteins as potential site-specific delivery systems for diagnostic and therapeutic agents. *J. Med. Chem.* 25, 1115.
- (3) van Berkel, T. J. C. (1993) Drug targeting: application of endogenous carriers for site-specific delivery of drugs. *J. Controlled Release* 24, 145.
- (4) Vitols, S. (1991) Uptake of low-density lipoprotein by malignant cells—possible therapeutic applications. *Cancer Cells* 3, 488.
- (5) de Smidt, P. C., and van Berkel, T. J. C. (1990) LDL-mediated drug targeting. *Crit. Revs. Thera. Drug Carrier Syst.* 7, 99.
- (6) Peterson, C., Masquelier, M., Rudling, M., Söderberg, K., and Vitols, S. (1991) Lipoproteins, malignancy and anticancer agents. *Targeted Diagn. Ther. (U.S.)* 5, 175.
- (7) Catapano, A. L. (1987) Transport of cytotoxic compounds to cells via the LDL receptor pathway. *Med. Sci. Res.* 15, 411.
- (8) Goldstein, J. L., Anderson, R. G. W., and Brown, M. S. (1979) Coated pits, coated vesicles and receptor-mediated endocytosis. *Nature* 279, 679.
- (9) Brown, M. S., Kovanen, P. T., and Goldstein, J. L. (1980) Evolution of the LDL receptor concept—from cultured cells to intact animals. *Ann. N. Y. Acad. Sci.* 348, 48.
- (10) Brown, M. S., Kovanen, P. T., and Goldstein, J. L. (1981) Regulation of plasma cholesterol by lipoprotein receptors. *Science* 212, 628.
- (11) Ponc, M., Havekes, L., Kempenaar, J., Lavrijsen, S., Wijsman, M., Boonstra, J., and Vermeer, B. J. (1985) Calcium-mediated regulation of the low density lipoprotein receptor and intracellular cholesterol synthesis in human epidermal keratinocytes. *J. Cell Physiol.* 125, 98.
- (12) Ho, Y. K., Smith, R. G., Brown, M. S., and Goldstein, J. L. (1978) Low-density lipoprotein (LDL) receptor activity in human acute myelogenous leukemia cells. *Blood* 52, 1099.
- (13) Vitols, S., Gahrton, G., and Peterson, C. (1984) Significance of the low-density lipoprotein receptor pathway for the in vitro accumulation of AD-32 incorporated into LDL in normal and leukemic white blood cells. *Cancer Treat. Rep.* 68, 515.
- (14) Vitols, S., Angelin, B., Ericsson, S., Gahrton, G., Juliusson, G., Masquelier, M., Paul, C., Peterson, C., Rudling, M., Söderberg-Reid, K., and Tidefelt, U. (1990) Uptake of low



- density lipoproteins by human leukemic cells in vivo: relation to plasma lipoprotein levels and possible relevance for selective chemotherapy. *Proc. Natl. Acad. Sci. U.S.A.* 87, 2598.
- (15) Vitols, S., Gahrton, G., Ost, A., and Peterson, C. (1984) Elevated low density lipoprotein receptor activity in leukemic cells with monocytic differentiation. *Blood* 63, 1186.
  - (16) Gal, D., Macdonald, P. C., Porter, J. C., and Simpson, E. R. (1981) Cholesterol metabolism in cancer cells in monolayer culture. III. Low-density lipoprotein metabolism. *Int. J. Cancer* 28, 315.
  - (17) Rudling, M. J., Reihner, E., Einarsson, K., Ewerth, S., and Angelin, B. (1990) Low density lipoprotein receptor-binding activity in human tissues: quantitative importance of hepatic receptors and evidence for regulation of their expression in vivo. *Proc. Natl. Acad. Sci. U.S.A.* 87, 3469.
  - (18) Rudling, M. J., Angelin, B., Peterson, C. O., and Collins, V. P. (1990) Low density lipoprotein receptor activity in human intracranial tumors and its relation to the cholesterol requirement. *Cancer Res.* 50, 483.
  - (19) Vitols, S., Peterson, C., Larsson, O., Holm, P., and Aberg, B. (1992) Elevated uptake of low density lipoproteins by human lung cancer tissue in vivo. *Cancer Res.* 52, 6244.
  - (20) Rudling, M. J., Collins, V. P., and Peterson, C. O. (1983) Delivery of a clacynomycin A to human glioma cells in vitro by the low-density lipoprotein pathway. *Cancer Res.* 43, 4600.
  - (21) Havekes, L., van Hinsbergh, V., Kempen, H. J., and Emeis, J. (1983) The metabolism in vitro of human low-density lipoprotein by the human hepatoma cell line hep G2. *Biochem. J.* 214, 951.
  - (22) Dashti, N., Wolfbauer, G., Koren, E., Knowles, B., and Alaupovic, P. (1984) Catabolism of human low-density lipoproteins by human hepatoma-cell line Hep G2. *Biochim. Biophys. Acta* 794, 374.
  - (23) Kerr, D. J., Hynds, S. A., Shepherd, J., Packard, C. J., and Kaye, S. B. (1988) Comparative cellular uptake and cytotoxicity of a complex of daunomycin-low density lipoprotein in human squamous lung tumour cell monolayers. *Biochem. Pharmacol.* 37, 3981.
  - (24) Simpson, E. R., Bilheimer, D. W., MacDonald, P. C., and Porter, J. C. (1979) Uptake and degradation of plasma lipoproteins by human choriocarcinoma cells in culture. *Endocrinology (Baltimore)* 104, 8.
  - (25) Norata, G., Canti, G., Ricci, L., Nicolini, A., Trezzi, E., and Catapano, A. L. (1984) In vivo assimilation of low density lipoproteins by a fibrosarcoma tumour line in mice. *Cancer Lett.* 25, 203.
  - (26) Welsh, J., Calman, K. C., Stuart, F., Glegg, J., Stewart, J. M., Packard, C. J., Morgan, H. G., and Shepherd, J. (1982) Low-density lipoprotein uptake by tumors. *Clin. Sci.* 63, 44P.
  - (27) Schroeder, F., Kier, A. B., Olson, C. D., and Dempsey, N. E. (1984) Correlation of tumor metastasis with sterol carrier protein and plasma membrane sterol levels. *Biochem. Biophys. Res. Commun.* 124, 283.
  - (28) Cambien, F., Ducimetiere, P., and Richard, J. (1980) Total serum cholesterol and cancer mortality in a middle-aged male population. *Am. J. Epidemiol.* 112, 388.
  - (29) Rudling, M. J., Ståhle, L., Peterson, C. O., and Skoog, L. (1986) Content of low density lipoprotein receptors in breast cancer tissue related to survival of patients. *Brit. Med. J.* 292, 580.
  - (30) Peterson, C., Vitols, S., Rudling, M., Blomgren, H., Edsmyr, F., and Skoog, L. (1985) Hypocholesterolemia in cancer patients may be caused by elevated LDL receptor activities in malignant cells. *Med. Oncol. Tumor Pharmacother.* 2, 143.
  - (31) Muller, C. P., Wagner, A. U., Maucher, C., and Steinke, B. (1989) Hypocholesterolemia, an unfavorable feature of prognostic value in chronic myeloid leukemia. *Eur. J. Haematol.* 43, 235.
  - (32) Zyada, L. E., Hassan, H. T., Rees, J. K. H., and Ragab, M. H. (1990) The relation between hypocholesterolemia and degree of maturation in acute myeloid leukemia. *Hematol. Oncol.* 8, 65.
  - (33) Ponc, M., Havekes, L., Kempenaar, J., Lavrisen, S., and Vermeer, B. J. (1984) Defective low-density lipoprotein metabolism in cultured, normal, transformed and malignant keratinocytes. *J. Invest. Dermatol.* 83, 436.
  - (34) Juliusson, G., and Vitols, S. (1988) Impaired low-density lipoprotein receptor activity in chronic B-lymphocytic leukemia cells. *Eur. J. Hematol.* 40, 18.
  - (35) Fabricant, M., and Broitman, S. A. (1990) Evidence for deficiency of low density lipoprotein receptor on human colonic carcinoma cell lines. *Cancer Res.* 50, 632.
  - (36) Clayman, R. V., Bilhartz, L. E., Spady, D. K., Buja, L. M., and Dietschy, J. M. (1986) Low density lipoprotein-receptor activity is lost in vivo in malignantly transformed renal tissue. *FEBS Lett.* 196, 87.
  - (37) Gal, D., Simpson, E. R., Porter, J. C., and Snyder, J. M. (1982) Defective internalization of low density lipoprotein in epidermoid cervical cancer cells. *J. Cell Biol.* 92, 597.
  - (38) Anderson, R. G. W., Brown, M. S., and Goldstein, J. L. (1981) Inefficient internalization of receptor-bound low density lipoprotein in human carcinoma A-431 cells. *J. Cell Biol.* 88, 441.
  - (39) Sainte-Marie, J., Vidal, M., Philippot, J. R., and Bienvenue, A. (1986) Internalization of low-density-lipoprotein-specific receptors in leukemic guinea pig lymphocytes. *Eur. J. Biochem.* 158, 569.
  - (40) Müller, H. G. (1939) Cholesterol metabolism in health and anemia. *Medicine* 9, 119.
  - (41) Rose, G., and Shipley, M. J. (1980) Plasma lipids and mortality: a source of error. *Lancet*, 523.
  - (42) Cambien, F., Ducimetiere, P., and Richard, J. (1980) Total serum cholesterol and cancer mortality in a middle-aged male population. *Am. J. Epidemiol.* 112, 388.
  - (43) Knekt, P., Reunanen, A., Aromaa, A., Heliövaara, M., Hakulinen, T., and Hakama, M. (1988) Serum cholesterol and risk of cancer in a cohort of 39,000 men and women. *Brit. J. Cancer*, 519.
  - (44) Hiatt, R. A., and Fireman, B. H. (1986) Serum cholesterol and the incidence of cancer in a large cohort. *J. Chron. Dis.* 39, 861.
  - (45) Kritchevsky, S. B., Wilcosky, T. C., Morris, D. L., Truong, K. N., and Tyroler, H. A. (1991) Changes in plasma lipid and lipoprotein cholesterol and weight prior to the diagnosis of cancer. *Cancer Res.* 51, 3198.
  - (46) Harris, T., Feldman, J. J., Kleinman, J. C., Ettinger, W. H., Jr., Makuc, D. M., and Schatzkin, A. G. (1992) The low cholesterol-mortality association in a national cohort. *J. Clin. Epidemiol.* 45, 595.
  - (47) Frank, J. W., Reed, D. M., Grove, J. S., and Benfante, R. (1992) Will lowering population levels of serum cholesterol affect total mortality? *J. Clin. Epidemiol.* 45, 333.
  - (48) Nomura, A. M. Y., Stemmerman, G. N., and Chyou, P.-H. (1991) Prospective study of serum cholesterol levels and large-bowel cancer. *J. Nat. Cancer Inst.* 83, 1403.
  - (49) Neaton, J. D., Blackburn, H., Jacobs, D., Kuller, L., Lee, D.-J., Sherwin, R., Shih, J., Stamler, J., and Wentworth, D. (1992) Serum cholesterol level and mortality findings for men screened in the multiple risk intervention trial. *Arch. Intern. Med.* 152, 1490.
  - (50) Schuit, A. J., Van Dijk, C. E. M. J., Dekker, J. M., Schouten, E. G., and Kok, F. J. (1993) Inverse association between serum total cholesterol and cancer mortality in Dutch civil servants. *Am. J. Epidemiol.* 137, 966.
  - (51) Chyou, P.-H., Nomura, A. M. Y., Stemmermann, G. N., and Kato, I. (1992) Prospective study of serum cholesterol and site-specific cancers. *J. Clin. Epidemiol.* 45, 287.
  - (52) Baptiste, M. S., Nasca, P. C., Doyle, J. T., Rothenberg, R. R., Maccubbin, P. A., Mettlin, C., Metzger, B. B., and Carlton, K. A. (1992) Cholesterol and cancer in a population of male civil-service workers. *Int. J. Epidemiol.* 21, 16.
  - (53) Brock, K. E., Hoover, R. N., and Hensley, W. J. (1989) Plasma cholesterol and in-situ cervical cancer—an Australian case control study. *J. Clin. Epidemiol.* 42, 87.
  - (54) Winawer, S. J., Flehinger, B. J., Buchalter, J., Herbert, E., and Shike, M. (1990) Declining serum cholesterol levels prior to diagnosis of colon cancer. *J. Am. Med. Assoc.* 263, 2083.
  - (55) Henriksson, P., Ericsson, S., Stege, R., Eriksson, M., Rudling, M., Berglund, R., and Angelin, B. (1989) Hypocholesterolemia and increased elimination of low-density lipoproteins in metastatic cancer of the prostate. *Lancet* II 1178.

- (56) Wald, N. J., Thompson, S. G., Law, M. R., Densem, J. W., and Bailey, A. (1989) Serum cholesterol and subsequent risk of cancer: results from the BUPA study. *Brit. J. Cancer* 59, 936.
- (57) Vitols, S., Gahrton, G., Björkholm, M., and Peterson, C. (1985) Hypocholesterolemia in malignancy due to elevated low-density-lipoprotein-receptor activity in tumor cells: evidence from studies in patients with leukemia. *Lancet* 1150.
- (58) Reverter, J. C., Sierra, J., Marti-Tutusa, J. M., Montserrat, E., Graña, A., and Rozman, C. Hypocholesterolemia in acute myelogenous leukemia. *Eur. J. Haematol.* 41, 317.
- (59) Venkatanarayanan, S., and Nagarajan, B. (1988) Association between tumor status and serum lipoprotein cholesterol in hematopoietic malignancy. *Biochem. Int.* 17, 499.
- (60) Alexopoulos, C. G., Pournaras, S., Vaslamatzis, M., Avgerinos, A., and Raptis, S. (1992) Changes in serum lipids and lipoproteins in cancer patients during chemotherapy. *Cancer Chemother. Pharmacol.* 30, 412.
- (61) Porta, C., Moroni, M., Nastasi, G., Invernizzi, R., and Bobbio-Pallavicini, E. (1991) Hypocholesterolemia and acute myeloid leukemia (AML). *Haematologica* 76, 348.
- (62) Miller, S. R., Tartter, P. I., Papatestas, A. E., Slater, G., and Aufses, A. H., Jr. (1981) Serum cholesterol and human colon cancer. *JNCI* 67, 297.
- (63) Budd, D., and Ginsberg, H. (1986) Hypocholesterolemia and acute myelogenous leukemia. *Cancer* 58, 1361.
- (64) Törnberg, S. A., Carstensen, J. M., and Holm, L.-E. (1988) Risk of stomach cancer in association with serum cholesterol and beta-lipoprotein. *Acta Oncol.* 27, 39.
- (65) Törnberg, S. A., Holm, L.-E., and Carstensen, J. M. (1988) Breast cancer risk in relation to serum cholesterol, serum beta-lipoprotein, height, weight, and blood pressure. *Acta Oncol.* 27, 31.
- (66) Kark, J. D., Smith, A. H., and Hames, C. G. (1980) The relationship of serum cholesterol to the incidence of cancer in Evans County, Georgia. *J. Chron. Dis.* 33, 311.
- (67) Schatzkin, A., Hoover, R. N., Taylor, P. R., Ziegler, R. G., Carter, C. L., Albanes, D., Larson, D. B., and Licitra, L. M. (1988) Site-specific analysis of total serum cholesterol and incident cancer in the national health and nutrition examination survey I epidemiologic follow-up study. *Cancer Res.* 48, 452.
- (68) Alexopoulos, C. G., Blatsios, B., and Avgerinos, A. (1987) Serum lipids and lipoprotein disorders in cancer patients. *Cancer* 60, 3065.
- (69) Williams, R. R., Sorlie, P. D., Feinleib, M., McNamara, P. M., Kannel, W. B., and Dawber, T. R. (1981) Cancer incidence by levels of cholesterol. *J. Am. Med. Assoc.* 245, 247.
- (70) Pekkanen, J., Nissinen, A., Punsar, S., and Karvonen, M. J. (1992) Short- and long-term association of serum cholesterol with mortality. *Am. J. Epidemiol.* 135, 1251.
- (71) Smith, G. D., Neaton, J. D., Benshlomo, Y., Shipley, M., and Wentworth, D. (1992) Serum-cholesterol concentration and primary malignant brain-tumors—a prospective study. *Am. J. Epidemiol.* 135, 259.
- (72) Forette, B., Tortrat, D., and Wolmark, Y. (1989) Cholesterol as risk factor for mortality in elderly women. *Lancet* 1 868.
- (73) Smith, G. D., and Shipley, M. J. (1989) Plasma cholesterol concentration and primary brain-tumors. *Brit. J. Med.* 299, 26.
- (74) Kritchevsky, S. B. (1992) Dietary lipids and the low blood cholesterol-cancer association. *Am. J. Epidemiol.* 135, 509.
- (75) Lackner, K. J., Schettler, G., and Kübler, W. (1989) Plasma Cholesterol, lipid lowering, and risk for cancer. *Klin. Woch.* 67, 957.
- (76) Burton, R., Eck, C. D., and Lloyd, J. B. (1975) The permeability properties of rat liver lysosomes to nucleotides. *Biochem. Soc. Trans.* 3, 1251.
- (77) Sainte-Marie, J., Vignes, M., Vidal, M., Phillipot, J. R., and Bienvenue, A. (1990) Effects of benzyl alcohol on transferrin and low density lipoprotein receptor mediated endocytosis in leukemic guinea pig B lymphocytes. *FEBS Lett.* 262, 13.
- (78) Krieger, M., Brown, M. S., Faust, J. R., and Goldstein, J. L. (1978) Replacement of endogenous cholesteryl esters of low density lipoprotein with exogenous cholesteryl linoleate. *J. Biol. Chem.* 253, 4093.
- (79) Krieger, M., McPhaul, M. J., Goldstein, J. L., and Brown, M. S. (1979) Replacement of neutral lipids of low density lipoprotein with esters of long chain unsaturated fatty acids. *J. Biol. Chem.* 254, 3845.
- (80) Krieger, M. Personal communication.
- (81) Masquelier, M., Vitols, S., and Peterson, C. (1986) Low-density lipoprotein as a carrier of antitumoral drugs: in vivo fate of drug-human low-density lipoprotein complexes in mice. *Cancer Res.* 46, 3847.
- (82) Walsh, M. T., Ginsburg, G. S., Small, D. M., and Atkinson, D. (1982) Apo B-lecithin-cholesterol ester complexes: reassembly of low density lipoprotein. *Arteriosclerosis* 2, 445a.
- (83) Lundberg, B., and Suominen, L. (1984) Preparation of biologically active analogs of serum low density lipoprotein. *J. Lipid Res.* 25, 550.
- (84) Ginsburg, G. S., Walsh, M. T., Small, D. M., and Atkinson, D. (1984) Reassembled plasma low density lipoproteins. *J. Biol. Chem.* 259, 6667.
- (85) Chun, P. W., Brumbaugh, E. E., and Shireman, R. B. (1986) Interaction of human low density lipoprotein and apolipoprotein-B with ternary lipid microemulsion. *Biophys. Chem.* 25, 223.
- (86) Lundberg, B. (1992) Assembly of prednimustine low-density-lipoprotein complexes and their cytotoxic activity in tissue culture. *Cancer Chemo. Pharm.* 29, 241.
- (87) de Smidt, P. C., and van Berkel, T. J. C. (1990) Prolonged serum half-life of antineoplastic drugs by incorporation into the low density lipoprotein. *Cancer Res.* 50, 7476.
- (88) Samadi-Boboli, M., Favre, G., Blancy, E., and Soula, G. (1989) Preparation of low density lipoprotein-9-methoxyellipticin complex and its cytotoxic effect against L1210 and P 388 leukemic cells in vitro. *Eur. J. Cancer Clin. Oncol.* 25, 233.
- (89) Samadi-Boboli, M., Favre, G., Bernadou, J., Berg, D., and Soula, G. (1990) Comparative study of the incorporation of ellipticine esters into low density lipoprotein (LDL) and selective cell uptake of drug-LDL complex via the LDL receptor pathway in vitro. *Biochem. Pharmacol.* 40, 203.
- (90) Samadi-Boboli, M., Favre, G., Canal, P., and Soula, G. (1993) Low density lipoprotein for cytotoxic drug targeting: improved activity of elliptinium derivative against B16 melanoma in mice. *Br. J. Cancer* 68, 319.
- (91) Halbert, G. W., Stuart, J. F. B., and Florence, A. T. (1985) A low density lipoprotein-methotrexate covalent complex and its activity against L1210 cells in vitro. *Cancer Chemo. Pharm.* 15, 223.
- (92) Laster, B. H., Kahl, S. B., Popenoe, E. A., Pate, D. W., and Fairchild, R. G. (1991) Biological efficacy of boronated low-density lipoprotein for boron neutron capture therapy as measured in cell culture. *Cancer Res.* 51, 4588.
- (93) Iwanik, M., Shaw, K. V., Ledwith, B., Yanovich, S., and Shaw, J. M. (1984) Preparation and interaction of a low-density lipoprotein:daunomycin complex with P388 leukemia cells. *Cancer Res.* 44, 1206.
- (94) Lestavel-Delattre, S., Martin-Nizard, F., Clavey, V., Testard, P., Favre, G., Doualin, G., Houssaini, H. S., Bard, J.-M., Duriez, P., Delbart, C., Soula, G., Lesieur, D., Lesieur, I., Cazin, J. C., and Fruchart, J.-C. (1992) Low-density lipoprotein for delivery of an acrylophenone antineoplastic molecule into malignant cells. *Cancer Res.* 52, 3629.
- (95) DeForge, L. E., Ruyan, M. K., Schwendner, S. W., Newton, R. S., and Counsell, R. E. (1991) Synthesis and evaluation of radiolabeled cholesteryl esters as lipoprotein probes. *Bioconjugate Chem.* 2, 254.
- (96) Shaw, J. M., Shaw, K. V., Yanovich, S., Iwanik, M., Futch, W. S., Rosowsky, A., and Schook, L. B. (1988) Delivery of lipophilic drugs using lipoproteins. *Ann. N. Y. Acad. Sci.* 252.
- (97) de Smidt, P. C., and van Berkel, T. J. C. (1992) Characteristics of association of oleoyl derivatives of 5-fluorodeoxyuridine and methotrexate with low-density lipoproteins (LDL). *Pharm. Res.* 9, 565.
- (98) Parks, J. S., Martin, J. A., Johnson, F. L., and Rudel, L. L. (1985) Fusion of low density lipoproteins with cholesterol ester-phospholipid microemulsions. *J. Biol. Chem.* 260, 3155.

- (99) Blomhoff, R., Drevon, C. A., Eskild, W., Helgerud, P., Norum, K., and Berg, T. (1984) Clearance of acetylated low density lipoprotein by rat liver endothelial cells. *J. Biol. Chem.* 259, 8898.
- (100) Craig, I. F., Via, D., Sherrill, B. C., Sklar, L. A., Mantulin, W. W., Gotto, A. M., Jr., and Smith, L. C. (1982) Incorporation of defined cholesteryl esters into lipoproteins using cholesteryl ester-rich microemulsion. *J. Biol. Chem.* 257, 330.
- (101) Krieger, M., Goldstein, J. L., and Brown, M. S. (1978) Receptor-mediated uptake of low density lipoprotein reconstituted with 25-hydroxycholesteryl oleate suppresses 3-hydroxy-3-methylglutaryl-coenzyme A reductase and inhibits growth of human fibroblasts. *Proc. Nat. Acad. Sci. U.S.A.* 75, 5052.
- (102) Mosley, S. T., Goldstein, J. L., Brown, M. S., Falck, J. R., and Anderson, R. G. W. (1981) Targeted killing of cultured cells by receptor-dependent photosensitization. *Proc. Nat. Acad. Sci. U.S.A.* 78, 5717.
- (103) Firestone, R. A., Pisano, J. M., Falck, J. R., McPhaul, M. M., and Krieger, M. (1984) Selective delivery of cytotoxic compounds to cells by the LDL pathway. *J. Med. Chem.* 27, 1037.
- (104) Lundberg, B. (1987) Preparation of drug-low density lipoprotein complexes for delivery of antitumoral drugs via the low density lipoprotein pathway. *Cancer Res.* 47, 4105.
- (105) Vitols, S. Personal communication.
- (106) Unpublished experiments with Dr. Gene Dubowchik.
- (107) Vitols, S., Söderberg-Reid, K., Masquelier, M., Sjöström, B., and Peterson, C. (1990) Low density lipoprotein for delivery of a water-soluble alkylating agent to malignant cells. In vitro and in vivo studies of a drug-lipoprotein complex. *Brit. J. Cancer* 62, 724.
- (108) Vitols, S., Gahrton, G., and Peterson, C. (1984) Significance of the low-density lipoprotein (LDL) receptor pathway for the in vitro accumulation of AD-32 incorporated into LDL in normal and leukemic white blood cells. *Cancer Treat. Repts.* 68, 515.
- (109) Vitols, S., Masquelier, M., and Peterson, C. (1985) Selective uptake of a toxic lipophilic anthracycline derivative by the low-density lipoprotein receptor pathway in cultured fibroblasts. *J. Med. Chem.* 28, 451.
- (110) Eley, J. G., Halbert, G. W., and Florence, A. T. (1990) The incorporation of estramustine into low density lipoprotein and its activity in tissue culture. *Int. J. Pharm.* 63, 121, Figure 1.
- (111) Eley, J. G., Halbert, G. W., and Florence, A. T. (1990) Incorporation of prednimustine into low density lipoprotein: activity against P388 cells in tissue culture. *Int. J. Pharm.* 65, 219.
- (112) Filipowska, D., Filipowski, T., Morelowska, B., Kazanowska, W., Laudanski, T., Lapinjo, S., Åkerlund, M., and Breeze, A. (1992) Treatment of cancer patients with a low-density-lipoprotein delivery vehicle containing a cytotoxic drug. *Cancer Chemother. Pharmacol.* 29, 396.
- (113) Mazière, J. C., Morlière, P., and Santus, R. (1991) New trends in photobiology. The role of the low density lipoprotein receptor pathway in the delivery of lipophilic photosensitizers in the photodynamic therapy of tumors. *J. Photochem. Photobiol.* 8, 351.
- (114) Jori, G. (1991) Low-density lipoproteins-liposome delivery systems for tumor photosensitizers in vivo. *Photodynamic Therapy* (B. W. Henderson, and T. J. Dougherty, Eds.) pp 173-186, Marcel Dekker, Inc., New York.
- (115) Mosley, S. T., Goldstein, J. L., Brown, M. S., Falck, J. R., and Anderson, R. G. W. (1981) Targeted killing of cultured cells by receptor-mediated photosensitization. *Proc. Nat. Acad. Sci. U.S.A.* 78, 5717.
- (116) Candide, C., Morlière, P., Mazière, J. C., Goldstein, S., Santus, R., Dubertret, S., Reyftmann, J. P., and Polonovski, J. (1986) In vitro interaction of the photoactive anticancer porphyrin derivative photofrin II with low density lipoprotein, and its delivery to cultured human fibroblasts. *FEBS Lett.* 207, 133.
- (117) de Smidt, P. C., Versluis, A. J., and van Berkel, T. J. C. (1993) Properties of incorporation, redistribution and integrity of porphyrin-low density lipoprotein complexes. *Biochemistry* 32, 2916.
- (118) Biade, S., Mazière, J. C., Mora, L., Santus, R., Mazière, C., Auclair, P., Morlière, P., and Dubertret, L. (1993) Lovastatin potentiates the photocytotoxic effect of Photofrin-II delivered to HT29 Human colonic adenocarcinoma cells by low density lipoprotein. *Photochem. Photobiol.* 57, 371.
- (119) Jiang, F. N., Allison, B., Liu, D., and Levy, J. G. (1992) Enhanced photodynamic killing of target cells by either monoclonal antibody or low density lipoprotein mediated delivery systems. *J. Contr. Release* 19, 41.
- (120) Barel, A., Jori, G., Perin, P., Pagnan, A., and Biffanti, S. (1986) Role of high-, low- and very low density lipoproteins in the transport and tumor delivery of hematoporphyrin in vivo. *Cancer Lett.* 32, 145.
- (121) Allison, B. A., Waterfield, E., Richter, A. M., and Levy, J. G. (1991) The effects of plasma-lipoproteins on in vitro tumor-cell killing and in vivo tumor photosensitization with benzoporphyrin derivative. *Photochem. Photobiol.* 54, 709.
- (122) Angelin, B., Raviola, C. A., Innerarity, T. L., and Mahley, R. W. (1983) Rapid regulation of apolipoprotein B,E receptors, but not of apolipoprotein E receptors, by intestinal lipoproteins and bile acids. *J. Clin. Invest.* 71, 816.
- (123) Hynds, S. A., Welsh, J., Stewart, J. M., Jack, A., Soukop, M., McArdle, C. S., Calman, K. C., Packard, C. J., and Shepherd, J. (1984) Low-density lipoprotein metabolism in mice with soft tissue tumours. *Biochim. Biophys. Acta* 795, 589.
- (124) Spady, D. K., and Dietschy, J. M. (1985) Dietary saturated triacylglycerols suppress hepatic low-density lipoprotein receptor activity in the hamster. *Proc. Nat. Acad. Sci. U.S.A.* 82, 4526.
- (125) Shimano, H., Aburatani, H., Mori, N., Ishibashi, S., Gotohda, T., Mokuno, H., Kawakami, M., Akanuma, Y., Takaku, F., Murase, T., and Yamada, N. (1988) Down-regulation of hepatic LDL receptor protein and messenger RNA in fasted rabbits. *J. Biochem.* 104, 712.
- (126) Fox, P. L., and DiCorleto, P. E. (1986) Modified low density lipoproteins suppress production of a platelet-derived growth factor-like protein by cultured endothelial cells. *Proc. Nat. Acad. Sci. U.S.A.* 83, 4774.
- (127) Pitas, R. E., Boyles, J., Mahley, R. W., and Bissell, D. M. (1985) Uptake of chemically modified low density lipoproteins in vivo is mediated by specific endothelial cells. *J. Cell Biol.* 100, 103.
- (128) Leitersdorf, E., Stein, O., and Stein, Y. (1985) Angiotensin II stimulates receptor-mediated uptake of LDL by bovine adrenal cortical cells in primary culture. *Biochim. Biophys. Acta* 835, 183.
- (129) Bilheimer, D. W., Grundy, S. M., Brown, M. S., and Goldstein, J. L. (1983) Mevinolin and colestipol stimulate receptor-mediated clearance of low density lipoprotein from plasma in familial hypercholesterolemia heterozygotes. *Proc. Nat. Acad. Sci. U.S.A.* 80, 4124.
- (130) Kovnen, P. T., Bilheimer, D. W., Goldstein, J. L., Jaramillo, J. L., and Brown, M. S. (1981) Regulatory role for hepatic low density lipoprotein receptors in vivo in the dog. *Proc. Nat. Acad. Sci. U.S.A.* 78, 1194.
- (131) Reihner, E., Angelin, B., Rudling, M., Ewerth, S., Björkhem, I., and Einarsson, K. (1990) Regulation of hepatic cholesterol metabolism in humans: stimulatory effects of cholestyramine on HMG-CoA reductase activity and low density lipoprotein receptor expression in gallstone patients. *J. Lipid Res.* 31, 2219.
- (132) Filipovic, I., and Buddecke, E. (1986) Calcium channel blockers stimulate LDL receptor synthesis in human skin fibroblasts. *Biochem. Biophys. Res. Commun.* 136, 845.
- (133) Harada, K., Shimano, H., Kawakami, M., Ishibashi, S., Gotoda, T., Mori, N., Takaku, F., and Yamada, N. (1990) Effect of tumor necrosis factor/cachectin on the activity of the low density lipoprotein receptor on human skin fibroblasts. *Biochem. Biophys. Res. Commun.* 172, 1022.
- (134) Nicholson, A. C., and Hajjar, D. P. (1992) Transforming growth factor- $\beta$  up-regulates low density lipoprotein receptor-mediated cholesterol metabolism in vascular smooth muscle cells. *J. Biol. Chem.* 267, 25982.
- (135) Hamanaka, R., Kohno, K., Seguchi, T., Okamura, K., Morimoto, A., Ono, M., Ogata, J., and Kuwano, M. (1992)

- Induction of low density lipoprotein receptor and a transcription factor SP-1 by tumor necrosis factor in human microvascular endothelial cells. *J. Biol. Chem.* 267, 13160.
- (136) Shaw, M. K., Newton, R. S., Sliskovic, D. R., Roth, B. D., Ferguson, E., and Krause, B. R. (1990) Hep-G2 cells and primary rat hepatocytes differ in their response to inhibitors of HMG-CoA reductase. *Biochem. Biophys. Res. Commun.* 170, 726.
- (137) Cohen, L. H., Griffioen, M., Havekes, L., Schouten, D., Van Hinsbergh, V., and Kempen, H. J. (1984) Effects of compactin, mevalonate, and low-density lipoprotein on 3-hydroxy-3-methylglutaryl-coenzyme A reductase activity and low-density-lipoprotein-receptor activity in the human hepatoma cell line Hep G2. *Biochem. J.* 222, 35.
- (138) Grove, R. I., Mazzucco, C. E., Radka, S. F., Shoyab, M., and Kiener, P. A. (1991) Oncostatin M Up-regulates low density lipoprotein receptors in HepG2 cells by a novel mechanism. *J. Biol. Chem.* 266, 18194.
- (139) Franceschini, G., Busnach, G., Calabresi, L., Chiesa, G., Gianfranceschi, G., Zoppi, F., Minetti, L., and Sirtori, C. R. (1991) Predictability of low-density lipoprotein levels during apheresis treatment of hypercholesterolemia. *Eur. J. Clin. Invest.* 21, 209.
- (140) Saal, S. D., Parker, T. S., Gordon, B. R., Studebaker, J., Hudgins, L., Ahrens, E. H., Jr., and Rubin A. L. (1986) Removal of low-density lipoproteins in patients by extracorporeal immunoadsorption. *Am. J. Med.* 80, 583.
- (141) Parker, T. S., Gordon, B. R., Saal, S. D., Rubin, A. L., and Ahrens, E. H., Jr. (1986) Plasma high density lipoprotein is increased in man when low density lipoprotein (LDL) is lowered by LDL-phoresis. *Proc. Nat. Acad. Sci. U.S.A.* 83, 777.
- (142) Goldstein, J. L., and Brown M. S. (1977) The low-density lipoprotein pathway and its relation to atherosclerosis. *Annu. Rev. Biochem.* 46, 897.
- (143) Havekes, L. M., De Wit, E. C. M., and Princen, H. M. G. (1987) Cellular free cholesterol in Hep G2 cells is only partially available for down-regulation of low-density-lipoprotein receptor activity. *Biochem. J.* 247, 739.
- (144) Salter, A. M., Ekins, N., Al-Seeni, M., Brindley, D. M., and Middleton, B. (1989) Cholesterol acidification plays a major role in determining low-density-lipoprotein receptor activity in primary monolayer cultures of rat hepatocytes. *Biochem. J.* 263, 255.
- (145) Wieland, H., and Seidel, D. (1983) A simple specific method for precipitation of low density lipoproteins. *J. Lipid Res.* 24, 904.
- (146) Behm, E., Loth, F., Toewe, D., Zshornig, O., Ernst, B., and Klinkmann, H. (1989) Low-density-lipoprotein binding by macroporous bead cellulose. *Biomed. Biochim. Acta* 48, 829.
- (147) Eriksson, M., Berg, B., Berglund, L., Lantz, B., and Angelin, B. (1989) Lipid lowering in severe familial hypercholesterolemia: efficacy and safety of a new regenerating system for selective apheresis of apolipoprotein B-containing lipoproteins. *J. Int. Med.* 225, 29.
- (148) Yamamoto, A., Kojima, S., Shibata-Harada, M., Kawaguchi, A., and Hatanaka, K. (1992) Assessment of the biocompatibility and long-term effect of LDL apheresis by dextran sulfate cellulose column. *Artif. Organs* 16, 177.
- (149) Williams, K. J., Vallabhajosula, S., Rahman, I. U., Donnelly, T. M., Parker, T. S., Weinrauch, M., and Goldsmith, S. J. (1988) Low density lipoprotein receptor-independent hepatic uptake of a synthetic, cholesterol-scavenging lipoprotein: implications for the treatment of receptor-deficient atherosclerosis. *Proc. Nat. Acad. Sci. U.S.A.* 85, 242.
- (150) Popovsky, M. A., Devine, P. A., and Taswell, H. F. (1985) Intraoperative autologous transfusion. *Mayo Clin. Proc.* 60, 125.
- (151) Schultis, H.-W., Von Baeyer, H., Neitzel, H., and Riedel, E. (1990) Functional characteristics of LDL particles derived from various LDL-apheresis techniques regarding LDL-drug-complex preparation. *J. Lipid Res.* 31, 2277.
- (152) Coppens, I., Bastin, P., Opperdoes, F. R., Baudhin, P., and Courtoy, P. J. (1992) Trypanosoma-brucei-brucei—antigenic stability of its LDL receptor and immunological cross-reactivity with the LDL receptor of the mammalian host. *Exp. Parasitol.* 74, 77.
- (153) Coppens, I., Baudhuin, P., Opperdoes, F. R., and Courtoy, P. J. (1988) Receptors for the host low density lipoproteins on the hemoflagellate Trypanosoma brucei: purification and involvement in the growth of the parasite. *Proc. Nat. Acad. Sci. U.S.A.* 85, 6753.
- (154) Coppens, I., Baudhuin, P., Opperdoes, F. R., and Courtoy, P. J. (1993) Role of acidic compartments in trypanosoma brucei, with special reference to low-density lipoprotein processing. *Molec. Biochem. Parasitol.* 58, 223.
- (155) Bennett, M. W., and Caulfield, J. P. (1991) Specific binding of human low-density lipoprotein to the surface of schistosoma of Schistosoma mansoni and ingestion by the parasite. *Am. J. Pathol.* 138, 1173.
- (156) Peterson, K. M., and Alderete, J. F. (1984) Trichomonas vaginalis is dependent on uptake and degradation of human low density lipoproteins. *J. Exp. Med.* 160, 1261.
- (157) Chaudhuri, G. (1989) Selective delivery of drugs to macrophages through a highly specific receptor. *Biochem. Pharmacol.* 38, 2995.

# ARTICLES

## Bifunctional Chelator for Facile Preparation of Neutral Technetium Complexes†

Kwamena E. Baidoo,\* Susan Z. Lever, and Ursula Scheffel

The Department of Environmental Health Sciences, Division of Radiation Health Sciences, The School of Hygiene and Public Health, The Johns Hopkins University, 615 North Wolfe Street, Baltimore, Maryland 21205-2179. Received August 27, 1993\*

The diaminedithiol (DADT) ligand system has proven to be useful as a carrier of technetium-99m in the preparation of a wide variety of site-specific radiopharmaceuticals. To expand the utility of the ligand system, we have designed and synthesized a bifunctional chelating agent based on the ligand system whose adducts generate a neutral technetium complex core and therefore can penetrate intact membranes. We have evaluated both the coupling of the thiolactone reactive moiety of the bifunctional chelate to benzylamine as a model as well as subsequent labeling with technetium-99m. Reaction with benzylamine was complete at room temperature within 2 h, producing the adduct in 74% isolated yield. On coordination of the benzylamine adduct to technetium-99m, one major product was obtained in high yield (>90%). The product was stable in serum and physiologic saline at 37 °C over a 20-h study period. The partition coefficient of the technetium complex was  $101 \pm 6.2$ , indicating that the complex was lipophilic. Biodistribution studies in mice showed that the brain concentration at 5 min postinjection was  $0.91 \pm 0.09\%$  injected dose/g indicating that the complex penetrates the intact blood-brain barrier. This is further evidence that the complex is neutral and lipophilic. This bifunctional chelate should facilitate the incorporation of technetium-99m into molecules of biological interest such as drugs, small peptides, and metabolic substrates.

### INTRODUCTION

Diaminedithiol (DADT) ligands form highly stable, neutral, and lipid-soluble technetium complexes capable of crossing intact membranes. The usefulness of the ligand derives from its ability to affect the biological properties of its technetium complexes through substituents on the chelate backbone. For example, while alkylamine (1, 2), benzylpiperazinyl (3), and diethyl ester (4) derivatives have been shown to be potentially useful for regional cerebral perfusion imaging, simple alkyl derivatives have shown high pulmonary accumulation (5). The ligand system has also shown utility in the preparation of technetium complexes that retain high binding affinity to receptors (6, 7). The development of  $^{99m}\text{Tc}$  radiopharmaceuticals can, therefore, greatly benefit from the versatility of the ligand system.

The usual preparation of diaminedithiol ligands, however, involves long linear synthesis and the use of strong reducing agents such as lithium aluminum hydride (LAH) to reduce the tertiary disulfide of the macrocyclic intermediates. The use of protected thiol intermediates has been evaluated as a means of avoiding strong reducing agents during the synthesis of DADT ligands (8, 9). However, reactivity of the nitrogens contained in these intermediates is much lower than expected, resulting in difficulties during alkylation in some instances (unpublished results). The development of a versatile precursor

to these DADT ligands would allow subsequent synthesis of several technetium-99m ( $^{99m}\text{Tc}$ ) derivatives for screening as potential tracers. Previously, we reported the synthesis and evaluation of a novel diaminedithiol bifunctional chelating agent (BCA), 1 (Figure 1), for stable incorporation of  $^{99m}\text{Tc}$  into proteins (10). This bifunctional chelating agent has substituents on both nitrogens and therefore results in the formation of positively charged Tc complex cores (11). Other bifunctional chelating agents reported for use with technetium also tend to form charged complexes (12, 13). These bifunctional chelating agents would be inappropriate for preparing radiopharmaceuticals intended for use in the uninjured brain. We have prepared a related bifunctional chelating agent, 2 (14), structurally modified to form neutral technetium complexes. In this paper, we report complete details of the synthesis, evaluation of the reaction of this thiolactone BCA using benzylamine as a model, and the subsequent complexation reaction with technetium.

### EXPERIMENTAL PROCEDURES

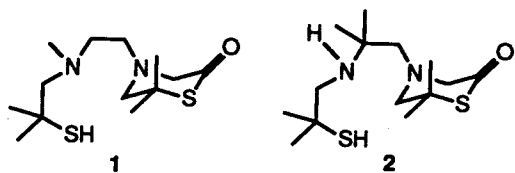
**Materials and Methods.** Solvents and chemicals were reagent grade and used as received unless specified. Glucoheptonate kits (Glucoscan) were purchased from Dupont, N. Billerica, MA.  $^{99m}\text{Tc}]/\text{NaTcO}_4$  was obtained as a saline solution from a  $^{99}\text{Mo}/^{99m}\text{Tc}$  generator purchased from Cintichem/Union Carbide. Male CD-1 mice were obtained from Charles River Laboratories.

Melting points were determined using a Thomas Hoover capillary melting point apparatus and are uncorrected. Compound 3 was synthesized according to previously published procedures (1). Centrifugation was performed on an IEC bench centrifuge Model HN-SII. HPLC was

\* Author to whom correspondence should be addressed.

† A preliminary communication of some of the material covered in this paper has been presented; see ref 14.

© Abstract published in *Advance ACS Abstracts*, January 15, 1994.



**Figure 1.** Bifunctional chelating agents derived from the diamine dithiol ligand system.

performed on either a Perkin-Elmer Series 2 instrument equipped with an LC-75 UV/vis detector or a Waters Associates Model 510EF pump equipped with a Model 490 UV absorbance detector; a 2-in. Cesium fluoride or sodium iodide flow-through scintillation detection system; EE & G/Ortec single-channel analyzer, amplifiers, and rate meters; and a Hewlett-Packard HP 3392A or Shimadzu CR3A integrating recorder.  $\gamma$ -Radioactivity was measured with a Capintec CRC-7 radioisotope dose calibrator or a Packard automated scintillation well detector. Infrared spectrophotometric determinations of neat liquids or KBr pellets were determined on a Perkin-Elmer 399B or Nicolet 205 FTIR, respectively.  $^1\text{H}$  NMR spectra were recorded in deuteriochloroform solution using an NR80 FT-NMR spectrometer (IBM Instruments, Inc.) or a Bruker WM 300-MHz spectrometer. Elemental analyses were performed by Atlantic Microlabs, Norcross, GA.

**Synthesis of 2,5,5,9-Tetramethyl-4,7-diaza-2,9-decanedithiol (4).** To a stirred mixture of  $\text{LiAlH}_4$  (5.0 g, 0.13 mol) in dry THF (100 mL, freshly distilled from sodium benzophenone ketyl under a slow stream of nitrogen) was added a solution of **3** (**1**) (10.20 g, 0.04 mol) in dry THF (140 mL) dropwise. The mixture was refluxed for 18 h and cooled to room temperature. The reaction was externally cooled at  $0^\circ\text{C}$  (ice bath) and quenched by slow dropwise addition of saturated  $\text{NH}_4\text{Cl}(\text{aq})$ . The mixture was then quickly triturated with ethanol ( $4 \times 50$  mL) and filtered. The filtrate was adjusted to pH 1 with  $\text{HCl}(\text{aq})$  (3 N), and volatile solvents were removed by evaporation under reduced pressure. Water (50 mL) was added to the residue, and the mixture was brought to pH 8 with aqueous sodium hydroxide (2.5 M). After extractive workup with ether, the organic layers were concentrated to about 50 mL under reduced pressure and then applied to a 93-g basic alumina column. The product was then eluted with ether. Concentration under reduced pressure and further drying under high vacuum provided **4** (8.0 g, 77%) as a colorless oil: IR (neat)  $\nu$  ( $\text{cm}^{-1}$ ) 3300 (NH); 2540 (SH);  $^1\text{H}$  NMR ( $\text{CDCl}_3$ )  $\delta$  1.06 (s, 6H), 1.36 (s, 12H), 1.72 (br s, 4H), 2.52 (s, 2H), 2.62 (s, 4H). For long-term storage, the free base was converted to the hydrochloride salt by redissolution of the oil in ethanol (30 mL) followed by saturation with dry  $\text{HCl}$  gas. The resulting warm solution was cooled to room temperature and the product precipitated with ether, filtered, washed, and dried under high vacuum to afford 4·2HCl as a white solid. Anal. Calcd for ( $\text{C}_{12}\text{H}_{28}\text{N}_2\text{S}_2\cdot 2\text{HCl}$ ): C, 42.72; H, 8.96; N, 8.30. Found: C, 42.91; H, 9.18; N, 8.26.

**2,5,5,9-Tetramethyl-4,7-diaza-2,9-bis[(*p*-methoxybenzyl)thio]decane (5).** Aqueous sodium hydroxide (100 mL, 2.5 M) was added to a stirred solution of **4** (19 g, 0.07 mol) in ethanol (150 mL). Neat *p*-methoxybenzyl chloride (34 g, 0.22 mol) was added, and stirring was continued at room temperature. After 1 h, TLC (silica, hexane/ether (50:50)) of the reaction mixture showed no evidence of starting thiol as evidenced by a negative Ellman's test. The ethanol was then distilled under reduced pressure. After extractive workup with ether, the organic extracts were dried over  $\text{MgSO}_4$ , filtered, and evaporated to leave

an oily residue which was redissolved in ethanol (10 mL). The mixture was adjusted to pH 2 with saturated ethanolic  $\text{HCl}$ . The warm mixture was cooled to room temperature, and the product was precipitated with ether. The precipitate was filtered and washed with ether to yield 5·2HCl as a white powder (35 g, 83%). For subsequent use, the free base was regenerated by treatment of the salt with aqueous sodium hydroxide (2.5 M) followed by extraction with ether: IR (free base, neat)  $\nu$  ( $\text{cm}^{-1}$ ) 3300 (NH);  $^1\text{H}$  NMR ( $\text{CDCl}_3$ )  $\delta$  1.00 (s, 6H), 1.32 (s, 12H), 1.53 (br s, 2H), 2.38 (s, 2H), 2.49 (s, 2H), 2.57 (s, 2H), 3.67 (s, 4H), 3.77 (s, 6H), 6.82, 7.23 (AB q,  $J = 8.8$  Hz, 8H). Anal. Calcd for ( $\text{C}_{28}\text{H}_{44}\text{N}_2\text{O}_2\text{S}_2$ ): C, 66.62; H, 8.79; N, 5.55; S, 12.70. Found: C, 66.57; H, 8.81; N, 5.51; S, 12.64.

**2,5,5,9-Tetramethyl-4,7-diaza-7-[(ethoxycarbonyl)methyl]-2,9-bis[(*p*-methoxybenzyl)thio]decane (6).** A solution of **5** as the free base (10.9 g, 0.0216 mol) and ethyl bromoacetate (3.61 g, 0.022 mol) in ethanol (20 mL) containing  $\text{K}_2\text{CO}_3$  (5.98 g, 0.043 mol) was heated at reflux for 18 h. Volatile solvents were removed by evaporation under reduced pressure. Water (50 mL) was added to the residue and the mixture extracted with ether ( $4 \times 30$  mL). The ether extracts were combined, dried over  $\text{MgSO}_4$ , filtered, and evaporated to an oily residue. The residue was dissolved in ether and made into a slurry with silica gel. The ether was evaporated and the powder applied to a short path silica gel column (3:1 hexane/ethyl ether to 100% ethyl acetate) to yield recovered **5** (3.30 g, 30.0%) and product **6** as a low-melting solid (3.84 g, 43.2%, corrected for recovered starting material): mp  $54.5\text{--}56.0^\circ\text{C}$ ; IR (neat)  $\nu$  ( $\text{cm}^{-1}$ ) 3300 (NH), 1730 (C=O);  $^1\text{H}$  NMR ( $\text{CDCl}_3$ )  $\delta$  1.03 (s, 6H), 1.23 (t, 3H), 1.28 (s, 6H), 1.33 (s, 6H), 1.80 (b s, 1H), 2.48 (s, 2H), 2.72 (s, 2H), 2.86 (s, 2H), 3.62 (s, 2H), 3.68 (s, 2H), 3.76 (s, 6H), 3.95 (s, 2H), 4.12 (q, 2H), 6.80, 7.22 (AB q,  $J = 5.7$  Hz, 8H). Anal. Calcd for ( $\text{C}_{32}\text{H}_{50}\text{N}_2\text{O}_4\text{S}_2$ ): C, 65.14; H, 8.47; N, 4.74; S, 10.85. Found: C, 64.85; H, 8.59; N, 4.73; S, 10.76.

**4-[2,5,5-Trimethyl-4-aza-2-mercaptohexyl]-6,6-dimethyl-2-thiomorpholinone (2).** A Teflon round-bottom flask containing **6** (2.0 g, 3.4 mmol) and anisole (0.9 g, 8.3 mmol) was cooled externally with a dry ice/acetone bath. Dry hydrogen fluoride gas (16.5 g) was condensed in the vessel and the dry ice/acetone bath replaced with an ice bath. The mixture was then stirred under a positive pressure of nitrogen for 2 h at  $0^\circ\text{C}$ . The HF was flushed with a stream of  $\text{N}_2$  into a KOH trap.  $\text{H}_2\text{O}$  (25 mL) was added to the residue, the pH of the mixture adjusted to 3 with NaOH (2.5 M), and the mixture extracted with methylene chloride ( $4 \times 20$  mL) and discarded. The pH of the aqueous fraction was adjusted to 8 with NaOH (2.5 M) and the mixture extracted with methylene chloride ( $4 \times 20$  mL). The combined methylene chloride extracts from the pH 8 extraction were dried with  $\text{Na}_2\text{SO}_4$ . The residue obtained after filtration and evaporation of solvent was chromatographed by silica short path chromatography to yield **2** (0.75 g, 73%) using 3:2 hexane/ether as solvent. The compound was stored under nitrogen at  $-20^\circ\text{C}$  and is stable for at least 1 year under these conditions: IR (neat)  $\nu$  ( $\text{cm}^{-1}$ ) 3300 (NH), 2540 (SH), 1655 (C=O);  $^1\text{H}$  NMR ( $\text{CDCl}_3$ )  $\delta$  1.06 (s, 6H), 1.32 (s, 6H), 1.51 (s, 6H), 2.39 (s, 2H), 2.52 (s, 2H), 2.84 (s, 2H), 3.94 (s, 2H). Anal. Calcd for ( $\text{C}_{14}\text{H}_{28}\text{N}_2\text{O}_2\text{S}_2$ ): C, 55.22; H, 9.27; N, 9.20; S, 21.06. Found: C, 55.38; H, 9.22; N, 9.28; S, 21.13.

**2,5,5,9-Tetramethyl-4,7-diaza-7-[(benzylcarbamoyl)methyl]-2,9-dithiadecane (7, Hex-DADT-BzA).** A solution of benzylamine (35.2 mg, 0.33 mmol) in acetonitrile (0.5 mL) was added to **2** (50 mg, 0.16 mmol) in a vial and stirred at room temperature for 2 h (Scheme 2). The



mixture was chromatographed by short path silica chromatography using 2:3 hexane/ether as solvent. Compound **7** was obtained in 74% yield (50 mg). For long-term storage, the oxalate salt was formed by addition of an ethanol solution of oxalic acid to an ethanolic solution of the free base: IR (free base, neat)  $\nu$  ( $\text{cm}^{-1}$ ) 3300 (NH), 2540 (SH), 1650 (C=O);  $^1\text{H}$  NMR ( $\text{CDCl}_3$ )  $\delta$  1.04 (s, 6H), 1.30 (s, 6H), 1.37 (s, 6H), 1.67 (br s, 3H), 2.50 (s, 2H), 2.65 (s, 2H), 2.74 (s, 2H), 3.49 (s, 2H), 4.5 (d,  $J = 6.1$  Hz, 2H), 7.28 (s, 5H), 8.10 (b, 5H). Anal. Calcd for  $(\text{C}_{21}\text{H}_{37}\text{N}_3\text{OS}_2)$ : C, 61.26; H, 9.05; N, 10.20; S, 15.57. Found: C, 61.38; H, 9.10; N, 10.16; S, 15.49.

**Synthesis of the Tc-99m Complex of **7** ( $^{99\text{m}}\text{Tc}$ -Hex-DADT-BzA).** A Glucoscan kit was reconstituted by the addition of  $[\text{}^{99\text{m}}\text{Tc}]\text{NaTcO}_4$  (3 mL, 12.3 mCi) from the generator and allowed to stand for 15 min. The resulting  $[\text{}^{99\text{m}}\text{Tc}]\text{Tc}$ -glucoheptonate (0.5 mL, 2.0 mCi) was transferred to a solution of **7**-oxalate (1 mg) in ethanol (0.5 mL) (Scheme 2). The mixture was vortexed for 1 min and then allowed to stand at room temperature for 10 min. The yield of  $^{99\text{m}}\text{Tc}$ -Hex-DADT-BzA was ascertained by reversed-phase HPLC (4.6  $\times$  250 mm Alltech Econosil C-18 column; solvent, acetonitrile/0.1 M ammonium formate (55:45), 4 mL/min) monitored on line by UV at 254 nm and radioactivity by scintillation. The retention time of  $^{99\text{m}}\text{Tc}$ -Hex-DADT-BzA under these conditions was 10.4 min.

**In Vitro Stability of  $^{99\text{m}}\text{Tc}$ -Hex-DADT-BzA.** The  $^{99\text{m}}\text{Tc}$ -Hex-DADT-BzA was purified by HPLC and volatile solvent removed by evaporation under reduced pressure. Physiologic saline was added to the residue, an aliquot of the mixture (1 mL) was added to human plasma (1 mL), and the mixture was incubated at 37  $^\circ\text{C}$ . Periodically, up to 20 h, an aliquot of the mixture was assayed by gel filtration HPLC. Another aliquot was added to an equal volume of ethanol to precipitate proteins, centrifuged, and the supernate assayed by reversed-phase HPLC.  $^{99\text{m}}\text{Tc}$ -Hex-DADT-BzA was also incubated in saline and treated similarly.

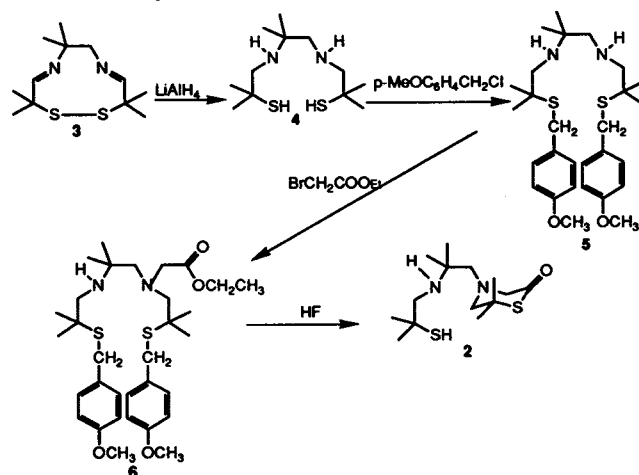
**Partition Coefficient of  $^{99\text{m}}\text{Tc}$ -Hex-DADT-BzA.** An aliquot of the HPLC-purified  $^{99\text{m}}\text{Tc}$ -Hex-DADT-BzA (0.1 mL) was added to a mixture of 1:1 octanol/phosphate buffer (0.1 M, pH 7) and vortexed for 1 min. The mixture was centrifuged at 2600 rpm for 10 min. An aliquot of the octanol phase (0.1 mL) was transferred to another mixture of 0.9 mL of octanol and 1 mL of phosphate buffer vortexed and centrifuged as before. The operation was repeated once more. After each centrifugation, equal aliquots of the aqueous and organic phases were counted in the scintillation counter. The process was repeated three times, and the counts were averaged for each phase.

**Biodistribution of  $^{99\text{m}}\text{Tc}$ -Hex-DADT-BzA.** Four groups of five male CD-1 mice were injected with HPLC purified and physiologic saline reconstituted  $^{99\text{m}}\text{Tc}$ -Hex-DADT-BzA (2.0  $\mu\text{Ci}$ , 0.2 mL each). At 5, 15, 30, and 60 min postinjection the mice were killed by cervical dislocation. Blood and organs of interest were removed, blotted, weighed, and counted in an automated scintillation  $\gamma$  counter for radioactivity. The counts were compared to standards prepared from the injectate and counted at the same time.

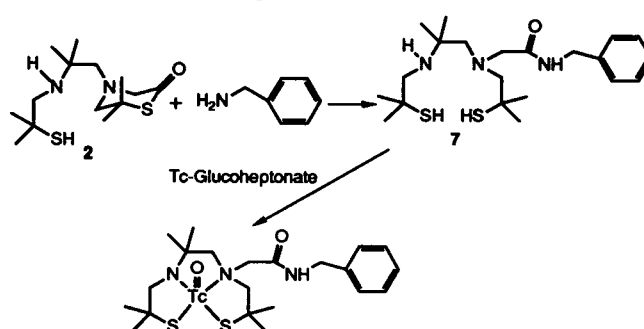
## RESULTS AND DISCUSSION

The design of the bifunctional chelating agent **2** was analogous to the features incorporated in **1** (10). Reaction of the thiolactone reactive functionality of these bifunctional chelating agents with appropriate nucleophiles results in the release of the previously masked thiol group

Scheme 1. Synthesis of BCA **2**

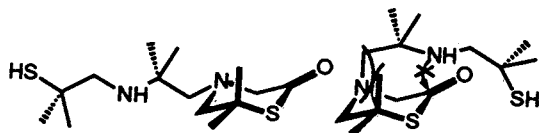


Scheme 2. Synthesis of the Benzylamine Adduct of BCA **2** and the Subsequent Chelation with Technetium



to complete the coordinate core of the diaminedithiol chelating ligand (Scheme 2). After reaction, the ligand becomes attached to its substrate through a two-carbon spacer. Thus, after complexation of the resulting adducts, the Tc complex core would be placed at some distance from sites that determine biological activity in the substrate. It is conceivable that agents could be prepared in which the biological activity of the substituent group is preserved. A critical difference between BCAs **1** and **2** is that one of the coordinating nitrogen atoms of **2** is maintained as a secondary amine. On complexation of adducts of **2** with technetium(V), the secondary amine deprotonates to obtain a neutral complex core as has been shown for several such diaminedithiol ligands (1, 15–17), unlike Tc complexes from adducts of **1** which are positively charged.

The bifunctional chelating agent was synthesized in five steps from known compounds (Scheme 1). The synthetic strategy first brought together the components of the eventual chelating backbone. By choice of the substituted ethylenediamine, a *gem*-dimethyl group was introduced next to one of the nitrogen atoms of the backbone. Hence, 2,2'-dithiobis(2-methylpropanal) was condensed with 1,2-diamino-2-methylpropane to yield **3**, the macrocyclic diimine disulfide (**1**). Reduction of **3** with LAH yielded **4**, the basic hexamethyl-substituted diaminedithiol. It is important during the workup of **4** to acidify the product as soon as possible in order to obtain the product in high yield and purity. We ensured this by triturating the inorganic residue with ethanol and filtering the ethanol triturate directly into aqueous HCl. The next step required selective alkylation at nitrogen. This was accomplished by temporary protection of the thiol groups of **4** as the *p*-methoxybenzyl thioethers in **5** followed by alkylation with ethyl bromoacetate. The presence of the *gem*-



**Figure 2.** Chair configurations of BCA 2 showing a 1,3 relationship between the *gem*-dimethyl group and the large substituent on nitrogen.

dimethyl group precluded alkylation at the adjacent nitrogen. Thus, overall selectivity was achieved, and the ultimate precursor 6 was obtained. We recovered a substantial portion of the unreacted starting material, 5, illustrating the limited reactivity of the amine. Deprotection of 6 in anhydrous HF yielded the target bifunctional chelating agent 2. Compound 2 has been stored under nitrogen at  $-20^{\circ}\text{C}$  for over 1 year without decomposition. Even though a secondary amine is present in 2, intermolecular reactions apparently did not occur. This may be due to the hinderance to attack at the carbonyl group of the thiolactone ring offered by the *gem*-dimethyl group  $\alpha$  to the secondary nitrogen. This would also hinder intramolecular  $\text{S} \rightarrow \text{N}$  transfer at least partially. The large substituent group on the nitrogen of the thiolactone ring is forced into an equatorial configuration since it is in a 1,3 relationship with the ring *gem* dimethyl group as depicted in Figure 2. This imparts a conformational restraint on the N-substituent placing the secondary nitrogen out of proximity for nucleophilic attack on the carbonyl group.

The reaction of the bifunctional chelating agent with benzylamine occurred smoothly and was practically complete within 2 h with an isolated yield of 74%. As anticipated, the resulting benzylamide derivative could be labeled efficiently ( $> 90\%$  yield) at the no carrier added  $^{99\text{m}}\text{Tc}$  level. As with any bimolecular reaction, the concentration of reactants is important in ensuring high yield in a short time period. We observed only one major product at a retention time 10.4 min. In contrast, in our work with BCA 1, we observed that at high concentrations a minor component which forms initially transforms into the major product with time. Therefore, the results we obtained on labeling with the BCA 2 adduct are consistent with labeling at high concentrations. More work is underway to test the hypothesis that the concentration of the DADT ligand affects the number of products obtained.

Studies of the stability of the complex *in vitro* indicated that the complex was stable in plasma and saline at  $37^{\circ}\text{C}$  over the 20-h study period with no indication of decomposition of the complex or hydrolysis of the amide bond. Thus, the amide linkage formed from the coupling of the thiolactone to the amine is stable in this biological system. This result is important especially with respect to the application of the BCA to molecules of biological interest such as peptides.

The partition coefficient ( $101 \pm 6.2$ ) of the  $^{99\text{m}}\text{Tc}$  complex formed from the benzylamine adduct was determined by the shake flask method. This compares very well with the well-characterized, neutral, basic Tc-diaminedithiol complex, (2,9-dimethyl-4,7-diaza-2,9-decanedithiolato)oxotechnetium(V), which has a partition coefficient of 97 (17). Further indication of the lipophilicity of the complex formed was obtained from biodistribution studies in normal male CD-1 mice (Table 1). These studies indicated that the concentration of  $^{99\text{m}}\text{Tc}$ -Hex-DADT-BzA in the brain was  $0.9 \pm 0.09\%$  injected dose/g at 5 min postinjection and the brain/blood ratio was 0.2. This is in contrast to the positively charged complex formed from the adduct of BCA 1 with benzylamine (10) which shows

**Table 1.** Biodistribution of  $^{99\text{m}}\text{Tc}$ -Hex-DADT-BzA in Male CD-1 Mice

organ	% injected dose/g time (min)			
	5	15	30	60
blood	$4.64 \pm 1.56$	$2.35 \pm 1.81$	$1.75 \pm 0.49$	$1.62 \pm 0.96$
brain	$0.91 \pm 0.09$	$0.38 \pm 0.10$	$0.31 \pm 0.04$	$0.33 \pm 0.02$
heart	$3.47 \pm 0.74$	$1.67 \pm 0.54$	$1.37 \pm 0.60$	$1.26 \pm 0.85$
lungs	$4.88 \pm 1.06$	$3.10 \pm 0.93$	$2.09 \pm 0.64$	$1.48 \pm 0.54$
liver	$17.79 \pm 5.32$	$11.30 \pm 2.13$	$10.19 \pm 1.40$	$11.10 \pm 1.18$
spleen	$2.21 \pm 0.33$	$1.30 \pm 0.19$	$0.81 \pm 0.11$	$0.70 \pm 0.14$
kidneys	$5.75 \pm 1.05$	$3.20 \pm 0.64$	$2.68 \pm 0.50$	$1.86 \pm 0.19$
stomach	$5.71 \pm 3.01$	$4.43 \pm 1.28$	$5.02 \pm 1.60$	$6.64 \pm 4.39$
intestines	$11.96 \pm 2.60$	$18.19 \pm 2.90$	$25.98 \pm 3.95$	$26.57 \pm 2.65$

a minimal brain concentration of  $0.09 \pm 0.03\%$  injected dose/g and a brain/blood ratio of 0.036. As a control, the brain concentration of pertechnetate, which is known not to cross the intact blood-brain barrier, was measured. At 5 min post injection the brain concentration was  $0.33\%$  injected dose/g, and the brain/blood ratio was 0.035 (data not shown). While the brain/blood ratio is low for  $^{99\text{m}}\text{Tc}$ -Hex-DADT-BzA, it is still more than 5-fold higher than either charged species. X-ray crystallographic studies are currently underway to unequivocally prove the neutrality of the complex.

In summary, we have synthesized a bifunctional chelating agent capable of generating neutral  $^{99\text{m}}\text{Tc}$  complexes that can penetrate the intact blood-brain barrier. The BCA is based on the strongly coordinating diaminedithiol chelating agent. Therefore, Tc complexes of its adducts are highly stable. Application of this BCA for the synthesis of high-affinity  $^{99\text{m}}\text{Tc}$ -labeled chemotactic oligopeptides capable of delineating focal sites of inflammation (7) has been reported. The BCA has also been used for the preparation of a benzovesamicol derivative as a potential marker for cholinergic neurons (18). Thus, this specially designed bifunctional chelate is proving useful for incorporation into drugs, small peptides, and metabolic substrates as a carrier of  $^{99\text{m}}\text{Tc}$  in the design of recognition site specific radiopharmaceuticals for scintigraphic applications.

#### ACKNOWLEDGMENT

This work was supported by USPHS grants NCI: 5 PO1 CA32845 and GM 27512.

#### LITERATURE CITED

- (1) Lever, S. Z., Burns, H. D., Kervitsky, T. M., Goldfarb, H. W., Woo, D. V., Wong, D. F., Epps, L. A., Kramer, A. V., and Wagner, H. N., Jr. (1985) Design, preparation, and biodistribution of a technetium-99m triaminedithiol complex to assess regional cerebral blood flow. *J. Nucl. Med.* 26, 1287-1294.
- (2) Scheffel, U., Goldfarb, H. W., Lever, S. Z., Gungon, R. L., Burns, H. D., and Wagner, H. N. (1988) Comparison of technetium-99m aminoalkyl diaminedithiol analogues as potential brain blood flow imaging agents. *J. Nucl. Med.* 29, 73-82.
- (3) Kung, H. F., Gao, Y.-Z., Yu, C.-C., Billings, J., Subramanyam, V., and Calabresse, J. C. (1989) New brain perfusion imaging agents based on  $^{99\text{m}}\text{Tc}$ -bis(aminoethanethiol) complexes: Stereoisomers and biodistribution. *J. Med. Chem.* 32, 433-437.
- (4) Cheesman, E. H., Blanchette, M. A., Ganey, M. V., Maheu, E. J., Miller, S. J., and Watson, A. D. (1988) Technetium-99m ECD: Ester derivatized diamine-dithiol Tc complexes for imaging brain perfusion. *J. Nucl. Med.* 29, 788 (abstract).
- (5) Baidoo, K. E., Epps, L. A., Scheffel, U., Burns, H. D., Lever, S. Z., Kramer, A. V., Goldfarb, H., Gungon, R., and Wagner, H. N. (1987) Pulmonary Accumulation of Tc-99m Diaminedithiol (DADT) Complexes. *J. Nucl. Med.* 28, 729 (abstract).
- (6) DiZio, J. P., Anderson, C. J., Davison, A., Ehrhardt, G. J., Carlson, K. E., Welch, M. J., and Katzenellenbogen, J. A. (1992)

- Technetium and rhenium-labeled progestins: Synthesis, receptor binding and *in vivo* distribution of an 11 $\beta$ -substituted progestin labeled with technetium-99m and rhenium-186. *J. Nucl. Med.* 33, 558–569.
- (7) Baidoo, K. E., Stathis, M., Scheffel, U., Lever, S. Z., and Wagner, H. N., Jr. (1993) High affinity Tc-labeled chemotactic peptides. *J. Nucl. Med.* 34, 18P. 1993 (abstract).
- (8) Baidoo, K. E., Lever, S. Z., Kramer, A. V., Epps, L. A., Burns, H. D., and Wagner, H. N., Jr. (1986) Synthesis of Tc-99m-N<sub>2</sub>S<sub>2</sub> Complexes via the *p*-Methoxybenzyl Protected Thiol Ligands. *J. Nucl. Med.* 27, 1050 (abstract).
- (9) Mach, R. H., Kung, H. F., Jungwiwattanaporn, P., and Guo, Y.-Z. (1989) A new synthesis of bis-aminoethanethiol (BAT) chelating agents containing a gamma carboxylate. *Tetrahedron Lett.* 30, 4069–4072.
- (10) Baidoo, K. E., and Lever, S. Z. (1990) Synthesis of a Diaminedithiol Bifunctional Chelating Agent for Incorporation of Technetium-99m into Biomolecules. *Bioconjugate Chem.* 1, 132–137.
- (11) Faggiani, R., Lock, C. J. L., Epps, L. A., Kramer, A. V., Brune (sic), D., and Burns, H. D. (1988) (3,6-Dimethyl-3,6-diazaoctan-1,8-dithiolato-S<sup>1</sup>, N<sup>3</sup>, N<sup>6</sup>, S<sup>8</sup>) oxotechnetium(V) pertechnetate. *Acta Crystallogr. C* 44, 777–779.
- (12) Fritzberg, A. R., Abrams, P. G., Baumier, P. L., Kasina, S., Morgan, A. C., Jr., Rao, T. N., Reno, J. M., Sanderson, J. A., Srinivasan, A., Wilbur, D. S., and Vanderheyden, J.-L. (1988) Specific and stable labeling of antibodies with technetium-99m with a diamide dithiolate chelating agent. *Proc. Natl. Acad. Sci. U.S.A.* 85, 4025–4029.
- (13) Lister-Jones, J., Weber, R. W., Boutin, R., Nedelman, M. A., and Dean, R. T. (1989) Site specifically Tc-99m labeled antibody-bifunctional chelator conjugates. *J. Nucl. Med.* 30, 793.
- (14) Baidoo, K. E., and Lever, S. Z. (1990) Design and synthesis of a versatile precursor to neutral technetium and rhenium complexes. *Tetrahedron Lett.* 31, 5701–5704.
- (15) Mahmood, A., Halpin, W. A., Baidoo, K. E., Sweigart, D. A., and Lever, S. Z. (1991) Structure of a neutral N-alkylated diamindithiol (DADT) <sup>99</sup>Tc(V) complex: *Syn* <sup>99</sup>TcO(NEt-TMDADT) *Acta Crystallogr. C* 47, 254–257.
- (16) Lever, S. Z., Baidoo, K. E., and Mahmood, A. (1990) Structure proof of *syn/anti* isomerism in N-alkylated diaminedithiol (DADT) complexes of technetium. *Inorg. Chim. Acta* 176, 183–184.
- (17) Epps, L. A. (1984) The chemistry of neutral, lipid soluble technetium(V) complexes of aminoalcohols and aminothiols. Ph.D. Thesis, The Johns Hopkins University, Baltimore.
- (18) del Rosario, R. B., Baidoo, K. E., Jung, Y.-W., Lever, S. Z., and Wieland, D. M. (1993) Synthesis and *in vivo* evaluation of Tc-99m-DADT-benzovesamicol: A potential marker for cholinergic neurons. *Nucl. Med. Biol.*, in press.

# Development and in Vitro Characterization of a Cationized Monoclonal Antibody against $\beta$ A4 Protein: A Potential Probe for Alzheimer's Disease<sup>1</sup>

Ulrich Bickel,\*<sup>†</sup> Virginia M. Y. Lee,<sup>‡</sup> John Q. Trojanowski,<sup>‡</sup> and William M. Pardridge<sup>†</sup>

Department of Medicine and Brain Research Institute, UCLA School of Medicine, Los Angeles, California 90024, and Medical Pathology Section, Hospital of the University of Pennsylvania, Philadelphia, Pennsylvania 19104. Received August 3, 1993\*

The blood–brain barrier (BBB) is impermeable to IgG. Therefore, a delivery strategy has to be applied in order to use monoclonal antibodies (mAb) as diagnostic or therapeutic agents in the brain. It has been demonstrated that cationization of IgG allows for the BBB penetration following peripheral administration. A cationized mAb against  $\beta$ A4-amyloid could be a sensitive and specific diagnostic tool for Alzheimer's disease (AD). The site-protected cationization and radiolabeling with <sup>111</sup>In of the specific anti  $\beta$ -amyloid mAb, AMY33, is described. The binding affinity of the antibody was retained after these procedures ( $K_d = 3.1 \pm 0.5$  nM), as determined by solid-phase immunoradiometric assay and immunocytochemistry on AD brain sections. The in vitro binding by isolated brain capillaries indicated that the cationized antibody may be delivered to the brain in vivo. The ability of the modified antibody to detect cerebral  $\beta$ -amyloid deposits in vivo can now be evaluated using single photon emission computed tomography (SPECT) and a suitable animal model for cerebral amyloidosis, such as non-human primates or aged canines.

## INTRODUCTION

Vascular amyloid deposits and senile plaques are among the neuropathologic hallmarks of Alzheimer's disease (AD).<sup>2</sup> The main constituent of these lesions is the 39–43 amino acid 4.2 kD  $\beta$  amyloid protein ( $\beta$ A4), which was originally characterized from meningeal blood vessels (1) and subsequently found in senile plaques (2) and cerebral cortical microvessels (3). It is derived from the amyloid precursor protein (APP) (4), and  $\beta$ A4 derivatives are released in small quantities into biological fluids (plasma, cerebrospinal fluid) in vivo (5). The APP consists of 695–770 amino acids depending on whether the APP isoform contains a Kunitz protease inhibitor-like insert. Soluble forms of APP are released from the membrane-bound APP pool, but these soluble forms do not contain the intact  $\beta$ A4 peptide moiety, which is found in the full-length form of membrane-bound APP. The measurement in CSF of the nonamyloidogenic, secreted form of APP, which appears to be the main product of physiologic APP-processing, has recently been suggested as a potential diagnostic test for AD (6, 7). However, despite the central role played by  $\beta$ A4 amyloid deposition in the etiology of Alzheimer's disease (8, 9), there is currently no noninvasive, in vivo diagnostic test for the presence of amyloid deposits within the central nervous system.

The availability of highly specific anti- $\beta$ A4 monoclonal antibodies (10–13) suggests their use in a diagnostic method such as radioimmunoimaging, analogous to the immunoscintigraphic methods in tumor diagnosis (14). Such a diagnostic method can be expected to be more specific and sensitive for AD than clinical criteria (15) or, e.g., the currently evaluated measurement of regional cerebral blood flow using <sup>99m</sup>Tc-HMPAO single photon emission-computed tomography (SPECT) (15, 16). However, not only parenchymal  $\beta$ A4 but also the cerebrovascular amyloid are localized beyond the endothelial cells of cerebral vessels (17), which comprise the blood–brain barrier (BBB) in vivo. Despite the demonstration of morphologic alterations of the BBB in AD (18, 19), there is no convincing functional evidence for a significant leakiness of the BBB in this disease (19, 20). Therefore, it cannot be anticipated that native antibodies or even Fab fragments will be useful in AD radioimaging (13), owing to the negligible transport of proteins through the brain capillary endothelial wall. On the other hand, it has been demonstrated that cationization of IgG allows for brain delivery of antibodies via absorptive-mediated transcytosis through the BBB following peripheral administration (21, 22). In the present paper we describe the cationization and in vitro characterization of the specific anti- $\beta$ A4 monoclonal antibody, AMY33 (11). The cationized antibody was then radiolabeled with an isotope suitable for SPECT, namely <sup>111</sup>In. The BBB permeability of the labeled cationized antibody was evaluated in vitro by measuring the uptake by isolated bovine brain capillaries, which represent an in vitro model of the BBB (23, 24).

## EXPERIMENTAL PROCEDURES

**Materials.**  $\beta$ A4<sup>1–28</sup> corresponding to the first 28 amino acids of the  $\beta$ -amyloid sequence as reported by Masters et al. (2) was synthesized using solid-phase methodology by the UCLA Peptide Synthesis Facility. Chromatographically purified mouse IgG (mIgG) and the mouse IgG1<sub>k</sub> mAb MOPC21 was purchased from Cappel (Durham, NC). Chloramine T was from MCB Reagents

\* Address correspondence to this author at UCLA c/o William M. Pardridge.

<sup>†</sup> UCLA School of Medicine.

<sup>‡</sup> Hospital of the University of Pennsylvania.

\* Abstract published in *Advance ACS Abstracts*, February 1, 1994.

<sup>1</sup> This work has been presented in part at the 22nd Meeting of the Society of Neuroscience, Anaheim, CA, Oct 25–30, 1992.

<sup>2</sup> Abbreviations used: AD, Alzheimer's disease;  $\beta$ A4,  $\beta$ -amyloid protein; APP, amyloid precursor protein; BBB, blood–brain barrier; IEF, isoelectric focusing; HMD, hexamethylenediamine; DTPA, diethylenetriaminepentaacetic acid; EDC, *N*-ethyl-*N'*-[3-(dimethylamino)propyl]carbodiimide; SPECT, single photon emission-computed tomography; IRMA, immunoradiometric assay; mAb, monoclonal antibody.

(Cincinnati, OH). C<sub>18</sub>-Sep Pak cartridges and Ultra-free 30 000 PLTK filtration units were obtained from Millipore (Bedford, MA). Superose 12HR fast protein liquid chromatography (FPLC) columns, protein G-Sepharose 4 fast flow, and ampholine PAG plate (pH = 3.5–9.5) isoelectric focusing (IEF) gels were purchased from Pharmacia (Piscataway, NJ). Maxisorp break-apart modules were obtained from Nunc (Naperville, IL). Biotinylated horse anti-mouse IgG and Vectastain ABC-elite reagents were obtained from Vector Labs (Burlingame, CA). Na<sup>125</sup>I was purchased from Amersham (Arlington Heights, IL) and <sup>111</sup>InCl<sub>3</sub> from New England Nuclear (Boston, MA). Hexamethylenediamine (HMD) and diethylenetriaminepentaacetic acid (DTPA) cyclic dianhydride were from Aldrich Chemical Co. (Milwaukee, WI). Centricon concentrators were supplied by Amicon (Danvers, MA). *N*-Ethyl-*N'*-[3-(dimethylamino)propyl]carbodiimide (EDC), Pristane, and all other reagents were obtained through Sigma Chemical Co. (St. Louis, MO). Female BALB/c mice were obtained from the Department of Laboratory Animal Medicine (UCLA).

**Production of AMY33 Antibody.** Pristane primed female BALB/c mice received 10<sup>7</sup> AMY33 hybridoma cells per animal ip. The IgG fraction was purified from the harvested ascites by affinity chromatography on a protein G Sepharose 4 fast flow affinity column. The antibody was eluted from the affinity column with 0.1 M glycine at pH 2.5 and immediately neutralized to pH 7 with 1 M Tris base. The elution from the column was monitored at 280 nm, and the IgG-containing fractions were pooled and dialyzed against 20 mM phosphate buffer/0.15 M NaCl (PBS, pH = 7.4). Protein was measured by the method of Lowry (25), and SDS-PAGE of the purified mAb was performed under reducing conditions followed by Coomassie blue staining. The nonspecific control IgG1 antibody, MOPC21, was similarly affinity purified from ascites on protein G sepharose.

**Cationization of IgG.** The cationization, as developed for albumin (24) and bovine IgG (21), was modified for the present experiments as follows: the IgG (AMY33, MOPC21, or nonimmune, chromatographically purified mouse IgG) was used at a concentration of 1 mg/mL in 20 mM PBS (pH = 7.4). Solutions of EDC (100 mg/mL, 0.52 M) and 2 M HMD were prepared in H<sub>2</sub>O. The HMD solution was adjusted to the desired pH for the cationization with concentrated HCl. The known amino acid composition of MOPC21 (26) was used to estimate the number of acidic amino acids (Asp, Glu) in the IgG molecules. There are 120 Asp and Glu residues per MOPC21 molecule. HMD and EDC were added to the IgG to give final molar ratios in the reaction mixture of HMD/EDC/COOH groups of 200:7:1 or 1000:35:1, respectively. The pH was adjusted to values of 7.8, 6.8, and 6.0 with 1 M HCl. Cationization was performed with or without site protection. Cationization under site protection of the antibody was performed after an overnight preincubation of AMY33 in PBS, pH 7.4, with a 10-fold molar excess of the synthetic peptide  $\beta$ A4<sup>1–28</sup> at 4 °C. For purification, the crude  $\beta$ A4<sup>1–28</sup> peptide had been dissolved in 90% formic acid and evaporated to dryness. It was then redissolved in 5 M guanidine/1 M acetic acid and injected onto a reversed-phase HPLC column (Vydac C<sub>4</sub>, 10 × 250 mm). Elution was performed with a linear gradient of acetonitrile in 0.1% trifluoroacetic acid at a flow rate of 3 mL/min and was monitored at 214 nm. The peptide peak was pooled and lyophilized. The purity of the HPLC-purified peptide has previously been confirmed

by amino acid sequencing (27). In addition, HPLC analysis following radioiodination yields a single, sharp peak (27).

The cationization was allowed to proceed for 3 h at room temperature under constant mixing, after which the reaction was quenched by the addition of a 20-fold (relative to EDC) excess of glycine (1 M in H<sub>2</sub>O, pH = 6.0 with HCl), followed by incubation for 1 h at room temperature. The final reaction volume was then adjusted to pH 2.5 with 1 M HCl, filtered, and injected onto a Superose 12HR FPLC column. The elution was performed with 0.1 M glycine at pH 2.5 at a flow rate of 0.5 mL/min. Elution under acidic conditions is required to separate the cationized AMY33 and the  $\beta$ A4<sup>1–28</sup> peptide. The elution was monitored at 280 nm, and the fractions corresponding to the molecular weight of IgG were immediately neutralized by the addition of an appropriate volume of 1 M Tris base. Isoelectric focusing (IEF) on polyacrylamide slab gels was used as described (21) to determine the isoelectric point (pI) of the native and cationized IgGs.

**Solid-Phase Immunoradiometric Assay (IRMA).** The binding affinity of the native and cationized antibodies to  $\beta$ A4<sup>1–28</sup> was tested in a solid-phase IRMA. The binding of <sup>125</sup>I-labeled AMY33 to the peptide antigen, which was absorbed to the surface of polystyrene microtiter wells, was competed with increasing concentrations of unlabeled IgG. Native AMY33, cationized AMY33 with and without site protection, native MOPC21, and cationized MOPC21 in concentrations between 0 and 67 nM were used as competitors. HPLC-purified  $\beta$ A4<sup>1–28</sup> was coated to NUNC Maxisorp microtiter wells overnight at 4 °C with 50  $\mu$ L per well of a 10  $\mu$ g/mL peptide solution in 0.1 M NaHCO<sub>3</sub> at pH 9. The peptide solution was removed by aspiration. Blocking of nonspecific binding was performed by incubating the wells for 2 h at room temperature with an aqueous 0.25% polylysine (126 kDa) solution. The wells were then washed three times with 200  $\mu$ L of 10 mM PBS (pH = 7.4).

Iodination of native AMY33 was achieved with a chloramine T technique: 20  $\mu$ g (0.13 nmol) of IgG in 50 mM PBS (pH 7.4) was labeled with 0.5 mCi Na <sup>125</sup>I by addition of 2 × 0.85 nmol chloramine T in 1-min intervals. The total reaction volume was 40  $\mu$ L. The reaction was stopped by addition of 2.5 nmol of Na<sub>2</sub>S<sub>2</sub>O<sub>5</sub> in 10  $\mu$ L of H<sub>2</sub>O. The iodinated antibody was purified by gel filtration on a 0.7 × 28-cm Sephadex G25 column and eluted with 50 mM PBS containing 0.01% bovine serum albumin. The specific activity of the tracer was calculated as 500 Ci/mmol.

For the binding experiments, the tracer was diluted to 50 000 dpm per 50  $\mu$ L (0.9 nM) in assay buffer (PBS with 0.5% gelatin, 0.1% Tween 20 and 10 U/mL heparin) and incubated in the microtiter wells in the presence or absence of unlabeled competitors overnight at 4 °C. After aspiration of the tracer solution, the wells were washed five times with 200  $\mu$ L of PBS, and the bound radioactivity was counted in a  $\gamma$ -counter. The binding data were expressed as fraction of total tracer bound to the wells and were evaluated by nonlinear regression analysis. The computer program used for the regression analysis employs the BMDP 3R program (28). It was developed for the evaluation of ligand binding assays, and one specific binding site and nonspecific binding was assumed (29). Nonspecific binding and binding capacities were assumed to be independent of the ligand species but were rescaled within each experiment to account for minor differences in antigen plating density of the microtiter wells between assays.

**Immunocytochemistry on Alzheimer's Disease**

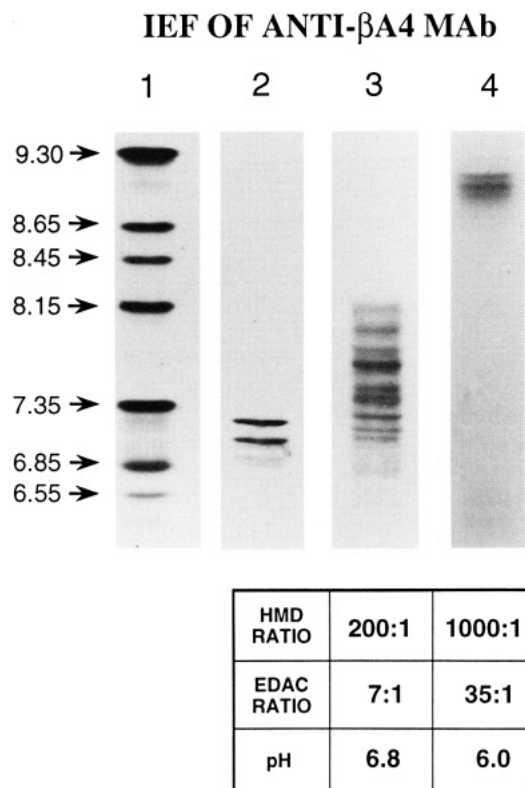
**Brain Sections.** Immunocytochemistry on 5- $\mu$ m paraffin sections of human AD brains were performed as described (30). Following deparaffinization in xylene and decreasing ethanol steps, the slides were incubated in 90% formic acid for 15 min followed by a tap water rinse (10 min) and treatment with 0.3%  $\text{H}_2\text{O}_2$  and again tap water for 5 min. After 5 min in TBS (50 mM Tris, pH 7.4, 0.9% NaCl), the sections were covered with 3% normal horse serum for 30 min. The excess serum was blotted from the sections, and the primary antibody was applied for 90 min at room temperature in concentrations of 5, 20, and 100  $\mu\text{g}/\text{mL}$  in TBS. Biotinylated horse anti-mouse IgG was used as secondary antiserum at a concentration of 50  $\mu\text{g}/\text{mL}$  for 30 min. The avidin-biotin-peroxidase complex (Vectastain ABC-Elite) was used according to the manufacturer's instructions. 3-Amino-9-ethylcarbazole (AEC) was used as a chromagen.

**DTPA Conjugation of Antibodies and Labeling with  $^{111}\text{In}$ .** A modification of the method described by Sakahara et al. (31) was used. Native and cationized antibodies were dialyzed against 0.1 M  $\text{NaHCO}_3$  and adjusted to a concentration of 1 mg/mL. DTPA cyclic dianhydride was dissolved in DMSO (5  $\mu\text{mol}/\text{mL}$ ) and added to the antibodies in a 30:1 molar excess. After 60 min at room temperature, the free, unconjugated DTPA was removed by repeated ultrafiltration on Centricon 30 filtration units (molecular weight cutoff 30 kDa). The initial reaction volume was concentrated to 10%, diluted 10-fold with 0.2 M Na citrate, and again concentrated to 10%. The DTPA-conjugated IgG was finally taken up into 0.2 M Na citrate at a concentration of 1 mg/mL. 5 mCi of  $^{111}\text{InCl}_3$  was diluted in 500  $\mu\text{L}$  of Na-citrate and added to the DTPA-conjugated antibody (200–300  $\mu\text{g}$  of IgG). After 60 min at room temperature, free  $^{111}\text{In}$  was removed by ultrafiltration on Centricon 30 concentrators as described above. 0.9% NaCl with 0.1% bovine albumin was used as a washing fluid.

**Binding Studies with Isolated Bovine Brain Capillaries.** Bovine brain capillaries were isolated by a mechanical homogenization technique as described (32). The cortex of fresh bovine brains was scraped off after removal of the pial membrane. Following addition of a 5-fold volume excess of Ringer-HEPES buffer (10 mM HEPES, 151 mM NaCl, 4 mM KCl, 2.8 mM  $\text{CaCl}_2$ ) containing 1% BSA, the tissue was homogenized with a hand-held Teflon homogenizer. The homogenate was then suspended in an equal volume 26% dextran (molecular weight = 60–90 kDa), followed by centrifugation at 5800g for 15 min at 4  $^\circ\text{C}$ . The vascular pellet was resuspended in buffer, and the microvessels were purified from nuclei and red cells by filtration over a 210- $\mu\text{m}$  nylon mesh and passage over a glass bead filtration column. The microvessels were finally resuspended in 0.25 M sucrose with 0.02 M Tris (pH = 7.4) containing 2 mM dithiothreitol and stored in liquid nitrogen. The binding assays were performed as described (21). Isolated capillaries corresponding to approximately 200  $\mu\text{g}$  of protein were incubated in a final volume of 450  $\mu\text{L}$  of Ringer-HEPES buffer and 1% BSA with 40 000 cpm radiolabeled antibodies at 37  $^\circ\text{C}$  for incubation times from 5 s to 30 min. At the end of the incubation, the mixture was microfuged at 10000g for 45 s. The supernatant was discarded, and the capillaries were solubilized in 0.5 mL of 1 M NaOH. Bound radioactivity was measured in a  $\gamma$  counter, and protein measurements were performed by the method of Lowry (25).

## RESULTS

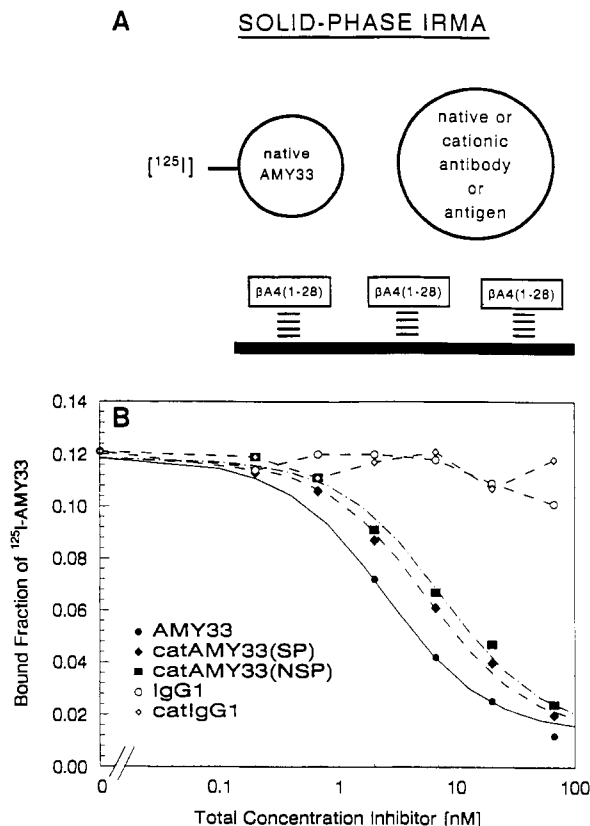
A total of 50 mg of AMY33 antibody was obtained by affinity chromatography on protein G Sepharose from 31



**Figure 1.** Coomassie blue staining of a polyacrylamide isoelectric focusing gel showing different degrees of cationization of AMY33 (lanes 3 and 4) as obtained by the reaction conditions indicated in the inset. The molar ratios are based on the amino acid composition of the mIgG1 mAb, MOPC21, and refer to the number of Asp and Glu residues in the antibody. The reaction time was 3 h at room temperature. pI standards (lane 1), native AMY33 (lane 2).

mL of ascites fluid produced in nine mice. SDS-PAGE confirmed the purity of the IgG by the demonstration of two sharp bands representing the heavy and light chain. The isoelectric points (pI) of native and cationized AMY33 are shown in the IEF in Figure 1. Native AMY33 yielded two bands corresponding to a pI of approximately 7. Cationization at pH 7.8 with a 200:7:1 molar ratio of HMD/EDC/COOH groups did not result in detectable cationization (data not shown). At pH 6.8 and with the same molar ratios, a partial cationization was observed with pI values ranging from 7 to 8. In contrast, molar ratios of 1000:35:1 (HMD/EDC/COOH groups) at pH 6.0 led to a homogeneous cationization resulting in a pI of 9 (lane 4 in Figure 1). These reaction conditions were applied in the subsequent experiments for AMY33, MOPC21, and the chromatographically purified mIgG. Cationization with or without site protection resulted in identical pI values. Native MOPC21 had a pI value of 6.5 and was cationized to a pI of > 9.5. Purified mIgG from mouse serum displayed a broad pI range between 5.5 and 7.5, which was converted by cationization to a homogeneous band corresponding to a pI of > 9.5. Purification of cationized AMY33, MOPC21, and mIgG on Superose 12HR did not reveal the presence of a significant peak in the high molecular weight range, indicating that there was no formation of high molecular weight aggregates due to the cationization procedure. 95% of the IgG eluted in a peak between 12 and 15 mL, corresponding to the retention volume of native IgG, as determined in standard chromatograms. In the case of the site-protected cationization of AMY33, the gel filtration chromatography also provided





**Figure 2.** (A) Principle of the solid-phase IRMA used for the measurement of the binding affinity of native and cationized AMY33. (B) Competition curves in the solid-phase IRMA for  $^{125}\text{I}$ -AMY33 binding to synthetic  $\beta\text{A4}^{1-28}$  peptide. SP and NSP refer to cationization of AMY33 with or without site protection, respectively. IgG1 refers to the mAb MOPC21. Data points are means of duplicates, and the curves were fitted by nonlinear regression analysis.

an efficient separation from the low molecular weight antigen  $\beta\text{A4}^{1-28}$ , which eluted in a retention volume of 19 mL.

Figure 2A shows the principle of the solid-phase IRMA, and Figure 2B shows the competition curves of native AMY33, cationized AMY33, and control antibody, MOPC-21. The  $K_d$  of native AMY33 was  $1.36 \pm 0.26$  nM. Cationization of AMY33 with and without site protection resulted in  $K_d$  values of  $3.06 \pm 0.49$  nM and  $4.20 \pm 0.67$  nM, respectively. Neither native nor cationized MOPC21 inhibited the specific binding of the  $^{125}\text{I}$ -AMY33 tracer within the covered concentration range.

$^{111}\text{In}$  labeling of the DTPA conjugated native and cationized antibodies resulted in specific activities of 1.5 mCi/nmol IgG. Challenge of the complex binding of  $^{111}\text{In}$  with an 18 000-fold molar excess of EDTA, followed by ultrafiltration on Ultrafree 30 000 PLTK filters, resulted in the recovery of less than 2.5% of the radioactivity in the ultrafiltrate.

Immunocytochemistry on AD brain sections with the native AMY33 antibody resulted in a strong specific staining of vascular amyloid deposits at all three concentrations of antibody used in these experiments. There was virtually no nonspecific background staining (Figure 3A). DTPA-conjugated native AMY33 exhibited the same specific staining pattern as unconjugated AMY33 at the same concentration, indicating that the DTPA conjugation had no effect on the binding affinity of the antibody. With cationized AMY33 and DTPA-conjugated cationized AMY33, the same vascular amyloid deposits could be detected on serial sections as with the native antibody

(Figure 3B), and the immunocytochemical results obtained with the derivatized AMY33 were nearly identical to those described earlier with native AMY33 (11, 33). When compared to native AMY33, the staining intensity was slightly decreased. A concentration of  $20 \mu\text{g/mL}$  of cationized AMY33 resulted in the same staining intensity as a concentration of  $5 \mu\text{g/mL}$  of native AMY33. There was a moderate increase in diffuse nonspecific background staining with the cationized AMY33 (Figure 3B). A comparable level of nonspecific background staining was present in control sections stained with the DTPA-conjugated cationized mIgG. However, the nonimmune mIgG did not label any amyloid deposits.

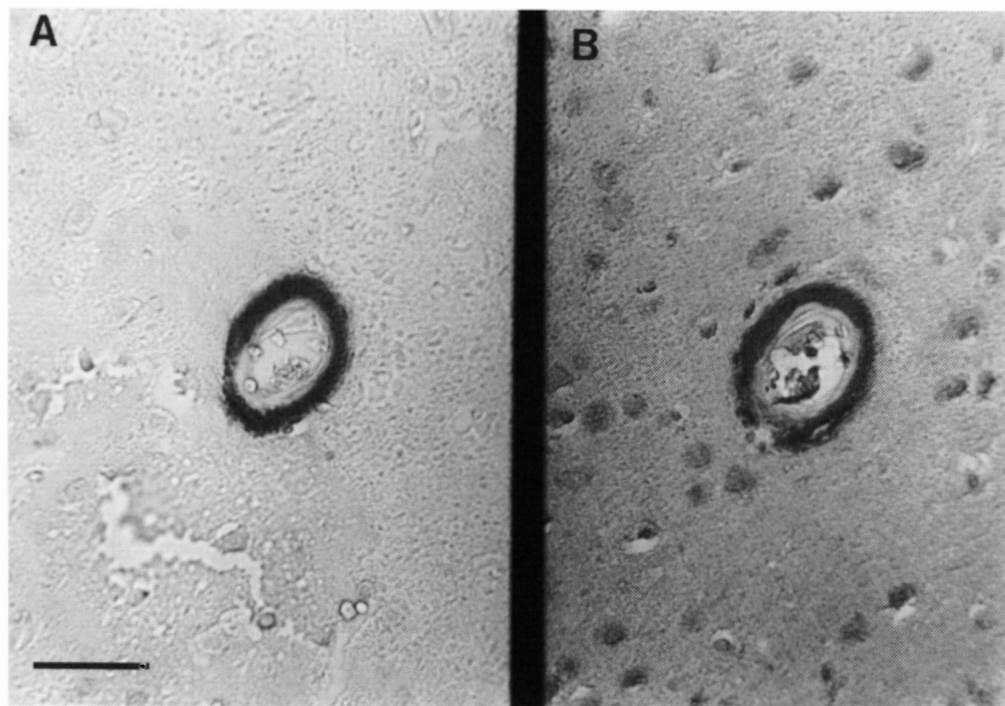
Incubation with  $^{111}\text{In}$ -labeled cationized AMY33 and cationized nonimmune mIgG with isolated bovine brain capillaries resulted in a time-dependent increase in tracer binding to the capillaries as compared to the native antibody (Figure 4). After 30 min, 71% of the cationized mIgG and 26% of the cationized AMY33 were bound per mg protein compared to 6% of the native AMY33.

## DISCUSSION

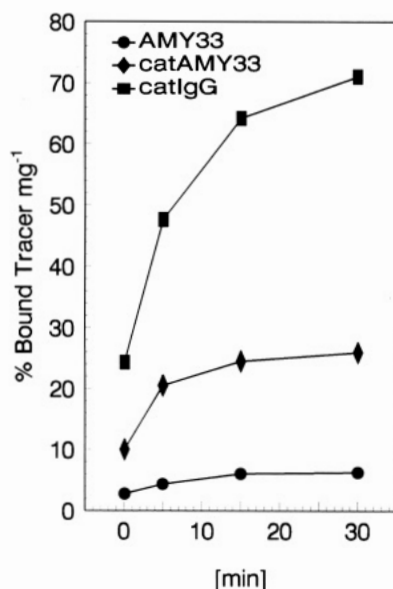
In the present study the mouse mAb, AMY33, was used, which has been raised against a synthetic peptide corresponding to the first 28 amino acids of the  $\beta\text{A4}$  sequence (2). The specificity of this antibody for  $\beta$ -amyloid protein in neuritic and diffuse plaques and cerebrovascular deposits has previously been demonstrated (11, 33). Sufficient quantities of the monoclonal antibody for the evaluation of the chemical modifications and subsequent *in vivo* studies were produced by ascites generation in pristane-primed mice, followed by affinity purification on protein G Sepharose. SDS-PAGE confirmed the purity of the obtained antibody.

Cellular uptake of IgG in general and transcytosis through the BBB in particular can be considerably enhanced by cationization, i.e., an increase of the pI of the molecule into the basic range (21, 22). Like other cationic proteins, such as cationized albumin (24), histone, and CD4 (34), cationized IgG penetrates the BBB by absorptive-mediated transcytosis. Cationized albumin also undergoes enhanced transport through the blood-cerebrospinal fluid barrier (35). It is apparently the process of cationization which enhances capillary uptake. In our experience, the absolute pI value alone is not crucial, but rather some structural modification introduced into the protein by cationization. As an example, there was no cellular uptake of a native mouse mAb generated against the ras oncogene, despite a pI of 8.8 (unpublished data). Therefore, even naturally basic antibodies cannot be expected to show BBB permeability, which may confound brain imaging attempts based on unmodified antibodies or Fab fragments (13).

The degree of the cationization involving the conversion of EDC-activated carboxyl groups on the protein into extended primary amino groups by HMD depends on the pH of the reaction (36), the availability of surface carboxyl groups (34), and the molar ratio of the reagents. In order to obtain significant cationization of AMY33, which has a neutral pI of 7, relatively higher concentrations of EDC and HMD and a lower pH value were required compared to the cationization of polyclonal bovine IgG (21). The number of amino groups added to the antibody molecule was not measured in the present study. However, estimates can be made based on the results obtained with another protein. The cationization of rat serum albumin, which resulted in a pI shift from 5 to 8.5 (comparable to the shift from 6.5 to >9.5 for MOPC21), introduced 30



**Figure 3.** Immunocytochemistry on serial sections from AD brain with native AMY33 (A) and DTPA-conjugated cationized AMY33 (B). The arteriole in the center shows circular amyloid disposition. Antibody concentration was 20  $\mu\text{g/mL}$  in both samples. B was lightly counterstained with hematoxylin and A is without counterstain. Scale bar = 50  $\mu\text{m}$ .



**Figure 4.** Binding of <sup>111</sup>In-labeled antibodies by isolated bovine brain capillaries (approximately 200  $\mu\text{g}$  of capillary protein per tube). Time course of the binding of native AMY33, cationized AMY33, and cationized nonspecific mIgG in serum-free assay buffer. The binding is normalized to percent bound per mg capillary protein. Data are means of duplicates, and the SE was below 5%.

new primary amino groups as determined with the amine detection reagent, 2,4,6-trinitrobenzene sulfonic acid (unpublished results).

Because the cationization is a random process which could potentially lower the affinity of the antibody in the presence of crucial Asp or Glu residues in the antigen binding site, the affinity of the cationized antibody has to be determined. It was necessary to develop the IRMA system with the unlabeled solid-phase absorbed antigen,  $\beta\text{A4}^{1-28}$ , because two alternative systems (solution phase RIA and ELISA, data not shown) proved to be unsuitable for this purpose. The solution-phase RIA experiments

showed that AMY33 does not recognize the peptide when the peptide is <sup>125</sup>I-labeled at either the Tyr<sup>10</sup> with chloramine T or Lys<sup>16</sup> with <sup>125</sup>I-Bolton-Hunter reagent. Together with the previous finding that AMY33 has no cross-reactivity with the peptide fragments  $\beta\text{A4}^{1-12}$  and  $\beta\text{A4}^{11-28}$  (11) and with the fact that post-translational modifications of Asp<sup>1</sup> or Asp<sup>7</sup> of  $\beta\text{A4}$  present in AD brain (37) apparently do not affect the recognition of  $\beta\text{A4}$  by this mAb, this further proves the high specificity of AMY33 against the midregion of  $\beta\text{A4}^{1-28}$ . The ELISA system resulted in high nonspecific background levels for the cationized IgG. This is due to nonspecific absorption of cationized proteins to solid-phase surfaces and has been described in other ELISA studies (38, 39). These high background levels prevented the quantitative evaluation of the ELISA for cationized AMY33. In contrast, nonspecific binding of the cationized antibody should not significantly interfere with the evaluation of the solid-phase IRMA as applied here. The unlabeled native or cationized antibody competes for binding to the solid-phase absorbed synthetic peptide antigen with the iodine-labeled native AMY33 tracer. Nonspecific binding of the cationized unlabeled competitor would not affect the signal, as long as the total free concentration of the unlabeled competitor is not significantly lowered. In this case, the determination of the  $K_d$  value would underestimate the true value. Therefore, the true  $K_d$  value of cationized AMY33 could be even closer to the  $K_d$  value of native AMY33. Site protection during the cationization reaction led to a decreased reduction of binding affinity compared to cationization without site protection ( $K_d$  3.06  $\pm$  0.49 nM versus 4.20  $\pm$  0.67 nM, respectively). In any case, the dissociation constant in the low nM range of the cationized AMY33 demonstrates that it is possible to cationize monoclonal antibodies without appreciable loss of affinity. Previously, this had only been demonstrated for polyclonal antibodies (40, 41). The beneficial effect of site-protection has to be evaluated for each individual monoclonal antibody. The relatively small  $K_d$  difference

between site-protected and non-site-protected cationization of AMY33 may be due to the absence of crucial carboxyl side chains in the antigen binding site. Similarly, cationization did not decrease the binding affinity of the monoclonal antibody MAb111 against the rev-protein of HIV (42), while this procedure led to a loss of antigen recognition of the mAb B72.3, which is directed against a colon carcinoma antigen (unpublished observations).

The choice of  $^{111}\text{In}$  as radioisotope was based on its photon energy and half-life, which are suitable for SPECT imaging (43). Although the liver accumulation of  $^{111}\text{In}$  and  $^{111}\text{In}$ -labeled antibodies may present problems in the imaging of abdominal organs (43), this would not interfere with the intended use for brain SPECT. Reaction conditions for the DTPA conjugation, such as those applied in the present study, have been shown to result in the incorporation of approximately one DTPA molecule per antibody molecule without affecting the antigen binding activity of monoclonal antibodies (31). Immunocytochemistry on AD brain sections provided evidence for retained binding affinity of DTPA-conjugated cationized AMY33 for tissue amyloid deposits. Therefore, the modified anti-amyloid antibody not only reacts with the synthetic peptide antigen  $\beta\text{A4}^{1-28}$  but is also able to recognize the full-length  $\beta\text{A4}$  protein, which will be the target in the in vivo application.

Uptake of the radiolabeled antibodies by isolated bovine brain capillaries was used as an in vitro model system for the BBB uptake of cationized proteins. This system only indicates binding to and endocytosis by endothelial cells, but not transcytosis. Nevertheless, in all cases of cationized proteins investigated so far, isolated capillary studies were predictive of BBB transcytosis in vivo (21, 24, 34, 44). The species from which the capillaries are isolated appears to be unimportant for binding experiments with cationized proteins, as can be concluded from studies with cationized rat serum albumin and isolated capillaries from rat or bovine brain (44). The binding values for native AMY33 were in the range previously found for native IgG (21), and they can be explained by physical trapping of the tracer inside the patent vascular lumen (23). The results for the cationized AMY33 and the cationized nonspecific mouse IgG are consistent with the previous data with  $^{125}\text{I}$ -labeled cationized bovine IgG (21). The cationized antibodies showed rapid initial binding to the capillaries which approximates a plateau after 30 min. The differences in the uptake between cationized AMY33 and cationized mouse IgG can be attributed to a higher degree of cationization of the latter. Similarly, cationization of bovine serum albumin to  $\text{pI} \geq 10$  resulted in a 5-fold higher capillary uptake compared to mild cationization ( $\text{pI} = 8.5-9$ ) (24). The lower in vitro uptake of cationized AMY33 may, however, not translate into a smaller brain uptake in an in vivo experiment. Tissue uptake in vivo is a function of both intrinsic organ clearance, represented by the permeability surface area (PS) product of the respective organ, and of the area under the plasma concentration-time curve (34). Previous studies have shown that highly cationic proteins with  $\text{pI}$  values above 10 are rapidly cleared from the plasma compartment. This is mainly due to uptake by peripheral organs such as liver, kidney, and lung and results in low AUC values (34).

In conclusion, the  $^{111}\text{In}$ -labeled cationized AMY33 has been developed as a tool for radioimmunoimaging of cerebral amyloid deposits using SPECT technology. The feasibility of the approach may now be evaluated in aged canines (45) or nonhuman primates (46), which develop brain lesions morphologically equivalent to human AD.

Similarly, cationized mAb targeted against other APP domains or cytoskeletal proteins found in senile plaques of AD (47) may be evaluated as diagnostic tools. Cationized proteins administered to humans may be pathogenic based on the immunogenicity of these modified proteins (48). However, the pathogenicity of cationized proteins has been observed in heterologous systems, wherein a protein with preexisting immunogenicity is cationized. Our previous studies have shown that cationized homologous proteins are not pathogenic and are weakly immunogenic (44). Therefore, the "humanization" of murine monoclonal antibodies prior to mAb cationization may facilitate the use of these proteins as neurodiagnostic or therapeutic agents in humans (49).

#### ACKNOWLEDGMENT

Harry V. Vinters (Department of Pathology, UCLA School of Medicine, Los Angeles) kindly provided human autopsy brain samples. Jody L. Buciak and Jing Yang provided expert technical assistance. Sherri J. Chien skillfully prepared the manuscript. This work was supported by California Department of Health Service Grant No. 90-11099. U.B. is recipient of a research stipend from the Deutsche Forschungsgemeinschaft.

#### LITERATURE CITED

- (1) Glenner, G. G., and Wong, C. W. (1984) Alzheimer's disease: initial report of the purification and characterization of a novel cerebrovascular amyloid protein. *Biochem. Biophys. Res. Commun.* 120, 885-890.
- (2) Masters, C. L., Simms, G., Weinman, N. A., Multhaup, G., McDonald, L. A., and Beyreuther, K. (1985) Amyloid plaque core protein in Alzheimer disease and Down syndrome. *Proc. Natl. Acad. Sci. U.S.A.* 82, 4245-4249.
- (3) Pardridge, W. M.; Vinters, H. V., Yang, J., Eisenberg, J., Choi, T. B., Tourtellotte, W. W., Huebner, V., and Shively, J. E. (1987) Amyloid angiopathy of Alzheimer's disease: amino acid composition and partial sequence of a 4,200-dalton peptide isolated from cortical microvessels. *J. Neurochem.* 49, 1394-1401.
- (4) Kang, J., Lemaire, H.-G., Unterbeck, A., Salbaum, J. M., Masters, C. L., Grzeschik, K.-H., Multhaup, G., Beyreuther, K., and Muller-Hill, B. (1987) The precursor of Alzheimer's disease amyloid  $\text{A}_4$  protein resembles a cell-surface receptor. *Nature* 325, 733-736.
- (5) Seubert, P., Vigo-Pelfrey, C., Esch, F., Lee, M., Dovey, H., Davis, D., Sinha, S., Schlossmacher, M., Whaley, J., Swindlehurst, C., McCormack, R., Wolfert, R., Selkoe, D., Lieberburg, I., and Schenk, D. (1992) Isolation and quantification of soluble Alzheimer's  $\beta$ -peptide from biological fluids. *Nature* 359, 325-327.
- (6) Farlow, M., Ghetti, B., Benson, M. D., Farrow, J. S., Van Nostrand, W. E., and Wagner, S. L. (1992) Low cerebrospinal fluid concentrations of soluble amyloid  $\beta$ -protein precursor in hereditary Alzheimer's disease. *Lancet* 340, 453-454.
- (7) Van Nostrand, W. E., Wagner, S. L., Shankle, W. R., Farrow, J. S., Dick, M., Rozemuller, J. M., Kuiper, M. A., Wolters, E. C., Zimmerman, J., Cotman, C. W., and Cunningham, D. D. (1992) Decreased levels of soluble amyloid  $\beta$ -protein precursor in cerebrospinal fluid of live Alzheimer disease patients. *Proc. Natl. Acad. Sci. U.S.A.* 89, 2551-2555.
- (8) Joachim, C. L., and Selkoe, D. J. (1992) The seminal role of  $\beta$ -amyloid in the pathogenesis of Alzheimer disease. *Alz. Dis. Assoc. Disorders* 6, 7-34.
- (9) Hardy, J., and Allsop, D. (1991) Amyloid deposition as the central event in the aetiology of Alzheimer's disease. *Trends Pharmacol. Sci.* 12, 383-388.
- (10) Wisniewski, H. M., Bancher, C., Barcikowska, M., Wen, G. Y., and Currie, J. (1989) Spectrum of morphological appearance of amyloid deposits in Alzheimer's disease. *Acta Neuropathol.* 78, 337-347.
- (11) Stern, R. A., Otvos, L., Jr., Trojanowski, J. Q., and Lee, V. M.-Y. (1989) Monoclonal antibodies to a synthetic peptide

- homologous with the first 28 amino acids of Alzheimer's disease  $\beta$ -protein recognize amyloid and diverse glial and neuronal cell types in the central nervous system. *Am. J. Pathol.* 134, 973-978.
- (12) Takahashi, H., Utsuyama, M., Kurashima, C., Mori, H., and Hirokawa, K. (1993) Monoclonal antibody to beta peptide, recognizing amyloid deposits, neuronal cells and lipofuscin pigments in systematic organs. *Acta Neuropathol.* 85, 159-166.
- (13) Majocha, R. E., Reno, J. M., Friedland, R. P., VanHaight, C., Lyle, L. R., and Marotta, C. A. (1992) Development of a monoclonal antibody specific for  $\beta$ /A4 amyloid in Alzheimer's disease brain for application to in vivo imaging of amyloid angiopathy. *J. Nucl. Med.* 33, 2184-2189.
- (14) Goldenberg, D. M. (1989) Future role of radiolabeled monoclonal antibodies in oncological diagnosis and therapy. *Sem. Nuclear Med.* 19, 332-339.
- (15) Dewan, M. J., and Gupta, S. (1992) Toward a definite diagnosis of Alzheimer's disease. *Comp. Psych.* 33, 282-290.
- (16) Holman, B. L., Johnson, K. A., Gerada, B., Carvalho, P. A., and Satlin, A. (1992) The scintigraphic appearance of Alzheimer's disease: A prospective study using technetium-99m-HMPAO SPECT. *J. Nucl. Med.* 33, 181-185.
- (17) Yamaguchi, H., Yamazaki, T., Lemere, C. A., Frosch, M. P., and Selkoe, D. J. (1992) Beta amyloid is focally deposited within the outer basement membrane in the amyloid angiopathy of Alzheimer's disease. An immunoelectron microscopic study. *Am. J. Pathol.* 141, 249-259.
- (18) Stewart, P. A., Hayakawa, K., Akers, M.-A., and Vinters, H. V. (1992) A morphometric study of the blood-brain barrier in Alzheimer's disease. *Lab. Invest.* 26, 734-742.
- (19) Kalaria, R. N. (1992) The blood-brain barrier and cerebral microcirculation in Alzheimer's disease. *Cerebrovas. Brain Metab. Rev.* 4, 226-260.
- (20) Schlageter, N. L., Carson, R. E., and Rapoport, S. I. (1987) Examination of blood-brain barrier permeability in dementia of the Alzheimer Type with [ $^{67}\text{Ga}$ ]EDTA and positron emission tomography. *J. Cereb. Blood Flow Metabol.* 7, 1-8.
- (21) Triguero, D., Buciak, J. B., Yang, J., and Pardridge, W. M. (1989) Blood-brain barrier transport of cationized immunoglobulin G. Enhanced delivery compared to native protein. *Proc. Natl. Acad. Sci. U.S.A.* 86, 4761-4765.
- (22) Triguero, D., Buciak, J. L., and Pardridge, W. M. (1991) Cationization of immunoglobulin G results in enhanced organ uptake of the protein after intravenous administration in rats and primate. *J. Pharmacol. Exp. Ther.* 258, 186-192.
- (23) Hjelle, J. T., Baird-Lambert, J., Cardinale, G., Spector, S., and Udenfriend, S. (1978) Isolated microvessels: the blood-brain barrier in vitro. *Proc. Natl. Acad. Sci. U.S.A.* 75, 4544-4548.
- (24) Kumagai, A. K., Eisenberg, J., and Pardridge, W. M. (1987) Absorptive-mediated endocytosis of cationized albumin and a  $\beta$ -endorphin-cationized albumin chimeric peptide by isolated brain capillaries. Model system of blood-brain barrier transport. *J. Biol. Chem.* 262, 15214-15219.
- (25) Lowry, O. H., Rosebrough, H. J., Farr, A. L., and Randall, R. J. (1951). Protein measurement with the Folin phenol reagent. *J. Biol. Chem.* 193, 262-275.
- (26) Kabat, E. A., Wu, T. T., Perry, H. M., Gottesman, K. S., and Foeller, C. (1991) Sequences of proteins of immunological interest. *NIH Publication No.* 91-3242.
- (27) Pardridge, W. M., Vinters, H. V., Miller, B. L., Tourtellotte, W. W., Eisenberg, J. L., and Yang, J. (1987) High molecular weight Alzheimer's disease amyloid peptide immunoreactivity in human serum and CSF is an immunoglobulin G. *Biochem. Biophys. Res. Comm.* 145, 241-248.
- (28) Dixon, W. J., Ed. (1990) *BMDP Statistical Software Manual*, pp 921-958, University of California Press, Berkeley.
- (29) Bickel, Y., Yoshikawa, T., Landaw, E. M., Faull, K. F., and Pardridge, W. M. (1993) Pharmacologic effects in vivo in brain by vector-mediated delivery of peptides. *Proc. Natl. Acad. Sci. U.S.A.* 90, 2618-2622.
- (30) Vinters, H. V., Pardridge, W. M., Secor, D. L., and Ishii, N. (1988) Immunohistochemical study of cerebral amyloid angiopathy. *Am. J. Pathol.* 133, 150-162.
- (31) Sakahara, H., Endo, K., Nakashima, T., Koizumi, M., Ohta, H., Torizuka, K., Furukawa, T., Ohmomo, Y., Yokoyama, A., Okada, K., Yoshida, O., and Nishi, S. (1985) Effect of DTPA conjugation on the antigen binding activity and biodistribution of monoclonal antibodies against  $\alpha$ -fetoprotein. *J. Nucl. Med.* 26, 750-755.
- (32) Pardridge, W. M., Eisenberg, J., and Yamada, T. (1985) Rapid sequestration and degradation of somatostatin analogues by isolated brain capillaries. *J. Neurochem.* 44, 1178-1184.
- (33) Arai, H., Lee, V. M. Y., Hill, W. D., Greenberg, B. D., and Trojanowski, J. Q. (1992) Lewy bodies contain beta-amyloid precursor proteins of Alzheimer's disease. *Brain Res.* 585, 386-390.
- (34) Bickel, U., Yoshikawa, T., and Pardridge, W. M. (1993) Delivery of peptides and proteins through the blood-brain barrier. *Adv. Drug Del. Rev.* 10, 205-245.
- (35) Griffin, D. F., and Giffels, J. (1982) Study of protein characteristics that influence entry into the cerebrospinal fluid of normal mice and mice with encephalitis. *J. Clin. Invest.* 70, 289-295.
- (36) Lambert, P. P., Doriaux, M., Sennesael, J., Vanholder, R., and Lammens-Verslijpe, M. (1983) The pathogenicity of cationized albumin in the dog. In *The Pathogenicity of Cationic Proteins* (P. P. Lambert, P. Bergmann, and R. Beauwens, Eds.), pp 307-317, Raven Press, New York.
- (37) Roher, A. E., Lowenson, J. D., Clarke, S., Wolkow, C., Wang, R., Cotter, R. J., Reardon, I. M., Zürcher-Neely, H. A., Heinrichson, R. L., Ball, M. J., and Greenberg, B. D. (1993) Structural alterations in the peptide backbone of  $\beta$ -amyloid core protein may account for its deposition and stability in Alzheimer's disease. *J. Biol. Chem.* 268, 3072-3083.
- (38) Pesce, A. J., Apple, R., Sawtell, N., and Michael, J. G. (1986) Cationic antigens: problems associated with measurement by ELISA. *J. Immunol. Meth.* 87, 21-27.
- (39) Pereira, H. A., Martin, L. E., and Spitznagel, J. K. (1989) Quantitation of cationic antimicrobial granule protein of human polymorphonuclear leukocytes by ELISA. *J. Immunol. Meth.* 117, 115-120.
- (40) Gauthier, V. J., Mannik, M., and Striker, G. E. (1982) Effect of cationized antibodies in performed immune complexes on deposition and persistence in renal glomeruli. *J. Exp. Med.* 156, 766-777.
- (41) Pardridge, W. M., Bickel, U., Buciak, J., Yang, J., and Diagne, A. Enhanced endocytosis and anti-HIV activity of anti-rev antibodies following cationization. *J. Infect. Dis.* (in press).
- (42) Pardridge, W. M., Bickel, U., Buciak, J., Yang, J., Diagne, A., and Aepinus, C. Treatment of human immunodeficiency virus-infected cells with a cationized monoclonal antibody directed against the rev protein. (Submitted for publication).
- (43) Gansow, O. A. (1991) Newer approaches to the radiolabeling of monoclonal antibodies by use of metal chelates. *Nucl. Med. Biol.* 18, 369-381.
- (44) Pardridge, W. M., Triguero, D., Buciak, J., and Yang, J. (1990) Evaluation of cationized rat albumin as a potential blood-brain barrier transport vector. *J. Pharmacol. Exp. Ther.* 255, 893-899.
- (45) Wisniewski, H., Johnson, A. B., Raine, C. S., Kay, W. J., and Terry, R. D. (1970) Senile plaques and cerebral amyloidosis in aged dogs. A histochemical and ultrastructural study. *Lab. Invest.* 23, 287-296.
- (46) Martin, L. J., Sisodia, S. S., Koo, E. H., Cork, L. C., Dellovade, T. L., Weidemann, A., Beyreuther, K., Masters, C., and Price, D. L. (1991) Amyloid precursor protein in aged nonhuman primates. *Proc. Natl. Acad. Sci. U.S.A.* 88, 1461-1465.
- (47) Arai, H., Lee, V. M.-Y., Otvos, Jr., L., Greenberg, B. D., Lowery, D. E., Sharma, S. K., Schmidt, M. L., and Trojanowski, J. Q. (1990) Defined neurofilament,  $\tau$ , and  $\beta$ -amyloid precursor protein epitopes distinguish Alzheimer from non-Alzheimer senile plaques. *Proc. Natl. Acad. Sci. U.S.A.* 87, 2249-2253.
- (48) Lambert, P. P., Bergmann, P., and Beauwens, R., Eds. (1983) *The Pathogenicity of Cationic Proteins*, Raven Press, New York.
- (49) Pardridge, W. M. (1991) *Peptide Drug Delivery to the Brain*, pp 235-236, Raven Press, New York.

## Cysteine Analogs of Recombinant Barley Ribosome Inactivating Protein Form Antibody Conjugates with Enhanced Stability and Potency *in Vitro*

Susan L. Bernhard,<sup>\*,†</sup> Marc Better,<sup>‡</sup> Dianne M. Fishwild,<sup>†</sup> Julie A. Lane,<sup>†</sup> Ann E. Orme,<sup>†</sup> Darryl A. Garrison,<sup>‡</sup> Cynthia A. Birr,<sup>†</sup> Shau-Ping Lei,<sup>‡</sup> and Stephen F. Carroll<sup>†</sup>

XOMA Corporation, 2910 Seventh Street, Berkeley, California 94710, and 1545 17th Street, Santa Monica, California 90404. Received August 6, 1993\*

Antibody immunoconjugates were made with native and recombinant forms of the type-I ribosome inactivating protein from barley (BRIP) and with three recombinant BRIP (rBRIP) analogs engineered to contain a unique cysteine residue near the C terminus (at amino acid 256, 270, or 277). rBRIP and all three cysteine analogs (rBRIP<sub>C256</sub>, rBRIP<sub>C270</sub>, and rBRIP<sub>C277</sub>) were produced in *E. coli*, with yields of soluble protein as high as 1 g/L, and were as active as native BRIP in inhibiting protein synthesis *in vitro*. Interestingly, the position of the engineered cysteine influenced not only the efficiency of conjugation to antibody but also the efficacy and disulfide bond stability of the immunoconjugates. Anti-CD5 antibody conjugates prepared with native and rBRIP were relatively inactive against antigen-positive target cells, while the conjugate made with rBRIP<sub>C277</sub> was 5-fold more cytotoxic. Anti-CD7 antibody conjugates made with rBRIP<sub>C277</sub> or rBRIP<sub>C270</sub> also exhibited improved potency and stability compared to the conjugate with native BRIP. These results indicate that engineering a cysteine residue into selected positions near the C-terminus of a type-I RIP such as BRIP can improve immunoconjugate yield, disulfide bond stability, and potency.

### INTRODUCTION

Plant leaves and seeds often contain a variety of proteins for defense against invasion by pathogens. One class of such proteins is the ribosome-inactivating proteins (RIP)<sup>1</sup> which enzymatically inhibit protein synthesis by hydrolyzing a single N-glycosidic bond in the 28 S rRNA of the eukaryotic ribosome (1, 2). Type-I RIP contain a single catalytic subunit (A chain). In addition to an A chain, type-II RIP contain a cell-binding lectin (B chain). There is considerable homology among RIP, especially for residues believed to be involved in catalysis (3). Best characterized of all RIP is the type-II protein ricin, and the X-ray crystal structure of ricin A chain (RTA) has recently been described (3).

These naturally occurring cytotoxic agents can be chemically coupled to antibodies or other cell-targeting agents to generate immunoconjugates capable of selectively killing antigen- or ligand-positive cells. Many antibody-RIP immunoconjugates have been evaluated *in vitro* and *in vivo* as potential therapeutic agents for cancer and autoimmune disease in man (4-7). Typically, such im-

munoconjugates have been constructed with the A chains of type-II RIP (such as RTA), which can be specifically targeted to cells *only* if the B chains are removed or inactivated.

Type-I RIP from cereal grains such as barley (BRIP) are attractive alternatives to the A chains of type-II RIP for the construction of targeted cytotoxic molecules. For example, BRIP is particularly nontoxic to intact cells (8) and is not glycosylated (9). This latter property may lead to reduced uptake and clearance by mannose receptors in the liver, resulting in prolonged serum residence time *in vivo* and, as a consequence, increased time to reach cellular targets. Moreover, BRIP conjugates of an IgG recognizing the transferrin receptor (10) and an IgG recognizing a melanoma antigen (11) are cytotoxic to antigen-positive human cell lines.

An important consideration for immunoconjugate assembly is the nature of the linkage between antibody and RIP. A disulfide linkage is usually thought to be essential for maximal cytotoxicity (12). RTA contains a single available cysteine, which can directly form a disulfide bond with an activated antibody thiol via a disulfide-exchange reaction. Type-I RIP, including BRIP, typically lack an unpaired cysteine, so disulfide-linked conjugates require modification of both antibody and RIP with heterobifunctional reagents. Unfortunately, the biological activity of many RIP (10, 13, 14) is diminished or destroyed by modification with the most commonly employed reagents. To address this issue, we have cloned and expressed BRIP and engineered several analogs of rBRIP to contain unique free cysteine residues for direct conjugation to antibody.

Three residues near the C-terminus of BRIP were selected as sites for amino acid substitution with cysteine. Comparison of the amino acid sequence of BRIP with the known primary and tertiary structure of RTA suggested that these sites should be on the surface of the molecule, and either at or proximal to the position of cysteine 259 in RTA. The enzymatic activity of each BRIP analog

\* To whom correspondence and reprint requests should be addressed.

<sup>†</sup> Berkeley, CA.

<sup>‡</sup> Santa Monica, CA.

\* Abstract published in *Advance ACS Abstracts*, January 15, 1994.

<sup>1</sup> Abbreviations: RIP, ribosome inactivating protein(s); BRIP, the barley ribosome inactivating protein; nBRIP, native BRIP; rBRIP, recombinant BRIP; PCR, polymerase chain reaction; PBMC, human peripheral blood mononuclear cell(s); mAb, monoclonal antibody; RTA, ricin toxin A chain; RTA<sub>30</sub>, M<sub>r</sub> 30 kDa glycoform of RTA; M2IT, 5-methyl-2-iminothiolane; DTNB, 5,5'-dithiobis(2-nitrobenzoic acid); TNB, 5-thio-2-nitrobenzoate anion; 2-ME, 2-mercaptoethanol; SPDP, 3-((N-succinimidyl-2-pyridyl)dithio)propionate; SDS-PAGE, sodium dodecyl sulfate polyacrylamide gel electrophoresis; RLA, rabbit reticulocyte assay; GSH, glutathione; PHA, phytohemagglutinin; DTT, dithiothreitol.



with its uniquely placed cysteine was examined, as was the effect of the cysteine position on conjugation yield, *in vitro* disulfide bond stability, and immunoconjugate potency.

## EXPERIMENTAL PROCEDURES

**Bacterial and Mammalian Cells.** The *E. coli* host for production of BRIP is an Ara<sup>-</sup> derivative of W3110 (American Type Culture Collection no. 27325). HSB2 is a CD5<sup>+</sup>, CD7<sup>+</sup> human T cell line (American Type Culture Collection CCL 120.1). PBMC were separated from whole blood of normal human donors by centrifugation through a discontinuous gradient (25).

**Antibodies H65 and 4A2.** H65 is a murine IgG1/k mAb that recognizes the human CD5 antigen (15). 4A2 is a murine IgG2a/k mAb that recognizes the human CD7 antigen on T cells (16). Concentrations of antibodies were determined for 1 mg/mL solutions by absorbance at 280 nm, using extinction coefficients of 1.25 for 4A2 and 1.30 for H65. For calculations, an approximate molecular weight of 150 000 was used for each mAb.

**Purification of nBRIP from Barley Seeds.** nBRIP (isoform II) was purified from pearled barley flour by a modification of the protocol of Asano et al. (9). Four kg of barley flour was extracted with 16 L of 10 mM NaPO<sub>4</sub>, 25 mM NaCl, pH 7.2 (extraction buffer), for 20 h at 4 °C. The sediment was removed by centrifugation, and 200 mL of packed S-Sepharose (Pharmacia, NJ) was added to adsorb the nBRIP. After 20 h at 4 °C with mixing, the resin was allowed to settle, rinsed several times with extraction buffer, and packed into a 2.6- × 40-cm column. The column was washed until the absorbance of the effluent approached zero. nBRIP was then eluted with a linear gradient of 0.025 to 0.3 M NaCl in extraction buffer. The nBRIP-containing fractions were pooled, concentrated, and chromatographed on a 2.6- × 100-cm column of Sephacryl S-200HR (Pharmacia, NJ) equilibrated in 10 mM NaPO<sub>4</sub>, 125 mM NaCl, pH 7.4 at 10 mL/h. The pure nBRIP was concentrated and stored at -70 °C.

**Cloning and Expression of rBRIP.** A cDNA expression library prepared from germinated barley seeds in  $\lambda$  ZAPII was purchased from Stratagene, La Jolla, CA. Approximately 700 000 phage plaques were screened with rabbit antibody raised against nBRIP, and six immunoreactive plaques were identified. DNA from one clone was isolated and sequenced with Sequenase (USB, Cleveland, OH). The cDNA contained therein was excised and subcloned into pUC18 (Pharmacia, NJ).

The pUC 18 clone containing the BRIP cDNA, pBS1, was used to construct a bacterial secretion vector. This process involved (1) introduction of a unique *Xho*I restriction site downstream of the BRIP termination codon, (2) addition of the *pelB* secretion signal to the 5'-end of the gene (18) and (3) positioning the BRIP gene under the control of the inducible *araB* promoter (19). The resulting plasmid was named pING3322. Details of vector construction and a schematic view of the expression vector are shown in Figure 1.

**Construction of rBRIP Analogs with a Free Cys Residue.** rBRIP analogs with introduced Cys codons were assembled by PCR amplification of the BRIP gene with mutagenic oligonucleotides followed by gene reassembly.

A plasmid capable of expressing a BRIP analog with a Cys in place of Leu at position 256 (rBRIP<sub>C256</sub>) was constructed using PCR to amplify the 3'-end of the gene while introducing an amino acid substitution. Plasmid pING3322 was amplified with 5'-TGTCTGTTTCGTG-GAGGTGCCG-3' and 5'-CGTTAGCAATTTAACTGT-

GAT-3'. The PCR product was treated with T4 polymerase and cut with *Xho*I, and the 87-bp fragment was purified. Plasmid pING3322 was also cut with *Bam*HI, treated with T4 polymerase, and cut with *Eco*RI, and the 891-bp fragment containing the BRIP gene was purified. These two gene fragments were then assembled into pING3322 to generate pING3801.

A plasmid for expression of a BRIP analog with Cys substituted for Ala at position 270 (rBRIP<sub>C270</sub>) was also generated by using PCR to amplify a new 3'-end segment with an altered residue. pING3322 was the template for PCR amplification with 5'-CCAAGTGTCTGGAGCT-GTTCCATGCGA-3' and 5'-CGTTAGCAATTTAACTGTGAT-3'. The PCR product was treated with T4 polymerase and cut with *Xho*I, and the 51-bp fragment was purified. This segment was cloned into pING3322 with the internal BRIP restriction fragment from *Sst*II to *Msc*I (151 bp) and the vector piece cut with *Sst*II and *Xho*I. The resulting plasmid was named pING3802.

A plasmid capable of expressing a BRIP analog in which the Ser at position 277 was converted to a Cys residue (rBRIP<sub>C277</sub>) was constructed by substituting the 3'-end of the BRIP gene in pING3322 with a DNA segment conferring this change. Oligonucleotides 5'-GCATTACATCCATGGCGGC-3' and 5'-GATATCTCGAGTTAACTATTTCACACACACGCATGGAACAGCTCCAGCGCCTTGCCACCGTC-3' were used to PCR amplify the BRIP gene. An 82-bp *Bam*HI to *Xho*I fragment containing the 3'-end of BRIP with the altered amino acid was purified on a 5% polyacrylamide gel, and this fragment was substituted into pING3322 in a three-piece ligation with the 891-bp *Eco*RI to *Bam*HI fragment containing the BRIP gene and the *Eco*RI and *Xho*I cut vector. This generated pING3803.

**Purification of rBRIP and rBRIP Cysteine Analogs.** rBRIP and rBRIP analogs were purified from concentrated bacterial fermentation broths. For rBRIP, concentrated broth from a 10-L fermentation batch was exchanged into 10 mM Tris-HCl, 20 mM NaCl, pH 7.5, applied to an S-Sepharose column, and eluted with a 20–500 mM NaCl linear gradient. Pooled rBRIP was further purified by affinity chromatography on Blue Toyopearl (Supelco, PA), equilibrated in 20 mM NaCl, and eluted with a 20–500 mM NaCl gradient in 10 mM Tris-HCl, pH 7.5. For the Cys analogs, concentrated fermentation broths were applied to a column of CM52 (Whatman) in 10 mM NaPO<sub>4</sub> buffer, pH 7.5, and eluted with a 0.0–0.3 M NaCl linear gradient. Further purification on Blue Toyopearl was as described above for rBRIP.

**Construction of BRIP Immunoconjugates.** For conjugation to mAb, nBRIP or rBRIP (3 mg/mL) was first modified with 0.5 mM 5-methyl-2-iminothiolane (M2IT) (20) and 1 mM DTNB in 25 mM triethanolamine-HCl, 150 mM NaCl, pH 8.0, for 3 h at 25 °C. The derivatized BRIP-(M2IT)-TNB was then desalted on a column of GF-05LS (IBF Biotechnics), and the number of thiol groups introduced was quantitated by measuring absorbance at 412 nm after the addition of 0.1 mM DTT. On average, each BRIP molecule contained 0.7 SH/mol. 4A2 or H65 antibody (4 mg/mL) in the same triethanolamine buffer was similarly incubated with M2IT (0.3 mM) and DTNB (1 mM) for 3 h at 25 °C. The modified antibody (for example, H65-(M2IT)-TNB) was then desalted, and the TNB/antibody ratio was determined. Typically, the number of linkers per antibody was in the range of 1.7 to 2.

To assemble the conjugate: (1) activated BRIP-(M2IT)-TNB was first reduced to BRIP-(M2IT)-SH with 5 mM



DTT for 1.5 h at 25 °C; (2) the reduced BRIP-(M2IT)-SH was desalted on GF-05LS to remove excess reducing agent and TNB leaving group, and (3) a 5-fold molar excess of BRIP-(M2IT)-SH was mixed with activated antibody-(M2IT)-TNB. After 3 h at 25 °C and an additional 18 h at 4 °C, an equimolar amount of mercaptoethylamine was added for 15 min at 25 °C to quench any unreacted linkers. The quenched conjugate was promptly applied to an Ultrogel AcA44 (IBF Biotechnics) equilibrated in 10 mM Tris-HCl, 100 mM NaCl, pH 7. The partially purified material was subsequently diluted with Tris-HCl, pH 7, and applied to a Blue Toyopearl column equilibrated in 10 mM Tris-HCl, 20 mM NaCl, pH 7, and eluted with 10 mM Tris-HCl, 0.5 M NaCl, pH 8. Conjugates prepared in this manner contain two M2IT linkers and are denoted MM, for example, 4A2-MM-nBRIP.

Prior to conjugation of the BRIP Cys analogs rBRIP<sub>C256</sub>, rBRIP<sub>C270</sub>, or rBRIP<sub>C277</sub>, each was treated with 50 mM DTT (2 h at 23 °C or 18 h at 4 °C) to expose the single sulfhydryl group and then desalted. Free sulfhydryl content was verified by reaction with DTNB as described above. To assemble each conjugate, M2IT-derivatized mAb was incubated with a 5-fold molar excess of freshly reduced rBRIP analog at 23 °C for 3 h and then 16 h at 4 °C. After being quenched with mercaptoethylamine, each conjugate was purified by sequential size exclusion and affinity chromatography as described above.

Samples of all immunoconjugates were examined by 5% SDS-PAGE under nonreducing conditions. Gels were stained with Coomassie R250 and scanned with a Shimadzu laser densitometer to quantitate the number of RIP molecules per mAb. The RIP to mAb ratio was 1.5 for 4A2-M-rBRIP<sub>C256</sub>, 0.93 for 4A2-M-rBRIP<sub>C270</sub>, 1.77 for 4A2-M-rBRIP<sub>C277</sub>, and 2 for 4A2-MM-nBRIP. The RIP to mAb ratio was 1.5 for H65-M-rBRIP<sub>C256</sub>, 1.43 for H65-M-rBRIP<sub>C270</sub>, 1.9 for H65-M-rBRIP<sub>C277</sub>, and 1.1 for H65-MM-rBRIP.

**Preparation of H65-RTA and 4A2-M-RTA<sub>30</sub>.** H65-RTA is an immunoconjugate composed of H65 mAb linked via SPDP to RTA (21, 22). The RIP to mAb ratio was 1.9 for H65-RTA. There was less than 5% free mAb in the H65-RTA preparation and no free RTA. 4A2-M-RTA<sub>30</sub> is an immunoconjugate composed of 4A2 mAb linked via M2IT to RTA<sub>30</sub>, the 30 kDa glycoform of RTA (16, 23). The RIP to mAb ratio was 1.1 for 4A2-M-RTA<sub>30</sub>. There was no detectable free mAb or RTA<sub>30</sub> in the 4A2-M-RTA<sub>30</sub>.

**Activities of RIP and Immunoconjugates.** The ability of RIP to inhibit protein synthesis in a cell-free system was examined in the rabbit reticulocyte lysate assay (RLA; 23, 24). The incorporation of <sup>3</sup>H-Leu was measured as a function of RIP concentration, and the concentration of RIP (in pM) which inhibited protein synthesis by 50% (the IC<sub>50</sub>) relative to untreated controls was calculated. All samples were tested in triplicate. The cytotoxicity of immunoconjugates or RIP for HSB2 cells or PHA-activated human peripheral blood mononuclear cells (PBMC) were examined as described (25, 26). Cells were incubated with increasing concentrations of immunoconjugates for a total of 24 h (HSB2 cells) or 90 h (PBMC), and inhibition of macromolecular synthesis was quantified. By comparison with untreated controls, the concentration of immunoconjugate (or RIP) that inhibited protein synthesis by 50% (the IC<sub>50</sub>) was calculated. Results are expressed in pM RIP, after multiplying the IC<sub>50</sub> (in pM) by the RIP to mAb ratio.

**HPLC Disulfide Bond Stability Assay.** Immunoconjugates (ca. 0.5 mg/mL) in 0.1 M NaPO<sub>4</sub>, 0.15 M NaCl,

**Table 1. Inhibition of Protein Synthesis in Vitro by BRIP and rBRIP Analogs**

	RLA <sup>a</sup> IC <sub>50</sub> <sup>c</sup> (pM)	cellular cytotoxicity <sup>b</sup> IC <sub>50</sub> (pM)
RTA <sub>30</sub>	3.1	20 000
nBRIP	15	170 000
rBRIP	18	170 000
rBRIP <sub>C256</sub>	23	260 000
rBRIP <sub>C270</sub>	20	300 000
rBRIP <sub>C277</sub>	24	>500 000

<sup>a</sup> Inhibition of protein synthesis in the cell-free rabbit reticulocyte lysate assay. <sup>b</sup> Inhibition of protein synthesis in intact HSB2 cells by RIP. <sup>c</sup> The IC<sub>50</sub> is the concentration of RIP (in pM) that inhibits protein synthesis by 50%.

1.5 mM EDTA, pH 7.5, were incubated at 37 °C for 1 h with increasing amounts of reduced GSH, (0.1–50 mM). A control reaction was incubated in the absence of reductant, and a 100% RIP release control sample was prepared by incubation in 60 mM 2-ME. The reduction was terminated by addition of iodoacetamide (final 100 mM) and incubation at 37 °C for 20 min. Samples were filtered (0.45 μm) and analyzed on a Waters HPLC system equipped with a TSK-G2000 (30 × 0.78-cm) size-exclusion column and a 280-nm detector. The column was eluted with 0.1 M Na<sub>2</sub>SO<sub>4</sub>, 0.02 M Na<sub>2</sub>PO<sub>4</sub>, pH 6.8, at 0.7 mL/min, and the absorbance of the effluent at 280 nm was recorded. The amount of RIP released from each conjugate after treatment with GSH was quantified by area integration and compared to a fully reduced (2-ME) sample. The percent of RIP released was plotted as a function of the log mM GSH concentration, and an RC<sub>50</sub> for each conjugate (the GSH concentration required to release 50% of the RIP) was calculated. The recovery of total RIP was consistently high (usually >80%) compared to the theoretical maximum calculated from the RIP to mAb ratios for each conjugate.

## RESULTS

**Characterization of nBRIP.** nBRIP was purified from barley seeds to assess (i) its ability to inhibit protein synthesis *in vitro* and (ii) its properties when conjugated to mAbs that recognize surface antigens on human T cells. As previously demonstrated (8–10, 27), nBRIP is a basic protein (pI ≈ 9.7) with an apparent *M<sub>r</sub>* of 30 kDa, based upon its mobility when analyzed by SDS-PAGE (data not shown). Consistent with earlier reports (27), the N-terminus of nBRIP was blocked. However, the amino acid sequence of BRIP fragments generated by limited proteolysis was consistent with that previously published (27) for isoform II from barley seeds.

The enzymatic activity of nBRIP relative to RTA<sub>30</sub> was examined in the RLA assay as shown in Table 1. In repeated assays nBRIP was about 5-fold less potent at inhibiting protein synthesis *in vitro* than was RTA<sub>30</sub>. Also shown in Table 1 is the nonspecific cytotoxicity of both nBRIP and RTA<sub>30</sub>, measured against intact human T cells. nBRIP was about 8-fold less cytotoxic to the HSB2 cell line than was RTA<sub>30</sub>.

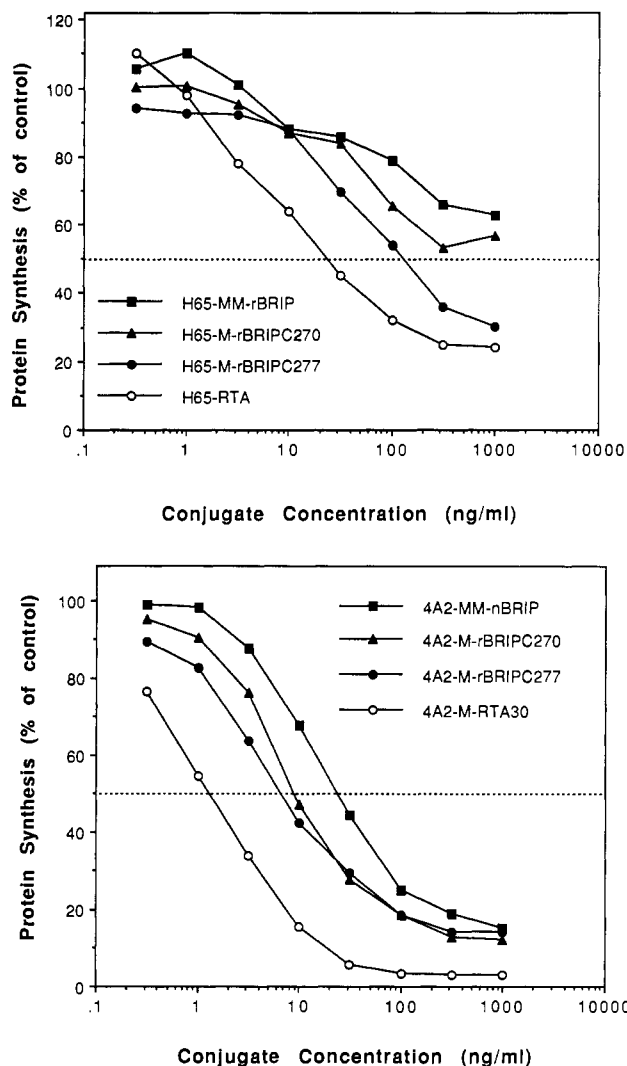
**Cloning, Expression, and Activity of rBRIP.** Although barley flour is readily available for the purification of nBRIP, we were interested in cloning the BRIP gene so that recombinant production and protein engineering of BRIP were possible. A BRIP cDNA clone was identified directly from a barley cDNA library in a phage λ vector. The DNA sequence of the BRIP cDNA we obtained was identical to the barley RIP isoform II cDNA (17; Genbank Accession no. M36990) and encodes a protein of 280 amino acids.



**Table 2. Disulfide Bond Stability of BRIP Conjugates<sup>a</sup>**

conjugate	RC <sub>50</sub> (mM GSH)	conjugate	RC <sub>50</sub> (mM GSH)
4A2-M-RTA <sub>30</sub>	4.4	H65-RTA	7.0
4A2-MM-nBRIP	3.3	H65-MM-rBRIP	2.8
4A2-M-rBRIP <sub>C270</sub>	53.0	H65-M-rBRIP <sub>C277</sub>	196.0
4A2-M-rBRIP <sub>C277</sub>	187.0		

<sup>a</sup> The relative disulfide bond stability of a series of BRIP conjugates was determined by measuring the amount of RIP released after 1 h of incubation with increasing amounts of GSH. The RC<sub>50</sub> for each conjugate is the concentration of reducing agent (GSH) needed to release 50% of RIP from a given conjugate (see also ref 29). A higher RC<sub>50</sub> indicates increased disulfide bond stability.



**Figure 3.** Cytotoxicity of BRIP immunoconjugates. The ability of several immunoconjugates to inhibit protein synthesis (incorporation of <sup>3</sup>H-Leu) in HSB2 cells was measured as described in the Experimental Procedures. A representative assay is shown. The H65 conjugates are shown in panel A and the 4A2 conjugates in panel B. The H65-M-rBRIP<sub>C256</sub> and 4A2-M-rBRIP<sub>C256</sub> conjugates were not tested in this assay.

M-rBRIP<sub>C277</sub> were 10–50 times more stable to reduction (RC<sub>50</sub>s 50–200 mM). It is likely that small variations in RIP to mAb ratios would have little impact in this assay, since different lots of H65-RTA containing RTA to H65 ratios between 1.0 and 3.0 gave identical RC<sub>50</sub> values (data not shown).

**In Vitro Cytotoxicity of BRIP Conjugates.** The 4A2- and H65-BRIP conjugates were tested for specific cytotoxicity against the human T cell line HSB2, which expresses both CD5 and CD7 antigens. Dose-response titration curves are shown in Figure 3A and B, where BRIP immunoconjugates are compared to H65-RTA (15, 25) or 4A2-M-RTA<sub>30</sub> (16) which are both cytotoxic to antigen

positive T cells. The IC<sub>50</sub> values and extend of kill are summarized in Table 3. Although 4A2-MM-nBRIP-inhibited protein synthesis in HSB2 cells with an IC<sub>50</sub> of 122 pM, it was about 10-fold less effective than 4A2-M-RTA<sub>30</sub>. 4A2 conjugates made with rBRIP<sub>C270</sub> or rBRIP<sub>C277</sub> were 2- to 3-fold more potent than 4A2-MM-nBRIP. In contrast, the conjugate made with rBRIP<sub>C256</sub> was less active than the native BRIP immunoconjugate.

The H65-MM-rBRIP conjugate was virtually noncytotoxic to HSB2 cells. At the highest concentration tested (1000 ng/mL), inhibition of protein synthesis was less than 50%. Two conjugates, H65-M-rBRIP<sub>C270</sub> and H65-M-rBRIP<sub>C256</sub>, were likewise not very effective at inhibiting translation in HSB2 cells. In contrast, H65-M-rBRIP<sub>C277</sub> showed enhanced potency toward the target cells, with an IC<sub>50</sub> only 8-fold less than that of the H65-RTA control, and approached 70% inhibition, compared to 78% for H65-RTA.

These conjugates were tested in similar experiments against human PBMC. As shown in Table 3, there was a trend toward enhanced cytotoxicity with some of the rBRIP Cys analog conjugates. 4A2-M-rBRIP<sub>C277</sub> and 4A2-M-rBRIP<sub>C270</sub> were, respectively, 10 and three times more cytotoxic than 4A2-MM-nBRIP. Both H65-M-rBRIP<sub>C270</sub> and H65-M-rBRIP<sub>C277</sub> were five times more cytotoxic than H65-MM-rBRIP.

## DISCUSSION

Nonspecific modification of proteins with cross-linking reagents can adversely affect their subsequent activity. Nevertheless, most immunoconjugates between antibodies and cytotoxic plant proteins such as the type-I RIP rely on chemical modification of both antibody and RIP lysine residues. Retention of biologic activity depends upon both the degree of modification and, unpredictably, the reactivity of active site or important structural amino acids. For example, modification of BRIP, the type-I RIP from barley, with 2-iminothiolane greatly inhibits its activity. An average of 1.4 thiols per BRIP was reported to reduce activity about 5-fold, while 4.0 thiols per molecule nearly abolished activity (10). Similar results have been observed with other cross-linking reagents and other type-I RIP including Bryodin, Gelonin, Momordin, Pokeweed antiviral protein, Saporin, and Trichosanthin (14). Immunoconjugates that result from such randomly derivitized RIP are heterogeneous with regard to the physical orientation of the two linked proteins. Thus, random derivitization of RIP can lead to decreased enzymatic activity and increased conjugate heterogeneity.

The complex nature of the immunoconjugate pool can be simplified if a single amino acid in the cytotoxic subunit is linked to antibody. For example, disulfide-linked RTA conjugates can be assembled using the available Cys residue at position 259. In previous experiments (28), we found that by genetic manipulation of the fungal protein mitogillin to expose an accessible cysteine immunoconjugates could also be generated without initial derivitization by nonspecific cross-linking agents. Like many

**Table 3. Cytotoxicity of BRIP Immunoconjugates for Human T Cells<sup>a</sup>**

conjugate	HSB2 cells		PBMC	
	IC <sub>50</sub> (pM RIP)	% inhibition	IC <sub>50</sub> (pM RIP)	% inhibition
4A2-M-RTA <sub>30</sub>	15 ± 3	95	34 (20–48)	89
4A2-MM-nBRIP	122 ± 6	85	744	80
4A2-M-rBRIP <sub>C256</sub>	464 ± 92	72	ND	ND
4A2-M-rBRIP <sub>C270</sub>	46 ± 3	85	226 (130–321)	80
4A2-M-rBRIP <sub>C277</sub>	57 ± 7	85	60 (45–74)	79
H65-RTA	150 ± 40	78	429 (46–1170)	70
H65-MM-rBRIP	>5000	<50	16 500	50
H65-M-rBRIP <sub>C256</sub>	>5000	<50	ND	ND
H65-M-rBRIP <sub>C270</sub>	>5000	<50	2220 (358 → 22 000)	54
H65-M-rBRIP <sub>C277</sub>	1176 ± 170	70	3040 (694 → 23 000)	62

<sup>a</sup> Cytotoxicity was measured as the inhibition of protein synthesis (incorporation of <sup>3</sup>H-Leucine) in HSB2 cells or as the inhibition of DNA synthesis (incorporation of <sup>3</sup>H-thymidine) in PBMC. Results are expressed in terms of pM RIP, in which the molar concentration of immunoconjugate that inhibited macromolecular synthesis by 50% (IC<sub>50</sub>) was multiplied by the RIP to antibody ratio. The IC<sub>50</sub>'s from representative HSB2 cell assays have been reported with the standard errors. For the PBMC assays, the median and range of IC<sub>50</sub> values have been tabulated, except in two cases where samples were tested once. The rBRIP<sub>C256</sub> conjugates were not tested against PBMC (ND). The percent inhibition was determined relative to the maximal inhibition of macromolecular synthesis of 1 µg/mL immunoconjugate.

type-I RIP, however, nBRIP does not contain any Cys free residues.

Here we show that BRIP can be engineered near its C-terminus to contain a single free Cys residue for site-specific conjugation, that these rBRIP Cys analogs are efficiently produced in *E. coli*, and that they retain enzymatic activity in the RLA assay. Moreover, positions for Cys have been identified which resulted in BRIP anti-CD5 and anti-CD7 immunoconjugates that were more potent than were the corresponding conjugates made with linker-modified BRIP. These results clearly demonstrate that modification of RIP with cross-linking reagents adversely affects not only their enzymatic activity but also the cytotoxicity of immunoconjugates made from them. As a consequence, it is likely that the potencies of immunoconjugates made with other linker-modified type-I RIP have also been underestimated.

Interestingly, immunoconjugates prepared with the rBRIP analog rBRIP<sub>C277</sub> were not only more potent than the corresponding conjugates made with nBRIP or rBRIP, they were also more efficiently synthesized and more stable to reduction. Although enhanced immunoconjugate potency can be explained by the retention of enzymatic activity with the rBRIP Cys analog relative to linker-modified BRIP, improved conjugation and disulfide bond stability cannot. Similarly, the enhanced activity of rBRIP<sub>C277</sub> conjugates compared to those made with other Cys analogs is not a reflection of their relative enzymatic activities.

Several hypotheses can be proposed to account for the observed differences. For example, the environment surrounding the conjugate disulfide bond (charge, hydrophobicity, etc.) may influence critical intracellular processes (reduction, trafficking, etc.) necessary for cytotoxicity. Alternatively, certain orientations of mAb and BRIP (such as those created with rBRIP<sub>C277</sub>) may more effectively present the RIP to cells, thereby facilitating access to the cytosol. Support for the latter view comes from the studies of Carayon et al. (30), who showed that variations in the cytotoxicity of anti-CD5 RTA conjugates resulted from different presentations of RTA epitopes to cells. It is also possible that conjugate binding to antigen may be differently affected by the BRIP analogs. Resolution of these alternatives will require further study.

Here we have shown that site-specific linkage of BRIP analogs to antibody affects conjugation yield, conjugate potency, and conjugate stability. Although we have focused on engineering Cys residues into the C-terminus of rBRIP, it is possible that introduction of a Cys at other

sites in rBRIP (or other RIP) may result in conjugates with even more desirable properties. Additionally, site-specific linkage of engineered RIP to antibody molecules via existing Cys residue(s) in the hinge region of antibody fragments (26), or via engineered surface-accessible Cys (31), should allow efficient production of homogenous immunoconjugates.

#### ACKNOWLEDGMENT

Special thanks are extended to Marcelo Ortigao for gene cloning and to Eddie Bautista, Maria Molina, and Hsiu-Mei Wu for *in vitro* assays. We thank Roy Yih, Charlotte Chang, Connie Galicia, and Grace Lam for preparation of immunoconjugates, Laz Agbowo for purification of nBRIP, and Maria Fang for consistently excellent support.

#### LITERATURE CITED

- Endo, Y., Mitsui, K., Motizuki, M., and Tsurugi, K. (1987) The mechanism of action of ricin and related toxic lectins on eukaryotic ribosomes. The site and the characteristics of the modification in 28 S ribosomal NRA caused by the toxins. *J. Biol. Chem.* 262, 5908–5912.
- Endo, Y., Tsurugi, K., and Ebert, R. F. (1988) The mechanism of action of barley toxin: a type 1 ribosome-inactivating protein with RNA N-glycosidase activity. *Biochim. Biophys. Acta* 954, 224–226.
- Katzin, B. J., Collins, E. J., and Robertus, J. D. (1991) Structure of ricin A-chain at 2.5 Å. *Proteins* 10, 251–259.
- Cobb, P. W., and LeMaistre, C. F. (1992) Therapeutic use of immunotoxins. *Seminars Hematol.* 29, 6–13.
- Ramakrishnan, S., Fryxell, D., Mohanraj, D., Olson, M., and Li, B.-Y. (1992) Cytotoxic conjugates containing translational inhibitory proteins. *Ann. Rev. Pharmacol. Toxicol.* 32, 579–621.
- Wawrzynczak, E. J. (1991) Rational design of immunotoxins: current progress and future prospects. *Anticancer Drug Des.* 7, 427–441.
- Byers, V. S., and Baldwin, R. W. (1991) Rationale for clinical use of immunotoxins in cancer and autoimmune disease. *Seminars Cell Biol.* 2, 59–70.
- Coleman, W. H., and Roberts, W. K. (1982) Inhibitors of animal cell-free protein synthesis from grains. *Biochim. Biophys. Acta* 696, 239–244.
- Asano, K., Svensson, B., and Poulsen, F. M. (1984) Isolation and characterization of inhibitors of animal cell-free protein synthesis from barley seeds. *Carlsberg Res. Commun.* 49, 619–626.
- Ebert, R. F., and Spryn, L. A. (1990) Immunotoxin construction with a ribosome-inactivating protein from barley. *Bioconjugate Chem.* 1, 331–336.

- (11) Ovadia, M., Hager, C. C., and Oeltmann, T. N. (1990) An antimelanoma-barley ribosome inactivating protein conjugate is cytotoxic to melanoma cells in vitro. *Anticancer Res.* 10, 671-675.
- (12) Blakey, D. C., Wawrzynczak, E. J., Wallace, P. M., and Thorpe, P. E. (1988) Antibody toxin conjugates: a perspective. *Prog. Allergy* 45, 50-90.
- (13) Lambert, J. M., Blattler, W. A., McIntire, G. D., Goldmacher, V. S., and Scott, C. F., Jr. (1988) Immunotoxins containing single chain ribosome-inactivating proteins. In *Immunotoxins* (A. E. Frankel, Ed.) pp 175-209, Kluwer Academic Publishers, Boston.
- (14) Battelli, M. G., Barbieri, L., and Stirpe, F. (1990) Toxicity of, and histological lesions caused by, ribosome-inactivating proteins, their IgG-conjugates, and their homopolymers. *APMIS* 98, 585-593.
- (15) Kernan, N. A., Knowles, R. W. Burns, M. J., Broxmeyer, H. E., Lu, L., Lee, H. M., Kawahata, R. T., Scannon, P. J., and Dupont, B. (1984) Specific inhibition of in vitro lymphocyte transformation by an anti-pan T cell (gp67) ricin A chain immunotoxin. *J. Immunol.* 133, 137-146.
- (16) Fishwild, D. M., Aberle, S., Bernhard, S. L., and Kung, A. H. (1992) Efficacy of an anti-CD7-ricin A chain immunconjugate in a novel murine model of human T-cell leukemia. *Cancer Res.* 52, 3056-3062.
- (17) Leah, R., Tommerup, H., Svendsen, I., and Mundy, J. (1991) Biochemical and molecular characterization of three barley seed proteins with antifungal properties. *J. Biol. Chem.* 266, 1564-1573.
- (18) Lei, S. P., Lin, H. C., Wang, S. S., Callaway, J., and Wilcox, G. (1987) Characterization of the *Erwinia carotovora* pelB gene and its product pectate lyase. *J. Bacteriol.* 169, 4379-4383.
- (19) Johnston, S., Lee, J. H., and Ray, D. S. (1985) High-level expression of M13 gene II protein from an inducible polycistronic messenger RNA. *Gene* 34, 137-145.
- (20) Goff, D. A., and Carroll, S. F. (1990) Substituted 2-iminothiolanes: reagents for the preparation of disulfide cross-linked conjugates with increased stability. *Bioconjugate Chem.* 1, 381-386.
- (21) Kernan, N. A., Byers, V., Scannon, P. J., Mischak, R. P., Brochstein, J., Flomenberg, N., Dupont, B., and O'Reilly, R. J. (1988) Treatment of steroid-resistant acute graft-vs-host disease by in vivo administration of an anti-T-cell ricin A chain immunotoxin. *JAMA, J. Am. Med. Assoc.* 259, 3154-3157.
- (22) Byers, V. S., Henslee, P. J., Kernan, N. A., Blazar, B. R., Gingrich, R., Phillips, G. L., LeMaistre, C. F., Gilliland, G., Antin, J. H., Martin, P., et al. (1990) Use of an anti-pan T-lymphocyte ricin A chain immunotoxin in steroid-resistant acute graft-versus-host disease. *Blood* 75, 1426-1432.
- (23) Trown, P. W., Reardan, D. T., Carroll, S. F., Stoudemire, J. B., and Kawahata, R. T. (1991) Improved pharmacokinetics and tumor localization of immunotoxins constructed with the Mr 30,000 form of ricin A chain. *Cancer Res.* 51, 4219-4225.
- (24) Press, O. W., Vitetta, E. S., and Martin, P. J. (1986) A simplified microassay for inhibition of protein synthesis in reticulocyte lysates by immunotoxins. *Immunol. Lett.* 14, 37-41.
- (25) Fishwild, D. M., Staskawicz, M. O., Wu, H. M., and Carroll, S. F. (1991) Cytotoxicity against human peripheral blood mononuclear cells and T cell lines mediated by anti-T cell immunotoxins in the absence of added potentiator. *Clin. Exp. Immunol.* 86, 506-513.
- (26) Better, M., Bernhard, S. L., Lei, S. P., Fishwild, D. M., Lane, J. A., Carroll, S. F., and Horwitz, A. H. (1993) Potent anti-CD5 ricin A chain immunconjugates from bacterially produced Fab' and F(ab')<sub>2</sub>. *Proc. Natl. Acad. Sci. U.S.A.* 90, 457-461.
- (27) Asano, K., Svensson, B., Svendsen, I., Poulsen, F. M., and Roepstorff, P. (1986) The complete primary structure of protein synthesis inhibitor II from barley seeds. *Carlsberg Res. Commun.* 51, 129-141.
- (28) Better, M., Bernhard, S. L., Lei, S. P., Fishwild, D. M., and Carroll, S. F. (1992) Activity of recombinant mitogillin and mitogillin immunconjugates. *J. Biol. Chem.* 267, 16712-16718.
- (29) Wawrzynczak, E. J., Cumber, A. J., Henry, R. V., May, J., Newell, D. R., Parnell, G. D., Worrell, N. R., and Forrester, J. A. (1990) Pharmacokinetics in the rat of a panel of immunotoxins made with abrin A chain, ricin A chain, gelonin, and momordin. *Cancer Res.* 50, 7519-7526.
- (30) Carayon, P., Bord, A., Gaillard, J. P., Vidal, H., Gros, P., and Jansen, F. K. (1993) Ricin-A Chain Cytotoxicity Depends on Its Presentation to the Cell Membrane. *Bioconjugate Chem.* 4, 146-162.
- (31) Lyons, A., King, D. J., Owens, R. J., Yarranton, G. T., Millican, A., Whittle, N. R., and Adair, J. R. (1990) Site-specific attachment to recombinant antibodies via introduced surface cysteine residues. *Protein Eng.* 3, 703-708.

# Modification of CD4 Immunoaderhin with Monomethoxypoly(ethylene glycol) Aldehyde via Reductive Alkylation

Steven M. Chamow,\*<sup>†</sup> Timothy P. Kogan<sup>‡,1</sup> Michael Venuti<sup>‡,2</sup> Thomas Gadek,<sup>‡</sup> Reed J. Harris,<sup>§</sup> David H. Peers,<sup>†</sup> Joyce Mordenti,<sup>⊥</sup> Steven Shak,<sup>||</sup> and Avi Ashkenazi<sup>▽</sup>

Departments of Process Science, Bioorganic Chemistry, Medicinal and Analytical Chemistry, Gene Therapy and Pulmonary Research, Experimental Therapeutics, and Molecular Biology, Genentech, Inc., 460 Point San Bruno Boulevard, South San Francisco, California 94080. Received September 8, 1993\*

CD4 immunoaderhin (CD4-IgG) is a chimeric glycoprotein molecule comprised of the gp120-binding portion of human CD4 fused to the hinge and Fc portions of human IgG. As a candidate for human therapeutic use, CD4-IgG represents an important advance over soluble CD4, insofar as the systemic clearance in humans of CD4-IgG is significantly slower. In an effort to prolong its *in vivo* residence time even further, we have modified CD4-IgG chemically by attaching monomethoxypoly(ethylene glycol) (MePEG) moieties to lysine residues via reductive alkylation. We synthesized MePEG aldehyde and investigated reaction conditions for adding a range of MePEG moieties per protein molecule. At neutral pH in the presence of sodium cyanoborohydride, the reaction was sufficiently slow to allow for significant control over the extent of MePEGylation. Addition of 7.7 or 14.4 MePEG moieties to CD4-IgG resulted in an approximately 4- or 5-fold increase, respectively, in the persistence of the protein in rats, as compared with unmodified CD4-IgG. These results suggest that the therapeutic utility of a human receptor IgG chimera can be improved by MePEGylation technology, provided that the modified immunoaderhin retains its biological activity *in vivo*. Such modification can lead to a significant additional increase in the *in vivo* residence time of the protein.

## INTRODUCTION

The value of a recombinant protein as a human therapeutic is determined, in significant part, by how rapidly the molecule is cleared from the body. Recombinant receptors are currently of great interest as candidates for protein therapeutics. One such protein is CD4, the primary receptor for human immunodeficiency virus type 1. CD4 is an integral membrane glycoprotein on the surface of lymphocytes and monocytes. By truncating a full-length cDNA to encode only the ectodomain of the receptor, CD4 was produced in a recombinant, soluble form (Smith et al., 1987). sCD4<sup>3</sup> binds to gp120, the envelope glycoprotein of HIV-1, with high affinity and inhibits infectivity *in vitro*. However, the short *in vivo* half-life and rapid clearance of sCD4 limits its potential for therapeutic use (Schooley et al., 1990).

To increase the *in vivo* residence time of sCD4, a human chimeric molecule, CD4 immunoaderhin, was designed

(Capon et al., 1989; Byrn et al., 1990; Chamow et al., 1992). In humans, this hybrid molecule was cleared from the blood approximately 25 times more slowly than sCD4 (Hodges et al., 1991; Kahn et al., 1990). This slower clearance results, in part, from the larger size of the chimeric protein dimer (91 kDa) relative to monomeric sCD4 (41 kDa). The increase in size reduces the rate of clearance of the protein via glomerular filtration in the kidney (Venkatachalam and Rennke, 1978). Although the half-life of CD4-IgG is markedly longer than that of sCD4, it is shorter than the half-life observed generally for human IgG, suggesting that further extension of its half-life by chemical means might be possible. Construction of immunoaderhins of several other soluble receptors has now been reported (reviewed in Ashkenazi et al. (1993)).

An additional means by which the *in vivo* residence time of proteins can be extended is by covalent modification with suitably activated hydrophilic polymers such as monomethoxypoly(ethylene glycol) (MePEG) (for a review, see Francis et al. (1992)). MePEGylation increases the Stokes radius, and thereby can be used to reduce the elimination of relatively small proteins via the kidney. In addition, MePEG can reduce the immunogenicity of modified proteins (Abuchowski et al., 1977a,b). The value of protein MePEGylation as a therapeutic design strategy is demonstrated by the clinical use of MePEG-modified adenosine deaminase for treatment of severe combined immunodeficiency disease caused by adenosine deaminase deficiency (Hershfeld et al., 1987).

Despite the overall structural similarity between CD4-IgG and human IgG, the half-life of the former is significantly shorter, suggesting that additional clearance mechanisms may exist that are relatively more efficient in removing the immunoaderhin versus an IgG antibody. We reasoned that MePEG modification of CD4-IgG might mask potential clearance-receptor binding sites and thus reduce the rate of the protein's clearance. To avoid excessive modification of CD4-IgG, which might compro-

\* Author to whom correspondence should be addressed.

<sup>†</sup> Department of Process Science.

<sup>‡</sup> Department of Bioorganic Chemistry.

<sup>§</sup> Department of Medicinal and Analytical Chemistry.

<sup>⊥</sup> Department of Experimental Therapeutics.

<sup>||</sup> Department of Gene Therapy and Pulmonary Research.

<sup>▽</sup> Department of Molecular Biology.

\* Abstract published in *Advance ACS Abstracts*, January 15, 1994.


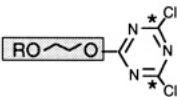
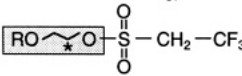
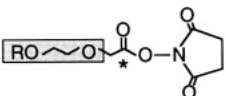
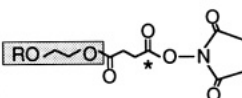
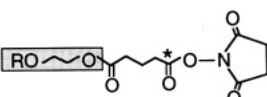
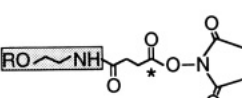
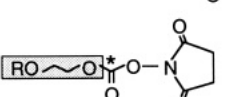
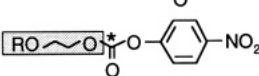
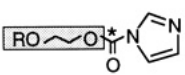
<sup>1</sup> Present address: Texas Biotechnology Corp., 7000 Fannin, Suite 1920, Houston, TX 77030.

<sup>2</sup> Present address: Parnassus Pharmaceuticals, 1501 Harbor Bay Parkway, Alameda, CA 94501.

<sup>3</sup> Abbreviations used: IDA, iminodiacetic acid; MePEG, monomethoxypoly(ethylene glycol); MePEG-CHO, monomethoxypoly(ethylene glycol) aldehyde; CD4-IgG, CD4 immunoaderhin; sCD4, recombinant, soluble form of CD4; HIV-1, human immunodeficiency virus type 1; SDS-PAGE, sodium dodecyl sulfate-polyacrylamide gel electrophoresis; HEPES, 4-(2-hydroxyethyl)-1-piperazineethanesulfonic acid; TCA, trichloroacetic acid; TNBS, 2,4,6-trinitrobenzenesulfonic acid; AUC, area under curve.



**Table 1. Activated Me-PEG Reagents That Are Reactive with Amines**

activated MePEG	structure of activated MePEG	amine linkage	ref
MePEG-OH			
<b>Alkylation</b>			
cyanurylate <sup>b</sup>		secondary amine	Abuchowski et al., 1977a; Jackson et al., 1987; Koide and Kobayashi, 1983
tresylate		secondary amine	Nilsson and Mosbach, 1984; Delgado et al., 1990
<b>Acylation</b>			
N-hydroxysuccinimide		amide	Buckmann et al., 1981
succinimidyl succinate		amide	Jopich and Luisi, 1979; Abuchowski et al., 1984
succinimidyl glutarate		amide	Katre et al., 1987; Kitamura et al., 1991
succinimidyl succinamide		amide	Boccu et al., 1983
succinimidyl carbonate		carbamate	Zalipsky et al., 1992
phenylcarbonate		carbamate	Veronese et al., 1985
imidazolyl formate		carbamate	Beauchamp et al., 1983

<sup>a</sup> Boxed structure is derived from MePEG; R = CH<sub>3</sub>(OCH<sub>2</sub>CH<sub>2</sub>)<sub>n</sub> as defined in Figure 1. Asterisk indicates reactive center where nucleophilic attack by amine nitrogen occurs. <sup>b</sup> Also reacts with Cys and Tyr.

mise its biological activity, we sought a means of MePEGylation for which the extent of reaction could be controlled.

Several chemistries have been described by which MePEG can be activated for protein modification (reviewed in Zalipsky and Lee, 1992). For this purpose, the hydroxyl group of MePEG has been activated and then coupled, via alkylation or acylation, to nucleophilic sites on proteins. Amino groups are the preferred sites of modification. MePEG cyanurylate has been used most commonly, but a number of other methods have also been developed for coupling MePEG to protein amino groups (Table 1). Our experience with reductive alkylation of proteins led us to seek an alkylating reagent that would be both easy to make and highly selective and one for which the extent of reaction could be controlled, so that partial modification is possible. Building on the initial work of Wirth et al. (1991) who reported modification of horseradish peroxidase with an aldehyde derivative of MePEG, we describe a modified synthesis of this reagent, and we extend the use of MePEG aldehyde to modification of the immunoadhesin CD4-IgG by reductive alkylation.

#### EXPERIMENTAL PROCEDURES

**Recombinant Proteins.** CD4-IgG was constructed and expressed in Chinese hamster ovary cells and was purified as described (Byrn et al., 1990). rgp120, a recombinant

form of the envelope glycoprotein of HIV-1<sub>IIIB</sub>, was similarly expressed and purified as described (Leonard et al., 1990).

**Synthesis of MePEG Aldehyde.** MePEG was oxidized using the Moffatt procedure (Figure 1) essentially as described by Harris et al. (1984) and Shak et al. (1989). Acetic anhydride (3 mL, 30 mmol) was added to dry DMSO (10 mL). In a separate stoppered flask, MePEG (10 g, 2 mmol) and DMSO (10 mL) were warmed to 50–60 °C to give a homogeneous solution and, after cooling to near-room temperature, were added to the acetic anhydride/DMSO solution. After the solution was stirred at ambient temperature for 24 h, further portions of acetic anhydride (3 mL, 30 mmol) and triethylamine (5 mL) were added, and the solution was stirred at room temperature for a further 24 h. Addition of ether (50 mL) and ethyl acetate (50 mL) and cooling the flask in the refrigerator resulted in precipitation of the product. The product was collected by filtration, triturated with ether (5×), and dried under vacuum. Extent of activation of the dried MePEG-CHO was quantitated by a colorimetric assay using alkaline 4-amino-3-hydrazino-5-mercapto-1,2,4-triazole (Aldrich) to detect aldehydes (Avigad, 1983), with acetaldehyde as the standard. A standard 5 mM solution of acetaldehyde was prepared by periodate oxidation of L-rhamnose, as described (Avigad, 1983). Absorbance was read at 542

nm. This assay method was linear in the range of 0.1–0.6 mM of acetaldehyde.

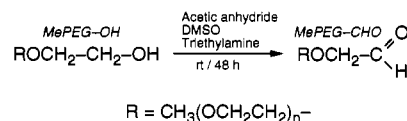
**Conjugation of MePEG to CD4-IgG and Removal of Residual MePEG.** Purified CD4-IgG (5 mg/mL; 0.055 mM) was incubated with an approximately 100-fold molar excess of MePEG-CHO (5.2 mM), 20 mM NaCNBH<sub>3</sub>, in 0.1 M HEPES pH 7.5, for various times at 0 or 23 °C; reactions were stopped by addition of ethanolamine to a final concentration of 50 mM. To recover MePEG-conjugated protein free of residual MePEG or MePEG-CHO, reaction mixtures were applied to IDA-Sepharose loaded with Cu<sup>2+</sup> and equilibrated in 10 mM Tris pH 8.0, 0.5 M NaCl. After the mixture was washed to remove residual MePEG and MePEG-CHO (Ingham and Ling, 1978), bound MePEG-conjugated protein was recovered by elution with the same pH 8.0 buffer containing 50 mM imidazole.

**Characterization of MePEG-Modified CD4-IgG and Quantitation of MePEG.** IDA-Sepharose pools were analyzed by SDS-PAGE, and the concentration of MePEG in each sample was determined by NMR (Jackson et al., 1987). Protein concentration was determined by assay using bicinchoninic acid (Smith et al., 1985) with bovine serum albumin as standard. Absorption of the protein at 280 nm ( $A_{0.1\%} = 1.34$ ) was also used to determine the CD4-IgG concentration. The concentrations determined by both methods agreed. For the NMR analysis, aqueous solutions (0.5 mL) were transferred to NMR tubes, diluted with D<sub>2</sub>O (0.2 mL), and placed in the instrument probe for 5 min at 20 °C prior to data acquisition. The intensity of the singlet MePEG signal at  $\delta = 3.7$  ppm was measured, and the concentration of MePEG in the sample was determined by comparing the signal intensity to intensities of known MePEG standards that were identically treated. The fraction of total amines in CD4-IgG that are potentially reactive was quantitated by TNBS assay (Fields, 1972).

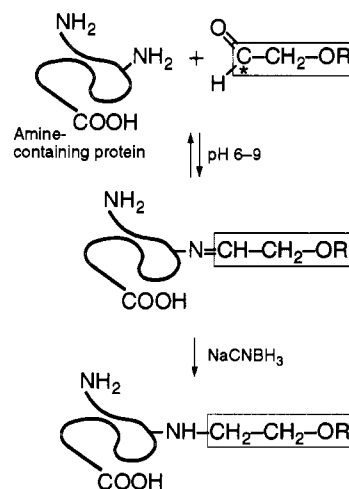
**N-Terminal Sequence Analysis and Peptide Mapping.** Desalted aliquots of selected IDA-Sepharose pools were inserted into an Applied Biosystems Model 477A sequencer reaction cartridge atop a preconditioned polybrene-coated filter. N-terminal sequence analysis was performed for five cycles using 500 pmol of CD4-IgG or MePEG<sub>5,8</sub>-modified CD4-IgG. Peptide mapping was performed on trypsin-digested S-carboxymethylated samples as described (Harris et al., 1990).

**gp120 Binding.** The ability of CD4-IgG and modified CD4-IgG to bind to rgp120 was determined as described previously (Chamow et al., 1990). Briefly, CD4-IgG was immobilized onto microtiter wells coated with anti-IgG antibody. Then, CD4-IgG or MePEG-CD4-IgG conjugates were added simultaneously with <sup>125</sup>I-labeled rgp120 (HIV-1<sub>IIIB</sub>), to determine the ability of added CD4-IgG (or derivatized CD4-IgG) to compete with the immobilized CD4-IgG for binding to labeled rgp120. The assays were done in triplicate; nonspecific binding was determined by omitting the first addition of CD4-IgG.

**Determination of in Vivo Clearance.** CD4-IgG, (MePEG)<sub>7,7</sub>-CD4-IgG, (MePEG)<sub>14,4</sub>-CD4-IgG, and human IgG (Jackson ImmunoResearch, West Grove, PA) were iodinated with Na<sup>[125]</sup>I using immobilized lactoperoxidase (Enzymobeads, Bio-Rad). Twelve male Sprague-Dawley-derived rats (295–335 g) received approximately 95  $\mu$ Ci/kg of labeled protein (specific activity 0.3  $\mu$ Ci/ $\mu$ g) as a bolus injection into a femoral vein catheter (three animals per group). Blood samples were collected from a jugular vein catheter at specified times over a 5-day period. The



**Figure 1.** Preparation of MePEG aldehyde (MePEG-CHO) from MePEG (MePEG-OH) via Moffatt oxidation. For MePEG-OH of MW = 5000,  $n \approx 110$ .



**Figure 2.** Conjugation of MePEG-CHO to protein amino groups via reductive alkylation. MePEG-CHO incubated with a protein at pH 6–9 results in reversible addition of MePEG to protein amino groups via Schiff's base formation. These linkages are converted to stable secondary amines by reduction with sodium cyanoborohydride.  $\epsilon$ -Amino groups of lysine residues, as well as the  $\alpha$ -amino group at the N-terminus, are targets for modification. The net charge of the modified protein does not change appreciably as a result of MePEGylation by this method, since primary amines are converted to secondary amines. Boxed region represents atoms derived from MePEG. R group and \* as defined in Table 1.

area under the TCA-precipitable radioactivity versus time curve (AUC) from 0 to 120 h was determined for each animal.

## RESULTS

**Synthesis.** MePEG-CHO was synthesized from commercially available monomethoxyPEG (5000 MW) via a Moffatt oxidation (Figure 1). The yield of MePEG-CHO was approximately 52% when assayed against an acetaldehyde standard. Thin-layer chromatography (3:17 CH<sub>3</sub>-OH/CH<sub>2</sub>Cl<sub>2</sub>) revealed a single spot with the same  $R_f$  as the MePEG-OH, implying that the remaining 48% was unoxidized MePEG-OH<sup>4</sup> (which does not participate in the subsequent alkylation reaction). Therefore, the concentration of MePEG-CHO was assumed to be 5.2 mM in a 10 mM solution of activated MePEG.

**Formation of Conjugates.** MePEG-CHO was conjugated to CD4-IgG via reductive alkylation to form a Schiff's base which, in the presence of NaCNBH<sub>3</sub>, was reduced to a stable secondary amine (Figure 2). Using the TNBS assay to quantitate primary amines, we determined that 34% of amino groups in CD4-IgG (26/

<sup>4</sup> Because of the heterogeneous nature of this polymer and the lack of a definitive assay for MePEG-OH (one which does not detect the enol form of the aldehyde or entrapped water), we cannot say with complete certainty that the remaining 48% of MePEG in this preparation is MePEG-OH. However, this conclusion seems only reasonable, considering the predicted course of the Moffatt oxidation, the aldehyde colorimetric analysis, and the thin-layer chromatographic result.

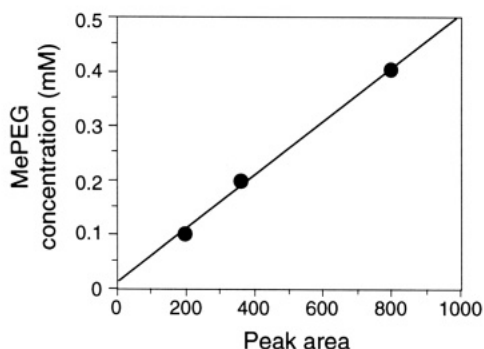
**Table 2. Quantitation of MePEG/CD4-IgG Ratio in Conjugates**

time <sup>a</sup> (h)	CD4-IgG		MePEG		MePEG/CD4-IgG
	mg/mL <sup>b</sup>	nmol	mM <sup>c</sup>	nmol	
0.5	1.24	9.54	0.040	28.1	2.9
1.0	1.87	14.38	0.073	51.2	3.6
1.5	0.92	7.08	0.051	36.0	5.1
2.0	1.78	13.69	0.114	79.9	5.8
2.5	1.84	14.15	0.132	92.1	6.5
3.0	1.69	13.00	0.137	95.8	7.4

<sup>a</sup> Reaction mixture (22 °C) contained 5 mg/mL of CD4-IgG, 5.2 mM of MePEG-CHO, 20 mM of NaCNBH<sub>3</sub>, 0.1 M HEPES pH 7.5.

<sup>b</sup> Determined by bicinchoninic acid assay (Smith et al., 1985) using bovine serum albumin as standard. CD4-IgG was assumed to have a molecular weight of 91 000, the size of the disulfide-linked dimer.

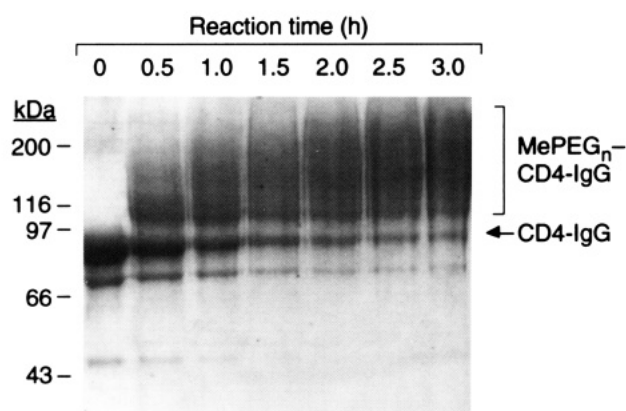
<sup>c</sup> Determined by NMR (Jackson et al., 1987). The slope of the line generated by the standard curve (Figure 3) was  $y = 0.000489x + 0.0118$ , where  $y$  = mM of MePEG and  $x$  = peak area.



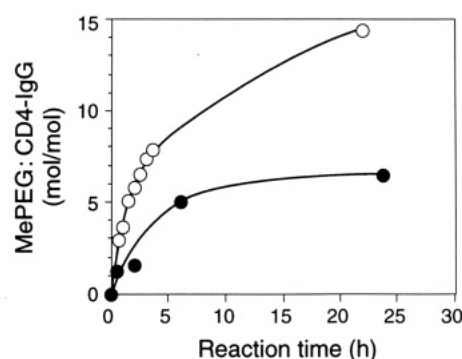
**Figure 3.** Quantitative assay of MePEG using NMR. The amount of MePEG covalently attached to CD4-IgG was determined by measuring the concentration of MePEG in a modified protein solution, after removal of residual MePEG-CHO from the reaction mixture by metal chelate chromatography. The intensity of the singlet MePEG signal at  $\delta = 3.7$  was measured, and peak areas were recorded for a series of MePEG standards of known concentration from 0.1–0.5 mM.

76)<sup>5</sup> are available for reaction (data not shown). Initially, we attempted to quantitate the extent of MePEGylation by this same procedure. However, we found that quantitation by NMR is a superior analytical method for this purpose. Among the reaction parameters that influenced the rate of MePEGylation of CD4-IgG were length of time, temperature of reaction, and molar excess of MePEG-CHO over protein. We found that in 0.5–3.0 h of reaction, at 22 °C and a 100-fold molar excess of MePEG-CHO over CD4-IgG, conjugates were produced with MePEG/CD4-IgG molar ratios ranging from 2.9 to 7.4 (Table 2). This represents reaction of 11–28% of the 26 available amino groups in CD4-IgG. Formation of MePEG-CD4-IgG conjugates generated after 0.5–3 h of reaction could also be followed by SDS-PAGE, a technique that we used to investigate molecular heterogeneity in reaction mixtures of modified CD4-IgG (Figure 4). Electrophoretic analysis indicated that MePEGylated forms of CD4-IgG began to appear after 0.5 h of reaction. At this short time point, a single, predominant, new band was observed at approximately 110 kDa, which presumably represents MePEG<sub>1</sub>-CD4-IgG. As the reaction time increased, we observed a shift toward the formation of higher molecular weight conjugates. At 3.0 h of reaction, a series of new high molecular weight species that stained intensely in the 130–

<sup>5</sup> Each CD4-IgG polypeptide contains 37 lysine residues (Harris et al., 1990); thus, the total number of amino groups per polypeptide is 38, or 76 amino groups per homodimer. CD4-IgG has a pI of 9.1.



**Figure 4.** SDS-PAGE analysis of MePEG-CD4-IgG conjugates. CD4-IgG (5 mg/mL; 0.055 mM) samples were incubated with MePEG-CHO (5.2 mM) and NaCNBH<sub>3</sub> (20 mM) in 0.1 M HEPES pH 7.5 for 0–3.0 h at 22 °C. Reactions were stopped, and samples were analyzed in 7.5% nonreduced gel, stained with Coomassie blue. Molecular weight standards in kDa are indicated at left. The designation “n” in “MePEG<sub>n</sub>-CD4-IgG” refers to the number of MePEG molecules incorporated into each polypeptide of CD4-IgG.



**Figure 5.** Reaction of MePEG-CHO with CD4-IgG slows with temperature. CD4-IgG (5 mg/mL; 0.055 mM) samples were incubated with MePEG-CHO (5.2 mM) and NaCNBH<sub>3</sub> (20 mM) in 0.1 M HEPES pH 7.5 for different lengths of time at 0 °C (●) and 22 °C (○). Reactions were stopped, and samples were recovered by metal chelate chromatography and analyzed to determine the extent of MePEG modification. The molar ratio of MePEG/protein, which is plotted on the y-axis, was determined by measuring the concentration of MePEG using NMR and the concentration of protein using bicinchoninic acid assay, for each sample.

250-kDa size range appeared, with a concomitant decrease in staining intensity of the CD4-IgG and MePEG<sub>1</sub>-CD4-IgG bands. Thus, electrophoretic analysis indicates that considerable heterogeneity is present in each reaction mixture, and that molecular heterogeneity of MePEG-CD4-IgG conjugates increases with increasing times of reaction. Molar ratios of MePEG/CD4-IgG, which we have derived from NMR and protein assay data (Figure 3 and Table 2), therefore represent an average degree of substitution in a MePEG/CD4-IgG mixture.

We investigated the effect of temperature on the reaction of MePEG-CHO with CD4-IgG and found that we could further reduce the amount of MePEG incorporated into CD4-IgG by lowering the temperature of reaction from 22 to 0 °C (Figure 5). At 22 °C, the amount of MePEG incorporated into CD4-IgG increased steadily (from 0 to 7.7 mol/mol) during the first 3.5 h of reaction, while after 23 h of reaction, the MePEG/CD4-IgG ratio was nearly 15 mol/mol (representing reaction of 55% of the 26 available amino groups). In contrast, a temperature of 0 °C slowed the reaction almost 2-fold. During the first 3.5 h of reaction, a MePEG/CD4-IgG molar ratio of approximately

**Table 3. N-Terminal Sequence Analysis of CD4-IgG and MePEG<sub>5.8</sub>-CD4-IgG<sup>a</sup>**

cycle no.	residue <sup>c</sup>	recovery <sup>b</sup> (%)	
		CD4-IgG	MePEG <sub>5.8</sub> -CD4-IgG
1	Lys	95	51
2	Lys	114	125
3	Val	104	115
4	Val	102	105
5	Leu	100	100

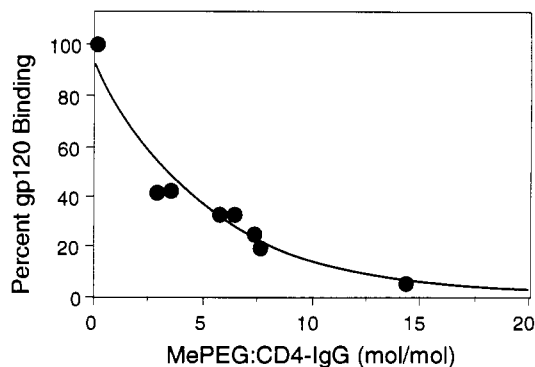
<sup>a</sup> 500 pmol of CD4-IgG or MePEG<sub>5.8</sub>-CD4-IgG (prepared as described for 2.0 h at 22 °C; see Table 2) was inserted into an Applied Biosystems Model 477A sequencer, and the recoveries of the first five amino acid residues were determined for each. <sup>b</sup> The values shown are relative recoveries of PTH-amino acids. Values are normalized to Leu-5 = 100%. <sup>c</sup> Confirms amino acid sequence reported for CD4-IgG by Harris et al. (1990).

4 was reached, with that ratio increasing to 6.5 after 24 h of reaction. A similar effect of temperature was seen for reductive methylation of albumin (Jentoft and Dearborn, 1979).

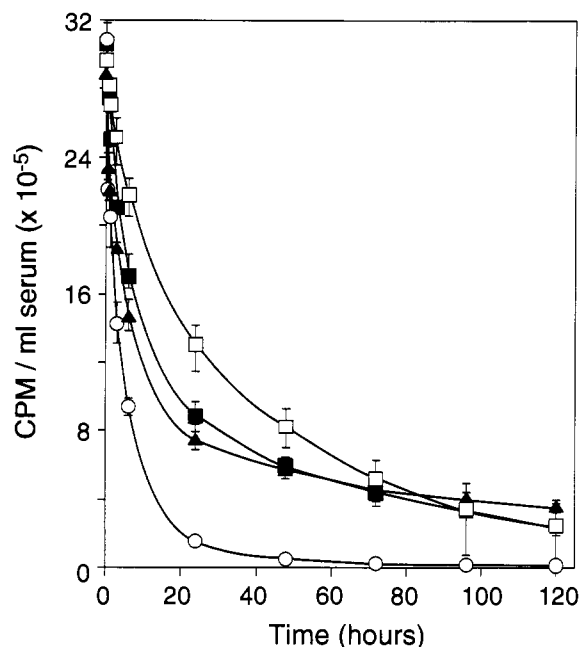
**Sites of Modification on CD4-IgG.** To determine the sites of modification, CD4-IgG containing an average of 5.8 MePEG molecules per CD4-IgG molecule was analyzed (Table 3). N-terminal sequence analysis showed a 50% yield of PTH-Lys at cycle 1, suggesting that 50% of Lys-1 residues were MePEG-modified. We assume that the reactive site in Lys-1 is the  $\alpha$ -amino group. Under the reaction conditions used (pH 7.5), the  $\alpha$ -amino group of the N-terminus is near its  $pK_a$  (~8.0) and thus a significant fraction is unprotonated and available for reaction, while the  $\epsilon$ -amino groups of Lys-1 and of lysine residues elsewhere in the protein remain almost completely protonated ( $pK_a$  = 9.5). No tryptic mapping differences were observed between control CD4-IgG and MePEG<sub>5.8</sub>-CD4-IgG, suggesting that the approximately six MePEG attachment sites were otherwise evenly distributed throughout the molecule. (Modification of the N-terminus would not be detected in the tryptic map, as it is found within a Lys-Lys sequence where cleavage after either of these two residues could generate free amino acids that would elute in the chromatographic void.) Although some reaction with  $\epsilon$ -amino groups must occur to account for the observed molar ratios, there appear to be no other unique sites that react to an extent approaching that of the  $\alpha$ -amino group.  $\epsilon$ -Amino groups of lysine residues in the protein appear to be indistinguishable in their reactivity with the MePEG-CHO reagent.

**Effect of MePEGylation on gp120 Binding.** We investigated whether MePEGylation of CD4-IgG affects gp120 binding affinity. Using a solid-phase radioreceptor assay, we observed a decrease in the ability of the modified protein to bind to rgp120 which correlates with the extent of MePEGylation (Figure 6). MePEG-CD4-IgG modified with 3.6, 7.7, and 14.4 mol of MePEG per mol of CD4-IgG displayed gp120 binding ability that was reduced to 42%, 19%, and 5.5%, respectively, of unmodified CD4-IgG. This result was not unexpected; in fact, similar decreases in the activity of other MePEGylated proteins have been reported (see Discussion).

**MePEGylation Decreases the Rate of Clearance of CD4-IgG.** To test whether the pharmacokinetic properties of CD4-IgG were affected by MePEGylation, the serum concentrations of radioiodinated CD4-IgG, MePEG<sub>7.7</sub>-CD4-IgG, MePEG<sub>14.4</sub>-CD4-IgG, and human IgG were measured for 5 days after intravenous injection into rats (Figure 7). As indicated by comparing the integrated area under the curve (AUC), the clearance rates of MePEG<sub>7.7</sub>-CD4-IgG and MePEG<sub>14.4</sub>-CD4-IgG were approximately



**Figure 6.** Binding of CD4-IgG conjugates to HIV-1 rgp120. CD4-IgG and its MePEGylated derivatives were tested for their ability to compete with immobilized CD4-IgG for the binding of <sup>125</sup>I-labeled rgp120. Plotted are points representing CD4-IgG and CD4-IgG modified with an average of 2.9, 3.6, 5.8, 6.5, 7.4, 7.7, and 14.4 MePEG molecules per CD4-IgG molecule. Percent rgp120 binding reflects the relative amount of competing molecule required to inhibit 50% of the binding to immobilized CD4-IgG.



**Figure 7.** MePEGylation decreases the serum clearance of CD4-IgG. Radioiodinated CD4-IgG (○), human IgG (▲), and CD4-IgG modified with an average number of 7.7 (■) or 14.4 (□) MePEG's per dimer, as determined by NMR quantitation, were injected intravenously into rats. Serum samples from three rats/group were taken over a 5-day period, and TCA-precipitable counts were measured. Approximate AUC values (h-cpm/mL) were  $1.96 \times 10^7$ ,  $7.90 \times 10^7$ ,  $8.18 \times 10^7$ , and  $1.05 \times 10^8$ , respectively.

4- and 5-fold slower, respectively, than that of CD4-IgG. Indeed, the rates of clearance of MePEGylated CD4-IgG are slightly lower than that of human IgG in the rat.

## DISCUSSION

Aldehyde groups react under mild aqueous conditions with aliphatic amines to form a Schiff's base (an imine) which can be reduced selectively by the mild reducing agent sodium cyanoborohydride to give a stable secondary amine (Jentoft and Dearborn, 1979). Although this method of amine modification (an alkylation) is not used in protein conjugations as frequently as the activated ester method (an acylation) (Bragg and Hou, 1975), it is mild, simple, and very effective. For these reasons, we chose to evaluate a MePEG aldehyde reagent for modification of

CD4-IgG. Using this reagent at 100-fold molar excess over protein (4-fold molar excess over amino groups), we were able to achieve modification of 11–55% of the available amino groups in CD4-IgG.

An important goal of adding MePEG groups to a therapeutic protein is an extension of the protein's persistence in circulating blood. Our results show that this indeed is the case for CD4-IgG, since the clearance of MePEGylated CD4-IgG (MePEG:protein = 7.7:1 or 14.4:1) was 4- to 5-fold slower than that of unmodified CD4-IgG. The resulting rate of clearance is, in fact, slightly lower than that observed for human IgG. For comparison, Kitamura et al. (1991) prepared a MePEG-modified monoclonal antibody (MePEG:protein = 5.1:1) and demonstrated less than 2-fold reduced clearance of the modified antibody in mice. The stabilizing effect of MePEGylation may be greater for the immunoadhesin, since its half-life prior to modification is shorter than that of the antibody. Notably, the more excessive modification (MePEG:protein = 14.4:1) resulted in only 20% further reduction in the rate of clearance. This result suggests that, at least for an antibody-like molecule such as CD4-IgG, the additional reduction in clearance that can be achieved by progressive MePEGylation is diminished at high degrees of modification.

By what mechanism might MePEGylation increase the *in vivo* residence time of CD4-IgG? We have determined that metabolic clearance of CD4-IgG occurs predominantly in the liver, and not in the kidney (J.M. and S.M.C., unpublished results). Clearance via glomerular filtration through the kidney is a principal route of elimination for globular proteins less than 60–70 kDa in size (Stokes radius of less than approximately 35 Å) (Venkatachalam and Rennke, 1978). It is believed that MePEGylation of small proteins, such as IL-2 (Knauf et al., 1988), increases their circulatory lifetimes *in vivo* by increasing their effective size, thus reducing filtration through the kidney. This is not the case for CD4-IgG, since its size (91 kDa) is beyond the limit for kidney filtration. However, since CD4-IgG contains a functional immunoglobulin Fc domain, at least some of its clearance may be caused by binding to Fc receptors on reticuloendothelial cells. MePEGylation of CD4-IgG, particularly at sites in the lysine-rich Fc region, may impair the interaction of CD4-IgG with Fc receptors, thus prolonging the serum stability of the modified molecule. Kitamura et al. (1991) suggest that, rather than affecting Fc receptor binding, MePEG may shield the antibody molecule from proteolysis and thereby inhibit catabolism. At least some characteristics of the Fc domain are changed by MePEGylation; for example, we found that while CD4-IgG binds well to *Staphylococcus aureus* Protein A, MePEGylated CD4-IgG binds only poorly to Protein A (data not shown). In addition, the binding of modified CD4-IgG to other chromatographic supports, such as ion-exchange media, is also adversely affected (data not shown). Similar changes in the physical properties of horseradish peroxidase were noted by Wirth et al. (1991) after modification of the protein with MePEG.

As reviewed in Francis (1992), MePEG-modified proteins have shown a modest to marked reduction in biological or enzymatic activity, almost without exception. Mercuripapain (Boccu et al., 1983),  $\alpha$ 2-macroglobulin (Beauchamp et al., 1983), L-glutaminase-L-asparaginase (Abuchowski et al., 1981), ribonuclease (Veronese et al., 1985), tissue plasminogen activator (Berger and Pizzo, 1988), and elastase (Koide and Kobayashi, 1983) all lost more than 50% of their activity upon modification with MePEG. MePEG modification of IgG caused complement

binding to be reduced but not binding to antigen (Suzuki et al., 1984), while modification of granulocyte-macrophage colony stimulating factor did not affect colony stimulating activity but enhanced neutrophil priming activity (Knusli et al., 1992).

We used an *in vitro* assay based on recombinant, soluble gp120 from the IIIB isolate of HIV-1 to evaluate the effect of MePEGylation on the ligand binding function of CD4-IgG. We observed a decrease in the ability of MePEG-modified CD4-IgG to bind to this form of gp120 that roughly correlates with the extent of MePEG modification. It should be noted, however, that this decrease in binding is not necessarily indicative of a decrease in the ability of modified CD4-IgG to neutralize HIV-1 *in vivo*. For example, the amino acid sequence of gp120 varies dramatically between different strains of HIV-1, and the changes in binding that we observe with gp120 from the IIIB strain may not be representative of other strains (Daar et al., 1990; Ashkenazi et al., 1991; Moore et al., 1992). Moreover, the structure of recombinant, soluble gp120 in solution is monomeric, whereas on the surface of virions it is oligomeric. Thus CD4-IgG, as a homodimer, may bind bivalently to each gp120 oligomer, which might stabilize the binding. Perhaps relevant to this issue is the example of adenosine deaminase, where a decrease in *in vitro* activity did not correlate with a lack of efficacy *in vivo*. MePEG-modified adenosine deaminase displayed a 40% decrease in enzymatic activity *in vitro* (Davis et al., 1981), yet the modified protein has proved to be efficacious *in vivo* (Hershfeld et al., 1987). Therefore, despite an apparent loss of rgp120 binding *in vitro*, the extension in *in vivo* residence time observed for MePEG-CD4-IgG may provide a significant therapeutic benefit.

As to the site(s) that may be responsible for this loss of binding activity, the rgp120 binding activity resides in the N-terminal immunoglobulin-like domain (residues 1–98) of the extracellular portion of CD4. In particular, Lys-46, positioned within the C' ridge of domain 1, is believed to be involved in such binding (Ashkenazi et al., 1990; Arthos et al., 1989; Brodsky et al., 1990). Since this residue is exposed to solvent (Wang et al., 1990; Ryu et al., 1990), it is possible—although we did not demonstrate this directly—that several of the lysines in this region, including Lys-46, are partially modified such that rgp120 binding is compromised. More generally, for proteins that do not contain active lysine residues, MePEGylation using this chemistry is less likely to compromise biological activity of the modified protein and, thus, may provide a greater therapeutic advantage.

In conclusion, we have applied a method of MePEGylation by reductive alkylation of amino groups to modification of an immunoadhesin. We synthesized an aldehyde derivative of MePEG and identified reaction conditions enabling the incorporation of MePEG into CD4-IgG in the range of approximately 3–15 mol of MePEG per mol of protein. MePEGylation resulted in a significant increase in the residence time of the protein in circulation, rendering it comparable to that of human IgG. While a reduction in *in vitro* binding of MePEG-CD4-IgG to soluble rgp120 was observed, the biological activity against intact virions of clinical strains of HIV remains to be investigated. The more general implication of our results is that MePEGylation by reductive alkylation can be a useful strategy, especially for proteins in which amino groups are not critical for biological activity.

#### ACKNOWLEDGMENTS

We wish to thank G. Osaka, E. Carlson, K. Thomsen, A. Nixon, and C. Baker for technical support, K. Andow,



W. Anstein, and L. Tamayo for preparation of figures, T. Somers and R. Ward for helpful suggestions, and T. Gregory for advice and support on the MePEGylation project.

## LITERATURE CITED

- Abuchowski, A., McCoy, J. R., Palczuk, N. C., van Es, T., and Davis, F. F. (1977a) Effect of covalent attachment of PEG on immunogenicity and circulating life of bovine liver catalase. *J. Biol. Chem.* 252, 3582-3586.
- Abuchowski, A., van Es, T., Palczuk, N. C., and Davis, F. F. (1977b) Alteration of immunological properties of bovine serum albumin by covalent attachment of PEG. *J. Biol. Chem.* 252, 3578-3581.
- Abuchowski, A., Davis, F. F., and Davis, S. (1981) Immunosuppressive properties and circulating life of *Achromobacter* glutaminase-asparaginase covalently attached to PEG in man. *Cancer Treat. Rep.* 65, 1077-1081.
- Abuchowski, A., Kazo, G. M., Verhoest, C. R., Jr., Van Es, T., Kafkewitz, D., Nucci, M. L., Viau, A. T., and Davis, F. F. (1984) Cancer therapy with chemically modified enzymes: Anti-tumor properties of PEG-asparaginase conjugates. *Cancer Biochem. Biophys.* 7, 175-186.
- Arthos, J., Deen, K. C., Chaikin, M. A., Fornwald, J. A., Sathe, G., Sattentau, Q. J., Clapham, P. R., Weiss, R. A., McDougal, J. S., Pietropaolo, C., Axel, R., Truneh, A., Maddon, P. J., and Sweet, R. W. (1989) Identification of the residues in human CD4 critical for binding of HIV. *Cell* 57, 469-481.
- Ashkenazi, A., Presta, L. G., Marsters, S. A., Camerato, T. R., Rosenthal, K. A., Fendly, B. M., and Capon, D. J. (1990) Mapping the CD4 binding site for human immunodeficiency virus by alanine-scanning mutagenesis. *Proc. Natl. Acad. Sci. U.S.A.* 87, 7150-7154.
- Ashkenazi, A., Smith, D. H., Marsters, S. A., Riddle, L., Gregory, T. J., Ho, D. D., and Capon, D. J. (1991) Resistance of primary isolates of HIV-1 to sCD4 is independent of CD4-rgp120 binding affinity. *Proc. Natl. Acad. Sci. U.S.A.* 88, 7056-7060.
- Ashkenazi, A., Capon, D. J., and Ward, R. H. R. (1993) Immunoaderhins. *Intern. Rev. Immunol.* 10, 219-227.
- Avigad, G. (1983) A simple spectrophotometric determination of formaldehyde and other aldehydes: Application to periodate-oxidized glycol systems. *Anal. Biochem.* 134, 499-504.
- Beauchamp, C. O., Gonias, S. L., Menapace, D. P., and Pizzo, S. V. (1983) A new procedure for the synthesis of MePEG-protein adducts: Effects on function, receptor recognition and clearance of superoxide dismutase, lactoferrin and alpha-2-macroglobulin. *Anal. Biochem.* 131, 25-33.
- Berger, H., and Pizzo, S. V. (1988) Preparation of PEG-tissue plasminogen activator adducts that retain functional activity: Characteristics and behavior in three animal species. *Blood* 71, 1641-1647.
- Boccu, E., Largajolli, R., and Veronese, F. M. (1983) Coupling of MePEGs to proteins via active esters. *Z. Naturforsch.* 38C, 94-99.
- Bragg, P. D., and Hou, C. (1975) Subunit composition, function, and spatial arrangement in the  $\text{Ca}^{2+}$ - and  $\text{Mg}^{2+}$ -activated adenosine triphosphatases of *Escherichia coli* and *Salmonella typhimurium*. *Arch. Biochem. Biophys.* 167, 311-321.
- Brodsky, M. H., Warton, M., Myers, R. M., and Littman, D. (1990) Analysis of the site in CD4 that binds to the HIV envelope glycoprotein. *J. Immunol.* 144, 3078-3086.
- Buckmann, A. F., Morr, M., and Johansson, G. (1981) Functionalization of PEG and monomethoxy-PEG. *Makromol. Chem.* 182, 1379-1384.
- Byrn, R. A., Mordenti, J., Lucas, C., Smith, D., Marsters, S. A., Johnson, J. S., Cossium, P., Chamow, S. M., Wurm, F. M., Gregory, T., Groopman, J. E., and Capon, D. J. (1990) Biological properties of a CD4 immunoaderhin. *Nature* 344, 667-670.
- Capon, D. J., Chamow, S. M., Mordenti, J., Marsters, S. A., Gregory, T., Mitsuya, H., Byrn, R. A., Lucas, C., Wurm, F. M., Groopman, J. E., Broder, S., and Smith, D. H. (1989) Designing CD4 immunoaderhins for AIDS therapy. *Nature* 337, 525-531.
- Chamow, S. M., Peers, D. H., Byrn, R. A., Mulkerrin, M. G., Harris, R. J., Wang, W. C., Bjorkman, P. J., Capon, D. J., and Ashkenazi, A. (1990) Enzymatic cleavage of a CD4 immunoaderhin generates crystallizable, biologically active Fd-like fragments. *Biochemistry* 29, 9885-9891.
- Chamow, S. M., Duliege, A. M., Ammann, A., Kahn, J. O., Allen, J. D., Eichberg, J. W., Byrn, R. A., Capon, D. J., Ward, R. H. R., and Ashkenazi, A. (1992) CD4 immunoaderhins in anti-HIV therapy: New developments. *Int. J. Cancer* 52, Suppl. 7, 69-72.
- Daar, E. S., Li, X. L., Moudgil, T., and Ho, D. D. (1990) High concentrations of sCD4 are required to neutralize primary HIV-1 isolates. *Proc. Natl. Acad. Sci. U.S.A.* 87, 6574-6578.
- Davis, S., Abuchowski, A., Park, Y. K., and Davis, F. F. (1981) Alteration of the circulating life and antigenic properties of bovine ADA in mice by attachment of PEG. *Clin. Exp. Immunol.* 46, 649-652.
- Delgado, C., Patel, J. N., Francis, G. E., and Fisher, D. (1990) Coupling of PEG to albumin under very mild conditions by activation with tresyl chloride: characterization of the conjugate by partitioning in aqueous two-phase systems. *Bio-technol. Appl. Biochem.* 12, 119-128.
- Fields, R. (1972) The rapid determination of amino groups with TNBS. *Meth. Enzymol.* 25, 464-468.
- Francis, G. E., Delgado, C., and Fisher, D. (1992) PEG-modified proteins. In: *Stability of Protein Pharmaceuticals: in vivo Pathways of Degradation and Strategies for Protein Stabilization*, T. J. Ahern, and M. Manning, (Eds.), Plenum Press, New York.
- Harris, J. M., Struck, E. C., Case, M. G., Paley, M. S., Yalpani, M., van Alstine, J. M., and Brooks, D. E. (1984) Synthesis and characterization of PEG derivatives. *J. Polymer Sci.: Polymer Chem. Ed.* 22, 341-352.
- Harris, R. J., Wagner, K. L., and Spellman, M. W. (1990) Structural characterization of a recombinant CD4-IgG hybrid molecule. *Eur. J. Biochem.* 194, 611-620.
- Hershfeld, M. S., Buckley, R. H., Greenberg, M. L., Melton, A. L., Schiff, R., Hatem, C., Kurtzberg, J., Markert, M. L., Kobayashi, R. H., Kobayashi, A. L., and Abuchowski, A. (1987) Treatment of adenosine deaminase deficiency with PEG-modified adenosine deaminase. *N. Engl. J. Med.* 316, 589-596.
- Hodges, T. L., Kahn, J. O., Kaplan, L. D., Groopman, J. E., Volberding, P. A., Ammann, A. J., Arri, C. J., Bouvier, L. M., Mordenti, J., Izu, A. E. and Allan, J. D. (1991) Phase 1 study of recombinant CD4-IgG therapy of patients with AIDS and AIDS-related complex. *Antimicrob. Agents Chemother.* 35, 2580-2586.
- Ingham, K. C., and Ling, R. C. (1978) A quantitative assay for PEG without interference by proteins. *Anal. Biochem.* 85, 139-145.
- Jackson, C. J. C., Charlton, J. L., Kuzminski, K., Lang, G. M., and Sehon, A. H. (1987) Synthesis, isolation and characterization of conjugates of ovalbumin with PEG using cyanuric chloride as the coupling agent. *Anal. Biochem.* 165, 114-127.
- Jentoft, J. E., and Dearborn, P. G. (1979) Labeling of proteins by reductive methylation using sodium cyanoborohydride. *J. Biol. Chem.* 254, 4359-4365.
- Joppich, M., and Luisi, P. L. (1979) Synthesis of glycyl-L-tryptophanyl-glycine substituted by PEG at both carboxyl and amino end groups. *Makromol. Chem.* 180, 1381-1384.
- Kahn, J. O., Allan, J. D., Hodges, T. L., Kaplan, L. D., Arri, C. J., Fitch, H. F., Izu, A. E., Mordenti, J., Sherwin, S. A., Groopman, J. E., and Volberding, P. A. (1990) The safety and pharmacokinetics of sCD4 in subjects with AIDS and AIDS-related complex. *Ann. Int. Med.* 112, 254-261.
- Katre, N. V., Knauf, M. J., and Laird, W. J. (1987) Chemical modification of recombinant interleukin 2 by PEG increases its potency in the murine Meth A sarcoma model. *Proc. Natl. Acad. Sci. U.S.A.* 84, 1487-1491.
- Kitamura, K., Takahashi, T., Yamaguchi, T., Noguchi, A., Noguchi, A., Takashina, K. I., Tsurumi, H., Inagake, M., Toyokuni, T., and Hakamori, S. (1991) Chemical engineering of the monoclonal antibody A7 by polyethylene glycol for targeting cancer chemotherapy. *Cancer Res.* 51, 4310-4315.
- Knauf, M. J., Bell, D. P., Hirtzer, P., Luo, Z. P., Young, J. D., and Katre, N. V. (1988) Relationship of effective molecular size to systemic clearance in rats of recombinant interleukin-2



- chemically modified with water-soluble polymers. *J. Biol. Chem.* 263, 15064–15070.
- Knusli, C., Delgado, C., Malik, F., Domine, M., Tejedor, M. C., Irvine, A. E., Fisher, D., and Francis, G. E. (1992) PEG modification of GM-CSF enhances neutrophil priming activity but not colony stimulating activity. *Brit. J. Haematol.* 82, 654–663.
- Koide, A., and Kobayashi, S. (1983) Modification of amino groups in porcine pancreatic elastase with PEG in relation to binding ability towards anti-serum and to enzymic activity. *Biochem. Biophys. Res. Commun.* 111, 659–667.
- Leonard, C. K., Spellman, M. W., Riddle, L., Harris, R. J., Thomas, J. N., and Gregory, T. J. (1990) Assignment of intrachain disulfide bonds and characterization of potential glycosylation sites of the type 1 recombinant HIV envelope glycoprotein expressed in Chinese hamster ovary cells. *J. Biol. Chem.* 265, 10373–10382.
- Moore, J. P., McKeating, J. A., Huang, Y., Ashkenazi, A., and Ho, D. D. (1992) Virions of primary HIV-1 isolates resistant to sCD4 neutralization differ in sCD4 binding and glycoprotein gp120 retention from sCD4-sensitive isolates. *J. Virol.* 66, 235–243.
- Nilsson, K., and Mosbach, K. (1984) Immobilization of ligands with organic sulfonyl chlorides. *Methods Enzymol.* 104, 56–69.
- Ryu, S. E., Kwong, P. D., Truneh, A., Porter, T. G., Arthos, J., Rosenberg, M., Dai, X., Xuong, N., Axel, R., Sweet, R. W., and Hendrickson, W. A. (1990) Crystal structure of an HIV-binding recombinant fragment of human CD4. *Nature* 348, 419–426.
- Schooley, R. T., Merigan, T. C., Gaut, P., Hirsch, M. S., Holodniy, M., Flynn, T., Liu, S., Byington, R. E., Henochoicz, S., Gubish, E., Spriggs, D., Kufe, D., Schindler, J., Dawson, A., Thomas, D., Hanson, D. G., Letwin, B., Liu, T., Gulino, J., Kennedy, S., Fisher, R., and Ho, D. D. (1990) Recombinant sCD4 therapy in patients with AIDS and AIDS-related complex. *Ann. Int. Med.* 112, 247–253.
- Shak, S., Capon, D. J., and Ward, R. H. R. (1989) CD4 polypeptide derivatives. European Patent Application #EP 0 372 752 A2.
- Smith, D. H., Byrn, R. A., Marsters, S. A., Gregory, T., Groopman, J. E., and Capon, D. J. (1987) Blocking of HIV-1 infectivity by a soluble, secreted form of the CD4 antigen. *Science* 238, 1704–1707.
- Smith, P. K., Krohn, R. I., Hermanson, G. T., Mallia, A. K., Gartner, F. H., Provenzano, M. D., Fujimoto, E. K., Goeke, N. M., Olson, B. J., and Klenk, D. C. (1985) Measurement of protein using bicinchoninic acid. *Anal. Biochem.* 150, 76–85.
- Suzuki, T., Kanbara, N., Tomono, T., Hayashi, N., and Shinohara, I. (1984) Physicochemical and biological properties of PEG-coupled immunoglobulin G. *Biochim. Biophys. Acta* 788, 248–255.
- Venkatachalam, M. A., and Rennke, H. G. (1978) The structural and molecular basis of glomerular filtration. *Circulation Res.* 43, 337–347.
- Veronese, F. M., Largajolli, R., Boccu, E., Benassi, C. A., and Schiavon, O. (1985) Activation of PEG by phenylchloroformates and modification of ribonuclease and superoxide dismutase. *Appl. Biochem. Biotech.* 11, 141–152.
- Wang, J., Yan, Y., Garrett, T. P. J., Liu, J., Rodgers, D. W., Garlick, R. L., Tarr, G. E., Husain, Y., Reinherz, E. L., and Harrison, S. C. (1990) *Nature* 348, 411–418.
- Wirth, P., Soupe, J., Tritsch, D., and Biellmann J. F. (1991) Chemical modification of horseradish peroxidase with ethanal-MePEG: Solubility in organic solvents, activity and properties. *Bioorganic Chem.* 19, 133–142.
- Zalipsky, S., and Lee, C. (1992) Use of functionalized PEGs for modification of polypeptides. In: *PEG Chemistry: Biotechnical and Biomedical Applications* (J. M. Harris, Ed.), pp 347–370, Plenum Press, New York.
- Zalipsky, S., Seltzer, R., and Menon-Rudolph, S. (1992) Evaluation of a new reagent for covalent attachment of PEG to proteins. *Biotechnol. Appl. Biochem.* 15, 100–114.

# Hexestrol Diazirine Photoaffinity Labeling Reagent for the Estrogen Receptor

Kathryn E. Bergmann, Kathryn E. Carlson, and John A. Katzenellenbogen\*

Department of Chemistry, University of Illinois, Urbana, Illinois 61801. Received October 4, 1993\*

3-Azibutyl (2*R*\*,3*S*\*)-2,3-bis(4-hydroxyphenyl)pentyl sulfide (1), a photoaffinity labeling reagent for the estrogen receptor (ER), has been prepared in unlabeled and in high specific activity tritium-labeled form (32 Ci/mmol) and has been shown to undergo selective and efficient photocovalent attachment to rat uterine ER. Diazirine 1 demonstrates high binding affinity for ER, as determined by both a competitive binding assay and a direct binding assay (relative binding: estradiol = 100; (1) = 17.  $K_d$ : estradiol = 0.19 nM; (1) = 0.98 nM, respectively). It is efficient in site-specific photoinactivation of ER, reaching the level of 31% after 5 min of irradiation at >315 nm. The tritium-labeled diazirine [<sup>3</sup>H]-1 undergoes specific photocovalent attachment to ER with an attachment efficiency of 29% and a selectivity of 90%. Both of these values are quite high for a photoaffinity reagent. SDS-polyacrylamide gel electrophoretic analysis of the photolabeled proteins shows specific labeling of a major species at  $M_r$  65 000, the same species that is labeled by [<sup>3</sup>H]tamoxifen aziridine, a well-characterized affinity label for ER. Hexestrol diazirine 1 is the first carbene-generating photoaffinity label that covalently labels ER with high efficiency and selectivity, and it should be useful in further studies on the hormone-binding domain of ER.

## INTRODUCTION

Affinity labeling is a technique that can be used to obtain structural information about binding sites in biomolecules, through the use of photochemically reactive or electrophilic derivatives of ligands that are capable of covalent attachment to the proteins (1). This technique has been used to label many binding proteins, such as hormone receptors, enzymes, and immunoglobins (2); affinity labels have also been used to investigate membrane structures (3).

We have developed molecular probes to study the ligand-binding domain of the estrogen receptor (ER) through the use of photoaffinity labels containing a wide variety of photoreactive functionalities: diazo ketones (4), aryl (1, 4a, 5), acyl (6) or alkyl (7) azides,  $\alpha,\beta$ -unsaturated ketones (8), aryl halides, (9) and nitro compounds (1, 4b). A photosensitive group that has not previously been employed in photoaffinity labels for ER is the diazirine heterocycle. Diazirines have shown favorable characteristics in many other photoaffinity labeling studies (10).

Diazirines absorb at 350–380 nm, well away from the absorption maxima of proteins (280 nm) and nucleic acids (260 nm) (11). (On the other hand, aryl azides, the most widely used photoactivatable group to date, absorb maximally at 250 nm (12).) Irradiation of diazirines generates carbenes that have sufficient lifetime to undergo C–H bond insertion reactions (11b), forming stable covalent bonds with many types of functional groups found in proteins. Diazirines can also undergo photochemical rearrangement to diazo compounds, which upon protonolytic diazotization give carbocations that can form covalent bonds by nucleophile capture (11a,c). Certain other photoaffinity reagents which undergo covalent attachment to proteins do not give reagent–receptor bonds that are stable during the chemical manipulations required to identify the site of attachment (e.g., proteolytic and chemical cleavage to peptides and Edman degradation) (12). Photoaffinity labels with a diazirine functional group, on the other hand,

have been shown to modify amino acids in several proteins in such a manner that these proteins do not undergo significant loss of label during the residue identification processes (13).

Both steroidal and nonsteroidal ligands for ER have been modified with photochemically reactive or electrophilic groups (1, 8, 14). Hexestrol (2), a nonsteroidal estrogen with a 3-fold higher affinity for ER than estradiol, has been functionalized with reactive groups as a biological probe for the ER, e.g., 3-azidohehexestrol (3) (4, 15) and ketononestrol aziridine (4) (16). 3-Azidohehexestrol (3) was found to have low photocovalent attachment to ER (ca. 10%), and its labeling selectivity was poor (4). Ketononestrol aziridine (4), an electrophilic labeling agent, is limited to reaction with highly reactive nucleophilic amino acid residues (17).

Recently, Kuhn et al. (18) described the preparation of a photolabile thioglycoside containing a dialkyldiazirine (5) as an analog of *N*-acetylhexosaminides and used it to specifically label both subunits of the enzyme  $\beta$ -hexosaminidase. On the basis of this favorable approach, we undertook the preparation of a hexestrol derivative substituted on the side chain with the same diazirine functionality. We report here the synthesis of the hexestrol diazirine photoaffinity label in unlabeled (1) and in high specific-activity tritium labeled forms ([<sup>3</sup>H]-1). We have found that this hexestrol diazirine demonstrates highly efficient and selective photocovalent attachment to ER.

## EXPERIMENTAL PROCEDURES

**A. Chemical Procedures. Materials.** The preparation of 2(*R*\*),3(*S*\*)-bis[4-[(*tert*-butyldimethylsilyloxy)-phenyl]pentanethiol (6) was reported previously (16b). 3-Azibutanol and its toluenesulfonate ester 7a were prepared according to the procedures of Church (19). Dry tetrahydrofuran (THF) was obtained by distillation from sodium benzophenone ketyl. All other chemicals and reagents were purchased from Aldrich Chemical Co. and were used without further purification.

**Methods.** All reactions were carried out under nitrogen atmosphere. In most cases, a standard procedure for

\* Abstract published in *Advance ACS Abstracts*, February 1, 1994.

product isolation and purification was used. Isolation consisted of quenching the reaction mixture in water or an aqueous solution, extracting with an organic solvent, drying over an anhydrous salt, filtering, and evaporating the solvent under reduced pressure. This is indicated in the text by the phrase "product isolation", which is followed by a list of the components in parentheses. The usual method for purification of reaction products consisted of flash chromatography performed according to standard methods (20) using Woelm 32–63- $\mu$ m silica gel. This is indicated in the text by the phrase "purification", with the eluting solvent given in parentheses. Elemental analyses were performed by the Microanalytical Laboratory at the University of Illinois and are within  $\pm 0.4\%$  of theory. High-performance liquid chromatography (HPLC) was performed isocratically for the unlabeled hexestrol diazirine using column A (a Whatman Partisil-10 silica gel preparative column (30 cm  $\times$  4.6 cm)) with a UV variable-wavelength detector set at 254 nm; the solvent system used was 35%  $\text{CH}_2\text{Cl}_2$ -*i*-PrOH (95:5) and 65% hexane at 5 mL/min. HPLC of [ $^3\text{H}$ ]hexestrol diazirine was performed isocratically using column B (a Supelcosil LC-CN semipreparative column (5  $\mu$ m, 25 cm  $\times$  10 mm) from Supelco, Inc., with a guard column packed with pellicular CN from Alltech) with a UV wavelength detector set at 254 nm and a Packard Flo-one  $\beta$  radiometric radiochromatography detector; the solvent systems used were 8% (2% MeOH-EtOAc) and 92% hexane (normal phase conditions using Flo-Scint I cocktail) and 30% or 40% water-MeOH (reversed phase conditions using Flo-Scint II cocktail).

**Chemical Synthesis of 3-Azibutyl 2,3-Bis(4-hydroxyphenyl)pentyl Sulfide.** 3-Azi-1-[(methylsulfonyl)oxy]butane (**7b**). 3-Azi-1-butanol, as well as its toluenesulfonate ester **7a**, were prepared as previously reported (19). The methanesulfonate ester **7b** was prepared as follows: 3-Azi-1-butanol (371 mg, 3.706 mmol) was dissolved in 7 mL of dry THF and cooled to 0 °C.  $\text{Et}_3\text{N}$  (1.03 mL, 7.390 mmol) was added to the solution, followed by slow addition of  $\text{CH}_3\text{SO}_2\text{Cl}$  (440  $\mu$ L, 5.569 mmol). A precipitate formed, and the solution turned a pale yellow. After the solution was stirred at 0 °C for 1 h, product isolation ( $\text{H}_2\text{O}$ , EtOAc,  $\text{MgSO}_4$ ) and purification (50% EtOAc/Hex) afforded 578 mg (88%) of the methanesulfonate ester **7b** as a clear oil:  $^1\text{H}$  NMR ( $\text{CDCl}_3$ )  $\delta$  1.11 (s, 3H,  $\text{CN}_2\text{CH}_3$ ), 1.80 (t, 2H,  $J = 6.2$  Hz,  $\text{CH}_2\text{CN}_2$ ), 3.07 (s, 3H,  $\text{OSO}_2\text{CH}_3$ ), 4.14 (t, 2H,  $J = 6.3$  Hz,  $\text{CH}_2\text{OSO}_2$ ); mass spectrum (CI)  $m/z$  (relative intensity) 178 (8), 152 (4), 111 (5), 109 (6), 97 (7), 67 (7), 55 (100). The molecular ion was too weak to be observed at high resolution.

3-Azibutyl (2*R*\*,3*S*\*)-2,3-Bis[4-[(*tert*-butyldimethylsilyl)oxy]phenyl]pentyl Sulfide (**8**). The oil was removed from  $\sim 40$  mg of KH (60% in oil, 5–10 fold excess) with dry THF, and the solid was cooled to  $-78^\circ\text{C}$ . erythro-Pentanethiol **6** (51.5 mg, 0.0996 mmol) and toluenesulfonate **7a** (30.7 mg, 0.1207 mmol) were dissolved in 1 mL of dry THF, and the solution was added to the KH slowly. The mixture was allowed to warm to room temperature slowly. After the mixture was stirred for an additional 5 h, product isolation (5% aqueous  $\text{Na}_2\text{HPO}_4$ , EtOAc,  $\text{MgSO}_4$ ) and purification (5% EtOAc/Hex) afforded 44.9 mg (75%) of the protected pentyl butyl sulfide **8** as an oily white solid: mp 44–49 °C;  $^1\text{H}$  NMR ( $\text{CDCl}_3$ )  $\delta$  0.21 (s, 12H,  $(\text{CH}_3)_2\text{Si}$ ), 0.53 (t, 3H,  $J = 7.3$  Hz,  $\text{CH}_2\text{CH}_3$ ), 0.90 (s, 3H,  $\text{CN}_2\text{CH}_3$ ), 0.98 (s, 9H,  $(\text{CH}_3)_3\text{C}$ ), 0.99 (s, 9H,  $(\text{CH}_3)_3\text{C}$ ), 1.2–1.5 (m, 4H,  $\text{CH}_2\text{CH}_3$  and  $\text{CH}_2\text{CH}_2\text{CN}_2$ ), 1.97 (t, 2H,  $J = 7.9$  Hz,  $\text{CH}_2\text{CH}_2\text{CN}_2$ ), 2.4–2.47 (m, 2H,  $\text{CHCH}_2\text{S}$ ), 2.54 (dt, 1H,  $J = 3.3, 10.6$  Hz,  $\text{CHCH}_2\text{S}$ ), 2.79

(dt, 1H,  $J = 4.9, 9.7$ ,  $\text{CHCH}_2\text{CH}_3$ ), 6.75–7.05 (m, 8H, ArH); MS (FAB)  $m/z$  (relative intensity) 599 ( $\text{M}^+ + 1$ , 2), 586 (2), 483 (2), 349 (5), 279 (23), 261 (35), 249 (50), 223 (38), 221 (25). Anal. Calcd for  $\text{C}_{33}\text{H}_{54}\text{N}_2\text{O}_2\text{SSi}_2$ : C, 66.17; H, 9.08; N, 4.68. Found: C, 66.32; H, 9.25; N, 4.62.

3-Azibutyl (2*R*\*,3*S*\*)-2,3-Bis(4-hydroxyphenyl)pentyl Sulfide (**1**). From the Bis(silyl)ether (**8**). To the solution of silyl-protected hexestrol diazirine **8** (17.7 mg, 0.0295 mmol) dissolved in 5 mL of THF was added 120  $\mu$ L of (*n*-Bu) $_4$ NF (0.120 mmol). After the solution was stirred for 30 min, a 10-fold excess of TsOH (56 mg, 0.294 mmol) was added to quench the phenolic ammonium salts. After being stirred 5 min, the solution was passed through a  $\text{SiO}_2$  plug, and the solvent was dried with  $\text{MgSO}_4$  and then was removed under reduced pressure. Purification (40% EtOAc/Hex) afforded 10.6 mg (97%) of the deprotected diazirine **1** as a white solid. Further purification by HPLC was accomplished using column A ( $t_R = 20.8$  min) before submission for binding analysis: mp 132–134 °C dec;  $^1\text{H}$  NMR (acetone- $d_6$ )  $\delta$  0.50 (t, 3H,  $J = 7.3$  Hz,  $\text{CH}_2\text{CH}_3$ ), 0.87 (s, 3H,  $\text{CN}_2\text{CH}_3$ ), 1.2–1.5 (m, 4H,  $\text{CH}_2\text{CH}_3$  and  $\text{CH}_2\text{CH}_2\text{CN}_2$ ), 2.0 (t, 2H,  $J = 7.8$  Hz,  $\text{CH}_2\text{CH}_2\text{CN}_2$ ), 2.45–2.5 (m, 2H,  $\text{CHCH}_2\text{S}$ ), 2.59 (dt, 1H,  $J = 3.6, 10.8$  Hz,  $\text{CHCH}_2\text{S}$ ), 2.81 (dt, 1H,  $J = 5.0, 8.6$ ,  $\text{CHCH}_2\text{CH}_3$ ), 6.75–7.15 (m, 8H, ArH), 8.15 (s, 2H, ArOH); IR (KBr pellet)  $\text{cm}^{-1}$  3302, 2955, 1599, 1512, 1236; UV (MeOH) nm ( $\epsilon$ ) 206 (26 500), 230 (20 900), 282 (3900); MS (FAB)  $m/z$  (relative intensity) 371 ( $\text{M}^+ + 1$ , 12), 279 (6), 261 (3), 250 (3), 195 (4), 169 (8); HRMS calcd for  $\text{C}_{21}\text{H}_{27}\text{N}_2\text{O}_2\text{S}$  371.1793, found 371.1785. Anal. Calcd C, 68.08; H, 7.07; N, 7.56; S, 8.65. Found: C, 68.04; H, 7.15; N, 7.52; S, 8.54.

From Reaction with 3-Azi-1-[(methylsulfonyl)oxy]butane (**7b**). The oil was removed from  $\sim 15$ –20 mg KH (60% in oil, 5–10 fold excess) with dry THF, and the solid was cooled to  $-78^\circ\text{C}$ . erythro-Pentanethiol **6** (20.8 mg, 0.0402 mmol) and methanesulfonate **7b** (36 mg, 0.202 mmol) were dissolved in 1 mL of dry THF, and the resulting solution was added to the KH slowly. The mixture was allowed to warm to room temperature. After the mixture was stirred for an additional 24 h, product isolation (5% aqueous  $\text{Na}_2\text{HPO}_4$ , EtOAc,  $\text{MgSO}_4$ ) and purification (40% EtOAc/Hex) afforded 5.4 mg (36%) of the deprotected pentyl butyl sulfide **1** as a white solid.

From the tetraiodohexestrol (**9**). The starting tetraiodide **9** (3.7 mg, 0.0042 mmol) was dissolved in 0.5 mL EtOAc. To the solution was added 5% Pd on alumina (22.5 mg) and  $\text{Et}_3\text{N}$  (5  $\mu$ L). The reaction was placed under hydrogen atmosphere. After 2.5 h, the solution was passed through a plug of Celite, and the solvent was removed in vacuo. Purification (40% EtOAc/Hex) afforded 1.4 mg (89%) of the expected protio product **1** and 0.6 mg of the corresponding ketone **13** (obtained by over reduction and hydrolysis of the diazirine).

3-Azibutyl (2*R*\*,3*S*\*)-2,3-Bis(3,5-diiodo-4-hydroxyphenyl)pentyl Sulfide (**9**). The starting bisphenol **1** (11.4 mg, 0.31 mmol) and molecular iodine (60 mg, 0.236 mmol) were dissolved in 2 mL of benzene. Morpholine (50  $\mu$ L, 0.573 mmol) was added to the solution, which turned from orange to clear. The mixture was allowed to stir at room temperature overnight. Product isolation (5% HCl, EtOAc, 20% aqueous  $\text{Na}_2\text{S}_2\text{O}_3$ ,  $\text{MgSO}_4$ ) and purification (30% EtOAc/Hex) afforded 21 mg (78%) of the tetraiodo product **9** as a pale yellow solid:  $^1\text{H}$  NMR (acetone- $d_6$ )  $\delta$  0.55 (t, 3H,  $J = 7.4$  Hz,  $\text{CH}_2\text{CH}_3$ ), 0.92 (s, 3H,  $\text{CN}_2\text{CH}_3$ ), 1.2–1.4 (m, 4H, contains (1.36, t, 2H,  $J = 7.3$  Hz,  $\text{CH}_2\text{CH}_2\text{CN}_2$ ) and  $\text{CH}_2\text{CH}_3$ ), 2.13 (t, 2H,  $J = 7.7$  Hz,  $\text{CH}_2\text{CH}_2\text{CN}_2$ ), 2.546 (AB quartet, 1H,  $J = 13.2$  Hz,  $\Delta\nu = 21.07$  Hz,  $\text{CHCHHS}$ ), 2.558 (AB quartet, 1H,  $J = 13.3$  Hz,  $\Delta\nu =$

36.99 Hz, CHCHHS), 2.65–2.8 (m, 1H, CHCH<sub>2</sub>S), 2.98 (dt, 1H,  $J = 3.8, 10.6$  Hz, CHCH<sub>2</sub>CH<sub>3</sub>), 7.73 (s, 2H, ArH), 7.76 (s, 2H, ArH); IR (KBr pellet) cm<sup>-1</sup> 3456, 2924, 1456; UV (MeOH) nm ( $\epsilon$ ) 224 (56 900), 292 (5900), 300 (5800); MS (FAB)  $m/z$  (relative intensity) 875 ( $M^+ + 1$ , 10), 748 (4), 419 (10), 387 (11), 359 (13), 345 (10), 223 (25), 195 (100); HRMS calcd for C<sub>21</sub>H<sub>23</sub>N<sub>2</sub>O<sub>2</sub>Si<sub>4</sub> 874.7659, found 874.7632.

**Radiochemical Synthesis of [<sup>3</sup>H]-3-Azibutyl 2,3-Bis(4-hydroxyphenyl)pentyl Sulfide ([<sup>3</sup>H]-1).** The conditions for tritiolysis of the tetraiodohexestrol diazirine **9** were based on those used for the hydrogenolysis of **9**, with the exception that the reaction time was doubled (to 90 min) in the hopes of ensuring complete reduction. A sample of the I<sub>4</sub>-hexestrol diazirine **9** (47.9 mg, 0.0548 mmol), purified by flash chromatography, was sent to Amersham Corp. (Arlington Heights, IL) where the radiochemical incorporation was performed according to the reported procedure.

"To a solution of I<sub>4</sub>-hexestrol **9** (47.9 mg, 0.0548 mmol) in 5 mL EtOAc was added 72  $\mu$ L Et<sub>3</sub>N (0.514 mmol) and 118 mg Pd on alumina (5%, 0.05545 mmol Pd). The solution was exposed to carrier-free tritium gas for 90 min at 25 °C and atmospheric pressure. The solution was then filtered through a 2 cm plug of Celite to remove the Pd catalyst and the residue was washed with 60% EtOAc/hexane (3  $\times$  2 mL). The solvent was removed in vacuo using low heat (tepid bath). Exchangeable tritium was removed using standard solvent exchange-evaporation cycles, but avoided warming above 40 °C. The resulting crude product was dissolved in ethanol and stored at -20 °C. The total amount of radioactivity produced was 1.75 Ci (28% of theoretical)."

The 100-mCi sample, obtained from Amersham, was examined by TLC and HPLC. Radio-TLC was difficult to interpret, and the reaction product was later determined to be unstable on silica. Analysis of the crude [<sup>3</sup>H]-hydrogenolysis products by normal and reversed-phase HPLC using cyanopropyl-substituted silica packing showed the presence of all iodinated intermediates, plus a small amount (<5%) of the fully tritiated product. A portion (ca. 30 mCi) of the 100-mCi sample (8 mL of the 25 mL) was concentrated in the dark under a gentle stream of N<sub>2</sub> and was taken up in 1:1 EtOAc/hexane in order to load onto the HPLC system. Normal-phase HPLC using semi-preparative cyanopropyl column B with 8% (5% MeOH in EtOAc)/92% hexane as the eluent at 5 mL/min was used to isolate the radioactive iodinated species ([<sup>3</sup>H]-<sup>3</sup>H<sub>3</sub>), for immediate further hydrogenation. These fractions ( $t_R = 22$ –36 min) were collected, removing the unreacted I<sub>4</sub>-hexestrol diazirine ( $t_R > 45$  min), and most of the solvent was removed under reduced pressure using low heat. The activity was taken up in 3 mL of EtOAc, and to the solution was added 5 mg of Pd catalyst (5% on alumina) and 10  $\mu$ L of Et<sub>3</sub>N. The solution was placed under a hydrogen atmosphere in the dark for 60 min, monitoring the reaction by HPLC (every 20 min) for disappearance of the radioactive iodinated species. The reaction was worked up by passing the mixture through a plug of Celite atop of silica, using 50% EtOAc/hexane as the eluting solvent. The solution was concentrated in vacuo, and the product was purified using the same conditions as before (cyanopropyl column, 8% (5% MeOH/EtOAc) in 92% hexane as the eluent), giving ~25 mCi, which corresponds to a radiochemical yield of ~80%.

The specific activity of [<sup>3</sup>H]hexestrol diazirine **1**, obtained from the tetraiodo precursor **9** by this two-stage tritiolysis-hydrogenolysis procedure, was determined to

be 32 Ci/mmol by Scatchard analysis (21). The radiochemical purity was evaluated by reinjection onto HPLC using both normal- and reversed-phase conditions; these analyses indicated a single peak of radioactivity (>90%) with a retention time of 37 min for normal phase (same conditions) and 14 min for reversed phase (40% H<sub>2</sub>O in MeOH), identical to the retention time of the unlabeled standard.

**B. Biological Procedures. Materials.** Biochemicals were obtained from the following sources: tritium-labeled estradiol ([6,7-<sup>3</sup>H]E<sub>2</sub>) (estra-1,3,5(10)-triene-3,17 $\beta$ -diol), 48 Ci/mmol, and [<sup>3</sup>H]tamoxifen aziridine (TAZ) ([ring-<sup>3</sup>H]-(Z)-[1-[4-[2-(N-aziridinyl)ethoxy]phenyl]]-1,2-diphenyl-1-butene), 20 Ci/mmol, were from Amersham Corp.; dextran, grade C, from Schwarz/Mann; 2-mercaptoethanol, ethylenedinitrilotetraacetic acid tetrasodium salt (EDTA), acrylamide, Photo-Flo 200, and *N,N'*-diallyltartardiamide were from Eastman Kodak Co.; Triton X-114 was from Chem Central-Indianapolis; bromophenol blue, *N,N,N',N'*-tetramethylethylenediamine (TEMED), sodium azide, and 1,4-bis(5-phenyloxazol-2-yl)benzene (POPOP) were from Aldrich Chemical Co.; sodium dodecyl sulfate (SDS) was from Matheson, Coleman, and Bell; ammonium peroxydisulfate and *N,N*-dimethylformamide (DMF) were from Fisher Scientific; periodic acid was from G. Frederick Smith Chemical Co.; unlabeled estradiol, leupeptin, phenylmethylsulfonyl fluoride (PMSF), activated charcoal, Trizma base, ovalbumin (MW 44 600), bovine serum albumin (MW 67 000), phosphorylase B (MW 97 400), and  $\beta$ -galactosidase (MW 116 000) were from Sigma Chemical Co.; Coomassie Brilliant Blue R-250 was from Colab Laboratories, Inc.; and 2,5-diphenyloxazole (PPO) was from Research Products International Corp. Rat and lamb uterine cytosols were prepared and stored as previously described (22). All experiments were done in TEA buffer (0.01 M Tris-HCl, 0.0015 M EDTA, and 0.02% sodium azide, pH 7.4 at 25 °C). Leupeptin (0.1 mg/mL) and PMSF (1 mM) were added to the cytosol to prevent proteolysis in samples for electrophoresis. The charcoal-dextran slurry used to remove unbound ligand was prepared as previously reported (15a) and was used at 1 part to 10 parts of cytosol solution.

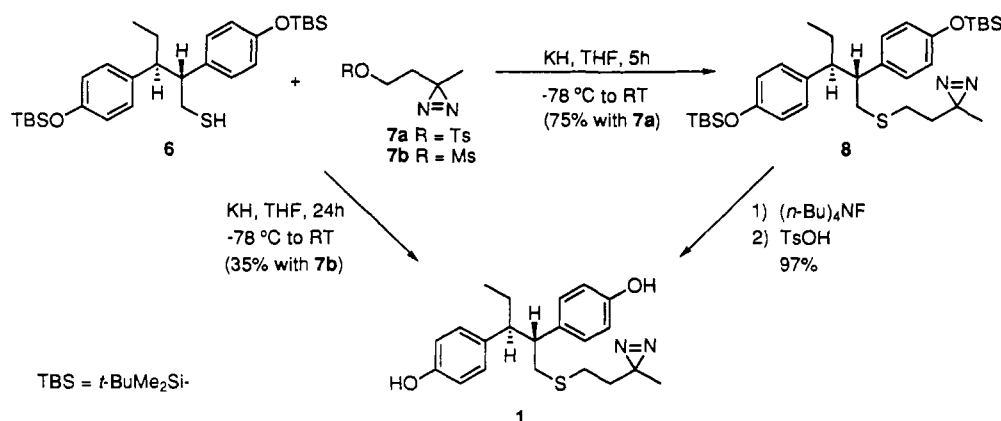
**Methods. Relative Binding Affinity (RBA).** Assays were performed as previously reported using lamb or rat uterine cytosol diluted to ~1.5 nM receptor (15a). Cytosol was incubated with buffer or several concentrations of unlabeled competitor together with 10 nM [<sup>3</sup>H]estradiol as tracer at 0 °C for 18–24 h. The unlabeled competitor was prepared in 1:1 dimethylformamide (DMF)/TEA to ensure solubility.

**Scatchard Assay.** Rat uterine cytosol was incubated at 0 °C for 4 h with various concentrations of [<sup>3</sup>H]ligand in the absence or presence of a 100-fold excess of unlabeled estradiol. Aliquots of the incubation solution were counted to determine the concentrations of total [<sup>3</sup>H]steroid. The incubation solutions were then treated with charcoal-dextran, and the bound [<sup>3</sup>H]steroid was determined. Data were processed according to the method of Scatchard (23).

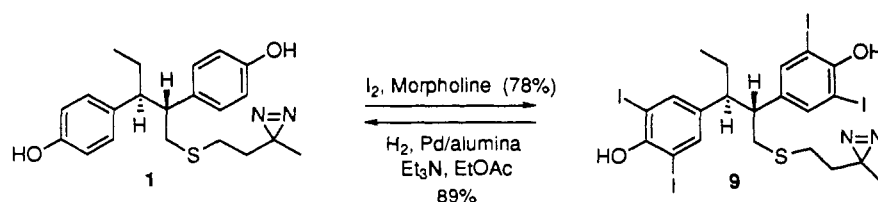
**Specific Activity.** A Scatchard plot for the [<sup>3</sup>H]diazirine ligand plotting Ci/mL was employed to determine the specific activity (21). The X-intercept gave  $6.347 \times 10^{-8}$  Ci/mL. From the parallel incubation assay of [<sup>3</sup>H]estradiol with the same receptor preparation, it was determined that there were 1.938 nM receptor sites. If one assumes that both the hexestrol diazirine and estradiol bind to the same sites, this corresponds to a specific activity of 32 Ci/mmol.

**Photolysis.** Photolysis was routinely carried out at >315

Scheme 1



Scheme 2



nm, using a 450-W mercury vapor lamp, Hanovia L679A, surrounded by a solution filter of saturated aqueous copper(II) sulfate at 2–4 °C, employing Pyrex reaction vessels, as previously described (4b).

**Inactivation Assay.** Covalent binding of nonradioactive ligands was estimated by a photolysis-exchange assay previously described for the estrogen receptor (4b).

**Attachment Assay.** Covalent binding of labeled ligands was measured directly by a filter disk assay previously described (24).

**Electrophoresis.** SDS electrophoresis samples and gels were prepared as previously reported (5c) with standard proteins of  $\beta$ -galactosidase (MW 116 000), phosphorylase B (MW 97 400), bovine serum albumin (MW 67 000), and ovalbumin (MW 44 600) to establish a molecular weight curve.

## RESULTS

**Synthesis of Hexestrol Diazirine (1).** The thioether linkage in the hexestrol diazirine derivative (1) could conceivably be formed from either side of the sulfur atom. However, since the protected *erythro*-pentanethiol **6** was readily available (16b) and the 3-azibutanol derivative **7a** had been previously synthesized (19), we selected the route shown in Scheme 1. Due to the low yields encountered in the preparation of 3-azi-1-[(*p*-tolylsulfonyl)oxy]butane (**7a**), we also prepared the methanesulfonate derivative, **7b**. Activation of the alcohol was accomplished by reaction with methanesulfonyl chloride (MsCl) in Et<sub>3</sub>N to form **7b** in high yield (88%). Coupling of the pentanethiol **6** with either of the activated azibutanols using KH as the base (Scheme 1) afforded either the protected thioether product **8** (75% yield from toluenesulfonate **7a**) or the deprotected product **1** (35% yield from the less reactive methanesulfonate, **7b**), the simultaneous deprotection in this case resulting from hydrolysis of the aryl silyl ethers during the more vigorous thioether synthesis. Deprotection of the aryl silyl ethers in **8** was accomplished by treatment with tetra-*n*-butylammonium fluoride (TBAF) to give the bisphenol diazirine **1** in 97% yield.

**Synthesis and Hydrogenation of Tetraiodohexestrol Diazirine (10).** The aromatic rings were selected

as sites for radiolabeling of the hexestrol diazirine. Iodination of both unprotected phenolic rings in **1** using iodine in morpholine (25) gave the tetraiodohexestrol **10** in good yield (Scheme 2). During the course of the reaction (after 1 h), only one intermediate was observed by TLC analysis; it most likely contained a mixture of iodinated hexestrols (I<sub>1</sub>–I<sub>3</sub> stage). Complete iodination to the I<sub>4</sub> stage was achieved after 8 h.

Palladium-catalyzed hydrogenolysis of aryl iodides is a standard method for tritiation of aromatic rings (16a, 17b,d, 26). However, in our system, the potential sensitivity of the diazirine to reduction was a concern (10). Hydrogenation of the tetraiodo diazirine under standard conditions (5% palladium on alumina with Et<sub>3</sub>N to scavenge HI) afforded the protiodiazirine **1** in good yield within 1 h. Extended reaction times or increased quantities of catalyst led to the formation of the methyl ketone **13**. In a time course study in which 1 mol % of palladium on alumina catalyst was used, the optimum reaction time for complete reduction of aryl iodide **9** without overreduction of the product diazirine **1** was 45 min.

A possible mechanism for the transformation of the diazirine to the ketone is outlined in Scheme 3. The diazirine is first reduced to the diaziridine **10**, which is cleaved to form the unstable  $\alpha$ -diamine **11** that would undergo hydrolysis to form the ketone **13**. Although hydrogenation with palladium on carbon is known to produce the alkyl amine and ammonia (27), we did not observe formation of the alkylamine **14** under our reduction conditions, indicating that the proposed imine intermediate **12** undergoes hydration in preference to hydrogenation.

**Radiochemical Synthesis and Purification of [<sup>3</sup>H]-Hexestrol Diazirine ([<sup>3</sup>H]-1).** A sample of the tetraiodohexestrol diazirine derivative and the palladium on alumina catalyst we had used were sent to Amersham Corp. to be labeled with carrier-free [<sup>3</sup>H]H<sub>2</sub>. While a 45-min reaction time had been optimal in our hands for hydrogenolysis, we recommended a 90-min reaction time for tritiation, in an attempt to compensate for an anticipated tritium isotope effect (26).

The radiolabeled sample returned from Amersham was

Scheme 3

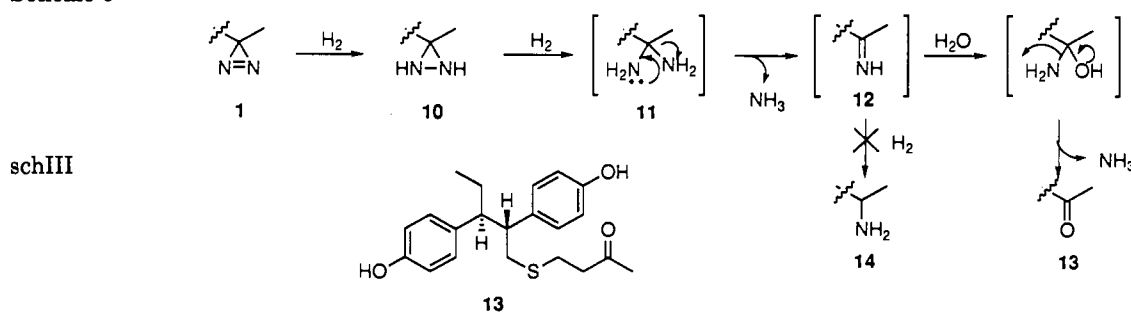


Table 1. Relative Binding Affinities and Inactivation Efficiencies (PIE) of Some Hexestrol Affinity Labels and Related Compounds

compd no.	substituents	RBA <sup>a</sup> $E_2 = 100\%$	inactivation efficiency <sup>b</sup> (%)
1	R = S(CH <sub>2</sub> ) <sub>2</sub> CN <sub>2</sub> CH <sub>3</sub>	17 (20) <sup>c</sup>	31 (29) <sup>c</sup>
15 <sup>d</sup>	= S(CH <sub>2</sub> ) <sub>3</sub> CH <sub>3</sub>	37	
16a <sup>e</sup>	= S(CH <sub>2</sub> ) <sub>n</sub> N $\triangle$ n = 2	5.8	0
16b <sup>e</sup>	n = 3	1.8	60–100
16c <sup>e</sup>	n = 4	0.30	ND <sup>f</sup>
17 <sup>g</sup>	= CH <sub>2</sub> OCOCHN <sub>2</sub>	55	ND
18 <sup>g</sup>	= COCHN <sub>2</sub>	2.8	ND
3 <sup>h</sup>	R' = H, R'' = H <sub>3</sub>	69	9, 15
19 <sup>h</sup>	R' = CH <sub>2</sub> COCHN <sub>2</sub> , R'' = H	1.8	15
4 <sup>e</sup>	R''' = (CH <sub>2</sub> ) <sub>4</sub> N $\triangle$	8.3	48–70
20 <sup>e</sup>	= S(CH <sub>2</sub> ) <sub>3</sub> CH <sub>3</sub>	44	
21 <sup>d,j</sup>	= CHN <sub>2</sub>	10.5	40
22 <sup>j</sup>	= CH <sub>2</sub> N <sub>3</sub>	38	ND

<sup>a</sup> The receptor binding affinity (RBA) was determined in a competitive radiometric binding assay with [<sup>3</sup>H]estradiol ( $E_2$ ) as the tracer. For further details, see the individual references designated. <sup>b</sup> The inactivation was determined by an exchange assay. The aziridines inactivated the estrogen receptor via nucleophilic addition, whereas the others were photoactivated. <sup>c</sup> The numbers in parentheses represent covalent photoattachment of the [<sup>3</sup>H]-labeled derivative. <sup>d</sup> K. E. Bergmann and J. A. Katzenellenbogen, unpublished results. <sup>e</sup> For preparation, see ref 16b. <sup>f</sup> ND = not determined. <sup>g</sup> J. T. Park and J. A. Katzenellenbogen, unpublished results. <sup>h</sup> For preparation, see ref 15a,b. <sup>i</sup> Values for photoinactivation at >315 and 254 nm, respectively. <sup>j</sup> S. W. Landvatter and J. A. Katzenellenbogen, unpublished results.

assayed by HPLC and was found to contain a mixture of all possible hydrogenolysis products: these include unreacted tetraiodide starting material ( $I_4$ ), iodinated intermediates ( $I_1$ – $I_3$ , seven of them are possible), and a small amount of the expected tetratritiohexestrol diazirine product [<sup>3</sup>H]-1 (9a). No significant amount of the reduced diazirine was observed. In order to obtain the desired product with the highest possible specific activity, the  $I_1$ – $I_3$  species and the  $I_0$  or  $^3H_4$  species (with a small amount of  $I_1$ ) were isolated as two separate fractions. Each of these fractions was exposed to hydrogen to complete the hydrogenolysis. The fraction with the mixture of  $I_1$ – $I_3$  species, which contained most (ca. 90%) of the total activity, was reduced smoothly, and the desired product was purified with high efficiency, by careful normal-phase HPLC on derivatized silica gel (see below). The fraction with the highest specific activity ( $I_0$ – $I_1$ ) (ca. 5% of the total activity), however, decomposed upon hydrogenation, and no expected product could be isolated.

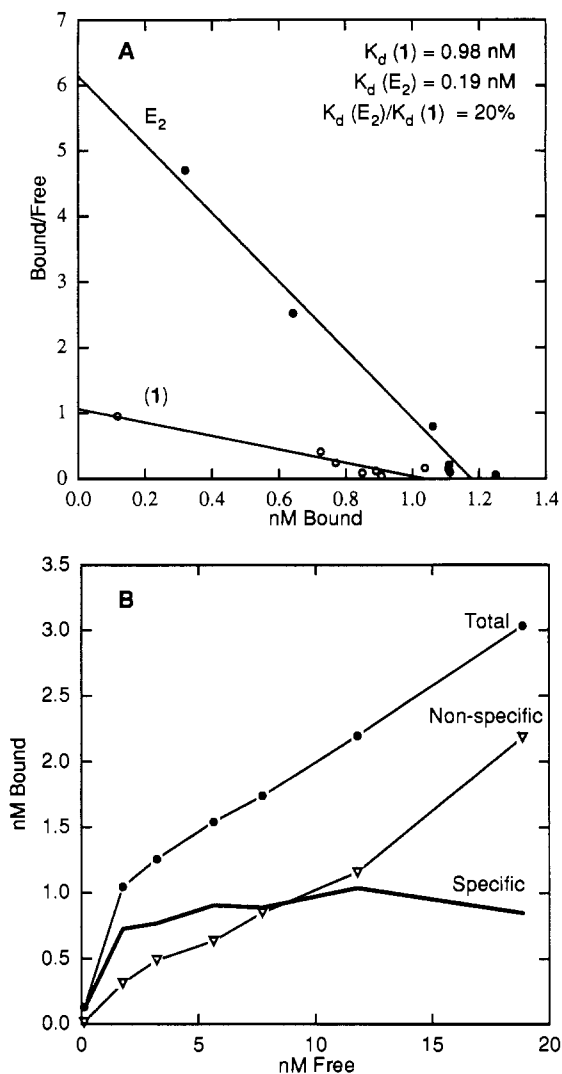
Traditional methods for determination of specific activity involve HPLC analysis. However, this could not be readily used for the [<sup>3</sup>H]hexestrol diazirine as its UV absorption at long wavelengths is too low to quantitate readily. The specific activity, determined indirectly by receptor binding analysis (see below), was 32.8 Ci/mmol, indicating an average of about one tritium atom per hexestrol molecule.

#### Estrogen Receptor Binding Studies on Hexestrol Diazirines 1 and [<sup>3</sup>H]-1. Relative binding affinities

(RBA) of the hexestrol diazirine 1, four similar hexestrol aziridines (16a–c, 4), and some structurally related side chain-substituted photolabile hexestrols (diazoketones 17, 18, and 21 and  $\beta$ -ketomethyl azide 22) for the estrogen receptor (ER) were determined by a competitive radiometric binding assay with [<sup>3</sup>H]estradiol as the radiotracer (15a). The data given in Table 1 are expressed relative to estradiol (100%,  $K_d = 0.19$  nM) (28). Hexestrol diazirine 1 has a moderately high RBA of 17%, which is higher than the hexestrol aziridines (16 and 4) with similar structures (0.3–8.3%). The photolabile hexestrol derivatives (all except 15, 16, 4, and 20) exhibit a wide range of binding affinities, ranging from the diazomethyl ketone 18 (2.8%) to the more extended diazoacetate 17 (55%). Placing a keto functionality at the C-2 position of hexestrol (29) has been shown to enhance binding affinity (butyl thioester 20 = 44% vs butyl sulfide 15 = 37% and C-2 diazomethyl ketone 21 = 10.5% vs C-3 diazomethyl ketone 18 = 2.8%). However, even though a thioester linkage might increase the binding affinity of the hexestrol diazirine for the receptor, their hydrolytic lability compared to the sulfide linkage makes them less desirable.

The binding affinity of [<sup>3</sup>H]hexestrol diazirine 1 to the estrogen receptor was determined directly using a binding titration assay. The direct binding plots for the [<sup>3</sup>H]-hexestrol diazirine (Figure 1, panel B) show moderate levels of nonspecific binding. This is consistent with the higher lipophilicity of this compound (measured as the octanol–water partition coefficient, log  $P$ ) compared to estradiol:

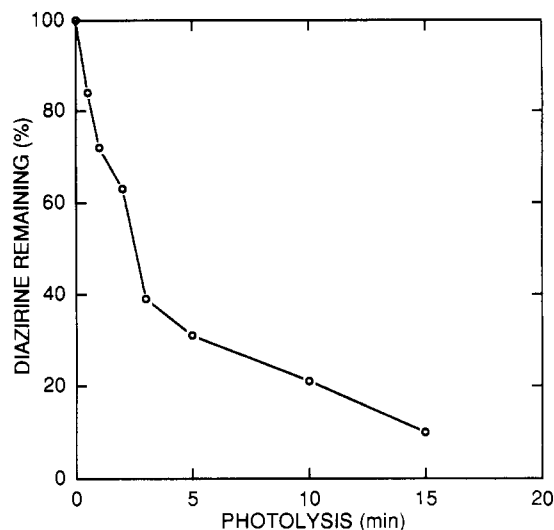




**Figure 1.** Binding assay for [<sup>3</sup>H]hexestrol diazirine 1. Rat uterine cytosol was incubated at 0 °C for 4 h with various concentrations of tritium-labeled ligand ([<sup>3</sup>H]-1 or [<sup>3</sup>H]-E<sub>2</sub>) in the absence (for total binding) or presence (for nonspecific binding) of a 100-fold excess of unlabeled estradiol. Aliquots of the incubation solution were counted to determine the concentration of total tritium-labeled ligand present. The incubation solutions were then treated with charcoal-dextran, and the concentration of the bound tritium-labeled ligand was determined. Specific binding is the difference between total and nonspecific binding. Data are presented as Scatchard (panel A) or direct (panel B) plots.

$\log P$  (estradiol) = 3.52;  $\log P$  (1) = 4.63. A direct comparison of the specific binding curves for the [<sup>3</sup>H]-hexestrol diazirine and for [<sup>3</sup>H]estradiol are presented as a Scatchard (23) plot (Figure 1, panel A). From this plot [<sup>3</sup>H]hexestrol diazirine 1 has an affinity of  $K_d$  = 0.98 nM for ER, or 20% that of [<sup>3</sup>H]estradiol. This value compares closely to that observed in the competitive binding assay (RBA = 17%).

**Solution Photolysis and Estrogen Receptor Photoinactivation by the Hexestrol Diazirine 1.** A preliminary investigation of the time course of photolysis of the hexestrol diazirine in solution was effected by irradiation with a mercury arc lamp through an aqueous CuSO<sub>4</sub> filter (effective  $\lambda$  > 315 nm) (4b). Hexestrol was added as the internal standard, and the progress of the photolysis was monitored by HPLC at 254 nm (Figure 2). Under these conditions, more than 70% of the diazirine has undergone photolysis by 5 min, with only 10% remaining at 15 min. Two minor products which increased with time of photolysis (to 25–30% of the expected maximum) had



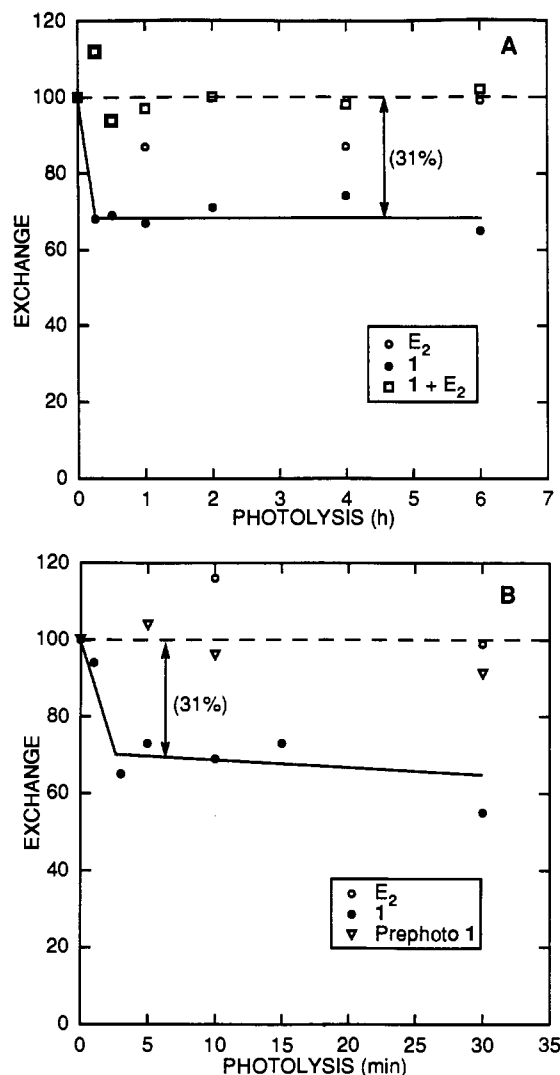
**Figure 2.** Time course of photolysis of hexestrol diazirine 1 ( $10^{-4}$  M in 5% DMF/TEA buffer). Photolysis was at >315 nm at 0 °C; aliquots were removed at various time points and extracted with EtOAc, and the quantity of hexestrol diazirine remaining was determined by reference to the internal standard (hexestrol) by HPLC.

retention times similar to the hexestrol butenes that might be produced from the carbene intermediate by a 1,2-hydrogen shift (11), but these were not identified definitively. No other significant products were observed. However, products that might have formed from insertion into water or buffer components might have been too polar to be observed under the normal-phase HPLC conditions we employed.

To investigate the photoinactivation efficiency (PIE) (4b) of the hexestrol diazirine 1 in the binding site of the estrogen receptor (ER), we photolyzed (at >315 nm) a receptor cytosol preparation that had been preincubated with the hexestrol diazirine. Upon photocovalent attachment, the receptor–ligand complex loses its capability for reversible binding. This is measured by a radiotracer exchange assay together with certain controls: (1) to monitor the stability of ER under photolysis conditions, (2) to monitor the nonspecific component of photoinactivation, and (3) to ensure no photoinactivation results from the photolysis products.

As shown in Figure 3, hexestrol diazirine reaches 31% photoinactivation within 30 min of photolysis, and the receptor is stable under these photolysis conditions for up to 6 h. No photoinactivation is observed when the receptor is incubated with either estradiol or the prephotolyzed hexestrol diazirine. Photolysis for shorter periods showed that most of the photoinactivation occurs within the first 5 min. (In order to determine the extent of photocovalent attachment of hexestrol diazirine to the ER and the extent of nonspecific attachment, it is necessary to study the photolysis with [<sup>3</sup>H]hexestrol diazirine 1; see below.) Inactivation efficiencies for hexestrol diazirine 1 and related hexestrol derivatives are given in Table 1. The percent inactivation of ER by hexestrol diazirine 1 (31%) was greater than the inactivation with the other photoactivatable derivatives (aryl azide 3 (9–15%) and diazo ketone 19 (15%)), although it was not as high as the inactivation by the electrophilic aziridines (4 and 16b; 50–100%).

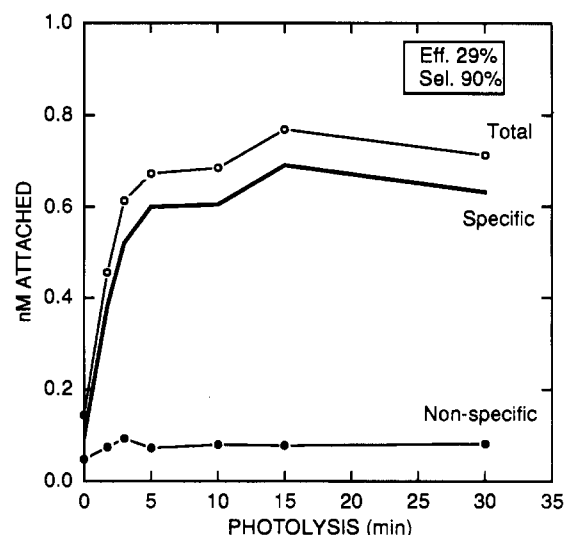
**Photolabeling of the Estrogen Receptor with Hexestrol Diazirine [<sup>3</sup>H]-1.** [<sup>3</sup>H]Hexestrol diazirine 1 was photolyzed at >315 nm in rat uterine cytosol preparations, and the percent of specific and nonspecific attachment



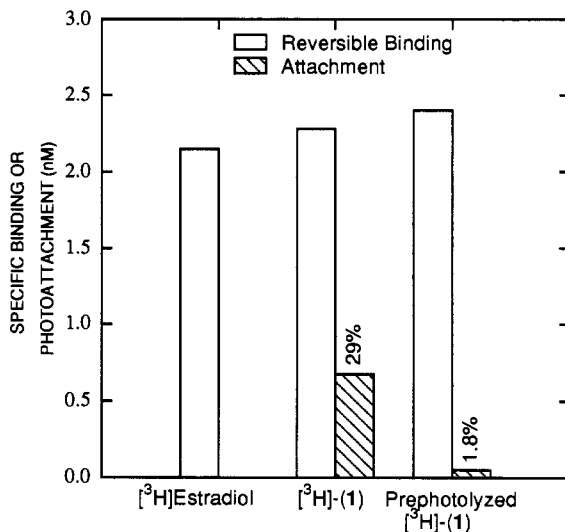
**Figure 3.** Photoinactivation of ER by hexestrol diazirine 1 during 6 h (panel A) or 30 min (panel B) of photolysis. Cytosol was incubated with diazirine 1 in the presence or absence of a 100-fold excess of estradiol for 1 h at 0 °C and then photolyzed at >315 nm for various times. Following charcoal-dextran treatment to remove free ligand, the cytosol was exchanged at room temperature for 20 h against [ $^3$ H]estradiol. Photoinactivation of reversible binding is seen as a loss of exchangeable sites and plotted as a percent of initial binding before photolysis. The percent specific photoinactivation is shown as a vertical double headed arrow, with a value given in parentheses. Control experiments included incubation with  $E_2$  alone to measure photodestruction of the protein and incubation with prephotolyzed 1 to measure inactivation by photoproducts.

was examined by a filter disk-solvent extraction assay (24). The binding was done in the presence of DMF (5%) (5c, 30), and the sample was pretreated with charcoal to remove excess free reagent before photolysis. Low concentrations of DMF reduce the extent of nonspecific binding of lipophilic ligands, thereby increasing the fraction of the ligand that is available for binding to the ER (30); this increases the extent and selectivity of ER labeling (5c). Photoattachment *efficiency* is defined as the amount of ER covalently labeled after photolysis as a percent of ER occupied reversibly by the affinity reagent; photoattachment *selectivity* is defined as the amount of ER labeled as a percent of the total protein covalently labeled upon photolysis (5c).

The time course of specific covalent attachment is shown in Figure 4. The specific attachment rises with time of photolysis and levels off after ~5 min. Diazirine 1 exhibits



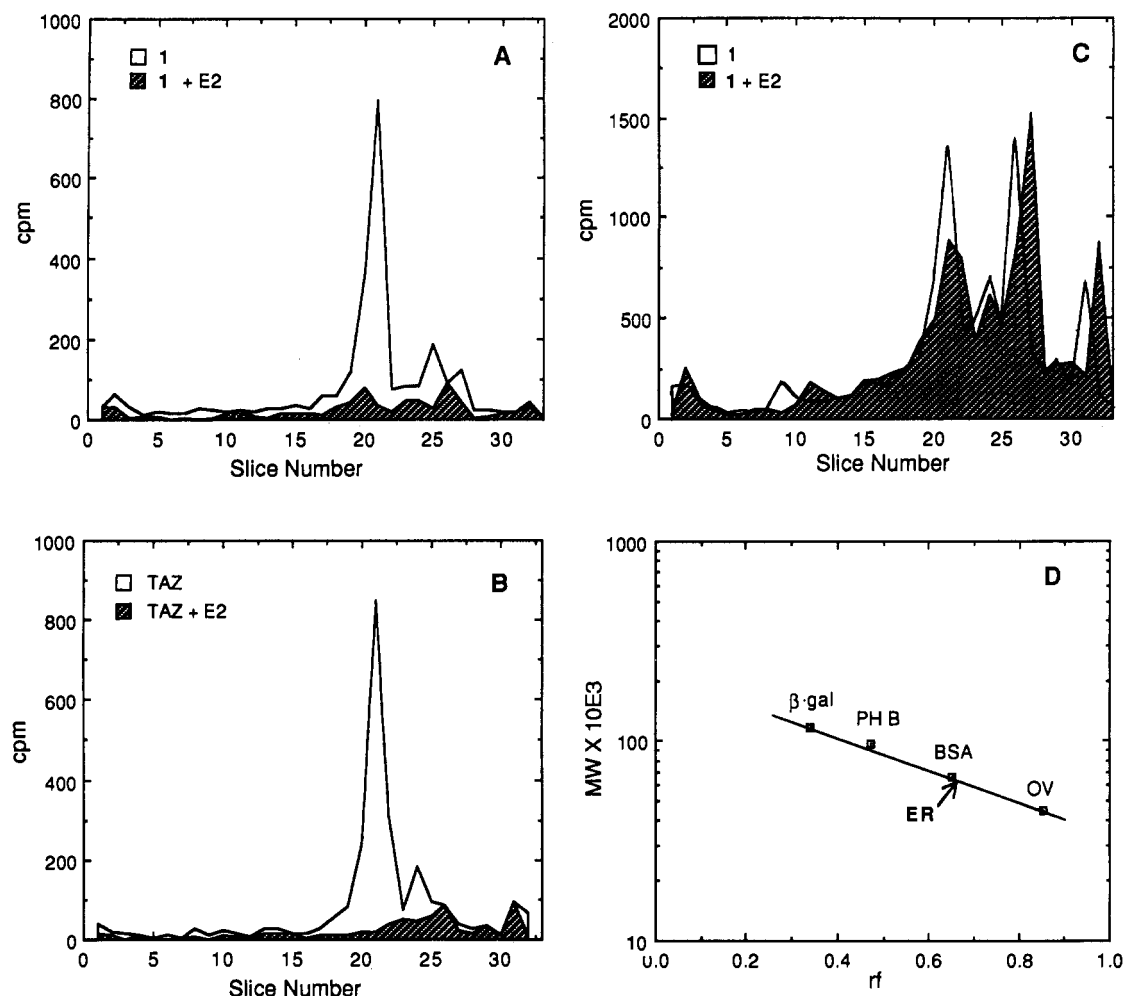
**Figure 4.** Time course of photoattachment of [ $^3$ H]hexestrol diazirine 1 with charcoal pretreatment. Rat uterine cytosol was incubated for 1 h at 0 °C in the dark in the absence (total) or presence (nonspecific) of an excess of unlabeled estradiol and then was photolyzed at >315 nm. Attachment was measured by the ethanol disk assay (see Experimental Procedures) for total attachment and nonspecific attachment; the specific attachment is the difference between the two values. Efficiency represents the attachment as a percentage of the reversible binding; selectivity is specific attachment as a percentage of total attachment.



**Figure 5.** Binding properties of [ $^3$ H]hexestrol diazirine 1 and prephotolyzed [ $^3$ H]hexestrol diazirine 1. A sample of [ $^3$ H]-hexestrol diazirine 1 was prephotolyzed for 30 min at >315 nm in ethanol. Rat uterine cytosol was incubated for 1 h at 0 °C in the dark with [ $^3$ H]hexestrol diazirine 1 and the prephotolyzed sample in the presence and absence of a 100-fold excess of unlabeled estradiol. After charcoal treatment to remove reversible binding, a portion was photolyzed at >315 nm for 30 min and assayed for photoattachment by ethanol disk assay.

moderate photoattachment efficiency (29%) and high photoattachment selectivity (90%) under these optimal conditions (5% DMF and charcoal treatment prior to photolysis). The attachment efficiency is comparable to the rate and extent predicted by the photolysis time course (Figure 2) and the photoinactivation assay (Figure 3, 31%), respectively.

The extent of ER binding and photolabeling by the photoproducts of [ $^3$ H]hexestrol diazirine 1 was also examined (Figure 5). A prephotolyzed sample, prepared by irradiating [ $^3$ H]hexestrol diazirine 1 in EtOH for 30



**Figure 6.** SDS-polyacrylamide gel electrophoresis of photoattached [ $^3\text{H}$ ]hexestrol diazirine 1 pretreated with charcoal-dextran (panel A) and without pretreatment (panel C) and [ $^3\text{H}$ ]tamoxifen aziridine (TAZ) (panel B). The calibration curve of standard proteins is shown in panel D. The standard proteins are  $\beta$ -galactosidase ( $\beta$ -gal), phosphorylase B (PH B), bovine serum albumin (BSA), and ovalbumin (OV). By linear regression the correlation coefficient of the line is 0.997.

min in a Pyrex tube at  $\lambda > 315$  nm, showed reversible ER binding equivalent to [ $^3\text{H}$ ]estradiol and [ $^3\text{H}$ ]hexestrol diazirine 1 but gave negligible photoattachment.

**Characterization of the ER Covalently Labeled with [ $^3\text{H}$ ]Hexestrol Diazirine.** SDS-polyacrylamide gel electrophoretic analysis of ER covalently labeled with [ $^3\text{H}$ ]hexestrol diazirine 1 in the presence and absence of excess estradiol, and with and without pretreatment with charcoal, is shown in Figure 6. The major peak migrates with a  $M_r$  of  $\sim 65\,000$  and corresponds to ER; a minor peak, at a  $M_r$  of  $\sim 53\,000$ , probably represents a proteolysis fragment of ER (31) (panel A). Similar results have been observed with [ $^3\text{H}$ ]tamoxifen aziridine, which is a well characterized electrophilic affinity label for the ER (panel B) (17a,b). The labeling of both fragments is blocked by addition of excess unlabeled estradiol. In the experiment in panel A, excess [ $^3\text{H}$ ]hexestrol diazirine was removed by treatment with charcoal prior to photolysis. If free ligand is not removed, the extent of nonspecific labeling is much greater (panel C).

## DISCUSSION

We have made a significant effort to develop affinity labeling agents for the estrogen receptor (ER) that will be efficient and selective in their labeling and will provide information about the composition of the ligand binding site of the receptor (4, 5, 8, 15–17). Such information is of great importance in elucidating structure-function

relationships of these receptors and has proven to be very useful in the development of three-dimensional models for hormone binding domains of these receptors (32).

The most successful affinity labeling agent for ER, prepared to date, is tamoxifen aziridine, an electrophilic derivative of an estrogen antagonist that labels ER with an efficiency approaching 100% and with selectivity as high as 90% (17a,b). The most promising photoaffinity label is a benzothiophene azide recently prepared by our group, which demonstrates high receptor binding affinity (66%), high specific photoinactivation efficiency (55%), and good photocovalent attachment (25%) (5c). Despite this promise, the photocovalent link of this reagent with ER appears to be chemically unstable (K. E. Carlson, J. A. Katzenellenbogen, unpublished results).

In this report, we present the synthesis and evaluation of a hexestrol-based photolabeling agent with a photo-sensitive diazirine group. Diazirines were initially developed to overcome some of the deficiencies of nitrene-yielding aryl azides (12), and their increasing use reflects their synthetic accessibility, their chemical and thermal stability, and their efficient photolabeling reaction via highly reactive carbene intermediates (11). We chose to attach the diazirine function to the nonsteroidal estrogen hexestrol because several hexestrol derivatives, functionalized on the side chain, still exhibit relatively high affinity for ER (23, 29, 33).

Hexestrol diazirine 1 showed a good binding affinity to

ER (17% that of estradiol) that was slightly less than a protio analog (butyl pentyl sulfide 15, 37%), but was higher than the aziridines of similar structure (16a-c; 5.8%, 1.8%, 0.3%, respectively). The specific binding of [<sup>3</sup>H]-1 to ER, relative to that of [<sup>3</sup>H]estradiol, determined by Scatchard analysis, was comparable at 20%.

The photolysis of diazirine 1 proceeds smoothly and rapidly at long wavelengths (>315 nm), where ER appears to be very stable to photodegradation. The photoattachment efficiency of [<sup>3</sup>H]diazirine 1 to ER (29%), determined directly, is almost exactly the same as the photoinactivation efficiency (31%), determined indirectly on unlabeled diazirine 1 by a photolysis exchange assay. While, in principle, these efficiencies may be equal, we have rarely found the attachment efficiency of a photoaffinity labeling agent to be equal to its photoinactivation efficiency, since many processes other than covalent attachment may contribute to the loss of exchangeable sites in the indirect photoinactivation assay (4b, 34). The 30% efficiency for [<sup>3</sup>H]-1 is also relatively high for steroid receptor photolabeling agents, and with proper experimental protocols (charcoal pretreatment), the labeling of ER is also very selective, approaching 90%, in rat uterine cytosol preparations, despite the relatively high lipophilicity of diazirine 1.

While competition for covalent labeling of ER by pretreatment with unlabeled estradiol is generally considered a good criterion for receptor specific labeling, the charcoal pretreatment protocol compromises this and requires additional verification of this selectivity. SDS-polyacrylamide gel electrophoretic analysis of [<sup>3</sup>H]diazirine 1 labeled ER shows a pattern equivalent to that obtained when ER is labeled with the well characterized electrophilic affinity labeling agent tamoxifen aziridine (17a,b).

Although photoaffinity labeling agents have been used to identify binding site residues in the progesterone receptor and the glucocorticoid receptor (35), in ER the only sites identified have been two cysteine residues labeled by the electrophilic agent tamoxifen aziridine (17a). The aziridine function in this reagent is weakly electrophilic, so the reagent labels only the most nucleophilic residue, cysteine. In the development of diazirine 1 and its use to label ER, we hope to be able to identify additional residues in the ligand binding site. Such work is currently underway.

#### ACKNOWLEDGMENT

We are grateful for support of this research through a grant from the National Institutes of Health (PHS 5R37 DK15556). High-resolution mass spectra were obtained on instruments supported by the National Institutes of Health (GM 27029), and <sup>1</sup>H NMR were obtained on a Varian QE 300 MHz instrument supported by the National Institutes of Health (PHS 1S10 RR 02299).

#### LITERATURE CITED

- (1) (a) Katzenellenbogen, J. A., Kilbourn, M. R., and Carlson, K. E. (1980) Photosensitive Steroids as Probes of Estrogen Receptors Sites. *Ann. N. Y. Acad. Sci.* 346, 18-30. (b) Knowles, J. R. (1972) Photogenerated Reagents for Biological Receptor-Site Labeling. *Acc. Chem. Res.* 5, 155-60. (c) Bayley, H. (1983) *Photogenerated Reagents in Biochemical and Molecular Biology*, Elsevier, Amsterdam.
- (2) (a) Plapp, B. V. (1982) Application of Affinity Labeling for Studying Structure and Function of Enzymes. *Methods Enzymol.* 87, 469-99. (b) Shih, L. B., and Bayley, H. (1985) A Carbene-Yielding Amino Acid for Incorporation into Peptide Photoaffinity Reagents. *Anal. Biochem.* 144, 132-41.
- (3) (a) Brunner, J., and Richards, F. M. (1980) Analysis of Membranes Photolabeled with Lipid Analogues. *J. Biol. Chem.* 255, 3319-28. (b) Delfino, J. M., Schreiber, S. L., and Richards, F. M. (1993) Design, Synthesis, and Properties of a Photoactivatable Membrane-Spanning Phospholipid Probe. *J. Am. Chem. Soc.* 115, 3458-74. (c) Lundblad, R. L., and Noyes, C. M. (1984) *Chemical Reagents for Protein Modification*, Vols. 1 and 2, CRC Press, Boca Raton, FL.
- (4) (a) Katzenellenbogen, J. A., Carlson, K. E., Johnson, H. J., and Myers, H. N. (1977) Estrogen Photoaffinity Labels II: Reversible Binding and Covalent Attachment of Photosensitive Hexestrol Derivatives to the Uterine Estrogen Receptor. *Biochemistry* 16, 1970-76. (b) Katzenellenbogen, J. A., Johnson, H. J., Carlson, K. E., and Myers, H. N. The Photoreactivity of Some Light Sensitive Estrogen Derivatives. The Use of an Exchange Assay to Determine Their Photoinactivation with Rat Uterine Estrogen Binding Protein. *Biochemistry* 13, 2986-94.
- (5) (a) Katzenellenbogen, J. A. (1978) Photoaffinity Labeling of Estrogen Receptor. *Fed. Proc.* 37, 174-78. (b) Pinney, K. G., and Katzenellenbogen, J. A. (1991) Synthesis of a Tetrafluoro-Substituted Aryl Azide and Its Protio Analogue as Photoaffinity Labeling Reagents for the Estrogen Receptor. *J. Org. Chem.* 56, 3125-33. (c) Pinney, K. G., Katzenellenbogen, B. S., and Katzenellenbogen, J. A. (1991) Efficient and Selective Photoaffinity Labeling of the Estrogen Receptor Using Two Nonsteroidal Ligands That Embody Aryl Azide or Tetrafluoroaryl Azide Photoreactive Functions. *Biochemistry* 30, 2421-31.
- (6) Pinney, K. G. Design, Synthesis, and Biochemical Evaluation of Novel Photoaffinity Labeling Reagents for the Estrogen and Progesterone Receptors. Ph. D. Thesis, University of Illinois at Urbana-Champaign, 1990. (Acyl azides were proposed as photoactivatable groups for affinity labels) (a) Sigman, M. E., Autrey, T., and Schuster, G. B. (1988) Arylnitrenes with Singlet Ground States: Photochemistry of Acetyl-Substituted Aryl and Aryloxycarbonyl Azides. *J. Am. Chem. Soc.* 110, 4297. (b) Melvin, T., and Schuster, G. B. (1990) The Photochemistry of Acetyl-Substituted Aryl Azides: The Design of Photolabeling Agents for Inert Sites in Hydrophobic Regions. *Photochem. Photobiol.* 31, 155; however, their lack of chemical stability greatly decreases their receptor attachment efficiency and selectivity.)
- (7) Link, R. P., Kutner, A., Schnoes, H. K., and DeLuca, H. F. (1987) Photoaffinity Labeling of Serum Vitamin D Binding Protein by 3-Deoxy-3-azido-25-hydroxyvitamin D<sub>3</sub>. *Biochemistry* 26, 3957-64.
- (8) Katzenellenbogen, J. A., and Katzenellenbogen, B. S. (1984) Affinity Labeling of Receptors for Steroid and Thyroid Hormones. *Vitamins and Hormones*, pp 213-74, Vol. 41, Academic, New York.
- (9) (a) Katzenellenbogen, J. A., and Hsiung, H. M. (1975) Iodohesterols I. The Synthesis and Photoreactivity of Iodinated Hexestrol Derivatives. *Biochemistry* 14, 1736-41. (b) Katzenellenbogen, J. A., Hsiung, H. M., Carlson, K. E., McGuire, W. L., Kraay, R. J., and Katzenellenbogen, B. S. (1975) Iodohesterols II. Characterization of the Binding and Estrogenic Activity of Iodinated Hexestrol Derivatives, In Vitro and In Vivo. *Biochemistry* 14, 1742-50.
- (10) Church, R. F. R., Kende, A. S., and Weiss, M. J. (1965) Diazirines. I. Some Observations on the Scope of the Ammonia-Hydroxylamine-O-sulfonic Acid Diaziridine Synthesis. The Preparation of Certain Steroid Diaziridines and Diazirines. *J. Am. Chem. Soc.* 87, 2665-71.
- (11) (a) *Chemistry of Diazirines* (1987) (M. T. H. Liu, Ed.) CRC Press, Boca Raton, FL. (b) Modarelli, D. A., Morgan, S., and Platz, M. S. (1992) Carbene Formation, Hydrogen Migration, and Fluorescence in the Excited States of Dialkyldiazirines. *J. Am. Chem. Soc.* 114, 7034-41. (c) Morgan, S., Jackson, J. E., and Platz, M. S. (1991) Laser Flash Photolysis Study of Adamantanylidene. *J. Am. Chem. Soc.* 113, 2782-3.
- (12) *Azides and Nitrenes* (1984) (E. F. V. Scriven, Ed.) Academic, Orlando, FL.
- (13) (a) Nakayama, T. A., and Khorana, H. G. (1990) Synthesis of a New Photoactivatable Analog of 11-*cis*-Retinal. *J. Org. Chem.* 55, 4953-6. (b) Van Ceunenbroeck, J. Cl., Krebs, J.,

- Hanssens, I., and Van Cauwelaert, F. H. (1986) Study of a Hydrophobic Site on Bovine  $\alpha$ -Lactalbumin by Labeling With [ $^{125}$ I]-TID. *J. Biochem. Biophys. Res. Commun.* 138, 604–10.
- (c) White, B. H., Howard, S., Cohen, S. G., and Cohen, J. B. (1991) The Hydrophobic Photoreagent 3-(Trifluoromethyl)-3-m-[( $^{125}$ I]iodophenyl)diazirine ([ $^{125}$ I]TID) Is a Novel Non-competitive Antagonist of the Nicotinic Acetylcholine Receptor. *J. Biol. Chem.* 266, 21595–607.
- (14) (a) Katzenellenbogen, B. S., and Katzenellenbogen, J. A. (1988) In *Affinity Labeling and Cloning of Steroid and Thyroid Hormone Receptors* (H. Gronemeyer, Ed.) pp 87–108, Ellis Horwood Ltd., Chichester, England. (b) Katzenellenbogen, J. A. (1977) In *Biochemical Actions of Hormones* (G. Litwack, Ed.) Vol. 4, Chapter 1, pp 1–84, Academic, New York.
- (15) (a) Katzenellenbogen, J. A., Johnson, H. J., Jr., and Myers, H. N. (1973) Photoaffinity Labels for Estrogen Binding Proteins of Rat Uterus. *Biochemistry* 12, 4085–92. (b) Katzenellenbogen, J. A., Myers, H. N., and Johnson, H. J., Jr. (1973) Reagents for Photoaffinity Labeling of Estrogen Binding Proteins. Synthesis of Some Azide and Diazo Derivatives of Estradiol, Estrone, and Hexestrol. *J. Org. Chem.* 38, 3525–33. (c) Katzenellenbogen, J. A., Myers, H. N., Johnson, H. J., Jr., Kempton, R. J., and Carlson, K. E. (1977) Estrogen Photoaffinity Labels I: Chemical and Radiochemical Synthesis of Hexestrol Diazoketone and Azide Derivatives: Photochemical Studies in Solution. *Biochemistry* 16, 1964–70.
- (16) (a) Elliston, J. F., Zablocki, J. A., Katzenellenbogen, B. S., and Katzenellenbogen, J. A. (1987) Ketononestrol Aziridine, an Agonistic Estrogen Receptor Affinity Label: Study of Its Bioactivity and Estrogen Receptor Covalent Labeling. *Endocrinology* 121, 667–76. (b) Zablocki, J. A., Katzenellenbogen, J. A., Carlson, K. E., Norman, M. J., and Katzenellenbogen, B. S. (1987) Estrogenic Affinity Labels: Synthesis, Irreversible Receptor Binding, and Bioactivity of Aziridine-Substituted Hexestrol Derivatives. *J. Med. Chem.* 30, 829–38.
- (17) (a) Harlow, K. W., Smith, D. M., Katzenellenbogen, J. A., Greene, G. L., and Katzenellenbogen, B. S. (1989) Identification of Cysteine-530 as the Covalent Attachment Site of an Affinity Labeling Estrogen (Ketononestrol Aziridine) and Antiestrogen (Tamoxifen Aziridine) in the Human Estrogen Receptor. *J. Biol. Chem.* 264, 17476–85. (b) Katzenellenbogen, J. A., Carlson, K. E., Heiman, D. F., Robertson, D. W., Wei, L. L., and Katzenellenbogen, B. S. (1983) Efficient and Highly Selective Labeling of the Estrogen Receptor with [ $^3$ H]Tamoxifen Aziridine. *J. Biol. Chem.* 258, 3487–95. (c) Salituro, F. G., Elliston, J. F., Carlson, K. E., Katzenellenbogen, B. S., and Katzenellenbogen, J. A. (1986) [ $^{125}$ I]Iododesethyl Tamoxifen Aziridine: Synthesis and Covalent Labeling of the Estrogen Receptor with an Iodine-Labeled Affinity Label. *Steroid* 48, 287–313. (d) Simpson, D. M., Elliston, J. J., and Katzenellenbogen, J. A. (1987) Desmethylnafoxidine Aziridine: An Electrophilic Affinity Label for the Estrogen Receptor with High Efficiency and Selectivity. *J. Steroid Biochem.* 28, 233–45.
- (18) Kuhn, C.-S., Lehmann, J., and Sandhoff, K. (1992) Efficient Photoaffinity Labeling of Human  $\beta$ -Hexosaminidase A. Synthesis and Application of 3-Azi-1-[(2-acetamido-2-deoxy-1- $\beta$ -D-glucopyranosyl)thio]- and -galactopyranosyl)thio]butane. *Bioconjugate Chem.* 3, 230–33.
- (19) Church, R. F. R., and Weiss, W. J. (1970) Diazirines. II. Synthesis and Properties of Small Functionalized Diazirine Molecules. Some Observations on the Reaction of A Diaziridine with Iodine–Iodine Ion System. *J. Org. Chem.* 35, 2465–71.
- (20) Still, W. C., Kahn, M., and Mitra, A. P. (1978) Rapid Chromatographic Technique for Preparative Separations With Moderate Resolution. *J. Org. Chem.* 43, 2923–25.
- (21) Bindal, R. D., Carlson, K. E., Reiner, G. C. A., and Katzenellenbogen, J. A. (1987) 11 $\beta$ -Chloromethyl- [ $^3$ H]estradiol-17 $\beta$ : A Very High Affinity, Reversible Ligand for the Estrogen Receptor. *J. Steroid Biochem.* 28, 361–370.
- (22) Carlson, K. E., Sun, L.-H. K., and Katzenellenbogen, J. A. (1977) Characterization of Trypsin-Treated Forms of the Estrogen Receptor From Rat and Lamb Uterus. *Biochemistry* 16, 4288–96.
- (23) Scatchard, G. (1949) The Attractions of Proteins for Small Molecules and Ions. *Ann. N. Y. Acad. Sci.* 51, 660–72.
- (24) Katzenellenbogen, J. A., Ruh, T. S., Carlson, K. E., Iwamoto, H. S., and Gorski, J. (1975) Ultraviolet Photosensitivity of the Estrogen Binding Protein from Rat Uterus, Wavelength and Ligand Dependence. Photocovalent Attachment of Estrogens to Protein. *Biochemistry* 14, 2310–16.
- (25) Southwick, P. L., and Kirchner, J. R. (1962) The Morpholine-Iodophenylacetylene Adduct or Charge-Transfer Complex. Formation and Conversion to N-Styrylmorpholine. *J. Org. Chem.* 27, 3305–8.
- (26) Evans, E. A. (1974) *Tritium and its Compounds*, pp 318–415, John Wiley and Sons, New York. (Other references which use this procedure: 17b,d and 16a.)
- (27) Schmitz, E., and Ohme, R. (1961) Preparation and Transformations of Diazirines. *Chem. Ber.* 94, 2166–73.
- (28) With electrophilic affinity labeling agents, such as the aziridine compounds 4, 16, and TAZ, the determination of the receptor binding affinity is probably distorted by simultaneous covalent attachment of these species to the estrogen receptor. Thus, these values should be considered “apparent” RBA values.
- (29) (a) Landvatter, S. W., and Katzenellenbogen, J. A. (1982) Nonsteroidal Estrogens: Synthesis and Estrogen Receptor Binding Affinity of Derivatives of (3R\*,4S\*)-3,4-Bis(4-hydroxyphenyl)hexane (Hexestrol) and (2R\*,3S\*)-2,3-Bis(4-hydroxyphenyl)pentane (Norhexestrol) Functionalized of the Side Chain. *J. Med. Chem.* 25, 1300–7. (b) Landvatter, S. W., and Katzenellenbogen, J. A. (1981) Stereochemical Considerations in the Binding of Non-Steroidal Estrogens to the Estrogen Receptor. *Molec. Pharmacol.* 20, 43–51.
- (30) Katzenellenbogen, J. A., Heiman, D. F., Carlson, K. E., and Lloyd, J. E. (1982) In *Receptor Binding Radiotracers* (W. C. Eckelman, Ed.) Vol. 1, pp 93–126. CRC Press, Boca Raton, FL.
- (31) (a) Sheen, Y. Y., and Katzenellenbogen, B. S. (1987) Antiestrogen Stimulation of the Production of a 37 000 Molecular Weight Secreted Protein and Estrogen Stimulation of the Production of a 32 000 Molecular Weight Secreted Protein in MCF-7 Human Breast Cancer Cells. *Endocrinology* 120, 1140–51. (b) Monsma, F. J., Jr., Katzenellenbogen, B. S., Miller, M. A., Ziegler, Y. S., and Katzenellenbogen, J. A. (1984) Characterization of the Estrogen Receptor and Its Dynamics in MCF-7 Human Breast Cancer Cells Using a Covalently Attaching Antiestrogen. *Endocrinology* 115, 143–53.
- (32) (a) Goldstein, R. A., Katzenellenbogen, J. A., Luthy-Schulten, A. Z. A., Seielstad, D. A., and Wolynes, P. G. (1993) Three-dimensional Model for the Hormone Binding Domains of Steroid Receptors. *Proc. Natl. Acad. Sci. U.S.A.* 90, 9949–9953. (b) Lemesle-Varloot, L., Ojasoo, T., Mornon, J. P., and Raynaud, J. P. (1992) A Model for the Determination of the 3D-Spatial Distribution of the Functions of the Hormone-Binding Domain of Receptors that Bind 3-Keto-4-ene Steroids. *J. Steroid Biochem. Molec. Biol.* 41, 369–88.
- (33) Goswami, R., Harsy, S. G., Heiman, D. F., and Katzenellenbogen, J. A. (1980) Estrogen Receptor-Based Imaging Agents 2. The Synthesis and Receptor Binding Affinity of Side-Chain Halogenated Hexestrol Derivatives. *J. Med. Chem.* 23, 1002–8.
- (34) Cridland, N. A., Wright, C. V. E., McKenzie, E. A., and Knowland, J. (1990) Selective Photochemical Treatment of Estrogen Receptor in a Xenopus Liver Extract Destroys Hormone Binding and Transcriptional Activation but not DNA Binding. *EMBO J.* 9, 1859–66.
- (35) (a) Carlstedt-Duke, J., Strömstedt, P.-E., Persson, B., Cederlund, E., Gustafsson, J. A., and Jörnvall, H. (1988) Identification of Hormone-Interacting Amino Acid Residues Within the Steroid-Binding Domain of the Glucocorticoid Receptor in Relation to Other Steroid Hormone Receptors. *J. Biol. Chem.* 263, 6842–6. (b) Strömstedt, P.-E., and Berkenstam, A., Jörnvall, H., Gustafsson, J. A., and Carlstedt-Duke, J. (1990) Radiosequence Analysis of the Human Progesterone Receptor Changes with [ $^3$ H]Promegestone. *J. Biol. Chem.* 265, 12973–7.

# N-Hydroxysuccinimide Ester Functionalized Perfluorophenyl Azides as Novel Photoactive Heterobifunctional Cross-Linking Reagents. The Covalent Immobilization of Biomolecules to Polymer Surfaces

Mingdi Yan,<sup>†</sup> Sui Xiong Cai,<sup>†,‡</sup> M. N. Wybourne,<sup>§</sup> and John F. W. Keana<sup>\*,†</sup>

Departments of Chemistry and Physics, University of Oregon, Eugene, Oregon 97403. Received September 28, 1993\*

The synthesis of *N*-hydroxysuccinimide (NHS) functionalized perfluorophenyl azides (PFPA) **2** and **3** is described together with a general method for the covalent modification of polymer surfaces using heterobifunctional, photoactivable cross-linking reagents **1** and **3**. The NHS-active ester group becomes covalently attached to the polymer surface via an efficient CH bond insertion reaction of the photogenerated, highly reactive nitrene intermediate derived from the PFPA. The NHS ester is capable of further reaction with a variety of primary amine-containing reagents including biomolecules by way of amide formation. The method is illustrated as follows. Photolysis of polystyrene (PS) and poly-(3-octylthiophene) (P3OT) thin films spin-coated with NHS PFPA ester **1** or **3** gave films **8** or **9**, respectively. Each film was then exposed to an aqueous solution of horseradish peroxidase (HRP), giving films **10** or **11**, respectively. The amounts of HRP immobilized on PS and P3OT were calculated from enzyme activity assays to be  $0.5 \pm 0.1$  ng/mm<sup>2</sup> for **10a**,  $1.0 \pm 0.2$  ng/mm<sup>2</sup> for **11a**,  $0.2 \pm 0.1$  ng/mm<sup>2</sup> for **10b**,  $0.3 \pm 0.1$  ng/mm<sup>2</sup> for **11b**. Using this surface functionalization methodology, biotin-streptavidin-biotin-HRP was constructed on the PS film. The storage stability of HRP thus immobilized through the extended linker, biotin-streptavidin-biotin, was enhanced as compared to that of HRP directly immobilized on the PS surface.

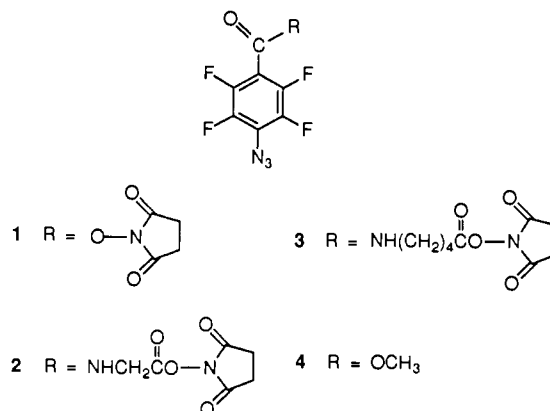
## INTRODUCTION

The conjugation of biologicals such as enzymes (**1**), antibodies (**2**), DNA (**3**), and cells (**4**) to solid supports is of importance in the areas of nucleotide synthesis (**5**), molecular recognition (**6**), polymeric drugs (**7**), and bio-sensors (**8**). The presence of suitably reactive functional groups on the surface is an essential feature in many of these applications. Thus, we became interested in developing a methodology for surface functionalization.

A series of functionalized perfluorophenyl azides (PF-PAs) was developed in our laboratory (**9,10**) and elsewhere (**11-13**) as a new class of photolabeling reagents with improved CH insertion efficiency over their nonfluorinated analogs. By incorporating a PFPA within a molecule that also contained a protein reactive group, there resulted a new series of photoactivated cross-linking reagents for bioconjugation (**14,15**). It occurred to us that functionalization of polymer surfaces ought to be possible through the use of a PFPA containing a second reactive functional group such as an *N*-hydroxysuccinimide (NHS) active ester elsewhere in the molecule. In the process of polymer surface modification, the NHS PFPA ester becomes covalently attached to the polymer surface by way of CH insertion of the highly reactive nitrene intermediate generated by photolysis of the PFPA. The covalently-attached NHS ester is then allowed to react with NHS-reactive groups such as primary amines in proteins or other biomolecules, resulting in the covalent immobilization of proteins or other biomolecules to polymer surfaces. Recently, we communicated the use of NHS-functionalized PFPA for the surface modification of polymers (**16**). By

combining this methodology with either deep-UV or electron beam lithography it is possible to generate micrometer-scale patterns of immobilized biomolecules on the polymer surface (**17**).

Herein, we detail the synthesis of NHS PFPA ester **2** as well as **3**, which has a six-atom spacer unit between the two reactive groups. We also detail the functionalization of polymer surfaces with **1** (**9**) and **3**. The surface



modification process involves a simple spin-coating technique followed by photolysis, providing an attractive alternative to the series of treatments with chemicals as described in other surface functionalization processes (**18**). We also demonstrate the efficient immobilization of the active enzyme horseradish peroxidase (HRP) to polystyrene (PS) and poly(3-octylthiophene) (P3OT) surfaces.

## EXPERIMENTAL PROCEDURES

**General.** Melting points were taken on a Mel-Temp melting point apparatus and are uncorrected. Preparative TLC was performed on Analtech GF precoated silica gel (1000  $\mu$ m) glass-backed plates (20  $\times$  20 cm). <sup>1</sup>H NMR spectra were recorded on a 300-MHz General Electric QE-

<sup>†</sup> Department of Chemistry.

<sup>‡</sup> Present address: Acea Pharmaceuticals, Inc., 1003 Health Science Road West, Irvine, CA 92715.

<sup>§</sup> Department of Physics.

\* Abstract published in *Advance ACS Abstracts*, January 15, 1994.



300. Chemical shifts are reported in  $\delta$  units referenced to residual proton signals of the deuterated solvents. Infrared spectra were obtained on a Nicolet 5DXB FT-IR spectrometer. UV-vis spectra were obtained on a Perkin Elmer Lambda 6 UV-vis spectrophotometer. Mass spectra were recorded on a VG ZAB-2-HF mass spectrometer with a VG-11-250 data system in the electron ionization mode (70 eV). Microanalyses were performed by Desert Analytics of Tucson, AZ. Spin-coating was performed with a Model 1-EC101D-R485 photoresist spinner (Headway Research Inc.) with the spin speed set at 1000 rpm. Baking was accomplished in an oven (Model 1410, VWR Scientific) preheated to 60 °C in air for 20 min. Photolysis was carried out at ambient temperature in a Rayonet photoreactor with 254 nm lamps (400 W) for 5 min.

**Materials.** Circular micro cover glasses (radius 10 mm) were purchased from VWR Scientific, Inc. Triethylamine, dicyclohexylcarbodiimide (DCC), *N*-hydroxysuccinimide (NHS), glycine ethyl ester hydrochloride, and 5-aminopentanoic acid were used as received from Aldrich. Polystyrene (PS) beads were used as received (MW 125 000–250 000, Polysciences Inc.). Poly(3-octylthiophene) (P3OT) was prepared following a known procedure (19). Horseradish peroxidase (HRP) was purchased as a salt-free powder (type IV-A, activity about 1,000 units/mg) from Sigma and used without further purification. Bovine serum albumin (BSA) (fraction V powder) was used as received from Sigma. 2,2'-Azinobis-(3-ethylbenzthiazoline-6-sulfonic acid) diammonium salt (ABTS) was purchased from Sigma and was used without further purification. *N*-(5-Aminopentyl)biotinamide, streptavidin, and biotin-HRP conjugate were used as received from Molecular Probes, Inc. (Eugene, OR). Hydrogen peroxide (30%) was used as received from J. T. Baker (20). NaHCO<sub>3</sub> buffer (0.1 M) was prepared by dissolving 8.4 g of NaHCO<sub>3</sub> in 1.0 L of doubly distilled water. Phosphate buffer (0.1 M, pH 7.0) was prepared from KH<sub>2</sub>PO<sub>4</sub>/K<sub>2</sub>HPO<sub>4</sub> in doubly distilled water. Tetrahydrofuran (THF) was dried over sodium/benzophenone ketyl. Dimethylformamide (DMF) was dried over molecular sieves. Nitromethane and chloroform (CHCl<sub>3</sub>) were dried over CaCl<sub>2</sub> pellets (4–8 mesh).

***N*-(4-Azido-2,3,5,6-tetrafluorobenzoyl)glycine Ethyl Ester (5).** A mixture of glycine ethyl ester hydrochloride (217 mg, 1.55 mmol) and triethylamine (158 mg, 1.56 mmol) in 7.0 mL of THF was stirred for 20 min. 4-Azido-2,3,5,6-tetrafluorobenzoic acid (9) (369 mg, 1.57 mmol) and DCC (324 mg, 1.57 mmol) were added, and the mixture was stirred overnight and filtered. The filtrate was evaporated, and the residue was treated with 20 mL of ethyl acetate. The mixture was filtered, and the filtrate was washed with 0.1 N HCl (2 × 10 mL). The solution was dried and evaporated to leave a solid which was purified by preparative TLC with 1:2 CHCl<sub>3</sub>–hexanes as the developing solvent to give 160 mg (32%) of 5 as a colorless powder, mp 85–86 °C: <sup>1</sup>H NMR (CDCl<sub>3</sub>)  $\delta$  1.32 (t, *J* = 7.1 Hz, 3 H), 4.24 (d, *J* = 4.8 Hz, 2 H), 4.27 (q, *J* = 7.1 Hz, 2 H), 6.54 (m, 1 H); FTIR 2128, 1744, 1686, 1649, 1523, 1488, 1225, 1001 cm<sup>-1</sup>. Anal. Calcd for C<sub>11</sub>H<sub>8</sub>F<sub>4</sub>N<sub>4</sub>O<sub>3</sub>: C, 41.26; H, 2.52; N, 17.50. Found: C, 41.46; H, 2.37; N, 17.66.

***N*-(4-Azido-2,3,5,6-tetrafluorobenzoyl)glycine (6).** To a solution of 5 (60 mg, 0.19 mmol) in 0.5 mL of methanol was added 1 N NaOH (0.25 mL, 0.25 mmol), and the solution was stirred for 1 h. The solution was acidified by addition of 2 N HCl to pH < 1, and the precipitate was filtered and dried to leave 23 mg of 6 as a white powder. The filtrate was extracted with THF/CHCl<sub>3</sub> (1:1, 3 × 3 mL), and the extracts were combined and evaporated to

give another portion (32 mg) of 6 as a white powder (combined yield 55 mg, 99%), mp 147–148 °C: <sup>1</sup>H NMR (CDCl<sub>3</sub> + DMSO-*d*<sub>6</sub>)  $\delta$  4.34 (d, *J* = 4.8 Hz, 2 H), 6.53 (m, 1 H); MS 292 (2, M<sup>+</sup>), 264 (20, M<sup>+</sup> – N<sub>2</sub>), 190 (20, NC<sub>6</sub>F<sub>4</sub>CO), 162 (100, NC<sub>6</sub>F<sub>4</sub>).

***N*-(4-Azido-2,3,5,6-tetrafluorobenzoyl)glycine *N*-Succinimidyl Ester (2).** A solution of 6 (39.3 mg, 0.134 mmol), DCC (29.3 mg, 0.142 mmol), and NHS (16.6 mg, 0.144 mmol) in 0.5 mL of THF was stirred at 25 °C overnight. The resulting mixture was filtered, and the filtrate was evaporated to leave a solid which was redissolved in 1.0 mL of CH<sub>2</sub>Cl<sub>2</sub> and filtered. The filtrate was evaporated to leave 42 mg (80%) of 2 as a white powder, mp 145–146 °C: <sup>1</sup>H NMR (CDCl<sub>3</sub>)  $\delta$  2.88 (s, 4 H), 4.64 (d, *J* = 5.4 Hz, 2 H), 6.55 (m, 1 H); FTIR 2129, 1792, 1748, 1718, 1699, 1649, 1520, 1489, 1204 cm<sup>-1</sup>; MS 389 (8, M<sup>+</sup>), 275 (60, M<sup>+</sup> – NHS), 247 (27, M<sup>+</sup> – NHS – N<sub>2</sub>), 218 (65, M<sup>+</sup> – CONHS – N<sub>2</sub> – H), 190 (45, NC<sub>6</sub>F<sub>4</sub>CO), 162 (100, NC<sub>6</sub>F<sub>4</sub>); high-resolution MS calcd for C<sub>13</sub>H<sub>7</sub>F<sub>4</sub>N<sub>5</sub>O<sub>5</sub> 389.0382, found 389.0405.

**5-(4-Azido-2,3,5,6-tetrafluorobenzamido)pentanoic Acid (7).** To a solution of 5-aminopentanoic acid (238 mg, 2.03 mmol) in 5 mL of 1 N NaOH was added 4-azido-2,3,5,6-tetrafluorobenzoyl chloride (9) (239 mg, 0.942 mmol). The mixture was stirred at 25 °C for 20 min and acidified with 2 N HCl to pH < 1. The white precipitate was filtered, washed with 0.1 N HCl (5 × 3 mL) and water (4 × 3 mL), and dried under reduced pressure to give 273 mg (87%) of 7 as a white powder, mp 160–161 °C: <sup>1</sup>H NMR (CDCl<sub>3</sub> + DMSO-*d*<sub>6</sub>)  $\delta$  1.44 (m, 4 H), 2.08 (t, *J* = 6.9 Hz, 2 H), 3.15 (q, *J* = 6.0 Hz, 2 H), 7.87 (s, 1 H); MS 334 (5, M<sup>+</sup>), 317 (4, M<sup>+</sup> – OH), 306 (40, M<sup>+</sup> – N<sub>2</sub>), 190 (15, NC<sub>6</sub>F<sub>4</sub>CO), 162 (100, NC<sub>6</sub>F<sub>4</sub>); high-resolution MS calcd for C<sub>12</sub>H<sub>10</sub>F<sub>4</sub>N<sub>4</sub>O<sub>3</sub> 334.0687, found 334.0710.

***N*-Succinimidyl 5-(4-Azido-2,3,5,6-tetrafluorobenzamido)pentanoate (3).** NHS PFPA ester 3 was prepared from 100 mg of acid 7 in a manner similar to 2 and was obtained as a white powder (yield 112 mg, 90%), mp 93–95 °C: <sup>1</sup>H NMR (CDCl<sub>3</sub>)  $\delta$  1.77 (m, 2 H), 1.85 (m, 2 H), 2.69 (t, *J* = 6.6 Hz, 2 H), 2.84 (s, 4 H), 3.51 (q, *J* = 6.2 Hz, 2 H), 6.22 (m, 1 H); FTIR 2127, 1817, 1786, 1742, 1681, 1649, 1602, 1526, 1487, 1260, 1209, 1069 cm<sup>-1</sup>; MS 431 (5, M<sup>+</sup>), 403 (3, M<sup>+</sup> – N<sub>2</sub>), 317 (22, M<sup>+</sup> – NHS), 289 (8, M<sup>+</sup> – NHS – N<sub>2</sub>), 162 (100, NC<sub>6</sub>F<sub>4</sub>); high-resolution MS calcd for C<sub>16</sub>H<sub>13</sub>F<sub>4</sub>N<sub>5</sub>O<sub>5</sub> 431.0850, found 431.0866.

**Surface Modification of PS with 1 and 3 To Give Films 8a and 9a.** PS beads (50.0 mg) were dissolved in 1.0 mL of xylenes to form a colorless solution. Two drops of the solution was placed on the surface of a circular micro cover glass, and the glass was spun at 1000 rpm for 2 min to give a smooth PS thin film. A solution of 2.5 mg of NHS PFPA ester 1 (9) or 3 in 0.5 mL of nitromethane was prepared. About 40  $\mu$ L of the solution was placed on top of the PS film, and the glass was spun at 1000 rpm for 1 min. The resulting film was baked for 20 min in an oven preheated to 60 °C and was photolyzed with 254-nm lamps for 5 min to give film 8a or 9a.

The decomposition of azide upon photolysis was monitored by FTIR using a NaCl disk as the support. The FTIR spectrum showed strong absorption at 2128 cm<sup>-1</sup> due to the azide group after the solution of 1 or 3 was spin-coated on the PS film. This absorption completely disappeared after the film was irradiated with 254-nm lamps for 5 min.

**Surface Modification of P3OT with 1 and 3 To Give Films 8b and 9b.** P3OT (20.0 mg) was dissolved in 1.0 mL of CHCl<sub>3</sub> to form a red solution. Four drops of the solution was placed on a circular micro cover glass and

was spun for 2 min to give a red thin film. About 40  $\mu\text{L}$  of a solution of 2.5 mg of 1 or 3 in 0.5 mL of methanol was placed on top of the P3OT film and was spun for 1 min. The resulting film was baked at 60  $^{\circ}\text{C}$  and photolyzed with 254-nm lamps for 5 min to give film 8b or 9b.

A control experiment using a NaCl disk as the support and FTIR to monitor the decomposition of the azido group was performed in a similar manner as described above. The IR spectrum showed strong azide absorption at 2128  $\text{cm}^{-1}$  after the solution of 1 or 3 was spin-coated on the P3OT film and complete disappearance of this absorption when the film was irradiated with 254-nm lamps for 5 min.

**Immobilization of HRP To Give Films 10 and 11.** HRP (2.0 mg) was dissolved in 1.0 mL of 0.1 M pH 8.2  $\text{NaHCO}_3$  buffer containing 10.0 mg of BSA to form a light brown solution (50  $\mu\text{M}$ ). The film obtained above (8 or 9) was incubated under this solution at 25  $^{\circ}\text{C}$  for 3 h and was washed thoroughly with  $\text{NaHCO}_3$  buffer followed by phosphate buffer to give film 10 or 11.

Two control experiments using PS as the polymer substrate were conducted. In the first experiment, a circular micro cover glass was spin-coated with 5% PS solution in xylenes for 2 min (for details see the spin-coating procedure above). The film was baked, photolyzed, incubated in 50  $\mu\text{M}$  HRP solution at 25  $^{\circ}\text{C}$  for 3 h and rinsed thoroughly with  $\text{NaHCO}_3$  buffer followed by phosphate buffer. In the second control experiment, a circular micro cover glass was spin-coated with 5% PS solution in xylenes, then with a solution of 0.5 wt % methyl 4-azido-2,3,5,6-tetrafluorobenzoate (4) in nitromethane on top of the PS film. The film was baked, photolyzed, incubated in 50  $\mu\text{M}$  HRP solution at 25  $^{\circ}\text{C}$  for 3 h, and rinsed thoroughly with  $\text{NaHCO}_3$  buffer followed by phosphate buffer.

A control experiment was performed using P3OT as the support. A circular micro cover glass was spin-coated with 2% P3OT solution in chloroform for 2 min, baked, photolyzed, incubated in 50  $\mu\text{M}$  HRP solution at 25  $^{\circ}\text{C}$  for 3 h, and rinsed thoroughly with  $\text{NaHCO}_3$  buffer followed by phosphate buffer.

**Preparation of PS-Biotin-Streptavidin-Biotin-HRP Conjugate.** A circular micro cover glass was spin-coated as described above with 5% PS solution in xylenes for 2 min and then with 0.5 wt % 1 solution in nitromethane on top of the PS film for 1 min. The film was baked and irradiated with 254-nm lamps for 5 min to give film 8a. *N*-(5-Aminopentyl)biotinamide (2.0 mg) was dissolved in 0.1 mL of DMF, and 0.5 mL of  $\text{NaHCO}_3$  buffer was added to form a colorless solution. Film 8a was immersed under this solution at 25  $^{\circ}\text{C}$  for 5 h and washed thoroughly with  $\text{NaHCO}_3$  buffer followed by phosphate buffer. The resulting film 12 was then incubated at 25  $^{\circ}\text{C}$  for 1 h in a premixed solution containing 2.6  $\mu\text{M}$  streptavidin and 0.52  $\mu\text{M}$  biotinylated HRP in pH 7.0 phosphate buffer (21). The film was washed thoroughly with phosphate buffer to give film 13.

**HRP Assays.** All HRP solutions and the dilutions were made in pH 7.0 phosphate buffer containing 10.0 mg/mL of BSA. ABTS solutions were prepared in pH 7.0 phosphate buffer and used at a concentration of 1.0 mg/mL throughout. Hydrogen peroxide was used at a concentration of 0.28% throughout.

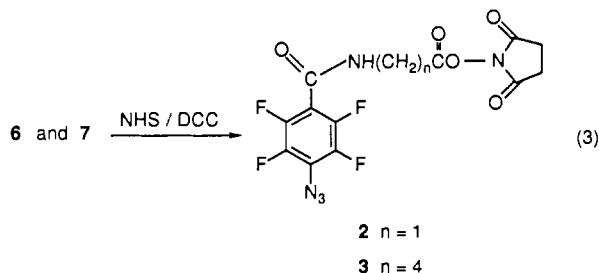
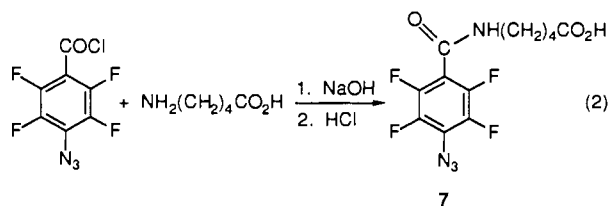
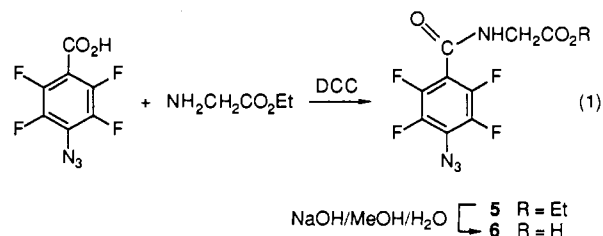
**Activity of Native HRP.** To a cuvette containing 2.0 mL of ABTS solution and 50.0  $\mu\text{L}$  of a HRP solution of various concentration was added 20.0  $\mu\text{L}$  of  $\text{H}_2\text{O}_2$  solution (final concentrations, 1.8 mM ABTS and 0.8 mM  $\text{H}_2\text{O}_2$ ). The absorbance of the resulting solution at 420 nm after

incubation at 25  $^{\circ}\text{C}$  for 10 min was read against pH 7.0 phosphate buffer.

**Assays for Immobilized HRP.** To a dish containing 10.0 mL of ABTS solution and film 10 or 11 or 13 was added 100.0  $\mu\text{L}$  of  $\text{H}_2\text{O}_2$  solution at 25  $^{\circ}\text{C}$  under stirring. Aliquots of about 2 mL of the resulting solution were taken at about 1 min time intervals, and the absorbances at 420 nm were recorded. Aliquots were returned to the dish after each measurement to keep the total volume constant.

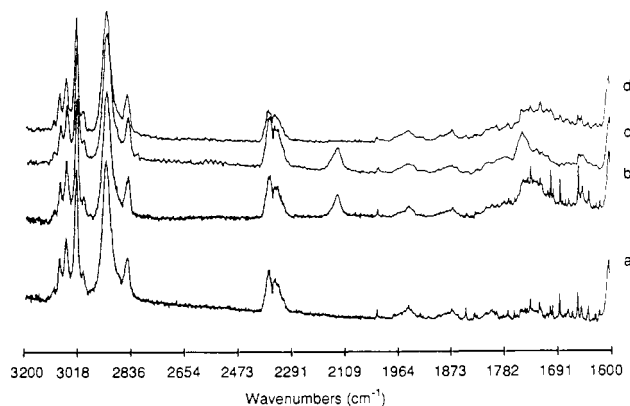
## RESULTS AND DISCUSSION

Syntheses of NHS PFPA esters 2 and 3 were accomplished as shown in eq 1–3. Reaction of 4-azido-2,3,5,6-



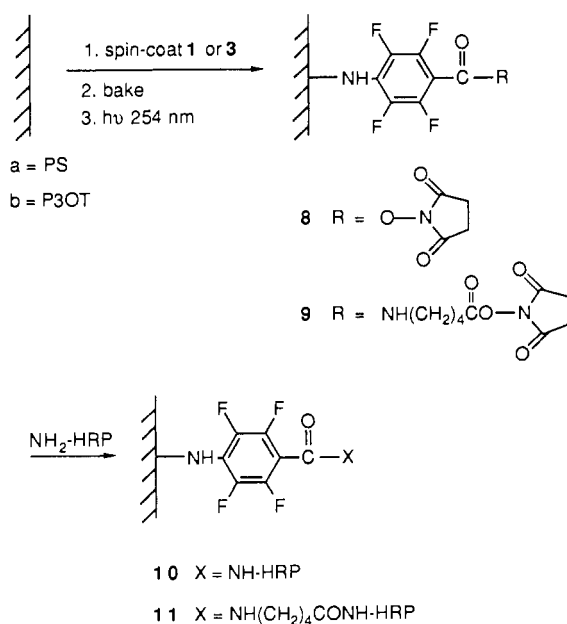
tetrafluorobenzoic acid (9) and glycine ethyl ester hydrochloride with DCC as the coupling reagent gave *N*-(4-azido-2,3,5,6-tetrafluorobenzoyl)glycine ethyl ester (5) in 32% yield. Hydrolysis of 5 with NaOH in methanol gave 6 as a white powder in 99% yield (eq 1). Treatment of 4-azido-2,3,5,6-tetrafluorobenzoyl chloride (9) with 5-aminopentanoic acid under basic conditions followed by acidification gave 5-(4-azido-2,3,5,6-tetrafluorobenzamido)pentanoic acid (7) as a white powder in 87% yield (eq 2). Reaction of 6 and 7 with NHS in the presence of DCC gave *N*-(4-azido-2,3,5,6-tetrafluorobenzoyl)glycine *N*-succinimidyl ester (2) and *N*-succinimidyl 5-(4-azido-2,3,5,6-tetrafluorobenzamido)pentanoate (3) as white powders in 80% and 90% yields, respectively (eq 3). Reagents, 2, 3, and *N*-succinimidyl 4-azido-2,3,5,6-tetrafluorobenzoate (1) (9), form a series of NHS-functionalized PFPA's differing in the lengths of the linker between the PFPA and the NHS ester group.

Surface modification of PS thin films with NHS-functionalized PFPA 1 and 3 was performed as follows. A circular micro cover glass was spin-coated with 5% PS solution in xylenes. The thickness of the film was measured as 0.5  $\mu\text{m}$  (22). Then a solution of 0.5 wt % 1 or 3 in nitromethane (PS is not soluble in nitromethane) was spin-coated on top of the PS film. In the control



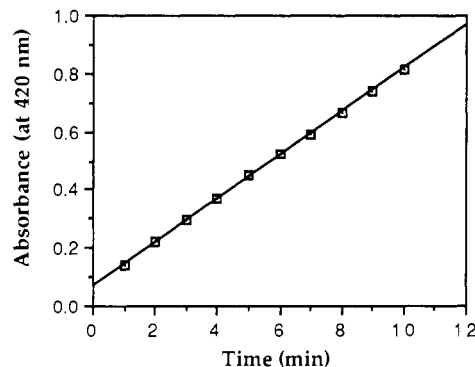
**Figure 1.** FTIR spectra of (a) a PS film, (b) a PS film spin-coated with 1 on top, (c) the resulting film baked at 60 °C for 20 min, and (d) the baked film photolyzed with 254-nm lamps for 5 min to give film 8a.

#### Scheme 1



experiment using a NaCl disk as the support, an IR spectrum showed the azide absorption at  $2138\text{ cm}^{-1}$  after 1 or 3 was spin-coated on the PS film (Figure 1b vs 1a). The film was then baked at 60 °C for 20 min. The baking process removed residual solvent present in the film and likely facilitated the diffusion of the surface-deposited NHS PFPA ester into the PS film, thus increasing the probability of CH bond insertion into the polymer surface of the nitrene intermediate generated in the next step. However, baking did not induce the thermodecomposition of the azide because the intensity of the absorption at  $2138\text{ cm}^{-1}$  after baking (Figure 1c) was essentially the same as that before baking (Figure 1b). Irradiation of the azide-containing film with 254-nm lamps for 5 min resulted in complete decomposition of the azide group in 1 or 3 as indicated by the absence of the  $2138\text{ cm}^{-1}$  absorption in the IR spectrum of the corresponding control sample (Figure 1d vs 1c). Photolysis of 1 and 3 generated the highly active nitrene intermediate (9, 11) which then underwent CH bond insertion into the PS surface, giving films 8a and 9a, respectively (Scheme 1). Since an NHS-active ester group is present in 1 and 3, it also becomes covalently attached to the PS surface.

As an example of the application of this surface functionalization technique for binding biomolecules to



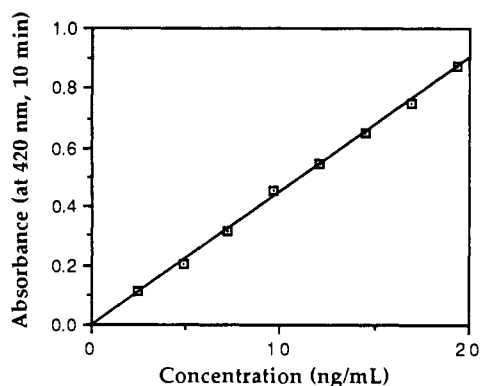
**Figure 2.** Time course of immobilized HRP reaction using 1 as the surface modification reagent. 1.8 mM ABTS/0.8 mM  $\text{H}_2\text{O}_2$  in 0.1 M pH 7.0 phosphate buffer. A least-squares fit gives absorbance  $A = 0.0693 + 0.0746t$ , where  $t$  is the time.

polymer surfaces, horseradish peroxidase (HRP) was immobilized on films 8a and 9a. The immobilization was accomplished via amide formation between the NHS active ester group and an amino group present in HRP. Since the NHS ester is slowly hydrolyzed by water (23), dilution of the HRP solution will result in competition between coupling and loss of the NHS ester group by hydrolysis. A concentration of 50  $\mu\text{M}$  HRP was used in order to minimize the loss of NHS ester caused by hydrolysis (24). Since only the unprotonated amino groups in HRP are reactive in the coupling reaction, it is necessary to maintain an alkaline pH at which a significant number of amino groups are unprotonated. However, hydrolysis of the NHS ester becomes competitive above pH 9. A pH 8.2  $\text{NaHCO}_3$  buffer was used since it was demonstrated to give excellent coupling results (24).

Immobilization of HRP on films 8a and 9a was carried out by separately incubating each film in a solution of 50  $\mu\text{M}$  HRP in  $\text{NaHCO}_3$  buffer at 25 °C for 3 h. The resulting films were washed thoroughly with  $\text{NaHCO}_3$  buffer followed by phosphate buffer to give films 10a and 11a.

In order to determine the immobilization efficiency, activities of the immobilized HRP and the native HRP were measured using the procedure of Groome (25). The activity of HRP was determined spectrophotometrically at 420 nm and 25 °C using 2,2'-azinobis(3-ethylbenzthiazoline-6-sulfonic acid) diammonium salt (ABTS) and hydrogen peroxide (1.8 mM ABTS/0.8 mM  $\text{H}_2\text{O}_2$ ). In a typical assay for immobilized HRP, film 10a or 11a was immersed in 10.0 mL of ABTS solution in phosphate buffer (1.0 mg/mL), and 100.0  $\mu\text{L}$  of  $\text{H}_2\text{O}_2$  solution (0.28%) was added with stirring. Aliquots of about 2 mL of the solution were taken at about 1-min time intervals, and absorbances at 420 nm were recorded. A representative curve for the immobilized HRP is shown in Figure 2.

Assays of the native HRP were carried out by incubating various HRP solutions of known concentration with 1.8 mM ABTS/0.8 mM  $\text{H}_2\text{O}_2$  in pH 7.0 phosphate buffer. Absorbances at 420 nm after 10 min incubation were read against pH 7.0 phosphate buffer. Figure 3 shows a linear relationship between the absorbance and the concentration of HRP. Making the assumption that the immobilized HRP has the same activity as the native HRP (25, 26), the amounts of HRP immobilized can be calculated. For example, using 1 as the surface modification reagent, the absorbance at 10 min was calculated to be 0.816 (Figure 2), corresponding to a concentration of 18.1 ng/mL (Figure 3). Since the total volume of the assay solution was 10.0 mL, the amount of HRP immobilized on the circular micro cover glass (radius = 10 mm) was 181 ng. This corresponds to 0.58 ng/ $\text{mm}^2$  of surface area.

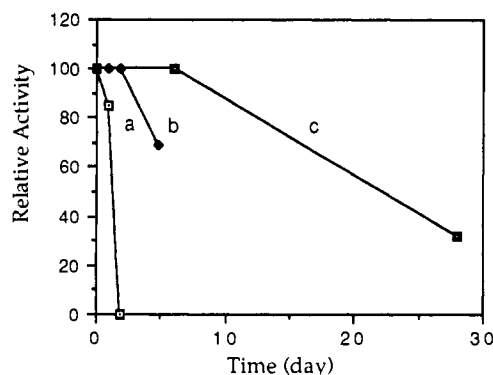


**Figure 3.** Relationship between absorbance and concentration of native HRP. 1.8 mM ABTS/0.8 mM  $\text{H}_2\text{O}_2$  in 0.1 M pH 7.0 phosphate buffer. Cuvettes were incubated at 25 °C for 10 min before reading the absorbances at 420 nm against pH 7.0 phosphate buffer blank. The least-squares fit gives absorbance  $A = 0.0746C$ , where  $C$  is the concentration.

From the four samples each of films 10a or 11a, the amount of HRP immobilized was calculated to be  $0.5 \pm 0.1 \text{ ng/mm}^2$  for film 10a and  $1.0 \pm 0.2 \text{ ng/mm}^2$  for film 11a. The amount of HRP immobilized using 3 was twice as much as that using 1 as the surface modification reagent. In the case of 3-functionalized PS film 9a, the NHS ester group is separated from the polymer surface by four methylene units as compared to 1-functionalized PS film 8a. The NHS ester separated from the PS surface by an extended spacer would be expected to experience less steric interference by the PS matrix, and consequently the reaction with the large HRP molecules should be more efficient.

A HRP molecule has been described as having an average molecular weight of 40 000 and a radius of 2.67 nm in the hydrated state (27). Considering a monolayer of densely packed HRP spheres on a flat surface, the maximum amount of HRP molecules laid on the surface is calculated to be  $2.7 \text{ ng/mm}^2$  (28). Therefore, the surface coverage of immobilized HRP is about 19% of the maximum coverage calculated using 1 and about 37% using 3 as the surface modification reagent, indicating a reasonable immobilization efficiency.

Two control experiments were carried out. In the first experiment, a PS film prepared by spin-coating 5% PS xylenes solution on a piece of micro cover glass was baked and photolyzed. After incubating in 50  $\mu\text{M}$  HRP solution at 25 °C for 3 h and washing thoroughly with  $\text{NaHCO}_3$  buffer followed by phosphate buffer, the film was subjected to the enzyme assay as described above. The result showed no enzyme activity, indicating that there was no detectable nonspecific adsorption of HRP molecules on the PS surface. In the second control experiment, the methyl PFPA ester 4 instead of the NHS PFPA ester 1 or 3 was used as the surface modification reagent. A piece of micro cover glass was spin-coated with 5% PS xylenes solution and then with a solution of 0.5 wt % methyl 4-azido-2,3,5,6-tetrafluorobenzoate (4) (9) in nitromethane on top of the PS film. The resulting film was baked, photolyzed, incubated in 50  $\mu\text{M}$  HRP solution at 25 °C for 3 h, and rinsed thoroughly with  $\text{NaHCO}_3$  buffer followed by phosphate buffer. No enzyme activity was detected, indicating that there was no reaction between the HRP molecule and the "unactivated" methyl PFPA ester-modified PS surface. Thus, HRP was likely immobilized on films 8a and 9a through covalent amide formation between the NHS active ester group and the amino group present in HRP.



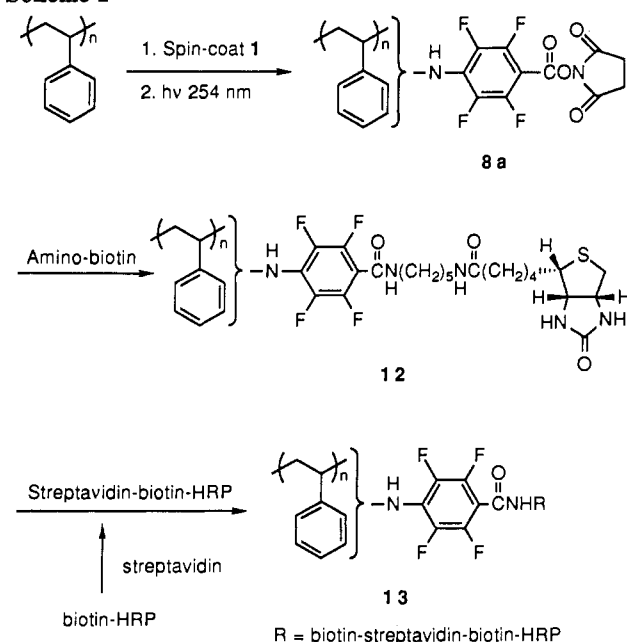
**Figure 4.** Storage stability of immobilized HRP at 4 °C in pH 7.0 phosphate buffer of film (a) 10a, (b) 11a, and (c) 13.

The generality of this methodology for polymer surface modification was extended to an organic conducting polymer, poly(3-octylthiophene) (P3OT). P3OT was prepared chemically from 3-octylthiophene using  $\text{FeCl}_3$  according to a known procedure (19). The functionalization of P3OT surface was performed by spin-coating a circular micro cover glass with 2% P3OT solution in chloroform followed by a solution of 0.5 wt % 1 or 3 in methanol on top of the P3OT film. Methanol was used as the solvent because it spread on P3OT film better than nitromethane and it does not dissolve the polymer film. In a control experiment using a NaCl disk as the support, the IR spectrum showed a strong azide absorption at 2138  $\text{cm}^{-1}$  after spin-coating of 1 or 3 onto P3OT. The film was then irradiated with 254-nm lamps for 5 min to give film 8b or 9b. The IR spectra of the corresponding control samples showed the complete disappearance of the azide absorption in 8b and 9b.

Immobilization of HRP on films 8b and 9b and the enzyme activity assays of the immobilized HRP on films 10b and 11b were carried out in the same manner as described above for films 8a, 9a and 10a, 11a. Similarly, by making the assumption that immobilized HRP has the same activity as the native HRP (25, 26), the amount of HRP immobilized was calculated as  $0.2 \pm 0.1 \text{ ng/mm}^2$  for film 10b and  $0.3 \pm 0.1 \text{ ng/mm}^2$  for film 11b. Again, the latter was larger than the former, the same result as observed in the case of using PS as the polymer substrate. A control experiment was carried out to determine whether there was nonspecific adsorption of HRP molecules on the P3OT surface. A P3OT film prepared by spin-coating 2% P3OT solution in chloroform was baked, photolyzed, and incubated in 50  $\mu\text{M}$  HRP solution at 25 °C for 3 h. After being rinsed thoroughly with  $\text{NaHCO}_3$  buffer followed by phosphate buffer, the film was subjected to the enzyme activity assay. No detectable enzyme activity was observed, indicating that there were no HRP molecules nonspecifically adsorbed on the P3OT film.

The stability of HRP immobilized on the PS film upon storage was also studied. Films 10a and 11a were stored at 4 °C in pH 7.0 phosphate buffer. HRP on film 10a lost essentially all of its initial activity after 1.8 days. HRP on film 11a retained 100% of its initial activity after 1.8 days but lost 31% of its initial activity after 4.8 days (Figure 4). It has been reported that enzymes tend to lose their biological activities after immobilization on solid matrices due to the masking of their active sites by the solid matrix or multipoint attachments which restrict the local movements necessary for the activities (29). In the case of film 10a, there was only a short spacer between HRP and PS. The polymer matrix may mask the active sites and/or alter the three-dimensional structure of HRP at its active sites

Scheme 2



by stretching the molecule. Multipoint attachment may also occur during the immobilization process; thus, the initial activity of the immobilized HRP was lower with 10a compared to 11a and the activity decreased rapidly over a 1–2-day period. In the case of film 11a, HRP was separated from the polymer matrix by four additional methylene units. The four methylene units act as a spacer to reduce the chance of masking of the active sites by the polymer matrix, resulting in a higher initial activity and enhanced storage stability of the immobilized HRP.

A multilayered system containing biotin–streptavidin–biotin–HRP was constructed on the PS surface in order to test whether further separation of HRP from the surface would lead to greater storage stability. Biotin (vitamin H) is known to bind strongly and specifically to the bacterial protein streptavidin with a binding constant of  $10^{15} \text{ M}^{-1}$ . The binding properties are only slightly influenced when biotin is functionalized (30). Since streptavidin has four binding sites for biotin situated on two opposite sides of the tetrameric protein, streptavidin can thus be used to link two different functions in the assembly (31). The PS–biotin–streptavidin–biotin–HRP assembly was constructed as shown in Scheme 2. Functionalization of the PS surface with 1 to give film 8a was performed in the same manner as described earlier. A solution of *N*-(5-aminopentyl)biotinamide in DMF (2.0 mg/0.1 mL) was prepared and was added to 0.5 mL of 0.1 M pH 8.2  $\text{NaHCO}_3$  buffer. Film 8a was immersed in the resulting solution at 25 °C for 5 h. After thorough rinsing with  $\text{NaHCO}_3$  buffer followed by phosphate buffer, the resulting film 12 was incubated at 25 °C for 1 h in a premixed solution of 2.6  $\mu\text{M}$  streptavidin and 0.52  $\mu\text{M}$  biotinylated HRP in pH 7.0 phosphate buffer. The film was then rinsed with the buffer to give film 13. Using the same method as described above to obtain the linear relationship between absorbance and the concentration of biotinylated HRP, the amount of biotinylated HRP immobilized on film 13 was calculated to be 0.25 ng/mm<sup>2</sup>.<sup>1</sup> The lower initial activity of film 13 as compared to that of film 10 is likely due to the fact that excess streptavidin was used in the conjugation step with

biotinylated HRP. Some free streptavidin molecules are present in the solution of streptavidin–biotin–HRP and will not contribute to the activity of film 13 after conjugation. An enzyme activity assay of film 13 stored at 4 °C showed that HRP immobilized in this manner retained 100% of its initial activity after 6 days and 38% of its initial activity after 28 days (Figure 4).

In conclusion, we present the synthesis of NHS functionalized PFPAs 2 and 3 and a general method using bifunctional cross-linking reagents such as 1 and 3 for the covalent modification of polymer surfaces. Application of this methodology for bioconjugation was demonstrated through covalently immobilization of HRP to the NHS PFFA ester-functionalized PS and P3OT surfaces. Utilization of the multilayer system, biotin–streptavidin–biotin–HRP, greatly enhanced the storage stability of the immobilized HRP. This new bioconjugation strategy may find application for the construction of novel micrometer-scale biosensors based on field-effect transistors and optical waveguides.

#### ACKNOWLEDGMENT

This work was supported by grants from the Office of Naval Research, the National Institute of General Medical Sciences (GM 27137), and the Oregon Resource Technology Development Corporation.

#### LITERATURE CITED

- (1) Shintaro, K., Shinji, M., and Akio, Y. (1993) A simple method of detecting amplified DNA with immobilized probes on microtiter wells. *Anal. Biochem.* 209, 63.
- (2) Pope, N. M., Kulcinski, D. L., Hardwick, A., and Chang, Y.-A. (1993) New application of silane coupling agents for covalently binding antibodies to glass and cellulose solid supports. *Bioconjugate Chem.* 4, 166.
- (3) Bottomley, L. A., Haseltine, J. N., Allison, D. P., Warmack, R. J., Thundat, T., Sachleben, R. A., Brown, G. M., Woychik, R. P., Jacobson, B., and Ferrell, T. L. (1992) Scanning tunneling microscopy of DNA: the chemical modification of gold surfaces for immobilization of DNA. *J. Vac. Sci. Tech. A* 10, 591.
- (4) Akashi, M., Maruyama, I., Fukudome, N., and Yashima, E. (1992) Immobilization of human thrombomodulin on glass beads and its anticoagulant activity. *Bioconjugate Chem.* 3, 363.
- (5) Maskos, U., and Southern, E. M. (1992) Oligonucleotide hybridisations on glass supports: a novel linker for oligonucleotide synthesis and hybridisation properties of oligonucleotides synthesised *in situ*. *Nucleic Acids Res.* 20, 1679.
- (6) Spinke, J., Liley, M., Guder, H.-J., Angermaier, L., and Knoll, W. (1993) Molecular recognition at self-assembled monolayers: the construction of multicomponent multilayers. *Langmuir* 9, 1821.
- (7) Maeda, H., Seymour, L. W., and Miyamoto, Y. (1992) Conjugates of anticancer agents and polymers: advantages of macromolecular therapeutics *in vivo*. *Bioconjugate Chem.* 3, 351.
- (8) Cass, A. E. G. (1990) *Biosensors a practical approach*, Oxford University Press, New York.
- (9) Keana, J. F. W., and Cai, S. X. (1990) New reagents for photoaffinity labeling: synthesis and photolysis of functionalized perfluorophenyl azides. *J. Org. Chem.* 55, 3640.
- (10) Cai, S. X., Glenn, D. J., and Keana, J. F. W. (1992) Toward the development of radiolabeled fluorophenyl azide-based photolabeling reagents: synthesis and photolysis of iodinated 4-azido-perfluorobenzoates and 4-azido-3,5,6-trifluorobenzoates. *J. Org. Chem.* 57, 1299.
- (11) Soundararajan N., and Platz, M. S. (1990) Descriptive photochemistry of polyfluorinated azides derivatives of methyl benzoate. *J. Org. Chem.* 55, 2034.
- (12) Pinney, K. G., and Katzenellenbogen, J. A. (1991) Synthesis of a tetrafluoro-substituted aryl azide and its protio analogue as photoaffinity labeling reagents for the estrogen receptor. *J. Org. Chem.* 56, 3125.

<sup>1</sup> A film was prepared in a similar manner as film 13 but using 3 as the surface modification reagent. The amount of immobilized biotinylated HRP was calculated to be 0.63 ng/mm<sup>2</sup>.

- (13) Poe, R., Schnapp, K., Young, M. J. T., Grayzar, J., and Platz, M. S. (1992) Chemistry and kinetics of singlet (pentafluorophenyl)nitrene. *J. Am. Chem. Soc.* 114, 5054.
- (14) (a) Aggeler, R., Cai, S. X., Keana, J. F. W., Koike, T., and Capaldi, R. A. (1993) The  $\gamma$  subunit of the *Escherichia coli*  $F_1$ -ATPase can be cross-linked near the glycine-rich loop region of a  $\beta$  subunit when ADP +  $Mg^{2+}$  occupies catalytic sites but not when ATP +  $Mg^{2+}$  is bound. *J. Biol. Chem.* 268, 20831. (b) Aggeler, R., Chicas-Cruz, K., Cai, S. X., Keana, J. F. W., and Capaldi, R. A. (1991) Introduction of reactive cysteine residues in the  $\epsilon$  subunit of *Escherichia coli*  $F_1$  ATPase, modification of these sites with tetrafluorophenylazido maleimides, and examination of changes in the binding of the  $\epsilon$  subunit when different nucleotides are in catalytic sites. *Biochemistry* 31, 2956.
- (15) Cai, S. X., and Keana, J. F. W. (1991) Diazo and azido functionalized glutaraldehydes as cross-linking reagents and potential fixatives for electron microscopy. *Bioconjugate Chem.* 2, 38.
- (16) Yan, M., Cai, S. X., Wybourne, M. N., and Keana, J. F. W. (1993) Photochemical functionalization of polymer surfaces and the production of biomolecule-carrying micrometer-scale structures by deep-UV lithography using 4-substituted perfluorophenyl azides. *J. Am. Chem. Soc.* 115, 814.
- (17) Wybourne, M. N., Wu, J. C., Yan, M., Cai, S. X., and Keana, J. F. W. (1993) The modification of polymer surfaces and the fabrication of submicron-scale functionalized structures by deep-UV and electron beam lithography. *J. Vac. Sci. Tech. B.* (in press).
- (18) Rozsnyai, L. F., Benson, D. R., Fodor, S. P. A., and Schultz, P. G. (1992) Photolithographic immobilization of biopolymers on solid supports. *Angew. Chem., Int. Ed. Engl.* 31, 759.
- (19) Cai, S. X., Nabity, J. C., Wybourne, M. N., and Keana, J. F. W. (1991) Conducting polymers as deep-UV and electron beam resists: direct production of micrometer-scale conducting structures from poly(3-octylthiophene). *J. Mol. Electron.* 7, 63.
- (20) The concentration was not standardized. According to ref 25, the concentration of  $H_2O_2$  from 0.1 to 0.8 mM has no influence on the absorbance.
- (21) Pantano, P., Morton, T. H., and Kuhr, W. G. (1991) Enzyme-modified carbon fiber microelectrodes with millisecond response times. *J. Am. Chem. Soc.* 113, 1832.
- (22) Cai, S. X., Kanskar, M., Wybourne, M. N., and Keana, J. F. W. (1992) Introduction of functional groups into polymer films via deep-UV photolysis or electron-beam lithography: modification of polystyrene and poly(3-octylthiophene) by a functionalized perfluorophenyl azide. *Chem. Mater.* 4, 879.
- (23) Lomants, A. J., and Fairbanks, G. (1976) Chemical probes of extended biological structures: synthesis and properties of the cleavable protein crosslinking reagent [ $^{35}S$ ]dithiobis-(succinimidyl)propionate. *J. Mol. Biol.* 104, 243.
- (24) Brinkley, M. (1992) A brief survey of methods for preparing protein conjugates with dyes, haptens, and cross-linking reagents. *Bioconjugate Chem.* 3, 2.
- (25) Groome, N. P. (1980) Superiority of ABTS over Trinder reagent as chromogen in highly sensitive peroxidase assays for enzyme linked immunoadsorbent assay. *J. Clin. Chem. Clin. Biochem.* 18, 345.
- (26) Nakane, P. K., and Kawaoi, A. (1974) Peroxidase-labeled antibody a new method of conjugation. *J. Histochem. Cytochem.* 22, 1084.
- (27) Steiner, H., and Dunford, H. B. (1978) Ionic strength dependence of the oxidation of iodide and ferrocyanide by compound I of horseradish peroxidase. *Eur. J. Biochem.* 82, 543.
- (28) Each sphere generates a void area of  $1/2 \times 5.34 \times (0.87 \times 5.34) - 3 \times 1/6 \times \pi(2.67)^2 = 1.15 \text{ nm}^2$ . Therefore, the number of HRP molecules densely packed on a flat surface of  $1 \text{ mm}^2$  is  $(1 \times 10^6)^2 / (\pi(2.67)^2 + 1.15) = 4.25 \times 10^{10}$ , which corresponded to  $4.25 \times 10^{10} / (6.02 \times 10^{23}) \times 40\,000 \times 10^9 = 2.7 \text{ ng of HRP/mm}^2$ .
- (29) Solomon, B., Hafas E., Koppel, R., Schwartz, F., and Fleminger, G. (1991) Highly active enzyme preparations immobilized via matrix-conjugated anti-Fc antibodies. *J. Chromatogr.* 539, 335.
- (30) Bayer, E. A., and Wilchek, M. (1980) The use of the avidin-biotin complex as a tool in molecular biology. *Methods of Biochemical Analysis* (D. Glick, Ed.) Vol. 26, p 1-46, John Wiley & Sons, New York.
- (31) Haussling, L., Michel, B., Ringsdorf, H., and Rohrer, H. (1991) Direct observation of streptavidin specifically adsorbed on biotin-functionalized self-assembled monolayer with the scanning tunneling microscope. *Angew. Chem., Int. Ed. Engl.* 30, 569.



# Synthesis of 2,6-Diazido-9-( $\beta$ -D-ribofuranosyl)purine 3',5'-Bisphosphate: Incorporation into Transfer RNA and Photochemical Labeling of *Escherichia coli* Ribosomes

Jacek Wower,<sup>†</sup> Stephen S. Hixson,<sup>‡</sup> Lee A. Sylvers,<sup>†,§</sup> Yide Xing,<sup>†,⊥</sup> and Robert A. Zimmermann<sup>\*†</sup>

Departments of Biochemistry and Molecular Biology and of Chemistry, University of Massachusetts, Amherst, Massachusetts 01003. Received October 20, 1993\*

2,6-Diazido-9-( $\beta$ -D-ribofuranosyl)purine was prepared by the reaction of 2,6-dichloro-9-( $\beta$ -D-ribofuranosyl)purine with sodium azide. The nucleoside was bisphosphorylated with pyrophosphoryl chloride to form 2,6-diazido-9-( $\beta$ -D-ribofuranosyl)purine 3',5'-bisphosphate. This product was labeled with <sup>32</sup>P using T4 polynucleotide kinase to exchange the 5' phosphate with the  $\gamma$  phosphate of [ $\gamma$ -<sup>32</sup>P]ATP. When yeast tRNA<sup>Phe</sup> containing 2,6-diazido-9-( $\beta$ -D-ribofuranosyl)purine at the 3' terminus was bound to the P site of the *Escherichia coli* ribosome in the presence of poly(U) and irradiated with 300-nm light, the photoreactive tRNA derivative became cross-linked exclusively to the 50S subunit. The label was attached to proteins L27 and L33 as well as to the 23S rRNA.

## INTRODUCTION

2-Azidoadenosine (2N<sub>3</sub>A) and 8-azidoadenosine (8N<sub>3</sub>A) phosphates have been extensively used for photoaffinity labeling of nucleotide binding sites in proteins (1–3). Recently, 2N<sub>3</sub>A and 8N<sub>3</sub>A have been incorporated at a number of specific positions throughout the tRNA molecule to probe the topography of tRNA binding sites on the ribosome (4–8). Such substitutions, which do not in general impair the biological activity of tRNA, yield derivatives that can be photoactivated with 300-nm light. Irradiation of tRNA-ribosome complexes at this wavelength results in very short (2–4 Å) cross-links between tRNA and ribosomes without adversely affecting ribosome activity (5). The photoaffinity labeling of ribosomes with azidoadenosine-containing tRNAs led us to advance a model of the tRNA-ribosome complex during the elongation phase of translation (6–8).

To gain additional information about the local environment of specific tRNA nucleosides on the ribosome, we have prepared 2,6-diazido-9-( $\beta$ -D-ribofuranosyl)purine 3',5'-bisphosphate,<sup>1</sup> a photoreactive purine nucleotide with azide moieties attached to both the 2 and 6 positions. Based on the spectroscopic properties of azidopurine bases (9) we expect tetrazole formation, which can reduce the efficiency of cross-linking at neutral pH, to be less significant for p2,6-diN<sub>3</sub>Rp than it is for p2N<sub>3</sub>Ap (3). At the same time, the glycosidic bond of p2,6-diN<sub>3</sub>Rp should assume the usual *anti* conformation, rather than the *syn*

conformation adopted by p8N<sub>3</sub>Ap. In this paper, we describe the synthesis of p2,6-diN<sub>3</sub>Rp, its incorporation into yeast tRNA<sup>Phe</sup>, and the cross-linking of [2,6-diN<sub>3</sub>-R76]tRNA<sup>Phe</sup> to the ribosome.

## EXPERIMENTAL PROCEDURES

**Materials.** Yeast tRNA<sup>Phe</sup>, calf intestine alkaline phosphatase, and puromycin were purchased from Boehringer Mannheim. T4 RNA ligase and 3'-phosphatase-free T4 polynucleotide kinase were obtained from Pharmacia. Ribonuclease T<sub>1</sub> was from Worthington. [ $\gamma$ -<sup>32</sup>P]-ATP (6000 Ci/mmol) was from New England Nuclear. Ribosomes from *E. coli* K12 cells were prepared according to Rheinberger et al. (10). PEI-cellulose plates were from Macherey and Nagel. All other chemicals were of reagent grade.

**Preparation of 2,6-Diazido-9-( $\beta$ -D-ribofuranosyl)purine 3',5'-Bisphosphate.** 2,6-Diazido-9-( $\beta$ -D-ribofuranosyl)purine (2) was prepared by reaction of 2,6-dichloro-9-( $\beta$ -D-ribofuranosyl)purine (1) (11) with sodium azide as described by Montgomery and Hewson (12) for the triacetate (Figure 1). Sodium azide, 256 mg (4.24 mmol), in 1.2 mL of H<sub>2</sub>O was added to a warm solution of 647 mg (2.02 mmol) of 2,6-dichloro-9-( $\beta$ -D-ribofuranosyl)purine in 16 mL of ethanol. The reaction mixture was refluxed 1 h, cooled, filtered, and concentrated *in vacuo* to a solid, which, upon crystallization from hot ethyl acetate, afforded 223 mg of 2,6-diazido-9-( $\beta$ -D-ribofuranosyl)purine as a white powder: mp 134–136 °C dec; IR (KBr) 3327, 2170, 2134, 1612, 1584, 1378, 1246, 1083 cm<sup>-1</sup>; <sup>1</sup>H-NMR (DMSO-d<sub>6</sub>)  $\delta$  8.69 (s, 0.8, H-8); UV (CH<sub>3</sub>OH)  $\lambda_{\max}$  244 ( $\epsilon$  19 000), 265, 294 nm; MS (electrospray) 335.1 (MH<sup>+</sup>).

The nucleoside was bisphosphorylated with pyrophosphoryl chloride according to Barrio et al. (13). After chromatography of the products on a DEAE-cellulose column, a mixture of 2,6-diazido-9-( $\beta$ -D-ribofuranosyl)purine 2',5'- and 3',5'-bisphosphates was obtained. The UV spectrum of p2,6-diN<sub>3</sub>Rp exhibited maxima at 244, 265, and 294 nm at pH 7.6. The major peak of the electrospray mass spectrum was at *m/z* 697.5 (calcd 697.6), corresponding to the (protonated) bis(triethylammonium) salt.

**Preparation of [5'-<sup>32</sup>P]p2,6-diN<sub>3</sub>Rp.** The 5'-phosphate of p2,6-diN<sub>3</sub>Rp was exchanged with the  $\gamma$ -phosphate of [ $\gamma$ -<sup>32</sup>P]ATP using 3'-phosphatase-free T4 polynucle-

\* To whom correspondence should be addressed.

<sup>†</sup> Department of Biochemistry and Molecular Biology.

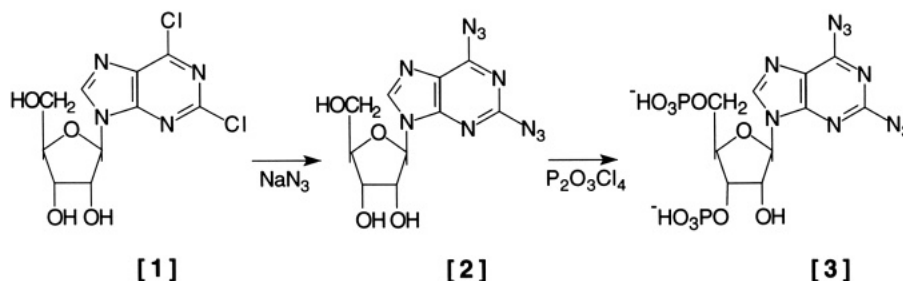
<sup>‡</sup> Department of Chemistry.

<sup>§</sup> Present address: Department of Molecular Biophysics and Biochemistry, Yale University, New Haven, CT 06511.

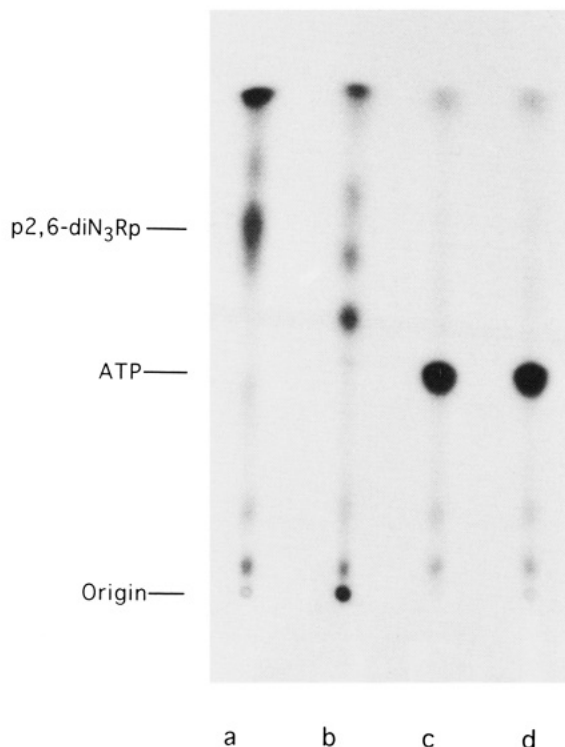
<sup>⊥</sup> Present address: DuPont/Merck Pharmaceutical Company, Chambers Works, Process Research Facility, Deepwater, NJ 08023.

\* Abstract published in *Advance ACS Abstracts*, February 15, 1994.

<sup>1</sup> Abbreviations: 2N<sub>3</sub>A, 2-azidoadenosine; 8N<sub>3</sub>A, 8-azidoadenosine; 2,6-diN<sub>3</sub>R, 2,6-diazido-9-( $\beta$ -D-ribofuranosyl)purine; pNp, nucleoside 3',5'-bisphosphate; [2,6-diN<sub>3</sub>R76]tRNA<sup>Phe</sup>, tRNA<sup>Phe</sup> containing 2,6-diazido-9-( $\beta$ -D-ribofuranosyl)purine at position 76; SDS-PAGE, sodium dodecyl sulfate-polyacrylamide gel electrophoresis; PEI, polyethyleneimine; TLC, thin-layer chromatography.



**Figure 1.** Synthesis of 2,6-diazido-9-( $\beta$ -D-ribofuranosyl)purine 3',5'-bisphosphate from 2,6-dichloro-9-( $\beta$ -D-ribofuranosyl)purine: (1) 2,6-dichloro-9-( $\beta$ -D-ribofuranosyl)purine, (2) 2,6-diazido-9-( $\beta$ -D-ribofuranosyl)purine, and (3) 2,6-diazido-9-( $\beta$ -D-ribofuranosyl)purine 3',5'-bisphosphate.



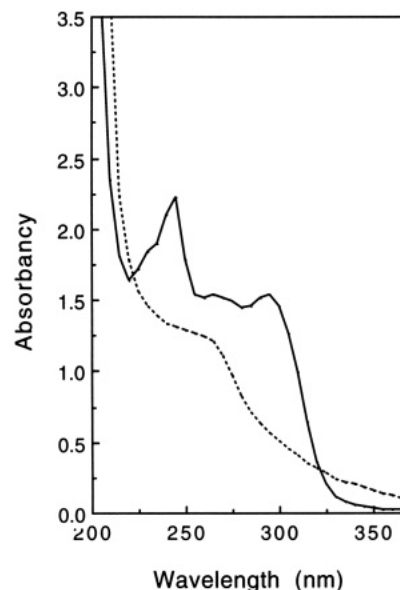
**Figure 2.** Preparation and photoreactivity of [ $5'$ - $^{32}$ P]p2,6-diN<sub>3</sub>Rp. Aliquots of the exchange reaction mixture containing [ $\gamma$ - $^{32}$ P]ATP, ADP, and p2,6-diN<sub>3</sub>Rp (a, b) and samples of [ $\gamma$ - $^{32}$ P]-ATP alone (c, d) were applied to a PEI-cellulose sheet. The material deposited at the origins of lanes b and d was then irradiated at 300 nm for 5 min. The PEI-cellulose sheet was developed by ascending chromatography in 0.75 M KH<sub>2</sub>PO<sub>4</sub>, pH 3.5 (14).

otide kinase (4). The products were analyzed by thin-layer chromatography on PEI-cellulose plates using 0.75 M KH<sub>2</sub>PO<sub>4</sub>, adjusted to pH 3.5 with HCl, as the mobile phase (14).

**Incorporation of [ $5'$ - $^{32}$ P]p2,6-diN<sub>3</sub>Rp into Position 76 of Yeast tRNA<sup>Phe</sup> and Cross-Linking of [2,6-diN<sub>3</sub>R76]tRNA<sup>Phe</sup> to the Ribosomal P Site.** The 3'-terminal adenosine at position 76 of yeast tRNA<sup>Phe</sup> was replaced with 2,6-diN<sub>3</sub>R by ligation of [ $5'$ - $^{32}$ P]p2,6-diN<sub>3</sub>Rp to tRNA<sup>Phe</sup> lacking A76 exactly as described by Wower et al. (5). The extent of incorporation of the photoreactive nucleotide was estimated by denaturing polyacrylamide gel electrophoresis. Noncovalent binding of the photoreactive tRNA derivative to the ribosomal P site and irradiation of the complex with 300-nm light were carried out as previously described (5).

## RESULTS AND DISCUSSION

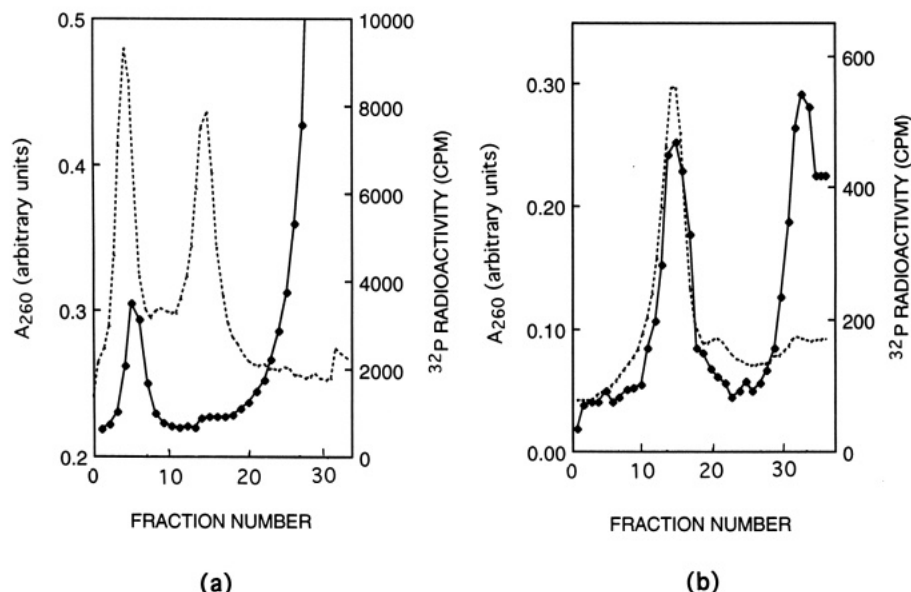
2,6-Diazido-9-( $\beta$ -D-ribofuranosyl)purine 3',5'-bisphosphate (3) was synthesized as depicted in Figure 1. 2,6-



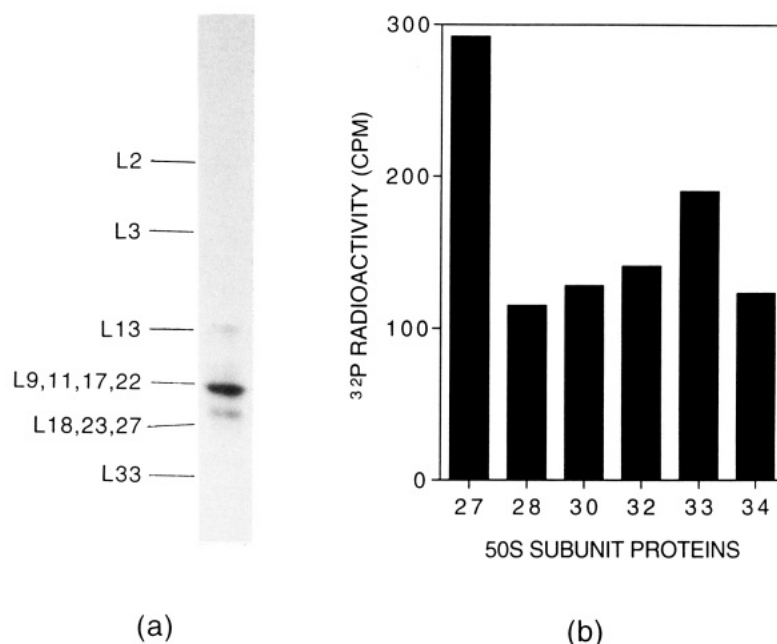
**Figure 3.** UV spectra of p2,6-diN<sub>3</sub>Rp before and after photolysis. Solutions of p2,6-diN<sub>3</sub>Rp in 50 mM Tris-HCl, pH 7.6, were irradiated for 10 min at 4 °C in a Rayonet photochemical reactor (Model RPR-100) equipped with four RPR-3000-Å lamps: (—) before irradiation; (---) after irradiation.

Dichloro-9-( $\beta$ -D-ribofuranosyl)purine (1) was reacted with sodium azide to give 2,6-diazido-9-( $\beta$ -D-ribofuranosyl)purine (2) (11, 12). The IR and <sup>1</sup>H-NMR spectra of 2 indicate that it exists predominantly in the azide form as had been previously found for the base, 2,6-diazidopurine (9). The nucleoside 2 was then bisphosphorylated with pyrophosphoryl chloride (13). The presence of the 3',5'-bisphosphate 3 in the reaction mixture was confirmed by the observation that T4 polynucleotide kinase was able to catalyze the exchange of the 5' phosphate with the  $\gamma$  phosphate of [ $\gamma$ - $^{32}$ P]ATP (Figure 2, lane a). The 2',5'-isomer in the bisphosphate mixture does not interfere with this procedure as it is neither labeled in the exchange reaction catalyzed by polynucleotide kinase nor does it act as a donor in the RNA ligase reaction used for incorporation of the photoreactive nucleotide into tRNA (13).

The photoreactivity of [ $5'$ - $^{32}$ P]p2,6-diN<sub>3</sub>Rp was assessed both by photolysis of the compound on a TLC plate and by spectrophotometry. In the first assay, [ $5'$ - $^{32}$ P]p2,6-diN<sub>3</sub>Rp was applied to the origin of a PEI-cellulose plate, which was irradiated with 300-nm light for 5 min before development. This procedure led to the formation of two new products, one immobilized at the origin and a second which migrated more slowly than unirradiated [ $5'$ - $^{32}$ P]p2,6-diN<sub>3</sub>Rp (Figure 2, lane b). This result is similar to that obtained with photolyzed p2N<sub>3</sub>Ap (4). Irradiation of the p2,6-diN<sub>3</sub>Rp in solution for 10 min completely abolished the absorption maxima at 244, 265, and 294 nm (Figure



**Figure 4.** Sucrose gradient analysis of cross-linked [2,6-diN<sub>3</sub>R76]tRNA<sup>Phe</sup>-ribosome complexes. (a) Noncovalent [<sup>32</sup>P][2,6-diN<sub>3</sub>R76]-tRNA<sup>Phe</sup>-ribosome complexes were irradiated and centrifuged through 10–30% sucrose gradients in 10 mM Tris-HCl, pH 7.6, 50 mM KCl, 0.25 mM MgCl<sub>2</sub>, and 0.05% 2-mercaptoethanol at 40 000 rpm for 135 min at 4 °C in a Beckman VTi50 rotor to resolve 50S and 30S ribosomal subunits. (b) The distribution of the cross-link between the 23S rRNA and 50S subunit proteins was assessed by centrifugation of the cross-linked 50S subunits through 5–20% sucrose gradients in a buffer containing 10 mM Tris-HCl, pH 7.6, 100 mM LiCl, 0.25 mM EDTA, and 0.5% (wt/vol) SDS at 40 000 rpm for 160 min at 10 °C in a VTi50 rotor.



**Figure 5.** Electrophoretic and immunological analysis of the [2,6-diN<sub>3</sub>R76]tRNA<sup>Phe</sup>-protein complex. (a) Covalent tRNA-protein complexes, isolated from the sucrose gradient depicted in Figure 4b, were digested with RNase T<sub>1</sub>, electrophoresed through an SDS-polyacrylamide gel, and visualized by autoradiography. The positions of the 50S subunit proteins, revealed by staining with Coomassie blue, are indicated at the left side of the autoradiogram. (b) The labeled proteins were eluted from the gel and screened for reaction with antibodies to ribosomal proteins as indicated. Selection of antibodies was based on the observation that all of the labeled proteins migrated to the “northwest” of proteins L27, L28, L33, and L34 upon two-dimensional polyacrylamide gel electrophoresis (see refs 5 and 7).

3). [5'-<sup>32</sup>P]p2,6-diN<sub>3</sub>Rp was ligated to the 3' end of yeast and *E. coli* tRNA<sup>Phe</sup> lacking the A residue at position 76 with a yield of 24% and 28%, respectively. Neither of the photoreactive tRNA derivatives was able to serve as a substrate for the cognate aminoacyl-tRNA synthetases.

When [<sup>32</sup>P][2,6-diN<sub>3</sub>R76]tRNA<sup>Phe</sup> was incubated with poly(U)-programmed 70S tight-couple ribosomes at a molar tRNA/ribosome input ratio of 1:4, 62% of the tRNA was noncovalently bound. Irradiation of the incubation mixture with 300-nm light for 10 min resulted in the covalent attachment of 10–16% of the bound tRNA to the ribosome, as judged by retention of tRNA on nitrocellulose

filters after dissociation of noncovalent complexes by exposure to low Mg<sup>2+</sup> concentration (5). Centrifugation of the irradiated tRNA-ribosome complexes through a sucrose gradient revealed that the tRNA was cross-linked exclusively to the 50S subunits (Figure 4a). The 50S-subunit fraction was then subjected to a second round of sucrose-gradient centrifugation in the presence of SDS and LiCl to dissociate the 50S-subunit proteins from the 23S rRNA. This analysis indicated that approximately 48% of the cross-linked tRNA was associated with the 3–5S protein fraction and 52% with 23S rRNA (Figure 4b).

To characterize the cross-linked protein(s), the 3-5S fraction was treated with RNase T<sub>1</sub>, and the proteins were resolved by SDS-PAGE. Autoradiography of the SDS-containing gel revealed two bands. The majority of the label migrated with a mobility corresponding to proteins L9, L11, L17, and L22 (Figure 5a). A smaller amount of the label migrated slightly slower than proteins L18, L23, and L27. Because a <sup>32</sup>P-labeled pentanucleotide remains attached to the cross-linked protein(s) after RNase T<sub>1</sub> digestion, its mobility undergoes a significant shift relative to its unlabeled counterpart. As a result, reliable identification of the labeled protein(s) cannot be made on the basis of one-dimensional polyacrylamide gels alone. To determine the identity of the cross-linked protein(s) conclusively, an immunological approach was used in which antibodies directed against individual ribosomal proteins were immobilized on agarose and mixed with an aliquot of the RNase-digested tRNA-protein complex. The radioactivity associated with each antibody on the agarose gel was then monitored by scintillation counting (15). The results, presented in Figure 5b, show that L27 and L33 were the proteins labeled by [2,6-diN<sub>3</sub>R76]tRNA<sup>Phe</sup>.

Protein L27 has previously been labeled from the P site by tRNA<sup>Phe</sup> derivatives containing either 2N<sub>3</sub>A or 8N<sub>3</sub>A at position 76 (5,6). Our present results add further evidence that L27 is a close neighbor of the 3' end of tRNA in the ribosomal P site. This protein is thus a likely structural and/or functional component of the peptidyl transferase center on the 50S subunit. Protein L33, on the other hand, has been cross-linked by tRNA probes bound to both the P and E sites (7, 16, 17). Labeling of protein L33 by [2,6-diN<sub>3</sub>R76]tRNA<sup>Phe</sup> is consistent with data on the relative positions of ribosomal proteins within the 50S ribosomal subunit (18, 19) and further underlines the proximity of the P and E sites suggested by our earlier studies (5-7).

Cross-linking of [2,6-diN<sub>3</sub>R76]tRNA<sup>Phe</sup> to the 23S rRNA is of considerable interest in view of recent evidence suggesting that the peptidyl transferase activity of the ribosome may be attributable to 23S rRNA (20). We previously reported that [2N<sub>3</sub>A76]tRNA<sup>Phe</sup> labeled the 23S rRNA nucleotide G1945 when bound to the P site (6). Since either of the azide groups of 2,6-diN<sub>3</sub>R can insert into adjacent bonds, we are characterizing the tRNA-23S rRNA cross-link described herein to further delineate nucleotides within the 23S rRNA that are in proximity to the 3' end of tRNA and thus of potential structural or functional importance at the peptidyl transferase center of the ribosome.

#### ACKNOWLEDGMENT

We are grateful to Dr. Richard Brimacombe for performing the immunological analysis of the tRNA-protein complexes and to Dr. George Dubay for obtaining the mass spectra. S.S.H. thanks Prof. Ned Porter and his co-workers for the use of their facilities at Duke University. This work was supported by NIH Grant GM22807.

#### LITERATURE CITED

- Haley, B. E. (1983) Development and utilization of 8-azidopurine nucleotide photoaffinity probes. *Fed. Proc.* 42, 2831-2836.
- Cusack, N. J., and Born, G. V. R. (1976) Effects of photolysable 2-azido analogues of adenosine, AMP and ADP on human platelets. *Proc. R. Soc. London* 197, 515-520.
- MacFarlane, D. E., Mills, D. C. B., and Srivastava, P. C. (1982) Binding of 2-azidoadenosine [ $\beta$ -<sup>32</sup>P]diphosphate to the receptor on intact human blood platelets which inhibits adenylate cyclase. *Biochemistry* 21, 544-549.
- Sylvers, L. A., Wower, J., Hixson, S. S., and Zimmermann, R. A. (1989) Preparation of 2-azidoadenosine 3',5'-[5'-<sup>32</sup>P]-bisphosphate for incorporation into transfer RNA: photoaffinity labeling of *Escherichia coli* ribosomes. *FEBS Lett.* 245, 9-13.
- Wower, J., Hixson, S. S., and Zimmermann, R. A. (1988) Photochemical cross-linking of yeast tRNA<sup>Phe</sup> containing 8-azidoadenosine at positions 73 and 76 to the *Escherichia coli* ribosome. *Biochemistry* 27, 8114-8121.
- Wower, J., Hixson, S. S., and Zimmermann, R. A. (1989) Labeling of the peptidyl transferase center of the *Escherichia coli* ribosome with photoreactive tRNA<sup>Phe</sup> derivatives containing azidoadenosine at the 3' end of the acceptor arm: a model of the tRNA-ribosome complex. *Proc. Natl. Acad. Sci. U.S.A.* 86, 5232-5236.
- Wower, J., Scheffer, P., Sylvers, L. A., Wintermeyer, W., and Zimmermann, R. A. (1993) Topography of the E site on the *Escherichia coli* ribosome. *EMBO J.* 12, 617-623.
- Wower, J., Sylvers, L. A., Rosen, K. V., Hixson, S. S., and Zimmermann, R. A. (1993) A Model of the tRNA Binding Sites on the *Escherichia coli* Ribosome, in *The Translational Apparatus* (K. H. Nierhaus, F. Franceschi, A. R. Subramanian, V. A. Erdmann, and B. Wittmann-Liebold, Eds.), pp 455-464, Plenum, New York.
- Temple, C., Jr., Kussner, C. L., and Montgomery, J. A. (1966) Studies on the azidoazomethine-tetrazole equilibrium. V. 2- and 6-azidopurines. *J. Org. Chem.* 31, 2210-2215.
- Rheinberger, H.-J., Geigenmüller, U., Wedde, M., and Nierhaus, K. H. (1988) Parameters for the preparation of *Escherichia coli* ribosomes and ribosomal subunits active in tRNA binding. *Methods Enzymol.* 164, 658-670.
- Gerster, J. F., and Robins, R. K. (1966) Purine Nucleosides. XIII. The synthesis of 2-fluoro- and 2-chloroinosine and certain derived purine nucleosides. *J. Org. Chem.* 31, 3258-3262.
- Montgomery, J. A., and Hewson, K. (1968) A convenient method for the synthesis of 2-fluoroadenosine. *J. Org. Chem.* 33, 432-434.
- Barrio, J. R., Barrio, M. C. G., Leonard, N. J., England, T. E., and Uhlenbeck, O. C. (1978) Synthesis of modified nucleoside 3',5'-bisphosphates and their incorporation into oligoribonucleotides with T4 RNA ligase. *Biochemistry* 17, 2077-2081.
- Reeve, A. E., and Huang, R. C. (1983) Synthesis and affinity purification of  $\beta$ -<sup>32</sup>P-labeled [ $\gamma$ -S]GTP. *Anal. Biochem.* 130, 14-18.
- Gulle, H., Hoppe, E., Osswald, M., Greuer, B., Brimacombe, R., and Stöffler, G. (1988) RNA protein cross-linking in *E. coli* 50S ribosomal subunits; determination of sites on 23S RNA that are cross-linked to proteins L2, L4, L24 and L27 by treatment with 2-iminothiolane. *Nucleic Acids Res.* 16, 815-832.
- Podkowinski, J., and Gornicki, P. (1989) Ribosomal proteins S7 and L1 are located close to the decoding site of *E. coli* ribosome-affinity labeling studies with modified tRNAs carrying photoreactive probes attached adjacent to the 3'-end of the anticodon. *Nucleic Acids Res.* 17, 8767-8782.
- Podkowinski, J., and Gornicki, P. (1991) Neighbourhood of the central fold of the tRNA molecule bound to the *E. coli* ribosome-affinity labeling studies with modified tRNAs carrying photoreactive probes attached to the dihydrouridine loop. *Nucleic Acids Res.* 19, 801-808.
- Walleczek, J., Martin, T., Redl, B., Stöffler-Meilicke, M., and Stöffler, G. (1989) Comparative cross-linking study on the 50S ribosomal subunit from *Escherichia coli*. *Biochemistry* 28, 4099-4105.
- Redl, B., Walleczek, J., Stöffler-Meilicke, M., and Stöffler, G. (1989) Immunoblotting analysis of protein-protein crosslinks within the 50S ribosomal subunit of *Escherichia coli*. *Eur. J. Biochem.* 181, 351-356.
- Noller, H. F., Hoffarth, V., and Zimniak, L. (1992) Unusual resistance of peptidyl transferase to protein extraction procedures. *Science* 256, 1416-1419.

# TECHNICAL NOTES

## Synthesis of a Lipid/Peptide/Drug Conjugate: $N^4$ -(Acylpeptidyl)-Ara-C

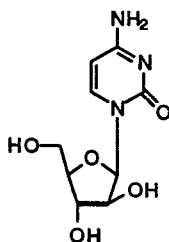
F. M. Menger,\* Y. Guo, and A. S. Lee

Department of Chemistry, Emory University, Atlanta, Georgia 30322. Received September 8, 1993\*

A lipid/peptide/drug conjugate,  $N^4$ -(acylpeptidyl)-ara-C, is synthesized under mild conditions to give an ara-C prodrug protected against cytidine deaminase-catalyzed deactivation. The compounds can be bound, *via* their hydrocarbon tails, to phospholipid membranes and examined for chymotrypsin-induced drug release. A tripeptide is too short to permit efficient enzyme/membrane contact and subsequent freeing of the drug. Faster rates can, presumably, be achieved by "fine tuning" the length and polarity of the peptide spacer attached to the drug.

### INTRODUCTION

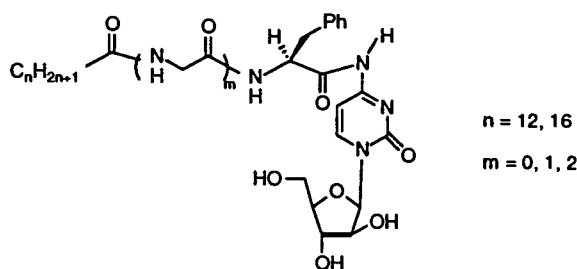
1-( $\beta$ -D-Arabinofuranosyl)cytosine (ara-C<sup>1</sup>) is one of the most important drugs for the treatment of human acute myeloblastic and lymphoblastic leukemia (1, 2). It is also



effective in combination-chemotherapy against solid tumors (3). Clinical activity of ara-C is, however, adversely affected by a cytidine deaminase-catalyzed  $\text{NH}_2$ -to-OH replacement that reduces the drug's half-life in the plasma (4).

Derivatives of ara-C with long-chain  $N^4$ -acyl groups have been reported to have greater chemotherapeutic activities than does ara-C itself (5). These derivatives are resistant to cytidine deaminase. In addition, they are more efficiently incorporated into cells, and maintained there for a longer time period, than the parent drug (6). We now describe the synthesis of  $N^4$ -(acylpeptidyl) derivatives of ara-C, a new class of ara-C prodrug having two key features: (a) The  $N^4$  amino group is protected *via* acylation by an enzyme-removable peptide. (b) At the distal end there is attached a long hydrocarbon chain to impart lipid solubility.

Two primary considerations motivated the design of these substances: (a) We wished to bind the compounds to an *in vitro* phospholipid bilayer (by means of their hydrocarbon tails) and to examine how the peptide structure affected enzyme-induced drug release at the membrane surface. Peptides are useful "spacers" in that



they can be readily modified in length and polarity. (b) We also wished to determine how *in vivo* activity depended upon the tail length and peptide sequence. These studies are in progress. For the present purposes, the focus will be mainly on the synthetic details involved in assembling lipid, peptide, nucleic acid base, and sugar (the four major building blocks of life) into a single unit.

In 1991, Wipf *et al.* (7) also synthesized  $N^4$ -peptidyl derivatives of ara-C, but their work differs from ours in two important ways. First, their compounds lack a lipid moiety. Second, their method for attaching the peptide to the drug involved reagents such as LiOH and BuLi that are too harsh for our more sensitive peptides.

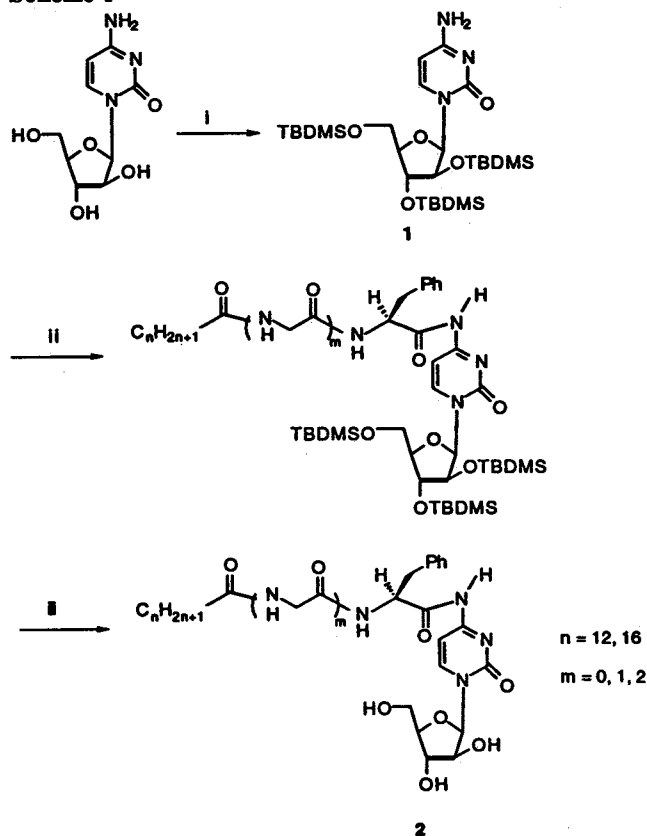
### RESULTS AND DISCUSSION

Acylpeptide was formed in 64–82% yield by treating a fatty acid with ethyl chloroformate and triethylamine for 20 min at 0 °C in THF (8). A 1:1 aqueous solution of peptide and NaOH was then added and the mixture stirred at room temperature for 19 h. Workup consisted of quenching with 10% aqueous HCl to pH 2, extraction into  $\text{CH}_2\text{Cl}_2$ , removal of solvent, and trituration with ether or  $\text{CH}_3\text{CN}$  to remove unreacted reagents. Products were characterized by NMR and elemental analysis. The remainder of the synthesis was carried out according to the three steps in Scheme 1: (a) ara-C was protected with TBDMSCl using the Wipf procedure (7), and (b) trisilylated nucleotide 1 thus obtained was reacted with an acylpeptide (1 equiv), EEDQ (1 equiv), and pyridine (6 equiv) in chloroform at 37 °C for 48 h (9). Removal of the solvent and pyridine under vacuum gave an oily product which was flash chromatographed on a silica column (20%  $\text{CH}_3\text{OH}$  in  $\text{CHCl}_3$  eluant). The resulting residue was treated, without further purification, with 1 M TBAF in THF (6 equiv) at room temperature for 2 h according to

\* Author to whom correspondence should be addressed.

\* Abstract published in *Advance ACS Abstracts*, January 15, 1994.

<sup>1</sup>Abbreviations used: ara-C, 1-( $\beta$ -D-arabinofuranosyl)cytosine; TBDMSCl, *tert*-butyldimethylsilyl chloride; EEDQ, 2-ethoxy-1-(ethoxycarbonyl)-1,2-dihydroquinoline; TBAF, tetrabutylammonium fluoride; DMAP, 4-(dimethylamino)pyridine; THF, tetrahydrofuran; 3-NBA, 3-nitrobenzyl alcohol.

Scheme 1<sup>a</sup>

<sup>a</sup> Key: (i) TBDMSCl, imidazole, DMAP, rt, 72 h; (ii) acylpeptide, EEDQ, py, 37 °C, 48 h; (iii) TBAF, rt, 2 h.

a procedure of Corey and Venkateswarlu (10). Flash chromatography on silica (20% CH<sub>3</sub>OH in CHCl<sub>3</sub>) afforded the final products **2** that were characterized by <sup>1</sup>H and <sup>13</sup>C NMR, elemental analysis, and MS (FAB, 3-NBA matrix). Although the overall yields in Scheme 1 were modest at best (21–47%), attempts to conjugate the weakly nucleophilic ara-C amino group to peptides by other methods were unsuccessful altogether.

All ara-C derivatives ( $n = 12, 16$ ;  $m = 0–2$ ) were too water-insoluble in the absence of a solubilizing entity (micelle, vesicle, etc.) to allow a study of their  $\alpha$ -chymotrypsin-catalyzed hydrolyses. In order to obtain "baseline" parameters, we used a short-chain analog ( $n = 5$ ,  $m = 0$ ) that was sufficiently water-soluble by itself. This substrate has a  $k_{\text{cat}} = 5.3 \text{ s}^{-1}$  and  $K_m = 1.4 \times 10^{-3} \text{ M}$  (pH = 7.0, 25.0 °C). When the long-chained lipid/peptide/ara-C compounds were adsorbed to phospholipid bilayers, the rate of drug release was too small to measure. The extraordinarily slow hydrolysis rates were even more evident with the membrane-bound *p*-nitrophenyl esters of our lipid-peptides. These hydrolysis rates were orders of magnitude slower than that of free phenylalanine *p*-nitrophenyl ester. It will be interesting to determine the number and structure of the amino acids required in the peptide spacer to achieve "normal" rates. These will depend upon the conformation of the peptide at the membrane surface and upon the minimum permissible enzyme/membrane contact distance. The work is now made possible by our synthetic route to lipid/peptide/drug conjugates described herein.

#### EXPERIMENTAL PROCEDURES

**General Methods.** Melting points were determined with a Thomas Hoover capillary melting point apparatus and are uncorrected. Fast atom bombardment (FAB) mass

spectra were obtained on a VG 70-S mass spectrometer using 3-nitrobenzyl alcohol (3-NBA) as the matrix. Elemental analyses were performed by Atlantic Microlab, Inc., P.O. Box 2288, Atlanta, GA. <sup>1</sup>H and <sup>13</sup>C NMR spectra were recorded on a QE-300 MHz spectrometer using CDCl<sub>3</sub> as the reference solvent unless otherwise indicated. Solvents were of reagent grade and dried over molecular sieves (4 Å). THF was distilled under N<sub>2</sub> from sodium benzophenone ketyl before use. All reactions were performed under N<sub>2</sub> unless otherwise noted.

**N-Tridecanoylphenylalanine.** To a solution of tridecanoic acid (4.29 g, 20 mmol) and triethylamine (2.8 mL, 20 mmol) in 50 mL of distilled THF at 0 °C under N<sub>2</sub> was added slowly ethyl chloroformate (2.1 mL, 22 mmol). After the solution was stirred at 0 °C for 20 min, an ice-cold solution of sodium salt of phenylalanine, prepared from phenylalanine (3.3 g, 20 mmol) and sodium hydroxide (800 mg, 20 mmol) in 40 mL of water, was added. The reaction mixture was warmed to room temperature, stirred for 19 h, and then acidified to pH ~2 with 10% aqueous HCl (8). The mixture was poured into water (250 mL) and extracted with CH<sub>2</sub>Cl<sub>2</sub> (3 × 50 mL). The combined organic extracts were extracted again with brine (100 mL), dried over MgSO<sub>4</sub>, filtered, and concentrated under reduced pressure. The crude residue was triturated with CH<sub>3</sub>CN and dried under vacuum to afford 4.82 g (67%) of *N*-tridecanoylphenylalanine (mp 91–92 °C). <sup>1</sup>H NMR (300 MHz, CDCl<sub>3</sub>):  $\delta$  0.88 (t,  $J = 6.6 \text{ Hz}$ , 3H), 1.15–1.65 (m, 20 H), 2.18 (t,  $J = 7.5 \text{ Hz}$ , 2 H), 3.10–3.20 (dd,  $J = 14.0 \text{ Hz}$ , 6.3 Hz, 1H), 3.20–3.30 (dd,  $J = 14.0 \text{ Hz}$ , 5.5 Hz, 1H), 4.90 (m, 1H), 6.00 (d,  $J = 7.1 \text{ Hz}$ , 1H), 7.05–7.20 (m, 5H). <sup>13</sup>C NMR (75.1 MHz, CDCl<sub>3</sub>):  $\delta$  14.1, 22.7, 25.5, 29.1, 29.3, 29.4, 29.5, 29.6, 31.9, 36.4, 37.2, 53.1, 127.2, 128.6, 129.3, 135.6, 173.9, 174.9. LRMS (FAB):  $m/z$  362 ( $M + H$ )<sup>+</sup>. Anal. Calcd for C<sub>22</sub>H<sub>35</sub>NO<sub>3</sub>: C, 73.09; H, 9.76; N, 3.87. Found: C, 72.99; H, 9.70; N, 3.87.

**N-Tridecanoylglycylphenylalanine.** To a solution of tridecanoic acid (4.29 g, 20 mmol) and triethylamine (2.8 mL, 20 mmol) in 45 mL of distilled THF at 0 °C under N<sub>2</sub> was added slowly ethyl chloroformate (2.1 mL, 22 mmol). After the solution was stirred at 0 °C for 35 min, an ice-cold solution of sodium salt of glycylphenylalanine, prepared from glycylphenylalanine (4.4 g, 20 mmol) and sodium hydroxide (800 mg, 20 mmol) in 50 mL of water, was added. The reaction mixture was warmed to room temperature, stirred for 19 h, and then acidified to pH ~2 with 10% aqueous HCl (8). The mixture was poured into water (300 mL) and extracted with CH<sub>2</sub>Cl<sub>2</sub>/CH<sub>3</sub>OH (3 × 70 mL). The combined organic extracts were extracted again with brine (100 mL), dried over MgSO<sub>4</sub>, filtered, and concentrated under reduced pressure. The crude residue was triturated with ether and dried under vacuum to afford 5.60 g (67%) of *N*-tridecanoylglycylphenylalanine (mp 112–113 °C). <sup>1</sup>H NMR (300 MHz, CDCl<sub>3</sub>):  $\delta$  0.88 (t,  $J = 6.6 \text{ Hz}$ , 3H), 1.20–1.70 (m, 20 H), 2.22 (t,  $J = 7.5 \text{ Hz}$ , 2 H), 2.95–3.25 (m, 2H), 3.60–4.00 (m, 2H), 7.10–7.30 (m, 5H). <sup>13</sup>C NMR (75.1 MHz, CDCl<sub>3</sub>):  $\delta$  13.5, 22.4, 25.4, 29.0, 29.1, 29.2, 29.4, 31.7, 35.7, 37.1, 42.3, 53.2, 126.6, 128.2, 129.1, 136.2, 169.6, 172.9, 175.1. LRMS (FAB):  $m/z$  419 ( $M + H$ )<sup>+</sup>. Anal. Calcd for C<sub>24</sub>H<sub>38</sub>N<sub>2</sub>O<sub>4</sub>·0.5H<sub>2</sub>O: C, 67.42; H, 9.19; N, 6.55. Found: C, 67.88; H, 9.03; N, 6.64.

**N-Tridecanoylglycylglycylphenylalanine.** To a solution of tridecanoic acid (3.22 g, 15 mmol) and triethylamine (2.1 mL, 15 mmol) in 60 mL of distilled THF at 0 °C under N<sub>2</sub> was added slowly ethyl chloroformate (1.6 mL, 16.5 mmol). After the solution was stirred at 0 °C for 150 min, an ice-cold solution of the sodium salt of glycylglycylphenylalanine, prepared from glycylglycyl-



phenylalanine (4.19 g, 15 mmol) and sodium hydroxide (600 mg, 15 mmol) in 50 mL of water, was added. The reaction mixture was warmed to room temperature, stirred for 21 h, and then acidified to pH  $\sim$ 2 with 10% aqueous HCl (8). The mixture was poured into water (150 mL) and extracted with  $\text{CH}_2\text{Cl}_2/\text{CH}_3\text{OH}$  ( $3 \times 50$  mL). The combined organic extracts were extracted again with brine (100 mL), dried over  $\text{MgSO}_4$ , filtered, and concentrated under reduced pressure. The crude residue was triturated with ether and dried under vacuum to afford 5.44 g (76%) of *N*-tridecanoylglycylglycylphenylalanine (mp 128–129 °C).  $^1\text{H}$  NMR (300 MHz,  $\text{CDCl}_3$ ):  $\delta$  0.88 (t,  $J$  = 6.6 Hz, 3H), 1.20–1.70 (m, 20 H), 2.27 (t,  $J$  = 7.5 Hz, 2H), 3.00–3.10 (dd,  $J$  = 14.0 Hz, 6.1 Hz, 1H), 3.15–3.30 (dd,  $J$  = 14.0 Hz, 5.0 Hz, 1H), 3.75–4.00 (m, 4H), 7.15–7.35 (m, 5H).  $^{13}\text{C}$  NMR (75.1 MHz,  $\text{CDCl}_3$ ):  $\delta$  13.0, 21.9, 24.9, 28.6, 28.8, 28.9, 31.2, 35.2, 36.6, 41.5, 42.0, 53.1, 126.1, 127.7, 128.5, 136.1, 169.1, 170.0, 172.6, 175.0. LRMS (FAB):  $m/z$  476 ( $M + \text{H}$ ) $^+$ . Anal. Calcd for  $\text{C}_{26}\text{H}_{41}\text{N}_3\text{O}_5 \cdot 0.5\text{H}_2\text{O}$ : C, 64.44; H, 8.74; N, 8.67. Found: C, 64.77; H, 8.76; N, 8.71.

***N*-Heptadecanoylphenylalanine.** To a solution of heptadecanoic acid (5.41 g, 20 mmol) and triethylamine (2.8 mL, 20 mmol) in 60 mL of distilled THF at 0 °C under  $\text{N}_2$  was added slowly ethyl chloroformate (2.1 mL, 22 mmol). After the solution was stirred at 0 °C for 20 min, an ice-cold solution of the sodium salt of phenylalanine, prepared from phenylalanine (3.3 g, 20 mmol) and sodium hydroxide (800 mg, 20 mmol) in 50 mL of water, was added. The reaction mixture was warmed to room temperature, stirred for 19 h, and then acidified to pH  $\sim$ 2 with 10% aqueous HCl (8). The mixture was poured into water (200 mL) and extracted with  $\text{CHCl}_3$  ( $3 \times 100$  mL). The combined organic extracts were extracted again with brine (200 mL), dried over  $\text{MgSO}_4$ , filtered, and concentrated under reduced pressure. The crude residue was triturated with  $\text{CCl}_4$  and dried under vacuum to afford 5.85 g (70%) of *N*-heptadecanoylphenylalanine (mp 74–75 °C).  $^1\text{H}$  NMR (300 MHz,  $\text{CDCl}_3$ ):  $\delta$  0.88 (t,  $J$  = 6.5 Hz, 3H), 1.15–1.65 (m, 28 H), 2.18 (t,  $J$  = 7.5 Hz, 2H), 3.10–3.20 (dd,  $J$  = 14.0 Hz, 6.2 Hz, 1H), 3.20–3.30 (dd,  $J$  = 14.0 Hz, 5.5 Hz, 1H), 4.90 (m, 1H), 5.98 (d,  $J$  = 7.3 Hz, 1H), 7.05–7.20 (m, 5H).  $^{13}\text{C}$  NMR (75.1 MHz,  $\text{CDCl}_3$ ):  $\delta$  14.1, 22.7, 25.6, 29.1, 29.3, 29.4, 29.5, 29.7, 31.9, 36.4, 37.3, 53.1, 127.2, 128.6, 129.3, 135.6, 174.0, 174.7. LRMS (FAB):  $m/z$  853 ( $M + 2\text{Li} - \text{H}$ ) $^+$ . Anal. Calcd for  $\text{C}_{26}\text{H}_{43}\text{NO}_3 \cdot 0.5\text{H}_2\text{O}$ : C, 73.20; H, 10.40; N, 3.28. Found: C, 73.77; H, 10.31; N, 3.33.

***N*-Heptadecanoylglycylphenylalanine.** To a solution of heptadecanoic acid (0.27 g, 1 mmol) and triethylamine (0.14 mL, 1 mmol) in 6 mL of distilled THF at 0 °C under  $\text{N}_2$  was added slowly ethyl chloroformate (97  $\mu\text{L}$ , 1 mmol). After the solution was stirred at 0 °C for 20 min, an ice-cold solution of sodium salt of glycylphenylalanine, prepared from glycylphenylalanine (0.22 g, 1 mmol) and sodium hydroxide (0.04 mg, 1 mmol) in 6 mL water, was added. The reaction mixture was warmed to room temperature, stirred for 19 h, and then acidified to pH  $\sim$ 2 with 10% aqueous HCl (8). The mixture was poured into water (30 mL) and extracted with  $\text{CH}_2\text{Cl}_2/\text{CH}_3\text{OH}$  ( $3 \times 10$  mL). The combined organic extracts were extracted again with brine (30 mL), dried over  $\text{MgSO}_4$ , filtered, and concentrated under reduced pressure. The crude residue was triturated with ether and dried under vacuum to afford 0.30 g (64%) of *N*-heptadecanoylglycylphenylalanine (mp 117–118 °C).  $^1\text{H}$  NMR (300 MHz,  $\text{CDCl}_3$ ):  $\delta$  0.88 (t,  $J$  = 6.6 Hz, 3H), 1.20–1.70 (m, 28 H), 2.22 (t,  $J$  = 7.5 Hz, 2H), 3.00–3.10 (dd,  $J$  = 14.0 Hz, 7.3 Hz, 1H), 3.15–3.25 (dd,  $J$  = 14.0 Hz, 5.2 Hz, 1H), 3.75–3.95 (m, 2H), 7.15–7.35 (m, 5H).  $^{13}\text{C}$  NMR (75.1 MHz,

$\text{CDCl}_3$ ):  $\delta$  14.2, 22.9, 25.8, 29.5, 29.6, 29.7, 29.9, 32.1, 36.3, 37.7, 42.7, 53.5, 127.1, 128.6, 129.5, 136.4, 169.6, 173.9, 175.1. LRMS (FAB):  $m/z$  476 ( $M + \text{H}$ ) $^+$ . Anal. Calcd for  $\text{C}_{28}\text{H}_{46}\text{N}_2\text{O}_4$ : C, 70.85; H, 9.77; N, 5.90. Found: C, 70.63; H, 9.83; N, 5.85.

***N*-Heptadecanoylglycylglycylphenylalanine.** To a solution of heptadecanoic acid (3.23 g, 11.9 mmol) and triethylamine (1.70 mL, 11.9 mmol) in 100 mL of distilled THF at 0 °C under  $\text{N}_2$  was added slowly ethyl chloroformate (1.15 mL, 11.9 mmol). After the solution was stirred at 0 °C for 50 min, an ice-cold solution of sodium salt of glycylglycylphenylalanine, prepared from glycylglycylphenylalanine (3.34 g, 11.9 mmol) and sodium hydroxide (478 mg, 11.9 mmol) in 70 mL of water, was added. The reaction mixture was warmed to room temperature, stirred for 20 h, and then acidified to pH  $\sim$ 2 with 10% aqueous HCl (8). The mixture was poured into water (200 mL) and extracted with  $\text{CH}_2\text{Cl}_2/\text{CH}_3\text{OH}$  ( $3 \times 70$  mL). The combined organic extracts were extracted again with brine (100 mL), dried over  $\text{MgSO}_4$ , filtered, and concentrated under reduced pressure. The crude residue was triturated with ether and dried under vacuum to afford 5.35 g (82%) of *N*-heptadecanoylglycylglycylphenylalanine (mp 142–143 °C).  $^1\text{H}$  NMR (300 MHz,  $\text{CDCl}_3$ ):  $\delta$  0.88 (t,  $J$  = 6.0 Hz, 3H), 1.20–1.70 (m, 28 H), 2.27 (t,  $J$  = 7.5 Hz, 2H), 3.00–3.10 (dd,  $J$  = 14.0 Hz, 6.1 Hz, 1H), 3.15–3.30 (dd,  $J$  = 14.0 Hz, 5.0 Hz, 1H), 3.75–4.00 (m, 4H), 7.15–7.35 (m, 5H).  $^{13}\text{C}$  NMR (75.1 MHz,  $\text{CDCl}_3$ ):  $\delta$  14.2, 22.8, 25.7, 29.5, 29.6, 29.8, 32.0, 36.2, 37.4, 42.6, 42.8, 53.7, 127.0, 128.5, 129.4, 136.5, 169.4, 170.4, 173.5, 175.2. LRMS (FAB):  $m/z$  532 ( $M + \text{H}$ ) $^+$ . Anal. Calcd for  $\text{C}_{30}\text{H}_{49}\text{N}_3\text{O}_5$ : C, 67.76; H, 9.29; N, 7.90. Found: C, 67.47; H, 9.31; N, 7.73.

**2',3',5'-Tri-*O*-TBDMS-ara-C.** A solution of ara-C (1.22 g, 5 mmol), TBDMSCl (4.56 g, 30 mmol), imidazole (2.04 g, 30 mmol), and DMAP (0.16 g, 1.25 mmol) in 40 mL of anhydrous  $\text{CH}_2\text{Cl}_2$  was stirred at room temperature for 4 days (7). The solvent was removed under reduced pressure, and the crude product was flash chromatographed on silica (20%  $\text{CH}_3\text{OH}/\text{CHCl}_3$ ) to afford 2.72 g of crude 2',3',5'-tri-*O*-TBDMS-ara-C. It was used in the following experiment without further purification.

***N*-(*N*-Tridecanoylphenylalanyl)-ara-C.** A solution of *N*-tridecanoylphenylalanine (564 mg, 1.56 mmol), tri-*O*-TBDMS-ara-C (914 mg, 1.56 mmol), EEDQ (386 mg, 1.56 mmol), and pyridine (760  $\mu\text{L}$ , 9.36 mmol) in 5 mL of anhydrous  $\text{CHCl}_3$  was heated at 37 °C under nitrogen for 48 h (9). The mixture was cooled to room temperature and concentrated under reduced pressure. The oily crude product was flash chromatographed on a silica column (20%  $\text{CH}_3\text{OH}/\text{CHCl}_3$ ). The resulting residue was treated, without further purification, with 1.0 M TBAF in THF (5.0 mL, 5.0 mmol) at room temperature for 2 h (10). Flash chromatography on silica (20%  $\text{CH}_3\text{OH}/\text{CHCl}_3$ ) afforded 190 mg (21%) of *N*-(*N*-tridecanoylphenylalanyl)-ara-C (mp 183–184 °C).  $^1\text{H}$  NMR (300 MHz,  $\text{CDCl}_3/\text{CD}_3\text{OD}$ , TMS = 0.0 ppm):  $\delta$  0.89 (t,  $J$  = 6.6 Hz, 3H), 1.15–1.60 (m, 20 H), 2.18 (t,  $J$  = 7.5 Hz, 2H), 2.90–3.30 (m, 2H), 3.75–3.95 (m, 2H), 4.05–4.35 (m, 3H), 6.23 (d,  $J$  = 5.0 Hz, 1H), 7.15–7.35 (m, 5H), 7.45 (d,  $J$  = 7.4 Hz, 1H), 8.27 (d,  $J$  = 7.4 Hz, 1H).  $^{13}\text{C}$  NMR (75.1 MHz,  $\text{CDCl}_3/\text{CD}_3\text{OD}$ ,  $\text{CDCl}_3$  = 77 ppm):  $\delta$  13.0, 21.9, 25.0, 28.4, 28.6, 28.7, 28.9, 31.2, 35.2, 36.7, 54.7, 54.8, 60.9, 74.4, 76.3, 85.4, 87.7, 95.5, 126.2, 127.7, 128.4, 135.6, 146.1, 155.7, 161.8, 171.8, 174.3. LRMS (FAB):  $m/z$  593 ( $M + \text{Li}$ ) $^+$ . Anal. Calcd for  $\text{C}_{31}\text{H}_{46}\text{N}_4\text{O}_7 \cdot \text{H}_2\text{O}$ : C, 61.57; H, 8.00; N, 9.26. Found: C, 61.64; H, 7.75; N, 9.09.

***N*-(*N*-Tridecanoylglycylphenylalanyl)-ara-C.** A

solution of *N*-tridecanoylglycylphenylalanine (628 mg, 1.5 mmol), tri-*O*-TBDMS-ara-C (879 mg, 1.5 mmol), EEDQ (371 mg, 1.5 mmol), and pyridine (728  $\mu$ L, 9.0 mmol) in 10 mL anhydrous  $\text{CHCl}_3$  was heated at 50  $^\circ\text{C}$  under nitrogen for 48 h (9). The mixture was cooled to room temperature and concentrated under reduced pressure. The oily crude product was flash chromatographed on a silica column (20%  $\text{CH}_3\text{OH}/\text{CHCl}_3$ ). The resulting residue was treated, without further purification, with 1.0 M TBAF in THF (10.0 mL, 10.0 mmol) at room temperature for 2 h (10). Flash chromatography on silica (20%  $\text{CH}_3\text{OH}/\text{CHCl}_3$ ) afforded 220 mg (23%) of *N*<sup>4</sup>-(*N*-tridecanoylglycylphenylalanyl)-ara-C (mp 120–121  $^\circ\text{C}$ ).  $^1\text{H}$  NMR (300 MHz,  $\text{CDCl}_3/\text{CD}_3\text{OD}$ , TMS = 0.0 ppm):  $\delta$  0.88 (t,  $J$  = 6.6 Hz, 3H), 1.20–1.70 (m, 20 H), 2.22 (t,  $J$  = 7.5 Hz, 2H), 2.95–3.25 (m, 2H), 3.75–4.35 (m, 7H), 4.80–5.00 (m, 1H), 6.23 (d,  $J$  = 5.0 Hz, 1H), 7.15–7.45 (m, 6H), 8.27 (d,  $J$  = 7.4 Hz, 1H).  $^{13}\text{C}$  NMR (75.1 MHz,  $\text{CDCl}_3/\text{CD}_3\text{OD}$ ,  $\text{CDCl}_3$  = 77 ppm):  $\delta$  13.4, 22.2, 25.2, 28.8, 28.9, 29.0, 29.1, 31.4, 35.6, 37.2, 42.1, 55.0, 61.1, 74.6, 85.5, 87.9, 95.8, 126.6, 128.1, 128.7, 135.4, 146.3, 155.8, 161.9, 169.6, 171.5, 174.8. LRMS (FAB):  $m/z$  644 ( $M + \text{H}$ )<sup>+</sup>. Anal. Calcd for  $\text{C}_{33}\text{H}_{49}\text{N}_5\text{O}_8 \cdot 0.5\text{H}_2\text{O}$ : C, 60.72; H, 7.72; N, 10.73. Found: C, 60.96; H, 7.69; N, 10.79.

***N*<sup>4</sup>-(*N*-Tridecanoylglycylglycylphenylalanyl)-ara-C.** A solution of *N*-tridecanoylglycylglycylphenylalanine (950 mg, 2.0 mmol), tri-*O*-TBDMS-ara-C (1.17 g, 2.0 mmol), EEDQ (494 mg, 2.0 mmol), and pyridine (970  $\mu$ L, 12.0 mmol) in 10 mL of anhydrous  $\text{CHCl}_3$  was heated at 50  $^\circ\text{C}$  under nitrogen for 51 h (9). The mixture was cooled to room temperature and concentrated under reduced pressure. The oily crude product was flash chromatographed on a silica column (20%  $\text{CH}_3\text{OH}/\text{CHCl}_3$ ). The resulting residue was treated, without further purification, with 1.0 M TBAF in THF (15.0 mL, 15.0 mmol) at room temperature for 2 h (10). Flash chromatography on silica gel (20%  $\text{CH}_3\text{OH}/\text{CHCl}_3$ ) afforded 435 mg (31%) of *N*<sup>4</sup>-(*N*-tridecanoylglycylglycylphenylalanyl)-ara-C (mp 122–123  $^\circ\text{C}$ ).  $^1\text{H}$  NMR (300 MHz,  $\text{CDCl}_3/\text{CD}_3\text{OD}$ , TMS = 0.0 ppm):  $\delta$  0.88 (t,  $J$  = 6.6 Hz, 3H), 1.15–1.75 (m, 20 H), 2.27 (t,  $J$  = 7.5 Hz, 2H), 3.00–3.30 (m, 2H), 3.75–4.35 (m, 7H), 4.75–4.95 (m, 1H), 6.23 (d,  $J$  = 5.0 Hz, 1H), 7.15–7.30 (m, 5H), 7.40 (d,  $J$  = 7.4 Hz, 1H), 8.27 (d,  $J$  = 7.4 Hz, 1H).  $^{13}\text{C}$  NMR (75.1 MHz,  $\text{CDCl}_3/\text{CD}_3\text{OD}$ ,  $\text{CDCl}_3$  = 77 ppm):  $\delta$  13.3, 14.3, 22.1, 25.1, 28.8, 28.9, 29.0, 29.1, 31.4, 35.4, 36.7, 42.0, 42.4, 55.4, 61.0, 65.4, 74.6, 76.3, 85.4, 87.8, 95.7, 126.4, 128.0, 135.8, 146.4, 155.7, 161.8, 169.8, 170.6, 171.5, 175.2. LRMS (FAB):  $m/z$  707 ( $M + \text{Li}$ )<sup>+</sup>. Anal. Calcd for  $\text{C}_{35}\text{H}_{52}\text{N}_6\text{O}_9 \cdot \text{H}_2\text{O}$ : C, 58.48; H, 7.57; N, 11.69. Found: C, 58.34; H, 7.64; N, 11.61.

***N*<sup>4</sup>-(*N*-Heptadecanoylphenylalanyl)-ara-C.** A solution of *N*-heptadecanoylphenylalanine (508 mg, 1.21 mmol), tri-*O*-TBDMS-ara-C (713 mg, 1.21 mmol), EEDQ (301 mg, 1.21 mmol), and pyridine (590  $\mu$ L, 7.3 mmol) in 5 mL of anhydrous  $\text{CHCl}_3$  was heated at 37  $^\circ\text{C}$  under nitrogen for 48 h (9). The mixture was cooled to room temperature and concentrated under reduced pressure. The oily crude product was flash chromatographed on a silica column (20%  $\text{CH}_3\text{OH}/\text{CHCl}_3$ ). The resulting residue was treated, without further purification, with 1.0 M TBAF in THF (7.0 mL, 7.0 mmol) at room temperature for 2 h (10). Flash chromatography on silica (20%  $\text{CH}_3\text{OH}/\text{CHCl}_3$ ) afforded 368 mg (47%) of *N*<sup>4</sup>-(*N*-heptadecanoylphenylalanyl)-ara-C (mp 161–162  $^\circ\text{C}$ ).  $^1\text{H}$  NMR (300 MHz,  $\text{CDCl}_3/\text{CD}_3\text{OD}$ , TMS = 0.0 ppm):  $\delta$  0.89 (t-like, 3H), 1.10–1.60 (m, 28 H), 2.18 (t-like, 2H), 2.80–3.30 (m, 2H), 3.70–4.40 (m, 5H), 4.60–5.00 (m, 1H), 6.23 (s, 1H), 7.00–7.50 (m, 6H), 8.24 (d,  $J$  = 7.4 Hz, 1H).  $^{13}\text{C}$

NMR (75.1 MHz,  $\text{CDCl}_3/\text{CD}_3\text{OD}$ ,  $\text{CDCl}_3$  = 77 ppm):  $\delta$  13.0, 21.9, 25.0, 28.4, 28.6, 28.7, 31.2, 35.1, 36.7, 54.7, 54.8, 60.9, 74.4, 76.3, 85.4, 87.6, 95.4, 126.2, 127.7, 128.4, 135.6, 146.1, 148.0, 155.7, 161.8, 171.8, 174.3. LRMS (FAB):  $m/z$  649 ( $M + \text{Li}$ )<sup>+</sup>. Anal. Calcd for  $\text{C}_{35}\text{H}_{54}\text{N}_4\text{O}_7 \cdot 2\text{H}_2\text{O}$ : C, 64.49; H, 8.50; N, 8.60. Found: C, 64.61; H, 8.41; N, 8.38.

***N*<sup>4</sup>-(*N*-Heptadecanoylglycylphenylalanyl)-ara-C.** A solution of *N*-heptadecanoylglycylphenylalanine (712 mg, 1.5 mmol), tri-*O*-TBDMS-ara-C (879 mg, 1.5 mmol), EEDQ (371 mg, 1.5 mmol), and pyridine (730  $\mu$ L, 9.0 mmol) in 10 mL of anhydrous  $\text{CHCl}_3$  was heated at 50  $^\circ\text{C}$  under nitrogen for 48 h (9). The mixture was cooled to room temperature and concentrated under reduced pressure. The oily crude product was flash chromatographed on a silica column (20%  $\text{CH}_3\text{OH}/\text{CHCl}_3$ ). The resulting residue was treated, without further purification, with 1.0 M TBAF in THF (10.0 mL, 10.0 mmol) at room temperature for 2 h (10). Flash chromatography on silica (20%  $\text{CH}_3\text{OH}/\text{CHCl}_3$ ) afforded 252 mg (24%) of *N*<sup>4</sup>-(*N*-heptadecanoylglycylphenylalanyl)-ara-C (mp 135–136  $^\circ\text{C}$ ).  $^1\text{H}$  NMR (300 MHz,  $\text{CDCl}_3/\text{CD}_3\text{OD}$ , TMS = 0.0 ppm):  $\delta$  0.88 (t,  $J$  = 6.6 Hz, 3H), 1.20–1.70 (m, 28 H), 2.22 (t,  $J$  = 7.5 Hz, 2H), 7.10–7.35 (m, 5H), 7.42 (d,  $J$  = 7.4 Hz, 1H), 8.27 (d,  $J$  = 7.4 Hz, 1H).  $^{13}\text{C}$  NMR (75.1 MHz,  $\text{CDCl}_3/\text{CD}_3\text{OD}$ ,  $\text{CDCl}_3$  = 77 ppm):  $\delta$  13.6, 22.3, 25.3, 29.0, 29.1, 29.2, 29.3, 31.6, 35.7, 37.2, 42.2, 55.1, 61.2, 74.7, 85.8, 88.0, 95.9, 126.7, 128.2, 128.9, 135.5, 146.4, 162.0, 162.9, 169.9, 171.5, 174.7. LRMS (FAB):  $m/z$  706 ( $M + \text{Li}$ )<sup>+</sup>. Anal. Calcd for  $\text{C}_{37}\text{H}_{57}\text{N}_5\text{O}_8 \cdot \text{H}_2\text{O}$ : C, 61.90; H, 8.28; N, 9.76. Found: C, 61.94; H, 8.17; N, 9.63.

***N*<sup>4</sup>-(*N*-Heptadecanoylglycylglycylphenylalanyl)-ara-C.** A solution of *N*-heptadecanoylglycylglycylphenylalanine (1.14 g, 1.5 mmol), tri-*O*-TBDMS-ara-C (880 mg, 1.5 mmol), EEDQ (372 mg, 1.5 mmol), and pyridine (730  $\mu$ L, 9.0 mmol) in 12 mL of anhydrous  $\text{CHCl}_3$  was heated at 50  $^\circ\text{C}$  under nitrogen for 72 h (9). The mixture was cooled to room temperature and concentrated under reduced pressure. The oily crude product was flash chromatographed on a silica column (20%  $\text{CH}_3\text{OH}/\text{CHCl}_3$ ). The resulting residue was treated, without further purification, with 1.0 M TBAF in THF (14.0 mL, 14.0 mmol) at room temperature for 2 h (10). Flash chromatography on silica (20%  $\text{CH}_3\text{OH}/\text{CHCl}_3$ ) afforded 360 mg (32%) of *N*<sup>4</sup>-(*N*-heptadecanoylglycylglycylphenylalanyl)-ara-C (mp 118–119  $^\circ\text{C}$ ).  $^1\text{H}$  NMR (300 MHz,  $\text{CDCl}_3/\text{CD}_3\text{OD}$ , TMS = 0.0 ppm):  $\delta$  0.88 (t,  $J$  = 6.6 Hz, 3H), 1.15–1.70 (m, 28 H), 2.27 (t,  $J$  = 7.5 Hz, 2H), 3.00–3.30 (m, 2H), 3.75–4.35 (m, 7H), 4.75–4.95 (m, 1H), 6.23 (d,  $J$  = 5.0 Hz, 1H), 7.15–7.35 (m, 5H), 7.42 (d,  $J$  = 7.4 Hz, 1H), 8.27 (d,  $J$  = 7.4 Hz, 1H).  $^{13}\text{C}$  NMR (75.1 MHz,  $\text{CDCl}_3/\text{CD}_3\text{OD}$ ,  $\text{CDCl}_3$  = 77 ppm):  $\delta$  13.3, 14.3, 22.1, 25.1, 28.8, 28.9, 29.0, 29.2, 35.4, 36.7, 42.0, 42.4, 55.3, 61.0, 65.4, 74.6, 76.4, 85.5, 87.8, 95.7, 126.4, 128.0, 128.7, 135.7, 146.4, 155.7, 161.8, 170.0, 170.5, 171.5, 175.1. LRMS (FAB):  $m/z$  764 ( $M + \text{Li}$ )<sup>+</sup>. Anal. Calcd for  $\text{C}_{39}\text{H}_{60}\text{N}_6\text{O}_9 \cdot 2\text{H}_2\text{O}$ : C, 59.07; H, 8.14; N, 10.60. Found: C, 58.71; H, 7.86; N, 10.47.

#### ACKNOWLEDGMENT

This work was supported by the National Institutes of Health (GM 21457).

#### LITERATURE CITED

- (1) Bodey, G. P., Freireich, E. J., Monto, R. W., and Hewlett, J. S. (1969) Cytosine Arabinoside (NSC-63878) Therapy for Acute Leukemia in Adults. *Cancer Chemother. Rep. (Part 1)* 53, 59.
- (2) Holland, J. F., and Glidewell, O. (1970) Complementary Chemotherapy in Acute Leukemia. *Recent Results Cancer Res.* 30, 95.

- (3) Kodama, K., Morozumi, M., Saitoh, K., Kuninaka, A., Yoshino, H., and Saneyoshi, M. (1989) Antitumor Activity and Pharmacology of 1- $\beta$ -D-Arabinofuranosylcytosine-5'-stearylphosphate: An Orally Active Derivative of 1- $\beta$ -D-Arabinofuranosylcytosine. *Jpn. J. Cancer Res.* 80, 679.
- (4) Rivera, G., Rhomes, J. A., Dahl, G. V., Pratt, C. B., Wood, A., and Avery, T. L. (1980) Combined VM-26 and Cytosine Arabinoside in Treatment of Refractory Childhood Lymphocytic Leukemia. *Cancer* 45, 1284.
- (5) Aoshima, M., Tsukagoshi, S., Sakurai, Y., Oh-ishi, J., Ishida, T., and Kobayashi, H. (1976) Antitumor Activities of Newly Synthesized N<sup>4</sup>-acyl-1- $\beta$ -D-Arabinofuranosylcytosine. *Cancer Res.* 36, 2726.
- (6) Tsuruo, T., Iida, H., Hori, K., Tsukagoshi, S., and Sakurai, Y. (1981) Membrane Affinity and Metabolism of N<sup>4</sup>-palmitoyl-1- $\beta$ -D-Arabinofuranosylcytosine into Cultured KB Cells. *Cancer Res.* 41, 4484.
- (7) Wipf, P., Li, W., and Sekhar, V. (1991) Synthesis of Chemoreversible Prodrugs of ara-C. *Bioorg. Med. Chem. Lett.* 1, 745.
- (8) Fieser, M., Fieser, L. F., Toromanoff, E., Hirata, Y., Heymann, H., Tefft, M., and Bhattacharya, S. (1956) Synthetic Emulsifying Agents. *J. Am. Chem. Soc.* 78, 2825.
- (9) Balleau, B., and Malek, G. (1968) A New Convenient Reagent for Peptide Synthesis. *J. Am. Chem. Soc.* 90, 1651.
- (10) Corey, E. J., and Venkateswarlu, A. (1972) Protection of Hydroxyl Groups as *tert*-Butyldimethylsilyl Derivatives. *J. Am. Chem. Soc.* 94, 6190.

# Synthesis of 3-Hydroxyestra-1,3,5(10)-trien-17-one and 3,17 $\beta$ -Dihydroxyestra-1,3,5(10)-triene 6 $\alpha$ -*N*-( $\epsilon$ -Biotinyl)caproamide, Tracer Substances for Developing Immunoassays for Estrone and Estradiol

Peter Luppa,\*† Christian Birkmayer,‡ and Hagen Hauptmann‡

Institute for Clinical Chemistry, Klinikum rechts der Isar, Technical University Munich, D-81675 Munich, Germany, and Institute for Organic Chemistry, University Regensburg, D-93053 Regensburg, Germany. Received October 5, 1993\*

We describe the synthesis of 3-hydroxyestra-1,3,5(10)-trien-17-one 6 $\alpha$ -*N*-( $\epsilon$ -biotinyl)caproamide and 3,17 $\beta$ -dihydroxyestra-1,3,5(10)-triene 6 $\alpha$ -*N*-( $\epsilon$ -biotinyl)caproamide from 3-hydroxyestra-1,3,5(10)-trien-17-one and 3,17 $\beta$ -dihydroxyestra-1,3,5(10)-triene, via the 6-keto estrogenic derivatives. The reductive amination of these compounds is an effective step toward an epimeric mixture of the respective amines, which are easily biotinylated by use of *N*-( $\epsilon$ -biotinylcaproyl)-*N*-hydroxysuccinimide ester. The 6 $\alpha$ -epimers could be isolated from the  $\alpha/\beta$ -composition by application of isocratic HPLC, and overall yields were about 20% for the epimeric end products. The structures of the stereoisomers could clearly be assigned through  $^1\text{H}$  NMR studies. The ratios of the respective isomers obtained from the reductive amination were found to be 3( $\alpha$ ):2( $\beta$ ). The biotinylated estrogens can be used as tracers in a novel immunoassay concept for the determination of these analytes in human serum. Ring position 6 was selected for derivatization because of its distance from the functionalized positions 3 and 17 and, therefore, of a negligible alteration of the tracer's structure in comparison to underivatized estrone or estradiol.

## INTRODUCTION

Numerous immunoassays based on nonradioactive labels for the determination of steroids in serum or other human body fluids were created in the last decade (1–4). Most of the competitive assays use either enzyme- or substrate-labeled steroid tracers. These assays often lack analytical sensitivity and specificity due to an altered structure of the respective steroid tracers (5–10). This effect is observed in cases in which steroids have been derivatized at the ring positions 3 or 17. By introducing the label in the same position as was used for the conjugation of the hapten steroid to a carrier protein for the purpose of antibody production, nearly identical recognition sites for the antisteroid antibody can be achieved. 3-Hydroxyestra-1,3,5(10)-trien-17-one (estrone, E1) and 3,17 $\beta$ -dihydroxyestra-1,3,5(10)-triene (estradiol, E2) are usually conjugated to carrier proteins via their benzylic 6-position using the *O*-(carboxymethyl)oximation (CMO) method (11–17). But little is reported about structural derivatizations at that or the vicinal 7-position for the development of labeled steroidal tracers.

Competitive nonradioactive immunoassays for E1 as well as E2 can be set up by using biotinylated estrogen tracers, which easily bind to a streptavidin reporter enzyme conjugate (18). With appropriate substrates, the enzyme-mediated signal subsequently indicates the concentration of the endogenous steroids of interest. The biotin residue must be attached via a defined spacer group to the steroid. According to ref 19, this is due to the importance of

diminishing sterical hindrances between the biotin moiety and the antiestrogen antibody. Additionally, the chemical structure of the spacer has a relevant impact on the antibody recognition: the structure must be similar to the *O*-(carboxymethyl)oxime linkage which is used in the immunization procedure.

6-Aminoestrogens were previously described by Hamacher and Christ (20, 21) and Chesne et al. (22) as intermediates for the synthesis of antineoplastics against the estrogen receptor. 6-Biotinylation of E2 was first reported by Tiefenauer and Bodmer, who described E2 tracers with different spacer groups between the E2 6-position and the biotin moiety and their potential use in enzyme immunoassays (19, 23–25). The aim of our work was to develop efficient syntheses of 3-hydroxyestra-1,3,5(10)-trien-17-one 6 $\alpha$ -*N*-( $\epsilon$ -biotinyl)caproamide (Bio-E1) and 3,17 $\beta$ -dihydroxyestra-1,3,5(10)-triene 6-*N*-( $\epsilon$ -biotinyl)caproamide (Bio-E2), including defined isolations and characterizations of the 6 $\alpha$ -epimers, for establishing new immunoassays for E1 and E2.

## EXPERIMENTAL PROCEDURES

**General Methods.** Melting points (uncorrected) were determined on a Reichert Thermovar.  $^1\text{H}$  NMR spectra were recorded on Beckman E 360 (60 MHz), Bruker AC 250 F (250 MHz), and Bruker ARX 400 (400 MHz). Me $_4$ -Si was used as the reference signal ( $\delta$  0.00 ppm). IR spectra were obtained from KBr on a Beckman spectrophotometer 24. UV spectra were measured in MeOH on a Hitachi spectrophotometer U 2000; dioxane was used for 11. MS analyses were performed for 70 eV EI with a Varian MAT 112S and for FAB/high-resolution MS with a Finigan MAT 90. For column chromatography silica gel (grain 0.063–0.200) was used, and TLC was performed using silica gel 60 F $_{254}$  (0.2 mm); both silica materials were obtained from E. Merck (Darmstadt, Germany). The preparative HPLC system consisted of an HPLC pump Knauer 64, a Vertex column (250 mm, 16-mm diameter), filled with LiChrosorb

\* Address correspondence to this author at: Institut für Klinische Chemie & Pathobiochemie, Klinikum rechts der Isar der TU München, Ismaninger Str. 22, D-81675 Munich, Germany. Phone 0049 89 4140 4751; Fax 0049 89 41 805 175.

† Technical University Munich.

‡ University Regensburg.

\* Abstract published in *Advance ACS Abstracts*, February 15, 1994.

100 (5  $\mu$ m), both from Knauer (Bad Homburg, Germany), and a UV detector ERC 7210 (ERC, Alteglofsheim, Germany). Chemicals were obtained from Merck, except for E1 and E2, which were purchased from Sigma (Deisenhofen, Germany), and *N*-( $\epsilon$ -biotinylcaproyl)-*N*-hydroxysuccinimide ester from Boehringer Mannheim (Mannheim, Germany).

**Preparation of 3-Hydroxyestra-1,3,5(10)-trien-17-one 6-*N*-( $\epsilon$ -Biotinyl)caproamide (6).**

**3-Hydroxyestra-1,3,5(10)-trien-17-one 17-(cyclic 1,2-ethanediyl acetal) (2)** was prepared from 1 according to ref 26 with a yield of 75%. Mp ( $^{\circ}$ C): 180–182 (lit. 26 mp ( $^{\circ}$ C) 182–185).

**3-Hydroxyestra-1,3,5(10)-trien-17-one 3-acetate 17-(cyclic 1,2-ethanediyl acetal) (3)** was prepared according to ref 27 with a yield of 70%. Mp ( $^{\circ}$ C): 103–104 (lit. (27) mp ( $^{\circ}$ C) 105–105.5).

**3-Hydroxyestra-1,3,5(10)-triene-6,17-dione 3-Acetate 17-(Cyclic 1,2-ethanediyl acetal) (4).** According to a method given by Garza and Rao (28), a stirred suspension of 2.8 g (28 mmol) of  $\text{CrO}_3$ /50 mL of  $\text{CH}_2\text{Cl}_2$  was cooled to  $-40^{\circ}\text{C}$  under  $\text{N}_2$ . A 2.58-g (28 mmol) portion of 3,5-dimethylpyrazole was added. After 15 min, 1.00 g (2.81 mmol) of 3 in 10 mL of  $\text{CH}_2\text{Cl}_2$  was added. The solution was stirred for 6 h at  $-25^{\circ}\text{C}$ . The residue was chromatographed on silica gel/petroleum ether using a petroleum ether/ethyl acetate eluent (4:1 v/v) ( $R_f$  = 0.2). A total of 518 mg (1.4 mmol, 50%) of the crude ketone was obtained. After recrystallization from MeOH, 310 mg (840  $\mu$ mol, 30%) of colorless ketone 4 was obtained. Mp ( $^{\circ}$ C): 161–163. IR ( $\text{cm}^{-1}$ ): 2945, 2880 (CH); 1755 (aliphatic ester C=O); 1675 (ketone); 1190 (cyclic ether (dioxolane)). MS (70 eV EI,  $m/z$ ): 370 (100,  $\text{M}^+$ ).  $^1\text{H}$  NMR (60 MHz,  $\text{CDCl}_3$ , ppm): 7.6 (d, 1H,  $J$  = 8 Hz); 7.5–7.0 (m, 2H, 2,4 CH); 3.8 (m, 4H, dioxolane CH); 2.2 (s, 3H, 17- $\text{OCOCH}_3$ ); 0.83 (s, 3H, 18-CH). UV: 245 nm,  $\log \epsilon$  = 3.84; 297 nm,  $\log \epsilon$  = 2.74. Anal. Calcd: C, 71.33; H, 7.08; O, 21.59. Found: C, 71.41; H, 6.84; O, 21.08.

**6-Amino-3-hydroxyestra-1,3,5(10)-trien-17-one 17-(Cyclic 1,2-ethanediyl acetal) (5).** A 370-mg (1 mmol) portion of the ketone 4 and 390 mg (6 mmol) of  $\text{NaCNBH}_3$  were dissolved under  $\text{N}_2$  in 4.5 mL of buffer (40.5 g of dried  $\text{NH}_4\text{OAc}$  in 150 mL of dry MeOH (24)) and refluxed at  $65^{\circ}\text{C}$  for 48 h. The clear reaction solution was worked up by removing the solvent and treating the residue with saturated aqueous  $\text{NaHCO}_3$  and diethyl ether. The combined aqueous phases were again extracted with diethyl ether. After the pooled ether phases were dried, the solvent was removed at room temperature (rt). A total of 250 mg of a slightly yellow amorphous product was obtained, corresponding to a 75% yield of the amine 5. IR ( $\text{cm}^{-1}$ ): 3340, 3320, 3260 (amine NH). MS (70 eV EI,  $m/z$ ): 329 (13,  $\text{M}^+$ ); 312 ( $\text{M}^+ - \text{NH}_3$ ).  $^1\text{H}$  NMR (250 MHz,  $\text{CDCl}_3$ , ppm): 7.14–6.65 (m, 4H, 1-CH, 2-CH, 3-COH, 4-CH); 3.97–3.44 (m, 5H, 6-CH, 17-C-dioxolane); 0.86, 0.85 (s, 3H, 18-CH) ( $\alpha/\beta$ -ratio: 1:1.5; epimeric excess: 20%). UV: 282 nm,  $\log \epsilon$  = 3.32; 218 nm,  $\log \epsilon$  = 3.88.

**3-Hydroxyestra-1,3,5(10)-trien-17-one 6-*N*-( $\epsilon$ -Biotinyl)caproamide (6).** A 53-mg (160  $\mu$ mol) portion of the amine 5, 87 mg (191  $\mu$ mol) of *N*-( $\epsilon$ -biotinylcaproyl)-*N*-hydroxysuccinimide ester, 32 mg (44  $\mu$ L,  $d$  = 0.73, 320  $\mu$ mol) of triethylamine, and 1 mL of DMF were stirred under  $\text{N}_2$  for 24 h at rt prior to evaporation of the solvent. The residue was treated with 2 mL of dry saturated methanolic hydrochloric acid (pH = 2) for 24 h at rt. All reaction compounds except 6 were removed by high vacuum. The substance was purified before HPLC on a

silica gel/petroleum ether column using a MeOH/ $\text{CH}_2\text{Cl}_2$  (1:4.5) (v/v) eluent ( $R_f$  = 0.5).

**Isolation of the 6 $\alpha$ -Epimer 6a from the 6 $\alpha/\beta$ -Epimeric Mixture 6.** Isocratic HPLC: eluent, 7% MeOH/93%  $\text{CH}_2\text{Cl}_2$ ; flow rate, 10 mL/min. **6a:** 13–14 min. **6b:** 14–20 min. **6a.** MS: HR-MS (PI-LISIMS) (glycerin/MeOH): calcd for  $\text{C}_{34}\text{H}_{49}\text{N}_4\text{O}_5\text{S}$  ( $\text{MH}^+$ ) 625.3424, found 625.3420; difference, 0.6 ppm.  $^1\text{H}$  NMR (400 MHz,  $\text{CDCl}_3$ , ppm): 9.70 (s, 1H); 7.26–6.69 (m, 3H, 1-CH, 2-CH, 4-CH); 6.37 (d, 1H,  $J_{\text{NH-6}}$  = 9 Hz, 6 $\alpha$ -CNH); 5.24 (ddd, 1H,  $J_{\text{NH-6}}$  = 9 Hz,  $J_{6-7}$  = 11.7 and 6.4 Hz, 6 $\beta$ -CH); 0.89 (s, 3H, 18-CH). UV: 279 nm,  $\log \epsilon$  = 3.54; 220 nm,  $\log \epsilon$  = 4.26.

**Preparation of 3,17 $\beta$ -Dihydroxyestra-1,3,5(10)-triene 6-*N*-( $\epsilon$ -Biotinyl)caproamide (12).**

**3,17 $\beta$ -Dihydroxyestra-1,3,5(10)-triene 3,17 $\beta$ -Diacetate (8)** was prepared from 7 according to the method of ref 29. The yield was 90%. Mp ( $^{\circ}$ C): 121–123 (lit. (21) mp ( $^{\circ}$ C) 123–125).

**3,17 $\beta$ -Dihydroxyestra-1,3,5(10)-trien-6-one 3,17-Diacetate (9).** Preparation was performed analogous to that of 4 from 8 with similar yields. Mp ( $^{\circ}$ C): 173 (lit. (21) mp ( $^{\circ}$ C) 173).

**3,17 $\beta$ -Dihydroxyestra-1,3,5(10)-trien-6-one (10)** was prepared from 9 according to ref 21 with a quantitative yield. Mp ( $^{\circ}$ C): 276–279 (lit. (21) mp ( $^{\circ}$ C) 282).

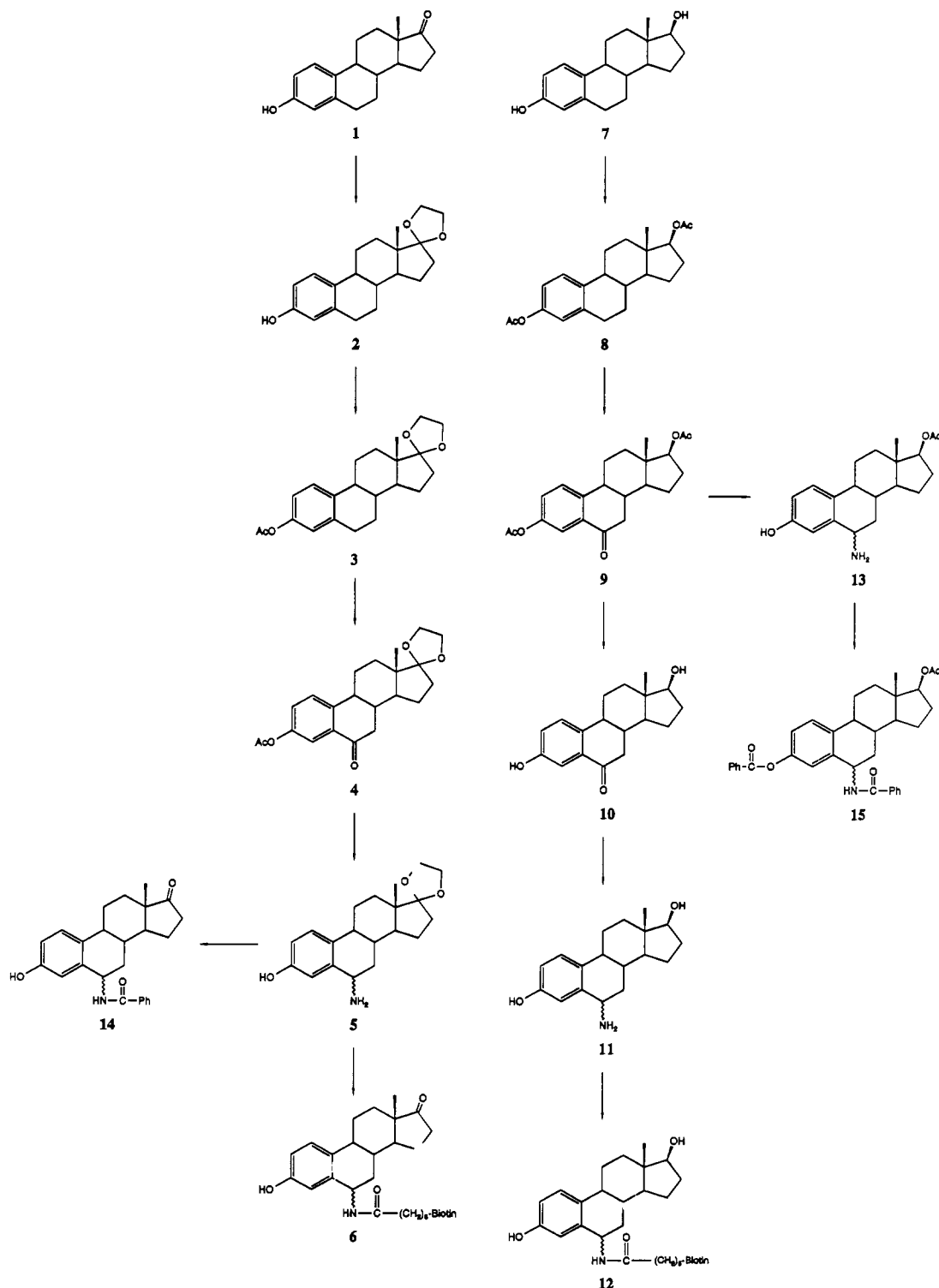
**6-Amino-3,17 $\beta$ -dihydroxyestra-1,3,5(10)-triene (11)** was prepared in a manner similar to the synthesis of 5 from 10 with a yield of 85% of the  $\alpha/\beta$ -mixture. IR ( $\text{cm}^{-1}$ ): 3420 (free OH); 3345, 3280 (amine NH); 2940 (CH aliphatic); 1600 ( $\text{NH}_{\text{def}}$ ) (24). MS (70 eV EI,  $m/z$ ): 287 (7,  $\text{M}^+$ ), 270 (100,  $\text{M}^+ - \text{NH}_3$ ) (24).  $^1\text{H}$  NMR (250 MHz,  $\text{CD}_3\text{OD}$ , ppm): 7.15–6.6 (m, 3H, 1,2,4-CH); 4.00 (m, 1H, 6-CH); 3.65 (m, 1H, 17-CH); 0.81, 0.75 (s, 1H, 18-CH) (24) ( $\alpha/\beta$ -ratio: 1:2.3; epimeric excess, 40%). UV (dioxane): 280 nm,  $\log \epsilon$  = 3.38; 222 nm,  $\log \epsilon$  = 4.03 (24).

**3,17 $\beta$ -Dihydroxyestra-1,3,5(10)-triene 6 $\alpha$ -*N*-( $\epsilon$ -Biotinyl)caproamide (12).** A 22-mg (76.7  $\mu$ mol) portion of the amine 11, 42 mg (92.5  $\mu$ mol) of *N*-( $\epsilon$ -biotinylcaproyl)-*N*-hydroxysuccinimide ester, 18.25 mg (25  $\mu$ L,  $d$  = 0.73) of triethylamine, and 1 mL of DMF were stirred under  $\text{N}_2$  for 24 h at rt prior to evaporation of the solvent. The residue was taken up with 1.5 mL of MeOH and purified on a chromatographic column filled with 7 g of silica gel/petroleum ether, using a benzene/MeOH eluent (4:1 v/v) ( $R_f$  = 0.24).

**Isolation of the 6 $\alpha$ -Epimer 12a from the 6 $\alpha/\beta$ -Epimeric Mixture 12.** Isocratic HPLC: eluent, 9% MeOH/91%  $\text{CH}_2\text{Cl}_2$ ; flow rate, 9.5 mL/min. **12a:** 17–17.75 min, 1.4 mg (2.23  $\mu$ mol). **12b:** 18.75–20 min, 1.7 mg (2.7  $\mu$ mol). **12a.** MS: HR-MS (PI-LISIMS) (glycerin/MeOH): calcd for  $\text{C}_{34}\text{H}_{51}\text{N}_4\text{O}_5\text{S}$  ( $\text{MH}^+$ ) 627.3581, found 627.3621; difference, 6.3 ppm; calcd for  $\text{C}_{34}\text{H}_{50}\text{N}_4\text{O}_5\text{SNa}$  ( $\text{MNa}^+$ ) 649.3399, found 649.3408; difference, 1.3 ppm (23).  $^1\text{H}$  NMR (400 MHz,  $\text{CDCl}_3$ , ppm): 9.43 (s, 1H); 7.52–6.76 (m, aromatic CH, OH); 6.26 (d, 1H,  $J_{\text{NH-6}}$  = 9 Hz, 6 $\alpha$ -NH); 6.01 (t, 1H,  $J$  = 6 Hz); 5.22 (ddd, 1H,  $J_{\text{NH-6}}$  = 9 Hz,  $J_{6-7}$  = 10 and 6 Hz, 6 $\beta$ -CH); 0.77 (s, 3H, 18-CH). UV: 280 nm,  $\log \epsilon$  = 3.13 (23).

**6-Amino-3,17 $\beta$ -dihydroxyestra-1,3,5(10)-triene 17 $\beta$ -Acetate (13)** was prepared in a manner analogous to that of 5 from 9 with a yield of 70%.

**Preparation of 3-Hydroxyestra-1,3,5(10)-trien-17-one 6-Benzamide (14) and 3,17 $\beta$ -Dihydroxyestra-1,3,5(10)-triene 17 $\beta$ -Acetate 6-Benzamide 3-Benzate (15).** **3-Hydroxyestra-1,3,5(10)-trien-17-one 6-benzamide (14).** A 22-mg (67  $\mu$ mol) portion of amine 5 and 40 mg (177  $\mu$ mol) of benzoic anhydride were stirred in 1 mL of pyridine for 24 h at rt. All reaction components except the steroid were removed by vacuum. The protecting

**Scheme 1. Biotinylation of 3-Hydroxyestra-1,3,5(10)-trien-17-one and 3,17β-Dihydroxyestra-1,3,5(10)-triene in the 6-Position**

groups were then removed successively by a dry methanolic hydrochloride solution (pH = 2) and a NaOH/MeOH solution (3 mL of saturated aqueous NaOH and 1 mL of MeOH).

**Isolation of the 6α-Epimer 14a from the 6α/β-Epimeric Mixture 14.** Isocratic HPLC conditions: eluent, 1% MeOH/CH<sub>2</sub>Cl<sub>2</sub>; flow rate, 10 mL/min. **14a**: 12.0–13.3 min, 1.196 mg. **14b**: 14.5–16.5 min, 0.45 mg. **14a**: MS (70 eV EI, *m/z*): 389 (3, M<sup>+</sup>); 312 (3, M<sup>+</sup> - Ph); 286 (100, M<sup>+</sup> - PhCONH<sub>2</sub>). UV: 278 nm, log ε = 2.45; 219 nm, log ε = 3.41. <sup>1</sup>H NMR (400 MHz, CDCl<sub>3</sub>, ppm): 7.77–

6.75 (m, 9H, 1-CH, 2-CH, benzoxy-aromate CH, OH); 6.35 (d, 1H, *J*<sub>NH-6</sub> = 9.5 Hz, NH); 5.55 (ddd, 1H, *J*<sub>6-NH</sub> = 9.5 Hz, *J*<sub>6-7</sub> = 6.11 Hz, 6β-CH); 0.92 (s, 3H, 18-CH). <sup>1</sup>H NMR (400 MHz, CD<sub>3</sub>OD, ppm): 7.95–6.63 (m, 8H, 1-CH, 2-CH, 4-CH, benzoxy-aromate CH); 5.43 (dd, 1H, *J*<sub>6-7</sub> = 6.1 and 11.2 Hz, 6β-CH); 0.96 (s, 3H, 18-CH).

**3,17β-Dihydroxyestra-1,3,5(10)-triene 17β-Acetate 6-Benzamide 3-Benzoate (15).** A 53-mg (161 μmol) portion of 13 and 75 mg (332 μmol) of benzoic anhydride were stirred for 20 h at rt in 1 mL of pyridine. After the solvent was removed, the crude product was purified on



a silica gel/petroleum ether column using petroleum ether/ethyl acetate (1:1 v/v), yielding 80 mg (150  $\mu$ mol, 92%) of purified **15**. IR (cm<sup>-1</sup>): 3065 (CH aromatic); 2920 (CH aliphatic); 1780 (3-benzoxycarbonyl); 1725 (17-acetoxy carbonyl); 1685 (amide I); 1660 (amide II).

**Isolation of the 6 $\alpha$ -Epimer 15a from the 6 $\alpha$ / $\beta$ -Mixture 15.** Eluent: 1.25% MeOH/CH<sub>2</sub>Cl<sub>2</sub>. Flow rate: 10 mL/min. **15a**: 8.0–9.5 min, 6.59 mg. **15b**: 9.5–10.3 min, 4.47 mg. **15a**: MS (70 eV EI, *m/z*): 537 (0.02, M<sup>+</sup>(I)); 433 (2, M<sup>+</sup>(II)); 416 (2, M<sup>+</sup> - PhCONH<sub>2</sub>); 312 (100, M<sup>+</sup>(II) - PhCONH<sub>2</sub>). <sup>1</sup>H NMR (400 MHz, CDCl<sub>3</sub>, ppm): 8.13–6.74 (m, 13H, 1-CH, 2-CH, 4-CH, 3-benzoxycarbonyl-H, 6-benzamide aromatic H); 6.32 (d, 1H, *J*<sub>NH-6</sub> = 9 Hz, NH); 5.52 (m, 1H), 4.69 (t, 1H, *J* = 8 Hz, 17-C-H); 2.06 (s, 3H, 17-OCOCH<sub>3</sub>); 0.84 (s, 3H, 18-CH). <sup>1</sup>H NMR (400 MHz, CD<sub>3</sub>OD, ppm): 7.98–6.62 (m, 8H, 1-CH, 2-CH, 4-CH, 6-benzamide aromatic H); 5.39 (dd, 1H, *J*<sub>6-7ax</sub> = 11 Hz, *J*<sub>6-7eq</sub> = 7 Hz, 6 $\beta$ -CH); 4.68 (t, 1H, *J* = 8 Hz, 17-CH); 2.04 (s, 3H, 17-OCOCH<sub>3</sub>); 0.90 (s, 3H, 18-CH). UV: 277 nm, log  $\epsilon$  = 2.64; 233 nm, log  $\epsilon$  = 3.33.

## RESULTS AND DISCUSSION

This paper describes the preparation of immunochemical tracer conjugates of estrogens by attaching biotin residues via a -NHCO(CH<sub>2</sub>)<sub>5</sub>NH- spacer arm to E1 and E2 at C-6. The five-step syntheses of the tracer substances **6** and **12** from the estrogens **1** and **7** are given in Scheme 1. The overall yields are 15% for **6** and 20% for **12**.

On the basis of syntheses of Garza (28) and Tiefenauer (24), our synthetic approaches for **6** and **12** exhibit the following features: the extractive procedure for the isolation of the epimeric amino compounds **5** and **11**, obtained by reductive amination of the respective 6-keto precursors, is convenient and simple. The biotinylation reaction was modified by employing approximately equimolar ratios of substrate and biotinylating agent with nearly quantitative yields. The separation of the respective biotinylated epimers was achieved by HPLC using an isocratic eluent system on a LiChrosorb 100 column.

To identify the exact stereochemistry at the benzylic ring position 6, HPLC-separable 6-benzamide derivatives **14** and **15** were synthesized. In the course of NMR investigations of the amines **5**, **11**, and **13**, we conclude that—in contrast to Tiefenauer *et al.* (24)—the reductive amination step is not characterized by  $\alpha$ -stereospecificity. Epimeric excesses for the  $\alpha$ -compounds of **5** and **11** were 20% and 40% as determined from their C-18 signals. To prove our assumption and to confirm the configuration of the tracers **6** and **12**, we set out to characterize the isolated 6 $\alpha$ -epimers by NMR spectroscopy. This approach is based on the work of Wintersteiner *et al.* (30), who found for the 6 $\beta$ -proton of the 3,6 $\alpha$ ,17 $\beta$ -estratriol triacetate epimer the coupling pattern of an ABX system with coupling constants of 5.5 and 8.5 Hz, while the AB part of the 6 $\alpha$ -proton's signal of the 6 $\beta$ -isomer gave the coupling constant of 3 Hz. The chromatographic separation of the amines was not feasible; therefore, we derivatized **5** and **13** with benzoic anhydride to obtain the stable benzamides **14** and **15**. The respective NMR-pure  $\alpha$ -epimers could be isolated by HPLC. We found that the amide proton also interacts with the 6-proton, thereby giving rise to complex signals. We removed the amide's interference by H/D exchange with CD<sub>3</sub>OD. A first-order evaluation of the four-line pattern found for the 6 $\beta$ -proton of **14a** and **15a**, according to Wintersteiner, resulted in coupling constants of 6.1, 11.3 Hz, and 6.6, 11.4 Hz, respectively. Analogous values were found for the 6-biotinylated estrogens: 11.7, 6.4 Hz for **6a**, as well as 6.0, 10.0 Hz for **12a**.

In summary, we propose effective synthetic pathways of both 6 $\alpha$ -biotinylated E1 and E2; the respective E1 derivative has not been described in literature. 6-Biotinylated E2 compounds, however, were already reported by Bodmer and Tiefenauer. But in contrast to data for the synthesis of these tracers compounds given in 24, and for the respective HPLC purifications, described in 19, 23, our synthetic pathway combined with the appropriate isocratic HPLC separation technique offers improved accessibility and yields stereochemical pure products.

Concerning the ability of the new tracers for E1 and E2 immunoassays, it must be considered that due to the mode of conjugation at C-6, the structural determinants of Bio-E1 and Bio-E2 are nearly unchanged in comparison to unsubstituted E1 and E2, since the position 6 in the B-ring is most distant from the prominent positions 3 and 17. Thus, the antiestrogen antibodies are unable to distinguish between the tracers and the endogenous steroids E1 or E2. By use of these compounds, a novel competitive immunoassay concept for the determination of E1 and E2 in serum could be realized. Results will be presented elsewhere. The E1 enzyme immunoassay is run with the following components: Bio-E1 tracer, polyclonal anti-E1 antibody, and reporter enzyme linked to streptavidin. In pilot experiments we checked the competitive character of the Bio-E1 tracer in competition to ring A-tritiated E1. It could be demonstrated that Bio-E1 adequately displaces tritiated E1 from the antibody in the expected competitive way (data not shown). As shown in ref 19, the -NHCO-(CH<sub>2</sub>)<sub>5</sub>NH- spacer arm, linking biotin to the estrogen, satisfactorily fulfills the structural requirements of optimal antigen-antibody interaction.

It is worth mentioning that biotinylated steroids, as stable immunochemical probes, in connection with streptavidin-conjugated reporter enzymes, should allow the development of a series of competitive immunoassays for the determination of the respective steroids in human serum as well as their potential application in steroid receptor studies.

## ACKNOWLEDGMENT

This article is dedicated to Prof. G. Märkl on the occasion of his 65th birthday. The authors thank Mrs. A. Rössner for technical assistance, Prof. E. Kuss for reading the manuscript, and the Fond der Deutschen Chemischen Industrie for financial support.

## LITERATURE CITED

- Pal, S. B., Ed. (1986) *Immunoassay technology*, Vol. 2, Walter de Gruyter, Berlin.
- Chan, D. W., and Perlstein, M. T., Eds. (1987) *Immunoassay. A practical guide*, Academic press, New York.
- Albertson, B. D., and Haseltine, F. P., Eds. (1988) *Non-radiometric assays. Technology and application in polypeptide and steroid hormone detection*, Alan R. Liss, New York.
- Gosling, J. P. (1990) A decade of development in immunoassay methodology. *Clin. Chem.* 36, 1408–1427.
- Folan, J., Gosling, J. P., and Fottrell, P. F. (1988) Solid-phase enzymeimmunoassay of estrone in serum. *Clin. Chem.* 34, 1843–1846.
- Folan, J., Gosling, J. P., Finn, M. F., and Fottrell, P. F. (1989) Solid-phase enzymeimmunoassay of estrone in saliva. *Clin. Chem.* 35, 569–572.
- Elder, P. A., Manley, L., and Lewis, J. G. (1990) Use of a monoclonal antibody to estrone-3-glucuronide in an enzyme-linked immunosorbent assay (ELISA). *J. Steroid Biochem.* 36, 439–443.
- Barnard, G., Kohen, F., Mikola, H., and Lövgren, T. (1989) Measurement of estrone-3-glucuronide in urine by rapid,

- homogeneous time-resolved fluoroimmunoassay. *Clin. Chem.* 35, 555-559.
- (9) Kim, J. B., Barnard, G. J., Collins, W. P., Kohen, F., Lindner, H. R., and Eshhar, Z. (1982) Measurement of plasma estradiol-17 $\beta$  by solid-phase chemiluminescence immunoassay. *Clin. Chem.* 28, 1120-1124.
- (10) De Boever, J., Kohen, F., Usanachitt, C., Vandekerckhove, D., Leyseele, D., and Vandewalle, L. (1986) Direct chemiluminescence immunoassay for estradiol in serum. *Clin. Chem.* 32, 1895-1900.
- (11) Kuss, E., Goebel, R., and Enderle, H. (1973) Influence of oxo-, and/or hydroxy-groups at C-16/C-17 of estrogens on affinity to anti-estrone, anti-estradiol-17 $\alpha$ - and anti-estradiol-17 $\beta$ -antisera. *Hoppe-Seyler's Z. Physiol. Chem.* 354, 347-364.
- (12) Doerr, P., Goebel, R., and Kuss, E. (1973) Specific radio-immunologic determination of plasma oestradiol in males without chromatography. *Acta Endocrinol. (Copenh.)* 72, Suppl. 173, 108.
- (13) Goebel, R., and Kuss, E. (1973) Radioimmunological determination of plasma estriol in pregnancy with anti-estriol-C6 conjugate-antiserum. *Acta Endocrinol. (Copenh.)* 72, Suppl. 173, 109.
- (14) Exley, D., Johnson, M. W., and Dean, P. D. G. (1971) Antisera highly specific for 17 $\beta$ -oestradiol. *Steroids* 18, 605-620.
- (15) Exley, D. (1972) Specificities of antibodies to oestrogens. *J. Steroid Biochem.* 3, 497-501.
- (16) Jeffcoate, S. L., and Searle, J. E. (1972) Preparation of a specific antiserum to estradiol-17 $\beta$  coupled to protein through the B-ring. *Steroids* 19, 181-188.
- (17) Lindner, H. R., Perel, E., Friedlander, A., and Zeitlin, A. (1972) Specificity of antibodies to ovarian hormones in relation to the site of attachment of the steroid hapten to the peptide carrier. *Steroids* 19, 357-375.
- (18) Diamandis, E. P., and Christopoulos, T. K. (1991) The biotin-(strept)avidin system: principles and applications in biotechnology. *Clin. Chem.* 37, 625-636.
- (19) Tiefenauer, L. X., and Andres, R. Y. (1990) Biotinyl-estradiol derivatives in enzyme immunoassays: structural requirements for optimal antibody binding. *J. Steroid Biochem.* 35, 633-639.
- (20) Hamacher, H. (1979) Potential antineoplastics. 4th Comm.: N-mustard derivatives of estrone. *Arzneim. Forsch./Drug Res.* 29, 463-466.
- (21) Hamacher, H., and Christ, E. (1983) Potential antineoplastics. 7th Comm.: Introduction of a nitrogen mustard group into the 6 $\alpha$ -position of estradiol. *Arzneim. Forsch./Drug Res.* 33, 347-352.
- (22) Chesne, C., Leclercq, G., Pointeau, P., and Patin, H. (1986) Synthesis and biological studies of aminoestradiol-platinum (II) conjugates. *Eur. J. Med. Chem.-Chim. Ther.* 21, 321-327.
- (23) Bodmer, D. M., Tiefenauer, L. X., and Andres, R. Y. (1989) Antigen- versus antibody-immobilized ELISA procedures based on a biotinyl-estradiol conjugate. *J. Steroid Biochem.* 33, 1161-1166.
- (24) Tiefenauer, L. X., Bodmer, D. M., Frei, W., and Andres, R. Y. (1989) Prevention of bridge binding in immunoassays: a general estradiol tracer structure. *J. Steroid Biochem.* 32, 251-257.
- (25) Bodmer, D. M., and Tiefenauer, L. X. (1990) Treatment of antibodies to reduce nonspecific binding in immunoassays using the avidin-biotin complex. *J. Immunoassays* 11, 139-145.
- (26) Buzby, G. C., Edgren, R. A., Fisher, J. A., Hughes, G. A., Jones, R. C., Leding, K., Pattison, T. W., Rees, R., Smith, H., Smith, L. L., Teller, D. M., and Wendt, G. R. (1964) Oxaestrapiene ketals as antilipemic agents. *J. Med. Chem.* 7, 755-758.
- (27) Nambara, T., Sudo, K., and Sudo, M. (1976) Synthesis of estretrol monoglucuronides. *Steroids* 27, 111-122.
- (28) Garza, G. A., and Rao, P. N. (1983) Chromic anhydride-3,5-dimethyl-pyrazole complex: an efficient reagent for oxidation of steroidal estrogens to 6-oxo-derivatives. *Steroids* 42, 469-474.
- (29) Dean, P. D. G., Exley, D., and Johnson, M. W. (1971) Preparation of 17 $\beta$  oestradiol-6-(O-carboxymethyl)oxime-bovine serum albumin conjugate. *Steroids* 18, 593.
- (30) Wintersteiner, D., Moore, M., and Cohen, A. J. J. (1963) Stereochemical studies on 6-7-substituted derivatives of estradiol. *J. Org. Chem.* 29, 1325.

# Bioconjugate Chemistry

MAY/JUNE 1994  
Volume 5, Number 3

© Copyright 1994 by the American Chemical Society

## REVIEWS

---

### Three-Dimensional Protein Models: Insights into Structure, Function, and Molecular Interactions

Jürgen Bajorath\*<sup>†</sup> and Alejandro Aruffo\*<sup>‡</sup>

Bristol-Myers Squibb, Pharmaceutical Research Institute, 3005 First Avenue, Seattle, Washington 98121, and Department of Biological Structure, University of Washington, Seattle, Washington 98195. Received October 19, 1993

Primary structures of proteins are being determined at a significantly higher rate than are tertiary structures. Only a relatively small number of protein structures of importance to molecular biologists and medicinal chemists are presently available in experimentally determined form. This is one of the reasons for the increasing interest in theoretical modeling of protein structures (1–4). Computer workstations, high-resolution computer graphic displays, and computational methods have become more readily available and are now widely used in biological and chemical research environments. Less than a decade ago, access to such instrumentation and methodology was more or less limited to a small number of groups of computational chemists and protein crystallographers. Given the computational resources that are currently available and the accessibility of protein sequences and three-dimensional structure data bases, computer modeling of proteins has become a fast and approachable technique for scientists who wish to use protein structure data for experimental design. How reliable is this discipline? How can structural models be assessed, analyzed, and used for the design and analysis of experiments? In this paper, we will discuss protein modeling methodology and, as a practical example, review recent work on P-selectin.

#### PROTEIN MODELING STRATEGIES

Protein modeling approaches can be divided into two classes. These are, first, methods that attempt the *de novo* prediction of protein structures from sequence data

(5, 6) and, second, methods that try to identify and utilize experimentally determined structures as templates for model building (7, 8). This latter structure-based approach is often called homology modeling or comparative modeling.

Methods which attempt to predict the structure of a protein *de novo* (i.e., without the use of an experimental structure as template) often start from secondary structure predictions based on a single sequence or multiple sequence alignments of homologous proteins (6, 9, 10) which (on a per residue basis) have an accuracy of ~70% (11, 12). Accurate predictions of the secondary structure elements in proteins have been reported for the cAMP-dependent protein kinase catalytic subunit (13), the Src homology 3 domain (14), and interleukin-2 (15). The spatial assembly of predicted secondary structure elements (5, 16) is required if a three-dimensional model is to be derived using this approach, and there is no obvious route to do so.

An alternative route to *de novo* tertiary structure prediction involves computer simulation of protein folding using lattice models. This approach does not start from secondary structure predictions but from a random coil representation of the protein on a lattice (17, 18). Theoretical models with protein backbone root mean square (rms) deviations of 2–3 Å relative to crystallographic models have been derived using this methodology (18). In general, three-dimensional models derived using *ab initio* prediction methods can be regarded as “lower resolution” models. The objective of *de novo* predictions, however performed, is often to understand the overall folding of a protein with unknown structure. For example, it may

\* To whom correspondence should be addressed.

<sup>†</sup> Bristol-Myers Squibb.

<sup>‡</sup> University of Washington.

be possible to understand that a protein has an all-helical structure and belongs to the four helix bundle folding type.

In structure-based or comparative modeling the initial goal is to assign protein sequences to families of structurally related proteins for which at least one structure has been experimentally determined (8, 19). If more than one experimentally known template is available, structurally conserved regions can be identified by structural comparison (19). The structure template to be used for modeling should be an experimental structure or a combination of the structurally conserved regions derived from several family members whose structures are known. Once the conserved protein core, which usually consists of well-ordered secondary structure elements, is defined, nonconserved loop regions are modeled by either incorporating related loops of other crystal structures (20) or employing theoretical methods such as conformational searching (21). Side chain replacements can be carried out using libraries of experimental side chain conformations (22) and combinatorial techniques (23). Finally, computational refinement of the initially built protein model utilizing molecular mechanics or dynamics calculations are employed to optimize the intramolecular contact and stereochemistry of the model. "Established" examples of comparative protein models with implications for inhibitor design include renin (24, 25) and HIV-protease (26, 27). Comparative models are in general more accurate than *ab initio* models provided that there is significant structural similarity between the template(s) and the protein which is modeled. In some cases, experimental accuracy may be approached (28, 29). In others, it may not even be possible to attempt comparative model building due to insufficient structural similarity between potential templates and the protein to be modeled. Most importantly, comparative model building is, in contrast to *ab initio* methods, unable to predict completely novel protein structures.

What are the more practical limitations of comparative protein models? The conformations of loop regions in protein models which cannot be assigned to known structural templates as well as the conformations of nonconservatively replaced side chains are usually the least reliable parts of the protein model. The overall quality of a model is dependent on the degree of structural similarity to the template structure and the template's crystallographic resolution and degree of structural refinement.

## PROTEIN SEQUENCES AND STRUCTURAL SIMILARITY

Protein structure types, characterized by defined spatial arrangements of secondary structure elements, are called protein folds. A common fold is often a characteristic feature of a family of proteins such as the trypsin family of the serine proteases. An example of a recently described and previously unobserved protein fold is the structure of the calcium-dependent lectin domain of the mannose binding protein (MBP) which is shown in Figure 1 (top). How many protein folds are known? How many are unknown? According to a recent estimate, the maximum number of protein families may be 1000 (30). Others have estimated that 500–700 protein folds with distinct topology may exist (31). Comparison of structures deposited in the Brookhaven Protein Data Bank (32, 33) through April 1992 has revealed the availability of approximately 150 nonhomologous protein folds (34). On the basis of these numbers, it may follow that 10–20% of the three-dimensional protein structure spectra are presently known.

However, protein structures represent much more a continuum (34) than a discrete spectrum, and the classification of structures into structure types or folds remains critically dependent on the criteria being applied. In any case, new folding motifs such as the recently described  $\beta$ -helix of pectate lyase C (35) are continuously being elucidated.

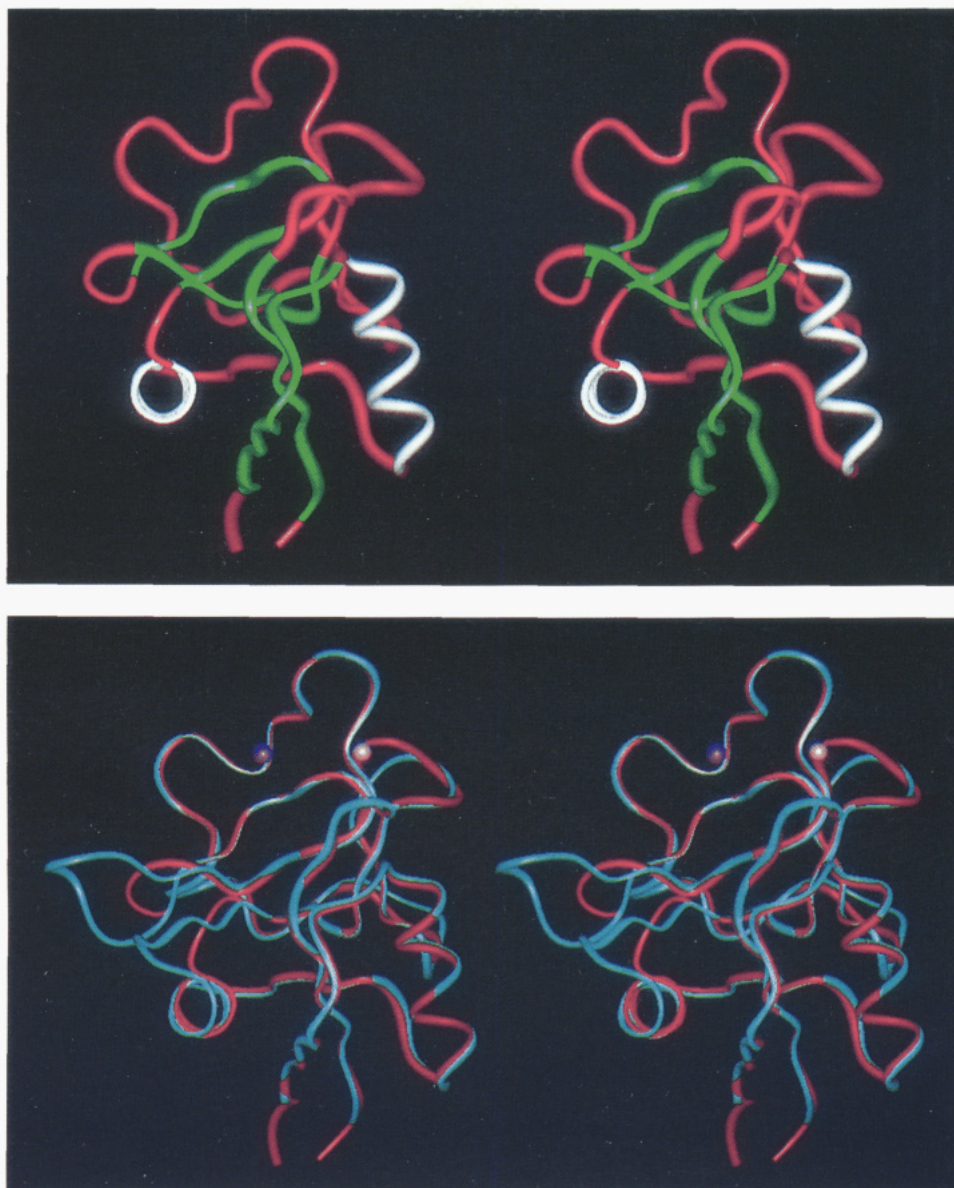
It is evident that the identification and assessment of structural similarities between proteins play a key role in protein modeling attempts that aim at generating detailed protein models. How can three-dimensional structural similarity be detected? The identification of structures similar to the protein to be modeled is straightforward if significant sequence similarity (40% or more) between the protein with unknown structure and the protein with known structure can be detected in sequence similarity searches and alignments. Significant sequence similarity directly correlates to structural similarity: The higher the sequence similarity, the more similar the three-dimensional structures (36). Template structures can be selected based on sequence similarity. Early examples of protein families which have been the subject of comparative model building, such as antibodies or serine proteases (19), usually show significant sequence similarity.

It is generally true that three-dimensional protein structure is significantly more conserved than sequence (36). In other words, sequences that fold into defined folding motifs, such as the immunoglobulin fold, may show great variability in their amino acid sequences. This means that sequence similarities of 20% or less may still indicate significant structural similarity. This has, for example, been shown for the heat shock protein fragment HSC70 and actin whose structures are very similar in spite of having less than 15% sequence identity (37). The three-dimensional structures of these proteins are also similar to hexokinase (38). At the same time, sequence similarities of approximately 20% may also be found in rather distantly related structures having major differences in their topologies. The presence of such similarities may therefore not be sufficient for the selections of structural templates and detailed comparative modeling. The tenuous relationship between structures having low sequence similarity and related tertiary structure requires that more detailed studies be performed to evaluate the degree of structural similarity.

In the case of moderate to low sequence similarity of approximately 25% or less, alignments of multiple sequences based on available three-dimensional structure(s) (39), often called structure-based sequence alignments or sequence-structure alignments, are considerably more informative than sequence alignments alone. Three-dimensional constraints can now be taken into account, and the conservation of key residues important for a particular protein fold may be detected or excluded. Tolerated sequence variance at given spatial positions can be assessed. Using this approach, it was found that 60% of the residues in two variant surface glycoproteins of *Trypanosoma brucei* are structurally equivalent despite the fact that there is only 16% sequence identity between these two molecules (40). Sequence-structure alignments have also allowed the generation of a detailed model of the CD40 ligand based on the structure of tumor necrosis factor (41).

In cases of very low or virtually no sequence similarity, structural similarity sufficient for the meaningful selection of template structures may still be detected using the so-called "inverse folding" methodology. This method evaluates the compatibility of protein sequences with a given





**Figure 1.** (Top) stereo representation of the fold of lectin domain of the mannose binding protein (MBP) from rat (78). MBP was the first calcium-dependent (C-type) mammalian lectin domain whose structure was solved experimentally. The structure revealed a previously unobserved protein fold which is shown here in solid ribbon representation. The  $\alpha$  helices in MBP are colored in white, and the  $\beta$  strands are colored in green. The view is along  $\alpha$  helix 2 (lower left corner). As can be seen, one of the striking features of this protein fold is its unusually high content of non- $\alpha$  helical or  $\beta$  strand secondary structure. Prominent loop regions can be seen, for example, in the upper part of the structure, colored in red. The fold of this C-type lectin domain represents a structural prototype for the protein family of mammalian C-type lectins which includes the ligand binding domains of the selectins. The N- and C-termini of the lectin domain are in close proximity (at the bottom of the picture). This spatial arrangement of the termini explains why C-type lectin domains can, as independent folding units or modules, be part of many multidomain cell surface proteins. (Bottom) superposition of the MBP crystal structure (red) and the model structure of the P-selectin ligand binding domain (blue). The view of the stereo comparison is according to Figure 1 (top). The position of a calcium ion whose coordination sphere is conserved in MBP and in the selectins is depicted as a purple ball, and the calcium binding site special to MBP and predicted to be not present in the selectins is shown in lavender. Major structural differences between MBP and P-selectin occur in loop regions. In contrast, the core regions are conserved in these proteins. In a way, this represents a result typical of comparative model building. Alignments of the sequences of the selectins and MBP based on the MBP crystal structure (sequence-structure alignments) suggested that P-selectin displays, despite the relatively low sequence similarity of approximately 25%, the same overall and previously unobserved fold as MBP. Figures 1 (top and bottom) may be viewed with stereo glasses to obtain the three-dimensional effect.

three-dimensional fold (42) by analyzing the residue environments in a three-dimensional structure (43, 44) or by threading sequences onto folds (45–48), followed by analysis of pairwise residues interaction energies (49). This technique does not depend on the initial presence of any sequence similarity. It is possible to screen protein sequences against a database of three-dimensional structures and *vice versa* to detect, for example, the structural similarities between HSC70, actin, and hexokinase, which as mentioned above, are structurally related.

No matter how structural similarities between proteins with known and unknown structure are identified, the assessment of the degree of similarity and the identification of dissimilar regions in protein structures represents a very important stage of the model-building process. A critical analysis of these aspects largely determines whether a meaningful model can be generated and where the limitations in the use of the model lie. Using inverse folding techniques, the compatibility of each residue with its environment in a given three-dimensional model can be

calculated (50). The global incompatibility of sequence and structure and some local inconsistencies such as, for example, a buried charged residue, can be detected using these methods. This analysis also provides further means to assess the confidence level of a structural model.

### PROTEIN MODELS TO AID DRUG DESIGN

Advances in macromolecular structure determination by crystallography, NMR, and computational chemistry have made structure-based drug design one of the current focal points of pharmaceutical research (51,52). A number of three-dimensional structures are now available which are of interest as targets for drug design (53). However, successes in structure-based drug design such as in the design and refinement of inhibitors of HIV protease (54), thymidylate synthase (55,56), and influenza virus sialidase (57) are still the exception rather than the rule. Although computational methods for the *de novo* design of inhibitors based on structural templates have been developed (58,59), it remains a difficult task to create a chemical lead based on a three-dimensional structure. If no structures of complexes with ligands are available, potential ligand binding or catalytic sites in the protein may have to be localized and characterized by chemical residue modification or mutagenesis. Many parameters such as the desolvation free energy of potential inhibitors critically influence protein-ligand interactions, and the structural details of these interactions are hard to rationalize in the absence of experimentally determined complexes. Once an initial lead is somehow discovered, iterative cycles of complex crystallographic analysis and lead compound modification may be required (55) to design a potent *in vitro* inhibitor.

Protein models are generally of lower accuracy than their crystallographic templates. If model structures are to be useful in the drug design process, a high degree of accuracy is essential as illustrated in studies on the design of renin inhibitors (25). Approximate models may still allow the outline of potential ligand binding sites in a protein but are unlikely to meaningfully aid computational ligand docking studies (60) where steric and chemical complementarity between binding sites in proteins and ligands are crucial criteria for the evaluation of test compounds.

A recent study by Cohen and colleagues (61) has shown that comparative protein models of parasitic serine and cysteine proteases can successfully be used in combination with a computational docking and database searching technique (62) to identify inhibitory compounds which bind to the target protein in the micromolar range. The active site geometries of serine and cysteine proteases are known and well described. Therefore, carefully built model structures of the catalytic domain of these enzymes should have a relatively high accuracy. As demonstrated by Cohen and colleagues, such models can, in the absence of crystallographic data, be useful in the design of inhibitors. For the application of structural models in drug design, two aspects seem to be very critical. These are the integration of structural studies into an experimental drug discovery effort (51,52) and the development of an understanding of which questions may be answered based on the analysis of structural models and which ones may not. Such decisions have to be made on a case-by-case basis since established procedures are not yet available.

In the following text we will discuss a specific example which may illustrate the critical stages, opportunities, and limitations of protein modeling and its implications for drug design. This example is the molecular model of the

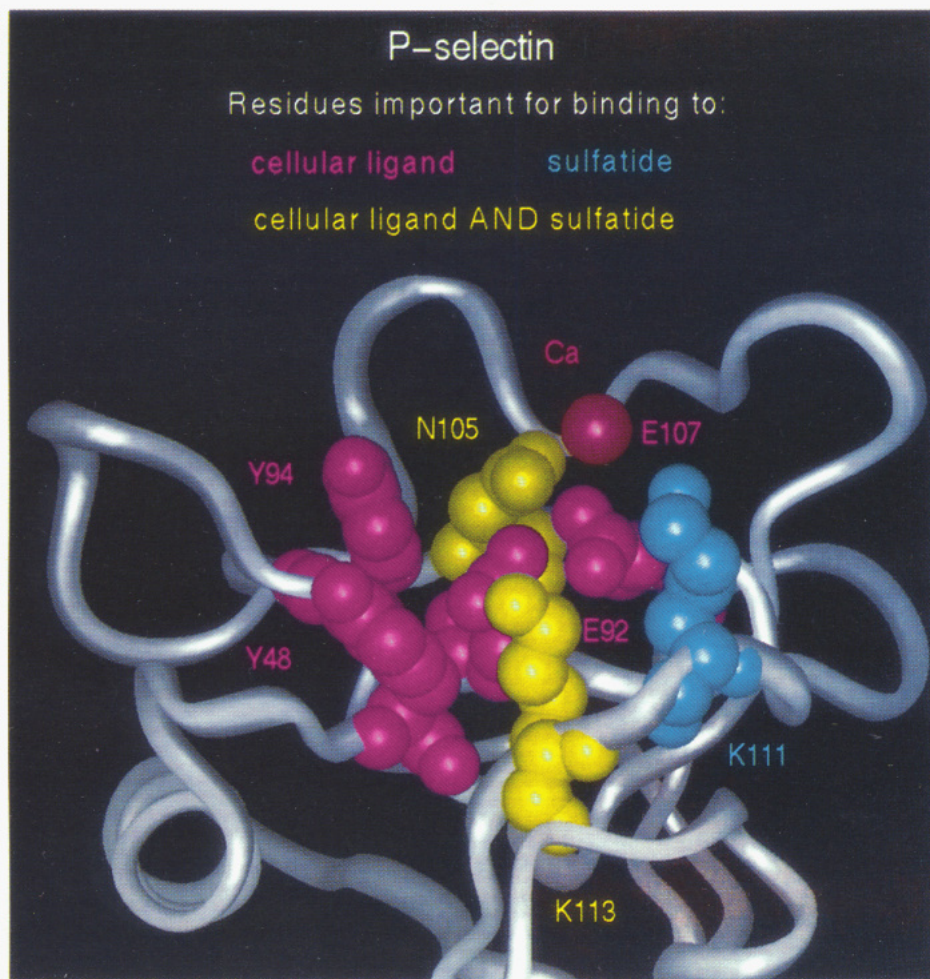
amino terminal extracellular domain of P-selectin and its application. The selectin family of cell adhesion molecules includes P-selectin (63, 64). This lectin is in part responsible for the initial attachment of leukocytes to activated vascular endothelium (65) which is one of the early events in an inflammatory response. The exact molecular nature of the physiological ligand of P-selectin is presently unknown. *In vitro* studies have shown that P-selectin is able to bind to Le<sup>x</sup> (66), sialylated Le<sup>x</sup> (67-69), sulfatide (70), sulfoglucuronylglycosphingolipids (71), and a ~250-kDa glycoprotein expressed by leukocytes (72). Considerable interest has surrounded studies of E- and P-selectin as targets to inhibit early events in the inflammatory responses such as the attachment of leukocytes to the vascular endothelium. Experimental structures (X-ray and/or NMR) of the selectin ligand binding domains have not yet been reported. We have focused our structure-function studies on P-selectin (73, 74). Experiments by others on E- (75) and P-selectin (76) have provided essentially the same conclusions regarding the location of the ligand binding site in the selectins and the identification of residues within the binding site which are critical for binding.

**Identification of a Structural Template.** Insight into the structural features of the lectin-like domain in P-selectin could not be obtained for a considerable time, since it was not possible to relate P-selectin to any known three-dimensional folds including plant lectins (77). This changed when the crystal structure of the lectin domain of a rat MBP, the first experimentally determined structure of a C-type lectin, became available (78). The sequence identity between the rat MBP and the selectin lectin domains is ~25%. Alignments of the selectin and MBP sequences relative to the crystallographic structure (74, 78) showed that residues in the hydrophobic core regions, the disulfide bonds, and the residues of at least one of the calcium binding sites in MBP are conserved in the selectins (78). This analysis strongly suggested the close similarity of the MBP and selectin structures. Figure 1 (top) outlines the previously unobserved fold of MBP which would have been hard, if not impossible, to predict from its amino acid sequence.

**Model Building.** The starting point for modeling P-selectin ligand binding domain was the MBP structures solved at 2.5-Å resolution. The atomic coordinates for this structure were obtained from the prerelease section of the Brookhaven Protein Data Bank (ref 33, entry "1MSB"). The conserved core region in MBP and P-selectin, including the disulfide bonds, and one fully conserved calcium coordination sphere provided the basis for the modeling of P-selectin. The conformation of loop regions in P-selectin which could not be modeled from known crystallographic structures were approximated by conformational search calculations. Amino acid replacements were carried out via computer graphics as similar as possible to the original conformation or, alternatively, in low-energy rotamer conformations (22). The initial model was refined using energy minimization calculations with harmonic constraints applied to the protein backbone and with the conserved calcium coordination sphere held fixed in space. Figure 1 (bottom) shows a superposition of the P-selectin model on the MBP structure. This Figure shows that amino acid insertions and deletions occur in surface loops but not in the core regions of the proteins which display a conserved spatial arrangement.

**Model Assessment.** Three-dimensional-profile analysis of the P-selectin model and its sequence relative to the MBP structure and its sequence showed that the sequence-





**Figure 2.** Ligand binding site in P-selectin. The P-selectin model structure is colored in silver and shown in the same orientation as in Figure 1. Residues important for ligand binding are shown in space-filling representation and color-coded according to their importance for binding to the cellular ligand of P-selectin on myeloid cells and for binding to sulfatide. The representation shows that the cellular ligand and sulfatide bind to an overlapping but not identical set of residues in P-selectin. The ligand binding site in P-selectin is located proximal to the conserved calcium position (shown as a red ball) which is functionally important and also thought to be vital for the structural integrity of the ligand binding domain. Residue asparagine 105 (N105), one of the residues of importance for the binding of both ligands, is part of the conserved calcium coordination sphere. Lysine 113 (K113) is an important residue for the binding to both ligands. The side chain of this residue is approximately 10 Å from the conserved calcium. The ligand binding site in P-selectin was identified based on the analysis of the P-selectin model. This analysis had led to an hypothesis regarding the location of the binding site region. On the basis of these studies, site-specific mutagenesis experiments revealed residues that are critical for binding of P-selectin to its cellular ligand (73). Subsequently, it was shown that the P-selectin binding sites for the cellular ligand and for sulfatide are overlapping (74).

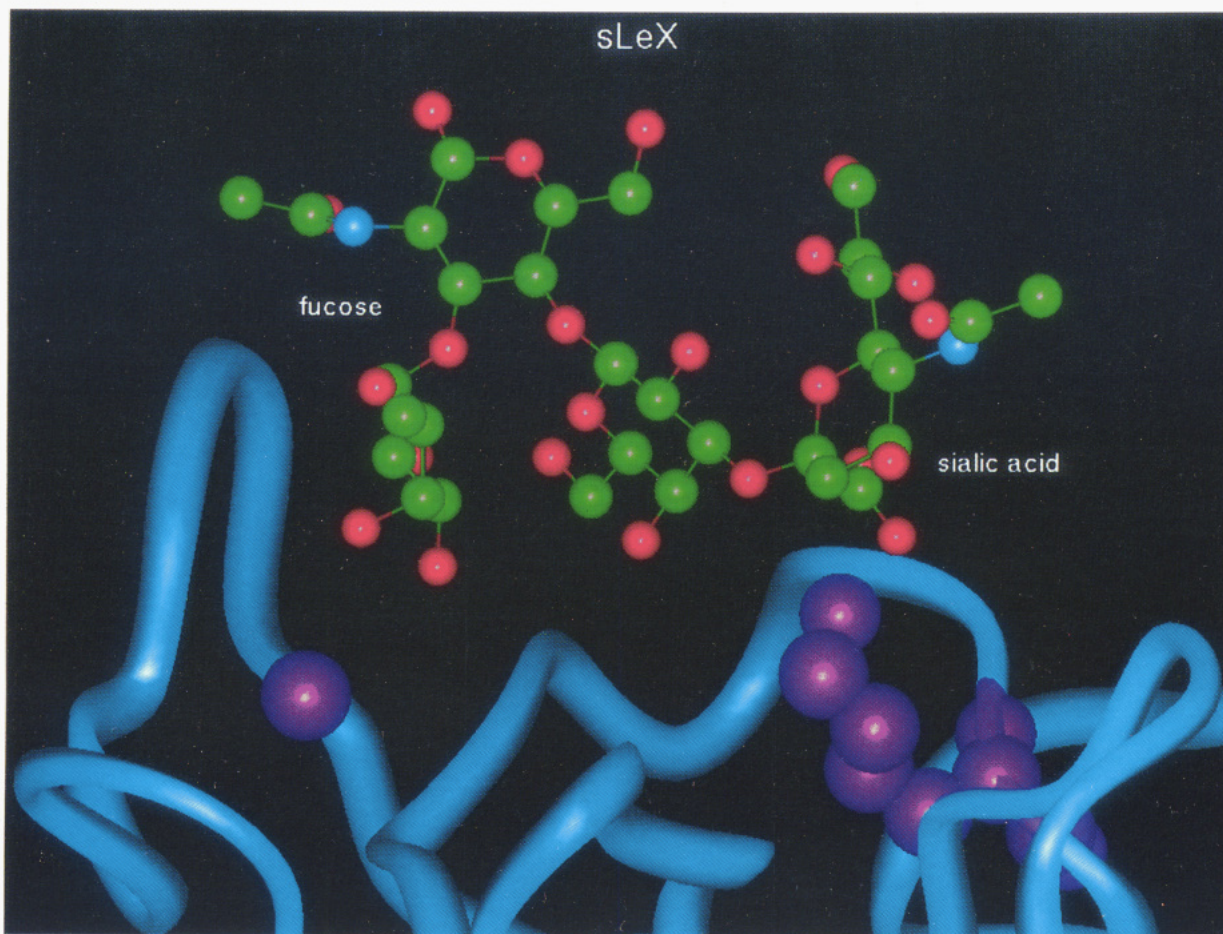
structure compatibility of the P-selectin model is comparable to the sequence-structure compatibility of MBP (73). The global stability of the P-selectin model was further confirmed by extensive molecular dynamics calculations where, after equilibration, correlated structural motions were observed equivalent to those found in simulations of MBP (79). The overall sequence-structure compatibility and stability of the P-selectin model is consistent with the proposed structure similarity between MBP and the selectins.

**Identification of the Ligand Binding Site.** Inspection of the P-selectin model suggested the presence of a shallow groove proximal to the conserved calcium binding site. This region of P-selectin was considered as a possible ligand binding site and subjected to site-specific mutagenesis experiments (73). The binding of wild-type P-selectin and P-selectin mutants to its cellular ligand on HL-60 cells was determined and compared. Mutation of amino acids within the putative ligand binding site of P-selectin resulted in the identification of a number of residues which when mutated significantly reduced or completely abolished binding of P-selectin to HL-60 cells.

In contrast, mutation of other residues on the surface of the P-selectin, distal to the putative binding site, had no effect on the binding of P-selectin to HL-60 cells. The residues which were found to participate in the formation of the P-selectin binding site for its cellular ligand are depicted in Figure 2. Residues Tyr 48, Tyr 94, and Lys 113 were found to be especially important for binding. Any mutation of these residues, for example, the changes of Tyr 48 and 94 to Phe, removing a single hydrogen bonding donor/acceptor moiety, abolished binding completely.

In the next step, binding of sulfatide to P-selectin was examined using the panel of P-selectin mutants which mapped the cellular ligand binding site of P-selectin. The results of these experiments are shown in Figure 2. Sulfatide was found to bind to the same site in P-selectin as the cellular ligand, utilizing an overlapping but not identical set of residues (74). Lys 113 is critical for binding of P-selectin to both the cellular ligand and to sulfatide. In contrast, Tyr 48 and Tyr 94, crucial for binding to myeloid cells, are not critical for binding to sulfatide. Lys 111, which was not critical for binding of P-selectin to the





**Figure 3.** Schematic model of sialylated Lewis<sup>x</sup> (sLe<sup>x</sup>) binding to the P-selectin ligand binding site. P-selectin is colored in blue and shown in a closeup side view. This orientation is obtained from the previous orientation by approximately 90° orientation around the *y*-axis. The carbohydrate ligand is shown with small spheres on its atoms and in standard atom coloring (carbon, green; oxygen, red; nitrogen, blue). The proposed "molecular anchors" in P-selectin are shown in space-filling representation and are colored in purple. These are the conserved calcium (on the left side of the picture) and residue lysine 113 (on the right side). These residues are spaced approximately 10 Å apart. We propose that the calcium interacts with the fucose moiety in sialylated Lewis<sup>x</sup> and that lysine 113 interacts with the negatively charged sialic acid moiety in sialylated Lewis<sup>x</sup>. The interaction between the calcium in P-selectin and the fucose was inferred from crystallographic data of MBP in complex with oligomannose (82). The interaction between the negatively charged sialic acid moiety and the positively charged lysine 113 was proposed based on mutagenesis experiments and based on the spatial separation of these potential molecular recognition sites. The use and the limitations of such schematic models are described in the text.

cellular ligand, is equally as important as Lys 113 for binding to sulfatide. As expected, the binding of both ligands was found to be strictly calcium-dependent (74).

In an independent study, the same region in E- and P-selectin was found to be responsible for binding of sLe<sup>x</sup> glycolipid (75). Recently, it has been reported that sLe<sup>x</sup> significantly reduced lung injury in a rat model of acute inflammation (80), presumably by blocking selectin function. Taken together, these results suggest that sLe<sup>x</sup> or related derivatives may provide a starting point for the design of specific selectin inhibitors which could be used in a clinical setting to block early events in inflammation.

**A Model of sLe<sup>x</sup> Binding to P-Selectin.** Given the information regarding the location of the ligand binding site in P-selectin, can a model of the sLe<sup>x</sup>-P-selectin interaction be developed? The accuracy of current model building methodology is insufficient to predict protein-carbohydrate complexes at the atomic level of detail (81) even if crystallographic structures of carbohydrate-binding proteins are available as starting points. For example, it is hard, if not impossible, to predict the role of water molecules which play an important role in mediating protein-carbohydrate interactions (81, 82). The great conformational flexibility of many oligosaccharides makes

it very difficult to approximate their binding conformations. Therefore, predicted protein-carbohydrate complexes are usually approximate at best.

In the case of P-selectin, further information has become available which allows a simple model of P-selectin-sLe<sup>x</sup> interactions to be constructed. Weis *et al.* (83) have determined the crystal structure of the C-type lectin domain of the rat MBP complexed with oligomannose. This structure revealed a previously unobserved mode of carbohydrate-protein interaction and explained the calcium dependence of carbohydrate binding to C-type mammalian lectins. It shows that a mannose residue directly coordinates with two equatorial hydroxyl groups to the calcium ion by replacing a water molecule in the calcium coordination sphere (83). The fact that this calcium binding site is rigorously conserved in the selectins suggests how a fucose residue, part of the sLe<sup>x</sup> ligand, can bind to the calcium in the selectins. An approximate conformation of sLe<sup>x</sup> can be modeled based on an NMR structure of Le<sup>x</sup> (84). In the modeled conformation, which uses the suggested calcium-fucose interaction as a molecular anchor point, the sLe<sup>x</sup> can be readily docked into the ligand binding site of the P-selectin model. The intermolecular interactions are optimized by constrained



molecular mechanics calculations. This schematic model is shown in Figure 3. The calcium–fucose interaction limits the possible orientations of the ligand in the binding site. A striking feature of this model complex is that the negatively charged group of the sialic acid moiety in sLe<sup>x</sup> is in a suitable position for ionic interactions with residue Lys 113 in P-selectin which, as discussed earlier, has been found to be essential for the binding of the selectin ligands.

This schematic model allows us to draw several conclusions about the interaction of P-selectin with one of its carbohydrate ligands. The mode of carbohydrate binding by P-selectin is different from previously reported carbohydrate–protein interactions (83, 84). The complex must be stabilized at the surface of P-selectin rather than in a cavity or groove, and likely important molecular recognition sites such as the conserved calcium and Lys 113 are ~10 Å apart. These predictions are consistent with results obtained in studies of the binding of E- and P-selectin to sLe<sup>x</sup> and its derivatives (75, 76, 85). Interestingly, only functional groups on one side of the ligand are involved in important contacts with the protein while the other side of the ligand remains completely exposed to solvent. In the absence of more detailed structural information, this limited model of selectin–carbohydrate binding can be applied to support inhibitor design. To take advantage of this model for the design of novel selectin ligands it should be understood that the focus is the functional groups most likely to interact with the P-selectin binding site. The spatial separation of residues important for binding and their proximity to functional groups in the ligand should be taken into account in the design of selectin inhibitors. In addition, compounds which may specifically interact with additional residues proximal to the binding site, taking advantage of the chemical nature of the residue side chain, should show enhanced binding affinity. Binding studies with compounds generated using these criteria may lead to the preparation of new inhibitory compounds with predictable binding characteristics.

## CONCLUSIONS

There is an ever-increasing interest in the prediction of three-dimensional protein structures and in the application of such protein models for the design of novel biologically active ligands. Fast computers and sophisticated computer graphic tools do not *per se* increase the quality of models. Currently, the most reliable models are being generated by comparative rather than *ab initio* modeling techniques. Comparative model building requires extensive analyses of structural relations and similarities to known structures. Methods which allow structural comparison of proteins with moderate to low sequence similarities significantly enhance the ability to identify structural templates for comparative model building. Methods which assess the sequence–structure compatibility of structural models are essential to assign a global confidence level to these models. The meaningful use of protein models for protein engineering and, even more so, drug design studies requires a high degree of model accuracy. Although some successful studies have now been reported, the use of model structures for drug design applications requires many approximations and is still in its infancy. Studies on the ligand binding domain of P-selectin have shown that a protein model can successfully be used for the design of mutagenesis experiments and that ideas for inhibitor design can be developed by rather simple and approximate model building of receptor–ligand complexes. This example also demonstrates how crucial the identification of a meaningful

structural template can be for the success of a protein modeling and engineering project.

## ACKNOWLEDGMENT

The authors are grateful to Peter Senter for critical review of the manuscript and many helpful suggestions and Debby Baxter for help in the preparation of this manuscript.

## NOTE ADDED IN PROOF

Recently, two publications have appeared which should be mentioned. The crystallographic structure of E-selectin (Graves et al. (1994) *Nature* 367, 532–538) has confirmed the proposed structural similarity of the C-type lectin domain of the mannose binding protein and the selectins. The results of the mutagenesis experiments on E-selectin by Graves et al. are consistent with the P-selectin binding site analysis. Furthermore, an instructive example of structure-based drug design has been reported by Lam et al. ((1994) *Science* 236, 380–384). These researchers have designed novel inhibitors of HIV protease which include a mimic of a structural water molecule found in previously reported crystal structures of HIV protease–inhibitor complexes.

## LITERATURE CITED

- (1) Fetrow, J. S., and Bryant, S. H. (1993) New programs for protein structure prediction. *Biotechnology* 11, 479–484.
- (2) Thornton, J. M. (1990) Tackling a loopy problem. *Nature* 343, 411–412.
- (3) Thornton, J. M., Flores, T. P., Jones, D. T., and Swindells, M. B. (1991) Prediction of progress at last. *Nature* 354, 105–106.
- (4) Bajorath, J., Stenkamp, R., and Aruffo, A. (1993) Knowledge-based model building of proteins: Concepts and Examples. *Protein Science* 2, 1798–1810.
- (5) Cohen, F. E., Richmond, T. J., and Richards, F. M. (1979) Protein folding: Evaluation of simple rules for the assembly of helices into tertiary structure with myoglobin as an example. *J. Mol. Biol.* 132, 275–288.
- (6) Benner, S. A. (1992) Predicting de novo the folded structure of proteins. *Curr. Opin. Struct. Biol.* 2, 402–412.
- (7) Blundell, T. L., Sibanda, B. L., Sternberg, M. J., and Thornton, J. M. (1987) Knowledge-based prediction of protein structures and the design of novel molecules. *Nature* 326, 347–352.
- (8) Greer, J. (1990) Comparative modeling methods: applications to the family of the mammalian serine proteases. *Proteins* 7, 317–334.
- (9) Garnier, J., Osguthorpe, D. J., and Robson, B. (1978) Analysis of the accuracy and implications of simple methods for predicting the secondary structure of globular proteins. *J. Mol. Biol.* 120, 97–120.
- (10) Bazan, J. F. (1990) Structural design and molecular evolution of a cytokine receptor family. *Proc. Natl. Acad. Sci. U.S.A.* 87, 6934–6938.
- (11) Rost, B., Schneider, R., and Sander, C. (1993) Progress in protein structure prediction? *Trends Biochem. Sci.* 18, 120–123.
- (12) Rost, B., and Sander, C. (1993) Prediction of protein secondary structure at better than 70% accuracy. *J. Mol. Biol.* 232, 584–599.
- (13) Benner, S. A., and Gerloff, D. (1991) Patterns of divergence in homologous proteins as indicators of secondary and tertiary structure: the catalytic domain of protein kinases. *Adv. Enz. Regul.* 31, 121–181.
- (14) Benner, S. A., Cohen, M. A., and Gerloff, D. (1993) Predicted secondary structure for the Src homology 3 domain. *J. Mol. Biol.* 229, 295–305.
- (15) Bazan, J. F. (1992) Unraveling the structure of IL-2. *Science* 257, 410–412.

- (16) Cohen, F. E., Sternberg, M. J. E., and Taylor, W. R. (1982) The analysis and prediction of the tertiary structure of globular proteins involving the packing of alpha helices against beta sheets: A combinatorial approach. *J. Mol. Biol.* 156, 821-862.
- (17) Skolnick, J., and Kolinsky, A. (1989) Computer simulations of globular protein folding and tertiary structure. *Ann. Rev. Phys. Chem.* 40, 207-235.
- (18) Skolnick, J., Kolinski, A., Brooks, C. L., III, Godzik, A., and Rey, A. (1993) A method for predicting protein structure from sequence. *Curr. Biol.* 3, 414-423.
- (19) Greer, J. (1991) Comparative modeling of homologous proteins. *Methods Enzymol.* 202, 239-252.
- (20) Jones, T. A., and Thirup, S. (1986) Using known substructures in protein model building and crystallography. *EMBO J.* 5, 819-822.
- (21) Bruccoleri, R. E., and Karplus, M. (1987) Prediction of the folding of short polypeptide segments by uniform conformational sampling. *Biopolymers* 26, 137-168.
- (22) Ponder, J. W., and Richards, F. M. (1987) Tertiary templates for proteins. Use of packing criteria in the enumeration of allowed sequences for different structural classes. *J. Mol. Biol.* 193, 775-791.
- (23) Bajorath, J., and Fine, R. M. (1992) On the use of minimization from many randomly generated loop structures in modeling antibody combining sites. *ImmunoMethods* 1, 137-146.
- (24) Blundell, T. L., Sibanda, B. L., and Pearl, L. (1983) Three-dimensional structure, specificity and catalytic mechanism of renin. *Nature* 304, 273-275.
- (25) Hutchins, C., and Greer, J. (1991) Comparative modeling of proteins in the design of novel renin inhibitors. *Crit. Rev. Biochem. Mol. Biol.* 26, 77-127.
- (26) Pearl, L. H., and Taylor, W. R. (1987) A structural model for the retroviral proteases. *Nature* 329, 351-354.
- (27) Weber, I. T., Miller, M., Jaskolski, M., Leis, J., Skalka, A. M., and Wlodawer, A. (1989) Molecular modeling of the HIV-1 protease and its substrate binding site. *Science* 243, 928-931.
- (28) Weber, I. T. (1990) Evaluation of homology modeling of HIV protease. *Proteins* 7, 172-184.
- (29) Chothia, C., Lesk, A. M., Tramontano, A., Levitt, M., Smith-Gill, S. J., Air, G., Sheriff, S., Padlan, E. A., Davies, D., Tulip, W. R., et al. (1989) Conformations of immunoglobulin hypervariable regions. *Nature* 342, 877-883.
- (30) Chothia, C. (1992) One thousand families for the molecular biologist. *Nature* 357, 543-544.
- (31) Blundell, T. L., and Johnson, M. S. (1993) Catching a common fold. *Protein Science* 2, 877-883.
- (32) Orengo, C. A., Brown, N. P., and Taylor, W. R. (1992). Fast structure alignment for protein databank searching. *Proteins* 14, 139-167.
- (33) Bernstein, F. C., Koetzle, T. F., Williams, G. J. B., Meyer, E. F., Brice, M. D., Rodgers, J. R., Kennard, O., Shimanouchi, T., and Tasumi, M. (1977) Protein Data Bank: a computer-based archival file for macromolecular structures. *J. Mol. Biol.* 112, 535-542.
- (34) Orengo, C. A., Flores, T. P., Taylor, W. R., and Thornton, J. M. (1993) Identification and classification of protein fold families. *Protein Eng.* 6, 485-500.
- (35) Yoder, M. D., Keen, N. T., and Jurnak, F. (1993) New domain motif: The structure of pectate lyase C, a secreted plant virulence factor. *Science* 260, 1503-1506.
- (36) Chothia, C., and Lesk, A. M. (1986) The relation between the divergence of sequence and structure in proteins. *EMBO J.* 5, 823-826.
- (37) Flaherty, K. M., McKay, D. B., Kabsch, W., and Holmes, K. C. (1991) Similarity of the three-dimensional structures of actin and the ATPase fragment of a 70-kDa heat shock cognate protein. *Proc. Natl. Acad. Sci. U.S.A.* 88, 5041-5045.
- (38) Bränden, C.-I. (1990) Founding fathers and families. *Nature* 346, 607-608.
- (39) Cygler, M., Schrag, J. D., Sussman, J. L., Harel, M., Silman, I., Gentry, A. K., and Doctor, B. P. (1993) Relationship between sequence conservation and three-dimensional structure in a large family of esterases, lipases, and related proteins. *Protein Sci.* 2, 366-382.
- (40) Blum, M. L., Down, J. A., Gurnett, A. M., Carrington, M., Turner, M. J., and Wiley, D. C. (1993) A structural motif in the variant surface glycoproteins of *Trypanosoma brucei*. *Nature* 362, 603-609.
- (41) Aruffo, A., Farrington, M., Hollenbaugh, D., Li, X., Milatovich, A., Nonoyama, S., Bajorath, J., Grosmaire, L. S., Stenkamp, R., Neubauer, M., et al. (1993) The CD40 ligand, gp39, is defective in activated T cells from patients with X-linked hyper-IgM syndrome. *Cell* 72, 1-20.
- (42) Wodak, S. J., and Rooman, M. J. (1993) Generating and testing protein folds. *Curr. Opin. Struct. Biol.* 3, 247-259.
- (43) Bowie, J. U., and Eisenberg, D. (1993) Inverted protein structure prediction. *Curr. Opin. Struct. Biol.* 3, 437-444.
- (44) Overington, J., Donnelly, D., Johnson, M. S., Sali, A., and Blundell, T. (1992) Environment-specific amino acid substitution tables: tertiary templates and prediction of protein folds. *Protein Sci.* 1, 216-226.
- (45) Jones, D. T., Taylor, W. R., and Thornton, J. M. (1992) A new approach to protein fold recognition. *Nature* 358, 86-89.
- (46) Godzik, A., and Skolnick, J. (1992) Sequence-structure matching in globular proteins: application to supersecondary and tertiary structure determination. *Proc. Natl. Acad. Sci. U.S.A.* 89, 12098-12102.
- (47) Bryant, S. H., and Lawrence, C. E. (1993) An empirical energy function for threading protein sequence through the folding motif. *Proteins* 16, 92-112.
- (48) Sippl, M. J., and Weitckus, S. (1992) Detection of native-like models for amino acid sequences of unknown three-dimensional structure in a database of known protein conformations. *Proteins* 13, 258-271.
- (49) Sippl, M. J. (1990) Calculation of conformational ensembles from potentials of mean force. An approach to the knowledge-based prediction of local structures in globular proteins. *J. Mol. Biol.* 216, 859-883.
- (50) Luthy, R., Bowie, J. U., and Eisenberg, D. (1992) Assessment of protein models with three-dimensional profiles. *Nature* 356, 83-85.
- (51) Kuntz, I. D. (1992) Structure-based strategies for drug design and discovery. *Science* 257, 1078-1082.
- (52) Navia, M. A., and Murcko, M. A. (1992) Use of structural information in drug design. *Curr. Opin. Struct. Biol.* 2, 202-210.
- (53) Walkinshaw, M. D. (1992) Protein targets for structure-based drug design. *Med. Res. Rev.* 12, 317-372.
- (54) Erickson, J., Neidhart, D. J., VanDrie, J., Kempf, D. J., Wang, X. C., Norbeck, D. W., Plattner, J. J., Rittenhouse, J. W., Turon, M., Wideburg, N., et al. (1990) Design, activity, and 2.8 Å crystal structure of a C<sub>2</sub> symmetric inhibitor complexed to HIV-1 protease. *Science* 249, 527-532.
- (55) Appelt, K., Bacquet, R. J., Bartlett, C. A., Booth, C. L., Freer, S. T., Fuhry, M. A., Gehring, M. R., Herrman, S. M., Howland, E. F., Janson, C. A., et al. (1991) Design of enzyme inhibitors using iterative protein crystallographic analysis. *J. Med. Chem.* 34, 1925-1934.
- (56) Shoichet, B. K., Stroud, R. M., Santi, D. V., Kuntz, I. D., and Perry, K. M. (1993) Structure-based discovery of inhibitors of thymidylate synthase. *Science* 259, 1445-1450.
- (57) von Itzstein, M., Wu, W.-Y., Kok, G. B., Pegg, M. S., Dyason, J. C., Jin, B., Phan, T. V., Smythe, M. L., White, H. F., Oliver, S. W., et al. (1993) Rational design of potent sialidase-based inhibitors of influenza virus replication. *Nature* 363, 418-423.
- (58) Böhm, H. J. (1992) The computer program LUDI: A new method for the *de novo* design of enzyme inhibitors. *J. Comput.-Aided Mol. Des.* 6, 61-78.
- (59) Rotstein, S. H., and Murcko, M. A. (1993) GroupBuild: A fragment-based method for *de novo* drug design. *J. Med. Chem.* 36, 1700-1710.
- (60) Burt, S. K., Hutchins, C. W., and Greer, J. (1991) Predicting receptor-ligand interactions. *Curr. Opin. Struct. Biol.* 1, 213-218.
- (61) Ring, C. S., Sun, E., McKerrow, J. H., Lee, G. K., Rosenthal, P. J., Kuntz, I. D., and Cohen, F. E. (1993) Structure-based inhibitor design by using protein models for the development of antiparasitic agents. *Proc. Natl. Acad. Sci. U.S.A.* 90, 3583-3587.

- (62) Kuntz, I. D., Blaney, J. M., Oatley, S. J., Landgride, R., and Ferrin, T. E. (1982) A geometric approach to macromolecule-ligand interactions. *J. Mol. Biol.* 161, 269-288.
- (63) Springer, T. A. (1990) Adhesion receptors of the immune system. *Nature* 346, 425-434.
- (64) Lasky, L. A. (1992) Selectins: interpreters of cell-specific carbohydrate information during inflammation. *Science* 258, 964-969.
- (65) Lawrence, M. B., and Springer, T. A. (1991) Leukocytes roll on a selectin at physiologic flow rates: distinction from and prerequisite for adhesion through integrins. *Cell* 65, 859-873.
- (66) Larsen, E., Palabrica, T., Sajer, S., Gilbert, G. E., Wagner, D. D., Furie, B. C., and Furie, B. (1990) PADGEM-Dependent adhesion of platelets to monocytes and neutrophils is mediated by a lineage-specific carbohydrate, LNF III (CD15). *Cell* 63, 467-474.
- (67) Foxall, C., Watson, S. R., Dowbenko, D., Fennie, C., Lasky, L. A., Kiso, M., Hasegawa, A., Asa, D., and Brandley, B. K. (1992) The three members of the selectin receptor family recognize a common carbohydrate epitope, the Sialyl Lewis<sup>x</sup> oligosaccharide. *J. Cell. Biol.* 117, 895-902.
- (68) Polley, M. J., Phillips, M. L., Wayner, E., Nudelman, E., Singhal, A. K., Hakomori, S.-I., and Paulson, J. C. (1991) CD62 and endothelial cell-leukocyte adhesion molecule 1 (ELAM-1) recognize the same carbohydrate ligand, sialyl-Lewis x. *Proc. Natl. Acad. Sci. U.S.A.* 88, 6224-6228.
- (69) Zhou, Q., Moore, K. L., Smith, D. F., Varki, A., McEver, R. P., and Cummings, R. D. (1991) The selectin GMP-140 binds to sialylated, fucosylated lactosaminoglycans on both myeloid and nonmyeloid cells. *J. Cell Biol.* 115, 557-564.
- (70) Aruffo, A., Kolanus, W., Walz, G., Fredman, P., and Seed, B. (1991) CD62/P-selectin recognition of myeloid and tumor cell sulfatides. *Cell* 67, 35-44.
- (71) Needham, L. K., Schnaar, R. L. (1993) The HNK-1 reactive sulfoglucuronyl glycolipids are ligands for L-selectin and P-selectin but not E-selectin. *Proc. Natl. Acad. Sci. U.S.A.* 90, 1359-1363.
- (72) Moore, K. L., Varki, A., and McEver, R. P. (1991) GMP-140 binds to a glycoprotein receptor on human neutrophils: evidence for a lectin-like interaction. *J. Cell Biol.* 112, 491-499.
- (73) Hollenbaugh, D., Bajorath, J., Stenkamp, R., and Aruffo, A. (1993) Interaction of P-selectin (CD62) and its cellular ligand: analysis of critical residues. *Biochemistry* 32, 2960-2966.
- (74) Bajorath, J., Hollenbaugh, D., King, G., Harte, W., Jr., Eustice, D. C., Darveau, R. P., and Aruffo, A. (1994) The CD62/P-selectin binding sites for myeloid cells and sulfatides are overlapping. *Biochemistry* 33, 1332-1339.
- (75) Erbe, D. V., Wolitzky, B. A., Presta, L. G., Norton, C. R., Ramos, R. J., Burns, D. K., Rumberger, J. M., Rao, B. N. N., Foxall, C., Brandley, B. K., and Lasky, L. A. (1992) Identification of an E-selectin region critical for carbohydrate recognition and cell adhesion. *J. Cell Biol.* 119, 215-227.
- (76) Erbe, D. V., Watson, S. R., Presta, L. G., Wolitzky, B. A., Foxall, C., Brandley, B. K., and Lasky, L. A. (1993) P- and E-selectin use common sites for carbohydrate recognition and cell adhesion. *J. Cell. Biol.* 120, 1227-1235.
- (77) Sharon, N. (1993) Lectin-carbohydrate complexes of plants and animals: an atomic view. *Trends in Biol. Sci.* 18, 221-226.
- (78) Weis, W. I., Kahn, R., Fourme, R., Drickamer, K., and Hendrickson, W. A. (1991) Structure of the calcium-dependent lectin domain from a rat mannose-binding protein determined by MAD phasing. *Science* 254, 1608-1615.
- (79) Harte, W., Jr., and Bajorath, J. (1994) Synergism of calcium and carbohydrate binding to mammalian lectin suggested by a dynamic model. Submitted.
- (80) Mulligan, M. S., Paulson, J. C., De Frees, S., Zheng, Z.-L., Lowe, J. B., and Ward, P. A. (1993) Protective effects of oligosaccharides in P-selectin-dependent lung injury. *Nature* 364, 149-151.
- (81) Bundle, D. R., and Young, N. M. (1992) Carbohydrate-protein interactions in antibodies and lectins. *Curr. Opin. Struct. Biol.* 2, 666-673.
- (82) Vyas, N. K. (1991) Atomic features of protein-carbohydrate interactions. *Curr. Opin. Struct. Biol.* 1, 732-740.
- (83) Weis, W. I., Drickamer, K., and Hendrickson, W. A. (1992) Structure of a C-type mannose-binding protein complexed with an oligosaccharide. *Nature* 360, 127-134.
- (84) Miller, K. E., Mukhopadhyay, C., Cagas, P., and Bush, A. C. (1992) Solution structure of the Lewis x oligosaccharide determined by NMR spectroscopy and molecular dynamics simulations. *Biochemistry* 31, 6703-6709.
- (85) Tyrrell, D., James, P., Rao, N., Foxall, C., Abbas, S., Dasgupta, F., Nashed, M., Hasegawa, A., Kiso, M., Asa, D., et al. (1991) Structural requirements for the carbohydrate ligand of E-selectin. *Proc. Natl. Acad. Sci. U.S.A.* 88, 10372-10376.

# ARTICLES

## Progestin Radiopharmaceuticals Labeled with Technetium and Rhenium: Synthesis, Binding Affinity, and in Vivo Distribution of a New Progestin N<sub>2</sub>S<sub>2</sub>-Metal Conjugate

James P. O'Neil,<sup>†,‡</sup> Kathryn E. Carlson,<sup>†</sup> Carolyn J. Anderson,<sup>§</sup> Michael J. Welch,<sup>§</sup> and John A. Katzenellenbogen<sup>\*,†</sup>

Department of Chemistry, University of Illinois, 600 South Mathews Avenue, Urbana, Illinois 61801, and Division of Radiation Sciences, Washington University Medical School, 600 South Kingshighway, St. Louis, Missouri 63110. Received December 27, 1993\*

We have prepared and evaluated three metal conjugates of a progestin-monoamine-monoamide (MAMA') bisthiol chelate system. These conjugates of rhenium and technetium-99 and -99m, are structural analogs of the bisamino-bisthiol (BAT) conjugates we have described recently, but the MAMA' chelate, being more polar than the BAT system, gives a conjugate that is much less lipophilic, having an octanol-water partition coefficient that is nearly 80-fold lower. In competitive binding assays, the Re- and <sup>99</sup>Tc-MAMA'-progestin conjugates bind to the progesterone receptor with affinities greater than that of progesterone itself, and in a direct binding assay, the equilibrium dissociation constant (*K*<sub>d</sub>) of the <sup>99m</sup>Tc-MAMA' conjugate was 0.97 nM. As is typical for 11 $\beta$ -substituted progestins, these conjugates also have substantial binding affinity for glucocorticoid receptors. In tissue distribution studies in immature female rats, the progestin-<sup>99m</sup>Tc-MAMA' conjugates show selective uptake for principal target tissue (such as uterus) over that of blood and nontarget tissue (such as muscle); these uptake ratios reach maximum levels of 5 and 4, respectively. Uptake by fat, liver, and kidney is quite high; however, only the uptake in uterus is displaceable upon coinjection of the selective progestin ORG2058. Metabolism studies show that the radioactivity in the uterus is essentially unmetabolized out to 4 h, while liver activity is completely due to metabolites. Other tissues show an intermediate fraction of unmetabolized conjugates that decreases with time. The in vivo behavior of the progestin-<sup>99m</sup>Tc-MAMA' conjugate is similar to that of the labeled BAT conjugate: its uptake selectivity is somewhat greater than that of the BAT conjugate, but its target tissue uptake is lower. Factors that may be responsible for limiting the target tissue uptake properties of these conjugates are their moderate affinity for progesterone receptor, their substantial binding to glucocorticoid receptors, and their large overall molecular size.

### INTRODUCTION

Because of its wide availability, convenient half-life, and appropriate  $\gamma$  energy, technetium-99m is frequently the radionuclide of choice in the development of diagnostic imaging agents (1). Nevertheless, there are certain situations in which it is difficult to utilize technetium-99m: being a metal, it requires a chelate system to form stable complexes (1, 2) and other systems of organometallic bonding, while intriguing in structure, are difficult to prepare at the no-carrier-added level, as is required for receptor-based imaging agents (3). Since the technetium complexes are large, generally having molecular weights in excess of 250, their incorporation into small ligands for receptors, such as steroid hormones and neurotransmitters, provides a formidable challenge: (1) metal complex substituents of this size can severely compromise the binding affinity of these receptor ligands, and (2) the bulk of these conjugates can alter the physicochemical properties of receptor ligands to such an extent that their receptor-

mediated biodistribution is limited by permeability barriers or overwhelmed by nonspecific uptake.

In a recent study in which we examined the receptor binding affinity of four progestin-metal conjugates, we reported the preparation of a conjugate **I** between a progestin related to the Roussel-Uclaf antiprogestin RU486 **IV** and a bisamine-bisthiol (BAT)-technetium complex that retained high affinity for the progesterone receptor (4). While we could demonstrate nanomolar receptor binding of this conjugate in in vitro assays, its nonspecific binding was high and its tissue distribution in vivo showed high uptake by nontarget tissues (5). We postulated that the poor distribution properties of **I** might be largely due to the very lipophilic character of the bisamine-bisthiol (BAT) chelate system that was used. To lower lipophilicity, we considered other more polar metal chelate systems, and we have recently described the preparation of a smaller and considerably less lipophilic monoamine-monoamide-bisthiol-metal chelate system **II** (MAMA') that forms stable, neutral complexes with rhenium and technetium (6). The MAMA'-metal chelate system is a structural isomer of the well known MAMA system (7, 8).

In this present report, we describe the preparation of a conjugate **III** of the RU486-related progestin with this

<sup>†</sup> University of Illinois.

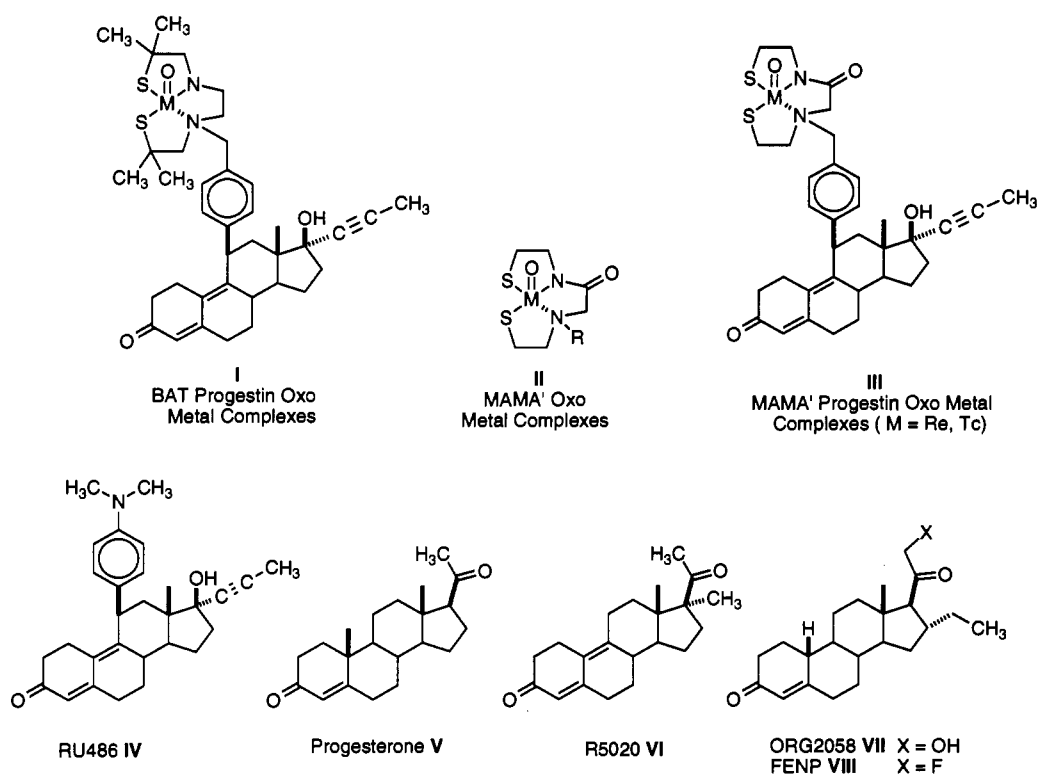
<sup>‡</sup> Current address: Center for Functional Imaging, Lawrence Berkeley Laboratory, 1 Cyclotron Rd., Berkeley, CA 94720.

<sup>§</sup> Washington University Medical School.

\* Abstract published in *Advance ACS Abstracts*, April 1, 1994.



Chart 1



new less lipophilic chelate system (9). The synthesis of the MAMA'-metal conjugates with rhenium and technetium-99 and -99m and an investigation of the progesterone receptor binding affinity, the measurement of lipophilicity, and the *in vivo* tissue distribution of these conjugates are presented. This new progesterone-metal conjugate represents the first metal-labeled steroid that retains nanomolar binding affinity for its receptor and has typical steroid-like lipophilicity; the *in vivo* tissue distribution characteristics of the <sup>99m</sup>Tc-MAMA' conjugate **III** are improved and show a higher component of receptor-mediated uptake than do the more lipophilic BAT congeners **I**.

## MATERIALS AND METHODS

**Biological Procedures. Materials.** Radioligands were obtained from the following sources: [17 $\alpha$ -methyl-<sup>3</sup>H]-promegestone (R5020), 86 Ci/mmol, and [6-methyl-<sup>3</sup>H]-11 $\beta$ ,17 $\beta$ -dihydroxy-6-methyl-17 $\alpha$ -(1-propynyl)androst-1,4,6-trien-3-one (RU28362), 77 Ci/mmol (DuPont New England Nuclear, Boston, MA). [<sup>3</sup>H]RU38486, 38 Ci/mmol, was a gift from Roussel-Uclaf, Romainville, France. Unlabeled ligands: promegestone and RU28362 (DuPont New England Nuclear, Boston, MA); 16 $\alpha$ -ethyl-21-hydroxy-19-norpregn-4-ene-3,20-dione (ORG2058) (Organon Corp., Oss, The Netherlands); RU486 (RU38486; Roussel-Uclaf, Romainville, France); hydrocortisone (Sigma Chemical Co., St. Louis, MO). Other chemicals were obtained from the following sources: activated charcoal, Trizma base, 3-(N-morpholino)propanesulfonic acid (MOPS), *n*-decylamine (Sigma Chemical Co., St. Louis, MO); dextran grade C (Schwarz/Mann, Orangeburg, NY); dimethylformamide (DMF) (Fisher Scientific, Fairlawn, NJ); (ethylenedinitrilo)tetraacetic acid tetrasodium salt (EDTA) and sodium azide (Eastman Organic Chemicals, Rochester, NY); sodium molybdate (Mallinckrodt Inc., St. Louis, MO); Triton X-114 (Central Solvents and Chemicals Co., Bedford Park, IL); 2,5-diphenyloxazole (PPO) (Research

Products International Corp., Mt. Prospect, IL); 1,4-bis-(5-phenyloxazol-2-yl)benzene (POPOP), 1-octanol (Aldrich Chemical Co., Milwaukee, WI); protosol (DuPont New England Nuclear, Boston, MA). All *in vitro* assays were done in the following buffer: 0.01 M Tris, 0.0015 M EDTA, 0.02 % NaN<sub>3</sub>, 20 mM Na molybdate, 20 % glycerol, pH 7.4 at room temperature.

**Cytosols.** Cytosols were prepared and stored as previously reported: rat PgR (10), rat liver GuR (11), and human PR from T<sub>47</sub>D tissue culture cells (12, 13).

**Relative Binding Affinity (RBA).** Assays were performed as previously reported (14). Several concentrations of unlabeled competitor or buffer, together with 10 nM tritiated tracer, were incubated with cytosol at 0 °C for 18–24 h. Unbound ligand was removed with charcoal-dextran. Competitor solutions were prepared in 1:1 DMF/buffer to ensure solubility. Progesterone receptor assays utilized either rat uterine cytosol from 3-day estrogen-primed immature rats or cytosol from T<sub>47</sub>D tissue culture cells (~1.5 nM receptor plus 1  $\mu$ M hydrocortisone to block any glucocorticoid receptor) and [<sup>3</sup>H]R5020 as the tracer. Glucocorticoid receptor assays utilized liver cytosol from 3-day adrenalectomized adult male rats (~1 nM type II sites) with [<sup>3</sup>H]RU28362 as the tracer.

Radioactivity was determined in a Nuclear Chicago Isocap 300 scintillation counter with adjustable windows, set to exclude 95 % of the <sup>99</sup>Tc counts from the tritium channel. The 5 % spill was subtracted from the tritium counts.

**Log P Determinations.** The log *P* values were estimated as previously reported (15) from the log *k'*<sub>w</sub> values determined by HPLC chromatography, following the recommendations of Minick (16), using an HPLC equipped with an autosampler and Spectra System software (Thermo Separation Products, Warrenville, IL).

**Direct Binding Assays.** Rat uterine cytosol containing ~1.5 nM progesterone receptor, preincubated with 1  $\mu$ M hydrocortisone, was incubated with various concentrations

of [ $^3\text{H}$ ](R5020 or RU486) or  $^{99\text{m}}\text{Tc}$  (MAMA' or BAT) progestin, in the absence or presence of a 100-fold excess of unlabeled R5020 (R5020 is used to block the progesterone receptor). Incubations were at 0 °C for 3–5 h. Unbound ligand was removed by charcoal–dextran. For all in vitro assays, the  $^{99\text{m}}\text{Tc}$  conjugate 7 was diluted with  $^{99\text{m}}\text{Tc}$  conjugate 6 to give a specific activity of  $\sim 86$  Ci/mmol.

The charcoal–dextran slurry used to remove unbound ligand was prepared as previously reported (14) and used in a ratio of 1 part charcoal–dextran slurry per 10 parts cytosol solution at 0 °C. Data were plotted according to the method of Scatchard (17). Radioactivity was determined in a Nuclear Chicago Isocap 300 scintillation counter with adjustable windows, set to exclude 95% of the  $^{99\text{m}}\text{Tc}$  counts from the tritium channel. The 5% spill was subtracted from the tritium counts.

**Animal Uptake Methods.** Immature female Sprague–Dawley rats (25 days old,  $\sim 50$  g except where noted) were injected (IV, lateral tail vein), under methoxyflurane (2,2-dichloro-1,1-difluoroethyl methyl ether) anesthesia, with ca. 25  $\mu\text{Ci}$  of  $^{99\text{m}}\text{Tc}$  conjugate 7 or 5  $\mu\text{Ci}$  of [ $^3\text{H}$ ]RU486 in a 4/1, physiological saline/ethanol solution. To ascertain whether the uptake was mediated by a high affinity, limited capacity system, in one set of animals 18  $\mu\text{g}$  of unlabeled ORG2058 (RBA = 170% relative to R5020) was coinjected with the radiopharmaceutical. Animals were sacrificed by decapitation at the times indicated, and samples of tissue and blood were weighed. Radioactivity in organ and standard samples was determined with a Beckman Gamma 8000 automatic well-type  $\gamma$  counter (Beckman Instruments, Fullerton, CA) (5, 18) for  $^{99\text{m}}\text{Tc}$ , while  $^3\text{H}$  radioactivity was determined following digestion using a previously reported protocol (19).

**Metabolism Studies.** The radiolabeled progestin 7 was extracted from blood or tissue samples at various time points with ethanol (15, 20). Blood samples (100  $\mu\text{L}$ ) were obtained by cardiac puncture, while tissue samples were dissected from various organs directly after sacrifice. The blood or tissue samples were weighed and their radioactivity measured; the samples were then diluted with EtOH (500  $\mu\text{L}$ ) and homogenized. After centrifugation (5 min, 2500 g), the pellet and supernatant were separated and counted. A 100- $\mu\text{L}$  aliquot of the supernatant was analyzed by TLC (5% iPrOH/ $\text{CH}_2\text{Cl}_2$ ) with comparison to an authentic sample of radiolabeled progestin 7. No attempt was made to identify the specific metabolites.

**Chemical Procedures. Materials.** Solvents and reagents were purchased from various commercial sources, Aldrich, Mallinckrodt, Sigma, Fisher, Baker, Eastman, or Alfa, and were used as received, unless otherwise noted.  $\text{Na}^{99\text{m}}\text{TcO}_4$  in saline solution was eluted from a  $^{99}\text{Mo}/^{99\text{m}}\text{Tc}$  generator purchased from DuPont or Mallinckrodt. [ $^{99}\text{Tc}$ ](*n*-Bu) $_4\text{NTcOCl}_4$  was prepared as previously described (5) from [ $^{99}\text{Tc}$ ](*n*-Bu) $_4\text{TcO}_4$  obtained from Alan Davison (MIT).  $^{99\text{m}}\text{Tc}$ –glucoheptonate kits (Glucoscan kits) were purchased from Du Pont, N. Billerica, MA.

**General.** Analytical thin layer chromatography (TLC) was performed using Merck silica gel F-254 glass-backed plates. Visualization was achieved by phosphomolybdic acid (PMA) or anisaldehyde spray reagents, iodine, or UV illumination. Flash chromatography refers to the method of Still et al. (21). Short silica plugs used Woelm silica gel (0.032–0.064 mm) or Merck silica gel (0.040–0.063 mm). High-performance liquid chromatography (HPLC) was performed isocratically with a preparative  $\text{SiO}_2$  column (Whatman Partisil M-9, 0.9 cm  $\times$  50 cm). The eluate was monitored by UV absorbance at 254 nm and a sodium

iodide scintillation flow detector, where appropriate. Proton magnetic resonance ( $^1\text{H}$  NMR) spectra at 400 MHz are reported downfield from a tetramethylsilane internal standard ( $\delta$  scale). Both low- and high-resolution fast atom bombardment (FAB) mass spectra were obtained employing a dithiothreitol matrix.

**11 $\beta$ -[ $\alpha$ -[*N*-[[[2-[(Triphenylmethyl)thio]ethyl]amino]carbonyl]methyl]-*N*-[2-[(triphenylmethyl)thio]ethyl]amino]-*p*-tolyl]-17 $\alpha$ -propynyl-17 $\beta$ -hydroxy-4,9-estradien-3-one (MAMA'-Tr $_2$ -Progestin Conjugate, 3).** To a stirring solution of 11 $\beta$ -[ $\alpha$ -[(methylsulfonyl)oxy]-*p*-tolyl]-17 $\alpha$ -propynyl-17 $\beta$ -hydroxy-4,9-estradien-3-one (1) (4) (115.2 mg, 0.23 mmol) in  $\text{CH}_2\text{Cl}_2$  (3 mL) in a Reactivial<sup>®</sup> was added a solution of *N*-[[[2-[(triphenylmethyl)thio]ethyl]amino]acetyl]-*S*-(triphenylmethyl)-2-aminoethanethiol (MAMA'-Tr $_2$ ) (2) (5) (332 mg, 0.49 mmol) in  $\text{CH}_2\text{Cl}_2$  (1 mL). The vial was flushed with nitrogen, sealed with a septum and cap, and placed in a 70 °C oil bath for 2 h. The crude reaction mixture was subjected to silica gel flash chromatography (2:1 EtOAc/hexanes) to provide the thiol-protected progestin–ligand conjugate 3 (156.5 mg, 62%) as a white foam:  $^1\text{H}$ -NMR ( $\text{CDCl}_3$ , 400 MHz)  $\delta$  7.55 (t, 1H,  $J$  = 5.7 Hz), 7.43–7.35 (m, 12 H, ArH), 7.25–7.13 (m, 20H, ArH), 7.02 (d, 2H,  $J$  = 9 Hz), 5.75 (s, 1H, 4-CH), 4.33 (d, 1H, 7.1 Hz, 11 $\alpha$ -CH), 3.40 (q, 2H,  $J$  = 13.4 Hz,  $\text{ArCH}_2\text{N}$ ), 3.10–2.89 (m, 2H), 2.86 (d, 2H,  $J$  = 4.2 Hz), 2.70 (dt, 1H,  $J$  = 14.6, 5.1 Hz), 2.56–2.18 (m, 14H), 2.20–1.84 (m, 3H), 1.91 (s, 3H,  $\text{C}\equiv\text{CCH}_3$ ), 1.78–1.64 (m, 3H), 1.50–1.18 (m, 2H), 0.46 (s, 3H, 18- $\text{CH}_3$ ); MS (LRFABMS)  $m/z$  (relative intensity) 1080 (28), 1079 (51), 1078 (61), 835 (13), 680 (14), 679 (26), 591 (27), 399 (26); HRFAB calcd for  $\text{C}_{72}\text{H}_{72}\text{N}_2\text{O}_3\text{S}_2$  ( $M + 1$ ) 1077.5063, found 1077.5076.

**11 $\beta$ -[ $\alpha$ -[*N*-[[[2-Mercaptoethyl]amino]carbonyl]methyl]-*N*-(2-mercaptoethyl)amino]-*p*-tolyl]-17 $\alpha$ -propynyl-17 $\beta$ -hydroxy-4,9-estradien-3-one (11 $\beta$ -MAMA'-Progestin Conjugate, 4).** To a solution of MAMA'-Tr $_2$ -progestin conjugate (3) (60 mg, 0.56 mmol) in ethyl acetate (1 mL) and ethyl alcohol (1 mL) was added a solution of  $\text{Hg}(\text{OAc})_2$  (44.4 mg, 0.139 mmol) in ethyl alcohol (2 mL). The mixture was heated to reflux for 10 min and then cooled to room temperature. Gaseous  $\text{H}_2\text{S}$  was bubbled through the solution until a dark black precipitate had formed, at which time the reaction vessel was capped and the solution allowed to stir for 5 min. The resulting heterogeneous mixture was filtered through Celite to remove the  $\text{HgS}$  residue, and the filtrate was concentrated to dryness in vacuo. Silica gel flash chromatography of the resulting yellow oil (EtOAc followed by 1:9 EtOH/EtOAc) provided, after concentration in vacuo, free bithiol conjugate 4 (12.2 mg, 37%) as a colorless oil. A standard solution of this compound was also prepared in nitrogen-degassed EtOH at a concentration of 1 mg/mL for use in the  $^{99\text{m}}\text{Tc}$  radiochemical labeling experiments.

**11 $\beta$ -[ $\alpha$ -[*N*-[[[2-Mercaptoethyl]amino]carbonyl]methyl]-*N*-(2-mercaptoethyl)amino]-*p*-tolyl]-17 $\alpha$ -propynyl-17 $\beta$ -hydroxy-4,9-estradien-3-one (4'-Joxorhenium(V) (MAMA'-Re(V)-Oxo-Progestin Conjugate, 5).** To a solution of MAMA'-Tr $_2$ -progestin conjugate (3) (150 mg, 0.139 mmol) in EtOAc (4 mL) was added a solution of  $\text{Hg}(\text{OAc})_2$  (11 mg, 0.034 mmol) in EtOH (3 mL). The mixture was heated to reflux for 20 min and then cooled to room temperature. Gaseous  $\text{H}_2\text{S}$  was bubbled through the solution until a black precipitate had formed, at which time the reaction vessel was capped and the solution allowed to stir for 5 min. The resulting heterogeneous mixture was filtered through Celite to remove the  $\text{HgS}$  residue, and the filtrate was concentrated to dryness in vacuo to provide the bithiol 4 as a yellow oil. To the free

ligand 4, diluted with MeOH (5 mL), was added NaOAc (1 N in MeOH, 2 mL) followed by (PPh<sub>3</sub>)<sub>2</sub>Re(O)Cl<sub>3</sub> (128 mg, 0.153 mmol). The reaction mixture was heated to 90 °C in a closed Reactivial® for 2 h and then cooled to room temperature. The resulting mixture was diluted with EtOAc (15 mL) and filtered through Celite. The purple solution was washed with water and the organic portion dried over MgSO<sub>4</sub>, filtered, and concentrated in vacuo. Silica gel flash chromatography of the resulting oil (gradient elution from 2:1 EtOAc/hexanes to 3:1 EtOAc/hexanes) provided 5 (33 mg, 0.067 mmol) as a purple solid. The two diastereomers about the tertiary amine of the ligand could be separated on the analytical scale by normal-phase HPLC (Whatman Si-5, 4.6 mm × 25 cm, 50% (1:20 iPrOH-CH<sub>2</sub>Cl<sub>2</sub>) 50% hexanes). <sup>1</sup>H-NMR (CDCl<sub>3</sub>, 400 MHz) δ 7.70–7.31 (m, 4H, ArH), 5.80 (s, 1H, 4-CH), 5.06 (d, 1H, *J* = 14.3 Hz), 4.96 (dd, 1H, *J* = 16.2, 2 Hz, ArCH<sub>2</sub>), 4.63 (d, 1H, *J* = 14.3 Hz), 4.58 (dd, 1H, *J* = 11.2, 6.6 Hz), 4.10 (d, 1H, *J* = 5.9 Hz, 11α-CH), 3.76 (d, 1H, *J* = 16.2 Hz, ArCH<sub>2</sub>), 3.69 (tt, 1H, *J* = 12.9, 2.7 Hz), 3.21 (m, 2H), 3.03 (ddd, 1H, *J* = 12.0, 9.5, 3.2 Hz), 2.88 (dt, 1H, *J* = 13.4, 4.4 Hz), 2.78 (dq, 1H, *J* = 14.9, 4.9 Hz), 2.61 (m, 2H), 2.50–2.18 (m, 6H), 2.12–1.15 (m, 10H), 1.90 (s, 3H, C≡CCH<sub>3</sub>), 0.45 (s, 1.5H, one diastereomer 18-CH<sub>3</sub>), 0.44 (s, 1.5H, other diastereomer 18-CH<sub>3</sub>); MS (LRFABMS) *m/z* (relative intensity) 794 (15) (*M* + 2), 793 (35) (*M* + 1), 791 (22) (*M* + 1, <sup>185</sup>Re), 615 (15), 613 (33), 581 (18), 463 (28), 461 (42), 459 (22), 309 (100), 279 (100); HRFAB calcd for C<sub>34</sub>H<sub>42</sub>N<sub>2</sub>O<sub>4</sub>S<sub>2</sub><sup>187</sup>Re (*M* + 1) 793.2144, found 793.2130.

[11β-[α-[N-[[[2-Mercaptoethyl]amino]carbonyl]-methyl]-N-(2-mercaptoethyl)amino]-*p*-tolyl]-17α-propynyl-17β-hydroxy-4,9-estradien-3-onato(4-)]oxo[<sup>99</sup>Tc]-technetium(V) (MAMA'-[<sup>99</sup>Tc]Tc(V)-Oxo-Progestin Conjugate, 6). Deprotection of the ligand system was performed in a manner similar to that described in the preparation of rhenium conjugate 5. Thus, bistirol 4 was prepared from protected compound 3 (44.6 mg, 0.41 mmol) and Hg(OAc)<sub>2</sub> (26 mg, 0.081 mmol). To the crude ligand in MeOH (2 mL) was added solid (*n*-Bu)<sub>4</sub>NTcOCl<sub>4</sub> (15 mg, 0.030 mmol) and NaOAc (0.400 mL, 1 N in MeOH). The mixture was allowed to react at room temperature for 20 min before the soluble product was isolated by filtration through Celite with EtOAc and washed with water. The organic extract was dried with MgSO<sub>4</sub> and concentrated by solvent evaporation under a stream of nitrogen. Silica gel flash chromatography (2:1 EtOAc:hexanes) provided 6 (16.6 mg, 78.3%) as a yellow solid. <sup>1</sup>H-NMR (CDCl<sub>3</sub>, 400 MHz) δ 7.39–7.30 (m, 4H, ArH), 5.81 (s, 1H, 4-CH), 5.07 (d, 1H, *J* = 14.2 Hz), 4.95 (dd, 1H, *J* = 16.1, 1.5 Hz, ArCH<sub>2</sub>), 4.63 (d, 1H, *J* = 14.2 Hz), 4.60 (dd, 1H, *J* = 10.7, 4.2 Hz), 4.48 (bd, 1H, *J* = 8 Hz, 11α-CH), 3.77 (d, 1H, *J* = 16.1 Hz, ArCH<sub>2</sub>), 3.70 (tt, 1H, *J* = 13.2, 3.2 Hz), 3.23 (m, 2H), 3.04 (ddd, 1H, *J* = 12.7, 10.3, 2.9 Hz), 2.90 (dt, 1H, *J* = 13.7, 4.4 Hz), 2.79 (dq, 1H, *J* = 14.9, 4.9 Hz), 2.62 (bm, 2H), 2.55–2.20 (m, 6H), 2.06 (dt, 1H, *J* = 12.9, 4.4), 1.95 (m, 1H), 1.91 (s, 3H, C≡CCH<sub>3</sub>), 1.81 (s, 1H), 1.74 (m, 2H), 1.65–1.18 (m, 5H), 0.46 (s, 1.5H, one diastereomer 18-CH<sub>3</sub>), 0.45 (s, 1.5H, other diastereomer 18-CH<sub>3</sub>); MS (LRFABMS) *m/z* (relative intensity) 706 (5) (*M* + 2), 705 (13) (*M* + 1), 613 (7), 463 (5), 461 (8), 406 (5), 399 (7), 391 (13); HRFAB calcd for C<sub>34</sub>H<sub>42</sub>N<sub>2</sub>O<sub>4</sub>S<sub>2</sub><sup>99</sup>Tc (*M* + 1) 705.1615, found 705.1632.

[11β-[α-[N-[[[2-Mercaptoethyl]amino]carbonyl]-methyl]-N-(2-mercaptoethyl)amino]-*p*-tolyl]-17α-propynyl-17β-hydroxy-4,9-estradien-3-onato(4-)]oxo[<sup>99m</sup>Tc]-technetium(V) (MAMA'-[<sup>99m</sup>Tc]Tc(V)-Oxo-Progestin Conjugate, 7). Water (5 mL) was added to a Glucoscan kit (200 mg glucoheptonate, 0.06 mg SnCl<sub>2</sub>·

2H<sub>2</sub>O), swirled, and allowed to stand for 10 min at room temperature. Na<sup>99m</sup>Tc(VII)O<sub>4</sub> (17.9 mCi) in saline (300 μL) was added to 500 μL of the previously prepared glucoheptonate solution, swirled, and allowed to stand for 15 min at room temperature. A solution of 11β-MAMA'-progesterin (4) (40 μg, 0.068 μmol) in EtOH (800 μL) was added to the Tc-glucoheptonate solution and stirred for 20 min at room temperature. The reaction mixture was extracted with CH<sub>2</sub>Cl<sub>2</sub> (3 × 1.5 mL), and the combined organic layers were dried over MgSO<sub>4</sub> and filtered. The solvents were removed in vacuo, and the residue was redissolved in CH<sub>2</sub>Cl<sub>2</sub> and applied to a short (2 cm) silica pipet column. The labeled progesterin was eluted from the column with CH<sub>2</sub>Cl<sub>2</sub> (2 mL) followed by 5% iPrOH/CH<sub>2</sub>Cl<sub>2</sub> (2 mL) and the solvent removed in vacuo. The residue was redissolved in 500 μL of 1/1 hexane/(5% iPrOH/CH<sub>2</sub>Cl<sub>2</sub>) and purified by normal-phase HPLC (Whatman M9, partisil 5, 9.4 mm × 50 cm), eluting with [60% (1:20 iPrOH-CH<sub>2</sub>Cl<sub>2</sub>)/40% hexanes] to provide 5.47 mCi (31%) of 11β-MAMA'-<sup>99m</sup>Tc-progesterin (7) (*t*<sub>R</sub> = 16.8 min) in a ligand-free form. This material (7) coeluted with the <sup>99</sup>Tc analog (6) by both normal phase and reversed-phase (H<sub>2</sub>O-acetonitrile gradient on C-18 silica gel) HPLC.

## RESULTS

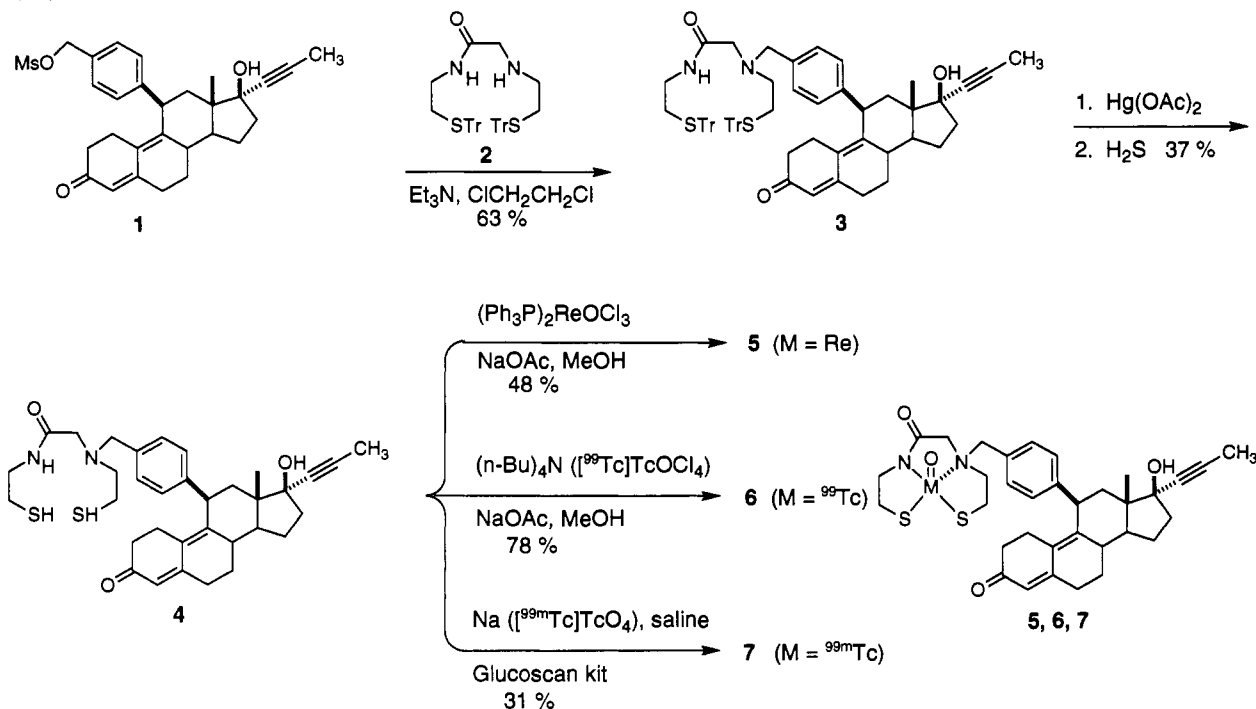
**Chemical Synthesis.** The synthesis of compounds 3–7 is shown in Scheme 1 and is described below. Each of the metal conjugates 5–7 was prepared from the same N<sub>2</sub>S<sub>2</sub> (MAMA')-progesterin conjugate (4). The progesterin conjugate 4 was prepared by N-alkylation of ligand 2 (4) with the methanesulfonate (mesylate) of the previously reported RU486 analog 1 (4), followed by removal of the triphenylmethane (trityl) sulfur-protecting groups. The metal conjugates 5 and 6, prepared at macroscopic levels, were characterized by standard analytical techniques, while the <sup>99m</sup>Tc conjugate 7, which could only be prepared at the tracer level, was identified by its coelution upon HPLC analysis with the previously characterized <sup>99</sup>Tc counterpart 6.

As was discussed in previous publications (4, 5), the insertion of a metal-oxo core into an N<sub>2</sub>S<sub>2</sub> ligand-progesterin system can result in four diastereomeric products. These are denoted as the syn and anti diastereomeric pairs, where syn and anti are defined by the orientation of the N-progesterin substituent relative to the metal-oxo bond. The syn diastereomeric pair is typically formed in far higher yield than the anti pair (4, 22); in fact, in these systems, the anti diastereomers could not be detected. All three metal-progesterin conjugates 5–7 could be isolated in ligand-free form by normal-phase HPLC, since the metal conjugates elute far ahead of the free ligand 4.

**S-Trityl-MAMA'-Progesterin (3).** The conjugate 3 was prepared by N-alkylation of the MAMA' ligand system (5) with the benzylic O-mesylate of the RU486 analog used in our previous work (4), under basic conditions provided by triethylamine. Extensive column chromatography was required to obtain analytically pure material, as the trityl protecting groups have a tendency to hydrolyze, thereby causing extensive streaking during chromatography.

**MAMA'-Progesterin (4).** S-deprotection of MAMA'-progesterin 3 was accomplished by treatment with Hg(OAc)<sub>2</sub> to displace the trityl protecting groups and form the steroidal mercury salt, followed by protonation with hydrogen sulfide (23) to provide free ligand 4. As the MAMA'-progesterin (4) is prone to disulfide formation under ambient conditions, this compound was used directly as described in the Chemical Procedures for the macroscopic preparations (conjugates 5 and 6) or was prepared

Scheme 1

**Table 1. Binding Affinity of the Progesterin-Metal Complexes and Related Ligands for the Progesterone Receptor (PR) and Glucocorticoid Receptor (GR) and Their Log *P* Values**

compd	RBA <sup>a</sup> (%)			log <i>P</i> (from <i>k'</i> <sub>w</sub> )
	PR (rat) <sup>b</sup> (R5020 = 100)	GR (rat) <sup>c</sup> (dexamethasone = 100)	PR (human) <sup>d</sup> (R5020 = 100)	
progesterone (V)	13 ± 1	1.08 ± 0.46	9 ± 3	3.87
RU486 (IV)	170 ± 5	319 ± 67	24 ± 7	4.69
ORG2058 (VII)	198 ± 39	1.98 ± 0.42	87 ± 3	4.21
R5020 (VI)	100	2.81 ± 1.60	100	4.34
FENP (VIII)	697 ± 88 <sup>e</sup>	1.42 ± 0.46	360 ± 18	4.41
BAT- <sup>99m</sup> Tc complex I (syn pair)	25 ± 1	56 ± 21	8 ± 3	6.41
BAT-Re complex I	25 ± 5 <sup>f</sup>	31 ± 8 <sup>f</sup>	5 ± 3	6.45
MAMA- <sup>99m</sup> Tc complex 6 (syn pair)	35 ± 8	100 ± 15	16 ± 3	5.25
MAMA-Re complex 5 (syn pair)	45 ± 8	117 ± 2	7.9 ± 0.1	4.90
syn A	28 ± 8	113 ± 46	not assayed	not assayed
syn B	52 ± 26	101 ± 65	not assayed	not assayed

<sup>a</sup> The receptor binding affinity is determined by a competitive radiometric binding assay. Values are the average of two or more determinations ± range (*n* = 2) or SD (*n* ≥ 3) and are expressed on a percent scale relative to the affinity of the tritium-labeled tracer (14). <sup>b</sup> Cytosol preparations were from estrogen-primed immature rat uterus, with [<sup>3</sup>H]R5020 as tracer (10). <sup>c</sup> Cytosol preparations were from saline perfused liver of 3-day adrenalectomized mature male rats with [<sup>3</sup>H]RU28362 as tracer (11). <sup>d</sup> Cytosol preparations were from human T47D breast cancer cells grown as previously described (13). <sup>e</sup> Data from ref 24. <sup>f</sup> Data from ref 4.

as a standard solution in degassed ethanol and stored at -20 °C for use in the tracer-level preparation of conjugate 7.

**MAMA'-Re-Oxo Conjugate 5.** The ReO core was inserted into the MAMA'-progesterin (4) through ligand exchange with (Ph<sub>3</sub>P)<sub>2</sub>Re(O)Cl<sub>3</sub> in basic (NaOAc) methanol. The product was purified by flash column chromatography and further examined by normal-phase HPLC. Only the syn diastereomeric pair could be detected. The two syn diastereoisomers could be partially separated by HPLC, but only at long elution times which provided broad peaks. Thus, the two syn diastereomers could be isolated for in vitro binding assays, but not on a time or quantity scale that would have been practical for in vivo biological studies.

**MAMA'-<sup>99m</sup>Tc-Oxo Conjugate 6.** The TcO core was inserted into the MAMA'-progesterin (4) through ligand exchange with an equimolar amount of (n-Bu)<sub>4</sub>N([<sup>99m</sup>Tc]TcOCl<sub>4</sub>) in basic (NaOAc) methanol. The syn diastereomeric pair was isolated by flash column chromatography

and further purified by normal-phase HPLC. No attempt was made to separate the two syn diastereomers, as their separation in the case of the rhenium conjugate 5 had proved to be a tedious task; also, previous work (4, 5) had shown that the ratio of in vitro binding affinities for the separate isomers is essentially equivalent for the Re and Tc compounds, and in our hands, the PR binding affinity of the two syn diastereomers of 5 differed by less than a factor of 2 (see below and Table 1).

**MAMA'-<sup>99m</sup>Tc-Oxo Conjugate 7.** Technetium-99m-progesterin 7 was prepared by a chelate exchange reaction with preformed <sup>99m</sup>Tc-glucoseheptonate and the MAMA'-progesterin (4) and was purified by normal-phase HPLC. Only the syn diastereomeric pair was detected, and these compounds were not separated (cf. discussion above for MAMA'-Re-progesterin 5). In order to maximize the exchange process, reaction conditions were adjusted to provide a much more dilute reaction in both aqueous medium (i.e., dilution of the Glucoscan kit), as well as organic medium (i.e., EtOH equal in volume to the aqueous

phase). Preparations were studied over a range of pH values (pH 4–11), and maximum incorporation was seen under slightly acidic conditions (pH 5), although for convenience the <sup>99m</sup>Tc–glucoheptonate obtained in kit form (pH 7) was found to provide satisfactory yields. Although the conjugate 7 was not formed as readily as the corresponding BAT–<sup>99m</sup>Tc compounds previously reported (5), the MAMA' conjugate appeared to be more stable to aqueous conditions and to concentration in vacuo than were the BAT conjugates.

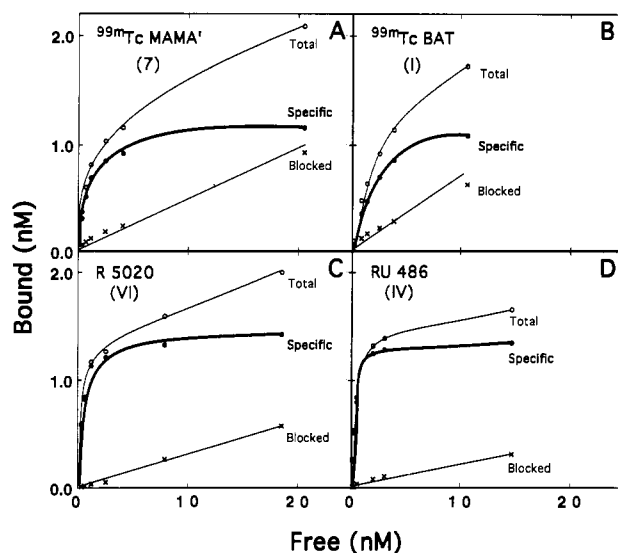
The sample of conjugate 7 used for the in vivo and in vitro studies had a radiochemical purity in excess of 95%, as determined by reversed-phase analytical HPLC. The specific activity of the preparation was estimated to be ca. 100 Ci/mmol, based on the history of the <sup>99</sup>Mo/<sup>99m</sup>Tc generator which was used (5). In vitro binding experiments were conducted with material that was diluted with the <sup>99</sup>Tc–progesterone 6 to a specific activity of 86 Ci/mmol.

**In Vitro Studies. Relative Binding Affinity of Metal/Progestin Conjugates III for the Progesterone Receptor (PR) and Glucocorticoid Receptor (GR).** The relative binding affinities (RBA) of the MAMA'–Re and –<sup>99</sup>Tc conjugates 5 and 6 as well as previously prepared BAT–Re and –<sup>99</sup>Tc conjugates (4,5) and some related compounds (cf. Scheme 1) to the progesterone receptor and the glucocorticoid receptor are shown in Table 1. The RBAs are determined by a competitive radiometric binding assay. Even though they are radioactive, the <sup>99</sup>Tc conjugates can be assayed in this competitive binding assay with a tritium-labeled tracer, using standard dual label scintillation counting methods (5); the specific activity (SA) of <sup>99</sup>Tc is low (0.0017 Ci/mmol) compared to the SA of tritiated tracer ligands (77–86 Ci/mmol), so the counts from the <sup>99</sup>Tc conjugates are appreciable only at the highest concentrations.

The RBA value of the <sup>99</sup>Tc conjugate 6 for the progesterone receptor is similar to that of the analogous unlabeled Re conjugate 5. This was observed previously with the BAT conjugates I (4) and is expected, since the Re and Tc complexes are similar in size and electron density distribution (25, 26). Both the MAMA'–Re and –<sup>99</sup>Tc conjugates assayed as syn pairs have rat PR binding affinities that are ca. three times greater than that of progesterone itself (35–45% vs 13%). When the syn diastereomers of the Re conjugate 5 are separated, one was found to have a binding affinity approximately two times greater than the other. The PR binding affinities of the MAMA' conjugates 5 and 6 for rat PR appear to be equivalent or marginally higher than those of the corresponding BAT conjugates I.

Many progestins and antiprogestins have markedly different binding affinities to the PR from different species (27–29). Almost uniformly, the compounds presented in Table 1 show lower affinity to the human PR than to rat PR (relative to R5020). The studies presented in this paper use the rat as the animal model, but the ultimate goal is to design compounds for use in humans. Therefore, binding affinity measurements in both human and rat are important.

In addition to PR, immature rat uterus contains substantial levels of glucocorticoid receptor (GR) and small levels of mineralocorticoid receptor (72% and 5%, relative to progesterone receptor = 100%) (K. E. Carlson, unpublished). All in vitro binding studies with PR included 1 μM of hydrocortisone to block these corticosteroid receptors. Since no attempt was made to block them in the in vivo tissue distribution experiments, this heterologous binding to other receptors may influence the results

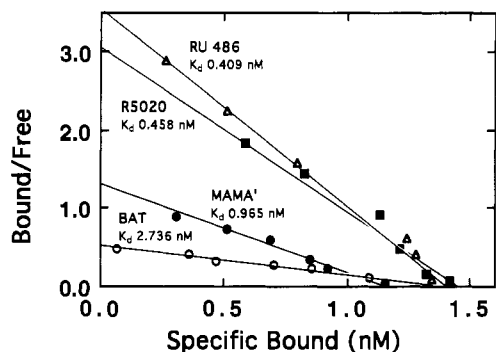


**Figure 1.** Binding curves for <sup>99m</sup>Tc–MAMA' (A), <sup>99m</sup>Tc–BAT (B), [<sup>3</sup>H]R5020 (C), and [<sup>3</sup>H]RU486 (D) in rat uterine cytosol. Shown is the total binding, the nonspecific binding (NS) (receptor blocked by 100× excess unlabeled R5020), and specific binding (difference between total and NS), after 3 h incubation at 0 °C. For comparison, the <sup>99m</sup>Tc–BAT conjugate is included, using data adapted from ref 5.

of the in vivo experiments. As shown in Table 1, the <sup>99</sup>Tc–BAT conjugates I have GR affinities comparable to their affinities for PR, while the Re– and <sup>99</sup>Tc–MAMA' conjugates 5 and 6 have GR affinities nearly three times higher than PR affinities. The GR affinities of these metal conjugates are ~10 times greater than those of the selective progesterone receptor ligands ORG2058 and R5020 but lower than that of the parent ligand, RU486.

**Lipophilicity Estimates (Log P).** Octanol/water partition coefficients (*P*), as a measure of lipophilicity, have been shown to correlate well with the nonspecific binding of steroids (30). The chromatographic method of Minick (16), to measure log *k'*<sub>w</sub>, has been found to accurately reproduce octanol/water partition values measured with the shake flask method. The regression line relating the chromatographically determined log *k'*<sub>w</sub> values of the standards to their measured log *P* values shows very high statistical reliability (15) and was extrapolated to the high log *k'*<sub>w</sub> values of the progestin conjugates, although no standards existed in this range. As shown in Table 1, the MAMA' conjugates have lower log *P* values than those of the corresponding BAT-substituted conjugates previously studied (4) and are in fact approximately 80 times less lipophilic. Unlike the BAT compounds, which show ca. 100-fold higher lipophilicities than those of simple steroidal progestins, the MAMA'–metal conjugates have log *P* values approaching those of the unsubstituted steroids themselves (V–VIII).

**Direct Binding Assays.** The direct assay of progesterone receptor binding with the tritium-labeled ligands R5020 (VI) and RU486 (IV) as well as <sup>99m</sup>Tc–MAMA'–progesterone conjugate 7 and the previously prepared <sup>99m</sup>Tc–BAT conjugate I is shown in Figure 1. All four ligands show high affinity (*K*<sub>d</sub> 0.46–2.74 nM), saturable binding to PR. The extent of nonspecific binding in this assay is evident from the slope of the “nonspecific” binding curve. The lipophilic BAT conjugate I shows the highest nonspecific binding, as was expected, since nonspecific binding typically correlates with lipophilicity. The nonspecific binding of the MAMA' conjugate is somewhat less, being more comparable to that of R5020.



**Figure 2.** Data shown in Figure 1 converted to Scatchard plots, showing  $K_d$  values for RU486 = 0.409 nM, R5020 = 0.458 nM,  $^{99m}\text{Tc}$ -MAMA' = 0.965 nM, and  $^{99m}\text{Tc}$ -BAT = 2.736 nM.

When the binding data are expressed as Scatchard plots (Figure 2), it is clear that the metal conjugates bind to nearly the same number of sites as do R5020 and RU486, consistent with their binding only to PR (glucocorticoid receptor was blocked with hydrocortisone). The small differences observed in site concentration for the MAMA' conjugate could be due to uncertainties in the estimated specific activities of the radioactive metals. The  $K_d$  for [ $^3\text{H}$ ]R5020 in these assays is 0.46 nM, while the  $K_d$  for  $^{99m}\text{Tc}$ -MAMA' conjugate 6 is 0.97 nM. The ratio of the dissociation constants for the metal conjugate vs R5020 ( $K_d(\text{R5020})/K_d(\text{conjugate})$ ) is analogous to an RBA value. For the  $^{99m}\text{Tc}$  conjugate, this ratio is 47%, very close to the RBA value of  $35\% \pm 8$  (Table 1). The concordance of  $K_d$  ratios with RBA values for metal conjugates is particularly significant, as it verifies that the RBA values obtained in the competitive binding assay (with  $^{99}\text{Tc}$  and unlabeled Re) are those of the intact metal conjugates and not the decomplexed steroid.

**In Vivo Tissue Distribution of  $^{99m}\text{Tc}$  Conjugate 7.** Tissue uptake studies were performed in immature female Sprague-Dawley rats, 21–25 days old, that were primed with estradiol to increase their uterine titer of PR (5, 10). The rats were injected IV (tail vein) with the radiopharmaceutical, and the uptake in various tissues was determined at the times indicated in Tables 2 and 3. Some rats were coinjected with a large dose (18  $\mu\text{g}$ ) of ORG2058 (RBA = 198% relative to R5020) to block PR sites. ORG2058 is one of the most selective ligands for PR (cf. Table 1); it should not block other receptors (glucocorticoid, mineralocorticoid) present in the rat tissues (11, 29). The tissue uptake data are presented as percent of injected dose per gram tissue (% ID/g) in Tables 2 and 3. Some of these data are shown in Figures 3–6.

The principal target organ for these radiolabeled progestins is the uterus, and there is substantial uterine uptake for the MAMA'- $^{99m}\text{Tc}$  conjugate (Table 2 and Figure 3). There is also high uptake in the nontarget organs (liver and kidney) involved in the metabolism and excretion of steroids. However, binding to GR may also account for some of the uptake into these organs, as they are rich in this receptor (29, 31–33). Fat also shows high uptake, suggesting that the nonspecific uptake may still be dominated by the lipophilicity of these metal conjugates. Nevertheless, the uptake in the uterus is higher than that in a nontarget tissue such as muscle, and the uterus to muscle ratio after 6 and 18 h is 4.1 and 2.9, respectively (Figure 4); uterus to blood ratios peak earlier, at 3 h, at even higher ratios.

When PR is blocked in vivo by coinjection of a large dose of ORG2058 (see Table 3 and Figure 5), only the uterus shows a significant decrease in uptake (55%, 60%,

and 71% at 1, 3, and 6 h, respectively), suggesting that the uterine uptake is PR-mediated. In this blocking experiment, the statistical significance of the changes in the various tissues was calculated by student's T-test (34),  $n = 5$ ; only the change in uterine activity is statistically significant at the 99% confidence level ( $0.01 > p > 0.001$ ) (cf. Figure 5). Thus, it appears that we are observing PR-mediated uptake of conjugate 7 in the uterus, as ORG2058 blocks PR, but is unlikely to block GR. The uterine uptake of the conjugate which cannot be blocked by ORG2058, however, might be due to its binding to GR, since the conjugate has substantial affinity for this receptor.

In order to make a critical evaluation of the chemical structure components affecting the animal uptake, we also conducted uptake studies using [ $^3\text{H}$ ]RU486, which is the parent ligand for both the BAT and MAMA' conjugates. The biodistribution of [ $^3\text{H}$ ]RU486 is presented in Table 4; its comparison with the two  $^{99m}\text{Tc}$  systems at 3 h is shown in Figure 6. The efficiency of ovarian and uterine uptake of [ $^3\text{H}$ ]RU486 was 2.7–4.3 times as great as that of the  $^{99m}\text{Tc}$ -MAMA' conjugate at 3 h ( $p < 0.05$ ). However, its uptake specificity (percent of uptake that can be blocked) is only marginally greater: 86% vs 60% at 3 h, respectively. Both of these properties are likely to be related to the binding affinity of the ligand to PR: RU486 has a 4.8 times greater affinity than the  $\text{Tc}$ -MAMA' complex. The  $^{99m}\text{Tc}$ -MAMA' is retained longer in the target tissues than is RU486: at 6 h, 35% of the initial  $^{99m}\text{Tc}$  MAMA' uptake remains in the uterus, while only 18% of the RU486 uptake remains. A slow clearance from the target tissues is a desirable characteristic for ligands designed for imaging (30).

Perhaps the best overall comparison among the three compounds can be seen at the 3 h time point shown in Figure 6. Here, the higher level of uterine uptake by RU486 and the improved uterus to muscle uptake ratio are evident. Liver and fat uptake of RU486, however, are still high and comparable to those of the two conjugates, suggesting that the progestin portion of the conjugate is mainly responsible for this uptake, not the metal chelate. A comparison between the two  $^{99m}\text{Tc}$  conjugates (MAMA' 7 and BAT I) at 3 h is also seen in Figure 6; the uterine uptake by the BAT conjugate is greater, as is its uterine to blood ratio, but relative to muscle and fat, uterine uptake is the same as for the MAMA' complex. The fraction of uterine activity displaced by ORG2058 is somewhat greater for the MAMA' 7 (70% at 6 h) compared to BAT I (63% at 6 h), but this difference is not statistically significant. It is notable that all three of the PR ligands show uterine uptake that is lower and less selective than 21-fluoro-16 $\alpha$ -ethyl-19-norprogesterone (FENP), where 1 h % ID/g levels are as follows: uterus, 6.43; muscle, 0.42; blood, 0.25; fat, 3.56; and liver, 3.34 (24).

**Metabolism Studies.** The in vivo stability of the  $^{99m}\text{Tc}$ -MAMA'-progestin conjugate 7 was investigated in immature rats. At various times after injection, blood and tissues were extracted with ethanol and the soluble activity analyzed by thin-layer chromatography to determine the percent activity that is unmetabolized. Correction is made for the extraction efficiency of the  $^{99m}\text{Tc}$ -MAMA'-progestin conjugate 7, and the results are shown graphically in Figure 7.

As has been noted with other receptor-binding radiopharmaceuticals (15, 19), the activity in the target tissue remains largely the administered compound, even out to 4 h, as receptor sequesters the tracer and prevents its metabolism. In contrast, even at the earliest time (1 h), liver activity is almost exclusively due to metabolites, while

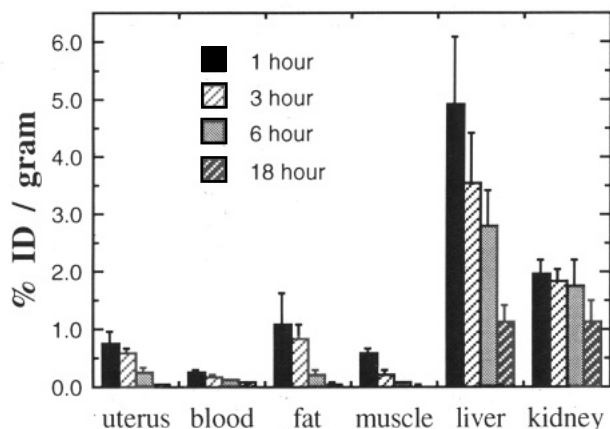


**Table 2. Biodistribution Data for 11 $\beta$ -MAMA'-<sup>99m</sup>Tc-Progesterin 7 at 1, 3, 6, and 18 h (% ID/g)<sup>a</sup>**

tissue	% ID/g $\pm$ SD (n = 10)			% ID/g $\pm$ SD (n = 5)
	1 h	3 h	6 h	18 h
blood	0.245 $\pm$ 0.027	0.155 $\pm$ 0.039	0.109 $\pm$ 0.021	0.073 $\pm$ 0.017
lung	0.655 $\pm$ 0.078	0.300 $\pm$ 0.046	0.166 $\pm$ 0.032	0.056 $\pm$ 0.010
liver	4.906 $\pm$ 1.190	3.528 $\pm$ 0.883	2.797 $\pm$ 0.640	1.140 $\pm$ 0.267
kidney	1.963 $\pm$ 0.259	1.830 $\pm$ 0.194	1.751 $\pm$ 0.475	1.108 $\pm$ 0.399
muscle	0.586 $\pm$ 0.088	0.226 $\pm$ 0.070	0.066 $\pm$ 0.019	0.016 $\pm$ 0.007
fat	1.094 $\pm$ 0.525	0.817 $\pm$ 0.270	0.203 $\pm$ 0.104	0.036 $\pm$ 0.030
uterus	0.753 $\pm$ 0.217	0.591 $\pm$ 0.082	0.266 $\pm$ 0.049	0.046 $\pm$ 0.014
ovaries	0.674 $\pm$ 0.181	0.535 $\pm$ 0.213	0.161 $\pm$ 0.063	0.041 $\pm$ 0.013
uterus/muscle	1.282 $\pm$ 0.364	2.680 $\pm$ 0.669	4.115 $\pm$ 0.808	2.875 $\pm$ 0.532
uterus/blood	3.166 $\pm$ 0.736	5.006 $\pm$ 1.111	2.529 $\pm$ 0.384	0.630 $\pm$ 0.241

<sup>a</sup> % ID/g: percent injected dose/gram tissue.**Table 3. Biodistribution Data for 11 $\beta$ -MAMA'-<sup>99m</sup>Tc-Progesterin 7 at 1, 3, and 6 h (% ID/g)<sup>a</sup>**

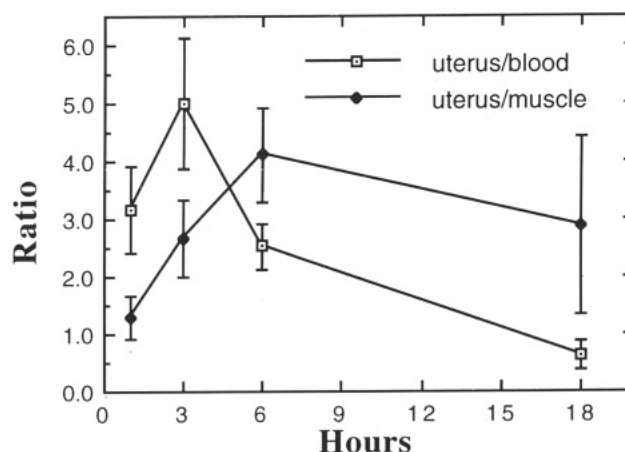
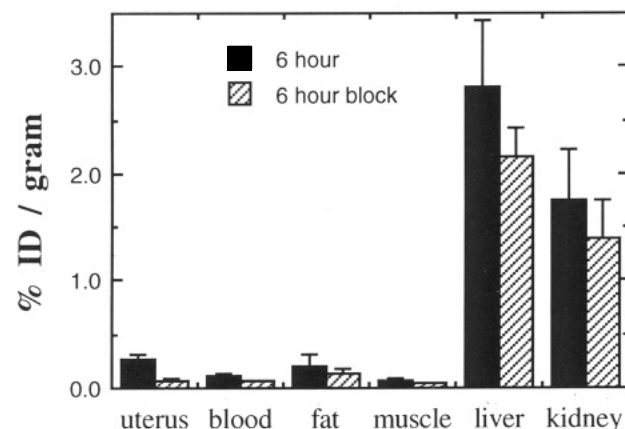
tissue	% ID/g $\pm$ SD (n = 10)		
	1 h (block)	3 h (block)	6 h (block)
blood	0.145 $\pm$ 0.031	0.098 $\pm$ 0.019	0.070 $\pm$ 0.006
lung	0.479 $\pm$ 0.145	0.209 $\pm$ 0.058	0.097 $\pm$ 0.016
liver	3.509 $\pm$ 0.806	3.021 $\pm$ 0.547	2.161 $\pm$ 0.260
kidney	1.453 $\pm$ 0.305	1.362 $\pm$ 0.289	1.394 $\pm$ 0.352
muscle	0.450 $\pm$ 0.116	0.214 $\pm$ 0.140	0.040 $\pm$ 0.012
fat	0.747 $\pm$ 0.173	0.438 $\pm$ 0.074	0.125 $\pm$ 0.046
uterus	0.339 $\pm$ 0.091	0.234 $\pm$ 0.019	0.076 $\pm$ 0.018
ovaries	0.461 $\pm$ 0.126	0.210 $\pm$ 0.028	0.077 $\pm$ 0.018
uterus/muscle	0.753 $\pm$ 0.280	1.093 $\pm$ 0.721	1.900 $\pm$ 0.726
uterus/blood	2.338 $\pm$ 0.802	2.388 $\pm$ 0.502	1.086 $\pm$ 0.274

<sup>a</sup> The rats used in these experiments were each coinjected with 18  $\mu$ g of ORG2058 (block). % ID/g: percent injected dose/gram tissue.**Figure 3.** Biodistribution of <sup>99m</sup>Tc-progesterin 7 in immature estrogen-primed female rats presented as percent injected dose/gram ( $\pm$ SD) of tissue at 1, 3, 6, and 18 h following injection. Data are taken from Table 2 and are decay corrected.

in the kidney and blood, the percent that is unmetabolized declines rather slowly from an initial value of 50%. This time course and pattern of metabolism is similar to that of the BAT conjugates (4).

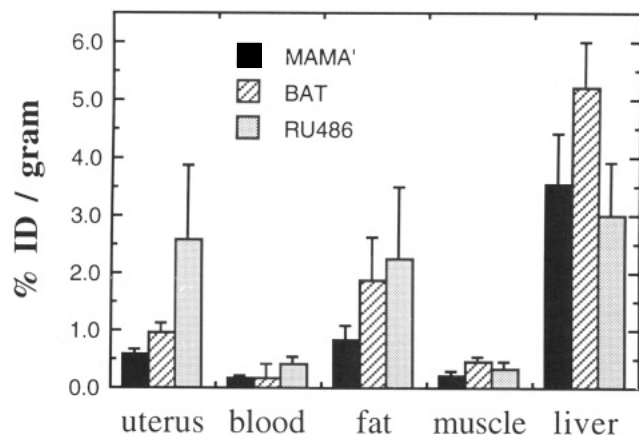
## DISCUSSION

In this paper, we describe the synthesis and evaluation of a new conjugate between a progestin with high affinity for the progesterone receptor (PR) and a new metal complex (MAMA'). This conjugate represents an extension of our recent work in which we described the preparation of the first receptor ligand labeled with technetium-99m that retains nanomolar receptor binding affinity (4, 5). While this first system, a progestin-<sup>99m</sup>Tc-BAT conjugate, displayed high receptor affinity, its nonspecific binding was high and its tissue distribution in

**Figure 4.** Time course of the change in the ratio ( $\pm$ SD) of target (uterus) to nontarget (blood or muscle) tissue uptake for <sup>99m</sup>Tc-progesterin 7. Data are taken from Table 2 and are decay corrected.**Figure 5.** Uptake of <sup>99m</sup>Tc-progesterin 7 at 6 h when unblocked or when the PR has been blocked by an excess of Org 2058, presented as percent injected dose/gram tissue ( $\pm$ SD). Data are taken from Tables 2 and 3.

vivo was not sufficiently selective for target tissues to be useful for imaging human breast tumors based on their content of steroid receptors (4, 5).

Because the BAT-metal conjugate system is very hydrophobic, we suspected that the high lipophilicity of this complex, which has an octanol-water partition coefficient nearly 100-fold higher than that of typical progestins, might be the principal reason for its reduced uptake selectivity. The progestin-MAMA'-metal conjugate described here is our first attempt to effect a substantial reduction in the lipophilicity of these progestin metal conjugate systems. Relative to the BAT chelate, the MAMA' system has four fewer methyl groups and has a carbonyl function in place of one methylene group.



**Figure 6.** Comparison of the biodistribution at 3 h of  $^{99m}\text{Tc}$ -MAMA' 7,  $^{99m}\text{Tc}$ -BAT I (taken from ref 5), and  $^3\text{H}$ RU486 (IV). Data presented as percent injected dose/gram tissue ( $\pm$ SD).

In a recent publication, we have described the preparation of the basic MAMA'-rhenium and -technetium chelates, and we have presented a detailed spectroscopic and structural analysis of both the syn and anti diastereomers of a simple *N*-benzyl derivative (6). This MAMA' system has many features similar to those of other conjugates of the well-studied  $\text{N}_2\text{S}_2$  class (7, 8). The preparation of the corresponding progestin-MAMA' conjugate proceeded in an analogous fashion to the preparation of the BAT conjugate and presented no particular difficulties, and the rhenium and technetium-99, and -99m conjugates could be readily prepared and purified. With the MAMA' conjugates, the syn diastereomers predominated over the anti to an even greater extent than with the BAT conjugates, so that only the syn isomers could be isolated and characterized.

The progestin-MAMA'-metal conjugates 5 and 6 have affinities for PR that are three to four times greater than the natural ligand (progesterone) for this receptor, as was also true for the progestin-BAT-metal conjugates I. With both of these systems, it is remarkable that a steroid conjugated to a metal complex of nearly equal size can retain such high affinity for receptor. It should be noted, however, that the affinity of these conjugates is lower than that of the synthetic ligands R5020, RU486, and ORG2058, a fact that may contribute to the moderate level of their receptor-mediated tissue distribution.

Both in the BAT and the MAMA' series, there is a significant reduction in affinity for human PR vs rat PR, relative to the tracer R5020. This is also true for progesterone and the synthetic ligands ORG2058 and RU486. Such species-dependent differences in PR ligand binding affinity and selectivity is well known (27-29), but the reason is unclear. The cDNA-deduced amino acid sequences for the rat and human PR ligand binding domains are 88-96% similar (35, 36); on the other hand, it is known that even a single amino acid change in PR can result in a profound alteration in ligand binding specificity (37).

There is considerable sequence homology between the hormone binding domains of PR and GR (38), and these two receptors (together with the mineralocorticoid and androgen receptors) are considered to be within the same evolutionary family (39). This sequence/structural similarity is reflected in the tendency of ligands for these receptors to exhibit considerable "receptor cross-talk" or "heterologous binding" (40, 41). In fact, the synthetic progestins R5020 and ORG2058 are useful as selective tracers for PR in *in vitro* binding assays because of their

high selectivity for PR vs GR, but this characteristic is not shared by most ligands with  $11\beta$  substituents, such as RU486 (28, 42). Both the BAT- and MAMA'-metal-progestin conjugates also demonstrate considerable binding affinity for the GR. This too may be a factor compromising the selectivity of their *in vivo* distribution.

One of our principal intents in developing the MAMA'-progestin conjugates was to create a system that would be similar to the BAT conjugates, but would have lower lipophilicity. We hoped that substitution of the MAMA' for the BAT-metal chelate would accomplish this without compromising the high PR binding affinity of the BAT conjugates. This was, in fact, borne out by experiment, where as expected, the MAMA' conjugates have octanol-water partition coefficients nearly 100-fold lower than those of the BAT systems, now being within the range that is typical for high affinity ligands for PR. This was achieved without a decrease in affinity for PR.

The *in vivo* tissue distribution of the progestin- $^{99m}\text{Tc}$ -MAMA' conjugate was quite similar to that of the corresponding BAT complex. Displaceable (receptor-mediated) uptake was only observed in the principal target tissue the uterus, and activity in this tissue was greater than in blood or muscle, but fat uptake and activity in liver and kidney was very high. The 80-fold lower lipophilicity of the MAMA' conjugate is not reflected in a dramatic way in its uptake behavior relative to the BAT complex: the uptake of the MAMA' conjugate into fat is only half that of the BAT complex, but the uterine uptake is also reduced by a similar fraction.

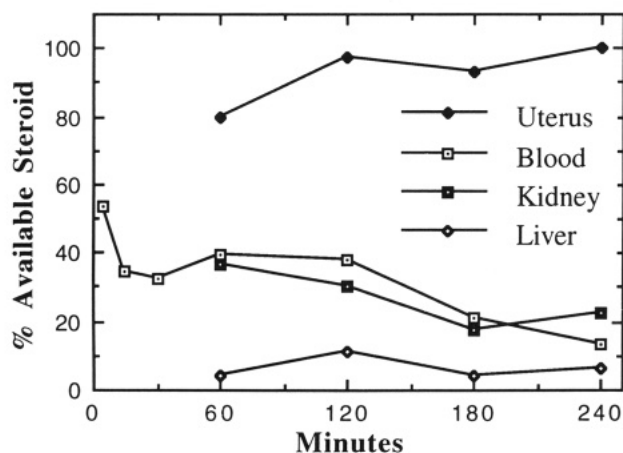
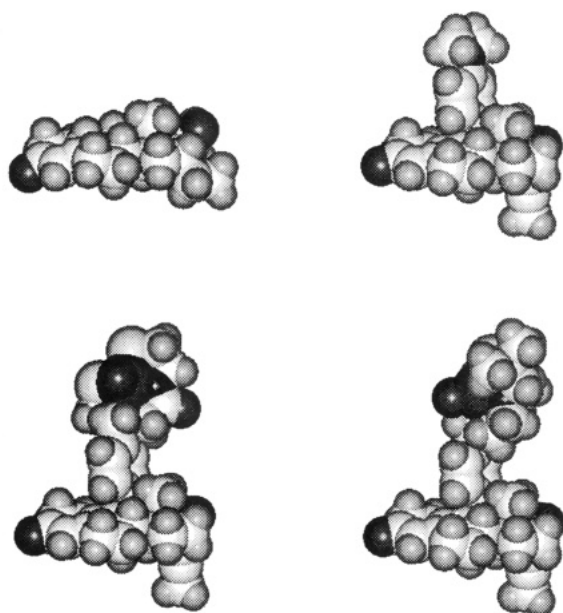
It is instructive to make a comparison of the tissue distribution of the BAT- and MAMA'-progestin conjugates with that of RU486 and other labeled progestins that we have studied earlier (19, 24, 43). As a class, the progestins tend to have lower target tissue uptake than, for example, the estrogens, and their uptake by fat and tissues involved in metabolism and clearance (liver and kidney) is relatively high. Nevertheless, the BAT- and MAMA'-metal conjugates have target tissue uptake efficiency and selectivity at the low end of all the compounds we have studied. The role that lipophilicity plays in uptake behavior as evidenced with the BAT and MAMA' conjugates does not seem to be a dominant one. The possibility that elevated liver uptake is due to their binding by GR in this tissue is unlikely, since metabolism studies on the two conjugates have shown that most of the activity in the liver is due to metabolites. Also, RU486, which has very high affinity for GR, does not show liver uptake that is very much greater than that of other PR tracers such as ORG2058, R5020, and FENP, which all have very low GR affinity. In fact, in other studies we have found that even tracers with very high GR binding affinity fail to show substantial receptor-mediated uptake by GR target tissues (44), indicating that the GR system itself may be poorly suited for selective ligand accumulation.

Two other factors that may account for the uptake behavior of the metal conjugates are receptor binding affinity and overall molecular size. Even though the BAT and MAMA' conjugates have nanomolar binding affinity for PR, exceeding that of progesterone several fold, their affinity for PR may still be too low to result in desirable distribution behavior. The affinity of progesterone itself is insufficient for target tissue uptake and retention, and it may be that affinities approaching those of FENP, ORG2058, and R5020 may be required. In fact, most progestins of moderate affinity for PR that we have studied have relatively poor target tissue uptake (5, 43, 45).

**Table 4.** Biodistribution Data for <sup>3</sup>H-RU486 at 1, 3, and 6 h (% ID/g)<sup>a</sup>

	tissue	% ID/g ± SD (n = 3)			
		1 h	3 h	6 h	3 h (block)
1	blood	0.550 ± 0.080	0.410 ± 0.140	0.390 ± 0.130	0.230 ± 0.100
2	lung	0.980 ± 0.360	0.440 ± 0.170	0.240 ± 0.040	0.190 ± 0.030
3	liver	5.240 ± 0.960	3.020 ± 0.890	1.140 ± 0.040	1.130 ± 0.230
4	spleen	0.820 ± 0.160	0.350 ± 0.130	0.210 ± 0.060	0.170 ± 0.030
5	muscle	0.940 ± 0.200	0.350 ± 0.100	0.190 ± 0.010	0.200 ± 0.070
6	fat	4.000 ± 1.600	2.270 ± 1.250	1.220 ± 0.200	1.570 ± 0.250
7	uterus	3.030 ± 1.670	2.570 ± 1.300	0.570 ± 0.160	0.360 ± 0.110
8	ovaries	2.940 ± 0.680	1.450 ± 0.600	0.520 ± 0.030	0.540 ± 0.140
9	uterus/muscle	3.223 ± 1.904	7.534 ± 4.377	3.000 ± 0.857	1.800 ± 0.836
10	uterus/blood	5.509 ± 0.582	6.268 ± 3.825	1.462 ± 0.637	1.565 ± 0.832

<sup>a</sup> One set of animals at 3 h was coinjected with 18 µg of ORG2058 (block). % ID/g: percent injected dose/gram tissue.

**Figure 7.** Metabolism of <sup>99m</sup>Tc progestin 7 in uterus and nontarget tissues, blood, kidney, and liver.**Figure 8.** Size comparison of FENP (upper left), RU486 (upper right), <sup>99m</sup>Tc-BAT I (lower left), and <sup>99m</sup>Tc-MAMA' 7 (lower right) using space-filling representations (46).

Finally, the issue of molecular size may be involved: The BAT and MAMA' conjugates as ligands for PR are nearly twice the size of a typical steroid, such as FENP, as shown in Figure 8. Differences in their transport and tissue permeability may compromise their target tissue uptake in ways that may not be apparent from a study of only steroid-sized ligands. The fact that RU486, which is a PR ligand midway in size between R5020 and the metal complex, has a target tissue uptake efficiency and selec-

tivity that is also intermediate between that of the steroids and the metal conjugates, suggests that the size of the tracer may be important.

In this study, we have determined that lipophilicity and heterologous binding to other receptors may be less important factors in tissue uptake than previously thought and the issues of overall molecular size and PR binding affinity more important. Our future investigations on technetium-labeled ligands for steroid receptors will address these considerations.

#### ACKNOWLEDGMENT

We are grateful for support of this research through grants from the Department of Energy (DE FG02 86ER60401 to J.A.K. and DE FG02 84ER60218 to M.J.W.). J.P.O. was partially supported through an NIH training fellowship (5T32CA09067). NMR spectra at 400 MHz and mass spectra were obtained on instruments supported by the National Science Foundation (CHE 90-01438EQ) and by the National Institutes of Health (GM27029, respectively). We wish to thank Donald Seielstad for insightful conversation regarding steroid receptor structure and Drs. James DiZio and Henry VanBrocklin for helpful discussions and assistance in the preparation of steroidal precursors. We also wish to thank Pam Roque and Henry Lee for their competent aid with the in vivo experiments and especially Tammy Pajean-Stinson for undertaking the biodistribution study of [<sup>3</sup>H]RU486.

#### LITERATURE CITED

- (1) Steigman, J., and Eckelman, W. C. (1992) *The Chemistry of Technetium in Medicine*, National Academy Press, Washington D.C. (b) *Technetium and Rhenium in Chemistry and Nuclear Medicine* (M. Nicolini, G. Bandoli, and U. Mazzi, Eds.) Vol. 3, pp 369-374, Raven Press, New York.
- (2) Lever, S. Z., and Wagner, H. M. (1990) The status and future of technetium-99m radiopharmaceuticals. In *Technetium and Rhenium in Chemistry and Nuclear Medicine* (M. Nicolini, G. Bandoli, and U. Mazzi, Eds.) Vol. 3, pp 648-659, Raven Press, New York.
- (3) Wenzel, M. (1992) Tc-99m-Markierung von Cymantren analogen Verbindungen mit verschiedenen Substituenten - Ein neuer Zugang zu Tc-99m Radiodiagnostika. (Technetium-99m labeling of cymantrene analogs with various substituents. A new preparation of technetium-99m radiodiagnostics). *J. Labelled Compound Radiopharm.* 31, 641-650.
- (4) DiZio, J. P., Fiaschi, R., Davison, A., and Katzenellenbogen, J. A. (1991) Progestin-rhenium complexes: Metal-labeled steroids with high receptor binding affinity, potential receptor-director agents for diagnostic imaging or therapy. *Bioconjugate Chem.* 2, 353-366.
- (5) DiZio, J. P., Anderson, C. J., Davison, A., Ehrhardt, G. J., Carlson, K. E., Welch, M. J., and Katzenellenbogen, J. A. (1992) Technetium- and rhenium-labeled progestins: synthesis, receptor binding and in vivo distribution of an 11β-substituted

- progesterin labeled with technetium-99 and rhenium-186. *J. Nucl. Med.* 33, 558-569.
- (6) O'Neill, J. P., Wilson, S. R., and Katzenellenbogen, J. A. (1994) Preparation and structural characterization of a monoamine-monoamide bithiol metal oxo complex with technetium(V) and rhenium(V). *Inorg. Chem.* 33, 319-323.
  - (7) Gustavson, L. M., Rao, T. N., Jones, D. S., Fritzberg, A. R., Srinivasan, A. (1991) Synthesis of a new class of Tc chelating agents:  $N_2S_2$  monoaminemonoamide (MAMA) ligands. *Tetrahedron Lett.* 32, 5485-5488.
  - (8) Rao, T. N., Gustavson, L. M., Srinivasan, A., Kasina, S., Fritzberg, A. R. (1992) Kinetics and mechanism of reactions of S-protected dithiol monoaminemonoamide (MAMA) ligands with technetium: Characterization of a technetium-thiolate-thioether-MAMA complex, a kinetic intermediate of the reaction. *Nucl. Med. Biol.* 19, 889-895.
  - (9) A preliminary account of this work was presented: O'Neill, J. P., Anderson, C. J., Carlson, K. E., Welch, M. J., and Katzenellenbogen, J. A. (1993) An Improved Progesterin-Techetium Complex as a Potential Imaging Agent for Steroid Receptors. *J. Nucl. Med.* 34, 18.
  - (10) Brandes, S. J., and Katzenellenbogen, J. A. (1987) Fluorinated androgens and progestins: molecular probes for androgen and progesterone receptors with potential use in positron emission tomography. *Molec. Pharmacol.* 32, 391-403.
  - (11) Pinney, K. G., Carlson, K. E., and Katzenellenbogen, J. A. (1990) [ $^3H$ ]DU41165: a high affinity ligand and novel photoaffinity labeling reagent for the progesterone receptor. *J. Steroid Biochem.* 35, 179-189.
  - (12) Carlson, K. E., Coppey, M., Magdelenat, H., and Katzenellenbogen, J. A. (1989) Receptor binding of NBD-labeled fluorescent estrogens and progestins in whole cells and cell-free preparations. *J. Steroid Biochem.* 32, 345-355.
  - (13) Eckert, R. L., and Katzenellenbogen, B. S. (1983) Modulation of progesterin binding activity in cultured human breast carcinoma cells: The effect of serum type and concentration. *J. Receptor Res.* 3, 599-621.
  - (14) Katzenellenbogen, J. A., Johnson, H. J., and Myers, H. N. (1973) Photoaffinity labels for estrogen binding proteins of rat uterus. *Biochemistry* 12, 4085-4092.
  - (15) Pomper, M. G., VanBrocklin, H. F., Thieme, A. M., Thomas, R. D., Kiesewetter, D. O., Carlson, K. E., Mathias, C. J., Welch, M. J., and Katzenellenbogen, J. A. (1990) 11 $\beta$ -methoxy-, 11 $\beta$ -ethyl- and 17 $\alpha$ -ethynyl-substituted 16 $\alpha$ -fluoroestradiols: Receptor-based imaging agents with enhanced uptake efficiency and selectivity. *J. Med. Chem.* 133, 3143-3155.
  - (16) Minick, D. J., Frenz, J. H., Patrick, M. A., and Brent, D. A. (1988) A comprehensive method for determining hydrophobicity constants by reversed-phase high-performance liquid chromatography. *J. Med. Chem.* 31, 1923-1933.
  - (17) Scatchard, G. (1949) The attractions of proteins for small molecules and ions. *Ann. N.Y. Acad. Sci.* 51, 660-672.
  - (18) Katzenellenbogen, J. A., McElvany, K. D., Senderoff, S. G., Carlson, K. E., Landvatter, S. W., and Welch, M. J. (1982) 16 $\alpha$ -[ $^{77}Br$ ]-Bromo-11 $\beta$ -methoxyestradiol-17 $\beta$ . A gamma-emitting estrogen imaging agent with high uptake and retention by target organs. *J. Nucl. Med.* 23, 411-419.
  - (19) Carlson, K. E., Brandes, S. J., Pomper, M. G., and Katzenellenbogen, J. A. (1988) Uptake of three [ $^3H$ ]Progestins by target tissues in vivo: Implications for the design of diagnostic imaging agents. *Nucl. Med. Biol.* 15, 403-408.
  - (20) Mathias, C. J., Welch, M. J., Katzenellenbogen, J. A., Brodack, J. W., Kilbourn, M. R., Carlson, K. E., and Kiesewetter, D. O. (1987) Characterization of the uptake of 16 $\alpha$ -([ $^{18}F$ ]-fluoro)-17 $\beta$ -estradiol in DMBA-induced mammary tumors. *Nucl. Med. Biol.* 14, 15-25.
  - (21) Still, W. C., Kahn, M., and Mitra, A. (1978) Rapid chromatographic technique for preparative separations with moderate resolution. *J. Org. Chem.* 43, 2923-2925.
  - (22) Baidoo, K. E., and Lever, S. Z. (1990) Evaluation of a diaminedithiol-based bifunctional chelate for labeling small molecules with  $^{99m}Tc$ . In *Technetium and Rhenium in Chemistry and Nuclear Medicine* (M. Nicolini, G. Bandoli, and U. Mazzi, Eds.) Vol. 3, pp 369-374, Raven Press, New York.
  - (23) Hiskey, R. G., Tomishige, M., and Igets, H. (1966) Sulfur-containing polypeptides. II. Selective removal of S-protective groups from some l-cysteinyl-l-cysteine derivatives. *J. Org. Chem.* 31, 1188-1192.
  - (24) Pomper, M. G., Katzenellenbogen, J. A., Welch, M. J., Brodack, J. W., and Mathias, C. J. (1988) 21-[ $^{18}F$ ]Fluoro-16 $\alpha$ -ethyl-19-norprogesterone: synthesis and target tissue selective uptake of a progesterin receptor based radiotracer for positron emission tomography. *J. Med. Chem.* 31, 1360-1363.
  - (25) Deutsch, E., Lisbon, K., Vanderheyden, J.-L., Ketring, A. R., and Maxon, H. R. (1986) The chemistry of rhenium and technetium as related to the use of isotopes of these elements in therapeutic and diagnostic nuclear medicine. *Nucl. Med. Biol.* 13, 465-477.
  - (26) Deutsch, E., Lisbon, L., and Vanderheyden, J. L. (1990) The inorganic chemistry technetium and rhenium as relevant to nuclear medicine. In *Technetium and Rhenium in Chemistry and Nuclear Medicine* (M. Nicolini, G. Bandoli, and U. Mazzi, Eds.) Vol. 3, pp 13-22, Raven Press, New York.
  - (27) Ojasso, T., Dore, J.-C., Gilbert, J., and Raynaud, J.-P. (1988) Binding of steroids to the progesterin and glucocorticoid receptors analyzed by correspondence analysis. *J. Med. Chem.* 31, 1160-1169.
  - (28) Garcia, T., Benhamou, B., Goffio, D., Vergez, A., Philibert, D., Chambon, P., and Gronemeyer, H. (1992) Switching agonistic, antagonistic, and mixed transcriptional responses to 11 $\beta$ -substituted progestins by mutation of the progesterone receptor. *Molec. Endocrinol.* 6, 2071-2078.
  - (29) Heubner, A., Pollow, K., Manz, B., Grill, H. J., and Belovsky, O. (1985)  $^3H$ -labelled RU38486: characterization of binding sites in human uterine cytosol. *J. Clin. Chem. Clin. Biochem.* 23, 265-276.
  - (30) Katzenellenbogen, J. A., Heiman, D. F., Carlson, K. E., and Lloyd, J. E. (1982) In vivo and in vitro steroid receptor assays in the design of estrogen radiopharmaceuticals. In *Receptor Binding Radiotracers* (W. C. Eckelman, Ed.) Vol. 1, pp 93-126, Chemical Rubber Co., Boca Raton.
  - (31) Manz, B., Grill, H.-J., and Pollow, K. (1982) Steroid side-chain modification and receptor affinity: binding of synthetic derivatives of corticoids to human spleen tumor and rat liver glucocorticoid receptors. *J. Steroid Biochem.* 17, 335-342.
  - (32) Sheppard, K. E., and Funder, J. W. (1987) Equivalent affinity of aldosterone and corticosterone for type I receptors in kidney and hippocampus: direct binding studies. *J. Steroid Biochem.* 28, 737-742.
  - (33) Pomper, M. G. (1989) Fluorine-18 labeled estrogens, progestins and corticosteroids for receptor-based imaging of breast tumors and target areas of the brain. Ph.D. thesis, University of Illinois.
  - (34) Swinscow, T. D. V. (1980) The T-tests. In *Studies at Square One*, pp 33-42, Mendip Press, Bath.
  - (35) Misrahi, R., Atger, M., D'Auriol, L., Loosfelt, H., Meriel, C., Fridlansky, F., Gwochon-Mantel, A., Galibert, F., and Milgrom, E. (1987) Complete amino acid sequence of the human progesterone receptor deduced from cloned cDNA. *Biochem. Biophys. Res. Commun.* 143, 740-748.
  - (36) Park, O.-K., and May, K. E. (1991) Transient expression of progesterone receptor messenger RNA in ovarian granulosa cells after the preovulatory luteinizing hormone surge. *Mol. Endocrinol.* 5, 967-978.
  - (37) Benhamou, B., Garcia, T., Lerouge, T., Vergez, A., Goffio, D., Bigogne, C., Chambon, P., and Gronemeyer, H. (1992) A single amino acid that determines the sensitivity of progesterone receptors to RU486. *Science* 255, 206-209.
  - (38) Carlstedt-Duke, J., Strömstedt, P.-E., Persson, B., Cederlund, E., Gustafsson, J.-A., and Jörnvall, H. (1988) Identification of hormone-interacting amino acid residues within the steroid-binding domain of the glucocorticoid receptor in relation to other steroid hormone receptors. *J. Biol. Chem.* 263, 6842-6846.
  - (39) Evans, R. M. (1988) The steroid and thyroid hormone receptor superfamily. *Science* 240, 889-894.
  - (40) Ojasoo, T., and Raynaud, J. P. (1978) Unique steroid congeners for receptor studies. *Cancer Res.* 38, 4186-4198.

- (41) Teutsch, G., Gaillard-Moguilewsky, M., Lemoine, G., Nique, F., and Philibert, D. (1991) Design of ligands for the glucocorticoid and progestin receptors. *Biochem. Soc. Trans.* 19, 901-908.
- (42) Belanger, A., Philibert, D., and Teutsch, G. (1981) Regio and stereospecificity of 11 $\beta$ -substituted 19-norsteroids. *Steroids* 37, 361-382.
- (43) Pomper, M. G., Pinney, K. G., Carlson, K. E., VanBrocklin, H. F., Mathias, C. J., Welch, M. J., and Katzenellenbogen, J. A. (1990) Target tissue uptake selectivity of three fluorine-substituted progestins: potential imaging agents for receptor positive breast tumors. *Nucl. Med. Biol.* 17, 309-319.
- (44) Pomper, M. G., Kochanny, M. J., Thieme, A. M., Carlson, K. E., VanBrocklin, H. F., Mathias, C. J., Welch, M. J., and Katzenellenbogen, J. A. (1992) Fluorine-substituted Corticosteroids: Synthesis and Evaluation as Potential Receptor-based Imaging Agents for Positron Emission Tomography of the Brain. *J. Nucl. Med. Biol.* 19, 461-480.
- (45) Kochanny, M. J., VanBrocklin, H. F., Kym, P. R., Carlson, K. E., O'Neil, J. P., Bonasera, T. A., Welch, M. J., and Katzenellenbogen, J. A. (1993) Fluorine-18-labeled progestin ketals: synthesis and target tissue uptake selectivity of potential imaging agents for receptor-positive breast tumors. *J. Med. Chem.* 36, 1120-1127.
- (46) Space filling models were constructed in the SYBYL 6.0 molecular modeling package (TRIPOS Assoc., St. Louis, MO) on a Silicon Graphics Indigo Elan computer system. Atomic coordinates for FENP and RU486 as well as the BAT-metal complex were obtained from the Cambridge Structural Database (Allen, F. H., Davies, J. E., Galloy, J. J., Johnson, O., Kennard, O., Macrae, C. F., Mitchell, E. M., Mitchell, G. F., Smith, J. M., and Watson, D. G. (1991) The development of versions 3 and 4 of the Cambridge Structural Database System. *J. Chem. Inf. Comp. Sci.* 31, 187-204). The progestin N<sub>2</sub>S<sub>2</sub> conjugates were constructed by merging the complex coordinates with those of RU486, replacing the dimethyl amino functionality. Atomic coordinates for the MAMA' structure were obtained directly from our previously published crystal structure (6).



# Characterization of Hapten Binding to Immunoconjugates by Electrospray Ionization Mass Spectrometry

Kenneth M. Straub<sup>\*†</sup> and Mark J. Levy<sup>‡</sup>

Syntex Discovery Research and Syva Co., 3401 Hillview Avenue, Palo Alto, California 94304. Received November 18, 1993<sup>\*</sup>

Electrospray ionization mass spectrometry (ESI-MS) has been used to characterize the covalent binding of different haptens to the enzyme glucose 6-phosphate dehydrogenase. The technique allows one to directly observe the relative amounts of each conjugated species present in a mixture, as well as the average hapten number. These measurements are useful for optimizing reaction conditions to yield a more precisely defined product for use in immunoassays. The results obtained show that ESI-MS with a quadrupole analyzer can be successfully used to analyze mixtures of derivatized proteins in the molecular weight range of 50–60 kDa, where the modifying hapten has a molecular weight as low as 130 Da.

## INTRODUCTION

There are numerous examples in protein chemistry where it is desirable to covalently modify the side chains of amino acid residues to give specifically derivatized macromolecules. For example, immunoconjugates comprised of haptens linked to carrier proteins are useful for eliciting the production of specific antibodies for use in immunoassays, and hapten-modified enzymes form the basis of many types of enzyme immunoassays. Conjugation of proteins with low molecular weight haptens gives a mixture of macromolecules that differ in the number and site of modified residues. The hapten number  $n$  describes the average number of covalently modified residues per protein and is a key parameter that must be carefully optimized when preparing enzyme tracers for use in immunoassays.

A number of analytical methods have been described that allow the determination of an average hapten number. Classical methods include the use of absorption spectroscopy and radiolabeled hapten. These techniques, while simple to apply, give an average hapten number but do not provide information on the actual distribution of modified macromolecules. These techniques can also overestimate the hapten number if noncovalently bound hapten is present in the sample. In addition, these methods suffer from a number of other limitations. Absorption spectroscopy requires that the hapten have a significant extinction coefficient over a useful range of wavelengths and is subject to uncertainty about changes in the absorbance of bound chromophores. The use of radiolabeled haptens requires the preparation of labeled material with a high specific activity.

Recently, matrix-assisted laser desorption ionization (MALDI) mass spectrometry has been used to estimate the hapten number of covalently modified proteins (1, 2). While this methodology appears to be a substantial improvement over conventional assays, the low mass resolution of the technique limits it to the determination of an average hapten modification number.

In principle, electrospray mass spectrometer (ESI-MS) is an ideal technique for this type of problem (3). Since ESI-MS can be implemented on quadrupole or magnetic sector mass spectrometers, the increased resolution afforded by these systems allows one to directly observe the relative amounts of each conjugated species present in a mixture, as well as the average hapten number. Knowing the amounts of each species present can help optimize reaction conditions to yield a more precisely defined product for use in immunoassays.

We have explored the use of ESI-MS to characterize the stoichiometry of covalent binding of different haptens to the enzyme glucose 6-phosphate dehydrogenase (G6PDH, EC 1.1.1.49). The homodimeric subunit of this enzyme has a molecular weight of 54.5 kDa and is widely used in enzyme-linked immunoassays. The results obtained show that ESI-MS with a quadrupole analyzer can be successfully used to analyze mixtures of derivatized proteins in the molecular weight range of 50–60 kDa where the modifying hapten has a molecular weight as low as 130 Da.

## EXPERIMENTAL SECTION

**Materials and Methods.** G6PDH was purchased from US Biochemicals. Digoxigenin 3-*O*-hemisuccinate succinimide ester (Figure 1, structure 2) was obtained from Boehringer-Mannheim Biochemicals. Desaminothyroxine (structure 1), 2,2-dipropylglutaric anhydride (structure 3), and 5-[*N*-(2'-carboxyethyl)carbamoyl]dibenz[*b,f*]azepine (structure 4) were synthesized as previously reported (4–6). Tritiated 5-[*N*-(2'-carboxyethyl)carbamoyl]dibenz[*b,f*]azepine had a specific activity of 7 Ci/mmol. All other chemicals were reagent grade or better.

**Preparation of Immunoconjugates.** The acidic haptens were activated for conjugation by formation of *N*-succinimidyl esters (7). Conjugation reactions were conducted in solutions containing 5 mg/mL of G6PDH, 100 mM NaHCO<sub>3</sub> (pH 8.0), and 20% dimethylformamide (DMF). Activated hapten dissolved in DMF was added to the enzyme solution while the solution was stirred on ice. A 25-fold molar excess (relative to G6PDH subunit) of desaminothyroxine and 10-fold excesses of digoxigenin and 2,2-dipropylglutaric anhydride were used in the conjugations. For the 5-[*N*-(2'-carboxyethyl)carbamoyl]dibenz[*b,f*]azepine conjugations, the molar excess was varied from 5-fold to 20-fold to achieve a variety of loadings.

<sup>\*</sup> To whom correspondence should be addressed. Tel (415) 855-5067; FAX (415) 354-7363.

<sup>†</sup> Syntex Discovery Research.

<sup>‡</sup> Syva Co.

<sup>\*</sup> Abstract published in *Advance ACS Abstracts*, March 15, 1994.



Unreacted hapten was removed after 1 h by chromatography over Biogel P6-DG resin (Bio-Rad) in 10 mM ammonium acetate buffer (pH 6.7). Residual salts were removed from the samples of three cycles of (1) dilution to 2 mL with 10 mM ammonium acetate buffer and (2) concentration to approximately 100  $\mu$ L using Centricon-30 microconcentrators (Amicon).

Labeling density of radioactive conjugates was determined by conventional methods. Aliquots of the purified conjugates were diluted to approximately 10  $\mu$ g/mL in water. Duplicate 800- $\mu$ L samples were taken from these common solutions for use in scintillation counting and protein assay. Protein assays were performed according to the method of Bradford by adding 200  $\mu$ L of dye reagent (Bio-Rad) to the samples and measuring absorbance at 595 nm (8). Unmodified G6PDH was used to generate a standard curve. Radioactivity was measured by adding 10 mL of Ready-Safe (Beckman) to each sample and counting on a Beckman scintillation counter.

**Mass Spectrometry.** Electrospray ionization mass spectra were obtained using a Finnigan-MAT TSQ700 (Finnigan-MAT) equipped with an electrospray ion source (Analytica of Branford). Samples were prepared at concentrations of 1–5 pmol/ $\mu$ L in 10 mM  $\text{NH}_4\text{OAc}$  containing 20–50% acetonitrile or methanol and infused directly into the source at 1–2  $\mu$ L/min. Ion source operating conditions were as follows: cylindrical electrode, –3.0 kV; capillary voltage, +50 V; tube lens, 150–195 V; drying gas temperature, 130  $^\circ\text{C}$ ; drying gas flow, ca. 6 L/min. The instrument was scanned over the  $m/z$  range 300–2000 in 3-s intervals. All data were acquired in profile mode, and successive scans were averaged until the required signal-to-noise ratio was obtained. Typically, 5–10-min averaging times were required to obtain useful data on samples at concentrations of 1–5 pmol/ $\mu$ L and an infusion rate of 1  $\mu$ L/min, corresponding to 5–50 pmol of sample consumed for each measurement.

Alternatively, samples in 0.05% trifluoroacetic acid–water were electrosprayed using a sheathing flow of 2-methoxyethanol (1  $\mu$ L/min) and a nebulizing flow of nitrogen (600 mL/min). Operating conditions were similar to what was employed for methanol–water or acetonitrile–water solutions, except that a higher drying gas temperature (255  $^\circ\text{C}$ ) and drying gas flow rate (40 mL/min) were employed. These conditions are useful for analyzing modified proteins that have reduced solubility in methanol–water or acetonitrile–water.

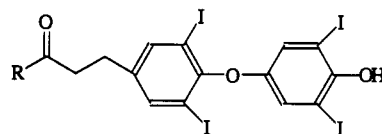
Multiply charged spectra were transformed to give molecular weights using the deconvolution program based on the algorithm described by Mann *et al.* (9). An implementation of this algorithm is supplied with the "BioSoft" software on the TSQ700 data system.

The hapten number ( $n$ ) was calculated from the observed molecular weight distribution as the sum of the product of the intensities  $I$  of each species  $j \rightarrow i$  and its hapten number  $n$  divided by the sum of the intensities for all components:

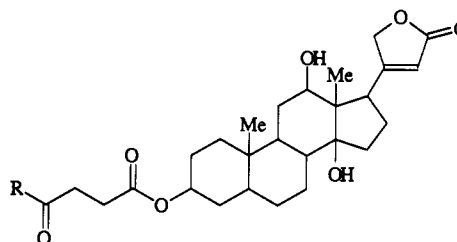
$$n = \frac{\sum_{j=0}^i n_j I_j}{\sum_{j=0}^i I_j}$$

## RESULTS

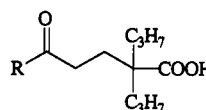
The general utility of ESI-MS for characterizing covalently modified proteins is demonstrated by the results of experiments using the enzyme glucose 6-phosphate



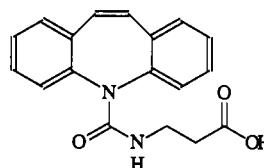
Desaminothyroxine hapten 1

 $\Delta m = 744$  Da

Digoxigenin hapten 2

 $\Delta m = 472$  Da

Valproic Acid hapten 3

 $\Delta m = 198$  Da

Carbamazepine hapten 4

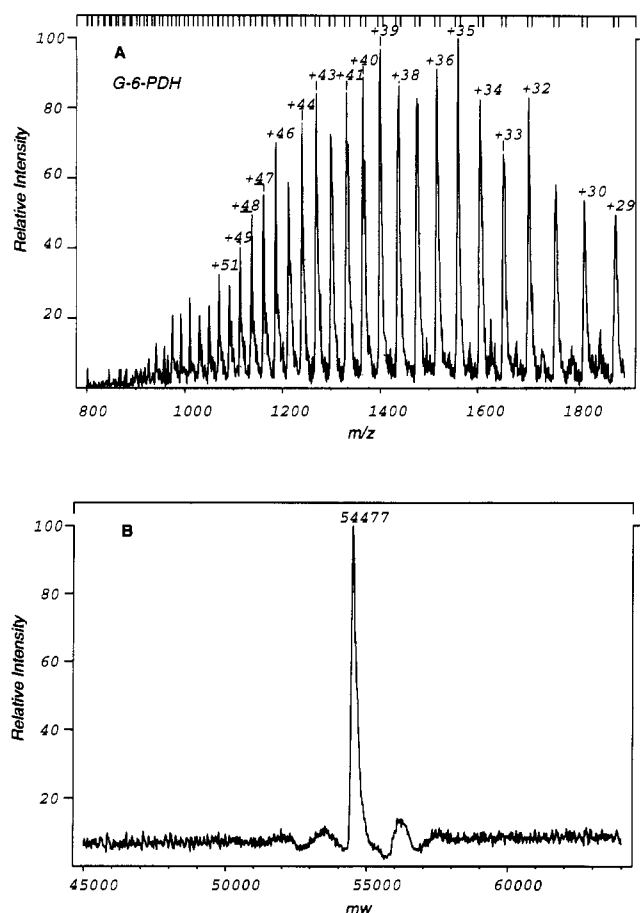
 $\Delta m = 290$  Da

**Figure 1.** Structures of haptens used for conjugation with glucose 6 phosphate dehydrogenase. Residue masses for each hapten following conjugation reaction are indicated.

dehydrogenase (G6PDH). This enzyme is widely used in commercially available enzyme-linked immunoassays. This type of assay requires covalently binding hapten to an enzyme while minimizing loss of catalytic activity.

A number of different G6PDH conjugates were prepared by using carboxylic acid-containing haptens with molecular weights of 300–700. The structures of these haptens are shown in Figure 1 and include analogues of thyroxine (structure 1), digoxigenin (structure 2), valproic acid (structure 3), and carbamazepine (structure 4). Covalent binding of these haptens to G6PDH, primarily by reaction with  $\epsilon$ -amino groups of lysine residues, yields a series of mixtures of modified proteins. Each of these proteins differs in molecular weight by the residue mass of the hapten. The corresponding residue mass differences for these haptens are 744 Da (thyroxine analogue), 472 Da (digoxigenin analogue), 198 Da (valproate analogue), and 290 Da (carbamazepine analogue).

When electrosprayed from a 30% methanol solution, G6PDH gives a typical ESI mass spectrum with a distribution of multiply charged species between +28 and

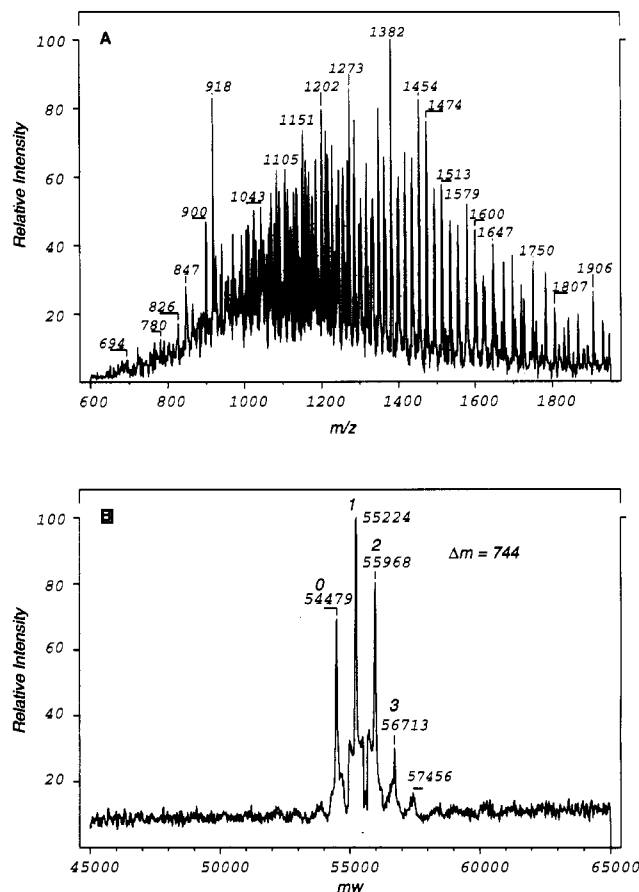


**Figure 2.** (A) ESI mass spectrum of G6PDH. (B) Deconvoluted spectrum obtained from data in A.

+70, as shown in Figure 2A. The multiply charged species are well resolved in this spectrum, and transformation of the data to molecular weight can be carried out by inspection or by application of a suitable algorithm such as that described by Mann *et al.* (9). Application of this algorithm gives the data presented in Figure 2B, which show that a single component of MW  $54477 \pm 5$  Da is present.

Modification of G6PDH by the thyroxine analogue 1 gives a mixture of proteins that yields an ESI mass spectrum in which each of the modified proteins independently contributes a series of multiply charged ions. The complexity of the resulting spectrum depends on both the modification number and the relative mass of the hapten. In the case of a low modification number and a large residue mass, the multiply charged ion series can still be resolved, and the deconvoluted spectrum shows a simple product distribution. For the thyroxine analogue, a mixture consisting predominantly of  $\text{Thyr}_0$ ,  $\text{Thyr}_1$ , and  $\text{Thyr}_2$  is obtained, where  $n = 1.2$  (Figure 3). As shown in Figure 3A, the raw data for the thyroxine conjugate consist of three to four sets of superimposed multiply charged species. A molecular weight profile can be determined either by inspection or by application of a transformation function.

As the mass of the hapten species decreases, the multiply charged species begin to overlap, eventually reaching a point where individual components can no longer be resolved. Simple inspection of the data is no longer sufficient for assigning multiply charged ions to the different series. This is shown by the data in Figures 4 and 5. For the digoxigenin-labeled enzyme (residue mass 472 Da; Figure 4), a series of products is obtained where  $n = 3$ –8. These products have an average modification



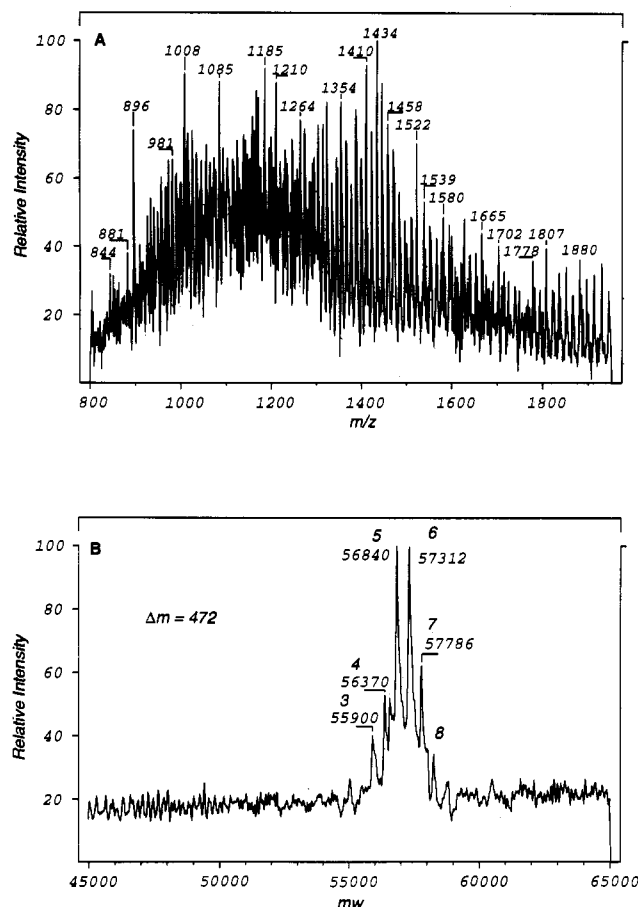
**Figure 3.** (A) ESI mass spectrum of G6PDH following conjugation with thyroxine (analogue 1). (B) Deconvoluted spectrum obtained from data in A. Hapten number of each component is indicated.

number of 6.4. The mass difference between the components corresponds to  $472 \pm 4$  Da, as expected for this hapten.

In the case of the valproate-labeled enzyme (Figure 5), the low residue mass ( $\Delta m = 198$ ) and increased degree of labeling results in significant overlap between the multiply charged species. Despite this overlap, complete deconvolution of the electrospray data to yield a molecular weight distribution is still possible, as shown in Figure 5B. In this example, components corresponding to  $n = 0$ –5 haptens are present, with an average modification number of 2.1. Note that the mass differences between the adjacent peaks are within the expected error of 0.01%.

Heterogeneity in the enzyme or protein can cause additional complexity. A common source of such heterogeneity is the partial removal of a methionine residue from the amino terminus of proteins that have been produced by recombinant techniques in bacteria, so that a mixture of two species differing by 131 Da is present. Figure 6, obtained from a digoxigenin analog-labeled G6PDH present in both Met and des-Met forms, is an example. The data shows that there are 10 species present, corresponding to five pairs of digoxigenin-labeled G6PDH where  $n = 1$ –5 with and without an N-terminal methionine.

**Comparison of Hapten Numbers Determined by ESI-MS and Radiolabeling.** Labeling density for G6PDH- $^3\text{H}$ -5-[*N*-(2'-carboxyethyl)carbamoyl]dibenz[*b,f*]azepine conjugate was determined for three different loadings of the hapten both by ESI-MS and by scintillation counting. Measurement of radioactivity and protein concentration yielded 1.5, 2.9, and 4.2 moieties per subunit for the three different conjugates A, B, and C. The



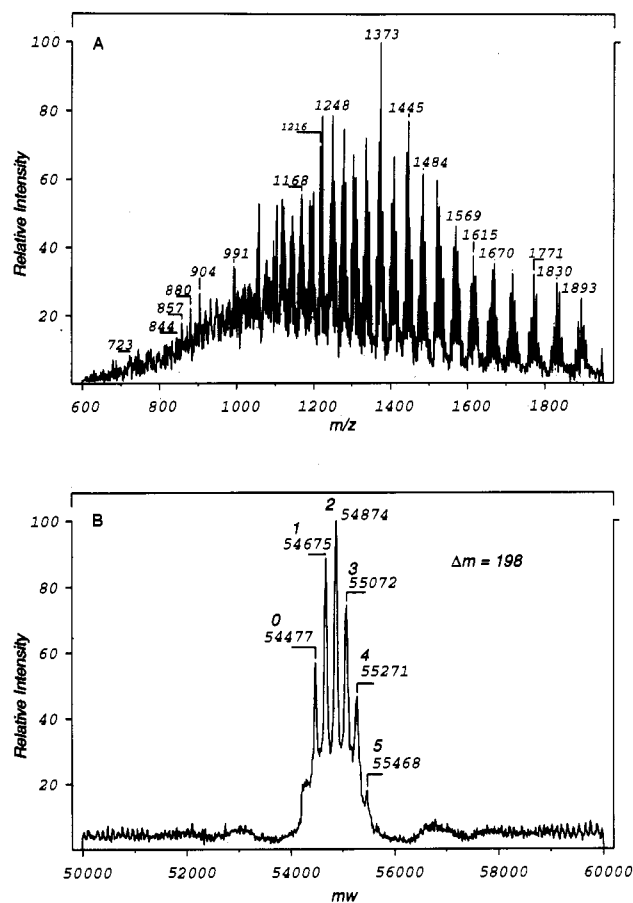
**Figure 4.** (A) ESI mass spectrum of G6PDH following conjugation with digoxigenin (analogue 2). (B) Deconvoluted spectrum obtained from data in A. Hapten number of each component is indicated.

respective labeling densities derived from the mass spectrometric determinations were 1.2, 2.6, and 3.4 (Table 1).

#### DISCUSSION

With a quadrupolar analyzer, a practical limit to analyzing these types of mixtures appears to occur for a 55-kDa protein at a modification number of *ca.* 8 and a hapten mass of approximately 130 Da. Mixtures that are more complex than this result in a degree of overlap between the various multiply charged species such that transformation of the data to yield a molecular weight profile becomes impractical.

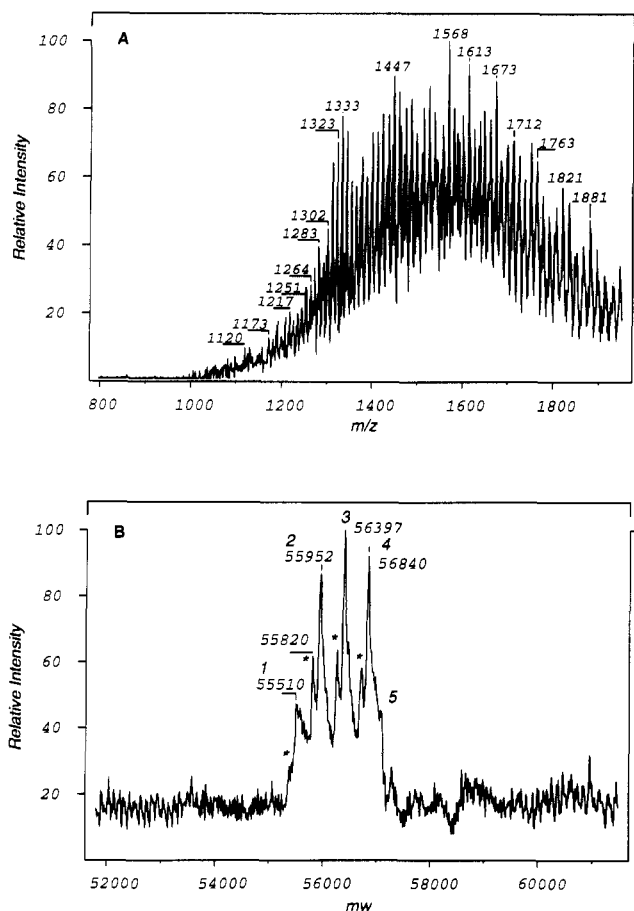
Improved mass resolution is the most obvious way to extend these measurements to more complex mixtures. Coupling ESI to magnetic sector or ICR-type instruments should result in improved resolution of the multiply charged ions contributing to each series (10, 11). For a quadrupole analyzer, increasing mass resolution does not always yield substantial improvements in the deconvoluted data since the resulting decrease in sensitivity offsets any real gain in signal. It is sometimes possible to improve the quality of the data by employing conditions that result in a shift of the entire envelope of multiply charged ions to higher *m/z* (lower charge number), where the *m/z* difference between successive charged species is larger. For example, use of water containing 0.1% trifluoroacetic acid in combination with 2-propanol or 2-methoxyethanol as a sheathing liquid will shift the distribution of charged ions for G6PDH from +40 out to +30, with ions observed up to *m/z* 3500. This technique is limited by the decreased sensitivity and resolution of quadrupole systems above *m/z* 2000.



**Figure 5.** (A) ESI mass spectrum of G6PDH following conjugation with valproic acid (analogue 3). (B) Deconvoluted spectrum obtained from data in A. Hapten number of each component is indicated.

In many instances, the major factor limiting resolution is not the analyzer performance but the presence of noncovalently bound adducts that contribute to broadening and attendant overlap of the multiply charged sample peaks. Alkali cations, primarily sodium, are particularly troublesome in this respect. Removal of these interfering substances using purification techniques such as ultrafiltration is sometimes successful, but severe loss of sample by irreversible adsorption limits this approach with many conjugated proteins.

The discrepancy observed between the hapten number as determined by the ESI-MS and radiolabeling methodologies can be attributed to the presence of noncovalently bound hapten in the samples despite extensive sample purification. This discrepancy would result in an overestimation of conjugation by the radiolabeling technique. A similar overestimation of hapten number as determined by absorption spectroscopy was noted by Wengatz *et al.* in their description of the use of MALDI for characterizing modified proteins (1). While it is also possible that ionization efficiencies may differ for proteins with different modification numbers, the evidence to date suggests that this is not the case. For example, it was observed during the course of these studies that the overall response factors for G6PDH modified with haptens 1–4 were essentially equivalent, despite the diversity of these functional groups. Another possible source of error is that proteins that are heavily modified with nonpolar moieties could have reduced solubility in the solvent used for electrospray ionization, so that components with large values of *n* would be lost prior to analysis. For the carbamazepine hapten, loadings that resulted in hapten



**Figure 6.** (A) ESI mass spectrum of a mixed G6PDH with and without an N-terminal methionine following conjugation with a digoxigenin analogue. (B) Deconvoluted ESI mass spectrum obtained from data in A. The hapten number of each component is indicated; desMet-forms are indicated with asterisk.

**Table 1.** Comparison of Hapten Numbers Determined by ESI-MS and Radiolabeling for Carbamazepine-Modified G6PDH

sample <sup>a</sup>	method	
	ESI-MS	scintillation counting
A	1.2	1.5
B	2.6	2.9
C	3.5	4.2

<sup>a</sup> Samples with different hapten numbers were prepared as described in the Experimental Section.

numbers greater than  $n = 6$  resulted in a product mixture that precipitated in the presence of 30% acetonitrile or methanol. This can be guarded against by monitoring the absorbance of the solution after centrifugation or ultrafiltration to verify that the total protein concentration has not changed.

Comparing the quality of the information obtained by ESI-MS with that afforded by conventional methods for determining hapten number is instructive. Absorption spectroscopy is restricted to haptens that absorb in a useable range of wavelengths, and the results are subject to uncertainty regarding changes in the extinction coefficient that bound material could undergo. As noted above, both absorption spectroscopy and the use of radiolabeled hapten can be complicated by the presence of noncovalently bound hapten that is not removed by the usual size-exclusion techniques. While it is possible to employ conditions in electrospray ionization that will preserve noncovalent interactions, the methodology described here yields ions from covalently bound species only (12).

The MALDI technique appears to be promising for determining the average modification number of conjugates, although the low mass resolution inherent to this type of analyzer makes resolution of individual conjugated species impractical. While some information about the distribution of species in a mixture can be obtained from a consideration of the peak width of the resulting data, such measurements can be misleading since noncovalently bound gas-phase clusters derived from sample matrix or other contaminants can contribute to increased peak width. It is unlikely, for example, that the presence of a des-Met analogue as shown in Figure 6 could have been detected by the MALDI technique.

In summary, ESI-MS is a relatively simple but powerful technique for characterizing covalently modified protein conjugates. Information can be readily obtained that describes both the average modification number as well as the relative amount of each species present in the sample.

#### ACKNOWLEDGMENT

The authors thank Dr. Michael Huster for the synthesis of desaminothyroxine and tritiated 5-[N-(2'-carboxyethyl)-carbamoyl]dibenz[b,f]azepine and Dr. Thomas Goodman for a sample of recombinant G6PDH.

#### LITERATURE CITED

- (1) Wengatz, I., Schmid, R. D., Kreissig, S., Wittmann, C., Hock, B., Ingendoh, A., and Hillenkamp, F. (1992) Determination of the hapten density of immunoconjugates by matrix-assisted UV laser desorption/ionization mass spectrometry. *Anal. Lett.* 25, 1993-1997.
- (2) Siegel, M. M., Hollander, I. J., Hamann, P. R., James, J. P., Hinman, L., Smith, B. J., Farnsworth, A. P. H., Phipps, A., King, D. J., Karas, M., Ingendoh, A., and Hillenkamp, F. (1991) Matrix-assisted UV-laser desorption/ionization mass spectrometric analysis of monoclonal antibodies for the determination of carbohydrate, conjugated chelator, and conjugated drug content. *Anal. Chem.* 63, 2470-2481.
- (3) Smith, R. D., Loo, J. A., Edmonds, C. G., Barinaga, C. J., and Udseth, H. R. (1990) New developments in biochemical mass spectrometry: electrospray ionization. *Anal. Chem.* 62, 882-899.
- (4) Kharasch, N., Kalfayan, S. H., and Arterberry, J. D. (1956) The synthesis of some methyl analogs of desaminothyroxine. *J. Org. Chem.* 21, 925-930.
- (5) Leung, D. K., and Singh, P. (1980) Valproate conjugation using dicarbonyls. U.S. Patent 4,238,389.
- (6) Singh, P. (1977) Tegretol antigens and antibodies. U.S. Patent 4,058,511.
- (7) Anderson, G. W., Zimmerman, J. E., and Callahan, E. M. (1964) The use of esters of N-hydroxysuccinimide in peptide synthesis. *J. Am. Chem. Soc.* 86, 1839.
- (8) Bradford, M. M. (1976) A rapid and sensitive method for the quantitation of microgram quantities of protein utilizing the principles of protein-dye binding. *Anal. Biochem.* 72, 248-254.
- (9) Mann, M., Meng, C. K., and Fenn, J. B. (1989) Interpreting mass spectra of multiply charged ions. *Anal. Chem.* 61, 1702-1708.
- (10) Meng, C.-K., McEwen, C. N., and Larsen, B. (1990) Electrospray ionization on a high-performance magnetic sector mass spectrometer. *Rapid Commun. Mass Spectrom.* 1, 147-150.
- (11) Beu, S. C., Senko, M. W., Quinn, J. P., Wampler, F. M., and McLafferty, F. W. (1993) Fourier-transform electrospray instrumentation for tandem high resolution mass spectrometry of large molecules. *Rapid Commun. Mass Spectrom.* 4, 557-565.
- (12) Li, Y.-T., Hsieh, Y.-L., Henion, J. D., and Ganem, B. (1993) Studies on heme binding in myoglobin, hemoglobin, and cytochrome c by ion spray mass spectrometry. *J. Am. Soc. Mass Spectrom.* 4, 631-637.

# Synthesis of an Acetylcholine Receptor-Specific Toxin Derivative Regioselectively Labeled with an Undecagold Cluster

P. Kessler,\*† F. Kotzyba-Hibert,‡ M. Leonetti,† F. Bouet,† P. Ringler,§ A. Brisson,§ A. Ménez,† M. P. Goeldner,‡ and C. Hirth<sup>‡</sup>

Département d'Ingénierie et d'Etudes des Protéines (DIEP), CEA, C.E. Saclay, 91191 Gif-sur-Yvette Cedex, France, Laboratoire de Chimie Bio-organique, URA CNRS 1386, BP24, 67401 Illkirch Cedex, France, and LGME-CNRS, U184 INSERM, Institut de Chimie Biologique, Faculté de Médecine, 11, rue Humann, 67085 Strasbourg Cedex, France. Received February 8, 1994\*

The regioselective modification of a snake curaremimetic toxin is described. Toxin- $\alpha$  from *Naja nigricollis* was derivatized with an electron-dense maleimido undecagold cluster 5. The cluster-bound obtained toxin 8 has a very high affinity for the cholinergic binding site ( $K_i = 70$  pM) of *Torpedo marmorata* nicotinic receptor. It is harboring a compact heavy atom core of about 8 Å which makes it very useful for electron microscopy experiments.

## INTRODUCTION

The nicotinic acetylcholine receptor is a pentameric membrane protein composed of four subunits with the stoichiometry  $\alpha_2\beta\gamma\delta$ , arranged symmetrically around a central pit, proposed to form the ion channel (1–3). A recent 9-Å resolution three-dimensional structure was determined by analysis of cryoelectron images (4). This study revealed that the subunits are arranged around a central channel, with approximately 55% of the mass of each subunit emerging outside the membrane in the synaptic space. A variety of ligands are known to interact with exposed areas of the receptor inducing either opening of the channel or its blocking in a resting state. It is well established that cholinergic agonists and competitive antagonists mainly interact with the  $\alpha$ -subunits (5, 6). However, a more precise three-dimensional localization of their interacting site is required for a better understanding of their action.

Some snake curaremimetic toxins are known to be efficient competitive antagonists for the AChR<sup>1</sup> binding sites (7, 8). These are small proteins that bind quasiirreversibly to AChR (affinity dissociation constants approximately equal to  $10^{-10}$  M). The binding domain of snake curaremimetic toxins with the AChR has been studied by chemical modifications (12–15), site-directed mutagenesis (15, 16), and photoaffinity labeling (17). These studies have revealed that the toxin binding domain is composed of at least 10 amino acids belonging to two of the three adjacent loops that are present in snake toxins (12–16). However, the site to which the toxin binds remain unclear. Previous attempts have been made to localize, by electron microscopy (9–11), the binding sites of such snake toxins. Such experiments made with native  $\alpha$ -bungarotoxin provided weak signals, even with two-dimensional crystalline arrangements. Enhancement of the contrast was previously

attempted using a toxin coupled to a biotin–avidin complex (11); however, the modification was achieved randomly on all nucleophilic amino acids of the toxin, leading to a heterogeneous population of derivatized toxin molecules. Moreover, the size of avidin (50 kDa) made difficult a precise localization of the bound toxin. New tools capable of improving the signal are therefore needed.

Here, we describe the synthesis of a toxin derivative in which a single and regioselective amino group (outside of the binding domain) was modified with an electron-dense undecagold cluster. This relatively small metal-containing cluster proved to be useful in low-dose electron microscopy experiments to localize cysteinyl residues on F-actin (18) and on cholera toxin (19). In this paper, we show that toxin labeling could be efficiently achieved in two steps. First, toxin derivatives harboring a single disulfide on various amino groups were generated. Second, the disulfide of a selected toxin derivative was reduced and the resulting sulfhydryl reacted with a monomaleimido undecagold cluster. The biological properties of the undecagold-cluster-modified toxin are described.

## EXPERIMENTAL PROCEDURES

Toxin- $\alpha$  was purified from *Naja nigricollis* venom (Pasteur Institute, Paris) and tritiated as previously described (20). SPDP was purchased from Pharmacia. Tri-*p*-tolylphosphine was purchased from STREM Chemical Co. Affi-Gel 401, Bio-Rex 70, and Bio-Gel P2 and P10 were obtained from Biorad. Dimethylformamide was dried over phosphorus pentoxide, distilled under reduced pressure ( $p < 10$  mbar), and kept on 4-Å molecular sieves. The other solvents were of commercial grade and used without further purification. NMR spectra were obtained on a BRUKER AC 200 spectrometer. Chemical shifts ( $\delta$ ) are given in ppm.

**Tris(*p*-carboxyphenyl)phosphine Oxide 1.** Tri-*p*-tolylphosphine (10 g; 32.9 mmol) was oxidized with an excess of  $\text{KMnO}_4$  (portions of 5 g were added until complete oxidation of the methyl groups was achieved) in a refluxing mixture of pyridine/water (100 mL:50 mL). The reaction was followed by TLC (eluent =  $\text{AcOEt}$ /acetone/water/ $\text{AcOH}$  (70:26:3:1)). At the end of the reaction,  $\text{MnO}_2$  was reduced with sodium disulfite in acidic conditions. The mixture was filtered and the precipitate washed with water and dried under vacuum to yield 8.1 g of a white solid

\* To whom correspondence should be addressed.

† Département d'Ingénierie et d'Etudes des Protéines.

‡ Laboratoire de Chimie Bio-organique.

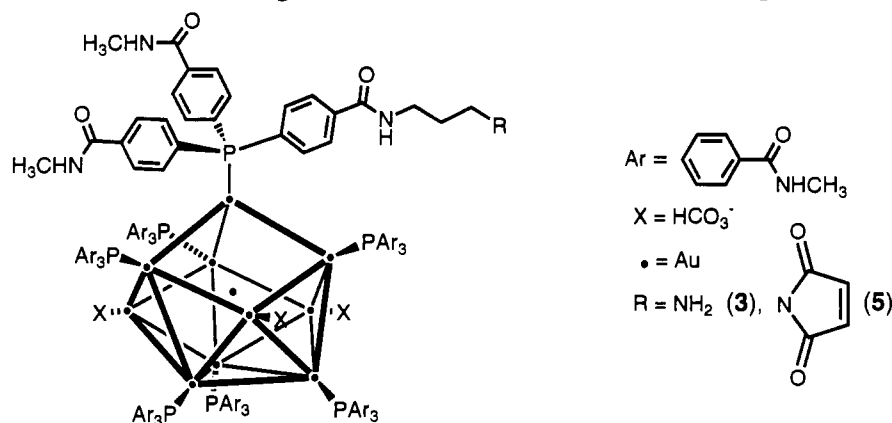
§ Institut de Chimie Biologique.

<sup>‡</sup> Deceased on May 28, 1992.

<sup>1</sup> Abbreviations: AChR, acetylcholine receptor; ACh, acetylcholine; SPDP, *N*-succinimidyl 3-(2-pyridyldithio)propionate;  $\text{AcOEt}$ , ethylacetate;  $\text{AcOH}$ , acetic acid;  $\text{AcONa}$ , sodium acetate; DTT, dithiothreitol; DTNB, 5,5'-dithiobis(2-nitrobenzoic acid).

\* Abstract published in *Advance ACS Abstracts*, April 1, 1994.

Chart 1. Structures of Monoamino Undecagold Cluster 3 and Monomaleimido Undecagold Cluster 5



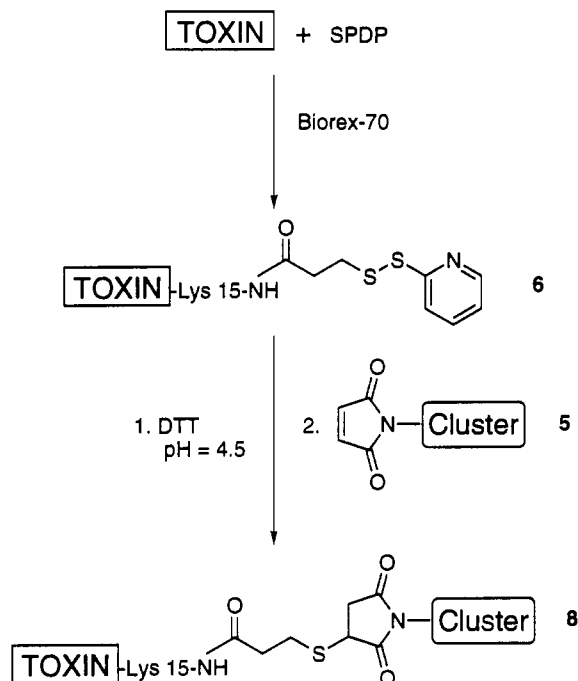
(60%). Mp: 340–357 °C (lit. (21) mp 347–357 °C).  $^1\text{H}$  NMR ( $\text{CD}_3\text{OD}$ ): ABX system (X = phosphorus)  $J_{\text{AB}} = 8.3$  Hz,  $J_{\text{AX}} = 2.6$  Hz,  $J_{\text{BX}} = 12$  Hz,  $\delta_{\text{A}} 7.80$  (2 H, ArH ortho to P),  $\delta_{\text{B}} 8.20$  (2 H, ortho to  $\text{COOH}$ ).

**Tris(*p*-carboxyphenyl)phosphine 2.** The phosphine oxide 1 (11.3 g; 27.5 mmol) was refluxed, under argon atmosphere, in 120 mL of dry toluene, in the presence of 60 mL (21 equiv) of trichlorosilane. After 60 h, the solvent was evaporated and the phosphine dissolved in concentrated ammonia. The mixture was filtered; the supernatant was acidified with concentrated hydrochloric acid to pH 1 and cooled in ice. The white precipitate was collected by filtration, washed with water, and dried under vacuum to yield 10.8 g (99.4%) of phosphine 2. Mp: 310–318 °C (lit. (21) mp 270–274 °C).  $^1\text{H}$  NMR ( $\text{CD}_3\text{OD}$ ): ABX system (X = phosphorus)  $J_{\text{AB}} = 8.2$  Hz,  $J_{\text{AX}} = 1.4$  Hz,  $J_{\text{BX}} = 8.2$  Hz,  $\delta_{\text{A}} 7.40$  (2 H, ArH ortho to P),  $\delta_{\text{B}} 8.02$  (2 H, ortho to  $\text{COOH}$ ).

**Monoamino Undecagold Cluster 3 (Chart 1).** The synthesis was achieved as described by Safer et al. (22) on 8.3 mmol of *N*-methyl-*N*-propylamine benzamide phosphine mixture, exchanging the  $\text{CN}^-$  ion in the gold clusters with  $\text{Cl}^-$  using DOWEX 1 $\times$ 2 resin. We used buffers with 20% of methanol to avoid precipitation of clusters. The yield of cluster 3 was 13.5% of the initial Au amount.  $^1\text{H}$  NMR ( $\text{CD}_3\text{OD}$ ):  $\delta$  1.72 (t broad, central methylene of the propylene group), 2.64 (t broad,  $\text{CH}_2\alpha$  to the amino group), 2.87 (s broad, 3 H,  $\text{CH}_3$ ), 3.40 (t broad,  $\text{CH}_2\alpha$  to the amido group), 7.30 (s broad, 4 H, ArH).  $^{31}\text{P}$  NMR ( $\text{CD}_3\text{OD}$ , external reference:  $\text{NaH}_2\text{PO}_4$  in  $\text{D}_2\text{O}$ ):  $\delta$  -54.3. Quantitative ninhydrin titration (23, 24): one amino group per gold cluster. Atomic absorption of gold: gold content = theoretical value obtained by UV spectrophotometry. The UV spectrum is in agreement with previous results (22).

***N*-(Methoxycarbonyl)maleimide 4.** Compound 4 was synthesized as previously described (25) and was obtained with 65% yield. Mp: 64–67 °C (lit. (25) mp 61–63 °C).  $^1\text{H}$  NMR ( $\text{CDCl}_3$ ):  $\delta$  3.92 (s, 3 H,  $\text{OCH}_3$ ), 6.86 (s, 2 H,  $\text{HC}=\text{CH}$ ).

**Monomaleimido Undecagold Cluster 5 (Chart 1).** The reaction and the purification were done at 4 °C to minimize the hydrolysis of the maleimido group. Cluster 3 (6  $\mu\text{mol}$ , determined by UV spectrophotometry) was stirred for 25 min in a mixture of MeOH (250  $\mu\text{L}$ ) and saturated sodium hydrogenocarbonate (100  $\mu\text{L}$ ) in the presence of 90 equiv (85 mg) of the maleimide 4. The purification was done, as described earlier (22), in buffer A (0.03 M triethanolamine-HCl, pH 7, 0.1 M NaCl). The yield was estimated, as previously described (22), by binding of the cluster 5 to a freshly reduced thiopropyl-agarose Affi-Gel 401 column (1 mL). Seventy-two percent

Scheme 1. Synthesis of Cluster-Modified Toxin- $\alpha$  8

of the cluster material remained covalently attached onto the resin. We observed a new resonance band at 6.8 ppm (singlet) in  $^1\text{H}$  NMR corresponding to the maleimido group.

**Monothiolated Toxin- $\alpha$  6 (Scheme 1).** Toxin- $\alpha$  was derivatized with SPDP using a method previously described (26). His-31 tritiated toxin- $\alpha$  (20) was added to the reactive medium (final specific radioactivity: 0.13 Ci·mmol $^{-1}$ ). The resulting derivatives were separated according to their isoelectric point by a cationic exchange chromatography (Bio-Rex 70,  $\text{Na}^+$ ) (Figure 2). The position of the modification for each monoderivative was determined by competition experiments using two toxin-specific monoclonal antibodies (13, 14) and by peptide sequencing.

Selective reduction of this newly introduced disulfide bond was achieved as described earlier (27). The (2-pyridyldithio)propionate moiety of the Lys-15 monomodified toxin- $\alpha$  (35 nmol) was reduced at room temperature, for 20 min, in 400  $\mu\text{L}$  of buffer (0.1 M AcONa, pH 4.5, NaCl 0.1 M, DTT 25 mM). The reduced toxin 7 was separated from the excess of reactant by gel filtration through a Bio-Gel P2 column eluted with degassed buffer (buffer B: 0.1 M  $\text{Na}_2\text{HPO}_4/\text{NaH}_2\text{PO}_4$ , pH 6, NaCl 0.1 M) and directly used for alkylation.



native toxin  
monomodified toxin  
  
dimodified toxin  
  
trimodified toxin



**Figure 1.** Migration pattern of each Biorex eluted fraction on an isoelectrofocusing gel pH 3.5–10.

**Isoelectrofocusing.** Ten  $\mu\text{g}$  of protein of each Biorex eluted fraction was applied to an 11-X 20-cm polyacrylamide gel (8% acrylamide, 0.2% *N,N'*-methylenebisacrylamide, 12% (w/v) sucrose, 2% (v/v) pH 3.5–10 Ampholine (LKB) and 0.15% ammonium persulfate). Electrophoresis was run at 4 °C for 75 min. Proteins were precipitated overnight with a trichloroacetic acid solution (20% w/v). The gel was then stained in a 20% (w/v) trichloroacetic acid solution containing 0.1% Coomassie blue.

**Toxin- $\alpha$ -Undecagold Cluster Covalent Complex 8 (Scheme 1).** Freshly reduced toxin (4  $\mu\text{M}$  final concentration), in solution in buffer B, was alkylated by freshly prepared cluster 5 (250  $\mu\text{M}$  final concentration), in solution in buffer A, for 2 h, at room temperature and under argon atmosphere. The mixture was concentrated up to 300  $\mu\text{L}$ , and the precipitate was centrifuged. The supernatant was applied on a Bio-Gel P10 column eluted with  $\text{H}_2\text{O}$ . The colored radioactive fractions were concentrated in a Speed-Vac apparatus.

**Biological Activity (Figure 5).** The binding of toxin- $\alpha$  to solubilized AChR (28) was done in a Tris buffer (Tris-HCl 10 mM, pH 7.4, NaCl 10 mM, 1% Triton X100). A constant amount of radioactive toxin (60 nM for SPDP-derivatized toxin and 200 nM for cluster-bound toxin) was incubated in the presence of increasing amounts of acetylcholine receptor (28–350 nM) in a total volume of 100  $\mu\text{L}$ , for 2.5 h at room temperature. Fifty  $\mu\text{L}$  of the solution were deposited on cationic filters (DE-81, Whatman). After 10 min, the filters were rinsed twice with Tris buffer, and the remaining radioactivity was measured on a liquid scintillation counter (LKB 1209 rackbeta).

**Apparent Dissociation Constant.** The measurement of the apparent dissociation constant of the modified toxin was realized as described earlier (8).

## RESULTS

**Maleimido Undecagold Cluster 5.** The maleimido undecagold cluster 5 was synthesized as previously described (22). We began the synthesis with tri-*p*-tolylphosphine, which was oxidized to tris(*p*-carboxyphenyl)-phosphine 2 with an overall yield of about 60%. The melting point of this compound was found to be 40 °C higher as compared to the one reported earlier (21). Gold cyanide was then reduced by sodium borohydride in the presence of a 1/20 mixture of *N*-propylamine/*N*-methylbenzamide-phosphines, obtained from 2 (22). Cluster 3 was purified by gel filtration and ion-exchange chromatography and was obtained with an overall yield of about 13%, according to the initial gold amount. It was converted into cluster 5 with 72% yield. The maleimido cluster was purified from excess of reactant by ion-exchange chromatography and immediately used.

The maleimido function is rather unstable in water solution, but the mixture can be precipitated by cold acetone and desalted by dissolving the clusters in MeOH. Component 5 can thus be conserved in a stable solid form in  $\text{CH}_2\text{Cl}_2$  for months at –80 °C.

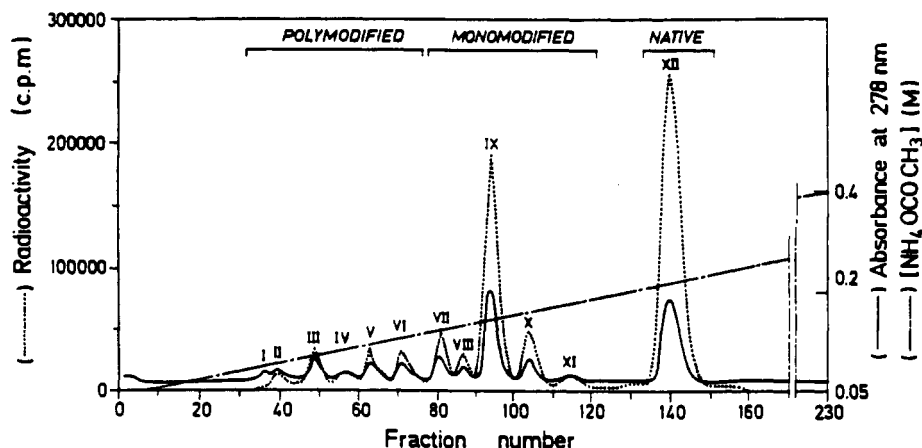
**Monomodified Toxin- $\alpha$ .** Due to the overlap of the UV spectra of the toxin and gold cluster, with a 15 times higher extinction coefficient for the latter, it is difficult to distinguish, by spectrophotometric measurement, the free from toxin-bound clusters. To facilitate the characterization of the covalent complex, we therefore used a radiolabeled toxin. Toxin- $\alpha$  from *Naja nigricollis* was tritiated on His-31 with a specific radioactivity of 0.13 Ci·mmol<sup>–1</sup>.

Toxin derivatives harboring a single additional disulfide were prepared by acylating toxin amino groups with SPDP. Toxin- $\alpha$  bears seven amino groups: the terminal  $\text{NH}_2$  group and lysines 15, 25, 26, 46, 50, and 58. The acylation of amino groups by SPDP induces an abolition of positive charges, and consequently the toxin isoelectric point decreases depending on the number of modified functions. The isoelectric point of the native toxin- $\alpha$  is higher than 10. Therefore, the resulting mixture was desalted and further submitted to chromatography on cation-exchange resin.

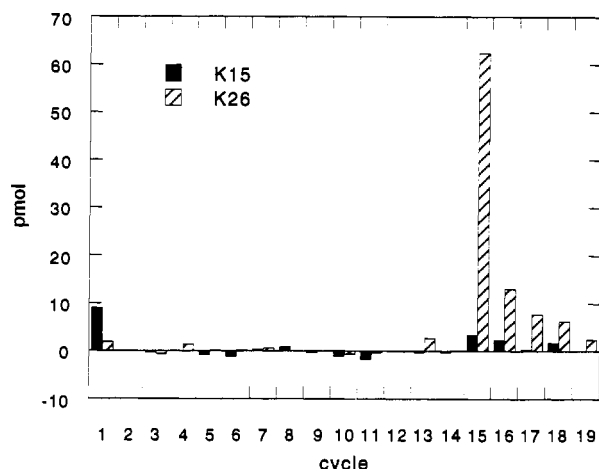
In a preliminary analytical experiment, we identified the different derivatives by gel isoelectrofocusing (Figure 1). The monomodified derivatives were found in four ion-exchange chromatography fractions. Their purity was checked by HPLC (data not shown). The first fraction was a mixture of two monoacylated toxins, whereas the three following fractions contained a single monomodified derivative.

In a preparative-scale experiment (60 mg of toxin), the fractionation was clearly improved (Figure 2). The first fractions (I–VI) contained polyacylated derivatives. The monoacylated derivatives were resolved into five fractions (VII–XI)—instead of four in the analytical experiment described above—and the last peak (XII) contained the native toxin. The purity of the fractions VII–XI was confirmed by reversed-phase HPLC. Fractions VII–IX were characterized by competition experiments using two toxin-specific monoclonal antibodies whose binding to the toxins is affected by well-defined modifications (data not shown) (13, 14). They contained derivatives of toxin- $\alpha$  monoacylated at Lys-50, Lys-46, and Lys-26, respectively. Fractions X and XI were shown by peptide sequencing to be the monoacylated derivatives respectively at Lys-15 (Figure 3) and at the terminal  $\text{NH}_2$  group.

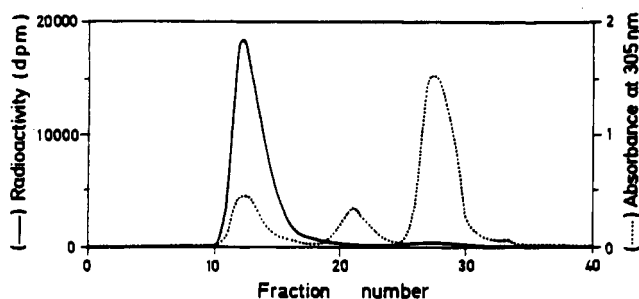
**Coupling of the Toxin with the Cluster.** The Lys-15 monoacylated derivative 6 was chosen for further coupling experiments with the maleimido cluster because competition data showed that lysine 15 is excluded from



**Figure 2.** Radioactive (---) and optical density (—) elution profiles of toxin derivatives modified with SPDP. Sixty mg of toxin was loaded on a Biorex 70 column (diameter: 2.5 cm,  $L = 46$  cm; gradient  $\text{NH}_4\text{OAc}$ , pH 7.7, 0.05 to 0.4 M in 16 h; flow rate  $1 \text{ mL} \cdot \text{min}^{-1}$ ). An aliquot ( $10 \mu\text{L}$ ) was taken, and radioactivity was counted in a liquid scintillator ( $10 \text{ mL}$ ). Optical density was measured directly at 278 nm.



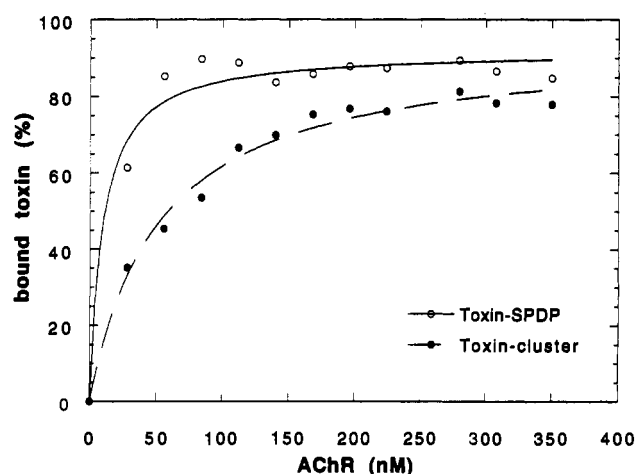
**Figure 3.** Lysine histogram of K15- and K26-SPDP-modified toxin. Microsequencing was done on 200 pmol of toxin.



**Figure 4.** Biogel P10 column: Radioactive (—) and optical density (---) elution profiles of cluster modified toxin- $\alpha 8$ . An aliquot ( $100 \mu\text{L}$ ) was taken, and radioactivity was counted in a liquid scintillator ( $5 \text{ mL}$ ). Optical density was measured directly at 305 nm ( $\epsilon$  cluster =  $100\,000 \text{ M}^{-1} \text{ cm}^{-1}$ ).

the toxin-AChR interacting domain (12, 13). The gold cluster covalently linked to this residue is anticipated not to impair the toxin recognition to its ACh binding area.

The disulfide bond introduced on Lys-15 was selectively reduced as described earlier (26). The toxin was separated from the excess of reactants by gel filtration (Biogel P2) and immediately coupled with a 60-fold excess of undecagold cluster 5 to ensure rapid and quantitative reaction in the micromolar range. The new covalent complex was purified by gel filtration (Biogel P10) (Figure 4). The reaction was quantitative since only one radioactive fraction, absorbing at 305 nm, eluted from the column



**Figure 5.** Binding experiments of modified toxins on AChR: [SPDP-modified toxin] = 60 nM; [cluster-modified toxin] = 200 nM; [AChR] = 28 nM to 350 nM.

(the molecular weight of the cluster-bound toxin was approximately 12 kDa). The first nonradioactive fraction had a similar UV spectrum as that of the gold cluster, but this component was not identified. The excess of gold cluster was eluted in the third fraction (MW = 5.3 kDa). The yield of recovery of modified toxin was approximately 30%, the rest being essentially lost in the concentration step before the gel filtration, because the gold cluster is not soluble in high concentration in water media. Its precipitation dragged down a good part of the toxin-cluster complex. No attempts were made to recover it. The stoichiometry cluster/toxin, calculated from the ratio  $\text{OD}_{420\text{nm}}/\text{radioactivity}$ , was found to be equal to 1.

**Binding of the Cluster-Bound Toxin to the Acetylcholine Receptor.** Binding experiments (Figure 5) revealed that 86% of the SPDP-derivatized toxin and 77% of the cluster-bound toxin bind to the acetylcholine receptor. We could thus assume that the biologic activity (active toxin amount)/(total toxin amount) of the two polypeptides were rather similar. The apparent dissociation constant of the complex was found to be 70 pM.

## DISCUSSION

Though regioselective introduction of a single label into a protein is usually a difficult task, successful mono-derivatizations of various snake toxin amino groups were previously reported, following a relatively simple procedure

(29, 30). Using an amino group specific reagent in appropriate stoichiometric conditions, a mixture of toxin derivatives can be generated and subsequently fractionated by ion-exchange chromatography, and series of mono- and polyderivatized toxins are thus readily separated (12). Following a similar approach and using SPDP as an amino group selective reagent we isolated, in a single step, five derivatives carrying each one additional disulfide at position 1, 15, 26, 46, or 50 of toxin- $\alpha$  from *Naja nigricollis* (Figure 2). The terminal NH<sub>2</sub> group is more embedded in the structure than the other amino groups, which could explain the low yield of modification. Lysines 15, 46, and 50 are well exposed to the solvent (31) and are equally modified. Lysine 26 was the most reactive residue, an observation which agrees with its low pK value (9.5) (32, 33). Lysines 25 and 58 were not modified, but the reason for the lack of reactivity is unclear. The additional disulfides introduced by the modification are readily susceptible to reduction, even at low pH (pH = 4.5), as compared to the four intrinsic toxin disulfides which require high concentration of reducing agents and higher pH (34). This property is due to the pyridyl moiety which is protonated at low pH values and is therefore a good leaving group (27). Thus, a thiol group could be generated on different toxin positions providing selective reactive moieties for maleimide containing reagents.

A monomaleimido undecagold cluster was synthesized according to a procedure previously described (22). We coupled this reagent with toxin- $\alpha$  derivatized with an additional thiol group at lys-15. A quantitative introduction of the undecagold cluster at this position had little effect on the binding affinity of the toxin, since the K<sub>d</sub> value for the cluster-bound derivative was equal to 70 pM instead of 20 pM for the native toxin.

We now have a new quasiirreversible antagonist of the nicotinic acetylcholine receptor which possesses a heavy atom core about 8 Å in diameter located at approximately 15–20 Å from the surface of the toxin. The electron-dense core has a smaller size as compared to avidin (30 Å) which was used as a contrast enhancer in previous electron microscopy experiments (11). Moreover, the label can be introduced at four other positions widely spread at the toxin surface. Two of them (positions 1 and 50), like position 15, are clearly excluded from the site by which the toxin interacts with the receptor (12), thus providing two possible additional derivatives with potential interest to study toxin-AChR complexes by electron microscopy.

Reconstructed images with a resolution of 9 Å were recently obtained with tubular crystalline arrangements of AChR (4). Such a resolution should allow a precise localization of our monomodified toxin on its binding site. Moreover, it could help us to elucidate respective positions of the high- and low-affinity ACh binding sites on the pentameric arrangement  $\alpha_2\beta\gamma\delta$ , as, for instance, by occupying the high affinity site with modified toxin and the other with native toxin.

#### ACKNOWLEDGMENT

We would like to acknowledge Dr. O. Trémeau for kind assistance, A. Staub and the microsequencing facility at the LGME, and the AFM, CNRS, and CEA for financial support.

#### LITERATURE CITED

(1) Reynold, J. A., and Karlin, A. (1978) Molecular weight in detergent solution of acetylcholine receptor from *Torpedo californica*. *Biochemistry* 17, 2035–2038.

(2) Raftery, M. A., Hunkapiller, M. H., Strader, C. D., and Hood, L. E. (1980) Acetylcholine receptor: complex of homologous subunits. *Science (Washington D.C.)* 208, 1454–1456.

(3) Brisson, A., and Unwin, P. N. T. (1984) Tubular crystals of acetylcholine receptor. *J. Cell. Biol.* 99, 1202–1211.

(4) Unwin, N. (1993) Nicotinic acetylcholine receptor at 9 Å resolution. *J. Mol. Biol.* 229, 1101–1124.

(5) Tzartos, S. J., and Changeux J. P. (1984) Lipid-dependent recovery of  $\alpha$ -bungarotoxin and monoclonal antibody binding to the purified  $\alpha$ -subunit from *Torpedo marmorata* acetylcholine receptor. *J. Biol. Chem.* 259, 11512–11519.

(6) Langenbuch-Cachat, J., Bon, C., Mulle, C., Goeldner, M. P., Hirth, C., and Changeux J.-P. (1988) Photoaffinity labeling by aryldiazonium derivatives of *Torpedo marmorata* acetylcholine receptor. *Biochemistry* 27, 2337–2345.

(7) Weber, M., and Changeux, J. P. (1974) Binding of *Naja nigricollis* <sup>3</sup>H  $\alpha$ -toxin to membrane fragments from *Electrophorus* and *Torpedo* electric organs. *Mol. Pharm.* 10, 1–40.

(8) Ishikawa, Y., Ménez, A., Hori, H., Yoshida, H., and Tamiya, N. (1977) Structure of snake toxins and their affinity to the acetylcholine receptor of fish electric organ. *Toxicon* 15, 477–488.

(9) Zingsheim, H. P., Barrantes, F. J., Franck, J., Hänicke, W., and Neugebauer, D. C. (1982) Direct structural localization of two toxin-recognition sites on an ACh receptor protein. *Nature* 299, 81–84.

(10) Kubalek, E., Ralston, S., Lindstrom, J., and Unwin, N. (1987) Location of subunits within the acetylcholine receptor by electron image analysis of tubular crystals from *Torpedo marmorata*. *J. Cell. Biol.* 105, 9–18.

(11) Holtzmann, E., Wise, D., Wall, J., and Karlin, A. (1982) Electron microscopy of complexes of isolated acetylcholine receptor, biotinyl-toxin, and avidin. *Proc. Natl. Acad. Sci. U.S.A.* 1982, 310–314.

(12) Faure, G., Boulain, J. C., Bouet, F., Montenay-Garestier, T., Fromageot, P., and Ménez, A. (1983) Role of indole and amino groups in the structure and function of *Naja nigricollis* toxin- $\alpha$ . *Biochemistry* 22, 2068–2076.

(13) Rousselet, A., Faure, G., Boulain, J. C., and Ménez A. (1984) The interaction of neurotoxin derivatives with either acetylcholine receptor or a monoclonal antibody. *Eur. J. Biochem.* 140, 31–37.

(14) Trémeau, O., Boulain, J. C., Couderc, J., Fromageot, P., and Ménez, A. (1986) A monoclonal antibody which recognizes the functional site of snake neurotoxins and which neutralizes all short-chain variants. *FEBS Lett.* 208, 236–240.

(15) Hervé, M., Pillet, L., Humbert, P., Trémeau, O., Ducancel, F., Hirth, C., and Ménez, A. (1992) Role and environment of the conserved Lys-27 of snake curaremimetic toxins as probed by chemical modifications, site-directed mutagenesis and photolabelling experiments. *Eur. J. Biochem.* 208, 125–131.

(16) Pillet, L., Trémeau, O., Ducancel, F., Drevet, P., Zinn-Justin, S., Pinkasfeld, S., Boulain, J.-C., and Ménez, A. (1993) Genetic engineering of snake toxins. *J. Biol. Chem.* 268, 909–916.

(17) Chatrenet, B., Trémeau, O., Bontems, F., Goeldner, M. P., Hirth, C. G., and Ménez, A. (1990) Topography of toxin-acetylcholine receptor complexes by using photoactivatable toxin derivatives. *Proc. Natl. Acad. Sci. U.S.A.* 87, 3378–3382.

(18) Milligan, R. A., Whittaker, M., and Safer, D. (1990) Molecular structure of F-actin and location of surface binding sites. *Nature* 348, 217–221.

(19) Schmutz, M. (1992) Localisation structurale de sites protéiques: localisation d'épitopes du récepteur nicotinique de l'acétylcholine par immuno-microscopie électronique; localisation de la cystéine N-terminale de la sous-unité A<sub>2</sub> de la toxine du choléra par couplage covalent à une sonde dense aux électrons. (Structural localization of proteic sites: localization of AChR epitopes by immunoelectron microscopy; localization of the N-terminal cysteine of the cholera toxin A<sub>2</sub> subunit by covalent coupling to an electron dense probe). Ph.D. thesis, Université Louis Pasteur, Strasbourg I, 22 Oct.

(20) Ménez, A., Morgat, J. L., Fromageot, P., Ronseray, A. M., Boquet, P., and Changeux, J. P. (1971) Tritium labelling of the  $\alpha$ -neurotoxin of *Naja nigricollis*. *FEBS Lett.* 17, 333–335.

- (21) Schiemenz, G. P., and Siebeneick, H. U. (1969) Phosphine mit mehreren Elektronenakzeptorsubstituenten. (Phosphines with several electron acceptor substituents). *Chem. Ber.* 102, 1883-1891.
- (22) Safer, D., Bolinger, L., and Leigh, J. S. (1986) Undecagold clusters for site-specific labeling of biological macromolecules: simplified preparation and model applications. *J. Inorg. Biochem.* 26, 77-91.
- (23) Moore, S., and Stein, W. H. (1948) Photometric ninhydrin method for use in the chromatography of amino acids. *J. Biol. Chem.* 176, 367-388.
- (24) Moore, S. (1968) Amino acid analysis: aqueous dimethyl sulfoxide as solvent for the ninhydrin reaction. *J. Biol. Chem.* 242, 6281-6283.
- (25) Keller, O., and Rudinger, J. (1975) Preparation and properties of maleimido acids and maleoyl derivatives of peptides. *Helv. Chim. Acta* 58, 531-541.
- (26) Léonetti, M., Pillet, L., Maillère, B., Lamthanh, H., Frachon, P., Couderc, J., and Ménez, A. (1990) Immunization with a peptide having both T cell and conformationally restricted B cell epitopes elicits neutralizing antisera against a snake neurotoxin. *J. Immunol.* 145, 4214-4221.
- (27) Carlsson, J. (1978) Protein thiolation and reversible protein-protein conjugation. *Biochem. J.* 173, 723-737.
- (28) Saitoh, T., and Changeux, J. P. (1980) Phosphorylation *in vitro* of membrane fragments from *Torpedo marmorata* electric organ. *Eur. J. Biochem.* 105, 51-62.
- (29) Karlsson, E., Eaker, D., and Ponterius, G. (1972) Modification of amino groups in *Naja naja* neurotoxins and the preparation of radioactive derivatives. *Biochim. Biophys. Acta* 257, 235-248.
- (30) Hori, H., and Tamiya, N. (1976) Preparation and activity of guanidinated or acetylated erabutoxins. *Biochem. J.* 153, 217-222.
- (31) Zinn-Justin, S., Roumestand, C., Gilquin, B., Bontems, F., Ménez, A., and Toma, F. (1992) Three-dimensional solution structure of a curaremimetic toxin from *Naja nigricollis* venom: a proton NMR and molecular modeling study. *Biochemistry* 31, 11335-11347.
- (32) Ménez, A., Montenay-Garestier, T., Fromageot, P., and Hélène, C. (1980) Conformation of two homologous toxins. Fluorescence and circular dichroism studies. *Biochemistry* 19, 5202-5208.
- (33) Ui, N., Takasaki, C., and Tamiya, N. (1982) Isoelectric points of erabutoxins and monoacyl derivatives of erabutoxin b. *Biochem. J.* 203, 427-433.
- (34) Ménez, A., Bouet, F., Tamiya, N., and Fromageot, P. (1976) Conformational changes in two neurotoxic proteins from snake venoms. *Biochem. Biophys. Acta* 453, 121-132.

# Pitfalls in Characterization of Protein Interactions Using Radioiodinated Crosslinking Reagents. Preparation and Testing of a Novel Photochemical $^{125}\text{I}$ -Label Transfer Reagent<sup>1</sup>

Troels Koch,<sup>†</sup> Elisabeth Suenson,<sup>‡</sup> Birgitte Korsholm,<sup>‡</sup> Ulla Henriksen,<sup>\*†</sup> and Ole Buchardt<sup>†</sup>

Research Center for Medical Biotechnology, Department of Organic Chemistry, The H. C. Ørsted Institute, University of Copenhagen, Universitetsparken 5, DK-2100 Copenhagen, Denmark, and Department of Clinical Biochemistry, Section for Hemostasis and Thrombosis, Rigshospitalet, Blegdamsvej 9, DK-2100 Copenhagen, Denmark. Received December 7, 1993\*

Much attention has been focused on the study of protein interactions with radioiodinated photo-crosslinking reagents, and pitfalls in using this methodology are discussed. A new photochemical and cleavable heterobifunctional crosslinking reagent, succinimidyl *N*-14-(2-hydroxybenzoyl)-*N*-11-(4-azidobenzoyl)-9-oxo-8,11,14-triaza-4,5-dithiatetradecanoate (SHAD) was prepared, and its potential as a label transfer reagent was tested in model systems. SHAD was radioiodinated, and the labeled reagent ( $^{125}\text{I}$ -SHAD) was converted to an amide ( $^{125}\text{I}$ -HADM, as a mimicry of conjugation to protein 1) and photolyzed. When compared to the widely used SASD reagent (sulfosuccinimidyl 2-[(4-azidosalicyl)-amino]ethyl]-1,3-dithiopropionate, Pierce), SHAD has a number of decisive advantages. The amide of  $^{125}\text{I}$ -SASD ( $^{125}\text{I}$ -ASDM) was generated and photolyzed, and it was found that at least 50% of the radioactivity is released from  $^{125}\text{I}$ -ASDM after 3 min of irradiation, whereas only approximately 10% is liberated from  $^{125}\text{I}$ -HADM under similar conditions. Furthermore,  $^{125}\text{I}$ -HADM was photolyzed in the presence of excess amine (mimicry of crosslinking to protein 2), and the product was cleaved by reduction (mimicry of label transfer). The transformations in the course of photolysis were monitored by UV spectroscopy and TLC analysis, and a high degree of reagent cleavage upon reduction was demonstrated.  $^{125}\text{I}$ -SHAD was used to crosslink Lys<sub>78</sub>-plasminogen and fibrin.  $^{125}\text{I}$ -SHAD was conjugated to Lys<sub>78</sub>-plasminogen in the dark. Fibrinogen and thrombin were added, and Lys<sub>78</sub>-plasminogen was crosslinked to the fibrin clot by exposure to light. Irradiation for 5 min caused very little labeling of fibrin not crosslinked to Lys<sub>78</sub>-plasminogen; the total recovery of radioactivity was high, and the efficiency of the crosslinking was 30%. Under reducing conditions, it was found that all radioactivity was depleted from the Lys<sub>78</sub>-plasminogen- $^{125}\text{I}$ -HAD conjugates in the dark, and label transfer showed that the labeling of the  $\alpha$ -chain was significantly higher than that of the  $\beta$ - and  $\gamma$ -chains. Analogous experiments with  $^{125}\text{I}$ -SASD revealed that this reagent is much less suitable for photocrosslinking and label transfer studies than  $^{125}\text{I}$ -SHAD. The reactions were followed by polyacrylamide gel electrophoresis.

## INTRODUCTION

Chemical crosslinking (irreversible formation of covalent bonds) has become increasingly popular in identifying the components of protein-protein interactions. The use of photoactivatable probes allows determination of the temporal course of dynamic protein interactions, and crosslinking with heterobifunctional reagents and subsequent cleavage of the linker, resulting in label transfer, is a powerful tool in mapping macromolecular protein-protein interactions (Schwartz et al., 1982; Ji, 1983; Denny and Blobel, 1984; Wollenweber and Morrison, 1985; Sørensen et al., 1986). Label transfer from the primary protein to the secondary protein domain(s) includes at least four successive steps: (1) introduction of the label into the reagent, (2) conjugation of the labeled reagent to the primary protein or ligand, (3) crosslinking to secondary, affinity protein(s), and (4) cleavage of the linker to provide label transfer. In order to obtain meaningful results, it is of utmost importance that the affinity protein(s) or

ligand(s) are labeled by transfer from the reagent and not by unspecific labeling. The most widely used label is  $^{125}\text{I}$ , which is readily introduced in the reagent; the labeled ligands can conveniently be followed by autoradiography, and  $^{125}\text{I}$  is easy to quantitate.

The most widely used photochemical heterobifunctional, cleavable crosslinking reagents are  $^{125}\text{I}$ -labeled in an azidophenyl group. These reagents have recently been shown to have multiple drawbacks. The photocrosslinking efficiency of the aryl azide is low, and the radioiodo label of aromatic azido compounds is released during photolysis and incorporated into surrounding macromolecules in a diffusion-controlled, nonspecific manner. That is, macromolecules or macromolecular domains other than those involved in ligand-affinity interactions become labeled (Watt et al., 1989). Furthermore, nonspecific labeling of the ligands has also been observed prior to photolysis. This "dark-labeling" is mainly due to the widely adopted iodination procedure with Iodo-Beads and can be avoided by purification of the radiolabeled reagent prior to use.

The photolability of the radioiodo label can be avoided (or significantly reduced) by separating the label site and the photoprobe (Henriksen and Buchardt, 1990). SHAD<sup>2</sup> (Scheme 1) was prepared, and its properties were examined and compared to those of the commercially available SASD reagent (Scheme 1) which has been used extensively in biological label transfer studies (Schwartz et al., 1982;

\* Corresponding author.

<sup>†</sup> Research Center for Medical Biotechnology, University of Copenhagen.

<sup>‡</sup> Department of Clinical Biochemistry, Rigshospitalet.

• Abstract published in *Advance ACS Abstracts*, April 15, 1994.

<sup>1</sup> This paper is dedicated to the memory of the late Dr. Elisabeth Suenson.

Wollenweber and Morrison, 1985; Sørensen et al., 1986). The design of SHAD and SASD is similar and the thermal probe and the cleavable linker are the same, but SASD is  $^{125}\text{I}$ -labeled in the photoprobe, whereas SHAD is  $^{125}\text{I}$ -labeled exclusively in the hydroxyphenyl ligand.

In order to obtain photoaffinity crosslinking with this type of reagent, several requirements must be met by the interacting proteins. The thermal probe is conjugated to proteins through lysine residues, and consequently, the primary protein must have an accessible lysine residue close to the binding domain but the residue must not be essential for the interaction studied. The photoprobe reacts with nucleophiles, and consequently, the secondary protein must have accessible nucleophilic side chains close to its binding domain. Furthermore, the time for the photocrosslinking reaction must be less than for dissociation of the protein complex; otherwise only so called "pseudo photoaffinity crosslinking" is observed. Another shortcoming is that the linker is cleaved under reductive conditions that also cleave disulfide bridges in the proteins. Furthermore, the distance between the thermal probe and the photoprobe is crucial in some cases. It has been shown that polyfluorination of the photoprobe (the phenyl azide) changes the photochemical behavior of the azide (Soundararajan and Platz, 1990). Polyfluorinated aryl azides react, contrary to their nonfluorinated analogues by C-H bond insertion, and this type of photoprobe is more effective when the binding site of the target protein consists of hydrophobic amino acid residues (Crocker et al., 1990; Drake et al., 1992).

The fibrinolytic system (Thorsen, 1992) has been extensively studied. It has been demonstrated that Lys-Pg shows enhanced affinity for fibrin, compared to the native Glu-Pg, and has an important function in the t-PA-mediated conversion of plasminogen into active plasmin (Thorsen et al., 1984; Suenson and Thorsen, 1988; Nesheim et al., 1990; Suenson et al., 1990; Fredenburgh and Nesheim, 1992). Fibrin, contrary to fibrinogen, binds both t-PA and plasminogen and stimulates plasminogen activation (Hoylaerts et al., 1982; Suenson et al., 1984; Bosma et al., 1988). The interaction between Lys-Pg and fibrin is consequently of great interest, and we used this system as a model for detailed testing of  $^{125}\text{I}$ -SHAD compared to  $^{125}\text{I}$ -SASD.

## EXPERIMENTAL PROCEDURES

**Materials and Methods.** SASD [sulfosuccinimidyl 2-[[[(4-azidosalicyl)amino]ethyl]-1,3-dithiopropionate] and

<sup>2</sup> Abbreviations used: DTE, dithioerythritol (*erythro*-1,4-dimercapto-2,3-butanediol); SASD, sulfosuccinimidyl 2-[[[(4-azidosalicyl)amino]ethyl]-1,3-dithiopropionate];  $^{125}\text{I}$ -SASD, iodinated sulfosuccinimidyl 2-[[[(4-azidosalicyl)amino]ethyl]-1,3-dithiopropionate];  $^{125}\text{I}$ -ASDM, iodinated 2-[[[(4-azidosalicyl)amino]ethyl]-1,3-dithiopropionamide]; SHAD, succinimidyl *N*-14-(2-hydroxybenzoyl)-*N*-11-(4-azidobenzoyl)-9-oxo-8,11,14-triaza-4,5-dithiatetradecanoate;  $^{125}\text{I}$ -SHAD, iodinated succinimidyl *N*-14-(2-hydroxybenzoyl)-*N*-11-(4-azidobenzoyl)-9-oxo-8,11,14-triaza-4,5-dithiatetradecanoate;  $^{125}\text{I}$ -HADM, iodinated *N*-14-(2-hydroxybenzoyl)-*N*-11-(4-azidobenzoyl)-9-oxo-8,11,14-triaza-4,5-dithiatetradecanamide; NHS, *N*-hydroxysuccinimide; DCC, *N,N'*-dicyclohexylcarbodiimide; THF, tetrahydrofuran; EtOAc, ethyl acetate; DMSO- $d_6$ , hexadeuteriodimethyl sulfoxide; MeOH, methanol; STB, Tris-HCl (0.05 M), NaCl (0.1 M), pH 7.7; SDS, sodium dodecyl sulfate; PAGE, polyacrylamide gel electrophoresis; NIH, National Institutes of Health units; Lys-Pg, Lys<sub>78</sub>-plasminogen, plasmin-modified plasminogen, mainly with N-terminal lysine (residues 78-790); Glu<sub>1</sub>-Pg, native human plasminogen; t-PA, tissue-type plasminogen activator; K1 + 2 + 3, K4, kringles 1-3 and kringles 4 of plasminogen; t-AMCA, *trans*-(4-aminomethyl)cyclohexanecarboxylic acid.

Iodo-Beads (*N*-chlorobenzenesulfamide immobilized on polystyrene) were purchased from Pierce Chemicals Co., Rockford, IL. Empore silica sheets were from 3M, St. Paul, MN. Silica gel, urea, SDS, and DTE were purchased from Merck, Darmstadt, Germany.  $\text{Na}^{125}\text{I}$  in sodium hydroxide pH 7-11 (84  $\mu\text{M}$ , 100 mCi/mL, carrier free) and  $^{14}\text{C}$ -methylated protein molecular weight markers were from Amersham, Buckinghamshire, England. Sephadex G 25F was from Pharmacia, Uppsala, Sweden. All standard chemicals were analytical grade and were used without further purification, except 3-aminopropanol which was distilled prior to use. TLC-solvents (v/v): solvent A, ethyl acetate/methanol 85/15; solvent B, chloroform/methanol/acetic acid 85/10/5. Phosphate buffer I: 6.93 mM, pH 8.00. Phosphate buffer II: 52.8 mM, pH 8.25. Phosphate buffer III: 0.5 M, pH 7.0.

**Proteins.** Preparations of human fibrinogen, thrombin, and Lys-Pg were those described previously. The concentrations of Lys-Pg and fibrinogen were determined spectrophotometrically at 280 nm (Suenson et al., 1984; Suenson and Thorsen, 1988). Aprotinin (Trasylol) was from Bayer, Leverkusen, Germany.

All manipulations with label transfer reagents were carried out in the dark, or with Kodak safe light filter No. 6B. Photolysis was done with one UV tube ( $\lambda_{\text{max}}$  310 nm) "TL" 20W/12 (Phillips, Eindhoven, the Netherlands) at a distance of 10 cm with Pyrex filter. UV spectra were recorded on a Hewlett-Packard diode array spectrophotometer 8452 A.  $^1\text{H}$  NMR spectra were recorded on a JEOL FX 90Q spectrometer. Radiolabeled samples were counted in an LKB 1282 Compugamma. Autoradiography of TLC plates and polyacrylamide gels was done with Agfa Cuprix RP-1 films in Agfa Cuprix MR 400 cassettes and developed in a Kodak RP X-Omat processor.

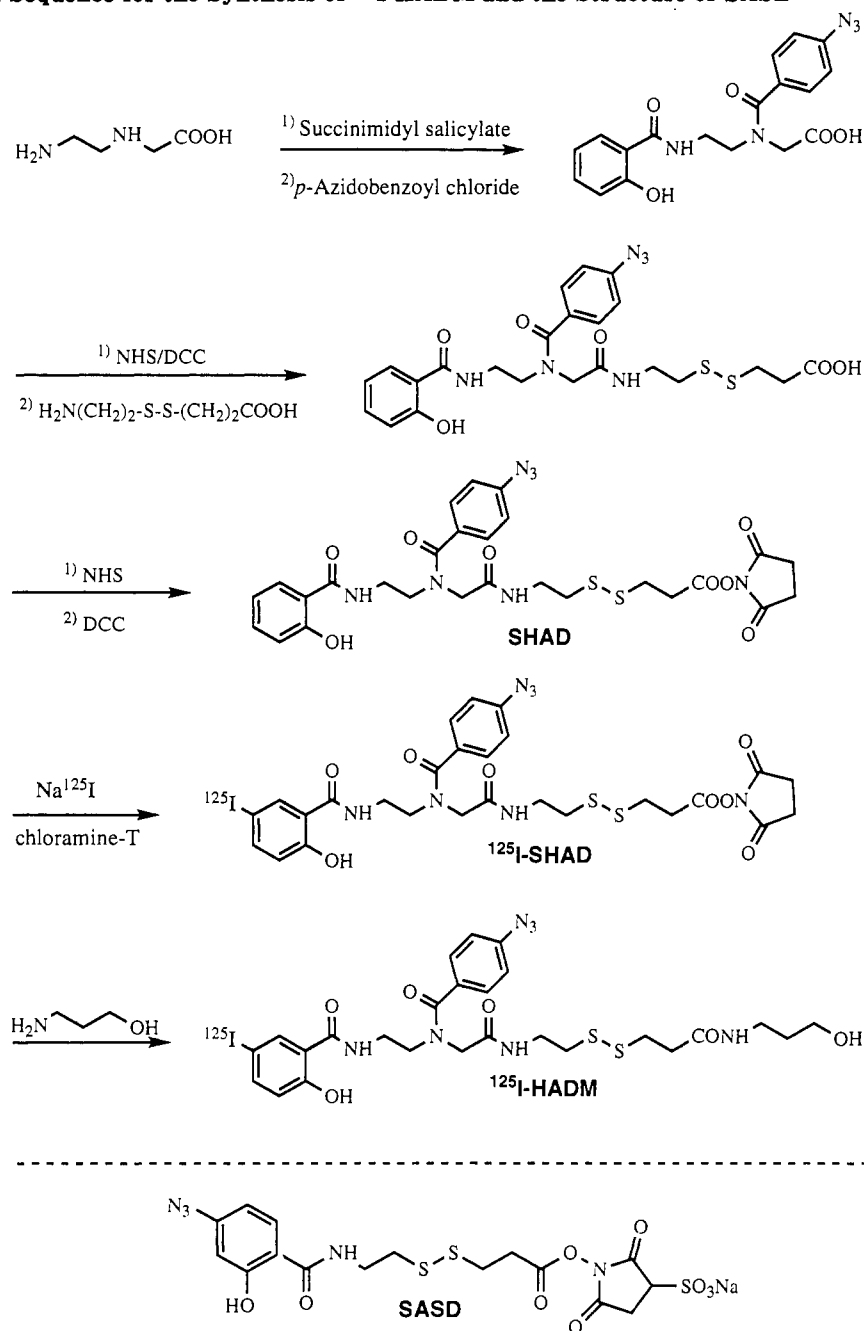
**Succinimidyl salicylate** was prepared from salicylic acid (5.0 g, 36.2 mmol), NHS (4.58 g, 39.8 mmol), and DCC (8.95 g, 43.4 mmol) in THF (80 mL) by a standard procedure (Koch et al., 1990). The product (7.81 g, 91%) was recrystallized from methanol:  $^1\text{H}$  NMR ( $\text{CDCl}_3$ )  $\delta$  9.49 (s, 1 H), 7.99 (d, 1 H), 7.59 (t, 1 H), 7.07-6.88 (m, 2 H), 2.90 (s, 4 H).

***N*-6-(2-Hydroxybenzoyl)-*N*-3-(4-azidobenzoyl)-3,6-diazaheptanoic Acid.** (Aminoethyl)glycine (Heimer et al., 1984) (6.58 g, 56 mmol) was dissolved in water, and triethylamine (23.5 mL) was added. After the mixture was cooled in an ice bath, succinimidyl salicylate (13.1 g, 56 mmol) in THF (300 mL) was added during 1 h. 4-Azidobenzoyl chloride (10.2 g, 56 mmol) in THF (100 mL) was added dropwise, and the mixture was then evaporated to half volume. The pH was adjusted to 10, the mixture was filtered, and the byproducts were extracted with EtOAc. After acidification, the aqueous layer was extracted with three portions of EtOAc, and the combined extracts were evaporated after drying. The product (15.2 g, 71%) was dissolved in EtOAc and precipitated with petroleum ether:  $^1\text{H}$  NMR ( $\text{DMSO}-d_6$ )  $\delta$  12.2 (broad, 2 H), 8.81 (broad, 1 H), 7.51 (t, 1 H), 7.42-6.80 (m, 8 H), 4.18 (s, 2 H), 3.46 (m, 4 H); MS (EI) 383 ( $\text{M}^+$ ).

**Succinimidyl *N*-6-(2-hydroxybenzoyl)-*N*-3-(4-azidobenzoyl)-3,6-diazaheptanoate** was prepared as described for succinimidyl salicylate and used without further purification.

***N*-14-(2-Hydroxybenzoyl)-*N*-11-(4-azidobenzoyl)-9-oxo-8,11,14-triaza-4,5-dithiatetradecanoic Acid.** Succinimidyl *N*-6-(2-hydroxybenzoyl)-*N*-3-(4-azidobenzoyl)-3,6-diazaheptanoate (1 equiv) was dissolved in THF; 7-amino-4,5-dithiaheptanoic acid (2 equiv) (Schnaar et al., 1985) and triethylamine (4 equiv) were added dropwise.



Scheme 1. Reaction Sequence for the Synthesis of  $^{125}\text{I}$ -HADM and the Structure of SASD

The mixture was stirred for 15 min, evaporated, and suspended in water. The pH was adjusted to 10 with triethylamine, and the byproducts were extracted with EtOAc. After acidification, the aqueous layer was extracted with three portions of EtOAc, and the combined extracts were evaporated after drying and used without further purification.

**Succinimidyl *N*-14-(2-hydroxybenzoyl)-*N*-11-(4-azidobenzoyl)-9-oxo-8,11,14-triaza-4,5-dithiatetradecanoate (SHAD)** was prepared from *N*-14-(2-hydroxybenzoyl)-*N*-11-(4-azidobenzoyl)-9-oxo-8,11,14-triaza-4,5-dithiatetradecanoic acid (1.05 g, 1.92 mmol), NHS (0.243 g, 2.11 mmol), and DCC (0.475 mg, 2.30 mmol) in THF (20 mL) by the standard procedure. The product (0.674 g, 55%) was passed through a silica gel column (elution with EtOAc:MeOH, 98:2). The product should be stored at  $-20^\circ\text{C}$ :  $^1\text{H}$  NMR ( $\text{CDCl}_3$ )  $\delta$  7.55–6.88 (m, 8 H), 4.08 (s, 2H), 3.71 (m, 6 H), 3.05 (s, 4 H), 2.84 (s, 4 H); MS (FAB $^+$ ) 644 ( $M + 1$ ).

**$^{125}\text{I}$ Iodination of SHAD.** To SHAD (3.75  $\mu\text{mol}$ ) in acetonitrile (600  $\mu\text{L}$ ) was added sodium phosphate buffer III (3.75  $\mu\text{L}$ ), NaI (100 mM) in acetonitrile (75  $\mu\text{L}$ ), and  $\text{Na}^{125}\text{I}$  (84  $\mu\text{mol}$ , 30  $\mu\text{L}$ , 100 mCi/mL) in NaOH (pH 8–11). Chloramine-T (15  $\mu\text{mol}$ ) in acetonitrile (300  $\mu\text{L}$ ) was added, and the mixture was placed on a rocking table for 10 min at room temperature. The iodinated reagent was purified by TLC on Empore Sheets (10  $\times$  10 cm). A 330- $\mu\text{L}$  portion of the reaction mixture was applied on each sheet in elongated bands, and the sheets were eluted with solvent A. The fastest moving band was cut out and extracted twice with EtOAc (10 mL). The extracts were combined, and the solvent was evaporated with a stream of nitrogen; 63% was obtained as purified iodinated label transfer reagent, and 31% of the total iodide used was incorporated. After evaporation the residue was dissolved in acetonitrile (1.5 mL).

**$^{125}\text{I}$ Iodination of SASD.** To SASD (0.1  $\mu\text{mol}$ ) dissolved in acetonitrile (50  $\mu\text{L}$ ) was added phosphate buffer III (10

$\mu\text{L}$ ), sodium iodide (5  $\mu\text{L}$ , 84  $\mu\text{M}$  containing 30  $\mu\text{Ci}$  of  $\text{Na}^{125}\text{I}$ ), and 1 Iodo-Bead. The mixture was incubated for 2 min at room temperature.

**Preparation of  $^{125}\text{I}$ -HADM and Characterization of Its Transitions during Photolysis.** To 1200  $\mu\text{L}$  of the solution of  $^{125}\text{I}$ -SHAD was added 3-aminopropanol (200  $\mu\text{mol}$ ), and after 2 min the mixture was purified by Empore Sheets as described above (as eluent was used solvent B). The fastest moving band was excised, and 3.9  $\mu\text{mol}$  of purified material was isolated.  $^{125}\text{I}$ -HADM (0.15  $\mu\text{mol}$ ) in acetonitrile (12  $\mu\text{L}$ ) was added to phosphate buffer I (1500  $\mu\text{L}$ ) and photolyzed. UV spectra were recorded, and aliquots (50  $\mu\text{L}$ ) were taken at time intervals of 0, 10, 20, 40, 60, 120, 180, 240, 600, 1200, 1800 s and applied on analytic TLC plates (eluent solvent B). The spots were excised and counted, and the total recovered radioactivity was calculated.

**Simulation of Label Transfer.**  $^{125}\text{I}$ -SHAD was dissolved in acetonitrile (500  $\mu\text{L}$ , 0.1 mM), DTE (to 100 mM) was added, and the mixture was refluxed for 2 min. To  $^{125}\text{I}$ -SHAD in acetonitrile (20  $\mu\text{L}$ , 7.63 mM) was added acetonitrile (80  $\mu\text{L}$ ), sodium phosphate buffer I (1.4 mL), and 3-aminopropanol (2  $\mu\text{L}$ ). After 2 min, the mixture was irradiated for 4 min, DTE (to 100 mM) was added, and the mixture was refluxed for 2 min. The reaction was followed by TLC (solvent B).

**Conjugation of  $^{125}\text{I}$ -SHAD and  $^{125}\text{I}$ -SASD to Lys-Pg.** To  $^{125}\text{I}$ -SHAD (76.3 nmol) in acetonitrile (10  $\mu\text{L}$ ) was added Lys-Pg (3.68 nmol) in sodium phosphate buffer II (150  $\mu\text{L}$ ). The mixture was incubated for 30 min on a rocking table, purified by gel filtration on Sephadex G 25 F (5 mL), and eluted with STB at 10 mL/h; only 0.85% of the radioactivity was found in nonconjugated material. When  $^{125}\text{I}$ -SASD was conjugated in the same way, 5.6% of the radioactivity was found in the nonconjugated material. The specific radioactivity was 274 MBq/ $\mu\text{mol}$  for the Lys-Pg- $^{125}\text{I}$ -HAD conjugate and 418/ $\mu\text{mol}$  for the Lys-Pg- $^{125}\text{I}$ -ASD conjugate.

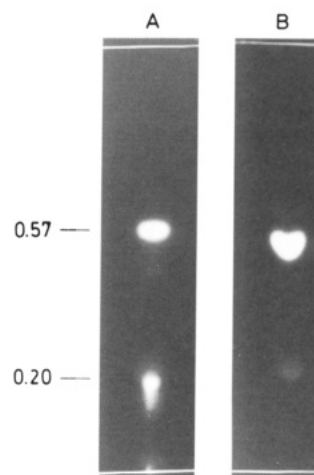
**Crosslinking Assay.** Aprotinin (5  $\mu\text{L}$  380  $\mu\text{M}$ , plasmin inhibitor), Lys-Pg- $^{125}\text{I}$ -HAD- or Lys-Pg- $^{125}\text{I}$ -ASD conjugate (30  $\mu\text{L}$  1.5  $\mu\text{M}$ ), fibrinogen (60  $\mu\text{L}$  7.5  $\mu\text{M}$ ), and thrombin (25  $\mu\text{L}$  6 NIHU/mL) were mixed in STB (180  $\mu\text{L}$ ). The mixture was incubated for 10 min in the dark at room temperature and irradiated for 5 min, and urea (to 6 M) and SDS (to 35 mM) were added to quench the reactions and dissolve the clot.

The conjugation and crosslinking were analyzed by SDS (3–5%) PAGE (Weber and Osborn, 1975). The gels were autoradiographed (Weisel et al., 1994), and the bands were subsequently excised and counted.

**Label Transfer.** Conjugation and crosslinking were performed as described above. Aliquots (100  $\mu\text{L}$ ) were taken, DTE (to 100 mM) was added, and the mixtures were refluxed for 2 min. The reactions were analyzed by SDS (7.5%) PAGE. The gels were autoradiographed, and the bands were subsequently excised and counted.

## RESULTS AND DISCUSSION

**Iodination of SHAD.** The iodination was preferentially performed in organic solvents instead of water in order to minimize hydrolysis of the succinimidyl probe (Shephard et al., 1988). In pilot experiments, the degree of reagent iodination was judged from autoradiographs of TLC analyses of the reaction mixtures. Acetonitrile and acetone were compared as solvents, and Iodo-Beads and nonimmobilized chloramine-T were compared as oxidizing agents. Optimal results were obtained using chloramine-T in acetonitrile. Nonimmobilized chloramine-T gave no-



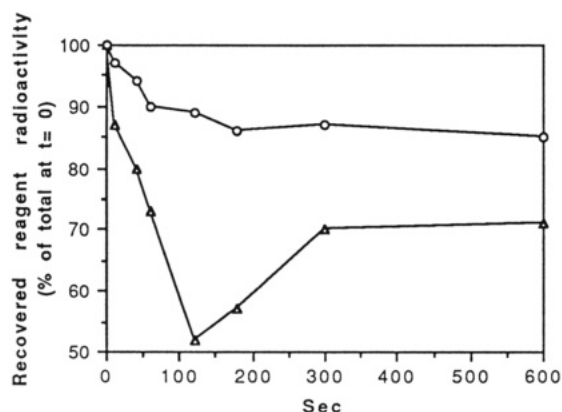
**Figure 1.** Autoradiography of the TLC analysis in EtOAc/MeOH (85/15) of (A)  $^{125}\text{I}$ -SHAD (reaction mixture) after 10 min incubation at room temperature and (B) purified  $^{125}\text{I}$ -SHAD.



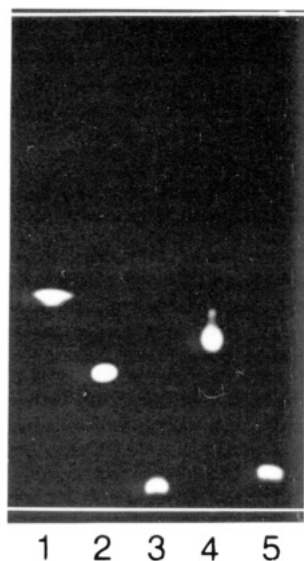
**Figure 2.** Autoradiography of the TLC analysis in  $\text{CHCl}_3/\text{MeOH}/\text{AcOH}$  (85/10/5) of the time course of photolysis of  $^{125}\text{I}$ -HADM. Lane 1:  $^{125}\text{I}$ -HADM (0.15  $\mu\text{mol}$ ) in phosphate buffer I (1500  $\mu\text{L}$ ). Lanes 2–8 represent photolysis for 10, 20, 40, 60, 120, 180, and 240 s, respectively.

tably higher yields and fewer byproducts than Iodo-Beads. When iodide and chloramine-T were present in equimolar concentrations, iodide was oxidized to iodine, and no reagent iodination was detected. Increasing the chloramine-T concentration to a 2 M excess accomplished aromatic electrophilic substitution (iodination) by giving rise to a more highly reactive iodine species (iodine chloride). Iodination of SHAD on a preparative scale with nonradiolabeled NaI and chloramine-T showed that no iodine is incorporated into the azidophenyl ligand and that the hydroxyphenyl ligand is iodinated almost exclusively in the 5-position.  $^{125}\text{I}$ -SHAD was purified after the iodination procedure to remove hydrolyzed reagent (the compound with  $R_f = 0.2$  in Figure 1A) and excess of iodination reagent that otherwise will be directly incorporated into tyrosine residues in a subsequent protein modification step. Autoradiography of the TLC analysis of  $^{125}\text{I}$ -SHAD is shown in Figure 1. Upon solvent evaporation and storage at  $-20^\circ\text{C}$ , the radiolabeled reagent is stable for at least 3 weeks.

**Reagent Photolysis and Resultant Deiodination.** The photostability of the radioiodine substituent of  $^{125}\text{I}$ -SHAD was investigated and compared to that of  $^{125}\text{I}$ -SASD. In order to simulate label transfer conditions,  $^{125}\text{I}$ -SHAD was reacted with excess 3-aminopropanol prior to photolysis in the aqueous system. The time course of



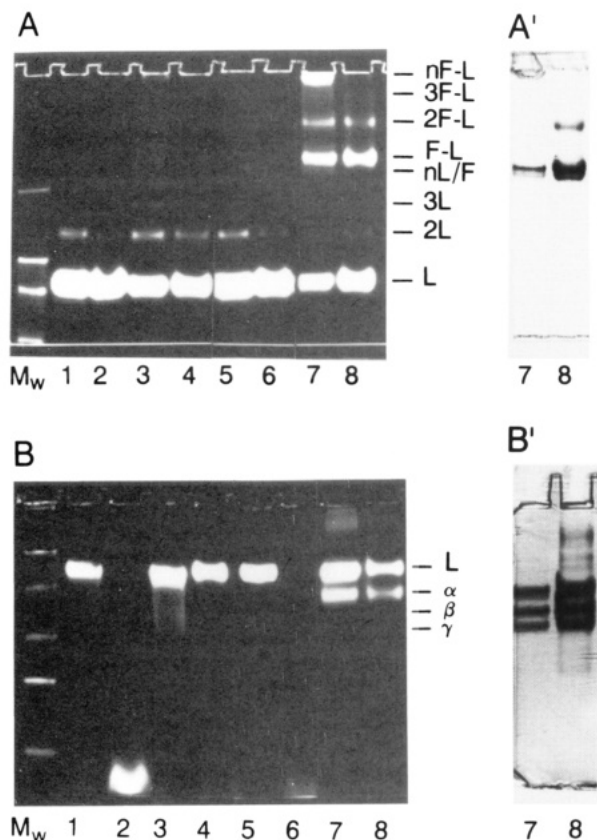
**Figure 3.** Recovered radioactivity: (O) total radioactivity recovered for  $^{125}\text{I}$ -HADM and its photolysis products. The spots displayed in Figure 2 were excised and counted. ( $\Delta$ ) Total radioactivity recovered for  $^{125}\text{I}$ -ASDM and its photolysis products from a similar experiment (the autoradiography is not shown). The results are representative of three trials.



**Figure 4.** Autoradiography of the TLC analysis of simulated label transfer with  $^{125}\text{I}$ -SHAD. Lane 1: nonphotolyzed  $^{125}\text{I}$ -SHAD in acetonitrile (0.1 mM, 500  $\mu\text{L}$ ). Lane 2: nonphotolyzed reaction mixture containing  $^{125}\text{I}$ -SHAD (7.63 mM, 20  $\mu\text{L}$ ), acetonitrile (80  $\mu\text{L}$ ), phosphate buffer I (1.4 mL), and 3-aminopropanol (2  $\mu\text{L}$ ), incubated for 2 min; this mixture is used in the following experiments. Lane 3: photolysis of the reaction mixture for 4 min. Lane 4: nonphotolyzed reaction mixture after reduction with DTE (100 mM). Lane 5: reduction of the photolyzed reaction mixture with DTE (100 mM).

photolysis was examined by UV spectroscopy (not shown) as well as by TLC analysis (Figure 2). UV spectroscopy showed typical azide photodegradation, yielding isosbestic points. These were maintained after 3–4 min of photolysis and thereafter slowly faded out. Photolysis was almost complete after 4 min, judging from both UV spectroscopy and TLC analysis.

On the basis of the autoradiograms, the  $^{125}\text{I}$  content in the organic species was determined (Figure 3). The radioactivity of the products and the unchanged amide during photolysis was determined and related to the activity of unphotolyzed amide. Eighty-five to 90% of the total reagent radioactivity is recovered in the products after 3–5 min of irradiation. Figure 3 shows that the deiodination is more pronounced in the initial minute of photolysis and decreases with product formation. The products may act as internal filters or quench the excited state that leads to deiodination, thus interfering with the



**Figure 5.** Panel A: autoradiography of SDS (3–5%) PAGE under nonreducing conditions of Lys-Pg conjugated to  $^{125}\text{I}$ -SASD (lanes with uneven numbers) or to  $^{125}\text{I}$ -SHAD (lanes with even numbers) and crosslinking of the Lys-Pg conjugates with fibrin.  $M_w$ : reduced mixture of  $^{14}\text{C}$ -labeled protein molecular weight standards ( $M_r$  = 200, 92.5, 69, and 46 kDa). Lane 1: Lys-Pg- $^{125}\text{I}$ -ASD conjugates, formed from  $^{125}\text{I}$ -SASD (73.9 nmol) and Lys-Pg (3.68 nmol) in phosphate buffer II (150  $\mu\text{L}$ ) after 30 min incubation in the dark and purified by gel filtration. Lane 2: Lys-Pg- $^{125}\text{I}$ -HAD conjugates, formed as described under lane 1. Lane 3: Lys-Pg- $^{125}\text{I}$ -ASD conjugates irradiated for 5 min. Lane 4: Lys-Pg- $^{125}\text{I}$ -HAD conjugates irradiated for 5 min. Lane 5: Lys-Pg- $^{125}\text{I}$ -ASD conjugates (0.15  $\mu\text{M}$ ), aprotinin (6.3  $\mu\text{M}$ ), fibrinogen (1.5  $\mu\text{M}$ ), and thrombin (0.5 MIHu/mL) in STB (300  $\mu\text{L}$ ) incubated for 10 min in the dark. Lane 6: Lys-Pg- $^{125}\text{I}$ -HAD conjugates, aprotinin, fibrinogen, and thrombin in STB as described under lane 5. Lane 7: the mixture described under lane 5 irradiated for 5 min. Lane 8: the mixture described under lane 6 irradiated for 5 min. nF-L: Lys-Pg- $^{125}\text{I}$ -reagent-n fibrin complexes ( $n > 3$ ). 3F-L: Lys-Pg- $^{125}\text{I}$ -reagent-3 fibrin complexes. 2F-L: Lys-Pg- $^{125}\text{I}$ -reagent-2 fibrin complexes. F-L: Lys-Pg- $^{125}\text{I}$ -reagent-fibrin complexes. nL/F:  $n$  Lys-Pg complexes or/and fibrin ( $n > 3$ ). 3L: Lys-Pg- $^{125}\text{I}$ -reagent trimer. 2L: Lys-Pg- $^{125}\text{I}$ -reagent dimer. L: Lys-Pg- $^{125}\text{I}$ -reagent conjugates. Panel A': as panel A but stained with Coomassie Brilliant Blue R250 (only lanes 7 and 8 are shown). Panel B: autoradiography of SDS (7.5%) PAGE under reducing conditions.  $M_w$ : reduced mixture of  $^{14}\text{C}$ -labeled protein molecular weight standards ( $M_r$  = 200, 92.5, 69, 46, 30, 21.5, and 14.3 kDa). The lanes correspond to those in panel A, except that all mixtures have been reduced with DTE prior to SDS-PAGE. L: Lys-Pg.  $\alpha$ -,  $\beta$ -, and  $\gamma$ :- the three polypeptide chains from reduced fibrin. Panel B': as panel B but stained with Coomassie Brilliant Blue R250 (only lanes 7 and 8 are shown).

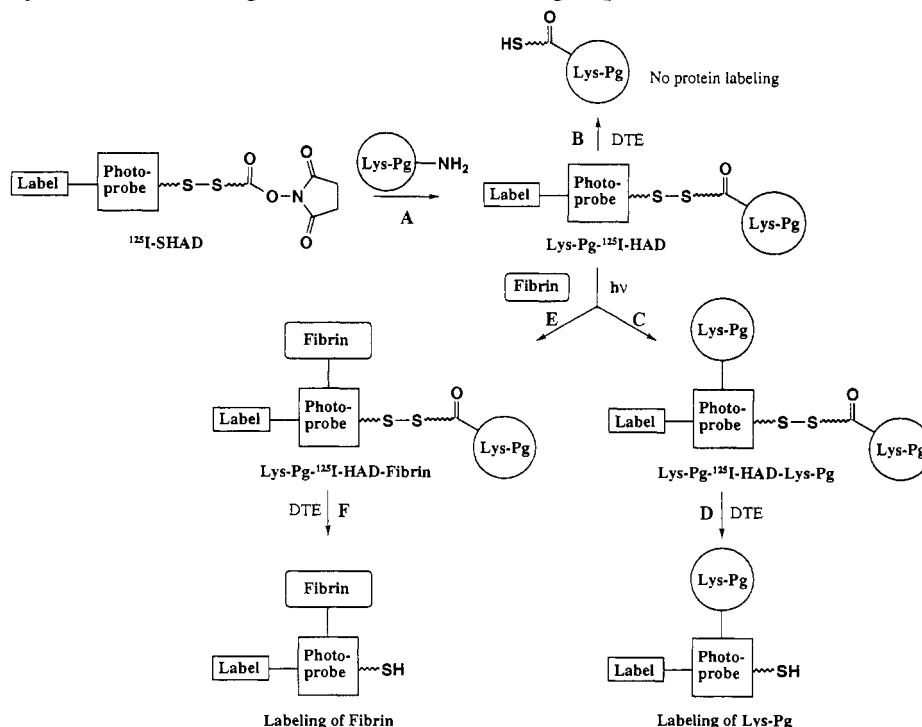
photodeiodination. Furthermore, a small amount of diiodinated reagent is present, and this compound loses iodine much faster than the monoiodinated reagent (Davidson et al., 1984). We performed a similar experiment with  $^{125}\text{I}$ -SASD and found that after 2 min only 50% was retained in the organic species. Further irradiation unexpectedly increased the recovered radioactivity by about 20%. This may be explained by massive initial  $^{125}\text{I}$ -release (Watt et al., 1989) and subsequent photo-

**Table 1. Recovered Radioactivity from SDS-PAGE of the Products from Crosslinking Lys-Pg and Fibrin with  $^{125}\text{I}$ -SASD and  $^{125}\text{I}$ -SATD<sup>a</sup>**

lane <sup>b</sup>	nonreducing conditions								reducing conditions							
	nF-L <sup>c</sup>	2F-L	nL	F-L	nL/F	3L	2L	L	total <sup>d</sup>	frct 1-4 <sup>e</sup>	L	$\alpha$ -	$\beta$ -	$\gamma$ -chain	frct 12-13 <sup>f</sup>	total <sup>d</sup>
1						1	4	49	56		6.5				1.5	10
2						0.5	3	69	75		0.5				2.5	3
3	5	3	2		4	3	6	29	59	2	11				2	17
4	1.5	1	1	1	4	3	7	40	62	2	7				2.5	13
5				0.5	2	1	4.5	64	74	1	7	0.5			1.5	12
6					0.5	0.5	3.5	89	97		0.5				3.5	5
7	15	7	2.5	10	2	0.5	1	16	56	5	8.5	4	1	1	2	23
8	12	10	2	18	4	1.5	3	40	94	5	8	6	1.5	1.5	4	23

<sup>a</sup> Percentage of the applied radioactivity corrected for gel background; the first part of the table is from SDS (3–5%) PAGE under nonreducing conditions, the second part from SDS (7.5%) PAGE under reducing conditions. The values given are from individual experiments, but the same trend was observed in a series of experiments. <sup>b</sup> The lanes correspond to those in Figure 5A and B. <sup>c</sup> Corresponds to the complexes given in the legend to Figure 5. <sup>d</sup> Total recovered radioactivity from the lanes. <sup>e</sup> High molecular weight unidentified proteins. <sup>f</sup> Low molecular weight unidentified compounds.

## Scheme 2. Pathways for the Plasminogen and Fibrin Crosslinking Experiments



chemical iodination of organic compounds in the reaction mixture, including photolyzed ASDM species and impurities.

Preparative photolysis of iodinated *N*-(4-azidobenzoyl)-tyrosine gave products with iodine retained (Henriksen and Buchardt, 1990), but a similar experiment with I-HADM revealed that iodine is released under these conditions. Furthermore, iodinated *N*-salicylyl-*N'*-(4-azidobenzoyl)-1,6-hexanediamine was photolyzed preparatively, and no iodine was observed in the products, indicating that it is the carbonyl group of the salicylyl ligand that is responsible for the deiodination on prolonged irradiation.

**Cleavage of  $^{125}\text{I}$ -HADM and the Photolysis Products by Reduction.** In order to simulate label transfer the reagent must be cleaved. This is in most cases done by adding mercapto compounds to the label transfer mixture. DTE was added to the native  $^{125}\text{I}$ -HADM and to the photolysis products (Figure 4). As seen from the autoradiograms, the disulfides are readily cleaved, yielding compounds with a slightly higher  $R_f$  value. Apparently only one product is formed on photolysis in the presence of 3-aminopropanol (Figure 4, lane 3), which corresponds

to reaction of the initially generated dehydroazepine with the amino group of 3-aminopropanol (Nielsen and Buchardt, 1982; Shields et al., 1988; Henriksen and Buchardt, 1990).

**Formation of Lys-Pg Conjugates with  $^{125}\text{I}$ -SHAD and  $^{125}\text{I}$ -SASD: Irradiation and Reduction of the Conjugates.** Autoradiography of SDS-PAGE analyses of the reaction profiles is shown in Figure 5, lanes 1–4, and the recovered radioactivity is summarized in Table 1.  $^{125}\text{I}$ -SHAD and  $^{125}\text{I}$ -SASD were conjugated to Lys-Pg (reaction A in Scheme 2) and 72% of the applied radioactivity was found in the bands representing the Lys-Pg- $^{125}\text{I}$ -HAD conjugates, versus 54% for the Lys-Pg- $^{125}\text{I}$ -ASD conjugates. Three to 4% of the radioactivity was found in bands presumably representing two crosslinked Lys-Pg. This is unexpected since the conjugates were not exposed to light. Disulfide exchange may be responsible for this dimer formation, since it is known that disulfide interchange occurs spontaneously in neutral and alkaline solution and is promoted by thiols and thiourea (Eager and Savige, 1963). After reduction of the Lys-Pg- $^{125}\text{I}$ -ASD conjugates, 6.5% of the radioactivity was still found in Lys-Pg indicating incomplete reduction or nonspecific labeling.

As expected, only 0.5% was found in Lys-Pg after reduction of the Lys-Pg-<sup>125</sup>I-HAD conjugates (reaction B in Scheme 2), indicating that the reduction of the disulfide is complete and that no nonspecific labeling of Lys-Pg occurs with this reagent. After irradiation of the Lys-Pg-<sup>125</sup>I-HAD- and the Lys-Pg-<sup>125</sup>I-ASD conjugates, 40 and 29%, respectively, of the radioactivity were still found in Lys-Pg, meaning that most of the photoprobes have reacted with the solvent, but complexes containing two (pathway C in Scheme 2), three, or more Lys-Pg were also observed, indicating a certain affinity between Lys-Pg molecules. After reduction, most of the recovered radioactivity was, as expected, found in Lys-Pg (reaction D in Scheme 2).

**Photocrosslinking of Fibrin and the Lys-Pg-<sup>125</sup>I-HAD and Lys-Pg-<sup>125</sup>I-ASD Conjugates and Reduction of the Complexes (Label Transfer).** Autoradiography of SDS-PAGE analyses of the reaction profiles is shown in Figure 5, lanes 5-8, and the recovered radioactivity is summarized in Table 1. The assignment of the bands was performed as described by Weisel et al. (1994). The Lys-Pg conjugates were mixed with fibrinogen in the dark, and clot formation was initiated with thrombin. A total of 93% of the applied radioactivity was found in the Lys-Pg-<sup>125</sup>I-HAD conjugates, and no nonspecific labeling of fibrin was observed. After reduction, no significant radioactivity was observed in either Lys-Pg or the  $\alpha$ -,  $\beta$ -, and  $\gamma$ -chains of fibrin. On the contrary, significant radioactivity was observed both in Lys-Pg and in the  $\alpha$ -,  $\beta$ -, and  $\gamma$ -chains when the Lys-Pg-<sup>125</sup>I-ASD conjugates were reduced in the presence of fibrin.

Photocrosslinking was accomplished by irradiation of the clot, but approximately 45% of the radioactivity was still found in the Lys-Pg-<sup>125</sup>I-HAD conjugates (40% in noncrosslinked Lys-Pg), and only approximately 40% in the Lys-Pg-<sup>125</sup>I-HAD-fibrin complexes (pathway E in Scheme 2). The high percentage of radioactivity found in noncrosslinked Lys-Pg could be expected, since only photoprobes close to the fibrin binding site(s) of Lys-Pg are effective in the crosslinking process. The K1 + 2 + 3, K4, and Val<sub>443</sub>-plasminogen domains are all modified with <sup>125</sup>I-SASD (Weisel et al., 1994). Complex formation between modified Lys-Pg and fibrin is inhibited by *t*-AMCA, showing that lysine binding sites are involved in a photoaffinity crosslinking process (Weisel et al., 1994).

Label transfer was then performed by reduction of the complexes (reaction F in Scheme 2), and 6% of the applied radioactivity was found in the  $\alpha$ -chain, 1.6% in the  $\beta$ -chain, and 1.7% in the  $\gamma$ -chain when <sup>125</sup>I-SHAD was used as photocrosslinker. A total of 8% of the radioactivity was found in Lys-Pg (from cleavage of crosslinked Lys-Pg molecules). Similar results were obtained when <sup>125</sup>I-SASD was used as crosslinker. The yield of label transfer to the  $\alpha$ -,  $\beta$ -, and  $\gamma$ -chains of fibrin is expected to be low since most of the radioactivity is found in Lys-Pg complexes before reduction. However, the observation that the labeling of the  $\alpha$ -chain of fibrin is four times the labeling of the  $\beta$ - and  $\gamma$ -chains is conclusive, since it was demonstrated that no nonspecific labeling of fibrin takes place when <sup>125</sup>I-SHAD was used as photocrosslinker.

## CONCLUSION

Substitution of the radioiodine into a separate hydroxybenzoyl group, or better a hydroxyphenyl group, instead of the photoreactive phenyl azide of SASD radically decreases photoinduced liberation of radioiodine. The yield of reduction of the disulfide linker is almost quantitative, a feature that is essential for high methodological sensitivity. Markedly reduced photodeiodination

as well as removal of oxidant and free radioiodide from the reagent after iodination potentially inhibit non-crosslinker related direct incorporation of radioiodine into protein tyrosine residues. In theory, both methodological sensitivity and specificity are thus markedly increased for SHAD compared to SASD. These potential advantages hold in parallel protein crosslinking experiments, indicating that the described TLC analyses of novel crosslinking reagents is highly advantageous in predicting their use in protein systems and in interpreting the results.

Fibrin has binding sites for both plasminogen and t-PA. The latter is bound to fibrin at the distal end of the coiled-coil regions, connecting the D-domains with the central E-domain (Schieren et al., 1991), and it seems reasonable to assume that plasminogen binds to fibrin in the vicinity of the activator. Although the yield of label transfer is low, we conclude that the labeling of the  $\alpha$ -chains of fibrin is significantly higher than for the  $\beta$ - and  $\gamma$ -chains, indicating that the plasminogen binding domain is located on the  $\alpha$ -chain, close to the coiled-coil regions.

## ACKNOWLEDGMENT

This work was supported by the Danish Natural Science Research Counsel (Grant No. 11-8133 to T.K.). We thank Dr. Michael Egholm for suggesting the use of (aminoethyl)-glycine and for donating a sample.

## LITERATURE CITED

- Bosma, P. J., Rijken, D. C., and Nieuwenhuizen, W. (1988) Binding of tissue-type plasminogen activator to fibrinogen fragments. *Eur. J. Biochem.* 172, 399-404.
- Crocker, P. J., Nobuyuki, I., Rajagopalan, K., Boggess, M. A., Kwiatkowski, S., Dwyer, L. D., Vanaman, T. C., and Watt, D. S. (1990) Heterobifunctional crosslinking Agents Incorporating Perfluorinated Aryl Azides. *Bioconjugate Chem.* 1, 419-424.
- Davidson, R. S., Gooden, J. W., and Kemp, G. (1984) The Photochemistry of Aryl Halides and Related Compounds, in *Advances in Physical Organic Chemistry* 20 (V. Gold, and D. Bethell, Eds.) pp 191-233, Academic Press, London.
- Denny, J. B., and Blobel, G. (1984) <sup>125</sup>I-labeled crosslinking reagent that is hydrophilic, photoactivable, and cleavable through an azo-linkage. *Proc. Natl. Acad. Sci. U.S.A.* 81, 5286-5290.
- Drake, R. R., Slama, J. T., Wall, K. A., Abramova, M., D'Souza, C., Elbein, A. D., Crocker, P. J., and Watt, D. S. (1992) Application of an *N*-(4-Azido-2,3,5,6-tetrafluorobenzoyl)tyrosine-Substituted Peptide as a Heterobifunctional Cross-Linking Agent in a Study of Protein O-Glycosylation in Yeast. *Bioconjugate Chem.* 3, 69-73.
- Eager, J. E., and Savige, W. E. (1963) Photolysis and Photo-oxidation of Amino Acids and Peptides-VI. A study of the Initiation of Disulfide Interchange by Light Irradiation. *Photochem. Photobiol.* 2, 25-37.
- Fredenburgh, J. C., and Nesheim, E. (1992) Lys-plasminogen Is a Significant Intermediate in the Activation of Glu-plasminogen during Fibrinolysis *in Vitro*. *J. Biol. Chem.* 267, 26150-26156.
- Heimer, E. P., Gallo-Torres, H. E., Felix, A. M., Ahmad, M., Lambros, T. J., Schiedl, F., and Meienhofer, J. (1984) Synthesis of analogs and oligomers of *N*-(2-aminoethyl)glycine and their gastrointestinal absorption in the rat. *I. J. Peptide Protein Res.* 23, 203-211.
- Henriksen, U., and Buchardt, O. (1990) Aryl Azides as Photolabels. Retention of Iodine During Photochemical Ring Expansion of an Iodinated Tyrosine Derivative. *Tetrahedron Lett.* 31, 2443-2444.
- Hoylaerts, M., Rijken, D. C., Lijnen, H. R., and Collen, D. (1982) Kinetics of the Activation of Plasminogen by Human Tissue Plasminogen Activator. *J. Biol. Chem.* 257, 2912-2919.

- Ji, T. H. (1983) Bifunctional Reagents, in *Methods of Enzymology* 91 (C. H. W. Hirs and S. A. Timashoff, Eds.) pp 580-609, Academic Press, New York.
- Koch, T., Suenson, E., Henriksen, U., and Buchardt, O. (1990) The Oxidative Cleavability of Protein Crosslinking Reagents Containing Organoselenium Bridges. *Bioconjugate Chem.* 2, 296-304.
- Nesheim, M., Fredenburgh, J. C., and Larsen, G. R. (1990) The Dissociation Constants and Stoichiometries of the Interactions of Lys-plasminogen and Chloromethyl Ketone derivatives of Tissue Plasminogen Activator and the Variant  $\Delta$ FEIX with Intact Fibrin. *J. Biol. Chem.* 265, 21541-21548.
- Nielsen, P. E., and Buchardt, O. (1982) Aryl Azides as Photoaffinity Labels. A Photochemical Study of Some 4-Substituted Aryl Azides. *Photochem. Photobiol.* 35, 317-323.
- Schielen, W. J. G., Adams, H. P. M., Voskuilen, M., Tesser, G. J., and Nieuwenhuizen, W. (1991) Structural requirements of position A $\alpha$ -157 in fibrinogen for the fibrin-induced rate enhancement of the activation of plasminogen by tissue-type plasminogen activator. *Biochem. J.* 276, 655-659.
- Schnaar, R. L., Langer, B. G., and Brandly, B. K. (1985) Reversible Covalent Immobilization of Ligands and Proteins on Polyacrylamide Gels. *Anal. Biochemistry* 151, 268-281.
- Schwartz, M. A., Das, O. P., and Hynes, R. O. (1982) A new radioactive crosslinking reagent for studying the interactions of proteins. *J. Biol. Chem.* 257, 2343-2349.
- Shephard, E. G., De Beer, F. C., von Holt, C., and Hapgood, J. P. (1988) The Use of Sulfosuccinimidyl-2-(p-azidosalicylamido)-1,3'-dithiopropionate as a Crosslinking reagent to Identify Cell Surface Receptors. *Anal. Biochem.* 168, 306-313.
- Shields, J. C., Falvey, D. E., Schuster, G. B., Buchardt, O., and Nielsen, P. E. (1988) Competitive singlet-singlet energy transfer and electron transfer activation of aryl azides: Application to photocrosslinking experiments. *J. Org. Chem.* 53, 3501-3507.
- Sørensen, P., Farber, N. M., and Krystal, G. (1986) Identification of the Interleukin-3 Receptor Using an Iodinatable, Cleavable, Photoactive Crosslinking Agent. *J. Biol. Chem.* 261, 9094-9097.
- Soundararajan, N., and Platz, S. (1990) Descriptive Photochemistry of Polyfluorinated Azide Derivatives of Methyl Benzoate. *J. Org. Chem.* 55, 2034-2044.
- Suenson, E., and Thorsen, S. (1988) The Course and Prerequisites of Lys-plasminogen Formation during Fibrinolysis. *Biochemistry* 27, 2435-2443.
- Suenson, E., Lutzen, O., and Thorsen, S. (1984) Initial plasmin-degradation of fibrin as the basis of a positive feed-back mechanism in fibrinolysis. *Eur. J. Biochem.* 140, 513-522.
- Suenson, E., Bjerrum, P., Holm, A., Lind, B., Meldal, M., Selmer, J., and Petersen, L. C. (1990) The Role of Fragment X Polymers in the Fibrin Enhancement of Tissue Plasminogen Activator-catalyzed Plasmin Formation. *J. Biol. Chem.* 265, 22228-22237.
- Thorsen, S. (1992) The mechanism of plasminogen activation and the variability of the fibrin effector during tissue-type plasminogen activator-mediated fibrinolysis. *Ann. N. Y. Acad. Sci.* 667, 52-63.
- Thorsen, S., Müllertz, S., Suenson, E., and Kok, P. (1984) Sequence of formation of molecular forms of plasminogen and plasmin-inhibitor complexes in plasma activated by urokinase or tissue-type plasminogen activator. *Biochem. J.* 223, 179-187.
- Watt, D. S., Kawada, K., Leyva, E., and Platz, M. S. (1989) Exploratory Photochemistry of Iodinated Aromatic Azides. *Tetrahedron Lett.* 30, 899-902.
- Weber, K., and Osborn, M. (1975) Proteins and sodium dodecyl sulfate. Molecular weight determination on polyacrylamide gels and related procedures, in *The Proteins 1* (H. Neurath, and R. L. Hill, Eds.) pp 179-223, Academic Press, New York/London.
- Weisel, J. W., Nagaswami, C., Korsholm, B., and Petersen, L. C. (1994) Interactions of Plasminogen and Polymerized Fibrin and its Derivatives Monitored with a Photoaffinity Crosslinker and Electron Microscopy. *J. Mol. Biol.* 235, 1117-1135.
- Wollenweber, H. W., and Morrison, D. C. (1985) Synthesis and Biochemical Characterization of a Photoactivable, Iodinatable, Cleavable Bacterial Lipopolysaccharide Derivative. *J. Biol. Chem.* 260, 15068-15074.



# Three-Dimensional Model of the BR96 Monoclonal Antibody Variable Fragment

Jürgen Bajorath

Bristol-Myers Squibb Pharmaceutical Research Institute, 3005 First Avenue, Seattle, Washington 98121.  
Received December 27, 1993\*

Molecular modeling was used to build a three-dimensional model of the variable regions of the tumor-reactive monoclonal antibody BR96. An immunoconjugate of this antibody with the anticancer drug doxorubicin is currently in a phase I clinical trial for the treatment of solid tumors. A model structure of the BR96 variable fragment was generated to guide site-specific mutagenesis experiments and further improve the affinity of the antibody. The model displayed a distinct groove-type binding site which contained a significant number of aromatic residues. The dimensions and nature of the proposed binding site were consistent with the binding of the Le<sup>y</sup> tetrasaccharide which was found to bind to BR96. On the basis of the model, some BR96 residues are proposed to be crucial for antigen binding. BR96 and its complex with the Le<sup>y</sup> determinant have recently been crystallized, and structure determination is currently underway. Therefore, the detailed prediction of the BR96 combining site will soon be assessed, as a "blind test", based on crystallographic data.

## INTRODUCTION

The murine mAb BR96 was originally raised against human breast carcinoma cells and was found to bind to a Le<sup>y</sup>-related antigen (Hellström et al., 1990). The Le<sup>y</sup>-tetrasaccharide (or determinant) is found on a variety of glycoproteins and glycolipids. The BR96 antigen is expressed at elevated levels (>200 000 molecules/cell) on >80% of human breast, colon, lung, and ovarian carcinomas and, at significantly lower levels, on some differentiated cells of the gastrointestinal epithelium and the pancreas (Hellström et al., 1990). Modified Le<sup>y</sup> antigens have been found associated with several human carcinomas (Hakamori et al., 1989). After binding to its antigen, BR96 is rapidly internalized into cells by receptor-mediated endocytosis and is ultimately degraded in endosomes and lysosomes (Garrigues et al., 1993). A chimeric form of BR96 was constructed by homologous recombination (Fell et al., 1989). The BR96 variable regions were cloned and sequenced, and the BR96 immunoglobulin V<sub>L</sub> was identified as a member of the murine  $\kappa$  class II family and the V<sub>H</sub> as a member of the V<sub>H</sub>7183 gene family (McAndrew et al., to be published). A chemical conjugate of chimeric BR96 with the anticancer drug doxorubicin was prepared (Willner et al., 1993; Trail et al., 1993). This immunoconjugate was found to induce complete regression of human carcinoma xenografts growing subcutaneously in athymic mouse and rat models (Trail et al., 1993) and is currently the subject of clinical trials.

Here, the generation and analysis of a three-dimensional BR96 model is reported. This model was generated using comparative model building (Greer, 1990; Bajorath et al., 1993), canonical CDR loop conformations (Chothia et al., 1989), and conformational search calculations (Brucoleri et al., 1988). The aim of this study was (a) to predict, prior to crystallographic analysis, the three-dimensional

structure of a novel antibody combining site and (b) to characterize the geometry and chemical nature of the antigen binding site of BR96. This latter analysis has enabled us to select BR96 binding site residues thought to be important for antigen binding and has provided the basis for mutagenesis studies.

A detailed prediction of an antibody combining site requires a discussion of the principal opportunities and limitations of such modeling. Different variable light and variable heavy chain structures can be combined, as structural templates, on the basis of the presence of highly conserved residues at the V<sub>L</sub>-V<sub>H</sub> domain interface (Novotny and Sharp, 1992). The conformations of canonical CDR loops can be predicted with some confidence (Chothia et al., 1989), and, in some cases, conformational search has successfully been used to reproduce CDR loop conformations, including the noncanonical H3 loop (Brucoleri et al., 1988; Bajorath and Fine, 1992). In combination, these techniques allow an approximation of the architecture and nature of a novel antibody combining site to be made. At the same time, current modeling methods are insufficient to allow the detailed prediction of antibody-antigen interactions or the assessment of conformational changes in antibodies upon antigen binding (Bhat et al., 1990; Wilson and Stanfield, 1993; Stanfield et al., 1993).

The BR96 model structure shows that BR96 displays a very distinctive groove-type binding site architecture with a prevalence of aromatic residues. On the basis of the dimensions of the groove, all four monosaccharide units of the Le<sup>y</sup> tetrasaccharide are likely to be involved in the binding, and selected tyrosine residues in BR96 are thought to be crucial for the interaction with Le<sup>y</sup>. It is suggested that CDR loop L2 does not participate in antigen binding. Recently, X-ray suitable crystals were obtained for the BR96 Fab fragment and for its complex with the Le<sup>y</sup> tetrasaccharide (Chang et al., 1994), and refined crystallographic coordinates will soon become available (S. Sheriff, personal communication). This makes the prediction of the BR96 combining site particularly attractive since we expect to soon have the opportunity to directly assess this prediction by comparison with a crystallographic model. Such "blind tests" (Chothia et al., 1986;

\* Abstract published in *Advance ACS Abstracts*, April 1, 1994.

Abbreviations: Å, angstrom; CDR, complementarity determining region; Fv, variable fragment; FRD, framework determinant; Le<sup>y</sup>, Lewis-Y; mAb, monoclonal antibody; rms, root mean square; V<sub>H</sub>, variable heavy chain; V<sub>L</sub>, variable light chain.

Chothia et al., 1989; Eigenbrot et al., 1993) which are still rare in the field of antibody modeling make it possible to assess the quality of structural predictions and, therefore, contribute to the assessment and improvement of predictive methods. Equally important, it will be possible to answer the question whether the model-based analysis of the BR96 combining site and the conclusions regarding carbohydrate binding to BR96 were valid.

## METHODS

The model structure of the BR96 variable regions was constructed using a strategy which included structure-based predictions and conformational search (Bajorath and Fine, 1992). In the first step, structural templates for the Fv framework regions were selected based on sequence similarity, and necessary residue replacements were carried out. In the second step, main-chain and side-chain conformations were included for those CDR loops which could unambiguously be assigned to known canonical conformations (Chothia et al., 1989). CDR loops which could not be modeled using known structural motifs were approximated by conformational search calculations (Brucoleri et al., 1988). Finally, the stereochemistry and intramolecular contacts of the initial model were refined by constrained energy minimization. This modeling protocol is not automated and requires interactive model building. In the following text, the different stages of the modeling procedure are described in more details. Rees and colleagues have developed an automated method (Martin et al., 1989; 1991) which also combines structure-based predictions of CDR loops with conformational search. The details of this method will be discussed later on.

Computer graphic model building was carried out using InsightII (Insight II, Version 2.0.0, Molecular Modeling Program, Biosym Technologies, Inc., San Diego). For energy minimization calculations, the Discover program (Discover, Version 2.7, Molecular Mechanics Program, Biosym Technologies, Inc., San Diego) was used. Conformational search calculations (Brucoleri et al., 1988) were carried out with CONGEN (Vers. 2, R. E. Brucoleri and Bristol-Myers Squibb Co., 1991). For modeling, the antibody combining site was divided into framework regions and the CDR loops according to Chothia and Lesk (Chothia and Lesk, 1987; Chothia et al., 1989). The confirmed sequence of the BR96 variable regions was made available by Dr. S. McAndrew, Bristol-Myers Squibb, Seattle.

The Brookhaven Protein Databank (Bernstein et al., 1977), including prerelease entries, was searched for framework structures with high sequence similarity to the BR96 variable regions. The crystallographic resolution and the degree of refinement were considered as additional criteria for the selection of template structures. The V<sub>L</sub> and V<sub>H</sub> chains of different antibodies were selected and combined based on a superposition of the most conserved structural framework segments (Novotny and Sharp, 1992).

The conformations of five CDR loops (L1–L3; the first, second, and third CDR loop of the V<sub>L</sub> chain; H1 and H2, the first and second CDR loop of the V<sub>H</sub> chain) were assigned to canonical structure types (Chothia et al., 1989). On the basis of these assignments, canonical (crystallographic) CDR loop conformations were selected and included in the model using interactive computer graphics. Often, CDR loops of antibodies different from the chosen V<sub>H</sub> or V<sub>L</sub> template structures are selected. It is then required to splice the backbone of these CDR loops into

the adjacent framework regions. This is accomplished using the SpliceLoop feature of Insight's Biopolymer module following superposition of the five N- and C-terminal framework residues of the loop on the corresponding framework residues of the structural template. The conformation of the noncanonical H3 CDR loop was approximated by systematic conformational search using CONGEN. Due to possible canonical conformation ambiguity, alternative H2 loop conformations were generated by conformational search using a previously described protocol (Brucoleri et al., 1988).

Side-chain replacements within framework regions were carried out in conformations as similar as possible. Side-chain replacements within the canonical CDR loops were modeled according to the side-chain conformations of residues at corresponding positions in other CDR loops belonging to the same canonical structure class. The side-chain conformations in the noncanonical H3 loop were modeled using iterative conformational search. The stereochemistry of the BR96 model structure was refined with a constrained energy minimization protocol using a distance-dependent dielectric constant (4 $r$ ) and a 14-Å cutoff distance for nonbonded interactions. Initially, harmonic constraints of 20 kcal/mol/Å<sup>2</sup> were applied to all protein backbone atoms but were subsequently reduced to 10 kcal/mol/Å<sup>2</sup>. The minimization was carried out until the rms derivative of the energy function was approximately 2 kcal/mol/Å. At this stage of the minimization, the average protein backbone rms deviation from the template structures was less than 0.3 Å. The H3 loop, which lacked any crystallographic template, was excluded from the rms comparison. The coordinates of the BR96 model structure were deposited, prior to crystallography of BR96, with Dr. R. Stenkamp, Department of Biological Structure, University of Washington, Seattle, WA, and Dr. S. Sheriff, Department Macromolecular Crystallography, Bristol-Myers Squibb, Princeton, NJ. The  $\alpha$  carbon coordinates for all 230 residues of the BR96 model are given in Table 1 (supplementary material).

## RESULTS

**The BR96 Model Structure.** Structural templates for the BR96 V regions were selected based on sequence similarity searches in the Brookhaven Protein Data Bank. The V<sub>L</sub> chain of BR96 is closely related (~87% sequence identity) to the fluorescein binding mAb 4-4-20 (Herron et al., 1989) which is only available in complex with fluorescein. The 4-4-20 V<sub>L</sub> chain was used as template structure for V<sub>L</sub> chain modeling. Coordinates of 4-4-20 refined to 1.75 Å resolution were a generous gift of Dr. J. Herron. The V<sub>H</sub> chain sequence of BR96 was found to share ~77% identity with the V<sub>H</sub> chain of 17/9 (Rini et al., 1992). The structure of 17/9 is available at 2.0-Å resolution in uncomplexed form and at 2.7-Å resolution in antigen-bound (peptide-bound) form. The unbound form was, therefore, selected as structural template for the BR96 V<sub>H</sub> chain. All parts of the crystallographic structure which were found to undergo some conformational changes upon antigen binding (Rini et al., 1992) were deleted prior to model building. On the basis of these selections, the BR96 model should, in principle, resemble the antigen-bound form of BR96 more closely than its uncomplexed form. The selected template structures were combined to a composite Fv template after superposition of the most conserved residues in antibody variable regions (Novotny and Sharp, 1992). Included in the superposition were the backbone of residues L40–L43, L91–L93, H36–

CDR	CDR loop residues												Framework residues							
L1	26	27	28	29	30	31	a	b	c	d	e	f	32	2	25	33	71			
BR96	S	Q	I	I	V	H	N	N	G	N	T		Y	V	S	L	F			
4-4-20	S	Q	S	L	V	H	S	N	G	N	T		Y	V	S	L	F			
L2	50	51	52												48	64				
BR96	K	V	S												I	G				
4-4-20	K	V	S												I	G				
L3	91	92	93	94	95	96												90		
BR96	G	S	H	V	P	F												Q		
4-4-20	S	T	H	V	P	W												Q		
H1	26	27	28	29	30	31	32												34	94
BR96	G	F	T	F	S	D	Y												M	R
17/9	G	F	S	F	S	S	Y												M	R
H2	52a	b	c	53	54	55												71		
BR96	Q			G	G	D												R		
17/9	N			G	G	G												R		
H3	95	96	97	98	99	100	a	b	101	102										
BR96	G	L	D	D	G	A	W	F	A	Y										

**Figure 1.** CDR loop sequences in BR96. The sequences of the five canonical CDR loops (L1-L3, H1-H2) (Chothia et al., 1989) and of the noncanonical H3 loop in BR96 are shown and numbered according to Kabat and Wu (1987). CDR loop H3 is defined according to Kabat and Wu (1987). The canonical CDR loops L1 to L3 in BR96 are aligned with the corresponding regions in 4-4-20 (Herron et al., 1989), and CDR loops H1 and H2 in BR96 are aligned with the corresponding loops in 17/9 (Rini et al., 1992). Structural determinant residues for canonical CDR loops in the framework regions (Chothia et al., 1989) are shown in italics. The single-letter code is used for the amino acid residues.

H39, and H96-H98 in 4-4-20 and the corresponding set of residues in 17/9 (L35-L38, L86-L88, H36-H39, and H90-H92). The rms deviation for the superposition of these residues was 0.5 Å.

Figure 1 shows the sequences of the CDR loops in BR96 according to the canonical structure model and the residues in the framework regions which are important for the conformation of single CDR loops (Chothia et al., 1989). The sequence of BR96 CDR loop L2 is identical to 4-4-20. The CDR loop L3 displays a sequence motif consistent with canonical structure class 1 (Chothia et al., 1989) for both BR96 and 4-4-20. CDR loops L1 in BR96 and 4-4-20 are unusually long but have the same length. BR96 displays structural determinant residues consistent with a canonical structure class 4 (Chothia et al., 1989). The L1 loops in 4-4-20 and BR96 are, therefore, similar. It should be considered, however, that the conformation of the tip of such long L1 loops (here with a six residue insertion relative to canonical structure class 1) may not be predictable (Steipe et al., 1992) since structural stabilization of the framework-distant portion of these loops is essentially absent. The nonstabilized portions of these loops can be expected to be somewhat flexible in their conformation. The CDR loops H1 in 17/9 and BR96 belong to canonical structure class 1. The four CDR loops L1-L3 and H1 could be unambiguously assigned to known canonical structure types. On the basis of the canonical assignments, it was possible to include the backbone of the three light chain CDR loops in 4-4-20 and the backbone of the H1 loop in 17/9 as templates for the corresponding CDR loops in BR96. Therefore, loop splicing was not required for these CDR loops in BR96.

An unambiguous assignment to a known canonical conformation was not possible for CDR loop H2 in BR96 although the loop is four residues long and displays a sequence motif consistent with a canonical conformation type 3 (Chothia et al., 1989). H2 loops belonging to this canonical structure type usually have a glycine residue at position 54 in the loop (capable of adopting unusual  $\phi/\psi$  torsion angles) and an arginine as structural determinant at position 71 in the framework. H2 in the crystallographic structure of 17/9 appears to adopt a canonical conformation type 3, although 17/9 has three glycine residues at positions 53-55. BR96 has two glycines at positions 53 and 54, both of which may adopt unusual  $\phi/\psi$  torsion angles and may have a local conformation different from the canonical structure. The backbone conformations of H2 in 17/9 was included in the BR96 model as a first approximation, and an alternative BR96 conformation of H2, including the six  $V_H$  residues 52-56, was generated using CONGEN conformational search calculations. The search produced 36 H2 conformations with acceptable conformational energies, with three of these conformations being within 2 kcal/mol of the energy minimum. The conformation with smallest solvent-accessible surface within this energy interval was selected. In contrast to the canonical conformation the selected conformation shows that the glycine at position 54 is in acceptable  $\phi/\psi$  regions but that the glycine at position 53 has usually unacceptable  $\phi/\psi$  torsional angles. This suggests the possibility of alternative H2 conformations in BR96. The backbone rms deviation between the H2 conformation found in 17/9 and the CONGEN-generated H2 conformation in BR96 is relatively small, approximately 1.2 Å.

The noncanonical H3 loop in BR96 was modeled using conformational searching. The conformational search over H3 was carried out as the final step of model building in the presence of the modeled framework regions and all CDR loops. A total of 145 conformations were generated but only two of these were within 10 kcal/mol of the energy minimum. The two loop conformations were similar (backbone rms of 0.35 Å). The energy minimum conformation was included in the model. The stereochemistry and the nonbonded interactions in the initial model were improved by application of a constrained energy minimization protocol. In the final model, backbone rms deviations relative to the crystallographic templates, excluding the CDR loops, were less than 0.3 Å.

**Proposed Architecture of the BR96 Combining Site.** Figure 2 (top left) shows a stereo representation of the  $\alpha$  carbon trace of the BR96 Fv model. The conformations of the single CDR loops can be seen and the geometry of the antigen-binding site proposed. The space-filling representation in Figure 2 (top right) emphasizes the most prominent feature of this combining site, the groove-type architecture. The architecture of the groove is determined by interactions of the CDR loops L1, L3, and H3. Residues of CDR loops H2, and to a lesser extent H1, form the bottom of the groove. BR96 has an average length H3 loop (10 residues) and a long L1 loop (12 residues). Interactions between these loops significantly contribute to the gross architecture of the binding site. The other prominent feature of the BR96 binding site is the significant number of aromatic residues which participate in the formation of the groove. These residues are depicted in Figure 2 (bottom right).

**Implications for Antigen Binding.** CDR loop L2 does not participate in the formation of the groove and is, therefore, not expected to be involved in antigen binding. We believe, as well as others (Bundle and Young, 1992), that the accuracy of current predictive methods is not sufficient to propose protein-carbohydrate complexes in detail. However, simple docking studies with model-built  $\text{Le}^y$  conformers suggest that the BR96 binding site groove is sufficiently large to bind all four monosaccharide units of the  $\text{Le}^y$  determinant. These studies also allow the identification of a number of residues in BR96 which may contact the carbohydrate. The following residues in BR96 are proposed to be likely carbohydrate contact residues and, therefore, thought to be important for antigen binding: L1, His31, Asn31a, Asn31b, Tyr32; L3, Phe96; H1, Tyr33, Tyr35; H2, Tyr50, Gln52a, Asp58; H3, Ala100. The analysis suggests that H3 residues in BR96 do not contribute significant side-chain contacts to the BR96- $\text{Le}^y$  interactions. Furthermore, it should be noted that four of the BR96 residues thought to be important for antigen binding (Tyr33H, Tyr35H, Trp50H, and Asp58H) are, according to the definition of Chothia and Lesk (1987), not CDR but framework residues. On the basis of the architecture of the BR96 binding site, these residues participate in the formation of the groove. The analysis of the three-dimensional model is essential for the selection of these residues.

## DISCUSSION

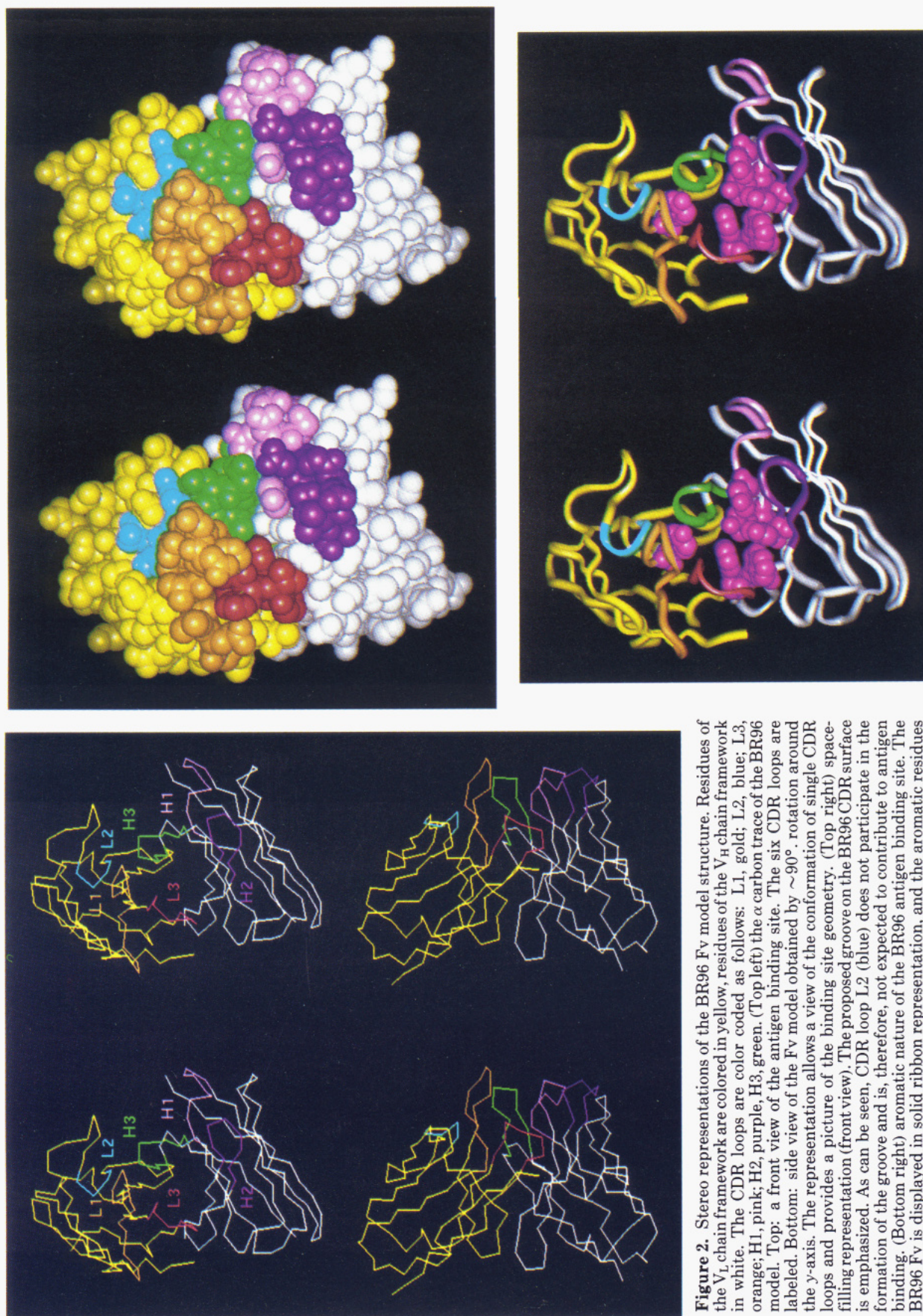
The BR96 Fv fragment was modeled with an emphasis on preference for structure-based predictions. A conformational search has been applied to approximate the conformations of CDR loops only when the assignment to known conformations was potentially ambiguous (H2) or impossible (H3). The identification of canonical conformational motifs for five of the six CDR loops in antibodies

by Chothia, Lesk, and colleagues (Chothia and Lesk, 1987; Chothia et al., 1989) has much enhanced the ability to carry out knowledge-based predictions of antibody combining sites. Canonical CDR loop motifs represent defined classes of conformations which are found in antibody crystal structures and are determined by the presence of a few key residues within the loop or within the framework regions. These motifs have been shown to be largely insensitive to sequence variations at other positions (Chothia et al., 1989). Therefore, five of six CDR loops in antibodies with unknown structure can frequently be assigned to known canonical conformations on the basis of the analysis of their sequences. In contrast, canonical conformations have not yet been identified for CDR loop H3. Approximation of H3 conformations in antibody modeling therefore remains usually dependent on the application of *ab initio* techniques such as conformational search. Major problems of structure-based CDR loop predictions presently include (a) the inability to identify canonical motifs for H3, (b) the remaining ambiguities in the assignment of sequences to known structural motifs, (c) the still limited database of crystallographic antibody structures refined to high resolution, and (d) the inability to take potential interactions between CDR loops into account. The major current problems of CDR loop predictions on the basis of conformational search are (a) the selection of the "right" conformation from an ensemble of generated conformations and (b) the computer time required for conformational search over longer loops.

A fully automated method to model CDR loop conformations by combining structure-based predictions and conformational search has been introduced by Rees and co-workers (Martin et al., 1989; 1991). These researchers essentially use the ( $\alpha$  carbon distance matrix) loop search technique of Jones and Thirup (1986) to extract loop conformations from the Brookhaven Protein Data Bank. For conformational search the CONGEN program (Brucoleri and Karplus, 1987; Brucoleri et al., 1988) is used. CDR loops consisting of up to five residues are modeled using CONGEN. CDR loops consisting of six or seven residues are modeled using the database loop search. For CDR loops of eight or more residues, database loop search is first applied, and then the midsection of the loop is remodeled with CONGEN. Generated conformations are filtered using solvent-modified potential functions (Martin et al., 1989). The approach depends on the assumptions (a) that the conformational space available to loops consisting of six to seven residues is sufficiently represented in the currently available protein structures, (b) that correct N- and C-terminal base segments for loops of eight or more residues can be extracted, and (c) that solvent-modified energy screening of generated conformations is capable of selecting the "right" conformation. Rees and colleagues also suggest the selection of framework regions based on sequence similarity and, furthermore, the inclusion of the assignment of CDR loops to canonical conformations if possible (Martin et al., 1991).

In the case of BR96, it was possible to identify structural templates for the framework regions which share significant sequence similarity. CDR loops L2, L3, and H1 were found to display well-established canonical conformations. Some uncertainty remains concerning the conformation of the distal part of CDR loop L1 (Steipe et al., 1992) and the canonical assignment of H2 for which an alternative (albeit similar) conformation was generated. This uncertainty is in spite of the fact that both CDR loops L1 and H2 are related to known structures. No H3 loop with identical length and significant sequence similarity to





**Figure 2.** Stereo representations of the BR96 Fv model structure. Residues of the V<sub>L</sub> chain framework are colored in yellow, residues of the V<sub>H</sub> chain framework in white. The CDR loops are color coded as follows: L1, gold; L2, blue; L3, orange; H1, pink; H2, purple; H3, green. (Top left) the  $\alpha$  carbon trace of the BR96 model. Top: a front view of the antigen binding site. The six CDR loops are labeled. Bottom: side view of the Fv model obtained by  $\sim 90^\circ$  rotation around the y-axis. The representation allows a view of the conformation of single CDR loops and provides a picture of the binding site geometry. (Top right) space-filling representation (front view). The proposed groove on the BR96 CDR surface is emphasized. As can be seen, CDR loop L2 (blue) does not participate in the formation of the groove and is, therefore, not expected to contribute to antigen binding. (Bottom right) aromatic nature of the BR96 antigen binding site. The BR96 Fv is displayed in solid ribbon representation, and the aromatic residues (Tyr32L, Phe96L, Tyr33H, Tyr35H, Trp47H, Tyr50H; colored in magenta) which are proposed to participate in the formation of the BR96 binding site are shown as space-filling models.

BR96 was found in the database of known antibody crystal structures, and therefore, conformational search calculations were carried out. To evaluate the conformational space available to H3 as well as its spatial position, we have simulated the conformation of H3 within the structural context provided by the BR96 model.

Crystallographic structures of the carbohydrate binding antibodies J539 (Suh et al., 1986) and Se155-4 (Cygler et al., 1991) show characteristic cavities or grooves as a prominent feature of their binding sites. The groove-type architecture proposed for the BR96 combining site is consistent with these crystallographic structures and represents a prominent feature of the BR96 model. The accuracy of current model building methodology is insufficient to explore the molecular details of antibody-carbohydrate interactions (Bundle and Young, 1992). This is primarily due to the conformational flexibility of carbohydrates and to the fact that the role of water molecules in carbohydrate-protein interactions (Vyas, 1991; Cygler et al., 1991) is difficult, if not impossible, to analyze in the absence of high-resolution crystallographic data (Bundle and Young, 1992). Analysis of the BR96 model strongly suggests a prevalence of aromatic residues involved in the formation of the binding site. Several of these residues, such as Tyr33H and Tyr50H, are very likely to represent carbohydrate contact residues. Such contacts suggest a different mode of carbohydrate binding than that frequently observed in other carbohydrate binding proteins, where charged and planar side-chains often dominate the interactions (Vyas, 1991). However, aromatic residue-carbohydrate interactions have been observed in the crystal structure of the Se155-4 antibody complexed with its carbohydrate epitope (Cygler et al., 1991). Tyrosine residues are frequently found in CDR loops of antibodies (Padlan, 1991), possibly due to their versatility in forming hydrogen bonds, van der Waals contacts, and aromatic interactions, in addition to their moderate loss of conformational entropy upon antigen binding. The proposed importance of aromatic residues in the formation of the BR96 antigen binding site is another prominent feature of the BR96 model structure.

The analysis of a proposed binding site can lead to the identification of residues crucial for antigen binding and may also allow conclusions regarding the nature of the antigen, if unknown, to be made. This was shown for the anticancer antibody L6 (Fell et al., 1992). The presence of a rather flat and irregular combining site was predicted for L6 (Fell et al., 1992). This led to the conclusion that L6 should recognize a protein surface rather than a carbohydrate epitope—a prediction that was subsequently experimentally confirmed (Fell et al., 1992). In contrast, BR96 is proposed to display a very distinct groove-type binding site architecture, consistent with the notion that it binds a carbohydrate antigen.

Comparison of crystallographic structures of uncomplexed and antigen-bound antibody fragments has shown that conformational changes occur in antibodies upon antigen binding (Bhat et al., 1990) which can be of significant magnitude (Wilson and Stanfield, 1993). These changes include segmental motions (Stanfield et al., 1990) and conformational changes of single (Rini et al., 1992) or several (Herron et al., 1991) CDR loops as well as changes in the relative  $V_L$ - $V_H$  domain orientation (Herron et al., 1991; Stanfield et al., 1993). The assessment of these possible conformational changes represents a major problem for antibody modeling attempts. The possibility and magnitude of such effects remains unpredictable and can only be determined by direct comparison of uncomplexed

and complexed structures. In the case of BR96, we may soon have the opportunity to evaluate the detailed prediction of the antibody-combining site with the crystallographic structures of the complexed and uncomplexed antibody and to assess the magnitude of potential conformational changes upon  $Le^x$  binding.

#### ACKNOWLEDGMENT

The author thanks Dr. Steven McAndrew for providing the sequence of the BR96 variable regions prior to publication. Furthermore, the author thanks Dr. Steven Sheriff and Dr. Jiri Novotny for many discussions and for support and Dr. Peter Senter for his critical review of the manuscript. The author is grateful to Dr. James Herron for providing high-resolution coordinates of 4-4-20 and to Debby Baxter for her help in the preparation of the manuscript.

**Supplementary Material Available:**  $\alpha$  carbon coordinates, sequence, and CDR loops for the BR96 Fv model structure (6 pages). Ordering information is given on any current masthead page.

#### LITERATURE CITED

- Bajorath, J., and Fine, R. M. (1992) On the use of minimization from many randomly generated loop structures in modeling antibody combining sites. *ImmunoMethods* 1, 137-146.
- Bajorath, J., Stenkamp, R., and Aruffo, A. (1993) Knowledge-based model building of proteins: Concepts and examples. *Protein Sci.* 2, 1798-1810.
- Bernstein, F. C., Koetzle, T. F., Williams, G. J. B., Meyer, E. F., Brice, M. D., Rodgers, J. R., Kennard, O., Shimanouchi, T., and Tasumi, M. (1977) The protein data bank: a computer-based archival file for macromolecular structures. *J. Mol. Biol.* 112, 535-542.
- Bhat, T. N., Bentley, G. A., Fischmann, T. O., Boulton, G., and Poljak, R. J. (1990). Small Rearrangements in Structures of Fv and Fab Fragments of Antibody D1.3 on Antigen Binding. *Nature* 347, 483-485.
- Brucoleri, R. E., and Karplus, M. (1987). Prediction of folding of short polypeptide segments by uniform conformational sampling. *Biopolymers* 26, 137-168.
- Brucoleri, R. E., Haber, E., and Novotny, J. (1988) Structure of antibody hypervariable loops reproduced by a conformational search algorithm. *Nature* 335, 564-568.
- Bundle, D. R., and Young, N. M. (1992) Carbohydrate-protein interactions in antibodies and lectins. *Curr. Opin. Struct. Biol.* 2, 666-673.
- Chang, C. Y., Jeffrey, P. D., Bajorath, J., Hellström, I., Hellström, K. E., and Sheriff, S. (1994) Crystallization and Preliminary X-ray Analysis of the Monoclonal Anti-Tumor Antibody BR96 and Its Complex with the  $Le^x$  Determinant. *J. Mol. Biol.* 235, 372-376.
- Chothia, C., and Lesk, A. M. (1987) Canonical structures for the hypervariable regions of immunoglobulins. *J. Mol. Biol.* 196, 901-971.
- Chothia, C., Lesk, A. M., Levitt, M., Amit, A. G., Mariuzza, R. A., Phillips, S. E. V., and Poljak, R. (1986). The Predicted Structure of Immunoglobulin D1.3 and Its Comparison with the Crystal Structure. *Science* 233, 755-758.
- Chothia, C., Lesk, A. M., Tramontano, A., Levitt, M., Smith-Gill, S. J., Air, G., Sheriff, S., Padlan, E. A., Davies, D., Tulip, W. R., Colman, P. M., Spinelli, S., Alzari, P. M., and Poljak, R. (1989) Conformations of immunoglobulin hypervariable regions. *Nature* 342, 877-883.
- Cygler, M., Rose, D. R., and Bundle, D. R. (1991) Recognition of a Cell-Surface Oligosaccharide of Pathogenic Salmonella by an Antibody Fab Fragment. *Science* 253, 442-445.



- Eigenbrot, C., Randal, M., Presta, L., Carter, P., and Kossiakoff, A. (1993) X-ray Structures of the Antigen-binding Domains from Three Variants of Humanized anti-p185<sup>HER2</sup> Antibody 4D5 and Comparison with Molecular Modeling. *J. Mol. Biol.* 229, 969–995.
- Fell, H. P., Yarnold, S., Hellström, I., Hellström, K. E., and Folger, K. (1989) Homologous recombination in hybridoma cells: heavy chain chimeric antibody produced by gene targeting. *Proc. Nat. Acad. Sci. U.S.A.* 86, 8507–8511.
- Fell, H. P., Gayle, M. A., Yelton, D., Lipsich, L., Schieven, G. L., Marken, M. S., Aruffo, A., Hellström, K. E., Hellström, I., and Bajorath, J. (1992) Chimeric L6 Anti-tumor Antibody: Genomic Construction, Expression, and Characterization of the Antigen Binding Site. *J. Biol. Chem.* 267, 15552–15558.
- Greer, J. (1990) Comparative Modeling Methods. Application to the Family of the Mammalian Serine Proteases. *Proteins: Struct., Funct., Genet.* 7, 317–334.
- Garrigues, J., Garrigues, U., Hellström, I., and Hellström, K. E. (1993) Le<sup>y</sup> Specific Antibody with Potent Anti-Tumor Activity Is Internalized and Degraded by Lysozymes. *Am. J. Pathol.* 142, 607–622.
- Hakamori, S. (1989) Aberrant Glycosylation In Tumors And Tumor-Associated Carbohydrate Antigens. *Adv. Cancer Res.* 52, 257–331.
- Hellström, I., Garrigues, H. J., Garrigues, U., and Hellström, K. E. (1990) Highly Tumor-reactive, Internalizing Mouse Monoclonal Antibodies to LeY-related Cell Surface Antigens. *Cancer Res.* 50, 2183–2190.
- Herron, J. N., He, X. M., Mason, M. L., Voss, W. E., Jr., and Edmundson, A. B. (1989) Three-Dimensional Structure of a Fluorescein-Fab Complex Crystallized in 2-Methyl-2,4-pentanediol. *Proteins: Struct., Funct., Genet.* 6, 271–280.
- Herron, J. N., He, X. M., Ballard, D. W., Blier, P. R., Pace, P. E., Bothwell, A. L. M., Voss, E. W. Jr., and Edmundson, A. B. (1991) An Autoantibody to Single-Stranded DNA: Comparison of the Three-Dimensional Structures of the Unliganded Fab and a Deoxynucleotide-Fab complex. *Proteins: Struct., Funct., Genet.* 11, 159–175.
- Jones, T. A., Thirup, S. (1986) Using Known Substructures in Protein Model Building and Crystallography. *EMBO J.* 5, 819–822.
- Kabat, E. A., Wu, T. T., Reid-Miller, M., Perry, H. M., and Gottesman, K. S. (1987) *Sequences of Proteins of Immunological Interest*, 4th ed., National Institutes of Health, Bethesda, MD.
- Martin, A. C. R., Cheetham, J. C., and Rees, A. R. (1989) Modeling antibody hypervariable loops: a combined algorithm. *Proc. Natl. Acad. Sci. U.S.A.* 86, 9268–9272.
- Martin, A. C. R., Cheetham, J. C., and Rees, A. R. (1991) Molecular Modeling of Antibody Combining Sites. *Meth. Enzymol.* 203, 121–151.
- Novotny, J., and Sharp, K. (1992) Electrostatic fields in antibodies and antibody/antigen complexes. *Prog. Biophys. Molec. Biol.* 58, 203–224.
- Padlan, E. A. (1991) On the nature of antibody combining sites: unusual structural features that may confer on these sites an enhanced capacity for ligand binding. *Proteins: Struct., Funct., Genet.* 7, 112–124.
- Rini, J. M., Schulze-Gahmen, U., and Wilson, I. A. (1992) Structural Evidence for Induced Fit as a Mechanism for Antibody–Antigen Recognition. *Science* 255, 959–965.
- Stanfield, R. L., Fieser, T. M., Lerner, R. A., and Wilson, I. A. (1990) Crystal Structures of an Antibody to a Peptide and Its Complex with Peptide Antigen at 2.8 Å. *Science* 248, 712–719.
- Stanfield, R. L., Takimoto-Kamimura, M., Rini, J. M., Profy, A. T., and Wilson, I. A. (1993) Major antigen-induced domain rearrangements in an antibody. *Structure* 1, 83–93.
- Steipe, B., Plückthun, A., and Huber, R. (1992) Refined Crystal Structure of a Recombinant Immunoglobulin Domain and a Complementarity-determining Region 1-grafted Mutant. *J. Mol. Biol.* 225, 739–753.
- Suh, S. W., Bhat, T. N., Navia, M. A., Cohen, G. H., Rao, D. N., Rudikoff, S., and Davies, D. R. (1986) The galactan-binding immunoglobulin Fab J539: an X-ray diffraction study at 2.6 Å resolution. *Proteins: Struct., Funct., Genet.* 1, 74–80.
- Trail, P. A., Willner, D., Lasch, D. J., Henderson, A. J., Casazza, A. M., Firestone, R. A., Hellström, I., and Hellström, K. E. (1993) Cure of Xenografted Human Carcinomas by BR96-Doxorubicin Immunoconjugates. *Science* 261, 212–215.
- Vyas, N. K. (1991) Atomic Features of Protein–Carbohydrate Interactions. *Curr. Opin. Struct. Biol.* 1, 732–740.
- Willner, D., Trail, P. A., Hofstead, S. J., King, H. D., Lasch, S. J., Braslawsky, G. R., Greenfield, R. S., Kaneko, T., and Firestone, R. A. (1993) (6-Maleimidocaproyl)hydrazones of Doxorubicin—A New Derivative for the Preparation of Immunoconjugates of Doxorubicin. *Bioconjugate Chem.* 4, 521–527.
- Wilson, I. A., and Stanfield, R. L. (1993) Antibody–antigen interactions. *Curr. Opin. Struct. Biol.* 3, 113–118.

# Monoclonal Antibody Fab' Fragment Cross-Linking Using Equilibrium Transfer Alkylation Reagents. A Strategy for Site-Specific Conjugation of Diagnostic and Therapeutic Agents with F(ab')<sub>2</sub> Fragments

D. Scott Wilbur,<sup>\*,†</sup> James E. Stray,<sup>‡</sup> Donald K. Hamlin,<sup>†</sup> Dena K. Curtis,<sup>‡</sup> and Robert L. Vessella<sup>†</sup>

Department of Radiation Oncology and Department of Urology, University of Washington, Seattle, Washington 98195. Received September 22, 1993\*

An investigation was conducted to evaluate the feasibility of site-selective addition of diagnostic and therapeutic agents to monoclonal antibody F(ab')<sub>2</sub> fragments through cross-linking of antibody Fab' fragments. In the investigation, *trifunctional* equilibrium transfer alkylation cross-link (ETAC) reagents, 4-[2,2-bis[(*p*-tolylsulfonyl)methyl]acetyl]benzoic acid, **1a**, *N*-[4-[2,2-bis[(*p*-tolylsulfonyl)methyl]acetyl]benzoyl]-4-(tri-*n*-butylstannyl)phenethylamine, **3a**, and *N*-[4-[2,2-bis[(*p*-tolylsulfonyl)methyl]acetyl]benzoyl]-4-[<sup>125</sup>I]iodophenethylamine, **3b**, were synthesized. The ETAC derivatives were reacted with Fab' fragments of an antirenal cell carcinoma antibody (A6H) produced from reduction of F(ab')<sub>2</sub> using 1,4-dithiothreitol. Cross-linking of Fab' was obtained to yield a radioiodinated modified F(ab')<sub>2</sub>, [mF(ab')<sub>2</sub>], fragment. The cross-linking reaction produced mixed addition products, requiring the desired mF(ab')<sub>2</sub> to be separated from radioiodinated Fab' by size exclusion HPLC. Tumor cell binding immunoreactivities varied (60–90%) for five isolated mF(ab')<sub>2</sub> preparations but were consistent with other radiolabeled antibody preparations tested on the same day. *In vitro* stability testing indicated that the mF(ab')<sub>2</sub> was reasonably stable toward loss of the ETAC cross-linking reagent, except under strongly basic conditions. Under reducing sodium dodecylsulfate–polyacrylamide gel electrophoresis (SDS–PAGE) analyses, protein bands believed to be cross-linked heavy chain dimers were observed. Biodistribution of purified radioiodinated A6H mF(ab')<sub>2</sub> was conducted in athymic mice bearing a renal cell carcinoma xenograft (TK-82). A nonmodified control A6H F(ab')<sub>2</sub>, radioiodinated as a *p*-[<sup>125</sup>I]iodobenzoyl conjugate, was coinjected for comparison. The radioiodinated mF(ab')<sub>2</sub> had a similar distribution to the radioiodinated control at 3.5, 19, and 43 h postinjection. In another study, the distribution of radioiodinated A6H Fab' was evaluated at 4 and 24 h to establish clearance and pharmacokinetics for comparison with the data obtained from the mF(ab')<sub>2</sub>. The biodistribution data indicated that A6H mF(ab')<sub>2</sub> was quite different from that of A6H Fab'. The results from this preliminary study suggest that it may be possible to attach (large polymeric) diagnostic or therapeutic agents to monoclonal antibody F(ab')<sub>2</sub> fragments through the use of ETAC reagents.

## INTRODUCTION

Monoclonal antibodies are being investigated as tumor-selective carriers of diagnostic reagents, such as radioisotopes or MRI enhancing reagents, and therapeutic reagents, such as drugs, toxins, and radioisotopes (1–4). In order to utilize monoclonal antibodies as carriers of diagnostic and therapeutic agents, these chemical entities must be coupled, or conjugated, to the antibody in a manner that does not significantly alter their binding affinity to tumor antigens, normal biodistribution, or pharmacokinetics. Fortunately, many different methods of conjugating diagnostic and therapeutic reagents to antibodies have been described (5–8). The majority of the conjugation methods involve reactions of functional groups, such as lysine amines or cysteine thiols, present on the antibody's polypeptide chain with a functional group present on the reagent to be conjugated. In general, such conjugations are nonspecific, leading to a mixture of antibody conjugates which have the reagent attached at a number of locations on the antibody. Although the reactions are not specific by nature, when one or two small molecules are conjugated the antibody's immunoreactivity

is often retained. This may be due to a higher reactivity (perhaps due to availability) of some amines at a location distant from the antigen binding site. While immunoreactivity is retained when nonspecifically conjugating a small molecule to an antibody, conjugation of several small molecules such as metal chelates or drug conjugates, or large molecules such as toxin conjugates or polymeric reagents, often results in loss of antibody immunoreactivity. Because of this problem investigators have sought to devise methods of site-specific conjugation of reagents to antibodies.

One method that has been described for "site-specific" conjugation to monoclonal antibodies is the use of equilibrium transfer alkylating cross-link (ETAC)<sup>1</sup> reagents (9). It has been reported that ETAC reagents can be site-selectively conjugated to intact antibodies through reaction with sulfhydryls produced by partial reduction of disulfide bonds in the hinge region of the antibody (10, 11). The ETAC reagents are unique among sulfhydryl reactive cross-

\* Address correspondence to this author at Department of Radiation Oncology, University of Washington, XD-48, 2121 N. 35th St., Seattle, WA 98103.

<sup>†</sup> Department of Radiation Oncology.

<sup>‡</sup> Department of Urology.

\* Abstract published in *Advance ACS Abstracts*, April 1, 1994.

<sup>1</sup> Abbreviations used: ETAC, equilibrium transfer alkylating cross-link; mF(ab')<sub>2</sub>, modified F(ab')<sub>2</sub>; SDS–PAGE, sodium dodecylsulfate–polyacrylamide gel electrophoresis; PIB, *N*-succinimidyl *p*-iodobenzoate; PBS, phosphate-buffered saline; MeOH, methanol; HOAc, acetic acid; CH<sub>3</sub>CN, acetonitrile; DMSO, dimethyl sulfoxide; NCS, *N*-chlorosuccinimide; THF, tetrahydrofuran; DTT, dithiothreitol; β-ME, 2-mercaptoethanol; ChT, chloramine-T; cpm, counts per minute.

linking reagents as they are reactive through a Michael-type addition reaction with an *in situ* generated  $\alpha,\beta$ -unsaturated ketone intermediate. The reaction proceeds by a stepwise addition of sulfhydryls, making it possible in theory to control the addition of the second sulfhydryl through carefully controlling the reaction conditions employed.

The unique trifunctional cross-linking nature of the ETAC reagents made them particularly attractive for application to conjugation of large peptides or polymers containing diagnostic or therapeutic agents. However, we were concerned that the method of conjugation previously described might not be applicable to large polymeric reagents due to the increase in antibody size (and shape), which could potentially affect the antibody's antigen binding by altering its tertiary structure. We postulated that conjugation of polymeric reagents to antibody fragments would diminish the problems associated with increased molecular size. It seemed apparent that the antibody fragment of choice was the F(ab')<sub>2</sub> fragment as the bivalent binding characteristics of the antibody would be retained, which results in maximizing the percent injected dose per gram (% ID/g) in the tumor. Thus, our hypothesis was that immunocompetent modified F(ab')<sub>2</sub> fragments could be prepared by removal of the nonessential Fc portion of the antibody with subsequent conjugation of a polymeric diagnostic or therapeutic reagent in its place.

Site-selective conjugation of reagents to F(ab')<sub>2</sub> fragments cannot be readily accomplished; however, site-selective conjugations with antibody Fab' fragments are possible due to the fact that free sulfhydryls are generated in the reduction of the bridging disulfides in the hinge region (12). Therefore, site-specific conjugation of a reagent to an antibody F(ab')<sub>2</sub> might be accomplished through site-selective cross-linking of two Fab' fragments with a trifunctional reagent. A general graphic representation of the envisioned method for reagent conjugation to monoclonal antibody F(ab')<sub>2</sub> fragments (of the IgG<sub>1</sub> subclass) is depicted in Figure 1. While not shown in Figure 1, the trifunctional reagent would be attached to the diagnostic or therapeutic reagent prior to cross-linking of the Fab's, such that the sulfhydryls present in the terminal protein segment (hinge region) would impart the site-specificity to the conjugation reaction. Since the methods of preparation of F(ab')<sub>2</sub> and Fab' are fairly standardized, it appeared that the single most important factor in the conjugation scheme was the choice of an appropriate trifunctional cross-linking reagent. Trifunctional ETAC compounds appeared to be ideal for this application.

Although the ultimate goal of our research was to develop a method for attaching large polymeric reagents to antibody F(ab')<sub>2</sub> fragments, the goal of this initial investigation was to ascertain whether the approach outlined in Figure 1 was feasible. We felt that feasibility of the approach could be established by demonstrating that reaction of Fab' fragments with simple ETAC compounds would form immunocompetent F(ab')<sub>2</sub> fragments. Conjugation of polymeric reagents is a complex problem that will require extensive studies for each specific reagent. Thus, reported herein is a preliminary investigation detailing the synthesis of a radioiodinated ETAC derivative (Figure 2) and the reaction conditions necessary to form a reannealed or modified F(ab')<sub>2</sub>. Also reported are the results of *in vitro* and *in vivo* evaluations of the radioiodinated modified F(ab')<sub>2</sub> [hereafter designated mF(ab')<sub>2</sub>].

#### EXPERIMENTAL PROCEDURES

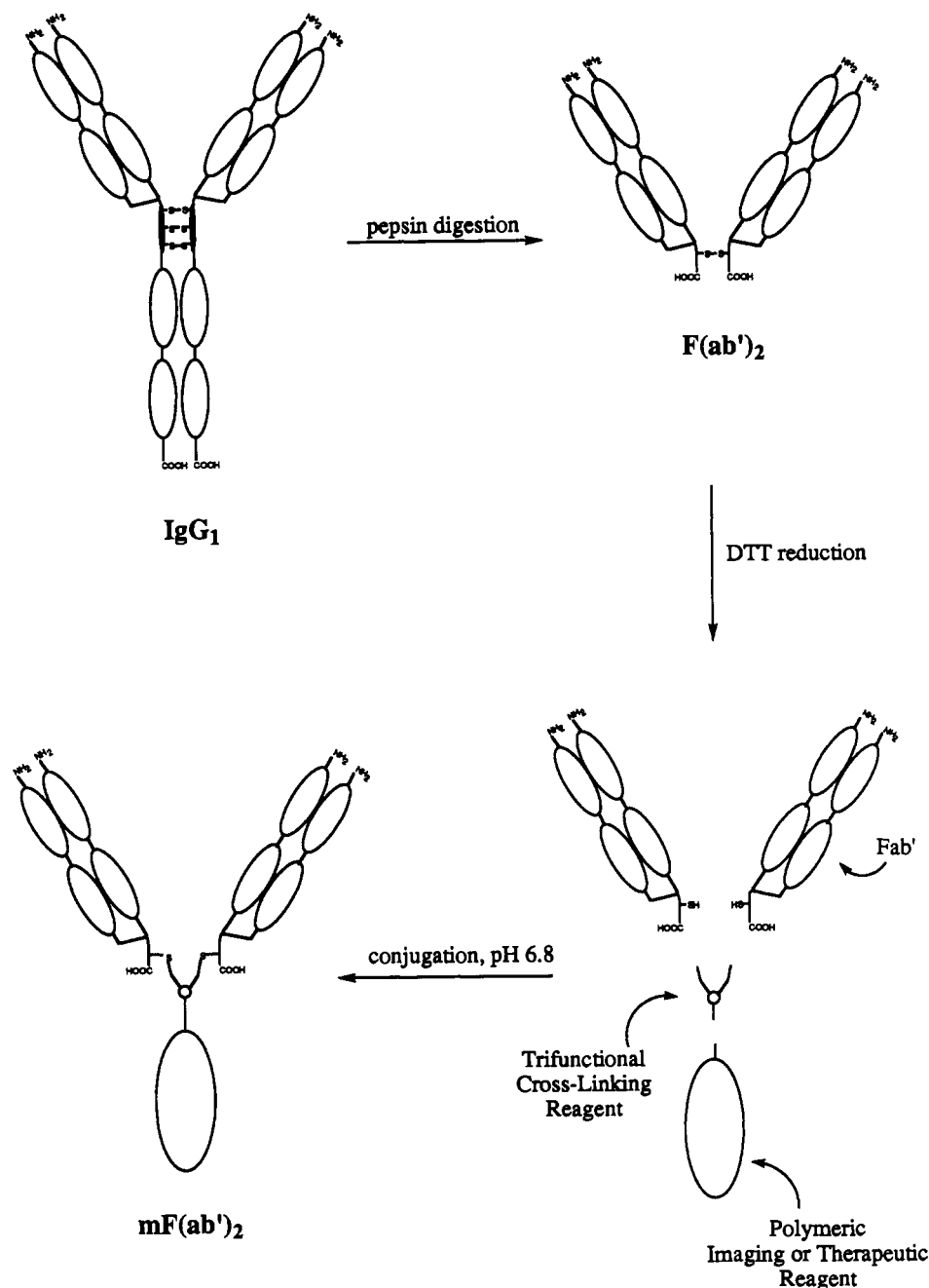
**General.** All chemicals purchased from commercial sources were analytical grade or better and were used

without further purification unless noted. HPLC solvents were obtained as HPLC grade and were filtered (0.2  $\mu$ m) prior to use. *p*-(Tri-*n*-butylstannyl)phenethylamine, **2**, was prepared and purified as previously described (13). Synthesis of the carboxyl ETAC reagent, 4-[2,2-bis[*p*-tolylsulfonyl)methyl]acetyl]benzoic acid, **1a**, was carried out as previously described (10). Sodium phosphate buffer, pH 6.8, was prepared by mixing equal quantities of 1 M solutions of Na<sub>2</sub>HPO<sub>4</sub> and NaH<sub>2</sub>PO<sub>4</sub> followed by adjustment of the pH with aqueous NaOH. Phosphate-buffered saline (PBS) was prepared by mixing 7.01 g of NaCl, 3.44 g of Na<sub>2</sub>HPO<sub>4</sub>, and 0.79 g of KH<sub>2</sub>PO<sub>4</sub> per liter of aqueous solution. Saline was obtained from Lyphomed (Deerfield, IL) as 0.9% NaCl in H<sub>2</sub>O. Column chromatography was conducted with 70–230-mesh 60-Å silica gel (Aldrich Chemical Co., Milwaukee, WI) or 40- $\mu$ m BAKERBOND C18 PrepLC reversed-phase packing (J.T. Baker, Inc., Phillipsburg, NJ). The monoclonal antibody A6H was obtained as previously described (14). Purification of radiolabeled A6H F(ab')<sub>2</sub> preparations was conducted by size exclusion gel chromatography using commercially available Sephadex G-25 (PD-10, Pharmacia) columns.

Na[<sup>125</sup>I]I and Na[<sup>131</sup>I]I were purchased from NEN/Dupont (Billerica, MA) as high concentration/high specific activity radioiodide in 0.1 N NaOH. Measurement of <sup>125</sup>I and <sup>131</sup>I was accomplished on the Capintec CRC-15R or a Capintec CRC-6A radioisotope calibrator. Tissue samples were counted in a LKB 1282  $\gamma$ -counter with the following window settings: channels 35–102 and 165–185 when <sup>125</sup>I and <sup>131</sup>I were counted together. *N*-Succinimidyl *p*-[<sup>125,131</sup>I]iodobenzoate, [<sup>125,131</sup>I]PIB, was prepared from *N*-succinimidyl *p*-(tri-*n*-butylstannyl)benzoate as previously described (15).

**Spectroscopic Data.** <sup>1</sup>H data were obtained on either a Varian VXR-300 (300 MHz) or a Bruker AC-200 (200 MHz). <sup>1</sup>H NMR data are referenced to tetramethylsilane as an internal standard ( $\delta$  = 0.0 ppm). IR data were obtained on a Perkin-Elmer 1420 infrared spectrophotometer and refer to absorptions of strong intensity unless otherwise noted for (m) medium intensity or (w) weak intensity. Mass spectral data (both low and high resolution) were obtained on a VG Analytical (Manchester, England) VG-70 SEQ mass spectrometer with associated 11250J data system. FAB<sup>+</sup> mass spectral data were obtained at 8 kV using a matrix of sodium salt of 3-nitrobenzyl alcohol or thioglycerol. FAB<sup>–</sup> mass spectral data were obtained at 8 kV in a matrix of thioglycerol. LC–MS were obtained on a HP 5989 mass spectrometer coupled to a HP 1090 liquid chromatograph using negative chemical ionization with methane.

**Analytical Chromatography.** HPLC separations of the nonradioactive and nonprotein compounds were obtained on either a Hewlett-Packard quaternary 1050 gradient pumping system with a multiple wavelength UV detector (220, 254, and 280 nm) or a Hewlett-Packard isocratic system consisting of a 1050 pump, variable-wavelength UV detector, and a Hewlett-Packard 1047A refractive index detector. Analyses of the HPLC data were conducted on a Hewlett-Packard Vectra QS/16S computer employing Hewlett-Packard HPLC ChemStation software. HPLC separations were conducted at a flow rate of 1 mL/min on a 5- $\mu$ m, 125- $\times$  4-mm C-18 column (LiChrospher 100 RP-18). Compounds were evaluated on a gradient system using an initial mixture of 60% MeOH/40% of an aqueous 1% HOAc solution. The gradient was held at the initial mixture for 3 min, increased to 100% MeOH over a 12-min period, and held at 100% MeOH for 10 min. Retention times for compounds using



**Figure 1.** Strategy for site specific conjugation of polymeric diagnostic and therapeutic reagents to antibody  $F(ab')_2$  fragments.

these conditions: **1a** = 1.4 min; **2** = 5.1 min; **3a** = 13.5 min; **3b** = 3.0 min; **4a** = 13.2 min; **4b** = 2.4 min.

HPLC conditions used in the HPLC-MS analysis of the mixture containing **3a** and **4a** were developed on the isocratic system described above. The optimized conditions employed an isocratic separation conducted on a 5- $\mu$ m (100- $\times$ 2.1-mm) ODS Hypersil column at a flow rate of 0.35 mL/min employing a 1:1 mixture of MeOH/1% aqueous HOAc.

The reaction mixtures from the radioiodination of **3a** were analyzed by HPLC using a 5- $\mu$ m C-18 column (Partisphere C-18, Whatman) eluting at a flow rate of 1 mL/min with a gradient beginning with 50% MeOH/50% of an aqueous HOAc solution. The gradient was held at the initial mixture for 5 min, increased to 100% MeOH over a 10-min period, and held at 100% MeOH for 10 min. The HPLC equipment used in the analyses of radioiodinated compounds (except proteins) consisted of two Beckman Model 110B pumps, a Beckman 420 controller,

a Beckman Model 153 UV detector (254 nm), and a Beckman Model 170 radioisotope detector. Retention times from UV detection on this system for **3b** and **4b** were 13.2 and 12.4 min. Retention times for detection of radioactivity were increased by approximately 0.5 min due to location of detector.

Proteins, including radiolabeled A6H  $F(ab')_2$ , were separated by size exclusion chromatography on a TSK-G2000-SW (7.5 $\times$ 60 cm, 10- $\mu$ m particle size, TOSO HAAS) column. The column was equilibrated, and proteins were eluted with 0.1 M sodium phosphate, pH 6.8, buffer (containing 1 mM EDTA + 5 mM  $NaN_3$ ) at a flow rates of 0.75 or 1.0 mL/min. Retention time for intact A6H  $F(ab')_2$  was 19.4 min, A6H  $Fab'$  was 22.4 min, and small molecule (e.g., free iodide) retention was 33.0 min at 1 mL/min. The  $mF(ab')_2$  had the same retention time as the unmodified  $F(ab')_2$ . The HPLC equipment used in this analysis consisted of two Model 302 Gilson pumps with 10SC pump heads, an ISCO Model V4 UV detector

(280 nm), a Beckman Model 170 radioisotope detector, a Gilson 621 Data Master, and an IBM 386 with Gilson 715 HPLC Controller software.

Thin-layer chromatography (TLC) of radiolabeled A6H F(ab')<sub>2</sub> was conducted on predried 1- × 6-cm silica gel impregnated glass-fiber strips eluting with 80% MeOH. Small aliquots of the labeled antibody were placed on a premarked spot (origin). After elution, the TLC strip was cut into six approximately equal sections, put into plastic tubes (12 × 75 mm), and counted. The percent of protein bound radioactivity (and radiochemical purity) was estimated from a calculation where the counts obtained from the origin section and two adjacent sections were divided by the cumulative counts from the entire plate (all six sections) multiplied by 100.

**N-[4-[2,2-Bis[(*p*-tolylsulfonyl)methyl]acetyl]benzoyl]-4-(tri-*n*-butylstannyl)phenethylamine, 3a.** To a dry 10-mL round-bottom flask was added 100 mg (2.0 mmol) of **1a** and 0.5 mL of SOCl<sub>2</sub> (0.89 g, 6.9 mmol). The solution was stirred at room temperature under argon for 24 h, and excess SOCl<sub>2</sub> was removed with a stream of Ar (captured in dry-ice cooled isopropyl alcohol). [Note: three additions of 5 mL of CHCl<sub>3</sub> followed by removal under Ar were conducted to completely remove the SOCl<sub>2</sub>.] The resultant crude solid, **1b**, was dissolved in 2 mL of anhydrous THF, and 50 μL of pyridine (0.69 mmol) was added. To this mixture was added 50 μL of neat stannylphenethylamine, **2** (0.12 mmol). The reaction mixture was stirred for 2 h and the THF removed under a stream of Ar. The residue was dissolved in 10 mL of CHCl<sub>3</sub> and washed with 10 mL of 0.1 N HCl and then 2 × 10 mL of H<sub>2</sub>O. The CHCl<sub>3</sub> solution was dried over MgSO<sub>4</sub> and evaporated to yield 151 mg (85%) of a tacky yellow-orange material. Analysis of the crude product by HPLC indicated that a mixture of closely eluting materials had been obtained in a 3:97 ratio. The crude material was dissolved in 1 mL of CH<sub>3</sub>CN, and a few drops of H<sub>2</sub>O were added (to cloudiness). This solution was eluted on a disposable C-18 column (Alltech Maxiclean, 300 mg) that had been pretreated with 10 mL of MeOH and then 10 mL of H<sub>2</sub>O. The effluent of the column was evaporated to yield 68 mg (38%) of a colorless tacky oil. HPLC analysis indicated that the proportions of the closely eluting peaks had changed to a 1:10 ratio.

An alternative method for purification was developed to obtain an analytical sample. In that purification, the crude material was dissolved in 2 mL of 1% HOAc in MeOH and was eluted on a reversed-phase C-18 column (5 g, 1 × 8 cm; preequilibrated with 1% HOAc in H<sub>2</sub>O). Fractions were collected from the column after elution with increasing concentrations of MeOH (20 mL of 1% HOAc in H<sub>2</sub>O; 10 mL 80% H<sub>2</sub>O/20% of 1% HOAc in MeOH; 30 mL 50% H<sub>2</sub>O/50% 1% HOAc in MeOH; 50 mL 30% H<sub>2</sub>O/70% of 1% HOAc in MeOH; 25 mL 5% H<sub>2</sub>O/95% 1% HOAc in MeOH) and flushed with 1% HOAc in MeOH. Collected fractions (6 mL) were evaluated by HPLC to assess purity. The fractions (32 and 33) containing pure compound were concentrated to yield 32 mg of a tacky colorless oil (no **4a** present by HPLC): IR (neat) 3375 (w, broad), 2945, 2915, 2863 (m), 2845 (m), 1687 (m), 1650, 1592 (m), 1530, 1312, 1300, 1145 (vs), 1134 (m), 926 (w), 860 (w), 813 (m), 739 (w); <sup>1</sup>H NMR (CDCl<sub>3</sub>) 7.7 (m, 8H), 7.44 (d, 2H, *J* = 7.7 Hz), 7.35 (d, 4H, *J* = 8.2 Hz), 7.20 (d, 2H, *J* = 7.7 Hz), 6.29 (t, 1H, *J* = 5.6 Hz), 4.34 (t, 1H, *J* = 6.2 Hz), 3.73 (dd, 2H, *J* = 6.8, 12.7 Hz), 3.61 (dd, 2H, *J* = 6.6, 14.3 Hz), 3.48 (dd, 2H, *J* = 6.0, 14.3 Hz), 2.92 (t, 2H, *J* = 6.9 Hz), 2.47 (s, 6H), 1.54 (m, 6H), 1.34 (m, 6H), 1.05 (m, 6H), 0.88 (t, 9H, *J* = 7.2 Hz); MS (FAB<sup>-</sup>,

isotopes, M - H) mass calcd for C<sub>45</sub>H<sub>58</sub>O<sub>6</sub>NS<sub>2</sub>Sn 888 (35), 889 (36), 890 (73), 891 (56), 892 (100), 893 (49), 894 (31), found 888 (32), 889 (42), 890 (72), 891 (68), 892 (100), 893 (73), 894 (46); MS (FAB<sup>+</sup>, M + Na) mass calcd for C<sub>45</sub>H<sub>58</sub>O<sub>6</sub>NS<sub>2</sub>SnNa 916 (100), Found 916 (100%) (with appropriate isotope envelope); HRMS (FAB<sup>+</sup>, M + H) calcd for C<sub>45</sub>H<sub>60</sub>O<sub>6</sub>NS<sub>2</sub>Sn (Sn 118) 892.2894, (Sn 119) 893.2907, (Sn 120) 894.2905, found (Sn 118) 892.2878, (Sn 119) 893.2895, (Sn 120) 894.2884.

A 60-mg quantity of the (Maxi-Clean column) purified **3a** was dissolved in 2.4 mL of dry CH<sub>3</sub>CN. Aliquots of 40 μL (1 mg) were placed into clean dry vials. The vials were placed in a vacuum desiccator, and the CH<sub>3</sub>CN was removed under vacuum. The oily residue in the vials was placed under an Ar atmosphere, capped, covered with aluminum foil, and stored desiccated in a freezer.

**N-[4-[2,2-Bis[(*p*-tolylsulfonyl)methyl]acetyl]benzoyl]-4-iodophenethylamine, 3b.** To a round-bottomed flask containing 80 mg (0.09 mmol) **3a** in 3 mL of 5% HOAc/MeOH was added 15 mg (0.26 mmol) of NaI and then 36 mg (0.26 mmol) of *N*-chlorosuccinimide (NCS). The mixture turned dark immediately and cleared within 30 s. After 30 min, the solvent was removed on a rotary evaporator. The residue was dissolved in 1 mL of 1% HOAc in MeOH, and a few drops of water were added until a cloudiness persisted. This material was added to the top of a C-18 reversed-phase column (5 g, 1 × 8 cm) that had been preequilibrated with 1% HOAc in H<sub>2</sub>O. Five-mL fractions were collected from the column eluting by step gradient from 1% HOAc in H<sub>2</sub>O (solvent A) to 1% HOAc in MeOH (solvent B). The elution was done as follows: 20 mL of A; 10 mL of 90% A/10% B; 10 mL of 80% A/20% B; 10 mL of 60% A/40% B; 10 mL of 40% A/60% B; 20 mL of 20% A/80% B; and 20 mL of B. Fractions 16 and 17 were combined to give 41 mg of the desired product by HPLC. The product, a white solid, had a faint alkyltin odor: <sup>1</sup>H NMR (CDCl<sub>3</sub>) 7.66 (m, 10 H), 7.35 (d, 4H, *J* = 8.2 Hz), 6.99 (d, 2H, *J* = 8.3 Hz), 6.40 (t, 1H, *J* = 5.8 Hz), 4.36 (m, 1H), 3.73–3.58 (m of d, 4H), 3.51–3.45 (m of d, 2H), 2.89 (t, 2H, *J* = 7.3 Hz), 2.48 (s, 6H) [<sup>1</sup>H NMR indicated that *n*-Bu<sub>3</sub>SnOH had coeluted with **4a** as an impurity; HRMS (FAB<sup>+</sup>, M + H) calcd for C<sub>33</sub>H<sub>33</sub>O<sub>6</sub>NS<sub>2</sub>I 730.0806, found 730.07941.

**Radioiodination of 3a, Preparation of [<sup>125</sup>I, <sup>131</sup>I]3b.** To a reaction vessel containing 50 μL of a 1 mg/mL solution of **3a** (50 μg, 5.6 × 10<sup>-5</sup> mmol) in 5% HOAc/MeOH was added 20 μL (20 μg, 1.5 × 10<sup>-4</sup> mmol) of a 1 mg/mL NCS in MeOH solution and 10 μL of PBS (or 5 μL of sodium phosphate buffer, pH 6.45). To this mixture was added 4–20 μL of the radioiodine solution (in 0.1 N NaOH). The reaction mixture was swirled and allowed to sit for 5 min. At that time, 20 μL of a 0.72 mg/mL aqueous solution of Na<sub>2</sub>S<sub>2</sub>O<sub>5</sub> was added. Further workup included removal of part or all of the solvent under a stream of Ar. A representative HPLC radioactivity trace of a crude reaction mixture is shown in Figure 3. A compilation of the labeling yields for several experiments is given in Table 1.

**Stability and Reactivity of ETAC Reagents.** (1) An experiment to study the stability of **3a** in some solvents of interest was conducted by preparing 1 mg/mL solutions and evaluating the solutions by HPLC at *t* = 0, 1, 2, 18–24 h and then daily for up to 12 days. The solvents studied were DMSO, CH<sub>3</sub>CN, and a mixture of 5% HOAc in MeOH. A 10-μL aliquot of the mixture was evaluated by HPLC at each time point, and the total area of the peaks was compared with the previous runs to account for changes in product composition or material lost to polymerization.

(2) A NMR experiment was conducted to evaluate the production and nature of the minor HPLC component (presumed to be **4a**). In the experiment, 25 mg (28  $\mu$ mol) of purified **3a** (by C-18 column) was dissolved in 1 mL of  $\text{CDCl}_3$ . After an initial NMR (300-MHz) spectrum was obtained, a 100- $\mu$ L aliquot of a 174  $\mu$ L/mL solution (17.4  $\mu$ L, 12.6 mg, 125  $\mu$ mol) of triethylamine in  $\text{CDCl}_3$  was added. NMR spectra were taken at 15 and 45 min postaddition. The contents of the NMR tube were then concentrated to an oil and dissolved in 2 mL of  $\text{CH}_3\text{CN}$ . The reaction mixture was analyzed by HPLC (isocratic, 254 nm; 87% MeOH/13% of a 1% HOAc aqueous solution). A 300- $\mu$ L aliquot of a 60 mg/mL solution of *N*-acetylcysteine (18 mg, 99  $\mu$ mol) in  $\text{CH}_3\text{CN}$  was then added. The reaction mixture was stirred at room temperature, and aliquots were taken at 5 min and 1 h for HPLC analysis.

(3) An experiment was conducted to examine the relative reactivity of the two iodinated ETAC compounds (**3b** and presumably **4b**) observed in the product mixture by HPLC. In that particular reaction the product mixture was taken to dryness under an Ar stream and was allowed to sit at room temperature in a concentrated form overnight. After that time, the oily residue was dissolved in 50  $\mu$ L of  $\text{CH}_3\text{CN}$  and was evaluated by HPLC. To the  $\text{CH}_3\text{CN}$  solution was added 10  $\mu$ L of a 1 M aqueous cysteine solution (1.2  $\mu$ g,  $10^{-2}$   $\mu$ mol) at room temperature. The reaction mixture was monitored by HPLC to see how its composition changed with time (10 min, 58 min, and 90 min). The results are shown graphically in Figure 4.

**Antibody Fragmentation.** Fragmentation of A6H was accomplished as previously described (14), except the reaction time was extended to 24 h. Briefly, purified A6H (1.67 mg/mL) was fragmented with pepsin (25 mg/mL) at 37 °C for 24 h. The  $\text{F(ab')}_2$  was dialyzed and passed over a DEAE column for purification. HPLC and SDS-PAGE analysis indicated that the  $\text{F(ab')}_2$  was pure of other protein contaminants (Figure 5A). The  $\text{F(ab')}_2$  was concentrated by ultrafiltration through PM-10 filters (Amicon) to 7.1 mg/mL, divided into 500- $\mu$ g quantities, and frozen at -80 °C until used.

**Preparation of A6H Fab'.** A frozen 500- $\mu$ g (74  $\mu$ L) aliquot of A6H  $\text{F(ab')}_2$  was thawed to room temperature, and 16  $\mu$ L of 0.1 M sodium phosphate, pH 6.8 containing 1 mM EDTA was added. To this solution was added 10  $\mu$ L of 10 mM dithiothreitol (DTT) in 0.1 M sodium phosphate, pH 6.8 containing 1 mM EDTA. Reduction of the  $\text{F(ab')}_2$  was followed by HPLC analysis of the reaction mixture. Typically, reduction was >95% complete within 2 h (see Figure 5C), and the reaction mixture was placed on ice. Separation of the generated Fab' from small molecules (e.g., excess DTT) was accomplished by centrifugal gel filtration through a 0.6-mL polypropylene microcentrifuge tube packed with Sephadex G-25 and equilibrated with 0.1 M sodium carbonate buffer, pH 6.8. This procedure was used to prevent dilution of the Fab' concentration by keeping the sample volumes small. Recovery of 70–80% (by weight) of the Fab' was obtained. Concentrations of 3–4 mg/mL were obtained, resulting in 350–400  $\mu$ g of Fab' in 90–130  $\mu$ L.

**Cross-Linking Experiments.** Cross-linking experiments were conducted on 175–200  $\mu$ g of A6H Fab' contained in 45–75  $\mu$ L of 0.1 M sodium carbonate, pH 6.8. An aliquot of 1, 5, or 10  $\mu$ L of a solution containing 50  $\mu$ g of the ETAC compound, **3a** or **3b**, in 25  $\mu$ L of  $\text{CH}_3\text{CN}$  (2  $\mu$ g/ $\mu$ L) was added to the Fab' solution. Reactions were conducted at room temperature for varying periods of time, and the progress of the cross-linking reactions was followed

by UV and radioisotope detection on HPLC (see Figure 5D–F). In several examples, purified  $\text{mF(ab')}_2$  was obtained by collection of samples from multiple injections of crude reaction mixture onto the HPLC. The  $\text{mF(ab')}_2$  collected in this manner was used without further purification for *in vitro* and *in vivo* studies.

**Cross-Linking with Iodoacetamide Blocking.** A 1-mg quantity of A6H  $\text{F(ab')}_2$  in 60  $\mu$ L of PBS was brought to 0.1 M Tris-HCl by the addition of 6.6  $\mu$ L of 1 M Tris-HCl, pH 8.8. To this solution was added 7  $\mu$ L of a 200 mM iodoacetamide solution in 0.1 M Tris-HCl and 1 mM EDTA, pH 8.8. The solution was incubated at 25 °C for 30 min, and then 7.5  $\mu$ L of a 20 mM solution of dithiothreitol (DTT) in 0.1 M phosphate buffer, pH 6.8, was added. The extent of reduction was measured after 2 h and found to be incomplete (in contrast with unmodified  $\text{F(ab')}_2$ ). The sample was stored cold overnight. The following day the buffer was exchanged to 0.1 M sodium carbonate, pH 6.8, and the DTT concentration was increased to 5 mM. Reduction was complete within 1 h. The sample was divided into two equal quantities. One sample (half-quantity) was desalted into 0.1 M sodium carbonate buffer, pH 6.8, containing 1 mM EDTA. The other sample was treated with Tris-HCl, pH 8.8, to make it 0.1 M in that reagent, and was subsequently retreated with 10 mM iodoacetamide for 30 min. The second sample was desalted into 0.1 M carbonate buffer, pH 6.8, containing 1 mM EDTA. Both samples were subsequently reacted with [ $^{131}\text{I}$ ]**3b**.

**In Vitro Stability of A6H  $\text{mF(ab')}_2$ .** Multiple injections of [ $^{131}\text{I}$ ]**3b**-cross-linked  $\text{mF(ab')}_2$  onto a size exclusion column (TSK G-2000; 7.6  $\times$  600 mm) resulted in isolation of 89  $\mu$ Ci (3.3 MBq) in 1.7 mL of 0.1 M sodium phosphate buffer, pH 6.8/1 mM EDTA. The isolated  $\text{mF(ab')}_2$  solution had a protein concentration of 46  $\mu$ g/mL and a specific activity of 1.14  $\mu$ Ci/ $\mu$ g (42 kBq/ $\mu$ g). Aliquots (110  $\mu$ L; 5  $\mu$ Ci or 0.19 MBq) of the isolated  $\text{mF(ab')}_2$  were added to 100  $\mu$ L of the following reagents: (1) 0.9% saline, (2) fresh human serum, (3) 1 M cysteine, (4) 1 M *N*- $\alpha$ -acetyl-L-lysine, and (5) 1 M sodium carbonate, pH 9.3. Tubes 1 and 2 were incubated at 37 °C, and tubes 3–5 were incubated at 25 °C. TLC was performed on silica gel impregnated strips, eluting with 80% MeOH.

**Electrophoresis.** Electrophoretic separations of proteins were conducted using conventional equipment (Hoefer Scientific) or a PhastSystem (Pharmacia, Uppsala, Sweden). Separations (using conventional equipment) on one-dimensional sodium dodecylsulfate-polyacrylamide gels (SDS-PAGE) were performed essentially as outlined previously (16, 17). Briefly, samples of purified  $\text{mF(ab')}_2$  (approximately 1  $\mu$ g of protein) or reaction mixtures containing  $\text{mF(ab')}_2$  (approximately 20  $\mu$ g of protein) were denatured by dilution in an equal volume of sample buffer containing 65 mM Tris-HCl, pH 6.8, 2% SDS, 10% glycerol, and 0.1% bromophenol blue. Some of the samples were treated under reducing conditions, which were achieved by addition of 5% 2-mercaptoethanol ( $\beta$ -ME) to the sample buffer. Samples were allowed to stand at room temperature for 10–30 min or were heated to 100 °C for 3 min prior to loading onto the gel. Molecular weight marker proteins (BioRad, Hercules, CA); myosin (200 kDa),  $\beta$ -galactoside (116 kDa), phosphorylase-b (97 kDa), bovine serum albumin (66 kDa), egg white ovalbumin (45 kDa), carbonic anhydrase (31 kDa), soybean trypsin inhibitor (22 kDa), and lysozyme (14 kDa) were treated with reducing denaturing conditions at 100 °C as described above. Samples were applied to the lanes of a 1.5-mm-thick 11% gel (30% T, 2.67% C), and electrophoresis was



carried out at constant current (25 mA stacking, 60 mA running) in Tris/glycine/SDS (3.0/14.4/1.0 g/L) buffer, pH 8.3. Following electrophoresis, gels were fixed for 2 h in 40% MeOH/10% HOAc and equilibrated for 1 h in 10% EtOH/5% HOAc.

Proteins were stained with silver as previously described (18). Briefly, proteins were oxidized by soaking the gel in a freshly prepared solution of 3.4 mM K<sub>2</sub>Cr<sub>2</sub>O<sub>7</sub>/3.2 mM HNO<sub>3</sub> for 10 min at room temperature. The gel was rinsed in deionized H<sub>2</sub>O until the yellow color of the dichromate solution was removed. The gel was then soaked in a solution containing 0.25 AgNO<sub>3</sub> for 30 min, followed by a brief 2-min rinse in deionized H<sub>2</sub>O. To visualize the bands, protein-bound silver was precipitated by immersing the gel in a solution containing 0.28 M Na<sub>2</sub>CO<sub>3</sub>/1% formaldehyde. Gel staining was stopped by immersion in 5% HOAc, 4% glycerol, after which they were dried on a heated vacuum manifold. Autoradiographic exposures were recorded on X-OMAT/AR film (Eastman Kodak; Rochester, NY). Optimal exposure times varied depending on the specific activity of the proteins analyzed. Figure 6 shows an autoradiographic exposure of a SDS-PAGE gel of unaltered radioiodinated F(ab')<sub>2</sub>. Figure 7 shows a silver-stained (A) and autoradiographic exposure (B) of a SDS-PAGE gel which compared crude reaction mixtures of radioiodinated mF(ab')<sub>2</sub> with purified mF(ab')<sub>2</sub>.

Proteins resolved on the PhastSystem were separated on 4–15% gradient SDS-polyacrylamide gels. Proteins were denatured by mixing four volumes of pure mF(ab')<sub>2</sub> (0.5–1 µg of protein) with one volume of concentrated sample buffer (5×) containing 10% SDS, 0.125 M Tris-HCl (pH 6.8), and 5 mM EDTA. Reducing conditions were achieved by addition of 25% β-ME to the sample buffer. Samples were allowed to stand at room temperature for 10–30 min or heated to 100 °C for 3 min prior to loading. Gels were prerun for 1 Vh (volt-hour) prior to loading, and then samples were loaded and resolved by applying a 10-mA current (<250 V) for 60 Vh at 15 °C. Gels were removed from the running chamber, placed immediately into the automated staining chamber, and silver stained. The PhastSystem gels were fixed in 12.5% freshly prepared glutaraldehyde, washed with H<sub>2</sub>O, and oxidized with 0.5% AgNO<sub>3</sub>. The gels were then washed with H<sub>2</sub>O, developed in 2.5% Na<sub>2</sub>CO<sub>3</sub>/0.015% formaldehyde, quenched in 10% HOAc/10% glycerol, and air dried. Autoradiographic exposures were obtained as described above. An example of an autoradiographic exposure of a SDS-PAGE gel run on the PhastSystem is shown in Figure 8.

**Antibody Cell Binding Assay.** Tumor cell binding immunoreactivity assays of the radiolabeled A6H F(ab')<sub>2</sub> were conducted as previously described (14). Briefly, each assay was conducted by addition of approximately 10 000 counts per min (cpm) of the F(ab')<sub>2</sub> or mF(ab')<sub>2</sub> preparation in 0.1 mL of 0.9% saline to 2 million trypsinized 7860 renal cell carcinoma cells suspended in 1 mL of PBS containing 1% BSA. (Trypsinization was carried out by treatment with 0.25% trypsin/0.03% sodium citrate solution at room temperature for 5 min). The actual number of cpm added to each tube was determined by quantification in a γ-counter. Cells were incubated at room temperature for 1 h with constant rotary inversion mixing, pelleted by centrifugation, decanted to remove supernatant, and resuspended in 1 mL of PBS. The cell suspension was then transferred to a new tube and recounted. The immunoreactivity estimation was taken as the counts remaining divided by initial total counts multiplied by 100.

**Animals and Tumor Model.** Male athymic mice (*nu/nu*), obtained from Simonson Laboratories (Gilroy, CA), were housed for 1 week in the isolator facility prior to beginning the study. Tumor pieces (5–10 mg) of TK-82 renal cell carcinoma (19) were implanted subcutaneously above the right shoulder of the mice using a protocol approved by the Animal Care Committee at the University of Washington. In the Fab' biodistribution study, the mice (*n* = 12) had an average weight of 26.6 ± 2.2 g and the TK-82 tumor xenografts had an average weight of 50 ± 19 mg. In the mF(ab')<sub>2</sub> biodistribution study, the mice (*n* = 18) had an average weight of 24.4 ± 2.1 g and the TK-82 tumor xenografts had an average weight of 140 ± 77 mg.

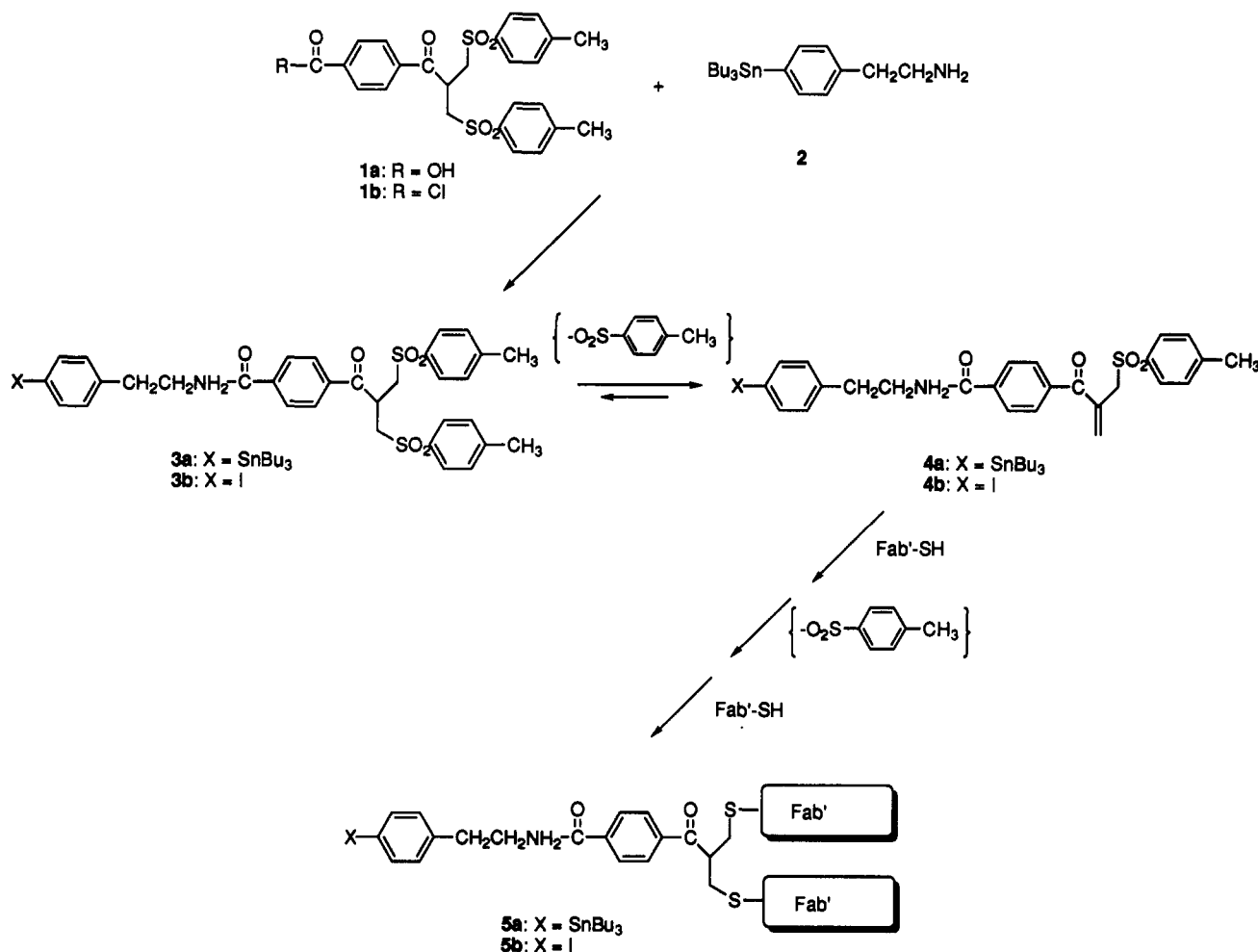
**Biodistribution Studies.** For the biodistribution of radioiodinated mF(ab')<sub>2</sub>, a 200-µL quantity of a mixture of [<sup>125</sup>I]PIB-labeled A6H F(ab')<sub>2</sub> (1.4 µCi (52 kBq) of <sup>125</sup>I on 6 µg) and [<sup>131</sup>I]3b-labeled A6H mF(ab')<sub>2</sub> (1.2 µCi (44 kBq) of <sup>131</sup>I on 8 µg) was injected into each of 18 athymic mice via the lateral tail vein. The actual amount of injectate administered to each animal was determined by weighing the administering syringe before and after injection. Six mice were sacrificed by cervical dislocation at 3.5, 19, and 43 h postinjection. The data obtained are given in Table 2. The biodistribution of radioiodinated A6H Fab' was conducted similarly, with approximately 130 µL of a mixture of [<sup>131</sup>I]PIB-labeled A6H Fab' (10.1 µCi (0.37 MBq) of <sup>131</sup>I on 11.2 µg) and <sup>125</sup>I-labeled A6H Fab' (17.4 µCi (0.64 MBq) of <sup>125</sup>I on 26 µg) being injected into each animal. Six mice were sacrificed at 4 and 24 h postinjection. The data obtained from this biodistribution are given in Table 3.

In the biodistributions, tissues were excised, blotted free of blood, weighed, and counted. Calculation of the percent injected dose per gram (% ID/g) in the tissues was accomplished using internal standards to compensate for decay, and the <sup>125</sup>I counts were compensated for spillover (14%) from <sup>131</sup>I.

## RESULTS

**Preparation of ETAC Compounds.** The synthetic steps involved in preparation of reagents and cross-linking of Fab' are depicted in Figure 2. The synthesis of the requisite carboxy-ETAC molecule, 1a, was accomplished as previously described (10). Oxidation of the bis-sulfide, following the reaction conditions described, did not give complete conversion to the bis-sulfone. Attempts at purification of the mixture resulted in increasing the percent of bis-sulfide rather than bis-sulfone. After HPLC conditions were developed which allowed the reaction to be followed more closely, it was found that longer reaction times and addition of more reagents did not improve the percent conversion. Interestingly, it was found that a complete conversion of the bis-sulfide to bis-sulfone could be obtained if the reaction was carried out in a tightly sealed vial.

Synthesis of the *p*-(tri-*n*-butylstannyl)phenethylamine adduct 3a was accomplished by reaction of 2 with crude acid chloride 1b, formed by reaction of 1a with thionyl chloride. Attempts to isolate 3a from other impurities by silica gel chromatography resulted in a large loss of material and caused the product mixture to become more complex by NMR analysis. Therefore, the crude light yellow product, which was >97% pure by HPLC, was initially stored neat in the refrigerator. However, it was found that the crude material completely polymerized in the refrigerator within a month. Because of the difficulties encountered on silica gel chromatography, reversed-phase chromatography was used to purify the crude product.



**Figure 2.** Chemical reactions for preparation of ETAC compounds (3a and 3b) and their cross-linking of monoclonal antibody Fab' fragments.

Since only small quantities were needed, purification of the crude product was possible by elution through a disposable reversed-phase C-18 syringe column (Alltech, Maxi-Clean). This removed the colored impurities to give a colorless (tacky) product. Even after purification, preparations of 3a contained a closely eluting minor component by HPLC analysis. NMR data indicated that the major component was the desired adduct 3a, but identification of the minor component could not be obtained readily. An alternate reversed-phase column chromatography purification method provided a pure sample (free of the minor contaminant) for characterization, but it was obtained in low yield (18%).

While the minor component present with 3a has not been unequivocally identified, it appears that it is the thiol-reactive  $\alpha,\beta$ -unsaturated ketone containing compound 4a based on spectroscopic evidence and its chemical reactivity. Initially, the similar elution characteristics of the minor component on HPLC was somewhat troubling, as it seemed that the lipophilicity of 4a might be considerably different from that of 3a. However, it was found that the 3a could be converted to the minor component by making the solution basic. To assist in the characterization of the minor component, a NMR experiment was conducted reacting triethylamine with isolated (purified) 3a in a NMR tube. After addition of Et<sub>3</sub>N, the NMR spectrum of 3a was altered by a decrease in integral of two multiplets (two protons each) at 3.48 and 3.61 ppm, with new singlets at 5.98 and 6.26 ppm being present, and with an increased complexity of peaks in the aromatic region (i.e., 7.1–7.9

ppm). Isolation of the reaction mixture from the NMR experiment and evaluation by (isocratic) HPLC analysis demonstrated that the minor component was present in approximately 1:2 ratio with 3a (from the starting ratio of 1:25). Stirring this mixture in CH<sub>3</sub>CN with *N*-acetylcysteine over a 1-h period provided evidence that reaction (of the sulfhydryl containing reagent) occurs predominately with the minor component, as might be expected for the  $\alpha,\beta$ -unsaturated keto compound 4a. Development of HPLC conditions provided a base-line separation of the two closely eluting components, which afforded an opportunity to evaluate each components' mass spectral characteristics by LC-MS analysis. The mass spectral data correlated well with the major peak being that of 3a (mass calcd 894; found 894) and the minor peak being 4a (mass calcd 738; found 738).

The stability of the ETAC molecules was of paramount importance in the cross-linking experiments. Therefore, stability of the carboxyl-ETAC 1a and the stannylphenethyl-ETAC reactive intermediate, 3a, was studied in DMSO, CH<sub>3</sub>CN, MeOH, MeOH/5% HOAc, and the buffer medium used in cross-linking experiments. The ETAC molecules were converted very rapidly to other species when dissolved in the buffer used in protein conjugations, but little change was observed in the original compound composition (or total peak area) over a 24-h period in the other solvents. At longer periods of time a difference was observed for the rate of disappearance of the peak corresponding to 3a in the different solvents. It was found that 3a was most stable in CH<sub>3</sub>CN, having essentially no

**Table 1.** Reaction Product Ratios and Overall Yields for Reaction of **3a**<sup>a</sup> with Radioiodine and NCS<sup>b</sup>

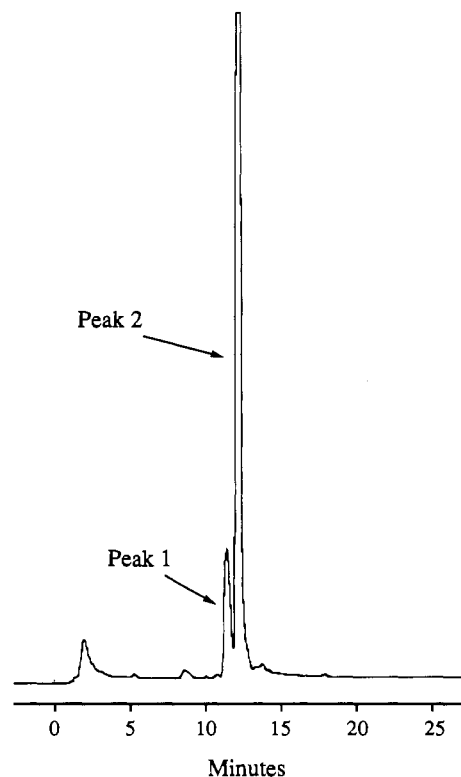
run	quantity of <b>3a</b> (μg)	radioiodine <sup>c</sup> quantity used	yield <sup>d,e</sup> (%) peak 1/peak 2 (total) <sup>f</sup>
1	50	20 μL, 1.17 mCi (43.3 MBq)	8/76 (84)
2	50	4 μL, 3.31 mCi (123 MBq)	8/86 (94)
3	5	5 μL, 2.10 mCi (77.8 MBq)	6/71 (77)
4	50	10 μL, 5.67 mCi (210 MBq)	8/86 (94)
5	50	5 μL, 5.77 mCi (214 MBq)	8/81 (88)
6	50	5 μL, 5.34 mCi (198 MBq)	7/85 (93)
7	50	4 μL, 0.370 mCi (13.7 MBq)	10/76 (86)
8	50	4 μL, 0.55 mCi (20.4 MBq)	8/80 (88)

<sup>a</sup> **3a**, *N*-[4-[2,2-bis[(*p*-tolylsulfonyl)methyl]acetyl]benzoyl]-4-(tri-*n*-butylstannyl)phenethylamine. <sup>b</sup> NCS, *N*-chlorosuccinimide. <sup>c</sup> <sup>131</sup>I was used in all experiments except 1, where <sup>125</sup>I was used. <sup>d</sup> Determined by HPLC. See Experimental Procedures for details. <sup>e</sup> All reaction product mixtures were used as obtained; runs 4–8 were concentrated under an Ar stream prior to reaction with A6H Fab'. <sup>f</sup> Percent of total radioactivity injected into HPLC.

change in composition after 12 days. ETAC derivative **3a** was least stable in 5% HOAc in MeOH and had an intermediate stability in DMSO. However, the stability was reasonably high even in 5% HOAc in MeOH as its peak area only decreased 25% in 3 days at room temperature. Interestingly, as the peak area for component **3a** decreased, its ratio with the minor peak **4a** did not change in these solvents, but a peak present in all chromatograms at 1.95 min, which may be the (*p*-methylphenyl)sulfinic acid, increased from 10% of the total peak areas to 26% of the total peak area over the 3-day period. No other new peaks were noted, suggesting perhaps that the intermediate formed might have polymerized. It was also noted that a sample had polymerized in acetone-*d*<sub>6</sub> prior to obtaining an NMR.

Evaluation of the cross-linking and stability of the ETAC molecules was facilitated by storing 1-mg samples of the stannylphenethyl-ETAC, **3a**. This was accomplished by dissolving a quantity of purified **3a** in dry CH<sub>3</sub>CN and aliquoting a predetermined volume into clean dry vials. The vials were placed in a vacuum desiccator, and the CH<sub>3</sub>CN was pulled off under vacuum. Argon was introduced into the desiccator, and after opening, the vials were capped and placed in an aluminum foil covered desiccator in the freezer. After 3 months storage under these conditions there did not appear to be any degradation of product by HPLC analysis.

**Iodination and Radioiodination.** Iodination of **3a** to form **3b** was accomplished by reaction with *N*-chlorosuccinimide (NCS) and NaI in 5% HOAc/MeOH solution. These reagents and reaction conditions were chosen as they had been used successfully for many previous high specific activity radioiodinations of arylstannanes (8, 20, 21). Reaction of the stannyl derivative as a mixture of the two closely eluting peaks by HPLC gave a nearly identical mixture ratio of two less lipophilic peaks (minor peak at 2.4 min and major peak at 3.0 min). Only the stoichiometry of reagents was changed for no-carrier-added radioiodinations, and a similar ratio of products was obtained. The radioiodination reactions were found to be quite facile, resulting in high overall yields (Table 1). A typical radioactivity trace is shown in Figure 3. A variance in the quantity of radioactivity used in the radioiodination reactions of **3a** did not appreciably alter the amount of **3b** obtained, except in the experiment where a much smaller quantity (i.e., 5 μg) of **3a** was used (see run 3 in Table 1). Aliquots of the initial radioiodination reaction mixtures (runs 1–3, Table 1) were used directly in the cross-linking experiments. However, concerns about controlling the

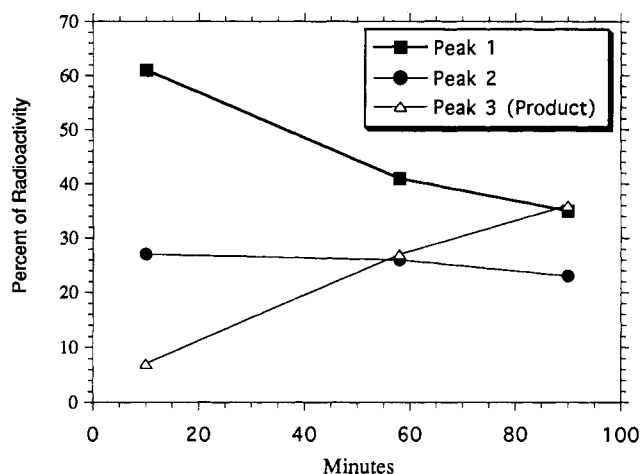


**Figure 3.** Radioactivity trace for HPLC separation of components from radioiodination reaction of **3a** (with some **3b** present). The separation was conducted on a 5-μm C-18 column eluting at a flow rate of 1 mL/min using a gradient mixture. The initial solvent mixture of 50% MeOH/50% of a 1% aqueous HOAc solution was held for 5 min and then increased to 100% MeOH over a 10-min period and held at 100% MeOH for 10 min. HPLC retention times correlate with peak 1 being that of the unknown minor component (believed to be [<sup>131</sup>I]**4b**), peak 2 being that of [<sup>131</sup>I]**3b**. The product compositions (peak 1/peak 2) for several radioiodinations are given in Table 1. For a description of the HPLC system used to separate (nonprotein) radioiodinated compounds see the Experimental Procedures.

pH of the coupling reaction with the addition of HOAc present in the radioiodination mixture led to removal of solvent from the crude radioiodination reaction mixture under a stream of Ar (runs 4–8, Table 1) prior to use in cross-linking experiments.

The radioiodinated product mixture was also evaluated for reaction with cysteine. In that experiment, the proportion of minor component had increased from <10% to >70% after removing the solvent under a stream of Ar and allowing the resultant film to set overnight at room temperature. Reaction of this product mixture with an aqueous cysteine solution provided data which indicated that the earlier eluting peak (Figure 3, peak 1), presumed to be **4b**, is considerably more reactive with cysteine than is **3b** (peak 2). The relative reactivities of the two components with cysteine, as determined by changes in the HPLC chromatogram, are plotted in Figure 4.

**Cross-Linking of Fab' Using the ETAC Molecules.** Studies of the cross-linking reactions of **1a**, **3a** (as a mixture with **4a**), and **3b** (as a mixture with **4b**) were carried out. In the experiments the reagents were cross-linked with Fab' at room temperature and 37 °C. Although a few of the coupling reactions were conducted at different pH values, evaluation of the products was only done on conjugates which had been cross-linked at pH 6.8 to assure that the primary reaction had been with the free sulfhydryl groups. The cross-linking of Fab' was conducted using varying molar equivalents of the ETAC derivative, but the target amount was 0.5 equiv such that excess ETAC



**Figure 4.** Plot of the change in chemical components present in the HPLC radioactive trace in the reaction of [ $^{131}\text{I}$ ]3b and [ $^{131}\text{I}$ ]4b in  $\text{CH}_3\text{CN}$  with 1 M aqueous cysteine as a function of time. HPLC retention times correlate with peak 1 being that of the unknown minor component (believed to be [ $^{131}\text{I}$ ]4b), peak 2 being that of [ $^{131}\text{I}$ ]3b, and peak 3 being a new (noncharacterized) cysteine reaction product. Figure 3 shows an example of a radioactivity trace similar to those obtained in the reaction with cysteine, but the percentages of peak 1 and peak 2 were as graphed. For a description of the HPLC system used to separate (nonprotein) radioiodinated compounds see the Experimental Procedures.

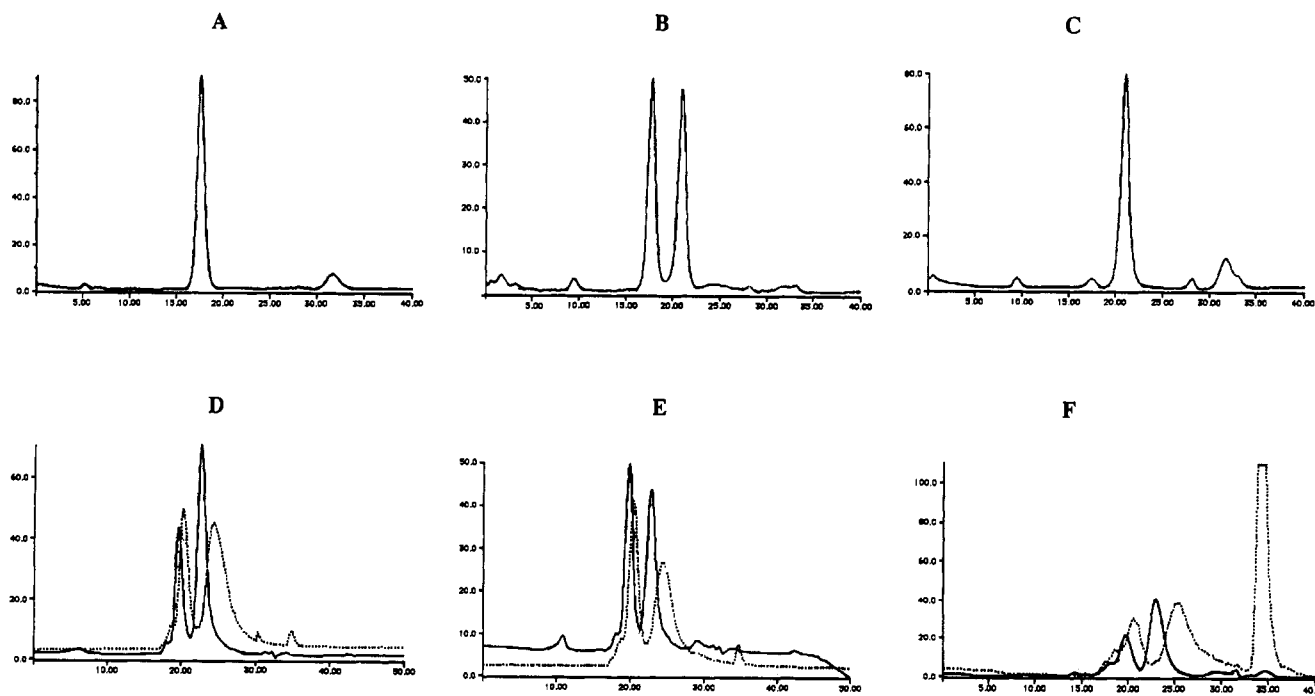
reagent would not be present to promote undesired side reaction products (e.g., polymer or aggregate formation).

The majority of cross-linking experiments were performed with 175–200  $\mu\text{g}$  of freshly reduced A6H Fab' contained in 75  $\mu\text{L}$  of 0.1 M sodium carbonate, pH 6.8. To the buffered Fab' solution was added a 1-, 5-, or 10- $\mu\text{L}$  aliquot containing 3a and/or 3b in  $\text{CH}_3\text{CN}$ . Reactions were allowed to proceed at room temperature or 37  $^\circ\text{C}$  for

various amounts of time, and the extent of cross-linking was determined by size-exclusion HPLC with UV and radioactivity detection. Coupling to Fab' and cross-linking could readily be observed by HPLC (Figure 5D–F). Yields of the cross-linked mF(ab')<sub>2</sub> ranged from 37 to 50% with most of the remaining radioactivity being associated with the Fab' peak when conducted at pH 6.8. The results obtained indicate that cross-linking of Fab' can be effected with minimal aggregate formation.

An experiment was conducted to determine if radioiodinated 3b would react with Fab' that had been previously treated with iodoacetamide for blocking sulfhydryls. In that experiment A6H F(ab')<sub>2</sub> was treated with iodoacetamide prior to reduction to the Fab' to block any highly reactive functional groups (e.g., amines and sulfhydryls) present. This was done to assure that the most reactive groups would be sulfhydryls in the hinge region (although there was no reaction of 3b with unmodified F(ab')<sub>2</sub> or iodoacetamide treated F(ab')<sub>2</sub>). The sample was then treated with DTT to form Fab'. After DTT treatment, half of that material was retreated with iodoacetamide to block the generated sulfhydryls and the other half was left untreated. Addition of the radioiodinated 3b to DTT reduced Fab' (treated prior to alkylation with iodoacetamide) resulted in cross-linking to form mF(ab')<sub>2</sub> as in the untreated Fab'. However, the sample that had been treated with iodoacetamide after reduction to Fab' did not add [ $^{131}\text{I}$ ]3b to the Fab' or cause cross-linking to form the mF(ab')<sub>2</sub>. It must be emphasized that while these results support the site selective cross-linking shown in Figure 1, they do not unequivocally establish that the cross-linking occurs (exclusively) in the hinge region.

**In Vitro Properties of the Cross-Linked mF(ab')<sub>2</sub>.** Retention of the tumor cell binding of the mF(ab')<sub>2</sub> was of paramount concern. Thus, cell binding assays were conducted on isolated preparations of mF(ab')<sub>2</sub>. Tumor



**Figure 5.** Size-exclusion HPLC chromatograms of A6H F(ab')<sub>2</sub> reduction to Fab' (A–C) and of product mixture for cross-linking of A6H Fab' with 3b (D–F): solid lines, obtained from UV detection; dashed lines, obtained from radioactivity detection. The HPLC pump was run at 1.0 mL/min for chromatograms A–C and 0.75 mL/min for D–F (resulting in differences in retention times). Chromatograms were obtained from the following: (A) A6H F(ab')<sub>2</sub> prior to reduction; (B) A6H F(ab')<sub>2</sub> after partial reduction to Fab'; (C) A6H Fab' after complete reduction of A6H F(ab')<sub>2</sub>; (D) cross-linking of A6H Fab' with 3b after 5 min reaction time; (E) cross-linking of A6H Fab' with 3b after 55 min reaction time; and (F) cross-linking of A6H Fab' with 3b at pH 6 for 24 h. For a description of the HPLC system used to separate radioiodinated proteins see Experimental Procedures.

**Table 2. Distribution of Radioactivity for Coinjected [<sup>131</sup>I]ETAC-mF(ab')<sub>2</sub>- and [<sup>125</sup>I]PIB-Labeled A6H F(ab')<sub>2</sub> in Athymic Mice with TK-82 Xenografts<sup>a</sup>**

tissues	3.5 h		19 h		43 h	
	<sup>131</sup> I	<sup>125</sup> I	<sup>131</sup> I	<sup>125</sup> I	<sup>131</sup> I	<sup>125</sup> I
blood	20.47 ± 2.30	19.93 ± 2.22	4.27 ± 0.84	4.73 ± 0.81	1.37 ± 0.15	1.03 ± 0.17
tumor	58.59 ± 5.97	53.69 ± 6.54	51.97 ± 3.27	80.38 ± 7.00	46.43 ± 1.69	63.17 ± 3.77
muscle	0.70 ± 0.07	0.71 ± 0.28	0.54 ± 0.06	0.43 ± 0.18	0.15 ± 0.03	0.12 ± 0.02
lung	9.89 ± 1.87	11.81 ± 3.35	2.28 ± 0.44	3.27 ± 0.95	1.14 ± 0.20	1.95 ± 0.91
kidney	11.15 ± 1.09	6.47 ± 0.90	4.29 ± 0.70	3.44 ± 0.73	2.02 ± 0.23	1.08 ± 0.13
spleen	3.16 ± 0.43	3.57 ± 0.50	1.03 ± 0.13	1.17 ± 0.24	0.48 ± 0.06	0.40 ± 0.07
liver	6.26 ± 0.66	5.84 ± 0.65	2.08 ± 0.19	1.50 ± 0.15	0.98 ± 0.12	0.60 ± 0.06
intestine	8.30 ± 2.06	3.23 ± 0.92	3.24 ± 1.20	1.34 ± 0.46	0.56 ± 0.06	0.26 ± 0.06
stomach	3.86 ± 2.76	7.73 ± 3.74	2.50 ± 0.93	3.50 ± 1.42	0.75 ± 0.32	1.01 ± 0.14
neck	4.49 ± 1.19	4.49 ± 1.28	1.11 ± 0.18	2.88 ± 2.53	0.36 ± 0.07	2.03 ± 2.93

<sup>a</sup> Results were obtained for *n* = 6 mice at each time point and are given as mean ± standard deviation of the percent injected dose/g (% ID/g).

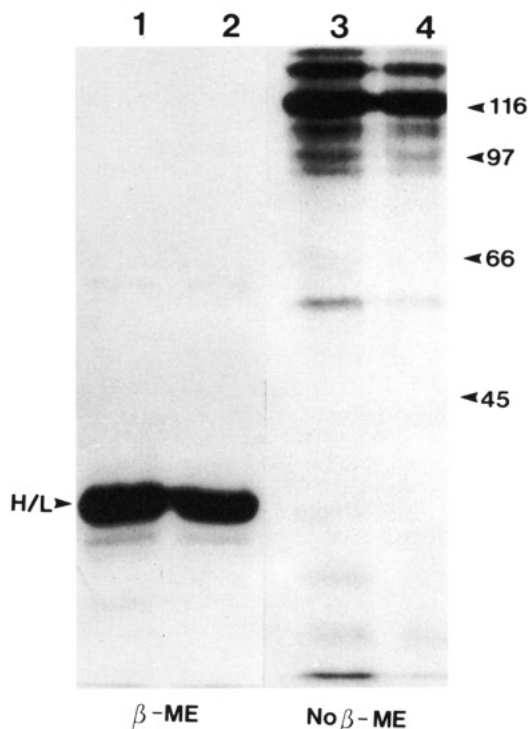
**Table 3. Distribution of Radioactivity for Coinjected [<sup>131</sup>I]PIB- and Na[<sup>125</sup>I]/ChT-Labeled A6H Fab' in Athymic Mice with TK-82 Xenografts<sup>a</sup>**

tissues	4 h		24 h	
	<sup>131</sup> I	<sup>125</sup> I	<sup>131</sup> I	<sup>125</sup> I
blood	7.52 ± 0.46	6.07 ± 0.34	0.41 ± 0.03	1.18 ± 0.12
tumor	27.04 ± 3.67	20.13 ± 3.28	5.90 ± 1.19	11.18 ± 2.85
muscle	0.47 ± 0.08	0.47 ± 0.08	0.06 ± 0.01	0.18 ± 0.03
lung	5.38 ± 1.83	2.87 ± 0.31	0.45 ± 0.15	0.82 ± 0.08
kidney	16.80 ± 2.41	4.39 ± 0.76	0.95 ± 0.22	0.80 ± 0.05
spleen	7.15 ± 0.66	1.15 ± 0.10	1.24 ± 0.35	0.37 ± 0.05
liver	6.77 ± 0.65	1.60 ± 0.15	1.17 ± 0.21	0.33 ± 0.05
intestine	1.60 ± 0.38	1.11 ± 0.13	0.12 ± 0.02	0.32 ± 0.06
stomach	3.36 ± 1.11	2.65 ± 0.61	0.20 ± 0.07	2.91 ± 1.04
neck	1.67 ± 0.57	1.40 ± 0.44	0.40 ± 0.38	1.24 ± 1.70

<sup>a</sup> Results were obtained for *n* = 6 mice at each time point and are given as mean ± standard deviation of the percent injected dose/g (% ID/g).

cell binding immunoreactivities of 60%, 90%, 77%, 75%, and 79% were obtained for the isolated A6H mF(ab')<sub>2</sub> in five separate experiments. The measured cell binding of the radioiodinated preparations used in the biodistribution study (Table 2) were 69% for the [<sup>131</sup>I]PIB-labeled A6H F(ab')<sub>2</sub> and 75% for the [<sup>125</sup>I]3b-labeled A6H mF(ab')<sub>2</sub>. The cell binding of radioiodinated preparations used in the Fab' biodistribution study (Table 3) were 50% for [<sup>131</sup>I]PIB-labeled Fab' and 51% for ChT/Na[<sup>125</sup>I]-labeled Fab'.

An evaluation of the *in vitro* stability of cross-linked A6H mF(ab')<sub>2</sub> toward release of radioactivity (presumably radiolabeled small molecules) was conducted. Samples of HPLC purified mF(ab')<sub>2</sub> were incubated with fresh human serum (37 °C), 0.9% saline (37 °C), 1 M carbonate buffer, pH 9.3, 1 M *N*-α-acetyl-L-lysine, and 1 M cysteine for 16–19 h. The reactions were monitored by denaturing TLC (80% MeOH), where protein-bound radioactivity remains at the origin and released radiolabeled small molecules (including free iodide) migrate with the solvent front. At 16–19 h incubation time there was no apparent change in the protein bound activity for saline or cysteine challenges, but a degradation of approximately 10% in carbonate buffer and 25% with the lysine challenge was noted. The TLC data obtained from incubation in human serum was inconclusive as the TLC plate smeared. The results suggest that under neutral conditions, no reversibility of the adduct occurs as cysteine would be expected to rapidly add to the released alkene. However, under basic conditions (pH 9.3) some degradation of the mF(ab')<sub>2</sub> occurred. Further, when the basic nucleophile lysine was present more degradation was noted, perhaps due to reaction with the α,β-unsaturated ketone intermediate prior to its reversible reaction with the Fab' sulfhydryl groups.

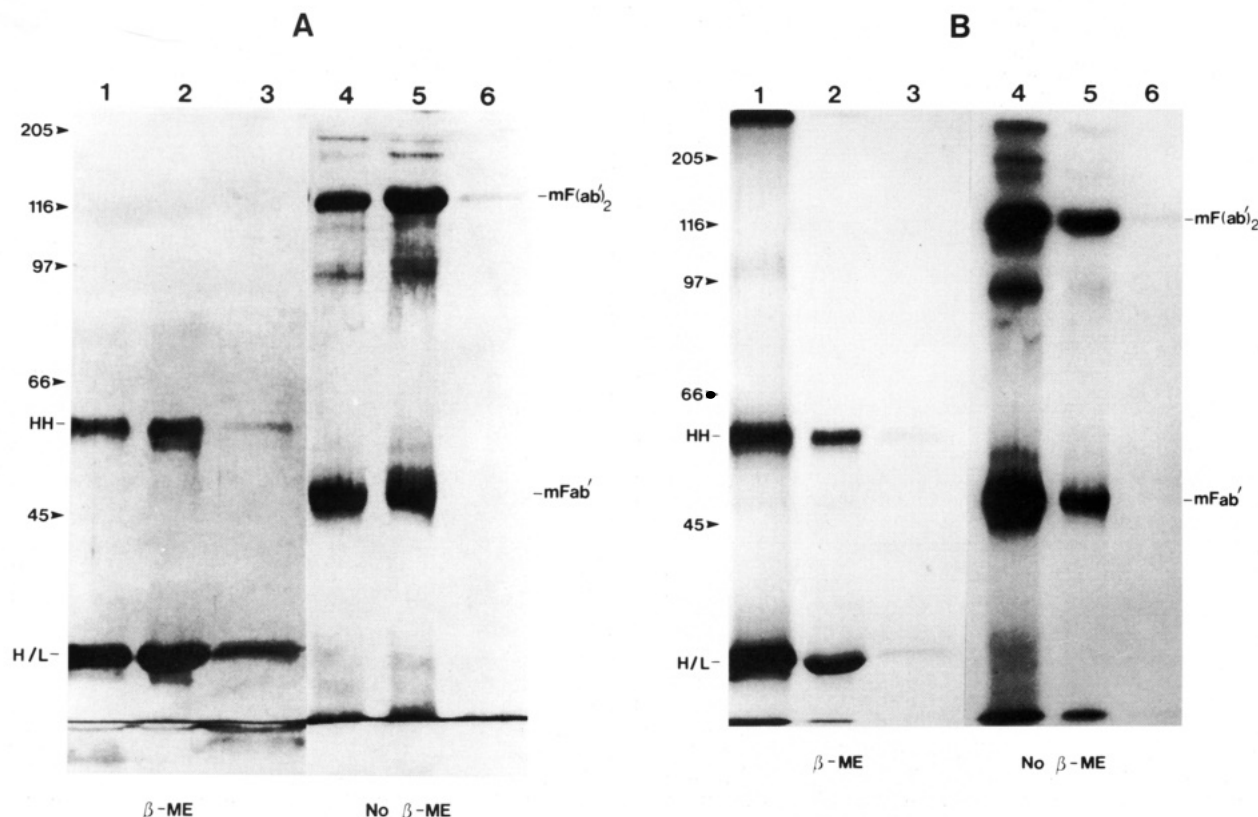


**Figure 6.** Autoradiograph of A6H F(ab')<sub>2</sub> radiolabeled with chloramine-T (lanes 1 and 3) or *N*-succinimidyl *p*-iodobenzoate (lanes 2 and 4). Samples applied to lanes 1 and 2 had been treated with 2-mercaptoethanol (β-ME), whereas samples applied to lanes 3 and 4 were not treated with β-ME. All lanes were loaded with approximately 20 μg of protein. Molecular weight markers were run to obtain estimations of sizes of proteins in the bands (see Experimental Procedures for description of markers).

SDS-PAGE analyses were conducted with samples of crude and/or isolated, purified A6H mF(ab')<sub>2</sub>, 5b. All SDS-PAGE analyses were conducted by treating the samples under nonreducing conditions (i.e., without 2-mercaptoethanol (β-ME)) and reducing conditions (i.e., with β-ME). A SDS-PAGE gel analysis of radioiodinated F(ab')<sub>2</sub> labeled with chloramine-T/Na<sup>125</sup>I and [<sup>131</sup>I]PIB was conducted for comparison with the mF(ab')<sub>2</sub> gels. An autoradiographic exposure of that gel is shown in Figure 6. Sample in lanes 1 and 2 were treated with β-ME. The reduced products had a masses consistent with heavy and/or light chain fragments. Samples in lanes 3 and 4 were not reduced with β-ME. There was a fair amount of heterogeneity apparent in the nonreduced radiolabeled F(ab')<sub>2</sub>, which was consistent with other F(ab')<sub>2</sub> fragments previously studied.

A silver-stained SDS-PAGE gel which was run to compare crude cross-linking reaction mixtures containing mF(ab')<sub>2</sub> with isolated, purified mF(ab')<sub>2</sub> is shown in Figure





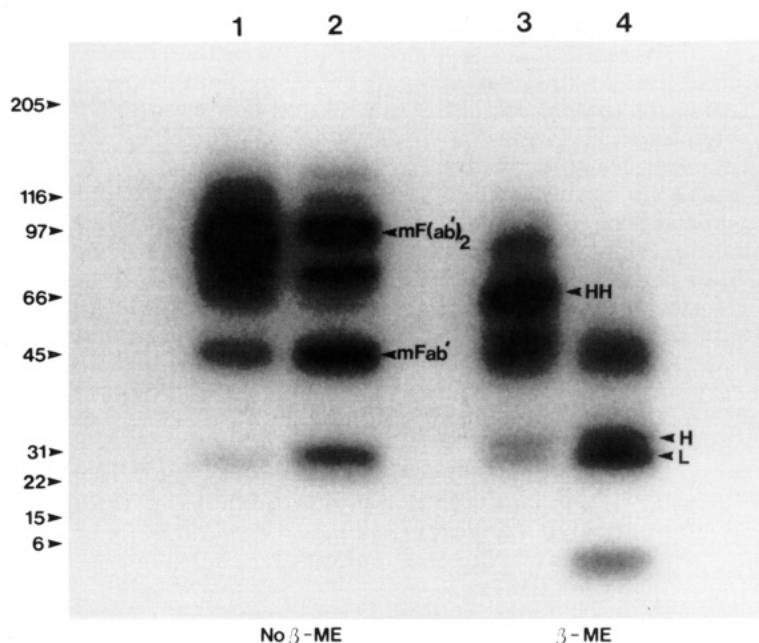
**Figure 7.** Silver-stained SDS-PAGE gel (A) and its autoradiograph (B) on which crude A6H m(Fab')<sub>2</sub> reaction mixtures and purified mF(ab')<sub>2</sub> was analyzed. Lanes 1–3 have been treated with 2-mercaptoethanol (β-ME), whereas lanes 4–6 have not been treated with β-ME. The samples applied to lanes 1, 3, 4, and 6 were obtained from cross-linking reactions conducted at 25 °C for 18 h, while samples applied to lanes 2 and 5 were from reactions run at 37 °C for 18 h. Lanes 1, 2, 4, and 5 were each loaded with approximately 20 μg of protein (crude reaction mixtures), and lanes 3 and 6 were each loaded with 1 μg of protein (purified mF(ab')<sub>2</sub>). The molecular weight markers (see Experimental Procedures) were run under reducing conditions and are marked on the reducing gel (A). The standards can serve only as a rough estimate of masses for the bands in the non-reducing gel (B).

7A. The autoradiograph of that gel is shown in Figure 7B. Samples in lanes 1–3 were run under reducing conditions (β-ME added), whereas samples applied to lanes 4–6 were run under nonreducing conditions. All samples were subjected to heat denaturation (i.e., 100 °C for 3 min) prior to running on the gel. Samples in lanes 1, 3, 4, and 6 were of reaction mixtures where the cross-linking was conducted at 25 °C for 18 h, whereas samples in lanes 2 and 5 were from reactions where the cross-linking was conducted at 37 °C for 18 h. The reducing gel (Figure 7; lanes 1–3) showed similar bands for all three samples. The crude reaction mixture applied to lane 1 (cross-linking at 25 °C) had four principal bands, which were interpreted to be (bottom to top) radiolabeled small molecule, heavy and/or light chains, heavy chain–heavy chain dimer, and aggregate. The crude reaction mixture applied to lane 2 (cross-linked at 37 °C) appeared very similar except only a minor amount of aggregate was present. The purified mF(ab')<sub>2</sub> applied to lane 3 had only two bands present under reducing conditions. These bands were most likely heavy chain–heavy chain dimer and heavy and/or light chains. The lanes run under nonreducing conditions (Figure 7; lanes 4–6) had substantially different bands from the reducing gel (i.e., different MW fragments). The reaction mixture applied to lane 4 (cross-linked at 25 °C) had two principal bands, believed to be the (bottom to top) mFab' and mF(ab')<sub>2</sub>. The autoradiographic trace (Figure 7B) for that lane appears to indicate that there is more heterogeneity in the radiolabeled species. However, this could be due to the extent of exposure needed to visualize the purified mF(ab')<sub>2</sub> in lanes 3 and 6 (only 1 μg of protein added vs 20 μg added in other lanes). While the silver stained and autoradiographic bands in lane 6 are

faint, it is important to note that the mFab' observed in the crude reaction mixtures was not present.

Reducing and nonreducing SDS-PAGE gels were run on the purified radioiodinated mF(ab')<sub>2</sub> that was used in the biodistribution study (PhastSystem). An autoradiographic exposure of the gels is shown in Figure 8. Samples applied to lanes 1 and 2 were run under nonreducing conditions (no β-ME), whereas samples in lanes 3 and 4 were run under reducing conditions (with added β-ME). Samples in lanes 1 and 3 were held at 25 °C prior to loading on the gel, but samples in lanes 2 and 4 were subjected to heat denaturation (100 °C for 3 min). The sample applied to lane 1 had the least manipulation (i.e., nonreducing conditions, no heat denaturation). The molecular weight markers on the gel indicated that the primary band in lane 1 was the mF(ab')<sub>2</sub>, but minor amounts of mFab' and other radiolabeled species were also present. The sample applied to lane 2 had been subjected to heat denaturation (100 °C) prior to loading. This treatment appeared to produce substantially more mFab', along with additional amounts of radiolabeled materials which are likely to be heavy chain–heavy chain dimer and heavy and/or light chain fragments. Lane 3 of the gel contained a sample which had not been denatured by heat but was run under reducing conditions. One major band was present in lane 3. This band was thought to be the heavy chain–heavy chain dimer, although it was present at a slightly lower (apparent) molecular weight than seen in the heat denatured sample of lane 2. Minor bands in lane 3 indicated that mFab' and mF(ab')<sub>2</sub> were also present. Lane 4 contained a sample that had been denatured by heat (100 °C) and run under reducing conditions. The autoradiographic bands indicate that these conditions were harsh





**Figure 8.** Autoradiograph of a SDS-PAGE gel (from PhastSystem running 4-15% gradient) of isolated, purified A6H mF(ab')<sub>2</sub>. Samples in lanes 1 and 2 were run under nonreducing conditions (i.e., no β-ME), and samples in lanes 3 and 4 were run under reducing conditions (i.e., treated with β-ME). Samples in lanes 1 and 3 were held at room temperature prior to loading, while those in lanes 2 and 4 were heated to 100 °C for 3 min prior to loading. Each lane had approximately 1 μg of protein loaded. Molecular weight markers were run to obtain estimations of sizes of proteins in the bands (see Experimental Procedures for description of markers).

enough to degrade the sample to heavy chain-heavy chain dimer and heavy/light chain fragments, and to even remove a small amount of the radiolabeled small molecule from the protein (band < 6 kDa).

**In Vivo Properties of A6H mF(ab')<sub>2</sub>.** Distribution and pharmacokinetics of the radioiodinated A6H mF(ab')<sub>2</sub> were examined in athymic mice carrying human TK-82 RCC tumor xenografts (19). Prior to administration to mice, the radioiodinated ETAC cross-linked mF(ab')<sub>2</sub> **5b** was purified by HPLC to remove the labeled monomeric mFab' (and other contaminants such as aggregates). This separation was necessary as one of the primary reasons for *in vivo* analysis to ascertain if the mF(ab')<sub>2</sub> was dissociating to Fab' *in vivo*. In the experiment, a control radioiodinated [<sup>125</sup>I]PIB-labeled A6H F(ab')<sub>2</sub> of similar quantity and specific activity was coinjected (15). Three groups of six male athymic mice were sacrificed at 3.5, 19, and 43 h postinjection in the dual label experiment.

The results of the biodistribution are given in Table 2. The calculated percent injected dose per gram (% ID/g) of the two radioisotopes in the blood appears to be similar at the three sacrifice times. Similar pharmacokinetics were also obtained in muscle and spleen. Some differences in the distributions of the two radioisotopes were seen in the kidney, liver, intestine and stomach, perhaps reflecting a difference in excretion routes of the catabolites. A substantial difference in radioiodine activities was observed at 3.5 h in the kidney, possibly indicating that the ETAC cross-linked mF(ab')<sub>2</sub> may be more susceptible to formation of Fab' than the native F(ab')<sub>2</sub> *in vivo*, or it may simply be reflective of the presence of a small amount of ETAC-conjugated Fab' in the injectate. The somewhat higher concentrations of <sup>125</sup>I (from control [<sup>125</sup>I]PIB-labeled F(ab')<sub>2</sub>) in the stomach were presumably brought about by contamination from free [<sup>125</sup>I]iodide in the preparation, as the neck (thyroid) accumulation is much higher at the later time points. The ETAC cross-linked A6H mF(ab')<sub>2</sub> appeared to target TK-82 xenograft tumors similar to that of A6H F(ab')<sub>2</sub>, but the retention of radioactivity at the tumor was decreased at 19 h in contrast

to the usual increase in accumulation observed with this antibody fragment and tumor system (14).

A separate biodistribution experiment was conducted where A6H F(ab')<sub>2</sub> was reduced to Fab' and radiolabeled with Na[<sup>131</sup>I]I/chloramine-T (ChT) and (separately) radiolabeled with [<sup>125</sup>I]PIB. No previous studies of radiolabeled A6H Fab' had been carried out. The two methods of radioiodination were performed to provide labeled Fab' for a dual label experiment. This was done so that the data obtained could be compared with that previously reported for radioiodinated Fab fragments (22). However, the primary purpose of the biodistribution experiment was to obtain data to compare the biodistribution and clearance kinetics of the Fab' fragment with those of the F(ab')<sub>2</sub> fragment and the reconstituted mF(ab')<sub>2</sub>. The biodistribution was evaluated in groups of 6 athymic mice sacrificed at 4 and 24 h postinjection. Data obtained from the biodistribution are tabulated in Table 3.

## DISCUSSION

The ultimate goal of our research is to develop a general method for site-specifically attaching polymeric diagnostic and therapeutic agents to monoclonal antibodies in a manner which does not adversely affect antibody binding to tumor cell antigens. The objective of this study was to obtain preliminary data on the use of equilibrium transfer alkylation cross-link (ETAC) reagents as a method of site-specific attachment of molecules to antibody F(ab')<sub>2</sub> fragments. The preliminary data sought included the following: (1) preparation of a radioiodinated trifunctional cross-linking reagent, *p*-[<sup>125</sup>,<sup>131</sup>I]iodophenethyl ETAC; (2) evaluation of reaction conditions necessary to achieve cross-linking of Fab'; (3) evaluation of the *in vitro* properties of the generated modified F(ab')<sub>2</sub>; and (4) evaluation of the *in vivo* properties of the modified F(ab')<sub>2</sub>.

Our strategy for constructing modified F(ab')<sub>2</sub> [termed mF(ab')<sub>2</sub>] fragments is shown in Figure 1. It was reasoned that a minimal detrimental affect might be expected when (large polymeric) diagnostic or therapeutic molecules were conjugated in place of the nonessential Fc portion of the

molecule. To accomplish the conjugation as depicted in Figure 1, a diagnostic or therapeutic reagent would have to be coupled with a *trifunctional* cross-linking reagent. Although a number of bifunctional cross-linking reagents have been described in the literature (23–25), few trifunctional cross-linking reagents have been described. It seemed that the reagent of choice should be heterobifunctional, containing one functional group that could be reacted with an amine containing compound and two functional groups that could subsequently be reacted with sulfhydryls on the Fab' to reform the F(ab')<sub>2</sub> moiety. Trifunctional reagents such as tris-maleimido compounds (26, 27) and tris(benzoyl chloride) (28) did not fulfill the heterobifunctional requirements and might have been expected to form a trimer of Fab'. Heterotrifunctional reagents, such as bis(isocyanatobenzoic acid) and its derivatives (29, 30), also did not fulfill the reagent requirements, as reactions with sulfhydryl groups were needed to impart a regiospecificity to the cross-linking process. At the time the study was initiated, the trifunctional cross-linking compounds that appeared to be most applicable were those described by Lawton et al. (9–11) as equilibrium transfer alkylation cross-link (ETAC) reagents. The ETAC compounds were particularly attractive as the addition of Fab's would be accomplished in a step-wise manner, potentially providing a means of forming bispecific F(ab')<sub>2</sub> constructs in later studies.

The carboxy-ETAC **1a** (Figure 2) was chosen as the reagent for cross-linking of Fab's. Reactions of **1a** with Fab' produced a small quantity of modified F(ab')<sub>2</sub> by HPLC analysis. This was encouraging as the Fab' by itself did not recombine to form F(ab')<sub>2</sub> under the same reaction conditions (data not shown). However, it became apparent in initial studies that a radiolabeled version of the ETAC reagent was needed since it could not be determined unequivocally that the cross-linked Fab' obtained from the study had come about from cross-linking with **1a** (versus reformation of a disulfide bond) nor could it be determined that addition of **1a** to the Fab' had occurred. The preparation of a radioiodinated ETAC molecule using an iodoaniline derivative had previously been described by Liberatore et al. (10), but the described procedure required manipulation of radioactive compounds, and resulted in very low yields (1.3%) of relatively low specific activity (50  $\mu$ Ci/ $\mu$ mol; 1.85 MBq/ $\mu$ mol) material. Thus, we chose to prepare a stannylphenethyl derivative of **1a** as a precursor which could be radioiodinated. On the basis of previous radioiodination studies with arylstannanes (8, 13–15) it was anticipated that a radioiodinated ETAC derivative could be prepared in high yield and high specific activity. Further, this approach was particularly attractive as it would allow preparation of the radioiodinated ETAC derivative (**3b**) in the final step prior to conjugation with the Fab' fragments.

Due to the differences in the masses of the antibody Fab' fragment (MW  $\approx$  50 000) and the iodinated ETAC reagent **3b** (MW = 582), radioiodinations to prepare **3b** were conducted at no-carrier-added levels of radioiodine (<sup>131</sup>I specific activity  $\approx$  1.3 mCi/ $10^{-3}$   $\mu$ mol; 48 MBq/ $10^{-3}$   $\mu$ mol). This allowed evaluation of cross-linking reactions employing small amounts (i.e., 200  $\mu$ g;  $4 \times 10^{-3}$   $\mu$ mol) of Fab'. The equivalents of **3b** used in the cross-linking reactions were dependent on a number of factors, including the amount of radioactivity aliquoted (see Table 1), actual specific activity of each particular radioiodine shipment and days from receipt before using (ranged from 1–1.6 mCi/ $10^{-3}$   $\mu$ mol; 37–59 MBq/ $10^{-3}$   $\mu$ mol), and quantity of CH<sub>3</sub>CN solution containing the radioiodinated **3b** used in

the coupling reactions. In most cross-linking reactions 10  $\mu$ L (40%) of the (standardized) 25- $\mu$ L CH<sub>3</sub>CN solution containing radioiodinated **3b** was added to 75  $\mu$ L of buffered Fab' solution. It was not possible to calculate the exact number of equivalents of radioiodinated **3b** employed due to uncertainties of introducing trace quantities of stable iodine, aliquoting, etc. However, an estimate of the equivalents of radioiodinated **3b** used in most cross-linking experiments could be made based on the HPLC radioactivity traces (total percent yield in Table 1) and the fact that 40% of the total radioactivity (radioiodine used in Table 1) was used in the reactions. As an example, in run 5 (Table 1) an estimated 88% of the 5.77 mCi (213 MBq) of <sup>131</sup>I used in the reaction, or 5.08 mCi (188 MBq), was present as **3b** (and **4b**). Of that total, 40% or 2.0 mCi (74 MBq) was aliquoted into the solution containing 200  $\mu$ g of Fab'. Thus, the quantity of **3b** aliquotted in that reaction was  $\approx 1.5 \times 10^{-3}$   $\mu$ mol (0.4–0.5 equiv). However, since the reaction is a dimerization, **3b** effectively contributes 0.8–1.0 equiv.

The cross-linking reactions were monitored by HPLC using size-exclusion chromatography with both UV and radioactivity detection. The conversion of the monomeric Fab' molecule to a mixture of radioiodinated Fab' and radioiodinated mF(ab')<sub>2</sub> under the cross-linking reaction conditions could be readily seen on the HPLC traces (see Figure 5D–F). It was anticipated that when 1 equiv (0.5 quantity) of **3b** was used the radiotracer would be similar to the UV trace, with perhaps a somewhat larger Fab'/mF(ab')<sub>2</sub> ratio in the UV trace than in the radioactivity trace, the expected differences being due to the fact that there should be some Fab' molecules with radioiodinated **3b** conjugated and some with no radioconjugate. This was found to be the case; however, we were surprised to find that a similar result was obtained in an experiment which employed 0.1–0.2 equiv of radioiodinated **3b**. This fact led us to examine the reaction of stannylphenethylamine-ETAC **3a** with Fab'. On the basis of previous studies with arylstannane antibody conjugation reactions (15), it was believed that this very lipophilic compound would not be soluble enough to react in aqueous solution. However, reaction with **3a** was found to result in cross-linking of Fab' to form mF(ab')<sub>2</sub> in approximately the same proportion as observed for the iodinated phenethyl derivative, **3b**. With the prospect of reaction of Fab' with **3a**, an evaluation of the amount of this reagent present in the reaction mixtures becomes important. In most radioiodination reactions, 50  $\mu$ g ( $56 \times 10^{-3}$   $\mu$ mol) of the stannylphenethylamine-ETAC reagent **3a** was used. Of that quantity, 40% or 20  $\mu$ g ( $22 \times 10^{-3}$   $\mu$ mol), or as many as 10 equiv, of **3a** was available for reaction with the Fab' in solution. The fact that reaction with **3a** occurs, and that **3a** is present in large excess, raised some questions about the cross-linking reactions. Of particular interest was the number of stannyl-ETAC molecules that have reacted with the Fab'. Another pertained to the location of the cross-linking if more than one ETAC molecule reacts with a Fab' fragment. Unfortunately, answers to these questions could not be obtained from these initial studies.

Site-specific cross-linking of an ETAC reagent with an antibody Fab' fragment is possible through selective reaction of free sulfhydryl groups in the hinge region, as depicted in Figure 1. In concept, this approach might be applied to all antibodies. However, general application of such an approach presumes that a Fab' can be prepared from any antibody, which is not the case. Immunoglobulins of the IgG class are globular in nature and contain inter- and intrachain disulfide bonds (31). Subclasses of

IgG molecules, and IgG molecules derived from different species, have differing numbers of interchain disulfide bonds. This difference in the hinge region disulfide bonds can affect the degradative enzymatic reactions used to prepare F(ab')<sub>2</sub> fragments. For example, antibodies of the IgG<sub>1</sub> and IgG<sub>2a</sub> subclasses are generally degraded by the enzyme pepsin or thiol-free "preactivated" papain to form the F(ab')<sub>2</sub> fragment (32), but antibodies of the IgG<sub>2b</sub> subclass are degraded by proteolytic enzymes (such as pepsin) to form the Fab fragment directly. Therefore, application of this approach may be limited to antibodies which can be enzymatically degraded to F(ab')<sub>2</sub> fragments.

The antibody used in this investigation was an antirenal cell carcinoma antibody of the IgG<sub>1</sub> subclass, designated as A6H (19, 33–36). The schematic representation of the A6H antirenal cell carcinoma antibody in Figure 1 has been drawn with three disulfide bonds between heavy chains as mouse derived IgG<sub>1</sub> antibodies have that number of interchain disulfide bonds in the hinge region (31). It is not generally known how many of the disulfide bonds are retained after the pepsin digestion. For simplicity only one disulfide bond is depicted in Figure 1. It should be noted that an immunocompetent A6H F(ab')<sub>2</sub> can be obtained from the pepsin digestion after only 2 h, but that F(ab')<sub>2</sub> fragment, although indistinguishable by size exclusion HPLC from that obtained after 24 h digestion, was not readily reduced to Fab' under the DTT reaction conditions employed in this investigation. The difference in DTT reactivity observed between the A6H F(ab')<sub>2</sub> molecules may be indicative of the extent of digestion in the hinge region.

A few cross-linking experiments were conducted at 37 °C. In those experiments, roughly the same amount of cross-linking was observed as had been seen at 25 °C. Cross-linking experiments were also conducted at lower pH values to determine what effect pH had on the cross-linking. At pH 6 (0.1 M sodium carbonate) about the same ratios of cross-linking occurred, but a large proportion of the radioactivity was present as radiolabeled small molecules (Figure 5F). At pH 5 (0.1 M sodium carbonate) very little of the activity was associated with Fab', and no cross-linking was seen. In the latter experiment, it appeared that the small amount of activity which was associated with protein might have come from reaction of the  $\alpha,\beta$ -unsaturated keto ETAC molecule, [<sup>131</sup>I]4b, introduced as an impurity with [<sup>131</sup>I]3b.

Some cross-linking experiments were conducted after pretreatment of the antibody fragment with iodoacetamide. These experiments were conducted to determine if sulfhydryl groups produced after reduction could be blocked, preventing addition of radioiodinated 3b. To ensure that only sulfhydryl groups produced from DTT reduction were present in the reactions, iodoacetamide capping (for preexisting sulfhydryl groups) was conducted prior to DTT treatment. The antibody F(ab')<sub>2</sub> fragment was then reduced with DTT to form Fab', and half of the quantity was treated a second time with iodoacetamide. The Fab' which had not been treated with iodoacetamide after reduction with DTT reacted with radioiodinated 3b, whereas Fab' treated with iodoacetamide after reduction did not react with 3b.

The A6H mF(ab')<sub>2</sub> had identical retention characteristics on size-exclusion HPLC analysis as that found for the A6H F(ab')<sub>2</sub>. Isolation of radioiodinated mF(ab')<sub>2</sub> was accomplished by collection of samples having the appropriate retention time from multiple injections (e.g., 2 or 3) on an analytical size exclusion HPLC column. This provided samples for *in vitro* and *in vivo* analysis of the

mF(ab')<sub>2</sub>. Several isolated samples were analyzed for their immunoreactivity (tumor cell binding), and little decrease was noted. Although there was a considerable range of immunoreactivities obtained, the range was consistent with day-to-day variability of the analysis, and other radiolabeled antibodies examined on the same day had similar cell binding values.

Results from SDS-PAGE analyses, which compared A6H F(ab')<sub>2</sub>, crude A6H mF(ab')<sub>2</sub>, and purified A6H mF(ab')<sub>2</sub>, indicated that cross-linked mF(ab')<sub>2</sub> was similar to unaltered F(ab')<sub>2</sub>. The autoradiograph of purified radioiodinated mF(ab')<sub>2</sub> SDS-PAGE gel (Figure 7B) appeared to have more heterogeneity than seen on the silver-stained protein (Figure 7A). Although the observed differences in heterogeneity may simply be an artifact of the exposure time (i.e., overexposure may bring out minor bands), this observation raised a question of whether there were cross-linked mF(ab')<sub>2</sub> species of different stabilities present in the radioiodinated product mixture. On the basis of the reactivity of 3a, it seems possible that a mixture of conjugated stannyl-ETAC 3a and radioiodinated-ETAC 3b species were formed in the cross-linking reactions. It is also possible that spontaneous reformation of disulfide-bonded F(ab')<sub>2</sub> might occur under the reaction conditions, but the latter possibility is unlikely as no cross-linking was observed under the reaction conditions employed without ETAC molecules being present.

Reversibility of addition is inherent in ETAC molecules and was of concern in our studies. Liberatore et al. were also concerned about reversible addition of ETAC molecules to antibodies and evaluated the stability of reduced (NaCNBH<sub>3</sub>) and nonreduced forms of antibody adducts (10). Those studies provided evidence that there was not a measurable difference in stability between the two. In our studies, we chose to evaluate the stability of the F(ab')<sub>2</sub> adducts by subjecting them to chemical challenges (i.e., incubation with reagents). The challenge experiments demonstrated that the purified A6H mF(ab')<sub>2</sub> was quite stable under neutral conditions (in saline) at physiological temperature (37 °C) for up to 20 h. The mF(ab')<sub>2</sub> was also found to be quite stable in a 1 M aqueous cysteine solution, where a detectable loss of radiolabeled ETAC might have been expected. Some reversibility of the radioiodinated ETAC was observed at room temperature (10% at 16–19 h) when mF(ab')<sub>2</sub> was mixed with 1 M carbonate buffer (pH 9.3). A higher percentage was lost (25% at 16–19 h) when challenged with 1 M aqueous *N*- $\alpha$ -acetyllysine, a nucleophilic base. From these results it was concluded that the A6H mF(ab')<sub>2</sub>, prepared by reaction with ETAC 3b, was stable enough to use without post-cross-linking modification (e.g., NaCNBH<sub>3</sub> reduction).

A biodistribution of purified mF(ab')<sub>2</sub> was conducted in athymic (nude) mice bearing a renal cell xenograft (TK-82) to ascertain how it compared *in vivo* with coinjected radiolabeled A6H F(ab')<sub>2</sub>. The data obtained (Table 2) suggest that the ETAC cross-linked mF(ab')<sub>2</sub> is nearly as stable as the F(ab')<sub>2</sub> *in vivo*, having a distribution more similar to a F(ab')<sub>2</sub> than a Fab' fragment (Table 3). Slightly higher concentrations of mF(ab')<sub>2</sub> were seen in the kidney and intestines at the three time points, and somewhat lower concentrations were seen in the tumor, lung, and stomach. The data in Table 2 correlate well with data obtained in a previous biodistribution employing PIB-labeled A6H F(ab')<sub>2</sub> as a control (14) and are quite different from data obtained from the radioiodinated A6H Fab' biodistribution study (Table 3).

In summary, we have found that trifunctional ETAC molecules can be readily prepared and modified for use

as Fab' cross-linking reagents. As a method of following the cross-linking reaction, a radioiodinated ETAC derivative, **3b**, was prepared in good yield and high specific activity. It was found that the ETAC molecules used were relatively stable but had to be handled and stored with care to avoid polymerization. Cross-linking experiments conclusively demonstrated that Fab' could be recombined to form mF(ab')<sub>2</sub> in moderate yields (30–50%). Since the cross-linking reactions did not go to completion, mF(ab')<sub>2</sub> had to be separated from Fab' prior to testing. The ETAC cross-linked mF(ab')<sub>2</sub> was found to be reasonably stable *in vitro* under a variety of conditions. The ETAC cross-linked mF(ab')<sub>2</sub> was also found to be reasonably stable *in vivo* as the distribution was similar to that of a co-injected iodobenzoyl labeled F(ab')<sub>2</sub>.

In this preliminary study, the conditions for radioiodination of F(ab')<sub>2</sub> via **3b** were not optimized, as we were primarily interested in determining if cross-linking could be accomplished. The investigation included studies of the stability of ETAC reagent in a number of solvents. However, more extensive studies need to be conducted with derivatized ETAC compounds to determine how long the reagents can be stored and to determine the best conditions for storage. HPLC analyses of the radiolabeling of the stannylphenethyl-ETAC **3a** indicated that it could be used in studies for up to 4 months, but it appeared that some of the radioactivity was being left on the HPLC column for the material stored over 1 month.

Many different applications of the conjugation method shown in Figure 1 can be envisioned. Although a number of other conjugate methods of radioiodination have already proven to be adequate (8), a polymeric reagent that has many sites for radioiodination is of interest. Such a reagent could be used to increase the specific activity achievable in therapeutic radiolabeling of antibody F(ab')<sub>2</sub> fragments. Another application of interest is preparation of an antibody conjugate which is coupled to a boronated polymer for application to boron neutron capture therapy (37). Many additional studies will have to be conducted before such goals can be realized.

#### ACKNOWLEDGMENT

We would like to thank Ed Arfman and Lisha Brown for their technical assistance in antibody characterization and immunoreactivity assays and Dr. Rajiv Srivastava for his helpful comments on the manuscript. We are very grateful to Steve Harnos and Hewlett-Packard for providing instrumentation and technical assistance in obtaining HPLC-MS data. We thank the University of Washington School of Medicine and NIH Biomedical Research Support Grant (RR05432), the Lucas Foundation, and the Medical Research Service of the Department of Veterans Affairs for financial assistance in the described research.

#### LITERATURE CITED

- Seiler, F. R., Gronski, P., Kurre, R., Luben, G., Harthus, H.-P., Ax, W., Bosslet, K. and Schwick, H. G. (1985) Monoclonal Antibodies: Their Chemistry, Functions, and Possible Uses. *Angew. Chem., Int. Ed. Engl.* 24, 139–160.
- Magerstadt, M. (1991) *Antibody Conjugates and Malignant Disease*, CRC Press, Boca Raton, FL.
- Srivastava, S. C., Ed. (1988) *Radiolabeled Monoclonal Antibodies for Imaging and Therapy*, Part III, pp 193–268, Plenum Press, New York.
- Vitetta, E. S., Fulton, R. J., May, R. D., Till, M., and Uhr, J. W. (1987) Redesigning Nature's Poisons to Create Anti-Tumor Reagents. *Science* 238, 1098–1104.
- Means, G. E., and Feeney, R. E. (1990) Chemical Modification of Proteins: History and Applications. *Bioconjugate Chem.* 1, 2–12.
- Pietersz, G. A. (1990) The Linkage of Cytotoxic Drugs to Monoclonal Antibodies for Treatment of Cancer. *Bioconjugate Chem.* 1, 89–95.
- Brinkley, M. (1992) A Brief Survey of Methods for Preparing Protein Conjugates with Dyes, Haptens, and Cross-Linking Reagents. *Bioconjugate Chem.* 3, 2–13.
- Wilbur, D. S. (1992) Radiohalogenation of Proteins: An Overview of Radionuclides, Labeling Methods, and Reagents for Conjugate Labeling. *Bioconjugate Chem.* 3, 433–470.
- Mitra S., and Lawton R. G. (1979) Reagents for the Cross-Linking of Proteins by Equilibrium Transfer Alkylation. *J. Am. Chem. Soc.* 101, 3097–3110.
- Liberatore, F. A., Comeau, R. D., Mckearin, J. M., Pearson, D. A., Belonga, B.Q., Brocchini, S. J., Kath, J., Phillips, T., Oswell, K., and Lawton, R. G. (1990) Site-Directed Chemical Modification and Cross-Linking of a Monoclonal Antibody Using Equilibrium Transfer Alkylating Cross-Link Reagents. *Bioconjugate Chem.* 1, 36–50.
- del Rosario, R. B., Wahl, R. L., Brocchini, S. J., Lawton, R. G., and Smith, R.H. (1990) Sulfhydryl Site-Specific Cross-Linking and Labeling of Monoclonal Antibodies by a Fluorescent Equilibrium Transfer Alkylation Cross-Link Reagent. *Bioconjugate Chem.* 1, 51–59.
- Ishikawa, E., Hashida, S., Kohno, T., Kotani, T., and Ohtaki, S. (1987) Modification of Monoclonal Antibodies with Enzymes, Biotin, and Fluorochromes and Their Applications. In *Monoclonal Antibody Production Techniques and Applications* (Schook, L. B., Ed.), Chapter 8, pp 113–137, Marcel Dekker, Inc., New York.
- Hylarides, M. D., Wilbur, D. S., Reed, M. W., Hadley, S. W., Schroeder, J. R., and Grant, L. M. (1991) Preparation and *In Vivo* Evaluation of an N-(p-[<sup>125</sup>I]iodophenethyl)maleimide-Antibody Conjugate. *Bioconjugate Chem.* 2, 435–440.
- Wilbur, D. S., Vessella, R. L., Stray, J. E., Goffe, D. K., Blouke, K. A., and Atcher, R. W. (1993) Preparation and Evaluation of para-[<sup>211</sup>At]Astatobenzoyl Labeled Anti-Renal Cell Carcinoma Antibody A6H F(ab')<sub>2</sub>. *In Vivo* Distribution Comparison with para-[<sup>125</sup>I]Iodobenzoyl Labeled A6H F(ab')<sub>2</sub>. *Nucl. Med. Biol.* 20, 917–927.
- Wilbur, D. S., Hadley, S. W., Hylarides, M. D., Abrams, P. G., Beaumier, P.L., Morgan, A. C., Reno, J., and Fritzberg, A. R. (1989) Development of a Stable Radioiodinating Reagent to Label Monoclonal Antibodies For Radiotherapy of Cancer. *J. Nucl. Med.* 30, 216–226.
- Laemmli, U. K. (1970) Cleavage of Structural Proteins During the Assembly of the Head of Bacteriophage T<sub>4</sub>. *Nature* 227, 680–685.
- Dunbar, B. S. (1987) Preparation of Slab Gels for One- or Two-Dimensional Polyacrylamide Sodium Dodecyl Sulfate Gel Electrophoresis. *Two-Dimensional Electrophoresis and Immunological Techniques*, Appendix 4, pp 243–247, Plenum Press, NY.
- Merril, C. R., Goldman, D., Sedman, S. A., and Ebert, M. H. (1981) Ultrasensitive Stain for Proteins in Polyacrylamide Gels Shows Regional Variation in Cerebrospinal Fluid Proteins. *Science* 211, 1437–1438.
- Vessella, R. L., Alvarez, V., Chiou, R.-K., Rodwell, J., Elson, M., Palme, D., Shafer, R., and Lange, P. (1987) Radioimmunoscintigraphy and Radioimmunotherapy of Renal Cell Carcinoma Xenografts. *NCI Monogr.* 3, 159–167.
- Coenen, H. H., Moerlein, S. M., and Stocklin, G. (1983) No-Carrier-Added Radiohalogenation Methods with Heavy Halogens. *Radiochim. Acta* 34, 47–68.
- Kabalka, G. W., and Varma, R. S. (1989) The Synthesis of Radiolabeled Compounds via Organometallic Intermediates. *Tetrahedron* 45, 6601–6621.
- Wilbur, D. S., Hadley, S. W., Grant, L. M., and Hylarides, M. D. (1991) Radioiodinated Iodobenzoyl Conjugates of a Monoclonal Antibody Fab Fragment. *In Vivo* Comparisons with Chloramine-T-Labeled Fab. *Bioconjugate Chem.* 2, 111–116.
- Lundblad, R. L., and Noyes, C. M. (1984) The Chemical Cross-Linking of Peptide Chains. *Chemical Reagents for Protein Modification*, Vol. II, Chapter 5, pp 123–139, CRC Press, Inc., Boca Raton, FL.

- (24) Peters, K., and Richards, F. M. (1977) Chemical Cross-Linking: Reagents and Problems in Studies of Membrane Structure. *Ann. Rev. Biochem.* 46, 523-551.
- (25) Das, M., and Fox, C. F. (1979) Chemical Cross-Linking in Biology. *Ann. Rev. Biophys. Bioeng.* 8, 165-193.
- (26) Schott, M. E., Frazier K. A., Pollock, D. K., and Verbanac, K. M. (1993) Preparation, Characterization, and in Vivo Biodistribution Properties of Synthetically Cross-Linked Multivalent Antitumor Antibody Fragments. *Bioconjugate Chem.* 4, 153-165.
- (27) Ahlem, C. N., Huang, A. E., and Anderson, L. D. (1991) Tris-maleimido compounds as intermediates in trifunctional antibody synthesis. Eur. Patent Appl. No. 91301962.6 (publication No. 0 446 071 A2).
- (28) Kluger, R., Song, Y., Wodzinska, J., Head, C., Fujita, T. S., and Jones, R. T. (1992) Trimesoyltris(3,5-dibromosalicylate): Specificity of Reactions of a Trifunctional Acylating Agent with Hemoglobin. *J. Am. Chem. Soc.* 114, 9275-9279.
- (29) Boring, D. L., Ji, X.-D., Zimmet, J., Taylor, K. E., Stiles, G. L., and Jacobson, K. A. (1991) Trifunctional Agents as a Design Strategy for Tailoring Ligand Properties: Irreversible Inhibitors of A<sub>1</sub> Adenosine Receptors. *Bioconjugate Chem.* 2, 77-88.
- (30) Jacobson, K. A., Olah, M. E., and Stiles, G. L. (1992) Trifunctional Ligands: A Radioiodinated High Affinity Acylating Antagonist for the A<sub>1</sub> Adenosine Receptor. *Pharmacol. Commun.* 1, 145-154.
- (31) Day, E. D. (1990) The Secondary, Tertiary, and Quaternary Structures of Assembled Immunoglobulins. *Advanced Immunochimistry*, 2nd ed., Chapter 3, pp 107-181, Wiley-Liss, New York.
- (32) Parham, P., Andrzejewicz, M. J., Brodsky, F. M., Holmes, N. J., and Ways, J. P. (1982) Monoclonal Antibodies: Purification, Fragmentation, and Application to Structural and Functional Studies of Class I MHC Antigens. *J. Immun. Methods* 53, 133-173.
- (33) Vessella, R. L. (1991) Radioimmunoconjugates in renal cell carcinoma. In *Immunotherapy of Renal Cell Carcinoma* (F. M. J. Debruyne, R. M. Bukowski, J. E. Pontes, and P. M. H. de Mulder, Eds.) pp 38-46, Springer-Verlag, Heidelberg.
- (34) Sands, H., Jones, P. L., Shah, S. A., Palme, D., Vessella, R. L., and Gallagher, B. M. (1988) Correlation of vascular permeability and blood flow with monoclonal antibody uptake by Clouser and renal cell xenografts. *Cancer Res.* 48, 188-193.
- (35) Vessella, R. L., Palme, D. F., Elson, M. K., Wessels, B. W., Chiou, R. K., and Lange, P. H. (1988) Radioiodinated monoclonal antibodies in the imaging and treatment of human renal cell carcinoma xenografts in nude mice. In *Targeted Diagnosis and Therapy* (J. Rodwell et al., Eds.) Chapter 9, pp 245-282, Marcel Dekker, Inc., New York.
- (36) Chiou, R. K., Vessella, R. L., Limas, C., Shafer, R. B., Elson, M. K., Arfman, E. W., and Lange, P. H. (1988) Monoclonal antibody-targeted radiotherapy of renal cell carcinoma using a nude mouse model. *Cancer* 61, 1766-1775.
- (37) Hawthorne, M. F. (1993) The Role of Chemistry in the Development of Boron Neutron Capture Therapy of Cancer. *Angew. Chem., Int. Ed. Engl.* 32, 950-984.

# Effect of Pegylation on the Structure and Function of Horse Cytochrome c

Patricia Ann Mabrouk

Department of Chemistry, Northeastern University, Boston, Massachusetts 02115. Received November 24, 1993\*

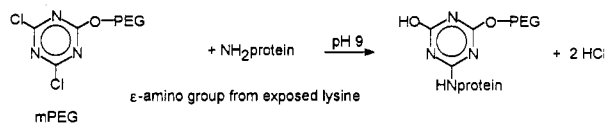
The preparation and spectrophotometric characterization of (both  $\text{Fe}^{2+}$  and  $\text{Fe}^{3+}$  forms) poly(ethylene glycol) (PEG; av FW 5000)-modified horse cytochrome c (cyt c(PEG)<sub>n</sub>) with different degrees of modification ( $n_{\text{av}} = 6, 19$ ) by UV-vis spectroscopy, circular dichroism spectroscopy, resonance Raman spectroscopy, and cyclic voltammetry are described. Extensive modification ( $n_{\text{av}} = 19$ ) of cyt c causes gross structural deformation of the heme as evidenced by major spectral changes in the UV-vis and circular dichroism spectral signatures of both the  $\text{Fe}^{2+}$  and  $\text{Fe}^{3+}$  forms. Modification of cyt c by six PEG residues, however, produces a protein in which the heme active site is structurally and functionally intact (UV-vis, circular dichroism, and resonance Raman) and which exhibits at least quasireversible direct electron transfer ( $E^{\circ'} = 338 \pm 5$  mV vs SHE;  $(2.1 \pm 0.6) \times 10^{-3}$  cm/s) at bis(4-pyridyl) disulfide-modified Au electrodes.

## INTRODUCTION

Recently, a number of reports have appeared describing the preparation and study of poly(ethylene glycol) (PEG)-modified proteins (1-6). PEG-modified proteins have a number of unique properties that make them of interest in a rather diverse range of applications. First, PEG is nonimmunogenic. Modification of proteins by PEG can change the natural immunological properties of the protein, rendering it invisible *in vivo*, (7-10). Thus, selected proteins are of interest in, for example, artificial blood, enzyme therapy, etc. (7-11). Secondly, covalent modification of enzymes by PEG produces enzyme derivatives that are soluble in nonaqueous solvents such as benzene (12, 13). Recently, enzymatic reactions have been shown to take place in organic solvents (14, 15). In organic media, enzymes have been found to exhibit remarkable new properties such as increased thermal stability (16), different substrate specificity (17), and novel chemo- (18, 19) and enantioselectivity (20, 21). Consequently, PEG-modified enzymes are of interest in the developing field of nonaqueous enzymology (22-25).

Limited spectroscopic characterization has been performed to date on PEG-modified proteins. It is likely that this is due to the highly heterogeneous nature of PEG-modified proteins (the size and conformation of the polymer, the uncertainty in the both the number of poly(ethylene glycol)s bound to the protein, and the identity of preferred protein binding sites).

One method of pegylation involves reaction of the protein's free amino groups with 2-methoxypoly(ethylene glycol)-substituted 4,6-dichloro-s-triazine:<sup>7</sup>



This approach is popular because pegylation can be accomplished readily under relatively mild reaction conditions (pH 9 at room temperature) in one step using a commercially available reagent. However, cyanuric chloride is toxic, partially inactivates some enzymes upon

coupling (26, 27), and has been shown to be somewhat promiscuous in its reactivity with functional groups other than amines (28). Recently, a number of other PEG-based reagents have been developed in an effort to circumvent these difficulties (29). Nonetheless, this strategy remains popular.

Cyt c, a heme redox protein involved in electron transfer in the mitochondrial respiratory chain (30), represents an excellent model biomolecule with which to study the effects of pegylation. Physicochemical characterization of cyt c (including UV-vis, CD, RR, and CV) has been extensive (31). Horse heart cyt c, perhaps the best characterized cyt c protein, has 22 lysines located primarily on the protein surface near the heme crevice (32, 33). Differences in the reactivity of singly substituted carboxydinitrophenyl (CDNP) cyt c derivatives, prepared by the chloroarylation of surface lysines, with cytochrome oxidase have been interpreted as evidence that these lysines play an important role in the electron-transfer activity of cyt c and have been used to define the effective domain of interaction between cyt c and cytochrome oxidase (34). For these reasons, horse cyt c represents an ideal model biomolecule with which to investigate the structural effects of pegylation.

In view of the aforementioned need for structural studies of pegylated proteins, the popularity of pegylation using 2-methoxypoly(ethylene glycol)-substituted 4,6-dichloro-s-triazine, and the attractiveness of cyt c as a model biomolecule, we wish to report our findings relating to the structure and reactivity in aqueous media of PEG-modified cyt c (both  $\text{Fe}^{2+}$  and  $\text{Fe}^{3+}$  forms) with several degrees of modification by UV-vis spectroscopy (UV-vis), circular dichroism spectroscopy (CD), resonance Raman spectroscopy (RR), and cyclic voltammetry (CV).

## MATERIALS AND METHODS

Horse heart cytochrome c, type VI, Sigma Chemical Co. was purified in the usual manner by ion-exchange chromatography (35) and subsequently desalted and repeatedly concentrated (more than five times—each time from an initial volume of 50 mL to a final volume of <5 mL) using an Amicon ultrafiltration cell (YM10 membrane) and distilled water. The purity of the cyt c was established by measurement of the ratio of the absorbance of  $\text{Fe}^{2+}$  cyt c at 550 nm to that of  $\text{Fe}^{3+}$  cyt c at 280 nm. Cyt c was deemed acceptable in this work if  $A_{550}/A_{280} \geq 1.15$ .

\* Abstract published in *Advance ACS Abstracts*, April 15, 1994.



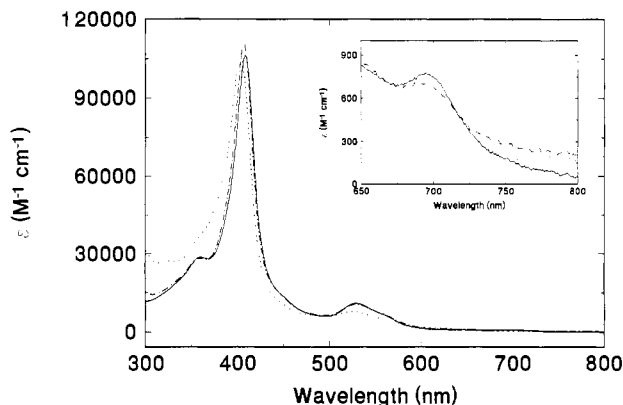
The following materials were obtained commercially and used as received: sodium phosphate monobasic monohydrate (Baker), sodium phosphate dibasic (Fisher), potassium perchlorate (Mallinckrodt), bis(4-pyridyl) disulfide (BPD; Sigma), methoxypoly(ethylene glycol) (av FW 5000) activated with cyanuric chloride (Sigma), sodium tetraborate decahydrate (Aldrich), and Silanor dimethyl sulfoxide- $d_6$  (MSD).

**Preparation of Cyt c(PEG)<sub>6</sub>.** Commercial methoxypoly(ethylene glycol) activated with cyanuric chloride (0.54 g;  $1.1 \times 10^{-4}$  mol) and purified horse cyt c (0.21 g;  $1.7 \times 10^{-5}$  mol) were stirred together in 20 mL of 0.1 M borate buffer, pH 9.2 for 3 h at 5 °C. The reaction was terminated by the addition of 50 mM phosphate buffer, pH 7.0, to the reaction mixture. Unreacted protein, PEG, and borate were removed by repeated concentration (more than five times—each time from an initial volume of 50 mL to a final volume of <5 mL) of the sample in an Amicon ultrafiltration cell (YM30 membrane) using distilled water. The final solution (<5 mL) was subsequently dialyzed (SpectraPor 7 MWCO 25,000) overnight against 500 mL of distilled water. Modified cyt c in the dry state was prepared by the lyophilization of this solution after it was determined that the UV-vis spectrum of the lyophilized protein upon immediate dissolution in water was identical to that of modified protein which had not been lyophilized. Most notably for cyt c(PEG)<sub>6</sub> the UV-vis spectrum of the lyophilized protein exhibited the 695-nm band upon immediate dissolution in water.

**Preparation of Cyt c(PEG)<sub>19</sub>.** Commercial methoxypoly(ethylene glycol) activated with cyanuric chloride (0.60 g;  $1.2 \times 10^{-4}$  mol) and purified horse cyt c (0.05 g;  $4.0 \times 10^{-6}$  mol) were stirred together in 20 mL of 0.1 M borate buffer, pH 9.2 for 3 h at 5 °C. The reaction was terminated by the addition of 50 mM phosphate buffer, pH 7.0, to the reaction mixture. Unreacted protein, PEG, and borate were removed by repeated concentration (more than five times—each time from an initial volume of 50 mL to a final volume of <5 mL) of the sample in an Amicon ultrafiltration cell (YM 100 membrane) using distilled water. The final solution (<5 mL) was subsequently dialyzed (SpectraPor 7 MWCO 50 000) overnight against 500 mL of distilled water. Modified cyt c in the dry state was prepared by the lyophilization of this solution.

**Optical Absorption and Circular Dichroism Measurements.** UV-vis spectra were recorded at room temperature on a Perkin-Elmer Lambda 9 UV-vis/NIR spectrophotometer. Circular dichroism spectra were obtained on a JASCO 500C spectropolarimeter. Rectangular Supracil cells (Hellma) of path length 0.1 and 1.0 cm were used for both UV-vis and CD measurements, depending on the protein concentration.

**Raman Spectroscopy.** Raman measurements were recorded on a home-built instrument. The system is based on a Coherent INNOVA 306 Argon ion laser, triplemate spectrometer (0.6 m, f/6.3), and a thermoelectrically cooled Princeton Instruments intensified PDA detector. A Spex 80386 computer controls the data acquisition. An uncoated broadband depolarizer (Optics for Research) was used in all measurements. Samples, contained in Kimax melting point tubes (1-mm i.d.), were typically excited with 100 mW or less of 514.5-nm light. The resolution of the spectrometer is ca.  $2 \text{ cm}^{-1}$  at the excitation wavelength used here. Fenchone was used to calibrate the Raman frequencies (36). All observed intensities are relative and not true intensities and have not been corrected for the spectral sensitivity of the instrument.



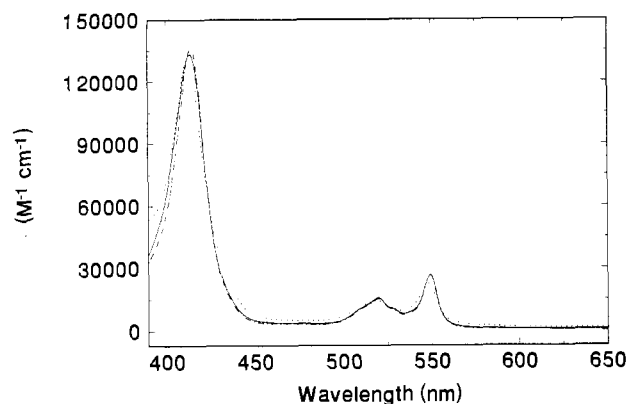
**Figure 1.** UV-vis spectra for native  $\text{Fe}^{3+}\text{cyt c}$  and  $\text{Fe}^{3+}\text{cyt c(PEG)}_n$  ( $n_{\text{av}} = 6, 19$ ) in 50 mM phosphate buffer, pH 7.0. (—) 12.5  $\mu\text{M}$  cyt c; (---) 87.5  $\mu\text{M}$  cyt c(PEG)<sub>6</sub>; (- - -) 75.0  $\mu\text{M}$  cyt c(PEG)<sub>19</sub>. Inset shows 695-nm band for these proteins.

**Electrochemistry.** Cyclic voltammetry measurements were made with a BAS 100B electrochemical workstation. The electrochemical cells were of the conventional three-electrode design. A single junction Ag/AgCl (3.0 M NaCl) reference electrode, a BPD-modified Au foil working electrode, and a Pt-gauze counter electrode were used in all experiments. The BPD-modified Au electrode was prepared by soaking an electrochemically cleaned (37) Au foil electrode for 5 min in a freshly prepared 1 mM BPD solution. The BPD-modified electrode was then rinsed and air dried. CV measurements were made in quiescent solution at room temperature  $23 \pm 1$  °C. The buffer solution was 50 mM sodium phosphate pH 7.0, saturated with  $\text{KClO}_4$ . All potentials are reported vs the standard hydrogen electrode (SHE). Background subtracted cyclic voltammograms (total current for all electroactive species minus current measured for buffer and electrolyte alone) were used in all quantitative analyses of the cyclic voltammetry data.

**Determination of Degree of PEG Modification.** The average extent of modification of amino groups in cyt c by 2-PEG-4,6-dichloro-s-triazine (av FW 5000) has been determined using a combination of UV-vis and  $^1\text{H}$  NMR. NMR spectra were recorded on a Varian XL-300 spectrometer. A calibration curve relating the average concentration of PEG ( $\delta = 3.49$  ppm) to that of the internal NMR standard tetramethylsilane, at constant known concentration, in  $\text{DMSO}-d_6$  was prepared and used to determine the concentration of PEG in actual cyt c(PEG)<sub>n</sub> samples. The average concentration of cyt c in the NMR samples was then determined by UV-vis, assuming that the molar absorptivities of the Soret and Q-bands, due to porphyrin-centered  $\pi \rightarrow \pi^*$  transitions (31), are unaffected upon modification by PEG. The average number of PEG's per cyt c was then determined from the ratio of the concentration of PEG (from the NMR analysis) to the concentration of cyt c (from the UV-vis). We estimate uncertainty in  $n$  as determined by this method to be better than  $\pm 1$ .

## RESULTS AND DISCUSSION

**Spectrophotometric Characterization of Cyt c(PEG)<sub>n</sub> in Aqueous Solution UV-vis.** Figure 1 shows the UV-vis spectra for two poly(ethylene glycol) (av FW 5000)-modified  $\text{Fe}^{3+}\text{cyt c}$ 's together with that for native cyt c. The absorption spectra of both pegylated derivatives exhibit the intense Soret (410 nm) and Q-band (500–550 nm) features,  $\pi \rightarrow \pi^*$  transitions characteristic of the cyt c heme active site.



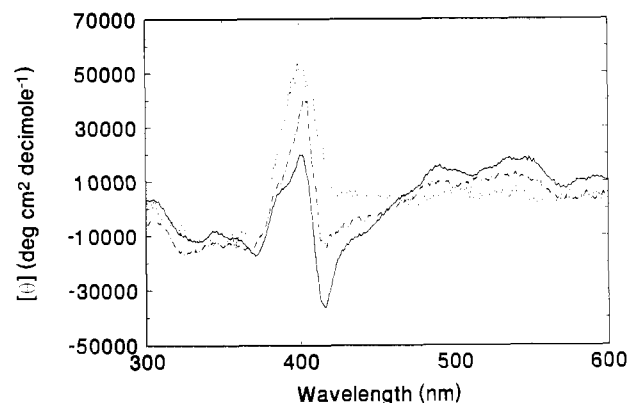
**Figure 2.** UV-vis spectra for native  $\text{Fe}^{2+}$ cyt c and  $\text{Fe}^{2+}$ cyt c(PEG) $_n$  ( $n_{\text{av}} = 6, 19$ ) in 50 mM phosphate buffer, pH 7.0: (—) 8.3  $\mu\text{M}$  cyt c; (---) 0.44 mM cyt c(PEG) $_6$ ; (···) 22  $\mu\text{M}$  cyt c(PEG) $_{19}$ . The  $\text{Fe}^{2+}$  form of these proteins was prepared by the addition of excess sodium dithionite.

The UV-vis spectrum for  $\text{Fe}^{3+}$ cyt c(PEG) $_6$  looks very similar to that of native ferricyt c both in terms of the energy and intensity of these absorption features. In addition, the UV-vis spectrum of cyt c(PEG) $_6$  shows the presence of the 695-nm band which is known to be a sensitive marker of cyt c conformation.

However, significant changes are apparent in the UV-vis spectra when the degree of PEG modification becomes extensive ( $n_{\text{av}} = 19$ ). In particular, the Soret and Q bands shift to slightly higher energy and gain intensity. Herskovits *et al.* (38) observed similar spectral changes in the Soret absorbance of cyt c in alcohol solutions. These spectral changes have previously been interpreted as evidence for loosening of the heme crevice and exposure of the heme to a more polar environment. In addition, in the UV-vis spectrum of cyt c(PEG) $_{19}$ , the intensity of the Q-bands decreases and the 695-nm band completely disappears. Loss of the 695-nm band is usually associated with weakening or rupture of the axial  $\text{Met80-Fe}^{3+}$  bond and an opening of the heme crevice (39, 40). Thus, taken together, the aforementioned UV-vis spectral changes observed for cyt c(PEG) $_{19}$  provide evidence that significant structural change has taken place in the heme active site of this pegylated derivative. Specifically, the spectral changes suggest that the axial  $\text{Met80-Fe}^{3+}$  bond has been broken and the heme crevice has opened exposing the heme active site to solution.

The UV-vis absorption spectra for the  $\text{Fe}^{2+}$  form of the cyt c(PEG) $_n$  derivatives were also investigated (Figure 2). The UV-vis spectra for the  $\text{Fe}^{2+}$ cyt c(PEG) $_n$ 's, prepared by chemical reduction in aqueous solution with either excess sodium dithionite or ascorbic acid, exhibited UV-vis spectra very similar to that of native ferrocyt c both in terms of the energy and intensity of the absorption features. The only detectable changes were observed for  $\text{Fe}^{2+}$ cyt c(PEG) $_{19}$ ; the Soret and Q-bands appear at slightly higher energy than for the unmodified  $\text{Fe}^{2+}$ cyt c. The similarity of the ferrous spectra for the pegylated derivatives to that of cyt c was not unexpected. The UV-vis spectrum for ferrous cyt c is known to be less sensitive to structural change than that of  $\text{Fe}^{3+}$  cyt c. For example, the addition of 6 mol % alcohol is known to produce significant changes in the UV-vis and CD spectra of  $\text{Fe}^{3+}$ cyt c while the addition of >50 mol % alcohol is required to produce any change in either the UV-vis or CD spectra of  $\text{Fe}^{2+}$  cyt c (41, 42).

**CD.** Figure 3 compares the visible CD spectra for two poly(ethylene glycol)-modified  $\text{Fe}^{3+}$  cyt c's ( $n_{\text{av}} = 6, 19$ )



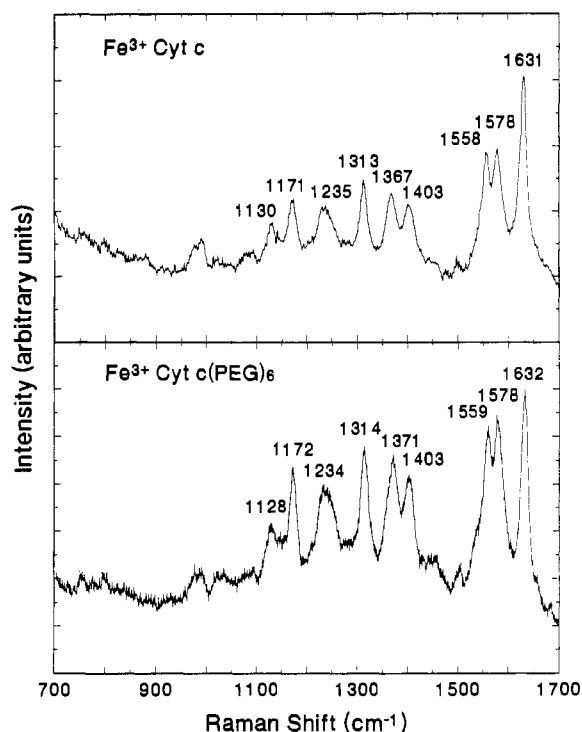
**Figure 3.** CD spectra for native  $\text{Fe}^{3+}$ cyt c and  $\text{Fe}^{3+}$ cyt c(PEG) $_n$  ( $n_{\text{av}} = 6, 19$ ) in 50 mM phosphate buffer, pH 7.0. (—) 14.2  $\mu\text{M}$  cyt c; (---) 19.6  $\mu\text{M}$  cyt c(PEG) $_6$ ; (···) 6.4  $\mu\text{M}$  cyt c(PEG) $_{19}$ .

with that of native cyt c. Significant changes in the CD spectra of cyt c(PEG) $_n$  are apparent as the degree of modification by PEG becomes extensive. In particular, the positive features at 490 and 530 nm and the negative troughs at 330, 370, and 417 nm disappear upon extensive modification of the protein by PEG.

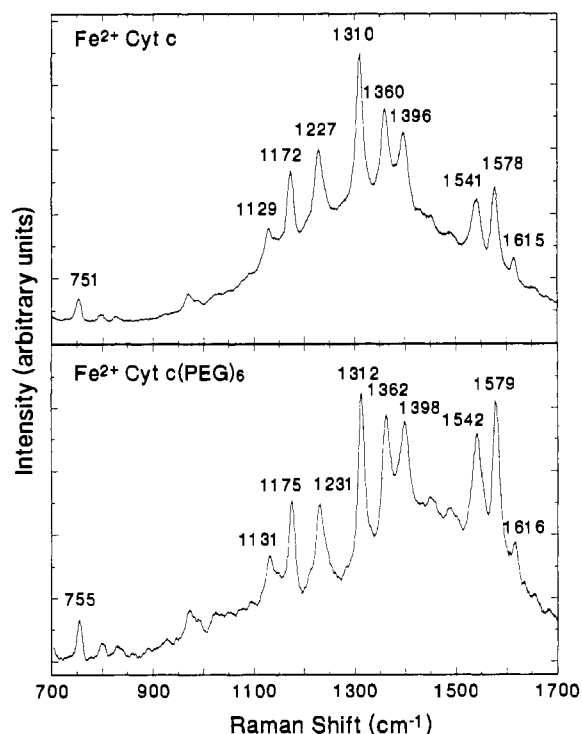
To investigate whether the spectral changes observed in the CD spectrum of  $\text{Fe}^{3+}$ cyt c(PEG) $_6$  are due to changes in local solvent polarity brought about by covalent attachment of the relatively hydrophobic PEG polymer to the protein, we prepared solutions of cyt c in 50 mM phosphate buffer containing different concentrations of PEG (5 mM–0.02 M). No detectable changes in energy or intensity of the Soret and Q-band features were observed in either the UV-vis or CD spectra (not shown) upon the addition of PEG to the protein suggesting that the differences in the Soret CD band shape observed for  $\text{Fe}^{3+}$ cyt c(PEG) $_n$  reflect genuine structural changes in the heme active site induced by covalent PEG binding. Furthermore, the observation of changes even in the CD spectra of cyt c(PEG) $_6$  suggests that the conformation of the cyt c heme active site may be affected by PEG modification even when the extent of pegylation is moderate.

**Resonance Raman.** Figures 4–6 show the resonance Raman spectra (700–1700  $\text{cm}^{-1}$ ) for native cyt c, cyt c(PEG) $_6$ , and cyt c(PEG) $_{19}$  upon laser excitation at 514.5 nm. At this excitation wavelength, resonant enhancement is expected primarily for in-plane heme vibrations in cyt c. The bands observed in the resonance Raman spectra for  $\text{Fe}^{3+}$  and  $\text{Fe}^{2+}$ cyt c (top of Figures 4 and 5, respectively) are known to be due to resonant enhancement of in-plane porphyrin modes involving C–C and C–N stretching as well as C–H bending at the methine bridges (43). The Raman data for  $\text{Fe}^{3+}$  and  $\text{Fe}^{2+}$ cyt c(PEG) $_6$  excited at this wavelength (bottom of Figures 4 and 5, respectively) appear remarkably similar to that of native cyt c both in terms of the frequencies and the relative intensity of the vibrational features observed for the native protein.

Several bands known as the oxidation state, spin-state, and core size marker bands have been demonstrated to be useful structural markers for cyt c (44). The so-called oxidation state marker band, principally an outer porphyrin ring breathing mode, is relatively insensitive to the nature of the spin state of the iron. The frequency of the oxidation state marker is known to decrease from 1375  $\text{cm}^{-1}$  for  $\text{Fe}^{3+}$  to 1360  $\text{cm}^{-1}$  for  $\text{Fe}^{2+}$ . A second feature known as the spin state marker band, mainly a methine bridge mode, is extremely sensitive to the nature of the iron spin state and decreases in frequency from 1585  $\text{cm}^{-1}$  for low-spin iron to 1555  $\text{cm}^{-1}$  for high-spin iron. A third useful



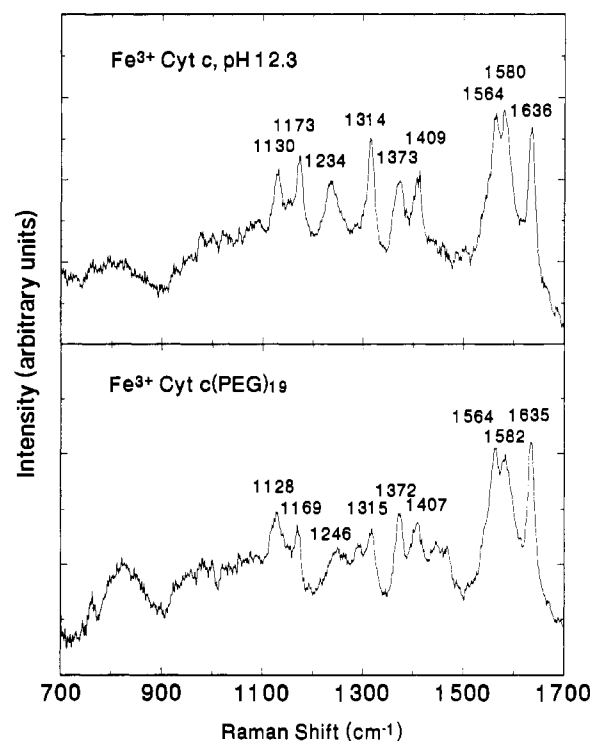
**Figure 4.** Resonance Raman spectra in 50 mM phosphate buffer, pH 7.0, of 7.0  $\mu$ M  $\text{Fe}^{3+}$  cyt c (top) and 0.45 mM  $\text{Fe}^{3+}$  cyt c(PEG)<sub>6</sub> (bottom). Spectral conditions: wavelength, 514.5 nm; power at sample,  $\approx$ 100 mW; integration time, 5 s/scan. The spectra are composites of 200 scans.



**Figure 5.** Resonance Raman spectra in 50 mM phosphate buffer, pH 7.0, of (top) 0.14 mM  $\text{Fe}^{2+}$  cyt c; (top) and 0.45 mM  $\text{Fe}^{2+}$  cyt c(PEG)<sub>6</sub> (bottom). Spectral conditions: wavelength, 514.5 nm; power at sample,  $\approx$ 100 mW; integration time, 5 s/scan. The spectra are composites of 200 scans. Excess sodium dithionite was added to ensure that the protein was in the reduced form.

marker band typically appearing at 1578  $\text{cm}^{-1}$  is a useful predictor of changes in the porphyrin core size.

Figures 4 and 5 show the key result that the frequency of the oxidation state marker band, the core size marker



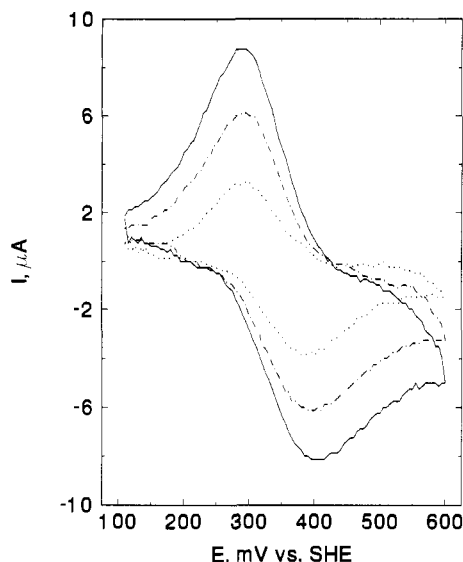
**Figure 6.** Resonance Raman spectra of 0.3 mM  $\text{Fe}^{3+}$  cyt c, pH 12.3 (top) and 0.4 mM  $\text{Fe}^{3+}$  cyt c(PEG)<sub>19</sub> in 50 mM phosphate buffer, pH 7.0 (bottom). Spectral conditions: wavelength, 514.5 nm; power at sample,  $\approx$ 100 mW; integration time, 5 s/scan. The spectra are composites of 200 scans.

band, and the spin state marker band for cyt c(PEG)<sub>6</sub> are the same as that found for the native protein within experimental error.

The most significant changes are differences in relative band in both redox forms of cyt c(PEG)<sub>6</sub>. For example, the intensity of the 1632  $\text{cm}^{-1}$  band for  $\text{Fe}^{3+}$  cyt c(PEG)<sub>6</sub> is attenuated compared to that for native  $\text{Fe}^{3+}$  cyt c. In addition, the intensity of spectral features at 1361, 1545, and 1580  $\text{cm}^{-1}$  of  $\text{Fe}^{2+}$  cyt c(PEG)<sub>6</sub> is somewhat greater compared to that for native  $\text{Fe}^{2+}$  cyt c. These intensity differences suggest that there are apparent differences in the polarization properties of these bands and signal small but real differences in the active site structure of cyt c(PEG)<sub>6</sub>.

Overall, the vibrational frequencies of the marker bands and the relative band intensities observed for cyt c(PEG)<sub>6</sub> provide strong evidence that the heme active site iron in cyt c(PEG)<sub>6</sub> assumes a hexacoordinated low-spin structure similar to that found in the native protein.

Figure 6 shows the resonance Raman spectrum for  $\text{Fe}^{3+}$ -cyt c(PEG)<sub>19</sub> in 50 mM phosphate buffer, pH 7.0, and  $\text{Fe}^{3+}$ -cyt c at pH 12.3. These Raman spectra appear remarkably similar both in terms of the observed intensities and frequencies of the vibrational features suggesting that the heme active site structure is similar in both systems. In the alkaline form of cyt c at pH 12.3, the heme active site axial methionine-80 sulfur-to-iron bond is known to be broken. Kitagawa *et al.* (45) have shown that the increase in frequency of the 1565  $\text{cm}^{-1}$  ( $\text{Fe}^{3+}$ ) Raman band and the decrease in the relative peak intensity of the 1636  $\text{cm}^{-1}$  line compared to that of the 1584  $\text{cm}^{-1}$  feature parallel the disappearance of the 695 nm band in the UV-vis spectrum of cyt c at alkaline pH and as such are useful indicators of the active site structural change. These spectral characteristics are observed in our Raman data for cyt c(PEG)<sub>19</sub>. Thus, our results provide strong evidence, in

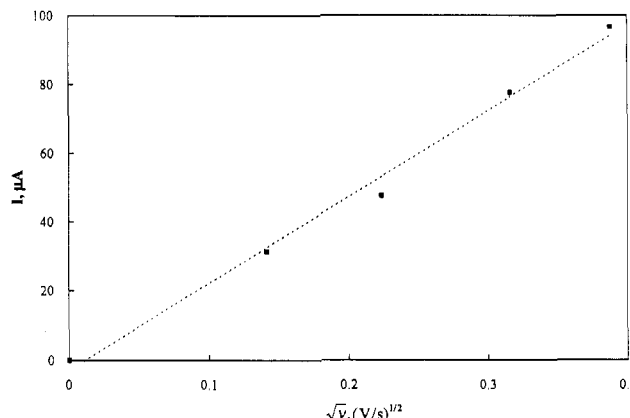


**Figure 7.** Background-subtracted cyclic voltammetry of 1.31 mM cyt c(PEG)<sub>6</sub> at a BPD-modified Au electrode in 50 mM phosphate buffer, pH 7.0 saturated with potassium perchlorate. Potential scan rates in mV/s are 50 (···), 100 (— · —), and 150 (—). Electrode area 0.70 cm<sup>2</sup>. The formal potential for cyt c(PEG)<sub>6</sub>, estimated from the cathodic and anodic peak potentials, is 338 ± 5 mV vs SHE.

agreement with our findings from UV-vis and CD spectroscopy, that the cyt c(PEG)<sub>19</sub> heme active site is non-native and similar to that in alkaline cyt c.

**Aqueous Direct Electrochemistry at Au.** The direct electrochemistry of cyt c(PEG)<sub>6</sub> at BPD-modified Au electrode has been investigated in aqueous phosphate buffer, pH 6.97. Figure 7 shows typical background-subtracted cyclic voltammograms for cyt c(PEG)<sub>6</sub> as a function of scan rate. The electrochemical response for cyt c(PEG)<sub>6</sub> at Au shows a well-defined redox wave that is stable with continuous cycling for at least 2 h. The formal potential for cyt c(PEG)<sub>6</sub>, estimated from the cathodic and anodic peak potentials, is 338 ± 5 mV vs SHE, 86 mV more positive than the value (252 ± 5 mV) for cyt c.

Between 10 and 250 mV/s, the peak-to-peak potential separations of the anodic and cathodic waves for the background subtracted data for cyt c(PEG)<sub>6</sub> are dependent on scan rate and are ca. 100–125 mV compared to 60 mV for native cyt c. The ratio of the anodic and cathodic peak currents was found to be 0.89 ± 0.08 based on all the scan rates studied. These data are consistent with a one-electron quasireversible diffusion-controlled electron-transfer process. Furthermore, both anodic and cathodic peak currents are linearly related to (scan rate)<sup>1/2</sup> for cyt c(PEG)<sub>6</sub> (Figure 8) as expected for a diffusion-controlled redox process. The average diffusion coefficient calculated from the slope of these plots is (1.4 ± 0.4) × 10<sup>-6</sup> cm<sup>2</sup>/s. This value is in good agreement with the accepted value of *D*<sub>o</sub> for native cyt c (1.0 × 10<sup>-6</sup> cm<sup>2</sup>/s) obtained by nonelectrochemical methods (46). The heterogeneous electron transfer rate constant was estimated by Nicholson's method (47) to be (2.1 ± 0.6) × 10<sup>-3</sup> cm/s. These results indicate that electron transfer between cyt c(PEG)<sub>6</sub> and BPD-modified Au electrodes in aqueous media is quasireversible in an electrochemical sense. Furthermore, the heterogeneous electron transfer rate for the modified protein compares well with that previously reported for native cyt c at BPD modified Au electrodes (ca. 5 × 10<sup>-3</sup> cm/s) (48–50). These results suggest that moderate modification of cyt c by PEG does not adversely affect the



**Figure 8.** Potential scan rate dependence of anodic CV peak responses taken from the cyclic voltammetry of 1.31 mM cyt c(PEG)<sub>6</sub> at a BPD-modified Au electrode in 50 mM phosphate buffer, pH 7.0 saturated with potassium perchlorate. The dotted curve represents the best fit (*D*<sub>o</sub> = (1.4 ± 0.4) × 10<sup>-6</sup> cm<sup>2</sup>/s; *r* = 0.99) to the data. Error bars for individual points are smaller than the symbol size used.

protein's ability to carry out its natural biological function, electron transport, at least at solid electrode surfaces.

In summary, we have found that moderate modification of cyt c by PEG produces a protein that is structurally, as characterized by UV-vis, CD, and RR spectroscopy, and functionally, as evidenced by demonstration of facile, reversible direct interfacial electron transfer at BPD modified Au, intact but which exhibits novel differences in both protein structure and redox function.

We have also shown that extensive modification adversely affects cyt c active site structure. Likely for cyt c this structural sensitivity toward pegylation is due to the location of the surface lysine residues available for pegylation near the heme active site. Studies are currently in progress to determine whether protecting the heme crevice during pegylation facilitates the preparation of derivatives in which the heme active site is structurally intact.

#### ACKNOWLEDGMENT

This work was supported by NIH Biomedical Research Support Grant 2 S07 RR07143 and NSF Grant CHE-9308680. P.A.M. wishes to thank Ed Takach and Drs. Jim Simms and Jeanne Owens of the M.I.T. Spectrometry Laboratory for access to the JASCO CD spectrometer.

#### LITERATURE CITED

- (1) Matsushima, A.; Okada, M.; Inada, Y. (1984) Chymotrypsin Modified with Polyethylene Glycol Catalyzes Peptide Synthesis Reaction in Benzene. *FEBS Lett.* 178, 275–277.
- (2) Ferjancic, A.; Puigserver, A.; Gaertner, H. (1988) Unusual Specificity of Polyethylene Glycol-Modified Thermolysin in Peptide Synthesis Catalyzed in Organic Solvents. *Biotechnol. Lett.* 10, 101–106.
- (3) Gaertner, H.; Puigserver, A. (1989) Kinetics and Specificity of Serine Proteases in Peptide Synthesis Catalyzed in Organic Solvents. *Eur. J. Biochem.* 181, 207–213.
- (4) Pina, C.; Clark, D.; Blanch, H. (1989) The Activity of PEG-Modified Chymotrypsin in Aqueous and Organic Media. *Biotechnol. Tech.* 3, 333–338.
- (5) Babonneau, M.; Jacquier, R.; Lazaro, R.; Viallefont, P. (1989) Enzymatic Peptide Syntheses in Organic Solvent Mediated by Modified α-Chymotrypsin. *Tetrahedron Lett.* 30, 2787–2790.

- (6) Wirth, P.; Soupe, J.; Tritsch, D.; Biellmann, J. (1991) Chemical Modification of Horseradish Peroxidase with Ethanol-Methoxypolyethylene Glycol: Solubility in Organic Solvents, Activity, and Properties. *Bioorg. Chem.* 19, 133-142.
- (7) Abuchowski, A.; van Es, T.; Palczuk, N. C.; Davis, F. F. (1977) Alteration of Immunological Properties of Bovine Serum Albumin by Covalent Attachment of Polyethylene Glycol. *J. Biol. Chem.* 252, 3578-3581.
- (8) Abuchowski, A.; McCoy, J. R.; Palczuk, N. C.; van Es, T.; Davis, F. F. (1977) Effect of Covalent Attachment of Polyethylene Glycol on Immunogenicity and Circulating Life of Bovine Liver Catalase. *J. Biol. Chem.* 252, 3582-3586.
- (9) Lee, W. Y.; Sehon, A. H. (1977) Abrogation of Reaginic Antibodies with Modified Allergens. *Nature* 267, 618-619.
- (10) Nishimura, H.; Takahashi, K.; Sakurai, K.; Fujinuma, K.; Imamura, Y.; Ooba, M.; Inada, Y. (1983) Modification of Batroxobin with Activated Polyethylene Glycol: Reduction of Binding Ability towards Anti-Batroxobin Antibody and Retention of Defibrinogenation Activity in Circulation of Preimmunized Dogs. *Life Sci.* 33, 1467-1473.
- (11) Pool, R. (1990) "Hairy Enzymes" Stay in Blood. *Science* 248, 305.
- (12) Takahashi, K.; Ajima, A.; Yoshimoto, T.; Inada, Y. (1984) Polyethylene Glycol-Modified Catalase Exhibits Unexpectedly High Activity in Benzene. *Biochem. Biophys. Res. Commun.* 125, 761-766.
- (13) Yoshimoto, T.; Takahashi, K.; Nishimura, H.; Ajima, A.; Tamaura, Y.; Inada, Y. (1984) Modified Lipase Having High Stability and Various Enzymic Activities in Benzene, and Its Use By Recovering From Benzene Solution. *Biotechnol. Lett.* 6, 337-340.
- (14) Klibanov, A. M. (1986) Enzymes That Work in Organic Solvents. *Chemtech.* 16, 354-359.
- (15) Kazandjian, R. Z.; Klibanov, A. M. (1985) Regioselective Oxidation of Phenols Catalyzed by Polyphenol Oxidase in Chloroform. *J. Am. Chem. Soc.* 107, 5448-5450.
- (16) Zaks, A.; Klibanov, A. M. (1984) Enzymatic Catalysis in Organic Media at 100 °C. *Science* 224, 1249-1251.
- (17) Zaks, A.; Klibanov, A. M. (1986) Substrate Specificity of Enzymes in Organic Solvents vs. Water Is Reversed. *J. Am. Chem. Soc.* 108, 2767-2768.
- (18) Zaks, A.; Klibanov, A. M. (1985) Enzyme-catalyzed Processes in Organic Solvents. *Proc. Natl. Acad. Sci. U.S.A.* 82, 3192-3196.
- (19) Rubio, E.; Fernandez-Mayorales, A.; Klibanov, A. M. (1991) Effect of the Solvent on Enzyme Regioselectivity. *J. Am. Chem. Soc.* 113, 695-696.
- (20) Sakurai, T.; Margolin, A. L.; Russell, A. J.; Klibanov, A. M. (1991) Control of Enzyme Enantioselectivity by the Reaction Medium. *J. Am. Chem. Soc.* 110, 7236-7237.
- (21) Fitzpatrick, P. A.; Klibanov, A. M. (1991) How Can the Solvent Affect Enzyme Enantioselectivity? *J. Am. Chem. Soc.* 113, 3166-3171.
- (22) Wong, C.-H. (1989) Enzymatic Catalysts in Organic Synthesis. *Science* 244, 1145-1152.
- (23) Klibanov, A. M. (1989) Enzymatic Catalysis in Anhydrous Organic Solvents. *Trends Biochem. Sci.* 14, 141-144.
- (24) Klibanov, A. M. (1990) Asymmetric Transformations Catalyzed by Enzymes in Organic Solvents. *Acc. Chem. Res.* 23, 114-1200.
- (25) Gupta, M. N. (1992) Enzyme Function in Organic Solvents. *Eur. J. Biochem.* 203, 25-32.
- (26) Ashihara, Y.; Kono, T.; Yamazaki, S.; Inada, Y. (1978) Modification of E. Coli L-Asparaginase with Polyethylene Glycol: Disappearance of Binding Ability to Anti-Asparaginase Serum. *Biochem. Biophys. Res. Commun.* 83, 385-391.
- (27) Abuchowski, A.; van Es, T.; Palczuk, N. C.; Davis, F. F. (1979) Treatment of L5178Y Tumor-Bearing BDF<sub>1</sub> Mice with a Nonimmunogenic L-Glutaminase-L-Asparaginase. *Cancer Treat. Rep.* 63, 1127-1132.
- (28) Matsushima, A.; Nishimura, H.; Ashihara, Y.; Yokota, Y.; Inada, Y. (1980) Modification of E. Coli Asparaginase with 2,4-bis(o-methoxypolyethylene glycol)-6-chloro-s-triazine(activated PEG<sub>2</sub>); Disappearance of binding ability towards anti-serum and retention of enzymic activity. *Chem. Lett.* 773-776.
- (29) Zalipsky, S.; Lee, C. (1990) Use of Functionalized Poly-(Ethylene Glycol)s for Modification of Polypeptides. *Poly-(Ethylene Glycol) Chemistry: Biotechnical and Biomedical Applications* (Harris, J. M., Ed.) pp 347-370, Plenum Press, New York.
- (30) Pettigrew, G. W.; Moore, G. R. (1987) *Cytochromes C: Biological Aspects*, Springer-Verlag, New York.
- (31) Moore, G. R.; Pettigrew, G. W. (1990) *Cytochromes C: Evolutionary, Structural and Physicochemical Aspects*. Springer-Verlag, New York.
- (32) Dickerson, R. E.; Takano, T.; Eisenberg, D.; Tallai, O. B.; Samson, L.; Cooper, A.; Margoliash, E. (1971) Ferricytochrome c. I. General Features of the Horse and Bonito Proteins at 2.8 Å Resolution. *J. Biol. Chem.* 246, 1511-1535.
- (33) Takano, T.; Dickerson, R. E. (1981) Conformation Change of Cytochrome c. 1. Ferrocycytochrome c Structure Refined at 1.5 Å Resolution. *J. Mol. Biol.* 153, 79-94.
- (34) Ferguson-Miller, S.; Brautigan, D. L.; Margoliash, E. (1978) Definition of Cytochrome c Binding Domains by Chemical Modification. III. Kinetics of Reaction of Carboxydinitrophenyl Cytochromes c with Cytochrome c Oxidase. *J. Biol. Chem.* 253, 149-159.
- (35) Brautigan, D. L.; Ferguson-Miller, S.; Margoliash, E. (1978) Mitochondrial Cytochrome c. *Methods Enzymol.* 33D, 131-132.
- (36) Yu, N.-T.; Srivastava, R. B. (1980) Resonance Raman Spectroscopy of Heme Proteins with Intensified Vidicon Detectors: Studies of Low Frequency Modes and Excitation Profiles in Cytochrome c and Hemoglobin. *J. Raman Spectrosc.* 9, 166-171.
- (37) Sawyer, D. T.; Roberts, J. L. (1974) *Experimental Electrochemistry for Chemists*, Wiley, New York.
- (38) Herskovits, T. T.; Gadegbeku, B.; Jaillet, H. (1970) On the Structural Stability and Solvent Denaturation of Proteins. I. Denaturation by the Alcohols and Glycols. *J. Biol. Chem.* 245, 2588-2598.
- (39) Smith, D. W.; Williams, R. J. P. (1969) The Spectra of Ferric Haems and Haemoproteins. *Struct. Bonding* 7, 1-45.
- (40) Schejter, A.; George, P. (1969) The 695-m $\mu$  Band of Ferricytochrome c and Its Relationship to Protein Conformation. *Biochemistry* 3, 1045-1049.
- (41) Kaminsky, L. S.; Davison, A. J. (1969) Effects of Organic Solvents on the Spectrum of Cytochrome c. *Biochemistry* 8, 4631-4637.
- (42) Kaminsky, L. S.; Yong, F. C.; King, T. E. (1972) Circular Dichroism Studies of the Perturbations of Cytochrome c by Alcohols. *J. Biol. Chem.* 247, 1354-1359.
- (43) Spiro, T. G. (1975) Resonance Raman Spectroscopic Studies of Heme Proteins. *Biochim. Biophys. Acta* 416, 169-189.
- (44) Spiro, T. G.; Strekas, T. C. (1974) Resonance Raman Spectra of Heme Proteins. Effects of Oxidation and Spin State. *J. Am. Chem. Soc.* 96, 338-345.
- (45) Kitagawa, T.; Ozaki, Y.; Kyogoku, Y.; Yamanaka, T. (1977) The pH Dependence of the Resonance Raman Spectra and Structural Alterations at Heme Moieties of Various c-Type Cytochromes. *Biochim. Biophys. Acta* 494, 100-114.
- (46) Theorell, H. (1936) Pure Cytochrome c. II. Preparation, Properties, Ionic Migration, Diffusion and Absorption Spectrum of Cytochrome c. *Biochem. Z.* 285, 207-218.
- (47) Nicholson, R. S. (1965) Theory and Application of Cyclic Voltammetry for Measurement of Electrode Reaction Kinetics. *Anal. Chem.* 37, 1351-1355.
- (48) Taniguchi, I.; Toyosawa, K.; Yamaguchi, H.; Yasukouchi, K. (1982) Voltammetric Response of Horse Cytochrome c at a Gold Electrode in the Presence of Sulfur Bridged Bipyridines. *J. Electroanal. Chem.* 140, 187-193.
- (49) Taniguchi, I.; Iseki, M.; Eto, T.; Toyosawa, K.; Yamaguchi, H.; Yasukouchi, K. (1984) The Effect of pH on the Temperature Dependence of the Redox Potential of Horse Cytochrome c at a Bis(4-Pyridyl)disulfide-Modified Gold Electrode. *Bioelectrochem. Bioenerg.* 13, 373-383.
- (50) Taniguchi, I.; Funatsu, T.; Iseki, M.; Yamaguchi, H.; Yasukouchi, K. (1985) The Temperature Dependence of the Redox Potential of Horse Cytochrome c at a Bis(4-Pyridyl)disulfide-Modified Gold Electrode in Sodium Chloride Solution. *J. Electroanal. Chem.* 193, 295-302.

# Synthesis of a Hybrid Protein Containing the Iron-Binding Ligand of Bleomycin and the DNA-Binding Domain of Hin

Martha G. Oakley, Kenneth D. Turnbull, and Peter B. Dervan\*

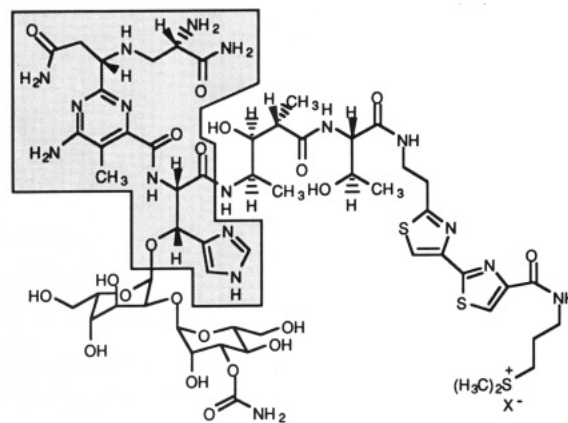
Arnold and Mabel Beckman Laboratories of Chemical Synthesis, Division of Chemistry and Chemical Engineering, California Institute of Technology, Pasadena, California 91125. Received February 16, 1994\*

The iron-binding and oxygen-activating domain of the natural product bleomycin [pyrimidoblastic acid- $\beta$ -hydroxy-L-histidine (PBA- $\beta$ -OH-His)] was attached to the NH<sub>2</sub> terminus of the DNA binding domain of Hin recombinase (residues 139-190). This hybrid 54-residue protein PBA- $\beta$ -OH-His-Hin(139-190) binds specifically to DNA at four distinct Hin binding sites with affinities comparable to those of the unmodified Hin(139-190). In the presence of dithiothreitol, Fe(II)-PBA- $\beta$ -OH-His-Hin(139-190) cleaves DNA with specificity remarkably similar to that of Fe(II)-EDTA-Hin(139-190). Analysis of the cleavage patterns suggests that site-specific DNA cleavage is mediated by a localized diffusible species, in contrast with cleavage by bleomycin, which occurs through a nondiffusible oxidant. This has implications for the design of second-generation artificial sequence specific DNA cleaving proteins and defines limitations in current efforts to create atom-specific chemistry on DNA.

## INTRODUCTION

Natural products have evolved over millions of years which are capable of high-yielding sequence-specific reactions at single atoms on double-helical DNA, *i.e.*, oxidation at C(4') by Fe(II)-bleomycin, alkylation of N(3) of adenine by CC-1065, and phosphate hydrolysis by restriction endonucleases. The design of *artificial* sequence-specific DNA-cleaving molecules requires the integration into a single molecule of two separate functions, recognition and cleavage. Early design of bifunctional molecules for sequence-specific oxidative cleavage of DNA relied on *nonnatural* cleaving moieties such as Fe(II)-EDTA which cleaves DNA by generating a diffusible species, most likely hydroxyl radical (1-4). It is of interest in the design field to explore whether the *architecturally more complex* cleavage domains of natural products are useful for the construction of second generation hybrid molecules capable of atom-specific cleavage reactions within a ligand-DNA complex.

**The Dioxygen Activating Domain, PBA- $\beta$ -OH-His.** Bleomycin cleaves double-stranded DNA in the presence of oxygen and Fe(II) at 5'-GC-3' and 5'-GT-3' sites (5, 6) by abstraction of the 4'-hydrogen of the pyrimidine deoxyribose (7). The bleomycin glycopeptide has traditionally been divided into several structural and functional domains (5, 6). The tripeptide pyrimidoblastic acid- $\beta$ -hydroxy-L-histidine (PBA- $\beta$ -OH-His) is necessary for iron binding and dioxygen activation (Figure 1) (8-10). The carbamoyl disaccharide moiety increases the efficiency of DNA cleavage, although deglycobleomycin cleaves DNA with similar specificity to that of bleomycin (8, 11, 12). A peptide linker region separates the iron-binding domain from the bithiazole and the positively charged tail, which appear necessary for sequence-specific recognition of DNA (10). A synthetically simplified peptide ligand (PYML-6), modeled on the bleomycin metal binding core, was attached to distamycin. In the presence



**Figure 1.** Bleomycin A<sub>2</sub>. The highlighted segment is PBA- $\beta$ -OH-His tripeptide.

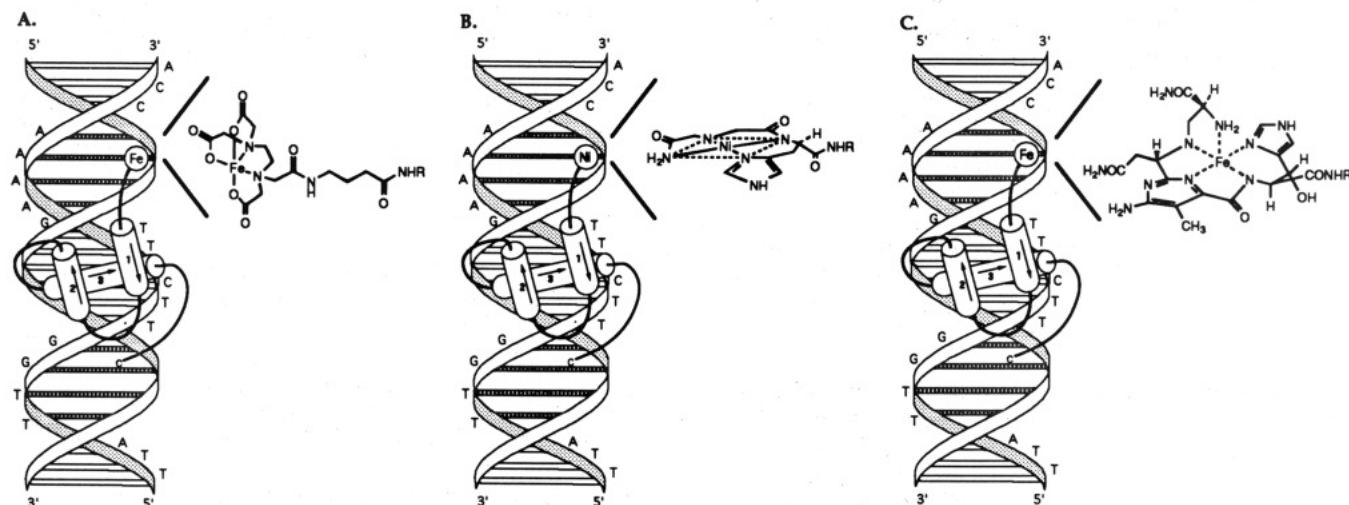
of Fe(II), this hybrid molecule cleaves DNA over several base pairs at each A,T-rich binding site, similar to the cleavage patterns produced by Fe(II)-EDTA-distamycin (13). To our knowledge, the tripeptide PBA- $\beta$ -OH-His from the natural product, bleomycin, has never been attached to other DNA binding domains presumably due to the prior lack of an efficient synthesis. It has not yet been tested whether the iron-binding domain *alone* is capable of mechanistically similar cleavage to that effected by bleomycin when it is attached to a heterologous DNA binding domain in the minor groove.

**The DNA Binding Domain, Hin(139-190).** Because of the precise spatial requirements for DNA degradation by atom-specific chemistry, we chose a DNA-binding domain that has been shown to support oxidative cleavage of DNA by both a diffusible and nondiffusible mechanism *in the minor groove*. Hin recombinase binds as a dimer to a number of similar DNA sites with the consensus sequence 5'-TTNTCNAACCA-3' (14, 15). A 52-amino acid peptide (residues 139-190) constitutes the sequence-specific DNA-binding activity of Hin (16). Attachment of Fe(II)-EDTA to the NH<sub>2</sub> terminus of Hin(139-190) affords specific oxidative degradation of the DNA at Hin binding sites via a *diffusible oxidant* proximal to the minor groove near the symmetry axis of Hin sites (17). A binding model for Hin(139-190) includes a helix-turn-helix-turn-

\* Correspondence address: Division of Chemistry and Chemical Engineering, 164-30, California Institute of Technology, Pasadena, CA, 91125. Phone: (818) 395-6002. Fax: (818) 683-8753.

\* Abstract published in *Advance ACS Abstracts*, April 15, 1994.





**Figure 2.** Schematic representations of models for hybrid proteins containing the Hin DNA-binding domain bound to one *hixL* half-site (IRLR). Putative  $\alpha$ -helices are shown as cylinders with an arrow pointing from the  $\text{NH}_2$  to the  $\text{CO}_2\text{H}$  terminus. (A)  $\text{Fe(II)}\cdot\text{EDTA}\cdot\text{Hin}(139\text{--}190)$ . (B)  $\text{Ni(II)}\cdot\text{GGH}\cdot\text{Hin}(139\text{--}190)$ . (C)  $\text{Fe(II)}\cdot\text{PBA-}\beta\text{-OH-His-Hin}(139\text{--}190)$ .

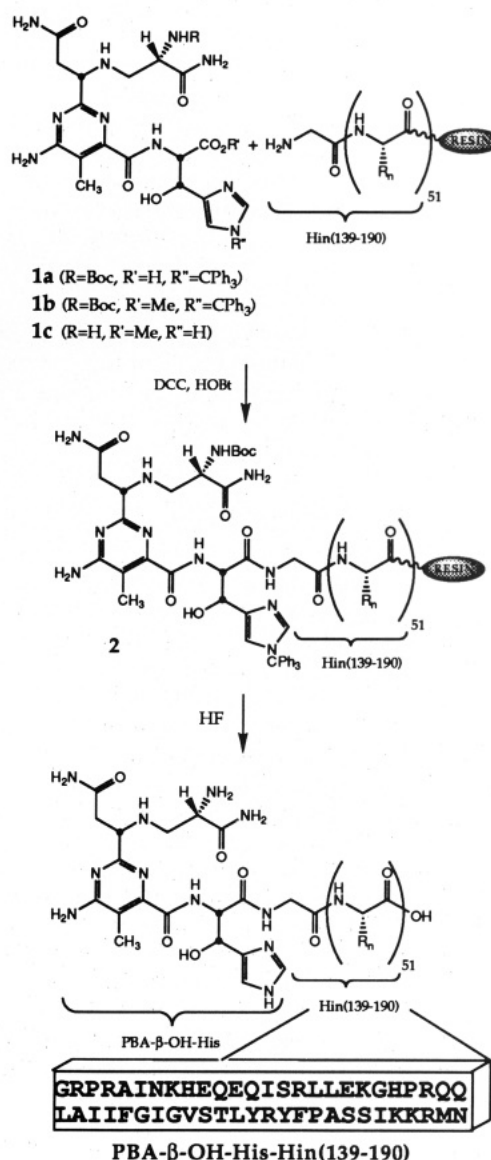
helix structure in the major groove with the  $\text{NH}_2$  terminus extending across the phosphodiester backbone and residues Gly139 and Arg140 making specific contacts in the minor groove (Figure 2A) (15, 17, 18).

Recently, the tripeptide Gly-Gly-His was also attached to the  $\text{NH}_2$  terminus of Hin(139–190) (Figure 2B) and shown to cleave DNA in the presence of Ni(II) and peracid predominantly at a *single deoxyribose position* at each Hin binding site (19, 20). Thus, the DNA-binding domain of Hin can support DNA cleavage in the adjacent minor groove by a reactive metal complex that reacts with DNA through a *nondiffusible oxidant*.

With the Hin DNA binding domain supporting both diffusible oxidant ( $\text{EDTA}\cdot\text{Fe}/\text{O}_2/\text{DTT}$ ) and nondiffusible oxidant ( $\text{GGH}\cdot\text{Ni}/\text{peracid}$ ) we are in a position to test mechanistically whether  $\text{PBA-}\beta\text{-OH-His-Fe(II)}$ , when bound in the minor groove of DNA by Hin(139–190), cleaves by a nondiffusible species in the presence of dioxygen and reducing agent. We describe here the solid-phase synthesis and DNA-cleaving properties of a 54-residue hybrid protein,  $\text{PBA-}\beta\text{-OH-His-Hin}(139\text{--}190)$ , comprising the DNA-binding domain of Hin recombinase and the putative iron-binding and oxygen-activating domain of bleomycin, pyrimidoblastic acid-*erythro*- $\beta$ -hydroxy-L-histidine.

## RESULTS

**Synthesis.** Pyrimidoblastic acid-*erythro*- $\beta$ -hydroxy-L-histidine was prepared in a diastereoselective synthesis according to the effective procedure recently described by Boger and co-workers (21). *tert*-Butyloxycarbonyl-protected (–)-pyrimidoblastic acid was prepared in eight steps from readily available starting materials and condensed with the triphenylmethyl-protected methyl ester of *erythro*- $\beta$ -hydroxy-L-histidine (prepared in seven steps) to afford  $\text{PBA-}\beta\text{-OH-His}$  dipetide **1a** in 64% yield upon hydrolysis of the methyl ester. Dipetide **1a** was coupled to the  $\text{NH}_2$  terminus of resin-bound, fully protected Hin(139–190) under standard peptide coupling conditions to afford **2** in 88% yield (Figure 3) (4, 17, 18, 22). The protein was deprotected and cleaved from the resin by treatment with anhydrous HF and purified by reversed-phase HPLC to afford  $\text{PBA-}\beta\text{-OH-His-Hin}(139\text{--}190)$  (Figures 2C and 3). The molecular weight of the hybrid protein was confirmed by laser desorption time-of-flight mass spectrometry. As a control to ensure that the  $\text{PBA-}\beta\text{-OH-His}$



**Figure 3.** Synthetic scheme for the attachment of the protected  $\text{PBA-}\beta\text{-OH-His}$  dipetide **1a** to the  $\text{NH}_2$  terminus of the Hin(139–190) resin by solid-phase methods.

dipeptide withstands HF treatment, the protected  $\text{PBA-}\beta\text{-OH-His}$  methyl ester, **1b**, was subjected to anhydrous

HF under the conditions used for peptide deprotection to afford **1c** in quantitative yield (Figure 3).

**DNA Binding and Cleaving Assays.** The DNA-binding and -cleaving properties of PBA- $\beta$ -OH-His-Hin(139-190) were investigated by DNase I footprinting and affinity cleaving on a  $^{32}$ P-end-labeled DNA fragment containing five 13 bp binding sites for Hin: two dimeric binding sites, *hix*L and *secondary*, and a lower affinity site, termed tertiary (Figures 4 and 5). The individual half sites are designated IRL (left) and IRR (right). In the presence of dithiothreitol (DTT), Fe(II)·PBA- $\beta$ -OH-His-Hin(139-190) at 10 mM (room temperature, pH 7.5) cleaves the restriction fragment at every Hin binding site, although with lower efficiency than Fe(II)·EDTA-Hin(139-190) (Figure 4C, lanes 11-14; Figure 5C,D). Additional cleavage is not observed at Fe(II)·bleomycin sites, indicating that the DNA-cleaving specificity of Fe(II)·PBA- $\beta$ -OH-His-Hin(139-190) is determined by the Hin DNA-binding domain alone (Figure 4C, lanes 17, 18; Figure 5F). As is the case with Fe(II)·EDTA-Hin(139-190), Fe(II)·PBA- $\beta$ -OH-His-Hin(139-190) cleavage occurs over several bases on each strand of DNA at each site. Relative association constants for Fe(II)·PBA- $\beta$ -OH-His-Hin(139-190) and PBA- $\beta$ -OH-His-Hin(139-190) were compared with those for the unmodified Hin(139-190) by quantitative DNase I footprint titration analyses (23). The relative binding affinities for all three proteins at four different sites are similar, indicating that the ligand-metal complex does not change the affinity or specificity of Hin(139-190) (24).

## DISCUSSION

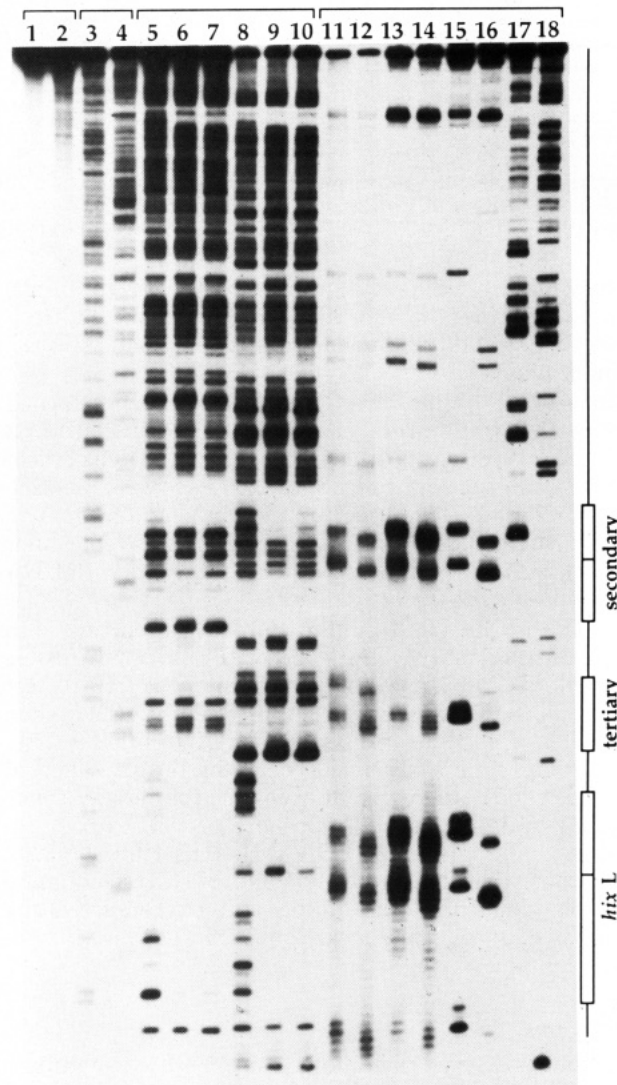
The hybrid protein Fe(II)·PBA- $\beta$ -OH-His-Hin(139-190) containing the nonheme metal-binding and oxygen-activating domain of bleomycin and DNA-binding domain of Hin cleaves DNA with the sequence-specificity of Hin(139-190). Cleavage at multiple nucleotide positions at each binding site is consistent with cleavage by a diffusible oxidant. Although a highly localized oxidant, such as a metal-oxo species, could react at a number of nucleotide positions if it is located on a flexible segment of the DNA-binding molecule, available evidence indicates that the NH<sub>2</sub> terminus of Hin(139-190) is anchored in the minor groove as in the case of Ni(II)·GGH-Hin(139-190). No reduction of binding affinity or specificity is observed with Fe(II)·PBA- $\beta$ -OH-His-Hin(139-190), implying that these contacts are not altered by the addition of the metal ligand.

The DNA end products generated by Fe(II)·PBA- $\beta$ -OH-His-Hin(139-190), analyzed by gel electrophoresis, are 5'- and 3'-phosphate, consistent with oxidative degradation of the deoxyribose backbone (24). The appearance of 3'-phosphate termini in the absence of base treatment demonstrates that DNA oxidation by Fe(II)·PBA- $\beta$ -OH-His-Hin(139-190) does not proceed through the same reaction pathway as Fe(II)·bleomycin.

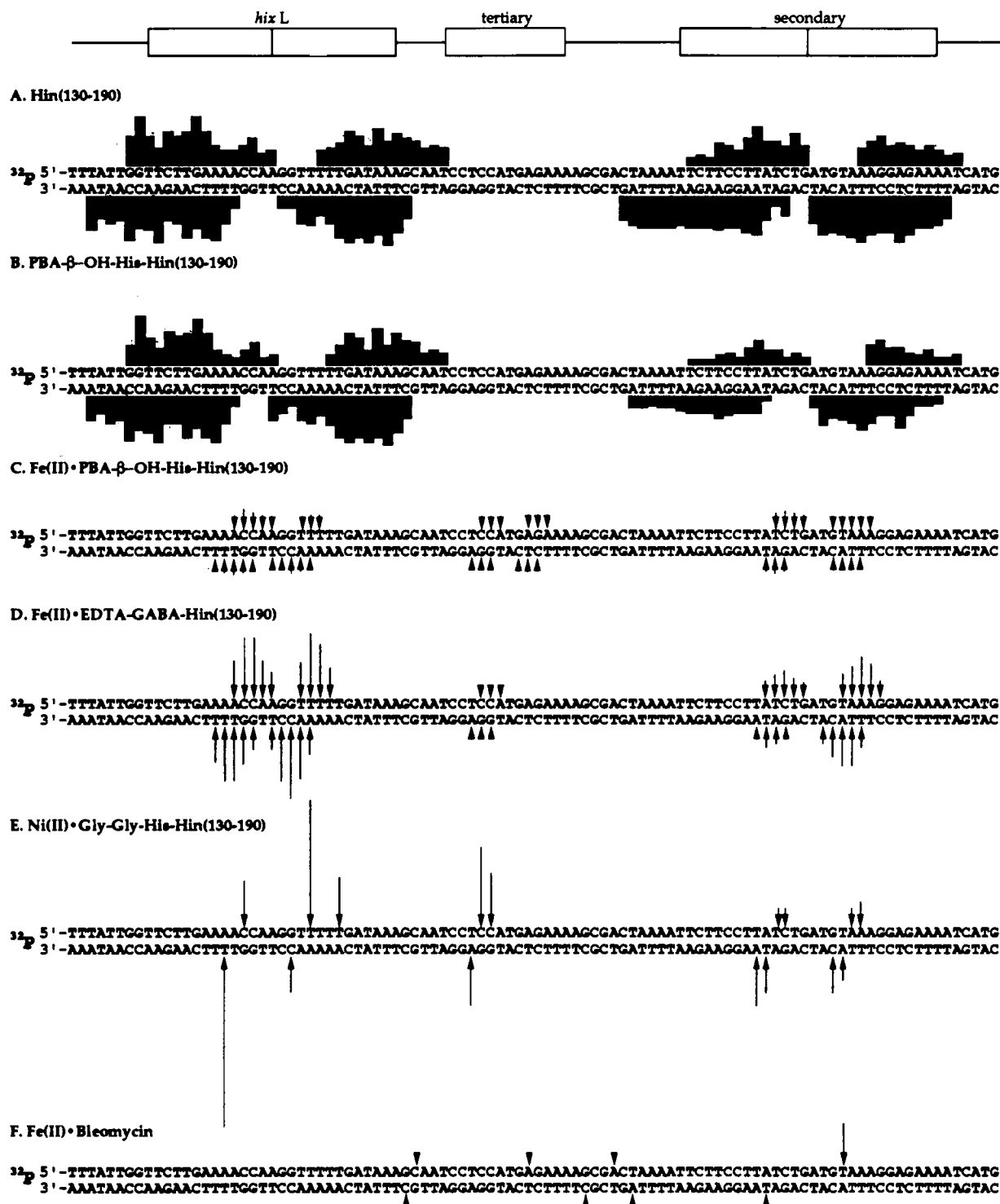
There are three possible mechanisms for cleavage by Fe(II)·PBA- $\beta$ -OH-His-Hin(139-190) through a diffusible oxidant rather than through the localized oxidant found in bleomycin. (1) The PBA- $\beta$ -OH-His ligand might be insufficient to form a stable iron-oxo complex. (2) The activated iron-oxo complex is formed but not held in the proper orientation to react as the nondiffusible oxidant with the deoxyribose backbone. Decomposition of a short-lived metal-oxo complex could then produce a diffusible oxidant which cleaves DNA proximal to the position of the metal complex. In this context, it will be interesting to reevaluate the importance of the dissacharide in the stability and lifetime of the metal-oxo species. (3) The

A. major minor  
5' - **TTNTC**NN**AA**ACCA - 3'

B.	Binding Site	Sequence
	Consensus	5' - <b>TTNTC</b> NN <b>AA</b> ACCA - 3'
	<i>hix</i> L IRL	5' - <b>TTCTT</b> GA <b>AA</b> ACCA - 3'
	<i>hix</i> L IRR	5' - <b>TTATC</b> AA <b>AA</b> ACCT - 3'
	secondary IRL	5' - <b>TCTTC</b> CT <b>TACT</b> CG - 3'
	secondary IRR	5' - <b>TTCTC</b> CT <b>TTAC</b> AT - 3'
	tertiary	5' - <b>TTTTC</b> T <b>CAT</b> GGAG - 3'



**Figure 4.** (A) Consensus half-site DNA binding sequence for Hin recombinase. Nucleotides implicated in major and minor groove contacts with the protein are printed in bold type (14-18). (B) Sequences of the five Hin half sites assayed. (C) Autoradiogram of a polyacrylamide gel showing DNase I footprinting reactions for Hin(139-190) and PBA- $\beta$ -OH-His-Hin(139-190) and affinity cleaving reactions for Fe(II)·PBA- $\beta$ -OH-His-Hin(139-190), Fe(II)·EDTA-Hin(139-190), Ni(II)·GGH-Hin(139-190), and Fe(II)·bleomycin. Lanes 1, 3, 5-7, 11, 13, 15, and 17 contain 5'- $^{32}$ P-end-labeled DNA; lanes 2, 4, 8-10, 12, 14, 16, and 18 contain 3'- $^{32}$ P-end-labeled DNA. Lanes 1 and 2, intact DNA; lanes 3 and 4, Maxam-Gilbert G-specific sequencing reactions; lanes 5 and 8, DNase control lanes; lanes 6 and 9, DNase I cleavage protection by Hin(139-190) (5 mM); lanes 7 and 10, DNase I cleavage protection by PBA- $\beta$ -OH-His-Hin(139-190) (5 mM); lanes 11 and 12, Fe(II)·PBA- $\beta$ -OH-His-Hin(139-190) at 10 mM; lanes 13 and 14, Fe(II)·EDTA-Hin(139-190) at 5 mM; lanes 15 and 16, Ni(II)·GGH-Hin(139-190) at 5 mM; lanes 17 and 18, Fe(II)·bleomycin at 2.5 mM.



**Figure 5.** Histogram representations of the data in Figure 4C. The sequence from left to right represents the data from the bottom to the middle of the gel. (A) Bars represent the extent of protection, derived from the ratio of cleavage at each band compared to the control lane, from DNase I cleavage in the presence of 5 mM Hin(139-190) (Figure 4C, lanes 6 and 9). (B) Bars represent the extent of protection from DNase I cleavage in the presence of 5 mM PBA-β-OH-His-Hin(139-190) (Figure 4C, lanes 7 and 10). (C) Arrows represent the extent of cleavage by 10 mM Fe(II)-PBA-β-OH-His-Hin(139-190) (Figure 4C, lanes 11 and 12). (D) Arrows represent the extent of cleavage by 5 mM Fe(II)-EDTA-Hin(139-190) (Figure 4C, lanes 13 and 14). (E) Arrows represent the extent of cleavage by 5 mM Ni(II)-GGH-Hin(139-190) (Figure 4C, lanes 15 and 16). (F) Arrows represent the extent of cleavage by 2.5 mM Fe(II)-bleomycin (Figure 4C, lanes 17 and 18).

metal binding ligand has sequence-specific requirements for DNA cleaving that are not met by the five Hin minor groove sites.

**Retrospective Analysis.** Future experiments on hybrid DNA-cleaving molecules containing the iron-binding domain of bleomycin might include a DNA binding site with bleomycin recognition sites proximal to the recogni-

tion sequence of the DNA-binding molecule. It may be necessary to design a *spacer domain* for suitable *orientation* of the bleomycin-derived DNA-cleaving tripeptide metal complex in the hybrid molecule. This will require significantly more structural information on the natural product than is currently available. It emphasizes the fact that design of bifunctional molecules truly requires

three domains, *i.e.*, spacer domains between recognition and cleavage functions for correct distance and orientation.

## EXPERIMENTAL SECTION

**Materials.** Asn-(phenylacetamido)methyl (PAM) resin, *N,N*-dimethylformamide (DMF), diisopropylethylamine, dicyclohexylcarbodiimide (DCC) in dichloromethane, *N*-hydroxybenzotriazole (HOBt) in DMF, trifluoroacetic acid (TFA), and protected amino acid derivatives were purchased from Applied Biosystems. Boc-L-His(DNP) was obtained from Fluka. Doubly distilled water was further purified through the Milli Q filtration system from Millipore. Sonicated, deproteinized calf thymus DNA was purchased from Pharmacia. Enzymes were obtained from Boehringer-Mannheim or New England Biolabs and used with the buffers supplied. Deoxyadenosine 5'-[ $\alpha$ - $^{32}$ P]-triphosphate and adenosine 5'-[ $\gamma$ - $^{32}$ P]triphosphate were obtained from Amersham. Bleomycin sulfate was purchased from Sigma, and solutions were prepared based on an extinction coefficient derived from an  $E_{1\%}^{1\text{cm}}$  of 105 at 292 nm and the molecular weight of bleomycin A<sub>2</sub> sulfate.

$^1\text{H}$  and  $^{13}\text{C}$  NMR spectra were recorded on a QE-300 NMR. Protein mass spectra were recorded at the Biotechnology Instrumentation Facility of the University of California, Riverside, on a laser desorption time-of-flight mass spectrometer. High-resolution mass spectra for other compounds were recorded using fast atom bombardment techniques at the Mass Spectrometry Facility of the University of California, Riverside. Optical rotations were measured on a JASCO DIP-180 digital polarimeter. Automated peptide synthesis was performed on an ABI 430A peptide synthesizer.

***N*<sup>6</sup>-[1-Amino-3-(*S*)-(4-amino-6-(amido-erythro- $\beta$ -hydroxy-L-histidine methyl ester)-5-methylpyrimidin-2-yl)propion-3-yl]-(*S*)- $\beta$ -aminoalanine Amide (1c).** Dipeptide 1b (21) (2.1 mg, 2.5 mmol), *p*-cresol (1 drop), and *p*-thiocresol (1 drop) were added to a Teflon tube equipped with a Teflon-coated magnetic stir bar. The reaction vessel was evacuated, cooled to  $-78^\circ\text{C}$ , and charged with HF ( $\sim 2.0$  mL). The mixture was allowed to stir at  $0^\circ\text{C}$  (1 h). HF was removed *in vacuo*, and the resulting yellow residue was taken up in  $\text{H}_2\text{O}$  (0.5 mL). The aqueous portion was extracted with  $\text{CHCl}_3$  ( $1 \times 0.5$  mL), and the organic portion was washed with  $\text{H}_2\text{O}$  ( $1 \times 0.5$  mL). The combined aqueous portions were concentrated *in vacuo* to afford an off-white foam. TLC (analytical RP-18,  $5 \times 10$  cm, 0.25-mm thickness, 25%  $\text{CH}_3\text{CN}/\text{H}_2\text{O}$ ) afforded a white powder which was dissolved in  $\text{H}_2\text{O}$  (1 mL) and filtered (0.2 mm) to remove particulate contaminants. Concentration *in vacuo* afforded 1c (1.2 mg, quantitative yield) as a white foam:  $[\alpha]_{\text{D}}^{25} = +12.2$  ( $c$  0.03,  $\text{CH}_3\text{OH}$ );  $^1\text{H}$  NMR (300 MHz,  $\text{D}_2\text{O}$ )  $\delta$  8.73 (s, 1H), 7.50 (s, 1H), 5.44 (d,  $J = 5.7$  Hz, 1H), 5.12 (d,  $J = 5.7$  Hz, 1H), 4.51 (m, 1H), 4.41 (m, 1H), 3.78 (s, 3H), 3.18 (m, 2H), 3.04 (m, 1H), 2.84 (m, 1H), 2.09 (s, 3H); IR (neat) 3384, 1736, 1664, 1460, 1380, 850, 698; FAB HRMS (SGly)  $m/e$  493.2272 (calcd  $\text{MH}^+$ ,  $\text{C}_{19}\text{H}_{29}\text{N}_{10}\text{O}_6$ , 493.2267).

**Protein Syntheses.** Hin(139–190) was synthesized by automated stepwise solid-phase chemical synthesis as previously reported (4, 17, 18, 22). Resin-bound peptide (ca. 50 mg, ca. 100 mmol/g, total peptide ca. 5 mmol) was placed in a 12- $\times$  80-mm reaction vessel. The terminal Boc protecting group was removed and the resin neutralized by standard procedures. Dipeptide 1a (21) (16.0 mg, 20 mmol) and HOBt (5.5 mg, 42 mmol) were dissolved in DMF (1 mL), and DCC (4.6 mg, 22 mmol) was added. The solution was allowed to stir at room temperature for 30 min and added to the peptide/resin with additional DMF

(1 mL). Ninhydrin analysis indicated 88% reaction with no further improvement in yield after 5 h. The resulting PBA- $\beta$ -OH-His-Hin(139–190) was deprotected and cleaved from the resin by treatment with anhydrous HF and purified by preparative reversed-phase HPLC as previously described (4, 17, 18, 22). Laser desorption time-of-flight mass spectrometry ( $\alpha$ -cyano-4-hydroxycinnamic acid matrix, 70% acetonitrile, 2% TFA in  $\text{H}_2\text{O}$ ) was consistent with the desired structure (calcd mass, 6495.5, obsd, 6493.3). A second, much smaller peak due to Hin(139–190) (calcd mass, 6036.1, obsd, 6035.6) was also apparent. Fe(II)-PBA- $\beta$ -OH-His-Hin(139–190) and Fe(II)-EDTA-Hin(139–190) were generated prior to use by equilibration of 250 mM protein with an equal volume of 250 mM ferrous ammonium sulfate for 15 min before dilution to the appropriate concentrations.

**DNA Manipulations.** The 450 bp *Xba* I-*Eco* RI restriction fragment of the plasmid pMFB36 was labeled at the 5' or 3' end and isolated by standard procedures. Maxam-Gilbert G-specific sequencing reactions were performed according to established protocols. All DNA-binding and -cleaving assays were performed at room temperature. DNase I footprinting reaction conditions were 20 mM phosphate, 20 mM NaCl, 10 mM  $\text{MgCl}_2$ , 100 mM DTT, 0.004 units DNase I, 100 mM calf thymus DNA, and  $\sim 20$  000 cpm labeled DNA, pH 7.5. The DNA binding hybrid proteins were allowed to equilibrate with the DNA for 15 min. Reactions were then initiated by the addition of a stock solution of DNase I,  $\text{MgCl}_2$ , and DTT and allowed to proceed 10 min at room temperature. Reactions were quenched by the addition of a 3 M ammonium acetate solution containing 250 mM EDTA followed by ethanol precipitation.

Fe(II)-PBA- $\beta$ -OH-His-Hin(139–190) and Fe(II)-EDTA-Hin(139–190) cleaving reactions were performed in 20 mM phosphate, 20 mM NaCl, 5 mM DTT, 100 mM calf thymus DNA,  $\sim 10$  000 cpm labeled DNA, and 5 mM Fe(II)-EDTA-Hin(139–190) or 10 mM Fe(II)-PBA- $\beta$ -OH-His-Hin(139–190), pH 7.5. Ni(II)-GGH-Hin(139–190) cleavage reactions were performed in 20 mM phosphate, 20 mM NaCl, 5 mM monoperoxyphthalic acid, 100 mM calf thymus DNA,  $\sim 10$  000 cpm labeled DNA, and 5 mM Ni(II)-GGH-Hin, pH 7.5. Fe(II)-bleomycin cleavage reactions were performed in 20 mM phosphate, 20 mM NaCl, 5 mM DTT, 100 mM calf thymus DNA,  $\sim 10$  000 cpm labeled DNA, and 2.5 mM Fe(II)-bleomycin, pH 7.5. All synthetic proteins were allowed to equilibrate with the DNA for 15 min before reactions were initiated with the addition of DTT or monoperoxyphthalic acid. Fe(II)-EDTA-Hin(139–190) and Ni(II)-GGH-Hin reactions were allowed to proceed for 1 h, Fe(II)-PBA- $\beta$ -OH-His-Hin(139–190) reactions for 6 h, and Fe(II)-bleomycin reactions for 15 min before they were terminated by ethanol precipitation. Residues were dried and resuspended in 100 mM Tris-borate-EDTA/80% formamide loading buffer. Reaction products were analyzed by electrophoresis on 6% polyacrylamide denaturing gels (5% crosslink, 7 M urea).

## ACKNOWLEDGMENT

This work was supported by the National Institutes of Health (GM-27681), a National Science Foundation predoctoral fellowship, a National Institutes of Health predoctoral traineeship, and a Glaxo Graduate Student Fellowship to M.G.O. and an American Cancer Society postdoctoral fellowship to K.D.T. We thank G. M. Hathaway (University of California, Riverside) for protein mass spectral analysis.

## LITERATURE CITED

- (1) Dervan, P. B. (1986) Design of Sequence Specific DNA Binding Molecules. *Science* 232, 464.
- (2) Dreyer, G. B.; Dervan, P. B. (1985) Sequence Specific Cleavage of Single Stranded DNA. Oligonucleotide-EDTA-Fe(II). *Proc. Natl. Acad. Sci. U.S.A.* 82, 968.
- (3) Moser, H. E.; Dervan, P. B. (1987) Sequence-Specific Cleavage of Double Helical DNA by Triple Helix Formation. *Science* 238, 645.
- (4) Sluka, J. P.; Horvath, S. J.; Bruist, M. F.; Simon, M. I.; Dervan, P. B. (1987) Synthesis of a Sequence-Specific DNA-Cleaving Peptide. *Science* 238, 1129.
- (5) Stubbe, J.; Kozarich, J. W. (1987) Mechanism of Bleomycin-Induced DNA Degradation. *Chem. Rev.* 87, 1107.
- (6) Hecht, S. M. (1986) The Chemistry of Activated Bleomycin. *Acc. Chem. Res.* 19, 383.
- (7) Kozarich, J. W.; Worth, L., Jr.; Frank, B. L.; Christner, D. F.; Vanderwall, D. E.; Stubbe, J. (1989) Sequence-Specific Isotope Effects on the Cleavage of DNA by Bleomycin. *Science* 245, 1396.
- (8) Sugiura, Y.; Suzuki, T.; Otsuka, M.; Kobayashi, S.; Ohno, M.; Takita, T.; Umezawa, H. (1983) Synthetic Analogues and Biosynthetic Intermediates of Bleomycin. *J. Biol. Chem.* 258, 1328.
- (9) Killkuskie, R. E.; Suguna, H.; Yellin, B.; Murugesan, N.; Hecht, S. M. (1985) Oxygen Transfer by Bleomycin Analogues Dysfunctional in DNA Cleavage. *J. Am. Chem. Soc.* 107, 260.
- (10) Umezawa, H.; Takita, T.; Sugiura, Y.; Otsuka, M.; Kobayashi, S.; Ohno, M. (1984) DNA-Bleomycin Interaction. Nucleotide Sequence-Specific Binding and Cleavage of DNA by Bleomycin. *Tetrahedron* 44, 501.
- (11) Sugiyama, H.; Killkuskie, R. E.; Hecht, S. M. (1985) An Efficient Site-Specific DNA Target for Bleomycin. *J. Am. Chem. Soc.* 107, 7765.
- (12) Sugiyama, H.; Ehrenfield, G. M.; Shipley, J. B.; Killkuskie, R. E.; Chang, L.-H.; Hecht, S. M. (1985) DNA Strand Scission by Bleomycin Group Antibiotics. *J. Nat. Prod.* 48, 869.
- (13) Otsuka, M.; Masuda, T.; Haupt, A.; Ohno, M.; Shiraki, T.; Sugiura, Y.; Maeda, K. (1990) Man-Designed Bleomycin with Altered Sequence Specificity in DNA Cleavage. *J. Am. Chem. Soc.* 112, 838.
- (14) Glasgow, A. C.; Bruist, M. F.; Simon, M. I. (1989) DNA-Binding Properties of the Hin Recombinase. *J. Biol. Chem.* 264, 10072.
- (15) Feng, J.-A.; Johnson, R. C.; Dickerson, R. E. (1994) Hin Recombinase Bound to DNA: The Origin of Specificity in Major and Minor Groove Interactions. *Science* 263, 348.
- (16) Bruist, M. F.; Horvath, S. J.; Hood, L. E.; Steitz, T. A.; Simon, M. I. (1987) Synthesis of a Site-Specific DNA-Binding Peptide. *Science* 235, 777.
- (17) Sluka, J. P.; Horvath, S. J.; Glasgow, A. C.; Simon, M. I.; Dervan, P. B. (1990) Importance of Minor-Groove Contacts for Recognition of DNA by the Binding Domain of Hin Recombinase. *Biochemistry* 29, 6551.
- (18) Mack, D. P.; Sluka, J. P.; Shin, J. A.; Griffin, J. H.; Simon, M. I.; Dervan, P. B. (1990) Orientation of the Putative Recognition Helix in the DNA-Binding Domain of Hin Recombinase Complexed with the Hix Site. *Biochemistry* 29, 6561.
- (19) Mack, D. P.; Dervan, P. B. (1990) Nickel-Mediated Sequence-Specific Oxidative Cleavage of DNA by a Designed Metalloprotein. *J. Am. Chem. Soc.* 112, 4604.
- (20) Mack, D. P.; Dervan, P. B. (1992) Sequence-Specific Oxidative Cleavage of DNA by a Designed Metalloprotein, Ni(II)-GGH(Hin139-190). *Biochemistry* 31, 9399.
- (21) Boger, D. L.; Menezes, R. F.; Honda, T. (1993) Total Synthesis of (-)-Pyrimidoblastic Acid and Deglycobleomycin A<sub>2</sub>. *Angew. Chem., Int. Ed. Engl.* 32, 273.
- (22) Kent, S. B. H. (1988) Chemical Synthesis of Peptides and Proteins. *Annu. Rev. Biochem.* 57, 957.
- (23) Brenowitz, M.; Senear, D. F.; Shea, M. A.; Ackers, G. K. (1986) Quantitative DNA Footprint Titration—A Method for Studying Protein-DNA Interactions. *Methods Enzymol.* 130, 132.
- (24) Oakley, M. G. (1994) Design, Synthesis and Characterization of Sequence-Specific DNA-Cleaving Metalloproteins. Ph.D. Thesis, California Institute of Technology.



## Enhanced Stability *in Vitro* and *in Vivo* of Immunoconjugates Prepared with 5-Methyl-2-iminothiolane

Stephen F. Carroll,\* Susan L. Bernhard,<sup>†</sup> Dane A. Goff,<sup>‡</sup> Robert J. Bauer, Will Leach, and Ada H. C. Kung

Departments of Biological Chemistry and Pharmacology/Toxicology, XOMA Corporation, 2910 Seventh Street, Berkeley, California 94710. Received December 3, 1993\*

Substituted 2-iminothiolanes (X2ITs) are new heterobifunctional crosslinking agents designed for the preparation of disulfide-linked conjugates with enhanced resistance to reduction. Based upon 2-IT substituted at the 4 and/or 5 position, these reagents appear to function by sterically protecting the conjugate disulfide bond from attack by thiolate nucleophiles. Here, we have used the X2ITs to prepare and evaluate a series of immunoconjugates (antibody-cytotoxin conjugates) between the murine monoclonal antibody 791/T36, which recognizes a 72-kDa surface antigen present on many human tumor cells, and RTA<sub>30</sub>, the naturally occurring 30-kDa glycoform of ricin A chain. The X2IT-linked conjugates were also compared to immunoconjugates prepared with *N*-succinimidyl 3-(2-pyridyldithio)propionate (SPDP) and 4-[(succinimidyl)oxy]carbonyl- $\alpha$ -methyl- $\alpha$ -(2-pyridyldithio)toluene (SMPT), as well as with methyl- and dimethyl-substituted structural analogs of SPDP. *In vitro*, 791-(X2IT)-TNB model compounds exhibited a 6000-fold range of stabilities. In contrast, the corresponding 791-(X2IT)-RTA<sub>30</sub> immunoconjugates were up to 20-fold more stable than conjugates made with unhindered linkages. These improvements resulted in immunoconjugates with prolonged serum half-lives in animals. Our data indicate that one of the crosslinking agents, 5-methyl-2-iminothiolane (M2IT), has optimal properties for the preparation of disulfide crosslinked immunoconjugates intended for therapeutic use in that (i) it is highly water soluble and reacts rapidly with protein amino groups at neutral pH, preserving the positive charge, (ii) it forms conjugates with RTA<sub>30</sub> efficiently, and (iii) its conjugates exhibit enhanced disulfide bond stability *in vitro* and *in vivo*. The potential utility of M2IT and other X2ITs for the preparation of controlled release protein-drug conjugates is also discussed.

### INTRODUCTION

Immunoconjugates (antibodies linked to cytotoxic proteins) represent a specialized class of protein-protein conjugates designed for therapeutic use (for a review, see refs 1 and 2). As such, they typically are prepared by covalently crosslinking an antibody molecule to a cytotoxin such as the A chain of ricin (RTA).<sup>1</sup> The antibody thus serves to target the action of the cytotoxic component to cells bearing the target antigen. Once internalized, the cytotoxin is released and then penetrates into the cytosol where it enzymically inactivates ribosomes, blocking protein synthesis and causing cell death. This approach for selective cellular elimination is currently being evaluated clinically for the treatment of autoimmune disorders and cancer (2-8).

Most of the RTA immunoconjugates prepared to date have utilized one of two crosslinking reagents, SPDP or 2IT, to generate a disulfide bond linking antibody to cytotoxin. That a reducible bond is required for maximal expression of cytotoxic activity has been demonstrated by numerous studies (1, 2, 9). However, many such conjugates are unstable in animals (10, 11), where cleavage of the disulfide bond regenerates free antibody and cytotoxin. For immunoconjugate therapy this deconjugation has two important consequences. First, it reduces the effective concentration of circulating immunoconjugate, and as a result, larger clinical doses may be required. Second, the released antibody may remain in circulation much longer than does conjugate, where it can compete for antigen binding sites on target cells. Thus, the disulfide bond linking antibodies to cytotoxin such as RTA must be sufficiently labile to facilitate intracellular cytotoxicity, but it must also be sufficiently stable to survive administration and delivery *in vivo*.

To address these issues, several new crosslinking reagents have been prepared and tested for immunoconjugate preparation, and the *in vitro* and *in vivo* properties of such conjugates have been studied. Each of these reagents contains one (12, 13) or two (14) methyl groups adjacent to the disulfide bond, and each has generated conjugates with enhanced stability (12-15) and improved efficacy (15) in animals. Thus, hindering access of reducing agents to the antibody-cytotoxin linkage results in immunoconjugates with improved *in vivo* stability and potency.

Recently, we described the synthesis and preliminary characterization of a new family of crosslinking reagents, termed X2ITs (16), which are based upon 2-iminothiolane (17). The X2ITs offer several advantages over other crosslinking reagents: (i) they react with primary amines

\* Current address: Chiron Corp., 4560 Horton Street, Emeryville, CA 94608.

<sup>†</sup> Current address: Gen Pharm Int., 297 N. Bernardo Ave., Mountain View, CA 94043.

\* Abstract published in *Advance ACS Abstracts*, March 15, 1994.

<sup>1</sup> Abbreviations: 2IT, 2-iminothiolane; 2-ME, 2-mercaptoethanol; 2TP, 2-thiopyridine; DTNB, dithionitrobenzoic acid; DTPO, 2,2'-dithiobis(pyridine *N*-oxide); DTDP, 2,2'-dithiodipyrindine; GSH, reduced glutathione; HPSEC, high-performance size-exclusion chromatography; MSPDP, the methyl-SPDP analog *N*-succinimidyl 3-(2-pyridyldithio)butyrate; RTA, ricin toxin A chain; RTA<sub>30</sub>, the 30-kDa glycoform of RTA; SAMBA, the dimethyl-SPDP structural analog *N*-hydroxysuccinimidyl 3-methyl-3-(acetylthio)butanoate; SMCC, succinimidyl 4-(*N*-maleimidomethyl)cyclohexane-1-carboxylate; SMPT, 4-[(succinimidyl)oxy]carbonyl- $\alpha$ -methyl- $\alpha$ -(2-pyridyldithio)toluene; SPDP, *N*-succinimidyl 3-(2-pyridyldithio)propionate; TNB, thionitrobenzoic acid; TPO, 2-thiopyridine *N*-oxide; X2IT, 2-iminothiolane substituted at the 4 and/or 5 position.



to form stable amidinium derivatives that retain the positive charge; (ii) inclusion of an aromatic disulfide (such as DTNB) in the reaction mixture both activates the newly exposed X2IT thiol and allows real-time spectrophotometric monitoring of the labeling reaction; and (iii) variation in the substituent at the 5-position (immediately adjacent to the linker thiol) alters the susceptibility of the resulting disulfide bond to reduction. For activated model compounds, these alterations in steric hindrance resulted in disulfide bonds that varied by over 4000-fold in their ability to be reduced by glutathione (16). The preparation and properties, both *in vitro* and *in vivo*, of RTA immunconjugates prepared with the X2IT reagents are the subject of this report.

## EXPERIMENTAL PROCEDURES

**Materials.** Solutions of DTNB (Sigma Chemical Co., St. Louis, MO) were prepared as described by Jocelyn (18). An  $E^{1\text{mM}}_{1\text{cm}}$  of 14.1 at 412 nm (19) was used to determine concentrations of the TNB anion. DTDP and DTPO were from Aldrich (Milwaukee, WI); the mM extinction coefficients (and wavelengths) used for 2TP (343 nm) and TPO (332 nm) were 7.06 and 4.16, respectively. Stock solutions of GSH (Sigma Chemical Co., St. Louis, MO) were prepared in PBS-EDTA (see below); prior to use, the concentration of free thiols was quantified by reaction with DTNB. DTT, 2-ME, Sephadex G25F, Phenyl-Sepharose (all from Sigma Chemical Co., St. Louis, MO), trisacryl GF-05LS, and Ultrogel AcA44 (both from IBF Biotechnics, France) were purchased as indicated. All other reagents were of analytical grade.

**Crosslinking Reagents.** 2IT, SMCC (both from Sigma Chemical Co., St. Louis, MO), and SPDP (Pierce Chemical, Rockford, IL) were obtained from the indicated sources. The X2IT crosslinking reagents, which have the structures shown in Table 1, were synthesized as described previously (16). Stock solutions were prepared in water; concentrations were determined spectrophotometrically by using appropriate extinction coefficients at 248 nm (16). In addition, three other crosslinkers were prepared for these studies. MSPDP and SMPT were synthesized according to Worrell et al. (12) and Thorpe et al. (13), respectively, with minor modifications. The structure of each linker was confirmed by  $^1\text{H}$  NMR. *N*-Hydroxysuccinimidyl 3-methyl-3-(acetylthio)butanoate (SAMBA), a dimethyl-substituted structural analog of SPDP, was prepared as follows: 3-Methyl-3-(acetylthio)butanoic acid (ref 10, 2.17 g, 12.3 mmol) in  $\text{CH}_2\text{Cl}_2$  (20 mL) was treated with *N*-hydroxysuccinimide (1.86 g, 16.2 mmol) and dicyclohexylcarbodiimide (3.34 g, 16.2 mmol) at room temperature for 66 h under  $\text{N}_2$ . The reaction mixture was filtered, concentrated *in vacuo*, and then subjected to flash chromatography on  $\text{SiO}_2$  with elution in hexane/EtOAc (80/20, v/v, then 50/50). The desired ester was obtained as a pale yellow oil (2.78 g, 82% yield) that gave a white solid upon standing at room temperature: mp 63 °C; TLC (hexane/EtOAc, 80/20, v/v)  $R_f$  = 0.27;  $^1\text{H}$  NMR (60 MHz,  $\text{CDCl}_3$ ) 3.23 (s, 2H), 2.80 (s, 4H, NHS ester), 2.27 (s, 3H, SAc), 1.60 (s, 6H).

**Preparation of Linker-Modified Antibody.** The murine IgG2b monoclonal antibody 791/T36 (791,  $M_r$  ca. 150 000) was produced in an Accusyst hollow fiber bioreactor (Endotronics, Minneapolis, MN) and purified as described (20). The purified antibody was derivatized with each crosslinker so as to incorporate an average of 1–1.5 linkers per mol of antibody. For modification with SPDP, MSPDP, SAMBA, or SMCC, 791 antibody at 2 mg/mL in reaction buffer (0.1 M  $\text{NaPO}_4$ , 0.1 M NaCl, pH 7.5) was first reacted with a 5- to 10-fold molar excess of

crosslinker (previously dissolved in absolute ethanol). Following a 20-min incubation at 20 °C, excess reagent and reaction byproducts were removed by size-exclusion chromatography on a GF-05LS column equilibrated in reaction buffer at 4 °C. The number of crosslinkers introduced into the antibody was determined by spectrophotometric analysis following DTT-induced release of the 2TP leaving group (21). For some experiments, the 2TP leaving groups were replaced with TNB by mild reduction of the linker-modified antibody (0.1 mM DTT, 30 min, 25 °C), followed by reaction with 2 mM DTNB (30 min, 25 °C). The TNB-activated antibody was then purified by size-exclusion chromatography on a column of G5-05LS equilibrated in phosphate buffered saline containing 1 mM EDTA, pH 7.4 (PBS-EDTA) and stored at 4 °C.

The reaction of 2IT and the X2ITs with 791 antibody was monitored spectrophotometrically as follows (16): 791 antibody (3 mg/mL; 20  $\mu\text{M}$ ) and DTNB (2.5 mM) in reaction buffer were equilibrated at 25 °C in a 1-cm disposable cuvette and placed in a dual-beam spectrophotometer. An identical solution prepared without antibody was placed in the reference position. To initiate the reaction, X2IT (freshly dissolved in water) was rapidly added to each cuvette with mixing to a final concentration of 0.5 mM, and the absorbance at 412 nm was monitored. When the  $A_{412}$  reached a value of 0.28 (20  $\mu\text{M}$  TNB, or 1 mol of TNB per mol of 791), the reaction mixture was rapidly desalted on a 1-cm  $\times$  20-cm column of Sephadex G25F equilibrated at 4 °C in PBS-EDTA. The excluded protein peak was pooled and stored at 4 °C. The number of linkers introduced per mole of antibody was determined spectrophotometrically as follows: The  $A_{280}$  of the linker-activated protein was first measured. Then, following reaction with 2 mM DTT, released TNB was quantified at 412 nm. The corrected protein  $A_{280}$  was calculated from the equation

$$A_{280}(\text{protein}) = A_{280}(\text{nonreduced}) - (0.33A_{412}(\text{reduced}))$$

and the concentration of 791 antibody was determined by using an  $E^{1\text{mM}}_{1\text{cm}}$  of 179 at 280 nm ( $E^{1\text{mg/mL}}_{1\text{cm}} = 1.2$ ). The linker/antibody ratio was then calculated from the molar values of TNB and protein.

**Preparation and Purification of Immunconjugates.** Immunconjugates containing SPDP-, SMPT-, and SMCC-activated 791 antibody and RTA<sub>30</sub> (the naturally occurring 30-kDa glycoform of RTA) were prepared essentially as described (16, 20). Briefly, linker-activated antibody (1–2 mg/mL) in PBS-EDTA was reacted with a 5-fold molar excess of freshly reduced RTA<sub>30</sub>. The disulfide exchange (SPDP, SMPT) or maleimide-based (SMCC) conjugation reactions proceeded for 16 h at 4 °C. For SAMBA-activated 791 antibody, the conjugation reaction proceeded differently. The free thiol on RTA<sub>30</sub> (5 mg/mL in reaction buffer) was first activated by reaction with 2 mM DTNB, and the RTA<sub>30</sub>-SS-TNB was purified by size-exclusion chromatography on Sephadex G25F. SAMBA-modified 791 antibody was then treated with 50 mM hydroxylamine (pH 7.5) for 30 min at 25 °C to remove the *S*-acetyl protecting group, and conjugation was initiated by the addition of RTA<sub>30</sub>-SS-TNB (3-fold molar excess).

Immunconjugates were separated from excess RTA<sub>30</sub> and reaction byproducts by chromatography on a 1-  $\times$  50-cm column of Ultrogel AcA44 equilibrated at 4 °C in reaction buffer. The number of RTA<sub>30</sub> molecules crosslinked to antibody was determined by densitometric analysis of samples following sodium dodecyl sulfate

polyacrylamide gel electrophoresis in 5% gels under nonreducing conditions (22) and Coomassie blue staining. The monoconjugate species (1 RTA per 791 antibody) of selected immunoconjugates was purified by hydrophobic interaction chromatography on Phenyl-Sepharose (20), so as to remove residual free antibody and immunoconjugates containing multiple RTA<sub>30</sub> moieties.

**Disulfide Bond Stability Assay.** The susceptibility of 791-RTA<sub>30</sub> immunoconjugates to reduction *in vitro* was evaluated in a high-performance size-exclusion chromatographic assay (HPSEC) which quantifies physical dissociation of the antibody-RTA<sub>30</sub> conjugate<sup>2</sup> (23). Immunoconjugates (0.23 mg/mL in PBS-EDTA) were incubated at 37 °C for 30 min with increasing concentrations of reduced glutathione (0–10 mM). Upon completion, free thiols were quenched by the addition of excess iodoacetic acid (pH 7.5; final concentration, 50 mM), and aliquots were chromatographed on a BioSil TSK-250 column (BioRad Labs, Richmond, CA) equilibrated at 25 °C in 50 mM NaPO<sub>4</sub>, 100 mM Na<sub>2</sub>SO<sub>4</sub>, pH 6.8. The flow rate was 1.0 mL/min, the column effluent was monitored at 280 nm, and the amount of RTA<sub>30</sub> released was quantified by area integration. By comparison to samples incubated with 50 mM 2-ME (which resulted in 100% deconjugation), plots were constructed correlating percent RTA<sub>30</sub> release with the concentration of glutathione in the incubation mixture. That concentration of glutathione which released 50% of the conjugated RTA<sub>30</sub> was termed the RC<sub>50</sub>.

**Cytotoxicity Assay.** The cytotoxicities of 791-RTA<sub>30</sub> immunoconjugates were determined using the 791T/M osteosarcoma cell line, which expresses the antigen recognized by 791 antibody (20). Cells (4 × 10<sup>5</sup>/mL) were incubated in a humidified 5% CO<sub>2</sub> incubator with increasing concentrations of immunoconjugates at 37 °C. After 42 h, <sup>3</sup>H-thymidine (1 μCi/well) was added, and incubation was continued for an additional 18 h. Upon completion, cell-associated radioactivity was determined by liquid scintillation counting. The IC<sub>50</sub> was calculated as the concentration of immunoconjugate necessary to inhibit incorporation of radioactivity by 50% relative to untreated controls. These IC<sub>50</sub> values were corrected for the number of RTA<sub>30</sub> molecules conjugated to antibody for each preparation by multiplying the conjugate IC<sub>50</sub> by the RTA/Ab ratio. These normalized values compensate for slight variations in the number of cytotoxins per antibody in the different preparations and are expressed in terms of pM RTA<sub>30</sub>.

**Pharmacokinetic Studies.** Pharmacokinetic studies of selected immunoconjugates were performed in 5-week-old male Sprague-Dawley rats (Simonsen Laboratories, Gilroy, CA) weighing an average of 149 g (range 122–175 g) at the initiation of dosing. All animals were delivered healthy to the XOMA animal care facility, where they were acclimated for at least 5 days prior to dosing, and were housed using standard NIH guidelines for husbandry procedures.

Only purified monoconjugates were used in these studies. Each monoconjugate was radiolabeled with <sup>125</sup>I by the Iodogen method (24) to a specific activity of 0.3–2 mCi/mg and was injected intravenously (33–50 μg/kg) into 42 rats per study (three rats per timepoint). At selected timepoints (0.05, 0.25, 0.5, 0.75, 2, 4, 8, 12, 18, 24, 36, 48, 72, and 96 h), blood samples were collected via the orbital sinus, and serum aliquots were counted in an LKB γ

**Table 1. Reaction of Substituted 2-Iminothiolanes with 791 Antibody<sup>a</sup>**

linker	substitution	structure	reaction rate <sup>a</sup> <i>k</i> × 10 <sup>5</sup>
2IT	(none)		5.0
M2IT	5-methyl		4.0
Ph2IT	5-phenyl		8.8
TB2IT	5-tert-butyl		7.4
DM2IT	5-dimethyl		4.6
S2IT	5-spiro		4.6
R2IT	4,5-ring		5.6

<sup>a</sup> Rates of reaction of X2ITs (0.5 mM) with 791 antibody (20 μM) as monitored by coupling the reaction with 2.5 mM DTNB in 0.1 M NaPO<sub>4</sub>, 0.1 M NaCl, pH 7.5, and monitoring the change in absorbance at 412 nm. First-order rate constants were determined from the linear slopes of plots for log [X2IT] against time.

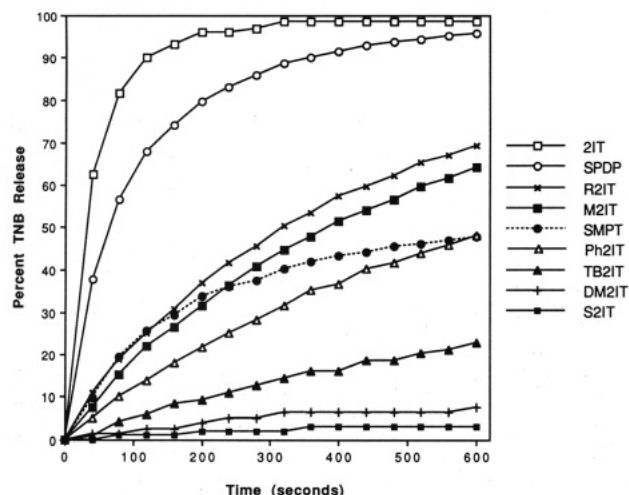
counter. Serum samples from each timepoint were also analyzed by SDS-PAGE and autoradiography to determine the fraction of intact monoconjugate prior to pharmacokinetic analysis (13). Pharmacokinetic parameters were determined from a two compartmental analysis using the program PCNONLIN (Statistical Consultants, Inc., Lexington, KY).

## RESULTS

**Reaction of X2ITs with Proteins.** The structures of the X2IT crosslinking reagents are summarized in Table 1. Prior studies had shown that the reactivity of the X2ITs with the amino group of glycine was relatively unaffected by the X2IT ring substituent (16). We therefore examined the reactivity of the X2ITs with protein amino groups, in preparation for conjugate production. Each X2IT (0.5 mM) was incubated at pH 7.5 with the murine IgG2b monoclonal antibody 791 (20 μM) in the presence of DTNB (2.5 mM), and changes in the absorbance at 412 nm were recorded. Following reaction of the X2ITs with the protein amino groups, DTNB undergoes disulfide exchange with the newly exposed X2IT thiol to yield a free TNB group (monitored at 412 nm) and an activated 791-(X2IT)-SS-TNB molecule. This coupling of the reactions between protein modification and TNB production simplifies the analysis of the rate and extent of the reaction. As was found for the reaction with glycine (16), reaction rates for the X2ITs with 791 antibody followed first-order kinetics and varied less than 2-fold for the entire series of crosslinkers (Table 1). Similar reaction conditions were therefore employed for the preparation of protein conjugates utilizing each X2IT linker.

**Stability of Model Disulfides.** The relative stability of X2IT model protein disulfides was assessed by measuring the rates of release of the TNB leaving group from 791-(X2IT)-SS-TNB molecules following incubation with 200 μM reduced glutathione (GSH). For comparison, two additional control analogs were examined. 791-(SPDP)-SS-TNB was prepared by derivatizing 791 antibody with the heterobifunctional crosslinking reagent SPDP and replacing the 2TP leaving group with TNB. A similar

<sup>2</sup> Carroll, S. F., Goff, D., Reardan, D., and Trown, P. W. (1989) Abstracts from the fourth international conference on monoclonal antibody immunoconjugates for cancer, San Diego, CA, p 161.



**Figure 1.** Glutathione-induced release of TNB from 791-TNB analogs. Samples of activated conjugates (791-(X)-SS-TNB, 10  $\mu$ M) in PBS-EDTA were placed in a cuvette at 25  $^{\circ}$ C, and at  $T = 0$   $^{\circ}$ C, reduced glutathione was added to a final concentration of 200  $\mu$ M. The release of TNB was monitored spectrophotometrically at 412 nm for 500 s, and 2-ME was then added to a final concentration of 200 mM to determine maximal release of TNB. Results were normalized by quantifying percent maximal release, as determined by dividing the absorbance at any timepoint by that obtained with 200 mM 2-ME and then multiplying the product by 100.

**Table 2.** Relative Stabilities of TNB-Activated 791 Antibody Analogs

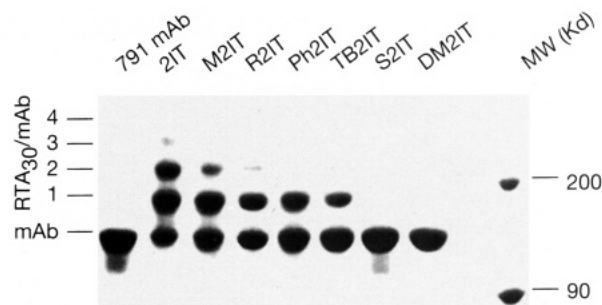
analog	TNB release rate <sup>a</sup> ( $k \times 10^4$ )	stability increase relative to	
		2IT <sup>b</sup>	SPDP <sup>c</sup>
791-(2IT)-SS-TNB	235	1.0	0.4
791-(R2IT)-SS-TNB	21.7	10.8	4.7
791-(M2IT)-SS-TNB	18.2	12.9	5.6
791-(Ph2IT)-SS-TNB	11.5	20.4	8.9
791-(TB2IT)-SS-TNB	4.5	52.2	22.7
791-(DM2IT)-SS-TNB	0.039	6030	2620
791-(S2IT)-SS-TNB	0.036	6530	2830
791-(SPDP)-SS-TNB	102	2.3	1.0
791-(SMPT)-SS-TNB	14.7	16.0	6.9

<sup>a</sup> Reaction mixtures contained 791-X-SS-TNB (20  $\mu$ M) and reduced glutathione (40–103 mM) and were incubated at 25  $^{\circ}$ C and monitored at 412 nm. Plots of  $\log [791-X-SS-TNB]$  vs time were linear for all analogs except 791-(SMPT)-SS-TNB. Pseudo-first-order reaction rates were calculated by computerized nonlinear curve fitting (GraFit, version 2.0, Erithacus Software Ltd., Staines, U.K.).

<sup>b</sup> Relative increase in disulfide stability compared to the 2IT analog.

<sup>c</sup> Relative increase in disulfide stability compared to the SPDP analog.

procedure was used to prepare 791-(SMPT)-SS-TNB, which incorporates the methyl-hindered crosslinking reagent developed by Thorpe et al. (13). Figure 1 indicates that the X2IT reagents create model protein disulfides which vary greatly in their susceptibility to reduction by GSH. However, each of the substituted X2ITs produced linkages that were significantly more stable than those produced by SPDP or 2IT. At appropriate concentrations of reductant, pseudo-first-order rate constants for TNB release were calculated (Table 2). Relative to 2IT, the most stable linkages (DM2IT and S2IT) were more than 6000-fold more resistant to reduction by GSH. The order from least to most stable was as follows: 2IT < R2IT < M2IT < Ph2IT < TB2IT < DM2IT < S2IT. For the most stable analogs (those made with DM2IT and S2IT), prolonged incubation (30–60 min) with 200 mM 2-ME was required for complete release of TNB. In this assay, the stability of the SMPT analog was intermediate between those of M2IT and Ph2IT.

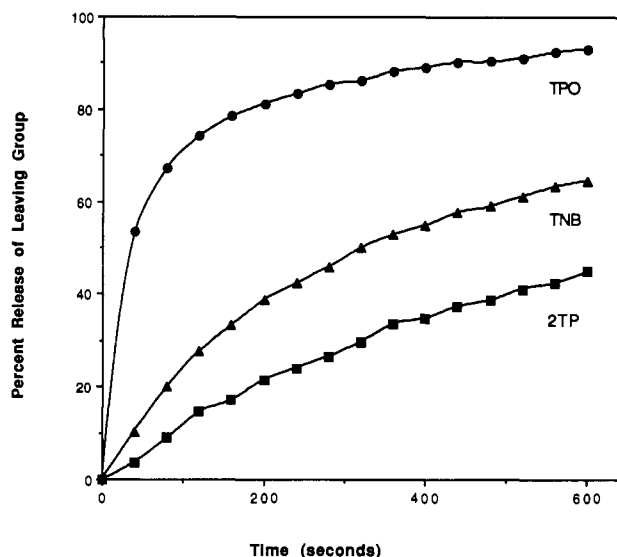


**Figure 2.** Conjugate formation by 791-TNB analogs. Each 791-(X2IT)-SS-TNB analog (1 TNB per 791 antibody) was incubated with a 5-fold molar excess of freshly reduced RTA<sub>30</sub> in PBS-EDTA. The final concentration for both 791-(X2IT)-TNB and RTA<sub>30</sub> was 1.6 mg/mL. After 16 h at 4  $^{\circ}$ C, aliquots (10  $\mu$ g) were analyzed by SDS-PAGE in a 5% gel under nonreducing conditions. Upon completion, the gel was stained with Coomassie blue.

**Preparation of RTA<sub>30</sub> Immunoconjugates.** Antibody-RTA immunoconjugates are typically prepared by performing a disulfide-exchange reaction between the free -SH group of RTA and an activated linker disulfide present on the antibody. Because this exchange reaction (like the stability assay described above) is essentially a reductive cleavage of the activated linker-SS-TNB bond, variations might be expected in the efficiency with which the linker-activated antibody is converted to immunoconjugate. Activated 791-(X2IT)-SS-TNB antibodies (1.0–1.3 linkers/Ab) were therefore individually reacted with a 5-fold molar excess of RTA<sub>30</sub> for 16 h at 4  $^{\circ}$ C and then aliquots were analyzed by SDS-PAGE. The results (Figure 2) suggest an inverse correlation between disulfide bond stability and the efficiency of conjugation, as determined by either the disappearance of the free antibody band or by the appearance of higher molecular weight conjugate bands. Utilizing densitometry to quantify the conversion of antibody into immunoconjugate, we found that the efficiency of conjugation followed the order 2IT > M2IT > R2IT = Ph2IT > TB2IT. Under identical conditions, SMPT-activated antibody was converted to immunoconjugate roughly as efficiently as was TB2IT-activated antibody (data not shown).

No immunoconjugates were detected in reaction mixtures containing DM2IT- or S2IT-modified antibody, suggesting that RTA<sub>30</sub> (like GSH and 2-ME) could not easily displace the TNB leaving group from these two linkers disubstituted at the 5 position (immediately adjacent to the disulfide bond). Similarly, little or no conjugation was detected with DM2IT- or S2IT-modified antibody even following prolonged incubation with RTA<sub>30</sub> for several months at 4  $^{\circ}$ C or after increasing the incubation temperature to 25 or 37  $^{\circ}$ C. Antibody activated by reaction with a dimethyl-substituted analog of SPDP (synthesized according to Worrell et al. (12)) was also incapable of making conjugates when incubated with an excess of RTA<sub>30</sub> (data not shown).

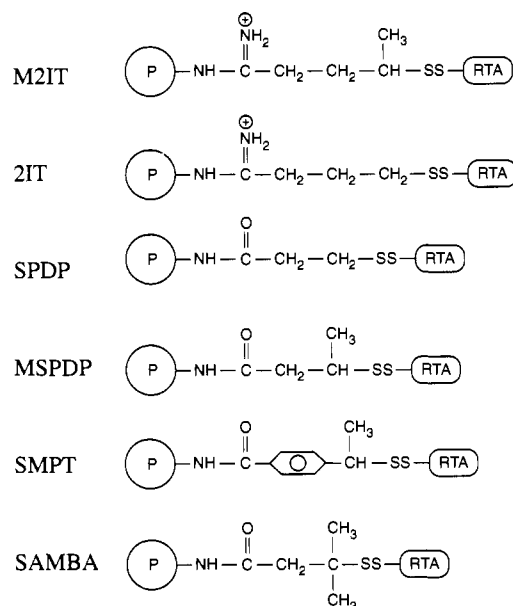
**Conjugation Efficiency Is Influenced by the Leaving Group.** Because the reactions of RTA<sub>30</sub> with DM2IT-TNB- or S2IT-TNB-activated antibodies were not productive, the effect of alternate leaving groups on conjugation efficiency was investigated. Initially, 791-(SPDP)-SS-2TP was studied, together with SPDP linkages activated by two additional diaryl disulfides. As before, the 2TP leaving group of SPDP was first removed by mild reduction, and the newly exposed linker thiol was then reacted with either DTNB or DTPO, thus generating 791-(SPDP)-SS-TNB and 791-(SPDP)-SS-TPO, re-



**Figure 3.** Glutathione-induced release of leaving groups from activated 791 antibody. Aliquots of 791-(SPDP)-SS-2TP were converted to the corresponding 791-(SPDP)-SS-TNB and 791-(SPDP)-SS-TPO analogs by mild reduction and subsequent reaction with the corresponding diaryl disulfide (DTNB and DTPO, respectively). The activated 791 antibodies were isolated by size-exclusion chromatography, and glutathione-induced release of the leaving groups was monitored as described in the legend for Figure 1. The final concentration of GSH in these assays was 40  $\mu$ M.

spectively. These compounds were then evaluated for their susceptibility to reduction by GSH. As shown in Figure 3, the TPO derivative was most easily reduced, followed by TNB and then 2TP. On the basis of first-order rate constants, the release of TPO was 8-fold faster than TNB and 15-fold faster than 2TP. When these activated antibodies were reacted with RTA<sub>30</sub>, conjugation efficiency was also highest for the TPO analog, followed again by TNB and then 2TP (data not shown). Essentially identical results were obtained with the M2IT-activated 791 antibody (791 reacted with M2IT in the presence of DTDP, DTNB, or DTPO); i.e., the TPO derivative was most easily reduced and was most efficiently conjugated with RTA<sub>30</sub> (data not shown). In fact, the conjugation efficiency of 791-(M2IT)-SS-TPO exceeded 95%, even when only a 3-fold molar excess of RTA<sub>30</sub> was used for conjugation. As before, however, no immunoconjugates were detected following reaction of 791-(DM2IT)-SS-TPO or 791-(S2IT)-SS-TPO with RTA<sub>30</sub> under any of the reaction conditions tested.

**Disulfide Bond Stability and Cytotoxicity of 791-RTA<sub>30</sub> Immunoconjugates *in Vitro*.** The *in vitro* stabilities of 791-RTA<sub>30</sub> immunoconjugates were analyzed directly by monitoring thiol-dependent release of RTA<sub>30</sub>. In addition to the conjugates described above, three additional immunoconjugates were also prepared, purified, and tested. 791-(MSPDP)-SS-RTA<sub>30</sub> (which incorporates a methyl-substituted analog of SPDP) and the thioether-linked conjugate 791-(SMCC)-CS-RTA<sub>30</sub> (which is not reducible) were prepared by standard reactions with linker-modified antibodies. The third conjugate was prepared in an effort to evaluate an immunoconjugate disubstituted at the carbon atom adjacent to the disulfide bond and, since conjugations with DM2IT- and S2IT-linked antibodies were unsuccessful, required alternate chemistries. An analog of SPDP was therefore prepared (SAMBA) which incorporated two methyl groups adjacent to the linker thiol and an S-acetyl protecting group instead of the usual 2TP moiety. Following reaction of the



**Figure 4.** Linkage structures formed by the different crosslinking agents. For the X2ITs, only M2IT is shown as an example.

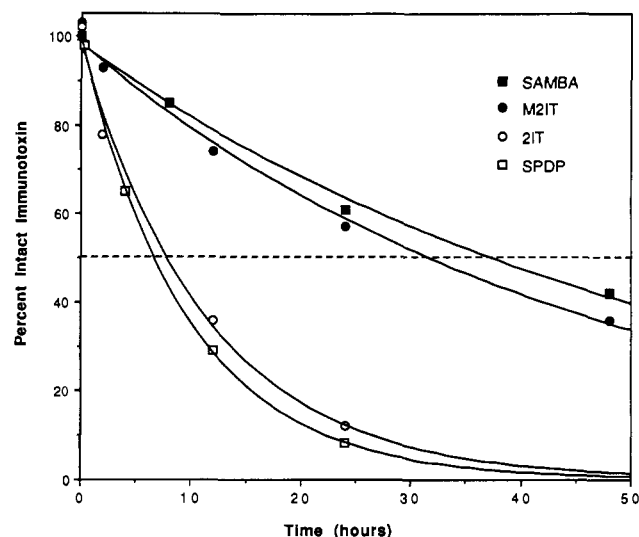
**Table 3. Stability and Cytotoxicity of 791-RTA<sub>30</sub> Immunoconjugates *in Vitro***

immunotoxin	stability increase relative to			IC <sub>50</sub> (pM RTA <sub>30</sub> )
	RC <sub>50</sub> <sup>a</sup>	2IT <sup>b</sup>	SPDP <sup>c</sup>	
791-(2IT)-SS-RTA <sub>30</sub>	1.9	1.0	0.6	70.6
791-(R2IT)-SS-RTA <sub>30</sub>	11.8	6.2	3.7	65.8
791-(M2IT)-SS-RTA <sub>30</sub>	26.2	13.8	8.3	69.0
791-(Ph2IT)-SS-RTA <sub>30</sub>	16.5	8.7	5.2	94.6
791-(TB2IT)-SS-RTA <sub>30</sub>	9.5	5.0	3.0	93.6
791-(SPDP)-SS-RTA <sub>30</sub>	3.2	1.7	1.0	89.1
791-(MSPDP)-SS-RTA <sub>30</sub>	11.8	6.2	3.7	72.2
791-(SAMBA)-SS-RTA <sub>30</sub>	32.9	17.3	10.4	89.6
791-(SMPT)-SS-RTA <sub>30</sub>	5.7	3.0	1.8	76.1
791-(SMCC)-CS-RTA <sub>30</sub>	nd <sup>e</sup>			9949.5

<sup>a</sup> The concentration of reduced glutathione, in mM, that releases 50% of the RTA<sub>30</sub> from the immunotoxin. <sup>b</sup> Obtained by dividing the RC<sub>50</sub> for each conjugate by 1.9, the value for 791-(2IT)-SS-RTA<sub>30</sub>. <sup>c</sup> Obtained by dividing the RC<sub>50</sub> value for each conjugate by 3.2, the value for 791-(SPDP)-SS-RTA<sub>30</sub>. <sup>d</sup> The concentration of immunotoxin that inhibited protein synthesis in 791T/M cells by 50%. The data are expressed in terms of RTA<sub>30</sub> equivalents. The RTA/Ab ratios varied between 1.1 and 1.5. <sup>e</sup> Not determined. The amount of RTA<sub>30</sub> released by reducing agents did not exceed 10%.

SAMBA NHS ester with antibody amino groups, a free -SH group was exposed on the linker by treatment with hydroxylamine. Thiol-activated RTA<sub>30</sub>-SS-TNB was then added, and conjugation occurred via disulfide exchange, thus producing 791-(SAMBA)-SS-RTA<sub>30</sub>. The linkage structures of these and other immunoconjugates are shown in Figure 4 (note that the linkage made by SAMBA is identical to that which would have been made by dimethyl-SPDP).

Following preparation and purification, the stability of the disulfide bond linking antibody and RTA<sub>30</sub> to reduction with GSH *in vitro* was then examined. The calculated RC<sub>50</sub> values (the concentration of GSH causing 50% release of RTA<sub>30</sub>) for all immunoconjugates are shown in Table 3. On the basis of these analyses, the dimethyl-substituted SAMBA conjugate was the most stable, followed closely by conjugates made with M2IT and Ph2IT. However, unlike the 791-TNB protein-leaving group compounds (which exhibited stabilities over an 6000-fold range), the



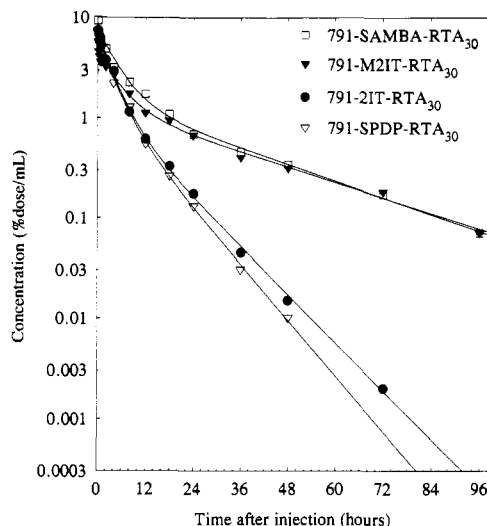
**Figure 5.** Stability of 791-RTA<sub>30</sub> immunoconjugates in rats. <sup>125</sup>I-labeled immunoconjugate monoconjugates were injected *iv* into rats as described in the Experimental Procedures. As a function of time thereafter, serum samples were collected and analyzed by SDS-PAGE and autoradiography. The percentage of radioactivity in serum associated with intact immunoconjugate at each timepoint was then quantified by densitometry.

increases in stability for the series of 791-RTA<sub>30</sub> protein-protein conjugates varied by less than a factor of 20. In all cases, the 2IT-linked forms were the least stable.

The cytotoxic activity of each 791 immunoconjugate was accessed against 791T/M cells in our standard 60-h assay (20). The IC<sub>50</sub> values calculated for all conjugates are presented in Table 4. Despite the 20-fold range of stabilities in the *in vitro* disulfide stability assay, each of the conjugates was highly cytotoxic and of similar potency for antigen-bearing target cells. Not unexpectedly, the thioether-linked conjugate (791-(SMCC)-CS-RTA<sub>30</sub>) was much less cytotoxic (ca. 100-fold) than the disulfide-linked conjugates.

**Pharmacokinetics of 791-RTA<sub>30</sub> immunoconjugates.** On the basis of the results of the *in vitro* stability studies, the two most stable (linked via SAMBA and M2IT) and the two least stable (linked via SPDP and 2IT) 791-RTA<sub>30</sub> immunoconjugates were selected for pharmacokinetic studies in rats. In order to simplify the interpretation of these studies, the monoconjugate species (1 RTA per antibody) of each immunoconjugate form was purified by hydrophobic interaction chromatography. Each monoconjugate was then radiolabeled with <sup>125</sup>I and injected *iv* into groups of rats. As a function of time thereafter, serum samples were collected and radioactivities were determined.

Rat serum aliquots were also analyzed for the presence of intact immunoconjugate by SDS-PAGE, autoradiography, and densitometry. These data were used to identify the fraction of radioactivity at each time point that was associated only with the intact monoconjugates (the remaining bands were primarily free 791 antibody). Figure 5 shows that the fraction of serum-associated radioactivity found in the immunoconjugate band varied greatly with the different conjugates. As was found *in vitro*, the 2IT- and SPDP-linked immunoconjugates appeared to deconjugate more quickly *in vivo*, with the fraction of counts present in the immunoconjugate bands decreasing to 50% within ca. 8 h. Similarly, the SAMBA- and M2IT-linked conjugates, which were significantly more stable *in vitro*, appeared to deconjugate more slowly *in vivo*. For these two conjugates, more than 50% of the radioactivity present



**Figure 6.** Pharmacokinetic serum elimination curves for 791-RTA<sub>30</sub> immunoconjugates. <sup>125</sup>I-labeled immunoconjugates were injected *iv* into rats as described in the Experimental Procedures, and serum samples were collected as a function of time thereafter. The percent injected dose corresponding to intact immunoconjugate was determined by  $\gamma$  counting and correction, based upon the data in Figure 5. Results are expressed as concentration of the monoconjugates (in percent of dose per mL of serum) vs time.

in the serum samples was still associated with intact immunoconjugate at 30 h.

The percentages of intact immunoconjugates at each time point, together with the total serum radioactivities, were then used to construct pharmacokinetic serum elimination curves for each of the immunoconjugates. As shown in Figure 6, two sets of clearance curves were obtained. The two conjugates most stable *in vitro* and *in vivo* (prepared with SAMBA and M2IT) were eliminated from the serum more slowly. Similarly, the two immunoconjugates least stable *in vitro* and *in vivo* (prepared with 2IT and SPDP) were cleared more rapidly. The pharmacokinetic parameters calculated from these data (Table 4) indicate that the conjugate serum mean residence times (sMRT) and AUCs were both increased by enhancing the stability of the linker. The elimination rate constants (CL<sub>c</sub>/V<sub>c</sub>) of the SAMBA- and M2IT-linked immunoconjugates (0.098 and 0.077 h<sup>-1</sup>, respectively) were decreased more than 2-fold relative to the 2IT- and SPDP-linked immunoconjugates (0.20 h<sup>-1</sup>).

## DISCUSSION

To be effective therapeutically, immunoconjugates made with cytotoxins such as RTA must possess two apparently conflicting properties; a labile disulfide bond linking the antibody and cytotoxin appears necessary for expression of full cytotoxic activity (1, 2, 9), but that disulfide bond must remain sufficiently stable *in vivo* to allow efficient delivery to target cells. Other studies have shown that reductive deconjugation of antibody-RTA immunoconjugates can occur in animals (10, 11) and that enhancing the stability of the linkage between antibody and cytotoxin improves immunoconjugate survival (12-15) and potency (15). The improved linkers used in these studies have had one (12, 13, 15) or two (14) methyl groups introduced immediately adjacent to the disulfide bond, suggesting that sterically hindering access to the antibody-cytotoxin linkage provides a simple means to enhance immunoconjugate stability and efficacy *in vivo*.

In an effort to more critically evaluate factors affecting immunoconjugate preparation and potency, we recently



**Table 4. Summary of Pharmacokinetic Parameters from a Two-Compartmental Analysis after Intravenous Administration of 791-RTA<sub>30</sub> Immunotoxins into Male Sprague-Dawley Rats**

parameter	unit	791-(SPDP)-SS-RTA <sub>30</sub>	791-(2IT)-SS-RTA <sub>30</sub>	791-(M2IT)-SS-RTA <sub>30</sub>	791-(SAMBA)-SS-RTA <sub>30</sub>
$T_{1/2\alpha}$	h	2.3 ± 0.36	2.4 ± 0.26	3.2 ± 0.57	3.2 ± 0.50
$T_{1/2\beta}$	h	6.5 ± 0.40	7.5 ± 0.24	23.2 ± 1.58	21.5 ± 1.55
AUC	% dose/mL·h	31.1 ± 1.26	34.3 ± 1.27	60.7 ± 2.08	76.8 ± 2.93
CLc	mL/h	3.2 ± 0.13	2.9 ± 0.11	1.6 ± 0.06	1.3 ± 0.05
V <sub>ss</sub>	mL	20.1 ± 1.09	19.8 ± 1.01	42.9 ± 2.41	28.2 ± 1.77
V <sub>c</sub>	mL	15.7 ± 0.92	14.5 ± 0.78	20.9 ± 1.27	13.3 ± 0.88
sMRT <sup>a</sup>	h	4.9 ± 0.29	5.0 ± 0.27	12.7 ± 0.82	10.2 ± 0.70
bMRT <sup>b</sup>	h	6.2 ± 0.17	6.8 ± 0.17	26.0 ± 1.16	21.7 ± 0.98

<sup>a</sup> Serum mean residence time (sMRT): The average time a molecule (the drug) resides in serum. Serum MRT is also the time it takes to clear approximately 63% of the drug from the serum. <sup>b</sup> Whole body mean residence time (bMRT): The average time a molecule (the drug) resides in the body, assuming drug is eliminated only from the central compartment. Body MRT is also the time it takes to clear approximately 63% of the drug from the body.

developed a new series of heterobifunctional crosslinking reagents, which we termed X2ITs (16). Based upon the structure of 2IT, a variety of analogs with substituents at the 4 and/or 5 position were synthesized, which, following reaction with an amino group and DTNB, places each substituent immediately adjacent to the linker-SS-TNB disulfide bond. For a series of model low molecular weight compounds (NH<sub>2</sub>-(X2IT)-SS-TNB), stability to reduction by GSH varied over 4000-fold; whereas linkages made with the parental 2IT were the least stable, those produced by DM2IT and S2IT (both disubstituted on the carbon adjacent to the disulfide bond) were very difficult to reduce. Overall, the stability of the series increased with increasing bulk (H < methyl < *tert*-butyl < dimethyl), suggesting that the X2IT substituents function by sterically protecting the disulfide bond from attack by thiolate nucleophiles.

The present studies have investigated the utility of the X2ITs to prepare protein-protein conjugates suitable for *in vivo* use. As was true for their reaction with glycine (16), the X2ITs reacted rapidly and with equal rates with 791 antibody, producing disulfide-activated 791-(X2IT)-SS-TNB analogs. And, like the small model analogs examined previously, the thiol-activated protein analogs also varied greatly (more than 6000-fold) in their susceptibility to reduction, with the DM2IT and S2IT analogs again being the most stable. In fact, activated disulfide bonds prepared with these two linkers required incubation with 200 mM 2-ME for more than 30 min to achieve maximal release of the TNB leaving groups.

Although the overall magnitudes of the TNB release rates for the protein analogs studied here are similar to those reported earlier for the small model analogs (16), differences were noted between the two systems. For example, most of the protein-X2IT-TNB analogs exhibited glutathione-induced TNB release rates nearly 4-fold slower than those measured for the corresponding NH<sub>2</sub>-X2IT-TNB compounds. Not surprisingly, this result suggests that the environment of the disulfide bond in the protein-TNB conjugates, or its accessibility to glutathione, differs from that in the NH<sub>2</sub>-TNB compounds.

The ability of the 791-(X2IT)-SS-TNB analogs to create immunoconjugate conjugates via disulfide-exchange reactions with RTA<sub>30</sub> was also markedly influenced by the nature of the X2IT substituent. Consistent with their relative ease of reduction, immunoconjugates were most easily produced with the parental 791-(2IT)-SS-TNB analog, whereas no conjugates were detected with either the disubstituted DM2IT or S2IT analogs. Even when a more efficient leaving group (TPO) was used in the conjugation reactions, no conversion of the DM2IT- or S2IT-activated antibodies to immunoconjugates were observed. High levels of conversion to immunoconjugate

were also observed with analogs such as 791-(M2IT)-SS-TNB, and efficiencies approaching 100% could be achieved with the corresponding TPO-activated analog. Thus, increasing the intrinsic stability of the activated protein disulfide had a detrimental effect on conjugate formation and yield, but these negative effects could (for some linkers) be reversed by appropriate selection of the leaving group.

Since immunoconjugates were not detected with the disubstituted X2IT-activated analogs, we prepared an immunoconjugate containing a new dimethyl-substituted analog of SPDP (SAMBA) and compared its properties to those of conjugates prepared with the remaining X2IT series, as well as to conjugates containing two other sterically hindered heterobifunctional crosslinkers, MSPDP (12) and SMPT (13). In animal models, immunoconjugates containing SMPT have exhibited improved potency, which has been attributed to their improved stability and prolonged serum half-lives (15). For each of the disulfide-linked 791-RTA<sub>30</sub> immunoconjugates, cytotoxicity for antigen-bearing cells was relatively unaffected by the linker substituents, whereas the activity of a nonreducible thioether-linked conjugate was decreased 100-fold. From these data we conclude that, as assayed herein, the linker substituents we have studied have little impact on the *in vitro* potency of the resulting immunoconjugates.

In contrast to the range of stabilities obtained with model 791-TNB analogs, the stability of the different 791-RTA<sub>30</sub> immunoconjugates varied by less than 20-fold *in vitro*. Thus, although the 791-(SAMBA)-SS-TNB analog was 2000-fold more resistant to reduction *in vitro* than was 791-(SPDP)-SS-TNB, the corresponding RTA<sub>30</sub> immunoconjugates (791-(SAMBA)-SS-RTA<sub>30</sub> and 791-(SPDP)-SS-RTA<sub>30</sub>) varied by only a factor of 10. Moreover, there was little difference between the relative stabilities of the SAMBA-linked and M2IT-linked conjugates (10.4-fold and 8.3-fold, respectively), whereas both the methyl-substituted SPDP conjugates (MSPDP and SMPT) appeared somewhat less stable. Clearly, adding a second methyl group immediately adjacent to the disulfide bond enhances the stability of model antibody-TNB compounds by more than 460-fold, whereas the corresponding antibody-RTA<sub>30</sub> immunoconjugates were much less affected (1.3-fold).

Similar trends were observed *in vivo*, where the M2IT-linked and SAMBA-linked conjugates exhibited comparable stabilities and their serum elimination profiles were essentially equivalent. Moreover, both conjugates were more stable and persisted longer than the corresponding conjugates made with 2IT and SPDP. Interestingly, the

<sup>3</sup> D. Fishwild and A. Kung, unpublished data.

<sup>4</sup> S.F. Carroll et al., unpublished data.



serum elimination curves for the M2IT- and SAMBA-linked immunoconjugates closely approached that of nonreducible thioether-linked conjugates,<sup>2</sup> and the improvements (relative to the unhindered linkers) were comparable to those reported for MSPDP (12) or SMPT (13, 15), as well as those reported for the dimethyl-substituted reagent sNHS-ATMBA (14). Thus, enhancing immunoconjugate disulfide bond stability beyond the level generated with M2IT would apparently provide little additional therapeutic benefit. Presumably, the differential magnitudes of stability noted with the antibody-RTA<sub>30</sub> conjugates reflect structural constraints imposed upon the linkages within protein-protein conjugates that are not present in the corresponding protein-TNB analogs.

Taken together, our results suggest that increasing the steric bulk of the X2IT substituent adjacent to the disulfide bond beyond that of a single methyl group offers little improvement in the *in vitro* and *in vivo* stability of protein-protein conjugates and that the stabilities of protein-protein conjugates (but not protein-TNB conjugates) to reduction *in vitro* are good indicators of stability *in vivo*. As a result of these evaluations, the M2IT crosslinker appears to possess many properties optimal for the preparation and therapeutic use of antibody-RTA immunoconjugates. Indeed, preliminary studies in animal models suggest that M2IT-linked immunoconjugates are more potent than conjugates prepared with SPDP.<sup>3</sup> Moreover, although the present studies were conducted with a single murine IgG2b monoclonal antibody, essentially equivalent results have been obtained with other murine (IgG1, IgG2a) and mouse/human chimeric antibodies and antibody fragments (25) as well as with other cytotoxins (26) and ribosome-inactivating proteins.<sup>4</sup>

It is noteworthy, however, that the therapeutic utility of M2IT (or the other X2ITs) is not limited to the preparation of protein-protein conjugates. For example, given the 6000-fold differences in stabilities noted with the antibody-TNB analogs, it should be possible to prepare protein-drug conjugates that exhibit a range of stabilities *in vivo*. Such conjugates may find use in the controlled, time-dependent release of active drug following systemic delivery or in the preparation of timed-release matrices for implantation.

#### ACKNOWLEDGMENT

We are grateful to Eddie Bautista, Charlotte Chang, Maria Fang, Bill Smith, and Will Leach for excellent assistance in the preparation and evaluation of conjugates and to Carroll Hess for assisting in manuscript preparation.

#### LITERATURE CITED

- (1) Ramakrishnan, S., Fryxell, D., Mohonraj, D., Olson, M., and Li, B.-Y. (1992) Cytotoxic conjugates containing translational inhibitory proteins. *Ann. Rev. Pharmacol. Toxicol.* 32, 579-621.
- (2) Vitetta, E. S., Thorpe, P. E., and Uhr, J. W. (1993) Immunotoxins: magic bullets or misguided missiles? *Immunol. Today* 14, 252-259.
- (3) Byers, V. S., Henslee, P. J., Kernan, N. A., Blazar, B. R., Gingrich, R., Phillips, G. L., LeMaistre, C. F., Gilliland, G., Antin, J. H., Martin, P., et al. (1990) Use of antipan T-lymphocyte ricin A chain immunotoxin in steroid-resistant graft-versus-host disease. *Blood* 75, 1426-1432.
- (4) Strand, V., Lipsky, P., Cannon, G., Calabrese, L., Wiesenhuber, C., Cohen, S., Olsen, N., Lee, M., Lorenz, T., Nelson, B., et al. (1993) Effects of administration of an anti-CD5 Plus immunoconjugate in rheumatoid arthritis. *Arthritis Rheum.* 36, 620-630.
- (5) Wacholtz, M. C., and Lipsky, P. E. (1992) Treatment of lupus nephritis with CD5 Plus, and immunoconjugate on an anti-CD5 monoclonal antibody and ricin A chain. *Arthritis Rheum.* 35, 837-838.
- (6) LeMaistre, C. F., Meneghetti, C., Rosenblum, M., Reuben, J., Parker, K., Shaw, J., Deisseroth, A., Woodsworth, T., and Parkinson, D. R. (1992) Phase I trial of an interleukin-2 (IL-2) fusion toxin (DAB486IL-2) in hematologic malignancies expressing the IL-2 receptor. *Blood* 79, 2547-2554.
- (7) Cobb, P. W., and LeMaistre, C. F. (1992) Therapeutic use of immunotoxins. *Sem. Hematol.* 29, suppl. 2, 6-13.
- (8) Pietersz, G. A., and McKenzie, I. F. C. (1992) Antibody conjugates for the treatment of cancer. *Immunol. Rev.* 129, 57-80.
- (9) Masuho, Y., Kishida, K., Saito, M., Umemoto, N., and Hara, T. (1982) Importance of the antigen-binding valency and the nature of the cross-linking bond in ricin A-chain conjugates with antibody. *J. Biochem.* 91, 1583-1591.
- (10) Worrell, N. R., Cumber, A. J., Parnell, G. D., Ross, W. C. J., and Forrester, J. A. (1986) Fate of an antibody-ricin A chain conjugate administered to normal rats. *Biochem. Pharmacol.* 35, 417-423.
- (11) Thorpe, P. E., Blakey, D. C., Brown, A. N. F., Knowles, P. P., Knyba, R. B., Wallace, P. M., Watson, G. J., and Wawrzynczak, E. J. (1987) Comparison of two anti-Thy 1.1-abrin A chain immunotoxins prepared with different cross-linking agent: Antitumor effects, *in vivo* fate, and tumor cell mutants. *J. Natl. Cancer Inst.* 79, 1011-1111.
- (12) Worrell, N. R., Cumber, A. J., Parnell, G. D., Mirza, A., Forrester, J. A., and Ross, W. C. J. (1986) Effect of linkage variation on pharmacokinetics of ricin A chain-antibody conjugates in normal rats. *Anti-Cancer Drug Design* 1, 179-188.
- (13) Thorpe, P. E., Wallace, P. M., Knowles, P. P., Relf, M. G., Brown, A. N. F., Watson, G. J., Knyba, R. E., Wawrzynczak, E. J., and Blakey, D. C. (1987) New coupling agents for the synthesis of immunotoxins containing a hindered disulfide bond with improved stability *in vivo*. *Cancer Res.* 47, 5924-5931.
- (14) Greenfield, L., Bloch, W., and Moreland, M. (1990) Thiol-containing cross-linking agent with enhanced steric hindrance. *Bioconjugate Chem.* 1, 400-410.
- (15) Thorpe, P. E., Wallace, P. M., Knowles, P. P., Relf, M. G., Brown, A. N. F., Watson, G. J., Blakey, D. C., Newell, D. R. (1988) Improved antitumor effects of immunotoxins prepared with deglycosylated ricin A-chain and hindered disulfide linkages. *Cancer Res.* 48, 6396-6403.
- (16) Goff, D. A., and Carroll, S. F. (1990) Substituted 2-Iminothiolanes: Reagents for the preparation of disulfide cross-linked conjugates with increased stability. *Bioconjugate Chem.* 1, 381-386.
- (17) Schramm, H. J., and Dülffer, T. (1977) The use of 2-Iminothiolane as a protein crosslinking reagent. *Hoppe-Syler's Z. Physiol. Chem.* 358, 137-139.
- (18) Jocelyn, P. C. (1987) Spectrophotometric assay of thiols. *Methods Enzymol.* 143, 44-67.
- (19) Riddles, P. W., Blakeley, R. L., and Zerner, B. (1979) Ellman's reagent: 5,5'-dithiobis(2-nitrobenzoic acid)—a re-examination. *Anal. Biochem.* 94, 75-81.
- (20) Trown, P. W., Reardan, D. T., Carroll, S. F., Stoudemire, J. B., and Kawahata, R. T. (1991) Improved pharmacokinetics and tumor localization of immunotoxins constructed with the Mr 30,000 form of ricin A chain. *Cancer Res.* 51, 4219-4225.
- (21) Carlsson, J., Drevin, H., and Axen, R. (1978) Protein thiolation and reversible protein-protein conjugation: N-succinimidyl-3-(2-pyridyldithio)propionate, a new heterobifunctional reagent. *Biochem. J.* 173, 723-737.
- (22) Laemmli, U. K. (1970) Cleavage of structural proteins during the assembly of the bacteriophage T4. *Nature* 227, 680-685.
- (23) Wawrzynczak, E. J., Cumber, A. J., Henry, R. V., May, J., Newell, D. R., Parnell, G. D., Worrell, N. R., and Forrester, J. A. (1990) Pharmacokinetics in the rat of a panel of immunotoxins made with abrin A chain, ricin A chain, gelonin, and momordin. *Cancer Res.* 50, 7519-7526.
- (24) Fraker, P. J., and Speck, J. D. (1978) Protein and cell membrane iodinations with a sparingly soluble chloroamide, 1,2,4,6-tetrachloro-3a,6a-diphenylglycouril. *Biochem. Biophys. Res. Commun.* 80, 849-857.

- (25) Better, M., Bernhard, S. L., Lei, S.-P., Fishwild, D. M., Lane, J. A., Carroll, S. F., and Horwitz, A. H. (1993) Potent anti-CD5 ricin A chain immunoconjugates from bacterially produced Fab' and F(ab')<sub>2</sub>. *Proc. Natl. Acad. Sci. U.S.A.* 90, 457-461.
- (26) Better, M., Bernhard, S. L., Lei, S.-P., Fishwild, D. M., and Carroll, S. F. (1992) Activity of recombinant mitogillin and mitogillin immunoconjugates. *J. Biol. Chem.* 267, 16712-16718.

# Fluorinated Proteins as Potential $^{19}\text{F}$ Magnetic Resonance Imaging and Spectroscopy Agents<sup>†</sup>

Vimal D. Mehta,\* Padmakar V. Kulkarni, Ralph P. Mason, Anca Constantinescu, and Peter P. Antich

Department of Radiology, University of Texas Southwestern Medical Center, Dallas, Texas 75235. Received December 17, 1993\*

Fluorinated proteins have been synthesized and characterized as potential *in vivo*  $^{19}\text{F}$  magnetic resonance imaging (MRI) and spectroscopy (MRS) agents. Proteins labeled with fluorine include bovine serum albumin,  $\gamma$ -globulin, and purified immunoglobulin (IgG). The amino groups in proteins were selectively trifluoroacetylated using *S*-ethyl trifluorothioacetate to synthesize fluorinated proteins (TFA-protein; 1-3). In another approach, trifluoroacetamidossuccinic anhydride has been used to prepare corresponding fluorinated derivatives of proteins (TFASA-protein; 4-6). The fluorinated proteins have been purified by exhaustive dialysis and isolated in good yields (55-76%). The fluorinated proteins exhibit useful NMR characteristics and the biocompatibility for *in vivo* studies. The initial investigations demonstrate the potential of these new fluorinated proteins as *in vivo* MRI/MRS probes.

## INTRODUCTION

Macromolecular carrier systems have been developed in an attempt to optimize the delivery of antineoplastic agents to tumors (1). Indeed, conjugation of antineoplastic drugs to carrier polymers and proteins may improve the biodistribution and therapeutic efficacy of drugs (2).

Macromolecules such as albumin, globulins, and synthetic polymers accumulate in tumor tissue because the vascular network shows both enhanced permeability of the neovasculature and lack of a lymphatic recovery system (3,4). Radionuclides have been attached to serum albumin in an effort to detect micrometastases using scintigraphy (5). In addition,  $^1\text{H}$  NMR paramagnetic tissue contrast agents have been conjugated to albumin with considerably enhanced vascular retention and improved contrast (6). Polyclonal human nonspecific IgG has been used as a carrier molecule ( $^{111}\text{In}$ -labeled) in clinical trials to detect areas of inflammation (7). Additionally, human polyclonal IgG attached to monodisperse iron oxides (MION) has been used to enhance MRI of inflammation (8). Kilbourn et al. have labeled proteins (HSA and IgA) with  $^{18}\text{F}$  and suggested that these approaches could be used for  $^{19}\text{F}$  labeling of proteins (9).

$^{19}\text{F}$  NMR offers a unique quantitative means of imaging infused agents, as there is essentially no  $^{19}\text{F}$  background signal in tissue. We have been developing both novel fluorine-labeled molecular probes (10,11) and enhanced MR techniques to exploit the exceptional characteristics of fluorine (12,13). Small fluorinated molecules, e.g., trifluoroacetylglucosamine, are subject to very rapid renal clearance (10). At the other extreme of molecular size, perfluorocarbon emulsions (nanoparticles) are subject to extensive uptake by the liver and spleen and exhibit excessive tissue retention (14). The development of fluorine-labeled probes with prolonged retention in the vascular compartment should facilitate  $^{19}\text{F}$  NMR investigations of lesions like tumor, ischemia, or inflammation. In addition, the fluorine-labeled proteins may permit quantification and characterization of the catabolic processes of proteins (15) in tissues *in vivo* that could not be achieved with conventional radiolabels.

The purpose of this study was to develop molecular probes with appropriate NMR characteristics and the biocompatibility for *in vivo* applications using magnetic resonance imaging (MRI) and spectroscopy (MRS). Albumin and the globulins have been used as model proteins for labeling with fluorine ( $^{19}\text{F}$ ). The fluorine-labeling procedures and  $^{19}\text{F}$  NMR characteristics of fluorinated conjugates are reported together with preliminary examinations of their biological behavior, such as blood clearance and *in vivo* spectroscopy.

## EXPERIMENTAL PROCEDURES

**Reagents and Materials.** Bovine serum albumin (BSA),  $\gamma$ -globulin, and purified immunoglobulin (IgG) were purchased from Sigma Chemical Co. *S*-Ethyl trifluorothioacetate, sodium trifluoroacetate ( $\text{CF}_3\text{COONa}$ ), sodium fluoride ( $\text{NaF}$ ), and sodium bicarbonate ( $\text{NaHCO}_3$ ) were purchased from Aldrich Chemical Co. Trifluoroacetamidossuccinic anhydride was synthesized by a literature-reported procedure (16) and stored under dry conditions. Spectra Por dialysis tubings (Fisher Scientific) with molecular weight cutoff (MWCO) 6-8 K and 12-14 K were used. All other reagents and solvents were reagent grade unless otherwise specified. Magnevist (Berlex Laboratories Inc., Wayne, NJ), a 0.5 M solution of *N*-methylglucamine salt of the gadolinium complex of diethylenetriamine pentaacetic acid (Gd-DTPA), was used as the paramagnetic relaxation agent.

**Equipment and Physical Measurements.**  $^{19}\text{F}$  NMR spectroscopy was performed using a 7 T (300 MHz,  $^1\text{H}$ ) Oxford magnet under control of a Techmag console. Imaging ( $^{19}\text{F}$  and  $^1\text{H}$ ) experiments were performed using an Omega CSI 4.7 T system with actively shielded gradients (Acustar, Bruker Instruments, Inc.). Infrared spectra (IR) were recorded in KBr on a Mattson Galaxy (2000) FT-IR spectrometer. Gel permeation chromatography (GPC) was carried out using a Waters HPLC system.

**Fluorine Labeling Procedures. Reaction of *S*-Ethyl Trifluorothioacetate with Proteins.** The appropriate protein (BSA,  $\gamma$ -globulin, or IgG) (50-100 mg) was dissolved in 0.1 M  $\text{NaHCO}_3$  (40-50 mL). *S*-Ethyl trifluorothioacetate (SETFA) (17) was added (50 molar excess) dropwise to the protein solution at 4 °C while a pH  $\sim$ 8.0 was maintained (by adding  $\text{NaHCO}_3$  solution).

\* To whom correspondence should be addressed.

<sup>†</sup> Presented at the 204th ACS National Meeting (Division of Medicinal Chemistry), Washington, D.C., Aug 23-28, 1992.

\* Abstract published in *Advance ACS Abstracts*, April 1, 1994.

The reaction was allowed to proceed overnight at room temperature. The reaction mixture was extensively dialyzed using MWCO 6-8-K and 12-14-K dialysis tubing (sequentially) against water to remove low molecular weight materials (excess of reagent) for not less than 72 h. The solution was lyophilized to yield trifluoroacetylated protein derivatives (TFA-protein; 1 and 3). Reaction of  $\gamma$ -globulin with SETFA resulted in water-insoluble product 2, which was isolated by centrifugation. During reaction and purification the temperature was maintained at 4 °C for IgG.

**Reaction of Trifluoroacetamidossuccinic Anhydride with Proteins.** The appropriate protein (BSA,  $\gamma$ -globulin, or IgG) (50–100 mg) was dissolved in 0.1 M NaHCO<sub>3</sub> (40–50 mL). Trifluoroacetamidossuccinic anhydride (16) was added (50 molar excess) in small lots to the protein solution at 4 °C while a pH  $\sim$ 8.0 was maintained (by adding NaHCO<sub>3</sub> solution). The reaction was allowed to proceed overnight at room temperature. The conjugate was extensively dialyzed using MWCO 6-8-K and 12-14-K dialysis tubing (sequentially) against water to remove low molecular weight materials (excess of reagent) for not less than 96 h. The solution was lyophilized to yield trifluorosuccinylated protein derivatives (TFASA-protein; 4–6). During reaction and purification the temperature was maintained at 4 °C for IgG.

**Gel Permeation Chromatography.** Gel permeation chromatography (GPC) was performed using Waters ultrahydrogel columns at 25 °C. Phosphate buffer (2M) was used for elution at a flow rate of 0.8 mL/min with a Waters 484 (UV/vis) and 410 differential refractometer.

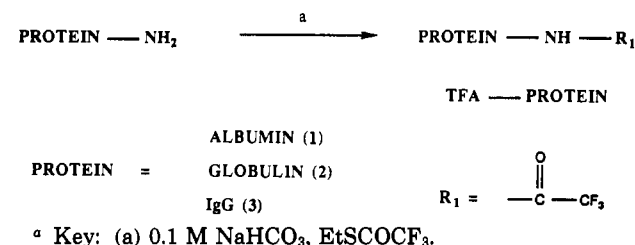
**<sup>19</sup>F NMR Spectroscopy and Sensitivity Measurements.** Typically, fluorinated protein (viz. 1;  $\sim$ 10 mg;  $\sim$ 0.28 M) was dissolved in water or fresh heparinized blood ( $\sim$ 500  $\mu$ L). The pH of the protein solution in water was adjusted to neutral (with NaOH solution) for NMR experiments. Sodium trifluoroacetate (CF<sub>3</sub>COONa; 0.46 M) and sodium fluoride (NaF; 0.1 M) in water were used as chemical shift reference standards. <sup>19</sup>F NMR detection sensitivity was estimated using NaF solution as an internal standard with relative sensitivity per mg material. *T*<sub>1</sub> and *T*<sub>2</sub> were estimated using standard pulse burst saturation recovery and Hahn spin-echo methods.

**In Vivo Evaluations. Blood Clearance Kinetics.** TFA-albumin (1, 11.3 mg) was injected iv in a group of six Balb/C mice. Blood samples were drawn from pairs of mice at 5 min, 2 h, 5 h, 48 h or 1 h, 4 h, 72 h or 2 h and 24 h to minimize blood volume loss for any given mouse. The concentration of fluorine in blood samples was estimated with <sup>19</sup>F NMR spectroscopy by comparison with an external standard of NaF.

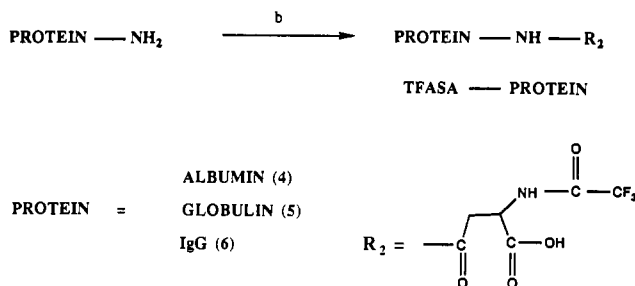
**In Vivo Spectroscopy.** TFA-albumin (1) was administered (iv) in two consecutive doses of 50 mg 2 h apart to a tumor-bearing mouse (Meth-A). The mouse was anesthetized [ketamine (100 mg/kg) + xylazine (5 mg/kg) (IM)], and a surface coil (1.8-cm diameter) was placed against the tumor. Spectra were acquired at 282.3 MHz using an 80- $\mu$ s pulse with 400 scans in 10 min and spectral width of 12 000 Hz. A 20-Hz exponential line broadening was applied prior to Fourier transformation.

**Phantom Imaging.** The phantom comprised three glass vials containing 40 mg of TFA-albumin (1) in 1 mL of water each. In addition, two of the vials had, respectively,  $\sim$ 5 and 10 mM Gd-DTPA. The phantom was placed in a 3-cm single turn solenoid <sup>1</sup>H/<sup>19</sup>F tunable coil. <sup>1</sup>H images were obtained at 200 MHz using TR = 250 ms and TE = 8 ms with two acquisitions at each of 64 increments for a total imaging time of 32 s. <sup>19</sup>F images

### Scheme 1



### Scheme 2



**Table 1. Characteristics of Fluorinated Proteins 1–6**

fluorinated proteins synthesized <sup>a</sup>	<sup>19</sup> F NMR sensitivity <sup>b</sup>	IR (KBr), cm <sup>-1</sup>	yield, <sup>c</sup> %
TFA-albumin (1)	10 mg/mg NaF	1658 (C=O), 1535 (NH)	76
TFA-IgG (3)	15 mg/mg NaF	1641 (C=O), 1529 (NH)	55
TFASA-albumin (4)	20 mg/mg NaF	1656 (C=O), 1539 (NH)	73
TFASA-globulin (5)	28 mg/mg NaF	1647 (C=O), 1535 (NH)	64
TFASA-IgG (6)	23 mg/mg NaF	1643 (C=O), 1531 (NH)	60

<sup>a</sup> All fluorinated proteins except 2 were water soluble and had a <sup>19</sup>F chemical shift coincident with CF<sub>3</sub>CO<sub>2</sub>Na and  $\sim$ 44.10 ppm downfield from NaF at neutral pH ( $\sim$ 7.0). <sup>b</sup> <sup>19</sup>F MR sensitivities obtained under fully relaxed conditions with respect to NaF (internal standard) at neutral pH ( $\pm$ 15–20% error). <sup>c</sup> Based on amount (mg) of protein recovered.

were obtained with TR = 150 ms and TE = 8 ms using a driven equilibrium sequence to enhance data collection efficiency (18) with 256 acquisitions at each of 32 gradient increments for a total imaging time of 20 min. Images were processed with sin<sup>2</sup> apodization prior to Fourier transformation.

## RESULTS AND DISCUSSION

We have used proteins which are readily available and occur naturally at high concentration in the body. In addition, bovine serum albumin and immunoglobulins were cost-effective model proteins for the development and standardization of fluorine-labeling procedures. We adopted two approaches to the fluorination of these proteins. In the first approach, the amino groups in the proteins were selectively trifluoroacetylated using *S*-ethyl trifluorothioacetate (SETFA) (TFA-protein; 1–3) (Scheme 1).  $\gamma$ -Globulin on reaction with SETFA produced a water-insoluble product (2). In an alternative approach we used trifluoroacetamidossuccinic anhydride (TFASAN) to prepare corresponding fluorinated derivatives of proteins (TFASA-protein; 4–6) (Scheme 2). The first approach, trifluoroacetylation of proteins, yielded products with higher fluorine labeling (i.e., proteins with higher <sup>19</sup>F detection sensitivity) as compared to labeling with trifluoroacetamidossuccinic anhydride (Table 1). This may be due to the competing hydrolysis reaction of anhydride with trifluorosuccinylation of proteins in aqueous solution. The additional free carboxylic acid groups introduced in

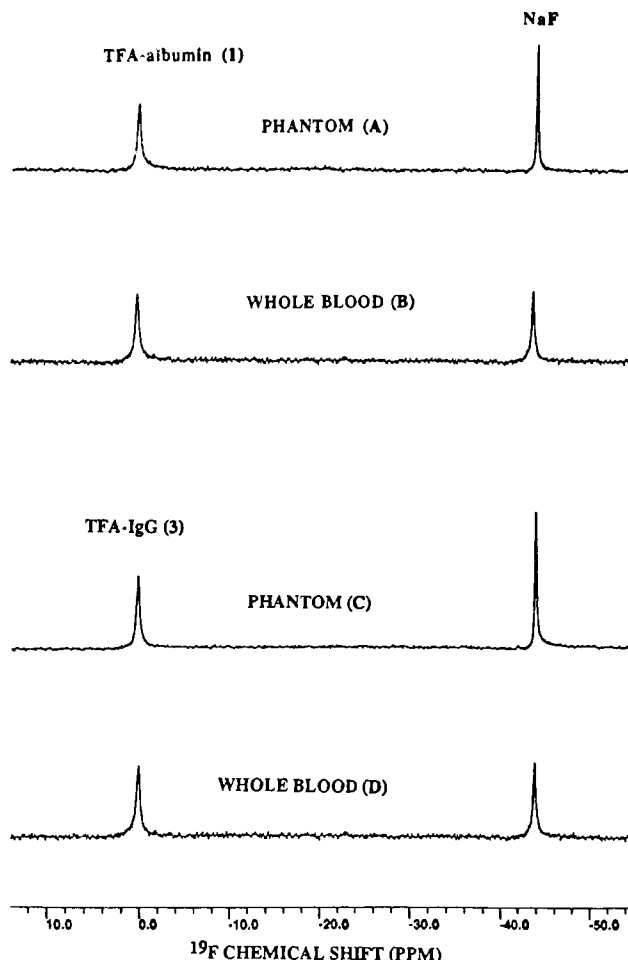
fluorinated proteins 4–6 using TFASAN may alter the charge on proteins and favorably enhance the water solubility, as is evident from  $\gamma$ -globulin derivative 5, which was obtained as a water-soluble product. For *in vivo* applications, it is desirable to minimize the injection volume. Usually, labeling of proteins with fluorinating agents involves the modification of amino acid side chain polar functional groups (e.g.,  $\text{NH}_2$  groups), which in turn results in reducing hydrophilicity of derivatized products. The introduction of polar groups simultaneously with fluorine labeling will maintain or even enhance the solubility of derivatized products.

The fluorinated proteins 1–6 were purified by exhaustive dialysis and isolated in good yields (55–76%; Table 1). A control experiment showed that dialysis successfully removed the reaction byproduct, trifluoroacetamidocacetic acid (TFASA), from proteins. A sample of TFASAN was first hydrolyzed to TFASA by adding to 0.1 M  $\text{NaHCO}_3$ . The TFASA solution was dialyzed independently and also after adding to albumin solution. Lyophilization of TFASA dialysate yielded no visible product. The dialysis solution containing albumin showed no  $^{19}\text{F}$  signal in the product obtained after lyophilization.

To evaluate the product purity and integrity of the proteins following the reaction, gel permeation chromatography (GPC) was performed. Analyses of fluorinated proteins showed a smooth GPC profile without formation of additional low or high molecular weight products. The IR spectra of TFA-protein 1–3 and TFASA-protein 4–6 showed two enhanced bands at 1641–1658 and 1529–1535  $\text{cm}^{-1}$  and 1643–1656 and 1531–1539  $\text{cm}^{-1}$ , respectively, compared to native proteins besides a broad band (2900–3500  $\text{cm}^{-1}$ ). The fluorinated proteins 1 to 6 exhibit a single sharp  $^{19}\text{F}$  NMR signal as demonstrated in Figure 1 for TFA-albumin (1) and TFA-IgG (3) with a typical line width of  $\sim 80$ –100 Hz. The chemical shifts of proteins 1–6 are essentially coincident with  $\text{CF}_3\text{COONa}$  and  $\sim 44.10$  ppm downfield from NaF.  $^{19}\text{F}$  spin-lattice relaxation time  $T_1 \approx 0.75$ –1.0 s and spin-spin relaxation time  $T_2 \approx 10$ –25 ms were obtained at 7 T for derivatized proteins 1–6 (19). The line width as well as relaxation parameters of derivatized proteins were significantly different from small molecular weight fluorinated compounds (e.g.,  $\text{CF}_3\text{COONa}$ , line width  $\sim 20$  Hz,  $T_1 \sim 2.9$  s,  $T_2 \sim 760$  ms) (19). The conjugation of the fluorinated moiety to macromolecules (e.g., proteins) results in a reduction of the relaxation times  $T_1$  and  $T_2$ . Reduced  $^{19}\text{F}$   $T_1$  is favorable for imaging experiments. It permits rapid data acquisition and thus shortens imaging time without sacrificing resolution. The NMR characteristics exhibited by derivatized proteins together with the other methods of characterization described above confirm the purity and identity of fluorinated proteins.

The observation of a single sharp  $^{19}\text{F}$  resonance for fluorine-labeled proteins 1–6 contrasts previous reports of protein labeling with fluorine (15), and facilitates imaging without chemical shift artifacts. We have determined the relative  $^{19}\text{F}$  NMR sensitivity of the fluorinated proteins compared to sodium fluoride (NaF). In other words, the relative sensitivity is defined as the number of mg of fluorinated protein needed to give the same intensity of  $^{19}\text{F}$  NMR signal as that obtained with 1 mg of NaF (Table 1). The NMR sensitivity provides an estimate for the relative efficiency of the labeling methods and *in vivo* NMR detectability of derivatized proteins.

The  $^{19}\text{F}$  signals from fluorinated proteins were readily observed when added to whole blood as shown for TFA-albumin (1) and TFA-IgG (3) in Figure 1B,D. They exhibit



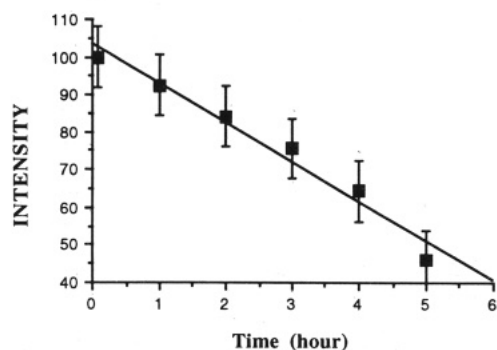
**Figure 1.** 282.3-MHz  $^{19}\text{F}$  NMR spectra of TFA-albumin (1) or TFA-IgG (3) and NaF. Fluorinated proteins 1 and 3 are shown, respectively, in water (A and C) and in whole rabbit blood (B and D). 1 and 3 both have a single sharp  $^{19}\text{F}$  signal, and there is no line broadening or change in chemical shift in blood.

a single sharp resonance without any substantial line broadening, change in signal intensity, or chemical shift in blood. TFA-albumin (1) was also detectable as a single resonance in blood drawn from an animal following iv infusion and, indeed, was detectable in excised tissues (liver and tumor) 72 h after administration (48 mg) to a tumor-bearing mouse.

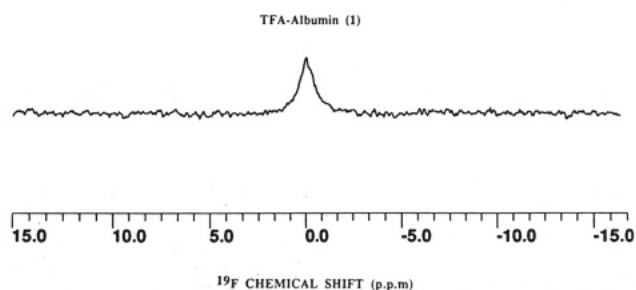
The blood clearance kinetics of TFA-albumin (1) in mice were investigated for a period of 6 h following iv injection (11.3 mg). Clearance of the agent from the blood as measured by the decrease in the intensity of  $^{19}\text{F}$  signal is shown in Figure 2. The signal to noise ratio of  $^{19}\text{F}$  signal ranged from  $\sim 11$  to 6 for blood samples at 5 min postinjection to 5 h. TFA-albumin (1) showed prolonged retention in the blood pool compared to monomeric molecules (10) and the half-life (4–5 h) is similar to Gd-DTPA-labeled albumin (20) and  $^{18}\text{F}$ -labeled human serum albumin (9). Clearance of TFA-albumin (1) appeared linear contrasting perfluorocarbon emulsions, which follow a nonlinear kinetic (21). Prolonged retention of TFA-albumin (1) in the intravascular space suggests enhanced probability of leakage of these agents into the tumor interstitium.

Although no formal toxicity studies have been performed, we have injected 40–50 mg of TFA-albumin (1) iv in tumor-bearing mice (Meth-A;  $n = 3$ ) without apparent acute toxicity. Similarly, in a rat there was no toxicity for 72 h following administration of 300 mg by combination of iv and ip. The TFA-albumin (1) has significantly lower

## BLOOD CLEARANCE KINETICS OF TFA-ALBUMIN (1)



**Figure 2.** Blood clearance profile of TFA-albumin (1) in Balb/C mice from 5 min to 5 h following iv injection (11.3 mg).



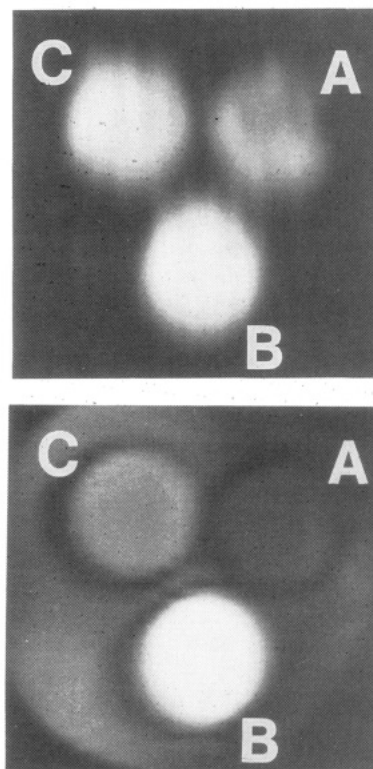
**Figure 3.**  $^{19}\text{F}$  MR spectrum of a Meth-A tumor obtained using a surface coil following administration of two consecutive doses of 50 mg each of TFA-albumin (1) iv 2 h apart. Spectra were acquired at 282.3 MHz using an 80- $\mu\text{s}$  pulse with 400 scans in 10 min and spectral width of 12 000 Hz. A 20-Hz exponential line broadening was applied prior to Fourier transformation.

toxicity than observed for fluorinated polylysines (10) and could be used at higher doses to provide the  $^{19}\text{F}$  NMR detection sensitivity for *in vivo* studies.

**In Vivo Spectroscopy.** Preliminary experiments using localized surface-coil spectroscopy showed  $^{19}\text{F}$  NMR signal from TFA-albumin (1) in the Meth-A tumor in a mouse following successive iv infusions (Figure 3). The concentration of 1 in the tumor remained constant over a period of  $\sim 2$  h as studied at 10-min intervals. This indicates the feasibility of *in vivo* investigations with fluorine-labeled proteins.

**Phantom Imaging.** We have determined the  $^{19}\text{F}$  NMR spin-lattice relaxation time  $T_1 \sim 620$  ms and spin-spin relaxation time  $T_2 \sim 70$  ms for TFA-albumin (1) at 4.7 T (22  $^\circ\text{C}$ ) to assess their imaging potential. Here, we show  $^{19}\text{F}$  and corresponding  $^1\text{H}$  MR images of a phantom of TFA-albumin (1) (Figure 4 (top and bottom)).  $^{19}\text{F}$  images were obtained with a S/N 10–20 using driven equilibrium. We have previously noted that addition of Gd-DTPA substantially reduces both  $T_1$  and  $T_2$  of the TFA-albumin (19). Use of driven equilibrium substantially enhances signal from the vial with longer  $T_1$  (no Gd-DTPA) but had relatively little effect on the two other vials (with Gd-DTPA). We note that reducing the  $T_1$  of TFA-albumin (1) with a paramagnetic contrast agent can have more significant impact on S/N than using driven equilibrium. However, excessive concentration of relaxation agent significantly shortens  $T_2$  (C) in Figure 4 (top and bottom), thereby reducing the benefits of the increased signal strength (22) caused by shortened  $T_1$  (B).

TFA-albumin (1) has been evaluated as a prototype macromolecular agent, and although it may not prove to be the optimal agent, it does provide an opportunity to investigate the applications of an intravascular  $^{19}\text{F}$  agent



**Figure 4.** (Top) driven equilibrium fluorine ( $^{19}\text{F}$ ) and (bottom) corresponding proton ( $^1\text{H}$ ) images of a phantom containing 40 mg of TFA-albumin (1) in 1 mL of water (A). Magnevist (Gd-DTPA) 20  $\mu\text{L}$  ( $\sim 5$  mM) and 40  $\mu\text{L}$  ( $\sim 10$  mM) has been added to B and C.  $^{19}\text{F}$  images were obtained with TR = 150 ms and TE = 8 ms using a driven equilibrium sequence to enhance data collection efficiency (18) with 256 acquisitions at each of 32 gradient increments for a total imaging time of 20 min. Corresponding  $^1\text{H}$  images were obtained at 200 MHz using TR = 250 ms, TE = 8 ms, and two acquisitions at each of 64 increments for total imaging time of 32 s. Images were processed with  $\sin^2$  apodization prior to Fourier transformation.

for MRI. Recently, we successfully conjugated  $^{19}\text{F}$  pH sensor to carrier polymers (23) without loss in pH sensing capability, providing the opportunity for tissue targeting of  $^{19}\text{F}$  physiological markers. The optimal macromolecular  $^{19}\text{F}$  agent must have appropriate NMR characteristics and prove to be safe and effective. The fluorinated macromolecular agents will be useful in the evaluation of tissue perfusion and for the diagnosis of ischemic and neoplastic disorders.

In summary, proteins have been successfully derivatized providing fluorine labeled biocompatible molecular probes with useful NMR characteristics. Our initial results demonstrate the potential of these new fluorinated proteins as MRI/MRS probes. However, more detailed studies with different proteins and fluorine labels involving biodistribution (plasma clearance and organ distribution), toxicity, metabolic fate, and immunologic consequences are necessary to establish their potential as *in vivo* MRI/MRS probes.

## ACKNOWLEDGMENT

This work was supported by Dallas Biomedical Corporation/Hartford Foundation, and MR studies were conducted at the Mary Nell & Ralph B. Rogers NMR center. We are grateful to Dr. H. Sinn (DKFZ, Heidelberg) for valuable discussions and thank Ms. P. Lea for help in the NMR experiments.



## LITERATURE CITED

- (1) Friend, D. R., and Pangburn, S. (1987) Site-specific drug delivery. *Med. Res. Rev.* 7, 53-106.
- (2) Maeda, H., Seymour, L. W., and Miyamoto, Y. (1992) Conjugates of anticancer agents and polymers: advantages of macromolecular therapeutics *in vivo*. *Bioconjugate Chem.* 3(5), 351-362.
- (3) Dvorak, H. F., Nagy, J. A., Dvorak J. T., and Dvorak, A. M. (1988) Identification and characterization of the blood vessels of solid tumors that are leaky to circulating macromolecules. *Am. J. Pathol.* 133, 95-109.
- (4) Jain, R. K. (1987) Transport of molecules across tumor vasculature. *Cancer Metastasis Rev.* 6, 559-593.
- (5) Sinn, H., Schrenk, H. H., Friedrich, E. A., Schilling, U., and Maier-Borst, W. (1990) Design compounds having an enhanced tumour uptake, using serum albumin as a carrier. Part I. *Nucl. Med. Biol.* 17(8), 819-827.
- (6) Ogan, M. D., Schmiedl, U., Moseley, M. E., Grodd, W., Paaanen, H., and Brasch, R. C. (1987) Albumin labeled with Gd-DTPA an intravascular contrast-enhancing agent for magnetic resonance blood imaging: preparation and characterization. *Invest. Radiol.* 22, 665-671.
- (7) Rubin, R. H., Fishman, A. J., and Callahan, R. J. (1989) <sup>111</sup>In-labelled nonspecific immunoglobulin scanning in the detection of focal infection. *N. Engl. J. Med.* 321, 935-940.
- (8) Weissleder, R., Lee, A. S., and Fischman, A. J. (1991) MR antibody imaging: polyclonal human IgG labelled with polymeric iron oxide. *Radiol.* 181, 245-249.
- (9) Kilbourn, M. R., Dence, C. S., Welch, M. J., and Mathias, C. J. (1987) Fluorine-18 labeling of proteins. *J. Nucl. Med.* 28(4), 462-470.
- (10) Mehta, V. D., Kulkarni, P. V., Rajur, S. B., Mason, R. P., Babcock, E. E., Constantinescu, A., and Antich P. P. (1992) Novel molecular probes for <sup>19</sup>F magnetic resonance imaging: synthesis & characterization of fluorinated polymers. *Biomed. Chem. Lett.* 2(6), 527-532.
- (11) Mehta, V. D., Kulkarni, P. V., Mason, R. P., and Antich, P. P. (1993) Fluorinated macromolecular probes for non-invasive assessment of pH by magnetic resonance spectroscopy. *Biomed. Chem. Lett.* 3(2), 187-192.
- (12) Mason, R. P., Bansal N., Babcock, E. E., Nunnally, R. L., and Antich, P. P. (1990) A novel editing technique for <sup>19</sup>F MRI: molecule-specific imaging. *Magn. Reson. Imaging* 8, 729-736.
- (13) Barker, B., Mason R. P., and Peshock, R. M. (1993) Echo planar imaging of perfluorocarbons. *Magn. Reson. Imaging* 11, 1165-1173.
- (14) Lutz, J., and Metzenauer, P. (1980) Effects of potential blood substituents on rat liver and spleen. *Pflugers Arch.* 387, 175-181.
- (15) Daugherty, A., Becker, N. N., Scherrer, L. A., Sobel, B. E., Ackerman, J. J. H., Baynes, J. W., and Thorpe, S. R. (1989) Non-invasive detection of protein metabolism *in vivo* by nmr spectroscopy. *Biochem. J.* 264, 829-835.
- (16) Lapidus, M., and Sweeney, M. (1973) L-4-Cyano-3-(2, 2, 2-trifluoroacetamido)succinallilic acid and related synthetic sweetening agents. *J. Med. Chem.* 16, 163-166.
- (17) Wolfrom, M. L., and Conigliaro, P. J. (1969) Trifluoroacetyl as an N-protective group in the synthesis of purine nucleosides of 2-amino-2-deoxy saccharides. *Carbohydr. Res.* 11, 63-76.
- (18) van Uijen, C. M. J., and Den Boef, J. H. (1984) Driven-equilibrium radiofrequency pulses in nmr imaging. *Magn. Reson. Med.* 1, 502-507.
- (19) Mehta, V. D., Mason, R. P., Kulkarni, P. V., Lea, P., Constantinescu, A., and Antich, P. P. (1994) <sup>19</sup>F MR characterization of fluorinated proteins and relaxation rate enhancement with Gd-DTPA for faster imaging. *Proceedings of the International Symposium on Chemists View of Imaging Centers* (A. M. Emran, Ed.) Plenum Press, New York, accepted for publication.
- (20) Schmiedl, U., Moseley, M. E., Ogan, M. D., Chew, W. M., and Brasch, R. C. (1987) Comparison of initial biodistribution patterns of Gd-DTPA and albumin-(Gd-DTPA) using rapid spin-echo imaging. *J. Comput. Assist. Tomogr.* 11, 306-13.
- (21) Malet-Martino, M. C., Betbeder, D., Lattes, A., Lopez, A., Martino, R., Francois, G., and Cros S. (1984) Fluosol 43 intravascular persistence in mice measured by <sup>19</sup>F NMR. *J. Pharm. Pharmacol.* 36, 556-559.
- (22) Ratner, A. V., Quay, S., Muller, B. B., Simpson, R., Hurd, R., and Young, S. W. (1989) <sup>19</sup>F relaxation rate enhancement and frequency shift with Gd-DTPA. *Invest. Radiol.* 24, 224-26.
- (23) Mehta, V. D., Aravind, S., Kulkarni, P. V., Mason, R. P., and Antich, P. P. (1993) Fluorinated macromolecular probes as biosensors for non-invasive assessment of pH with magnetic resonance spectroscopy. *J. Nucl. Med.* 34(5), 124.

# Synthesis and Characterization of Monoclonal Antibody- $\beta$ -Lactamase Conjugates

Håkan P. Svensson,\* Philip M. Wallace, and Peter D. Senter

Bristol-Myers Squibb Pharmaceutical Research Institute, 3005 First Avenue, Seattle, Washington 98121. Received December 17, 1993\*

$\beta$ -Lactamase from *Enterobacter cloacae* ( $\beta$ L) was conjugated to the Fab'<sub>2</sub> fragment of the monoclonal antibody L6 through a thioether linkage. Although L6-Fab'<sub>2</sub>- $\beta$ L was capable of activating the antitumor prodrug, 7-(phenylacetamido)cephalosporin mustard, it was impaired in its ability to bind to antigens on the H2981 human lung adenocarcinoma cell line. As a result, studies were undertaken to prepare conjugates with preserved binding activities. L6-Fab'- $\beta$ L and a dimeric conjugate consisting of two individual L6-Fab' units linked to a single  $\beta$ L molecule (dimeric L6- $\beta$ L) were prepared by linking L6-Fab'-SH to maleimide-substituted  $\beta$ L. Analysis of these conjugates by SDS-PAGE indicated that the linkage involved heavy-chain thiol groups on L6 that are most likely in the hinge region and are therefore removed from the antigen binding site of the antibody. Cell binding studies revealed that the monovalent conjugate L6-Fab'- $\beta$ L bound as well as L6-Fab'. Dimeric L6- $\beta$ L displayed slightly less binding than L6-Fab'<sub>2</sub>, but bound substantially better than L6-Fab'<sub>2</sub>- $\beta$ L. Lower concentrations of dimeric L6- $\beta$ L compared to L6-Fab'<sub>2</sub>- $\beta$ L were required to convert the prodrug 7-(phenylacetamido)-cephalosporin mustard into the cytotoxic drug phenylenediamine mustard. Localization studies were performed in nude mice with H2981 subcutaneous tumor xenografts. At 96 h post conjugate treatment, there was no significant difference in tumor concentration between L6-Fab'<sub>2</sub>- $\beta$ L and dimeric L6- $\beta$ L. In contrast, the blood and normal tissue levels of dimeric L6- $\beta$ L were lower than L6-Fab'<sub>2</sub>- $\beta$ L, resulting in improved tumor to blood and tumor to normal tissue ratios. Thus, the conjugation methodology described here may be of use for targeting strategies in which high tumor to nontumor conjugate ratios are required in order to minimize nonspecific toxicity.

## INTRODUCTION

The efficacy of monoclonal antibody (mAb<sup>1</sup>) based strategies for the treatment and detection of cancer is often dependent on the ability of the mAb to localize in tumor masses and to achieve high tumor to non-tumor ratios (1). Many studies have demonstrated that valency, avidity, and molecular weight (2-4) can play important roles in mAb in vivo distribution. Consequently, a great deal of research has been directed toward optimizing these properties in order to enhance mAb and mAb-conjugate tumor localization, to accelerate clearance from the blood, and to minimize exposure to normal tissues (5, 6). For certain applications of mAb conjugates (6-8), these factors are critical.

A number of recent reports have described the use of mAb-enzyme conjugates for the conversion of relatively nontoxic drug precursors (prodrugs) into active anticancer drugs (reviewed in refs 6 and 8). This is a two-step approach to cancer therapy in which a mAb-enzyme conjugate is administered, and after allowing enough time for tumor uptake and systemic clearance to take place, an anticancer prodrug is then given. The targeted enzyme converts the relatively nontoxic prodrug into an active anticancer drug. Considerable evidence has accumulated

suggesting that optimal effects require high tumor to blood conjugate ratios (8-10), which presumably can be affected by the chemistry used for conjugate preparation.

Several groups have utilized  $\beta$ -lactamases for the activation of cephalosporin-containing prodrugs (11-13). Recently, we described the in vivo activities of a Fab'<sub>2</sub> conjugate of *Enterobacter cloacae*  $\beta$ -lactamase ( $\beta$ L) against a subcutaneous human tumor xenograft in nude mice (12). A significant level of antitumor activity was obtained in spite of the fact that the conjugate was impaired in its ability to bind to cell surface antigens. In this report, we describe new conjugation methodology that preserves mAb binding activity and correlate this with the ability of the conjugate to activate prodrug and specifically localize into subcutaneous tumors in vivo.

## EXPERIMENTAL PROCEDURES

**Materials.** Crude *E. cloacae* penicillinase was obtained from Sigma Chemical Co., St. Louis, MO, and purified according to established procedures, using boronic acid affinity chromatography (12, 14). The synthesis of 7-(phenylacetamido)cephalosporin mustard has been reported elsewhere (15). Nitrocefin and PADAC were purchased from Beckton Dickinson Microbiology Systems, Beckton Dickinson and Company, Cockeysville, MD, and Calbiochem, La Jolla, CA, respectively. The mAbs L6 and P1.17 are both of the IgG<sub>2a</sub> isotype. L6 was purified by protein A chromatography from the supernatant of an L6-producing hybridoma cell line (16). P1.17 was purified from mouse ascites on a protein A column. L6 binds to antigens on a variety of human carcinomas, including the lung adenocarcinoma cell line H2981 (16). P1.17 shows no detectable binding to these cells. The Fab'<sub>2</sub> fragments of the mAbs were obtained by digestion with pepsinogen as described previously (15), and purified by affinity

\* To whom correspondence should be addressed.

\* Abstract published in *Advance ACS Abstracts*, April 15, 1994.

<sup>1</sup> Abbreviations used:  $\beta$ L, *Enterobacter cloacae*  $\beta$ -lactamase; dimeric mAb- $\beta$ L, (mAb-Fab')<sub>2</sub>- $\beta$ L; DTT, DL-dithiothreitol; FITC, fluorescein isothiocyanate; IC<sub>50</sub>, concentration that gives 50% cell kill; LFE, linear fluorescence equivalence; mAb, monoclonal antibody; PBS, phosphate-buffered saline, pH 7.4; SDS-PAGE, sodium dodecyl sulfate polyacrylamide gel electrophoresis; SMCC, *N*-succinimidyl 4-(maleimidomethyl)cyclohexane-1-carboxylate.

chromatography on a protein A column and size-exclusion chromatography on Sephacryl S-300. L6-Fab' was obtained by reduction of the interchain disulfides of L6-Fab'<sub>2</sub>, followed by addition of 5,5'-dithiobis(2-nitrobenzoic acid) (17).

**Conjugate Preparation.** The preparation of mAb-Fab'- $\beta$ L conjugates has been described previously (12). Briefly, maleimide-substituted mAb (from reaction with *N*-succinimidyl 4-(maleimidomethyl)cyclohexane-1-carboxylate, SMCC, Pierce Chemical Co., Rockford, IL) was allowed to react with  $\beta$ L that had been modified with 2-iminothiolane to contain free sulfhydryl groups. The conjugate was purified using a two-step procedure that involved size-exclusion and boronic acid affinity chromatographies.

MAB-Fab'- $\beta$ L and (mAb-Fab')<sub>2</sub>- $\beta$ L (dimeric mAb- $\beta$ L) conjugates were prepared using a method based on previously published procedures (17, 18). SMCC was dissolved in dimethylformamide at 20.0 mM and added to  $\beta$ L solutions at 4–5 mg/mL in phosphate-buffered saline (PBS) to give a final SMCC concentration of 1.0 mM. The mixture was incubated for 30 min at 30 °C, followed by removal of unreacted SMCC and reaction byproducts by gel filtration chromatography at 4 °C through Sephadex G-25M (PD-10, Pharmacia, Piscataway, NJ), equilibrated in N<sub>2</sub>-purged 40 mM sodium phosphate, pH 7.4, containing 0.6 M NaCl.

DL-Dithiothreitol (DTT, Sigma Chemical Co.) was dissolved in PBS at 10.0 mM and added to solutions of mAb-Fab'<sub>2</sub> at 5–10 mg/mL in PBS, containing 15 mM sodium borate, pH 8.0, to give a final DTT concentration of 0.5 mM. The solution was incubated for 60 min at 30 °C, followed by purification of the reduced mAb by gel filtration at 4 °C on a PD-10 column which was equilibrated in N<sub>2</sub>-purged 40 mM sodium phosphate (pH 7.4) containing 0.6 M NaCl. The number of free sulfhydryl groups obtained using this procedure (determined using 5,5'-dithiobis(2-nitrobenzoic acid)) (19) was 3.8–4.4.

The maleimide-substituted enzyme was added to the reduced mAb at a 1:2–3 molar ratio of  $\beta$ L:mAb-Fab'. The mixture was incubated at ambient temperature for 60 min, followed by the addition of *trans*-4,5-dihydroxy-1,2-dithiane (Sigma Chemical Co.) dissolved at 60 mM in H<sub>2</sub>O (final concentration of 5 mM). Incubation was continued for 60 min at ambient temperature and then 18 h at 4 °C. Subsequent manipulations were all carried out at 4 °C. The conjugate was subjected to purification by affinity chromatography on a boronic acid affinity column of the hydrophilic type (L-type, 14), equilibrated in 20 mM triethanolamine hydrochloride at pH 7.0, containing 0.5 M NaCl, followed by washing of the column with the above buffer until A<sub>280</sub>  $\approx$  0. The bound material was eluted off with 0.5 M sodium borate at pH 7.0, containing 0.5 M NaCl. Fractions were analyzed for relative enzymatic activity, and those that eluted with sodium borate and had high enzymatic activities were pooled, concentrated by ultrafiltration, and applied to a Sephacryl S-300 (Pharmacia) size-exclusion column (equilibrated in PBS). The fractions were analyzed by sodium dodecyl sulfate polyacrylamide gel electrophoresis (SDS-PAGE) and by their relative enzymatic activities. Two pools, consisting of the purified mAb-Fab'- $\beta$ L and dimeric mAb- $\beta$ L conjugates, were concentrated by ultrafiltration, filtered through 0.2- $\mu$ m filters, and stored at -70 °C. The concentrations of the preparations were determined spectrophotometrically at 280 nm using an E<sup>1%</sup> of 14.0 and 15.3 (12) for the mAbs and the enzyme, respectively.

**Enzyme Activity. Specific Activity.** The enzymatic activities of the purified enzyme and the mAb conjugates were determined using either nitrocefin (12, 20) or PADAC (18) as substrates. (1) Nitrocefin:  $\beta$ L-containing solutions (5.0 ng of enzyme/mL) in PBS containing 12.5  $\mu$ g/mL bovine serum albumin were incubated with nitrocefin (50  $\mu$ M) in a cuvette at ambient temperature. The rate of hydrolysis was estimated from the increase in absorbance at 490 nm ( $\Delta\epsilon = 19\,500\text{ M}^{-1}\text{ cm}^{-1}$ ) that occurs when the  $\beta$ -lactam ring is opened. (2) PADAC:  $\beta$ L-containing solutions (25–50 ng of enzyme/mL) in PBS/bovine serum albumin (as above) were incubated with PADAC (25  $\mu$ M) in a cuvette at ambient temperature. Hydrolysis rates were estimated from the increase of absorbance at 450 nm ( $\Delta\epsilon = 14\,700\text{ M}^{-1}\text{ cm}^{-1}$ ). The specific activity of each conjugate was compared to the specific activity of the  $\beta$ L sample used for the conjugate preparation. The data represent the mean specific activity ratio from at least three preparations of each conjugate, except in the case of P1.17-Fab'- $\beta$ L, which was only prepared once.

**Relative Activity.** Fractions from boronic acid and size-exclusion chromatography were tested for relative enzymatic activities. An aliquot of each fraction was diluted 2000–8000-fold in a 0.1 mg/mL bovine serum albumin solution in PBS and incubated at ambient temperature with nitrocefin (final concentration of 50  $\mu$ M) in a 96-well microtiter plate. The absorbance at 490 nm (using 630 nm as a reference wavelength) was read 5–10 min after the initiation of the reaction on an EL 312 Bio-Kinetics Reader (Bio-Tek Instruments, Inc.). Reaction conditions were chosen such that the value of the fraction with the highest absorbance fell within a range of 0.10–0.25.

**Cell Binding.** L6- $\beta$ L conjugates were tested for their abilities to bind to H2981 cells relative to L6-Fab'<sub>2</sub> and L6-Fab' in a competition assay (15). H2981 cells ( $0.5 \times 10^6$ ) in Iscove's modified Dulbecco's medium with 10% fetal bovine serum were incubated with the test sample and fluorescein isothiocyanate labeled whole L6 (L6-FITC) such that the combined L6-Fab' concentration (test sample + L6-FITC) was 800 nM. The ratio of test sample to L6-FITC ranged from 0 to 1. After the sample was incubated for 30 min on ice, the cells were washed and analyzed on a fluorescence activated cell sorter. The mean channel number of fluorescence was converted into linear fluorescence equivalence (LFE) and percent of binding was calculated using the following formula: % binding =  $100 - 100[(\text{LFE}_{100\% \text{ L6-FITC}} - \text{LFE}_{\text{sample}})/(\text{LFE}_{100\% \text{ L6-FITC}} - \text{LFE}_{\text{no mAb}})]$ .

**In Vitro Cytotoxicity.** H2981 cells in Iscove's modified Dulbecco's medium with 10% fetal bovine serum were plated out at 8000 cells/well into 96-well plates and allowed to adhere overnight at 37 °C. The cells were incubated with varying concentrations of  $\beta$ L or  $\beta$ L conjugates for 30–45 min at 4 °C. After unbound material was washed off, the cells were treated with 10  $\mu$ M 7-(phenylacetamido)-cephalosporin mustard for 60 min at 37 °C. The cells were then washed, and incubation was continued for 18 h at 37 °C. This was followed by a 6-h pulse with [<sup>3</sup>H]-thymidine (1  $\mu$ Ci/well). The cells were washed with PBS, detached by treatment with trypsin/EDTA, harvested onto filtermats (LKB WALLAC 1295-001 Cell Harvester), and counted on an LKB WALLAC 1205 liquid scintillation counter. The incorporation of [<sup>3</sup>H]thymidine was calculated as the percentage of treated cells relative to untreated controls.

**In Vivo Biodistribution. Radiolabeling of Conjugates.** L6-Fab'- $\beta$ L and dimeric L6- $\beta$ L were labeled with <sup>125</sup>I using Iodogen (Pierce Chem. Co.). Both conjugates

were separated from low molecular weight material by gel filtration on PD-10 columns equilibrated in PBS. Previous studies with such columns and elution conditions yielded 90% protein recovery, which was therefore used as the assumed recovery of radiolabeled conjugates. The specific activities in terms of radioactivity were 1.6  $\mu\text{Ci}/\mu\text{g}$  for L6-Fab' $_2$ - $\beta\text{L}$  and 0.9  $\mu\text{Ci}/\mu\text{g}$  for dimeric L6- $\beta\text{L}$ .

**Immunoreactivity.** The radiolabeled conjugates were tested for their abilities to bind to H2981 cells in a competition assay. Cells were grown to confluence in a 96-well plate in Iscove's modified Dulbecco's medium supplemented with 10% fetal bovine serum. Each conjugate was added to the cells at a constant concentration of conjugate, while the ratio of labeled to unlabeled material was varied. The cells were incubated for 30 min at 4 °C, washed with PBS, detached with trypsin/EDTA, and counted with a  $\gamma$ -counter.

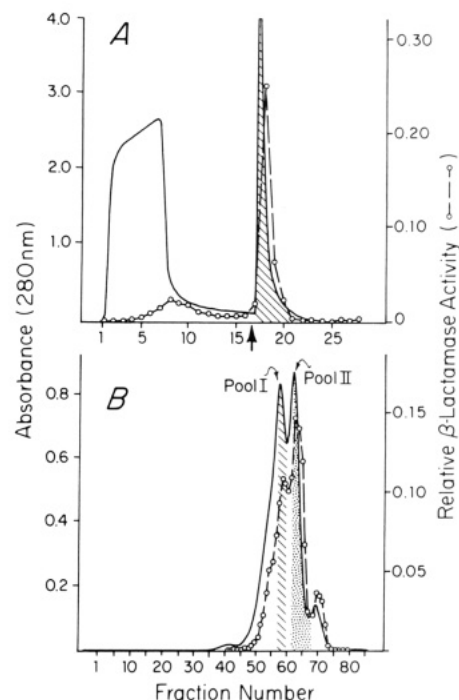
**In Vivo Distribution.** In vivo studies were performed in 6–10 week old female athymic nu/nu mice (Harlan-Sprague-Dawley, Indianapolis, IN). The mice were implanted subcutaneously with in vivo passaged H2981 tumors. When tumor growth was established and the tumors had reached a size of 100–175 mg, groups of three to four mice were injected intravenously with radiolabeled conjugates at a dose of 0.5 mg (265–310  $\mu\text{Ci}$ ) of L6 component/kg (10 mL/kg), using 1.0 mg/mL bovine serum albumin in PBS as the diluent. At 96 h post conjugate treatment the mice were bled and sacrificed. Tissues were collected and weighed immediately following excision and then counted with a  $\gamma$ -counter.

**Trichloroacetic Acid Precipitation.** The in vivo stabilities of the radiolabeled conjugates in tumors and blood were monitored by trichloroacetic acid precipitation. Tumors were homogenized with a pestle, and protein was precipitated with 500  $\mu\text{L}$  of a 10% aqueous (wt:vol) solution of trichloroacetic acid for 30 min at ambient temperature. Plasma proteins were similarly precipitated. The samples were centrifuged, and the supernatant from each of these was removed. The pellets were resuspended in 500  $\mu\text{L}$  of a 5% solution of trichloroacetic acid. After centrifugation, the supernatants were pooled, and the pellets and supernatants were counted with a  $\gamma$ -counter.

## RESULTS AND DISCUSSION

**Preparation and Structures of mAb- $\beta\text{L}$  Conjugates.** L6-Fab' $_2$ - $\beta\text{L}$  and P1.17-Fab' $_2$ - $\beta\text{L}$  conjugates were prepared by linking the two proteins via a thioether bond as previously described (12). Briefly, this involved combining thiol-containing  $\beta\text{L}$  with mAb-Fab' $_2$  that had been modified with maleimide groups. The conjugate thus formed was purified by size-exclusion and affinity chromatography, using Sephacryl S-300 and immobilized boronic acid, respectively. This conjugation method yielded 1:1 adducts (>95% purity) of mAb-Fab' $_2$ : $\beta\text{L}$  with an apparent molecular weight of 150 kDa. The overall yield was 13–15%, based on the amount of thiol-containing  $\beta\text{L}$  used for the preparation. Analysis of L6-Fab' $_2$ - $\beta\text{L}$  for binding to L6 antigens on the H2981 human lung adenocarcinoma cell line revealed a reproducible and significant loss in binding activity (12). This was in contrast to similarly prepared conjugates between L6-Fab' $_2$  and *Bacillus cereus*  $\beta$ -lactamase (II) (15), in which the binding activity of L6 was preserved (15). Consequently, studies were undertaken to prepare conjugates of  $\beta\text{L}$  having preserved binding activities.

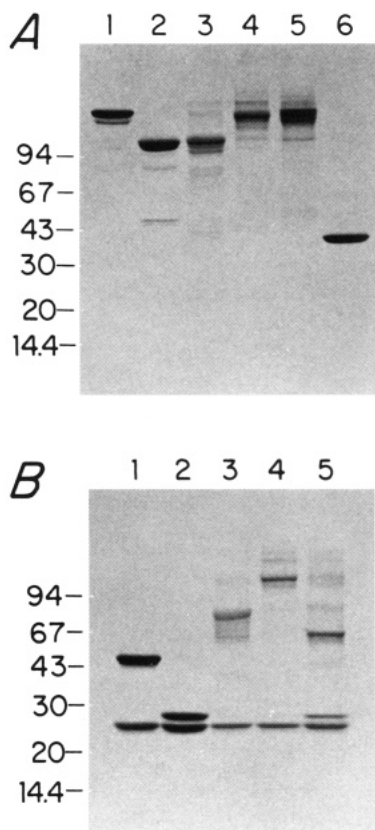
Conjugates of L6 and  $\beta\text{L}$  were prepared by reacting reduced L6-Fab' $_2$  with maleimide-substituted enzyme. SDS-PAGE analysis indicated that complete reduction



**Figure 1.** Purification of  $\beta\text{L}$  conjugates. (A) The unpurified conjugation mixture was loaded on a boronic acid affinity column, and bound material was eluted off with a sodium borate buffer (indicated by an arrow). Shaded area of protein peak shows the fractions that were pooled. (B) The conjugates were further purified by size-exclusion chromatography on a Sephacryl S-300 column. Two pools were obtained (shaded).

of interchain disulfides took place when DTT was used as the reducing agent (data not shown). The reduced mAb was reacted with maleimide-substituted enzyme at an L6-Fab' $_2$ : $\beta\text{L}$  molar ratio of 2–3:1 and then subjected to purification using a modification of a previously described two-step procedure (12). In the first step, the reaction mixture was applied to a boronic acid affinity column and eluted with sodium borate (Figure 1A). Analysis of the fractions for enzymatic activity indicated that most of the activity was present in the fractions that bound to the column and eluted with sodium borate. Fractions that had high enzymatic activity (fractions number 17–21, Figure 1A) were pooled and concentrated. SDS-PAGE analysis (data not shown) indicated the presence of material with distinct apparent molecular weights of 40, 110, and 150 kDa, respectively. Adducts of higher molecular weights were also present. The concentrated pool was applied to a Sephacryl S-300 size-exclusion column (Figure 1B). Three peaks were obtained in the elution of the conjugate mixture, all of which had  $\beta$ -lactamase activity. SDS-PAGE analysis showed that the first two peaks (pools I and II, Figure 1B) contained fractions with apparent molecular weights of 150 and 110 kDa, respectively. The fractions that eluted immediately prior to pool I contained higher molecular weight adducts. The peak that eluted last had a molecular weight of 40 kDa, which corresponds to unreacted  $\beta\text{L}$ .

The pooled conjugate-containing fractions were analyzed by SDS-PAGE under nonreducing conditions, which showed that the conjugates were at least 90% pure (Figure 2A). L6-Fab' $_2$ - $\beta\text{L}$  (Figure 2A, lane 5) had an apparent molecular weight of 150 kDa, corresponding to the expected molecular weight for a mAb-Fab' $_2$  fragment attached to a single  $\beta\text{L}$  molecule. Pool I had the same apparent molecular weight (Figure 2A, lane 4). Pool II (Figure 2A, lane 3) had a molecular weight of approximately 110 kDa,

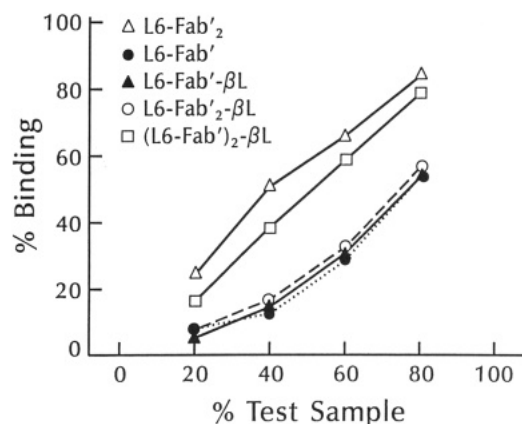


**Figure 2.** SDS-PAGE analyses (4–20%) of  $\beta$ L conjugates under nonreducing (A) and reducing (B) conditions: lane 1, whole L6; lane 2, L6-Fab'<sub>2</sub>; lane 3, L6-Fab'- $\beta$ L; lane 4, dimeric L6- $\beta$ L; lane 5, L6-Fab'<sub>2</sub>- $\beta$ L; lane 6,  $\beta$ L. Molecular weight markers (in kDa) are indicated on the left.

which is close to the theoretical molecular weight (95 kDa) for a monomeric Fab'- $\beta$ L adduct.

Further structural information of the conjugates was derived by subjecting the conjugates to SDS-PAGE under reducing conditions. It was found that the heavy (30 kDa) and light (25 kDa) chains of L6-Fab'<sub>2</sub> could be distinguished due to their different mobilities on the SDS gel (Figure 2B, lane 2). The two chains stained with approximately the same intensity using Coomassie blue. Under the reducing conditions, both heavy and light chains were released from the L6-Fab'<sub>2</sub>- $\beta$ L conjugate (Figure 2B, lane 5). Most, if not all, of the  $\beta$ L was conjugated to the heavy chain, since there is approximately twice as much light chain released as heavy chain. The identity of the light chain released from the conjugate rests on the fact that it has the same apparent molecular weight as the light chains from either whole L6 or L6-Fab'<sub>2</sub> (Figure 2B, lanes 1 and 2).

Pools I and II (Figure 1B) did not appear to contain disulfide-linked heavy chains that could be released upon reduction, indicating that the  $\beta$ L is attached only to the heavy chains of these conjugates. The structure of the conjugate obtained in pool I (Figure 1B) therefore is consistent with the covalent attachment of two individual L6-Fab' fragments to maleimides on  $\beta$ L. The attachment is most likely through a heavy chain cysteine in the hinge region. Further evidence to support the proposed dimeric structure of this conjugate (chemically represented as (L6-Fab')<sub>2</sub>- $\beta$ L and designated as dimeric L6- $\beta$ L) is based on the fact that it has the same apparent molecular weight as L6-Fab'<sub>2</sub>- $\beta$ L under nonreducing conditions on SDS-PAGE (Figure 2A, lanes 4 and 5). Finally, similar analyses of pool II (Figure 1B) under both nonreducing (Figure 2A,



**Figure 3.** Cell binding assay. H2981 cells were exposed to conjugated or unconjugated L6 in various mixtures with L6-FITC, while the L6-Fab' concentration was kept constant at 800 nM. Fluorescence intensity was determined by fluorescence-activated cell sorter analysis. Dimeric L6- $\beta$ L is represented as (L6-Fab')<sub>2</sub>- $\beta$ L.

lane 3) and reducing (Figure 2B, lane 3) conditions indicate that the conjugate is L6-Fab'- $\beta$ L, in which the L6 heavy chain is linked to maleimides on the enzyme. Conjugates were also made with the control mAb P1.17 using the same methods as described above for L6. The purities and mobilities by SDS-PAGE were similar to that of the L6- $\beta$ L conjugates. On the basis of the amount of maleimide-containing  $\beta$ L used in the conjugate preparation, the overall yields were 10–25% for the mAb-Fab'- $\beta$ L conjugates and 8–13% for the (mAb-Fab')<sub>2</sub>- $\beta$ L conjugates.

**Conjugate Activities.** A competition assay was used to assess the effects that the different conjugation methods had on the binding characteristics of the  $\beta$ L conjugates to H2981 human lung adenocarcinoma cell surface antigens (Figure 3). Cells were incubated with conjugates or unconjugated mAbs in various mixtures with whole L6-FITC. It was found that dimeric L6- $\beta$ L was only slightly less effective than L6-Fab'<sub>2</sub> in competing for binding to cell surface antigens. The monovalent conjugate, L6-Fab'- $\beta$ L, showed a substantially lower level of binding in this assay, but the level was identical to L6-Fab'. Since there were no differences in binding between the L6-Fab' and the L6-Fab'- $\beta$ L conjugate, it is likely that the enzyme is conjugated to a site on the L6 such that it does not interfere with the binding to cell surface antigens. In contrast to these two examples, L6-Fab'<sub>2</sub>- $\beta$ L exhibited significantly impaired binding to H2981 cells compared to unmodified L6-Fab'<sub>2</sub>. This is consistent with previous findings (12), and is probably due to either the site at which *E. cloacae*  $\beta$ L binds to L6-Fab'<sub>2</sub> and/or to interactions between the antigen binding site on L6 with the enzyme. P1.17 has been shown previously to give no detectable binding on H2981 cells.

The  $\beta$ L conjugates were also tested for  $\beta$ -lactamase enzyme activities using either nitrocefin or PADAC as substrates. With nitrocefin, the specific activity of  $\beta$ L was  $405 \pm 43$   $\mu$ mol/min/mg, and with PADAC, the activity was  $23.1 \pm 1.9$   $\mu$ mol/min/mg. The results showed that the enzymatic activities of all the conjugates were similar to that of unconjugated  $\beta$ L (Table 1). Thus, it appears that the methods for conjugation and purification had little effect on enzyme activity. This is consistent with previous observations for a variety of  $\beta$ -lactamase conjugates (12, 15, 18).

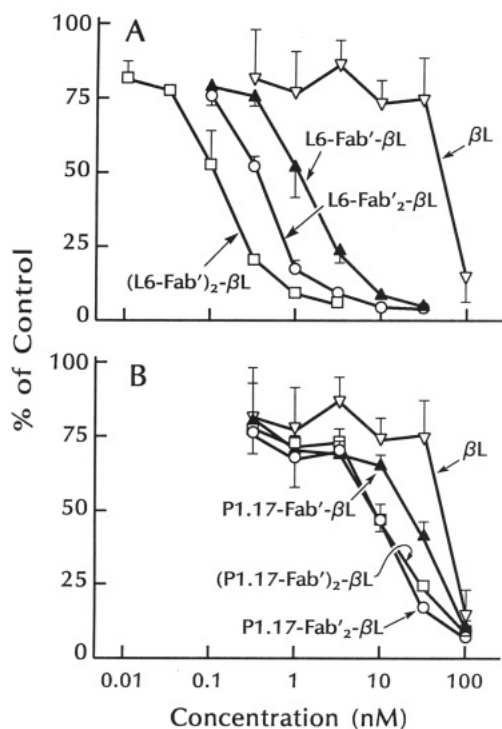
**In Vitro Prodrug Activation.** To establish the effects that the conjugation methods had on in vitro prodrug activation, cytotoxicity studies were performed with the



**Table 1. Enzymatic Activities of  $\beta$ L Conjugates**

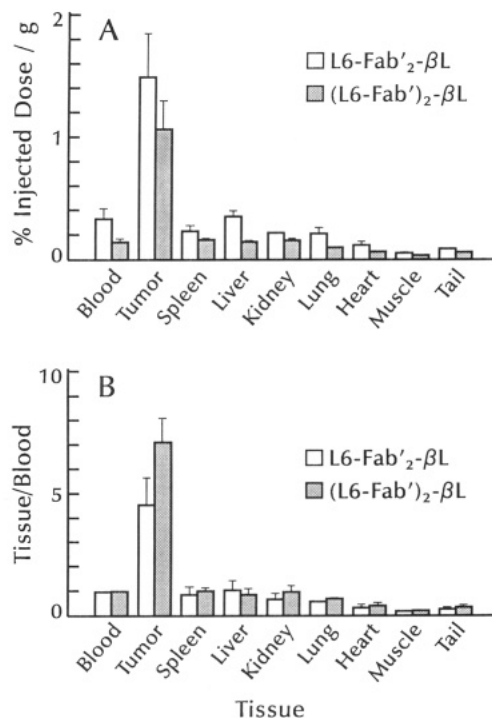
conjugate	rel activity <sup>a</sup> (%) (no. of preparations)
L6-Fab'- $\beta$ L	108 $\pm$ 12 (5)
(L6-Fab') <sub>2</sub> - $\beta$ L <sup>b</sup>	107 $\pm$ 12 (4)
L6-Fab'- $\beta$ L	110 $\pm$ 17 (3)
P1.17-Fab'- $\beta$ L	119 $\pm$ 24 (4)
(P1.17-Fab') <sub>2</sub> - $\beta$ L <sup>b</sup>	124 $\pm$ 33 (4)
P1.17-Fab'- $\beta$ L	110 <sup>c</sup> (1)

<sup>a</sup> The activity of each conjugate is expressed relative to the particular  $\beta$ L sample that was used for the conjugate preparation. The numbers in parentheses indicate the number of independently prepared conjugates that were tested. <sup>b</sup> These are referred to in the text as dimeric mAb- $\beta$ L conjugates. <sup>c</sup> No standard deviation was obtained, since this conjugate was only prepared once.



**Figure 4.** In vitro prodrug activation. H2981 cells (L6 positive, P1.17 negative) were exposed to varying concentrations of  $\beta$ L conjugates or unconjugated  $\beta$ L, washed, and treated with 7-(phenylacetamido)cephalosporin mustard (10  $\mu$ M). Cell viability was measured by [<sup>3</sup>H]thymidine incorporation and is expressed as a percentage of untreated control cells. The dimeric conjugates are represented as (mAb-Fab')<sub>2</sub>- $\beta$ L.

conjugates in combination with 7-(phenylacetamido)-cephalosporin mustard, a prodrug that was previously shown to be a substrate for  $\beta$ L (12). Upon enzymatic hydrolysis of the  $\beta$ -lactam ring of the prodrug, the cytotoxic agent phenylenediamine mustard is released (15). H2981 cells were incubated with various concentrations of  $\beta$ L-containing conjugates or unconjugated enzyme. The cells were washed and then incubated with a nontoxic concentration (10  $\mu$ M) of 7-(phenylacetamido)cephalosporin mustard. The highest degree of immunospecific activation was obtained with the dimeric mAb- $\beta$ L conjugates, in which there was an 80-fold difference between the L6 and P1.17 conjugates (Figure 4). In this respect, the dimeric L6- $\beta$ L conjugate was superior to L6-Fab'- $\beta$ L and L6-Fab'- $\beta$ L, which had smaller degrees (20-fold) of immunologically specific activation. The finding that both L6- and P1.17-Fab'- $\beta$ L conjugates showed a greater degree of prodrug activation compared to their respective mAb-Fab'- $\beta$ L counterparts (Figure 4) may be attributable to a slightly higher degree of non-specific binding to H2981 cells.



**Figure 5.** In vivo biodistribution. L6-Fab'- $\beta$ L and (L6-Fab')<sub>2</sub>- $\beta$ L (dimeric L6- $\beta$ L) were labeled with <sup>125</sup>I and administered to nude mice with subcutaneous H2981 xenografts. At 96 h post treatment, the mice were bled and sacrificed. The data were calculated as a percentage of the injected dose per gram tissue (A) and as tissue to blood concentration ratios (B).

Since the conjugates had similar enzymatic activities (Table 1), the level of prodrug activation was expected to be dependent on the amount of conjugate that bound to cells. Therefore, higher concentrations of conjugates would be needed to activate the prodrug, if the conjugate is impaired in its ability to bind to cell surface antigens. Dimeric L6- $\beta$ L effected prodrug activation at the lowest concentration compared to the other conjugates (Figure 4). The concentration of dimeric L6- $\beta$ L needed to achieve an IC<sub>50</sub> value with the prodrug (0.1 nM) was 4 and 10 times lower than L6-Fab'- $\beta$ L and L6-Fab'- $\beta$ L, respectively (Figure 4A).

**In Vivo Biodistribution.** The in vivo distribution of L6-Fab'- $\beta$ L and dimeric L6- $\beta$ L to H2981 tumors was investigated in mice with subcutaneous H2981 tumor xenografts. The conjugates were radiolabeled (<sup>125</sup>I) without any loss of immunoreactivity, as measured by a competition cell binding assay. Autoradiograms from SDS-PAGE analysis of the radiolabeled materials suggested that the conjugates were homogeneously labeled and stable to the radiolabeling procedure (data not shown). At 96 h post conjugate administration, tissues were removed and counted for radioactivity. Additional experiments confirmed that >90% of the radioactivity measured was precipitable with trichloroacetic acid and was therefore associated with protein.

Figure 5A shows the concentration of the conjugates in various tissues 96 h post conjugate administration. This particular timepoint was chosen since it coincides with the schedule used in a previously reported in vivo therapeutic efficacy study involving L6-Fab'- $\beta$ L and was determined to be an appropriate time for prodrug administration in mice receiving this conjugate (12). Analysis of the tissue to blood concentration ratios (Figure 5B) indicated that dimeric L6- $\beta$ L had a 50% higher tumor to blood ratio than L6-Fab'- $\beta$ L (*P* value of 0.03). The tumor levels of dimeric L6- $\beta$ L and L6-Fab'- $\beta$ L were not



statistically different ( $P$  value of 0.17) even though the blood concentration of dimeric L6- $\beta$ L was half that of L6-Fab'- $\beta$ L ( $P$  value of 0.01). In all other tissues examined, the amount of radioactivity associated with dimeric L6- $\beta$ L was lower than that of L6-Fab'- $\beta$ L (Figure 5B). Thus, a modest, but significant, improvement in conjugate tumor to blood ratio is achieved with dimeric L6- $\beta$ L compared to L6-Fab'- $\beta$ L, and this is accompanied with reduced conjugate levels in nontarget tissues. On the basis of this, we are now utilizing dimeric mAb- $\beta$ L conjugates in combination with anticancer prodrugs for in vivo therapy studies.

## CONCLUSION

L6-Fab'- $\beta$ L and dimeric L6- $\beta$ L conjugates were conveniently prepared by linking one and two individual L6-Fab' units to maleimide-substituted  $\beta$ L, respectively. Analyses of these conjugates by SDS-PAGE indicated that linkage occurred through heavy-chain thiols on L6 that are most likely located in the hinge region of the mAb and are removed from the antigen binding site. A greater degree of control was therefore used in the preparation of these conjugates compared to L6-Fab'- $\beta$ L, which was prepared by random modification of L6-Fab' with maleimide groups. As a result, the dimeric L6- $\beta$ L conjugate displayed better binding characteristics, increased potency in prodrug activation, and improved in vivo localization characteristics compared to L6-Fab'- $\beta$ L. Although the absolute amount of intratumoral conjugate was not increased using dimeric L6- $\beta$ L relative to L6-Fab'- $\beta$ L the amount in the blood and in nontarget tissues was reduced. This constitutes an improvement for the targeting strategy described here, in which high tumor to nontumor conjugate ratios are required to minimize toxicities due to adventitious drug release.

## ACKNOWLEDGMENT

We wish to thank Vivekananda Vrudhula for providing the prodrug used in this study, David Kerr for enzyme purification, Nathan Siemers for his comments on the manuscript, and Karl Erik and Ingegerd Hellström for their continued support of the project.

## LITERATURE CITED

- (1) LoBuglio, A. F., and Saleh, M. N. (1992) Advances in monoclonal antibody therapy of cancer. *Am. J. Med. Sci.* 304, 214-224.
- (2) Pack, P., Kajau, M., Schroeckh, V., Knüpfer, U., Wenderoth, R., Riesenberger, D., and Plückthun, A. (1993) Improved bivalent miniantibodies, with identical avidity as whole antibodies, produced by high cell density fermentation of *Escherichia coli*. *Bio/Technology* 11, 1271-1277.
- (3) Schott, M. E., Frazier, K. A., Pollock, D. K., and Verbanac, K. M. (1993) Preparation, characterization, and in vivo biodistribution properties of synthetically cross-linked multivalent antitumor antibody fragments. *Bioconjugate Chem.* 4, 153-165.
- (4) Holton, O. D., III, Black, C. D. V., Parker, R. J., Covell, D. G., Barbet, J., Sieber, S. M., Talley, M. J., and Weinstein, J. N. (1987) Biodistribution of monoclonal IgG1, F(ab')<sub>2</sub> and Fab' in mice after intravenous injection. *J. Immunol.* 139, 3041-3049.
- (5) Vitetta, E. S., Thorpe, P. E., and Uhr, J. W. (1993) Immunotoxins: magic bullets or misguided missiles? *Immunol. Today* 14, 252-258.
- (6) Bamias, A., and Epenetos, A. A. (1992) Two-step strategies for the diagnosis and treatment of cancer with bioconjugates. *Antibody Imm. Radiopharm.* 5, 385-395.
- (7) Goldenberg, D. M. (1993) Monoclonal antibodies in cancer detection and therapy. *Am. J. Med.* 94, 297-312.
- (8) Senter, P. D., Wallace, P. M., Svensson, H. P., Vrudhula, V. M., Kerr, D. E., Hellström, I., and Hellström, K. E. (1993) Generation of cytotoxic agents by targeted enzymes. *Bioconjugate Chem.* 4, 3-9.
- (9) Sharma, S. K., Bagshawe, K. D., Springer, C. J., Burke, P. J., Rogers, G. T., Boden, J. A., Antoniow, P., Melton, R. G., and Sherwood, R. F. (1991) Antibody directed enzyme prodrug therapy (ADEPT): A three phase system. *Dis. Markers* 9, 225-231.
- (10) Wallace, P. M., MacMaster, J. F., Smith, V. F., Kerr, D. E., Senter, P. D., and Cosand, W. L. (1994) Intratumoral generation of 5-fluorouracil mediated by an antibody-cytosine deaminase conjugate in combination with 5-fluorocytosine. *Cancer Res.*, in press.
- (11) Meyer, D. L., Jungheim, L. N., Law, K. L., Mikolajczyk, S. D., Shepherd, T. A., Mackensen, D. G., Briggs, S. L., and Starling, J. J. (1993) Site-specific prodrug activation by antibody- $\beta$ -lactamase conjugates: Regression and long-term growth inhibition of human colon carcinoma xenograft models. *Cancer Res.* 53, 3956-3963.
- (12) Vrudhula, V. M., Svensson, H. P., Kennedy, K. A., Senter, P. D., and Wallace, P. M. (1993) Antitumor activities of a cephalosporin prodrug in combination with monoclonal antibody- $\beta$ -lactamase conjugates. *Bioconjugate Chem.* 4, 334-340.
- (13) Alexander, R. P., Beeley, N. R. A., O'Driscoll, M., O'Neill, F. P., Millican, T. A., Pratt, A. J., and Willenbrock, F. W. (1991) Cephalosporin nitrogen mustard carbamate prodrugs for "ADEPT". *Tetrahedron Lett.* 32, 3269-3272.
- (14) Cartwright, S. J., and Waley, S. G. (1984) Purification of  $\beta$ -lactamases by affinity chromatography on phenylboronic acid-agarose. *Biochem. J.* 221, 505-512.
- (15) Svensson, H. P., Kadow, J. F., Vrudhula, V. M., Wallace, P. M., and Senter, P. D. (1992) Monoclonal antibody- $\beta$ -lactamase conjugates for the activation of a cephalosporin mustard prodrug. *Bioconjugate Chem.* 3, 176-181.
- (16) Hellström, I., Horn, D., Linsley, P. S., Brown, J. P., Brankovan, V., and Hellström, K. E. (1986) Monoclonal antibodies raised against human lung carcinoma. *Cancer Res.* 46, 3917-3923.
- (17) Goshorn, S. C., Svensson, H. P., Kerr, D. E., Somerville, J. E., Senter, P. D., and Fell, H. P. (1993) Genetic construction, expression and characterization of a single chain anti-carcinoma antibody fused to  $\beta$ -lactamase. *Cancer Res.* 53, 2123-2127.
- (18) Meyer, D. L., Jungheim, L. N., Mikolajczyk, S. D., Shepherd, T. A., Starling, J. J., and Ahlem, C. (1992) Preparation and characterization of  $\beta$ -lactamase-Fab' conjugates for the site specific activation of oncolytic agents. *Bioconjugate Chem.* 3, 42-48.
- (19) Riddles, P. W., Blakeley, R. L., and Zerner, B. (1979) Ellman's reagent: 5,5'-Dithiobis(2-nitrobenzoic acid)—a re-examination. *Anal. Biochem.* 94, 75-81.
- (20) Madgwick, P. J., and Waley, S. G. (1987)  $\beta$ -Lactamase I from *Bacillus cereus*. *Biochem. J.* 248, 657-662.

# Europium-Labeled Oligonucleotide Hybridization Probes: Preparation and Properties

Patrik Dahlén, Liisa Liukkonen,<sup>†</sup> Marek Kwiatkowski,<sup>‡</sup> Pertti Hurskainen,<sup>\*</sup> Antti Iitiä,<sup>†</sup> Harri Siitari, Jyrki Ylikoski,<sup>§</sup> Veli-Matti Mikkala, and Timo Lövgren<sup>†</sup>

Wallac Oy, P.O. Box 10, FIN-20101 Turku, Finland, Department of Biochemistry, University of Turku, FIN-20520 Turku, Finland, and Department of Medical Genetics, Biomedical Center, University of Uppsala, P.O. Box 589, S-75123 Uppsala, Sweden. Received August 20, 1993<sup>\*</sup>

A chemical method for labeling of oligonucleotide probes with europium chelates is presented. A modified deoxycytidine phosphoramidite is used to introduce multiple reactive amino groups to the oligonucleotide during the synthesis phase. Upon deprotection and purification of the modified oligonucleotide, an isothiocyanate derivative of a stable Eu chelate is reacted with the primary amino groups. The labeling technology enables the coupling of a high number of Eu chelates to a single probe. The melting temperatures and hybridization efficiencies of the oligonucleotides are not significantly altered by the labeling process. However, hybridization kinetics of the oligonucleotides are affected by the introduction of multiple modified deoxycytidine residues. In a solid-phase hybridization assay, up to  $10^7$  target molecules can be detected.

## INTRODUCTION

Synthetic oligonucleotides have become important tools in both research and diagnostic applications as probes for the detection of specific nucleic acid sequences. Oligonucleotides are easy to produce and use, and as a result of the recent development of highly efficient *in vitro* amplification methods, such as the polymerase chain reaction (PCR) (1, 2), oligonucleotides have become popular as hybridization probes. Most commonly, oligonucleotides are labeled with radioactive labels, such as  $^{32}\text{P}$ . However, due to the health hazards and short shelf-lives associated with radioactive labels, several alternative nonradioactive labeling methods have been developed. Oligonucleotides can be directly labeled with enzymes, fluorophores, or chemiluminescent markers (3-5). Indirect labeling procedures including biotin and hapten labels have also been described (6, 7).

Time-resolved fluorometry (TRF) is a nonradioactive measurement technology that enables the sensitive detection of lanthanide chelates (for review see ref 8). The TRF technology has been used in DNA hybridization assays in a wide variety of applications (9-18). Several methods of directly labeling oligonucleotides with lanthanide chelates have been presented (13, 16, 17).

Here we describe in detail a method for the preparation of Eu-labeled oligonucleotides. This method involves the use of a 1,6-diaminohexane-modified deoxycytidine phosphoramidite which is coupled in a multiple fashion to the oligonucleotide. Upon deprotection and purification of the modified oligonucleotide, the primary amino groups are labeled with Eu in a reaction with an isothiocyanate derivative of a stable Eu chelate (13). Thus a high number of Eu chelates can be conjugated to one oligonucleotide. We have investigated the effect of various degrees of

modifications on the dissociation temperatures ( $T_d$ 's) and on the hybridization properties of the Eu-labeled probes.

## MATERIALS AND METHODS

**Synthesis of Diaminohexane-Modified Deoxycytidine Phosphoramidite.** Diaminohexane-modified deoxycytidine phosphoramidite was synthesized as described earlier (4) with some modifications. The hydroxyl groups of deoxycytidine hydrochloride (5.27 g, 20 mmol) were protected with 1,3-dichloro-1,1,3,3-tetraisopropylideneisiloxane (8.2 g, 26 mmol) in dry pyridine (200 mL). The protected deoxycytidine was tosylated (19) as follows. Toluene-4-sulfonyl chloride (6.1 g, 32 mmol) and dry diisopropylethylamine (5.5 mL, 32 mmol) were added. The reaction mixture was stirred at room temperature overnight, and the red mixture was poured into saturated  $\text{NaHCO}_3$  and extracted with  $\text{CHCl}_3$  ( $3 \times 200$  mL). The organic phase was evaporated and coevaporated with toluene. The residue was then purified by short silica gel (40-63  $\mu\text{m}$ , Merck G60) column chromatography using 2% ethanol in  $\text{CHCl}_3$  in the mobile phase. The product, 4-*N*-(*p*-tolylsulfonyl)-3',5'-*O*-(1,1,3,3-tetraisopropylideneisiloxane-1,3-diyl)deoxycytidine, has an  $R_f$  value of 0.60 using thin-layer chromatography on precoated silica gel plates (60 F254, Merck) with a  $\text{MeOH}/\text{CHCl}_3$ , 10/90 (v/v), solvent system. Yield: 10.25 g (82%).  $^1\text{H-NMR}$  ( $\text{CDCl}_3$ ): 1.00-1.10 (m, 28 H); 2.26 (dd,  $J = 7.0, 13.1$  Hz, 1 H); 2.42 (s, 3 H); 2.48-2.57 (m, 1 H); 3.75-3.79 (m, 1 H); 4.00 (dd,  $J = 2.7, 13.4$  Hz, 1 H); 4.14 (d,  $J = 13.4$  Hz, 1 H); 4.36-4.43 (m, 1 H); 5.98 (d,  $J = 6.1$  Hz, 1 H); 7.30 (2  $\times$  d,  $J = 7.9$  Hz, 4 H); 7.82 (d,  $J = 7.9$  Hz, 2 H); 7.84 (d,  $J = 7.9$  Hz, 2 H). Anal. Calcd for  $\text{C}_{28}\text{H}_{45}\text{N}_3\text{O}_7\text{Si}_2$ : C, 53.91; H, 7.28; N, 6.74; O, 17.96; Si, 5.13. Found: C, 53.79; H, 7.47; N, 6.56. The synthesis was continued by protecting the aliphatic primary amino group with trifluoroacetic anhydride and deprotecting the hydroxyl groups with tetrabutylammonium fluoride. Subsequently, the hydroxyl group in the 5'-position was protected with 4,4'-dimethoxytrityl chloride, and the 3'-hydroxyl group was phosphitylated according to standard procedure (20) to give 4-*N*-[6-(trifluoroacetamido)hexyl]-5'-*O*-(4,4'-

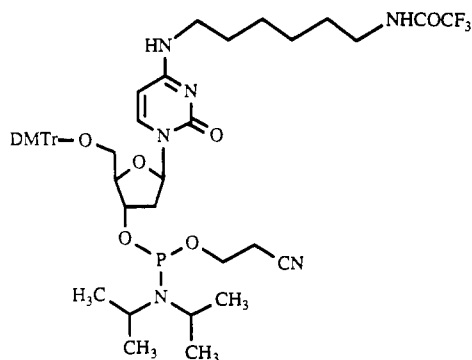
\* To whom correspondence should be addressed at Wallac Oy. Tel. Int+358-21-678 439, Fax Int+358-21-678380.

<sup>†</sup>University of Turku.

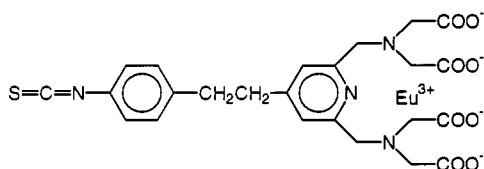
<sup>‡</sup>University of Uppsala.

<sup>§</sup> Present address: Perkin-Elmer Oy, P.O. Box 34, FIN-02271 Espoo, Finland.

<sup>\*</sup> Abstract published in *Advance ACS Abstracts*, April 15, 1994.



**Figure 1.** Structure of the diaminohexane-modified deoxycytidine phosphoramidite.



**Figure 2.** Structure of the Eu chelate for labeling oligonucleotides.

dimethoxytrityl)deoxycytidine 3'-(2-cyanoethyl)-*N,N*-diisopropylphosphoramidite (Figure 1) with a total yield of 35%.

**Syntheses and Europium Labeling of Oligonucleotides.** Diaminohexane-modified deoxycytidine phosphoramidite was used for DNA synthesis (scale 0.2  $\mu$ mole) in the Gene Assembler Plus (Pharmacia LKB Biotechnology, Uppsala, Sweden) at 0.1 M concentration in acetonitrile according to standard procedures. The oligonucleotides containing the diaminohexane-modified deoxycytidine base ( $\text{NH}_2\text{C}$ ) were deprotected in concentrated ammonia at 55  $^\circ\text{C}$  overnight. Purification of these oligonucleotides was done on a 10% urea polyacrylamide gel (21). The buffer of the eluted pure oligonucleotide was changed to water by gel filtration.

The probing sequences of the oligonucleotides were selected from the exon V region of human  $\alpha$ -1-antitrypsin gene: 14mers (N14), ATCGACGAGAAAGG; 18mers (N18), CCATCGACGAGAAAGGGA; 21mers (N21), AC-CATCGACGAGAAAGGGACT; 28mers (N28), CTGAC-CATCGACGAGAAAGGGACTGAAG. A series of oligonucleotides (Table 1) were synthesized containing 10 (C10), 25 (C25), and 40 (C40)  $\text{NH}_2\text{C}$ 's at the 5' end. These oligonucleotides were labeled with europium as follows. One to 4 nmol of the purified oligonucleotide was dried and resuspended in 50  $\mu\text{L}$  of  $\text{H}_2\text{O}$ . The pH was adjusted to 9.5 by adding  $\text{Na}_2\text{CO}_3$  to a final concentration of 50 mM. Eu chelate of 4-[2-(4-isothiocyanatophenyl)ethyl]-2,6-bis[[*N,N*-bis(carboxymethyl)amino]methyl]pyridine (12, 13) (Figure 2) (Wallac Oy, Turku, Finland), which contains an isothiocyanate as the reactive group, was added in a 10 molar excess over available  $\text{NH}_2\text{C}$ 's (unless otherwise stated). The reaction was allowed to proceed overnight at 4  $^\circ\text{C}$ . The final product was purified on a Sephadex G-50 DNA Grade column (50  $\times$  1 cm) using 10 mM Tris-HCl pH 7.5, 50  $\mu\text{M}$  ethylenediaminetetraacetic acid (EDTA) as elution buffer. The fractions containing the labeled oligonucleotide were pooled. The Eu concentration was measured in a time-resolved fluorometer, 1230 Arcus (Wallac Oy) against a  $\text{EuCl}_3$  standard. The amount of oligonucleotide was determined at 260 nm using a correction factor for the absorption of Eu chelate at that wavelength. The extinction coefficient at 260 nm for the reacted Eu chelate is 16 600.

**Biotinylation of Oligonucleotide N39C1.** Ten nmol of the oligonucleotide N39C1 (5'  $\text{NH}_2\text{CAGCAGC-TTCAGTCCCTTTCTCGTCGATGGTCAGCACAGC}$  3') containing a single  $\text{NH}_2\text{C}$  base at the 5' end was biotinylated as described earlier (14).

**Preparation of Radioactive Oligonucleotides.** The oligonucleotides were enzymatically labeled to  $1.0 \times 10^9$  cpm/ $\mu\text{g}$  using [ $\gamma$ - $^{32}\text{P}$ ]ATP (Amersham) and T4 polynucleotide kinase (21).

**Fluorescence Measurements.** The Eu fluorescence was measured in a 1232 DELFIA fluorometer (Wallac Oy) from microtitration plates in a 200- $\mu\text{L}$  volume of DELFIA enhancement solution (Wallac Oy) after a 25-min shaking at room temperature (RT).

**Hybridizations.** The hybridizations were performed on streptavidin-coated microtitration strips (14) as follows. The biotinylated target oligonucleotide N39C1Bio (amounts as indicated) was immobilized onto the surface of microtitration strip wells in a 2-h incubation at RT with shaking in 200  $\mu\text{L}$  per well of DELFIA assay buffer (Wallac Oy). The hybridization solution was obtained by mixing DELFIA assay buffer (50 mM Tris-HCl pH 7.75, 0.9% NaCl, 0.5% bovine serum albumin, 0.05% bovine globulin, 0.05%  $\text{Na}_2\text{S}_2\text{O}_8$ , 20  $\mu\text{M}$  diethylenetriaminepentaacetic acid, 0.01% Tween-20), supplemented with 1 M NaCl, with an equal volume of water. The actual hybridization was carried out using Eu-labeled oligonucleotides at  $5 \times 10^{10}$  molecules per reaction (200  $\mu\text{L}$  per well). The hybridization temperature was 35  $^\circ\text{C}$  for N14 probes and 45  $^\circ\text{C}$  for N18, N21, and N28 probes. The strips were washed six times using DELFIA wash solution (10 mM Tris-HCl pH 7.75, 0.9% NaCl, 0.005% Tween-20, 0.05%  $\text{Na}_2\text{S}_2\text{O}_8$ ; Wallac Oy) at RT in a DELFIA 1294-024 platelasher (Wallac Oy), and the Eu fluorescence was subsequently measured as mentioned above.

**Dissociation Temperature Analysis.** The biotinylated target oligonucleotide N39C1Bio ( $5 \times 10^{10}$  molecules per well) was hybridized to Eu-labeled probes ( $5 \times 10^{10}$  molecules per well) on streptavidin-coated strips at 45  $^\circ\text{C}$  (N14 probes at 32  $^\circ\text{C}$ ) for 1 h. After being washed at RT the hybrids were washed by stepwise increasing the temperature (3  $\times$  5 min at each temperature) and using prewarmed wash buffer, 50 mM HEPES pH 7.5 containing 15 mM NaCl, 100  $\mu\text{M}$  EDTA, and 0.05% Tween-20. The N14 probes were washed with the same wash buffer but containing 150 mM NaCl. At each temperature the remaining Eu-probe was determined by measuring the Eu fluorescence.

When  $^{32}\text{P}$ -labeled probes were used, the procedure was identical, but the individual wells were counted in a scintillation counter (1219 Rackbeta, Wallac Oy) after they were dissolved in LipoLuma scintillation solution (Lumax, Landgraaf, The Netherlands).

## RESULTS

**Syntheses of Europium-Labeled Oligonucleotide Probes.** The diaminohexane-modified deoxycytidine phosphoramidite was coupled in the oligonucleotide synthesis with high efficiency (98% or higher), fully comparable to unmodified phosphoramidites as judged by monitoring the dimethoxytrityl release. Oligonucleotides, with 10 and 25  $\text{NH}_2\text{C}$ 's at the 5' end, were made at the 0.2  $\mu\text{mol}$  scale with good yields, i.e., 6–20 nmol of pure oligonucleotide (Table 1). It is noteworthy that the oligonucleotides containing 40  $\text{NH}_2\text{C}$ 's were synthesized with low yields even though the coupling efficiencies and the UV-shadowing inspection during purification indicated otherwise.

Table 1. Synthesized and Labeled Oligonucleotides

name	length of		synthesis yield <sup>a</sup> (nmol)	labeling degree (Eu/oligo)
	probing sequence	NH <sub>2</sub> C tail		
N14C10Eu8	14	10	20	8
N14C25Eu20	14	25	12	20
N18	18		22	
N18C10Eu2	18	10	20	2
N18C10Eu5	18	10		5
N18C10Eu10	18	10		10
N18C25Eu9	18	25	6.1	9
N18C25Eu14	18	25		14
N18C25Eu25	18	25		25
N18C40Eu23	18	40	1.0	23
N21C10Eu10	21	10	22	10
N21C25Eu20	21	25	8.9	20
N21C40Eu22	21	40	1.0	22
N28C10Eu10	28	10	19	10
N28C25Eu20	28	25	9.9	20
N28C40Eu26	28	40	4.5	26

<sup>a</sup> The amount of synthesized oligonucleotides before Eu labeling.

The number of Eu chelates that could be coupled to the oligonucleotides was studied by varying the molar excess of the chelate in the labeling reaction. The oligonucleotide with a probing sequence of 18 nucleotides and a tail of 10 NH<sub>2</sub>C's was labeled using a 0.5-, 2-, and 10-fold molar excess of the chelate per NH<sub>2</sub>C, giving incorporations of two (N18C10Eu2), five (N18C10Eu5), and 10 (N18C10Eu10) Eu chelates, respectively. The oligonucleotide with a tail of 25 NH<sub>2</sub>C's was reacted with a 1-, 10- and 20-fold molar excess of the chelate per NH<sub>2</sub>C, resulting in the coupling of nine (N18C25Eu9), 14 (N18C25Eu14), and 25 (N18C25Eu25) chelates, respectively. Thus, it was possible to label all available primary aliphatic amino groups when the length of the NH<sub>2</sub>C tail was 10 or 25. However, oligonucleotides with 40 NH<sub>2</sub>C's were not completely labeled (maximum 26 Eu/oligo, Table 1).

**Properties of Eu-Labeled Oligonucleotides.** To study the effect of Eu labeling on the properties of the oligonucleotide probes, oligonucleotides carrying probing sequences of 14, 18, 21, and 28 bases were made (Table 1). Each probe was synthesized containing a tail of 10, 25, and 40 NH<sub>2</sub>C's. In addition, 18mer probes containing a varying number of Eu chelates (but otherwise identical) were made (N18C10Eu2, N18C10Eu5, N18C10Eu10 and N18C25Eu9, N18C25Eu14, N18C25Eu25). We studied the dissociation temperatures (*T<sub>d</sub>*'s) and hybridization properties of the Eu-labeled oligonucleotides.

The melting temperature analysis could not be carried out by UV hyperchromicity measurement due to the strong UV absorbance of Eu chelate. Therefore, we performed the dissociation temperature experiments by washing immobilized hybrids at increasing temperatures in microtitration wells. The remaining probe was measured in a time-resolved fluorometer. In order to ensure that the biotinylated target oligonucleotide was not released from the streptavidin-coated surface in the *T<sub>d</sub>* experiments, the solid phase was subjected to a washing test performed under stressed conditions. After the first hybridization of Eu-labeled oligonucleotide to the biotinylated target the obtained specific signal was 51735 cps (100%). After washing at 70 °C, reprobing gave 98% of the previous specific signal. After an additional washing (70 °C) and hybridization the specific signal was 103% of the specific signal obtained in the first hybridization. To verify that the Eu-labeled probe was removed during the washes at 70 °C, the remaining probe was measured after two cycles of hybridization/washing (70 °C), and only 3% was still hybridized to the biotinylated target oligonucleotide. In

Table 2. Properties of Eu-Labeled Oligonucleotides

name	<i>T<sub>d</sub></i> <sup>a</sup> (°C)	kinetics <sup>b</sup>	hybridization	bg <sup>d</sup> (cps)	efficiency <sup>e</sup> (%)
		<i>t</i> <sub>50%</sub> (min)	sensitivity <sup>c</sup> (molecules)		
N14C10Eu8	41	14	5 × 10 <sup>7</sup>	509	20
N14C25Eu20	41	23	1 × 10 <sup>7</sup>	846	18
N18	(44)				
N18C10Eu2	42	18	4 × 10 <sup>7</sup>	397	27
N18C10Eu5	42	18	3 × 10 <sup>7</sup>	412	29
N18C10Eu10	43 (44)	18	3 × 10 <sup>7</sup>	520	25
N18C25Eu9	44	20	3 × 10 <sup>7</sup>	542	25
N18C25Eu14	43	23	2 × 10 <sup>7</sup>	660	28
N18C25Eu25	44	20	1 × 10 <sup>7</sup>	715	21
N18C40Eu23	42	42	2 × 10 <sup>7</sup>	1388	24
N21C10Eu10	47 (46)		2 × 10 <sup>7</sup>	544	29
N21C25Eu20	49		1 × 10 <sup>7</sup>	831	31
N21C40Eu22	49		1 × 10 <sup>7</sup>	1587	35
N28C10Eu10		25	3 × 10 <sup>7</sup>	1149	31
N28C25Eu20		37	2 × 10 <sup>7</sup>	1511	30
N28C40Eu26		43	3 × 10 <sup>7</sup>	2333	30

<sup>a</sup> *T<sub>d</sub>* values were determined at 15 mM NaCl with the exception of N14C10Eu8 and N14C25Eu20, which were washed in 150 mM NaCl. The values in parentheses were obtained using <sup>32</sup>P as a label.

<sup>b</sup> N14 probes were hybridized at 35 °C, N18 and N28 probes at 45 °C. The amount of immobilized target N39C1Bio was 5 × 10<sup>10</sup> molecules per well. The *T*<sub>50%</sub> value expresses the time when 50% of maximum signal has been achieved. <sup>c</sup> The amount of immobilized biotinylated target oligonucleotide that could be detected. Sensitivity limit was determined as 2 × background. <sup>d</sup> Background, no target immobilized on the surface, expressed as counts per second. <sup>e</sup> The hybridization efficiency calculation was based on the obtained specific signal (from 1 × 10<sup>9</sup> target molecules on the standard curve) on a Eu standard and taking into account the Eu/oligo ratio.

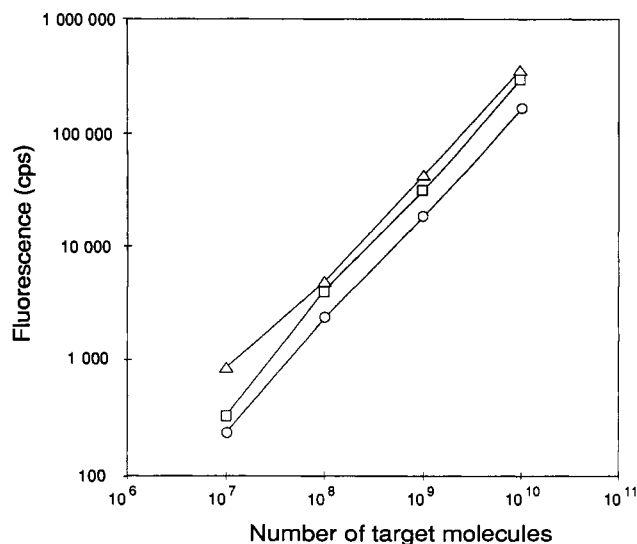
addition, oligonucleotides labeled with <sup>32</sup>P (N18, N18C10Eu10, and N21C10Eu10) were used in *T<sub>d</sub>* experiments and measured in a scintillation counter, in order to establish the validity of our *T<sub>d</sub>* measurement experimental setting. Theoretical *T<sub>m</sub>* values were calculated (22) to be 41, 43, and 46 °C for 14mer, 18mer, and 21mer, respectively. Our results showed that neither the tail of NH<sub>2</sub>C's nor the Eu/oligo ratio affected the *T<sub>d</sub>*'s of the probing sequences (Table 2).

The hybridization kinetics of the Eu-labeled oligonucleotides were studied in a solid-phase system. As shown in Table 2, the length of the NH<sub>2</sub>C tail affected the hybridization kinetics of the probe: the rate of hybridization decreased as the length of the tail increased. Oligonucleotides differing only in regard to the number of the coupled Eu chelates (N18C10Eu2, N18C10Eu5, N18C10Eu10 and N18C25Eu9, N18C25Eu14, N18C25Eu25) hybridized at the same rate.

The hybridization efficiency of Eu-labeled probes can be calculated if the Eu/oligo ratio of the probe and the amount of target on the solid support are known. The 14mers and 18mers showed hybridization efficiencies of about 20% and 25%, respectively, and those of the 21mers and 28mers were about 30% (Table 2). We observed some variation in the hybridization efficiencies between oligonucleotides of the same probing sequence length. However, there was no clear tendency indicating that the hybridization efficiency of the oligonucleotides was affected by the length of the NH<sub>2</sub>C tail or by the number of incorporated Eu chelates.

With a view to investigating the smallest detectable amount of Eu-labeled oligonucleotides, these were diluted in 200 μL/microtitration well of DELFIA enhancement solution and measured by TR fluorometry. The detection limit was directly dependent on the Eu/oligo ratio. Two attomol of oligonucleotide with 25 Eu chelates (N18C25Eu25) could be detected (data not shown).

The practical detection limit of Eu-labeled oligonucleotides was studied in a solid-phase hybridization assay.



**Figure 3.** Standard curves of N18C25 oligonucleotides with different Eu incorporation. N18C25Eu9 (circles), N18C25Eu14 (squares), and N18C25Eu25 (triangles) were hybridized at 10 ng/mL against varying amounts of immobilized N39C1Bio. Backgrounds (542 cps, 660 cps, and 715 cps for N18C25Eu9, N18C25Eu14, and N18C25Eu25, respectively) were subtracted from the obtained cps values.

The best sensitivity obtained was  $10^7$  target molecules (Table 2 and Figure 3). All the probes showing this high sensitivity contained at least 20 Eu chelates. Another important factor affecting the detection limit was background. Eu-labeled oligonucleotides exhibited a very low nonspecific binding (about  $1/10^7$  of the added probe). However, as shown in Table 2, the background was slightly elevated when oligonucleotides with a high Eu/oligo ratio were used. Eu-labeled oligonucleotides also gave a linear response in hybridization assays making quantitative analysis possible (Figure 3).

## DISCUSSION

The development and a closer characterization of a labeling method for the direct coupling of europium chelates to oligonucleotides was the initiative of this study. Directly Eu-labeled oligonucleotides are well-suited for many applications, e.g., as Eu-labeled hybridization probes and PCR primers (14, 23).

The synthesis of diaminohexane-modified deoxycytidine phosphoramidite is straightforward. A similar product has been described (4), but although most of the synthetic steps were identical, the present work utilized the relatively stable *N*-4-tosyl nucleoside as an intermediate for the introduction of a diaminohexane moiety (19). Due to its stability, large amounts of *N*-4-tosyl nucleoside could be prepared and stored as starting material.

The use of diaminohexane-modified deoxycytidine phosphoramidite allows preparation of multiply labeled oligonucleotides and insertion of  $\text{NH}_2\text{C}$  at any position(s) in the sequence during synthesis. Oligonucleotides with an  $\text{NH}_2\text{C}$  tail were synthesized with good yields with the exception of oligonucleotides with a tail of 40  $\text{NH}_2\text{C}$ 's. The reason for the low overall yield of oligonucleotides with 40  $\text{NH}_2\text{C}$ 's is not known. It is noteworthy that the methodology described herein can be used with commercial supports according to standard protocols. Alternatively, it is possible to use a modification of the phosphoramidite described by Nelson et al. (24), which is the UniLink aminomodifier (Clontech, Palo Alto, CA), for introduction of multiple amino groups to the oligonucleotide.

An important factor contributing to the high sensitivity of the presented labeling technology is the fact that several Eu chelates can be coupled to a single probe. In this study we were able to add up to 26 Eu chelates to an oligonucleotide. The Eu/oligonucleotide ratio could potentially be increased by adding a larger excess of Eu chelate to the labeling reaction when labeling oligonucleotides containing 40  $\text{NH}_2\text{C}$ 's. Using conventional fluorophores, such as fluorescein, it is not advantageous to employ multilabel procedures due to self-quenching (25). For europium chelates, which have a large Stokes' shift, self-quenching is not a problem. The hybridization sensitivity of Eu-labeled oligonucleotides ( $10^7$  target molecules) is at least as high as with other oligonucleotide-based detection systems (4).

The properties of Eu-labeled oligonucleotides were investigated in relation to dissociation temperature as well as hybridization kinetics and efficiency on solid support. The labeling procedure caused no apparent change in the  $T_d$ 's of the Eu-oligonucleotides. This was interesting since the molecular weight of the largest introduced modification in oligonucleotides used in the  $T_d$  analysis was in total about 30 000. Oligonucleotides labeled with the enzyme alkaline phosphatase have been reported to show a decrease of 5–10 °C in the melting temperature (3). The solid-phase hybridization kinetics of Eu oligonucleotides were affected. One possible explanation is that the increased molecular size affects the diffusion of the Eu-oligonucleotide to the surface of the well. However, closer examination of oligonucleotides differing only in the number of incorporated Eu chelates suggests that the higher molecular weight is not the main reason for slower hybridization kinetics. For example, the molecular weights of N18C10Eu2 and N18C10Eu10 are 11 000 and 17 000, respectively. Despite the considerable difference in the molecular weights, these two oligonucleotides hybridized at the same rate. Oligonucleotides N18C25Eu9 and N18C25Eu25 (molecular weights 22 000 and 33 000, respectively) were also kinetically similar with each other. A more plausible explanation is the effect of the total number of nucleotides in Eu-labeled oligonucleotides, that is the sequence complexity. As the total number of nucleotides in the probing sequence and  $\text{NH}_2\text{C}$  tail increased, the hybridization rate decreased. This is in agreement with the knowledge of the effect of sequence complexity on the hybridization kinetics (26).

The hybridization efficiency of Eu-labeled oligonucleotides was not detectably altered by the labeling process. It was evident that the length of the probing sequence was reflected in the hybridization efficiency. Eu-labeled oligonucleotides with a probing sequence of 21 or 28 nucleotides (N21 and N28) hybridized more efficiently than shorter ones. Additionally, the hybridization temperature (45 °C) for the longer probes (N28) was not optimum and thus the hybridization efficiencies achieved with the longer probes were not the actual best efficiencies obtainable with these probes.

## ACKNOWLEDGMENT

We thank Ms. Minna Alkio, Ms. Liisa Meriö, and Mr. Matti Wahlsten for technical assistance. We are indebted to Ms. Teija Ristelä for revising the language. This work was supported by the Finnish National Fund for Research and Development and the Finnish Technology Development Center.

## LITERATURE CITED

- (1) Saiki, R. K., Scharf, S., Faloona, F., Mullis, K. B., Horn, G. T., Erlich, H. A., and Arnheim, N. (1985) Enzymatic



- amplification of  $\beta$ -globin genomic sequences and restriction site analysis for diagnosis of sickle cell anemia. *Science* 230, 1350-1354.
- (2) Saiki, R. K., Gelfand, D. H., Stoffel, S., Scharf, S. J., Higuchi, R., Horn, G. T., Mullis, K. B., and Erlich, H. A. (1988) Primer directed enzymatic amplification of DNA with a thermostable DNA polymerase. *Science* 239, 487-491.
- (3) Jablonski, E., Moomaw, E. W., Tullis, R. H., and Ruth, J. L. (1986) Preparation of oligonucleotide-alkaline phosphatase conjugates and their use as hybridization probes. *Nucleic Acids Res.* 14, 6115-6128.
- (4) Urdea, M. S., Warner, B. D., Running, J. A., Stempien, M., Clyne, J., and Horn, T. (1988) A comparison of nonradioisotopic hybridization assay methods using fluorescent, chemiluminescent and enzyme-labeled synthetic oligodeoxyribonucleotide probes. *Nucleic Acids Res.* 16, 4937-4956.
- (5) Septak, M. (1989) Acridinium ester-labeled DNA oligonucleotide probes. *J. Biolumin. Chemilumin.* 4, 351-356.
- (6) Agrawal, S., Christodoulou, C., and Gait, M. J. (1986) Efficient methods for attaching nonradioactive labels to the 5' ends of synthetic oligodeoxyribonucleotides. *Nucleic Acids Res.* 14, 6227-6245.
- (7) Schmitz, G. G., Walter, T., Seibl, R., and Kessler, C. (1991) Nonradioactive labeling of oligonucleotides *in vitro* with hapten digoxigenin by tailing with terminal transferase. *Anal. Biochem.* 192, 222-231.
- (8) Soini, E., and Lövgren, T. (1987) Time-resolved fluorescence of lanthanide probes and applications in biotechnology. *CRC Crit. Rev. Anal. Chem.* 18, 105-153.
- (9) Syvänen, A.-C., Tchen, P., Ranki, M., and Söderlund, H. (1986) Time-resolved fluorometry: a sensitive method to quantify DNA-hybrids. *Nucleic Acids Res.* 14, 1017-1028.
- (10) Dahlén, P., Syvänen, A.-C., Hurskainen, P., Kwiatkowski, M., Sund, C., Ylikoski, J., Söderlund, H., and Lövgren, T. (1987) Sensitive detection of genes by sandwich hybridization and time-resolved fluorometry. *Mol. Cell. Probes* 1, 159-168.
- (11) Oser, A., Roth, W. K., and Valet, G. (1988) Sensitive non-radioactive dot-blot hybridization using DNA probes labeled with chelate group substituted psoralen and quantitative detection by europium ion fluorescence. *Nucleic Acids Res.* 16, 1181-1196.
- (12) Hurskainen, P., Dahlén, P., Ylikoski, J., Kwiatkowski, M., Siitari, H., and Lövgren, T. (1991) Preparation of europium-labeled DNA probes and their properties. *Nucleic Acids Res.* 19, 1057-1061.
- (13) Sund, C., Ylikoski, J., Hurskainen, P., and Kwiatkowski, M. (1988) Construction of europium ( $\text{Eu}^{3+}$ ) labeled oligo DNA hybridization probes. *Nucleosides Nucleotides* 7, 655-659.
- (14) Dahlén, P. O., Iitiä, A. J., Skagius, G., Frostell, A., Nunn, M. F., and Kwiatkowski, M. (1991) Detection of Human Immunodeficiency Virus Type 1 by using the polymerase chain reaction and a time-resolved fluorescence-based hybridization assay. *J. Clin. Microbiol.* 29, 798-804.
- (15) Prat, O., Lopez, E., and Mathis, G. (1991) Europium(III) Cryptate: A fluorescent label for the detection of DNA hybrids on solid support. *Anal. Biochem.* 195, 283-289.
- (16) Oser, A., Collasius, M., and Valet, G. (1990) Multiple end labeling of oligonucleotides with terbium chelate-substituted psoralen for time-resolved fluorescence detection. *Anal. Biochem.* 191, 295-301.
- (17) Bush, C. E., Di Michele, L. J., Peterson, W. R., Sherman, D. G., and Godsey, J. H. (1992) Solid-phase time-resolved fluorescence detection of Human Immunodeficiency Virus polymerase chain reaction amplification products. *Anal. Biochem.* 202, 146-151.
- (18) Gudgin Templeton, E. F., Wong, H. E., Evangelista, R. A., Granger, T., and Pollak, A. (1991) Time-resolved fluorescence detection of enzyme-amplified lanthanide luminescence for nucleic acid hybridization assays. *Clin. Chem.* 37, 1506-1512.
- (19) Kierzek, R., and Markiewicz, W. T. (1987) Synthesis of 5'-O-dimethoxytrityl-4-N-(trifluoroacetamidohexyl)-2'-deoxycytidine and its application in the synthesis of biotin-labeled oligonucleotides. *Nucleosides Nucleotides* 6, 403-405.
- (20) Sinha, N. D., Biernat, J., McManus, J., and Köster, H. (1984) Polymer support oligonucleotide synthesis XVIII: use of  $\beta$ -cyanoethyl-N,N-dialkylamino-N-morpholino phosphoramidite deoxynucleosides for the synthesis of DNA fragments simplifying deprotection and isolation of the final product. *Nucleic Acids Res.* 12, 4539-4557.
- (21) Sambrook, J., Fritsch, E. F., and Maniatis, T. (1989) *Molecular Cloning: A laboratory manual*, Cold Spring Harbor Laboratory Press, Cold Spring Harbor.
- (22) Rychlik, W., and Rhoads, R. E. (1989) A computer program for choosing optimal oligonucleotides for filter hybridization, sequencing and *in vitro* amplification of DNA. *Nucleic Acids Res.* 17, 8543-8551.
- (23) Dahlén, P., Iitiä, A., Mikkala, V.-M., Hurskainen, P., and Kwiatkowski, M. (1991) The use of europium ( $\text{Eu}^{3+}$ ) labeled primers in PCR amplification of specific target DNA. *Mol. Cell. Probes* 5, 143-149.
- (24) Nelson, P. S., Sherman-Gold, R., and Leon, R. (1989) A new and versatile reagent for incorporating multiple primary aliphatic amines into synthetic oligonucleotides. *Nucleic Acids Res.* 17, 7179-7186.
- (25) Haralambidis, J., Angus, K., Pownall, S., Duncan, L., Chai, M., and Treager, G. W. (1990) The preparation of polyamide-oligonucleotide probes containing multiple nonradioactive labels. *Nucleic Acids Res.* 18, 501-505.
- (26) Meinkoth, J., and Wahl, G. (1984) Hybridization of nucleic acids immobilized on solid supports. *Anal. Biochem.* 138, 267-284.

# TECHNICAL NOTES

## Peroxidase Labeling of IgMs Fragment of ABO Blood Group Specific Mouse Monoclonal IgM

Nobuhiro Yukawa, Hirokazu Matsuda, Yasuhisa Seo, Katsutoshi Suetomi, and Keiichi Takahama\*

Department of Legal Medicine, Miyazaki Medical College, Kiyotake, Miyazaki 889-16, Japan.

Received January 14, 1994\*

A method for peroxidase labeling of the monomeric subunit (IgMs) of ABO blood group specific mouse monoclonal IgM is described. IgM was purified from a commercial monoclonal anti-B blood grouping reagent by a combination of salt precipitation, euglobulin precipitation, and gel filtration. IgM was mildly reduced with L-cysteine to yield SH-bearing IgMs. Finally, IgMs was conjugated to horseradish peroxidase, into which SH-reacting maleimide groups had been introduced using *N*-succinimidyl 6-maleimidohexanoate, through the selective reaction between SH of IgMs and maleimide groups of peroxidase.

### INTRODUCTION

Being produced under the requirement for efficient hemagglutination activity, most commercial monoclonal ABO blood grouping reagents are of the IgM class. By combining ABO-specific mouse monoclonal IgM with an enzyme-labeled (anti-mouse IgM) IgG, forensic and medico-legal investigators developed many indirect enzyme immunoassays for ABH blood group substances in body fluids (1-3), and these have been proven to work quite accurately and reliably (4, 5). The encouraging results achieved by the indirect enzyme immunoassays evoked expectations for a simpler and more convenient direct enzyme immunoassay employing enzyme-labeled ABO-specific monoclonal IgM. This prompted us to develop a peroxidase-labeling method suitable for ABO-specific monoclonal IgM.

### EXPERIMENTAL PROCEDURES

Scheme 1 illustrates the principle of the method. Mouse IgM consists of five monomeric subunits (IgMs,  $H_2L_2$ )<sup>1</sup> and one J chain joined by disulfide bonds at the penultimate cysteine of the H chain (6). The J chain, which accounts for approximately 2% of the total molecular weight of IgM (7), is not depicted in the scheme.

Throughout the experiments, column chromatography (gel filtration) was performed at room temperature. Buffers used for equilibrating and running columns were degassed by an aspirator vacuum under sonication for 15-20 min. The other buffers were not degassed.

**Purification of Monoclonal IgM.** Mouse monoclonal IgM was purified by a combination of neutral salt

precipitation, euglobulin precipitation upon dialysis under very low ionic strength conditions, and gel filtration described by Hayzer and Jatton (8). The amount of IgM was calculated from the absorbance at 278 nm by taking the extinction coefficient to be  $1.35 \text{ g}^{-1} \cdot \text{L} \cdot \text{cm}^{-1}$  (9).

One hundred mL of Bioclone anti-B (Lot No. BBB512D-1, Ortho Diagnostics, Raritan, NJ) was precipitated with 20 g of  $\text{Na}_2\text{SO}_4$ . The precipitate was dissolved in 4.0 mL of 0.155 mol/L NaCl and then thoroughly dialyzed against distilled water at 4 °C. The precipitate which formed was dissolved in 3.0 mL of 50 mmol/L tris(hydroxymethyl)-aminomethane Tris-HCl buffer, pH 8.0, containing 0.5 mol/L NaCl and subjected to gel filtration on a column ( $1.6 \times 70 \text{ cm}$ ) of Ultrogel AcA 22 (IBF biotechnics, Villeneuve-la-Garenne, France) using the same buffer (Figure 1). The amount of IgM obtained was 6.1 mg.

**Preparation of Maleimide-Peroxidase.** Maleimide groups were introduced into peroxidase using *N*-succinimidyl 6-maleimidoheptanoate according to Hashida et al. (10). The amount of maleimide-peroxidase was calculated from the absorbance at 403 nm by taking the extinction coefficient and the molecular weight to be  $2.275 \text{ g}^{-1} \cdot \text{L} \cdot \text{cm}^{-1}$  and 40 000, respectively (11).

Horseradish peroxidase (6.7 mg, Grade I, Boehringer-Mannheim GmbH, Mannheim, FRG) in 1.0 mL of 0.1 mol/L sodium phosphate buffer, pH 7.0, was mixed with 0.10 mL of 27.5 mmol/L *N*-succinimidyl 6-maleimidoheptanoate (Dojindo, Kumamoto, Japan) in *N,N*-dimethylformamide. After incubation at 30 °C for 45 min, the reaction mixture was subjected to gel filtration on a column ( $1.0 \times 30 \text{ cm}$ ) of Sephadex G-25 medium (Pharmacia Fine Chemicals AB, Uppsala, Sweden) using 20 mmol/L sodium phosphate buffer, pH 6.8, containing 0.14 mol/L NaCl and 2 mmol/L ethylenediaminetetraacetate (EDTA). The average number of maleimide groups introduced per one peroxidase molecule was 1.5 (11).

**Mild Reduction of IgM To Yield Monomeric Subunit (IgMs).** IgM was mildly reduced with L-cysteine to yield IgMs according to Hashimoto et al. (12). The amount of IgMs was calculated from the absorbance at 280 nm by taking the extinction coefficient and the molecular weight to be  $1.29 \text{ g}^{-1} \cdot \text{L} \cdot \text{cm}^{-1}$  (13) and 180 000 (12), respectively.

\* Abstract published in *Advance ACS Abstracts*, April 15, 1994.

<sup>1</sup>Abbreviations used: IgMs, monomeric subunit of IgM pentamer; H and L, heavy and light (chains); Tris, tris(hydroxymethyl)aminomethane; EDTA, ethylenediaminetetraacetate; PBS, phosphate-buffered saline (10 mmol/L sodium phosphate buffer, pH 7.3, containing 0.145 mol/L NaCl); NC membrane, nitrocellulose membrane; Tween 20, polyoxyethylene sorbitan monolaurate; SDS-PAGE, sodium dodecyl sulfate-polyacrylamide gel electrophoresis.

IgM (5.0 mg) in 1.2 mL of 0.2 mol/L Tris-HCl buffer, pH 8.6, was mixed with 0.12 mL of 550 mmol/L L-cysteine (Nacalai Tesque Ltd., Kyoto, Japan) in the same buffer.<sup>2</sup> After incubation at 27 °C for 10 min, the reaction mixture was cooled on ice and immediately subjected to gel filtration on a column (1.5 × 45 cm) of Ultrogel AcA 34 (IBF biotechnics) using 20 mmol/L sodium phosphate buffer, pH 6.8, containing 0.14 mol/L NaCl and 2 mmol/L EDTA at a flow rate of 21 mL/h (Figure 2). Fractions containing IgMs were pooled, concentrated with an ultrafiltration membrane (Diaflo PM-30, 25 mm in diameter, Amicon Corp., Danvers, MA), and immediately subjected to conjugation to maleimide-peroxidase. The amount of IgMs obtained was 1.7 mg.

**Conjugation of IgMs to Maleimide-Peroxidase.** IgMs was reacted with maleimide-peroxidase to produce IgMs-peroxidase conjugate. The amount of IgMs-peroxidase conjugate was calculated from the absorbance at 280 nm and 403 nm (11) by taking the extinction coefficient of IgMs (1.29 g<sup>-1</sup>·L·cm<sup>-1</sup> at 280 nm) (13) together with the molecular weight of IgMs (180 000) (12) and the extinction coefficient of peroxidase (0.73 g<sup>-1</sup>·L·cm<sup>-1</sup> at 280 nm and 2.275 g<sup>-1</sup>·L·cm<sup>-1</sup> at 403 nm) together with the molecular weight of peroxidase (40 000) (11).

IgMs (1.7 mg) in 1.5 mL of 20 mmol/L sodium phosphate buffer, pH 6.8, containing 0.14 mol/L NaCl and 2 mmol/L EDTA was mixed with maleimide-peroxidase (1.1 mg) in 0.43 mL of the same buffer and then concentrated at 4 °C with a microconcentrator (Centricon 30, Amicon Corp.) to a final volume of 0.26 mL. The concentration of IgMs and maleimide-peroxidase in the reaction mixture were 30 μmol/L and 90 μmol/L, respectively. After incubation at 4 °C for 16 h, the reaction mixture was subjected to gel filtration on the Ultrogel AcA 34 column (1.5 × 45 cm) using 100 mmol/L sodium phosphate buffer, pH 6.5. Fractions containing immunoreactive IgMs-peroxidase (Figure 3, fractions 35–48), which were determined as described below, were pooled. The amount of IgMs-peroxidase obtained was 1.5 mg (1.01 mg as IgMs and 0.51 mg as peroxidase). The molar ratio of peroxidase to IgMs in the conjugate was hence calculated to be 2.3.

**Dot Immunoblotting.** Fractions containing immunoreactive anti-B IgMs-peroxidase conjugate from gel filtration on an Ultrogel AcA 34 column were determined using the dot immunoblotting method (3), with modifications. Saliva from a blood group B ABH-secreter was diluted 100- to 3000-fold with phosphate-buffered saline (PBS), and 2 μL of the diluent was applied on a nitrocellulose (NC) membrane (0.45 μm, Bio-Rad laboratories, Richmond, CA). After blocking with a commercial buffer solution for an enzyme immunoassay containing casein (Block Ace, Snow Brand Co. Ltd., Sapporo, Japan), the NC membrane was incubated with anti-B IgMs-peroxidase conjugate from each fraction (3.0 μg/mL as peroxidase) in Block Ace diluted 10-fold with distilled water at room temperature for 1 h. After the NC membrane was washed three times with 50 mmol/L Tris-HCl buffer, pH 7.5, containing 0.5 mol/L NaCl and 0.1 % Tween 20 (polyoxyethylene sorbitan monolaurate), peroxidase activity bound on the NC membrane was visualized

with a commercial immunostain kit for peroxidase (Konika HRP, Konika Corp., Tokyo, Japan).<sup>3</sup>

After the fractions containing immunoreactive anti-B IgMs-peroxidase conjugate (Figure 3, fractions 35–48) were pooled, the antigen-binding activity of the anti-B IgMs-peroxidase conjugate was compared with that of the initial anti-B IgM by the dot blotting method. Blood group O, A, B, and AB ABH-secreter saliva samples diluted with 10- to 30 000-fold with PBS were used as antigens. As for the anti-B IgMs-peroxidase conjugate, the procedure was the same as described above, and the concentration of IgMs-peroxidase conjugate was 5.9 μg/mL as IgMs or 3.0 μg/mL as peroxidase. As for anti-B IgM, an indirect method, in which IgM was used as primary antibody and affinity-purified goat (anti-mouse IgM) IgG-peroxidase conjugate (Tago, Inc., Burlingame, CA) was used as secondary antibody, was adopted. The concentration of IgM was 5.9 μg/mL and the dilution of IgG-peroxidase conjugate was 1/500. The incubation times of the first incubation (IgM) and the second incubation (IgG-peroxidase) were both 1 h.

**Purity and Stability of IgMs.** IgMs prepared from another lot of Bioclone anti-B (100 mL, Lot No. BBB-533A21, Ortho Diagnostics) was used for characterizing IgMs. In this lot, 2.3 mg of IgMs was obtained from 4.8 mg of IgM.

The purity of IgMs was assessed by sodium dodecyl sulfate-polyacrylamide gel electrophoresis (SDS-PAGE) under reducing conditions (14). The separation on an 8–25 % gradient gel followed by staining with Coomassie Brilliant Blue was performed using Phast System (Pharmacia Fine Chemicals AB). The gel was scanned at 660 nm using a Beckman spectrophotometer (DU-65) with Soft-Pac modules for determination of area and molecular weight (Beckman Instruments, Inc., Fullerton, CA).

SH content and elution profile of gel filtration were examined for assessing the stability of IgMs in 20 mmol/L sodium phosphate buffer, pH 6.8, containing 0.14 mol/L NaCl and 2 mmol/L EDTA. IgMs eluted from an Ultrogel AcA 34 column (1.5 × 45 cm) at a flow rate of 21 mL/h (Figure 5a, fractions 40–50)<sup>4</sup> were pooled (0.24 mg/mL), concentrated to a volume of 1.5 mL (1.5 mg/mL), and then left standing on ice for 6 h, during which time the SH content in the IgMs was determined using 4,4'-dithiodipyridine (11, 15) as described below. Finally, the concentrated IgMs was mixed with *N*-ethylmaleimide (5 mmol/L in the mixture, Nacalai Tesque Ltd.) for blocking the remaining SH groups and subjected to gel filtration on the same column at the same flow rate.

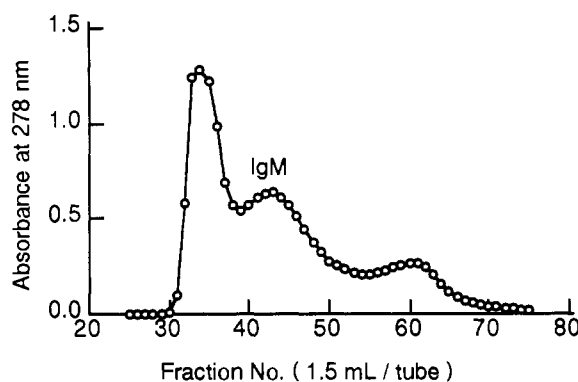
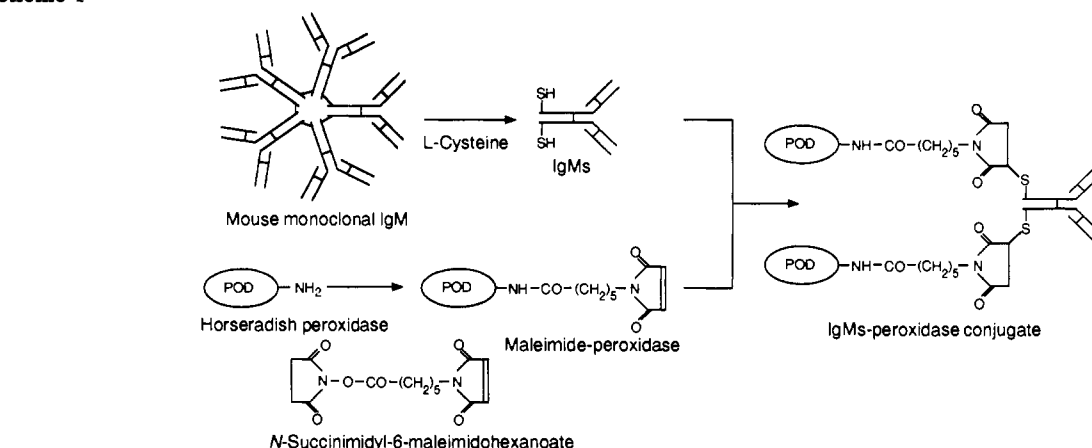
Twenty μL of 5 mmol/L 4,4'-dithiodipyridine (Nacalai Tesque Ltd.) was added to 0.6 mL of the pooled IgMs before (0.24 mg/mL) and after concentration (rediluted to a concentration of 0.19 mg/mL from 1.5 mg/mL) in 20 mmol/L sodium phosphate buffer, pH 6.8, containing 0.14 mol/L NaCl and 2 mmol/L EDTA or to the same buffer as a reference. After 10 min incubation at 30 °C, the absorbance at 324 nm was measured and the number of

<sup>3</sup>A dark blue color was developed by the heterocoupling reaction between a naphthol derivative and an aromatic amine derivative under the presence of H<sub>2</sub>O<sub>2</sub>. The exact chemical formulas of the derivatives were not available to the users.

<sup>4</sup>IgMs was eluted more rapidly from a column of Ultrogel AcA 34 purchased recently (57 % of the column volume, Figure 5) than from that purchased a few years before (65 %, Figure 2). Although this difference might be inevitable variation in gel filtration, we felt that some physicochemical properties of Ultrogel AcA 34 had been modified as we had similar experiences for Ultrogel AcA 44.

<sup>2</sup>L-Cysteine solution was prepared just prior to use by dissolving L-cysteine (not L-cysteine monohydrochloride monohydrate) in 0.2 mol/L Tris-HCl buffer, pH 8.6. The pH of the solution was not measured.

## Scheme 1



**Figure 1.** Elution profile of crude IgM on an Ultrogel AcA 22 column ( $1.6 \times 70$  cm). IgM was eluted in the second peak (fractions 40–47).

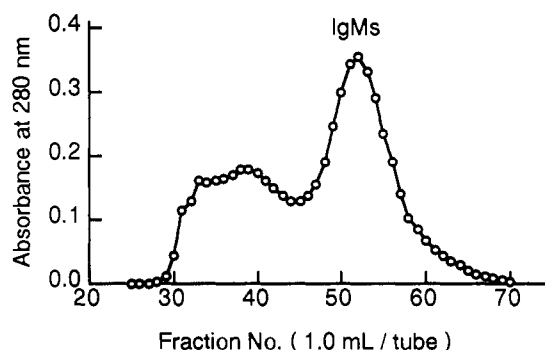
SH groups per one IgMs molecule was calculated by taking the molar extinction coefficient of 4-mercaptopyridine to be 19 800 (15). The initial IgM was also examined and found to have no free SH groups.

## RESULTS AND DISCUSSION

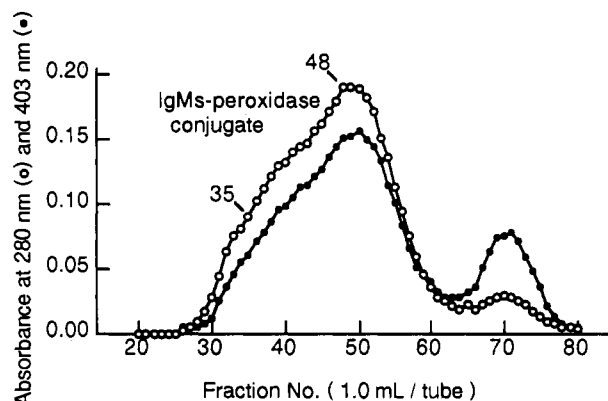
**Development of the Method.** Ishikawa and co-workers (16, 17) established an excellent method, the so-called “hinge method”, for the labeling of IgG with enzymes through the selective reaction between SH in the hinge of the Fab’ fragment of IgG and maleimide groups introduced into enzymes. A similar strategy was used for the coating of liposome with IgG by Martin and Papahadjopoulos (18). They introduced maleimide groups into the liposome membrane and coupled the liposome to the Fab’ fragment of IgG. By the replacement of Fab’ with the monomeric subunit (IgMs) of IgM, Hashimoto et al. (12, 19) were able to coat liposome with monoclonal IgM. The present method has been developed from a modification of these methods (Scheme 1).

**Monoclonal IgM.** After enrichment by physicochemical means, the final purification of IgM was performed by gel filtration on an Ultrogel AcA 22 column. IgM was eluted in the second peak (Figure 1). IgM was subjected to mild reduction without further purification.

**Preparation of Monomeric Subunit (IgMs) of IgM.** IgMs was prepared from IgM by mild reduction with L-cysteine, followed by gel filtration on an Ultrogel AcA 34 column. IgMs was eluted in the second peak (Figure 2). Hashimoto et al. (12) stated that it was necessary to seek the optimal concentration of IgM or L-cysteine in order to achieve a good yield of IgMs for each monoclonal IgM. In this experiment, the yield of the IgMs was 34%,



**Figure 2.** Elution profile of mildly reduced IgM on an Ultrogel AcA 34 column ( $1.5 \times 45$  cm). IgMs was eluted in the second peak (fractions 48–57).

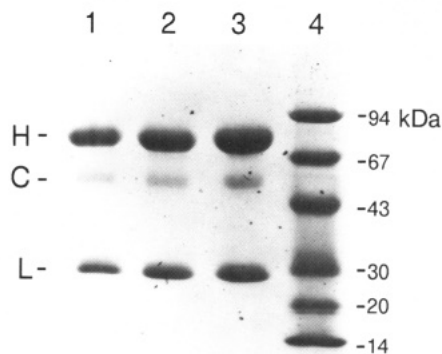


**Figure 3.** Elution profile of the reaction mixture of IgMs and maleimide-peroxidase on an Ultrogel AcA 34 column ( $1.5 \times 45$  cm). Fractions 35–48 contained immunoreactive IgMs-peroxidase conjugate.

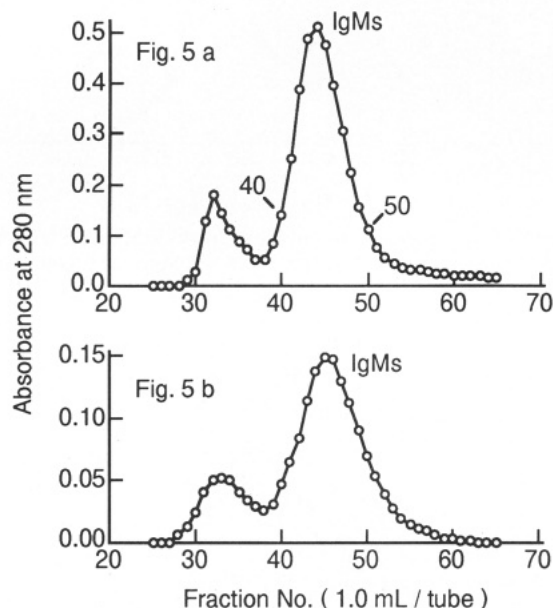
which was lower than that previously obtained (50%) (12) but was sufficient for performing conjugation. Thus, we did not optimize the reducing conditions with trial and error.

**Purity and Stability of IgMs.** SDS-PAGE of IgMs under reducing conditions showed H and L chain migrating at molecular masses of 79 and 27 kDa, respectively, which were similar to those (80 and 25 kDa) reported by Knutson et al. (20), and one contaminant migrating at a molecular mass of 58 kDa (Figure 4). The nature of the contaminant was unknown. By densitography, the purity of the IgMs (H and L chains) was estimated to be 91–92%.

The stability of IgMs before conjugation was assessed as follows. (1) Fractions containing IgMs eluted from an Ultrogel AcA 34 column (Figure 5a) were pooled and



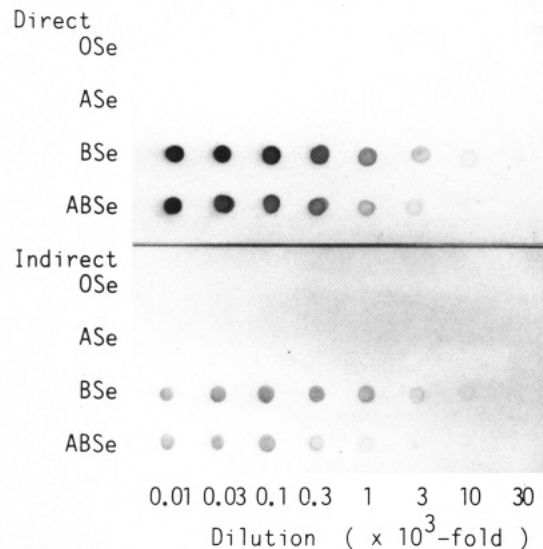
**Figure 4.** SDS-PAGE of IgMs under reducing conditions using an 8–25% gradient gel. Lanes 1, 2, and 3: IgMs (1, 2, and 3  $\mu$ g per lane, respectively). Lane 4: markers. For 1  $\mu$ g of IgMs, the areas of H chain (H), L chain (L), and a contaminant (C) on the densitogram comprised 61.7%, 31.0%, and 7.3%, respectively, and the purity of IgMs was hence calculated to be 92%. Almost the same value (91%) was obtained for 2  $\mu$ g, but a somewhat lower value (87%) was obtained for 3  $\mu$ g probably due to a nonlinear increase in the areas.



**Figure 5.** Changes in elution profile of IgMs after 6 h storage (b). IgM was mildly reduced and subjected to an Ultrogel AcA 34 column (1.5  $\times$  45 cm), and fractions containing IgMs (40–50) (a) were pooled and concentrated. After being left on ice for 6 h, the concentrated IgMs was resubjected to the same column (b).

concentrated to a volume suitable for conjugation. The number of SH groups per one IgMs molecule was 7.2 for the pooled IgMs and was decreased to 6.6 after concentration. The concentrated IgMs was then left standing on ice for 6 h, during which time the values were found to remain essentially unchanged (6.5–6.7). (2) After 6 h of standing on ice, the IgMs was resubjected to gel filtration on the Ultrogel AcA 34 column (Figure 5b). The chromatogram showed a major peak corresponding to IgMs and a minor peak with larger molecular mass. The areas of the major and the minor peaks comprised 79% and 21%, respectively. These results (1 and 2) indicated that IgMs was relatively stable, though some IgMs seemed to reassemble by oxidation.

The number of SH per IgMs ( $H_2L_2$ ) were larger (6.6–7.2) than that (2) expected from Scheme 1. Part of the difference (two SH per IgMs) seemed to be well explained by Clem and co-workers' observations (21, 22) that IgMs



**Figure 6.** Direct dot immunoblotting for O, A, B, and AB ABH-secreter saliva samples (OSe, ASe, BSe, and ABSe) using anti-B IgMs-peroxidase conjugate (top) and indirect dot immunoblotting for the same samples using the initial anti-B IgM with (anti-mouse IgM) IgG-peroxidase conjugate (bottom). Dilutions of saliva samples were from 10- to 30 000-fold. The detection limits both by the direct method and those by the indirect method were approximately 3000-fold dilution for BSe and 1000-fold dilution for ABSe.

prepared by mild reduction of IgM consisted of two covalent H–L chain halfmers which were noncovalently bound together. Cleavage of disulfide bonds within and between the H and L chains with resultant formation of smaller fragments (e.g.,  $H_2L$ ) might also contribute to the difference.

**IgMs–Peroxidase Conjugate.** IgMs was conjugated to maleimide–peroxidase through the selective reaction between SH of IgMs and maleimide groups of peroxidase and then subjected to gel filtration on an Ultrogel AcA 34 column. IgMs–peroxidase conjugate (the first broad peak) was separated from unconjugated peroxidase (the second peak) but not separated from unconjugated IgMs (Figure 3). The antigen-binding activity of IgMs–peroxidase conjugate tended to be less in the lower half section from the top (fraction 49) of the first broad peak. This decrease might be due to less or nonimmunoreactive complexes (e.g.,  $H_2L$ –peroxidases) with smaller sizes than IgMs ( $H_2L_2$ )–peroxidase conjugate. The fractions from the upper half section (fractions 35–48) were pooled and used in the following experiment in order to confirm the conservation of antigen-binding activity of anti-B IgMs–peroxidase conjugate.

**Antigen-Binding Activity of IgMs–Peroxidase Conjugate.** Blood group O, A, B, and AB ABH-secreter saliva samples were diluted 10- to 30 000-fold with PBS and were then subjected to both a direct dot immunoblotting using anti-B IgMs–peroxidase conjugate and an indirect dot immunoblotting using the initial anti-B IgM with (anti-mouse IgM) IgG–peroxidase conjugate. There was no significant difference between the detection limits by the direct method and those by the indirect method (Figure 6). This indicated that no significant decrease in antigen-binding activity occurred for most part of the monoclonal anti-B IgM during conjugation.

Fujiwara et al. (21) succeeded in  $\beta$ -galactosidase-labeling of monoclonal anti-Lewis<sup>x</sup> IgM, in which maleimide groups were introduced into IgM by the use of amino groups of IgM and then reacted with SH of  $\beta$ -galactosidase. The random use of amino groups, however, may possibly cause

a decrease in antigen-binding activities of some monoclonal IgM due to the modification of amino groups which are located within or in close proximity to antigen binding sites (22). In the present method, although precise locations of SH groups used for conjugation were not determined, the SH groups released from disulfide bonds between monomeric subunits (IgMs) seemed much more accessible to maleimide-peroxidase than those released from other disulfide bonds (e.g., SH groups released from disulfide bonds between two H-L chain halfmers seemed hidden by noncovalent association of the two halfmers). Antigen-binding activities of most monoclonal IgM would thereby be conserved, and we hope the present method is applicable to other ABO blood group specific monoclonal IgM.

**Anti-A IgMs-Peroxidase Conjugate.** Mouse monoclonal anti-A IgM purified from Bioclone anti-A (Lot No. BAA 116G-1, Ortho Diagnostics) also could be labeled with peroxidase, and the results were briefly described. Anti-A IgM (7.9 mg) was reduced with L-cysteine at 27 °C for 10 min, in which the concentrations of IgM and L-cysteine were 3.8 mg/mL and 50 mmol/L, respectively. All IgMs obtained (3.6 mg) were reacted three times (mol/mol) with maleimide-peroxidase and resulted in 2.2 mg of immunoreactive anti-A IgMs-peroxidase conjugate (1.41 mg as IgMs and 0.76 mg as peroxidase). The molar ratio of IgMs to peroxidase in the conjugate was hence calculated to be 2.4.

#### ACKNOWLEDGMENT

We are profoundly grateful to Professor Dr. Eiji Ishikawa, Dr. Takeyuki Kohno, Dr. Seiichi Hashida, and Dr. Koichiro Tanaka for their kind advice. We also thank to Professor Dr. Minoru Hamada and Dr. Hitoshi Takenaka for the use of a Beckman spectrophotometer.

#### LITERATURE CITED

- (1) Bolton, S., and Thorpe, J. W. (1986) Enzyme-linked immunosorbent assay for A and B water soluble blood group substances. *J. Forensic Sci.* 31, 27-35.
- (2) Takizawa, N., Ohba, Y., Mukoyama, R., Komuro, T., Mukoyama, H., and Takei, T. (1989) Determination of ABO blood groups from saliva and saliva stains by an indirect enzyme-linked immunosorbent assay (ELISA) using monoclonal antibodies. *Nippon Hoigaku Zasshi* 43, 294-302.
- (3) Pflug, W., Bässler, G., and Eberspächer, B. (1989) ABO and Lewis typing of secretion stains on nitrocellulose membranes using a new dot-blot-ELISA technique. *Forensic Sci. Int.* 43, 171-182.
- (4) Bolton, S., and Thorpe, J. (1988) An examination of a contaminated seminal stain using absorption-elution and enzyme-linked immunosorbent assay (ELISA). *J. Forensic Sci.* 33, 797-800.
- (5) De Soyza, K. (1991) Evaluation of an enzyme linked immunosorbent assay (ELISA) method for ABO and Lewis typing of body fluids in forensic samples. *Forensic Sci. Int.* 52, 65-76.
- (6) Davis, A. C., Roux, K. H., and Shulman, M. J. (1988) On the structure of polymeric IgM. *Eur. J. Immunol.* 18, 1001-1008.
- (7) Koshland, M. E. (1985) The coming of age of the immunoglobulin J chain. *Ann. Rev. Immunol.* 3, 425-453.
- (8) Hayzer, D. J., and Jaton, J.-C. (1985) Immunoglobulin M (IgM). *Methods Enzymol.* 116, 26-36.
- (9) Dombink-Kurtzman, M. A., and Voss, E. W. (1988) Cryoprecipitation properties of a high-affinity monoclonal IgM anti-fluorescein antibody. *Mol. Immunol.* 25, 1309-1320.
- (10) Hashida, S., Imagawa, M., Inoue, S., Ruan, K.-H., and Ishikawa, E. (1984) More useful maleimide compounds for the conjugation of Fab' to horseradish peroxidase through thiol groups in the hinge. *J. Appl. Biochem.* 6, 56-63.
- (11) Ishikawa, E., Imagawa, M., Hashida, S., Yoshitake, S., Hamaguchi, Y., and Ueno, T. (1983) Enzyme-labeling of antibodies and their fragments for enzyme immunoassay and immunohistochemical staining. *J. Immunoassay* 4, 209-327.
- (12) Hashimoto, Y., Sugawara, M., Kamiya, T., and Suzuki, S. (1986) Coating of liposomes with subunits of monoclonal IgM antibody and targeting of the Liposomes. *Methods Enzymol.* 121, 817-828.
- (13) Sunamoto, J., Sato, T., Hirota, M., Fukushima, K., Hiratani, K., and Hara, K. (1987) A newly developed immunoliposome—An egg phosphatidylcholine liposome coated with pullulan bearing both a cholesterol moiety and an IgMs fragment. *Biochim. Biophys. Acta* 898, 323-330.
- (14) Laemmli, U. K. (1970) Cleavage of structural proteins during the assembly of the head of bacteriophage T4. *Nature* 227, 680-685.
- (15) Grassetti, D. R., and Murray, J. F., Jr. (1967) Determination of sulfhydryl groups with 2,2'- or 4,4'- dithiodipyridine. *Arch. Biochem. Biophys.* 119, 41-49.
- (16) Yoshitake, S., Yamada, Y., Ishikawa, E., and Masseyeff, R. (1979) Conjugation of glucose oxidase from *Aspergillus niger* and rabbit antibodies using *N*-hydroxysuccinimide ester of *N*-(4-carboxycyclohexylmethyl)-maleimide. *Eur. J. Biochem.* 101, 395-399.
- (17) Ishikawa, E. (1987) Development and clinical application of sensitive enzyme immunoassay for macromolecular antigens—A review. *Clin. Biochem.* 20, 375-385.
- (18) Martin, F. J., and Papahadjopoulos, D. (1982) Irreversible coupling of immunoglobulin fragments to preformed vesicles—An improved method for liposome targeting. *J. Biol. Chem.* 257, 286-288.
- (19) Hashimoto, Y., Sugawara, M., and Endoh, H. (1983) Coating of liposomes with subunits of monoclonal IgM antibody and targeting of the liposomes. *J. Immunol. Methods* 62, 155-162.
- (20) Knutson, V. P., Buck, R. A., and Moreno, R. M. (1991) Purification of a murine monoclonal antibody of the IgM class. *J. Immunol. Methods* 136, 151-157.
- (21) Fujiwara, K., Matsumoto, N., Yagisawa, S., Tanimori, H., Kitagawa, T., Hirota, M., Hiratani, K., Fukushima, K., Tomonaga, A., Hara, K., and Yamamoto, K. (1988) Sandwich enzyme immunoassay of tumor-associated antigen sialosylated Lewis<sup>x</sup> using  $\beta$ -D-galactosidase coupled to a monoclonal antibody of IgM isotype. *J. Immunol. Methods* 112, 77-83.
- (22) O'Shannenssy, D. J., and Quarles, R. H. (1987) Review article—Labeling of the oligosaccharide moieties of immunoglobulins. *J. Immunol. Methods* 99, 153-161.
- (23) Giles, R. C., Klapper, D. G., and Clem, L. W. (1983) Intramolecular heterogeneity of ligand binding by two IgM antibodies derived from murine hybridomas. *Mol. Immunol.* 20, 737-744.
- (24) Pascual, D., and Clem, L. W. (1988) Ligand binding by murine IgM antibodies: Intramolecular heterogeneity exists in certain, but not all, cases. *Mol. Immunol.* 25, 87-94.



# Synthesis of Europium(III) Chelates Suitable for Labeling of Bioactive Molecules

Harri Takalo,\*<sup>†</sup> Veli-Matti Mukkala,<sup>‡</sup> Heikki Mikola,<sup>‡</sup> Päivi Liitti,<sup>†</sup> and Ilkka Hemmilä

Wallac Oy, P. O. Box 10, FIN-20101 Turku, Finland, Department of Chemistry, University of Turku, FIN-20500 Turku, Finland, and Centre for Biotechnology, P. O. Box 123, FIN-20521 Turku, Finland.

Received March 30, 1993\*

Two different kinds of europium(III) chelates, luminescent and nonluminescent, were prepared. The chelates were coupled to bioanalytical reagents, such as antibodies, after activations of the amino group on the chelates with thiophosgene, 2,4,6-trichloro-1,3,5-triazine, or iodoacetic anhydride. The reactivities of the activated luminescent chelates in the labeling of antibodies as well as the effects of both the coupling ratio and the linkage group to the luminescence quantum yield of the antibody-bound chelate were studied in aqueous buffer solution.

## INTRODUCTION

Due to their unique luminescence properties lanthanide chelates have recently been developed and used as labels both in immunological and in DNA hybridization assays (1, 2). The types of chelates synthesized include lanthanide cryptates (3), macrocyclic Schiff bases (4), and polyaminopolycarboxylates (2, 5-11).

The commonly used commercial system, DELFIA (Wallac Oy, Turku, Finland), is based on the use of non-luminescent europium(III) chelates (2, 5-7) as the labels. After completion of the specific binding reaction the lanthanide ions are dissociated from the nonluminescent transporting chelates, and the luminescence is enhanced in a micellar chelating environment. In DELFIA-type immunoassays, the label is a lanthanide (Eu(III), Sm(III), or Tb(III)) chelate of *N*-(isothiocyanatobenzyl)diethylenetriamine-*N,N',N'',N'''*-tetrakis(acetic acid) (5) whereas in DNA hybridization assays the chelate is composed of 2,2',2'',2'''-[[4-[2-(4-isothiocyanatophenyl)ethyl]pyridine-2,6-diyl]bis(methylenenitrilo)]tetrakis(acetic acid) (10a in Scheme 1) because that chelate better tolerates conditions used in hybridization (6, 7).

The marker release prohibits the application of DELFIA labels in areas where the luminescence signals have to be localized, e.g., *in situ* immunostaining, *in situ* and Southern blot nucleic acid hybridization, DNA sequencing, or in cytofluorometry. The other way to utilize lanthanide chelates is to use a free luminogenic ligand as a label and saturate the ligand afterwards with the ion (12). There are, however, numerous reasons why a stable luminescent chelate would be preferred. The ligands which can be used as luminogenic labels are generally only three dentate, and before measurement the surface has to be dried to avoid aqueous quenching (13). In addition, the use of free ligand requires an additional step in the indirect staining process to avoid ligand contamination with endogenous ions originating from the sample and the final luminescence depends, amongst other things, on the chelate stoichiometry and humidity of the surface. A stable, multidentate, luminescent chelate would eliminate all these problems and make the staining simple and the response quantitative.

A large number of ligands capable of forming stable and luminescent complexes with lanthanides have been prepared (14-18). As a part of these studies, the europium(III) chelate of 2,2',2'',2'''-[[4-[2-(4-isothiocyanatophenyl)ethynyl]pyridine-2,6-diyl]bis(methylenenitrilo)]-tetrakis(acetic acid) (13a in Scheme 1) was used as a luminescent label in time-resolved fluorescence microscopy for localization of antigens, mRNAs and gene sequences on the cell and tissue level (9).

As yet, though, a good preparation method of the europium(III) chelate 10a (DELFI DNA labeling chelate) has not been reported, and the only reported synthesis of ligand 8 contains many steps (19). The present work describes in detail the preparation of 13a and gives a simple method for the synthesis of 10a from the same key intermediate 6 (18). In the present work we have also used different activation methods including 2,4,6-trichloro-1,3,5-triazine (DTA) and iodoacetic anhydride (I-Acet) in addition to thiophosgene (NCS) for coupling the chelates to biomolecules. The effect of both coupling ratio (chelates per biomolecule) and the chemical linkage between the chelate and a biomolecule to luminescence properties were studied by conjugating luminescent chelates 13a-c to an antibody, rabbit anti-mouse IgG.

## EXPERIMENTAL PROCEDURES

**General Comments.** All reagents were purchased from Aldrich-Chemie GmbH & Co. KG, Steinheim, and used without further purification. The solvents employed were of reagent grade and were used as received. <sup>1</sup>H NMR spectra were recorded at 400 MHz on a Jeol-GX-400 spectrometer with TMS as a standard. UV and IR spectra were recorded on Shimadzu-UV-2100 and Perkin-Elmer 1600 FTIR spectrophotometers, respectively. Elemental analyses were recorded on the Perkin-Elmer 2400 CHNS/O elemental analyzer.

**Tetra(*tert*-butyl) 2,2',2'',2'''-[[4-[2-(4-Aminophenyl)ethyl]pyridine-2,6-diyl]bis(methylenenitrilo)]tetrakis(acetate) (7).** A mixture of tetra(*tert*-butyl) 2,2',2'',2'''-[[4-[2-(4-aminophenyl)ethynyl]pyridine-2,6-diyl]bis(methylenenitrilo)]tetrakis(acetate) (18) (6; 3.45 g, 5.00 mmol), 10% Pd on carbon (0.5 g), and MeOH (40 mL) was stirred in a hydrogen atmosphere (0.69 MPa) for 6 h. After filtration, the filtrate was evaporated and the residue purified by flash chromatography on silica gel by eluting with petroleum ether (40-60 °C)/ethyl acetate (5:3) to give 7 (3.10 g, 89%). IR (film): 1716, 1368, 1157 cm<sup>-1</sup> ν(C=O

\* Wallac Oy and Centre for Biotechnology.

<sup>†</sup> Wallac Oy and University of Turku.

\* Abstract published in *Advance ACS Abstracts*, April 15, 1994.

and CO). UV (EtOH): 294, 271 (sh), 239 nm.  $^1\text{H}$  NMR:  $\delta$  (DMSO- $d_6$ ) 1.42 (36 H, s), 2.66–2.72 (2 H, m), 2.74–2.80 (2 H, m), 3.39 (8 H, s), 3.85 (4 H, s), 4.83 (2 H, s), 6.47 (2 H, d,  $J$  = 8.6 Hz), 6.85 (2 H, d,  $J$  = 8.6 Hz), 7.24 ppm (2 H, s). Anal. Calcd for  $\text{C}_{39}\text{H}_{60}\text{N}_4\text{O}_8\cdot\text{H}_2\text{O}$ : C, 64.09; H, 8.55; N, 7.67. Found: C, 64.10; H, 8.48; N, 7.59.

**2,2',2'',2'''-[[4-[2-(4-Aminophenyl)ethyl]pyridine-2,6-diyl]bis(methylenenitrilo)]tetrakis(acetic acid) (8).** A solution of compound 7 (3.15 g, 4.4 mmol) in trifluoroacetic acid (120 mL) was stirred for 1.5 h at room temperature. After evaporation, the residue was triturated with diethyl ether and filtered to give 8 (3.50 g, 96%). IR (KBr pellet): 1735, 1671, 1413, 1197  $\nu$ (C=O, CO), 1197  $\text{cm}^{-1}$   $\nu$ (CF). UV ( $\text{H}_2\text{O}$ ): 268 (sh), 261 nm.  $^1\text{H}$  NMR:  $\delta$  (DMSO- $d_6$ ) 2.84–2.92 (2 H, m), 2.97–3.05 (2 H, m), 3.57 (8 H, s), 3.89 (4 H, s), 4.18 (2 H, s), 6.82 (2 H, d,  $J$  = 7.8 Hz), 7.07 (2 H, d,  $J$  = 7.8 Hz), 7.57 ppm (2 H, s). Anal. Calcd for  $\text{C}_{23}\text{H}_{28}\text{N}_4\text{O}_8\cdot 3\text{CF}_3\text{OOH}$ : C, 41.94; H, 3.76; N, 6.75. Found: C, 41.64; H, 3.96; N, 6.28.

**Synthesis of Europium(III) Chelates 9 and 12.** Tetraacid (8 or 11 (18), 6.7 mmol) was dissolved in water (75 mL) and pH was adjusted to 6.5 with solid  $\text{NaHCO}_3$ . Europium(III) chloride (2.7 g, 7.4 mmol) in water (30 mL) was added over 15 min and the pH was maintained in the range 5–7. After the mixture was stirred for 1.5 h, the pH was raised to 8.5 with 1 M NaOH and the precipitate was filtered off. Acetone was added, and the precipitate was filtered and washed with acetone.

**Europium(III) Chelate of 2,2',2'',2'''-[[4-[2-(4-Aminophenyl)ethyl]pyridine-2,6-diyl]bis(methylenenitrilo)]tetrakis(acetic acid) (9).** Yield: 82%. IR (KBr pellet): 1602, 1403  $\text{cm}^{-1}$   $\nu$ (C=O and CO). UV ( $\text{H}_2\text{O}$ ): 263, 235 nm. Anal. Calcd for  $\text{C}_{23}\text{H}_{24}\text{N}_4\text{O}_8\text{EuNa}\cdot 6\text{H}_2\text{O}\cdot 2\text{NaCl}$ : C, 31.24; H, 4.10; N, 6.34. Found: C, 31.85; H, 3.37; N, 6.36.

**Europium(III) Chelate of 2,2',2'',2'''-[[4-[(4-Aminophenyl)ethynyl]pyridine-2,6-diyl]bis(methylenenitrilo)]tetrakis(acetic acid) (12).** Yield: 77%. IR (KBr pellet): 2196  $\nu$ (C $\equiv$ C), 1597, 1406  $\text{cm}^{-1}$   $\nu$ (C=O and CO). UV ( $\text{H}_2\text{O}$ ): 341, 261 nm. Anal. Calcd for  $\text{C}_{23}\text{H}_{20}\text{N}_4\text{O}_8\text{EuNa}\cdot 7\text{H}_2\text{O}\cdot 2\text{NaCl}$ : C, 30.75; H, 3.81; N, 6.24. Found: C, 30.24; H, 3.32; N, 6.61.

**Synthesis of Chelates 10a and 13a.** An aqueous solution (15 mL) of amino chelate (9 or 12, 0.91 mmol) was added over 15 min to a mixture of thiophosgene (115  $\mu\text{L}$ , 3.66 mmol),  $\text{NaHCO}_3$  (380 mg, 4.57 mmol), and  $\text{CHCl}_3$ . After the mixture was stirred for 0.5–1 h, the phases were separated and the water phase was washed with  $\text{CHCl}_3$  (3  $\times$  15 mL). The aqueous solution was extracted with phenol (about 3 g), and the phenol phase was treated with water (3 mL) and diethyl ether (60 mL). The water phase was separated and washed with diethyl ether (15 mL). The pH was adjusted to 7 with 1 M acetic acid, and acetonitrile was added ( $\text{H}_2\text{O}/\text{MeCN}$ , 1:2). The mixture was filtered through silica gel by elution with  $\text{H}_2\text{O}/\text{MeCN}$  (1:2). The solution was evaporated to 1–2 mL and treated with acetone. The precipitate was filtered and washed with acetone.

**Europium(III) Chelate of 2,2',2'',2'''-[[4-[2-(4-Isothiocyanatophenyl)ethyl]pyridine-2,6-diyl]bis(methylenenitrilo)]tetrakis(acetic acid) (10a).** Yield: 69%. IR (KBr pellet): 2115  $\nu$ (SCN), 1618, 1401  $\text{cm}^{-1}$   $\nu$ (C=O and CO). UV ( $\text{H}_2\text{O}$ ): 278 (sh), 268, 223 nm. Anal. Calcd for  $\text{C}_{24}\text{H}_{22}\text{N}_4\text{SO}_8\text{EuNa}\cdot 6\text{H}_2\text{O}$ : C, 35.61; H, 4.23; N, 6.92. Found: C, 35.51; H, 3.82; N, 7.06.

**Europium(III) Chelate of 2,2',2'',2'''-[[4-[(4-Isothiocyanatophenyl)ethynyl]pyridine-2,6-diyl]bis(methylenenitrilo)]tetrakis(acetic acid) (13a).** Yield: 73%.

IR (KBr pellet): 2190  $\nu$ (C $\equiv$ C), 2096  $\nu$ (SCN), 1610, 1405  $\text{cm}^{-1}$   $\nu$ (C=O and CO). UV ( $\text{H}_2\text{O}$ ): 334, 321, 300 (sh), 285 (sh), 225 nm. Anal. Calcd for  $\text{C}_{24}\text{H}_{18}\text{N}_4\text{SO}_8\text{EuNa}\cdot 6\text{H}_2\text{O}$ : C, 35.79; H, 3.75; N, 6.96. Found: C, 36.19; H, 3.65; N, 6.79.

**Synthesis of Compounds 10b and 13b.** A solution of 2,4,6-trichloro-1,3,5-triazine (18 mg, 0.1 mmol), acetone (1.0 mL) and water (1.0 mL), was added to a solution of amino chelate (9 or 12, 0.1 mmol) and 0.1 M NaOAc (1.5 mL, pH 4.9). After being stirred for 30 min, the reaction mixture was treated with acetone, and the precipitate was filtered and washed with acetone.

**Europium(III) Chelate of 2,2',2'',2'''-[[4-[2-[4-[(4,6-Dichloro-1,3,5-triazin-2-yl)amino]phenyl]ethyl]pyridine-2,6-diyl]bis(methylenenitrilo)]tetrakis(acetic acid) (10b).** Yield: 72%. IR (KBr pellet): 1601, 1400  $\text{cm}^{-1}$   $\nu$ (C=O and CO). UV ( $\text{H}_2\text{O}$ ): 270 nm. Anal. Calcd for  $\text{C}_{26}\text{H}_{23}\text{Cl}_2\text{N}_7\text{O}_8\text{EuNa}\cdot 6\text{H}_2\text{O}$ : C, 34.11; H, 3.85; N, 10.71. Found: C, 34.75; H, 3.68; N, 10.17.

**Europium(III) Chelate of 2,2',2'',2'''-[[4-[[4-[(4,6-Dichloro-1,3,5-triazin-2-yl)amino]phenyl]ethynyl]pyridine-2,6-diyl]bis(methylenenitrilo)]tetrakis(acetic acid) (13b).** Yield 78%. IR (KBr pellet): 2208  $\nu$ (C $\equiv$ C), 1601, 1405  $\text{cm}^{-1}$   $\nu$ (C=O and CO). UV ( $\text{H}_2\text{O}$ ): 325 nm. Anal. Calcd for  $\text{C}_{26}\text{H}_{19}\text{Cl}_2\text{N}_7\text{O}_8\text{EuNa}\cdot 6\text{H}_2\text{O}$ : C, 34.26; H, 3.43; N, 10.76. Found: C, 34.14; H, 3.74; N, 10.95.

**Europium(III) Chelate of 2,2',2'',2'''-[[4-[[4-(Iodoacetamido)phenylethynyl]pyridine-2,6-diyl]bis(methylenenitrilo)]tetrakis(acetic acid) (13c).** A solution of iodoacetic anhydride (165 mg, 0.47 mmol) and  $\text{CHCl}_3$  (1.5 mL) was added to a solution of chelate 12 (51 mg, 0.078 mmol),  $N,N$ -diisopropylethylamine (81  $\mu\text{L}$ , 0.47 mmol), and water (1.5 mL). After the mixture was stirred for 1 h, the phases were separated and the water phase was washed with  $\text{CHCl}_3$  (2  $\times$  4 mL). The aqueous solution was treated with acetone, and the precipitate was filtered and washed with acetone. Yield: 65 mg (90%). IR (KBr pellet): 2207  $\nu$ (C $\equiv$ C), 1600, 1406  $\text{cm}^{-1}$   $\nu$ (C=O and CO). UV ( $\text{H}_2\text{O}$ ): 317 nm. Anal. Calcd for  $\text{C}_{26}\text{H}_{21}\text{IN}_4\text{O}_9\text{EuNa}\cdot 6\text{H}_2\text{O}$ : C, 32.24; H, 3.57; N, 6.02. Found: C, 32.06; H, 3.33; N, 5.65.

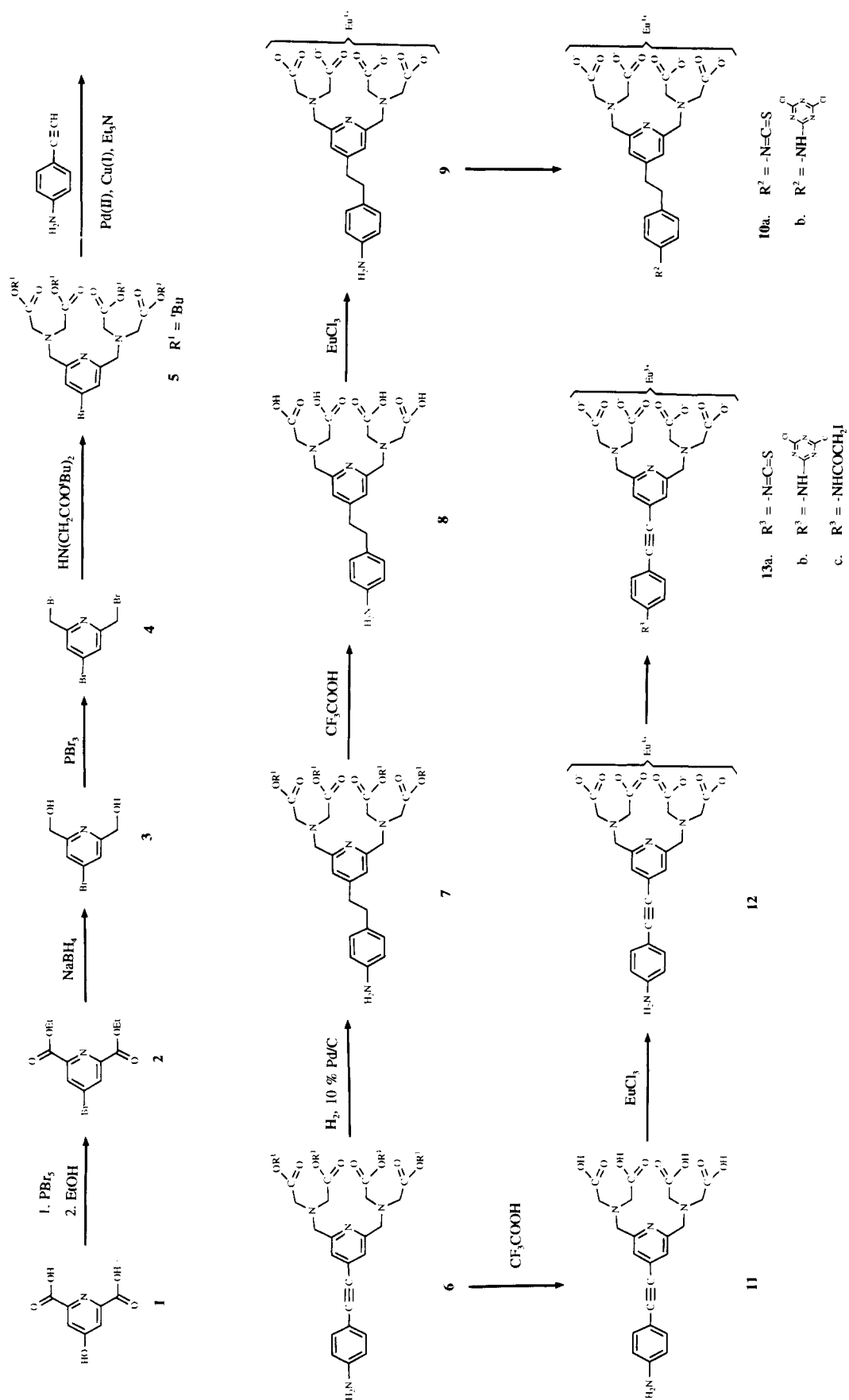
**Conjugation of the Europium(III) Chelates 13a-c to an Antibody.** The IgG fraction of rabbit anti-mouse IgG (Dako, Copenhagen, Denmark) was coupled with increasing amounts of the chelate 13a by incubating the protein with the chelate at different molar ratios in carbonate buffer, pH 9.3, at room temperature for 16 h. The protein-chelate conjugates were purified by gel chromatography and the labeling ratio analyzed by DELFIA system (20). The labeling efficiency test was performed by using fixed concentrations of the chelates 13a-c (at a 35-fold molar excess) during the labeling.

**Luminescent Properties of the Antibody Conjugates.** Luminescent properties (excitation and emission spectra, decay times, and emission intensities) of the Eu-labeled antibodies were investigated using a Perkin-Elmer Model LS 5 spectrofluorometer (Beaconsfield, UK). The luminescent properties were analyzed in an aqueous buffer, Tris-HCl buffer, pH 7.5.

## RESULTS AND DISCUSSION

Europium(III) chelates 9 and 12 were prepared according to the routes shown in Scheme 1. The synthesis of the common intermediate, tetra(*tert*-butyl) 2,2',2'',2'''-[[4-(4-aminophenyl)ethynyl]pyridine-2,6-diyl]bis(methylenenitrilo)]tetrakis(acetate) (6) (18), started from 4-hydroxypyridine-2,6-dicarboxylic acid (1), which reacted with phosphorus pentabromide to yield 4-bromopyridine-2,6-

Scheme 1



dicarboxylic dibromide (21, 22). Treatment with EtOH generated the corresponding ester 2. Reduction with sodium borohydride resulted in the bis(methanol) 3, and bromination with phosphorus tribromide gave the bis(bromomethyl) derivative 4. After its reaction with di-(*tert*-butyl) iminobis(acetate), the 4-bromo atom of compound 5 reacted with 4-aminophenylacetylene in the presence of a palladium catalyst and copper(I) iodide. The triple bond was easily reduced with hydrogen and palladium on carbon. The reduction of the triple bond of compound 6 can be seen from the disappearance of  $\nu$ -(C $\equiv$ C) at about 2210  $\text{cm}^{-1}$  in the IR spectra. This synthesis of compound 7 is much more convenient and shorter than the previously reported method (19). Moreover, we can prepare both the luminescent (12 and 13a-c) and nonluminescent chelate (9 and 10a-b) from the same intermediate 6.

The ester groups of compounds 6 and 7 were hydrolyzed with trifluoroacetic acid. Finally, europium(III) chelates 9 and 12 as well as their activated products 10 and 13 with thiophosgene, iodoacetic anhydride (5), and 2,4,6-trichloro-1,3,5-triazine (11) were prepared in accordance with standard methods. According to TLC, the activated reactions were nearly quantitative. After the activation reaction with thiophosgene, the products were purified from inorganic salts by phenol extraction (23). Usually, activated chelates contain inorganic impurities and are difficult to purify. We found that simple phenol extraction can be used for desalting the chelates. The formation of an isothiocyanato group can be seen from the appearance of  $\nu$ (S=C=N) at about 2100  $\text{cm}^{-1}$  in the IR spectra. After the activation of chelate 12, the products 13a-c gave strong red luminescence both in solution and on TLC. Phenol extraction cannot be done with chelates activated by 2,4,6-trichloro-1,3,5-triazine because of the high reactivity of the products.

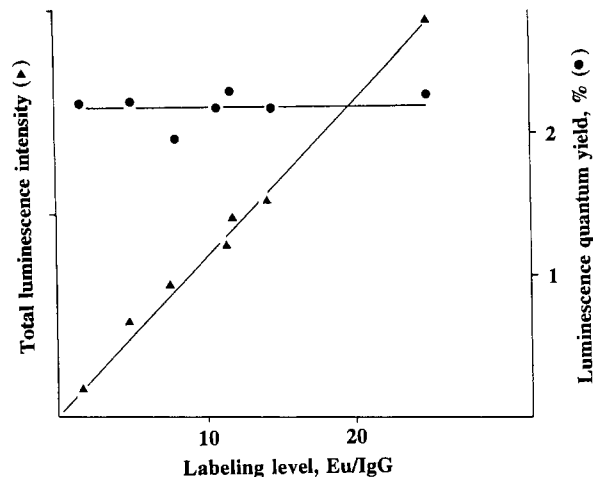
The efficiencies of the activated groups in forming covalent bonds with a protein were elucidated by labeling of a model antibody. The dichlorotriazinyl group produced clearly the most efficient labeling reagent with a labeling level of 12 Eu/IgG, the isothiocyanato group yielded under same conditions 6.5 Eu/IgG, and the iodoacetamido group yielded 1.2 Eu/IgG. Another important factor relating to the choice of reaction is its effect on the affinity and nonspecific binding properties of the used antibodies, which has to be elucidated for each particular antibody to be labeled. The most strongly reactive intermediate, dichlorotriazinyl activated chelate, may also cause decreased affinities when used in high excess conditions.

It is generally assumed that, because of the very long Stokes' shift of the chelates, there is no problem of inner-filter quenching. This was verified by labeling IgG with up to 25 chelates per IgG and studying the respective luminescence quantum yields. As shown in Figure 1, the increasing amount of chelates in a protein does not have any major effect on quantum yield. Accordingly, the total luminescence can be increased by more efficient labeling as long as immunoreactivity is retained.

The effect of different activated groups and different linkages between the chelate and the protein on the luminescent properties of Eu-chelates is shown in Table 1. Only the isothiocyanato group has a slightly negative effect on luminescence quantum yield and decay time.

#### ACKNOWLEDGMENT

The financial support of the Academy of Finland is gratefully acknowledged.



**Figure 1.** Effect of labeling level (Eu<sup>3+</sup>/IgG) to total luminescence intensity (▲) (arbitrary units) and to luminescence quantum yield (●).

**Table 1.** Effect of Linkage Group on the Luminescence of Eu Chelates (13) Coupled to an Antibody

chelate	active group	$\lambda_{\text{exc.}}$ , nm	$\tau$ , $\mu\text{s}$	$\epsilon\Phi$	$\Phi$
13	NCS	330	380	550	0.025
13b	DTA	341	400	1100	0.05
13c	I-Acet	330	395	1150	0.05

#### LITERATURE CITED

- (1) Soini, E., and Hemmilä, I. (1979) Fluoroimmunoassay: present status and key problems. *Clin. Chem.* 25, 353-361.
- (2) Hemmilä, I. (1991) *Application of fluorescence in immunoassays*, pp 215-217, Wiley Interscience, New York.
- (3) Prat, O., Lorez, E., and Mathis, G. (1991) Europium(III) cryptates: a fluorescent label for the detection of DNA hybrids on solid support. *Anal. Biochem.* 195, 283-289.
- (4) Leif, R. C., and Vallarino, L. M. (1992) Rare-earth chelates as fluorescent marker in cell separation and analysis. *ACS Symp. Ser.* 464, 41-58.
- (5) Mikkala, V.-M., Mikola, H., and Hemmilä, I. (1989) The synthesis and use of activated *N*-benzyl derivatives of diethylenetriaminetetraacetic acids: alternative reagents for labeling of antibodies with metal ions. *Anal. Biochem.* 176, 319-325.
- (6) Sund, C., Ylikoski, J., Hurskainen, P., and Kwiatkowski, M. (1988) Construction of europium (Eu<sup>3+</sup>)-labeled oligo DNA hybridization probes. *Nucleosides Nucleotides* 7, 655-659.
- (7) Hurskainen, P., Dahlén, P., Ylikoski, J., Kwiatkowski, M., Siitari, H., and Lövgren, T. (1991) Preparation of europium-labeled DNA probes and their properties. *Nucleic Acids Res.* 19, 1057-1061.
- (8) Dakubu, S., Hale, R., Lu, A., Quick, J., Solas, D., and Weinberg, J. (1988) Time-resolved pulsed fluorescence immunometric assays of carcinoembryonic antigen. *Clin. Chem.* 34, 2337-2340.
- (9) Seveus, L., Väisälä, M., Syrjänen, S., Sandberg, M., Kuusisto, A., Harju, R., Salo, J., Hemmilä, I., Kojola, H., and Soini, E. (1992) Time-resolved fluorescence imaging of europium chelate label in immunohistochemistry and *in situ* hybridization. *Cytometry* 13, 329-338.
- (10) Kankare, J., Haapakka, K., Kulmala, S., Nantö, V., Eskola, J., and Takalo, H. (1992) Immunoassay by time-resolved electrogenerated luminescence. *Anal. Chim. Acta* 266, 205-212.
- (11) Mikkala, V.-M., Helenius, M., Hemmilä, I., Kankare, J., and Takalo, H. (1993) Development of luminescent europium(III) and terbium(III) chelates of 2,2':6',2''-terpyridine derivatives for protein labelling. *Helv. Chim. Acta* 76, 1361-1378.
- (12) Diamandis, E. P., and Christopoulos, T. K. (1990) Europium chelate labels in time-resolved fluorescence immunoassays and DNA hybridization assays. *Anal. Chem.* 62, 1149A-1157A.

- (13) Evangelista, R. A., Pollak, A., Allore B., Templeton E. F., Morton, R. C., and Diamandis, E. P. (1988) A new europium chelate for protein labelling and time-resolved fluorometric applications. *Clin. Biochem.* 21, 173-178.
- (14) Kankare, J., Latva, M., and Takalo, H. (1991) Fluorescence intensities of Eu(III) complexes with substituted 4-phenylethynylpyridines as ligands. *Eur. J. Solid State Inorg. Chem.* 28, 183-186.
- (15) Mikkala, V.-M., and Kankare, J. (1992) New 2,2'-bipyridine derivatives and their luminescence properties with europium(III) and terbium(III) ions. *Helv. Chim. Acta* 75, 1578-1592.
- (16) Mikkala, V.-M., Sund, C., Kwiatkowski, M., Pasanen, P., Högberg, M., Kankare, J., and Takalo, H. (1992) New heteroaromatic complexing agents and luminescence of their europium(III) and terbium(III) chelates. *Helv. Chim. Acta* 75, 1621-1632.
- (17) Mikkala, V.-M., Kwiatkowski, M., Kankare, J., and Takalo, H. (1993) Influence of chelating groups on the luminescence properties of europium(III) and terbium(III) chelates in the 2,2'-bipyridine series. *Helv. Chim. Acta* 76, 893-899.
- (18) Takalo, H., Hänninen, E., and Kankare, J. (1993) Luminescence of europium(III) chelates of substituted 4-phenylethynylpyridines as ligands. *Helv. Chim. Acta* 76, 877-883.
- (19) Kwiatkowski, M., Sund, C., Ylikoski, J., Mikkala, V.-M., and Hemmälä, I. (1987) Metal-chelating 2,6-substituted pyridine compounds and their use. Eur. Pat. 298939B1.
- (20) Hemmälä, I., Dakubu, S., Mikkala, V.-M., Siitari, H., and Lövgren, T. (1984) Europium as a label in time-resolved immunofluorometric assays. *Anal. Biochem.* 137, 335-343.
- (21) Takalo, H., and Kankare, J. (1987) Synthesis of dimethyl and diethyl 4-(phenylethynyl)-2,6-pyridinedicarboxylate. *Acta Chem. Scand. B* 41, 219-221.
- (22) Takalo, H., Pasanen, P., and Kankare, J. (1988) Synthesis of 4-(phenylethynyl)-2,6-bis[*N,N*-bis(carboxymethyl)amino-methyl]pyridine. *Acta Chem. Scand. B* 42, 373-377.
- (23) Anton, D. L., Hogenkamp, H. P. C., Walker, T. E., and Matwiyoff, N. A. (1980) Carbon-13 nuclear magnetic resonance studies of the monocarboxylic acids of cyanocobalamin. Assignments of the b-, d-, and e-monocarboxylic acids. *J. Am. Chem. Soc.* 102, 2215-2219.

# Bioconjugate Chemistry

JULY/AUGUST 1994  
Volume 5, Number 4

© Copyright 1994 by the American Chemical Society

## LETTERS

---

### Stabilization of L-Asparaginase Modified with Comb-Shaped Poly(ethylene glycol) Derivatives, in Vivo and in Vitro

Yoh Kodera, Taichi Sekine, Tohru Yasukohchi, Yoshihiro Kiri, Misao Hiroto, Ayako Matsushima, and Yuji Inada\*

Toin Human Science and Technology Center, Department of Materials Science and Technology, Toin University of Yokohama, 1614 Kurogane-cho, Midori-ku, Yokohama 225, Japan. Received February 4, 1994\*

---

L-Asparaginase from *Escherichia coli* was coupled with two types of comb-shaped copolymer of poly(ethylene glycol) derivative and maleic anhydride (activated PM), having molecular weights of 13 000 and 100 000 (activated PM<sub>13</sub> and PM<sub>100</sub>, respectively) with multivalent reaction sites. After single intravenous injections of PM<sub>100</sub>-asparaginase and nonmodified asparaginase into rats, the enzymic activity of PM<sub>100</sub>-asparaginase in serum was well retained for at least 11 days, and the serum L-asparagine concentration remained undetectable for 27 days. The half-lives of PM<sub>100</sub>-asparaginase and nonmodified asparaginase were 50 and 1.5 h, respectively. Stabilization of L-asparaginase toward heat, urea, and acidity was caused by modifying the enzyme with activated PM<sub>13</sub> and PM<sub>100</sub>. Especially, PM<sub>100</sub>-asparaginase retained high enzymic activity toward heat and urea, compared with PM<sub>13</sub>-asparaginase. It was suggested that these modifiers with a comb-shaped form and with multivalent reactive sites cover the whole surface of the asparaginase molecule and stabilize its conformation possibly through multiple covalent bindings and through various noncovalent interactions.

---

L-Asparaginase from *Escherichia coli* has been used clinically for the therapy of acute lymphocytic leukemia and lymphosarcoma (1, 2). The disadvantage of this therapy lies in short circulation time in blood and in immunological side effects ranging in severity from mild allergic reactions to anaphylactic shock, as the enzyme is a protein foreign to humans. To overcome these drawbacks, L-asparaginase was modified with poly(ethylene glycol) derivatives with a chain-shaped form (3-5) or a comb-shaped form (6). PEG<sub>2</sub>-asparaginase<sup>1</sup> lost its immunoreactivity with retention of its enzymic activity (4) and also caused the prolongation of clearance time in blood

(7). This manipulation of protein modifications could improve the properties of native proteins. Recently, we explored comb-shaped copolymers of a poly(ethylene glycol) derivative and maleic anhydride with molecular weights of 13 000 (activated PM<sub>13</sub>) and 100 000 (activated PM<sub>100</sub>) as modifiers (6). This concept was further extended to biotechnological process. PM<sub>13</sub>-lipase was soluble and

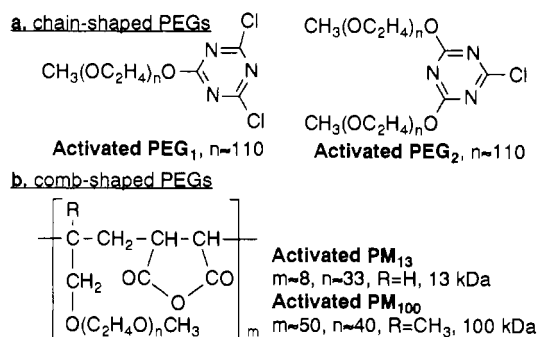
---

\* To whom correspondence should be addressed. Fax: +81-45-972-5972.

© Abstract published in *Advance ACS Abstracts*, June 15, 1994.

<sup>1</sup> Abbreviations: activated PM<sub>13</sub>, copolymer of poly(oxyethylene) allyl methyl diether and maleic anhydride (13 kDa); activated PM<sub>100</sub>, copolymer of poly(oxyethylene) 2-methyl-2-propenyl methyl diether and maleic anhydride (100 kDa); PEG, poly(ethylene glycol); activated PEG<sub>1</sub>, 2-[O-methoxypoly(ethylene glycol)]-substituted 4,6-dichloro-s-triazine; activated PEG<sub>2</sub>, 2,4-bis[O-methoxypoly(ethylene glycol)]-substituted 6-chloro-s-triazine.





**Figure 1.** Structures of activated PEGs and PMs: activated PEG<sub>1</sub>, 2-[O-methoxypoly(ethylene glycol)]-substituted 4,6-dichloro-s-triazine; activated PEG<sub>2</sub>, 2,4-bis[O-methoxypoly(ethylene glycol)]-substituted 6-chloro-s-triazine; activated PM<sub>13</sub>, copolymer of poly(oxyethylene) allyl methyl diether and maleic anhydride; activated PM<sub>100</sub>, copolymer of poly(oxyethylene) 2-methyl-2-propenyl methyl diether and maleic anhydride. The values of *n* and *m* were calculated from the average molecular weights of the PEG monomer (MW 5000 for activated PEGs, 1500 for PM<sub>13</sub>, and 1900 for PM<sub>100</sub>) and of the copolymer (MW 13 000 for PM<sub>13</sub> and 100 000 for PM<sub>100</sub>), respectively.

active in organic solvents and catalyzed the reverse reactions of hydrolysis, ester synthesis, and ester exchange reactions with high enzymic activity in benzene (8). The present paper deals with the stabilization of L-asparaginase by the modification with comb-shaped copolymers, activated PM<sub>13</sub> and PM<sub>100</sub>, *in vivo* and *in vitro*.

L-Asparaginase from *E. coli* has 92 amino groups in the molecule with a molecular weight of 136 000 and consists of four identical subunits (9). Figure 1 shows the structures of activated PM<sub>13</sub> and PM<sub>100</sub> together with activated PEG<sub>1</sub> and PEG<sub>2</sub>. Amino groups in the asparaginase molecule were reacted with acid anhydrides in activated PM molecules to form amide bonds.<sup>2</sup> The degrees of modification of the amino groups in L-asparaginase molecule were 50% for PM<sub>13</sub>-asparaginase and 34% for PM<sub>100</sub>-asparaginase. The enzymic activity of PM<sub>13</sub>- and PM<sub>100</sub>-asparaginases were 91 IU/mg and 168 IU/mg, respectively. As activated PM has many reactive sites in a molecule, a protein can be modified with activated PM through multipoint attachments between amino groups in the protein molecule and acid anhydrides in the modifier.

In our previous study, it was reported that *E. coli* L-asparaginase modified by activated PEG<sub>2</sub> with a chain-shaped form and with a monovalent reactive site does not cross-react with antiasparaginase serum in the precipitation reaction (4). The half-lives of the modified and nonmodified asparaginases were 56 and 2.9 h, respectively, after each asparaginase was intraperitoneally injected into rats (7). Quite recently, we reported that PM<sub>100</sub>-asparaginase retained its enzymic activity (85.3% of the original activity) very well, even when its immunoreactivity was completely lost (6).

Figure 2a shows the clearance time of PM<sub>100</sub>-asparaginase and nonmodified asparaginase administered intravenously into rats. After PM<sub>100</sub>-asparaginase was injected, the enzymic activity was retained at least 11 days in blood circulation (curve A) and the L-asparagine concentration in serum remained undetectable (limit of

**Table 1.** Activity, Immunoreactivity, and Half-life in Blood of *E. coli* L-Asparaginase Modified with Activated PEGs and PMs

modifying reagent (mw)	degree of enzymic modification (%)	enzymic activity (%)	immuno- reactivity (%)	half-life in blood (h)
nonmodified asparaginase	0	100	100	1.5, <sup>a</sup> 2.9 <sup>b</sup>
activated PEG <sub>1</sub> (5000)	79	0.9	0	
activated PEG <sub>2</sub> (10 000)	57	11.0	0	56 <sup>b</sup>
activated PM <sub>13</sub> (13 000)	50	45.5	0	
activated PM <sub>100</sub> (100 000)	34	85.3	0	50 <sup>a</sup>

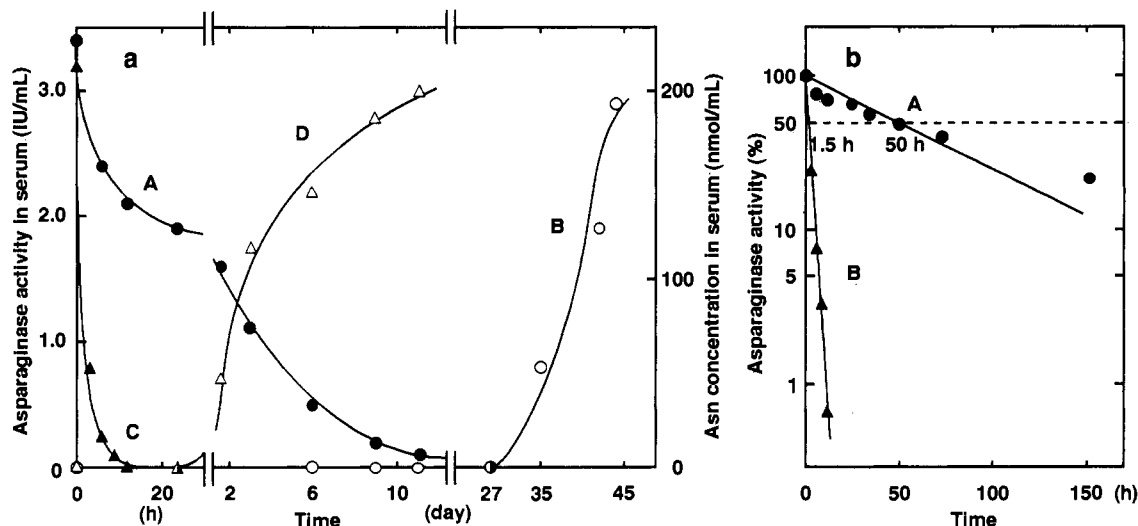
<sup>a,b</sup> The half-lives of the enzyme in blood were measured after intraperitoneal (7) and intravenous injections into rats, respectively.

detection: 5 μM) for 27 days. After 27 days, the concentration of L-asparagine in serum was markedly increased with time (curve B). In the case of nonmodified asparaginase, its enzymic activity was kept for less than 1 day (curve C), during which time L-asparagine was not detected in serum. After 1 day, the L-asparagine concentration in serum was sharply increased with time (curve D). Figure 2b shows semilogarithmic plots of the enzymic activity of modified (curve A) and nonmodified (curve B) asparaginases against time after the injection. From the figure, the half-lives of the modified and nonmodified asparaginases were calculated to be 50 and 1.5 h, respectively.

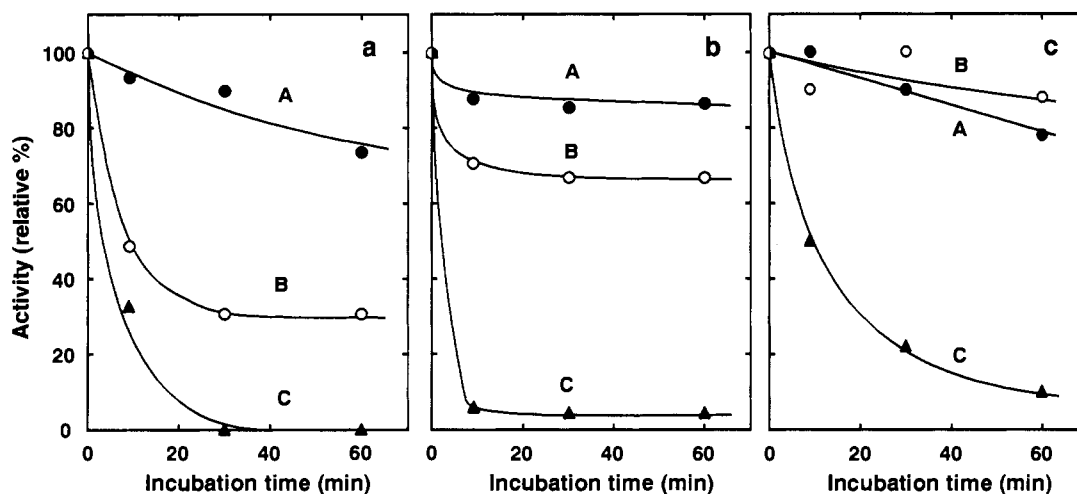
Table 1 shows the summary of properties of asparaginases modified with PEG derivatives with a chain-shaped form (activated PEG<sub>1</sub> and PEG<sub>2</sub>) and with a comb-shaped form (activated PM<sub>13</sub> and PM<sub>100</sub>). In Table 1, the degree of modification of amino groups in the asparaginase molecule, enzymic activity, immunoreactivity toward antiasparaginase serum and half-life in the blood circulation are included. From the results obtained in previous (3, 4, 6, 7) and the present studies, it is concluded that PM<sub>100</sub>-asparaginase has a reduced immunoreactivity with a lower degree of modification (34%) and with higher enzymic activity (85.3%) in comparison with PM<sub>13</sub>- and PEG-asparaginases. Furthermore, the half-life of asparaginase was prolonged by modification with both activated PEG<sub>2</sub> and PM<sub>100</sub>.

The effect of the modification with activated PM<sub>13</sub> and PM<sub>100</sub> on the stabilization of asparaginase was tested, *in vitro*, toward heat, urea, and acidity. The results are shown in Figure 3. In the heat-stability test at 65 °C (Figure 3a), the enzymic activity of nonmodified asparaginase was completely lost after a 30-min incubation (curve C). On the other hand, PM<sub>13</sub>- and PM<sub>100</sub>-asparaginases retained their enzymic activities of 35% and 90%, respectively, at the same incubation time at 65 °C (curves B and A). It is well-known that urea with a high concentration disrupts the higher-order structure of protein molecules. Using 4.0 M urea, the stabilities of modified and nonmodified asparaginases were tested, which are shown in Figure 3b. Although nonmodified asparaginase almost lost the enzymic activity with 4.0 M urea in 10 min (curve C), PM<sub>13</sub>- and PM<sub>100</sub>-asparaginases retained 70% and 85% of the initial activities, respectively (curves B and A). The stabilization test was also performed with acidity (Figure 3c). At pH 4.0, the enzymic activity of nonmodified asparaginase decreased markedly to 10% of the original activity by the 60-min incubation. The PM<sub>13</sub>- and PM<sub>100</sub>-asparaginases retained approximately 80% of their enzymic activities as shown by curves B and A, respectively. In the case of PEG<sub>2</sub>-asparaginase, similar stabilizing phenomena toward high temperature and acidity were never observed (12), probably because activated PEG<sub>2</sub> is a chain-shaped form with a monovalent reactive site.

<sup>2</sup> Crystallized L-asparaginase (EC 3.5.1.1) from *E. coli* (specific activity, 200 IU/mg of protein) and two types of comb-shaped copolymers, activated PM<sub>13</sub> and PM<sub>100</sub>, were gifts from Kyowa Hakko Kogyo Co. (Tokyo, Japan) and from NOF Co. (Tokyo, Japan), respectively. PM<sub>13</sub>- and PM<sub>100</sub>-asparaginases were prepared as described previously (6). Protein concentration was determined by the biuret method (10).



**Figure 2.** Prolongation of clearance time of PM<sub>100</sub>-asparaginase compared with that of nonmodified asparaginase. (a) Curves A and B: the enzymic activity and the L-asparagine concentration in the serum after PM<sub>100</sub>-asparaginase was intravenously injected, respectively. Curves C and D: the same plotting after nonmodified asparaginase was injected, respectively. (b) Semilogarithmic plots of the enzymic activity of modified (curve A) and nonmodified (curve B) asparaginases against time after the injection. PM<sub>100</sub>-asparaginase and nonmodified asparaginase were injected once intravenously at 100 IU/kg into male albino rats (Wistar strain). Blood (200  $\mu$ L) was taken from the tail vein, and a sample of serum (50  $\mu$ L) was subjected to assay for the enzymic activity by the GOT method (11). The remaining serum (50  $\mu$ L) was deproteinized with sulfosalicylic acid, and the concentration of L-asparagine was determined with an amino acid analyzer Hitachi L-8500 (Tokyo, Japan).



**Figure 3.** Stabilization of L-asparaginase modified with activated PMs toward heat at 65 °C (a), 4.0 M urea (b), and acidity of pH 4.0 (c). Curves A, B, and C: PM<sub>100</sub>-asparaginase, PM<sub>13</sub>-asparaginase, and nonmodified asparaginase, respectively. Asparaginase solutions (6.7, 4.0, and 3.0 IU/mL for PM<sub>13</sub>-asparaginase, PM<sub>100</sub>-asparaginase, and nonmodified asparaginase, respectively) were incubated at 65 °C or 4.0 M urea (in borate buffer, 50 mM, pH 8.5) or pH 4.0 (in the mixed buffer composed of 0.5 M borate, citrate, and phosphate). At a given time, to 5  $\mu$ L of a sample enzyme solution were added 3.0 mL of L-asparagine (3 mg/mL). The mixture was incubated at 37 °C for 20 min, and then the amount of released ammonia was determined by the Nessler method (11).

These results mentioned above indicate that the stabilization of asparaginase is caused by the modification with activated PMs. This may be due to the interaction with covalent bonds and/or noncovalent bonds between PMs and the protein molecule. The former is amide bonds probably with multipoint attachments between carboxyl groups in activated PMs and amino groups in the enzyme molecule. The latter is various noncovalent bonds between many PEG chains in PMs and the protein surface; ionic bonds between negative charges of carboxyl groups in PMs and positive charges in the enzyme molecule may also contribute to the stabilization. Therefore, the comb-shaped modifiers, activated PMs, may cover the whole surface of the asparaginase molecule having four subunits. Resistance of PM<sub>100</sub>-asparaginase toward heat or urea denaturation was superior to PM<sub>13</sub>-asparaginase. The lengths of the main chain of activated PM<sub>13</sub> and PM<sub>100</sub> are

calculated to be 4 and 26 nm, respectively. The value of 26 nm is enough to cover the whole surface of the asparaginase molecule ( $8.7 \times 6.3 \times 5.8$  nm) (13), if the main chain of the modifier is stretched. The same effective modification with activated PM<sub>100</sub> was also demonstrated to reduce the immunoreactivity of bovine serum albumin (14) with a molecular weight of 67 000 and with an ellipsoid form ( $14 \times 4$  nm) (15). Although PM-asparaginase exhibits prominent properties in comparison with nonmodified enzyme, problems yet remain to be clarified: identification of binding sites between acid anhydrides in PMs and amino groups in a protein molecule and possibility inter- or intramolecular bindings between protein molecules through the activated PM molecule.

Since Abuchowski *et al.* (16, 17) had reported the modification of bovine serum albumin and catalase by activated PEG<sub>1</sub> with the purpose of the reduction of

immunoreactivity in 1977, the same line of work has markedly developed for application to biomedical and biotechnological processes. In fact, PEG-adenosine deaminase (18) is the first PEG-protein drug, which gained Food and Drug Administration approval in 1991. The technique of PEG-modification has been further expanded by us since 1984; as PEG is an amphipathic macromolecule, PEG-enzymes become soluble in organic solvents and exhibit the enzymic activity in them (19). A mutant of purine nucleoside phosphorylase, in which three arginine residues were substituted with lysine residues by genetic engineering, exhibited the enhanced epitope-shielding effect of the PEG-modification (20). Its effective process would be replaced by the chemical modification with activated PMs, as activated PM has many PEG chains with a comb-shaped form and also with multivalent reactive sites.

Experiments are now in progress to clarify the physicochemical properties of PMs-modified proteins in relation to their functions. We believe that this novel technique may open a new avenue to biomedical and biotechnological fields.

#### LITERATURE CITED

- (1) Clarkson, B., Krakoff, I., Burchenal, J., Karnofsky, D., Golbey, R., Dowling, M., Oettgen, H., and Lipton, A. (1970) Clinical results of treatment with *E. coli* L-asparaginase in adults with leukemia, lymphoma and solid tumors. *Cancer* 25, 279-305.
- (2) Ertel, I. J., Nesbit, M. E., Hammond, D., Weiner, J., and Sather, H. (1979) Effective dose of L-asparaginase for induction of remission in previously treated children with acute lymphocytic leukemia: a report from a children's cancer study group. *Cancer Res.* 39, 3893-3896.
- (3) Ashihara, Y., Kono, T., Yamazaki, S., and Inada, Y. (1978) Modification of *E. coli* L-asparaginase with polyethylene glycol: Disappearance of binding ability to anti-asparaginase serum. *Biochem. Biophys. Res. Commun.* 83, 385-391.
- (4) Matsushima, A., Nishimura, H., Ashihara, Y., Yokota, Y., and Inada, Y. (1980) Modification of *E. coli* asparaginase with 2,4-bis(*O*-methoxypolyethylene glycol)-6-chloro-*s*-triazine(activated PEG<sub>2</sub>); Disappearance of binding ability towards anti-serum and retention of enzymic activity. *Chem. Lett.* 773-776.
- (5) Abuchowski, A., Kazo, G. M., Verhoest Jr., C. R., van Es, T., Kafkewitz, D., Nucci, M. L., Viau, A. T., and Davis, F. F. (1984) Cancer therapy with chemically modified enzymes. I. Antitumor properties of polyethylene glycol-asparaginase conjugates. *Cancer Biochem. Biophys.* 7, 175-186.
- (6) Kodera, Y., Tanaka, H., Matsushima, A., and Inada, Y. (1992) Chemical modification of L-asparaginase with a comb-shaped copolymer of polyethylene glycol derivative and maleic anhydride. *Biochem. Biophys. Res. Commun.* 184, 144-148.
- (7) Kamisaki, Y., Wada, H., Yagura, T., Matsushima, A., and Inada, Y. (1980) Reduction in immunogenicity and clearance rate of *Escherichia coli* L-asparaginase by modification with monomethoxypolyethylene glycol. *J. Pharmacol. Exp. Ther.* 216, 410-414.
- (8) Hiroto, M., Matsushima, A., Kodera, Y., Shibata, Y., and Inada, Y. (1992) Chemical modification of lipase with a comb-shaped synthetic copolymer of polyoxyethylene allyl methyl diether and maleic anhydride. *Biotechnol. Lett.* 14, 559-564.
- (9) Maita, T., Morokuma, K., and Matsuda, G. (1974) Amino acid sequence of L-asparaginase from *Escherichia coli*. *J. Biochem.* 76, 1351-1354.
- (10) Layne, E. (1957) Spectrophotometric and turbidimetric methods for measuring proteins. *Methods Enzymol.* 3, 474-454.
- (11) Jayaram, H. N., Cooney, D. A., Jayaram, S., and Rosenblum, L. (1974) A simple and rapid method for the estimation of L-asparaginase in chromatographic and electrophoretic effluents: Comparison with other methods. *Anal. Biochem.* 59, 327-346.
- (12) Yoshimoto, T., Nishimura, H., Saito, Y., Sakurai, K., Kamisaki, Y., Wada, H., Sako, M., Tsujino, G., and Inada, Y. (1986) Characterization of polyethylene glycol-modified L-asparaginase from *Escherichia coli* and its application to therapy of leukemia. *Jpn. J. Cancer Res.* 77, 1264-1270.
- (13) Itai, A., Yonei, M., Mitsui, Y., and Iitaka, Y. (1976) Crystallographic study on the orthorhombic crystal of L-asparaginase from *Escherichia coli* HAP. *J. Mol. Biol.* 105, 321-325.
- (14) Sasaki, H., Ohtake, Y., Matsushima, A., Hiroto, M., Kodera, Y., and Inada, Y. (1993) Reduction of immunoreactivity of bovine serum albumin conjugated with comb-shaped polyethylene glycol derivatives. *Biochem. Biophys. Res. Commun.* 197, 287-291.
- (15) Peters, T., Jr. (1985) Serum albumin. *Adv. Protein Chem.* 37, 161-245.
- (16) Abuchowski, A., van Es, T., Palczuk, N. C., and Davis, F. F. (1977) Alteration of immunological properties of bovine serum albumin by covalent attachment of polyethylene glycol. *J. Biol. Chem.* 252, 3578-3581.
- (17) Abuchowski, A., McCoy, J. R., Palczuk, N. C., van Es, T., and Davis, F. F. (1977) Effect of covalent attachment of polyethylene glycol on the immunogenicity and circulating life of bovine liver catalase. *J. Biol. Chem.* 252, 3582-3586.
- (18) Levy, Y., Hershfield, M. S., Fernandez-Mejia, C., Polmar, S. H., Scudiero, D., Berger, M., and Sorensen, R. U. (1988) Adenosine deaminase deficiency with late onset of recurrent infections: Response to treatment with polyethylene glycol-modified adenosine deaminase. *J. Pediatrics* 113, 312-317.
- (19) Inada, Y., Matsushima, A., Kodera, Y., and Nishimura, H. (1990) Polyethylene glycol(PEG)-protein conjugates: Application to biomedical and biotechnological processes. *J. Bioactive Compatible Polym.* 5, 343-364.
- (20) Hershfield, M. S., Chaffee, S., Koro-Johnson, L., Mary, A., Smith, A., and Short, S. (1991) Use of site-directed mutagenesis to enhance the epitope-shielding effect of covalent modification of proteins with polyethylene glycol. *Proc. Natl. Acad. Sci. U.S.A.* 88, 7185-7189.

# REVIEWS

## Selection and Transplantation of Hematopoietic Stem and Progenitor Cells

Karen Auditore-Hargreaves,\* Shelly Heimfeld, and Ronald J. Berenson

CellPro, Inc., 22322 20th Avenue SE, Bothell, Washington 98021. Received December 6, 1993

The mammalian hematopoietic system is composed of multiple cell types that provide vital infection-fighting, blood-clotting, and oxygen-carrying abilities to the body. These cells arise in the bone marrow and migrate to the periphery as they mature. The hematopoietic system represents a spectrum of differentiation encompassing, at one end, mature, morphologically identifiable cells that have little or no ability to divide. At the opposite end is a rare, but self-sustaining population of stem cells that have the ability to give rise to cells of all the hematopoietic lineages. In between these two extremes are cells termed progenitor cells which, although committed to a specific lineage, are functionally immature and retain a limited capacity for proliferation.

The antigenic profile of hematopoietic cells changes during the course of differentiation, with some antigens lost and others gained (Beverley et al., 1980; Fitchen et al., 1981; Civin and Loken, 1987). This heterogeneity enables one to discriminate among and isolate cells at different points in the continuum, paving the way to a variety of research and clinical applications for the various subsets of cells. This review will focus on methods, especially immunologically based techniques, for the isolation of human hematopoietic stem and progenitor cells and will summarize clinical experience using these cells for bone marrow transplantation and gene therapy.

### BONE MARROW TRANSPLANTATION

Approximately 25 years ago, E. Donnall Thomas and colleagues pioneered bone marrow transplantation to reconstitute the hematopoietic system of patients exposed to myeloablative doses of chemotherapy and/or radiation for the treatment of malignancy (reviewed by Thomas et al. (1975)). Today, two types of bone marrow transplantation are practiced, autologous and allogeneic. In an autologous transplant, a portion of the patient's own marrow is removed prior to myeloablation, stored frozen, and reinfused at the completion of the patient's treatment. In an allogeneic transplant, marrow is obtained from a donor, usually a relative and preferably one whose HLA type matches that of the transplant recipient, and infused into a patient whose own marrow has been destroyed by radiation and/or chemotherapy.

The application of allogeneic bone marrow transplantation has been limited by the inability to transplant across a major histocompatibility barrier and by the occurrence of severe, often life-threatening graft versus host disease (GVHD) in approximately one-third to one-half of transplant recipients. The severity of GVHD, which is caused at least in part by T cells present in the graft, is directly related to the degree of mismatch between donor and recipient. The availability of potent immunosuppressive drugs, such as cyclosporine, has helped to control the incidence and severity of GVHD, but it has not eliminated the problem.

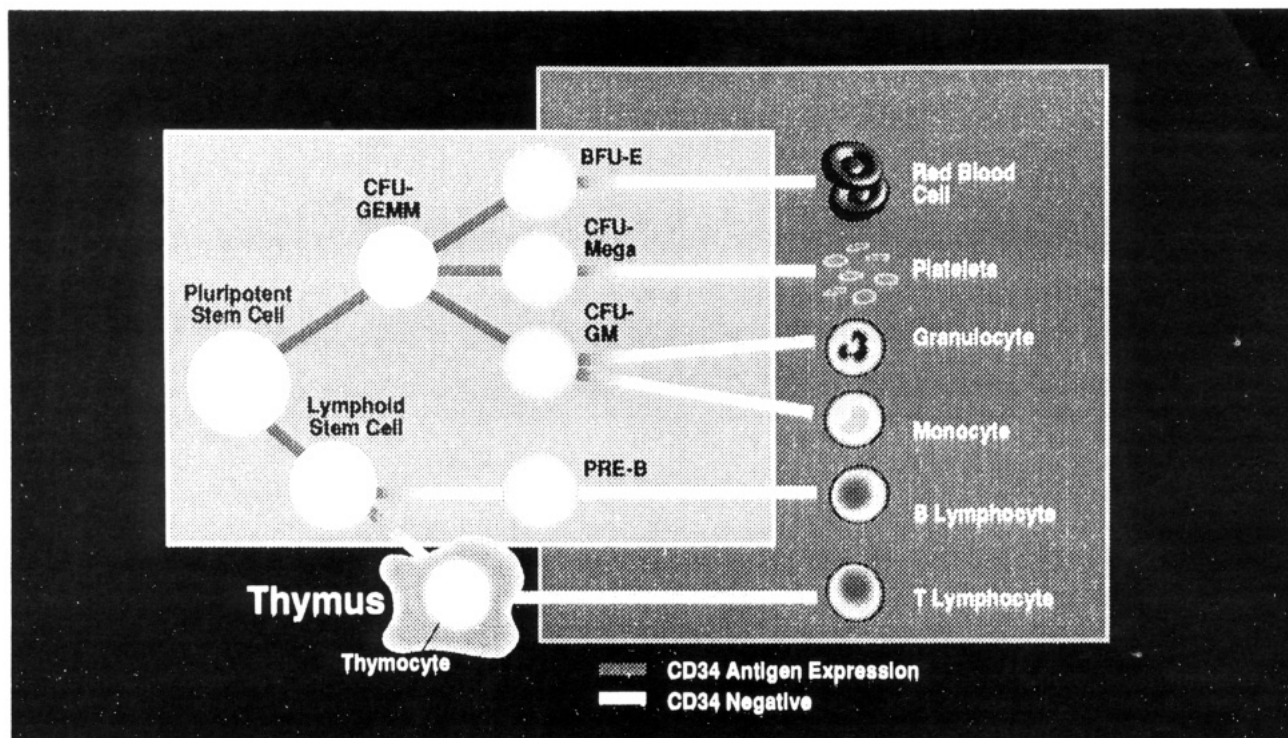
Autologous transplantation does not suffer from these limitations; however, it may not always be an alternative, especially in patients whose tumor involves the bone marrow. With improved methods of detection, such as immunocytochemical staining, it has become clear that tumor cell contamination of the marrow is more common than was thought when diagnosis was made by routine histology. For example, marrow metastases have been detected in 17-54% of patients with solid tumors whose marrows appeared histologically normal at the time of harvest (Berendsen et al., 1988; Cote et al., 1988; Porro et al., 1988; Moss et al., 1991).

Bone marrow is obtained by aspiration from the pelvis or sternum of anesthetized patients or donors. Between 5 and 25 mL of marrow are removed at each aspiration, with the needle moved to a new site between aspirations. A typical transplant involves collecting 1-2 L of marrow and processing that by centrifugation to yield 200-500 mL of buffy coat. Until relatively recently, this entire volume of buffy coat was then infused into the patient. Although only the stem cells in marrow are necessary for engraftment and although these constitute only a small fraction (less than 1%) of the total cells in marrow, there was no clinically practicable method to identify and isolate these rare cells from among the much larger number of unnecessary cells.

**Human Stem Cell Markers.** A cell surface marker unique to human hematopoietic stem cells has not yet been discovered, but several markers are known to be shared among stem cells and early progenitor cells. One such marker, the CD34 antigen, identifies a population of cells capable of mediating sustained reconstitution of the hematopoietic system. A large number of monoclonal antibodies have been identified that collectively define at least three epitopes on the human CD34 antigen (Civin et al., 1984; Tindle et al., 1984, 1985; Andrews et al., 1986; Fina et al., 1990). These epitopes are distinguished by their sensitivity to various enzymes (Sutherland et al., 1992).

The CD34 antigen is a 115 kDa glycoprotein present on 1-3% of human bone marrow cells, including virtually all committed progenitor cells, as well as more primitive progenitors, such as the long-term culture-initiating cell, detected by *in vitro* assays. It is not expressed at detectable levels on mature blood cells, including lymphocytes, granulocytes, erythrocytes, and platelets, nor is it expressed on most malignant cell types, with the exception of certain leukemias (reviewed in Sutherland and Keating, 1992). The CD34 antigen shows no sequence homology with any other previously described molecules at either the protein level (Sutherland et al., 1988) or the DNA level (Simmons et al., 1992), and little is known about its function in the cell membrane.

Berenson and colleagues, working initially in a baboon model (Berenson et al., 1988) and subsequently in humans



**Figure 1.** CD34 antigen expression in hematopoiesis. The CD34 antigen is a 115 kDa glycoprotein which is expressed on pluripotent stem cells and committed progenitor cells in human bone marrow (depicted in the left-hand box). The level of CD34 expression gradually declines as cells differentiate along a given lineage, such that mature cells in the blood (right-hand box) are uniformly CD34 negative.

(Berenson et al., 1991; Shpall et al., 1992a,b), were the first to show that CD34<sup>+</sup> cells could reconstitute the hematopoietic system following myeloablative treatment. These *in vivo* studies were critical to the validation of CD34 as a stem cell marker, as there is no definitive *in vitro* assay for the human stem cell.

**Sources of CD34<sup>+</sup> Cells. Bone Marrow.** The bone marrow is a particularly rich source of CD34<sup>+</sup> cells. Figure 1 shows a schematic representation of the distribution of the CD34 antigen on hematopoietic cells in the bone marrow. The majority of these CD34<sup>+</sup> cells are committed progenitors, rather than true stem cells. True stem cells probably represent only about 1 in 10<sup>5</sup> bone marrow cells.

The fact that the CD34 antigen identifies both the stem cell and progenitor populations is an advantage for clinical applications such as bone marrow transplantation. Several studies in mice have shown that engraftment is delayed when marrow depleted of progenitor cells is transplanted, thus placing the recipient at increased risk of bleeding and infectious complications (Jones et al., 1989, 1990). These same studies demonstrated that transplantation of marrow lacking stem cells leads to rapid, but transient, engraftment. Thus, stem cells as well as progenitor cells are necessary to accomplish both rapid and sustained engraftment of transplant patients. Since CD34 marks both populations, it is an ideal antigen for therapeutic protocols.

**Peripheral Blood.** Numerous studies in animals (Cavins et al., 1964; Nothdurft et al., 1977; Flidner et al., 1979; Storb et al., 1977; Carbonell et al., 1984) and man (Korbling et al., 1981, 1986; Reiffers et al., 1986) have demonstrated that hematopoietic stem cells circulate in peripheral blood and can reconstitute hematopoiesis completely and permanently. The number of stem cells normally present in the peripheral circulation is small compared with marrow (Kessinger et al., 1986; Bell et al., 1986; Bender et al., 1991). However, their number can be increased dramati-

cally by pretreatment with an agent that mobilizes stem and progenitor cells from the bone marrow. G-CSF (Duhrsen et al., 1988), GM-CSF (Gianni et al., 1989), and cyclophosphamide (Siena et al., 1989; To et al., 1989) have all been used successfully to increase the CD34 content of peripheral blood. Consequently, it is now possible to isolate by an apheresis procedure sufficient quantities of engrafting cells from the peripheral blood to transplant myelosuppressed or ablated patients (Korbling and Martin, 1988).

**Umbilical Cord Blood.** CD34<sup>+</sup> stem and progenitor cells have also been obtained from umbilical cord blood at parturition (Broxmeyer et al., 1989, 1991, 1992). The use of cord blood CD34<sup>+</sup> cells for transplant is attractive because the material is readily available and matching of donor and recipient may be less important than when adult cells are employed.

Several groups have reported success in treating children with malignant (Vilmer et al., 1992; Wagner et al., 1992) and nonmalignant diseases (Gluckman et al., 1989) using these cells. More recently, two children with severe combined immunodeficiency disease (SCID) have been transplanted with cord blood stem cells genetically modified to express adenosine deaminase (ADA), the enzyme missing in this disease (Kohn et al., 1993). Several groups have advocated the banking of cord blood for future use in transplantation or gene therapy (Wagner, 1993).

## METHODS OF CELL SELECTION

Methods for fractionating heterogeneous mixtures of cells into subpopulations include techniques based on the cells' physical properties, such as size and density, and specific binding methods, in which cells are identified by their expression of surface markers. The technique of choice for a given application is dictated by the frequency of the cells of interest in the starting population, the degree



of enrichment required, the desired yield, and the intended use of the selected cells.

Selection of hematopoietic stem and progenitor cells is a particularly demanding application of cell selection technology because these cells are so rare in the tissues from which they are typically isolated. The less frequently a cell type occurs in a given tissue, the larger the amount of that tissue which must be processed in order to obtain a desired number of the target cell type. In order to obtain an engrafting dose of CD34+ cells, approximately 20 billion nucleated marrow cells must be processed.

It is also self-evident that in any cell fractionation procedure there is a trade-off between purity and yield which must be balanced. In the stem cell transplant setting, there is probably a threshold number of CD34+ cells below which the recipient will not engraft in a clinically acceptable time frame. However, for ethical reasons, the expected dose-response relationship has been difficult to demonstrate in humans. In clinical transplantation studies with CD34-selected cells, engraftment has been seen with as few as  $0.5 \times 10^6$  CD34-selected cells/kg (Shpall et al., 1994), but it is likely that the actual threshold dose is even lower. In the mouse, where there are fewer ethical constraints, studies indicate that the LD<sub>50</sub> for survival of lethally irradiated animals is approximately 30 "true" stem cells (Spangrude et al., 1988).

Both the number and the nature of nontarget cells contaminating a target cell preparation are important in a cell selection process where the cells are to be used clinically. The number of CD34-negative cells which can be tolerated in a CD34-selected preparation is dependent on whether or not those CD34-negative cells are clinically neutral. If they are clinically neutral, a relatively high proportion of them may be tolerated in the enriched product. In the allogeneic stem cell transplant setting, for example, the presence of granulocytes in the CD34-enriched fraction is clinically inconsequential. However, contamination of this fraction with T lymphocytes is highly significant, as these cells contribute to the development of GVHD in the recipient and thus influence clinical outcome.

**Physical Separation Methods.** Physical methods of cell separation include velocity sedimentation, density gradient centrifugation, counterflow centrifugal elutriation, and related techniques (reviewed in Kumar and Lykke, 1984). Velocity sedimentation, using automated or semiautomated cell-separating centrifuges, has been used to separate the red cells and plasma from the nucleated cells in marrow (Gilmore et al., 1983; Faradji et al., 1988) and peripheral blood (Korbling and Martin, 1988; Williams et al., 1990). This technique reduces the volume of material by about 10-fold and recovers 60–80% of nucleated cells. Density gradient separations can also be accomplished on these machines (English et al., 1989; Humblet et al., 1988).

Human hematopoietic stem cells, as assayed by their ability to form colonies in methyl cellulose, are lighter (1.060–1.070 g/mL) than most other mononuclear cells in bone marrow (Lasky and Zanjani, 1985; Francis et al., 1983; Ellis et al., 1984). Thus, a density separation method can afford a modest (2- to 10-fold) enrichment of colony-forming cells relative to other cells in the marrow. Colony-forming cells in cord blood are thought to be more dense than those in marrow (Broxmeyer et al., 1991; reviewed in Flomenberg and Keever, 1992); hence, use of the typical density media (Ficoll, Percoll) to fractionate cord blood may result in loss of 50–90% of committed progenitor

cells (Broxmeyer et al., 1989, 1990, 1991; Nakahata and Ogawa, 1982).

In counterflow centrifugal elutriation, a cell suspension is pumped into a spinning chamber in a direction opposite to the centrifugal field. Either the pump speed or the rotor speed is varied gradually, causing cells of increasing sedimentation rate to elute out of the chamber in a centripetal direction. Studies by Noga and colleagues have shown that when this technique is applied to human bone marrow, CD34+ cells are recovered predominantly in the 100 mL/min and rotor-off fractions, where the majority of CFU-GM are also found (Gao et al., 1987; Noga et al., 1986a,b). Unfortunately, the majority of lymphocytes are found in these same fractions, making elutriation of limited utility for the purification of allogeneic marrows, because the T cells that mediate GVHD are enriched to approximately the same extent as the stem and progenitor cells.

Generally speaking, the degree of purification of stem cells achieved with physical separation methods is low (<1–1.5 logs) compared to that which can be achieved by specific binding methods (2.5–3 logs). Consequently, physical separation methods are used most often as adjuncts or preenrichment steps to specific binding methods. By performing a physical preenrichment step, the volume of marrow or blood that must be processed is reduced, simplifying handling and reducing the amount of specific binding agent needed for subsequent enrichment steps. However, multiple preenrichment steps are undesirable, as some loss of target cells, due to physical heterogeneity among the cells or to nonspecific binding to glass or plastic, is unavoidable at each step.

**Specific Binding Methods.** Specific binding methods, based on the affinity of a receptor for a ligand on the cell surface, can be used to select cells from a heterogeneous population on either a negative or a positive basis. In a negative selection method, the cells of interest (the target cells) are excluded from the specific binding reaction, while in a positive selection method, the target cells are included and nontarget cells are excluded. Although antibody/antigen pairs are the most widely used in specific binding reactions, many other ligand/receptor interactions have been employed, including lectin agglutination (Edelman et al., 1971; Hellstrom et al., 1976), erythrocyte rosette formation (Bianco et al., 1970; Wormmeester et al., 1984), and growth factor/receptor interactions (Juckett and Hultquist, 1983).

Positive selection methods intuitively afford a higher degree of enrichment for the target cells than negative selection methods. This is because the nontarget cells do not usually represent a single cell type, but many cell types that are heterogeneous with respect to the properties used to select them. Hence, the degree of depletion that can be attained in a single negative selection step is generally much less than the degree of enrichment that can be attained in a single positive selection step. However, if it was practical to select against every nontarget cell type in a cell suspension, negative selection could yield, in theory, the same degree of enrichment as positive selection.

Negative selection methods are placed at an even greater disadvantage relative to positive selection methods when the frequency of the target cell in the starting population is low. This occurs for two reasons. First of all, a large quantity of specific binding agent(s) is necessary to ensure depletion of a significant fraction of the nontarget cells. Secondly, assuming that two selection methods, one negative and one positive, are equivalent in efficiency of capture and recovery, the negative selection method will



yield a less enriched product than the positive selection method when the target cells are much less frequent than the nontarget cells. This is because the number of cells bound in a single selection step represents a smaller fraction of the total cells in the population undergoing fractionation.

**Flow Cytometry.** Flow cytometry has proven to be an extremely useful tool for the analysis and separation of heterogeneous mixtures of cells. It has been applied extensively to the study of hematopoietic stem cells from several species, including rat (Goldschneider et al., 1980; Castagnola et al., 1981; McCarthy et al., 1985), mouse (Visser et al., 1984; Spangrude et al., 1988), monkey (Gerritsen et al., 1988), and human (Beverley et al., 1980; Bodger et al., 1981; Andrews et al., 1983; Griffin et al., 1983; Civin and Loken, 1987; Visser, 1990; Civin and Gore, 1993).

Since flow cytometry techniques have been reviewed recently (Bauer et al., 1993), they will not be discussed in detail here. Suffice it to say that cells can be labeled with multiple antibodies, each bearing a different fluorescent tag, allowing them to be analyzed on the basis of their level of expression on multiple antigens at the same time. The cells' light scatter properties can also be analyzed simultaneously, providing information regarding cell volume and complexity, in addition to antigen expression. DNA binding dyes can be utilized to provide information on ploidy. Other fluorescent dyes can be used to assess viability, calcium flux, and mitochondrial activity. By electrically charging those droplets which contain fluorescence, labeled cells can be sorted from unlabeled cells, allowing the isolation of essentially pure populations of cells.

Using these techniques, we know that the most primitive stem cells in human bone marrow are small, relatively agranular cells which are CD34-bright, CD38-dull and, HLA-DR-dull, while the more mature progenitor cells are CD34-bright, CD38-bright, and HLA-DR-bright (Civin et al., 1987; Andrews et al., 1989; Civin and Gore, 1993). Heterogeneity of expression by CD34+ cells for other markers, such as CD45 (Lansdorp et al., 1990), rhodamine-123 (Udomsakdi et al., 1990), and CD33 (Andrews et al., 1989; Bender et al., 1991), has also been shown by flow cytometry.

Flow cytometry is an exquisitely sensitive analytic tool because it looks at one cell at a time, but it is not a clinically practicable method for the isolation of stem cells from blood or marrow for transplantation. This is because of the length of processing time required, the complexity of the equipment, and the difficulty of sterilizing the instrument between patient samples. To process the approximately 20 billion nucleated cells present in a typical marrow harvest would require about 1 month of sorting time at generally attainable sorting rates of 2500–5000 cells/s. Even with the development of high-speed sorters (Van den Engh and Stokdijk, 1989), capable of processing two to four times as many cells, sorting times will still exceed 400 h per marrow or apheresis product. This is clearly an impractical technology for the clinic.

**Solid-Phase Methods.** Specific binding methods in which the antibody is immobilized on a solid phase offer the potential for processing larger numbers of cells in substantially shorter times than can be accomplished by flow cytometry. Furthermore, it is more feasible to develop single-use devices which can be disposed after use, thus reducing or eliminating infection-control and cross-contamination concerns that are important in a clinical setting.

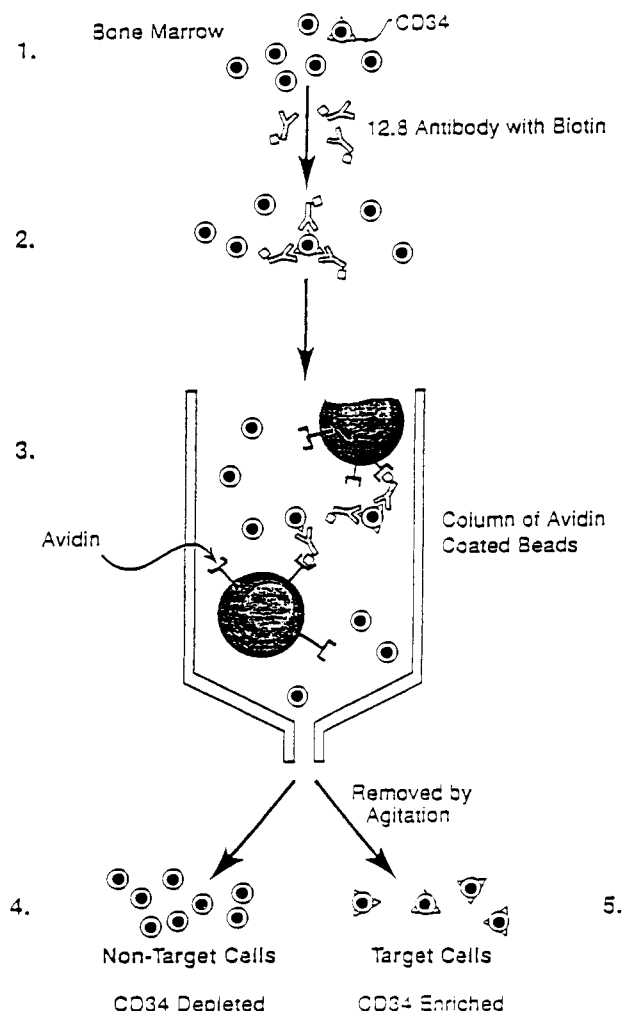
The major disadvantage of solid-phase methods is the difficulty of removing the target cells from the solid phase when positive selection is employed. Solvent, pH, and chaotropic elution methods may work well for soluble protein antigens, which are reversibly denatured by these agents, but they are generally unsuitable for the elution of specifically bound cells because they result in unacceptable losses of viability and biological activity. To circumvent this problem, linkers which can be cleaved, either chemically (Bonnafeous et al., 1983; Thomas et al., 1989) or enzymatically (Civin et al., 1990), as well as supports that can be melted or dissolved (Gold et al., 1974; Haas and von Boehmer, 1978) have been employed. However, less complicated options, such as ligand elution (Wofsy et al., 1971; Cammisuli and Wofsy, 1976; Wofsy et al., 1978) and simple mechanical release (Juckett and Hultquist, 1983; Berenson et al., 1986; Colter et al., 1992), can also be used with comparable or better efficiency and with substantially less risk of damage to the cells than denaturing methods of release.

Specific binding techniques using immobilized ligands have been reviewed recently (Hermanson et al., 1992). Briefly, major technical considerations include the choice of support material, the chemistry immobilizing the ligand to the support, flow rates and incubation times, and the method of elution of the cells from the support (positive selection mode). Solid phases employed in specific binding methods include various chromatographic media (such as beaded agarose, polystyrene, polyacrylamide, and copolymers thereof), formed surfaces (such as Petri dishes, dipsticks, microtiter wells, microscope slides, and tissue culture flasks), magnetic beads, and microfiltration membranes. Immobilization chemistries employed to bind the antibody or ligand to the solid phase include both covalent and noncovalent methods. Among the various functional groups exploited for covalent immobilization are carbohydrate groups, amine, carboxylate, and sulfhydryl groups. For the most part, solid-phase binding techniques have been developed using soluble, rather than cell-associated antigens. However, the same considerations generally apply to both, except that the range of options is more limited in the case of cells. This is particularly true with regard to the method of elution.

Several solid-phase methods of selecting CD34+ cells from marrow or blood have been described. These include a magnetic bead method (Civin et al., 1990; Hardwick et al., 1992; Hardwick et al., 1993; Law et al., 1993), a panning method (Lebkowski et al., 1992; Okarma, 1992; Okarma et al., 1992), and an avidin-biotin column chromatography method (Berenson et al., 1986, 1987, 1992). However, only the column chromatography method has been reported to have been applied clinically (Berenson et al., 1991; Sphall et al., 1992a,b, 1994).

**Avidin-Biotin Column Chromatography.** This method utilizes immobilized avidin and directly or indirectly biotinylated antibody to enrich antigen-positive cells from blood or marrow (Berenson et al., 1986; Lemoli et al., 1988, 1989). In this method (Figure 2), a bone marrow buffy coat is incubated with a biotinylated anti-CD34 antibody (12.8) and then passed through a column of avidin-coated polyacrylamide or agarose beads. The column is washed to remove unbound cells, and then the bound CD34+ cells are eluted by mechanical agitation of the column bed, using a magnetically driven stirring bar.

Because of the high binding affinity between avidin and biotin, the chromatographic separation step can be performed under continuously flowing conditions that minimize nonspecific binding without compromising the



**Figure 2.** Direct avidin-biotin immunoadsorption. A buffy coat is prepared from bone marrow (step 1), and the resultant cell suspension is incubated with a biotinylated, mouse monoclonal antibody to the CD34 antigen (step 2). The cell suspension is then passed through a column containing 40 mL of polyacrylamide beads to which avidin has been covalently attached (step 3). CD34+ cells adhere to the beads by virtue of the biotinylated antibody with which they are labeled, while CD34- cells flow through the column without binding (step 4). The contents of the column are agitated using a magnetically-driven stirring bar to release the bound CD34+ cells from the beads, and these cells are washed out of the column and collected (step 5).

capture of CD34+ cells. Mechanical release of the bound cells has little or no effect on viability and, more importantly, on repopulating ability of the CD34+ cells. This has been shown by both *in vitro* assays of colony-forming ability and *in vivo* transplantation studies. Furthermore, the bound cells are eluted largely free of antibody. This is believed to be due to the tight binding between avidin and the biotin groups on the antibody, resulting in breakage of the chain attaching the cells to the solid phase at the chain's weakest link, that is, between antibody and antigen. That the CD34 antigen remains on the cell surface is evidenced by the ability to restrain the selected cells with an anti-CD34 antibody.

With any positive selection method, there is a potential concern that binding of antibody to the cell surface may activate or inhibit the cells in ways which are undesirable. However, recent studies using avidin-biotin column chromatography to positively select T cell subsets from human blood diminish this concern. These studies show that such positively-selected T cells behave normally in *in vitro* assays of activation and proliferation, suggesting

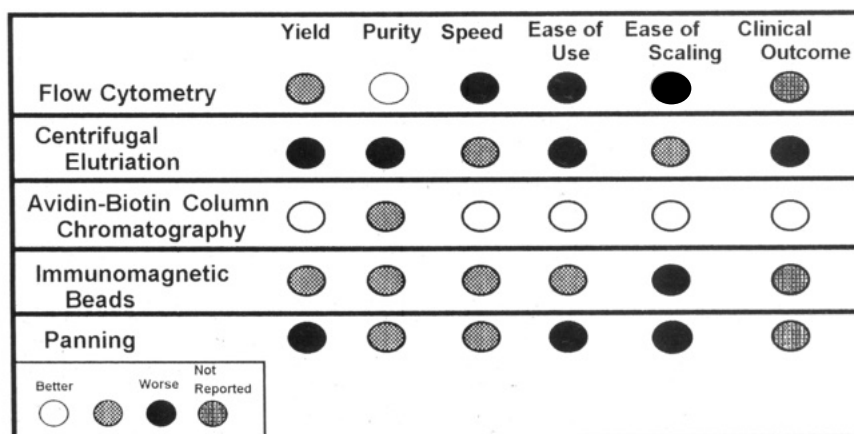
that they are neither inhibited nor stimulated by the quantity of antibody used to bind them to the support (L. S. Davis et al., unpublished results). Positively-selected CD34 cells also behave normally, as shown by their ability to grow in *in vitro* colony forming assays and to repopulate marrow *in vivo*.

From a practical standpoint, the entire marrow processing procedure takes less than two hours from collection of the marrow to elution of the CD34+ cells, while the actual column chromatography step takes only about 30 min. Operation of the column chromatography system is computer-controlled, and the columns themselves are single-use disposable items, each capable of processing at least 60 billion cells.

To date, more than 200 patients worldwide have been transplanted with CD34+ cells enriched using this system. The system has been used to select CD34+ cells from growth factor-primed peripheral blood (Heimfeld et al., 1992, 1993; Shpall et al., 1992a), bone marrow (Berenson et al., 1991; Shpall et al., 1992a,b), and umbilical cord blood (Hervatin et al., 1993; DeBruyn et al., 1993), and has been used in both the allogeneic (Noga et al., 1993) and autologous transplant settings to treat breast cancer (Shpall et al., 1992a,b, 1994), neuroblastoma (Berenson et al., 1991), non-Hodgkin's lymphoma (Douay et al., 1993), and chronic myelogenous leukemia (Deisseroth et al., 1992, 1993).

**Immunomagnetic Separation.** In the magnetic bead method, a mononuclear cell fraction of marrow or blood is incubated with an anti-CD34 antibody (Civin et al., 1990). After the cell fraction is washed to remove excess antibody, the antibody-labeled cells are mixed with paramagnetic (ferric oxide-treated polystyrene) beads coated with sheep anti-mouse Ig. The resultant mixture is separated into rosetted (CD34+) and nonrosetted (CD34-) populations by applying magnets to the sides of the vessel in which the cells are contained. The non-rosetted cells are washed out of the vessel by gravity flow, while the rosetted cells are pulled to the container's walls. After a series of washing steps, the rosetted cells are released from the beads, using the protease chymopapain to effect release. This method has been used to enrich CD34+ cells from growth factor-primed peripheral blood, marrow, and umbilical cord blood (Law et al., 1993). However, there are no published reports of transplantation and engraftment of patients with CD34+ cells isolated by this method.

There are two concerns with immunomagnetic enrichment of cells intended for clinical application. The first is the magnetic beads. These must be completely removed from the cells prior to reinfusion or they will be removed from the circulation by the reticuloendothelial system, preventing engraftment (Kemshead, 1991). Free beads which elude the reticuloendothelial system can lodge in the capillaries, where there is a theoretical possibility that they may lead to the formation of emboli. The beads are also potentially subject to movement from one location in the body to another if the patient is placed in a magnetic field, such as in magnetic resonance imaging. Since the beads are not biodegradable, the potential for them to cause side effects in the patient continues indefinitely. Immunomagnetic beads have been used for negative selection for many years with no reports, to our knowledge, of adverse events; this suggests that the reinfusion of free beads can be controlled to an extent sufficient to prevent significant side effects. Insufficient data are available at present on the likelihood and severity of side effects which



**Figure 3.** Comparison of stem cell selection technologies. Six different methods of stem cell selection are ranked, relative to each other, with respect to cell yield, cell purity, speed of processing, ease of use, ease of scaling up to clinically relevant volumes, and ability to support engraftment (clinical outcome).

may be associated with the reinfusion of cells positively selected using immunomagnetic beads.

The second concern is the effect of chymopapain treatment on the enriched cells. Chymopapain alters the cell surface and may compromise the functional activity of the cells upon transplantation (Lansdorp and Thomas, 1991), affecting their homing properties, their response to growth factors, and their adhesion properties, among others. Enzyme-digested cells may also be less tolerant of freezing, a potential problem in the autologous transplant setting where the cells are stored prior to reinfusion. The capacity of chymopapain-treated CD34<sup>+</sup> cells to generate colony forming cells *in vitro* does not appear to be impaired (Silvestri et al., 1992). However, the more critical test, whether or not the cells can engraft *in vivo*, has yet to be published.

**Panning.** CD34<sup>+</sup> cells have also been enriched from marrow by panning, a technique originally described by Wysocki and Sato (1978) and Mage et al. (1977) for the enrichment of lymphocyte subsets. A two-step procedure has been described in which bone marrow mononuclear cells are panned with a soybean agglutinin (SBA)-coated polystyrene flask, followed by panning of the SBA-negative fraction with anti-CD34 antibody (IC33)-coated flask (Okarma, 1992; Okarma et al., 1992; Lebkowski et al., 1992). The bound CD34<sup>+</sup> cells are mechanically released from the flask. This method has been applied to peripheral blood as well as marrow, but there are, as yet, no published reports of transplantation and engraftment of patients with CD34<sup>+</sup> cells isolated by this method.

The major limitation to panning methods of cell selection is the large amount of surface area required to process clinically useful quantities of cells. Consequently, two pre-enrichment steps, a density gradient separation and a negative lectin adherence step, are performed prior to CD34 selection in order to reduce the volume of marrow cells that must be processed. Whether this magnitude of manipulation will be acceptable in the clinical setting remains to be tested. More importantly, the multiplicity of steps performed is expected to result in a comparatively lower yield of CD34<sup>+</sup> cells, since there is inevitably cell loss at each step. However, yield data are not always reported for CD34<sup>+</sup> selection because of the low frequency of CD34<sup>+</sup> cells in the starting material and the weak staining intensity of the cells (Lebkowski et al., 1992).

Figure 3 compares counterflow centrifugal elutriation, flow cytometry, avidin-biotin column chromatography, immunomagnetic separation, and panning with respect

to a number of practically important considerations for the selection of CD34<sup>+</sup> cells from marrow or blood. The comparisons are subjective because patient-to-patient variability and differences in the scale on which marrow has been processed make quantitative comparisons meaningless. Nonetheless, the various methods are clearly differentiated from each other in clinical practicality, including ease of use, speed, and adaptability to collections of clinically meaningful quantities of cells.

#### CLINICAL EXPERIENCE WITH STEM CELL TRANSPLANTS

**Rationale for CD34 Selection.** Isolating CD34<sup>+</sup> stem and progenitor cells has numerous clinical benefits in the field of transplantation. In the autologous setting, CD34 selection may result in depletion of tumor cells, often to levels undetectable by immunocytochemical staining (Shpall et al., 1994). This is accomplished without resort to pharmacologic agents, such as 4-hydroperoxycyclophosphamide (4-HC) or immunotoxins, which may damage engrafting cells as well as tumor cells (Shpall et al., 1992b; Vredenburg et al., 1992). However, it should be noted that some acute leukemias are CD34<sup>+</sup>, in which case CD34 selection will not result in tumor depletion, but may rather result in tumor enrichment. A further advantage of CD34 selection with respect to depletion of CD34<sup>+</sup> tumor cells relates to the reduction in volume of the material to be transfused. This means that additional, post-positive-selection, purging steps are more feasible, because the total number of cells which must be manipulated is now much smaller. Hence, one can envision a stem cell selection system in which CD34<sup>+</sup> cells are positively selected from marrow or blood in a first step and purged of tumor cells by negative selection, in a second step, using a cocktail of antibodies reactive with a given tumor.

Transplantation of CD34<sup>+</sup> cells also has the potential to reduce the infusional toxicity experienced by autologous transplant patients. The majority of infusional toxicity is believed to be attributable to the use of the cryoprotective agent dimethyl sulfoxide (DMSO) to preserve the patient's marrow. When the marrow is thawed, the DMSO in which it was frozen is infused along with the cells, potentially causing nausea, vomiting, headaches, hypertension, and bradycardia. More significant complications, such as serious cardiac arrhythmias, renal failure, and respiratory decompensation can also occur (Davis et al., 1990; Stroncek et al., 1991; Smith et al., 1987). Removal of DMSO by washing the thawed cells is not usually considered an option, because of the loss of stem cells that inevitably

accompanies the washing steps. Since the amount of DMSO used to preserve a marrow is proportional to its volume, the smaller the volume in which the cells are stored, the less the likelihood of serious infusional toxicity.

Infusional toxicity is also believed to be due to lysis of red blood cells and aggregation of granulocytes which occur during the freeze-thaw cycle. Since these cells are depleted by the CD34 selection, the patient can be expected to experience less hemoglobinuria, due to red cell lysis, and fewer pulmonary emboli, due to granulocyte clumps, after infusion.

Volume reduction is also an important consideration in and of itself, regardless of its effect on infusional toxicity. As the number of autologous transplants increases, the demand for frozen storage space becomes critical. CD34-selected cells can be frozen in a single 5-mL vial, versus the 100–200-mL bags in which unselected marrow is frozen. If in the future cord blood is banked for transplantation, the importance of volume reduction will continue to grow.

In gene therapy, retrovirus-mediated transfection is facilitated by selection of CD34+ cells. Transfection of unfractionated marrow requires as much as 80 L of retroviral supernatant, while the smaller volume in which CD34+ cells are contained can be transfected with as little as 1–2 L of supernatant (Cassel et al., 1993). Transduction efficiency has also been reported to be higher for CD34+ cells than for unfractionated marrow (Cassel et al., 1993).

In the allogeneic transplant setting, an important advantage of CD34 selection is the depletion of T cells which contribute to GVHD. This effect has been shown already in non-human primates (Andrews et al., 1991) and is currently being studied in humans, using CD34 cells selected by avidin-biotin column chromatography. Other methods of T cell depletion, such as negative selection, complement-mediated lysis, and counterflow centrifugal elutriation, have been complicated by graft failure and/or an increased rate of relapse. It has been suggested that positive selection for CD34+ cells may avoid these problems, while retaining the clinical benefit of T cell depletion (Martin, 1990, 1992).

**Transplantation of Autologous CD34-Selected Cells from Marrow.** A pilot study was performed in which nine patients (seven with stage IV breast cancer and two with stage IV neuroblastoma) were transplanted after marrow ablative therapy with autologous CD34+ cells, selected from bone marrow using the avidin-biotin column chromatography method. All evaluable patients in this study engrafted (Berenson et al., 1991). On the basis of these results, a Phase I/II clinical study was initiated.

In this study, 43 patients with poor-prognosis breast cancer were transplanted, after marrow ablative therapy, with autologous CD34+ cells, selected from marrow (25 patients), peripheral blood (7 patients), or both (11 patients), using the avidin-biotin column chromatography method. All but two patients achieved trilineage engraftment, as defined by recovery of peripheral blood counts, similar to historical controls who received marrow buffy coats. Two patients experienced delayed platelet engraftment, one of whom died of recurrent disease and the other of whom remained platelet-dependent, despite infusion of her backup marrow. There were no late engraftment failures (median followup 9 months, longest followup 24 months), and no acute toxicity was observed in any of the study participants. In addition, from one to greater than four logs of breast cancer cell depletion was observed in the CD34+ fraction, for patients in whom tumor was initially detected (Shpall et al., 1994).

**Peripheral Blood Stem Cell Transplantation.** Transplantation of stem and progenitor cells enriched from peripheral blood is an attractive alternative to bone marrow aspiration. The latter is an unpleasant and expensive inpatient procedure performed under general anesthesia. By contrast, one or two apheresis collections can yield sufficient CD34+ cells from growth factor-mobilized peripheral blood for transplantation of an average 70 kg adult. At present, nearly one-half of all stem cell transplants performed in Europe use peripheral blood stem cells. The number is smaller in the U.S., but is growing rapidly.

Recent data suggest that hematologic recovery may be faster in patients transplanted with CD34+ peripheral blood stem cells than in patients transplanted with CD34+ cells derived from marrow (Heimfeld et al., 1993; Shpall et al., 1992a; Shpall et al., 1994). Median time to neutrophil engraftment was approximately the same (10–11 days) in patients who received G-CSF post-transplant and either peripheral blood CD34+ cells (7 patients) or marrow CD34+ cells (10 patients). Median time to platelet recovery, however, was significantly shorter in the cohort which received peripheral blood CD34+ cells (10 days) versus the cohort which received marrow CD34+ cells (23 days) (Shpall et al., 1994). If this trend is supported by studies of larger numbers of patients, peripheral blood stem cell transplants may well replace marrow transplants entirely.

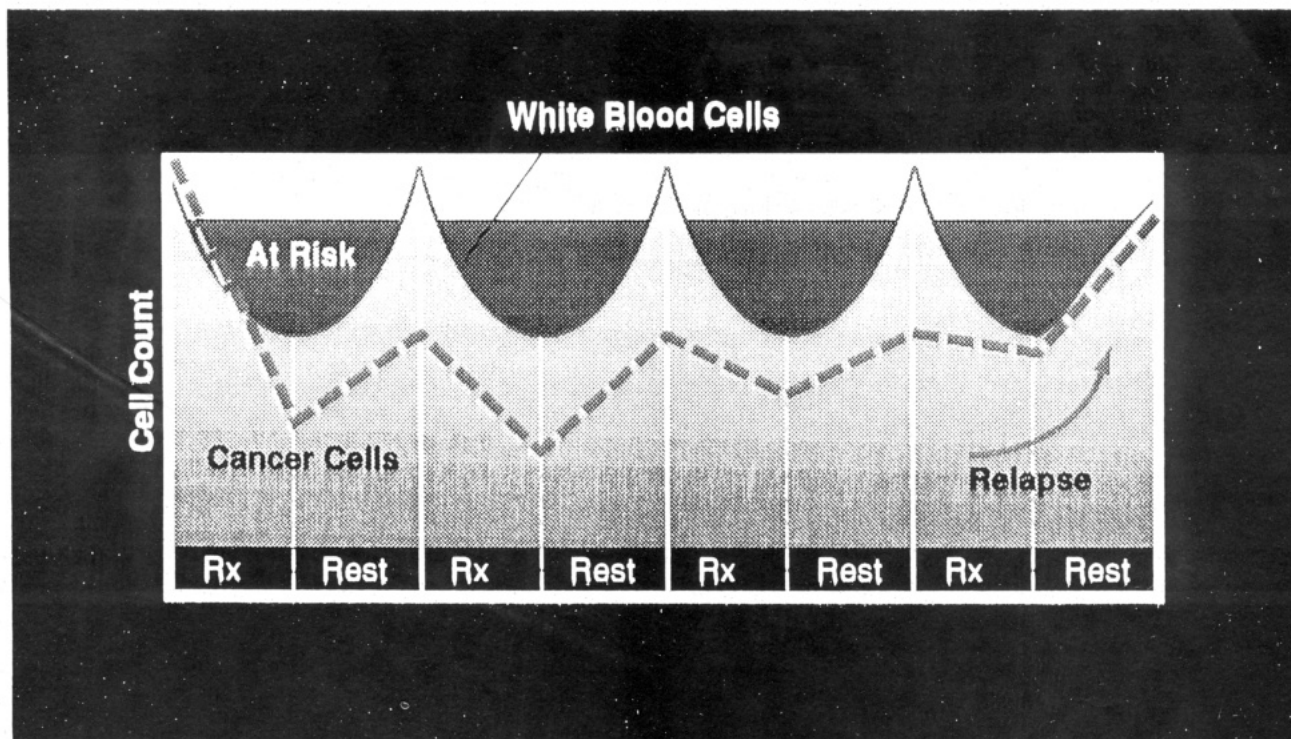
**Multiple Cycles of High-Dose Chemotherapy with Stem Cell Support.** Bone marrow suppression is the major dose-limiting toxicity of most chemotherapeutic regimens. Consequently, chemotherapy is administered in cycles, comprised of a treatment period and a withdrawal period, the latter designed to allow the bone marrow time to recover (Figure 4). Unfortunately, the malignant cells also recover during the withdrawal period. Data are accumulating that suggest the likelihood of achieving a cure of the patient's cancer would be substantially increased, if chemotherapy could be given in larger doses and/or shorter cycles (Vose et al., 1992; Antman et al., 1992).

Autologous stem cell support, combined with growth factors, may enable high-dose chemotherapy to be administered safely, by promoting the recovery of peripheral blood cell counts. This cannot be accomplished with growth factors alone, since growth factors are only effective if they have enough progenitor cells on which to act. It is now feasible to collect and freeze sufficient CD34+ cells from one or two apheresis procedures to support multiple cycles of high-dose therapy.

**Stem Cells as Targets for Gene Therapy.** Gene therapy is a viable option for treating many single gene diseases, such as ADA deficiency, Gaucher's disease, and  $\beta$ -thalassemia and has been proposed for the treatment of various malignancies and viral diseases as well (reviewed by Karlsson (1991) and Gutierrez et al. (1992)). The ideal target cell for gene therapy is widely agreed to be the hematopoietic stem cell because of its transplantability; stem cells can continuously renew themselves and differentiate into a much larger number of circulating progeny cells. Gene therapy is also more practical using CD34-selected cells because smaller volumes of viral supernatant can be used for transfection.

CD34+ cells selected by avidin-biotin column chromatography have been transfected with viral vectors expressing the genes for glucocerebrosidase, the defective enzyme in Gaucher's disease (Nimgaonkar et al., 1993), ADA, the defective enzyme in severe combined immu-





**Figure 4.** Conventional chemotherapy. Most chemotherapeutic agents are toxic to the bone marrow as well as to tumor cells. Therefore, chemotherapy is generally given in cycles, each cycle consisting of a period of treatment (Rx), followed by a period of withdrawal or rest. During the treatment period, both the tumor cells and the white blood cells decline in number, the decline in the latter putting the patient at risk for infection and bleeding. The rest period permits the white blood cells to recover, but at the price of the cancer cells recovering as well. With time, chemotherapy becomes progressively less effective, killing fewer tumor cells as they develop resistance, until eventually the patient relapses.

nodeficiency disease (Kohn et al., 1993), and with various marker genes, useful for determining the source of relapse in cancer patients treated by bone marrow transplantation (Deisseroth et al., 1992, 1993).

#### FUTURE CLINICAL APPLICATIONS OF ENRICHED CELLS

**Stem Cell Expansion.** The ability to select CD34+ cells from marrow or blood makes it feasible to consider expanding these cells in culture. Previously, the presence of inhibitory accessory cells in marrow or blood limited the degree of expansion in the progenitor compartment which could be attained *ex vivo*. Also, practical considerations, such as the large volume of cells which had to be handled and the quantities of medium and growth factors necessary for their maintenance, adversely impacted the prospects for *ex vivo* expansion.

There are several reasons why stem cell expansion might be important. The most obvious is that it should be possible to achieve an engrafting dose of cells from a much smaller initial harvest. Presumably, the ability to donate cells without having to undergo the discomfort and inconvenience of a full marrow harvest or apheresis procedure would expand the potential donor pool.

Transplantation of *ex vivo* expanded cells may lead to faster hematologic recovery because of the higher content of committed progenitor cells in the graft. Mice transplanted with bone marrow that had been expanded *ex vivo* recovered peripheral blood counts more rapidly than animals transplanted with bone marrow that had not been expanded, and fewer expanded cells were necessary for engraftment than unexpanded cells (Muench and Moore, 1992).

It has also been postulated that *ex vivo* culture of marrow stem cells differentially supports the growth of normal

progenitors, while inhibiting the growth of malignant cells. This phenomenon has been demonstrated in CML (Barnet et al., 1989; Coulombel et al., 1983) and acute non-lymphocytic leukemia (Chang et al. 1989; Eaves et al., 1987).

Lineage-directed, *ex vivo* expansion of CD34+ cells is also possible, at least in theory. The goal of this work would be to generate mature cells to help the patient through the post-transplant period of pancytopenia. Of particular interest in this regard is the generation of neutrophils and platelets, since the majority of post-transplant morbidity and mortality in the autologous setting is due to infection and bleeding episodes. Currently, the average time to neutrophil recovery in a patient undergoing bone marrow transplantation and receiving post-transplant growth factors is 10 to 19 days (Nemunaitis et al., 1991; Devereaux et al., 1989) and for platelet recovery, 26 to 40 days (Sheridan et al., 1992; Nemunaitis et al., 1991).

Stem cell expansion is also important in gene therapy, both for the initial transfection and subsequently for the selection of transfected cells. Gene transfer using viral vectors occurs more readily in cells that are cycling than in non-cycling cells. Even at high efficiencies of transfection, there will inevitably be some cells that have not taken up the gene. A post-transfection selection for those cells which have taken up the gene, followed by *ex vivo* expansion of this population, may improve the outcome of gene therapy by increasing the likelihood that patients will be repopulated with stem cells expressing the introduced gene.

**Stem Cell Therapy of Autoimmune Diseases.** It is possible that marrow ablation of individuals with autoimmune conditions, to eliminate autoreactive lymphocytes and their precursors, will be curative when

followed by reconstitution with CD34-selected stem cells. However, there are conflicting data on the role of bone marrow transplantation in the management of autoimmune diseases. In some cases, marrow transplantation has been reported to transfer autoimmunity from the donor to the recipient, suggesting an underlying defect in the stem cell compartment (reviewed by Marmont (1992) and Van Bekkum (1993)). In other cases, allogeneic bone marrow transplantation, performed for a coexisting, life-threatening condition, has been reported to cure such autoimmune phenomena as psoriasis (Eedy et al., 1990; Liu Yin and Jowitt, 1992), ulcerative colitis (Liu Yin and Jowitt, 1992), and rheumatoid arthritis (Jacobs et al., 1986).

There are several reasons to think myeloblation followed by autologous stem cell transplantation will cure at least certain autoimmune diseases. Hematopoietic reconstitution is probably oligoclonal, so even if autoimmunity is due to an underlying stem cell defect, there is a reasonable likelihood that the offending clones will not be reconstituted following transplantation. Furthermore, it is possible that the agent which incited the autoimmune response initially will no longer be present in the patient's environment and thus disease will fail to develop, regardless of the pattern of reconstitution.

**Tolerization of Solid Organ Graft Recipients Using Enriched Stem Cells.** More than 10 thousand solid organ grafts are performed in the United States every year. Although the development of immunosuppressive drugs, especially cyclosporine, has enhanced graft survival, it is estimated that 20% of kidney allografts still fail within the first year post-transplant and that 80% fail within 10 years. Furthermore, chronic administration of immunosuppressive drugs can lead to toxicity, increased incidence of infections, and malignancy in the host.

Studies performed about 40 years ago demonstrated that tolerance to allografts could be induced in fetal and neonatal animals by exposure to donor lymphoid cells, this exposure leading to a state of mixed chimerism (Owen, 1945; Billingham et al., 1953). These studies provided the impetus for numerous attempts to induce antigen-specific tolerance in adult allograft recipients by means of donor bone marrow transfusions (Barber, 1990; Barber et al., 1991).

It is possible that solid organ graft recipients can be made tolerant to donor antigens using CD34-selected bone marrow to establish a mixed chimeric state, thus prolonging graft survival and reducing or eliminating the need for chronic immunosuppressive treatment. This approach offers several theoretical advantages. Since CD34+ stem cells are capable of self-renewal, they should sustain a long-term state of mixed chimerism. Furthermore, by virtue of their ability to give rise to all of the mature elements of the hematopoietic system, stem cells should be able to mediate tolerance by more than one mechanism. Finally, by transfusing only CD34-selected cells, which are functionally immature, the possibility of sensitizing the host and precipitating acute graft rejection is diminished, as is the likelihood of eliciting GVHD, both these phenomena being mediated by mature cells.

**Other Rare Cell Therapies.** The technologies developed for CD34 selection are also applicable, with minor modifications, to the selection of other cell types that may be useful for therapy or diagnosis. Therapeutic applications include the selection of tumor-specific or virus-specific T-cells from tumor-bearing or virus-infected patients; these cells can be activated and expanded *ex vivo* and ultimately reinfused into the patient with the

hope that they will sustain an effective cell-mediated immune response.

**Rare Cell Diagnostics.** The ability to identify and capture rare cells also enables the development of new methods for prenatal and cancer diagnosis. Prenatal diagnosis currently involves obtaining fetal cells by amniocentesis or chorionic villus sampling. These are invasive procedures which entail a measurable risk of fetal injury or spontaneous abortion. It has been known for a number of years now that fetal cells circulate in maternal peripheral blood (Schroder, 1975; Schroder and de la Chappelle, 1972; Schroder and Herzenberg, 1979). However, the frequency of these cells is so low, about one in 1 million, that it has not been clinically practicable to isolate them. Cell selection technology, using antibodies which bind preferentially to fetal cells, can be used to capture these extremely rare fetal cells from the maternal circulation. Circulating tumor cells can also be enriched from peripheral blood using cell selection technology (Hall et al., 1993), enabling early diagnosis of hematologic malignancies, detection of metastasis, and determination of chemosensitivity of the tumor *in vitro*.

## CONCLUSIONS

Bone marrow transplantation has been an accepted treatment modality for a number of malignant diseases, as well as other disorders in which bone marrow function is abnormal, for many years now. The transplantation of hematopoietic stem and progenitor cells, enriched from marrow or peripheral blood, represents the next logical step in the evolution of this therapy.

The CD34 antigen is a convenient marker for the selection of these cells, as it identifies both the pluripotent stem cell and committed progenitor cells, enabling rapid hematologic recovery as well as long-term reconstitution. Several methods of selecting CD34+ cells have been developed, one of which has been successfully implemented in the clinic.

The advantages which flow from transplantation with CD34 selected cells, such as reduced infusional toxicity, volume reduction, and potential reductions in tumor cell burden and GVHD, have widened the applications for stem cell transplants in support of high-dose chemotherapy and in gene therapy of congenital disorders. In the future, cell selection technology can be expected to lead to additional advances in cancer therapy and diagnosis, prenatal diagnosis, and therapy of organ failure and autoimmune diseases.

## LITERATURE CITED

- Andrews, R. G., Torok-Storb, B., and Bernstein, I. D. (1983) Myeloid-associated Differentiation Antigens on Stem Cells and their Progeny Identified by Monoclonal Antibodies. *Blood* 62, 124-132.
- Andrews, R. G., Singer, J. W., and Bernstein, I. D. (1986) Monoclonal Antibody 12-8 Recognizes a 115-kd Molecule Present on both Unipotent and Multipotent Hematopoietic Colony-Forming Cells and their Precursors. *Blood* 67, 842-845.
- Andrews, R. G., Singer, J. W., and Bernstein, I. D. (1989) Precursors of Colony-forming Cells in Humans can be Distinguished from Colony-forming Cells by Expression of the CD33 and CD34 Antigens and Light Scatter Properties. *J. Exp. Med.* 169, 1721-1731.
- Andrews, R. G., Bartelmez, S. H., Knitter, G. H., Bryant, E., Longen, K., Bensinger, W. I., D. Y., Strong, M., and Bernstein, I. D. (1991) Isolated Allogeneic CD34+ Marrow Cells Engraft



- and Reconstitute Hematopoiesis in Lethally Irradiated Baboons. *Blood* 78, 257a.
- Antman, K., Corringham, R., de Vries, E., Elfenbein, G., Gianni, A. M., Gisselbrecht, C., Herzig, R., Juttner, C., Kaizer, H., Kennedy, M. J., Kessinger, A., Kotasek, D., Lazarus, H., Ljungman, P., Maraninchi, D., Nabholz, J., Niederwieser, D., Ogawa, M., Patrone, F., Peters, W., Rosti, G., Rouesse, J., Schilcher, R., Selby, G., Shea, T., Shpall, E., Spitzer, G., Sweet, D., Tajima, T., Vaughan, W., Williams, S., and Wolff, S. (1992) Dose Intensive Therapy in Breast Cancer. *Bone Marrow Transplant.* 10 (Suppl. 1), 67-73.
- Barber, W. H. (1990) Induction of Tolerance to Human Renal Allografts with Bone Marrow and Antilymphocyte Globulin. *Transplant Rev.* 4, 68-78.
- Barber, W. H., Mankin, J. A., Laskow, D. A., Deierhoi, Julian, B. A., Curtis, J. J., and Diethelm, A. G. (1991) Long-term Results of a Controlled Prospective Study with Transfusion of Donor-specific Bone Marrow in 57 Cadaveric Renal Allograft Recipients. *Transplantation* 51, 70-75.
- Barnet, M. J., Eaves, C. J., Phillips, G., Kalousek, D. K., Klingemann, H. G., Lansdorp, P. M., Reece, D. E., Sheperd, J. D., Shaw, G. J., and Eaves, A. C. (1989) Successful Autografting in Chronic Myelogenous Leukemia after Maintenance of Marrow in Culture. *Bone Marrow Transplant.* 4, 345-351.
- Bauer, K. D., Duque, R. E., and Shankey, T. V. (Eds.) (1993) *Clinical and Flow Cytometry. Principles and Application*, Williams and Wilkins, Baltimore.
- Bell, A. J., Hamblin, T. J., and Oscier, D. G. (1986) Circulating Stem Cell Autografts. *Bone Marrow Transplant.* 1, 103-110.
- Bender, J. G., Unverzagt, K. L., Walker, D. E., Lee, W., Van Epps, D. e., Smith, d. H., Stewart, C. C., and To, L. B. (1991) Identification and Comparison of CD34-positive Cells and Their Subpopulations from Normal Peripheral Blood and Bone Marrow using Multicolor Flow Cytometry. *Blood* 77, 2591-2596.
- Berendsen, H. H., De Leij, L., Postmus, P. E., Ter Haar, J. G., Poppema, S., and The, T. H. (1988) Detection of Small Cell Lung Cancer Metastases in Bone Marrow Aspirates using Monoclonal Antibody Directed against Neuroendocrine Differentiation Antigen. *J. Clin. Pathol.* 41, 273-276.
- Berenson, R. J., Bensinger, W. I., and Kalamasz, D. (1986) Positive Selection of Viable Cell Populations using Avidin-Biotin Immunoadsorption. *J. Immunol. Meth.* 91, 11-19.
- Berenson, R. J., Bensinger, W. I., Kalamasz, D., Schuening, F., Deeg, H. J., and Storb, R. (1987) Avidin-Biotin Immunoadsorption: A Technique to Purify Cells and its Potential Applications, in *Progress in Bone Marrow Transplantation* (R. P. Gale and R. Champlin, Eds.), pp 423-428, Alan R. Liss, New York.
- Berenson, R. J., Andrews, R. G., Bensinger, W. I., Kalamasz, D. F., Knitter, G., Buckner, C. D., and Bernstein, I. D. (1988) Antigen CD34+ Marrow Cells Engraft Lethally Irradiated Baboons. *J. Clin. Invest.* 81, 951-955.
- Berenson, R. J., Bensinger, W. I., Hill, R. S., Andrew, R. G., Garcia-Lopez, J., Kalamasz, D. F., Still, B. J., Spitzer, G., Buckner, C. D., Bernstein, I. D., and Thomas, E. D. (1991) Engraftment after Infusion of CD34+ Marrow Cells in Patients with Breast Cancer or Neuroblastoma. *Blood* 77, 1717-1722.
- Berenson, R. J., Bensinger, W. I., Kalamasz, D., Heimfeld, S., Goffe, R. A., Berninger, R. W., Peterson, D. R., Thompson, P., and Strong, D. M. (1992) Transplantation of Stem Cells Enriched by Immunoadsorption, in *Advances in Bone Marrow Purging and Processing* (D. A. Worthington-White, A. P. Gee, and S. Gross, Eds.), pp 449-459, Wiley-Liss, New York.
- Beverly, P. C. L., Linch, D., and Delia, D. (1980) Isolation of Human Hematopoietic Progenitor Cells using Monoclonal Antibodies. *Nature* 287, 332-333.
- Bianco, C., Patrick, R., and Nussenzweig, V. (1970) A Population of Lymphocytes Bearing a Membrane Receptor for Antigen-Antibody-Complement Complexes. I. Separation and Characterization. *J. Exp. Med.* 132, 702-706.
- Billingham, R. E., Brent, L., Medawar, P. B. (1953) Actively Acquired Tolerance of Foreign Cells. *Nature* 172, 603-606.
- Bodger, M. P., Francis, G. E., Delia, D., Granger, S. M., and Janossy, G. (1981) A Monoclonal Antibody Specific for Immature Human Hemopoietic Cells and T Lineage Cells. *J. Immunol.* 127, 2269-2274.
- Bonnafous, J.-C., Dornand, J., Favero, J., Sizes, M., Boschetti, E., and Mani, J.-C. (1983) Cell Affinity Chromatography with Ligands Immobilized through Cleavable Mercury-Sulfur Bonds. *J. Immunol. Meth.* 58, 93-107.
- Broxmeyer, H. E., Douglas, G. W., Hangoc, G., Cooper, S., Bard, J., English, D., Arny, M., Thomas, L., Boyse, E. A. (1989) Human Umbilical Cord Blood as a Potential Source of Transplantable Hematopoietic Stem/Progenitor Cells. *Proc. Natl. Acad. Sci. U.S.A.* 86, 3828-3832.
- Broxmeyer, H. E., Gluckman, E., Auerbach, A., Douglas, G. W., Friedman, H., Cooper, S., Hangoc, G., Kurtzberg, J., Bard, J., and Boyse, E. A. (1990) Human Umbilical Cord Blood: A Clinically Useful Source of Transplantable Hematopoietic Stem/Progenitor Cells. *Int. J. Cell Cloning* 8, 76-89.
- Broxmeyer, H. E., Kurtzberg, J., Gluckman, E., Auerbach, A. D., Douglas, G., Cooper, S., Falkenburg, J. H. F., Bard, J., and Boyse, E. A. (1991) Umbilical Cord Blood Hematopoietic Stem and Repopulating Cells in Human Clinical Transplantation. *Blood Cells* 17, 313-329.
- Broxmeyer, H. E., Hangoc, G., Cooper, S., Ribeiro, R. C., Graves, V., Yoder, M., Wagner, J., Vadhad-Raj, S., Rubinstein, P., and Broun, E. R. (1992) Growth Characteristics and Expansion of Human Umbilical Cord Blood and Estimation of its Potential for Transplantation of Adults. *Proc. Natl. Acad. Sci. U.S.A.* 89, 4109-4113.
- Cammisuli, S., and Wofsy, L. (1976) Hapten-sandwich Labeling. III. Bifunctional Reagents for Immunospecific Labeling of Cell Surface Antigens. *J. Immunol.* 117, 1965-1704.
- Carbonell, F., Calvo, W., Flidner, T. M., Kratt, E., Gerhartz, H., Korbling, M., Nothdurft, W., and Ross, W. M. (1984) Cytogenetic Studies in Dogs after Total Body Irradiation and Allogeneic Transfusion with Cryopreserved Blood Mononuclear Cells: Observations in Long-term Chimeras. *Inter. J. Cell Cloning* 2, 81-88.
- Cassel, A., Cottler-Fox, M., Doren, S., and Dunbar, C. E. (1993) Retroviral-mediated Gene Transfer into CD34-enriched Human Peripheral Blood Stem Cells. *Exp. Hematol.* 21, 585-591.
- Castagnola, C., Visser, J., Boersma, W., van Bekkum, D. W. (1981) Purification of Rat Pluripotent Hemopoietic Stem Cells. *Stem Cells* 1, 250-260.
- Cavins, J. A., Scheer, S. C., Thomas, E. D., and Feerebee, J. W. (1964) The Recovery of Lethally Irradiated Dogs Given Infusions of Autologous Leukocytes Preserved at -80°C. *Blood* 23, 38-43.
- Chang, J., Morgenstern, G., Coutinho, L. H., Scarffe, J. H., Carr, T., Deakin, D. P., Testa, N. G., and Dexter, T. M. (1989) The Use of Bone Marrow Cells Grown in Long-term Culture for Autologous Bone Marrow Transplantation in Acute Myeloid Leukemia: An Update. *Bone Marrow Transplant.* 4, 5-9.
- Civin, C. I., and Loken, M. R. (1987) Cell Surface Antigens on Human Marrow Cells: Dissection of Hematopoietic Development Using Monoclonal Antibodies and Multiparameter Flow Cytometry. *Int. J. Cell Cloning* 5, 267-288.
- Civin, C. I., and Gore, S. D. (1993) Antigenic Analysis of Hematopoiesis: A Review. *J. Hematother.* 2, 137-144.
- Civin, C. I., Strauss, L. C., Brovall, C., Fackler, M. J., Schwartz, J. F., and Shaper, J. H. (1984) Antigenic Analysis of Hematopoiesis III. A Hematopoietic Progenitor Cell Surface Antigen defined by a Monoclonal Antibody raised against KG1a Cells. *J. Immunol.* 133, 157-165.
- Civin, C. I., Banquerigo, M. L., Strauss, L. C., and Loken, M. R. (1987) Antigenic Analysis of Hematopoiesis. VI. Flow Cytometric Characterization of My-10-positive Progenitor Cells in Normal Human Bone Marrow. *Exp. Hematol.* 15, 10-17.
- Civin, C. I., Strauss, L. C., Fackler, M. J., Trischmann, T. M., Wiley, J. M., and Loken, M. R. (1990) Positive Stem Cell Selection—Basic Science, in *Bone Marrow Purging and Processing* (S. Gross, A. P. Gee, and D. A. Worthington-White, Eds.) pp 387-402, Alan R. Liss, New York.
- Colter, M., Fogarty, B., McGuire, K., Berenson, R. J., and Heimfeld, S. (1992) Rapid Isolation of CD4 or CD8 T-cell

- Subsets using the CEPRATE® LC Laboratory Cell Separation System. *Transplant. Proc.* 24, 2801-2802.
- Cote, R. J., Rosen, P. P., Hakes, T. B., Sedira, M., Bazinet, M., Kinne, D. W., Old, L. J., and Osborne, M. P. (1988) Monoclonal Antibodies Detect Occult Breast Carcinoma Metastases in the Bone Marrow of Patients with Early Stage Disease. *Am. J. Surg. Pathol.* 12, 333-340.
- Coulombel, L., Kalousek, D. K., Eaves, C. J., Gupta, C. M., and Eaves, A. C. (1983) Long-term Marrow Culture Reveals Chromosomally Normal Hematopoietic Progenitor cells in Patient with Philadelphia Chromosome-Positive Chronic Myelogenous Leukemia. *N. Engl. J. Med.* 308, 1493-1498.
- Davis, J. M., Rowley, S. D., Braine, H. G., Piantadosi, S., and Santos, G. W. (1990) Clinical Toxicity of Cryopreserved Bone Marrow Graft Infusion. *Blood* 75, 781-786.
- DeBruyn, C., Stryckmans, P., Bernier, M., Massy, M., Ley, P., Deguelde, M., Bron, D., and Delforge, A. (1993) Amplification of Cord Blood CD34+ Purified Cells on Stromal Cell-Free Long Term Cultures in Presence of Growth Factors (GFs). *Exp. Hematol.* 21, 1134.
- Deisseroth, A. B., Korbli, M., Reading, C., Hester, J., Heimfeld, S., Talpaz, M., Kantarijan, H., O'Brien, S., Feldman, E., Claxton, D., Etkin, M., Ellerson, D., Durett, A., Thomas, M., Champlin, R., and Berenson, R. J. (1992) Selection and Transplantation of CD34+ Progenitor Cells Following Retroviral Marking in Autologous Bone Marrow Transplantation in Chronic Myelogenous Leukemia (CML). *Blood* 80, 232a.
- Deisseroth, A., Kantarijan, H., Talpaz, M., Fu, S. Q., Hanania, E., Ellerson, D., Zu, Z., Calvert, L., Thomas, M., Durett, A., Reading, C., Hester, J., Berenson, R. J., Heimfeld, S., Claxton, D., Andreeff, M., and Champlin, R. (1993) Retroviral Marking of CD34 Stem cells to Monitor Purging in Chronic Myelogenous Leukemia Autologous Transplants. *Proc. Am. Assoc. Cancer Res.* 34, 215.
- Devereaux, S., Linch, D. C., Gribben, J. G., McMillan, A., Patterson, K., and Goldstone, A. H. (1989) GM-CSF Accelerates Neutrophils Recovery after Autologous Bone Marrow Transplantation for Hodgkin's Disease. *Bone Marrow Transplant.* 4, 49-54.
- Douay, L., Lopez, M., Laporte, J. P., Quitter, P. H., Lessage, S., and Gorin, N. C. (1993) Autologous Bone Marrow Transplantation with CD34 Positive Selected Cells in Patients with Non-Hodgkin's Lymphoma. *Exp. Hematol.* 21, 1066.
- Duhrsen, U., Villeval, J. L., Boyd, J., Kannourakis, G., Morstyn, G., and Metcalf, D. (1988) Effects of Recombinant Human Granulocyte Colony Stimulating factor on Hematopoietic Progenitor Cells in Cancer Patients. *Blood* 72, 2074-2081.
- Eaves, A. C., Cashman, J. D., Gaboury, L. A., and Eaves, C. J. (1987) Clinical Significance of Long-term Cultures of Myeloid Blood Cells. *CRC Crit. Rev. Oncol. Hematol.* 7, 125-138.
- Edelman, G. M., Rutishauser, U., and Millette, C. F. (1971) Cell Fractionation and Arrangement on Fibers, Beads, and Surfaces. *Proc. Natl. Acad. Sci. U.S.A.* 68, 2153-2157.
- Eedy, D. J., Burrows, D., Bridges, J. M., and Jones, F. G. (1990) Clearance of Severe Psoriasis after Allogeneic Bone Marrow Transplantation. *Br. Med. J.* 300, 908-909.
- Ellis, W. M., Georgios, G. M., Robertson, D. M., and Johnson, G. R. (1984) The Use of Discontinuous Percoll Gradients to Separate Populations of Cells from Human Bone Marrow and Peripheral Blood. *J. Immunol. Meth.* 66, 9-16.
- English, D., Lamberson, R., Graves, V., Akard, L. P., McCarthy, L. J., and Jansen, J. (1989) Semiautomated Processing of Bone Marrow Grafts for Transplantation. *Transfusion* 29, 12-16.
- Faradji, A., Andreu, G., Pillier-Loriette, C., Bohbot, A., Nicod, A., Autran, D., Gergerat, J. P., Rio, B., Leblond, V., Binet, J. L., Zittoun, R., and Oberling, F. (1988) Separation of Mononuclear Bone Marrow Cells Using the Cobe 2997 Blood Cell Processor. *Vox Sang.* 55, 133-138.
- Fina, L., Molgaard, H. V., Robertson, D., Bradley, J. J., Monaghan, P., Delia, D., Sutherland, D. R., Baker, M. A., and Greaves, M. F. (1990) Expression of the CD34 Gene in Vascular Endothelial Cells. *Blood* 75, 2417-2426.
- Fitchen, J. H., Foon, K. A., and Cline, M. A. (1981) The Antigenic Characteristics of Hematopoietic Stem Cells. *N. Engl. J. Med.* 305, 17-25.
- Fliedner, T. M., Calvo, W., Korbli, M., Nothdurft, W., Pflieger, H., and Ross, W. (1979) Collection, Storage and Transfusion of Blood Stem Cells for the Treatment of Hemopoietic Failure. *Blood Cells* 5, 313-328.
- Flomenberg, N., and Keever, C. A. (1992) Cord Blood Transplants: Potential Utility and Potential Limitations. *Bone Marrow Transplant.* 10 (Suppl. 1), 115-119.
- Francis, G. E., Wing, M. A., Berney, J. J., and Gutmaras, J. E. T. (1983) CFU-GEMM, CFU-GM, CFU-MK Analysis by Equilibrium Density Centrifugation. *Exp. Hematol.* 11, 481-489.
- Gao, I. K., Noga, S. J., Wagner, J. E., Cremo, C. A., Davis, J., and Donnenberg, A. D. (1987) Implementation of a Semiclosed Large Scale Counterflow Centrifugal Elutriation System. *J. Clin. Apheresis* 3, 154-160.
- Gerritsen, W. R., Wagemaker, G., Jonker, M., Kenter, M. J. H., Wielenga, J. J., Hale, G., Waldmann, H., van Bekkum, D. W. (1988) The Repopulation Capacity of Bone Marrow Grafts following Pretreatment and Monoclonal Antibodies against T-lymphocytes in Rhesus Monkeys. *Transplantation* 45, 301-307.
- Gianni, A. M., Siena, S., Bregni, M., Tarella, C., Stern, A. C., Pileri, A., and Bonadonna, G. (1989) Granulocyte-macrophage Colony-stimulating Factor to Harvest Circulating Haemopoietic Stem Cells for Autotransplantation. *Lancet* ii, 580-585.
- Gilmore, M. J., Prentice, H. G., Corringham, R. E., Blacklock, H. A., and Hoffbrand A. V. (1983) A Technique for the Concentration of Nucleated Bone Marrow Cells for *in vitro* Manipulation or Cryopreservation using the IBM 2991 Blood Cell Processor. *Vox Sang.* 45, 294-302.
- Gluckman, E., Broxmeyer, H. E., Auerbach, A. D., Friedman, H. S., Douglas, G. W., Devergie, A., Esperous, H., Thierry, D., Socie, G., Lehn, P., Cooper, S., English, E., Kurtzberg, J., Bard, J., and Boyse, E. A. (1989) Hematopoietic Reconstitution in a Patient with Fanconi's Anemia by Means of Umbilical-Cord Blood from a HLA-identical Sibling. *N. Engl. J. Med.* 321, 1174-1178.
- Gold, E. F., Kleinman, R., and Bon-Efraim, S. (1974) A Heat-digestible Cell-immunoadsorbent Made by Coupling Hapten to Gelatin. *J. Immunol.* 4, 431-437.
- Goldschneider, I., Metcalf, D., Battye, F., and Mandel, T. (1980) Analysis of Rat Hemopoietic Cells on the Fluorescence-activated Cell Sorter. I. Isolation of Pluripotent Hemopoietic Stem Cells and Granulocyte-macrophage Progenitor Cells. *J. Exp. Med.* 152, 419-437.
- Griffin, J. D., Ritz, J., Beveridge, R. P., Lipton, J. M., Daley, J. F., and Schlossman, S. F. (1983) Expression of MY7 Antigen on Myeloid Precursor Cells. *Int. J. Cell Cloning* 1, 33-49.
- Gutierrez, A. A., Lemoine, N. R., and Sikora, K. (1992) Gene Therapy for Cancer. *Lancet* 339, 715-721.
- Haas, W., and von Boehmer, H. (1978) Techniques for Separation and Selection of Antigen-specific Lymphocytes. *Curr. Topics Microbiol.* 84, 1-120.
- Hall, J. M., Moles, D., and Layton, T. (1993) Use of RNA-PCR for Quantitative Evaluation of Breast Tumor Cells in Blood and Bone Marrow after Enrichment using an Avidin-Biotin Immunoaffinity System. *Breast Cancer Treat. Res.* 27, A171.
- Hardwick, R. A., Law, P., Mansour, V., Kulcinski, D., Ishizawa, L., and Gee, A. P. (1992) Development of a Large-scale Immunomagnetic Separation System for Harvesting CD34-Positive Cells from Bone Marrow, in *Advances in Bone Marrow Purging and Processing* (D. A. Worthington-White, A. P. Gee, S. Gross, Eds.) pp 583-589, Wiley-Liss, New York.
- Hardwick, R. A., Kulcinski, D., Mansour, V., Ishizawa, L., Law, P., and Gee, A. P. (1993) Design of Large-scale Separation Systems for Positive and Negative Immunomagnetic Selection of Cells using Superparamagnetic Microspheres. *J. Hematother.* 1, 379-386.
- Heimfeld, S., Fogarty, B., McGuire, K., Williams, S., and Berenson, R. J. (1992) Peripheral Blood Stem Cell Mobilization after Stem Cell Factor or G-CSF Treatment: Rapid Enrichment for Stem and Progenitor Cells Using the CEPRATE® Immunoaffinity Separation System. *Transplant. Proc.* 24, 2818.

- Heimfeld, S., Shpall, E. J., Jones, R. B., and Berenson, R. J. (1993) Clinical Transplantation of CD34+ Cells. *Exp. Hematol.* 21, 1066.
- Hellstrom, U., Hammarstrom, S., Dillner, M. L., Perlmann, H., and Perlmann, P. (1976) Fractionation of Human Blood Lymphocytes on *Helix pomatia* A Hemagglutinin Coupled to Sepharose Beads. *Scand. J. Immunol.* 5, 45-55.
- Hermanson, G. T., Mallia, A. K., and Smith, P. K. (1992) *Immobilized Affinity Ligand Techniques*, Academic Press, San Diego.
- Hervatin, F., LeNiger, C., Thierry, D., Traineau, R., Benbunan, M., Carosella, E., and Gluckman, E. (1993) Enrichment of CD34+ Cells from Cord Blood and Bone Marrow. *Exp. Hematol.* 21, 1068.
- Humblet, Y., Lefebvre, P., Jacques, J. L., Bosly, A., Feyens, A. M., Sekhavat, M., Agalotis, D., and Symann, M. (1988) Concentration of Bone Marrow Progenitor Cells by Separation on a Percoll Gradient using the Haemonetics Model. *Bone Marrow Transplant.* 3, 63-67.
- Jacobs, P., Vincent, M. D., and Martell, R. W. (1986) Prolonged Remission of Severe Refractory Rheumatoid Arthritis following Allogeneic Bone Marrow Transplantation for Drug-induced Aplastic Anaemia. *Bone Marrow Transplant.* 1, 237-239.
- Jones, R. J., Celano, P., Sharkis, S. J., and Sensenbrenner, L. L. (1989) Two Phases of Engraftment Established by Serial Bone Marrow Transplantation in Mice. *Blood* 73, 397-401.
- Jones, R. J., Wagner, J. E., Celano, P., Zicha, M. S., and Sharkis, S. J. (1990) Separation of Pluripotent Haematopoietic Stem Cells from Spleen Colony-forming Cells. *Nature* 347, 188-189.
- Juckett, D. A., and Hultquist, D. E. (1983) Chromatography of Erythroblasts on Immobilized Transferrin. *Proc. Soc. Expt. Biol. Med.* 172, 79-83.
- Karlsson, S. (1991) Treatment of Genetic Defects in Hematopoietic Cell Function by Gene Transfer. *Blood* 78, 2481-2492.
- Kemshead, J. T. (1991) The Immunomagnetic Manipulation of Bone Marrow, in *Bone Marrow Processing and Purging* (A. P. Gee, Ed.) pp 293-305, CRC Press, Boca Raton, FL.
- Kessinger, A., Armitage, J. O., Landmark, J. D., and Weisenburger, D. D. (1986) Reconstitution of Human Hematopoietic Function with Autologous Cryopreserved Circulating Stem Cells. *Exp. Hematol.* 14, 192-196.
- Kohn, D. B., Weinberg, K., Parkman, R., Lenarsky, C., Crooks, G. M., Hanley, M. B., Annett, G., Brooks, J. S., Lawrence, K., Wara, D., Elder, M., Bowen, T., Herschfield, M., Moen, R. C., Mullen, C., Berenson, R. J., Blaese, R. M. (1993) Gene Therapy for Neonates with Adenosine Deaminase (ADA)-Deficiency (SCID) by Retroviral-mediated Transfer of the Human ADA cDNA into Umbilical Cord CD34+ Cells. *Blood* 82, 315a.
- Korbling, M., and Martin, H. (1988) Transplantation of Hemapheresis-derived Hemopoietic Stem Cells: A New Concept in the Treatment of Patients with Malignant Lymphohemopoietic Disorders. *Plasma Ther. Transfus. Technol.* 9, 119-132.
- Korbling, M., Burke, P., Braine, H., Elfenbein, G., Santos, B. W., and Kaizer, H. (1981) Successful Engraftment of Blood Derived Normal Hemopoietic Stem Cells in Chronic Myelogenous Leukemia. *Exp. Hematol.* 9, 684-690.
- Korbling, M., Dorken, B., Ho, A. D., Pezzutto, A., Hunstein, W., and Flidner, T. M. (1986) Autologous Transplantation of Blood-Derived Hemopoietic Stem Cells after Myeloablative Therapy in a Patient with Burkitts Lymphoma. *Blood* 67, 529-532.
- Kumar, R. K., and Lykke, A. W. (1984) Cell Separation: A Review. *Pathology* 16, 53-62.
- Lansdorp, P. M. and Thomas, T. E. (1991) Selection of Human Hemopoietic Stem Cells, in *Bone Marrow Processing and Purging* (A. P. Gee, Ed.) pp 351-362, CRC Press, Boca Raton, FL.
- Lansdorp, P. M., Sutherland, H. J., and Eaves, C. J. (1990) Selective Expression of CD45 Isoforms on Functional Subpopulations of CD34+ Hemopoietic Cells from Human Bone Marrow. *J. Exp. Med.* 172, 363-366.
- Lasky, L. C., and Zanjani, E. D. (1985) Size and Density Characterization of Human Committed and Multipotent Hematopoietic Progenitors. *Exp. Hematol.* 13, 680-684.
- Law, P., Ishizawa, L., van de Ven, C., Burgess, J., Hardwick, A., Plunkett, M., Gee, A. P., and Cairo, M. (1993) Immunomagnetic Positive Selection and Colony Culture of CD34+ Cells from Blood. *J. Hematother.* 2, 247-250.
- Lebkowski, J. S., Schain, L. R., Okrongly, D., Levinsky, R., Harvey, M., Okarma, T. B. (1992) Rapid Isolation of Human CD34 Hematopoietic Stem cells: Purging of Human Tumor Cells. *Transplantation* 53, 1011-1019.
- Lemoli, R. M., Gobbi, M., Tazzari, P. L., Grassi, G., Dinota, A., Gherlinzonei, F., Mazza, P., and Tura, S. (1988) Avidin-biotin Immunoabsorption for *Ex Vivo* Bone Marrow Purging: Effect of Percentage of Target Cells and Flow Rate. *Haematologica* 73, 183-185.
- Lemoli, R. M., Gobbi, M., Tazzari, P. L., Tassi, C., Dinota, A., Visani, G., Grassi, G., Mazza, P., Cavo, M. and Tura, S. (1989) Bone Marrow Purging for Multiple Myeloma by Avidin-Biotin Immunoabsorption. *Transplantation* 47, 385-387.
- Liu, Yin, J. A., and S. N. Jowitt (1992) Resolution of Immune-mediated Diseases following Allogeneic Bone Marrow Transplantation for Leukaemia. *Bone Marrow Transplant.* 9, 31-33.
- Mage, M. G., McHugh, L. L., and Rothstein, T. L. (1977) Mouse Lymphocytes with and without Surface Immunoglobulin: Preparative Scale Separation in Polystyrene Tissue Culture Dishes Coated with Specifically Purified Anti-immunoglobulin. *J. Immunol. Meth.* 15, 47-56.
- Marmont, A. M. (1992) Autoimmunity and Allogeneic Bone Marrow Transplantation. *Bone Marrow Transplant.* 9, 1-3.
- Martin, P. J. (1990) The Role of Donor Lymphoid Cells in Allogeneic Marrow Engraftment. *Bone Marrow Transplant.* 6, 283-289.
- Martin, P. J. (1992) Determinants of Engraftment after Allogeneic Marrow Transplantation. *Blood* 79, 1647-1650.
- McCarthy, K. F., Hale, M. L., and Fehnel, P. L. (1985) Rat Colony-forming Unit Spleen is OX7 Positive, W3/13 Positive, OX1 Positive and OX22 Negative. *Exp. Hematol.* 13, 847-854.
- Moss, T. J., Reynolds, C. P., Reisfeld, R. A., Sather, H. N., Hammond, G. D., and Seeger, R. C. (1991) Prognostic Value of Immunocytologic Detection of Bone Marrow Metastases in Neuroblastoma. *N. Engl. J. Med.* 324, 219-226.
- Muench, M. O., and Moore, M. A. S. (1992) Accelerated Recovery of Peripheral Blood Cell Counts in Mice Transplanted with *In Vitro* Cytokine-expanded Hematopoietic Progenitors. *Exp. Hematol.* 20, 611-618.
- Nakahata, T., and Ogawa, M. (1982) Hemopoietic Colony-forming Cells in Umbilical Cord Blood with Extensive Capability to Generate Mono- and Multipotential Hemopoietic Progenitors. *J. Clin. Invest.* 70, 1324-1328.
- Nemunaitis, J., Rabinowe, S. N., Singer, J. W., Bierman, P. J., Vose, J. M., Feedman, A. S., Onetto, N., Gillis, S., Oette, D., and Gold, M. (1991) Recombinant Granulocyte-Macrophage Colony Stimulating Factor after Autologous Bone Transplantation for Lymphoid Cancer. *N. Engl. J. Med.* 324, 1773-1778.
- Nimgaonkar, M., Bahnson, A., Boggs, S., Robbins, P. D., Patrene, K., Fei, Y., Barranger, J. A., Ball, E. D. (1993) G-CSF Primed Peripheral Blood Stem Cells as Targets for Gene Therapy in Gaucher Disease. *Exp. Hematol.* 21, 1160.
- Noga, S. J., Cremo, C. A., Duff, S. C., Schwartz, C. L., Melaragno, A., Civin, C. I., Donnenberg, A. D. (1986a) Large Scale Separation of Human Bone Marrow by Counterflow Centrifugation Elutriation. *J. Immunol. Meth.* 92, 211-218.
- Noga, S. J., Donnenberg, A. D., Schwartz, C. L., Strauss, L. C., Civin, C. I., and Santos, G. W. (1986b) Development of a Simplified Counterflow Centrifugation Elutriation Procedure for Depletion of Lymphocytes from Human Bone Marrow. *Transplantation* 41, 220-229.
- Noga, S. J., Jones, R. J., Davis, J. M., Berenson, R. J., Sharkis, S. J., Hess, A. D., Vogelsang, G. B., and Santos, G. W. (1993) Using CD34 Augmentation of the Lymphocyte Depleted Allograft to Improve the Kinetics of Engraftment. *Exp. Hematol.* 21, 1060.
- Nothdurft, W., Bruch, C., Flidner, T. M., and Ruber, E. (1977) Studies on the Regeneration of the CFU-C Population in Blood and Bone Marrow of Lethally Irradiated Dogs after Autologous

- Transfusion of Cryopreserved Mononuclear Blood Cells. *Scand. J. Haematol.* 19, 470-481.
- Okarma, T. B. (1992) Stem Cell Selection for Autologous Bone Marrow Transplantation. *Sem. Hematol.* 29 (Suppl. 1), 9-20.
- Okarma, T., Lebkowski, J., Schain, L., Harvey, M., Tricot, G., Srour, E., Meyer, W. G., Burnett, A., Sniecinski, I., and O'Reilly, R. J. (1992) The AIS Collector: A New Technique for Stem Cell Purification, in *Advances in Bone Marrow Purging and Processing*. (D. A. Worthington-White, A. P. Gee, and S. Gross, Eds.), pp 449-459, Wiley-Liss, New York.
- Owen, R. D. (1945) Immunogenetic Consequences of Vascular Anastomoses between Bovine Twins. *Science* 102, 400-401.
- Porro, B., Menard, S., Tagliabue, E., Orefice, S., Salvadori, B., Squicciarini, P., Andreola, S., Rilke, F., and Colnaghi, M. I. (1988) Monoclonal Antibody Detection of Carcinoma Cells in Bone Marrow Biopsy Specimens from Breast Cancer Patients. *Cancer* 61, 2407-2411.
- Reiffers, J., Bernard, P., David, B., Vezon, G., Sarraz, A., Marit, G., Moulinier, J., and Broustet, A. (1986) Successful Autologous Transplantation with Peripheral Blood Hemopoietic Cells in a Patient with Acute Leukemia. *Exp. Hematol.* 14, 312-315.
- Schroder, J. (1975) Transplacental Passage of Blood Cells. *J. Med. Genet.* 12, 230-242.
- Schroder, J., and de la Chapelle, A. (1972) Fetal Lymphocytes in the Maternal Blood. *Blood* 39, 153-162.
- Schroder, J., and Herzenberg, L. A. (1979) Fetal Cells in the Maternal Circulation. Prenatal Diagnosis by using a Fluorescence-activated Cell-sorter (FACS), in *Genetic Disorders and the Fetus* (A. Mitulsky, Ed.) pp 541-555, Plenum Press, New York.
- Sheridan, W. P., Begley, C. G., Juttner, C. A., Szer, J., To, L. B., Maher, D., McGrath, K. M., Morstyn, G., and Fox, R. M. (1992) Effect of Peripheral-blood Progenitor Cells Mobilized by Filgrastim (G-CSF) on Platelet Recovery after High-dose Chemotherapy. *Lancet* 339, 640-644.
- Shpall, E. J., Jones, R. B., Franklin, W., Curiel, T., Bearman, S. I., Stemmer, S., Hami, L., Petsche, D., Taffs, S., Heimfeld, S., Hallagain, J., Berenson, R. J. (1992a) CD34+ Marrow and/or Peripheral Blood Progenitor Cells (PBPCs) Provide Effective Hematopoietic Reconstitution of Breast Cancer Patients Following High-dose Chemotherapy with Autologous Hematopoietic Progenitor Cell Support. *Blood* 80, (Suppl. 1), 24a.
- Shpall, E. J., Stemmer, S. M., Johnston, C. F., Hami, L., Bearman, S. I., Berenson, R. J., and Jones, R. B. (1992b) Purging of Autologous Bone Marrow for Transplantation: The Protection and Selection of the Hematopoietic Progenitor Cell. *J. Hematother.* 1, 45-54.
- Shpall, E. J., Jones, R. B., Franklin, W. A., Archer, P. G., Curiel, T., Bitter, M., Claman, H., Bearman, S., Stemmer, S., Purdy, M., Myers, S., Hami, L., Taffs, S., Heimfeld, S., Hallagan, J., and Berenson, R. J. (1994) Transplantation of Enriched CD34-Positive Autologous Marrow into Breast Cancer Patients Following High-dose Chemotherapy: Influence of CD34+ Peripheral Blood Progenitors and Growth Factors on Engraftment. *J. Clin. Oncol.* 12, 28-36.
- Siena, S., Bregni, M., Brando, B., Ravagnani, F., Bonadonna, B., and Gianni, A. M. (1989) Circulation of CD34+ Hematopoietic Stem Cells in the Peripheral Blood of High-dose Cyclophosphamide-treated Patients: Enhancement by Intravenous Recombinant Human Granulocyte-Macrophage Colony-stimulating Factor. *Blood* 74, 1905-1914.
- Silvestri, F., Banavali, S., Yin, M., Gopal, V., Savignano, C., Baccarani, M., and Preisler, H. D. (1992) CD34-Positive Cell Selection by Immunomagnetic Beads and Chymopapain. *Haematologica* 77, 307-310.
- Simmons, D. L., Satterthwaite, A. B., Tenen, D. G., and Seed, B. (1992) Molecular Cloning of a cDNA encoding CD34, a Sialomucin of Human Hematopoietic Stem Cells. *J. Immunol.* 148, 267-271.
- Smith, D. M., Weisenburger, D. D., Bierman, P., Kessinger, A., Vaughn, W. P., and Armitage, J. O. (1987) Acute Renal Failure Associated with Autologous Bone Marrow Transplantation. *Bone Marrow Transplant.* 2, 195-201.
- Spangrude, G. J., Heimfeld, S., and Weissman, I. L. (1988) Purification and Characterization of Mouse Hematopoietic Stem Cells. *Science* 241, 58-62.
- Storb, R., Graham, R. C., Epstein, R. B., Sale, G. E., and Thomas, E. D. (1977) Demonstration of Hemopoietic Stem Cells in the Peripheral Blood of Baboons by Cross Circulation. *Blood* 50, 537-542.
- Stroncek, D. F., Fautsch, S. K., Lasky, L. C., Hurd, D. D., Ramsay, N. K., McCullough, J. (1991) Adverse Reactions in Patients Transfused with Cryopreserved Marrow. *Transfusion* 31, 521-526.
- Sutherland, D. R., and A. Keating (1992) The CD34 Antigen: Structure, Biology and Potential Clinical Applications. *J. Hematother.* 1, 115-129.
- Sutherland, D. R., Watt, S. M., Dowden, G., Karhi, K., Baker, M. A., Greaves, M. F., and Smart, J. S. (1988) Structural and Partial Amino Acid Sequence Analysis of the Human Hemopoietic Progenitor Cell Antigen CD34. *Leukemia* 2, 793-803.
- Sutherland, D. R., Marsh, J. C. W., Davidson, J., Baker, M. A., Keating, A., and Mellors, A. (1992) Differential Sensitivity of CD34 Epitopes to Cleavage by *Pasteurella haemolytica* Glycoprotease: Implications for Purification of CD34-Positive Progenitor Cells. *Exp. Hematol.* 20, 590-599.
- Thomas, E. D., Storb, R., Clift, R. A., Fefer, A., Johnson, L., Heiman, P. E., Lerner, K. G., Glucksberg, H., and Buckner, C. D. (1975) Bone-marrow Transplantation (second of two parts). *N. Engl. J. Med.* 292, 895-902.
- Thomas, T. E., Sutherland, H. J., and Lansdorp, P. M. (1989) Specific Binding and Release of Cells from Beads using Cleavable Tetrameric Antibody Complexes. *J. Immunol. Meth.* 120, 221-231.
- Tindle, R. W., Nichols, R. A. B., Catovsky, D., and Janossy, G. (1984) A Novel Anti-Myeloid Monoclonal Antibody BI-3C5 recognizes Early Myeloid and some Lymphoid Precursors, and Sub-Classifies Human Acute Leukemias. *Hybridoma* 3, 106a.
- Tindle, R. W., Nichols, R. A. B., Chan, L., Campana, D., Catovsky, D., and Birnie, G. D. (1985) A Novel Monoclonal Antibody BI-3C5 recognizes Myeloblasts and non-Bnon-T Lymphoblasts in Acute Leukemias and CGL Blast Crises and Reacts with Immature Cells in Normal Bone Marrow. *Leuk. Res.* 9, 1-9.
- To, L. B., Haylock, D. N., Thorp, D., Dyson, P. G., Branford, A. L., Ho, J. Q., Dart, G. D., Roberts, M. M., Horvath, N., and Bardy, P. (1989) The Optimization of Collection of Peripheral Blood Stem Cells for Autotransplantation in Acute Myeloid Leukaemia. *Bone Marrow Transplant.* 4, 41-47.
- Udomsakdi, C., Sutherland, H. J., Eaves, C. J., and Lansdorp, P. E. (1990) Separation of Functional Subpopulations of Primitive Hemopoietic Cells in Normal Human Marrow using Rhodamine-123. *Exp. Hematol.* 18, 33a.
- Van Bakkum, D. W. (1993) BMT in Experimental Autoimmune Diseases. *Bone Marrow Transplant.* 10, 183-187.
- Van den Engh, G., and Stokdijk, W. (1989) Parallel Processing Data Acquisition System for Multilaser Flow Cytometry and Cell Sorting. *Cytometry* 10, 282-293.
- Vilmer, E., Sterkers, G., Rahimy, C., Elion, J., Broyart, A., Lescœur, B., Gerota, J., and Blot, P. (1992) HLA-mismatched Cord Blood Transplantation in a Patient with Advanced Leukemia. *Transplantation* 53, 1155-1157.
- Visser, J. W. M. (1990) Analysis and Sorting of Blood and Bone Marrow Cells, in *Flow Cytometry and Sorting*, 2nd ed. (M. R. Melamed, T. Lindmo, and M. L. Mendelsohn, Eds.) pp 669-683, Wiley-Liss, New York.
- Visser, J. W. M., Bauman, J. G. L., Mulder, A. H., Eliason, J. F., and de Leeuw, A. M. (1984) Isolation of Murine Pluripotent Hemopoietic Stem Cells. *J. Exp. Med.* 159, 1576-1590.
- Vose, J. M., Bierman, P. J., Anderson, J. R., Kessinger, A., Pierson, J., Nelson, J., Frappier, B., Schmit-Pokorny, K., Weisenburger, D. D., and Armitage, J. O. (1992) Progressive Disease after High-dose Therapy and Autologous Transplantation for Lymphoid Malignancy: Clinical Course and Patient Follow-Up. *Blood* 80, 2142-2148.
- Vredenburg, J. J., Shpall, E. J., and Ross, M. (1992) Immunopharmacologic Bone Marrow Purging and High Dose Chemotherapy with Autologous Bone Marrow Support (ABMS)

- for Patients with Metastatic Breast Cancer. *Proc. Am. Soc. Clin. Oncol.* 11, 58.
- Wagner, J. E. (1993) Umbilical Cord Blood Stem Cell Transplantation: Current Status and Future Prospects. *J. Hematother.* 2, 225-228.
- Wagner, J. E., Broxmeyer, H. E., and Cooper, S. (1992) Umbilical Cord and Placental Blood Hematopoietic Stem Cells: Collection, Cryopreservation and Storage. *J. Hematother.* 1, 167-173.
- Williams, S. F., Bitran, J. D., Richards, J. M., DeChristopher, P. J., and Orlina, A. R. (1990) Peripheral Blood-derived Stem Cell Collections for Use in Autologous Transplantation after High Dose Chemotherapy: An Alternative Approach. *Prog. Clin. Biol. Res.* 333, 461-469.
- Wofsy, L., Henry, C., and Cammisuli, S. (1978) Hapten-sandwich Labeling of Cell-surface Antigens. *Contemp. Top. Mol. Immunol.* 7, 215-237.
- Wofsy, L., Kimura, J., and Truffa-Bachi, P. (1971) Cell Separation on Affinity Columns: The Preparation of Pure Populations of Anti-hapten specific Lymphocytes. *J. Immunol.* 107, 725-729.
- Wormmeester, J., Stiekma, F., and de Groot, K. (1984) A Simple Method for Immunoselective Cell Separation with the Avidin-Biotin System. *J. Immunol. Meth.* 67, 389-394.
- Wysocki, L. J., and Sato, V. L. (1978) Panning for Lymphocytes: A Method for Cell Selection. *Proc. Natl. Acad. Sci. U.S.A.* 75, 2844-2848.

# ARTICLES

## Biotinylation of an Enkephalin-Containing Heptapeptide via Various Spacer Arms. Synthesis, Comparative Binding Studies toward Avidin, and Application as Substrates in Enzymatic Reactions

Ajoy Basak, François Jean, Hermann Dugas,<sup>†</sup> and Claude Lazure\*

Laboratory of Structure and Metabolism of Neuropeptides, Clinical Research Institute of Montréal (Affiliated with the Université de Montréal), 110 Pine Ave West, Montréal, Québec, Canada H2W 1R7, and Department of Chemistry, Université de Montréal, Montréal, Québec, Canada H3C 3J7. Received November 5, 1993\*

The preparation of an enkephalin-containing heptapeptide of the sequence Tyr-Gly-Gly-Phe-Leu-Arg-Arg-OH with a biotinyl moiety linked to the carboxy terminus is described. A series of biotinylated derivatives, each containing a different linker (LC) moiety between the biotin function and the carboxy-terminal Arg residue, were synthesized by solution-phase chemistry following the coupling of the side chain protected peptide with previously prepared appropriate biotinylamine derivative. Both linear and flexible spacer arms of variable chain lengths [LC = (CH<sub>2</sub>)<sub>x</sub>, *x* = 2, 4, or 6] as well as semirigid cyclohexyl spacers (racemic 1,2-cyclohexane, *cis* or *trans*) were incorporated. The relative binding aptitudes of these molecules toward the glycoprotein, avidin, either in immobilized form or in solution were compared using both <sup>125</sup>I-labeled and unlabeled peptide derivatives and were found to be in the following order, *trans* ≥ 6C > 4C > 2C > *cis*. The potential application of these materials as substrates for enzymatic analysis is illustrated for one of the derivatives, namely the LC-2C analogue.

### INTRODUCTION

The remarkably high affinity (*K*<sub>d</sub> = 10<sup>-15</sup> M<sup>-1</sup>) of the vitamin biotin for the glycoprotein avidin has been exploited as a powerful tool in a wide variety of bioanalytical applications (reviewed in 1-3). These include studies involving cytochemical localization, isolation of receptor, affinity chromatography, radioimmunoassay and molecular biology techniques. The usefulness of the biotin/avidin system is based upon the fact that if one modifies chemically any biologically active target molecule through biotinylation, the biological and physiological properties of the conjugate will not be changed significantly, thereby allowing unimpeded interaction with avidin. An extensive number of biotinylating agents are now commercially available for the covalent attachment of the biotin moiety to protein and peptides (2) mostly at a free amino group.

Recently, we have developed a solid-phase assay for detecting minute levels of endopeptidase activities using radiolabeled immobilized peptide derivatives (4). This approach was further extended by incorporating to a peptide containing a radiolabeled NH<sub>2</sub>-terminal Tyr residue a biotinyl function through coupling to the ε-NH<sub>2</sub> group of a carboxy-terminal Lys residue (5). Both methods are based on the release of a free radiolabeled peptide fragment into solution following proteolytic digestion. In an effort to further pursue and expand this approach, we have constructed a series of Leu-enkephalin-containing heptapeptide derivatives of the type Boc-Tyr-Gly-Gly-Phe-Leu-Arg-Arg-LC-biotin where LC represents linear carbon chains containing two, four, or six carbons or semirigid 1,2-*trans*- and 1,2-*cis*-cyclohexane rings as spacer molecules. The present paper describes their synthesis, chemical characterization, and comparative avidin binding properties; in addition, the proposed use of one analog in the context of enzymatic assays is also described.

### EXPERIMENTAL PROCEDURES

All amino acid derivatives (L-form) and the peptide coupling reagents were purchased from Institut Armand Frappier (Laval, Québec, Canada) and Chemical Dynamics Corporation (South Plainfield, NJ). All solvents were freshly distilled over nitrogen. Silica gel (column chromatography, 230-400 mesh) and (+)-biotin were from Aldrich (Milwaukee, WI) and Sigma (St. Louis, MI) Chemical Companies, respectively. <sup>1</sup>H-NMR spectra (done in DMSO-*d*<sub>6</sub> unless otherwise mentioned) and FAB-MS were recorded on Varian Associate Bruker 400 MHz and MS-50 HMTCTA (FAB or CI mode) instruments, respectively. Melting points, determined in open capillaries with a digital apparatus (electrothermal), were uncorrected. Amino acid analyses following 18 h hydrolysis

\* To whom all correspondence and reprint requests should be addressed. Tel: 514-987-5593; Fax: 514-987-5542.

<sup>†</sup> Department of Chemistry.

\* Abstract published in *Advance ACS Abstracts*, May 1, 1994.

Abbreviations used: *n*BuOH, *n*-butyl alcohol; Bz, benzyl; CHCl<sub>3</sub>, chloroform; CI-MS, chemical ionization mass spectroscopy; *p*-DACA, *p*-(dimethylamino)cinnamaldehyde; DCC, dicyclohexylcarbodiimide; DMF, *N,N*-dimethylformamide; DMSO, dimethyl sulfoxide; EtOAc, ethyl acetate; FAB-MS, fast atom bombardment mass spectroscopy; HABA, 4-hydroxyazobenzene-2-carboxylic acid; HOAc, acetic acid; HOBT, 1-hydroxybenzotriazole; IBC, isobutyl chloroformate; LC, linker; MeOH, methanol; mp, melting point; NHS, *N*-hydroxysuccinimide; NMM, *N*-methylmorpholine; <sup>1</sup>H-NMR, proton nuclear magnetic resonance spectroscopy; Py, pyridine; RP-HPLC, reversed-phase high-pressure liquid chromatography; TFA, trifluoroacetic acid; THF, tetrahydrofuran; TLC, thin-layer chromatography; Z, benzyloxycarbonyl.



in 5.7 N HCl at 110 °C *in vacuo* were obtained using a modified Beckman 120C autoanalyzer equipped with a Varian DS 604 integrator/plotter. Reversed-phase high-pressure liquid chromatography was performed with an analytical Vydac 218TP510 C<sub>18</sub> column (The Separation Group, Hesperia, 25 × 0.5 cm). The buffer system consisted of an aqueous 0.1% (V/V) TFA solution and an organic phase made of acetonitrile also containing 0.1% TFA (V/V). In all cases, the elution was carried out using a linear gradient from 5% to 60% organic phase in 55 min, at a flow rate of 1 mL/min; elution was monitored using UV absorbance at 225 nm. TLC was performed on silica gel precoated (0.25-mm thickness) aluminum sheets (Kiesel gel, Merck Co.) with the following solvent systems: (A) CHCl<sub>3</sub>/MeOH (4:1), (B) CHCl<sub>3</sub>/MeOH (6:1), (C) EtOAc/MeOH (2:3), (D) EtOAc/MeOH (1:2), (E) nBuOH/HOAc/H<sub>2</sub>O (4:1:1), (F) nBuOH/HOAc/H<sub>2</sub>O/Py (15:3:12:10), and (G) nBuOH/HOAc/H<sub>2</sub>O/Py (30:3:12:10). The peptide spots were revealed under illumination by UV or by spraying the TLC plates with ammonium molybdate/sulfuric acid, ninhydrin, or *p*-DACA/sulfuric acid reagent (6).

**Synthesis of the Various Biotinyl-LC-NH<sub>2</sub> Derivatives.** (+)-Biotin (244.3 mg, 1 mmol) was dissolved by warming in DMF (5 mL) and then brought back to ambient temperature. NHS (127 mg, 1.1 mmol) and DCC (226 mg, 1.1 mmol) were then added. The mixture was stirred for 30 min at 0 °C and then for 3 h at ambient temperature. The insoluble dicyclohexylurea was filtered off, and the filtrate was added slowly (over a 10 min period) to a solution of the appropriate diamine (1.1 mmol) in DMF (5 mL). The reaction was stirred for 3 h at ambient temperature, and the precipitated white material was collected by filtration. The filtrate was diluted with excess diethyl ether (100 mL), resulting in the production of another crop of precipitate. The combined solid was dissolved in methanol (70 mL) and purified by silica gel column chromatography (18 × 2 cm). Elution of the column with MeOH/CHCl<sub>3</sub> (1:1) yielded the side product, bis-biotinyl-LC-diamide, with a 20–25% yield. Subsequent elution with MeOH/CHCl<sub>3</sub> (2:1) furnished the sought after biotin-LC-NH<sub>2</sub> derivatives (65–75%). Representative <sup>1</sup>H-NMR data are given for the biotinyl derivative (I) whereas, in the case of mass spectra, the value of each analog molecular ion observed together with its theoretical value is given.

*N*-(6-Amino-*n*-hexyl)-1-biotinamide (I): mp 207–209 °C dec; TLC homogenous, *R*<sub>f</sub> 0.56 (D); <sup>1</sup>H-NMR δ 7.74 (1 H, t, *J* = 5.5 Hz, CONH), 6.44 (1 H, s, H-3), 6.37 (1 H, s, H-1), 4.30 (1 H, dd, *J* = 5.3 Hz, H-3a), 4.12 (1 H, m, H-6a), 3.38 (2 H, m, H-6'), 3.09 (1 H, m, H-4), 3.0 (2 H, q, *J* = 6.6 Hz, H-1'), 2.81 (1 H, dd, *J*<sub>1</sub> = 5.1 Hz, *J*<sub>2</sub> = 12.4 Hz, H-6α), 2.55 (1 H, d, *J* = 12.5 Hz, H-6β), 2.04 (2 H, t, *J* = 7.4 Hz, biotin side chain αH), 1.65–1.40 (6 H, m, biotin side chain βγδH), 1.40–1.20 (10 H, br m, 2', 3', 4', 5' H + NH<sub>2</sub>); CI-MS *m/z* 342 (M)<sup>+</sup> (theor 342.55).

*N*-(4-Amino-*n*-butyl)-1-biotinamide (II): mp 220–223 °C dec; TLC homogenous, *R*<sub>f</sub> 0.49 (D); FAB-MS: *m/z* 315 (M + H)<sup>+</sup> (theor 314.49).

*N*-(2-Aminoethyl)-1-biotinamide (III): mp 235–237 °C dec; TLC homogenous, *R*<sub>f</sub> 0.41 (D); CI-MS *m/z* 286 (M)<sup>+</sup> (theor 286.43).

*trans*-*N*-(1-Aminocyclohexyl)-2-biotinamide (IV): mp 265 °C dec; TLC homogenous, *R*<sub>f</sub> 0.58 (D), 0.49 (C); CI-MS *m/z* 341 (M + H)<sup>+</sup> (theor 340.53).

*cis*-*N*-(1-Aminocyclohexyl)-2-biotinamide (V): mp 127–129 °C dec; TLC homogenous, *R*<sub>f</sub> 0.57 (D); CI-MS *m/z* 341 (M + H)<sup>+</sup> (theor 340.53).

**Synthesis of the Heptapeptide Boc-Tyr-Gly-Gly-Phe-Leu-Arg-Arg-OH (VIII).** The synthesis of the Boc-Tyr-Gly-Gly-Phe-Leu fragment was conducted in steps by solution-phase chemistry following either carbodiimide or mixed anhydride mediated coupling reactions as previously described (7); therefore, only the last three steps yielding VIII are described. The <sup>1</sup>H-NMR data as well as the fragmentation pattern observed in mass spectrometry are not described but are entirely consistent with the proposed structures. Some of the coupling reactions are accompanied by a small amount of racemization which, as estimated by <sup>1</sup>H-NMR, never exceeded 10%.

*Z*-Arg(NO<sub>2</sub>)-Arg(NO<sub>2</sub>)-COOBz (VI) was prepared by coupling *Z*-Arg(NO<sub>2</sub>)-OH with H-Arg(NO<sub>2</sub>)-COOBz·2Tos with DCC/HOBT: mp 129–132 °C; TLC homogenous, *R*<sub>f</sub> 0.28 (B); FAB-MS *m/z* 645 (M + H)<sup>+</sup> (theor 642.59).

*Boc*-Tyr(OBz)-Gly-Gly-Phe-Leu-Arg(NO<sub>2</sub>)-Arg(NO<sub>2</sub>)-COOBz (VII). *Z*-Arg(NO<sub>2</sub>)-Arg(NO<sub>2</sub>)-COOBz (270 mg, 0.42 mmol) was deprotected with 32% HBr/HOAc (7) and coupled to the protected pentapeptide Boc-Tyr(OBz)-Gly-Gly-Phe-Leu-OH (228 mg, 0.31 mmol) in 5% DMF/THF (3.2 mL) using IBC (42 mg, 0.31 mmol) and NMM (31 mg, 0.31 mmol) at –20 °C in N<sub>2</sub> atmosphere (6). Column chromatography (silica gel, 23 × 2.5 cm) yielded a white crystalline solid (eluted with 25% MeOH/CHCl<sub>3</sub>), 205 mg (54% yield): mp 127–129 °C; TLC homogenous, *R*<sub>f</sub> 0.48 (A), 0.38 (B); amino acid analysis Tyr<sub>0.95</sub> (1), Gly<sub>2.09</sub> (2), Phe<sub>1.00</sub> (1), Leu<sub>0.96</sub> (1), Arg<sub>1.83</sub> (2); FAB-MS *m/z* 1147 (M<sup>+</sup> – Bz) (theor 1146.31).

*Boc*-Tyr-Gly-Gly-Phe-Leu-Arg-Arg-OH (VIII). The protected heptapeptide (VII) (190 mg, 0.164 mmol) following hydrogenolysis with Pd-black (200 mg)/H<sub>2</sub> in 0.5% HOAc/DMF (5 mL) yielded on silica gel column chromatography (23 × 2 cm) a white solid [eluted with CHCl<sub>3</sub>/MeOH/HOAc (25:25:0.1)], 141 mg (88% yield): mp 245–247 °C; TLC homogenous, *R*<sub>f</sub> 0.11 (E); amino acid analysis Tyr<sub>0.89</sub> (1), Gly<sub>2.19</sub> (2), Phe<sub>1.00</sub> (1), Leu<sub>0.93</sub> (1), Arg<sub>1.78</sub> (2); FAB-MS *m/z* 969 (M + H)<sup>+</sup> (theor 968.10).

**Synthesis of the Boc-peptidyl-LC-biotinyl Derivatives (IXa–IXe).** The heptapeptide VIII (50 mg, 0.044 mmol) was coupled to the various biotinyl-LC (I–V, 0.05 mmol) using IBC/NMM (each 0.044 mmol). The product Boc-peptidyl-LC-biotin derivative was recovered by silica gel column chromatography (24 × 2 cm) upon elution with 25% MeOH/CHCl<sub>3</sub> in 40–55% isolated yield. The <sup>1</sup>H-NMR data and the observed fragmentation patterns were in full agreement with the proposed structures.

*Boc*-Tyr-Gly-Gly-Phe-Leu-Arg-Arg-CONH-(CH<sub>2</sub>)<sub>6</sub>-NHCO-biotin: TLC homogenous, *R*<sub>f</sub> 0.75 (F); <sup>1</sup>H-NMR δ 9.28 (1H, m, Tyr OH), 8.70 (1H, m, CONH), 8.50 (1H, m, 2CONH), 8.39 (2H, m, 2CONH), 8.24 (2H, m, 2CONH), 8.2–8.1 (2H, m, 2CONH), 8.2–7.3 (10H, m, Gn NH), 7.32–7.18 (5H, m, aromatic), 7.0 (2H, d, *J* = 8.6 Hz, Tyr<sub>2,6</sub> H), 7.05 (1H, m, Boc NH), 6.67 (2H, d, *J* = 8.6 Hz, Tyr<sub>3,5</sub> H), 6.44 (1H, s, biotin H-3), 6.39 (1H, s, biotin H-1), 4.55 (1H, m, Leu αH), 4.4–4.25 (3H, m, 2Arg αH + biotin H-3a), 4.20 (1H, m, Tyr αH), 4.14 (1H, m, biotin H-6a), 3.78 (1H, m, Phe αH), 3.61 (4H, m, 2Gly αH), 3.10 (4H, finely splitted d, *J* = 6.0 Hz, 2Arg δH), 3.0 (2H, m, Tyr βH), 2.90–2.70 (2H, m, Phe βH), 2.81 (1H, dd, *J*<sub>1</sub> = 5.05 Hz, *J*<sub>2</sub> = 12.43 Hz, biotin H-6α), 2.57 (1H, d, *J* = 12.2 Hz, biotin H-6β), 2.29, 2.04 (2H, t, *J* = 7.2 Hz), 1.91 (6H, s, 2OAc), 1.30 (9H, s, Boc), 1.85–1.20 (25H, m, biotin 14H + Arg, Leu, βγH), 0.89 (3H, q, *J* = 6.4 Hz, γCH<sub>3</sub> Val), 0.87 (3H, t, *J* = 6.3 Hz, γ'CH<sub>3</sub> Val); FAB-MS *m/z* 1293 (M + H)<sup>+</sup> (theor 1292.64); RP-HPLC *t*<sub>R</sub> 37.2 min (42% CH<sub>3</sub>CN).

*Boc-Tyr-Gly-Gly-Phe-Leu-Arg-Arg-CONH-(CH<sub>2</sub>)<sub>4</sub>-NHCO-biotin*: FAB-MS *m/z* 1265 (*M* + *H*)<sup>+</sup> (theor 1264.58); RP-HPLC *t<sub>R</sub>* 39.1 min (44% CH<sub>3</sub>CN).

*Boc-Tyr-Gly-Gly-Phe-Leu-Arg-Arg-CONH-(CH<sub>2</sub>)<sub>2</sub>-NHCO-biotin*: FAB-MS *m/z* 1237 (*M* + *H*)<sup>+</sup> (theor 1236.51); RP-HPLC *t<sub>R</sub>* 36.9 min (42% CH<sub>3</sub>CN).

*Boc-Tyr-Gly-Gly-Phe-Leu-Arg-Arg-CONH-trans-1,2-diamidocyclohexyl-NHCO-biotin*: FAB-MS *m/z* 1063 (*M* - biotin)<sup>+</sup> (theor 1063.42); RP-HPLC *t<sub>R</sub>* 37.7 min (43% CH<sub>3</sub>CN).

*Boc-Tyr-Gly-Gly-Phe-Leu-Arg-Arg-CONH-cis-1,2-diaminocyclohexyl-NHCO-biotin*: FAB-MS *m/z* 1063 (*M* - biotin)<sup>+</sup> (theor 1063.42); RP-HPLC *t<sub>R</sub>* 38.9 (44% CH<sub>3</sub>CN).

**Radiolabeling of Boc-Tyr-Gly-Gly-Phe-Leu-Arg-Arg-LC-biotin.** All the biotinyl peptide derivatives were radiolabeled with <sup>125</sup>I using a modified chloramine T method (5). The radiolabeled products were recovered from the iodination mixture by elution from a Sep-Pak cartridge with 60% CH<sub>3</sub>CN/H<sub>2</sub>O (2 mL) directly into a tube containing some free biotin (50 μg) in order to minimize oxidation of the biotin function.

**Binding Studies of Biotinyl Peptide Derivatives to Avidin.** Three separate methods were used in order to investigate the avidin binding profile of the biotinylated peptide analogs.

(a) In the first method, each biotinylated peptide derivative (20 μg, 14–18 nmol) was dissolved in 4.4% DMSO in 100 mM potassium phosphate, pH 7.4 (400 μL) and shaken in a rotary shaker with immobilized avidin (avidin-agarose gel, 200 μL packed gel capable of binding 41 nmol of biotin) for 1 h at ambient temperature. The suspension was then centrifuged for 10 min at 3000 rpm, and a constant aliquot of the supernatant (100 μL) was injected into an analytical RP-HPLC column. The rate of disappearance of the peptide peak provided a direct measurement of the avidin binding capacities of the various analogs.

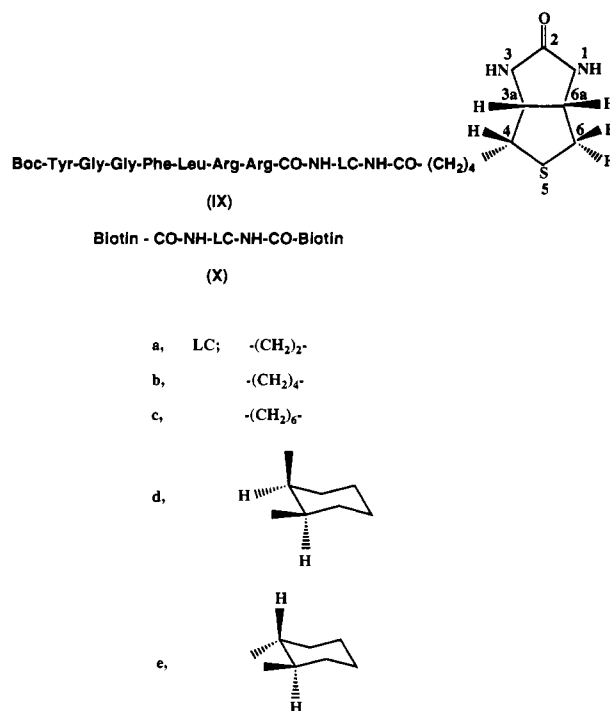
(b) In an alternate method, the avidin binding capacity was measured following displacement of the dye, HABA, previously bound to immobilized avidin as described (8, 9).

(c) The binding was followed by measuring the amount of radioactivity retained on a fixed quantity of avidin-agarose gel upon incubation with radiolabeled biotinyl peptide derivatives as a function of time.

**Enzymatic Assays.** All enzymatic assays and analysis of the resulting digests were conducted according to procedures described previously (4, 5).

## RESULTS

**Synthesis of Biotinyl-LC-Leu-enkephalin Derivatives.** The heptapeptide, Tyr-Gly-Gly-Phe-Leu-Arg-Arg-OH, was selected as a model peptide since, in the past, similar peptide analogues have been shown to be excellent substrates for a large number of endopeptidases, especially the serine proteinases (4, 5). This peptide was obtained following liquid-phase chemistry as the Boc N-terminally blocked form. The various biotinylamines were prepared by reacting the respective diamines with freshly made biotin-*N*-hydroxysuccinimide. The latter reaction was accompanied by the formation of the bis-biotinyldiamide derivative as a major secondary product. However, its formation can be kept at a minimum level (less than 30%) by adding slowly the preformed solution of biotinyl succinimide ester to the solution of the diamine in equimolar quantities. Each biotinyl-LC-amine was next coupled to the Boc-protected Leu-enkephalin heptapep-



**Figure 1.** Structures of the various biotinyl derivatives prepared in this study.

tide via its carboxy terminus using the mixed anhydride chemistry. The overall yield for the latter step was found in all cases to be between 55 and 65%.

**Chemical Characterization of the Biotinyl Peptides.** All the biotinylated peptide analogs exhibited the correct amino acid composition. Furthermore, the presence of the biotin function was clearly established by positive color reaction with *p*-DACA (6) and their binding ability to immobilized avidin. In addition, these analogs were further characterized by <sup>1</sup>H-NMR where the characteristic signals for the biotinyl moiety, mostly unaffected following conjugation, are consistent with those reported previously (10, 11). In addition, the signals for the protons belonging to the peptide chain were easily identified and also remained unaffected upon coupling to the respective spacer arms.

While some of the biotinyl peptide derivatives displayed sharp molecular ion peaks, others failed to show any such peaks, as, for example, the LC-trans analog. However, their characteristic fragmentation patterns observed in mass spectrometry greatly facilitated their characterization.

**Comparative Studies of the Biotinyl Peptide Derivatives Binding to Avidin.** Three separate procedures were used to explore the relative binding capacities toward avidin of the various biotinyl derivatives, whose structures are summarized in Figure 1. These include (i) monitoring spectrophotometrically the displacement of the dye HABA from its 1:1 complex with avidin, (ii) following by RP-HPLC the gradual disappearance of the biotin containing sample upon incubation with immobilized avidin, and finally (iii) measuring the radioactivity bound on immobilized avidin upon incubation with a known quantity of radiolabeled biotinyl sample.

As indicated in Table 1, it is apparent that while the unmodified peptide failed to displace any significant amount of HABA from its complex with avidin, all the biotinyl peptides as well as biotin itself and bis-biotinyl derivatives were able to displace the dye from the complex in a quantitative fashion. The bis-biotinyl derivatives were

**Table 1. Displacement of HABA from Preformed Avidin-HABA Complex by Various Synthetic Biotinyl Derivatives**

compd	spacer arm (LC)	half-maximal displacement value <sup>a</sup> (nmol)
biotin	none	8.1
VIII	none	
IXa	-(CH <sub>2</sub> ) <sub>2</sub> -	25.5
IXb	-(CH <sub>2</sub> ) <sub>4</sub> -	15.2
IXc	-(CH <sub>2</sub> ) <sub>6</sub> -	11.9
IXd	<i>cis</i> -cyclohexyl	39.6
IXe	<i>trans</i> -cyclohexyl	12.5
Xa	-(CH <sub>2</sub> ) <sub>2</sub> -	9.3
Xb	-(CH <sub>2</sub> ) <sub>4</sub> -	9.6
Xc	-(CH <sub>2</sub> ) <sub>6</sub> -	8.3

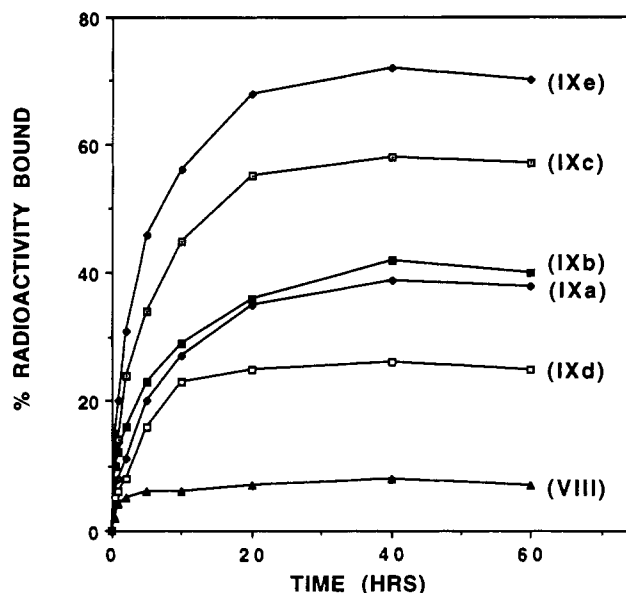
<sup>a</sup> The amounts shown represent the amount of peptides (nmol) necessary to displace 50% of the HABA bound to the immobilized avidin.

found to be almost as potent as biotin itself with a half-maximal value of between 8.3 and 9.6 nmol compared to 8.1 nmol for biotin. Though less potent, all the biotinyl peptide derivatives exhibited half-maximal values ranging from 11.9 to 39.6 nmol. Among the five derivatives tested, the LC-6C analogue (IXc) emerges as the most potent whereas the LC-*cis*-cyclohexyl analogue (IXd) is the least.

Similar conclusions were also reached from RP-HPLC analysis following incubation with a constant amount of immobilized avidin. Thus, under conditions where biotin binding is optimal, less than 9% of the underivatized peptide (VIII) binds to the immobilized avidin. Under identical conditions, 54% of the LC-*cis*-cyclohexyl (IXd) and 74% of the LC-2C (IXa) derivatives were bound to immobilized avidin whereas the three other analogs (IXb, IXc, and IXe) were all bound in excess of 90% (data not shown). It is worth noting that, for example, using the LC-2C derivative (IXa), the extent of binding to immobilized avidin can be increased from 25% to a maximum of 65% by addition of higher amount of avidin-agarose gel (from 250  $\mu$ L to 2.0 mL) (data not shown).

Finally, considering that such compounds were designed for application in enzymatic assays, their binding properties were further verified following radiolabeling. Under the conditions where less than 7% of radiolabeled unmodified peptide bound to immobilized avidin, the LC-6C (IXc) and LC-*trans*-cyclohexyl (IXe) derivatives displayed the highest affinity toward immobilized avidin when compared to the rest of the derivatives (Figure 2). This result appears to confirm the assumption that no significant changes on the affinity is introduced upon using the iodination procedure outlined in the previous section. Indeed, when 200  $\mu$ L of avidin-agarose gel (capable of binding 0.1–0.2  $\mu$ mol biotin/mL) was shaken with an identical amount of <sup>125</sup>I-biotinylated peptides (~15 ng, 300 000 cpm), between 25% to 72% of the radioactivity, depending on the derivatives used, was retained by the gel even after extensive washing.

**Application of Biotinyl-LC-Leu-Enkephalin Peptide as Enzyme Substrate.** In order to investigate the usefulness of these biotinyl peptide derivatives as enzyme substrates either in solution or in solid-phase, the LC-2C (IXa) derivative was incubated in the presence of trypsin. Upon digestion, besides the unreacted material ( $t_R$  = 36.9 min in RP-HPLC), two major products identified by amino acid composition as Boc-Tyr-Gly-Gly-Phe-Leu-Arg-OH ( $t_R$  = 32.4 min) and Arg-CONH-CH<sub>2</sub>-CH<sub>2</sub>-NH-biotin ( $t_R$  = 20.4 min) were obtained, the identity of the latter being further confirmed by its strong avidin binding property (data not shown). It is important to note that a longer related peptide, acetyl-Tyr-Gly-Gly-Phe-Leu-Arg-Arg-



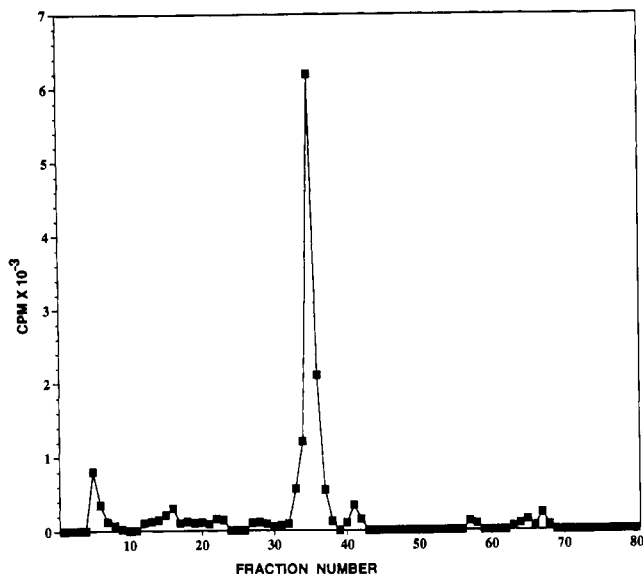
**Figure 2.** Time-dependent binding of the radiolabeled biotinyl peptide derivatives to immobilized avidin. In each case, the amount of immobilized avidin used was 200  $\mu$ L and the amount of radioactivity used corresponded to 300 000 cpm. Each line represents the biotinyl peptide derivative identified as described in Table 1 and the Experimental Procedures.

Phe-Leu-Lys, prepared by solid-phase synthesis and containing a biotinyl moiety linked to the  $\epsilon$ -amino group of Lys, was cleaved carboxy-terminal to either of the Arg residues (5) contrary to what is observed here as the cleavage appears to be solely restricted to the site in between the two basic residues. Identical results were obtained upon digestion of <sup>125</sup>I-labeled material ( $t_R$  = 39.3 min), in which case a single other radioactive peak in addition to the remaining undigested starting material appearing at  $t_R$  = 34.9 min is generated.

Alternatively, the incubation with the enzyme can be accomplished by using the immobilized substrate. Thus, when the same biotinyl LC-2C peptide analog with or without labeling with <sup>125</sup>I was immobilized on avidin-agarose and the resulting gel was incubated with trypsin, the amino-terminal peptide Boc-Tyr-Gly-Gly-Phe-Leu-Arg-OH was released into the medium as identified by RP-HPLC using either UV (data not shown) or radioactivity measurement (as shown in Figure 3). These results are similar to those reported earlier (4). In all our conditions, no leakage of the biotinyl substrate from the bound solid matrix was observed, thus permitting sensitive assay of proteolytic activity by direct measurement of the released fragment in the supernatant and identification of the cleavage site following RP-HPLC.

## DISCUSSION

In the past, researchers have routinely employed a six-atom (amino caproyl) linker chain between the biotin and peptide moiety in various biochemical applications with great success (1–3). Consequently, biotinylation reagents incorporating such a linker are commercially available as they allow relatively easy modification of any free amino function. On the other hand, preparation of C-terminally biotinyl peptides was comparatively less easy as it frequently involved either incorporation of an extra C-terminal Lys residue so as to allow the use of the biotinyl-N-hydroxysuccinimide ester reagent, as we have done in the past (5), modification of the free COOH group with a suitable biocytin reagent (12), or coupling biocytinamide through the use of an enzyme such as carboxypeptidase



**Figure 3.** RP-HPLC chromatogram of the digestion products obtained following an overnight incubation of  $^{125}\text{I}$ -labeled analogue IXa immobilized on avidin-agarose (0.5 mL of gel containing  $3 \times 10^6$  cpm) with trypsin at 25 °C. The major peak corresponds to the elution position of  $^{125}\text{I}$ -labeled Boc-Tyr-Gly-Gly-Phe-Leu-Arg.

Y (13). Here, we decided to use a fragment condensation approach which allowed us to modify the sole free C-terminal residue present in the fully side-chain protected peptide which is coupled in solution with a preformed appropriate biotinyl-linker synthesized independently. Such fully side chain protected peptides can be obtained by liquid phase synthesis but also, nowadays, by synthesis on special resins such as the Rink, the HMPB or the Sasrin resins (reviewed in 14). As shown herein, this approach is efficient even though it does suffer from two inherent problems. Firstly, as mentioned, coupling between the preformed biotinyl-linker and the peptide chain must be carried out prior to deprotection of the peptide if it contains internal Asp or Glu residues since side chain biotinylation might occur in addition to C-terminal modification. Secondly, because coupling is carried out in solution and with activating agents such as IBC, racemization is likely to happen though in variable amounts at the site of coupling. In this instance, the residue occupying the C-terminus, namely the Arg7, could indeed racemize since this residue is activated for coupling to the biotinyl-linker.

Using linkers of different chain length and/or flexibility, we were able to demonstrate that for optimal binding between a carboxy-terminally biotinyl peptide and avidin, one requires a chain length of at least four-carbon atoms or that the peptide backbone and the biotin moiety are spatially disposed anti to one another. Thus, for sensitive application such as enzymatic assays, the ones with optimum binding capacity such as the LC-*trans*-cyclohexyl or LC-6C derivatives are preferred. Finally, while these compounds were studied, Ghealen *et al.* (15) described a general procedure for preparation of peptides biotinylated at the C-terminus which essentially offers a solution to problems noticed during the present study. Another solid-phase approach for COOH-terminal biotinylation of Met-enkephalin via a six-carbon spacer was also reported (16). It thus appears now that the usefulness of the biotin/avidin methodology can be extended in a rather straight-

forward manner to most peptides by modifying specifically any amino or carboxyl group with biotin.

#### ACKNOWLEDGMENT

We wish to thank Dr. B. Marsden (IRCM) and Dr. M. Evans (Chemistry Department, University of Montréal) for providing the  $^1\text{H}$ -NMR and FAB-MS analyses, respectively. We would like to thank Dany Gauthier for technical assistance. C.L. is a "Chercheur-boursier" of the "Fonds de la Recherche en Santé du Québec" and F.J. is a recipient of a studentship from the "Fonds pour la Formation de Chercheurs et l'Aide à la Recherche". This study was made possible by a Program Grant (PG-11474) from the Medical Research Council of Canada.

#### LITERATURE CITED

- (1) Wilchek, M., and Bayer, E. A. (1990) Introduction to avidin-biotin technology. *Methods Enzymol.* 184, 5-45.
- (2) Wilchek, M., and Bayer, E. A. (1988) The avidin-biotin complex in bioanalytical applications. *Anal. Biochem.* 171, 1-32.
- (3) Green, N. M. (1975) Avidin. *Adv. Protein Chem.* 29, 85-133.
- (4) Jean, F., Basak, A., Chrétien, M., and Lazure, C. (1991) Detection of endopeptidase activity and analysis of cleavage specificity using a radiometric solid-phase enzymatic assay. *Anal. Biochem.* 194, 399-406.
- (5) Basak, A., Boudreault, A., Jean, F., Chrétien, M., and Lazure, C. (1993) Radiolabeled biotinylated peptides as useful reagents for the study of proteolytic enzymes. *Anal. Biochem.* 209, 306-314.
- (6) McCormick, D. B., and Roth, J. A. (1970) Specificity, Stereochemistry, and Mechanism of the color reaction between p-Dimethylamino cinnamaldehyde and Biotin analogs. *Anal. Biochem.* 34, 226-236.
- (7) Basak, A., Gong, Y. T., Cromlish, J. A., Paquin, J., Jean, F., Lazure, C., Seidah, N. G., and Chrétien, M. (1990) Synthesis of argininal semicarbazone containing peptides and their applications in the affinity chromatography of serine proteinases. *Int. J. Pept. Protein Res.* 36, 7-17.
- (8) Hochhaus, G., Gibson, B. W., and Sadée, W. (1988) Biotinylated human  $\beta$ -endorphins as probes for the opioid receptors. *J. Biol. Chem.* 263, 92-97.
- (9) Green, N. M. (1970) Spectrophotometric determination of avidin and biotin. *Methods Enzymol.* 18, 418-424.
- (10) Bonnafous, J. C., Tence, M., Seyer, R., Marie, J., Aumelas, A., and Jard, S. (1988) New probes for angiotensin II receptors. Synthesis, radioiodination and biological properties of biotinylated and haptenated angiotensin derivatives. *Biochem. J.* 251, 873-880.
- (11) Seyer, R., Aumelas, A., Tence, M., Marie, J., Bonnafous, J. C., Jard, S., and Castro, B. (1989) Synthesis of a biotinylated, iodinated and photoactivatable probe for angiotensin receptors. *Int. J. Peptide Protein Res.* 34, 235-245.
- (12) Hofmann, K., Finn, F. M., and Kiso, Y. (1978) Avidin-biotin affinity columns. General methods for attaching biotin to peptides and proteins. *J. Am. Chem. Soc.* 100, 3585-3590.
- (13) Schwarz, A., Wandrey, C., Bayer, E. A., and Wilchek, M. (1990) Enzymatic C-terminal biotinylation of proteins. *Methods Enzymol.* 184, 160-162.
- (14) Fields, G. B., and Noble, R. L. (1990) Solid phase synthesis utilizing 9-fluorenylmethoxycarbonyl amino acids. *Int. J. Pept. Protein Res.* 35, 161-214.
- (15) Geahlen, R. L., Loudon, G. M., Paige, L. A., and Lloyd, D. (1992) A general method for preparation of peptides biotinylated at the carboxy terminus. *Anal. Biochem.* 202, 68-70.
- (16) Leftheris, K., and Mapelli, C. (1993) Facile methods for the C-terminal biotinylation of peptides, in *Peptides 1992* (C. H. Schneider, and A. N. Eberle, Eds.) Leiden. pp 349-350, ESCOM.

## Preparation of Asialoorosomucoid-Polylysine Conjugates

Timothy D. McKee,<sup>†</sup> Mary E. DeRome,<sup>†</sup> George Y. Wu,<sup>‡</sup> and Mark A. Findeis<sup>\*†</sup>

TargeTech, Inc., 290 Pratt Street, Meriden, Connecticut 06450, and University of Connecticut Health Center, Division of Gastroenterology AM-044, #1845, 263 Farmington Avenue, Farmington, Connecticut 06030. Received September 29, 1993\*

Asialoorosomucoid-polylysine (ASOR-PL) conjugates have been recently developed as carriers of electrostatically bound DNA for targeted delivery to the hepatic asialoglycoprotein receptor (ASGPr) for gene therapy. Using acid-urea gel electrophoresis we have found that previously reported procedures for the fractionation of ASOR-PL conjugates do not efficiently remove noncovalently bound polylysine (PL) from ASOR-PL. DNA complexes prepared with these conjugates have low solubilities, which limits their usefulness for subsequent experimentation, particularly *in vivo*. For ASOR-PL made by carbodiimide-mediated crosslinking with 5-kDa PL, dialysis against 1 M guanidine hydrochloride is effective to remove the low molecular weight unbound PL. Dialysis is not feasible when using higher molecular weight PLs, but preparative elution acid-urea gel electrophoresis was used to isolate crude ASOR-PL fractions free of unbound PL. ASOR-PL freed of PL by dialysis or electrophoresis was further fractionated by cation-exchange HPLC on carboxymethyl-functionalized columns eluted with a mixed pH-salt gradient. Early-eluting ASOR-PL fractions isolated by a combination of preparative elution acid-urea gel electrophoresis and cation-exchange HPLC were found to be preferred for the formation of soluble DNA complexes.

### INTRODUCTION

The transfer to human cells of DNA containing therapeutic genes (gene therapy) has undergone a transition in recent years from a laboratory technique to a variety of experimental applications in the clinic (1, 2). Most of the gene-transfer protocols that have been developed are based on the use of retroviral vectors to transfect cells outside of the patient. The modified cells are subsequently transferred back to the patient after transfection. Amidst concern over the complexity and efficacy of these strategies, researchers have investigated ways to introduce therapeutic DNAs directly into patients in the manner of a more traditional pharmaceutical agent such as by intravenous injection. To improve the efficiency of this strategy techniques have been developed to use receptor-mediated endocytosis to carry DNA into cells (3, 4).

The liver has been recognized as a useful site for highly hepato-selective targeted delivery via the asialoglycoprotein receptor (ASGPr)<sup>1</sup> for over a decade (5). Early experiments focused on the delivery of agents covalently bound to asialoglycoproteins such as asialofetuin (6-8) and asialoorosomucoid (9) or galactose-terminated neoglycoproteins (10, 11). ASGPr-mediated endocytosis of the glycoproteins carried the bound agent into cells. More

recently, this strategy has been expanded to the use of asialoorosomucoid-polylysine (ASOR-PL) conjugates to carry DNA into hepatocytes as a strategy for gene therapy (5). DNA is bound in a tight electrostatic complex by ASOR-PL. The ASGPr recognizes the ASOR in the complex, binds and internalizes the ASOR, and brings the DNA into the cell at the same time. This technique has been used successfully for the delivery of DNAs containing a variety of genes *in vitro* (12-15) and *in vivo* (16-20) including the gene for the low-density lipoprotein receptor (LDLR) in Watanabe rabbits. Expression of the delivered LDLR gene resulted in transiently lowered serum cholesterol levels (19).

ASOR is readily available by isolation of orosomucoid (OR, also referred to as  $\alpha_1$ -acid glycoprotein) from human plasma (21) followed by desialylation to expose penultimate galactosyl groups. Orosomucoid is quite a robust protein and can be desialylated by acid treatment with heating thus avoiding the expense of using neuraminidase to cleave sialic acid residues (22). Poly-L-lysine (PL) is available commercially with varying molecular weight ranges. Conjugates formed by crosslinking PL with proteins have been reported using carbodiimide-mediated amide bond formation (14, 15) and thiol reagents (12, 13, 23). The product mixtures obtained in the formation of conjugates of this type are both very heterogeneous and highly charged. Previously described methods for the preparation of ASOR-PL for targeted delivery to the ASGPr-bearing cells have used dialysis (9), gel filtration (9, 12), and ion-exchange HPLC (14, 23) for purification of the conjugate from reaction byproducts and unconsumed starting materials. To be able to conduct gene delivery experiments *in vivo*, both larger quantities of targeting conjugates and higher concentrations of complexed DNA are needed in comparison with the usual experiments conducted *in vitro*. We have found ASOR-PL conjugates prepared by the previously detailed methods to be of variable quality with respect to the solubility of DNA complexes made with them. When solubility of complexed DNA is low it is not practical to inject animals with sufficient DNA to observe gene expression in a

\* Author to whom correspondence should be addressed. Tel: (203) 235-5600. Fax: (203) 237-8539.

<sup>†</sup> TargeTech, Inc., a wholly owned subsidiary of The Immune Response Corporation of Carlsbad, CA 92008.

<sup>‡</sup> University of Connecticut Health Center.

\* Abstract published in *Advance ACS Abstracts*, May 15, 1994.

<sup>1</sup> Abbreviations used: ASGPr, asialoglycoprotein receptor; ASOR, asialoorosomucoid; ASOR-PL, asialoorosomucoid-polylysine conjugate; AUGE, acid-urea gel electrophoresis; CEHPLC, cation-exchange high-performance liquid chromatography; DEAE, (diethylamino)ethyl; EDC, 1-[3-(dimethylamino)propyl]-3-ethylcarbodiimide; MW, molecular weight; MWCO, molecular weight cutoff; NaOAc, sodium acetate; OR, orosomucoid; PEAGE, preparative elution acid-urea gel electrophoresis; PL, poly-L-lysine; SDS-PAGE, sodium dodecyl sulfate-polyacrylamide gel electrophoresis; TEMED, *N,N,N',N'*-tetramethylethylenediamine.

reproducible manner. In this study we report our investigation of the use of the combination of acid-urea gel electrophoresis and cation-exchange chromatography to analyze and purify ASOR-PL conjugates to be used in the formation of soluble targetable DNA complexes.

#### EXPERIMENTAL PROCEDURES

**General.** Human plasma was obtained from the American Red Cross Blood Services, Farmington, CT. DEAE-cellulose was purchased from Sigma. Poly-L-lysine was obtained from Sigma, and 1-[3-(dimethylamino)propyl]-3-ethylcarbodiimide (EDC) was from Aldrich. MWs of PL are expressed as the average MW determined by viscosity measurements. Agarose for electrophoresis was from International Biotechnologies, Inc. Water was purified with a Barnstead Nanopure System. DNA plasmid pSVHBV<sub>2</sub> containing the gene for hepatitis B virus surface antigen was provided by Dr. Henry Chiou (TargeTech, Inc.). Assays for surface antigen expression were performed using the corresponding Abbott Auszyme monoclonal antibody assay kit according to the manufacturer's instructions. Concentrations of DNA were based on an extinction coefficient of 20 mL mg<sup>-1</sup> cm<sup>-1</sup> at 260 nm, and agarose gel electrophoresis of DNA was performed as described by Sambrook (24). Dialysis tubing (12–14 kDa MWCO) was from Spectrum. Dialyses were performed in 20-L tanks of water for 2 days at 4 °C with one change of water after 1 day.

**Orosomucoid ( $\alpha_1$ -Acid Glycoprotein).** OR was isolated using an adaptation of a previous report (21). Buffers used in this isolation were made up to the stated concentration in sodium acetate (NaOAc) with glacial acetic acid added to obtain the desired pH: buffer 1, 0.05 M NaOAc, pH 4.5; buffer 2, 0.10 M NaOAc, pH 4.0; buffer 3, 0.05 M NaOAc, pH 3.0. DEAE-cellulose (84 g) was suspended in water, allowed to swell for  $\geq 2$  h, and then washed successively with 0.5 N HCl, 0.5 N NaOH, and 0.01 M EDTA (25). The DEAE-cellulose was poured to a bed volume of 5 cm  $\times$  25 cm in a Waters AP-5 column. Using a peristaltic pump (10 mL/min flow rate) the column was equilibrated with buffer 1 until the pH of the column eluate was 4.5.

Pooled human plasma (4 units,  $\sim 1.2$  L) was transferred to dialysis tubing (12–14 kDa MWCO) and dialyzed overnight at 4 °C against 20 L of buffer 1. The dialyzed plasma was then centrifuged at 14 000 rpm in a Beckman JA-14 rotor (30000g) for 10 min at 4 °C. The supernatant was then filtered through Whatman #4 paper, and the precipitate was discarded, followed by an additional filtration through a 0.2- $\mu$ m filter (Zapcap, Schleicher & Schuell). The dialyzed and filtered plasma was applied to the DEAE-cellulose column which was then washed with buffer 1 until the eluate had an absorbance at 280 nm of less than 0.10. The column was then eluted with buffer 2. The eluate was collected starting when the  $A_{280}$  began to increase and ending after the  $A_{280}$  had peaked and was  $< 0.10$ . After the orosomucoid-rich fraction had been eluted and collected, the column was washed with buffer 3 (1 L) and reequilibrated with buffer 1.

The orosomucoid-rich eluate was brought to 50% saturation with ammonium sulfate (313 g/L of eluate) and stirred overnight at 4 °C. This solution was then centrifuged in the JA-14 rotor (14 000 rpm  $\times$  15 min, 4 °C) and the supernatant retained. Ammonium sulfate (320 g/L of 50% saturation supernatant) was slowly added to bring the solution to 92% saturation. This solution was then stirred for at least 4 h at 4 °C and then centrifuged (14 000 rpm  $\times$  30 min, 4 °C). The pellet was retained and dissolved in a minimal volume of water and transferred

Table 1.

A. Solution To Prepare for Use in Casting Acid-Urea Gels		
8 M urea	48 g plus H <sub>2</sub> O to 100 mL	
Running gel buffer (RGB)	48 mL of 1 M potassium hydroxide 17.2 mL of glacial acetic acid water to 100 mL	
4X sample buffer (4XSB)	1.34 g of potassium hydroxide 2 mL of glacial acetic acid water to 100 mL	
10X running buffer (10XRB)	311.8 g of $\beta$ -alanine 80.4 mL of acetic acid water to 1 L	
30% bis/acrylamide	30 g of acrylamide 0.8 g of bisacrylamide 100 mL of H <sub>2</sub> O	
10% ammonium persulfate	100 mg in 1 mL of H <sub>2</sub> O	
methyl green stock	0.1% methyl green in 1:3 (4XSB:8M urea)	
Coomassie stain	1 g/L in 40% ethanol, 10% acetic acid in H <sub>2</sub> O	
destaining solution	10% ethanol, 7.5% acetic acid in H <sub>2</sub> O	
B. Gel Recipe (for 10% Running Gel, 4% Stacking Gel) <sup>a</sup>		
	running gel (mL)	stacking gel (mL)
30% bis/acrylamide	13.3	1.3
buffer	5 RGB	2.5 4XSB
8 M urea	20	5
H <sub>2</sub> O	1.2	1.3
10% ammonium persulfate	0.3	0.1
TEMED	0.2	0.012

\* Proportions of solutions in A to use for casting running gels and stacking gels, respectively.

to dialysis tubing, leaving a 3-fold volume for expansion of the dialysate, and dialyzed for 2 days at 4 °C against 20 L of water (the water was changed after 1 day). The resulting dialysate was lyophilized and stored at -20 °C. The OR was run on SDS-PAGE and showed a single band at an apparent MW of 44 kDa. OR has a MW of 36 800 as determined by mass spectrometry (26) but runs on SDS-PAGE with a higher apparent MW (27, 28). The typical yield of lyophilized salt-free OR using this procedure is 400 mg.

**Asialoorosomucoid (22).** OR (10 mg/mL) isolated as above was dissolved in water. An equal volume of 0.1 N H<sub>2</sub>SO<sub>4</sub> was added to the OR solution, and the resulting mixture was heated at 80 °C for 1 h in a water bath to hydrolyze sialic acids from the protein. The acidolysis mixture was removed from the water bath, neutralized with NaOH, dialyzed against water for 2 days, and then lyophilized. The thiobarbituric acid assay of Warren (29) or of Uchida (30) was then used to verify desialylation of the OR. Samples used for thiobarbituric acid assay were subjected to the same acid hydrolysis conditions as used to form ASOR. A standard reference curve was prepared using sialic acid samples subjected to the same conditions. Targetability of ASOR samples was verified by labeling with <sup>125</sup>I and measuring liver uptake in mice (16).

**Analytical Acid-Urea Gel Electrophoresis (31, 32).** Analytical gels (15 cm H  $\times$  17.5 cm W plates with 2-mm spacers) were prepared using the recipe in Table 1. Prior to the addition of TEMED, all acrylamide solutions were degassed under vacuum ( $\sim 20$  mmHg) for 10 min. Samples were prepared in 8 M urea-4X sample buffer (3:1 v/v) and loaded on previously cast gels. Electrophoresis was run from anode to cathode (electrodes connected in *reverse* polarity from the norm) with 1X running buffer. Voltage was at 90–150 V. Methyl green can be used as a tracking dye in these gels although we usually omit it. Gels were stained with 0.1% Coomassie Brilliant Blue R250 in



ethanol-acetic acid-water (40:10:50 v/v) and destained with ethanol-acetic acid-water (10:7.5:82.5).

**Preparative Acid-Urea Gel Elution Electrophoresis.** Preparative gels were cast and run in the Bio-Rad Model 491 Prep Cell apparatus (gel recipe, Table 1) in a manner similar to that used for analytical gels and as described in the directions for the apparatus. Running gel solutions were degassed under vacuum, poured into the gel holder, and allowed to stand overnight to ensure full polymerization. Stacking gel solutions were degassed under vacuum and allowed to polymerize for 30 min. After assembly of the elution electrophoresis apparatus with the electrodes connected in *reverse* polarity, the elution chamber was eluted with 1X running buffer at 1 mL/min using a peristaltic pump. Lyophilized crude ASOR-PL was dissolved in 8 M urea-4X sample buffer (3:1 v/v) with a total sample volume equal to one-half the stacking gel volume. Sample was loaded and electrophoresis conducted at 11 W for small (40-mL) gels and 22 W for large (80-mL) gels. The eluate was passed through a UV detector operating at 280 nm. Fractions (10 mL) were collected starting after the ion front (first sharp peak) was eluted from the gel.

**Cation-Exchange HPLC Fractionation of ASOR-PL.** CEHPLC was performed in a manner similar to that described previously using a 1 cm D  $\times$  10 cm L Waters AP-1 column filled with Waters CM 15HR packing material (14). The gradient described in Table 2 was used to chromatograph ASOR-PL mixtures that had been freed of noncovalently bound PL by preparative electrophoresis or dialysis. Fractions of interest were eluted after the buffer pH was lowered to 2.3 and the salt concentration was initially increased. The first major peak observed under these conditions from the first conjugate peak off the preparative gel had the best properties for DNA binding, resulting in high recoveries of ASOR-PL-DNA complexes after filtration.

**ASOR-PL Conjugate Synthesis.** Carbodiimide-mediated coupling of ASOR with PL was performed in a manner similar to a previous description with important changes (18). A typical synthesis of an ASOR-PL conjugate used weight ratios of ASOR:PL:EDC of 1.0:0.22:0.45. ASOR (165.7 mg) was dissolved in water (5 mL), and the solution was filtered through a 0.45- $\mu$ m syringe filter (Acrodisc, Gelman). The filter was washed with water (5 mL), the filtrates were combined, and the pH was adjusted to 7.4 with 0.1 N NaOH. Poly-L-lysine (36.6 mg, 25 Kd, as the HBr salt) was dissolved in water (5 mL), and the pH of the solution was adjusted to 7.4 with 0.1 N NaOH. EDC (25 mg) was dissolved in water (0.33 mL) and added directly to the ASOR solution. The PL solution was added to the ASOR-EDC solution, and the pH was readjusted to 7.4 with 0.1 N NaOH. The reaction mixture was covered, stirred, and maintained at 37 °C. Two additional aliquots of EDC (25 mg) were dissolved in water (0.33 mL) and added at 2.3 h and 3.2 h. After 72 h at 37 °C the reaction mixture was transferred to 12–14-kDa MWCO dialysis tubing and dialyzed at 4 °C against water (20 L) for 2 days with one change of water. The dialysate was lyophilized, and the recovered material (169 mg) was preparatively electrophoresed through an 80-mL preparative acid-urea gel with a 10-mL stacking gel (Figure 1). The two large peaks eluting after the polylysine-ion front were collected, dialyzed, and lyophilized as above. Both front and back peaks (27.0 mg and 42.8 mg) were then fractionated by cation-exchange chromatography (Figure 2). The resulting fractions were then dialyzed and lyophilized as above and analyzed by acid-urea gel electrophoresis (Figure 3).

**Gel Retardation Assay.** Different amounts of purified conjugate were added to 15- $\mu$ g aliquots of plasmid DNA (300  $\mu$ g DNA/mL and 0.15 M NaCl final concentrations) to result in conjugate-to-DNA ratios (wt/wt) of 4.0, 3.5, 3.0, 2.5, 2.0, 1.5, 1.0, and 0. After a 15-min room-temperature incubation, the eight samples were run on a 1% agarose gel in 1X TPE at 50 V for 45 min. The optimum conjugate:DNA ratio for complex formation was determined as the lowest ratio that gave near to full retardation of DNA in the wells (Figure 4A) (13).

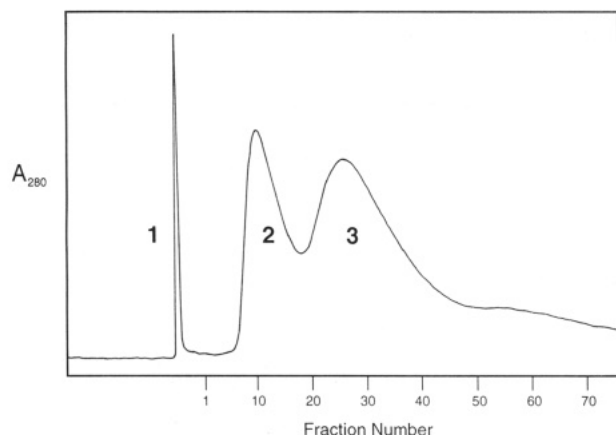
**DNA-Conjugate Complex Formation.** An ASOR/PL/DNA complex was formed at a 3:1 conjugate:DNA ratio, as determined by gel retardation assay, by slowly adding 3.0 mg of purified conjugate (as a 5 mg/mL aqueous solution) to 1 mg of pSV-HBV<sub>2</sub> DNA (300  $\mu$ g DNA/mL and 0.15 M NaCl final concentrations). After complete addition the complex was filtered through a 0.45- $\mu$ m filter (Acrodisc, Gelman Sciences), and the concentration was found to be 251  $\mu$ g/mL by UV absorbance. An aliquot of the complex was then run on a 1% agarose gel to confirm full retardation of the DNA (Figure 4B).

**DNA Expression *in Vivo* (15).** BALB/c mice (Harlan Sprague Dawley) were pretreated intraperitoneally with chloroquine (800  $\mu$ g) and colchicine (15  $\mu$ g) and after 1 h injected with complexed DNA in a volume of 1 mL via the tailvein. Blood samples were obtained periodically and assayed for HBV surface antigen expression.

## RESULTS AND DISCUSSION

Previous reports on the preparation of ASOR-PL conjugates have referred to the use of neuraminidase-treated OR to prepare ASOR. A well-documented property of OR is its relative stability to low pH and elevated temperature to allow acidolytic cleavage of sialic acid residues (22). We have used ASOR prepared in this manner exclusively and encountered no problems in using it alone or in a conjugate as a ligand for targeting to the ASGPr. Preparation of ASOR by acidolysis of OR is much more convenient than using neuraminidase digestion. Care should be exercised, however, in not overexposing OR to low pH and heat as the remaining carbohydrate moieties of ASOR may be damaged providing a less effective ligand to the ASGPr. For those unfamiliar with the Warren and Uchida assays for sialic acid it is important to remember that these assays are for free sialic acid. Prior to conducting an assay for removal of sialic acid from OR, the protein has to be subjected to acid hydrolysis (or neuraminidase treatment) to liberate any protein-bound sialic acid.

Using the previously reported protocol (14) for cation-exchange chromatography of ASOR-PL mixtures we found the major portion of the product mixture to be strongly retained on the column and eluted at low pH with little resolution. We ascribed our differing results to column-to-column variation in manufacturing or prior use. As an alternative HPLC method we developed a mixed pH-salt gradient (Table 2) to elute ASOR-PL in several well-resolved peaks. Even with these HPLC "purified" fractions we experienced variability in the DNA-binding properties of different samples of ASOR-PL and the solubility of the resulting DNA complexes. Using analytical acid-urea gel electrophoresis we were able to observe that CEHPLC alone was incomplete at separating free PL from ASOR-PL (data not shown). Attempts to improve resolution of PL from ASOR-PL with different buffer and gradient conditions have so far been unsatisfactory. The presence of free PL in ASOR-PL fractions was worrisome since complexes of DNA formed with PL alone have lower solubility than those made with ASOR-PL suggesting that the presence of free PL in ASOR-PL



**Figure 1.** Elution profile from PEAUGE. The sample was a crude product mixture (169 mg) from the coupling of ASOR and 25-kDa PL with EDC as described in the text. Fractions (10 mL) were collected starting between peaks 1 and 2. Peaks 2 (fractions 5–17, 27.0 mg) and 3 (fractions 19–43, 42.8 mg) were collected, pooled, dialyzed against water, and lyophilized before further fractionation by CEHPLC.

**Table 2.**

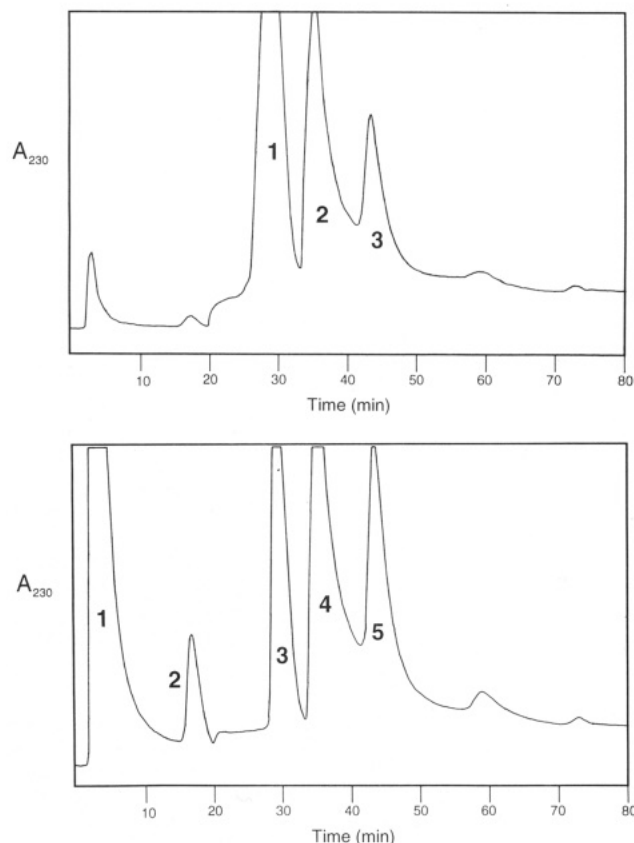
<i>t</i> (min)	HPLC gradient <sup>a</sup>				<i>t</i> (min)	HPLC gradient <sup>a</sup>			
	% A	% B	% C	% D		% A	% B	% C	% D
0	25	0	75	0	50	0	25	65	10
8	25	0	75	0	51	0	25	60	15
9	0	25	75	0	65	0	25	60	15
20	0	25	75	0	66	0	25	55	20
21	0	25	70	5	80	0	25	55	20
35	0	25	70	5	81	0	25	25	50
36	0	25	65	10	95	0	25	25	50

<sup>a</sup> For cation-exchange chromatography on Waters CM 15HR packing in a 10-mm-diameter × 100-mm-length column. Flow rate = 1.8 mL/min. Buffers: (A) 0.4 M sodium acetate, pH 5.0; (B) 0.4 M sodium acetate, pH 2.3; (C) water; (D) 2 M NaCl. buffers are made up to the stated concentration in sodium acetate. pH is adjusted by adding HCl.

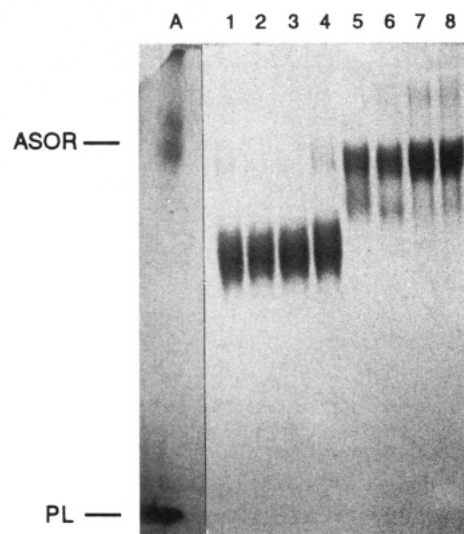
**Table 3. Comparison of DNA-Complex Solubilities with Various ASOR–PL Fractions and PL Alone**

polycation	ratio (μg) polycation:μg DNA	theoretical concn of DNA (μg/mL)	final concn of DNA (μg/mL)	% recovery of DNA based on A <sub>260</sub>
69-kDa PL	0.4:1	685	177	26.9
peak 1, Figure 2A	3.0:1	300	251	83.8
peak 2, Figure 2A	1.3:1	300	157	52.3
peak 3, Figure 2A	1.3:1	300	113	37.8

was deleterious to the formation of soluble ASOR–PL–DNA complexes (Table 3). Having observed that analytical acid–urea gels could resolve PL from ASOR–PL we attempted preparative electrophoresis for this purpose using a commercially available elution electrophoresis apparatus in which a flow-cell allows recovery of fractions as they elute from an electrophoresis gel (Figure 1). Indeed, using this technique we were able to preparatively isolate ASOR–PL fractions free of unbound PL (Figure 3). Pooled ASOR–PL isolated by preparative electrophoresis was still somewhat heterogeneous, and we used ion-exchange chromatography to further fractionate this material (Figure 2). Thus, by subjecting crude ASOR–PL mixtures to a combination of preparative electrophoresis to remove free PL and partially fractionate the ASOR–PL, followed by ion-exchange HPLC to further purify ASOR–PL, we were able to obtain ASOR–PL fractions with reduced heterogeneity that formed soluble DNA complexes with high recoveries (Table 4). Important to the preparation of these preferred ASOR–PL fractions is the removal of



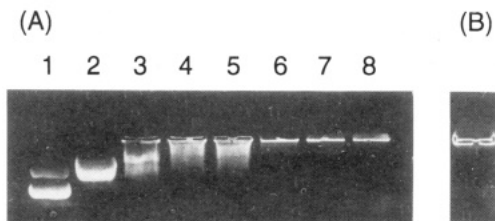
**Figure 2.** CEHPLC chromatograms of ASOR–PL from (top) peak 2 of Figure 1 and (bottom) peak 3 of Figure 1 (see Table 2 for HPLC gradient conditions).



**Figure 3.** Analytical acid–urea gel electrophoresis of peaks collected from PEAUGE and CEHPLC (Figures 1 and 2). Lane A is a mixture of ASOR and 41-kDa PL. Lanes 1 and 5 correspond to prep gel peaks 2 and 3, respectively, in Figure 1. Lanes 2, 3, and 4 correspond to HPLC peaks 1, 2, and 3, respectively, in Figure 2A. Lanes 6, 7, and 8 correspond to CEHPLC peaks 3, 4, and 5 in Figure 2B. All samples are free of noncovalently bound PL, and the amount of material streaking to the top portion of the gel increases with HPLC retention times.

free PL and the more highly cross-linked ASOR–PL components that have lower mobility in the gels and chromatography.

An alternative approach to the removal of free PL is dialysis, and this procedure is feasible only for those reactions in which a low average MW PL is used so that the higher MW PLs in the MW distribution of the PL are

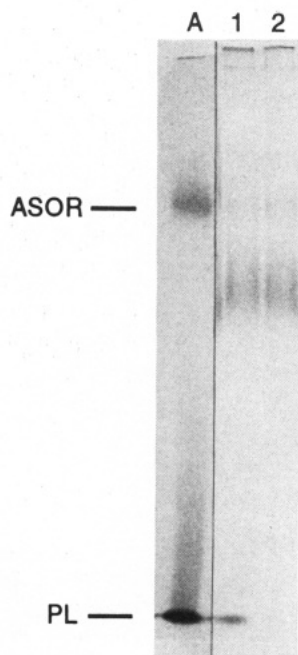


**Figure 4.** (A) Gel retardation assay of the binding of ASOR-PL synthesized and purified as described in the text in complex with plasmid DNA. Lane 1 is plasmid in the absence of conjugate. Lanes 2–8 contain weight ratios of ASOR-PL to DNA of 1.0, 1.5, 2.0, 2.5, 3.0, 3.5, and 4.0, respectively. (B) Agarose gel electrophoresis of an ASOR-PL-DNA complex prepared at a ratio of 3:1 as described in the text showing fully complexed DNA.

**Table 4. Expression of HBV Surface Antigen (HBsAg) in Mice Resulting from Injection of ASOR-PL-Complexed pSVHBV<sub>2</sub> Plasmid**

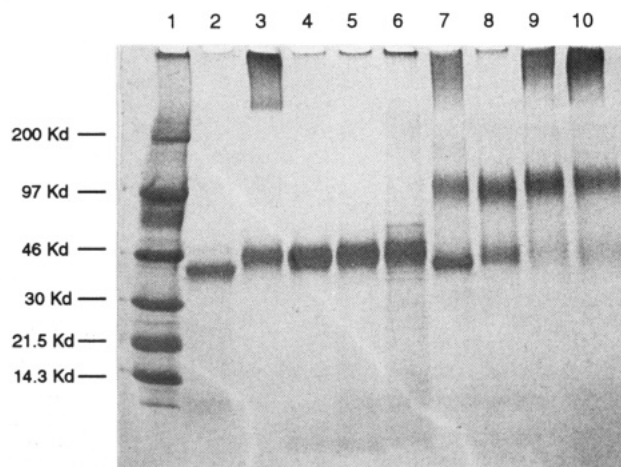
mouse no.	ASOR-PL	DNA dose	HBsAg
1	peak 1 <sup>a</sup>	251 $\mu$ g	0.266 <sup>b</sup>
2	peak 1 <sup>a</sup>	251 $\mu$ g	0.067
3	peak 1 <sup>a</sup>	251 $\mu$ g	0.012
4	peak 2 <sup>c</sup>	157 $\mu$ g	0.023
5	peak 2 <sup>c</sup>	157 $\mu$ g	0.011
6	peak 2 <sup>c</sup>	157 $\mu$ g	0.004

<sup>a</sup> Peak 1 fraction from CEHPLC of the leading ASOR-PL peak obtained following PEAUGE (see Figure 2A). <sup>b</sup> Arbitrary units from HBsAg assay, the cutoff for positive gene expression in these experiments was a value of 0.033. <sup>c</sup> Peak 2 fraction from CEHPLC (see Figure 2A).



**Figure 5.** Acid-urea gel electrophoresis of a crude product mixture between ASOR and 5-kDa PL before (lane 1) and after (lane 2) guanidine dialysis. Lane A; ASOR and PL mixture.

small enough to be resolved from the other components of the reaction product mixture. Dialysis against water of an ASOR-PL product mixture based on a 5-kDa PL was ineffective as removing the unbound PL. We reasoned that electrostatic interactions between PL and ASOR in low ionic-strength solution might be responsible for this result. On inclusion of 1 M guanidine hydrochloride in the dialysis buffer, however, we were able to remove the unbound PL (Figure 5). Further fractionation of the resulting dialyzed product mixture by ion-exchange afforded PL-free conjugate suitable for formation of DNA complexes. SDS-PAGE analysis of this material (Figure



**Figure 6.** SDS-PAGE. Lane 1, MW standards; lane 2, ASOR; lane 3, Figure 1, peak 2; lane 4, Figure 2A, peak 1; lane 5, Figure 2A, peak 2; lane 6, Figure 2A, peak 3; lane 7, Figure 1, peak 3; lane 8, Figure 2B, peak 3; lane 9, Figure 2B, peak 4; lane 10, Figure 2B, peak 5.

6) reveals a mobility for the main ASOR-PL fraction corresponding to a MW of 46 kDa (globular protein MW standards). The "tethered" nature of a 2:1 (ASOR)<sub>2</sub>-PL species may allow greater mobility in electrophoresis gels, and resolution of this question will require further investigation. Crosslinking of the macromolecular components of ASOR-PL conjugates results in product mixtures that are inherently heterogeneous. This heterogeneity is exacerbated by the polydisperse nature of the PL prepared by polymerization by standard methods. To maintain reasonable yields of ASOR-PL, any practically useful preparation will have to contain a moderate degree of heterogeneity.

The suitability of the more soluble DNA complexes for delivery of functional DNA is illustrated by the results presented in Table 4. The data show levels of gene expression obtained using ASOR-PL fractions corresponding to peaks 1 and 2 in Figure 2A. The peak 1 material resulted in observable gene expression in two out of three mice. In the mouse expressing the higher level of surface antigen, expression above background was detected out to 15 days. In the three mice that received DNA complexed with peak 2 material there was no gene expression detectable above the background level of the assay.

#### SUMMARY

With the techniques described here, we routinely prepare ASOR-PL based on different MW PLs purified by PEAUGE and CEHPLC. For the purpose of forming soluble targetable DNA complexes, ASOR-PL isolated in the two steps as the first ASOR-PL peak off of the prep gel, and the first ASOR-PL peak off of the ion-exchange column is a preferred fraction. This material is characterized by an intermediate band position on analytical gels of approximately one-third of the separation from ASOR to PL (an  $R_f$  of 0.45 overall where free PL is at 1.0). DNA complexes prepared with this ASOR-PL fraction have good solubilities and effectively deliver functional plasmid DNA (as measured by protein expression, data not shown) in experiments comparable to those previously reported (12–14, 16). Further details of the use of ASOR-PL conjugates prepared in this manner will be reported elsewhere (H. C. Chiou, J. R. Merwin, and G. L. Spitalny, unpublished results).

There is considerable flexibility within the general procedures detailed above. We have prepared conjugates

using PLs over a wide range of average molecular weights (4–58 kDa) with similar results in DNA binding and delivery. The ratios of the ASOR, PL, and EDC in the reaction mixture can be widely varied as well. We have recently used an ASOR:PL:EDC ratio of 1:1:0.45 in reactions conducted at pH 6.0 for 2 h with good results (M. E. DeRome and M. A. Findeis, unpublished data). Proper purification of the ASOR-PL from these reaction product mixtures is important to allow the formation of a soluble DNA complex. For applications *in vivo*, the ASOR-PL should be free of both unbound PL and the highly crosslinked ASOR-PL species which migrate more slowly in the acid-urea gels. ASOR-PL purified in this manner allows the formation of DNA complexes at a concentration suitable for intravenous injection into experimental animals (typically 0.25–0.50 mg/mL DNA). For *in vitro* experimentation complexes can be made up at lower concentrations and it is possible (though not preferable) to use less rigorously purified ASOR-PL to prepare soluble targetable complexes. Complexes of oligonucleotides (14) are more soluble (to greater than 10 mg/mL oligonucleotide) than those of plasmid DNAs and also may be prepared with less highly purified ASOR-PL.

#### ACKNOWLEDGMENT

We thank Drs. Henry C. Chiou, June Rae Merwin, and George L. Spitalny for sharing their preliminary data on the targetability and bioactivity of ASOR-PL-DNA complexes prepared in our laboratory. Kim Wimler and Michelle Salafia provided the gene expression data. We also thank Dr. Catherine H. Wu for helpful discussions during the development of the procedures described in this paper.

#### LITERATURE CITED

- Mulligan, R. C. (1993) The Basic Science of Gene Therapy. *Science* 260, 926–932 and references cited therein.
- Friedman, T. (1993) Gene therapy—a new kind of medicine. *Trends Biotechnol.* 11, 156–159.
- Findeis, M. A., Merwin, J. R., Spitalny, G. L., and Chiou, H. C. (1993) Targeted delivery of DNA for gene therapy. *Trends Biotechnol.* 11, 202–205.
- Chiou, H. C., Spitalny, G. L., Merwin, J. R., and Findeis, M. A. (1994) In Vivo Gene Therapy Via Receptor-Mediated DNA Delivery. In *Gene Therapeutics: Methods and Applications of Direct Gene Transfer* (J. A. Wolff, Ed.) pp 143–156, Birkhäuser, Boston.
- Wu, G. Y., and Wu, C. H., Eds. (1991) *Liver Diseases, Targeted Diagnosis and Therapy Using Specific Receptors and Ligands*, Marcel Dekker, Inc., New York.
- Wu, G. Y., Wu, C. H., and Stockert, R. J. (1983) Model for specific rescue of normal hepatocytes during methotrexate treatment of hepatic malignancy. *Proc. Natl. Acad. Sci. U.S.A.*, 80, 3078–3080.
- Wu, G. Y., Wu, C. H., and Rubin, M. I. (1985) Acetaminophen Hepatotoxicity and Targeted Rescue: A Model for Specific Chemotherapy of Hepatocellular Carcinoma. *Hepatology*, 5, 709–713.
- Keegan-Rogers, V., and Wu, G. Y., (1990) Targeted protection of hepatocytes from galactosamine toxicity in vivo. *Cancer Chemother. Pharmacol.* 26, 93–96.
- Wu, G. Y., Keegan-Rogers, V., Franklin, S., Midford, S., and Wu, C. H. (1988) Targeted Antagonism of Galactosamine Toxicity in Normal Rat Hepatocytes *in Vitro*. *J. Biol. Chem.* 263, 4719–4723.
- Ponzetto, A., Fiume, L., Forzani, B., Song, S. H., Busi, C., Mattioli, A., Spinelli, C., Marinelli, M., Smedile, A., Chiaberge, E., Bonino, F., Gervasi, G. B., Rapicetta, M., and Verme, G. (1991) Adenine Arabinoside Monophosphate and Acyclovir Monophosphate Coupled to Lactosaminated Albumin Reduce Woodchuck Hepatitis Virus Viremia at Doses Lower than do the Unconjugated Drug. *Hepatology* 14, 16–24.
- Fiume, L., Busi, C., Mattioli, A., Balboni, P. G., and Barbanti-Brodano, G. (1981) Hepatocyte targeting of adenine-9- $\beta$ -D-arabinofuranoside 5'-monophosphate (ara-AMP) coupled to lactosaminated albumin. *FEBS Lett.* 129, 261–264.
- Wu, G. Y., and Wu, C. H. (1987) Receptor-mediated *in Vitro* Gene Transformation by a Soluble DNA Carrier System. *J. Biol. Chem.* 262, 4429–4432.
- Wu, G. Y., and Wu, C. H. (1988) Evidence for Targeted Delivery to Hep G2 Hepatoma Cells *in Vitro*. *Biochemistry* 27, 887–892.
- Wu, G. Y., and Wu, C. H. (1992) Specific Inhibition of Hepatitis B Viral Gene Expression *in Vitro* by Targeted Antisense Oligonucleotides. *J. Biol. Chem.* 267, 12436–12439.
- Cristiano, R. J., Smith, L. C., and Woo, S. L. C. (1993) Hepatic gene therapy: Adenovirus enhancement of receptor-mediated gene delivery and expression in primary hepatocytes. *Proc. Natl. Acad. Sci. U.S.A.* 90, 2122–2126.
- Wu, G. Y., and Wu, C. H. (1988) Receptor-mediated Gene Delivery and Expression *in Vivo*. *J. Biol. Chem.* 263, 14621–14624.
- Wu, G. Y., Wilson, J. M., and Wu, C. H. (1989) Targeting Genes: Delivery and Persistent Expression of a Foreign Gene Driven by Mammalian Regulatory Elements *in Vivo*. *J. Biol. Chem.* 264, 16985–16987.
- Wu, G. Y., Wilson, J. M., Shalaby, F., Grossman, M., Shafritz, D. A., and Wu, C. H. (1991) Receptor-mediated Gene Delivery *in Vivo*. *J. Biol. Chem.* 266, 14338–14343.
- Wilson, J. M., Grossman, M., Cabrera, J. A., Wu, C. H., Chowdhury, N. R., Wu, G. Y. and Chowdhury, J. R. (1992) Hepatocyte-directed Gene Transfer *in Vivo* Leads to Transient Improvement of Hypercholesterolemia in Low Density Lipoprotein Receptor-deficient Rabbits. *J. Biol. Chem.* 267, 963–967.
- Wilson, J. M., Grossman, M., Cabrera, J. A., Wu, C. H., and Wu, G. Y. (1992) A Novel Mechanism for Achieving Transgene Persistence *in Vivo* after Somatic Gene Transfer into Hepatocytes. *J. Biol. Chem.* 267, 11483–11489.
- Whitehead, P. H., and Sammons, H. G. (1966) A simple technique for the isolation of orosomucoid from normal and pathological sera. *Biochim. Biophys. Acta* 124, 209–211.
- Schmid, K., Polis, A., Hunziker, K., Fricke, R., and Yayoshi, M. (1967) Partial Characterization of the Sialic Acid-Free Forms of  $\alpha_1$ -Acid Glycoprotein from Human Plasma. *Biochem. J.* 104, 361–368.
- Wagner, E., Zenke, M., Cotten, M., Beug, H., and Birnstiel, M. L. (1990) Transferrin-polycation conjugates as carriers for DNA uptake into cells. *Proc. Natl. Acad. Sci. U.S.A.* 87, 3410–3414.
- Sambrook, J., Fritsch, E. F., and Maniatis, T. (1989) *Molecular Cloning*, 2nd ed., Chapter 6, Cold Spring Harbor Laboratory Press: Cold Spring Harbor.
- Cooper, T. G. (1977) *The Tools of Biochemistry*, Chapter 6, John Wiley & Sons, Inc., New York.
- Chait, B. T., and Kent, S. B. H. (1992) *Science* 257, 1885–1894.
- Schmid, K. (1976)  $\alpha_1$ -Acid Glycoprotein. In *The Plasma Proteins*, (F. W. Putnam, Ed.) 2nd ed., Vol. 1, pp 183–228, Academic Press, New York.
- Schmid, K. (1989) Human Plasma  $\alpha_1$ -Acid Glycoprotein—Biochemical Properties, The Amino Acid Sequence and the Structure of the Carbohydrate Moiety, Variants and Polymorphism. *Alpha<sub>1</sub>-Acid Glycoprotein: Genetics, Biochemistry, Physiological Functions, and Pharmacology*, pp 7–22, Alan R. Liss, Inc., New York.
- Warren, L. (1959) The Thiobarbituric Acid Assay of Sialic Acids. *J. Biol. Chem.* 234, 1971–1975.
- Uchida, Y., Tsukada, Y., and Sugimori, T. (1977) Distribution of Neuraminidase in *Arthrobacter* and Its purification by Affinity Chromatography. *J. Biochem.* 82, 1425–1433.
- Hames, B. D. (1981) Introduction to PAGE, In *Gel Electrophoresis of Proteins* (B. D. Hames, and D. Rickwood, Eds.), p 68, IRL Press, Oxford and Washington, D.C.
- Panyim, S., and Chalkley, R. (1969) High Resolution Acrylamide Gel Electrophoresis of Histones. *Arch. Biochem. Biophys.* 130, 337–346.

# Preparation of Vitamin B<sub>6</sub>-Conjugated Peptides at the Amino Terminus and of Vitamin B<sub>6</sub>-Peptide-Oligonucleotide Conjugates

Tianmin Zhu and Stanley Stein\*

Center for Advanced Biotechnology and Medicine, 679 Hoes Lane, Piscataway, New Jersey 08854, and Department of Chemistry, Rutgers University, Piscataway, New Jersey 08854. Received February 23, 1994\*

A series of *N*-(4'-pyridoxyl)peptides has been made by standard Fmoc chemistry and a solid-phase coupling procedure. The last Fmoc group of the peptide was removed on the synthesizer, and the free amino group was then condensed with pyridoxal. The Schiff base formed was selectively reduced using sodium cyanoborohydride. The product was cleaved from the resin using a standard procedure. No deleterious effects were found when using the protected amino acids Fmoc-L-Ala, Fmoc-L-Arg(Pmc), Fmoc-L-Asp(OtBu), Fmoc-L-His(Trt), Fmoc-L-Ser(tBu), Fmoc-L-Thr(tBu), and Fmoc-L-Cys(Trt) for peptide synthesis. A vitamin B<sub>6</sub>-peptide-oligonucleotide conjugate could be synthesized using a cysteinyl peptide and a suitably activated oligonucleotide.

## INTRODUCTION

In contrast to attaining a pharmacologic response by binding to an extracellular receptor, certain compounds may require access to intracellular compartments. Co-transport of a compound as a conjugate with vitamin B<sub>6</sub> has been shown to be an attractive option (1). Virtually all eukaryotic cells have a receptor-mediated transport system for vitamin B<sub>6</sub>, which also accepts secondary amine conjugates at position 4 of pyridoxal (1). Following uptake into the cytosol, the conjugate can be enzymatically altered by phosphorylation and oxidation to release pyridoxal phosphate and the original amine-containing compound. In previous studies (1), several amines were reacted with pyridoxal to form the Schiff base, which was subsequently reduced with sodium borohydride. These compounds were able to effectively compete for binding to the vitamin B<sub>6</sub> receptor and be taken up by cells in culture.

We are interested in using vitamin B<sub>6</sub> to facilitate the cell uptake of peptides and peptide-oligonucleotide conjugates. A convenient solid-phase synthesis of *N*-(4'-pyridoxyl)peptide at the amino terminus has been established. A series of *N*-(4'-pyridoxyl)peptides has been made by standard Fmoc<sup>1</sup> chemistry and a solid-phase coupling procedure prior to cleavage from the resin. It was then possible to covalently link a suitably activated oligonucleotide to the vitamin B<sub>6</sub>-peptide conjugate using a previously developed procedure (2).

## EXPERIMENTAL PROCEDURES

**Reagents.** *N*- $\alpha$ -Boc-L-ornithine and (benzotriazol-1-yloxy)tris(dimethylamino)phosphonium hexafluorophosphate (BOP reagent) were from Bachem (Torrance, CA). Most peptide synthesis reagents were from Milligen/Bioscience (Burlington, MA). Anisole, ethanedithiol, 1-hydroxybenzotriazole hydrate (HOBt), *N*-[(9-fluorenylmethoxycarbonyl)oxy]succinimide (Fmoc reagent), trifluoroacetic acid (TFA), pyridoxal hydrochloride, and sodium cyanoborohydride were from Aldrich (Milwaukee,

WI). Water was purified by a Milli-Q Water System from Millipore. *N*- $\alpha$ -Boc-*N*- $\delta$ -Fmoc-L-ornithine was prepared by the method described previously (3).

**Peptide Synthesis.** The peptides were synthesized in a Milligen/Bioscience Model Excess instrument. The *N*- $\alpha$ -Boc-*N*- $\delta$ -Fmoc-L-ornithine cartridge was packed with *N*- $\alpha$ -Boc-*N*- $\delta$ -Fmoc-L-ornithine (227 mg, 0.5 mmol), BOP reagent (221.3 mg, 0.5 mmol), and HOBt (67.5 mg, 0.5 mmol). The PAL support for peptide amide (0.1 mmol synthesis) was used to synthesize the carboxy-terminal amide, and Fmoc-L-Lys(Boc) PAC support was used for preparing the carboxy-terminal acid. Fmoc-L-amino acid/BOP + HOBt cartridges such as Fmoc-L-Ala, Fmoc-L-Arg(Pmc), Fmoc-L-Asp(OtBu), Fmoc-L-His(Trt), Fmoc-L-Ser(tBu), Fmoc-L-Thr(tBu), and Fmoc-L-Cys(Trt) were used. The recommended conditions were followed, except that the coupling time for the ornithine derivative was extended to 90 min. The last protecting Fmoc group on the N-terminal residue of each peptide was removed. The peptides synthesized for these studies were ( $\delta$ -Orn)<sub>*n*</sub>-Cys-NH<sub>2</sub>, where *n* = 1, 3, 8, 12, and Ala-Arg-His-Thr-Asp-Thr-Lys-OH.

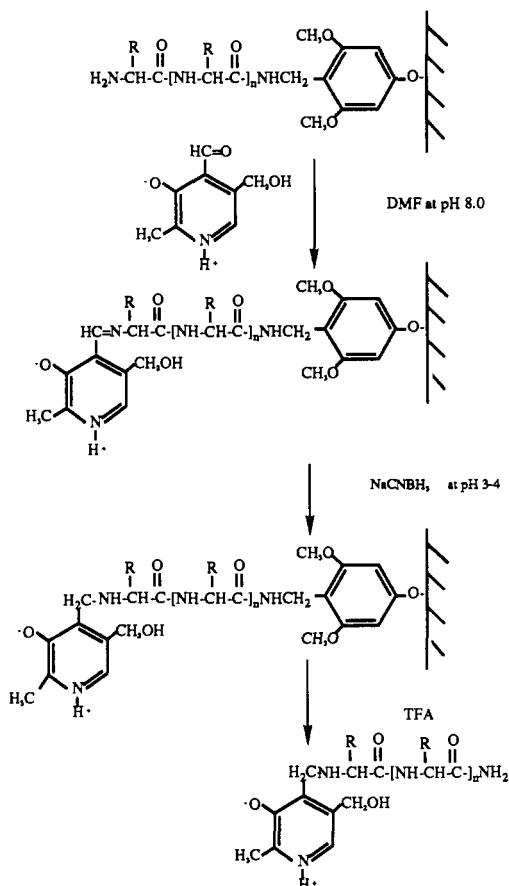
**Solid-Phase Coupling of Pyridoxal to Peptide (Scheme 1).** The peptide-resin in the synthesis cartridge, after removal of the final Fmoc protecting group, was removed from the machine and swelled with DMF for 10 min. Then 0.5 mmol of pyridoxal hydrochloride, dissolved in 5 mL of DMF and adjusted to pH 8 with 1 N NaOH, was added. The pyridoxal solution was added to the solid support cartridge by syringe, and the reaction was carried out overnight at room temperature. Excess pyridoxal was removed by syringe, and the solid support was washed three times with 5 mL of DMF and once with 5 mL of methanol. The solid support was swelled with DMF again and reacted with 0.5 mmol of sodium cyanoborohydride, dissolved in 5 mL DMF, and adjusted to pH 3-4 with 2 N HCl. The reduction reaction was at room temperature for 7 h (the yellow color of the solid support faded). The excess sodium cyanoborohydride was removed by syringe, and the solid support was washed three times with 5 mL of DMF and three times with 5 mL of methanol. The solid support was dried under vacuum, and the peptide was cleaved with 5 mL of TFA containing 20  $\mu$ L of ethanedithiol for 3 h at room temperature. The solid support was filtered through a Pasteur pipet filled with glass wool and washed with 1 mL of TFA. The filtrate

\* Abstract published in *Advance ACS Abstracts*, June 15, 1994.

<sup>1</sup> Abbreviations: Boc, *tert*-butoxycarbonyl; BOP, (benzotriazol-1-yloxy)tris(dimethylamino)phosphonium hexafluorophosphate; tBu, *tert*-butyl; OtBu, *tert*-butyl ester; Fmoc, 9-fluorenylmethoxycarbonyl; HOBt, hydroxybenzotriazole hydrate; Pmc, 2,2,5,7,8-pentamethylchroman-6-sulfonyl; TFA, trifluoroacetic acid; Trt, trityl.



Scheme 1. Solid-Phase Synthesis of Pyridoxylpeptide

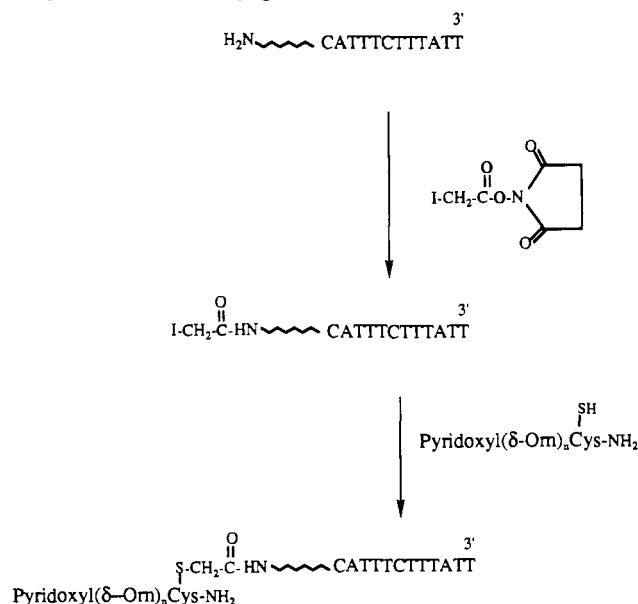


was collected and blown to near dryness under nitrogen. The oily residue was precipitated by adding ethyl ether. The precipitate was filtered with a 10–15 M sintered glass filter and washed thoroughly with ethyl ether to obtain the dry product.

**Purification of Vitamin B<sub>6</sub>-Peptide Conjugates.** The conjugates were purified by HPLC on a Vydac (Hesperia, CA) 218TP1022, 10- $\mu$ m, reversed-phase C-18 column (2.2  $\times$  25 cm) using a gradient of 0–10 min 100% A and 10–45 min from 100% A to 75% A at a flow rate of 4 mL/min. Mobile phase A was 0.1% TFA in water, mobile phase B was 0.1% TFA in acetonitrile:isopropanol:water (70:20:10). The yield of vitamin B<sub>6</sub>-peptides was about 90% by weight. The structure of each peptide was confirmed by fast atom bombardment mass spectrometry and one of them was by <sup>1</sup>H-NMR.

**Preparation of *N*-(4'-Pyridoxyl)peptide-Oligonucleotide Conjugates (Scheme 2).** These conjugates could be prepared by reaction of an iodo group on the oligonucleotide and a thiol group on the peptide (2). Oligonucleotide with 5' amino linker (4 units, A<sub>260</sub>) and 2 mg of *N*-iodoacetoxy succinimide, dissolved in 50  $\mu$ L of DMSO, were mixed in 100  $\mu$ L of 0.1 M sodium bicarbonate solution for 2 h. The unreacted *N*-iodoacetoxy succinimide and byproducts were removed by anion-exchange chromatography on a Nucleogen 60–7 DEAE column (4  $\times$  125 mm) from the Nest Group (Southboro, MA). Mobile phase A was 60% 20 mM sodium acetate, pH 6.5, and 40% acetonitrile. Mobile phase B was mobile phase A containing 0.7 M lithium chloride. The gradient was 100% A for 10 min, 100% A to 88% A for 20 min and 88% A to 50% A in 1 min. The flow rate was 1 mL/min. The eluent corresponding to the peak at 35 min, which was iodo-activated DNA (iodoacetyl-DNA), was collected. About 2 mg of pyridoxyl( $\delta$ -Orn)<sub>8</sub>Cys-NH<sub>2</sub> dissolved in

Scheme 2. Synthesis of Pyridoxylpeptide-Oligonucleotide Conjugate



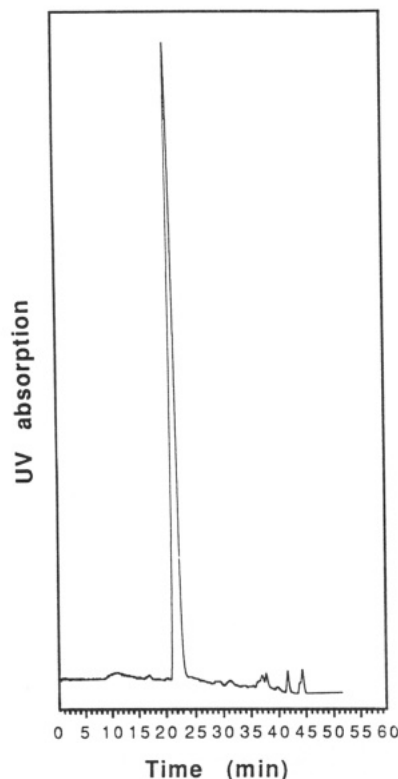
water was added into the iodoacetyl-DNA solution from the anion-exchange chromatography. The mixture was reacted for 12 h at room temperature and then put under vacuum to remove acetonitrile. The product, *N*-(4'-pyridoxyl)peptide-oligonucleotide, was isolated by anion-exchange chromatography using the same column and mobile phase, but the gradient was 1% B/min. The flow rate was 1 mL/min. The final product was desalted by reversed-phase chromatography on a PRP-1 column (4.1  $\times$  150 mm) from VWR (Piscataway, NJ) using a gradient of acetonitrile in 0.1 M triethylammonium acetate, pH 9.7. After the buffer was removed under vacuum overnight, the conjugates were redissolved in water. The yield was 55% based on A<sub>260</sub> (2.2 units).

**Polyacrylamide Gel Electrophoresis (PAGE).** The pyridoxylpeptide-oligonucleotide and peptide-oligonucleotide conjugates were analyzed on a native 20% polyacrylamide gel. The running buffer was 40 mM MOPS and 10 mM sodium acetate (pH 7.0, adjusted with sodium hydroxide). The samples were suspended in 20  $\mu$ L of loading buffer (99% formamide), heated to 90  $^{\circ}$ C for 2 min, chilled on ice, and loaded on the gel. The pictures were taken by Polaroid 667 film under UV shadowing using a green filter from Eastman Kodak Co. (Rochester, NY).

## RESULTS

Vitamin B<sub>6</sub> can be appended to the amino-terminus of a peptide prior to cleavage from the solid support. The advantage of this approach is that only the amino-terminal amine is free to condense with pyridoxal, while the other potentially active side chain groups are still protected. The Schiff base was formed and then selectively reduced to the stable secondary amine with sodium cyanoborohydride. To test the utility of this approach, a trial of the synthesis was carried out to construct a pyridoxyl- $\delta$ -Orn-Cys-NH<sub>2</sub> conjugate. Excess pyridoxal and sodium cyanoborohydride were readily removed by filtration in the synthesis cartridge using a syringe. Following cleavage of the peptide from the resin and removal of protecting groups by TFA, the vitamin B<sub>6</sub>-containing peptide was analyzed by reversed-phase HPLC (Figure 1). The modified peptide eluted from the column as a single major peak, accounting for >93% of total peak area at 220 nm. Analysis of the peptide by FAB-MS (*M* + 1) revealed the expected mass



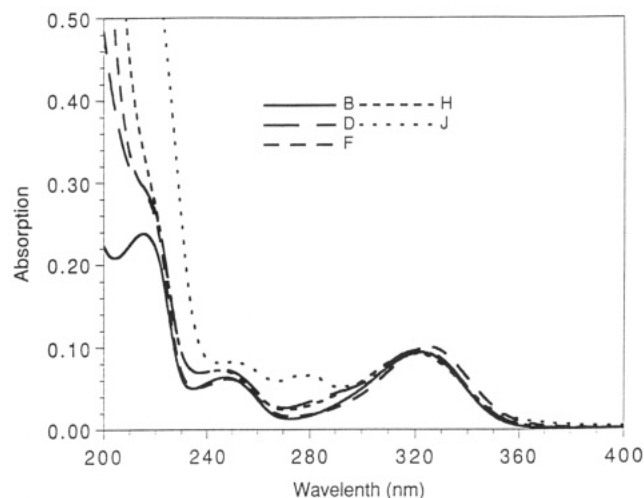


**Figure 1.** HPLC chromatography of pyridoxyl- $\delta$ -Orn-Cys on a Vydac C18 column.

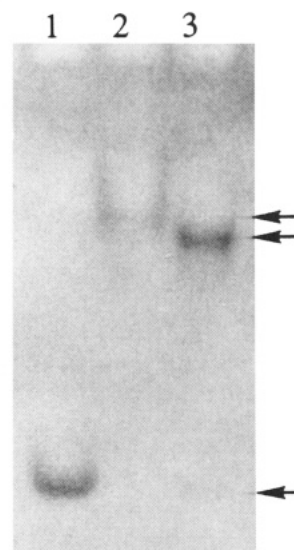
(calcd 386, found 386.2). The structure of the conjugate was also assigned on the basis of its  $^1\text{H-NMR}$  spectrum for pyridoxyl- $\delta$ -Orn-Cys- $\text{NH}_2$  ( $\text{CD}_3\text{OD}$ ):  $\delta = 1.9\text{--}2.1$  (b, 4H), 2.69 (s, 3H,  $\text{CH}_3$ ), 2.85–3.0 (m, 2H), 3.15–3.2 (m, 2H), 3.95–4.1 (b, 1H), 4.45–4.6 (m, 3H), 4.8 (s, 2H), 8.2 (s, 1H). These data indicate that the vitamin  $\text{B}_6$  group had been linked to the peptide in the expected way and remained stably attached and unmodified during synthesis, cleavage, and deprotection. The result showed that condensation can be performed under biphasic conditions.

A series of similar isopeptides with different lengths of the ornithine chain was attempted and each gave the correct product according to FAB-MS ( $M + 1$ ) pyridoxyl-( $\delta$ -Orn) $_3$ -Cys- $\text{NH}_2$  (calcd 614, found 614.3), pyridoxyl-( $\delta$ -Orn) $_8$ -Cys- $\text{NH}_2$  (calcd 1184, found 1184.5), pyridoxyl-( $\delta$ -Orn) $_{12}$ -Cys- $\text{NH}_2$  (calcd 1641, found 1640.8). Next a model peptide with aliphatic, aromatic, basic, acidic, and hydroxyl-containing side chains, Ala-Arg-His-Thr-Asp-Tyr-Lys, was attempted. The usual amino acid protecting groups,  $t\text{Bu}$ ,  $\text{OtBu}$ ,  $\text{Trt}$  and  $\text{Pmc}$  were used. Vitamin  $\text{B}_6$ -linked Ala-Arg-His-Thr-Asp-Tyr-Lys was prepared and found to have the expected mass ( $M + 1$ ) (calcd 1041, found 1041.5). Furthermore, the UV spectra demonstrated the presence of the pyridoxyl group (Figure 2). Thus, this method for coupling vitamin  $\text{B}_6$  to a peptide prior to cleavage from the solid support is generally applicable for the synthesis of vitamin  $\text{B}_6$ -peptide conjugates.

A model pyridoxylpeptide-oligonucleotide conjugate, pyridoxyl-( $\delta$ -Orn) $_8$ -Cys-CATTTCTTTATT, was synthesized by conjugation of the pyridoxylpeptide with the oligonucleotide. The purification was by anion-exchange chromatography. Excess pyridoxyl-( $\delta$ -Orn) $_8$ -Cys- $\text{NH}_2$  was eluted within the void volume, and the  $N$ -(4'-pyridoxyl)-peptide-oligonucleotide conjugate peak was at 30 min. This conjugate had the characteristic UV spectrum for both DNA and vitamin  $\text{B}_6$  (not shown). The conjugate was also analyzed by PAGE. The mobility of pyridoxyl-peptide-oligonucleotide conjugate was retarded by the



**Figure 2.** UV spectra of pyridoxylpeptide conjugates. B, pyridoxyl- $\delta$ -Orn-Cys- $\text{NH}_2$ ; D, pyridoxyl-( $\delta$ -Orn) $_3$ -Cys- $\text{NH}_2$ ; F, pyridoxyl-( $\delta$ -Orn) $_8$ -Cys- $\text{NH}_2$ ; H, pyridoxyl-( $\delta$ -Orn) $_{12}$ -Cys- $\text{NH}_2$ ; J, pyridoxyl-Ala-Arg-His-Thr-Aps-Tyr-Lys-OH.



**Figure 3.** Electrophoretic analysis of conjugates. Lane 1 is 12-mer DNA with 5' amino linker. Lane 2 is ( $\delta$ -Orn) $_8$ -Cys- $\text{NH}_2$  (5' 12-mer DNA). Lane 3 is pyridoxyl-( $\delta$ -Orn) $_8$ -Cys- $\text{NH}_2$  (5' 12-mer DNA).

positively charged peptide, although it migrated slightly faster than a similar peptide-oligonucleotide conjugate without the pyridoxyl group (Figure 3).

## DISCUSSION

Transmembrane delivery into cells of certain pharmacologic compounds may be achieved through utilization of unrelated transport mechanisms. According to this approach, a conjugate of the pharmacologic compound and the delivery vehicle is prepared. Generally, the vehicle represents a ligand that binds to a cell surface receptor which is internalized through an endocytic pathway. Examples include cellular uptake of ricin A-chain coupled to human chorionic gonadotropin (4), asialoglycoprotein-polylysine conjugates for delivery of DNA into hepatocytes (5), mannose 6-phosphate for uptake of low density lipoproteins (6), and cholera toxin binding subunit for transport of insulin (7). The problem of lysosomal entrapment of the pharmacologic agent has been addressed by the use of transferrin-adenovirus-polylysine conjugates for gene delivery (8), based on the lysosomal disruption ability of adenovirus.

Cellular uptake of low molecular weight compounds, such as water-soluble vitamins, is by a process referred to as potocytosis, as opposed to endocytosis (9). This mechanism has been examined for folate uptake (10), and it may also be applicable to vitamin B<sub>6</sub>. McCormick and colleagues have suggested the utilization of the uptake system for several vitamins, including riboflavin, ascorbic acid, biotin, and vitamin B<sub>6</sub> (1). In their studies on the vitamin B<sub>6</sub> adducts, it was suggested that positively charged groups should be placed near the pyridoxyl group to enhance receptor binding and internalization. Accordingly, the polyornithine bridge between the oligonucleotide and pyridoxyl portion of our conjugate may play a beneficial role. In conclusion, our procedure for conjugating vitamin B<sub>6</sub> specifically at the amino-terminus of peptides, especially the possibility of reduction with tritiated cyanoborohydride, provides a foundation for studying the cellular uptake, intracellular localization, and metabolism of such conjugates.

#### ACKNOWLEDGMENT

This work was funded by Gene Shears (Australia) Pty. Ltd.

#### LITERATURE CITED

- (1) Zhang, Z., and McCormick, D. B. (1991) Uptake of N-(4'-pyridoxyl)amines and release of amines by renal cells: A model for transporter-enhanced delivery of bioactive compounds. *Proc. Natl. Acad. Sci. U.S.A.* 88, 10407-10410.
- (2) Zhu, T., Tung, C.-H., Dickerhof, W. A., Breslauer, K. J., and Stein, S. (1993) Preparation and Physical Properties of Conjugates of Oligodeoxynucleotides with Poly( $\delta$ )ornithine Peptides. *Antisense Res. Dev.* 3, 349-356.
- (3) Zhu, T., Wei, Z., Tung, C.-H., Dickerhof, W. A., Breslauer, K. J., Georgopoulos, D. E., Leibowitz, M. J., and Stein, S. (1993) Oligonucleotide-Poly-L-ornithine Conjugates: Binding to Complementary DNA and RNA. *Antisense Res. Dev.* 3, 265-275.
- (4) Oeltmann, T. N., and Heath, E. C. (1979) A Hybrid Protein Containing the Toxic Subunit of Ricin and the Cell-specific Subunit of Human Chorionic Gonadotropin. *J. Biol. Chem.* 254, 1028-1032.
- (5) Wu, G. Y., and Wu, C. H. (1987) Receptor-mediated *in Vitro* Gene Transformation by a Soluble DNA Carrier System. *J. Biol. Chem.* 262(10), 4429-4432.
- (6) Murray, G., and Neville, D. M. (1980) Mannose 6-Phosphate Receptor-mediated Uptake of Modified Low Density Lipoprotein Results in Down Regulation of Hydroxymethylglutaryl-CoA Reductase in Normal Familial Hypercholesterolemic Fibroblasts. *J. Biol. Chem.* 255(24), 11941-11948.
- (7) Roth, R. A., and Maddox, B. (1983) Insulin-Cholera Toxin Binding Unit Conjugate: A Hybrid Molecule With Insulin Biological Activity and Cholera Toxin Binding Specificity. *J. Cell Phys.* 115, 151-158.
- (8) Wagner, E., Zatloukal, K., Cotten, M., Kirlappos, H., Mechtler, K., Curiel, D. T., and Birnstiel, M. L. (1992) Coupling of adenovirus to transferrin-polylysine/DNA complexes greatly enhances receptor-mediated gene delivery and expression of transfected genes. *Proc. Natl. Acad. Sci. U.S.A.* 89, 6099-6103.
- (9) Anderson, R. G. W., Kamen, B. A., Rothberg, K. G., and Lacey, S. W. (1992) Potocytosis: Sequestration and Transport of Small Molecules by Caveolae. *Science* 255, 410-411.
- (10) Rothberg, K. G., Ying, Y., Kolhouse, J. F., Kamen, B. A., and Anderson, R. G. W. (1990) The Glycophospholipid-linked Folate Receptor Internalizes Folate Without Entering the Clathrin-coated Pit Endocytic Pathway. *J. Cell Biol.* 110, 637-649.

# Platinum(II)-Adenosine Phosphothiorate Complexes: Kinetics of Formation and Phosphorus-31 NMR Characterization Studies

Lori L. Slavin,<sup>†</sup> Elizabeth H. Cox,<sup>‡</sup> and Rathindra N. Bose\*

Chemistry Department, Kent State University, Kent, Ohio 44242. Received October 5, 1993\*

Reactions of chloro(diethylenetriamine)platinum(II) chloride with adenosine 5'-O-thiomonophosphate, adenosine 5'-O-(2-thiodiphosphate), and adenosine 5'-O-(3-thiotriphosphate) yielded exclusively (phosphothiorato)platinum(II) complexes. Phosphorus-31 NMR data for the coordinated phosphothiorate phosphorus atom exhibited about 15-20 ppm upfield chemical shift compared to chemical shifts for free nucleotides. Uncoordinated phosphate groups exhibited insignificant changes in the chemical shift upon complexation. Likewise, proton NMR data indicate no significant changes in chemical shift for the purine or ribose protons. Reactions between phosphothiorates and the platinum complex predominately take place through a second-order process, first order with respect to each of the reactants indicating that the aquated pathway contributes insignificantly toward complexation. The second-order rate constants,  $1.9 \pm 0.1 \text{ M}^{-1} \text{ s}^{-1}$  for the AMP-S,  $2.4 \pm 0.2 \text{ M}^{-1} \text{ s}^{-1}$  for the ADP- $\beta$ -S, and  $2.7 \pm 0.2 \text{ M}^{-1} \text{ s}^{-1}$  for the ATP- $\gamma$ -S reactions were evaluated at pH 6.5 and at 25 °C. These rate data were compared with those reactions of adenosine 5'-monophosphate (AMP) and guanosine 5'-monophosphate (GMP) with the same platinum(II) complex. These reactions proceed through the direct interaction between the starting platinum complex and nucleotides as well as through the reaction between the aquaplatinum complex and nucleotides. The rate constant for the aquation process was evaluated to be  $(2.0 \pm 0.1) \times 10^{-4} \text{ s}^{-1}$  for both AMP and GMP reactions. Second-order rate constants for the direct reaction with the chloro complex were calculated to be  $(1.5 \pm 0.1) \times 10^{-2} \text{ M}^{-1} \text{ s}^{-1}$  for the GMP and  $(6.0 \pm 0.3) \times 10^{-3} \text{ M}^{-1} \text{ s}^{-1}$  for the AMP reaction at 40 °C.

## INTRODUCTION

A great deal of effort has been devoted to understanding the role of metal ions in phosphate hydrolyses catalyzed by many metalloenzymes--ranging from phosphokinases to polymerases (1-5). Inert metal ions such as Cr(III), Co(III), and Rh(III) have been utilized to understand the roles played by metals in ATP hydrolysis (1-5, 6, 7). All these metal ions promote hydrolysis in highly basic solutions, but none of these metals catalyze hydrolysis significantly at or near physiological pH (6). Earlier, we showed that platinum(II) catalyzes the hydrolysis of inorganic polyphosphates in acidic solutions (8). Recently, it has been demonstrated that platinum complexes promote hydrolytic cleavages of peptides (9). Since platinum(II) aqua complexes are fairly acidic, presumably these hydrolyses are initiated through the hydroxyl transfer reactions from the metal center to the phosphate moiety. These coordinated acidic water molecules offer a unique advantage over the other tripositive inert metal centers in that mechanistic ambiguities between the coordinated hydroxyl transfer and involvement of the free hydroxide can be removed. Platinum(II), however, cannot be utilized in promoting the hydrolysis of NTP since nitrogen of the purine and pyrimidine bases favor coordination over the phosphate and coordination to the phosphate moiety is a prerequisite for hydrolysis. In order to circumvent the base coordination, a phosphothiorate group can be introduced to the adenosine nucleoside to facilitate platinum binding through the sulfur atom. Here, we report the kinetics of formation and the phosphorus-31 NMR characterization of platinum(II)phosphothiorate

complexes utilizing AMP-S, ADP- $\beta$ -S, and ATP- $\gamma$ -S (Figure 1) and compare these rate data with those of AMP and GMP coordinations.

Platinum(II)-phosphothiorate chemistry has been exploited in several areas of cell and molecular biology. Lippard and co-workers (10) have explored the application of platinum-bound phosphothiorate nucleotides for DNA sequencing by using electron microscopy. Chou and Orgel (11) have used *trans*-diamminedichloroplatinum(II) to cross-link double-stranded oligonucleotides. These workers also used  $\text{PtCl}_4^{2-}$  to promote covalent cross-linking between double-stranded DNA and protein. The extent of platinum(II)-phosphothiorate complex formation and the roles played by this metal center to cross-link proteins and nucleotides are not understood. Phosphorus-31 NMR presented here would be useful to characterize platinum-phosphothiorate complexes, and their possible roles in cross-linking oligonucleotides and nucleotide-protein can be explored.

## EXPERIMENTAL METHODS

**Reagents.** Chloro(diethylenetriamine)platinum(II) chloride was synthesized following the literature method (13). The corresponding aqua complex was prepared *in situ* by adding 2 equiv of  $\text{AgNO}_3$  or  $\text{AgClO}_4$ . This aqua complex was generated in acidic solution (pH  $\sim$  2) to avoid dimerization. All nucleotides, AMP, GMP, AMP-S, ADP- $\beta$ -S, and ATP- $\gamma$ -S (Sigma) were of the highest quality available and used without further purification. Nuclear magnetic resonance experiments were carried out in  $\text{D}_2\text{O}$  (99% atom) (Sigma). Sodium perchlorate was prepared by neutralization of  $\text{HClO}_4$  with  $\text{Na}_2\text{CO}_3$ .

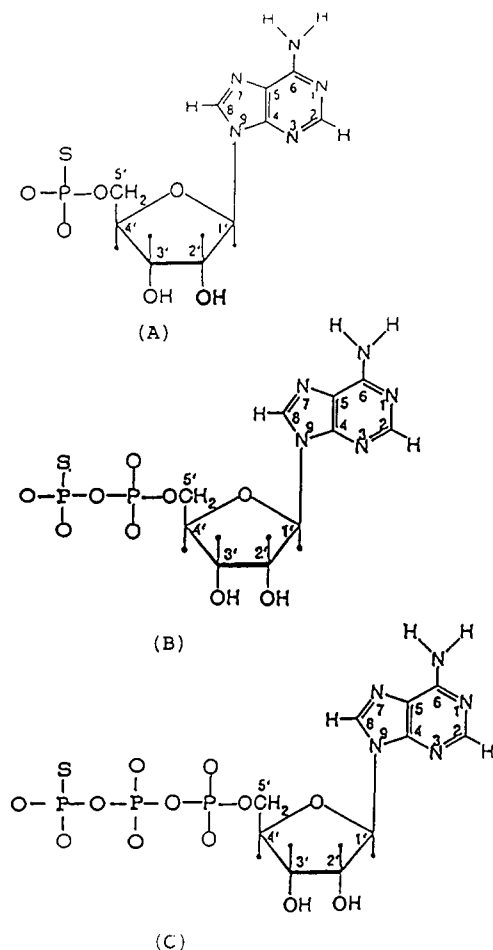
**Physical Measurements. Rate Measurements.** Reactions between nucleotides and platinum complexes were followed on a UV-vis spectrophotometer (Perkin-Elmer, Lambda 600) at 260 and 300 nm. The temperature was

\* To whom correspondence should be addressed.

<sup>†</sup> Present address: Department of Chemistry, Austin Peay State University, Clarksville, TN.

<sup>‡</sup> Undergraduate participant.

\* Abstract published in *Advance ACS Abstracts*, June 15, 1994.



**Figure 1.** Structures of the phosphothiorate analogues of adenosine nucleotides: (A) adenosine 5'-O-thiomonophosphate (AMP-S), (B) adenosine 5'-O-(2-thiodiphosphate) (ADP-β-S), and (C) adenosine 5'-O-(3-thiotriphosphate) (ATP-γ-S).

kept constant at  $25.0 \pm 0.1$  °C by an Isotemp thermostat (Fisher). Reactions were followed under both pseudo-first- and -second-order conditions utilizing excess nucleotides over the platinum complex. For the first-order kinetic curves, the rate constants were evaluated from an iterative nonlinear least-squares fit of absorbance as a function of time according to the equation

$$A = (A_0 - A_\infty)e^{-k_0 t} + A_\infty \quad (1)$$

where  $A_0$ ,  $A$ , and  $A_\infty$  are absorbances at time  $t = 0$ , at time  $t$ , and at infinite time, respectively, and  $k_0$  is the first-order rate constant. For the second-order reactions, eq 2

$$A = A_0 + \frac{k_2[B](A_\infty - A_0)e^{-(k_2[B] - k_2[A])t} - 1}{k_2[B]e^{k_2[B]t} - k_2[A]} \quad (2)$$

was utilized to fit the absorbance-time data. Platinum and nucleotide concentrations are expressed by  $[A]$  and  $[B]$ , and  $k_2$  is the second-order rate constant.

**NMR Measurements.** Nuclear magnetic resonance spectra were obtained on a GE 300-MHz (GN 300) instrument. Proton signals were internally referenced with respect to the H-O-D resonance at 4.67 ppm, and the P-31 signals were referenced with respect to 85%  $H_3PO_4$ . For a typical P-31 experiment, usually a 90° pulse for 25 μs was applied with a delay time interval of 1.0 s. Frequency windows of 4000–10 000 Hz with 8–16 K data

**Table 1.** Rate Data<sup>a</sup> for the Reaction of  $Pt(dien)Cl^+$  with Adenosine Phosphothiorate<sup>b</sup> Nucleotides

thio-nucleotide	[Pt], mM	[Nu], mM	$k_2$ , $M^{-1} s^{-1}$
AMP-S	1.0	4.0	1.7
	2.0	4.0	2.0
	2.0	6.0	1.9
ADP-β-S	2.0	4.0	2.5
	2.0	4.0	2.2
	5.0	15.0	2.6
ATP-γ-S	2.0	4.0	2.7
	2.0	6.0	2.6
	5.0	15.0	2.8

<sup>a</sup> Determined by a nonlinear least-squares computer fit of eq 2.  
<sup>b</sup> At pH 6.8,  $T = 25.0$  °C,  $\mu = 0.50$  M  $NaClO_4$ .

**Table 2.** Rate Data<sup>a</sup> for the Reactions of  $Pt(dien)Cl^+$  with AMP and GMP at 40 °C, pH = 6.8,  $\mu = 0.50$  M ( $NaClO_4$ )

nucleotide	[nucleotide], $\times 10^3$ M	$k_0 \times 10^4$ , $s^{-1}$
AMP	10.0	2.7
	20.0	2.9
	30.0	3.5
GMP	10.0	3.8
	20.0	4.9
	30.0	6.4

<sup>a</sup> Platinum concentrations lie in the range  $(1.0\text{--}2.0) \times 10^{-3}$  M. Nucleotide concentrations were at least 10-fold excess over the platinum complex.

points were selected. Acquisition times lie in the range 200–500 ms, and 500 transients were usually necessary to observe a signal with  $S/N > 10$  using 2.0 mM nucleotide solutions. A line-broadening factor of 2 or 3 Hz was introduced before Fourier transformation. A much longer delay time between pulses was employed to ensure  $>95\%$  relaxation when P-31 resonances were subject to integration. For the proton spectra, smaller pulse widths of 12 μs with a narrower window of 2000 Hz were utilized; 32–64 accumulations were sufficient to generate spectra of  $S/N > 10$  for solutions containing 2.0 mM nucleotides.

The pH of the reaction mixture was adjusted with dilute NaOD and  $DNO_3$  solutions in  $D_2O$ . The pH correction was made by applying the relationship (14)  $pH = pD + 0.4$ , where pD is the pH meter reading in  $D_2O$  solution consisting of 99% deuterium atom.

The  $pK_a$  values of thionucleotide complexes were estimated from the pH-δ profile according to (15)

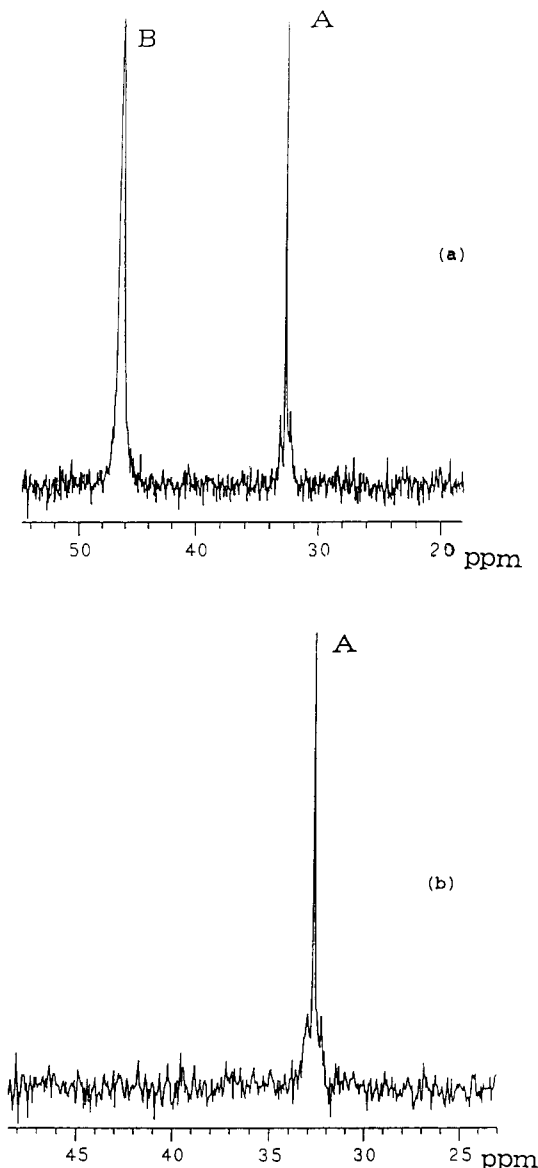
$$\delta = \frac{\delta_1[H_3O^+] + \delta_2 K_a}{K_a + [H_3O^+]} \quad (3)$$

where δ is the observed chemical shift, and  $\delta_1$  and  $\delta_2$  are the chemical shifts of the protonated and deprotonated forms. Equation 3 was derived assuming a monoprotic behavior (15).

## RESULTS

Reactions of  $Pt(dien)Cl^+$  with AMP-S, ADP-β-S, and ATP-γ-S exhibited increases in absorbance at 300 and 260 nm. The absorbance-time traces with 2–3-fold excess of thionucleotides over the platinum complex can be adequately fitted to the second-order rate expression, eq 2. Second-order rate constants (Table 1) for the phosphothiorate reactions with the platinum complex are evaluated to be  $1.9 \pm 0.1 M^{-1} s^{-1}$ ,  $2.4 \pm 0.2 M^{-1} s^{-1}$ , and  $2.7 \pm 0.2 M^{-1} s^{-1}$  for the AMP-S, ADP-β-S, and ATP-γ-S reactions.

Reactions of  $Pt(dien)Cl^+$  with AMP and GMP were carried out under pseudo-first-order conditions utilizing excess nucleotide. First-order rate constants,  $k_0$ , as



**Figure 2.** (a) Proton-decoupled phosphorus-31 NMR (121.5 Mz) spectrum of a reaction mixture containing 4.0 mM [Pt(dien)-Cl]Cl and 6.0 mM AMP-S at pH 6.5 after 10 min of mixing. The signal B is for the free AMP-S and A is for the Platinum(II)-S-AMP complex. (b) Spectrum of the same reaction mixture at equimolar concentration (10 mM each). Note that no unreacted AMP-S remained as evidenced by the complete depletion of the signal B. Platinum-195 satellites are exhibited around A.

functions of [AMP] and [GMP] exhibited a familiar two-term rate law 16

$$k_o = k_a + k_2[\text{Nu}] \quad (4)$$

where [Nu] represents the nucleotide concentration. The value of  $k_a$  obtained for the AMP reaction,  $(2.0 \pm 0.1) \times 10^{-4} \text{ s}^{-1}$ , agrees closely with the same value evaluated for the GMP reaction. The constant,  $k_a$ , can be taken as the rate constant for the equation of the platinum complex. The values of the second-order rate constants ( $k_2$ ) for GMP and AMP reactions,  $(1.5 \pm 0.1) \times 10^{-2} \text{ s}^{-1}$  and  $(6.0 \pm 0.3) \times 10^{-3} \text{ M}^{-1} \text{ s}^{-1}$  were evaluated. Note that the value of  $k_2$  for the GMP reaction is about 2.5 times higher than that of the AMP reaction.

The magnitude of the second-order rate constant for the thionucleotide is about 50 times greater than that for the GMP and AMP reactions. Since  $k_2/[\text{thionucleotide}]$

**Table 3.** Phosphorus-31 Chemical Shifts for the Pt(dien) (AMP-S) Complex as a Function of pH

pH	chemical shift of the complex, ppm	coordination chemical shift, <sup>a</sup> ppm
1.04	40.85	-19.04
1.10	40.68	-18.40
1.30	40.44	-17.71
1.70	40.05	-17.09
2.08	37.45	-17.63
2.96	33.43	-20.72
4.30	32.64	-19.60
5.79	32.70	-15.10
6.23	32.70	-13.70
7.34	32.71	-13.30 <sup>b</sup>
9.14	32.17	-13.30 <sup>b</sup>

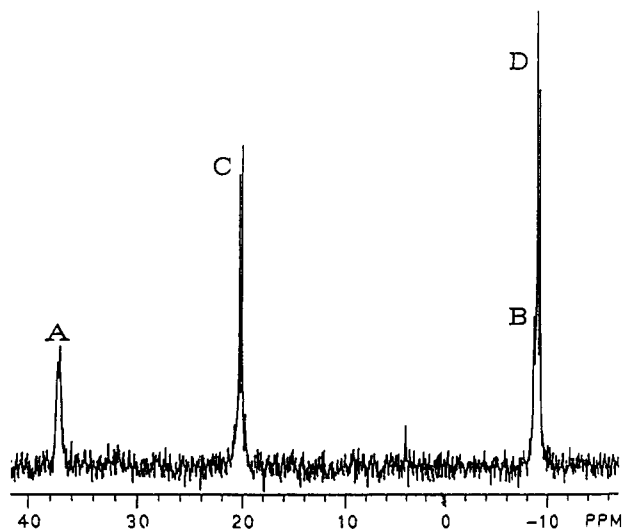
<sup>a</sup> Coordination chemical shift =  $\delta_{\text{complex}} - \delta_{\text{free ligand}}$ . <sup>b</sup> Free ligand appeared as a broad signal.

at its lowest concentration is greater than  $k_a$  by a factor of 30, inclusion of a parallel first-order path contributes insignificantly to the data-fitting procedure outlined earlier.

Products were characterized by proton and phosphorus-31 NMR spectroscopy. The proton NMR spectrum of GMP exhibits a signal at 8.02 ppm for the H(8) of the purine ring. When the reaction of Pt(dien)Cl<sup>+</sup> with GMP was followed at various time intervals, a new signal at 8.56 ppm grew initially at the expense of the peak at 8.02 ppm and then leveled off after 6 h. This new signal at 8.56 ppm is taken as evidence of GMP coordination through N7 of the purine ring (17). Similarly, AMP complexation is accompanied by the appearance of a new resonance at 8.76 ppm for the H(8) of the coordinated AMP molecule at the expense of the H(8) resonance of free AMP at 8.15 ppm.

The reactions of phosphothiorate were essentially over in the time required to mix the reactants, place samples in the NMR tube, and record spectra. Free AMP-S exhibits a P-31 resonance at 46.40 ppm at pH 6.63 (Figure 2a). When 10.0 mM Pt(dien)Cl<sup>+</sup> was mixed with equal concentration of the phosphothiorate, a new signal at 32.70 ppm appeared, and no unreacted nucleotide was observed by P-31 spectroscopy (Figure 2b). When a 2–3-fold excess of nucleotide over the platinum complex was employed, no additional resonances for the product other than the one at 32.70 ppm were observed (Figure 2a). Furthermore, integrated peak areas indicate that the reaction essentially follows 1:1 stoichiometry. The proton NMR spectra recorded at regular time intervals did not exhibit any alteration of the H(8) signal. No changes in chemical shifts of ribose protons were apparent during the reactions. Furthermore, a direct coordination through the phosphate oxygen in a monodentate fashion can be ruled out since such a coordination is accompanied by a 4–10 ppm downfield shift of the P atom of the coordinated phosphate group (18). Proton and phosphorus NMR data indicate that nitrogen atoms of the purines are not involved in coordination. The signal at 32.70 ppm can be attributed to the Pt(dien)-S-AMP complex in which the nucleotide is coordinated through the sulfur atom. The chemical shift of the P-31 resonance of Pt(dien)-S-AMP complex decreases with pH up to pH 5 but levels off above pH 5. These data were utilized to estimate the  $K_a$  value of the complex by using eq 3. The pH chemical shift data are shown in Table III.

Figure 3 shows the P-31 spectrum recorded for ADP- $\beta$ -S (6 mM) and Pt(dien)Cl<sup>+</sup> (5 mM) 10 min after mixing. Two doublets, A and B, at 37.8 and -8.6 ppm are for the  $\beta$ - and  $\alpha$ -phosphorus atoms of the unreacted nucleotide, and C and D at 20.23 and -9.09 ppm are the corresponding



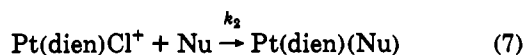
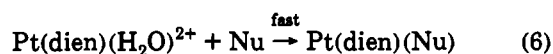
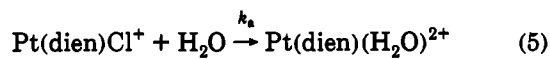
**Figure 3.** Proton-decoupled 121.5-MHz phosphorus-31 spectrum of [Pt(dien)Cl]Cl (5.0 mM) and ADP- $\beta$ -S (6.0 mM) reaction mixture at pH 6.5. Doublets A and B are for the free ligands, and C and D are for the Pt(II)-S-ADP complex.

doublets for the complex. Like the AMP-S system, coordination through the sulfur atom has shifted the resonance of the  $\beta$ -phosphorus atom about 17 ppm upfield. Very little change in the chemical shift of  $\alpha$ -phosphorus atom is observed since this phosphate group did not coordinate the platinum and was virtually unaffected by the  $\beta$ -phosphothiorate coordination. We were unable to determine the pH-chemical shift profile for this complex owing to the precipitation at pH < 4 due to its limited solubility.

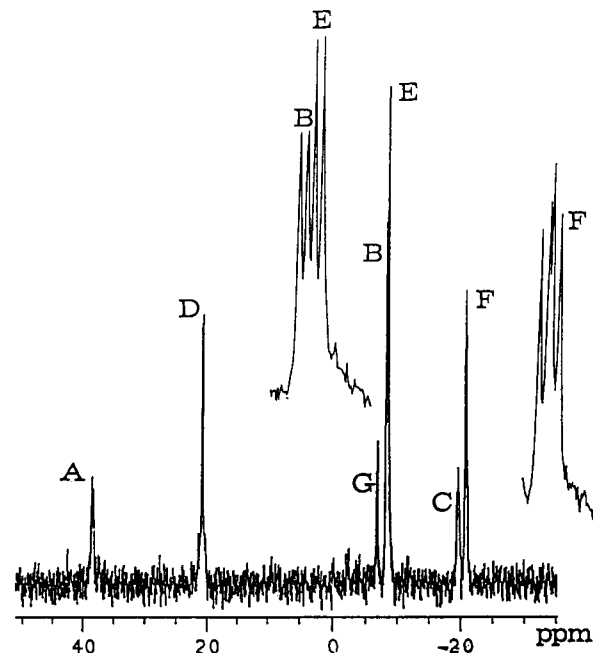
The reaction of ATP- $\gamma$ -S also afforded a complex in which the sulfur atom of the phosphothiorate group is coordinated to platinum(II) as evidenced by P-31 NMR data (Figure 4). Free ATP- $\gamma$ -S exhibits two doublets at 37.57 and -8.08 ppm for the  $\gamma$ - and  $\alpha$ -phosphorus atoms at pH 7.0. The  $\beta$ -phosphorus atom shows doublet of doublets centered at -19.43 ppm due to the coupling with both  $\alpha$ - and  $\gamma$ -phosphorus atoms. As for the AMP-S and ADP- $\beta$ -S reactions with Pt(dien)Cl<sup>+</sup>, the signals for the coordinated  $\gamma$ -phosphorus atom shifted 18 ppm upfield to 20 ppm. The  $\alpha$ - and  $\beta$ -phosphorus atoms show about 1 ppm upfield shift as well.

## DISCUSSION

The complexations of AMP and GMP with Pt(dien)Cl<sup>+</sup> follow the familiar two-term rate law (eq 4), consistent with a sequence of reactions shown in eqs 5-7:



The value of  $k_a$  was determined to be  $(2.0 \pm 0.1) \times 10^{-4} \text{ s}^{-1}$  for both the AMP and GMP reactions at 40 °C. This value can be compared with  $5 \times 10^{-5} \text{ s}^{-1}$  at 25 °C reported by Belluco et al. (16). The magnitude of  $k_2$  for the GMP reaction is about 2.5 times larger than that for the AMP reaction which is consistent with the established kinetic preference toward guanine bases in DNA binding to platinum(II) (17).



**Figure 4.** Proton-decoupled 121.5-MHz phosphorus-31 NMR spectrum of [Pt(dien)Cl]Cl (5.0 mM) and ATP- $\gamma$ -S (6.0 mM) reaction mixture at pH 6.5. Peaks A, B, and C are for the  $\gamma$ -,  $\alpha$ -, and  $\beta$ -phosphorus atoms of free ligand. Doublets D and E and doublet of doublets F are for the  $\gamma$ -,  $\alpha$ -, and  $\beta$ -phosphorus atoms of ATP- $\gamma$ -S bound to platinum(II). Note that Pt-195 satellites are barely visible near the base of peak D. Peak G is due to an unidentified hydrolyzed product. The inset exhibits the expansion of signals abbreviated by B and E.

In principle, phosphothiorate complexation should follow the same reactions as shown in eqs 5-7. However, these complexes are formed mainly through the direct reactions with the chloro complex. The contribution from the aquated pathway is insignificant, as can be judged by comparing the relative magnitudes of  $k_a$  and  $k_2$ . The values of  $k_2$  for all phosphothiorates lie in the range  $1.9\text{--}2.7 \text{ M}^{-1} \text{ s}^{-1}$ . These values are close to those found for the cysteine and glutathione reactions with the same platinum(II) complex (19). It is interesting to note that the value of  $k_2$  is largest for ATP- $\gamma$ -S complexation. This relatively higher reactivity may be associated with a higher nucleophilicity of the phosphothiorate group in the ATP- $\gamma$ -S due to significant deprotonation of the triphosphate moiety. Reactions at lower acidities would have helped us to understand how deprotonated oxygens modulate the reactivity of the phosphothiorate group. Unfortunately, precipitation of the (phosphothiorato)platinum complexes at lower pH prevented us from establishing a pH-rate profile. All phosphothiorate complexes exhibited 15-20 ppm upfield chemical shifts compared to free nucleotides. This upfield shift of the coordinated phosphothiorate group may be due to the  $d\pi\text{--}d\pi \text{ Pt} \rightarrow \text{S}$  backbonding which in turn enriches the electron density around the phosphorus atom. There were no significant changes in the chemical shift of purine or ribose protons upon complexation with Pt(II). This is primarily due to the fact that remote phosphothionate coordination has little or no influence to the electronic environment of these protons.

In conclusion, the present study establishes that platinum(II) exclusively coordinates to the phosphothiorate group of thionucleotides even when purine nitrogens are available for coordination. This selectivity toward phosphothiorate groups can be exploited in elucidating mechanisms of intramolecular hydroxyl transfer reactions by



utilizing platinum(II) complexes that offer coordinated water molecules adjacent to the Pt-S bond.

#### ACKNOWLEDGMENT

Funding of this research in part through the Biomedical Research Support Grant (NIH) is gratefully acknowledged. We also thank Prof. Roger Gregory for reading the manuscript and making valuable suggestion and Johnson Matthey, Inc., for the generous loan of  $K_2PtCl_4$ .

#### LITERATURE CITED

- (1) Mertes, M. P., and Mertes, K. B. (1990) *Acc. Chem. Res.* 23, 413.
- (2) Cornelius, R. D., and Cleland, W. W. (1978) *Biochemistry* 17, 3279. Norman, P. R., and Cornelius, R. D. (1982) *J. Am. Chem. Soc.* 104, 2356.
- (3) Masoud, S. S., and Milburn, R. M. (1990) *J. Inorg. Biochem.* 39, 337-49.
- (4) Hendry, P., and Sargson, A. M. (1990) *Inorg. Chem.* 29, 97-104; (1990) *In Progress in Inorganic Chemistry* (S. J. Lippard, Ed.) Wiley, New York.
- (5) Kramer, P., and Nowak, T. J. (1988) *Inorg. Biochem.* 32, 135.
- (6) Kim, J. H., and Chin, J. (1992) *J. Am. Chem. Soc.* 29, 97-104.
- (7) Lu, Z., Shorter, A. L., Lin, I., and Duhaway-Mariano, D. (1988) *Inorg. Chem.* 27, 4135.
- (8) Bose, R. N., Viola, R. E., and Cornelius, R. D. (1984) *Inorg. Chem.* 23, 1181; (1985) 24, 4403.
- (9) Burgeson, E. E., and Kostic, N. M. (1991) *Inorg. Chem.* 30, 4299.
- (10) Strothkamp, K. G., and Lippard, S. J. (1976) *Proc. Natl. Acad. Sci. U.S.A.* 2536-2540.
- (11) Szalda, S. J., Eckstein, F., Sternbach, H., and Lippard, S. J. (1979) *J. Inorg. Biochem.* 11, 279-282.
- (12) Chu, B. C. F., and Orgel, L. E. (1992) *Nucleic Acid. Res.* 20, 2497-2502; (1990) *DNA Cell Biol.* 9, 70-76.
- (13) Mahal, G., and Van Eldik, R. (1987) *Inorg. Chim Acta* 127, 203-208.
- (14) Glasoe, P. K., and Long, F. A. (1960) *J. Phys. Chem.* 64, 118.
- (15) Slavin, L. L., and Bose, R. N. (1990) *J. Inorg. Biochem.* 40, 339-347.
- (16) Belluco, U., Cattalini, L., Basolo, F., Pearson, R. G., and Turco, A. (1965) *J. Am. Chem. Soc.* 87, 241.
- (17) See, for example: Sherman, S. E., and Lippard, S. J. (1987) *Chem. Rev.* 87, 1153.
- (18) Bose, R. N., Slavin, L. L., Cameron, J. W., Luellen, D. L., and Viola, R. E. (1993) *Inorg. Chem.* 32, 1795. Slavin, L. L., Bose, R. N. (1990) *J. Chem. Soc., Chem. Commun.* 1256. Bose, R. N., Viola, R. E., and Cornelius, R. D. (1984) *J. Am. Chem. Soc.* 106, 3336.
- (19) Moghaddas, S., Cox, E. H., and Bose, R. N. (1994) *Inorg. Chem.* (submitted).

# Mutations of Two Lysine Residues in the CDR Loops of a Recombinant Immunotoxin That Reduce Its Sensitivity to Chemical Derivatization

Itai Benhar, Ulrich Brinkmann, Keith O. Webber, and Ira Pastan\*

Laboratory of Molecular Biology, Division of Cancer Biology, Diagnosis and Centers, National Cancer Institute, National Institutes of Health, 9000 Rockville Pike, Building 37, Room 4E16, Bethesda, Maryland 20892. Received January 18, 1994\*

B3(Fv)-PE38 is a recombinant single-chain immunotoxin in which the Fv region of monoclonal antibody B3 is connected to a truncated form of *Pseudomonas* exotoxin. It would be desirable to use the lysine residues of the molecule for chemical modification so that it can be derivatized with poly(ethylene glycol) to achieve reduced immunogenicity or with the Bolton-Hunter reagent for biodistribution studies. We found that derivatizing lysine residues of B3(Fv)-PE38 causes a marked loss of specific target cell cytotoxicity and/or immunoreactivity. Here we show that two lysine residues in the antibody-combining region of B3(Fv)-PE38 can be replaced with arginines, with only a small loss of cytotoxicity and no change in specificity. This mutant molecule is 3-fold more resistant to inactivation by derivatization with succinimidyl 4-(*N*-maleimidomethyl)cyclohexane 1-carboxylate (SMCC) or Bolton-Hunter reagent.

## INTRODUCTION

B3(Fv)-PE38 is a recombinant single-chain immunotoxin composed of the variable regions from the heavy and light chains of the B3 monoclonal antibody connected by a flexible peptide linker and joined to a truncated form of *Pseudomonas* exotoxin A (1). B3(Fv)-immunotoxins bind to a carcinoma-associated carbohydrate antigen present on many human breast, colon, gastric, lung, and other carcinomas and specifically kill carcinoma cells *in vitro* and cause complete regression of tumor xenografts in athymic mice. Thus, they are potential agents for cancer therapy in humans (2). To improve these immunotoxins for future therapeutic applications, we plan to modify B3(Fv)-PE38 by attaching poly(ethylene glycol) (PEG)<sup>1</sup> to reduce its immunogenicity and to prolong its survival in the circulation. Attachment of PEG commonly targets the  $\alpha$  amino group of the lysines either directly, using activated PEG, or following chemical modification of the lysine with a heterobifunctional reagent. We have found that directly coupling PEG onto B3(Fv)-PE38, or modifying B3(Fv)-PE38 with the heterobifunctional reagent SMCC for subsequent PEGylation, resulted in the inactivation of the immunotoxin. We observed a similar inactivation when we attempted to label B3(Fv)-PE38 with radioactive Bolton-Hunter reagent for biodistribution assays. These results suggest that chemical modification of some of the lysine residues in B3(Fv)-PE38 with large molecules such as PEG (MW 6000) or even with small molecules such as SMCC or Bolton-Hunter reagent (MW 380) may be deleterious to one or more of its biological functions. There are 14 lysine residues in B3(Fv)-PE38; three of these are in the C-terminus of PE38, and 11 are in the B3(Fv) portion of which two are in the binding region of B3(Fv). One is in CDR2 of V<sub>H</sub>, and the other is in CDR2 of V<sub>L</sub>. Both of these lysines are probably

exposed on the surface of the protein and therefore are good targets for chemical derivatization. Modification of these lysines in the binding region could account for the loss of binding and activity of B3(Fv)-immunotoxins either because the lysines directly contribute to antigen binding or because such a modified lysine interferes with antigen binding in another part of the binding cleft. Also, lysines in the toxin moiety of the immunotoxin, particularly near or at the C-terminus, might cause reduced immunotoxin activity if they become modified. This paper evaluates these possibilities by making mutant immunotoxins in which the lysines in PE are mutated to glutamines and/or the Fv CDR lysines are mutated to arginines.

## EXPERIMENTAL PROCEDURES

**Materials.** Succinimidyl 4-(*N*-maleimidomethyl)cyclohexane-1-carboxylate (SMCC) was obtained from Pierce (Rockford, IL). Oligodeoxynucleotides were obtained from BioServe Biotechnologies (Laurel, MD). Other reagents were obtained from standard sources.

**Construction of Plasmids for Expression of B3(Fv)-PE38 Derivatives.** Plasmid pULI7 encodes the parental B3(Fv)-PE38 single-chain immunotoxin. The schematic structure of pULI7 and the amino acid sequence of B3(Fv)-PE38 are described in Figure 1. Lysine codons that were mutated in this work are in boldface in Figure 1B, with the replacing residues indicated below them. All the plasmids encoding B3(Fv)-PE38 derivatives were obtained either by site-specific mutagenesis according to Kunkel (3) using single-stranded pULI7 DNA as template or by subcloning (4). All the mutations were confirmed by DNA dideoxy sequencing (5). In plasmid pULI26, lysine codon 66 in V<sub>H</sub> CDR2 and lysine codon 190 in V<sub>L</sub> CDR2 were changed to arginine codons. The encoded protein is named B3(Fv)-PE38RR. In plasmid pULI14, PE38 lysine codons 575 and 591 were mutated to glutamine codons, and the 3' end lysine codon 598 was mutated to an amber (TAG) stop codon. The encoded protein is named B3(Fv)-PE38QQ $\Delta$ . Plasmid pITA27 carries the Fv CDR lysine to arginine mutation derived from pULI26 and the PE38 lysine to glutamine mutations and 3' end lysine-stop codon mutation derived from pULI14. The protein it encodes

\* To whom all correspondence should be sent. Phone (301) 496-4797, fax (301) 402-1344.

\* Abstract published in *Advance ACS Abstracts*, June 1, 1994.

<sup>1</sup> Abbreviations: CDR, complementarity determining region; SMCC, succinimidyl 4-(*N*-maleimidomethyl)cyclohexane-1-carboxylate; PE, *Pseudomonas* exotoxin A; PEG, poly(ethylene glycol); BES, [*N,N*-bis(2-hydroxyethyl)-2-amino]ethanesulfonic acid; BSA, bovine serum albumin.

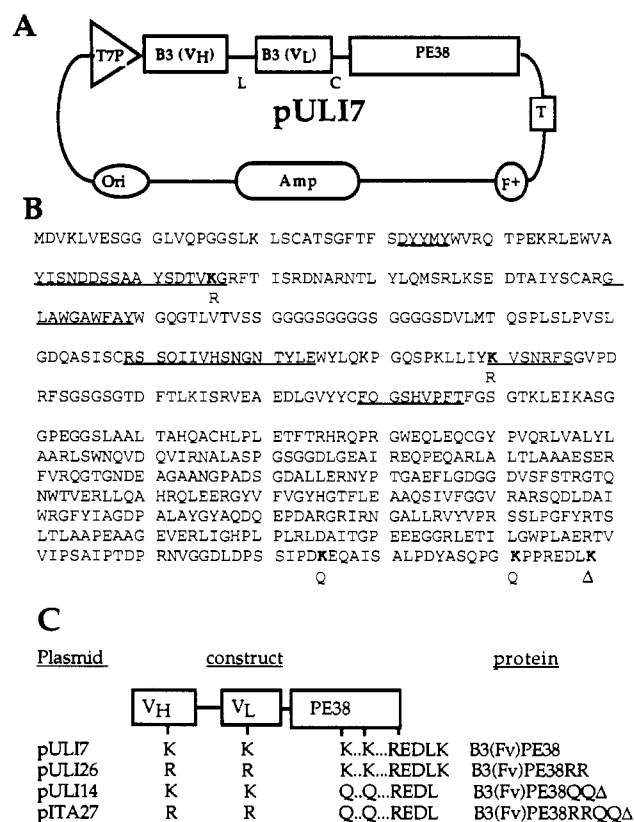
is named B3(Fv)-PE38RRQQΔ. A scheme of the plasmids and their respective encoded proteins is given in Figure 1C.

**Expression and Purification of Recombinant Proteins.** Expression plasmids encoding B3(Fv)-PE38 or its mutated derivatives were introduced into *E. coli* strain BL21 (λDE3) (6) by transformation, and the recombinant proteins were expressed as inclusion bodies as described (1). The single-chain immunotoxins were obtained by solubilization and refolding of inclusion body protein as described (8). Properly refolded proteins were separated from contaminating proteins and aggregates by ion-exchange chromatography on Mono Q (Pharmacia) followed by size exclusion chromatography on a TSK G3000SW (TosoHaas) column.

**Derivatization of Immunotoxins.** Purified immunotoxins stored in phosphate-buffered saline were derivatized with a 30-fold molar excess of SMCC for 1 h at 25 °C. Typically, 200 μg of protein was mixed with 30 μg of SMCC (Pierce) in a 1-mL reaction. Following derivatization, the immunotoxins were desalted, and aggregates were removed by size exclusion chromatography on a TSK G3000SW (TosoHaas) column. Fractions containing monomeric immunotoxin were pooled and used for further analysis. To estimate the number of derivatized residues per toxin molecule, aliquots of the SMCC-derivatized proteins were reduced with a 30-fold molar excess of 2-mercapto ethanol for 60 min at 37 °C, which was followed by determination of free sulfhydryl using Ellman's reagent (Pierce) (9).

**Antigen Binding and Cytotoxicity of Recombinant Immunotoxins.** Relative binding affinities of the immunotoxins were determined by competition against [<sup>125</sup>I]-labeled B3 IgG for binding to A431 adenocarcinoma cells at 4 °C. Cells [in RPMI media (GIBCO) supplemented with 5% fetal calf serum] were plated at 1 × 10<sup>5</sup> cells/well in 24-well plates on the day prior to assay. Cells were washed with RPMI, 1% BSA, 50 mM BES, pH 7.0 and then blocked with 5% BSA in RPMI, 50 mM BES, pH 7.0 for 30 min. After the blocking solution was washed off, competitors and labeled tracer (0.01 μCi, 10 fmol labeled with moniodo [<sup>125</sup>I]-Bolton-Hunter reagent (New England Nuclear, Boston, MA) were added in a total volume of 100 μL and rocked gently for 2 h at 4 °C. Unbound tracer was removed by washing the cells twice with RPMI/BSA/BES. Cells were lysed with 0.5% SDS in 10 mM Tris-HCl, 1 mM EDTA, pH 8.0, and the total lysate was counted in a Beckman Model 5500B γ counter. The cytotoxic activities of B3(Fv)-PE38 and mutated derivatives were tested by determination of their ability to inhibit protein synthesis in cultured cells as described (1).

**Immunoreactivity of [<sup>125</sup>I]-Labeled Immunotoxins.** The immunoreactivity of [<sup>125</sup>I]-labeled B3(Fv)-PE38 and B3(Fv)-PE38RRQQΔ were tested by binding to A431 adenocarcinoma cells at 4 °C. Cells [in RPMI media (GIBCO) supplemented with 5% fetal calf serum] were plated at 2 × 10<sup>4</sup>, 5 × 10<sup>4</sup>, 1 × 10<sup>5</sup>, 2 × 10<sup>5</sup>, 5 × 10<sup>5</sup>, 7.5 × 10<sup>5</sup>, and 10<sup>6</sup> cells/well in six-well plates on the day prior to assay. Cells were washed with RPMI, 1% BSA, 50 mM BES, pH 7.0 and then blocked with 5% BSA in RPMI, 50 mM BES, pH 7.0 for 30 min. After the blocking solution was washed off, labeled immunotoxins (0.01 μCi, 3.3 fmol) labeled with moniodo [<sup>125</sup>I]-Bolton-Hunter reagent (New England Nuclear, Boston, MA) according to the suppliers' recommendations were added in a total volume of 250 μL and rocked gently for 2 h at 4 °C. Unbound immunotoxin was removed by washing the cells twice with RPMI/BSA/BES. Cells were lysed with 0.5% SDS in 10 mM Tris-

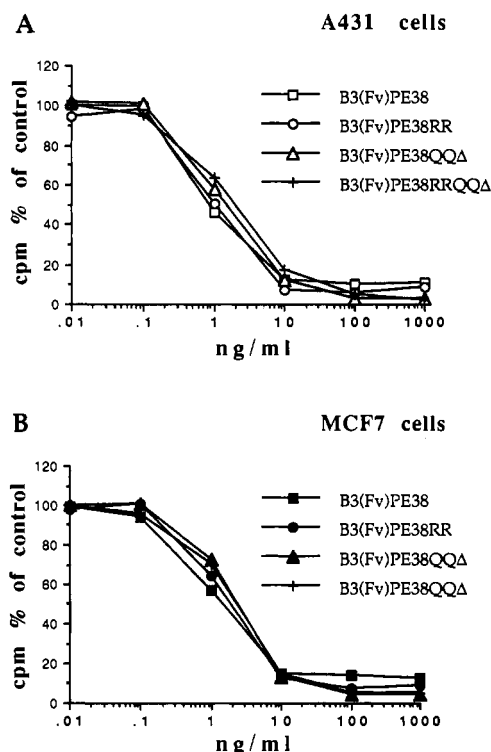


**Figure 1.** Expression of B3(Fv)-PE38. (A) The expression plasmid pULI7 was derived from pULI9 (10) by replacing the 3' end sequence encoding the KDEL C-terminus with a sequence encoding the wild-type C-terminus of PE, REDLK. T7P is a T7 promoter, L is the (gly4ser)×3 linker, C is the C3 connector, T is a transcription terminator, and F+ is a filamentous phage origin of replication. (B) Amino acid sequence of B3(Fv)-PE38. The Fv sequence is double spaced and the PE38 sequence is single spaced. The six CDRs are underlined. Lysines that were mutated in this study are in bold type with the replacing residue indicated below them. (C) Scheme showing the plasmids and their respective encoded B3(Fv)-PE38 derivatives used; shown are the positions of the mutated residues and the corresponding replacing residues.

HCl, 1 mM EDTA, pH 8.0, and the total lysate was counted in a Beckman Model 5500B γ counter.

## RESULTS

**Plasmid Construction and Production of Mutated Derivatives of B3(Fv)-PE38.** The parental plasmid, pULI7 (Figure 1A), encodes B3(Fv)-PE38 (Figure 1B), a single-chain immunotoxin composed of the B3 heavy-chain variable domain linked via a (Gly4Ser)<sub>3</sub> peptide linker to the B3 light-chain variable domain, which is fused through a C3 connector to PE38, a truncated form of *Pseudomonas* exotoxin. B3(Fv)-PE38 is almost identical to B3(Fv)-PE38KDEL (1), except that the carboxyl terminus ends with the REDLK (the wild-type *Pseudomonas* exotoxin carboxyl terminus) instead of the mutant KDEL sequence. It has a molecular weight of 63 kDa and contains 598 amino acids. Other plasmids used in this study are all pULI7 derivatives (Figure 1C). In pULI26, V<sub>H</sub> CDR2 lysine codon 66 (Figure 1B, line 2, in boldface) and V<sub>L</sub> CDR2 lysine codon 190 (Figure 1B, line 4, in boldface) were mutated to arginine codons. Arginine was chosen as the replacing amino acid in order to maintain the charge of the molecule. In pULI14, PE38 lysine codons 575 and 591 (Figure 1B bottom line in boldface) were mutated to glutamine codons, and the 3' end lysine codon 598 (codon 613 in native PE) was mutated to an amber (TAG) stop codon. This



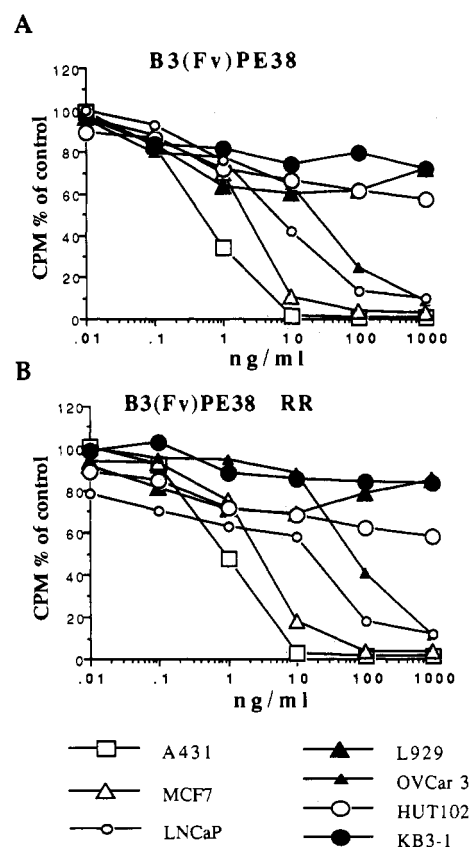
**Figure 2.** Cytotoxicity of B3(Fv)-PE38 and its mutants toward two B3 antigen-positive human carcinoma cell lines: (A) A431, (B) MCF7. Assays were performed as described in the Experimental Procedures.

combination of carboxyl-terminal replacements was previously shown by Chaudhary *et al.* (7) to preserve the cytotoxic activity of *Pseudomonas* exotoxin. Plasmid pTA27 carries the mutations of both pULI26 and pULI14 and thus has no lysine in the PE portion and the two CDR lysines of the Fv mutated to arginines.

Cultures of BL21(λDE3) (6) transformed with each plasmid were used to produce immunotoxins. Following IPTG induction, the overproduced proteins accumulated in inclusion bodies. These were isolated, and the recombinant protein was solubilized, reduced, and refolded as previously described (8). Active immunotoxins were recovered from the refolded proteins by ion exchange and size exclusion chromatography, as described in the Experimental Procedures.

**Specific Binding and Specific Cytotoxicity of B3(Fv)-PE38 and B3(Fv)-PE38RR.** The cytotoxic activity of B3(Fv)-PE38 and of its mutated derivatives was measured by incubation of various human carcinoma cell lines with serial dilutions of the immunotoxin in PBS containing 0.2% BSA and measuring the incorporation of [<sup>3</sup>H]leucine as previously described (10). As shown in Figure 2, B3(Fv)-PE38 has an IC<sub>50</sub> of 1.0 ng/mL on A431 cells and 1.2 ng/mL on MCF7 cells. Both are B3 antigen expressing cells. The mutant B3(Fv)-PE38RR had the same cytotoxic activity on these cells. B3(Fv)-PE38QQΔ and B3(Fv)-PE38RRQQΔ appear to have slightly lower cytotoxicities than B3(Fv)-PE38. B3(Fv)-PE38QQΔ and B3(Fv)-PE38RRQQΔ have cytotoxicities similar to each other.

To test whether mutating CDR residues caused a change in specificity, the same assays were done on additional cell lines. As shown in Figure 3 and Table 1, both B3(Fv)-PE38 and B3(Fv)-PE38RR had the same spectrum of recognition and cytotoxicity against the cell lines used. These cell lines differ in their level of B3 antigen expression (11). This result indicates that the antigen-binding



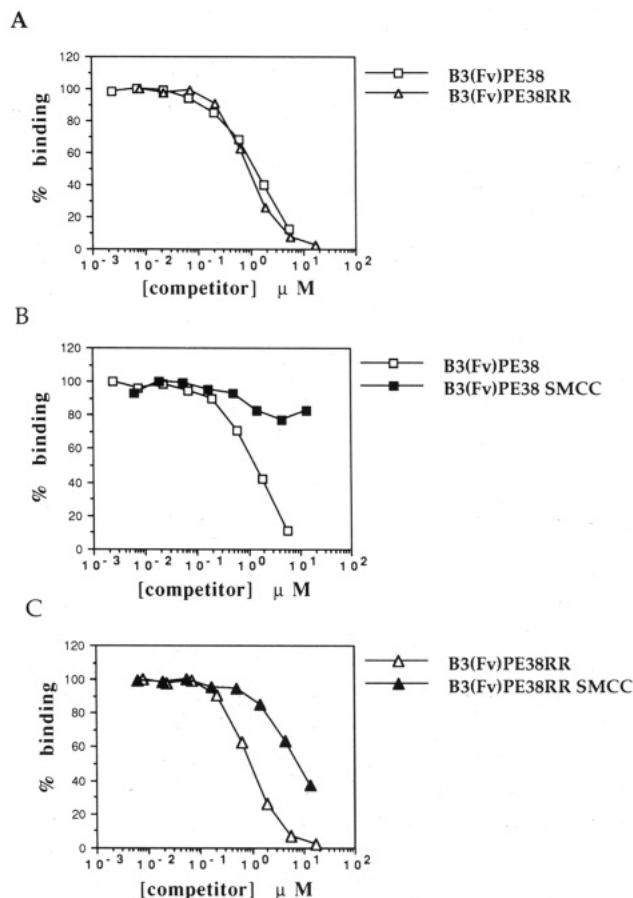
**Figure 3.** Specific cytotoxicity of B3(Fv)-PE38 and B3(Fv)-PE38RR towards different cell lines (see Table 1). The cytotoxicity of B3(Fv)-PE38 (A) or B3(Fv)-PE38RR (B) was tested on B3 antigen strongly positive (A431, MCF7), weakly positive (LNCaP), or negative (OVCAR3, KB3-1, HUT102, and L929) cell lines.

**Table 1. Cytotoxicity of Recombinant B3(Fv) Immunotoxins toward Various Cell Lines**

cell line <sup>b</sup>	B3 antigen source	expression	cytotoxicity IC <sub>50</sub> <sup>a</sup> ng/mL	
			B3(Fv)-PE38	B3(Fv)-PE38RR
A431	epidermoid carcinoma	+++	0.6	0.9
MCF7	breast carcinoma	+++	2.0	2.9
LnCap	prostate carcinoma	+	8.0	17.0
OVCAR3	ovarian carcinoma	-	24.0	70.0
KB 3-1	cervical carcinoma	-	>1000	>1000
HUT102	T-cell leukemia	-	>1000	>1000
L929	mouse fibroblast	-	>1000	>1000

<sup>a</sup> Cytotoxicity data are given as IC<sub>50</sub> values, the concentration of immunotoxin that causes a 50% inhibition of protein synthesis following its incubation on the cells for 16 h. Expression level estimation of the B3 antigen is based on immunofluorescence: +++, strong; +, weak; -, not detected. <sup>b</sup> All the cell lines except L929 are of human origin.

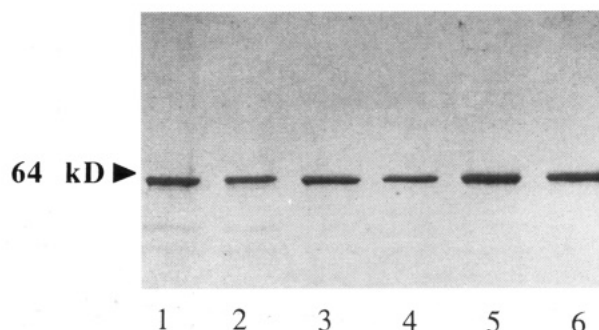
specificity of the B3(Fv) was not altered by mutating the CDR lysines to arginines. The specific antigen binding of B3(Fv) immunotoxins was further analyzed by determination of the binding affinity of B3(Fv)-PE38 or B3(Fv)-PE38RR to the B3 antigen by a competition assay in which increasing concentrations of either immunotoxin were used to compete out binding of iodinated B3 IgG to A431 cells at 4 °C. As shown in Figure 4A, both B3(Fv)-PE38 and B3(Fv)-PE38RR competed for the binding of [<sup>125</sup>I]-B3 antibody to A431 cells by 50% at about 1.1 μM. This result implies that the antigen-binding affinities of the two Fv parts of the two immunotoxins are similar and that antigen binding is not impaired by the lysine to arginine CDR mutations.



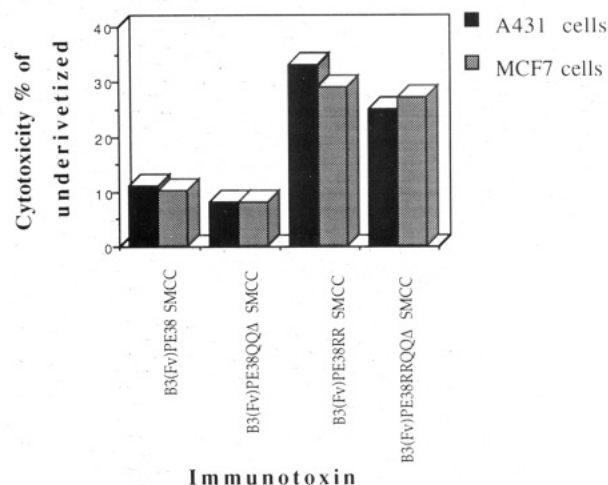
**Figure 4.** Inhibition of B3 IgG binding to antigen positive A431 cells by competing immunotoxins. Iodinated B3 IgG was bound to cells in the presence of varying concentrations of competitors as described in the Experimental Procedures. (A) Competition with B3(Fv)-PE38 or B3(Fv)-PE38RR. (B) Competition with unmodified or SMCC-modified B3(Fv)-PE38. (C) Competition with unmodified or SMCC-modified B3(Fv)-PE38RR.

**Activities of SMCC Derivatized Immunotoxins.** To determine the effect of modifying lysine residues and other amino groups on activity, the B3(Fv)-PE38 immunotoxins were derivatized with a 30-fold molar excess of SMCC as described in the Experimental Procedures. This ratio was chosen to achieve a 2–3 SMCC to 1 lysine ratio because using a lower ratio (i.e., 10–15-fold) resulted in a low level of derivatization and lower inactivation of the immunotoxins. For example, using 5-fold SMCC over protein to modify B3(Fv)-PE38 resulted in derivatization of two to three lysines and 3-fold loss in cytotoxicity. The mutant B3(Fv)-PE38RR was not inactivated at all at that level (data not shown). Thus, 6–10 residues per protein molecule were modified when a 30-fold molar excess of SMCC over protein was used (data not shown). Derivatization with SMCC resulted in a moderate amount of aggregation (5–10% of the protein). Such aggregates form when B3(Fv)-PE38 immunotoxins are incubated at 37 °C in buffers of low ionic strength. These were removed by size exclusion chromatography. Fractions containing monomeric proteins were pooled and used for further analyses. The recovery of monomer was 80–90% of the input protein. As shown in Figure 5, nonreducing SDS-PAGE shows that pure monomers were obtained.

Samples from SMCC-derivatized proteins were tested for cytotoxic activity as described above. Underivatized proteins were subjected to the same treatment, excluding the SMCC, and were tested in parallel. The results are presented in Figure 6. Derivatized B3(Fv)-PE38 and B3(Fv)-PE38RR retained 8–10% of their cytotoxic



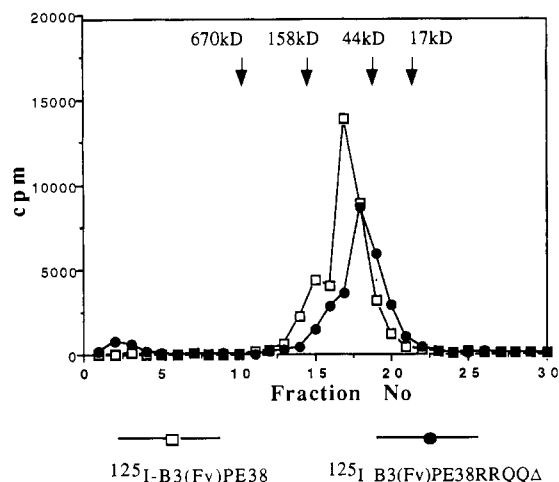
**Figure 5.** SDS-PAGE of SMCC derivatized B3(Fv)-PE38 derivatives. B3(Fv)-PE38, B3(Fv)-PE38RR, and B3(Fv)-PE38RRRQQA were derivatized with a 30-fold molar excess of SMCC, as described in the Experimental Procedures. Following derivatization, both unmodified and modified proteins were subjected to size exclusion chromatography to isolate the monomer fraction. Since improperly refolded B3(Fv) immunotoxins have a strong tendency to aggregate (7), monomers obtained by size exclusion are predominantly of the correct active conformation. Lane 1: B3(Fv)-PE38. Lane 2: B3(Fv)-PE38-SMCC. Lane 3: B3(Fv)-PE38RR. Lane 4: B3(Fv)-PE38RR-SMCC. Lane 5: B3(Fv)-PE38RRRQQA. Lane 6: B3(Fv)-PE38RRRQQA-SMCC.



**Figure 6.** Effect of SMCC derivatization on the cytotoxicity of B3(Fv)-PE38 and its mutated derivatives. Immunotoxins were treated with a 30-fold molar excess of SMCC and purified as described in Experimental Procedures. The cytotoxicities of the derivatized immunotoxins were compared to their respective activities in the unmodified form.

activity relative to their corresponding underivatized proteins. In contrast, B3(Fv)-PE38RR and B3(Fv)-PE38RRRQQA retained 30–40% of their cytotoxic activity relative to their corresponding underivatized proteins. In another experiment, immunotoxins were incubated with a 30-fold molar excess of 2-mercaptoethanol following SMCC derivatization. This was done in order to block the reactive groups introduced by SMCC onto the immunotoxins, thereby preventing them from making non-specific interactions with media components or cells. However, there was no difference in the activity of the SMCC-derivatized immunotoxins with or without the subsequent 2-mercaptoethanol treatment.

**SMCC Derivatization Causes a Loss of Antigen Binding, but Not Specificity.** B3(Fv)-PE38 and B3(Fv)-PE38RR, both underivatized or derivatized with a 30-fold molar excess of SMCC as described above, were also tested for binding in competition assays. As shown in Figure 4B, SMCC derivatization caused a loss of more than 100-fold in antigen binding by B3(Fv)-PE38. However, as shown in Figure 4C, the loss in antigen binding



**Figure 7.** Profile of TSK G3000SW chromatography of Bolton-Hunter labeled immunotoxins. Labeled immunotoxins were mixed with gel-filtration molecular weight standards (Bio-Rad), whose sizes and elution positions are indicated above the chromatograms.

of B3(Fv)-PE38RR was about 8-fold. SMCC-derivatized B3(Fv)-PE38RR was also tested for specificity by cytotoxic assays on cell lines which differ in their sensitivity to B3(Fv)-PE38 due to different levels (high to none) of the B3 antigen. B3(Fv)-PE38RR and SMCC-derivatized B3(Fv)-PE38RR had the same spectrum of activity on the various cell lines used (data not shown).

**Immunoreactivity of Bolton-Hunter Labeled Immunotoxins.** To determine the effect of modifying B3(Fv)-PE38 lysine residues with the Bolton-Hunter reagent on immunoreactivity, B3(Fv)-PE38 and B3(Fv)-PE38RRQQΔ were labeled with the Bolton-Hunter reagent as described in the Experimental Procedures. Like SMCC, Bolton-Hunter reagent targets amino groups. Aliquots of labeled immunotoxins were subjected to analytical gel filtration on a TSK G3000SW (TosoHaas) column in order to determine whether the treatment caused aggregation. As shown in Figure 7, both labeled proteins eluted from the column as a monomeric peak with a leading shoulder, indicating that little aggregation occurred. The immunoreactivities of [ $^{125}$ I]-B3(Fv)-PE38 and [ $^{125}$ I]-B3(Fv)-PE38RRQQΔ were tested by checking their respective binding to A431 cells at 4 °C as described in the Experimental Procedures. The immunoreactivity of [ $^{125}$ I]-B3(Fv)-PE38 was 4–6%, whereas that of [ $^{125}$ I]-B3(Fv)-PE38RRQQΔ was 10–17%. For each labeled immunotoxin, the binding was maximal and similar for the three highest cell densities used, indicating that antigen was in excess over immunotoxin for those densities. Under similar radioiodination conditions, B3 IgG has 60–70% immunoreactivity. Thus, B3(Fv)-PE38 is about 10-fold more sensitive to loss of immunoreactivity than the whole IgG, whereas B3(Fv)-PE38RRQQΔ is 3–4-fold more sensitive to loss of immunoreactivity than the whole IgG. Therefore, it is also about 3-fold less sensitive than the wild-type B3(Fv)-PE38 immunotoxin.

## DISCUSSION

In this study we have constructed a mutated form of the single-chain immunotoxin B3(Fv)-PE38 in which the only two lysines in the CDR regions were mutated to arginines. Additionally, we found that while the parental molecule is 90% inactivated by both treatment with the bifunctional reagent SMCC or by iodination with the Bolton-Hunter reagent, the mutated form is more resistant to such inactivation. We found that replacing the CDR lysines

with arginine residues did not result in any significant changes in antigen binding, specificity, or specific cytotoxicity of the mutated immunotoxin.

Chemical conjugation is a well-established method of producing antibody-toxin conjugates (12 and references cited therein) or for conjugation of other macromolecules to antibodies or to their fragments (13–15). In some cases, chemical modification has led to loss of antigen binding by the modified antibody (16, 17). Chemical conjugation was used to prepare the first-generation immunotoxin B3-PE38, in which the whole B3 IgG which contains lysine residues was conjugated to PE38. This conjugate binds almost as well as the underivatized antibody to target cells and is very active (18). Radioiodination of proteins for use in a wide variety of basic and clinical investigations is another example of chemical modification of proteins (19, 20). We have routinely labeled the B3 IgG to be used as a tracer in our antigen-binding competition assays, with retention of about 60–70% of the immunoreactivity.<sup>2</sup> It is thus evident that the whole antibody and PE38 are relatively resistant to chemical modification. B3(Fv)-PE38, however, contains only the Fv part of the IgG, so it is more likely that a functionally important lysine will be modified following chemical derivatization with a possible loss of activity. Because general chemical modification is *a-priori* not usually position-specific (21), emphasis should be placed on modifying proteins on a predetermined position using site-directed mutagenesis. We have found that the single-chain immunotoxin B3(Fv)-PE38 can be site-specifically modified on cysteine residues that replace surface-exposed residues in either domain II or III of PE38.<sup>3</sup> Among residues replaced and derivatized without activity loss were lysine 575 and lysine 591. In this study they were replaced with glutamine because previous data indicated that such replacements would not impair the immunotoxins' cytotoxicity (7). Also it has been shown that the C-terminal lysine of *Pseudomonas* exotoxin can be deleted or replaced with arginine without significant activity loss, but replacement with other amino acids reduces activity (7). Therefore, chemical modification of the C-terminal lysine could interfere with the toxin's activity. The similar sensitivity of B3(Fv)-PE38 and B3(Fv)-PE38QQΔ to inactivation following chemical derivatization on the one hand, and the similar resistance of B3(Fv)-PE38RR and B3(Fv)-PE38RRQQΔ on the other hand, implies that loss of activity does not result from chemical modification of the PE38 part of B3(Fv)-PE38. The same results further suggest that the immunotoxins' sensitivity to such inactivation resides mainly in one or both of its CDR lysines. The modification of framework lysines in the Fv or of the amino terminal  $\alpha$ -amino group may also interfere with the formation of the optimal configuration for antigen binding or, indirectly, with the antigen binding itself, as implied by the residual loss of activity of B3(Fv)-PE38RR and B3(Fv)-PE38RRQQΔ following SMCC treatment or radioiodination. However, most of the interference with antigen binding following chemical derivatization of B3(Fv)-PE38 results from the fact that either the CDR lysines are directly involved in antigen binding or the bound reagent sterically hinders a binding interaction between a neighboring CDR residue and the B3 antigen. The fact that both lysines can be mutated to arginines without a significant activity loss suggests that the latter is the more likely explanation. Both lysine 65 in V<sub>H</sub> CDR2 (Kabat No. 64) (22) and lysine 190 in V<sub>L</sub> CDR2 (Kabat No. 50)

<sup>2</sup> Benhar and Webber, 1993 (unpublished data).

<sup>3</sup> Benhar *et al.*, 1993 (manuscript in preparation).



(22) are on the framework-CDR boundary and are conserved in murine immunoglobulin genes belonging to the same structural group (22). This suggests that they may not be directly involved in antigen binding but rather have a structural role so that they can be replaced with arginine residues that have properties similar to the original lysines.

#### LITERATURE CITED

- (1) Brinkmann, U., Pai, L. H., FitzGerald, D. J., Willingham, M., and Pastan, I. (1991) B3(Fv)-PE38KDEL, a single-chain immunotoxin that causes complete regression of a human carcinoma in mice. *Proc. Natl. Acad. Sci. U.S.A.* 88, 8616-8620.
- (2) Pastan, I., Pai, L. H., Brinkmann, U., and FitzGerald, D. J. (1993) Recombinant toxins: New therapeutic agents for cancer. *Annals N. Y. Acad. Sci.* (in press).
- (3) Kunkel, T. A. (1985) Rapid and efficient site-directed mutagenesis without phenotypic selection. *Proc. Natl. Acad. Sci. U.S.A.* 82, 488-492.
- (4) Sambrook, J., Fritsch, E. F., and Maniatis, T. (1989) *Molecular cloning, a Laboratory Manual*, 2nd ed., Cold Spring Harbor Laboratory Press, Cold Spring Harbor, New York.
- (5) Sanger, F., Nicklen, S., and Coulson, A. R. (1977) DNA sequencing with chain-terminating inhibitors. *Proc. Natl. Acad. Sci. U.S.A.* 74, 5463-5467.
- (6) Studier, F. W., and Moffat, B. A. (1986) Use of bacteriophage T7 polymerase to direct selective expression of cloned gene. *J. Mol. Biol.* 189, 113-130.
- (7) Chaudhary, V. K., Jinno, Y., FitzGerald, D. J., and Pastan, I. (1990) *Pseudomonas* exotoxin contains a specific sequence at the carboxyl terminus that is required for cytotoxicity. *Proc. Natl. Acad. Sci. U.S.A.* 87, 308-312.
- (8) Buchner, J., Pastan, I., and Brinkmann, U. (1992) A method to increase the yield of properly folded recombinant fusion proteins, e.g., single-chain immunotoxins from renaturations of bacterial inclusion bodies. *Anal. Biochem.* 205, 267-270.
- (9) Ellman, G. L. (1958) A colorimetric method for determining low concentrations of mercaptans. *Arch. Biochem. Biophys.* 74, 443-450.
- (10) Jinno, Y., Chaudhary, V. K., Kondo, T., Adhya, S., FitzGerald, D. J., and Pastan, I. (1988) Mutational analysis of domain I of *Pseudomonas* exotoxin: Mutations in domain I of *Pseudomonas* exotoxin that reduce cell binding and animal toxicity. *J. Biol. Chem.* 263, 13203-13207.
- (11) Brinkmann, U., Reiter, Y., Jung, S.-H., Lee, B., and Pastan, I. (1993) A recombinant immunotoxin containing a disulfide-stabilized Fv fragment (dsFv). *Proc. Natl. Acad. Sci. U.S.A.* 90, 7538-7542.
- (12) Cumber, A. J., Forrester, J. A., Foxwell, B. M. J., Ross, W. C. J., and Thorpe, P. E. (1985) Preparation of antibody-toxin conjugates. *Methods Enzymol.* 112, 207-225.
- (13) Meares, C. F., and Goodwin, D. A. (1984) Linking radiometals to proteins with bifunctional chelating agents. *J. Protein Chem.* 3, 215-228.
- (14) Byers, V., and Baldwin, R. (1988) Therapeutic strategies with monoclonal antibodies and immunoconjugates. *Immunology* 65, 329-335.
- (15) Lyons, A., King, D. J., Owens, R. J., Yarranton, G. T., Millican, A., Whittle, N. G., and Adair, J. R. (1990) Site-specific attachment to recombinant antibodies via introduced surface cysteine residues. *Protein Eng.* 3, 703-708.
- (16) Lindmo, T., Boven, E., Cuttitta, F., Fedorko, J., and Bunn, P. A., Jr. (1984) Determination of the immunoreactive fraction of radiolabeled monoclonal antibodies by linear extrapolation to binding at infinite antigen excess. *J. Immunol. Methods* 72, 77-89.
- (17) Rodwell, J. D., Alvarez, V. L., Lee, C., Lopez, A. D., Goers, J. W., King, H. D., Powsner, H. J., and McKearn, T. J. (1986) Site-specific covalent modification of monoclonal antibodies: *in vitro* and *in vivo* evaluations. *Proc. Natl. Acad. Sci. U.S.A.* 83, 2632-2636.
- (18) Pai, L. H., Batra, J. K., FitzGerald, D. J., Willingham, M. C., and Pastan, I. (1991) Anti-tumor activities of immunotoxins made of monoclonal antibody B3 and various forms of *Pseudomonas* exotoxin. *Proc. Natl. Acad. Sci. U.S.A.* 88, 3358-3362.
- (19) Langone, J. J. (1989) Radioiodination by use of the Bolton-Hunter and related reagents. *Methods Enzymol.* 70, 221-247.
- (20) Vaidyanathan, G., Affleck, D. J., and Zalutsky, M. R. (1993). Radioiodination of proteins using *N*-Succinimidyl 4-Hydroxy-3-iodobenzoate.
- (21) Smith, R. A. G., Dewdney, J. M., Fears, R., and Foste, G. (1993) Chemical derivatization of therapeutic proteins. *TIBTECH* 11, 397-403.
- (22) Kabat, E. A., Wu, T. T., Perry, H. M., Gottesman, K. S., and Foeller, C. (1991) *Sequences of proteins of immunological interest*, 5th ed., U.S. Department of Health and Human Services, Public Health Service, National Institutes of Health, Bethesda, MD.

# DNA-Linked RNase H for Site-Selective Cleavage of RNA<sup>†</sup>

Yohtaro Uchiyama,<sup>†,§</sup> Hideo Inoue,<sup>||</sup> Eiko Ohtsuka,<sup>\*,||</sup> Chieko Nakai,<sup>⊥</sup> Shigenori Kanaya,<sup>⊥</sup> Yoshio Ueno,<sup>†,§</sup> and Morio Ikehara<sup>§,⊥</sup>

Faculty of Pharmaceutical Sciences, Science University of Tokyo, Tokyo 162, Japan, Research Institute for Biosciences, Science University of Tokyo, Noda 278, Japan, Faculty of Pharmaceutical Sciences, Hokkaido University, Sapporo 060, Japan, and Protein Engineering Research Institute, Suita, Osaka 565, Japan. Received December 15, 1993\*

A DNA-linked RNase H (Hybrid Enz-1) (Kanaya et al. (1992) *J. Biol. Chem.* 267, 8492-8498), in which dGTCATCTCC was attached to *E. coli* RNase H via a covalent linker of 21 Å, was altered to improve the site-specific RNA cleavage by increasing the linker length. The sizes of the linkers on these hybrid enzymes (Hybrid Enz-2, -3, and -4) differed by 3 Å, the axial rise of the DNA/RNA hybrid, to give 18-, 24-, and 27-Å lengths. The conjugate with a size of 27 Å was able to cleave a synthetic 22mer RNA (5'-rAAGAUGUCUACGGAGAUGACCA-3'), containing the complementary 9mer RNA sequence (underlined), at one position, A16-U17. The kinetic parameters of Hybrid Enz-1, -2, -3, and -4 were examined using a 9mer RNA target. The results showed that longer linkers produced higher  $K_m$ ,  $k_{cat}$ , and  $k_{cat}/K_m$  values, and the  $k_{cat}/K_m$  value of the conjugate with the 27-Å linker reached 83% of that of the wild-type RNase H. Hybrid Enz-4 was found to be useful as an RNA restriction endonuclease.

To cleave RNA site-specifically, investigators have reported several methods. These include chemical cleavage, with compounds such as Fe(II)-bleomycin (Carter et al., 1990), and enzymatic cleavage with ribozymes (Symons, 1992), staphylococcal nuclease-DNA conjugate (Zuckermann et al., 1988; Zuckermann and Schultz, 1989), and RNase A-DNA conjugate (Zuckermann and Schultz, 1988). In the approaches using RNase H,<sup>1</sup> short oligodeoxynucleotides or modified oligonucleotides, such as 2'-modified oligonucleotides (Hayase et al., 1990; Monia et al., 1993) and mixed-phosphate-backbone oligodeoxynucleotides (Agrawal et al., 1990), were used as the complementary strand.

RNase H, which participates in DNA replication and repair (Crouch and Derksen, 1982; Crouch, 1990), endonucleolytically degrades the RNA moiety of a DNA/RNA hybrid, in the presence of Mg<sup>2+</sup> or Mn<sup>2+</sup>, to produce 5'-phosphates at the hydrolysis sites (Miller et al., 1973; Berkower et al., 1973). The enzyme consists of a single polypeptide chain with 155 amino acid residues (Kanaya and Crouch, 1983), and the sequence is similar to the RNase H domains of the reverse transcriptases from retroviruses, including human immunodeficiency virus (Johnson et al., 1986; Doolittle, 1989). Site-directed mutagenesis experiments and computer analysis of the homology of the amino acid sequence between RNase H and the C-terminal domains of the reverse transcriptases from many species suggest that the residues of the active site are Asp-10,

Glu-48, and Asp-70. The three-dimensional structure of RNase H was determined by X-ray crystallographic studies (Katayanagi et al., 1990; Yang et al., 1990) and showed that Mg<sup>2+</sup> binds close to the three acidic amino acids within the active site.

RNase H has a slight specificity for the base sequence of the hybrid. For cleavage of RNA at single site, a DNA-linked RNase H (Hybrid Enz-1) (Kanaya et al., 1992) has been constructed using the mutant RNase H (C135/RNase H) (Kanaya et al., 1990) in which all three Cys residues were replaced by Ala, and Glu-135 was replaced by Cys. The 9mer DNA (dGTCATCTCC) was linked with a 21-Å covalent linker including maleimide at the 5'-terminus of the DNA and then attached to Cys-135 of the mutant RNase H. In the conjugate, the DNA portion plays the role of cleavage site recognition and the RNase H portion catalyzes the hydrolysis of the RNA that hybridizes with the DNA portion. In the presence of the 9mer DNA, the wild-type enzyme and C135/RNase H cleaved the 9mer RNA (rGGAGAUGAC) at the A5-U6 and U6-G7 positions and the 22mer RNA (5'-rAAGAUGUCUACGGAGAUG-ACCA-3') containing the complementary 9mer RNA sequence (underlined) at the A16-U17 and U17-G18 positions (corresponding to the 9mer RNA). On the other hand, Hybrid Enz-1 with the 9mer DNA attached via a 21-Å linker cleaved the complementary 9mer RNA at a single site (A5-U6) and cleaved the 22mer RNA at two positions (A14-G15 and A16-U17). Cleavage by Hybrid Enz-1 at A14-G15, the site the nonconjugated enzymes did not cleave, was thought to be caused by the shorter linker length.

In this study, the linker length was altered by 3 Å, which is equal to the axial rise of a DNA/RNA hybrid (Saenger, W., 1984), and three hybrid enzymes with linkers of different lengths (18, 24, and 27 Å) were constructed. Hybrid Enz-4 (Figure 1), whose linker size was 6 Å (the axial rise of two bases) longer than that of Hybrid Enz-1, was found to cleave the 22mer RNA almost site-selectivity at A16-U17. The effect of the linker length on the activity was examined by measuring the kinetic parameters ( $K_m$  and  $k_{cat}$  values) for the cleavage of the 9mer RNA.

<sup>†</sup> This work was supported in part by a Grant-in-Aid from the Ministry of Education, Science and Culture, Japan.

\* Author to whom correspondence should be addressed. Tel: +81-11-706-4979; FAX: +81-11-706-4989.

<sup>†</sup> Faculty of Pharmaceutical Sciences, Science University of Tokyo.

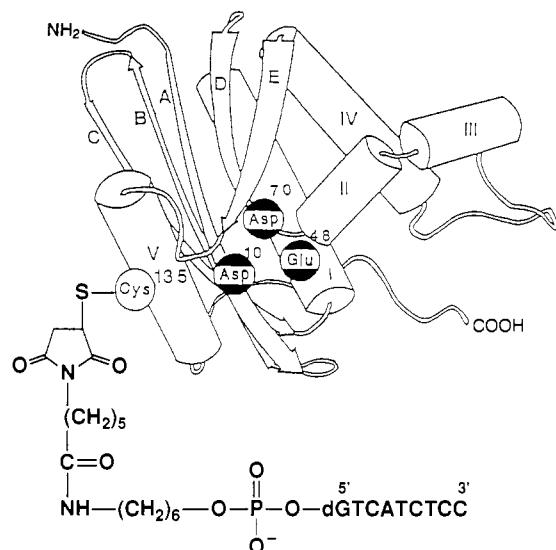
<sup>§</sup> Research Institute for Biosciences.

<sup>||</sup> Faculty of Pharmaceutical Sciences, Hokkaido University.

<sup>⊥</sup> Protein Engineering Research Institute.

\* Abstract published in *Advance ACS Abstracts*, June 1, 1994.

<sup>1</sup> Abbreviations: RNase H, ribonuclease H; EDTA, ethylenediaminetetraacetic acid; SDS, sodium dodecyl sulfate; PAGE, polyacrylamide gel electrophoresis; kDa, kilodaltons.



**Figure 1.** Model of Hybrid Enz-4.  $\beta$ -Strands and  $\alpha$ -helices are represented by arrows and cylinders, respectively. The three acidic residues required for activity are shown by solid circles with residue numbers.

## MATERIALS AND METHODS

**Materials.** Aminomodifier II (*N*-Fmoc-*O*<sup>1</sup>-(dimethoxytrityl)-*O*<sup>2</sup>-[(cyanoethoxy)(diisopropylamino)phosphinyl]-3-amino-1,2-propanediol) was purchased from Clontech Co., Ltd., and aminolink 2 (*N*-(trifluoroacetyl)-*O*-[methoxy(diisopropylamino)phosphinyl]-6-aminoheptan-1-ol) was from Applied Biosystems Inc. *N*-[( $\epsilon$ -Maleimidocaproyl)-oxy]succinimide (EMCS) and *N*-[( $\gamma$ -maleimidobutyryl)-oxy]succinimide (GMBS) were purchased from Dojindo Laboratories. *Crotalus durissus* phosphodiesterase was purchased from Boehringer Mannheim. The 9mer RNA (rGGAGAUGAC) and the 9mer DNA (dGTCATCTCC) have been described previously (Kanaya et al., 1992).

**Synthesis of the 22mer RNA (rAAGAUGUCUACG-GAGAUGACCA).** Oligonucleotides were synthesized on an Applied Biosystems 394 DNA/RNA Synthesizer using the standard phosphoramidite method (Caruthers, 1985) with commercially available reagents (MilliGen Biosearch for RNA). The products were deprotected and purified to give single peaks on reversed-phase and anion-exchange HPLC. Reversed-phase HPLC was carried out on an Inertsil ODS-2 column (4.6 mm  $\times$  250 mm) from GL Sciences Inc. For the 22mer RNA, elution was performed with a linear gradient of acetonitrile in 0.1 M triethylammonium acetate buffer, pH 7.0, from 9.0 to 14% (v/v) over 25 min at a flow rate of 1.0 mL/min at 50  $^{\circ}$ C. The retention time was 14.7 min. Anion-exchange HPLC was carried out on a DEAE 2SW column (4.6 mm  $\times$  250 mm) from Tosoh Co., Ltd. Elution was performed with a linear gradient from 0.4 to 0.9 M ammonium formate in 20% acetonitrile for 25 min at a flow rate of 1.0 mL/min at 50  $^{\circ}$ C. The retention time was 20.2 min.

**Labeling of the 5'-Ends of the 9mer and 22mer RNAs.** The 5'-ends of the 9mer and 22mer RNAs were <sup>32</sup>P-labeled with T4 polynucleotide kinase from *E. coli* strain A19 and [ $\gamma$ -<sup>32</sup>P]ATP and were purified on a NENSORB 20 column (DuPont).

**Preparation of Hybrid Enz-1, -2, -3, and -4.** Hybrid Enz-1 (d9-C135/RNase H) with a 21-Å linker was prepared as described (Kanaya et al., 1992). Hybrid Enz-2 with an 18-Å linker was prepared by the same procedure used for Hybrid Enz-1, except GMBS and Aminomodifier II were used. Hybrid Enz-3 (24 Å) and -4 (27 Å) were prepared

using GMBS plus aminolink 2 and EMCS plus aminolink 2, respectively.

The 5'-end amino group was introduced into the 9mer DNA (dGTCATCTCC) in the last step of the DNA synthesis. After the protecting groups were removed, the product was then allowed to react with the bifunctional reagent in dimethylformamide in the presence of 50 mM phosphate buffer, pH 7.5, at room temperature for 1 h. The product was purified by gel filtration on Sephadex G-25 in water. The purity was checked by reversed-phase HPLC. Elution was performed with a linear gradient of acetonitrile in 0.1 M triethylammonium acetate buffer, pH 7.0, from 0 to 38% (v/v) over 25 min at a flow rate of 1.0 mL/min at 50  $^{\circ}$ C. The retention times of the linker-DNAs were 21.5 min for Hybrid Enz-1, 19.6 min for Hybrid Enz-2, 21.2 min for Hybrid Enz-3, and 23.1 min for Hybrid Enz-4.

The coupling reaction of the mutant RNase H, the C135/RNase H (10 nmol), and the linker-9mer DNA (10 nmol) was carried out in 100  $\mu$ L of Tris-HCl buffer, pH 7.0, at room temperature for 1 h. The resultant hybrid enzymes were purified by cation-exchange HPLC on an Asahipack ES 502C column (7.5 mm  $\times$  100 mm) from Asahi Chemical Industries Co., Ltd. The column was equilibrated with 20 mM sodium phosphate buffer, pH 6.5, and elution was performed by a linear gradient from 0.0 to 0.3 M Na<sub>2</sub>SO<sub>4</sub> in 20 mM sodium phosphate buffer, pH 6.5, over 30 min. The retention times were 22.8 min for Hybrid Enz-1, 23.2 min for Hybrid Enz-2, 22.8 min for Hybrid Enz-3, and 22.4 min for Hybrid Enz-4.

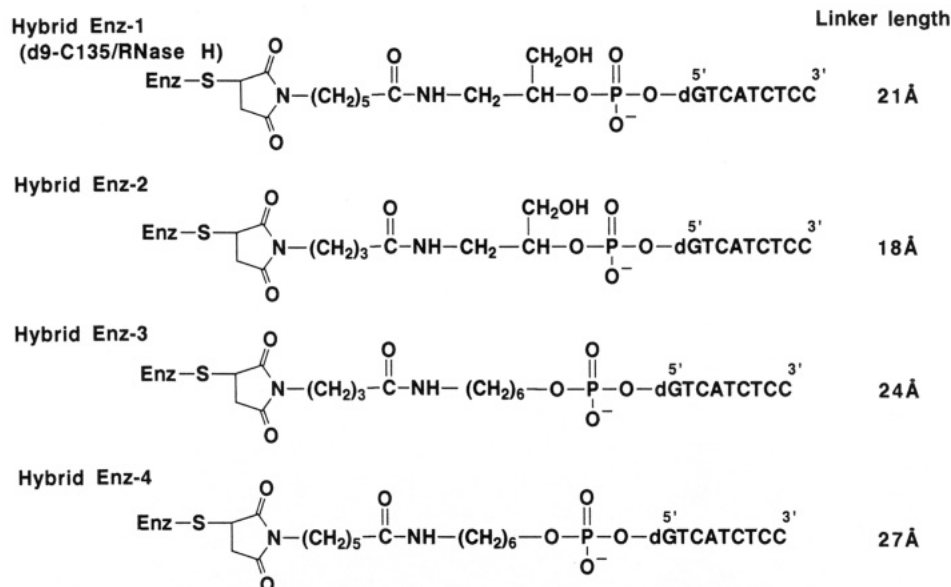
**Assay for Hybrid Enz-1, -2, -3, and -4.** The substrate for the wild-type and C135/RNase H was either a 9mer RNA/9mer DNA or a 22mer RNA/9mer DNA hybrid duplex, and that of the hybrid enzymes was either a single-stranded 9mer RNA or 22mer RNA.

The substrate (10 pmol) was hydrolyzed with enzymes (0.02 pmol) at 30  $^{\circ}$ C for 15 min in 10  $\mu$ L of 10 mM Tris-HCl buffer, pH 8.0, containing 10 mM MgCl<sub>2</sub>, 50 mM NaCl, 1 mM 2-mercaptoethanol, and 0.01% bovine serum albumin. The reaction was stopped by the addition of 20  $\mu$ L of loading buffer (10 M urea, 50 mM EDTA), and the hydrolysates were fractionated on polyacrylamide sequencing gels (19:1 acrylamide/bis(acrylamide)) with 7 M urea (0.3 mm  $\times$  40 cm). A 20% gel was used for the 9mer, and a 15% gel was used for the 22mer. They were identified by comparing the degraded products with those of a <sup>32</sup>P-5'-end-labeled 9mer RNA treated with snake venom phosphodiesterase (Jay et al., 1974). The amount of each hydrolysate was directly quantitated by measuring the radioactivity with a Fujix BA1000 bioimage analyzer.

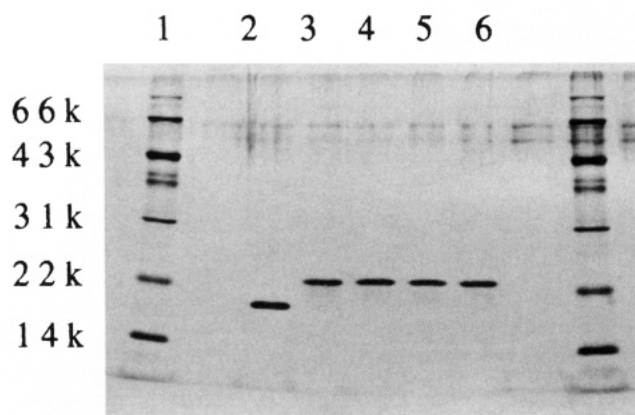
**Determination of the Kinetic Parameters of Hybrid Enz-1, -2, -3, and -4 with 9mer RNA.** The hydrolysis was carried out at 30  $^{\circ}$ C in the same buffer solution as described. The substrate concentrations were varied from 0.2 to 20.0  $\mu$ M, and the hydrolysate concentration was <10% of the original 9mer RNA.

## RESULTS

**Preparation of Hybrid Enzymes.** Hybrid enzymes with different linker lengths (Figure 2) were constructed by the procedure used for the previously described 21-Å linker Hybrid Enz-1. The linker length was changed by two-atom increments, with a size of 3 Å. The linker length containing the maleimide group was calculated assuming that all distances between two atoms were 1.5 Å and a linker arm extended. The maleimide group of the linker was attached to the unique Cys135 of the mutant enzyme, Cys135/RNase H (Kanaya et al., 1992).



**Figure 2.** Structures of the four hybrid RNase H proteins with linkers of different lengths. Hybrid Enz-1 is identical to d9-C135/RNase H (Kanaya et al., 1992).

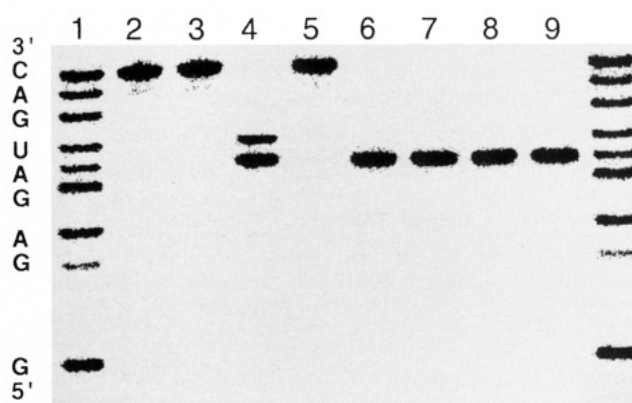


**Figure 3.** SDS-PAGE of the four hybrid RNase H proteins after HPLC. Samples (0.1  $\mu\text{g}$ ) were subjected to electrophoresis on a 15% polyacrylamide gel and silver stained: lane 1, SDS-PAGE low molecular weight standards (Bio-Rad Laboratories) containing phosphorylase b (98k), bovine serum albumin (66k), ovalbumin (43k), carbonic anhydrase (31k), trypsin inhibitor (22k), and lysozyme (14k); lane 2, unmodified C135/RNase H; lane 3, purified Hybrid Enz-1; lane 4, purified Hybrid Enz-2; lane 5, purified Hybrid Enz-3; lane 6, purified Hybrid Enz-4.

After the cross-linking reaction, the resultant hybrid RNase H proteins were purified by cation-exchange HPLC. The materials in the 23-min retention time peak gave a single band of 23 kDa on SDS-PAGE, as shown in Figure 3. (The material in the 30-min time peak was identified as the unmodified enzyme, which gave a band of 20 kDa on SDS-PAGE.)

**Cleavage of 9mer RNA with Hybrid Enz-2, -3, and -4.** Complete cleavage of the 9mer (rGGAGAUGAC) RNA was observed under the described conditions. The (C135/RNase H) cleaved at the two positions, A5-U6 and U6-G7. All of the hybrid enzymes cleaved at one position, A5-U6. Regardless of the linker length, no change in specificity for the hydrolysis of the 9mer RNA was observed (Figure 4).

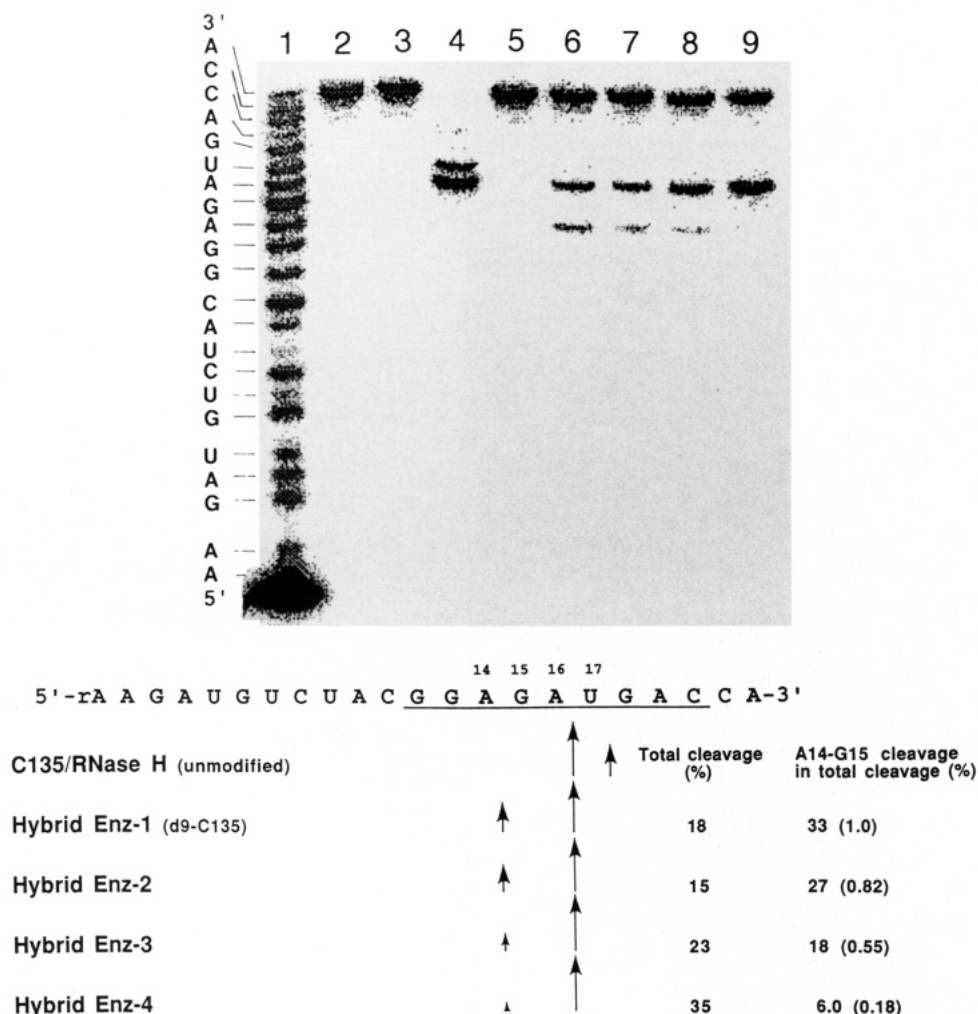
**Cleavage of 22mer RNA with Hybrid Enz-1, -2, -3, and -4.** The unmodified enzyme (C135/RNase H) cleaved the 22mer RNA (rAAGAUGUCUACGGAGAUGACCA) containing the 9mer sequence (underlined) in the presence of the complementary 9mer DNA at two positions, A16-U17 and U17-G18, which were the same positions as in



**Figure 4.** Cleavage pattern of the 9mer RNA. Autoradiograph of cleavage reactions: lane 1, partial digest of the 9mer RNA with snake venom phosphodiesterase; lanes 2 and 3, the duplex of the 9mer RNA/9mer DNA (dGTCATCTCC) and the single-stranded 9mer RNA treated under reaction conditions without enzyme, as described in the Materials and Methods; lane 4, hydrolysates of the duplex of 9mer RNA/9mer DNA with the C135/RNase H (unmodified); lane 5, the single-stranded 9mer RNA with C135/RNase H (unmodified); lane 6, the single-stranded 9mer RNA with Hybrid Enz-1(d9-C135/RNase H); lane 7, the RNA with Hybrid Enz-2; lane 8, the RNA with Hybrid Enz-3; lane 9, the RNA with Hybrid Enz-4.

the case of the 9mer RNA. The hybrid enzymes cleaved the 22mer RNA at two positions, A16-U17 (corresponding to A5-U6 in the 9mer) as the major site and A14-G15 (corresponding to A3-G4 in the 9mer) as the minor site, in a different manner from C135/RNase H (Figure 5). The percentages of cleavage at A14-G15 in each hybrid enzyme are shown in Figure 5. The amounts of the A14-G15 product in the reaction with the four hybrid enzymes were different. The yield of the minor product decreased as the linker length increased (33% for Hybrid Enz-1 to 6.0% for Hybrid Enz-4). The linker length affected the cleavage pattern of the 22mer RNA. The ratio of the major product to the minor product in Hybrid Enz-4 with the 27- $\text{\AA}$  linker was 8.3-fold higher than Hybrid Enz-1, and Hybrid Enz-4 cleaved the 22mer RNA almost exclusively at a single position (A16-U17).

**Kinetic Parameters ( $K_m$  and  $k_{cat}$ ) of Hybrid Enzymes for the 9mer RNA.** Since the four hybrid enzymes with linkers of different sizes cleaved the 9mer RNA at



**Figure 5.** Cleavage pattern of the 22mer RNA. (Top) autoradiograph of cleavage reactions: lane 1, partial digest of the 22mer RNA with snake venom phosphodiesterase; lanes 2 and 3, the duplex of 22mer RNA/9mer DNA (dGTCATCTCC) and the single-stranded 9mer RNA treated under reaction conditions without enzyme, as described in the Materials and Methods; lane 4, hydrolysates of the duplex of 22mer RNA/9mer DNA with the C135/RNase H (unmodified); lane 5, the single-stranded 22mer RNA with C135/RNase H (unmodified); lane 6, the single-stranded 22mer RNA with Hybrid Enz-1(d9-C135/RNase H); lane 7, the RNA with Hybrid Enz-2; lane 8, the RNA with Hybrid Enz-3; lane 9, the RNA with Hybrid Enz-4. (Bottom) illustrations of cleavage patterns. The cleavage percentages are shown at the arrows.

**Table 1. Summary of the Kinetic Parameters<sup>a</sup>**

	$K_m$ ( $\mu\text{M}$ )	$k_{\text{cat}}$ ( $\text{min}^{-1}$ )	$k_{\text{cat}}/K_m$ ( $\text{min}^{-1} \mu\text{M}^{-1}$ )
wild type	$0.67 \pm 0.04$ (1.0)	$5.0 \times 10^2 \pm (3 \times 10)$ (1.0)	$7.5 \times 10^2$ (1.0)
C135/RNase H	$11 \pm 2.1$ (16)	$1.5 \times 10^3 \pm (3 \times 10^2)$ (3.1)	$1.4 \times 10^2$ (0.19)
Hybrid Enz-1 (d9-C135/RNase H)	$0.42 \pm 0.01$ (0.63)	$1.6 \times 10^2 \pm 3$ (0.31)	$3.8 \times 10^2$ (0.50)
Hybrid Enz-2	$0.24 \pm 0.02$ (0.36)	$5.1 \times 10 \pm 4$ (0.10)	$2.1 \times 10^2$ (0.28)
Hybrid Enz-3	$1.0 \pm 0.04$ (1.5)	$4.9 \times 10^2 \pm (2 \times 10)$ (0.98)	$4.9 \times 10^2$ (0.63)
Hybrid Enz-4	$1.4 \pm 0.1$ (2.1)	$8.8 \times 10^2 \pm (6 \times 10)$ (1.8)	$6.3 \times 10^2$ (0.83)

<sup>a</sup> Values are from the mean of four experiments. Relative values are in parentheses.

the same position, the net effect of the linker length could be examined independent of the base sequence. It was reported that the hydrolysis rates of different homopolymeric RNA/DNA hybrids varied (Berkower et al., 1973). The A5–U6 cleavage reaction of the 9mer RNA (rGG-AGAUGAC) with the hybrid enzymes followed Michaelis-Menten kinetics. The kinetic constants of A5–U6 cleavage were obtained from the Lineweaver–Burk plots using the procedure described for C135/RNase H and Hybrid Enz-1 (Kanaya et al., 1992). The  $K_m$  value of the hybrid enzyme increased as the linker length increased ( $0.42 \mu\text{M}$  for Hybrid Enz-1 to  $1.4 \mu\text{M}$  for Hybrid Enz-4) (Table 1). The RNA substrate-binding of Hybrid Enz-4 was only 0.3-fold of that of Hybrid Enz-1. The  $k_{\text{cat}}$  values of the hybrid enzymes increased as the linker length increased ( $160 \text{ min}^{-1}$  for hybrid Enz-1 to  $880 \text{ min}^{-1}$  for Hybrid Enz-4) (Table

1). The turnover number of Hybrid Enz-4 increased to 5.5-fold of the Hybrid Enz-1 value. The  $K_m/k_{\text{cat}}$  values of the hybrid enzymes increased as the linker length increased ( $380 \text{ min}^{-1} \mu\text{M}^{-1}$  for Hybrid Enz-1 to  $630 \text{ min}^{-1} \mu\text{M}^{-1}$  for Hybrid Enz-4) (Table 1). The catalytic efficiency of Hybrid Enz-4 was 1.7-fold higher than Hybrid Enz-1 and 83% of that of the wild-type enzyme, which should be sufficient for most practical purposes.

## DISCUSSION

The wild-type enzyme and Cys135/RNase H cleaved the 9mer RNA at A5–U6 and U6–G7 and the 22mer RNA at A16–U17 and U17–G18. The hybrid enzymes cleaved the 9mer RNA at one position, A5–U6. However, they cleaved the 22mer RNA at two positions: A16–U17 as the major site and A14–G15 as the minor cleavage site, which



is different from the minor site cleaved by the nonconjugated enzymes. When the longer RNA was used as the substrate, the minor cleavage product increased. When the linker length was increased by 3 Å, the amount of the minor product (A14–G15 cleavage) decreased. The linker of Hybrid Enz-4 is 27 Å, which is about 6 Å longer (equal to the axial rise of two bases of a DNA/RNA hybrid) than that of Hybrid Enz-1, and the amount of the A14–G15 product with Hybrid Enz-4 cleavage of the 22mer RNA was 6.0% of the total cleavage (Figure 5). The hybrid enzymes with shorter linkers seem to enforce cleavage at A14–G15, but in Hybrid Enz-4 there is little cleavage restraint. The hybrid enzymes did not cleave at U17–G18 in the 22mer and U6–G7 in the 9mer, which is in contrast to the nonconjugated enzymes. The linkers in these hybrid enzymes were not long enough for the linked DNA to bind the RNA for cleavage at these positions. It seems that the 27-Å linker anchored the duplex to enable the specific hydrolysis. Linkers with a certain length seem to be required for selective cleavage. It appeared that the 9mer RNA was too short to be cleaved at the A3–G4 site (corresponding to A14–G15 in the 22mer RNA). The substrate RNA apparently requires about four or five bases in the 5'-region of the cleavage site (data not shown). The 132mer RNA containing the complementary 9mer RNA sequence was also cleaved with Hybrid Enz-1 (d9-C135/RNase H). Although a difference between the cleavage patterns of the 9mer and that of the 22mer RNA was observed, it was found that the cleavage site of the 132mer RNA was the same as that of the 22mer RNA (Nakai et al., 1994). The model of RNase H complexed with a 21mer DNA/RNA hybrid duplex, which was built based on the X-ray crystallography, NMR, and site-directed mutagenesis experiments, shows that the interface of the enzyme covers roughly two turns of a double helix (Katayanagi et al., 1992). This indicates that the length of the RNA that interacts with RNase H and affects the specificity is less than the 22mer RNA. Therefore, the 22mer RNA was long enough for the characterization of the site specificity of the enzymes.

The effects of the linker length on the cleavage rate of the hybrid enzymes were examined by measuring the kinetic parameters ( $K_m$  and  $k_{cat}$  values). The  $K_m$  values of the hybrid enzymes may be affected by the following factors: the interaction of a substrate RNA with the DNA attached to the enzyme and the binding of the duplex with the enzyme protein. The 9mer DNA linked to the enzyme is thought to have increasing flexibility as the linker length is increased. This may result in larger  $K_m$  values for the hybrid enzymes with longer linkers. The  $k_{cat}$  values of the hybrid enzymes reflect the turnover number. The hybrid Enz-4 with a long linker may release the product more easily, thereby increasing the turnover number of the enzyme for the substrate. Consequently, the  $k_{cat}$  value was increased.

The longer the linker length, the higher the  $k_{cat}/K_m$  value obtained for these four hybrid enzymes, and it was revealed that the linker length had a greater effect on the turnover of the enzyme than on the affinity for the substrates. The  $k_{cat}/K_m$  value of the Hybrid Enz-4 was 83% of that of the wild type and 1.7-fold higher than that of Hybrid Enz-1.

If the hybrid enzyme reaction is bimolecular, there may be two sites of cleavage for the 9mer RNA, as found with the unmodified enzyme. Since these hybrid enzymes cleaved the 9mer RNA at a single site, the reaction seems to be unimolecular.

The three-dimensional structure of RNase H from *E. coli* was determined by X-ray crystallography (Katayanagi

et al., 1990; Yang et al., 1990); however, no crystals of the complex of DNA/RNA and the enzyme, or of the hybrid enzyme, have been obtained. Models of hydrolysis with these complexes will provide some structural information on the mechanism of RNA cleavage by RNase H.

Staphylococcal nuclease–DNA and RNase A–DNA conjugates were designed for site-specific endoribonucleases, but they were shown to degrade the substrate in a manner reflecting the nonspecific natures of staphylococcal nuclease and RNase A (Zuckermann and Schultz, 1988; Zuckermann et al., 1988; Zuckermann and Schultz, 1989). On the other hand, Hybrid Enz-4 cleaved the RNA at single site within the target region. Ribozymes were shown to cleave RNA site-specifically (Symons, 1992). However, Hybrid Enz-4 was catalytically more active, with a  $k_{cat}$  value of 750 min<sup>-1</sup>, as compared to that of a ribozyme, with a  $k_{cat}$  value of less than 1 min<sup>-1</sup> (Haseloff and Gerlach, 1988).

In conclusion, Hybrid Enz-4 with the 27 Å linker was found to cleave RNA site-selectively and with high efficiency. This kind of hybrid RNase H will provide sequence specific cleavage of RNAs as a restriction enzyme for RNA and, because the cleavage reaction does not need the addition of DNA splints, the product purification may be easier. The hybrid RNase H can be useful to study the structure and function of RNAs. In addition, a hybrid RNase H, consisting of a thermostable mutant and a linked DNA, may be useful for cleavage of RNAs at high temperatures, where RNA secondary and tertiary structures can be melted.

#### LITERATURE CITED

- Agrawal, S., Mayrand, S. H., Zamecnik, P. C., and Pederson, T. (1990) Site-specific excision from RNA by RNase H and mixed-phosphate-backbone oligodeoxynucleotides. *Proc. Natl. Acad. Sci. U.S.A.* 87, 1401–1405.
- Berkower, I., Leis, J., and Hurwitz, J. (1973) Isolation and characterization of an endonuclease from *Escherichia coli* specific for ribonucleic acid in ribonucleic acid–deoxyribonucleic acid hybrid structures. *J. Biol. Chem.* 248, 5914–5921.
- Carter, B. J., de Vroom, E., Long, E. C., van der Marel, G. A., van Boom, J. H., and Hecht, S. M. (1990) Site-specific cleavage of RNA by Fe(II)-bleomycin. *Proc. Natl. Acad. Sci. U.S.A.* 87, 9373–9377.
- Caruthers, M. H. (1985) Gene synthesis machines: DNA chemistry and its uses. *Science* 230, 281–285.
- Crouch, R. J. (1990) Ribonuclease H: from discovery to 3D structure. *New Biol.* 2, 771–777.
- Crouch, R. J., and Derksen, M.-L. (1982) in *Nuclease* (Linn, S. M., and Roberts, R. J., Eds.) pp 211–241, Cold Spring Harbor Laboratory, Cold Spring Harbor, New York.
- Dash, P., Lotan, I., Knapp, M., Kandel, E. R., and Goelet, P. (1987) Selective elimination of mRNAs *in vivo*: Complementary oligodeoxynucleotides promote RNA degradation by an RNase H-like activity. *Proc. Natl. Acad. Sci. U.S.A.* 84, 7896–7900.
- Doolittle, R. F., Feng, D. F., Johnson, M. S., and McClure, M. A. (1989) Origins and evolutionary relationships of retroviruses. *Quart. Rev. Biol.* 64, 1–30.
- Haseloff, J., and Gerlach, W. L. (1988) Simple RNA enzymes with new and highly specific endoribonuclease activities. *Nature* 334, 585–591.
- Hayase, Y., Inoue, H., and Ohtsuka, E. (1990) Secondary structure in formylmethionine tRNA influences the site-directed cleavage of ribonuclease H using chimeric 2'-O-methyl oligodeoxyribonucleotides. *Biochemistry* 29, 8793–8797.
- Jay, E., Bambara, R., Padmanabhan, R., and Wu, R. (1974) DNA sequence analysis: a general, simple and rapid method for sequencing large oligodeoxyribonucleotide fragments by mapping. *Nucleic Acids Res.* 1, 331–353.
- Johnson, M. S., McClure, M. A., Feng, D. F., Gray, J., and Doolittle, R. F. (1986) Computer analysis of retroviral pol



- genes: Assignment of enzymatic functions to specific sequences and homologies with nonviral enzymes. *Proc. Natl. Acad. Sci. U.S.A.* 83, 7648–7652.
- Kanaya, S., and Crouch, R. J. (1983) DNA sequence of the gene coding for *Escherichia coli* ribonuclease H. *J. Biol. Chem.* 258, 1276–1281.
- Kanaya, S., Kimura, S., Katsuda, C., and Ikehara, M. (1990) Role of cysteine residues in ribonuclease H from *Escherichia coli*. *Biochem. J.* 271, 59–66.
- Kanaya, S., Nakai, C., Konishi, A., Inoue, H., Ohtsuka, E., and Ikehara, M. (1992) A hybrid ribonuclease H. *J. Biol. Chem.* 267, 8492–8498.
- Katayanagi, K., Miyagawa, M., Kanaya, S., Ikehara, M., Matsuzaki, T., and Morikawa, K. (1990) Three-dimensional structure of ribonuclease H from *E. coli*. *Nature* 347, 306–309.
- Katayanagi, K., Miyagawa, M., Matsushima, M., Ishikawa, M., Kanaya, S., Nakamura, H., Ikehara, M., Matsuzaki, T., and Morikawa, K. (1992) Structural details of ribonuclease H from *Escherichia coli* as refined to an atomic resolution. *J. Mol. Biol.* 223, 1029–1052.
- Miller, H. I., Riggs, A. D., and Gill, G. N. (1973) Ribonuclease H (hybrid) in *Escherichia coli*. *J. Biol. Chem.* 248, 2621–2624.
- Minshall, J., and Hunt, T. (1986) The use of single-stranded DNA and RNase H to promote quantitative hybrid arrest of translation of mRNA/DNA hybrids in reticulocyte lysate cell-free translations. *Nucleic Acids Res.* 14, 6433–6451.
- Monia, B. P., Lesnik, E. A., Gonzalez, C., Lima, W. F., McGee, D., Guinosso, C. J., Kawasaki, A. M., Cook, P. D., and Freier, S. M. (1993) Evaluation of 2'-modified oligonucleotides containing 2'-deoxy gaps as antisense inhibitors of gene expression. *J. Biol. Chem.* 268, 14514–14522.
- Nakai, C., Konishi, A., Komatsu, Y., Inoue, H., Ohtsuka, E., and Kanaya, S. (1994) Sequence-specific cleavage of RNA by a hybrid ribonuclease H. *FEBS Lett.* 339, 67–72.
- Saenger, W. (1984) in *Principles of Nucleic Acid Structure* (Cantor, C. R., Ed.) p 234, Springer-Verlag, New York.
- Saison-Behmoaras, T., Tocqué, B., Rey, I., Chassignol, M., Thuong, N. T., and Hélène, C. (1991) Short modified antisense oligonucleotides directed against Ha-ras point mutation induce selective cleavage of the mRNA and inhibit T24 cells proliferation. *EMBO J.* 10, 1111–1118.
- Symons, R. H. (1992) Small catalytic RNAs. *Annu. Rev. Biochem.* 61, 641–671.
- Walder, R. Y., and Walder, J. A. (1988) Role of RNase H in hybrid-arrested translation by antisense oligonucleotides. *Proc. Natl. Acad. Sci. U.S.A.* 85, 5011–5015.
- Yang, W., Hendrick, W. A., Crouch, R. J., and Satow, Y. (1990) Structure of ribonuclease H phased at 2 Å resolution by MAD analysis of the selenomethionyl protein. *Science* 249, 1398–1405.
- Zuckermann, R. N., and Schultz, P. G. (1988) A hybrid sequence-selective ribonuclease S. *J. Am. Chem. Soc.* 110, 6592–6594.
- Zuckermann, R. N., and Schultz, P. G. (1989) Site-selective cleavage of structured RNA by a staphylococcal nuclease-DNA hybrid. *Proc. Natl. Acad. Sci. U.S.A.* 86, 1766–1770.
- Zuckermann, R. N., Corey, D. R., and Schultz, P. G. (1988) Site-selective cleavage of RNA by a hybrid enzyme. *J. Am. Chem. Soc.* 110, 1614–1615.

# Site-Specific Religation of G-CSF Fragments through a Thioether Bond

Hubert F. Gaertner,\*† Robin E. Offord,† Ron Cotton,‡ David Timms,‡ Roger Camble,‡ and Keith Rose†

Département de Biochimie Médicale, Centre Médical Universitaire, 1, rue Michel Servet, 1211 Geneva 4, Switzerland, and Zeneca Pharmaceuticals, Mereside, Alderley Park, Macclesfield Cheshire SK 10 4TG, U.K. Received February 9, 1994\*

A new approach is described for linking, through a thioether bond, the C-terminus of one unprotected polypeptide with the N-terminus of another. Homocysteine thiolactone is attached to the C-terminus of one polypeptide by reverse proteolysis and provides through hydroxylamine treatment a free sulfhydryl group. The  $\alpha$ -amino group of a second polypeptide is selectively iodoacetylated by reaction with iodoacetic anhydride at pH 6.0 or the *N*-hydroxysuccinimide ester derivative at pH 7.0. Coupling of the two modified fragments occurs in a spontaneous alkylation reaction under mild conditions. After preliminary experiments with small peptides, this approach was extended to large protein fragments derived from recombinant analogs of G-CSF by enzymatic digestion. This approach provides a means of making head-to-tail protein chimeras or introducing noncoded structural elements into a protein.

## INTRODUCTION

In recent years several chemical or chemoenzymatic tools have been successfully developed for the construction of protein analogs and the introduction of noncoded structural elements as a means of modulating protein stability and activity. Those approaches that show the most general applicability involve the use of nonpeptide links formed by the spontaneous and specific reaction of two functional groups that have been introduced at the end of the fragments to be joined. For example, formation of a hydrazone bond was shown to be a powerful way to site-specifically relink protein fragments resulting from the enzymatic digestion of a recombinant analog of G-CSF (Gaertner et al., 1992) or to incorporate a synthetic peptide into the protein backbone (Gaertner et al., 1994). Other means already investigated for the construction of protein chimeras or analogs involve relinking through a disulfide bridge which is a procedure used since the beginning of synthetic studies on proteins (Humphries et al. and references cited therein, 1991), an oxime bond (Rose, 1994), or a thioester or a thioether bond (Schnölzer and Kent, 1992, 1993). However, in the case of Schnölzer and Kent's analogs of HIV-1 protease both fragments were made by total synthesis so that the positioning of the reactive groups was not a problem.

In this paper, we describe an approach for relinking unprotected protein fragments through a stable, thioether bond, using as an example the two polypeptides resulting from enzymatic cleavage of tailored recombinant analogs of G-CSF containing a single lysine residue at specified positions (Gaertner et al., 1992). This strategy involves two distinct modifications. In one, a reactive cysteine derivative, homocysteine thiolactone, was introduced at the C-terminal lysine of the terminal fragment by reverse proteolysis, using the same enzyme as was used for cleavage of the tailored analog at that point. The grafted residue is subsequently opened with hydroxylamine to liberate a thiol group ready for alkylation. For the second modification, an  $\alpha$ -haloacetyl moiety is specifically grafted to the N-terminus of the second fragment, owing to the absence of any  $\epsilon$ -amino group. To exemplify the method, we describe the conjugation of two small peptides bearing

these functional groups at the ends to be joined and the extension of this chemistry to larger polypeptides for the construction of several protein analogs of G-CSF.

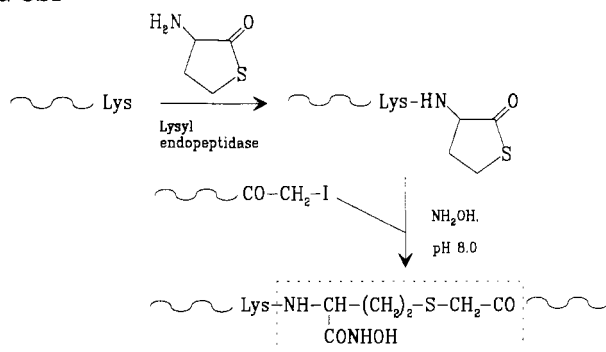
## EXPERIMENTAL PROCEDURES

**Materials and General Methods.** Iodoacetic anhydride was from Aldrich Chemical Co. and Ser-Leu-Leu from Bachem (Bubendorf, Switzerland). Boc-GlyONSu, iodoacetate, bromoacetate, sodium lauroyl sarcosinate (Sarcosyl), and homocysteine thiolactone (HCTL) were purchased from Fluka (Buchs, Switzerland). *Achromobacter lyticus* protease (lysyl endopeptidase) was from Wako Pure Chemical Co., Osaka, Japan.

Boc-Gly-HCTL was synthesized by adding 82 mg of Boc-Gly-ONSu (300  $\mu$ mol) to 50 mg of HCTL (325  $\mu$ mol) dissolved in 1 mL of anhydrous DMSO. *N*-methylmorpholine was added to an apparent pH of 9.0 (measured externally using pH paper prewetted with water). After 3 h at room temperature, the reaction mixture was diluted with 25 volumes of 0.1% TFA and applied on a Chromabond C<sub>18</sub> cartridge, bed volume 2 mL, previously washed with MeOH and equilibrated with 0.1% TFA. After the Chromabond was thoroughly washed with 0.1% TFA containing 5% acetonitrile, the product was eluted with 25 mL of 0.1% TFA containing 50% acetonitrile and dried under vacuum (weight, 66 mg; yield, 80%). The product was characterized by electrospray ionization mass spectrometry (ESI-MS) (calcd  $M + H$ ,  $m/z$  275.2, found  $m/z$  275.3).

ICH<sub>2</sub>COONSu was obtained by reaction of 1 equiv of ICH<sub>2</sub>COOH with 1 equiv of *N*-hydroxysuccinimide (NSu) and 1 equiv of dicyclohexylcarbodiimide dissolved in a small volume of ethyl acetate. After 4 h incubation, dicyclohexylurea was discarded by filtration and the solvent evaporated. An analogous procedure was used to prepare the bromoacetyl derivative. HPLC was performed on a Waters 625 LC system equipped with a Wisp 712 sample processor and a Model 441 UV detector. For analytical work, a column 250  $\times$  4 mm i.d. (Nucleosil 300-Å 5- $\mu$ m C8, Macherey Nagel, Oensingen, Switzerland) was used at a flow rate of 0.6 mL/min and the effluent monitored at 214 nm. For preparative work, a column 250  $\times$  10-mm i.d. of Nucleosil 300-Å 5- $\mu$ m C4 or C8 (Macherey Nagel) was used at a flow rate of 3 mL/min.

\* Abstract published in *Advance ACS Abstracts*, June 1, 1994.

**Scheme 1. Construction of the Thioether Analog of G-CSF**

Solvent A was 1 g of trifluoroacetic acid (Pierce) added to 1 L of water (MilliQ system). Solvent B was prepared by adding 1 g of trifluoroacetic acid to 100 mL of water and making up to 1 L with acetonitrile (Lichrosolv, Merck).

The N-terminal fragments (1-62, 1-75, 1-98) and C-terminal fragments (63-174, 76-174, 99-174) were obtained by enzymatic digestion with *Achromobacter* protease of three recombinant analogs of G-CSF produced in *E. coli* as previously described (Gaertner et al., 1992). These analogs are known as TG116 (Cys 17 → Ser; Lys 16, 23, 34, 40 → Arg; Ser62 → Lys), TG 117 (Cys17 → Ser; Lys16, 23, 34, 40 → Arg; Leu75 → Lys), and TG47 (Cys17 → Ser; Lys16, 23, 34, 40 → Arg; Glu98 → Lys). Each contains a single lysine residue for proteolytic cleavage, and ligation of resulting large protein fragments can be achieved, as already shown with TG116 and TG117 fragments, through a hydrazone linkage (Gaertner et al., 1992).

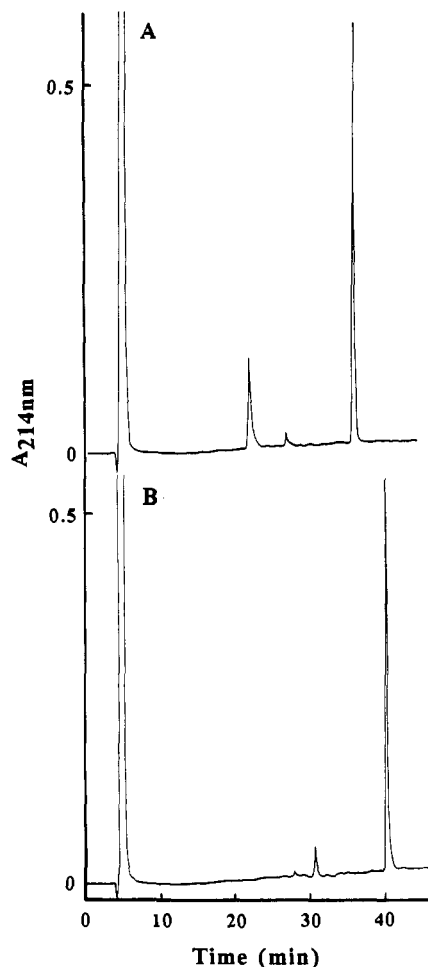
**Enzymatic Coupling of Homocysteine Thiolactone.** HCTL was attached to fragments 1-75, 1-62, and 1-98, all of which have a C-terminal lysine, by reverse reaction of *Achromobacter* protease. A solution of HCTL (0.5M) was prepared in 80% butanediol, and the apparent pH was adjusted to 5.5 with *N*-methylmorpholine using an uncorrected glass electrode calibrated with aqueous standards. The protein fragment was dissolved in the HCTL solution at 20 mg/mL. *Achromobacter* protease was added as a freshly prepared solution in water (20 mg/mL) at an enzyme/substrate ratio of 1:20 (w/w) and the sample incubated at room temperature for 3 h. The extent of modification was followed by analytical HPLC of samples quenched in excess 0.1% TFA using a linear gradient from 40% to 60% B over 40 min for fragments 1-75 and 1-62 and 45% to 65% B over 40 min for fragment 1-98. In both cases, the HCTL derivative eluted later than the unmodified fragment. The modified fragment was recovered by acidification with two volumes of pure acetic acid and dilution with 10 volumes of 0.1% TFA followed by adsorption to a Sep-Pak C<sub>18</sub> cartridge, previously washed with methanol and equilibrated with 0.1% TFA. After being washed with 5 mL of 0.1% TFA containing 20% CH<sub>3</sub>CN, the sample was eluted with 5 mL of 0.1% TFA containing 80% CH<sub>3</sub>CN. Solvent was removed in the vacuum centrifuge and the mixture of modified and unmodified fragments lyophilized and taken up in water at a 2 mM concentration for the condensation reaction.

**Iodoacetylation and Bromoacetylation.** Derivatization of the tripeptide Ser-Leu-Leu with iodoacetic anhydride was performed according to the method of Wood and Wetzel (1992a). Briefly, to 1 mL of Ser-Leu-Leu (10 mM in a 0.1 M 2-(*N*-morpholino)ethanesulfonic acid (MES) buffer at pH 6.0) were added under vortex mixing

three 60-μL additions of iodoacetic anhydride (0.25 M in dry THF) at 3-min intervals. The reaction was stopped after 10 min at 0 °C by the addition of 2 equiv of acetic acid and the product purified by HPLC on the 250 × 10-mm i.d. column using a flow rate of 3 mL/min and a linear gradient of 20–40% (by vol) B over 20 min. The product gave the expected molecular weight, as determined by FAB-MS (calcd M + H, *m/z* 500.3, found *m/z* 500.6).

The protein fragments 76–174 and 99–174 were dissolved (2 mg/mL) in a 0.1 M sodium phosphate buffer (pH 7.0) in the presence of 0.3% Sarcosyl and were modified with the *N*-hydroxysuccinimide ester of iodo- or bromoacetic acid, since the derivatization with iodoacetic anhydride was in this case inefficient, as monitored by analytical HPLC using a linear gradient of 50%–80% (by vol) B over 30 min in the case of fragment 76–174 and 45%–85% B over 40 min in the case of fragment 99–174. Eight to 10 additions of 5 equiv of the active ester were made over 30 min to the fragment solution at 0 °C and the reaction stopped after 45 min. In the case of 76–174, this was done by desalting the derivatized fragment on a 10-mL Biorad column packed with Biogel P6 and equilibrated in 0.1 M sodium phosphate pH 8.0 in the presence of 0.1% Sarcosyl. The excluded protein fraction was used for the alkylation reaction after concentration on a Centricon 100 concentrator to about 2 mg/mL. In case of α-haloacetylated 99–174, which is less soluble than derivatized 76–174, the reaction was stopped by a pH shift to 5.3 with acetic acid and the excess of reagent removed by dialysis against a 20 mM NaOAc buffer, pH 5.3, containing 0.1% sarcosyl during 7 h. Since working up the iodoacetylation reaction as quickly as possible was found to be essential, as already reported (Wood & Wetzel, 1992b), HPLC purification would have been the best way to isolate the iodo- or bromoacetyl products. However, the very low recoveries with this method, probably due to the high hydrophobicity of these particular compounds, led us to adopt the alternative conditions of purification described. The condensation reaction was started without delay.

**Condensation Reaction.** In the case of model peptides, equimolar amounts of Boc-Gly-HCTL and ICH<sub>2</sub>CO-Ser-Leu-Leu were mixed to obtain a 1 mM solution in 0.1 M sodium phosphate, pH 8.0, which was brought to 0.1 M NH<sub>2</sub>OH and incubated at room temperature. The conjugation was followed by analytical HPLC, using a linear gradient of 10% to 50% (by vol) B over 40 min, and all the peaks were collected and characterized by electrospray ionization mass spectrometry. In the case of coupling the iodoacetyl tripeptide to the C-terminal-derivatized fragment 1-75 from TG117, a 2-fold molar excess of the alkylating peptide over the latter compound was used. In case of derivatized protein fragment, conjugation was carried out with a 2–3-fold excess of HCTL-derivatized N-terminal fragment (2 mM in water, initially) over the α-haloacetylated C-terminal fragment in a 0.1 M sodium phosphate buffer, pH 8.0, and brought to 1 mM EDTA and 0.1 M NH<sub>2</sub>OH. The 99–174 derivative which was previously dialyzed against 20 mM NaOAc buffer, pH 5.3, was mixed with a 1/10 volume of 1 M sodium phosphate buffer, pH 8.0, and the pH adjusted to 8.0 with NaOH before the addition of the other reagents. After 15 h incubation at room temperature, the reaction mixture was analyzed by SDS-PAGE under reducing conditions and the coupled product was separated from unreacted fragments and side products by reversed-phase HPLC using a linear gradient from 50% to 80% B over 30 min in case of the TG117 analog and 45% to 70% B over 50 min in case of the TG47 analog.



**Figure 1.** Reversed-phase HPLC chromatograms of (A) the reaction mixture of Boc Gly-HCTL preincubated 1 h with 0.1 M  $\text{NH}_2\text{OH}$  and iodoacetylated Ser-leu-Leu at pH 2.0 and (B) the reaction mixture of iodoacetylated Ser-Leu-Leu and Boc-Gly-HCTL after 15 h incubation at pH 8.0, in the presence of 0.1 M  $\text{NH}_2\text{OH}$ . The conjugation product elutes at  $t_R = 40$  min while the peak that eluted at  $t_R = 32$  min corresponds to the side product of the coupling reaction. In A, Boc-Gly-HCTL and  $\text{ICH}_2\text{CO-Ser-Leu-Leu}$  elute at  $t_R = 26$  and 35 min, respectively, and the  $\text{NH}_2\text{OH}$ -opened thiolactone derivative at 22 min.

**SDS-PAGE.** SDS-PAGE under reducing conditions (5%, by vol  $\beta$ -mercaptoethanol) was performed on a Phast-System electrophoresis apparatus (Pharmacia) using 20% polyacrylamide gels. Proteins were applied to the gel for 90 Vh at 15 °C and visualized by silver staining. Protein standards were from Pharmacia: phosphorylase b (94 kDa), albumin (67 kDa), ovalbumin (43 kDa), carbonic anhydrase (30 kDa), soybean trypsin inhibitor (20.1 kDa), and  $\alpha$ -lactalbumin (14.4 kDa).

**Mass Spectrometry.** The molecular weight of the different derivatives obtained at each step of the constructions was measured by mass spectrometry. Equipment and operating conditions were as previously described (Gaertner et al., 1992).

## RESULTS AND DISCUSSION

**Peptide Coupling through a Thioether Linkage.** Homocysteine thiolactone was chemically attached to Boc-Gly in order to introduce a thiol functionality at the C-terminus and study the site-specific conjugation with iodoacetylated Ser-Leu-Leu. This strategy of conjugation through a thioether bond involves two reaction steps, the deprotection of the masked sulfhydryl group and its subsequent alkylation. As shown in Figure 1B, the

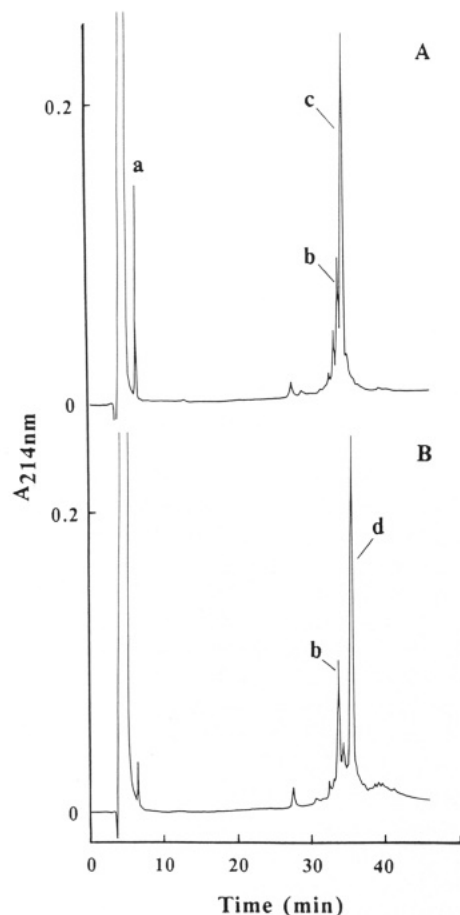
coupling reaction proceeds cleanly. A 1-h preincubation of the HCTL derivative with  $\text{NH}_2\text{OH}$  (0.1 M) at pH 8.0, which releases a free sulfhydryl group at the C-terminus (Figure 1A), is in fact not necessary to carry out the alkylation; this procedure only improves the rate of the coupling reaction, which is almost complete after 5 h incubation at room temperature (results not shown). The same profile was obtained when  $\text{NH}_2\text{OH}$  treatment and alkylation were carried out at the same time (Figure 1B) with a 15 h incubation in a 0.1 M sodium phosphate buffer, pH 8.0, containing 0.1 M  $\text{NH}_2\text{OH}$ . These conditions were expected to reduce the occurrence of unwanted side reactions (i.e., disulfide formation or disulfide bond exchange) when conjugation involves polypeptides containing either cysteine residues or disulfide bridges.

The conjugation product had the expected molecular weight, as determined by FAB-MS (calcd  $M + H$   $m/z$  679.32, found  $m/z$  679.26). The earlier-eluting product ( $t_R = 32$  min), was identified by FAB-MS as the *N*-alkylated derivative of Gly-HCTL (calcd  $M + H$   $m/z$  546.25, found  $m/z$  546.31). This side product could be detected under all conditions of conjugation tried and was shown to be especially prominent when the concentration of  $\text{NH}_2\text{OH}$  was very low (<20 mM). The coupling reaction is pH dependent: while no coupling occurred at pH 6.0, a maximum coupling yield was obtained at pH 8.0 in the presence of 0.1 M  $\text{NH}_2\text{OH}$ .

**Enzymatic Coupling of Homocysteine Thiolactone.** The high resistance of G-CSF analogs to organic solvents (Gaertner et al., data not shown) and the ability to obtain a solution of homocysteine thiolactone at a relatively high concentration (0.5 M) in butane-1,4-diol allowed us to explore enzymatic coupling by reverse proteolysis (Offord, 1990) as a means of appending a masked thiol group to the C-terminus of isolated protein fragments 1-62, 1-75, and 1-98. HCTL was considered as the most appropriate reagent to site-specifically introduce a masked sulfhydryl group in the protein fragment while avoiding side reactions that might occur with unmasked thiol derivatives when used at high concentration. Though HCTL has a rather high  $pK$  value when compared to hydrazides, a satisfactory conjugation yield could be still obtained at pH 5.5 owing to the presence of a high proportion of organic solvent in the medium. Attempts to shift the equilibrium even more toward synthesis by further increasing the pH resulted in HCTL precipitation and thiolactone hydrolysis. The use of pH values lower than 5.5 led to esterification of the fragment with butane-1,4-diol.

When the reaction was carried out in the presence of 80% butane-1,4-diol as cosolvent at an enzyme:substrate ratio of 1:20 (w/w), equilibrium in the coupling reaction was reached within 2-3 h with a conjugation yield of approximately 70%. Figure 2A, which is in fact a control of the next step of construction, reflects the extent of enzymatic coupling. The product was characterized by ESI-MS (calcd  $m/z$  8277.6, found  $m/z$  8278.1  $\pm$  0.5). Prolongation of the incubation time should be avoided, so as to preclude the formation of overreaction products which were eluted at the same time as the expected product and were identified by ESI-MS as 1-75-(Hcys)<sub>2</sub> and 1-75-(Hcys)<sub>2</sub>-HCTL.

This specific derivatization does not require isolation of the coupled product from uncoupled fragment as this latter is not able to react with the iodoacetylated peptide. Adsorption on to a C18 Sep-Pak cartridge, which separates the excess of HCTL from protein fragment, was therefore sufficient.

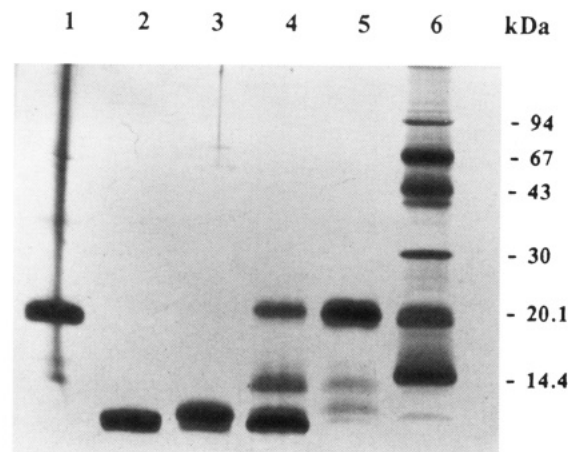


**Figure 2.** HPLC chromatograms of coupling between fragment (1-75)-HCTL and iodoacetylated Ser-Leu-Leu. Panel A: reaction mixture of ICH<sub>2</sub>CO-Ser-Leu-Leu (a) and (1-75)-HCTL (c) at pH 2.0. Panel B: reaction mixture of ICH<sub>2</sub>CO-Ser-Leu-Leu (a) and (1-75)-HCTL (b) at pH 8.0 after 15 h at room temperature, in the presence of 0.1 M NH<sub>2</sub>OH. ICH<sub>2</sub>CO-Ser-Leu-Leu (a), fragment 1-75 (b), (1-75)-HCTL (c), and the thioether derivative (d) elute at 6.5, 33.0, 34.0, and 35.0 min, respectively.

**Iodoacetylation and Bromoacetylation of the Protein Fragment N-Terminus.** Fragments 76-174 and 99-174 were iodoacetylated specifically at the N-terminus upon addition of at least a 50-fold molar excess of the *N*-hydroxysuccinimide ester derivative over the fragment in a 0.1 M sodium phosphate buffer at pH 7.0. ICH<sub>2</sub>CO-(76-174), which eluted later than the unmodified fragment, could be characterized by ESI-MS (calcd *m/z* 10 917.2, found *m/z* 10 916.0 ± 1.9).

In the case of fragment 99-174, iodoacetylation and bromoacetylation were run in parallel under the same conditions as previously described. Modified fragments were purified by dialysis, and the two resulting derivatives were compared in the conjugation reaction.

**Conjugation of Protein Fragments.** Reactions with protein fragments were carried out at lower concentrations than when linking two small model peptides. Perhaps as a consequence, it was found that conjugation of ICH<sub>2</sub>CO-Ser-Leu-Leu to fragment 1-75-HCTL only occurred efficiently if the alkylation was performed at the same time as sulfhydryl deprotection. Moreover, all solutions were previously flushed with N<sub>2</sub> to avoid disulfide formation. Under these conditions, when using a 2-fold excess of ICH<sub>2</sub>CO-Ser-Leu-Leu over (1-75)-HCTL in the presence of 0.1 M NH<sub>2</sub>OH, a high coupling yield could be obtained (Figure 2B). The conjugation product (1-75)-NH-CH(CONHOH)(CH<sub>2</sub>)<sub>2</sub>SCH<sub>2</sub>CO-Ser-Leu-Leu was isolated and characterized by ESI-MS (calcd *m/z* 8682.1,



**Figure 3.** SDS-polyacrylamide gel electrophoresis of coupling between fragment (1-75)-HCTL and iodoacetylated fragment 76-174: lane 1, G-CSF analog TG 117; lane 2, fragment 1-75; lane 3, fragment 76-174; lane 4, incubation of ICH<sub>2</sub>CO-(76-174) with (1-75)-HCTL after 15 h; lane 5, (1-75)-(76-174) thioether analog after HPLC purification; lane 6, protein markers.

found *m/z* 8682.1 ± 0.8) which is consistent with NH<sub>2</sub>-OH-promoted thiolactone ring opening and formation of the thioether linkage at the C-terminus of the protein fragment.

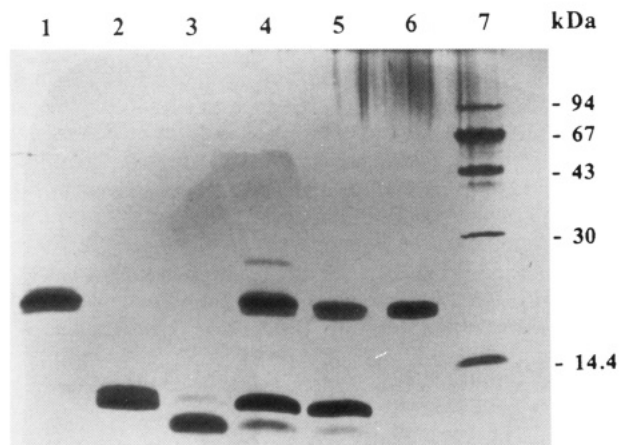
The same reaction was carried out with ICH<sub>2</sub>CO-(76-174) by using a 2-3-fold molar excess of the HCTL derivative over the iodoacetylated fragment. As shown in Figure 3, the coupling reaction led to a G-CSF protein analog containing a thioether bond, which is supported by ESI-MS data (calcd *m/z* 19 099.9, found *m/z* 19 103.1 ± 3.5). However, the conjugation reaction also resulted in some byproducts with defined masses (18 432.4 ± 2.0; 15 211.0 ± 7.3), which must involve splitting of one of the initial derivatized fragments. The structure of these polypeptides was not further investigated.

According to the HPLC profile, the reaction yield was estimated to be about 50%. The coupling efficiency is likely to be related to the accessibility of the activated end groups. Indeed, our attempts to recouple fragments 1-62 and 63-174 resulting from the enzymatic digestion of TG116 were disappointing (yield <10%), whereas the (1-62)-NHCH(CONHOH)(CH<sub>2</sub>)<sub>2</sub>SCH<sub>2</sub>CO-(76-174) analog lacking the disulfide loop could be constructed with a high yield (results not shown) and characterized by ESI-MS (calcd *m/z* 17 855.5, found *m/z*, 17 861.8 ± 3.8). In the same way, as shown in Figure 4, this procedure gave quite high coupling yields in the conjugation of 1-98-HCTL and ICH<sub>2</sub>CO-(99-174). Similarly, at least 70% coupling yield based on BrCH<sub>2</sub>CO-(99-174) was obtained, indicating that both iodo- and bromoacetylated derivatives are efficient for protein fragment conjugation. In both cases, some side products could be detected by overloading the gel (results not shown), so both were equally suited for the coupling step. The resulting thioether analog was characterized by ESI-MS (calcd *m/z* 19 084.1, found *m/z* 19 088.9 ± 6.6).

This strategy of ligation involves the insertion of -NHCH(CONHOH)CH<sub>2</sub>CH<sub>2</sub>SCH<sub>2</sub>CO-, which has to be taken into account in the design of the product to be assembled. The stable thioether bond introduced might exhibit higher flexibility between the joined fragments than does the hydrazone bond (Gaertner et al., 1994).

With respect to the biological response, the specific activity of the thioether analog of TG117 (Table 1, sample 6) in the *in vitro* assay, was comparable to that of the





**Figure 4.** Conjugation reaction of fragment (1-98)-HCTL with either iodoacetylated or bromoacetylated fragment 99-174: lane 1, G-CSF analog TG47; lane 2, fragment 1-98; lane 3, fragment 99-174; lane 4, incubation of  $\text{ICH}_2\text{CO}$ -(99-174) with (1-98)-HCTL after 15 h; lane 5, incubation of  $\text{BrCH}_2\text{CO}$ -(99-174) with (1-98)-HCTL after 15 h; lane 6, (1-98)-(99-174) thioether analog after HPLC purification; lane 7, protein markers.

**Table 1. Biological Activity (Units/mg Protein) of G-CSF Recombinant Proteins, Their Fragments, and Recoupled Thioether Analogs**

sample	specific activity <sup>a</sup>
1. TG 117	$1.5 (\pm 1.0) \times 10^5$
2. TG 47	$5.3 (\pm 0.9) \times 10^6$
3. (1-75) + (76-174) from TG 117	trace
4. (1-62) + (76-174) from TG 116 and TG 117	0
5. (1-98) + (99-198) from TG 47	trace
6. (1-75)-NHCH(CONHOH) $\text{CH}_2\text{CH}_2$ -SCH <sub>2</sub> CO-(77-174)	$1.3 (\pm 0.5) \times 10^5$
7. (1-62)-NHCH(CONHOH) $\text{CH}_2\text{CH}_2$ -SCH <sub>2</sub> CO-(77-174)	$1.8 (\pm 1.2) \times 10^5$
8. (1-98)-NHCH(CONHOH) $\text{CH}_2\text{CH}_2$ -SCH <sub>2</sub> CO-(99-174)	$5.8 (\pm 5.0) \times 10^5$

<sup>a</sup> The values are means  $\pm$ SD ( $n = 4$ ).

starting protein. While initial fragments had no activity of their own (Table 1, samples 3-5) the regain of activity was of the same order of magnitude as that obtained for fragments joined by a hydrazone bond ( $2.0 (\pm 0.4) \times 10^5$ , Gaertner et al., 1994). The same feature is observed for the thioether analog lacking the Cys<sup>64</sup>-Cys<sup>74</sup> disulfide loop (Table 1, sample 7) when compared to (1-62)-NHN=CHCO-(77-174) and corresponding carbo and adipo hydrazone (Gaertner et al., 1994). The thioether analog of TG47 (Table 1, sample 8) exhibits a specific biological activity which is only 1 order of magnitude lower than that of the initial protein. But it is important to bear in mind that biosynthetic mutation of Glu<sup>98</sup> to Lys has already produced a decrease of 1-2 orders of magnitude in the specific activity of the mutant form TG47.

These preliminary results illustrate the potential applications of this approach for fragment coupling or introducing segments containing unusual residues.

## CONCLUSION

The procedure described here provides a new means to construct analogs of proteins which either naturally or through engineering contain a single lysine residue. The two fragments obtained by enzymatic cleavage of such a protein with the lysine specific protease from *Achromobacter Lyticus* are relinked through a thioether bond. This approach involves the site-specific modification of the ends to be joined so that the ligation reaction occurs unambi-

gously. For this purpose, reverse proteolysis was shown to afford a unique way to append a protected sulfhydryl group at the C-terminus of one fragment. Specific N-terminal modification with an  $\alpha$ -haloacetyl moiety was easily achieved with a protein fragment having a unique reactive amino group. However, the very different basic strength of  $\alpha$ - and  $\epsilon$ -amino groups (Means & Feeney, 1990) allows proteins containing lysine residues to be more or less selectively derivatized through their N-terminal amino groups by means of acylation reactions in slightly acidic media and/or use of certain types of reagents (Wetzel et al., 1990). Indeed, such a selectivity has already been demonstrated with peptides bearing both  $\alpha$ - and  $\epsilon$ -amines via pH-controlled modification with iodoacetic anhydride (Wood & Wetzel, 1992a,b).

The chemoselective ligation, which constitutes the second step of this strategy, takes advantage of the high reactivity of iodo- or bromoacetamido groups toward sulfhydryl anions in neutral or slightly basic media when compared to that of the side-chain nucleophilic groups of Met, His, Lys, and Arg. This technique has already been investigated in order to prepare conjugates involving peptides (Bernatowicz & Matsueda, 1986; Wood & Wetzel, 1992a). Our experiments show that this strategy is also powerful for the site-specific ligation of large protein fragments. One of the major limitations of this approach is the overall low conjugation yield which is due to the instability of iodoacetylated fragments during isolation at neutral pH but is easily overcome for modified fragments soluble at acidic pH. Unfortunately, the derivatized fragment used in excess cannot be recycled as it is in the case of ligation through a hydrazone bond (Gaertner et al., 1992). Nevertheless, this technique seems particularly appropriate for the incorporation of small unprotected building blocks into the polypeptide chain and extends the range of tools already available for protein backbone engineering (Balaram, 1992; Gaertner et al., 1994). But in all cases these constructions take advantage of a careful design of the sequence by site directed mutagenesis techniques.

## ACKNOWLEDGMENT

This work was supported by the Strategic Research Fund of Zeneca Pharmaceuticals (Macclesfield, U.K.). We thank the Fonds National de la Recherche Scientifique and the Sandoz Stiftung for support of the Geneva mass spectrometry facility and P. O. Regamey for mass spectrometric analyses.

## LITERATURE CITED

- Balaram, P. (1992) Non-standard amino acids in peptide design and protein engineering. *Curr. Opin. Struct. Biol.* 2, 845-851.
- Bernatowicz, M. S., and Matsueda, G. R. (1986) Preparation of peptide-protein immunogens using N-succinimidyl bromoacetate as a heterobifunctional crosslinking reagent. *Anal. Biochem.* 155, 95-102.
- Gaertner, H. F., Rose, K., Cotton, R., Timms, D., Camble, R., and Offord, R. E. (1992) Construction of protein analogues by site-specific condensation of unprotected fragments. *Bioconjugate Chem.* 3, 262-268.
- Gaertner, H. F., Offord, R. E., Cotton, R., Timms, D., Camble, R., and Rose, K. (1994) Chemo-enzymic backbone engineering of proteins: site specific incorporation of synthetic peptides that mimic the 64-74 disulfide loop of G-CSF. *J. Biol. Chem.* 269, 7224-7230.
- Humphries, J., Offord, R. E., and Smith, A. G. (1991) Chemical methods of protein synthesis and modification. *Curr. Opin. Biotech.* 2, 539-543.



- Means, G. E., and Feeney, R. E. (1990) Chemical modifications of proteins: history and applications. *Bioconjugate Chem.* 1, 2-12.
- Offord, R. E. (1990) in Protein Design and the Development of New Therapeutics and Vaccines (J. B. Hook, and G. Poste, Eds.) pp 253-282, Plenum, New York.
- Rose, K. (1994) Facile synthesis of homogenous artificial proteins. *J. Am. Chem. Soc.* 116, 30-33.
- Schnölzer, M., and Kent, S. B. H. (1992) Constructing proteins by dovetailing unprotected synthetic peptides: backbone-engineered HIV protease. *Science* 256, 221-225.
- Schnölzer, M., and Kent, S. B. H. (1993) Chemoselective ligation of unprotected peptide segments: backbone engineered HIV-1 protease. *Peptides* 1992 (C. H. Schneider and A. N. Eberle, Eds.) pp 237-238, ESCOM, Leiden, The Netherlands.
- Wetzel, R., Halualani, R., Stults, J. T., and Quan, C. (1990) A general method for highly selective cross-linking of unprotected polypeptides via pH-controlled modification of N-terminal  $\alpha$ -amino groups. *Bioconjugate Chem.* 1, 114-122.
- Wood, S. J., and Wetzel, R. (1992a) A novel method for the incorporation of glycoprotein-derived oligosaccharides into neoglycoproteins. *Bioconjugate Chem.* 3, 391-396.
- Wood, S. J., and Wetzel, R. (1992b) Novel cyclisation chemistry especially suited for biological derived, unprotected peptides. *Int. J. Peptide Protein Res.* 39, 533-539.

# Functionalized Derivatives of Hyaluronic Acid Oligosaccharides: Drug Carriers and Novel Biomaterials

Tara Pouyani and Glenn D. Prestwich\*

Department of Chemistry, University at Stony Brook, Stony Brook, New York 11794-3400. Received November 12, 1993\*

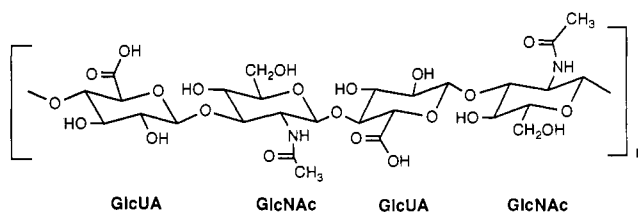
Oligosaccharides derived from hyaluronic acid (HA), a naturally occurring linear polysaccharide composed of repeating disaccharide units of *N*-acetyl-D-glucosamine and D-glucuronic acid, can be chemically modified to introduce a pendant amine-like functionality (patent application pending). Covalent attachment of steroidal and nonsteroidal antiinflammatory drugs to functionalized HA oligosaccharides was accomplished with the incorporation of hydrolytically labile bonds. Further derivatization of the pendant group with homobifunctional crosslinkers allowed the introduction of covalent crosslinks. Chemically-modified HA oligosaccharides were unambiguously characterized in solution by high-resolution  $^1\text{H}$  NMR spectroscopy.

## INTRODUCTION

Hyaluronic acid (HA) is a viscoelastic biomaterial composed of repeating disaccharide units of *N*-acetyl-D-glucosamine (GlcNAc) and D-glucuronic acid (GlcUA) (Figure 1). It is a major component of the extracellular matrix, and has been recently shown to participate in a number of important biological processes such as cell motility (1), cell differentiation (2), wound healing (3), and cancer metastasis (4). Its biocompatibility, high viscoelasticity, and nonimmunogenicity make it a medically important biomaterial. Highly-purified, high molecular weight (MW) HA sodium salt, often referred to as sodium hyaluronate or hyaluronan, is currently used in viscosurgery and viscosupplementation (5). HA is frequently used as a surgical aid in ophthalmic surgery, where advantage is taken of its lubricating and shock-absorbing properties (6). The use of hyaluronate as a potential therapy for osteoarthritis has shown beneficial effects in humans (7, 8).

The importance of hyaluronate as a potentially useful biomedical polymer has elicited research directed toward developing methodology for its chemical modification. For example, covalently-crosslinked derivatives of hyaluronate (hydrogels) could show enhanced rheological and mechanical properties and increased resistance to degradation by hyaluronidases. The covalent attachment of drugs to HA in order to create polymeric prodrugs has also received considerable attention. HA would be an excellent candidate as a drug-delivery agent. In addition to being both biocompatible and nonimmunogenic, it is also subject to degradation by enzymes widely distributed throughout the body. Moreover, both carboxyl and hydroxyl groups offer potential sites for covalent modification.

Efforts at chemical modification of hyaluronate have targeted both the hydroxyl and the carboxylate functionalities. Crosslinked derivatives of HA have been prepared by reaction with divinyl sulfone (9) and homobifunctional glycidyl ethers (10) under highly basic conditions. Esterification of HA salts with alkyl halides in organic media has resulted in the production of modified HA species showing altered physical characteristics (11). The generation of a free amino group on HA has also been the subject of much research. Hydrazinolysis of high MW HA resulted



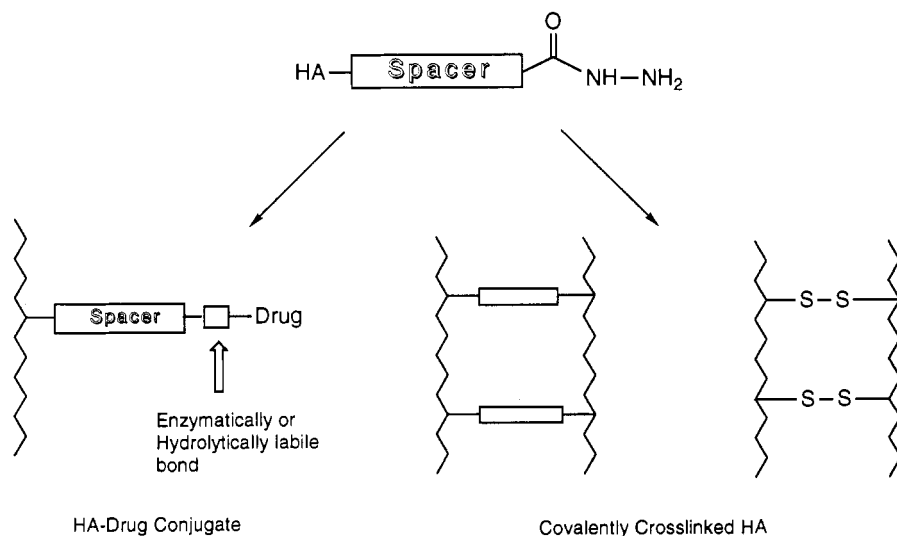
**Figure 1.** Structure of hyaluronic acid (HA) showing two disaccharide repeat units.

in *N*-deacetylation and the generation of a free amino group on the HA backbone; however, extensive degradation of HA was observed under the experimental conditions employed (12, 13). None of the heterogeneous final products of these chemical modifications were fully characterized by spectroscopic analysis. We reasoned that a mild and versatile chemical methodology was still needed. Such a methodology would (a) allow coupling of pharmacophores under mild, aqueous conditions, (b) allow crosslinking under mild conditions, (c) preserve the molecular size distribution of the HA used, and (d) produce materials that could be characterized spectroscopically.

We first focused our attention on the preparation of HA bearing a spacer with a terminal hydrazido group. The pendant hydrazido group would offer a highly versatile and sterically accessible functional group for further coupling and crosslinking (Figure 2). Initial studies were performed with HA oligomers of defined length ranging in size from 2 to 20 disaccharide units in order to facilitate unambiguous characterization of the resultant modified HA species by solution  $^1\text{H}$  NMR. We planned to extend this methodology to high MW HA ( $1.5 \times 10^6$  Da) following optimization of the chemistry.

In earlier work, solid-state NMR analysis of the reaction products obtained from the reaction of high MW hyaluronate with isotopically-labeled 1-ethyl-3-[3-(dimethylamino)propyl]carbodiimide (EDC) showed the production of two isomeric *N*-acylureas in unequal amounts (14). This confirmed earlier results obtained during unsuccessful attempts to couple diamines to HA using EDC (15). The putative *O*-acylurea intermediate rearranged in preference to trapping by the diamine nucleophiles. To take advantage of the presence of this reactive intermediate for the further functionalization of HA, a different strategy was required. Dihydrazides, by virtue of the low  $\text{pK}_a$  values (2.0–3.0) of their conjugate acids, maintain their nucleo-

\* Abstract published in *Advance ACS Abstracts*, May 1, 1994.



**Figure 2.** General strategy for generating functionalized derivatives of HA.

philicity at pH = 4.75 relative to normal protonated aliphatic or aromatic diamines with  $pK_a$  values above 9. The hydrazido  $NH_2$  could add to the *O*-acylurea intermediate to provide hydrazido-functionalized HA derivatives (16, 17). We report the preparation and characterization of HA oligosaccharides functionalized with three commercially-available dihydrazides. We demonstrate the versatility of the linker in allowing further coupling by covalent attachment of steroidal and nonsteroidal anti-inflammatory drugs and by the introduction of covalent crosslinks.

## EXPERIMENTAL PROCEDURES

**General.** High-resolution 1-D and 2-D  $^1H$  spectra were recorded on a Bruker AMX-600 MHz spectrometer. Chemical shifts are given in ppm using residual  $H_2O$  (4.80 ppm) as an internal standard, unless otherwise indicated. Water suppression was achieved by low-power selective irradiation of the  $H_2O$  resonance for 1.5–2.0 s. Phase-sensitive DQF-COSY spectra (18) were acquired in TPPI mode with standard-phase cycling schemes. In the F1 and F2 dimensions, 256 and 1024 data points were used, respectively. Hyaluronic acid (Amvisc), obtained as its sodium salt (sodium hyaluronate), was provided by MedChem Products, Inc. (Woburn, MA). Ibuprofen, hydrocortisone-hemisuccinate, and hyaluronidase (type VI-S) were purchased from Sigma Chemical Co. (St. Louis, MO). Adipic dihydrazide, succinic dihydrazide, dicyclohexylcarbodiimide (DCC), 1-ethyl-3-[3-(dimethylamino)propyl]carbodiimide (EDC), and *N*-hydroxysuccinimide (NHS) were obtained from Aldrich Chemical Co. (Milwaukee, WI). Suberic dihydrazide was purchased from Lancaster Synthesis, Inc. (Windham, NH). Homobifunctional crosslinkers bis(sulfosuccinimidyl)suberate (BS<sup>3</sup>), 3,3'-dithiobis(sulfosuccinimidyl propionate) (DTSSP), dimethyl suberimidate-2HCl (DMS), and ethylene glycolbis(sulfosuccinimidyl succinate) (sulfo-EGS) were obtained from Pierce Chemical Co. (Rockford, IL). All solvents used were Optima (HPLC grade), obtained from Fisher Chemical Co. (Pittsburgh, PA). HA fragments of defined length were generated by either limited or exhaustive digestion with testicular hyaluronidase and were separated, purified, and characterized according to published procedures (19–21). HA oligosaccharides were assayed using the carbazole method (22) with glucuronolactone as the standard. Biogel P-2 (fine), Biogel P-6 (fine),

and Biogel P-30 (superfine) were purchased from Bio-Rad Laboratories (Richmond, CA).

**General Procedure for Coupling of HA with Dihydrazides.** Fragments of hyaluronate (typically 10–15 mg) were dissolved in water to a concentration of 4 mg/mL. To this mixture was added a 20–40-fold molar excess of dihydrazide. The pH of the reaction mixture was adjusted to 4.75 by addition of 0.1 N HCl. A 4-fold molar excess of EDC was dissolved in ca. 1 mL of water and added to the reaction mixture. An increase in pH was typically observed after addition of the carbodiimide. The pH of the reaction was consistently maintained at 4.75 by addition of 0.1 N HCl, and the reaction was allowed to proceed at room temperature for 2 h or until no further change in pH was observed. The pH of the reaction mixture was then adjusted to 7.0 with 0.1 N NaOH, concentrated by rotary evaporation, redissolved in 1.5 mL of  $H_2O$ , and applied directly to a column of Biogel P-2 (30  $\times$  1.5 cm). The mixture was separated by gel filtration chromatography using water as eluant at a flow rate of 30 mL/h. Typically, 40 fractions of 2 mL each were collected and assayed for glucuronic acid content using the carbazole method. Fractions that tested positive were pooled and lyophilized and subsequently analyzed by high-resolution  $^1H$  NMR spectroscopy in  $D_2O$ .

**Coupling Products of HA Fragments with Dihydrazides (1a–c).** The above-described general procedure was adopted in preparing the hydrazide-functionalized HA derivatives. The details of selected individual reactions and the analytical results are given below for several different HA oligosaccharides.

**Succinyl Derivative 1a.** HA tetrasaccharide (15 mg, 0.036 mmol) was subjected to the coupling reaction. The molar ratio of HA tetrasaccharide:succinic dihydrazide was 1:30, and the ratio of HA:EDC was 1:3. The reaction was conducted at 50  $^{\circ}C$  to improve succinic dihydrazide solubility in water. The recovery of modified HA after gel filtration was 13.0 mg (86% recovery); 2 mg of 1a was dissolved in 500  $\mu$ L of  $D_2O$  for  $^1H$  NMR. Proton resonances were assigned by comparison of the modified HA spectrum to unmodified HA and to an admixture of unmodified HA and the succinic dihydrazide reagent alone:  $^1H$  NMR ( $D_2O$ )  $\delta$  2.50–2.80 (m, 4H,  $-NHNHC(O)CH_2CH_2C(O)-NHNH_2$ ).

**Adipic Dihydrazide Derivative 1b.** HA hexasaccharide (10 mg, 0.025 mmol) was subjected to the coupling reaction at room temperature. The molar ratio of HA hexasac-

charide:adipic dihydrazide was 1:40, and the ratio of HA:EDC was 1:4. The recovery of modified HA after gel filtration was 8.0 mg (80% recovery).  $^1\text{H}$  NMR assignments were made as described for 1a:  $^1\text{H}$  NMR ( $\text{D}_2\text{O}$ )  $\delta$  2.29–2.31 (t, 2H,  $J = 6.3$  Hz,  $-\text{NHNHC}(\text{O})\text{CH}_2$ ), 2.16–2.25 (t, 2H,  $J = 6.4$  Hz,  $-\text{NHNHC}(\text{O})\text{CH}_2$ ), 2.11–2.15 (m, 2H,  $-\text{CH}_2\text{C}(\text{O})\text{NHNH}_2$ ), 1.53–1.54 (m, 2H,  $-\text{CH}_2\text{CH}_2\text{CH}_2\text{C}(\text{O})\text{NHNH}_2$ ), 1.55–1.57 (m, 2H,  $-\text{CH}_2\text{CH}_2\text{C}(\text{O})\text{NHNH}_2$ ).

**Suberic Dihydrazide Derivative 1c.** HA octasaccharide (10 mg, 0.025 mmol) was subjected to the coupling reaction. The molar ratio of HA octasaccharide:suberic dihydrazide was 1:40, and the ratio of HA:EDC was 1:4. The reaction was run at 70 °C to promote the solubility of suberic dihydrazide in water. The recovery of modified HA after gel filtration was 8.0 mg (80% recovery).  $^1\text{H}$  NMR assignments were made as described for 1a and 1b:  $^1\text{H}$  NMR ( $\text{D}_2\text{O}$ )  $\delta$  2.25–2.28 (t, 2H,  $J = 7.3$  Hz,  $-\text{NHNHC}(\text{O})\text{CH}_2$ ), 2.16–2.25 (t, 2H,  $J = 7.4$  Hz,  $-\text{NHNHC}(\text{O})\text{CH}_2$ ), 2.11–2.15 (m, 2H,  $-\text{CH}_2\text{C}(\text{O})\text{NHNH}_2$ ), 1.53–1.58 (m, 2H,  $-\text{NHNHC}(\text{O})\text{CH}_2\text{CH}_2$ ), 1.49–1.51 (t, 2H,  $J = 7.5$  Hz,  $-\text{CH}_2\text{CH}_2\text{C}(\text{O})\text{NHNH}_2$ ), 1.24–1.27 (m, 4H,  $\text{CH}_2\text{CH}_2\text{CH}_2\text{C}(\text{O})\text{NHNH}_2$ ).

**Synthesis of *N*-Succinimidyl Ibuprofen (2).** Ibuprofen (100 mg, 0.48 mmol) was dissolved in 2 mL of dry glyme. To this mixture was added an equimolar amount of NHS (56.0 mg, 0.48 mmol). The reaction mixture was cooled to 4 °C, and DCC (99.0 mg, 0.48 mmol) was added. A white precipitate formed, and the reaction was allowed to stir overnight at 4 °C. The reaction mixture was filtered and then concentrated by rotary evaporation to give 120 mg of the NHS ester of Ibuprofen. The compound was used without further purification in the coupling reaction with hydrazido-modified HA:  $^1\text{H}$  NMR (300 MHz,  $\text{CDCl}_3$ )  $\delta$  7.12–7.20 (dd, 4H, ArH), 3.90–4.08 (q, 1H,  $\text{CHCOOH}$ ), 2.78 (s, 4H,  $\text{C}(\text{O})\text{CH}_2\text{CH}_2\text{C}(\text{O})$ ), 2.43–2.45 (d, 3H,  $\text{CH}_3\text{CHCOOH}$ ), 1.80–1.90 (m, 1H,  $(\text{CH}_3)_2\text{CHCH}_2$ ), 1.60–1.63 (d, 2H,  $(\text{CH}_3)_2\text{CHCH}_2$ ), 0.85–0.89 (d, 6H,  $(\text{CH}_3)_2\text{CHCH}_2$ ).

**Synthesis of *N*-Succinimidyl Hydrocortisone-Hemisuccinate (4).** Hydrocortisone-hemisuccinate (100 mg, 0.216 mmol) was dissolved in 2 mL of dimethyl formamide (DMF). To this mixture was added NHS (25.0 mg, 0.216 mmol). Next, DCC (45.0 mg, 0.216 mmol) was added to the mixture, and the reaction was allowed to stir at room temperature for 16 h. The precipitated dicyclohexylurea was removed by filtration, and the mixture was concentrated by rotary evaporation. The NHS derivative was used without any further purification in the coupling reaction with hydrazido-functionalized HA 1b.

**General Procedure for Coupling of *N*-Hydroxysuccinimide Derivatives of Hydrocortisone-Hemisuccinate and Ibuprofen to HA Functionalized with Adipic Dihydrazide 1b.** HA fragments of defined length functionalized with adipic dihydrazide as described above were dissolved in 0.1 M  $\text{NaHCO}_3$  buffer (pH = 8.50) to a concentration of 5 mg/mL. To this mixture was added the NHS ester dissolved in sufficient DMF to give a homogeneous solution. The reaction was stirred at room temperature for 18 h, concentrated by rotary evaporation, redissolved in 2 mL of  $\text{H}_2\text{O}$ , and subjected to gel filtration on a column of Biogel P-2 (30 cm  $\times$  1.5 cm) using water as eluant at a flow rate of 30 mL/h. Typically, 40 fractions of 2 mL each were collected and assayed for glucuronic acid content. The fractions that tested positive were pooled, lyophilized, and analyzed spectroscopically by high-resolution  $^1\text{H}$  NMR in  $\text{D}_2\text{O}$  at 600 MHz.

**Coupling Products of Adipic Dihydrazide-Functionalized HA with NHS-Ibuprofen and NHS-Hy-**

**drocortisone-Hemisuccinate.** The general procedure above was used for the coupling of Ibuprofen and hydrocortisone-hemisuccinate to adipic dihydrazide functionalized HA. The details of the individual reactions and the spectroscopic results follow.

**Ibuprofen-HA 3 (Scheme 2).** Hydrazido-functionalized HA octasaccharide (5.0 mg, 0.013 mmol) was coupled with NHS-Ibuprofen (18.0 mg, 0.063 mmol) dissolved in 2 mL DMF. The molar ratio of hydrazido-HA:NHS-Ibuprofen was 1:5. The recovery of Ibuprofen-linked HA after gel filtration chromatography was 3.0 mg (60% recovery). The modified sample was dissolved in 500  $\mu\text{L}$  of  $\text{D}_2\text{O}$ ; diagnostic peaks that do not overlap with the HA and linker resonances are reported:  $^1\text{H}$  NMR ( $\text{D}_2\text{O}$ )  $\delta$  7.20–7.30 (dd, 4H, ArH), 2.50 (m, 2H,  $-\text{CH}_2\text{C}(\text{O})\text{NHNH}-$ ), 1.60–1.70 (m, 4H,  $\text{CH}_2\text{CH}_2\text{CH}_2\text{C}(\text{O})\text{NHNH}-$ ), 1.55 (d, 2H,  $(\text{CH}_3)_2\text{CHCH}_2$ ), 0.90 (d, 6H,  $-\text{CH}(\text{CH}_3)_2$ ); UV (0.1 M  $\text{NaHCO}_3$ )  $\lambda_{\text{max}}$  266 nm.

**Hydrocortisone-HA 5 (Scheme 3).** Hydrazido-functionalized HA decasaccharide (3.0 mg, 0.008 mmol) was allowed to react with NHS-hydrocortisone-hemisuccinate (42.0 mg, 0.075 mmol) dissolved in 1 mL of DMF. The molar ratio of hydrazido HA:NHS-hydrocortisone-hemisuccinate was 1:10. The recovery of hydrocortisone-linked HA after gel filtration was 2.80 mg (93% recovery):  $^1\text{H}$  NMR ( $\text{D}_2\text{O}$ )  $\delta$  5.80 (s, 1H,  $\text{C}(\text{O})\text{CH}=\text{C}$ ), 1.65–1.80 (m, 4H, linker  $\beta\text{-CH}_2$  groups), 1.45 (s, 3H,  $\text{CH}_3$  of hydrocortisone), 0.90 (s, 3H,  $\text{CH}_3$  of hydrocortisone); UV (0.1 M  $\text{NaHCO}_3$ )  $\lambda_{\text{max}}$  246 nm.

**General Procedure for Crosslinking of Hydrazido-Functionalized HA with Homobifunctional Crosslinkers.** Hydrazido-functionalized HA fragments were dissolved in 0.1 M  $\text{NaHCO}_3$  buffer (pH = 8.50) at a concentration of 8 mg/mL. To this mixture was added a slight molar excess of the homobifunctional crosslinker in solid form. The structures of the four crosslinkers employed (BS<sup>3</sup>, DMS, DTSSP, sulfo-EGS) are shown in Scheme 4. The homogeneous reaction mixture was allowed to stir at room temperature for 16–18 h. The reaction mixture was applied directly to a column of Biogel P-2 (30  $\times$  1.5 cm) and chromatographed using water as eluant at a flow rate of 30 mL/h. Typically, 40 fractions of 2 mL each were collected and assayed for glucuronic acid content using the carbazole method. Fractions that tested positive were pooled, lyophilized, and subsequently analyzed spectroscopically by  $^1\text{H}$  NMR in  $\text{D}_2\text{O}$  at 600 MHz.

**Crosslinked Products of Adipic Dihydrazide Functionalized HA with Homobifunctional Crosslinkers (Scheme 5).** The procedure described above was employed to prepare crosslinked derivatives of HA from adipic dihydrazide-functionalized HA 1b. The details of the individual reactions and the spectroscopic results follow.

**BS<sup>3</sup>-HA (6).** Hydrazido-functionalized HA oligosaccharide (6.0 mg, 0.02 mmol) was dissolved in 1 mL of 0.1 M  $\text{NaHCO}_3$  (pH = 8.50). The molar ratio of hydrazido-HA:BS<sup>3</sup> was 1.0:7.0. The recovery of crosslinked HA after gel filtration was 4.8 mg (80% recovery). The sample was dissolved in 500  $\mu\text{L}$  of  $\text{D}_2\text{O}$  for spectroscopic analysis. Diagnostic peaks from the crosslinker that do not overlap with the HA resonances are reported:  $^1\text{H}$  NMR ( $\text{D}_2\text{O}$ )  $\delta$  2.25–2.50 (m, 12H, all  $\text{CH}_2\text{C}(\text{O})\text{NHNH}$ ,  $\alpha\text{-CH}_2$  groups of linker and crosslinker), 1.60–1.80 (m, 12H, all  $\text{CH}_2\text{CH}_2\text{CH}_2\text{C}(\text{O})\text{NHNH}$ ,  $\beta\text{-CH}_2$  groups of linker and crosslinker), 1.35–1.43 (m, 4H,  $\gamma\text{-CH}_2$  groups of crosslinker).

**DMS-HA (7).** Hydrazido-functionalized HA oligosaccharide (3.8 mg, 0.10 mmol) was subjected to the crosslinking reaction. The molar ratio of hydrazido-HA:DMS was 1.0:3.5. The recovery of crosslinked HA after purification

was 3.0 mg (79% recovery):  $^1\text{H}$  NMR ( $\text{D}_2\text{O}$ )  $\delta$  2.25–2.56 (m, 12H, all  $\text{CH}_2\text{C}(\text{O})\text{NHNH}$  and  $-\text{CH}_2\text{C}(\text{NH}_2)^+$ ),  $\alpha\text{-CH}_2$  groups of linker and crosslinker), 1.69–1.77 (m, 12H, all  $\text{CH}_2\text{CH}_2\text{CH}_2\text{C}(\text{O})\text{NHNH}$ -,  $\beta\text{-CH}_2$  groups of linker and crosslinker), 1.31–1.48 (m, 4H,  $\gamma\text{-CH}_2$  groups of crosslinker).

**DTSSP-HA (8).** Hydrazido-functionalized HA oligosaccharide (4.0 mg, 0.10 mmol) was dissolved in 0.5 mL of 0.1 M  $\text{NaHCO}_3$  buffer. The molar ratio of hydrazido-HA:DTSSP was 1.0:3.5. The recovery of crosslinked HA after purification was 3.20 mg (80% recovery):  $^1\text{H}$  NMR ( $\text{D}_2\text{O}$ )  $\delta$  2.38–2.49 (m, 8H,  $\alpha\text{-CH}_2$  groups of linker), 1.69–1.79 (m, 8H,  $\beta\text{-CH}_2$  groups of linker).

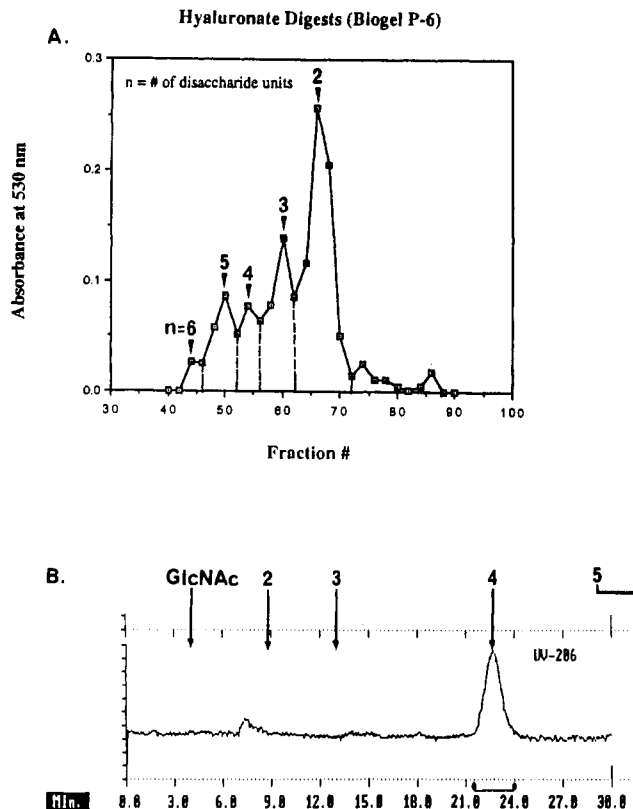
**EGS-HA (9).** Hydrazido-functionalized HA oligosaccharide (3.5 mg, 0.009 mmol) was subjected to the crosslinking reaction. The reaction mixture was allowed to stir at room temperature for 3 h. The molar ratio of hydrazido-HA:sulfo-EGS was 1.0:4.5. The recovery of crosslinked HA after purification was 2.8 mg (80% recovery):  $^1\text{H}$  NMR ( $\text{D}_2\text{O}$ )  $\delta$  2.62–2.79 (m, 12H,  $\alpha$  and  $\beta\text{-CH}_2$  groups of crosslinker), 2.36–2.52 (m, 8H,  $\alpha\text{-CH}_2$  groups of linker), 1.63–1.76 (m, 8H,  $\beta\text{-CH}_2$  groups of linker).

## RESULTS

**Preparation of HA Oligosaccharides.** Hyaluronate fragments of defined length were generated primarily by digestion of high MW HA ( $1.5 \times 10^6$  Da) with testicular hyaluronidase. This enzyme degrades HA to generate a series of even-numbered oligosaccharides with the *N*-acetylglucosamine moiety placed at the reducing terminus (23). Incubation of a solution of 1.0 g of high MW HA in 0.05 M  $\text{NaOAc}$  buffer in 0.15 M  $\text{NaCl}$  (pH = 5.50) with testicular hyaluronidase for 24 h at 37 °C resulted in the formation of a nonviscous mixture of HA oligosaccharides. These digestion conditions were optimal for the formation of oligosaccharides ranging in size from two to six disaccharide units.

The HA oligomers were separated by gel filtration chromatography on Biogel P-6 (240  $\times$  1.5 cm) using pyridinium acetate (pH = 6.50) as eluant (19). The fractions were assayed for glucuronic acid content by the carbazole method using glucuronolactone as the standard. A column profile was generated based on these data (Figure 3a), and the fractions corresponding to each number of disaccharide units were pooled. Further characterization of the fragments was accomplished by HPLC on an amino-modified silica gel column using 0.1 M  $\text{KH}_2\text{PO}_4$  buffer (pH = 4.75) as the mobile phase (21). This column allows the separation of HA fragments up to six disaccharide units. The HPLC traces of the pooled fractions (compared with those of known standards) verified the length of the oligosaccharides and indicated that the fragments exhibited a high degree of homogeneity. The HPLC trace of a purified HA octasaccharide (i.e., four disaccharide units) is depicted in Figure 3b.

**Functionalization of HA Fragments.** The preparation of tethered HA derivatives is outlined in Scheme 1. HA fragments of defined length were dissolved in water to a concentration of 4 mg/mL, and a 40-fold molar excess of dihydrazide was added. The pH of the reaction mixture was adjusted to 4.75 by addition of 0.1 N  $\text{HCl}$ . Next, a four-fold molar excess of solid EDC was added to the reaction, and an increase in pH was observed corresponding to proton uptake. The pH of the reaction mixture was maintained at 4.75 by addition of 0.1 N  $\text{HCl}$ , known to be optimal for carbodiimide coupling reactions. The reaction was allowed to proceed for 2 h or until no further increase in pH was observed. The reaction mixture was concen-

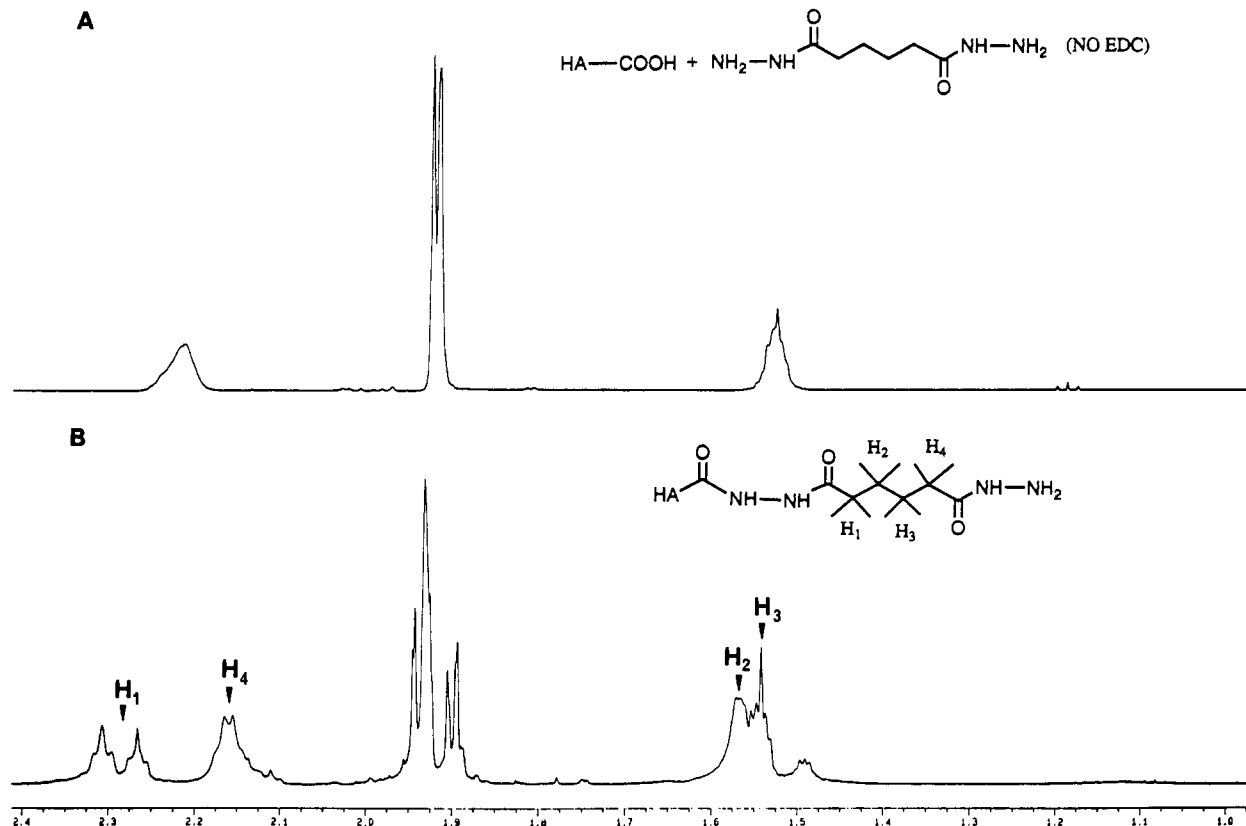


**Figure 3.** (A) Gel filtration elution profile of HA oligosaccharides generated by exhaustive digestion with testicular hyaluronidase. (B) HPLC trace of a purified HA octasaccharide.

trated *in vacuo*, redissolved in 1.5 mL  $\text{H}_2\text{O}$ , and separated by gel filtration on a column of Biogel P-2. The collected fractions were assayed for glucuronic acid content, and positive fractions were pooled and lyophilized. The modified HA fragments were isolated as white fibrous materials in approximately 80–86% yield.

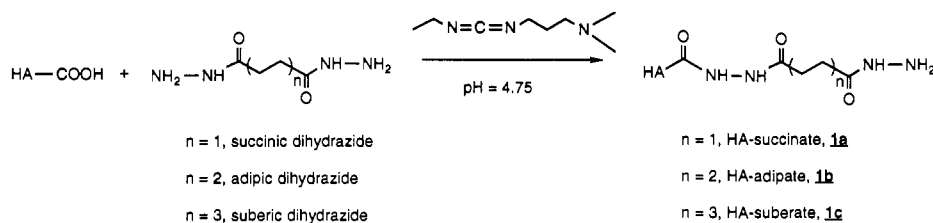
Three commercially-available dihydrazides (succinic, adipic, and suberic) were attached to the HA backbone in this study (Scheme 1). Since the optimal results were obtained with adipic dihydrazide, this example is described in detail first. HA hexasaccharide and a large excess of adipic dihydrazide were reacted in the presence of EDC as described above. The equivalency ratio of HA:adipic dihydrazide:EDC was 1:40:4. The purified product was studied by  $^1\text{H}$  NMR spectroscopy in  $\text{D}_2\text{O}$  at 600 MHz. Analysis of the  $^1\text{H}$  NMR spectrum of HA-adipate **1b** (Figure 4) suggested that adipic dihydrazide was covalently bound to the HA backbone without any appreciable crosslink formation. This conclusion was reached by examining the changes in the NMR resonances of the methylene protons of the hydrazide linkers as discussed below.

The admixture of HA hexasaccharide with adipic dihydrazide in the absence of carbodiimide showed two broad multiplets in a 1:1 ratio. The upfield multiplet contained the internal methylene (H-2, H-3) protons of adipic dihydrazide, while the downfield multiplet comprised the H-1 and H-4 methylene protons. Upon covalent attachment to the HA backbone, splitting of these peaks was observed: the H-1 methylene protons in the dihydrazide linkage became distinguishable from the terminal methylene protons (H-4). Moreover, the H-1 protons become diastereotopic as a result of restricted rotation. The upfield multiplet, centered at  $\delta$  = 1.55 ppm, also lost its degeneracy and resolved into separate resonances for the H-2 and H-3 methylenes. These assignments could



**Figure 4.** (A)  $^1\text{H}$  NMR spectrum of native HA hexasaccharide mixed with adipic dihydrazide in  $\text{D}_2\text{O}$  at 600 MHz. (B)  $^1\text{H}$  NMR spectrum in of HA hexasaccharide covalently bound to adipic dihydrazide **1b** in  $\text{D}_2\text{O}$  at 600 MHz.

#### Scheme 1. Coupling of HA Oligosaccharides to Aliphatic Dihydrazides



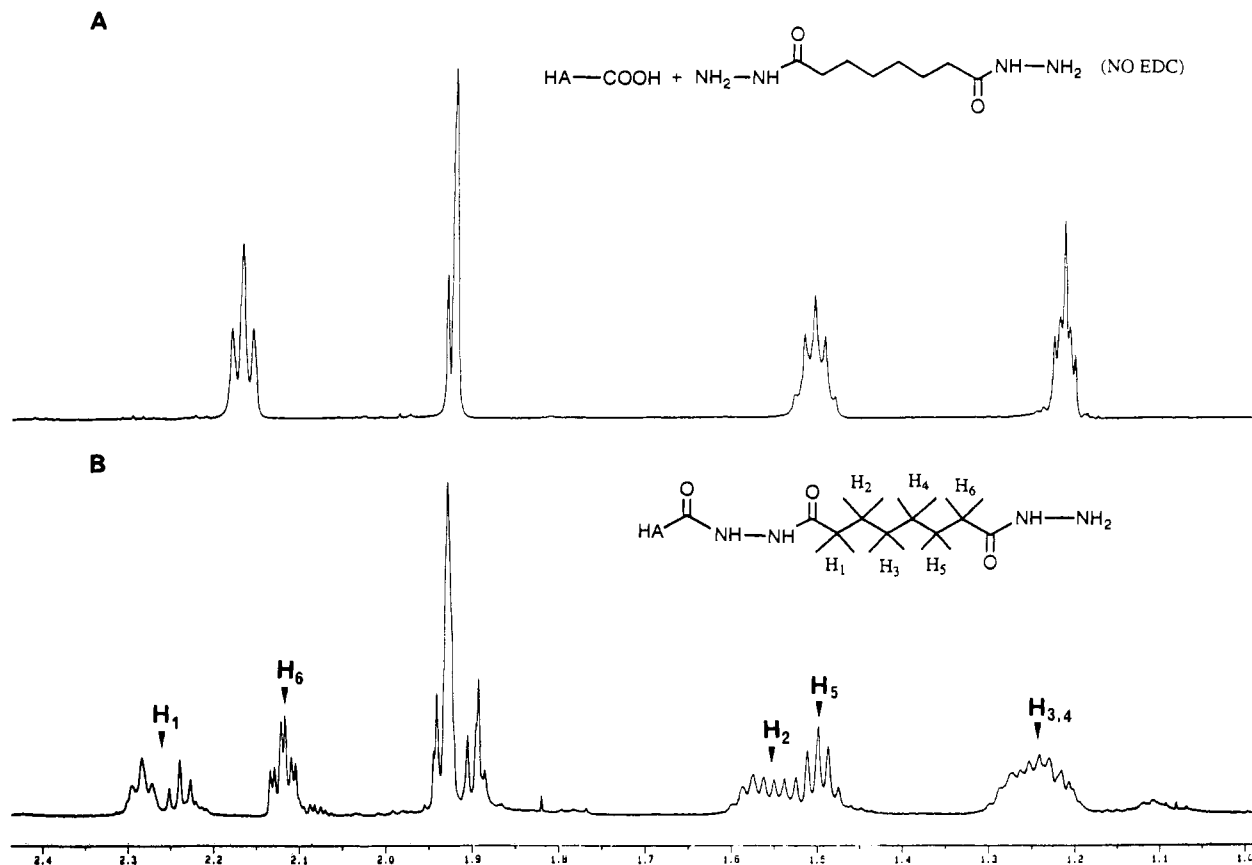
be made unambiguously by observing cross peaks in a double-quantum filtered COSY experiment (24). The absence of symmetrical peaks at a detectable level strongly suggested that crosslinking did not occur during the hydrazide functionalization, which was confirmed by subsequent chemical reactions as described below. The degree of coupling was determined by integration of the linker methylene signals (H-4) using as an internal standard the methyl resonances ( $\delta = 1.85\text{--}1.95$  ppm) of the acetamido moiety of the *N*-acetyl-D-glucosamine residue of known fragments of HA. NMR integration shows that 56% coupling of adipic dihydrazide to the HA hexasaccharide had occurred under these conditions. That is, approximately 1.6 out of 3.0 carboxylates per hexasaccharide were modified.

Suberic dihydrazide was coupled to an HA octasaccharide at  $70^\circ\text{C}$  to increase the solubility of the reagent. Purification of the complex **1c** was accomplished by gel filtration chromatography. Analysis of the  $^1\text{H}$  NMR spectrum in  $\text{D}_2\text{O}$  at 600 MHz showed univalent attachment of suberic dihydrazide to the HA backbone. The proton NMR spectrum (Figure 5a) of the HA-suberic dihydrazide mixture shows three symmetrical multiplets for the three sets of methylene protons in the reagent. By contrast, Figure 5b clearly shows that all methylene protons acquire different chemical shifts upon covalent attachment to the

HA backbone. The terminal methylene protons (H-1 and H-6), which appear as a distinct triplet at  $\delta = 2.15$  ppm in suberic dihydrazide, split into two separate sets of peaks upon binding to HA. The H-1 methylene protons appear as two adjacent triplets, suggesting that the two protons are now diastereotopic in a manner similar to that observed with **1b**. The H-6 methylenes appear as a multiplet at  $\delta = 2.12$  ppm. The methylene protons of H-2 and H-5 that appear as a multiplet centered at  $\delta = 1.50$  ppm are split into two distinct multiplets upon univalent binding of suberic dihydrazide to the HA backbone. The assignments of H-2 and H-5 were made by observing crosspeaks in a double-quantum filtered COSY experiment (24). The methylene protons corresponding to H-3 and H-4 appear as a multiplet in suberic dihydrazide; however, this multiplet ( $\delta = 1.25$  ppm) becomes significantly broadened upon binding of suberic dihydrazide to the HA oligosaccharides. The amount of coupling, estimated by NMR integration of the H-6 linker methylenes against the *N*-acetyl methyl peaks ( $\delta = 1.85\text{--}1.95$  ppm) of the HA octasaccharide as an internal standard, was approximately 46%.

Succinic dihydrazide was coupled to the HA tetrasaccharide at  $50^\circ\text{C}$  to promote its solubility in water. The molar equivalency ratio of HA:succinic dihydrazide:EDC was 1:30:3. The HA-succinate complex **1a** was purified





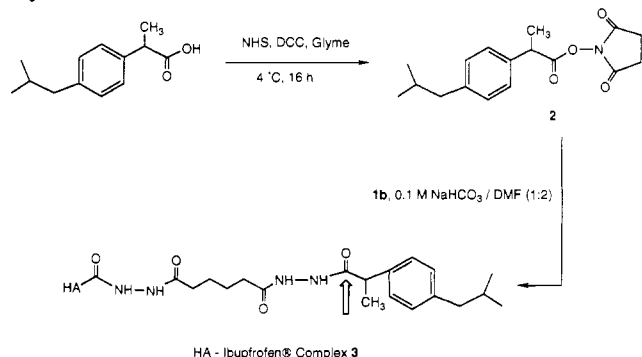
**Figure 5.** (A)  $^1\text{H}$  NMR spectrum in of native HA octasaccharide mixed with suberic dihydrazide in  $\text{D}_2\text{O}$  at 600 MHz. (B)  $^1\text{H}$  NMR spectrum of HA octasaccharide covalently bound to suberic dihydrazide **1c** in  $\text{D}_2\text{O}$  at 600 MHz.

by gel filtration chromatography. Characterization of the HA-succinate derivative **1a** was achieved in a manner similar to that described for **1b** and **1c**. The  $^1\text{H}$  NMR spectrum of **1c** in  $\text{D}_2\text{O}$  at 600 MHz is denoted by the appearance of a multiplet at  $\delta = 2.50\text{--}2.80$  ppm. The degree of coupling was estimated to be 30% by NMR integration under the experimental conditions employed.

**Drug Attachment to Functionalized HA.** Ibuprofen was selected as a model nonsteroidal antiinflammatory drug. Reaction of Ibuprofen with NHS in the presence of the coupling agent DCC resulted in the preparation of the NHS derivative **2** in quantitative yield (25). The NHS derivative of Ibuprofen was then coupled to hydrazido-HA **1b** in 0.1 M  $\text{NaHCO}_3$  buffer at pH = 8.50 using DMF as a cosolvent. Purification by gel filtration on Biogel P-2 using water as eluant (Scheme 2) provided Ibuprofen linked to HA **3** through a hydrazide bond. The Ibuprofen-HA complex **3** was characterized by  $^1\text{H}$  NMR in  $\text{D}_2\text{O}$  at 600 MHz. The characteristic phenyl peaks of Ibuprofen were observed in the  $^1\text{H}$  NMR spectrum at  $\delta = 7.25$  ppm providing unambiguous proof for the formation of the covalent Ibuprofen-HA adduct **3**. The UV spectrum of the complex showed a  $\lambda_{\text{max}}$  at 266 nm. The degree of coupling of Ibuprofen to HA was determined to be 24% based on NMR integration of the phenyl protons against the hyaluronate GlcNAc methyl peaks ( $\delta = 2.0$  ppm).

Hydrocortisone was selected as a prototypical steroidal antiinflammatory drug, and the hemisuccinate derivative allowed preparation of the metabolically-labile form of the drug using an activated ester. Thus, the terminal carboxylate of hydrocortisone hemisuccinate was converted to the NHS-ester derivative **4** by reaction with NHS in the presence of DCC in DMF at room temperature. The hydrocortisone hemisuccinate-NHS-ester derivative **4** was then coupled to hydrazido-HA **1b** in 0.1 M  $\text{NaHCO}_3$

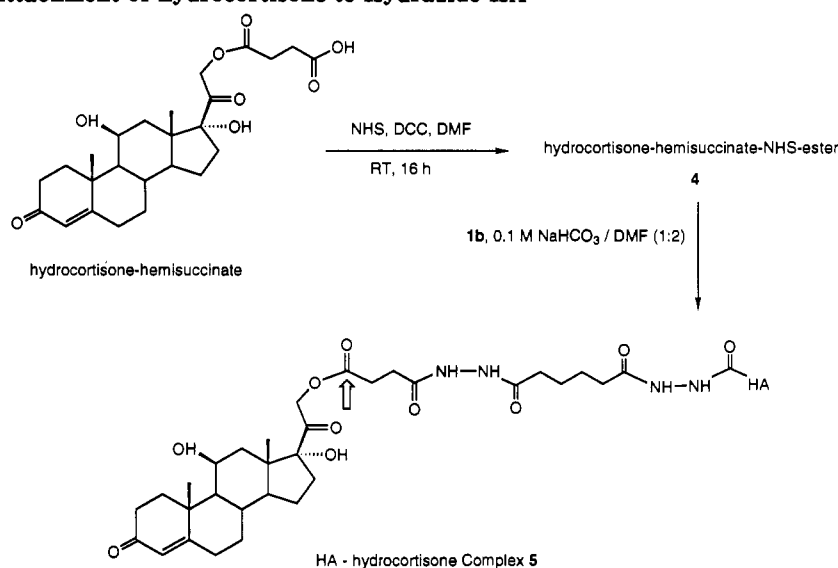
#### Scheme 2. Covalent attachment of Ibuprofen to Hydrazido-HA<sup>a</sup>



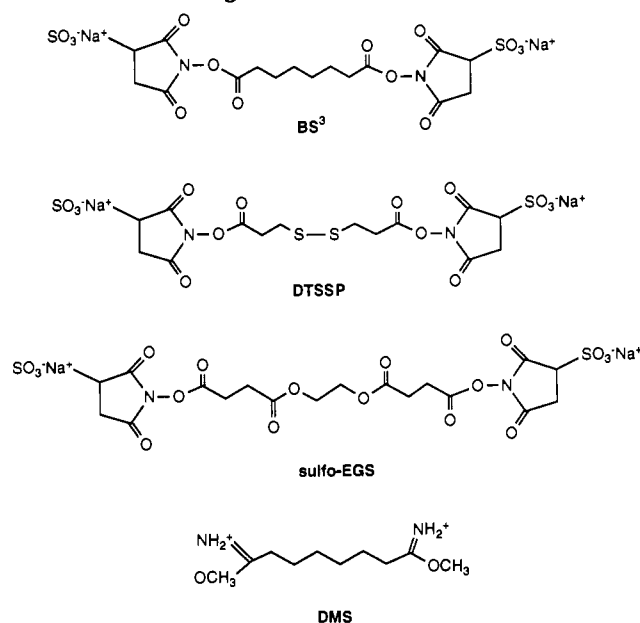
<sup>a</sup> The arrow indicates the site for release of free drug by chemical or enzymatic hydrolysis.

buffer (pH = 8.50) using DMF as a cosolvent (Scheme 3). The HA-hydrocortisone complex **5** was purified by gel filtration chromatography on Biogel P-2 and studied by  $^1\text{H}$  NMR in  $\text{D}_2\text{O}$  at 600 MHz. Peaks that are characteristic of the hydrocortisone moiety appear at  $\delta = 0.90$ , 1.41, and 5.80 ppm. The UV spectrum of the complex **5** shows a  $\lambda_{\text{max}}$  at 246 nm. The amount of hydrocortisone attached to the HA backbone was estimated by UV to be 25%.

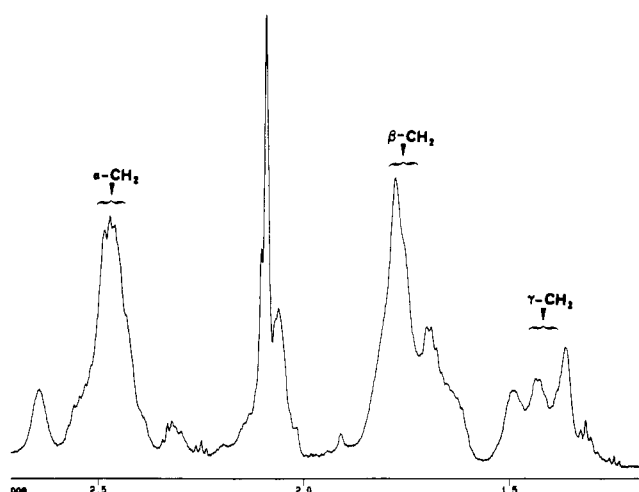
**Crosslinking of HA.** The presence of a reactive hydrazido moiety on the HA backbone enabled the introduction of a variety of covalent reversible and irreversible crosslinks between individual HA strands using commercially-available amine-specific homobifunctional crosslinkers (Scheme 4). Hydrazido-HA **1b** was dissolved in 0.1 M  $\text{NaHCO}_3$  buffer (pH = 8.50) at a concentration of 8 mg/mL. This concentration was chosen to maximize the number of interstrand crosslinks as opposed to

**Scheme 3. Covalent Attachment of hydrocortisone to Hydrazido-HA<sup>a</sup>**

<sup>a</sup> The arrow indicates the site for release of free drug by chemical or enzymatic hydrolysis.

**Scheme 4. Homobifunctional Crosslinking Reagents Used for Generating Crosslinked Derivatives of HA**

intrastrand crosslinks that would be favored under more dilute conditions. To this mixture was added a slight excess of the homobifunctional crosslinker in solid form. The equivalency ratios of hydrazido-HA:crosslinker were typically 1:3.5. The reaction was allowed to proceed at room temperature for 16–18 h, and the mixture was then directly applied to a column of Biogel P-2 for purification using H<sub>2</sub>O as eluant. The crosslinked HA complexes 6–9 (Scheme 5) were characterized by <sup>1</sup>H NMR in D<sub>2</sub>O at 600 MHz. A common feature of the <sup>1</sup>H NMR spectra is the downfield shift of the multiplet at  $\delta = 2.15$  ppm that is assigned to H-4 in 1b. Upon covalent binding of the terminal hydrazido group to the homobifunctional crosslinkers, the H-4 methylene protons become chemical shift equivalent with H-1 protons, and these peaks now appear as a broad multiplet centered at  $\delta = 2.50$  ppm. The upfield region of the <sup>1</sup>H NMR spectrum of hydrazido-HA crosslinked with dimethyl suberimidate (DMS) 7 in D<sub>2</sub>O is shown in Figure 6. The significant line broadening observed in the region of the sugar ring protons ( $\delta = 3.20$ –



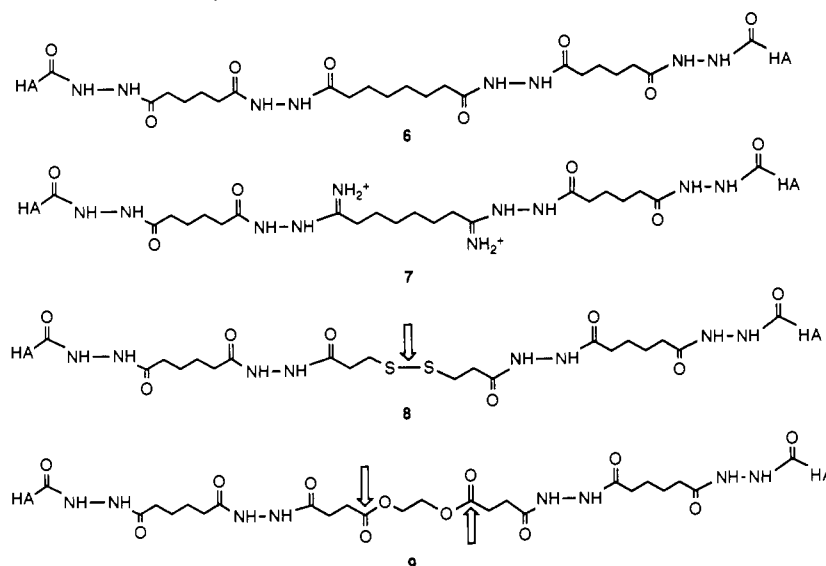
**Figure 6.** Upfield region of the <sup>1</sup>H NMR (600 MHz) spectrum of crosslinked HA 7 (HA-DMS) in D<sub>2</sub>O.

4.20) ppm also suggested the formation of a high MW species as anticipated if extensive interstrand crosslinks had formed.

**DISCUSSION**

The major objective of this study was the development of a convenient methodology for the covalent attachment of a pendant hydrazido group on the HA backbone. The approach described in this paper was based on an observation made earlier in our laboratory. We noticed that attempted coupling of aliphatic and aromatic diamines to the HA carboxylate group (MW =  $1.5 \times 10^6$  Da) using EDC as an activating agent at pH = 4.75 had resulted only in the formation of *N*-acylurea adducts of HA and EDC (15). On the basis of these results, we documented that the putative *O*-acylurea intermediates rapidly rearranged to the more stable *N*-acylurea isomers (14). A similar phenomenon was observed at the oligomer level using HA fragments ranging in size from two to six disaccharide units (24). To take advantage of the high reactivity of HA toward EDC, we refocused our attention on the aliphatic dihydrazides as linkers for HA. The low pK<sub>a</sub> values of 2.0–3.0 for the protonated forms of these dihydrazides meant that over 99% of the hydrazide amino

Scheme 5. Crosslinked Derivatives of Hydrazido-HA



groups would be present as unprotonated nucleophiles at the coupling pH value of 4.75 (25). When present in sufficient excess, the dihydrazides could add to the electrophilic *O*-acylurea in competition with intramolecular rearrangement to the more stable *N*-acylurea. Thus, the success of this approach would be attributed to increasing the rate of *intermolecular* coupling to obtain the desired tethered HA derivatives with a reactive hydrazido group.

The presence of a pendant hydrazido group on the HA molecule at defined positions offers a number of advantages. The low  $pK_a$  of the protonated form of the pendant hydrazido group allowed subsequent coupling and cross-linking reactions to be conducted under conditions of neutral pH that were not detrimental to the MW integrity of the HA molecule. Furthermore, the pendant hydrazido moiety was highly reactive toward a number of amine-specific probes that were commercially available or that could be readily prepared in the laboratory. The presence of the four-, six-, or eight-carbon spacer ensured the steric accessibility of the pendant groups for further reactions. Due to its superior solubility properties in water, adipic dihydrazide became the linker of choice for further modifications of HA.

The pendant hydrazido group was next exploited for the covalent attachment of drugs to the HA backbone through the intermediacy of hydrolytically and/or enzymatically labile bonds. This approach would allow the preparation of controlled-release HA-drug formulations for the potential treatment of osteoarthritis. Currently, local injections of high MW native HA in its noninflammatory form into the joint are used in the treatment of osteoarthritis. Combinations of corticosteroids and native HA injections have been used in veterinary medicine for the treatment of joint dysfunction in race horses (26). Covalent attachment of drugs to polymeric supports is known to retard drug release, and especially in the case of topical applications can provide highly improved therapeutic benefits (27, 28). Given the history and potential of HA in the treatment of joint dysfunction and arthritis, ibuprofen and hydrocortisone were selected as models for steroidal and nonsteroidal antiinflammatory drugs for attachment to the HA backbone. Ibuprofen was linked to hydrazido-HA 1b through a hydrazide bond. Hydrocortisone was linked to the HA backbone through the intermediacy of a hydrolytically labile ester linkage.

These model reactions demonstrate the feasibility of covalent drug attachment to the modified HA through the intermediacy of a variety of bond types.

Crosslinked derivatives of HA have a wide range of potential biomedical applications. The introduction of covalent crosslinks between the individual strands of HA molecules could lead to the production of "hydrogels", i.e., macromolecular networks swollen in water (29). These hydrogels could have great value as biomaterials for a variety of applications such as sustained drug delivery and for the prevention of postsurgical adhesions. The reaction of hydrazido-functionalized HA 1b with the commercially-available homobifunctional crosslinkers depicted in Scheme 4 led to the isolation of crosslinked HA derivatives 6–9, which were characterized by <sup>1</sup>H NMR. The different types of linkers provide a series of crosslinked HA derivatives with different physical properties that could degrade in response to a variety of biological stimuli. Recently, inflammation-responsive HA gels, which degrade in response to the presence of the hydroxy radical produced as a result of the onset of the inflammatory state, have been reported (30).

## CONCLUSIONS

Hydrazido-HA allows the attachment of carboxyl-containing drugs and for the introduction of covalent crosslinks into the HA molecule. This methodology is versatile in permitting a number of manipulations on the HA molecule from a single precursor that can be readily prepared in one step. Furthermore, the mild reaction conditions prevent the degradation of HA, which is known to be unstable and undergo extensive degradation below pH 4 and above pH 9. Unlike previous modifications of HA, this approach offers the advantage that the modified species have been characterized by high-resolution <sup>1</sup>H NMR methods.

We have thus presented a convenient and versatile method for the chemical modification and functionalization of HA that facilitates subsequent attachment of antiinflammatory drugs and the introduction of covalent reversible and irreversible crosslinks. We have extended this crosslinking methodology to high MW hyaluronate ( $1.5 \times 10^6$  Da) to prepare a series of novel hydrogels. These results will be described in detail elsewhere.

## ACKNOWLEDGMENT

We thank the Center for Biotechnology supported by New York State Foundation for Science and Technology for financial support of this project. Initial supplies of sodium HA (Amvisc) were kindly provided by J.-w. Kuo and D. A. Swann, MedChem Products, Inc. We thank M. K. Cowman for helpful discussions concerning the generation and characterization of HA fragments. We are grateful to G. B. Crull and B. A. Clark for their help in obtaining the 600-MHz 1-D and 2-D  $^1\text{H}$  NMR spectra and to J. F. Marecek for helpful discussions throughout the course of this work. The Bruker AMX-600 was acquired with instrument grants from NIH (RR05547A) and the NSF (CHE8911350), with additional support from the University at Stony Brook and the Center for Biotechnology.

## LITERATURE CITED

- (1) Hardwick, C., Hoare, K., Owens, R., Hohn, H. P., Hook, M., Moore, D., Cripps, V., Austen, L., Nance, D. M., and Turley, E. A. (1992) *J. Cell Biol.* 117, 1343-1350.
- (2) Toole, B. P., Munaim, S. F., Welles, S., and Knudson, C. B. (1989) *Ciba Found. Symp.* 143, 138-149.
- (3) LeBoeuf, R. D., Raja, R. H., Fullert, G. M., and Weigel, P. H. (1986) *J. Biol. Chem.* 261, 12586-12592.
- (4) Turley, E. A. (1984) *Cancer Met. Rev.* 3, 325-339.
- (5) Balazs, E. A., and Denlinger, J. L. (1989) *Ciba Found. Symp.* 143, 265-275.
- (6) Balazs, E. A. (1986) in *Ophthalmic Viscosurgery—a Review of Standards, Techniques, and Applications* (G. Eisner, Ed.) pp 3-19, Medicopea, Montreal, Canada.
- (7) Kopp, S., Wenneberg, B., Haraldson, T., and Gunnar, C. E. (1985) *J. Oral Maxillofac. Surg.* 43, 429-435.
- (8) Punzi, L., Schiavon, F., Ramonda, R., Malatesta, V., Gambari, P., and Silvano, T. (1988) *Curr. Ther. Res.* 43, 643-647.
- (9) Balazs, E. A., and Leshchiner, A. (15 Apr 1986) US Patent 4,582,865 A.
- (10) Balazs, E. A., and Leshchiner, A. (15 Dec 1987) US Patent 4,713,448.
- (11) (a) Della Valle, F., and Romeo, A. (1 Apr 1987) Eur. Patent Appl. 86305233.8. (b) Joshi, H. N., Stella, V. J., and Topp, E. M. (1992) *J. Controlled Release* 20, 109-122.
- (12) Dahl, L. B., Laurent, T. C., and Smedsrod, B. (1988) *Anal. Biochem.* 175, 397-407.
- (13) Curvall, M., Lindberg, B., and Lonngren, J. (1975) *Carbohydr. Res.* 41, 235-239.
- (14) Pouyani, T., Kuo, J.-w., Harbison, G. S., and Prestwich, G. D. (1992) *J. Am. Chem. Soc.* 114, 5972-5976.
- (15) Kuo, J.-w., Swann, D. A., and Prestwich, G. D. (1991) *Bioconjugate Chem.* 2, 232-241.
- (16) Inman, J. K., and Dintiz, H. M. (1969) *Biochemistry* 8, 4074-4082.
- (17) Rakestraw, S. L., Tompkins, R. G., and Yarmush, M. L. (1990) *Bioconjugate Chem.* 1, 212-221.
- (18) Piantini, U., Sorensen, O. W., and Ernst, R. R. (1982) *J. Am. Chem. Soc.* 104, 6800-6801.
- (19) Cowman, M. K., Slahetka, M. F., Hittner, D. M., Kim, J., Forino, M., and Gadelrab, G. (1984) *Biochem. J.* 221, 707-716.
- (20) Turner, R. E., and Cowman, M. K. (1985) *Arch. Biochem. Biophys.* 237, 253-260.
- (21) Nebinger, P., Koel, M., Franz, A., and Werries, E. (1983) *J. Chromatogr.* 265, 19-25.
- (22) Balazs, E. A., Bernsten, K. O., Karossa, J., and Swann, D. A. (1965) *Anal. Biochem.* 12, 547-558.
- (23) Meyer, K. (1971) in *The Enzymes* (P. D. Boyer, Ed.) Vol. 2, pp 307-320, Academic Press, New York.
- (24) Pouyani, T. (1993) Ph.D. Dissertation, University at Stony Brook.
- (25) Rakestraw, S. L., Tompkins, R. G., and Yarmush, M. L. (1990) *Proc. Natl. Acad. Sci. U.S.A.* 87, 4217-4221.
- (26) Rydell, N. W., Butler, J., and Balazs, E. A. (1970) *Acta. Vet. Scand.* 11, 139-155.
- (27) Langer, R. (1990) *Science* 249, 1473-1624.
- (28) Duncan, R., and Kopecek, J. (1984) *Adv. Polym. Sci.* 57, 53-101.
- (29) Peppas, N. A. (1986) *Hydrogels in Medicine and Pharmacy*, Vol. 1, CRC Press, Inc., Boca Raton, FL.
- (30) Yui, N., Okano, T., and Sakurai, Y. (1992) *J. Controlled Release* 22, 105-116.

## A Sensitive Assay for Maleimide Groups

Rajeeva Singh

ImmunoGen, Inc., 148 Sidney St., Cambridge, Massachusetts 02139. Received November 24, 1993\*

A sensitive spectrophotometric assay has been developed for maleimide groups incorporated into proteins. The assay involves the reaction of maleimide with an excess of cysteine and quantitation of the remaining cysteine using an enzymatic assay that is based on the stoichiometric conversion of an inactive disulfide form of papain to the active enzyme. The restored enzymatic activity is then measured using a chromogenic substrate. The amount of maleimide is calculated as the difference between the amounts of initial cysteine and assayed remaining cysteine. The limits of detection of this assay are about 0.1 nmol maleimide in a final assay volume of 1.2 mL. This assay is about 100-fold more sensitive than a similar assay using Ellman's reagent.

### INTRODUCTION

Maleimide groups rapidly and selectively react with thiols, forming stable thioether bonds. This characteristic has led to their widespread use in the formation of stable protein conjugates (1, 2). Maleimide groups are typically incorporated in proteins by random modification of their lysine amino groups. Sensitive assays of maleimide and thiol groups are required for the efficient conjugation of proteins that are expensive and available only in small amounts.

Maleimides can be directly assayed spectrophotometrically at 302 nm, having an extinction coefficient  $\epsilon_{302\text{nm}}$  of  $620 \text{ M}^{-1} \text{ cm}^{-1}$  (3). However, the small  $\epsilon_{302\text{nm}}$  renders this assay not very sensitive, and the assay is further complicated by the protein absorbance at the same wavelength. Indirectly, maleimide groups can be assayed by first reacting them with a known amount of thiol present in excess and then assaying the remaining unreacted thiol using Ellman's reagent (2, 4, 5). The amount of maleimide is calculated as the difference between the initial amount of thiol and the amount of unreacted thiol after complete reaction of all maleimide groups. The sensitivity of this indirect assay is limited by that of the Ellman's assay ( $\epsilon_{412\text{nm}} = 14\,150 \text{ M}^{-1} \text{ cm}^{-1}$ ) (6, 7); this assay reaches its limit of accurate detection for large proteins (e.g., antibodies,  $M_r$  160 000) modified with an average of one maleimide group, requiring concentrations of greater than 1 mg/mL to measure a change in the absorbance of 0.1 unit (in a cuvet of 1-cm pathlength).

We have previously described an enzymatic assay for thiol groups that is based on the stoichiometric activation of papain-SSCH<sub>3</sub> and that is about 100-fold more sensitive than Ellman's assay (8). In this paper we extend the use of this assay to the measurement of maleimide groups incorporated into proteins.

### EXPERIMENTAL PROCEDURES

**Materials.** Papain (EC 3.4.22.2; 2 × crystallized suspension in 50 mM sodium acetate, pH 4.5, containing 0.01% thymol), avidin (egg white), 4-(*N*-maleimidomethyl)cyclohexane-1-carboxylic acid *N*-hydroxysuccinimide ester (SMCC), *N*-ethylmaleimide, and *N*-benzoyl-L-arginine-*p*-nitroanilide hydrochloride were purchased from Sigma (St. Louis, MO). The murine monoclonal antibody anti-B4 (IgG<sub>1</sub>,  $M_r$  160 000;  $A_{0.1\%}^{0.1\text{cm}} = 1.4$  at 280 nm) was purified from hybridoma culture supernatants by affinity

chromatography on protein A followed by ion-exchange chromatography. All other reagents were of commercial reagent grade. The compositions of buffers frequently used were as follows: buffer A (10 mM potassium phosphate, 150 mM NaCl, 1 mM EDTA, pH 7.2); buffer B (5 mM sodium acetate, 50 mM NaCl, 0.5 mM EDTA, pH 4.7); buffer C (50 mM sodium phosphate, 1 mM EDTA, pH 7.0).

Papain-SSCH<sub>3</sub> was prepared as described before (8). Commercial papain contains about 90% inactive mixed disulfide papain-SS-cysteine (8). Briefly, homogeneous samples of papain-SSCH<sub>3</sub> were prepared by first reducing commercial papain with cysteine and then treating with methyl methanethiosulfonate. Such preparations of papain-SSCH<sub>3</sub> were used in the experiments described below and in Figure 1. Other experiments were performed with mixtures of papain-SS-cysteine and papain-SSCH<sub>3</sub> that had been obtained by reaction of commercial papain with methyl methanethiosulfonate. Although the results were found to be similar using either preparation, we recommend usage of the homogeneous preparation of papain-SSCH<sub>3</sub> (8).

**Modification of Proteins with Maleimide Groups.** A 0.6 mM solution of SMCC in ethanol/water (1/1, v/v) was freshly prepared by first dissolving SMCC in ethanol using sonication and then adding water. The concentration of maleimide in the solution was determined by measuring its absorbance at 302 nm ( $\epsilon_{302} = 620 \text{ M}^{-1} \text{ cm}^{-1}$ ) (3). A 1.5 molar excess of SMCC (135  $\mu\text{L}$  of the above solution, 81 nmol) was added to a prewarmed antibody solution [715  $\mu\text{L}$  of an antibody solution in 50 mM sodium phosphate, 50 mM NaCl, pH 7; 8.5 mg IgG<sub>1</sub>, 53 nmol] at 30 °C (9). After incubation at 30 °C for 30 min, the reaction mixture was purified by gel filtration using a Sephadex G-25 (fine) column equilibrated with buffer A. The concentration of pooled antibody fraction was determined from its absorbance at 280 nm. This modification resulted in an average incorporation of 0.9 maleimide group per antibody molecule (Table 1).

**Assay for Maleimide Groups Using Cysteine and Papain-SSCH<sub>3</sub>.** All solutions were degassed as described before (8). Typically, protein samples containing maleimide in the range 0.7–0.3 nmol (based on estimate from Ellman's assay) were incubated with a 2- to 5-fold molar excess of cysteine (Table 1). In a test sample the maximum theoretical amount of maleimide can also be estimated from the molar excess of SMCC used during modification. In the experiment described below, for the

\* Abstract published in *Advance ACS Abstracts*, May 1, 1994.

smallest measurement of maleimide in this study, the test samples (in quadruplicate) contained 10  $\mu\text{L}$  of the sample (1.66 mg/mL maleimide-modified antibody in buffer A; 17  $\mu\text{g}$  or 0.1 nmol antibody,  $\sim 0.1$  nmol maleimide) and an excess of cysteine (9  $\mu\text{L}$  of a 0.097 mM solution in buffer B; 0.87 nmol). Separate tubes containing standard samples of cysteine (0.29, 0.58, 0.87, and 1.17 nmol) were prepared by addition of cysteine [3, 6, 9 (in two tubes, equal to the initial amount of cysteine in test sample), and 12  $\mu\text{L}$ , respectively, of a 0.097 mM solution of cysteine in buffer B] followed by addition of 10  $\mu\text{L}$  of buffer A. Blanks (in triplicate) contained only 10  $\mu\text{L}$  of buffer A and no cysteine. To all tubes was then added 240  $\mu\text{L}$  of 40 mM sodium phosphate, 2 mM EDTA, pH 7.6. Buffer B was then added to bring the total volume in each tube to 262  $\mu\text{L}$ . The tubes were then incubated for about 40 min. The value of the pH during the initial incubation of maleimide sample with excess cysteine was  $\sim 7.6$ .

Papain-SSCH<sub>3</sub> (0.25 mL of a 1.18 mg/mL solution in 5 mM sodium acetate, 50 mM NaCl, pH 4.5; 0.3 mg papain-SSCH<sub>3</sub>, 12.6 nmol) (8) was then added, and the tubes were further incubated for about 40 min (pH  $\sim 7.6$ ). Substrate (0.7 mL of a 3.4 mM *N*-benzoyl-L-arginine-*p*-nitroanilide solution in 50 mM bis-Tris-HCl, 1 mM EDTA, 5% v/v DMSO, pH 6.3) was then added at 1-min intervals between successive tubes. The value of pH during the incubation with substrate was  $\sim 6.3$ . The absorbance values (410 nm) of all samples were measured at about 1 h after the addition of substrate, at the same 1 min intervals between successive tubes.

The value of absorbance for the blank was subtracted from those for the cysteine standards and for the test samples. The  $\Delta A_{410\text{nm}}$  values for the cysteine standard solutions were then plotted *vs* the amounts of cysteine initially added. The remaining cysteine in the test samples was then determined using this standard curve. The amount of maleimide in the test samples was calculated as the difference between the amount of initially added cysteine and that of the remaining cysteine (Figure 1).

The final substrate concentration was 2 mM; the final volume was 1.2 mL. All volume measurements of  $< 25$   $\mu\text{L}$  were performed using a Gilson positive-displacement pipet. All incubations were done at room temperature.

**Assay for Maleimide Groups Using Cysteine and Ellman's Reagent.** Two tubes were each set up with 800  $\mu\text{L}$  of a 1.66 mg/mL solution of maleimide-modified antibody (1.33 mg, 8.31 nmol antibody) in buffer A, and to each tube was added 100  $\mu\text{L}$  of a 0.4 mM solution of cysteine (40 nmol) in buffer C. In two separate tubes, 800  $\mu\text{L}$  of buffer A was incubated with 100  $\mu\text{L}$  of a 0.4 mM cysteine solution in buffer C. Another tube containing 800  $\mu\text{L}$  of buffer A and 100  $\mu\text{L}$  of buffer C served as the blank. All tubes were incubated at 30  $^{\circ}\text{C}$  for 5 min and then at room temperature for 15–20 min.

Ellman's reagent (100  $\mu\text{L}$  of a 5 mM solution in buffer C, freshly prepared from a 100 mM stock in DMSO) was added to all tubes, at 1-min intervals between successive tubes. The absorbance values at 412 nm of all solutions were measured at 1-min intervals, about 8–10 min after the addition of Ellman's reagent. The value of the absorbance of the blank tube was subtracted from the values of absorbance of all tubes. The average values of  $\Delta A$  were calculated for the tubes containing cysteine and for those initially containing cysteine and maleimide-modified antibody. The value of maleimide in the antibody sample was calculated from the difference in the average values of  $\Delta A$  for the above two sets of tubes. The value of  $\Delta A$  was corrected for the trace absorbance at 412

nm of the maleimide-modified antibody solution (before addition of cysteine and Ellman's reagent).

**Kinetics of Reaction between Thiols and *N*-Ethylmaleimide.** The reactions of several thiols and *N*-ethylmaleimide (NEM) in 0.2 M sodium acetate, 0.5 mM EDTA, pH 5.0, were studied at 22  $^{\circ}\text{C}$  by measuring the rate of decrease of absorbance at 302 nm ( $\epsilon_{\text{NEM}} = 620 \text{ M}^{-1} \text{ cm}^{-1}$ ) (10). The initial concentrations ( $c$ , 0.4–1.5 mM) of thiol and NEM were set to be equal, and the apparent rate constant ( $k_{\text{app}}$ ,  $\text{M}^{-1} \text{ min}^{-1}$ ) was calculated using the integrated second-order rate equation:  $k_{\text{app}} = (1/c_{\text{final}} - 1/c_{\text{initial}})/t$  (11). The values of absolute rate constants ( $k_{\text{RS}}$ ,  $\text{M}^{-1} \text{ min}^{-1}$ ) based on thiolate concentration were then calculated using published  $\text{p}K_{\text{a}}$  values of thiols (cysteine methyl ester,  $\text{p}K_{\text{a}}$  7.3; cysteamine,  $\text{p}K_{\text{a}}$  8.46; cysteine,  $\text{p}K_{\text{a}}$  8.54;  $\beta$ -mercaptoethanol,  $\text{p}K_{\text{a}}$  9.61; 3-mercaptopropanoic acid,  $\text{p}K_{\text{a}}$  10.84) (12, 13) and the equation  $k_{\text{RS}} = k_{\text{app}}[1 + 10^{(\text{p}K_{\text{a}} - \text{pH})}]$  (14). A Brønsted plot was established for  $\log k_{\text{RS}}$  *vs*  $\text{p}K_{\text{a}}$  of thiol, and a linear equation ( $R^2 = 0.989$ ) was obtained:  $\log k_{\text{RS}} = 2.118 + 0.534\text{p}K_{\text{a}}$ . This Brønsted correlation was similar to that obtained by Bednar (10).

## RESULTS

**A Sensitive Assay of Maleimide Using Cysteine and Papain-SSCH<sub>3</sub>.** The values of maleimide for several maleimide-modified protein samples and for samples of *N*-ethylmaleimide were determined by addition of a known amount of cysteine present in excess and then assaying the remaining cysteine using an enzymatic assay based on stoichiometric regeneration of active papain (papain-SH) from its inactive mixed disulfide (papain-SSCH<sub>3</sub>) (Table 1). Typically, assay samples containing about 17–80  $\mu\text{g}$  of protein were used. The concentration of each stock solution of maleimide was also determined by an assay using cysteine and Ellman's reagent (Table 1). The assay using Ellman's reagent required a significantly larger amount of protein (about 0.6–1.3 mg) than that using papain-SSCH<sub>3</sub>.

The concentration of a stock solution of *N*-ethylmaleimide (NEM) was determined by assaying a sample containing about 8 nmol of maleimide using Ellman's reagent. Two samples of NEM (0.30 and 0.60 nmol, based on Ellman's assay) from the same stock solution were then assayed using papain-SSCH<sub>3</sub>. The values of maleimide obtained using papain-SSCH<sub>3</sub> ( $0.31 \pm 0.01$  nmol and  $0.61 \pm 0.02$  nmol, respectively) were similar to those expected from Ellman's assay (Table 1). Furthermore, the concentration of the NEM stock solution could also be determined from its absorbance at 302 nm using an extinction coefficient of  $620 \text{ M}^{-1} \text{ cm}^{-1}$  (3) and was found to be in agreement with the results of the above two assays.

All maleimide assays for the maleimide-modified antibody and maleimide-modified avidin samples using papain-SSCH<sub>3</sub> gave results similar to those obtained using Ellman's reagent (Table 1). A stock solution of maleimide-modified antibody was assayed by Ellman's reagent using about 1.3 mg of antibody. From the same stock solution of maleimide-modified antibody, the smallest sample that was then assayed using papain-SSCH<sub>3</sub> contained 17  $\mu\text{g}$  of antibody (0.10 nmol maleimide, based on Ellman's assay). The result obtained using papain-SSCH<sub>3</sub> ( $0.09 \pm 0.01$  nmol maleimide) was similar to that expected from Ellman's assay of the stock solution (Table 1). The determination of maleimide by the assay using papain-SSCH<sub>3</sub> was therefore sensitive, accurate, and precise.

**Comparison of Sensitivities of Maleimide Detection Using Papain-S-SCH<sub>3</sub> *vs* That Using Ellman's Reagent.** For each maleimide determination with the new



**Table 1.** Assay of Maleimide by Addition of Excess Cysteine and Estimation of Remaining Cysteine Using Papain-SSCH<sub>3</sub> or Ellman's Reagent

sample	maleimide (based on papain assay) <sup>a</sup> (nmol)	maleimide (based on Ellman's assay) <sup>b</sup> (nmol)	$\Delta A_{410\text{nm}}^c$ (papain assay, 1 h)	$\Delta A_{412\text{nm}}^d$ (Ellman's assay, calcd values)	sensitivity ratio <sup>e</sup> ( $\Delta A(\text{papain})/$ $\Delta A(\text{Ellman})$ )
<i>N</i> -ethylmaleimide	0.31 ± 0.01	0.30	0.34	0.004	100
	0.61 ± 0.02	0.60	0.66	0.007	100
antibody-maleimide <sup>f</sup>	0.09 ± 0.01	0.10	0.09 <sup>g</sup>	0.001	80 <sup>h</sup>
antibody-maleimide <sup>h</sup>	0.28 ± 0.01	0.27	0.36	0.003	110
	0.48 ± 0.02	0.51	0.61	0.006	100
antibody-maleimide <sup>i</sup>	0.34 ± 0.01	0.33	0.42	0.004	110
	0.67 ± 0.01	0.66	0.82	0.008	110
avidin-maleimide <sup>j</sup>	0.33 ± 0.01	0.35	0.42	0.004	100
	0.64 ± 0.01	0.70	0.83	0.008	100

<sup>a</sup> The values of maleimide were determined by assaying unreacted cysteine (after the initial incubation of excess cysteine and maleimide) using papain-SSCH<sub>3</sub>. For the maleimide-modified protein samples, about 20–80  $\mu\text{g}$  of protein was typically used in the assay. Each value is an average of at least three experiments, and standard deviations are given. <sup>b</sup> The concentration of the stock solution of maleimide was determined by the assay using Ellman's reagent in a separate experiment using a significantly large amount of protein (about 1.3 mg of maleimide-modified antibody or about 8 nmol maleimide in a final assay volume of 1 mL). <sup>c</sup> The  $\Delta A_{410\text{nm}}$  values in the papain assay were determined 1 h after the addition of 2 mM substrate. <sup>d</sup> The  $\Delta A_{412\text{nm}}$  values (decrease in absorbance due to loss of thiol) from Ellman's assay are hypothetical values calculated for the same amount of sample as used in the papain assay in the same final volume (1.2 mL), assuming  $\epsilon_{412\text{nm}} = 14\,150\text{ M}^{-1}\text{ cm}^{-1}$ . <sup>e</sup> The sensitivity ratio is calculated as the ratio of  $\Delta A_{410\text{nm}}$  of the papain assay (1 h after addition of substrate) and the calculated  $\Delta A_{412\text{nm}}$  value for Ellman's assay. <sup>f</sup> Antibody (IgG<sub>1</sub>) was modified at a concentration of 10 mg/mL (pH 7) using a 1.5-fold molar excess of SMCC (30 min, 30 °C), resulting in an average of  $\sim 0.92$  maleimide group per antibody molecule (based on Ellman's assay). <sup>g</sup> The  $\Delta A_{410\text{nm}}$  values in this papain assay were measured 53 min after the addition of 2 mM substrate. <sup>h</sup> Antibody was modified at a concentration of 9.5 mg/mL (pH 7) using a 1.4-fold molar excess of SMCC (30 min, 30 °C), resulting in an average of  $\sim 0.94$  maleimide group per antibody molecule (based on Ellman's assay). <sup>i</sup> Antibody was modified at a concentration of 9.5 mg/mL (pH 7) using a 2.1-fold molar excess of SMCC (30 min, 30 °C), resulting in an average of  $\sim 1.35$  maleimide groups per antibody molecule (based on Ellman's assay). <sup>j</sup> Avidin ( $M_r$  68 000; tetramer;  $A_{0.1\%}^{280\text{nm}} = 1.57$  at 280 nm) was modified at a concentration of 5 mg/mL (pH 7.6) using a 1.4-fold molar excess of SMCC (30 min, 30 °C), resulting in an average of  $\sim 0.81$  maleimide group per avidin tetramer (based on Ellman's assay).

papain-SSCH<sub>3</sub> assay, the expected value of  $\Delta A_{412\text{nm}}$  from the assay using Ellman's reagent was calculated. Table 1 shows that the experimentally observed changes in absorbance with the papain-SSCH<sub>3</sub> assay (1 h after the addition of substrate) are about 100-fold higher than the theoretically achievable values with the Ellman's assay. The determination of maleimide using papain-SSCH<sub>3</sub> is therefore significantly more sensitive than that using Ellman's reagent.

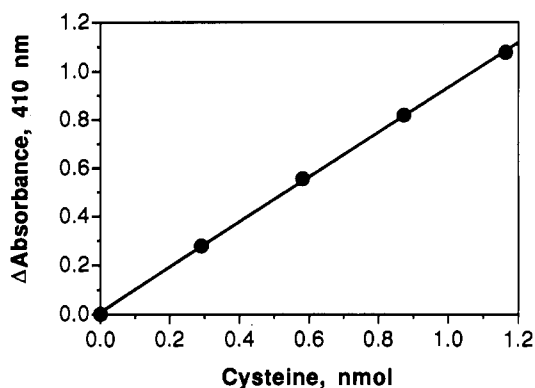
**Estimation of Incubation Times for the Assay of Maleimide Using Cysteine and Papain-SSCH<sub>3</sub>.** The assay of maleimide is based on the complete reaction of maleimide with cysteine (or another thiol of known  $pK_a$ ) and then the complete reaction of the remaining cysteine with papain-SSCH<sub>3</sub>. The necessary reaction times for both conversions can be calculated using the values of apparent rate constants for the reactions.

On the basis of the Brønsted plot and the equations described in the Experimental Procedures, the apparent rate constant ( $k_{\text{app}}$ ) for the reaction of cysteine and *N*-ethylmaleimide at pH 7.6 was calculated as  $4.9 \times 10^5\text{ M}^{-1}\text{ min}^{-1}$  (22 °C). On incubation of 0.10 nmol (0.38  $\mu\text{M} = B_0$ ) of maleimide and 0.87 nmol of cysteine (3.3  $\mu\text{M} = A_0$ ) in a volume of 0.26 mL at pH 7.6, the time for 95% completion of reaction (i.e.,  $B_t = 0.019\text{ }\mu\text{M}$ , and  $A_t = 2.94\text{ }\mu\text{M}$ ) was calculated using the integrated second-order rate equation:  $t = [\ln[(A_t B_0)/(A_0 B_t)]]/[(A_0 - B_0)k_{\text{app}}]$  (11). The time ( $t$ ) for 95% completion of the reaction between maleimide and cysteine was therefore calculated as 2 min.

In the following incubation of the remaining cysteine (0.77 nmol; 1.5  $\mu\text{M} = B_0$ ) with papain-SSCH<sub>3</sub> (12.6 nmol; 24.7  $\mu\text{M} = A_0$ ) at pH 7.6 in a volume of 0.51 mL ( $k_{\text{app}} = 10^4\text{ M}^{-1}\text{ min}^{-1}$ ) (15, 16), the reaction should be 95% complete (i.e.,  $B_t = 0.075\text{ }\mu\text{M}$  and  $A_t = 23.3\text{ }\mu\text{M}$ ) in 13 min. In the experiments described here and for routine assays, we chose incubation times of 40 min at room temperature for both reactions.

## DISCUSSION

In our experiments on conjugation of proteins using thiol and maleimide groups as the reactive moieties (17), we



**Figure 1.** Standard plot of changes in absorbance at 410 nm vs initial amounts of cysteine incubated with papain-SSCH<sub>3</sub>. A sample of maleimide-modified protein was initially incubated with a known amount of cysteine present in excess, and the amount of unreacted remaining cysteine was determined using this standard plot. The amount of maleimide was calculated as the difference between the amounts of initial cysteine and assayed remaining cysteine (see Experimental Procedures for details).

were often at the limit of sensitivity of detection of these functional groups. We therefore devised a sensitive assay for the thiol group based on the stoichiometric reactivation of inactive papain (8). In this paper, we have developed a similar assay for maleimide groups by quenching it with a known amount of cysteine present in excess, and determining the remaining unreacted cysteine using the papain-based assay.

Proteins are subject to proteolytic cleavage by papain during the assay. The assay of thiols using papain-SSCH<sub>3</sub> was, however, unaffected by the addition of a significant amount (160  $\mu\text{g}$ ) of unmodified antibody (8), and we concluded that the activity of papain toward the chromogenic substrate (*N*-benzoyl-L-arginine-*p*-nitroanilide) is not inhibited by antibody. We recommend that before assaying new maleimide-modified proteins, similar control experiments should be done to demonstrate that the protein itself does not interfere in the assay of cysteine using papain-SSCH<sub>3</sub>. We have also used an alternative

approach, in which the unmodified protein was added to the tubes containing cysteine standards and to the blank without cysteine, at an amount equivalent to that of the modified protein in the test sample.

The amplified response of this assay is due to the catalytic activity of papain that is regenerated by the reaction of thiol with the inactive mixed disulfide of papain (8). The signal obtained in the assay can be increased by (i) increasing the time of incubation with substrate and (ii) increasing the concentration of substrate (18). The assay has been shown to be linear for 2 h after the addition of substrate (8). In the experiments described here, the values of absorbance of all samples were measured 1 h after the addition of substrate, so that the maximum changes in the absorbance were less than 1.5 unit (Figure 1). Small amounts of maleimide (0.1 nmol) in a sample of antibody were measured accurately and precisely (Table 1). We recommend the lower limit of 0.1 nmol for the assay because of the cumulative errors possible (i) in volume measurements and (ii) in estimation of the difference between the amounts of cysteine initially added to the maleimide sample and of the remaining cysteine.

#### ACKNOWLEDGMENT

I am thankful to Drs. Walter A. Blättler, Albert R. Collinson, John M. Lambert, and Yeldur P. Venkatesh for helpful discussions.

#### LITERATURE CITED

- (1) Ji, T. H. (1983) Bifunctional reagents. *Methods Enzymol.* 91, 580–609.
- (2) Yoshitake, S., Yamada, Y., Ishikawa, E., and Masseyeff, R. (1979) Conjugation of glucose oxidase from *Aspergillus niger* and rabbit antibodies using *N*-hydroxysuccinimide ester of *N*-(4-carboxycyclohexylmethyl)-maleimide. *Eur. J. Biochem.* 101, 395–399.
- (3) Gregory, J. D. (1955) The stability of *N*-ethylmaleimide and its reactions with sulfhydryl groups. *J. Am. Chem. Soc.* 77, 3922–3923.
- (4) Roberts, E., and Rouser, G. (1958) Spectrophotometric assay for reaction of *N*-ethylmaleimide with sulfhydryl groups. *Anal. Chem.* 30, 1291–1292.
- (5) Alexander, N. M. (1958) Spectrophotometric assay for sulfhydryl groups using *N*-ethylmaleimide. *Anal. Chem.* 30, 1292–1294.

- (6) Riddles, P. W., Blakeley, R. L., and Zerner, B. (1983) Reassessment of Ellman's reagent. *Methods Enzymol.* 91, 49–60.
- (7) Ellman, G. L. (1959) Tissue sulfhydryl groups. *Arch. Biochem. Biophys.* 82, 70–77.
- (8) Singh, R., Blättler, W. A., and Collinson, A. R. (1993) An amplified assay for thiols based on reactivation of papain. *Anal. Biochem.* 213, 49–56.
- (9) Yoshitake, S., Imagawa, M., Ishikawa, E., Niitsu, Y., Urushizaki, I., Nishiura, M., Kanazawa, R., Kurosaki, H., Tachibana, S., Nakazawa, N., and Ogawa, H. (1982) Mild and efficient conjugation of rabbit Fab' and horseradish peroxidase using a maleimide compound and its use for enzyme immunoassay. *J. Biochem.* 92, 1413–1424.
- (10) Bednar, R. A. (1990) Reactivity and pH dependence of thiol conjugation to *N*-ethylmaleimide: Detection of a conformational change in chalcone isomerase. *Biochemistry* 29, 3684–3690.
- (11) Atkins, P. W. (1982) *Physical Chemistry*, 2nd ed., Chapter 27, Freeman, San Francisco.
- (12) Wilson, J. M., Wu, D., Motiu-DeGrood, R., and Hupe, D. J. (1980) A spectrophotometric method for studying the rates of reaction of disulfides with protein thiol groups applied to bovine serum albumin. *J. Am. Chem. Soc.* 102, 359–363.
- (13) Roberts, D. D., Lewis, S. D., Ballou, D. P., Olson, S. T., and Shafer, J. A. (1986) Reactivity of small thiolate anions and cysteine-25 in papain toward methyl methanethiosulfonate. *Biochemistry* 25, 5595–5601.
- (14) Singh, R., and Whitesides, G. M. (1993) Thiol-disulfide interchange. *Supplement S: The Chemistry of Sulphur-Containing Functional Groups* (S. Patai and Z. Rappoport, Eds.) pp 633–658, Wiley, London.
- (15) Shaked, Z., Szajewski, R. P., and Whitesides, G. M. (1980) Rates of thiol-disulfide interchange reactions involving proteins and kinetic measurements of thiol  $pK_a$  values. *Biochemistry* 19, 4156–4166.
- (16) Singh, R., and Whitesides, G. M. (1991) A reagent for reduction of disulfide bonds in proteins that reduces disulfide bonds faster than does dithiothreitol. *J. Org. Chem.* 56, 2332–2337.
- (17) Lambert, J. M., Goldmacher, V. S., Collinson, A. R., Nadler, L. M., and Blättler, W. A. (1991) An immunotoxin prepared with blocked ricin: A natural plant toxin adapted for therapeutic use. *Cancer Res.* 51, 6236–6242.
- (18) Mole, J. E., and Horton, H. R. (1973) Kinetics of papain-catalyzed hydrolysis of  $\alpha$ -*N*-benzoyl-L-arginine-*p*-nitroanilide. *Biochemistry* 12, 816–822.

# Improved Synthesis of *N*-Succinimidyl 4-[<sup>18</sup>F]Fluorobenzoate and Its Application to the Labeling of a Monoclonal Antibody Fragment

Ganesan Vaidyanathan\* and Michael R. Zalutsky

Department of Radiology, Duke University Medical Center, Durham, North Carolina 27710. Received February 3, 1994\*

Our previously reported method for the <sup>18</sup>F labeling of antibodies using *N*-succinimidyl 4-[<sup>18</sup>F]-fluorobenzoate (SFB) involved a rather long synthesis time. Here we present an improved method for the synthesis of SFB which reduces the synthesis time by about 45 min. A reaction time of 5-8 min (versus 25 min for the original procedure) was sufficient in the fluorination step to form 4-[<sup>18</sup>F]-fluorobenzaldehyde in high yield. In the original method, 30-35 min was necessary to convert 4-[<sup>18</sup>F]-fluorobenzoic acid to SFB using dicyclohexylcarbodiimide and *N*-hydroxysuccinimide. When *N,N'*-disuccinimidyl carbonate was used, facile conversion of 4-fluorobenzoic acid to SFB was seen at a micromolar level. At a tracer level, no product was formed at room temperature; however, complete consumption of starting material was observed. Heating at 150 °C resulted in the formation of SFB in more than 80% yield in 1-3 min. HPLC purification of SFB was necessary since use of crude SFB, or SFB purified using a silica solid-phase cartridge column, resulted in lower protein coupling yields. Furthermore, use of crude SFB resulted in cross-linking and lower immunoreactivity of antibody. Largely as a result of the considerable reduction in total labeling time, these modifications have increased the amount of <sup>18</sup>F-labeled antibody available per 100 mCi of [<sup>18</sup>F]fluoride by 30-35%.

## INTRODUCTION

Monoclonal antibodies (mAbs)<sup>1</sup> labeled with radionuclides have been used extensively for diagnostic and therapeutic applications (1). In general, radioimmuno-scintigraphy has been successful in detecting greater than 70% of lesions (2, 3). However, less favorable results have been observed for smaller tumors and when lesions are located in regions with high normal tissue uptake. Utilization of tomographic imaging methods is one of the approaches to improve radioimmunodetection. For example, encouraging results were obtained in clinical investigations using single photon emission computed tomography (SPECT) with <sup>123</sup>I-labeled anticarcinoembryonic antigen mAb fragments (4). Further improvements in tumor detection might be achieved by combining the potential tumor specificity of mAbs with the imaging advantages of positron emission tomography (PET).

Of the several positron-emitting nuclides available, <sup>18</sup>F is attractive because of its routine availability and widespread clinical use. Several methods have been reported for the <sup>18</sup>F labeling of proteins in general, and mAbs in particular (5-9). We recently reported a method for labeling mAbs with <sup>18</sup>F using *N*-succinimidyl 4-[<sup>18</sup>F]-fluorobenzoate, SFB (10, 11). This method offers several advantages in comparison to other methods for labeling proteins with <sup>18</sup>F. First, it yields a labeled template on the mAb that is structurally analogous to iodo- and astatobenzoates which have been developed for the radioiodination and astatination of mAbs (12, 13). Second, mAb fragments labeled with <sup>18</sup>F using this method exhibit

better tumor to normal tissue ratios as a consequence of lower normal tissue uptake (11). However, labeling mAbs using SFB required a longer time for preparation of the labeled mAb than desirable for use with 2-h half-life <sup>18</sup>F. For this reason, we sought to make the SFB method more amenable to clinical evaluation by attempting to reduce the total synthesis time in order to increase the available level of <sup>18</sup>F-labeled mAb fraction.

## EXPERIMENTAL PROCEDURES

**Materials and Methods.** All reagents were purchased from Aldrich Chemical Co. Mel-14 F(ab')<sub>2</sub> was obtained as a gift from Dr. Darell Bigner of the Department of Pathology, Duke University Medical Center. This mAb is an IgG<sub>2a</sub> and is reactive with the tumor-associated chondroitin sulfate proteoglycan present in melanomas, gliomas, and medulloblastomas (14). Thin-layer chromatography (TLC) was performed using EM Science silica gel analytical plates. Melting points were determined on a Fischer-Johns melting point apparatus and are uncorrected. The NMR spectrum was recorded on a General Electric Midfield GN-300 spectrometer. Tetramethylsilane was used as an internal reference ( $\delta = 0.00$ ). The mass spectrum was obtained on a JEOL SX-102 high-resolution mass spectrometer. High-pressure liquid chromatography (HPLC) was conducted with two LKB Model 2150 pumps, a LKB Model 2152 control system, a LKB Model 2138 fixed-wavelength (254 nm) UV detector, and a Beckman Model 170 radioisotope detector (the detectors were connected in series in that order). Peak analysis was performed using a Nelson Analytical software package on an IBM computer. Normal-phase HPLC was performed using an Alltech silica gel column (Partisil silica 10  $\mu$ m, 250  $\times$  4.6 mm) eluted with hexane:ethyl acetate:acetic acid (70:30:2 v/v/v) at a flow rate of 1 mL/min. Gel filtration HPLC was performed using a Bio-Rad TSK column (300  $\times$  7.5 mm) and eluted with phosphate-buffered saline, pH 7.2 at 1 mL/min.

\* Abstract published in *Advance ACS Abstracts*, June 1, 1994.

<sup>1</sup> Abbreviations: SFB, *N*-succinimidyl 4-[<sup>18</sup>F]fluorobenzoate; DCC, dicyclohexylcarbodiimide; NHS, *N*-hydroxysuccinimide; DSC, *N,N'*-disuccinimidyl carbonate; mAb, monoclonal antibody; TSTU, *N,N,N',N'*-tetramethyl(succinimido)uronium tetrafluoroborate; SFBs, *N*-succinimidyl 8-[(4'-<sup>18</sup>F]fluorobenzyl)amino]suberate; SPECT, single photon emission computed tomography; PET, positron emission tomography; sFv, single-chain antibody fragment.

**Preparation of [<sup>18</sup>F]Fluoride Ion.** [<sup>18</sup>F]Fluoride ion was produced using the <sup>18</sup>O(p,n)<sup>18</sup>F reaction by irradiating [<sup>18</sup>O]H<sub>2</sub>O in a small volume (300 μL) silver target (15). The activity was delivered to a solution of Kryptofix (10 mg in 1 mL of CH<sub>3</sub>CN) and potassium carbonate (1 mg in 5 μL water) in a glass tube and then evaporated in an automated drying unit. The dried activity was resublimized in 100–200 μL of dry DMSO.

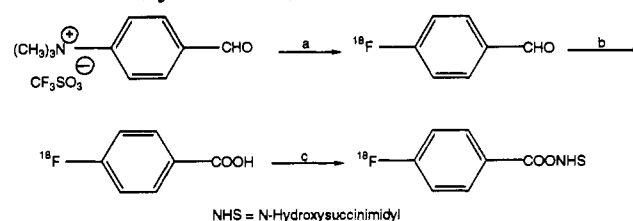
**Disuccinimidyl Carbonate-Mediated Microscale Synthesis of *N*-Succinimidyl 4-Fluorobenzoate.** Solutions (0.1 M) of each 4-fluorobenzoic acid, disuccinimidyl carbonate, and pyridine were prepared in Sure Seal acetonitrile (Aldrich). The esterification reaction was conducted by mixing 10 μL each of the above solutions in a Reacti vial and left at room temperature. The reaction was followed by TLC (50:50 ethyl acetate:hexane; *R<sub>f</sub>* of SFB = 0.4) and normal-phase HPLC (*t<sub>R</sub>* of SFB = 14–15 min) and was complete in 10 min. The product formed in this reaction was isolated by preparative thick-layer chromatography and characterized. The melting point and the mixed melting point with the SFB prepared using *N*-hydroxysuccinimide/DCC route were identical to that of the latter: <sup>1</sup>H-NMR (CDCl<sub>3</sub>) δ 2.91 (s, 4H), 7.19 (m, 2H), 8.18 (m, 2H); MS (CI, NH<sub>3</sub>) *m/z* 255 (M + NH<sub>4</sub>)<sup>+</sup>, 238 (MH<sup>+</sup>), 140, 123; HRMS (FAB<sup>+</sup>) calcd for C<sub>11</sub>H<sub>9</sub>FNO<sub>4</sub> (MH<sup>+</sup>) *m/z* 238.0515, found 238.0525.

***N*-Succinimidyl 4-[<sup>18</sup>F]Fluorobenzoate.** The first two steps involved for the preparation of the title compound were similar to those reported earlier (10). The yield for the fluorination of 4-formyl-*N,N,N*-trimethylanilinium triflate to form 4-[<sup>18</sup>F]fluorobenzaldehyde was essentially complete using a reaction time of only 5–8 min. To the acid (0.1–40.0 mCi) in a Reacti vial were added 100 μL of Sure Seal acetonitrile followed by 30 μL each of 0.1 M DSC and pyridine in acetonitrile. The vial was tightly capped and placed on a hot plate kept at 150 °C. The yield of the reaction was determined at 1, 3, and 5 min by injecting an aliquot onto HPLC (normal phase). The product was purified either by HPLC or by using a Waters silica gel Sep Pak cartridge column. For HPLC, acetonitrile from the reaction mixture was evaporated using a stream of argon, and the activity was reconstituted in a small volume (50–100 μL) of ethyl acetate. For the solid-phase extraction, the residual activity after removing acetonitrile was taken in about 100 μL of 70:30:2 (v/v/v) hexane:ethyl acetate:acetic acid and loaded onto the Sep Pak cartridge. The activity was eluted with the same solvent. A 2-mL fraction and several 1-mL fractions was collected. The fractions containing the ester activity were identified by HPLC. Generally, the ester activity elutes in fractions 3–7.

For mAb labeling, the organic solvents were evaporated from the appropriate HPLC or Sep Pak fractions containing the SFB activity to a small volume. This solution was transferred to a 0.5 dram vial and evaporated to dryness. In the case of crude activity, the acetonitrile from the reaction mixture was removed by evaporation with argon. The activity was transferred to another 0.5 dram vial with 70:30:2 (v/v/v) hexane:ethyl acetate:acetic acid solvent. The solvents were evaporated to dryness.

**Coupling of SFB with Mel-13 F(ab')<sub>2</sub>.** Either the crude, the Sep Pak-purified, or the HPLC-purified SFB activity was used for the coupling reaction. To the activity (0.3–7.0 mCi) contained in a 0.5 dram vial was added 50 μL of Mel-14 F(ab')<sub>2</sub> in 0.1 M borate buffer (6 mg/mL). This mixture was incubated at room temperature for 15 min. The coupling was stopped by the addition of 300 μL of 0.2 M glycine in borate buffer. The labeled mAb was

### Scheme 1. Synthesis of SFB<sup>a</sup>



<sup>a</sup> Key: (a) [<sup>18</sup>F]KF, Kryptofix, DMSO, 150 °C, 5–8 min (25 min); (b) KMnO<sub>4</sub>, NaOH, 150 °C, 3 min; (c) DSC, pyridine, CH<sub>3</sub>CN, 1–3 min, 150 °C (NHS, DCC, THF, room temperature).

purified by passing through a G-25 Sephadex column eluted with phosphate-buffered saline. When crude and Sep Pak-purified SFB were used, coupling yields were based on the amount of SFB activity, determined by HPLC, present in the mixture.

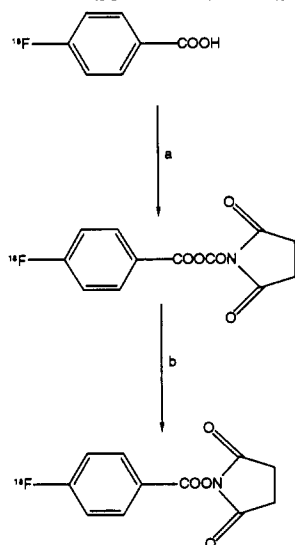
**In Vitro Analyses of <sup>18</sup>F-Labeled mAb Fragment.** The protein-associated activity was determined by 20% trichloroacetic acid precipitation. The homogeneity of the labeled mAb was determined by gel filtration HPLC. In vitro specific binding was determined using a single-point assay (10). About 100 ng of labeled mAb was added in triplicate to 250 mg of both antigen-positive D-54 MG human glioma and antigen-negative rat liver or brain homogenates. After a 90-min incubation at room temperature, the homogenates were washed three times and counted for <sup>18</sup>F activity in an automated γ-counter. Specific binding is defined as the percentage of activity bound to tumor minus the percentage bound to control homogenates.

**Biodistribution of <sup>18</sup>F-Labeled Mel-14 F(ab')<sub>2</sub>.** Tissue distribution of Mel-14 F(ab')<sub>2</sub> labeled with <sup>18</sup>F using both crude (A) and HPLC-purified SFB (B) was compared in mouse. Mice, weighing 20–25 g, were injected via the tail vein with 3–4 μg (5 μCi) of B and another group of mice with 20–21 μg (5 μCi) of A. A half hour after injection, the mice (five in each group) were killed with halothane overdose. After dissection, the tissues of interest were removed, washed with saline, and counted for <sup>18</sup>F activity.

### RESULTS AND DISCUSSION

With the generation of smaller mAb fragments such as sFv (16–18) and the renewed interest in labeled peptide imaging (19), the potential of <sup>18</sup>F as a protein and peptide label for PET has increased significance. Because <sup>18</sup>F has a half-life of only 110 min, it is important that the labeling methods for this nuclide be fast and of high yield. Three aspects of the original method for preparing SFB (Scheme 1) were investigated in order to reduce the total time of synthesis. These were the fluorination step, esterification step, and purification of SFB. In our original method, we adapted the conditions reported by Haka *et al.* (20) for the fluorination. These investigators used a period of 25 min for this reaction. However, the yield obtained by conducting the reaction for 5–8 min was similar to that obtained for a 25-min reaction, resulting in a saving of about 20 min in the synthesis time.

In the original method, we utilized the DCC-mediated coupling of *N*-hydroxysuccinimide to convert 4-[<sup>18</sup>F]-fluorobenzoic acid to SFB. A yield versus esterification time study revealed that a reaction time of 30–35 min was necessary to achieve an optimum yield. Generally, DCC-mediated esterification is slow, needing 15–20 h for the preparation of unlabeled SFB. Alternative approaches such as the use of disuccinimidyl carbonate (21) or *N,N,N',N'*-tetramethyl(succinimido)uronium tetrafluoroborate (TSTU; 22) for the preparation of *N*-hydrox-

**Scheme 2. Possible Pathway for the DSC-Mediated Conversion of 4-Fluorobenzoic Acid to SFB<sup>a</sup>**

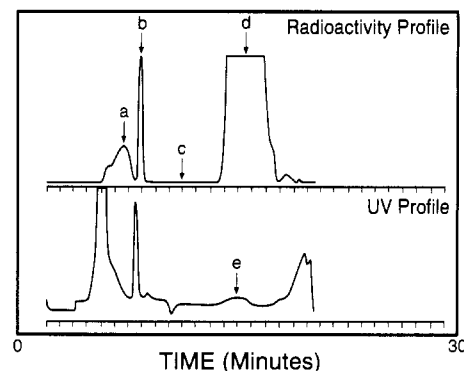
<sup>a</sup> Key: (a) DSC/pyridine/acetonitrile; (b) 150 °C.

ysuccinimide esters have been reported. These methods require only very short reaction periods. Our attempts to prepare labeled SFB using TSTU were not successful.

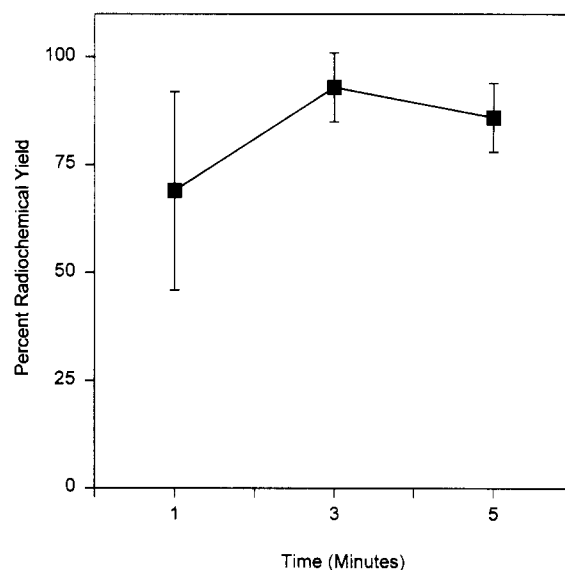
Initially, we evaluated the utility of the DSC-mediated approach in the preparation of unlabeled SFB at a micromolar scale. The reaction was essentially complete in 10 min. Encouraged by this result, we adapted the DSC method for the preparation of no-carrier-added SFB. Analysis of the reaction mixture by HPLC showed the complete disappearance of the starting material, 4-[<sup>18</sup>F]fluorobenzoic acid ( $t_R$  = 8–9 min), in as early as 5 min; however, no formation of SFB ( $t_R$  = 15.0–15.5 min) was observed. Most of the activity was associated with a rapidly eluting peak in HPLC ( $t_R$  = 6.5–7.0 min). It was reasoned that the intermediate carbonate shown in Scheme 2 was formed but was not converted to the product at tracer level. To demonstrate that the intermediate is indeed the carbonate, a method was sought to prepare it.

An ideal reagent for the conversion of 4-fluorobenzoic acid to this carbonate would be *N*-succinimidyl chloroformate. A literature search revealed that not only has this reagent been made but also that it has been used to convert *N*-protected amino acids to the type of mixed carbonate discussed above (23). Further, the same authors report that heating of the intermediate converted them to *N*-hydroxysuccinimide esters. Encouraged by this, the esterification reaction was conducted at 150 °C which resulted in the conversion of the intermediate to SFB. A typical HPLC profile of this reaction mixture is shown in Figure 1. A study of the effect of time on yield (Figure 2) showed that only 1–3 min was required for more than 80% conversion of the acid to the ester. While our work was in progress, Gohlke *et al.* also reported on the preparation of active esters of <sup>18</sup>F-labeled carboxylic acids using DSC and other similar agents (24).

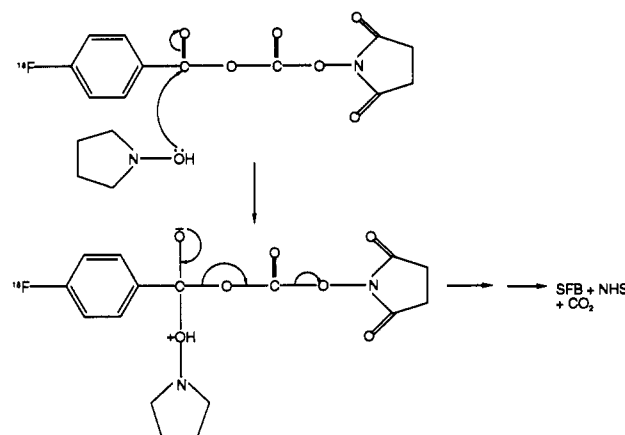
The hypothesized carbonate intermediate was not stable in carrier level reactions, yet it was difficult to convert it to SFB at a no-carrier-added level. The most probable mechanism for the formation of SFB from this intermediate is by the nucleophilic attack of *N*-hydroxysuccinimide (a byproduct formed in the first step) at the benzoyl carbonyl carbon (Scheme 3). The difference in the results at carrier level and no-carrier-added level is most likely related to concentration-dependent kinetics. Due to the large amount of DSC present in the reaction mixture,



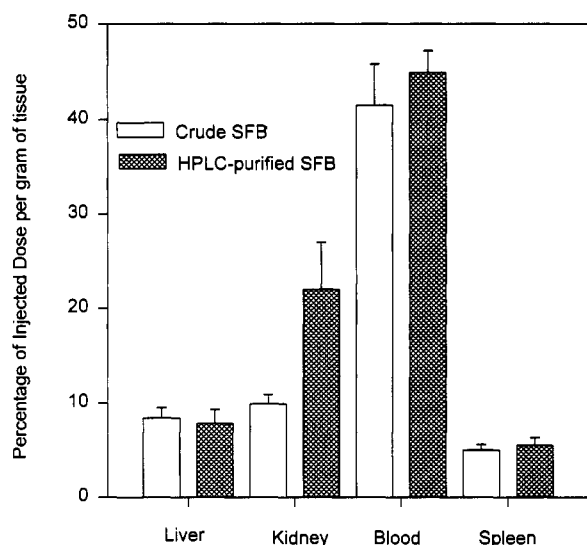
**Figure 1.** UV and radioactivity HPLC profiles of the reaction of mixture of [<sup>18</sup>F]SFB preparation: (a) 4-[<sup>18</sup>F]fluorobenzaldehyde;  $t_R$  = 5–6 min; (b) mixed carbonate intermediate;  $t_R$  = 7 min; (c) 4-[<sup>18</sup>F]fluorobenzoic acid;  $t_R$  = 8–9 min; (d) [<sup>18</sup>F]SFB;  $t_R$  = 15–16 min; (e) carrier SFB;  $t_R$  = 14–15 min.



**Figure 2.** Yield as a function of time in the DSC-mediated formation of SFB.

**Scheme 3. Proposed Mechanism for the Conversion of the Mixed Carbonate to SFB**

conversion of 4-[<sup>18</sup>F]fluorobenzoic acid to the mixed carbonate might not have been a problem. On the other hand, subsequent conversion of the carbonate to SFB might be difficult as both the carbonate and *N*-hydroxysuccinimide were available only in trace amounts. Attempts to force this conversion by use of excess *N*-hydroxysuccinimide (addition after 1-min reaction) in the reaction mixture were not successful. However, one should



**Figure 3.** Uptake of Mel-14 F(ab')<sub>2</sub> labeled with <sup>18</sup>F using HPLC-purified and crude SFB in mouse liver, kidney, blood, and spleen.

**Table 1.** Effect of SFB Purification Method on Labeling Mel-14 F(ab')<sub>2</sub> with <sup>18</sup>F

mode of purification	coupling yield (%)	specific binding (%)	high mol wt species present
none	27 ± 17	29.5 ± 1.6	10–15%
Sep Pak	13–17	30.0 ± 2.2	none detected
HPLC	51 ± 6	50.7 ± 0.8	none detected

realize that excess *N*-hydroxysuccinimide may also prevent the formation of the intermediate itself. HPLC analysis of the above reaction mixture showed the presence of the intermediate and acid in about 60:40 ratio. We also tried unsuccessfully to couple the intermediate directly to mAb fragment. Attempts to prepare the carbonate intermediate or its *N*-hydroxyphthalimido analog from 4-fluorobenzoic acid and *N*-succinimidyl or phthalimidyl chloroformate were not successful either. Formation of SFB in these reactions was noticed by TLC.

Purification of SFB using HPLC requires an additional 15–20 min of preparation time. For this reason, the possibility of coupling crude SFB, or SFB purified by a silica solid-phase extraction cartridge column, was investigated. The results of these studies are summarized in Table 1. Irrespective of the quality of SFB, the protein-associated activity, determined by trichloroacetic acid precipitability, of the labeled mAb was more than 96% in all cases. Compared to HPLC-purified SFB, the coupling efficiency of crude SFB to mAb was generally lower. Immunoreactivity of the labeled mAb was also lower when crude SFB was used. Furthermore, with the crude SFB-labeled mAb, protein cross-linking (low *t<sub>R</sub>* shoulder in gel filtration HPLC; about 10–15%) was observed, presumably caused by unreacted DSC. Garg *et al.* (9) have shown that it is necessary to purify the <sup>18</sup>F labeling agent SFBS by HPLC in order to obtain good quality of labeled mAb in good coupling yields. Labeling of an antimyosin Fab with crude SFBS provided a labeled mAb preparation with about 15% of high molecular weight impurities which in turn resulted in higher liver and spleen uptake and lower blood pool activity.

The quality of the mAbs labeled using crude and HPLC-purified SFB was further evaluated by performing a tissue distribution in mice. As shown in Figure 3, no significant (*p* > 0.05) difference in liver uptake (an indicator of cross-linking) was observed. The uptake was also similar in most other organs except in the kidney, where a substantial reduction in uptake was seen for the fragment labeled

with crude SFB. It is not clear why the high molecular weight species did not alter the liver, spleen, and blood uptakes. The difference in the kidney uptake could very well be explained as a result of high molecular weight species. Generally, molecules of the size of Fab and F(ab')<sub>2</sub> are cleared through the kidney whereas IgG are not (25). The higher molecular weight species, formed when crude SFB was used, should have a molecular weight equal to or higher than that of an IgG and hence cannot accumulate in renal cells.

When silica Sep Pak-purified SFB was used, no high molecular weight species was formed. However, the coupling efficiency was rather poor with this method of purification. This could have been caused by some impurity which might not have been separated from the activity by this mode of purification. Moreover, using this purification method, there was no improvement in the percent specific binding of the labeled mAb either. These results confirm the need to purify SFB by HPLC for better coupling efficiencies and immunoreactivities.

In conclusion, we were able to reduce the total synthesis time of pure SFB by about 45 min, increasing the amount of available <sup>18</sup>F-labeled mAb by about 35%. Although crude SFB could be coupled to mAbs, this is accompanied by reduced coupling yields and poor quality of labeled mAb. The additional time needed for HPLC purification will result in the loss of about 12% of the total activity by decay. On the other hand, HPLC purification of SFB increases the available activity by 47%, because of higher coupling efficiency, and provides a good quality labeled mAb. Using this improved method, we have labeled a chemotactic peptide (26) and are currently evaluating its potential in the PET imaging of bacterial infections.

#### ACKNOWLEDGMENT

The excellent technical assistance of Donna Affleck and Susan Slade is greatly appreciated. The authors wish to thank Sandra Gatling for her help in preparing this manuscript. The research was funded by Department of Energy Grant DE-FG05-89ER60789 and National Institutes of Health Grants CA 14236 and NS 20023.

#### LITERATURE CITED

- (1) Zalutsky, M. R. (1989) *Antibodies in Radiodiagnosis and Therapy*, CRC Press, Boca Raton, FL.
- (2) Carrasquillo, J. A. (1989) Radioimmunoassay with polyclonal or monoclonal antibodies. In *Antibodies in Radiodiagnosis and Therapy* (M. R. Zalutsky, Ed.) pp 169–198, CRC Press, Boca Raton, FL.
- (3) Larson, S. M. Clinical Radioimmunoassay. (1990) 1978–1988: overview and suggestion for standardization of clinical trials. *Cancer Res. (Suppl.)* 50, 892s–898s.
- (4) Lind, P., Lechner, P., Arian-Schad, K., Klimpfinger, M., Cesnik, H., Kammerhuber, F., and Eber, O. (1991) Anticarcinoma embryonic antigen immunoscintigraphy (technetium-99m-monoclonal antibody BW 431/26) and serum CEA levels in patients with suspected with primary and recurrent colorectal carcinoma. *J. Nucl. Med.* 32, 1319–1325.
- (5) Müller-Platz, C. M., Kloster, G., Legler, G., and Stöcklin, G. (1982) <sup>18</sup>F-Fluoroacetate: An agent for introducing no-carrier-added fluorine-18 into urokinase without loss of biological activity. *J. Labelled Compd. Radiopharm.* 19, 1645–1646.
- (6) Kilbourn, M. R., Dence, C. S., Welch, M. J., and Mathias, C. J. (1987) Fluorine-18 labeling of proteins. *J. Nucl. Med.* 28, 462–470.



- (7) Shiue, C.-Y., Wolf, A. P., and Hainfield, J. F. (1988) Synthesis of  $^{18}\text{F}$ -labeled *N*-(*p*-[ $^{18}\text{F}$ ]fluorophenyl)maleimide and its derivatives for labelling monoclonal antibody with  $^{18}\text{F}$  (Abstract). *J. Labelled Compd. Radiopharm.* 26, 287-289.
- (8) Shai, Y., Kirk, K. L., Channing, M. A., Dunn, B. B., Lesniak, M. A., Eastman, R. C., Finn, R. D., Roth, J., and Jacobson, K. A. (1989)  $^{18}\text{F}$ -labeled insulin: a prosthetic group methodology for incorporation of a positron emitter into peptides and proteins. *Biochemistry* 28, 4801-4806.
- (9) Garg, P. K., Garg, S., and Zalutsky, M. R. (1991) Fluorine-18 labeling of monoclonal antibodies and fragments with preservation of immunoreactivity. *Bioconjugate Chem.* 2, 44-49.
- (10) Vaidyanathan, G., and Zalutsky, M. R. (1992) Labeling proteins with fluorine-18 using *N*-succinimidyl 4-[ $^{18}\text{F}$ ]fluorobenzoate. *Nucl. Med. Biol.* 19, 275-281.
- (11) Vaidyanathan, G., Bigner, D. D., and Zalutsky, M. R. (1992) Fluorine-18-labeled monoclonal antibody fragments: a potential approach for combining radioimmunoassay and positron tomography. *J. Nucl. Med.* 33, 1535-1541.
- (12) Zalutsky, M. R., and Narula, A. S. (1987) A method for the radiohalogenation of proteins resulting in decreased thyroid uptake of radioiodine. *Appl. Radiat. Isot.* 38, 1051-1055.
- (13) Zalutsky, M. R., and Narula, A. S. (1988) Astatination of proteins using an *N*-succinimidyl tri-*n*-butylstannyl benzoate intermediate. *Appl. Radiat. Isot.* 39, 227-232.
- (14) Carrel, S., Accolla, R. S., Carmagnola, A. L., and Mach, J.-P. (1980) Common human melanoma-associated antigen(s) detected by monoclonal antibodies. *Cancer Res.* 40, 2523-2528.
- (15) Wieland, B. W., Hendry, G. O., Schmidt, D. G., Bida, G., and Ruth, T. J. (1986) Efficient small-volume O-18 water targets for producing F-18 fluoride with low energy protons. *J. Labelled Compd. Radiopharm.* 23, 1202-1204.
- (16) Bird, R. E., Hardman, K. D., Jacobson, J. W., Johnson, S., Kaufman, B. M., Lee, S.-M., Lee, T., Pope, S. H., Riordan, G. S., and Whitlow, M. (1989) Single-chain antigen-binding proteins. *Science* 242, 423-426.
- (17) Milenic, D. E., Yokota, T., Filpula, D. R., Finkelman, M. A. J., Dodd, S. W., Wood, J. F., Whitlow, M., Snoy, P., and Schlom, J. (1991) Construction, binding properties, metabolism and tumor penetration of a single-chain Fv derived from pancreatic carcinoma monoclonal antibody CC49. *Cancer Res.* 51, 6363-6371.
- (18) Yokota, T., Milenic, D. E., Whitlow, M., and Schlom, J. (1992) Rapid tumor penetration of a single chain Fv and comparison with other immunoglobulin forms. *Cancer Res.* 52, 3402-3408.
- (19) Fischman, A. J., Babich, J. W., and Strauss, H. W. (1993) A ticket to ride: Peptide Radiopharmaceuticals. *J. Nucl. Med.* 34, 2253-2263.
- (20) Haka, M. S., Kilbourn, M. R., Watkins, G. L., and Toorongan, S. A. (1989) Aryltrimethylammonium trifluoromethanesulfonates as precursors to aryl [ $^{18}\text{F}$ ]fluorides: Improved synthesis of [ $^{18}\text{F}$ ]GBR-13119. *J. Labelled Compd. Radiopharm.* 27, 823-833.
- (21) Bannworth, W., and Knorr, R. (1991) Formation of carboxamides with *N,N,N',N'*-tetramethyl(succinimido)uronium tetrafluoroborate in aqueous/organic solvent systems. *Tetrahedron Lett.* 32, 1157-1160.
- (22) Ogura, H., Kobayashi, T., Kazumasa, K., and Takeda, K. (1979) A novel active ester synthesis reagent (*N,N'*-disuccinimidyl carbonate). *Tetrahedron Lett.* 4745-4746.
- (23) Gross, V. H., and Bilk, L. (1967) *N,N*-Disubstituted derivatives of *O*-chloroformylhydroxylamines as reagents for peptide synthesis. *Angew. Chem.* 79, 532-533.
- (24) Gohlke, S., Coenen, H. H., and Stöcklin, G. (1993) [ $^{18}\text{F}$ ]-Fluoroacetic acid and [ $^{18}\text{F}$ ]fluoropropionic acid derivatives as reactive fluoroacylation agents (Abstract). *J. Labelled Compd. Radiopharm.* 32, 108-110.
- (25) Mack, T., Park, C. H., and Camargo, M. J. F. Renal filtration, transport, and metabolism of proteins. (1992) In *The Kidney: Physiology and Pathophysiology* D. W. Seldin, and G. Giebisch, Eds.) 2nd ed., pp 3005-3038, Raven Press Ltd., New York.
- (26) Vaidyanathan, G., Affleck, D. A., Welsh, P., and Zalutsky, M. R. (1994) Fluorine-18 labeled chemotactic peptide: A potential agent for the PET imaging of focal infection (Abstract). *J. Labelled Compd. Radiopharm.* 35, 365-367.

# Monoclonal Antibodies to Thioguanine: Influence of Coupling Position on Fine Specificity

Vibeke Mortensen Nerstrøm,<sup>\*,†</sup> Ulla Henriksen,<sup>‡</sup> Peter E. Nielsen,<sup>§</sup> Ole Buchardt,<sup>‡</sup> Kjeld Schmiegelow,<sup>±</sup> and Claus Koch<sup>†</sup>

Research Center for Medical Biotechnology, Department of Immunology, Statens Seruminstitut, Artillerivej 5, DK-2300 Copenhagen S, Denmark, Research Center for Medical Biotechnology, Department of Organic Chemistry, The H.C. Ørsted Institute, University of Copenhagen, Universitetsparken 5, DK-2100 Copenhagen Ø, Denmark, Research Center for Medical Biotechnology, Department of Biochemistry B, The Panum Institute, University of Copenhagen, Blegdamsvej 3, DK-2200 Copenhagen N, Denmark, and Department of Pediatrics, Rigshospitalet, University Hospital, Blegdamsvej 9, DK-2100 Copenhagen Ø, Denmark. Received November 17, 1993\*

Thioguanine derivatives with reactive ester groups at positions 6, 7, or 9 of the purine ring were synthesized and coupled to a protein carrier. The purified protein derivative of tuberculin was used as the carrier for immunizing bacillus Calmette-Guerin primed mice. This led to high antibody titers against the homologically coupled hapten, and spleen cells from the immunized mice were used to produce monoclonal antibodies against thioguanine. All monoclonal antibodies were selected for their ability to recognize free thioguanine and were analyzed for their fine specificity by inhibition experiments with a panel of thiopurine derivatives. The specificity of the monoclonal antibodies showed a strong dependence on the coupling position of the thioguanine. Within each group of monoclonal antibodies, raised against one of the three different conjugates, there was a high degree of heterogeneity, with antibodies differing in their binding according to the substitution on the thioguanine analogues used in the inhibition experiments. This panel of antibodies may be used for quantitative assays of thiopurines and their metabolites in patients undergoing treatment with thioguanine, 6-mercaptopurine, and azathioprine.

## INTRODUCTION

The thiopurines azathioprine (6-((1-methyl-4-nitroimidazol-5-yl)thio)purine), thioguanine (2-amino-6-purinethione), and 6-mercaptopurine (6-purinethione) are used for the treatment of systemic connective tissue diseases, leukemia, and lymphomas. Catalyzed by the hypoxanthine guanine phosphoribosyl transferase these antineoplastic agents are converted to thioguanine nucleotides which mediate the cytotoxic effect of the thiopurines through incorporation into DNA and RNA. In addition, the thiopurines inhibit de-novo purine synthesis, thus enhancing the incorporation of thioguanine nucleotides through the purine salvage pathway (Tidd et al., 1974). Treatment with thiopurines may, however, cause certain side effects, most of which are dose-related (McCormack and Johns, 1990).

It is therefore of clinical interest to establish quantitative assays, not only for thioguanine itself, but also for thioguanine metabolites in blood samples from patients undergoing treatment with thioguanine. Current methods are mostly based on the extraction of thioguanine from plasma or blood, followed by HPLC analysis, and they are thus both cumbersome and time consuming (Bruunshuus and Schmiegelow, 1989). An attractive alternative would be to set up assays based on the use of immunological reagents, provided antibodies can be prepared that recognize intact thioguanine. Also, antibodies that recognize relevant metabolites of thioguanine would be useful.

From an immunological point of view, thioguanine is a hapten (MW 167 Da) and has to be coupled onto an

immunogenic carrier protein in order to be recognized as an antigen. A reactive linking group therefore must be introduced which can subsequently be employed for the coupling reaction. The coupling of the hapten to the carrier must be strong and stable, and the position of the reactive group may influence the fine specificity of the resulting antibodies.

We have used three different coupling positions on thioguanine to obtain series of monoclonal antibodies against this hapten, and we have analyzed the reactivity of these antibodies to thioguanine and a series of 6-purinethiono and 6-purinethiolo derivatives.

## EXPERIMENTAL PROCEDURES

**Materials and Methods.** Chemicals for syntheses were obtained from Aldrich, Steirheim, Germany. Chemicals for conjugations were obtained from Merck. The protein carrier PPD<sup>1</sup> and rabbit antibodies against OA were from Statens Seruminstitut, Copenhagen, Denmark, and OA was from Sigma, St. Louis, MO. Compounds used for the screening of antibody specificity were obtained from Sigma or prepared as described. The derivatives are listed in Scheme 1 and Chart 1. Peroxidase-labeled rabbit anti-mouse immunoglobulin and antibodies for mouse immunoglobulin subclass determination were from DAKO, Ballerup, Denmark, and Zymed, San Francisco, CA, respectively. Microtiter plates (Maxisorp) were from NUNC, Roskilde, Denmark.

<sup>1</sup> Abbreviations used: BCG, bacillus Calmette-Guerin; DCC, *N,N'*-dicyclohexylcarbodiimide; DMF, dimethylformamide; DMSO, dimethyl sulfoxide; ELISA, enzyme-linked immunosorbent assay; EtOAc, ethyl acetate; EtOH, ethanol; MeCN, acetonitrile; MeOH, methanol; NHS, *N*-hydroxysuccinimide; OA, ovalbumin; OPD, 1,2-phenylenediamine hydrochloride; PBS, phosphate-buffered saline; PPD, purified protein derivative.

<sup>†</sup> Statens Seruminstitut.

<sup>‡</sup> The H.C. Ørsted Institute.

<sup>§</sup> The Panum Institute.

<sup>±</sup> The University Hospital.

\* To whom correspondence should be addressed. Tel: +45 32683595; Fax: +45 32683149.

© Abstract published in *Advance ACS Abstracts*, June 15, 1994.



filtration, the product was precipitated with ether, collected, and washed with MeOH and ether (155 mg, 0.48 mmol, 48%). The compound could not be purified further because of hydrolysis: MS (FAB<sup>+</sup>)  $m/z$  323 ( $M + 1$ ).

**2-Amino-7-(carboxymethyl)-6-purinethione (6)** was prepared from 2-amino-7-(carboxymethyl)-6-chloropurine (4) (595 mg, 2.62 mmol) and thiourea (239 mg, 3.14 mmol) as described for 5 (450 mg, 2 mmol, 77%): MS (FAB<sup>+</sup>)  $m/z$  226 ( $M + 1$ ). Anal. Calcd for  $C_7H_7N_5O_2S \cdot 0.5H_2O$ : C, 35.89; H, 3.44; N, 30.03. Found: C, 35.94; H, 3.21; N, 29.78.

**Succinimidyl Thioguanin-7-ylacetate (8)** was prepared from 2-amino-7-(carboxymethyl)-6-purinethione (6) (123 mg, 0.55 mmol), NHS (76 mg, 0.66 mmol), and DCC (135 mg, 0.66 mmol) as described for 7 (45 mg, 0.14 mmol, 26%): MS (FAB<sup>+</sup>)  $m/z$  323 ( $M + 1$ ).

**Succinimidyl 4-(Bromomethyl)benzoate.** 4-(Bromomethyl)benzoic acid (1.18 g, 5.5 mmol) and NHS (0.76 g, 6.6 mmol) were dissolved in anhydrous dioxane (15 mL). DCC (1.35 g, 6.6 mmol) was added, and the mixture was left overnight at room temperature, filtered, and evaporated to dryness. The product (1.21 g, 3.9 mmol, 71%) was recrystallized from 2-propanol: <sup>1</sup>H NMR (CDCl<sub>3</sub>)  $\delta$  8.11 (d, 2 H,  $J = 8$  Hz), 7.53 (d, 2 H,  $J = 8$  Hz), 4.50 (s, 2 H), 2.90 (s, 4 H).

**Succinimidyl 4-(((2-Amino-6-puriny)thio)methyl)benzoate (9).** Succinimidyl 4-(bromomethyl)benzoate (343 mg, 1.1 mmol), thioguanine (1) (167 mg, 1 mmol), and excess Et<sub>3</sub>N were mixed in anhydrous DMF (5 mL) with stirring. After 3 h at room temperature, the mixture was filtered, and the product was precipitated with ether, collected, and washed with CHCl<sub>3</sub> (300 mg, 0.75 mmol, 75%): MS (FAB<sup>+</sup>)  $m/z$  399 ( $M + 1$ ). Anal. Calcd for  $C_{17}H_{14}N_6O_4S \cdot 2.5H_2O$ : C, 46.05; H, 4.32; N, 18.95; S, 7.23. Found: C, 45.84; H, 4.34; N, 18.73; S, 7.19.

**2,4-Diamino-5-acetamido-6-hydroxypyrimidine (10a)** and **2,4-diamino-5-benzamido-6-hydroxypyrimidine (10b)** were prepared as previously described (Wilson, 1948).

**2-Amino-6-chloro-8-methylpurine (11a).** 2,4-Diamino-5-acetamido-6-hydroxypyrimidine (10a) (986 mg, 5.39 mmol) was refluxed in POCl<sub>3</sub> (25 mL) for 5 min, benzyltriethylammonium chloride (2.46 g, 10.4 mmol) in MeCN (25 mL) was added, and refluxing was continued for 4 h. The mixture was evaporated to an oil, poured on ice-water, neutralized with concentrated ammonium hydroxide, and boiled for 5 min. The product (500 mg, 2.75 mmol, 51%) was precipitated by adjusting the pH to 3 with concentrated HCl, collected, and used without further purification.

**2-Amino-6-chloro-8-phenylpurine (11b).** 2,4-Diamino-5-benzamido-6-hydroxypyrimidine (10b, 826 mg, 3.37 mmol) was refluxed in POCl<sub>3</sub> (15 mL) for 1 h, benzyltriethylammonium chloride (1.54 g, 6.76 mmol) was added, and refluxing was continued for 1 h. The product was collected after cooling, suspended in water, neutralized with concentrated ammonium hydroxide, boiled for 5 min, chilled, collected, and used without further purification (480 mg, 1.96 mmol, 58%) (modification of the method by Elion et al., 1951).

**2-Amino-8-methyl-6-purinethione (12a)** was prepared from 2-amino-6-chloro-8-methylpurine (11a) (260 mg, 1.42 mmol) and thiourea (129 mg, 1.7 mmol) as described for 5, except that Na<sub>2</sub>CO<sub>3</sub> was used in the purification instead of NaHCO<sub>3</sub> (193 mg, 1.07 mmol, 75%): MS (FAB<sup>+</sup>)  $m/z$  182 ( $M + 1$ ). (11a has been prepared previously by different methods (Daves, Jr., et al., 1960).)

**2-Amino-8-phenyl-6-purinethione (12b)** was prepared from 2-amino-6-chloro-8-phenylpurine (11b) (150 mg, 0.61 mmol) and thiourea (56 mg, 0.73 mmol) analogously to 12a (100 mg, 0.41 mmol, 68%): MS (FAB<sup>+</sup>)  $m/z$  244 ( $M + 1$ ).

**Conjugation of Activated Thioguanine Derivatives to Carrier Proteins.** The activated thioguanine derivatives 7–9 were dissolved in DMSO at 40 mg/mL and were conjugated with PPD and OA. The protein solutions were adjusted to 1 mg/mL and dialyzed against 0.1 M NaHCO<sub>3</sub>, pH 8.3. Ten  $\mu$ L of thioguanine derivative was added per milliliter of protein solution and allowed to react for 2 h at room temperature under gentle mixing. The conjugate was finally dialyzed against PBS, pH 7.2, for 24 h with three buffer changes.

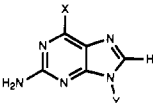
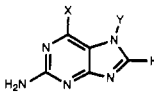
**Immunization Procedure.** The thioguanine–PPD conjugates were adsorbed onto an Al(OH)<sub>3</sub> suspension to give a vaccine that contained 10  $\mu$ g of PPD and 1 mg of Al in 0.5 mL of vaccine. CF1xBALB/c mice that had been sensitized with two human doses of BCG 1 month previously were injected intraperitoneally with 0.5 mL of vaccine per immunization. Five mice were immunized with each conjugate. After 2 weeks, they were reimmunized with the same dose, and mouse sera were assayed for antibody levels 10 days after the second immunizations. Four days prior to fusion the mice received a final intraperitoneal boost with the same vaccine.

**Fusion and Screening Procedure.** Fusions were performed essentially as described by Köhler and Milstein with slight modifications (Köhler and Milstein, 1975; Reading, 1982). The spleen cells from immunized mice were fused with the myeloma cell line X63.Ag8.653. Selected clones were recloned by limiting dilution at least three times to ascertain monoclonality.

Culture supernatants were screened for antibody activity against thioguanine by a capture ELISA, in which microtiterplates were coated with a rabbit antiserum to OA, at 10  $\mu$ g/mL in 0.05 M sodium carbonate buffer, pH 9.6, followed by the respective thioguanine derivative coupled to OA at 10–50 ng/mL in dilution buffer (PBS, pH 7.2 containing 1% w/v bovine albumin and 0.05% v/v Triton X-100). This was followed by incubation with dilutions of culture supernatant, horse radish peroxidase-labeled rabbit anti-mouse immunoglobulin (Code P260) diluted 1:1000, and finally with H<sub>2</sub>O<sub>2</sub> and OPD substrate solution in phosphate-acetate buffer, pH 5.0. (Engvall and Perlmann, 1971; Tijssen, 1985). Culture supernatants which tested positive in the above system were immediately assayed for inhibition of the reaction with free thioguanine, and only those cultures whose reactions could be inhibited were further propagated.

**Assay for the Fine Specificity of the Monoclonal Antibodies.** The fine specificities of the monoclonal antibodies were analyzed by inhibition experiments with a series of thiopurines (depicted in Chart 1). The density of the thioguanine–OA conjugates on rabbit anti-OA-coated plates was adjusted to give a maximal signal of about 3.5 OD at 490 nm in ELISA. Variations in titers of the monoclonal antibodies were adjusted by diluting the individual culture supernatants to give an OD signal of 2.0. The monoclonal antibodies were incubated overnight with varying concentrations from  $3 \times 10^{-5}$  to  $6 \times 10^{-9}$  M of the respective thiopurines before the mixture was transferred to the antigen-coated ELISA plate. The further procedure was as described above. The inhibitory potential was calculated as inhibition (%) =  $((OD_{\text{control}} -$

Table 1.  $^1\text{H}$  NMR and UV Data of 2-Aminopurines

compd	X	Y	 or 		H-8 <sup>a</sup>	(2)NH <sub>2</sub> <sup>a</sup>	$\lambda_{\text{max}}$ <sup>c</sup>
			$\delta^a$ (X or N(1)H <sup>b</sup> )	$\delta$ (Y) <sup>a</sup>			
3	Cl	CH <sub>2</sub> COOH		(9)CH <sub>2</sub> : 4.88 s	8.10 s	6.96	243; 310
4	Cl	CH <sub>2</sub> COOH		(7)CH <sub>2</sub> : 5.13 s	8.32 s	6.65	243; 320
7	SH	CH <sub>2</sub> CONHS	11.98	(9)CH <sub>2</sub> : 5.40 s NHS, C <sub>2</sub> H <sub>4</sub> : 2.82 s	7.98 s	6.92	256; 344
8	SH	CH <sub>2</sub> CONHS	12.1	(7)CH <sub>2</sub> : 5.97 s NHS, C <sub>2</sub> H <sub>4</sub> : 2.80 s	8.28 s	6.58	262; 348
9	SCH <sub>2</sub> C <sub>6</sub> H <sub>4</sub> CONHS	H	CH <sub>2</sub> : 4.67 s C <sub>6</sub> H <sub>4</sub> : 7.76 d; 8.03 d ( $J = 8$ Hz) NHS, C <sub>2</sub> H <sub>4</sub> : 2.89 s	12.5	7.90 s	6.43	242; 314

<sup>a</sup>  $\delta$ -values in DMSO-*d*<sub>6</sub>. <sup>b</sup> For 7 and 8. <sup>c</sup> nm in MeOH.

OD<sub>expl</sub>/OD<sub>control</sub>)100. Subclasses of individual monoclonal antibodies were determined by ELISA using a commercial kit.

## RESULTS

**Chemical Synthesis of Thioguanine Derivatives for Coupling to Proteins.** The reaction sequences are shown in Scheme 1 and described in the Materials and Methods. Alkylation of 2-amino-6-chloropurine with bromoacetic acid resulted in a mixture of 9- and 7-carboxymethyl isomers with 2-amino-9-(carboxymethyl)-6-chloropurine (3) as the major product. The assignment, 7- or 9-isomer, was done by  $^1\text{H}$  NMR and UV spectroscopy (Table 1). The signals from H(8) and N-CH<sub>2</sub> are shifted upfield for the 9-isomers relative to the corresponding signals from the 7-isomers, whereas the (2)NH<sub>2</sub> signals appear at lower field for the 9-isomers (Kjellberg and Johansson, 1986; Green et al., 1990). The longest wavelength absorption maximum in the UV spectra exhibits a bathochromic shift for the 7-isomers compared to the 9-isomers (Green et al., 1990).

The 6-chloro substituent of purines is exchangeable with nucleophiles, and treatment of the 9- and 7-(carboxymethyl) isomers with thiourea gave the corresponding thiono derivatives 5 and 6. The reactive succinimidyl esters, 7 and 8, were then obtained by reacting 5 and 6 with NHS and DCC.

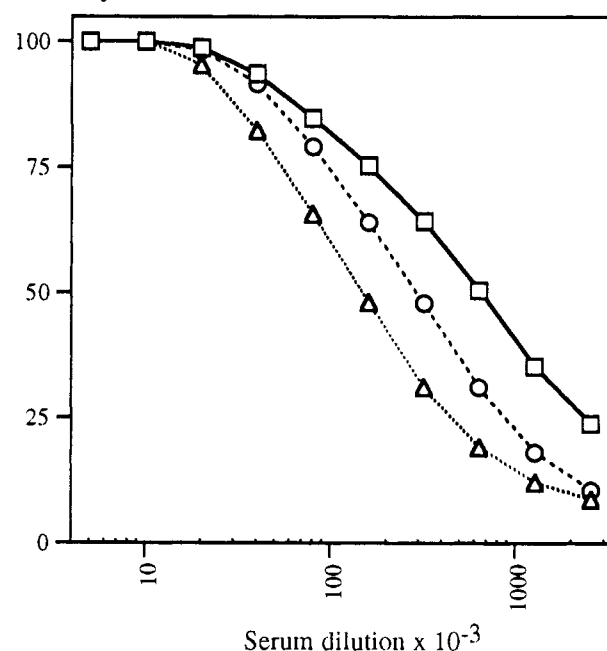
Attempts to react 2-amino-6-chloropurine (2) or thioguanine (1) directly with succinimidyl bromoacetate failed, but reaction of thioguanine with the less reactive succinimidyl 4-(bromomethyl)benzoate led to a usable thioguanine derivative reactive at position 6 (9 in Scheme 1).

**Immune Responses to the Thioguanine Conjugates.** All three conjugates of the differently activated thioguanine derivatives induced a high antibody response (Figure 1). When defined as the reciprocal of the dilution giving half maximum signal value, the mean titers for five mice from each group were 150 000, 320 000, and 640 000 for the 7-, 9-, and S-substituted thioguanines, respectively.

**Monoclonal Antibodies against S-Substituted Thioguanine (the 138 Series).** Sixty-eight positive clones were found, of which around 30% produced antibodies inhibitable with free thioguanine. Fourteen of these mAbs were selected, nine of which were analyzed in detail for their fine specificity.

The pattern of cross-reactivities for this series of mAbs is displayed in Figure 2, showing the results for three representative antibodies, all of the IgG2a subclass. The antigen used for immunization was conjugated through the sulfur atom and could be regarded as a substituted thiol (structures c and d in Scheme 2), but screening was

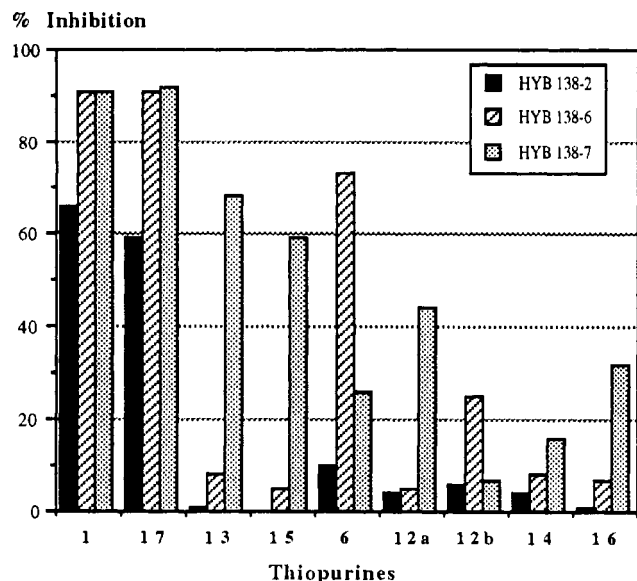
Arbitrary units



**Figure 1.** Immune response against thioguanine conjugated to a carrier protein through three different positions as measured in ELISA. Each curve represents mean responses in groups of five mice. Arbitrary units of 100 represent maximum response in the individual ELISA assays.  $\Delta$ : 7-conjugated thioguanine.  $\circ$ : 9-conjugated thioguanine.  $\square$ : S-conjugated thioguanine.

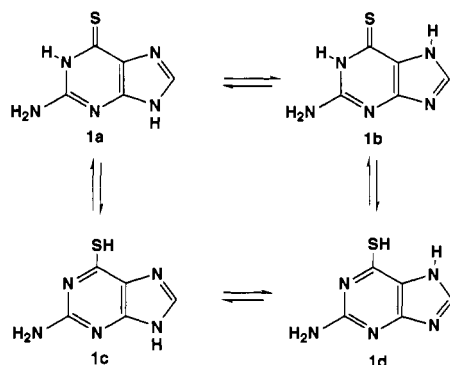
performed with thioguanine, which is best represented by the thiono form (structure a or b in Scheme 2). Both 6-thiono- and 6-thiolo derivatives (i.e., (methylthio)guanine (17)) are thus recognized by this series of antibodies. Changes at position 2 have varying effects on reactivity. Exchange of the amino group with hydrogen (i.e., 6-purinethione (13)) or introduction of oxygen at position 2 (i.e., 6-thioxanthine (15)) only affected the reactivity of antibody 138-7 marginally, whereas it completely abolished the reactivity of the other two antibodies. Compounds with substituents at positions 7, 8, or 9 were markedly restricted in their reactivity with these antibodies, but to varying degrees. Thus, substitution at position 7 (6) hardly affected the reactivity of 138-6, whereas 138-2 lost most and 138-7 part of their reactivities. Substitution at position 8 (12a and 12b) diminished reactivity depending on the substituent. Substitution at position 9 further diminished reactivity of 138-7; compare 13 with 14.

**Monoclonal Antibodies against 9-Substituted Thioguanine (the 125 Series).** One fusion gave a yield of 600 antigen-specific hybridomas, which were all inhib-



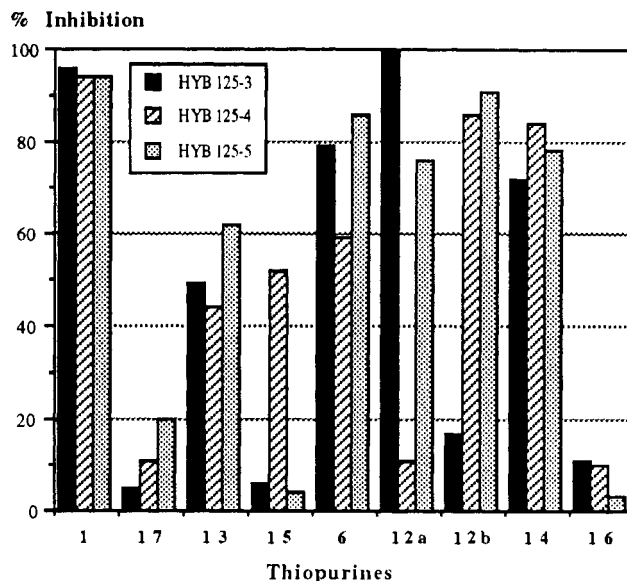
**Figure 2.** Cross-reactivity pattern for three representative monoclonal antibodies raised against thioguanine conjugated to the carrier protein at position 6. The numbers are the different thioguanine analogues ( $3 \times 10^{-5}$  M) used in the inhibition assay and refer to Chart 1.

#### Scheme 2

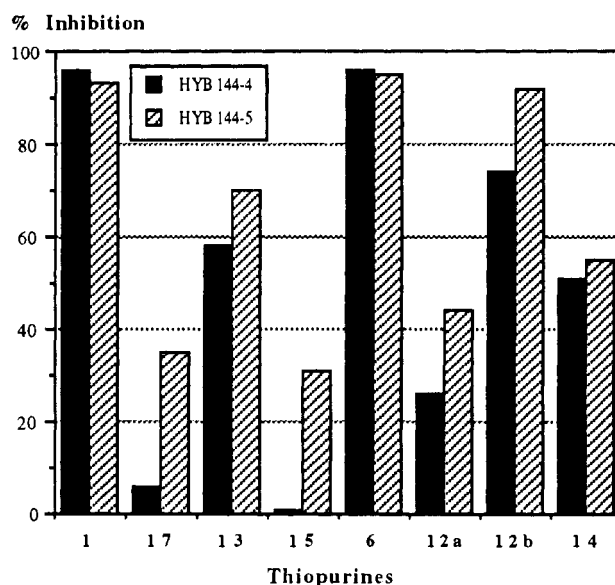


itable by free thioguanine. Six clones were subjected to repeated reclonings, and the resulting antibodies were analyzed for their fine specificity in the inhibition assay. The cross-reactivity patterns for this group of monoclonal antibodies is shown in Figure 3, where three antibodies, all of the IgG2a subclass, have been selected to represent the observed patterns of binding specificity. It appears that reactivity was primarily dependent on the structure of the pyrimidine ring. The S-substituted derivative (17) had markedly reduced reactivity. Changes at position 2 interfered with reactivity: exchange of the amino group with hydrogen (13) diminished the reactivities of the three antibodies, and introduction of oxygen at position 2 (15) practically abolished reactivity with antibodies 125-3 and 125-5, whereas antibody 125-4, as an exception, maintained some reactivity. Substitution at position 7 (6) did not influence reactivity, whereas substitution at position 8 appeared to affect the reactivity differently (compare the reactivity of 12a and 12b for the three antibodies mentioned). Substitution with ribose at position 9 (14) seemed almost to restore the reactivity lost by removal of the amino group (13) but did not restore the reactivity lost by S-substitution (16).

**Monoclonal Antibodies against 7-Substituted Thioguanine (the 144 Series).** Fusions gave a very large number of positive clones, of which almost all the antibodies could be inhibited by free thioguanine. Sixteen



**Figure 3.** Cross-reactivity pattern for three representative monoclonal antibodies raised against thioguanine conjugated to the carrier protein in position 9. The numbers are the different thioguanine analogues ( $3 \times 10^{-6}$  M) used in the inhibition assay and refer to Chart 1.



**Figure 4.** Cross-reactivity pattern for two representative monoclonal antibodies raised against thioguanine conjugated to the carrier protein in position 7. The numbers are the different thioguanine analogues ( $3 \times 10^{-5}$  M) used in the inhibition assay and refer to Chart 1.

mAbs were selected and further analyzed. This group of mAbs showed a higher degree of homogeneity than the two other. The general pattern of reactivity is represented by 144-4 (IgG1) and 144-5 (IgG2a) in Figure 4.

The binding activity for the 144 series was mostly influenced by the structure of the pyrimidine ring. Thus, S-substitution (17) profoundly reduced reactivity, and changes at position 2 diminished reactivity, either slightly when the amino group was exchanged with hydrogen (13) or more profoundly with 6-thioxanthine (15).

Substitution in the imidazole ring seemed to be less important. Compound 6 with substitution at position 7 inhibited just as well as thioguanine, as might be expected from the fact that this is the site of substitution in the immunizing conjugate. With substitution at position 8, the reactivity depended on the substituent (compare 12a



and 12b), and substitution at position 9 did not seem to have much impact on reactivity (compare 13 and 14).

Antibody 144-5 from this series showed a somewhat extraordinary reactivity pattern, in that almost all the thiopurines possessed some reactivity, though with different affinities.

## DISCUSSION

When the reactive thioguanine derivatives were allowed to react with free amino groups on a carrier protein (PPD), immunogenic hapten-carrier conjugates were obtained that led to the production of antibodies which recognized derivatives of thioguanine differentially depending on the structure of the exposed part of the molecule.

Previous experience suggests that immunization of animals pretreated with live BCG vaccine with hapten conjugated to PPD gives rise to a remarkably potent carrier effect (Lachmann et al., 1986). This has been demonstrated when merthiolat was used as hapten<sup>2</sup> and also in systems involving peptides (Lussow et al., 1991) or low-immunogenic proteins.<sup>3</sup> The mechanism is presumed to involve the induction of a strong T-cell immunity to mycobacterial antigens by the BCG treatment, followed by the exploitation of these educated T cells as T helper cells in the subsequent proliferation of specific B cells presenting the hapten linked to fragments of mycobacterial protein (PPD). In the present experiments, BCG-pre-vaccinated mice responded after only two immunizations with anti-hapten antibody titers high enough to warrant cell fusion after a final boost.

The initial screening of the mouse sera was performed with the homologous thioguanine derivative coupled onto an irrelevant carrier, OA. Thus, at this stage, we did not analyze whether the antibody response was directed against free or coupled forms of thioguanine. However, during the screening of hybridomas secreting antibodies against the homologous hapten-carrier conjugate, we immediately selected those for which antibody binding to the solid phase was completely inhibited by free thioguanine in solution.

Several types of tautomerism have been proposed for thioguanine and related compounds (Pullman and Pullman, 1973; Elguero et al., 1976). The most important ones are shown in Scheme 2, i.e., 9-7 tautomerism, e.g.,  $\mathbf{a} \rightleftharpoons \mathbf{b}$ , and thiono-thiolo tautomerism, e.g.,  $\mathbf{a} \rightleftharpoons \mathbf{c}$ . Thioguanine has primarily the thiono structure ( $\mathbf{a}$  or  $\mathbf{b}$ ), both in the solid state and in solution. A pronounced difference is observed in the UV spectra of thiono ( $\lambda_{\max} = 350$  nm) and thiolo forms ( $\lambda_{\max} = 320$  nm) (cf. Table 1; Elion et al., 1959). Thioguanine is best represented by the canonical form  $\mathbf{b}$  in the solid state (Bugg and Thewalt, 1970). Little is known about the 9-7 tautomerism in solution, but thioguanine is probably best represented by a mixture of the canonical forms  $\mathbf{a}$  and  $\mathbf{b}$  in solution, by analogy with guanine (Pfleiderer, 1961).

The fine specificity of the selected monoclonal antibodies was analyzed through inhibition experiments with a series of thiopurine derivatives, substituted at various positions. The specificity was strongly dependent on the position used for coupling to the carrier molecule.

When the S-position was chosen as the coupling site, the reactivity of the resulting antibodies was not influenced

by substitution at the sulfur atom. The reactivities of these antibodies were strongly influenced by the substituents at positions 2, 7, 8, and 9. When the 7- or 9-positions were used for conjugation, the reactivities of the resulting antibodies were mostly dependent on the structure of the pyrimidine ring and less influenced by substitutions at positions 7, 8, and 9.

However, for all three series of mAbs we observed a high degree of heterogeneity, i.e., the influence of substitutions at various positions varied from no inhibition to complete inhibition of the homologous interaction with the antigen used for immunization.

Among the structures used to define the fine specificity of the thioguanine-specific antibodies are some which are known to be metabolites of thioguanine in man and experimental animals after the injection or therapeutic use of thioguanine as an antimetabolite. The finding that such metabolites are recognized differently by the monoclonal antibodies that we have obtained provides the opportunity to measure thioguanine and certain of its metabolites in clinical samples. The present series of antibodies will therefore be employed in assays to monitor the treatment of patients with thioguanine.

## ACKNOWLEDGMENT

This study has been supported by grants from The Industry and Trade Development Council, The Ville Heise Foundation, and The Rosalie Petersen Foundation.

## LITERATURE CITED

- Brunshuus, I., and Schmiegelow, K. (1989) Analysis of 6-mercaptopurine, 6-thioguanine nucleotides, and 6-thiouric acid in biological fluids by high-performance liquid chromatography. *Scand. J. Clin. Lab. Invest.* 49, 779-784.
- Bugg, C. E., and Thewalt, U. (1970) The Crystal and Molecular Structure of 6-Thioguanine. *J. Am. Chem. Soc.* 92, 7441-7445.
- Daves, G. D., Jr., Noell, C. W., Robins, R. K., Koppel, H. C., and Beaman, A. G. (1960) Potential Purine Antagonists. XXII. The Preparation and Reactions of Certain Derivatives of 2-Amino-6-purinethiol. *J. Am. Chem. Soc.* 82, 2633-2640.
- Elguero, J., Marzin, C., Katritzky, A. R., and Linda, P. (1976) Purines and Other Condensed Five-Six Ring Systems with Heteroatoms in Both Rings. *The Tautomerism of Heterocycles. Advances in Heterocyclic Chemistry*, Suppl. 1, pp 502-525, Academic Press, London.
- Elion, G. B., Burgi, E., and Hitchings, G. H. (1951) Studies on Condensed Pyrimidine Systems. VII. Some 8-Arylpurines. *J. Am. Chem. Soc.* 73, 5235-5239.
- Elion, G. B., Goodman, I., Lange, W., and Hitchings, G. H. (1959) Condensed Pyrimidine Systems. XX. Purines Related to 6-Mercaptopurine and Thioguanine. *J. Am. Chem. Soc.* 81, 1898-1902.
- Engvall, E., and Perlmann, P. (1971) Enzyme-linked immunosorbent assay (ELISA) quantitative assay of Immunoglobulin G. *Immunochimistry* 8, 871-874.
- Green, G. R., Grinter, T. J., Kinsey, P. M., and Jarvest, R. L. (1990) The Effect of The C-6 Substituent on The Regioselectivity of N-Alkylation of 2-Aminopurines. *Tetrahedron* 46, 6903-6914.
- Hitchings, G. H., and Elion, G. B. (1954) The chemistry and biochemistry of purine analogues. *Ann. N.Y. Acad. Sci.* 60, 195-199.
- Kjellberg, J., and Johansson, N. G. (1986) Characterization of N7 and N9 Alkylated Purine Analogues by <sup>1</sup>H and <sup>13</sup>C NMR. *Tetrahedron* 42, 6541-6544.
- Köhler, G., and Milstein, C. (1975) Continuous cultures of fused cells secreting antibody of predefined specificity. *Nature* 256, 495-497.

<sup>2</sup> Klausen, J., Weiss Bentzon, M., and Koch, C. Immunization of BCG-pretreated mice with merthiolat conjugated to Purified Protein Derivative (PPD) of Tuberculin gives rise to high titre antibodies. (Manuscript in preparation).

<sup>3</sup> Unpublished observation.

- Lachmann, P. J., Strangeways, L., Vyakarnam, A., and Evan, G. (1986) Raising antibodies by coupling peptides to PPD and immunizing BCG-sensitized animals. Synthetic peptides as antigens. *Ciba Foundation Symposium 119* (R. Porter, and R. Whelan, Eds.) pp 25-57, J. Wiley and Sons, Chichester.
- Lussow, A. R., Barrios, C., Van Embden, J., Van der Zee, R., Verdini, A. S., Pessi, A., Louis, J. A., Lambert, P. H., and del Giudice, G. (1991) Mycobacterial heat-shock proteins as carrier molecules. *Eur. J. Immunol.* 21, 2297-2302.
- McCormack, J. J., and Johns, D. G. (1990) Purine and Purine Nucleoside Antimetabolites. *Cancer Chemotherapy: Principles and Practice*. (B. A. Chabner, and J. M. Collins, Eds.) pp 234-252, J. B. Lippincott Company, Philadelphia.
- Pfleiderer, W. (1961) Purine IV. Über die Methylierung des 9-Methyl-guanins und die struktur des Herbigolins. *Ann. Chem.* 647, 167-173.
- Pullman, B., and Pullman, A. (1973) Electronic Aspects of Purine Tautomerism. *Advances in Heterocyclic Chemistry* 13 (A. R. Katritzky, and A. J. Boulton, Eds.) pp 77-156, Academic Press, London.
- Reading, C. L. (1982) Theory and methods for immunization in culture and monoclonal antibody production. *J. Immunol. Methods* 53, 261-291.
- Tidd, D. M., Paterson, A. R. P. (1974) A biochemical mechanism for delayed cytotoxic action of 6-mercaptopurine. *Cancer Res.* 34, 738-746.
- Tijssen, P. (1985) Practice and theory of enzyme immunoassays. *Laboratory techniques in biochemistry and molecular biology* R. H. Burdon, and P. H. van Knippenberg, Eds.) Vol. 15, pp 9-20, Elsevier, Amsterdam.
- Wilson, W. (1948) Some 2,4-Diamino-5-acylamido-6-hydroxypyrimidines. *J. Chem. Soc.* 1157-1161.

## 2-Substituted Thioadenine Nucleoside and Nucleotide Analogues: Synthesis and Receptor Subtype Binding Affinities (1)

Ahmad Hasan,<sup>\*,†</sup> Tahir Hussain,<sup>‡</sup> S. Jamal Mustafa,<sup>‡</sup> and Prem C. Srivastava<sup>§</sup>

Health Sciences Research Division, Oak Ridge National Laboratory, Oak Ridge, Tennessee 37831-6229, and Department of Pharmacology, School of Medicine, East Carolina University, Greenville, North Carolina 27858. Received February 4, 1994<sup>\*</sup>

The design, synthesis, and receptor subtype binding affinities of several 2-substituted thioadenosine nucleoside and nucleotide analogues are described. Alkylation of 2-thioadenosine (1) with iodopentylboronic acid followed by iododeboronation gave 2-((*E*)-1-iodo-1-penten-5-yl)thioadenosine (9). Compound 1 on treatment with 4-nitrobenzyl bromide and propargyl bromide furnished compounds 3 and 5, respectively. The 5'-monophosphate analogues of compounds 3, 5, 7, and 9 were prepared similarly using 2-thioadenosine 5'-monophosphate (2). Treatment of 1 with bromoethylamine hydrobromide provided 2-[(aminoethyl)thio]adenosine (11) which on coupling with *N*-succinimidyl 3-(4-hydroxyphenyl)propionate gave 2-[[[3-(4-hydroxyphenyl)propionamido]ethyl]thio]adenosine (12). Iodination of 12 gave 2-[[[3-(4-hydroxy-3-iodophenyl)propionamido]ethyl]thio]adenosine (13). Compounds 3-13 were evaluated for their affinities toward A<sub>1</sub> and A<sub>2</sub> adenosine receptors in rat brain cortex and striatum, respectively using [<sup>3</sup>H]DPCPX and [<sup>3</sup>H]CGS 21680 as ligands. The nucleotide analogues 4, 6, 8, and 10 inhibited binding of [<sup>3</sup>H]DPCPX by 10-20% and of [<sup>3</sup>H]CGS 21680 by 40-50% at a concentration of 100 μM suggesting weak affinity toward adenosine receptors. The nucleoside analogues 3, 5, 7, 9, 12, and 13 inhibited the A<sub>2</sub> receptor binding of [<sup>3</sup>H]CGS 21680 with K<sub>i</sub> values of 1.2-3.67 μM, while A<sub>1</sub> receptor binding of [<sup>3</sup>H]DPCPX was inhibited with K<sub>i</sub> values 10-17 μM. The A<sub>1</sub>/A<sub>2</sub> ratios suggest 4-8-fold A<sub>2</sub> receptor selectivity.

### INTRODUCTION

Adenosine is an effective mediator of a wide variety of physiological functions including vasodilation, cardiac depression, inhibition of platelet aggregation, inhibition of lymphocyte functions, inhibition of insulin release and potentiation of glucagon release in the pancreas, and inhibition of lipolysis (2). Many of these effects are mediated by extracellular receptor subtypes, A<sub>1</sub> and A<sub>2</sub>, linked to adenylate cyclase in an inhibitory and stimulatory manner, respectively. These two receptor subtypes can be distinguished on the basis of structure-activity relationships (3-5) using receptor binding assays (6, 7).

Substitutions on the adenine base have been found to alter the affinity of adenosine for its receptors (8-14). For example, *N*<sup>6</sup>-cyclopentyladenosine (8, 9) is a potent and selective agonist at the A<sub>1</sub> adenosine receptor (7, 10). The availability of *N*<sup>6</sup>-substituted adenosine analogues has aided in the development of models for the A<sub>1</sub> adenosine receptor (10, 15), and also for the A<sub>2</sub> adenosine receptor (16, 17), and a large number of *N*<sup>6</sup>-substituted purine nucleosides have been prepared. Even though several early studies of adenosine receptor of the platelet (18-20) and the coronary artery (21, 22) indicate greater selectivity of 2-substituted adenosine analogues as agonist at the A<sub>2</sub> subtype, the synthesis and biological evaluation of this class of compounds has been less vigorously pursued.

Several 2-CH-, 2-O-, 2-NH-, and 2-S-alkyl-, and aryl-modified adenine nucleosides have been reported (18-30). The aralkoxy substitution at the 2 position of adenosine appears to enhance the A<sub>2</sub> receptor affinity. The A<sub>2</sub> receptor affinity of phenethoxy adenosine has been further optimized by substitution of the phenyl ring with F, Cl, CH<sub>3</sub> and CH<sub>3</sub>O- functional groups (26). This led us to synthesize the new 2-substituted thioadenine nucleoside and nucleotide analogues for biological evaluation described in this paper.

### EXPERIMENTAL PROCEDURES

**General Methods.** All solvents, chemicals, and reagents were analytical grade and were used without further purification unless otherwise indicated. The melting points (mp) were determined on a Thomas-Hoover apparatus in open capillary tubes and were uncorrected. <sup>1</sup>H spectra were recorded on a Varian Gemini-200 spectrometer and reported in ppm downfield from the internal tetramethylsilane (TMS = 0) standard. The signals are expressed as s (singlet), d (doublet), t (triplet), m (multiplet), or br (broad). The presence of exchangeable protons was confirmed by visualization with deuterium oxide followed by reintegration of the NMR spectrum. UV spectra were recorded on Beckman DU-64 spectrophotometer. Baker analyzed silica gel (60-200 mesh) was used for column chromatography. Thin-layer chromatography (TLC) was performed using 250-μm layers of silica gel GF precoated glass plates (Analtech, Inc.). Spots on the TLC plates were detected by visualization under short wave ultraviolet (UV) light, exposure to iodine vapors, or heating the chromatogram at 100 °C after spraying with a solution of 5% sulfuric acid in methanol. The TLC solvent systems used were (A) isobutyric acid:water:conc'd ammonium hydroxide (33:17:0.5 v/v), (B) methanol:chloroform (1:5 v/v), (C) ethyl acetate:2-propanol:water (7:1:2 v/v, top layer), and (D) methanol:chloroform (2:8 v/v). The paper

\* Author to whom correspondence should be addressed.

<sup>†</sup> Current address: Department of Chemistry, Box 90349, Duke University, Durham, NC 27708-0349. Phone (919)-660-1553; Fax (919)-660-1605.

<sup>‡</sup> East Carolina University.

<sup>§</sup> Work was done during the tenure at ORNL. Current address: Medical Applications and Biophysical Research Division, ER-73; US Department of Energy, Washington, D.C.

\* Abstract published in *Advance ACS Abstracts*, June 1, 1994.

chromatography was performed using Whatman no. 1 cellulose paper in an ascending technique with solvent system A. The elemental analyses were determined by Galbraith Laboratories (Knoxville, TN), and the results are within  $\pm 4\%$  of the theoretical value except where noted.

**2-[(4-Nitrobenzyl)thio]adenosine (3).** Compound 3 was prepared by slight modification (NaH and DMF) of literature procedure (18) in 46% yield, mp 152 °C [shrinks at 126–127 °C (lit. (18) 130.5–132 °C)].  $^1\text{H}$  NMR (DMSO- $d_6$ ):  $\delta$  8.27 (s, 1H, H-8), 8.15 (d,  $J$  = 8.5 Hz, 2H, Ar-H), 7.78 (d,  $J$  = 8.8 Hz, 2H, Ar-H), 7.46 (s, 2H,  $\text{NH}_2$ ), 5.87 (d,  $J$  = 5.6 Hz, 1H, H-1'), 5.45 (d,  $J$  = 5.86 Hz, 1H, OH), 5.20 (d,  $J$  = 5.9 Hz, 1H, OH), 5.06 (t,  $J$  = 5.5 Hz, 1H, OH), 4.5 (m, 1H, H-2'), 4.12 (m, 1H, H-3'), 3.96 (d,  $J$  = 3.66 Hz, 1H, H-4'), 3.60 (m, 2H, H-5'), 3.14 (s, 2H,  $-\text{CH}_2-$ ). Anal. Calcd for ( $\text{C}_{17}\text{H}_{18}\text{N}_6\text{O}_6\text{S}\cdot\text{CH}_3\text{OH}$ ): C, 46.35; H, 4.72; N, 18.03. Found: C, 46.66; H, 4.89; N, 17.78.

**2-[(4-Nitrobenzyl)thio]adenosine 5'-Monophosphate (4).** Sodium methoxide (540 mg, 10 mmol) was added to a suspension of 2-thioadenosine 5'-monophosphate (32) (1.0 g, 2.6 mmol) in methanol (200 mL) under an argon atmosphere. The reaction mixture was stirred at room temperature for 30 min after which 4-nitrobenzyl bromide (570 mg, 2.6 mmol) was added, and the stirring was continued for 10 h at room temperature. Solvents were removed under reduced pressure, and the residue was dissolved in water. The solution was adjusted to pH 2 with 2 N hydrochloric acid. The crude product was collected by filtration, washed with cold water, and purified by dissolution in 1 N sodium hydroxide followed by adjusting the solution to pH 2 with 1 N hydrochloric acid. The mixture was kept at room temperature overnight, and the crystalline solid that separated was collected by filtration to yield 4 (570 mg, 42%), mp 192–194 °C.  $^1\text{H}$  NMR (DMSO- $d_6$ ):  $\delta$  8.4 (s, 1H, H-8), 8.17 (d,  $J$  = 7.86 Hz, 2H, Ar-H), 7.79 (d,  $J$  = 7.89 Hz, 2H, Ar-H), 6.02 (d,  $J$  = 4.48 Hz, 1H, H-1'), 4.42 (m, 2H, H-2', H-3'), 4.15 (bs, 2H,  $-\text{CH}_2-$ ), 4.01 (bm, 3H, H-4', H-5'). UV (pH 1):  $\lambda_{\text{max}}$  269. Anal. Calcd for ( $\text{C}_{17}\text{H}_{19}\text{N}_6\text{O}_9\text{SP}\cdot\text{H}_2\text{O}$ ): C, 37.09; H, 4.18; N, 15.27. Found: C, 36.94; H, 3.90; N, 15.06.

**2-[(Propargyl)thio]adenosine (5).** Sodium hydride (40 mg, 1 mmol, 60% suspension in oil) was added to a suspension of compound 1 (299 mg, 1 mmol) in anhydrous DMF (10 mL) under an argon atmosphere. The mixture was stirred at room temperature until evolution of hydrogen gas ceased ( $\sim 25$  min). A solution of propargyl bromide (2 mL, 80% solution in toluene) in anhydrous DMF (5 mL) was added to the reaction mixture, and stirring was continued overnight. Solvent was removed under reduced pressure, and the residue was triturated with water, filtered, and washed with cold water. The crude product was purified by silica gel column chromatography. The column was eluted with ethyl acetate followed by 5% methanol in ethyl acetate, and the fractions ( $R_f$  = 0.46, silica gel TLC in solvent C) containing the major product were combined, and solvent was removed to yield 5 (277 mg, 82%), mp 121 °C (78–80 °C shrinks).  $^1\text{H}$  NMR ( $\text{CDCl}_3 + \text{CD}_3\text{OD}$ ):  $\delta$  7.94 (s, 1H, H-8), 5.8 (d,  $J$  = 6.06 Hz, 1H, H-1'), 4.79 (t,  $J$  = 5.5 Hz, 1H, H-2'), 4.37 (m, 1H, H-3'), 4.2 (m, 1H, H-4'), 3.79 (m, 2H, H-5'), 3.40 (s, 2H,  $-\text{CH}_2-$ ), 2.25 (t,  $J$  = 2.6 Hz, 1H,  $\text{C}\equiv\text{CH}$ ). Anal. Calcd for ( $\text{C}_{13}\text{H}_{15}\text{N}_5\text{O}_4\text{S}\cdot\text{CH}_3\text{OH}$ ): C, 45.53; H, 5.15; N, 18.97. Found: C, 45.82; H, 4.90; N, 19.12.

**2-[(Propargyl)thio]adenosine 5'-Monophosphate (6).** Compound 6 was prepared following the procedure described for 4, using 2 (230 mg, 0.6 mmol), sodium methoxide (125 mg, 2.3 mmol), and propargyl bromide (250 mg, 80% wt solution in toluene) in methanol at 60

°C for 12 h. The residue was dissolved in water (2 mL), and the solution was adjusted to pH 2 with dilute hydrochloric acid. The crude product was collected by filtration, washed with water, dried under vacuum, and crystallized from water to yield 6 (75 mg, 30%), mp 218–220 °C.  $^1\text{H}$  NMR (DMSO- $d_6$ ):  $\delta$  8.44 (s, 1H, H-8), 5.9 (d,  $J$  = 5.49 Hz, 1H, H-1'), 4.65 (t,  $J$  = 4.8 Hz, 1H, H-2'), 4.18–4.0 (m, 5H, H-3', H-4', and H-5'), 3.9 (s, 2H,  $-\text{CH}_2-$ ), 2.5 (t,  $J$  = 1.75 Hz, 1H,  $\text{C}\equiv\text{CH}$ ). UV (pH 1):  $\lambda_{\text{max}}$  269.6. Anal. Calcd for ( $\text{C}_{13}\text{H}_{16}\text{N}_5\text{O}_7\text{SP}\cdot\text{H}_2\text{O}$ ): C, 35.86; H, 4.14; N, 16.09. Found: C, 35.85; H, 3.96; N, 16.07.

**2-[(*E*)-1-Borono-1-penten-5-yl]thio]adenosine (7).** Compound 7 was prepared following the procedure described for 5, using 1 (299 mg, 1 mmol), sodium hydride (40 mg, 1 mmol, 60% dispersion in oil), and (1-iodo-5-penten-5-yl)boronic acid (242 mg, 1 mmol) in DMF. The residue was dissolved in hot water and filtered. The solution was adjusted to pH 5.5 with glacial acetic acid. The solvent was evaporated to dryness, and the residue was purified by silica gel column chromatography. The column was eluted with 8–12% methanol in ethyl acetate, the fractions ( $R_f$  = 0.27, silica gel TLC in solvent C) were collected, and solvent was removed to yield 7 (238 mg, 58%), mp 229–233 °C.  $^1\text{H}$  NMR (DMSO- $d_6$ ):  $\delta$  8.19 (s, 1H, H-8), 7.4 (bs, 2H,  $\text{NH}_2$ ), 6.65 (bm, 1H,  $\text{HC}=\text{CH}$ ), 6.12 (d,  $J$  = 14.1 Hz, 1H,  $\text{HC}=\text{CH}$ ), 5.64 (d,  $J$  = 5.2 Hz, 1H, H-1'), 3.5 (m, 2H,  $\text{CH}_2$ ), 2.55 (m, 2H,  $\text{CH}_2$ ), 1.89 (m, 2H,  $\text{CH}_2$ ). UV (pH 1):  $\lambda_{\text{max}}$  268. Anal. Calcd for ( $\text{C}_{15}\text{H}_{22}\text{BN}_5\text{O}_6\text{S}$ ): C, 43.80; H, 5.35; N, 17.03. Found: C, 44.16; H, 5.22; N 17.44. \*N: calcd 17.03, found 17.44.

**2-[(*E*)-1-Iodo-1-penten-5-yl]thio]adenosine (9).** Compound 7 (155 mg, 0.37 mmol) was dissolved in 50% aqueous THF (4.0 mL). Sodium iodide (84 mg, 1.5 equiv) was added followed by addition of a solution of chloramine-T (126 mg, 0.55 mmol) in 50% aqueous THF (2 mL). The reaction mixture was stirred in the dark at room temperature for 1 h and quenched with a saturated solution of sodium thiosulfate (50 mg in 0.5 mL water). The solvent was evaporated, and the residue was dissolved in water (10 mL) and extracted with ethyl acetate (5  $\times$  20 mL). The ethyl acetate portion was dried (sodium sulfate), filtered, and evaporated. The crude product was crystallized from hot methanol to yield 9 (145 mg, 78%), mp 89–91 °C (methanol and water). TLC:  $R_f$  = 0.68, silica gel, solvent C.  $^1\text{H}$  NMR (DMSO- $d_6$ ):  $\delta$  8.23 (s, 1H, H-8), 7.38 (bs, 2H,  $\text{NH}_2$ ), 6.66 (dt,  $J$  = 14.2 and 7.1 Hz, 1H,  $\text{HC}=\text{CH}$ ), 6.2 (d,  $J$  = 14.3 Hz, 1H,  $\text{HC}=\text{CH}$ ), 5.81 (d,  $J$  = 5.5 Hz, 1H, H-1'), 4.61 (d,  $J$  = 6.3 Hz, 1H, H-2'), 4.1 (d,  $J$  = 4.8 Hz, 1H, H-3'), 3.9 (d,  $J$  = 3.1 Hz, 1H, H-4'), 3.5 (m, 2H, H-5'), 3.18 (d,  $J$  = 5.1 Hz, 2H,  $\text{CH}_2$ ), 2.15 (m, 2H,  $\text{CH}_2$ ), 1.75 (m, 2H,  $\text{CH}_2$ ). UV (pH 1):  $\lambda_{\text{max}}$  268.8. Anal. Calcd for ( $\text{C}_{15}\text{H}_{20}\text{IN}_5\text{O}_4\text{S}\cdot 0.5\text{H}_2\text{O}$ ): C, 35.85; H, 4.18; N, 13.94. Found: C, 35.93; H, 4.30; N, 13.91.

**2-[(*E*)-1-Borono-1-penten-5-yl]thio]adenosine 5'-Monophosphate (8).** Iodopentenylboronic acid (37.6 mg, 0.16 mmol) was added to a mixture of 2 (50 mg 0.13 mmol) and sodium methoxide (27 mg, 0.5 mmol) in DMF (2 mL) under an argon atmosphere. The mixture was stirred at room temperature for 18 h. The solvent was removed under reduced pressure and the residue was dissolved in water ( $\sim 2$  mL). The solution was adjusted to pH 2 with 2 N hydrochloric acid. The mixture was passed through a column (1  $\times$  10 cm) packed with AG50 WX1 resin. The column was eluted with water (75 mL) followed by 45% acetic acid in water. The fractions ( $R_f$  = 0.44, paper chromatography in solvent A) were combined, and the solvent was evaporated to yield 8 (27 mg, 42%), mp >300 °C. The compound was highly insoluble in deuteriosol-

vents at a suitable concentration for NMR; hence, NMR data is not included for this compound. Anal. Calcd for ( $C_{15}H_{23}BN_5O_9SP \cdot H_2O$ ): C, 35.36; H, 4.91; N, 13.75. Found: C, 35.60; H, 4.81; N, 13.69.

**2-[(*E*)-1-Iodo-1-penten-5-yl]thio]adenosine 5'-Monophosphate (10).** A solution of chloramine-T (17.3 mg, 76  $\mu$ mol) in aqueous THF (1 mL) was added to a mixture of 8 (25 mg, 50  $\mu$ mol) and sodium iodide (11.4 mg, 76  $\mu$ mol) in 50% aqueous THF (2 mL). The reaction mixture was stirred at room temperature for 24 h in the dark and quenched by addition of a saturated solution of sodium thiosulfate (~1 mL). The solvent was removed under reduced pressure, and the residue was dissolved in water (2 mL) and filtered. The filtrate was adjusted to pH 2 with 2 N hydrochloric acid. The crude product separated as a solid was filtered and washed with cold water. The crude product was crystallized from a mixture of water and ethanol to yield 10 (18 mg, 62%), mp 169–171 °C. TLC:  $R_f$  = 0.76, paper chromatography, solvent A.  $^1H$  NMR (DMSO- $d_6$ ):  $\delta$  8.28 (s, 1H, H-8), 6.55 (dt,  $J$  = 14.2 and 7.0 Hz, 1H, HC=CHI), 6.3 (d,  $J$  = 14.33 Hz, 1H, HC=CHI), 5.9 (d,  $J$  = 5.2 Hz, 1H, H-1'), 2.5 (m, 2H,  $CH_2$ ), 2.2 (m,  $CH_2$ ), 1.82 (m, 2H,  $CH_2$ ). UV (pH 1):  $\lambda_{max}$  268. Anal. Calcd for ( $C_{21}H_{25}IN_5PO_7S \cdot 2H_2O$ ): C, 29.56; H, 4.11; N, 11.49. Found: C, 29.42; H, 3.99; N, 11.26.

**2-[(Aminoethyl)thio]adenosine (11).** Compound 11 was prepared following the procedure described for 5, using 1 (448.5 mg, 1.5 mmol), sodium hydride (60 mg, 1.5 mmol, 60% dispersion in oil), and 2-bromoethylamine hydrobromide (307 mg, 1.5 mmol) in DMF. The residue was dissolved in water and adjusted to pH 8 with 1 N sodium hydroxide. The solvent was evaporated to dryness, and the residue was purified by silica gel column chromatography. The column was eluted with 6–10% methanol in chloroform and the fractions ( $R_f$  = 0.46, TLC in solvent B) were combined. The solvent on evaporation gave 11 (380 mg, 74%), mp 198–205 °C dec.  $^1H$  NMR (CD $_3$ OD):  $\delta$  8.25 (s, 1H, H-8), 6.0 (d,  $J$  = 6.2 Hz, 1H, H-1'), 4.7 (t,  $J$  = 5.4 Hz, 1H, H-2'), 4.38 (m, 1H, H-3'), 4.15 (m, 1H, H-4'), 3.85 (m, 2H, H-5'), 3.4 (bm, 4H,  $(CH_2)_2$ ).

**2-[[[3-(4-Hydroxyphenyl)propionamido]ethyl]thio]adenosine (12).** A solution of *N*-succinimidyl 3-(4-hydroxyphenyl)propionate (65.3 mg, 0.25 mmol) in DMF (1 mL) was slowly added to a solution of 11 (85.5 mg, 0.25 mmol) in DMF (2 mL). The reaction mixture was stirred at room temperature for 24 h. The solvent was removed under reduced pressure, and the mixture was purified using preparative TLC (solvent D). The UV-vis band ( $R_f$  = 0.46, silica gel TLC in solvent D) was scrapped and eluted with a solution of chloroform and methanol. The solvent was evaporated to yield 12 (35 mg, 29%), mp 110 °C (methanol).  $^1H$  NMR (CD $_3$ OD):  $\delta$  8.23 (s, 1H, H-8), 7.01 (d,  $J$  = 8.4 Hz, 2H, Ar-H), 6.68 (d,  $J$  = 8.4 Hz, 2H, Ar-H), 6.0 (d,  $J$  = 5.7 Hz, 1H, H-1'), 4.7 (t,  $J$  = 5.33 Hz, 1H, OH), 4.4 (t,  $J$  = 3.58 Hz, 1H, H-2'), 4.18 (t,  $J$  = 2.55 Hz, 1H, H-3'), 3.85 (m, 2H, H-4' and OH), 3.5 (m, 2H, H-5'), 3.55 (m, 2H,  $CH_2$ ), 3.2 (t,  $J$  = 6.6 Hz, 2H,  $CH_2$ ), 2.75 (t,  $J$  = 7.24 Hz,  $CH_2$ ), 2.46 (t,  $J$  = 7.02 Hz, 2H,  $CH_2$ ). UV (pH 1):  $\lambda_{max}$  268.6. The compound was analyzed as the corresponding iodide derivative 13.

**2-[[[3-(4-Hydroxy-3-iodophenyl)propionamido]ethyl]thio]adenosine (13).** Sodium iodide (53 mg, 0.35 mmol) was added to a solution of 12 (172 mg, 0.35 mmol) in 50% aqueous THF (5 mL). Subsequently, a solution of chloramine-T (80 mg, 0.35 mmol) in THF (1 mL) was added, and the reaction mixture was stirred in the dark for 1 h. A solution of sodium thiosulfate (50 mg in 0.5 mL water) was added, and the solvent was removed under

reduced pressure. The resulting residue was extracted with chloroform and washed with water. The organic layer was dried (sodium sulfate) and filtered, and the residue obtained after evaporation of the solvent was purified using preparative TLC (solvent C). The major band visible under UV light was scrapped and eluted with a solution of chloroform and methanol (1:1 v/v). The solvent was removed to yield 13 (150 mg, 56%). A portion of this was crystallized from a mixture of water and ethanol to yield an analytical sample, mp 190–192 °C.  $^1H$  NMR (CD $_3$ OD):  $\delta$  8.23 (s, 1H, H-8), 7.53 (d,  $J$  = 2.2 Hz, 1H, Ar-H), 6.99 (dd,  $J$  = 8.2 and 2.1 Hz, 1H, Ar-H), 6.77 (d,  $J$  = 8.2 Hz, 1H, Ar-H), 6.04 (d,  $J$  = 5.6 Hz, 1H, H-1'), 4.42 (t,  $J$  = 3.58 Hz, 1H, H-2), 4.19 (d,  $J$  = 3.11 Hz, 1H, H-3'), 3.86 (m, 3H, H-4' and H-5'), 3.53 (m, 2H,  $CH_2$ ), 3.23 (t,  $J$  = 5.5 Hz, 2H,  $CH_2$ ), 2.7 (m, 2H,  $CH_2$ ), 2.39 (m, 2H,  $CH_2$ ). Anal. Calcd for ( $C_{21}H_{25}IN_5O_6S \cdot 2H_2O$ ): C, 38.65; H, 4.45; I, 19.48; N, 12.88. Found: C, 38.48; H, 4.33; I, 19.41; N, 12.76.

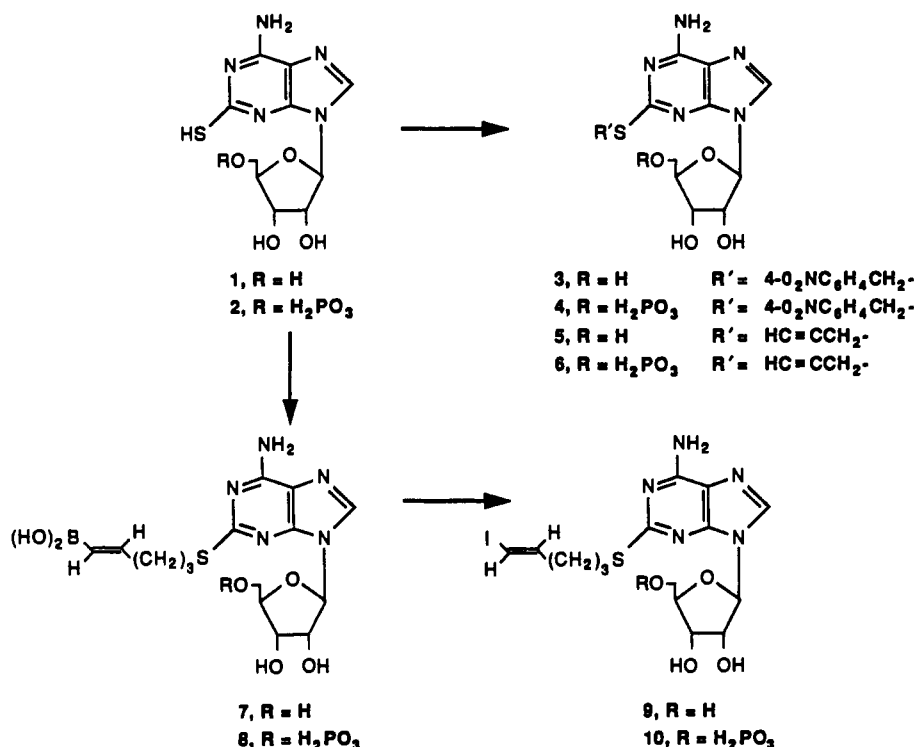
**Biological Studies. Membrane Preparation.** The membranes from male Wistar rat (170–200 g) cerebral cortex and striatum were prepared as described (33). Protein was measured according to the method described by Bradford (34).

**Radioligand Binding Assays.** Radioligand binding of  $A_1$  receptors from rat cortical membranes was measured as described (35) for the  $A_1$  antagonist [ $^3H$ ]DPCPX. [ $^3H$ ]-CGS 21680 was used to measure  $A_2$  receptor binding in rat striatal membranes (36) containing approximately 100  $\mu$ g of protein in a total volume of 250  $\mu$ L at 25 °C. Cold (*R*)-PIA (10  $\mu$ M) and CGS 21680 (10  $\mu$ M) were used to define the non specific binding for  $A_1$  and  $A_2$  receptor, respectively. The values of inhibition constant ( $K_i$ ) were calculated using EBDA computer program. This program uses the  $IC_{50}$  values for calculating  $K_i$  according to the equation of Cheng and Prusoff (37).

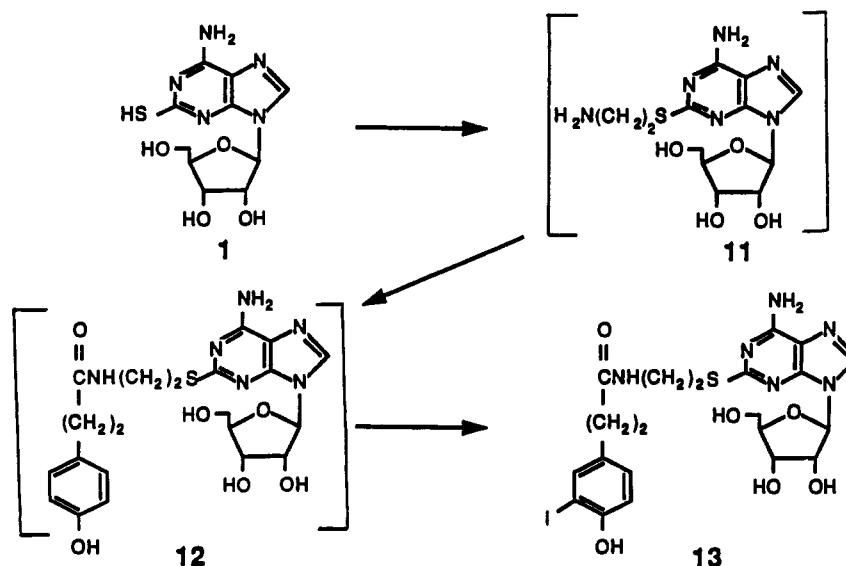
## RESULTS AND DISCUSSION

**Chemistry.** The viable intermediate compounds, 2-thioadenosine (1) and 2-thioadenosine 5'-monophosphate (2), were prepared as reported (31, 32), starting with adenosine and adenosine 5'-monophosphate, respectively. Boronovinyl (Scheme 1) and phenol (Scheme 2) moieties were introduced in 2-thioadenosine substrate sites for selective and easy iodination and potentially for radioiodination for receptor characterization studies. Alkylation of the sodium salt of 2-thioadenosine with (iodopentenyl)boronic acid (38) in anhydrous DMF gave 7. The S-alkylation was supported by UV spectrometry (21). Iodination of 7 with sodium iodide and chloramine-T in anhydrous THF furnished 2-[(*E*)-1-iodo-1-penten-5-yl]thio]adenosine (9) in 78% yield. Our attempts to directly phosphorylate (39–42) the 5'-OH of either 7 or 9 were futile, and unchanged starting material was recovered in each case. It is possible that the steric nature of the 2-substituent obscures the nucleoside conformation making selective phosphorylation impossible. This led us to investigate an alternate route for the synthesis of compounds 8 and 10. Treatment of 2 with (iodopentenyl)boronic acid in the presence of 3.1 molar equiv of sodium methoxide in DMF gave 2-[(*E*)-1-borono-1-penten-5-yl]thio]adenosine 5'-monophosphate (8). Iododeboronation of 8 with sodium iodide and chloramine-T gave 2-[(*E*)-1-iodo-1-penten-5-yl]thio]adenosine 5'-monophosphate (10). The *E*-isomeric configuration of the vinylic iodide moiety in compounds 9 and 10 was established on the basis of  $^1H$  NMR spectroscopy. In the  $^1H$  NMR spectrum of 9, the signals for the vinylic protons appeared as a doublet at  $\delta$  6.20 ( $J$  = 14.3 Hz) ppm and a set of triplets at  $\delta$  6.66 ( $J$  = 14.20 and 7.10 Hz) ppm,

Scheme 1



Scheme 2



consistent with the literature report (38). Treatment of compounds 1 and 2 with 4-nitrobenzyl bromide under basic conditions (NaH) gave compounds 3 (18) and 4 in 46% (lit. (18) 36%) and 42% yield, respectively. Similarly, alkylation of 1 with propargyl bromide (80% solution in toluene) in the presence of sodium hydride gave 2-[(propargyl)thio]adenosine (5). Compounds 3-6 were prepared as precursors for iodination. Our attempts to convert compound 5 to the corresponding tributyltin derivative following the literature procedure (43) resulted in desulfurization.

The synthesis of a phenyl-substituted 2-thioadenosine analogue (13) containing a larger carbon chain interposition between the terminal phenyl group and the C-2 subregion of purine is outlined in Scheme 2. Reaction of 1 with 2-bromoethylamine hydrobromide in the presence of sodium hydride in DMF gave 2-[(aminoethyl)thio]adenosine (11) in 74% yield. Coupling of 11 with *N*-suc-

cinimidyl 3-(4-hydroxyphenyl)propionate in DMF gave 12. The incorporation of the phenolic moiety in compound 12 was confirmed by the <sup>1</sup>H NMR spectrum in which the signal for aromatic protons (phenyl ring) appeared as doublets at δ 7.01 (*J* = 8.40 Hz, 2H) and at δ 6.68 (*J* = 8.4 Hz, 2H) ppm. Iodination of 12 with sodium iodide and chloramine-T in THF gave 2-[[[3-(4-hydroxy-3-iodophenyl)propionamido]ethyl]thio]adenosine (13) in 56% yield. In the <sup>1</sup>H NMR spectrum of 13 the signals for aromatic protons (phenyl ring) appeared as a doublet at δ 7.53 (*J* = 2.2 Hz, 1H) ppm, a set of doublets at δ 6.98 (*J* = 8.2 and 2.1 Hz, 1H) ppm, and another doublet at δ 6.77 (*J* = 8.2 Hz, 1H) ppm.

**Biological Evaluation.** The effects of a series of 2-substituted thioadenosine nucleoside and nucleotide analogues were evaluated on the adenosine receptors using radioligand binding in competition assays, and the results are given in Table 1. Affinities for A<sub>2</sub> receptors were



**Table 1.**  $K_i$  Values for  $A_1$  and  $A_2$  Receptor Binding Affinities for 2-Substituted Thioadenine Nucleoside and Nucleotide Analogues<sup>a</sup>

compd	$K_i$ ( $\mu$ M), $A_2$ binding <sup>b</sup>	$K_i$ ( $\mu$ M), $A_1$ binding <sup>c</sup>	selectivity $A_1/A_2$
(R)-PIA	$0.4 \pm 0.06$	$0.0013 \pm 0.00042$	0.0032
CGS 21680	$0.011 \pm 0.0009$	$1.4 \pm 0.92$	127
3	$2.4 \pm 0.16$	$15.7 \pm 1.3$	6.5
5	$2.0 \pm 0.10$	$9.2 \pm 1.2$	4.6
7	$3.67 \pm 0.30$	$15.0 \pm 1.4$	4.1
9	$3.67 \pm 0.25$	$17.2 \pm 2.5$	4.6
12	$2.04 \pm 0.08$	$16.0 \pm 1.0$	7.8
13	$1.2 \pm 0.09$	$10.0 \pm 0.9$	8.3

<sup>a</sup> The assays were performed three times in triplicate and values represent mean  $\pm$  SE. (R)-Phenylisopropyladenosine ((R)-PIA) and 2-[[4-(2-Carboxyethyl)phenethyl]amino]adenosine 5'-N-ethyluronamide (CGS 21680) were used at  $10^{-11}$ – $10^{-4}$  M while compounds were used at  $10^{-9}$ – $10^{-4}$  M for the competition experiments. <sup>b</sup> [<sup>3</sup>H]CGS 21680. <sup>c</sup> [<sup>3</sup>H]8-Cyclopentyl-1,3-dipropylxanthine ([<sup>3</sup>H]DPCPX).

determined in radioligand assays for the receptors of rat striatum using [<sup>3</sup>H]CGS 21680 as the radioligand. Affinities for  $A_1$  receptors were determined in radioligand competition assays for the receptors of rat cortex using [<sup>3</sup>H]DPCPX as radioligand. CGS 21680 and (R)-PIA were used as reference compounds, for  $A_2$  and  $A_1$ , respectively.

The  $K_i$  values of (R)-PIA and CGS 21680 for  $A_1$  and  $A_2$  receptors, respectively, were found in accordance with the earlier reports (44) suggesting the validity of the receptor binding assays. The nucleotides 4, 6, 8, and 10 exhibited poor affinities for both  $A_1$  and  $A_2$  receptors (10–20% inhibition of [<sup>3</sup>H]DPCPX binding and approximately 40–50% inhibition of [<sup>3</sup>H]CGS 21680 binding) at 100  $\mu$ M concentrations. It could be expected since the nucleotide, AMP, had been reported earlier to be a less potent on adenosine receptors (45). Compounds 3, 5, 7, 9, 12, and 13 have  $K_i$  1.2–3.6  $\mu$ M for the  $A_2$  receptor and 10–17  $\mu$ M for the  $A_1$  receptor suggesting low affinities but with 4–8-fold higher selectivity for  $A_2$  as compared to  $A_1$ . The  $A_2$  selectivity of these compounds was apparently based on the accepted notion (46) that adenosine with N<sup>6</sup> substituents is more selective for  $A_1$  receptor while those with the C-2 substituents are more selective for  $A_2$  receptor. However, the difference in  $A_2$  selectivity of compounds 12 and 13 (8-fold) and compound 3 (6-fold) may be explained on the basis of the carbon chain length and the nature of substituents on the phenyl ring. The presence of a phenyl group increases the hydrophobicity of these compounds resulting in higher selectivity. The decrease in hydrophobicity of compounds 5, 7, and 9 compared to compounds 3, 12, and 13 led to a slight attenuation in  $A_2$  selectivity (4-fold). The presence of a boronic acid moiety in compound 7 or iodine in compound 9 apparently made no significant difference in either the affinity or selectivity of these compounds. Also, it appears that alkylvinyl and alkyl phenyl moieties seriously perturb the adenosine molecule and impair its ability for  $A_1/A_2$  receptor selectivity. The agonist activity of these compounds was tested in isolated rat aortic rings (for  $A_2$  response in terms of vasorelaxation) and left atria (for  $A_1$  response in terms of inotropic effect) using the organ bath technique (47). Compound 3 produced vasorelaxation with an  $IC_{50}$  of 7.5  $\mu$ M. The force of contraction (inotropic effect) was inhibited by 20% at 100  $\mu$ M concentration of compound 3. These data suggest that the compound exhibits the agonist activity as well as the  $A_2$  selectivity. A similar pattern of agonist activity and selectivity was observed with other compounds. These preliminary data did not support pursuing radiolabeling of these compounds with

<sup>123</sup>I for receptor imaging application by single photon emission computed tomography.

In summary, the binding affinities observed for 2-substituted thioadenine nucleoside and nucleotide analogues indicate that introduction of the sulfur atom at the C-2 position of adenosine does not contribute toward the affinity or selectivity of these compounds. However, the presence of a hydrophobic group at the C-2 position appears to increase the  $A_2$  receptor selectivity.

#### ACKNOWLEDGMENT

Research supported by the Office of Health and Environmental Research, U.S. Department of Energy, under Contract DE-AC05-84OR21400 with Martin Marietta Energy Systems, Inc.

#### LITERATURE CITED

- (1) Presented in part (as an abstract) at the 204th American Chemical Society National Meeting, Washington, D. C.; Aug 23–28, 1992.
- (2) Stone, T. W. (1989) Purine receptors and their pharmacological roles. In *Advances in Drug Research*, Vol. 18, pp 291–429, Academic Press Limited: New York.
- (3) van Calcar, D., Muller, M., and Hamprecht, B. (1979) Adenosine regulates via two different types of receptors, the accumulation of cyclic AMP in cultured brain cells. *J. Neurochem.* 33, 999–1005.
- (4) Londos, C., Cooper, D. M. F., and Wolff, J. (1980) Subclasses of external adenosine receptors. *Proc. Natl. Acad. Sci. U.S.A.* 77, 2551–2554.
- (5) Hamprecht, B., and van Calcar, D. (1985) Nomenclature of adenosine receptor. *Trends Pharmacol. Sci.* 6, 153–154.
- (6) Yeung, S. M. H., and Green, R. D. (1984) [<sup>3</sup>H]5'-N-ethylcarboxamidoadenosine binds to both  $R_A$  and  $R_I$  adenosine receptors in rat striatum. *Naunyn-Schmiedeberg's Arch. Pharmacol.* 325, 218–225.
- (7) Bruns, R. F., Lu, G. H., and Pugsley, T. A. (1986) Characterization of the  $A_2$  adenosine receptor labeled by [<sup>3</sup>H]NECA in rat striatal membranes. *Mol. Pharmacol.* 29, 331–346.
- (8) Kusachi, S., Thompson, R. D., Bugni, W. J., Yamada, N., and Olsson, R. A. (1985) Dog coronary artery adenosine receptor: Structure of the N<sup>6</sup>-alkyl subregion. *J. Med. Chem.* 28, 1636–1643.
- (9) Moos, W. H., Szotek, D. L., and Bruns, R. F. (1985) N<sup>6</sup>-Cycloalkyladenosines. Potent,  $A_1$ -selective adenosine agonist. *J. Med. Chem.* 28, 1383–1384.
- (10) Daly, W. J., Padgett, W., Thompson, R. D., Kusachi, S., Bugni, W. J., and Olsson, R. A. (1986) Structure-activity relationships for N<sup>6</sup>-substituted adenosine at a brain  $A_1$ -adenosine receptor with a comparison to an  $A_2$ -adenosine receptor regulating coronary blood flow. *Biochem. Pharmacol.* 35, 2467–2481.
- (11) Bridges, A. J., Bruns, R. F., Ortwine, D. F., Pirebe, S. F., Szotek, D. L., and Trivedi, B. K. (1988) N<sup>6</sup>-[2-(3,5-Dimethoxyphenyl)-2-(2-methylphenyl)ethyl]adenosine and its uronamide derivatives. Novel adenosine agonist with both high affinity and high selectivity for the adenosine  $A_2$  receptor. *J. Med. Chem.* 31, 1282–1285.
- (12) Trivedi, B. K., Bristol, J. A., Bruns, R. F., Haleen, S. J., and Steffen, R. P. (1988) N<sup>6</sup>-(Arylalkyl)adenosine. Identification of N<sup>6</sup>-(9-fluorenylmethyl)adenosine as a high potent agonist for the adenosine  $A_2$  receptor. *J. Med. Chem.* 31, 271–273.
- (13) Cristalli, G., Eleuteri, A., Vittori, S., Volpini, R., Lohse, M. J., and Klotz, K. N. (1992) 2-Alkynyl derivatives of adenosine and adenosine-5'-N-ethyluronamide as selective agonist at  $A_2$  adenosine receptors. *J. Med. Chem.* 35, 2363–2368.
- (14) Olsson, R. A., Kusachi, S., Thomson, R. D., Ukena, D., Padgett, W., and Daly, D. T. (1986) N<sup>6</sup>-Substituted N-alkyladenosine-5'-uronamides: bifunctional ligands having recognition groups for  $A_1$  and  $A_2$  adenosine receptors. *J. Med. Chem.* 29, 1683–1689.

- (15) van Galen, P. J. M., Leusen, F. J. J., IJzerman, A. P., and Soudijn, W. (1989) Mapping the N<sup>6</sup>-region of the adenosine A<sub>1</sub> receptor with computer graphics. *Eur. J. Pharmacol.-Mol. Pharmacol. Sect.* 172, 19-27.
- (16) Kusachi, S., Thompson, R. D., Yamada, N., Daly, D. T., and Olsson, R. A. (1986) Dog coronary artery adenosine receptor: Structure of the N<sup>6</sup>-aryl subregion. *J. Med. Chem.* 29, 989-996.
- (17) Ortwine, D. F., Bridges, A. J., Humblet, C., Trivedi, B. K. (1990) In *Purines in Cellular Signaling* (K. A. Jacobson, J. W. Daly, V. Manganiello, Eds.) pp 152-157, Springer Verlag, Berlin.
- (18) Kikugawa, K., Suehiro, H., and Ichino, M. (1973) Platelet aggregation inhibitors. 2-Thioadenosine derivatives. *J. Med. Chem.* 16, 1381-1388.
- (19) Kikugawa, K., Suehiro, H., Yanase, R., and Aoki, A. (1977) Platelet aggregation inhibitors: 1X. Chemical transformation of adenosine into 2-thioadenosine derivatives. *Chem. Pharm. Bull.* 25, 1959-1969.
- (20) Kikugawa, K., Suehiro, H., and Ichino, M. (1973) Platelet aggregation inhibitors. S-Substituted 2-thioadenosine 5'-monophosphate. *J. Med. Chem.* 16, 1389-1391.
- (21) Maguire, M. H., Nobbs, D. M., Einstein, R., and Middleton, J. C. (1971) 2-Alkylthioadenosines, specific coronary vasodilator. *J. Med. Chem.* 14, 415-420.
- (22) Marumoto, R., Yoshioka, Y., Miyashita, O., Shima, S., Imai, K., Kawazoe, K., and Honjo, M. (1975) Synthesis and coronary vasodilating activity of 2-substituted adenosine. *Chem. Pharm. Bull.* 23, 759-774.
- (23) Ueda, M., Thompson, R. D., Arroyo, L. H., and Olsson, R. A. (1991) 2-Alkoxyadenosines: Potent and selective agonist at the coronary artery A<sub>2</sub> adenosine receptor. *J. Med. Chem.* 34, 1334-1339.
- (24) Homma, H., Watanabe, Y., Abiru, T., Murayama, T., Nomura, Y., and Matsuda, A. (1992) Nucleosides and nucleotides. 112. 2-(1-Hexyn-1-yl) adenosine-5'-uronamides: A new entry of selective A<sub>2</sub> adenosine receptor agonist with potent antihypertensive activity. *J. Med. Chem.* 35, 2881-2890.
- (25) Hutchison, A. J., Williams, M., de Jesus, R., Yokoyama, R., Oei, H. H., Ghai, G. R., Webb, R. L., Zoganas, H. C., Stone, G. A., and Jarvis, M. F. (1990) 2-(Arylalkylamino)adenosine 5'-uronamides: A new class of highly selective adenosine A<sub>2</sub> receptor ligands. *J. Med. Chem.* 33, 1919-1924.
- (26) Ueda, A., Thompson, R. D., Arroyo, L. H., and Olsson, R. A. (1991) 2-Aralkoxyadenosines: Potent and selective agonist at the coronary artery A<sub>2</sub> adenosine receptor. *J. Med. Chem.* 34, 1340-1344.
- (27) Fransis, J. E., Webb, R. L., Ghai, G. R., Hutchison, A. J., Moskal, M. A., de Jesus, R., Yokoyama, R., Rovinski, S. L., Contardo, N., Dotson, R., Barclay, B., Stone, G. A., and Jarvis, M. F. (1991) Highly selective adenosine A<sub>2</sub> receptor agonist in the series of N-alkylated 2-aminoadenosines. *J. Med. Chem.* 34, 2570-2579.
- (28) Matsuda, A., Shinozaki, M., Yamaguchi, T., Homma, H., Nomoto, R., Miyasaka, T., Watanabe, Y., and Abiru, T. (1992) Nucleosides and nucleotides, 103. 2-Alkynyladenosines: A novel class of selective adenosine A<sub>2</sub> receptor agonist with potent antihypertensive effects. *J. Med. Chem.* 35, 241-252.
- (29) Abiru, T., Yamaguchi, T., Watanabe, Y., Kogi, K., Aihara, K., and Matsuda, A. (1991) The antihypertensive effect of 2-alkynyladenosines and their selective affinity for adenosine A<sub>2</sub> receptors. *Eur. J. Pharmacol.* 196, 69-76.
- (30) Stiles, G. L., Daly, D. T., and Olsson, R. A. (1985) The A<sub>1</sub> adenosine receptor. *J. Biol. Chem.* 260, 10806-10811.
- (31) Kikugawa, K., and Suehiro, H. A. (1975) A facile synthesis of 2-thioadenosine. *J. Carbohydr. Nucleosides Nucleotides* 2, 159-164.
- (32) Kapetanovic, E., Bailey, J. M., and Colman, R. F. (1985) 2-[(4-Bromo-2,3-dioxobutyl)thio]adenosine-5'-monophosphate, a new nucleotide analogue that acts as affinity label of pyruvate kinase. *Biochemistry* 24, 7586-7593.
- (33) Olah, M., and Stiles, G. L. (1990) Agonist and antagonists recognize different but overlapping populations of A<sub>1</sub> adenosine receptors: Modulation of receptor number by MgCl<sub>2</sub>, solubilization, and guanine nucleotides. *J. Neurochem.* 55, 1432-1438.
- (34) Bradford, M. M. (1976) A rapid and sensitive method for the quantitation of microgram quantities of protein utilizing the principle of protein dye binding. *Anal. Biochem.* 72, 248-254.
- (35) Bruns, R. F., Fergus, J. H., Badger, E. W., Bristol, J. A., Santay, L. A., Hartman, J. D., Hays, S. J., and Huang, C. C. (1987) Binding of the A<sub>1</sub> selective adenosine antagonist, 8-cyclopentyl-1,3-dipropylxanthine to rat brain membranes. *Naunyn-Schmiedeberg's Arch. Pharmacol.* 335, 59-63.
- (36) Jarvis, M. F., Schulz, R., Hutchison, A. J., Do, U. H., Sills, M. A., and Williams, M. (1989) [<sup>3</sup>H] CGS 21680, A selective A<sub>2</sub> adenosine receptor agonist directly labels A<sub>2</sub> receptors in rat brain. *J. Pharmacol. Exp. Ther.* 251, 888-893.
- (37) Cheng, Y. C., and Prusoff, W. J. (1973) Relationship between the inhibition constant (K<sub>i</sub>) and the concentration of inhibitor which causes 50 percent inhibition (I<sub>50</sub>) of an enzymatic reaction. *Biochem. Pharmacol.* 22, 3099-3108.
- (38) Knapp, F. F., Jr., Goodman, M. M., Callahan, A. P., Ferren, L. A., Kabalka, G. W., and Sastry, K. A. R. (1983) New myocardial imaging agents: Stabilization of radioiodine as a terminal vinyl iodide moiety on tellurium fatty acids. *J. Med. Chem.* 26, 1293-1300.
- (39) Macfarlane, D. E., Srivastava, P. C., and Mills, D. C. B. (1983) 2-Methylthioadenosine [<sup>32</sup>P] diphosphate. An agonist and radioligand for the receptor that inhibits the accumulation of cyclic AMP in intact blood platelets. *J. Clin. Invest.* 71, 420-428.
- (40) Yamazaki, A., Kumashiro, I., and Takenishi, T. (1968) Synthesis of 2-alkylthioinosine 5'-monophosphate and N<sup>2</sup>-methylated guanine 5'-phosphate. *Chem. Pharm. Bull.* 16, 338-344.
- (41) Gough, G., Maguire, M. H., and Michal, F. (1969) 2-Chloroadenosine 5'-phosphate and 2-chloroadenosine 5'-diphosphate, pharmacologically active nucleotide analogs. *J. Med. Chem.* 12, 494-498.
- (42) Sowa, T., and Ouchi, S. (1975) The facile synthesis of 5'-nucleotides by the selective phosphorylation of a primary hydroxyl group of nucleosides with phosphoryl chloride. *Bull. Chem. Soc. Jpn.* 48, 2084.
- (43) Hasan, A., Srivastava, P. C. (1992) Synthesis and biological studies of unsaturated acyclonucleoside analogues of S-adenosine-L-homocysteine hydrolase inhibitors. *J. Med. Chem.* 35, 1435-1439.
- (44) Daly, J. W., Padgett, W. L., Secunda, S. I., Thompson, R. D., and Olsson, R. A. (1993) Structure-activity relationships for 2-substituted adenosine at A<sub>1</sub> and A<sub>2</sub> adenosine receptors. *Pharmacology*, 46, 91-100.
- (45) Burnstock, G., and Brown, C. M. (1981) An introduction to purinergic receptors. In *Purinergic Receptors*, (G. Burnstock, Ed.) Series 2, pp 1037, London and New York, Chapman Hall.
- (46) van Galen, P. J. M., Stiles, G. L., Michael, G., and Jacobson, K. A. (1992) Adenosine A<sub>1</sub> and A<sub>2</sub> receptors: structure-function relationships. *Med. Res. Rev.* 12, 423-471.
- (47) (a) Nakagawa, Y., Gudenzi, M., and Mustafa, S. J. (1986) Calcium entry blocking activity of dilazep and other adenosine potentiating compounds in guinea-pig atria. *Eur. J. Pharmacol.* 122, 51-58. (b) Hussain, T., Leigh, J. H. and Mustafa, S. J. (1994) Regulation of adenosine receptor function by theophylline in rat aorta. *J. Cardiovasc. Pharmacol.* (in press).

# TECHNICAL NOTES

## Biotinylated Hyaluronic Acid: A New Tool for Probing Hyaluronate-Receptor Interactions

Tara Pouyani and Glenn D. Prestwich\*

Department of Chemistry, University at Stony Brook, Stony Brook, New York 11794-3400.

Received November 12, 1993\*

Hyaluronic acid (HA) is a linear polysaccharide composed of repeating disaccharide units of D-glucuronic acid (GlcUA) and N-acetyl-D-glucosamine (GlcNAc). Hyaluronate plays an important role in many biological processes as mediated by its interactions with a number of HA-binding proteins (the "hyaladherins") and with the cell surface HA-receptor, CD44. Studies of hyaluronate-hyaladherin interactions would be greatly facilitated by the availability of molecular probes derived from HA. We recently reported a convenient chemical modification of hyaluronate that introduces multiple pendant amine functionalities onto the HA carboxylate residues. We now report the preparation of biotinylated hyaluronic acid (molecular weight =  $1.2 \times 10^6$  Da) as a probe for histochemical and immunochemical characterization of HA-binding proteins. Approximately one-third of the available HA glucuronate residues could be readily biotinylated in high molecular weight HA.

### INTRODUCTION

Modification of biopolymers with reporter groups has become a powerful research tool in immunology, cell biology, and histochemistry (1). Generally, this strategy involves binding small molecules with specific reporter properties, e.g., fluorophores, antigens, or radioisotopes, to the biopolymer. The targeted biological macromolecule often has primary amino ( $\text{NH}_2$ ), thiol ( $\text{SH}$ ), or other pendant functionality that is readily derivatized with group-specific reagents.

Hyaluronic acid (HA), usually isolated as sodium hyaluronate, is a biologically important biopolymer (Figure 1) that plays important roles in diverse processes such as cell motility (2), wound repair (3), and cancer metastasis (4). The availability of hyaluronate probes would greatly facilitate the study of the interactions of HA with its binding proteins (hyaladherins) and could potentially allow the localization of these proteins. Ideally, one would want to use either HA oligosaccharides or high molecular weight HA, and one would want precise control of the degree and chemistry of derivatization. A number of research groups have reported the use of biotinylated HA as a probe for HA binding proteins. However, a reliable and versatile method for preparing biotinylated HA probes is currently unavailable (5,6). Three methods are currently used. First, biotinylated HA was prepared by modification of a small number of putative free amino groups believed to be present on native hyaluronate (7). A second approach for the preparation of polysaccharide probes used cyanogen bromide activation of the hydroxyl groups. This has the disadvantage that it introduced random modifications along the polymer backbone (8). Third, HA has one "reducing-end" sugar per molecule; this could be reductively coupled to a diamine and used to prepare HA probes. Unfortunately, derivatization of a single reporter group to a  $M_r$   $1.5 \times 10^6$  Da molecule gave a probe with low sensitivity of detection (9).

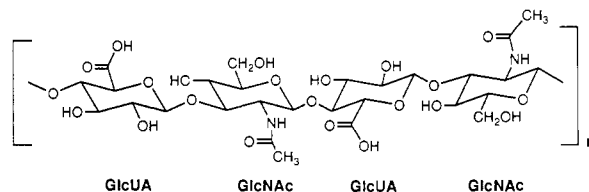


Figure 1. Structure of hyaluronic acid (HA) showing two disaccharide repeat units.

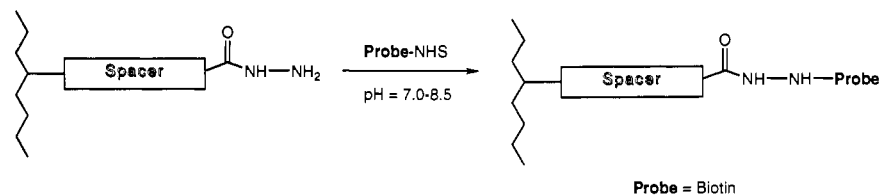
We recently described a convenient methodology that allows the controlled attachment of a pendant hydrazido moiety to the glucuronic acid residues of the HA backbone via a variable-length spacer (Figure 2) (10-12). We now report extension of this methodology to prepare biotinylated native HA ( $M_r$  =  $1.2 \times 10^6$  Da) through the reaction of the pendant hydrazido group with sulfo-NHS-biotin. The technique is general and can be applied to HA oligosaccharides in any size range.

### EXPERIMENTAL PROCEDURES

**Materials.** Sodium hyaluronate (Cristalhyal) was provided by Collaborative Laboratories, Inc. (East Setauket, NY). Adipic dihydrazide and 1-ethyl-3-[3-(dimethylamino)propyl]carbodiimide (EDC) were purchased from Aldrich Chemical Co. (Milwaukee, WI). Sulfo-NHS-biotin, 2-(4'-hydroxyphenylazo)benzoic acid (HABA), and avidin were purchased from Pierce Chemical Co. (Rockford, IL). Spectrapor membrane tubing ( $MW_{\text{cutoff}}$  = 3500 Da) was obtained from Fisher Chemical Co. (Pittsburgh, PA).

**Preparation of Hydrazido-HA (1).** Sodium hyaluronate (200 mg, 0.50 mmol) was dissolved in water such that the concentration of the HA solution was approximately 4 mg/mL. To this mixture was added a 30-fold molar excess of adipic dihydrazide (3.5 g, 20 mmol). The pH of the reaction mixture was then adjusted to 4.75 using 0.1 N HCl. To this mixture was added EDC (382 mg, 2.0 mmol) in solid form. The pH of the reaction

\* Abstract published in *Advance ACS Abstracts*, May 1, 1994.



**Figure 2.** General strategy for generating molecular probes of hyaluronate.

mixture was maintained at 4.75 by addition of 0.1 N HCl. The reaction was allowed to proceed for 2 h or until no further rise in pH was observed. The pH of the reaction mixture was then raised to 7.0 by addition of 1 N NaOH. For purification, the reaction mixture was transferred to the prewetted dialysis tubing and was dialyzed exhaustively against water. The clear and viscous final mixture was placed on the lyophilizer for 48 h.

**Preparation of Biotinylated Hyaluronate (3).** Hydrazido-HA (1) (11 mg, 0.028 mmol) was dissolved in 0.1 M NaHCO<sub>3</sub> to a concentration of 7 mg/mL. To this solution was added sulfo-NHS-biotin (2) (50 mg, 0.11 mmol) in solid form, and the resulting turbid reaction mixture was stirred for 18 h at ambient temperature. The mixture was then diluted 10-fold with water, transferred to pretreated dialysis tubing, and dialyzed exhaustively against water. The biotinylated hyaluronate probe 3 was isolated as a white fiber after lyophilization.

The degree of substitution was determined by a displacement assay according to the manufacturer's protocol (Pierce). Briefly, 900  $\mu$ L of avidin-HABA reagent was placed in a 1-mL cuvette. The absorbance at 500 nm was recorded. To this mixture was added 100  $\mu$ L of a 0.25 mg/mL sample of biotin-HA (3) in phosphate-buffered saline. After thorough mixing the absorbance at 500 nm was recorded. These data were used to calculate the degree of substitution using the reported value for the extinction coefficient of biotin (34  $\mu$ mol/mL). An average value of 0.33 mol of biotin/mol of HA was obtained from three separate measurements on a single preparation.

## RESULTS

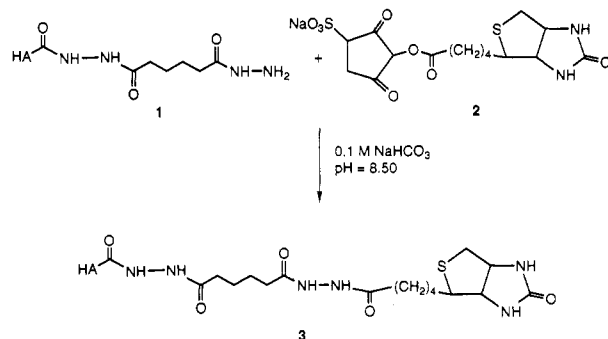
Native hyaluronate was dissolved in water to a final concentration of 4 mg/mL, and adipic dihydrazide was added in 20–50-fold excess. The pH of the reaction mixture was adjusted to 4.75, and the coupling reagent EDC was added to the mixture in solid form. The pH of the reaction was maintained at 4.75 by addition of 0.1 N HCl and was allowed to proceed for 2 h or until no further increase in pH was observed. The mixture was dialyzed exhaustively against water, and hydrazido-HA 1 was isolated as a white fiber after lyophilization.

The hydrazido-modified HA 1 was then dissolved in 0.1 M NaHCO<sub>3</sub> at a concentration of 7 mg/mL. Sulfo-NHS-biotin (2) was added to this clear solution in solid form. After the reaction mixture was stirred for 18 h at ambient temperature, the mixture was diluted 10-fold with water and dialyzed exhaustively against water. The biotinylated-HA probe 3 (Scheme 1) was isolated in quantitative yield after lyophilization. The degree of substitution was determined by a spectrophotometric displacement assay to be 0.33 mol biotin/mol of HA.

## DISCUSSION

The major objective of this paper is to present a convenient and reproducible method for the preparation of a biotinylated-HA probe. Methodology that we had

## Scheme 1. Preparation of Biotinylated Hyaluronic Acid



previously developed for HA oligosaccharides of defined length was extended to high molecular weight hyaluronate ( $1.2 \times 10^6$  Da) to provide hydrazido-HA (1). The pendant hydrazido group represents a highly versatile functionality that can react with a number of commercially-available amine-specific reagents with reporter functions. Reaction of the hydrazido-functionalized HA 1 with sulfo-NHS-biotin (2) in 0.1 M NaHCO<sub>3</sub> (pH = 8.50) resulted in the formation of the HA-biotin complex (3).

We have described a convenient, simple, and reproducible method for preparing biotinylated HA (3). This technique has five important advantages over earlier methods. First, all reaction components are water-soluble, eliminating the need for the use of cosolvents. Second, all reactions are conducted between pH 4.75 and 8.5; these mild reaction conditions prevent the degradation of HA. Third, the presence of the six-carbon spacer of the adipate moiety further ensures the availability of biotin to the binding site of avidin, affording increased sensitivity of detection. Fourth, the degree of substitution can be readily varied by keeping a large excess of dihydrazide relative to HA and varying the proportion of EDC to HA during the initial coupling reaction. Finally, this methodology allows the introduction of high levels of biotin since there are multiple attachment sites on the HA backbone. Up to one-third of the glucuronate moieties could be derivatized using this method. Alternatively, reducing the modification of the HA would provide a lower loading of biotin groups.

## ACKNOWLEDGMENT

We thank the Center for Biotechnology funded through the New York State Science and Technology Foundation for financial support of this project. Sodium hyaluronate (Cristalhyal) was kindly provided by Dr. James Hayward of Collaborative Laboratories, Inc.

## LITERATURE CITED

- (1) Brinkley, M. (1992) *Bioconjugate Chem.* 3, 2–13.
- (2) Banerjee, S. D., and Toole, B. P. (1992) *J. Cell Biol.* 119, 643–652.
- (3) LeBoeuf, R. D., Raja, R. H., Fullert, G. M., and Wiegel, P. H. (1986) *J. Biol. Chem.* 261, 12586–12592.
- (4) Turley, E. (1984) *Cancer Met. Rev.* 3, 325–339.

- (5) Hardwick, C., Hoare, K., Owens, R., Hohn, H. P., Hook, M., Moore, D., Cripps, V., Austen, L., Nance, D. M., and Turley, E. A. (1992) *J. Cell Biol.* 117, 1343-1350.
- (6) Yang, B., Zhang, L., and Turley, E. A. (1993) *J. Biol. Chem.* 268, 8617-8623.
- (7) Hardingham, T. E., and Fosang, A. J. (1992) *FASEB J.* 6, 861-870.
- (8) Glabe, C. G., Harty, P. K., and Rosen, S. D. (1983) *Anal. Biochem.* 130, 287-294.
- (9) Raja, R. H., LeBoeuf, R. D., Stone, G. W., and Weigel, P. H. (1984) *Anal. Biochem.* 139, 168-177.
- (10) Pouyani, T., and Prestwich, G. D. (1994) *Bioconjugate Chem.*, in press.
- (11) Pouyani, T., Harbison, G. S., and Prestwich, G. D. (1993) *J. Am. Chem. Soc.*, submitted.
- (12) Pouyani, T., and Prestwich, G. D. Functionalized derivatives of hyaluronic acid. Patent Appl. Nov, 1993.

# Routine Preparation of Thiol Oligonucleotides: Application to the Synthesis of Oligonucleotide-Peptide Hybrids

Nicholas J. Ede, Geoffrey W. Tregear, and Jim Haralambidis\*

Howard Florey Institute of Experimental Physiology and Medicine, University of Melbourne, Parkville, Victoria 3052, Australia. Received February 18, 1994\*

Oligonucleotide-peptide hybrids have potential for use as antisense inhibitors of gene expression, with the peptide helping to increase the intracellular concentration of the active oligonucleotide. The preparation of such hybrids can be achieved by the coupling of thiol-derivatized oligonucleotides with maleimido-peptides. We have developed reliable methods for preparing 5'-thiol oligonucleotides in good yields using phosphoramidite chemistry and coupling 6-(tritylthio)hexyl phosphoramidite as the 5'-terminal residue. The use of highly pure thiol phosphoramidite as well as a manual iodine treatment after this coupling were found to be important. Oligonucleotide-peptide hybrids were prepared in high yield (85%) by reacting freshly purified 5'-thiol oligonucleotides with peptides derivatized at their N-terminus with a maleimido functionality.

## INTRODUCTION

Synthetic oligonucleotides are useful tools in molecular biology as probes and as antisense inhibitors of gene expression (1-3). For the latter application, the oligonucleotide must enter the cell and bind to its target mRNA to inhibit its translation. However, oligonucleotides do not cross cell membranes readily, and it is thus difficult to achieve high intracellular concentrations. We have devised a novel series of oligonucleotide-peptide hybrid molecules in which the peptide segment is designed to enhance the ability of the oligonucleotide to enter the cell. In a previous report we described a total synthesis method of preparing oligonucleotide-peptide hybrids on a controlled pore glass (CPG) solid-phase support (4). The peptide is synthesized first, a derivatized linker attached, and the oligonucleotide assembled onto the linker by standard DNA synthesis methods. However, this method is unsuitable for the preparation of some oligonucleotide-peptide molecules in good yield. Therefore, we have investigated methods for the specific linking of peptides and oligonucleotides, prepared and purified separately.

Conjugation of DNA and peptide synthons can be achieved if the 5'-terminus of the synthetic oligonucleotide is derivatized with a thiol group (5-9). The thiol group is introduced at the 5' terminus during the solid-phase synthesis procedure by reaction with commercially available thiol-linker phosphoramidites. Peptides can be synthesized separately containing the thiol-reactive maleimido group.

Our initial attempts to conjugate thiol oligonucleotides to maleimido-peptides by this approach were not satisfactory. However, we have now developed improved procedures for the preparation of large amounts of thiol oligonucleotides and their conjugation to maleimido-derivatized peptides to give oligonucleotide-peptide hybrids in high yield.

## MATERIALS AND METHODS

All melting points are uncorrected.  $^1\text{H}$  NMR spectra were recorded at 300 MHz on a Bruker AM300 spectrometer.  $^{31}\text{P}$  NMR spectra were recorded at 121.5 MHz on the same spectrometer. Amino acid analyses were

performed on a Beckman System 6300 analyzer after the samples had been hydrolyzed *in vacuo* for 24 h at 130 °C, with HCl/0.1% phenol. High-performance liquid chromatography (HPLC) was performed on a Waters liquid chromatography system, consisting of a Waters 600 multisolute delivery system with a variable-wavelength detector. The thiol-oligonucleotide and hybrid molecules were purified using one of the following Synchrom columns: RP  $\text{C}_{18}$  250  $\times$  4.6 mm (column A),  $\text{C}_4$  250  $\times$  10 mm (column B), or  $\text{C}_{18}$  250  $\times$  21.2 mm (column C). Buffer A was 0.1 M triethylammonium acetate (TEAA) in water, buffer B  $\text{CH}_3\text{CN}$ , and a gradient of 0-50% B over 30 min with flow rates of 1.5, 3, or 10 mL/min for columns A, B, and C, respectively, were used with detection at 260 nm. Peptides were purified using a Vydac  $\text{C}_4$  250  $\times$  10 mm reversed-phase column (cat. no. 214TP1010) buffer A water (0.1% TFA); buffer B  $\text{CH}_3\text{CN}$  (0.1% TFA) with a flow rate of 3 mL/min and detection at 214 nm. The purity of both peptides was confirmed with a Vydac analytical  $\text{C}_{18}$  column, 250  $\times$  4.6 mm (cat. no. 218TP54) buffer A water (0.1% TFA); buffer B  $\text{CH}_3\text{CN}$  (0.1% TFA) with a flow rate of 1.0 mL/min and detection at 214 nm. Flash chromatography was carried out using silica gel 60, 40-63  $\mu\text{m}$  (230-400 mesh) (E. Merck cat. no. 9385) using solvent systems indicated in the text. Analytical thin-layer chromatography (TLC) was performed on Merck SG-60 precoated plastic plates.

**Chemicals.** Unless otherwise stated, solvents were BDH analytical grade. Dimethylformamide (DMF) and trifluoroacetic acid (TFA) were of peptide synthesis grade (Auspep, Melbourne, Australia). Maleic anhydride was obtained from Pierce Chemicals,  $\beta$ -alanine from BDH, dicyclohexylcarbodiimide (DCC), 1-hydroxybenzotriazole (HOBt), trinitrobenzenesulfonic acid (TNBSA), thioanisole, and diisopropylethylamine (distilled from  $\text{CaH}_2$  prior to use) from Fluka, *N*-Hydroxysuccinimide (NHS), (benzotriazol-1-yloxy)trispyrrolidinophosphonium hexafluorophosphate (pyBOP), *O*-benzotriazolyl-*N,N,N',N'*-tetramethyluronium hexafluorophosphate (HBTU) from Auspep, 4-methylmorpholine (NMM) from E. Merck, and triphenylmercaptan, 6-chlorohexanol, and 2-cyanoethyl *N,N*-diisopropylchlorophosphoramidite from Aldrich Chemical.

**Succinimido 3-Maleimidopropanoate (3).** The method of Nielsen and Buchardt (10) was adapted. Thus,

\* Abstract published in *Advance ACS Abstracts*, May 15, 1994.



Table 1. Characterization Data

compd	HPLC $t_R$ (min)	yield (%)	amino acid analysis	oligonucleotide/ peptide ratio
peptide 1	27.94 <sup>a</sup>	90 <sup>e</sup>	Ala 3.03 (3) Leu 6.07 (6) Arg 2.90 (3)	
peptide 2	21.20 <sup>b</sup>	78 <sup>e</sup>	Asn 1.13 (1) Thr 2.00 (2) Ser 1.16 (1) Thr 4.07 (4) Pro 0.80 (1) Val 1.04 (1) Tyr 0.92 (1) Phe 0.88 (1) Arg 1.99 (2)	
conjugate 9	29.19 <sup>c</sup>	84 <sup>f</sup>	Ala 2.93 (3) Leu 6.10 (6) Arg 2.97 (3)	0.98
conjugate 10	16.98 <sup>d</sup>	85 <sup>f</sup>	Asn 1.06 (1) Thr 1.96 (2) Ser 1.00 (1) Thr 4.29 (4) Pro 0.92 (1) Val 0.92 (1) Tyr 1.00 (1) Phe 0.93 (1) Arg 1.92 (2)	1.09

<sup>a</sup> Vydac analytical C<sub>18</sub>, 250 × 4.6 mm, buffer A water (0.1% TFA); B CH<sub>3</sub>CN (0.1% TFA), 0–100% B over 30 min. <sup>b</sup> Vydac analytical C<sub>18</sub>, 250 × 4.6 mm, buffer A water (0.1% TFA); B CH<sub>3</sub>CN (0.1% TFA), 0–50% B over 30 min. <sup>c</sup> Synchrom C<sub>4</sub> 250 × 10 mm, buffer A (0.1 M TEAA); B CH<sub>3</sub>CN 0–50% B over 30 min. <sup>d</sup> Synchrom C<sub>18</sub> 250 × 4.6 mm, buffer A (0.1 M TEAA); B CH<sub>3</sub>CN 0–50% B over 30 min. <sup>e</sup> Based on weight of crude isolated peptide. <sup>f</sup> Based on amount of pure thiol oligonucleotide read at 260 nm.

$\beta$ -alanine (0.91 g, 10 mmol) was added to a solution of maleic anhydride (1.00 g, 10 mmol) in DMF (12 mL) and the mixture stirred for 2 h. The resulting solution was cooled in an ice bath, and *N*-hydroxysuccinimide (1.44 g, 12.5 mmol) was added followed by DCC (4.12 g, 20 mmol). After approximately 5 min the ice bath was removed and the solution stirred overnight. The resulting dicyclohexylurea (DCU) was filtered and the filtrate poured into water (60 mL) and extracted with CH<sub>2</sub>Cl<sub>2</sub> (3 × 20 mL). The organic phase was washed with water (20 mL), 5% NaHCO<sub>3</sub> (2 × 20 mL), and brine (20 mL) and dried (Na<sub>2</sub>SO<sub>4</sub>). The solution was filtered and the solvent evaporated (reduced pressure). The residue was dissolved in CH<sub>2</sub>Cl<sub>2</sub> (3 mL), and addition of petroleum ether precipitated 3 as a white solid (1.10 g, 41%); mp 162–163 °C (lit. (10) 164–166 °C).

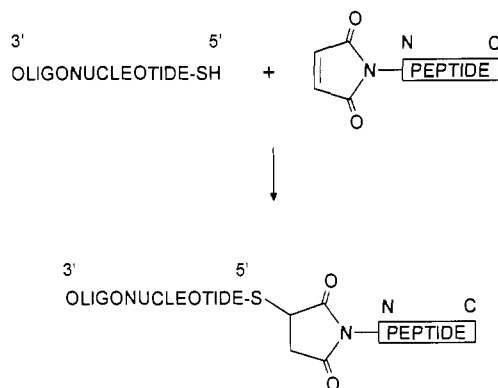
**6-(Tritylthio)hexanol (5).** The method of Connolly and Rider (5) was adapted. Sodium hydroxide (0.88 g, 22 mmol) was dissolved in water (5 mL) and added to a mixture of triphenylmercaptan (5.52 g, 20 mmol) in ethanol (30 mL) with stirring. Following this, 6-chlorohexanol (1.25 mL, 11 mmol) was added and the mixture stirred at room temperature overnight. It was then filtered, the filtrate collected, and the solvent removed (reduced pressure). The residue was redissolved in CH<sub>2</sub>Cl<sub>2</sub> (50 mL) and washed with water (3 × 30 mL). The organic extract was dried (Na<sub>2</sub>SO<sub>4</sub>) and evaporated (reduced pressure) to yield an oil which was flash chromatographed (CHCl<sub>3</sub>) to yield a clear oil which crystallized from ether/petroleum ether to give 5 as a white solid (1.25 g, 30%); mp 68–69 °C (lit. (11) 70–72 °C). No starting material could be detected by <sup>1</sup>H NMR: TLC (CHCl<sub>3</sub>)  $R_f$  = 0.30; <sup>1</sup>H NMR (CDCl<sub>3</sub>) 7.40 (15H, m, ArH), 3.58 (2H, t,  $J$  = 6.58 Hz, OCH<sub>2</sub>), 2.15 (2H, t,  $J$  = 7.25 Hz, SCH<sub>2</sub>), 1.53–1.22 (8H, m, CH<sub>2</sub>).

**6-(Tritylthio)hexanol, 2-Cyanoethyl *N,N*-Diisopropylphosphoramidite (6).** The method of Connolly and Rider (5) was adapted. 6-(Tritylthio)hexanol (5) (0.70 g, 1.86 mmol) was coevaporated twice with 10% pyridine in CH<sub>2</sub>Cl<sub>2</sub> (10 mL) and dried overnight under vacuum. Under argon, distilled diisopropylethylamine (1.30 mL, 7.44 mmol) was added followed by CH<sub>2</sub>Cl<sub>2</sub> (5 mL). The resulting solution was cooled in an ice bath, and 2-cyanoethyl *N,N*-diisopropylchlorophosphoramidite (1.04 mL, 4.65 mmol) was added (by syringe). After 2 h the solvent was evaporated by bubbling argon. The residue was dissolved in ethyl acetate (20 mL) and washed with 5% NaHCO<sub>3</sub> (2 × 20 mL) and water (2 × 20 mL). The organic phase was dried (Na<sub>2</sub>SO<sub>4</sub>) and the solvent evaporated (reduced pressure) to yield a clear oil. The product was then purified according to the method of Sinha and Striepeke (11). A flash column was packed with silica gel using 25% ethyl acetate in hexane containing 5% pyridine. The column was first washed with one volume of 25% ethyl acetate in hexane. The crude product was loaded

dissolved in 50% ethyl acetate in hexane and the column eluted with 30% ethyl acetate in hexane to yield pure 6 as a clear oil (0.92 g, 86%); TLC (ethyl acetate/hexane, 50/50)  $R_f$  = 0.75; <sup>31</sup>P NMR (CD<sub>2</sub>Cl<sub>2</sub>)  $\delta$  147.63.

**Peptide Synthesis.** Continuous flow solid-phase peptide synthesis was carried out using a CRB manual Synthesizer on Pepsyn K100 resin (CRB). An internal standard (glycine) and an acid-labile handle (hydroxymethyl)phenoxyacetic acid, from Novabiochem) were attached before peptide synthesis was commenced. Fmoc amino acids were obtained from Auspep. Standard solid-phase peptide synthesis protocols for Fmoc/*t*-Bu chemistry were employed (12). All couplings were carried out in DMF using a 3-fold excess of amino acid, HBTU (peptide 1), or pyBOP (peptide 2) and HOBt. A 5-fold excess of NMM was used. The maleimido reagent 3, with an equimolar amount of HOBt, was coupled to the *N*-terminus of the resin-bound peptides to give (after cleavage, deprotection, and purification) peptides 1 and 2. The peptide-resins were cleaved at room temperature for 3 h with 95% trifluoroacetic acid/5% thioanisole. The cleavage mixture was filtered, and the volume of the filtrate was reduced to approximately 2 mL (reduced pressure). The crude peptides were precipitated by the addition of cold ether. After the peptides were stored overnight at 0 °C the ether was decanted and the peptides washed with fresh ether (3 × 20 mL). After the final decantation of ether, the peptides were dissolved in 25% aqueous CH<sub>3</sub>CN and freeze-dried. After dissolution of the peptides in 65% CH<sub>3</sub>CN (3 mL) they were purified by HPLC, using gradients of 0–100% B (peptide 1) or 0–50% B over 30 min (peptide 2). The purity of all peptides was confirmed by analytical C<sub>18</sub> HPLC (see Table 1 for conditions) and amino acid analysis.

**Thiol Oligonucleotide Synthesis.** Oligonucleotides 7 and 8 were synthesized on an Applied Biosystems 380A DNA Synthesizer using standard  $\beta$ -cyanoethyl-protected phosphoramidites (Applied Biosystems, Foster City, CA) (13) on a 10  $\mu$ mol scale. The thiol linker phosphoramidite 6 (50 mg, 85  $\mu$ mol) was dissolved in the appropriate volume of acetonitrile for the program being used, e.g., 1.5 mL for a 10  $\mu$ mol scale, and attached to a spare port on the DNA synthesizer. The amidite was then applied to the reaction column using a 10  $\mu$ mol program. The coupling was followed by an acetonitrile wash and reverse flush, the column was removed immediately, and the resin was transferred to a sintered reaction vessel. It was then treated with iodine (0.05 M in THF:pyridine:water 7:1:2) for 30 s, washed with CH<sub>3</sub>CN (3 × 20 mL), and dried under a stream of argon. The oligonucleotide was immediately cleaved by treatment with 30% ammonia for 6 h and the resulting solution heated at 50 °C for 18 h to effect base deprotection. The ammonia was removed by a stream of argon and the resulting aqueous solution purified immediately by HPLC using column C. Fractions containing



**Figure 1.** Oligonucleotide-peptide synthesis *via* the thiol oligonucleotide and maleimido-peptide conjugation reaction.

the pure trityl-ON oligonucleotide were pooled and freeze-dried. The trityl group was removed after purification according to published methods (5). Thus, trityl-ON oligonucleotide **7a** (10 mg, 333 OD units) was dissolved in 0.1 M TEAA (20 mL), 1 M silver nitrate (2.1 mL) added, and the mixture vortexed and allowed to react for 30 min. Following this, 1 M dithiothreitol (DTT, 2.5 mL) was added and the reaction mixture vortexed and allowed to react for a further 20 min. The yellow mixture was centrifuged and the supernatant collected. The precipitated silver salt was washed twice more with 0.1 M TEAA and centrifuged and the supernatants were pooled. The thiol oligonucleotide/DTT mixture can be stored frozen until the conjugation experiment.

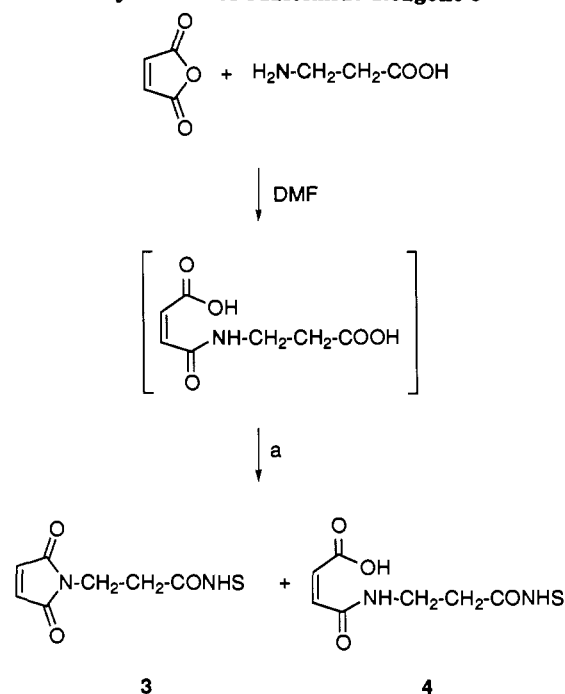
**Oligonucleotide-Peptide Hybrid Synthesis.** The previously prepared and purified peptide maleimides were reacted with thiol oligonucleotide immediately after removal of the excess DTT by HPLC. A sample synthesis follows. Trityl-ON thiol oligonucleotide **7a** (3.0 mg) was deprotected as described in the previous section. Excess DTT was removed by HPLC (column B) to give pure thiol oligonucleotide **7b** with a retention time of 15.24 min, 2.56 mg as read at 260 nm. The purified thiol oligonucleotide, still in HPLC buffer ( $\approx 7$  mL), was reacted immediately with peptide maleimide **1** which was dissolved in 20% 0.1 M TEAA/acetonitrile (1 mL). The molar ratio of peptide to oligonucleotide was 10:1. The mixture was incubated at 37 °C for 2 h, after which time an analytical HPLC indicated complete reaction. The mixture was purified by HPLC (column B) immediately and dialyzed (Spectrapor 6 dialysis tubing, MW cutoff 2000) against 0.1 M NaCl (4  $\times$  3 h) and water (4  $\times$  3 h) to give the desired hybrid **9**, retention time 29.19 min, 2.16 mg (85% yield) as read at 260 nm. Analytical data are shown in Table 1.

## RESULTS AND DISCUSSION

Our primary objective is to develop oligonucleotide-peptide hybrids as antisense agents. In order to prepare these hybrids efficiently, we have investigated methods for conjugating separately prepared peptides and oligonucleotides. The conjugation of a 5'-thiol oligonucleotide with a peptide containing a maleimide functionality at the *N*-terminus, reported by Eritja *et al.* (6), was a logical route to these hybrid molecules. The conjugation of these two motifs is shown in Figure 1. The conjugation of an oligonucleotide to a peptide can also be achieved by derivatizing the 5'-terminus of the oligonucleotide with a maleimido group and reacting this with a cysteine-containing peptide (9).

The incorporation of a thiol group into oligonucleotides is achieved commonly with 6-(tritylthio)hexyl phosphor-

## Scheme 1. Synthesis of Maleimido Reagent 3<sup>a</sup>

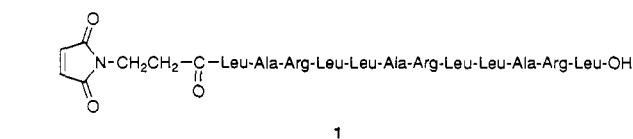


<sup>a</sup> Key: (a) *N*-hydroxysuccinimide (NHS), DCC, DMF.

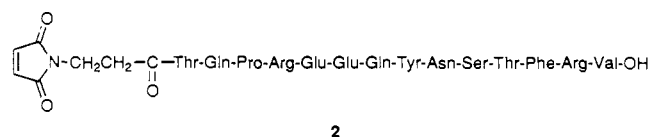
amidite **6**. This reagent is available commercially and is coupled to the 5'-terminus of the oligonucleotide as the last coupling. The retardation of the resulting trityl-containing oligonucleotides on RP HPLC facilitates purification. The trityl group is removed by reaction with silver nitrate and the product isolated by RP HPLC after treatment with dithiothreitol (DTT). The process has been reported to work well for short oligonucleotides (12mers) but yields decrease significantly for the preparation of longer thiol oligonucleotides (5, 8).

In this report we describe the preparation of conjugates composed of either a 20mer sequence antisense to human immunodeficiency virus (HIV-1) (14) or a 20mer antisense to rat  $\alpha$ -fetoprotein (rAFP) (15). The peptides that were conjugated to these oligonucleotides include the  $\alpha$ -helical peptide **1** (16) and an F<sub>c</sub> receptor binding peptide **2** derived from the putative receptor binding site of rat IgG  $\gamma$ 2b (residues 289–302) (17). The corresponding sequence in the human IgG C<sub>H</sub>2 domain has high binding affinity for the F<sub>c</sub> receptor (18).

**Preparation of maleimidopeptides.** For the synthesis of peptides **1** and **2**, standard solid-phase peptide synthesis methodology for Fmoc/*t*-Bu chemistry was employed (12).

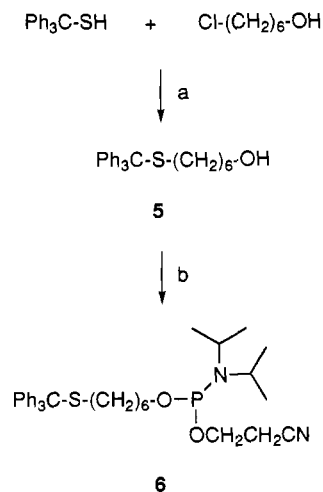


**1**



**2**

The maleimido reagent **3** was synthesized by adapting the method of Nielsen and Buchardt (10) (Scheme 1). We found it necessary to include a base wash to remove any uncyclized maleimido intermediate **4**. The presence of

**Scheme 2. Synthesis of Protected Thiol Linker Reagent 6<sup>a</sup>**

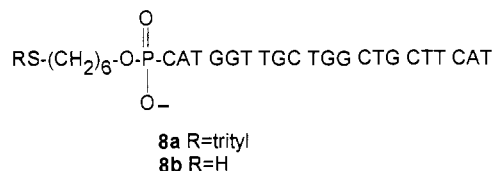
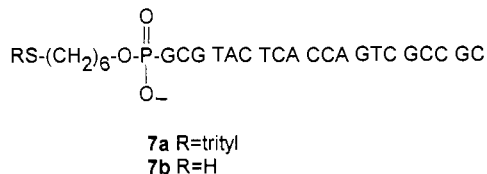
<sup>a</sup> Key: (a) NaOH, EtOH; (b) CIP(OCH<sub>2</sub>CH<sub>2</sub>CN)N(iPr)<sub>2</sub>, (iPr<sub>2</sub>)NEt, CH<sub>2</sub>Cl<sub>2</sub>.

this byproduct was confirmed by <sup>1</sup>H NMR. The maleimide reagent 3, with an equimolar amount of 1-hydroxybenzotriazole (HOBt), couples to the *N*-terminus of the peptide-resin within 20 min (as judged by the TNBSA test (19)). The crude (isolated peptide) yields of peptides 1 and 2 were 90 and 78% respectively. For both peptides, purity of the crude cleaved product was good (≥85%) and amino acid analysis gave satisfactory ratios (Table 1), including a peak for β-alanine, derived from the maleimido reagent 3. The maleimido containing peptides are stable if stored dry.

**Preparation of Thiol-Containing Oligonucleotides.** The successful preparation of large amounts (>1 mg) of thiol oligonucleotides depends largely on the purity of the (tritylthio)hexyl phosphoramidite 6 and to a lesser extent on the workup procedure used. Most laboratories require only small amounts of thiol oligonucleotide for labeling studies and use the commercially available reagent. However if larger amounts are required, for example, for antisense studies, then it may be more economical to undertake synthesis of the reagent 6.

The preparation of 6-(tritylthio)hexanol (5) and the corresponding phosphoramidite 6 was adapted from the method of Connolly and Rider (5) and is outlined in Scheme 2. We found that reacting approximately equimolar amounts of triphenylmercaptan with 6-chlorohexanol resulted in substantial amounts of 6-chlorohexanol being retained in the final product. The product 5 and 6-chlorohexanol coeluted by TLC but the presence of the starting material could be clearly seen by <sup>1</sup>H NMR. To ensure complete conversion of 6-chlorohexanol to the product 5 a 2-fold excess of triphenylmercaptan was used. <sup>1</sup>H NMR confirmed the purity of 5. The synthesis of the phosphoramidite was relatively straightforward, but the purity of this product is important to the success of thiol oligonucleotide synthesis. The purification method described by Sinha and Striepeke (11) was found to give the cleanest product. The purified phosphoramidite 6 was stored under argon at -20 °C.

Our early attempts at thiol oligonucleotide synthesis were not successful. For the HIV-1 thiol oligonucleotide 7, the apparent "trityl ON" material 7a coeluted with unmodified "trityl OFF" oligonucleotide (this had been previously synthesized), suggesting the absence of the trityl group. The isolated product (after treatment with silver nitrate and DTT) was not reactive to maleimido peptide

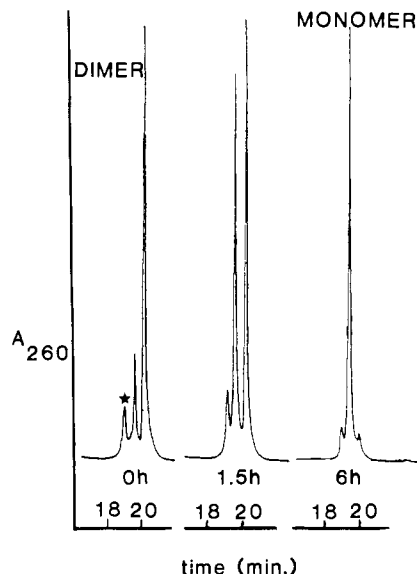


1, suggesting that the 5'-terminus did not contain a thiol functional group. Yields for the preparation of thiol oligonucleotides utilizing phosphoramidite chemistry have been reported to be low (5, 8). Dimerization of the thiol oligonucleotide has been considered as a cause for the low yields, although attempts to reduce the dimer back to a reactive thiol with DTT were not successful (8). In the present study, treatment of the unreactive thiol oligonucleotide with DTT resulted in no change in maleimido peptide reactivity, suggesting that the low yields were not related to dimerization but more likely resulted from chemical modification of the 5'-thiol terminus.

Phosphorus NMR spectroscopy of the amidite 6 used in the synthesis indicated that approximately 5% hydrolysis had occurred. The amidite reagent was repurified, the homogeneity confirmed by <sup>31</sup>P NMR, and the thiol oligonucleotide resynthesized. A high yield of "trityl ON" thiol oligonucleotide 7a was obtained, validating the importance of the purity of phosphoramidite 6. The yield is further improved by executing the final iodine oxidation manually. This improves the yield (for a 10 μmol synthesis) by another 20–30%. This iodine oxidation was done manually to ensure that all the resin received an equally short treatment since, for a 10 μmol column, this is not possible when using the synthesizer. After manual oxidation the resin was washed with acetonitrile and cleaved with aqueous ammonia immediately. This results in substantial amounts (>60%) of the required "trityl ON" thiol oligonucleotide.

The exact effect of the impure (85–95% purity) phosphoramidite 6 on coupling efficiency is unclear. Even though HPLC analysis of the crude cleaved oligonucleotides indicates no "trityl ON" material, small-scale experiments on the prepared resin suggest otherwise. Addition of TFA to trityl oligonucleotide which is still resin-bound liberates a bright yellow color (presumably the trityl cation) into solution. In addition, after attachment of the tritylthio phosphoramidite 6 with *no capping step*, further nucleoside phosphoramidite couplings are completely negative. This is indicative of full coupling of the amidite 6. These results suggest that loss of trityl group occurs postsynthesis.

Immediately following iodine oxidation, the resins were washed and dried before being treated with 30% aqueous ammonia at room temperature for 6 h. The cleaved oligonucleotide was deprotected by heating at 55 °C overnight. Purification by preparative HPLC was always carried out immediately following resin cleavage and base deprotection. The HPLC-purified trityl S-oligonucleotides 7a and 8a were treated with silver nitrate to cleave the trityl group, followed by DTT to liberate the free thiol oligonucleotides. When working with larger

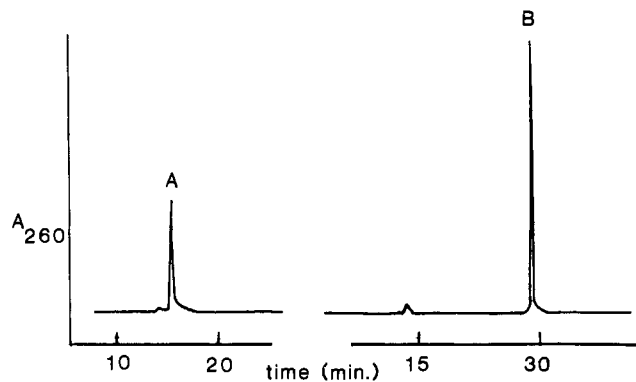


**Figure 2.** Time course of the reaction between the dimer from thiol oligonucleotide **8b** (19.80 min) and dithiothreitol to give monomer **8b** (18.39 min): \*, unknown impurity.

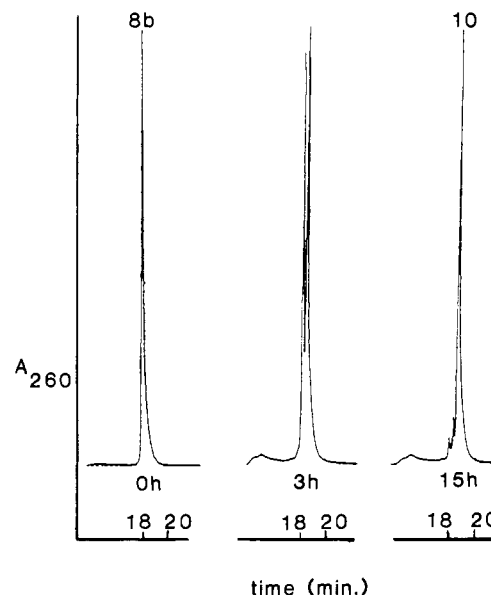
amounts of thiol oligonucleotide (>2–3 mg), dilution of the silver nitrate reaction mixture with 0.1 M TEAA (up to 25 mL) is essential to prevent precipitation of the thiol oligonucleotide silver salt (a white solid). Liberation of the free thiol oligonucleotide can be as low as 15% if the oligonucleotide is not in solution. The thiol oligonucleotide/DTT mixture can be stored until all or some of the thiol oligonucleotide is required.

**Preparation of the Oligonucleotide–Peptide Hybrids.** Thiol oligonucleotides **7b** and **8b** were stored in the DTT solution and can be separated from excess DTT by HPLC. The peptide conjugation must be performed immediately following this step because the purified free thiol forms a dimer in the HPLC eluent within 1–2 h. This was evident from some early experiments with **8b** in which the purified thiol oligonucleotide was freeze-dried in order to reduce the volume for the conjugation reaction. This resulted in no reaction with maleimido-peptides taking place. Addition of DTT to the purified unreactive thiol oligonucleotide resulted in conversion of the dimer back to the free thiol oligonucleotide. This is evidenced by a shorter HPLC retention time as shown in Figure 2. The dimer has a retention time of 19.80 min whereas the reduced monomer elutes at 18.39 min. Purification and reaction of this converted dimer (to free thiol oligonucleotide **8b**) with maleimido peptide **2** resulted in full conjugation to give conjugate **10**. The conjugate prepared from the reduced dimer had an identical HPLC retention time to conjugate prepared from thiol oligonucleotide that had not previously dimerized.

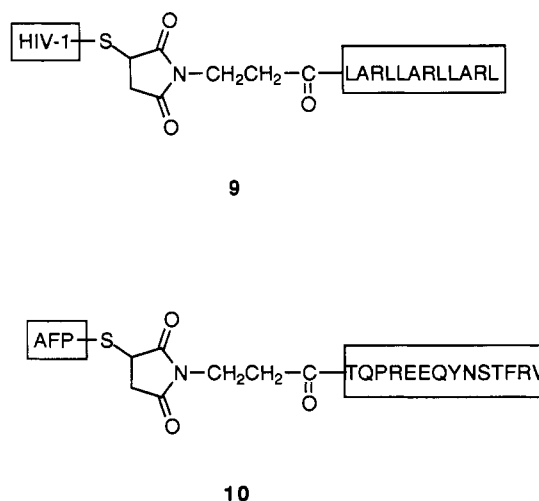
The maleimido peptides (dissolved in 0.1 M TEAA/CH<sub>3</sub>CN, 60:40) must be directly added to the HPLC eluent containing the thiol oligonucleotide, the volume of which has no significant effect on the conjugation reaction. In each oligonucleotide–peptide conjugation the peak corresponding to the starting oligonucleotide disappears and a new peak appears with a different retention time. The time required for complete reaction is dependant on the nature of the peptide. The conjugations of the thiol oligonucleotides **7b** and **8b** with the  $\alpha$ -helical and Fc peptide maleimides **1** and **2**, respectively, are shown in Figures 3 and 4. The oligonucleotide–peptide hybrids **9** and **10** (Figure 5) were obtained after HPLC purification and were characterized spectrophotometrically and by



**Figure 3.** Conjugation of thiol oligonucleotide **7b** (retention time 15.24 min) with maleimido-peptide **1** to give conjugate **9** (retention time 29.13 min): A, purified **7b** (no peptide); B, reaction mixture after 1.5 h.



**Figure 4.** Time course of the reaction between thiol oligonucleotide **8b** (retention time 16.28 min) and maleimido-peptide **2** to give conjugate **10** (retention time 16.98 min).



**Figure 5.** Oligonucleotide–peptide hybrid molecules prepared. HIV-1 is the 20mer oligonucleotide from **7a** and AFP the 21mer oligonucleotide from **8a**. The peptides are those derived from **1** and **2**.

amino acid analysis. The conjugation reactions have yields of greater than 80%, based on the amount of the starting thiol oligonucleotide. These yields include HPLC puri-

fication and dialysis. Results for the conjugation reactions are shown in Table 1.

## CONCLUSION

In this study, we have developed improved methods for preparing and reacting thiol oligonucleotides. The 6-(tritylthio)hexyl phosphoramidite must be pure in order to obtain any significant "trityl ON" product. Due to the inherent design of the automated DNA synthesizer, a manual iodine treatment of the resin is advisable to improve the yield of the tritylated oligonucleotide. The purified thiol oligonucleotide must be reacted with a thiol reactive molecule as soon as it is eluted from the HPLC column to avoid formation of the unreactive dimer. The protocol described here has been found to proceed efficiently for several other examples of oligonucleotide and peptide combinations and provides a practical and reliable method for the synthesis of hybrids in high yield.

## ACKNOWLEDGMENT

This work was supported by the Commonwealth AIDS Research Grants Council. The Howard Florey Institute is supported by an Institute block grant from the National Health and Medical Research Council of Australia.

## LITERATURE CITED

- (1) Agrawal, S. (1989) Antisense oligonucleotides as antiviral agents. *TIBTECH* 10, 152-158.
- (2) Crooke, S. T. (1992) Therapeutic applications of oligonucleotides. *BIO/Technology* 10, 882-886.
- (3) Matsukura, M., Shinozuka, K., Zon, G., Mitsuya, H., Reitz, M., Cohen, J. S., and Broder, S. (1987) Phosphorothioate analogues of oligodeoxynucleotides: inhibitors of replication and cytopathic effects of human immunodeficiency virus. *Proc. Natl. Acad. Sci. U.S.A.* 84, 7706-7710.
- (4) Haralambidis, J., Duncan, L., Angus, K., and Tregear, G. W. (1990) The synthesis of polyamide-oligonucleotide conjugate molecules. *Nucleic Acids Res.* 18, 493-499.
- (5) Connolly, B. A., and Rider, P. (1985) Chemical synthesis of oligonucleotides containing a free sulphhydryl group and subsequent attachment of thiol specific probes. *Nucleic Acids Res.* 13, 4485-4502.
- (6) Eritja, R., Pons, A., Escarceller, M., Giralt, E., and Albericio, F. (1991) Synthesis of defined peptide-oligonucleotide hybrids containing a nuclear transport signal sequence. *Tetrahedron* 47, 4113-4120.
- (7) Li, P., Medon, P. P., Skingle, D. C., Lanser, J. A., and Symons, R. H. (1987) Enzyme-linked synthetic oligonucleotide probes: non-radioactive detection of enterotoxigenic *Escherichia coli* in faecal specimens. *Nucleic Acid Res.* 15, 5275-5287.
- (8) Sinha, N. D., and Cook, R. M. (1988) The preparation and application of functionalized synthetic oligonucleotides: III. Use of H-phosphonate derivatives of protected amino-hexanol and mercapto-propanol or -hexanol. *Nucleic Acids Res.* 16, 2659-2669.
- (9) Tung, C.-H., Rudolph, M. J., and Stein, S. (1991) Preparation of Oligonucleotide-Peptide Conjugates. *Bioconjugate Chem.* 2, 464-465.
- (10) Nielsen, O., and Buchardt, O. (1991) Facile synthesis of reagents containing a terminal maleimido ligand linked to an active ester. *Synthesis* 819-821.
- (11) Sinha, N. D., and Striepeke, S. (1991) Oligonucleotides with reporter groups attached to the 5'-terminus. *Oligonucleotides and Analogues: A Practical Approach* (F. Eckstein, Ed.) pp 185-210, Oxford University Press, New York.
- (12) Atherton, E., and Sheppard, R. C. (1989) *Solid-phase peptide synthesis: A practical approach*, IRL Press, Oxford, England.
- (13) Beaucage, S. L., and Iyer, R. P. (1992) Synthesis of oligonucleotides by the phosphoramidite Approach. *Tetrahedron* 48, 2223-2311.
- (14) Goodchild, J., Agrawal, S., Civeira, M. P., Sarin, P. S., Sun, D., and Zamecnik, P. C. (1988) Inhibition of human immunodeficiency virus replication by antisense oligodeoxynucleotides. *Proc. Natl. Acad. Sci. U. S. A.* 85, 5507-5511.
- (15) Turcotte, B., Guertin, M., and Belanger, L. (1985) Rat  $\alpha_1$ -fetoprotein messenger RNA: 5'-end sequence and glucocorticoid-suppressed liver transcription in an improved nuclear run-off assay. *Nucleic Acids Res.* 13, 2387-2398.
- (16) Lee, S., Mihara, H., Aoyagi, H., Kato, T., Izumiya, W.-J. O., Ito, A., Omura, Y., Uzu, S., and Nakajima, T. (1986) Effect of amphiphilic model peptides on biomembranes and mast cells. *Peptide Chemistry 1985* (Y. Kiso, Ed.) pp 317-320, Protein Research Foundation, Osaka.
- (17) Bruggemann, M. (1988) Evolution of rat immunoglobulin gamma heavy-chain gene family. *Gene* 74, 473-482.
- (18) Sarmay, G., Benczur, M., Petranyi, E. K., Kahn, M., Stanworth, D. R., and Gergely, J. (1984) Ligand inhibition studies on the role of Fc receptors in antibody-dependent cell-mediated cytotoxicity. *Mol. Immunol.* 21, 43-51.
- (19) Hancock, W. S., and Battersby, J. E. (1976) A new micro-test for the detection of incomplete coupling reactions in solid phase peptide synthesis using 2,4,6-trinitrobenzenesulphonic acid. *Anal. Biochem.* 71, 260-264.

# Bioconjugate Chemistry

SEPTEMBER/OCTOBER 1994  
Volume 5, Number 5

© Copyright 1994 by the American Chemical Society

## LETTERS

---

### Redox Reaction of Poly(ethylene oxide)-Modified Hemoglobin in Poly(ethylene oxide) Oligomers at 120 °C

Hiroyuki Ohno\* and Natsue Yamaguchi

Department of Biotechnology, Tokyo University of Agriculture & Technology, Koganei, Tokyo 184, Japan.  
Received March 4, 1994<sup>§</sup>

---

Human hemoglobin, modified with poly(ethylene oxide) with average molecular weight of 3500 (PEO-Hb) was dissolved in PEO<sub>200</sub> (molecular weight of 200) containing 0.5 M KCl. A quasi-reversible redox reaction of the PEO-Hb was found in PEO oligomers by alternately changing the potential polarity ( $\pm 1.2$  V vs Ag). The PEO-Hb showed redox reactions in PEO<sub>200</sub> even at 120 °C. PEO modification was concluded to give the thermal stability in some extent. In phosphate buffer at 70 °C, the electrochemical redox reaction of native Hb was not observed spectroscopically, but that of PEO-Hb was detected. The most effective factor was, however, concluded to be the use of PEO oligomers as a solvent. The molecular motion of PEO oligomers should be milder than that of water at higher temperature. This lower molecular motion was suggested to keep the redox activity of PEO-Hb in the PEO oligomer at 120 °C. However, the PEO-Hb in PEO<sub>200</sub> was stable in the oxidized form at 30 °C; it was reduced without giving potential at 120 °C. Cyclic voltammetry revealed that this autoreduction was attributed to the shift of redox potential with elevating temperature.

---

There have been various studies on the direct electron transfer to heme proteins with the aim of some applications to biomaterials *in vitro* (1). While the electrochemistry of electron transport proteins such as cytochrome *c* has been reported (2–4), there are only a few reports of direct electron transfer reactions of other heme proteins besides cytochrome *c*. Recently, the quasi-reversible redox reaction of horse heart myoglobin at an indium tin oxide coated glass electrode was reported (5, 6). A new attempt was reported to control the electrochemical response of proteins in a solid film (7). The solid-state electrochemistry of heme proteins would also attract considerable attention from the viewpoint of molecular devices.

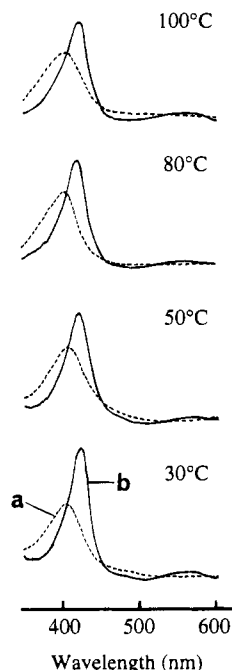
Poly(ethylene oxide)-modified hemoglobin (PEO-Hb) is a typical bioconjugate which has been designed as an artificial blood component (8). On the other hand, poly(ethylene oxide) (PEO) is known as a nontoxic synthetic polymer but also a typical base material for ion conductive polymers. As counterion migration is required to compensate the charge change of the substrate for the electron transfer reaction in solid state, we expected that PEO-modified heme protein would exhibit the redox reaction in ion conductive polymers as well. Indeed, myoglobin and hemoglobin were soluble in PEO oligomers after PEO modification and were redox active in PEO derivatives (9–11). We report here the first demonstration of excellent thermal stability and quasi-reversible redox reaction of PEO-modified hemoglobin in PEO with molecular weight of 200 (PEO<sub>200</sub>) up to 120 °C.

---

\* To whom correspondence should be addressed.

§ Abstract published in *Advance ACS Abstracts*, July 1, 1994.





**Figure 1.** Visible spectra of PEO-modified Hb (PEO-Hb) ( $1.0 \times 10^{-4}$  M) in PEO<sub>200</sub> containing 0.5 M KCl at different temperatures. (a, dotted line) oxidized form of PEO-Hb; (b, solid line) reduced form of PEO-Hb which was obtained after reduction by applying  $-1.2$  V (vs Ag) to an indium tin oxide (ITO) glass electrode. The cell temperature was controlled by circulating hot water up to  $80^\circ\text{C}$ . For experiments above  $80^\circ\text{C}$ , a sample-containing quartz cell was heated in an oil bath for 20 min and immediately put in a cell holder to measure the visible spectra.

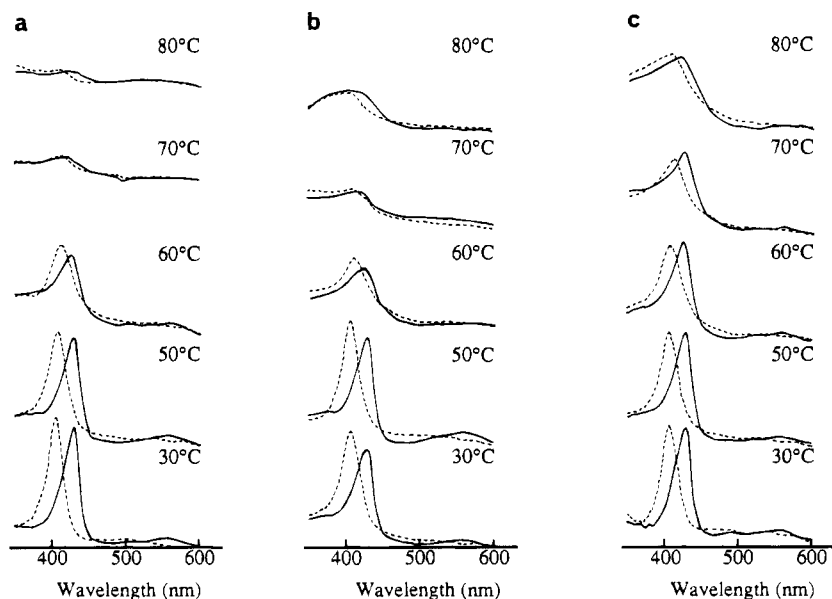
PEO-Hb (8) was a gift from Ajinomoto Co. Ltd. PEO was activated with *N*-hydroxysuccinimide to react with amino groups on the surface of hemoglobin. We used PEO-Hb having six PEO chains with a molecular weight of 3500. The redox reactions of PEO-Hb were analyzed spectroscopically. Potential was given until no visible spectral change was found using a thin-layer cell (light path length:  $150\ \mu\text{m}$ ) composed of an indium tin oxide (ITO) glass electrode as working electrode under potential (9). Ag and Pt wires were used as reference and counter

electrode, respectively. Negative potential was applied on ITO glass electrode until PEO-Hb was reduced completely. All experiments were carried out under nitrogen gas atmosphere to avoid the contribution of oxygen to form an oxygen adduct.

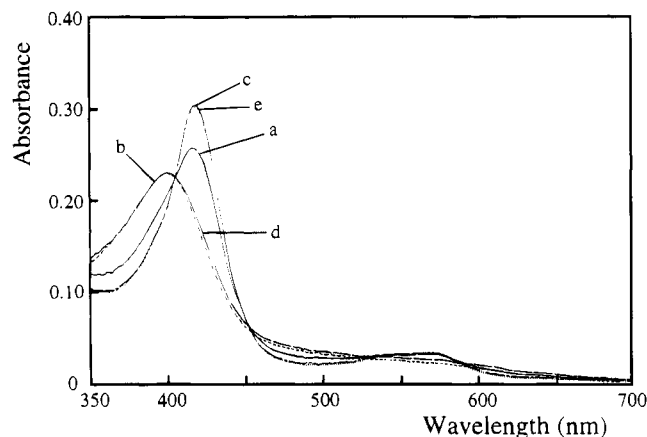
The maximum absorption intensity ( $\lambda_{\text{max}} = 403.4\ \text{nm}$ ) for oxidized PEO-Hb (Figure 1a) was gradually decreased and that for reduced PEO-Hb ( $\lambda_{\text{max}} = 423.4\ \text{nm}$ ) (Figure 1b) was increased in PEO<sub>200</sub> by applying  $-1.2$  V (vs Ag). Several isosbestic points were found during reduction, suggesting a single electron transfer reaction forming no oxygen adduct. Visible spectral change for electrochemical reduction of PEO-Hb in PEO<sub>200</sub> was also seen by applying  $-1.2$  V (vs Ag) at  $50$ ,  $80$ , and  $100^\circ\text{C}$  (Figure 1). It is remarkable that PEO-Hb was reduced in PEO at even  $100^\circ\text{C}$ . The reduction rate seemed to be accelerated by elevating the temperature.

Native hemoglobin (Hb) was also electrochemically reduced by applying negative potential in phosphate buffer at various temperatures. Native Hb shows no characteristic spectrum in phosphate buffer above  $60^\circ\text{C}$  because of thermal denaturation and precipitation (Figure 2a). PEO-Hb was cross-linked by pyridoxalated 5-phosphate (PLP) to avoid Hb from dissociating into subunits (8). PLP bridges were initially considered to be one of major factors to improve the thermal stability of PEO-Hb in PEO<sub>200</sub>. However, the thermal stability of the pyridoxalated hemoglobin without PEO modification was almost the same as that of native Hb in phosphate buffer (Figure 2b). The oxidized PEO-Hb ( $\lambda_{\text{max}} = 405.2\ \text{nm}$ ) in phosphate buffer was also reduced by applying negative potential to show the absorption maximum at  $430.0\ \text{nm}$ . The thermal stability of PEO-Hb was slightly improved over that of Hb. The visible spectral change was found in phosphate buffer at even  $70^\circ\text{C}$ , but the absorbance was, however, reduced (Figure 2c). Neither Hb nor PEO-Hb was stable in phosphate buffer at  $80^\circ\text{C}$ . Only PEO-Hb was stable and redox-active at  $100^\circ\text{C}$  in PEO<sub>200</sub> (Figure 1).

The visible spectra of PEO-Hb in PEO<sub>200</sub> containing  $0.5\ \text{M}$  KCl were also measured after heating at temperatures above  $100^\circ\text{C}$ . The absorption maximum at  $418.4\ \text{nm}$  was observed after heating at  $120^\circ\text{C}$  for 20 min without applying a potential (Figure 3a). A new absorp-



**Figure 2.** Effect of temperature on the visible spectra of hemoglobin ( $2.0 \times 10^{-5}$  M) in  $0.1\ \text{M}$  phosphate buffer (pH 7.0) containing  $0.2\ \text{M}$  KCl. (a) native hemoglobin; (b) pyridoxalated hemoglobin; and (c) PEO-modified hemoglobin. Dotted line: oxidized form of heme protein. Solid line: reduced form of heme protein which was obtained by applying  $-0.8$  V (vs Ag).



**Figure 3.** Reversible spectral changes of PEO-Hb ( $1.0 \times 10^{-4}$  M) in PEO<sub>200</sub> containing 0.5 M KCl at 120 °C. These spectra were obtained by applying the potential with the following sequence: (a, —) open circuit → (b, - -) + 0.5 V → (c, - · -) - 0.5 V → (d, - -) + 0.5 V → (e, - · -) - 0.5 V. Similar results (d and e) were obtained after further potential cycling.

tion signal was seen at a shorter wavelength by applying +0.5 V (vs Ag) with a maximum absorption at 400.6 nm for the oxidized PEO-Hb (Figure 3b). Then, the spectrum with absorption maximum at 420.2 nm for the reduced PEO-Hb was obtained by applying -0.5 V (vs Ag) (Figure 3c). Since the initial spectrum of PEO-Hb (Figure 3a) showed a quite similar absorption maximum but smaller intensity than that of fully reduced PEO-Hb (Figure 3c), a part of PEO-Hb was considered to be automatically reduced by heating at 120 °C. The same spectral change of PEO-Hb was also observed at 140 °C in PEO<sub>200</sub>. The redox potential of PEO-Hb, determined by cyclic voltammetry, was -113.5 and -60 mV (vs Ag) at 25 and 80 °C. Further, the redox potential was +26.5, +37.0, and +75.5 mV (vs Ag) at 100, 120, and 140 °C, respectively. This supported that the PEO-Hb was reduced automatically due to the shift of redox potential with elevating temperature. In an aqueous medium, similar shifts of redox potentials for cytochrome *c* and myoglobin with increasing temperature have been reported (12–14). The redox reactions of PEO-Hb in PEO<sub>200</sub> at 120 °C were revealed to be quasi-reversible. After the reduction, the spectrum of PEO-Hb for the oxidized form was obtained by applying +0.5 V (vs Ag) for 3 min (Figure 3d). Similarly, PEO-Hb was reduced again by applying -0.5 V (vs Ag) after the reoxidation (Figure 3e). These spectra were alternately obtained by further switching of potential polarity.

The iron protoporphyrin IX (heme) would not come away from the globin domain at higher temperatures. However, heme was soluble in PEO<sub>200</sub> and it kept its redox activity in PEO<sub>200</sub> (15); the visible spectrum of heme for the oxidized form ( $\lambda_{\text{max}} = 384.5$  nm) in PEO<sub>200</sub> was different from that of PEO-Hb in PEO<sub>200</sub> from 30 to 140 °C. This strongly suggests that heme was retained in the globin domain of PEO-Hb up to 140 °C in PEO<sub>200</sub>.

The most essential difference between water and PEO as solvent was considered to be the thermal molecular motion. As the mobility of PEO was much smaller than that of water, this difference should be the main reason for the thermal stability of PEO-Hb in PEO<sub>200</sub>. Drastic mobility of water may cause the denaturation of proteins at higher temperatures. The effect of water molecules on the denaturation of proteins at higher temperatures was also supported by the improved stability of the

membrane proteins in a dry film at 140 °C reported by Shen *et al.* (16). The present study might be a model for functionalization of proteins in polymer solvents and showed an effectiveness of the polymer solvents for biomaterials at higher temperatures.

#### ACKNOWLEDGMENT

The authors would like to thank Dr. Yuji Iwashita, Central Research Center, Ajinomoto Co., Ltd., for supplying the PEO-Hb and PLP-Hb. This study was supported by the Grant-in-Aid for Scientific Research from the Ministry of Education, Science and Culture, Japan, and Asahi Glass Foundation.

#### LITERATURE CITED

- (1) Armstrong, F. A., Hill, H. A. O., and Walton, N. J. (1988) Direct electrochemistry of redox properties. *Acc. Chem. Res.* 21, 407–413.
- (2) Yeh, P., and Kuwana, T. (1977) Reversible electrode reaction of cytochrome *c*. *Chem. Lett.* 1145–1148.
- (3) Bowden, E. F., Hawkridge, F. M., Chlebowski, J. F., Bancroft, E. E., Thorpe, C., and Blount, H. N. (1982) Cyclic voltammetry and derivative cyclic voltabsorptometry of purified horse heart cytochrome *c* at tin-doped indium oxide optically transparent electrodes. *J. Am. Chem. Soc.* 104, 7641–7644.
- (4) Niki, K., Yagi, T., Inokuchi, H., and Kimura, K. (1979) Electrochemical behavior of cytochrome *c*<sub>3</sub> of *Desulfovibrio vulgaris*, strain Miyazaki, on the mercury electrode. *J. Am. Chem. Soc.* 101, 3335–3340.
- (5) King, B. C., Hawkridge, F. M., and Hoffman, B. M. (1992) Electrochemical studies of cyanometmyoglobin and metmyoglobin: implications for long-range electron transfer in proteins. *J. Am. Chem. Soc.* 114, 10603–10608.
- (6) Taniguchi, I., Watanabe, K., Tominaga, M., and Hawkridge, F. M. (1992) Direct electron transfer of horse heart myoglobin at an indium oxide electrode. *J. Electroanal. Chem.* 333, 331–338.
- (7) Oliver, B. N., Egekeze, J. O., and Murray, R. W. (1988) "Solid-state" voltammetry of a protein in a polymer solvent. *J. Am. Chem. Soc.* 110, 2321–2322.
- (8) Iwashita, Y. (1991) Pyridoxalated hemoglobin-polyoxyethylene conjugate (PHP) as an oxygen carrier. *Artif. Organs Today* 1, 89–114.
- (9) Ohno, H., and Tsukuda, T. (1992) Electron-transfer reaction of polyethylene oxide-modified myoglobin in polyethylene oxide oligomers. *J. Electroanal. Chem.* 341, 137–149.
- (10) Ohno, H., and Tsukuda, T. (1994) Electron transfer reaction of poly(ethylene oxide)-modified myoglobin coated on an ITO electrode in poly(ethylene oxide) oligomers. *J. Electroanal. Chem.* 367, 189–194.
- (11) Ohno, H., Yamaguchi, N., and Watanabe, M. (1993) Electron transfer reaction of poly(ethylene oxide)-modified hemoglobin on the ITO electrode in solid polymer electrolytes. *Polym. Adv. Technol.* 4, 133–138.
- (12) Koller, K. B., and Hawkridge, F. M. (1985) Temperature and electrolyte effects on the electron-transfer reactions of cytochrome *c*. *J. Am. Chem. Soc.* 107, 7412–7417.
- (13) Koller, K. B., and Hawkridge, F. M. (1988) The effects of temperature and electrolyte at acidic and alkaline pH on the electron transfer reactions of cytochrome *c* at In<sub>2</sub>O<sub>3</sub> electrodes. *J. Electroanal. Chem.* 239, 291–306.
- (14) Yuan, X., Hawkridge, F. M., and Chlebowski, J. F. (1993) Thermodynamic and kinetic studies of cytochrome *c* from different species. *J. Electroanal. Chem.* 350, 29–42.
- (15) Shi, G., and Ohno, H. (1991) Electrochemical behaviors of porphyrins incorporated into solid polymer electrolytes. *J. Electroanal. Chem.* 314, 59–69.
- (16) Shen, Y., Safinya, C. R., Liang, K. S., Ruppert, A. F., and Rothschild, K. J. (1993) Stabilization of the membrane protein bacteriorhodopsin to 140 °C in two-dimensional films. *Nature* 366, 48–50.

# REVIEWS

## Gene Transfer with Synthetic Cationic Amphiphiles: Prospects for Gene Therapy

Jean-Paul Behr

Laboratoire de Chimie Génétique, CNRS URA 1386, Faculté de Pharmacie de Strasbourg, B.P. 24, F-67401 Illkirch Cedex, France. Received February 9, 1994

The introduction of genes into cells of various origins is a major technique of cell biology research. Gene transfer indeed is the most straightforward way to study gene and protein function and regulation, from an *in vitro* isolated cell context up to *in vivo* multicellular processes such as embryogenesis or through the creation of animal models of human diseases. Besides being a powerful research tool, transfection also has important economic implications through the genetic engineering of microorganisms, plants, and animals, for the production of proteins as well as for crop and livestock improvement. The diversity of gene transfer uses has resulted in the development of a variety of artificial techniques, such as direct DNA microinjection, DNA coprecipitation with inorganic salts or with polycations, DNA encapsulation into liposomes, and cell membrane perturbation by chemicals (organic solvents, detergents, polymers, enzymes) or by physical means: mechanic (particle gun), osmotic, thermic, and electric (electroporation) shocks.

This sustained interest in gene transfer techniques has recently exploded with the advent of gene therapy. As a conceptually new therapeutic approach, gene therapy, besides raising an unprecedented media interest, is intellectually appealing to a very widespread population of scientists and clinicians, who join their efforts for the development of techniques that can be used in humans. Indeed, the weak link of gene therapy paradoxically is the vehicle rather than the "drug" itself. Many ongoing clinical protocols (1) make use of recombinant retroviruses which are by far the most efficient vehicles to integrate foreign DNA into the genome of dividing cells. On the other hand, adenoviral vectors have been shown recently to efficiently transfect a large variety of post-mitotic cells. These and other currently developed biological vectors (HSV, AAV), however, raise unassessable long term risks and have a limited capacity to carry foreign genetic material.

In addition to these natural vectors, designed synthetic vectors are being developed (2–4), which in principle could solve the aforementioned questions, provided they are efficient enough *in vivo*. Two classes of molecules have been described so far:

Cationic polypeptides chemically linked to cell surface-binding ligands such as asialoorosomucoid, insulin, or transferrin bind ionically to DNA and trigger targeted cell entry of the complex (4). Receptor-mediated endocytosis, however, leads to low transfection efficiencies since DNA remains essentially entrapped (or is degraded) in endosomes. This technique has greatly improved with the addition of endosomolytic components such as inactivated viruses or fusogenic peptides, leading to synthetic virus-like particles (4). Other related cationic peptides (5) or dendrimeric polymers (6) also have been used to efficiently transfect eucaryotic cells *in vitro*.

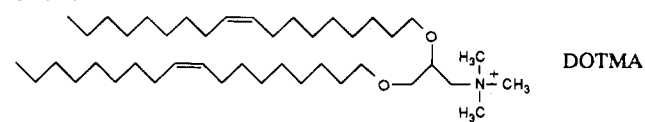
Cationic amphiphiles do not require a specific cell surface receptor. These transfection vehicles are most often erroneously called "cationic liposomes", and al-

though many true liposome-based DNA delivery systems have been described (7, 8), the latter do not compare favorably with cationic amphiphiles (9) unless viral fusion proteins are included (10). "Cationic liposomes" is a confusing term, since it implicitly suggests both the occurrence during transfection of lipid particles with an aqueous interior and a DNA encapsulation step, none of which is needed. Rather, cationic amphiphiles bind cooperatively to DNA and coat it with a cationic layer which in turn interacts with anionic residues on the cell surface. Subsequent cell membrane destabilization is an intrinsic property of the amphiphilic gene carrier. This mechanism will be discussed in detail below, following a chronological description of the various systems which have been developed up to now.

**Various Cationic Amphiphile Structures Transfect Cells.** The rational design of such synthetic gene carriers is recent (3, 4), and within a few years, several groups reported on the synthesis or the use of already commercially available cationic, DNA binding, amphiphiles for gene transfer purposes.

Felgner and co-workers synthesized the quaternary ammonium amphiphile DOTMA ((dioleoyloxypropyl)-trimethylammonium bromide, see Chart 1) and were the first to describe DNA (11) as well as RNA (12) transfer into eukaryotic cell lines following *mixing* of the nucleic acid with a cationic lipid (as opposed to *encapsulation* into a liposome). This new technique was shown to be up to 100-fold more efficient than calcium phosphate or DEAE-dextran coprecipitation. DOTMA was commercialized (Lipofectin, GIBCO-BRL) as a one to one mixture with dioleoylphosphatidylethanolamine (DOPE) and has been widely used since to transfect a large variety of animal and plant eukaryotic cells (13–31). Our own

Chart 1



efforts were directed toward the design of cationic amphiphiles able to *compact* genomic DNA, namely, lipopolyamines (32). The metabolizable parent lipids DOGS and DPPES (see Chart 2) were shown to transfect (2 orders of magnitude better than Ca phosphate) established cell lines as well as primary neuronal cultures. Most importantly, *DNA coating with excess cationic lipid* (rather than liposome binding to the nucleic acid) and subsequent binding of the resulting particle to the negatively charged cell surface via ionic forces was inferred (33). Such an excess of lipid cationic charges over the DNA anionic phosphates is a general requirement for optimal *in vitro* transfection with cationic lipids (see below). DOGS also has been commercialized (Transfectam, Promega) and has been shown to transfect many animal cells very efficiently (33–53).

Chart 2

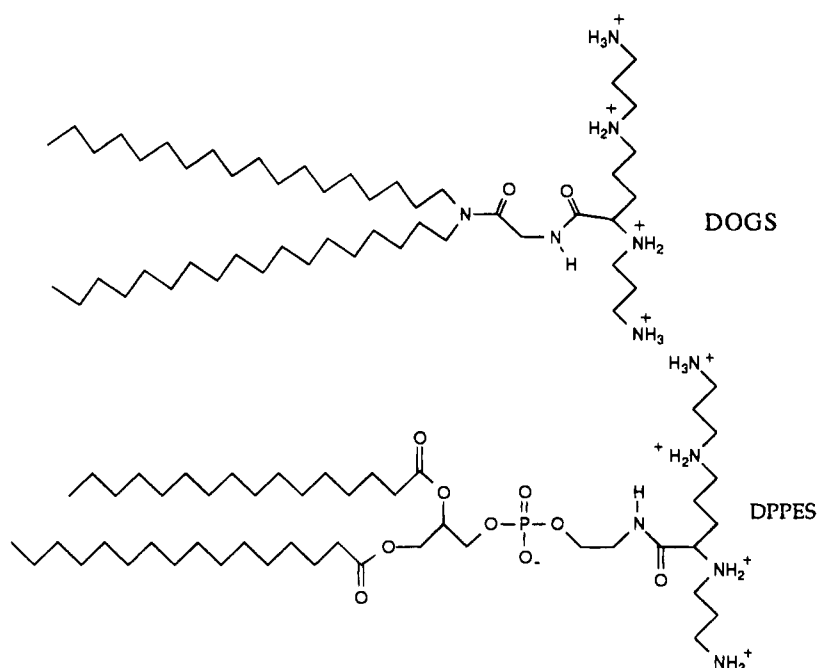
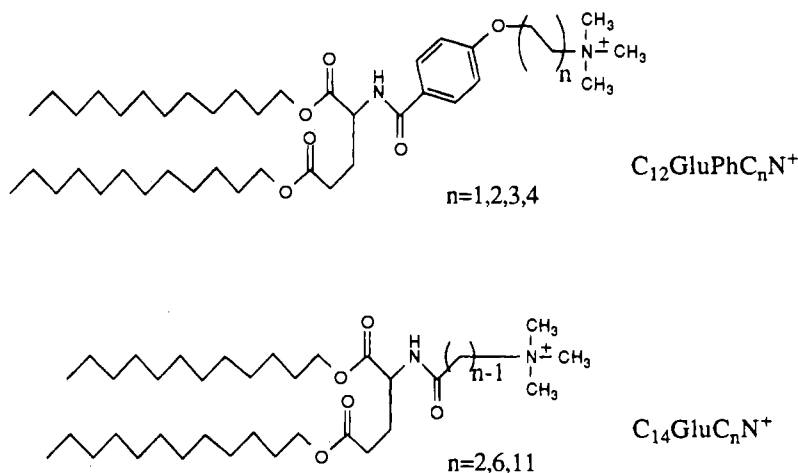


Chart 3



Kunitake et al. (54) synthesized a whole series of lipophilic glutamate diesters with pendent trimethylammonium heads (Chart 3). Whereas transfection properties were similar for dodecyl and tetradecyl esters, they decreased drastically as the link between the lipidic and cationic moieties increased.  $\text{C}_{12}\text{GluPhC}_2\text{N}^+$  was as efficient as Lipofectin.

In an effort to reduce the cytotoxicity of DOTMA, Silvius et al. (55) synthesized a series of metabolizable quaternary ammonium salts, some of which (DOTB, DOTAP dioleoyl esters, Chart 4) had efficiencies comparable to that of Lipofectin when dispersed with DOPE. Mixtures with cholesterol-derived cations (ChoTB, ChoSC) and, most surprisingly, the dioleoyl ester with a slightly longer head group spacer (DOSC) were much less efficient. DOTAP also is now available (Boehringer, Mannheim).

Huang et al. (56) thought along the same lines and synthesized DC-Chol (Chart 5) having a hydrolyzable dimethylethylenediamine headgroup. DOPE/DC-Chol one to one mixtures were able to transfect several cell lines, with efficiencies slightly better than with Lipofectin. The same group also reported about lipophilic polylysines (LPLL) (57), which were up to 3-fold more

efficient than Lipofectin, but only when the fibroblast cells were mechanically scraped following the transfection period.

Meanwhile, biologists had discovered that some commercial cationic detergents, when mixed with true lipids, could also function as transfection agents. Loyter et al. (58) showed that DEBDA hydroxide (Chart 6) added to excess phosphatidylcholine/cholesterol is able to introduce tobacco mosaic virus-RNA into tobacco and petunia protoplasts. Unfortunately, no comparison was made with the classical calcium/poly(ethylene glycol) technique for transfection of plant protoplasts.

Huang et al. (59) compared the transfection properties of several quaternary ammonium detergents (Chart 7) on fibroblasts and found that CTAB/DOPE mixtures were the most efficient, although somewhat less than Lipofectin.

Yagi et al. (60) used a lipophilic diester of glutamic acid (TMAG, Chart 8) with DOPE and found it to be as efficient as calcium phosphate for fibroblast transfection.

Rose et al. (61) compared commonly used detergents of diverse structures: CTAB, DEBDA (see structures above), DDAB (Chart 9), and stearylamine in admixture with phosphatidylethanolamine. Comparative transfection

Chart 4

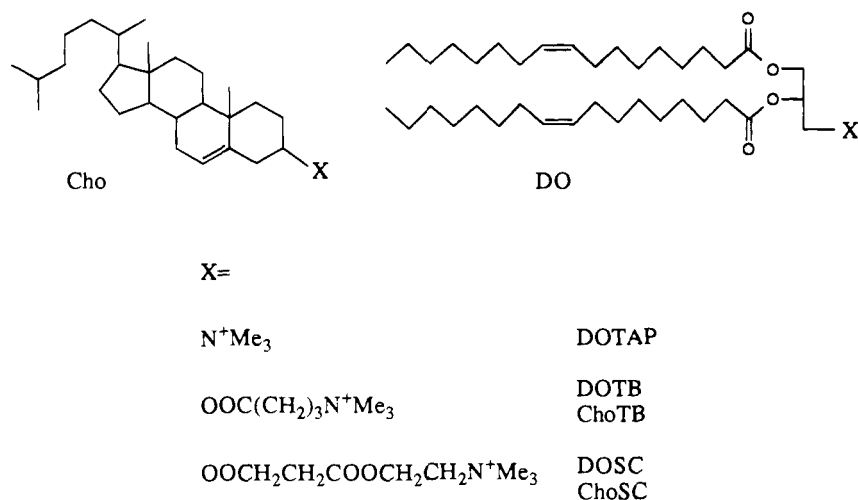


Chart 5

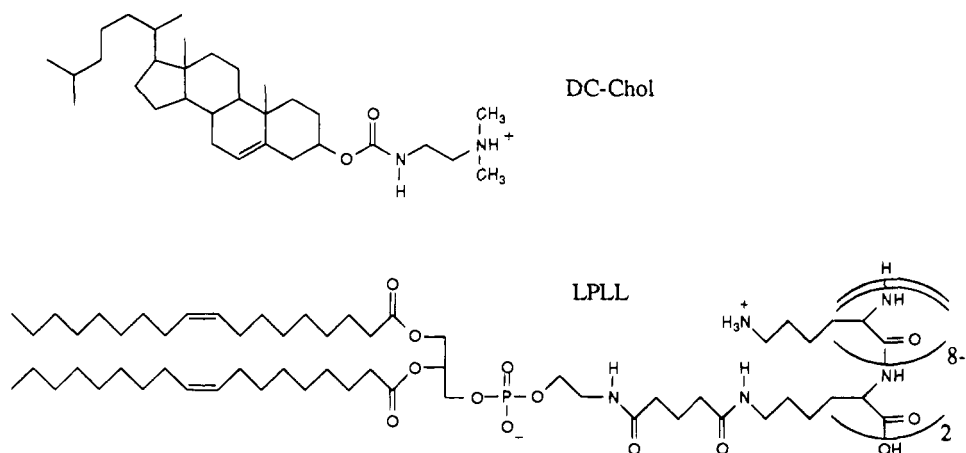


Chart 6

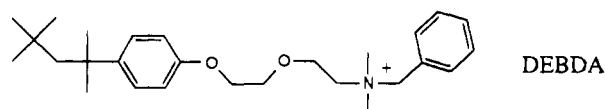


Chart 7

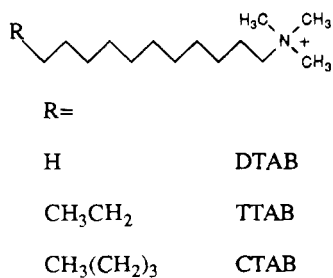


Chart 8

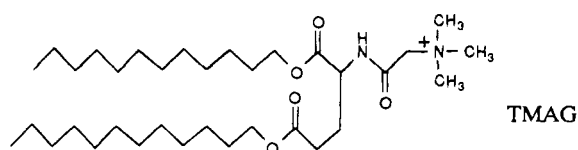
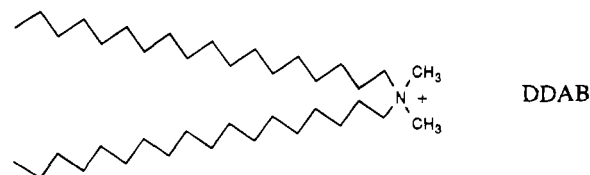


Chart 9



**Comparative Efficiencies.** The level of transfection is best assessed by using a gene which is absent from the cells to be transduced (reporter gene), driven by a strong viral promoter/enhancer element. Normally, this exo-gene must reach the eukaryotic cell nucleus where it is transiently transcribed; alternatively, "stable" expression may be selected out from a subpopulation of daughter cells. In any case the net result is the synthesis of a foreign protein, which may be detected immunologically or enzymatically. Widely used reporter genes include those for the following enzymes:

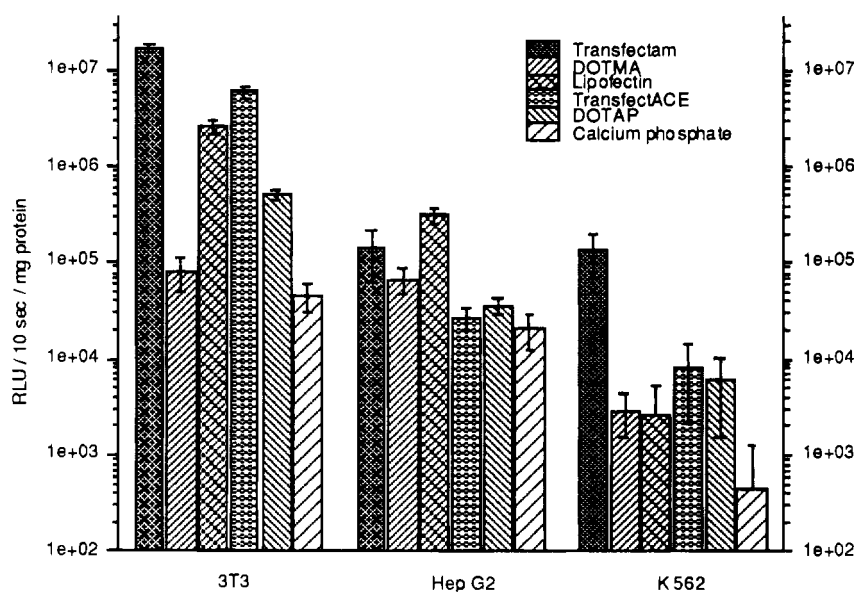
(1) the bacterial chloramphenicol-acetyltransferase (CAT) with either radioactive or fluorescent detection of acetylchloramphenicol or immunochemical ELISA quantitation of the CAT protein; (2) the bacterial  $\beta$ -galactosidase ( $\beta$ -Gal), sometimes bearing a nuclear localization signal, which is mostly used for in vivo histochemical visualization of transfected cells: a synthetic substrate (X-Gal) is diffused into the fixed tissue, leading to precipitation of a deep blue product in cells expressing high levels of  $\beta$ -Gal; and (3) the firefly luciferase (Luc) which is quantitated in the cell extract by photon

tion efficiencies were highly variable with the cell line; DDAB (which was shown earlier to be efficient (33), albeit very toxic) seemed to be the most promising, and the DDAB/DOPE formulation was patented (TransfectACE, GIBCO BRL).

**Table 1. Gene Transfer Efficiencies of Various Cationic Amphiphiles**

cationic amphiphile	reporter gene <sup>a</sup>	cell type	± ratio <sup>b</sup>	efficiency	ref
<b>lipid</b>					
DOTMA	CAT	CV1, COS7...	>2	5-100× DEAE dextran	11
	Neo	LMTK, $\psi$ 2...		10-30× calcium phosphate	
DOGS	CAT	primary neurons, CHO, S49...	4	>10× calcium phosphate	33
	DHFR	CHO...		10-100× calcium phosphate	
DDAB	CAT	primary neurons	3	<DOGS	33
C <sub>12</sub> GluC <sub>2</sub> N <sup>+</sup>	Cyt c <sub>5</sub>	COS1	>2	~DOTMA	54
DOTAP	CAT	CV1, 3T3	2.5	20-200× DEAE dextran, ~DOTMA	55
LPLL	CAT	L929, HeLa...	6	3× DOTMA	57
<b>detergent/neutral lipid</b>					
DEBDA 1/lecithin 1.3/Chol. 0.7	TMV-RNA	tobacco, petunia protoplasts	>10		58
DC-Chol 1/DOPE 1	CAT	A431, L929...	~1	2× DOTMA	56
CTAB 1/DOPE 4	CAT	L929	~1	<DOTMA	59
TMAG 1/lecithin 4	$\beta$ -Gal	COS1	3	~calcium phosphate	60
DDAB 1/PE 2	VSV-G protein	VTF 7-3 infected HeLa, BHK <sup>c</sup>	1.5	~DOTMA	61

<sup>a</sup> CAT (chloramphenicol-acetyltransferase), Neo (neomycin), DHFR (dihydrofolate reductase), Cyt c<sub>5</sub> (cytochrome c<sub>5</sub>), TMV (tobacco mosaic virus),  $\beta$ -Gal ( $\beta$ -galactosidase), VSV (vesicular stomatitis virus). <sup>b</sup> The molar ratio of cationic amphiphile to anionic DNA phosphate, as estimated from concentration data given in the corresponding reference. <sup>c</sup> These cells express bacteriophage T7 RNA polymerase in their cytoplasm.



**Figure 1.** Comparison of transfection efficiencies of various commercially available cationic lipids to that of the calcium phosphate method. 3T3 (murine fibroblasts), HepG2 (human hepatoma), and K562 (human leukaemia) derived cell lines (ca.  $10^5$  cells/15 mm well) were transfected with 2  $\mu$ g of pGL2-Luc plasmid (Promega) and a 4-fold charge excess of cationic lipid, following essentially the manufacturer's protocol. Control values (250 RLU for DNA alone) were subtracted; the bars are the mean of three experiments.

counting of a phosphorescent product it catalytically generates; this technique has by far the highest dynamic range (ca. 7 orders of magnitude).

Besides the vehicle and the nucleic acid, transfection also depends to a large extent on the cell type as well as on many other (often unpredictable) factors (37, 57). Efforts to draw up a hit-parade of gene transfer vectors seem therefore hopeless. The best transfection experiments described with each of the cationic amphiphiles mentioned above have nonetheless been summarized in Table 1, for several pertinent conclusions emerge from such an overview.

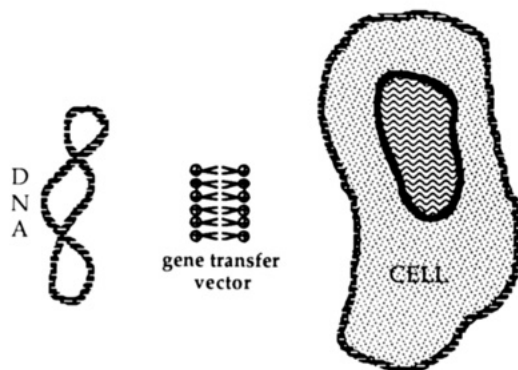
The extent of electrical neutralization of DNA anionic charges by the cationic amphiphile has been calculated from the concentration data given for each system ( $\pm$  ratio in Table 1). It shows that regardless of the structure and number of charges borne by the molecule, in vitro transfection becomes really efficient only when the nucleolipidic particles have a net mean positive charge (33). Transfection efficiency increases with the cationic lipid/DNA ratio up to the onset of cytotoxicity. Bilayer-disrupting detergents and DDAB are among the most toxic, which limits their performances.

True double chain cationic lipids (upper part of Table 1) are active by themselves, whereas cationic detergent-like molecules require an additional excess of neutral lipid; the detergent/lipid ratio is such that nonmicellar structures prevail. Such a behavior suggests that cationic amphiphiles act as gene transfer vectors by providing a cationic multimolecular surface which glues anionic DNA to the anionic cell surface (see next paragraph).

A dangling cationic head seems to be a penalty for a vector, as seen in the series C<sub>12</sub>GluPhC<sub>n</sub>N<sup>+</sup>, C<sub>14</sub>GluC<sub>n</sub>N<sup>+</sup>, and DOTB/DOSC, where the shortest spacers lead to the highest surface charge density, hence the best transfection efficacy.

The new vectors have been compared to popular techniques such as calcium phosphate or DEAE-dextran coprecipitation or to the widely distributed DOTMA (Lipofectin). Efficiencies are at least that of classical coprecipitation techniques, and most often raise 1–2 orders of magnitude over that of calcium phosphate. Surprisingly, several compounds of quite different structures, including DOTMA, seem roughly equivalent to each other (see Table 1). In order to check whether this truly reflects an upper limit to the transfection level obtainable





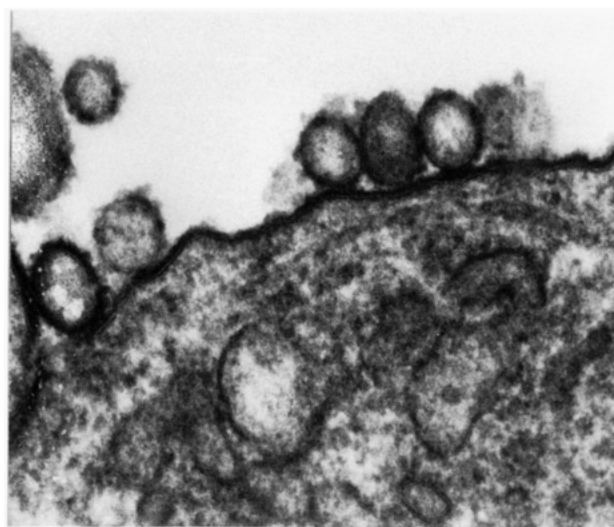
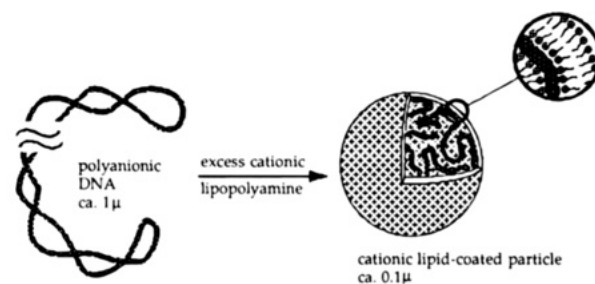
**Figure 2.** "Doubly faced sticky tape" hypothesis of anionic DNA binding to the anionic cell surface.

with the cationic lipid method (rather than saturation of the detection method which was used), several commercially available compounds were compared using the luciferase reporter gene which has a very extended measurement range. Results (62) obtained with various cell types (Figure 1) favor the second hypothesis: relative efficiencies now are split indeed over more than 1 order of magnitude. The order of efficiencies varies with the cell type, emphasizing the precautions already mentioned above, yet invariably the DNA-compacting lipopolyamine is found to be at least as efficient as the quaternary ammonium lipids (notice the efficiency scale is logarithmic). These results shed some light on the way cationic lipids help a gene to enter a cell.

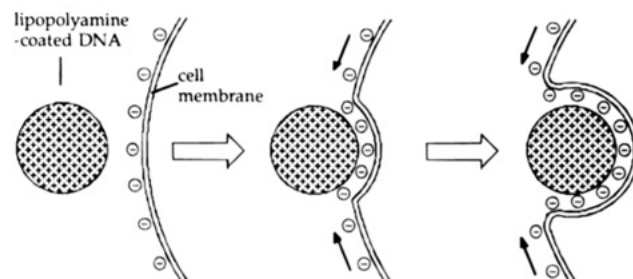
**Gene Transfer Mechanism.** Broadly speaking, a gene is a huge piece of DNA, typically of micron size and  $10^4$  anionic charges, which gives it two good reasons *not* to enter a cell of comparable size surrounded by an itself negatively charged lipid bilayer. Consequently, a synthetic gene transfer vector should be designed to compact DNA and to bind it to the cell surface in such a way as to favor membrane destabilization or endocytosis. As schematically depicted in Figure 2, aggregated cationic lipids could provide a kind of "doubly-faced sticky tape" to glue the anionic DNA to the anionic cell surface.

Our own efforts toward the development of synthetic gene carriers were directed along the following lines (33): The simplest natural organic cations able to condense DNA are the polyamines spermidine and spermine. Regardless of its size, DNA is condensed into toroids and rods of ca. 70–100 nm with stoichiometric amounts of spermine in low salt (63). Under physiological conditions, however, this interaction is quickly reversed. We therefore designed *lipopolyamines*, i.e., amphiphiles with a self-aggregating hydrocarbon tail linked to a polycationic DNA-compacting headgroup, and showed them to be able to stably condense DNA into discrete particles (32). Particularly when DNA is mixed with an excess of lipopolyamines such as DOGS and DPPES, the nucleic acid is condensed into ca. 100 nm size nucleolipidic particles surrounded by a lipid bilayer, as confirmed by electron microscopy (64) and quasielastic light scattering (65) (Figure 3). Such particles are clearly not liposomes since their interior is composed of several compacted plasmid molecules glued together with the lipopolyamine.

The lipid composition of cytoplasmic membranes is highly variable, yet natural lipids are either zwitterionic or anionic, *never cationic*. It is therefore conceivable that submicron size particles with a high cationic surface charge density bind cooperatively to anionic residues on the cell surface (Figure 4). This hypothesis (38) would explain the common transfection property shared by



**Figure 3.** Upper part: lipopolyamines condense several extended plasmids into a small nucleolipidic particle. Lower part: electron microscopy picture of nucleolipidic particles bound to the cytoplasmic membrane of a human meningioma cell (64); scale: 80 nm for 1 cm.

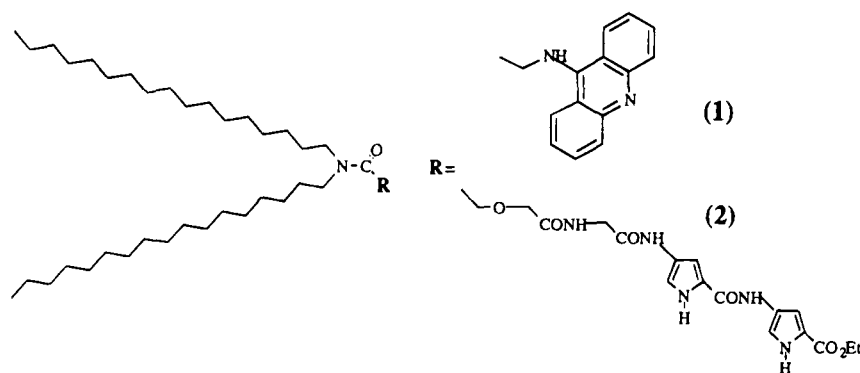


**Figure 4.** Spontaneous "zipper" engulfment of a rigid cationic particle.

vehicles as different as high molecular weight cationic polymers (DEAE-dextran, polybrene), a mineral cationic particle (asbestos fiber), alkaline-earth insoluble salts (e.g., calcium phosphate), and aggregated cationic amphiphiles: they all can provide a cationic surface for binding DNA to the cell membrane. There, a combination of lateral diffusion of cellular lipids with cytoplasmic membrane deformability (as opposed to the hard cationic particle) results in engulfment of the latter (3) (Figure 4). Subsequent cell entry may then depend on many factors such as cell type or the particle nature and size. Cationic lipid-coated particles may take either of two routes reminiscent of viral infection (66): membrane fusion at the most curved edge of the cell surface in contact with the particle or, more probably, spontaneous endocytosis. The intracellular fate of the DNA-containing particles is even more obscure (but see below); however, some of the nucleic acid must reach the nucleus and become uncoated at some stage, since active exogene transcription is observed.

This rather putative view of the mechanism by which

Chart 10



the nucleolipidic particles enter a cell is consistent with the aforementioned general observations (i.e., the requirement for positively charged particles, and the inability of cationic detergents to promote transfection by themselves). Furthermore, lipids with other strong DNA-binding heads (see Chart 10) which either intercalate between base pairs (1) or fill the minor groove (2) are unable to transfect cells (65).

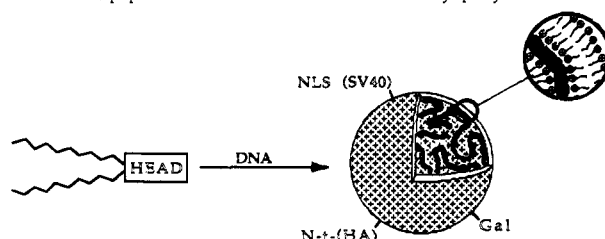
More speculative arguments go along the same lines: DOGS-, DDAB-, and oleoyl-containing lipids (DOTMA, DOPE, DOTAP, LPLL) do not form stable bilayer liposomes in the presence of DNA and in high salt physiological media; a similar behavior probably holds for cationic detergents/DOPE mixtures. This property favors several independent lipidic structures initially bound to a plasmid (as dewdrops on a spider's thread) to merge into a lipid-coated DNA particle. It also may destabilize cytoplasmic and internal endosomal and nuclear membranes, thus helping the particles to sequentially reach the cytoplasm and the nucleus. There, uncoating may simply be the result of a competitive distribution of the cationic lipid between DNA from exogenous plasmids and that from a large pool of chromatin.

The consistently higher transfection efficiency observed with lipopolyamines, as compared to quaternary ammonium-bearing lipids (Figure 1) may be a consequence of the high charge density of  $\text{NH}^+$  as compared to the more diffuse  $\text{N}(\text{CH}_3)_3^+$  cation where the charge is spread over some 10 aliphatic hydrogens (hence a weaker interaction of the latter with the cell membrane phosphate or carboxylate groups). Furthermore, the least basic secondary amine of DOGS ( $\text{pK}_a$  ca. 5.4) is able to buffer acidic lysosomes (as dendrimeric polymers probably do (6)), thus protecting DNA from degradation. Finally, polyamines, in contrast to the other cationic headgroups, possess the unique property of DNA compaction (DOTMA, although coating DNA, seems to do so without significant size reduction (67)).

**Conclusion.** Cationic lipid-mediated gene transfer has become a very attractive alternative to other *in vitro* techniques: it is as straightforward as calcium phosphate coprecipitation (requiring only mixing of DNA with the lipid); it is of general use with respect to cell type and DNA size, since it is entirely driven by nonspecific ionic interactions; and it may be of low toxicity if the carrier is designed to be biodegradable. As such, cationic lipids are being widely used in cell biology research as well as in gene therapy protocols where *ex vivo* transfection is possible (13–31, 33–53).

Efficient *in vivo* gene transfer with amphiphilic vectors is a much harder task to achieve: the nucleolipidic particles interact with circulating serum proteins (heparin, albumin, ...) as well as with the anionic tissue matrix, and except for endothelial cells, particles must

Lipid Headgroup	Property	Function
$\text{Sper}^{4+}$	DNA condensation	core particle
$(\text{Gal})_n$	receptor binding	cell targeting
(N-t-HA) peptide	fusogenic	cytoplasm entry
(NLS-SV40) peptide	nuclear localization	caryophily



**Figure 5.** Self-assembly of several "programmed" lipids with DNA leads to a transfecting particle having the useful properties of a virus. N-t-HA, N-terminal peptide of hemagglutinin; NLS-SV40, nuclear localization signal of SV40 large T antigen.

penetrate a tissue. In spite of several successful reports (35, 40, 68–80), real advances in this field will probably arise from novel formulations of already existing molecules, or from vectors based on a different principle. The several orders of magnitude wide gap between the efficiencies of viruses and that of synthetic vectors remains a challenge to chemists (3, 4). One way to take up this challenge is to develop a modular transfection system, where each molecular component is in charge of a key step of viral entry.

Such a system is still based on a (neutral) lipopolyamine/DNA core particle (Figure 5). Self-aggregation and intermixing of lipids allows one to add new properties to this particle via other lipids: Hepatic cell targeting has been achieved recently with an additional oligogalactose-bearing lipid (81). Virus-derived fusion and nuclear localization peptide headgroups should help the particles to cross the cytoplasmic and nuclear membranes. Thus, upon mixing these various lipids with a gene, only the lipopolyamine component will interact with DNA and condense it. Concentrated at the resulting particle's surface will be molecular signals for cell targeting, entry into the cytoplasm, and finally trafficking toward the nucleus, a process reminiscent of programmed molecular self-organization (82) leading to a virus.

#### ACKNOWLEDGMENT

I thank my colleagues V. Mordvinov, H. Perron, J. S. Remy, and C. Sirlin for references to unpublished experiments and Prof. B. Spiess for  $\text{pK}$  measurements. This work was supported by the Centre National de la Recherche Scientifique, Association Francaise contre les Myopathies, Association Francaise de Lutte contre la Mucoviscidose, and Association pour la Recherche contre le Cancer.

## LITERATURE CITED

- (1) Miller, A. D. (1992) Human gene therapy comes of age. *Nature* 357, 455–460. Lehn, P. (1993) General principles of retroviral-mediated gene transfer. *Path. Biol.* 41, 658–662. Briand, P., and Kahn, A. *Ibid.* 663–671. Blaese, R. M., Mullen, C. A., and Ramsey, W. J. *Ibid.* 672–676.
- (2) Monsigny, M., Midoux, P., and Roche, A.-C. (1993) Perspectives ex vivo et in vivo, pour la thérapie génique, de la transfection sélective à l'aide de complexes plasmide-polylysine ciblés (Targeted Plasmid Polylysine Complexes as Putative Tools to Selectively Transfer Genes ex-Vivo and in-Vivo). *Médecine/Sciences* 9, 441–449.
- (3) Behr, J. P. (1993) Synthetic gene transfer vectors. *Acc. Chem. Res.* 26, 274–278.
- (4) Cotten, M., and Wagner, E. (1993) Non-viral approaches to gene therapy. *Curr. Op. Biotech.* 4, 705–710.
- (5) Legendre, J.-Y., and Szoka, F. C., Jr. (1993) Cyclic amphipathic peptide–DNA complexes mediate high-efficiency transfection of adherent mammalian cells. *Proc. Natl. Acad. Sci. U.S.A.* 90, 893–897.
- (6) Haensler, J., and Szoka, F. C. (1993) Polyamidoamine Cascade Polymers Mediate Efficient Transfection of Cells in Culture. *Bioconjugate Chem.* 4, 372–379.
- (7) Nicolau, C., Legrand, A., and Grosse, E. (1987) Liposomes as carriers for in vivo gene transfer and expression. *Methods Enzymol.* 149, 157–176.
- (8) Mannino, R. J., and Gould-Fogerite, S. (1988) Liposome-mediated gene transfer. *Biotechniques* 6, 682–690.
- (9) Legendre, J. Y., and Szoka, F. C. (1992) Delivery of plasmid DNA into mammalian cell lines using pH-sensitive liposomes: comparison with cationic liposomes. *Pharm. Res.* 9, 1235–1242.
- (10) Gould-Fogerite, S., Mazurkiewicz, J. E., Raska, K., Voelkerding, K., Lehman, and J. M., Mannino, R. J. (1989) Chimerasome-mediated gene transfer in vitro and in vivo. *Gene* 84, 429–438.
- (11) Felgner, P. L., Gadek, T. R., Holm, M., Roman, R., Chan, H. W., Wenz, M., Northrop, J. P., Ringold, G. M., and Danielsen, M. (1987) Lipofection: a highly efficient, lipid-mediated DNA-transfection procedure. *Proc. Natl. Acad. Sci. U.S.A.* 84, 7413–7417.
- (12) Malone, R. W., Felgner, P. L., and Verma, I. M. (1989) Cationic liposome-mediated RNA transfection. *Proc. Natl. Acad. Sci. U.S.A.* 86, 6077–6081.
- (13) Brigham, K. L., Meyrick, B., Christman, B., Berry, L. C., Jr., and King, G. (1989) Expression of a prokaryotic gene in cultured lung endothelial cells after lipofection with a plasmid vector. *Am. J. Respir. Cell Mol. Biol.* 1, 95–100.
- (14) Lu, L., Zeitlin, P. L., Guggino, W. B., and Craig, R. W. (1989) Gene transfer by lipofection in rabbit and human secretory epithelial cells. *Pflügers Arch.* 415, 198–203.
- (15) Welsh, N., Öberg, C., Hellerström, C., and Welsh, M. (1990) Liposome-mediated in vitro transfection of pancreatic islet cells. *Biomed. Biochim. Acta* 12, 1157–1164.
- (16) Antonelli, N. M., and Stadler, J. (1990) Genomic DNA can be used with cationic methods for highly efficient transformation of maize protoplasts. *Theor. Appl. Genet.* 80, 395–401.
- (17) Innes, C. L., Smith, P. B., Langenbach, R., Tindall, K. R., and Boone, L. R. (1990) Cationic liposomes (Lipofectin) mediate retroviral infection in the absence of specific receptors. *J. Virol.* 64, 957–961.
- (18) Rippe, R. A., Brenner, D. A., and Leffert, H. L. (1990) DNA-mediated gene transfer into adult rat hepatocytes in primary culture. *Mol. Cell. Biol.* 10, 689–695.
- (19) Muller, S. R., Sullivan, P. D., Clegg, D. O., and Feinstein, S. C. (1990) Efficient transfection and expression of heterologous genes in PC12 cells. *DNA Cell Biol.* 9, 221–229.
- (20) Brant, M., Nachmansson, N., Norrman, K., Regnell, and Bredberg, A. (1991) Shuttle vector plasmid propagation in human peripheral blood lymphocytes facilitated by liposome-mediated transfection. *DNA Cell Biol.* 10, 75–79.
- (21) Spörlein, B., and Koop, H.-U. (1991) Lipofectin: direct gene transfer to higher plants using cationic liposomes. *Theor. Appl. Genet.* 83, 1–5.
- (22) Parker-Ponder, K., Dunbar, R. P., Wilson, D. R., Darlington, G. J., and Woo, S. (1991) Evaluation of relative promoter strength in primary hepatocytes using optimized lipofection. *Hum. Gene Ther.* 2, 41–52.
- (23) Jiang, C.-K., Connolly, D., and Blumenberg, M. (1991) Comparison of methods for transfection of human epidermal keratinocytes. *J. Invest. Dermatol.* 98, 969–973.
- (24) Jarnagin, W. R., Debs, R. J., Wang, S.-S., and Bissell, D. M. (1992) Cationic lipid-mediated transfection of liver cells in primary culture. *Nucl. Acids Res.* 20, 4205–4211.
- (25) Ray, J., and Gage, F. H. (1992) Gene transfer into established and primary fibroblast cell lines: comparison of transfection methods and promoters. *Biotechniques* 13, 598–603.
- (26) Yeoman, L. C., Danels, Y. J., and Lynch, M. J. (1992) Lipofectin enhances cellular uptake of antisense DNA while inhibiting tumor cell growth. *Antisense Res. Develop.* 2, 51–59.
- (27) Li, A. P., Myers, C. A., and Kaminski, D. L. (1992) Gene transfer in primary cultures of human hepatocytes. *In Vitro Cell. Dev. Biol.* 28, 373–375.
- (28) Bennett, C. F., Chiang, M.-Y., Chan, H., Shoemaker, J. E. E., and Mirabelli, C. K. (1992) Cationic lipids enhance cellular uptake and activity of phosphorothioate antisense oligonucleotides. *Mol. Pharmacol.* 41, 1023–1033.
- (29) Jiao, S. S., Williams, P., Safda, N., Schultz, E., and Wolff, J. A. (1993) Co-Transplantation of Plasmid-Transfected Myoblasts and Myotubes into Rat Brains Enables High Levels of Gene Expression Long-Term. *Cell Transplant* 2, 185–192.
- (30) Gao, X., and Huang, L. (1993) Cytoplasmic Expression of a Reporter Gene by Co-delivery of T7 RNA Polymerase and T7 Promoter Sequence with Cationic Liposomes. *Nucleic Acids Res.* 21, 2867–2872.
- (31) Watson, M. E. E., and Moore, M. (1993) A Quantitative Assay for Trans-Activation by HIV-1 TAT, Using Liposome-Mediated DNA Uptake and a Parallel ELISA System. *AIDS Res. Hum. Retroviruses* 9, 861–867.
- (32) Behr, J. P. (1986) DNA strongly binds to micelles and vesicles containing lipopolyamines or lipointercalants. *Tetrahedron Lett.* 27, 5861–5864.
- (33) Behr, J. P., Demeneix, B., Loeffler, J. P., and Perez-Mutul, J. (1989) Efficient gene transfer into mammalian primary endocrine cells with lipopolyamine-coated DNA. *Proc. Natl. Acad. Sci. U.S.A.* 86, 6982–6986.
- (34) Loeffler, J. P., Barthel, F., Feltz, P., Behr, J. P., Sassone-Corsi, P., and Feltz, A. (1990) Lipopolyamine-mediated transfection allows gene expression studies in primary neuronal cells. *J. Neurochem.* 54, 1812–1815.
- (35) Demeneix, B. A., Fredriksson, G., Lezoual'ch, F., Daugeras-Bernard, N., Behr, J. P., and Loeffler, J. P. (1991) Gene transfer into intact vertebrate embryos. *Int. J. Dev. Biol.* 35, 481–484.
- (36) Barthel, F., Boutillier, A. L., Giraud, P., Demeneix, B. A., Behr, J. P., and Loeffler, J. P. (1992) Gene regulation analysis by lipopolyamine-mediated DNA transfer in primary neurons. In *Methods in Neurosciences*, (P. M. Conn, Ed.) Vol. 9, pp 291–312.
- (37) Loeffler, J. P., and Behr, J. P. (1993) Gene transfer into primary and established mammalian cell lines with lipopolyamine-coated DNA in *Methods in Enzymology Recombinant DNA* (R. Wu, Ed.) Vol. 217, pp 599–618, Academic Press, New York.
- (38) Barthel, F., Remy, J. S., Loeffler, J. P., and Behr, J. P. (1993) Gene transfer optimization with Lipospermine-coated DNA. *DNA Cell Biol.* 12, 553–560.
- (39) Staedel, C., Remy, J. S., Hua, Z., Broker, T. R., Chow, L. T., and Behr, J. P. (1994) High efficiency transfection of primary human keratinocytes with positively charged lipopolyamine:DNA complexes. *J. Invest. Dermatol.* 102, 768–772.
- (40) Demeneix, B. A., Abdel-Taweb, H., Benoit, C., Seugnet, I., and Behr, J. P. (1994) Temporal and spatial expression of lipospermine-compacted genes transferred into chick embryos in vivo. *Biotechniques* 16, 496–498.
- (41) Demeneix, B. A., Kley, N., and Loeffler, J. P. (1990) Differentiation to a neuronal phenotype in bovine chromaffin cells is repressed by protein kinase C and is not dependent on c-Fos oncoproteins. *DNA Cell Biol.* 9, 335–345.
- (42) Boutillier, A. L., Sassone-Corsi, P., and Loeffler, J. P. (1991) The protooncogene c-Fos is induced by corticotropin-releasing

- factor and stimulates proopiomelanocortin gene transcription in pituitary cells. *Mol. Endocrinol.* 5, 1301–1310.
- (43) Giraud, P., Kowalski, C., Barthel, F., Bequet, D., Renard, M., Grinau, M., Boudouresque, F., and Loeffler, J. P. (1991) Striatal proenkephalin turnover and gene transcription are regulated by cAMP and protein kinase C related pathways. *Neuroscience* 43, 67–79.
- (44) Schweighoffer, F., Barlat, I., Chevallier-Multon, M. C., and Tocque, B. (1992) Implication of GAP in Ras-dependent transactivation of a polyoma enhancer sequence. *Science* 256, 825–827.
- (45) Schenborn, E., and Goiffon, V. (1992) Greatly increased transfection efficiency of NIH 3T3 and HeLa cells using Transfectam reagent. *J. NIH Res.* 4, 79.
- (46) Bejanin, S., Habert, E., Berrard, S., Dumas Milne Edwards, J. B., Loeffler, J. P., and Mallet, J. (1992) Promoter elements of the rat choline acetyltransferase gene allowing nerve growth factor inducibility in transfected primary cultured cells. *J. Neurochem.* 58, 1580–1583.
- (47) Boutillier, A. L., Barthel, F., Loeffler, J. P., Hassan, A., and Demeneix, B. A. (1992) Genetic analysis in neurons and neural crest-derived post mitotic cells. *Prog. Neuro-Psychopharmacol. and Biol. Psychiat.* 16, 959–968.
- (48) Boutillier, A. L., Barthel, F., Roberts, J. L., and Loeffler, J. P. (1992)  $\beta$ -adrenergic stimulation of c-Fos via protein kinase A is mediated by CREB dependent and tissue specific CREB independent mechanisms in corticotrope cells. *J. Biol. Chem.* 267, 23520–23526.
- (49) Kley, N., Chung, R. Y., Fay, S., Loeffler, J. P., and Seizinger, B. R. (1992) Specific repression of the basal c-Fos promoter by wild-type p53. *Nucleic Acids Res.* 20, 4083–4087.
- (50) Barthel, F., and Loeffler, J. P. (1993) Characterization and genetic analysis of functional corticotropin releasing hormone receptors in primary cerebellar cultures. *J. Neurochem.* 60, 696–703.
- (51) Lezoualc'h, F., Hassan, A. H. S., Giraud, P., Loeffler, J. P., Lee, S. L., and Demeneix, B. A. (1992) Assignment of the  $\beta$ -thyroid hormone receptor to 3,5,3'-triiodothyronine-dependent inhibition of transcription from the thyrotropin-releasing hormone promoter in chick hypothalamic neurons. *Mol. Endocrinol.* 6, 1797–1804.
- (52) Bading, H., Ginty, D. D., and Greenberg, M. E. (1993) Regulation of gene expression in hippocampal neurons by distinct calcium signalling pathways. *Science* 260, 181–186.
- (53) Perron, H., Suh, M., Lalande, B., Gratacap, B., Laurent, A., Stoeber, P., and Seigneurin, J. M. (1993) Herpes simplex virus ICP0 and ICP4 immediate early proteins strongly enhance expression of a retrovirus harboured by a leptomeningeal cell line from a patient with multiple sclerosis. *J. Gen. Virol.* 74, 65–72.
- (54) Ito, A., Miyazoe, R., Mitoma, J., Akao, T., Osaki, T., and Kunitake, T. (1990) Synthetic cationic amphiphiles for liposome-mediated DNA transfection. *Biochem. Inter.* 22, 235–241.
- (55) Leventis, R., and Silvius, J. R. (1990) Interactions of mammalian cells with lipid dispersions containing novel metabolizable cationic amphiphiles. *Biochim. Biophys. Acta* 1023, 124–132.
- (56) Gao, X., and Huang, L. (1991) A novel cationic liposome reagent for efficient transfection of mammalian cells. *Biochem. Biophys. Res. Comm.* 179, 280–285.
- (57) Zhou, X., Klibanov, A. L., and Huang, L. (1991) Lipophilic polylysines mediate efficient DNA transfection in mammalian cells. *Biochim. Biophys. Acta* 1065, 8–14.
- (58) Ballas, N., Zakai, N., Sela, I., and Loyter, A. (1988) Liposomes bearing a quaternary ammonium detergent as an efficient vehicle for functional transfer of TMV-RNA into plant protoplasts. *Biochim. Biophys. Acta* 939, 8–18.
- (59) Pinnaduwa, P., Schmitt, L., and Huang, L. (1989) Use of a quaternary ammonium detergent in liposome mediated DNA transfection of mouse L-cells. *Biochim. Biophys. Acta* 985, 33–37.
- (60) Koshizaka, T., Hayashi, Y., and Yagi, K. (1989) Novel liposomes for efficient transfection of beta-galactosidase gene into COS-1 cells. *J. Clin. Biochem. Nutr.* 7, 185–192.
- (61) Rose, J. K., Buonocore, L., and Whitt, M. A. (1991) A new cationic liposome reagent mediating nearly quantitative transfection of animal cells. *Biotechniques* 10, 520–525.
- (62) Remy, J. S., Mordvinov, V., Kichler, A., and Behr, J. P. (to be published).
- (63) Wilson, R. W., and Bloomfield, V. A. (1979) Counterion-induced condensation of DNA. A light-scattering study. *Biochemistry* 18, 2192–2196.
- (64) Perron, H., and Brambilla, E. (unpublished results).
- (65) Remy, J. S., Sirlin, C., Vierling, P., and Behr, J. P. (1994) Gene transfer with a series of lipophilic DNA-binding molecules (submitted).
- (66) Haywood, A. M. (1975) 'Phagocytosis' of Sendai virus by model membranes. *J. Gen. Virol.* 29, 63–68.
- (67) Gershon, H., Ghirlando, R., Guttman, S. B., and Minsky, A. (1993) Mode of formation and structural features of DNA-cationic liposome complexes used for transfection. *Biochemistry* 32, 7143–7151.
- (68) Nabel, E. G., Plautz, G., and Nabel, G. J. (1992) Transduction of a foreign histocompatibility gene into the arterial wall induces vasculitis. *Proc. Natl. Acad. Sci. USA* 89, 5157–5161.
- (69) Ono, T., Fujino, Y., Tsuchita, T., and Tsuda, M. (1990) Plasmid cDNAs directly injected into mouse brain with lipofectin can be incorporated and expressed by brain cells. *Neurosci. Lett.* 117, 259–263.
- (70) Jiao, S., Acsadi, G., Jani, A., Felgner, P. L., and Wolf, J. A. (1992) Persistence of plasmid DNA and expression in rat brain cells in vivo. *Exper. Neurol.* 115, 400–413.
- (71) Brigham, K. L., Meyrick, B., Christman, B., Magnuson, M., King, G., Berry, L. C., Jr. (1989) In vivo transfection of murine lungs with a functioning prokaryotic gene using a liposome vehicle. *Am. J. Med. Sci.* 298, 278–281.
- (72) Holt, C. E., Garlick, N., and Cornel, E. (1990) Lipofection of cDNAs in the embryonic vertebrate central nervous system. *Neuron* 4, 203–214.
- (73) Yoshimura, K., Rosenfeld, M. A., Nakamura, H., Scherer, E. M., Pavirani, A., Lecocq, J.-P., and Crystal, R. G. (1992) Expression of the human cystic fibrosis transmembrane conductance regulator gene in the mouse lung after in vivo intratracheal plasmid-mediated gene transfer. *Nucl. Acids Res.* 20, 3233–3240.
- (74) Stribling, R., Brunette, E., Liggitt, D., Gaensler, K., and Debs, R. (1992) Aerosol gene delivery in vivo. *Proc. Natl. Acad. Sci. U.S.A.* 89, 11277–11281.
- (75) Hyde, S. C., Gill, D. R., Higgins, C. F., Trezise, A. E. O., Mac Vinish, L. J., Cuthbert, A. W., Ratcliff, R., Evans, M. J., and Colledge, W. H. (1993) Correction of the ion transport defect in cystic fibrosis transgenic mice by gene therapy. *Nature* 362, 250–255.
- (76) Alino, S. F., Bobadilla, M., Garciasanz, M., Lejarreta, M., Unda, F., and Hilario, E. (1993) In vivo Delivery of Human alpha-1-Antitrypsin Gene to Mouse Hepatocytes by Liposomes. *Biochem. Biophys. Res. Commun.* 192, 174–181.
- (77) Jiao, S. S., Williams, P., Safda, N., Schultz, E., and Wolff, J. A. (1993) Co-Transplantation of Plasmid-Transfected Myoblasts and Myotubes into Rat Brains Enables High Levels of Gene Expression Long-Term. *Cell Transplant.* 2, 185–192.
- (78) Plautz, G. E., Yang, Z. Y., Wu, B. Y., Gao, X., Huang, L., and Nabel, G. J. (1993) Immunotherapy of Malignancy by In Vivo Gene Transfer into Tumors. *Proc. Natl. Acad. Sci. U.S.A.* 90, 4645–4649.
- (79) Zhu, N., Liggitt, D., Liu, Y., and Debs, R. (1993) Systemic Gene Expression After Intravenous DNA Delivery into Adult Mice. *Science* 261, 209–211.
- (80) Alton, E. W. F. W., Middleton, P. G., Caplen, N. J., Smith, S. N., Steel, D. M., Munkonge, F. M., Jeffery, P. K., Geddes, D. M., Hart, S. L., Williamson, R., Fasold, K. I., Miller, A. D., Dickinson, P., Stevenson, B. J., McLachlan, G., Dorin, J. R., and Porteous, D. J. (1993) Non-Invasive Liposome-Mediated Gene Delivery Can Correct the Ion Transport Defect in Cystic Fibrosis Mutant Mice. *Nat. Genet.* 5, 135–142.
- (81) Remy, J. S., Kichler, A., Mordvinov, V., Schuber, F., and Behr, J. P. (to be published).
- (82) Lehn, J. M. (1993) Supramolecular chemistry—Molecular information and the design of supramolecular materials. *Makromol. Chem., Macromol. Symp.* 69, 1–17; Supramolecular Chemistry. *Science* 260, 1762–1763.

# ARTICLES

## Conjugates of Double-Stranded Oligonucleotides with Poly(ethylene glycol) and Keyhole Limpet Hemocyanin: A Model for Treating Systemic Lupus Erythematosus

David S. Jones,\* John P. Hachmann, Stephen A. Osgood, Merle S. Hayag, Paul A. Barstad, G. Michael Iverson, and Stephen M. Coutts

La Jolla Pharmaceutical Company, 6455 Nancy Ridge Drive, San Diego, California 92121. Received March 22, 1994<sup>®</sup>

Two types of oligonucleotides were synthesized with linker groups attached at the 5'-end. Both were repeating dimers of deoxyribocytidine and deoxyriboadenosine. A 20-mer was prepared with a thiol-containing linker, masked as a disulfide, and a 50-mer was prepared with a vicinal diol-containing linker. A tetraiodoacetylated poly(ethylene glycol) (PEG) derivative was synthesized and reacted with the thiol-containing 20-mer to provide an oligonucleotide PEG conjugate of precisely four oligonucleotides on each PEG carrier. The vicinal diol on the 50-mer was oxidized to an aldehyde and conjugated to keyhole limpet hemocyanin (KLH) to provide an oligonucleotide-KLH conjugate by reductive alkylation. The conjugates were annealed with complementary (TG)<sub>n</sub> strands. While the double-stranded oligonucleotide-KLH conjugate is an immunogen, eliciting the synthesis of antibodies against oligonucleotides, the PEG conjugate has the biological property of specifically suppressing (tolerizing) B cells which make antibodies against the immunizing oligonucleotide.

### INTRODUCTION

Multiple copies of a hapten attached covalently to a nonimmunogenic polymeric backbone can down regulate, or tolerize, B cells which produce antibody toward the hapten, rendering them nonresponsive to haptened immunogens (Nossal et al., 1973; Liu et al., 1979). The result is a decrease in the amount of antibody produced against the hapten. Molecules such as these, which suppress antibody production by B cells, are called toleragens. For example, 2,4-dinitrophenyl (DNP) groups attached to D-lysine-containing polymers can suppress IgG production in animals which have been immunized with DNP-derivatized proteins. Such findings suggested a therapeutic approach for treatment of autoimmune disorders by tolerizing B cells. Systemic lupus erythematosus (SLE) is characterized by antibodies to a number of nuclear antigens. Specifically, antibodies to double-stranded DNA (anti-ds-DNA) are thought to cause lupus nephritis (Smeenk et al., 1988). We have shown that synthetic double-stranded oligonucleotides (ds-ON) cross react with anti-ds-DNA (Conrad and Coutts, 1994). Our approach toward a therapy for SLE involves the use of ds-ON conjugates with nonimmunogenic carriers to inactivate B cells which synthesize anti-ds-DNA.

Conjugates of synthetic oligonucleotides with both large and small molecules have been reported. Oligonucleotides have been modified at the 5'-end with a carboxylic acid or aldehyde and attached to latex microspheres containing hydrazide residues (Kremsky et al., 1987). Oligonucleotides were attached to biotin and fluorophores at the 5'-end, using either an oxidation of a 5'-ribouridine moiety with periodate followed by reduction in the presence of biotin hydrazide or attachment of

a fluorenylmethoxycarbonyl amino group at the 5'-end (Agrawal et al., 1986). Similarly, oligonucleotides have been attached to antibodies (Kuijpers et al., 1993). Oligonucleotides were attached to poly-L-lysine using oxidation of a 3'-ribonucleotide followed by reductive amination (Leonetti et al., 1988). Amino and, subsequently, thiol groups have been introduced at the 5'-end of oligonucleotides (Gaur, 1991). Trityl-protected thiols have been attached to the 5'-end of oligonucleotides using phosphoramidite chemistry, with subsequent detritylation using silver nitrate (Connolly, 1985; Ansorge et al., 1987; Sproat et al., 1987). Thiols have been generated at the 3'-end of oligonucleotides by reduction of a disulfide bond, generating a 3'-linked thiol which was used, subsequently, to attach the oligonucleotide to alkaline phosphatase (Li et al., 1987). Similarly, Thuong reported the preparation of an oligonucleotide with a 3'-linked thiol (Asseline et al., 1992).

We have developed two new types of ds-ON conjugates to study the tolerization, or suppression, of an anti-ds-DNA immune response. The first conjugate, in which multiple oligonucleotides are attached to an immunogenic protein, keyhole limpet hemocyanin (KLH), was synthesized to provide a reagent for eliciting an antibody response in immunized mice. DNA does not contain T cell activating structures (epitopes), and alone will not provoke an antibody response. When DNA is attached to a protein, which contains T cell epitopes, it becomes immunogenic. We developed such a conjugate in which the oligonucleotide is attached to lysine  $\epsilon$ -amino groups on KLH, via a new vicinal diol linkage, which is attached to the 5'-end of an oligonucleotide in the last step of an automated synthesis. This linker can be used, in theory, to attach oligonucleotides to any amine-containing compound. The 5'-end is desirable for modification, because only full length oligonucleotides will receive the linker. The vicinal diol is oxidized with periodate prior to

\* Abstract published in *Advance ACS Abstracts*, July 15, 1994.



conjugation, resulting in the formation of an aldehyde on the linker and the loss of formaldehyde, which is removed by alcohol precipitation. The aldehyde-containing oligonucleotide is then treated with pyridine–borane complex in the presence of KLH. This results in a stable, single-stranded oligonucleotide–KLH conjugate by reductive alkylation of the lysine  $\epsilon$ -amines with the aldehyde linker. Finally, a complementary oligonucleotide is annealed to the conjugate to form a double-stranded oligonucleotide–KLH conjugate. This conjugate was used to immunize mice, eliciting an antibody response against the ds-ON. A conjugate of oligonucleotides with the 60/40 copolymer of D-glutamic acid and D-lysine (D-EK) was also prepared using the same methodology as the KLH conjugate. After a complementary strand was annealed, the resulting double-stranded conjugate (LJP 105) was used in an antibody-forming cell assay.

The second type of conjugate was developed in which precisely four oligonucleotides are attached to a poly(ethylene glycol) (PEG) backbone. This conjugate is prepared using a new thiol-containing linker. Thioether formation between thiols and haloacetyl groups is known to be facile and capable of high yields (Bernatowicz and Matsueda, 1986; Inman et al., 1991). We chose to avoid the silver-assisted detritylation of a trityl-protected thiol and rely instead on the reductive cleavage of a disulfide, linked to the 5'-end, to generate the thiol after automated synthesis. The linker is attached to the 5'-end of the oligonucleotide as a disulfide in the last step of an automated synthesis. The disulfide is subsequently reduced to a thiol, which is reacted with haloacetyl groups in a modified PEG derivative, to form a stable conjugate in which the oligonucleotides are attached to the modified PEG *via* thioether bonds. A complementary oligonucleotide is annealed to the conjugate to form a double-stranded oligonucleotide–PEG conjugate LJP 249 (compound **21**), which is used to tolerize ds-ON immunized mice.

## EXPERIMENTAL PROCEDURES

Imidazole, 5-hexen-1-ol, *tert*-butyldimethylsilyl chloride (TBDMSCl), *N*-methylmorpholine *N*-oxide (NMMO), osmium tetroxide (2.5% in *tert*-butyl alcohol), benzoyl chloride, tetrabutylammonium fluoride (TBAF), tetrazole, *O*-cyanoethyl *N,N,N',N'*-tetra isopropylphosphorodiamidite, 2-cyanoethyl *N,N*-diisopropylchlorophosphoramidite, 6-chloro-1-hexanol, thiourea, iodine, triphenylmethyl chloride (trityl chloride), 3,5-diaminobenzoic acid, dicyclohexylcarbodiimide (DCC), *N*-hydroxysuccinimide (NHS), and iodoacetic anhydride were purchased from Aldrich Chemical Co. Nucleoside phosphoramidites (dA, dC, dG, and dT) and derivatized controlled pore glass (CPG) supports were purchased from Milligen. Keyhole limpet hemocyanin (KLH) was purchased from Pacific Bio-Marine, Venice, CA. D-EK, the copolymer consisting of 40% D-lysine and 60% D-glutamic acid, was purchased from Damon Biotech, Inc., Needham Heights, MA (acquired by Abbott Laboratories, Abbott Park, IL). All solvents and reagents were used as received from the manufacturer unless otherwise specified.

Silica gel (230–400 Mesh ASTM) was purchased from Baxter. Basic alumina (aluminum oxide, activated, basic, Brockman I) was purchased from Aldrich Chemical Co. Q-Sepharose was purchased from Pharmacia. Fractogel EMD–DEAE 650(S) (particle size 0.025–0.040 mm) was purchased from EM, a subsidiary of E. Merck. Sephacryl S-200 was purchased from Pharmacia. Macro-Prep High Q was purchased from BioRad. The GEN-PAK FAX HPLC column was purchased from Waters. TLC was performed on silica gel TLC plates (5554) manufactured

by EM Separations. Phosphate-buffered saline (PBS) was prepared by dissolving 175 g of NaCl, 6.5 g of NaH<sub>2</sub>PO<sub>4</sub>·H<sub>2</sub>O, and 40.9 g of Na<sub>2</sub>HPO<sub>4</sub>·7H<sub>2</sub>O in H<sub>2</sub>O and diluting to a final volume of 20 L.

Melting points are reported uncorrected. NMR spectra were recorded on a Bruker AC-300 spectrometer with broad band probe. DNA synthesis was performed on a Milligen 8800 Prep Scale DNA synthesizer following the manufacturer's protocols for DNA phosphoramidite synthesis. UV absorbances were made on a Perkin-Elmer Lambda 4 spectrophotometer. Quantities of oligonucleotides and oligonucleotide conjugates were estimated by absorbance at 260 nm.<sup>1</sup> Melt curves and hyperchromicity were determined on a Varian Cary 3E spectrophotometer. Elemental analyses were performed by Desert Analytics of Tucson, AZ. Mass spectra were obtained from the Mass Spectroscopy Lab, Department of Chemistry, University of California, Berkeley, CA.

***O*-(*tert*-Butyldimethylsilyl)-5-hexenol, 1.** To a solution of 12.5 mL (10.4 g, 104 mmol) of 5-hexen-1-ol in 104 mL of DMF was added 15.7 g (230 mmol) of imidazole and 20.0 g (130 mmol) of TBDMSCl. The mixture was stirred at room temperature for 4 h and partitioned between 200 mL of EtOAc and 100 mL of saturated NaHCO<sub>3</sub> solution. The EtOAc layer was washed with 100 mL of saturated NaHCO<sub>3</sub> solution, 100 mL of saturated NaCl solution, dried (MgSO<sub>4</sub>), filtered, and concentrated to a volume of approximately 100 mL. Distillation under vacuum provided 70.1 g (90%) of **1**: bp 130–143° 100 mmHg; <sup>1</sup>H NMR (CDCl<sub>3</sub>)  $\delta$  0.11 (s, 6H), 0.95 (s, 9H), 1.48 (m, 2H), 1.57 (m, 2H), 2.11 (dt, 2H), 3.66 (t, 2H), 5.03 (m, 2H), 5.86 (m, 1H); <sup>13</sup>C NMR (CDCl<sub>3</sub>)  $\delta$  –5.25, 18.40, 25.21, 26.01, 32.35, 33.60, 63.09, 114.40, 138.92. Anal. Calcd for C<sub>12</sub>H<sub>26</sub>OSi: C, 67.22; H, 12.22. Found: C, 66.96; H, 12.16.

**1-*O*-(*tert*-Butyldimethylsilyl)-1,5,6-hexanetriol, 2.** To a solution of 9.86 g (46.0 mmol) of **1** in 92 mL of acetone was added a solution of 6.46 g (55.2 mmol) of NMMO in 23 mL of H<sub>2</sub>O. To the mixture was added 443  $\mu$ L of a 2.5% solution of OsO<sub>4</sub> in *tert*-butyl alcohol (360 mg of solution, 9.0 mg of OsO<sub>4</sub>, 35  $\mu$ mol) and 50  $\mu$ L of 30% H<sub>2</sub>O<sub>2</sub>. The mixture was stirred for 16 h, and a solution of 474 mg of sodium dithionite in 14 mL of H<sub>2</sub>O was added. After another 0.5 h the mixture was filtered through Celit. The filtrate was dried with MgSO<sub>4</sub> and filtered through 1 in. of silica gel in a 150-mL Buchner funnel using 250-mL portions of EtOAc. Fractions containing product were concentrated to provide 11.0 g (96%) of **2** as a viscous oil: TLC *R*<sub>f</sub> 0.2 (1:1 hexane/EtOAc); <sup>1</sup>H NMR (CDCl<sub>3</sub>)  $\delta$  0.05 (s, 6H), 0.89 (s, 9H), 1.25 (m, 4H), 1.55 (m, 2H), 3.41 (dd, 2H), 3.62 (t, 2H), 3.71 (m, 1H); <sup>13</sup>C NMR (CDCl<sub>3</sub>)  $\delta$  –5.23, 18.42, 21.91, 26.02, 32.68, 32.81, 63.16, 66.74, 72.24; HRMS (FAB, MH<sup>+</sup>), calcd for C<sub>12</sub>H<sub>26</sub>O<sub>3</sub>Si 249.1886, found: 249.1889.

**5,6-Di-*O*-benzoyl-1-*O*-(*tert*-butyldimethylsilyl)-1,5,6-hexanetriol, 3.** To a solution of 5.29 g (21.3 mmol) of **2** in 106 mL of pyridine was added 6.18 mL (7.48 g, 53.2 mmol) of benzoyl chloride. The mixture was stirred for 18 h and concentrated on the rotary evaporator. The mixture was partitioned between 100 mL of cold 1 N HCl and 100 mL of EtOAc. The pH of the aqueous layer was checked to make sure it was acidic. The EtOAc layer was washed successively with 100 mL of H<sub>2</sub>O and 100 mL of saturated NaCl, dried (MgSO<sub>4</sub>), filtered, and concentrated

<sup>1</sup> Single-stranded oligonucleotides were estimated to contain 33  $\mu$ g of oligonucleotide in 1 mL of solution which has unit absorbance in pH 7.2 PBS. Double-stranded oligonucleotides were estimated to contain 50  $\mu$ g of oligonucleotide in 1 mL of a solution which has unit absorbance in pH 7.2 PBS.



to provide 10.33 g (99%) of **3** as a viscous yellow oil: TLC  $R_f$  0.45 (1:4 EtOAc/hexanes);  $^1\text{H}$  NMR ( $\text{CDCl}_3$ )  $\delta$  0.05 (s, 6H), 0.88 (s, 9H), 1.59 (m, 4H), 1.85 (m, 2H), 3.14 (t, 2H), 4.49 (dd, 1H), 4.59 (dd, 1H), 5.54 (m, 1H), 7.45 (m, 4H), 7.58 (m, 2H), 8.05 (m, 4H).

**5,6-Di-O-benzoyl-1,5,6-hexanetriol, 4.** To a solution of 2.62 g (5.36 mmol) of **3** in 10.9 mL of THF was added 10.7 mL (10.7 mmol) of a 1 N solution of TBAF in THF. The mixture was allowed to stir for 16 h. The mixture was partitioned between 25 mL of saturated  $\text{NaHCO}_3$  solution and  $3 \times 25$  mL of EtOAc. The combined EtOAc extracts were washed with saturated NaCl solution, dried ( $\text{MgSO}_4$ ), filtered, and concentrated to a viscous oil which was purified by silica gel chromatography (1:1 hexane/EtOAc) to provide 823 mg (41%) of **4** as a viscous oil:  $R_f$  0.14 (1:1 hexane/EtOAc);  $^1\text{H}$  NMR ( $\text{CDCl}_3$ )  $\delta$  1.58 (m, 2H), 1.68 (m, 2H), 1.88 (m, 2H), 3.68 (t, 2H), 4.52 (dd, 1H), 4.62 (dd, 1H), 5.56 (m, 1H), 7.46 (m, 4H), 7.58 (m, 2H), 8.05 (m, 4H);  $^{13}\text{C}$  NMR ( $\text{CDCl}_3$ )  $\delta$  22.08, 31.20, 31.30, 32.88, 62.92, 66.17, 72.63, 128.93, 130.19, 130.57, 133.62, 166.72, 166.86; HRMS (FAB,  $\text{MH}^+$ ) calcd for  $\text{C}_{20}\text{H}_{25}\text{O}_5$  343.1545, found: 343.1553.

**1-O-[5,6-Bis-O-(benzoyloxy)hexyl] 1'-O'-(2'-Cyanoethyl) N,N-Diisopropylphosphoramidite, 5.** To a solution of 1.02 g (2.98 mmol) of **4** and 255 mg (1.49 mmol) of diisopropylammonium tetrazolide (prepared by mixing acetonitrile solutions of diisopropylamine and tetrazole in a 1:1 mole ratio and concentrating to a white solid) in 14.9 mL of  $\text{CH}_2\text{Cl}_2$  was added a solution of 989 mg (3.28 mmol) of *O*-cyanoethyl *N,N,N',N'*-tetraisopropylphosphorodiamidite in 2.0 mL of  $\text{CH}_2\text{Cl}_2$ . The mixture was stirred for 4 h and partitioned between 25 mL of  $\text{CH}_2\text{Cl}_2$  and 25 mL of chilled saturated  $\text{NaHCO}_3$  solution. The  $\text{CH}_2\text{Cl}_2$  layer was washed with saturated NaCl solution, dried ( $\text{Na}_2\text{SO}_4$ ), filtered, and concentrated. Purification by filtration through a 2-in. plug of basic alumina in a 25-mm column, eluting with 9:1 EtOAc/ $\text{Et}_3\text{N}$ , provided 1.5 g (93%) of **5** as a viscous oil:  $^1\text{H}$  NMR ( $\text{CDCl}_3$ )  $\delta$  1.19 (m, 12H), 1.62 (m, 2H), 1.73 (m, 2H), 1.90 (m, 2H), 2.62 (dd, 2H), 3.53–3.92 (m, 6H), 4.53 (dd, 1H), 4.62 (dd, 1H), 5.58 (m, 1H), 7.48 (m, 4H), 7.60 (m, 2H), 8.09 (m, 4H);  $^{31}\text{P}$  NMR ( $\text{CDCl}_3$  with 15%  $\text{H}_3\text{PO}_4$  internal standard)  $\delta$  148.2; HRMS (FAB,  $\text{MH}^+$ ) calcd for  $\text{C}_{29}\text{H}_{40}\text{O}_6\text{N}_2\text{P}$  543.2624, found 543.2619.

**Coupling of 5 to (CA)<sub>25</sub> as the Final Step of Automated Synthesis: Synthesis of 6.** Forty-nine sequential steps were carried out using alternating dC and dA phosphoramidites beginning with 10 g of DMT-d-bzA-CPG support (Milligen) with a nucleoside loading of 30  $\mu\text{mol/g}$ . The DMT blocking group was removed, and 40 mL of activator solution (Milligen, Cat. No. MBS 5040) and 800 mg of **5** were added to the reaction mixture. The suspension was mixed for 8 min by argon ebullition and subjected to the usual oxidation step. The support-bound oligonucleotide was removed from the reaction vessel, air dried, and treated with 100 mL of concentrated ammonia for 40 h at 55 °C. When cool, the mixture was filtered through a 10- $\mu\text{m}$  polypropylene filter, and the filtrate was then purified by ion-exchange chromatography on Q Sepharose (gradient, 0.4 M NaCl adjusted to pH 12 with NaOH to 1.0 M NaCl adjusted to pH 12 with NaOH). Fractions which absorbed at 260 nm were further analyzed by polyacrylamide gel electrophoresis after [ $^{32}\text{P}$ ] 3'-labeling (Cozzarelli et al., 1969), and those containing pure product were combined and precipitated with 2-propanol to provide 510 mg (31.9  $\mu\text{mol}$ , 10%) of **6**.

**Synthesis of Single-Stranded Oligonucleotide-KLH Conjugate, 7a.** A 500- $\mu\text{L}$  aliquot (100  $\mu\text{mol}$ ) of a 200 mM solution of  $\text{NaIO}_4$  was added to a solution of 1.0

g (estimated to be 400 mg of full length, 25  $\mu\text{mol}$ )<sup>2</sup> of **6** in 19.5 mL of  $\text{H}_2\text{O}$  at 0 °C in the dark. The mixture was kept at 0 °C for 40 min, and 50 mL of EtOH was added. The mixture was kept at -20 °C for 30 min and centrifuged for 5 min at 2000 rpm. The supernatant was discarded, and the pellet was dried under vacuum. The pellet was dissolved in 3.3 mL of  $\text{H}_2\text{O}$ , and to the resulting solution was added a solution of 166 mg (1.66  $\mu\text{mol}$ ) of KLH in 8.5 mL of 0.5 M  $\text{NaHCO}_3$  and 2.0 mL of pH 8.0 0.5 M sodium borate. To the resulting solution was added 250  $\mu\text{L}$  (50  $\mu\text{mol}$ ) of a 0.2 M solution of pyridine-borane complex in MeOH, and the mixture was kept at 37 °C for 4 days. The product was purified by chromatography on Sephacryl S-200 (isocratic, 10 mM pH 8 sodium borate) to give 200 mL of a solution of **7a** which contained 85 mg of DNA as determined by absorbance at 260 nm. The ratio of DNA molecules to KLH molecules was determined to be approximately 5:1 from the ratio of absorbance at 230 nm to absorbance at 260 nm, assuming a molecular weight of  $10^6$  Da and comparing to the 230-nm/260-nm absorbance ratios of standard mixtures of unconjugated (CA)<sub>25</sub> and KLH. The yield of **7a** was calculated to be 140 mg (46%).

**Hybridization of 7a with (TG)<sub>25</sub>, 8a.** The synthesis of (TG)<sub>25</sub> was carried out in a manner essentially the same as for the synthesis of (TG)<sub>10</sub>. A solution of 140 mg of **7a** in 200 mL of 10 mM pH 8.0 sodium borate was added to 89 mg (5.5  $\mu\text{mol}$ ) of (TG)<sub>25</sub> and the mixture was heated at 85 °C for 10 min and allowed to cool to room temperature over 1 h. The double-stranded conjugate, **8a**, contained a total of 174 mg of DNA;  $T_m$  79°, hyperchromicity 28% (PBS, pH 7.2).

**Synthesis of Single-Stranded Oligonucleotide-D-EK Conjugate, 7b.** A 1.00-mL aliquot (200  $\mu\text{mol}$ ) of a 200 mM solution of  $\text{NaIO}_4$  was added to a solution of 2.01 g (estimated to be 803 mg of full length, 50  $\mu\text{mol}$ ) of **6** in 35 mL of  $\text{H}_2\text{O}$  and 4.01 mL of 1 M pH 7.5 sodium phosphate solution at 0 °C in the dark. The mixture was kept at 0 °C for 40 min, and 40 mL of isopropyl alcohol was added. The mixture was kept at -20 °C for 30 min and centrifuged for 20 min at 3000 rpm. The supernatant was discarded, and the pellet was dried under vacuum. The pellet was dissolved in 11.8 mL of  $\text{H}_2\text{O}$ , and to the resulting solution was added a solution of 86.3 mg (5.0  $\mu\text{mol}$ ) of D-EK<sup>3</sup> in 1.15 mL of  $\text{H}_2\text{O}$  and 0.80 mL of pH 8.0, 1.0 M sodium borate. This was followed by the addition of 500  $\mu\text{L}$  (100  $\mu\text{mol}$ ) of a 0.2 M solution of pyridine-borane complex in MeOH, and the mixture was kept at 37 °C for 48 h. The product, **7b**, was purified by chromatography on Sephacryl S-200 (isocratic, 10 mM pH 8 sodium borate) to give single-stranded conjugate, which contained 306 mg of DNA, as determined by absorbance at 260 nm,<sup>1</sup> at a concentration of 0.81 mg/mL. Amino acid analysis of the conjugate, was used to determine the amount of lysine and glutamic acid in a sample containing 50  $\mu\text{g}$  ( $3.25 \times 10^{-9}$  mol) of oligonucleotide: lysine,  $15.9 \times 10^{-9}$  mol; and glutamic acid,  $23.7 \times 10^{-9}$  mol. The ratio of oligonucleotide to D-EK was

<sup>2</sup> The estimated yield of full length oligonucleotide with linker is 40% based on 50 steps of approximately 98% efficiency. The remaining 600 mg is comprised mostly of failure sequences which do not contain the linker on the 5'-end.

<sup>3</sup> D-EK was purified on a Bio-Gel P-100 column (BioRad) eluting with pH 8.0 50 mM sodium borate, 100 mM NaCl. The leading edge of the peak detected at 220 nm was discarded, and the first half of the peak was collected and dialyzed against  $\text{H}_2\text{O}$ . The resulting solution was lyophilized to a white solid. The average molecular weight was determined to be 17 200 by sedimentation equilibrium.

calculated to be approximately 11:1 using an average molecular weight of 17 200 for D-EK.

**Hybridization of 7b with (TG)<sub>25</sub>, 8b (LJP 105).** A solution of 306 mg of **7b** in 378 mL of 10 mM pH 8.0 sodium borate was added to 306 mg of (TG)<sub>25</sub>, and the mixture was heated to 90 °C and allowed to cool to room temperature. The double-stranded conjugate was precipitated by adding 42 mL of 3 M NaCl and 420 mL of isopropyl alcohol. The mixture was kept at -20 °C for 1 h and centrifuged at 3000 rpm for 20 min. The pellet was dissolved in 0.5 × PBS to give 756 mg of LJP 105 at a concentration of 100 mg/mL; *T<sub>m</sub>* 77 °C, hyperchromicity 29% (PBS, pH 7.2).

**S-(6-Hydroxyhexyl)isothiuronium Chloride, 9.** To a solution of 16.6 mL (20.0 g, 146 mmol) of 6-chlorohexanol in 49 mL of ethanol was added 11.1 g (146 mmol) of thiourea, and the mixture was refluxed for 24 h. The mixture was cooled to 0 °C and the product crystallized. The crystals were collected by vacuum filtration and dried to give 28.4 g (92%) of **9** as a white solid: mp 122–124 °C; <sup>1</sup>H NMR (DMSO) δ 1.40 (m, 4H), 1.65 (m, 2H), 3.21 (t, 2H), 3.41 (t, 2H), 9.27 and 9.33 (overlapping broad singlets, 4H). Anal. Calcd for C<sub>7</sub>H<sub>17</sub>ClN<sub>2</sub>OS: C, 39.51; H, 8.06; N, 13.17; S, 15.07. Found: C, 39.69; H, 8.00; N, 13.01; S, 15.16.

**6-Mercaptohexan-1-ol, 10.** To a solution of 17.8 mg (83.6 mmol) of **9** in 120 mL of H<sub>2</sub>O and 120 mL of EtOH was added 9.25 g of NaOH pellets. The mixture was refluxed for 4 h. The mixture was carefully concentrated to approximately 75 mL, and the concentrate was purified by vacuum distillation to provide 7.4 g (66%) of **10**: bp 95–105 °C (5 mmHg); <sup>1</sup>H NMR (CDCl<sub>3</sub>) δ 1.41 (m, 9H), 2.59 (dt, 2H), 3.69 (t with underlying brd s, 3H); <sup>13</sup>C NMR (CDCl<sub>3</sub>) δ 24.5, 25.2, 28.0, 32.5, 33.9, 62.7. Anal. Calcd for C<sub>6</sub>H<sub>14</sub>OS: C, 53.68; H, 10.51; S, 23.89. Found: C, 53.35; H, 10.72; S, 23.60.

**Bis(6-hydroxyhexyl) Disulfide, 11.** To a solution of 4.26 g (31.7 mmol) of **10** in 10 mL of MeOH and 13.7 mL (9.97 g, 98.5 mmol) of Et<sub>3</sub>N under N<sub>2</sub> atmosphere and cooled in an ice bath was added dropwise over 10 min a solution of 4.02 g (15.8 mmol) of I<sub>2</sub> in 90 mL of MeOH. The cooling bath was removed, and the mixture was stirred at room temperature for 4 h. The mixture was concentrated on a rotary evaporator and purified by silica gel chromatography (1:1 hexane/EtOAc) to provide 3.12 g (73%) of **11** as a pale yellow solid: TLC *R<sub>f</sub>* 0.18 (1:1 hexane/EtOAc); mp 38–48 °C; <sup>1</sup>H NMR (CDCl<sub>3</sub>) δ 1.15–2.20 (m, 16H), 2.73 (t, 4H), 3.70 (t, 4H). Anal. Calcd for C<sub>12</sub>H<sub>26</sub>S<sub>2</sub>O<sub>2</sub>: C, 54.09; H, 9.84; S, 24.06. Found: C, 54.85; H, 9.86; S, 24.11.

**Mono-O-(triphenylmethyl) Bis(6-hydroxyhexyl) Disulfide.** Trityl chloride (60 g, 0.21 mol) was added to a solution of 57 g (0.21 mol) of compound **11** in 60 mL of pyridine. The mixture was stirred at room temperature for 16 h. The mixture was filtered, and the filtrate was diluted with 300 mL of CH<sub>2</sub>Cl<sub>2</sub> and extracted with 200 mL of saturated sodium bicarbonate. The CH<sub>2</sub>Cl<sub>2</sub> layer was dried (Na<sub>2</sub>SO<sub>4</sub>), filtered, and concentrated to an oil. Purification by silica gel chromatography (gradient, 9/1 hexane/EtOAc to 3/1 hexane/EtOAc) yielded 55 g (50%) of **12** as a viscous oil: TLC *R<sub>f</sub>* 0.36 (1/1 heptane/EtOAc); <sup>1</sup>H NMR (CDCl<sub>3</sub>) δ 1.38 (m, 8H), 1.63 (m, 8H), 2.66 (m, 4H), 3.04 (t, 2H), 3.62 (t, 2H), 7.25 (m, 9H), 7.42 (m, 6H); <sup>13</sup>C NMR (CDCl<sub>3</sub>) δ 25.3, 25.8, 28.2, 28.3, 29.1, 29.8, 32.5, 38.9, 39.0, 62.7, 63.4, 66.2, 126.7, 127.6, 128.3, 144.4; HRMS (FAB, M<sup>+</sup>) calcd for C<sub>31</sub>H<sub>40</sub>O<sub>2</sub>S<sub>2</sub> 508.2470, found 508.2482.

**1-O-[14-(triphenylmethoxy)-7,8-dithiatetradecyl] 1'-O'-(2'-Cyanoethyl) N,N-Diisopropylphosphoramidite, 13.** To a solution of 10 g (19.7 mmol) of **12** and

6.3 mL (36.2 mmol) of diisopropylethylamine in 90 mL of CH<sub>2</sub>Cl<sub>2</sub> at 0 °C under argon was slowly added 4.5 mL (20.2 mmol) of 2-cyanoethyl N,N-diisopropylchlorophosphoramidite. The mixture was stirred for 90 min and extracted twice with 100 mL of saturated sodium bicarbonate solution. The combined CH<sub>2</sub>Cl<sub>2</sub> layers were dried (Na<sub>2</sub>SO<sub>4</sub>), filtered, and concentrated to an oil. Purification by basic alumina chromatography (75/24/1 hexanes/EtOAc/triethylamine) provided 11.3 g (81%) of **13** as a viscous oil: <sup>1</sup>H NMR (CDCl<sub>3</sub>) δ 1.18 (m, 12H), 1.13 (m, 8H), 1.62 (m, 8H), 2.60 (m, 6H), 3.04 (t, 2H), 3.60 (m, 4H), 3.82 (m, 2H), 7.26 (m, 6H), 7.44 (m, 9H); <sup>31</sup>P NMR (CDCl<sub>3</sub>) δ 147.9; HRMS (FAB, MH<sup>+</sup>) calcd for C<sub>40</sub>H<sub>58</sub>N<sub>2</sub>O<sub>3</sub>-PS<sub>2</sub> 709.3626, found 709.3621.

**3,5-Bis(iodoacetamido)benzoic Acid, 14.** To a stirred suspension of 572 mg (3.76 mmol) of 3,5-diaminobenzoic acid in 19 mL of dioxane at room temperature under N<sub>2</sub> atmosphere was added 2.93 g (8.28 mmol) of iodoacetic anhydride. The mixture was stirred in the dark for 20 h and partitioned between 50 mL of EtOAc and 50 mL of 1 N HCl solution. The EtOAc layer was washed with brine, dried (MgSO<sub>4</sub>), filtered, and concentrated under vacuum to give a tan solid. Purification by silica gel chromatography (94/5/1 CH<sub>2</sub>Cl<sub>2</sub>/MeOH/HOAc) yielded 992 mg (54%) of **14** as a white solid: mp >220 °C dec; <sup>1</sup>H NMR (DMSO) δ 3.84 (s, 4H), 7.91 (s, 2H), 8.14 (s, 1H), 10.56 (s, 2H). Anal. Calcd for C<sub>11</sub>H<sub>10</sub>N<sub>2</sub>O<sub>4</sub>I<sub>2</sub>: C, 27.07; H, 2.06; N, 5.74; I, 52.01. Found: C, 26.55; H, 2.23; N, 5.29; I, 52.71.

**3,5-Bis(iodoacetamido)benzoic Acid, N-Hydroxysuccinimide Ester, 15.** DCC (309 mg, 1.5 mmol) was added to a solution of 488 mg (1.0 mmol) of **14** and 126 mg (1.1 mmol) of NHS in 10 mL of anhydrous THF. The mixture was stirred for 2.5 h, and eight drops of acetic acid was added. The mixture was kept in a -20 °C freezer for 16 h, and the solids were removed by filtration. The filtrate was concentrated to give 722 mg of yellow foamy solid. Purification by silica gel chromatography (gradient 50/50/1 EtOAc/hexanes/HOAc to 75/25/1 EtOAc/hexanes/HOAc) yielded 511 mg of foamy solid. Recrystallization from EtOAc/hexanes gave 385 mg (66%) of **15** as a white powdery solid: mp 146–147 °C dec; <sup>1</sup>H NMR (MeOH) δ 2.90 (s, 4H), 3.88 (s, 4H), 8.11 (s, 2H), 8.26 (s, 1H). Anal. Calcd for C<sub>15</sub>H<sub>13</sub>N<sub>3</sub>O<sub>6</sub>I<sub>2</sub>: C, 30.79; H, 2.24; N, 7.18; I, 43.38. Found: C, 30.46; H, 2.62; N, 6.81; I, 43.08.

**N,N'-Bis[3,5-bis(iodoacetamido)benzoyl] Derivative of α,ω-Bis[N-(2-aminoethyl)carbamoyl]poly(ethylene glycol), 17.** A solution of 335 mg (0.10 mmol, 3350 g/mol) of α,ω-bis[N-(2-aminoethyl)carbamoyl]poly(ethylene glycol) (Sigma), **16**, and 16.8 mg (0.20 mmol) of NaHCO<sub>3</sub> in 1.0 mL of H<sub>2</sub>O was cooled to 0 °C. A solution of 146 mg (0.25 mmol) of **15** in 0.5 mL of dioxane was added, followed by 0.5 mL of EtOH. The resulting slurry was stirred for 1 h at 0 °C, and 10 mL of 2 N H<sub>2</sub>SO<sub>4</sub> was added. The mixture was extracted with two 10-mL portions of CH<sub>2</sub>Cl<sub>2</sub>. The CH<sub>2</sub>Cl<sub>2</sub> layers were dried (Na<sub>2</sub>SO<sub>4</sub>), filtered, and concentrated to yield 442 mg of crude solid. Purification by chromatography on silica gel (step gradient 8/92 MeOH/CH<sub>2</sub>Cl<sub>2</sub> to 14/86 MeOH/CH<sub>2</sub>Cl<sub>2</sub>) yielded 239 mg (54%) of **17** as a white solid: <sup>1</sup>H NMR (CDCl<sub>3</sub>) δ 3.40 (bd m, 8H), 3.59 (bd s, (CH<sub>2</sub>CH<sub>2</sub>O)<sub>n</sub>, integral too large to integrate in relation to other integrals), 3.80 (bd m, 4H), 3.91 (s, 8H), 7.49 (bd m, 2H), 7.77 (bd m, 2H), 7.82 (bd s, 4H), 8.27 (bd s, 2H), 8.90 (bd m, 4H). Iodoacetyl determination (Thorpe et al., 1984): calcd, 0.92 mmol/g, found 0.96 mmol/g. Anal. Calcd for C<sub>126</sub>H<sub>326</sub>N<sub>8</sub>O<sub>82</sub>I<sub>4</sub>: C, 48.32; H, 7.51; N, 2.56. Found: C, 48.42; H, 7.61; N, 2.54.

**Coupling of 13 to (CA)<sub>10</sub> as the Final Step of**

**Automated Synthesis: Synthesis of 18.** Nineteen sequential steps were carried out using alternating dC and dA phosphoramidites beginning with 10 g of DMT-d-bzA-CPG support (Milligen) with a nucleoside loading of 30.0  $\mu\text{mol/g}$ . The DMT blocking group was removed, and 45 mL of activator solution (Milligen, Cat. No. MBS 5040) and 385 mg of **13** were added to the reaction mixture. The suspension was mixed for 8 min by argon ebullition, and the oligomer was subjected to the usual oxidation step. The support bound oligonucleotide was removed from the reaction vessel, air dried, and treated with 100 mL of concentrated ammonia for 16 h at 55 °C. When cool, the mixture was filtered through a 10- $\mu\text{m}$  polypropylene filter, and the filtrate was then purified by ion-exchange chromatography on Q Sepharose (gradient, 0.2 M NaCl adjusted to pH 12 with NaOH to 1.3 M NaCl adjusted to pH 12 with NaOH). Fractions which absorbed at 260 nm were [ $^{32}\text{P}$ ] 3'-labeled and analyzed by polyacrylamide gel electrophoresis followed by autoradiography. Fractions containing pure product were combined and precipitated with 2-propanol to provide 498 mg (62.2  $\mu\text{mol}$ , 20%) of **18**.

**Synthesis of Single-Stranded Oligonucleotide-PEG Conjugate, 20.** A solution of 500 mg (78  $\mu\text{mol}$ ) of **18** in 12.5 mL of water was treated with 388  $\mu\text{L}$  (315 mg, 1.56 mmol) of tributylphosphine for 1 h at room temperature with agitation. The reduced oligonucleotide was precipitated by adding 1.39 mL of 3 M NaCl and 17.5 mL of isopropyl alcohol. The mixture was kept at -20 °C for 1 h and centrifuged at 5 °C for 20 min at 3000 rpm. The supernatant was removed, and the pellet was dissolved in 8.44 mL of water. A second precipitation was performed with 937  $\mu\text{L}$  of 3 M NaCl and 11.82 mL of isopropyl alcohol. The mixture was kept at -20 °C for 1 h and centrifuged at 5 °C for 20 min at 3000 rpm. The supernatant was removed, and the oily pellet was placed under vacuum for 16 h to give crude **19** as a foamy solid, which was dissolved in 4.5 mL of helium sparged water. The mixture was kept under Ar, and 500  $\mu\text{L}$  of pH 7.8 1 M sodium phosphate buffer and 555  $\mu\text{L}$  of MeOH were added. To the stirred solution was added a solution of 57 mg (13  $\mu\text{mol}$ ) of **17** in 0.55 mL of MeOH, and the mixture was stirred for 22 h. The mixture was purified by chromatography on Macro-Prep High Q (gradient, 0.45 M NaCl, 10% MeOH, adjusted to pH 11 with NaOH to 0.70 M NaCl, 10% MeOH, adjusted to pH 11 with NaOH), and the fractions were combined which were pure as evidenced by polyacrylamide gel electrophoresis after [ $^{32}\text{P}$ ] 3'-labeling and by HPLC on a GenPAK FAX column (gradient, A 0.01 M pH 7.5 sodium phosphate, 10% MeOH; B 0.01 M pH 7.5 sodium phosphate, 1 M NaCl, 10% MeOH; 30% B to 70% B; 1 mL/min; retention time 15.0 min). The pure fractions were combined and precipitated with an equal volume of isopropyl alcohol at -20 °C. The pelleted precipitate was dialyzed against PBS to give 6.7 mL of a solution of **20** (74 mg) at a concentration of 11 mg/mL.

**Hybridization of 20 with (TG)<sub>10</sub>, To Yield 21 (LJP 249).** (TG)<sub>10</sub> was synthesized by standard phosphoramidite chemistry. The protecting groups were removed, and the product was liberated from the CPG solid phase by treatment with concentrated  $\text{NH}_4\text{OH}$  at 55 °C for 16 h. The full length oligonucleotide with trityl protecting groups on the 5'-end was purified by ion-exchange chromatography on Q Sepharose (gradient; 0.8 M NaCl adjusted to pH 12 with NaOH to 1.2 M NaCl adjusted to pH 12 with NaOH). Fractions containing product were identified by HPLC on a Gen-PAK column (0.75 mL/min; 260 nm; gradient, A 0.05 M pH 7.5 sodium phosphate, 10% MeOH; B 0.05 M pH 7.5 sodium phosphate, 1 M

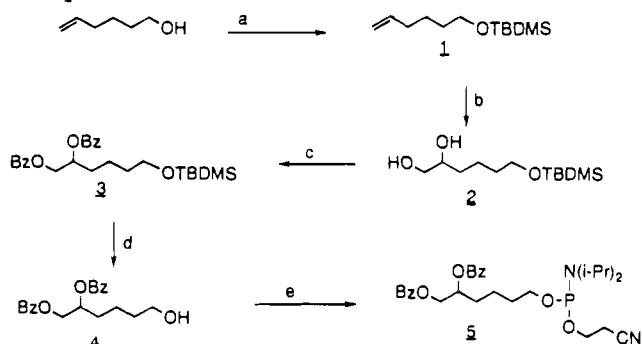
NaCl, 10% MeOH; 0–25 min, 20–80% B; retention time 17.0 min) and precipitated with an equal volume of isopropyl alcohol. The solid, which was collected by centrifugation and decantation of the supernatant, was dried under vacuum and treated with 80/20 HOAc/ $\text{H}_2\text{O}$  for 20 min to remove the trityl protecting groups. Two precipitations from 0.3 M NaCl using isopropyl alcohol yielded (TG)<sub>10</sub>. A 5% excess (69.3 mg) of (TG)<sub>10</sub> was added to a solution of 66 mg of **20** in 9.8 mL of PBS. The mixture was heated at 90 °C for 10 min and allowed to cool to room temperature over 1.5 h. Precipitation with isopropyl alcohol yielded 135 mg of **21** (LJP 249);  $T_m$  68.1 °C, hyperchromicity 25.0% (0.15 M NaCl, 0.01 M sodium citrate, pH 6.8).

**Immunization and Tolerization of Mice.** Female C57Bl/6 mice, 6–8 weeks of age, were obtained from Jackson Laboratories and housed in accordance with NIH guidelines. The mice were primed as previously described (Iverson, 1986). Briefly, mice were injected, ip, with 100  $\mu\text{g}$  of compound **8a** precipitated on Alum (aluminum hydroxide gel) along with  $2 \times 10^9$  *B. pertussis* organisms (obtained from Massachusetts Department of Public Health, State Laboratory Institute, Boston, MA) as an adjuvant. Three weeks after priming with compound **8a**, the mice were divided into groups and injected, ip, with graded doses of **21** (LJP 249). One group was treated with saline and served as the nontreated control. For serological experiments the mice were divided into groups of five mice per group and for plaque-forming cell (pfc; equivalent to antibody-forming cells) experiments they were divided into three mice per group. Five days after treatment with the toleragen **21** (LJP 249) all of the mice, including the controls, were boosted with 50  $\mu\text{g}$  of **8a**. For serological experiments the mice were bled from the tail 7 days after the boost. For pfc experiments the mice were sacrificed 4 days after the boost.

**Biological Activity Assays.** For serological experiments the sera were analyzed for anti-ds-ON antibodies by the Farr assay (Garvey et al., 1977) at a final antigen concentration of  $10^{-8}$  M. A 5'-hydroxyphenyl containing (CA)<sub>25</sub> oligonucleotide strand was prepared as described (Fontanel et al. 1993) and annealed with a complementary (TG)<sub>25</sub> strand. The duplex was radiolabeled with  $^{125}\text{I}$  as also described by Fontanel. Antigen binding capacity was determined as described (Mitchison, 1971). For pfc experiments spleens were analyzed for the number of IgG anti-ds-ON antibody-forming cells by a standard indirect plaque forming cell assay (Henry, 1980). Indicator cells were prepared, as described (Henry, 1980), by coating sheep red blood cells (SRBC) with LJP 105 using 1-[3-(dimethylamino)propyl]-3-ethylcarbodiimide hydrochloride.

<sup>4</sup> The convention used herein to describe repeating dimers of deoxyribonucleotides is exemplified as follows. The 20-mer ON, (CA)<sub>10</sub>, is an alternating sequence of deoxycytidine and deoxyadenosine with deoxycytidine at the 5'-end. The 50-mer ON, (CA)<sub>25</sub>, is an alternating sequence of deoxycytidine and deoxyadenosine with deoxycytidine at the 5'-end. Similarly, (TG)<sub>10</sub> is a 20-mer ON with deoxythymidine at the 5'-end, and (TG)<sub>25</sub> is a 50-mer ON with deoxythymidine at the 5'-end.

<sup>5</sup> Experiments with different sequences of synthetic oligonucleotide duplexes demonstrated sequence-dependence on binding to anti-ds-DNA from lupus mice and humans, as detected by competitive inhibition assays with high molecular weight DNA. This is apparently related to the stability of the duplex and its propensity to assume the B DNA conformation. The duplex formed from (CA)<sub>25</sub> and (TG)<sub>25</sub> assumes the B DNA conformation as evidenced by CD spectroscopy. There is also a modest length dependence on the ability of a B DNA duplex to bind anti-ds-DNA. The  $\text{IC}_{50}$  in the 40-mer duplex (CA)<sub>20</sub>(TG)<sub>20</sub> is five times smaller than the  $\text{IC}_{50}$  in the 60-mer duplex (CA)<sub>30</sub>(TG)<sub>30</sub>.

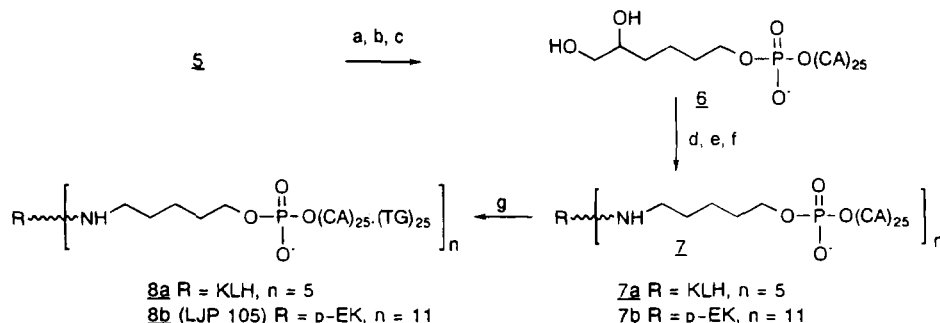
**Scheme 1. Synthesis of Vicinal Diol Containing Phosphoramidite<sup>a</sup>**

<sup>a</sup> Key: (a) TBDMSCl, imidazole, DMF; (b) *N*-methylmorpholine *N*-oxide, OsO<sub>4</sub> (cat.), acetone, H<sub>2</sub>O; (c) benzoyl chloride, pyridine; (d) tetrabutylammonium fluoride, THF; (e) 2-cyanoethyl *N,N,N',N'*-tetraisopropylphosphorodiamidite, diisopropylammonium tetrazolidine, CH<sub>2</sub>Cl<sub>2</sub>.

ride (Aldrich). Spleen cells, from individual mice, were mixed with indicator cells, rabbit anti-mouse immunoglobulin, and guinea pig serum as a source of complement. This mixture was then placed in a Cunningham chamber and incubated for 1 h at 37 °C and the number of plaques were counted by light microscopy. Each spleen cell preparation was also tested against SRBC that had not been coated with LJP 105. This number of nonspecific plaques, always less than 1% of the number of specific plaques, was subtracted to give the number of ds-ON specific IgG plaque forming cells. Knowing the number of spleen cells in the mixture allowed a determination of the number of IgG anti-ds-ON antibody forming cells per 10<sup>6</sup> spleen cells. The percent reduction in anti-ds-ON antibody forming cells was determined by subtracting the number of pfc in the experimental group from those of the control group, followed by division by the number of pfc in the nontreated control group and multiplying by 100.

**RESULTS AND DISCUSSION**

A conjugate of double-stranded oligonucleotides on KLH, **8a**, was designed to immunize mice to elicit antibodies against double-stranded DNA. A duplex consisting of 25 repeating CA<sup>4</sup> units and 25 repeating TG units was used, based on the ability of unconjugated duplexes to bind human SLE serum and murine (MRL) serum (Conrad & Coutts, 1994).<sup>5</sup> The vicinal diol linker was designed to attach oligonucleotides to polymers or proteins with multiple amino groups. The availability of **8a** enabled the development of an immunized mouse model and the testing of nonimmunogenic conjugates for tolerance.

**Scheme 2. Synthesis of KLH Conjugate<sup>a</sup>**

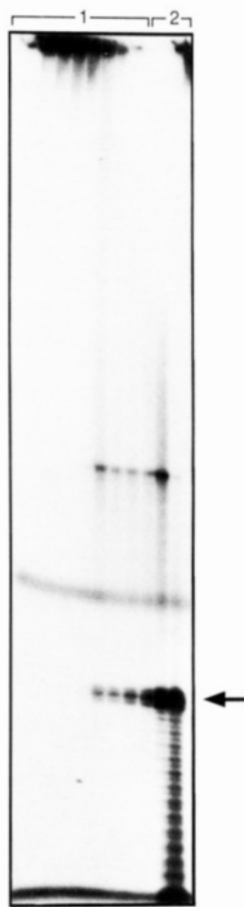
<sup>a</sup> Key: (a) (CA)<sub>25</sub>-CPG, tetrazole, CH<sub>3</sub>CN; (b) I<sub>2</sub>, pyridine, H<sub>2</sub>O, THF; (c) concd NH<sub>4</sub>OH; (d) NaIO<sub>4</sub>, H<sub>2</sub>O; (e) keyhole lipet hemocyanin (KLH or D-EK); (f) BH<sub>3</sub>/pyridine, NaHCO<sub>3</sub>, H<sub>2</sub>O; (g) (TG)<sub>25</sub>.

Toleragens having varying lengths of duplexes of repeating CA units and repeating TG units on nonimmunogenic carriers, including conjugate **21** (LJP 249), were designed, synthesized, and studied in the immunized mouse model. These studies indicated that there was little length dependence on the ability of these conjugates to tolerize, as evidence by their ability to suppress antibody titers, and that conjugates containing oligonucleotides of 20–50 base pairs are essentially equivalent (data not shown). Conjugates containing duplexes of 20 base pairs are biologically active and thermally stable, having *T<sub>m</sub>*'s > 65 °C (pH 6.8, 0.15 M NaCl).

The synthesis of the dibenzoylated vicinal diol-containing phosphoramidite, **5**, is diagrammed in Scheme 1. Protection of the hydroxyl group of 5-hexen-1-ol, as its *tert*-butyldimethylsilyl (TBDMS) ether, was accomplished using TBDMSCl and imidazole in DMF to provide compound **1**. Hydroxylation of **1** with *N*-methylmorpholine *N*-oxide and a catalytic amount of osmium tetroxide in aqueous acetone led to vicinal diol **2**, which was benzoylated by treating with benzoyl chloride in pyridine to give **3**. The TBDMS protecting group was removed with tetrabutylammonium fluoride in THF to provide the alcohol **4**. Finally, the phosphoramidite, **5**, was prepared using *O*-cyanoethyl *N,N,N',N'*-tetraisopropylphosphorodiamidite and diisopropylammonium tetrazolidine in CH<sub>2</sub>Cl<sub>2</sub> (Caruthers et al., 1987; Nielsen et al., 1986).

The syntheses of the KLH conjugate, **8a**, and the D-EK conjugate, **8b** (LJP 105), are diagrammed in Scheme 2. In the final step of automated synthesis, phosphoramidite **5** was added, instead of a nucleoside phosphoramidite, to the alternating (CA)<sub>25</sub> chain. After standard oxidation with iodine and treatment with ammonia to remove protecting groups and cleave the oligonucleotide from the solid support, compound **6** was obtained and partially purified by ion-exchange chromatography. Oxidation of **6** with periodate, followed by treatment with a 1:1 complex of pyridine and borane in the presence of KLH, yielded single-stranded conjugate **7a**. Purification was accomplished by gel filtration. Polyacrylamide gel electrophoresis of [<sup>32</sup>P] 3'-labeled material, followed by autoradiography, was used to monitor the conjugation reaction and purification (see Figure 1). Analysis by UV absorbance ratio A<sub>260</sub>/A<sub>230</sub> indicated a ratio of five oligonucleotides to one molecule of KLH. The conjugate was annealed with a second oligonucleotide consisting of alternating (TG)<sub>25</sub> to provide **8a**.

An oligonucleotide D-EK conjugate, **8b** (LJP 105), was prepared in an essentially similar manner to the KLH conjugate. The single-stranded conjugate, **7b**, was purified by gel filtration. Polyacrylamide gel electrophoresis of [<sup>32</sup>P] 3'-labeled material, followed by autoradiography,

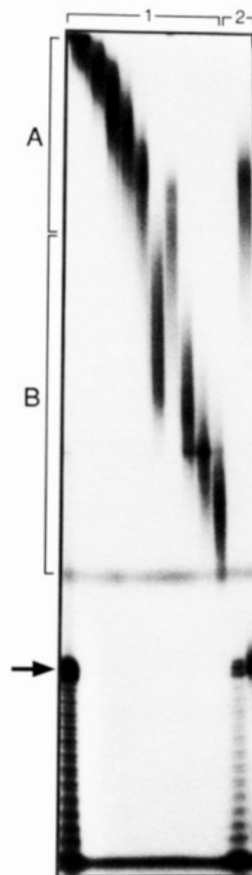


**Figure 1.** Assay of fractions containing single-stranded conjugate **7a** from a Sephacryl S-200 column. Autoradiogram of an 8% polyacrylamide gel, 3'-end labeled with  $^{32}\text{P}$  and terminal deoxytransferase: far right lane, crude compound **6** as used in conjugation reaction (arrow indicates 50-mer); lanes under bracket 1, conjugate **7a**; lanes under bracket 2, mostly unconjugated oligonucleotide. Bands between bottom third and top third are unidentified.

was used to monitor the conjugation reaction and purification (see Figure 2). The fractions which contained higher molecular weight conjugate, region A in Figure 2, were combined as purified **7b**. A ratio of 11 oligonucleotides to one D-EK molecule was determined from the absorbance at 260 nm and amino acid analysis. The conjugate was annealed with a second oligonucleotide consisting of  $(\text{TG})_{25}$  to provide LJP 105, which was used as the antigen in the antibody-forming cell assay.

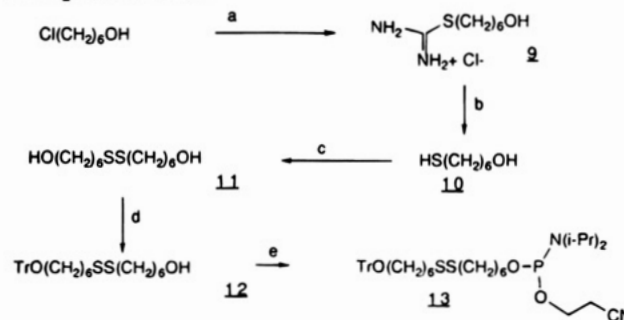
The rationale for choosing to attach four copies of the oligonucleotide to the nonimmunogenic carrier was based on the strategy of cross linking surface antibodies on B cells. While an oligovalent conjugate was desired, the valency was limited by the need to synthesize a discrete, isolatable compound. Since there are possible side reactions in the conjugation step, the more reactive attachment points there are, the more difficult it becomes to achieve a reasonable yield of fully substituted and fully characterizable material. By branching each end of PEG, we were able to attach four copies of oligonucleotides.

PEG was chosen as a molecular platform because it is nonimmunogenic, nontoxic, and water soluble. A diamino-substituted PEG (molecular weight 3350 Da), compound **16**, is commercially available and a convenient starting material for attachment of a branching moiety at both ends of the polymeric chain, via an amide bond. Iodoacetylated 3,5-diaminobenzoic acid was selected as the branching functionality, because its carboxylic acid provided a facile coupling moiety to the terminal amines



**Figure 2.** Assay of fractions containing **7b** from a Sephacryl S-200 column. Autoradiogram of an 8% polyacrylamide gel, 3'-end labeled with  $^{32}\text{P}$  and terminal deoxytransferase: far left lane, crude compound **6** as used in conjugation reaction (arrow indicates 50-mer); lanes under bracket 1, conjugates of decreasing molecular weight from left to right; region A, fractions of **7b** used to prepare LJP 105; region B, less substituted conjugates; left lane under bracket 2, unconjugated oligonucleotide; right lane under bracket 2, irrelevant.

### Scheme 3. Synthesis of Disulfide-Containing Phosphoramidite<sup>a</sup>

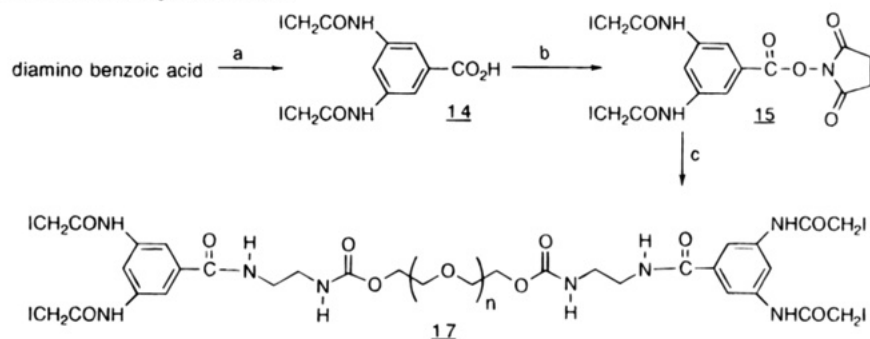


<sup>a</sup> Key: (a) thiourea, EtOH, reflux; (b) NaOH, EtOH, reflux; (c)  $\text{I}_2$ , Et<sub>3</sub>N, MeOH; (d) trityl chloride, pyridine; (e) 2-cyanoethyl *N,N*-diisopropylchlorophosphoramidite, diisopropylethylamine,  $\text{CH}_2\text{Cl}_2$ .

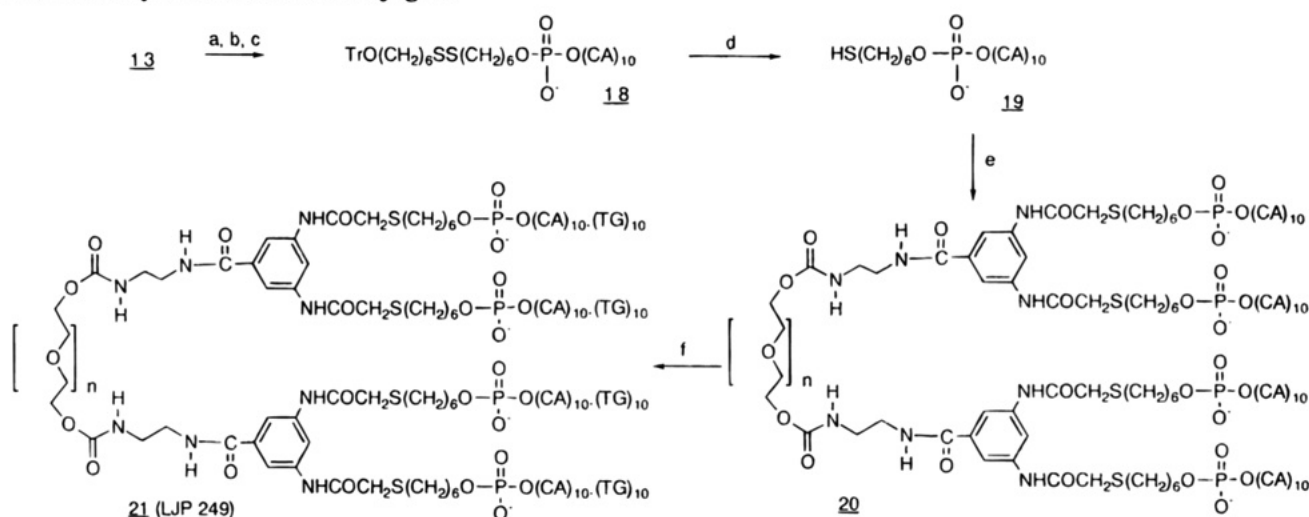
on the PEG and because it is analogous to iodoacetylated 4-aminobenzoic acid (IAB), which has been used to attach sulfhydryl containing molecules to proteins (Weltman et al., 1983).

The synthesis of the PEG conjugate, **21** (LJP 249) (Scheme 5), began with the synthesis of the disulfide-containing phosphoramidite **13**, which is diagrammed in Scheme 3. Reaction of 6-chlorohexan-1-ol with thiourea provided the isothiuronium salt **9**. Alkaline hydrolysis of **9** provided the mercapto alcohol, **10**, which was subsequently converted to the symmetrical disulfide, **11**,



**Scheme 4. Synthesis of Iodoacetylated PEG<sup>a</sup>**

<sup>a</sup> Key: (a) iodoacetic anhydride, dioxane; (b) NHS, DCC, THF; (c)  $\text{H}_2\text{N}(\text{CH}_2)_2\text{NHCO}_2(\text{CH}_2\text{CH}_2\text{O})_n\text{CH}_2\text{CH}_2\text{O}_2\text{CNH}(\text{CH}_2)_2\text{NH}_2$  (compound 16, average  $n$  = approximately 76, synthesized from PEG of average MW 3350),  $\text{NaHCO}_3$ ,  $\text{H}_2\text{O}$ , dioxane, EtOH.

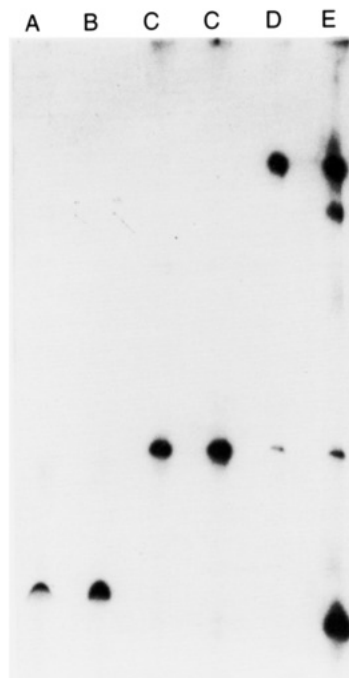
**Scheme 5. Synthesis of PEG Conjugate<sup>a</sup>**

<sup>a</sup> Key: (a)  $(\text{CA})_{10}$ -CPG, tetrazole,  $\text{CH}_3\text{CN}$ ; (b)  $\text{I}_2$ , pyridine,  $\text{H}_2\text{O}$ , THF; (c) concd  $\text{NH}_4\text{OH}$ ; (d) tributylphosphine, pH 5 100 mM sodium acetate; (e) 17, pH 7.8 0.1 M sodium phosphate, 10% MeOH; (f) (TG)<sub>10</sub>.  $n$  = approximately 76 (derived from an average molecular weight of 3350 g/mol for PEG).

by oxidation with methanolic iodine. Treatment of 11 with a limited amount of trityl chloride in pyridine provided a mixture from which the monotritylated compound, 12, was isolated. Phosphitylation of 12 was accomplished using *O*-cyanoethyl *N,N*-diisopropylchlorophosphoramidite and diisopropylethylamine in  $\text{CH}_2\text{Cl}_2$  to provide phosphoramidite 13.

PEG of average molecular weight 3350 g/mol and derivatized with amino containing end groups, 16 (Sigma), was modified to produce a tetraiodoacetylated species, 17, as shown in Scheme 4. Thus, 3,5-diaminobenzoic acid was iodoacetylated with iodoacetic anhydride in dioxane to provide compound 14. Treatment of compound 14 with NHS and DCC provided the *N*-hydroxysuccinimide ester, 15. Acylation of 16 with 15 in the presence of  $\text{NaHCO}_3$  in aqueous dioxane provided compound 17, a tetraiodoacetylated PEG derivative.

The conjugate of four oligonucleotides on a PEG platform was prepared as described in Scheme 5. The disulfide-containing phosphoramidite, 13, was attached to the 5'-end of the oligonucleotide in the last step of an automated synthesis. The usual iodine oxidation step was followed by removal of protecting groups and cleavage from the support with ammonia to provide 18. Compound 18 was reduced to thiol 19 with tributylphosphine, and compound 17 was added to 6 equiv of 19 in pH 7.8 phosphate buffer to provide the single-stranded conjugate 20. Purification was accomplished by ion-exchange chromatography. Polyacrylamide gel electrophoresis of [ $^{32}\text{P}$ ] 3'-labeled material (Cozzarelli et al.,



**Figure 3.** Autoradiogram of an 8% polyacrylamide gel, 3'-end labeled with  $^{32}\text{P}$  and terminal deoxytransferase: lane A, compound 18; lane B, (TG)<sub>10</sub>; lane C, disulfide dimer (formed by oxidative dimerization of 19); lane D, purified conjugate, 20; lane E, crude conjugate.



**Table 1. Reduction in the Serum Antibody Levels of Mice Treated with Compound 21 (LJP 249)**

dose <sup>b</sup> (nmol)	antigen binding capacity (ABC) <sup>a</sup>	
	mean (SD) <sup>c</sup>	reduction (%)
none	5.75 (1.88)	
4.383	2.91 (0.81)	66.8*
1.461	2.29 (0.46)	81.4*
0.487	3.23 (1.77)	59.3
0.162	2.88 (0.83)	67.5*
0.054	3.19 (1.59)	60.2
0.018	4.93 (1.54)	19.3

<sup>a</sup> All sera were tested at three dilutions. The ABC was calculated for each dilution, and the mean ABC was determined.

<sup>b</sup> Dose of **21** (LJP 249) per mouse (average molecular weight calculated to be approximately 57 000 g/mol). <sup>c</sup> The data were analyzed by analysis of variance (ANOVA). The groups that were significantly different from the control group are marked with an \*;  $P = 0.002$ .

**Table 2. Reduction in the Number of Double-Stranded Oligonucleotide Specific, IgG, Antibody-Forming Cells in Mice Treated with Compound 21 (LJP 249)**

dose <sup>b</sup> (nmol)	antibody-forming cells per 10 <sup>6</sup> spleen cells <sup>a</sup>			
	expt 1 <sup>c</sup>		expt 2 <sup>c</sup>	
	mean (SD)	reduction	mean (SD)	reduction (%)
none	6223 (2425)		3616 (305)	
4.383	2873 (657)	53.8*	1395 (332)	61.4*
1.461	2322 (1282)	62.7*	2273 (416)	37.1*
0.487	2566 (237)	58.8*	1558 (743)	56.9*
0.162	4182 (766)	32.8	1910 (599)	47.2*
0.054	5364 (1051)	13.8	3159 (130)	12.8
0.018	4838 (1644)	22.2	2993 (252)	17.2
0.006	6020 (1627)	3.3	4309 (213)	-19.0

<sup>a</sup> The number of ON-specific antibody-forming cells was determined in two separate experiments. <sup>b</sup> Dose of **21** (LJP 249) per mouse (average molecular weight calculated to be approximately 57 000 g/mol). <sup>c</sup> The data were analyzed by analysis of variance (ANOVA). The groups that were significantly different from the control group are marked with an \*. For experiment 1,  $P = 0.0117$ , and for experiment 2,  $P = 0.0001$ .

1969), followed by autoradiography, was used to monitor the conjugation reaction and purification (see Figure 3). Annealing with a second strand of (TG)<sub>10</sub> provided the double-stranded conjugate **21** (LJP 249).

**In vivo Biology.** Mice (C57BL/6) were immunized with KLH conjugate **8a** and 3 weeks later were injected with **21** (LJP 249). A control group was injected with saline after the immunizations. Five days later mice in both groups were boosted with compound **8a**. Seven days later the mice were bled and their sera analyzed for anti-ds-ON antibodies. The results are shown in Table 1. The amount of anti-ds-ON antibodies was significantly reduced in the mice which were treated with **21** (LJP 249), as compared to the saline-treated control group. However, the anti-KLH response was not reduced (data not shown), demonstrating the specificity of the intervention. This experiment was repeated, with the exception that the number of anti-ds-ON antibody forming cells was determined, rather than the serum levels of anti-ds-ON antibodies, to rule out the possibility that **21** (LJP 249) was merely adsorbing the serum antibody. The results, shown in Table 2, show that the treatment of mice, which were immunized with **8a**, with **21** (LJP 249) significantly reduced the number of anti-ds-ON antibody-forming cells in a dose-dependent manner. Thus, these mice were rendered unresponsive (tolerant) to further challenge with an immunogenic form of the oligonucleotide.

## SUMMARY AND CONCLUSIONS

Two methods of attaching oligonucleotides to a common carrier molecule have been developed. One method relies

on a sulfhydryl linker at the 5'-end of an oligonucleotide which reacts with iodoacetylated amino groups on the carrier to form conjugates through a thioether bond. This method was used to prepare a well-defined conjugate of four (CA)<sub>10</sub> oligonucleotides attached to one modified PEG carrier. The other method utilizes a vicinal diol linker which is oxidized to an aldehyde and reacts with amines under reducing conditions to form conjugates through reductive alkylation. This method was used to prepare a conjugate of approximately five (CA)<sub>25</sub> oligonucleotides attached to each molecule of KLH. Both conjugates were annealed with a complementary TG strand to provide double-stranded oligonucleotide conjugates. The double-stranded KLH conjugate was used to immunize mice to elicit antibodies against the synthetic oligonucleotides. The double-stranded PEG toleragen, LJP 249 (compound **21**), was used to suppress the anti-ds-ON response as a model for down regulating anti-DNA antibodies in lupus patients.

## LITERATURE CITED

- Agrawal, S., Christodoulou, C., and Gait, M. J. (1986) Efficient Methods for Attaching Non-radioactive Labels to the 5' Ends of Synthetic Oligodeoxyribonucleotides. *Nucleic Acids Res.* 14, 6227-6245.
- Ansorge, W., Sproat, B., Stegemann, J., Schwager, C., and Zenke, M. (1987) Automated DNA Sequencing: Ultrasensitive Detection of Fluorescent Bands During Electrophoresis. *Nucleic Acids Res.* 15, 4593-4602.
- Asseline, U., Bonfils, E., Kurtürst, R., Chassignol, M., Roig, V., and Thuong, N. T. (1992) Solid-Phase Preparation of 5',3'-Heterobifunctional Oligodeoxyribonucleotides Using Modified Solid Supports. *Tetrahedron* 48, 1233-1254.
- Bernatowicz, M. S., and Matsueda, G. R. (1986) Preparation of Peptide-Protein Immunogens Using N-Succinimidyl Bromoacetate as a Heterobifunctional Crosslinking Reagent. *Anal. Biochem.* 155, 95-102.
- Caruthers, M. H., Brill, W., and Dellinter, D. J. (1987) Phosphoramidites as Synthons for Polynucleotide Synthesis. *Phosphorus Sulfur* 30, 549-553.
- Connolly, B. A. (1985) Chemical Synthesis of Oligonucleotides Containing a Free Sulfhydryl Group and Subsequent Attachment of Thiol Specific Probes. *Nucleic Acids Res.* 13, 4485-4502.
- Conrad, M. J. and Coutts, S. M. (1994) Conjugates of Biologically Stable Polyfunctional Molecules and Polynucleotides for Treating Systemic Lupus Erythematosus. US Patent 5,272,013.
- Cozzarelli, N. R., Kelly, R. E., and Kornberg (1969) Enzymatic Synthesis of DNA. XXXIII: Hydrolysis of a 5'-Triphosphate Terminated Polynucleotide in the Active Center of DNA. *J. Mol. Biol.* 45, 513.
- Fontanel, M. L., Bazin, H., Roget, A., Teoule, R. (1993) Synthesis and Use of 4-Hydroxyphenyl Derivatized Phosphoramidites in the Selective Radioiodination of Oligonucleotide Probes. *J. Labelled Compd. Radiopharm.* 33, 717-724.
- Garvey, J. S., Cremer, N. E., and Sussdorf, D. H. (1977) *Methods in Immunology*, 3rd ed., pp 301-312, W. A. Benjamin, Inc., Reading, MA.
- Gaur, R. K. Introduction of 5' Terminal Amino and Thio Groups into Synthetic Oligonucleotides (1991). *Nucleosides Nucleotides* 10, 895-909.
- Henry, C. (1980) Hemolytic Plaque Assay. *Selected Methods in Cellular Immunology* (B. B. Mishell, S. M. Shiigi, Eds.) Chapter 3, pp 69-123, W. H. Freeman and Co., San Francisco.
- Inman, J. K., Highet, P. F., Kolodny, N., and Robey, F. A. (1991) Synthesis of N<sup>α</sup>-(tert-Butoxycarbonyl)-N<sup>ε</sup>-[N-(bromoacetyl)-β-alanyl]-L-lysine: Its Use in Peptide Synthesis for Placing a Bromoacetyl Cross-Linking Function at Any Desired Sequence Position. *Bioconjugate Chem.* 2, 458-463.
- Iverson, G. M. (1986) Assay for *in vivo* adoptive immune

- response. *Handbook of Experimental Immunology, Volume 2: Cellular Immunology* (D. M. Eir, L. A. Herzenberg, C. Blackwell, L. A. Herzenberg, Eds.) 4th ed., Chapter 67, pp 67.1–67.8, Blackwell Scientific Publications, Oxford.
- Kremsky, J. N., Wooters, J. L., Dougherty, J. P., Meyers, R. E., Collins, M., and Brown, E. L. (1987) Immobilization of DNA via Oligonucleotides Containing an Aldehyde or Carboxylic Acid Group at the 5' Terminus. *Nucleic Acids Res.* 15, 2891–2909.
- Kuijpers, W. H. A., Bos, E. S., Kaspersen, F. M., Veeneman, G. H., and van Boeckel, C. A. A. (1993) Specific Recognition of Antibody–Oligonucleotide Conjugates by Radiolabeled Antisense Nucleotides: A Novel Approach for Two-Step Radioimmunotherapy of Cancer. *Bioconjugate Chem.* 4, 94–102.
- Leonetti, J. P., Rayner, B., Lemaitre, M., Gagnor, C., Milhaud, P. G., Imbach, J.-L., and Lebleu, B. (1988) Antiviral Activity of Conjugates Between Poly (L-lysine) and Synthetic Oligodeoxyribonucleotides. *Gene* 72, 323–332.
- Li, P., Medon, P., Skingle, D. C., Lanser, J. A., and Symons, R. H. (1987) Enzyme-linked Synthetic Oligonucleotide Probes: Non-radioactive Detection of Enterotoxigenic *Escherichia Coli* in Faecal Specimens. *Nucleic Acids Res.* 15, 5275–5287.
- Liu, F.-T., Zinnecker, M., Hamaoka, and Katz, D. H. (1979) New Procedures for Preparation and Isolation of Conjugates of Proteins and a Synthetic Copolymer of D-Amino Acids and Immunochemical Characterization of Such Conjugates. *Biochemistry* 18, 690–697.
- Mitchison, N. A. (1971) The Carrier Effect in the Secondary Response to Hapten-Protein Conjugates. (1) Measurement of the Effect and Objections to the Local Environment Hypothesis. *Eur. J. Immunol.* 1, 10.
- Nielsen, J., Marrug, J. E., Taagaard, M., van Boom, J. H., and Dahl, O. (1986) Polymer-Supported Synthesis of Deoxyoligonucleotides Using in-situ Prepared Deoxynucleoside 2-Cyanoethyl Phosphoramidites. *Recl. Trav. Chim. Pays-Bas* 105, 33–34.
- Nossal, G. J. V., Pike, B. L., and Katz, D. H. (1973) Induction of B Cell Tolerance *in vitro* to 2,4-Dinitrophenyl Coupled to a Copolymer of D-Glutamic Acid and D-Lysine (DNP-D-GL). *J. Exptl. Med.* 138, 312–317.
- Smeenk, R. J. T., Brinkman, K., van den Brink, H. G., and Westgeest, A. A. A. (1988) Reaction Patterns of Monoclonal Antibodies to DNA. *J. Immunol.* 140, 3786–3792.
- Sproat, B. S., Beigher, B., Rider, P., and Neuner, P. (1987) The Synthesis of Protected 5'-Mercapto-2',5'-dideoxyribonucleoside-3'-O-phosphoramidites; Uses of 5'-Mercapto-oligodeoxyribonucleotides. *Nucleic Acids Res.* 15, 4837–4848.
- Thorpe, P. E., Ross, W. C. J., Brown, A. N. F., Myers, C. C., Cumber, A. J., Foxwell, B. M. J., and Forrester, J. T. (1984) Blockade of the Galactose-binding Sites of Ricin by its Linkage to Antibody: Specific Cytotoxic Effects of the Conjugates. *Eur. J. Biochem.* 140, 63–71.
- Weltman, J. K., Johnson, S.-A., Langevin, J., and Riester, E. F. (1983) N-Succinimidyl (4-Iodoacetyl) Aminobenzoate: A New Heterobifunctional Crosslinker. *Bio. Techniques* 1, 148–152.

# Fluorescent Derivatives of Diphenyl [1-(*N*-Peptidylamino)alkyl]phosphonate Esters: Synthesis and Use in the Inhibition and Cellular Localization of Serine Proteases

Ahmed S. Abuelyaman, Dorothy Hudig,<sup>†</sup> Susan L. Woodard,<sup>†</sup> and James C. Powers\*

School of Chemistry and Biochemistry, Georgia Institute of Technology, Atlanta, Georgia 30332-0400, and The School of Medicine and The College of Agriculture, Howard Building, University of Nevada, Reno, Nevada 89557-0046. Received April 5, 1994<sup>§</sup>

Three fluorescein- and one Texas Red-labeled derivatives of [1-(*N*-dipeptidylamino)alkyl]phosphonate diphenyl esters were synthesized and evaluated as inhibitors of serine proteases. The two fluorophores, FITC and TXR, were attached to the peptide phosphonates via an  $\epsilon$ -aminocaproyl unit that acts as a spacer group and facilitates the binding of the phosphonate inhibitor to the targeted enzymes. These derivatives are potent and specific inhibitors of chymotrypsin, porcine pancreatic elastase (PPE), and human leukocyte elastase (HLE). FTC-Aca-Phe-Leu-Phe<sup>P</sup>(OPh)<sub>2</sub> (**3**) inhibited chymotrypsin very potently ( $k_{\text{obsd}}/[\text{I}] = 9500 \text{ M}^{-1} \text{ s}^{-1}$ ) and 600-fold better than it did PPE ( $k_{\text{obsd}}/[\text{I}] = 16 \text{ M}^{-1} \text{ s}^{-1}$ ). FTC-Aca-Ala-Ala-Met<sup>P</sup>(OPh)<sub>2</sub> (**1**) was a more effective inhibitor of chymotrypsin ( $k_{\text{obsd}}/[\text{I}] = 190 \text{ M}^{-1} \text{ s}^{-1}$ ) than PPE and HLE ( $k_{\text{obsd}}/[\text{I}] = 13$  and  $22 \text{ M}^{-1} \text{ s}^{-1}$ , respectively). Only HLE and PPE were inhibited by FTC-Aca-Ala-Ala-Ala<sup>P</sup>(OPh)<sub>2</sub> (**2**) ( $k_{\text{obsd}}/[\text{I}] = 41$  and  $22 \text{ M}^{-1} \text{ s}^{-1}$ , respectively). The specificity of these inhibitors toward the targeted serine proteases depends on the sequence of the tripeptide portion and was not affected by the presence of the fluorescent label. Trypsin, for instance, was not inhibited by any of these compounds. In some cases, the inhibitory potency was increased by the fluorescent label. For example, chymotrypsin was inhibited by the fluorescent compounds, FTC-Aca-Ala-Ala-Met<sup>P</sup>(OPh)<sub>2</sub> (**1**) and FTC-Aca-Phe-Leu-Phe<sup>P</sup>(OPh)<sub>2</sub> (**3**), more potently than by the nonfluorescent compounds, Boc-Ala-Ala-Met<sup>P</sup>(OPh)<sub>2</sub> (**5**) and Z-Phe-Leu-Phe<sup>P</sup>(OPh)<sub>2</sub> (**7**). Initial experiments with cytotoxic lymphocytes indicate that FTC-Aca-Ala-Ala-Met<sup>P</sup>(OPh)<sub>2</sub> labels discrete granule-like regions where the serine proteases of the NK cell line, RNK-16, are stored.

## INTRODUCTION

The lymphocyte serine proteases, which are also known as granzymes, are a group of proteolytic enzymes found in specialized granules of natural killer (NK)<sup>1</sup> cells and cytotoxic T lymphocytes (Tschoep et al., 1988). Studies with synthetic substrates revealed that at least five different substrate specificities are present among these proteases, namely, tryptase (trypsin-like, cleaving after arginine or lysine), Asp-ase (cleaving after aspartic acid), chymase (chymotrypsin-like, cleaving after phenylalanine, tryptophan, or tyrosine), Met-ase (cleaving after methionine), and Ser-ase (cleaving after serine) (Hudig et al., 1991). Upon killing, T and NK lymphocytes release the pore-forming protein, perforin, and several serine proteases which are believed to be essential for lymphocyte-mediated cytotoxicity. It is not clear if all the granzymes are involved in lymphocyte-mediated cytotoxicity, but in-

vestigations with inhibitors showed that the chymotrypsin-like proteases of the lymphocyte granules play an important role in perforin-dependent cytotoxicity (Ewoldt et al., 1992; Hudig et al., 1993). However, despite a considerable amount of research effort, the exact role of the serine proteases in cytotoxicity is unknown. In this paper, we report several fluorescent derivatives which should be useful in elucidating the biological role of granzymes in cytotoxicity.

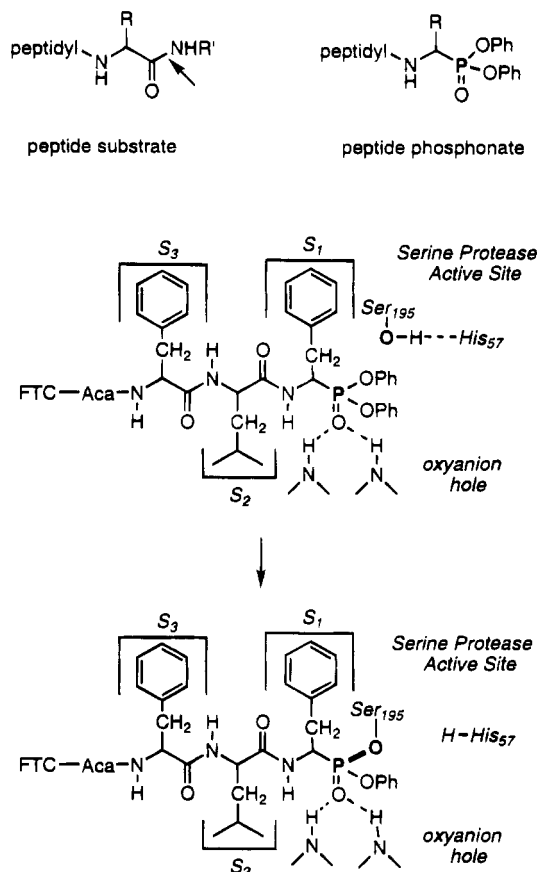
Diphenyl [1-(*N*-peptidylamino)alkyl]phosphonate esters are potent irreversible serine protease inhibitors (Oleksyszyn and Powers, 1991). In these inhibitors, the scissile peptide bond of a substrate is replaced by a diphenyl phosphonate functional group (Figure 1). Peptide phosphonates are highly specific inhibitors since proper interactions with the S<sub>1</sub> pocket of the target serine protease are prerequisites for nucleophilic attack by the active site serine hydroxyl group on the phosphorus atom. This attack gives, via a pentacoordinate intermediate, a very stable phosphoryl derivative (Powers et al., 1993). The selection of the right peptide sequence in these inhibitors produces an important direct effect on the specificity and the rate of their interactions with serine proteases. For example, Z-Phe<sup>P</sup>(OPh)<sub>2</sub> and Suc-Val-Pro-Phe<sup>P</sup>(OPh)<sub>2</sub> inhibited chymotrypsin potently with  $k_{\text{obsd}}/[\text{I}]$  of 1200 and 44 000 M<sup>-1</sup> s<sup>-1</sup>, respectively, but they did not inhibit porcine pancreatic or human leukocyte elastase (designated PPE or HLE, respectively) (Oleksyszyn and Powers, 1991). The unaffected elastases cleave after Val, Leu, or Ile. The inhibitor Boc-Val-Pro-Val<sup>P</sup>(OPh)<sub>2</sub>, on the other hand, inhibited PPE with an inhibition rate of 11 000 M<sup>-1</sup> s<sup>-1</sup> and HLE with 27 000 M<sup>-1</sup> s<sup>-1</sup>, but did not inhibit chymotrypsin. Phosphonate inhibitors also have a number of other advantages. They are unreactive

<sup>†</sup> University of Nevada.

\* To whom correspondence should be addressed.

<sup>§</sup> Abstract published in *Advance ACS Abstracts*, July 1, 1994.

<sup>1</sup> Abbreviations: Ac, acetyl; Aca, 6(or  $\epsilon$ )-aminocaproyl; Boc, *tert*-butoxycarbonyl; DCC, *N,N'*-dicyclohexylcarbodiimide; DCU, dicyclohexylurea; DMF, *N,N*-dimethylformamide; FAB, fast atom bombardment; FITC, 5-fluorescein isothiocyanate; FTC, 5-fluoresceinyl(thiocarbamoyl); Hepes, *N*-(2-hydroxyethyl)piperazine-*N'*-2-ethanesulfonic acid; HLE, human leukocyte elastase; HOBt, 1-hydroxybenzotriazole; Me, methyl; MeO, methoxy; Me<sub>2</sub>SO, dimethyl sulfoxide; NK, natural killer lymphocyte; NMM, *N*-methylmorpholine; Ph, phenyl; pNA, *p*-nitroanilide; PPE, porcine pancreatic elastase; rt, room temperature; Suc, succinyl; T cell, thymus-derived lymphocyte; TEA, triethylamine; TXR, Texas Red, 9-[2(or 4)-(chlorosulfonyl)-4(or 2)sulfophenyl]-2,3,6,7,12,13,16,17-octahydro-1*H*,5*H*,11*H*,15*H*-xantheno[2,3,4-*ij*:5,6,7-*i'**j'*]diquinolizin-18-ium hydroxide, inner salt; TLC, thin layer chromatography; Z, benzyloxycarbonyl.



**Figure 1.** Comparison of the structure of a peptide substrate for a serine protease and a peptidyl phosphonate inhibitor (top) and illustration of the inhibitor-enzyme complex formed with compound **3** (bottom). In the top illustration, the arrow indicates the scissile bond of the substrate. The phosphorus atom in the phosphonate is shown in bold throughout. The tetracovalent bond between the phosphonate and the enzyme active site serine in the enzyme-inhibitor complex is shown in bold. The interactions between the peptide amino acid residues and the enzyme sites S<sub>1</sub>, S<sub>2</sub>, and S<sub>3</sub> are numbered using the nomenclature of Schechter and Berger (Schechter and Berger, 1967).

toward most other nucleophiles, nontoxic to cells, stable under physiological conditions, and form stable phosphonylated enzyme derivatives upon reaction with serine proteases.

Fluorescent derivatives of proteins, synthetic peptides, and inhibitors are important tools for the detection, localization, and quantification of numerous cellular constituents in biological systems. For example, fluorochrome-labeled gene probes are used for the rapid and quantitative detection of homologous RNA at the single cell level (Pachmann et al., 1991). Proteins and antibodies labeled with fluorescein isothiocyanate (FITC) and the sulfonyl chloride of sulforhodamine 101 (commercially designated as Texas Red) have been used to study the distribution of the receptors for IgE and IgG on basophilic leukemia cells (Titus et al., 1982). In many cases, proteins and synthetic peptides did not lose their biological activity after being labeled with FITC and Texas Red (TXR). These two fluorophores have the advantage that the excitation and emission spectra of their conjugates are widely separated from each other, a characteristic that permits them to be detected simultaneously. For example, to determine that T cells have Ig receptors, human peripheral blood leukocytes were treated with unlabeled normal rabbit IgG, washed, and then treated with Texas Red-conjugated goat anti-rabbit IgG antibodies together with FITC-conjugated mouse anti-human T

cell hybridoma 3A1 antibodies. Both fluors were then detected together on individual cells identified as simultaneous, two-color fluorescent events using dual-parameter flow microfluorometry (Titus et al., 1982).

In this paper we report the synthesis of several tripeptide phosphonate inhibitors labeled with FITC or TXR and the kinetics of their inhibition of several serine proteases. The fluorophores were coupled to the peptidyl phosphonates using an  $\epsilon$ -aminocaproyl unit as a spacer group between the peptide and the fluorophore. We expected that the spacer would prevent unfavorable steric interactions between the fluorophore and the active site of the protease. We found that the four new inhibitors with the fluor-spacer-peptide-phosphonate structure are reactive and selective among serine proteases of different specificities. In addition, we report that FTC-Aca-Ala-Ala-Met<sup>P</sup>(OPh)<sub>2</sub> irreversibly labels discrete granule-like regions of the NK cell line, RNK-16. The properties of these fluorophores indicate that these peptide phosphonates will be excellent tools for the study of the distribution of serine proteases in lymphocytes and their role during killing. Use of these inhibitors with different peptide sequences with varying specificities and different fluorophores will allow the simultaneous detection of different proteases in cytotoxic lymphocytes as well as in other biological systems.

## MATERIALS AND METHODS

**Materials.** 5-Fluorescein isothiocyanate (FITC), sulforhodamine 101, 6-aminocaproic acid (Aca), and all common reagents and solvents were purchased from Aldrich Chemical Co., Milwaukee, WI. Porcine pancreatic elastase (PPE) was obtained from United States Biochemical Corp., Cleveland, OH. Human leukocyte elastase (HLE) was obtained from Athens Research and Technology, Inc., Athens, GA. Hepes was obtained from Research Organics, Inc., Cleveland, OH. Bovine trypsin was purchased from Sigma Chemical Co., St. Louis, MO. Preparative thin-layer chromatography was performed with plates precoated with 2 mm of silica gel G.F. and were obtained from EM Separations, Gibbstown, NJ 08027. NMR spectra were recorded on a Varian GEMINI 300. Elemental analyses were performed by the Atlantic Microlabs, Atlanta, GA. Diphenyl [1-(*N*-dipeptidylamino)alkyl]phosphonate esters were synthesized as previously described (Oleksyszyn and Powers, 1991; A. Abuelyaman, D. Jackson, D. Hudig, and J. Powers (unpublished results)). The sulfonyl chloride of sulforhodamine 101 (Texas Red) was prepared as previously described (Titus et al., 1982) and was used without further isolation in coupling reactions.

**6-[5-Fluoresceinyl(thiocarbamoyl)amino]caproic Acid [FTC-Aca-OH].** 5-Fluorescein isothiocyanate (0.20 g, 0.51 mmol) was dissolved in 5 mL of DMF. A solution of methyl 6-aminocaproate (0.15 g, 1.03 mmol) in 1 mL of DMF was added at rt, and the mixture was stirred for 0.5 h. The solvent was removed *in vacuo*. The residue was purified on a silica gel column eluted with CHCl<sub>3</sub>:MeOH (4:1). Fractions with *R<sub>f</sub>* = 0.38 were collected and concentrated to give a dark orange oily residue which was triturated with H<sub>2</sub>O to give FTC-Aca-OME as an orange sheetlike solid: yield 88%; one spot on TLC (*R<sub>f</sub>* = 0.70, CHCl<sub>3</sub>:MeOH:HOAc, 16:3:1); <sup>1</sup>H NMR (DMSO-*d*<sub>6</sub>)  $\delta$  10.38–10.05 (m, 3H), 8.32 (bs, 1H), 8.24 (s, 1H), 7.73 (dd, 1H), 7.16 (dd, 1H), 6.70–6.52 (m, 6H), 3.59 (s, 3H), 3.47 (bs, 2H), 2.32 (t, 2H), 1.65–1.50 (m, 4H), 1.40–1.25 (m, 2H); high-resolution FAB-MS, *m/e* (*M* + *H*) calcd 535.1539, found 535.1560. Anal. Calcd for C<sub>28</sub>H<sub>26</sub>N<sub>2</sub>O<sub>7</sub>S·H<sub>2</sub>O: C, 60.86; H, 5.11; N, 5.07; S, 5.80. Found: C, 60.53; H, 5.11; N, 5.05; S, 5.73.

A solution of 1 N NaOH (3.0 mL) was added to FTC-Aca-OMe followed by a minimum of MeOH to give a clear solution that was stirred at rt for 1 h. Most of the MeOH was removed *in vacuo*, and the aqueous solution was placed in an ice bath. Drops of concentrated HCl were added with stirring until the mixture became just acidic (pH = 3–4). The orange suspension that formed was cooled for 3 additional h. The solid was isolated by vacuum filtration and dried to give FTC-Aca-OH as an orange solid: yield 95%; one spot on TLC ( $R_f$  = 0.51,  $\text{CHCl}_3$ :MeOH:HOAc, 16:3:1);  $^1\text{H}$  NMR (DMSO- $d_6$ )  $\delta$  12.00 (bs, 1H), 10.15 (s, 2H), 9.90 (bs, 1H), 8.30 (s, 1H), 8.15 (bs, 1H), 7.80 (d, 1H), 7.20 (d, 1H), 6.75–6.52 (m, 6H), 3.60–3.40 (bs, 2H), 2.25 (t, 2H), 1.62–1.48 (m, 4H), 1.42–1.27 (m, 2H); MS (FAB $^+$ )  $m/e$  521 ( $M + 1$ ). Anal. Calcd for  $\text{C}_{27}\text{H}_{24}\text{N}_2\text{O}_7\text{S} \cdot 0.5\text{H}_2\text{O}$ : C, 61.24; H, 4.76; N, 5.29; S, 6.05. Found: C, 61.42; H, 4.58; N, 5.14; S, 6.00.

**Diphenyl [1-[[[6-[5-Fluoresceinyl(thiocarbamoyl)amino]caproyl]alanyl]alanyl]amino]-3-(methylthio)propyl]phosphonate [FTC-Aca-Ala-Ala-Met $^P$ -(OPh) $_2$ , 1] (General Procedure).** FTC-Aca-OH (0.13 g, 0.25 mmol) and the hydrochloride of H-Ala-Ala-Met $^P$ -(OPh) $_2$  (0.13 g, 0.25 mmol) were dissolved in 25 mL of DMF followed by addition of 1 equiv of TEA. The solution was stirred in an ice bath for 15 min, and then DCC (0.05 g, 0.25 mmol) was added and the mixture was stirred at 0 °C for 4 h and at rt for 48 h. The solvent was removed *in vacuo*, and the residue was purified on a silica gel column eluted with  $\text{CHCl}_3$ :MeOH (9:1). Fractions containing product were combined and concentrated *in vacuo* to give a yellow oil that was triturated with water to give a bright yellow solid: yield 25%;  $^1\text{H}$  NMR (DMSO- $d_6$ )  $\delta$  10.15 (s, 2H), 9.95–9.82 (bs, 1H), 8.45 (d, 1H), 8.25 (s, 1H), 8.18–7.98 (m, 3H), 7.73 (d, 1H), 7.49–7.35 (m, 4H), 7.30–7.10 (m, 7H), 6.73–6.52 (m, 6H), 4.89–4.67 (m, 1H), 4.42–4.20 (m, 2H), 3.58–3.42 (bs, 2H), 2.72–2.32 (m, 2H), 2.22–1.92 (m and s, 7H), 1.63–1.42 (m, 4H), 1.38–1.10 (m, 8H); MS (FAB $^+$ )  $m/e$  1004 ( $M + \text{Na}$ ). Anal. Calcd for  $\text{C}_{49}\text{H}_{52}\text{N}_5\text{O}_{11}\text{PS}_2 \cdot 1.5\text{H}_2\text{O}$ : C, 58.32; H, 5.49; N, 6.94; S, 6.35. Found: C, 58.43; H, 5.72; N, 6.68; S, 6.01.

**Diphenyl [1-[[[6-[5-Fluoresceinyl(thiocarbamoyl)amino]caproyl]alanyl]alanyl]amino]ethyl]phosphonate [FTC-Aca-Ala-Ala-Ala $^P$ (OPh) $_2$ , 2].** The general procedure for compound 1 was used, starting with H-Ala-Ala-Ala $^P$ (OPh) $_2$ . Crude product was purified on a silica gel preparative TLC plate using  $\text{CHCl}_3$ :MeOH (85:15) as the eluting solvent to give a yellow solid: yield 35%;  $^1\text{H}$  NMR (DMSO- $d_6$ )  $\delta$  10.30–10.05 (bs, 2H), 9.98–9.85 (bs, 1H), 8.55 (t, 1H), 8.25 (s, 1H), 8.18–7.95 (m, 3H), 7.75 (d, 1H), 7.48–7.32 (m, 4H), 7.28–7.08 (m, 7H), 6.75–6.52 (m, 6H), 4.78–4.55 (m, 1H), 4.45–4.18 (m, 2H), 3.58–3.38 (m, 2H), 2.12 (t, 2H), 1.62–1.05 (m, 15H); MS (FAB $^+$ )  $m/e$  921 ( $M$ ). Anal. Calcd for  $\text{C}_{47}\text{H}_{48}\text{N}_5\text{O}_{11}\text{PS}_2$ : C, 60.06; H, 5.37; N, 7.50; S, 3.40. Found: C, 60.04; H, 5.35; N, 7.36; S, 3.39.

**Diphenyl [1-[[[6-[5-Fluoresceinyl(thiocarbamoyl)amino]caproyl]phenylalanyl]leucyl]amino]-2-phenylethyl]phosphonate [FTC-Aca-Phe-Leu-Phe $^P$ -(OPh) $_2$ , 3].** The general procedure for compound 1 was used, starting with H-Phe-Leu-Phe $^P$ (OPh) $_2$ : yield 36%;  $^1\text{H}$  NMR (DMSO- $d_6$ )  $\delta$  10.15 (s, 2H), 9.85 (bs, 1H), 8.87 (d, 1H), 8.77 (d, 1H), 8.25 (s, 1H), 8.10–7.90 (m, 3H), 7.75 (d, 1H), 7.45–7.05 (m, 21H), 6.72–6.52 (m, 6H), 4.92–4.75 (m, 1H), 4.62–4.32 (m and m, 2H), 3.50–2.55 (m, 6H), 2.09–1.92 (m, 2H), 1.60–0.90 (m, 9H), 0.85–0.65 (m, 6H); MS (FAB $^+$ )  $m/e$  389.9 (100%,  $M^+$  – fluoresceinyl-NHCS), 1116 (20%,  $M + 1$ ). Anal. Calcd for  $\text{C}_{62}\text{H}_{62}\text{N}_5\text{O}_{11}\text{PS}_2 \cdot \text{H}_2\text{O}$ : C, 65.66; H, 5.69; N, 6.17; S, 2.82. Found: C, 65.98; H, 5.68; N, 6.21; S, 2.80.

**6-[4(or 2)-[9-[2,3,6,7,12,13,16,17-octahydro-1H,5H,-11H,15H-xantheno[2,3,4- $\bar{i}j$ :5,6,7- $\bar{i}j$ ]diquinoliziny]-18-ium]]-3(or 5)-sulfo-1-phenylsulfonamido]caproic Acid, Hydroxide, Inner Salt [TXR-Aca-OH].** The intermediate TXR-Aca-OMe was synthesized from a freshly prepared dry Texas Red solution in  $\text{CHCl}_3$  (Titus et al., 1982) and 1 equiv of 6-aminocaproic acid methyl ester in the presence of 1 equiv of NMM. After being stirred at 0 °C for 0.5 h and at rt overnight, the mixture was concentrated *in vacuo* to give a dark solid that was purified on a silica gel preparative plate using  $\text{CHCl}_3$ :MeOH:HOAc (16:3:1) to give TXR-Aca-OMe: yield, 67%; one spot on TLC ( $R_f$  = 0.71,  $\text{CHCl}_3$ :MeOH:HOAc, 16:3:1);  $^1\text{H}$  NMR (DMSO- $d_6$ )  $\delta$  8.42 (d, 1H), 7.98–7.85 (m, 2H), 7.35 (d, 1H), 6.52 (s, 2H), 3.60–3.40 (s and m, 11H), 3.05–2.95 (m, 4H), 2.92–2.80 (m, 2H), 2.67–2.55 (m, 4H), 2.27 (t, 2H), 2.11–1.75 (m, 8H), 1.55–1.18 (m, 6H); high-resolution FAB-MS,  $m/e$  ( $M + \text{H}$ ) calcd 734.2570; found 734.2568. Anal. Calcd for  $\text{C}_{38}\text{H}_{43}\text{N}_3\text{O}_8\text{S}_2 \cdot 2.5\text{H}_2\text{O}$ : C, 58.60; H, 6.21; N, 5.39; S, 8.23. Found: C, 58.41; H, 5.83; N, 5.33; S, 8.09.

An excess solution of 1 N NaOH was added to TXR-Aca-OMe followed by a few drops of MeOH. The mixture was stirred at rt for 2 h and then cooled in an ice bath. Concentrated HCl was added carefully until a dark solid completely precipitated. The solid was isolated by vacuum filtration and then purified on a preparative plate to give TXR-Aca-OH: yield, 85%; one spot on TLC ( $R_f$  = 0.55,  $\text{CHCl}_3$ :MeOH:HOAc, 16:3:1);  $^1\text{H}$  NMR (DMSO- $d_6$ )  $\delta$  8.40 (d, 1H), 8.05–7.88 (m, 2H), 7.37 (d, 1H), 6.50 (s, 2H), 3.60–3.40 (m, 8H), 3.05–2.95 (m, 4H), 2.90–2.80 (m, 2H), 2.68–2.58 (m, 4H), 2.10–1.95 (m, 6H), 1.90–1.78 (m, 4H), 1.50–1.15 (m, 6H); high-resolution FAB-MS  $m/e$  ( $M + \text{H}$ ) calcd 720.2435; found 720.2413.

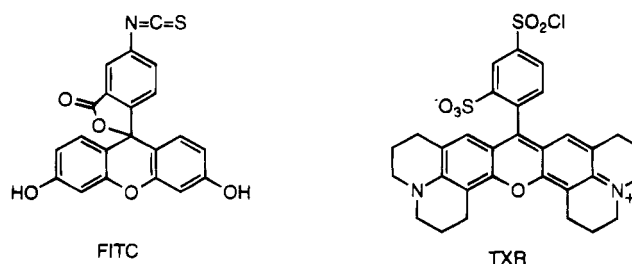
**Diphenyl [1-[[[6-[4(or 2)-[9-[2,3,6,7,12,13,16,17-octahydro-1H,5H,11H,15H-xantheno[2,3,4- $\bar{i}j$ :5,6,7- $\bar{i}j$ ]diquinoliziny]-18-ium]]-3(or 5)-sulfo-1-phenylsulfonamido]caproyl]phenylalanyl]leucyl]amino]-2-phenylethyl]phosphonate, Hydroxide, Inner Salt [TXR-Aca-Phe-Leu-Phe $^P$ (OPh) $_2$ , 4].** This compound was prepared from TXR-Aca-OH (0.084 g, 0.12 mmol) and H-Phe-Leu-Phe $^P$ (OPh) $_2$  hydrochloride (0.084 g, 0.13 mmol) using the DCC/HOBt method in the presence of TEA. The reaction was carried out in  $\text{CHCl}_3$  at 0 °C for 2 h and at rt for 48 h. The crude product was purified on a silica gel preparative TLC plate using  $\text{CHCl}_3$ :MeOH:AcOH (16:3:1) as the eluting solvent. The isolated product was dissolved in 20 mL of  $\text{CHCl}_3$  and extracted twice with 10 mL of 5% aqueous  $\text{NaHCO}_3$  and then with 10 mL of  $\text{H}_2\text{O}$ . The organic layer was dried ( $\text{Na}_2\text{SO}_4$ ) and then concentrated to give a dark purple solid: yield, 25–35%; one spot on TLC,  $R_f$  = 0.79,  $\text{CHCl}_3$ :MeOH:AcOH (16:3:1); NMR spectrum was recorded and was consistent with the proposed structure; high-resolution FAB-MS,  $m/e$  ( $M + \text{H}$ ) calcd 1315.501, found 1315.495. Anal. Calcd for  $\text{C}_{72}\text{H}_{79}\text{N}_6\text{O}_{12}\text{PS}_2 \cdot 2\text{H}_2\text{O}$ : C, 63.98; H, 6.18; N, 6.22; S, 4.74. Found: C, 63.62; H, 6.03; N, 6.39; S, 4.87.

**Enzyme Assays.** The hydrolysis of peptide *p*-nitroanilide substrates, catalyzed by chymotrypsin, PPE, HLE, and trypsin was measured in 0.1 M Hepes and 0.5 M NaCl (0.01 M  $\text{CaCl}_2$  for trypsin), pH 7.5 buffer containing 5–10%  $\text{Me}_2\text{SO}$  at 25 °C. Stock solutions of substrates were prepared in  $\text{Me}_2\text{SO}$  (20 mM) and stored at –20 °C. Final substrate concentrations were 0.24 mM. Chymotrypsin activity was assayed with Suc-Val-Pro-Phe-pNA (Tanaka et al., 1985). PPE was assayed with Suc-Ala-Ala-Ala-pNA (Bieth et al., 1974). HLE was assayed with MeO-Suc-Ala-Ala-Pro-Val-pNA (Nakajima et al., 1979) and trypsin was assayed with Z-Arg-pNA (Kanaoka et al., 1977). The initial rates of hydrolysis

were measured at 410 nm ( $\epsilon_{410} = 8800 \text{ M}^{-1} \text{ cm}^{-1}$  (Erlander et al., 1961)) on a Beckman 35 spectrophotometer after 25–50  $\mu\text{L}$  of an enzyme stock solution was added to a cuvette containing 2.0 mL of buffer and 25  $\mu\text{L}$  of substrate.

**Inhibition Kinetics—Incubation Method.** Each inhibition reaction was initiated by adding a 50- $\mu\text{L}$  aliquot of inhibitor (100–5000  $\mu\text{M}$  in  $\text{Me}_2\text{SO}$ ) to 0.5 mL of a 0.1 M Hepes, 0.5 M NaCl (0.01 M  $\text{CaCl}_2$  for trypsin), pH 7.5 buffer containing 50  $\mu\text{L}$  of a stock enzyme solution at 25  $^\circ\text{C}$ . The enzyme stock solutions were 20  $\mu\text{M}$  chymotrypsin, trypsin, and PPE in 1 mM HCl (pH 3) and 0.4–4  $\mu\text{M}$  HLE in 0.25 M NaAc and 1 M NaCl at pH 5.5. All the enzyme stock solutions were stored at  $-20^\circ\text{C}$  prior to use. Aliquots (25  $\mu\text{L}$ ) were withdrawn at various intervals, and the residual enzymatic activity was measured spectrophotometrically as described above. Pseudo-first-order inactivation rate constants ( $k_{\text{obsd}}$ ) were obtained from plots of  $\ln v/v_0$  vs time and had correlation coefficients greater than 0.98. Each  $k_{\text{obsd}}$  was calculated from 5–10 activity determinations which extended to 2–3 half-lives. Control experiments were carried out in the same way as described above except  $\text{Me}_2\text{SO}$  was added in place of the inhibitor solution in  $\text{Me}_2\text{SO}$ . The initial rates of substrate hydrolysis did not change during the first 60 min of incubation. These initial rates were used as  $v_0$  in the calculation of the inhibition rate constants.

**Cell Labeling and Imaging.** Cells of the NK line RNK-16 (Ward and Reynolds, 1983) were labeled as live cells, washed, treated with methanol as a fixative and permeabilizing agent, and then examined by confocal microscopy. The cells were treated at  $1 \times 10^7$  cells/mL in RPMI 1640 culture media (Sigma Chemical Co., St. Louis, MO) containing 10 mM Hepes with 0.1 mM FTC-Aca-Ala-Ala-Met<sup>P</sup>(OPh)<sub>2</sub> for 30 min at 37  $^\circ\text{C}$ . Control cells were treated with the same volume of DMSO required to deliver the inhibitor (typically 1% final concentration). Cells were then washed several times with phosphate-buffered saline (PBS) to remove excess inhibitor. They were suspended overnight in cold 80% methanol to permeabilize the membrane. The cells were washed free of MeOH into PBS and fixed onto poly-L-lysine (Sigma) coated microscope slides using 3% paraformaldehyde. Fixed slides were washed in PBS, coated with Vectashield (Vector Laboratories, Inc., Burlingame, CA) to prevent fluorescence fading, and topped with a coverslip. Fluorescent laser scanning confocal microscopy was done with a Bio-Rad MRC 600 confocal system utilizing a Zeiss Axiophot microscope and equipped with



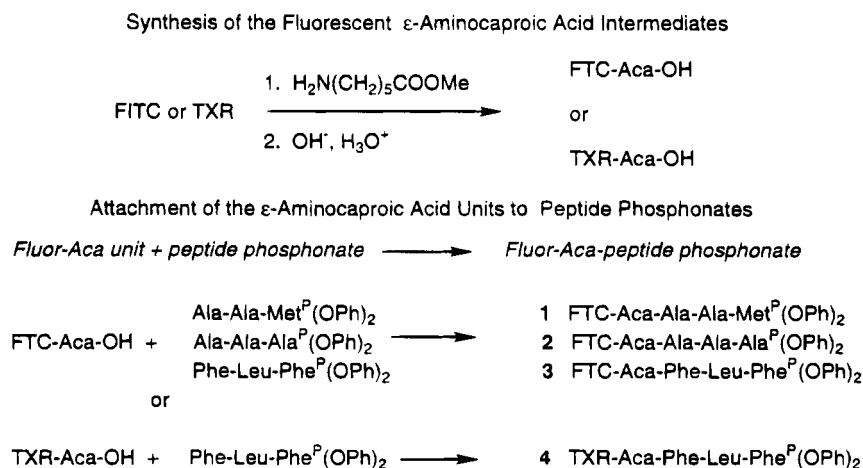
**Figure 2.** Structures of fluorescein isothiocyanate (FITC) and Texas red (TXR).

a mixed-gas argon/krypton ion laser using 488-nm excitation for fluorescein.

## RESULTS AND DISCUSSION

**Synthesis.** Three fluorescein labeled and one Texas Red labeled diphenyl tripeptidylphosphonate esters were synthesized. They were made by joining two synthetic intermediates: a fluorophore- $\epsilon$ -aminocaproic acid unit and a tripeptide phosphonate. The  $\epsilon$ -aminocaproyl acts as a spacer group to facilitate the correct binding of the phosphonate inhibitors to the targeted serine proteases. The fluorophores, FITC and TXR (Figure 2), were incorporated into the  $\epsilon$ -caproyl units as follows. In the case of the FITC derivatives, commercially available fluorescein isothiocyanate, FITC, was coupled to methyl 6-aminocaproate, followed by saponification of the ester group to give FTC-Aca-OH. The TXR derivative, TXR-Aca-OH, was obtained from coupling the sulfonyl chloride functional group in Texas Red with methyl 6-aminocaproate in presence of 1 equiv of TEA. Hydrolysis of the methyl ester resulted in TXR-Aca-OH. The procedure we used in preparing these two intermediates was very efficient and resulted in high yields (70–80%). Both FTC-Aca-OH and TXR-Aca-OH were then coupled to the hydrochloride salts of tripeptidyl phosphonates using the DCC/HOBt method in the presence of TEA (Figure 3). The products were purified on silica gel preparative plates. The final products were characterized by NMR, mass spectroscopy and elemental analysis. The isolated Texas Red derivative compound (4) was initially isolated as a mixture of the zwitterionic form and as an acetate salt mixture, a result that was evident from the NMR and elemental analysis. Pure zwitterionic form was obtained after dissolving the crude product in  $\text{CHCl}_3$  and then extracting with 5% aqueous  $\text{NaHCO}_3$ .

**Kinetic Studies.** The specificity of these phosphonate inhibitors is dependent upon the amino acid sequence in



**Figure 3.** Scheme for the synthesis of FITC and TXR labeled peptidyl phosphonates.



**Table 1. Inhibition of Serine Proteases by Fluorescent Peptide Phosphonates<sup>a</sup>**

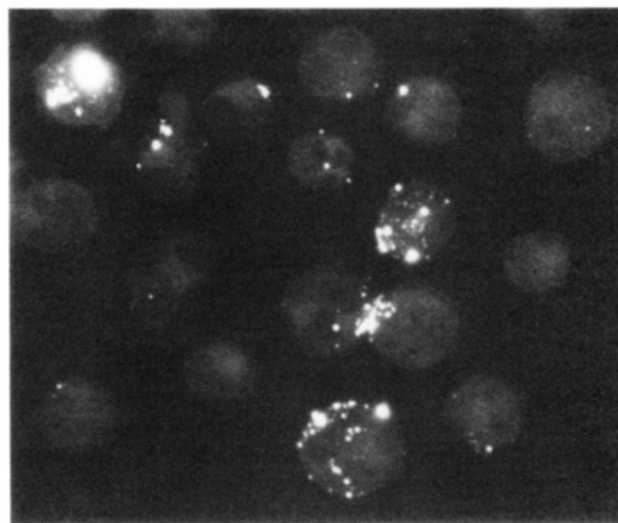
inhibitor	[I] ( $\mu$ M)	$k_{\text{obsd}}/[\text{I}]$ ( $\text{M}^{-1} \text{s}^{-1}$ )		
		chymo- trypsin	PPE	HLE
FTC-Aca-Ala-Ala-Met <sup>P</sup> (OPh) <sub>2</sub> (1)	8.3	190	13	22
FTC-Aca-Ala-Ala-Ala <sup>P</sup> (OPh) <sub>2</sub> (2)	8.3	NI <sup>b</sup>	22	41
FTC-Aca-Phe-Leu-Phe <sup>P</sup> (OPh) <sub>2</sub> (3)	8.3	9500	16	252
TXR-Aca-Phe-Leu-Phe <sup>P</sup> (OPh) <sub>2</sub> (4)	8.3	15	11	96
Boc-Ala-Ala-Met <sup>P</sup> (OPh) <sub>2</sub> (5)	210	3	3	2
Z-Ala-Ala-Ala <sup>P</sup> (OPh) <sub>2</sub> (6)	41.7	NI	30	38
Z-Phe-Leu-Phe <sup>P</sup> (OPh) <sub>2</sub> (7)	10.4	110	NI	27

<sup>a</sup> Inhibition kinetics were measured in 0.1 M Hepes, 0.5 M NaCl, pH 7.5 buffer, 5–10% Me<sub>2</sub>SO and at 25 °C. <sup>b</sup> No inhibition after 40 min of incubation of inhibitor and enzyme. No inhibition was observed with trypsin after 1 h of incubation of the enzyme and the inhibitor in 0.1 M Hepes, 0.01 M CaCl<sub>2</sub>, pH 7.5.

the tripeptide portion of the inhibitor. In each case, the amino acid sequence was chosen based on the specific sequence of a good substrate or inhibitor for the target enzyme. For example, previous studies showed that human Q31 chymase, cathepsin G, and related chymotrypsin-like enzymes have significant hydrolysis activity toward Suc-Phe-Leu-Phe-SBzl and were potently inhibited by the corresponding peptide chloromethyl ketone, Suc-Phe-Leu-Phe-CH<sub>2</sub>Cl (Otake et al., 1991). Likewise, the *p*-nitroanilide substrates Suc-Ala-Ala-Ala-*p*NA and Boc-Ala-Ala-Ala-*p*NA were hydrolyzed effectively by PPE (Bieth et al., 1973, 1974) and peptide chloromethyl ketones such as Ac-Ala-Ala-Ala-Ala-CH<sub>2</sub>Cl are good inhibitors of HLE (Tuhy and Powers, 1975).

The fluorescent compounds were evaluated as inhibitors of chymotrypsin, PPE, and HLE and were found to be potent and very specific with inactivation rate constants ( $k_{\text{obsd}}/[\text{I}]$ ) as high as 9500 M<sup>-1</sup> s<sup>-1</sup> (Table 1). For instance, the Phe derivative, compound 3, inhibited chymotrypsin very potently ( $k_{\text{obsd}}/[\text{I}] = 9,500 \text{ M}^{-1} \text{s}^{-1}$ ) and 600 times faster than it inhibited HLE ( $k_{\text{obsd}}/[\text{I}] = 16 \text{ M}^{-1} \text{s}^{-1}$ ). Chymotrypsin was also inhibited by FTC-Aca-Ala-Ala-Met<sup>P</sup>(OPh)<sub>2</sub> (1) more effectively ( $k_{\text{obsd}}/[\text{I}] = 190 \text{ M}^{-1} \text{s}^{-1}$ ) than HLE and PPE ( $k_{\text{obsd}}/[\text{I}] = 22$  and  $13 \text{ M}^{-1} \text{s}^{-1}$ , respectively). Compound 2, FTC-Aca-Ala-Ala-Ala<sup>P</sup>(OPh)<sub>2</sub>, inhibited PPE and HLE with  $k_{\text{obsd}}/[\text{I}]$  of 22 and 41 M<sup>-1</sup> s<sup>-1</sup>, respectively, but did not inhibit chymotrypsin. As expected, none of these phosphonates inhibited trypsin.

The presence of the fluorescein fluorophore in these inhibitors resulted in either better or the same inhibitory potency compared to their nonfluorescent analogs. For example, with chymotrypsin, the presence of the fluorophores increased the potency of these inhibitors. The fluoresceinylated Phe analog 3 inhibited chymotrypsin very potently with  $k_{\text{obsd}}/[\text{I}]$  of 9500 M<sup>-1</sup> s<sup>-1</sup>, while the nonfluoresceinylated analog, Z-Phe-Leu-Phe<sup>P</sup>(OPh)<sub>2</sub> (7), inhibited chymotrypsin but less potently with  $k_{\text{obsd}}/[\text{I}]$  of 110 M<sup>-1</sup> s<sup>-1</sup> (A. Abuelyaman, D. Jackson, D. Hudig, and J. Powers (unpublished results)). Compound 1, FTC-Aca-Ala-Ala-Met<sup>P</sup>(OPh)<sub>2</sub>, was found to be a better inhibitor of chymotrypsin and HLE,  $k_{\text{obsd}}/[\text{I}] = 190$  and  $22 \text{ M}^{-1} \text{s}^{-1}$  respectively, than Boc-Ala-Ala-Met<sup>P</sup>(OPh)<sub>2</sub> (5),  $k_{\text{obsd}}/[\text{I}] = 3$  and  $2 \text{ M}^{-1} \text{s}^{-1}$ , respectively. In contrast to FTC enhancement of the inhibitory potency of the chymotrypsin-directed inhibitors with chymotrypsin, the presence of FTC did not alter the efficacy of the elastase-directed inhibitor with the two elastases. FTC-Aca-Ala-Ala-Ala<sup>P</sup>(OPh)<sub>2</sub> (2) and its analog Z-Ala-Ala-Ala<sup>P</sup>(OPh)<sub>2</sub> (6) inhibited HLE with almost equal rate constant values,  $k_{\text{obsd}}/[\text{I}] = 38$  and  $41 \text{ M}^{-1} \text{s}^{-1}$ , respectively. Compound 2 also showed similar efficacy with PPE as compound 6,  $k_{\text{obsd}}/[\text{I}] = 22$  and  $30 \text{ M}^{-1} \text{s}^{-1}$ , respectively. Fluorescent

**Figure 4.** RNK-16 cytotoxic lymphocytes labeled with FTC-Aca-Ala-Ala-Met<sup>P</sup>(OPh)<sub>2</sub>.

Met and Phe derivatives 1 and 3 are better inhibitors of PPE ( $k_{\text{obsd}}/[\text{I}] = 13$  and  $16 \text{ M}^{-1} \text{s}^{-1}$ , respectively) compared to their nonfluorescent analogs, compounds 5 ( $k_{\text{obsd}}/[\text{I}] = 3 \text{ M}^{-1} \text{s}^{-1}$ ) and 7 (no inhibition). The fluoresceinylated Ala analog, compound 2, on the other hand, showed almost the same inhibitory effect with PPE as did its nonfluorescent analog, Z-Ala-Ala-Ala<sup>P</sup>(OPh)<sub>2</sub> (6),  $k_{\text{obsd}}/[\text{I}] = 22$  and  $30 \text{ M}^{-1} \text{s}^{-1}$ , respectively.

Addition of the Texas Red fluorophore resulted in a less effective compound in comparison with an analogous compound with the FTC-fluorophore. The TXR-labeled derivative, TXR-Aca-Phe-Leu-Phe<sup>P</sup>(OPh)<sub>2</sub> (4), showed less inhibition with all three enzymes compared to FTC-Aca-Phe-Leu-Phe<sup>P</sup>(OPh)<sub>2</sub> (3). However, when TXR-Aca-Phe-Leu-Phe<sup>P</sup>(OPh)<sub>2</sub> (4) was compared with nonfluorescent Z-Phe-Leu-Phe<sup>P</sup>(OPh)<sub>2</sub> (7), the effects varied with the different enzymes. Inhibition of chymotrypsin was less with TXR-Aca-Phe-Leu-Phe<sup>P</sup>(OPh)<sub>2</sub> (4) while inhibition of HLE and PPE was greater (Table 1).

From the results discussed above, it can be concluded that attaching the fluorophores in these phosphonate inhibitors resulted in either a similar or equal inhibitory potency with HLE and PPE. In the case of chymotrypsin, the presence of the FTC fluorophore increased the potency of these inhibitors substantially, an observation that implies interactions between this fluorophore and chymotrypsin. It is also clear that the specificities of these fluorescent compounds are parallel to those of nonfluorescent analogs and are dependent on the sequences of the peptide portions.

**Cell Labeling.** Fluorescent peptide phosphonates inactivated and labeled intracellular granzymes. They traversed the membranes of living cells and of their granules and irreversibly labeled the cells for subsequent analyses. The inhibitor FTC-Aca-Ala-Ala-Met<sup>P</sup>(OPh)<sub>2</sub> reacted with distinct, granule-like regions of the cytotoxic lymphocytes cell line RNK-16 (Figure 4), similar to granules as observed in living cells by differential interference contrast microscopy (Yannelli et al., 1986). Examination of individual sections through the cells (not illustrated) indicated that these fluorescent regions are interspersed in the cytoplasm. The fluorescent regions had a granule-like morphology similar to that detected by granzyme reactivity with the reversible serine protease inhibitor soybean trypsin inhibitor (Burkhardt et al., 1989). In the latter experiments, the cells were fixed and permeabilized before the macromolecular inhibitor was used. Thus, the fluorescent phosphonate compounds

offer technical advantages over previous approaches. The new reagents also have far greater specificity: soybean trypsin inhibitor inactivated both tryptases and chymases of cytotoxic lymphocytes (Hudig et al., 1987) whereas the FTC-Aca-Ala-Ala-Met<sup>P</sup>(OPh)<sub>2</sub> inactivated RNK-16 chymase and little Asp-ase or tryptase granule protease activities (Woodard et al., unpublished results).

## SUMMARY

The synthesis of four different peptidyl phosphonates labeled with two fluorophores, TXR and FITC, was accomplished from two synthetic intermediates. The intermediates TXR-Aca-OH and FTC-Aca-OH were prepared and then coupled to tripeptidyl phosphonates using the DCC method. The inhibitory potency of these compounds, as serine protease inhibitors, was evaluated using inactivation rate constants ( $k_{\text{obsd}}/[\text{I}]$ ) with the representative enzymes chymotrypsin, PPE, and HLE. These inhibitors were found to be very potent and specific irreversible inhibitors. The most potent inhibitor-enzyme interaction was between FTC-Aca-Phe-Leu-Phe<sup>P</sup>(OPh)<sub>2</sub> (**3**) and chymotrypsin ( $k_{\text{obsd}}/[\text{I}] = 9500 \text{ M}^{-1} \text{ s}^{-1}$ ). Specificity was indicated by the observation that chymotrypsin was inhibited 600 times faster than HLE by this inhibitor (**3**). FTC-Aca-Ala-Ala-Ala<sup>P</sup>(OPh)<sub>2</sub>, on the other hand, inhibited only HLE and PPE and did not inhibit chymotrypsin. None of these compounds inhibited trypsin. It is also noteworthy that the specificity of these inhibitors was unaffected by the presence of the fluorescent tags. Initial experiments with the inhibitor, FTC-Aca-Ala-Ala-Met<sup>P</sup>(OPh)<sub>2</sub>, and rat RNK-16 cytotoxic lymphocytes indicate that granzymes can be labeled within living cells. Thus, these compounds are expected to be excellent reagents for the identification of fully mature cytotoxic lymphocytes within tissues and for the comparison of the granzyme contents of individual cells.

## ACKNOWLEDGMENT

This research was supported by a grant, RO1 GM42212 (to D.H. and J.C.P.), from the National Institutes of Health. We thank the Texaco Corp. for a graduate fellowship awarded to A.S.A. We also thank Dr. Chih-Min Kam for assistance with the kinetic experiments.

## LITERATURE CITED

- Bieth, J., and Wermuth, C. G. (1973) The Action of Elastase on *p*-Nitroanilide Substrates. *Biochem. Biophys. Res. Commun.* **53** (2), 383–390.
- Bieth, J., Siess, B., and Wermuth, C. G. (1974) Synthesis and Analytical Use of a Highly Sensitive and Convenient Substrate of Elastase. *Biochem. Med.* **11**, 350–357.
- Burkhardt, J. K., Hester, S., and Argon, Y. (1989) Two Proteins Targeted to The Same Lytic Granule Compartment Undergo Very Different Posttranslational Processing. *Proc. Natl. Acad. Sci. U.S.A.* **86**, 7128–7132.
- Erlanger, B. F., Kokowsky, N., and Cohen, W. (1961) Preparation and Properties of Two Chromogenic Substrates of Trypsin. *Arch. Biochem. Biophys.* **95**, 271–278.
- Ewoldt, G. R., Winkler, U. W., Powers, J. C., and Hudig, D. (1992) Sulfonyl Fluoride Serine Srotease Inhibitors inactivate RNK-16 Lymphocyte Granule Proteases and Reduce Lysis by Granule Extracts and Perforin. *Mol. Immunol.* **29**, 713–721.
- Hudig, D., Gregg, N. J., Kam, C.-M., and Powers, J. C. (1987) Lymphocyte Granule-Mediated Cytolysis Requires Serine Protease Activity. *Biochem. Biophys. Res. Commun.* **149**, 882–888.
- Hudig, D., Allison, N. J., Pickett, T. M., Winkler, U., Kam, C.-M., and Powers, J. C. (1991) The Function of Lymphocyte Proteases: Inhibition and Restoration of Granule Mediated Lysis with Isocoumarin Serine Protease Inhibitors. *J. Immunol.* **147**, 1360–1368.
- Hudig, D., Ewoldt, G. R., and Woodard, S. L. (1993) Proteases and Lymphocyte Cytotoxic Killing Mechanism. *Curr. Opin. Immunol.* **5**, 90–96.
- Kanaoka, Y., Takahashi, T., Nakayama, H., Takada, K., Kimura, T., and Sakakibara, S. (1977) Synthesis of a Key Fluorogenic Amide, L-Arginine-4-methylcoumaryl-7-amide (L-Arg-MCA) and Its Derivatives. Fluorescence Assays for Trypsin and Papain. *Chem. Pharm. Bull.* **25**, 3126–3128.
- Nakajima, K., Powers, J. C., Ashe, B. M., and Zimmerman, M. (1979) Mapping the Extended Substrate Binding Site of Cathepsin G and Human Leukocyte Elastases. Studies with Peptide Substrates Related to  $\alpha_1$ -Protease Inhibitor Reactive Site. *J. Biol. Chem.* **254**, 4027–4032.
- Odake, S., Kam, C.-M., Narasimhan, L., Poe, M., Blake, J. T., Krahenbuhl, O., Tschopp, J., and Powers, J. C. (1991) Human and Murine Cytotoxic T Lymphocyte Serine Proteases: Subsite Mapping with Peptide Thioester Substrates and Inhibition of Enzyme Activity and Cytolysis by Isocoumarins. *Biochemistry* **30**, 2217–2227.
- Oleksyszyn, J., and Powers, J. C. (1991) Irreversible Inhibition of Serine Proteases by Peptide Derivatives of ( $\alpha$ -Aminoalkyl)-phosphonate Diphenyl Esters. *Biochemistry* **30**, 485–493.
- Pachmann, K., Reinecke, K., Emmerich, B., and Thiel, E. (1991) Highly Fluorochrome Labeled Gene Probes for Quantitative Tracing of RNA in Individual Cells by *in situ* Hybridization. *Bioconjugate Chem.* **2** (1), 19–25.
- Powers, J. C., Odake, S., Oleksyszyn, J., Hori, H., Ueda, T., Boduszek, B., and Kam, C.-M. (1993) Proteases-Structures, Mechanism, and Inhibitors. In: *Proteases, Protease Inhibitors and Protease-Derived Peptides* (J. C. Cheronis, and J. E. Repine, Eds.) pp 3–19, Birkhäuser Verlag, Basel, Boston, Berlin.
- Schechter, I., and Berger, A. (1967) On the Size of the Active Site in Protease. 1 Papain. *Biochem. Biophys. Res. Commun.* **27**, 157–162.
- Tanaka, T., Minematsu, Y., Reilly, C. F., Travis, J., and Powers, J. C. (1985) Human Leukocyte Cathepsin G. Subsite Mapping with 4-Nitroanilide, Chemical Modification and Effect of Possible Cofactors. *Biochemistry* **24**, 2040–2047.
- Titus, J. A., Haugland, R., Sharrow, S. O., and Segal, D. M. (1982) Texas Red, A Hydrophilic, Red-emitting Fluorophore for Use with Fluorescein in Dual Parameter Flow Microfluorometric and Fluorescence Microscopic Studies. *J. Immunol. Methods* **50** (2), 193–204.
- Tschopp, J., and Jongeneel, C. V. (1988) Cytotoxic T Lymphocyte Mediated Cytolysis. *Biochemistry* **27**, 2641–2646.
- Tuhy, P. M., and Powers, J. C. (1975) Inhibition of Human Leukocyte Elastase by Peptide Chloromethyl Ketones. *FEBS Lett.* **50** (3), 359–361.
- Ward, J. M., and Reynolds, C. W. (1983) Large Granular Lymphocyte Leukemia. A Heterogeneous Lymphocytic Leukemia in F344 Rats. *Am. J. Path.* **111**, 1–11.
- Yannelli, J. R., Sullivan, J. A., Mandell, G. L., and Engelhard, V. H. (1986) Reorientation and Fusion of Cytotoxic T Lymphocyte Granules after Interaction With Target Cells as Determined by High Resolution Cinemicrography. *J. Immunol.* **136**, 377–382.

# Complete Inactivation of Target mRNA by Biotinylated Antisense Oligodeoxynucleotide–Avidin Conjugates

Ruben J. Boado\* and William M. Pardridge

Department of Medicine, Brain Research Institute, UCLA School of Medicine, Los Angeles, California 90024.  
Received February 10, 1994<sup>®</sup>

Biotinylation of phosphodiester oligodeoxynucleotides (PO-ODN) allows for conjugation to avidin-based transcellular delivery systems. In addition, biotinylation of PO-ODN at the 3'-terminus provides complete protection against serum 3'-exonuclease degradation. The present study was undertaken to determine if antisense 3'-biotinylated PO-ODN–avidin constructs are able to recognize and inactivate the target mRNA through RNase H-mediated degradation. A 21-mer antisense PO-ODN complementary to the *tat* gene encompassing nucleotides 5402–5422 of the HIV-1 genome was synthesized with biotin conjugated to the 3'-terminus (bio-*tat*). Gel mobility assays using [5'-<sup>32</sup>P]-labeled bio-*tat* ODN and avidin showed that the bio-*tat* ODN was fully monobiotinylated. Aliquots of [<sup>32</sup>P]-labeled sense or antisense *tat* RNA (337 and 351 nucleotides, respectively) were prepared from transcription plasmids and were preincubated with an excess of bio-*tat* ODN with or without avidin constructs and digested with RNase H. Products were resolved with sequencing gel and analyzed by autoradiography. Complete conversion to predicted RNA fragments resulting from RNase H digestion of the RNA–ODN duplex (53 and 263 nucleotides) was observed when [<sup>32</sup>P]-*tat* sense RNA was incubated with antisense bio-*tat* ODN or conjugated to avidin or an avidin-cationized human serum albumin (cHSA) complex. Conversely, no degradation of [<sup>32</sup>P]-*tat*-antisense RNA was observed after incubation with antisense bio-*tat* ODN and RNase H. In addition, the avidin–cHSA complex significantly increased (84-fold) the uptake of [<sup>32</sup>P]-internally labeled bio-*tat* ODN and its stability against cellular nuclease degradation in peripheral blood lymphocytes. In conclusion, biotinylated antisense ODN–avidin constructs induce complete inactivation of target mRNA by RNase H. Therefore, 3'-biotinylated PO-ODNs have the advantages of (a) resistance to serum and cellular 3'-exonuclease, (b) conjugation by avidin-based transcellular delivery systems, and (c) inactivation of target mRNA via RNase H degradation.

## INTRODUCTION

Antisense oligodeoxynucleotides (ODN) are potential therapeutics for the treatment of cancer, viral infections, and other pathological disorders (1–3). A principal mechanism of action by which phosphodiester ODN (PO-ODN) inactivates the target mRNA is through degradation of an antisense ODN–RNA duplex by activation of RNase H, an intracellular enzyme (4, 5). However, the efficacy of antisense ODN *in vivo* is limited by the minimal transcapillary transport or cellular uptake of these highly charged molecules and the rapid degradation by serum nucleases (6, 7), which are mainly comprised of 3'-exonucleases (8, 9). Modification of the ODN backbone, such as with methylphosphonate (MP-ODN) or phosphorothioate (PS-ODN) oligomers provides resistance to nuclease degradation (8, 10, 11). However, MP-ODN–RNA duplexes are unable to activate RNase H (12, 13) and exhibit weaker affinity for RNA (14). PS-ODNs are inhibitors of RNase H activity at PS-ODN concentrations above 100 nM, resulting in protection of the complementary RNA from degradation (5, 15).

The optimal ODN therapeutic may be one in which the ODN is both protected from 3'-exonuclease and is able to activate RNase H without inhibition; in addition, it is desirable to conjugate the ODN to a transcellular delivery system (16, 17). These three goals may be achieved by the use of 3'-biotinylated PO-ODNs coupled to conjugates of avidin and transcellular delivery vectors. The latter are monoclonal antibodies or proteins that undergo

receptor- or absorptive-mediated transcytosis through capillary endothelium and endocytosis into target cells. The use of avidin-based cell delivery systems for ODN therapeutics is optimized by biotinylation of the 3'-terminus of the PO-ODN. Recent studies have shown that 3'-biotinylation affords complete protection from serum 3'-exonuclease (9). Similarly, incorporation of phosphodiester linkages (for example, hexanol or acridine) (18) or phosphopropylamine (19) at the 3'-terminus protects ODNs against serum 3'-exonuclease degradation. However, to date it is not known whether 3'-biotinylated PO-ODN, conjugated to avidin-based vectors, will activate RNase H at high molar ratios of oligomers. This was investigated in the present studies using the *tat* mRNA of human immunodeficiency virus (HIV)-1 as a model target mRNA (20). The cleavage of this mRNA by RNase H was measured in the presence of a 3'-biotinylated 21-mer PO-ODN coupled to a conjugate of avidin and cationized human serum albumin (cHSA). The latter is a modified protein that undergoes absorptive-mediated endocytosis and serves as a transcellular delivery system (21). In addition, the effect of the avidin–cHSA complex on the uptake and stability of 3'-biotinylated ODN was also investigated in human peripheral blood lymphocytes.

## EXPERIMENTAL PROCEDURES

**Materials.** [ $\gamma$ -<sup>32</sup>P]adenosine 5'-triphosphate (ATP) (3000 Ci/mmol) and [ $\alpha$ -<sup>32</sup>P]uridine 5'-triphosphate (UTP) (800 Ci/mmol) were purchased from Dupont-NEN (Boston, MA). T4 polynucleotide kinase, RNasin, and *E. coli* RNase H were obtained from Promega Corp. (Madison, WI). T7 and T3 RNA polymerase and the plasmid Bluescript M13+ were obtained from Stratagene (San

\* Author to whom correspondence should be addressed.  
Phone: (310) 825-8858. Fax: (310) 206-5163.

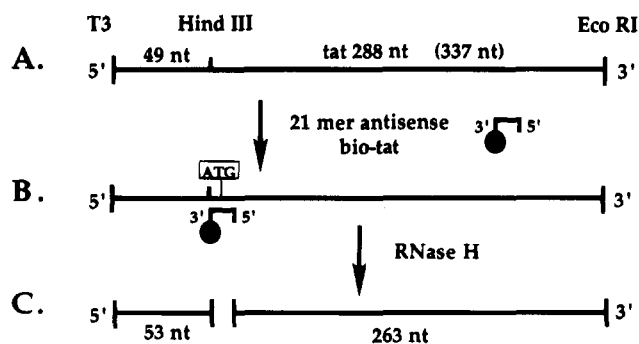
<sup>®</sup> Abstract published in *Advance ACS Abstracts*, July 1, 1994.

Diego, CA). Restriction endonucleases EcoRI and HindIII were obtained from United States Biochemical (Cleveland, OH). Sephadex G-25 spin columns and RNase free/DNase I were purchased from Broehringer Mannheim (Indianapolis, IN). Competent *E. coli* DH5 $\alpha$  cells and low molecular size RNA ladders were obtained from BRL Life Technology (Bethesda, MD). Low melting point agarose NUSIEVE-GTG was obtained from FMC Bioproducts (Rocklin, ME). Acrylamide, *N,N'*-methylenebisacrylamide, urea, and ammonium persulfate were purchased from Stewarts/Mann Biotech. (Cleveland, OH). Avidin and all other reagents were obtained from Sigma Chemical Co. (St. Louis, MO). The plasmid pUC18 containing the HIV-1 *tat* designer gene in *E. coli* DH5 $\alpha$  (catalog no. 827) was obtained from the AIDS Research and Reference Reagent Program, NIAID (Rockville, MD). Customized oligodeoxynucleotides were obtained from Genesis Biotechnologies, Inc. (The Woodlands, TX).

**Biotinylated Oligodeoxynucleotides.** A 21-mer antisense PO-ODN complementary to the *tat* gene and nucleotides 5402–5422 of the HIV-1 genome (20) was synthesized with a 3'-amino modifier CPG [[1-dimethoxytrityl]oxy]-3-[(fluorenylmethoxycarbonyl)amino]propan-2-succinoyl]-long chain alkylamino-CPG (Glen Research, Hendron, VA) and was biotinylated with *N*-hydroxysuccinimide ester-XX (X = 6-aminohexanoyl) of biotin (Glen Research) by the manufacturer as previously described (9). This yielded the following oligodeoxynucleotide: 5'-TACTGGCTCCATTCTTGCTC-biotin-3' (bio-*tat* ODN). The size of this oligodeoxynucleotide was determined by the manufacturer by comparing migration distances with that of the parallel oligodeoxynucleotide standard using a 20% polyacrylamide/7 M urea gel electrophoresis. The 3'-biotinylated oligodeoxynucleotide was purified by high-pressure liquid chromatography using a 5- $\mu$ m C18 reversed phase column (9). In addition, the bio-*tat* ODN 5'-GACTGGTTC-CATGGCAGGTAA-biotin-3' complementary to nucleotides 5–25 of the HIV-1 *tat* designer gene was also synthesized as described above.

**Preparation of [<sup>32</sup>P]-Labeled Oligodeoxynucleotide and Gel-Shift Mobility Assay.** In order to determine if the bio-*tat* ODN was fully biotinylated, gel-shift mobility assays were performed with 5'-[<sup>32</sup>P]-3'-bio-*tat* ODN and avidin. Aliquots of 15 pmol bio-*tat* ODN were labeled at the 5'-end with 50  $\mu$ Ci of [ $\gamma$ -<sup>32</sup>P]ATP and T4 polynucleotide kinase as previously described (9), to a specific activity = 1.25  $\mu$ Ci/pmol. For the [<sup>32</sup>P]ODN mobility assays, 14.5 fmol (= 40 000 dpm) of 5'-[<sup>32</sup>P]bio-*tat* ODN was incubated with an excess of avidin (25 pmol) in a total volume of 12  $\mu$ L of PBS (PBS = 10 mM Na<sub>2</sub>HPO<sub>4</sub>, pH 7.5/150 mM NaCl) containing 0.8 mg/mL of tRNA for 10 min at room temperature. Following the addition of glycerol to a final concentration of 5%, samples were resolved in a 4% nondenaturing polyacrylamide gel electrophoresis (PAGE) for 2 h at 400 V. Autoradiograms were performed overnight at room temperature with Kodak-XOMat AR film. In order to disrupt any possible secondary structure of the bio-*tat* ODN, the 5'-[<sup>32</sup>P]bio-*tat* ODN was incubated for 2 min at 98 °C followed by 2 min on ice immediately before the experiment.

**Synthesis of Sense and Antisense [<sup>32</sup>P]-*tat*-RNA.** To synthesize [<sup>32</sup>P]-labeled *tat* sense or antisense mRNA, a DNA fragment corresponding to the entire *tat* open reading frame was subcloned in the plasmid bluescript using standard cloning techniques described elsewhere (22). Briefly, the 288 base pair (bp) *tat* cDNA was released from the HIV-1 *tat* designer gene pUC18 plasmid by double digestion with EcoRI and HindIII. The



**Figure 1.** Strategy for RNase H assays. (A) *tat* sense RNA (337 nt) is comprised of 288 nucleotides corresponding to the HindIII/EcoRI *tat* cDNA fragment and 49 nucleotides of the plasmid multiple cloning site. T3 denotes the T3 RNA polymerase promoter region. (B) The 21-mer antisense 3'-biotinylated *tat* ODN (bio-*tat*) is complementary to nucleotides 54–74 of the synthetic *tat* sense RNA. (C) Following annealing of *tat* sense RNA with bio-*tat* ODN, RNase H treatment will produce two RNA fragments of 53 and 263 nucleotides, respectively.

DNA fragment was isolated by 2% low melting point agarose gel electrophoresis, phenol/chloroform extraction, and ethanol precipitation as previously described (22). Ligation into EcoRI/HindIII-digested Bluescript was performed overnight at 15 °C in a total volume of 10  $\mu$ L of ligation buffer (50 mM Tris pH 7.6, 10 mM magnesium chloride, 5 mM DTT, 0.1 mM spermidine, 0.1 mM EDTA, 1 mM ATP) containing 2 units of T4 ligase. Following transformation of *E. coli* DH5 $\alpha$  cells with the newly synthesized plasmid, the plasmid DNA was isolated by the alkaline method (23) and characterized by restriction mapping. For the synthesis of [<sup>32</sup>P]-labeled sense and antisense RNA, the plasmid was linearized with EcoRI and HindIII and RNA was synthesized with T3 and T7 RNA polymerase, respectively. The labeling reaction was performed in a 25- $\mu$ L volume containing 40 mM Tris (pH = 8), 8 mM magnesium chloride, 2 mM spermidine, 50 mM sodium chloride, 0.4 mM of each ATP, CTP, and GTP, 40  $\mu$ M UTP, 50  $\mu$ Ci [ $\alpha$ -<sup>32</sup>P]UTP, 30 mM DTT, 40 units of RNasin, and 25 units of T3 or T7 RNA polymerase for 30 min at 37 °C. The reaction was stopped by the addition of 10 units of RNase free/DNase I and incubation for 15 min at 37 °C. [<sup>32</sup>P]-RNA was purified by electrophoresis on a 5% denaturing PAGE/7 M urea gel and recovered by passive elution for 5 h at room temperature as previously described (9). The percentage of incorporation was determined by absorption to DE-81 filters (Whatman International, Ltd., Mainstone, England) as reported previously (9). The specific activity of the [<sup>32</sup>P]-labeled RNA, calculated as the amount of radioactivity used ( $\mu$ Ci)  $\times$  number of UTP residues (71 and 88 for sense and antisense, respectively)/mass of UTP in the reaction (pmol), was 3.6 and 4.4  $\mu$ Ci/pmol for the sense and antisense RNA, respectively.

**RNase H Assays.** The strategy for RNase H assays is summarized in Figure 1. The synthetic sense mRNA contains 337 nucleotides (nt) with 288 *tat* RNA nt and 49 nt of the multiple cloning site of the vector. The 21-mer *tat* antisense ODN hybridizes to nucleotides 54–74 of the entire synthetic mRNA, which corresponds to nucleotides 5–25 of the actual *tat* mRNA. The synthetic antisense mRNA contains 351 nt with 288 *tat* RNA nt and 63 nt of the multiple cloning region. Aliquots (4.5 fmol, approximately 40 000 cpm) of [<sup>32</sup>P]-labeled sense or antisense *tat* RNA were preincubated with or without an excess of bio-*tat* ODN (30 pmol) for 2 min at 65 °C followed by 5 min at room temperature in a total volume of 7.3  $\mu$ L containing 100 mM potassium chloride/0.1 mM EDTA/20 units of RNasin. Following hybridization, 2



units of RNase H were added in 40  $\mu$ L of 50 mM Tris pH 7.5/80 mM potassium chloride/12.5 mM magnesium chloride/1.25 mM DTT/625  $\mu$ g/mL BSA, and incubated for 30 min at 37 °C. The reaction was stopped by incubation for 5 min at 95 °C and 2 min on ice. Following extraction with phenol:chloroform (1:1) (22), samples were precipitated with ethanol (22) and resolved in a sequencing gel (5% polyacrylamide/7 M urea). Autoradiograms were performed as described previously (9). For the avidin-construct experiments, bio-*tat* ODN was preincubated with 15 pmol of avidin or avidin-cHSA for 5 min at room temperature prior to hybridization with [ $^{32}$ P]-labeled RNA. Avidin was conjugated to cHSA with a thiol-ether linkage as previously described (21), and the number of sites available for biotin binding was determined to be 2.8 per avidin-cHSA conjugate (21). The unmodified avidin tetramer has four biotin binding sites (24).

**Stability and Uptake of Bio-*tat*-ODN in Cells in Vitro.** In order to determine if avidin-cHSA increases uptake and protects 3'-biotinylated PO-ODNs against 3'-exonuclease in cultured cells, 3'-bio-*tat* and non-bio-*tat* PO-ODNs that were  $^{32}$ P-labeled were incubated overnight in primary cultures of human peripheral blood lymphocytes (PBLs) in the presence or absence of avidin-cHSA. However, 5'-[ $^{32}$ P]-labeling of the PO-ODN may lead to removal of the  $^{32}$ P by cell phosphatases. Therefore, internally [ $^{32}$ P]-labeled bio-*tat* ODN was prepared (19). The 21-mer bio-*tat* ODN was labeled with [ $^{32}$ P] at the 5' end with T4 polynucleotide kinase as described above. This 5'-[ $^{32}$ P]-bio-*tat* ODN and a second antisense 15-mer PO-ODN complementary to nucleotides 5422–5437 of the *tat* gene (5'-CTCTAGGCTAGGATC-3', DNA International Inc., Lake Oswego, OR) were hybridized to a third 36-mer synthetic single stranded template PO-ODN corresponding to the sense nucleotide sequence of both 15-mer and 21-mer 3'-bio-*tat*, for 2 min at 95 °C and 5 min at room temperature. The 36-mer template was synthesized by Keystone Labs (Menlo Park, CA) with the following nucleotide sequence: 5'-TTACCTGCCATGGAACAGTCGATCCTAGCCTAGAG-3'. Following ligation with 2 units of T4 ligase overnight at 15 °C, single-stranded internally labeled bio-*tat* ODN was isolated from the template by a 12% sequencing/7 M urea gel and passive elution as described above.

Aliquots of the [ $^{32}$ P]<sub>21</sub>bio-*tat* ODN (0.50  $\mu$ Ci) with and without avidin-cHSA (2.6  $\mu$ g) were incubated with  $2 \times 10^6$  peripheral blood lymphocytes in 125  $\mu$ L of RPMI for 24 h at 37 °C. Media was removed by centrifugation, and cells were washed once in cold PBS buffer (10 mM phosphate, pH = 7.4/0.15 M NaCl) and lysed in 200  $\mu$ L of 10 mM Hepes, pH 7.4/3 mM magnesium chloride/5% glycerol/1% NP40. Aliquots of media and cell lysates were collected for trichloroacetic acid (TCA) precipitation and determination of cellular uptake. The percent of medium [ $^{32}$ P] CPM taken up per  $10^7$  cells was calculated, and this "total uptake" value was multiplied by the percent TCA-precipitable cell radioactivity to give the "corrected uptake" per  $10^7$  PBLs.

[ $^{32}$ P]-labeled ODNs present in the cells at the end of the incubation were analyzed by urea/PAGE. The final cell lysates were heated for 5 min at 95 °C and cooled 2 min on ice, nucleic acids were precipitated with ethanol, and samples were resolved in a 12% sequencing/7 M urea gel, as described previously (9). For comparison, parallel experiments were also performed with the [ $^{32}$ P]-labeled nonbiotinylated 36-mer template. Autoradiograms were performed using a PhosphorImager (Molecular Dynamics, Sunnyvale, CA) for 4 days at room temperature. Area



**Figure 2.** Shift mobility assay of [ $^{32}$ P]bio-*tat* ODN. The bio-*tat* ODN was labeled at the 5'-end with [ $\gamma$ - $^{32}$ P]ATP and T4 polynucleotide kinase, and incubated in the presence or absence of avidin for 10 minutes at room temperature. Samples were resolved in a 4% non-denaturing PAGE gel for 2 h at 400 V. Autoradiogram was performed overnight at room temperature.

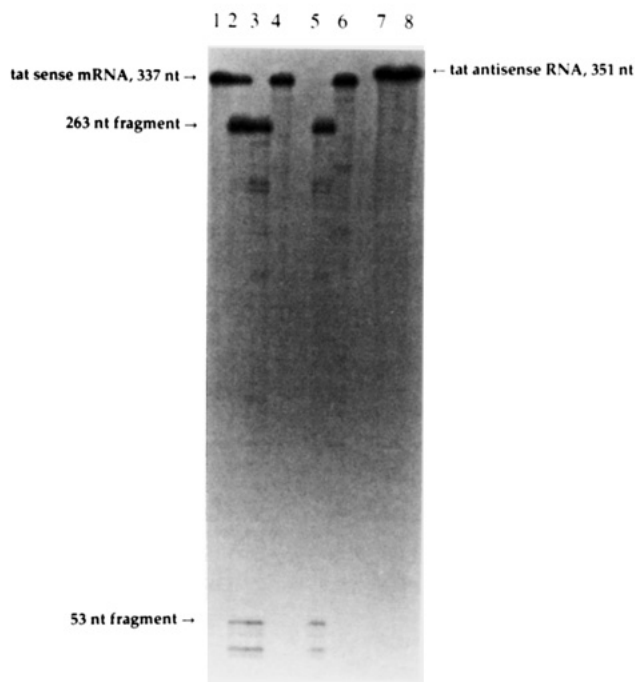
and integrated density were obtained using the NIH Image 1.45 program.

## RESULTS

**Gel Shift Mobility Assays.** To determine whether the bio-*tat* ODN was fully biotinylated, labeled bio-*tat* ODN-shift mobility assay was performed with avidin and the result from a representative autoradiogram is depicted in Figure 2. Incubation with avidin induced a complete shift in the mobility of the 5'-[ $^{32}$ P] 3'-bio-*tat* ODN. Similar results were obtained with the 3'-bio ODN to the HIV-*tat* designer gene (data not shown). On the other hand, parallel experiments performed with a non-biotinylated ODN showed no shift in the mobility of [ $^{32}$ P]-ODN in the presence of avidin (data not shown).

**RNase H Assays.** RNase H induced no degradation of either [ $^{32}$ P]-*tat* sense RNA incubated without bio-*tat* ODN (lane 1, Figure 3), or [ $^{32}$ P]-*tat* antisense RNA incubated with or without the bio-*tat* ODN (lanes 7 and 8, Figure 3). Bio-*tat* ODN converted the labeled *tat* sense RNA to the predicted RNA fragments (Figure 1) after RNase H digestion of the RNA-ODN duplex (lane 2, Figure 3). Similarly, complete formation of the 263 and 53 nt *tat* RNA fragments was observed in samples incubated with both avidin (lane 3, Figure 3) and avidin-cHSA conjugate (lane 5, Figure 3). In addition, no degradation of [ $^{32}$ P]-*tat* sense RNA was seen by incubation with avidin (lane 4, Figure 3) or cHSA-avidin (lane 6, Figure 3), without bio-*tat* ODN. The formation of two intermediate additional bands of RNA was observed in samples incubated with bio-*tat* ODN-avidin complexes (Figure 3, lanes 3 and 5). The 51 nt fragment observed following incubation of bio-*tat* ODN with [ $^{32}$ P]-sense *tat* RNA was probably due to the presence of a -2 nt [ $^{32}$ P]-target RNA.

**Stability and Uptake of ODN in PBL.** To determine the effect of the avidin-cHSA complex on the uptake and stability of 3'-bio-*tat* ODN in primary cultures of PBL cells, both the internally labeled [ $^{32}$ P]<sub>21</sub>-3'-bio-*tat* PO-ODN and a nonbiotinylated [ $^{32}$ P]ODN were incubated with and without avidin-cHSA in PBL cells for 24 h. The avidin-cHSA complex significantly increased (~6-fold) the cellular uptake of [ $^{32}$ P]bio-*tat* ODN compared to the



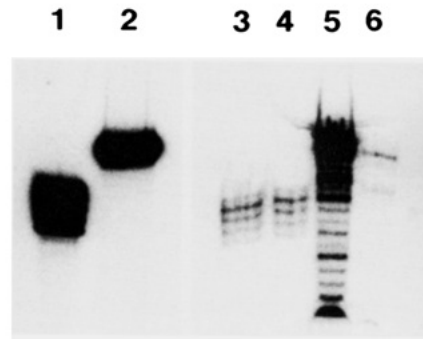
**Figure 3.** Effect of avidin and avidin-chSA on RNase H cleavage of *tat* sense or antisense mRNA. [ $^{32}$ P]-sense (lanes 1–6) and antisense (lanes 7 and 8) *tat* RNA were incubated with or without antisense 3'-biotinylated-*tat* PO-ODN (21-mer anti-bio-*tat*), avidin, or chSA-avidin conjugate. Following treatment with RNase H, RNA was extracted with phenol/chloroform, ethanol precipitated, and resolved in a 5% polyacrylamide/7 M urea gel; lane 1, sense RNA; lane 2, sense RNA + anti-bio-*tat* ODN; lane 3, sense RNA + anti-bio-*tat* ODN + avidin; lane 4, sense RNA + avidin; lane 5, sense RNA + anti-bio-*tat* ODN + avidin-chSA; lane 6, sense RNA + avidin-chSA; lane 7, antisense RNA control; lane 8, antisense RNA + anti-bio-*tat* ODN. Autoradiogram was performed overnight at room temperature. The predicted RNA fragments resulting from RNase H digestion of RNA-ODN duplex (Figure 1) are depicted on the left- and right-hand sides. The size of the RNA fragment was estimated by comparing fragment mobility to the migration of an RNA size ladder (530, 400, 280, and 160 nucleotides), as well as the migration of xylene cyanol and bromophenol blue dyes, which migrate as 132 and 27 nucleotides, respectively, in a 5% sequencing gel (22).

**Table 1.** Effect of Avidin-chSA on PBL Uptake of [ $^{32}$ P]ODNs<sup>a</sup>

ODN	avidin-chSA	cellular % TCA	% total uptake per 10 <sup>7</sup> cells	% corrected uptake per 10 <sup>7</sup> cells
[ $^{32}$ P]ODN <sub>36</sub>	–	17.7 ± 1.2	6.24 ± 0.16	1.10 ± 0.08
[ $^{32}$ P]ODN <sub>36</sub>	+	19.1 ± 0.8	7.36 ± 0.64	1.41 ± 0.14
[ $^{32}$ P]bio-ODN <sub>36</sub>	–	17.7 ± 0.8	7.20 ± 0.48	1.27 ± 0.10
[ $^{32}$ P]bio-ODN <sub>36</sub>	+	34.0 ± 1.5 <sup>b</sup>	18.32 ± 0.96 <sup>b</sup>	6.22 ± 0.43 <sup>b</sup>

<sup>a</sup> Mean ± SE ( $n = 4$ ). Corrected uptake = [(% cell TCA)(% total uptake)]/100. <sup>b</sup> Analysis of variance, Scheffe's test,  $p < 0.001$ .

bio-*tat* ODN alone measured as trichloroacetic precipitable material (Table 1). On the contrary, the avidin vector induced no changes in the uptake of [ $^{32}$ P]-non-biotinylated ODN, and the cell uptake values were comparable to the low percentage of uptake of [ $^{32}$ P]bio-*tat* ODN without vector. Autoradiograms of sequencing gels showed no ethanol-precipitable degradation products in the medium at the end of the incubation (data not shown). The ethanol-precipitable cell associated [ $^{32}$ P]-labeled ODNs were examined; as shown in Figure 4, the size of labeled ODNs in these samples was identical to the respective [ $^{32}$ P]-labeled control. Although degradation products were observed in cell lysates of samples incubated with [ $^{32}$ P]bio-*tat* ODN/avidin-chSA (Figure 4, lane 5), the integrated density obtained for the intact 36-



**Figure 4.** Effect of avidin-chSA on the cellular uptake and stability of [ $^{32}$ P]-labeled bio-*tat* and nonbiotinylated *tat* ODN in peripheral blood lymphocytes (PBL). [ $^{32}$ P]-labeled ODNs were incubated with PBL cells for 24 h, media were removed by centrifugation and washing, and cell extract was resolved in 12% sequencing/7 M urea gel. Autoradiogram obtained using a PhosphorImager is shown: lane 1, 5'-[ $^{32}$ P] 36-mer nonbiotinylated ODN control (this ODN was slightly contaminated with up to ~4 nucleotide fragments); lane 2, [ $^{32}$ P]<sub>21</sub>-internally labeled 36-mer 3'-bio-*tat* ODN standard; lane 3, cell extract of 5'-[ $^{32}$ P]-non-bio 36-mer plus avidin-chSA; lane 4, cell extract of 5'-[ $^{32}$ P]-non-bio 36-mer alone; lane 5, cell extract of [ $^{32}$ P]<sub>21</sub>bio-*tat* ODN plus avidin-chSA; lane 6, cell extract of [ $^{32}$ P]<sub>21</sub>bio-*tat* ODN alone. There was a consistent slightly slower migration of labeled products through the gel in samples obtained from cell extracts.

mer was 84.5-fold greater in the bio-*tat* ODN/avidin-chSA complex compared to the bio-*tat* ODN alone (arbitrary densitometric units: 1.69 versus 0.02, respectively). The amounts of [ $^{32}$ P]-labeled ODN in lanes 3, 4, and 6 of Figure 4 are identical and may represent [ $^{32}$ P]-labeled ODN derived from medium contamination of the washed cellular lysate.

## DISCUSSION

The present investigation, using the HIV-*tat* gene as a target model, demonstrates that the complexes of PO-ODN biotinylated at the 3'-terminus and avidin (avidin alone or avidin-chSA) are able to recognize and completely inactivate the target mRNA through RNase H-mediated activation. In addition, these complexes of bio-*tat* ODN and avidin appear to be more effective in regard to inducing RNase H-mediated digestion of the labeled *tat* mRNA, as compared to the bio-*tat* ODN alone, which induced incomplete RNase H-degradation of *tat* mRNA (Figure 3). It is possible that avidin samples were contaminated with other ribonucleases (i.e., RNase A). However, the reaction tubes contained 20 units of the ribonuclease inhibitor RNasin, and incubation with either avidin or avidin-chSA without bio-*tat* ODN induced no degradation of *tat* mRNA (Figure 3). Therefore, avidin may induce conformational changes in the target RNA, possibly due to the cationic nature of avidin (24), that makes the RNA molecule more susceptible to RNase H activation. This is supported by the formation of 2 additional RNA bands exclusively in samples incubated with bio-*tat*-ODN-avidin complexes (Figure 3, lanes 3 and 5).

PS-ODN may inhibit mRNA expression and increase its degradation at low concentrations through a sequence-specific mechanism (15). However, when PS-ODN are used in excess molar concentrations relative to the target RNA, these molecules inhibit RNase H activation, protecting the complementary RNA from degradation (15, 25). In the present study, a 6000-fold molar excess of PO-ODN-avidin vector conjugates over target RNA was employed in order to ensure full inactivation of the *tat* mRNA, resulting in complete inactivation of complemen-



tary RNA. Interestingly, neither inactivation of RNase H nor recognition of nonspecific nucleotide sequence was observed. For example, incubation of [ $^{32}$ P]-antisense *tat* RNA with severalfold excess of bio-*tat* ODN induced no RNase H-mediated degradation of RNA (Figure 3, lane 8).

The avidin-cHSA complex markedly increased the cellular uptake of [ $^{32}$ P]-bio-*tat* ODN, and this effect was specific for the biotinylated oligomer (Table 1 and Figure 4). On the basis of the TCA assay (Table 1), the avidin-cHSA vector increased cell uptake 6-fold, and based on the autoradiography (Figure 4), the vector increased cell uptake 84.5-fold. However, the actual increase in cell uptake caused by the avidin-cHSA vector may have been greater since the amount of ODN associated with the cell extract in the absence of the vector was very low (Table 1, Figure 4) and may represent medium contamination of the cell extract. Even though the great majority of the cellular [ $^{32}$ P]-bio-*tat* ODN was found to be in the 36-mer form at 24 h of incubation with the avidin-cHSA vector (Figure 4, lane 5), the presence of some degradation products was observed in cell extracts, suggesting that the 3'-bio-*tat* ODN may be subject to endonuclease and/or 5'-exonuclease activity in peripheral lymphocytes.

In summary, the present investigations extend previous studies with serum *in vitro* (9) to cultured cells and show that 3'-biotinylation and binding to an avidin-cHSA complex results in protection of PO-ODNs against cellular 3'-exonucleases, and in a marked increase in cellular uptake. Similarly, other 3'-modifications protect PO-ODNs in cultured cells (18). However, the use of 3'-biotinylation has the advantage of facilitating the conjugation of the PO-ODN to avidin-based vectors which have the dual capacity to fully activate RNase H (Figure 3) and to mediate transcellular delivery (Figure 4, Table 1).

#### ACKNOWLEDGMENT

The authors are indebted to Sherri J. Chien for skillful preparation of the manuscript. The following reagent was obtained through the AIDS Research and Reference Reagent Program, Division of AIDS, NIAID, NIH: HIV-1 Tat Designer Gene. This work was supported by NIH Grant R01-AI28760.

#### LITERATURE CITED

- Weintraub, H., Izant, J. G., and Harland, R. M. (1985) Antisense RNA as a Molecular Tool for Genetic Analysis. *Trends Genet.* 1, 22-25.
- Mirabelli, C. K., Bennett, C. F., Anderson, K., and Crooke, S. T. (1991) *In Vitro* and *In Vivo* Pharmacologic Activities of Antisense Oligonucleotides. *Anti-Cancer Drug Des.* 6, 647-661.
- Cohen, J. S. (1991) Antisense Oligonucleotides as Antiviral Agents. *Antiviral Res.* 16, 121-133.
- Neckers, L., Whitesell, L., Rosolen, A., and Geselowitz, D. A. (1992) Antisense Inhibition of Oncogene Expression. *Crit. Rev. Oncogen.* 3, 175-231.
- Stein, C. A., and Cheng, Y.-C. (1993) Antisense Oligonucleotides as Therapeutic Agents - Is the Bullet Really Magical? *Science* 261, 1004-1012.
- Wickstrom, E. (1986) Oligodeoxynucleotide Stability in Subcellular Extracts and Culture Media. *J. Biochem. Biophys. Method* 13, 97-102.
- Tidd, D. M. and Varenus, H. M. (1989) Partial Protection of Oncogene, Anti-Sense Oligodeoxynucleotides Against Serum Nuclease Degradation Using Terminal Methylphosphonate Groups. *Br. J. Cancer* 60, 343-350.
- Smith, C. C., Aurelian, L., Reddy, M. P., Miller, P. S., and Ts'o, P. O. P. (1986) Antiviral Effect of an Oligonucleoside methylphosphonate Complementary to the Splice Junction of Herpes Simplex Virus Type 1 Immediate Early Pre-mRNAs 4 and 5. *Proc. Natl. Acad. Sci. U.S.A.* 83, 2787-2791.
- Boado, R. J., and Pardridge, W. M. (1992) Complete Protection of Antisense Oligonucleotides against Serum Nuclease Degradation by an Avidin-Biotin System. *Bioconjugate Chem.* 3, 519-523.
- Marcus-Sekura, C. J., Woerner, A. M., Shinozuka, K., Zon, G., and Quinlan, G. V., Jr. (1987) Comparative Inhibition of Chloramphenicol Acetyltransferase Gene Expression by Antisense Oligonucleotide Analogues Having Alkyl Phosphotriester, Methylphosphonate and Phosphorothioate Linkages. *Nucl. Acids Res.* 15, 5749-5763.
- Matsukura, M., Shinozuka, K., Zon, G., Mitsuya, H., Reitz, M., Cohen, J. S., and Broder, S. (1987) Phosphorothioate Analogs of Oligodeoxynucleotides: Inhibitors of Replication and Cytopathic Effects of Human Immunodeficiency Virus. *Proc. Natl. Acad. Sci. U.S.A.* 84, 7706-7710.
- Cagnor, C., Bertrand, J.-R., Thenet, S., Lemaitre, M., Morvan, F., Rayner, B., Malvy, C., Lebleu, B., Imbach, J.-L., and Paoletti, C. (1987)  $\alpha$ -DNA VI: Comparative Study of  $\alpha$ - and  $\beta$ -Anomeric Oligodeoxynucleotides in Hybridization to mRNA and in Cell Free Translation Inhibition. *Nucl. Acids Res.* 15, 10419-10436.
- Furdon, P. J., Dominski, Z., and Kole, R. (1989) RNase H Cleavage of RNA Hybridized to Oligonucleotides Containing Methylphosphonate, Phosphorothioate and Phosphodiester Bonds. *Nucl. Acids Res.* 17, 9193-9204.
- Maher, L. J., III, and Dolnick, B. J. (1988) Comparative Hybrid Arrest by Tandem Antisense Oligodeoxyribonucleotides or Oligodeoxyribonucleoside Methylphosphonates in a Cell-Free System. *Nucl. Acids Res.* 16, 3341-3358.
- Gao, W.-Y., Han, F.-S., Storm, C., Egan, W., and Cheng, Y.-C. (1992) Phosphorothioate Oligonucleotides are Inhibitors of Human DNA Polymerases and RNase H: Implications for Antisense Technology. *Molec. Pharmacol.* 41, 223-229.
- Pardridge, W. M., and Boado, R. J. (1991) Enhanced Cellular Uptake of Biotinylated Antisense Oligonucleotide or Peptide Mediated by Avidin, a Cationic Protein. *FEBS Lett.* 288, 30-32.
- Pardridge, W. M., Boado, R. J., and Buciak, J. L. (1993) Drug Delivery of Antisense Oligonucleotides or Peptides to Tissues *In Vivo* Using an Avidin-Biotin System. *Drug Delivery* 1, 43-50.
- Gamper, H. B., Reed, M. W., Cox, T., Viroso, J. S., Adams, A. D., Gall, A. A., Scholler, J. K., and Meyer, R. B., Jr. (1992) Facile Preparation of Nuclease Resistant 3' Modified Oligodeoxynucleotides. *Nucl. Acids Res.* 21, 145-150.
- Zendegui, J. G., Vasquez, K. M., Tinsley, J. H., Kessler, D. J., and Hogan, M. E. (1992) *In vivo* Stability and Kinetics of Absorption and Disposition of 3' Phosphopropyl Amine Oligonucleotides. *Nucl. Acids Res.* 20, 307-314.
- Arya, S. K., Guo, C., Josephs, S. F., and Wong-Staal, F. (1985) Trans-Activator Gene of Human T-Lymphotropic Virus Type III (HTLV-III). *Science* 229, 63-73.
- Kang, Y.-S., and Pardridge, W. M. (1994) Brain Delivery of Biotin Bound to a Conjugate of Neutral Avidin and Cationized Human Albumin. *Pharm. Res.* (in press).
- Sambrook, J., Fritsch, E. F., and Maniatis, T. (1989) *Molecular Cloning: A Laboratory Manual*, Cold Spring Harbor Laboratory Press, Cold Spring Harbor.
- Davis, L. G., Dibner, M. D., and Battey, J. F. (1986) *Basic Methods in Molecular Biology*, Elsevier, New York.
- Green, N. M. (1975) Avidin. *Adv. Protein Chem.* 29, 85-133.
- Cazenave, C., Stein, C. A., Loreau, N., Thuong, N. T., Neckers, L. M., Subasinghe, C., Hélène, C., Cohen, J. S., and Toulmé, J.-J. (1989) Comparative Inhibition of Rabbit Globin mRNA Translation by Modified Antisense Oligodeoxynucleotides. *Nucl. Acids Res.* 17, 4255-4273.

# Site-Specific Conjugation of an Enzyme and an Antibody Fragment

Raymond C. Werlen,<sup>\*,†</sup> Mervi Lankinen,<sup>†</sup> Keith Rose,<sup>†</sup> David Blakey,<sup>‡</sup> Helen Shuttleworth,<sup>§</sup> Roger Melton,<sup>§</sup> and Robin E. Offord<sup>†</sup>

Département de Biochimie Médicale, Centre Médical Universitaire, 1 rue Michel Servet, CH 1211 Geneva 4, Switzerland, Cancer Research Department, Zeneca Pharmaceuticals, Mereside, Alderley Park, Macclesfield, Cheshire SK 10 4TG, U.K., and Division of Biotechnology, PHLS/CAMR, Porton Down, Salisbury, Wiltshire SP4 0JG, U.K. Received February 3, 1994<sup>®</sup>

A site-specific immunoconjugate was prepared between an F(ab')<sub>2</sub>-like fragment of the monoclonal anti-CEA murine IgG1 A5B7 and a mutant of the dimeric enzyme carboxypeptidase G2 possessing an N-terminal Thr in place of Ala. First an aldehyde was introduced at the N-terminus of the enzyme by mild periodate oxidation and a residue of carbohydrazide was specifically introduced at the C-terminus of the truncated heavy chain of the F(ab')<sub>2</sub>-like fragment by reverse proteolysis. Then the two modified proteins were conjugated by the formation of a hydrazone bond between the hydrazide and the aldehyde groups. The conjugate obtained retained both enzymic activity and antigen-binding capacity. The antigen-binding capacity was better than that of a similar conjugate made conventionally by random reaction with side chains.

## INTRODUCTION

Antibody-directed enzyme prodrug therapy (ADEPT)<sup>1</sup> is a technique which uses a conjugate consisting of an antibody (or antibody fragment) bound to an enzyme to enhance the therapeutic benefit of chemotherapy by converting *in situ* a nontoxic prodrug to a toxic drug (for a recent review, see Senter et al. (1993)). At present, most immunoconjugates are prepared by introducing complementary reactive groups into the protein partners via acylation of lysine side chains with heterobifunctional reagents (for a recent review of this technology, see Brinkley (1992)). By controlling the extent of acylation and then purifying the conjugate according to its size, useful heterodimers can be prepared. However, the conjugates obtained through this approach consist generally of a mixture of isomers each linked through different residues, and each isomer may potentially have a different biological activity. Recently, techniques have been described which permit the introduction of a hydrazide group selectively at C-termini of proteins by reverse proteolysis (Rose et al., 1991; Fisch et al., 1992) and the introduction of an aldehyde group at the N-terminus of a protein (when this is occupied by Ser or Thr, see Scheme 1) through mild periodate oxidation of the 1,2 amino-ol characteristic of these residues when in the N-terminal position (Geoghegan and Stroh, 1992, and references cited therein). As shown in Scheme 2, hydrazide and aldehyde groups are able to react specifically with each other to give a hydrazone, and this can be exploited in the construction of protein conjugates (Rose et al., 1991). The combination of these two techniques allows the construction, via hydrazone formation, of

homogeneous proteins with a new backbone (Gaertner et al., 1992) by head-to-tail conjugation without the need of any protecting groups. In the present paper, we have applied this approach to the preparation of a conjugate designed for ADEPT. We describe the conjugation of an F(ab')<sub>2</sub>-like fragment of the monoclonal anti-CEA IgG1 murine antibody A5B7 to the enzyme carboxypeptidase G2 (CPG2), which is known to be able to convert nontoxic prodrugs into toxic drugs (Bagshawe et al., 1988). Conjugates of these two proteins have already been shown to be of interest for ADEPT (Sharma et al., 1991). Conjugation is achieved via the formation of a hydrazone bond between the C-terminus of the truncated heavy chain of the F(ab')<sub>2</sub> and the N-terminus of a mutant of the carboxypeptidase having an N-terminal threonine.

## MATERIALS AND METHODS

**Materials.** Except where otherwise specified, solvent and reagents were of analytical grade or better, were obtained from commercial sources, and were used without further purification. The pH of solutions was adjusted at room temperature (about 22 °C). Urea was purified by passing an 8 M solution through a column packed with Serdolite MB3 (Serva) just prior to use. Lysyl endopeptidase (2.3 U/mg, amidase activity using *N*<sup>α</sup>-benzoyl-DL-lysine-*p*-nitroanilide as substrate) from *Achromobacter lyticus* was obtained from Wako Pure Chemical Co (Neuss, Germany). The A5B7 IgG1 murine antibody was obtained from CRC (Sutton, U.K.) as a 5.4 mg/mL solution in phosphate-buffered saline.

**General Methods.** The enzymic activity of CPG2 was assayed as previously described (Sherwood et al., 1985) except that the reaction was carried out at room temperature.

The binding activity of the conjugate was measured in a competitive binding assay using an alkaline phosphatase-labeled A5B7 standard. Briefly, 96-well ELISA plates were coated with CEA (0.1 µg/well) followed by the addition of mixtures of conjugate (10–0.5 µg/mL) and labeled A5B7 (1 µg/mL). After 90 min unbound antibody was removed and the amount of labeled A5B7 bound was determined by addition of *p*-nitrophenyl phosphate (Sigma) and measurement of the absorbance at 405 nm. The ability of the conjugate to compete with the labeled A5B7

<sup>†</sup> Centre Médical Universitaire.

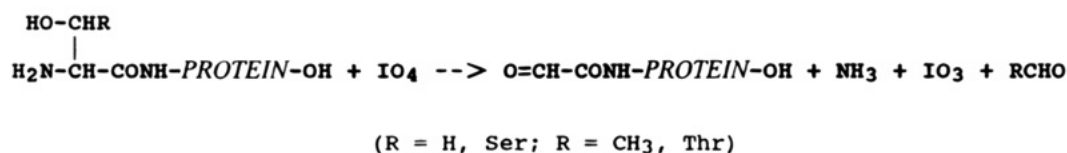
<sup>‡</sup> Zeneca Pharmaceuticals.

<sup>§</sup> PHLS/CAMR.

<sup>®</sup> Abstract published in *Advance ACS Abstracts*, July 15, 1994.

<sup>1</sup> Abbreviations: ADEPT, antibody-directed enzyme prodrug therapy; DAI, des-Ala<sup>B30</sup> porcine insulin; CPG2, carboxypeptidase G2; ESMS, electrospray ionization mass spectrometry; SDS-PAGE, sodium dodecyl sulfate polyacrylamide gel electrophoresis; AU, absorption unit; MES, morpholino ethyl sulfonate; CEA, carcino embryonic antigen; PCR, polymerase chain reaction.

## Scheme 1



## Scheme 2



for binding to CEA was compared to intact unlabeled A5B7 to give a percent binding activity relative to unconjugated antibody.

Protein solutions were concentrated on Centrprep 10 or Centricon 10 devices following the instructions of the manufacturer (Amicon). Since glycerol could interfere with periodate oxidation, when necessary, the glycerol present as protecting agent for the membrane was removed by rinsing the concentrator three times with water and three times with the buffer to be used for the concentration and then by passing fresh buffer through the membrane twice prior to the concentration step.

Electrophoresis on polyacrylamide gels in SDS (SDS-PAGE) was performed on Pharmacia Phast system using 8–25% gradient gels, and proteins were detected with the silver nitrate procedure according to the recommendations of the manufacturer.

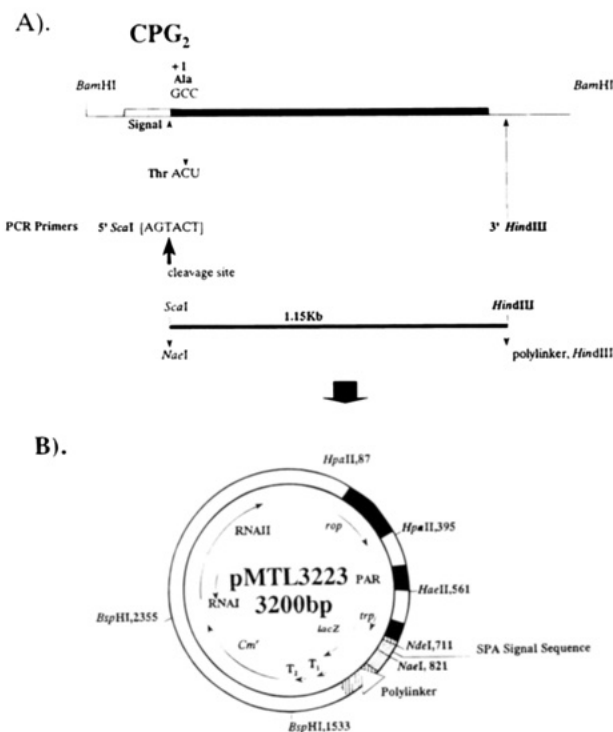
Desalting was performed on a Pharmacia FPLC system using a HR10/10 fast desalting column. The same system was used for gel filtration using a Superose 12 HR 10/30 column and for ion exchange chromatography with a Mono S HR5/5 column.

The samples for electrospray ionization mass spectrometry (ESMS) were dialyzed against 10 mM dithiothreitol. ESMS was performed as previously described (Vilaseca et al., 1993).

#### Preparation of the Threonine N-Terminal CPG2.

The N-terminal Ala was replaced by a Thr using standard PCR technology (McPherson et al., 1993) with two mutagenic oligonucleotides: a 26bp oligonucleotide complementary to the DNA sequence immediately downstream of the CPG2 translational terminus, which introduced a mutagenic *Hind* III restriction site, and a second 30bp oligonucleotide complementary to the nucleotide sequence of the 5' end of CPG2 gene, which coded for the Ala to Thr codon change and also introduced a *Sca* I restriction site across the DNA coding for the peptidase cleavage site of the immature CPG2 (see Figure 1). The presence of these two unique restriction enzyme sites facilitated the cloning of the 1.15 kb (threonine mutant) CPG2 gene into the *Nae* I–*Hind* III sites of a specifically designed secretion vector: pMTL3223 (manuscript in preparation) to give the recombinant vector pCPS3. The mutant CPG2 was expressed in *E. coli* MC1061 transformed with pCPS3. Cultures were grown overnight in 1 L of L-broth containing 30 µg/mL of chloramphenicol. The cells were harvested by centrifugation (6000g for 20 min) and then resuspended in 10 mL of 10 mM sodium acetate pH 5.5 and sonicated (MSE soniprep 150, 3 × 20 s, amp 18 µm). The cell debris was removed by centrifugation (17000g for 45 min) and the supernatant containing CPG2 collected for further purification.

**Purification of Mutant CPG<sub>2</sub>.** The enzyme was purified to homogeneity, as judged by SDS-PAGE (Figure 2, lane 8), from the cell supernatant by a two-step ion-exchange chromatography method. The obtained mutant enzyme had a specific activity indistinguishable from the wild-type enzyme (manuscript in preparation). The presence of the threonine N-terminus was confirmed

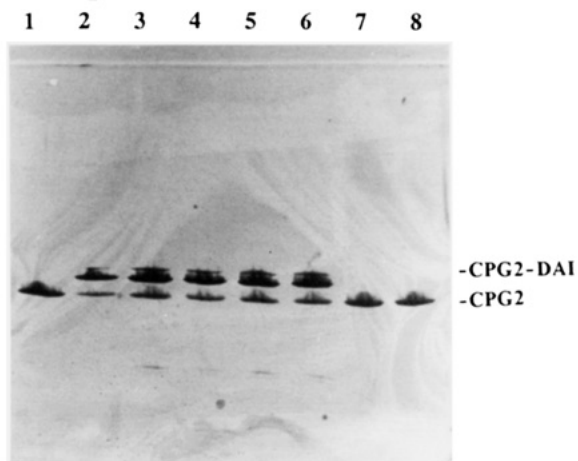


**Figure 1.** Insertion of the mutated CPG2 gene into an *E. coli* expression vector: A, the position of the mutagenic PCR primers to the CPG2 gene and the nucleotides involved in the mutation of Ala (wild-type) to Thr; B, restriction enzyme map of the expression vector pMTL3223 indicating the insertional sites of CPG2 gene.

by pulsed liquid phase N-terminal sequencing on an ABI 477 sequencer. The mass observed by ESMS was 41 727.29 Da ± 3.47 (expected 41 725.8 Da).

#### Periodate Oxidation of N-Terminal Threonine.

The carboxypeptidase G2 mutant possessing N-terminal threonine was buffer-exchanged into freshly made 0.1 M NH<sub>4</sub>HCO<sub>3</sub> by gel filtration on a fast desalting column or a NAP-5 column (Pharmacia). It was then concentrated on a Centrprep 10 concentrator (extensively washed; see General Methods) to about 8.4 mg/mL. All estimates of CPG2 concentrations and quantities given in this paper are based on optical density at 280 nm, assuming an absorption of 0.4 AU for a 1 mg/mL solution. A concentration of 8.4 mg/mL corresponds to about 200 µmol/L N-terminal Thr. Thirty equiv of methionine (0.2 M in water) were added followed by 10 equiv of periodic acid (20 mM in 0.1 M NH<sub>4</sub>HCO<sub>3</sub>). After 10 min at room temperature, the reaction was stopped by addition of 0.5 M 1,3-diaminopropan-2-ol (in 90% 1,4-butanediol) to give a final concentration of 50 mM. After a further 20 min at room temperature, the protein was separated from excess reagents and small molecular weight aldehydes by gel filtration on a fast desalting column in 0.1 M sodium acetate pH 4.6 (0.1 M sodium acetate, pH adjusted to 4.6 with acetic acid). The aldehydic protein was then concentrated to 10 mg/mL and could be kept



**Figure 2.** SDS-PAGE analysis of the oxidation of CPG2 and its conjugation with DAI-carbohydrazide: lane 1, 75  $\mu$ M CPG2, 20 equiv of periodate, 10 min; lane 2, 78  $\mu$ M CPG2, 10 equiv of periodate, 20 min; lane 3, 78  $\mu$ M CPG2, 10 equiv of periodate, 10 min; lane 4, 78  $\mu$ M CPG2, 10 equiv of periodate, 5 min; lane 5, 75  $\mu$ M CPG2, 20 equiv of periodate, 10 min; lane 6, 75  $\mu$ M CPG2, 20 equiv of periodate, 10 min; lane 7, 80  $\mu$ M CPG2 not oxidized incubated with 20 equiv of DAI-carbohydrazide; lane 8, 80  $\mu$ M CPG2 not oxidized. Lanes 2–6: CPG2 was incubated with 20 equiv of DAI-carbohydrazide after oxidation.

at 4 °C from 1 to 14 days until needed for the conjugation. The mass of the aldehydic protein observed by ESMS was  $41\,713.44 \pm 7.37$  (see Discussion).

The reactivity of the aldehyde was checked by incubation of 1 to 2  $\mu$ L of sodium acetate pH 4.6 containing about 0.1 nmol of oxidized CPG2 (8.4  $\mu$ g of protein, 0.2 nmol of aldehyde as the protein is a homodimer (Sherwood et al. 1985)) with 4  $\mu$ L of the same buffer containing 1 nmol per  $\mu$ L of des-Ala<sup>B30</sup>-insulin carrying a carbohydrazide group on the C-terminus of the B chain (DAI-carbohydrazide). The DAI-carbohydrazide was prepared by reverse proteolysis as previously described (Rose et al., 1991). After 20 h at 37 °C, the samples were analyzed by SDS-PAGE, and the degree of conjugation between the oxidized enzyme and the insulin derivative gave a measure of the aldehydic reactivity of the former.

**Digestion with Lysyl Endopeptidase.** Four 1-mL portions of the A5B7 solution (see Materials) were buffer-exchanged into 50 mM Tris pH 8.4 (pH adjusted with HCl) by gel filtration on a fast desalting column and then concentrated on a Centrprep 10 to a final concentration of about 5 mg/mL (the concentration of A5B7 antibody and of its fragments was estimated from the optical density at 280 nm assuming an absorption of 1.25 AU for a 1 mg/mL solution). Lysyl endopeptidase (10 mg/mL in water) was added to give a 3% w/w enzyme-substrate ratio and the mixture incubated at 37 °C for about 20 h.

**Ion-Exchange Chromatography.** After centrifugation in a bench-top centrifuge to remove some precipitate the digest was diluted with 4 volumes of 50 mM sodium acetate pH 4.6 (adjusted with HCl) and loaded on a SP-trisacryl column (10  $\times$  1.5-cm diameter) equilibrated in the same buffer. The column was washed with the same buffer and developed with a 400-mL salt gradient from 0 to 400 mM NaCl, still in the same buffer, at a flow rate of 0.34 mL/min. The fractions containing F(ab')<sub>2</sub> were pooled, concentrated, buffer-exchanged into 10 mM Tris-HCl pH 8.0 on the fast desalting column, and concentrated again. The typical yield of this preparation was 35–40% of the theoretical maximum for F(ab')<sub>2</sub>.

**Reverse Proteolysis.** Solid carbohydrazide was added to the purified F(ab')<sub>2</sub> (typically about 5 mg protein in

700  $\mu$ L 10 mM Tris pH 8.0) to get a final carbohydrazide concentration of 2.5 M. The pH was then lowered to 5.5 by addition of glacial acetic acid prior to addition of lysyl endopeptidase (10 mg/mL in water, enzyme:F(ab')<sub>2</sub> ratio of 5% w/w). The amounts of carbohydrazide and acetic acid were calculated as follows: the sum of the volumes, in  $\mu$ L, of the F(ab')<sub>2</sub> and of the enzyme solutions was multiplied by 0.265 to obtain the amount of carbohydrazide (in mg) and by 0.023 to obtain the amount of acetic acid (in  $\mu$ L) required. These quantities had been determined by tests on larger volumes without protein and take into account the volume increase due to carbohydrazide. The mixture was allowed to stand at room temperature for 3 h whereupon the reaction was stopped by addition of Trasylol (100 mg/mL in water, 30-fold mass excess over the lysyl endopeptidase). The mixture was then gel-filtered on a Superose 12 column in 0.1 M sodium acetate pH 4.6 (adjusted with acetic acid) at a flow rate of 0.6 mL/min. The peak corresponding to F(ab')<sub>2</sub> was collected in a tube containing Trasylol (10-fold mass excess over the quantity of peptidase used for the reverse proteolysis), concentrated, and made 10 mM in urea by adding 1 M urea in water. After 1 h at room temperature, the sample was desalted on a fast desalting column equilibrated in the same sodium acetate buffer. The protein recovery was quantitative.

The incorporation of carbohydrazide was quantified by incubating 100  $\mu$ g of F(ab')<sub>2</sub>-carbohydrazide with 5 nmol of O=CHC<sub>6</sub>H<sub>4</sub>-*m*-CH=NOCH<sub>2</sub>CO-ferrioxamine labeled with <sup>55</sup>Fe, as described by Fisch et al. (1992).

**Conjugation (Hydrazone Formation).** The F(ab')<sub>2</sub>-carbohydrazide obtained as described above was mixed with the aldehydic CPG2 (0.8 mg of CPG2 for 1 mg of F(ab')<sub>2</sub>-carbohydrazide, which corresponds to about four aldehyde groups per hydrazide). The mixture was concentrated in a Centrprep 10 concentrator to a final volume of about 700  $\mu$ L and was then allowed to stand at room temperature for about 60 h, after which time it was gel filtered (in two portions) on Superose 12 in phosphate-buffered saline (PBS: 8 g/L of NaCl, 0.2 g/L of KCl, 1.44 g/L of Na<sub>2</sub>HPO<sub>4</sub>·2H<sub>2</sub>O, 0.2 g/L of KH<sub>2</sub>PO<sub>4</sub>, pH 7.4) at a flow rate of 0.4 mL/min. The fractions containing the conjugate were pooled and concentrated in a Centrprep 10 concentrator. The conjugate can be stored at -20 °C. The yield of the conjugation was typically about 33%. The overall yield of the conjugate preparation was 10–15% based on starting IgG and 30% based on starting CPG2.

## RESULTS AND DISCUSSION

**Preparation of Aldehydic CPG2.** An aldehyde group was introduced at the N-terminus of carboxypeptidase G2. The homodimeric mutant, which had threonine N-terminal, was subjected to mild oxidation at pH 8.3 (the pH of freshly prepared 0.1 M NH<sub>4</sub>HCO<sub>3</sub>) with 10 molar equiv of periodic acid per N-terminal Thr (i.e., 20 equiv per molecule of the dimeric enzyme). The presence of the aldehyde was detected by the formation of a hydrazone with DAI-carbohydrazide: after 20 h at pH 4.6 and 37 °C, analysis by SDS-PAGE shows that while in a nonoxidized control, the enzyme still migrates as a single band at 41 kDa (Figure 2, lane 7), reaction with oxidized enzyme leads to two bands (lane 2–6), the lower band representing less than 50% of the staining intensity, corresponds to the unconjugated enzyme, while the upper band corresponds to the CPG2-DAI conjugate. This result shows that N-termini of both subunits of CPG2 are accessible to the oxidation and hydrazone formation with DAI-carbohydrazide.



The enzymic activity of CPG2 was not altered by the oxidation of N-terminal threonine: the specific activity of the oxidized enzyme was found to be 126 U/mg which is not significantly different from the 131 U/mg of the unoxidized mutant enzyme. It is thus possible to introduce an aldehyde at the N-terminus of the CPG2 without altering its activity.

Both oxidized and unoxidized enzymes were analyzed by ESMS. For the unoxidized mutant enzyme, the observed mass ( $41\,727.29\text{ Da} \pm 3.47$ ) was in agreement with the expected mass ( $41\,725.8\text{ Da}$ ). For the oxidized enzyme, the observed mass ( $41\,713.44\text{ Da} \pm 7.37$ ) was significantly higher than the expected mass for the aldehydic protein ( $41\,680.8\text{ Da}$ ) and for the hydrated aldehyde ( $41\,698.8$ ), but was in agreement with the mass expected for the methanol hemiacetal of the aldehydic enzyme ( $41\,713.8\text{ Da}$ ). The hemiacetal was seen instead of the aldehyde because for ESMS analysis the samples were diluted to produce a solvent mixture containing water/methanol/acetic acid (49.5:49.5:1, by volume). The oxidation of the N-terminal Thr to an aldehyde could thus be achieved without affecting other groups in the protein.

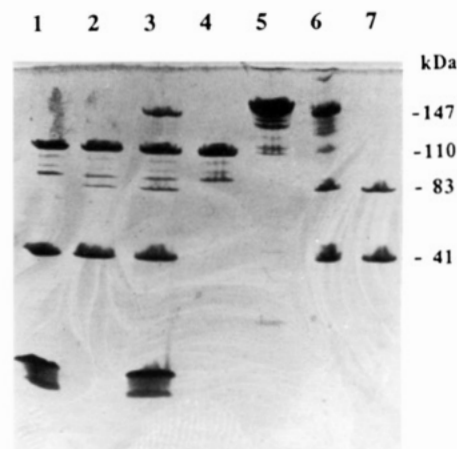
Geoghegan and Stroh (1992) studied the oxidation of a peptide containing Tyr, His, Met, and Trp at slightly basic pH, such as we use: only methionine was seen to be affected, and that only to a very slight degree. Cysteine was not tested, but is not of interest here since CPG2 does not contain cysteine. To protect the six methionine residues contained in CPG2 (Minton et al., 1984), the oxidation was performed in presence of a 30-fold excess of methionine. There were thus five molecules of free methionine for each methionyl residue in the protein and 3 mol of methionine per mole of periodate added. This tactic has been shown to prevent oxidation of the Met residues of G-CSF under similar conditions to those described here (Gaertner et al., 1993).

It is important to avoid contamination of the oxidation solution by the glycerol present as a preserving agent on the concentrator membrane. The extensive washing procedure described is sufficient for this purpose, in that oxidation succeeded where it had previously failed without the wash.

In other experiments (data not shown), variations in protein concentration (40 to  $200\text{ }\mu\text{mol/L}$  in terms of N-terminal Thr), and excess of periodate (5 to 20-fold) gave similar results in the conjugation test with DAI-carbohydrazide and had no effect on the enzymic activity of the oxidized enzyme. The procedure described in the Experimental section was found to work routinely leading to a conjugation with DAI-carbohydrazide close to 90% as determined by SDS-PAGE.

**Preparation of  $\text{F(ab')}_2$ -Carbohydrazide.** The A5B7 antibody, which is a murine IgG1  $\kappa$ , can be slowly digested to a  $\text{F(ab')}_2$  fragment with lysyl endopeptidase at pH 8.4. It is important to remove intact antibody at this stage because it is more difficult to remove it from the final conjugate. The  $\text{F(ab')}_2$  was thus purified by cation-exchange chromatography. After purification, the  $\text{F(ab')}_2$  was transferred to a buffer with low salt to avoid any interference of sodium ions (from the salt gradient) with the reverse proteolysis: sodium ions are known to inhibit cleavage by lysyl endopeptidase ( $K_i = 15\text{ mM}$ , technical information sheet from Wako) even if this effect has not been proven for reverse proteolysis.

Reverse proteolysis was then performed as described in the Experimental Section. The conditions are the optimal conditions of (Fisch et al., 1992). It is important to keep the  $\text{F(ab')}_2$ -carbohydrazide, once isolated, in the presence of a large excess of Trasyol to avoid the action of traces of lysyl endopeptidase which would cleave the



**Figure 3.** SDS-PAGE analysis of the conjugation of  $\text{F(ab')}_2$ -carbohydrazide with oxidized CPG2: lane 1,  $\text{F(ab')}_2$ -carbohydrazide with unoxidized CPG2; lane 2, control  $\text{F(ab')}_2$  (reverse proteolysis with Trasyol instead of lysyl endopeptidase) with oxidized CPG2; lane 3,  $\text{F(ab')}_2$ -carbohydrazide with oxidized CPG2; lane 4,  $\text{F(ab')}_2$ ; lane 5, IgG; lane 6, purified conjugate; lane 7, oxidized CPG2 incubated with 1 equiv of carbohydrazide.

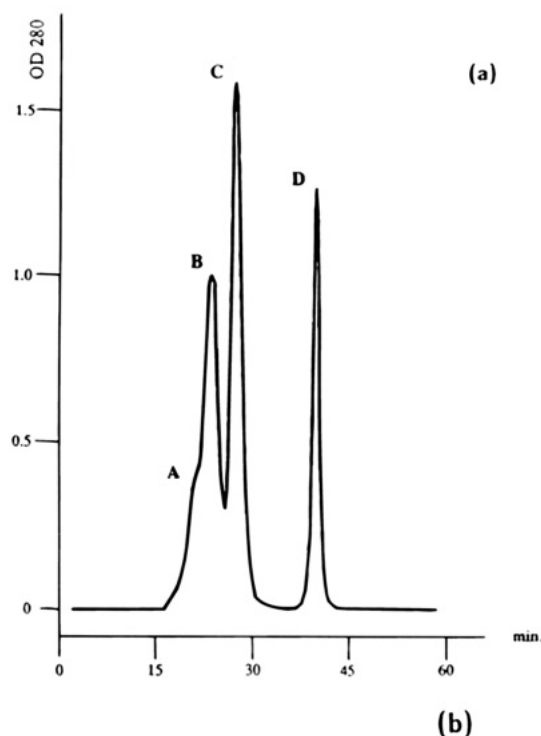
carbohydrazide once the conditions forcing the equilibrium in favor of synthesis (pH 5.5 and  $2.5\text{ M}$  carbohydrazide) no longer remain.

Typically, the incorporation of carbohydrazide obtained with antibody A5B7 is about 0.5 carbohydrazide per  $\text{F(ab')}_2$ , as determined by incorporation of  $^{55}\text{Fe}$  labeled aldehyde. If, as expected, the distribution of  $\text{F(ab')}_2$ ,  $\text{F(ab')}_2$ -carbohydrazide,  $\text{F(ab')}_2$ -(carbohydrazide) $_2$  follows a binomial distribution, this corresponds to 56% of unmodified  $\text{F(ab')}_2$ , 37% of  $\text{F(ab')}_2$ -carbohydrazide, and 6%  $\text{F(ab')}_2$ -(carbohydrazide) $_2$ . The species we are most interested in is the monocarbohydrazide derivative because it should lead to a single conjugate with a monovalent partner (see later). The yield of this species would be optimal at 1 carbohydrazide per  $\text{F(ab')}_2$ , but then the proportion of dicarbohydrazide derivative would be 25%. In principle, the unmodified  $\text{F(ab')}_2$  can be recycled (recoupled with carbohydrazide) but this was not attempted.

IgG,  $\text{F(ab')}_2$ , and  $\text{F(ab')}_2$ -carbohydrazide were analyzed by ESMS after reduction of disulfide bridges by dialysis in  $10\text{ mM}$  dithiothreitol. In all three samples, two main signals were obtained corresponding to the light and heavy chain. The light chain had the same mass in all three samples ( $23\,189$ – $23\,194\text{ Da}$ ) indicating that the light chain is not modified by this procedure. The heavy chain mass was  $26\,416\text{ Da}$  in the  $\text{F(ab')}_2$  and  $26\,489\text{ Da}$  in the  $\text{F(ab')}_2$ -carbohydrazide. The 73-Da difference between the two heavy chains is in agreement with the 72-Da increment expected by the incorporation of one carbohydrazide.

**Conjugation.** SDS-PAGE (see Figure 3, lane 3) shows that a conjugate with a mass of 147 kDa is produced when  $\text{F(ab')}_2$  after reverse proteolysis is incubated with 1 equiv of oxidized mutant CPG2 dimer (i.e., 4 aldehyde per hydrazide) at pH 4.6 for 60 h at room temperature. In contrast, no conjugate is formed when the same  $\text{F(ab')}_2$  is incubated with unoxidized CPG2 (lane 1) or if oxidized CPG2 is incubated with  $\text{F(ab')}_2$  that has been incubated in  $2.5\text{ M}$  carbohydrazide as for reverse proteolysis but with the lysyl endopeptidase replaced by Trasyol (lane 2).

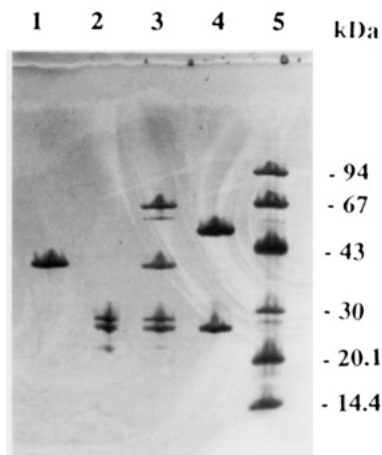
When analyzed by gel filtration, the conjugation mixture gives the profile shown in Figure 4a: a shoulder (A) and three peaks (B–D). Gel electrophoresis of these fractions (Figure 4b) shows that peak B corresponds to



**Figure 4.** (a) Purification of the  $F(ab')_2$ -CPG2 conjugate on Superose 12: A, shoulder containing aggregated material and conjugates of higher molecular weight; B, peak containing the  $F(ab')_2$ -CPG2 conjugate; C, peak containing unreacted  $F(ab')_2$  and CPG2; D, Trasylol. (b) SDS-PAGE analysis of the Superose 12 fractions of the conjugation: lane 1, peak C; lane 2, peak B; lane 3, shoulder A; lane 4, CPG2; lane 5,  $F(ab')_2$ .

the conjugate (lane 2: observed  $147 \pm 8$  kDa, expected 153 kDa). Since one of the two enzyme subunits is noncovalently linked to the conjugate, the other major band in lane 2, corresponding to free enzyme, was to be expected. Peak C corresponds to unreacted  $F(ab')_2$  and CPG2 (lane 1). Electrophoresis for a shorter time (not shown) indicated that peak D contains the Trasylol (approx. 6 kDa) which was present to prevent the  $F(ab')_2$ -carbohydrazide being converted back to  $F(ab')_2$  by residual traces of protease. The shoulder A (lane 3) also contained a little conjugate and we suppose that it might in addition contain more complex conjugates where, for instance, two  $F(ab')_2$  are linked to a CPG2 dimer (or two CPG2 dimers linked to one  $F(ab')_2$ ).

If one incubates the oxidized enzyme with 1 equiv of carbohydrazide at pH 4.6, a new band is seen, corresponding to an apparent  $M_r$  of 83 kDa (Figure 3, lane 7). The simplest explanation of this band is that two aldehydic subunits (42 kDa) have been covalently linked



**Figure 5.** Characterization of the  $F(ab')_2$ -CPG2 conjugate by SDS-PAGE: lane 1, CPG2; lane 2, reduced and carboxymethylated  $F(ab')_2$ ; lane 3, reduced and carboxymethylated conjugate; lane 4, reduced and carboxymethylated IgG; lane 5, reduced and carboxymethylated molecular weight markers.

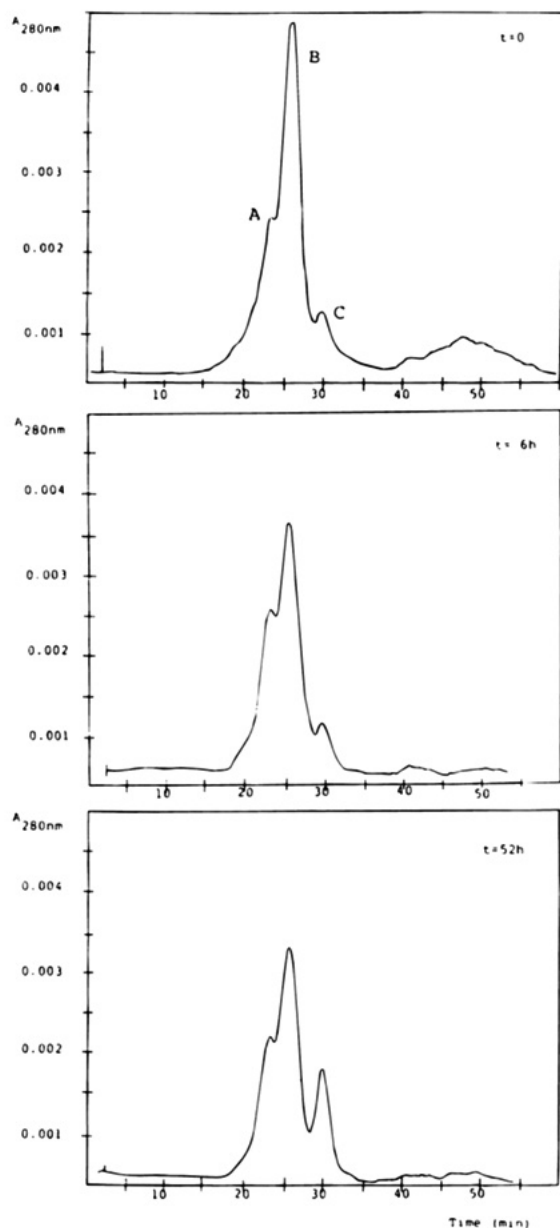
through hydrazone bonds by a single carbohydrazide molecule. Since the new component elutes from Superose 12 under nondenaturing conditions at a position corresponding to approximately 160 kDa, the most likely hypothesis is that it consists of two dimers linked by a single covalent bond: dissociation in SDS would then give both the 83-kDa and the 42-kDa band, which is what is seen.

SDS-PAGE analyses of early preparations of the conjugate showed the same 83-kDa band to a quite significant extent (data not shown), and we concluded that some carbohydrazide had been introduced in the conjugate reaction mixture, having been noncovalently bound to the  $F(ab')_2$ -carbohydrazide sufficient tightly to accompany it on gel filtration. The experiment described in the previous paragraph shows that very small quantities of carbohydrazide would be enough to promote the formation of the cross-linked byproduct. The noncovalent binding must be quite strong, since repeated gel filtration did not suffice to solve this problem. Therefore, based on the structural similarity between carbohydrazide ( $CO-(NHNH_2)_2$ ) and urea, we sought to displace the carbohydrazide by pretreatment of the  $F(ab')_2$ -carbohydrazide with a dilute solution of urea (10 mM). This operation had the hoped-for result, effectively abolishing the 83-kDa band in analyses of the conjugate. It was essential to carry out this urea treatment, since the cross-linked enzyme coelutes with the conjugate on gel filtration (data not shown) and it would have persisted as a contaminant.

**Characterization of the Conjugate.** The purified conjugate was also analyzed by reducing SDS-PAGE (Figure 5). On reducing SDS-PAGE (Figure 5 lane 3) the conjugate shows, as expected, four bands: one at  $70 \pm 5$  kDa corresponding to the truncated heavy chain linked to a CPG2 subunit, a second at 41 kDa corresponding to the noncovalently bound CPG2 subunit, a third at  $28 \pm 2$  kDa corresponding to the unconjugated truncated heavy chain (present in reduced  $F(ab')_2$ , lane 2, but not in reduced IgG, lane 4), and a fourth at  $26 \pm 2$  kDa corresponding to the intact antibody light chain (present in reduced  $F(ab')_2$  and in reduced IgG).

The majority of the conjugate appears to have the wanted structure of one  $F(ab')_2$  linked to one CPG2 dimer. On strong overloaded nonreducing gels, (a faint band seen at 185 kDa indicates some small quantities of larger structures (two molecules of  $F(ab')_2$  or two of CPG2 dimer). Given the fact that there are two aldehydic groups per CPG2 dimer (one per subunit) and some



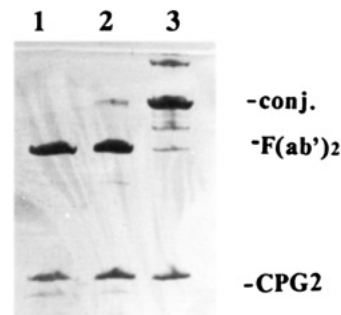


**Figure 6.** Stability of the  $F(ab')_2$ -CPG2 conjugate. The conjugate (1.4 mg/mL in PBS, pH 7.4) was incubated at 37 °C for the indicated time and then analyzed on Superose 12.

$F(ab')_2$  molecules have two carbonyl groups, it is not surprising to see them. That they are found in only relatively small amounts is probably due to steric hindrance between the close pairs of identical reactive groups.

Figure 6 shows the stability of the conjugate when incubated at 37 °C at pH 7.4. Peak B (the conjugate with the one  $F(ab')_2$  linked to one CPG2 dimer structure) diminishes slowly in favor of the shoulder, suggesting that an equilibrium exists between the wanted conjugate and conjugates of higher molecular weight. After 1 day or more, both peak B and the shoulder decrease in favor of peak C suggesting that the hydrazone bond is very slowly hydrolyzed. No significant changes are seen on SDS-PAGE after up to 24 h at pH 7.4 and 37 °C (data not shown). The rate of decomposition is slow enough not to be an obstacle to the use of the conjugate in ADEPT. Indeed, preliminary experiments in the nude-mouse xenograft system (data not shown) show a clear therapeutic effect of this conjugate.

As a confirmation of the proposed structure of the conjugate, Figure 7 shows that the bond between the



**Figure 7.** SDS-PAGE analysis of the digestion of the conjugate.  $F(ab')_2$ -CPG2 (1.2 mg/mL) was incubated with lysyl endopeptidase (1% w/w) in PBS (pH 7.4) at 37 °C: lane 1, 60 min; lane 2, 30 min; lane 3, undigested conjugate.

$F(ab')_2$  and the CPG2 is the one most susceptible to lysyl endopeptidase in the conjugate: it can be cleaved by 1% Achromobacter protease in 30 min before the CPG2 is degraded. Under these conditions, the  $F(ab')_2$  is resistant to proteolysis.

The enzymic activity of the conjugate was found to be 45 U/mg conjugate which corresponds to 101 U/mg CPG2. This represents 75% of the activity of the unmodified mutant CPG2.

The binding activity of the conjugate was found to be  $122 \pm 43\%$  (mean  $\pm$  SD for 4 conjugate samples) in a competitive binding assay where the ability of the conjugate to compete with binding of an A5B7-alkaline phosphatase conjugate to CEA is compared with intact A5B7. Thus, the A5B7  $F(ab')_2$ -CPG2 conjugate prepared by reverse proteolysis retains full binding activity. Similar conjugates prepared using conventional linker technology only retain approximately 70% binding activity in this assay suggesting that the head-to-tail conjugation described here leads to improved retention of antigen binding activity over conventional linker technology.

## CONCLUSION

The linking of a large antibody fragment to a homodimeric enzyme can potentially yield a very complex mixture of products. Restriction of protein modification to the C-terminus of the heavy chain of the antibody fragment, and to the N-terminus of the enzyme subunit, limits the number of possible products and permitted us to prepare a head-to-tail immunoconjugate between a  $F(ab')_2$ -like fragment of the monoclonal anti-CEA murine IgG1 A5B7 and a mutant of carboxypeptidase G2 with retention of both the antigen binding and the enzymic activity.

## ACKNOWLEDGMENT

We thank Zeneca Pharmaceuticals and la Fondation du Centenaire de la Société suisse d'Assurances générales sur la Vie humaine pour la Santé publique et les Recherches médicales for financial support and the Fonds National Suisse de la Recherche Scientifique for funding the analytical facilities used in this project.

## LITERATURE CITED

- Bagshawe, K. D., Springer, C. J., Searle, F., Antoniow, P., Sharma, S. K., Melton, R.G., and Sherwood, R. F. (1988) A cytotoxic agent can be generated selectively at cancer sites. *Br. J. Cancer* 58, 700-703.
- Brinkley, M. (1992) A Brief Survey of Methods for Preparing Protein Conjugates with Dyes, Haptens, and Cross-Linking Reagents. *Bioconjugate Chem.* 3, 2-13.
- Fisch, I., Künzi, G., Rose, K., and Offord, R. E. (1992) Site-Specific Modification of a Chimeric Monoclonal Antibody Using Reverse Proteolysis. *Bioconjugate Chem.* 3, 147-153.

- Gaertner, H. F., Rose, K., Cotton, R., Timms, D., Camble, R., and Offord, R. E. (1992) Construction of Protein Analogues by Site-Specific Condensation of Unprotected Fragments. *Bioconjugate Chem.* 3, 262–268.
- Gaertner, H. F., Rose, K., Cotton, R., Timms, D., Camble, R., and Offord, R. E. (1993) Construction of Protein Analogues by Site-Specific Condensation of Unprotected Fragments. In *Peptides 1992* (C. H. Schneider, and A. N. Eberle, Eds.) pp 239–240, ESCOM, Leiden, The Netherlands.
- Geoghegan, K. F., and Stroh, J. G. (1992) Site-Directed Conjugation of Nonpeptide Groups to Peptides and Proteins via Periodate Oxidation of a 2-Amino Alcohol. Application to Modification at N-Terminal Serine. *Bioconjugate Chem.* 3, 138–146.
- McPherson, M. J., Quirke, P., and Taylor, G. R., Eds. (1993) *PCR A practical approach*, IRL Press, Oxford University Press.
- Minton, N. P., Atkinson, T., Bruton, C. J., and Sherwood, R. F. (1984) The Complete Nucleotide Sequence of the *Pseudomonas* Gene Coding for Carboxypeptidase G2. *Gene* 31, 31–38.
- Rose, K., Vilaseca, A., Werlen, R., Meunier, A., Fisch, I., Jones, R. M. L., and Offord, R. E. (1991) Preparation of Well-Defined Protein Conjugates Using Enzyme-Assisted Reverse Proteolysis. *Bioconjugate Chem.* 2, 154–159.
- Senter, P. D., Wallace, P. M., Svensson, H. P., Vrudhula, V. M., Kerr, D. M., and Hellström, I. (1993) Generation of Cytotoxic Agents by Targeted Enzymes. *Bioconjugate Chem.* 4, 3–9.
- Sharma, S. K., Bagshawe, K. D., Springer, C. J., Burke, P. J., Rogers, G. T., Boden, J. A., Antoniow, P., Melton, R. G., and Sherwood, R. F. (1991) Antibody Directed Enzyme Prodrug Therapy (ADEPT): a Three Phase System. *Dis. Markers* 9, 225–231.
- Sherwood, R. F., Melton, R. G., Alwan, S. M., and Hughes, P. (1985) Purification and Properties of Carboxypeptidase G2 from *Pseudomonas* sp. Strain RS-16. *Eur. J. Biochem.* 148, 447–453.
- Vilaseca, A., Rose, K., Werlen, R., Meunier, A., Offord, R. E., Nichols, C. L., Scott, W. L. (1993) Protein Conjugates of Defined Structure: Synthesis and Use of a New Carrier Molecule. *Bioconjugate Chem.* 4, 515–520.

# Glutamyl- $\beta$ -alanyl Spacer Group for Haptenic Coupling to Proteins. Preparation of Immunogens for Antibody Production against Polychlorinated Biphenyls

David J. W. Goon,<sup>†</sup> Herbert T. Nagasawa,<sup>\*,†</sup> Daniel E. Keyler,<sup>‡</sup> Catherine A. Ross,<sup>‡</sup> and Paul R. Pentel<sup>†,§</sup>

Departments of Medicinal Chemistry and of Medicine, University of Minnesota, Minneapolis, Minnesota 55455, and VA Medical Center and Hennepin County Medical Center, Minneapolis, Minnesota 55417.

Received March 3, 1994<sup>\*</sup>

By use of a glutamyl- $\beta$ -alanyl spacer group, a hapten for the polychlorinated biphenyl, 2,2',4,4',5,5'-hexachlorobiphenyl (**1**), viz., 2-amino-2',4,4',5,5'-pentachlorobiphenyl (**2**), was successfully conjugated to carrier proteins to provide immunogens with high hapten/protein molar substitution ratios (MSR's). The procedure allows for the incorporation of  $\beta$ -[<sup>3</sup>H]-alanine into the immunogen, thereby providing an accurate radiochemical method for the quantitative assessment of MSR. The use of the glutamyl spacer group was prompted by the observation that the corresponding succinamyl group was subject to side reactions manifested by succinimide formation during the carboxyl activation step to an activated ester for subsequent coupling to proteins, thus severely compromising the coupling yields. The glutamyl- $\beta$ -alanyl spacer group should be generally applicable for protein conjugation of any hapten with an amino functional group in the molecule.

## INTRODUCTION

Polychlorinated biphenyls (PCB's), dioxins, and dichlorodiphenyltrichloroethane (DDT) are ubiquitous environmental contaminants that have very long elimination half-lives in animals and humans. Exposure to these compounds therefore results in an accumulated body burden that persists for months to years (1, 2). Since these PCB's are not only toxic (3, 4), but induce the hepatic microsomal enzymes that metabolize xenobiotics (5), their presence in tissues may lead to adverse drug reactions and/or premature inactivation of drugs in therapeutic use. It is anticipated that understanding the mechanisms responsible for the long elimination half-lives of PCB's and their toxicologic consequences may aid in the development of new strategies for diagnosis and/or treatment of excessive exposure.

We therefore wished to prepare PCB-specific antibody Fab fragments as pharmacokinetic probes to study the redistribution of tissue-deposited 2,2',4,4',5,5'-hexachlorobiphenyl (**1**, Chart 1). It has been reported that the succinamylated hapten **2**, viz., *N*-(2',4,4',5,5'-pentachlorobiphenyl-2-yl)succinamic acid (**3**), was successfully conjugated to human serum albumin using a water-soluble carbodiimide to produce antibodies specific to **1** (6). Using this procedure, we coupled **3** to bovine serum albumin (BSA) and, after vigorous purification to remove low molecular weight products, attempted to estimate the extent of hapten incorporation into BSA by UV spectrometry as reported (6), but were unable to distinguish any differential UV absorption due to overlapping bands. Moreover, when rabbits were immunized with this antigen, serum antibody titers to **1** were marginal, as determined in vitro by competitive ELISA and by bioassay in rats.

We therefore studied this reaction in detail and found that difficulties are encountered in the use of the succinamyl spacer group to link **2** to BSA. This was shown to be due to the propensity of the succinamyl group to side reactions during the coupling procedure, thus lowering the coupling yields or nullifying it entirely. These inherent problems with the succinamyl linker have not previously been described, and we wish to alert other readers of this Journal of this potential pitfall.

In its stead, we introduce the glutamyl- $\beta$ -alanyl spacer group for the successful conjugation of hapten **2** to carrier proteins. The  $\beta$ -alanyl spacer not only extends the linker by four atoms but also allows for the incorporation of radioactivity into the immunogen using  $\beta$ -[<sup>3</sup>H]-alanine, thereby providing an accurate quantitative measure of hapten/protein molar substitution ratios (MSR's).

## EXPERIMENTAL PROCEDURES

Melting points were determined using a Fisher-Johns melting point apparatus and are uncorrected. <sup>1</sup>H NMR spectra were recorded on either a Varian T-60A, Nicolet NT-300WB, or a Varian Gemini 300 spectrometer. IR spectra were recorded on Bio-rad/Digilab FTS-40 or Nicolet 740 FT-IR spectrometers, and a Kratos MS 25 mass spectrometer was used to record the mass spectra. Elemental analyses were performed by Galbraith Laboratories, Inc., Knoxville, TN, or M-H-W Laboratories, Phoenix, AZ.

The following chemicals were purchased from commercial vendors: 2,4,5-trichloroaniline, 1,2-dichlorobenzene, anhydrous toluene, anhydrous acetonitrile, anhydrous ethyl acetate, 1,3-dicyclohexylcarbodiimide (DCC), glutaric anhydride, *N*-hydroxysuccinimide, and  $\beta$ -alanine. Succinic anhydride was purified by sublimation before use. Bis(trimethylsilyl)trifluoroacetamide (BSTFA) was purchased from Sigma Chemical Co., St. Louis, MO, and  $\beta$ -[<sup>3</sup>H]-alanine from DuPont NEN Research Products, Boston, MA. Silica gel GF plates (Analtech, Inc.) were used for TLC analyses. 2-Amino-2',4,4',5,5'-pentachlorobiphenyl (**2**) was synthesized using procedures pat-

\* To whom correspondence should be addressed.

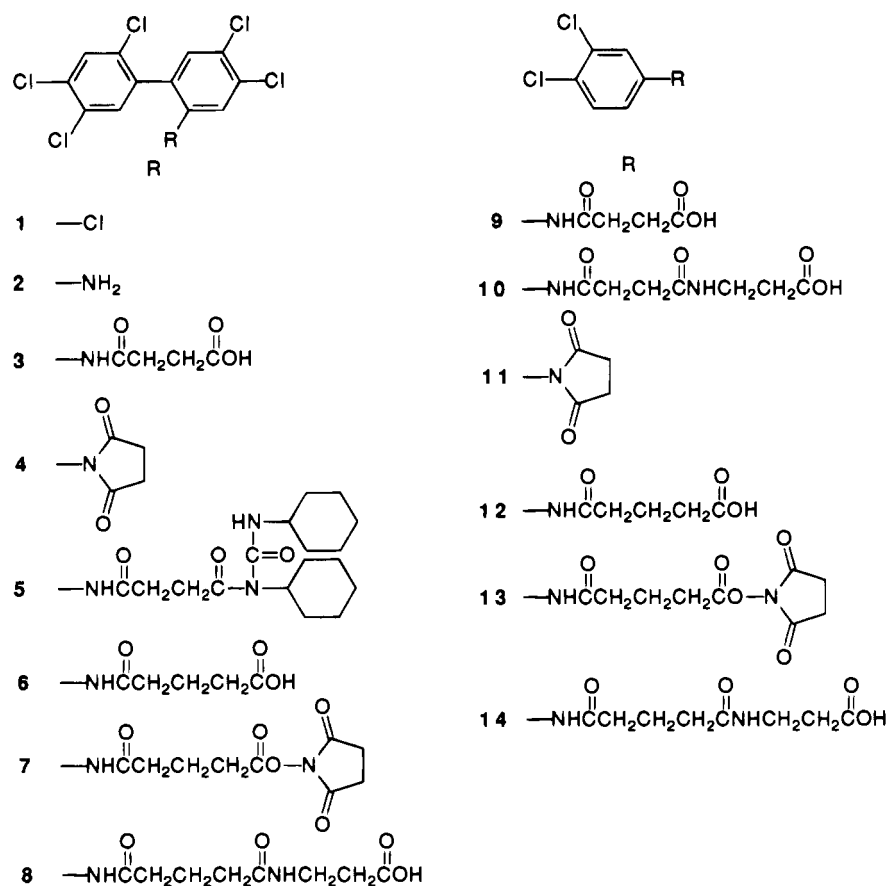
<sup>†</sup> Department of Medicinal Chemistry, University of Minnesota.

<sup>‡</sup> Department of Medicine, University of Minnesota.

<sup>§</sup> Hennepin County Medical Center.

<sup>\*</sup> Abstract published in *Advance ACS Abstracts*, July 15, 1994.

Chart 1



turned after those described by Newsome and Shields (6). Thus, 2,3',4,4',5-pentachlorobiphenyl was prepared by diazotization of 2,4,5-trichloroaniline and subsequent coupling to 1,2-dichlorobenzene and then nitrated to give 2-nitro-2',4,4',5,5'-pentachlorobiphenyl. The latter was reduced to **2** using stannous chloride and hydrochloric acid and isolated and purified by preparative TLC.

**N-(2',4,4',5,5'-Pentachlorobiphenyl-2-yl)succinamic Acid (3).** To a solution of **2** (138.5 mg, 0.406 mmol) and anhydrous toluene (8 mL) was added succinic anhydride (44.6 mg, 0.446 mmol), and the mixture was heated and stirred under reflux for 26 h. Since TLC analysis (methylene chloride:hexane, 1:1) showed considerable unreacted amine remaining, additional succinic anhydride (42.2 mg, 0.442 mmol) was added, and the reaction was allowed to proceed for another 18 h. The solvent was then evaporated in vacuo to give 236 mg of solids which contained succinic anhydride (by NMR analysis). This was removed (34.2 mg) by sublimation at 74 °C (50 mm Hg). The residual solids were recrystallized from ethyl acetate–hexane to give 104 mg (58.0% yield) of **3**: mp 185–7 °C; <sup>1</sup>H NMR (CDCl<sub>3</sub>, 300 MHz)  $\delta$  8.38 (s, 1 H), 7.63 (s, 1 H), 7.38 (s, 1 H), 7.22 (s, 1 H), 7.01 (s, 1 H), 2.72 (t,  $J$  = 6.3 Hz, 2 H), 2.50 (t,  $J$  = 6.3 Hz, 2 H); IR (KBr) 3091, 1709, 1566, 1504, 1452 cm<sup>-1</sup>. Anal. Calcd for C<sub>16</sub>H<sub>10</sub>NO<sub>3</sub>Cl<sub>5</sub>: C, 43.53; H, 2.28; N, 3.17. Found: C, 43.47; H, 2.24; N, 3.17. A second crop, 49.7 mg, had mp 185–7 °C (85.7% total yield).

**N-(3,4-Dichlorophenyl)succinamic Acid (9).** A mixture of 3,4-dichloroaniline (0.64 g, 4.0 mmol), succinic anhydride (0.42 g, 4.2 mmol), and anhydrous toluene (20 mL) was stirred and heated under reflux for 1.5 h. Most of the solids dissolved within the first 15 min of reflux, and the product precipitated soon thereafter. After the

mixture was cooled to room temperature, the crude product (1.03 g) was collected and recrystallized from ethyl acetate–hexane (decolorized with C) to give 0.88 g (84% yield) of **9**: mp 164–5.5 °C; IR (KBr) 3290, 3097, 1699, 1666, 1589 cm<sup>-1</sup>; <sup>1</sup>H NMR (acetone-*d*<sub>6</sub>, 300 MHz)  $\delta$  9.52 (s, 1 H), 8.11 (s, 1 H), 7.53 (m, 2 H), 2.72 (s, 4 H). Anal. Calcd for C<sub>10</sub>H<sub>9</sub>NO<sub>3</sub>Cl<sub>2</sub>: C, 45.83; H, 3.46; N, 5.34. Found: C, 45.96; H, 3.58; N, 5.37.

**Reaction of N-(3,4-Dichlorophenyl)succinamic Acid (9) with DCC.** A solution of **9** (0.26 g, 0.99 mmol) and anhydrous acetonitrile (20 mL) was cooled in an ice bath, and DCC (0.23 g, 1.1 mmol) was added all at once. Within 1 min following dissolution of the DCC, the reaction mixture became cloudy. The reaction mixture was stirred for 2 h in the ice bath and at room temperature for 15 min. The solids (dicyclohexylurea, DCU) were collected (0.17 g, 77% yield, mp 224–230 °C), the filtrate was concentrated in vacuo, and the residue was crystallized from ethyl acetate–hexane (additional 0.02 g of insoluble DCU was removed) to give 0.12 g of crude **11**; mp 180–7 °C; IR (KBr) 1708 cm<sup>-1</sup> (imide C=O). Further recrystallization from ethyl acetate–hexane gave **11** in two crops 0.04 g; mp 189–190 °C, and 0.06 g, mp 194–6 °C (lit. (7) mp 194–6 °C, lit. (8) mp 171–2 °C); <sup>1</sup>H NMR (CDCl<sub>3</sub>, 300 MHz) spectra of both crops were identical  $\delta$  7.53 (m, 2 H), 7.22 (m, 1 H), 2.92 (s, 4 H); EIMS  $m/z$  = 243 (MO<sup>+</sup>) with isotopic cluster consistent with two Cl atoms (9); CIMS  $m/z$  = 244 (MH<sup>+</sup>) with isotopic cluster consistent with two Cl atoms. Anal. Calcd for C<sub>10</sub>H<sub>7</sub>NO<sub>2</sub>Cl<sub>2</sub>: C, 49.21; H, 2.89; N, 5.74. Found: C, 49.41; H, 2.96; N, 5.75.

**Reaction of N-(2',4,4',5,5'-Pentachlorobiphenyl-2-yl)succinamic Acid (3) with DCC.** A solution of **3** (58.0 mg, 0.131 mmol) in anhydrous acetonitrile (10 mL) was cooled in an ice bath, and DCC (30.5 mg, 0.148 mmol)

was added. After the mixture was stirred in the cold for 1.5 h (a white precipitate formed within the first 0.5 h) and at room temperature for 2 h, the precipitate of DCU was collected, 21.2 mg (72% yield). The filtrate was concentrated in vacuo, and the residue was triturated with ethyl acetate. Additional DCU which did not dissolve (3.0 mg) was removed, the concentrated filtrate was applied to a preparative TLC plate, and the plate was developed in chloroform. Visualization with UV (254 nm) light showed three fluorescence quenching spots, one of which was at the origin. Each band was removed and extracted with ethyl acetate, and the extract was concentrated in vacuo. The most mobile band yielded 26.3 mg of a solid which on recrystallization from ethyl acetate–hexane gave 18.6 mg of the succinimide **4**: mp 182–3 °C; <sup>1</sup>IR (KBr) 1722 (imide C=O), 1487, 1456, 1393 cm<sup>-1</sup>; <sup>1</sup>H NMR (CDCl<sub>3</sub>, 300 MHz)  $\delta$  7.52 (s, 1 H), 7.48 (s, 1 H), 7.40 (s, 1 H), 7.31 (s, 1 H), 2.69 (m, 4 H); EIMS isotopic cluster consistent for five Cl atoms (9) with the most intense peak at  $m/z$  = 423 [(M + 2)<sup>+</sup>]; CIMS (isobutane): isotopic cluster consistent for five Cl atoms with the most intense peak at  $m/z$  424 [(MH + 2)<sup>+</sup>]. Anal. Calcd for C<sub>16</sub>H<sub>8</sub>NO<sub>2</sub>Cl<sub>5</sub>: C, 45.38; H, 1.90; N, 3.31. Found: C, 45.65; H, 1.90; N, 3.32. The second most mobile band yielded 18.9 mg of solids which, on recrystallization from ethyl acetate/hexane, gave 11.5 mg of compound **5**: mp 195–9 °C; IR (KBr) 3014, 2932, 2853, 1677, 1648 cm<sup>-1</sup>; <sup>1</sup>H NMR (CDCl<sub>3</sub>, 300 MHz)  $\delta$  8.39 (s, 1 H), 7.63 (s, 1 H), 7.56 (s, 1 H), 7.38 (s, 1 H), 7.22 (s, 1 H), 6.55 (s, 1 H), 2.69 (t, 2 H), 2.56 (t, 2 H), 1.48 (m, 22 H); EIMS isotopic cluster consistent with five Cl atoms (9) with the most intense peak at  $m/z$  522 [(M + 2 – C<sub>6</sub>H<sub>11</sub>NCO)<sup>+</sup>]; CIMS (isobutane) isotopic cluster consistent with five Cl atoms (9) with the most intense peak at  $m/z$  523 [(MH + 2 – C<sub>6</sub>H<sub>11</sub>NCO)<sup>+</sup>]; FABMS (glycerol) isotopic cluster (5 Cl) with most intense peak at  $m/z$  648 [(MH + 2)<sup>+</sup>]. The third band at the origin gave 4.4 mg of a white solid which was not characterized.

***N*-(2',4,4',5,5'-Pentachlorobiphenyl-2-yl)glutaramic Acid (6)**. A solution of **2** (261 mg, 0.472 mmol) and glutaric anhydride (59.0 mg, 0.518 mmol) in anhydrous toluene (8 mL) was heated under reflux with stirring for 24 h. Solids formed when the reaction mixture was allowed to stand overnight at room temperature. After the mixture was cooled in an ice bath, the solids were collected and dried in a vacuum desiccator to give 152 mg of crude **6**. Recrystallization from ethyl acetate–hexane yielded 113 mg (52.6% yield) of **6**: mp 141–2 °C; <sup>1</sup>H NMR (CDCl<sub>3</sub>, 300 MHz)  $\delta$  8.39 (s, 1 H), 7.63 (s, 1 H), 7.38 (s, 1 H), 7.22 (s, 1 H), 6.81 (s, 1 H), 2.39 (t,  $J$  = 7 Hz, 2H), 2.30 (t,  $J$  = 7 Hz, 2H), 1.93 (m, 2 H). Anal. Calcd for C<sub>17</sub>H<sub>12</sub>NO<sub>3</sub>Cl<sub>5</sub>: C, 44.82; H, 2.66; N, 3.07. Found: C, 45.02; H, 2.73; N, 2.97.

***N*-(2',4,4',5,5'-Pentachlorobiphenyl-2-yl)glutaramic Acid *N*-hydroxysuccinimide Ester (7)**. To an ice-cooled solution of **6** (80.3 mg, 0.176 mmol) in anhydrous acetonitrile (10 mL) was added with stirring DCC (40.4 mg, 0.196 mmol) followed 5 min later by *N*-hydroxysuccinimide (22.6 mg, 0.196 mmol). Solids appeared within 10 min after the addition of the *N*-hydroxysuccinimide. After 110 min, the solids were collected and washed with ethyl acetate (1 mL) to give 12.8 mg of DCU. The combined filtrate and wash were concentrated

on a rotary evaporator to give 141 mg of solid residue, which on recrystallization from ethyl acetate–hexane (additional 27.8 mg of DCU was removed giving a total of 41.6 mg or 94.5% yield) gave 86.1 mg of **7** (88.5% yield): mp 188–191 °C; <sup>1</sup>H NMR (CDCl<sub>3</sub>, 300 MHz)  $\delta$  8.35 (s, 1 H), 7.60 (s, 1 H), 7.37 (s, 1 H), 7.30 (s, 1 H), 7.20 (s, 1 H), 2.80 (s, 4 H), 2.61 (m, 2 H), 2.33 (t, 2 H), 2.11 (m, 2 H).

***N*-(2',4,4',5,5'-Pentachlorobiphenyl-2-yl)glutaramyl- $\beta$ -alanine (8)**. A mixture of  $\beta$ -alanine (10.8 mg, 0.121 mmol), BSTFA (35 mL, 0.13 mmol), and anhydrous acetonitrile (5 mL) was heated under reflux with stirring for 0.5 h. Additional BSTFA (35 mL) was added, and the reaction was allowed to proceed for another 40 min. After the mixture was cooled in an ice bath, a solution of the *N*-hydroxysuccinimide ester **7** (50.0 mg, 0.0905 mmol) in anhydrous ethyl acetate (6 mL) was added all at once, and the reaction mixture was stirred with cooling for 1 h and at room temperature for 1 h. Solids (4.1 mg) which had formed were removed by filtration, and the filtrate was concentrated in vacuo to give 102 mg of a slightly yellow oil. To this was added water (5 mL), and the mixture was stirred for 1 h to solvolyze the silyl ester and then extracted with ethyl acetate (3  $\times$  10 mL). The extract was dried (Na<sub>2</sub>SO<sub>4</sub>) and concentrated in vacuo to give 69.9 mg of solids mixed with oil. Recrystallization (twice) from ethyl acetate–hexane gave 34.8 mg of **8** (73.0% yield): mp 202–204 °C; <sup>1</sup>H NMR (300 MHz, CD<sub>3</sub>-OD)  $\delta$  7.89 (s, 1 H), 7.74 (s, 1 H), 7.52 (s, 1 H), 7.44 (s, 1 H), 3.39 (t, 2 H), 2.48 (t, 2 H), 2.24 (t, 2 H), 2.13 (s, 2 H), 1.79 (m, 2H). Anal. Calcd for C<sub>20</sub>H<sub>17</sub>N<sub>2</sub>O<sub>4</sub>Cl<sub>5</sub>: C, 45.61; H, 3.25; N, 5.32. Found: C, 45.79; H, 3.50; N, 5.35.

***N*-(2',4,4',5,5'-Pentachlorobiphenyl-2-yl)glutaramyl- $\beta$ -[3-<sup>3</sup>H]alanine**.  $\beta$ -[3-<sup>3</sup>H]-Alanine (0.0540  $\mu$ mol, 92.60 Ci/mmol) in 2% aqueous ethanol (5.0 mL) was mixed with unlabeled  $\beta$ -alanine (10.7 mg, 0.120 mmol), and the mixture was lyophilized. The coupling procedure above was followed except that H<sub>2</sub>O (3 mL) and 10% aqueous Na<sub>2</sub>CO<sub>3</sub> (3 mL) were used to solvolyze the intermediate silyl ester for approximately 15 min. The mixture was then adjusted to pH 2 with 2 M HCl and worked up as above. Recrystallization of the crude product from ethyl acetate–hexane gave 23.9 mg of radioactive **8** (50.1% yield, sp act = 4.35 mCi/mmol). A second crop, 9.9 mg (20.8%), was obtained by concentration of the filtrate. TLC (*n*-PrOH:H<sub>2</sub>O (7:3) or CHCl<sub>3</sub>:HOAc (4:1)) showed only one spot for both crops.

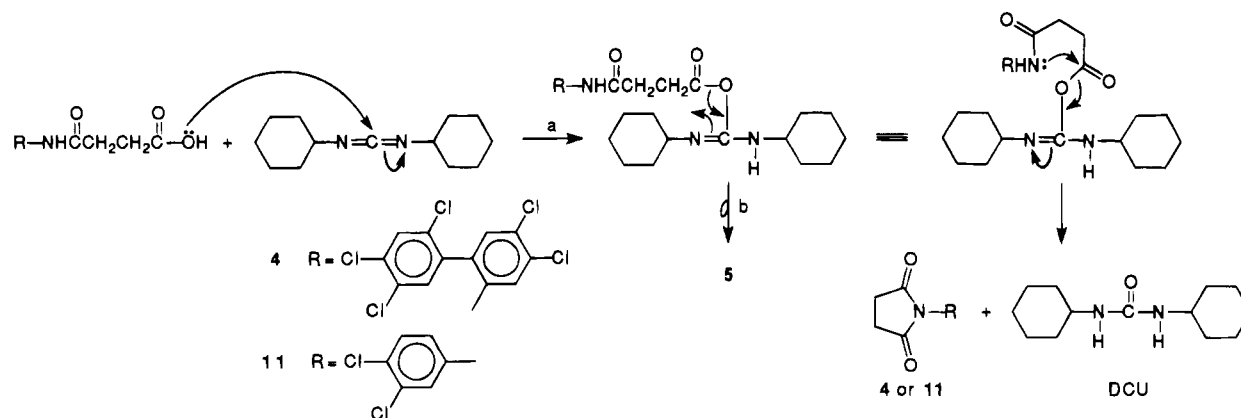
## RESULTS AND DISCUSSION

Spacer groups are often used to separate a xenobiotic hapten from the carrier protein in order to facilitate the production of antibodies to the xenobiotic substance (10). The function of such groups is to hold the hapten away from the protein to which it is covalently bonded so that the lymphocytes can distinguish this antigenic determinant from the protein, thus producing antibodies specific to the epitope. The succinamyl group is one such commonly used linking group (11–14), and we have alluded to our unsuccessful attempts to prepare antibodies against **1** using the succinamyl linker group to join the hapten **2** to serum albumin.

At that juncture, we envisioned that extension of the succinamyl spacer group with a  $\beta$ -alanine linker might achieve two goals, viz., (a) a more potent immunogen might result due to this four-atom extension, and (b) radioactivity could be incorporated into this extended linker for the quantitative assessment of the degree of conjugation to carrier protein. Since the multistep synthesis of hapten **2** (6) was labor intensive and its supply was limited, *N*-(3,4-dichlorophenyl)succinamic

<sup>1</sup> A succinimide, ostensibly compound **4**, was reported to be produced when **2** was reacted with succinic anhydride in the presence of H<sub>2</sub>SO<sub>4</sub> (6). However, no physical chemical properties of this succinimide were reported. In fact, these authors actually prepared **3** by hydrolysis of the succinimide with methanolic NaOH.

Scheme 1



acid (**9**, Chart 1) was prepared as a model compound (albeit with a less sterically hindered amino group) to work out the chemical procedures involved. However, several attempts to prepare the *N*-hydroxysuccinimide ester of compound **9** (for subsequent coupling to  $\beta$ -alanine) by reacting it with DCC in the presence of *N*-hydroxysuccinimide had either very limited success or failed to yield the desired ester. Reactions between compound **9** and 1-hydroxybenzotriazole in the presence of DCC in acetonitrile or dimethylformamide also failed to yield the desired ester. Activation of compound **9** with isobutyl chloroformate using triethylamine or 4-(dimethylamino)pyridine as base followed by reaction with trimethylsilylated  $\beta$ -alanine was also not successful in yielding the desired compound **10**. Small-scale attempts to prepare the *N*-hydroxysuccinimide ester of the succinamylated PCB hapten **3** also failed.

It was observed that when DCC was added to a solution of compound **9** in acetonitrile, solids formed within minutes after mixing *even before the addition of N-hydroxysuccinimide*. These solids were identified to be dicyclohexylurea (DCU) on the basis of the melting point and IR spectrum, suggesting that DCC was effecting the cyclodehydration of the succinamylated compound **9**. Indeed, workup of the filtrate gave a solid whose IR, NMR, and mass spectra were consistent with the *succinimide* **11**. When **3** was treated similarly with DCC in acetonitrile, the succinimide **4** as well as the *N*-acylated dicyclohexylurea **5** were produced. These products were isolated by preparative TLC and characterized by their IR, NMR, and mass spectra and also by elemental analyses for **11** and **4**.

The IR spectra of compounds **11** and **4** exhibited intense carbonyl bands at 1708 and 1722  $\text{cm}^{-1}$ , respectively, characteristic of succinimides, while their NMR spectra showed marked shifts in the positions of some of the aromatic protons relative to the parent succinamic acids as might be expected by their proximity to the succinimide carbonyls. Finally, the EI and CI mass spectra of compounds **11** and **4** showed the correct calculated molecular ions and characteristic isotopic clusters near their molecular ions due to the presence of multiple chlorines (**9**); moreover, the EI mass spectrum of **11** was in good agreement with a published spectrum (**8**).

The mechanism of formation of these products is outlined in **Scheme 1**. It is generally accepted that the initial adduct between DCC and the carboxylic acid to be activated is an *O*-acylisourea (step a), but *O,N*-intramolecular acyl migrations to produce *N*-acylureas

(step b, compound **5**) have also been shown to occur (**15**). However, succinimides such as **11** and **4** have not been reported as byproducts of the reaction of carbodiimides with succinamylated compounds (**11**, **13**, **14**). We recognize, of course, that these succinimides can only be formed from hemisuccinylated *primary* amines. It is likely that the formation of the stable succinimides **11** and **4** from **9** and **3** during the carboxyl activation step abrogated the formation of the desired activated *N*-hydroxysuccinimide *esters* and, by analogy, may have interfered in the coupling of the succinamylated hapten **3** with BSA.

Having recognized this unique problem with the succinamyl spacer group, we investigated the use of the homologous glutaramyl spacer group and found that under similar conditions the glutaramylated model compound **12** readily coupled to  $\beta$ -alanine in good yield. Application of this reaction to **6** yielded the glutaramyl- $\beta$ -alanyl-extended hapten **8** which when coupled to carrier proteins by use of a water-soluble carbodiimide resulted in the preparation of highly potent immunogens (**16**).

Thus, 2-amino-2',4,4',5,5'-pentachlorobiphenyl (**2**) was condensed with glutaric anhydride to give the glutaramyl derivative **6**. Compound **6** was treated with DCC and *N*-hydroxysuccinimide to give the activated ester **7**, which in turn was reacted with trimethylsilylated  $\beta$ -alanine or  $^3\text{H}$ -labeled  $\beta$ -alanine to produce the unlabeled or radiolabeled compound **8**. These reactions proceeded in acceptable to excellent yields. When radiolabeled compound **8** was conjugated with keyhole-limpet hemocyanin, thyroglobulin, and BSA, MSR's of 371:1, 39:1, and 29:1, respectively, were achieved. The use of these immunogens to prepare antibody Fab fragments and application of the latter in the study of the pharmacokinetics of the redistribution and urinary excretion of PCB **1** in rats are being reported elsewhere (**16**).

In summary, we have shown that the glutaramyl- $\beta$ -alanyl spacer group is a highly satisfactory linker arm with general applicability for the conjugation of haptens that contain an amino functional group to carrier proteins and is amenable to incorporation of radioactivity in the linker for the quantitative assessment of the degree of conjugation. The succinamyl group, on the other hand, can lead to byproduct formation during the activation/coupling step which obviates the formation of viable coupling products.

#### ACKNOWLEDGMENT

This work was supported by NIMH Grant MH42799, Hennepin Faculty Associates Grant EIP 111, and in part by the Department of Veterans Affairs. We are indebted



to Thomas P. Krick of the Mass Spectrometry Laboratory (which is maintained by the Minnesota Agricultural Experiment Station) of the Department of Biochemistry, University of Minnesota, St. Paul, for the EI, CI, and FAB mass spectra and for some of the 300-MHz NMR spectra. We thank James A. Elberling and Yul Yost of the Minneapolis VA Medical Center for some of the IR spectra and for the synthesis of initial samples of compound **2**, respectively. Finally, we thank Dr. Gary O. Rankin of Marshall University School of Medicine, Huntington, WV, for directing our attention to refs 7 and 8.

**Supplementary Material Available:** Experimental details for the preparation of the model compounds **12–14** (2 pages). Ordering information is given on any current masthead page.

#### LITERATURE CITED

- (1) Phillips, D. L., Smith, A. B., Burse, V. W., Steele, G. K., Needham, L. L., and Hannon, W. H. (1989) Half-life of polychlorinated biphenyls in occupationally exposed workers. *Arch. Environ. Health* **44**, 351–354.
- (2) Luotamo, M., Jarvisalo, J., and Aitio, A. (1991) Assessment of exposure to polychlorinated biphenyls: analysis of selected isomers in blood and adipose tissue. *Environ. Res.* **54**, 121–134.
- (3) Kimbrough R. D. (1987) Human health effects of polychlorinated biphenyls (PCBs) and polybrominated biphenyls (PBBs). *Ann. Rev. Pharmacol. Toxicol.* **27**, 87–111.
- (4) Rogan, W. J., and Gladen B. C. (1992) Neurotoxicology of PCBs and related compounds. *Neurotoxicol.* **13**, 27–36.
- (5) Snyder, R., and Remmer, H. (1982) Classes of hepatic microsomal mixed function oxidase inducers. *Hepatic Cytochrome P-450 Monooxygenase System* (J. B. Schenkman, and D. Kupfer, Eds.) Chapter 8, pp 227–268, Pergamon Press, New York.
- (6) Newsome, W. H., and Shields, J. B. (1981) Radioimmunoassay of PCBs in milk and blood. *Int. J. Environ. Anal. Chem.* **10**, 295–304.
- (7) Fujinami, A., Ozaki, T., Nodera, K., and Tanaka, K. (1972) Studies on biological activity of cyclic imide compounds. Part II. Antimicrobial activity of 1-phenylpyrrolidine-2,5-diones and related compounds. *Agric. Biol. Chem.* **36**, 318–323.
- (8) Arjmand, M., and Saudermann, Jr., H. (1987) *N*-(Chlorophenyl)-succinimides: A novel metabolite class isolated from *Phanerochaete chrysosporium*. *Pesti. Biochem. Physiol.* **27**, 173–181.
- (9) McLafferty, F. W. (1966) *Interpretation of Mass Spectra*, pp 20–23, W. A. Benjamin, Inc., New York.
- (10) Mäkelä, O., and Seppälä, I. J. T. (1986) Haptens and carriers. *Handbook of Experimental Immunology, Vol. 1: Immunochemistry* (D. M. Weir, Ed.; L. A. Herzenberg, C. Blackwell, and L. A. Herzenberg, Co-Eds.) Chapter 3, pp 3.1–3.13, Blackwell Scientific Publications, Boston.
- (11) Van Vunakis, H., Freeman, D. S., and Gjika, H. B. (1975) Radioimmunoassay for anileridine, meperidine and other *N*-substituted phenylpiperidine carboxylic acid esters. *Res. Commun. Chem. Path. Pharmacol.* **12**, 379–387.
- (12) Brunswick, D. J., Needelman, B., and Mendels, J. (1978) Radioimmunoassay of imipramine and desmethylinipramine. *Life Sci.* **22**, 137–146.
- (13) Trouet, A., Masquelier, M., Baurain, R., and Deprez-De Campeneere, D. (1982) A covalent linkage between daunorubicin and proteins that is stable in serum and reversible by lysosomal hydrolases, as required for a lysosomotropic drug-carrier conjugate: *In vitro* and *in vivo* studies. *Proc. Natl. Acad. Sci. U.S.A.* **79**, 626–629.
- (14) Henn, T. F. G., Garnett, M. C., Chhabra, S. R., Bycroft, B. W., and Baldwin, R. W. (1993) Synthesis of 2'-deoxyuridine and 5-fluoro-2'-deoxyuridine derivatives and evaluation in antibody targeting studies. *J. Med. Chem.* **36**, 1570–1579.
- (15) Bodanszky, M., Klausner, Y. S., and Ondetti, M. A. (1976) Formation of the peptide bond. *Peptide Synthesis*, 2nd ed., Chapter 5, pp 85–136, John Wiley and Sons, New York.
- (16) Keyler, D. E., Goon, D. J. W., Shelver, W. L., Ross, C. A., Nagasawa, H. T., St. Peter, J. V., and Pentel, P. R. Redistribution and enhanced urinary excretion of 2,2',4,4',5,5'-hexachlorobiphenyl (HCB) in rats using HCB-specific IgG and Fab fragments. *Biochem. Pharmacol.*, in press.

# Characterization of Ribosome-Inactivating Proteins Isolated from *Bryonia dioica* and Their Utility as Carcinoma-Reactive Immunoconjugates

Clay B. Siegall,\* Susan L. Gawlak, Dana Chace, Edith A. Wolff, Bruce Mixan, and Hans Marquardt†

Molecular Immunology Department, Bristol-Myers Squibb, Pharmaceutical Research Institute, 3005 First Avenue, Seattle, Washington 98121. Received March 25, 1994\*

Two ribosome-inactivating proteins (RIPs) were isolated and characterized from the roots of *Bryonia dioica*. One of these was a novel 27-kDa protein termed bryodin 2 (BD2), while the second was a previously reported RIP, referred to here as bryodin 1 (BD1). The amino-terminal sequence obtained for BD2 was similar, but distinct from BD1, ricin A chain, trichosanthin, and momorcharin. BD2-specific monoclonal antibodies were generated and found not to react with BD1 or ricin A chain. Purified BD1 and BD2 RIP inhibited protein synthesis in a cell-free *in vitro* translation assay at EC<sub>50</sub> values of 7 and 9 pM, respectively. Intravenous administration of BD1 was less toxic to mice than BD2, with LD<sub>50</sub> values of >40 for BD1 and 10–12 mg/kg for BD2. Primary human endothelial cells were 5–8-fold less sensitive to BD1 and BD2 than compared to ricin A chain. BD1 and BD2 were constructed as immunoconjugates with the chimeric form of BR96 (chiBR96), a carcinoma-reactive, internalizing antibody. ChiBR96–BD1 and chiBR96–BD2 were found to bind to and kill BR96 antigen-positive carcinoma cells while not killing antigen-negative carcinoma cells. Bryodins represent RIPs that may be useful in constructing immunotoxin conjugates with reduced toxicity and vascular sensitivity, as compared to ricin A chain immunotoxins.

## INTRODUCTION

Plant ribosome-inactivating proteins (RIPs)<sup>1</sup> have been placed into two groups based on their structure (1, 2). Type I RIPs (i.e., gelonin, saporin, and trichosanthin) contain a single chain that has enzymatic activity but no binding domain. Type II RIPs (i.e., ricin and abrin) contain two chains, an A chain that is catalytically active and a B chain that contains a cell binding domain and lectin properties, and are thereby cytotoxic to many cell types. Both types of RIPs inhibit protein synthesis by inactivating the 60S subunit of eukaryotic ribosomes through cleavage of the N-glycosidic bond of adenine at position 4324 of 28S rRNA (3–6).

The ribosome-inactivating protein bryodin (BD) was initially identified as a 30-kDa type I RIP isolated from the plant *Bryonia dioica* (7). Three additional species from the plant family Cucurbitaceae have also been found to contain RIPs, *Momordica charantia* (8–10), *Trichosanthes kirilowii* (11–15), and *Luffa cylindrica* (16–18). The RIPs identified from these plants include  $\alpha$ - and  $\beta$ -momorcharin ( $\alpha$ -MMC,  $\beta$ -MMC) from *Momordica charantia*; trichosanthin (TCS),  $\alpha$ -trichosanthin ( $\alpha$ -TCS), and trichokirin from *Trichosanthes kirilowii*; and  $\alpha$ -luffin, luffin-a, and luffin-b from *Luffa cylindrica*. All of these proteins display properties that are characteristic of Type I RIPs, namely a single-chain protein of approximately 25–30 kDa, and an isoelectric point ranging between 9.0 and 10.0 (1, 2).

The linkage of toxic proteins including ribosome-

inactivating proteins isolated from plants and bacterial toxins with antibody molecules results in antigen-specific cytotoxic agents referred to as immunotoxins (19). Immunotoxins have been prepared using a variety of RIPs, including BD (7, 20–22), ricin (23, 24), saporin (25), and pokeweed antiviral protein (26). Type I RIPs offer advantages over Type II RIPs or bacterial toxins such as diphtheria toxin or *Pseudomonas* exotoxin A in that removal of the toxin-binding domain is not required to gain target selectivity (27).

Ricin has been the most widely employed RIP for immunotoxin clinical trials. Despite the significant antitumor responses obtained in trials using ricin-based immunotoxins (28), there are still difficulties in administering these reagents. One such difficulty is vascular leak syndrome, a common toxicity associated with ricin A chain-immunotoxins (29). Thus, the isolation of new RIPs that are less harmful to human vasculature may be useful in preparing immunotoxins that either cause no or reduced vascular leak syndrome.

In this report, we describe the characterization of two novel RIP activities from the roots of *Bryonia dioica*. One of these, a newly isolated BD form referred to as BD2, was compared to the previously identified form referred to as BD1 regarding N-terminal amino acid sequence and reactivity to a BD2-specific monoclonal antibody. Additionally, *in vitro* protein synthesis inhibition activity (cell-free), *in vitro* endothelial cell sensitivity, and *in vivo* toxicity were determined for BD1, BD2, and the RIPs ricin A chain, pokeweed antiviral protein, and gelonin. Lastly, cell-killing activity in the form of BD1 and BD2 immunotoxin conjugates with a carcinoma-reactive antibody were determined against four human carcinoma cell lines.

## EXPERIMENTAL PROCEDURES

**Reagents.** 4-[(Succinimidyl)oxy]carbonyl- $\alpha$ -methyl- $\alpha$ -(2-pyridyldithio) toluene (SMPT) and 2-iminothiolane (2-IT) were purchased from Pierce Chemical Corp. (Rock-

\* To whom correspondence should be addressed: Tel. 206-727-3542; Fax 206-727-3603.

† Biochemistry Department.

\* Abstract published in *Advance ACS Abstracts*, July 15, 1994.

<sup>1</sup> Abbreviations: RIP, ribosome-inactivating protein; BD1, bryodin 1; BD2, bryodin 2; ELISA, enzyme-linked immunosorbent assay; rt = room temperature; mAb, monoclonal antibody; SMPT, 4-[(succinimidyl)oxy]carbonyl- $\alpha$ -methyl- $\alpha$ -(2-pyridyldithio)-toluene; IMDM, iscoves modified dulbecco medium.

ford, IL). Hypoxanthine-aminopterin-thymidine was purchased from Sigma Chemical Corp. (St. Louis, MO). Gelonin, pokeweed antiviral protein-S, and ricin A chain were purchased from Inland Laboratories, Inc. (Austin, TX). ABC immunoblot kits were purchased from Vector Laboratories (Burlingame, CA). Goat anti-mouse HRP was purchased from Tago (Camarillo, CA). [ $^3\text{H}$ ]Leucine was purchased from New England Nuclear (Boston, MA). Gamma Bind Plus, CM-Sepharose, Blue-Sepharose, and S-Sepharose were purchased from Pharmacia (Uppsala, Sweden). TSK-3000 columns were purchased from Tosoh-Haas, Inc. (Philadelphia, PA). Chimeric BR96 monoclonal antibody (chiBR96) was provided by Drs. I. and K. E. Hellström (30).

**Cell Lines and Culture Conditions.** H3396 human breast carcinoma cells and H3747 and H3719 human colon carcinoma cells were provided by Drs. I. and K. E. Hellström, Bristol-Myers Squibb Pharmaceutical Research Institute (Seattle, WA). H3396 cells were derived from a metastatic human breast carcinoma. H3747 and H3719 cells were established from primary human colon carcinomas. The three tumor cell lines were established at Bristol-Myers Squibb (Seattle, WA) and cultured as monolayers in IMDM supplemented with 10% FBS and 1% penicillin/streptomycin. MDA-MB-453 human breast carcinoma cells were purchased from the American Type Culture Collection (Rockville, MD). Human aortic (HAEC), pulmonary artery (HPAEC), and umbilical vein (HUVEC) endothelial cells were purchased as primary cultures from Clonetics, Inc. (San Diego, CA) and cultured in endothelial growth medium (EGM). EGM is composed of modified MCDB 131 media, 10 ng/mL of EGF, 1.0  $\mu\text{g/mL}$  of hydrocortisone, 2% FBS, 0.4% bovine brain extract, 0.05 mg/mL of gentamycin, 0.05  $\mu\text{g/mL}$  of amphotericin-B.

**Purification of Plant Protein.** *Bryonia dioica* roots were purchased from Poyntzfield Herb Nursery in Black Isle by Dingwall, Ross-shire, U.K. Total root protein was obtained from the roots of *Bryonia dioica* through a series of four steps: (1) the cleaned root sample was peeled, shredded, and homogenized in PBS (1 L per 550 g of plant material), (2) the slurry was stirred at low speed for 16 h at 4 °C and strained through cheesecloth, (3) the sample was centrifuged at 5000g for 15 min at 4 °C to remove large particulates followed by a second centrifugation at 50000g for 20 min to clarify, and (4) the sample was filtered through a sterile 0.22- $\mu\text{m}$  filter and dialyzed against 5 mM sodium phosphate buffer, pH 6.5.

Plant proteins were purified based on charge and size differences using a five-step procedure: (1) the protein was applied to CM-Sepharose equilibrated with 5 mM sodium phosphate, pH 6.5, and eluted with a 0–0.3 M NaCl gradient, (2) chromatography fractions were evaluated by electrophoresis using 12% SDS–PAGE, (3) fractions containing 27–30-kDa protein bands were pooled and concentrated using a Centriprep 10 column (Amicon, Bedford, MA) to less than 8 mL, (4) the sample was applied to a TSK-3000 column (size-exclusion) in an isocratic fashion using PBS as eluant, and (5) fractions were analyzed by electrophoresis using 12% SDS–PAGE. The fractions associated with 29- and 27-kDa bands were pooled and quantitated.

The highest yield of intact BD RIPs was isolated when using younger root sections (root diameter <3 cm) and starting with approximately 235–652 g of root material. Elution of protein from CM-Sepharose resulted in approximately 100-mg (fractions containing BD1 and BD2). A final yield of 10.5–21.6 mg of BD1 and 13.4–35.7 mg of BD2 was obtained following size-exclusion chromatography.

**Amino Acid Sequence Analysis.** Proteins were recovered from SDS–polyacrylamide gels by electroblotting onto a Problott membrane (Applied Biosystems, Foster City, CA) using a Mini-Transblot electrophoretic transfer cell (Bio-Rad Laboratories), as previously described (31). The membrane was stained with Coomassie brilliant blue and then destained, and the 29- and 27-kDa bands were excised for subsequent amino terminal sequence analysis.

Samples were sequenced in a pulsed-liquid protein sequencer (Model 476A, Applied Biosystems) equipped with a vertical cross-flow reaction cartridge using manufacturer-released cycle programs. (Phenylthio)hydantoin amino acid derivatives were analyzed by reversed-phase HPLC with a PTH C18 column (Applied Biosystems) using a sodium acetate/tetrahydrofuran/acetonitrile gradient for elution (32). Data reduction and quantitation were performed using Model 610A chromatogram analysis software (Applied Biosystems).

**Generation of Monoclonal Antibodies to Bryodin Proteins.** Four- to six-week old female BALB/c mice were initially immunized with two subcutaneous injections (0.1 mL) and one intraperitoneal injection (0.2 mL) of a 50:50 mixture of purified BD protein (BD1 and BD2; 200  $\mu\text{g}$  total protein) and Ribi adjuvant (Ribi Immunochemical, Hamilton, MT), with Montanide ISA 50 oil (Seppic, Paris, France) followed by a 0.3-mL intraperitoneal injection of BD protein, 60  $\mu\text{g}$ , in ISA 50 oil on week 4 and then another 0.3-mL intraperitoneal injection of 60  $\mu\text{g}$  of RIP protein on week 7 to boost immunization. Spleen cells from an immunized mouse were removed 3 days after the final immunization and fused with the myeloma, Ag8.653, at a ratio of 3:1 with 40% poly(ethylene glycol) 1450. The fused mixture was plated in HAT (hypoxanthine-aminopterin-thymidine) medium with approximately  $2 \times 10^6$  thymocytes/mL (BALB/c) at 0.2 mL/well into 10 96-well plates.

Positive hybridomas were selected by ELISA. Briefly, Immulon II plates (Dynatech, Chantilly, VA) were coated with 0.3  $\mu\text{g/mL}$  of BD1 or BD2 overnight at 4 °C in 0.1 mL/well of carbonate buffer (0.1 M sodium carbonate/sodium bicarbonate, pH 9.6). Plates were washed with phosphate-buffered saline (PBS), blocked with 200  $\mu\text{L}$ /well of specimen diluent (Genetic Systems Corp., Redmond, WA) for 2 h at 4 °C, and rewashed with PBS. Sample supernatant and specimen diluent (0.05 mL each) were added to each well, incubated at 4 °C for 2 h, and washed three times in PBS. Goat anti-mouse HRP (0.1 mL/well), used at 1:3000 dilution in conjugate diluent (Genetic Systems Corp.), was incubated for 1 h at room temperature and washed four times before addition of 0.1 mL/well of substrate (TMB chromogen in buffered substrate; Genetic Systems) and further incubated for 10 min. The reaction was stopped with 0.1 mL/well of 1.3 M  $\text{H}_2\text{SO}_4$  and the o.d. quantified at 450 nm on a Biotek microplate reader (Winooski, VT).

Positive hybridomas were cloned by two rounds of limiting dilution and retested for reactivity by ELISA as described above. Hybridomas that tested positive for BD2 were cultured in IMDM, 10% FCS, 1% penicillin/streptomycin. Antibodies were purified from culture supernatant by affinity chromatography using Gamma Bind Plus antibody purification columns (Pharmacia). Protein concentration was determined by OD<sub>280</sub>.

Immunoblot analysis was used to confirm the specificity of purified anti-BD2 antibody 50-44-3. SDS–PAGE of BD1, BD2, ricin A chain, and gelonin was performed in duplicate using 12% gels. One of the gels was stained with Coomassie brilliant blue, and the other was trans-

ferred to nitrocellulose, probed with 1  $\mu\text{g/mL}$  50-44-3 mAb, and detected using a mouse Vectastain ABC kit.

**In Vitro Protein Synthesis Inhibition Assay.** Inhibition of protein synthesis was determined using a cell-free rabbit reticulocyte lysate translation system (Promega Biotec, Madison, WI). Briefly, toxin proteins were mixed in a volume of 25  $\mu\text{L}$  with rabbit reticulocyte lysate (70% of reaction volume), a mixture of all amino acids (minus leucine) at 1 mM, 0.5 mCi/mL of [ $^3\text{H}$ ]leucine, and Brome Mosaic Virus RNA (33) as substrate (0.5  $\mu\text{g}$ ). The reaction was incubated at 30  $^{\circ}\text{C}$  for 5 min and terminated by adding 1 M NaOH, 2%  $\text{H}_2\text{O}_2$ . The translation product was precipitated using ice-cold 25% trichloroacetic acid (TCA) and 2% casamino acids on ice for 30 min. The radiolabeled proteins were harvested on glass fiber filters, rinsed with 5% TCA, rinsed with ethanol, dried, and quantitated using a scintillation counter.

**Toxicity of RIPs in Mice.** Six- to eight-week old female athymic mice (nu/nu) were purchased from Harlan Sprague-Dawley (Indianapolis, IN). Toxicity of BD1, BD2, ricin A chain, gelonin, and pokeweed antiviral protein was determined by intravenous (via the tail vein) administration. The purified RIPs were diluted in PBS to reach final administered doses of 1–40 mg/kg, depending on RIP used. Animals were monitored for at least 7 days following injection of RIP. For comprehensive necropsy analysis, animals were intravenously injected with 20 mg/kg BD RIP and sacrificed after 24 h and the tissues analyzed using gross and microscopic techniques by Dr. Denny Liggitt, University of Washington, Seattle, WA, Department of Comparative Medicine.

**Human Endothelial Cell Sensitivity to RIPs.** Inhibition of protein synthesis by BD1, BD2, gelonin, pokeweed-antiviral protein, and ricin A chain on human endothelial cells was studied. Endothelial cells ( $10^5$  cells/mL) in EGM were added to 96-well flat bottom tissue culture plates (0.1 mL/well) and incubated at 37  $^{\circ}\text{C}$  for 16 h. Dilutions of RIPs (BD1, BD2, gelonin, pokeweed-antiviral protein, and ricin A chain) were made in EGM, and 0.1 mL was added to each well for 20 h at 37  $^{\circ}\text{C}$ . Each dilution was done in triplicate. The cells were pulsed with [ $^3\text{H}$ ]leucine (1  $\mu\text{Ci/well}$ ) in leucine-free RPMI with 10% FBS, for an additional 8 h at 37  $^{\circ}\text{C}$ . They were then lysed by freeze-thawing and harvested using a Tomtec cell harvester (Orange, CT). Incorporation of [ $^3\text{H}$ ]leucine into cellular protein was determined using an LKB Beta-Plate liquid scintillation counter.  $\text{EC}_{50}$  is the amount of RIP required to inhibit 50% of protein synthesis as determined by [ $^3\text{H}$ ]leucine incorporation into cellular protein and represent averages of two to three experiments done in triplicate.

**Immunotoxin Construction, Purification, and Binding Analysis.** Chimeric BR96 (15.6 mg/mL) (30, 34, 35) was thiolated by addition of a 3-fold molar excess of 2-IT in 0.2 M sodium phosphate buffer (pH 8.0), 1 mM EDTA for 1 h at 37  $^{\circ}\text{C}$ . BD1 and BD2 (4.6 mg/mL) were derivatized with a 3-fold molar excess of SMPT in 0.2 M sodium phosphate buffer (pH 8.0), 1 mM EDTA at room temperature for 60 min, and conjugation was done as previously described (36).

Immunotoxin conjugates were applied to size-exclusion columns (TSK-3000) and separated from free toxin. The immunotoxin (180 kDa) and free antibody (150 kDa) eluted together and were further purified by Blue-Sepharose affinity chromatography in 0.1 M sodium phosphate pH 7.0 (wash buffer) and adsorbed to Blue-Sepharose (5 mL of resin/5 mg of conjugate) for 16 h at 4  $^{\circ}\text{C}$ . The mixture was packed in a 5-mL Econocolumn (Bio-Rad, Richmond, CA), and 1-mL fractions were eluted with a two-step gradient of increasing NaCl concentra-

tions in wash buffer (400 mM NaCl, step 1; 800 mM NaCl, step 2). Immunotoxin conjugates were quantitated at  $\text{OD}_{280}$  (1.4 = 1 mg/mL) and analyzed by nonreducing SDS-PAGE.

BR96 immunoconjugates were tested for their ability to bind BR96 antigen using H3396 human breast carcinoma cell membranes as previously described (37).

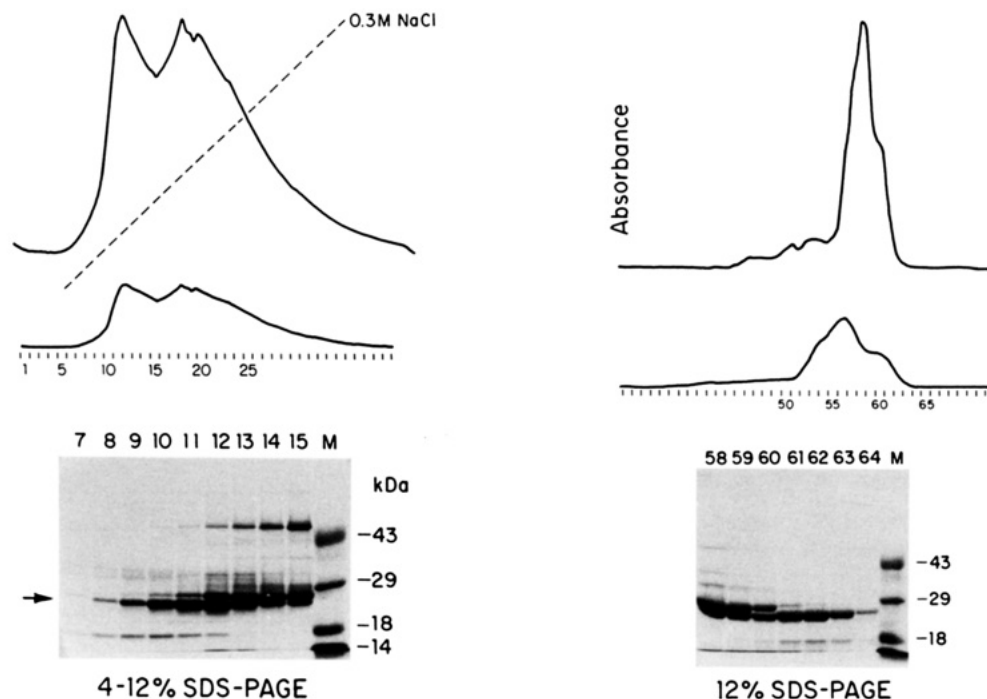
**Cytotoxicity Analysis of chiBR96-BD RIP Immunotoxins.** Tumor cells were plated onto 96-well flat bottom tissue culture plates ( $1 \times 10^4$  cells/well) and kept at 37  $^{\circ}\text{C}$  for 16 h. Dilutions of immunoconjugate or immunoconjugate components were made in culture media, and 0.1 mL was added to each well for 96 h at 37  $^{\circ}\text{C}$ . Each dilution was done in triplicate. After treatment, the wells were washed twice with PBS, 200  $\mu\text{L/well}$  of 1.5  $\mu\text{M}$  calcein-AM (Molecular Probes Inc., Eugene, OR) was added, and the plates were incubated for 40 min at room temperature. Hydrolysis of calcein-AM by intracellular esterases yields the fluorescent product calcein. Following incubation with calcein-AM, fluorescence was determined using a fluorescence concentration analyzer (Baxter Healthcare Corp., Mundelein, IL) at excitation/emission wavelengths of 485/530 nm. The results are presented as percent cell killing for each treatment [ $100 - [(\text{sample signal} - \text{background signal}) / (\text{maximal signal} - \text{background signal}) \times 100]$ ]. The background signal was measured from cells treated with Triton X-100, and the maximal signal was measured from nonimmunotoxin-treated cells.

## RESULTS

**Purification of 29- and 27-kDa Proteins from *Bryonia dioica*.** Roots from *Bryonia dioica* were homogenized in PBS and clarified by centrifugation and filtration. The total root protein was chromatographed using CM-Sepharose, and fractions were evaluated by SDS-PAGE (Figure 1 (left)). Fractions containing proteins migrating at 27–29 kDa were pooled (fractions 9–15) and applied to a TSK-3000 column (Figure 1 (right)). The peak fractions associated with the 29- and 27-kDa bands were separated (fractions 58 and 63, respectively) and quantitated. SDS-PAGE was visualized with Coomassie-blue staining.

**Amino Acid Sequence of Bryodin Proteins.** The amino terminal sequence of the 27- and 29-kDa proteins was determined. The 29-kDa protein had the same N-terminal sequence as previously reported for bryodin (7), herein referred to as bryodin 1 (BD1), while the sequence of the 27-kDa protein encoded the sequence of a novel RIP which we call bryodin 2 (BD2). Figure 2 shows a comparison of the N-terminal amino acid sequence of BD2 with previously identified plant RIPs. The N-terminus of BD2 has 48.3% homology with the A chain of the plant RIP ricin in a 29 amino acid overlap (BD2 residues 1–29 and ricin A residues 7–35). BD2 is slightly less related to BD1 and trichosanthin (TCS), with a 46.4% homology (amino acids 2–29 of BD2 and 1–28 of both BD1 and TCS). Additionally, BD2 shares 39.3% homology with both  $\alpha$ -momorcharin ( $\alpha$ -MMC) and luffin a (Figure 2).

**Generation of mAbs Specific for BD2.** BALB/c mice were immunized and boosted over a 7-week span with a mixture (50:50) of BD1 and BD2, as described in the Experimental Procedures. Briefly, spleen cells were removed from an immunized animal, fused with Ag8.653 myeloma cells, and plated in HAT medium. Hybridomas secreting anti-BD RIP antibodies were selected by ELISA using plates coated with BD1 or BD2. Two BD2-reactive antibodies were cloned by two rounds of limiting dilution and purified by antibody affinity chromatography. We



**Figure 1.** Chromatography and SDS-PAGE analysis of protein isolated from *Bryonia dioica*. (Left) CM-Sepharose chromatography (0–0.3 M NaCl gradient) and Coomassie blue stained, 12% SDS-PAGE (reducing). Fractions containing 27 and 29 kDa protein bands were pooled (fractions 9–15) and concentrated. The smooth line tracing corresponds to eluted protein and the dashed line corresponds to the NaCl gradient. (Right) TSK-3000 chromatography and analysis of concentrated 27- and 29-kDa protein. Absorbance at 280 nm was determined.

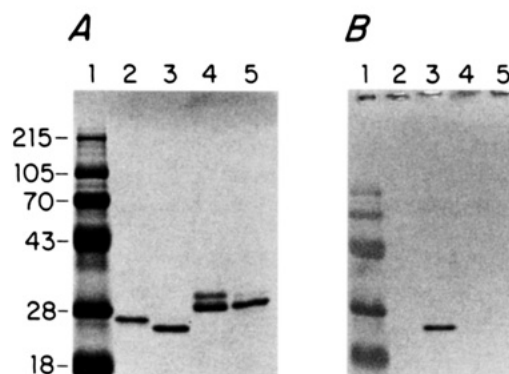
BD2		V	D	I	N	F	S	L	I	G	A	T	G	A	T	K	T	F	I	R	N					
BD1			D	V	S	F	R	L	S	G	A	T	T	S	Y	G	V	F	I	K	N					
RA	I	F	P	K	Q	Y	P	I	I	N	F	T	A	G	A	T	V	Q	S	Y	T	N	F	I	R	A
$\alpha$ -MMC			D	V	S	F	R	L	S	G	A	D	P	R	S	Y	G	M	F	I	K	D				
TCS			D	V	S	F	R	L	S	G	A	T	S	S	S	Y	G	V	F	I	S	N				
Luffin a			D	V	R	F	S	L	S	G	S	S	T	S	Y	S	K	F	I	G	D					

**Figure 2.** Amino acid sequence of 27-kDa (BD2) and 29-kDa (BD1) proteins isolated from *Bryonia dioica*. N-Terminal sequences were determined from electroblotted plant protein, as described in the Experimental Procedures. Comparison of BD2 amino acid sequence with other plant RIPs sequences: RA = ricin A chain;  $\alpha$ -MMC =  $\alpha$ -momorcharin; TCS =  $\alpha$ -trichosanthin.

could not identify any BD1-reactive antibodies from the same fusion.

Once antibodies were isolated that were reactive to BD2, the specificity of this interaction was investigated. One of the BD2 reactive antibodies (50-44-3) was tested by immunoblot analysis against BD1, BD2, ricin A chain, and gelonin. The 50-44-3 anti-BD2 antibody only recognized BD2, as determined by positive immunoblot staining (Figure 3). A second antibody (50-43-1) that reacts similarly was also isolated, although 50-44-3 has a slightly higher level of reactivity with BD2 than does 50-43-1 (data not shown).

**Protein Synthesis Inhibition Activity of BD RIPs.** Both isolated protein toxins, BD1 and BD2, were tested for inhibition of protein synthesis using a cell-free, rabbit reticulocyte lysate assay in which an exogenously added RNA transcript (Brome Mosaic Virus RNA) was used as a translation template for protein synthesis. BD1 and BD2 were found to be potent inhibitors of protein synthesis with  $EC_{50}$  values of 7 and 9 pM, respectively (Table 1). Three other plant ribosome inhibitory proteins were tested for protein synthesis inhibitory activity, gelonin, pokeweed antiviral protein, both type 1 RIPs similar to BD1 and BD2, and ricin A chain. These RIPs inhibited cell-free protein synthesis with  $EC_{50}$  values of 42, 6, and 3 pM, respectively.



**Figure 3.** SDS-PAGE (12%) and immunoblot analysis of BD RIPs (A) stained with Coomassie brilliant blue or (B) transferred to nitrocellulose and probed with anti-BD2 antibody 50-44-3: lanes 1, molecular weight marker; lanes 2, BD1; lanes 3, BD2; lanes 4, ricin A chain; lanes 5, gelonin.

**RIP Toxicity in Mice.** The toxicity of BD1 and BD2 was determined by intravenous administration into female athymic mice. Following administration, the animals were monitored for survival. The single dose  $LD_{50}$  for BD1 and BD2 was determined to be >40 mg/kg and 10–12 mg/kg, respectively (Table 1). For comparison, the single-dose  $LD_{50}$  was also determined for ricin A chain (5 mg/kg), pokeweed antiviral protein (2.5 mg/kg), and gelonin (>40 mg/kg).

Comprehensive necropsy revealed that liver toxicity was the cause of death in mice receiving lethal administration (20 mg/kg, i.v.) of BD2. Histopathologic analysis of tissue from injected animals showed liver lesions and elevated serum glutamic-oxaloacetic transaminase (SGOT) and serum glutamic-pyruvic transaminase (SGPT), indicative of liver damage (data not shown). No other toxicity was identified.

**Endothelial Cell Sensitivity to BD RIPs.** Since ricin A chain is toxic to vascular endothelium, a finding which has been suggested to explain the vascular leak

**Table 1. Protein Synthesis Inhibition and *in Vivo* Toxicity of Various RIPs<sup>a</sup>**

RIP	EC <sub>50</sub> (pM)	LD <sub>50</sub> (mg/kg)
BD1	7	>40
BD2	9	11
RA	3	5
GM	42	>40
PAP-S	6	2.5

<sup>a</sup> *In vitro* protein synthesis inhibition in a cell-free rabbit reticulocyte translation assay. EC<sub>50</sub> represents the amount of RIP required to inhibit 50% of protein synthesis as determined by [<sup>3</sup>H]leucine incorporation versus nontreated translation products. The EC<sub>50</sub> results represents averages of two to three experiments done in duplicate. For LD<sub>50</sub> determination, animals (20–25 g) were observed for survival for >7 days following intravenous injection of RIPs (in PBS vehicle). For each LD<sub>50</sub> value, 10–40 animals were used. RA = ricin A chain (from *Ricinus communis*; GM = gelonin (from *Gelonium multiflorum*); PAP-S = pokeweed antiviral protein-seeds (from *Phytolacca americana*).

**Table 2. Inhibition of Protein Synthesis in Primary Human Endothelial Cells<sup>a</sup>**

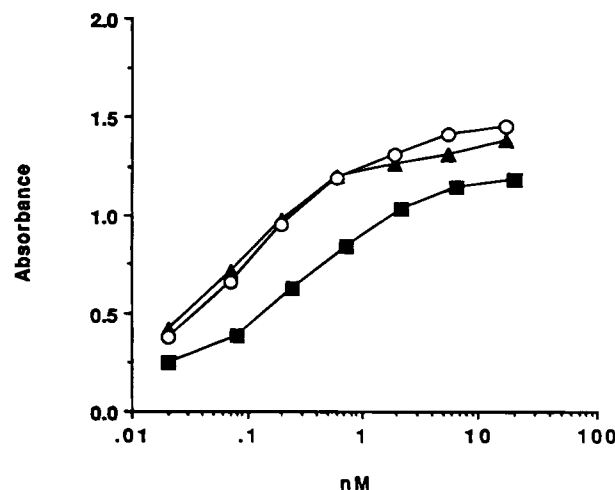
RIP	EC <sub>50</sub> (μM)		
	HPAEC	HAEC	HUVEC
BD1	>3	1.3	2
BD2	1.65	1.3	1.5
RA	0.38	0.24	0.4
GM	>3	2.9	1.7
PAP-S	2.3	0.2	0.4

<sup>a</sup> HPAEC = human pulmonary artery endothelial cells; HAEC = human aortic endothelial cells; HUVEC = human umbilical vein endothelial cells.

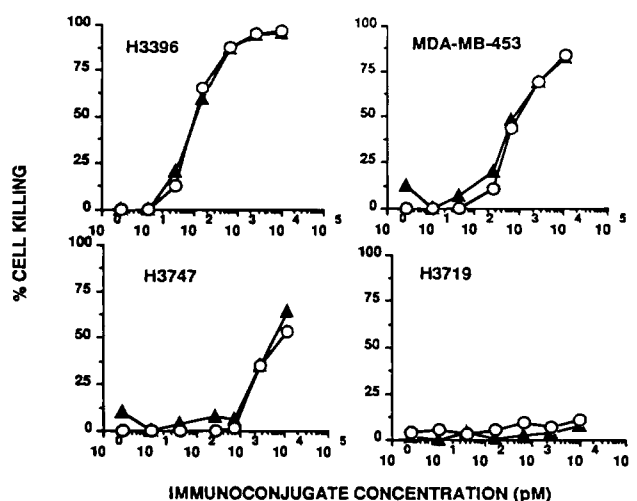
syndrome seen in patients given ricin A-immunotoxins (29), we determined the cytotoxic effects of BD1, BD2, gelonin, pokeweed antiviral protein, and ricin A chain against human endothelium. Cultured primary aortic, pulmonary, and umbilical vein endothelial cells (Clonetics, San Diego, CA) were exposed to RIPs for 20 h, washed free of toxin, and pulsed with [<sup>3</sup>H]leucine for 8 h to measure cellular protein synthesis. The most potent RIPs at inhibiting protein synthesis in endothelium were ricin A chain (0.24 μM) and pokeweed antiviral protein (0.2 μM), both against human aortic endothelium (Table 2). BD1, BD2, and gelonin were able to inhibit cellular protein synthesis in endothelial cell cultures, but with 5–8-fold less potency than ricin A chain or pokeweed antiviral protein (Table 2). Comparing the five RIPs tested, BD1 and gelonin were overall the least potent in inhibiting protein synthesis in endothelial cell cultures.

**Binding of chiBR96-Immunoconjugates to H3396 Membranes.** Antigen binding activity of chiBR96-BD1 and chiBR96-BD2 immunotoxin conjugates was studied using H3396 membranes. Bound chiBR96-immunotoxin was detected by goat anti-human antibodies as previously described (37). Both chiBR96-BD1 and chiBR96-BD2 conjugates bound to H3396 membranes similarly to unconjugated chiBR96 antibody (Figure 4). A slightly increased binding activity in the conjugate may be due to the presence of chiBR96 aggregates caused by the conjugation procedure, since it has previously been shown that increased binding activity can be associated with dimers of chiBR96 (38).

**Cytotoxicity Analysis of chiBR96-BD Immunoconjugates.** Cell-killing activity of chiBR96-BD1 and chiBR96-BD2 immunoconjugates was determined by fluorescent measurement of calcein that is produced following a 96 h incubation of the immunotoxins with cells as described in the Experimental Procedures. ChiBR96-BD1 and chiBR96-BD2 were found to be equally cytotoxic toward BR96 antigen positive H3396 and MDA-



**Figure 4.** Binding analysis of BR96-immunoconjugates. Binding of BR96-immunoconjugates was determined using H3396 cell membranes. Specific antigen binding was detected with goat anti-human IgG HRP. Data represents average of duplicate data points: ■, chiBR96; ○, chiBR96-BD2; ▲, chiBR96-BD1. Absorbance was measured at 405 nm.



**Figure 5.** Cytotoxicity of BR96-BD1 and BR96-BD2 immunoconjugates. Cell killing was determined following incubation of BR96-BD1 and BR96-BD2 immunoconjugates with H3396 and MDA-MB-453 breast carcinomas (antigen positive), H3747 colon carcinoma (antigen positive), and H3719 colon carcinoma (antigen negative) cells for 96 h. Cell killing was determined by measuring calcein-AM hydrolysis into fluorescent calcein: ○, chiBR96-BD2; ▲, chiBR96-BD1.

MB-453 human breast carcinoma cells (EC<sub>50</sub> = 100 pM and 600 pM, respectively) and H3747 human colon carcinoma cells (EC<sub>50</sub> = 4000 pM) (Figure 5). H3719 colon carcinoma cells, displaying undetectable levels of BR96 antigen, were relatively insensitive to both chiBR96-BD1 and chiBR96-BD2 (EC<sub>50</sub> > 5 × 10<sup>4</sup> pM) (Figure 5). The cell lines tested were not sensitive to native BD1 and BD2 at amounts > 1 × 10<sup>4</sup> pM (data not shown).

## DISCUSSION

The plant RIP bryodin, referred to as BD1 in this paper, was previously isolated and partially characterized from *Bryonia dioica* of the Cucurbitaceae family (7). It was found to be a single-chain Type I RIP of approximately 30 kDa in size with an LD<sub>50</sub> in mice of 12.1 mg/kg (39). Bryodin has been reported to inhibit the growth of HIV infected cells and to reduce HIV production (40). The N-terminal amino acid sequence of BD has



homology with other RIPs of the Cucurbitaceae family, specifically TCS and  $\alpha$ -MMC (41). In this paper, two similar but distinct RIPs, BD1 and BD2, were identified and characterized from *Bryonia dioica*.

Since BD2 was chromatographically separated from BD1, we were able to accurately evaluate the biological activities of both proteins. The N-terminal amino acid sequence of BD2 is more similar to ricin A chain than to BD1. Antibodies were generated that were specific for BD2 and not reactive with BD1 or ricin A chain (Figure 3). This further demonstrated the uniqueness of BD2, since BD1 would have stained positive in Western analysis using the anti-BD2 mAb 50-44-3 if BD2 was a processed fragment of BD1.

We determined that BD1, BD2, pokeweed antiviral protein, and ricin A chain were within 3-fold in terms of potency in inhibiting cell-free protein synthesis (Table 1). In contrast, gelonin was more than 5-fold less potent. Pilot toxicology studies performed in mice determined that BD1 and gelonin were the least toxic RIPs tested. In fact, we were unable to establish an LD<sub>50</sub> value for BD1 and gelonin with administrations up to 40 mg/kg. An LD<sub>50</sub> value of 10–12 mg/kg was established for BD2 (Table 1), with toxicity most likely due to liver damage as seen histochemically by liver lesions and by increased liver protein in a blood chemistry screen (data not shown). Similar liver necrosis was also found in toxicity studies with other type I RIPs (22). Ricin A chain and pokeweed antiviral protein were considerably more lethal to mice than BD1, gelonin, or BD2 (Table 1) and, as a result, may be less desirable to utilize in immunoconjugates constructed for clinical use.

Vascular leak syndrome has been an obstacle in human clinical trials of immunotoxins. While it cannot be excluded that complications due to vascular leak are sometimes caused by antibody-mediated immunotoxin-binding to endothelial cells (or neutrophils releasing vasoactive substances), it has been demonstrated that ricin A chain is toxic to cultured endothelial cells and that this toxicity may cause vascular leak *in vivo* (29). The isolation of RIPs or toxins that have less direct effects on endothelial cells may reduce the toxicity of immunotoxins. In cellular protein synthesis inhibition studies, BD1 and BD2 (and gelonin) were found to be >5-fold less active versus cultured aortic endothelial cells than ricin A chain and pokeweed antiviral protein (Table 2). Continued examination of BD1, BD2, and other RIPs or toxins, as well as the immunotoxins themselves, as to their effects on human endothelium, may ultimately enable immunotoxins to be constructed with minimum possible side effects, especially vascular leak syndrome.

Conjugates between chiBR96–BD1 and chiBR96–BD2 were constructed using hindered disulfide linkers. Both immunoconjugates were purified and found to be equally active in killing human carcinoma cells that display BR96 antigen (Figure 5). Since the *in vitro* potency of BD1 and BD2 was similar, it was not unexpected that the conjugates would have similar activity. Chimeric BR96 has previously been conjugated with a binding defective form of *Pseudomonas* exotoxin A (42), LysPE40, and found to inhibit protein synthesis in tumor cell lines that display BR96 antigen. BR96 has also been prepared as a single-chain immunotoxin fusion protein with PE40 (37, 43, 44) and as a drug conjugate with doxorubicin (45).

Immunotoxin conjugates of BD1 and BD2, and ultimately antibody–BD1 or –BD2 fusion proteins constructed by recombinant technology, perhaps requiring an appropriate translocation domain for activity, are of interest for therapeutic application in preclinical *in vivo* models. Both BD RIPs are less toxic *in vivo* than many

other RIPs including ricin A chain and pokeweed antiviral protein, and they are more potent at inhibiting protein synthesis once inside cells than other RIPs including gelonin. This may provide for wider therapeutic windows than are possible with immunoconjugates using more commonly available toxins such as ricin A chain and pokeweed antiviral protein.

#### ACKNOWLEDGMENT

The authors thank Drs. P. Fell, K. E. Hellström, P. Senter, and J. Somerville for helpful discussions and/or critical review of the manuscript, Dr. I. Hellström, B. Nevin, and U. Garrigues for mAb production, Dr. D. Liggitt for histopathology analysis, M. Stebbins for mAb purification, and E. P. Walker for assistance with plant procurement.

#### LITERATURE CITED

- (1) Stirpe, F., and Barbieri, L. (1986) Ribosome-inactivating proteins up to date. *FEBS Lett.* 195, 1–8.
- (2) Jimenez, A., and Vasquez, D. (1985) Plant and fungal protein and glycoprotein toxins inhibiting eukaryotic protein synthesis. *Ann. Rev. Microbiol.* 39, 649–672.
- (3) Endo, Y., Tsurugi, K., and Lambert, J. M. (1988) The site of action of six different ribosome-inactivating proteins from plants on eukaryotic ribosomes: The RNA N-glycosidase activity of the proteins. *Biochem. Biophys. Res. Commun.* 150, 1032–1036.
- (4) Endo, Y., Mitsui, K., Motizuki, M., and Tsurugi, K. (1987) The mechanism of action of ricin and related toxic lectins on eukaryotic ribosomes. *J. Biol. Chem.* 262, 5908–5912.
- (5) Stirpe, F., and Hughes, C. (1989) Specificity of ribosome-inactivating proteins with RNA N-glycosidase activity. *Biochem. J.* 257, 723–727.
- (6) Stirpe, F., Bailey, S., Miller, S. P., and Bodley, J. W. (1988) Modification of ribosomal RNA by ribosome-inactivating proteins from plants. *Nucleic Acid Res.* 16, 1349–1357.
- (7) Stirpe, F., Barbieri, L., Battelli, M. G., Falasca, A. I., Abbondanza, A., Lorenzoni, E., Stevens, W. A. (1986) Bryodin, a ribosome-inactivating protein from the roots of *Bryonia dioica* L. (white bryony). *Biochem. J.* 240, 659–665.
- (8) Barbieri, L., Zamboni, M., Lorenzoni, E., Montanaro, L., Sperti, S., and Stirpe, F. (1980) Inhibition of protein synthesis *in vitro* by proteins from the seeds of *Momordica Charantia* (bitter melon). *Biochem. J.* 186, 443–452.
- (9) Yeung, H. W., Ng, T. B., Li, W. W., and Cheung, W. K. (1987) Partial chemical characterization of alpha- and beta-momorcharins. *Planta Med.* 53, 164–166.
- (10) Yeung, H. W., Li, W. W., Law, L. K., Chan, W. Y., and Ng, T. B. (1986) Alpha and beta momorcharins. Abortifacient proteins from the seeds of the bitter melon *Momordica charantia* (family Cucurbitaceae). *Int. J. Pept. Prot. Res.* 28, 518–524.
- (11) Wang, Y., Quin, R. Q., Gu, Z. W., Jin, S. W., Zhang, L. Q., Xia, Z. X., Tian, G. Y., and Ni, C. Z. (1986) Scientific evaluation of Tian Hua Fen (THF)-history, chemistry and application. *Pure. Appl. Chem.* 58, 798–798.
- (12) Zhang, X., and Wang, J. (1986) Homology of trichosanthin and ricin A chain. *Nature* 321, 477–478.
- (13) Maraganore, J. M., Joseph, M., and Bailey, M. C. (1987) Purification and characterization of trichosanthin. Homology to ricin A chain and implications as to mechanism of abortifacient activity. *J. Biol. Chem.* 262, 11628–11633.
- (14) Collins, E. J., Robertus, J. D., LoPresti, M., Stone, K. L., Williams, K. R., Wu, P., Hwang, K., and Piatak, M. (1990) Primary amino acid sequence of  $\alpha$ -trichosanthin and molecular models for abrin A-chain and  $\alpha$ -trichosanthin. *J. Biol. Chem.* 265, 8665–8669.
- (15) Casellas, P., Dussossoy, D., Falasca, A. I., Barbieri, L., Guillemot, J. C., Ferrara, P., Bolognesi, A., Cenini, P., and Stirpe, F. (1988) Trichokirin, a ribosome-inactivating protein from the seeds of *Trichosanthes kirilowii* Maximowicz. Purification, partial characterization and use for the preparation of immunotoxins. *Eur. J. Biochem.* 176, 581–588.

- (16) Kishida, K., Masudo, Y., and Hara, T. (1993) Protein-synthesis inhibitory protein from seeds of *Luffa cylindrica* Roem. *FEBS Lett.* **153**, 209–212.
- (17) Kanenosono, M., Nishida, H., and Funatsu, G. (1988) Isolation and characterization of two luffins, protein-biosynthesis inhibitory proteins from the seeds of *Luffa cylindrica*. *Agric. Biol. Chem.* **54**, 2967–2978.
- (18) Kataoka, J., Habuka, N., Miyano, M., Masuta, C., and Koizumi, A. (1992) Nucleotide sequence of cDNA encoding  $\alpha$ -luffin, a ribosome-inactivating protein from *Luffa cylindrica*. *Plant Mol. Biol.* **18**, 1199–1202.
- (19) Vitetta, E. S., Fulton, R. L., May, R. D., Till, M., and Uhr, J. W. (1987) Redesigning nature's poisons to create anti-tumor reagents. *Science* **238**, 1098–1104.
- (20) Bolognesi, A., Tazzarini, P. L., Tassi, C., Gromo, G., Gobbi, M., and Stirpe, F. (1992) A comparison of anti-lymphocyte immunotoxins containing different ribosome-inactivating proteins and antibodies. *Clin. Exp. Immunol.* **89**, 341–346.
- (21) Stirpe, F., Wawrzynczak, E. J., Brown, A. N. F., Knyba, R. E., Watson, G. J., Barbieri, L., Thorpe, P. E. (1988) Selective cytotoxic activity of immunotoxins composed of a monoclonal anti-Thy 1.1 antibody and the ribosome-inactivating proteins bryodin and momordin. *Br. J. Cancer.* **34**, 418–425.
- (22) Battelli, M. G., Barbieri, L., and Stirpe, F. (1990) Toxicity of, and histological lesions caused by, ribosome-inactivating proteins, their IgG-conjugates, and their homopolymers. *APMIS.* **98**, 585–593.
- (23) Till, M., Ghetie, V., Gregory, T., Patzer, E., Porter, J. P., Uhr, J. W., Capon, D. J., and Vitetta, E. S. (1988) HIV-infected cells are killed by rCD4-ricin A chain. *Science* **242**, 1166–1168.
- (24) Fishwild, D. M., Aberle, S., Bernhard, S. L., and Kung, A. H. (1992) Efficacy of an anti-CD7-ricin A chain immunotoxin conjugate in a novel murine model of human T-cell leukemia. *Cancer Res.* **52**, 3056–3062.
- (25) Thorpe, P. E., Brown, A. N., Bremmer, J. A., Jr., Fowell, B. M., and Stirpe, F. (1985) An immunotoxin composed of monoclonal anti-Thy 1.1 antibody and a ribosome-inactivating protein from *Saponaria officinalis*: Potent anti-tumor effects *in vitro* and *in vivo*. *J. Natl. Cancer Inst.* **75**, 151–159.
- (26) Uckun, F. M., Chelstrom, L. M., Irvin, J. D., Finnegan, D., Gunther, R., Young, J., Kuebelbeck, V., Myers, D. E., and Houston, L. L. (1992) *In vivo* efficacy of B43 (anti-CD19)-pokeweed antiviral protein immunotoxin against BCL-1 murine B-cell leukemia. *Blood* **79**, 2649–2661.
- (27) Robertus, J. D. (1992) The structure of plant toxins as a guide to rational design. In *Genetically Engineered Toxins* (A. E. Frankel, Ed.) pp 133–150, New York, Marcel Dekker.
- (28) Vitetta, E. S., Thorpe, P. E., and Uhr, J. W. (1993) Immunotoxins: magic bullets or misguided missiles? *Immunol. Today* **14**, 252–259.
- (29) Soler-Rodriguez, A. M., Ghetie, M. A., Marks, N. O., Uhr, J. W., and Vitetta, E. S. (1993) Ricin A chain and ricin A-chain immunotoxins rapidly damage human endothelial cells: implications for vascular leak syndrome. *Exp. Cell Res.* **206**, 227–234.
- (30) Hellström, I., Garrigues, H. J., Garrigues, U., and Hellström, K. E. (1990) Highly tumor-reactive, internalizing, mouse monoclonal antibodies to Le<sup>y</sup>-related cell-surface antigens. *Cancer Res.* **50**, 2183–2190.
- (31) Matsudaira, P. (1987) Sequence from picomole quantities of proteins electroblotted onto polyvinylidene difluoride membranes. *J. Biol. Chem.* **262**, 10035–10038.
- (32) Tempst, P., and Riviere, L. (1989) Examination of automated polypeptide sequencing using standard phenyl isothiocyanate reagent and subpicomole high-performance liquid chromatographic analysis. *Anal. Biochem.* **183**, 290–300.
- (33) Shih, D. S., and Kaesberg, P. (1973) Translation of bromo mosaic viral ribonucleic acid in a cell-free system derived of wheat embryo. *Proc. Natl. Acad. Sci. U.S.A.* **70**, 1799–1803.
- (34) Garrigues, J., Garrigues, U., Hellström, I., and Hellström, K. E. (1993) Le<sup>y</sup> specific antibody with potent anti-tumor activity is internalized and degraded in lysosomes. *Am. J. Path.* **2**, 607–621.
- (35) Schreiber, G. J., Hellström, K. E., and Hellström, I. (1992) An unmodified anticarcinoma antibody, BR96, localizes to and inhibits the outgrowth of human tumors in nude mice. *Cancer Res.* **52**, 3262–3266.
- (36) Thorpe, P., Wallace, P., Knowles, P., Relf, M., Brown, A., Watson, G., Knyba, R., Wawrzynczak, E., and Blakely, D. (1987) New coupling agents for the synthesis of immunotoxins containing a hindered disulfide bond with improved stability *in vivo*. *Cancer Res.* **47**, 5924–5931.
- (37) Siegall, C. B., Chace, D., Mixan, B., Garrigues, U., Wan, H., Paul, L., Wolff, E., Hellström, I., and Hellström, K. E. (1994) *In vitro* and *in vivo* characterization of BR96 sFv-PE40. *J. Immunol.* **152**, 2377–2384.
- (38) Wolff, E. A., Schreiber, G. J., Cosand, W. L., and Raff, H. V. (1993) Monoclonal antibody homodimers: enhanced anti-tumor activity in nude mice. *Cancer Res.* **53**, 2560–2565.
- (39) Barbieri, L., Battelli, M. G., and Stirpe, F. (1990) Blood clearance and organ distribution and tissue concentration of native, homopolymerized and IgG-conjugated ribosome-inactivating proteins. *Xenobiotica* **20**, 1331–1341.
- (40) Wachinger, M., Samtleben, R., Gerhauser, C., Wagner, H., and Erfle, V. (1993) Bryodin, a single-chain ribosome-inactivating protein, selectively inhibits the growth of HIV-1 infected cells and reduces HIV-1 production. *Res. Exp. Med.* **193**, 1–12.
- (41) Montecucci, P. C., Lazzarini, A. M., Barbieri, L., Stirpe, F., Soria, M., and Lappi, D. (1989) N-terminal sequence of some ribosome-inactivating proteins. *Int. J. Peptide Protein Res.* **33**, 263–267.
- (42) Siegall, C. B., Gawlak, S. L., Chin, J. J., Zoeckler, M. E., Kadow, K. F., Brown, J. P., and Braslawsky, G. R. (1992) Cytotoxicity of chimeric (human-murine) monoclonal antibody BR96, F(ab')<sub>2</sub> and Fab' conjugated to *Pseudomonas* exotoxin. *Bioconjugate Chem.* **3**, 302–307.
- (43) Friedman, P. N., McAndrew, S. J., Gawlak, S. L., Chace, D., Trail, P. A., Brown, J. P., and Siegall, C. B. (1993) BR96 sFv-PE40, a potent single-chain immunotoxin that selectively kills carcinoma cells. *Cancer Res.* **53**, 334–339.
- (44) Friedman, P. N., Chace, D. F., Trail, P. A., and Siegall, C. B. (1993) Anti-tumor activity of the single-chain immunotoxin BR96 sFv-PE40 against established breast and lung tumor xenografts. *J. Immunol.* **150**, 3054–3061.
- (45) Trail, P. A., Willner, D., Lasch, S. J., Henderson, A. J., Casazza, A. M., Firestone, R. A., Hellström, I., and Hellström, K. E. (1993) Cure of xenografted human carcinomas by BR96-doxorubicin immunoconjugates. *Science* **261**, 212–215.

# Targeting Glucose Oxidase at Aspartate and Glutamate Residues with Organic Two-Electron Redox Mediators

Fernando Battaglini, Maria Koutroumanis, Ann M. English,\* and Susan R. Mikkelsen\*

Department of Chemistry and Biochemistry, Concordia University, 1455 de Maisonneuve Boulevard West, Montreal, Quebec, Canada H3G 1M8. Received February 9, 1994\*

The bimolecular rate constants for the reactions of five organic two-electron redox mediators with reduced glucose oxidase (GOx) were determined by measuring voltammetric electrocatalytic currents at glassy carbon electrodes in the presence of excess glucose under anaerobic conditions. The mediators studied were thionine, brilliant cresyl blue, azure A, daunomycin, and dopamine, and the bimolecular rate constants for electron transfer between GOx and the oxidized mediator ( $M^{-1} s^{-1}$ ) are  $1.6 \times 10^4$ ,  $4.0 \times 10^2$ ,  $9.8 \times 10^2$ ,  $9.0 \times 10^3$ , and  $1.2 \times 10^6$ , respectively. GOx was covalently derivatized using 1-ethyl-3-[3-(dimethylamino)propyl]carbodiimide and *N*-hydroxysulfosuccinimide to form amide bonds between the aliphatic primary amine groups on daunomycin and dopamine and carboxylate side chains of aspartate and glutamate residues. Derivatives with  $2.5 \pm 0.1$  daunomycin groups and  $4 \pm 1$  dopamine groups were obtained, with activities of 50% and 75%, respectively, relative to native GOx in a dye-peroxidase assay. Although the daunomycin derivative did not show measurable intramolecular electron-transfer rates, the dopamine derivative rapidly transfers electrons from active-site FADH<sub>2</sub> groups to the oxidized (quinone) form of dopamine. Because the heterogeneous oxidation of dopamine is relatively slow, the currents measured at +0.75 V vs Ag/AgCl were not at their limiting (plateau) values, and only a minimum value of the intramolecular rate constant ( $4.5 s^{-1}$ ) could be determined. This value is >20 times larger than values obtained for GOx-ferrocene derivatives in which surface lysine residues were covalently modified using identical coupling reagents and similar reaction conditions. This work shows that targeting GOx carboxylate groups with electron-transfer mediators may represent a promising approach to the design of reagentless glucose biosensors.

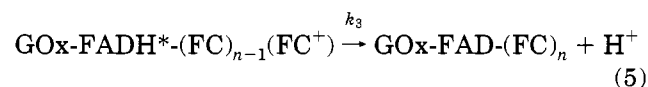
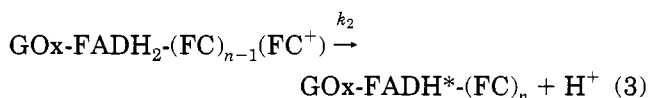
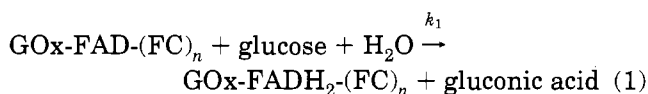
## INTRODUCTION

Quantitative *in vivo* applications of amperometric oxidase-based biosensors generally involve the detection of H<sub>2</sub>O<sub>2</sub> produced by oxidation at high potential ( $\sim 0.7$ – $1$  V vs Ag/AgCl). Possible interference from species such as ascorbic acid in biological fluids is of a major concern at such high potentials, and suitable membranes are used to prevent access of interfering species to the electrode surface (1). However, this generally results in a decrease in the efficiency of H<sub>2</sub>O<sub>2</sub> oxidation at the electrode surface and escape of H<sub>2</sub>O<sub>2</sub> into the surrounding medium, which may be harmful over time. A second, more recent approach has been aimed at replacing oxygen as an electron acceptor by small molecular weight mediators such as ferrocenes which are readily oxidized at lower potentials. For *in situ* applications two problems are foreseen using this approach. One is the containment of small freely-diffusing mediators while allowing access of the substrate, and the second is competition with molecular oxygen present in the sample. For glucose oxidase (GOx), the first problem has been addressed by binding the redox mediators either to an immobilized polymer (2) or directly to the enzyme (3–6). To circumvent the second problem, it is necessary that the mediated reaction be rapid with respect to the reaction with oxygen (6).

Our studies toward reagentless glucose sensors based on GOx have focused on protein derivatization (6). GOx covalently modified with one-electron mediators, such as

ferrocenes (FC), undergoes anaerobic electrocatalytic oxidation in the presence of glucose according to Scheme 1:

### Scheme 1



In this scheme, the fully reduced enzyme, GOx-FADH<sub>2</sub>-(FC)<sub>n</sub>, undergoes two one-electron oxidations of the flavin adenine dinucleotide (FADH<sub>2</sub>), first to the semiquinone (FADH\*) and then to the quinone form (FAD), following one-electron electrochemical oxidation of a bound ferrocene (FC) to ferricinium (FC<sup>+</sup>). In the presence of excess glucose, limiting electrocatalytic currents, *i*<sub>max</sub>, are measured as a function of enzyme concentration to determine the intramolecular electron-transfer rate con-

\* Authors to whom correspondence should be addressed. Fax: (514) 848–2868.

\* Abstract published in *Advance ACS Abstracts*, August 1, 1994.

stant,  $k$ , according to<sup>6</sup>

$$i_{\max} = 2FA[\text{GOx}]_T(D_{\text{GOx}}k)^{1/2} \quad (6)$$

where  $F$  is Faraday's constant,  $A$  the electrode area,  $[\text{GOx}]_T$  the total modified enzyme concentration,  $D_{\text{GOx}}$  the diffusion coefficient of the modified enzyme, and  $k = k_2k_3/(k_2^{1/2} + k_3^{1/2})^2$ .

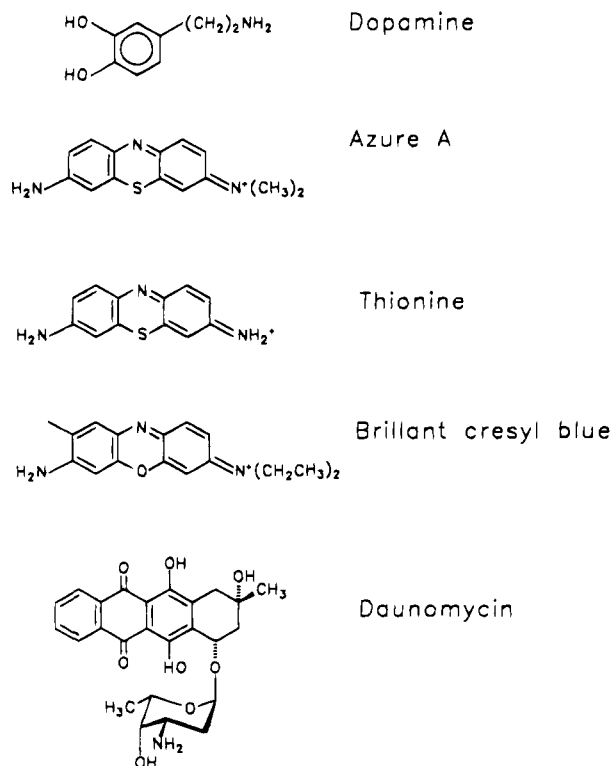
Targeting of GOx at lysine residues with carboxylic acid derivatives of ferrocene resulted in catalytically active products capable of intramolecular mediation.<sup>6</sup> However, the observed intramolecular electron-transfer rate constants ( $<0.2 \text{ s}^{-1}$ ) are 3 orders of magnitude too low to overcome the bimolecular reaction with oxygen. With these derivatives, the rate-limiting step involves electron transfer from the active-site flavin to bound ferricinium groups; this conclusion was reached because electrocatalytic waves observed in the presence of excess glucose show facile heterogeneous electron transfer and well-defined plateau currents. The crystal structure of deglycosylated GOx (7) reveals large distances ( $\geq 23 \text{ \AA}$ ) between active-site FAD/FADH<sub>2</sub> prosthetic groups buried within the 160 kD homodimer and the 30 lysine residues located mainly on the hydrophilic surface of the enzyme, consistent with the slow intramolecular mediation observed for the lysine-targeted derivatives.

Each GOx monomer possesses 66 amino acid residues with carboxylate side chains (aspartate and glutamate). Ten of these are located less than 16 Å from the active-site flavin (7), so derivatization of GOx at carboxylate groups with facile redox mediators should result in mediated FADH<sub>2</sub> oxidation rates that are faster than the competing bimolecular reaction with oxygen.

We began our work toward carboxylate modification by measuring bimolecular electron-transfer rate constants for the oxidation of FADH<sub>2</sub> groups in GOx by mediators containing quinone or phenoxazine structures. Kulys and C  nas (8) have studied quinoidal mediators, and their work shows a linear relationship between the logarithm of the bimolecular rate constants for GOx oxidation (ranging from  $1.5 \times 10^3$  to  $1.5 \times 10^6 \text{ M}^{-1} \text{ s}^{-1}$ ) and formal redox potential (quinone mediators with  $E^\circ$  values between 0.02 and 0.36 V vs NHE were studied); however, none of these mediators possesses functional groups that would allow covalent binding to GOx carboxylate groups. The mediators studied in this work are shown in Figure 1; all possess primary amino groups that could be used to form amide bonds with protein carboxylic acid groups, and all undergo two-electron redox reactions in aqueous media. Two of these mediators, daunomycin and dopamine, were subsequently used for the covalent modification of GOx. The modified enzymes were characterized by measuring mediator:enzyme stoichiometry, aerobic activity relative to native GOx, and anaerobic electrocatalytic behavior in the presence of excess glucose. Our results indicate that intramolecular electron transfer from FADH<sub>2</sub> to the oxidized mediator is rapid in the case of dopamine-modified glucose oxidase; however, heterogeneous electron transfer from enzyme-bound dopamine to the glassy carbon electron surface is slow.

## EXPERIMENTAL SECTION

**Materials and Instrumentation.** Glucose oxidase (Grade II, E.C. 1.1.3.4 from *A. niger*) was obtained from Boehringer Mannheim. Peroxidase (E.C. 1.11.1.7 from horseradish), 1-ethyl-3-[3-(dimethylamino)propyl]carbodiimide (EDC), and *o*-dianisidine dihydrochloride were obtained from Sigma. Daunomycin, dopamine, thionine, azure A, brilliant cresyl blue, and  $\alpha$ -D-glucose were



**Figure 1.** Structures of the two-electron mediators used in this work.

purchased from Aldrich. *N*-Hydroxysulfosuccinimide (NHS) was obtained from Pierce. BioRad supplied Coomassie Brilliant Blue G-250 protein assay dye reagent, sodium dodecylsulfate polyacrylamide gels (7.5%), bromophenol blue, and protein molecular weight markers. Potassium phosphate (mono- and dibasic), anhydrous FeCl<sub>3</sub>, and platinum wire for auxiliary electrodes (0.5-mm diameter) were purchased from Fisher. Potassium citrate was obtained from Mallinckrodt. Glassy carbon working electrodes (0.30-cm diameter), Ag/AgCl reference electrodes, and polishing alumina (0.3  $\mu\text{m}$ ) were obtained from Bioanalytical Systems. Ultrafiltration membranes (YM 30, 30 000-MW cutoff) and cells were purchased from Amicon, and Sephadex G-15 gel filtration resin ( $\leq 1500$  MW fractionation range) was obtained from Pharmacia. All solutions were prepared using nanopure water (Barnstead).

UV-vis absorption spectra were recorded on a Cary 1 double-beam spectrophotometer (Varian). A BAS-100A potentiostat (Bioanalytical Systems) and a conventional thermostatted (25  $^\circ\text{C}$ ) three-electrode cell were used for voltammetric experiments. SDS-PAGE was done using a Mini-Protein II Cell (BioRad).

**Methods. Voltammetry.** Immediately following gel filtration on a  $1.5 \times 10\text{-cm}$  column, 500  $\mu\text{L}$  of GOx solution (native or modified) was transferred to the electrochemical cell and deoxygenated under N<sub>2</sub>. Deoxygenated, mutarotated glucose solutions and deoxygenated solutions of free mediator, where required, were added to the cell with a gas-tight syringe. Voltammograms were recorded from 0.0 to 0.8 V vs Ag/AgCl at 2 mV/s under a continuous N<sub>2</sub> purge. Glassy carbon working electrodes were polished with an alumina slurry and sonicated prior to each run.

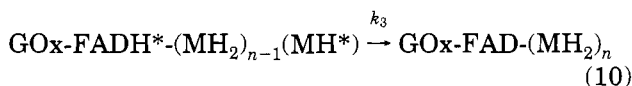
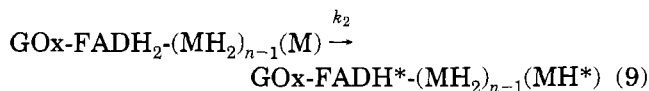
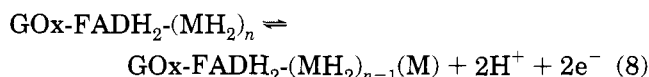
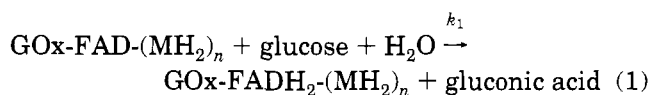
Bimolecular rate constants were determined by voltammetry following consecutive dilutions of a solution of GOx, mediator, and 0.1 M glucose in 0.1 M phosphate buffer, pH 7.0, with a solution of 0.1 M glucose in the same buffer. For freely-diffusing, two-electron redox

mediators, the electrocatalytic plateau current,  $i_{\max}$ , is related to the concentrations of mediator and GOx as shown below (9)

$$i_{\max} = 2FA[M](D_M k'_{\text{obs}}[\text{GOx}])^{1/2} \quad (7)$$

where  $[M]$  and  $D_M$  are the concentration and diffusion coefficient of the mediator,  $k'_{\text{obs}}$  is the bimolecular rate constant for the two-electron oxidation of active-site  $\text{FADH}_2$  by mediator, and  $[\text{GOx}]$  is the concentration of catalytically active FAD (measured by UV-vis difference spectroscopy of the oxidized and fully reduced enzyme (10)).

Rate constants for the intramolecular oxidation by covalently-bound mediator of active-site  $\text{FADH}_2$  in GOx derivatives were determined as described above, but in the absence of free mediator. For rate-limiting intramolecular electron transfer following the two-electron electrochemical oxidation of bound mediator ( $\text{MH}_2$ ), eq 11 describes the dependence of electrocatalytic current on enzyme concentration



$$i_{\max} = 2FA[\text{MGOx}](D_{\text{GOx}}k_{\text{obs}})^{1/2} \quad (11)$$

where  $\text{MGOx}$  is the covalently modified enzyme,  $D_{\text{GOx}}$  is the diffusion coefficient of the enzyme, and  $k_{\text{obs}} = k_2k_3/(k_2 + k_3)$ . Although the studied mediators are all capable of accepting two electrons in a single step, individual one-electron transfers are considered because the semiquinone,  $\text{FADH}^*$ , is known to exist (11). The derivation of this expression is very similar to that reported for eq 6.<sup>6</sup>

**Covalent Modification of GOx.** (a) *Daunomycin.* To 15 mL of 0.25 mM daunomycin and 10  $\mu\text{M}$  GOx in 0.1 M phosphate buffer, pH 7.0, were added 300 mg of EDC and 16 mg of NHS, yielding final concentrations of 100 mM EDC and 5 mM NHS. After the mixture was stirred at 4 °C for 4 h, excess reagents were removed by ultrafiltration, followed by gel filtration on a 1.5-  $\times$  40-cm column with 0.1 M phosphate buffer. The modified enzyme eluted in the first band, an aliquot of which was immediately studied by voltammetry, and the remainder stored at 4 °C.

(b) *Dopamine.* The same procedure was used for GOx modification with dopamine, except that the final reagent concentrations were 5 mM dopamine, 50  $\mu\text{M}$  GOx, 100 mM EDC, and 10 mM NHS, and the reaction was allowed to continue at 4 °C for 12 h.

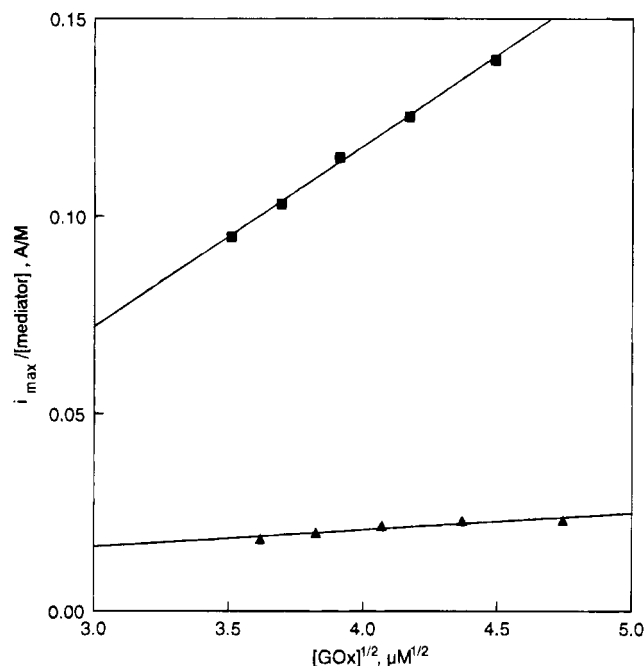
For both modification procedures, control reactions were carried out in the absence of EDC and NHS. These reactions were necessary to test for the adsorption of mediator to GOx, since this is known to occur with hydroquinone sulfonate (12).

**Characterization of Covalently Modified GOx.** Total protein concentrations were determined following gel filtration, using the Coomassie Blue dye-binding assay (13), with native GOx as a calibration standard, following the procedure recommended by BioRad. Mediator:GOx stoichiometries were determined spectrophotometrically. In the case of daunomycin-modified GOx, the molar absorptivities of free daunomycin at 476 nm ( $9620 \text{ M}^{-1} \text{ cm}^{-1}$ ) and 550 nm ( $5560 \text{ M}^{-1} \text{ cm}^{-1}$ ) were used, and measurements were made on  $\text{N}_2$ -purged solutions of modified enzyme in 0.1 M glucose to eliminate absorbance due to FAD. Dopamine was determined at 584 nm ( $178 \text{ M}^{-1} \text{ cm}^{-1}$ ) following color development in the reaction with the  $\text{Fe(III)}$ -citrate complex;<sup>14</sup> dopamine quantitation was done after protein quantitation, so that dopamine calibration standards could be prepared with the same concentration of native GOx. In this assay, 100  $\mu\text{L}$  of a stock solution containing 0.015 M  $\text{FeCl}_3$  and 0.37 M citrate (pH 7.0) was combined with 900  $\mu\text{L}$  of a standard containing a known dopamine concentration and added native GOx in 0.1 M phosphate buffer, pH 7.0; after 5 min,  $A_{584}$  was measured. A typical dopamine calibration curve followed the equation  $A_{584} = 178[\text{dopamine}] + 0.027$ , with  $R = 0.991$ . The catalytic activities of the modified GOx species were determined relative to native GOx, using the coupled peroxidase-o-dianisidine assay (15) in  $\text{O}_2$ -saturated 0.1 M phosphate (pH 7.0) at 23 °C. SDS-PAGE was used to confirm that no crosslinking of GOx occurred during modification. Electrophoresis of samples (modified and native GOx) containing the tracking dye bromophenol blue was performed for 30 min at 100 V, and the gels were stained with Coomassie Blue.

## RESULTS AND DISCUSSION

Bimolecular rate constants for the reaction of native GOx with five two-electron mediators were determined so that a facile mediator could be chosen for the covalent modification of GOx. Voltammetric dilution experiments performed on anaerobic solutions containing excess glucose yielded a linear dependence of  $i_{\max}/[M]$  on  $[\text{GOx}]^{1/2}$ , as expected from eq 7. Figure 2 shows these plots for dopamine and thionine, and the bimolecular rate constants for all five mediators are given in Table 1, along with their formal redox potentials and the potentials at which  $i_{\max}$  values were measured or estimated. The quinone form of dopamine is clearly the best mediator of the five, with a rate constant 2–4 orders of magnitude larger than the other mediators. At pH 7, however,  $E^{\circ'}$  for dopamine is 0.17 V but a measurable current is observed only at potentials  $>0.5$  V, revealing irreversible electrochemical behavior indicative of slow heterogeneous electron transfer. Nonetheless, the broad electrocatalytic wave observed in the presence of GOx and glucose (Figure 3) approaches a diffusion-limited plateau at the measurement potential of +0.70 V, allowing a lower limit of  $1.2 \times 10^6 \text{ M}^{-1} \text{ s}^{-1}$  to be estimated for  $k'_{\text{obs}}$  using eq 7. More precise determinations of voltammetric plateau currents, and hence of  $k'_{\text{obs}}$ , would require applied potentials extreme enough to oxidize amino acid and carbohydrate residues present in GOx.

GOx was covalently modified with dopamine and daunomycin by amide bond formation between GOx carboxylates and the aliphatic primary amino groups present on the mediators. The activities and mediator:enzyme stoichiometries of these derivatives were measured, and the results are summarized in Table 2. Control reactions performed in the absence of the EDC and NHS coupling reagents yielded active enzyme with



**Figure 2.** Plots of normalized voltammetric plateau current ( $i_{\max}/[M]$ ) against  $[\text{GOx}]^{1/2}$  according to eq 7: (■) [dopamine]/[GOx] = 5.9, initial [GOx] = 20  $\mu\text{M}$ ; (Δ) [thionine]/[GOx] = 6.3, initial [GOx] = 23  $\mu\text{M}$ . Voltammograms (2 mV/s) were recorded in 0.1 M phosphate buffer, pH 7.0, containing 100 mM glucose. The diffusion-limited electrocatalytic plateau was not reached using dopamine as a mediator, so  $i_{\max}$  was approximated by the current measured at +0.70 V (see text).

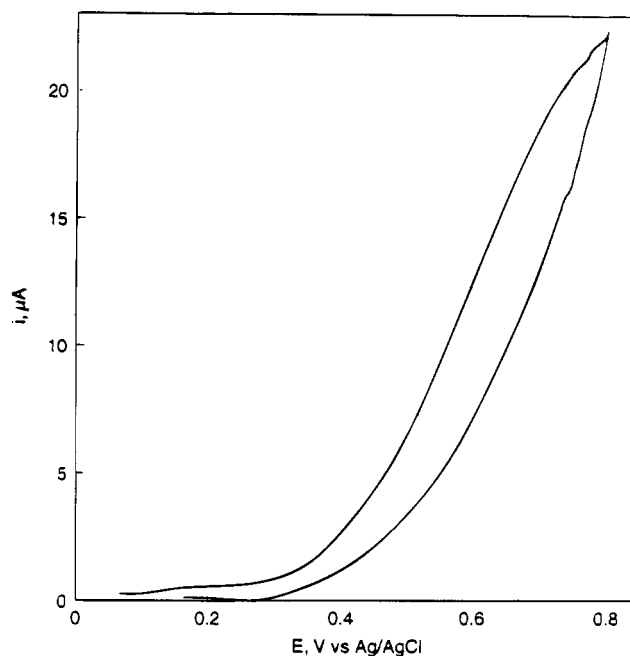
**Table 1. Observed Bimolecular Rate Constants for the Oxidation of GOx by Freely-Diffusing Two-Electron Mediators ( $k'_{\text{obs}}$ )<sup>a</sup>**

mediator	$k'_{\text{obs}}$ ( $\text{M}^{-1} \text{s}^{-1}$ )	$E^0$ , V vs Ag/AgCl	working potential <sup>d</sup> V vs Ag/AgCl
brilliant cresyl blue	$4.0 \times 10^2$	-0.27 <sup>b</sup>	-0.15
azure A	$9.8 \times 10^2$	-0.22 <sup>b</sup>	-0.25
thionine	$1.6 \times 10^4$	-0.18 <sup>b</sup>	-0.10
dopamine	$1.2 \times 10^6$	+0.17 <sup>c</sup>	+0.70
daunomycin	$9.0 \times 10^3$	+0.37 <sup>b</sup>	+0.60

<sup>a</sup> Experimental conditions: 0.1 M phosphate buffer, pH 7.0; initially,  $[M] \approx 1.0 \times 10^{-4} \text{ M}$  and  $[\text{GOx}] \approx 1.0 \times 10^{-5} \text{ M}$ ; scan rate = 2 mV/s;  $T = 25^\circ \text{C}$ ;  $k'_{\text{obs}}$  from eq 7. <sup>b</sup> Values were estimated from the average of the anodic and cathodic peak potentials in aqueous phosphate buffer (0.1 M, pH 7.0) in the absence of GOx. <sup>c</sup> Reported by Tse and Kuwana (17). <sup>d</sup> Voltammetric electrocatalytic plateau currents ( $i_{\max}$ ) were observed at these working potentials for all the mediators except dopamine (see text).

no detectable mediator following gel filtration, indicating that neither daunomycin nor dopamine adsorb to GOx, unlike hydroquinone sulfonate (12). SDS-PAGE showed that no crosslinking of GOx occurred during the coupling reactions. Attempts to modify GOx with the phenoxazine mediator thionin in a similar reaction were unsuccessful, probably because the aromatic amine group of thionin is a poor nucleophile. Only strong nucleophiles, such as aliphatic primary amines, are reactive toward the NHS ester intermediate formed in the GOx coupling reaction.

It is interesting to compare the extent of GOx carboxylate derivatization with amine-containing mediators to results obtained previously for the targeting of lysines with carboxylate-containing mediators, since the same coupling chemistry was used in both studies. Our previous work showed that ferrocenemonocarboxylic acid can be covalently bound to 12 of the 32 primary amino groups present in GOx (6), whereas this work shows that under similar conditions, dopamine binds to an average of only four of the 132 carboxylate-containing Asp and



**Figure 3.** Voltammogram (2 mV/s) of 100  $\mu\text{M}$  dopamine in the presence of 20  $\mu\text{M}$  GOx and 100 mM glucose in 0.1 M phosphate buffer, pH 7.0.

**Table 2. Stoichiometries and Activities of Covalently Modified GOx**

mediator	mediator:GOx stoichiometry <sup>a</sup>	relative activity <sup>b</sup>
none	0	100
daunomycin	$2.5 \pm 0.2$	50
dopamine	$4 \pm 1$	73

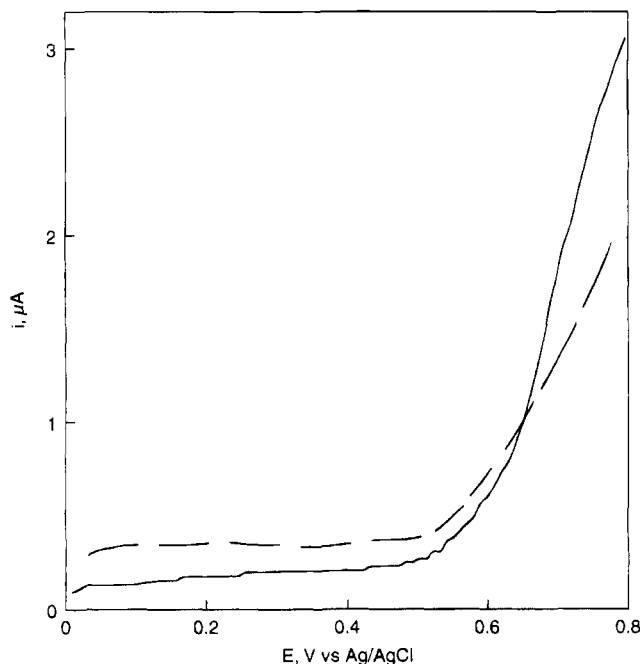
<sup>a</sup> Determined as outlined in the Experimental Section. <sup>b</sup> Homogeneous activity with oxygen mediation as measured by the coupled peroxidase-*o*-dianisidine activity assay (15).

Glu residues in the enzyme. A previous study of GOx carboxylate modification with glycine methyl ester has shown that extreme conditions are required to achieve significant levels of modification (250 mg of EDC and 1 g of glycine methyl ester in 15 mL of 40  $\mu\text{M}$  GOx yields 38% derivatization) (16). Our results with dopamine and daunomycin demonstrate the lack of reactivity of GOx carboxylates toward amide bond formation.

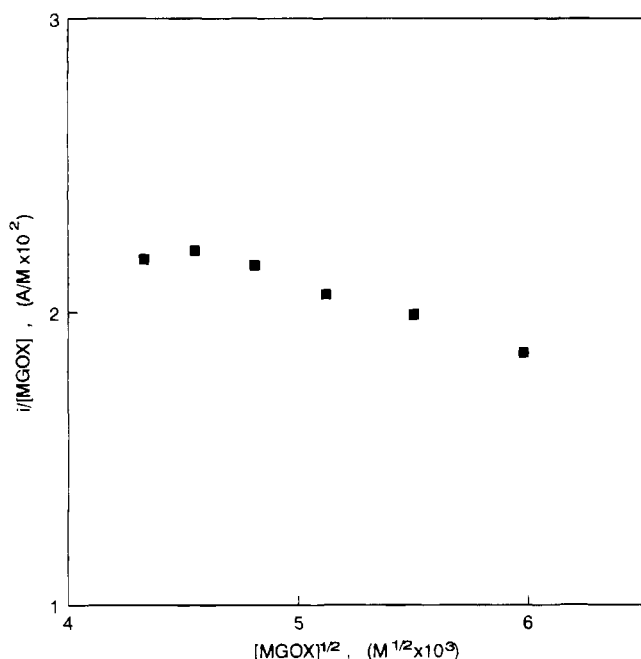
Although the dopamine derivative of GOx has 4:1 stoichiometry while the daunomycin derivative has a lower degree of substitution at 2.5:1, the dopamine derivative shows significant greater activity in the dye-peroxidase assay, with oxygen as cosubstrate. Derivatization of carboxylate residues in or near the substrate access channel could conceivably account for this difference in activity, since a larger group such as daunomycin would more effectively block the substrate channel.

Figures 4 and 5 show the results of voltammetric dilution experiments on anaerobic solutions of dopamine-modified GOx. The electrocatalytic wave observed in the presence of glucose (Figure 4) occurs at a more positive potential in the dopamine-GOx derivative than with free dopamine and native GOx, probably because of the reduced electron-donating ability of the dopamine substituent following amide bond formation. Electrocatalytic currents were measured at +0.75 V rather than at +0.70 V as in the case of free dopamine and were used to construct the plot of  $i/[MGOx]$  vs  $[MGOx]^{1/2}$  shown in Figure 5. The normalized electrocatalytic current does not increase with increasing enzyme concentration as is observed in the presence of freely-diffusing mediators (Figure 2). In fact, the slight decrease in normalized





**Figure 4.** Voltammogram (2 mV/s) of 75  $\mu$ M dopamine-modified GOx (MGOx) in 0.1 M phosphate buffer, pH 7.0, in the absence (---) and presence (—) of 100 mM glucose.



**Figure 5.** Plot of normalized voltammetric current,  $i$ , measured at +0.75 V (vs Ag/AgCl) against the square root of the dopamine-modified GOx concentration  $[MGOx]^{1/2}$  in 0.1 M phosphate buffer, pH 7.0, with 100 mM glucose. Diffusion-limited electrocatalytic plateau currents ( $i_{max}$ ) were not obtained using GOx-bound dopamine as a mediator, so the currents measured at +0.75 V (see text) were used as estimates of  $i_{max}$ .

current with increasing MGOx concentration observed in Figure 5 is attributed to protein aggregation as was seen previously for GOx modified with ferrocenes (6).

Under saturating glucose, the electrocatalytic activity is dependent on the rates of the heterogeneous (eq 8) and the homogeneous intramolecular electron transfers in eqs 9 and 10. The average value of  $k_{obs}$  calculated from eq 11 is  $4.5 \text{ s}^{-1}$ , and as in the case of free dopamine, this value represents a *lower limit* for  $k_{obs}$  since limiting currents were not observed in Figure 4 due to the

irreversible electrochemical behavior of dopamine as discussed above. In a scheme involving this type of electrochemical behavior,  $k_{obs}$  will be less than  $k_2k_3/(k_2 + k_3)$  (9); thus, the *lower limit* for  $k_2$  or  $k_3$  for active-site  $FADH_2$  intramolecular oxidation by enzyme-bound mediator is  $4.5 \text{ s}^{-1}$ . Nonetheless, even this minimum value is  $>20$  times larger than the value of  $0.17 \text{ s}^{-1}$  obtained for ferrocene-GOx conjugates prepared by targeting lysine residues using EDC and NHS (6).

The targeting of carboxylate groups in GOx may be an appropriate strategy for the development of a reagentless glucose sensor. GOx derivatization at lysine residues resulted in facile electrochemical kinetics for the generation of ferricinium groups but slow intramolecular electron transfer from the active site to surface-bound mediators (6). The results of this study show that fast intramolecular electron transfer can be obtained following derivatization at carboxylate groups, although dopamine electrochemical oxidation is slow. Work is now in progress toward GOx derivatization with transition metal complexes that undergo facile electrochemical kinetics as well as rapid intramolecular electron transfer following GOx carboxylate derivatization.

#### ACKNOWLEDGMENT

Financial support from the Natural Sciences and Engineering Research Council of Canada is gratefully acknowledged.

#### LITERATURE CITED

- (1) Moussy, F., Harrison, D. J., O'Brien, D. W., and Rajotte, R. V. (1993) Performance of Subcutaneously Implanted Needle-Type Glucose Sensors Employing a Novel Trilayer Coating. *Anal. Chem.* 65, 2072–2077.
- (2) Vreeke, M., Maidan, R., and Heller, A. (1992) Hydrogen peroxide and  $\beta$ -nicotinamide adenine dinucleotide sensing amperometric electrodes based on electrical connection of horseradish peroxidase redox centers to electrodes through a three-dimensional electron relaying polymer network. *Anal. Chem.* 64, 3084–3090.
- (3) Degani, Y., and Heller, A. (1987) Direct electrical communication between chemically modified enzymes and metal electrodes. 1. Electron transfer from glucose oxidase to metal electrodes via electron relays, bound covalently to the enzyme. *J. Phys. Chem.* 91, 1285–1289.
- (4) Heller, A. (1990) Electrical wiring of redox enzymes. *Acc. Chem. Res.* 23, 128–134.
- (5) Bartlett, P. N., Bradford, V. Q., and Whitaker, R. G. (1991) Enzyme electrode studies of glucose oxidase modified with a redox mediator. *Talanta* 38, 57–63.
- (6) Badia, A., Carlini, R., Fernandez, A., Battaglini, F., Mikkelsen, S. R., and English, A. M. (1993) Intramolecular electron-transfer rates in ferrocene-derivatized glucose oxidase. *J. Am. Chem. Soc.* 115, 7053–7060.
- (7) Hecht, H.-J., Kalisz, H. M., Hendle, J., Schmid, R. D., and Schomburg, D. (1993) Crystal structure of glucose oxidase from *Aspergillus niger* refined at 2.3 Å resolution. *J. Mol. Biol.* 229, 153–172.
- (8) Kulys, J. J., and Cénas, N. K. (1983) Oxidation of glucose oxidase from *Penicillium vitale* by one- and two-electron acceptors. *Biochim. Biophys. Acta* 744, 57–63.
- (9) Nicholson, R. S., and Shain, I. (1964) Theory of stationary electrode polarography. *Anal. Chem.* 36, 706–723.
- (10) Duke, F. R., Weibel, M., Page, D. S., Bulgrin, V. G., and Luthy, J. (1969) The glucose oxidase mechanism. Enzyme activation by substrate. *J. Am. Chem. Soc.* 91, 3904–3909.
- (11) Stankovich, M. T., Schopfer, L. M., and Massey, V. (1978) Determination of glucose oxidase oxidation–reduction potentials and the oxygen reactivity of fully reduced and semiquinoid forms. *J. Biol. Chem.* 253, 4971–4979.

- (12) Kajiya, Y., and Yoneyama, H. (1992) Electron transfer between an electron mediator-adsorbed glucose oxidase and an electrode. *J. Electroanal. Chem.* 328, 259–269.
- (13) Bradford, M. M. (1976) A rapid and sensitive method for the quantitation of microgram quantities of protein utilizing the principle of protein-dye binding. *Anal. Biochem.* 72, 248–254.
- (14) Cheronis, N. D., and Entrikin, J. B. (1955) *Semimicro Qualitative Organic Analysis*, pp 117–145, T. Y. Crowell Co., New York.
- (15) (1972) *Worthington Enzyme Manual*, p 19, Worthington Biochemical Corp., New Jersey.
- (16) Jones, M. N., Manley, P., and Wilkinson, A. (1982) The dissociation of glucose oxidase by sodium *n*-dodecyl sulfate. *Biochem. J.* 203, 285–291.
- (17) Tse, D. C. and Kuwana, T. (1978) Electrocatalysis of dihydronicotinamide adenosine diphosphate with quinones and modified quinone electrodes. *Anal. Chem.* 50, 1315–1318.

# Synthesis and Characterization of Conjugates Formed between Periodate-Oxidized Ribonucleotides and Amine-Containing Fluorophores

Ronald E. Hileman, Kay Martin Parkhurst, Naba K. Gupta, and Lawrence J. Parkhurst\*

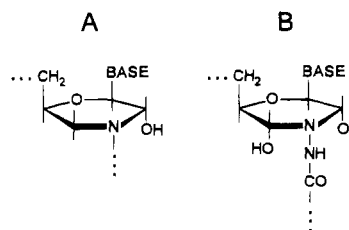
Department of Chemistry, University of Nebraska—Lincoln, Lincoln, Nebraska 68588-0304. Received January 19, 1994\*

The synthesis and purification of new fluorescently labeled derivatives of GDP and ATP are described. The fluorescent groups are coupled initially through amine-containing linker arms to periodate-oxidized nucleotides. Reduction of the initial product yields primarily a six-membered morpholine-like ring. Fluorescein-labeled GDP, rhodamine-labeled GDP, and fluorescein-labeled ATP were characterized by absorbance spectroscopy and TLC. NMR and FAB-MS studies were carried out on a single nucleotide derivative formed by reacting periodate-oxidized guanosine and benzylamine with subsequent reduction to establish the modification to the ribose moiety. The synthesis of the guanosine–benzylamine conjugate led to a mixture of products that were separated. The predominant product (70%) resulted in conversion of the ribose moiety to a six-membered morpholine-like ring having no hydroxyl group, and the minor product (30%) resulted in an open ring structure having one hydroxyl. When NaCNBH<sub>3</sub> was used as the sole reductant, only the product with the morpholine-like ring was formed. These probes were prepared for use in solution studies of the interactions of eukaryotic initiation factor-2 with other components of mammalian protein synthesis initiation.

## INTRODUCTION

Fluorescent dyes have been used extensively as probes to study the microscopic environment of proteins (1–3). In mammalian protein synthesis, the protein eIF-2<sup>1</sup> plays an essential role in initiation. Its function has been characterized using radioactive filter assays (4, 5), and it is known to be required for both ternary (eIF-2·GTP·Met-tRNA<sup>Met</sup>) and 40S complex (40S·mRNA·Met-tRNA<sup>Met</sup>) formation.

Our interest in monitoring the behavior of eIF-2 in solution and in quantitating the interaction of eIF-2 with other components of the protein synthesis initiation process prompted our attempts to label eIF-2 directly with the 5-(and 6)-*N*-hydroxysuccinimidyl ester of rhodamine. This labeling resulted in inactivation of the eIF-2. Since eIF-2 is known to bind GDP and had been reported to bind ATP with high affinity (6), we opted to attach a dye to these nucleotides and label the eIF-2 indirectly. Previous investigators had reported that modification of the ribose has no apparent effect on the binding of these nucleotides to various proteins. For example, the 2',3'-*O*-(2,4,6-trinitrocyclohexadienylidene)-adenosine derivatives have been characterized to act as substrates for adenosine deaminase, alkaline phosphatase, adenylate kinase, myosin subfragment 1, and gastric H<sup>+</sup>,K<sup>+</sup>-ATPase (7–10). The natural product guanosine 3',5'-bispyrophosphate has been implicated to act as a competitive inhibitor for enzymes involved in prokaryotic protein synthesis, in both the initiation and



**Figure 1.** Previously proposed structures formed by the reaction of a periodate-oxidized nucleotide with (A) an amine with subsequent reduction and (B) a hydrazine without subsequent reduction.

elongation steps (11, 12). Moreover, periodate-oxidized guanine nucleotides have been shown to bind to the prokaryotic elongation factor G (EF-G) and the 70S ribosome (13). GTP labeled by dansyl through the 2' (and 3') ribose hydroxyl has been shown to bind to eIF-2 and histone H1 proteins (14).

Formation of Schiff base adducts by the reaction of periodate-oxidized ribonucleotides (or polyribonucleotides) with amines (or hydrazines) has been previously reported (15–17). No structural studies were carried out to clarify the modification at the ribose ring. On the other hand, Khym (18) reported that the reaction of methylamine with periodate-oxidized adenosine and subsequent borohydride reduction yielded a 6-membered morpholine derivative with a hydroxyl group at the 2' position (Figure 1A). Girshovich *et al.* (19) proposed an alternative structure having a hydroxyl group at both the 2' and 3' positions when periodate-oxidized GTP and 2-nitro-4-azidobenzoylhydrazine are reacted in the absence of reducing agents (Figure 1B). Hansske *et al.* (20) also proposed that a morpholine-like structure having 2'- and 3'-hydroxyl groups resulted from the reaction of periodate-oxidized adenosine or adenosine monophosphate with carboxylic acid anhydrazides in the absence of reducing agents (Figure 1B).

We report here the synthesis of GDP- and ATP-fluorescein (GDP\*F<sup>1</sup> and ATP\*F, respectively) and GDP-rhodamine (GDP\*R) prepared by reducing the Schiff base

\* Author to whom correspondence should be addressed.

† Abstract published in *Advance ACS Abstracts*, August 1, 1994.

<sup>1</sup> Abbreviations: GDP\*F, fluorescein-labeled GDP; GDP\*FH, fluorescein hydrazine-labeled GDP; ATP\*F, fluorescein-labeled ATP; GDP\*R, rhodamine-labeled GDP; oxG, periodate-oxidized guanosine; oxGDP, periodate-oxidized GDP; oxATP, periodate-oxidized ATP; GBA, the adduct(s) formed from the synthesis using oxG and benzylamine; GDP-BA, the adduct formed between oxGDP and benzylamine; eIF-2, eukaryotic initiation factor-2; Tris, tris(hydroxymethyl)aminomethane.

formed in the reaction of the 2',3'-dialdehyde of a periodate-oxidized nucleotide with amino derivatives of the dyes. In order to understand the structure of the labeled nucleotides, specifically, the nature of the ribose ring following the incorporation of the dye derivative, we synthesized a guanosine benzylamine derivative (GBA). The synthesis of this material was entirely analogous to that for the labeled nucleotides but gave NMR and mass spectra that were significantly simpler to interpret.

#### EXPERIMENTAL PROCEDURES

**Materials.** The reactive fluorophores purchased from Molecular Probes (Eugene, OR) were 5-((2-aminoethyl)-thioureidyl)fluorescein<sup>2</sup> (catalog no. A-458), 5-((2-((carbohydrazinomethyl)thio)acetyl)amino)fluorescein (C-356), and 5-(and 6)-((N-(5-aminopentyl)amino)carbonyl)tetramethylrhodamine<sup>3</sup> "rhodamine cadaverine" (A-1318). Periodate-oxidized GDP, ATP, and guanosine, as well as NaCNBH<sub>3</sub>, trichloroacetic acid, *N,N*-dimethylformamide, sephadex G-25 superfine, DEAE-sephacel, and the colorimetric inorganic phosphorus determination kit were from Sigma (St. Louis, MO). Silica gel 60 f<sub>254</sub> TLC plates were from EM Science (Darmstadt, Germany), extra fine Biogel P-2 was from BioRad (Richmond, CA), and NaBH<sub>4</sub> and benzylamine were from Aldrich Chemical Co. (Milwaukee, WI). All other materials used were reagent grade or better.

**Buffers used:** buffer A, 10 mM Tris-Cl, pH 8.0; buffer B, 20 mM Tris-Cl, pH 7.8, 100 mM KCl, 5 mM  $\beta$ -mercaptoethanol, and 10% (v/v) glycerol; buffer C, 50 mM Tris-Cl, pH 7.8, 100 mM KCl, 1 mM MgCl<sub>2</sub>, 5 mM  $\beta$ -mercaptoethanol, and 10% (v/v) glycerol.

**Instrumentation and Data Analysis.** All purification was done using an FPLC system that consisted of an LCC-500 Plus gradient programmer, two P-500 pumps, P-1 peristaltic pump, UV-1 monitor, FRAC-100 fraction collector and REC 481 chart recorder (Pharmacia, Uppsala, Sweden) unless otherwise noted. The Pharmacia columns used were Mono-Q HR 5/5, PepRPC 5/5 or 10/10, and G-25 SF HR10/10 fast desalting columns. Absorbance measurements were made using a Hewlett-Packard photodiode array spectrophotometer HP 8452A (Palo Alto, CA).

All NMR and FAB mass spectra were obtained from the instrument facilities at the University of Nebraska—Lincoln Chemistry Department. The NMR spectra were acquired using a General Electric Omega-500 NMR system operating at 500.1 MHz for proton observation. The mass spectra were obtained using an Analytical Instruments VG ZAB-T B<sub>1</sub>E<sub>1</sub>B<sub>2</sub>E<sub>2</sub> configured mass spectrometer with a Cs-Ion gun for FAB desorption or a Kratos MS50 E<sub>1</sub>BE<sub>2</sub> configured mass spectrometer with an Ar-Ion Saddle-Field gun for FAB desorption. The matrix used was either 50:50 (v/v) 3-nitrobenzyl alcohol: glycerol or 1% (v/v) trifluoroacetic acid in glycerol.

For steady-state measurements, the fluorimeter (AlphaScan, Photon Technology, Inc.) with single excitation and emission f4.4 ruled monochromators was fitted with a 150-W Xenon compact arc lamp and a Lexel Model 75 Argon ion laser as light sources with a reference cell quantum counter. Emission scans were collected through PTT's Alphascan software (version 2.060). The background fluorescence from the buffer alone was subtracted for all data reported. Each scan was corrected for dilution when necessary.

Fluorescence anisotropy measurements were made using the method of Meuser and Parkhurst (14), a modification of the Desa and Wampler method (21) with modulation of the exciting light. The same fluorimeter described above was used with a Lexel Model 75 argon ion laser (Palo Alto, CA) with 488-nm light as the excitation light source. A photoelastic modulator (Model 01 01 PEM 80, Hinds International, Inc., Portland, OR) was positioned between the laser and the cuvette in order to modulate the excitation light (14). The laser power supply was set between 5.5 and 6.5 A.

For each emission anisotropy measurement 100 data points were collected in 1 s, first for unmodulated excitation, followed immediately by modulated excitation, with the emission monochromator set at 518 nm for fluorescein or 575 nm for rhodamine. The PEM 80 dial setting was 595.4 nm (retardation 1.22 $\pi$  radians, since the instrument setting corresponds to  $\lambda$  in nm for  $\pi$  retardation). Each set of points was fit by linear regression analysis; the last point of the fitted line was recorded as the emission intensity for the unmodulated reading, and the first point of the fitted line was used for the second, modulated, case. The very slight effect of photobleaching of the fluorescein by the exciting light was thus essentially eliminated. The cuvette holder was thermostated at 15 °C (Lauda K-2/R constant temperature circulating bath). Typically, 250  $\mu$ L of the fluorescein-labeled material was thermally equilibrated in the cuvette, and three to five anisotropy measurements were taken, recorded, and averaged. The corrections to the anisotropy due to scattering were calculated as described earlier (14) and were found to be negligible (less than 0.001).

(1) *Synthesis of Fluorescein-Labeled GDP.* (A) A modification of the method of Ingham and Brew (22), which describes a method for labeling the periodate-oxidized sialic acid moiety of glycoproteins with dansylethylenediamine, fluoresceinamine, or dansylhydrazine, was used for the synthesis of GDP\*F. Our conditions reflect those that were found to be optimal in that work (22). Preliminary PepRPC 10/10 chromatography (conditions described below) of oxGDP was done to ascertain purity; four peaks were obtained (relative amounts given in parentheses) based on the absorbance at 280 nm: oxGDP (83%), oxGMP (9%), oxG (8%), and unknown (<0.4%). The third chromatographic peak of oxGDP had the same retention time as oxG (Sigma) under the same conditions, and the second peak was thus assumed to be oxGMP. All reactions were carried out at room temperature and in the dark to minimize photobleaching. Eighteen  $\mu$ mol of 5-((2-aminoethyl)thioureidyl)fluorescein (8.7 mg) dissolved in 0.4 mL of DMF was added at once to 6  $\mu$ mol (3.0 mg) of periodate-oxidized GDP dissolved in 0.8 mL of 100 mM sodium phosphate buffer, pH 7.1, while stirring. The reaction mixture was stirred for 30 min at room temperature in a fume hood. After the addition of 120  $\mu$ mol (7.5 mg) of solid NaCNBH<sub>3</sub>, the solution was stirred another 30 min followed by the addition of 120  $\mu$ mol of NaBH<sub>4</sub> (120  $\mu$ L of a freshly prepared 1 M NaBH<sub>4</sub> solution in 10 mM NaOH) for a final NaBH<sub>4</sub> concentration of 90 mM. The solution was stirred for 1 h at room temperature and then acidified to pH 5.0 to remove any excess NaCNBH<sub>3</sub> and NaBH<sub>4</sub> by the addition 150  $\mu$ L of 1.0 M acetic acid. The pH was then adjusted to 7.8 with 1 M Tris base, and the solution was left overnight on ice in order to fully oxidize any remaining trace amounts of NaCNBH<sub>3</sub> and NaBH<sub>4</sub>.

In our modification, the reaction mixture was loaded onto a PepRPC 10/10 column (0.5 mL for each sample injection) previously equilibrated with 1% (w/v) potas-

<sup>2</sup> Fluorescein, 2-(3,6-dihydroxy-9H-xanthen-9-yl)benzoic acid.

<sup>3</sup> Tetramethylrhodamine, *N*-[9-(2-carboxyphenyl)-6-(dimethylamino)-3H-xanthen-3-ylidene]-*N*-methylaminium chloride.

sium acetate in water, pH 7.8 at 6 °C. A 10-mL linear gradient of 0 → 45% methanol in 1% (w/v) potassium acetate in water was run, followed by a 40-mL linear gradient of 45 → 90% methanol in 1% (w/v) potassium acetate in water, at a flow rate of 0.5 mL/min. Unlabeled GDP was eluted at 0% methanol in potassium acetate, free fluorescein at approximately 45% methanol and fluorescein-labeled GDP at approximately 75% methanol. One-mL fractions were collected, and an absorbance spectrum from 230–650 nm was obtained for each fraction. The concentrations of GDP and fluorescein were calculated using the following extinction coefficients: GDP, pH 7.8,  $13.7 \text{ mM}^{-1} \text{ cm}^{-1}$  at 252 nm (23), fluorescein, pH 7.8,  $72.6 \text{ mM}^{-1} \text{ cm}^{-1}$  at 492 nm, and  $32.3 \text{ mM}^{-1} \text{ cm}^{-1}$  at 252 nm. The extinction coefficient for fluorescein at 252 and 492 nm were calculated for pH 7.8 buffer using the extinction coefficients of  $75 \text{ mM}^{-1} \text{ cm}^{-1}$  at 492 nm in 20 mM Tris-Cl, pH 9.0 (24). All fractions with a mole ratio of GDP to fluorescein between 0.9 and 1.5 were dried by vacuum centrifugation, weighed (approximately 1 mg product was obtained), and redissolved in a minimum volume of H<sub>2</sub>O (total of 0.2 mL) and stored at -80 °C. A 20–21% yield was achieved based on the initial moles of oxGDP and calculated from the ratio of the product absorbance to that of the starting material at 252 nm (for oxGDP) correcting for the contribution of \*F (for GDP\*F) to the absorbance. For the molar absorptivity of oxidized nucleotides in the 252-nm region, we used the values for the intact nucleotides. The spectra of oxGDP and GDP could be scaled to overlay exactly throughout this region. The labeled GDP was stored frozen at -80 °C and remained stable for at least 4 months through repeated freeze-thaw cycles.

(B) A second procedure for preparing fluorescein-labeled GDP was developed for the 5-((2-((carbohydrazinomethyl)thio)acetyl)amino)fluorescein (\*FH, hydrazine derivative of fluorescein) that followed closely the procedure of Wells and Cantor (25) who describe the preparation of dansyl-labeled tRNA but only used dialysis to purify the labeled material. The motivation for this alternative method was to improve the product yield since the hydrazine moiety forms the relatively stable hydrazone intermediate (compared to the relatively unstable Schiff base formed from amines) (24). Purification was performed using silica gel TLC and size-exclusion chromatography instead of reversed-phase chromatography as in the GDP\*F synthesis described in procedure 1A. All reactions were carried out at room temperature in a fume hood and in the dark. Twelve  $\mu\text{mol}$  of fluorescein hydrazine (6 mg, weighed on an analytical balance) were added to 8  $\mu\text{mol}$  (4 mg) of periodate-oxidized GDP dissolved in 2 mL of 100 mM sodium phosphate buffer, pH 7.1. The reaction was monitored by TLC using silica gel 60 f<sub>254</sub> plastic-backed plates and 80% acetonitrile in water as the solvent. A new fluorescent spot appeared at  $R_f = 0.15$  as the reaction progressed. The optimal reaction time (room temperature) for maximum product formation was 4.5 h. A 10-fold molar excess (NaCNBH<sub>3</sub>:fluorescein) of solid NaCNBH<sub>3</sub> (7 mg) was added at once, and the reaction mixture was stirred for 1 h and then stored at 4 °C overnight before preparative TLC purification was carried out.

Using 25- × 25-cm Kieselgel-60 0.2-mm coated plastic TLC plates, 0.4–0.5 mL of the above reaction mixture, which was stored overnight, was applied by repeated applications followed by drying under a stream of nitrogen. The plates were developed using a 20% water/80% acetonitrile mixture. The newly appearing band ( $R_f = 0.15$ , visualized by room light or a 365-nm lamp) was cut

out from each plate with a razor blade and scraped into a 30-mL siliconized Corex tube. UV-vis absorption measurements later showed that this band corresponded to 1:1 guanosine nucleotide:fluorescein. Fluorescent bands (and the relative amounts estimated visually given in parentheses) were observed at  $R_f = 0.15$  (40%), 0.3 (20%), 0.5 (20%), 0.68 (10%), and 0.75 (10%). Elution of the GDP\*FH was performed using four successive extractions using 5 mL of 20% water in acetonitrile followed by centrifugation at 2000 rpm for 5 min in an SA-600 rotor (DuPont). No visible fluorescein remained in the gel after the fourth extraction. The pooled material was dried to completion by vacuum centrifugation, resuspended in a minimum volume of water (0.75 mL), and loaded onto a 1- × 60-cm Biogel P-2 column preequilibrated with sterile water. A P-1 pump (Pharmacia) was used to maintain a flow rate of 0.02 mL/h while collecting 1-mL fractions. The major fluorescein-containing peak eluted in the void volume of 21 mL and was dried by vacuum centrifugation and weighed. The material was dissolved in 1 mL of water, and an absorbance spectrum was obtained from 230 to 550 nm. The concentration of GDP was calculated from the absorbance at 252 nm, correcting for the contribution of fluorescein at that wavelength and using the extinction coefficients given in procedure 1A. Based on the absorbance at 252 nm (for GDP), 38% of the initial oxGDP was recovered as GDP\*FH. The material was stored at -80 °C.

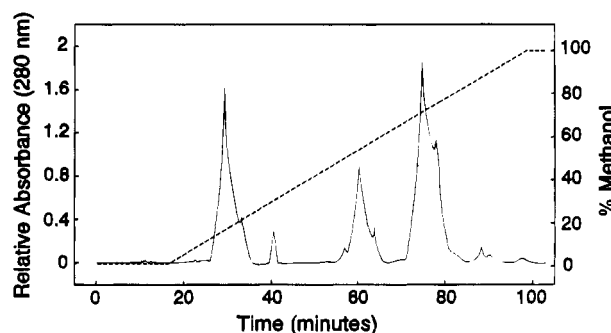
(2) *Synthesis of Fluorescein-Labeled ATP.* The quality of the oxATP starting material was ascertained by PepRPC 10/10 chromatography; two peaks were obtained (relative amounts given in parentheses) based on the absorbance at 280 nm: oxATP (98%), unknown (2%). This synthesis was identical to that used for GDP\*F, procedure A, through the step calling for the solution to be stored overnight on ice to ensure complete oxidation of any remaining borohydride. A different chromatographic method was used, however, since ATP\*F and free fluorescein nearly coelute on the PepRPC 5/5 column under the conditions for the fluorescein-GDP preparation. First, nearly all the free fluorescein was removed as follows. The solution (after sitting on ice overnight) was diluted to 100 times the reaction volume by the addition of water to 200 mL and loaded onto a 1.0- × 7.0-cm gravity flow DEAE-Sephacel anion exchange column preequilibrated with buffer A (10 mM Tris-Cl, pH 8.0). The column was washed at a flow rate of 0.5 mL/min with buffer A until no absorbance at 492 nm could be detected (approximately 50 mL of buffer A was required). Both the ATP\*F and unlabeled ATP were then eluted with 0.4 M NaCl in buffer A by batch elution. The eluant (3 mL total) was loaded in separate runs (0.5 mL for each sample injection) directly onto a PepRPC 5/5 column preequilibrated with 1% (w/v) potassium acetate in water and washed with 5 mL of the same solution. A 70-mL linear gradient from 0 to 80% methanol in 1% (w/v) potassium acetate solution at a flow rate of 0.2 mL/min was used and resulted in four major peaks at the following methanol concentrations: 0% (reduced ATP), 60% (free fluorescein), 70% (ATP\*F), and 85% (unknown, fluorescein:ATP ratio approximately 4:1 based on absorbances at 492 and 258 nm). One-mL fractions were collected and an absorption spectrum obtained for each from 230 to 650 nm. The ratio of ATP to fluorescein was calculated using the following extinction coefficients. The concentration of ATP was determined from the absorbance at 258 nm, using  $\epsilon_{258 \text{ nm}}$  (pH 7.8) of  $15.4 \text{ mM}^{-1} \text{ cm}^{-1}$  (23), and the concentration of fluorescein from the absorbance at 492 nm, using  $\epsilon_{492 \text{ nm}}$  (pH 7.8) of  $72.6 \text{ mM}^{-1} \text{ cm}^{-1}$  and  $\epsilon_{258 \text{ nm}}$  of  $28.3 \text{ mM}^{-1} \text{ cm}^{-1}$ . The extinction

coefficients for fluorescein at 258 and 492 nm were determined as before in the GDP\*F preparation using  $75 \text{ mM}^{-1} \text{ cm}^{-1}$  at 492 nm in pH 9.0 (24). Fractions that eluted at  $70 \pm 1\%$  methanol in 1% (w/v) potassium acetate solution and that had a molar ratio of ATP:fluorescein from 0.9 to 1.5 were pooled, dried by vacuum centrifugation, weighed (approximately 1 mg of product), and redissolved in a minimum volume of sterile water (0.2 mL). A 24% yield was calculated based on the initial amount of oxATP, with  $\epsilon_{\text{oxATP}} = \epsilon_{\text{ATP}}$  at 258 nm. The material was stored at  $-80^\circ \text{C}$  and was stable for up to 4 months through repeated freeze-thaw cycles.

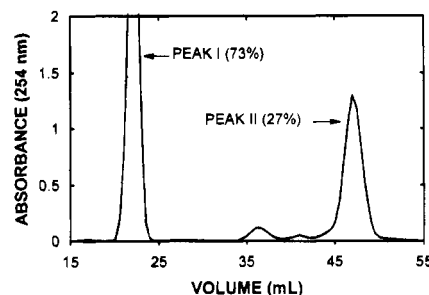
(3) *Synthesis of Rhodamine-Labeled GDP*. This synthesis followed the same protocol used to prepare ATP\*F, with the following exceptions: A 2-fold molar excess of tetramethylrhodamine cadaverine to oxGDP (12 and 6  $\mu\text{mol}$ , respectively) was used. A  $1.0 \times 5.0\text{-cm}$  gravity flow DEAE-Sephacel column was equilibrated with buffer A, the sample was applied, and the absorbance of the eluant was monitored at 556 nm to determine when the unreacted rhodamine had been nearly all removed (approximately 25 mL was required) before elution of the product, as in procedure 2 above. Purified rhodamine-GDP was obtained by PepRPC 5/5 chromatography. The column was preequilibrated with 5% methanol in 1% (w/v) potassium acetate in water, and the total sample (2 mL) was loaded. A 40-mL linear gradient of 5  $\rightarrow$  95% methanol in 1% (w/v) potassium acetate solution at a flow rate of 0.4 mL/min was used. Under these conditions, two peaks were obtained from the column. Unlabeled GDP does not bind and elutes in the void volume, and GDP\*R elutes at approximately 40% methanol. The fractions containing GDP\*R were determined by absorption spectroscopy, using values for  $\epsilon_{556 \text{ nm}}$  of  $70 \text{ mM}^{-1} \text{ cm}^{-1}$  (24) and  $\epsilon_{252 \text{ nm}}$  of 25.9 (pH 7.8) for rhodamine and a value for  $\epsilon_{252 \text{ nm}}$  of  $13.7 \text{ mM}^{-1} \text{ cm}^{-1}$  for GDP (23). These fractions were pooled, dried by vacuum centrifugation, and redissolved in a minimum volume (0.4 mL) of 10% ethanol in  $\text{H}_2\text{O}$ . The purified material was stored frozen at  $-80^\circ \text{C}$ .

(4) *Synthesis of the Guanosine-Benzylamine Derivative*. (A) This synthesis was similar to that used for GDP\*F, procedure 1A. Ten mg of oxG (33  $\mu\text{mol}$ ) was dissolved in 1 mL of 100 mM sodium phosphate buffer, pH 7.1, and added to 36  $\mu\text{L}$  (330  $\mu\text{mol}$ ) of benzylamine mixed into 2 mL of the same buffer. This resulted in a solution that was 110 mM in benzylamine and 11 mM in oxG (10:1, benzylamine:oxG). While the solution was stirring, the progress of the reaction was monitored by spotting 2–5  $\mu\text{L}$  at 20-min intervals on silica gel 60  $f_{254}$  plastic-backed TLC plates, using an 80% (v/v) acetonitrile in water as the mobile phase. A new spot was observed using a 254-nm lamp at  $R_f = 0.78$  ( $R_f$  values for oxG and benzylamine were 0.52 and 0.42, respectively). After the solution was stirred for 1 h, 10 mg of  $\text{NaCNBH}_3$  was added and the solution stirred for 1 h. Ten mg of  $\text{NaBH}_4$  was added and the solution stirred for another 1 h. The solution was acidified to pH 6.0 (measured by the color change after spotting 5  $\mu\text{L}$  on pH paper) by the addition of 50  $\mu\text{L}$  of 4 M acetic acid and stirred for 10 min and the pH adjusted to pH 9.5 (also measured by pH paper) with 75  $\mu\text{L}$  of 1 M NaOH.

Reversed-phase chromatography using the PepRPC 10/10 column was performed using a 0  $\rightarrow$  100% methanol gradient in water over 40 mL while 1-mL fractions were collected at a flow rate of 1 mL/min. Six runs (0.5 mL each) were required to apply the total sample of 3 mL. As shown in Figure 2, three major peaks were obtained by monitoring absorbance at 280 nm, corresponding to reduced oxG at 20% methanol, benzylamine at 50%



**Figure 2.** Reversed-phase chromatography of the crude guanosine-benzylamine mixture using a PepRPC 10/10 column as described in the Experimental Procedures. The relative absorbance is shown as a solid line and the percent methanol as a dotted line.

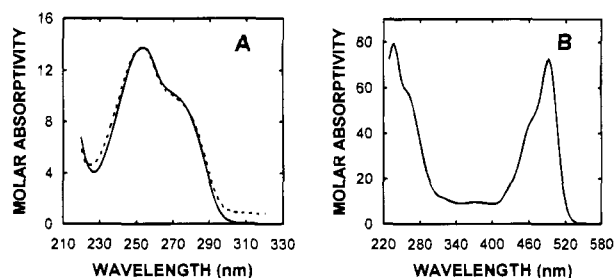


**Figure 3.** Separation of the two major products formed during the guanosine-benzylamine synthesis using a Biogel P-2 column.

methanol, and guanosine-benzylamine at 70% methanol, as identified by the  $R_f$  values on silica TLC of an aliquot from each fraction. Five fractions from each of the six runs that eluted between 65–75% methanol (total volume 30 mL) were pooled and concentrated to approximately 2 mL by vacuum centrifugation. This solution (1 mL/injection) was rechromatographed on the same column using a linear gradient from 0 to 40% methanol in water over 5 mL followed by a 40  $\rightarrow$  90% linear gradient over 70 mL at a flow rate of 2.0 mL/min. Elution was monitored by absorbance at 280 nm, and 1-mL fractions were collected. The predominant absorbance peak occurred at  $70 \pm 1\%$  methanol, and these fractions were spotted and checked for purity on silica TLC. The four fractions that yielded a spot at  $R_f = 0.78$  were pooled, dried by vacuum centrifugation, and redissolved in 0.5 mL water, and the absorption spectrum was obtained. A 38.3% yield was achieved based on the initial oxG, calculated from the absorbance at 254 nm for guanosine ( $\epsilon_{254 \text{ nm}} = 13.7 \text{ mM}^{-1} \text{ cm}^{-1}$ ) and benzylamine ( $\epsilon_{254 \text{ nm}} = 1.2 \text{ mM}^{-1} \text{ cm}^{-1}$ , (26)).

The results of the initial  $^1\text{H}$  NMR analysis suggested that two different products were present. Two peaks (which when integrated) with a ratio of 7:3 were seen for the characteristic guanylyl H-8 downfield chemical shift (approximately 8 ppm) as well as for the anomeric ribosyl H-1' (approximately 5.7 ppm). Further purification was obtained by Biogel P-2 size-exclusion chromatography. The total sample (0.5 mL) was applied to a  $1.5 \times 25\text{-cm}$  column previously equilibrated with water. Fractions of 1 mL each were collected at a flow rate of 0.08 mL/min and were analyzed by absorbance scans from 230 to 350 nm. Two major peaks were observed in the chromatogram when monitored at 254 nm: the first (I) eluted at 24 mL and the second (II) at 46 mL water (see Figure 3). The fractions eluting at 20–23 mL were pooled, and fractions eluting at 45–49 mL were pooled and labeled as GBA (I) and GBA (II), respectively. The





**Figure 4.** (A) Absorption spectra of the Biogel P-2-separated components of the guanosine benzylamine (GBA) synthesis. GBA I (solid line) and GBA II (dotted line) correspond to the major product (peak I) and the minor product (peak II), respectively. (B) Absorption spectra of ATP\*F. The y-axes units are  $\text{mM}^{-1} \text{cm}^{-1}$ .

two small peaks eluting in fractions 34 to 44 mL were discarded. The UV absorption spectra are shown in Figure 4. Both GBA (I) and (II) were submitted for NMR and FAB-MS analysis.

(B) In a second procedure, the synthesis of the guanosine-benzylamine derivative was carried out with the following changes to procedure 4A. The reaction was carried out using 100 mM sodium phosphate buffer, pH 6.5, and  $\text{NaBH}_4$  was omitted. Following PepRPC 10/10 chromatography, the predominant peak material occurring at approximately 70% methanol was submitted for FAB-MS analysis.

(C) In a third procedure, to determine whether phosphates were lost during the reaction, oxGDP was reacted with benzylamine and the resulting product used for phosphate analysis. The same procedure described in section 1A for the synthesis of GDP\*F was used with the following changes. In order to obtain sufficient product for analysis, both the volume and amount of reactants were scaled up. Benzylamine (300 mmol) dissolved in 4 mL of DMF was added at once to 60 mmol of oxGDP dissolved in 8 mL of 100 mM sodium phosphate buffer, pH 7.1, while stirring. Similarly, the amounts of reductants added were scaled up, using 1.2 mmol of solid  $\text{NaCNBH}_3$  and 1.2 mmol of  $\text{NaBH}_4$  (1.2 mL of a 1 M  $\text{NaBH}_4$  solution in 10 mM NaOH). The GDP-BA derivative was isolated as a single peak at approximately 60% methanol from the PepRPC 10/10 chromatography. The product was dried by vacuum centrifugation and redissolved in 4 mL of  $\text{H}_2\text{O}$ .

Silica gel TLC of the nucleotide derivatives was extremely useful during the synthesis to check the progress of reaction and after each chromatographic step to check the purity. Table 1 summarizes the  $R_f$  value(s) for each material and the method of detection used to visualize the plate.

**Inorganic Phosphorus Determination.** The GDP-BA derivative prepared in section 4C above was subjected to acid and enzymatic hydrolysis in order to release inorganic phosphorus as follows. To 124.8 nmol of GDP-BA (determined from the absorbance at 254 nm) was added  $\text{H}_2\text{SO}_4$  to a final concentration of 0.5 M in a total volume of 1.30 mL and the mixture incubated at 100 °C for 1 h. Acid hydrolysis of 1 mol of GDP results in 1 mol of guanine, 1 mol of ribose 5-phosphate, and 1 mol of inorganic phosphorus (23). After treatment, the acid-hydrolyzed sample was analyzed using the colorimetric inorganic phosphorus kit by comparison with a  $\text{KH}_2\text{PO}_4$  standard curve. Measured at 660 nm, for each inorganic phosphate standard (0, 65.1, 130.2, 195.3, 259.9, and 325.5 nmol, each in 2.625 mL) the absorbance values were 0, 0.0841, 0.1762, 0.2671, 0.3556, and 0.4465, respectively. The acid-hydrolyzed GDP-BA sample re-

**Table 1. Summary of TLC Results<sup>a</sup>**

compd	$R_f$ value(s)	
	detected by 365-nm excitation	detected by 254-nm excitation
oxGDP		0
oxATP		0
oxG		0.52
*F	0.18 0.30 0.55 0.68 0.72 0.75	
*FH	0.18 0.30 0.55 0.68 0.72 0.75	
*R	0.19 0.54 0.63	
benzylamine		0.42
GDP*F	0.15	
GDP*FH	0.15	
GDP*R	0.15	
ATP*F	0.10	
GBA (I)		0.78
GBA (II)		0.13

<sup>a</sup> All values were observed using acetonitrile/water 8:2 as the mobile phase.

sulted in an  $A_{660 \text{ nm}}$  value of 0.1729. The sample was compared to the standard curve (correlation coefficient,  $r$ , of 0.9999).

**Purification of eIF-2.** The preparation of both four-(eIF-2 containing the 67-kDa subunit in addition to the three subunits,  $\alpha$ ,  $\beta$ , and  $\gamma$ ) and three-subunit eIF-2 was described earlier (5, 27).

**Labeling eIF-2 with Fluorescein-GDP or Fluorescein-ATP.** The eIF-2 preparations were labeled with a dye-labeled nucleotide by adding a 30-fold molar excess of fluorescein-labeled GDP (GDP\*F) or ATP\*F to eIF-2 as follows. Ten or 20  $\mu\text{L}$  of 1.5 mM ATP\*F in water was added to 0.5 or 1.0 nmol (72 or 144  $\mu\text{g}$ ) of eIF-2 in buffer B (20 mM Tris-Cl, pH 7.8, 100 mM KCl, 5 mM  $\beta$ -mercaptoethanol and 10% (v/v) glycerol), respectively, in a total volume of 0.2 mL, and incubated for 15 min at 37 °C in the dark. All subsequent steps were carried out at 6 °C. The incubation mixture was centrifuged at 15 000 rpm for 10 min and loaded onto a Sephadex G-25 10/10 superfine fast desalting column equilibrated with buffer C (50 mM Tris-Cl, pH 7.8, 100 mM KCl, 1 mM  $\text{MgCl}_2$ , 5 mM  $\beta$ -mercaptoethanol, and 10% (v/v) glycerol) at a flow rate of 0.2 mL/min. The eluant was collected in 0.5-mL fractions and monitored for absorbance at 280 nm. Fluorescently labeled ATP\*F·eIF-2 or eIF-2·GDP\*F eluted in the void volume of 4.5 mL, well separated from the peak of excess ATP\*F or GDP\*F which eluted at 12–13 mL. Although near-base-line resolution was obtained based on the chromatogram (monitored at 280 nm), the fluorescence intensity was commonly 10% above background in the interpeak fractions. The labeled eIF-2 was freshly prepared at the beginning of each set of fluorescence experiments. The portion of material not used immediately was kept on ice and used within 2–3 h or discarded.

Attempts were made to optimize the labeling procedure by varying the incubation conditions: time, temperature, and nucleotide/protein concentrations. An increase in steady-state anisotropy ( $\langle r \rangle$ ) of the chromatographic peak from the gel filtration separation was used as the criterion to determine the optimal conditions. Incubation with greater than a 30-fold molar excess of GDP\*F or ATP\*F over eIF-2 reduced the resolution of the chromatography. Typical  $\langle r \rangle$  values ranged from 0.1 to 0.15 for ATP\*F labeling when a 60-fold molar excess was used, approximately 40% less than the optimal 0.205. Using less than a 30-fold excess only reduced the yield of labeled eIF-2. When a 10-fold molar excess of ATP\*F was used over eIF-2, the measured  $I_F$  value was approximately 50% less than that obtained for a 30-fold excess, but the

anisotropy was normally greater than 0.160. Millipore filtration assays were performed to measure eIF-2 ternary complex activity. When eIF-2 was incubated at 37 °C for 1 h, then used to form ternary complex by addition of GTP and [<sup>35</sup>S]Met-tRNA<sub>f</sub> as described elsewhere (5), a 30% loss of ternary complex activity was observed (compared to a control where the same eIF-2 was stored on ice for the same time period). Thus, to maintain eIF-2 activity, incubation times greater than 15 min at 37 °C were not tried for labeling. When the temperature was lowered to 0 °C, long incubation times could be tried without harm to eIF-2 activity. However, incubation of a 30-fold molar excess of ATP\*F over eIF-2 for 12 h on ice resulted in essentially no binding, with  $\langle r \rangle = 0.060$ .

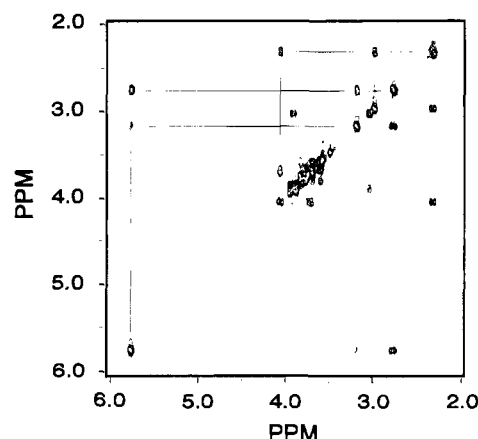
## RESULTS

**Synthesis of Nucleotide Conjugates.** Reaction of amine-containing dyes with periodate-oxidized nucleotides with subsequent reduction produced nucleotide labeled through the ribose (rather than the base). The absorption spectra of the benzylamine derivatives of guanosine and a representative dye-labeled nucleotide (ATP\*F) synthesized at pH 7.1 using both NaCNBH<sub>3</sub> and NaBH<sub>4</sub> reductants are shown in Figure 4. The absorption spectra of both Biogel P-2-purified GBA (I) and (II) are essentially identical. The GDP\*F, GDP\*FH, and GDP\*R spectra are very similar to that of ATP\*F and are therefore not shown. A 1:1 molar ratio was calculated for fluorescein:ATP based on the absorbance values at 492 and 258 nm. When the reductive amination was carried out with only NaCNBH<sub>3</sub> at pH 6.5 (see Experimental Procedures section 4B), only one product was obtained corresponding to GBA (I).

**Inorganic Phosphorus Determination.** To address the possibility of base-catalyzed  $\beta$ -elimination of the phosphate moiety, a GDP-BA derivative was isolated and analyzed using a quantitative inorganic phosphorus colorimetric method. Analysis of the acid hydrolysis of 125 nmol of GDP-BA yielded a value of 127 nmol of inorganic P from the standard curve.

**FAB-MS Analysis.** For GBA (I), positive ion low-resolution FAB in 50:50 (v/v) 3-nitrobenzyl alcohol:glycerol showed  $m/z = 357$ . Identification of the molecular ion species was accomplished after doping the matrix with Na<sub>2</sub>CO<sub>3</sub> for which  $m/z = 379$  for (M + Na)<sup>+</sup>. For GBA (II), low-resolution FAB in both 50:50 (v/v) 3-nitrobenzyl alcohol:glycerol and 1% (v/v) trifluoroacetic acid in glycerol showed  $m/z = 375$ . Similarly, identification of the molecular ion species was accomplished after doping (separately) the matrix with Na<sub>2</sub>CO<sub>3</sub> and KI for which  $m/z = 397$  (M + Na)<sup>+</sup> and  $m/z = 413$  (M + K)<sup>+</sup>, respectively. Two separate high-resolution FAB-MS analyses for each GBA (I) and (II) were performed using CsI as the standard. A search for C, H, O, and N-containing compounds within 10 ppm of the observed mass was also done to obtain the following: GBA (I), (M + H)<sup>+</sup> = 357.168 30 and 357.166 90, predicted formula C<sub>17</sub>H<sub>21</sub>N<sub>6</sub>O<sub>3</sub> (calculated mass = 357.167 513 745, deviation = 2.2 ppm and -1.7 ppm, respectively) and C<sub>19</sub>H<sub>23</sub>N<sub>3</sub>O<sub>4</sub> (calculated mass = 357.168 856 435, deviation = -1.5 ppm and -5.4 ppm, respectively); GBA (II), (M + H)<sup>+</sup> = 375.176 60 and 375.178 30, predicted formula C<sub>17</sub>H<sub>23</sub>N<sub>6</sub>O<sub>4</sub> (calculated mass = 375.178 078 459, deviation = -3.9 ppm and 0.5 ppm, respectively) and C<sub>19</sub>H<sub>25</sub>N<sub>3</sub>O<sub>5</sub> (calculated mass = 375.179 421 149, deviation = -7.5 ppm and -2.9 ppm, respectively).

The low-resolution FAB-MS analysis of the GBA derivative synthesized at pH 6.5 using only NaCNBH<sub>3</sub> resulted in a (M + H)<sup>+</sup> of 357.2, corresponding to GBA (I) from the synthesis at pH 7.1 with both reductants.



**Figure 5.** <sup>1</sup>H-COSY spectrum of Biogel P-2 purified GBA (I) in D<sub>2</sub>O.

**Table 2.** Measured Steady-State Anisotropy Values of the Free Labeled Nucleotides and after Binding to 3-Subunit eIF-2<sup>a</sup>

material	measured anisotropy
GDP*F	0.050 ± 0.001
GDP*R	0.055 ± 0.002
ATP*F	0.045 ± 0.001
eIF-2-GDP*F	0.103 ± 0.005
eIF-2-GDP*R	0.110 ± 0.004
eIF-2-ATP*F	0.172 ± 0.007

<sup>a</sup> Excitation was 488 nm for both \*F and \*R, emission was detected at 518 nm for \*F and 575 nm for \*R. The sample volume was 250 μL for all measurements.

No GBA (II) product was detected from the modified synthesis procedure.

**NMR Analysis.** The proton assignments for the one-dimensional <sup>1</sup>H NMR spectra of GBA (I) and (II) in D<sub>2</sub>O are as follows. GBA (I):  $\delta$  (ppm) 7.94 (s, 1 H, guanylyl H-8), 7.48–7.38 (m, 5 H, benzyl H), 5.73 (d,  $J = 10.5$  Hz, 1 H, ribosyl H-1'), 4.04–4.01 (m, 1 H, ribosyl H-4'), 3.89–3.55 (bm, 4 H, ribosyl H-5' CH<sub>2</sub> and benzylamine CH<sub>2</sub>), 3.15 (d,  $J = 12.1$  Hz, 1 H, ribosyl H-2', equatorial), 2.96 (d,  $J = 12.5$  Hz, 1 H, ribosyl H-3', equatorial), 2.73 (t,  $J = 10.9$  Hz, 1 H, ribosyl H-2', axial), 2.30 (t,  $J = 11.7$  Hz, 1 H, ribosyl H-3', axial). GBA (II):  $\delta$  (ppm) 7.96 (s, 1 H, guanylyl H-8), 7.48–7.38 (m, 5 H, benzyl H), 5.38 (d,  $J = 10.5$  Hz, 1 H, ribosyl H-1'), 4.28–4.26 (m, 1 H, ribosyl H-4'), 3.92–3.46 (bm, 6 H, ribosyl H-5' CH<sub>2</sub>, H-2' CH<sub>2</sub>, and benzylamine CH<sub>2</sub>), 3.02–2.99 (dd,  $J = 2.8$  Hz, 1 H, ribosyl H-3'), 1.93 (s, 1 H, ribosyl H-3'). The assignments for the ribosyl protons were made possible from the <sup>1</sup>H-COSY NMR spectrum (Figure 5) of GBA (I) which was used to further characterize the material.

**Labeling eIF-2 with GDP\*F, GDP\*R, and ATP\*F.** The fluorescent nucleotide derivatives synthesized have been demonstrated to bind to 3-subunit eIF-2. Both GDP\*F and ATP\*F have also been shown to bind 4-subunit eIF-2 (28). Incubation using a 30-fold molar excess of labeled nucleotide over eIF-2 and subsequent size-exclusion chromatography to remove unbound labeled nucleotide resulted in a significant increase in anisotropy above that for the labeled nucleotide (see Table 2).

## DISCUSSION

Initially, PepRPC 10/10-purified GDP\*F and Biogel P-2-purified GDP\*FH were submitted for analysis by NMR. The spectra obtained were complex and ambiguous with regard to the nature of the ribose ring and the position of the dye. The three main factors contributing

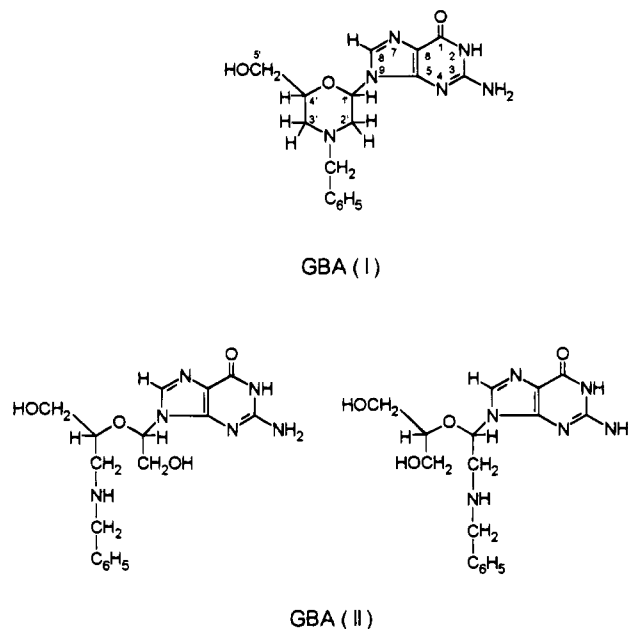
to the complexity were as follows: (1) the peaks were too crowded, overlapped, and not sufficiently resolved, (2) the  $^1\text{H}$  NMR spectrum of \*F alone (not shown) integrated to a total of 28 protons, when only 13 would be expected for \*F in  $\text{D}_2\text{O}$  (this indicated that \*F was impure), TLC analysis of \*F (Table 1) showed several fluorescent species of different mobilities (a spectrum of pure \*F was needed to facilitate analysis of  $\text{GDP*F}$ ), and (3) the  $\text{GDP*F}$  (and \*F) NMR spectra showed a large number of aromatic and heteroaromatic proton peaks between 8.3 and 6.4 ppm as well as  $\alpha$ -monosubstituted aliphatic proton peaks between 4.4 and 2.4 ppm, making it difficult to identify the guanylyl H-8 peak at  $\sim 8$  ppm and any ribosyl protons in the anticipated morpholine-like structure (expected between 5 and 2 ppm).

A similar synthesis using periodate-oxidized guanosine and benzylamine was chosen for the following reasons: (1) the chemistry of the synthesis was expected to be very similar since the  $\text{pK}_a$  of benzylamine and the fluorescein amine derivative are approximately equal ( $\text{pK}_a \approx 9$ ), (2) both benzylamine and the fluorescein amine derivative have similar solubility properties, (3) the expected product would have a relatively small molecular weight, facilitating FAB-MS studies, (4) benzylamine can be obtained in much greater purity than the fluorescein amine derivative, and (5)  $\beta$ -elimination of the phosphates need not be considered.

Periodate-oxidized nucleotides can undergo  $\beta$ -elimination, a reaction catalyzed by base (29–31). Near pH 7, however,  $\beta$ -elimination can be prevented (32). Lowe and Beechey (33) have reported no loss of inorganic P over a period of 1 h when at pH 8–9 during the  $\text{NaBH}_4$  reduction of oxATP. Hansske *et al.* (20) measured the half-lives of oxAMP decomposition (due to  $\beta$ -elimination) at 4, 20, and 37  $^\circ\text{C}$  (pH 7) to be 17 days and 45 and 15 h, respectively. In our procedure, reaction materials are at pH 7.1 at room temperature for no more than 90 min, through the final reduction. Inorganic phosphorus analysis of the purified GDP-BA product synthesized at pH 7.1 yielded 2 mol of  $P_i$  per mole of GDP-BA. Thus,  $\beta$ -elimination appears to be insignificant under our conditions.

The guanosine–benzylamine derivative gave significantly simpler NMR and mass spectra from which we have drawn several conclusions.

(1) Following the described synthesis and purification procedure to the PeprRPC 10/10 stage leads to a mixture of products (Experimental Procedures section 4A). The mixture was separated using a Biogel P-2 size-exclusion column. By comparing the total absorbance (at 254 nm) found in peak I (GBA I) and peak II (GBA II), the mixture was calculated to be 73% I and 27% II. The two relatively insignificant peaks eluting before GBA (II) were not included in GBA (II) or in the above percentages. In a modified synthesis (Experimental Procedures section 4B) where only  $\text{NaCNBH}_3$  was used in the reaction at pH 6.5, only one product was synthesized, corresponding to GBA (I). Fluorescent dyes have been coupled as the amine (15) or as the thiosemicarbazide (17) to oxidized polyribonucleotides without subsequent reduction. Although there are several reports that describe the use of only  $\text{NaBH}_4$  during the reduction step (18, 30, 31, 34, 35), the synthesis method we chose to follow was based on the use of  $\text{NaCNBH}_3$  and  $\text{NaBH}_4$  (22). When Ingham and Brew (22) used only  $\text{NaBH}_4$  during the reduction step, they obtained low yields of a relatively unstable product, but when both  $\text{NaCNBH}_3$  and  $\text{NaBH}_4$  were used, a greater yield of a thermally stable product was obtained. Other authors have also reported the use of both  $\text{NaBH}_4$  and  $\text{NaCNBH}_3$  in similar reductive amination procedures



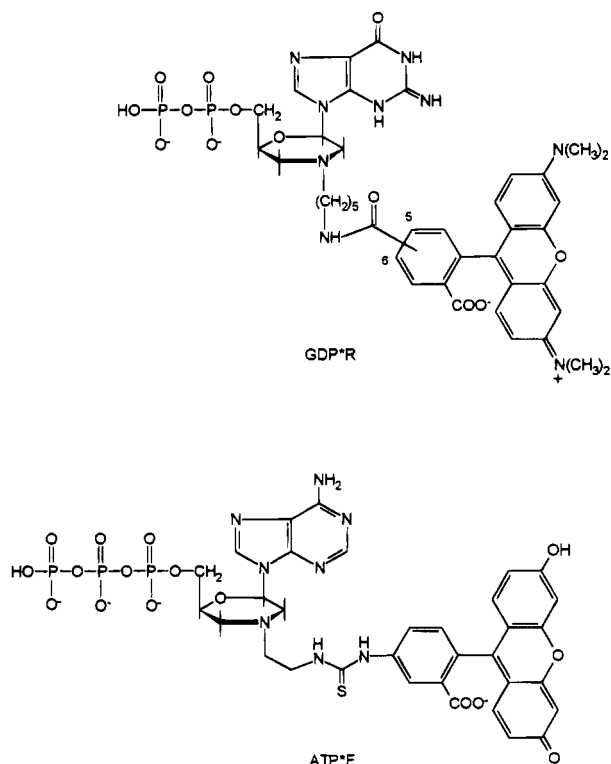
**Figure 6.** Proposed structures for GBA (I) and GBA (II) from the synthesis starting from periodate-oxidized guanosine and benzylamine.

(32, 36). Wells and Cantor (25) described a procedure to label periodate-oxidized tRNA with dansyl hydrazine using only a single reductant,  $\text{NaCNBH}_3$ . Stirchak *et al.* (37) used  $(\text{NH}_4)_2\text{B}_4\text{O}_7$ , also with only  $\text{NaCNBH}_3$ , to form a morpholine nucleoside for incorporation into nucleoside oligomers. Our observations show that the use of both  $\text{NaCNBH}_3$  and  $\text{NaBH}_4$  results in formation of a second product, GBA (II).

(2) On the basis of the high-resolution FAB mass spectra, GBA (I) had a molecular ion mass consistent with two possible  $(M + H)^+$  formulas for GBA (I),  $\text{C}_{17}\text{H}_{21}\text{O}_3\text{N}_6$  and  $\text{C}_{19}\text{H}_{23}\text{O}_4\text{N}_3$ , the latter of which is not possible from the synthesis because of the two additional carbon atoms. Similarly, GBA (II) had a molecular ion mass consistent with two possible  $(M + H)^+$  formulas,  $\text{C}_{17}\text{H}_{23}\text{O}_4\text{N}_6$  and  $\text{C}_{19}\text{H}_{25}\text{O}_3\text{N}_5$ , the latter of which is again not possible because of the two additional carbon atoms. These results suggest one structure for the major product GBA (I) in which the ribose moiety has been converted to a morpholine ring structure (Figure 6). The two possible isomers for the minor product, GBA (II), that are consistent with the predicted formula are also shown in Figure 6.

(3) The predominant product, GBA (I), as well as the minor product, GBA (II), contained one guanosine per benzylamine based on  $^1\text{H}$  NMR analyses. No free aldehyde group remained on the ribose moiety, indicated by the absence of the characteristic downfield chemical shift for aldehydic protons at 9–10 ppm.

(4) Further analysis performed on GBA (I) using COSY  $^1\text{H}$  NMR (Figure 5) was used to assign chemical shift values to each proton and was completely consistent with the structure proposed from the high-resolution FAB-mass spectra analysis of GBA (I). The diagonal peaks (from the lower left to upper right corners) represent the one-dimensional spectrum. The guanylyl H-8 ( $\sim 8$  ppm, region not shown) is expected to appear downfield since it is on a carbon adjacent to two electronegative nitrogen atoms which would deshield the proton. The ribosyl H-1' peak (5.7 ppm) is correlated to two cross-peaks at 3.1 and 2.7 ppm which must therefore correspond to the two nonequivalent ribosyl H-2' protons. Furthermore, since the cross-peak at 2.7 ppm is larger, we may assign it as



**Figure 7.** Proposed structures of GDP\*R and ATP\*F corresponding to GBA (I).

the axial H-2' proton and the 3.1 ppm cross-peak as the equatorial H-2' proton. The peak at 4.0 ppm was assigned as the H-4' proton since it would be deshielded by the adjacent oxygen (thus shifted downfield) and would be expected to show complex splitting patterns due to the adjacent H-3' and H-5' protons. Indeed, the peak at 4.0 ppm ( $x$ -axis) in the one-dimensional spectrum has cross-peaks that connect peaks in the one-dimensional spectrum ( $y$ -axis) both in the 3.9–3.6 ppm range (assigned as the two ribosyl H-5' protons) as well as the 2.3 ppm peak (assigned as the axial H-3' proton because of the large cross-peak size). The smaller cross-peak to the equatorial H-3' is not seen due to suppression of axial peaks. However, the H-3' peak at 2.3 ppm has a cross-peak to 3.0 ppm, which was thus assigned as the equatorial ribosyl H-3' proton. The assignments given for the H-2' and H-3' protons are reinforced by the fact that they show the same splitting patterns: H-2', doublet and triplet (3.1 and 2.7 ppm, respectively); H-3', doublet and triplet (3.0 and 2.3 ppm, respectively).

In contrast to previously reported work involving periodate-oxidized nucleotides and their reactions with amines (18) or carboxylic hydrazides (19, 20) the ribose moiety of the major product, following reduction, *does not* contain a hydroxyl on either the 2' or 3' carbon. The minor product, however, does contain one hydroxyl group.

By inference, we propose that the structure(s) of the fluorescent nucleotide conjugates are the same as for that of the guanosine benzylamine conjugate(s) in regard to the modification at the ribose ring. In Figure 7, we show putative structures for GDP\*R and ATP\*F corresponding to GBA (I). Since a mixture of products was obtained from the guanosine benzylamine synthesis with two reductants, we also infer that a similar mixture is obtained for the fluorescent nucleotide conjugates. Similarly, we presume that only the ring structures shown in Figure 7 should be formed when only the single reductant NaCNBH<sub>3</sub> is used. It is unknown at this point

whether only one or both forms are recognized by the eIF-2 nucleotide binding site. The form in which the ribose ring remains open, however, is expected to have added flexibility compared to the morpholine-like closed ring derivative, and could facilitate binding. These fluorescent nucleotide derivatives have been very useful probes for studies involving eIF-2 interactions with several of the components necessary for the initiation of eukaryotic protein synthesis using steady-state fluorescence anisotropy (28).

#### ACKNOWLEDGMENT

The authors are grateful to Dr. Patrick A. Dussault for discussions concerning the syntheses, Dr. Richard Shoemaker and Dr. Charles A. Kingsbury for discussions and technical assistance concerning NMR, and Dr. Michael L. Gross and Dr. Ronald Cerny for discussions and technical assistance concerning FAB-MS. This work was supported by grants from the Center for Biotechnology, University of Nebraska—Lincoln, and by NIH Grant GM 22079 (N.K.G.) and NIH Grant DK 36288 (L.J.P.).

#### LITERATURE CITED

- (1) Lakowicz, J. R. (1983) *Principles of Fluorescence Spectroscopy*, Plenum Press, New York.
- (2) Churchich, J. E., (1976) Fluorescent Probe Studies of Binding Sites in Proteins and Enzymes. In *Modern Fluorescent Spectroscopy* (E. L. Wehry, Ed.) pp 217–237, Plenum Press, New York.
- (3) Guilbault, G. G. (1973) *Practical Fluorescence: Theory, Methods and Techniques*, Marcel Dekker, Inc., New York.
- (4) Gupta, N. K., Roy, A. L., Nag, M. K., Kinzy, T. G., MacMillan, S., Hileman, R. E., Dever, T. E., Wu, S., Merrick, W. C., and Hershey, J. W. B. (1990) New insights into an old problem: Ternary complex (Met-tRNA<sub>i</sub>eIF-2-GTP) formation. In *Post-Translational Control of Gene Expression* (J. E. G. McCarthy and M. F. Tuite, Eds.) pp 521–526, Vol. H49, NATO ASI Series, Springer-Verlag, Berlin, Heidelberg.
- (5) Roy, A. L., Chakrabarti, D., Datta, B., Hileman, R. E., and Gupta, N. K. (1988) Natural mRNA is required for directing Met-tRNA<sub>i</sub> binding to 40S ribosomal subunits in animal cells: Involvement of Co-eIF-2A in natural mRNA-directed initiation complex formation. *Biochemistry* 27, 8203–8209.
- (6) Gonsky, R., Lebendiker, M. A., Harary, R., Banai, Y., and Kaempfer, R. (1990) Binding of ATP to eukaryotic initiation factor 2. *J. Biol. Chem.* 265, 9083–9089.
- (7) Hiratsuka, T. (1982) Biological activities and spectroscopic properties of chromophoric and fluorescent analogs of adenosine nucleoside and nucleotides, 2',3'-O-(2,4,6-trinitrocyclohexadienylidene) adenosine derivatives. *Biochim. Biophys. Acta* 719, 509–517.
- (8) Hiratsuka, T. (1983) New ribose-modified fluorescent analogs of adenine and guanine nucleotides available as substrates for various enzymes. *Biochim. Biophys. Acta* 742, 496–508.
- (9) Cremo, C. R., Neuron, J. M., and Yount, R. G. (1990) Interaction of myosin subfragment I with fluorescent ribose-modified nucleotides. A comparison of vanadate trapping and SH<sub>1</sub>-SH<sub>2</sub> cross-linking. *Biochemistry* 29, 3309–3319.
- (10) Faller, L. D. (1990) Binding of the fluorescent substrate analogue 2',3'-O-(2,4,6-trinitrocyclohexadienylidene) adenosine 5'-triphosphate to the gastric H<sup>+</sup>,K<sup>+</sup>-ATPase: Evidence for cofactor-induced conformational changes in the enzyme. *Biochemistry* 29, 3179–3186.
- (11) Svitil, A. L., Cashel, M., and Zyskind, J. W. (1993) Guanosine tetraphosphate inhibits protein synthesis *in vivo*: A possible protective mechanism for starvation stress in *Escherichia coli*. *J. Biol. Chem.* 268, 2307–2311.
- (12) Dix, D. B., and Thompson, R. C. (1986) Elongation factor Tu:guanosine 3'-diphosphate 5'-diphosphate complex increases the fidelity of proofreading in protein biosynthesis:

- Mechanism for reducing translational errors introduced by amino acid starvation. *Proc. Natl. Acad. Sci. U.S.A.* **83**, 2027–2031.
- (13) Bodley, J. W., and Gordon, J. (1974) Interactions of periodate-oxidized guanine nucleotides with *E. coli* elongation factor G and the ribosome. *Biochemistry* **13**, 3401–3415.
- (14) Mueser, T. C., and Parkhurst, L. J. (1993) Synthesis of dansylribonucleotides and their use in steady-state fluorescence anisotropy studies of nucleotide binding by initiation factor-2 (eIF-2) and histone H1. *J. Int. Biochem.* **25**, 1689–1696.
- (15) Millar, D. B. S., and Steiner, R. F. (1965) Fluorescent conjugates of biosynthetic polyribonucleotides. *Biochim. Biophys. Acta* **102**, 571–589.
- (16) Czworkowski, J., Odom, O. W., and Hardesty, B. (1991) Fluorescent study of the topology of messenger RNA bound to the 30S ribosomal subunit of *Escherichia coli*. *Biochemistry* **30**, 4821–4830.
- (17) Odom, O. W., Robbins, D. J., Lynch, J., Dottavio-Martin, D., Kramer, G., and Hardesty, B. (1980) Distances between 3' ends of ribosomal ribonucleic acids reassembled into *Escherichia coli* ribosomes. *Biochemistry* **19**, 5947–5954.
- (18) Khym, J. X. (1963) The reaction of methylamine with periodate-oxidized adenosine 5'-phosphate. *Biochemistry* **2**, 344–350.
- (19) Girshovich, A. S., Pozdnyakov, V. A., and Ovchinnikov, Y. A. (1974) Ribose-modified photoactivated GTP analog. *Meth. Enzymol.* **46**, 656–658.
- (20) Hansske, F., Sprinzl, M., and Cramer, F. (1974) Reaction of the ribose moiety of adenosine and AMP with periodate and carboxylic acid anhydrazides. *Bioorg. Chem.* **3**, 367–376.
- (21) Desa, R. J., and Wampler, J. E. (1973) On-line spectrophotometer for collection and manipulation of absorbance spectra. *Appl. Spectrosc.* **27**, 279–284.
- (22) Ingham, K. C., and Brew, S. A. (1981) Fluorescent labeling of the carbohydrate moieties of human chorionic gonadotropin and  $\alpha_1$ -acid glycoprotein. *Biochim. Biophys. Acta* **670**, 181–189.
- (23) Dawson, R. M. C., Elliot, D. C., Elliot, W. H., and Jones, K. M. (1986) *Data for Biochemical Research*, 3rd ed., pp 89–109, Oxford University Press, New York.
- (24) Haugland, R. P. (1992) In *Handbook of Fluorescent Probes and Research Chemicals* (K. D. Larison, Ed.) Molecular Probes, Inc., Eugene, OR.
- (25) Wells, B. D., and Cantor, C. R. (1977) A strong ethidium binding site in the acceptor stem of most or all transfer RNAs. *Nuc. Acids Res.* **4**, 1667–1680.
- (26) Standard Ultraviolet Spectra Collection, Sadtler Research Laboratories (1980), UV 266.
- (27) Wu, S., Gupta, S., Chatterjee, N., Hileman, R. E., Chakrabarti, D., Denslow, N., Merrick, W. C., Kinzy, T. G., Osterman, J., and Gupta, N. K. (1993) Cloning and characterization of complementary DNA encoding the eukaryotic initiation factor-2 associated 67 kDa polypeptide (p<sup>67</sup>). *J. Biol. Chem.* **268**, 10796–10801.
- (28) Hileman, R. E. (1993) Ph.D. Dissertation, University of Nebraska, Lincoln.
- (29) Schwartz, D. E., and Gilham, P. T. (1972) The sequence of polyribonucleotides by stepwise chemical degradation. A method for the introduction of radioactive label into nucleoside fragments after cleavage. *J. Am. Chem. Soc.* **94**, 8921–8922.
- (30) Steinschneider, A. (1971) Effect of methylamine on periodate-oxidized adenosine 5'-phosphate. *Biochemistry* **10**, 173–178.
- (31) King, M. M., and Colman, R. F. (1983) Affinity labeling of nicotinamide adenine dinucleotide dependent isocitrate dehydrogenase by the 2',3'-dialdehyde derivative of adenosine 5'-diphosphate. Evidence for the formation of an unusual reaction product. *Biochemistry* **22**, 1656–1665.
- (32) Löw, A., Faulhammer, H. G., and Sprinzl, M. (1992) Affinity labeling of GTP-binding proteins in cellular extracts. *FEBS Lett.* **303**, 64–68.
- (33) Lowe, P. N., and Beechey, R. B. (1982) Preparation, structure and properties of periodate-oxidized ATP, a potential affinity labeling reagent. *Bioorg. Chem.* **11**, 55–71.
- (34) Abraham, G., and Low, P. S. (1980) Covalent labeling of specific membrane carbohydrate residues with fluorescent probes. *Biochim. Biophys. Acta* **597**, 285–291.
- (35) Lee, J. A., and Fortes, P. A. G. (1985) Labeling of the glycoprotein subunit of (Na,K)ATPase with fluorescent probes. *Biochemistry* **24**, 322–330.
- (36) Atha, D. H., Brew, S. A., and Ingham, K. C. (1984) Interaction and thermal stability of fluorescent labeled derivatives of thrombin and antithrombin III. *Biochim. Biophys. Acta* **785**, 1–6.
- (37) Stirchak, E. P., Summerton, J. E., and Weller, D. D. (1989) Uncharged stereoregular nucleic acid analogs: 2. Morpholino nucleoside oligomers with carbamate internucleoside linkages. *Nuc. Acids Res.* **17**, 6129–6141.

# Double-Stranded Cyclic Oligonucleotides with Non-Nucleotide Bridges

H. Gao,\*† N. Chidambaram,‡ B. C. Chen,‡ D. E. Pelham,† R. Patel,† M. Yang,† L. Zhou,‡ A. Cook,† and J. S. Cohen‡

PharmaGenics, Inc., Allendale, New Jersey 07401, and Cancer Pharmacology Section, Georgetown University Medical Center, Washington, DC. Received April 22, 1994\*

A series of double-stranded, cyclic oligodeoxynucleotides with non-nucleotide bridges have been synthesized, and their physicochemical properties and susceptibility to enzymes have been investigated. These bridged duplexes are of potential interest for their binding properties to transcription factors and other DNA-binding proteins. Triethylene glycol has been employed as the bridge to alter the lipophilicity of the duplex and avoid the potential for enzymatic cleavage. The synthetic route involved the synthesis of a 3'-phosphorylated, nicked double-stranded precursor with the final internucleotide bond being formed chemically using a water soluble carbodiimide. These bridged duplexes have high thermal dissociation temperatures, and the  $T_m$  for a triethylene-bridged 20 base pair duplex was higher than that for the corresponding pentathymidylate-bridged duplex. EcoR I endonuclease cleaved a ligated, bridged duplex at a slower rate than the corresponding unmodified duplex, whereas the unligated, bridged duplex was cleaved more rapidly. Sufficient amounts of the bridged octamer and dodecamer were prepared for proton NMR spectroscopic studies, and 2D COSY and NOESY spectra were obtained. The results indicate that the ligated duplex has a B-form conformation.

## INTRODUCTION

Oligonucleotide-based therapeutics are of considerable interest as a potentially new approach to drug design. Although the most common oligonucleotide-based approaches involve the targeting of RNA (the antisense approach) or DNA (the antigene or triplex approach), a less explored route is to target essential DNA-binding regulatory proteins, such as transcription factors, with short sequences of double-stranded oligonucleotides. Since unmodified oligonucleotides are rapidly degraded in serum and cell extracts (1, 2), the attachment of non-nucleotide linkers to the ends of a duplex might provide an advantage by reducing the rate of degradation, especially by exonucleases. A further advantage might be that the enhanced thermal stability of these bridged duplexes as compared with their natural counterparts ensures that relatively short recognition sequences are more effectively held in a duplex conformation and thus available for recognition. In this report we describe methodology for the synthesis of examples of these compounds, together with a brief study of their physicochemical properties.

The earliest report of the study of the properties of a double-stranded cyclic oligonucleotide or dumbbell was described by Scheffler et al., who investigated the physical properties of a series of linear and cyclic d(AT) oligomers and showed that the circular molecules possessed unexpectedly higher thermal denaturation temperatures (3). Wemmer and Benight (4) subsequently described the preparation of a duplex bridged by two tetranucleotide loops and again showed that the closed, circular duplex exhibited considerably greater stability than the unligated sequence. Erie et al. (5) reported the synthesis of a covalently closed, double-stranded se-

quence by enzymatic ligation of a nicked duplex using T<sub>4</sub> DNA ligase, with five thymidylate residues being employed for each of the bridges or loops. Previous work by the same group (6) showed that a similar sequence with only four thymidylate residues in each bridge could not be enzymatically ligated. A related approach was taken by Ashley and Kushlan (7) who synthesized double-stranded cyclic oligonucleotides with four thymidylate residues in the bridges using a purely chemical route. Ligation was found to be most effective for 3'-phosphorylated nicked sites flanked by two purine bases. Circular oligonucleotides which are capable of forming triple-stranded structures by binding single-stranded DNA or RNA have also been reported (8,9), and in these sequences the bridges were constructed either from a sequence of natural nucleotides or from hexaethylene glycol linkers. More recently, a series of 17 DNA dumbbells were constructed with duplex regions ranging in length from 14 to 18 base pairs, linked at the ends by four thymidylate residues as bridges. The thermal denaturation profiles of members of this series of oligonucleotides were investigated in a study of nearest neighbor interactions (10). The stability of dumbbell DNA in serum has been studied, and it was shown that the nucleotides in the single-stranded loops were preferentially nicked (11). The regulation of specific gene expression by double-stranded dumbbell oligonucleotides possessing pentathymidylate loops has been reported (12) and a report of bridged RNA duplexes with nucleotide and non-nucleotide bridges has also recently been published (13).

Several groups have described the synthesis of hairpin molecules with non-nucleotide bridges. An oligonucleotide hairpin containing a hexaethylene glycol bridge has been reported (14), and its properties were compared to an oligonucleotide in which the hexaethylene glycol was replaced by four thymidine residues and to a duplex of the same sequence without the bridge. An aromatic terephthalimide group has been used as a bridge to connect two complementary oligonucleotide strands, and a marked increase in the stability of the duplex was

\* To whom correspondence should be addressed. Tel: 201-818-1000. Fax: 201-818-9044.

† PharmaGenics, Inc.

‡ Georgetown University Medical Center.

© Abstract published in *Advance ACS Abstracts*, August 1, 1994.



observed with this conjugate as compared to the same duplex without the bridge (15). Two thymidylate strands connected by this type of linker also showed enhanced affinity for oligo(dA) strands, presumably by triplex formation.

Glycol or propanediol linkers have been used to connect noncomplementary oligonucleotide sequences (16, 17). These molecules were used as probes to bind to two separate, noncontiguous regions of an RNA target molecule. Doubly bridged molecules containing terephthalimide or hexaethylene glycol bridges have also been prepared (15, 18). In both cases, the oligonucleotide was able to fold back on itself twice to form a triple helix at low temperature. A recent report described the synthesis of a series of hammerhead-like synthetic RNA molecules containing glycols in one of the loops, some of which were shown to possess catalytic, ribozyme-like activity (19). Only two examples of a doubly bridged duplex containing non-nucleotide bridging groups have been described. In the first example the molecule was linked via disulfide bridges attached to the bases rather than the phosphodiester backbone (20), and in the second example RNA molecules with glycol bridges were obtained by enzymatic ligation (13).

Since DNA-binding proteins such as transcription factors provide an attractive target for binding by modified, double-stranded oligonucleotides we describe the synthesis and physicochemical properties of DNA duplexes in which the termini of the phosphodiester backbones are connected by triethylene glycol bridges, together with an initial study of their physicochemical and enzymatic properties.

## EXPERIMENTAL PROCEDURES

**Materials and Methods.** Oligonucleotides shown in Figure 1 were synthesized using an Applied Biosystems Model 390B or 394 DNA synthesizer using a 1  $\mu$ mol synthesis cycle (trityl-on mode). Unmodified oligos were purified by reversed-phase HPLC on a C<sub>18</sub> column, lyophilized, and detritylated using 0.1 M aqueous acetic acid for 30–40 min, extracted with ethyl acetate (3 $\times$ ) followed by ether (3 $\times$ ), lyophilized to dryness, and converted into the sodium form. The chemical phosphorylation reagent and the triethylene glycol phosphoramidite were purchased from Glen Research. HPLC purifications were performed using a Waters 600E system controller equipped with a multisolvent delivery system and a Model 991 photodiode array detector. Unless otherwise stated, analytical reversed-phase HPLC was performed using a Waters Delta-Pak C<sub>4</sub> cartridge (8  $\times$  100 mm, 15  $\mu$ m, 300 Å), and a Delta-Pak C<sub>4</sub> cartridge (25  $\times$  100 mm, 15  $\mu$ m, 300 Å) was employed for preparative use. A linear gradient of 0.1 M triethylammonium acetate buffer pH 7.0 (TEAA, solvent A)/acetonitrile (solvent B) was employed for all reversed-phase separations. Unless otherwise stated, anion exchange chromatography was performed on a Dionex NucleoPac PA-100 column (4  $\times$  250 mm, Dionex Corporation, Sunnyvale, CA) using a linear gradient of 25 mM Tris-HCl, pH 8.0 containing 0.5% CH<sub>3</sub>CN (solvent A), increasing to 25 mM Tris-HCl/1M NH<sub>4</sub>Cl, pH 8.0 containing 0.5% CH<sub>3</sub>CN (solvent B), with a flow rate of 1.5 mL/min. Ultraviolet spectra were obtained with a Shimadzu UV 160U spectrophotometer using 1-mL quartz cuvettes. Unless otherwise stated, polyacrylamide gel electrophoresis (PAGE) was performed using a 12% polyacrylamide gel containing 7 M urea with 0.09 M Tris borate/EDTA (1 $\times$  TBE) buffer, pH 8; bands were detected by UV shadowing. Oligonucleotides were converted into their sodium salts

by passage through a short column of Dowex AG50W-X8 resin, sodium form.

### Synthesis of the Unligated Dodecamer Duplex 1.

Fourteen syntheses were carried out on a 1  $\mu$ mol scale (trityl-on) and combined for purification purposes. The 3'-phosphate was introduced using (2-cyanoethoxy)[2'-[[[O-4,4'-dimethoxytrityl]oxy]ethyl]sulfonyl]ethoxy](*N,N*-diisopropylamino)phosphine as the phosphoramidite (21), the reagent being coupled directly to controlled pore glass solid support to which a deoxycytidine residue was attached (i.e., a C-column). After addition of the required nucleotides using conventional cyanoethyl phosphoramidites, the triethylene glycol bridging groups were introduced using [[[4,4'-dimethoxytrityl]oxy]triethylene]oxy[2-cyanoethoxy](*N,N'*-diisopropylamino)phosphine (14) at the appropriate positions. After completion of the synthesis and cleavage from the solid support, the aqueous ammonia solution of the crude oligonucleotide from the synthesizer was heated at 55 °C for 15 h to remove the protecting groups, and ammonia was removed by passing a stream of nitrogen over the solution. The solution was lyophilized, and the residue was dissolved in 0.02 M triethylammonium bicarbonate, pH 7.6. The crude, trityl-on oligonucleotide was purified by preparative reversed-phase HPLC, gradient 2–15% B over 4 min and then 15–40% over 45 min, followed by 40–80% B over 3 min. The peak eluting between 26 and 33 min, corresponding to the tritylated oligonucleotide, was collected and lyophilized to remove buffer, detritylated by treatment with 0.1 M acetic acid solution for 40 min at room temperature, and extracted with ethyl acetate (3 $\times$ ) followed by ether (6 $\times$ ). After lyophilization to dryness, the residue was converted into the sodium salt. The eluate was evaporated to dryness to give the unligated oligonucleotide 1, 628 OD<sub>260</sub>. Anion exchange HPLC analysis (gradient: 15–30% B over 1.5 min and then 30–80% B 2–27 min) showed a single peak with a retention time of 16.5 min.

**Formation of the Bridged Duplex 2.** The unligated oligonucleotide 1 (Figure 1), 100 OD<sub>260</sub> units, was dissolved in sodium 4-morpholinoethanesulfonate buffer (MES, 0.05 M, pH 6.0, 30 mL) containing 20 mM magnesium chloride and treated with 1-[3-(dimethylamino)propyl]-3-ethylcarbodiimide hydrochloride (EDC, 2 g). The mixture was briefly vortexed, stored at 4 °C for 3 days, and analyzed by HPLC using a Waters C<sub>4</sub> column (Delta Pak 5  $\mu$ m, 300 Å, 3.9  $\times$  150 mm). Buffer A: 0.1 M TEAA pH 7. Buffer B: CH<sub>3</sub>CN, flow rate 1.5 mL/min, gradient 2–15% B over 20 min, then 15–20% B from 21–24 min. Virtually no starting material remained after 3 days. Using a similar procedure, an additional 116 OD<sub>260</sub> units of 1 were ligated with similar results. These two reaction mixtures were combined, evaporated to dryness, precipitated from ethanol, and purified on a C<sub>4</sub> preparative reversed-phase column using a linear gradient of 0.1 M TEAA/CH<sub>3</sub>CN, with the concentration of B being varied from 2 to 15% over 40 min. The product peak eluting between 10 and 13.5 min was collected, lyophilized to dryness, and converted into the sodium salt. The eluate was evaporated to dryness to give the ligated oligonucleotide 2, 122 OD<sub>260</sub>. Analysis by 15% PAGE showed a single band with higher mobility than the starting material 1.

**Synthesis of the Unligated Octanucleotide Duplex 3.** Twenty syntheses (1  $\mu$ mol scale) were performed with trityl-on and auto cleavage as the ending method. After storage in concentrated aqueous ammonia at 55 °C for approximately 8 h, the ammonia was removed by partial evaporation, and the resulting aqueous solution was filtered through a 0.22- $\mu$ m Millex filter unit which

was rinsed with water (0.5 mL). The filtrate and washings were combined and purified by reversed-phase HPLC using a Hamilton PRP-1 preparative column (21.5 × 250 mm). Gradient: 20–30% B over 24 min then 30% B over 40 min, flow rate 10 mL/min. The eluate containing the desired component, which eluted at 18 min, was collected and evaporated, and the residue was detritylated by treatment with 6% acetic acid for 10 min. The solution was washed with ethyl acetate and the aqueous layer was evaporated to dryness. The residue was purified by reverse phase HPLC using a Hamilton Semi-Prep PRP-1 column (10  $\mu$ , 7 × 305 mm), flow rate 1.5 mL/min, gradient: 2–80% B. The desired component, which eluted after 19 min, was collected, evaporated, and desalted over BioRad P2 gel (2 × 82 cm, 0.001 M Na<sub>2</sub>HPO<sub>4</sub>). The fraction containing the desired oligomer was collected and evaporated to give 400 OD<sub>260</sub> units of **3**. Analysis by 15% PAGE showed a single band with higher mobility than the starting material **1**. A sample was lyophilized twice from D<sub>2</sub>O for NMR purposes.

**Chemical Ligation of **3**.** A solution of oligonucleotide **3** (202 OD<sub>260</sub>) in MES buffer pH 6.0 (0.05 M, 40.4 mL) containing 20 mM MgCl<sub>2</sub> was cooled on ice and treated with EDC (6.06 g) with stirring. The reaction was stirred at 4 °C for 3 days, and oligonucleotide was precipitated by addition of absolute ethanol (180 mL) followed by storage overnight at –80 °C. The solid was collected by centrifugation at –5 °C, dissolved in a minimum amount of water and filtered through a 0.22- $\mu$ m filter. The eluate was purified by HPLC using a Hamilton semipreparative PRP-1 column, and the fractions containing ligated material, which eluted at 17 min, were combined, evaporated, and desalted (2 × 82 cm, 0.001 M Na<sub>2</sub>HPO<sub>4</sub>) to obtain a pure ligated material **4** (100 OD<sub>260</sub>). The purity of a sample was analyzed by PAGE and HPLC. For NMR, a sample was lyophilized twice with 0.4 mL of D<sub>2</sub>O and dissolved in D<sub>2</sub>O (0.4 mL) containing 10 mM phosphate and 100 mM NaCl, pH 7.4.

**Synthesis of the 20-mer Duplexes **5**, **6**, **11**, and **12**.** Synthesis and HPLC purification of the unligated 20-mer duplex **5** were similar to the procedures described for the unligated dodecamer duplex **1**. The product **5** was analyzed by PAGE, and a single band was detected by UV shadowing. The unligated oligonucleotide **5** (23 OD<sub>260</sub>) was dissolved in 50 mM MES–NaOH, pH 6.0, 20 mM MgCl<sub>2</sub> (2 mL), and after addition of EDC (0.2 g) the resulting mixture was stirred at 4 °C for 3 days. A further portion of EDC (0.15 g) was added, and after reaction for an additional 3 days, analysis by PAGE indicated that most of the starting material (>90%) was converted into a faster migrating, ligated oligonucleotide **6**. The product was separated by PAGE and extracted from the gel by crushing the frozen gel slice, followed by soaking overnight in 0.3 M sodium acetate (0.5 mL) containing 2 mM EDTA (1 mL, pH 8.0). The mixture was filtered, and the solids were washed with 2 mM EDTA (1.5 mL). The filtrate and washings were combined, concentrated to dryness, precipitated from ethanol, and converted into the sodium form to give **6** (4 OD<sub>260</sub>).

The unligated oligonucleotide **11** was synthesized and purified as described for **5**, except that five additions of thymidine phosphoramidite were substituted for each addition of the triethylene glycol phosphoramidite. The ligation of **11** was carried out as described for **5**.

**Thermal Denaturation Experiments.** These were performed on a Gilford Response II temperature-controlled spectrophotometer by monitoring the changes in absorbance at 260 nm versus temperature, with a heating rate of 1 °/min from 25 to 100 °C. Extinction coefficients used to calculate the molar ratios of oligonucleotides were

obtained by the method of Rychlik and Rhoads (22). Melting curves were determined in 10 mM Na<sub>2</sub>HPO<sub>4</sub>, pH 7.0. Transition temperatures were obtained from the first-order derivative plot of absorbance versus temperature.

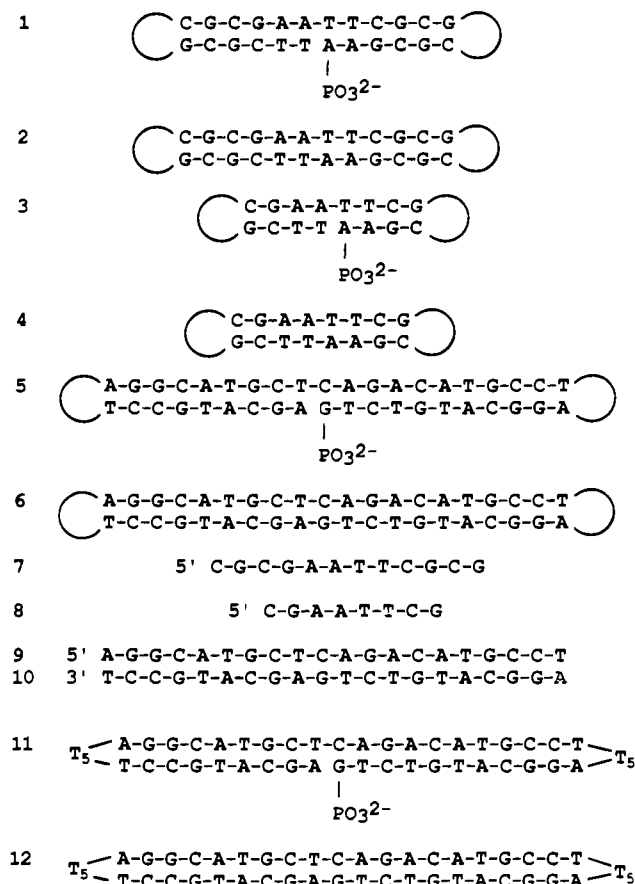
**Enzyme Digestion to Monomers.** Each oligomer (0.5 OD<sub>260</sub> units) was dissolved in water (66  $\mu$ L), and 0.1 M Tris–HCl buffer, pH 7.5 (0.2  $\mu$ L) and MgCl<sub>2</sub> (1.2  $\mu$ L) were added. The solution was treated with crude snake venom diesterase (0.037 units in 3.6  $\mu$ L) and alkaline phosphatase (0.5 units in 5.8  $\mu$ L) and incubated for 12 h at 37 °C. The reaction was centrifuged, and the supernatant was filtered through a 0.22- $\mu$ m filter membrane and analyzed by HPLC using a Beckman C<sub>18</sub> reversed-phase column (5  $\mu$ m, 0.46 × 25 cm) with a flow rate of 1.5 mL/min. Gradient: 1–10% B from 0–15 min, then 10–20% B over 10 min, followed by 20–100% B over 10 min.

**Incubation of Dodecamers with EcoR 1 Endonuclease.** Samples of the oligonucleotides **1**, **2**, and **7** (1 OD<sub>260</sub>) were each dissolved in buffer (50 mM NaCl, 100 mM Tris–HCl, 10 mM MgCl<sub>2</sub>, 0.025% Triton X-100, pH 7.5, 540  $\mu$ L) and treated with EcoR 1 restriction endonuclease (60  $\mu$ L, 20 units/ $\mu$ L, New England BioLabs, Beverly, Ma). Each solution was incubated at 37 °C, and aliquots were removed, quenched by addition of 0.5 M EDTA, and heated at 75 °C for 15 min to destroy the enzyme. Each aliquot was extracted with phenol/chloroform (1:1, pH 8), chloroform, and ether, concentrated to dryness, and precipitated from ethanol. The products were examined by 20% PAGE.

**NMR Studies.** The proton one-dimensional spectra, the two-dimensional pure absorption-phase NOESY spectra, and the two-dimensional double quantum-filtered COSY (DQF-COSY) spectra were acquired on a General Electric GN-400 or a Varian XL-400 instrument. The proton spectra were referenced to sodium 3-(trimethylsilyl)propionate-2,2,3,3-*d*<sub>4</sub> (TSP; from MSD Isotopes) at 0 ppm. The <sup>1</sup>H one-dimensional spectra of the dodecamers and octamers were acquired with a sweep width of 4000 Hz and 32K data points, with a relaxation delay of 3.0 s. The data were processed with a line broadening of 0.5 Hz.

The two-dimensional pure absorption phase NOESY spectra of the dodecamers and octamers were acquired at two mixing times (500 and 150 ms) for the assignment of the proton NMR spectra. The NOESY spectra were acquired with a sweep-width of 4000 Hz in both the *t*<sub>1</sub> and *t*<sub>2</sub> dimensions. The spectrum was collected as 512 FID's (*t*<sub>1</sub>) by 1024 complex points (*t*<sub>2</sub>). A relaxation delay of 4.5 s was used. Sixteen transients were collected for each of the *t*<sub>1</sub> values. The experiments were processed with 2K of zero-filling in the *t*<sub>2</sub> dimension and 1K of zero-filling in the *t*<sub>1</sub> dimension for a final matrix size of 1K × 1K. A Gaussian apodization function was applied in both the *t*<sub>1</sub> and *t*<sub>2</sub> dimensions to generate resolution enhancement. The spectra were collected without spinning the sample. The HDO solvent signal was saturated with the decoupler during the recycle delay.

The DQF-COSY spectra were acquired to assign the H<sub>5</sub>–H<sub>6</sub> cytosine protons through their COSY coupling crosspeaks. The DQF-COSY spectrum was measured with a sweep-width of 4000 Hz in both the *t*<sub>1</sub> and *t*<sub>2</sub> dimensions. The spectrum was collected with 1024 complex points in *t*<sub>2</sub> and 128 *t*<sub>1</sub> values. Eight transients were collected for each *t*<sub>1</sub> value, and a relaxation delay of 2 s was used. The spectra were collected without sample spinning. The spectra were zero-filled to 4K in the *t*<sub>1</sub> dimension and 2K in the *t*<sub>2</sub> dimension for a final matrix size of 2K × 2K. Spectra were apodized using a



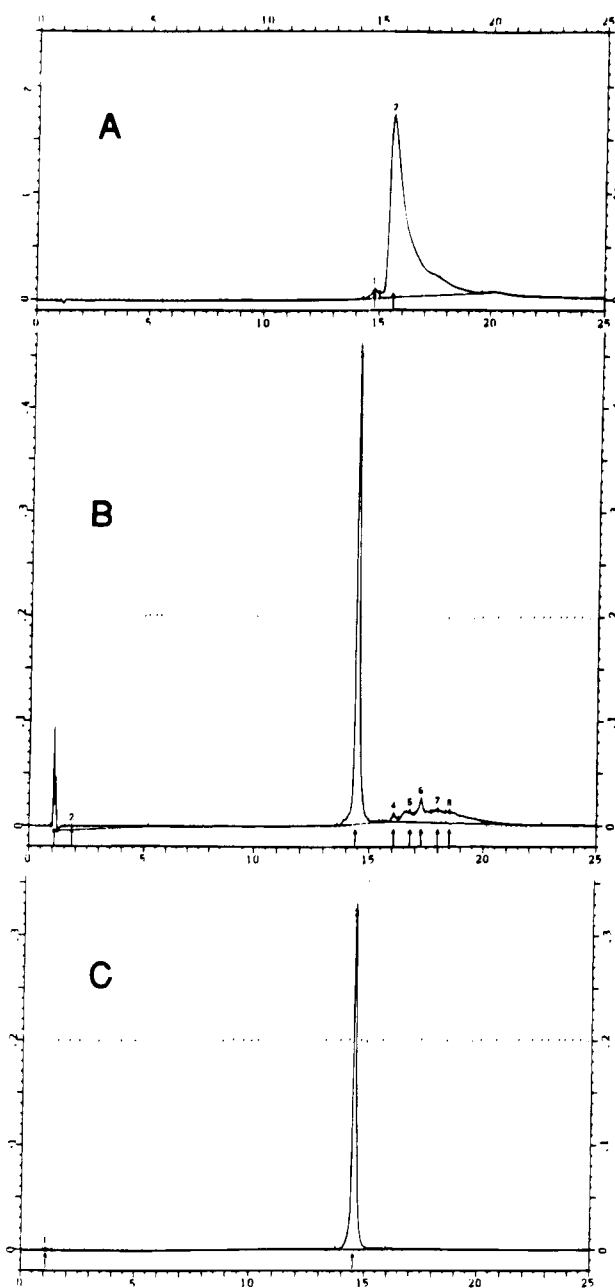
**Figure 1.** Structures of oligodeoxynucleotide duplexes, the triethylene glycol bridges are indicated by the open circles.

sine-bell function in both the  $t_1$  and  $t_2$  dimensions to enhance resolution.

## RESULTS AND DISCUSSION

**Synthetic Strategy.** The basic strategy for the synthesis of these double-stranded, circular molecules relies on the chemical ligation of an open chain, double-stranded (nicked dumbbell) precursor. This strategy was followed by Ashley and Kushlan (7) in the synthesis of dumbbells with pentathymidylate loops and takes advantage of the fact that part of the sequence acts as a template for the nucleotides adjacent to the site to be ligated. The nicked dumbbell precursor 1 (Figure 1) was prepared on a DNA synthesizer using the phosphorylation reagent of Horn and Urdea (21) to generate a 3'-phosphate upon cleavage from the support and deprotection. Positioning of the phosphate at the 3'-terminus allowed for the dimethoxytrityl to be retained at the 5'-terminus, thus facilitating purification by conventional reversed-phase trityl-on HPLC. The full length tritylated oligonucleotide was well separated from failure sequences on a C<sub>4</sub> column and was collected and detritylated using dilute acid. The unligated material was converted into the sodium salt in order to remove the bulky triethylammonium cations which might potentially interfere with ligation.

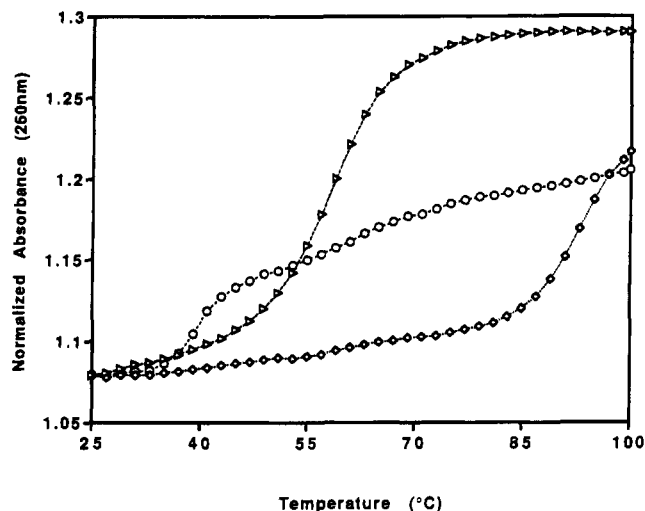
Ligation employed the water-soluble carbodiimide EDC as the condensing agent, and the preferred conditions employed a large excess of condensing agent and a reaction time of 3 days. Repeated addition of smaller amounts of EDC was found to be less effective, and this reagent was found to be more satisfactory than others such as cyanogen bromide/imidazole. Ligation was very efficient under these conditions since an analysis of the



**Figure 2.** HPLC chromatograms of the unligated and ligated duplexes. Panel A: unligated duplex 1. Panel B: ligation reaction mixture. Panel C: purified, ligated duplex 2.

crude reaction mixtures by gel electrophoresis usually showed that only small amounts of starting material remained. The ligated material was isolated by reversed-phase HPLC using a C<sub>4</sub> column, although a polystyrene-based reversed-phase column was also found to be suitable for separation of **2** from unligated material. Figure 2 shows HPLC traces of the unligated oligonucleotide **1** (panel A), the ligation reaction mixture (panel B), and the ligated material **2** (panel C). The synthesis and purification of the octamer duplex **3** closely paralleled the procedure for the dodecamer except that a polystyrene-based HPLC column was employed for purification. The ligation reaction also paralleled that for **1** and yielded approximately 100 OD<sub>260</sub> units.

The 20 base pair duplex examined in this study corresponds to the DNA binding site of the p53 tumor suppressor gene (23) and consists of two copies of the 10 base pair motif PuPuPuCATGPyPyPy. The synthesis of this oligonucleotide closely paralleled that for **2**, except

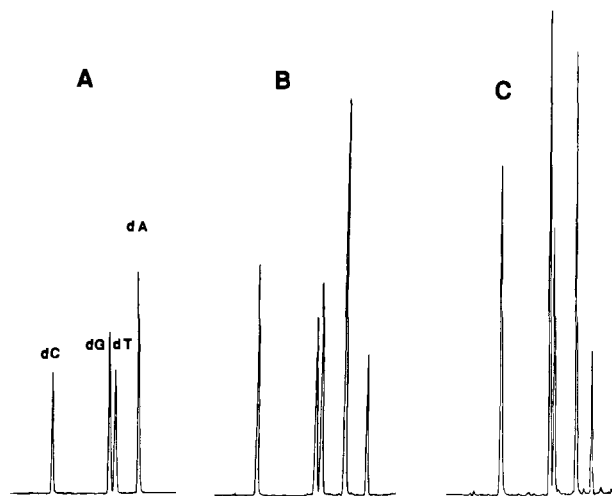


**Figure 3.** Thermal dissociation curves of dodecamer duplexes in 10 mM  $\text{Na}_2\text{HPO}_4$ . Unmodified duplex 7:  $-\circ-$ . Unligated duplex 1:  $-\triangle-$ . Ligated duplex 2:  $-\diamond-$ .

that the separation of the ligated duplex 6 from unreacted starting material 5 was not possible by HPLC. The reaction mixture was therefore purified by preparative gel electrophoresis, since the ligated material could be clearly observed as a faster migrating band which was well separated from starting material. Elution of the gel slice provided sufficient material for enzymatic and thermal dissociation experiments. The corresponding sequence with pentathymidylate bridges (compound 12) was prepared by a similar method.

**Thermal Denaturation Experiments.** The thermal denaturation profiles of the unligated and ligated oligonucleotides were determined in sodium phosphate buffer and compared to those of the unmodified duplexes. The denaturation of the unmodified duplex of the dodecamer 7 showed a biphasic rather than a standard sigmoidal curve, due to transitions involving duplex, hairpin, and single-stranded structures as has been previously described (24). The unligated duplex 1 was considerably more stable than its unmodified counterpart 7 and gave a monophasic curve with a  $T_m$  of 59.5 °C in 10 mM  $\text{Na}_2\text{HPO}_4$ . The increase in melting temperature is similar to those previously reported for thymidylate bridged sequences versus sequences without bridges (4, 5, 25). A further, large increase in dissociation temperature to approximately 93 °C was observed for the ligated, bridged duplex 2, and the plateau corresponding to the fully dissociated form was not reached at 100 °C. The melting curves for these three oligonucleotides are shown in Figure 3. The biphasic nature of the curve for 7 presumably represents formation, then melting, of a hairpin conformation of this self-complementary sequence as has been previously described (24). Similar melting curves have been reported for other self-complementary sequences (4). Melting curves were also obtained for the octamer duplexes 3 and 4, with an especially large increase in  $T_m$  of over 50 °C being observed for the ligated species versus the natural duplex. The results are summarized in Table 1.

Since a number of duplexes with thymidylate bridges have been previously described and shown to be quite stable toward thermal denaturation, it was of interest to investigate the difference in thermal stability between a duplex with triethylene glycol bridges versus the same sequence with nucleotide bridges. This comparison was investigated for the 20 base pair duplexes 5 and 6 having triethylene glycol bridges versus 11 and 12 possessing



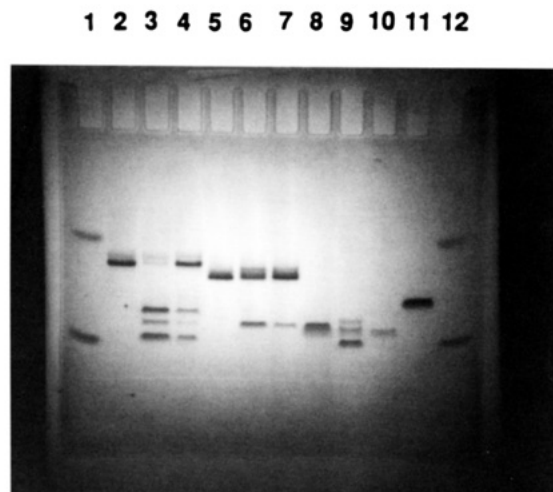
**Figure 4.** HPLC chromatograms of the products of digestion of oligonucleotide duplexes with snake venom phosphodiesterase and bacterial alkaline phosphatase. Panel A: natural duplex 8. Panel B: unligated duplex 3. Panel C: ligated duplex 4.

**Table 1.** Comparison of Thermal dissociations of Bridged Duplexes vs Their Unmodified Counterparts

compd	oligonucleotide	$T_m$ (°C) in 10 mM $\text{Na}_2\text{HPO}_4$
7	natural (unbridged) dodecamer	39.5
1	unligated dodecamer	58.5
2	ligated dodecamer	93
8	natural (unbridged) octamer	22
3	unligated octamer	32
4	ligated octamer	77.5
9 + 10	natural (unbridged) 20mer duplex	62
5	unligated 20mer	68
6	ligated 20mer	89.5
11	unligated 20mer, $T_5$ bridges	61.5
12	ligated 20mer, $T_5$ bridges	82.5

pentathymidylate bridges. In both cases the duplexes with triethylene glycol bridges exhibited greater stability than those with the pentathymidylate bridges, with the melting temperature differential between the two being approximately 7 °C. Although the magnitude of this difference is probably not of significance for longer sequences, the greater stability of the triethylene glycol bridges might be more important for stabilization of short duplexes.

**Enzyme Degradation.** Samples of the octamers 3 and 4 were digested to monomers using a mixture of crude snake venom phosphodiesterase and bacterial alkaline phosphatase in order to confirm that the monomer components and the backbone had not been unexpectedly modified under the conditions of synthesis. A digestion of the natural sequence 8 served as the control. Aliquots were examined by HPLC, and the results are displayed in Figure 4. Digestion of the unmodified sequence 8 produced four peaks corresponding to the component nucleosides (dC, dG, dT and dA, panel A), whereas digestion of 3 or 4 produced five peaks (panels B and C), four corresponding to the standard nucleosides together with a later eluting peak presumably due to the monomer to which the triethylene glycol linker is attached. Evidence for the identity of the later eluting peak was obtained by the synthesis of the dimer d-Gp-triethylene glycol-pC followed by enzyme degradation with snake venom diesterase and alkaline phosphatase. HPLC analysis showed that the retention time of the later eluting peak from the digestion of 3 or 4 was identical to that from the digestion of dGp-triethylene glycol-pdC. Since snake venom is known to cleave



**Figure 5.** Treatment of **1**, **2**, and **7** with EcoR I restriction endonuclease. Lanes 1 and 12: bromophenol blue and xylene cyanol dye markers. Lane 2: **1**. Lanes 3 and 4: **1** + EcoR I overnight, 3 h, respectively. Lane 5: **2**. Lanes 6 and 7: **2** + EcoR I overnight, 3 h. Lane 8: **7**. Lanes 9 and 10: **7** + EcoR I overnight, 3 h, respectively. Lane 11: 12-mer marker.

phosphodiesterases to produce 5'-monoesters, the later eluting cleavage product is expected to be dG-3'-phosphoryl-ethylene glycol. Similar enzyme degradation experiments (not shown) were performed on the dodecamers **1**, **2**, and **7**, with identical results.

**Cleavage by EcoR I Restriction Endonuclease.** EcoR I is a restriction endonuclease which cleaves double-stranded DNA between the G and A residues of the recognition site GAATTC. Since such a recognition site exists in the dodecamers **1**, **2**, and **7**, it was of interest to examine the effect of the enzyme on these oligonucleotides, especially in view of the potential constraint introduced by the triethylene glycol bridges. When the natural duplex of **7** was incubated with EcoR I and the products examined by gel electrophoresis (Figure 5), the starting material was partially degraded after overnight incubation to give a faster running species (lane 9), which would be expected for symmetrical cleavage between the G and A residues, together with a slower species of unknown origin. It should also be noted that the mobility of **7** (lane 8) is faster than that of a random sequence 12-mer (lane 11), which suggests that the former exhibits secondary structure even under the denaturing conditions of the gel.

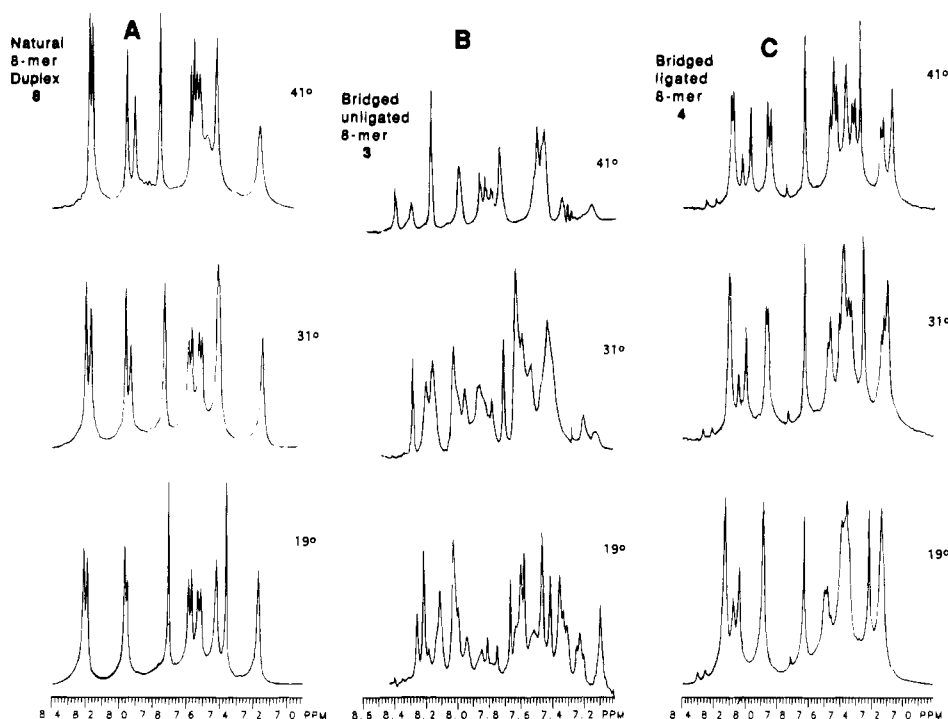
When the unligated, bridged duplex **1** was treated under the same conditions, virtually no starting material remained and three faster running species were produced (lane 3). Cleavage between the G and A residues of both strands of the molecule would be expected to give 12-mer and 10-mer hairpin sequences, whereas cleavage of only one strand would give rise to 14-mer and 10-mer structures. In the former case, the dinucleotide AA would also be generated by cleavage between the G and A residues adjacent to the nick; this dimer was not observed, presumably because of migration off the gel. Thus, the gel results indicate that the presence of the glycol bridges has no inhibitory effect on enzymatic cleavage and that both single- and double-strand cleavage occurs. The ligated oligonucleotide **2** was less readily degraded but could be cleaved slowly to give a single new species (lane 6), which would be expected because of the symmetry of the starting material and cleavage of both strands. The structure of this new species was confirmed as the expected 12 base hairpin with one triethylene glycol loop by independent synthesis and comparison by gel electrophoresis. One possible reason for the much

slower cleavage of **2** may be related to its resistance to denaturation, so that partial unwinding or "breathing" to allow for binding to the active site of the enzyme is less likely. A second possibility is that the helix may be distorted, and the NMR spectrum of **2** does in fact provide evidence for distortion in the region of the bridges.

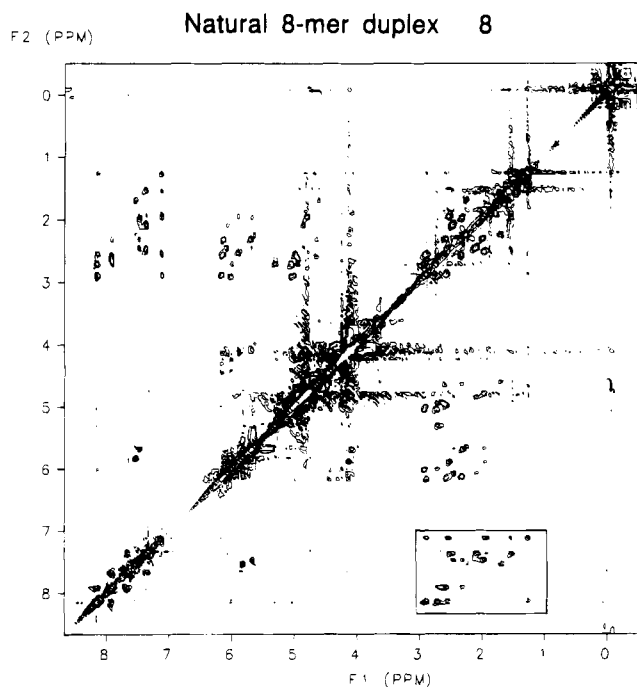
**Nuclear Magnetic Resonance Studies. 1D Spectra.** The one-dimensional spectra in D<sub>2</sub>O of the aromatic protons of the self-complementary duplex **8** and its bridged derivatives **3** and **4** are shown in Figure 6. The spectrum of the bridged, unligated octamer duplex **3** is the broadest and most complex at lower temperature compared to the natural duplex **8** and the ligated duplex **4**. This is indicative of asymmetry of the structure and the possible presence of multiple equilibria between unpaired, partially base-paired, and fully paired species. The unligated compound is asymmetric because of the the CGAA and TTCG segments, this asymmetry being removed upon ligation. Similar results (not shown) were obtained with the natural 12-mer duplex **7** as compared with the unligated analog **1**.

**2D Spectra.** The COSY spectrum of **8** (not shown) was used for the assignment of cross peaks following previous approaches (26–28). The pyrimidine bases were readily identified by the off-diagonal cross peaks of the aromatic protons since the only aromatic scalar-coupled protons in the molecule were the H<sub>5</sub> and H<sub>6</sub> of cytosine. Hence, the two strong aromatic cross peaks immediately identified the H<sub>5</sub> and H<sub>6</sub> protons of two cytosines in this sequence. The weak cross peak connecting the 7 ppm region to the 1 ppm region was the result of four-bond coupling between the methyl and H<sub>6</sub> protons and served to identify the protons of the two thymine residues. Thus, the two cytosine and two thymine residues in the sequence could be identified through the COSY spectrum. The remaining peaks in the aromatic region of the spectrum were from the purines, i.e., guanine H<sub>8</sub> and adenine H<sub>8</sub> and H<sub>2</sub>. The couplings among the sugar protons were also clearly seen in the COSY spectrum and grouped the sugar protons into sets belonging to a single residue. Each H<sub>1'</sub> in the 5.4 to 6.2 ppm region coupled to H<sub>2'</sub> and H<sub>2''</sub>. Similarly, each H<sub>3'</sub> proton was scalar-coupled to its H<sub>4'</sub> proton, which, in turn, was coupled to the H<sub>5'</sub> and H<sub>5''</sub> protons, which were poorly resolved and overlapped the chemical shifts of H<sub>4'</sub> protons. Thus, the COSY spectrum permitted the grouping of resonances according to the base, or to a single sugar, without giving any information about the position of these residues in the sequence.

The NOESY spectrum of d(CGAAATTCG)<sub>2</sub> **8** is presented as a contour plot in Figure 7. In right-hand helical DNA, the purine H<sub>8</sub> or pyrimidine H<sub>6</sub> is close to the H<sub>1'</sub> proton of its own sugar and to the H<sub>1'</sub> of the 5-terminal sugar of each strand. This provides a way to connect adjacent residues. In addition, the H<sub>2''</sub> proton of the 5-terminal residue is also close to the H<sub>5</sub>/H<sub>6</sub> of the 3-terminus of the same strand. The two thymine methyl resonances at 1.28 and 1.53 ppm represent a convenient starting point for the sequential assignments. The H<sub>6</sub> protons of thymine to which a given methyl group belongs were revealed through the weak four-bond scalar coupling to the CH<sub>3</sub> resonance. Thus, the 7.16 and 7.44 ppm aromatic protons were the H<sub>6</sub> protons of the two thymines, with the 7.16 ppm H<sub>6</sub> weakly coupled to the higher field (1.28 ppm) methyl group. The assignments of the scalar-coupled H<sub>6</sub> and CH<sub>3</sub> pairs to their specific thymine residues were based on the fact that one of the methyl resonances generated NOESY cross peaks to both thymine H<sub>6</sub> protons whereas the other thymine CH<sub>3</sub> cross-saturated its own H<sub>6</sub> and another aromatic resonance at



**Figure 6.** 1D 400-MHz NMR spectra of the octamer **8** duplex and its bridged and ligated derivatives **3** and **4** as a function of temperature.



**Figure 7.** 2D-NOESY NMR spectrum at 400 MHz of the duplex of the natural octamer **8**. The boxed region highlights the  $H_{2'}$ ,  $H_{2''}$ -base interactions.

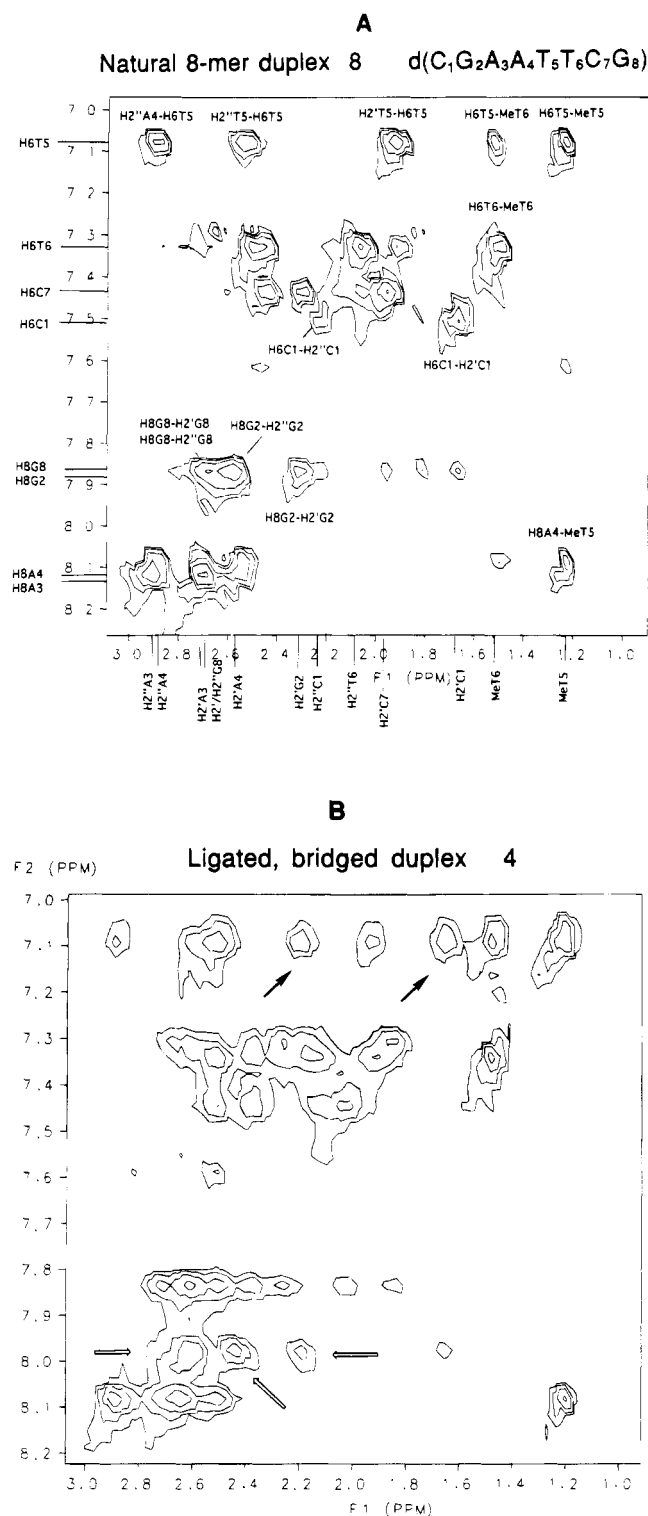
8.14 ppm. The only neighbors of the thymine in the duplex were the  $A_4$ , and the absence of any scalar coupling involving the 8.14 ppm resonance identified it as an  $H_8$  of adenine. The fact that the  $T_5$  aromatic proton was near both the  $T_5$  and  $T_6$  methyls independently established that the helix was right-handed without any prior assumptions. Having identified the  $H_6$  and methyl resonances of  $T_5$  and  $T_6$ , one can proceed along the helix in either direction using the  $H_{1'}$  proton to aromatic proton NOE's to complete the assignments. It should be noted that the NOESY spectrum of **8** showed clear evidence for the existence of a duplex, even though the tempera-

ture of the NMR experiment (approximately 25 °C) is close to its dissociation temperature as determined by UV measurement. Presumably, the much higher concentration of sample used in the NMR experiment as compared with the very dilute sample in the thermal denaturation experiment was sufficient to favor formation of the duplex rather than the single-stranded form.

Once the base and  $H_{1'}$  protons have been assigned, the COSY spectrum generally sufficed to assign all of the remaining sugar protons. Both  $H_{2'}$  and  $H_{2''}$  protons were strongly coupled to their  $H_{1'}$ ; however, any given  $H_{2''}$  was nearer to its  $H_{1'}$  than is  $H_{2'}$  and, hence, gave a much stronger NOESY cross peak, which made the 2' and 2'' relatively easy to distinguish. Since the sugar proton  $H_{2'}/H_{2''}$  resonances in two thymines were heavily overlapped, it was not possible to assign their chemical shifts by the NOE cross peaks between base protons and  $H_{2'}/H_{2''}$  in the 5' end, even though this distance was about 2.2 Å in B-form DNA. The distance between  $H_{2'}/H_{2''}$  to the methyl group at the 3' end was used as an alternative, this distance being about 2.9–3.4 Å. As can be seen from Figure 7, well-resolved cross peaks between the methyl and  $H_{2'}/H_{2''}$  protons were observed. Since the chemical shifts of  $H_{2'}$  and  $H_{2''}$  of  $T_5$  and  $T_6$  were almost overlapped, the cross peaks between methyl and  $H_{2'}/H_{2''}$  protons could be used to make these assignments (Figure 7).

**Comparison of the 2D-NOESY Spectra of **4** and **8**.** The expanded regions of the deoxyribose-base interactions of the unmodified octamer **8** (panel A) and the ligated duplex **4** (panel B) are shown in Figure 8. A comparison of the two revealed a few obvious differences. It is remarkable that 19 peaks were unaltered in position, although their intensities may have changed. Five peaks were clearly shifted; the two indicated by solid arrows represent the  $C_1$  cross peaks, indicating that the chemical shift of  $H_6C_1$  has changed from 7.51 ppm to 7.08 ppm. The two cross peaks indicated by open arrows arose from a shift of the  $H_8$  proton of  $G_8$  (from 7.87 to 7.99 ppm). Remarkably, the only major shifts were associated with  $C_1$  and  $G_8$ , at the termini where the bridges were





**Figure 8.** Expanded regions of the 400-MHz 2D-NOESY NMR spectra of **8** (panel A) and **4** (panel B) showing the  $H_2', H_2''$ -base interactions.

attached, and helped to confirm the presence of the bridge. These shifts could have arisen from (a) the mere presence of the bridging group, (b) a conformational change at the terminus, i.e., buckling of the base pairs due to distortion produced by the presence of the bridge, or (c) a more restricted conformational status (less fraying) for the bridged duplex than the natural duplex. Since the positions of NOE cross peaks provided a fingerprint of the conformation, these results (19 out of 26 cross peaks unshifted, and five shifted at termini)

would indicate that no major conformational change has occurred, and thus it can be deduced that the ligated duplex **4** is likely to possess a B-form structure. The cross peaks associated with  $A_4$ - $T_5$  interactions were either absent or much weaker in the spectrum of the unligated sample (not shown), and might indicate the absence of strong interactions between  $A_4$  and  $T_5$  due to breathing at the nick site. A spectrum obtained at 600 MHz (not shown) of the reaction mixture from the ligation reaction of the unbridged unligated dodecamer **1** to give the bridged duplex **2** gave results consistent with the above analysis for the 400-MHz 2D-NOESY spectrum of the ligated octamer **4**, including the presence of  $C_1$ - and  $G_{12}$ -shifted resonances.

#### ACKNOWLEDGMENT

We thank Ad Bax, NIH, for running a 600-MHz NMR spectrum. Fellowships to N.C. and L.Z. from Pharmagenics, Inc., are gratefully acknowledged.

#### LITERATURE CITED

- (1) Shaw, J.-P., Kent, K., Bird, J., Fishback, J., and Froehler, B. (1991) Modified Deoxyoligonucleotides Stable to Exonuclease Degradation in Serum. *Nucleic Acids Res.* **19**, 747-750.
- (2) Akhtar, S., Kole, R., and Juliano, R. L. (1991) Stability of Antisense DNA Oligodeoxynucleotide Analogs in Cellular Extracts and Sera. *Life Sci.* **49**, 1793-1801.
- (3) Scheffler, I. E., Elson, E. L., and Baldwin, R. L. (1970) Helix Formation by d(TA) Oligomers II. Analysis of the Helix-Coil Transitions of Linear and Circular Oligomers. *J. Mol. Biol.* **48**, 145-171.
- (4) Wemmer, D. E., and Benight, A. S. (1985) Preparation and Melting of Single Strand Circular DNA Loops. *Nucleic Acids Res.* **13**, 8611-8621.
- (5) Erie, D. A., Jones, R. A., Olson, W. K., Sinha, N. K., and Breslauer, K. J. (1989) Melting Behavior of a Covalently Closed, Single-Stranded Circular DNA. *Biochemistry* **28**, 268-273.
- (6) Erie, D. A., Sinha, N. K., Olson, W. K., Jones, R. A., and Breslauer, K. J. (1987) A Dumbbell-Shaped, Double Hairpin Structure of DNA: A Thermodynamic Investigation. *Biochemistry* **26**, 7150-7159.
- (7) Ashley, G. W., and Kushlan, D. M. (1991) Chemical Synthesis of Oligodeoxynucleotide Dumbbells. *Biochemistry* **30**, 2927-2933.
- (8) Kool, E. (1991) Molecular Recognition by Circular Oligonucleotides: Increasing the Selectivity of DNA Binding. *J. Am. Chem. Soc.* **113**, 6265-6266.
- (9) Rumney, S. and Kool, E. T. (1992) Recognition by Hybrid Oligoether Oligodeoxynucleotide Macrocycles. *Angew. Chem., Int. Ed. Engl.* **31**, 1617-1619.
- (10) Doktycz, M. J., Goldstein, R. F., Paner, T. M., Gallo, F. J., and Benight, A. S. (1992) Studies of DNA dumbbells. 1. Melting Curves of 17 DNA Dumbbells with Different Duplex Stem Sequences Linked by T4 Endloops: Evaluation of the Nearest-Neighbor Stacking Interactions in DNA. *Biopolymers* **32**, 849-864.
- (11) Chu, B. C. F., and Orgel, L. E. (1992) The stability of different forms of double-stranded decoy DNA in serum and nuclear extracts. *Nucleic Acids Res.* **20**, 5857-5858.
- (12) Clusel, C., Ugarte, E., Enjolras, N., Vasseur, M., and Blumenfeld, M. (1993) Ex Vivo Regulation of Specific Gene Expression by Nanomolar Concentration of double-stranded Dumbbell Oligonucleotides. *Nucleic Acids Res.* **21**, 3405-3411.
- (13) Ma, M. Y.-X., McCallum, K., Climie, L. S., Kuperman, R., Lin, W. C., Sumner-Smith, M., and Barnett, R. W. (1993) Design and Synthesis of RNA Miniduplexes via a Synthetic Linker Approach. 2. Generation of Covalently Closed, Double-stranded Cyclic HIV-1 TAR Analogs with High Tat-binding Affinity. *Nucleic Acids Res.* **21**, 2585-2589.
- (14) Durand, M., Chevre, K., Chassignol, M., Thuong, N. T., and Maurizot, J. C. (1990) Circular dichroism Studies of an

- Oligodeoxyribonucleotide containing a Hairpin Loop made of a Hexaethylene Glycol Chain: Conformation and Stability. *Nucl. Acids Res.* 18, 6353–6359.
- (15) Salunkhe, M. S., Wu, T., and Letsinger, R. L. (1992) Control of Folding and Binding of Oligonucleotides by Use of a Non-nucleotide Linker. *J. Am. Chem. Soc.* 114, 8768–8772.
- (16) Cload, S. T., and Schepartz, A. (1991) Polyether Tethered Oligonucleotide Probes. *J. Am. Chem. Soc.* 113, 6324–6326.
- (17) Richardson, P. L., and Schepartz, A. (1991) Tethered Oligonucleotide Probes. A Strategy for the Recognition of Structured RNA. *J. Am. Chem. Soc.* 113, 5109–5111.
- (18) Durand, M., Peloille, S., Thuong, N. T., and Maurizot, J. C. (1992) Triple-Helix Formation by an Oligonucleotide Containing One (dA)<sub>12</sub> and Two (dT)<sub>12</sub> Sequences Bridged by Two Hexaethylene Glycol Chains. *Biochemistry* 31, 9197–9204.
- (19) Benseler, F., Fu, D., Ludwig, J., and McLaughlin, L. W. (1993) Hammerhead-like Molecules Containing Non-Nucleoside Linkers are Active RNA Catalysts. *J. Am. Chem. Soc.* 115, 8483–8484.
- (20) Glick, G. D., Osborne, S. E., Knitt, D. S., and Marino, J. P. (1992) Trapping and Isolation of an Alternate DNA Conformation. *J. Am. Chem. Soc.* 114, 5447–5448.
- (21) Horn, T., and Urdea, M., (1986) A Chemical 5'-Phosphorylation of Oligodeoxyribonucleotides that can be Monitored by Trityl Cation Release. *Tetrahedron Lett.* 27, 4705–4708.
- (22) Rychlik, W., and Rhoads, R. E. (1989) A Computer Program for Choosing Optimal Oligonucleotides for Filter Hybridization, Sequencing and in vitro Amplification of DNA. *Nucleic Acids Res.* 17, 8543–8551.
- (23) El-Deiry, W. S., Kern, S. E., Pietenpol, J. A., Kinzler, K. W., and Vogelstein, B. (1992) Human Genomic Sequences Define a Consensus Binding Site for p53. *Nature Genet.* 1, 45–49.
- (24) Marky, L. A., Blumenfeld, K. S., Kozlowski, S., and Breslauer, K. J. (1983) Salt-Dependent Conformational Transitions in the Self-Complementary Deoxydodecanucleotide d(CGCGAATTCGCG): Evidence for Hairpin Formation. *Biopolymers* 22, 1247–1257.
- (25) Rentzeperis, D., Ho, J., and Marky, L. A. (1993) Contribution of Loops and Nicks to the Formation of DNA Dumbbells: Melting Behaviour and Ligand Binding. *Biochemistry* 32, 2564–2572.
- (26) Feigon, J., Leupin, W., Denny, W. A., and Kearns, D. R. (1983) Two-Dimensional Proton NMR Investigation of the Synthetic Deoxyribonucleic Acid Decamer d(ATATCGATAT)<sub>2</sub>. *Biochemistry* 22, 5943–5951.
- (27) Hare, D. R., Wemmer, D. E., Chou, H. H., Drobny, G., and Reid, B. R. (1983) Assignment of the Non-exchangeable Proton Resonances of d(CGCGAATTCGCG) using Two-dimensional Nuclear Magnetic Resonance Methods. *J. Mol. Biol.* 171, 319–336.
- (28) Weiss, M. A., Patel, D. J., Sauer, R. T., and Karplus, M. (1984). Two-dimensional <sup>1</sup>H NMR study of the λ operator site O<sub>1</sub>: A sequential assignment strategy and its application. *Proc. Natl. Acad. Sci. U.S.A.* 81, 130–134.

# Fluorogenic *N*-Nitrosoamides: Active-Site Labeling Reagents for Chymotrypsin-like Proteases

Min Li<sup>†</sup> and Emil H. White<sup>\*</sup>

Department of Chemistry, The Johns Hopkins University, Baltimore, Maryland 21218. Received February 17, 1994<sup>\*</sup>

Two fluorogenic *N*-nitrosoamides, *N*-nitroso-*N*-((7-methoxycoumarin-4-yl)methyl)-*N'*-isobutyrylalaninamide (**6a**) and *N*-nitroso-*N*-((6-methoxyquinolin-2-yl)methyl)-*N'*-isobutyrylalaninamide (**6b**), were synthesized. Both *N*-nitrosoamides inhibited  $\alpha$ -chymotrypsin irreversibly; they show promise as labeling reagents for the active sites of chymotrypsin-like proteases.

## INTRODUCTION

*N*-Nitrosoamide derivatives of amino acids are active-site-directed enzyme-activated inhibitors ("suicide inhibitors") for hydrolytic enzymes (White et al., 1975; 1977a; 1977b; 1981; 1990; Donadio et al., 1985; White and Chen, 1993). Because of the extremely high reactivity of the carbocations (White et al., 1968; 1973; 1978) released during enzyme-catalyzed hydrolyses, they can serve as relatively indiscriminating active-site labeling reagents (eq 1, Scheme 1). The alkylation by the carbocations can occur at the amide linkages as well as the side chains (except alkyl groups) within the active site of a targeted enzyme (Donadio et al., 1985; White et al., 1990). No other affinity or "suicide" reagents, except photoaffinity labeling reagents (White et al., 1978), have comparable reactivity. We report here the synthesis of two fluorogenic labeling reagents for chymotrypsin-like proteases based on the nitrosoamide functional group. Upon enzymatic activation (hydrolysis), these reagents deliver fluorescent labels (methoxycoumarin or quinoline moieties) to the amide linkages and/or the side chains of amino acid residues in the active site (eq 1). The identification of the alkylated sites should be facilitated by the facile detection of fluorescent peptides produced in a subsequent hydrolysis of the inhibited (labeled) enzyme.

## RESULTS AND DISCUSSION

The general synthetic route employed is outlined in Scheme 2.

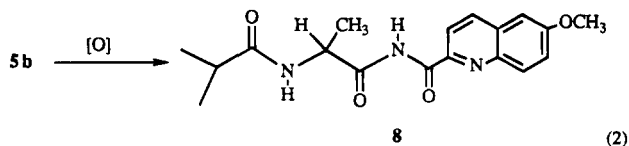
In the "b" series, the bromomethyl intermediate required (**2b**) was obtained through bromination of 6-methoxyquinaldine (**1b**) with *N*-bromosuccinimide (NBS) in CCl<sub>4</sub>. In addition to the desired mono- $\alpha$ -bromination, ring- and presumably di- $\alpha$ -bromination also occurred. The bromination was terminated, therefore, before the latter side reactions became important. In the second step of the synthesis, only the mono- $\alpha$ -brominated compound (**2b**) reacted with hexamethylenetetramine (Blazevic et al., 1979) to form a complex salt (**3b**), which precipitated as a white powder in rather pure form.

The salts **3a,b**, formed upon reacting **2a,b** with hexamethylenetetramine, were hydrolyzed (Nodiff et al., 1974; Blazevic et al., 1979) to give the amines **4a,b** in high yields (~90%). The subsequent coupling reactions

between the amines **4a,b** and isobutyrylalanine were effected by using 1-(3-(dimethylamino)propyl)-3-ethylcarbodiimide hydrochloride (EDC) (Sheehan et al., 1965). In attempts to make optically pure **5b**, however, a racemized product was obtained. This was first detected by the unusually small values of the optical rotation for the amides formed: D-**5b**,  $[\alpha]^{23.5}_D -1.5^\circ$  (c 4.08, CHCl<sub>3</sub>); L-**5b**,  $[\alpha]^{23.5}_D +0.6^\circ$  (c 2.14, CHCl<sub>3</sub>). The racemization was confirmed via the <sup>1</sup>H-NMR spectrum of D-**5b** in the presence of a chiral shift reagent, tris[3-((trifluoromethyl)hydroxymethylene)-D-camphorato]europium(III) derivative (Goering et al., 1974); two methoxy peaks of approximately equal intensity were observed. It has been reported that carbodiimide type coupling reagents can lead to a substantial amount of racemization of the peptides formed (Anderson and Callahan, 1958; Williams and Young, 1963).

In the nitrosation step (Scheme 2) (White, 1955), approximately equal amounts of the mononitroso (**6a,b**) and dinitroso (**7a,b**) products were formed. It appears that the difference in steric hindrance between the two potential nitrosation sites is not large enough to substantially reduce the formation of the dinitroso compounds. The mono and dinitroso compounds, however, were readily separated on silica gel columns.

In the EDC coupling step to make the quinoline amide (**5b**), it was found that when the reaction mixture was not protected from air and the reaction time was long (33 h) the initially formed amide **5b** underwent an oxidation reaction to give compound **8** with an imide grouping (eq 2). <sup>1</sup>H-NMR spectra showed that the signal



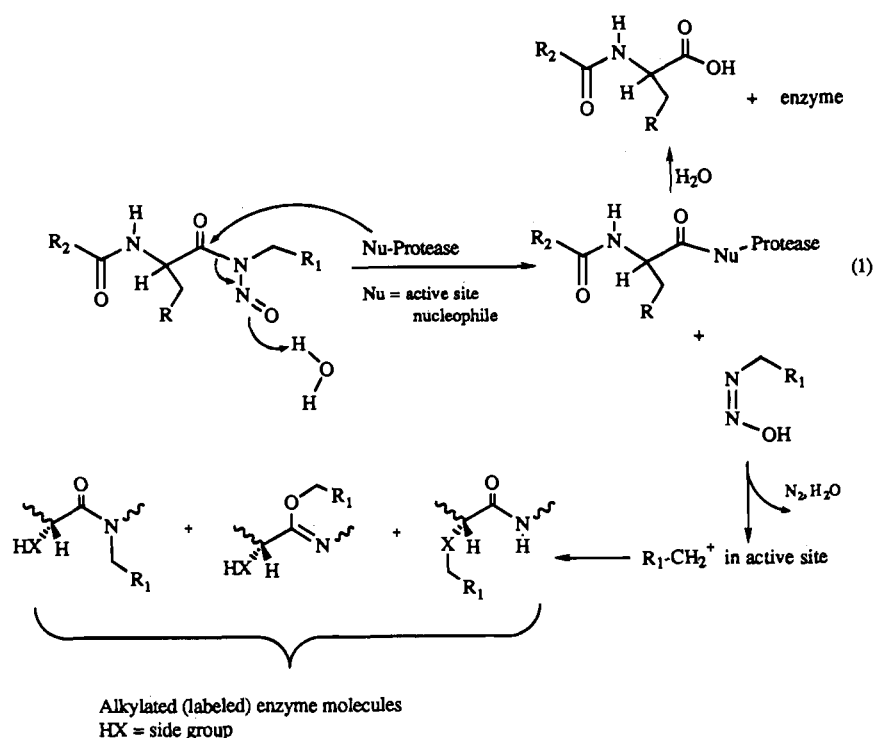
for the two methylene protons in **5b** (4.71–4.65 ppm) disappeared as a result of the oxidation, while the signal for one of the amide protons shifted from 7.52 ppm to 10.93 ppm. The mass spectrum was even more informative (Figure 1); in addition to the parent ion at *m/z* 343, it showed fragmentation peaks at 230, 229, 202, 186, 158, and 114.

Preliminary labeling tests with  $\alpha$ -chymotrypsin showed that 40% of the enzyme was irreversibly inhibited (or labeled) by a 70-fold molar excess of **6b**, where time-dependent inhibition was clearly demonstrated (Figure 2). There appears to be no doubt that the enzyme was

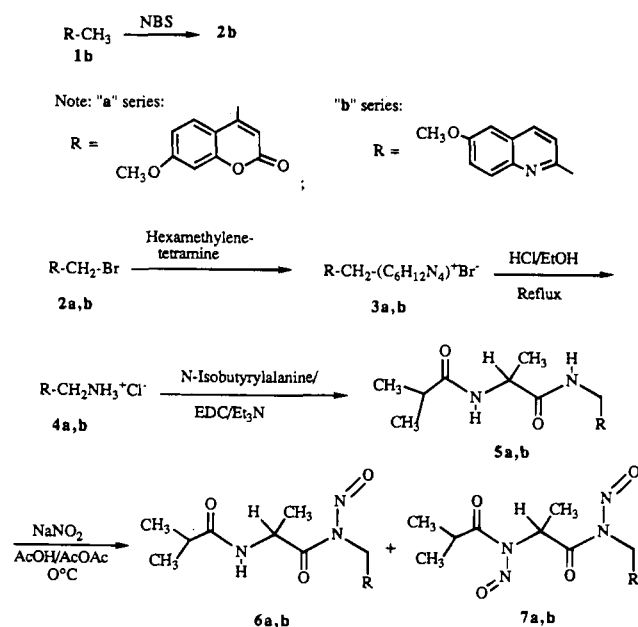
<sup>†</sup> Present address: Department of Medicinal Chemistry & Pharmacognosy (M/C 781), University of Illinois at Chicago, 833 South Wood Street, Chicago, IL 60612.

<sup>\*</sup> Abstract published in *Advance ACS Abstracts*, August 1, 1994.

## Scheme 1



## Scheme 2. Synthesis of Fluorogenic Inhibitors



irreversibly inhibited; no regeneration of enzyme activity was observed during an incubation period of ~10 h. With the same amount of **6a**, 10% of the enzyme was labeled (Figure 3). It is assumed that in both cases only the D-isomers would be responsible for the observed inhibition, according to a previous study by White et al. (1977a). That is, in reality, the "active" nitrosoamide/enzyme ratio used was 35 rather than 70. Since **6a** and **6b** contain aromatic groups at the P1 position and since it is expected that they will not be highly selective (no group is present beyond P2), it is reasonable for us to speculate that these two compounds would also label other proteases that have a specificity for aromatic side chains similar to that of chymotrypsin.

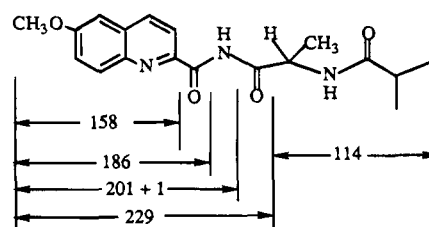
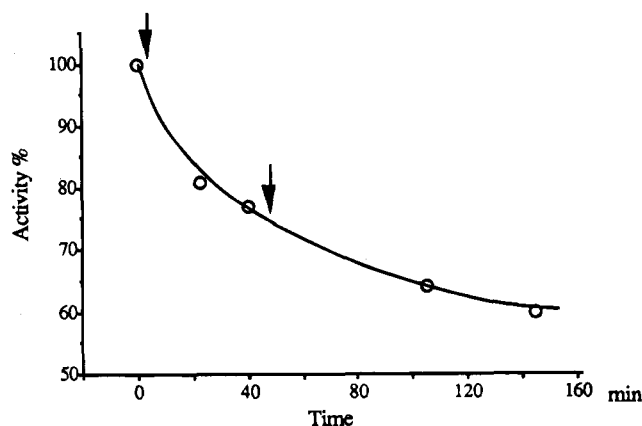


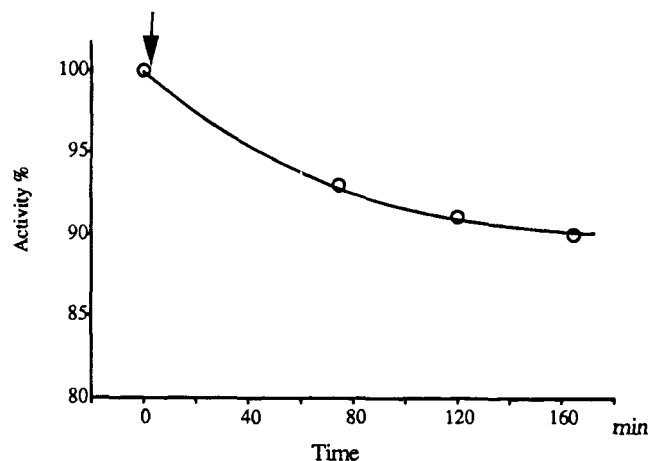
Figure 1. MS cracking peaks for imide 8.



**Figure 2.** Inhibition of chymotrypsin with **6b**. The inhibitor (70-fold total molar excess) in acetonitrile was divided equally into two portions and added dropwise at 0 and 46 min, respectively. The arrows indicate the beginning of each addition. The activities shown are corrected for the activity loss due to autolysis (control run).

## EXPERIMENTAL PROCEDURES

**Materials and Methods.** 7-Methoxy-4-(bromomethyl)coumarin, 6-methoxyquinoline, and 1-(3-(dimethylamino)propyl)-3-ethylcarbodiimide hydrochloride (EDC) were obtained from Aldrich Chemical Co.  $\alpha$ -Chymotrypsin (type I-S) was purchased from Sigma Chemical Co. All other reagents were of the highest purity avail-



**Figure 3.** Inhibition of chymotrypsin with **6a**. The inhibitor (70-fold molar excess) in acetonitrile was added dropwise over a 45-min period. The arrow indicates the beginning of the addition. The activities shown are corrected for the activity loss due to autolysis (control run).

able. Melting points were measured on a Thomas/Hoover Unimelt apparatus and were not corrected.

<sup>1</sup>H- and <sup>13</sup>C-NMR spectra were acquired on a Varian Associates XL-400 NMR spectrometer. Tetramethylsilane (TMS) was used as an internal reference in organic solvents. Infrared spectra were recorded on a Perkin-Elmer 1600 Series FTIR spectrometer. A Beckman Model 25 UV-vis spectrophotometer was used for recording UV-vis spectra. Mass spectra of organic compounds were acquired on a VG 70-S mass spectrometer.

**4-((Hexamethylenetetraminiumyl)methyl)-7-methoxycoumarin Bromide (3a).** Hexamethylenetetramine (HMTA) (0.527 g, 3.76 mmol) in 80 mL of CHCl<sub>3</sub> and 15 mL of acetone was added dropwise into a solution of compound **2a** (1.011 g, 3.76 mmol in 500 mL of acetone) within a period of ~20 min at room temperature. About 10 min after the complete addition of the HMTA solution, the reaction mixture turned cloudy and a white precipitate began to form. The reaction solution was stirred for 4 h at room temperature and then allowed to stand overnight. A white fine powder (1.37 g, 3.35 mmol, 89%) was obtained, mp 200 °C dec. <sup>1</sup>H-NMR (DMSO-*d*<sub>6</sub>): δ 8.08 (d, 1 H, *J* = 8.8 Hz), 7.14 (d, 1 H, *J* = 2.5 Hz), 7.07 (dd, 1 H, *J*<sub>1</sub> = 8.8 Hz, *J*<sub>2</sub> = 2.5 Hz), 6.60 (s, 1 H), 5.20 (s, 6 H), 4.54 (AB quartet, 6 H, *J*<sub>1</sub> = *J*<sub>2</sub> = 12.6 Hz), 4.22 (s, 2 H), 3.90 (s, 3 H). IR (KBr): 1718, 1613, 1300, 1148, and 1010 cm<sup>-1</sup>.

**4-(Aminomethyl)-7-methoxycoumarin Hydrochloride (4a).** Compound **3a** (500 mg, 1.22 mmol) was suspended in 27 mL of concd HCl in EtOH made up in a 1/15 ratio (v/v). The reaction mixture was refluxed for 2.5 h and then cooled to room temperature. Fine white crystals formed at room temperature; they were collected by filtration to yield the product (280 mg, 95%), mp 234 °C dec. NMR (DMSO-*d*<sub>6</sub>): δ 8.75 (s, 3 H), 7.72 (d, 1 H, *J* = 8.8 Hz), 7.07 (d, 1 H, *J* = 2.5 Hz), 7.1 (dd, 1 H, *J*<sub>1</sub> = 8.8 Hz, *J*<sub>2</sub> = 2.5 Hz), 4.36 (s, 2 H), 3.88 (s, 3 H). IR (KBr): 3030 (broad), 1731, 1682, 1618, 1405, and 1149 cm<sup>-1</sup>. Anal. Calcd for C<sub>11</sub>H<sub>12</sub>NO<sub>3</sub>Cl·0.5H<sub>2</sub>O: C, 52.71; H, 5.23; N, 5.59. Found: C, 52.98; H, 5.06; N, 5.96.

**N-Isobutyrylalanine.** The title compound was synthesized according to the procedures of Doherty and Popenoe (1951). <sup>1</sup>H-NMR (DMSO-*d*<sub>6</sub>): δ 8.00 (d, 1 H, *J* = 7.2 Hz), 4.17 (m, 1 H), 2.41 (m, 1 H), 1.25 (d, 3 H, *J* = 7.3 Hz), 0.99 (dd, 6 H, *J*<sub>1</sub> = 7.0 Hz, *J*<sub>2</sub> = 6.8 Hz). DL-Racemate: mp 124–126 °C (lit. (Doherty and Popenoe, 1951) mp 129–130 °C). D-Isomer: mp 150–152 °C.

[α]<sub>D</sub><sup>27</sup>: +32.5° (c 0.080, EtOH). L-Isomer: mp 147–149 °C. [α]<sub>D</sub><sup>23</sup>: -33.2° (c 0.266, EtOH).

**DL-N-((7-Methoxycoumarin-4-yl)methyl)-N'-isobutyrylalaninamide (5a).** To 10 mL of CH<sub>2</sub>Cl<sub>2</sub> was added compound **4a** (150 mg, 0.621 mmol), N-isobutyryl-L-alanine (101 mg, 0.635 mmol), Et<sub>3</sub>N (90 μL, 0.647 mmol), and EDC (133 mg, 0.645 mmol). After being stirred at room temperature for 24 h, the reaction mixture was mixed with another 20 mL of CH<sub>2</sub>Cl<sub>2</sub> and then washed with H<sub>2</sub>O (2×), 3% HCl, 5% NaHCO<sub>3</sub>, and H<sub>2</sub>O, respectively. The washed solution was dried over anhydrous Na<sub>2</sub>SO<sub>4</sub>, and the solvent was removed to give 145 mg (0.419 mmol, 67.5%) of crude product as a yellowish solid, which was recrystallized (90%) from ethyl acetate/hexane for use in the next step, mp 205 °C dec. NMR (CDCl<sub>3</sub>): δ 7.7 (s, 1 H), 7.48 (d, 1 H, *J* = 8.8 Hz), 6.85 (dd, 1 H, *J*<sub>1</sub> = 8.8 Hz, *J*<sub>2</sub> = 2.5 Hz), 6.79 (d, 1 H, *J* = 2.5 Hz), 6.4 (d, 1 H, *J* = 7 Hz), 6.16 (s, 1 H), 4.64 (m, 2 H), 4.51 (m, 1 H), 3.87 (s, 3 H), 2.41 (m, 1 H), 1.41 (d, 3 H), 1.14 (t, 6 H, *J* = 7.0 Hz). IR (KBr): 3278, 1726, 1637, 1618, 1542, and 1292 cm<sup>-1</sup>. Anal. Calcd for C<sub>18</sub>H<sub>22</sub>O<sub>5</sub>N<sub>2</sub>·0.25H<sub>2</sub>O: C, 61.63; H, 6.42. Found: C, 61.74; H, 6.22.

**Nitrosation of DL-N-((7-Methoxycoumarin-4-yl)methyl)-N'-isobutyrylalaninamide (5a).** Coumarin amide **5a** (24.5 mg, 0.071 mmol) was dissolved in a mixture of acetic acid (306 μL, 5.39 mmol) and acetic anhydride (1.52 mL, 16.1 mmol), and the solution was cooled in an ice-water bath. Sodium nitrite (114 mg, 1.65 mmol) was added to the amide solution at once with strong magnetic stirring. After the starting material had disappeared (~60 min; TLC), the reaction mixture was diluted with 20 mL of CH<sub>2</sub>Cl<sub>2</sub> and then washed with cold 5% NaHCO<sub>3</sub> solution (2×) and H<sub>2</sub>O. The washed solution was dried over anhydrous Na<sub>2</sub>SO<sub>4</sub>, and the solvent was removed *in vacuo*. The residue was applied in ethyl acetate to a short silica gel column; elution occurred with ethyl acetate/hexane (1/2, v/v). The fast-moving yellow band (6 mg, 21%) (*R*<sub>f</sub> = 0.7) was found to be the dinitroso compound (**7a**); no NH signals were observed in the <sup>1</sup>H-NMR spectrum (CDCl<sub>3</sub>): δ 7.44 (d, 1 H, *J* = 8.8 Hz), 6.88 (dd, 1 H, *J*<sub>1</sub> = 8.8 Hz, *J*<sub>2</sub> = 2.5 Hz), 6.83 (d, *J* = 2.5 Hz), 6.03 (q, 1 H, *J* = 7.0 Hz), 5.51 (s, 1 H), 4.95 (AB quartet, *J*<sub>1</sub> = *J*<sub>2</sub> = 16 Hz), 3.88 (s, 3 H), 3.78 (m, 1 H), 1.47 (d, 3 H, *J* = 7.0 Hz), 1.26 (d, 3 H, *J* = 6.9 Hz), 1.23 (d, 3 H, *J* = 6.8 Hz). After the first band had been collected, ethyl acetate was used to elute the desired mononitroso compound **6a** (*R*<sub>f</sub> = 0.4). Extra pressure was employed during the separation to ensure that the whole process was complete within 10–15 min, as longer times led to decomposition of the nitroso compounds. After removal of the solvents, a yellow oil (**6a**) was obtained (6.8 mg, 26%). <sup>1</sup>H-NMR (CDCl<sub>3</sub>): δ 7.37 (d, 1 H, *J* = 8.8 Hz), 6.81 (dd, 1 H, *J*<sub>1</sub> = 8.8 Hz, *J*<sub>2</sub> = 2.5 Hz), 6.76 (d, 1 H, *J* = 2.5 Hz), 6.18 (d, 1 H, *J* = 7 Hz), 5.77 (m, 1 H), 5.51 (s, 1 H), 4.95 (s, 2 H), 3.81 (s, 3 H), 2.42 (m, 1 H), 1.55 (d, 3 H, *J* = 7.2 Hz), 1.14 (d, 3 H, *J* = 6.9 Hz), 1.13 (d, 3 H, *J* = 7.0 Hz).

Nitrosations were also conducted at -13 °C [same ratio of acetic anhydride/acetic acid (v/v) as used above: 5/1], as well as at different ratios of acetic anhydride/acetic acid such as 2/1 and 1/1 (0 °C), in an attempt to minimize the amount of dinitroso compound. Under these conditions, however, the product distribution was essentially the same; i.e., the mononitroso/dinitroso ratio was ~1.

**2-(Bromomethyl)-7-methoxyquinoline (2b) and 2-((Hexamethylenetetraminiumyl)methyl)-6-methoxyquinoline Bromide (3b).** To 434 mL of CCl<sub>4</sub> was added 6-methoxyquinaldine (**1b**) (7.24 g, 41.8 mmol), NBS (7.44 g, 41.8 mmol), and benzoyl peroxide (290 mg,

1.20 mmol), and the mixture was refluxed for 2 h. After the reaction mixture was cooled to room temperature, the succinimide formed and unreacted NBS were removed by filtration. Removal of  $\text{CCl}_4$  yielded a brown oil, which was dissolved in 45 mL of  $\text{CHCl}_3$ . TLC [silica gel; ethyl acetate/hexane, 1/1, (v/v)] showed that four compounds were present in the solution with  $R_f$ s of 0.18, 0.27, 0.51, and 0.60. The compound with  $R_f$  0.27 fluoresced very strongly; it was shown to be the starting material (**1b**). The compound with  $R_f$  0.51 appeared initially as a strong dark spot which quickly turned strongly fluorescent, suggesting that it was the desired product (**2b**). The spot with  $R_f$  0.18 was very weak and never became fluorescent, indicating a possible ring bromination. The spot with  $R_f$  0.60, almost equally weak, quickly turned fluorescent suggesting a possible dibromination on the methyl group. It has been known that an introduction of heavy atoms such as bromine into a fluorescent chromophore results in loss of fluorescence (heavy atom effect) (Wehry, 1973). Apparently, the bromination on the ring or at the  $\alpha$  position had the same effect in terms of quenching the fluorescence. The mixture was also analyzed by HPLC [ $\mu$ -Bondapak C-18 column under isocratic conditions: 50% A solution (0.1% TFA in acetonitrile) and 50% B solution (50% MeOH in  $\text{H}_2\text{O}$ )] with UV detection at 333 nm; two peaks were observed at  $R_f$  3.7 and 4.6 min, respectively, with a relative ratio of 3/1. The relative area of the peak at  $R_f$  4.6 min represented a 25% yield of compound **2b**. Thus, to the above mixture was added 1.46 g of hexamethylenetetramine (25%  $\times$  41.8 mmol) in 30 mL of  $\text{CHCl}_3$ . The resulting mixture was heated at 52 °C for 5 min; a white precipitate formed, which was collected by filtration (1.94 g). Condensation and cooling of the mother liquor yielded another 1.53 g of the white solid. Therefore, a total of 3.47 g of **3b** was obtained (21% yield from compound **1b**), mp 172 °C dec.  $^1\text{H-NMR}$  ( $\text{DMSO}-d_6$ ):  $\delta$  8.41 (d, 1 H,  $J = 8.4$ ), 8.00 (d, 1 H,  $J = 9.2$  Hz), 7.62 (d, 1 H,  $J = 8.4$  Hz), 7.50–7.47 (m, 2 H), 5.23 (s, 6 H), 4.52 (AB quartet, 6 H,  $J_1 = J_2 = 12.6$  Hz), 4.26 (s, 2 H), 3.92 (s, 3 H). IR (KBr): 1620, 1500, 1266, 1241, 999, and 812  $\text{cm}^{-1}$ . Anal. Calcd for  $\text{C}_{17}\text{H}_{22}\text{N}_5\text{OBr} \cdot 0.25\text{H}_2\text{O}$ : C, 51.46; H, 5.72; N, 17.65. Found: C, 51.42; H, 5.59; N, 17.97.

The bromination of **1b** with NBS was also tried in  $\text{CHCl}_3$ , instead of  $\text{CCl}_4$ . After being refluxed for 4 h, the reaction solution was checked by TLC; it showed a strong nonfluorescent spot at  $R_f$  0.18 (a ring bromination product) and a very weak spot at  $R_f$  0.51 (**2b**), in addition to the strong fluorescent spot of the starting material **1b** at  $R_f$  0.27. Therefore, the bromination of **1b** in  $\text{CHCl}_3$  appeared to favor ring bromination over bromination at the  $\alpha$  position; it was thus not useful for the desired synthesis.

**2-(Aminomethyl)-6-methoxyquinoline (4b).** Using a method similar to that used for the synthesis of **4a**, compound **3b** (3.47 g, 8.85 mmol) was dissolved in 195 mL of a solution of concd HCl in EtOH (1/15, v/v), and the solution was refluxed for 1.5 h. The precipitate formed was collected by filtration (2.36 g);  $^1\text{H-NMR}$  spectrum showed that it contained 87% of the desired compound (corresponding to an 89% yield) and 13% of  $\text{NH}_4\text{Cl}$  (w/w).  $^1\text{H-NMR}$  ( $\text{DMSO}-d_6$ ):  $\delta$  8.93 (s, 3 H, br), 8.61 (d, 1 H,  $J = 8.4$  Hz), 8.10 (d, 1 H,  $J = 9.2$  Hz), 7.87 (d, 1 H,  $J = 8.4$  Hz), 7.58–7.55 (m, 2 H), 7.43 (t, 4 H,  $J = 50$  Hz,  $\text{NH}_4\text{Cl}$ ), 4.46 (s, 2 H), 3.90 (s, 3 H). This solid (2.18 g) was dissolved in 20 mL of  $\text{H}_2\text{O}$  and 2 N NaOH was used to adjust the solution to pH 14. The basic solution was extracted with  $\text{CH}_2\text{Cl}_2$  (4 $\times$ , 150 mL total) and the extract was dried over KOH. Removal of  $\text{CH}_2\text{Cl}_2$  yielded 1.18 g of amine (6.28 mmol, 71% from **3b**),

mp 74 °C (began to decompose), 97 °C (crystals collapsed and turned opaque), 119 °C, full melting.  $^1\text{H-NMR}$  ( $\text{DMSO}-d_6$ ):  $\delta$  8.19 (d, 1 H,  $J = 8.4$  Hz), 7.85 (d, 1 H,  $J = 9.2$  Hz), 7.55 (d, 1 H,  $J = 8.4$  Hz), 7.38–7.32 (m, 2 H), 3.92 (s, 2 H), 3.87 (s, 3 H). IR (KBr): 3351, 1622, 1601, 1501, and 1233  $\text{cm}^{-1}$ .

**N-((6-Methoxyquinolin-2-yl)methyl)-N'-isobutyrylalaninamide (5b).** The DL isomers were synthesized from **4b** and DL-isobutyrylalanine following the same method outlined for **5a**. In attempts to synthesize optically pure **5b**, D- and L-isobutyrylalanines were utilized in lieu of the DL racemate. Both D-**5b** and L-**5b**, giving identical  $^1\text{H}$  NMR spectra to that of DL-**5b**, had very low values of optical rotation. D-**5b**.  $[\alpha]^{23.5}_D$ :  $-1.5^\circ$  (c 4.08,  $\text{CHCl}_3$ ). L-**5b**.  $[\alpha]^{23.5}_D$ :  $+0.6^\circ$  (c 2.14,  $\text{CHCl}_3$ ).  $^1\text{H-NMR}$  ( $\text{CDCl}_3$ ):  $\delta$  8.03 (d, 1 H,  $J = 8.6$  Hz), 7.94 (d, 1 H,  $J = 9.2$  Hz), 7.52 (s, 1 H, br), 7.38 (dd, 1 H,  $J_1 = 9.2$  Hz,  $J_2 = 2.8$  Hz), 7.28 (d, 1 H,  $J = 8.6$  Hz), 7.08 (d, 1 H,  $J = 2.8$  Hz), 6.24 (d, 1 H,  $J = 6.8$  Hz), 4.71–4.65 (m, 3 H), 3.94 (s, 3 H), 2.43 (m, 1 H), 1.47 (d, 3 H,  $J = 7.2$  Hz), 1.190 (d, 3 H,  $J = 6.8$  Hz), 1.186 (d, 3 H,  $J = 6.8$  Hz). IR (KBr): 3270, 1639, 1547, 1501, 1235, and 832  $\text{cm}^{-1}$ . The elementary analysis for D-**5b** was satisfactory. Anal. Calcd for  $\text{C}_{16}\text{H}_{23}\text{N}_3\text{O}_3$ : C, 65.63; H, 7.04; N, 12.76. Found: C, 65.63; H, 7.06; N, 12.38.

**DL-N-((6-Methoxyquinolin-2-yl)carbonyl)-N'-isobutyrylalaninamide (8).** In an attempted synthesis of DL-**5b** during which the reaction was carried out in air for a prolonged time (33 h), it was found that a fluorescent side product was formed [ $R_f$  0.78 on a silica gel TLC plate eluted with BuOH/AcOH/ $\text{H}_2\text{O}$  (4/1/1, v/v/v); compound DL-**5b** had an  $R_f$  of 0.37 under the same conditions]. The side product was separated from DL-**5b** on a silica gel column (elution was carried out with ethyl acetate until the first compound was eluted and then with acetone).  $^1\text{H-NMR}$  and EIMS spectra indicated that this side product stemmed from the oxidation of the 2-methylene carbon of the quinoline moiety.  $^1\text{H-NMR}$  ( $\text{CDCl}_3$ ):  $\delta$  10.93 (s, 1 H), 8.28 (d, 1 H,  $J = 8.4$  Hz), 8.24 (d, 1 H,  $J = 8.4$  Hz), 8.05 (d, 1 H,  $J = 9.2$  Hz), 7.47 (dd, 1 H,  $J_1 = 9.2$  Hz,  $J_2 = 2.8$  Hz), 7.14 (d, 1 H,  $J = 2.8$  Hz), 6.29 (d, 1 H,  $J = 6.8$  Hz), 5.47 (m, 1 H), 3.98 (s, 3 H), 2.45 (m, 1 H), 1.54 (d, 3 H,  $J = 6.8$  Hz), 1.21 (d, 3 H,  $J = 6.8$  Hz), 1.20 (d, 3 H,  $J = 6.8$  Hz). EIMS:  $m/z$  343 (15,  $\text{M}^+$ ), 230 (33), 229 (32), 202 (20), 186 (40), 158 (100), and 114 (13) (Figure 1).

**Nitrosation of Quinoline Amide DL-5b.** The procedure described for the nitrosation of coumarin amide **5a** was followed. Dinitroso- (**7b**) and mononitrosoquinoline amides (**6b**) were formed in approximately equal quantities and separated on a silica gel column as described for **7a** and **6a**. Dinitroso **7b**. NMR ( $\text{CDCl}_3$ ):  $\delta$  7.96 (d, 1 H,  $J = 8.4$  Hz), 7.84 (d, 1 H,  $J = 9.0$  Hz), 7.32 (dd, 1 H,  $J_1 = 9.0$  Hz,  $J_2 = 2.6$  Hz), 7.08 (d, 1 H,  $J = 8.4$  Hz), 7.01 (d, 1 H,  $J = 2.6$  Hz), 6.08 (q, 1 H,  $J = 6.8$  Hz), 5.15 (AB quartet, 2 H,  $J_1 = J_2 = 15.2$  Hz), 3.91 (s, 3 H), 3.80 (m, 1 H), 1.50 (d, 3 H,  $J = 6.8$  Hz), 1.24 (t, 6 H,  $J = 7.0$  Hz). Mononitroso **6b**. NMR ( $\text{CDCl}_3$ ):  $\delta$  7.98 (d, 1 H,  $J = 8.5$  Hz), 7.77 (d, 1 H,  $J = 9.2$  Hz), 7.30 (dd, 1 H,  $J_1 = 9.2$  Hz,  $J_2 = 2.8$  Hz), 7.14 (d, 1 H,  $J = 8.5$  Hz), 7.02 (d, 1 H,  $J = 2.8$  Hz), 6.32 (d, 1 H,  $J = 7.0$  Hz), 5.99 (m, 1 H), 5.21 (AB quartet, 2 H,  $J_1 = J_2 = 15.5$  Hz), 3.91 (s, 3 H), 2.48 (m, 1 H), 1.68 (d, 3 H,  $J = 7.0$  Hz), 1.21 (d, 3 H,  $J = 7.0$  Hz), 1.22 (d, 3 H,  $J = 7.0$  Hz).

**Inhibition of  $\alpha$ -Chymotrypsin with Coumarin Inhibitor 6a.** Chymotrypsin (12 mg,  $4.8 \times 10^{-4}$  mmol) was dissolved in 3.24 mL of pH 7.8, 50 mM phosphate buffer with gentle magnetic stirring at 23 °C and the resulting solution was designated the "enzyme solution". Coumarin inhibitor **6a** (10 mg,  $2.7 \times 10^{-2}$  mmol) in 0.3



mL of acetonitrile was then added to 2.70 mL of the "enzyme solution" (containing 10 mg of chymotrypsin,  $4.0 \times 10^{-4}$  mmol) over a 45-min period. At the same time a control solution was prepared by mixing 0.27 mL of "enzyme solution" with 0.03 mL of acetonitrile. Aliquots (5  $\mu$ L) were taken from both the inhibition and control solutions for enzymatic activity assay (Hummel, 1959) (Figure 3).

**Inhibition of  $\alpha$ -Chymotrypsin with Quinoline Inhibitor 6b.** Chymotrypsin (5 mg,  $2 \times 10^{-4}$  mmol) was dissolved in 1 mL of pH 7.8, 50 mM phosphate buffer with gentle magnetic stirring at 25 °C. After the enzyme had dissolved, three 5- $\mu$ L aliquots were taken and added to three 1-mL volumes of pH 3 HCl for the enzymatic activity assay (Hummel, 1959). Quinoline nitrosamide **6b** (5 mg,  $1.4 \times 10^{-2}$  mmol) was dissolved in 0.111 mL of acetonitrile, and half of the solution was added to the enzyme solution over a period of 4 min. The remaining half of the inhibitor solution was added 46 min later (inhibitor/enzyme = 70). The decreasing enzymatic activity was followed by assaying aliquots (5  $\mu$ L) from the inhibition solution (Figure 2). A 10-fold molar excess of DFP (10  $\mu$ L of 0.2 M solution in acetonitrile) was added 70 min after the second batch of **6b** had been added. Immediately prior to the addition of DFP, two aliquots were taken out of the enzyme solution, and they were allowed to stand at 25 °C for another 8 h and then assayed. A control run in the absence of **6b** was performed at the same time. The DFP-treated **6b**-inhibited enzyme was gravity filtered through Whatman #1 filter paper to yield a clear, strongly fluorescent solution. The filter paper was washed with ~0.5 mL of water, and the washing solution was combined with the enzyme filtrate. The filtrate was transferred to dialysis tubing with a molecular weight cutoff of 3500 and dialyzed against pH 3 HCl solution for 40 h at 4 °C with four bath changes (500 mL every 10 h). The dialyzed enzyme solution was still strongly fluorescent.

#### ACKNOWLEDGMENT

We would like to thank the Institute of General Medical Sciences of the U.S. Public Service for financial support (Grant 21450) and the D. Mead Johnson Foundation for a fellowship to M.L.

#### LITERATURE CITED

- Anderson, G. W., and Callahan, F. M. (1958) Racemization by the dicyclohexylcarbodiimide method of peptide synthesis. *J. Am. Chem. Soc.* **80**, 2902–2903.
- Blazevic, N., Kolbah, D., Belin, B., Sunjic, V., and Kajtez, F. (1979) Hexamethylenetetramine, a versatile reagent in organic synthesis. *Synthesis* **3**, 161–176.
- Doherty, D. G., and Popenoe, E. A., Jr. (1951) The resolution of amino acids by asymmetric enzymatic synthesis. *J. Biol. Chem.* **189**, 447–460.
- Donadio, S., Perks, H. M., Tsuchiya, K., and White, E. H. (1985) Alkylation of amide linkages and cleavage of the C chain in the enzyme-activated-substrate inhibition of  $\alpha$ -chymotrypsin with N-Nitrosoamides. *Biochemistry* **24**, 2447–2458.
- Goering, H. L., Eikengerry, J. N., Koerner, G. S., and Lattimer, J. (1974) Direct determination of enantiomeric compositions with optically active nuclear magnetic resonance lanthanide shift reagents. *J. Am. Chem. Soc.* **96**, 1493–1501.
- Hummel, B. C. W. (1959) A modified spectrophotometric determination of chymotrypsin, trypsin, and thrombin. *Can. J. Biochem. Physiol.* **37**, 1393–1399.
- Nodiff, A. E., Hulsier, J. M., and Tanable, K. (1974) Simple syntheses for the 4-O-methyl derivatives of epinephrine, norepinephrine and N-methylepinephrine. *Chem. Ind. (London)* 962–963.
- Sheehan, J. C., Preston, J., and Cruickshank, P. A. (1965) A rapid synthesis of oligopeptide derivatives without isolation of intermediates. *J. Am. Chem. Soc.* **87**, 2492–2493.
- Wehry, E. L. (1973) *Practical Fluorescence* (G. G. Guilbault, Ed.) Chapter 3, Marcel Dekker, Inc., New York.
- White, E. H. (1955) The chemistry of the N-alkyl-N-nitrosoamides. I. methods of preparation. *J. Am. Chem. Soc.* **77**, 6008–6010.
- White, E. H., and Chen, Y. (1993) The synthesis of N'-4-dimethylamino-1-butyl-[1-<sup>13</sup>C]-N-nitrosobenzamide, an inhibitor of trypsin-cyanide does not exchange with acetonitrile. *J. Labelled Compd. Radiopharm.* **33**, 96–104.
- White, E. H., Tiwari, H. P., and Todd, M. J. (1968) Interception of carbonium ions in the deamination of 1-norbornylamine. *J. Am. Chem. Soc.* **90**, 4734–4736.
- White, E. H., McGirk, R. H., Aufdermarsh, C. A., Jr., Tiwari, H. P., and Todd, M. J. (1973) The deamination of bridgehead amines via the nitroso- and nitroamide approach. *J. Am. Chem. Soc.* **95**, 8107–8113.
- White, E. H., Roswell, D. F., Politzer, I. R., and Branchini, B. R. (1975) Active site directed inhibition of enzymes utilizing deaminatively produced carbonium ions. Application to chymotrypsin. *J. Am. Chem. Soc.* **97**, 2290–2291.
- White, E. H., Jelinski, L. W., Perks, H. M., Burrows, E. P., and Roswell, D. F. (1977a) Preferential inhibition of  $\alpha$ -chymotrypsin by the D form of an amino acid derivative, N'-isobutyl-N-benzyl-N-nitrosophenylalaninamide (**1a**). *J. Am. Chem. Soc.* **99**, 3171–3173.
- White, E. H., Roswell, D. F., Politzer, I. R., and Branchini, B. R. (1977b) Active site-directed inhibition with substrates producing carbonium ions: chymotrypsin. *Methods Enzymol.* **46**, 216–220.
- White, E. H., Perks, H. M., and Roswell, D. F. (1978) Labeling of amide linkages in active site mapping: carbonium ion and extended photoaffinity labeling approaches. *J. Am. Chem. Soc.* **100**, 7421–7423.
- White, E. H., Jelinski, L. W., Politzer, I. R., Branchini, B. R., and Roswell, D. F. (1981) Active-site-directed inhibition of  $\alpha$ -chymotrypsin by deaminatively produced carbonium ions: an example of suicide or enzyme-activated-substrate inhibition. *J. Am. Chem. Soc.* **103**, 4231–4239.
- White, E. H., Li, M., Cousins, J. P., and Roswell, D. F. (1990) Multiple alkylation of the active site of  $\alpha$ -chymotrypsin by carbonium ions generated with active-site-directed enzyme-activated nitrosoamide substrates. *J. Am. Chem. Soc.* **112**, 1956–1961.
- Williams, M. W., and Young, G. T. (1963) Amino-acids and peptides. part XVI. Further studies of racemisation during peptide synthesis. *J. Chem. Soc.* 881–889.

# Immunoassay Reagents for Thyroid Testing. 1. Synthesis of Thyroxine Conjugates

Maciej Adamczyk,\* Lynnmarie Fino, Jeffrey R. Fishpauqh, Donald D. Johnson, and Phillip G. Mattingly

Divisional Organic Chemistry Research, Diagnostics Division, Abbott Laboratories, D9NM, Building AP20, One Abbott Park Road, Abbott Park, Illinois 60064-3500. Received April 5, 1994\*

Immunoreagents were designed to improve the performance of a commercial fluorescent polarization immunoassay for thyroxine. The thyroxine immunogen was prepared by selective coupling of *N*-acetyl-L-thyroxine to BSA via an aminocaproic acid spacer arm. The fluorescent tracer was prepared by a multistep reaction sequence which relied on extensive use of orthogonol protecting groups.

## INTRODUCTION

The amino acid 3,5,3',5'-tetraiodo-L-thyronine (thyroxine or T<sub>4</sub>, 1), is the predominant iodothyronine secreted from the thyroid gland. T<sub>4</sub> is responsible for regulating diverse biochemical processes throughout the body, which are essential for normal metabolic and neural activity. The measurement of serum T<sub>4</sub> concentration has become the common initial test in the diagnosis of altered thyroid function (1).

The concentration of thyroxine in the bloodstream is extremely low and can only be detected with very sensitive techniques. Approximately 0.05% of the total circulating thyroxine is physiologically active (i.e., free thyroxine). The remaining circulating thyroxine is bound to proteins, primarily thyroxine binding globulin (TBG). Thyroxine will also bind to other binding proteins, particularly, thyroxine binding prealbumin and albumin (1).

Radioimmunoassay (RIA) has proved to be a sensitive, specific technique for measuring T<sub>4</sub> (2, 3). More recently, fluorescent polarization immunoassay (FPIA) has been used to assay for T<sub>4</sub> (4). Fluorescent polarization techniques are based on the principle that a fluorescent labeled compound when excited by linearly polarized light will emit fluorescence having a degree of polarization inversely related to its rate of rotation. Therefore, when a fluorescent labeled tracer-antibody complex is excited with linearly polarized light, the emitted light remains highly polarized because the fluorophore is constrained from rotating between the time light is absorbed and emitted. When a "free" tracer compound (i.e., unbound to an antibody) is excited by linearly polarized light, its rotation is much faster than the corresponding tracer-antibody conjugate and the molecules are more randomly oriented; therefore, the emitted light is depolarized. Thus, fluorescent polarization provides a quantitative means for measuring the amount of tracer-antibody conjugate produced in a competitive binding immunoassay (5).

FPIA has advantages over RIA in that there are no radioactive substances to dispose of and the assay is homogenous and can be easily automated. However, it has been reported that in isolated individuals, the commercially available Abbott TDx T<sub>4</sub> FPIA (6) assay resulted in a low T<sub>4</sub> value which did not conform to RIA measurement and the clinical symptoms of hypothyroid-

ism (7). It was postulated that the FPIA tracer used in the assay might be binding to endogenous immunoglobulin G in the patient sample.

In this work we present the synthesis of new thyroxine conjugates which served in the development of a new TDx/IMx Total T<sub>4</sub> FPIA which more closely correlates with RIA and clinical symptoms (8, 9).

## EXPERIMENTAL PROCEDURES

**General Comments.** All reagents were purchased from Aldrich Chemical Co., Inc., Milwaukee, WI, and were used without further purification, except where noted. Solvents employed were of reagent or HPLC grade and were used as received. <sup>1</sup>H NMR spectra were recorded at 200 MHz on a Chemagnetics A-200 spectrometer or at 300 MHz on a Varian Gemini 300 in CDCl<sub>3</sub> with TMS as a standard. Mass spectra were recorded on a Nermag 3010 MS-50 mass spectrometer. HPLC was carried out using a Waters RCM C18 (8 × 10) reversed phase column eluting at 1 mL/min with the solvent indicated.

**Synthesis of the L-Thyroxine Immunogen (8).** L-Thyroxine (1) as the sodium salt, pentahydrate (10 g, 11 mmol) was nearly completely dissolved in ethanol/2 N ammonium hydroxide (1/1, v/v, 400 mL) and filtered and the filtrate poured into 5% HCl (425 mL). The resulting precipitate was isolated by vacuum filtration and dried under high vacuum to afford a white solid. This material was dissolved in dimethylformamide (160 mL); acetic anhydride (100 mL, 1.06 mol) was added. The reaction mixture was stirred for 1.5 h, diluted with water (850 mL), and allowed to stand at 4 °C for 16 h. The resulting precipitate was isolated by filtration, dissolved in ethanol (350 mL) containing 1 N NaOH (41 mL), and stirred for 2.5 h. HCl (5%, 680 mL) was added and the mixture allowed to stand at 4 °C for 16 h. The resulting precipitate was isolated by vacuum filtration and dried under high vacuum to yield 8.1 g (90%) of the desired *N*-acetyl-L-thyroxine (5) (10) as a white solid: <sup>1</sup>H NMR (200 MHz, CD<sub>3</sub>OD) (δ) 7.8 (s, 2H), 7.1 (s, 2H), 4.6-4.7 (m, 1H), 2.8-3.0 (m, 2H), 2.0 (s, 3H); MS (FAB) (M + H)<sup>+</sup> *m/z* 820.

*N*-Acetyl-L-thyroxine (5) (1.0 g, 1.2 mmol) was dissolved in tetrahydrofuran (50 mL). *N*-Hydroxysuccinimide (170 mg, 1.5 mmol) and 1,3-dicyclohexylcarbodiimide (300 mg, 1.5 mmol) were added and the reaction stirred under nitrogen for 3 days. The reaction mixture was then vacuum filtered to remove insoluble urea, affording 40 mL of filtrate. Half the filtrate volume (20 mL, 0.6 mmol) was combined with 6-aminocaproic acid (80 mg, 0.6

\* Abstract published in *Advance ACS Abstracts*, August 1, 1994.

mmol). The pH was adjusted to 9 with triethylamine, and the reaction was allowed to stir under nitrogen for 2 days. The solvent was then removed *in vacuo* and the crude product purified by chromatography [Chromatotron, Harrison Research, Palo Alto, CA], eluting with methylene chloride/methanol/acetic acid (90/10/0.2, v/v), to yield 300 mg (54%) of the desired product (**6**) as a yellow oil: MS (FAB) ( $M + H$ )<sup>+</sup>  $m/z$  933; <sup>1</sup>H NMR (200 MHz, CDCl<sub>3</sub>/CD<sub>3</sub>OD, 9:1)  $\delta$  7.81 (s, 2H), 7.13 (s, 2H), 4.54 (t, 1H,  $J = 13$  Hz), 3.32–2.80 (m, 4H), 2.25 (t, 2H,  $J = 13$  Hz), 1.99 (s, 3H), 1.70–1.20 (m, 6H); HPLC [Waters  $\mu$ -Porasil, 3.9  $\times$  150; 6% methanol in methylene chloride; 254 nm; 1 mL/min] retention time 8.07 min, 98.9%.

The acid **6** (300 mg, 0.322 mmol) was dissolved in THF (25 mL); *N*-hydroxysuccinimide (45 mg, 0.39 mmol) and 1,3-dicyclohexylcarbodiimide (80 mg, 0.39 mmol) were added and the reaction mixture stirred for 16 h under nitrogen. The reaction mixture was then vacuum filtered to remove insoluble 1,3-dicyclohexylurea, affording 16 mL of filtrate. Then 4 mL (0.08 mmol) of the filtrate containing the active ester (**7**) was added to a stirred solution of bovine serum albumin (250 mg, 0.0037 mmol) dissolved in 0.05 M sodium phosphate (10 mL, pH = 8.0) and DMF (10 mL). After being stirred for 3 days the reaction was dialyzed against 0.05 M sodium phosphate (4 L, pH = 8.0) for 24 h and then water (4 L) for 24 h. The dialyzed solution was then lyophilized to afford the desired L-thyroxine immunogen (**8**) (297 mg).

**Synthesis of the L-Thyroxine Tracer (16).** L-Thyroxine (**1**) sodium salt, pentahydrate (22.0 g, 24.7 mmol) and sodium carbonate (7.85 g, 74.1 mmol) were stirred in THF/water (1/1, v/v, 960 mL). 9-Fluorenylmethyl chloroformate (7.04 g, 27.2 mmol) was added, and the reaction mixture was stirred for 30 min. The reaction mixture was then diluted with 1 N HCl (170 mL) and extracted with ethyl acetate (3  $\times$  700 mL). The organic extracts were combined, dried over anhydrous Na<sub>2</sub>SO<sub>4</sub>, filtered, and evaporated *in vacuo* to afford *N*-FMOC-L-thyroxine (**9**, 26.3 g) as a beige solid: <sup>1</sup>H NMR (300 MHz, DMSO-*d*<sub>6</sub>)  $\delta$  9.29 (s, 1H), 7.08–7.89 (m, 12H), 4.19–4.29 (m, 4H), 3.06–3.16 (m, 1H), 2.82 (t, 1H,  $J = 13$  Hz); MS (FAB) ( $M + Na$ )<sup>+</sup> calcd for C<sub>30</sub>H<sub>21</sub>NO<sub>6</sub>I<sub>4</sub>Na 1021.7441, found 1021.7448; HPLC [15:85:0.4 water:methanol:acetic acid; 220 nm] retention time 10.4 min, 98.9%.

*N*-FMOC-L-thyroxine (**9**, 26.3 g, 23.2 mmol) was dissolved in THF (150 mL) and treated with acetic anhydride (3.28 mL, 34.8 mmol) and 4-(*N,N*-dimethylamino)pyridine (283 mg, 2.32 mmol). The reaction was stirred under nitrogen for 45 min and then poured into water (400 mL) and extracted with chloroform (3  $\times$  400 mL). The chloroform extracts were combined, dried over anhydrous Na<sub>2</sub>SO<sub>4</sub>, filtered, and evaporated *in vacuo*. The residue was then purified by silica gel column chromatography, eluting with methylene chloride/methanol/acetic acid (90/10/0.4, v/v), to yield *O*-acetyl-*N*-FMOC-L-thyroxine (**10**, 21.95 g, 91%) as a beige solid: <sup>1</sup>H NMR (300 MHz, DMSO-*d*<sub>6</sub>)  $\delta$  7.12–7.91 (m, 12H), 4.07–4.31 (m, 4H), 3.07–3.19 (m, 1H), 2.82 (t, 1H,  $J = 13$  Hz), 2.29–2.40 (m, 3H); MS (FAB) ( $M + Na$ )<sup>+</sup>  $m/z$  1064; HPLC [Waters RCM  $\mu$ -porasil 8  $\times$  10; 95:5:0.2 methylene chloride:methanol:acetic acid; 240 nm] retention time, 4.54 min, 90%.

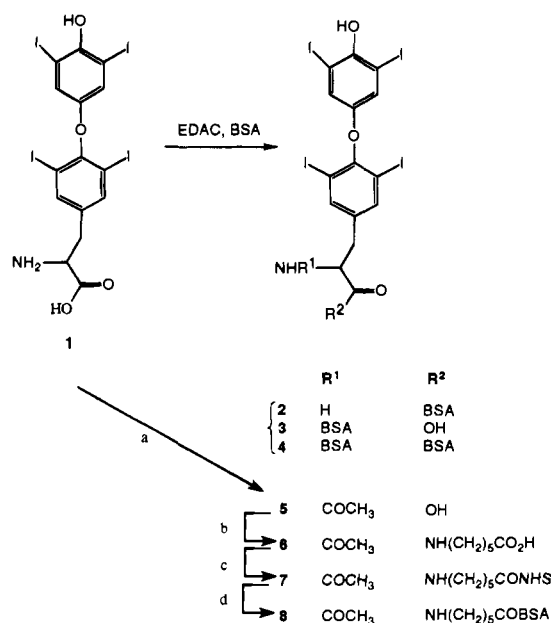
*O*-Acetyl-*N*-FMOC-L-thyroxine (**10**, 21.70 g, 19.17 mmol) was dissolved in methylene chloride (250 mL), cooled to 0 °C, and treated with *O*-*tert*-butyl-*N,N'*-diisopropylisourea (**11**, **12**) (19.20 g, 95.85 mmol) in methylene chloride (50 mL) dropwise. The reaction mixture was stirred overnight under nitrogen, at room temperature, and vacuum filtered to remove insoluble impurities, and the filtrate solvent was removed *in vacuo*. The resulting

residue was stirred in ethyl acetate/hexane (300 mL, 40/60, v/v) for 4 h and vacuum filtered to remove insoluble impurities, and filtrate solvent was removed *in vacuo*. The residue was then purified by silica gel column chromatography, eluting with ethyl acetate/hexane (40/60, v/v), to afford *tert*-butyl *O*-acetyl-*N*-FMOC-L-thyroxine (**11**, 9.64 g, 46%) (**2**) as a beige solid: <sup>1</sup>H NMR (300 MHz, CDCl<sub>3</sub>)  $\delta$  7.18–7.82 (m, 12H), 4.21–4.57 (m, 4H), 3.05 (s, 2H), 2.39 (s, 3H), 1.33–1.54 (m, 9H); MS (FAB) ( $M + H$ )<sup>+</sup>  $m/z$  1098; HPLC [Waters RCM  $\mu$ -Porasil 8  $\times$  10; 20:80 ethyl acetate:hexane; 256 nm] retention time, 9.13 min, 89%.

*tert*-Butyl *O*-acetyl-*N*-FMOC-L-thyroxine (**11**, 9.59 g, 8.04 mmol) was dissolved in dimethylformamide (40 mL), triethylamine (1.12 mL, 8.04 mmol) was added, and the reaction mixture was stirred overnight under nitrogen. Ethyl bromoacetate (1.78 mL, 16.1 mmol) followed by triethylamine (1.12 mL, 8.04 mmol) were added. The reaction mixture was stirred an additional 2 h under nitrogen and then poured into water (200 mL) and extracted with ethyl acetate (3  $\times$  200 mL). The ethyl acetate extracts were combined, dried over anhydrous MgSO<sub>4</sub>, and evaporated *in vacuo*. The resulting oil was purified initially by silica gel column chromatography, eluting with ethyl acetate/hexane (40/60, v/v), and then purified a second time by preparative silica gel HPLC, eluting with ethyl acetate/hexane (20/80, v/v), to yield *tert*-butyl *O*-acetyl-*N*-(carboxymethyl)-L-thyroxine (**13**, 3.77 g, 49%) as a white solid: <sup>1</sup>H NMR (300 MHz, CDCl<sub>3</sub>)  $\delta$  7.75 (s, 2H), 7.19 (s, 2H), 4.20 (q, 2H,  $J = 5$  Hz), 3.39–3.49 (m, 3H), 2.80–2.98 (m, 2H), 2.39 (s, 3H), 1.42 (s, 9H), 1.27 (t, 3H,  $J = 5$  Hz); MS (FAB) ( $M + H$ )<sup>+</sup> calcd for C<sub>25</sub>H<sub>28</sub>NO<sub>7</sub>I<sub>4</sub> 961.8040, found 961.8046; HPLC [Waters RCM  $\mu$ -Porasil 8  $\times$  10; 30:70 ethyl acetate:hexane; 260 nm, 1.5 mL/min] retention time, 6.8 min, 98%.

The ethyl ester intermediate (**13**, 3.73 g, 3.88 mmol) was dissolved in methanol (85 mL) containing 10% sodium hydroxide (12.4 mL, 31 mmol). The reaction mixture was stirred for 40 min and poured into water (250 mL). The pH of the solution was adjusted to 4 with 1 N HCl and then extracted with ethyl acetate (3  $\times$  250 mL). The ethyl acetate extracts were combined, dried over anhydrous MgSO<sub>4</sub>, and evaporated *in vacuo* to afford *tert*-butyl *N*-(carboxymethyl)-L-thyroxine (**14**, 3.29 g, 95%) (**3**) as a white solid: <sup>1</sup>H NMR (300 MHz, DMSO-*d*<sub>6</sub>)  $\delta$  7.81 (s, 2H), 7.07 (s, 2H), 3.52 (m, 1H), 3.32 (s, 2H), 2.89–2.98 (m, 1H), 2.20–2.31 (m, 1H), 1.32 (s, 9H); MS (FAB) ( $M + H$ )<sup>+</sup> calcd for C<sub>21</sub>H<sub>22</sub>NO<sub>6</sub>I<sub>4</sub> 891.7621, found 891.7622; HPLC [20:80:0.4 water:methanol:acetic acid; 240 nm] retention time, 7.3 min, 95%.

*tert*-Butyl *N*-(carboxymethyl)-L-thyroxine (**14**, 1.78 g, 2.00 mmol) was dissolved in dimethylformamide (20 mL) and treated with *N*-hydroxysuccinimide (230 mg, 2.00 mmol) and 1,3-dicyclohexylcarbodiimide (413 mg, 2.00 mmol). The reaction mixture was stirred for 16 h under nitrogen and then vacuum filtered. The filtrate was combined with 5-(aminomethyl)fluorescein hydrobromide (**13**) (884 mg, 2.00 mmol) and triethylamine (1.8 mL, 13 mmol), and the reaction was stirred for 16 h, under nitrogen, in the dark. The solvent was removed *in vacuo*, and the residue was purified by preparative reversed phase C18 HPLC, eluting with water/methanol/acetic acid (25/75/0.4, v/v), to afford 1.51 g (61%) of the desired *tert*-butyl ester protected tracer as an orange solid: <sup>1</sup>H NMR (300 MHz, DMSO-*d*<sub>6</sub>)  $\delta$  10.13 (s, 2H), 9.29 (s, 1H), 8.43 (m, 1H), 7.85 (s, 1H), 7.83 (s, 2H), 7.68 (d, 1H,  $J = 5$  Hz), 7.12–7.28 (m, 2H), 7.07 (s, 2H), 6.68 (s, 2H), 6.54 (s, 4H), 4.36–4.61 (m, 2H), 3.26–3.50 (m, 3H), 2.94–3.04 (m, 1H), 2.71–2.82 (m, 1H), 1.33 (s, 9H); MS (FAB) ( $M$ )<sup>+</sup> calcd for C<sub>42</sub>H<sub>34</sub>N<sub>2</sub>O<sub>10</sub>I<sub>4</sub> 1234.8466, found 1234.8465;

Scheme 1<sup>a</sup>

<sup>a</sup> Key: (a) Ac<sub>2</sub>O; (b) DCC, NHS, 6-aminocaproic acid; (c) EDAC, NHS; (d) BSA.

HPLC [20:80:0.4 water:methanol:acetic acid; 240 nm] retention time 12.7 min, 98%.

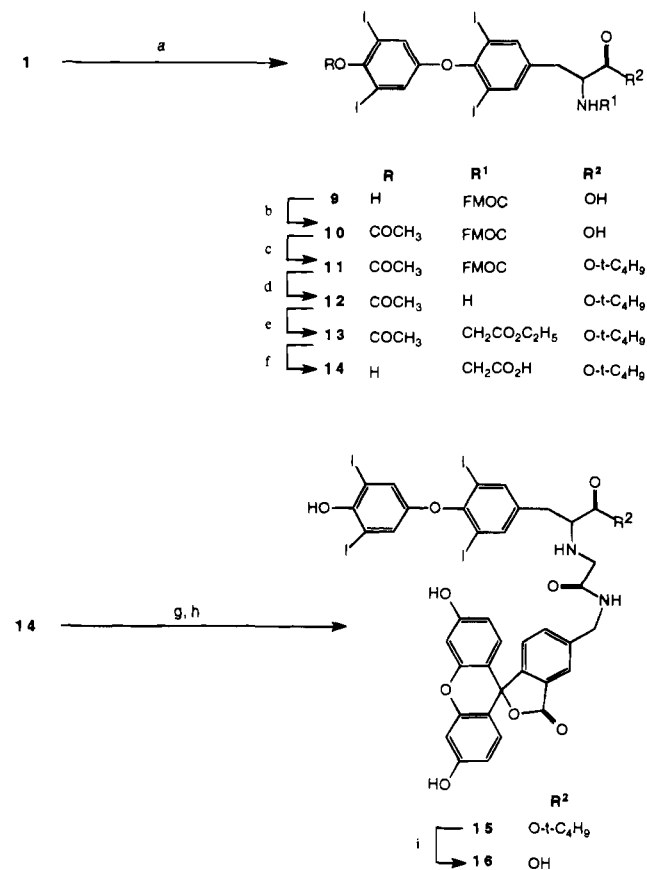
The *tert*-butyl ester protected tracer (**15**, 1.464 g, 1.19 mmol) was dissolved in methylene chloride/trifluoroacetic acid (30 mL 1/1, v/v) and stirred for 5 h, and the solvent was removed *in vacuo*. The crude product was purified by preparative reversed phase C18 HPLC, eluting with water/methanol/acetic acid (25/75/0.4, v/v) to yield 1.01 g (72%) of the desired L-thyroxine tracer (**16**) as an orange solid: <sup>1</sup>H NMR (300 MHz, DMSO-*d*<sub>6</sub>) δ 10.0–10.3 (broad s, 2H), 8.31 (t, 1H, *J* = 2 Hz), 7.86 (s, 2H), 7.83 (s, 1H), 7.64 (d, 1H, *J* = 7 Hz), 7.15–7.30 (m, 2H), 7.08 (s, 2H), 6.68 (s, 2H), 6.55 (s, 4H), 4.31–4.59 (m, 2H), 3.28–3.55 (m, 3H), 2.82–2.99 (m, 2H); MS (FAB) (*M* + *H*)<sup>+</sup> calcd for C<sub>38</sub>H<sub>27</sub>N<sub>2</sub>O<sub>10</sub>I<sub>4</sub> 1178.7840, found 1178.7834; HPLC [25:75:0.4, water:methanol:acetic acid; 240 nm] retention time 8.1 min, 99%.

## RESULTS

The first step toward improvement of the T<sub>4</sub> immunoassay was to prepare a well-defined immunogen (**14**, **15**). This was accomplished by the selective conjugation of L-T<sub>4</sub> to BSA through the carboxyl group. Initially, the α-amino group of T<sub>4</sub> was acetylated to give compound **5**. Activation of the carboxyl group with DCC and NHS followed by coupling to 6-aminocaproic acid resulted in L-T<sub>4</sub> hapten **6**. The terminal carboxyl group of the L-T<sub>4</sub> hapten was finally activated with a water soluble carbodiimide (EDAC), and NHS in DMF then conjugated to BSA to produce the desired immunogen, **8**. Analysis by TNBS titration showed 48% of the available amino groups of BSA had been substituted by the hapten (**16**).

Contrary to the obvious practice of using an analogous tracer, the L-T<sub>4</sub> tracer was prepared by conjugating the fluorescent label through the amino group of L-T<sub>4</sub>, not through the carboxyl group as done in the immunogen preparation.

The multiple step synthesis of the L-T<sub>4</sub> fluorescent tracer is shown in Scheme 2. The first step was the selective protection of the amino group with fluoromethyl chloroformate (FMOC-Cl) to give *N*-FMOC-L-T<sub>4</sub>, **9**. The phenolic group was acetylated with acetic anhydride and the carboxyl group protected as the *tert*-butyl ester to give

Scheme 2<sup>a</sup>

<sup>a</sup> (a) FMOC-Cl, Na<sub>2</sub>CO<sub>3</sub>, H<sub>2</sub>O/THF; (b) Ac<sub>2</sub>O, DMAP, THF; (c) *O*-*tert*-butyl-*N,N'*-diisopropylisourea, CH<sub>2</sub>Cl<sub>2</sub> (d) Et<sub>3</sub>N, DMF; (e) BrCH<sub>2</sub>CO<sub>2</sub>Et, Et<sub>3</sub>N, DMF; (f) 10% NaOH, MeOH; (g) NHS, DCC, DMF; (h) 5-(aminomethyl)fluorescein HBr, Et<sub>3</sub>N, DMF; (i) TFA, CH<sub>2</sub>Cl<sub>2</sub>.

**11.** Next the FMOC group was selectively removed by triethylamine in DMF. The unmasked amino group was alkylated *in situ* with ethyl bromoacetate to produce compound **13**. Simultaneous removal of the acetyl and ethyl ester protecting groups was achieved in methanolic sodium hydroxide. *tert*-Butyl *N*-(carboxymethyl)-L-T<sub>4</sub>, **14**, was conjugated to 5-(aminomethyl)fluorescein (**13**) and the *tert*-butyl ester subsequently removed in the presence of trifluoroacetic acid to give the tracer, **16**.

## DISCUSSION

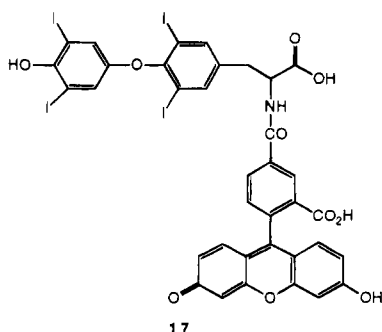
When preparing specific antibodies and complementary labeled haptens, one needs to consider the chemical structure of both the immunogen used to elicit the antibody response and the labeled hapten. Traditionally, one attaches the hapten to the carrier protein through a site on the hapten that is remote from the unique features of the hapten that are critical for achieving selective antibodies. Likewise, when preparing a labeled hapten able to bind to such antibodies, it is customary to attach the label to the hapten through the same site as the carrier protein. The immunogen and tracer prepared by this design are homologous. One reason for choosing the homologous approach in immunoreagent design is that the carrier protein sterically blocks access of the immune system to that part of the hapten closest to the point of attachment. Normally, the complementary labeled hapten is synthesized by attaching its label to the same site on the hapten as the immunogen uses for attachment of its carrier protein, so as not to interfere with antibody binding to the critical features of the

hapten. In the case of T<sub>4</sub> the unique feature important for antibody recognition is the tetraiodosubstituted diphenyl ether system.

A second approach to immunoreagent design is the heterologous approach. In this approach, the immunogen and tracer do not share a common point of attachment on the hapten. The heterologous approach has sometimes been used successfully to improve assay performance (17). A heterologous free T<sub>4</sub> assay has recently been described (18).

The reason that this approach is superior only in some cases has not been fully elucidated. One rationalization might be that in some homologous systems the antibody binds the tracer too tightly, preventing effective competition with the analyte to be measured. A heterologous tracer which does not share the same hapten as the immunogen would be expected to bind less tightly, restoring effective competition and improving the assay performance.

The Abbott TDx T<sub>4</sub> FPIA, used in the Levine (7) report, was developed using an antibody to an immunogen represented by structures 2–4, the result of a nonspecific coupling of L-T<sub>4</sub> through both the carboxyl and amino groups to the carrier protein, bovine serum albumin (BSA). The FPIA was optimized using D-T<sub>4</sub> tracer 17. In a sense this tracer was heterologous to all the immunogen structures produced, since the D enantiomer was used.



17

In the present work, the immunogen of structure 8 was produced in which the amino group of L-T<sub>4</sub> was permanently blocked with an acetyl group. Thus, two modifications to the parent L-T<sub>4</sub> structure were introduced in making the immunogen; i.e., the carboxylic acid was converted to an amide and the amino group was acetylated. Neither modification alters the critical tetraiodo-substituted diphenyl ether system. The tracer 16 was prepared from L-T<sub>4</sub> through a multistep sequence resulting in the fluorescent label attached to the  $\alpha$ -amino group via a carboxymethyl spacer arm.

Thus, in this paper we have described the synthesis of a new immunogen 8 and fluorescent tracer 16 for

thyroxine. We have successfully utilized these two reagents in the development of a new FPIA (9) on the TDx analyzer which has replaced the assay used in the Levine study and alleviates the problem noted in that study. We will describe the full details of the assay optimization and performance elsewhere.

#### LITERATURE CITED

- (1) Alexander, N. M. (1984) Thyroid function tests. *Clin. Chem.* 30, 827–828.
- (2) Siebert, G. R., and Armstrong, J. (1987) Monoclonal Antibodies recognizing L-Thyroxine. US Patent 4,636,478.
- (3) Siebert, G. R., and Armstrong, J. (1989) Monoclonal Antibodies recognizing L-Thyroxine. US Patent 4,888,296.
- (4) Fino, J. F., and Kirkemo, C. L. (1984) Substituted carboxy-fluoresceins. US Patent 4,476,229.
- (5) Blecka, L. J., and Jackson, G. J. (1987) Immunoassays in therapeutic drug monitoring. *Clin. Lab. Med.* 7, 357–70.
- (6) (1992) Abbott Laboratories TDx Operation Manual.
- (7) Levine, S., Noth, R., Loo, A., Chopra, I. J., and Klee, G. G. (1990) Anomalous Serum Thyroxine Measurements with the Abbott TDx Procedure. *Clin. Chem.* 36, 1838–1840.
- (8) Kabadi, U. M., Fox, I. S., and Cook, P. (1994) Falsely Low Serum Thyroxine Concentration Measured with the Abbott TDx. *Clin. Chem.* 40, 337–338.
- (9) Lewis, C. A., and Clarisse, D. (1994) A response to "Falsely Low Serum Thyroxine Concentration Measured with the Abbott TDx". *Clin. Chem.* 40, 338.
- (10) Pitt-Rivers, R. (1948) The Oxidation of Diiodotyrosine Derivatives. *Biochem. J.* 43, 223–231.
- (11) Mathias, L. J. (1979) Esterification and Alkylation Reactions Employing Isoureas. *Synthesis* 561–576.
- (12) Schmidt, E., and Moosmueller, F. (1955) Zur Kenntnis aliphatischer Carbodiimide, IX. *Mitt. Liebigs Ann. Chem.* 597, 235–240.
- (13) Mattingly, P. G. (1992) Preparation of 5 and 6-(Amino-methyl)fluorescein. *Bioconjugate Chem.* 3, 430–431.
- (14) Adamczyk, M., Fishpaugh, J., Harrington, C., Hartter, D., Johnson, D., and Vanderbilt, A. (1993) Immunoassay reagents for psychoactive drugs. I. The method for the development of antibodies specific to amitriptyline and nortriptyline. *J. Immunol. Methods*, 162, 47–58.
- (15) Adamczyk, M., Fishpaugh, J., Harrington, C., Johnson, D., and Vanderbilt, A. (1993) Immunoassay reagents for psychoactive drugs. II. The method of the development of antibodies specific to imipramine and desipramine. *J. Immunol. Methods* 163, 187–197.
- (16) Shinoda, T., and Tsuzukida, Y. (1974) Identification of rapidly trinitrophenylating amino groups of human Bence-Jones proteins modified by incubating for 45 minutes at 37 °C before measuring UV absorbance. *J. Biochem.* 75, 23.
- (17) Kasson, B. G., Bai, S., Liu, J., Tobin, C., and Kessel, B. (1993) Characterization of a rapid and sensitive enzyme immunoassay (EIA) for progesterone applied to conditioned cell culture media. *J. Immunoassay* 14, 33–49.
- (18) Khosravi, M. J., and Papanastasiou-Diamandi, A. (1993) Hapten–heterologous conjugates evaluated for application to free thyroxine immunoassays. *Clin. Chem.* 39, 256–262.

# Use of Psoralens for Covalent Immobilization of Biomolecules in Solid Phase Assays

Henrik I. Elsner\* and Søren Mouritsen

M&E, Lersø, Parkallé 40, 2100 Copenhagen, Denmark. Received April 7, 1994\*

The ability of compounds to adsorb passively to hydrophobic polymer surfaces composed of, e.g., polystyrene generally is restricted to limited types of molecules such as proteins. Some proteins, many peptides, polysaccharides, oligonucleotides, and small molecules as well as pro- and eucaryotic cells cannot adsorb directly to such surfaces. Also, solid phase adsorbed antigens, antibodies, or gene probes may not be recognized by its corresponding ligand due to denaturation or steric hindrance of the molecular tertiary structure. Covalent binding, on the other hand, orientates all immobilized compounds in a defined way on the solid phase, thereby exposing the interacting sites on the enzymes, antibodies, gene probes, etc. Here we describe a method for modifying a polymer surface by contacting the polymer with derivatives of psoralen under irradiation with long-wavelength UV light. The psoralen derivatives were immobilized covalently on the polymer surface by this process. The psoralen molecules were conjugated to appropriate chemical linkers, incubated in aqueous solutions, and irradiated with UV light. This resulted in solid phase introduction of functional groups such as, e.g., amino groups on the polystyrene surface. The functional groups could subsequently be used for immobilization of biomolecules using conventional cross-linker technology. The method only involved premodification of the psoralens to be immobilized whereas no pretreatment of the polymer was required. Psoralen modified microtiter plates seems to have future application for the development of solid phase hybridization and immunoassays.

## INTRODUCTION

The usual way to immobilize biomolecules such as antibodies or protein antigens in solid phase assays is by passive adsorption on, e.g., polystyrene or poly(vinyl chloride) surfaces (1). Many molecules, microorganisms, and cells cannot, however, be immobilized by this method. Polysaccharides, peptides, gene probes, small organic molecules, viruses, and pro- and eukaryotic cells generally have to be immobilized by other techniques. Furthermore, passive adsorption is not an irreversible process (2), which may affect the reproducibility of the immunoassays, especially when the antigen/antibody coated solid phase is stored in dry form.

The nature of passive adsorption predominantly involves multiple hydrophobic interactions between the solid phase and the biomolecule. Passive adsorption may therefore interfere with the structure and function of adsorbed antigens and antibodies (3, 4). Also, solid phase adsorbed antigen may not be recognized by its corresponding antibody due to denaturation of the antigen tertiary structure (5, 6). Epitopes of, e.g., peptides may be hidden and prevented from recognition by antibodies (7), and the biological activity of passively adsorbed antibodies or enzymes may decline with time (8).

Covalent binding, in contrast to passive adsorption, orientates all immobilized compounds in defined ways on the solid phase, thereby exposing defined areas on, e.g., antigens, antibodies, or enzyme catalytic sites to the fluid phase. The antigen epitopes or active sites on these compounds will therefore probably be more conserved. Irreversible immobilization of molecules may furthermore be advantageous in relation to storage of the immobilized compounds.

In order to immobilize biomolecules covalently on microtiter wells, these surfaces must possess some kind of functional groups. Methods to introduce amino groups

have been described previously (9), but large scale production of modified microtiter plates using these methods generally has been impractical. Here we describe a method for covalent immobilization of biomolecules on polystyrene microtiter wells, which can be used for immobilization of many kinds of molecules. Functional groups on the polymer surface are introduced by contacting the polymer with derivatives of psoralen under irradiation with long-wavelength UV light.

The herein described method for introducing secondary amino groups on polystyrene surfaces is currently being used by Nunc A/S (Roskilde, Denmark), and microtiter plates are being marketed under the name CovaLink. Several papers reporting the usefulness of these plates have been published.

## EXPERIMENTAL PROCEDURES

**Materials and General Procedures.** All chemicals for preparation of buffers were of analytical grade unless noted, and chemicals for synthesis were standard commercial. Elemental analyses were performed at the Microanalytical Laboratory of The H. C. Ørsted Institute at The University of Copenhagen. Thin-layer chromatography was performed on silica gel 60 F<sub>254</sub> precoated aluminum sheets (layer thickness, 0.2 mm) from E. Merck, Darmstadt, Germany. The plates were visualized by UV light (254 nm). <sup>1</sup>H-NMR were recorded at 90 MHz on a Jeol FX 90 Q spectrometer. Chromatography was performed on a 60 × 1.5 cm column using silica gel grade 60 from E. Merck, Darmstadt, Germany. Polystyrene microtiter plates (Maxisorp) were from Nunc A/S, Roskilde, Denmark. All experiments have been performed at least three times in duplicate, and the values shown in Figures 1-5 are mean values.

***N,N'*-Dimethyl-*N*-[3-(psoralen-8-yloxy)propyl]-*N'*-(*tert*-butoxycarbonyl)hexanediamine (I).** 3-Bromo-1-(psoralen-8-yloxy)propane (10, 11), (2.3 g, 8.2 mmol) and *N*-(*tert*-butoxycarbonyl)-*N,N'*-dimethylhexanediamine (12) (1.75 g, 8.2 mmol) were mixed in acetone (100 mL)

\* Abstract published in *Advance ACS Abstracts*, August 1, 1994.



with potassium carbonate (2.7 g) and refluxed for 72 h, whereupon the mixture was filtered and evaporated in vacuum. The residue was purified on a silica gel column using methanol in methylene chloride as eluent giving rise to **I** (1.7 g, 3.5 mmol, 43%). <sup>1</sup>H NMR (CDCl<sub>3</sub>): 7.73–6.17 (5H, m, psoralen), 4.44 (2H, t, OCH<sub>2</sub>), 3.54 (2H, q, CH<sub>2</sub>), 3.07 (4H, q, CH<sub>2</sub>), 2.70 (3H, s, CH<sub>3</sub>), 2.53 (4H, m, CH<sub>2</sub>), 2.25 (2H, m, CH<sub>2</sub>), 2.13 (3H, s, CH<sub>3</sub>), 1.90 (4H, m, CH<sub>2</sub>), 1.35 (9H, s, Boc). Anal. Calcd for C<sub>27</sub>H<sub>38</sub>N<sub>2</sub>O<sub>6</sub>: C, 66.66; H, 7.82; N, 5.76. Found: C, 66.57; H, 7.88; N, 5.77. TLC: *R<sub>f</sub>* = 0.25, 10% CH<sub>3</sub>OH in CH<sub>2</sub>Cl<sub>2</sub>.

***N,N'*-Dimethyl-*N*-[3-(psoralen-8-yloxy)propyl]hexanediamine (**II**).** **I** (1.7 g, 3.5 mmol) was suspended in hydrochloric acid (35 mL, 4 M), and after 1 h the solution was evaporated in vacuum, and the main product (**II**) was purified on a silica gel column using triethylamine and ethanol as eluent (1.4 g, 28 mmol, 77%). <sup>1</sup>H NMR (D<sub>2</sub>O, DCl): 7.73–6.09 (5H, m, psoralen), 4.32 (2H, t, OCH<sub>2</sub>), 3.45–2.97 (6H, m, CH<sub>2</sub>), 2.86 (3H, s, CH<sub>3</sub>), 2.65 (3H, s, CH<sub>3</sub>), 1.99–1.41 (10H, q, CH<sub>2</sub>). Anal. Calcd for C<sub>22</sub>H<sub>30</sub>N<sub>2</sub>O<sub>4</sub>: C, 68.39; H, 7.78; N, 7.26. Found: C, 68.16; H, 7.82; N, 7.04. TLC: *R<sub>f</sub>* = 0.30, 50% CH<sub>3</sub>OH, 50% N(CH<sub>3</sub>CH<sub>2</sub>)<sub>3</sub>.

***N,N'*-Dimethyl-*N*-[3-(psoralen-8-yloxy)propyl]-*N'*-biotinylohexanediamine (**III**).** **II** (0.62 g, 1.34 mmol) was solubilized in DMF whereupon triethylamine (1 mL, 7.2 mmol) and *N*-hydroxysuccinimide-biotin (0.46 g, 1.34 mmol) were added under stirring. The next day the solution was evaporated in vacuum, and the main product (**III**) was purified on silica gel as described above (0.4 g, 0.60 mmol, 45%). <sup>1</sup>H NMR (DMSO): 8.24–6.40 (5H, m, psoralen), 4.60 (2H, t, OCH<sub>2</sub>), 4.55–4.01 (2H, m), 3.50–2.93 (9H, m), 2.81 (3H, s, CH<sub>3</sub>), 2.77 (3H, s, CH<sub>3</sub>), 2.19–1.01 (18H, m). Anal. Calcd C<sub>32</sub>H<sub>44</sub>N<sub>4</sub>O<sub>6</sub>S: C, 66.73; H, 7.19; N, 9.15. Found: C, 65.97; H, 7.43; N, 9.06. TLC: *R<sub>f</sub>* = 0.90, 50% CH<sub>3</sub>OH, 50% N(CH<sub>3</sub>CH<sub>2</sub>)<sub>3</sub>.

**Photochemical Modification of Polystyrene.** (a) **Binding of *N,N'*-Dimethyl-*N*-[3-(psoralen-8-yloxy)propyl]-*N'*-biotinylohexanediamine (**III**) to Microtiter Wells.** A stock solution of **II** (10 mg/mL in DMSO) could be stored for months at –4 °C. Ten-fold dilutions in distilled water were made from this stock in concentrations ranging from 0.1 to 1000 µg/mL, and 100 µL/well of each dilution was added to the wells of polystyrene microtiter wells. The wells were then irradiated for 2 h at room temperature with long-wavelength ( $\lambda > 350$  nm) UV light from a Phillips TL 20W/09N lamp placed 20 cm above the microtiter wells. Subsequently, the wells were washed three times with 200 µL of washing buffer (pH, 7.2, 0.1 M phosphate, 0.5 M NaCl (PBS), 1% Triton X-100). The same experiment was done without irradiation. For detection of immobilized biotin on the solid phase, a solution of 100 µL/well of horse radish peroxidase conjugated avidin (HRP-avidin, Sigma, St. Louis, MO) was added to the wells (25 µg of HRP-avidin, 100 mg of BSA, 10 mL of washing buffer) and incubated at 37 °C for 1 h. The wells were then washed three times with washing buffer and 100 µL/well of a solution of the chromogenic substrate *O*-phenyldiamine (OPD, 10 mg) and hydrogen peroxide (1 µL, 35%) in citrate/phosphate buffer (0.1 M, 10 mL, pH 5.0) was added. After approximately 3 min the colored reaction was stopped with sulfuric acid (100 µL, 1 M), and the optical density (OD) was read on a Titertek Multiscan ELISA-photometer.

(b) **The Influence of Irradiation Times on the Solid-Phase Binding of *N,N'*-Dimethyl-*N*-[3-(psoralen-8-yloxy)propyl]-*N'*-biotinylohexanediamine (**III**).** A stock solution of **III** (10 mg/mL, DMSO) was diluted in water to a concentration of 10 µg/mL and 100 µg/mL, respectively. One hundred µL/well of each dilution was transferred to

microtiter wells, UV-irradiated for different time periods, and subsequently treated as described above.

(c) **Binding of *N,N'*-Dimethyl-*N*-[3-(psoralen-8-yloxy)propyl]hexanediamine (**II**) to Microtiter Wells.** A solution of **II** (500 µg/mL) in phosphate-buffered saline (0.1 M, pH 8.2, 2 M NaCl) was made. One hundred µL per well was added, and the microtiter plates were irradiated for 1 h as described above. Each well was washed three times with demineralized water, and solutions of *N*-hydroxysuccinimide-biotin (NHS-biotin, Hoechst, lot no. 410074, Calbiochem) in carbonate buffer (pH 9.6, 0.005 M) was then added in 2-fold dilution series starting at 125 µg/mL. Subsequently, the microtiter wells were incubated for 2 h at room temperature, and each well was washed three times with washing buffer. The coupling efficiency of biotin was visualized using HRP-avidin as described above.

(e) **Binding of 5-[(Trimethylammonio)[<sup>1</sup>H]methyl]-8-methoxypsoralen Bromide of Microtiter Wells.** Aqueous solutions of 5-[(trimethylammonio)[<sup>1</sup>H]methyl]-8-methoxypsoralen bromide (**13**) were added to polystyrene microtiter wells (100 µL, 1 mg/mL, 3 800 000 cpm) and diluted 10-fold in distilled water to a final concentration of 0.01 µg/mL. The wells were then irradiated for 2 h at room temperature and washed eight times with 200 µL of washing buffer. The same experiment was performed without UV irradiation. The wells were emptied, separated mechanically, and transferred to scintillation vials. Ten mL of scintillation fluid (Instagel, Packard) was added, and the samples were analyzed in a scintillation counter (Beckman LS7000).

(d) **Treatment of Microtiter Wells with *N*-(4-Azido-2-nitrophenyl)-*N'*-[3-(biotinylamino)propyl]-*N'*-methyl-1,3-propanediamine (Photobiotin).** It was also attempted to biotinylate polystyrene using *N*-(4-azido-2-nitrophenyl)-*N'*-[3-(biotinylamino)propyl]-*N'*-methyl-1,3-propanediamine (photobiotin, Sigma cat. no. A 7667). This reagent contains a photoreactive aryl azide group connected to a chemical linker similar to the one used for **III**.

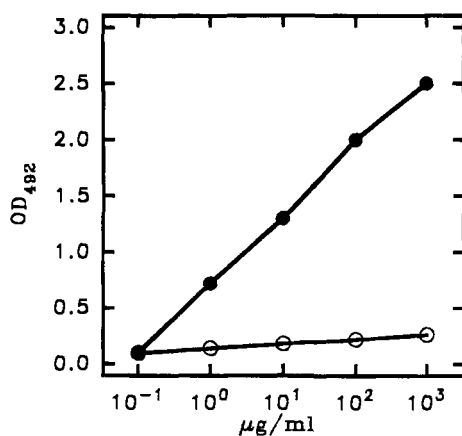
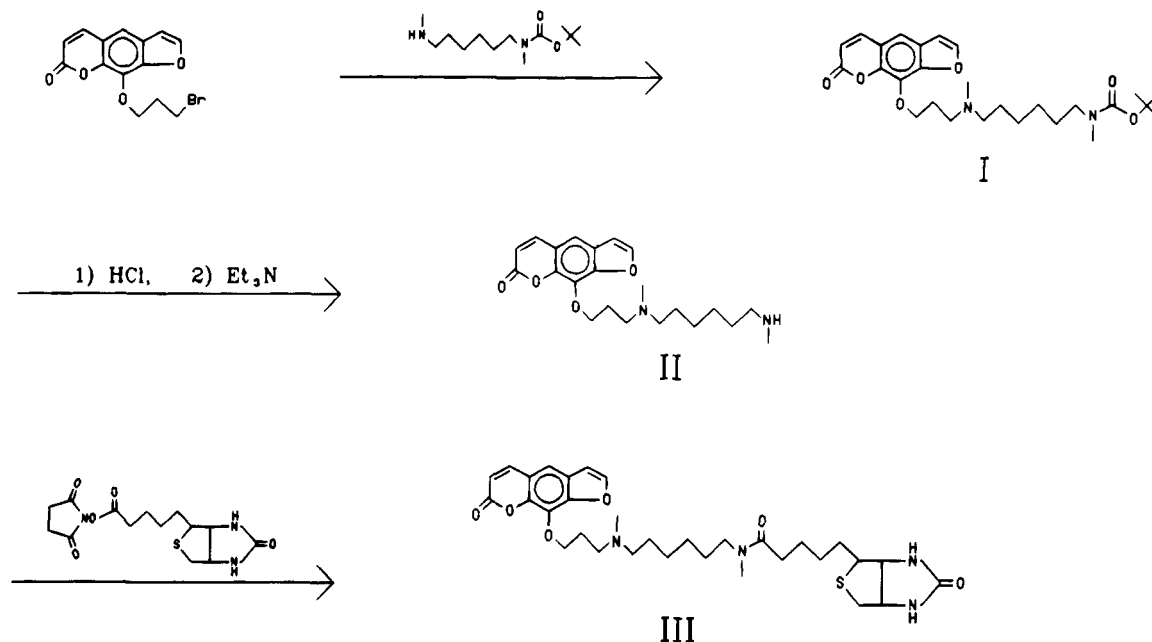
**The Stability of the Psoralen-Modified Surface.** One hundred µL of the following aqueous solutions were added to microtiter wells modified with **II** as described above: 1 M NaOH; 1 M HCl; 1% Triton X-100; 10% acetic acid; 0.1 M citrate, pH 5.5; 0.1 M PBS pH 7.2, 0.1 M Carbonate buffer pH 9.6, 10% ethanol; 10% methanol; 1% DMSO, 1% DMF, water, washing buffer, and absolute ethanol. After 2 h the wells were emptied and washed five times with water. Detection of secondary amino groups on the surface was performed as described above.

## RESULTS

**Preparation of Derivatives of 8-(Propyloxy)psoralen.** Three psoralen derivatives were synthesized starting from 3-bromo-1-(psoralen-8-yloxy)propane and *N*-(*tert*-butoxycarbonyl)-*N,N'*-dimethylhexanediamine, one derivative with a Boc-group (**I**), one with a secondary amine (**II**), and one conjugated to biotin (**III**) (Scheme 1). **II** and **III** were used for photomodification of polystyrene surfaces. All three compounds were characterized by elemental analysis, TLC, and <sup>1</sup>H NMR.

**Photobinding of *N,N'*-Dimethyl-*N*-[3-(psoralen-8-yloxy)propyl]-*N'*-biotinylohexanediamine (**III**) to Microtiter Wells.** By using HRP-avidin it was shown that **III** bound to polystyrene under irradiation of UV light. When no UV light was used no significant binding of **III** could be observed (Figure 1). The amount of **III** that could be detected depended on the added amount, and this relationship was almost linear in concentrations of ranging from 0 to 1 mg/mL. The influence of the UV irradiation time was most pronounced in a time range

**Scheme 1.** Synthesis of *N,N'*-Dimethyl-*N*-[3-(psoralen-8-yloxy)propyl]-*N'*-(*tert*-butoxycarbonyl)hexanediamine (I), *N,N'*-Dimethyl-*N*-[3-(psoralen-8-yloxy)propyl]hexanediamine (II), and *N,N'*-Dimethyl-*N*-[3-(psoralen-8-yloxy)propyl]-*N'*-biotinylhexanediamine (III)

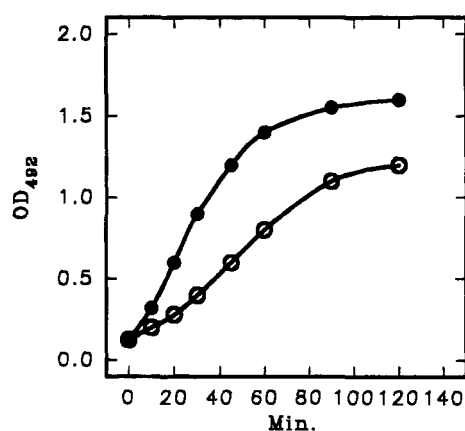


**Figure 1.** Binding of *N,N'*-dimethyl-*N*-[3-(psoralen-8-yloxy)propyl]-*N'*-biotinylhexanediamine (III) to microtiter wells with (●) and without irradiation (○) of UV light.

from 0 to 90 min (Figure 2). Longer irradiation periods did not increase the amount of immobilized biotin, although the used amount of III influenced the maximal amount of biotin which could be detected.

**Photobinding of *N,N'*-Dimethyl-*N*-(3-psoralen-8-yloxy)hexanediamine (III) to Microtiter Wells.** A clear correlation could be demonstrated between the added amounts of *N*-hydroxysuccinimide-biotin and the signal level obtained with HRP-avidin on microtiter wells modified with this psoralen derivative (Figure 3). Addition of *N*-hydroxysuccinimide-biotin (125 μg/mL) to nonmodified wells gave an average signal level of only 0.077 OD units.

**Photobinding of 5-[(Trimethylammonio)[<sup>3</sup>H]-methyl]-8-methoxypsoralen Bromide to Microtiter Wells.** Using a solution of 1 mg/mL of 5-[(trimethylammonio)[<sup>3</sup>H]-methyl]-8-methoxypsoralen bromide, it could be demonstrated that 87 ng were photochemically immobilized on the polymer surface, whereas only 17 ng were immobilized in nonirradiated wells. When using a concentration of 5-[(trimethylammonio)[<sup>3</sup>H]-methyl]-8-methoxypsoralen bromide of 100 μg/mL, 48 ng were immobilized to the solid phase whereas nonirradiated



**Figure 2.** Influence of irradiation time on the binding of *N,N'*-dimethyl-*N*-[3-(psoralen-8-yloxy)propyl]-*N'*-biotinylhexanediamine (III) to microtiter wells using concentrations of 100 μg/mL (●) and 10 μg/mL (○), respectively.

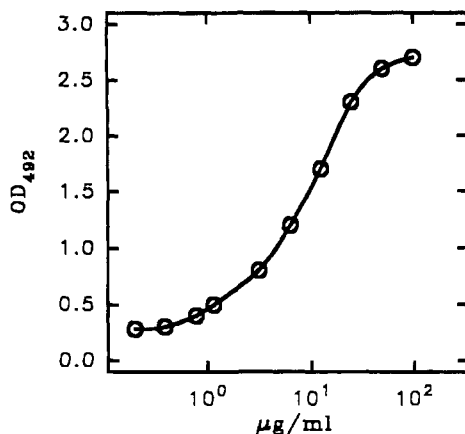
wells showed near-background values (12 ng) (Figure 4). At concentrations lower than 100 μg/mL no significant immobilization of 5-[(trimethylammonio)[<sup>3</sup>H]-methyl]-8-methoxypsoralen bromide could be detected (Figure 4).

**Binding of Photobiotin.** The same experiments were performed as for III, but no biotinylation of the polystyrene solid phase could be detected.

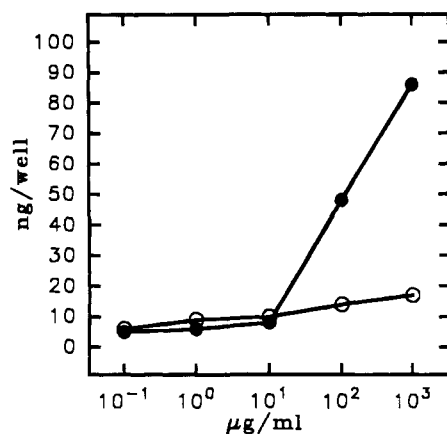
**The Stability of the Psoralen-Modified Surface.** Treatment of microtiter wells modified with II using different buffers and solvents had no significant effect on the amount of secondary amino groups which subsequently could be detected on the surface (Figure 5).

## DISCUSSION

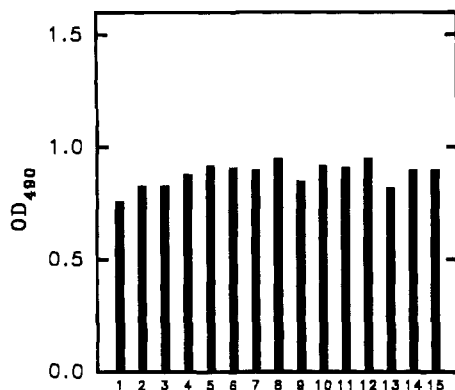
We describe here an easy method for introduction of functional groups on polymer surfaces. Such groups were introduced using the psoralen derivative as the surface reactive compound. Secondary amino groups were immobilized on the surface through an appropriate linkage to the psoralen moiety, and these functional groups could subsequently be used for chemical coupling of, e.g., activated biotin.



**Figure 3.** Binding of *N*-hydroxysuccinimide-biotin to microtiter wells modified with *N,N'*-dimethyl-*N*-[3-psoralen-8-yloxy]-propyl]hexanediamine (**II**).



**Figure 4.** Binding of 5-[(trimethylammonio)[<sup>1</sup>H]methyl]-8-methoxypsoralen bromide to microtiter wells with (●) and without irradiation (○) of UV light.



**Figure 5.** Treatment of psoralen-modified surfaces with 1 M NaOH (1), 1 M HCl (2), 1% Triton X-100 (3), 10% acetic acid in water (4), 0.1 M citric acid buffer pH 5.5 (5), 0.1 M PBS pH 7.2 (6), 0.1 M carbonate buffer pH 9.6 (7), 10% ethanol in water (8), 10% methanol in water (9), 1% DMSO in water (10), 1% DMF in water (11), water (12), washing buffer (13), absolute ethanol (14), no treatment (15).

A clear correlation between the added amounts of **III** and the detectable amounts of solid phase immobilized biotin was seen after irradiation with UV light (Figure 1). Without irradiation only a small amount of biotin could be detected, showing that the surface modification of polystyrene was caused by a photochemical reaction. The process depended on the amounts of psoralen derivative used and on the irradiation time. When using concentrations of 100 and 10 µg/mL, respectively, the

amounts of immobilized psoralen derivative were in linear proportion to the irradiation time in an interval from 0 to 90 min (Figure 2).

A psoralen derivative containing a secondary amine **II** was synthesized for purpose of introduction of secondary amines on the polystyrene surface using the same protocol as for photobinding of **III**. These amino groups could be confirmed using an active ester of biotin and HRP-avidin. A dose-dependent relation was seen between the added amounts of NHS-biotin and the immobilized peroxidase activity, and as expected NHS-biotin itself was not able to react with nonmodified wells (Figure 4).

The amount of psoralen derivative immobilized by the method was estimated using radioactively labeled 5-[(trimethylammonio)[<sup>1</sup>H]methyl]-8-methoxypsoralen bromide. The maximum amount, which could be immobilized of this compound—although different from **II** and **III**—was 87 ng/well (0.28 nmol/well) when using a solution of 1000 µg/mL (Figure 5). At concentrations less than 100 µg/mL no significant immobilization of 5-[(trimethylammonio)[<sup>1</sup>H]methyl]-8-methoxypsoralen bromide could be detected. The amount of secondary groups introduced on polystyrene with **II** has also been determined using a colorimetric method (14). Approximately the same result was obtained corresponding to about 10<sup>14</sup> amino groups per well.

The psoralen-modified surfaces were treated with different strong aqueous eluents in order to examine the nature of binding to the surface. Neither detergents, strong acid, strong base, buffers, high salt concentrations, alcohols, 1% DMSO, nor 1% DMF in water were able to remove the introduced secondary amino groups (Figure 5). This suggests that the mechanism of binding involves covalent bonds between the psoralen derivative and the polystyrene surface.

It is well known that psoralens are able to photoreact with DNA through a cycloaddition between the double-bond of the coumarin/furan in the psoralen molecule and the 5,6 double bond in thymine (15). It has recently been shown that psoralens are capable of making photocycloaddition to pyrimidine (16). These reactions take place under irradiation of long-wavelength UV light, and since we previously have shown that this wavelength interval also is optimal for the herein described method (data not shown), it seems likely that the observed photobinding of the psoralen derivatives to polystyrene was established through a similar mechanism. Perhaps a photocyclization takes place between the coumarin/furan part of a psoralen molecule and a styrene group on the polymer surface. Two psoralen molecules are furthermore able to react with each other under formation of dimers (17) resulting in further modification of the surface.

Others have premodified polystyrene surfaces with UV light (18, 19) and with UV light in combination with cerium ammonium nitrate (20). The nature of the introduced functional groups was, however, not characterized, and the mechanisms seemed to be entirely different from the herein described method, where the introduced functional groups were known to be secondary amino groups. This enables the use of crosslinking reagents for subsequent, well-defined immobilization of biomolecules.

A known photoreactive derivative of biotin, in which the active compound was arylazide (21), was also examined. This compound did, however, not bind to polystyrene, which may be due to an immediate reaction between the photoreactive azide and the aqueous solvent. Psoralens, on the other hand, do not react with water.

Psoralen-modified surfaces containing secondary amines were shown to be able to react with a succinimide ester of biotin, but other active compounds have been shown by others to react with this surface. Crosslinking reagents such as 1-[3-(dimethylamino)propyl]-3-ethylcarbodiimide (EDC) and succinimidyl 4-(*N*-maleimidomethyl)-cyclohexane-1-carboxylate (SMCC) have been shown to react selectively with the modified surface (22). Oligonucleotides (23), peptides (22, 24), and biotin (22) have been immobilized on **II** modified surfaces using EDC as the coupling reagent. The immobilized oligonucleotides could subsequently be used in solid phase hybridization assays where it was possible to detect very low amounts of hybridized DNA (23). Peptides were immobilized with EDC on the same surface for the development of an ELISA for detection of peptide antibodies (24), and an even smaller molecule (a steroid) could be immobilized on **II** modified microtiter wells (25) and subsequently detected with antibodies.

Photomodification of microtiter wells using derivatives of psoralen may solve many of the problems concerning immobilization and detection of small molecules. These surfaces may furthermore have many future interesting applications within the field of automated solid phase DNA hybridization.

#### LITERATURE CITED

- (1) Engvall, E., and Perlmann, P. (1971) Enzyme-linked immunosorbent assay (ELISA). Quantitative assay of immunoglobulin G. *Immunochemistry* 8, 871–874.
- (2) Lehtonen, O. P., and Viljanen, M. K. (1980) Antigen attachment in ELISA. *J. Immunol. Methods* 34, 61–70.
- (3) Darst, A. S., Robertson, C. R., and Berzofsky, J. A. (1988) Adsorption of the protein antigen myoglobin affects the binding of conformation-specific monoclonal antibodies. *Biophys. J.* 53, 533–535.
- (4) Dierks, S. E., Butler, J. E., and Richerson, H. B. (1986) Altered recognition of surface-adsorbed compared to antigen-bound antibodies in the ELISA. *Molec. Immunol.* 23, 403–411.
- (5) Kurki, P. and Virtanen, I. (1984) The detection of human antibodies against cytoskeletal components. *J. Immunol. Methods* 67, 209–23.
- (6) Butler, J. E., Nessler, Ni, L., Nessler, R., Joshi, K. S., Suter, M., Rosenberg, Chang, J., Brown, W. R., and Cantarero, L. A. (1992) The physical and functional behaviour of capture antibodies adsorbed on polystyrene. *J. Immunol. Methods* 150, 77–90.
- (7) Wood, W. G., and Gadow, A. (1983) Immobilisation of Antibodies and Antigens on Macro Solid Phases—A Comparison Between Adsorptive and Covalent Binding. *J. Clin. Chem. Clin. Biochem.* 21, 789–797.
- (8) Ansari, A. A., Hattikudur, N. S., Joshi, S. R., and Medeira, M. A. (1985) ELISA Solid Phase: Stability and Binding Characteristics. *J. Immunol. Methods* 84, 117–124.
- (9) Neurath, A. R., and Strick, N. (1981) Enzyme-linked fluorescence immuno assays using beta-galactosidase and antibodies covalently bound to polystyrene plates. *J. Virol. Methods* 3, 155–65.
- (10) Elsner, H. I., Buchardt, O., Moeller, J., and Nielsen, P. E. Photochemical crosslinking of protein and DNA in chromatin. Synthesis and application of psoralen–cystamine–arylazido photocrosslinking reagents. *Anal. Biochem.* 149, 575–81.
- (11) Henriksen, U., Buchardt, O., and Nielsen, P. E. (1991) Azidobenzoyl-, azidoacridinyl-, diazocyclopentadienylcarbonyl- and 8-propyloxypsoralen photobiotinylation reagents. Syntheses and photoreactions with DNA and protein. *J. Photochem. Photobiol.* 57, 331–42.
- (12) Hansen, J. B., Nielsen, M. C., Ehrbar, U., and Buchardt, O. (1985) Partially Protected Polyamines. *Synthesis* 5, 404–405.
- (13) Buchardt, O., Ebbesen, P., Kantrup, A., Karup, G., Knudsen, P. H., Nielsen, P., Hansen, J. B., Bjerring, P. E., Nielsen, M. C., Norden, B., and Ygge, B. (1985) Psoralenamines synthesis, pharmacological behavior and DNA binding of 5-(aminomethyl)-8-methoxy-, 5-([3-aminopropyl]oxy)methyl- and -[(3-aminopropyl)oxy]psoralen derivatives. *J. Med. Chem.* 28, 1001–10.
- (14) Kakabakos, S. E., Tyllianakis, P. E., Evangelatos, G. P., and Ithakissios, D. S. (1993) Colorimetric Determination of Amino Groups of Covalink NH Microwells. *Nunc Bull.* 11, 1–2.
- (15) Parsons, B. J. (1980) Psoralen photochemistry. *Photochem. Photobiol.* 32, 813–21.
- (16) Bisagni, E. (1992) Synthesis of psoralens and analogs. *J. Photochem. Photobiol.* 14, 23–46.
- (17) Shim, S. C., Lee, S. S., and Choi, S. J. (1990) The C4-photocyclodimers of 4,5',8-trimethylpsoralen (TMP). *J. Photochem. Photobiol.* 51, 1–7.
- (18) Zouali, M., and Stollar, B. D. (1986) A rapid ELISA for measurement of antibodies to nucleic acid antigens using UV-treated polystyrene microplates. *J. Immunol. Methods* 90, 105–10.
- (19) Boudet, F., Theze, J., and Zouali, M. (1991) UV-treated polystyrene micro-titer plates for use in an ELISA to measure antibodies against synthetic peptides. *J. Immunol. Methods* 142, 73–82.
- (20) Buchardt, O., Jørgensen, W. A., Henriksen, U., Rasmussen, M., Lohse, C., Løvborg, U., Bjerrum, O. J., and Nielsen, P. E. (1993) Photochemical surface modification of polystyrene in the presence of cerium(IV) ammonium nitrate: improved binding of proteins, amines and mercaptans in the presence of detergent. *Biotechnol. Appl. Biochem.* 17, 223–237.
- (21) Forster, A. C., McInnes, J. L., Skingle, D. C., and Symons, R. H. (1985) Non-radioactive hybridization probes prepared by the chemical labeling of DNA and RNA with a novel reagent, photobiotin. *Nucleic Acids Res.* 13, 745–61.
- (22) Rasmussen, S. E. (1990) Covalent immobilization of biomolecules onto polystyrene MicroWells for use in biospecific assays. *Ann. Biol. Clin.* 48, 647–650.
- (23) Rasmussen, S. R., Larsen, M. R., and Rasmussen, S. E. (1991) Covalent Immobilization of DNA onto Polystyrene Microwells: The Molecules Are Only Bound at the 5'End. *Anal. Biochem.* 198, 138–142.
- (24) Søndergård-Andersen, J., Lauritzen, E., Lind, K., and Holm, A. (1990) Covalently linked peptides for enzyme-linked immunosorbent assay. *J. Immunol. Methods* 131, 99–104.
- (25) Yonezawa, S., Kambegawa, A., and Tokudome, S. (1993) Covalent coupling of steroid to microwell plates for use in a competitive enzyme-linked immunosorbent assay. *J. Immunol. Methods* 166, 55–61.

# Synthesis of Oligoarginine–Oligonucleotide Conjugates and Oligoarginine-Bridged Oligonucleotide Pairs

Ziping Wei,<sup>†,‡</sup> Ching-Hsuan Tung,<sup>†</sup> Tianmin Zhu,<sup>†,‡</sup> and Stanley Stein<sup>\*,†,‡</sup>

Center for Advanced Biotechnology and Medicine, 679 Hoes Lane, Piscataway, New Jersey 08854, and Department of Chemistry, Rutgers University, Piscataway, New Jersey 08855. Received May 3, 1994\*

Conjugates consisting of oligoarginine peptides linked to oligodeoxynucleotides have been synthesized, including a new type of conjugate, in which a pair of oligonucleotides is bridged by a cationic peptide. Two different 9-mer oligonucleotides were conjugated to the terminal cysteine residues of the peptide series H-Cys-(Arg)<sub>n</sub>-Cys-NH<sub>2</sub> ( $n = 3, 5, 7$ ). Different thiol protecting groups were utilized on the amino- and carboxy-terminal cysteine residues of the peptide to allow selective attachment to the 3'- or 5'-terminus of each specific oligonucleotide. The conjugates containing oligoarginine peptides were purified by anion-exchange chromatography, and their structures were confirmed by polyacrylamide gel electrophoresis and amino acid analysis.

## INTRODUCTION

Synthetic oligonucleotides provide a new approach for controlling cellular or viral gene expression at the transcription or translation level (reviewed in 1–3). However, oligonucleotides are highly sensitive to nucleases and ineffective in passing through the cellular membrane. In order to meet the requirements for therapeutic applications, chemically modified oligonucleotides have attracted great interest (4, 5).

One form of modification is to append non-nucleic acid moieties to the oligonucleotides. For example, oligonucleotides have been conjugated to different peptides, such as cationic polylysine (6) or hydrophobic polytryptophan (7), to enhance cellular uptake. Metal chelate peptides have been appended to generate specific cleavage of nucleic acids (8). Multifunctional polyamides have been incorporated for attaching labels and reporter groups (9). Recently, non-nucleic acid moieties have been used to link short oligonucleotides to alter their hybridization properties (10–12). These tethered oligonucleotides were made by machine synthesis using phosphoramidite chemistry. The tethers were constructed from poly(phosphodiester) or poly(ethylene glycol) units, which were either negatively charged or neutral. Automated synthesis with standard protecting schemes, however, limited the range of functional groups which could be introduced on the tethers. Such functional groups might be useful for altering the properties of this class of compounds.

In recent years, arginine-rich motifs have been found in many RNA binding proteins, such as antiterminators, Gag proteins, ribosomal proteins, and human immuno-

deficiency virus (HIV) Rev protein (13). In one example, the arginine-rich region of Tat specifically binds a 3-nucleotide bulge structure in the stem-loop region of TAR RNA of HIV-1 (14, 15). Small arginine-containing peptides and even arginine itself showed specific TAR RNA recognition (16). The group I self-splicing intron of Tetrahymena pre-rRNA has been reported to stereospecifically bind arginine in a competitive manner at the guanosine nucleotide binding site (17). Random oligonucleotides selected for arginine binding activity revealed three additional small RNA motifs capable of binding to arginine but without homology to the arginine binding site of group I introns (18). Physical evidence of such arginine–RNA interaction was also found in the cocrystal structure of glutamyl tRNA synthetase–tRNA (19). Arginine residues play important roles in the activity of nucleases and other enzymes and were found in the active sites of staphylococcal nuclease (20), lactate dehydrogenase (21), and yeast inorganic pyrophosphatase (22). Arginine peptides are expected to have strong interaction with the phosphate groups and the bases of nucleic acids (16). Highly specific and strong binding of an oligoarginine–oligonucleotide conjugate might be useful for antisense inhibition of certain RNA targets. Here, we report a general method for synthesizing single-linked oligoarginine–oligonucleotide conjugates and oligonucleotide pairs bridged by oligoarginine peptides, using the peptide series H-Cys-(Arg)<sub>n</sub>-Cys-NH<sub>2</sub> as the bridge. The C-terminal and N-terminal cysteines provide for selective attachment of the peptide to two different oligonucleotides having any desired sequences.

## EXPERIMENTAL PROCEDURES

**Materials.** TFA and 5'-amino-modifier-C6-TFA were from Applied Biosystems (Foster City, CA). Iodoacetic acid, Bu<sub>3</sub>P, anisole, ethanedithiol, and lithium chloride were obtained from Aldrich Chemical Co. (Milwaukee, WI). Fmoc-L-Cys(S-*t*-Bu)-OH and Fmoc-D-Arg(Pmc)-OH were from Bachem California (Torrance, CA). Acetic acid, sodium acetate, and sodium bicarbonate were from EM Science (Gibbstown, NJ). The ISS oligo staining system was from Integrated Separation Systems (Natick, MA). Acetonitrile and methylene chloride were from J. T. Baker (Philipsburg, NJ), and triethylamine and ethyl ether were from Fisher Scientific (Springfield, NJ). DMT-C6-3'-amino-ON CPG was from Clontech Laboratories (Palo Alto, CA). BOP, HOBT, PAL support (0.1

\* To whom correspondence should be addressed at the Center for Advanced Biotechnology and Medicine. Tel: 908-235-5319. Fax: 908-235-4850.

<sup>†</sup> Center for Advanced Biotechnology and Medicine.

<sup>‡</sup> Rutgers University.

\* Abstract published in *Advance ACS Abstracts*, August 1, 1994.

<sup>1</sup> Abbreviations: Arg, arginine; BOP, (benzotriazol-1-yloxy)-tris(dimethylamino)phosphonium hexafluorophosphate; Bu<sub>3</sub>P, tributylphosphine; Cys, cysteine; DMT, dimethoxytrityl; DTNB, 5,5'-dithiobis(2-nitrobenzoic acid); Fmoc, 9-fluorenylmethyloxycarbonyl; HOBT, 1-hydroxybenzotriazole hydrate; MOPS, 3-(*N*-morpholino)propanesulfonic acid; NHS, *N*-hydroxysuccinimide; Pmc, 2,2,5,7,8-pentamethylchroman-6-sulfonyl; S-*t*-Bu, *tert*-butyl thiol; TFA, trifluoroacetic acid; Trt, trityl.

Table 1. Names of the Compounds and Their Retention Times

compsds	name	overall charges	$t_R^a$ (min)	$t_R^b$ (min)
oligonucleotides				
5'-TAA TGT GAT-3' with 5' amino linker	9-mer I	-8	29	21
5'-GAC TAG GTG-3' with 3' amino linker	9-mer II	-8	29	21
acetylated 9-mer I, or 9-mer II		-9	30	25–26
single-linked conjugates				
Cys-(L-Arg) <sub>3</sub> -Cys-9-mer I	R <sub>3</sub> I	-5	25	
Cys-(L-Arg) <sub>5</sub> -Cys-9-mer I	R <sub>5</sub> I	-3	23	31
Cys-(L-Arg) <sub>7</sub> -Cys-9-mer I	R <sub>7</sub> I	-1	21	
bridged oligonucleotide pairs				
9-mer II-Cys-(L-Arg) <sub>3</sub> -Cys-9-mer I	IIR <sub>3</sub> I	-14	35	
9-mer II-Cys-(L-Arg) <sub>5</sub> -Cys-9-mer I	IIR <sub>5</sub> I	-12	33	
9-mer II-Cys-(L-Arg) <sub>7</sub> -Cys-9-mer I	IIR <sub>7</sub> I	-10	32	
9-mer II-Cys-L-Arg-D-Arg-L-Arg-Cys-9-mer I	IID/LR <sub>3</sub> I	-14	35	25–26
9-mer II-Cys-(L-Arg-D-Arg) <sub>2</sub> -L-Arg-Cys-9-mer I	IID/LR <sub>5</sub> I	-12	33	
9-mer I-Cys-(L-Arg) <sub>3</sub> -Cys-Cys-(L-Arg) <sub>3</sub> -Cys-9-mer I	IR <sub>3</sub> R <sub>3</sub> I	-10	32	

<sup>a</sup> Retention time on a Nucleogen DEAE 60-7 column. Gradient: 100% A for 5 min, 100% A to 60% A in 40 min. <sup>b</sup> Retention time on a Hamilton PRP-1 column. Gradient: 100% A for 5 min, 100% A to 80% A in 40 min.

mmol each) as well as Fmoc-L-Cys(Trt)-OH/BOP+HOBT and Fmoc-L-Arg(Pmc)-OH/BOP+HOBT cartridges (0.5 mmol each) were from Milligen/Bioscience (Milford, MA). NHS, 6 N hydrochloric acid, and dimethyl sulfoxide were from Pierce Chemical Co. (Rockford, IL). DTNB was from Sigma Chemical Co. (St. Louis, MO); MOPS and glycerol were from United States Biochemical Corp. (Cleveland, OH).

**Preparation of H-Cys(S-*t*-Bu)-(Arg)<sub>*n*</sub>-Cys-NH<sub>2</sub>.** The peptides, having a free amino-terminus but an amidated carboxy-terminus, were synthesized in a 9400 Excell peptide synthesizer (Milligen/Bioscience, Burlington, MA) using the Fmoc chemistry on a 0.1 mmol scale. Pre-packed amino acid cartridges were used directly, except for Fmoc-L-Cys(S-*t*-Bu)-OH (215.8 mg, 0.5 mmol) and Fmoc-D-Arg(Pmc)-OH (331 mg, 0.5 mmol), which were packed with BOP reagent (221.3 mg, 0.5 mmol) and HOBT (67.5 mg, 0.5 mmol) separately before use. After synthesis, the peptides were cleaved from the resin with 5 mL of TFA/anisole/ethanedithiol (95/4/1, v/v), precipitated from ethyl ether, and purified by reversed-phase HPLC on a Vydac 218TP1022, 10  $\mu$ m, C<sub>18</sub> column (2.2  $\times$  25 cm) (Separation Group, Hesperia, CA) using a gradient of acetonitrile in 0.1% trifluoroacetic acid at a flow rate of 4 mL/min. The structures of the purified peptides were verified by fast atom bombardment mass spectroscopy (FAB): H-Cys(S-*t*-Bu)-(Arg)<sub>3</sub>-Cys-NH<sub>2</sub>, 781 (M + 1); H-Cys(S-*t*-Bu)-(Arg)<sub>5</sub>-Cys-NH<sub>2</sub>, 1093 (M + 1); H-Cys(S-*t*-Bu)-(Arg)<sub>7</sub>-Cys-NH<sub>2</sub>, 1405 (M + 1). Ellman assay with DTNB (23) showed 0.9 mol of free thiol group per mole peptide, based on peptide weight.

**Preparation of Oligonucleotides.** The oligonucleotides were synthesized by phosphoramidite methodology using a Model 380B DNA synthesizer (Applied Biosystems, Foster City, CA) on a 1  $\mu$ mol scale. The DNA 9-mers were coupled to amino linkers at either the 5' or 3' terminus with either 5'-amino-modifier-C6-TFA or DMT-C6-3'-amino-ON CPG on the synthesizer. The 9-mer with a 5'-amino linker (9-mer I, Table 1) was purified by anion-exchange chromatography on a Nucleogen DEAE 60-7 column (4  $\times$  125 mm) (Nest Group, Southborough, MA). The product was desalted by reversed-phase chromatography on a Hamilton PRP-1, 10  $\mu$ m, C<sub>18</sub> column (4.1  $\times$  150 mm) (VWR Scientific, Piscataway, NJ) using a gradient of acetonitrile with aqueous 0.1 M triethylammonium acetate, pH 7.0 at a flow rate of 1 mL/min. Trityl-on and Trityl-off two-step purifications (24) on the PRP-1 column were done for 9-mer II (Table 1) using a similar acetonitrile gradient.

**Synthesis of Iodoacetylated Oligonucleotides.** Iodoacetic acid and *N*-hydroxysuccinimide were used to

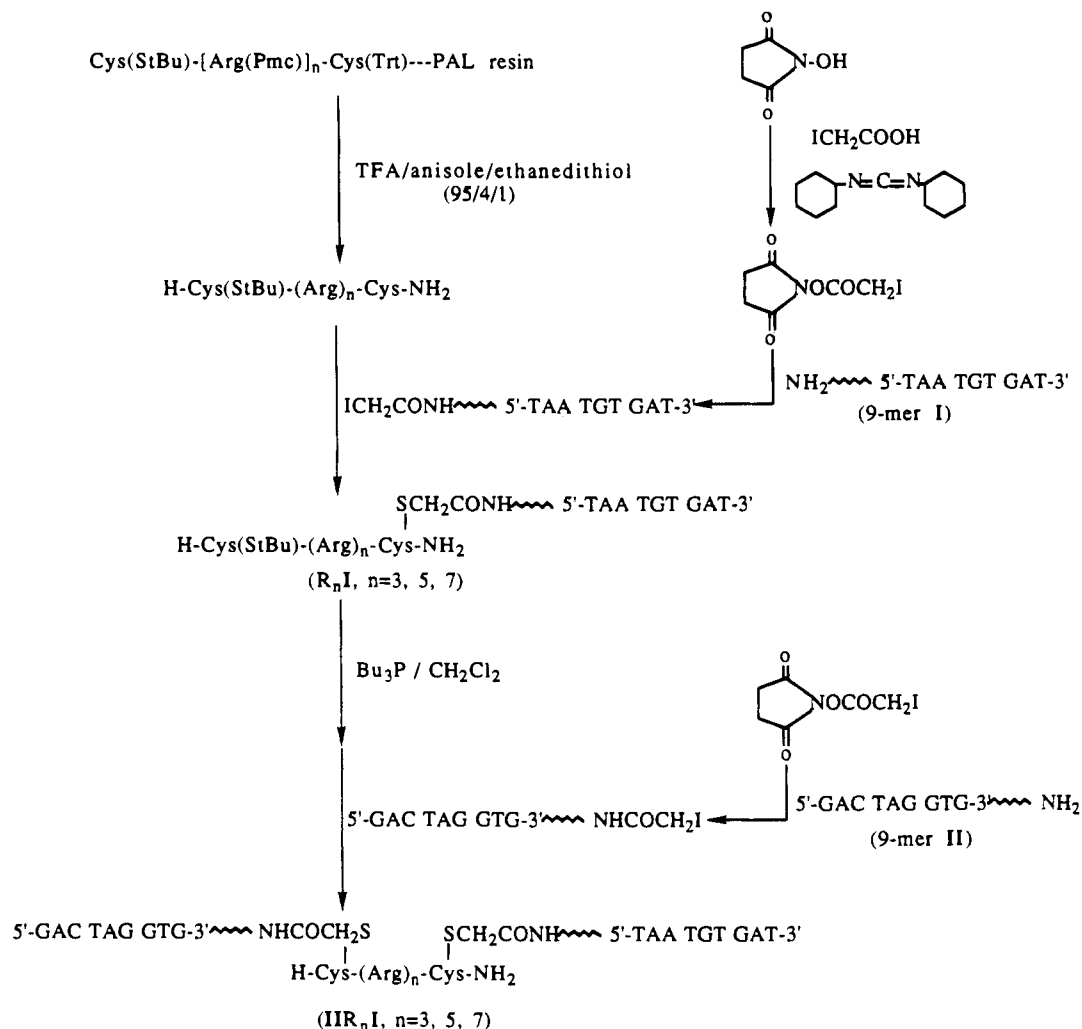
synthesize *N*-[(iodoacetyl)oxy]succinimide (25). Oligonucleotide 9-mer I (5 units, A<sub>260</sub>) in 100  $\mu$ L of 0.1 M NaHCO<sub>3</sub> and 2 mg of *N*-[(iodoacetyl)oxy]succinimide (150 equiv) in 100  $\mu$ L of dimethyl sulfoxide were mixed and reacted in the dark at room temperature for 2 h. The mixture of unreacted and iodoacetylated oligonucleotide was freed of unreacted *N*-[(iodoacetyl)oxy]succinimide by anion-exchange chromatography on a Nucleogen DEAE 60-7 column. Mobile phase A was 60% 20 mM sodium acetate (pH 7.0), 40% acetonitrile. Mobile phase B was mobile phase A containing 0.7 M lithium chloride. The flow rate was 1 mL/min. The gradient was 100% A for 5 min, 100% A to 88% A in 30 min, 88% A to 50% A in 1 min. The eluent at 35 min was collected and put under vacuum for 20 min to evaporate acetonitrile and was then ready for conjugation to the peptide.

Iodoacetylated 9-mer II was prepared in a similar manner, except that sodium bicarbonate (NaHCO<sub>3</sub>) was added to a final concentration of 0.1 M after acetonitrile was removed under vacuum.

**Synthesis of Oligoarginine–Oligonucleotide Conjugates.** The synthesis scheme is outlined in Figure 1. Iodoacetylated 9-mer I in eluent buffer was reacted overnight with 1 mg of H-Cys(S-*t*-Bu)-(Arg)<sub>3</sub>-Cys-NH<sub>2</sub> (25 equiv) dissolved in 50  $\mu$ L of water under nitrogen, in the dark, at room temperature. The reaction mixture was diluted and purified on a Nucleogen DEAE 60-7 column in two or three purification runs (Figure 2, A). Mobile phase A was 20 mM sodium acetate (pH 7.0), 40% acetonitrile. Mobile phase B was buffer A containing 0.7 M lithium chloride. The gradient was 100% A for 5 min and 100% A to 60% A in 40 min at a flow rate of 1 mL/min. The chromatogram showed a new major peak (peptide-9-mer I conjugate, referred to as R<sub>3</sub>I), as well as small peaks at 29 min (unreacted 9-mer I) and 30 min (unreacted iodoacetylated 9-mer I). The unreacted peptide eluted with the solvent front at 1.5 min, as detected by UV absorption and Ellman's reagent (DTNB). The new major peak was collected and reduced in volume to 200  $\mu$ L under vacuum and was then ready for conjugation to the 9-mer II. In another preparation, the peptide-9-mer I was also desalted on the PRP-1 column. Mobile phase A was 95% 0.1 M triethylammonium acetate (pH 8.0), 5% acetonitrile. Mobile phase B was 5% 0.1 M triethylammonium acetate (pH 8.0), 95% acetonitrile. The gradient was 100% A for 5 min and 100% A to 80% A in 40 min at a flow rate of 1 mL/min. The peak at 31 min was collected and dried, giving a 60% yield (3 units, A<sub>260</sub>).

**Synthesis of Oligoarginine-Bridged Oligonucleotide Pairs.** R<sub>3</sub>I conjugate (3 units, A<sub>260</sub>) in 200  $\mu$ L of concentrated eluent buffer (from the Nucleogen DEAE





**Figure 1.** Synthesis scheme for oligoarginine-oligonucleotide conjugates and oligoarginine-bridged oligonucleotide pairs.

60-7 column) was adjusted to pH 8.3 (final concentration of 0.1 M  $\text{NaHCO}_3$ ), and then stirred vigorously with 10  $\mu\text{L}$  of  $\text{Bu}_3\text{P}$  (1300 equiv) (26) in 200  $\mu\text{L}$  of methylene chloride under nitrogen at room temperature for 4 h to cleave the *tert*-butyl thiol protecting group on cysteine. The iodoacetylated 9-mer II (3 units,  $A_{260}$ , 1 equiv), in 800  $\mu\text{L}$  of eluent buffer containing 0.1 M  $\text{NaHCO}_3$ , was added, and the reaction mixture was stirred overnight under nitrogen, in the dark, at room temperature. The aqueous layer was then separated and washed four times with 0.5 mL of methylene chloride. The aqueous phase was diluted and resolved by ion-exchange chromatography in several purification runs, as above (Figure 2B). The R<sub>3</sub>I peak, 9-mer II peak (29 min) and iodoacetylated 9-mer II peak (30 min) were all small. A new later-eluting peak was collected, dried, and desalted on the PRP-1 column. The major peak (25–26 min) was dried, giving a 50% yield of IIR<sub>3</sub>I (3 units,  $A_{260}$ ). The bridged oligonucleotide pairs IIR<sub>3</sub>I, IIR<sub>7</sub>I, IIR<sub>10</sub>I, and IIR<sub>13</sub>I (see Table 1) were prepared similarly as above.

**Control Experiments.** The disulfide-linked dimer, IR<sub>3</sub>R<sub>3</sub>I, was synthesized for comparison using a method similar to the above, but with the following modifications. After the *tert*-butyl thiol group was removed from cysteine on R<sub>3</sub>I, the aqueous phase was washed with methylene chloride and stirred overnight to allow disulfide bond formation. The purification step was the same as that for bridged oligonucleotide pairs. A peak at 32 min was observed on the Nucleogen DEAE 60-7 column (50% yield). When R<sub>3</sub>I conjugate, without removing the

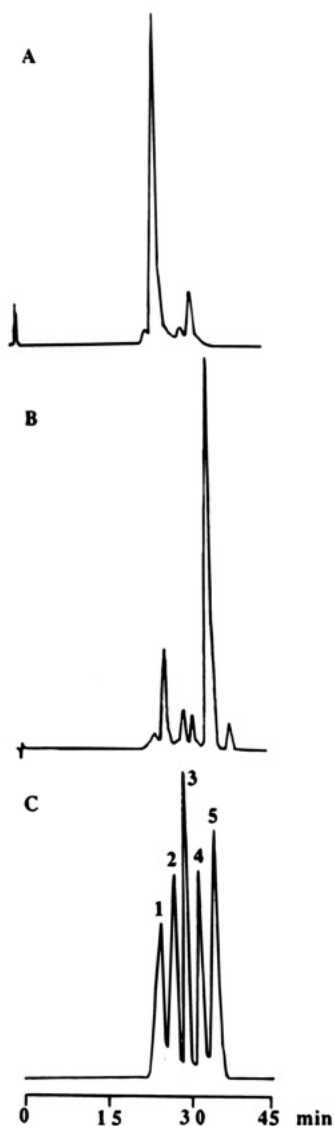
*tert*-butyl thiol group, was stirred with a second iodoacetylated 9-mer overnight, no reaction occurred, as indicated by ion-exchange chromatography.

**Polyacrylamide Gel Electrophoresis (PAGE).** The oligonucleotide conjugates and pairs were analyzed on a native 20% polyacrylamide gel. The running buffer was 40 mM MOPS and 10 mM sodium acetate (pH 7.0, adjusted with sodium hydroxide). The samples (0.01 units,  $A_{260}$ ) were suspended in 20  $\mu\text{L}$  of loading buffer (30% glycerol) and heated at 90 °C for 2 min. Other lanes were loaded with 20  $\mu\text{L}$  of 30% glycerol, 0.05% xylene cyanol, and 0.05% bromophenol blue as markers. The bands were visualized by silver staining with an ISS oligo staining system kit. The gel was photographed with Polaroid film (Figure 3).

**Amino Acid Analysis.** The samples (0.1 units,  $A_{260}$ ) were hydrolyzed in 6 N hydrochloric acid/4% thioglycolic acid in the gas phase in a vacuum desiccator at 110 °C for 24 h, as described (27). Amino acid analysis was based on reverse phase separation on a Chroma Bond MC-18, 3  $\mu\text{m}$  column (4.6  $\times$  100 mm), followed by *o*-phthalaldehyde (OPA) postcolumn derivatization (27).

## RESULTS

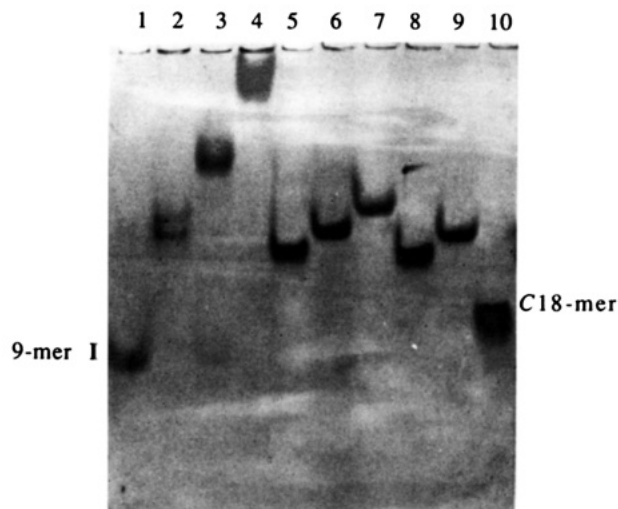
**Synthesis of Polyarginine-Oligonucleotide Conjugates and Polyarginine-Bridged Oligonucleotide Pairs.** In the synthesis scheme, two cysteines with two different protecting groups, trityl (cleavable by TFA) and *tert*-butyl thiol (cleavable by  $\text{Bu}_3\text{P}$ ), were utilized to



**Figure 2.** Chromatography on a Nucleogen DEAE 60-7 column: (A) purification of  $R_3I$  conjugate; (B) purification of  $IIR_3I$  bridged oligonucleotide pair; (C) coinjection of five components, (1)  $R_3I$  (25 min), (2) 9-mer I (29 min), (3) iodoacetylated 9-mer I (30 min), (4)  $IR_3R_3I$  (32 min), (5)  $IIR_3I$  (35 min). Chromatographic conditions are given in the Experimental Procedures. Detection was at 260 nm.

control the selective attachment of oligonucleotides to the peptide (Figure 1). Each peptide was deprotected in TFA/anisole/ethanedithiol (95/4/1) (28). This condition did not lead to reduction of the *tert*-butyl thiol-protected cysteine, which is resistant to acids like TFA and bases, but cleavable by mild reagents such as thiols or phosphines (29). In the absence of 1% ethanedithiol scavenger, the desired product cannot be obtained, and an unidentified product with a mass of 82 greater and nonreactive in the Ellman assay for thiols was found to be formed. The synthesis of peptide-9-mer I conjugate was performed at neutral pH in order to prevent the loss of the *tert*-butyl thiol protecting group. However, a basic pH (0.1 M  $NaHCO_3$ ) was found to be necessary for high yields of bridged oligonucleotide pairs. If only the single-linked oligoarginine–oligonucleotide conjugate is desired, there is no need for the peptide to contain N-terminal cysteine, which is necessary for the synthesis of bridged oligonucleotide pairs.

Oligonucleotides can be prepared with amino groups at either the 5' or 3' end for attachment to the peptide. The primary amine groups on oligonucleotides are con-



**Figure 3.** Photograph of a native 20% polyacrylamide gel after silver staining: (1) 9-mer I, (2)  $R_3I$ , (3)  $R_5I$ , (4)  $R_7I$ , (5)  $IIR_3I$ , (6)  $IIR_5I$ , (7)  $IIR_7I$ , (8)  $IID_1LR_3I$ , (9)  $IID_1LR_5I$ , (10) C18-mer (its sequence is the combination of 9-mer I and 9-mer II, 5'-TAA TGT GAT GAC TAG GTG-3').

verted to the iodoacetamide moiety by iodoacetylation and are readily reacted with the free thiol group on the peptide. The single-linked oligoarginine–oligonucleotide conjugate can be simply achieved this way. Then, the other cysteine on the peptide is deprotected and reacted with the second oligonucleotide to achieve the oligoarginine-bridged oligonucleotide pair.

All conjugation reactions were performed in lithium chloride salt solution because peptide-9-mer I conjugates have low solubility in water due to strong interaction of arginine side chains and phosphate groups. In salt solution, this interaction is weakened, making the conjugate readily soluble. The bridged oligonucleotide pairs can be readily dissolved in water because they have an excess of phosphate groups compared to arginine residues.

A sequential one-pot method, which was used in quantitative reduction (with  $Bu_3P$ ) and alkylation of wool (30, 31), as well as conjugation of synthetic peptides to proteins (32), was applied to the synthesis of these peptide-bridged oligonucleotide pairs. First, the peptide in the conjugate was reduced. Subsequently, the alkylating agent was added to the reaction bath in the presence of excess reducing agent. It was found to be necessary to allow the initial reduction step to go to completion, since iodoacetic acid and its amides react with  $Bu_3P$  to form a quarternary phosphonium salt, which is much less reactive than  $Bu_3P$  (26).

The reducing reagent  $Bu_3P$  has two advantages over the widely used dithiothreitol (DTT) in this application. First, DTT must be removed after reduction of the disulfide bond, which requires an additional separation step. Second, a substantial amount of the disulfide-linked dimer side product, 9-mer I-peptide-peptide-9-mer I, was found to be formed in the DTT procedure. The presence of  $Bu_3P$  during this conjugation prevented this undesirable dimer formation, thereby increasing the yield of the final product. A large excess of  $Bu_3P$  was used, since it is readily oxidized in air. Due to the limited aqueous solubility of  $Bu_3P$ , a two-phase reaction was performed, and the organic phase containing most of the  $Bu_3P$  was removed after the reaction was completed.

**Chromatographic Purifications.** The purification of conjugates was successfully achieved by anion-exchange chromatography on a Nucleogen DEAE 60-7 column (Figure 2). The separations are based on the

interaction of the negative charges on short oligonucleotides with the positive charges on the column packing. The fractionation of the mixture components is governed by the difference in their net charges. Organic solvent in the eluent (40% acetonitrile) minimized nonionic interactions between the oligonucleotides and packing materials. Figure 2 shows the purification chromatogram of **IIR<sub>3</sub>I** conjugate. The retention time of the 9-mer with an amino linker (with an overall charge of -8) was 29 min. After iodoacetylation, the new molecule eluted 1 min later, at 30 min. This was possibly due to the elimination of one positive charge on the primary amino group by amide bond formation. After conjugation to the peptide containing three arginine residues, which had four positive charges, the **R<sub>3</sub>I** (with an overall charge of -5) eluted much earlier, at 25 min (Figure 2A). The **IIR<sub>3</sub>I** oligonucleotide pair, comprised of two 9-mers and one peptide (with an overall charge of -14), eluted at 35 min (Figure 2B). The control compound, **IR<sub>3</sub>R<sub>3</sub>I** disulfide-linked dimer, comprised of two 9-mers and two peptides (with an overall charge of -10) eluted at 32 min. Thus, the retention times of the conjugates are proportional to their net negative charges (Figure 2C). The single-linked conjugates **R<sub>3</sub>I**, **R<sub>5</sub>I**, and **R<sub>7</sub>I** eluted at 25, 23, and 21 min, respectively. The bridged oligonucleotide pairs **IIR<sub>3</sub>I** (and **IID<sub>L</sub>R<sub>3</sub>I**), **IIR<sub>5</sub>I** (and **IID<sub>L</sub>R<sub>5</sub>I**), and **IIR<sub>7</sub>I** eluted at 35, 33, and 32 min, respectively. The relative elution times are consistent with the overall charge of each compound. In all cases, the products are well resolved from the reactants. The retention times of all the compounds are included in Table 1.

The conjugates were desalted on a Hamilton PRP-1 column using a TEAA buffer system. Certain separations can also be achieved on this reversed-phase column, but purification of single-linked conjugates from reaction mixtures cannot be performed by reversed-phase chromatography due to precipitation of the conjugates in the column in the presence of a large excess of positively charged peptides. In the anion-exchange column, this problem is solved because peptides elute with the solvent front. The bridged oligonucleotide pairs have almost the same retention times as acetylated 9-mers and, therefore, cannot be purified on the reversed-phase column, either. Therefore, the Fmoc-on/Fmoc-off purification step we previously developed (33, 34) is not applicable for this purpose.

**Gel Electrophoresis.** Gel electrophoresis allows separation of macromolecules according to charge and size. Each conjugate gave only one band on the gel, confirming its purity (Figure 3). The gel was run at neutral pH to maintain the negative charges on the oligonucleotides and positive charges on the peptides. The peptide-9-mer **I** conjugates migrated much more slowly than 9-mer **I**, due to the influence of the positive charges on the peptide. The positions of peptide-9-mer **I** conjugates were dependent on their charges. **R<sub>3</sub>I** had two less positive charges than **R<sub>5</sub>I** and four less than **R<sub>7</sub>I** and migrated faster than **R<sub>5</sub>I**, which migrated faster than **R<sub>7</sub>I**. **R<sub>7</sub>I**, having only one net negative charge, barely moved in the gel. Such an effect was also found in oligonucleotides bearing positively charged  $\omega$ -aminohexyl groups (35). The bridged oligonucleotide pairs ran faster than peptide-9-mer **I** and had the same order of electrophoretic mobility as single-linked conjugates. Although the bridged oligonucleotide pair has a larger size, the additional negative charges have a greater influence on migration. The stereoisomer pairs, **IIR<sub>3</sub>I** and **IID<sub>L</sub>R<sub>3</sub>I**, as well as **IIR<sub>5</sub>I** and **IID<sub>L</sub>R<sub>5</sub>I** (Table 1), migrated to the same positions. Compared with an unmodified 18-mer (C18-mer), the oligonucleotide pairs had slower mobility

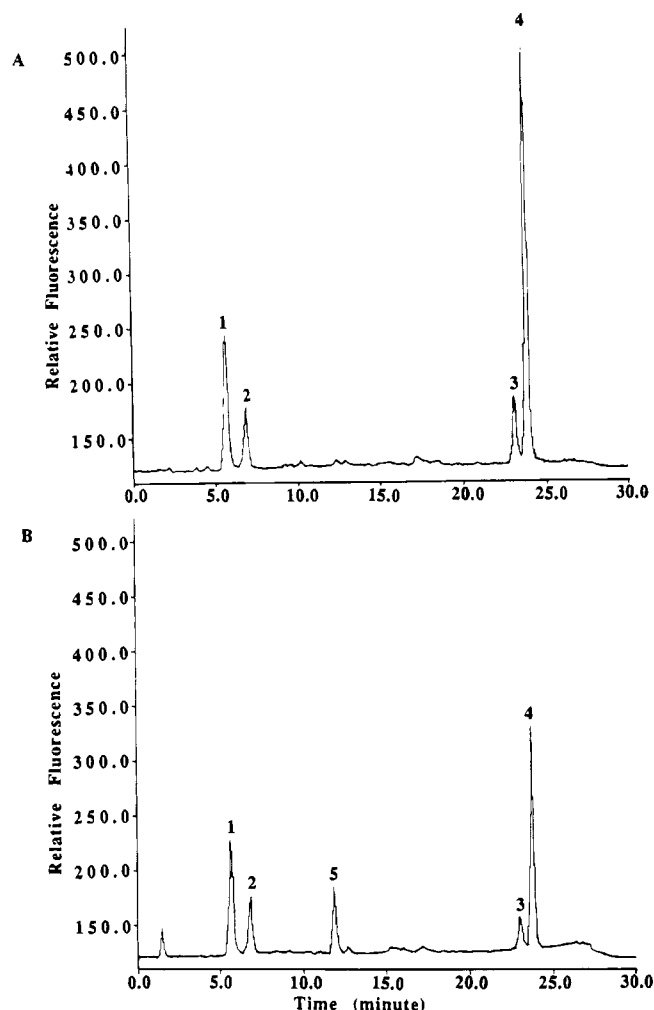
because of the positive charges of the peptides. The disulfide-linked dimer **IR<sub>3</sub>R<sub>3</sub>I**, had an even slower mobility than **R<sub>3</sub>I**, due to increased molecular size (data not shown). In summary, the electrophoretic migration order is 9-mer > C18-mer > bridged oligonucleotide pair > single-linked conjugate > disulfide-linked dimer (for each peptide). Thus, gel electrophoresis shows striking variations in mobility among the set of conjugates and is a powerful tool for distinguishing these compounds.

**Amino Acid Analysis.** The amount of each oligonucleotide was determined by absorption at 260 nm based on the extinction coefficient calculated from dimer and monomer values by using the nearest-neighbor method (36, 37). The amount of peptide was determined by amino acid analysis of an acid hydrolysis. The peptide-9-mer **I** and the disulfide-linked dimer, 9-mer **I**-peptide-peptide-9-mer **I**, should give 1:1 molar ratio of 9-mer to peptide, whereas the oligonucleotide pairs should give 2:1 ratio of 9-mer to peptide. The measured values of 9-mer to peptide from **R<sub>3</sub>I**, **R<sub>5</sub>I**, **R<sub>7</sub>I**, **IR<sub>3</sub>R<sub>3</sub>I**, **IIR<sub>3</sub>I**, **IIR<sub>5</sub>I**, and **IIR<sub>7</sub>I** were 1.0, 1.0, 1.0, 0.9, 1.9, 1.9, and 1.9, respectively, within experimental error of the expected integer ratios. Unmodified oligonucleotide hydrolysates were found to generate a single peak at the glycine position. It has been found that a glycine peak is derived from deoxyadenosine hydrolysis by amino acid analysis (38). Hydrolysates of 9-mer **I** with 5' amino linker and 9-mer **II** with 3' amino linker had extra peaks at 23.0 and 11.8 min, respectively, derived from the amino linkers. An *S*-(carboxymethyl)cysteine peak appeared at 6.8 min (Figure 4A) in the hydrolysate of the single-linked conjugate **R<sub>3</sub>I**. The *S*-(carboxymethyl)-cysteine peak released upon acid hydrolysis was previously reported for quantitating the coupling ratio of synthetic peptides to carrier proteins (26). The arginine peak (23.8 min) was from the conjugated peptide. As shown in Figure 4A, the **R<sub>3</sub>I** conjugate gave four peaks: glycine, *S*-(carboxymethyl)cysteine, 5'-amino linker, and arginine in amino acid analysis. The bridged oligonucleotide pair **IIR<sub>3</sub>I** generated one more peak at 11.8 min (Figure 4B), which was from the 3'-amino linker on 9-mer **II**. The relative ratios of these peaks were consistent with the structures of the single-linked conjugates and bridged oligonucleotide pairs.

## DISCUSSION

We have developed a convenient method for synthesizing and purifying oligoarginine-oligonucleotide conjugates and oligonucleotide pairs containing positively charged peptides as the bridge. This pathway can be applied to synthesize conjugates linked or bridged by a peptide, pseudopeptide, or polyamine containing one or more positive charges. Similarly, conjugates linked or bridged by negatively charged components should also be amenable to the anion-exchange purification procedure, since there is a change in net charges of the compounds.

The properties of arginine-containing oligonucleotide conjugates and pairs are the subject of a forthcoming article (39). In summary, we have found that there is an increase of 2.0 °C in  $T_m$  per arginine residue in the duplex of **R<sub>n</sub>I** with a complementary single-stranded DNA in a buffer of 10 mM sodium phosphate (pH 7.0) containing 100 mM sodium chloride and 0.1 mM EDTA. Hybridization of compounds of the class **IIR<sub>n</sub>I** were shown to bind in a cooperative manner to complementary single-stranded DNA or RNA. Enhanced thermal stability of the complex between **IIR<sub>n</sub>I** and complementary single-stranded DNA results, in part, from favorable interactions between the negatively charged nucleic acid target



**Figure 4.** Chromatograms of amino acid analysis: (A) single-linked conjugate R<sub>3</sub>I, (B) bridged oligonucleotide pair IIR<sub>3</sub>I, (1) glycine (5.6 min), (2) S-(carboxymethyl)cysteine (6.9 min), (3) 5'-amino linker (23.0 min), (4) arginine (23.8 min), (5) 3'-amino linker (11.8 min).

and the positively charged peptide bridge. Our data suggest the usefulness of these compounds in antisense strategies.

#### ACKNOWLEDGMENT

We thank Henry Lackland and Ying Peng for amino acid analysis. Oligonucleotides were synthesized by Elizabeth Flores in Dr. Michael J. Leibowitz's lab of UMDNJ-Robert Wood Johnson Medical School. This research was supported by a grant to S. Stein from Gene Shears (Australia) Pty. Ltd.

#### LITERATURE CITED

- (1) Uhlmann, E., and Peyman, A. (1990) Antisense oligonucleotides. A new therapeutic principle. *Chem. Rev.* 90, 543–584.
- (2) Stein, C. A., and Cohen, J. S. (1989) Antisense compounds: Potential role in cancer therapy. *Important Advances In Oncology* (V. T. DeVita, S. Hellman, and S. A. Rosenberg, Eds.) pp 79–97, J. B. Lippincott, Philadelphia.
- (3) Cooney, M., Czernuszewicz, G., Postel, E. H., Flint, S. J., and Hogan, M. E. (1988) Site-specific oligonucleotide binding represses transcription of the human c-myc gene *in vitro*. *Science* 241, 456–489.
- (4) Zon, G. (1988) Oligonucleotide analogues as potential chemotherapeutic agents. *Pharm. Res.* 5, 539–549.
- (5) Croke, S. T. (1992) Therapeutic applications of oligonucleotides. *Bio/Technology* 10, 882–886.
- (6) Leonetti, J.-P., Degols, G., and Lebleu, B. (1990) Biological activity of oligonucleotide-poly(L-lysine) conjugates: Mechanism of cell uptake. *Bioconjugate Chem.* 1, 149–153.
- (7) Juby, C. D., Richardson, C. D., and Brousseau, R. (1991) Facile preparation of 3' oligonucleotide-peptide conjugates. *Tetrahedron Lett.* 32, 879–882.
- (8) Mack, D. P., and Dervan, P. B. (1990) Nickel-mediated sequence-specific oxidative cleavage of DNA by a designed metalloprotein. *J. Am. Chem. Soc.* 112, 4604–4606.
- (9) Haralambidis, J., Duncan, L., Angus, K., and Tregear, G. W. (1990) The synthesis of polyamide-oligonucleotide conjugate molecules. *Nucleic Acids Res.* 18, 493–499.
- (10) Richardson, P. L., and Scherpatz, A. (1991) Tethered oligonucleotide probes. A strategy for the recognition of structured RNA. *J. Am. Chem. Soc.* 113, 5109–5111.
- (11) Cload, S. T., and Scherpatz, A. (1991) Polyether tethered oligonucleotide probes. *J. Am. Chem. Soc.* 113, 6324–6326.
- (12) Durand, M., Pelloille, S., Thuong, N. T., and Maurizot, J. C. (1992) Triple-helix formation by an oligonucleotide containing one (dA)<sub>12</sub> and two (dT)<sub>12</sub> sequences bridged by two hexaethylene glycol chains. *Biochemistry* 31, 9197–9204.
- (13) Lazinski, D., Grzadziska, E., and Das, A. (1989) Sequence-specific recognition of RNA hairpins by bacteriophage anti-terminators requires a conserved arginine-rich motif. *Cell* 59, 207–218.
- (14) Calnan, B. J., Biancalana, S., Hudson, D., and Frankel, A. D. (1991) Analysis of arginine-rich peptides from the HIV Tat proteins reveals unusual features of RNA-protein recognition. *Genes Dev.* 5, 201–210.
- (15) Roy, S., Delling, U., Chen, C.-H., Rosen, C. A., and Sonenberg, N. (1990) A bulge structure in HIV-1 TAR RNA is required for Tat binding and Tat-mediated trans-activation. *Genes Dev.* 4, 1365–1373.
- (16) Frankel, A. D. (1992) Peptide models of the Tat-TAR protein-RNA interaction. *Protein Sci.* 1, 1539–1542.
- (17) Michel, G., Hanna, M., Green, R., Bartel, D. P., and Szostak, J. W. (1989) The guanosine binding site of the *Tetrahymena* ribozyme. *Nature* 342, 391–395.
- (18) Connell, G. J., Illangsekare, M., and Yarus, M. (1993) Three small ribooligonucleotides with specific arginine sites. *Biochemistry* 32, 5497–5502.
- (19) Rould, M. A., Perona, J. J., Soll, D., and Steitz, T. A. (1989) Structure of *E. coli* glutamyl-tRNA synthetase complexed with tRNA<sup>Gln</sup> and ATP at 2.8 Å resolution. *Science* 246, 1135–1142.
- (20) Cotton, F. A., Hazen, E. A., and Legg, M. J. (1979) Staphylococcal nuclease: proposed mechanism of action based on structure of enzyme-thymidine 3',5'-biphosphate-calcium ion complex at 1.5 Å resolution. *Proc. Natl. Acad. Sci. U.S.A.* 76, 2551–2555.
- (21) Adams, M. J., Buehner, M., Chandrasekner, K., Ford, G. C., Hackert, M. L., Liljas, A., Rossmann, M. G., Smiley, I. E., Allison, W. S., Everse, J., Kaplan, N. O., and Taylor, S. S. (1973) Structure-function relationships in lactate dehydrogenase. *Proc. Natl. Acad. Sci. U.S.A.* 70, 1968–1972.
- (22) Cooperman, B. S., and Chiu, N. Y. (1973) Yeast inorganic pyrophosphatase. III. Active-site mapping by electrophilic and binding measurements. *Biochemistry* 12, 1676–1682.
- (23) Riddles, P. W., Blakeley, R. L., and Zerner, B. (1979) Ellman's Reagent: 5,5'-Dithiobis(2-nitrobenzoic acid)—a re-examination. *Anal. Biochem.* 94, 75–81.
- (24) Ebright, Y., Tous, G. I., Tsao, J., Fausnaugh, J., and Stein, S. (1988) Chromatographic purification of non-ionic methylphosphonate oligodeoxyribonucleosides. *J. Liquid Chromatogr.* 11, 2005–2017.
- (25) Schmidt, F. J., and Bock, R. M. (1972) Chemical modification of transfer-RNA species-Heavy atom derivatization of aminoacyl transfer-RNA. *Biochem. Biophys. Res. Commun.* 48, 451–456.
- (26) Ruegg, U. T., and Rudinger, J. (1977) Reductive cleavage of cysteine disulfides with tributylphosphine. *Methods Enzymol.* 47, 111–126.
- (27) Melter, N. M., Tous, G. I., Gruber, S., and Stein, S. (1987) Gas-phase hydrolysis of proteins and peptides. *Anal. Biochem.* 160, 356–361.

- (28) McCurdy, S. N. (1989) The investigation of Fmoc-cysteine derivatives in solid phase peptide synthesis. *Peptide Res.* 2, 147–152.
- (29) Eritja, R., Ziehler-Martin, J. P., Walker, P. A., Lee, T. D., Legesse, K., Albericio, F., and Kaplan, B. E. (1987) *Tetrahedron* 43, 2675–2680.
- (30) Friedman, M., and Noma, A. T. (1970) Cysteine content of wool. *Textile Res. J.* 40, 1073–1078.
- (31) Maclaren, J. A. (1971) Quantitative reduction and alkylation of wool. *Textile Res. J.* 41, 713.
- (32) Kolodny, N., and Robey, F. A. (1990) Conjugation of synthetic peptides to proteins: Quantitation from S-carboxymethylcysteine released upon acid hydrolysis. *Anal. Biochem.* 187, 136–140.
- (33) Tung, C.-H., Rudolph, M. J., and Stein, S. (1991) Preparation of oligonucleotide-peptide conjugates. *Bioconjugate Chem.* 2, 464–465.
- (34) Zhu, T., Tung, C.-H., Breslauer, K. L., Dickerhof, A. W., and Stein, S. (1993) A general method for preparation of deoxyoligonucleotide with single and double end conjugated to a peptide and physicochemical properties study of the conjugates. *Antisense Res. Dev.* 3, 349–356.
- (35) Hashimoto, H., Nelson, M. G., and Switzer, C. (1993) Zwitterionic DNA. *J. Am. Chem. Soc.* 115, 7128–7134.
- (36) Cantor, C. R., and Warshaw, M. M. (1970) Oligonucleotide interactions. 3. Circular-dichroism studies of conformation of deoxyoligonucleotides. *Biopolymers* 9, 1059–1077.
- (37) Dunn, D. B., and Hall, R. H. (1975) Optical properties of nucleic acids, absorption, and circular dichroism spectra. *Handbook of Biochemistry and Molecular Biology* (G. P. Fasman, Ed.) pp 589, CRC Press, Cleveland, OH.
- (38) Zhu, T., Peng, Y., Lackland, H., and Stein, S. (1993) Confirmation of peptide-oligonucleotide structure by amino acid analysis. *Anal. Biochem.* 214, 585–587.
- (39) Wei, Z., Tung, C.-H., Zhu, T., Dickerhof, W. A., Breslauer, K. J., Georgopoulos, D. E., Leibowitz, M. J., and Stein, S.: Hybridization properties of oligodeoxynucleotide pairs bridged by polyarginine peptides to single-stranded DNA and RNA targets. (Manuscript in preparation).

# Antitumor Combilexin. A Thiazole-Containing Analogue of Netropsin Linked to an Acridine Chromophore

Bertrand Plouvier,<sup>†</sup> Raymond Houssin,<sup>†</sup> Bernard Hecquet,<sup>‡</sup> Pierre Colson,<sup>§</sup> Claude Houssier,<sup>§</sup> Michael J. Waring,<sup>⊥</sup> Jean-Pierre Hénichart,<sup>†,||</sup> and Christian Bailly<sup>\*,⊥,▽</sup>

Institut de Chimie Pharmaceutique, rue Laguesse, 59045 Lille, France, Centre Anticancéreux Oscar Lambret, 59020 Lille, France, Laboratoire de Chimie Macromoléculaire et Chimie Physique, Université de Liège au Sart-Tilman 4000 Liège, Belgium, Department of Pharmacology, University of Cambridge, Tennis Court Road, Cambridge CB2 1QJ, England, UCB Pharmaceuticals, Chemin du Foriest, 1420 Braine-l'Alleud, Belgium, and INSERM U124, Institut de Recherches sur le Cancer, Place de Verdun 59045 Lille, France. Received December 27, 1993\*

We report the synthesis, DNA-binding properties and antitumor activity of ThiaNetGA, a hybrid molecule in which are conjugated a thiazole-lexitropsin and an intercalating anilinoacridine chromophore. This combilexin molecule binds to DNA via a bimodal process involving minor groove binding of the lexitropsin moiety and intercalation of the acridine moiety. The uptake and distribution of the hybrid in L1210 leukemia cells were investigated by ESR spectroscopy using a spin-labeled derivative. The nitroxide-containing conjugate accumulates preferentially in the cell nuclei and rapidly saturates the nuclear receptor sites. Both *in vitro* and *in vivo* assays indicate that the drug is practically nontoxic but exhibits moderate antitumor activity against P388 leukemia cells in mice.

In recent years the concept of synthesizing biconjugates having mixed DNA-binding functionalities has attracted growing interest. The antiviral antibiotics netropsin and distamycin which bind to the minor groove of DNA have served as lead compounds for extensive chemical modifications intended to modulate their sequence selectivity, hopefully to confer higher pharmacological activities. Essentially two different drug design strategies have been undertaken: the first is the lexitropsin approach pioneered by Dickerson (1) and extensively exploited by Lown (2) and others (3) which deals with the replacement of the pyrrole rings of netropsin and distamycin by other heterocycles including imidazole, thiazole, oxazole, pyrazole, and pyridine. The second strategy involves equipping the oligo-*N*-methylpyrrolecarboxamide moiety with a reactive group capable of reacting irreversibly with DNA (4) and/or with an intercalating chromophore (5) intended to confer higher affinity for DNA and to facilitate the penetration and transport of the drug into cells. This latter approach has been actively pursued in our laboratory with the design of so-called combilexin molecules (6). Here we report the synthesis, DNA-binding properties, intracellular distribution, and antitumor activity of a hybrid molecule, ThiaNetGA, in which are conjugated a minor groove-binding thiazole-containing analog of netropsin ThiaNet and an intercalating glycyl-anilino-9-amino-acridine chromophore GA (Figure 1). This bifunctional molecule thus combines features of both the lexitropsin and combilexin approaches.

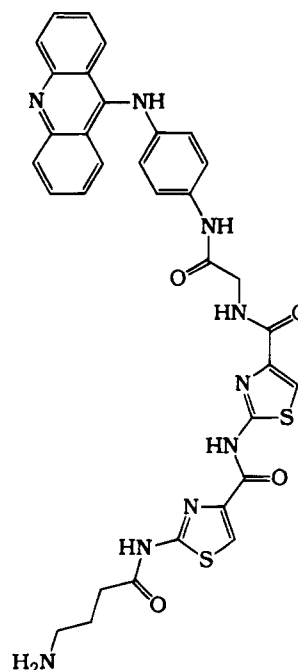


Figure 1. Structure of the hybrid ThiaNetGA.

## EXPERIMENTAL PROCEDURES

The IR spectra were obtained on a Perkin-Elmer 177 spectrophotometer in KBr pellets. <sup>1</sup>H-NMR spectra were recorded on a Bruker AM 400 WB spectrophotometer. Chemical shifts are reported in ppm from tetramethylsilane as an internal standard and are given in  $\delta$  units. FAB mass spectra were determined on a Kratos MS-50 RF mass spectrometer arranged in an EBE geometry. The sample was bombarded using a beam of xenon with a kinetic energy of 7 keV. The mass spectrometer was operated at 8 kV accelerating voltage with a mass resolution of 3000. Glycerol, thioglycerol, or nitrobenzyl alcohol were used as matrices. Thin layer chromatography (TLC) was carried out using Merck 60F-254 silica gel (0.25 mm thick) precoated UV-sensitive plates. Spots

<sup>†</sup> Institut de Chimie Pharmaceutique.

<sup>‡</sup> Centre Oscar Lambret.

<sup>§</sup> Université de Liège.

<sup>⊥</sup> University of Cambridge.

<sup>||</sup> UCB Pharmaceuticals.

<sup>▽</sup> INSERM U124.

\* To whom correspondence should be addressed at INSERM U124. Fax: (33) 20.57.70.83. Present address: Department of Pharmacology, University of Cambridge, Tennis Court Road CB2 1QJ Cambridge, England. Fax: (44) 223 33 40 40.

© Abstract published in *Advance ACS Abstracts*, August 15, 1994.



were visualized by inspection under UV light at 254 nm and after exposure to vaporized I<sub>2</sub> and/or ninhydrin. Kiesegel 60 (230–400 mesh) from Merck was used for column chromatography.

**Synthesis.** To synthesize the hybrid ThiaNetGA, the N-protected [(aminobutyl)amino]bis-thiazolecarboxylic acid moiety (7) was coupled with the anilinoacridine chromophore (8) in the presence of dicyclohexylcarbodiimide and 4-(dimethylamino)pyridine as catalyst. 4-(9-Acridinylamino)-N-[2-[[[2'-(4-aminobutyl)amino]thiazol-4'-ylcarbonyl]amino]thiazol-4-ylcarbonyl]glycylaniline, dihydrobromide (ThiaNetGA): mp 211–213 °C; <sup>1</sup>H-NMR (Me<sub>2</sub>SO-*d*<sub>6</sub>)  $\delta$  1.73 (m, 2H, CH<sub>2</sub>), 2.35 (m, 2H, CH<sub>2</sub>CO), 2.84 (m, 2H, CH<sub>2</sub>NH<sub>3</sub><sup>+</sup>), 4.19 (m, 2H, CH<sub>2</sub>), 7.45–8.00 (m, 15H, 12CHAr, NH<sub>3</sub><sup>+</sup>, 8.21 (m, 2H, NH), 7.92, 8.31 (2s, 2H, 2CHThz), 10.45 (s, 1H, CONH), 12.00 (s, 1H, CONH), 12.51 (s, 1H, CONH), 14.02 (s, 1H, NH<sup>+</sup>); MS (FAB<sup>+</sup>) 680 (M<sup>+</sup> + 1). Anal. Calcd for C<sub>33</sub>H<sub>31</sub>Br<sub>2</sub>N<sub>9</sub>O<sub>4</sub>S<sub>2</sub>: C, 47.10; H, 3.71; N, 14.98. Found: C, 47.35; H, 3.60; N, 14.95.

**Drugs.** Netropsin was purchased from Serva (Heidelberg, Germany). Hoechst 33258 and ethidium bromide were purchased from Sigma Chemical Co. Fluorouracil was purchased from Laboratories Roche (France). Amsacrine (m-AMSA) was obtained by a modification of the original procedure (8). The syntheses of compounds GA, ThiaNet, and NetGA together with complete spectral characterization has been described previously (7–9). Drug concentrations were determined spectroscopically in 10 mm pathlength quartz cuvettes using the following molar extinction coefficients (in M<sup>-1</sup> cm<sup>-1</sup>): 21 500 for netropsin at 296 nm; 12 000 for amsacrine at 434 nm; 6300 for ethidium bromide at 480 nm; 42 000 for Hoechst 33 258 at 338 nm; and 10 900 for ThiaNetGA at 440 nm. All other chemicals were analytical grade reagents, and solutions were prepared with doubly distilled water.

**DNA and Restriction Fragments.** Calf thymus (CT) DNA (highly polymerized sodium salt) was purchased from Sigma Chemical Co., deproteinized twice with sodium dodecyl sulfate (SDS), and precipitated with ethanol. DNA concentrations were determined applying a molar extinction coefficient of 6600 M<sup>-1</sup> cm<sup>-1</sup> at 260 nm. The restriction fragments used in the footprinting experiments were prepared as follows: the 160 base pair *tyr T* DNA was obtained by digestion of the plasmid pKMA-98 (10) with *Eco*RI and *Ava*I; the 117-mer and 265-mer fragments were obtained by digestion of the plasmid pBS (Stratagene, La Jolla, CA) with *Eco*RI and *Pvu*II. All three DNA fragments were 3'-[<sup>32</sup>P]-end labeled using  $\alpha$ -[<sup>32</sup>P]-dATP (6000 Ci/mmol, New England Nuclear) and AMV reverse transcriptase (Pharmacia). The digestion products were separated on a 6% polyacrylamide gel under native conditions. After autoradiography, the band containing DNA was excised, crushed, and soaked in elution buffer (500 mM ammonium acetate, 10 mM magnesium acetate) overnight at 37 °C. This suspension was filtered through a Millipore 0.22  $\mu$ m filter, and the DNA was precipitated with ethanol. Following washing with 70% ethanol and vacuum drying of the precipitate, the labeled DNA was resuspended in 10 mM Tris adjusted to pH 7.0 containing 10 mM NaCl.

**Fluorescence measurements** were carried out on a Jobin-Yvon J-Y-3 spectrofluorimeter. All measurements were made using a 10 mm lightpath cuvette in a 0.01 M ionic strength buffer (9.3 mM NaCl, 2 mM Na acetate, 0.1 mM EDTA) using 20  $\mu$ M DNA and 2  $\mu$ M ethidium bromide or Hoechst 33258 (11). The DNA–ethidium complex was excited at 546 nm and the fluorescence measured at 595 nm. For Hoechst 33258, excitation was at 353 nm and fluorescence was measured at 465 nm.

**Electric Linear Dichroism (ELD).** This electro-

optical method exploits the fact that, under the influence of a short electric field pulse, the DNA molecules become oriented, rendering the solution optically anisotropic. Measurements were carried out as previously described (12). The optical set-up consisting of a high sensitivity T-jump spectrometer equipped with a Glan polarizer was used under the following conditions: bandwidth 3 nm, sensitivity limit 0.001 in  $\Delta A/A$ , response time 3  $\mu$ s. Electric field pulses in the range 0–13 kV/cm were applied to the samples in a 10 mm optical pathlength Kerr cell with a distance between the platinum electrodes of 1.5 mm. The pulse duration was carefully adjusted to reach the steady-state orientation of the molecule (50–100  $\mu$ s, depending on the electric field strength) without degrading or denaturing it. Sample heating under the electric pulses was negligible. Linear dichroism  $\Delta A$  is defined as the difference between the absorbance for light polarized parallel ( $A_{||}$ ) and perpendicular ( $A_{\perp}$ ) to the applied field at a given wavelength. The reduced dichroism is  $\Delta A/A = (A_{||} - A_{\perp})/A$ , where  $A$  is the isotropic absorbance of the sample measured in the absence of field at the same wavelength and with the same pathlength. Because of axial symmetry around the electric field direction, the changes in absorbance  $\Delta A_{||} = A_{||} - A$  and  $\Delta A_{\perp} = A_{\perp} - A$  are related by  $\Delta A_{||} = 2\Delta A_{\perp}$ ; thus, measurement of  $\Delta A_{||}$  or  $\Delta A_{\perp}$  or  $\Delta A_{||}$  alone suffices for the calculation of the reduced dichroism  $\Delta A/A$ .  $\Delta A_{||}$  was chosen for its higher sensitivity. When DNA solutions are exposed to the electric field pulses, the absorbance of 260 nm light polarized parallel to the electric field vector is lower than the absorbance of light polarized perpendicularly ( $A_{||} < A_{\perp}$ ), indicative of a negative dichroism. Similar negative signals are observed with intercalator–DNA complexes in the absorption band of the ligand. In contrast, when rectangular electric pulses are applied to a solution of a minor groove ligand bound to DNA, the change of the absorption of light in the ligand absorption band is different ( $A_{||} > A_{\perp}$ ) indicative of a positive dichroism of the complex. Therefore, on the basis of the sign and the amplitude of the observed signals, this technique can reveal the binding mode of the ligand via an estimation of its orientation with respect to the helical axis. All experiments were conducted in 1 mM sodium cacodylate buffer adjusted to pH 6.5, at room temperature (20 °C). The conductivity of all the solutions was measured directly in the electro-optical cell with Metrohm conductimeter Model E527 and never exceeded 2 mS.

**DNAase I Footprinting and Electrophoresis.** Cleavage reactions (total volume 10  $\mu$ L) catalyzed by DNAase I were performed essentially according to the original protocols (13). Samples (3  $\mu$ L) of the labeled DNA fragment were incubated with 5  $\mu$ L of the buffer solution containing the desired drug concentration. After 30–60 min incubation at 37 °C to ensure equilibration of the binding reaction, the digestion was initiated by the addition of 2  $\mu$ L of the endonuclease solution whose concentration was adjusted to limit the digestion to less than 30% of the starting material so as to minimize the incidence of multiple cuts in any strand (“single-hit” kinetic conditions). Optimal enzyme dilutions were established in preliminary calibration experiments. Typically, DNAase I experiments included 0.01 unit/mL of enzyme, 20 mM NaCl, 2 mM MgCl<sub>2</sub>, 2 mM MnCl<sub>2</sub>, pH 7.3. At the end of the reaction time (routinely 3 min at room temperature), the digestion was stopped by freeze-drying. After lyophilization the sample was washed once with deionized water and then lyophilized again prior to resuspending in 3  $\mu$ L of an 80% formamide solution containing tracking dyes (0.1% bromophenol blue–xylene

cyanol purchased from Sigma). Samples were generally electrophoresed immediately, but they can be stored (at 4 °C for about 24 h) prior to resuspending in the dye solution. Samples were heated to 90 °C for 4 min and then chilled in an ice-bath just before being loaded on to a sequencing gel capable of resolving DNA fragments differing in length by one nucleotide. The chemical identities of the digestion products were assigned by coelectrophoresis of dimethyl sulfate/piperidine G markers. Cleavage products were separated on 0.3 mm thick, 8% (w/v) polyacrylamide gels containing 8 M urea. After 2 h electrophoresis in TBE buffer (89 mM Tris base, 89 mM Boric acid, 2.5 mM Na<sub>2</sub> EDTA, pH 8.3) at 60 W, the gels were soaked in 10% acetic acid for 15 min, transferred to Whatman 3MM paper, dried under vacuum at 80 °C, and subjected to autoradiography at -70 °C.

**Spin-Labeling, Cell Fractionation, and Electron Spin Resonance (ESR).** The spin-labeled derivative SL-ThiaNetGA was synthesized by coupling the nitroxide moiety with the hybrid ThiaNetGA. A solution of 3-carboxy-2,2,5,5-tetramethyl-1-pyrrolidinyloxy (3-carboxy-PROXYL, Aldrich) (10 mg; 0.054 mmol) in dimethylformamide was mixed with solutions of dicyclohexyl carbodiimide (12 mg, 0.058 mmol) and hydroxybenzotriazole (9 mg, 0.058 mmol) in dimethylformamide/CH<sub>2</sub>Cl<sub>2</sub> (1:1, v:v, 5 mL). The reaction mixture was stirred for 2 h at 0 °C to form the HOBt-activated ester of the spin-label derivative. The hybrid ThiaNetGA (45 mg, 0.054 mmole) was dissolved in dimethylformamide (10 mL) in the presence of triethylamine (15  $\mu$ L, 0.108 mmole) and then added directly to the reaction vessel, and stirring was continued for 2 h in ice. The reaction, followed by TLC, was allowed to take place for 12 h at room temperature. The organic solvents were evaporated to dryness, and the spin-label conjugate SL-ThiaNetGA was purified by flash chromatography using MeOH/CHCl<sub>3</sub> (20:80, v:v) as eluent (*R<sub>f</sub>*: 0.41). 4-(9-Acridinylamino)-N-[2-[[2'-[[4-[(2,2,5,5-tetramethyl-1-pyrrolidinyloxy)-3-carbonyl]amino]butyryl]-amino]thiazol-4'-ylcarbonyl]amino]thiazol-4-ylcarbonyl]glycylaniline, dihydrobromide (30 mg, 65% yield): mp > 250 °C; MS (FAB<sup>+</sup>) 849 (M<sup>+</sup> + 2).

SL-ThiaNetGA was added to 50 mL cell cultures at a final concentration of 25  $\mu$ M for various incubation times. At intervals, cells were collected by low-speed centrifugation, and the pellet was washed twice with 30 mL of NaCl solution (9 g/L). Cell disruption was effected with a Dounce homogenizer. Cell fractionations were performed as previously described (14). The purity of the nuclear and cytoplasmic fractions was assessed by both morphological examination under an electron microscope and by appropriate marker enzyme activities: 5'-nucleotidase, glucose-6-phosphatase, and catalase markers, respectively, for the plasma membrane, endoplasmic reticulum, and peroxisomes-lysosomes. ESR measurements were recorded on a Varian E109 X-band spectrometer with an E238 cavity operating in the TM110 mode. A 100 KHz high frequency modulation was used with 20 mW microwave power. The samples were examined in a flat quartz cell.

**Cell Cultures and Growth Inhibition.** L1210 Leukemia cells were grown in suspension culture in RPMI 1640 medium supplemented with 10% fetal calf serum (v:v) in a humidified atmosphere of 5% carbon dioxide in air at 37 °C. Fresh aliquots, stored in liquid nitrogen, of cells were frequently thawed. Cultures used to assess drug effects were in exponential growth (doubling time 15–18 h). The drug at the appropriate concentration was added to cell cultures (5 mL) for 4 days without renewal of the medium. Every day, the cells were diluted with

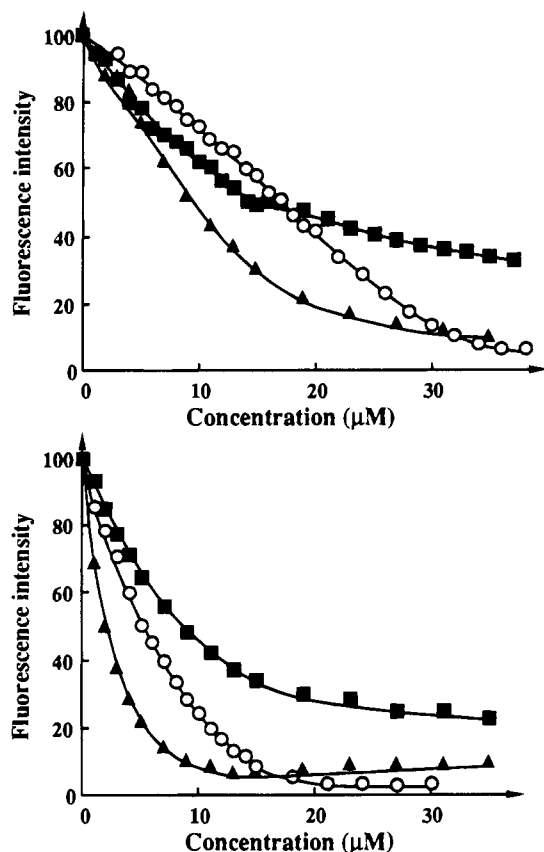
trypan blue and counted. Assays were carried out in triplicate and the results averaged.

**Toxicity Studies and Antitumor Activity.** Toxicity studies were performed in healthy female Swiss mice (median weight: 30 g, range 28–31 g). The drug was administered ip in 0.4 mL of sterile physiological saline. The drug was tested by daily administration (25 mg/kg/day) from day 1 to day 5. Toxicity was evaluated both by the evolution of animal weights and by 30 day survival. Antitumor activity was evaluated in P388-bearing DBA/2 female mice (Charles River, France) (median weight: 24 g, range 23–25g). Mice were housed six per cage, with free access to food and water. Inoculum consisted of 0.1 mL of diluted (sterile physiological saline) ascitic fluid containing 10<sup>6</sup> leukemic cells drawn from a leukemic mouse. The day of ip tumor inoculation was designated as day 0. The drug was administered ip (25 mg/kg/day) in 0.2 mL of sterile physiological saline from day 1 to day 5. Untreated controls and positive controls were performed by ip administration of sterile physiological saline (0.2 mL, day 1 to day 5) and 5-fluorouracil (20 mg/kg/day) in 0.4 mL, day 1 to day 5, respectively. Median and range of survival time were reported for each group. Antitumor activity was evaluated by calculating  $T/C\% = (\text{test group median survival time}/\text{control median}) \cdot 100$ . Comparison between groups was performed using the nonparametric Mann–Whitney U-test.

## RESULTS AND DISCUSSION

**Interaction with DNA.** Upon binding to DNA, the absorption spectrum of the ligand underwent a hypochromic shift in the 250–280 nm band and also in the acridine band centered at 430 nm, together with a 3–5 nm red shift in the latter band which is indicative of an increased delocalization of the  $\pi$ -electrons in the ligand as a consequence of its interaction with the double helix. No isosbestic point was observed upon titration of the drug with DNA suggesting that different types of binding sites exist. We sought for means to verify that both parts of the combilexin molecule are involved in the binding to DNA. It is known that netropsin and its thiazole analogue diminish the fluorescence of Hoechst 33258 bound to DNA complex which thus can serve to probe for minor groove binding. It is also known that amsacrine competes with ethidium for binding to DNA which can serve accordingly as a probe for intercalative binding. On this basis we examined the ability of the combilexin to affect the fluorescence of these two probes. Figure 2 shows typical fluorescence quenching curves obtained under high DNA–low fluorophore conditions (11) for the hybrid and each of its constituents. The conjugate strongly reduces the fluorescence of both Hoechst 33258 and ethidium bound to DNA, consistent with the belief that each part of the hybrid does indeed participate in the binding reaction.

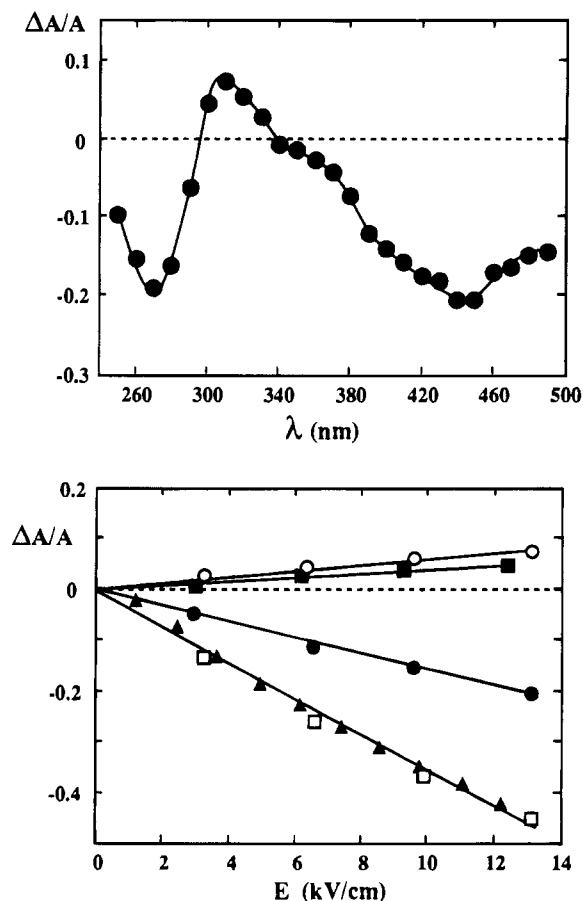
Further evidence that both linked functionalities of the hybrid are engaged in the binding reaction comes from electric linear dichroism experiments. This electro-optical method has proved most useful as a means of determining the orientation of drugs bound to DNA and has the additional advantage that it senses only the orientation of the polymer-bound ligand: free ligand is isotropic and does not contribute to the signal (12). Figure 3 reports the wavelength and the field-strength dependence of the reduced dichroism  $\Delta A/A$  for the ThiaNetGA–DNA complex. Such an ELD spectrum is characteristic of a bimodal binding process, with the 380–490 nm negative band due exclusively to the acridine moiety of the hybrid and the 300–330 nm positive band due to the bis-thiazole moiety, with a minor contribution



**Figure 2.** Percent quenching of fluorescence intensity of (top) ethidium- and (bottom) Hoechst 33258-DNA complexes by the hybrid ThiaNetGA (○) compared to its constituents ThiaNet (■), and the anilinoacridine derivative GA (▲). Experimental conditions: 20  $\mu$ M calf thymus DNA, 2  $\mu$ M ethidium bromide ( $\lambda_{\text{exc}} = 546$  nm,  $\lambda_{\text{em}} = 595$  nm) or 2  $\mu$ M Hoechst 33258 ( $\lambda_{\text{exc}} = 353$  nm,  $\lambda_{\text{em}} = 465$  nm) in 0.01 M ionic strength buffer (9.3 mM NaCl, 2 mM Na acetate, 0.1 mM EDTA) (8).

from the anilinoacridine moiety. The field strength dependence at 310 nm is identical for the hybrid ThiaNetGA and its parent compound ThiaNet. This implies that the acridine portion of the conjugate does not impede minor groove binding of the attached bis-thiazole unit. By contrast, the reduced dichroism measured at 440 nm with the hybrid is much lower than that obtained with the anilino-9-aminoacridine compound. The reduced dichroism of the DNA bases at 260 nm in the absence of ligand was found to be  $-0.45$  (at 13 kV/cm). The value for the compound GA bound to DNA ( $\Delta A/A = -0.43$  at 430 nm and under the same electric field) is nearly the same as that of the DNA bases indicating that the transition moment, located in the plane of the acridine chromophore, lies parallel to the plane of the DNA base pairs, as expected for an intercalating agent. For the hybrid, the maximum ELD value at 430 nm was found to be  $-0.2$  which corresponds to an orientation inclined at about  $65^\circ$  to the helix axis.<sup>1</sup> A similar tilt of the acridine ring with respect to the plane of the base pairs was noticed previously with a netropsin-acridine hybrid (15). Thus, the ELD experiments reveal that the hybrid molecule interacts with DNA in a geometrically well-defined fashion, placing its thiazole-

<sup>1</sup> The angle is estimated from a comparison of the reduced dichroism at 13 kV/cm for the DNA bases and for the hybrid in their respective absorption bands, assuming a theoretical angle of  $90^\circ$  for the DNA bases with respect to the orientation axis of the particles. The angle is  $62^\circ$  assuming an experimental angle of  $72^\circ$  for the DNA bases. Details in ref 12a.



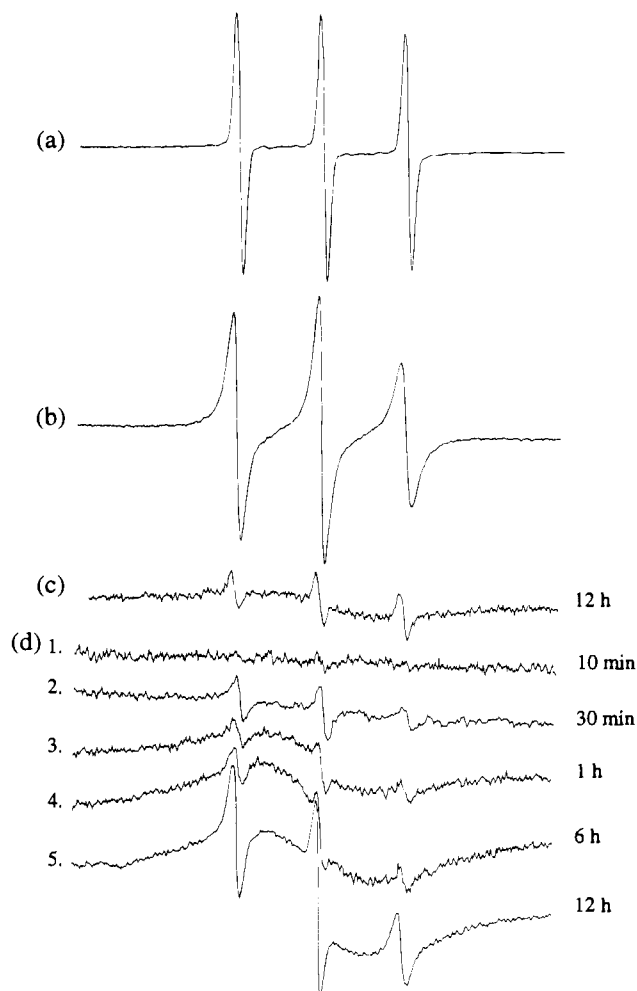
**Figure 3.** (Top) electric linear dichroism spectrum of the ThiaNetGA-DNA complex at 13 kV/cm. (Bottom) electric field dependence of the reduced dichroism ( $\Delta A/A$ ) measured for calf thymus DNA alone at 260 nm (□) compared to that of its complex with ThiaNetGA at 440 nm (●) and 310 nm (○) or with ThiaNet at 310 nm (■) or compound GA at 440 nm (△). Experimental conditions: drug-DNA ratio of 0.1; 1 mM Na cacodylate buffer, pH 6.5.

containing netropsin moiety in the minor groove and with the acridine chromophore oriented at an angle consistent with its insertion into a distorted DNA structure. Indeed, in the crystal structure of the anilinoacridine chromophore the plane of the anilino group is oriented at about  $70^\circ$  to the plane of the acridine ring (16), so when the ThiaNet moiety of the hybrid is lodged within the minor groove full intercalation of the acridine ring could well be precluded on steric grounds. The short size of the glycol linker between the two moieties of the conjugate may also serve to constrain the acridine ring to intercalate only partially between the DNA base pairs, leaving a part of the tricyclic nucleus outside the DNA helix. This model in which the acridine ring partially protrudes outside the intercalation site would account satisfactorily for the linear dichroism measurements, and was predicted in a molecular modeling analysis of the complex between DNA and the netropsin-acridine hybrid which bears exactly the same anilinoacridine moiety (15). Moreover, studies on the DNA binding properties of a distamycin-ellipticine hybrid (17) have revealed that in this case also the ellipticine chromophore is associated with significant bending of the helix at the intercalation site such that the ellipticine ends up inclined at about  $65^\circ$  with respect to the macromolecular axis.<sup>2</sup>

Attempts were made to determine if the combilexin molecule might bind to specific sequences in DNA. The thiazole lexitropsin ThiaNet is known to be capable of selectively recognizing alternating purine-pyrimidine

sequences containing both A·T and G·C base pairs (19). Two different footprinting methodologies, using DNAase I and MPE-Fe<sup>II</sup> as DNA cleaving agents, and three DNA fragments of varied composition (117 and 265 base pair fragments from plasmid pBS and the 160 base-pair *tyr* T DNA fragment containing the tyrosine tRNA promoter) were tested but in all cases the hybrid failed to inhibit the cleavage of DNA in such a manner as to yield identifiable footprints. Thus, the sequence preferences (if any) associated with binding of the hybrid combilexin to DNA cannot readily be determined by these means, in common with the antitumor-active parent compound amsacrine and other anilinoacridines (20).

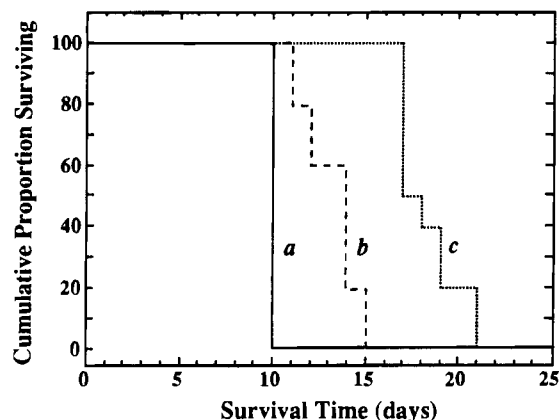
**Cellular Distribution.** DNA may be expected to serve as a critical target for the biological actions of the hybrid providing that the drug can effectively reach the genome in the cell nuclei. It is worth mentioning that netropsin exhibits no antitumor properties but its toxicity is increased by a factor of 200 when the cell membrane is permeabilized; it then becomes as toxic as the clinically used anticancer drug actinomycin (21). Netropsin penetrates slowly into cells (22) and that surely constitutes a limiting factor which prevents the antibiotic exerting its potential cytotoxicity. Given the expected relationship between the ability of the drug to penetrate into cells and its probable efficacy we chose to study the uptake and cellular distribution of the conjugate by electron spin resonance (ESR) spectroscopy using a spin-labeled derivative of the hybrid, SL-ThiaNetGA, which can easily be detected within cells. The ESR spectrum of a nitroxide spin-label reflects its rotational motion, and the constraints upon that motion produced by the immediate environment are readily discernible. Figure 4 shows a series of ESR spectra of the spin-labeled hybrid in different environments. The ESR spectrum of the free drug in solution is isotropic ( $a_N = 15$  G) and results from the anisotropic hyperfine interaction between the unpaired electron and the nuclear spin of the nitrogen atom. In the presence of a large excess of purified calf thymus DNA, the ESR spectrum remains essentially isotropic indicating that the trailing nitroxide attached at the very end of the aminobutrylamino side chain is still free to rotate when the drug is bound to DNA. However, the broadening of the bands and the significant decrease in the intensity of the low field band attest to a certain degree of restricted motion of the spin label. Such a spectrum is consistent with location of the spin label group in the minor groove, which is expected to reduce but not block the rotation of the paramagnetic nitroxide. For the spectra shown in Figure 4c and d SL-ThiaNetGA was incubated with L1210 leukemia cells for various lengths of time. At intervals cells were collected and fractionated, and the ESR spectra of the drug-containing cytoplasmic and nuclear fractions were recorded. Appropriate controls were performed to verify negligible redistribution of spin-labeled drug during the separation process (14a). The spectra of the cytoplasmic fractions always consisted of a triplet of weak intensity even after 12 h incubation (Figure 4c). This indicates that the drug penetrates into cells but does not accumulate in the cytoplasm. The ESR spectra of the nuclear fraction obtained after 1–12 h of incubation with the drug are characteristic of the presence of two different species: (i) unrestricted molecules which give rise to a triplet as



**Figure 4.** ESR spectra of (a) SL-ThiaNetGA in solution, (b) SL-ThiaNetGA-DNA complex at a calf thymus DNA/drug ratio of 120, (c) the cytoplasmic fraction, and (d) the nuclear fraction of L1210 leukemia cells incubated with the spin-labeled drug. Incubation times are indicated. Instrumental conditions: field set 3375 G; scan range 100 G; time constant 0.25 s; modulation amplitude 8 G; modulation frequency 100 KHz; microwave power 10 mW; microwave frequency 9.44 GHz; receiver gain (a)  $4 \times 10^3$ , (b)  $1 \times 10^4$ , (c)  $4 \times 10^4$ , (d) (spectra 1–4)  $4 \times 10^4$ , (spectrum 5)  $2.5 \times 10^4$ .

observed for the cytoplasmic fractions and (ii) completely immobilized molecules characterized by a powder-type spectrum. Such a broad ESR signal reflects spin-spin interactions due to the close proximity of clustered spin-labeled molecules. The drug molecules must either condense to form intranuclear aggregates or be closely stacked in association with some kind of macromolecular support such as a membrane or part of the cytoskeleton. In view of the isotropic spectrum obtained for the drug-DNA complex, it is unlikely that the powder-type spectrum simply reflects the formation of drug-chromatin complexes. The penetration of the drug into L1210 cells is fast since an anisotropic spectrum is obtained after only 1 h of incubation. By comparison with previous studies, the kinetics of penetration and nuclear translocation of SL-ThiaNetGA are much faster than found for netropsin (22) and comparable to the rates observed with the netropsin-acridine hybrid (23). These data reinforce the view that the acridine chromophore serves as a powerful vector to carry the minor groove binding entity to the nuclear receptor sites (6). An effect of this sort has been well characterized with oligonucleotide-acridine conjugates (24).

<sup>2</sup> Despite the commonly held view that the base pairs are essentially orthogonal to the helical axis of B-form DNA, linear dichroism measurements have shown that the bases in natural DNAs do not lie perpendicular to the helix axis, not even in the B-form. The angles of base inclination vary from 16° to 25° (18).



**Figure 5.** Antitumor effect *in vivo* of (b) ThiaNetGA at 25 mg/kg/day ( $N = 6$ ) compared to (c) 5-fluorouracil at 20 mg/kg/day ( $N = 6$ ), relative to (a) untreated animals ( $N = 6$ ). DBA/2 female mice were inoculated ip with 0.1 mL of diluted ascitic fluid containing  $10^6$  P388 leukemic cells (day 0). The drug was administered ip from day 1 to day 5. Median and range of survival times were recorded for each group. Comparison between groups was performed using the nonparametric Mann-Whitney U-test.

**Antitumor Activity.** L1210 leukemia cells were also used to evaluate the cytotoxic properties of the hybrid *in vitro*. Under the conditions used, an  $IC_{50}$  value of 10  $\mu M$  was measured for ThiaNetGA while, under the same conditions, values of 0.5 and 2.5  $\mu M$  were obtained for amsacrine and compound GA, respectively. The thiazole-containing netropsin ligand ThiaNet was totally inactive ( $IC_{50} > 100 \mu M$ ). The hybrid is thus weakly toxic for L1210 leukemia cells. To screen the antitumor potency of the hybrid drug *in vivo* P388 leukemia cells were inoculated intraperitoneally into DBA/2 mice and grown. The sensitivity of the leukemia to the hybrid can be seen in Figure 5. At 25 mg/kg/day of ThiaNetGA, a noticeable increase in life span was observed, expressed by a % T/C (test group median survival time/control median) of 140. The hybrid exhibits improved antitumor activities over the netropsin-acridine hybrid NetGA ( $T/C = 132$ , (15b)) although it still falls short of what can be achieved with amsacrine in a comparable assay ( $T/C = 178$  at 8.9 mg/kg/dose (25)). However, it is very important to emphasize that the hybrid drug is safe since it has not revealed any type of toxicity to healthy mice (at the same dose and by the same ip route). Thus, in respect to its activities *in vivo* the ThiaNetGA hybrid successfully combines the desired properties of its parent compounds without their major defects, *viz.* the antitumor activity of the acridine moiety (the ThiaNet compound has none) plus the low toxicity of the thiazole lexitropsin (as opposed to the toxicity of the acridine compound GA toward mice which has precluded assessment of its potential antitumor activity).

## CONCLUSION

The combilexin molecule ThiaNetGA clearly exhibits potentially useful antileukemic properties *in vivo*. It is likely that the capacity of the hybrid to bind to DNA and perhaps to some other constituents of the nucleus contributes significantly to its biological properties. Other targets such as topoisomerases may well be involved in the whole mechanism of action of the drug. On the basis on these data, further hybrid molecules are now being synthesized with the aim of finding congeners endowed with superior antitumor properties but remaining as nontoxic as the conjugate reported here. Evaluation of their therapeutic potential will demand consideration of

both range of activity and cytotoxicity for each tested compound. These first combilexin results reported here encourage us to believe that this new approach to DNA-targeted pharmacology has the potential to yield important developments in the search for new and better anticancer drugs.

## ACKNOWLEDGMENT

This work was supported by grants from the INSERM and the ARC (France), the CFB and the FNRS (Belgium), the Cancer Research Campaign (U.K.), and the Association for International Cancer Research.

## LITERATURE CITED

- (1) (a) Goodsell, D., and Dickerson, R. E. (1986) Isohelical analysis of groove-binding drugs. *J. Med. Chem.* 29, 727–733. (b) Kopka, M. L., and Larsen, T. A. (1992) Netropsin and the lexitropsins. The search for sequence-specific minor-groove-binding ligands. In *Nucleic Acid Targeted Drug Design* (C. L. Propst and T. J. Perun, Eds.), pp 303–374, Marcel Dekker, Inc., New York.
- (2) (a) Lown, J. W. (1988) *Lexitropsins*: rational design of DNA sequence reading agents as novel anti-cancer agents and potential cellular probes. *Anti-Cancer Drug Design* 3, 25–40. (b) Lown, J. W. (1993) Design of sequence-specific agents: lexitropsins. *Molecular Aspects of Anticancer Drug-DNA Interactions* (S. Neidle and M. J. Waring, Eds.), Vol. 2, pp 322–355, Macmillan, London.
- (3) (a) Dervan, P. B. (1986) Design of sequence-specific DNA-binding molecules. *Science* 232, 464–471. (b) Zakrzewska, K., and Pullman, B. (1988) Theoretical study of the sequence selectivity of isoxetins, isohelical DNA groove binding ligands. Proposal for GC minor groove specific compounds. *J. Biomol. Struct. Dyn.* 5, 1043–1058. (c) Lee, H. H., Boyd, M., Gravatt, G. L., and Denny, W. A. (1991) Pyrazole analogues of the bispyrrolecarboxamide anti-tumor antibiotics: synthesis, DNA binding and anti-tumor properties. *Anti-Cancer Drug Design* 6, 501–517. (d) Mrksich, M., Wade, W. S., Dwyer, T. J., Geierstanger, B. H., Wemmer, D. E., and Dervan, P. B. (1992) Antiparallel side-by-side dimeric motif for sequence-specific recognition in the minor groove of DNA by the designed peptide 1-methylimidazole-2-carboxamide netropsin. *Proc. Natl. Acad. Sci. U.S.A.* 89, 7586–7590. (e) Wade, W. S., Mrksich, M., and Dervan, P. B. (1992) Design of peptides that bind in the minor groove of DNA at 5'-(A,T)G(A,T)C(A,T)-3' sequences by a dimeric side-by-side motif. *J. Am. Chem. Soc.* 114, 8783–8794.
- (4) (a) Baker, B. F., and Dervan, P. B. (1985) Sequence-specific cleavage of double-helical DNA. N-bromoacetyldistamycin. *J. Am. Chem. Soc.* 107, 8366–8368. (b) Krowicki, K., Balzarini, J., De Clercq, E., Newman, R. A., and Lown, J. W. (1988) Novel DNA groove binding alkylators: design, synthesis, and biological evaluation. *J. Med. Chem.* 31, 341–345. (c) Church, K. M., Wurdeman, R. L., Zhang, Y., and Gold, B. (1990) N-(2-chloroethyl)-N-nitrosoureas bound to nonionic and monocationic lexitropsin dipeptides. Synthesis, DNA affinity binding characteristics, and reactions with  $^{32}P$ -end-labeled DNA. *Biochemistry* 29, 6827–6838. (d) Otsuka, M., Masuda, T., Haupt, A., Ohno, M., Shiraki, T., Sugiura, Y., and Maeda, K. (1990) Man-designed bleomycin with altered sequence specificity in DNA cleavage. *J. Am. Chem. Soc.* 112, 838–845. (e) Broggini, M., Erba, E., Ponti, M., Ballinari, D., Geroni, C., Spreafico, F., and D'Incalci, M. (1991) Selective DNA interaction of the novel distamycin derivative FCE 24517. *Cancer Res.* 51, 199–204. (f) Nicolaou, K. C., and Dai, W.-M. (1991) Chemistry and biology of the enediyne anticancer antibiotics. *Angew. Chem., Int. Ed. Engl.* 30, 1387–1416. (g) Zhang, Y., Chen, F.-X., Mehta, P., and Gold, B. (1993) Groove- and sequence-selective alkylation of DNA by sulfonate esters tethered to lexitropsins. *Biochemistry* 32, 7954–7965. (h) He, G.-X., Browne, K. A., Groppe, J. C., Blaskò, A., Mei, H.-Y., and Bruice, T. C. (1993) Microgonotropens and their interactions with DNA. I. Synthesis of the tripyrrole peptides dien-microgonotropen-a, -b, and -c and characterization of their interactions with dsDNA.

- J. Am. Chem. Soc.* **115**, 7061–7071. (i) Grokhovskii, S. L., Nikolaev, V. A., Zubarev, V. E., Surovaya, A. N., Zhuze, A. L., Chernov, B. K., Sidorova, N. Y., Zasedatelev, A. S., and Gurskii, G. V. (1993) Specific DNA cleavage by a netropsin analog containing a copper(II)-chelating peptide Gly-Gly-His. *Molecular Biol.* **6**, 839–855. (j) Tokuda, M., Fujiwara, K., Gomibuchi, T., Hiramata, M., Uesugi, M., and Sugiyura, Y. (1993) Synthesis of a hybrid molecule containing neocarzinostatin chromophore analogue and minor groove binder. *Tetrahedron Lett.* **34**, 669–672.
- (5) (a) Eliadis, A., Phillips, D. R., Reiss, J. A., and Skorobogaty, A. (1988) The synthesis and DNA footprinting of acridine-linked netropsin and distamycin bifunctional mixed ligands. *J. Chem. Soc., Chem. Commun.* 1049–1052. (b) Subra, F., Carreau, S., Pager, J., Paoletti, J., Paoletti, C., Auclair, C., Mrani, D., Gosselin, G., and Imbach, J. L. (1991) Bis-(pyrrolicarboxamide) linked to intercalating chromophore oxazopyridocarbazole (OPC): selective binding to DNA and polynucleotides. *Biochemistry* **30**, 1642–1650.
- (6) (a) Bailly, C., and Hénichart, J. P. (1991) DNA recognition by intercalator-minor groove binder hybrid molecules. *Bioconjugate Chem.* **2**, 379–393. (b) Bailly, C., and Hénichart, J. P. (1994) Molecular Pharmacology of intercalator-minor groove binder hybrid molecules. *Molecular Aspects of Anti-cancer Drug-DNA Interactions* (S. Neidle and M. J. Waring, Eds.), Vol. 2, pp 162–196, Macmillan, London.
- (7) (a) Plouvier, B., Bailly, C., Houssin, R., and Hénichart, J. P. (1989) Synthesis and DNA-binding study of a thiazole-containing analog of netropsin. *J. Heterocycl. Chem.* **26**, 1643–1647. (b) Plouvier, B., Bailly, C., Houssin, R., and Hénichart, J. P. (1991) Synthesis of two new thiazole-containing oligopeptides as potential DNA minor groove binding analogs of netropsin. *Heterocycles* **32**, 693–701.
- (8) Hénichart, J. P., Bernier, J. L., and Catteau, J. P. (1982) Interaction of 4'-(9-acridinylamino)aniline and derivatives with DA. Influence of a lysyl glycyl side chain on the binding parameters. *Hoppe Seyler's Z. Physiol. Chem.* **363**, 835–841.
- (9) Bailly, C., Pommery, N., Houssin, R., and Hénichart, J. P. (1989) Design, synthesis, DNA-binding and biological activity of a series of DNA minor groove binding intercalating drugs. *J. Pharm. Sci.* **78**, 910–917.
- (10) Lamond, A. I., and Travers, A. A. (1983) Requirement for an upstream element for optimal transcription of a bacterial tRNA gene. *Nature* **305**, 248–250.
- (11) Baguley, B. C., Denny, W. A., Atwell, G. J., and Cain, B. F. (1981) Potential antitumor agent. 34. Quantitative relationships between DNA binding and molecular structure for 9-anilino-acridines substituted in the anilino ring. *J. Med. Chem.* **24**, 170–177.
- (12) (a) Houssier, C. (1981) Investigating nucleic acids, nucleoproteins, polynucleotides, and their interactions with small ligands by electro-optical systems. *Molecular Electro-Optics* (S. Krause, Ed.) pp 363–398, Plenum Publishing Corporation, New York. (b) Bailly, C., Hénichart, J. P., Colson, P., and Houssier, C. (1992) Drug-DNA sequence-dependent interactions analysed by electric linear dichroism. *J. Mol. Recognit.* **5**, 155–171.
- (13) Low, C. M. L., Drew, H. R., and Waring, M. J. (1984) Sequence-specific binding of echinomycin to DNA: evidence for conformational changes affecting flanking sequences. *Nucleic Acids Res.* **12**, 4865–4877.
- (14) (a) Lemay, P., Bernier, J. L., Hénichart, J. P., and Catteau, J. P. (1983) Subcellular distribution of a nitroxide spin-labeled 9-aminoacridine in living KB cells. *Biochem. Biophys. Res. Commun.* **111**, 1074–1081. (b) Bailly, C., Beauvillain, J. C., Bernier, J. L., and Hénichart, J. P. (1990) Plasma membrane perturbations of KB<sub>3</sub> cells induced by the bleomycin-iron complex. *Cancer Res.* **50**, 385–392.
- (15) (a) Bailly, C., Helbecque, N., Hénichart, J. P., Colson, P., Houssier, C., Rao, K. E., Shea, R. G., and Lown, J. W. (1990) Molecular recognition between oligopeptides and nucleic acids. DNA sequence specificity and binding properties of an acridine-linked netropsin hybrid ligand. *J. Mol. Recognit.* **3**, 26–35. (b) Bailly, C., Collyn-d'Hooghe, M., Lantoine, D., Fournier, C., Hecquet, B., Fosse, P., Saucier, J. M., Colson, P., Houssier, C., and Hénichart, J. P. (1992) Biological activity and molecular interaction of a netropsin-acridine hybrid ligand with chromatin and topoisomerase II. *Biochem. Pharmacol.* **43**, 457–466. (c) Bailly, C., Sun, J. S., Colson, P., Houssier, C., Hélène, C., Waring, M. J., and Hénichart, J. P. (1992) Design of a sequence-specific DNA-cleaving molecule which conjugates a copper-chelating peptide, a netropsin residue, and an acridine chromophore. *Bioconjugate Chem.* **3**, 100–103. (d) Flock, S., Bailly, F., Bailly, C., Waring, M. J., Hénichart, J. P., Colson, P., and Houssier, C. (1994) Interaction of two peptide-acridine conjugates containing the SPKK peptide motif with DNA and chromatin. *J. Biomol. Struct. Dyn.* **11**, 881–900.
- (16) Neidle, S., Webster, G. D., Baguley, B. C., and Denny, W. A. (1986) Nucleic acid binding drugs. XIV. The crystal structure of 1-methylamsacrine hydrochloride; relationships to DNA binding ability and anti-tumor activity. *Biochem. Pharmacol.* **35**, 3915–3921.
- (17) (a) Bailly, C., OhUigin, C., Houssin, R., Colson, P., Houssier, C., Rivalle, C., Bisagni, E., Hénichart, J. P., and Waring, M. J. (1992) DNA-binding properties of a distamycin-ellipticine hybrid molecule. *Mol. Pharmacol.* **41**, 845–855. (b) Bourdouxhe, C., Colson, P., Houssier, C., Sun, J.-S., Montenay-Garestier, T., Hélène, C., Rivalle, C., Bisagni, E., Waring, M. J., Hénichart, J. P. and Bailly, C. (1992) Binding of a distamycin-ellipticine hybrid molecule to DNA and chromatin: spectroscopic, biochemical and molecular modeling investigations. *Biochemistry* **31**, 12385–12396. (c) Bailly, C., Leclère, V., Pommery, N., Colson, P., Houssier, C., Rivalle, C., Bisagni, E., and Hénichart, J. P. (1993c) Binding to DNA, cellular uptake and biological activity of a distamycin-ellipticine hybrid molecule. *Anti-Cancer Drug Design* **8**, 145–164.
- (18) Chou, P.-J., and Johnson, W. C., Jr. (1993) Base inclinations in natural and synthetic DNAs. *J. Am. Chem. Soc.* **115**, 1205–1214.
- (19) Plouvier, B., Bailly, C., Houssin, R., Rao, K. E., Lown, J. W., Hénichart, J. P., and Waring, M. J. (1991) DNA-sequence specific recognition by a thiazole analogue of netropsin: a comparative footprinting study. *Nucleic Acids Res.* **21**, 5821–5829.
- (20) Bailly, C., Denny, W. A., Mellor, L., Wakelin, L. P. G., and Waring, M. J. (1992) Sequence-specificity of the binding of 9-aminoacridine- and amsacrine-4-carboxamides to DNA studied by DNase I footprinting. *Biochemistry* **31**, 3514–3524.
- (21) Orlowski, S., Belehradek, J., Jr., Paoletti, C., and Mir, L. M. (1988) Transient electroporation of cells in culture. Increase in the cytotoxicity of anticancer drugs. *Biochem. Pharmacol.* **37**, 4727–4733.
- (22) Bailly, C., Catteau, J. P., Hénichart, J. P., Reszka, K., Shea, R. G., Krowicki, K., and Lown, J. W. (1989) Subcellular distribution of a nitroxide spin-labeled netropsin in living KB cells. *Biochem. Pharmacol.* **38**, 1625–1630.
- (23) Bailly, C., and Hénichart, J. P. (1990) Subcellular distribution of a nitroxide spin-labeled netropsin-acridine hybrid in living KB cells. *Biochem. Biophys. Res. Commun.* **167**, 798–806.
- (24) Hélène, C., Montenay-Garestier, T., Saison, T., Takasugi, M., Toulmé, J. J., Asseline, U., Lancelot, G., Maurizot, J. C., Toulmé, F., and Thuong, N. T. (1985) Oligodeoxynucleotides covalently linked to intercalating agents: a new class of gene regulatory substances. *Biochimie* **67**, 777–783.
- (25) Baguley, B. C., Holdaway, K. M., and Fray, L. M. (1990) Design of DNA intercalators to overcome topoisomerase II-mediated multidrug resistance. *J. Natl. Cancer Inst.* **82**, 398–402.



# Fc Site-Specific Labeling of Immunoglobulins with Calf Intestinal Alkaline Phosphatase<sup>†</sup>

Mazhar Husain\* and Christopher Bieniarz

Department of Immunochemistry, Diagnostics Division, Abbott Laboratories, Abbott Park, Illinois 60064.  
Received April 11, 1994\*

A strategy is described for the site-specific conjugation of alkaline phosphatase to the Fc region of immunoglobulins. Mild oxidation of immunoglobulins by sodium periodate followed by reductive amination with excess cystamine and sodium cyanoborohydride covalently attaches cystamine specifically to the oligosaccharide chains of the antibody's Fc region. The disulfide bonds of the conjugated cystamine moieties are then reduced to free thiols with a low concentration of dithiothreitol. The thiol-modified antibodies (typically containing three to four thiols per Fc region) are then brought into contact with maleimide-functionalized alkaline phosphatase to form antibody-alkaline phosphatase conjugates. The Fc site-specific conjugation methodology was optimized and successfully applied to a number of different monoclonal and polyclonal antibodies. The conjugates prepared show assay performances superior to those prepared by more conventional means. Evidence obtained indicates that this superior conjugate performance results from total retention of the antibody's antigen binding activity following the Fc site-specific conjugation procedure.

## INTRODUCTION

The ability to produce active and stable enzyme-antibody and enzyme-antigen conjugates is of paramount importance in immunoassays. Several methods for covalently coupling enzyme labels to antibodies are known (1-3). The majority of these coupling methods fall in two categories, (i) periodate coupling procedures and (ii) coupling procedures based on the use of bifunctional cross-linking reagents. In the periodate method carbohydrate chains on the surface of enzymes are oxidized by treatment with sodium periodate to generate aldehyde groups. The oxidized enzyme is allowed to react with antibody resulting in the formation of Schiff's bases between aldehyde groups on the enzyme and amino groups on the antibody. The coupling is stabilized by reduction of the initially formed imine to the secondary amine with sodium borohydride or sodium cyanoborohydride. The periodate method has been used with horseradish peroxidase (4), glucose oxidase (5), and alkaline phosphatase (6).

Bifunctional cross-linkers are extremely useful for protein structural studies and for the coupling of small molecules such as haptens and peptides to carrier proteins, as well as for the linking of enzymes labels to Igs.<sup>1</sup> Glutaraldehyde, an amine reactive homobifunctional cross-linker, has been extensively used to couple enzymes to antibodies (7-9). However, because control

of intra- versus intermolecular cross-linking is very difficult to achieve with glutaraldehyde and other homobifunctional cross-linkers, the products are generally heterogenous, high molecular weight aggregates with greatly reduced enzyme and antibody activities. In recent years, the use of heterobifunctional cross-linkers has greatly increased, mainly to fulfill the need for more controlled coupling between two different biomolecules, such as antibody and enzyme, without formation of homodimers and oligomers.

Heterobifunctional cross-linking reagents having reactive groups with different selectivities at each end of the molecule provide greater control of the coupling reaction so as to enhance the yield of the heteroconjugates, such as antibody-enzyme conjugates. The vast majority of heterobifunctional cross-linking reagents contains a primary amine-reactive group and a thiol or a thiol-reactive group. Heterobifunctional linkers which are frequently used for the purpose of introducing thiol, protected thiol, and thiol-reactive groups into proteins include Traut's reagent (iminothiolane) (10,11), succinimidyl (acetylthio)acetate (SATA) (12,13), succinimidyl 3-(2-pyridyldithio)propionate (SPDP) (14, 15), and succinimidyl *trans*-4-(*N*-maleimidylmethyl)cyclohexane-1-carboxylate (SMCC) (13, 16). One major problem with the use of these heterobifunctional linkers, however, is the random distribution of amino groups throughout the entire Ig molecule including the antigen binding region. Thus, these cross-linking agents may react with Ig at a site close to the antigen binding region and, thus, interfere with the binding of IgG. Therefore, coupling methods that utilize amine-reactive heterobifunctional cross-linking reagents yield heterogeneous immunoconjugates with either partial or complete loss of antigen binding activity (17, 18). In contrast, carbohydrate moieties of antibodies, which are located away from the antigen binding region, can be modified by periodate treatment without significant impairment of the antigen binding function (17, 19, 20). The use of carbohydrate moieties for site-specific labeling has been exploited in spin-labeling work for Ig structural studies (21), to prepare mAb-drug conjugates for chemotherapeutic applications (19, 22, 23), and only on a limited basis for labeling Ig with enzymes (24). The

<sup>†</sup> This paper is dedicated to the memory of our friend and colleague, Dr. Howard E. Bond.

\* Abstract published in *Advance ACS Abstracts*, August 15, 1994.

<sup>1</sup> Abbreviations: SDS-PAGE, sodium dodecyl sulfate polyacrylamide gel electrophoresis; DTNB, 5,5'-dithiobis(2-nitrobenzoic acid); EDTA, ethylenediaminetetraacetic acid; HPLC, high-performance liquid chromatography; DTT, dithiothreitol; TEA, triethanolamine; NEM, *N*-ethylmaleimide; DMF, dimethylformamide; SMTCC, succinimidyl 4-[(*N*-maleimidomethyl)tricarboxamidocyclohexane-1-carboxylate]; PBS, phosphate-buffered saline; MEIA, microparticle capture enzyme immunoassay; CEA, carcinoembryonic antigen; Ig, immunoglobulin; IgG, immunoglobulin G; Fc, crystallizable fragment; CA19-9, carbohydrate antigen recognized by the monoclonal antibody, 19-9; Alk Phos, alkaline phosphatase; mAb, monoclonal antibody.

site-specific labeling of Ig by oxidation of their carbohydrate moieties with periodate followed by reaction of the exposed aldehyde groups with an amine on the enzyme label under reducing conditions has been reported for the labeling of rabbit and goat IgG molecules with lysozyme and horseradish peroxidase (24). Although the use of rabbit anti-human IgG-peroxidase Fc conjugate prepared by this method for the detection of human IgG by enzyme immunoassay was demonstrated (24), no data were reported on comparison of the Fc conjugate with conjugates prepared by conventional methods. It should be noted that formation of IgG-IgG oligomers is a serious drawback of the direct Fc coupling method (24). A 40-fold molar excess of peroxidase was required to minimize the Schiff's base formation between IgG molecules (24). The use of such a large excess of enzyme label renders the direct Fc coupling method very cost ineffective and purification of conjugate by gel filtration very cumbersome, particularly with phosphatase as the label. The carbohydrate-based site-specific labeling of Igs has been reviewed by O'Shannessy and Quarles (25). The increasing role of immunoconjugates in diagnostic and therapeutic applications has created a need for methods of labeling antibodies that will yield well-defined conjugates with minimal effect on immunoreactivity.

In this paper we describe a method for site-specific labeling of Igs with calf intestinal alkaline phosphatase by introducing thiols in the Fc region of Igs and subsequently reacting site-specifically thiolated Igs with the enzyme suitably modified with maleimides. The site-specific thiolation of an Ig consists of periodate oxidation of the oligosaccharide moiety located in the Fc region, subsequent reaction of the aldehyde groups with cystamine, and reduction of the resultant imine with sodium cyanoborohydride to yield cystamine-functionalized Ig. The cystamine-derivatized Ig with cystamine covalently bound to the Fc region is finally subjected to mild reduction with a low concentration of dithiothreitol to yield the site-specifically thiolated Ig. We have successfully used the method for site-specific thiolation of a number of polyclonal and monoclonal Igs and their subsequent conjugation to calf intestinal alkaline phosphatase. The functionalization procedure was shown to have no effect on the immunochemical reactivity of the modified antibody, and conjugates prepared by this site-specific conjugation procedure usually gave assay performance superior than those prepared by conventional methods. The work presented in this paper has recently been disclosed in a U.S. patent (26).

## EXPERIMENTAL PROCEDURES

**Materials.** Cystamine dihydrochloride, L-cystine, sodium periodate, sodium cyanoborohydride, 5,5'-dithiobis-(2-nitrobenzoic acid), *p*-nitrophenyl phosphate bis(2-amino-2-ethyl-1,3-propanediol) salt, and bovine serum albumin were obtained from Sigma (St. Louis, MO). Oxidized glutathione, *N*-ethylmaleimide, Sephadex G-25 (100–300  $\mu$ m), and dithiothreitol were obtained from Aldrich (Milwaukee, WI). 2-Iminothiolane was purchased from Pierce (Rockford, IL). Calf intestinal alkaline phosphatase (EC 3.2.1.23, enzyme immunoassay grade) was obtained from Boehringer Mannheim (Indianapolis, IN). Centricon-30 microconcentrators (MW cut-off 30 kDa) were purchased from Amicon Corp. (Danvers, MA). The extended heterobifunctional maleimide active ester, succinimidyl 4-[(*N*-maleimidomethyl)tricaproamido]cyclohexane-1-carboxylate (SMTCC linker) was prepared as previously described (27). Complete Freund's adjuvant was obtained from DIFCO Laboratories (Detroit, MI). The monoclonal antibody against the tumor-

associated carbohydrate antigen, CA 19–9, was obtained from Centocor (Malvern, PA).

**Isolation and Purification of Anti-CEA IgG.** Purified carcinoembryonic antigen (CEA) (20–50  $\mu$ g/mL) in PBS buffer 1 (10 mM sodium phosphate, 0.15 M NaCl, pH 7.2) was emulsified with 1 mL of Freund's complete adjuvant and was injected subcutaneously in the axillary and inguinal regions of goats. A second injection was administered 30 days later and a third injection given 30 days after that. Two weeks after the third injection, a blood sample was drawn and the serum tested for the presence of anti-CEA IgG. When the antibody titer reached an acceptable level, the goat was put on a production bleeding schedule and the serum was pooled. The purification was accomplished as follows. The pooled serum was subjected to ammonium sulfate fractionation, and the precipitate containing the IgG fraction was suspended in and extensively dialyzed against PBS buffer 1. The dialyzed IgG fraction was then applied over a CEA-specific affinity column which was washed with PBS buffer 1 until the absorbance of the effluent at 280 nm was zero. Anti-CEA antibody was eluted with 0.1 M sodium citrate, pH 3.0, and the absorbance of each fraction was monitored at 280 nm. The eluted IgG fractions were pooled, immediately neutralized, and dialyzed overnight against PBS buffer 1. The protein concentration was calculated from the absorbance at 280 nm using an extinction coefficient ( $E_{1\text{cm}}^{1\%}$ ) of 13.9 (28), and the antibody was stored at  $-20^\circ\text{C}$  until used.

**Preparation of the Conventional Conjugates Using Iminothiolane and SMTCC Linker.** CEA- and CA19–9-specific IgGs (5 mg, 33.3 nmol) in 1 mL of PBS buffer 2 (0.1 M sodium phosphate, 0.1 M NaCl, pH 7.0) were treated with 50- and 15-fold molar excess of SMTCC linker, respectively. After 30 min of incubation at ambient temperature, derivatized IgGs were recovered by gel filtration with a Sephadex G-25 column (1  $\times$  45 cm) equilibrated with PBS buffer 2.

The phosphatase (6 mg, 40 nmol) in 1 mL of PBS buffer 3 (0.1 M sodium phosphate, 0.1 M NaCl, 1 mM  $\text{MgCl}_2$ , 0.1 mM  $\text{ZnCl}_2$ , pH 7.0) was thiolated by treatment with a 500-fold molar excess of iminothiolane (184  $\mu$ L of a 15 mg/mL solution in PBS buffer 2) for 30 min at ambient temperature. The derivatized phosphatase was recovered by gel filtration with a Sephadex G-25 column (1  $\times$  45 cm) equilibrated with PBS buffer 3. The concentration of the enzyme was calculated by its absorbance at 280 nm using an extinction coefficient ( $E_{1\text{cm}}^{1\%}$ ) of 10 (29). Prior to activation and coupling to CEA specific IgG, the phosphatase was modified as follows. The enzyme was treated with 20 mM sodium periodate in 0.2 M sodium acetate–0.2 M sodium phosphate buffer, pH 4.5, containing 0.1 M NaCl, 1 mM  $\text{MgCl}_2$ , and 0.1 mM  $\text{ZnCl}_2$ . After 3 h of gentle stirring at ambient temperature in the dark, the enzyme was dialyzed against 10 mM sodium acetate, pH 4.5, containing 0.1 M NaCl, 1 mM  $\text{MgCl}_2$ , and 0.1 mM  $\text{ZnCl}_2$ . The pH of the dialyzed enzyme was raised to about 9.0, and ethanolamine (40 mM) was added to 1 mM final concentration. The resulting solution was gently stirred for 5 h at ambient temperature and then extensively dialyzed against PBS buffer 2 to remove excess ethanolamine. The pretreatment of the phosphatase was found to be necessary in order to overcome the nonspecific background observed with some patient samples.

Thiolated phosphatase was combined with maleimide-functionalized CEA and CA 19–9 specific IgGs at a molar ratio of 1.5:1 and 1:1, enzyme to antibody, respectively, and incubated 18 h at  $2-8^\circ\text{C}$ . Unreacted thiol groups were then capped by addition of 5 mM NEM to 0.3 mM

final concentration in order to prevent any undesirable cross-linking.

**Fc Site-Specific Conjugation of Alkaline Phosphatase to IgGs.** The antibodies were activated by introducing thiol groups site-specifically in the Fc region as follows. The antibody (5 mg, 33.3 nmol) in 1 mL of 0.1 M triethanolamine (TEA) buffer, pH 8.0, containing 0.16 M sodium chloride was placed in an amber vial. A freshly prepared solution of sodium periodate in the TEA buffer (200 mM, 110  $\mu$ L) was added, and after 1 h at 5  $^{\circ}$ C, the reaction mixture was gel filtered with a Sephadex G-25 column (1  $\times$  45 cm) equilibrated with PBS buffer 2. The fractions containing the oxidized antibody were pooled and concentrated to 1 mL using Centricon-30. Aliquots of cystamine dihydrochloride (0.75 M in PBS buffer 2, 250  $\mu$ L) and sodium cyanoborohydride (0.3 M in PBS buffer 2, 65  $\mu$ L) were added to the antibody pool in that order, and the resulting solution was incubated overnight at ambient temperature. The cystamine-derivatized antibody was recovered by gel filtration with a Sephadex G-25 column (1  $\times$  45 cm) equilibrated with PBS buffer 4 (0.1 M sodium phosphate, 0.1 M NaCl, 2 mM EDTA, pH 7.0). The fractions containing the antibody were pooled, concentrated to 1 mL as before, and then treated with DTT (40 mM in PBS buffer 4, 50  $\mu$ L; final concentration 2 mM) for 15 min at ambient temperature. EDTA was included in the buffer during reduction to chelate any metal ions that might catalyze the oxidation of free thiol groups (30). The activated antibody containing thiol groups in the Fc region was recovered by gel filtration with a Sephadex G-25 column (1  $\times$  45 cm) equilibrated with PBS buffer 4. The fractions containing the reduced antibody were pooled and the concentration of the antibody in the pool was calculated from its absorbance at 280 nm (28). The activated antibodies were stored on ice and used for conjugation, usually within 30 min. No significant decrease in the thiol content was observed during storage as judged by the reaction of modified antibodies with DTNB.

The maleimide derivatization of phosphatase (6 mg, 40 nmol) in 1 mL of PBS buffer 3 was accomplished by treatment with a 30-fold molar excess of SMTCC linker (in 150  $\mu$ L of DMF) for 30 min at ambient temperature. The derivatized enzyme was recovered by gel filtration with a Sephadex G-25 column (1  $\times$  45 cm) equilibrated with PBS buffer 3. The phosphatase coupled to CEA specific IgG was pretreated prior to activation as described above.

The maleimide functionalized phosphatase was combined with Fc thiolated CEA and CA 19-9 specific IgGs at molar ratios of 2:1 and 1.5:1, enzyme to antibody, respectively, and incubated overnight at 2-8  $^{\circ}$ C. Unreacted thiol groups were capped with NEM as mentioned above.

**Assay Performance of Conjugates:** The assay performance of the Fc as well the conventional conjugates was evaluated with the Abbott IMx automated immunoassay analyzer based on the microparticle capture enzyme immunoassay (MEIA) technology (31), generally used for assays of high-molecular-mass analytes. In the MEIA technology, antibody-coated microparticles capture the analyte and are then reacted with an alkaline phosphatase labeled antibody conjugate, which completes the "sandwich". The nonfluorescent substrate, 4-methylumbelliferyl phosphate, is added, and the rate of the appearance of the fluorescence signal due to formation of the fluorescent product (methylumbelliferone) is measured. Six CEA (0, 4, 10, 60, 100, and 200  $\mu$ g/mL) and six CA 19-9 (0, 30, 90, 180, 320, and 500 units/mL) standards were used to generate standard curves for

concentration vs the rate of fluorescence increase expressed in arbitrary units of counts/s/s. The CA19-9 unit is an arbitrary activity corresponding to approximately 0.8 ng of purified antigenic material (32).

**Immunoreactivity of the Native and the Fc-functionalized Anti-CA 19-9 IgG.** The effect of the site-specific Fc functionalization procedure on the immunoreactivity of anti-CA 19-9 antibody was determined by competitive inhibition assays performed using an Abbott IMx immunoassay analyzer. The sequence of steps performed by the instrument was as follows. The F calibrator, containing 500 units of human CA 19-9/mL, the specimen diluent, and the anti-CA 19-9 IgG-coated microparticles were combined in the reaction cell. An aliquot of the reaction mixture containing the antibody-antigen complex bound to the microparticles was transferred to the glass fiber matrix. The microparticles bound irreversibly to the glass fiber matrix which was washed to remove unbound materials. A limiting and fixed amount of anti-CA 19-9 IgG-alkaline phosphatase conjugate with varying amount of the native or the Fc-functionalized anti-CA 19-9 IgG was dispensed onto the matrix. The matrix was washed to remove unbound materials. The substrate, 4-methylumbelliferyl phosphate, was added to the matrix, and the rate of fluorescent product formation was measured in arbitrary units of counts/s/s. Each point was run in duplicate, and the mean value was used in the plot.

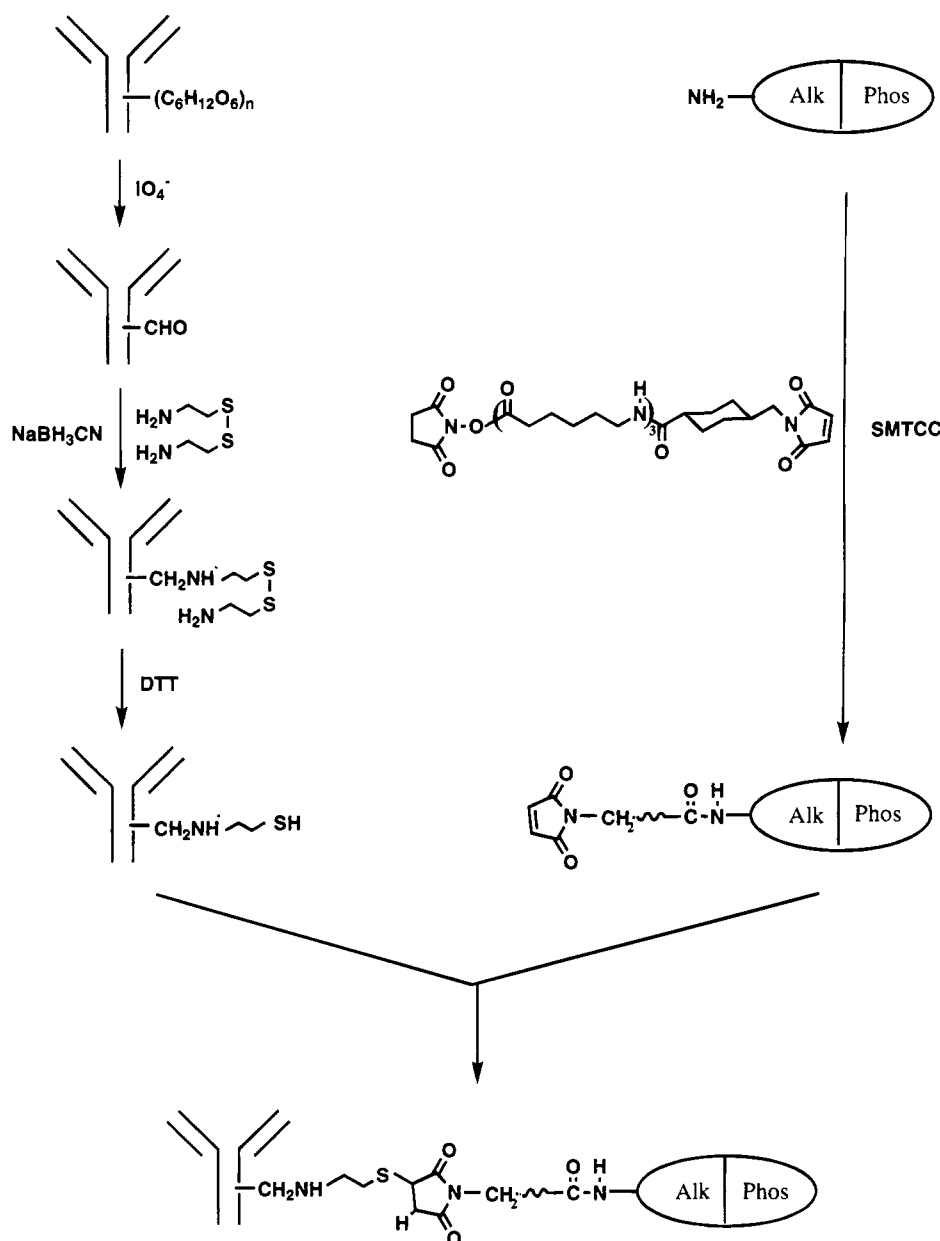
**Quantitation of Thiol and Maleimide Groups.** The thiol group content of proteins was quantitated spectrophotometrically by reaction with DTNB (33) using the experimentally determined molar extinction coefficient of 13 000 M $^{-1}$  cm $^{-1}$  with cysteine at pH 7.0. For the quantitation of maleimide groups, samples of the derivatized alkaline phosphatase were incubated with 50  $\mu$ M 2-mercaptoethylamine in a final volume of 1 mL of PBS buffer 4 at ambient temperature. After 15 min of incubation, the remaining thiol content was measured by the method described above.

**Alkaline Phosphatase Assay.** The enzymatic activity of alkaline phosphatase and the antibody-alkaline phosphatase conjugates was assayed spectrophotometrically by following the hydrolysis of 0.1 mM *p*-nitrophenyl phosphate in 0.5 M diethanolamine, 1 mM MgCl $_2$ , 0.1 mM ZnCl $_2$ , pH 10.2, at 410 nm.

## RESULTS

**Site-Specific Thiolation of Antibodies.** The approach used for the site-specific introduction of thiols in the Fc region of Igs and the subsequent coupling of the thiolated Igs to the maleimide derivatized calf intestinal alkaline phosphatase is depicted in Scheme 1. Igs were oxidized under mild conditions and then subjected to reductive amination in the presence of excess cystamine and sodium cyanoborohydride. A series of experiments was carried out using varying concentrations of periodate and cystamine, pH, and incubation times during this procedure to determine the conditions required to achieve a minimum incorporation of 1-2 cystamine/Ig without any adverse effect on immunoreactivity. The size-exclusion HPLC profiles of the native and the cystamine-derivatized Igs were identical, indicating the absence of oligomerization due to intermolecular cross-linking (data not shown). The large excess of cystamine, in addition to driving the amination reaction, serves to block the aldehydes from attacking lysine residues on adjacent Ig molecules, which would be an undesirable reaction. The cystamine-modified Igs were finally treated with 2 mM DTT generating covalently bound thiols from reduction of the cystamine disulfide bonds. No thiols were gener-

Scheme 1



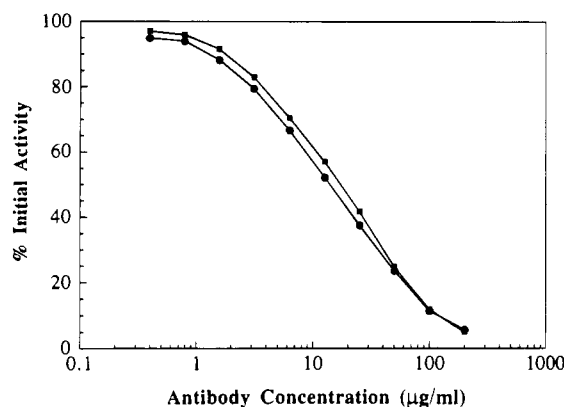
ated in a control experiment when anti-CA19-9 IgG was treated with cystamine and DTT but without prior oxidation with periodate. These results suggest that the generation of thiols is related to incorporation of cystamine into IgG during Fc-functionalization instead of reduction of intrinsic disulfide bonds. Higher concentration of DTT (25–50 mM) and longer incubation periods (30–60 min) are required to reduce the intrinsic disulfide bonds.

The Fc site-specific functionalization procedure was successfully used to derivatize about a dozen different antibodies, including both monoclonal and polyclonal types. Typically, three to four thiols were incorporated per IgG molecule. However, in a few cases, the thiol content was as high as eight to ten groups per IgG molecule. The derivatized anti-CA 19-9 and anti-CEA antibodies contained four and seven thiol groups per molecule, respectively.

**Determination of Antibody Activity.** A competitive binding assay was used to establish how effectively the Fc-functionalized anti-CA19-9 IgG could bind to the multiepitopic CA19-9 antigen already captured by anti-

CA19-9 IgG immobilized on microparticles. In this assay, microparticles/anti-CA19-9 IgG/CA19-9 antigen complex was exposed to different ratios of the Fc-functionalized or unmodified antibody and anti-CA19-9 IgG-alkaline phosphatase conjugate. The data presented in Figure 1 show that the Fc-functionalized and unmodified anti-CA19-9 IgGs were virtually equal in their ability to compete with anti-CA19-9 IgG-alkaline phosphatase conjugate.

**Introduction of Maleimide Groups into Calf Intestinal Alkaline Phosphatase.** Initially, in order to establish the conditions required for the controlled introduction of maleimide groups into alkaline phosphatase, identical aliquots of the enzyme were treated with different concentrations of the 30-atom maleimide linker. The extent of the modification was followed by treatment of the derivatized enzyme with excess cysteamine, followed by titration of the unreacted thiol groups with DTNB (33). The effect of the linker derivatization on the enzyme activity was also evaluated. It can be seen from the results presented in Table 1 that the number of maleimide groups incorporated into alka-



**Figure 1.** Effect of Fc-functionalization on the immunoreactivity of CA 19-9 specific IgG. Inhibition by unmodified (squares) and Fc functionalized antibody (circles).

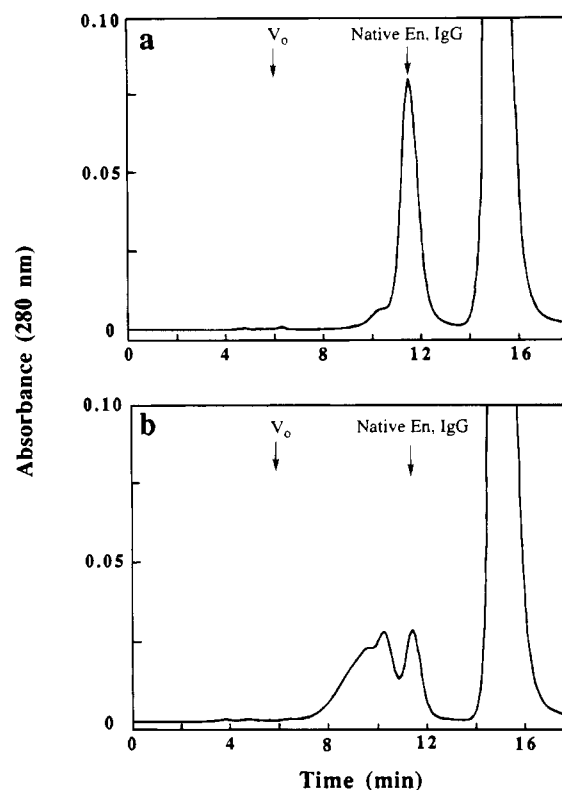
**Table 1. Number of Maleimide Groups Introduced into Calf Intestinal Alkaline Phosphatase as a Function of the SMTCC Linker and the Enzyme Stoichiometry**

equiv of the linker/enzyme used	maleimide groups introduced	% starting activity retained
15	3	93
30	6	93
45	8	90
60	12	80

line phosphatase was directly dependent on the amount of linker used, varying between three and 12 groups per enzyme molecule at linker to enzyme ratios of 15 and 60, respectively. Analysis of the activity of the linker-derivatized alkaline phosphatase showed that introduction of up to eight maleimide groups per molecule had a small effect on enzymatic activity, and even at 13 maleimide groups per molecule, the loss observed was only 20% of the starting activity. A linker to alkaline phosphatase ratio of 30 was found to be optimum for the preparation of Fc site-specific IgG-alkaline phosphatase conjugates as judged by the absence of undesirable high molecular weight aggregates generally observed with conventional conjugates, as well as the overall assay performance.

**Preparation and Characterization of Site-Specific Anti-CA19-9 IgG-Alkaline Phosphatase and Anti-CEA IgG-Alkaline Phosphatase Conjugates.** Anti-CA 19-9 and anti-CEA IgGs were covalently and Fc site-specifically coupled to alkaline phosphatase through stable thioether bonds (Scheme 1). This was achieved by combining site-specifically thiolated IgGs with the enzyme prefunctionalized with 30-atom extended length heterobifunctional maleimide active ester (SMTCC linker). In an earlier work we demonstrated that this extended length coupling agent, succinimidyl 4-[(*N*-maleimidomethyl)tricaproamido]cyclohexane-1-carboxylate, offers several advantages as a coupling agent over the shorter, more hydrophobic heterobifunctional reagents used in the past (27). The general procedure described in the Experimental Section for the preparation of anti-CA19-9 IgG-alkaline phosphatase and anti-CEA IgG-alkaline phosphatase site-specific conjugates as well as other site-specific IgG-alkaline phosphatase was developed such that 80–90% of the starting IgG was consumed during coupling reaction.

Alkaline phosphatase was first derivatized with a 30-fold molar excess of SMTCC linker, and following removal of the unreacted linker by size exclusion chromatography, the derivatized enzyme containing five to six maleimide groups/enzyme was stored on ice until conjugation. However, because the maleimide ring is known to have



**Figure 2.** Analytical size-exclusion HPLC profiles of the site-specific anti-CA 19-9 antibody-alkaline phosphatase conjugates (a) immediately after the two activated proteins were combined and (b) after 18 h of incubation at 2–8 °C. Size-exclusion HPLC analyses were performed on a Spectra-Physics instrument equipped with a SP8490 dual-wavelength detector using a Bio-Rad Bio-Sil SEC 400 column (7.8 × 300 mm) fitted with a Bio-Rad Bio-Sil guard column (7.8 × 80 mm). The columns were equilibrated and eluted with PBS buffer 2 at a flow rate of 1 mL/min, and absorbance was monitored at 280 nm.

limited stability at neutral pH (34), the maleimide-functionalized enzyme was never stored longer than a few hours. Anti-CA19-9 IgG, site-specifically thiolated as described above, was recovered from size exclusion chromatography following DTT reduction, the last step in the Fc functionalization procedure, and was immediately reacted with the maleimide-derivatized enzyme. The reaction of the freshly thiolated anti-CA19-9 IgG with DTNB indicated incorporation of three to four thiols/IgG. The coupling reaction of the thiolated anti-CA19-9 IgG with the maleimide-derivatized alkaline phosphatase was monitored by size-exclusion HPLC. Figure 2, panel a, is an HPLC profile of the derivatized enzyme and IgG immediately after they were combined in a molar ratio of 1.5:1, respectively. The peak at 11.8 min corresponds to both the unconjugated, derivatized IgG and the enzyme; both calf intestinal alkaline phosphatase and IgG are known to exist as 150 kDa proteins. The small leading shoulder just ahead of the free enzyme and the antibody peak indicates the start of the coupling reaction. The conjugation reaction between anti-CA19-9 and alkaline phosphatase proceeds relatively slowly, requiring several hours for completion. Figure 2, panel b, is an HPLC profile after 18 h when the conjugation reaction was complete. The peak corresponding to the free enzyme and the antibody is considerably diminished, and new peaks at about 9.8 and 10.3 min are observed corresponding to enzyme-IgG conjugates with molecular weights ranging between 300 and 700 kDa. The major peak at about 15 min in both panels a and b is an artifact related to the presence of EDTA, MgCl<sub>2</sub>, and ZnCl<sub>2</sub> in

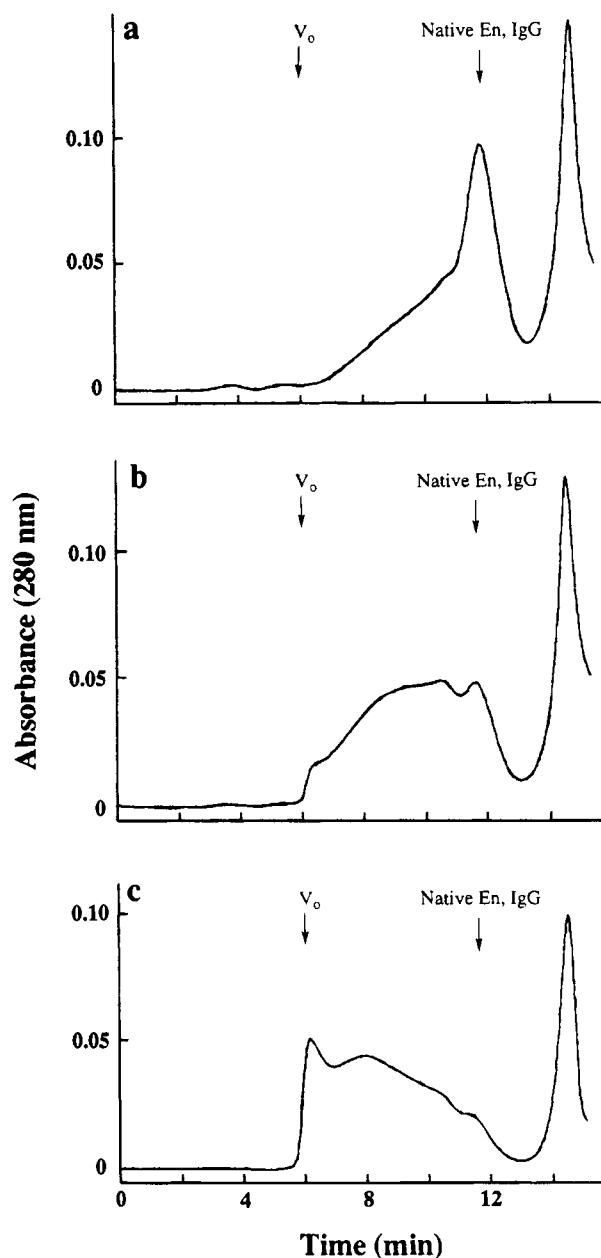
PBS buffers 3 and 4, used for the activation of enzyme and antibody, respectively. From the relative areas of the proteins peaks, the yield of the conjugation reaction was estimated to be 67%. Coupling at higher molar ratios of enzyme to antibody, such as 2:1 and 3:1, results in higher amounts of the free enzyme present at the end of reaction, as judged by the size-exclusion HPLC and SDS-PAGE data (not shown).

As mentioned above, site-specific thiolation of anti-CEA IgG leads to introduction of six to seven thiols/IgG, considerably higher than a typical incorporation of three to four thiols/IgG, observed with the majority of IgGs used, including anti-CA19-9 IgG. When the thiolated anti-CEA IgG was reacted with the maleimide-functionalized alkaline phosphatase, the conjugation reaction, as monitored by size exclusion HPLC, proceeded at a much faster rate than that observed between anti-CA19-9 IgG and alkaline phosphatase. Figure 3, panel a, is an HPLC profile of the derivatized enzyme and IgG, immediately after they were combined together in a molar ratio of 2:1, respectively. Clearly, a considerable amount of coupling between the two activated proteins took place, as indicated by the broad shoulder associated with the free enzyme and IgG peak. After 90 min of mixing (Figure 3, panel b), about 80% of the starting enzyme and the IgG were consumed in conjugation reaction. Finally, after 18 h, nearly all the starting enzyme and the IgG were consumed in conjugation (Figure 4, panel c). Furthermore, as indicated by the broad and complex profile, the final conjugation product consisted of mostly high molecular weight adducts of the enzyme and the IgG, a considerable amount eluting in the void volume.

The performance of anti-CA19-9 IgG/alkaline phosphatase and anti-CEA IgG/alkaline phosphatase conjugates prepared by the site-specific and conventional conjugation methods were evaluated with IMx, an automated immunoassay analyzer, using microparticle capture enzyme immunoassay technology (MEIA) and a direct sandwich-type assay format (31). According to this assay format, latex microparticles covalently coupled with capture antibody are incubated first with sample containing known or unknown amounts of analyte and then with alkaline phosphatase-labeled antibody conjugate. Unadsorbed materials are removed at each step by capillary action and buffer washes. Following the removal of unbound conjugate, the enzyme substrate methylumbelliferyl phosphate is added and the increase in the rate of fluorescence due to the alkaline phosphatase-catalyzed formation of the product, 4-methylumbelliferone, is measured.

The data in Figure 4 compare the performance of the Fc site-specific anti-CEA IgG-alkaline phosphatase conjugate prepared as described above with that of the conventional conjugate prepared by combining iminothiolane-activated enzyme with SMTCC linker-activated antibody. Six IMx CEA calibrators (0, 4, 10, 60, 100, and 200 ng/mL) were used to generate the standard curves for concentration vs the signal measured as rate of fluorescence increase in arbitrary units of counts/s/s due to methylumbelliferone formation. The substrate, 4-methylumbelliferyl phosphate, is dephosphorylated to 4-methylumbelliferone by alkaline phosphatase. Approximately a 200% increase in signal is observed with the Fc site-specific conjugate at 0.5  $\mu\text{g/mL}$  compared to conventional conjugate at 1.0  $\mu\text{g/mL}$ , generating an improvement in overall assay performance of approximately 400%.

Figure 5 shows standard curves which were generated with the Fc site-specific and conventional anti-CA19-9 IgG/alkaline phosphatase conjugates, at final conjugate



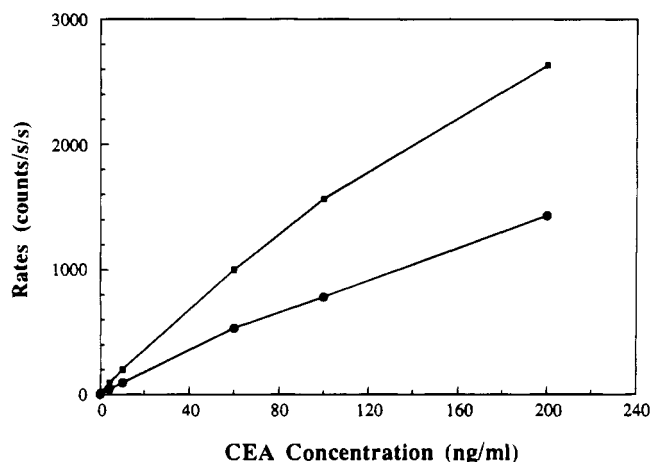
**Figure 3.** Analytical size-exclusion HPLC profiles of the site-specific anti-CEA antibody-alkaline phosphatase conjugates (a) immediately after the two activated proteins were combined (b) after 90 min of incubation at 2–8 °C, and (c) after 18 h of incubation at 2–8 °C. The analyses were performed as described in the legend to Figure 2.

concentrations of 1 and 4  $\mu\text{g/mL}$ , respectively, using the six IMx CA19-9 calibrators (0, 30, 90, 180, 320, and 500 units/mL). The results demonstrate approximately 600% improvement in an overall assay performance with the Fc site-specific conjugate compared to the conventional conjugate.

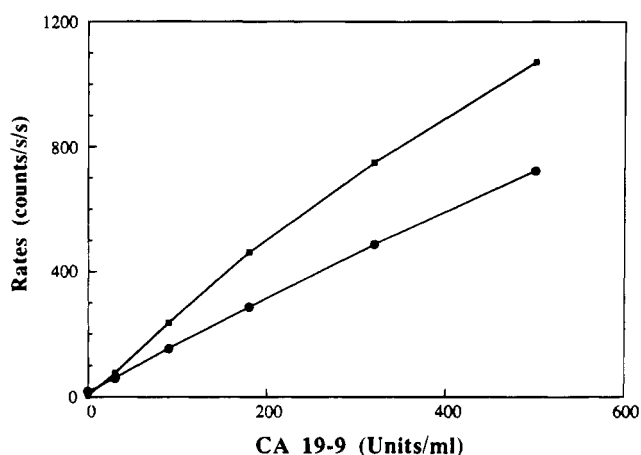
## DISCUSSION

Because most of the diagnostic and therapeutic applications of immunoglobulins (Ig) require their conjugation to other substances, there is a continuing need for improved methods of covalent modifications that will allow labeling of a wide variety of Igs without compromising their antigen binding activity as well as the activity of the labeling agent. The Fc site-specific Ig labeling methodology described here offers several advantages. (1) The methodology is based on the chemistry





**Figure 4.** Comparison of the standard curves obtained using conventional and Fc site-specific anti-CEA antibody-alkaline phosphatase conjugates: Fc site-specific at 0.5 µg/mL (squares) vs conventional at 1.0 µg/mL (circles). The rate of fluorescence increase is expressed in arbitrary instrument units of counts/s/s.



**Figure 5.** Comparison of the standard curves obtained using conventional and Fc site-specific anti-CA19-9 antibody-alkaline phosphatase conjugates: Fc site-specific at 1 µg/mL (squares) vs conventional at 4 µg/mL (circles). The CA19-9 unit is an arbitrary activity corresponding to approximately 0.8 ng of purified antigenic material.

that is targeted at the carbohydrate moieties of Ig, localizing the site of modification away from the antigen binding region, with no effect on the antigen binding activity. Conversely, conventional methods which are usually based on chemistries that utilize lysine residues randomly distributed throughout the entire Ig molecule, including the antigen binding region, often compromise the immunoreactivity. (2) Unlike conventional conjugation methods that lack site specificity and generate heterogeneous products with respect to site of coupling, the method presented here allows Fc site-specific labeling of Igs. (3) Use of the extended arm 30-atom maleimide linker for functionalization of proteins, such as antibodies, has been shown to significantly improve the signal in the immunoassays, presumably by reducing the steric hindrance. (4) The labeling method generates Fc site-specifically thiolated Ig as an intermediate which can be coupled to a wide variety of molecules after their appropriate derivatization with either maleimide or  $\alpha$ -halocarbonyl functionalities. In the work presented here, however, we have focused on the use of the Fc site-specific conjugation methodology for labeling Igs with calf intestinal alkaline phosphatase. (5) The site-specific methodology exploits thiol and maleimide-based chemistry

which is clearly superior to other conjugation chemistries with respect to specificity, rate and stoichiometry of reaction, and stability of the reactive groups in aqueous solvents, as well as the stability of the thioether bond formed as result of the reaction between a thiol and a maleimide group (35, 36). Additionally, although the work presented here focuses on the use of cystamine and SMTCC linker for the site-specific labeling, these reagents can be substituted with a variety of diamino disulfide compounds and heterobifunctional cross-linkers, thereby providing a high degree of freedom in the design of labeled Igs. (6) Finally, because carbohydrate moieties of Igs are at least in part believed to participate in Fc receptor interactions, conjugates prepared by the Fc conjugation methodology may help reduce the "nonspecific" assay background observed with some patient samples.

We have used the Fc site-specific conjugation methodology to couple calf intestinal alkaline phosphatase to about a dozen different monoclonal and polyclonal IgG molecules using the method described in the Experimental Section for the preparation of Fc site-specific anti-CA 19-9 IgG/alkaline phosphatase conjugate. Although the possibility of an Ig, particularly the monoclonal type, without any carbohydrate moiety exists, we were able to thiolate each Ig by the Fc functionalization procedure, as judged by reaction of the derivatized Igs with Ellman's reagent. Additionally, the thiolation of Ig was found to be dependent on prior oxidation of Ig with periodate, clearly indicating the crucial role of the carbohydrate moiety in the generation of thiols during the Fc functionalization of Ig. The degree of thiolation following Fc derivatization varies considerably, ranging from 3–4 mol of thiols/mol Ig observed with the majority of the Igs that were subjected to the Fc functionalization, to as many as 8–10 mol of thiols with some Igs. As expected, the Igs with the higher thiol content react with maleimide derivatized alkaline phosphatase at a much faster rate than Igs with lower thiol content.

An important objective of the present study was to compare conjugates prepared by the Fc site-specific conjugation methodology (Fc conjugates) with those prepared by conventional methods (conventional conjugates). Conventional conjugates were prepared by the following two methods: (1) by activation of alkaline phosphatase and Igs with iminothiolane and SMTCC linker, respectively, followed by coupling as described in the experimental section and (2) by oxidation of alkaline phosphatase with periodate, subsequent incubation with Ig, followed by reduction of the resultant imine group with sodium cyanoborohydride. The conditions for the preparation of conventional conjugates were optimized with each individual Ig with respect to the overall assay performance. In general, the Fc conjugates exhibited sensitivity 200–400% higher than conventional conjugates. Because of the high potency, Fc conjugates could be used in assays at much lower concentration without sacrificing the signal. This often resulted in lowering of the nonspecific assay background and consequently considerable improvement in analytical sensitivity. In a few cases, however, the performance of the Fc conjugate was equivalent to that of conventional conjugate.

The use of a low molecular weight reagent such as cystamine, which can be used at high concentration to drive the covalent modification was very advantageous for our strategy. Only oxidized cystamine could be utilized for the Fc-functionalization of Igs. When cysteamine (reduced cystamine) was used, the functionalized Ig could not be conjugated to the maleimide-derivatized alkaline phosphatase, most probably due to the formation

of thiazolidine ring (37). We also examined the use of cystine and oxidized glutathione in the Fc-functionalization of Igs. Both reagents were effective, in that the site-specific conjugates prepared with cystine and oxidized glutathione gave assay performance nearly equivalent to those prepared with cystamine.

The increasing role of antibodies as highly specific reagents for delivering toxins, drugs, or radiolabels to a variety of cell populations including tumors, as well as for many diagnostic applications, calls for conjugation methods that will not only preserve the full antigen binding activity and specificity of antibody but also reduce the nonspecific binding problems. We believe that the approach described here for the Fc site-specific labeling of antibodies is of fairly general applicability, and we hope that it will help many research endeavors.

#### ACKNOWLEDGMENT

We are grateful to Dr. R. Ganson of Abbott Diagnostics Division for his help with CA 19-9 assays.

**Supplementary Material Available:** Comparison of the signal generated with anti-CA125 microparticles by using linkers of various lengths and structures of various linkers (2 pages). Ordering information is available on any current masthead page.

#### LITERATURE CITED

- (1) Avrameas, S., Ternynck, T., and Guesdon, J. L. (1978) Coupling of enzyme to antibodies and antigens. *Scand. J. Immunol.* 8, 7-23.
- (2) O'Sullivan, M. J., Bridges, J. W., and Marks, V. (1979) Enzyme immunoassay: a review. *Annals of Clin. Biochem.* 16, 221-240.
- (3) Blake, C., and Gould, B. J. (1984) Use of enzymes in immunoassay techniques: a review. *Analyst* 109, 533-547.
- (4) Nakane, P. K., and Kawaoi, A. (1974) Peroxidase labeled antibody. A new method of conjugation. *J. Histochem. Cytochem.* 22, 1084-1091.
- (5) Johnson, R. B., and Nakamura, R. M. (1980) In *Immunoassays: Clinical Laboratory Techniques for the 1980s* (R. M. Nakamura, W. R. Dito, and E. S. Tucker, Eds.) pp 144, A. R. Liss, New York.
- (6) Hazlett, D. T. G., and Garner, P. (1981) A new method for labeling antibodies with alkaline phosphatase for use in the enzyme-linked immunosorbent assay. *Afr. J. Clin. Exp. Immunol.* 2, 325-336.
- (7) Avrameas, S. (1969) Coupling of enzymes to proteins with glutaraldehyde. Use of the conjugates for the detection of antigens and antibodies. *Immunochemistry* 6, 43-52.
- (8) Korn, A. H., Fearheller, S. H., and Filachione, E. M. (1972) Glutaraldehyde: nature of the reagent. *J. Mol. Biol.* 65, 525-529.
- (9) Hardy, P. M., Nicholls, A. C., and Rydon, N. H. (1976) The nature of the crosslinking of proteins by glutaraldehyde. Part 1. Interaction of glutaraldehyde with the amino group of 6-aminohexanoic acid and of  $\alpha$ -N-acetyl lysine. *J. Chem. Soc., Perkin Trans. 1*, 958-962.
- (10) Jue, R., Lambert, J. M., Pierce, L. R., and Traut, R. R. (1978) Addition of sulfhydryl groups to *Escherichia coli* ribosomes by protein modification with 2-iminothiolane (methyl 4-mercaptobutyrimidate) *Biochemistry* 17, 5399-5405.
- (11) McCall, M. J., Diril, H., and Meares, C. F. (1990) Simplified method for conjugating macrocyclic bifunctional chelating agents to antibodies via 2-iminothiolane. *Bioconjugate Chem.* 1, 222-226.
- (12) Julian, R., Duncan, S., Weston, P. D., and Wriglesworth, R. (1983) A new reagent which may be used to introduce sulfhydryl groups into proteins, and its use in the preparation of conjugates for immunoassay. *Anal. Biochem.* 132, 68-73.
- (13) Ghetie, V., Till, M. A., Ghetie, M., Tucker, T., Porter, J., Patzer, E. J., Richardson, J. A., Urh, J. W., and Vitetta, A. (1990) Preparation and characterization of conjugates of recombinant CD4 and deglycosylated ricin A chain using different cross-linkers. *Bioconjugate Chem.* 1, 24-31.
- (14) Carlsson, J., Drevin, H., and Axen, R. (1978) Protein thiolation and reversible protein-protein conjugation. *Biochem. J.* 173, 723-737.
- (15) Cumber, J. A., Forrester, J. A., Foxwell, B. M. J., Ross, W. C. J., and Thorpe, P. E. (1985) Preparation of antibody-toxin conjugates. *Methods Enzymol.* 112, 207-225.
- (16) Freytag, J. W., Lau, H. P., and Wadsley, J. J. (1984) Affinity column-mediated immunoenzymatic assays: influence of affinity column ligand and valency of antibody-enzyme conjugates. *Clin. Chem.* 30, 1494-1498.
- (17) Ghose, T. I., Blair, A. H., and Kulkarni, P. N. (1983) Preparation of antibody-linked cytotoxic agents. *Methods Enzymol.* 93, 280-333.
- (18) Petrella, E. C., Wilkie, S. D., Smith, C. A., Morgan, A. C., Jr., and Vogel, C. W. (1987) *J. Immunol. Methods* 104, 159-172.
- (19) Rodwell, J. D., Alvarez, V. L., Lee, C., Lopes, A. D., Goers, J. W. F., King, H. D., Powsner, H. J., and McKearn, T. J. (1986) Site-specific covalent modification of monoclonal antibodies: *in vitro* and *in vivo* evaluations. *Proc. Natl. Acad. Sci. U.S.A.* 83, 2632-2636.
- (20) Chua, M.-M., Fan, S.-T., and Karush, F. (1984) Attachment of immunoglobulin to liposomal membrane via protein carbohydrate. *Biochim. Biophys. Acta* 800, 291-300.
- (21) Nezlin, R. S., and Sykulev, Y. K. (1982) Structural studies of immunoglobulins spin-labeled at the carbohydrate moiety. *Mol. Immunol.* 19, 347-356.
- (22) Pochon, S., Buchegger, F., Pelegrin, A., Mach, J. P., Offord, R. E., Ryser, J. E., and Rose, K. (1989) A novel derivative of the chelon desferrioxamine for site-specific conjugation to antibodies. *Int. J. Cancer* 43, 1188-1194.
- (23) Webb, R. R., and Kaneko, T. (1990) Synthesis of 1-(aminoxy)-4-[(3-nitro-2-pyridyl)dithio]butane and 1-(aminoxy)-4-[(3-nitro-2-pyridyl)dithio]but-2-ene, novel heterobifunctional cross-linking reagents. *Bioconjugate Chem.* 1, 96-99.
- (24) Murayama, A., Shimada, K., and Yamamoto, T. (1978) Modification of immunoglobulin G using specific reactivity of sugar moiety. *Immunochemistry* 15, 523-528.
- (25) O'Shannessy, D. J., and Quarles, R. H. (1987) Labeling of the oligosaccharide moieties of immunoglobulins. *J. Immunol.* 139, 153-161.
- (26) Bieniarz, C., Husain, M., and Bond, H. E. (1993) Site-specific conjugation of immunoglobulins and detectable labels. U.S. Patent No. 5,191,066.
- (27) (a) Bieniarz, C., Welch, C. J., and Barnes, G. (1991) Heterobifunctional Coupling Agents. U.S. Patent No. 4,994,385. (b) Bieniarz, C., Welch, C. J., Barnes, G., and Schlesinger, C. A. (1991) Covalent Attachment of Antibodies and Antigens to Solid Phases Using Extended Length Heterobifunctional Coupling Agents. U.S. Patent No. 5,002,883. (c) Bieniarz, C., Welch, C. J., and Barnes, G. (1991) Heterobifunctional Maleimide Containing Coupling Agents. U.S. Patent No. 5,053,520. (d) Bieniarz, C., Welch, C. J., Barnes, G., and Schlesinger, C. A. (1991) Covalent Attachment of Antibodies and Antigens to Solid Phases Using Extended Length Heterobifunctional Coupling Agents. U.S. Patent No. 5,063,109.
- (28) Johnstone, A., and Thorpe, R. (1982) *Immunochemistry in Practice*, Blackwell Scientific, Oxford.
- (29) Personal communication from Boehringer Mannheim.
- (30) Gross, J., Carlson, R. I., Brauer, A. W., Margolies, M. N., Warshaw, A. L., and Wands, J. R. (1985) Isolation, characterization, and distribution of an unusual pancreatic human secretory protein. *J. Clin. Invest.* 76, 2115-2126.
- (31) Fiore, M., Mitchell, J., Doan, T., Nelson, R., Winter, G., Grandone, C., Zeng, K., Haraden, R., Smith, J., Harris, K., Leszczynski, J., Berry, D., Stafford, S., Barnes, G., Scholnick, A., and Ludington, K. (1988) The Abbott IMx automated benchtop immunochemistry analyzer system. *Clin. Chem.* 34, 1726-1732.
- (32) Del Villano, B. C., Brennan, S., Brock, P., Bucher, C., Liu, V., McClure, M., Rake, B., Space, S., Westrick, B., Schoemaker, H., and Zurawski, V. R., Jr. (1983) Radioimmuno-metric assay for a monoclonal antibody-defined tumor marker, CA 19-9. *Clin. Chem.* 29, 549-552.

- (33) Ellman, G. L. (1959) Tissue sulphhydryl groups. *Arch. Biochem. Biophys.* 82, 70–77.
- (34) (a) Gregory, J. D. (1955) The stability of *N*-ethylmaleimide and its reaction with sulfhydryl groups. *J. Am. Chem. Soc.* 77, 3922–3923. (b) Kitagawa, T., Shimozone, T., Aikawa, T., Yoshida, T., and Nishimura, H. (1981) Preparation and characterization of heterobifunctional crosslinking reagents for protein modification. *Chem. Pharm. Bull.* 29, 1130–1135. (c) Hamaguchi, Y., Yoshitake, S., Ishikawa, E., Endo, Y., and Ohtaki, S. (1979) Improved procedure for the conjugation of rabbit IgG and Fab' antibodies with beta galactosidase from *Escherichia coli* using *N,N'*-o-phenylenedimaleimide. *J. Biochem.* 85, 1289–1300.
- (35) Yoshitake, S., Yamada, Y., Ishikawa, E., and Masseyeff, R. (1979) Conjugation of glucose oxidase from *Aspergillus niger* and rabbit antibodies using *N*-hydroxysuccinimide ester of *N*-(4-carboxycyclohexylmethyl)maleimide. *Eur. J. Biochem.* 101, 395–399.
- (36) Ji, T. H. (1983) Bifunctional reagents. *Methods Enzymol.* 91, 580–609.
- (37) Greene, T. W., and Wuts, P. G. M. (1991) *Protective Groups in Organic Synthesis*, pp 219, 292, John Wiley & Sons, Inc., New York.

# TECHNICAL NOTES

## Improved Method for Preparing *N*-Hydroxysuccinimide Ester-Containing Polymers for Affinity Chromatography

M. Wilchek,\* K. L. Knudsen, and T. Miron

Department of Membrane Research and Biophysics, The Weizmann Institute of Science, Rehovot 76100, Israel.  
Received May 10, 1994\*

*N,N,N',N'*-Tetramethyl(succinimido)uronium tetrafluoroborate is proposed as a reagent of choice for the activation of carboxyl groups and formation of *N*-hydroxysuccinimide esters on polymers. Unlike conventional methods which generate unstable gels, the reaction is appropriate for hydroxy-containing resins like Sepharose, cellulose, and dextran. The yields of activation and subsequent coupling capacity for ligands and proteins are very high. The respective columns can be used for affinity chromatography and immobilization of proteins.

### INTRODUCTION

*N*-Hydroxysuccinimide (NHS) esters are widely used as coupling agents for protein modification (1, 2) and as a means to immobilize ligands containing amino groups (e.g., proteins) onto solid supports for affinity chromatography (3, 4). NHS-activated polymers are commercially available and commonly used.

Several years ago (5), we demonstrated that the standard procedure to prepare NHS esters (namely *N*-hydroxysuccinimide and carbodiimides) leads to the formation of unstable immobilized compounds on polymers that also contain hydroxyl groups. This phenomenon is due to the formation of a  $\beta$ -alanine derivative which binds to the hydroxy-containing polymer, resulting in an unstable bond (5). In the latter study, we suggested alternative approaches to overcome this problem, including a two-step procedure and the use of trifluoroacetyl-NHS (6). In all cases, however, reduced yields of NHS ester were obtained.

*N,N,N',N'*-Tetramethyl(succinimido)uronium tetrafluoroborate (TSTU) was recently introduced as a reagent to produce NHS esters for carboxamide formation (7, 8) without accompanying side reactions. In the present study we adapted TSTU for the rapid activation in high yields of carboxyl groups on Sepharose and other carriers, which also contain hydroxyl groups. The resultant columns are appropriate for use in affinity chromatography and protein immobilization. The reaction proceeds without the side reactions which characterize classical methods.

### EXPERIMENTAL PROCEDURES

**Materials.** *N,N,N',N'*-Tetramethyl(succinimido)uronium tetrafluoroborate (TSTU) and 4-(dimethylamino)pyridine (DMAP) were obtained from Fluka (Buchs, Switzerland). *N,N*-Dimethylformamide (DMF) and 1,4-

dioxane were from Merck (Darmstadt, Germany). Cl-Sepharose 4B- $\epsilon$ -amino caproic acid was prepared as described previously (5).

**Activation Procedure.** Cl-Sepharose 4B- $\epsilon$ -aminocaproic acid was washed with 0.3 N HCl and water and dehydrated gradually by increasing concentrations of dioxane (25%, 50%, and 100%). The filtered gel was found to contain about 50  $\mu$ mol of carboxyl groups per gram, as determined by amino acid analysis ( $\epsilon$ -aminocaproic acid) after total hydrolysis.

The dehydrated gel (1 g) was suspended in 0.1 M TSTU in DMF (0.5 mL). DMAP was added dropwise (0.1 M in DMF, 0.5 mL), and about 2 mL of additional solvent (DMF or dioxane) was then added. The reaction mixture was stirred for 1 h at room temperature, filtered, and washed successively with DMF, methanol, and isopropanol. The gel was stored in 2-propanol at 4 °C.

The yield of activation was quantitative (49–55  $\mu$ mol/g) as determined by spectroscopic titration (9). After total hydrolysis, the sole amino acid observed was  $\epsilon$ -aminocaproic acid; no  $\beta$ -alanine could be detected.

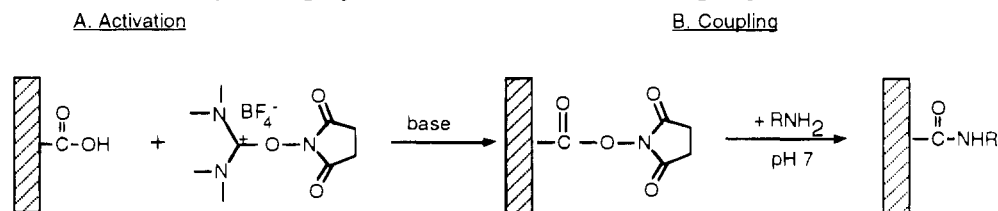
**Coupling of Proteins.** A suspension of the activated gel (containing about 1 g of filtered gel) was washed with cold water to remove the 2-propanol. The gel was then added immediately to a solution of protein (between 1–10 mg in 0.1 M phosphate buffer, pH 7.0) and shaken overnight at 4 °C. The conjugate was filtered and washed extensively with phosphate buffer.

The amount of coupled protein was determined either by amino acid analysis or spectroscopically by assessing the amount of uncoupled protein after acidification of the resin. The yields were very high—usually over 90%. For example, 5–7 mg of avidin could be coupled per g of wet gel. Depending on their solubility, low-molecular-weight ligands were coupled either in organic solvents or in buffer.

### RESULTS AND DISCUSSION

The structure of TSTU and its interaction with a carboxyl group for peptide synthesis was originally

\* Abstract published in *Advance ACS Abstracts*, August 1, 1994.

**Scheme 1. Activation of Carboxyl Group by TSTU (A) and Its Use in Coupling of Proteins (B)**

described by Knorr et al. (7, 8). The reaction is depicted in Scheme 1.

In order to apply TSTU on polymeric carriers for immobilization purposes, experiments were performed using different reaction conditions and different concentrations of reagents. Optimization experiments demonstrated that a 1-h reaction period at room temperature, using a ratio of carboxyl:TSTU:base of 1:1:1, gives quantitative yields of NHS ester.

We recommend using DMAP as base, since diisopropylethylamine or triethylamine caused extensive discoloration of carriers such as Sepharose. After coupling of protein or ligand, a small amount of black residue was left in solution. On the other hand, when the base was DMAP, white (colorless) gels were obtained.

Recently, it was shown that NHS esters can also be prepared in a mixed aqueous/organic solvent system using TSTU (8). This makes the system even more attractive since the solvents do not have to be dehydrated.

The method was also applied to prepare NHS esters in high yields on other polymers which contain carboxyl and hydroxyl groups, such as (carboxymethyl)cellulose and (carboxymethyl)dextran. NHS esters of poly(ethylene glycols), which contain carboxyl groups, were also prepared by this method, but we found that for isolation purposes, the conventional approach using *N*-hydroxysuccinimide and diisopropylcarbodiimide is preferable in this case.

Due to the high yield of activation, efficient coupling of proteins and ligands was obtained. When reacted with

1–5 mg of protein per g (wet-weight) of gel, coupling yields of about 90% for proteins were easily obtained with near-complete retention of biological activity.

**LITERATURE CITED**

- (1) Bauminger, S., and Wilchek, M. (1980) The use of carbodiimide in the preparation of immunizing conjugates. *Methods Enzymol.* 70, 151–159.
- (2) Becker, J. M., and Wilchek, M. (1972) Inactivation by avidin of biotin-modified bacteriophage. *Biochim. Biophys. Acta* 264, 165–170.
- (3) Cuatrecasas, P., and Parikh, I. (1972) Adsorbents for affinity chromatography. Use of *N*-hydroxysuccinimide esters of agarose. *Biochemistry* 11, 2291–2299.
- (4) Wilchek, M., Miron, T., and Kohn, J. (1984) Affinity chromatography. *Methods Enzymol.* 104, 3–55.
- (5) Wilchek, M., and Miron, T. (1987) Limitations of *N*-hydroxysuccinimide esters in affinity chromatography and protein immobilization. *Biochemistry* 26, 2155–2161.
- (6) Sakakibara, S., and Inukai, N. (1965) The trifluoroacetate method of peptide synthesis. I. The synthesis and use of trifluoroacetate reagents. *Bull. Chem. Soc. Jpn.* 38, 1979–1984.
- (7) Knorr, R., Trzeciak, A., Bannwarth, W., and Gillesen, D. (1989) New coupling reagents in peptide chemistry. *Tetrahedron Lett.* 30, 1927–1930.
- (8) Bannwarth, W., and Knorr, R. (1991) Formation of carboxamides with *N,N,N',N'*-tetramethyl(succinimido)uronium tetrafluoroborate in aqueous/organic solvent systems. *Tetrahedron Lett.* 32, 1157–1160.
- (9) Miron, T., and Wilchek, M. (1982) A spectrophotometric assay for soluble and immobilized *N*-hydroxysuccinimide esters. *Anal. Biochem.* 126, 433–435.

# Bioconjugate Chemistry

NOVEMBER/DECEMBER 1994  
Volume 5, Number 6

© Copyright 1994 by the American Chemical Society

## LETTERS

---

### New Amphipatic Polymer–Lipid Conjugates Forming Long-Circulating Reticuloendothelial System-Evading Liposomes

Martin C. Woodle, Charles M. Engbers, and Samuel Zalipsky\*

Liposome Technology, Inc., 960 Hamilton Court, Menlo Park, California 94025. Received August 8, 1994\*

---

Lipid-conjugates of two amphipatic polymers, poly(2-methyl-2-oxazoline) (PMOZ) and poly(2-ethyl-2-oxazoline) (PEOZ) (degree of polymerization  $\approx 50$ ) were synthesized by linking glutarate esters of the polymers to distearoylphosphatidylethanolamine (DSPE) or alternatively by termination of the polymerization process with DSPE. Surface-modified liposomes ( $90 \pm 5$  nm) prepared from either conjugate (5 mol % of total lipid) were injected into rats and followed by blood level and tissue distribution measurements. Both polymers PEOZ and PMOZ were found to convey long circulation and low hepatosplenic uptake to liposomes to the same extent as polyethylene glycol (PEG), the best known material for this purpose. This is the first demonstration of protection from rapid recognition and clearance conveyed by alternative polymers, which is equal to the effect of PEG.

---

Suppression or evasion of biological recognition mechanisms is of primary importance for successful use of implant devices and macromolecular or particulate drug delivery systems. Specifically, in the case of liposomal drug delivery, until recently, most applications were hampered by very short blood lifetimes of conventional lipid vesicles, their preferential accumulation in organs of the reticuloendothelial system (RES<sup>1</sup>), mainly liver and spleen, and dose-dependent pharmacokinetics. In the last few years several liposomal surface modifiers were

introduced, which addressed these problems to some extent. Among the various lipid derivatives used to prepare surface modified vesicles were dicarboxylic acid–lipid adducts, synthetic polymer conjugates, and natural (e.g., GM1) and synthetic glycolipids (for recent reviews see refs 1 and 2). Best RES-avoiding vesicles were obtained when poly(ethylene glycol) (PEG)–lipids (3) were incorporated into liposomes (4–12). Such liposomes exhibit dose-independent pharmacokinetics accompanied with remarkable persistence *in vivo* ( $t_{1/2} \geq 48$  h in humans). While several manuscripts attempted to explain this phenomenon (9–12), heretofore no other liposomal surface modifiers were identified that are as efficient as PEG in producing these beneficial properties. We report here for the first time dramatic RES-evasion and prolonged circulation effects brought about by the incorporation of lipid conjugates of two amphiphatic polyoxazolines into liposomes. Furthermore, the effect produced by both polymers described in this paper, poly-

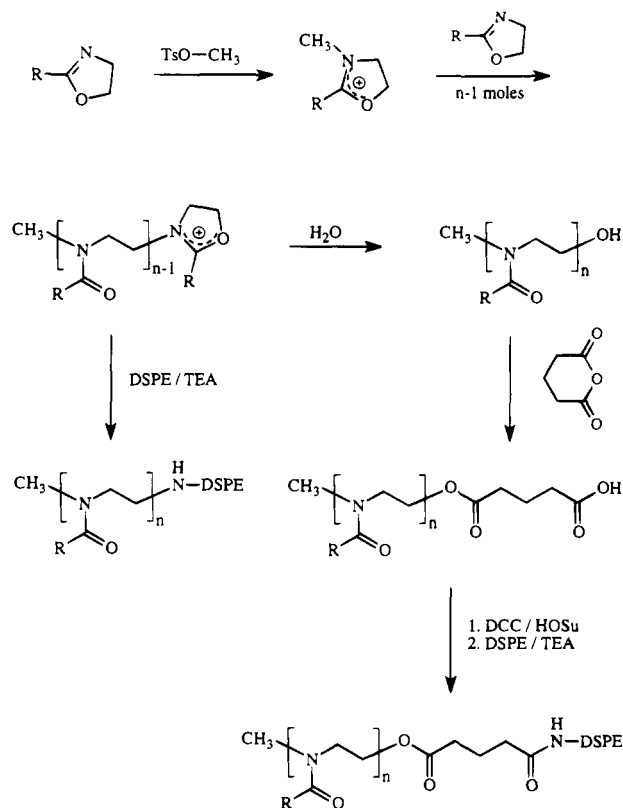
---

\* To whom correspondence should be addressed. Tel. (415) 323-9011; Fax (415) 617-3080.

\* Abstract published in *Advance ACS Abstracts*, October 15, 1994.

<sup>1</sup> Abbreviations: RES, reticuloendothelial system; PEG, poly(ethylene glycol); POZ, poly(oxazoline); PEOZ, poly(ethyloxazoline); PMOZ, poly(methyloxazoline); DSPE, distearoylphosphatidylethanolamine; EPC, egg phosphatidylcholine; EPG, egg phosphatidylglycerol; TsO, *p*-toluenesulfonate; DP, degree of polymerization; DCC, dicyclohexylcarbodiimide; HOSu, *N*-hydroxysuccinimide.



**Scheme 1. Preparation of Poly(oxazoline) Conjugates of DSPE<sup>a</sup>**

<sup>a</sup> Key: R =  $\text{CH}_3$  for PMOZ; R =  $\text{C}_2\text{H}_5$  for PEOZ; DP =  $n \approx 50$ .

(ethyloxazoline) (PEOZ) and poly(methyloxazoline) (PMOZ), are quantitatively comparable to the effect of PEG.

The synthesis of POZ-lipid conjugates is shown in Scheme 1. The polymers were prepared by methyl *p*-toluenesulfonate-initiated reactions of 2-methyl- and 2-ethyl-2-oxazolines following the previously published procedures (13–17). Since oxazoline polymerization is known to proceed via a cationic ring-opening mechanism yielding living polymers (for a review see ref 13), we used initiator–monomer ratios of 1:50, aiming for the same degree of polymerization as PEG of molecular weight 2000 (DP  $\approx 46$ ). The latter polymer was previously identified as optimal for preparation of long-circulating liposomes (5). Hydroxyl-terminated POZs of low dispersity ( $M_w/M_n \approx 1.1$ –1.4) were obtained after aqueous workup, followed by dialysis and lyophilization. The molecular weights of the polymers used in conjugation with lipid were 4000 for PMOZ and 5000 for PEOZ, as determined by GPC using PEG molecular weight standards (18). Pyridine-catalyzed reaction of PEOZ with glutaric anhydride in refluxing benzene was used to introduce the carboxylic acid end-group onto the polymer. Since PMOZ is insoluble under these conditions (Table 1), acetonitrile was used as a solvent for preparation of PMOZ-glutarate under otherwise same conditions. The glutarate derivatives of POZs<sup>2</sup> were converted into reactive succinimidyl esters and then coupled with distearoylphosphatidylethanolamine (DSPE) in chloroform in the presence of triethylamine (TEA). To assure complete conversion of DSPE into the conjugates the

**Table 1. Comparative Solubility of PEG, PEOZ, and PMOZ<sup>a</sup>**

solvent	polarity index <sup>b</sup>	PEG	PEOZ	PMOZ
petroleum ether	0.1	–	–	–
benzene	2.7	+	±	–
ethyl ether	2.8	–	–	–
<i>n</i> -butanol/2-propanol	3.9	–	+	+
tetrahydrofuran	4.0	±	+	–
chloroform	4.1	+	+	+
ethyl acetate	4.4	±	+	–
acetonitrile	5.8	+	+	+
dimethylformamide	6.4	+	+	+
water	10.2	+	+	+

<sup>a</sup> Solubilities of the polymers (DP  $\approx 45$ –50) were tested qualitatively. Key: +, soluble; –, insoluble; ±, soluble only upon warming, yet remain in solution at 25 °C. <sup>b</sup> Taken from ref 30.

reactive polymers were used in slight excess to DSPE<sub>3</sub>. Taking advantage of very low critical micelle concentration of distearoyl lipids, the conjugates were purified by removing excess of free polymer and other reactants by dialysis through 300 000 MWCO membrane (7, 19).

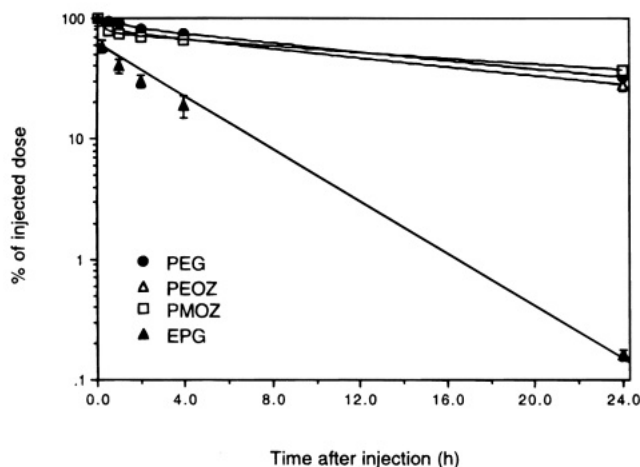
An alternative approach to POZ–DSPE conjugates involved direct termination of living oxazolinium-terminated polymers obtained in chloroform (14–16) with DSPE in the presence of TEA. This unoptimized procedure, while considerably simpler, was accompanied by very low recoveries of conjugates (yields  $\leq 5\%$ ). However, the purified conjugates (characterized by NMR and TLC)<sup>3</sup> obtained by both methods produced equivalent results in animal experiments with liposomal formulations described below.

Liposomes containing POZ–DSPE conjugates (or for comparison PEG–DSPE), egg phosphatidylcholine (EPC), and cholesterol were prepared as described previously (5, 6), labeled with <sup>67</sup>Ga, and injected intravenously into rats (20). Each liposomal preparation contained 5 mol % of the corresponding polymer–lipid conjugate. Figure 1 illustrates the persistence of the <sup>67</sup>Ga-labeled liposomes in the bloodstream. The behavior of a conventional liposomal preparation containing (for the total charge equivalence) egg phosphatidylglycerol (EPG) instead of polymer–lipid conjugate is also shown. The performance of both POZ-grafted liposomes ( $t_{1/2} \geq 15$  h) was similar to PEG–DSPE-containing vesicles. A striking similarity was also observed in biodistribution data (Figure 2). Low uptake by the liver and spleen was observed for the polymer-grafted liposomes with the largest portion of the dose remaining in the bloodstream after 24 h, in sharp contrast to the control preparation of conventional liposomes. Of the three polymer grafted vesicles compared here, PMOZ-containing liposomes produced slightly better results (Figures 1 and 2). However, the relative superiority of one polymer over another could be formulation dependent; e.g., each of the polymers might have a different optimal molecular weight. Therefore, a definite statement on this point has to be delayed until our ongoing studies fully examine the interrelationship of all the relevant formulation variables.

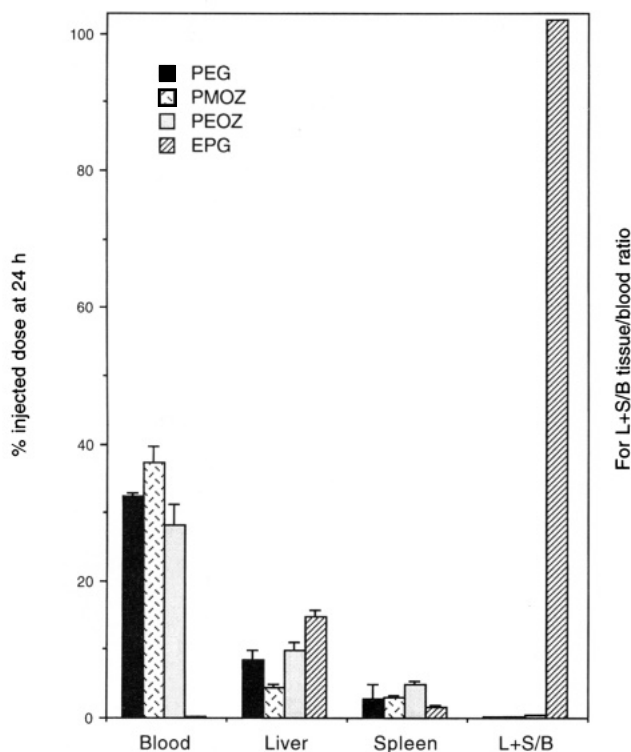
The ability of PEG to elicit its beneficial effect when grafted onto the surface of liposomes has been explained by its chains' high mobility associated with conforma-

<sup>2</sup> Glutarates of POZs obtained by terminating 2-oxazoline polymerization with glutaric acid were described by Miyamoto *et al.* (29).

<sup>3</sup> The conjugation reactions were followed by TLC on silica gel G (for PMOZ derivatives:  $\text{CHCl}_3/\text{EtOH}/30\%$  aqueous ammonia 3:7:1; for PEOZ  $\text{CHCl}_3/\text{MeOH}/\text{water}$  80:18:2; and 130:70:8 for derivatives of both POZs). Being only slightly soluble in chloroform, DSPE completely dissolved in the process of the polymer coupling reaction. Characteristic signals of both polymer and lipid components were clearly identifiable on H-NMR ( $\text{CDCl}_3$ ) spectra of the purified POZ–DSPE conjugates.



**Figure 1.** Blood lifetimes of  $^{67}\text{Ga}$ -labeled liposomes ( $90 \pm 5$  nm) prepared (5, 20) from the EPC, cholesterol, and DSPE conjugate of either PEG, PMOZ, or PEOZ, or as a control EPG, in a molar ratio of 1.85:1:0.15. Four Sprague–Dawley rats were injected with each liposomal preparation via the tail vein. Samples obtained by retro-orbital bleeding at various time points were used to determine radioactivity in the blood.



**Figure 2.** Selected tissue distribution at 24 h. The animals treated as described in legend for Figure 1 were sacrificed after 24 h and tissues removed for determination of radioactive content. Ratio of summed liver and spleen to blood levels (L + S/B) is a commonly used measure for RES uptake (5, 6, 8).

tional flexibility and water-binding ability—all of which contribute to the so-called steric stabilization effect, which results in the well-known propensity of PEG to exclude proteins, other macromolecules, and particulates from its surroundings (9–12). Taking advantage of these properties, PEG grafting has been widely used in other systems as a method for reduction of various undesirable consequences of biological recognition manifested by immunogenicity and antigenicity in the case of proteins (21–23), and thrombogenicity, cell adherence, and protein adsorption in the case of artificial biomaterials (24, 25).

Polyoxazolines, despite their low toxicity and superb

chemical versatility (13) have been considerably less studied than PEG, and only a few biomedical applications of these polymers were heretofore contemplated (26–29). However, the above-mentioned properties thought to be responsible for the “PEG-effect” could be reasonably attributable to the POZs as well. For example, similar to PEG, they have carbon–carbon–heteroatom repeating units, with tendency to be engaged in hydrogen bonds, which explains similarity in solubility properties of PEG and the two PEOZs (see Table 1).

The PEOZ and PMOZ conjugates described in this paper are the first polymers to be able to convey long circulation and low hepatosplenic uptake to liposomes to the same extent as PEG. Since previous efforts to identify liposomal surface modifiers other than PEG to exert measurable protection from biological recognition had only very limited success (1, 2, 4), our findings not only have important practical implications, but they should also help to advance the understanding of the properties that these amphiphatic polymers exert on the surfaces modified by them.

#### ACKNOWLEDGMENT

The authors are grateful to Ms. Jan Oaks and Ms. Bhagya Puntambekar for their enthusiastic and skillful technical assistance and Liposome Technology, Inc., for support and release for publication of this work.

#### LITERATURE CITED

- (1) Allen, T. (1994) The use of glycolipids and hydrophilic polymers in avoiding rapid uptake of liposomes by the mononuclear phagocyte system. *Adv. Drug Delivery Rev.* 13, 285–309.
- (2) Sunamoto, J., Akiyoshi, K., and Sato, T. (1993) Effective transport of bioactive materials to cell using specifically modified liposomes. *New Functionality Materials* (T. Tsuruta, M. Doyama, M. Seno, and Y. Imanishi, Eds.) pp 203–210, Elsevier Science, Amsterdam.
- (3) Zalipsky, S. (1995) Polyethylene glycol–lipid conjugates. *Stealth Liposomes* (D. Lasic, and F. Martin, Eds.) CRC Press, Boca Raton, FL (in press).
- (4) Woodle, M. C., and Lasic, D. D. (1992) Sterically stabilized liposomes. *Biochim. Biophys. Acta* 1113, 171–199.
- (5) Woodle, M. C., Matthay, K. K., Newman, M. S., Hidayat, J. E., Collins, L. R., Redemann, C., Martin, F. J., and Papahadjopoulos, D. (1992) Versatility in lipid compositions showing prolonged circulation with sterically stabilized liposomes. *Biochim. Biophys. Acta* 1105, 193–200.
- (6) Papahadjopoulos, D., Allen, T. M., Gabizon, A., Mayhew, E., Matthay, K., Huang, S. K., Lee, K.-D., Woodle, M. C., Lasic, D. D., Redemann, C., and Martin, F. J. (1991) Sterically stabilized liposomes: Improvements in pharmacokinetics and antitumor therapeutic efficacy. *Proc. Natl. Acad. Sci. U.S.A.* 88, 11460–11464.
- (7) Klivanov, A. L., Maruyama, K., Beckerleg, A. M., Torchilin, V. P., and Huang, L. (1991) Activity of amphipathic poly(ethylene glycol) 5000 to prolong the circulation time of liposomes depends on the liposome size and is unfavorable for immunoliposome binding to target. *Biochim. Biophys. Acta* 1062, 142–148.
- (8) Allen, T. M., Hansen, C., Martin, F., Redemann, C., and Yau-Young, A. (1991) Liposomes containing synthetic derivatives of poly(ethylene glycol) show prolonged circulation half-lives in vivo. *Biochim. Biophys. Acta* 1066, 29–36.
- (9) Lasic, D. D., Martin, F. J., Gabizon, A., Huang, S. K., and Papahadjopoulos, D. (1991) Sterically stabilized liposomes: A hypothesis on the molecular origin of the extended circulation times. *Biochim. Biophys. Acta* 1070, 187–192.
- (10) Blume, G., and Cevc, G. (1993) Molecular mechanism of the lipid vesicle longevity in vivo. *Biochim. Biophys. Acta* 1146, 157–168.

- (11) Needham, D., McIntosh, T. J., and Lasic, D. D. (1992) Repulsive interactions and mechanical stability of polymer-grafted lipid membranes. *Biochim. Biophys. Acta* 1108, 40–48.
- (12) Torchilin, V. P., and Papisov, M. I. (1994) Why do polyethylene glycol-coated liposomes circulate so long? *J. Liposome Res.* 4, 725–739.
- (13) Kobayashi, S. (1990) Ethyleneimine polymers. *Prog. Polym. Sci.* 15, 751–823.
- (14) Kobayashi, S., Uyama, H., Higuchi, N., and Saegusa, T. (1990) Synthesis of a nonionic polymer surfactant from cyclic imino ethers by the terminator method. *Macromolecules* 23, 54–59.
- (15) Kobayashi, S., Kaku, M., Sawada, S., and Saegusa, T. (1985) Synthesis of poly(2-methyl-2-oxazoline) macromonomers. *Polym. Bull.* 13, 447–451.
- (16) Chujo, Y., Ihara, E., Kure, S., and Saegusa, T. (1993) Synthesis of triethoxysilyl-terminated polyoxazolines and their cohydrolysis polymerization with tetraethoxysilane. *Macromolecules* 26, 5681–5686.
- (17) Sinai-Zingde, G., Verma, A., Liu, Q., Brink, A., Bronk, J. M., Mirand, H., McGrath, J. E., and Riffle, J. S. (1991) Polyoxazoline containing polymers useful as emulsifiers for polymer blends. *Macromol. Chem. Macromol. Symp.* 42/43, 329–343.
- (18) Nathan, A., Zalipsky, S., Erthel, S. I., Agathos, S. N., Yarmush, M. L., and Kohn, J. (1993) Copolymers of lysine and polyethylene glycol: A new family of functionalized drug carriers. *Bioconjugate Chem.* 4, 54–62.
- (19) Zalipsky, S. (1993) Synthesis of an end-group functionalized polyethylene glycol–lipid conjugate for preparation of polymer-grafted liposomes. *Bioconjugate Chem.* 4, 296–299.
- (20) Woodle, M. C. (1993) Gallium-67-labeled liposomes with prolonged circulation: Preparation and potential as nuclear imaging agents. *Nucl. Med. Biol.* 20, 149–155.
- (21) Delgado, C., Francis, G. E., and Fisher, D. (1992) The uses and properties of PEG-linked proteins. *Crit. Rev. Therap. Drug Carrier Syst.* 9, 249–304.
- (22) Katre, N. V. (1993) The conjugation of proteins with polyethylene glycol and other polymers. Altering properties of proteins to enhance their therapeutic potential. *Adv. Drug Delivery Rev.* 10, 91–114.
- (23) Zalipsky, S., and Lee, C. (1992) Use of functionalized polyethylene glycols for modification of polypeptides. *Poly(ethylene glycol) Chemistry: Biotechnical and Biomedical Applications* (J. M. Harris, Ed.) pp 347–370, Plenum Press, New York.
- (24) Merrill, E. W. (1992) Poly(ethylene oxide) and blood contact: A chronicle of one laboratory. *Poly(Ethylene Glycol) Chemistry: Biotechnical and Biomedical Applications* (J. M. Harris, Ed.) pp 199–220, Plenum Press, New York.
- (25) Llanos, G. R., and Sefton, M. V. (1993) Review. Does polyethylene oxide possess a low thrombogenicity? *J. Biomater. Sci. Polym. Edn.* 4, 381–400.
- (26) Goddard, P., Hutchinson, L. E., Brown, J., and Brookman, L. J. (1989) Soluble polymeric carriers for drug delivery. Part 2. Preparation and in vivo behaviour of N-acyl ethyleneimine copolymers. *J. Controlled Release* 10, 5–16.
- (27) Desai, N. P., and Hubbell, J. A. (1991) Solution technique to incorporate polyethylene oxide and other water-soluble polymers into surfaces of polymeric biomaterials. *Biomaterials* 24, 144–153.
- (28) Velander, W. H., Madurawe, R. D., Subramanian, A., Kumar, G., Sinai-Zingde, G., and Riffle, J. S. (1992) Polyoxazoline-peptide adducts that retain antibody avidity. *Biotechnol. Bioengin.* 39, 1024–1030.
- (29) Myamoto, M., Naka, K., Shiozaki, M., Chujo, Y., and Saegusa, T. (1990) Preparation and enzymatic activity of poly-[(N-acylimino)ethylene]-modified catalase. *Macromolecules* 23, 3201–3205.
- (30) Snyder, L. R. (1978) Classification of the solvent properties of common liquids. *J. Chromatogr. Sci.* 16, 223–234.

# Target-Promoted Alkylation of DNA

Tianhu Li,<sup>†</sup> Qinqing Zeng, and Steven E. Rokita\*

Department of Chemistry, State University of New York at Stony Brook, Stony Brook, New York 11794.  
Received June 30, 1994<sup>®</sup>

Inducible and selective alkylation of DNA was accomplished under neutral conditions by use of a silyl-protected phenol that served as a precursor for a highly reactive quinone methide. As expected, addition of fluoride triggered reaction of a model compound, 3-(*tert*-butyldimethylsiloxy)-4-[(*p*-nitrophenoxy)methyl]benzamide, and its oligodeoxynucleotide conjugate. Surprisingly, the silyl phenol was also specifically yet more slowly activated by the environment of duplex DNA in the absence of fluoride. This alternative process was associated with the hybridization of probe and target strands, and single-stranded DNA was unable to induce a similar activation. Therefore, DNA appears to effect its own alkylation by promoting the formation of an electrophilic and nondiffusible intermediate.

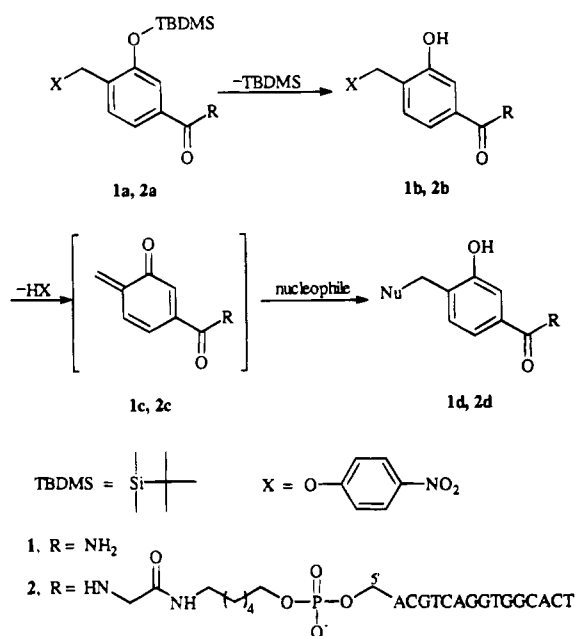
DNA alkylation is central to the action of many anticancer therapeutics despite its inherent lack of specificity. Most efforts to enhance the selectivity have relied on the technique of affinity modification (1–3) in which an electrophile is attached to a DNA-binding ligand. Much greater specificity would be possible through the use of mechanism-based inactivation. In this case, selective modification could be controlled by the binding and catalytic properties of a target as widely applied in enzymology (4). Extension of this to the field of nucleic acids is currently restricted by the limited reactions catalyzed by this class of molecules. For DNA, only the hydrolysis of benzo[ $\alpha$ ]pyrenediol epoxide has been investigated repeatedly (5–8), but other reports now indicate that DNA can also chemically activate the antitumor antibiotics CC-1065 (9, 10) and neocarzinostatin chromophore (11). For RNA, splicing reactions (12–14) and most recently esterase activity (15, 16) have received considerable attention. This letter reports the discovery of a silyl phenol ether that is converted by the environment of duplex DNA to a reactive electrophile available for alkylation of a target sequence.

Quinone methide formation is often employed in the design of enzyme inactivators (17–20) and is also associated with the biological activity of DNA-targeted drugs such as mitomycin (21–24) and anthracyclins (25–27). Our laboratory has recently studied model systems that form related intermediates under control of local pH (28, 29), reducing agents (30), and near-UV irradiation (30). A silyl-protected phenol provided a complementary source of quinone methide (Scheme 1). Stability of such a precursor is greatest at physiological pH (31), and quinone methide generation is easily triggered by addition of fluoride (32). Affinity modification based on this chemistry exhibited the expected properties: (a) only a target sequence of DNA was alkylated; (b) modification was initiated by fluoride; and (c) the alkylating species was produced transiently (33). Surprisingly, target modification was also evident when fluoride was replaced with chloride, bromide, phosphate, or perchlorate (33). This result has since been investigated below and shown to depend uniquely on the duplex formed by hybridization of probe and target strands.

<sup>†</sup> Current address: Department of Chemistry, Scripps Research Institute.

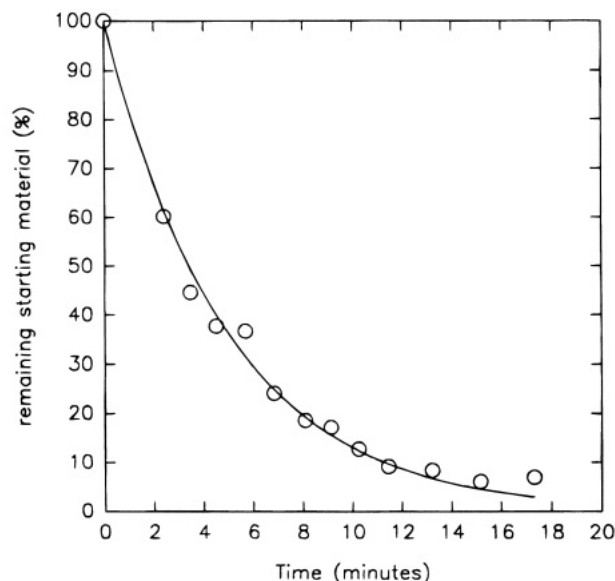
<sup>®</sup> Abstract published in *Advance ACS Abstracts*, October 1, 1994.

Scheme 1



To distinguish between the intrinsic and inducible reactivity of the silyl phenol ether, its stability and modification were examined first in the absence of DNA, and then attached to a single-stranded oligodeoxynucleotide, and finally held adjacent to duplex DNA. In each system, the fluoride-dependent activity served as a positive control for generating the quinone methide (Scheme 1). In the presence of 4 mM KF, desilylation of the low molecular weight model **1a** occurred with a half-life of 4 min as observed by  $^1\text{H}$  NMR (Figure 1). The resulting phenol **1b** was moderately stable under these conditions and could even be isolated after silica gel flash chromatography albeit in low yield (unoptimized, 9%).<sup>1</sup> Elimination of nitrophenol ( $t_{1/2} > 60$  h) and addition of water to form **1d** proceeded slowly under conditions equivalent to those of Figure 1.<sup>2</sup> Thus, as expected, the silyl phenol moiety was chemically competent for fluoride-induced reaction in the absence of DNA.

<sup>1</sup> Synthesis and characterization of **1a**, **1b**, and **1d** are included in the supplementary material. Preparation of **2a** was reported previously (33).

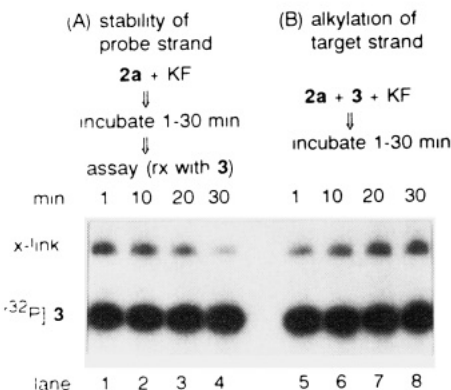


**Figure 1.** Fluoride dependent reaction of **1a**. Conversion of **1a** to **1b** was monitored by integrating the NMR signals of the benzylic protons of these compounds (5.21 and 5.16 ppm, respectively). Remaining starting material was determined as the fraction of **1a**/(**1a** + **1b**) and this was fit to a first order process using nonlinear regression (—). Reaction was initiated by adding 4 mM KF to a solution of **1a** (0.5 mM), 70 mM morpholinoethansulfonate (MES) and 2.5 M CD<sub>3</sub>CN in D<sub>2</sub>O pD 6.5 at 20 °C.

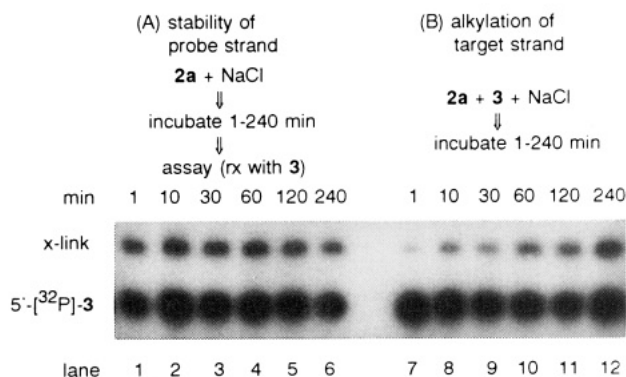
The fluoride-initiated activity of the oligonucleotide conjugate **2a** alone and in complex with a complementary target, **3**, 5'-d(AGTGCCACCTGACGTCTAAG), was also consistent with the activation process outlined in Scheme 1. In the absence of a target strand, the electrophilic intermediate **2c** was consumed via solvent, and possibly intramolecular, reaction. This process was illustrated by treating **2a** with fluoride for 1–30 min and then observing the mixture's diminished ability to form interstrand cross-links upon subsequent addition of **3** (Figure 2A). Both the decomposition of single strand **2a** and the cross-linking of duplex **2a** + **3** (Figure 2B) were induced by fluoride with similar efficiency. This suggests the common transformation of **2a** to **2c** controlled both reactions independent of the surrounding DNA structure.

In contrast, neither the model silyl phenol (**1a**) nor its single-stranded derivative (**2a**) exhibited any intrinsic or ion-inducible reactivity in the absence of fluoride. Compound **1a** did not undergo modification when another salt such as LiClO<sub>4</sub> (4–100 mM) replaced KF under the conditions described in Figure 1. NMR analysis of such incubations revealed that **1a** persisted beyond 10 days (20 °C) without change, and no trace of desilylation or substitution was detected. A related model lacking the carboxamide group was also inert in the presence of 100 mM LiClO<sub>4</sub> or NaCl (34). Similarly, these salts did not promote any of the possible solvent and intramolecular reactions that consumed the single-stranded reagent **2a** after its exposure to KF. Incubation of **2a** with NaCl in place of KF did not diminish its later ability to alkylate **3** (Figure 3A). Consequently, the silyl-protected phenol of **2a** expressed no spontaneous reactivity as a single strand.

<sup>2</sup> Reaction of the model **1b** proceeded more slowly than the related reaction of **2b**, oligodeoxynucleotide cross-linking, in part due to solvent effects (Q. Zeng, unpublished observations). The solubility of **1** was limited under aqueous conditions, and therefore, a mixed organic/aqueous system was used during its investigation. The oligodeoxynucleotide derivative **2** was examined under aqueous conditions.



**Figure 2.** Autoradiograms of denaturing polyacrylamide (20%) gels used to monitor nonproductive consumption of single-stranded **2a** vs interstrand cross-linking of **2a** + **3** in the presence of fluoride. For lanes 1–4, **2a** (9 nM) was preincubated with 200 mM KF in 1 mM MES pH 7 for the indicated times before addition of 5'-[<sup>32</sup>P]-**3** (9 nM). These final solutions were quenched after 30 min. For lanes 5–8, oligodeoxynucleotides **2a** and 5'-[<sup>32</sup>P]-**3** (9 nM each) were hybridized for one min in 1 mM MES pH 7 before addition of 200 mM KF. Samples were then incubated under ambient temperature and quenched (33) at the indicated times.

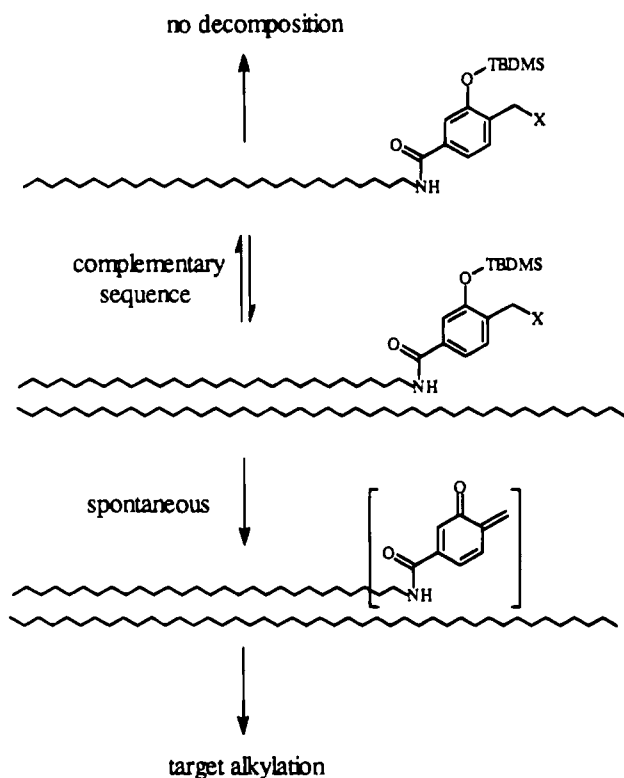


**Figure 3.** Autoradiograms of denaturing polyacrylamide (20%) gels used to monitor nonproductive consumption of single-stranded **2a** vs interstrand cross-linking of **2a** + **3** in the presence of NaCl. For lanes 1–6, **2a** (9 nM) was preincubated with 200 mM NaCl in 1 mM MES pH 7 for the indicated times before addition of 5'-[<sup>32</sup>P]-**3** (9 nM). These final solutions were quenched after 240 min. For lanes 7–12, oligodeoxynucleotides **2a** and 5'-[<sup>32</sup>P]-**3** (9 nM each) were hybridized for one min in 1 mM MES pH 7 before addition of 200 mM NaCl. Samples were then incubated under ambient temperature and quenched (33) at the indicated times.

Duplex formation played an obligatory role in the activation of the phenol derivative when fluoride was excluded. Hybridization of **2a** and its complement **3** effected strand cross-linking under conditions that did not promote any reaction of single-stranded **2a** (Figure 3A vs 3B). Probe-target modification was observed in the presence of NaCl (Figure 3B) albeit at a rate lower than that induced by KF at equivalent ionic strength. Ultimately, both conditions produced the same yield of cross-linking (ca. 30%) (33).

These results are not consistent with simple affinity modification since **1a** and **2a** exhibited no intrinsic reactivity that could be directed to a DNA sequence. Furthermore, a mechanism involving direct displacement could not explain both the similar reactivity of **2a** and **2a** + **3** in the presence of fluoride and the dissimilar reactivity of **2a** and **2a** + **3** in the absence of fluoride. Instead, the structure established by **2a** + **3** most likely converted the attached silyl phenol ether into an electrophilic intermediate for target alkylation. This transformation could mimic the fluoride-dependent mechanism

Scheme 2



by effecting loss of the silyl group and formation of the quinone methide (Scheme 1). Such an analogous pathway would also account for the similarity in cross-linking yields induced by fluoride and strand hybridization.

Selective modification of DNA is traditionally based on preferential binding and orientation of reactive functional groups (35). However, the intrinsic activity of such groups often causes in vivo modification of nontargeted components of a cell or organism. The inducible alkylation demonstrated here should now minimize these undesirable events since the reactive species is generated only after target recognition (Scheme 2).

#### ACKNOWLEDGMENT

This research was generously supported by the Center for Biotechnology, State University of New York at Stony Brook, in conjunction with the New York State Science and Technology Foundation. We thank the Mass Spectrometry Facility of UC Riverside for mass spectral analysis.

**Supplementary Material Available:** Preparation and characterization of **1a**, **1b**, and **1d** (4 pages). Ordering information is given on any current masthead page.

#### LITERATURE CITED

- (1) Dervan, P. B. (1991) Characterization of Protein-DNA Complexes by Affinity Cleaving. *Methods Enzymol.* 208, 497-513.
- (2) Uhlmann, E., and Peyman, A. (1990) Antisense Oligonucleotides: A New Therapeutic Principle. *Chem. Rev.* 90, 543-584.
- (3) Sigman, D. S., Bruice, T. W., Mazumder, A., and Sutton, C. L. (1993) Targeted Chemical Nucleases. *Acc. Chem. Res.* 26, 98-104.
- (4) Silverman, R. B. (1988) *Mechanism-Based Enzyme Inactivation: Chemistry and Enzymology*, Vols. I and II, CRC Press, Boca Raton.
- (5) Kootsra, A., Haas, B. L., and Slaga, T. J. (1980) Reaction of Benzo[ $\alpha$ ]-pyrene Diol-Epoxides with DNA and Nucleosomes in Aqueous Solution. *Biochem. Biophys. Res. Commun.* 94, 1432-1438.
- (6) Geacintov, N. E., Yoshida, H., Ibanez, V., and Harvey, R. G. (1982) Noncovalent Binding of 7 $\beta$ ,8 $\alpha$ -Dihydroxy-9 $\alpha$ ,10 $\beta$ -epoxytetrahydrobenzo[ $\alpha$ ]pyrene to Deoxyribonucleic Acid and Its Catalytic Effect on the Hydrolysis of the Diol Epoxide to Tetrol. *Biochemistry* 21, 1864-1869.
- (7) Michaud, D. P., Gupta, S. C., Whalen, D. L., Sayer, J. M., and Jerina, D. M. (1983) Effects of pH and Salt Concentration on the hydrolysis of a Benzo[ $\alpha$ ]pyrene 7,8-Diol-9,10-Epoxide Catalyzed by DNA and Polyadenylic Acid. *Chem.-Biol. Interact.* 44, 41-52.
- (8) Huang, C.-R., Milliman, A., Price, H. L., Urnao, S., Fetzer, S. M., and LeBreton, P. R. (1993) Photoemission Probes of Catalysis of Benzo[ $\alpha$ ]pyrene Epoxide Reactions in Complexes with Linear, Double-Stranded and Closed-Circular, Single-Stranded DNA. *J. Am. Chem. Soc.* 115, 7794-7805.
- (9) Lin, C. H., Beale, J. M., and Hurley, L. H. (1991) Structure of the (+)-CC-1065-DNA Adduct: Critical Role of Ordered Water Molecules and Implications for Involvement of Phosphate Catalysis in the Covalent Reaction. *Biochemistry* 30, 3597-3602.
- (10) Boger, D. L., Munk, S. A., Zarrinmayeh, H. (1991) (+)-CC-1065 DNA Alkylation: Key Studies Demonstrating a Non-covalent Binding Selectivity Contribution to the Alkylation Selectivity. *J. Am. Chem. Soc.* 113, 3980-3983.
- (11) Kappen, L. S., Goldberg, I. H. (1993) DNA Conformation-induced Activation of an Ene-diyne for Site-Specific Cleavage. *Science* 261, 1319-1321.
- (12) Cech, T. R. (1990) Self-Splicing of Group I Introns. *Annu. Rev. Biochem.* 59, 259-271.
- (13) Pace, N. R., and Smith, D. (1990) Ribonuclease P: Function and Variation. *J. Biol. Chem.* 265, 3587-3590.
- (14) Symons, R. H. (1992) Small Catalytic RNAs. *Annu. Rev. Biochem.* 61, 641-647.
- (15) Noller, H. F., Hoffarth, V., and Zimniak, L. (1992) Unusual Resistance of Peptidyl Transferase to Protein Extraction Procedures. *Science* 256, 1416-1419.
- (16) Piccirilli, J. A., McConnell, T. S., Zaug, A. J., Noller, H. F., and Cech, T. R. (1992) Aminoacyl Esterase Activity of the Tetrahymena Ribozyme. *Science* 256, 1420-1424.
- (17) Béchet, J.-J., Dupaix, A., Yon, J., Wakselman, M., Robert, J. C., and Vilkas, M. (1973) Inactivation of  $\alpha$ -Chymotrypsin by a Bifunctional Reagent, 3,4-Dihydro-3,4-dibromo-6-bromomethyl Coumarin. *Eur. J. Biochem.* 35, 527-59.
- (18) Harper, J. W., and Powers, J. C. (1985) Reaction of Serine Proteases with Substituted 3-Alkoxy-4-chloroisocoumarines and 3-Alkoxy-7-amino-4-chloroisocoumarines: New Reactive Mechanism-Based Inhibitors. *Biochemistry* 24, 7200-7213.
- (19) Lee, C.-H., and Skibo, E. B. (1987) Active-Site-Directed Reductive Alkylation of Xanthine Oxidase by Imidazo[4,5-*g*]quinazoline-4,9-diones Functionalized with a Leaving Group. *Biochemistry* 26, 7355-7362.
- (20) Myers, J. K., and Widlanski, T. S. (1993) Mechanism-Based Inactivation of Prostatic Acid Phosphatase. *Science* 262, 1451-1453.
- (21) Tomasz, M., and Lipman, R. (1981) Reductive Metabolism and Alkylating Activity of Mitomycin C Induced by Rat Liver Microsomes. *Biochemistry* 20, 5056-5061.
- (22) Egbertson, M., and Danishefsky, S. J. (1987) Modeling of the Electrophilic Activation of Mitomycins: Chemical Evidence for the Intermediacy of a Mitosene Semiquinone as the Active Electrophile. *J. Am. Chem. Soc.* 109, 2204-2205.
- (23) Tomasz, M., Chawla, A. K., and Lipman, R. (1988) Mechanism of Monofunctional and Bifunctional Alkylation of DNA by Mitomycin C. *Biochemistry* 27, 3182-3187.
- (24) Han, I., Russell, D. J., and Kohn, H. (1992) Studies on the Mechanism of Mitomycin C (1) Electrophilic Transformations: Structure-Reactivity Relationships. *J. Org. Chem.* 57, 1799-1807.
- (25) Fisher, J., Ramakrishnan, K., and Becvar, J. E. (1983) Direct Enzyme-Catalyzed Reduction of Anthracyclines by Reduced Nicotinamide Adenine Dinucleotide. *Biochemistry* 22, 1347-1355.



- (26) Gaudiano, G., Frigerio, M., Bravo, P., and Koch, T. H. (1990) Intramolecular Trapping of the Quinone Methide from Reductive Cleavage of Daunomycin with Oxygen and Nitrogen Nucleophiles. *J. Am. Chem. Soc.* **112**, 6704–6709.
- (27) Schweitzer, B. A., and Koch, T. H. (1993) Synthesis and Redox Chemistry of 5-Deoxydaunomycin. A Long-Lived Hydroquinone Tautomer. *J. Am. Chem. Soc.* **115**, 5440–5445.
- (28) Woolridge, E. M., Rokita, S. E. (1991) 6-(Difluoromethyl)-tryptophan as a Probe for Substrate Activation during the Catalysis of Tryptophanase. *Biochemistry* **30**, 1852–1857.
- (29) Woolridge, E. M., and Rokita, S. E. (1991) The Use of 6-(Difluoromethyl)indole to Study the Activation of Indole by Tryptophan Synthase. *Arch. Biochem. Biophys.* **286**, 473–480.
- (30) Chatterjee, M., and Rokita, S. E. (1994) The Role of a Quinone Methide in the Sequence Specific Alkylation of DNA. *J. Am. Chem. Soc.* **116**, 1690–1697.
- (31) Shirai, N., Moriya, K., and Kawazoe, Y. (1986) pH Dependence of Hydrolytic Removal of Silyl Group from Trialkylsilyl Ethers. *Tetrahedron* **42**, 2211–2214.
- (32) Marino, J. P., and Dax, S. L. (1984) An Efficient Desilylation Method for the Generation of *o*-Quinone Methides: Application to the Synthesis of (+)- and (–)-Hexahydrocannabinol. *J. Org. Chem.* **49**, 3671–3672.
- (33) Li, T., and Rokita, S. E. (1991) Selective Modification of DNA Controlled by an Ionic Signal. *J. Am. Chem. Soc.* **113**, 7771–7773.
- (34) Li, T. (1992) *Sequence Selective Modification of DNA with a Silyl Phenol Ether–Oligodeoxynucleotide Conjugate*, Ph.D. Dissertation, The State University of New York at Stony Brook.
- (35) Warpehoski, M. A., and Hurley, L. H. (1988) Sequence Selectivity of DNA Covalent Modification. *Chem. Res. Toxicol* **1**, 315–333.

# Synthesis and Primer Properties of Oligonucleotides Containing 3'-Deoxy-psicothymidine Units, Labeled with Fluorescein at the 1'-Position

Andrei Guzaev, Elena Azhayeva, Jari Hovinen, Alex Azhayev,\* and Harri Lönnberg

Department of Chemistry, University of Turku, FIN-20500 Turku, Finland. Received May 9, 1994\*

Several analogues of the standard M13 sequencing primer that contain up to five 3'-deoxy-psicothymidines, or one or two such units labeled with fluorescein at the 1'-position, have been prepared. All these oligonucleotides have been shown to prime the DNA-polymerase-catalyzed synthesis of DNA.

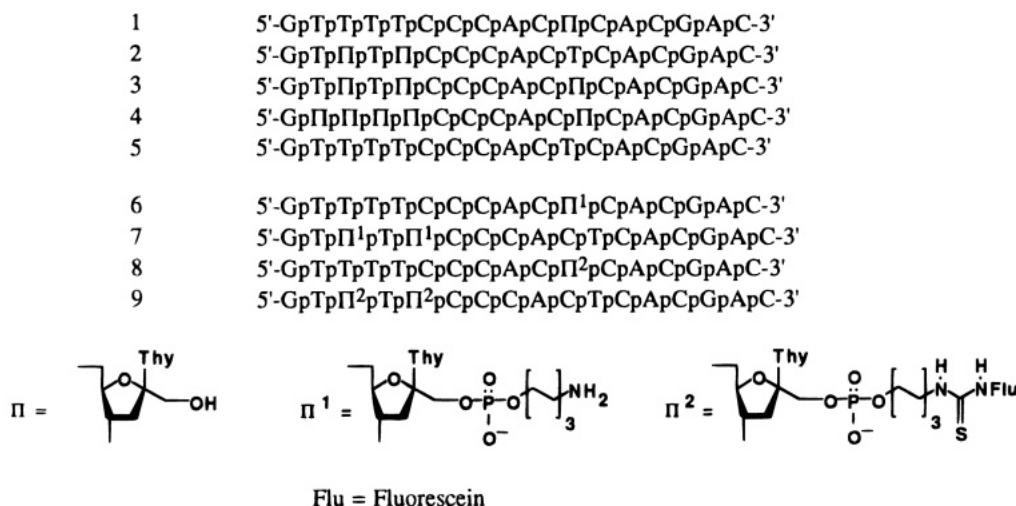
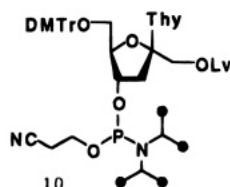
Oligonucleotide conjugates bearing reporter groups have recently found an increasing number of applications as versatile tools in basic research in molecular biology (1, 2), as diagnostic probes (2), and as regulators of gene expression (3, 4). Usually aminoalkyl tethers are employed to introduce reporter groups at the 5'- or 3'-terminus of the oligonucleotide (1–3, 5), at heterocyclic nucleic bases (6, 7), or at internucleosidic phosphodiester bonds (8). All these methods suffer from some shortcomings. 3'- and/or 5'-terminal conjugate groups prevent the enzymatic extension or ligation of the labeled oligonucleotide. Tethers attached to the nucleic bases sometimes weaken the base-pairing (9), and substitution of the phosphodiester bond gives rise to two diastereomers about phosphorus, which are not always easily resolved (10). Recently, several groups have reported on preparation of sugar moiety tethered oligonucleotides that upon hybridization place the reporter group at the minor groove (11–15). This approach leaves all the ionic and tautomeric properties as well as the functional groups of 2'-deoxynucleoside units unchanged and minimizes the steric hindrance for duplex formation. Manoharan *et al.* (11) and Sproat *et al.* (12) attached a linker to the 2'-position of a ribonucleoside unit and used the tether for subsequent labeling of the oligonucleotide. Matsuda *et al.* (13, 14) employed 3'-deoxy-psicouridine (1'-(hydroxymethyl)-2'-deoxyuridine) for the same purpose. Both approaches involve a multistep preparation of the phosphoramidite building block, carrying the protected aminoalkyl linker at the sugar moiety, and subsequent use of these monomers in the solid phase DNA synthesis. We have previously reported on derivatization of the 1'-position of 3'-deoxy-psicothymidine (1'-(hydroxymethyl)-2'-deoxythymidine) (16) during the course of oligonucleotide synthesis (15). This approach is advantageous, since a normal thymine base is used instead of uracil (13, 14), and the length and reactivity of the linker may be adjusted according to the requirements of the further derivatization without synthesis of new building blocks.

The present report describes the synthesis of oligonucleotides containing up to five 3'-deoxy-psicothymidine units  $\Pi$  (oligonucleotides 1–4) or up to two such units labeled with either an aminoalkyl group ( $\Pi^1$ , oligonucleotides 6, 7) or fluorescein at the 1'-position ( $\Pi^2$ , oligonucleotides 8, 9). Moreover, their ability to prime DNA-polymerase-catalyzed synthesis of DNA is demonstrated. All the oligonucleotides were analogues of the standard

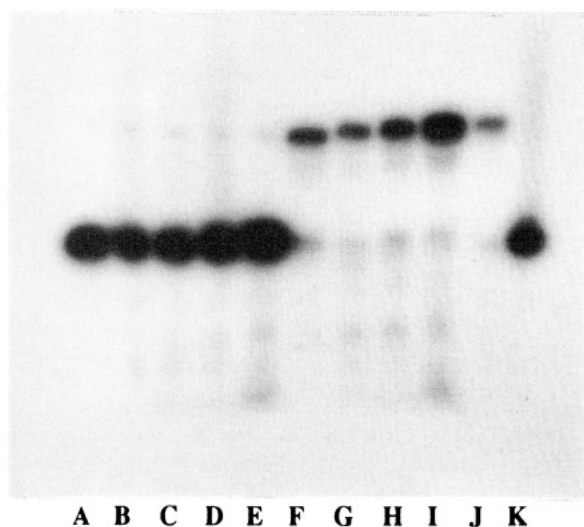
M13 primer 5, which is widely used in DNA sequencing (17) (Figure 1).

We have described previously the preparation of building block 10 (Figure 2) derived from 3'-deoxy-psicothymidine and demonstrated its efficiency in the oligonucleotide condensation (15). However, since the introduction of several modified units may bring additional sterical hindrance in the growing oligonucleotide chain, and hence decrease the coupling efficiency, the ABI 392 DNA synthesizer was programmed to use a longer coupling step (180 s) when the oligonucleotide chain was elongated with 10. The coupling yield of each psicothymidine unit proved to be about 98%, as determined by a trityl assay. After the chain assembly was completed, oligonucleotides 1–4 were deblocked in the conventional manner. Modified oligomers 6 and 7 were obtained as follows. The reaction columns were removed from the synthesizer upon completion of the chain elongation (DMTr-On synthesis) (18), 1'-O-levulinyl groups were cleaved (15), and the reaction columns were reinstalled to the synthesizer. The aminoalkyl phosphate groups were introduced using a commercial Aminolink-2 and a prolonged coupling step (180 s) as part of the standard protocol (18). For the preparation of 6 one coupling was sufficient. To obtain 7, two couplings, separated by acetonitrile wash and argon flush, were applied. Upon iodine oxidation, 6 and 7 were deblocked in a usual manner. All oligonucleotides prepared were isolated by successive anion exchange and reversed phase HPLC and finally desalted by gel filtration (15). The HPLC analysis of the oligonucleotides 1–4, 6, and 7, digested with a mixture of phosphodiesterases I and II in the presence of alkaline phosphatase (15), verified the presence of expected nucleosides in the correct ratio. Oligonucleotides 6 and 7 were finally reacted with FITC using two different methods. In method A the labeling was performed in a sodium carbonate buffer at pH 10.3 under standard conditions (13). The isolated yield of monolabeled oligonucleotide 8 was repeatedly 50–60% and that of the double labeled 9 30–40%. In method B acetylated long chain (alkylamino)-CPG was used as a carrier of oligonucleotides. Compounds 6 and 7 (2–3 OD) were dried in the presence of the carrier (2–3 mg), and the labeling was performed with a 3% solution of FITC in a mixture of pyridine–*N,N*-diisopropylethylamine–water (8:1:1, 100  $\mu$ L). After the reaction was completed (12 h, rt), the carriers and the adsorbed oligonucleotides were washed with dioxane (1.5 mL), dioxane–pyridine (19:1, 5  $\times$  1.5 mL), and finally with ether (1.5 mL). Labeled oligonucleotides were then dissolved in water, purified

\* Abstract published in *Advance ACS Abstracts*, September 15, 1994.

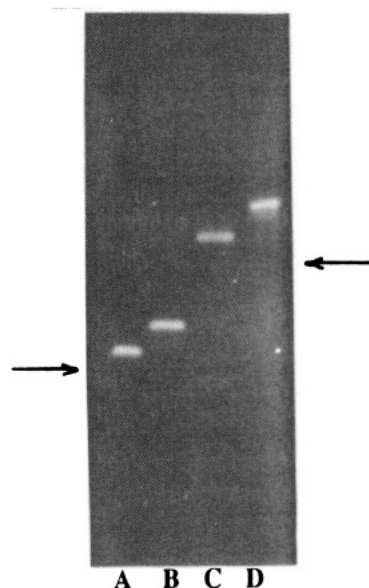
**Figure 1.** Structures of oligonucleotides 1–9.

Thy = thymine-1-yl; DMTr = 4,4'-dimethoxytrityl; Lv = levulinyl.

**Figure 2.** Structure of the building block 10.**Figure 3.** Autoradiogram of 20% PAGE: lines A, K,  $^{32}$ P-labeled commercial 17nt standard M13 sequencing primer 5; lines B–E,  $^{32}$ P-labeled 1–4; line F, enzymatic elongation of  $^{32}$ P-labeled commercial standard M13 sequencing primer 5 on 27nt matrix; lines G–J, enzymatic elongation of  $^{32}$ P-labeled 1–4 on 27nt matrix.

by a successive anion exchange and reversed-phase HPLC, and finally desalted. The isolated yield of **8** was 80–90% and that of double labeled **9** was 70–80% repeatedly. The UV–vis absorption spectra of the labeled **8** and **9** exhibited the characteristic fluorescein absorption at 490 nm and oligonucleotide absorption at 260 nm, the ratio A (490 nm)/A (260 nm) observed with **9** being approximately 2-fold compared to that of **8**.

Matsuda *et al.* (13, 14) have shown that oligonucleotides containing a 1'-derivatized 3'-deoxypsycouridine unit hybridize with complementary DNA strands. The aim of this work was to test the ability of the oligonucleotides 1–4, as well as that of the FITC-labeled **8** and **9**,

**Figure 4.** Photograph of 20% PAGE under the long wavelength UV: lines A, B, **8** and **9**; lines C, D, enzymatic elongation of **8** and **9** on 27nt matrix. The arrow on the left indicates the position of  $^{32}$ P-labeled commercial 17nt standard M13 sequencing primer 5; the arrow on the right indicates the position of enzymatically elongated  $^{32}$ P-labeled commercial standard M13 sequencing primer 5 on 27nt matrix.

to prime the DNA–polymerase-catalyzed reaction and to compare their priming ability to that of commercial standard M13 sequencing primer 5. 5'- $^{32}$ P-Labeled (19) derivatives 1–4 and FITC-labeled **8** and **9** were annealed to the synthetic 27-nt. complementary strand, and the polymerase reaction, employing Sequenase version 2.0, was performed.<sup>1</sup> The products were analyzed with PAGE. Figure 3 shows the autoradiography of PAGE,

<sup>1</sup> The elongation reaction mixtures contained the following: 1.25 pmol of  $^{32}$ P-labeled 1–5, annealed to an equal amount of synthetic matrix 5'-GTTTACAACTGCTGACTGGGAAAAC-3'; 1–2 units of Sequenase version 2.0; 0.06 M 1,4-dithio-D,L-threitol; 75  $\mu$ M each 2'-deoxynucleoside 5'-triphosphate, 40 mM Tris–HCl pH 7.5; 20 mM MgCl<sub>2</sub>; 50 mM NaCl. The chain elongation reaction of FITC-labeled primers contained 60 pmol of **8** and **9** and an equal amount of synthetic matrix. After 10 min at 37 °C reactions were stopped by 10 times dilution with "stop-solution" (95% formamide, 20 mM EDTA, 0.05% bromophenol blue, 0.05% xylene cyanol). Products of the chain elongation reactions were analyzed with 20% PAGE.

referring to the experiment with primers 1–5. Figure 4 demonstrates the photograph of PAGE taken under the long wavelength UV and referring to the DNA–polymerase reaction with luminescent primers 8 and 9. It is clearly seen that oligonucleotides containing up to five 3'-deoxypsicothymidine units are all able to serve as efficient primers in the DNA–polymerase synthesis of DNA, analogously to the commercial M13 sequencing primer 5. The attachment of one or two fluorescein molecules *via* (aminoalkyl)phospho-linker to the 1'-position of 3'-deoxypsiconucleoside still does not prevent the oligonucleotide analogues to hybridize with the complementary DNA and prime the enzymatic reaction.

In summary, the introduction of 1'-modified nucleosides and the subsequent tethering may easily be performed on an automated DNA synthesizer. Neither several 3'-deoxypsicothymidine units nor their derivatives tethered with bulky substituents at O-1' abolish the ability of modified oligonucleotide to hybridize the complementary DNA strand and prime the polymerase reaction. The data presented demonstrate an alternative approach for the labeling of DNA with reporter groups.

#### ACKNOWLEDGMENT

Financial support from the Research Council for Natural Sciences, the Academy of Finland, is gratefully acknowledged.

#### LITERATURE CITED

- (1) Eckstein, F. (Ed.) (1991) *Oligonucleotides and Analogues. A Practical Approach*, IRL Press, Oxford.
- (2) English, U., and Gauss, D. H. (1991) Chemically Modified Oligonucleotides as Probes and Inhibitors. *Angew. Chem., Int. Ed. Engl.* 30, 613–629.
- (3) Cohen, J. S., Ed. (1989) *Oligodeoxynucleotides. Antisense Inhibitors of Gene Expression*, The Macmillan Press Ltd., London.
- (4) Thuong, N. T., and Helene, C. (1993) Sequence-Specific Recognition and Modification of Double-Helical DNA by Oligonucleotides. *Angew. Chem., Int. Ed. Engl.* 32, 666–690.
- (5) Beaucage, S. L., and Iyer, R. P. (1993) The Functionalization of Oligonucleotides Via Phosphoramidite Derivatives. *Tetrahedron* 49, 1925–1963.
- (6) Goodchild, J. (1990) Conjugates of Oligonucleotides and Modified oligonucleotides: A Review of Their Synthesis and Properties. *Bioconjugate Chem.* 1, 165–187.
- (7) Markiewicz, W. T.; Gröger, G., Rösch, R., Zebrowska, A., and Seliger, H. (1992) A New Method of Synthesis of Fluorescently

- Labeled Oligonucleotides and their Application in DNA Sequencing. *Nucleosides Nucleotides* 11, 1703–1711.
- (8) Agrawal, S. (1994) Functionalization of Oligonucleotides with Amino Groups and Attachment of Amino Specific Reporter Groups. *Methods in Molecular Biology: Protocols for Oligonucleotide Conjugates* (Agrawal, S., Ed.) Vol. 26, pp 93–120, Humana Press, Totowa, NY.
  - (9) Tesler, J., Kruickshank, K. A., Morrison, L. E., and Netzel, T. L. (1989) Synthesis and Characterization of DNA Oligomers and Duplexes Containing Covalently Attached Molecular Labels: Comparison of Biotin, Fluorescein, and Pyrene Labels by Thermodynamic and Optical Spectroscopic Measurements. *J. Am. Chem. Soc.* 111, 6966–6976.
  - (10) O'Donnell, M., Hebert, N., and McLaughlin, L. W. (1994) The Stereospecific Introduction of Reporter Groups to Oligodeoxynucleotides by the Labeling of Individual Phosphorus Diastereomers. *BioMed. Chem. Lett.* 4, 1001–1004.
  - (11) Manoharan, M., Guinosso, Ch. J., and Cook, P. D. (1991) Novel Functionalization of the Sugar Moiety of Nucleic Acids for Multiple Labeling in the Minor Groove. *Tetrahedron Lett.* 32, 7171–7174.
  - (12) Douglas, M. E., Beijer, B., and Sproat, B. S. (1994) An Approach towards Thiol Mediated Labeling in the Minor Groove of Oligonucleotides. *BioMed. Chem. Lett.* 4, 995–1000.
  - (13) Dan, A., Yoshimura, Y., Ono, A., and Matsuda, A. (1993) Nucleosides & Nucleotides. 118. Synthesis of Oligonucleotides Containing a Novel 2'-Deoxyuridine Analogue that Carries an Aminoalkyl Tether at 1'-Position; Stabilization of Duplex Formation by an Intercalating Group Accommodated in the Minor Groove. *BioMed. Chem. Lett.* 3, 615–618.
  - (14) Ono, A., Dan, A., and Matsuda, A. (1993) Nucleosides & Nucleotides. 121. Synthesis of Oligonucleotides Carrying Linker Groups at the 1'-Position of Sugar Residues. *Bioconjugate Chem.* 4, 499–508.
  - (15) Azhaye, A., Guzaev, A., Hovinen, J., Azhaye, E., and Lönnberg, H. (1993) Analogues of Oligonucleotides Containing 3'-Deoxy- $\beta$ -D-Psicothymidine. *Tetrahedron Lett.* 34, 6435–6438.
  - (16) Azhaye, A., Guzaev, A., Hovinen, J., Mattinen, J., Sillanpää, R., and Lönnberg, H. (1994) Synthesis and Properties of 3'-Deoxypsiconucleosides: Anomeric 1-(3-Deoxy-D-erythro-2-hexulofuranosyl)thymine and 9-(3-Deoxy-D-erythro-2-hexulofuranosyl)adenine. *Synthesis* 4, 396–400.
  - (17) USB (1992) *Molecular Biology Reagents/Protocols*, 236.
  - (18) Applied Biosystems (1988) *User Bulletin* 49.
  - (19) Culagina, M., Scaptsova, N., Batchikova, N., Kurkin, A., and Azhaye, A. (1990) H-Phosphonate Method in the Synthesis of the Human Interleukin 4 Gene. (in Russian) *Bioorgan. Khim.* 16, 625–634.

# Site-Specific Conjugation of a Temperature-Sensitive Polymer to a Genetically-Engineered Protein<sup>†</sup>

Ashutosh Chilkoti,<sup>‡</sup> Guohua Chen,<sup>§</sup> Patrick S. Stayton,<sup>\*,‡</sup> and Allan S. Hoffman<sup>\*,§</sup>

Center for Bioengineering, University of Washington, WD-12/FL-20,  
Seattle, Washington 98195. Received June 8, 1993<sup>®</sup>

A genetically-engineered mutant of cytochrome b<sub>5</sub>, incorporating a unique cysteine residue, was conjugated to maleimide-terminated oligo(*N*-isopropylacrylamide). The conjugation of the protein by reaction of the cysteine residue, precisely positioned by site-directed mutagenesis techniques, with an activated oligomer containing only one reactive end group in the oligomer chain permits the site-specific and stoichiometric conjugation of the oligomer with the protein. The protein–oligomer conjugate was shown to exhibit lower critical solution temperature (LCST) behavior, similar to the free oligomer. Furthermore, the LCST behavior of the protein–oligomer conjugate is reversible and allows selective precipitation of the conjugate above its LCST.

Poly(*N*-isopropylacrylamide) (poly(NIPAAm)) is a temperature-sensitive polymer that exhibits lower critical solution temperature (LCST) behavior in water. Below its LCST of 32 °C, poly(NIPAAm) is readily soluble in water, while above its LCST the polymer sheds much of its bound water and becomes hydrophobic, which leads to collapse and aggregation of the polymer chains and subsequent precipitation of the polymer (1). This phenomenon is reversible and occurs within a sharp transition range (typically 1–2 °C) (1). The LCST behavior of poly(NIPAAm) is fully maintained upon conjugation to proteins (2), making such protein–polymer conjugates attractive for affinity separations and immunoassays (3–8).

Conventional protein–polymer conjugation schemes utilize the reactive amino group of lysine residues to attach proteins to activated soluble polymers. Limitations in controlling the conjugation chemistry frequently arise because the number and location of lysine residues vary greatly in natural proteins and because the location of reactive groups along the polymer chain is random. Thus, the stoichiometry of the protein–polymer conjugate and the attachment site(s) of the polymer to the protein cannot be precisely controlled, factors that may have important implications for protein stability and function. These limitations may be circumvented by appropriate design of both the protein and the activated polymer.

Protein engineering techniques permit the design of unique attachment sites on the protein surface for polymer conjugation. The synthesis of a polymer with one activated group per polymer chain, and at one end of the molecule, then allows the stoichiometrically-precise attachment of the polymer to the protein of interest. Furthermore, genetic engineering techniques allow the attachment site to be precisely defined on the protein molecule using site-directed mutagenesis techniques.

We report here the stoichiometrically-precise, site-specific attachment of oligo(NIPAAm) by one end group only to a genetically-engineered protein containing a unique thiol functionality at a defined surface site. The protein is conjugated by reaction of the protein sulfhydryl group with a polymer containing a single maleimide end group. The protein selected for these experiments is cytochrome b<sub>5</sub>, a small (molecular mass: ~11 000 Da), bis-imidazole-ligated heme protein (9–11). The absence of cysteine residues in the native protein, and the availability of detailed structural information for this protein (12, 13), make it an attractive candidate for the design of site-directed cysteine mutants. Furthermore, the unique electronic and optical properties associated with the heme prosthetic group provide a convenient spectroscopic probe to monitor the thermally induced reversible precipitation of the protein–polymer conjugate (14).

A unique thiol group was introduced by the replacement of a threonine residue at amino acid position 8 with a cysteine utilizing site-directed mutagenesis (T8C) (15, 16). The maleimide (MI)-terminated oligo(NIPAAm) (MI-oligo(NIPAAm))<sup>1</sup> was conjugated to T8C in solution; the reaction scheme is shown in Figure 1.<sup>2</sup> Native cytochrome b<sub>5</sub> did not react with MI-oligo(NIPAAm)

<sup>1</sup> The maleimide-terminated oligo(NIPAAm) [MI-oligo(NIPAAm)] was synthesized as follows: first, the amino-terminated oligo(NIPAAm) [A-oligo(NIPAAm)] with a molecular weight of 1900 was synthesized by free radical polymerization of NIPAAm using 2,2'-azobisisobutyronitrile and 2-aminoethanethiol hydrochloride as initiator and chain transfer reagent, respectively, at 60 °C for 4 h. Then, the amino end group was reacted with succinimidyl 4-(*N*-maleimidomethyl)cyclohexane-1-carboxylate, resulting in MI-oligo(NIPAAm).

<sup>2</sup> The following procedure was performed to conjugate T8C to MI-oligo(NIPAAm). Typically, 160 µL of a 1 mM protein solution in 50 mM phosphate, 1 mM EDTA buffer, pH 8.0 was reduced with 1 mM dithiothreitol (DTT) for 10 min at 4 °C. The mixture was passed over a Sephadex G-25 gel filtration column equilibrated with the same buffer to recover the protein free of DTT. The protein band was collected in a 15 mL centrifuge tube containing a 10-fold molar excess of MI-oligo(NIPAAm). The reaction was allowed to proceed for 4 h at room temperature with gentle shaking to ensure complete mixing of the reactants. The T8C/MI-oligo(NIPAAm) conjugate was separated from unreacted T8C by the following procedure: 10% (v/v) saturated (NH<sub>4</sub>)<sub>2</sub>SO<sub>4</sub> was added to the mixture to depress the LCST from

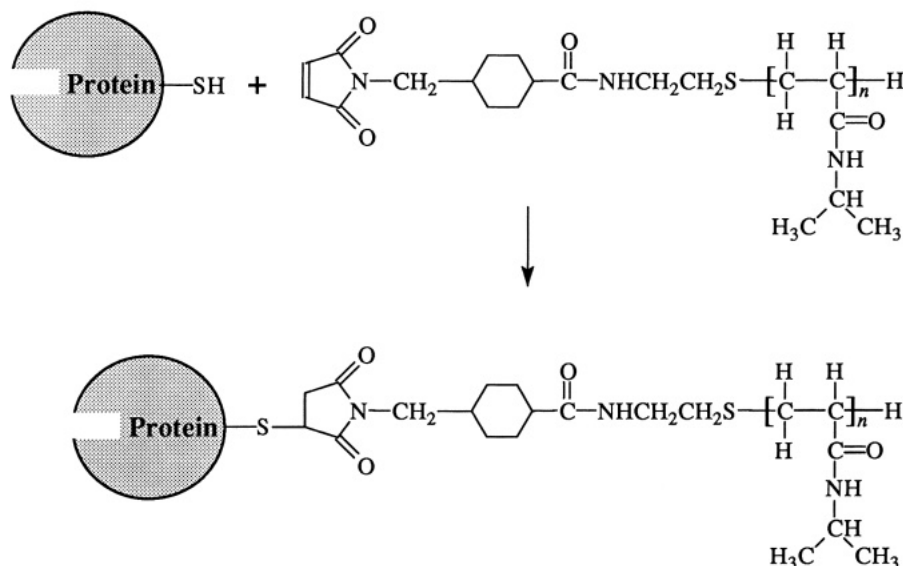
\* Authors to whom correspondence should be addressed. Tel (P.S.S.): (206) 685-8148. Tel (A.S.H.): (206) 543-9423. Fax: (206) 685-3300.

<sup>†</sup> Supported by Whitaker Foundation (P.S.S) and NSF Grant No. BCS-9101716 (A.S.H).

<sup>‡</sup> WD-12.

<sup>§</sup> FL-20.

<sup>®</sup> Abstract published in *Advance ACS Abstracts*, August 15, 1994.



**Figure 1.** Reaction scheme of stoichiometrically-precise conjugation of a protein to activated poly(NIPAAm) by reaction of the protein sulfhydryl group with a maleimide group, located at one end of the polymer chain.

under the reaction conditions utilized,<sup>3</sup> indicating that the maleimide end groups react selectively with thiol groups in the protein. Given the presence of only one thiol group in T8C, these results strongly suggest a 1:1 stoichiometry of protein and oligomer in the T8C-oligo(NIPAAm) conjugate.

These conclusions are supported by matrix-assisted laser desorption ionization-time of flight (MALDI-TOF) mass spectrometry (MS).<sup>4</sup> MALDI-TOF MS of T8C/MI-oligo(NIPAAm) conjugate showed a peak at ~11 000 Da [ $(M + H)^+$ ], and a minor peak at ~13 000 Da. The latter peak was not observed in the spectrum of protein alone (native b5, T8C) or the spectrum of a physical mixture of native b5 and MI-oligo(NIPAAm). The MALDI-TOF MS spectrum of MI-oligo(NIPAAm) displays a range of peaks differing by 113 Da, suggesting that they can be assigned to  $[nM + H]^+$  ions where M is the monomer

(minus the maleimide endgroup). The observation of these peaks is consistent with the distribution of oligomer chain lengths expected from free radical polymerization. More importantly, however, the molecular weight distribution of the oligomer is centered at ~1900 Da, which is consistent with the difference in mass of the protonated protein and the unique peak at ~13 000 Da (11 000 + 1900 Da) observed only in the spectrum of the conjugate. These results strongly support an oligomer:protein stoichiometry of 1:1. We note that, given the distribution of oligomer chain lengths, we would expect a series of peaks corresponding to oligomers with different chain lengths conjugated to T8C but the low signal to noise in the mass spectrum of the conjugate precludes their assignment.

The LCST of the T8C/MI-oligo(NIPAAm) conjugate in water, determined spectrophotometrically by cloud point measurement,<sup>5</sup> was 32 °C, which is in agreement with the free oligomer LCST. The reversible precipitation of the T8C/MI-oligo(NIPAAm) conjugate, monitored by the solution absorbance of the heme group at 412 nm, is shown in Figure 2.<sup>6</sup> The T8C/MI-oligo(NIPAAm) conjugate was cooled at 4 °C, and the absorbance at 412 nm was measured to determine the concentration of the conjugate (cooling cycle 1, filled bar). The T8C/MI-oligo(NIPAAm) conjugate was then heated at 37 °C for 5 min, followed by centrifugation at room temperature at 10000g for 10 min to precipitate the T8C/MI-oligo(NIPAAm) conjugate. The fraction of unprecipitated T8C/MI-oligo(NIPAAm) conjugate was then determined by measuring the absorbance at 412 nm of the supernatant (heating cycle 1, filled bar). A mixture of T8C and amino-terminated oligo(NIPAAm) [A-oligo(NIPAAm)] was simi-

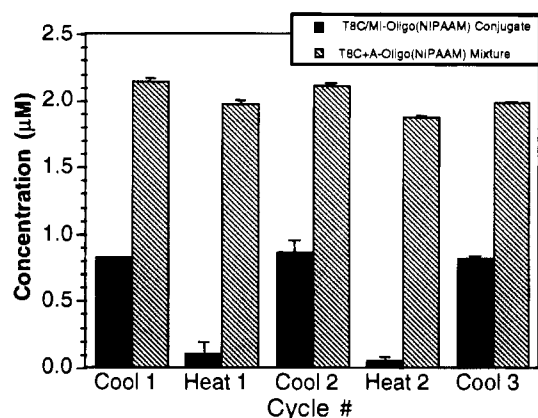
32 °C to ~20 °C, and the reaction mixture was warmed to 37 °C (> LCST) to selectively precipitate the T8C/MI-oligo(NIPAAm) conjugate. The precipitate was then separated by centrifugation (10000g, ambient temperature) to produce a pink-colored pellet. The pellet was redissolved in buffer, and the precipitation step was repeated twice to ensure complete removal of the unreacted T8C. There is probably some unreacted oligo(NIPAAm) that is precipitated along with the T8C/MI-oligo(NIPAAm) conjugate.

<sup>3</sup> One hundred  $\mu$ L of 0.84 mM native cytochrome b<sub>5</sub> was mixed with a 10-fold molar excess of MI-oligo(NIPAAm) following the same procedure as for T8C conjugation. No conjugation of MI-oligo(NIPAAm) with native b<sub>5</sub> was achieved, based on the absence of a visible peak at 412 nm in the redissolved pellet, indicating that no protein was entrapped in the precipitated polymer.

<sup>4</sup> MALDI-TOF mass spectra were acquired on a Finnigan MAT LaserMAT LD-TOF instrument. Samples were prepared by depositing ~1  $\mu$ L of sample on the center of a gold-plated metal target. All samples were at 5–10  $\mu$ M concentration in distilled, deionized water except the T8C/MI-oligo(NIPAAm) conjugate, which was at a concentration of 1  $\mu$ M. The matrix used was 2,5-dihydroxybenzoic acid, dissolved in 60% acetonitrile, 40% 0.1% TFA at a concentration of ~5–10 mg/mL. The molar ratio of analyte to matrix was typically 1:10 000. The samples were allowed to air dry and placed in the spectrometer. Multiple laser shot spectra were acquired after spectral optimization, which involved determining the minimum laser power density required to observe analyte ions from one of four predefined target positions. The instrument was calibrated using sperm whale apomyoglobin as a calibrant.

<sup>5</sup> The cloud point of the T8C/MI-oligo(NIPAAm) conjugate was measured spectrophotometrically in deionized-distilled water with a temperature rate increase of 0.4 °C min<sup>-1</sup>. The temperature at 90% light transmittance (at 500 nm) was defined as the cloud point. Because (NH<sub>4</sub>)<sub>2</sub>SO<sub>4</sub> depresses the LCST of the conjugate, and the presence of free oligomer (precipitated and collected along with the conjugate by thermally-induced precipitation and centrifugation at 37 °C) can interfere with the measurement of the LCST of the protein-oligomer conjugate, (NH<sub>4</sub>)<sub>2</sub>SO<sub>4</sub> and unreacted MI-oligo(NIPAAm) were removed from the T8C/MI-oligo(NIPAAm) conjugate by ultrafiltration through a 10 000 MW cutoff filter (Amicon).





**Figure 2.** Concentration of the T8C/MI-oligo(NIPAAM) conjugate (filled bars) and the control, a mixture of T8C and A-oligo(NIPAAM) (hatched bars) plotted versus cycle number. For the cooling cycles 1–3, the sample was assayed below the LCST, and for heating cycles 1 and 2, the sample was assayed above its LCST (see footnotes 6 and 7 for details).

larly assayed<sup>7</sup> as a control for the effect of physical coprecipitation of the protein due to the presence of A-oligo(NIPAAM) and  $(\text{NH}_4)_2\text{SO}_4$  (17) (hatched bar, cooling cycle 1 and heating cycle 1, respectively). This process was then repeated twice to examine the reversibility of this phenomenon and the short term stability of the protein-oligomer conjugate.

Three important observations can be derived from these data. First, the T8C/MI-poly(NIPAAM) conjugate can be precipitated above the LCST of the protein-oligomer conjugate. Below its LCST, the protein-oligomer conjugate is soluble (cooling cycle 1, filled bar). Upon heating at 37 °C the conjugate precipitates, which is shown by the significantly lower concentration of the conjugate in the supernatant (heating cycle 1, filled bar). This process is ~90% efficient in selectively fractionating the protein-oligomer conjugate from the aqueous phase, as shown by the difference in the concentration of soluble protein-oligomer conjugate in cycles 2 and 3 (filled bars). Second, this behavior is fully reversible, shown by the repeated cycling of the same sample between the hydrated, water-soluble state and the precipitated, insoluble state. Third, this phenomenon requires covalent conjugation of the oligomer and protein, as shown by the much lower (<10%) degree of precipitation of a physical mixture of protein (T8C) and A-oligo(NIPAAM), even with added

$(\text{NH}_4)_2\text{SO}_4$ . Finally, we note that the degree of conjugation required for precipitation of protein-poly(NIPAAM) conjugates has, heretofore, been difficult to control, largely due to the inherent lack of control in the number and location of the active sites on the oligomer chains and their subsequent reaction with native proteins. The results in this study provide clear evidence that a 1:1 conjugation of poly(NIPAAM) with an average molecular weight approximately 6-fold smaller than the protein is sufficient to allow efficient (>90%) and reversible precipitation of the protein-oligomer conjugate.

#### ACKNOWLEDGMENT

We thank Stephen G. Sligar and Mark McLean (Department of Biochemistry, University of Illinois at Urbana-Champaign, Urbana, IL) for providing native cytochrome  $b_5$  and the T8C mutant. The oligomer synthesis and end-conjugation to native proteins has been developed under support of the National Science Foundation, Grant No. BCS-9101716 (A.S.H.). We also thank John Yates (National Science Foundation Center for Molecular Biotechnology, Department of Molecular Biotechnology, University of Washington) for access to the MALDI-TOF MS instrumentation.

#### LITERATURE CITED

- (1) Heskins, M., and Guillet, J. E. (1968) Solution properties of poly(*N*-isopropylacrylamide). *J. Macromol. Sci. Chem.* A2-(8), 1441.
- (2) Chen, J. P., Yang, H. J., Hoffman, A. S. (1990) Polymer-protein conjugates I. Effect of protein conjugation on the cloud point of poly(*N*-isopropylacrylamide). *Biomaterials* 11, 625.
- (3) Hoffman, A. S. (1987) Applications of thermally reversible polymers and hydrogels in therapeutics and diagnostics. *J. Controlled Release* 6, 297.
- (4) Monji, N., and Hoffman, A. S. (1987) A novel immunoassay system and bioseparation process based on thermal phase separation polymers *Appl. Biochem. Biotechnol.* 14, 107.
- (5) Chen, J. P., and Hoffman, A. S. (1990) Protein-polymer conjugates II. Affinity precipitation separation of immunoglobulin by a poly(*N*-isopropylacrylamide)-protein A conjugate *Biomaterials* 11, 631.
- (6) Chen, G. H., and Hoffman, A. S. (1993) Preparation and properties of thermoreversible, phase-separating enzyme-oligo(isopropylacrylamide) conjugates. *Bioconjugate Chem.* 4, 509.
- (7) Chen, G. H., and Hoffman, A. S. (1994) Synthesis of carboxylated poly(NIPAAM) oligomers and their application to form thermo-reversible polymer-enzyme conjugates. *J. Biomat. Sci. Polym. Ed.* 5, 371.
- (8) Takei, Y. G., Aoki, T., Sanui, K., Ogata, N., Okano, T., and Sakurai, Y. (1993) Temperature-responsive bioconjugates. 1. Synthesis of temperature-responsive oligomers with reactive end groups and their coupling to biomolecules. *Bioconjugate Chem.* 4, 42.
- (9) Salemme, F. R. (1976) A hypothetical structure for an intermolecular complex of cytochrome *c* and  $b_5$ . *J. Mol. Biol.* 102, 563.
- (10) Poulos, T. L., and Mauk, A. G. (1983) Models for the complexes formed between cytochrome  $b_5$  and the subunits of methemoglobin. *J. Biol. Chem.* 258, 7369.
- (11) Wendolski, J. J., Mathew, J. B., Weber, P. C., and Salemme, F. R. (1987) Molecular dynamics of a cytochrome *c*-cytochrome  $b_5$  electron transfer complex. *Science* 238, 794.
- (12) Mathew, F. S., Levine, M., and Argos, P. (1972) Three dimensional Fourier synthesis of calf liver cytochrome  $b_5$  at 2.8 Å resolution. *J. Mol. Biol.* 64, 229.
- (13) Pochapsky, T. C., Sligar, S. G., McLachlan, S. J., and La Mar, G. N. (1990) Relationship between heme binding site

<sup>6</sup> A 0.95 mL portion of 0.8 μM T8C/MI-oligo(NIPAAM) conjugate in 50 mM phosphate, 1 mM EDTA, pH 8.0 buffer with 10% (v/v)  $(\text{NH}_4)_2\text{SO}_4$  was cooled at 4 °C for 5 min. The saturated  $(\text{NH}_4)_2\text{SO}_4$  (10% v/v) was added to prevent resolubilization of the conjugate during centrifugation at room temperature. A 0.5 mL portion of this solution was pipetted into a cuvette, and the absorbance at 412 nm was determined spectrophotometrically (cooling cycle 1, filled bar). The T8C/MI-oligo(NIPAAM) conjugate solution was then carefully removed from the cuvette and added back to the original sample. The sample was then warmed to 37 °C for 10 min to precipitate the conjugate, followed by centrifugation at room temperature. A 0.5 mL portion of the supernatant was assayed spectrophotometrically at room temperature to determine the concentration of the conjugate that remained in solution (heating cycle 1, filled bar). The supernatant was then added back to the original sample and the conjugate was redissolved by cooling to 4 °C, and the process was repeated twice to monitor the reversible precipitation of the protein-oligomer conjugate (cycles 2 and 3).

<sup>7</sup> A physical mixture of 1 mg of A-oligo(NIPAAM) and 50 μL of 1 mM T8C in 1 mL of buffer (50 mM phosphate, 1 mM EDTA, pH 8.0) with 10% (v/v) saturated  $(\text{NH}_4)_2\text{SO}_4$  was similarly assayed (hatched bars, Figure 1) as in footnote 6.

- structure and heme orientation of two ferrocycytochrome b<sub>5</sub>s. A study in prosthetic group recognition. *J. Am. Chem. Soc.* **112**, 5258.
- (14) Gouterman, M. (1978) In *The Porphyrins* (D. Dolphin, Ed.) pp 1–165, Academic Press Inc., New York.
- (15) Beck von Bodman, S., Schuler, M. A., Jollie, D. R., Sligar, S. G. (1986) Synthesis, bacterial expression and mutagenesis of the gene coding for mammalian cytochrome b<sub>5</sub>. *Proc. Natl. Acad. Sci. U.S.A.* **83**, 9443–9447.
- (16) Stayton, P. S., Fisher, M. T., and Sligar, S. G. (1988) Determination of cytochrome b<sub>5</sub> association reactions. Characterization of methemoglobin and cytochrome P-450<sub>cam</sub> binding to genetically engineered cytochrome b<sub>5</sub>. *J. Biol. Chem.* **263**, 13544.
- (17) Yang, H. J. (1989) Investigation into an affinity precipitation system based on the thermally reversible solution behavior of poly(*N*-isopropylacrylamide). Ph.D. dissertation, University of Washington.

## Synthesis of Uridine Phosphoramidite Analogs: Reagents for Site-Specific Incorporation of Photoreactive Sites into RNA Sequences

Kavita Shah, Hongyan Wu, and Tariq M. Rana\*

Department of Pharmacology, Robert Wood Johnson Medical School, University of Medicine and Dentistry of New Jersey, 675 Hoes Lane, Piscataway, New Jersey 08854. Received December 17, 1993\*

The synthesis of three new photoactive RNA phosphoramidites, 5-bromouridine, 5-iodouridine, and *O*<sup>4</sup>-triazolouridine, is reported. The 5' OH of bromouridine and iodouridine were protected as dimethoxytrityl ether using dimethoxytrityl chloride and pyridine. Selective protection of 2' OH was achieved as the corresponding *tert*-butyldimethylsilyl ether. Protected ribonucleosides were converted to phosphoramidites using 2-cyanoethyl *N,N*-diisopropylchlorophosphoramidite. *O*<sup>4</sup>-Triazolouridine phosphoramidite monomer was prepared in one step from uridine phosphoramidite. These phosphoramidites were used to incorporate photoprobes at any chosen sites in the RNA sequences during chemical syntheses. The modified monomers were incorporated into RNA oligomers with coupling yields >98%. After chemical synthesis, *O*<sup>4</sup>-triazolouridine was converted to 4-thiouridine by the addition of thiolacetic acid during standard deprotection methods. The extent of thiation and incorporation of modified nucleotides into RNA sequences were confirmed by nuclease digest, HPLC, and gel electrophoresis.

RNA plays a central role in cellular processes, including regulation and catalysis. Since the discovery of RNA enzymes, there has been an increasing interest in RNA structure (1). The multiple functions of RNA must reflect diversity in its three-dimensional structure. Despite the importance of RNA function, very little is known about its structure. Knowledge of the three-dimensional structure and general rules for RNA folding will be valuable to infer a more detailed mechanism of RNA function. X-ray crystallography provides high-resolution structures, and a few crystal structures of RNA have been determined (2, 3). Recently, high-resolution NMR techniques have been developed to elucidate RNA structures in solution (4). There is a need for new methods to determine higher order RNA structure under physiological conditions (5, 6).

Recent advances in chemical synthesis of DNA have opened a new field of DNA applications as structural probes and inhibitors. Oligonucleotides can be covalently linked to a dye, enzyme, or other biological macromolecule (for a recent review on chemically modified DNA see ref 7). Important biomedical applications of modified oligonucleotides include the detection and localization of messenger RNA, detection of bacterial or viral sequences, inhibition of RNA translation, and control of DNA replication. Recently, Xu et al. (8) described a strategy for postsynthetic modification of DNA at the 4-position of thymine. There is a variety of modified monomer phosphoramidites commercially available for automated synthesis of DNA. On the other hand, chemical synthesis of RNA is a much more challenging task due to the presence of a 2'-hydroxyl group. During chemical synthesis of RNA, the 2'-hydroxyl group has to be protected until all other protecting groups have been removed. Due to the synthetic difficulties, modified monomers for

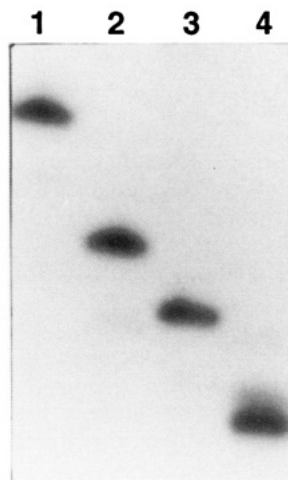
chemical synthesis of RNA are not common for structural studies.

Photochemical cross-linking has been widely used to study RNA–RNA and RNA–protein interactions (9–13). Recently, Ebright and co-workers have exploited photocrosslinking reactions mediated by site-specifically placed bromouracil to identify an amino acid–base contact in GCN4–DNA and Myc–DNA complexes (14, 15). Photochemical crosslinking can trap transient association of macromolecules, which might not be possible by available physical methods. In the case of dynamic structures such as ribozyme–substrate interactions, these methods are extremely valuable. However, this technique faces the challenge of how to site-specifically incorporate photoprobes into the internal sequences of RNA. To meet this challenge, we have synthesized phosphoramidites of 5-bromouridine, 5-iodouridine, and *O*<sup>4</sup>-triazolouridine.

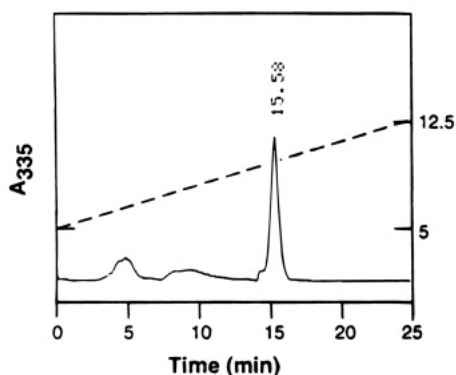
These new phosphoramidites were used to incorporate photo probes at chosen sites in the RNA sequence during chemical syntheses. The following four sequences were synthesized on an automated DNA synthesizer: (1) 5'-AUU AAU U<sup>B</sup>AG-3'; (2) 5'-CGC UGU<sup>I</sup>CA-3'; (3) 5'-AUU CU<sup>Thio</sup>U G-3'; and (4) 5'-GCC GUU UUU UC-3' (unmodified control sequence). RNAs containing bromouridine and iodouridine were cleaved from the support, deprotected, and desalted according to standard procedures. Modified RNA phosphoramidites were incorporated into RNA oligomers with more than 98% coupling efficiencies. After chemical synthesis, *O*<sup>4</sup>-triazolouridine was converted to 4-thiouridine by the addition of thiolacetic acid during deprotection methods. To analyze the stability of RNA, crude modified oligoribonucleotides were 5' labeled with <sup>32</sup>P and run on 20% polyacrylamide–8 M urea gels. Results of this analysis are shown in Figure 1. Three crude sequences containing modified monomers gave single bands on the gel, indicating that modification or deprotection conditions had no effect on the stability of RNA (lanes 2–4, Figure 1). One unmodified control sequence was synthesized and deprotected under similar conditions. Stability of control sequence is shown in lane

\* To whom correspondence should be addressed. Phone: (908) 235-4590. Fax: (908) 235-4073. E. Mail: rana@mbcl.rutgers.edu.

\* Abstract published in *Advance ACS Abstracts*, October 1, 1994.



**Figure 1.** Analysis of the chemically synthesized crude RNA sequences by 8 M urea–20% polyacrylamide gel electrophoresis. All RNA sequences were labeled at the 5' end with  $^{32}\text{P}$ . Labeling reactions were carried out at rt for 30 min in a mixture containing 10  $\mu\text{M}$  RNA, 10 mM  $\text{MgCl}_2$ , 0.5  $\mu\text{M}$  [ $\gamma\text{-}^{32}\text{P}$ ] ATP (6000 Ci/mmol), and 4 units of T4 polynucleotide kinase in 50 mM Tris–HCl (pH 7.4). Autoradiogram of a typical gel is shown: unmodified control sequence, 5'-GCC GUU UUU UC-3' (lane 1); bromouridine containing sequence, 5'-AUU AAU U<sup>Br</sup>AG-3' (lane 2); iodouridine containing sequence, 5'-CGC UGU<sup>I</sup> CA-3' (lane 3); and RNA sequence modified with 4-thiouridine, 5'-AUU CU<sup>ThioU</sup> G-3' (lane 4).



**Figure 2.** HPLC profile of crude RNA modified with  $O^4$ -triazolouridine. RNA sequence, 5'-AUU CU<sup>ThioU</sup> G-3', was deprotected as described in the Experimental Procedures and chromatographed on a  $\text{C}_8$  reversed phase column (Zorbax 300 SB, 4.6 mm  $\times$  25 cm). A 25 min linear gradient, from 0.1 M triethylammonium acetate in 5% acetonitrile, pH 6.4, to 12.5% acetonitrile, was used with a flow rate of 1.0 mL/min. The shape of the solvent gradient is shown by the dashed line. Retention time of the major peak at 15.58 min is also indicated.

1, Figure 1. These results clearly indicate that there were no significant degradation products during deprotection procedures of modified RNA sequences.

During the development of postsynthetic RNA modification methods, the major concern was the stability of RNA toward nonconventional deprotection conditions. To address this question, we synthesized sequence 3 and modified the 4-position of uridine by postsynthetic substitution. After deprotection, the RNA oligomer was analyzed by HPLC. The presence of 4-thiouridine in deprotected sequence 3 was confirmed by monitoring at 335 nm. As shown in Figure 2, crude sequence 3 RNA gave only one major peak with retention time of 15.58 min. The extent of thiation was calculated by measuring the absorbance of sequence 3 at 330 and 260 nm, which showed 97% transformation of  $O^4$ -triazolouridine into 4-thiouridine. Incorporation of 5-bromouridine and 5-iodouridine in oligomers was assessed by nuclease digest analyses. Quantification of HPLC data showed

1.0 nucleoside of 5-bromouridine and 0.92 nucleoside of 5-iodouridine in sequences 1 and 2, respectively.

The synthetic methodology presented in this report is the first example of chemical synthesis of RNA containing bromouridine, iodouridine, and 4-thiouridine at a predetermined site and postsynthetic substitution of RNA. An important application of single site RNA modification is the use of these photoprobes for structural studies of ribozymes. Synthesis of RNA with longer sequences can be accomplished by using T7 RNA polymerase *in vitro* with oligonucleotide DNA templates (16). Site-specifically modified RNA can be prepared by synthesizing short sequences of modified RNA on automated synthesizer and ligating it into longer pieces of RNA with the use of bacteriophage T4 DNA ligase (17). By the use of this method, RNA can be labeled with photoprobes at predetermined sites in the ribozyme and substrate sequences.

## EXPERIMENTAL PROCEDURES

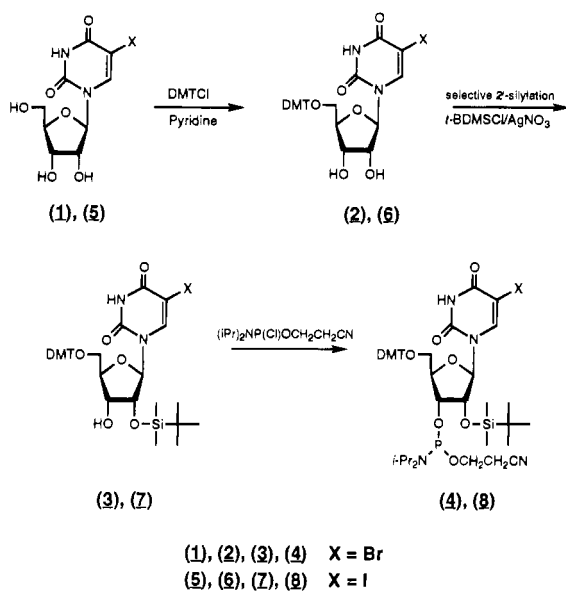
(-)-5-Bromouridine, (-)-5-iodouridine, uridine, dimethoxytrityl chloride (DMTCl), *tert*-butyldimethylsilyl chloride (*t*-BDMSCl), 2-cyanoethyl *N,N*-diisopropylchlorophosphoramidite, 1,2,4-triazole, phosphorus oxychloride, triethylamine, tetrabutylammonium fluoride (1 M solution in THF), 2,4,6-collidine, thiolacetic acid, DBU, anhydrous *N*-methylimidazole, dry THF, and pyridine were purchased from Aldrich. 2,4,6-Collidine was dried over 4 Å molecular sieves. The CPG linked monomers and the chemicals for synthesizer were obtained from Glen Research (VA). Sep Pak  $\text{C}_{18}$  plus cartridges were purchased from Waters (Millipore). Snake venom phosphodiesterase I (1 mg/0.5 mL) and alkaline phosphatase (1000 U/mL) were obtained from Boehringer Mannheim (Indianapolis, IN). Solvents were HPLC grade and were degassed immediately before use.

$^1\text{H}$  NMR spectra were recorded at 200 MHz on a Gemini 200 spectrometer (Varian). All spectra were taken in  $\text{CDCl}_3$ . Mass spectra were recorded using fast atom bombardment (FAB) ionization. TLC were performed with precoated 0.2 mm silica gel 60 F-254 TLC plates (EM Reagents, Darmstadt, FRG). Plates were visualized under short wave UV light and with iodine vapors. Dimethoxytrityl-containing compounds were visualized by exposing the TLC plate to concentrated HCl vapors. Column chromatography was performed with silica gel (70–230 mesh, 60 Å) purchased from Aldrich. Reversed-phase HPLC analysis of oligomers was carried out on Beckman 344 with a variable wavelength detector (Beckman Model 165). Reagent grade chemicals were used without purification unless otherwise stated. All the reactions involving (-)-5-bromouridine and (-)-5-iodouridine were performed in the dark.

**Synthesis of (-)-5-Bromouridine Phosphoramidite (4).** The synthesis of phosphoramidite 4 is delineated in Scheme 1. The 5' OH of bromouridine 1 was protected as DMT ether 2 using DMTCl and pyridine, followed by selective 2' OH protection as the corresponding *t*-BDMS ether 3 using Ogilvie's method (18). Finally, nucleoside 3 was converted to the phosphoramidite 4 using 2-cyanoethyl *N,N*-diisopropylchlorophosphoramidite (19).

**5'-O-[(4,4'-Dimethoxyphenyl)methyl]-(-)-5-Bromouridine (2).** To a solution of (-)-5-bromouridine (323 mg, 1 mmol) in dry pyridine (4 mL) was added DMTCl (350 mg, 1.03 mmol) and the reaction mixture was stirred overnight under  $\text{N}_2$  atmosphere. Methanol (1 mL) was added, and after 15 min the solution was concentrated to dryness under reduced pressure. A 5%  $\text{NaHCO}_3$  solution (10 mL) was added, the resulting solution was extracted with ethyl acetate (2  $\times$  15 mL), and the organic

Scheme 1



layer was dried over molecular sieves and reconcentrated to yield a gum, which was purified by column chromatography (ethyl acetate). Nucleoside **2** was obtained as a white solid (413 mg, 0.66 mmol; 66%).  $^1\text{H NMR}$  ( $\text{CDCl}_3$ )  $\delta$  (ppm): 8.09 (1H, s,  $\text{H}_6$ ), 7.41–7.17 (9H, m, aromatic), 6.82 (4H, d, aromatic,  $J = 8.7$  Hz), 5.90 (1H, d,  $\text{H}_1$ ,  $J = 4.04$  Hz), 4.46 (1H, dd,  $\text{H}_2$ ,  $J = 4.2$  Hz), 4.41 (1H, t,  $\text{H}_3$ ), 4.23 (1H, d,  $\text{H}_4$ ,  $J = 3.08$  Hz), 3.75 (6H, s,  $\text{OCH}_3$ ), 3.40 (2H, br s,  $\text{H}_5$  and  $\text{H}_5'$ ). MS ( $\text{NaI} + \text{MNBA}$ ):  $m/e$  647 ( $\text{M} - \text{H} + \text{Na}^+$ ). TLC (ethyl acetate):  $R_f$  0.33.

**5'-O-[(4,4'-Dimethoxyphenyl)methyl]-2'-O-(tert-butyl-dimethylsilyl)-(-)-5-bromouridine (3).** To a solution of nucleoside **2** (312 mg, 0.5 mmol) in dry THF (5 mL) was added dry pyridine (0.4 mL, 5 mmol) and silver nitrate (102 mg, 0.6 mmol). The reaction mixture was stirred for 15 min, followed by the addition of *tert*-butyldimethylsilyl chloride (98 mg, 0.65 mmol). Stirring was continued for an additional 2 h, followed by filtration into 5%  $\text{NaHCO}_3$  solution (10 mL). The aqueous layer was extracted with ethyl acetate ( $3 \times 10$  mL), dried over molecular sieves, and evaporated under reduced pressure. Column purification (ethyl acetate:benzene 1:9) provided 2'-silylnucleoside **3** as a white solid (249 mg, 0.33 mmol, 67.5%).  $^1\text{H NMR}$  ( $\text{CDCl}_3$ )  $\delta$  (ppm): 8.17 (1H, s,  $\text{H}_6$ ), 7.45–7.23 (9H, m, aromatic), 6.85 (4H, d, aromatic,  $J = 8.78$  Hz), 6.01 (1H, d,  $\text{H}_1$ ,  $J = 5.16$  Hz), 4.51 (1H, t,  $\text{H}_2$ ,  $J = 5.14$  Hz), 4.32 (1H, q,  $\text{H}_3$ ,  $J = 4.04$  Hz), 4.19 (1H, d,  $\text{H}_4$ ,  $J = 3.14$  Hz), 3.80 (6H, s,  $\text{OCH}_3$ ), 3.44 (2H, d,  $\text{H}_5$  and  $\text{H}_5'$ ,  $J = 2.12$  Hz), 0.93 (9H, s, *t*-butyl), 0.17 (6H, s,  $\text{CH}_3$ ). MS ( $\text{NaI} + \text{MNBA}$ ):  $m/e$  761 ( $\text{M} - \text{H} + \text{Na}^+$ ). TLC (ethyl acetate:benzene 1:1):  $R_f$  0.83.

**5'-O-[(4,4'-Dimethoxyphenyl)methyl]-2'-O-(tert-butyl-dimethylsilyl)-(-)-5-iodouridine 3'-O-[2-cyanoethyl *N,N*-(diisopropylamino)phosphoramidite] (4).** To a stirred solution of nucleoside **3** (200 mg, 0.27 mmol) in dry THF (5 mL) was added dry 2,4,6-collidine (0.26 mL, 2.02 mmol), followed by *N*-methylimidazole (0.01 mL, 0.135 mmol). 2-Cyanoethyl *N,N*-diisopropylchlorophosphoramidite (45  $\mu\text{L}$ , 0.20 mmol) in dry THF (1 mL) was added dropwise over a period of 5 min at rt. Stirring was continued for 1 h at rt. The reaction mixture was worked up by diluting it with ethyl acetate (25 mL) and washing the organic phase with 5%  $\text{NaHCO}_3$  solution (5 mL) and brine (5 mL). Evaporation followed by column purification (ethyl acetate:benzene 1:9, 0.05%  $\text{Et}_3\text{N}$ ) yielded phosphoramidite **4** as a white solid (215 mg, 0.22 mmol,

85%).  $^1\text{H NMR}$  ( $\text{CDCl}_3$ )  $\delta$  (ppm): 8.15 (1H, s,  $\text{H}_6$ ), 7.39–7.24 (9H, m, aromatic), 6.83 (4H, d, aromatic,  $J = 8.83$  Hz), 5.99 (1H, d,  $\text{H}_1$ ), 4.61–4.44 (2H, m,  $\text{H}_3$  and  $\text{H}_2$ ), 4.29–4.00 (3H, m,  $\text{H}_4$  and  $\text{OCH}_3$ ), 3.77 (6H, s,  $\text{OCH}_3$ ), 3.61–3.29 (4H, m,  $\text{H}_5$ ,  $\text{H}_5'$  and 2CH), 2.75 (2H, t,  $\text{CH}_2\text{-CN}$   $J = 6.22$  Hz), 1.27 (12 H, m, isopropyl), 0.88 (9H, s, *tert*-butyl), 0.10 (6H, s,  $\text{CH}_3$ ). MS ( $\text{NaI} + 2$ -hydroxyethyl disulfide):  $m/e$  963 ( $\text{M} + \text{Na}^+$ ). TLC (ethyl acetate: dichloromethane 1:4):  $R_f$  0.73, 0.58 (two diastereomers).

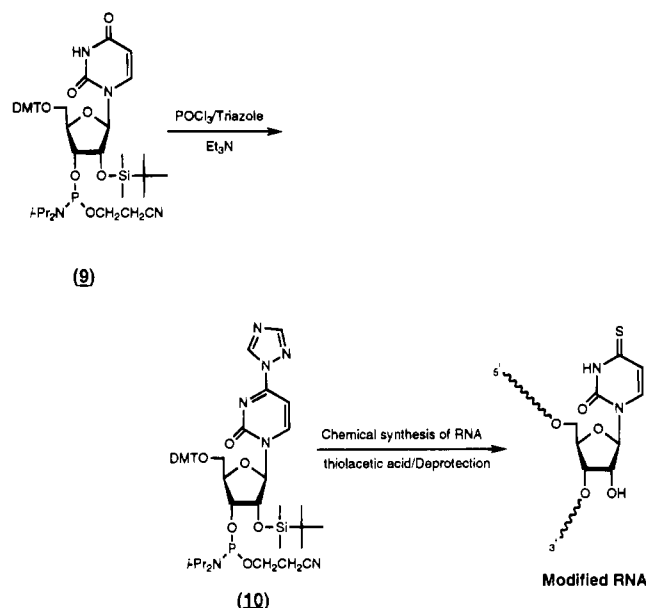
**Synthesis of (-)-5-Iodouridine phosphoramidite (8).** The synthesis of phosphoramidite **8** is outlined in Scheme 1. The 5' OH of iodouridine **5** was protected as DMT ether **6** using DMTCl and pyridine, followed by selective 2' OH protection as the corresponding *t*-BDMS ether **7**. Finally, nucleoside **3** was converted to the phosphoramidite **8** using 2-cyanoethyl *N,N*-diisopropylchlorophosphoramidite.

**5'-O-[(4,4'-Dimethoxyphenyl)methyl]-(-)-5-iodouridine (6).** A solution of (-)-5-iodouridine (370 mg, 1 mmol) and DMTCl (340 mg, 1 mmol) in dry pyridine (4 mL) was stirred for 6 h at rt. Methanol (1 mL) was added, and after 15 min the solution was concentrated to dryness under reduced pressure. A 5%  $\text{NaHCO}_3$  solution (10 mL) was added, the resulting solution was extracted with ethyl acetate ( $2 \times 15$  mL), and the organic layer was dried over molecular sieves and reconcentrated to yield a gum, which was purified by column chromatography (ethyl acetate:benzene 1:1) to yield 5'-DMT ether **6** as a white solid (417 mg, 0.62 mmol, 62%).  $^1\text{H NMR}$  ( $\text{CDCl}_3$ )  $\delta$  (ppm): 8.10 (1H, s,  $\text{H}_6$ ), 7.44–7.18 (9H, m, aromatic), 6.83 (4H, d, aromatic,  $J = 8.8$  Hz), 5.94 (1H, d,  $\text{H}_1$ ,  $J = 4.18$  Hz), 4.50 (1H, t,  $\text{H}_2$ ,  $J = 4.46$  Hz), 4.42 (1H, t,  $\text{H}_3$ ,  $J = 4.46$  Hz), 4.22 (1H, br s,  $\text{H}_4$ ), 3.73 (6H, s,  $\text{OCH}_3$ ), 3.40 (2H, br s,  $\text{H}_5$  and  $\text{H}_5'$ ). MS ( $\text{NaI} + \text{MNBA}$ ):  $m/e$  695 ( $\text{M} + \text{Na}^+$ ). TLC (ethyl acetate):  $R_f$  0.42.

**5'-O-[(4,4'-Dimethoxyphenyl)methyl]-2'-O-(tert-butyl-dimethylsilyl)-(-)-5-iodouridine (7).** To a solution of nucleoside **6** (269 mg, 0.4 mmol) in dry THF (5 mL) was added dry pyridine (0.16 mL, 2.0 mmol) and silver nitrate (82 mg, 0.48 mmol). The reaction mixture was stirred for 15 min, followed by the addition of *tert*-butyldimethylsilyl chloride (79 mg, 0.52 mmol). Stirring was continued for an additional 2 h, followed by filtration into 5%  $\text{NaHCO}_3$  solution (10 mL). The aqueous layer was extracted with ethyl acetate ( $3 \times 10$  mL), dried over molecular sieves, and evaporated under reduced pressure. The 2'-*t*-BDMS ether **7** was obtained as a white solid (270 mg, 0.34 mmol, 85.5%) after column purification (ethyl acetate:benzene 1:9).  $^1\text{H NMR}$  ( $\text{CDCl}_3$ )  $\delta$  (ppm): 8.23 (1H, s,  $\text{H}_6$ ), 7.47–7.25 (9H, m, aromatic), 6.87 (4H, d, aromatic,  $J = 8.82$  Hz), 6.05 (1H, d,  $\text{H}_1$ ,  $J = 5.4$  Hz), 4.52 (1H, t,  $\text{H}_2$ ,  $J = 5.12$  Hz), 4.30 (1H, q,  $\text{H}_3$ ,  $J = 3.94$  Hz), 4.21 (1H, br s,  $\text{H}_4$ ), 3.81 (6H, s,  $\text{OCH}_3$ ), 3.50 (2H, d,  $\text{H}_5$ ,  $J = 9.36$  Hz), 3.40 (2H, d,  $\text{H}_5'$ ,  $J = 9.78$  Hz), 0.94 (9H, s, *tert*-butyl), 0.16 (6H, s,  $\text{CH}_3$ ). MS ( $\text{NaI} + \text{MNBA}$ ):  $m/e$  809 ( $\text{M} + \text{Na}^+$ ). TLC (benzene:ethyl acetate 1:1):  $R_f$  0.76.

**5'-O-[(4,4'-Dimethoxyphenyl)methyl]-2'-O-(tert-butyl-dimethylsilyl)-(-)-5-iodouridine 3'-O-[2-Cyanoethyl (*N,N*-diisopropylamino)phosphoramidite] (8).** To a stirred solution of nucleoside **7** (78 mg, 0.1 mmol) in dry THF (2 mL) was added dry 2,4,6-collidine (0.1 mL, 0.75 mmol), followed by *N*-methylimidazole (4  $\mu\text{L}$ , 0.05 mmol). 2-Cyanoethyl *N,N*-diisopropylchlorophosphoramidite (45  $\mu\text{L}$ , 0.20 mmol) in dry THF (1 mL) was added dropwise over a period of 5 min at rt. Stirring was continued for 1 h at rt. The reaction mixture was worked up by diluting it with ethyl acetate (25 mL) and washing the organic phase with 5%  $\text{NaHCO}_3$  solution (5 mL) and brine

## Scheme 2



(5 mL). Evaporation followed by column purification (ethyl acetate:benzene 2:8, 0.05%  $\text{Et}_3\text{N}$ ) yielded phosphoramidite **8** as a white solid (78 mg, 0.8 mmol, 80%).  $^1\text{H}$  NMR ( $\text{CDCl}_3$ )  $\delta$  (ppm): 8.18 (1H, s,  $\text{H}_6$ ), 7.35–7.26 (9H, m, aromatic), 6.83 (4H, d, aromatic,  $J = 7.7$  Hz), 5.99 (1H, m,  $\text{H}_{1'}$ ), 4.61–4.35 (2H, m,  $\text{H}_3'$  and  $\text{H}_2'$ ), 4.21–4.03 (3H, m,  $\text{H}_4'$  and  $\text{OCH}_2$ ), 3.77 (6H, s,  $\text{OCH}_3$ ), 3.50–3.15 (4H, m,  $\text{H}_5'$ ,  $\text{H}_{5''}$  and 2CH), 2.80–2.55 (2H, m,  $\text{CH}_2\text{CN}$ ), 1.27 (12 H, m, isopropyl), 0.88 (9H, s, *tert*-butyl), 0.05 (6H, s,  $\text{CH}_3$ ). MS ( $\text{NaI} + \text{MNBA}$ ):  $m/e$  1010 ( $\text{M} + \text{Na}$ ) $^+$ . TLC (ethyl acetate:dichloromethane 3:7)  $R_f$  0.62, 0.50 (two diastereomers).

**Synthesis of  $\text{O}^4$ -Triazolouridine Phosphoramidite (10).** The synthesis of triazolouridine phosphoramidite **10** is outlined in Scheme 2. Triazolouridine phosphoramidite (**10**) was obtained from commercially available uridine phosphoramidite **9** by using triazole,  $\text{POCl}_3$ , and triethylamine (20).

**5'-O-[(Dimethoxyphenyl)methyl]-2'-O-(*tert*-butyldimethylsilyl)triazolouridine 3'-O-[2-Cyanoethyl *N,N*-(diisopropylamino)phosphoramidite] (10).** To an ice-cooled stirred suspension of 1,2,4-triazole (209 mg, 3.03 mmol) in dry acetonitrile (4 mL) was added  $\text{POCl}_3$  (0.06 mL), followed by dry  $\text{Et}_3\text{N}$  (0.45 mL). After 30 min a solution of nucleoside **9** (43 mg, 0.05 mmol) in dry acetonitrile (1 mL) was added over a period of 15 min and stirring continued for 2 h. The reaction was stopped with saturated  $\text{NaHCO}_3$  solution (5 mL), the aqueous layer extracted with ethyl acetate ( $3 \times 10$  mL), the organic layer washed with saturated  $\text{NaHCO}_3$  (5 mL) and brine (5 mL) and dried over molecular sieves, and solvent removed under reduced pressure. The crude compound thus obtained was purified by column chromatography (ethyl acetate:benzene 8:2). Yield: 28 mg, 0.03 mmol, 62%.  $^1\text{H}$  NMR ( $\text{CDCl}_3$ )  $\delta$  (ppm): 8.82–8.52 (1H, m,  $\text{H}_6$ ), 8.22 (2H, s, aromatic), 7.36–7.19 (9H, m, aromatic), 6.86–6.80 (4H, m, aromatic), 6.68–6.38 (1H, m,  $\text{H}_{1'}$ ), 6.05–5.80 (1H, m,  $\text{H}_5$ ), 4.70–4.06 (5H, m,  $\text{H}_2'$ ,  $\text{H}_3'$ ,  $\text{OCH}_2$  and  $\text{H}_4'$ ), 3.90–3.30 (4H, m, 2CH,  $\text{H}_5'$  and  $\text{H}_{5''}$ ), 3.79 (6H, s,  $\text{OCH}_3$ ), 2.80–2.50 (2H, m,  $\text{CH}_2\text{CN}$ ), 1.30–1.20 (12 H, m, isopropyl), 0.91–0.74 (9H, m, *tert*-butyl), 0.22–0.03 (6H, m,  $\text{CH}_3$ ). MS ( $\text{NaI} + 2$ -hydroxyethyl disulfide):  $m/e$  937 ( $\text{M} + \text{Na} + \text{H}_2$ ) $^+$ . TLC (ethyl acetate:dichloromethane 2:3):  $R_f$  0.46, 0.35 (two diastereomers).

**RNA Synthesis and Deprotection.** All RNA syntheses were performed on ABI synthesizer Model 392

using standard protocols. All the monomers of (2-cyanoethyl)phosphoramidites were obtained from Glen Research. The fully protected (with 5'-DMT removed) sequence 3, 5'-AUU CU<sup>Triaz</sup>U G-3' attached to the CPG support was treated with 10% thiolacetic acid/acetonitrile (1 mL) overnight at rt. Resin was filtered, washed with excess acetonitrile, and dried. Cleavage from the support and deprotection was carried out with 10% DBU/methanol (1 mL) for 16 h at rt. Product was filtered and purified by Sep Pak  $\text{C}_{18}$  cartridge by standard methods. Purified and 2'-protected RNA was dried and further treated with 0.5 mL of TBAF (1.0 M solution in THF) for 24 h at rt. The reaction was quenched with 1.0 mL of 0.1 M TEAA, pH 7.0, and dried to a total volume of 1.0 mL. Desalting was achieved by Sep Pak  $\text{C}_{18}$  cartridge purification. The other three sequences of RNA were deprotected using 10% DBU/methanol (1 mL) followed by TBAF treatment and purification as described above.

**Enzymatic Digestion of Oligonucleotides.** Enzymatic digestion was carried out by incubating 0.24<sub>260</sub> unit of purified oligonucleotide at 37 °C overnight with 6  $\mu\text{L}$  (12  $\mu\text{g}$ ) of snake venom phosphodiesterase and 2  $\mu\text{L}$  (2 units) of alkaline phosphatase in a total volume of 78.2  $\mu\text{L}$  of 32 mM Tris, pH 7.5, and 15 mM  $\text{MgCl}_2$  (21). Nucleosides were recovered by adding 10  $\mu\text{L}$  of 3 M  $\text{NaOAc}$ , pH 5.2, and 234  $\mu\text{L}$  of 95% ethanol, mixing and chilling to  $-80$  °C for 30 min. After centrifugation at 13 000 rpm for 20 min at 4 °C, the supernatant was taken and dried in Speed-Vac (Savant) and redissolved in 200  $\mu\text{L}$  of water for HPLC analysis.

**HPLC Analysis of Oligonucleotides.** Nucleosides were chromatographed on a  $\text{C}_{18}$  reversed phase column (Beckman 5  $\mu\text{m}$  4.6 mm  $\times$  25 cm, Ultrasphere). Solvent A: 97.5% 0.01 M  $\text{KH}_2\text{PO}_4$  (pH 5), 2.5% methanol; Solvent B: 80% 0.01 M  $\text{KH}_2\text{PO}_4$  (pH 5.1), 20% methanol. Gradient: at 0 min, 0% B; at 7 min, start ramp to 10% B over 5 min; at 12 min, start ramp to 25% B over 3 min; at 15 min, start ramp to 60% B over 5 min; at 20 min, start ramp to 62% B in 2.5 min; at 22.5 min, start ramp to 100% B over 6 min; at 28.5 min, continued 100% B for 10 min. UV absorbance of nucleosides was monitored at 254 nm. Retention times for ribonucleosides (in min) were as follows: C, 7.19; U, 10.44; G, 22.47; 5-bromo-U, 24.9; 5-iodo-U, 28.14; A, 31.25. Quantitation of HPLC data was performed by comparison to authentic nucleoside standards and integration of the absorbance as described by Eadie et al. (21).

## ACKNOWLEDGMENT

We wish to thank Dr. Edward Browning for his help in HPLC analysis of oligonucleotides and Dr. Narayan C. Chaudhuri for helpful discussions. This research was supported by a Research Grant AI 34785 from the National Institutes of Health.

## LITERATURE CITED

- (1) Cech, T. R. (1991) Self splicing of RNA. *Curr. Opin. Cell. Biol.* 59, 543–568.
- (2) Dock-Bregeon, A. C., Chevrier, B., Podjarny, A., Johnson, J., De Bear, J. S., Gough, G. R., Gilham, P. T., and Moras, D. (1989) Crystallographic structure of an RNA helix: [U(UA)-6A]<sub>2</sub>. *J. Mol. Biol.* 209, 459–474.
- (3) Holbrook, S. R., Cheong, C., Tinoco, I., Jr., and Kim, S.-H. (1991) Crystal structure of an RNA double helix incorporating a track of non-Watson-Crick base pairs. *Nature* 353, 579–581.
- (4) Varani, G., and Tinoco, I., Jr. (1991) RNA structure and NMR spectroscopy. *Q. Rev. Biophys.* 24, 479–532.



- (5) Wang, J. F., and Cech, T. R. (1992) Tertiary structure around the guanosine-binding site of the tetrahymena ribozyme. *Science* 256, 526–529.
- (6) Chow, C. S., and Barton, J. K. (1990) Shape-selective cleavage of transfer RNA Phe by transition-metal complexes. *J. Am. Chem. Soc.* 112, 2839–2841.
- (7) Englisch, U., and Gauss, D. H. (1991) Chemically Modified Oligonucleotides as probes and Inhibitors. *Angew. Chem., Int. Ed. Engl.* 30, 613–629.
- (8) Xu, Y.-Z., Zheng, Q., and Swann, P. F. (1992) Synthesis of DNA containing modified bases by postsynthetic substitution. Synthesis of oligomers containing 4-substituted thymine: O<sup>4</sup>-alkyl thymine, 5-methylcytosine, N<sup>4</sup>-(dimethylamino)-5-methylcytosine, and 4-thiothymine. *J. Org. Chem.* 57, 3839–3845.
- (9) Woisard, A., Favre, A., Clivio, P., and Fourrey, J.-l. (1992) Hammerhead ribozyme tertiary folding: Intrinsic photo-labeling studies. *J. Am. Chem. Soc.* 114, 10072–10074.
- (10) Hanna, M. M. (1989) Photoaffinity crosslinking methods for studying RNA–protein interactions. *Methods Enzymol.* 180, 383–409.
- (11) Bartholomew, B., Meares, C. F., and Dahmus, M. E. (1990) Photoaffinity labeling of RNA polymerase III transcription complexes by nascent RNA. *J. Biol. Chem.* 265, 3731–3737.
- (12) Willis, M. C., Hicke, B. J., Uhlenbeck, O. C., Cech, T. R., and Koch, T. H. (1993) Photocrosslinking of 5-Iodouracil-Substituted RNA and DNA to Proteins. *Science* 262, 1255–1257.
- (13) Meares, C. F. (1991) Mapping the path of a growing ribonucleic acid molecule. *Acc. Chem. Res.* 24, 183–190.
- (14) Blatter, E. E., Ebright, Y. W., and Ebright, R. H. (1992) Identification of an Amino Acid–Base contact in the GCN4–DNA Complex by bromouracil-Mediated Photocrosslinking. *Nature* 359, 650–652.
- (15) Dong, Q., Blatter, E. E., Ebright, Y. W., Bister, K., and Ebright, R. H. (1994) Identification of an Amino Acid–Base contact in the Myc-DNA Complex by Site-Specific bromouracil-Mediated Photocrosslinking. *Embo J.* 13, 200–204.
- (16) Milligan, J. F., Groebe, D. R., Witherell, G. W., and Uhlenbeck, O. C. (1987) Oligoribonucleotide Synthesis Using T7 Polymerase and Synthetic DNA Templates. *Nucl. Acids. Res.* 15, 8783–8798.
- (17) Moore, M. J., Sharp, P. A. (1992) Site-Specific Modification of Pre-mRNA: The 2'-Hydroxyl Groups at the Splice Sites. *Science* 256, 992–997.
- (18) Hakimelahi, G. H., Proba, Z. A., and Ogilvie, K. (1982) New catalysts and procedures for the dimethoxytritylation and selective silylation of ribonucleosides. *Can. J. Chem.* 60, 1106–1113.
- (19) Scaringe, S. A., Francklyn, C., and Usman, N. (1990) Chemical Synthesis of Biologically Active Oligoribonucleotides using b-Cyanoethyl Protected Ribonucleoside Phosphoramidites. *Nucl. Acids Res.* 18, 5433–5441.
- (20) Xu, Y.-Z., Zheng, Q., and Swann, P. F. (1991) Simple Synthesis of 4-Thiothymidine, 4-Thiouridine and 6-Thio-2'-deoxyguanosine. *Tetrahedron Lett.* 32, 2817–2820.
- (21) Eadie, J. S., McBride, L. J., Efcavitch, J. W., Hoff, L. B., and Cathcart, R. (1987) High Performance Liquid Chromatographic Analysis of Oligodeoxynucleotides Base Composition. *Anal. Biochem.* 165, 442–447.

# REVIEWS

## RNA Degradation by Bleomycin, a Naturally Occurring Bioconjugate

Sidney M. Hecht

Departments of Chemistry and Biology, University of Virginia, Charlottesville, Virginia 22901. Received March 23, 1994

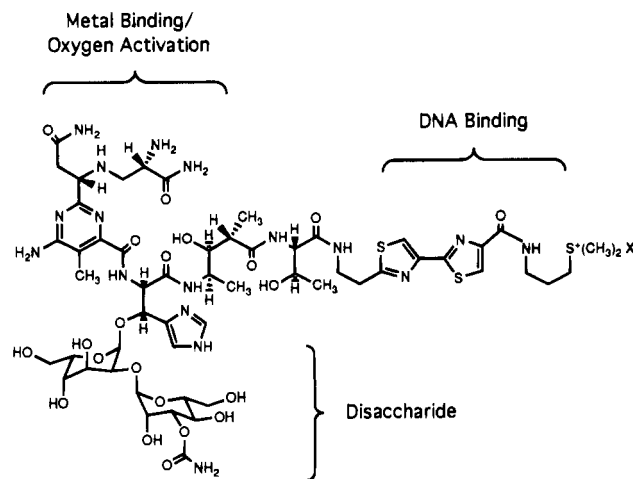
The antitumor antibiotic bleomycin (BLM) has now been the focus of structural (1), synthetic (2–7), mechanistic (8–10), and therapeutic studies (11, 12) for 30 years. At a biochemical level, the most intensively studied property of bleomycin is its ability to mediate the oxidative destruction of DNA, a transformation that involves several steps including metal ion binding, di-oxygen binding and activation, DNA binding, and the actual chemical transformation of DNA in a sequence-selective fashion (8–10).

Detailed analysis of the structural elements in bleomycin responsible for the individual steps leading to DNA degradation have made it clear that BLM is a bioconjugate; as indicated in Figure 1, the N-terminus of this polypeptide-derived antibiotic is responsible for metal binding as well as oxygen binding and activation, while the C-terminus participates in DNA binding (8–10). The disaccharide moiety may also provide a metal ligand (10) and may possibly be involved additionally in cell surface recognition by bleomycin. At the level of noncovalent binding, BLM also participates in the formation of other conjugates, i.e., with metal ions such as Fe and Cu, with O<sub>2</sub>, and ultimately with its polynucleotide substrates.

While early mechanistic studies considered several potential therapeutic targets for bleomycin, including DNA and RNA polymerases, DNA ligase, and DNA and RNA nucleases (13–16), the discovery that BLM could mediate DNA cleavage both *in vitro* (8–10) and *in vivo* (17–19) led to increasing efforts in the characterization of this facet of bleomycin action. The subsequent finding that DNA cleavage was sequence-selective, and could result in both single- and double-stranded breaks, prompted intensive efforts to understand the molecular basis for this sequence-selective cleavage. It has seemed reasonable to assume that the principles so derived could be used for the design of new structural classes of antitumor agents that employ the same biochemical strategy as bleomycin.

An inevitable consequence of the focus on DNA as a therapeutic target for bleomycin is that less attention has been given to other biochemical and biological effects of the drug. For example, BLM mediates lipid peroxidation (20–23), a logical consequence of its characterized properties in small molecule oxidation/oxygenation (24–26). It has also been shown that a bleomycin analog rendered dysfunctional for DNA cleavage by chemical modification was able to inhibit the growth of cultured mammalian cells in the presence of the local anesthetic dibucaine (27).

Of special interest in this regard are studies of RNA degradation by bleomycin. Early studies failed to detect RNA cleavage by bleomycin (28–32). In retrospect, this is not entirely surprising as much of this work was done before it was appreciated that BLM-mediated polynucleotide degradation requires a metal ion cofactor and oxygen. Also noted was the inability of certain RNA's to



**Figure 1.** Structure of bleomycin A<sub>2</sub>. The functional domains of the molecule are indicated.

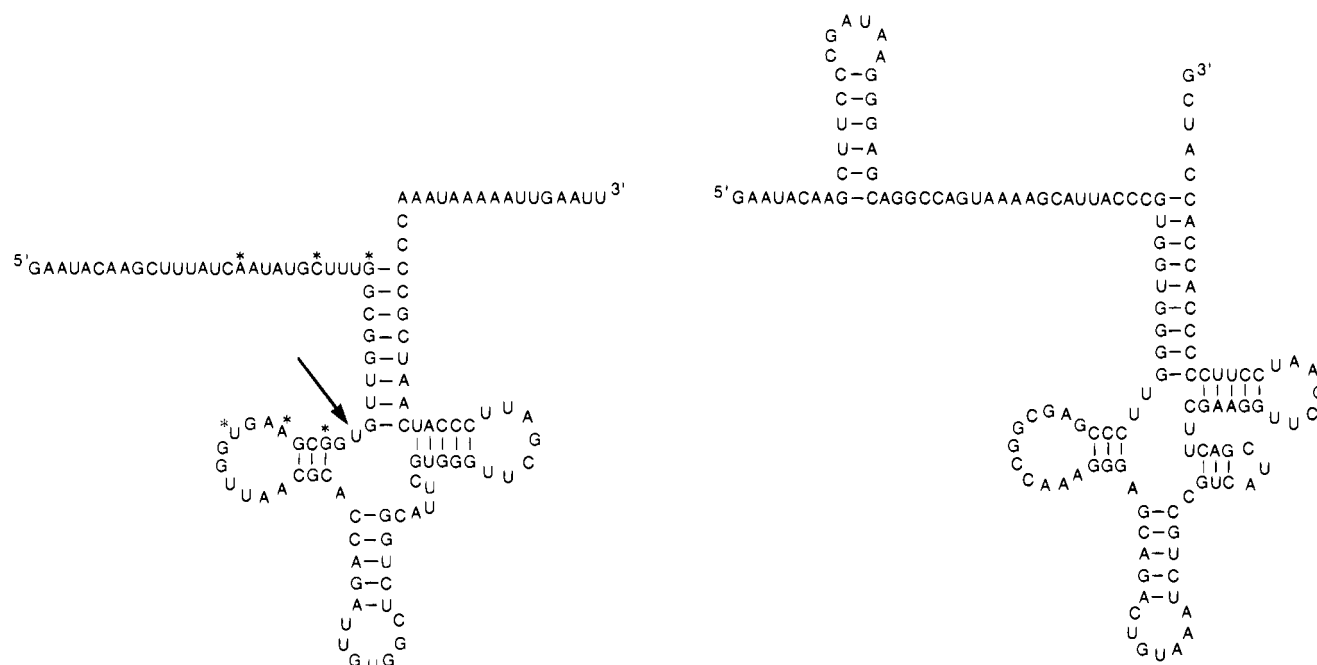
inhibit BLM-mediated DNA degradation, suggesting that bleomycin did not bind to RNA (32).

The first evidence in support of the ability of Fe·BLM to degrade RNA was reported by Magliozzo et al. (33). They demonstrated that titration of solutions containing 20 μM bleomycin with tRNA or DNA (0.2–0.6 mM) gave comparable quenching of the fluorescence of the bithiazole moiety of bleomycin, indicating that BLM would bind to tRNA. At a high (0.3 mM) concentration of activated Fe·BLM, limited degradation of yeast tRNA<sup>Phe</sup> and a few other tRNA isoacceptors was noted.

### A SURVEY OF RNA CLEAVAGE BY BLEOMYCIN

#### Transfer RNA's and tRNA Precursor Transcripts.

The first systematic study of RNA cleavage by BLM was carried out by Carter et al. (34–36), using Fe(II)·BLM A<sub>2</sub> that was activated aerobically in the absence of any added reducing agent. A survey of several tRNA precursor transcripts and mature tRNA's indicated that most were not cleaved by activated Fe·BLM; however, a 118-nucleotide *Bacillus subtilis* tRNA<sup>His</sup> precursor transcript was cleaved efficiently in the presence of 3 μM Fe(II)·BLM A<sub>2</sub>, i.e., under conditions comparable to those required to produce DNA damage. Relative to the cleavage of B-DNA by Fe·bleomycin, which is selective for 5'-G-pyr-3' sites, but typically results in the production of many DNA lesions with varying efficiencies even in duplexes of modest length, the cleavage of the tRNA<sup>His</sup> precursor was remarkable in two ways. First, the RNA was cleaved only at a single site at the lowest concentration of Fe·BLM employed; even at higher concentrations of added drug, cleavage at this site predominated. The other unusual feature associated with this substrate became apparent when the site of cleavage was identified by RNA sequence



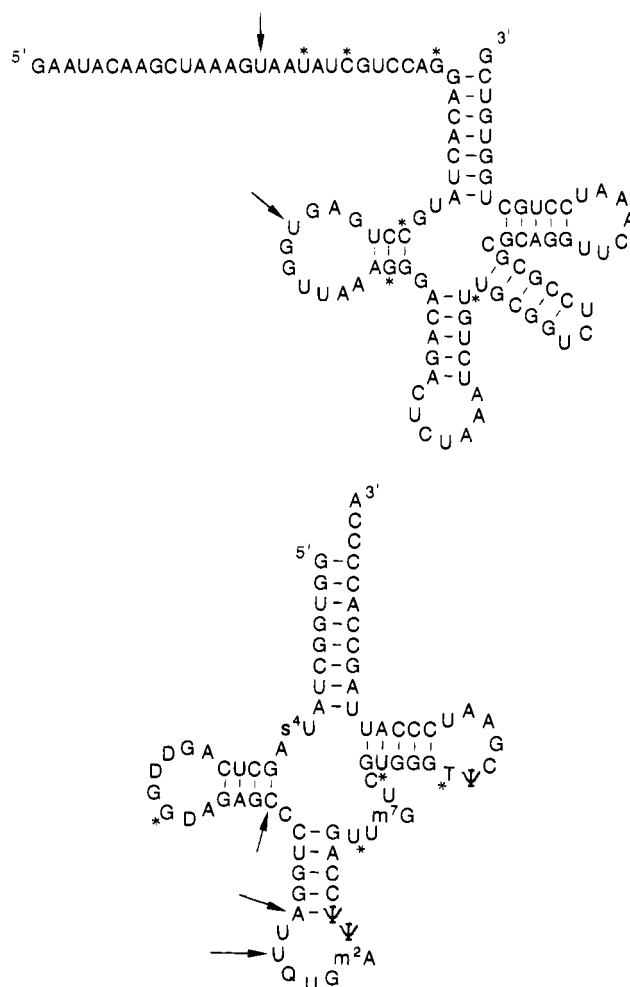
**Figure 2.** Structures of *Bacillus subtilis* tRNA<sup>His</sup> precursor (left) and *Escherichia coli* tRNA<sup>Trp</sup> precursor (right). The major Fe-BLM cleavage site is denoted with an arrow, the minor sites with asterisks.

analysis. As illustrated in Figure 2, the primary site of cleavage was at uridine<sub>35</sub>. While this nucleotide was part of a 5'-GU-3' cleavage site, it was in a region of the molecule believed to be single-stranded, by analogy with the folding of other structurally characterized tRNA's. Further, the minor sites of cleavage in the tRNA<sup>His</sup> precursor substrate exhibited no clear sequence selectivity. Treatment of tRNA<sup>His</sup> precursor with BLM congeners that produce more DNA damage than BLM A<sub>2</sub>, such as BLM A<sub>5</sub>, gave enhanced cleavage of tRNA<sup>His</sup> precursor and resulted in the appearance of a few additional minor sites. Otherwise, these species produced the same effects as BLM A<sub>2</sub> (C. E. Holmes and S. M. Hecht, unpublished data).

In comparison with the tRNA<sup>His</sup> precursor, an *in vitro* RNA transcript corresponding to *Escherichia coli* tRNA<sup>Trp</sup> precursor was refractory to cleavage by activated Fe-BLM (34). In spite of the ostensible structural similarities between these two tRNA precursor transcripts (Figure 2), only minimal damage was noted for the tRNA<sup>Trp</sup> precursor, even when the BLM:tRNA ratio was 5000-fold greater than that required to produce cleavage of tRNA<sup>His</sup> precursor (C. E. Holmes and S. M. Hecht, unpublished data). That this apparent difference in susceptibility to BLM was not an experimental artifact was verified by repeating the cleavage experiment using a reaction mixture that contained both tRNA precursor transcripts; again, only tRNA<sup>His</sup> precursor was cleaved.

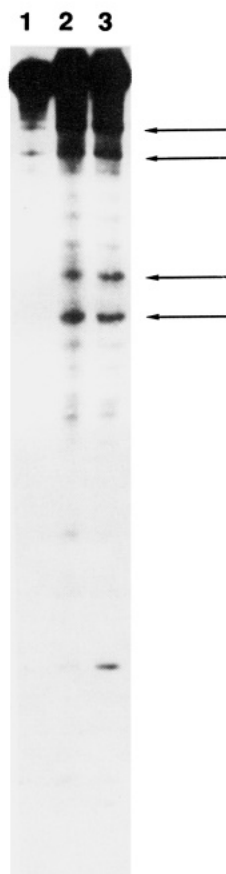
Numerous additional tRNA precursor transcripts and mature tRNA's have now been tested as substrates for cleavage by Fe-bleomycin. Those species that were cleaved included a *Schizosaccharomyces pombe* amber suppressor tRNA<sup>Ser</sup> construct and mature *E. coli* tRNA<sup>His</sup> (Figure 3) (37), as well as *E. coli* tRNA<sup>SeCys</sup> precursor construct (37) and a yeast cytoplasmic tRNA<sup>Asp</sup> precursor construct (C. E. Holmes and S. M. Hecht, unpublished data). Hüttenhofer et al. (38) have reported their findings using yeast tRNA<sup>Phe</sup> as a substrate for Fe-BLM and have also reported that an *E. coli* tRNA<sup>Asp</sup> precursor transcript and *E. coli*<sub>Leu</sub> were cleaved, although the sites of cleavage for the last two RNA's were not given.

A comparison of the sites cleaved in these substrates indicated that cleavage involved 5'-GN-3' sites, but that



**Figure 3.** Structures of *Schizosaccharomyces pombe* amber suppressor tRNA<sup>Ser</sup> construct (top) and mature *E. coli* tRNA<sup>His</sup> (bottom). The major sites of Fe-BLM-induced cleavage are indicated by arrows, the minor sites by asterisks.

other sequences (notably 5'-UU-3' in *E. coli* tRNA<sup>His</sup> (37) and 5'-UG-3' in yeast tRNA<sup>Phe</sup> (38)) were also cleaved.

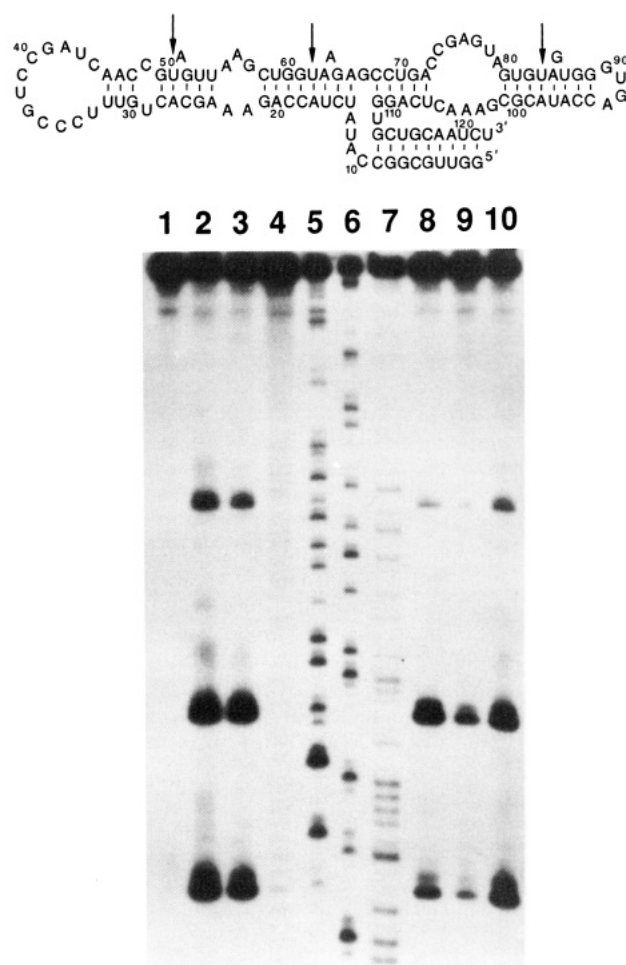


**Figure 4.** Bleomycin-mediated cleavage of an RNA transcript corresponding to the 5'-end of HIV-1 reverse transcriptase mRNA. The 5'-<sup>32</sup>P end-labeled RNA was prepared by *in vitro* transcription of a *Sca* I-linearized DNA plasmid; lane 1, RNA alone; lane 2, 100  $\mu$ M Fe(II)-BLM A<sub>2</sub>; lane 3, 500  $\mu$ M Fe(II)-BLM A<sub>2</sub>.

As in the case of *B. subtilis* tRNA<sup>His</sup> precursor, a number of cleavage sites were located at positions believed to occur at a junction between single- and double-stranded regions of the molecule, but some cleavage sites (see, e.g., Figure 3) were in regions that are nominally single-stranded.

**Other RNAs.** Although most of the work reported to date has involved transfer RNAs and tRNA precursor constructs prepared by *in vitro* transcription, other types of RNA substrates have also been studied. This included a substrate 347 nucleotides in length corresponding to the 5'-end of HIV-1 reverse transcriptase mRNA that was prepared by *in vitro* transcription from an expression plasmid following linearization of the plasmid with restriction endonuclease *Sca* I (34). As shown in Figure 4, this RNA was cleaved at least in four places by Fe(II)-BLM A<sub>2</sub>.

Recently, Dix et al. (39) have utilized activated Fe-BLM as a reagent for characterizing structural changes in the iron regulatory element (IRE) of ferritin mRNA from bullfrog. The wild-type RNA was cleaved at a single site (U<sub>17</sub>) within the IRE, at a 5'-GU-3' sequence believed to be at the junction between a single- and double-stranded region in the stem-loop structure. Interestingly, a mutant substrate associated with decreased translational regulation by the endogenous regulatory protein, in which the flanking region contiguous with the IRE was altered by disrupting a phylogenetically conserved triplet set of base pairs, was cleaved at A<sub>10</sub> and A<sub>11</sub> by Fe-BLM, rather than U<sub>17</sub>. The latter two sites were the first two bases within the double-stranded region on the opposite



**Figure 5.** Fe(II)-bleomycin A<sub>2</sub>-mediated cleavage of yeast 5S ribosomal RNA. The secondary structure of the yeast 5S rRNA is shown at the top of the figure, with the three sites of cleavage shown by arrows. The polyacrylamide gel at the bottom illustrates the cleavage of the 5'-<sup>32</sup>P end-labeled RNA: lane 1, rRNA alone ( $\sim 1 \mu$ M final nucleotide concentration); lane 2, 250  $\mu$ M Fe(II)-BLM A<sub>2</sub>; lane 3, 125  $\mu$ M Fe(II)-BLM A<sub>2</sub>; lane 4, alkali-treated RNA; lane 5, G-lane, lane 6, A > G lane; lane 7, U + A lane; lane 8, 250  $\mu$ M Fe(II)-BLM A<sub>2</sub> + 100 mM NaCl; lane 9, 250  $\mu$ M Fe(II)-BLM A<sub>2</sub> + 5 mM Mg<sup>2+</sup>; lane 10, 250  $\mu$ M Fe(II)-BLM A<sub>2</sub> + 1 mM Mg<sup>2+</sup>.

side of the stem-loop structure from that cleaved in the wild-type IRE.

The cleavage of yeast 5S ribosomal rRNA by Fe(II)-BLM A<sub>2</sub> has also been studied. This substrate was of interest both because it represented a member of the third major class of RNA molecules and also because the structure has been conserved evolutionarily and characterized in detail using chemical and enzymatic probes. As shown in Figure 5, treatment of this rRNA with Fe(II)-BLM A<sub>2</sub> afforded three cleavage bands. RNA sequence analysis indicated that all three sites of cleavage involved the uridine nucleotide in a 5'-GUA-3' sequence; all of these sequences also have a one-base bulge one or two nucleotides to the 3'-side of the cleavage site. It is interesting that the sites in the 5S rRNA cleaved by Febleomycin represent three of the four 5'-GUA-3' sequences in the RNA; all three are believed to be present within helical regions of the RNA and to contribute to stabilization of RNA tertiary structure (37, 40).

One additional RNA substrate of special interest is an RNA-DNA heteroduplex, a species that is formed during both forward and reverse transcription. An RNA-DNA heteroduplex suitable for study was prepared by reverse transcription of *E. coli* 5S rRNA using a suitable DNA

primer. The RNA and DNA strands of the heteroduplex were uniquely end labeled in parallel experiments so the cleavage of each could be studied. Treatment with Fe(II)-BLM under aerobic conditions resulted in cleavage of both the RNA and DNA strands at a limited number of sites and at comparable concentrations. Further, the sites of cleavage of the RNA strand of the heteroduplex were different than those of the rRNA from which it was formed by reverse transcription, indicating that cleavage of the RNA strand involved recognition and cleavage of the heteroduplex per se (41).

**Characteristics of Bleomycin-Mediated RNA Cleavage.** At a descriptive level, there are several facets of BLM-mediated RNA strand scission that are worth noting. In addition to the observation made initially, i.e., that not every RNA studied has been a substrate for cleavage by bleomycin, none of the substrate RNA's have been cleaved at large numbers of sites. Further, unlike DNA (oligonucleotide) substrates for Fe-bleomycin, to date no RNA substrate has undergone double-strand cleavage or cleavage toward the end of an RNA strand (*vide infra*). Although most of the survey work carried out in the Hecht laboratory has employed relatively high concentrations of bleomycin to facilitate the identification of authentic substrates, not all of the substrate RNA's so identified exhibit comparable susceptibility to cleavage. Three RNA's studied thus far, including *B. subtilis* tRNA<sup>His</sup> precursor, yeast 5S rRNA, and the RNA-DNA heteroduplex formed by reverse transcription of *E. coli* 5S rRNA, were found to undergo cleavage readily at 1–3  $\mu$ M FeBLM concentrations when the final RNA nucleotide concentrations were ~1–5  $\mu$ M. The sensitivity of these RNA's to FeBLM was thus at least several-fold greater than that of the other RNA substrates.

The experiments carried out with RNA have employed conditions less complex than those which obtain in a cellular environment. In order to ensure that the observations made in these experiments could be obtained under physiological conditions, the effects of agents such as NaCl, spermidine, and MgCl<sub>2</sub> on BLM-mediated RNA cleavage have been studied (37, 42). It was found that the cleavage of most RNA's diminished sharply in the presence of cations such as spermidine and Mg<sup>2+</sup>; the structural basis for this is discussed below. However, the three RNA's that had been found to act as efficient substrates for FeBLM (*vide supra*) were still cleaved efficiently even at >1 mM Mg<sup>2+</sup> concentration. Remarkably, as demonstrated convincingly for some RNA substrates (see, e.g., Figure 5), the presence of salt and Mg<sup>2+</sup> actually further increased the *selectivity* of RNA cleavage by bleomycin. While no study of the intracellular cleavage of RNA has been reported thus far, it seems likely that it may prove to be a highly selective process.

#### THE CHEMISTRY OF RNA CLEAVAGE BY BLEOMYCIN

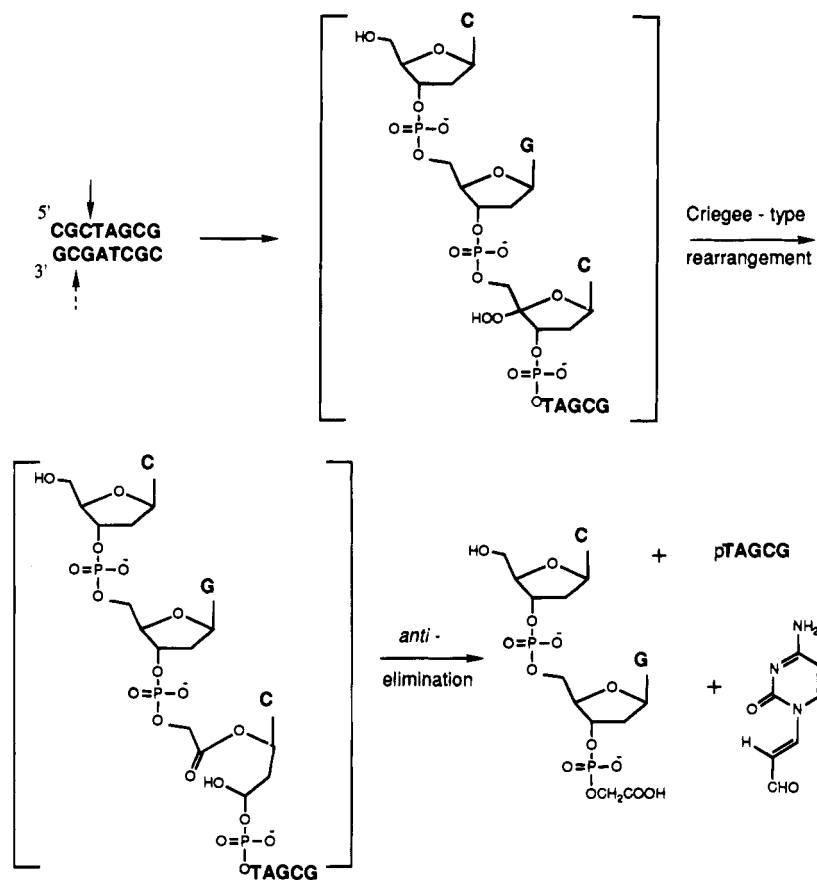
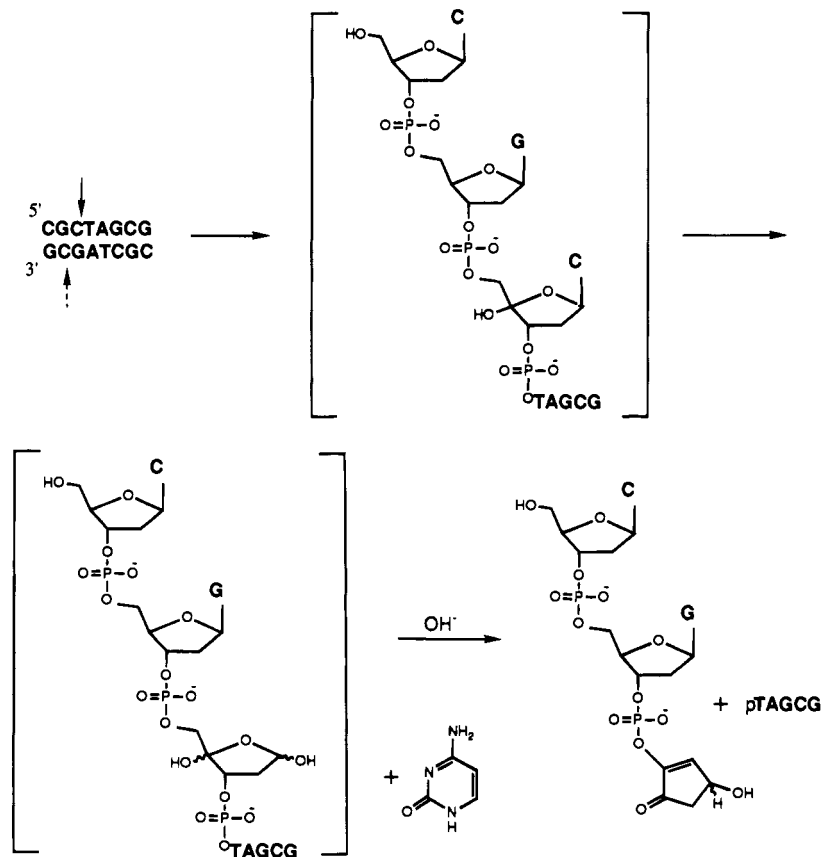
Several lines of evidence suggest that the mechanism of Fe(II)-BLM-mediated RNA strand scission, like that of DNA, involves oxidative transformation of the polynucleotide. These include the observations that RNA cleavage by bleomycin was supported by Fe(II), but not Fe(III), and that cleavage was potentiated by reducing agents such as ascorbate and dithiothreitol (37). In common with DNA cleavage, Fe(II)-BLM-mediated RNA strand scission also required O<sub>2</sub>. It has been shown by several investigators that Fe(III)-bleomycin can be activated for DNA strand scission via the agency of H<sub>2</sub>O<sub>2</sub> in a process formally analogous to the peroxide shunt mechanism established for cytochrome P<sub>450</sub> (8–10). RNA cleavage was also observed following admixture of Fe(III)-BLM and H<sub>2</sub>O<sub>2</sub>; the sequence selectivity was the

same as that noted following aerobic activation (C. E. Holmes and S. M. Hecht, unpublished data).

**Product Analysis.** The actual chemical products of bleomycin-mediated RNA degradation have been shown to include the nucleic acid bases adenine and uracil, as shown by TLC (33) and HPLC analyses (34). By the use of a tRNA<sup>His</sup> precursor transcribed in the presence of [<sup>3</sup>H]-UTP and then 5'-<sup>32</sup>P end labeled via the agency of [<sup>32</sup>P]-ATP + polynucleotide kinase, it has been shown that strand breaks at U<sub>35</sub> (34–37) were roughly stoichiometric with the release of free [<sup>3</sup>H]uracil (R. J. Duff, C. E. Holmes, and S. M. Hecht, manuscript in preparation).

During the studies of bleomycin-mediated DNA degradation, one particularly effective tool involved the use of oligonucleotide substrates that underwent oxidative transformation at one site, or a small number of sites, thereby facilitating product analysis (8–10). This was especially true for substrates that underwent cleavage near the ends of the oligonucleotide strand, as low molecular weight products amenable to direct analysis were thereby obtained (43, 44). For example, by the use of this strategy, the self-complementary octanucleotide 5'-CGCTAGCG-3' was found to undergo FeBLM-mediated degradation almost exclusively at deoxycytidine<sub>3</sub> and deoxycytidine<sub>7</sub>; strand scission at the former position afforded the dinucleotide CpGpCH<sub>2</sub>COOH, in which the glycolate moiety must have been derived from C-4' and C-5' of the sugar moiety of deoxycytidine<sub>3</sub> (Scheme 1). As noted in Scheme 1, Febleomycin-mediated DNA degradation also results in the formation of base propenals, which in this case is believed to contain C-1', C-2', and C-3' of the sugar moiety of deoxycytidine<sub>3</sub>. As indicated, it is possible to rationalize the formation of these products as arising from initial abstraction of C-4' H of deoxyribose (8–10). Another set of products involves the formation of a C-4' OH apurinic acid (the alkali labile lesion (45–47)) with concomitant release of free base (Scheme 2). It may be noted that the latter pathway does not lead directly to strand scission; an additional chemical treatment is required to obtain cleavage (8–10, 45–47).

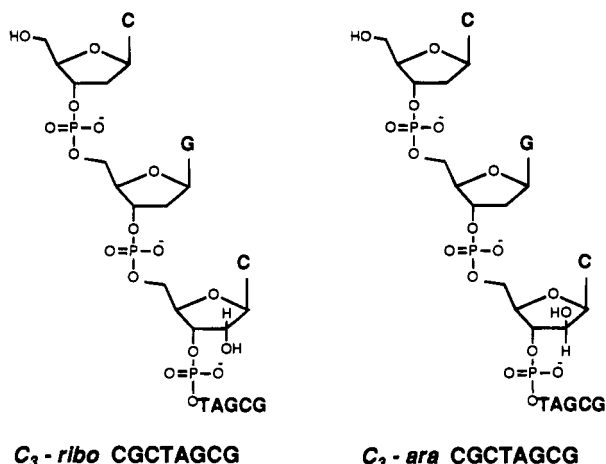
Although the strategy outlined in Scheme 1 has worked well for the analysis of BLM-mediated DNA cleavage products, to date no RNA substrate has been observed to undergo cleavage near the end of an oligonucleotide, thus precluding the use of this approach for the analysis of the chemistry of RNA cleavage. In order to determine whether a ribonucleoside could undergo FeBLM-mediated oxidative damage analogous to that observed for deoxyribonucleosides, the chimeric oligonucleotides shown in Figure 6 were employed as substrates for Fe(II)-BLM A<sub>2</sub>. As illustrated in Scheme 3, both of these oligonucleotides afforded CpGpCH<sub>2</sub>COOH, suggesting strongly that both had undergone oxidative transformation initiated by abstraction of C-4' H from the sugar moiety of ribocytidine<sub>3</sub> and *ara*-cytidine<sub>3</sub>, respectively (34). It may be noted that no base propenal formation was detected following tRNA degradation (33, 34), as expected. The hydroxylated base propenal, whose formation might have been anticipated following the degradation of the chimeric oligonucleotides shown in Figure 6, has not been detected. This is not entirely unexpected, as the hydroxylated base propenal might be anticipated to be unstable, undergoing facile hydrolysis to afford the free nucleic acid base. In fact, the appearance of free bases has been reported (33, 34); as noted above for *B. subtilis* tRNA<sup>His</sup> precursor, the formation of uridine was roughly stoichiometric with tRNA cleavage at uridine<sub>35</sub> (C. E. Holmes, R. J. Duff, and S. M. Hecht, manuscript in preparation). In the case of the chimeric oligonucleotides,

**Scheme 1. Strand Scission Products Resulting from Treatment of CGCTAGCG with Fe-Bleomycin**

**Scheme 2. Alkali-Labile Lesion Resulting from Treatment of CGCTAGCG with Fe-Bleomycin**


the amount of free cytosine released was in excess of that anticipated from the characterized oligonucleotide cleav-

age mechanisms (8-10, 43-47) and was studied further (*vide infra*).





**Figure 6.** Self-complementary chimeric octanucleotides used as substrates for Fe(II)-bleomycin.

As noted above, Fe·BLM-mediated DNA strand scission produces alkali-labile lesions in addition to strand breaks (45–47); both sets of products are believed to derive from a common C-4' deoxyribose radical (8–10). Because the strand scission products formed from RNA appear to be analogous to those formed from DNA, it is logical to think that RNA degradation may also proceed via a C-4' ribose radical. The possible existence of a second set of RNA products, analogous to the alkali lesion in DNA, seems not unlikely, but has not yet been demonstrated experimentally due to the inherent lability of RNA to treatment with alkali.

#### Cleavage of Double-Labeled Ribosomal RNA.

Although no detailed structural analysis of the Fe·BLM-mediated cleavage of any RNA molecule has been re-

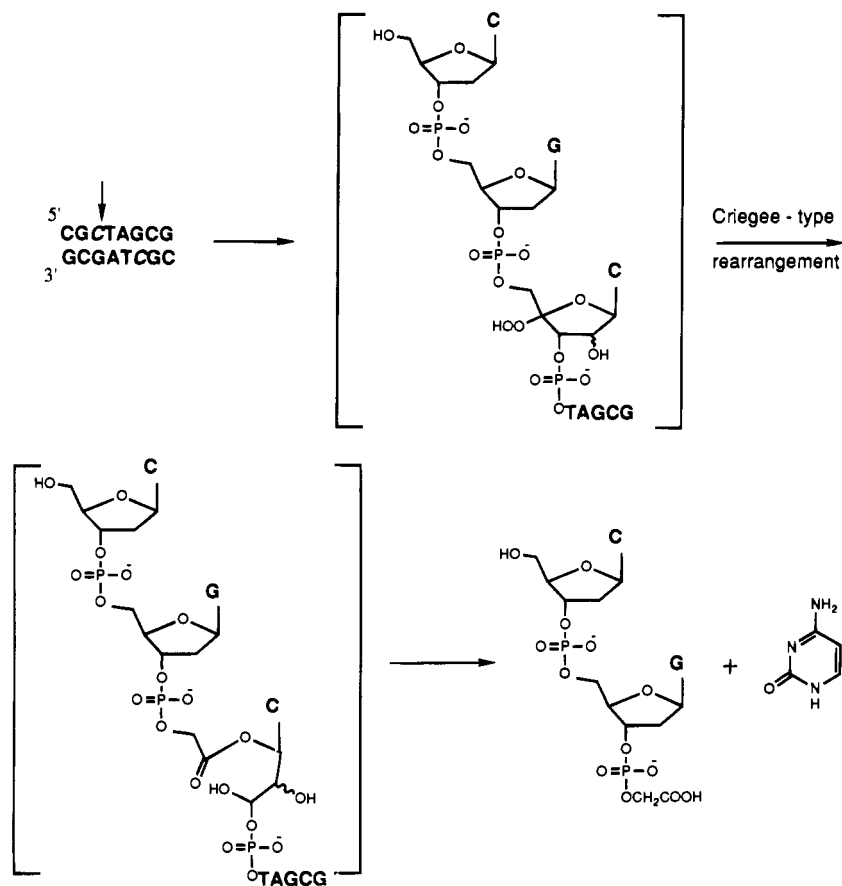
ported to date, some useful data fully consistent with the chemistry outlined in Scheme 3 have been obtained using yeast 5S ribosomal RNA.

As shown in Figure 5, the cleavage of this rRNA by activated Fe·bleomycin was carried out using both 5'- and 3'-end-labeled rRNA's in parallel experiments. In addition to verifying the absence of double-strand cleavage of this substrate (37), the analysis indicated that each of the three cleavage sites was a primary site. This experiment also provided some information about the chemical nature of the cleavage products.

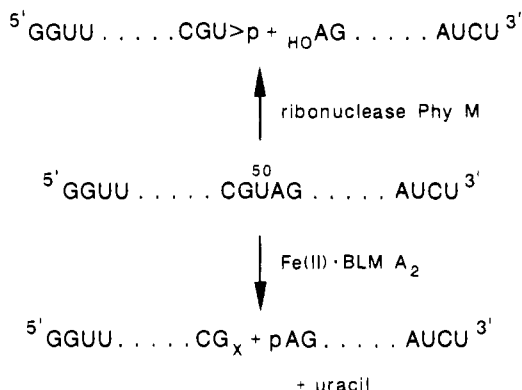
Scheme 4 illustrates the nature of the products that would form as a result of cleavage of the 5S rRNA at uridine<sub>50</sub> if the chemical mechanism of cleavage were analogous to that which is obtained for DNA (cf. Schemes 1 and 3). In particular, it would be anticipated that the 5'-end-labeled rRNA would afford a product having a phosphoroglycolate moiety at the 3'-terminus (34). If actually formed as a reaction product, this species would migrate farther on a polyacrylamide gel than the corresponding band in the sequencing lane which has a 2',3'-cyclic phosphate at its 3'-terminus. As shown in Figure 5, this was actually observed. Likewise, cleavage of the 3'-<sup>32</sup>P end-labeled rRNA by Fe·BLM gave bands that migrated slightly faster than the corresponding bands in the U-lane of the sequencing gel, the latter of which are known to have 5'-OH termini. As shown in Scheme 4, this is entirely consistent with cleavage of the RNA by the same oxidative mechanism as DNA, which is known to afford 5'-phosphate termini (8–10).

**Oxidation of RNA at C-1' of Ribose.** Prior to the definitive characterization of C-4' of deoxyribose as the site of oxidation of DNA by activated Fe·BLM, it was suggested that oxidation of C-1' was reasonable from a chemical perspective and could potentially explain some

#### Scheme 3. Oxidative Degradation of Chimeric Octanucleotides Initiated by Abstraction of C-4' H



**Scheme 4. Putative Chemistry of 5S rRNA Cleavage by Fe(II)-Bleomycin, Illustrated for the Lesion Produced at Uridine<sub>50</sub>**



of the experimental observations that had been made (48). In fact, this site has subsequently been shown to be oxidized by other DNA damaging agents (49–51). On the basis of the earlier observation (52) that poly-(dA)-poly(rU) gave more free adenine production (relative to adenine propenal) than would have been expected from oxidation of C-4' H of deoxyribose with bleomycin, as might be anticipated from analogous oxidation processes operating at C-1' (48) (cf. Schemes 1 and 2), Absalon et al. (53) studied the possible involvement of C-1' chemistry in DNA degradation. For the substrates studied, they excluded the involvement of C-1' chemistry convincingly.

Recently, Long et al. (54) have shown that structural alteration of a DNA substrate, in a fashion that leads to altered conformation, can alter the ratio of products

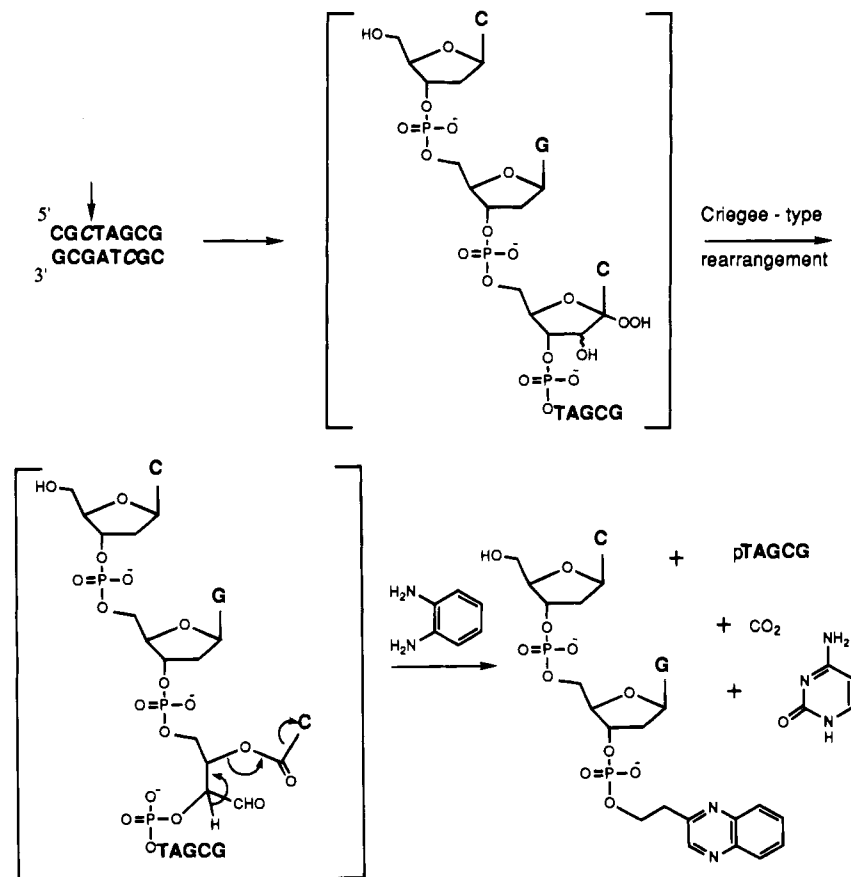
formed from that substrate upon treatment with bleomycin. Because the amount of free cytosine released upon treatment of *C3-ara* CGCTAGCG was greater than would have been anticipated from the degradation processes shown in Schemes 1 and 2, and because this oligonucleotide is known to have a conformation different from that of B-DNA (55), we explored the possibility that it might undergo oxidation at C-1'. The strategy, outlined in Scheme 5, involved capture of putative intermediate **i**, which would form via Criegee-type rearrangement of a C-1' hydroperoxide intermediate, with diaminobenzene. In fact, the derived quinoxaline was shown to form, as judged by HPLC comparison with an authentic synthetic standard. Further verification of the structure of the bleomycin-induced product, as well as quantification of the amount of quinoxaline formed, was accomplished both by analysis of the UV spectrum of the product, which has a  $\lambda_{\text{max}}$  at 320 nm ( $\epsilon$  5900), and also by the use of [<sup>14</sup>C]-1,2-diaminobenzene of known specific activity. It was found that the pathway outlined in Scheme 5 afforded 58% of the products derived from degradation of cytidine<sub>3</sub> in *C3-ara* CGCTAGCG and about 10% of those produced from *C3-ribo* CGCTAGCG (56).

Not yet resolved experimentally is the issue of whether C-1' oxidation is also accompanied by formation of a C-1' hydroxide intermediate analogous to that depicted in Scheme 2, as originally suggested for oxidative damage to DNA (48).

**POLYNUCLEOTIDE BINDING AND DEGRADATION**

In spite of the fact that bleomycin-mediated polynucleotide degradation has been studied intensively for a number of years, surprisingly little is known about the

**Scheme 5. Oxidative Degradation of Chimeric Octanucleotides Initiated by Abstraction of C-1' H**



strategy employed by BLM to select and destroy its polynucleotide substrates. Although the preferential cleavage of DNA, and to some extent RNA, at certain 5'-G-pyr-3' sites has been well documented (8-10, 57-59), it is uncertain why those preferred sites are chosen. Further, while Fe-BLM-mediated damage to DNA occurs in the minor groove (8-10), it is still not certain whether the mode of association of BLM with DNA involves minor groove binding (60), intercalation (61-63), or both.

Nonetheless, on the basis of the accumulated data, a number of inferences can be drawn about the way in which BLM selects its preferred binding sites and associates with them prior to their oxidative destruction. On the assumption that the recognition and binding of RNA by BLM is fundamentally analogous to that of DNA (*vide infra*), recent experiments with RNA allow further observations to be made.

**Characteristics of Polynucleotide Binding by Bleomycin.** The equilibrium binding constant for the association of bleomycin and certain metalbleomycins with DNA is on the order of  $10^5 \text{ M}^{-1}$ , as demonstrated under a variety of experimental conditions (10). The lifetimes of the DNA complexes have been measured for Cu(II)-BLM and Fe(III)-BLM; they were 0.1 and 22 s, respectively (64). (Metallo)bleomycins can unwind DNA and cause helix elongation, although it is not certain whether this results from (partial) intercalation of the bithiazole moiety, ionic interactions between bleomycin and the phosphate ester backbone of DNA, or both (65).

The preference of bleomycin for cleaving DNA at 5'-GC-3' and 5'-GT-3' sites has been attributed to a specific hydrogen bonding interaction between the bithiazole moiety of BLM and the guanine nucleotide at the cleavage site (60). However, recent studies of the intrinsic preference of the bithiazole moiety for specific sites on DNA suggest that it has little sequence specificity and that any preference that it may have is unlike that of bleomycin (66, 67). Further, at least three lines of evidence suggest strongly that it is the metal-binding domain of BLM that is responsible for the sequence selectivity of DNA cleavage by bleomycin. These include (i) the observation that BLM congeners having the same C-terminus, but altered metal-binding domains, exhibited altered strand selectivity of DNA cleavage (44), (ii) the finding that a series of deglycobleomycin analogs in which the metal-binding domain and bithiazole moiety was separated by semirigid spacers of increasing length all cleaved DNA substrates the same site, albeit with varying efficiencies (68), and (iii) the discovery that PMAH, a model for the metal-binding domain of BLM, exhibited similar sequence selectivity of DNA cleavage to that of BLM itself (69). It may be noted, however, that other analogs having metal-binding domains similar to that of BLM failed to produce sequence selective cleavage (7, 70).

In the context of the foregoing observations, it may be pertinent to note that 5'-G-pyr-3' sequences constitute the widest part of the minor groove of B-DNA (71), which is the preferred substrate for BLM (8-10, 72). Molecular modeling studies in the Hecht laboratory suggest that the chelated metal binding domain of bleomycin may be somewhat too large to fit within the (unperturbed) minor groove of B-form DNA; the somewhat greater width of the minor groove at GC as compared with AT sequences (~6 Å vs 4 Å, respectively) could well facilitate the DNA binding of the BLM metal binding domain at 5'-GC-3'. Consistent with this suggestion were the observations that Fe-BLM cleaved DNA preferentially at the sites of bulges (73) and (partially) perturbed duplexes (74) *regardless of DNA sequence*, as such sites would necessarily

have somewhat wider minor grooves. As noted above, a number of the sites at which activated Fe-BLM has been noted to cleave RNA involve one-nucleotide bulges (37) or the junction between single- and double-strand regions; the "minor groove" of RNA in such regions is also very likely to be somewhat wider than that of a normal A-form duplex.

**Factors That Limit the Efficiency of Cleavage of DNA and RNA by Bleomycin.** Depending on the way that individual experiments are performed, any of several factors can limit the amount of polynucleotide damage mediated by bleomycin. These include the omission, or use of a suboptimal amount, of some cofactor required for cleavage such as metal ions, oxygen, or a reducing agent (8-10, 75). The facility of substrate degradation can also be influenced by factors such as pH (75, 76), temperature (35, 36, 76), and the timing and order of addition of reagents (77). Ironically, it has also been shown that large amounts of DNA substrate can inhibit cleavage by bleomycin (75, 78-81), apparently reflecting the fact that activation of Fe(II)-BLM under aerobic conditions occurs more readily in solution before the activated species binds to DNA (81).

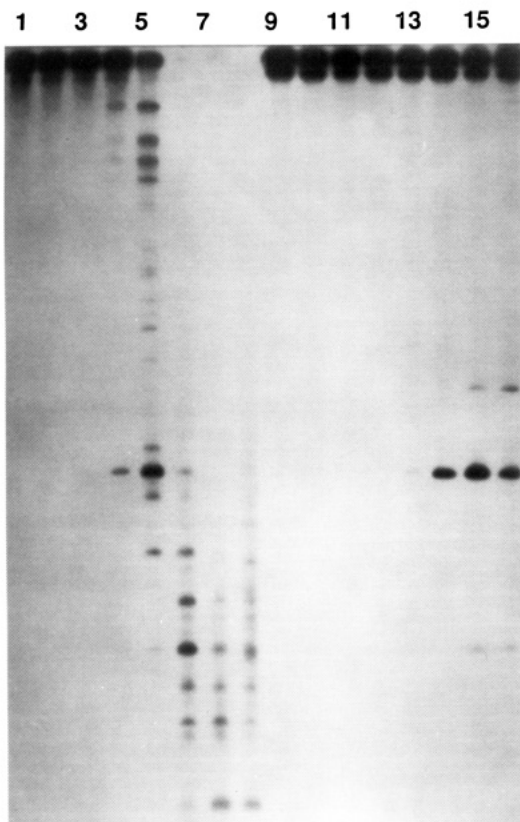
Even under conditions optimal for substrate degradation, one or more steps must limit the efficiency of the overall process. A few lines of evidence suggest that one of the limiting steps involves the actual chemical transformations that lead to DNA and RNA degradation. These include the observations that (i) some polynucleotide substrates are cleaved with efficiencies much greater than others of ostensibly similar structure (34, 37, 43, 44), (ii) there is a primary isotope effect associated with the abstraction of C-4' H from deoxyribose by Fe-BLM (82) which can vary from site to site on DNA (83), (iii) the association/dissociation of BLM from DNA would seem to be fast relative to cleavage (64), and (iv) there appear to be BLM molecules bound to DNA at sites that do not lead to (efficient) DNA degradation (84, 85).

Recently, we carried out an experiment to define the reasons for the greater selectivity of RNA cleavage by BLM as compared with DNA cleavage; the results were surprising and provided important insights into the nature of BLM-polynucleotide interaction.

**Cleavage of a tRNA Precursor and Its Corresponding tDNA.** The initial observation that *B. subtilis* tRNA<sup>His</sup> precursor was cleaved at a single major site by activated Fe-BLM, and that a number of other tRNA's and tRNA precursor constructs were not cleaved at all, suggested that bleomycin-mediated cleavage of RNA must differ fundamentally from that of DNA. The results of the survey of RNA cleavage summarized above have tended to lessen the distinction, as both DNA and RNA are cleaved primarily at 5'-G-pyr-3' sites, but the cleavage of RNA clearly does occur in a much more highly selective fashion than that of DNA.

While it seemed at first that the differences in bleomycin-mediated cleavage must be due to the fact that DNA and RNA are constituted from different types of mononucleotides, it was also recognized that DNA's do not ordinarily assume secondary and tertiary structures analogous to those believed to obtain for the tRNA's and tRNA precursors that had been studied most intensively as substrates for Fe-BLM. Accordingly, we prepared a DNA identical in primary sequence with *B. subtilis* tRNA<sup>His</sup> precursor.

Although there was no direct evidence for the secondary and tertiary structure of either of these species, it seemed highly likely that they would be quite similar based on reports of the behavior of pairs of tRNA's and tDNA's studied earlier. For example, *E. coli* tRNA<sup>Met</sup>



**Figure 7.** Comparison of the cleavage of tRNA<sup>His</sup> and tDNA<sup>His</sup> precursor substrates by Fe(II)-BLM. The reactions were run with the tRNA and tDNA substrates at 7–8  $\mu$ M nucleotide concentrations; lane 1, tDNA only; lane 2, 1.25  $\mu$ M BLM A<sub>2</sub>; lanes 3–8, 0.25, 0.5, 1.25, 2.5, 25, and 250  $\mu$ M Fe(II)-BLM A<sub>2</sub>, respectively; lane 9, tRNA only; lane 10, 1.25  $\mu$ M BLM A<sub>2</sub>; lanes 11–16, 0.25, 0.5, 1.25, 2.5, 25, and 250  $\mu$ M Fe(II)-BLM A<sub>2</sub>, respectively.

and its corresponding tDNA, the latter of which contained a 3'-terminal riboadenosine, were both substrates for methionyl-tRNA synthetase (86). It was also shown that tDNA analogs of *E. coli* tRNA<sup>Phe</sup> and tRNA<sup>Lys</sup> were capable of inhibiting tRNA activation by the cognate aminoacyl-tRNA synthetases, and also acting as substrates for the same activating enzymes (87).

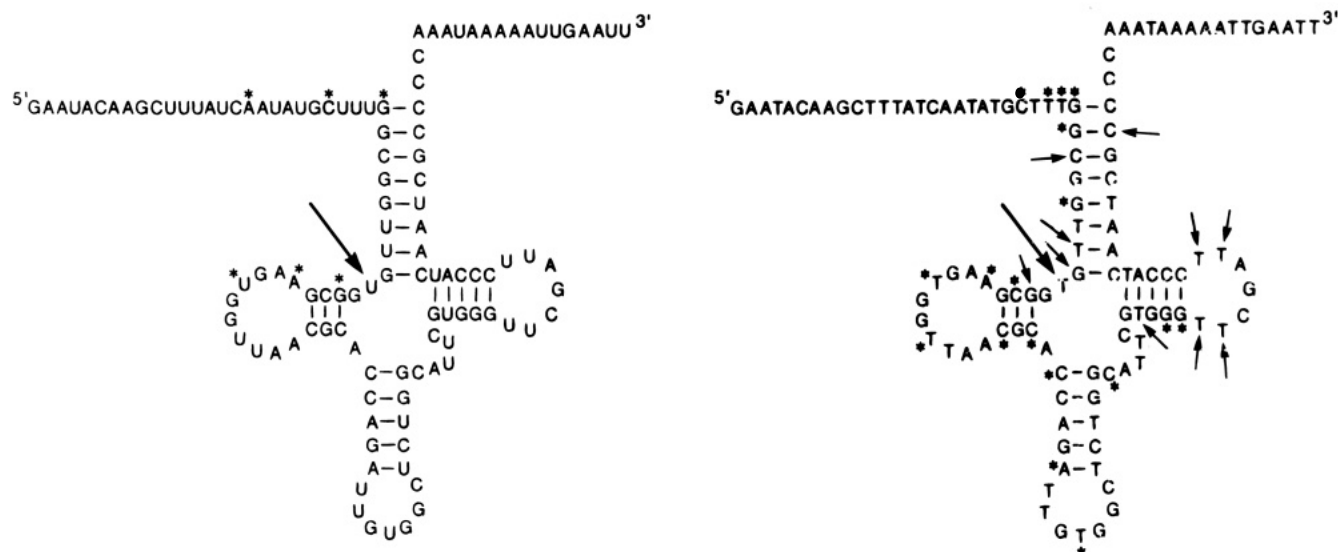
Initially, *B. subtilis* tRNA<sup>His</sup> precursor and its corresponding tDNA were treated with Fe(II)-BLM A<sub>2</sub>, under

aerobic conditions. Cleavage of the tDNA was detected readily following treatment with 500 nM Fe(II)-BLM A<sub>2</sub>; tRNA<sup>His</sup> cleavage was slightly less facile, being detectable at 1.25  $\mu$ M concentration and readily apparent at 2.5  $\mu$ M (Figure 7). Remarkably, at low concentrations of added Fe-BLM, cleavage of the tDNA occurred predominantly at a single site, identical with the primary site of cleavage of tRNA<sup>His</sup> precursor (42)! This observation argues strongly that the recognition of DNA and RNA by activated Fe-BLM must be fundamentally analogous and relies primarily on recognition of nucleic acid structure and conformation, rather than the nature of the constituent mononucleotides.

Treatment of the tDNA with higher concentrations of Fe(II)-BLM A<sub>2</sub> resulted in increasing amounts of degradation and the appearance of additional cleavage bands. The additional sites of cleavage, summarized in Figure 8, reinforce the view that cleavage of the tDNA was analogous to that of tRNA<sup>His</sup> precursor, as several of the additional sites of cleavage of the tDNA were identical to the minor sites of cleavage of tRNA<sup>His</sup> precursor. Also similar was the inhibition of cleavage of the tDNA and tRNA substrates upon admixture of Mg<sup>2+</sup>, demonstrating that nucleic acid secondary and tertiary structure determine the susceptibility of a BLM substrate to inhibition by Mg<sup>2+</sup> (42).

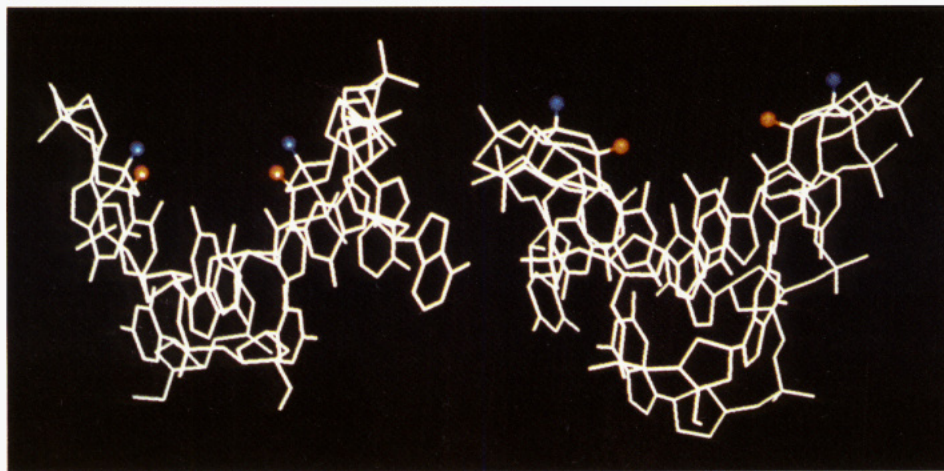
The cleavage of the tDNA and tRNA did differ in one important respect, however, i.e., in the results obtained when higher concentrations of Fe-BLM were employed. As shown in Figure 7, the tDNA (present at 7–8  $\mu$ M nucleotide concentration) was consumed completely in the presence of 2.5  $\mu$ M Fe(II)-BLM A<sub>2</sub>; even more extensive degradation was apparent at 25  $\mu$ M Fe-BLM. In comparison, the extent of tRNA<sup>His</sup> cleavage obtained using 2.5  $\mu$ M Fe(II)-BLM did not change dramatically in the presence of greater concentrations of the drug, even when 250  $\mu$ M Fe(II)-BLM was employed (42).

In the belief that this difference must reflect the greater affinity of Fe-BLM for the tDNA, a competition experiment was carried out. In this experiment radiolabeled tDNA or tRNA substrates having the same specific activity were treated with Fe(II)-BLM A<sub>2</sub> in the presence of varying concentrations of unlabeled tRNA<sup>His</sup> or tDNA. Unexpectedly, unlabeled tRNA<sup>His</sup> was much more effective than unlabeled tDNA in inhibiting the Fe-BLM-induced degradation of both radiolabeled sub-

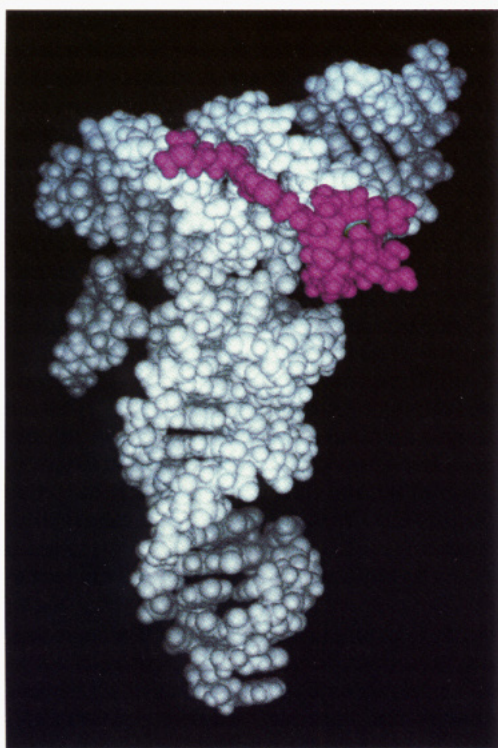


**Figure 8.** Structures of *B. subtilis* tRNA<sup>His</sup> precursor and a tDNA arbitrarily folded in the same secondary structure. In addition to the major sites of cleavage at U<sub>35</sub> (T<sub>35</sub>), denoted by large arrows, other significant sites of tDNA cleavage are indicated by small arrows. Minor sites of cleavage of both substrates are denoted by asterisks.





**Figure 9.** Structures of 5'-CGCGAATTCGCG-3', a B-DNA (88), and 5'-GGGGCCCC-3', an A-DNA (89). Both species are viewed along the minor groove at the site of cleavage actually established for the dodecanucleotide (left) in comparison with the corresponding GC sequence for the octanucleotide (right). The relevant C-1' H's are shown in red; the C-4' H's are in blue.



**Figure 10.** Structure of yeast cytoplasmic tRNA<sup>Asp</sup> (90) with Fe-bleomycin (91) bound in an orientation consistent with the observed chemistry of C-4' H abstraction.

strates. Unless the kinetics of binding are dramatically different for the two substrates, or there is some RNA-specific mechanism for BLM deactivation, the inescapable conclusion is that *Fe-BLM binds more tightly to the RNA substrate than to its DNA counterpart*.

**Why Is the Cleavage of RNA More Selective Than That of DNA?** Given the likelihood that bleomycin actually binds more tightly to RNA than to DNA, the observation that RNA cleavage occurs less frequently is intriguing. There are two possible explanations for this phenomenon, either or both of which could account for the experimental observation. The first is that Fe-BLM produces RNA damage much of which does not lead to RNA strand scission. The second is that bleomycin binds to RNA in an orientation not conducive to the production of strand breaks.

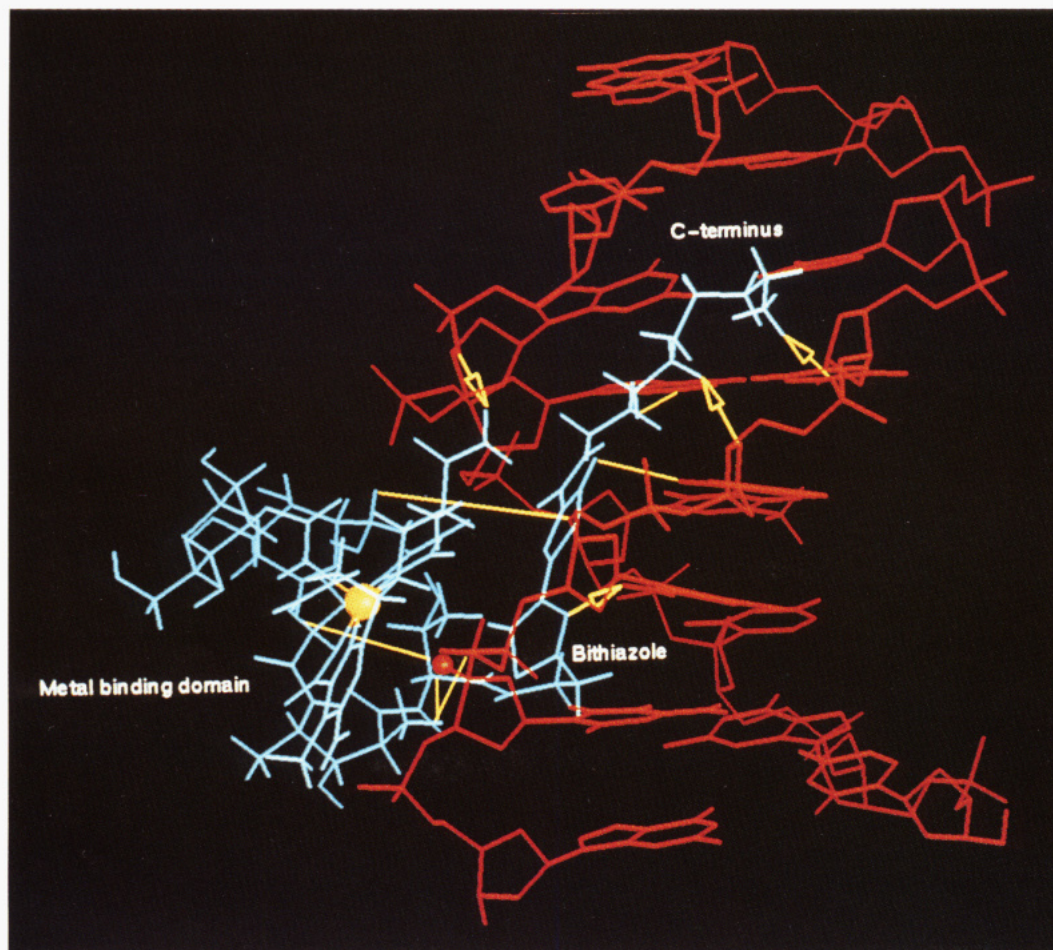
Much of what is known about the actual chemistry of RNA cleavage at present relies on the experiments

described above involving the use of *C<sub>3</sub>-ribo* CGCTAGCG as a substrate for Fe-BLM. Assuming that this is a valid model for RNA degradation, RNA strand scission results from initial abstraction of C-4' H of ribose, i.e., the same mechanism employed for DNA strand scission. RNA may also be degraded by a process involving initial abstraction of C-1' H of ribose, but this would probably not lead directly to strand scission (Scheme 5). Both of the mechanisms for octanucleotide degradation that have been established experimentally involve hydroperoxy intermediates (cf. Schemes 1 and 5). For DNA, the initially formed C-4' radical resulting from H abstraction can also be converted to a C-4' OH intermediate, which is believed to lead to the formation of the alkali labile lesion (Scheme 2) (8–10). In principle, C-4' and C-1' ribose radicals in RNA could also afford the respective hydroxylated ribose intermediates. Collapse of such species would presumably occur without RNA strand scission (cf. Scheme 2 and ref 48); the unmasking of these possible lesions in BLM-treated RNA is complicated by the intrinsic lability of the RNA backbone to reagents such as alkali.

At present, it is difficult to assess the extent to which the apparent selectivity of RNA cleavage by BLM may reflect the production of lesions that do not lead to strand scission. However, one may note that three of the foregoing four mechanisms for RNA degradation are predicted to afford free nucleic acid bases concomitant with production of the lesion, and the fourth (Scheme 3) would also do so by hydrolysis of a putative hydroxylated base propenal, which is anticipated to be unstable. Therefore, if the extent of strand breakage is compared with base release, the importance of lesions that do not lead to strand scission can be estimated. This has been done both for *B. subtilis* tRNA<sup>His</sup> precursor and for *C<sub>3</sub>-ribo* CGCTAGCG. In both cases, the strand scission product would seem to be the major product (R. J. Duff, C. E. Holmes, and S. M. Hecht, manuscript in preparation) arguing that selectivity of RNA cleavage is not due primarily to the formation of lesions that do not lead to strand scission. On the other hand, given the conformational variability of RNA, it may be the case that some sites susceptible to Fe-BLM-mediated oxidation do not produce strand breaks.

The second possible reason for selectivity of RNA cleavage, i.e., the inability of BLM to oxidize the RNA substrate from the orientation in which it is bound, is supported by a few experimental observations. These





**Figure 11.** Model of the Zn(II)-BLM A<sub>5</sub>-d(CGCTAGCG)<sub>2</sub> complex. BLM (light blue) is positioned in the minor groove of the B-form octamer (red). The six intermolecular NOEs are shown as yellow lines; the apparent length differences are due to perspective only. H bonding contacts are shown as yellow arrows pointing toward the hydrogen atoms. The metal ion (gold ball) is 3.3 Å from the C<sub>7</sub> H4' (red ball).

include the evidence that certain metallobleomycins bind to DNA at more sites than those at which they produce oxidative damage (84, 85). The finding of a primary isotope effect associated with the abstraction of C-4' H from deoxyribose (82, 83) also argues that chemical transformation of the DNA substrate is rate-limiting. It would not be surprising if RNA cleavage exhibited the same characteristics, limiting the amount of products that can be formed.

In this context, it may be noted that RNA exists in an A-form conformation, which could be less conducive to oxidative transformation than B-DNA. This is illustrated in Figure 9, which shows the X-ray crystallographic structures determined for 5'-CGCGAATTCGCG-3' (88), a B-DNA structure, and 5'-GGGGCCCC-3' (89), an A-DNA structure. The structure of the dodecanucleotide, which is cleaved by Fe-BLM at cytidine<sub>3</sub> and cytidine<sub>11</sub> (M. Morgan, unpublished results), highlights the nature of the minor groove at the site actually cleaved by Fe-BLM; both the C-4' H (blue) and C-1' H (red) atoms are clearly accessible within the minor groove, although BLM apparently abstracts only C-4' H (8-10, 53). In comparison, the minor groove of 5'-GGGGCCCC-3' at the analogous GC site is wider and shallower but has C-4' H displaced out of the groove where it may be more difficult for BLM to abstract. Interestingly, C-1' H is still prominent within the minor groove of this A-DNA and presumably also within A-RNA helices as well. Although the susceptibility of the C-1' H to abstraction by BLM is clearly less than that of C-4' H where both are available in the minor groove (8-10, 53), the lesser accessibility

of C-4' H in the minor groove of A-DNA and RNA might permit the (occasional) abstraction of C-1' H. This would be entirely consistent with the observation (*vide supra*) that Fe-BLM afforded a product from C<sub>3</sub>-ribo and C<sub>3</sub>-ara CGCTAGCG whose formation must involve abstraction of C-1' H from the sugar moiety of cytidine<sub>3</sub> (56).

#### X-RAY CRYSTALLOGRAPHICALLY DEFINED RNA SUBSTRATES FOR BLEOMYCIN

An important goal in the study of bleomycin-mediated RNA degradation is better definition of the way in which the antitumor agent binds to RNA. In addition to more detailed structural analysis of known RNA substrates for bleomycin, it would also be helpful to determine whether Fe-BLM can mediate the cleavage of RNA's whose structures are known at high resolution. In this regard, the recent report by Hüttenhofer et al. (38) is of special interest, as it identifies two major sites of cleavage of yeast tRNA<sup>Phe</sup> by Fe-BLM.

In collaboration with the laboratory of Prof. Richard Giegé, Université Louis Pasteur, we have shown that yeast cytoplasmic tRNA<sup>Asp</sup> is cleaved at a single major site, cytidine<sub>67</sub>, by Fe-BLM. On the basis of this observation, as well as a consideration of the locations at which BLM cleaves a number of other tRNA and tRNA precursor substrates, we have constructed a model that provides a working hypothesis for the way in which Fe-BLM might bind to tRNA<sup>Asp</sup>. As shown in Figure 10, this model employs the X-ray crystallographic coordinates for yeast tRNA<sup>Asp</sup> (90) and a structure for Fe-BLM based on a set



of metal binding ligands described by Oppenheimer et al. (91). Fe-BLM was docked to the "minor groove" formed by the T $\psi$ /CG stem-loop structure, adjusting the interaction to permit potential hydrogen bonding interactions between the bithiazole N-atoms and N<sup>2</sup> H of guanosine, as well as electrostatic interaction between the dimethylsulfonium moiety of the BLM A<sub>2</sub> C-substituent and a phosphate oxygen anion. This orientation would permit the abstraction of C-4' H from the ribose moiety of cytidine<sub>67</sub> in a spatially reasonable fashion (92). Although the structure proposed in Figure 10 is not supported at present by direct physical measurement, the essential correctness of the mode of interaction is suggested by the recent report of the solution structure of Zn(II)-bleomycin A<sub>5</sub> bound to the DNA octanucleotide duplex 5'-CGCTAGCG-3' (Figure 11) (93). The latter complex was characterized structurally using two-dimensional NMR experiments and molecular dynamics calculations.

#### RNA AS A THERAPEUTICALLY RELEVANT TARGET FOR BLEOMYCIN

Bleomycin is commonly thought to exert its therapeutic effects at the level of DNA degradation. In fact, treatment of cultured mammalian cells with bleomycin causes extensive DNA damage, growth inhibition, and diminished clonogenic potential; these effects all increase with increasing amounts of BLM employed, or as the time of treatment is lengthened (17–19, 94). On the basis of numerous studies, it seems clear that DNA constitutes a critical locus for the therapeutic action of bleomycin.

However, there are a number of observations that seem difficult to reconcile with the action of bleomycin at this single locus. These include the relatively poor correlation between the extent of BLM-induced DNA damage and growth inhibition of KB cells for a series of BLM congeners (94) and the remarkably facile cellular repair of bleomycin-mediated damage to chromatin (94).

The possible effects of the cell membrane on the expression of cytotoxicity by bleomycin are also of interest. Poddevin et al. (95) demonstrated that introduction of bleomycin into cultured Chinese hamster fibroblast cells by electroporabilization greatly enhanced the cytotoxic potential of bleomycin. In addition to the implication that the nuclear membrane could also constitute a barrier to bleomycin, suggesting the involvement of some cytoplasmic target, the finding that bleomycin crosses the cell membrane inefficiently raises the possibility that the drug may actually react with the membrane. In fact, bleomycin has been shown to mediate lipid peroxidation, an effect that could contribute to cytotoxicity (20–23). It has also been shown that the local anesthetic dibucaine, which increases membrane fluidity, rendered cultured KB cells susceptible to inhibition by a bleomycin congener dysfunctional in DNA degradation (27).

In this regard, RNA represents a potentially attractive therapeutic target for bleomycin for several reasons. RNA's are present in the cytoplasm of eukaryotic cells, where they would be more accessible to exogenous agents; representative examples of all three major classes of RNA's, as well as an RNA–DNA heteroduplex, have been shown to act as substrates for cleavage by activated Fe-BLM. RNA cleavage by bleomycin is more highly selective than that of DNA and is anticipated to be even more so under physiological conditions due to the effects of Mg<sup>2+</sup> and polyamines noted above. In addition, the apparent paucity of mechanisms for RNA repair suggests that damage to one or more RNA's essential for cell

function could create an insufficiency of an RNA, or some derived protein, required for cell viability.

At present, it is not known whether the cytotoxic effects of bleomycin are mediated (in part) via oxidative damage to RNA. While the studies carried out to date in cell free systems have been helpful in defining the parameters conducive to RNA degradation, it is essential that the effects of BLM on RNA in cultured mammalian cells be determined. Likewise, since mRNA can undergo cleavage by bleomycin, it is also possible that the cellular level of proteins whose turnover is fast relative to mRNA production could also be reduced. This possibility should also be addressed experimentally.

#### ACKNOWLEDGMENT

I acknowledge with gratitude the contributions of my co-workers to these studies. Their names appear in the references; special thanks are due to Dr. Barbara Carter, Dr. Robert Duff, Dr. Chris Holmes, Mr. Michael Morgan, and Dr. Richard Manderville. I also thank my collaborators, including Drs. Jacques van Boom and Gijs van der Marel (University of Leiden), Dr. Christine Debouck (SmithKline Beecham Pharmaceuticals), and Drs. Richard Giegé and Catherine Florentz (Université Louis Pasteur). This work was supported at the University of Virginia by Research Grants CA27603, CA38544, and CA53913, awarded by the National Cancer Institute, DHHS, and by NATO Travel Grant CRG900204.

#### LITERATURE CITED

- (1) Takita, T. (1979) Review of the structural studies on bleomycin. *Bleomycin: Chemical, Biochemical and Biological Aspects* (S. M. Hecht, Ed.) pp 37–47, Springer-Verlag, New York.
- (2) Takita, T., Umezawa, Y., Saito, S., Morishima, H., Nagawara, H., Umezawa, H., Tsuchiya, T., Miyake, T., Kageyama, S., Umezawa, S., Muraoka, Y., Suzuki, M., Otsuka, M., Narita, M., Kobayashi, S., and Ohno, M. (1982) Total synthesis of bleomycin A<sub>2</sub>. *Tetrahedron Lett.* 23, 521–524.
- (3) Aoyagi, Y., Katano, K., Suguna, H., Primeau, J., Chang, L.-H., and Hecht, S. M. (1982) Total synthesis of bleomycin. *J. Am. Chem. Soc.* 104, 5537–5538.
- (4) Otsuka, M., Masuda, T., Haupt, A., Ohno, M., Shiraki, T., Sugiura, Y., and Maeda, K. (1990) Man-designed bleomycin with altered sequence specificity in DNA cleavage. *J. Am. Chem. Soc.* 112, 838–845.
- (5) Boger, D. L., Menezes, R. F., and Dang, Q. (1992) Synthesis of desacetamidopyrimidoblastic acid and deglyco desacetamidoblastic acid. *J. Org. Chem.* 57, 4333–4336.
- (6) Boger, D. L., and Honda, T. (1994) Total synthesis of bleomycin A<sub>2</sub> and related agents. Synthesis of the disaccharide subunit: 2-O-(3-O-carbamoyl- $\alpha$ -D-mannopyranosyl)-L-gulopyranose and completion of the total synthesis of bleomycin A<sub>2</sub>. *J. Am. Chem. Soc.* 116, 5647–5656.
- (7) Hamamichi, N., Natrajan, A., and Hecht, S. M. (1992) On the role of individual bleomycin thiazoles in oxygen activation and DNA cleavage. *J. Am. Chem. Soc.* 114, 6278–6291.
- (8) Hecht, S. M. (1986) The chemistry of activated bleomycin. *Acc. Chem. Res.* 19, 383–391.
- (9) Stubbe, J., and Kozarich, J. W. (1987) Mechanisms of bleomycin-induced DNA degradation. *Chem. Rev.* 87, 1107–1136.
- (10) Natrajan, A., and Hecht, S. M. (1993) Bleomycin: mechanism of polynucleotide recognition and oxidative degradation. *Molecular Aspects of Anticancer Drug–DNA Interactions* (S. Neidle, and M. Waring, Eds.) pp 197–242, MacMillan, London.
- (11) Carter, S. K., Crooke, S. T., and Umezawa, H., Eds. (1978) *Bleomycin: Current Status and New Developments*, Academic Press, New York.

- (12) Sikic, B. I., Rozenzweig, M., and Carter, S. K., Eds. (1985) *Bleomycin Chemotherapy*, Academic Press, New York.
- (13) Tanaka, N., Yamaguchi, H., and Umezawa, H. (1963) Mechanism of action of phleomycin. I. Selective inhibition of the DNA synthesis in *E. coli* and HeLa cells. *J. Antibiot.* 16A, 86–91.
- (14) Falaschi, A., and Kornberg, A. (1964) Phleomycin, an inhibitor of DNA polymerase. *Fed. Proc.* 23(1), 940–945.
- (15) Mueller, W. E., and Zahn, R. K. (1976) Effect of bleomycin on DNA, RNA, protein, chromatin and on cell transformation by oncogenic RNA viruses. *Prog. Biochem. Pharmacol.* 11, 28–47.
- (16) Ohno, T., Miyaki, M., Taguchi, T., and Ohashi, M. (1976) Actions of bleomycin on DNA ligase and polymerases. *Prog. Biochem. Pharmacol.* 11, 48–58.
- (17) Barranco, S. C., and Humphrey, R. M. (1971) Effects of bleomycin on survival and cell progression in Chinese hamster cells. *Cancer Res.* 31, 1218–1223.
- (18) Hittelman, W. N., and Rao, P. N. (1974) Bleomycin-induced damage in prematurely condensed chromosomes and its relation to cell cycle progression in CHO [chinese hamster ovary] cells. *Cancer Res.* 34, 3433–3439.
- (19) Barlogie, B., Drewinko, B., Schumann, J., and Freireich, E. J. (1976) Pulse cytophotometric analysis of cell cycle perturbation with bleomycin *in vitro*. *Cancer Res.* 36, 1182–1187.
- (20) Gutteridge, J. M. C., and Fu, X.-C. (1981) Enhancement of bleomycin-iron free radical damage to DNA by antioxidants and their inhibition of lipid peroxidation. *FEBS Lett.* 123, 71–74.
- (21) Ekimoto, H., Takahashi, K., Matsuda, A., Takita, T., and Umezawa, H. (1985) Lipid peroxidation by bleomycin-iron complexes *in vitro*. *J. Antibiot.* 38, 1077–1082.
- (22) Nagata, R., Morimoto, S., and Saito, I. (1990) Iron-peplomycin catalyzed oxygenation of linoleic acid. *Tetrahedron Lett.* 31, 4485–4488.
- (23) Kikuchi, H., and Tetsuka, T. (1992) On the mechanism of lipoxigenase-like action of bleomycin-iron complexes. *J. Antibiot.* 45, 548–555.
- (24) Murugesan, N., Ehrenfeld, G. M., and Hecht, S. M. (1982) Oxygen transfer from bleomycin-metal complexes. *J. Biol. Chem.* 257, 8600–8603.
- (25) Murugesan, N., and Hecht, S. M. (1985) Bleomycin as an oxene transferase. Catalytic oxygen transfer to olefins. *J. Am. Chem. Soc.* 107, 493–500.
- (26) Natrajan, A., Hecht, S. M., van der Marel, G. A., and van Boom, J. H. (1990) Activation of iron(III)-bleomycin by 10-hydroperoxy-8,12-octadecadienoic acid. *J. Am. Chem. Soc.* 112, 4532–4538.
- (27) Berry, D. E., Kilkuskie, R. E., and Hecht, S. M. (1985) Damage induced by bleomycin in the presence of dibucaine is not predictive of cell growth inhibition. *Biochemistry* 24, 3214–3219.
- (28) Suzuki, H., Nagai, K., Akutsu, E., Yamaki, H., Tanaka, N., and Umezawa, H. (1970) On the mechanism of action of bleomycin: strand scission of DNA caused by bleomycin and its binding to DNA *in vitro*. *J. Antibiot.* 23, 473–480.
- (29) Müller, W. E. G., Yamazaki, Z., Breter, H.-J., and Zahn, R. K. (1972) Action of bleomycin on DNA and RNA. *Eur. J. Biochem.* 31, 518–525.
- (30) Haidle, C. W., Kuo, M. T., and Weiss, K. K. (1972) Nucleic acid-specificity of bleomycin. *Biochem. Pharmacol.* 21, 3308–3312.
- (31) Haidle, C. W., and Bearden, J., Jr. (1975) Effect of bleomycin on an RNA-DNA hybrid. *Biochem. Biophys. Res. Commun.* 65, 815–821.
- (32) Hori, M. (1979) Interaction of bleomycin with DNA. *Bleomycin: Chemical, Biochemical and Biological Aspects* (S. M. Hecht, Ed.) pp 195–206, Springer-Verlag, New York.
- (33) Magliozzo, R. S., Peisach, J., and Ciriolo, M. R. (1989) Transfer RNA is cleaved by activated bleomycin. *Mol. Pharmacol.* 35, 428–432.
- (34) Carter, B. J., de Vroom, E., Long, E. C., van der Marel, G. A., van Boom, J. H., and Hecht, S. M. (1990) Site-specific cleavage of RNA by Fe(II)-bleomycin. *Proc. Natl. Acad. Sci. U.S.A.* 87, 9373–9377.
- (35) Carter, B. J., Reddy, K. S., and Hecht, S. M. (1991) Polynucleotide recognition and strand scission by Fe-bleomycin. *Tetrahedron* 47, 2463–2474.
- (36) Carter, B. J., Holmes, C. E., Van Atta, R. B., Dange, V., and Hecht, S. M. (1991) Metal-catalyzed polynucleotide strand scission. *Nucleosides Nucleotides* 10, 215–227.
- (37) Holmes, C. E., Carter, B. J., and Hecht, S. M. (1993) Characterization of iron(II)-bleomycin-mediated RNA strand scission. *Biochemistry* 32, 4293–4307.
- (38) Hüttenhofer, A., Hudson, S., Noller, H. F., and Mascharak, P. K. (1992) Cleavage of tRNA by Fe(II)-bleomycin. *J. Biol. Chem.* 267, 24471–24475.
- (39) Dix, D. J., Lin, P.-N., McKenzie, A. R., Walden, W. E., and Theil, E. C. (1993) The influence of the base-paired flanking region on structure and function of the ferritin mRNA iron regulatory element. *J. Mol. Biol.* 231, 230–240.
- (40) McDougall, J., and Nazar, R. N. (1983) Tertiary structure of the eukaryotic ribosomal 5S RNA: accessibility of phosphodiester bonds to ethylnitrosurea modification. *J. Biol. Chem.* 258, 5256–5259.
- (41) Morgan, M., and Hecht, S. M. (1994) Iron(II)-bleomycin-mediated degradation of a DNA-RNA heteroduplex. *Biochemistry* 33, 10286–10293.
- (42) Holmes, C. E., and Hecht, S. M. (1993) Fe-bleomycin cleaves a transfer RNA precursor and its “transfer DNA” analog at the same major site. *J. Biol. Chem.* 268, 25909–25913.
- (43) Sugiyama, H., Kilkuskie, R. E., Hecht, S. M., van der Marel, G. A., and van Boom, J. H. (1985) An efficient, site-specific DNA target for bleomycin. *J. Am. Chem. Soc.* 107, 7765–7767.
- (44) Sugiyama, H., Kilkuskie, R. E., Chang, L.-H., Ma, L.-T., Hecht, S. M., van der Marel, G. A., and van Boom, J. H. (1986) DNA strand scission by bleomycin: catalytic cleavage and strand selectivity. *J. Am. Chem. Soc.* 108, 3852–3854.
- (45) Sugiyama, H., Xu, C., Murugesan, N., and Hecht, S. M. (1985) Structure of the alkali-labile product formed during Fe(II)-bleomycin-mediated DNA strand scission. *J. Am. Chem. Soc.* 107, 4104–4105.
- (46) Rabow, L. E., Stubbe, J., Kozarich, J. W., and Gerlt, J. A. (1986) Identification of the alkali-labile product accompanying cytosine release during bleomycin-mediated degradation of d(CGCGCG). *J. Am. Chem. Soc.* 108, 7130–7131.
- (47) Sugiyama, H., Xu, C., Murugesan, N., Hecht, S. M., van der Marel, G. A., and van Boom, J. H. (1988) Chemistry of the alkali-labile lesion formed from iron(II)-bleomycin and d(CGCTTTAAAGCG). *Biochemistry* 27, 58–67.
- (48) Hecht, S. M. (1979) Summary of the bleomycin symposium. *Bleomycin: Chemical, Biochemical and Biological Aspects* (S. M. Hecht, Ed.) pp 1–23, Springer-Verlag, New York.
- (49) Uesugi, S., Shida, T., Ikehara, M., Kobayashi, Y., and Kyogoku, Y. (1982) Identification of degradation products of d(C-G) by a 1,10-phenanthroline-copper ion complex. *J. Am. Chem. Soc.* 104, 5494–5495.
- (50) Sigman, D. S. (1990) Chemical nucleases. *Biochemistry* 29, 9097–9105.
- (51) Goldberg, I. H. (1991) Mechanism of neocarzinostatin action: role of DNA microstructure in determination of chemistry of bistranded oxidative damage. *Acc. Chem. Res.* 24, 191–198.
- (52) Krishnamoorthy, C. R., Vanderwall, D. E., and Kozarich, J. W. (1988) Degradation of DNA-RNA hybrids by bleomycin: evidence for DNA strand specificity and for possible structural modification of chemical mechanism. *J. Am. Chem. Soc.* 110, 2008–2009.
- (53) Absalon, M. J., Krishnamoorthy, C. R., McGall, G., Kozarich, J. W., and Stubbe, J. (1992) Bleomycin mediated degradation of DNA-RNA hybrids does not involve C-1' chemistry. *Nucleic Acids Res.* 20, 4179–4185.
- (54) Long, E. C., Hecht, S. M., van der Marel, G. A., and van Boom, J. H. (1990) Interaction of bleomycin with a methylated DNA oligonucleotide. *J. Am. Chem. Soc.* 112, 5272–5276.
- (55) Pieters, J. M. L., de Vroom, E., van der Marel, G. A., van Boom, J. H., Koning, T. M. G., Kaptein, R., and Altona, C. (1990) Hairpin structures in DNA containing arabinofuranosylcytosine. A combination of nuclear magnetic resonance and molecular dynamics. *Biochemistry* 29, 788–799.

- (56) Duff, R. J., de Vroom, E., Geluk, A., Hecht, S. M., van der Marel, G. A., and van Boom, J. H. (1993) Evidence for C-1' hydrogen abstraction from modified oligonucleotides by Febleomycin. *J. Am. Chem. Soc.* 115, 3350–3351.
- (57) D'Andrea, A. D., and Haseltine, W. A. (1978) Sequence specific cleavage of DNA by the antitumor antibiotics neocarzinostatin and bleomycin. *Proc. Natl. Acad. Sci. U.S.A.* 75, 3608–3612.
- (58) Takeshita, M., Grollman, A. P., Ohtsubo, E., and Ohtsubo, H. (1978) Interaction of bleomycin with DNA. *Proc. Natl. Acad. Sci. U. S. A.* 75, 5983–5987.
- (59) Mirabelli, C. K., Ting, A., Huang, C.-H., Mong, S., and Crooke, S. T. (1982) Bleomycin and talisomycin sequence-specific strand scission of DNA: a mechanism of double-strand cleavage. *Cancer Res.* 42, 2779–2785.
- (60) Kuwahara, J., and Sugiura, Y. (1988) Sequence-specific recognition and cleavage of DNA by metalbleomycin: minor groove binding and possible interaction mode. *Proc. Natl. Acad. Sci. U.S.A.* 85, 2459–2463.
- (61) Povirk, L. F., Hogan, M., and Dattagupta, N. (1979) Binding of bleomycin to DNA: intercalation of the bithiazole rings. *Biochemistry* 18, 96–101.
- (62) Lin, S. Y., and Grollman, A. P. (1981) Interactions of a fragment of bleomycin with deoxyribodinucleotides: nuclear magnetic resonance studies. *Biochemistry* 20, 7589–7598.
- (63) Hénichart, J.-P., Bernier, J.-L., Helbecque, N., and Houssin, R. (1985) Is the bithiazole moiety of bleomycin a classical intercalator? *Nucleic Acids Res.* 13, 6703–6717.
- (64) Povirk, L. F., Hogan, M., Dattagupta, N., and Buechner, M. (1981) Copper(II)-bleomycin, iron(III)-bleomycin, and copper(II)-phleomycin: comparative study of deoxyribonucleotide acid binding. *Biochemistry* 20, 665–671.
- (65) Levy, M. J., and Hecht, S. M. (1988) Copper(II) facilitates bleomycin-mediated unwinding of plasmid DNA. *Biochemistry* 27, 2647–2650.
- (66) Quada, J. C., Jr., Levy, M. J., and Hecht, S. M. (1993) Highly efficient DNA strand scission by photoactivated chlorobithiazoles. *J. Am. Chem. Soc.* 115, 12171–12172.
- (67) Kane, S. A., Natrajan, A., and Hecht, S. M. (1994) On the role of the bithiazole moiety in sequence selective DNA cleavage by Febleomycin. *J. Biol. Chem.* 269, 10899–10904.
- (68) Carter, B. J., Murty, V. S., Reddy, K. S., Wang, S.-N., and Hecht, S. M. (1990) A role for the metal binding domain of bleomycin in determining the DNA sequence selectivity of Fe-bleomycin. *J. Biol. Chem.* 265, 4193–4196.
- (69) Guajardo, R. J., Hudson, S. E., Brown, S. J., and Mascharak, P. K. (1993)  $[\text{Fe}(\text{PMA})]^{n+}$  ( $n = 1, 2$ ): Good models of Fe-bleomycins and examples of mononuclear non-heme iron complexes with significant  $\text{O}_2$ -activation capabilities. *J. Am. Chem. Soc.* 115, 7971–7977.
- (70) Boger, D. L., Honda, T., Menezes, R. F., Colletti, S. L., Dang, Q., and Yang, W. (1994) Total synthesis of (+)-P-3A, *epi*-(-)-P-3A, and (-)-desacetamido P-3A. *J. Am. Chem. Soc.* 116, 82–92.
- (71) Dickerson, R. E. (1990) What do we really know about B-DNA? *Structure and Methods*, vol. 3; *DNA and RNA. Proceedings of the Sixth Conversation in Biomolecular Stereodynamics* (R. H. Sarma, and M. H. Sarma, Eds.) pp 1–38, Adenine Press, Schenectady, New York.
- (72) Hertzberg, R. P., Caranfa, M. J., and Hecht, S. M. (1988) Degradation of structurally modified DNA's by bleomycin group antibiotics. *Biochemistry* 27, 3164–3174.
- (73) Williams, L. D., and Goldberg, I. H. (1988) Selective strand scission by intercalating drugs at DNA bulges. *Biochemistry* 27, 3004–3011.
- (74) Gold, B., Dange, V., Moore, M. A., Eastman, A., van der Marel, G. A., van Boom, J. H., and Hecht, S. M. (1988) Alteration of bleomycin cleavage specificity in a platinated DNA oligomer of defined structure. *J. Am. Chem. Soc.* 110, 2347–2349.
- (75) Natrajan, A., Hecht, S. M., van der Marel, G. A., and van Boom, J. H. (1990) A study of oxygen versus hydrogen peroxide-supported activation of iron-bleomycin. *J. Am. Chem. Soc.* 112, 3997–4002.
- (76) Sausville, E. A., Stein, R. W., Peisach, J., and Horwitz, S. B. (1978) Properties and products of the degradation of DNA by bleomycin and iron(II). *Biochemistry* 17, 2746–2754.
- (77) Ehrenfeld, G. M., Shipley, J. B., Heimbrook, D. C., Sugiyama, H., Long, E. C., van Boom, J. H., van der Marel, G. A., Oppenheimer, N. J., and Hecht, S. M. (1987) Copper-dependent cleavage of DNA by bleomycin. *Biochemistry* 26, 931–942.
- (78) Burger, R. M., Peisach, J., Blumberg, W. E., and Horwitz, S. B. (1979) Iron-bleomycin interactions with oxygen and oxygen analogues. *J. Biol. Chem.* 254, 10906–10912.
- (79) Albertini, J. P., Garnier-Suillerot, A., and Tosi, L. (1982) Iron-bleomycin-DNA-system. Evidence of a long-lived bleomycin iron oxygen intermediate. *Biochem. Biophys. Res. Commun.* 104, 557–563.
- (80) Ciriolo, M. R., Magliozzo, R. S., and Peisach, J. (1987) Microsome-stimulated activation of ferrous bleomycin in the presence of DNA. *J. Biol. Chem.* 262, 6290–6295.
- (81) Van Atta, R. B., Long, E. C., Hecht, S. M., van der Marel, G. A., and van Boom, J. H. (1989) Electrochemical activation of oxygenated iron-bleomycin. *J. Am. Chem. Soc.* 111, 2722–2724.
- (82) Wu, J. C., Kozarich, J. W., and Stubbe, J. (1985) Mechanism of bleomycin: evidence for a rate-determining 4'-hydrogen abstraction from poly(dA-dU) associated with the formation of both free base and base propenal. *Biochemistry* 24, 7562–7568.
- (83) Kozarich, J. W., Worth, L., Jr., Frank, B. L., Christner, D. F., Vanderwall, D. E., and Stubbe, J. (1989) Sequence-specific isotope effects on the cleavage of DNA by bleomycin. *Science* 245, 1396–1399.
- (84) McLean, M. J., Dar, A., and Waring, M. J. (1989) Differences between sites of binding to DNA and strand cleavage for complexes of bleomycin with iron or cobalt. *J. Mol. Recognition* 1, 184–192.
- (85) Nightingale, K. P., and Fox, K. R. (1992) Interaction of bleomycin with a bent DNA fragment. *Biochem. J.* 284, 929–934.
- (86) Perreault, J. P., Pon, R. T., Jiang, M., Usman, N., Pika, J., Ogilvie, K. K., and Cedergren, R. (1989) The synthesis and functional-evaluation of RNA and DNA polymers having the sequence of *Escherichia coli* tRNA<sup>Met</sup>. *Eur. J. Biochem.* 186, 87–93.
- (87) Khan, A. S., and Roe, B. A. (1988) Aminoacylation of synthetic DNAs corresponding to *Escherichia coli* phenylalanine and lysine tRNAs. *Science* 241, 74–79.
- (88) Drew, H. R., Samson, S., and Dickerson, R. E. (1982) Structure of a B-DNA dodecamer at 16K. *Proc. Natl. Acad. Sci. U.S.A.* 79, 4040–4044.
- (89) McCall, M., Brown, T., and Kennard, O. (1985) The crystal structure of d(GGGGCCCC). A model for poly(dG)·poly(dC). *J. Mol. Biol.* 183, 385–396.
- (90) Westhof, E., Dumas, P. H., and Moras, D. (1988) Restrained refinement of two crystalline forms of yeast aspartic acid and phenylalanine transfer RNA crystals. *Acta Cryst. A* 44, 112–123.
- (91) Oppenheimer, N. J., Rodriguez, L. O., and Hecht, S. M. (1979) Structural studies of "active complex" of bleomycins: assignment of ligands to the ferrous ion in a ferrous-bleomycin-carbon monoxide complex. *Proc. Natl. Acad. Sci. U.S.A.* 76, 5616–5620.
- (92) Holmes, C. E. (1993) RNA recognition and cleavage by Fe(II)-bleomycin. Ph.D. Thesis, University of Virginia, pp 150–160.
- (93) Manderville, R. A., Ellena, J. F., and Hecht, S. M. (1994) Solution structure of a Zn(II)-bleomycin A<sub>5</sub>-d(CGCTAGCG)<sub>2</sub> complex. *J. Am. Chem. Soc.* (in press).
- (94) Berry, D. E., Chang, L.-H., and Hecht, S. M. (1985) DNA damage and growth inhibition in cultured human cells by bleomycin congeners. *Biochemistry* 24, 3207–3214.
- (95) Poddevin, B., Orłowski, S., Belehradek, J., Jr., and Mir, L. M. (1991) Very high cytotoxicity of bleomycin introduced into the cytosol of cells in culture. *Biochem. Pharmacol.* 42, S-67–S-75.

# ARTICLES

## Psoralen-Containing Vinyl Monomer for Conjugation of Double-Helical DNA with Vinyl Polymers

Mizuo Maeda,\* Chitoshi Nishimura, Daisuke Umeno, and Makoto Takagi

Department of Chemical Science and Technology, Faculty of Engineering, Kyushu University, 6-10-1, Hakozaki, Higashi-ku, Fukuoka 812, Japan. Received May 31, 1994\*

We have synthesized a vinyl monomer having a psoralen moiety, which can form a photoadduct with double-helical DNA. The monomer 1 was proved to have an ability to crosslink DNA double strands through a photochemical reaction when irradiated by UV light. The resulting DNA having vinyl groups was copolymerized with a comonomer such as acrylamide and *N*-isopropylacrylamide to give rise to a DNA-vinyl polymer conjugate. A conjugation based on covalent bondings was verified by using gel electrophoresis; the conjugation efficiency was found to be dependent upon concentration of the monomer which had been used in the antecedent photochemical reaction. This monomer will be a useful tool when anchoring double-helical DNA on polymeric materials for separating and sensing DNA-binding substances.

### INTRODUCTION

Hybridization of biological macromolecules with synthetic polymers has received considerable attention in view of modulation and utilization of the biological functions (1). For example, modification of proteins by connecting with poly(ethylene glycol) made the proteins nonimmunogenic (2). A conjugate between protein and poly(*N*-isopropylacrylamide) (polyNIPAAm) was demonstrated to have temperature-responsive functions due to the polyNIPAAm chains (3).

However, there have been no reports on such a semi-synthetic conjugate which comprises DNA as a counterpart. Recently, we reported the first example of DNA-containing semisynthetic conjugates: double-helical DNA modified with vinyl polymers. A DNA-intercalative molecule having a polymerizable vinyl group was employed to connect DNA with vinyl polymers (4). The conjugation between DNA and polymer chains was confirmed to be based on noncovalent, intercalative binding (5). The conjugates exhibited a peculiar migration behavior in gel electrophoresis due to the modifying polymer chains, as was visualized by fluorescence microscopy (6). The conjugate comprising polyNIPAAm chains was exploited for the thermally-induced "affinity" separation of a DNA-binding protein (7).

In the present paper, we describe a vinyl monomer having a psoralen moiety, which can form a photoadduct with double-helical DNA (8); the monomer 1 was designed to be bound covalently to DNA, endowing a polymerizable function to it (Scheme 1, c). The resulting DNA furnished with vinyl groups can be copolymerized with a comonomer to give rise to a DNA-vinyl polymer conjugate (Scheme 1, d). In contrast to the DNA-intercalative monomer which has been adopted in our previous studies (4-7), the present monomer endorses a stable conjugation. Therefore, the psoralen-containing monomer will be a useful tool for anchoring double-helical DNA on polymeric materials when applying the DNA as

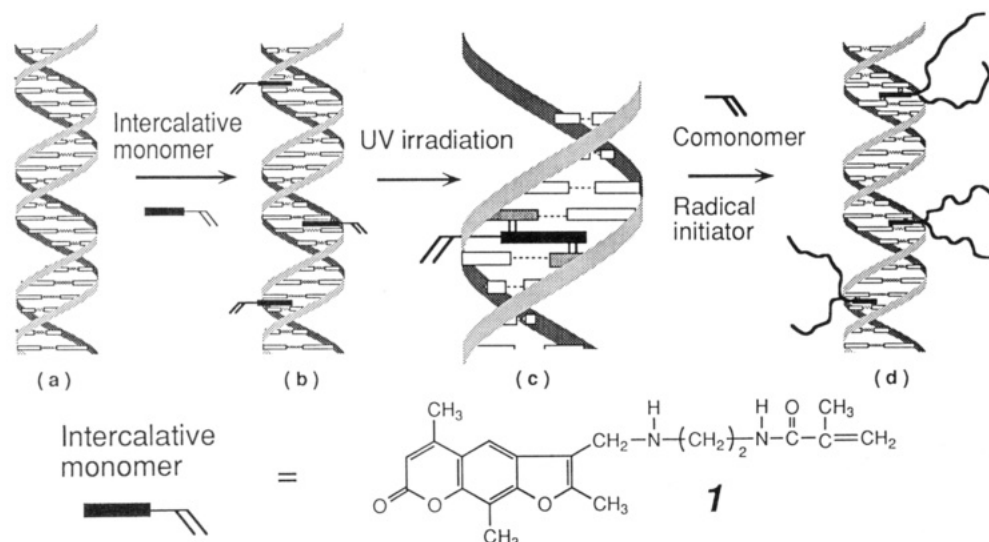
an affinity ligand for bioseparation and bioanalysis. In addition, conjugation of DNA with vinyl polymers which carry reporter groups such as biotin would be promising for highly sensitive detection of DNA, since the present method should allow a large number of labels on DNA.

### EXPERIMENTAL PROCEDURES

**Materials.** Acrylamide (AAM) was obtained from Wako Pure Chemicals (electrophoresis grade) and used without purification. *N*-Isopropylacrylamide (NIPAAm) was obtained from Tokyo Kasei Kogyo and recrystallized from a mixture of benzene and hexane. pBR322 DNA was purchased from Takara Shuzo.  $\lambda$  Phage DNA and Hind III were purchased from Nippon Gene. Trioxalen was obtained from Aldrich.

**Synthesis of Psoralen-Containing Monomer 1.** 4'-[[*N*-(2-Aminoethyl)amino]methyl]-4,5',8-trimethylpsoralen (0.40 g, 1.33 mmol), which was synthesized according to a method described by Lee et al. (9), was reacted with 0.25 g (1.34 mmol) of *N*-methacryloyl succinimide (Tokyo Kasei Kogyo) in pyridine-DMF (1:7, v/v) for 1 d at ambient temperature. After evaporation of the solvent, the diethyl ether soluble fraction of the residue was subjected to column chromatography (silica gel; eluent, CHCl<sub>3</sub>-MeOH in which MeOH content was varied from 0 to 20%). The main fraction was collected and evaporated to give a slightly-yellowish residue. The residue was washed with ethyl acetate-hexane (1:2, v/v) and dried in vacuo to give a white powder (yield: 41%). The product showed a single spot on a thin-layer chromatogram (silica gel, *R<sub>f</sub>* 0.35 for CHCl<sub>3</sub>-MeOH (9:1, v/v)). Mp: 124-126 °C. Anal. Found: C, 66.31; H, 6.35; N, 7.24. Calcd for C<sub>21</sub>H<sub>24</sub>N<sub>3</sub>O<sub>4</sub> + 0.67H<sub>2</sub>O: C, 66.29; H, 6.36; N, 7.36. <sup>1</sup>H NMR (400 MHz, CDCl<sub>3</sub>)  $\delta$ : 7.61 (s, arom H-5), 6.40 (bs, amide NH; D<sub>2</sub>O exchange), 6.22 (d, *J* = 0.92 Hz, arom H-3), 5.58 (s, trans HC=), 5.25 (t, *J* = 1.22 Hz, cis HC=), 3.92 (s, 4'-CH<sub>2</sub>N), 3.44 (q, *J* = 5.50, 5.80 Hz; t, *J* = 5.80 Hz on D<sub>2</sub>O exchange; CH<sub>2</sub>-amide side), 2.84 (t, *J* = 5.80 Hz; CH<sub>2</sub>-amine side), 2.54 (s, 5'-CH<sub>3</sub>), 2.49 (m, 4-CH<sub>3</sub> and 8-CH<sub>3</sub>), 2.28 (bs, amine NH; D<sub>2</sub>O exchange), 1.88 (t, *J* = 1.22 Hz; CH<sub>3</sub>C=C).

\* Abstract published in *Advance ACS Abstracts*, October 1, 1994.

**Scheme 1. Conjugation of Double-Helical DNA with Vinyl Polymers with the Aid of a Psoralen-Containing Vinyl Monomer 1<sup>a</sup>**

<sup>a</sup> Key: (a) double-helical DNA, (b) intercalative binding, (c) light-induced crosslinking, (d) conjugation with vinyl polymers

Since **1** was poorly soluble in water, an ethanol solution of **1** (10 mM) was diluted with TE buffer (10 mM Tris-HCl, 1 mM EDTA, pH 7.9) to give a stock solution (100  $\mu$ M) containing 1 vol % of ethanol. A PE (8 mM Na<sub>2</sub>HPO<sub>4</sub>, 2 mM NaH<sub>2</sub>PO<sub>4</sub>, 1 mM EDTA, pH 7.4) solution of **1** was prepared similarly.

**Photoreaction of **1** with DNA.** Plasmid pBR322 DNA was linearized with Hind III, and the DNA was purified by phenol extraction, followed by ethanol precipitation and resuspension in TE buffer at 100  $\mu$ g/L. To 2  $\mu$ L of the DNA solution in a micro test tube (Eppendorf, 1.5 mL) was added a TE solution of **1** from the stock. The total volume was 12  $\mu$ L. The final concentration of the DNA was 51  $\mu$ M (in nucleotide). The concentration of **1** was varied in the range of 1.7 and 83  $\mu$ M. Each solution was irradiated (ca. 60 mW/cm<sup>2</sup>) on an ice bath with a 500-W ultra-high-pressure Hg lamp equipped with a high-pass filter (Toshiba, UV-31) for 10 min.

To the reaction mixture was added 3  $\mu$ L of aqueous NaOH (1.2 M) in order to make the DNA denatured, and then the mixture was analyzed by gel electrophoresis: the mixture was combined with 3  $\mu$ L of gel-loading solution consisting of glycerin and water (7:3, v/v). The mixture was loaded on a 1% agarose gel, and the gel electrophoresis was performed at 7 V/cm for 1 h in TAE buffer (80 mM Tris-acetate, 1 mM EDTA, pH 7.6). After electrophoresis, DNA in the gel was stained by ethidium bromide.

**Polymerization.** Before polymerization, photoreaction was made as follows: in a micro test tube were charged a TE solution of  $\lambda$  DNA (150  $\mu$ g/mL; 5  $\mu$ L) and a PE solution of **1** (100  $\mu$ M; 1–10  $\mu$ L). With the addition of PE buffer, the total volume was made to be 20  $\mu$ L; the concentrations of DNA and **1** were 115 and 5–50  $\mu$ M, respectively. Then the mixture was irradiated by UV light in a manner similar to that described above. The reaction mixture was extracted twice by chloroform-isoamyl alcohol (3-methylbutanol) (24:1, v/v) in order to remove **1** which was not covalently bound to the DNA.

After the photoreaction, a PE solution of AAm (0.35 M; 40  $\mu$ L), a PE solution of *N,N,N',N'*-tetramethylethylenediamine (TEMED), and aqueous ammonium peroxydisulfate were successively introduced to the mixture under nitrogen atmosphere. The total volume of the reaction mixture was 0.1 mL (TE:PE = 1:19, v/v) with the addition of PE buffer. At the polymerization, the

concentration of the respective component was as follows: DNA, 22.5  $\mu$ M (in nucleotide); AAm, 140 mM; ammonium peroxydisulfate, 0.3 mg/mL; TEMED, 10 mg/mL. The reaction was carried out at 24  $^{\circ}$ C for 1 h.

After the polymerization, the mixture was analyzed by gel electrophoresis: a 10  $\mu$ L portion of each of the sample solutions was combined with 8  $\mu$ L of gel-loading solution consisting of glycerin and water (1:1, v/v). The mixture was loaded on a 0.5% agarose gel, and the gel electrophoresis was performed at 7 V/cm for 1 h in TBE buffer (89 mM Tris-borate, 2.5 mM EDTA, pH 8.0). After electrophoresis, DNA in the gel was stained by ethidium bromide.

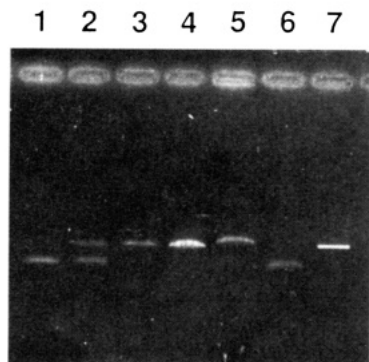
**Modification with PolyNIPAAm.** The polymerization of NIPAAm was carried out similarly, except that gel electrophoresis for the analysis was performed at 10  $^{\circ}$ C since precipitation of polyNIPAAm and its conjugates takes place from aqueous glycerin (25%) at ambient temperature (7). Another difference in the polymerization procedure for NIPAAm was that an extraction of the post-polymerization mixture was made by chloroform in order to remove the vinyl polymers which were not covalently bound to DNA: the reaction mixture just after polymerization (0.1 mL) was combined with 0.1 mL of chloroform. After vortex-mixing, the mixture was centrifuged (10 000 rpm, 1 min), and the aqueous phase was collected to be subjected to gel electrophoresis. The DNA band having the same mobility as native  $\lambda$  DNA was evaluated by scanning densitometry to give a modification efficiency.

In addition, the post-polymerization mixture from  $\lambda$  DNA and NIPAAm was examined from a viewpoint of thermally-induced precipitation. The mixture was centrifuged (15 000 rpm, 30 min) at 35  $^{\circ}$ C in order to precipitate the DNA-polyNIPAAm conjugates. After centrifugation, the supernatant was collected and subjected to gel electrophoresis. The DNA band having the same mobility as the native one was evaluated by scanning densitometry in order to estimate a precipitation efficiency.

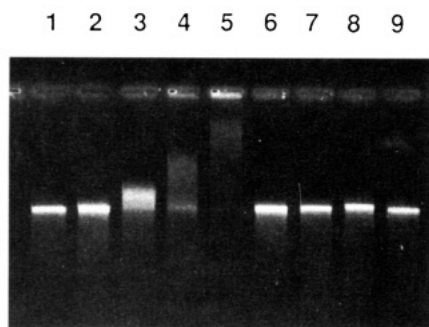
## RESULTS AND DISCUSSION

**Light-Induced Binding of **1** with DNA.** It was reported that psoralens intercalate into DNA double strands in the dark and form covalent bonds at their 3,4





**Figure 1.** DNA crosslinking by the psoralen-containing monomer **1**. Linear pBR322 DNA (51  $\mu$ M) was irradiated by UV light in the presence of increasing amounts of **1**. Samples are alkali denatured and then loaded on a nondenaturing gel from 1% agarose: lane 1, [**1**] = 0; lane 2, [**1**] = 1.7  $\mu$ M; lane 3, [**1**] = 8.3  $\mu$ M; lane 4, [**1**] = 16.7  $\mu$ M; lane 5, [**1**] = 83  $\mu$ M; lane 6, [**1**] = 83  $\mu$ M, but no UV irradiation; lane 7, DNA alone, but no alkali denaturation.



**Figure 2.** Gel electrophoresis of DNA-polyAAM conjugates.  $\lambda$  DNA (115  $\mu$ M) was irradiated by UV light in the presence of **1**. After unbound **1** was removed, samples were coinubated in the polymerization mixture of AAM and then loaded on 1% agarose gel: lanes 1 and 9, DNA alone (control); lane 2, [**1**] = 0; lanes 3 and 6, [**1**] = 5  $\mu$ M; lanes 4 and 7, [**1**] = 20  $\mu$ M; lanes 5 and 8, [**1**] = 50  $\mu$ M. For lanes 6–8, no polymerization was made. The concentrations of **1** ([**1**]) represent those at the antecedent photochemical reaction.

and 4',5' double bonds with pyrimidines upon near-UV irradiation (8). If both sites of the psoralen are reacted, the result is an interstrand DNA crosslink; both strands are connected to each other. The ability of **1** to form DNA crosslinks (Scheme 1, b to c) was tested according to the literature (10) by reacting linear double-stranded plasmid DNA with **1** and near-UV light.

The photoreacted DNA was alkali denatured and loaded onto a nondenaturing agarose gel. Crosslinked DNA immediately renatures in the neutral gel buffer (pH 7.6) and runs as the double-stranded form, while non-crosslinked DNA remains single-stranded and runs with greater mobility. As seen in Figure 1, an increasing amount of **1** resulted in increased levels of crosslinking after UV irradiation (lanes 2–5), while even the highest concentration of **1** produced no crosslinking in the absence of light (lane 6). Thus, the monomer **1** was proved to be bound covalently to double-helical DNA through a photochemical reaction when irradiated by UV light.

**Modification of DNA with Polyacrylamide.**  $\lambda$  DNA which had been reacted photochemically with **1** was coinubated in the polymerization system of acrylamide (AAM) (Scheme 1, c to d). The gel electrophoresis of the product showed retarded migration as well as broadening of the DNA band, as seen in Figure 2, lanes 3–5. The degree of retardation appears to increase with increasing concentration of **1** in the photoreaction mixture. In

contrast, as seen in lanes 6–8, the light-induced binding of **1** with  $\lambda$  DNA did not affect the migration significantly in the concentration range examined here. Since the mobility in gel electrophoresis is primarily a function of size and charge, the retarded migration is ascribed to the increase in size or the "fattening" of the migrating species brought about by the modification of DNA with nonionic polyAAM chains.

On the other hand, lane 2 for the control in which the DNA was not derivatized with **1** showed no retardation after the polymerization; the migration profile of the DNA was the same as that for native DNA (lanes 1 and 7). This indicates that the control sample was a simple mixture of DNA and the homopolymer of AAM; direct conjugation of vinyl polymers on DNA does not take place. Thus, the vinyl-derivatized DNA incubated in the polymerization system of AAM is concluded to be conjugated with polyAAM by means of **1** residues, which had been previously introduced in the DNA and then took part in copolymerization with AAM.

It should be noted that, in lanes 3 and 4, some portion of DNA was seen at the same mobility as native one. This indicates that the post-polymerization mixture contained DNA strands which were not conjugated with polyAAM chains; a part of the vinyl-derivatized DNA did not take part in the polymerization. The population of the unpolymerized DNA is discussed below.

**Modification with PolyNIPAAm.** Modification of DNA with poly(*N*-isopropylacrylamide) (polyNIPAAm) was also possible;  $\lambda$  DNA which had been reacted photochemically with **1** was coinubated in the polymerization system of NIPAAm. The gel electrophoresis of the product showed migration behaviors quite similar to those in Figure 2.

Since polyNIPAAm is somewhat more hydrophobic than polyAAM and is soluble in chloroform, an additional experiment was conducted for NIPAAm after polymerization; an extraction of the post-polymerization mixture was made by chloroform in order to separate the unpolymerized DNA. When the post-polymerization mixture was combined with chloroform, the NIPAAm polymers which were not covalently bound to DNA should transfer to chloroform phase. At the same time, white turbid was found to appear at the interface. This is ascribed to DNA-polyNIPAAm conjugates which gathered or "anchored" at the interface; it was dissolved again in aqueous phase when the chloroform phase was carefully removed.

From the two-phase system was collected the aqueous phase, which was then subjected to gel electrophoresis. As a result, the DNA bands having the same mobility as native  $\lambda$  DNA were observed; the bands are due to the DNA strands which were not conjugated with polyNIPAAm chains. The result is in accord with the case of modification by polyAAM as described above; there remained unmodified DNA. The bands due to the unmodified DNA were evaluated by scanning densitometry, and the percentage with respect to the DNA initially added was plotted against the concentration of **1** at the photochemical reaction (Figure 3). The amount of the unmodified DNA is seen to be dependent on the modification conditions; it decreased with increasing concentration of **1** in the antecedent photoreaction mixture. The modification efficiency of DNA with polyNIPAAm was 85% when 50  $\mu$ M of **1** was used; more than 80% of DNA strands initially fed took part in the polymerization, being conjugated covalently with polyNIPAAm.

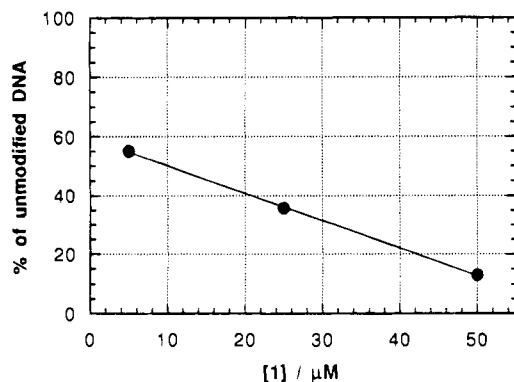
The modification of DNA with polyNIPAAm should make the conjugate temperature-responsive since polyNIPAAm as the modifying chains has a property to precipitate from aqueous media above the transition



**Table 1. Temperature-Responsiveness of  $\lambda$  DNA-PolyNIPAAm Conjugates**

[1] at photoreaction <sup>a</sup> ( $\mu$ M)	precipitation % $\pm$ SEM ( $n = 4$ ) <sup>b</sup>
5	48.3 $\pm$ 12.1
25	45.6 $\pm$ 9.9
50	57.5 $\pm$ 11.2

<sup>a</sup> The concentration of **1** at the photochemical reaction with  $\lambda$  DNA (115  $\mu$ M) prior to copolymerization with NIPAAm. <sup>b</sup> The polymerization mixture was centrifuged at 35  $^{\circ}$ C, and the supernatant was analysed by gel electrophoresis to estimate the amount of unprecipitated DNA, which was then converted to the percent of precipitation of the conjugates.



**Figure 3.** Amount of  $\lambda$  DNA which was not covalently bound to polyNIPAAm; amount of the DNA released from the conjugates upon chloroform extraction, expressed in percent to the DNA originally added, is plotted against the concentration of **1** at the antecedent photochemical reaction.

temperature around 31  $^{\circ}$ C. Such temperature-responsive bioconjugates would be useful as intelligent biomaterials (3). A preliminary experiment was made to evaluate the temperature-responsiveness of the present conjugates; the reaction mixture after polymerization was centrifuged at 35  $^{\circ}$ C so that the precipitation of the DNA-polyNIPAAm conjugate should take place. The supernatant was analyzed by gel electrophoresis to estimate the amount of unprecipitated DNA. As seen in Table 1, 45–58% of DNA was found to acquire the temperature-responsive property when 5–50  $\mu$ M of **1** was used at the photochemical reaction. However, the values for four experiments had considerable variation. In addition, the yield of temperature-responsive DNA was smaller than that expected from the result of the modification efficiency in Figure 3. The reason for this is not clear at present. Structural polydispersity of the conjugates in terms of number and length of the modifying polyNIPAAm chains may account for the result. More intensive study on conditions of modification as well as thermally-induced separation should be required before practical application of the conjugate is available.

#### Photoreaction of **1**-AAm Copolymer with DNA

Copolymerization of the **1**-derivatized DNA with some reporter monomers is of much interest since this makes it possible to put a large number of labels on DNA; monomers which carry a conventional label such as fluorescent dyes, electrochemical probes, and affinity ligands like biotin may be used for highly sensitive detection of DNA. For practical purposes, however, a more convenient way for a user is to obtain a copolymer of **1** with such a reporter monomer and apply it to various DNA of one's interest, if the copolymer can react with DNA photochemically to give a conjugate.

In order to know the feasibility, copolymerization of **1** with AAm was carried out in the absence of DNA and the resulting copolymer was examined whether it is bound to DNA when irradiated by UV light. However,

the conjugate formation was not observed for the copolymers which had been prepared by using **1** with the concentration between 5 and 100  $\mu$ M in the copolymerization mixture (the concentration of AAm was 140 mM); the photoirradiation of the copolymers with  $\lambda$  DNA (22.5  $\mu$ M) did not make any retardation of the DNA band on gel electrophoresis (results not shown). An explanation may be that **1** moieties in the copolymer are rather hydrophobic and are surrounded by polyAAm chains. This structure should prevent the interaction of **1** with DNA, resulting in no conjugation.

**Synthetic Scheme for DNA-Vinyl Polymer Conjugate.** Although the experiment described in the previous subsection was not successful, it in fact proved that the prior introduction of **1** to DNA (Scheme 1, a to b) is a prerequisite for obtaining DNA-vinyl polymer conjugates. It should also be noted that a conjugate formation does not take place when the copolymerization of **1** with a comonomer is carried out in the presence of  $\lambda$  DNA under similar concentration conditions (results not shown); gel electrophoresis of the mixture did not show any detectable retardation of DNA bands when **1** had not been reacted photochemically with DNA prior to polymerization. Although the psoralen-containing monomer **1** should be bound to the DNA by intercalative binding (Scheme 1, a to b) and some of these intercalating monomers on the DNA may take part in copolymerization with the comonomer, a conjugate thus formed seems to be very weak and dissociable upon gel electrophoresis. The light-induced derivatization of DNA by **1** prior to polymerization (Scheme 1, b to c) is concluded to be essential to obtain a stable conjugate. Thus, the synthetic procedure shown in Scheme 1 is exclusive for the monomer **1** to give DNA-vinyl polymer conjugates.

In conclusion, we have developed a synthetic method to semisynthetic bioconjugates from DNA and vinyl polymer by taking advantage of the psoralen-containing monomer **1** which consists of a psoralen moiety, connected to polymerizable vinyl group by a positively charged linker. **1** was proved to retain an ability due to its psoralen moiety to crosslink double-helical DNA through a photochemical reaction when irradiated by UV light. The resulting DNA having vinyl groups was copolymerized with a comonomer such as acrylamide or *N*-isopropylacrylamide to give rise to a DNA-vinyl polymer conjugate. A conjugation based on covalent bondings was verified by using gel electrophoresis; the conjugation efficiency was found to be dependent on the concentration of the monomer used in the photochemical reaction.

The psoralen-containing monomer should be a useful tool for immobilizing or anchoring double-helical DNA on polymeric materials with the intention of separating and sensing DNA-binding substances (11, 12). Conjugation of DNA with vinyl polymers carrying reporter groups would serve as a highly efficient method of DNA labeling. In addition, the DNA-polyNIPAAm conjugate presented here seems promising for separating a DNA-binding protein by the thermally-induced affinity precipitation.

#### ACKNOWLEDGMENT

The authors are grateful to Dr. Toshihiro Ihara and Ms. Akiko Inenaga of Kyushu University for helpful discussions. This work was supported in part by The Naito Foundation. Financial support by a Grant-in-Aid for Scientific Research from the Ministry of Education, Science and Culture of Japan is also acknowledged.

## LITERATURE CITED

- (1) Imanishi, Y., Ed. (1992) *Synthesis of Biocomposite Materials: Chemical and Biological Modifications of Natural Polymers*, CRC Press, Boca Raton, FL.
- (2) Abuchowski, A., van Es, T., Palczuk, N. C., and Davis, F. F. (1977) Alteration of immunological properties of bovine serum albumin by covalent attachment of polyethylene glycol. *J. Biol. Chem.* 252, 3578–3581.
- (3) Takei, Y. G., Aoki, T., Sanui, K., Ogata, N., Okano, T., and Sakurai, Y. (1993) Temperature-responsive bioconjugates. 2. Molecular design for temperature-modulated bioseparations. *Bioconjugate Chem.* 4, 341–346.
- (4) Maeda, M., Hirai, A., and Takagi, M. (1989) Gel electrophoretic demonstration of pseudo-grafting of polyacrylamide onto  $\lambda$  phage DNA. *Chem. Lett.* 1831–1834.
- (5) Maeda, M., Hirai, A., and Takagi, M. (1991) Pseudo-grafting of polyacrylamide onto Hind III restriction fragments of  $\lambda$  DNA. *Reactive Polym.* 15, 103–109.
- (6) Minagawa, K., Matsuzawa, Y., Yoshikawa, K., Masubuchi, Y., Matsumoto, M., Doi, M., Nishimura, C., and Maeda, M. (1993) Change of the higher order structure of DNA induced by the complexation with intercalating synthetic polymer, as is visualized by fluorescence microscopy. *Nucleic Acids Res.* 21, 37–40.
- (7) Maeda, M., Nishimura, C., Inenaga, A., and Takagi, M. (1993) Modification of DNA with poly(N-isopropylacrylamide) for thermally induced affinity separation. *Reactive Polym.* 21, 27–35.
- (8) Cimino, D. G., Gamper, H. B., Isaacs, S. T., and Hearst, J. E. (1985) Psoralens as photoactive probes of nucleic acid structure and function: Organic chemistry, photochemistry, and biochemistry. *Ann. Rev. Biochem.* 54, 1151–1193.
- (9) Lee, B. L., Murakami, A., Blakes, K. R., Lin, S.-B., and Miller, P. S. (1988) Interaction of psoralen-derivatized oligodeoxyribonucleoside methylphosphonates with single-stranded DNA. *Biochemistry* 27, 3197–3203.
- (10) Saffran, W. A., Welsh, J. T., Knobler, R. M., Gasparro, F. P., Cantor, C. R., and Edelson, R. L. (1988) Preparation and characterization of biotinylated psoralen. *Nucleic Acids Res.* 16, 7221–7231.
- (11) Kashiwagi, S., Ohmori, K., Maeda, M., and Takagi, M. (1992) Efficient coupling of DNA on a silica support with psoralen derivatives as anchoring agents for high-performance liquid affinity chromatography. *Anal. Sci.* 8, 261–263.
- (12) Maeda, M., Mitsuhashi, M., Nakano, K., and Takagi, M. (1992) DNA-Immobilized gold electrode for DNA-binding drug sensor. *Anal. Sci.* 8, 83–84.

## Analysis of Sequences Required for the Cytotoxic Action of a Chimeric Toxin Composed of *Pseudomonas* Exotoxin and Transforming Growth Factor $\alpha$

Ako Kihara and Ira Pastan\*

Laboratory of Molecular Biology, Division of Cancer Biology, Diagnosis and Centers, National Cancer Institute, National Institutes of Health, 9000 Rockville Pike, Building 37, Room 4E16, Bethesda, Maryland 20892. Received April 27, 1994\*

Chimeric toxins composed of transforming growth factor  $\alpha$  fused to mutant forms of *Pseudomonas* exotoxin bind to the EGF receptor and kill cells bearing these receptors. In early experiments, the binding domain of *Pseudomonas* exotoxin was deleted and replaced with TGF $\alpha$  to make TGF $\alpha$ -PE40. This chimeric toxin required proteolytic processing within the target cell to be converted to its active form (Siegal *et al.* (1989) *FASEB J.* 3, 2647-2652). Subsequently, recombinant toxins that do not require proteolytic processing were constructed by inserting TGF $\alpha$  near the carboxyl terminus of domain III and deleting toxin residues up to the processing site at position 280. In addition, the carboxyl terminus of this toxin was converted from REDLK to KDEL to increase its activity. Recombinant toxins of this type, termed PE37/TGF $\alpha$ /KDEL, are about 100-fold more potent than TGF $\alpha$ -PE40. To determine if other sequences can be removed from such chimeric toxins to make a smaller molecule that can penetrate tissues better, we have carried out a deletion analysis of sequences present within domains II and Ib. We find that all of domain Ib and a portion of domain II can be deleted without significant loss of cytotoxic activity, but larger deletions extending further into domain II lose cytotoxic activity. We also find that inserting a small linking peptide (Gly)<sub>4</sub>Ser between residual sequences in domain II and domain III, in molecules with diminished cytotoxic activity, enhances cytotoxicity suggesting that one role of domain Ib is to prevent undesirable interactions between domains II and III. These new chimeric toxins are very active on A431 epidermoid carcinoma cells which contain many EGF receptors. One of these was also tested in animals and showed strong antitumor activity against A431 tumors growing in nude mice.

### INTRODUCTION

Recombinant toxins are chimeric proteins composed of a targeting domain and a cytotoxic domain (1). The toxins used to make recombinant toxins are *Pseudomonas* exotoxin A (PE) and diphtheria toxin. Both are bacterial toxins. To make a recombinant toxin, the binding domain of the toxin is deleted and it is replaced by a growth factor, an antibody combining site, or another targeting molecule (1, 2). The chimeric gene encoding the chimeric toxin is then expressed in *E. coli* when the recombinant protein is produced. Native PE is composed of three domains and has a molecular weight of 66 kDa (3). One of the earliest chimeric toxins produced is composed of transforming growth factor  $\alpha$  (TGF $\alpha$ ) fused to a truncated form of PE termed PE40 to reflect its molecular weight of 40 kD (4, 5). TGF $\alpha$ -PE40 was shown to be very cytotoxic to cell lines displaying large numbers of EGF receptors and had very little cytotoxic activity toward cell lines without EGF receptors. TGF $\alpha$  contains three disulfide bonds, and PE40 contains two additional disulfide bonds. In PE40, one disulfide bond lies in domain II (amino acids 253-364), which is the translocation domain (6). The other lies in domain Ib (amino acid 365-399). This domain has no known function. Domain III (amino acids 400-613) is the ADP-ribosylation domain and has no disulfide bonds. When TGF $\alpha$ -PE4 is produced in *E. coli*, some improper disulfide bonds form diminishing the binding of TGF $\alpha$  to its

receptor (5). Therefore, a modified molecule, TP40, was constructed in which both disulfide bonds are removed by substituting alanine for cysteine residues at positions 265, 287, 372, and 379. TP40 is also selectively cytotoxic to cells bearing EGF receptors (7). TP40 is active in animals and has been shown to cause regression of EGF receptor-bearing tumors growing in nude mice. These include an epidermoid carcinoma, a prostate carcinoma, and a glioblastoma (8, 9).

Bladder cancer is the fourth most frequent cancer in American males in the United States. Fifty thousand patients annually develop this form of cancer (10). The current therapy of human bladder cancer includes the administration of chemotherapeutic agents and immunomodulators. Bacillus Calmette-Guerin (BCG) is an effective treatment in patients with superficial bladder cancer and is the treatment of choice for carcinoma *in situ* (11), but not all superficial bladder cancers are controlled by BCG. Furthermore, all drugs, including BCG, that are used for intravesical therapy have side effects that necessitate their judicious application to patients (12). An alternative treatment for bladder cancer is to target the epidermal growth factor receptor (EGFR) which is present on normal urothelium and in increased amounts in bladder cancer. Epidermal growth factor is a protein mitogen excreted in the urine at very high levels (13). The density of the receptor for EGF is closely related to tumor grade and is present on both "pre-malignant" and neoplastic urothelium (15). On the basis of these findings, a phase I trial was carried out in which TP40, which targets the EGF receptor, was infused weekly for 6 weeks into the bladder of patients with superficial bladder carcinomas (16).

\* Author to whom correspondence should be addressed. Phone: (301) 496-4797. Fax: (301) 402-1344.

\* Abstract published in *Advance ACS Abstracts*, October 15, 1994.

**Table 1. Oligonucleotides Used in Polymerase Chain Reactions for Two Linker Inserted Deletion Toxins ( $\Delta$ 11L2 and  $\Delta$ 12L2)**

A1	5' TAA TAC GAC TCA CTA TAG GGA GAC CAC AAC 3'
A2	5' ACT TCC GCC ACC TCC GGA GCC GCC ACC TCC GCG GAT CAC CTG GTC GAC CTG GTT C3'
A3	5' ACT TCC GCC ACC TCC GGA GCC GCC ACC TCC CTG CTC GCG GAT CGC TTC GCC CAG G 3'
A4	5' GGA GGT GGC GGC TCC GGA GGT GGC GGA AGT CCC ACT GGC GCG GAG TCC CTA GGC GAC 3'
A5	5' AGG CTC GAG CGC GGC ACA TAG ACC CGC AGC 3'

One of the difficulties that must be overcome in using cytotoxic proteins for cancer treatment is the inability of these large molecules to penetrate into tissues and solid cancers (17). It is well known that large molecules, such as IgM, leave the circulatory system extremely slowly and that even immunoglobulins (MW 165 000) penetrate tissues and tumors slowly and poorly (18). In general, the smaller the protein the better its tissue and tumor penetration (17–19). TP40 (MW 46 000) is much smaller than an antibody and therefore should penetrate into tumors better. Yet it would be desirable to have an even smaller molecule to enhance tissue and tumor penetration. One way that this could be accomplished is to delete all unnecessary residues within TGF $\alpha$ –PE40 or TP40.

In order to kill target cells, TP40 and other chimeric toxins must be internalized by endocytosis, proteolytically processed to an active form and carried to the right compartment where translocation into the cytosol can occur. In the case of PE, the proteolytic step is a cleavage between amino acids 279 and 280 in domain II (20). The carboxyl terminal fragment that is generated then appears to be carried to the endoplasmic reticulum from which it translocates to the cytosol (21, 22). To circumvent the need for proteolytic cleavage, we have synthesized a new recombinant form of PE which begins at amino acid 280, the site of proteolytic processing, and also contains a deletion of a portion of domain Ib (23). To direct this molecule to the EGF receptor, TGF $\alpha$  was inserted at the end of domain III just prior to the carboxyl terminus (23, Figure 1). This molecule (PE35/TGF $\alpha$ /KDEL) was extremely cytotoxic to target cells. In the current study, we have continued our efforts to make as small a cytotoxic molecule as possible by deleting additional sequences from domain Ib and domain II and replacing these sequences with a linker peptide in order to enable domains II and III to fold and function independently.

## MATERIALS AND METHODS

**Materials.** Restriction endonucleases were obtained from New England Biolabs (Beverly, MA). As a template DNA, PE35/TGF $\alpha$ /KDEL (pCT12) was a gift from Charles Theuer (Torrance, CA). Oligonucleotide-directed mutagenesis was carried out by a modification of the method of Kunkel (24). Oligonucleotides with one mutation each, with a new restriction site introduced, were synthesized by Bioserve Biotechnology (Laurel, MD). Single-stranded DNA prepared from first cycle phage in uridine-containing medium was used as a template for *in vitro* mutagenesis. To insert two linkers such as (GGGGGS)<sub>2</sub>, PCR technique was used (25). PCR was carried out using 10 ng of pCT12 as template and reagents as per the manufacturer's instruction (Gene Amp; Perkin-Elmer Cetus Instruments), and 100 pmol of primer's A1, A2, A3, A4, and A5 (Table 1). Each polymerase chain reaction totaled 30 cycles consisting of denaturation at 94 °C for 1 min, annealing at 50 °C for 90 s and polymerization at 72 °C for 2 min in each cycle. The amplified fragments were purified on 1.5% low melting point agarose (SeaPlaque, FMC). The sequences of all mutant plasmids were confirmed by DNA sequencing. The A431 cell line was previously described (4).

**Plasmids.** All the plasmids utilize a lactose-inducible T7 promoter expression system (26). Mutant plasmids were directly expressed in the T7 promoter based expression system in BL21 as previously described unless otherwise stated. Cells were incubated for 90 min following induction with isopropyl 1-thio- $\beta$ -D-galactopyranoside. The fusion proteins were purified from inclusion bodies.

**Protein Purification.** Inclusion bodies were dissolved in guanidine and renatured by rapid dilution into phosphate-buffered saline. Proteins were purified by sequential use of Q-Sepharose, Mono Q HR5/5 (Pharmacia LKB Biotechnology, Inc.) and TSK-250 columns (27). SDS–PAGE was used to analyze column fractions. All proteins were at least 95% homogeneous (Figure 2).

**Protein Synthesis Inhibition Assay.** Cytotoxic assays were generally performed as described previously (28). Cells were placed 24 h prior to toxin addition to 16 000 cells/well in 96-well plates. Toxins or control proteins diluted in 0.2% human serum albumin–phosphate–buffer saline were added to a final volume of 200  $\mu$ L/well. After a 16–20 h incubation with toxins, [<sup>3</sup>H]-leucine (2  $\mu$ Ci per well) was added for 90–120 min, and incorporation into cellular protein was measured. Data were obtained from the average of triplicates, which varied from the mean by 5–10%. Results were calculated by a percentage of incorporated cpm of cells incubated without toxin.

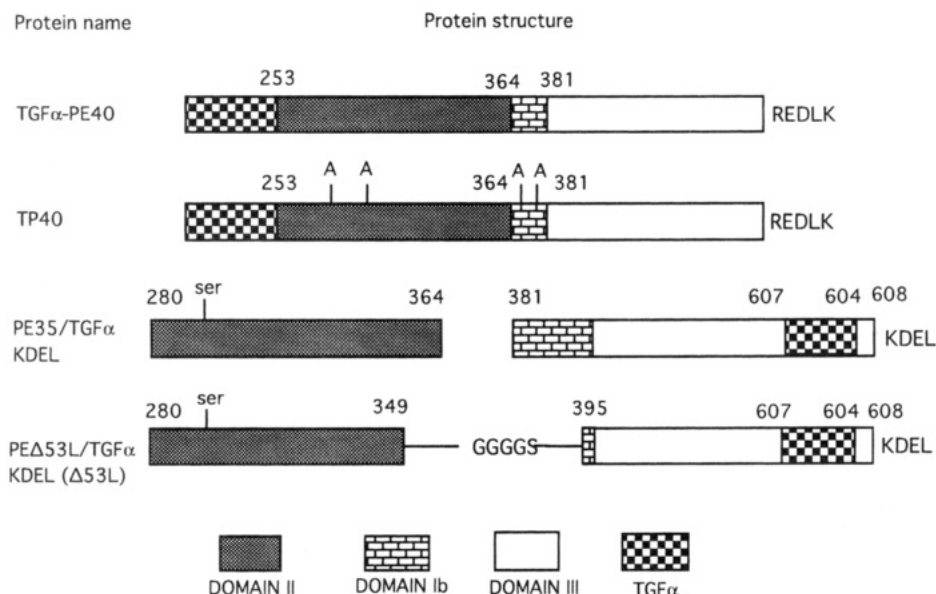
**ADP-Ribosylation Assay.** ADP-ribosylation activity of protein samples was measured by the procedure of Collier and Kandel using wheat germ extract enriched in elongation factor 2 (29).

**[<sup>125</sup>I]-EGF Displacement Studies.** A431 cells were plated at 8000 cells/well in 1 mL of medium in 24-well plates. After 24 h, the cells were washed twice with binding buffer (Dulbecco's modified Eagle's medium) containing 50 mM BES (pH 6.8) and 1 mg/mL of bovine serum albumin and treated with 200  $\mu$ L of binding buffer containing 0.5 ng (0.05  $\mu$ Ci) of [<sup>125</sup>I]-EGF, combined with either 0, 0.8, 4, 20, or 100 pmol of chimeric toxin. After equilibration for 90 min on a rocker at 4 °C, the cells were washed with binding buffer, lysed with 10 mM Tris–HCl (pH 7.4) containing 0.5% SDS and 1 mM EDTA, and bound ligand counted with a  $\gamma$  detector (30).

**In Vivo Study.** Four- to six-week old female athymic nude mice were supplied by the Frederick Cancer Research Center, National Cancer Institute. LD<sub>50</sub> studies were performed by the tail vein injection, and the number of dead animals was determined daily for 7 days following immunotoxin administration.

**Osmotic Pumps.** Miniosmotic pumps (Model 1007, delivering 0.5  $\mu$ L/h for 7 days) were obtained from Alza Corp. and used as recommended by the manufacturer. Pumps were filled with a solution containing TGF $\alpha$  chimeric toxins at different concentrations in sterile phosphate-buffered saline containing 0.2% human serum albumin in sterile phosphate buffer or phosphate-buffered saline alone.

**Surgical Procedure.** Animals were anesthetized with Metofane (methoxyflurane). The skin was cleaned with 70% alcohol (v/v), and a midline incision less than 1 cm long was made in the lower abdomen. The peritoneal cavity was opened carefully, and a filled pump was



**Figure 1.** Structures of TGFα-PE40, TP40, PE35/TGFα/KDEL, and PEΔ53L/TGFα/KDEL.

inserted. The musculo-peritoneal layer was closed with 4-0 silk sutures, and the skin was closed with two wound clips. The procedure was performed in a laminar flow hood under stringent sterile conditions.

**Stability of TGFα Chimeric Toxins at 37 °C.** Chimeric toxins were analyzed for their stability at 37 °C prior to the initiation of its use in animal experiments. A solution containing TGFα chimeric toxins at 100 μg/mL and 0.2% human serum albumin was kept at 37 °C for 7 days. A small aliquot was taken daily and analyzed for its cytotoxic activity on A431 cells.

**LD<sub>50</sub> for TGFα Chimeric Toxins in Nude Mice.** Osmotic pumps containing escalating doses of TGFα chimeric toxins calculated to deliver 40, 80, and 100 μg/kg/day were placed i.p. as described in groups of two mice. The number of dead animals was determined on days 2, 4, 6, 8, and 10.

**Antitumor Activity of Chimeric Toxins in Nude Mice Bearing Human Carcinoma.** A431 cells ( $3 \times 10^6$ ) were injected s.c. on day 0 into female nude mice, and tumors about 50 mm<sup>3</sup> in size reproducibly developed in all mice by day 5. Treatment of mice with chimeric toxins was started on day 5 after tumor implantation. Each group consisted of five animals. Tumors were measured with a caliper every 2 days, and the volume of the tumor was calculated by using the following:

$$\text{tumor volume (in mm}^3\text{)} = \text{length} \times (\text{width})^2 \times 0.4$$

All statistical comparisons were made using the Wilcoxon rank sum test. Error bars are standard deviation, and we used five mice for each point. To ensure that tumors were uniform at the beginning of treatment, extra mice were injected with tumors and only mice with tumors very similar in size were used.  $SD = [(V - A)^2 + (V - B)^2 + (V - C)^2 + (V - D)^2 + (V - E)^2]^{1/2}/5$  where  $V$  is the average size and  $A-E$  are individual tumor sizes.

## RESULTS

Figure 1 shows the structure of TGFα-PE40 and its analog TP40 which is missing two disulfide bonds as well as the structure of a variety of mutant molecules in which TGFα is inserted near the carboxyl terminus and the toxin begins at amino acid 280. Theuer et al. had previously shown that PE35/TGFα/KDEL is a very potent cytotoxic agent when tested on cell lines with EGF

receptors (31). Using this molecule as a starting point, we made a series of deletions removing increasing amounts of the carboxyl end of domain Ib. It had been previously shown using PE and TGFα-PE40 that a large portion of domain Ib could be deleted without loss of activity but that larger deletions caused significant loss of activity (33). We found it was possible to delete amino acids up to position 395 without a significant loss in cytotoxic or ADP-ribosylation activity. However, deletion of amino acids 395-400 led to a molecule with very low cytotoxic activity, even though ADP-ribosylation activity remained at 80%. We also made a series of deletions extending toward the amino end of the molecule and found that sequences up to position 365 could be deleted without loss of cytotoxic activity (Table 2). This indicates that a large part of domain Ib is not required for the cytotoxic activity of these molecules. However, when the deletion extended one or six amino acids further, a very large loss of cytotoxic activity was observed. These data indicate that a large part of domain Ib can be deleted without loss of cytotoxic activity.

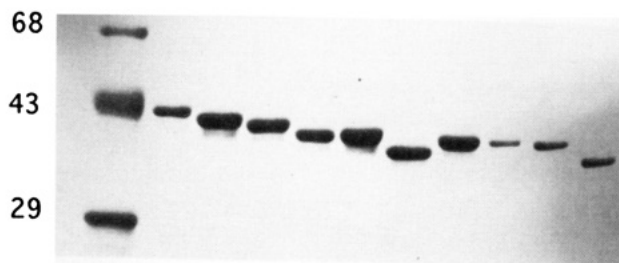
**Construction with Peptide Linker Insertions.** Because domain Ib connects domain II to domain III, we reasoned that deletion of domain Ib may lead to molecules in which domains II or III are folded improperly or interact in some abnormal manner. Therefore, we chose the three molecules shown in Table 2 with deletions within domain Ib and II in which to insert a short flexible linking peptide. The sequence GGGGS was chosen because it is flexible and its estimated length which is 13.5 Å would permit domains on either side of it to fold independently. Furthermore, it would minimize their interactions with each other. Each of these molecules was expressed in *E. coli* and purified to near homogeneity (Figure 2). In each case the introduction of a linking peptide increased activity. In the case of Δ3, which is already an extremely active molecule ( $IC_{50} \sim 0.004$  ng/mL), the increase in activity was only about 2-fold. In the case of Δ53 ( $IC_{50}$  0.05 ng/mL), the increase in activity was about 11-fold, and in the case of Δ13 the increase in activity was about 7-fold. We also found that introduction of the linking peptide increased the ADP-ribosylation activity measured in cell free extracts using wheat germ EF2 as an acceptor molecule (Table 2). These results indicate that direct fusion of domain II to domain III results in a molecule with diminished cytotoxic activity.



**Table 2. ADP-Ribosylation and Cell Killing Activity of Various Mutant Forms of PE35/TGF $\alpha$ KDEL**

plasmid	amino acids deleted in <i>Pseudomonas</i> exotoxin in region from 280 to 613	IC <sub>50</sub> on A431 (ng/mL)	rel ADP-ribosylation activity (%)
PE35/TGF $\alpha$ KDEL	365–380	0.005	100
$\Delta$ 3	365–394	0.004	100
$\Delta$ 9	365–399	0.3	80
$\Delta$ 4	360–386	0.015	100
$\Delta$ 5	349–386	0.025	80
$\Delta$ 53	350–394	0.05	30
$\Delta$ 13	344–394	7	20
with a peptide linker			
$\Delta$ 53L	350–394/GGGGS	0.004	160
$\Delta$ 17L	350–395/GGGGS	0.02	120
$\Delta$ 14L	350–397/GGGGS	0.7	150
$\Delta$ 16L	349–394/GGGGS	0.1	25
$\Delta$ 15L	347–394/GGGGS	0.025	60
$\Delta$ 13L	344–394/GGGGS	1	80
$\Delta$ 12L	333–394/GGGGS	7	50
$\Delta$ 12L2	333–394/(GGGGS)2	40	<1
$\Delta$ 11L2	314–394/(GGGGS)2	100	<1

kD    STD   1   2   3   4   5   6   7   8   9   10



**Figure 2.** SDS-PAGE (14% reducing) of various deletion mutant proteins stained with Coomassie blue. The position of standards is indicated in the left margin: lane 1, STD; 2, PE35/TGF $\alpha$ KDEL; 3,  $\Delta$ 1; 4,  $\Delta$ 3; 5,  $\Delta$ 5; 6,  $\Delta$ 9; 7,  $\Delta$ 13; 8,  $\Delta$ 53L; 9,  $\Delta$ 17L; 10,  $\Delta$ 12L2; 11,  $\Delta$ 11L2.

**Deletions Extending into Domain II.** We next made a series of large deletions, most of which started at amino acid 395 at the carboxyl end and extended into domain II. The longest of these terminated at amino acid 313. In all of these a GGGGS linking peptide was inserted in place of the deleted sequences. As shown in Table 2, amino acids 350–394 could be deleted without significant loss of activity. However, when the deletion extended to amino acid 346 as in  $\Delta$ 15L, a 10-fold loss in activity was noted. Nevertheless, this molecule is very active with an IC<sub>50</sub> on A431 cells of 0.025 ng/mL. Extending the deletion further into domain II resulted in molecules with much less activity (see  $\Delta$ 13L and  $\Delta$ 12L). We also attempted to increase the length of the linker to determine if this would increase the activity of molecules with relatively low cytotoxicity. However, in the case of  $\Delta$ 12L2 the longer peptide led to a decrease in cytotoxic activity and also loss of ADP-ribosylation activity. Furthermore, molecules beginning at amino acid 313 and ending at 395 which contained a longer linker also had very low ADP-ribosylating activity and very little cytotoxicity. These last two results suggest that the longer linker either itself or in concert with the remaining portion of domain II interacts with domain III in such a manner that EF2 or NAD cannot bind to domain III.

**EGF Receptor Binding.** A loss of cytotoxicity can be due to diminished binding to the EGF receptor, failure of the molecule to be transported to the right compartment for translocation, or a defect in translocation itself. To assess the effect of the various mutations on binding, we carried out displacement assays on A431 cells with two of the chimeric toxins using [<sup>125</sup>I]-EGF as a ligand.

The results of these binding studies are shown in Figure 3 and are summarized in Table 3. In the two cases examined,  $\Delta$ 13L and  $\Delta$ 53L, the presence of the linking peptide led to an increase in the binding of the chimeric toxin to the EGF receptor. The increase was about 3-fold in the case of  $\Delta$ 13 and about 4-fold in the case of  $\Delta$ 53.

**Toxicity and LD<sub>50</sub> of Chimeric Toxins.** Miniosmotic pumps have been used to successfully administer a wide variety of biological agents (32). Preliminary experiments have shown that half of the animals died when given a single i.v. injection of 50  $\mu$ g/kg of  $\Delta$ 53L. To determine how much chimeric toxin could be given to mice by continuous infusion, these toxins were delivered over 7 days by osmotic pumps implanted in the peritoneal cavity at doses of 40, 80, and 100  $\mu$ g/kg/day. Table 4 shows that half of the animals died when given approximately 90  $\mu$ g/kg/day of  $\Delta$ 53L. This result shows that when using osmotic pumps, more recombinant toxin can be given than by a single injection.

**Antitumor Experiments with  $\Delta$ 53L.** Having established the LD<sub>50</sub>,  $\Delta$ 53L was tested for its ability to inhibit the growth of A431 tumors growing in nude mice. On day 5, after tumor implantation subcutaneously, miniosmotic pumps were placed in the mice. At this time, the tumor size was approximately 50 mm<sup>3</sup>. In the control group in which the pumps were filled with PBS, the tumors grew rapidly and reached 1800 mm<sup>3</sup> by day 20–22 (Figure 4). In the group treated from days 5–11 with  $\Delta$ 53L, there was a definite antitumor effect that was dose related over the dose range 20–80  $\mu$ g/kg/day without any animal deaths. TP40 at 400  $\mu$ g/kg/day also showed an antitumor effect but this was less than  $\Delta$ 53L at 20  $\mu$ g/kg/day, despite the fact that the concentration of TP40 used was 80% of the LD<sub>50</sub>.

## DISCUSSION

To determine the function of sequences present in domains Ib and II of PE and to make a small molecule with potentially improved tissue penetration, we performed a deletion analysis on a very active chimeric toxin, PE37/TGF $\alpha$ KDEL. As described previously, deletion of various regions in domain II results in loss of cytotoxicity indicating that domain II is essential for full expression of cytotoxicity (33). In contrast, deletion of the amino terminus of domain Ib (amino acids 365–380) indicates domain Ib is not essential for the cytotoxic effect of TGF $\alpha$ -PE40. On the basis of these results, we made a variety of new deletion mutants and made these in a molecule that did not require proteolysis for activation



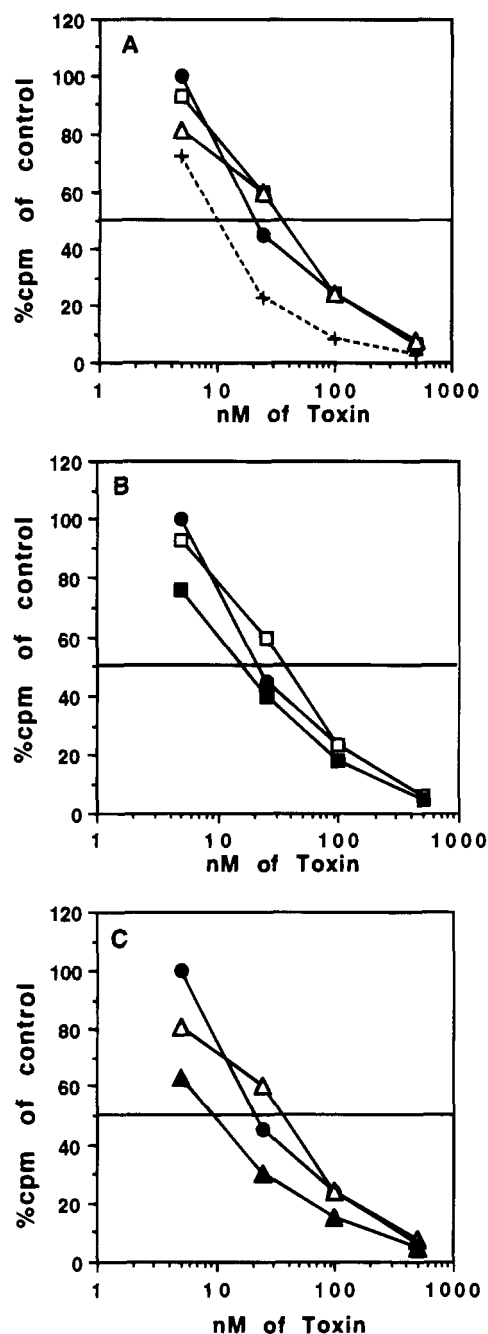
**Table 3. Relative Inhibition of EGF Binding by Various Deletion Mutants<sup>a</sup>**

proteins	rel binding (%)
PE35/TGF $\alpha$ /KDEL	100
$\Delta 13$	58
$\Delta 13L$	138
$\Delta 53$	63
$\Delta 53L$	230

<sup>a</sup> The data are derived from Figure 3. The concentrations of each protein that gives a 50% inhibition of binding are compared with PE35/TGF $\alpha$ /KDEL, which is set at 100%.

of its cytotoxic activity. Thus, any effects of mutations on the proteolytic processing step are excluded from our analysis. We find that all of domain Ib and a portion of domain II can be deleted without significant loss of cytotoxic activity (Figure 1). However, deletions which remove large amounts of domain II have significantly diminished cytotoxic activity (Table 2). Examination of the three-dimensional structure of PE reveals that domains II and III are intimately related to each other with many interacting amino acids (3). Deletion of residues within domain Ib and the carboxyl end of domain II produce molecules in which the relationship with domain II to domain III is disrupted. Therefore, we chose two deletions ( $\Delta 53$  and  $\Delta 13$ ) to determine whether insertion of a flexible linking peptide that might allow the two domains to fold independently and interact with less strain would affect the cytotoxicity of the recombinant toxins. As shown in Table 2, the introduction of sequences that are about 13.5 Å in length led in each case to an increase in cytotoxic activity. The increase in activity ranged from 7-fold ( $\Delta 13$ ) to 12-fold ( $\Delta 53$ ). This suggested that deletion of amino acids from Ib without the insertion of a linking peptide did create abnormal interactions between domains II and III. However, abnormal folding could also interfere with the ability of TGF $\alpha$  to fold properly to interact with this reaction. Thus, we measured the binding of these chimeric toxins to the EGF receptor in a competition assay format and observed up to a 3-fold change in binding (Figure 3 and Table 3). The molecules containing a linking peptide had better binding than the parental molecules. The increase in binding was not sufficient to account entirely for the increase in cytotoxicity in  $\Delta 13L$  and  $\Delta 53L$ . Therefore, the introduction of the linker probably has two effects. One is to increase binding of TGF $\alpha$  to its receptor. The second is to enable domains II and III to interact in a favorable manner to allow optimal expression of their cytotoxic activity.

**Size and Antitumor Activity of Recombinant of Toxins.** It has been emphasized by Dedrick (18) and Yokota (17) that the penetration of proteins into tissues is strongly dependent on their molecular weight. To enable recombinant toxins to penetrate tumors more effectively, it is desirable to produce molecules with as small a molecular weight as possible. Therefore, we have attempted to delete all unnecessary sequences from recombinant toxins. We have used TGF $\alpha$  containing toxins as a model for this study. We have previously shown that increased cytotoxicity could be produced by inserting TGF $\alpha$  near the carboxyl terminus of domain III and deleting amino acids 1–279 of PE. This chimeric toxin has a molecular weight of 41.0 kD. We next analyzed the function of sequences between domains II and III. Beginning with a molecule which has a partial deletion of Ib, termed PE35/TGF $\alpha$ /KDEL, we have made a series of larger deletions. We find that we can delete amino acids 350–394 without significant loss of cytotox-

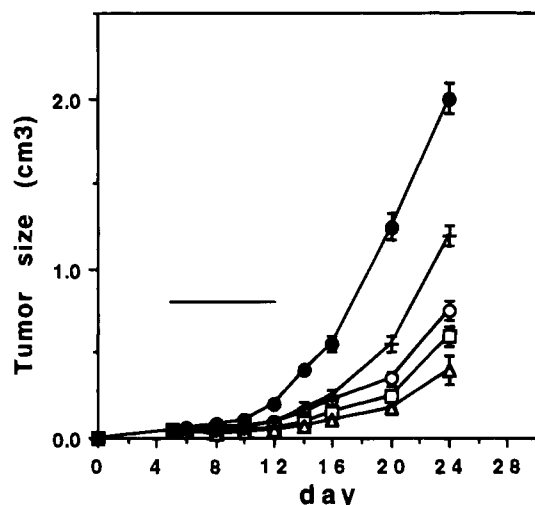


**Figure 3.** Displacement of [<sup>125</sup>I]-EGF by various deletion mutant proteins. Protein concentrations were estimated by Bradford assay. [<sup>125</sup>I]-EGF bound to A431 cells was measured as cpm and expressed as percentage of cpm of cells incubated without toxin. Key: (A) TP40 (+), PE35/TGF $\alpha$ /KDEL (●),  $\Delta 13$  (□),  $\Delta 53$  (Δ); (B) PE35/TGF $\alpha$ /KDEL (●),  $\Delta 13$  (□),  $\Delta 13L$  (■); (C) PE35/TGF $\alpha$ /KDEL (●),  $\Delta 53$  (Δ),  $\Delta 53L$  (▲).

**Table 4. LD<sub>50</sub> of PE $\Delta 53L$ /TGF $\alpha$ /KDEL Delivered i.p. by Osmotic Pump**

dose ( $\mu$ g/kg/day for 7 days)	no. death/no. mice				
	day 2	day 4	day 6	day 8	day 10
PE $\Delta 53L$ /TGF $\alpha$ /KDEL					
40	0/2	0/2	0/2	0/2	0/2
80	0/2	0/2	0/2	0/2	0/2
100	0/2	0/2	1/2	2/2	0/2

icity, if replaced by the linker, GGGGS. The molecular weight of this molecule ( $\Delta 53L$ ) is 38.4 kD, and it is 17% smaller than TP40 and 6.4% smaller than PE35/TGF $\alpha$ /KDEL. TP40 is the TGF $\alpha$ -containing recombinant toxin



**Figure 4.** Effect of PE $\Delta$ 53L/TGF $\alpha$ /KDEL on the growth of A431 tumors in nude mice. Animals received injections of  $3 \times 10^6$  cells on day 0. Osmotic pumps were placed i.p. on day 5 to deliver PE $\Delta$ 53L/TGF $\alpha$ /KDEL 20  $\mu$ g/kg/day (○), 40  $\mu$ g/kg/day (□), 80  $\mu$ g/kg/day (Δ), and TP40 400  $\mu$ g/kg/day (+) for 7 days. The control groups received phosphate-buffered saline (●). Bars, standard deviation.

that is currently undergoing clinical evaluation in bladder cancer. Not only is  $\Delta$ 53L significantly smaller than TP40, but it is also 125 times more active on A431 cells (Table 2). To determine if  $\Delta$ 53L was active on animals, it was administered intraperitoneally to mice bearing A431 tumors. A clear dose dependent antitumor effect was observed over the range of 20–80  $\mu$ g/kg/day (Figure 4). Even at the 20  $\mu$ g/kg/day level,  $\Delta$ 53L was more active than TP40 given at 400  $\mu$ g/kg/day.

**Conclusion.** In this paper we have been able to delete all of domain Ib (amino acids 365–394) and retain very high cytotoxic activity. Deletion of additional sequences in domain II results in a loss of activity but this loss of activity can be partly prevented by placing a flexible linker GGGGS, about 13.5 Å in length between the two molecules. These findings must be considered when trying to assign a specific function to each domain of PE and its chimeric derivatives. One difference between conventional cytotoxic drugs and recombinant toxins is size. Conventional drugs penetrate into tumors rapidly whereas proteins do not. Although the decrease in size of the molecules described here is relatively modest, the change in size may be nevertheless useful. Furthermore, the approach taken to decrease size may be extended to other toxins.

#### ACKNOWLEDGMENT

We thank E. Lovelace and A. Harris for cell culture assistance, D. Heimbrook of Merck and Co. for a gift of TP40, C. P. Theuer for a gift of the plasmid (pCT12), L. H. Pai for her helpful technical advice on antitumor experiments, and J. Evans and A. Jackson for editorial assistance.

#### LITERATURE CITED

- (1) Pastan, I., Chaudhary, V. K., and FitzGerald, D. J. (1992) Recombinant toxins as novel therapeutic agents. *Ann. Rev. Biochem.* 61, 331–354.
- (2) Chaudhary, V. K., Mizukami, T., Fuerst, T. R., FitzGerald, D. J., Moss, B., Pastan, I., and Berger, E. A. (1988) Selective killing of HIV-infected cells by a recombinant human CD4-*Pseudomonas* exotoxin hybrid protein. *Nature* 335, 369–372.
- (3) Allured, V., Collier, R. J., Carroll, S. F., and McKay, D. B. (1986) Structure of exotoxin A of *Pseudomonas aeruginosa*

- at 3.0 Angstrom resolution. *Proc. Natl. Acad. Sci. U.S.A.* 83, 1320–1324.
- (4) Chaudhary, V. K., FitzGerald, D. J., Adhya, S., and Pastan, I. (1987) Activity of a recombinant fusion protein between transforming growth factor alpha and *Pseudomonas* toxin. *Proc. Natl. Acad. Sci. U.S.A.* 84, 4538–4542.
- (5) Siegall, C. B., Xu, Y.-H., Chaudhary, V. K., Adhya, S., FitzGerald, D., and Pastan, I. (1989) Cytotoxic activities of a fusion protein comprised of TGF $\alpha$  and *Pseudomonas* exotoxin. *FASEB J.* 3, 2647–2652.
- (6) Hwang, J., FitzGerald, D. J. P., Adhya, S., and Pastan, I. (1987) Functional domains of *pseudomonas* exotoxin identified by deletion analysis of the gene expressed in *E. coli*. *Cell* 48, 129–136.
- (7) Heimbrook, D. C., Stirdivant, S. M., Ahern, J. D., Balishin, N. L., Patrick, D. R., Edwards, G. M., Defeo-Jones, D., FitzGerald, D. J., Pastan, I., and Oliff, A. (1990) Transforming growth factor-alpha *Pseudomonas* exotoxin fusion protein prolongs survival of nude mice bearing tumor xenografts. *Proc. Natl. Acad. Sci. U.S.A.* 87, 4697–4701.
- (8) Pai, L. H., Gallo, M. G., FitzGerald, D. J., and Pastan, I. (1991) Anti-tumor activity of a transforming growth factor alpha-*Pseudomonas* exotoxin fusion protein (TGF $\alpha$ -PE40). *Cancer Res.* 51, 2808–2812.
- (9) Kunwar, S., Pai, L. H., and Pastan, I. (1993) Cytotoxicity and antitumor effects of growth factor-toxin fusion proteins on human glioblastoma multiforme cells. *J. Neurosurg.* 79, 569–576.
- (10) Boring, C. C., Squires, T. S., and Tong, T. (1993) Cancer statistics. 1993. *CA Cancer J. Clin.* 43, 7–26.
- (11) Lamm, D. L., Blumenstein, B. A., Crawford, E. D., Montie, J. E., Scardino, P., Grossman, H. B., Staniscic, T. H., Smith, J. A., Jr., Sullivan, J., Sarosdy, M. F., Crissman, J. D., and Coltman, C. A. (1991) A randomized trial of intravesical doxorubicin and immunotherapy with bacille Calmette-Guerin for transitional cell carcinoma of the bladder. *N. Engl. J. Med.* 325, 1205–1209.
- (12) Lamm, D. L., Stogdill, V. D., Stogdill, B. J., and Crispen, R. G. (1986) Complications of bacillus Calmette-Guerin immunotherapy in 1278 patients with bladder cancer. *J. Urol.* 135, 272–274.
- (13) Smith, K., Fennelly, J. A., Neal, D. E., Hall, R. R., and Harris, A. L. (1989) Characterization and quantitation of the epidermal growth factor receptor in invasive and superficial bladder tumors. *Cancer Res.* 49, 5810–5815.
- (14) Neal, D. E., Smith, K., Fennelly, J. A., Bennett, M. K., Hall, R. R., and Harris, A. L. (1989) Epidermal growth factor receptor in human bladder cancer: a comparison of immunohistochemistry and ligand binding. *J. Urol.* 141, 517–521.
- (15) Messing, E. M., Hanson, P., Ulrich, P., and Erturk, E. (1987) Epidermal growth factor interactions with normal and malignant urothelium: *in vivo* and *in situ* studies. *J. Urol.* 138, 1329–1335.
- (16) Goldberg, M. R., Heimbrook, D. C., Russo, P., Sarosdy, M. F., Greenberg, R. E., Linehan, M. J., Fisher, H. A. G., Messing, E., Crasford, E. D., Oliff, A. I., and Pastan, I. H. (1993) Transforming growth factor- $\alpha$ -*Pseudomonas* exotoxin – 40 (TP40): antitumor activity in a phase I study in patients with superficial bladder cancer. *J. Urol.* (submitted).
- (17) Yokota, T., Milenic, D. E., Whitlow, M., Wood, J. F., Hubert, S. L., and Schlom, J. (1993) Microautoradiographic analysis of the normal organ distribution of radioiodinated single-chain Fv and other immunoglobulin forms. *Cancer Res.* 53, 3776–3783.
- (18) Dedrick, R. L., and Flessner, M. F. (1989) Pharmacokinetic considerations on monoclonal antibodies. *Immun. Cancer* 2, *Proc. Conf.* 2nd 429–438.
- (19) Sung, C., Dedrick, R. L., Hall, W. A., Johnson, P. A., and Youle, R. J. (1993) The spatial distribution of immunotoxins in solid tumors: assessment by quantitative autoradiography. *Cancer Res.* 53, 2092–2099.
- (20) Ogata, M., Fryling, C. M., Pastan, I., and FitzGerald, D. J. (1992) Cell mediated cleavage of *Pseudomonas* exotoxin between Arg279 and Gly280 generates the enzymatically active fragment which translocates to the cytosol. *J. Biol. Chem.* 267, 25396–25401.

- (21) Ogata, M., Chaudhary, V. K., Pastan, I., and FitzGerald, D. J. (1990) Processing of *Pseudomonas* exotoxin by a cellular protease results in the generation of a 37,000-Da toxin fragment that is translocated to the cytosol. *J. Biol. Chem.* 265, 20678–20685.
- (22) Theuer, C. P., Buchner, J., FitzGerald, D., and Pastan, I. (1993) The N-terminal region of the 37 kD translocated fragment of *Pseudomonas* exotoxin A aborts translocation by promoting its own export following microsomal membrane insertion. *Proc. Natl. Acad. Sci. U.S.A.* 90, 7774–7778.
- (23) Theuer, C. P., FitzGerald, D. J., and Pastan, I. (1992) A recombinant form of *Pseudomonas* exotoxin directed at the epidermal growth factor receptor that is cytotoxic without requiring proteolytic processing. *J. Biol. Chem.* 267, 16872–16877.
- (24) Kunkel, T. A. (1985) Rapid and efficient site-specific mutagenesis without phenotypic selection. *Proc. Natl. Acad. Sci. U.S.A.* 83, 488–492.
- (25) Saiki, R. K., Scarf, S. J., Faloona, F., Mullis, K. B., Horn, G. T., Erlich, H. A., and Arnheim, N. (1988) Enzymatic amplification of beta-globin genomic sequences and restriction site analysis for diagnosis of sickle cell anemia. *Science* 239, 487–491.
- (26) Chaudhary, V. K., Batra, J. K., Gallo, M., Willingham, M. C., FitzGerald, D. J., and Pastan, I. (1990) A rapid method of cloning functional variable region antibody genes in *E. coli* as single chain immunotoxins. *Proc. Natl. Acad. Sci. U.S.A.* 87, 1066–1070.
- (27) Buchner, J., Pastan, I., and Brinkmann, U. (1992) A method to increase the yield of properly folded recombinant fusion proteins, e.g., single-chain immunotoxins, from renaturations of bacterial inclusion bodies. *Anal. Biochem.* 205, 263–270.
- (28) Prior, T. I., FitzGerald, D. J., and Pastan, I. (1991) Barnase toxin – A new chimeric toxin composed of *pseudomonas* exotoxin-A and barnase. *Cell* 64, 1017–1023.
- (29) Collier, R., and Kandel, J. (1971) Structure and activity of diphtheria toxin. I. Thiol-dependent dissociation of a fraction of toxin into enzymatically active and inactive fragments. *J. Biol. Chem.* 246, 1496–1503.
- (30) Kreitman, R. J., Chaudhary, V. K., Siegall, C. B., FitzGerald, D. J., and Pastan, I. (1992) Rational chemotherapeutic design of *Pseudomonas* exotoxin: an intramolecular location for the insertion of transforming growth factor alpha as a targeting ligand. *Bioconjugate Chem.* 3, 58–62.
- (31) Theuer, C. P., FitzGerald, J. P., and Pastan, I. (1993) A recombinant form of *Pseudomonas* exotoxin A containing transforming growth factor alpha near its carboxyl terminus for the treatment of bladder cancer. *J. Urol.* 149, 1626–1632.
- (32) Leichman, C. G., Corbett, T., and Leichman, L. (1985) Improved treatment results in murine colon tumors treated with infusion 5 FU versus standard bolus schedule. *Proc. Am. Assoc. Cancer Res.* 26, 355.
- (33) Siegall, C. B., Chaudhary, V. K., FitzGerald, D. J., and Pastan, I. (1989) Functional analysis of domains II, Ib and III of *Pseudomonas* exotoxin. *J. Biol. Chem.* 264, 14256–14261.

## Expression of Oligohistidine-Tagged Ricin B Chain in *Spodoptera frugiperda*

Lawrence B. Afrin, Heather Gulick, Joseph Vesely, Mark Willingham, and Arthur E. Frankel\*

Departments of Medicine and Pathology, Medical University of South Carolina, Charleston, South Carolina 29425. Received June 7, 1994\*

DNA encoding ADPGH<sub>6</sub>G was fused to the 5'-end of RTB DNA and subcloned as a BamHI-EcoRI DNA cassette into the baculovirus transfer vector, pAcGP67A. *Spodoptera frugiperda* Sf9 cells were cotransfected with pAcGP67A-ADPGH<sub>6</sub>G-RTB DNA and BaculoGold AcNPV DNA, and recombinant baculovirus was isolated by two cycles of limiting dilution assay followed by dot blot analysis with <sup>32</sup>P-dCTP random primer labeled RTB DNA. Recombinant virus was purified and amplified to obtain stocks at titers of 10<sup>7</sup> infectious particles/mL. Sf9 cells grown in serum-free medium were then infected at an moi of 3 in the presence of 25 mM  $\alpha$ -lactose. After 5 days, supernatants and cell pellets were harvested and assayed by an asialofetuin ELISA for recombinant RTB protein. Fusion RTB protein was produced in the supernatant at 5 mg/L and in the cell pellet at 1 mg/L. Recombinant protein was purified to >80% homogeneity using either a monoclonal antibody affinity matrix with alkaline elution or a Ni<sup>2+</sup>-NTA matrix with imidazole elution. The purified protein bound asialofetuin similarly to plant RTB. N-terminal sequencing confirmed the oligohistidine tag. SDS-PAGE confirmed the 1,000 Da increase in mass relative to "wild-type" recombinant RTB produced in Sf9 cells. Immunoblots confirmed reactivity with polyclonal and monoclonal antibodies to plant RTB. The fusion protein reassociated with plant RTA similarly to plant RTB. The recombinant reassociated heterodimer not only demonstrated cytotoxicity to HPB-MLT human leukemia cells (ID<sub>50</sub> 10<sup>-12</sup>M) similar to ricin and reassociated plant RTA-plant RTB but also bound Ni<sup>2+</sup>-NTA resin, suggesting preservation of function of RTA, RTB, and the new ligand fused to RTB. Thus, the recombinant fusion of new ligands to RTB may represent a novel and practical method for developing new immunotoxins.

### INTRODUCTION

An immunotoxin is a conjugate of a targeting ligand (e.g., antibodies, cytokines, etc.) covalently linked to a moiety which intoxicates the targeted cell (1). For example, ricin toxin A chain (RTA) has been conjugated to an antibody directed against the lymphocyte surface marker CD22 to produce an immunotoxin targeting B lymphocytes (2), and *Pseudomonas* exotoxin (PE) has been linked to OVB3, a monoclonal antibody directed against a cell surface antigen on ovarian carcinomas (3). The ID<sub>50</sub> (concentrations of immunotoxin which reduce cellular protein synthesis by 50%) for anti-CD22-RTA on the Daudi B lymphoma cell line was 10<sup>-12</sup> M, which was similar to the ID<sub>50</sub> of ricin on Daudi cells (10<sup>-11</sup> M). Similarly, the ID<sub>50</sub>'s of OVB3-PE and PE were both 10<sup>-12</sup> M on the OVCAR3 ovarian carcinoma cell line. Many immunotoxins with *in vitro* activity have also demonstrated preclinical *in vivo* activity. SCID mice bearing human Daudi tumors were treated with four intravenous injections of anti-CD22-RTA. Survival was doubled from 45 to 87 days representing a four log kill of tumor cells (4). Nude mice with growing human OVCAR-3 ascites tumors were given three intraperitoneal injections of OVB3-PE (3). Median survival was quadrupled from 50 to 193 days.

Several immunotoxins with demonstrated preclinical activity have also been evaluated in humans with consistently less encouraging results than seen in animal models. Extending the previously cited examples, two to 12 doses of anti-CD22-RTA were infused intrave-

nously into patients with refractory B-cell lymphoma (5). One complete response and five partial responses occurred out of 24 patients but the responses were transient lasting 1–3 months and the dose-limiting toxicity, vascular leak syndrome, was observed early. Twenty-three patients with refractory ovarian cancer were treated with intraperitoneal escalating doses of OVB3-PE (6). No responses were seen, and dose-limiting toxic encephalopathy occurred in three patients. Many factors were postulated to bear influence on these observed clinical outcomes, including (a) limited tumor penetration due to the large sizes of the immunotoxin conjugates (7), (b) cross-reactive, nonspecific binding of the ligand or toxin moieties to bystander cells with consequent damage to normal tissues (5, 6, 8), (c) conjugate heterogeneity due to varying chemical modifications (9), and (d) altered toxin structure in the conjugate, causing diminished cytosolic translocation efficiency (10).

In the setting where both toxin and ligand are peptides (as in the above examples), one approach to overcoming some of these barriers is to genetically engineer an amide linkage between the two moieties. Such a recombinant gene not only allows for expression of a homogeneous product (a "fusion toxin") but also provides a base line model for pursuing systematic investigation of mutations which might improve targeting specificity, translocation efficiency, or other pharmacologic parameters. Examples of fusion toxins developed to date include the diphtheria toxin (DT) fusions with IL-2 (DAB<sub>486</sub>IL-2 and DAB<sub>389</sub>IL-2) (11, 12) and PE with the single chain antibody to the IL-2 receptor (anti-Tac(Fv)-PE40) (13). DAB<sub>486</sub>IL-2 and DAB<sub>389</sub>IL-2 had an ID<sub>50</sub> of 10<sup>-11</sup> M on the human T leukemia cell line, HUT102. Similarly, anti-Tac(Fv)-PE40 had an ID<sub>50</sub> of 10<sup>-12</sup> M on HUT102 cells. In contrast, anti-Tac monoclonal antibody chemically linked to PE40 or RTA had ID<sub>50</sub>'s of 10<sup>-10</sup> M on the same

\* To whom correspondence should be addressed: Hollings Cancer Center Room 311, Medical University of South Carolina, 171 Ashley Avenue, Charleston, SC 29425.

\* Abstract published in *Advance ACS Abstracts*, October 1, 1994.

HUT102 cells (13, 14). Thus, this fusion protein was 10–100-fold more potent *in vitro* than its chemically coupled conjugate counterpart. Few comparisons have been made between fusion toxins and antibody–toxin chemical conjugates in animal models (15–18). Nude mice bearing human epidermoid carcinoma cells transfected with a plasmid encoding the IL-2 receptor  $\alpha$  subunit (4 days postinoculation) were treated with three daily doses of anti-Tac(Fv)–PE38KDEL or a chemical conjugate between anti-Tac(IgG) and truncated PE. The fusion toxin was able to cure mice whereas the chemical conjugate had much less antitumor activity. C57BL/6 mice inoculated with murine CP3 leukemia cells were treated 24 h later with 10 daily doses of DAB<sub>486</sub>IL-2 or DAB<sub>389</sub>IL-2. DAB<sub>486</sub>IL-2 doubled mean survival time from 30 to 60 days, while DAB<sub>389</sub>IL-2 cured 90% of the animals. Using a different animal model for anti-CD25-RTA, the L540 human Hodgkin's disease cell line was inoculated into SCID mice, followed by anti-CD25-RTA treatment 24 h later. This regimen resulted in a cure rate of 70%. Small phase I/II clinical trials have been conducted with DAB<sub>486</sub>IL-2, DAB<sub>389</sub>IL-2, and anti-CD5-RTA in cutaneous T cell lymphoma (CTCL) and with anti-Tac-PE in adult T cell leukemia (ATL). Again, better activity was observed with the fusion toxins. DAB<sub>486</sub>IL-2 given by five daily intravenous boluses to patients with CTCL produced one complete response and two partial responses in five patients lasting 4 months to over 3 years (19). DAB<sub>389</sub>IL-2 given similarly produced five partial responses in 11 patients with CTCL (20). The chemical conjugate anti-CD5-RTA was given daily intravenously for 10 days to CTCL patients (21). Only four of 14 patients showed partial responses lasting 3–8 months, and toxicity related to vascular leak syndrome was significant. Anti-Tac antibody conjugated to PE yielded no responses in four patients and produced early dose-limiting hepatotoxicity (22).

Fusion toxins based on ricin may have advantages over DT- and PE-based fusion proteins. Ricin is a class II ribosome inactivating protein naturally found in the castor bean seed of the plant *Ricinus communis*. The toxin is a heterodimer consisting of an enzymatically toxic A chain (RTA) disulfide-linked to a lectin B chain (RTB) which has two galactose-specific binding sites (23). The mechanism of ricin cytotoxicity, namely the N-glycosylation of the 28S ribosomal RNA at the binding site for elongation factors (24), is distinct and independent from that of DT and PE (ADP-ribosylation of elongation factor 2 (25)). Thus, ricin-based fusion toxins are non-cross-resistant with DT- and PE-based chimeric proteins. Additionally, ricin-based fusion toxins should not exhibit a similar immunogenicity profile as compared with fusion proteins containing either DT or PE.

DNA encoding the ricin gene was simultaneously isolated from both a genomic library and a cDNA library (26, 27). Preproricin DNA has no introns, thus simplifying construction of gene expression vectors. RTA has been expressed in bacteria (28) and yeast (29), while RTB has been expressed in bacteria (30), yeast (31), *Xenopus* oocytes (32), mammalian COS cells (33), and recently, *Spodoptera frugiperda* Sf9 insect cells (34). Ricin-based fusion toxins developed to date include RTA fused to protein A (35), RTA–IL-2 (36), and proricin containing an alternate Factor X cleavable linker peptide (37). Problems encountered with ricin-based fusion toxins thus far have included inadequate intracellular heterodimer cleavage and poor production yields.

We have approached the design of ricin-based fusion toxins by production and modification of recombinant RTB (rRTB) which can be reassociated with native RTA.

The recombinant heterodimer can then be purified and tested. To this end, we subcloned the RTB gene into a baculovirus expression vector at the 3' end of the gp67 signal peptide leader DNA (34). rRTB was isolated in Sf9 culture supernatant at 3 mg/L. Purification was performed by means of an immunoaffinity matrix. The purified rRTB bound galactose and reassociated with plant RTA to form heterodimers equally cytotoxic as native ricin.

We now describe the introduction of a new ligand at the N-terminus of RTB by genetic modification. This site was chosen because X-ray crystallographic studies of ricin show the N-terminus of RTB to lie in disordered structure (accessible to the solvent) and without apparent interaction with either the RTA–RTB interface or the galactose-binding sites on RTB (38). To be potentially useful, any introduced ligand must retain its original function, and thus for our first such construction we chose a ligand whose function would be simple to test and simultaneously might demonstrate the applicability of a purification method for RTB-based chimeric proteins distinct from the usual immunologically based approaches. This report documents the production of ADPGH<sub>6</sub>G–RTB (oligohistidine-tagged or His-tag RTB) at a level comparable to that of rRTB and also demonstrates preservation in His-tag RTB–RTA of both cytotoxicity and ligand-binding functions (oligohistidine affinity for nickel as well as RTB affinity for galactose). These results not only suggest a novel and practical method for developing recombinant ricin-based immunotoxins but also demonstrate that the oligohistidine–nickel affinity system can be used in the purification of such toxins.

## EXPERIMENTAL PROCEDURES

**Reagents.** Materials used for construction and characterization of pAcGP67A–GH<sub>6</sub>G–RTB were the same as those used for construction and characterization of pAcGP67A–RTB (34). Additionally, Ni<sup>2+</sup>–NTA resin was obtained from Qiagen (Chatsworth, CA), and imidazole was obtained from Sigma (St. Louis, MO). TFTB1 hybridoma producing monoclonal antibody to RTB was obtained from the American Type Culture Collection (Rockville, MD).

**Construction of pAcGP67A–GH<sub>6</sub>G–RTB.** A baculovirus transfer vector was prepared containing DNA encoding a gp67 signal peptide followed by ADPGH<sub>6</sub>G–RTB. The construction was based on the previously described baculovirus transfer vector pAcGP67A–RTB (34). To construct the RTB variant DNA, a polymerase chain reaction (PCR) was performed as previously described (34) using two oligonucleotide primers (5'-GCTCATGAGGATCCCGGGCATCATCACCACC-ACCACGGAGCTGATGTTTGTATGGAC-3' and 5'-GAG-TTTTGTGTTCTTGCCGGGTCCCAG-3') which introduce sequences encoding GH<sub>6</sub>G at the 5' end and sequences encoding two stop codons and an *Eco*RI site at the 3' end. Oligonucleotides were synthesized on an Applied Biosystems 380B DNA synthesizer and desalted with *n*-butanol. The PCR product was purified and *Eco*RI/*Bam*HI-restricted according to the manufacturer's instructions and then subcloned into pAcGP67A. This DNA was then transformed into INV $\alpha$ F' cells, and clones were selected on LB-ampicillin plates. Dideoxy sequencing confirmed the correct construction. pAcGP67A–GH<sub>6</sub>G–RTB DNA was then purified by cesium chloride density gradient centrifugation.

**Construction, Isolation, and Amplification of Recombinant Baculovirus.** As previously detailed for pAcGP67A–RTB (34), standard techniques were used in the maintenance of an Sf9 cell line as well as construction

and isolation of recombinant baculovirus by homologous recombination between pAcGP67A-GH<sub>6</sub>G-RTB and BaculoGold DNA. In dot blot assays of limiting dilutions, positive wells were identified and the corresponding supernatants reassayed by limiting dilution until all wells were positive up to a  $10^{-7}$  dilution. Recombinant virus in supernatants was then amplified by infecting Sf9 cells at a multiplicity of infection (moi) of 0.1 and collecting supernatants at day 7 for another round of amplification. Three rounds of amplification were performed.

**Expression and Purification of His-tag RTB.** Amplified virus at a titer of  $10^7$ /mL was added to Sf9 cell cultures (moi = 1.5–3) in a manner identical to that done previously for the expression of rRTB (34). Also, methods detailed previously for harvesting, concentration, and dialysis of rRTB culture supernatant as well as lysing and storage of cell pellets (34) were again used, without alteration, in this work with His-tag RTB. Immunoaffinity column preparation (monoclonal anti-RTB antibody P2) was also identical. Of note, just as found for rRTB (34), His-tag RTB eluted with 0.1 M triethylamine pH 11.0 (and was immediately neutralized with 1/10 volume of 1 M sodium phosphate pH 4.8). RTB protein concentration was determined by absorbance at 280 nm based on an absorbance of 1.44 for a 1 mg/mL solution of plant RTB and a 1 cm pathlength.

**Characterization of His-tag RTB.** Except for nickel affinity testing, all characterization of His-tag RTB and reassociated His-tag RTB-RTA heterodimer was performed as described previously for rRTB (34). The molecular weight of His-tag RTB was determined by 15% reducing SDS-PAGE. The N-terminal sequence of His-tag RTB was determined by Edman degradation. Immunological characterization was performed by immunofluorescent microscopy (monoclonal anti-RTB antibodies P2 and P10) and immunoblots (polyclonal anti-RTB antibodies and monoclonal anti-RTB antibodies P2, P10, and TFTB1). Lectin activity was tested via the previously described asialofetuin ELISA (34) as well as passage over a lactosyl acrylamide matrix (elution performed with NTEA buffer (50 mM NaCl, 25 mM Tris pH 8, 1 mM EDTA, 0.01% sodium azide) plus 50 mM  $\alpha$ -lactose, also as previously described for rRTB (34)). Eluted fractions were assayed for optical density at 280 nm and binding to asialofetuin by the same ELISA assay as referenced above. To assess immunoreactivity under nondenaturing conditions, an ELISA was performed identically to the asialofetuin ELISA except the plate coat was done with monoclonal antibody (P2, P10, or TFTB1) at 10  $\mu$ g/mL. To characterize His-tag RTB-RTA heterodimer reassociation, 30  $\mu$ g of His-tag RTB, rRTB, or plant RTB (pRTB) was mixed with 90  $\mu$ g of plant RTA in NTEA plus 50 mM lactose and placed on an orbital shaker for 4 h at room temperature. The reaction mixture was then analyzed by a ricin ELISA as previously described (34). Heterodimer cytotoxicity to HPB-MLT human T leukemia cells was then assessed via a standard [<sup>3</sup>H]leucine incorporation-based assay as described previously (34), using dilutions of ricin, plant RTA (pRTA)-pRTB, rRTB-pRTA, His-tag RTB-pRTA, or pRTA or His-tag RTB alone. Wells receiving dilutions of media alone served as controls. All assays were performed in triplicate. In some experiments, duplicate samples were incubated in the presence of 50 mM  $\alpha$ -lactose. The ID<sub>50</sub> was the concentration of protein which inhibited protein synthesis by 50% compared to control.

**Nickel-Binding of rRTB, His-tag RTB, and Recombinant Heterodimers.** Media supernatants from Sf9 cells infected with RTB or His-tag RTB encoding

recombinant baculovirus were collected, adjusted to 0.01% sodium azide, concentrated by vacuum dialysis, dialyzed against 1 M NaCl, 25 mM Tris pH 8, 0.01% sodium azide, and 25 mM  $\alpha$ -lactose (HNTAL-"H" for high salt concentration). Samples were then ultracentrifuged at 100000g for 1 h and adjusted to 5 mM  $\beta$ -mercaptoethanol and 1% Tween-20.

rRTB-pRTA and His-tag RTB-pRTA reassociated heterodimers were diluted into 5 mL of HNTAL and adjusted to 1% Tween-20.

Four 1 mL Ni<sup>2+</sup>/nitrilotriacetic acid (NTA)/agarose matrices were prepared per supplier's instructions and equilibrated with 10 mL of HNTAL. Supernatants or recombinant reassociated heterodimers were passed over the columns four times, and then the columns were washed with 10 mL of HNTAL. Nickel-binding proteins were then eluted with HNTAL containing 10, 20, 30, 40, 50, 100, 200, 500, and 1000 mM imidazole. Eluates were assayed for RTB or heterodimer by the asialofetuin ELISA or ricin ELISA, respectively. Immunoblots of eluate fractions from rRTB and His-tag RTB supernatants were performed as described above.

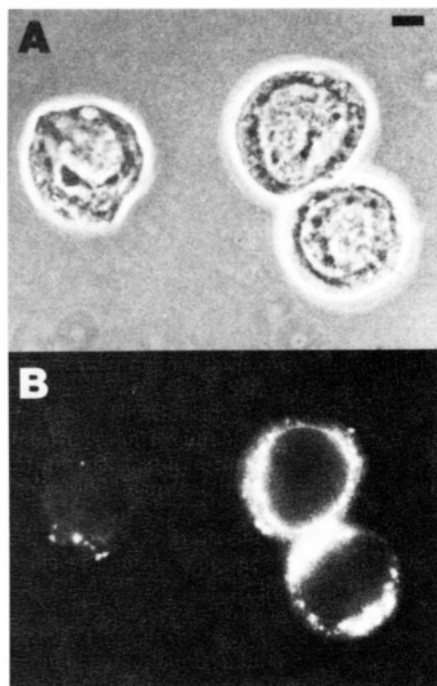
## RESULTS

**Production of Recombinant Baculovirus.** pAcGP67A-GH<sub>6</sub>G-RTB DNA was cotransfected with BaculoGold AcNPV DNA into Sf9 insect cells. Day 5 supernatants had a viral titer of  $10^5$ /mL by limiting dilution assay. Supernatant was selected from a positive well at  $10^{-5}$  dilution, and the limiting dilution assay was repeated to yield a titer of  $10^7$ /mL. Virus amplification was then performed on a positive well at  $10^{-7}$  dilution. Supernatants collected from all three stages of virus amplification (5, 50, and 150 mL) continued to show virus titers of  $10^7$ /mL.

**Expression of His-tag RTB.** Day 5 supernatants from Sf9 cells infected at an moi of 1.5–3 were assayed by the asialofetuin ELISA. His-tag RTB was present at 5.8  $\mu$ g/mL. Cell lysates yielded 1.4  $\mu$ g of His-tag RTB/mL cell culture. Immunofluorescent staining of 48 h postinfection Sf9 cells revealed intracellular accumulation of His-tag RTB (Figure 1).

**Purification and Characterization of His-tag RTB.** The total concentration of protein in the Ex-Cell 400 Sf9 postinfection supernatants was 6 mg/mL, and His-tag RTB represented 0.1% of the total protein. We initiated a purification scheme to enrich the recombinant product nearly 1000-fold. First, the supernatants were concentrated 10-fold by vacuum dialysis with 10 000 M<sub>r</sub>-cutoff membranes. Yields of His-tag RTB after vacuum dialysis were close to 100%. After dialysis into NTEA plus 25 mM  $\alpha$ -lactose and ultracentrifugation, 80% of the recombinant protein remained soluble and biologically active. Binding of His-tag RTB to the P2 monoclonal antibody affinity matrix was then tested. Less than 5% of the recombinant protein loaded remained in the column flow-through. His-tag RTB eluted with pH 11 triethylamine and was neutralized with sodium phosphate buffer. Approximately 200–400  $\mu$ g of His-tag RTB from 100 mL of supernatants was recovered after immunoaffinity chromatography. Thus, the yield of His-tag RTB from starting supernatants was 60–80%. The protein remained biologically active stored at -20 °C in the triethylamine-sodium phosphate buffer. SDS-PAGE showed His-tag RTB as the major band with minor bands corresponding to the P2 monoclonal antibody heavy and light chains which eluted to a minor degree from the matrix (Figure 2). Purity was in excess of 75% for each preparation based on densitometry performed on Coomassie-stained SDS-PAGE gels.





**Figure 1.** Immunofluorescence of Sf9 insect cells infected with AcNPV baculovirus or recombinant baculovirus. Cells were attached to poly-lysine coated tissue culture dishes and fixed with 3.7% formaldehyde in PBS followed by 0.1% Triton X-100 in PBS, washed with 2 mg/mL of BSA in PBS and then PBS plus BSA plus monoclonal antibody P10 at 10  $\mu$ g/mL. The cells were then washed with PBS and incubated with affinity purified goat anti-mouse Ig coupled to rhodamine (Jackson ImmunoResearch) at 25  $\mu$ g/mL, rewashed, and postfixed in 3.7% formaldehyde in PBS. Sf9 cells infected with AcNPV baculovirus showed no fluorescence (data not shown). (A) Sf9 cells infected with recombinant baculovirus examined at 200 $\times$  under phase contrast. (B) Sf9 cells infected with recombinant baculovirus examined for fluorescence.

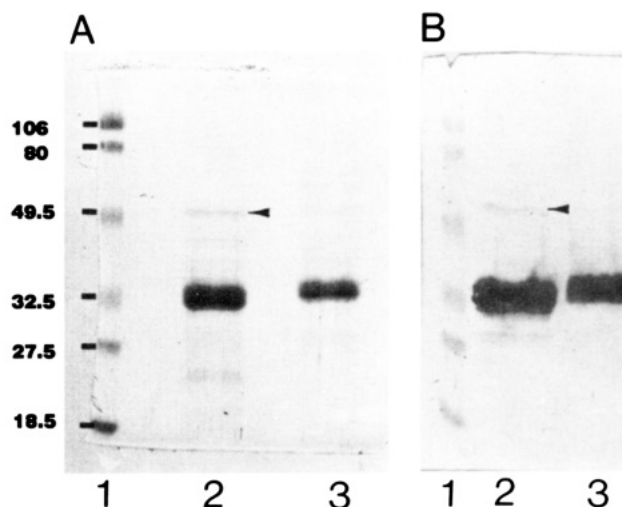
The molecular weight of insect His-tag RTB was 34 500 Da based on reducing Coomassie-stained SDS-PAGE gels and the prestained low molecular weight protein standards from BioRad. This compares with a molecular weight of 33 500 Da for insect rRTB. The N-terminal sequence of the His-tag RTB was shown to be ADPGH<sub>6</sub>-GA. Immunoblots of His-tag RTB, rRTB, and pRTB with polyclonal rabbit antiricin antibody (Figure 2B) and murine monoclonal antibodies P2, P10, and TFTB1 all yielded a single strong band at molecular weight of 34 500 Da (data not shown). An ELISA testing the immunoreactivity of each of pRTB, rRTB, and His-tag RTB with each of P2, P10, and TFTB1 showed that P2 bound His-tag RTB 46% and 71% as well as pRTB or rRTB, respectively. The relative binding affinities for P10 were 41% and 100%, respectively, and for TFTB1, 10% and 22% (data not shown).

His-tag RTB bound asialofetuin and lactose on a molar basis 80–100% as well as pRTB. Asialofetuin binding was assessed by ELISA; lactose binding was measured by yields of His-tag RTB in fractions from the lactosyl acrylamide matrix. Fifty percent of pRTB or His-tag RTB bound to immobilized lactose and was eluted with 50 mM lactose.

#### Characterization of Recombinant Heterodimers.

Incubation of His-tag RTB at 10<sup>-6</sup> M with pRTA at 3  $\times$  10<sup>-6</sup> M for 4 h at room temperature yielded 50% re-associated heterodimer. Similar levels of reassociation were seen using pRTB or rRTB with pRTA at the same concentrations. The heterodimer concentrations were quantitated by ricin ELISA.

The ID<sub>50</sub>'s of ricin, reassociated pRTB-RTA, reassoci-



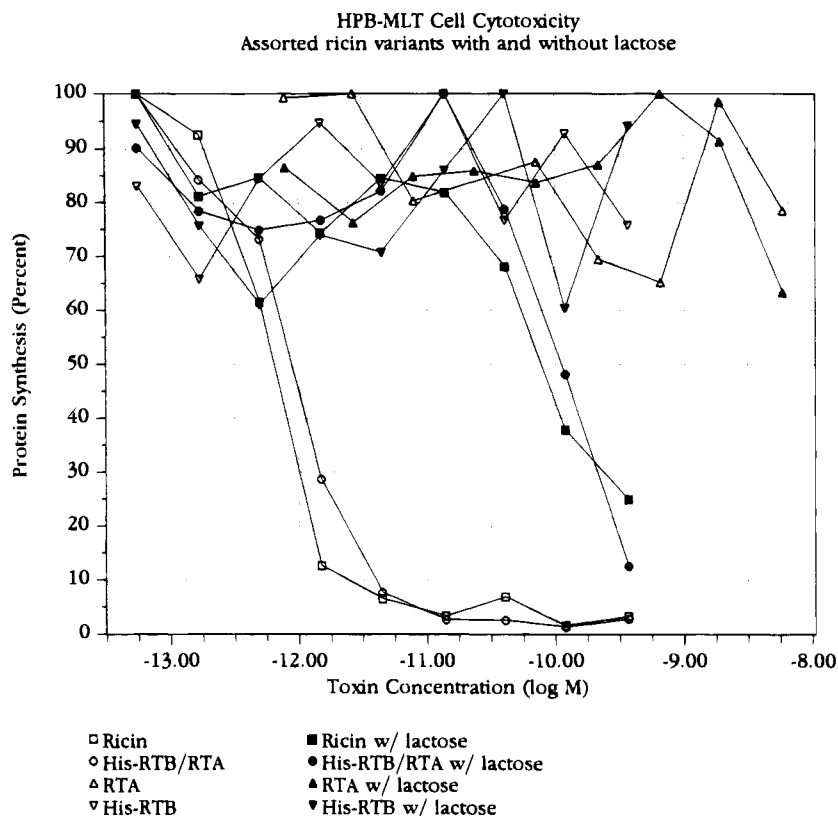
**Figure 2.** 15% reducing SDS-PAGE of immunoaffinity purified His-tag RTB and rRTB. Recombinant protein for His-tag RTB was prepared as described in the text. rRTB protein was isolated as previously described (33). (A) Coomassie stained gel. Lane 1: BioRad prestained low molecular weight protein standards (106, 80, 49.5, 32.5, 27.5, and 18.5 kDa). Lane 2: rRTB. Lane 3: His-tag RTB. (B) Immunoblot using rabbit polyclonal antiricin antibody. Lane 1: BioRad prestained low molecular weight protein standards. Lane 2: rRTB. Lane 3: His-tag RTB. The double-band appearance of rRTB and His-tag RTB on Coomassie stained gels reflect two major glycosylation patterns of RTB produced in Sf9 cells (33). The Coomassie stained gel shows the approximately 1000 Da increase in mass of His-tag RTB relative to rRTB. The faint band in both Coomassie stained gels and immunoblots at approximately 60 000 Da represents homodimers resulting from incomplete reduction during incubation with  $\beta$ -mercaptoethanol-containing sample buffer prior to SDS-PAGE. The monoclonal antibody immunoblots gave similar patterns as the polyclonal antibody immunoblot (data not shown).

ated rRTB-RTA, and reassociated His-tag RTB-RTA were all approximately 7  $\times$  10<sup>-13</sup> M, with a two-log increase in ID<sub>50</sub> seen in each case in the presence of 50 mM  $\alpha$ -lactose (Figure 3). His-tag RTB alone was completely nontoxic at the concentrations tested.

#### Nickel-Binding of His-tag RTB and Recombinant Heterodimers.

Day 5 supernatants of Sf9 cells infected with recombinant baculovirus encoding rRTB or His-tag RTB were harvested, vacuum concentrated, dialyzed into HNTAL, and ultracentrifuged. Supernatants were then adjusted to 1% Tween-20 and 5 mM  $\beta$ -mercaptoethanol, passed four times through Ni<sup>2+</sup>-NTA agarose, washed, and eluted with increasing concentrations of imidazole. Asialofetuin ELISA (Figure 4), Coomassie-stained gels, and immunoblots demonstrated complete binding of His-tag RTB to the Ni<sup>2+</sup>-NTA matrix and elution with 20 mM imidazole or greater. The greatest yield was at 30 mM imidazole, and the highest purity (95%) was at 40–100 mM imidazole. In contrast, rRTB from supernatants failed to bind to Ni<sup>2+</sup>-NTA and was not observed in fractions eluted with 20 mM or greater imidazole.

In recombinant heterodimer testing, 200  $\mu$ g of His-tag RTB-RTA or rRTB-RTA was diluted into separate 5 mL quantities of HNTAL with 1% Tween-20 (but without  $\beta$ -mercaptoethanol) and passed four times over freshly prepared nickel affinity matrices. After each matrix was washed with HNTAL, elutions were again performed with increasing concentrations of imidazole. His-tag RTB-RTA bound identically to His-tag RTB, while rRTB-RTA behaved similarly to rRTB and failed to bind to the nickel matrix (Figure 5).



**Figure 3.** HPB-MLT cell cytotoxicity.  $2 \times 10^5$  cells were incubated with varying concentrations of heterodimers, RTA, or His-tag RTB in the presence or absence of 50 mM  $\alpha$ -lactose for 20 h at 37 °C, 5% CO<sub>2</sub>, and then 1  $\mu$ Ci/well of [<sup>3</sup>H]leucine was added for 4 h. Cells were harvested on glass fiber filters and washed. Filters were dried and counted in a liquid scintillation counter: □, ricin; ○, His-tag RTB-RTA; △, RTA; ▽, His-tag RTB; ■, ricin plus 50 mM  $\alpha$ -lactose; ●, His-tag RTB-RTA plus 50 mM  $\alpha$ -lactose; ▲, RTA plus 50 mM  $\alpha$ -lactose; ▼, His-tag RTB plus 50 mM  $\alpha$ -lactose.

## DISCUSSION

Recombinant baculovirus encoding His-tag RTB was isolated after only two rounds of selection. The rapid generation and selection of recombinant baculovirus was facilitated by using an AcNPV derivative with a deletion in ORF1629 (39). The transfer vector contains sequences which complement the essential downstream gene, and thus only recombinant baculoviruses are viable. We observed similar efficient selection for recombinant baculovirus encoding RTB (34).

Levels of expression and secretion of His-tag RTB into infected insect cell supernatants were comparable to that previously observed with rRTB and far higher than previously reported levels of recombinant RTB from eukaryotic expression systems including yeast, monkey kidney, and *Xenopus* (31–33). The 4-fold higher level of His-tag RTB in media versus intracellular levels suggests efficient secretion and processing of the recombinant protein with the gp67 leader peptide and minimal proteolytic degradation in the medium after release. Also, the N-terminal sequence of His-tag RTB was ADPGH<sub>6</sub>-GA. These results further support efficient and proper processing of the gp67 leader peptide, as the predicted cleavage site at the C-terminal end of this leader is between the adjacent alanines in HSFAADP. These results agree with those observed for rRTB (34). The oligohistidine tag did not alter the stability or proteolytic sensitivity of the recombinant product.

Immunoaffinity chromatography was used as a single step purification method for His-tag RTB. The high overall yields and homogeneity of the product suggest that monoclonal antibody affinity matrices are well suited for isolation of recombinant proteins from baculovirus-infected insect cell supernatants. Alkaline conditions for

elution were also found optimal for purification of rRTB (34) and may be generally useful for proteins with low pI's.

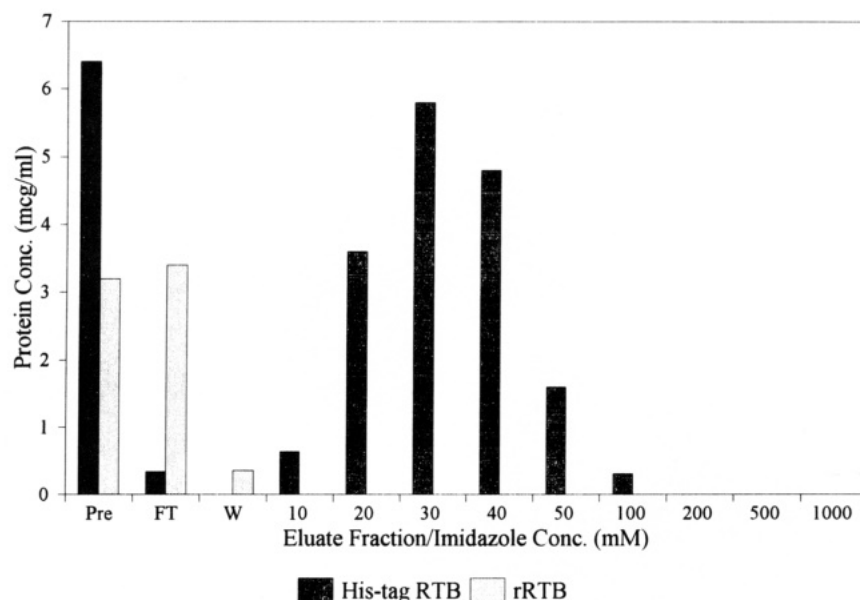
The observed molecular weight of 34 500 Da corresponds to the predicted molecular weight of 34 478 Da, consisting of ADP-RTB, two Man<sub>9</sub>GlcNac<sub>2</sub> oligosaccharides, and the GH<sub>6</sub>G N-terminal peptide sequence.

Reducing SDS-PAGE was performed using equivalent amounts of His-tag RTB, rRTB, and pRTB. The proteins were transferred to nitrocellulose and probed with polyclonal antibody to ricin and three different monoclonal antibodies to RTB. Immunoreactivity of His-tag RTB was minimally different from pRTB or rRTB. Further, ricin ELISA yielded similar reading on equivalent amounts of pRTB-RTA, rRTB-RTA, and His-tag RTB-RTA. These results suggest His-tag RTB is folded similarly to rRTB and pRTB. The only secondary structural elements in RTB are  $\Omega$ -loops and are formed within each subdomain of RTB. They consist of compact, contiguous peptide segments with a "loop-shaped" path in three-dimensional space. The  $\Omega$ -loops are stabilized by sets of hydrogen bonds between the backbone nitrogen and carbonyl oxygen atoms.  $\Omega$ -loops in the  $\alpha$  and  $\beta$  subdomains have disulfide bonds securing the neck of the loops. RTB also has a core with residues contributed by hydrophobic residues from each subdomain. All of the amino acid residues critical both to core formation and  $\Omega$ -loop stabilization are distant from the N-terminus. The oligohistidine tag comprising the N-terminus was not expected to interrupt RTB folding and the evidence supports this prediction.

The lectin activity of His-tag RTB was similar to rRTB and pRTB. Again, the sugar binding sites in subdomains 1 $\alpha$  and 2 $\gamma$  of RTB are structurally distant from the

### Nickel Affinity: His-tag RTB vs. rRTB

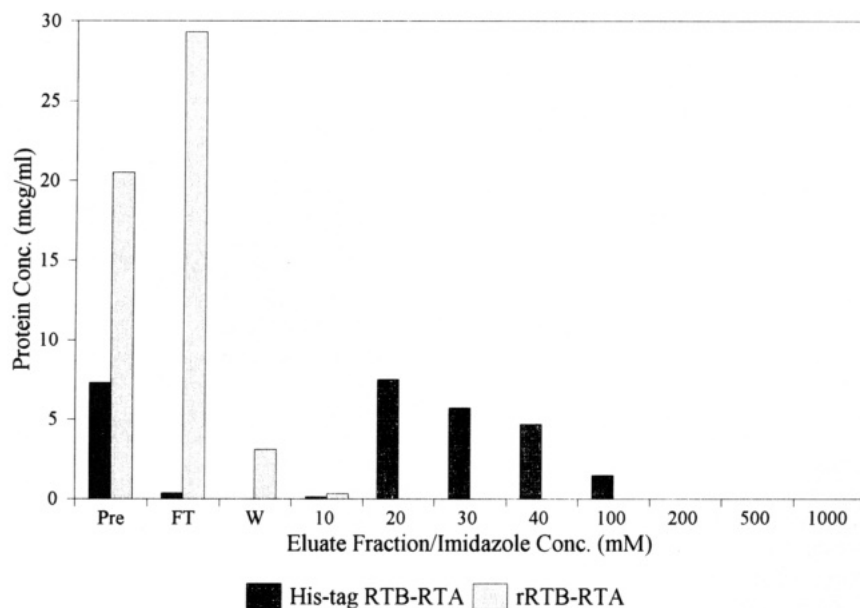
Asialofetuin ELISA



**Figure 4.** Binding of recombinant lectins to  $\text{Ni}^{2+}$ -NTA-agarose. Supernatants from Sf9 cells infected with recombinant baculovirus encoding His-tag RTB or rRTB were concentrated, dialyzed into HNTAL, ultracentrifuged, adjusted to 1% Tween-20 and 5 mM  $\beta$ -mercaptoethanol, and passed four times over a 1 mL  $\text{Ni}^{2+}$ -NTA-agarose column. The column was washed with HNTAL and then eluted with increasing concentrations of imidazole in HNTAL. Total RTB in the different fractions was measured by the asialofetuin ELISA described in the text. Lightly shaded bars are rRTB fractions. Darkly shaded bars are His-tag RTB fractions: Pre, material prior to passage on the matrix; FT, flowthrough or material which did not bind the nickel matrix; W, HNTAL wash following passage of recombinant protein; 10–1000, 5 mL eluates from the nickel matrix with the specified imidazole concentration (mM).

### Nickel Affinity of Heterodimers

Asialofetuin ELISA



**Figure 5.** Binding of recombinant heterodimers to  $\text{Ni}^{2+}$ -NTA-agarose. Two hundred  $\mu\text{g}$  each of His-tag RTB-RTA and rRTB-RTA were separately diluted into 5 mL of HNTAL, adjusted to 1% Tween-20, passed through 1 mL of  $\text{Ni}^{2+}$ -NTA-agarose columns, washed with HNTAL, and eluted with increasing concentrations of imidazole in HNTAL. Total heterodimer concentration in the different fractions was measured by the ricin ELISA described in the text. Lightly shaded bars are rRTB-RTA fractions. Darkly shaded bars are His-tag RTB-RTA fractions: Pre, material prior to passage on the matrix; FT, flowthrough or material which did not bind the nickel matrix; W, HNTAL wash following passage of recombinant protein; 10–1000 5 mL eluates from the nickel matrix with the specified imidazole concentration (mM).

N-terminus. Thus, the addition of 11 amino acid residues to the N-terminus should not modify lectin activity, and our results support this hypothesis. Accurate measurements of sugar binding affinity require 10–1000  $\mu\text{g}$  of

protein for equilibrium dialysis measurements or the BIAcore surface plasmon resonance system (40). With scaleup of the recombinant baculovirus-Sf9 expression system, adequate quantities of recombinant RTB proteins

are now available for comparative studies in different laboratories and potentially for efforts to crystallize the proteins and determine structure–function relationships.

Plant RTA reassociated equally well with His-tag RTB, rRTB, and pRTB. Amino acid residues critical for interaction of RTB with RTA include C4, which forms a disulfide bridge with C259 of RTA. The disulfide bond functions to maintain chain association at very low toxin concentrations. The ability of the ricin ELISA to measure intact His-tag RTB–RTA at ng/mL concentration and the cytotoxicity of His-tag RTB–RTA to HPB–MLT cells at  $<10^{-12}$  M suggests the disulfide bond is intact in the recombinant heterodimer. Most of the interactions of RTB and RTA are due to hydrophobic interactions between aliphatic sidechains and aromatic rings, although some polar contacts are made. Interface RTB residues include A1, D2, D94, V141, F140, K219, F218, N220, P260, and F262, all of which are preserved in His-tag RTB. The first three amino acid residues of RTB in ricin crystals have less ordered structure and spend a significant fraction of time floating in the solvent. The 11 amino acid oligohistidine tag was expected to remain free in the solvent and not bond with amino acid residues in the area of contact with RTA. The similar free energy for the association of His-tag RTB with RTA and pRTB with RTA corroborates these hypotheses.

The potent cytotoxicity of His-tag RTB–RTA suggests that the fusion of the oligohistidine peptide to the N-terminus of RTB did not affect cell intoxication. Since the translocating and enzymatic domains of ricin appear to reside on RTA (23, 41), we anticipated full cytotoxicity for the His-tag RTB–RTA heterodimer. The lower potencies for *Xenopus* proricin with a factor X cleavage site, *E. coli* RTA with a diphtheria toxin disulfide loop fused to protein A, and *E. coli* RTA fused directly to protein A was likely due to poor cleavage and release of RTA intracellularly (35–37). In contrast, the linkage of RTA to His-tag RTB uses the native disulfide bond and RTA–RTB interface and displays cytotoxicity similar to native ricin. Further, the recombinant protein expressed within insect cells is recovered at much higher yields than *Xenopus* proricin.

Potentially useful fusion ricin toxins must demonstrate the new ligand specificity on the heterodimer. We tested His-tag RTB alone, rRTB alone, His-tag RTB–RTA, and rRTB–RTA for binding to a nickel affinity matrix. Both free His-tag RTB and His-tag RTB–RTA bound nickel and were eluted with 20–100 mM imidazole buffers. In contrast, rRTB and rRTB–RTA, which lack oligohistidine sequences, failed to bind nickel. These observations are similar to other insect–derived recombinant proteins with introduced oligohistidine tags (42, 43). Taken together, these results suggest that, as with the oligohistidine tag reported here, a new N-terminal ligand is likely to be free in the solvent and accessible for novel binding specificities. These results also suggest that oligohistidine-tagging of an N-terminal RTB fusion peptide might provide a purification method (nickel affinity) which may be particularly useful if RTB mutants are engineered which fail to bind both sugar and the common anti-RTB antibodies. The preparation of milligram quantities of fully active ricin fusion protein with intact novel specificity makes possible genetic engineering of ricin similar to that reported previously for DT (12) and PE (13). Other peptide ligands can be substituted for the oligohistidine tag (or interposed between the oligohistidine tag and RTB) and the fusion protein reassociated with pRTA or rRTA to provide a smaller and more homogeneous product for therapeutic studies.

## ACKNOWLEDGMENT

This work was supported by NIH grant R01CA54116 and an American Cancer Society Clinical Oncology Fellowship Award. I wish to acknowledge the assistance of the Protein Chemistry Facility and Oligonucleotide Synthesis Facility at MUSC. We also thank Dr. Walter Blattler for the P2, P10, and  $\alpha$ BR12 monoclonal antibodies.

## LITERATURE CITED

- (1) Pastan, I., and FitzGerald, D. (1991) Recombinant toxins for cancer therapy. *Science* 254, 1173–1177.
- (2) Shen, G., Li, J., Ghetie, M., Ghetie, V., May, R., Till, M., Brown, A., Relf, M., Knowles, P., Uhr, J., Janossy, G., Amlot, P., Vitetta, E., and Thorpe, P. (1988) Evaluation of four CD22 antibodies as ricin A chain-containing immunotoxins for the in vivo therapy of human B-cell leukemias and lymphomas. *Int. J. Cancer* 42, 792–797.
- (3) FitzGerald, D., Idziorek, T., Batra, J., Willingham, M., and Pastan, I. (1990) Antitumor activity of a thioether-linked immunotoxin: OVB3-PE. *Bioconjugate Chem.* 1, 264–268.
- (4) Ghetie, M., Richardson, J., Tucker, T., Jones, D., Uhr, J., and Vitetta, E. 1991. Antitumor activity of Fab' and IgG-anti-CD22 immunotoxins in disseminated human B lymphoma grown in mice with severe combined immunodeficiency disease: effect on tumor cells in extranodal sites. *Cancer Res.* 51, 5876–5880.
- (5) Amlot, P., Stone, M., Cunningham, D., Fay, J., Newman, J., Collins, R., May, R., McCarthy, M., Richardson, J., Ghetie, V., Ramilo, O., Thorpe, P., Uhr, J., and Vitetta, E. (1993) A phase I study of an anti-CD22-deglycosylated ricin A chain immunotoxin in the treatment of B-cell lymphomas resistant to conventional therapy. *Blood* 82, 2624–2633.
- (6) Pai, L., Bookman, M., Ozols, R., Young, R., Smith, J., Longo, D., Gould, B., Frankel, A., McClay, E., Howell, S., Reed, E., Willingham, M., FitzGerald, D., and Pastan, I. (1991) Clinical evaluation of intraperitoneal *Pseudomonas* exotoxin immunconjugate OVB3-PE in patients with ovarian cancer. *J. Clin. Oncol.* 9, 2095–2103.
- (7) Hertler, A., Schlossman, D., Borowitz, M., Laurent, G., Jansen, F., Schmidt, C., and Frankel, A. (1988) A phase I study of T101-ricin A chain immunotoxin in refractory chronic lymphocytic leukemia. *J. Biol. Response Modif.* 7, 97–113.
- (8) Gould, B., Borowitz, M., Groves, E., Carter, P., Anthony, D., Weiner, J., and Frankel, A. (1989) A phase I study of a continuous infusion anti-breast cancer immunotoxin: report of a targeted toxicity not predicted by animal studies. *JNCI* 81, 775–781.
- (9) Grossbard, M., Lambert, J., Goldmacher, V., Blattler, W., and Nadler, L. (1992) Correlation between in vivo toxicity and preclinical in vitro parameters for the immunotoxin anti-B4-blocked ricin. *Cancer Res.* 52, 4200–4207.
- (10) Manske, J., Buchsbaum, D., and Valleria, D. (1989) The role of ricin B chain in the intracellular trafficking of anti-CD5 immunotoxins. *J. Immunol.* 142, 1755–1766.
- (11) Williams, D., Parker, K., Bacha, P., Bishai, W., Borowski, M., Genbauffe, F., Strom, T., and Murphy, J. (1987) Diphtheria toxin receptor binding domain substitution with interleukin-2: genetic construction and properties of a diphtheria toxin-related interleukin-2 fusion protein. *Protein Eng.* 1, 493–498.
- (12) Williams, D., Snider, C., Strom, T., and Murphy, J. (1990) Structure/function analysis of interleukin-2 toxin (DAB486-IL-2). *J. Biol. Chem.* 265, 11885–11889.
- (13) Chaudhary, V., Queen, C., Junghans, R., Waldmann, T., FitzGerald, D., and Pastan, I. (1990) A recombinant immunotoxin consisting of two antibody variable domains fused to *Pseudomonas* exotoxin. *Nature* 339, 394–397.
- (14) Kronke, M., Depper, J., Leonard, W., Vitetta, E., Waldmann, T., and Greene, W. (1985) Adult T cell leukemia: a potential target for ricin A chain immunotoxins. *Blood* 65, 1416–1421.
- (15) Friedman, P., McAndrew, S., Gawlak, S., Chace, D., Trail, P., Brown, J., and Siegal, C. (1993) BR96 sFv-PE40, a potent

- single-chain immunotoxin that selectively kills carcinoma cells. *Cancer Res.* 53, 334–339.
- (16) Kreitman, R., Bailon, P., Chaudhary, V., FitzGerald, D., and Pastan, I. (1994) Recombinant immunotoxins containing anti-Tac(Fv) and derivatives of *Pseudomonas* exotoxin produce complete regression in mice of an interleukin-2 receptor-expressing human carcinoma. *Blood* 83, 426–434.
- (17) Bacha, P., Forte, S., McCarthy, D., Estis, L., Yamada, G., and Nichols, J. (1991) Impact of interleukin-2-receptor-targeted cytotoxins on a unique model of murine interleukin-2-receptor-expressing malignancy. *Int. J. Cancer* 49, 96–101.
- (18) Winkler, U., Gottstein, C., Schon, G., Kapp, U., Wolf, J., Hansmann, M., Bohlen, H., Thorpe, P., Diehl, V., and Engert, A. (1994) Successful treatment of disseminated human Hodgkin's disease in SCID mice with deglycosylated ricin A-chain immunotoxins. *Blood* 83, 466–475.
- (19) Hesketh, P., Caguioa, P., Koh, H., Dewey, H., Facada, A., McCaffrey, R., Parker, K., Nysten, P., and Woodworth, T. (1993) Clinical activity of a cytotoxic fusion protein in the treatment of cutaneous T-cell lymphoma. *J. Clin. Oncol.* 11, 1682–1690.
- (20) LeMaistre, C., Kuzel, T., Foss, F., Hesketh, P., Saleh, M., Platanias, L., Schwartz, G., Craig, F., Tolson, K., and Woodworth, T. (1994) DAB389IL-2 is well tolerated at doses inducing responses in IL-2 receptor expressing lymphomas. *Blood* 82, Suppl. 1, 137a.
- (21) LeMaistre, C., Rosen, S., Frankel, A., Kornfeld, S., Saria, E., Meneghetti, C., Drajesk, J., Fishwild, D., Scannon, P., and Byers, V. (1991) Phase I trial of H65-RTA immunconjugate in patients with cutaneous T-cell lymphoma. *Blood* 78, 1173–1182.
- (22) Waldman, T., Pastan, I., Gansow, O., and Junghans, R. (1992) The multichain interleukin-2 receptor: a target for immunotherapy. *Ann. Intern. Med.* 116, 148–160.
- (23) Olsnes, S., and Pihl, A. (1973) Different biological properties of the two constituent peptide chains of ricin, a toxic protein inhibiting protein synthesis. *Biochemistry* 12, 3121–3126.
- (24) Endo, Y., and Tsurugi, K. (1987) RNA N-glycosidase activity of ricin A-chain. *J. Biol. Chem.* 262, 8128–8130.
- (25) Middlebrook, J., and Dorland, R. (1984) Bacterial toxins: cellular mechanisms of action. *Microbiol. Rev.* 48, 199–221.
- (26) Halling, K., Halling, A., Murray, E., Ladin, B., Houston, L., and Weaver, R. (1985) Genomic cloning and characterization of a ricin gene from *Ricinus communis*. *Nucleic Acids Res.* 13, 8019–8032.
- (27) Lamb, F., Roberts, L., and Lord, J. (1985) Nucleotide sequence of cloned cDNA for preprorin. *Eur. J. Biochem.* 148, 265–270.
- (28) Piatak, M., Lane, J., Laird, W., Bjorn, M., Wang, A., and Williams, M. (1988) Expression of soluble and fully functional ricin A chain in *Escherichia coli* is temperature-sensitive. *J. Biol. Chem.* 263, 4837–4843.
- (29) Frankel, A., Schlossman, D., Welsh, P., Hertler, A., Withers, D., and Johnston, S. (1989) Selection and characterization of ricin toxin A-chain mutations in *Saccharomyces cerevisiae*. *Mol. Cellular Biol.* 9, 415–420.
- (30) Hussain, K., Bowler, C., Roberts, L., and Lord, J. (1989) Expression of ricin B chain in *Escherichia coli*. *FEBS Lett.* 244, 383–387.
- (31) Richardson, P., Roberts, L., Gould, J., Smith, A., and Lord, M. (1987) The expression of ricin B-chain in *Saccharomyces cerevisiae*. *Biochem. Soc. Trans.* 15, 903–904.
- (32) Richardson, P., Gilmartin, P., Colman, A., Roberts, L., and Lord, J. (1988) Expression of functional ricin B chain in *Xenopus* oocytes. *BioTechnology* 6, 565–570.
- (33) Chang, M., Russell, D., Uhr, J., and Vitetta, E. (1987) Cloning and expression of recombinant, functional ricin B chain. *Proc. Natl. Acad. Sci. U.S.A.* 84, 5640–5644.
- (34) Frankel, A., Gulick, H., Afrin, L., Vesely, J., and Willingham, M. (1994) Expression of ricin B chain in *Spodoptera frugiperda*. *Biochem. J.* (in press).
- (35) Kim, J., and Weaver, R. Construction of a recombinant expression plasmid encoding a staphylococcal protein A-ricin A fusion protein. *Gene* 68, 315–321.
- (36) O'Hare, M., Brown, A., Hussain, K., Gebhardt, A., Watson, G., Roberts, L., Vitetta, E., Thorpe, P., and Lord, J. (1990) Cytotoxicity of a recombinant ricin A-chain fusion protein containing a proteolytically-cleavable spacer sequence. *FEBS Lett.* 273, 200–204.
- (37) Westby, M., Argent, R., Pitcher, C., Lord, J., and Roberts, L. (1992) Preparation and characterization of recombinant proricin containing an alternative protease-sensitive linker sequence. *Bioconjugate Chem.* 3, 375–381.
- (38) Rutenber, E., and Robertus, J. (1991) Structure of ricin B-chain at 2.5 Angstrom resolution. *Proteins* 10, 260–269.
- (39) Kitts, P., and Possee, R. (1993) A method for producing recombinant baculovirus expression vectors at high frequency. *BioTechniques* 14, 810–816.
- (40) Mayo, C., and Hallock, R. (1989) Immunoassay based on surface plasmon oscillations. *J. Immunol. Methods* 120, 105–114.
- (41) Herschman, H. (1984) The role of binding ligand in toxic hybrid proteins: a comparison of EGF-ricin, EGF-ricin A-chain and ricin. *Biochem. Biophys. Res. Commun.* 124, 551–557.
- (42) Taussig, R., Quarumby, L., and Gilman, A. (1993) Regulation of purified type I and type II adenylylases by G protein  $\beta\gamma$  subunits. *J. Biol. Chem.* 268, 9–12.
- (43) Gearing, K., Gottlicher, M., Teboul, M., Widmark, E., and Gustafsson, J. (1993) Interaction of the peroxisome-proliferator-activated receptor and retinoid X receptor. *Proc. Natl. Acad. Sci. U.S.A.* 90, 1440–1444.

# Arabinogalactan for Hepatic Drug Delivery

Ernest V. Groman, Philip M. Enriquez, Chu Jung, and Lee Josephson\*

Advanced Magnetix, Inc., 61 Mooney Street, Cambridge, Massachusetts 02138. Received February 21, 1994\*

Arabinogalactan, a polysaccharide from the tree *Larix occidentalis*, has been purified and its biological and physical properties described. Intravenous injection of radiolabeled arabinogalactan (4 mg/kg) in rats resulted in 52.5% of the dose being present in the liver, while prior injection of asialofetuin (100 mg/kg) reduced hepatic radioactivity to 3.54%. Gel chromatography indicates arabinogalactan is a single species of 19 kDa, while light scattering gave a molecular weight of 40 kDa. Glycosyl linkage analysis of arabinogalactan is consistent with a highly branched structure comprising a backbone of 1,3-linked galactopyranose connected by 1,3-glycosidic linkages, comprised of 3,4,6-, 3,6-, and 3,4- as well as 3-linked residues. In the carbon-13 NMR spectra, the major resonances of arabinogalactan are assigned to  $\beta$ -galactopyranose,  $\beta$ -arabinofuranose, and  $\beta$ -arabinopyranose. Arabinogalactan produced no adverse reactions in single intravenous dose (mouse, 5000 mg/kg) and repeat dose toxicity studies (rats, 500 mg/kg/day, 90 days). When tritiated arabinogalactan was injected, radioactivity cleared from the liver with a half-life of 3.42 days. Arabinogalactan has properties that make it suitable as a carrier for delivering diagnostic or therapeutic agents to hepatocytes via the asialoglycoprotein receptor.

## INTRODUCTION

Delivery of diagnostic or therapeutic agents to hepatocytes has often been achieved by attachment of the agent to carrier molecules that bind the asialoglycoprotein receptor (1). Carriers have included asialoglycoproteins of natural origin, synthesized neoglycoproteins, and synthetic polymers modified to contain galactose residues (2-6). Another approach in the design of carriers binding the asialoglycoprotein receptor involves the synthesis of low molecular weight compounds containing multiple galactose residues (7, 8). Recently, it was reported that a superparamagnetic iron oxide covered with arabinogalactan, a polysaccharide from the plant *Larix occidentalis*, was removed from blood by the asialoglycoprotein receptor of hepatocytes (9). This observation suggested that arabinogalactan might serve as a carrier for targeting diagnostic or therapeutic agents to the liver.

While preclinical research on targeted drug delivery can be conducted with a variety of carriers, many carriers are not fully satisfactory for clinical applications. For example, a conjugate of adenine arabinoside monophosphate with lactosylated albumin, designed to be taken up by the asialoglycoprotein receptor, has been tested for the treatment of hepatitis B in humans (3). However, conjugates utilizing protein-based carriers have deficiencies. Chemical modification of plasma proteins like albumin can make them susceptible to uptake by scavenger receptors on cells other than the hepatocyte (10). Immunogenicity and the formation of hepatic vacuoles have also been reported with lactosylated albumin (11, 12). Problems of protein carriers for drug delivery have been recently reviewed (13).

In this paper we demonstrate that a naturally occurring polysaccharide, purified arabinogalactan, can serve as a carrier for the delivery of a model compound, a cobalt chelate of diethylenetriamine pentaacetic acid, to the liver via the asialoglycoprotein receptor. Our results with purified arabinogalactan and the asialoglycoprotein re-

ceptor suggest that naturally occurring polysaccharides can be used for the receptor-mediated delivery of diagnostic and therapeutic agents.

The eventual use of purified arabinogalactan as a carrier for the delivery of diagnostic or therapeutic agents in humans requires a clear understanding of its physical and chemical properties. Unfortunately, as described below, the properties of materials referred to as "arabinogalactan" in the literature vary significantly. Therefore, we undertook the characterization of the purified arabinogalactan used in these studies.

## EXPERIMENTAL PROCEDURES

All materials were obtained from common commercial sources unless stated otherwise.

**1. Demonstration of Receptor Interaction: Biodistribution and Receptor Binding Studies with Purified Arabinogalactan.** *Purification of Arabinogalactan.* Arabinogalactan was purchased from Champion Corp. (Tacoma, WA) as Stractan 2. In a typical purification, crude arabinogalactan (100 g) was dissolved in 2 L of water and purified by ultrafiltration with 100 000 and 10 000 Da membranes. The concentrated solution was filtered through a 0.22  $\mu$ m filter and lyophilized. Eighty-five g of purified arabinogalactan, denoted pAG, was obtained.

*Synthesis of Arabinogalactan-DTPA.* pAG (20.0 g, 0.50 mmol based on a molecular weight of 40 kDa, see below) and the dianhydride of diethylenetriaminepentaacetic acid (2.15 g, 6.02 mmol) were dissolved in dimethyl sulfoxide (200 mL) at 60 °C. After 0.5 h, the clear solution was added to 500 mL of H<sub>2</sub>O. The solution was filtered on a YM3 ultrafiltration membrane (Amicon, Beverly, MA) and washed with water (2  $\times$  400 mL). The retentate, about 70 mL, was lyophilized to yield a white powder (18.8 g). Titration of an aqueous solution of this conjugate with 0.01 N NaOH indicated the presence of 0.117 mmol of DTPA per gram of product, corresponding to the presence of 4.68 DTPA's per mole of pAG.

*Synthesis of <sup>57</sup>Co-DTPA.* A solution of Na<sub>5</sub>DTPA (4.75 mM, 0.20 mL, pH 9.8) was added to a sterile, graduated centrifuge tube. <sup>57</sup>CoCl<sub>2</sub> solution in 0.1 N HCl (0.11 mL, 128  $\mu$ Ci/g, 100  $\mu$ g/mL) was added. <sup>57</sup>CoCl<sub>2</sub> was obtained

\* Corresponding author. Phone: 617-497-2070. Fax: 617-547-2445.

\* Abstract published in *Advance ACS Abstracts*, September 1, 1994.



from Amersham (Arlington Heights, IL). The solution was adjusted to pH 6.85 with NaOH and diluted to 2.0 mL with saline.

**Synthesis of Arabinogalactan- $^{57}\text{Co}$ -DTPA.** A solution of  $^{57}\text{CoCl}_2$  (see above, 0.31 mL, 40  $\mu\text{Ci}$ ) was added to arabinogalactan-DTPA (16.7 mg, 1.95  $\mu\text{mol}$  DTPA) in saline (1.0 mL). The solution was adjusted to pH 6.87 with NaOH and the volume raised to 4.0 mL with saline. The molar ratio of pAG,  $^{57}\text{Co}$ , and DTPA is 1.0:0.0012:4.68. The conjugate assumes a negative charge at physiological pH, due to the negative carboxyl groups of DTPA.

**Stability of Arabinogalactan- $^{57}\text{Co}$ -DTPA in Rat Serum.** The stability of the AG- $^{57}\text{Co}$ -DTPA conjugate was evaluated by incubation of the conjugate in rat serum at 37  $^{\circ}\text{C}$ , followed by analysis on Sephadex G-50 (9.5  $\times$  300 mm; 0.1%  $\text{NaN}_3$  at 0.33 mL/min flow rate).

**Biodistribution of Arabinogalactan- $^{57}\text{Co}$ -DTPA and  $^{57}\text{Co}$ -DTPA.** The rats used in all studies were male Crl: CD-BR from Charles River Laboratories, Wilmington, MA. Six rats weighing between 330 and 389 grams were anesthetized with Inactin (100 mg/kg body weight, Promonta, Hamburg, Germany). The femoral artery and vein were exposed and the animal received via femoral vein injection 4 mg/kg body weight of arabinogalactan- $^{57}\text{Co}$ -DTPA (9.5  $\mu\text{Ci}$   $^{57}\text{Co}$ ). Two additional groups of three rats each were anesthetized and prepared as above. The first group of animals was injected with 100 mg/kg body weight asialofetuin (type II, Sigma Chemical Co., St. Louis, MO), an asialoglycoprotein receptor ligand, 5 min prior to administration of 4 mg/kg of arabinogalactan- $^{57}\text{Co}$ -DTPA. The second group of rats was injected with  $^{57}\text{Co}$ -DTPA, 0.48  $\mu\text{mol}$  of  $\text{Na}_5\text{DTPA}$ /kg body weight (7  $\mu\text{Ci}$   $^{57}\text{Co}$ /kg), which is the amount of chelate injected with the 4 mg/kg body weight of arabinogalactan- $^{57}\text{Co}$ -DTPA. After 90 min, a blood sample was collected by syringe and 26 gauge needle, and the animals were exsanguinated *via* the cut femoral artery and vein. Aliquots of the liver, spleen, and the bladder content, also collected by syringe and 26 gauge needle, were placed into tared snap-cap polyethylene vials and weighed. All samples were counted in a GammaTrac 1193 counter (TM Analytical, Inc., Elk Grove, IL). A weighed aliquot of injectate was counted to serve as a standard for calculation of the percent of the injected dose present in the tissues.

**Receptor Assay.** Asialoglycoprotein receptor from rat liver was isolated following the method of Hudgin et al. (14) and stored frozen until used. The tracer, a tyramine derivative of arabinogalactan (hereafter tyramine-arabinogalactan), was prepared by activating arabinogalactan with cyanogen bromide (15), followed by reaction with tyramine. The tyramine-arabinogalactan was then radioiodinated with chloramine T to give a specific activity of about 20 mCi/mg (16). The iodinated material was purified on a Sephadex G-25 column (Pharmacia LKB Biotechnology, Piscataway, NJ).

To perform the assay, samples and standards were dissolved in 0.01 M phosphate buffer (pH 7.4) containing 0.1% bovine serum albumin and 0.1% sodium azide. Sample or standard (0.1 mL) was added to [ $^{125}\text{I}$ ]tyramine-arabinogalactan (0.4 mL containing 100 000 dpm per tube), followed by receptor sufficient to produce between 15 and 20% binding of total counts. The solutions were incubated for 25 min at 25  $^{\circ}\text{C}$  and transferred to an ice bath for 5 min. Next, 0.5 mL of 20% poly(ethylene glycol) (dissolved in 0.5 M phosphate buffer containing 0.15 M sodium chloride and 0.1% bovine gamma globulin) was added, and the tubes were chilled to 4  $^{\circ}\text{C}$ , vortexed, and incubated at 4  $^{\circ}\text{C}$  for 5 min. The samples were trans-

ferred onto 0.22  $\mu\text{m}$  filters presoaked with assay buffer, and liquid was removed by suction. The filters were washed three times with assay buffer, and the radioactivity retained on the filters was quantitated by  $\gamma$  counting.

**2. Chemical Characterization of pAG.** **Size Exclusion Chromatography and Light Scattering.** Solutions of pAG, dextran T-10, and dextran T-40 (Pharmacia, Piscataway, NJ) were prepared in a buffer of 20 mM potassium phosphate, 150 mM sodium chloride, and 0.1% sodium azide, pH 7.2 to give a final concentration of 15–30 mg/mL. Samples were filtered (0.45  $\mu\text{m}$ ) and injected into a CL-300 Cellufine column (0.5  $\times$  30 cm, Amicon Corp., Beverly, MA). For determination of molecular weight by size exclusion chromatography, a flow rate of 0.3 mL/min was used with detection by a differential refractometer. The molecular weight of pAG was estimated using dextran standards (Pharmacosmos, Viby Sj. Denmark).

For light scattering measurements, samples were chromatographed on the CL-300 Cellufine column above, and refractive index and molecular weight were obtained by passing the effluent through a differential refractometer and a flow cell light scattering detector (Precision Detectors, Amherst, MA). The molecular weight at the peak of refractive index was then calculated using the Precision detector software taking a value of 0.145 as the refractive index for pAG.

The monosaccharide composition of pAG was determined at the University of Georgia Center for Carbohydrate Research (Athens, GA). Compositional analysis, the alditol acetate method, and the trimethylsilyl (TMS) methylglycoside method were minor modifications of previously described procedures (17).

**Alditol Acetate Assay.** pAG (300  $\mu\text{g}$ ), spiked with 100 nmol of inositol internal standard, was hydrolyzed in 2 M trifluoroacetic acid for 2 h at 120  $^{\circ}\text{C}$ . The acid and water were removed under a stream of nitrogen, and the glycosyl residues were reduced to the corresponding alditols with the addition of sodium borohydride. The alditols were per-*O*-acetylated to the corresponding alditol acetates by treatment with acetic anhydride in pyridine. The alditol acetates were then extracted into methylene chloride. Methylene chloride was removed by evaporation and the solid residue dissolved in acetone. The alditol acetates were analyzed by GC/MS using an SP2330 capillary column (Supelco, Bellefonte, PA).

**Trimethylsilyl (TMS) Methylglycoside Assay.** pAG (300  $\mu\text{g}$ ), spiked with 100 nmol of inositol internal standard, was hydrolyzed in 1 M hydrochloric acid in methanol for 15 h at 80  $^{\circ}\text{C}$ . This reaction converts the polysaccharide to methyl glycosides. After removal of hydrochloric acid by evaporation, the methyl glycosides were silylated with hexamethyldisilane and trimethylchlorosilane in pyridine at 80  $^{\circ}\text{C}$  for 20 min. The products,  $\alpha$ - and  $\beta$ -trimethylsilyl methylglycosides, were extracted into hexane for analysis by GC/MS using a 30 m capillary DB1 column (J & W Scientific, Folsom, CA).

**Endotoxin Determination.** Endotoxin levels were determined using the *Limulus amoebocyte lysate* (LAL) assay kit (Associates of Cape Cod, Falmouth, MA).

**Elemental Analysis.** Elemental analysis (C, H, N), heavy metals (As, Pb, Hg), and ash content were determined by Galbraith Laboratories, Inc. (Knoxville, TN).

**Amino Acid Analysis.** Amino acid analysis was performed at AAA Laboratories, Mercer Island, WA. Samples containing a crystal of phenol were hydrolyzed for 20 h in 6 N HCl with 0.05% mercaptoethanol at 115  $^{\circ}\text{C}$ .

**Carbon-13 NMR.** Fourier transform  $^1\text{H}$  (300 MHz) and  $^{13}\text{C}\{^1\text{H}\}$  NMR (75 MHz) spectra of pAG were measured

in D<sub>2</sub>O solution using a Varian XL300 spectrometer (Varian Corp., Palo Alto, CA) at  $21 \pm 1$  °C. Chemical shifts were referenced to internal 1% DSS (sodium 2,2-dimethyl-2-silapentyl sulfonate).

**FTIR.** Fourier-transform infrared spectroscopy spectra were measured using a Galaxy 5020 spectrometer (Matteson Instruments, Madison, WI). Samples were mixed with KBr, ground with an agate mortar and pestle, and dried for 1 h at 110 °C before they were transferred to a Harrick Praying Mantis diffuse reflectance cell (Harrick Corp., Ossining, NY). Spectra were recorded over the frequency range from 400 to 4000 cm<sup>-1</sup> (256 scans at 2 cm<sup>-1</sup> resolution). The spectra were ratioed against KBr.

**Lectin Binding Assay.** pAG (0.1 g), dissolved in 0.02 mL of 0.01 M potassium phosphate, 0.15 M sodium chloride at pH 7.4 (PBS), was applied to a 1 mL *Ricinus communis* agglutinin affinity column (Sigma, St. Louis, MO) equilibrated with PBS. A total of 14 1 mL fractions were collected and assayed for carbohydrate using the phenolsulfuric acid method (18).

**Linkage Analysis.** The linkage analysis procedure was a modification of York (17). pAG (0.5 mg) was dissolved in 0.5 mL of DMSO, butyllithium reagent (Aldrich Chemical, Milwaukee, WI) was added, and the mixture was stirred for 4 h at room temperature. Methyl iodide reagent (0.5 mL) was added and again stirred for 18 h at room temperature. Methyl iodide was removed under a stream of nitrogen, and the procedure was repeated, starting with the addition of butyllithium. The final product mixture was placed on a C-18 Sep-Pak Column (Millipore Bedford, MA), washed with water, and then eluted with acetonitrile. The solvent was removed by evaporation under a stream of nitrogen gas. The per-*O*-acetylated polysaccharide was then converted to alditol acetates as described above. The partially per-*O*-methylated alditol acetates were then analyzed by GC/MS, using a Supelco SP2300 column, to identify and provide peak areas for each of the components.

### 3. Metabolic and Toxicological Studies of pAG.

**Synthesis of [<sup>3</sup>H]pAG.** pAG (10 g) was dissolved in 50 mL of 0.1 M sodium phosphate buffer, pH 6.0. Galactose oxidase (225 units) dissolved in 2.5 mL of the same buffer was added. The reaction was allowed to proceed for 24 h at 25 °C. Catalase (20 mg) was added to the reaction solution and incubated for 12 h. Mixed bed ion exchange resin (10 g) was added to the reaction solution and mixed for 60 min. The resin was removed by filtration. The product was purified by ultrafiltration (YM-3 membrane, Amicon, Beverly, MA), and the polyaldehydic pAG was isolated by ethanol precipitation. The polyaldehydic pAG (5 g) was dissolved in deionized water (15 mL) and cooled to 0 °C. Sodium borotritide (5 mCi, 490 mCi/mmol) in cold 0.01 M sodium hydroxide (2 mL) was added, and the reaction was stirred at 25 °C. Thirty min after the borotritide addition, sodium borohydride (500 mg) was added and reacted for 2 h. The reaction was quenched by the addition of 1 mL of acetone. The product was purified by repeated ultrafiltration and isolated by lyophilization.

**Clearance of [<sup>3</sup>H]Arabinogalactan from the Liver.** Rats were injected *via* the tail vein with 5 mg and 0.54 μCi [<sup>3</sup>H]arabinogalactan per kg body weight. Initial weights were chosen so that at the time of sacrifice the rats were between 300 and 400 grams. After 30 min, 1, 3, 5, 7, 14, or 28 days postinjection, three animals at each time period, with the exception of the 30 min period ( $n = 4$ ), were anesthetized with 35 mg/kg body weight sodium pentobarbital, the animals were exsanguinated, and the livers were removed and weighed. Approximately 100 mg aliquots of tissue were added to tared glass scintil-

lation vials containing 1 mL of 0.5 M tissue solubilizer solution (Solvable, NEN Research Products, Boston, MA) and weighed. The samples were incubated for 3 h at 50 °C in a shaking water bath. The digest was decolorized with 0.3 mL of 30% H<sub>2</sub>O<sub>2</sub> added to each sample and incubated an additional hour. Samples were cooled, and 15 mL of scintillation cocktail (Aquasol, NEN Research Products, Boston, MA) was added. Finally, 0.5 mL of 0.5 N HCl was added to minimize chemiluminescence. All samples were counted in a Packard liquid scintillation counter (Packard Instruments, Inc., Downers Grove, IL). A weighed aliquot of injectate was processed similarly to serve as a standard for calculation of the percent of the injected dose present in the tissues. Counting efficiency was determined using [<sup>3</sup>H]toluene as an internal standard.

The half-life disappearance of <sup>3</sup>H from the liver was calculated according to the general first order equation

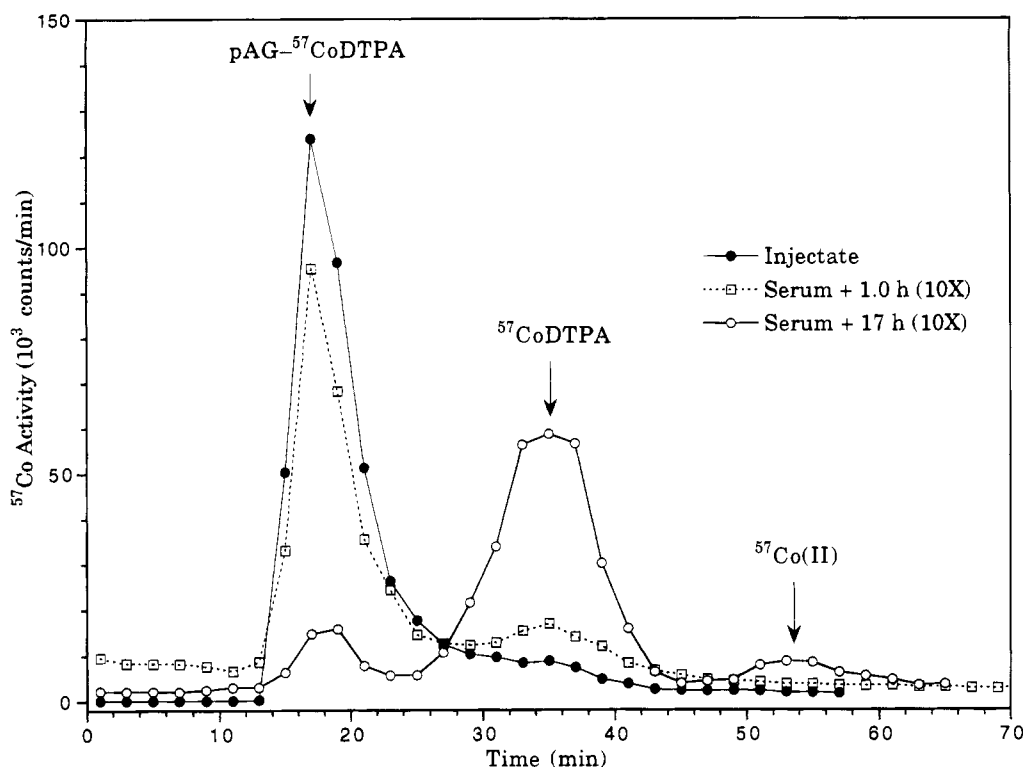
$$A/A_0 = e^{-kt} \quad (1)$$

where  $A/A_0$  is the calculated fraction of the injected radioactivity remaining in the liver at any time ( $t$ ) postinjection and  $k$  is the first order rate constant.

**Acute Toxicity of pAG in the Rodent.** pAG was administered to female CD-1 mice ( $n = 5$ , Charles River Laboratories, Wilmington MA, approximately 25 g body weight) and male CD rats ( $n = 5$ ; 225–300 g body weight) intravenously via the tail vein at a dose level of 5000 mg/kg body weight. The animals were observed for clinical signs and symptoms of toxicity for up to 48 h post-treatment. The signs and symptoms recorded included respiration, neurological function (e.g., motor, convulsions), autonomic nervous system function (e.g., salivation, defecation), and behavior. All animals were sacrificed by CO<sub>2</sub> asphyxiation and exsanguination at study termination.

**Repeat-Dose Toxicity in Rats with pAG.** pAG was administered over 90 days to the rat by intravenous injection via the tail vein. Three groups of 10 male rats per group were administered pAG at dose levels of 31.25, 125, and 500 mg/kg/day. A control group of 10 rats received 0.9% saline at a dose volume of 10 mL/kg/day. All animals were observed daily for clinical signs and symptoms of toxicity. Body weights were obtained upon study initiation, weekly thereafter, and at study termination. At the conclusion of the treatment period, all animals were anesthetized with an intraperitoneal injection of sodium pentobarbital and exsanguinated. Gross necropsies were conducted on each animal by trained personnel using procedures approved by a board-certified pathologist, and organ weights (brain, heart, liver, spleen, kidney, adrenals, and testes with epididymides) were obtained. Gross necropsy included examination of the external surface, all orifices, the cranial cavity, carcass, external surface of the brain and spinal cord, cut surfaces of the brain, the thoracic, abdominal, and pelvic cavities and their viscera, and the cervical tissues and organs. Tissues retained for possible future evaluation were preserved in 10% buffered formalin. The livers from the control (saline treated) group and the high dose group (pAG at 500 mg/kg/day) were evaluated by microscopic examination for pathological changes. The histopathological evaluation of the livers was performed by Lynd L. Pippin, D.V.M., of Pathology Associates, Inc., Frederick, MD. Two sections from each of the livers of the 10 control rats and the 10 rats receiving 500 mg/kg/day were trimmed and processed as above.

**Hepatotoxicity of pAG.** pAG (50 mg/mL in 0.9% saline) was administered intravenously via the tail vein at a dose



**Figure 1.** Chromatograms of arabinogalactan- $^{57}\text{Co}$ -DTPA after 1 and 17 h at 37 °C in rat serum. The 1 and 17 h curves were expanded 10 $\times$  for comparative purposes.

level of 500 mg/kg body weight to both male CD-1 mice and male CD rats. Twenty-four hours postinjection, all animals were sacrificed by  $\text{CO}_2$  asphyxiation and exsanguination. The livers were excised and preserved in 10% buffered formalin. The histopathological evaluation of the mouse livers was performed by Lynd L. Pippin, D.V.M., of Pathology Associates, Inc., Frederick, MD. Two sections from each of the livers of the three mice receiving 500 mg/kg/day were trimmed, processed through paraffin, cut at approximately 6  $\mu\text{m}$ , stained with hematoxylin and eosin, and examined microscopically.

The histopathological evaluation of the rat livers was performed by Roderick T. Bronson, D.V.M., of Tufts University, School of Veterinary Medicine, Veterinary Diagnostic Laboratory, North Grafton, MA. Two or more sections from each of the livers of the six rats receiving 500 mg/kg/day were trimmed and processed as above.

## RESULTS

**1. Demonstration of Receptor Interaction: Biodistribution and Receptor Binding Studies with Purified Arabinogalactan.** The fate of pAG after intravenous injection into rats was examined by obtaining the biodistribution of the arabinogalactan- $^{57}\text{Co}$ -DTPA conjugate 90 min after injection. Arabinogalactan- $^{57}\text{Co}$ -DTPA was present in the liver (52.5% of injected dose) and urine (30.0% injected dose); see Table 1. When asialofetuin was coinjected with arabinogalactan- $^{57}\text{Co}$ -DTPA, hepatic uptake decreased to 3.54%. For comparison,  $^{57}\text{Co}$ -DTPA undergoes largely renal elimination, with 1.22% accumulating in the liver. Thus, the attachment of  $^{57}\text{Co}$ -DTPA to pAG affected a 40-fold increase in hepatic biodistribution (52.5/1.22).

The stability of the arabinogalactan- $^{57}\text{Co}$ -DTPA conjugate in rat serum was examined as shown in Figure 1. Under these conditions, the retention times for the arabinogalactan- $^{57}\text{Co}$ -DTPA conjugate,  $^{57}\text{Co}$ -DTPA, and  $\text{Co(II)}$  were 17, 35, and 53 min, respectively. Inte-

**Table 1. Biodistribution of Arabinogalactan- $^{57}\text{Co}$ -DTPA and  $^{57}\text{Co}$ -DTPA: Percent Injected Dose in Selected Organs<sup>a</sup>**

tissue	arabinogalactan- $^{57}\text{Co}$ -DTPA	arabinogalactan- $^{57}\text{Co}$ -DTPA + asialofetuin	$^{57}\text{Co}$ -DTPA
liver	52.5 (5.8)	3.54 (1.0)	1.22 (0.19)
spleen	<1	<1	<1
urine	30.0 (4.4)	39.8 (5.1)	83.1 (6.5)
blood	<1	18.8 (2.7)	1.9 (0.2)

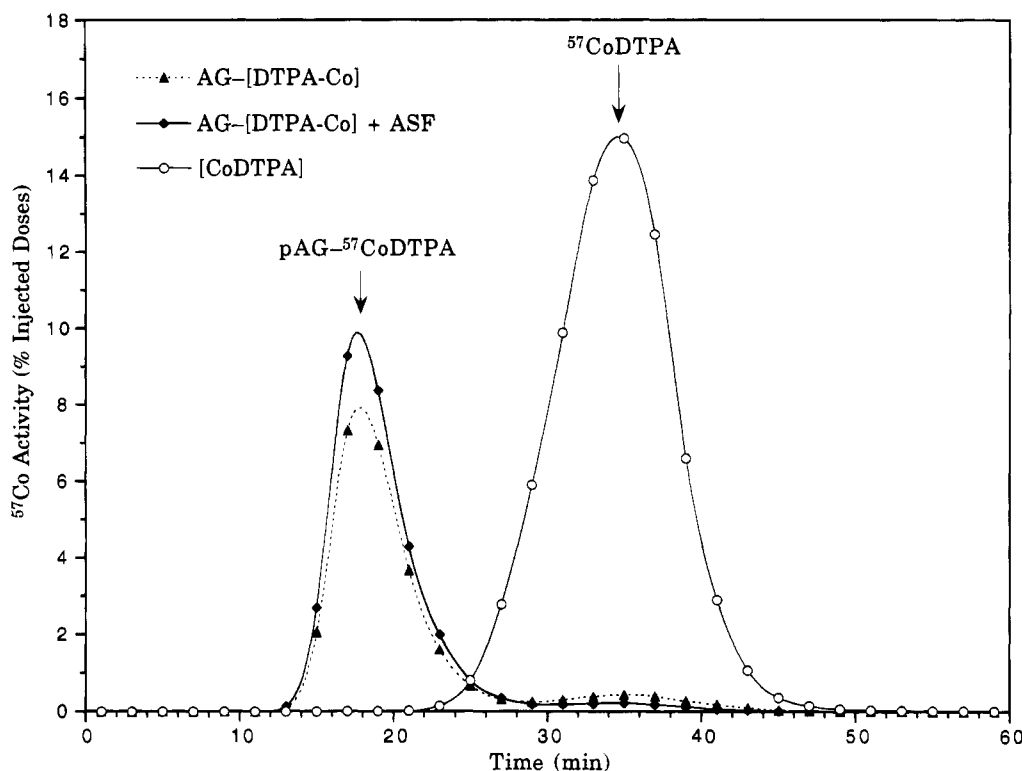
<sup>a</sup> 90 min post iv injection,  $n = 6$ , standard error in parentheses.

**Table 2. Binding of Ligands to Purified Asialoglycoprotein Receptor**

compd	$\text{IC}_{50}$ (M)
arabinogalactan (pAG)	$2.0 \times 10^{-6}$
asialofetuin	$1.3 \times 10^{-7}$
lactosylated BSA	$1.9 \times 10^{-7}$
galactan	$>1 \times 10^{-4}$
galactose	$>2 \times 10^{-2}$
arabinogalactan-DTPA	$2.6 \times 10^{-6}$
T-40 dextran	$>6.4 \times 10^{-4}$

gration of the curves showed <10% and 75%  $^{57}\text{Co}$ -DTPA after 1.0 and 17 h in rat serum, respectively. A peak at 53 min (11%) was present in the 17 h sample, due to a very low molecular weight, nonchelated form of cobalt. Figure 2 shows the chromatograms of the urine from rats on which biodistribution data was obtained (Table 1), using the same chromatographic system as for Figure 1. With or without asialofetuin, radioactivity was seen at the retention times of arabinogalactan- $^{57}\text{Co}$ -DTPA and  $^{57}\text{Co}$ -DTPA.

The interaction of pAG with the asialoglycoprotein receptor was examined with an in vitro assay using a purified preparation of the asialoglycoprotein receptor. Table 2 compares the ability of arabinogalactan and other ligands to inhibit the binding of [ $^{125}\text{I}$ ]tyramine arabinogalactan to the receptor. Data in Table 2 are expressed as  $\text{IC}_{50}$ , the molar concentration necessary to displace 50%



**Figure 2.** Chromatograms of rat urine samples after injection with arabinogalactan- $^{57}\text{Co}$ -DTPA, with and without asialofetuin, and  $^{57}\text{Co}$ -DTPA. Values are averages for six, three, and three rats, respectively, in each group.

**Table 3. Linkage Analysis of Purified Arabinogalactan<sup>a</sup>**

linkages	mol %
galactose	
3,4,6-	2.2 ± 0.3
2,3,6-	1.6 ± 0.1
3,6-	30.7 ± 0.8
3,4-	2.3 ± 0.3
6-	19.4 ± 0.6
3-	1.6 ± 0.1
terminal pyranose	26.8 ± 0.9
% total of galactose	84.5 ± 1.34
arabinose	
furanose 3-	3.9 ± 0.1
terminal furanose	7.4 ± 1.0
terminal pyranose	5.2 ± 0.3
% total of arabinose	15.5 ± 1.4

<sup>a</sup>  $n = 15$ ; values ± 1 standard deviation.

of the tracer from the receptor. When pAG was reacted with DTPA, the resulting molecule had a slightly higher  $\text{IC}_{50}$ , indicating that the reaction with DTPA does not greatly alter interaction with the receptor. Asialofetuin and lactosylated bovine serum albumin have about a 5-fold lower  $\text{IC}_{50}$  than arabinogalactan, while with the galactan and galactose, 50% displacement of the [ $^{125}\text{I}$ ]-tyramine derivative of arabinogalactan could not be achieved at the highest concentration that could be employed.

**2. Chemical Characterization of pAG.** Size exclusion chromatography of pAG yields a single peak corresponding to a molecular weight of 19 kDa using dextran standards. Molecular weight determinations of pAG using static light scattering methods generated a molecular weight of 40 kDa.

The TMS methylglycoside assay to determine glycoside composition indicated the only residues detected in pAG were arabinose and galactose. On the basis of the detection limits of the assay, these two sugars account for greater than 99% of the total glycosyl content. The

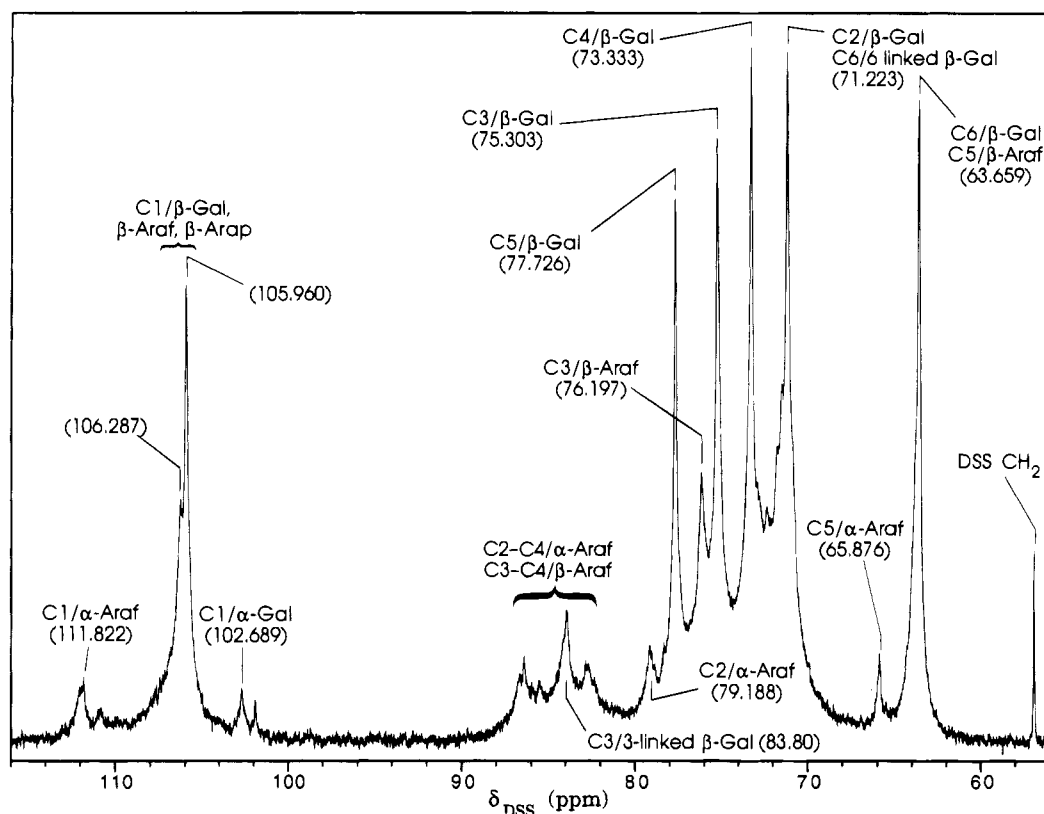
ratio of galactose to arabinose determined from 15 determinations was  $5.45 \pm 0.6$ . With the alditol acetate method the only residues detected were galactose and arabinose, and the ratio of galactose to arabinose was  $5.13 \pm 1.7$ .

The carbon-13 spectrum of pAG is shown in Figure 3. Resonances were assigned by comparison with published data (19–24). The major resonances are assigned to  $\beta$ -galactopyranose,  $\beta$ -arabinofuranose, and  $\beta$ -arabinopyranose. Minor resonances (<ca. 10%) attributable to  $\alpha$ -conformers were also observed. Treatment of pAG with  $\text{NaBH}_4$  did not affect the  $\alpha$ -conformers. This observation is in accord with the FTIR spectrum of pAG, which contained characteristic  $\beta$ -pyranose ring deformation modes at ca. 882 and 775  $\text{cm}^{-1}$  (25). The 300 MHz proton NMR spectrum of pAG showed no evidence of noncarbohydrate substituents such as acetyl, pyruval, or fatty acyl groups.

Elemental analysis (C, H, N) revealed trace amounts of nitrogen (<0.01%) and less than 1 ppm of lead, mercury, and arsenic, while the ash content was less than 0.1%. No amino acids were detected in three preparations of pAG. Three preparations of pAG showed less than 0.03 endotoxin units/mg (EU/mg) of pAG.

To further assess homogeneity, pAG was applied to a *Ricinus communis* agglutinin (RCA lectin) affinity column. Less than 0.1% of the total carbohydrate eluted after two column volumes, demonstrating the preparation was uniform with respect to lectin binding. The RCA lectin has a specificity for terminal galactose residues and has been reported to bind arabinogalactans (26).

Glycosyl linkage analysis was performed by per-*O*-methylation followed by hydrolysis, borohydride reduction, and then alditol acetylation (Table 3). Our data are consistent with a structure of pAG with a backbone of 1,3-linked galactopyranose connected by 1,3-linked glycosidic linkages, comprised of 3,4,6-, 2,3,6-, 3,6-, 3,4-, and 3-linked residues. These residues comprise 38.4 mol % ( $2.2 + 1.6 + 30.7 + 2.3$ ) of the total glycosyl residues in



**Figure 3.**  $^{13}\text{C}$  NMR spectrum of purified arabinogalactan.

**Table 4. Summary of Physical Properties of Purified Arabinogalactan**

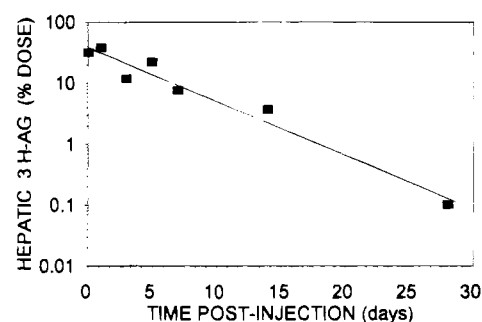
property	result
nitrogen content, %	<0.01
endotoxin units/mg	<0.03
size, chromatography, kDa	19
size, light scattering, kDa	40
branching	high, terminal galactoses and arabinoses (Figure 3, Table 3)
$^{13}\text{C}$ -NMR	galactose and arabinose exclusively (Figure 3)
galactose/arabinose ratio	
alditol method	$5.13 \pm 1.7$
galactose/arabinose ratio	
TMS glycoside	$5.45 \pm 0.6$
RCA lectin binding, %	>99.9

purified arabinogalactam. Of these backbone residues, essentially all have a branch point. Terminal glycosyl residues consist of arabinofuranose and galactopyranose, comprising 38.4 mol % ( $26.8 + 7.4 + 4.2$ ) of total residues. The 6-linked galactopyranose and 3-linked arabinofuranose connect terminal sugars to the backbone. These residues comprise 23.3 mol % ( $19.4 + 3.9$ ) of the total residues.

A summary of the physical properties of pAG is presented in Table 4.

**3. Metabolic and Toxicological Properties of pAG.** *Clearance of [ $^3\text{H}$ ]Arabinogalactan.* To be practical as a carrier for the delivery of diagnostic or therapeutic agents to the liver, the carrier must be readily degraded and cleared from the liver. To examine the clearance of pAG after hepatic uptake, we injected [ $^3\text{H}$ ]pAG into rats.

After intravenous injection of 5 mg/kg of [ $^3\text{H}$ ]pAG, radioactivity decreased from the blood with a half-life of 3.8 min (data not shown). At 30 min postinjection 31.1% of the injected dose was found in the liver, 39.3% in the bladder urine, and less than 0.1% in the spleen. The radioactivity remaining in the liver after injection of



**Figure 4.** Elimination of hepatic radioactivity after injection of  $^3\text{H}$ -purified arabinogalactan.

tritiated pAG is shown in Figure 4. Hepatic radioactivity declined following first order kinetics with a half-life of 3.42 days.

*Acute Toxicity Studies.* pAG did not cause mortality in either the rat or mouse during the 48 h observation period following the intravenous administration of 5000 mg/kg, nor were there signs or symptoms of toxicity evident in either species during the in-life phase of the study.

*Repeat-Dose Toxicity.* There were no overt clinical signs or symptoms of toxicity related to test material administration, excluding an irritability postinjection exhibited by the high dose group. All animals gained weight over the 90-day dosing period with no difference observed among the four groups; however, there was some short-term weight loss during the course of the study in three animals in the control group, two in the 31.25 mg/kg/day dose group, and four each in the 125 and 500 mg/kg/day dose groups. Any demonstrated weight loss was regained during the following week. Gross necropsy showed no abnormalities in any animal. No differences between treatment groups were observed in the mean organ weights. All liver sections from the

**Table 5. Summary of Biological Properties of Purified Arabinogalactan**

study	species, dose	result	data
biodistribution after IV injection	rat, 4 mg/kg	clearance to liver, urine	Table 1
receptor interaction	rat liver	strong	Table 2
clearance	rat, 5 mg/kg	hepatic clearance	Figure 4
acute dose toxicology	mouse, 5000 mg/kg	no effect	text
	rat, 5000 mg/kg	no effect	text
repeat dose toxicology	rat, 500 mg/kg/ 90 days	no effect	text
hepatotoxicity	mouse, 500 mg/kg	no effect	text
	rat, 500 mg/kg	no effect	text

control and high dose groups examined microscopically for histopathological changes were considered to be within normal limits.

**Hepatotoxicity.** There were no overt signs of toxicity during the 24 h postdosing in the mice and rats receiving 500 mg of pAG/kg. There was no evidence of hepatic damage or alteration, in particular, abnormal vacuolization, in either the rat or mouse livers.

A summary of the biological properties of pAG is presented in Table 5.

## DISCUSSION

In this paper we describe the biological and chemical properties of purified arabinogalactan, denoted pAG, a polysaccharide of interest because it exhibits many properties of asialoglycoproteins.

**1. Demonstration of Receptor Interaction: Biodistribution and Receptor Binding of Purified Arabinogalactan.** The biodistribution of pAG was determined as the presence of  $^{57}\text{Co}$  in tissues after the injection of arabinogalactan- $^{57}\text{Co}$ -DTPA (Table 1). At 90 min postinjection, arabinogalactan was present in the liver (52.5% injected dose), with less than 1% in the spleen, consistent with uptake being due to the uptake of arabinogalactan- $^{57}\text{Co}$ -DTPA by the asialoglycoprotein receptor of hepatocytes. The injection of asialofetuin (100 mg/kg) with arabinogalactan- $^{57}\text{Co}$ -DTPA decreased hepatic uptake from 52.5 to 3.54%, a decrease of more than 90%, indicating that the hepatic clearance of  $^{57}\text{Co}$ -DTPA-arabinogalactan was mediated by the asialoglycoprotein receptor. It can be inferred that at least 48% (52.5–3.54%) of the  $^{57}\text{Co}$  remained associated with arabinogalactan for this result to have been obtained. Asialofetuin also increased blood radioactivity (1% to 18.8%), which resulted in increased urinary elimination (30.0 to 39.8%) due to the presence of increased conjugate in the blood.

Also shown in Table 1 is the biodistribution of  $^{57}\text{Co}$ -DTPA, which undergoes rapid renal elimination. By comparing the biodistribution of  $^{57}\text{Co}$ -DTPA and arabinogalactan- $^{57}\text{Co}$ -DTPA, the effect of attaching  $^{57}\text{Co}$ -DTPA to arabinogalactan is illustrated. That is, hepatic radioactivity increased from 1.22 to 52.5% of the injected dose or approximately 40-fold.

The stability of the arabinogalactan- $^{57}\text{Co}$ -DTPA is shown by incubating the conjugate in rat serum followed by chromatographic analysis (Figure 1). After 1 h in rat serum, greater than 90% of the radioactivity was found to have a retention time of 17 min, the retention time of arabinogalactan- $^{57}\text{Co}$ -DTPA. After 17 h, the predominate species was  $^{57}\text{Co}$ -DTPA, reflecting hydrolysis of the ester formed when the anhydride of DTPA reacts with the hydroxyl groups of pAG. A small amount of radioactivity was seen at 53 min, the retention time of aqueous  $\text{Co(II)}$ .

The urine of the rats from the biodistribution study (Table 1) was obtained and subjected to chromatographic analysis as shown in Figure 2. When arabinogalactan- $^{57}\text{Co}$ -DTPA conjugate was injected, urinary radioactivity, 30% of the injected dose, had the retention time of the conjugate. When  $^{57}\text{Co}$ -DTPA was injected, urinary radioactivity, 83.1% of the injected dose, had the retention time of the chelate. Thus, when either the arabinogalactan- $^{57}\text{Co}$ -DTPA conjugate or the  $^{57}\text{Co}$ -DTPA were injected, urinary  $^{57}\text{Co}$  was associated with the intact chelate.

The interaction of arabinogalactan with the asialoglycoprotein receptor was also evident with *in vitro* receptor binding studies. Though asialofetuin and lactosylated bovine albumin interact about 5–10 times more strongly with the receptor than arabinogalactan-DTPA (Table 2), the interaction of arabinogalactan-DTPA with the receptor was sufficient to permit 52.5% of the arabinogalactan-DTPA- $^{57}\text{Co}$  to be taken up by the liver (Table 1). Galactan did not interact detectably with the receptor. Though galactan is a high molecular weight polymer of galactose, the galactose residues are not in an appropriate configuration to bind the receptor. As expected based on the results of Lee et al. (34), galactose interacted weakly with the receptor. We characterized the interaction of dextran with the receptor because of a recent report that the hepatic uptake of dextran was inhibited by galactosyl-bovine serum albumin, suggesting that dextran might interact with this receptor (27). The interaction of dextran with the receptor was weak.

**2. Chemical Characterization of pAG.** pAG had a molecular weight of 19 kDa by size exclusion chromatography and 40 kDa by light scattering. Molecular weight determinations by light scattering are independent of a molecular conformation (28), while gel filtration estimates of molecular weight depend upon the radius of gyration of the molecule and, hence, conformation (29–31). The discrepancy in the estimates of molecular weight between the two methods suggests that arabinogalactan is a more compact molecule than dextran, which would be expected from the highly branched structure proposed for arabinogalactan.

The chemical properties of materials described as arabinogalactan vary considerably in the scientific literature. This may result in part from different sources, since arabinogalactans are present in a wide variety of plants, or from different methods of purification. However, there are literature reports for the arabinogalactan from *Larix occidentalis*, the source of pAG, at variance with our results. Larch arabinogalactan has been often reported to consist of two components of different molecular weights, while in contrast pAG consists of a single molecular weight species. A review of the literature by Clarke and co-workers states: "The larch arabinogalactans generally occur as two components, one high MW with values recorded in the range of 37 000–100 000 (70–95%) and a second component with a lower MW with values in the range 7500–18 000 (5–30%)" (32). Given that the molecular weight of pAG was quite different from earlier materials described as larch arabinogalactan, studies on the composition and structure of pAG were conducted.

pAG is composed of two glycosides, D-galactose and L-arabinose, in a ratio of 5.45 by the TMS glycoside assay and 5.13 by the alditol method.  $^{13}\text{C}$  NMR spectra failed to demonstrate other glycosides, consistent with the presence of only galactose and arabinose in pAG. Our linkage data (Table 3) are consistent with a structure where arabinogalactan has a backbone of (1→3) linked galactose, evident from the 38.4 mol % of the total



glycosyl residues that are linked at the 3 position of galactose. A highly branched structure is apparent from the 38.4 mol % present as terminal galactose or arabinose. Our results are consistent with the structure for arabinogalactan from *Larix occidentalis* used elsewhere; see Figure 2 of the review by Clarke (32). Another reported variation in arabinogalactans concerns the presence of amino acids. Arabinogalactan can exist as an arabinogalactan protein, with covalently attached amino acids (32, 33). On the basis of the lack of elemental nitrogen and amino acid analysis, pAG lacks amino acids. The composition and structure of pAG are consistent with earlier reports, while the molecular weight and molecular weight distribution differ from earlier reports.

A number of observations suggest that the arabinogalactan prepared here is highly pure. Carbon-13 and proton NMR spectra of pAG provided no evidence of acetyl, pyruvyl, or lignin residues. NMR acquisition times and sample concentrations were adjusted to detect less than 0.5% by weight of these impurities in our pAG preparation. Greater than 99.9% of the applied pAG was retained by the RCA lectin affinity support, which recognizes terminal galactose residues. The nitrogen content of pAG was less than 0.01%, while the endotoxin was less than 0.03 EU/mg. The nitrogen and endotoxin levels in pAG are similar to those in clinical grade dextran T-40 (less than 0.005% nitrogen and 0.05 EU/mg). The levels of these contaminants in pAG are sufficiently low to permit its use in parenteral pharmaceutical applications.

The reason for the strong interaction of arabinogalactan with the asialoglycoprotein receptor may lie in its highly branched structure and numerous terminal galactose and arabinose residues. Since arabinose also interacts with the asialoglycoprotein receptor (34), all terminal sugars on pAG contribute to its receptor binding. On the basis of a molecular weight of 40 kDa, there are approximately 68 terminal galactose and 19 terminal arabinose residues per mole of pAG. Closely spaced, terminal monosaccharide residues may form clusters similar to those found in natural asialoglycoproteins; such clusters possess a high affinity for the asialoglycoprotein receptor (8). Supporting this interpretation is the fact that galactan, a linear polymer of galactose, fails to interact with the receptor (Table 2).

The presence of 87 terminal residues on each molecule of pAG (68 + 19, see above) may be why pAG tolerates covalent modification, such as the reaction with DTPA or tyramine, with retention of receptor binding. For example, attachment of 4.68 DTPA's per molecule of pAG, the number attained in this paper, leaves 82 terminal residues unmodified.

### 3. Metabolic and Toxicological Studies of pAG.

Thirty min after intravenous injection of [ $^3\text{H}$ ]pAG, 31.1% was found in the liver, while bladder urine had 39.3%. The renal elimination obtained was consistent with the molecular weight of pAG, which was 19 and 40 kDa by chromatography and light scattering, respectively. Ninety min after the injection of arabinogalactan- $^{57}\text{Co}$ -DTPA, 52.5% was found in the liver, while bladder urine had 30.0% of the radioactivity. The negatively charged arabinogalactan- $^{57}\text{Co}$ -DTPA is expected to have a somewhat lower glomerular filtration rate, and higher hepatic uptake, than neutral [ $^3\text{H}$ ]pAG, due to the role of charge in determining glomerular filtration rate (36). Arabinogalactan- $^{57}\text{Co}$ -DTPA is negatively charged because of the many DTPA groups are not chelated with  $^{57}\text{Co}$ , see above, while pAG is assumed to be neutral based on its composition exclusively of arabinose and galactose.

For dextrans of a given volume, modification to make them negatively charged decreased glomerular filtration rate, while modification to make them positively charged increased glomerular filtration rate (36).

The hepatic radioactivity resulting from the injection of [ $^3\text{H}$ ]pAG decreased with a half-life of 3.42 days, Figure 4, indicating pAG is eliminated from the liver after uptake. The catabolism of pAG may be faster than 3.42 days, with the half-life obtained reflecting the loss of [ $^3\text{H}$ ]pAG degradation products from the liver. Alternatively, the catabolism of pAG may occur more slowly than 3.42 days, with the half-life obtained reflecting the transport of pAG from the liver by some mechanism.

pAG has low toxicity as shown by single and repeated dose studies in rats and mice. Administration of pAG produced no signs of hepatotoxicity upon histopathological examination.

It might be argued that pAG is of little interest as a carrier for hepatic delivery because the hepatic accumulation of arabinogalactan- $^{57}\text{Co}$ -DTPA is less than, and urinary elimination greater than, that achieved with asialoglycoproteins or neoglycoproteins. For arabinogalactan- $^{57}\text{Co}$ -DTPA hepatic uptake was 52.5% and urinary elimination 30.0%. The hepatic uptake achieved by lactosylated human serum albumin was 75%, with less than 1% urinary excretion (4). Similarly, with [ $^3\text{H}$ ]pAG, hepatic uptake was only 31.1% and urinary excretion was 39.3%. In spite of the urinary elimination of arabinogalactan, we believe it is of interest as a carrier for delivering agents to the asialoglycoprotein receptor for the reasons given below.

First, as indicated by Table 1, the attachment of  $^{57}\text{Co}$ -DTPA to arabinogalactan effected a 40-fold increase in the hepatic accumulation of chelate (52.5/1.22). The increase in the hepatic uptake of  $^{57}\text{Co}$ -DTPA suggests that therapeutic agents with properties similar to  $^{57}\text{Co}$ -DTPA, i.e., low molecular weight and high water solubility, a combination which favors renal elimination, should undergo increased hepatic uptake by virtue of their attachment to pAG. An example of such a therapeutic agent would be an antiviral nucleotide vidarabine (araAMP); see ref 3. However, the renal elimination of some fraction of injected drug, as might occur if araAMP were attached to pAG, does not present a problem in pharmaceutical development, provided the basic criteria of drug safety and efficacy are met.

Second, if pAG is used as a carrier in hepatic drug delivery, the biodistribution obtained is that of the conjugate not pAG. In some cases molecular weight will be greatly increased by the chemistry employed, preventing urinary excretion. Arabinogalactan has been employed as a carrier for delivering a superparamagnetic iron oxide colloid as an asialoglycoprotein receptor directed MR contrast agent to hepatocytes (9). Since the arabinogalactan covers iron oxide crystals about 5 nm in diameter, the arabinogalactan covered iron oxide is too large for glomerular filtration and is retained in the vascular compartment until taken up by the liver. A second strategy for decreasing urinary elimination is the production of negatively charged conjugates of pAG, as explained above.

Third, hepatic uptake may depend on dose, with higher doses producing higher levels of receptor saturation and smaller percentages of the injected dose going to the liver. Doses of ligand for the asialoglycoprotein receptor vary widely with application. With scintigraphic labels small amounts of carrier are used, e.g., 0.05 mg of lactosylated albumin per kg (4). When the antiviral nucleotide araAMP is attached to the same carrier, and used in

humans, a dose of 35 mg/kg was used (3). Our studies utilized 4 mg/kg (Table 1).

Finally, it should be noted pAG binds the asialoglycoprotein receptor in its naturally occurring form, and in manner that is sufficiently strong to be useful in the hepatic delivery of diagnostic (9) and possibly therapeutic agents (see above). Currently used protein-based carriers for the asialoglycoprotein receptor require the synthetic attachment of saccharides, to make so-called neoglycoproteins, or removal of sialic acid, to make asialoglycoproteins. The fact that pAG binds the receptor in its naturally occurring form may lead to substantial cost savings, important in those applications where carrier usage is high.

On the basis of these studies, pAG has properties that make it suitable as a carrier for targeting diagnostic or therapeutic agents *via* the asialoglycoprotein receptor to hepatocytes. pAG is pure and homogeneous and therefore suitable for use as a raw material in the synthesis of parenteral pharmaceutical products. The increase in hepatic uptake of  $^{57}\text{Co}$ -DTPA afforded by attachment to pAG suggests that coupling therapeutic agents to arabinogalactan will increase their hepatic biodistribution significantly. pAG is nontoxic and leaves the liver after hepatic uptake. Thus, pAG has an array of properties that make it suitable for hepatic drug delivery.

#### ACKNOWLEDGMENT

The authors wish to thank Joseph V. Rutkowski, Ph.D., Howard Bengel, Ph.D., James Prescott, Ph.D., and Lorraine Murphy, B.S., for their technical assistance and Debra Gaw, B.A., for the preparation of the manuscript. The assistance of Daniel Kolker and Stephen Plouff in performing some of these experiments is also appreciated. Analyses performed at the University of Georgia Center for Carbohydrate Research (Athens, GA) were supported in part by the USDA/DOE/NSF Plant Science Centers program; this particular center has been funded by the Department of Energy Grant DE-FG09-87-ER13810.

#### LITERATURE CITED

- Meijer, D. K. F., Molema, G., Jansen, R. W., and Mollenaar, J. F. (1990) Design of cell-specific drug targeting preparations for the liver: where cell biology and medicinal chemistry meet. In *Trends in Drug Research* (V. Claassen, Ed.) Vol. 13, pp 303-332, Elsevier, Amsterdam.
- Wu, G. Y., and Wu, C. H. (1991) Targeted delivery and expression of foreign genes in hepatocytes. *Targeted Diagn. Ther.* 4, 127-49.
- Fiume, L., Cerenzia, M. R., Bonino, F., Busi, C., Mattioli, A., Brunetto, M. R., Chiaberge, E., and Verme, G. (1988) Inhibition of hepatitis B virus replication by vidarabine monophosphate conjugated with lactosaminated serum albumin. *Lancet* 2, 13-5.
- Stadalnik, R. C., Vera, D. R., Woodle, E. S., Trudeau, W. L., Porter, B. A., Ward, R. E., Krohn, K. A., and O'Grady, L. F. (1985) Technetium-99m NGA functional hepatic imaging: preliminary clinical experience. *J. Nucl. Med.* 26, 1233-42.
- Virgolini, I., Kornek, G., Hobart, J., Li, S. R., Raolerer, M., Bergmann, H., Scheithauer, W., Pantev, T., Angelberger, P., and Sinzinger, H. (1993) Scintigraphic evaluation of functional hepatic mass in patients with advanced breast cancer. *Br. J. Cancer* 68, 549-54.
- Wedge, S. R., Duncan, R., and Kopeckova, P. (1991) Comparison of the liver subcellular distribution of free daunomycin and that bound to galactosamine targeted N-(2-hydroxypropyl) methacrylamide copolymers, following intravenous administration in the rat. *Br. J. Cancer* 63, 546-549.
- Kempen, J. M., Hoss, C., Bloom, J. H. v., Spanjer, H. H., Lange, J. D., Langendoen, A., and Berkel, T. J. C. v. (1984) A water-soluble cholesteryl-containing trisgalactoside: synthesis, properties, and use in directing lipid-containing particles to the liver. *J. Med. Chem.* 27, 1306-1312.
- Lee, Y. C. (1978) Synthesis of some cluster glycosides suitable for attachment to proteins or solid matrices. *Carbohydr. Res.* 67, 509-514.
- Josephson, L., Groman, E. V., Menz, E., Lewis, J. M., and Bengel, H. (1990) A functionalized superparamagnetic iron oxide colloid as a receptor directed MR contrast agent. *Magn. Reson. Imag.* 8, 637-46.
- van der Sluijs, P., Bootsma, H. P., Postema, B., Moolenaar, F., and Meijer, D. K. (1986) Drug targeting to the liver with lactosylated albumins: does the glycoprotein target the drug or is the drug targeting the glycoprotein? *Hepatology* 6, 723-8.
- Fiume, L., Busi, C., Preti, P., and Spinosa, G. (1987) Conjugates of ara-AMP with lactosaminated albumin: a study on their immunogenicity in mouse and rat. *Cancer Drug Deliv.* 4, 145-50.
- Fiume, L., Betts, C. M., Busi, C., Corzani, S., Derenzini, M., DiStefano, G., and Mattioli, A. (1992) The pathogenesis of vacuoles produced in rat and mouse liver cells by a conjugate of adenine arabinoside monophosphate with lactosaminated albumin. *J. Hepatol.* 15, 314-22.
- Meijer, D. F. K., Jansen, R. W., and Molema, G. (1992) Drug targeting systems for antiviral agents: options and limitations. *Antiviral Res.* 18, 215-258.
- Hudgin, R. L., William, E., Pricer, J., Ashwell, G., Stockert, R. J., and Morell, A. G. (1974) The isolation and properties of a rabbit liver binding protein specific for asialoglycoproteins. *J. Biol. Chem.* 249, 5536-5543.
- Kohn, J., and Wilchek, M. (1984) The use of cyanogen bromide and other novel cyanylating agents for the activation of polysaccharide resins. *Appl. Biochem. Biotechnol.* 9, 285-305.
- Hunter, W. M., and Greenwood, F. C. (1962) Preparation of iodine-131 labeled human growth hormone of high specific activity. *Nature* 194, 495-497.
- York, W. S. (1985) Isolation and characterization of plant cell wall components. In *Methods in Enzymology*, Vol. 118, pp 3-40, Academic Press, New York.
- Dubois, M., Gilles, K. A., Hamilton, J. K., Rebers, P. A., and Smith, F. (1956) Colorimetric method for determination of sugars and related substances. *Anal. Chem.* 28, 350-356.
- Gorin, P. A. J., Mazurek, M., Duarte, H. S., Iacomini, M., and Duarte, J. H. (1982) Properties of carbon-13 NMR spectra of O-(1-carboxyethylidene) derivatives of methyl  $\beta$ -D-galactopyranoside: models for determination of pyruvic acid acetal structures in polysaccharides. *Carbohydr. Res.* 100, 1-15.
- Jarrell, H. C., Conway, T. F., Moyna, P., and Smith, I. C. P. (1979) Manifestation of anomeric form, ring structure, and linkage in the carbon-13 NMR spectra of oligomers and polymers containing D-fructose: maltulose, isomaltulose, sucrose, leucrose, 1-kestose, nystose, inulin, and grass levan. *Carbohydr. Res.* 76, 45-57.
- Saito, H., Ohki, T., and Sasaki, T. (1979) A carbon-13 nuclear magnetic resonance study of polysaccharide gels. Molecular architecture in the gels consisting of fungal, branched (1 $\rightarrow$ 3)-b-D-glucans (lentinan and schizophyllan) as manifested by conformational changes induced by sodium hydroxide. *Carbohydr. Res.* 74, 227-40.
- Serrianni, A. S., and Barker, R. (1984)  $^{13}\text{C}$ -Enriched tetroses and tetrofuranosides: an evaluation of the relationship between NMR parameters and furanosyl ring conformation. *J. Org. Chem.* 49, 3292-300.
- Stipanovic, A. J., and Stevens, E. S. (1981) Carbon-13 NMR of (1 $\rightarrow$ 6)-b-D-glucan (pustulan). *Makromol. Chem., Rapid Commun.* 2, 339-41.
- Vignon, M., Michon, F., Joseleau, J. P., and Bock, K. (1983) Molecular motion of branched-chain polysaccharides studied by carbon-13 NMR spin-lattice relaxation rates. *Macromolecules* 16, 835-8.
- Nakanishi, K. (1962) *Infrared Absorption Spectroscopy*, pp 34-35, Holden-Day, San Francisco.
- Majumdar, T., and Surolia, A. (1978) Cross-linked arabinogalactan: a new affinity matrix for the purification of Ricinus communis lectins. *Experientia* 34, 979-980.

- (27) Nishikawa, M., Yamashita, F., Takakura, Y., Hasida, M., and Sezaki, H. (1992) Demonstration of the receptor-mediated hepatic uptake of dextran in mice. *J. Pharm. Pharmacol.* **44**, 396–401.
- (28) Tanford, C. (1961) *Physical Chemistry of Macromolecules*, p 275, John Wiley and Sons, New York.
- (29) Cervenka, A., and Bates, T. W. (1970) Characterization of polydisperse polymers by means of gel permeation chromatography. *J. Chromatog.* **53**, 85–93.
- (30) Andrews, P. (1970) *Methods of Biochemical Analysis*, Vol. 18, pp 1–53, Interscience Publishers, New York.
- (31) Fischer, L. (1980) *Laboratory Techniques in Biochemistry and Molecular Biology, an introduction to gel chromatography*, pp 159–167, Elsevier, Amsterdam.
- (32) Clarke, A. E., Anderson, R. L., and Stone, B. A. (1979) Form and function of arabinogalactans and arabinogalactan proteins. *Phytochemistry* **18**, 521–540.
- (33) Fincher, G. B., and Stone, B. A. (1983) Arabinogalactan-proteins: structure, biosynthesis, and function. *Annu. Rev. Plant Physiol.* **34**, 47–70.
- (34) Lee, H., Kelm, S., Terno, Y., and Schauer, R. (1988) Carbohydrate specificity of the galactose-recognizing receptor of rat peritoneal macrophage. *Biol. Chem. Hoppe-Seyler* **369**, 705–714.
- (35) Sjostrom, E. (1993) *Wood Chemistry, Fundamentals and Applications*, 2nd ed., p 67, Academic Press, New York.
- (36) Valtin, H. (1983) *Renal Function, Mechanisms Preserving Fluid and Solute Balance in Health*, 2nd ed., pp 48–9, Little Brown and Company, Boston.

# Synthesis and Characterization of Oligomeric *nido*-Carboranyl Phosphate Diester Conjugates to Antibody and Antibody Fragments for Potential Use in Boron Neutron Capture Therapy of Solid Tumors

Charng-Jui Chen,<sup>†</sup> Robert R. Kane,<sup>‡</sup> F. James Primus,<sup>†</sup> György Szalai,<sup>†</sup> M. Frederick Hawthorne,<sup>‡</sup> and John E. Shively<sup>\*,†</sup>

Division of Immunology, Beckman Research Institute of the City of Hope, Duarte, California 91010, and Department of Chemistry and Biochemistry, University of California, Los Angeles, California 90024. Received July 22, 1994<sup>§</sup>

Antibodies conjugated to oligomeric carboranyl compounds have a high potential as target species for boron neutron capture therapy (BNCT) of solid tumors. As a first step toward developing conjugates with BNCT capabilities, an oligomeric *nido*-carboranyl phosphate diester (Kane, R. R., Dreschel, K., and Hawthorne, M. F. (1993) *J. Am. Chem. Soc.* 115, 8853-8854), CB10 (10 *nido*-carboranes containing 90 boron atoms) with a pseudo-5'-terminal amino group, was conjugated to the anticarcinoembryonic antigen antibody T84.66 and its F(ab') fragment. The homobifunctional linker disuccinimidyl suberate (DSS) was coupled to CB10 via its 5'-terminal amino group followed by removal of excess linker with organic solvent extraction and conjugation with intact antibody. Similarly, the heterobifunctional linker, *m*-maleimidobenzoyl-*N*-hydroxysuccinimide (MBS), was coupled to CB10 and conjugated to the hinge region sulfhydryl of the F(ab') fragment of T84.66. The extent of reaction was monitored by the mobility shift of CB10-antibody conjugate on native polyacrylamide gels and the increased susceptibility of the CB10-antibody conjugate to staining with silver nitrate. CB10 was also labeled with radioiodine (<sup>131</sup>I) in a solid phase reaction with iodogen and used in double-label studies with <sup>125</sup>I-labeled antibody. Although free CB10 bound very tightly to gel filtration media such as Sephadex G-25, the CB10-antibody conjugate passed through freely. After separation of CB10-antibody conjugate from free CB10 on Sephadex G-25, molar incorporations of CB10 were calculated. At a molar ratio of 10:1 (CB10:T84.66), greater than 90% of T84.66 and 30% of its F(ab') fragment were conjugated to CB10. The amount of CB10 covalently incorporated into mT84.66 ranged from 1.2 to 6.2 (moles per mole), with retention of immunoreactivity in the range of 80-90%. Biodistribution studies in Balb/C mice revealed high uptake of free CB10 or CB10-mT84.66 conjugate in the liver followed by rapid clearance presumably via a dehalogenation or biliary clearance mechanism. Tumor uptake at 48 h was 6.6% ID/g for CB10-mT84.66 conjugate compared to 33% ID/g in mT84.66 controls. These studies demonstrate reliable methods for the routine conjugation of oligomeric *nido*-carboranyl phosphate diesters to both antibody and antibody fragments, but suggest that the resulting conjugates are captured by the liver rendering them inefficient for tumor-targeting. Current chemical studies are being directed toward the synthesis of a variety of oligomeric carboranyl phosphate diester trailers expected to provide more acceptable biodistributions.

## INTRODUCTION

Antibody-targeted boron neutron capture therapy is a binary approach to cancer therapy based on the concept that a tumor-specific antibody can deliver selectively large amounts of the stable isotope boron-10 to the targeted tumor. Boron-10 has a great propensity to capture thermal neutrons resulting in the emission of high energy, cytotoxic particles (<sup>10</sup>B (n, α) <sup>7</sup>Li, 2.3 MeV). Since the emitted helium and lithium nuclei have a translational path of about one cell diameter, high selectivity is expected following the deposition of significant amounts of boron in the tumor mass. It has been estimated that approximately 10-30 μg of boron-10/g of tumor is needed to attain an acceptable therapeutic advantage (1). Therefore, a successful approach requires an efficient tumor-specific antibody carrying large numbers of boron-10 nuclei. We have chosen an antibody

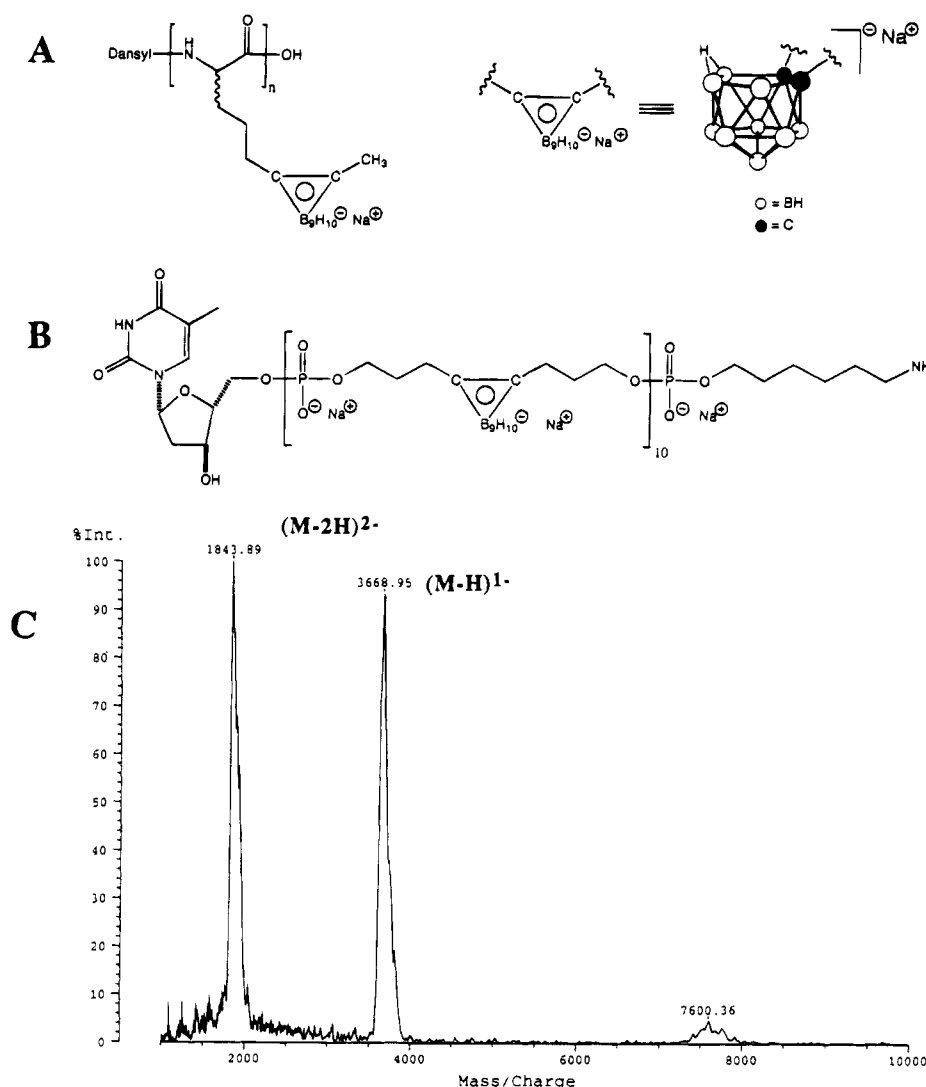
(mT84.66)<sup>1</sup> directed to carcinoembryonic antigen (CEA), a well-characterized human tumor marker antigen which has been widely used for the *in vitro* diagnosis of human colon cancer (2). The mT84.66 has a high affinity constant for CEA,  $K_{\text{aff}} = 2.6 \times 10^{10} \text{ M}^{-1}$  (3), and when radiolabeled with <sup>111</sup>In can provide up to 35% ID/g uptake in tumors in a human xenograft nude mouse model (4) and 48% sensitivity in presurgical imaging of human colon cancers (5). We have also generated a mouse/human chimeric antibody, cT84.66, which bears the mT84.66 variable region joined to human constant regions for use in human cancer diagnosis and therapy (6). In previous studies we have demonstrated the conjugation of up to 600 boron atoms to mT84.66 using homogeneous *nido*-carborane-containing peptides (Figure 1A). These conjugates exhibited high liver and low tumor uptake compared to unmodified antibody when tested in

<sup>†</sup> Beckman Research Institute of the City of Hope.

<sup>‡</sup> University of California.

<sup>§</sup> Abstract published in *Advance ACS Abstracts*, November 1, 1994.

<sup>1</sup> Abbreviations: BNCT, boron neutron capture therapy; CEA, carcinoembryonic antigen; DSS, disuccinimidylsuberate; MBS, maleimidobenzoyl-*N*-hydroxysuccinimide ester; PBS, phosphate-buffered saline; cT84.44, chimeric anti-CEA antibody; mT84.66, murine anti-CEA antibody.



**Figure 1.** Structure and mass spectrometric analysis of CB10. A. Structure of carboranyl peptide. B. Structure of carboranyl oligophosphate C. MALDI-TOF mass spectrometric analysis of carboranyl oligophosphate (CB10). The mass spectrum shows the doubly charged ( $MH^{2-}$ ), singly charged ( $MH^{1-}$ ), and singly charged dimer ( $m/z = 7600$ ) species.

an animal model (7–9). The hydrophobicity of the boron cages present in the peptide reagent was believed to adversely affect the conjugates' biodistributions. In order to increase the hydrophilicity of the boron-rich conjugation reagents, *nido*-carborane cages were coupled using phosphate diesters as the linking groups (Figure 1B). Homogeneous oligomeric phosphate diesters containing up to 400 boron atoms have been synthesized, and these highly charged species exhibit extensive water solubility (10). The present report describes the preparation and characterization of the *nido*-carboranyl phosphate diester-whole antibody conjugates as well as related F(ab')-conjugates. The biodistribution of a oligomeric *nido*-carboranyl oligophosphate diester-whole antibody conjugate in an animal model is also described.

#### EXPERIMENTAL PROCEDURES

**General.** An oligomeric *nido*-carboranyl phosphate diester (Figure 1B, hereafter called "CB 10") containing a pseudo-5'-terminal amino group was synthesized by Midland Certified Reagent Company, Midland, TX, as described previously (10). The ammonium salt was converted to the sodium form by passage over Dowex 50W-A2 (sodium form) and dried in 200 nmol aliquots. Anti-CEA monoclonal antibody (mT84.66) was purified

from ascites by 40% ammonium sulfate precipitation and protein A affinity chromatography. Anti-CEA chimeric antibody, cT84.66 (6), was produced in a Unisyn bioreactor and purified by ion-exchange and protein G affinity chromatography. Disuccinimidyl suberate (DSS), maleimidobenzoic acid *N*-hydroxysuccinimide ester (MBS), Iodogen, and Ellman's reagent were purchased from Pierce Chemical Co. Cysteine, silver nitrate, and *N,N'*-dimethylformamide (DMF) were obtained from Sigma. Ethyl acetate was supplied from Burdick & Jackson Labs.

**Mass Spectrometry.** Matrix-assisted laser desorption-time of flight mass spectrometry (MALDI-TOF) was performed on a Kratos Kompact III mass spectrometer. The sample (dissolved in water, 10 pmol in 0.5  $\mu$ L) was applied to the metal stage, mixed with 0.5  $\mu$ L of matrix (a saturated solution of 3-hydroxypicolinic acid in 30% acetonitrile/70% water containing 0.1% TFA), and analyzed in the negative ion mode according to Wu et al. (11). The  $MH^-$  and  $(MH_2)^{2-}$  peaks of an oligonucleotide were used to calibrate the instrument ( $m/z = 5735, 2867$ ).

**Silver Nitrate Spot Test.** Samples containing CB10 (2  $\mu$ L, 1.0 mM) were spotted on Whatman 3 filter paper and air dried. Five  $\mu$ L of 10% silver nitrate solution prepared in 30% ammonium hydroxide were added to the same spot. In the presence of *nido*-carborane derivatives, brown color develops within 1 min.

**Introduction of Linker Groups into CB10.** The CB10 oligomer was dissolved in 50 mM sodium borate buffer, pH 7.0, to a final concentration of 1 mM. Bifunctional linkers (DSS or MBS) were dissolved in ice cold DMF to a final concentration of 100 mM. Fifty  $\mu\text{L}$  of 1 mM CB10 was incubated with 25  $\mu\text{L}$  of 100 mM bifunctional linker at room temperature for 2 h with occasional stirring. The excess unreacted bifunctional linker was removed by three extractions with 750  $\mu\text{L}$  of ethyl acetate. The aqueous phase, containing linker-activated CB10, was used for conjugation with whole antibody or an antibody fragment.

**Preparation of CB10–mT84.66 Conjugate.** Various amounts of DSS–CB10 were mixed with mT84.66 (1 mg/mL in PBS) at room temperature for 2 h. The reaction was terminated by the addition of one-tenth volume 1 M Tris buffer, pH 8.0. The control reaction was carried out under the same conditions except the DSS–CB10 was quenched by reaction with Tris (10  $\mu\text{L}$  of 1 M Tris–HCl, pH 8) for 30 min prior to the addition of mT84.66.

**Preparation of F(ab') and CB10–Fab' Conjugate.** Anti-CEA cT84.66 (30 mg in 10 mL of 0.1 M sodium acetate, pH 4.2 buffer) was digested with pepsin employing an antibody to pepsin ratio of 100:30 (w/w) at 37 °C for 4 h. The reaction was terminated with 2 mL of 2 M Tris base. The F(ab')<sub>2</sub> fragment was purified on a Pharmacia Superose 12 column equilibrated in PBS and concentrated by ultrafiltration with an Amicon membrane to a final concentration of 10 mg/mL. The F(ab') fragment was prepared by reduction of F(ab')<sub>2</sub> with 10 mM cysteine in 40 mM ammonium carbonate, pH 8.0, at 37 °C for 2 h. The reduced F(ab') was purified by a Sephadex G-25 column equilibrated in 50 mM ammonium citrate, pH 6.3, containing 2 mM EDTA and 100 mM NaCl. The free sulphydryl content was quantitated with Ellman's reagent according to the manufacturer's instructions (Pierce). Maleimide groups in samples of CB10 activated with MBS were determined by reacting an aliquot of the sample with a fixed amount of cysteine (in excess) and back-titrating the residual sulphydryl groups with Ellman's reagent. All buffers used for the preparation of F(ab') were thoroughly degassed and saturated with nitrogen. The reduced F(ab') was mixed with MBS–CB10 at a molar ratio of 1:10. The conjugation reaction was carried out under a nitrogen atmosphere for 2 h at room temperature and subsequently terminated with a 10-fold excess of iodoacetamide.

**Analysis of Conjugation Reactions.** An aliquot from each reaction mixture was analyzed by gel electrophoresis on a Pharmacia Phastsystem using 7.5% or 10–15% gradient native or SDS polyacrylamide gels. Gels were stained for protein with Coomassie Blue only or stained briefly with silver stain (Pharmacia kit) for carboranes followed by protein staining with Coomassie Blue. The staining procedures were carried out manually following the manufacturer's instructions.

**Radioiodination of CB10 and Antibodies.** Radioiodination of CB10, mT84.66, and cT84.66 F(ab') was performed as follows: The sample (10–20  $\mu\text{g}$  of protein or oligomeric carboranyl phosphate diester in 10–20  $\mu\text{L}$  of PBS) was added to a 1.2 mL polyethylene tube coated with 10–50  $\mu\text{g}$  of Iodogen (10–50  $\mu\text{L}$  of 1 mg/mL reagent in chloroform, vacuum dried and rinsed with 10–50  $\mu\text{L}$  of PBS). The tube was enclosed in a 4 mL Reacti-Vial (Pierce) and sealed with a silicone septum. The radioiodine (0.5–1.0 mCi in 5–10  $\mu\text{L}$  of PBS; <sup>125</sup>I or <sup>131</sup>I) was injected into the vial using a Hamilton syringe and allowed to react for 2 min at room temperature. The radiolabeled sample was removed with a syringe along

with two to three rinses of 20  $\mu\text{L}$  each of PBS and, in the case of antibody or its fragments, further purified by gel filtration on a Pharmacia PD10 column in PBS. Radio-labeled CB10 was not further purified because of its high binding to Sephadex G25 and other gel permeation media.

**Purification of CB10–mT84.66 Conjugate.** In a typical experiment, 5  $\mu\text{L}$  of the <sup>125</sup>I–CB10–antibody conjugate or control reaction were loaded onto 100  $\mu\text{L}$  of Sephadex G-25 gel packed in a small pipette tip. The sample was eluted with 250  $\mu\text{L}$  of PBS, followed by another 200  $\mu\text{L}$  of PBS containing 0.05% Triton X-100 in PBS. Fractions (50  $\mu\text{L}$ ) were collected and counted. For the preparation of larger amounts of conjugate, a 1 mL Sephadex G-25 column was used to remove the free CB10.

**Determination of CB10 Content in CB10–mT84.66 Conjugates.** Variable amounts of DSS–<sup>131</sup>I–CB10 were mixed with a fixed amount of <sup>125</sup>I–mT84.66 (1 mg/mL) at room temperature for 2 h. The reaction mixture was terminated by adding 1/10 volume of 1 M Tris buffer, pH 8.0. The control reaction was carried out under the same conditions except the DSS–CB10 was inactivated with Tris–buffer, pH 8, for 30 min before mixing with antibody. An aliquot from each control and conjugation reaction mixture was analyzed on a Phastsystem 7.5% native or SDS polyacrylamide gel. The CB10 content of the CB10–antibody conjugate was determined by differential monitoring of radioactivity of the conjugated band cut from the SDS gel. The remainder of the reaction mixture was loaded onto a Sephadex G-25 column and eluted with PBS. The radioactivity of the eluate was measured and calculated as the percentage of total input.

**Immunoreactivity of CB10–mT84.66 Conjugates.** CEA coupled to Sepharose 4B (0.5 mL) was equilibrated in PBS in a spin column. The double-labeled conjugate (<sup>131</sup>I–CB10, <sup>125</sup>I–mT84.66, or <sup>125</sup>I–cT84.66 F(ab')) or the control samples purified from Sephadex G-25 were loaded to each column, incubated for 15 min at 37 °C, and washed three times with PBS containing 1% BSA. The percent of the reactivity was calculated as the percentage of the counts bound to the column to the total number of counts added.

**Biodistribution Studies.** Biodistribution studies were carried out in female athymic nude mice (NCR-nu, Simonsen, Gilroy, CA) under approval of the Institutional Research Animal Care Committee. Animals were injected sc with  $1 \times 10^6$  LS-174T colon carcinoma cells (ATCC, Rockville, MD). Seven days after tumor inoculation, approximately 4  $\mu\text{Ci}$  of dual <sup>131</sup>I- and <sup>125</sup>I-labeled control or conjugate preparations were administered by tail vein injection. Animals were euthanized at 24 and 48 h after injection of the radioiodinated preparations and blood, tumor, and normal tissues were removed. Radioactivity was determined in a multichannel  $\gamma$  counter with counts appearing in the <sup>125</sup>I channel corrected for <sup>131</sup>I cross-over.

## RESULTS

**Characterization of CB10.** CB10 is an oligomeric *nido*-carboranyl phosphate diester with an amino group at the pseudo-5'-terminus and a thymidine at the pseudo-3'-terminus (Figure 1B). It was synthesized by adding 10 carboranyl monomers, followed by a hexylamine linker residue, to a thymidine-derivatized resin using standard phosphoramidate chemistry on a DNA synthesizer (10). The oligomer was removed from the resin and deprotected by treatment with concentrated ammonium hydroxide (30 min at 80 °C). The ammonium hydroxide treatment also converted the *closo*-carborane structure



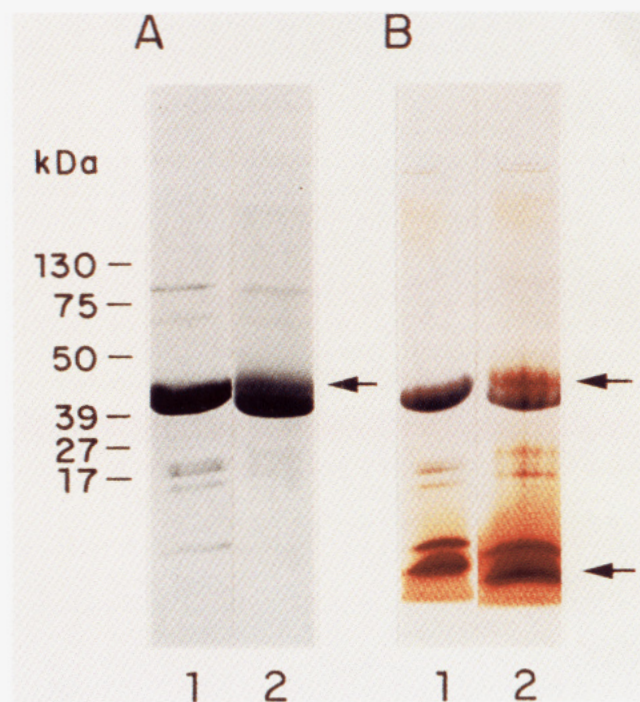
to the corresponding anionic *nido*-cage. The initially isolated ammonium salt of CB10 was converted to its corresponding sodium salt on Dowex 50W-A2 resin (sodium form) and was used directly for coupling to crosslinkers. Both the sodium and ammonium salts of CB10 were extremely water soluble.

The mass of CB10 as determined by negative ion MALDI-TOF MS was 3669 (Figure 1C). The predicted mass of fully protonated CB10 is 3514.9 while that of its sodium salt is 3956.5. The intermediate value of 3669 probably corresponds to a mixture of species differing in their relative contents of sodium and proton neutralized structures. The unusual peak width may be due to this phenomenon as well as the abundant (20%)  $^{10}\text{B}$  isotope.

**Coupling of Linkers to CB10.** Because of difficulties in purifying CB10 or CB10-linker conjugates (CB10 bound strongly to dextran and polyacrylamide-based gel permeation media as well as silica-based C18 media), a simple organic solvent extraction method was developed to separate excess linker from free or linker-coupled CB10. The efficiency of the extraction of the MBS bifunctional linker with ethyl acetate was tested by back titration of underivatized cysteine with Ellman's reagent after a fixed amount of cysteine was allowed to react with MBS in the aqueous phase (1:3 molar ratio of MBS to cysteine). After three extractions with ethyl acetate (10 vol), MBS was completely removed. The recovery of CB10 during extraction was monitored either by a silver nitrate spot test or by counting of radiolabeled CB10. The recovery of CB10 was >95%. The bifunctional linker DSS was also removed efficiently by ethyl acetate extraction. The aqueous phase which contained CB10-coupled linker was used for whole antibody or antibody fragment conjugation.

**Preparation and Analysis of CB10-F(ab') Conjugate.** The  $\text{F(ab')}_2$  fragments were generated by pepsin treatment of cT84.66 and reduced with 10 mM cysteine for 2 h at 37 °C. Excess reducing reagent was removed by gel filtration. Greater than 90% of  $\text{F(ab')}_2$  fragments were reduced to  $\text{F(ab')}$  when analyzed by nonreducing SDS gel electrophoresis. The reduced  $\text{F(ab')}$  fragment contained 1.8 equiv of the sulhydryl function per mole of  $\text{F(ab')}$  fragment as measured by Ellman's reagent. The sulhydryl content decreased significantly upon storage (50% in 2 days), but remained in a monomeric  $\text{F(ab')}$  form when analyzed by SDS polyacrylamide gel electrophoresis. The CB10-F(ab') conjugate was prepared by the addition of MBS-CB10 at a molar ratio of 10:1 to  $\text{F(ab')}$  (2 mg/mL) immediately after the removal of excess reducing agent and analyzed by SDS gel electrophoresis. The CB10-F(ab') conjugate migrated more slowly than the unconjugated  $\text{F(ab')}$  during SDS gel electrophoresis (Figure 2A). When the gel was stained briefly with silver nitrate followed by Coomassie Blue, the CB10-F(ab') stained intensively as a broad brown band immediately above the blue band corresponding to the unconjugated  $\text{F(ab')}$  fragment. Unconjugated CB10 migrated at the dye front as one or two bands. The best yield for the conjugation of CB10 to  $\text{F(ab')}$  was about 30% as judged by the Coomassie Blue staining (Figure 2, Panel A, lane 2). Although a wide variety of conditions were explored to increase the conjugation efficiency, including higher concentrations of  $\text{F(ab')}$  and higher molar ratios of CB10 to  $\text{F(ab')}$ , the maximum yield obtained was about 30%. The low conjugation efficiency might be a result of the tendency of the  $\text{F(ab')}$  fragment to form intramolecular disulfide bonds, as judged by its rapid loss of free sulhydryl content without  $\text{F(ab')}_2$  fragment formation.

**Preparation and Analysis of CB10-mT84.66 Conjugate.** A 5–15-fold molar excess of DSS-CB10 was



**Figure 2.** Dual stain analysis of the CB10-F(ab') conjugate on SDS gel electrophoresis.  $\text{F(ab')}$  (2 mg/mL) prepared from anti-CEA cT84.66 was mixed with MBS-CB10 at a molar ratio of 1:10. The conjugation reaction was carried out in the presence of 50 mM ammonium acetate, pH 6.3, containing 2 mM EDTA, 100 mM NaCl for 2 h at room temperature. Lane 1: control reaction,  $\text{F(ab')}$  was alkylated with iodoacetamide prior to mixing with MBS-CB10. Lane 2: conjugation reaction. Panel A: staining with Coomassie Blue. Panel B: the gel was stained briefly with silver nitrate and followed by Coomassie Blue staining. The upper arrow indicates the CB10-F(ab') conjugate, which was detected as a broad brown band on the top of the unconjugated  $\text{F(ab')}$  band. The bottom arrow indicates free CB10.

incubated with mT84.66 (1 mg/mL) in PBS at room temperature for 2 h. When an aliquot of the conjugation mixture was analyzed by SDS polyacrylamide gel under nonreducing conditions, no significant difference in mobility was observed between conjugated and unconjugated antibody (data not shown). However, when the CB10-mT84.66 conjugation mixtures were analyzed on a native gel, the mobility of the CB10-mT84.66 conjugate was markedly retarded (Figure 3, lanes 2–4). Unconjugated CB10 migrated at the dye front. At higher molar ratios (15:1) of DSS-CB10 to mT84.66 the conjugate exhibited less retardation compared to free mT84.66 (Figure 3, lane 2). The reason for the lessened mobility shift at higher CB10 incorporation levels is not clear. When the gel was stained briefly with silver nitrate prior to Coomassie Blue, the CB10-mT84.66 conjugate stained brown and unconjugated antibody stained blue, similar to the pattern observed for the CB10-F(ab') conjugate. This staining pattern is due to the facile reduction of silver ion by incorporated CB10 (under these conditions proteins are not stained with silver nitrate). The mobility shift together with the unique silver staining pattern provided a convenient method with which to monitor the conjugation reaction. As shown in Figure 3, lane 2, when the DSS-CB10 to mT84.66 ratio increased to 15:1, more than 90% of the mT84.66 was conjugated to CB10.

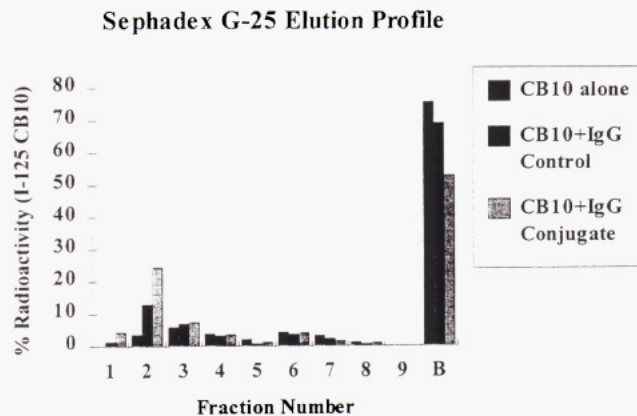
**Partial Purification of CB10-mT84.66 Conjugate.** In preliminary experiments, we investigated the use of gel filtration media to remove excess unconjugated CB10 from CB10-antibody conjugate. Since we already knew that low concentrations of CB10 bind tightly to Sephadex G-25, we reasoned that excess CB10 would be bound to



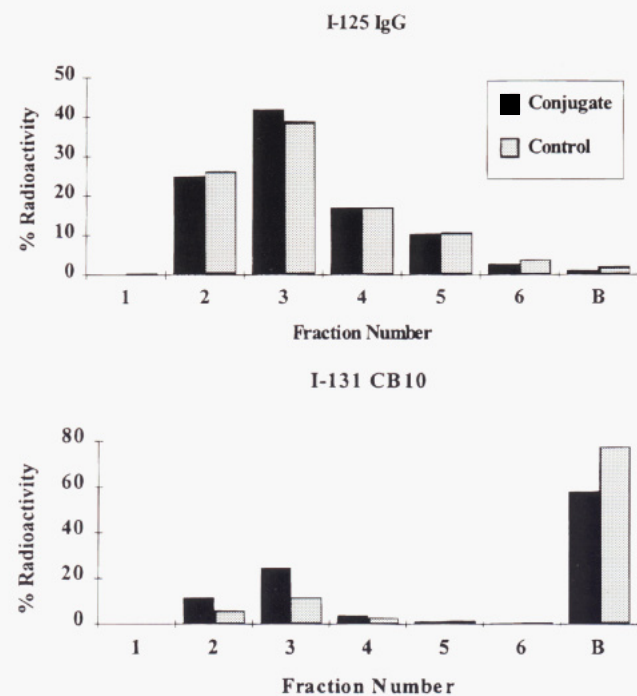


**Figure 3.** Analysis of the CB10–mT84.66 conjugate by native polyacrylamide gel electrophoresis. The CB10–mT84.66 conjugate and the control reaction mixtures were analyzed by electrophoresis on a Phast-system 7.5% native polyacrylamide gel. The gel was stained briefly with silver stain and followed by Coomassie Blue stain. Lane 1: Control reaction. Lane 2–4: the conjugation reactions were carried out at a DSS–CB10/antibody molar ratio of 15 (lane 2), 10 (lane 3), and 5 (lane 4). The top left arrow indicates the CB10–antibody conjugates. The bottom left arrow indicates free CB10. The right arrow indicates unconjugated antibody.

the column, while conjugated CB10 would be eluted with the antibody. To test this possibility, five  $\mu\text{L}$  of the  $^{125}\text{I}$ -labeled CB10–antibody conjugate reaction mixture was loaded onto a 100  $\mu\text{L}$  bed volume of Sephadex G-25 in a micropipette tip and was eluted with PBS followed by PBS containing 0.05% Triton X-100. Two control reactions were carried out under the same conditions, one with  $^{125}\text{I}$ -CB10 only, and another with a mixture of inactivated  $^{125}\text{I}$ -CB10 and antibody. When CB10 alone was loaded to the column, about 15% of the radioactivity was eluted from the column, while 85% was bound to the resin. The addition of Triton X-100 did not improve the dissociation of CB10 from the Sephadex G-25 once the CB10 had bound (Figure 4). When the conjugation reaction mixture was loaded onto the Sephadex G-25 column, approximately 40% of the labeled CB10 eluted from the column, while 53% bound to the column. An additional 7% was eluted by 0.05% Triton X-100 in PBS. The control mixture containing unconjugated CB10 and antibody gave 23% of the counts in the eluate, an 8% increase over the CB10 only control. These results indicate that CB10 can noncovalently bind to mT84.66, thus complicating the analysis of the reaction mixture by Sephadex gel filtration. Furthermore, it is possible that a small percentage of the CB10–mT84.66 conjugate was irreversibly bound to the column. In order to investigate this possibility, double labeled CB10–mT84.66 conjugate was prepared in which mT84.66 was  $^{125}\text{I}$  labeled, and the CB10 was  $^{131}\text{I}$  labeled. As shown in Figure 5, greater than 98% of the doubled labeled  $^{131}\text{I}$ -CB10- $^{125}\text{I}$ -mT84.66 conjugate passed through the column. The remaining counts bound to the column were solely due to free  $^{131}\text{I}$ -CB10. This was further confirmed by analysis of the conjugation reaction mixture before and



**Figure 4.** Analysis of  $^{125}\text{I}$ -CB10–mT84.66 conjugate by Sephadex G-25 chromatography. DSS– $^{125}\text{I}$ -CB10 was mixed with mT84.66 (1 mg/mL in PBS) at a molar ratio of 10:1. After 2 h of incubation, 5  $\mu\text{L}$  of the conjugation mixture was loaded onto a 100  $\mu\text{L}$  Sephadex G-25 column and was eluted with 250  $\mu\text{L}$  of PBS, followed by 200  $\mu\text{L}$  of PBS containing 0.05% Triton X 100. Tris buffer inactivated DSS– $^{125}\text{I}$ -CB10 was used in the control reaction. Counts for each fraction (50  $\mu\text{L}$ ) and counts irreversibly bound to the column (B) were measured and plotted as the percentage of the total input.

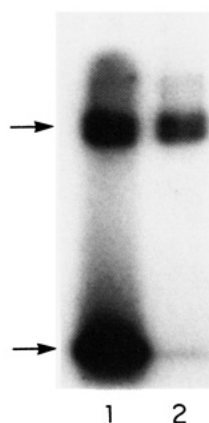


**Figure 5.** Profile of double-labeled CB10–mT84.66 conjugate on Sephadex G-25. The experimental procedures were the same as described in Figure 4 (CB10 to antibody molar ratio of 10:1), except that mT84.66 was labeled with  $^{125}\text{I}$  and CB10 with  $^{131}\text{I}$ . The control and conjugation reaction mixture was loaded onto a Sephadex column and eluted with PBS. The counts for each fraction (50  $\mu\text{L}$ ) and the counts irreversibly bound to the column (B) were measured and plotted as the percentage of the total input. Upper panel:  $^{125}\text{I}$  counts (mT84.66). Lower panel:  $^{131}\text{I}$  counts (CB10).

after passing through Sephadex G-25 resin by SDS gel electrophoresis followed by the autoradiography (Figure 6). These results show that the gel filtration purified sample contains no unconjugated CB10 and confirm that gel filtration is an appropriate method for the removal of excess CB10 from CB–mT84.66 conjugate.

**Determination of CB10 Content in Conjugates.** Double-labeled CB10–mT84.66 conjugate was used for the determination of the nonspecific binding of CB10 and quantitation of the incorporation of CB10 into mT84.66.





**Figure 6.** SDS-PAGE analysis of  $^{125}\text{I}$ -CB10-mT84.66 conjugate before and after Sephadex G-25 filtration. The unfractionated conjugation mixture and the second fraction of eluate from the Sephadex G-25 column (Figure 4) were analyzed on a Phastsystem 10–15% gradient SDS gel, followed by autoradiography. Lane 1: the conjugation reaction mixture of  $^{125}\text{I}$ -CB10 and antibody. Lane 2: the peak fraction eluted from the Sephadex G-25 column. Upper arrow indicates the radioactive band which corresponds to the CB10 conjugated antibody. The lower arrow indicates free CB10.

Increasing amounts of DSS-CB10 were incubated with a fixed amount of mT84.66 at room temperature for 2 h. An aliquot from each control and conjugation reaction mixture was analyzed by electrophoresis on a 7.5% native and SDS polyacrylamide gel. The rest of the reaction mixture was partially purified by passing through a 1 mL Sephadex G-25 column. The calculated CB10 incorporation of control and CB10-mT84.66 conjugates after removal of free CB10 is shown in Table 1. The moles of CB10 incorporated per mole into mT84.66 was dependent on the molar ratio of CB10 to mT84.66 used in the conjugation reaction. When the molar ratio of CB10/mT84.66 in the conjugation reaction was increased from 5 to 25, the amount of CB10 incorporated into mT84.66 was increased from 2.4 to 11.3 mol/mol of mT84.66. However, the nonspecific binding also increased from 1.2 to 5.1 mol of CB10/mol of mT84.66. Thus, the moles of CB10 covalently incorporated into the CB10-mT84.66

conjugate ranged from 1.2 to 6.2 (difference between conjugate and control). In addition, the control and conjugate were analyzed by SDS polyacrylamide gel electrophoresis by excising and counting the gel bands corresponding to conjugated and unconjugated mT84.66 (Table 2). The calculated CB10 incorporation for both the nonspecific binding control and specific binding conjugate were lower but comparable with the CB10 content measured from the Sephadex G-25 gel filtrate.

#### Immunoreactivity of CB10-mT84.66 Conjugate.

After removal of excess CB10 from the conjugate by Sephadex G-25 chromatography, the immunoreactivity of the modified antibodies was tested by binding to a CEA-Sepharose 4B spin column. The double labeled ( $^{131}\text{I}$ -CB10,  $^{125}\text{I}$ -mT84.66, or  $^{125}\text{I}$ -F(ab')) conjugates and the control samples (mixture of inactivated CB10 and mT84.66 purified from Sephadex G-25) were loaded onto the CEA affinity column, and washed three times with PBS containing 1% BSA. The percent immunoreactivity was calculated as the percentage of the counts bound to the column over input counts. As shown in Table 3, the immunoreactivity of the control sample was 92%. This suggests that the nonspecific association of CB10 with antibody did not alter its immunoreactivity. The CB10-mT84.66 conjugate retained greater than 80% of immunoreactivity even for the highest levels of CB10 incorporation. The CB10-F(ab') conjugate gave essentially the same immunoreactivity (ca. 60%) as control F(ab'). In this case, the loss of immunoreactivity was due to radioiodination conditions.

**Biodistribution of CB10-mT84.55 Conjugates.** Because the yields of Fab' conjugates were low, biodistribution studies with double-labeled whole antibody conjugates were carried out in tumor-bearing nude mice. Radioiodinated whole mT84.66-CB10 conjugate was prepared as described above using a 15:1 ratio of  $^{125}\text{I}$ -labeled CB10 to  $^{131}\text{I}$ -mT84.66. A control preparation consisting of a mixture of radioiodinated CB10 and mT84.66 was also produced as described above. The CEA binding properties of the control and conjugate preparations were very similar to that shown in Table 3. The distribution of mT84.66 and CB10 in blood and selected tissues at 24 h after injection is shown in Figure 7. The

**Table 1.** CB10 Incorporation into the CB10-mT84.66 Conjugate after Separation by Sephadex G-25 Filtration<sup>a</sup>

input molar ratio	$^{131}\text{I}$ -CB10 eluate/input (%)		$^{125}\text{I}$ -mT84.66 eluate/input (%)		CB10/mT84.66 output molar ratio	
	control	conjugate	control	conjugate	control	conjugate
5	23	48	97	99	1.2	2.4
10	19	45	95	96	2.0	4.5
15	19	46	97	96	2.3	7.2
20	20	46	98	96	4.1	10.0
25	20	44	96	97	5.1	11.3

<sup>a</sup> The antibody was  $^{125}\text{I}$  labeled and CB10 was  $^{131}\text{I}$  labeled and reacted with DSS as described in the Experimental Procedures. After mT84.66 and DSS-CB10 were reacted at the indicated input molar ratios (CB10/mT84.66; column 1), conjugate was separated from unconjugated material on a 1 mL Sephadex column and output molar ratios were calculated (columns 6 and 7). Controls are treated in the same way, except that the DSS-CB10 was treated with Tris base to prevent covalent coupling to mT84.66.

**Table 2.** CB10 Incorporation into CB10-mT84.66 Conjugate after Separation by SDS Polyacrylamide Gel Electrophoresis<sup>a</sup>

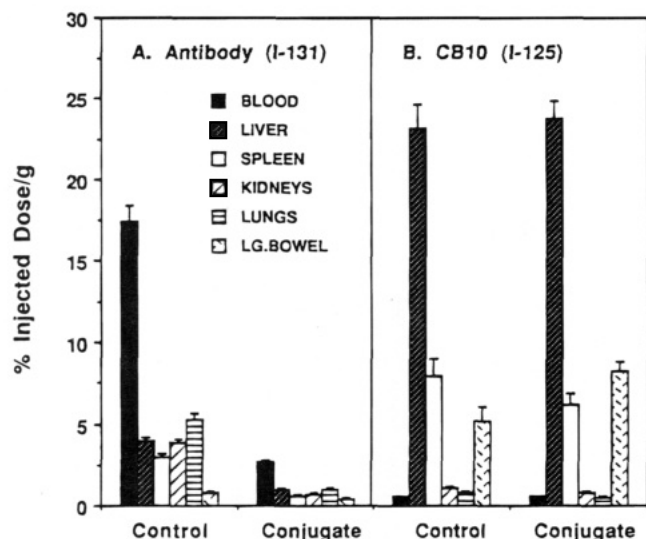
input molar ratio	$^{131}\text{I}$ -CB10-mT84.66/Input (%)		$^{125}\text{I}$ -mT84.66/input (%)		CB10/mT84.66 output molar ratio	
	control	conjugate	control	conjugate	control	conjugate
5	21	27	81	82	1.2	1.5
10	20	24	80	81	2.0	3.1
15	16	23	79	82	2.7	5.1
20	14	28	82	76	3.7	6.3
25	15	33	81	81	5.2	10.0

<sup>a</sup> The double-labeled sample was prepared as described in Table 1 and analyzed by SDS gel electrophoresis under nonreducing conditions. The gel bands corresponding to antibody were excised and the radioactivity for each band was measured. The percentage of the radioactivity compared to the total input was calculated. CB10 incorporation into the antibody was calculated based on the measurement of the ratios of  $^{125}\text{I}$  to  $^{131}\text{I}$  in the excised conjugate band (columns 6 and 7).

**Table 3.**  $^{125}\text{I}$ -mT84.66 or F(ab') Binding (Immunoreactivity) and  $^{131}\text{I}$ -CB10 Binding to a CEA Affinity Column<sup>a</sup>

input molar ratio CB10–mT84.66	immunoreactivity (%)	
	control	conjugate
5	93	82
10	104	85
15	92	90
20	100	86
25	102	84

<sup>a</sup> The conjugates were synthesized with  $^{125}\text{I}$ -mT84.66 or F(ab') and  $^{131}\text{I}$ -CB10. The immunoreactivity was calculated as the percentage of the  $^{125}\text{I}$  counts bound to a CEA-Sepharose 4B spin column. The control was  $^{125}\text{I}$ -labeled mT84.66 or the F(ab') fragment. The input ratio for F(ab') was 10 with 61% immunoreactivity for the control and 64% for the conjugate.



**Figure 7.** Biodistribution of CB10–mT84.66 conjugate in athymic nude mice bearing LS-174T colon carcinoma xenografts. The control group consisted of animals injected with a mixture of  $^{131}\text{I}$ -labeled antibody plus  $^{125}\text{I}$ -labeled CB10. The conjugate was prepared with  $^{125}\text{I}$ -labeled CB10 and  $^{131}\text{I}$ -labeled antibody, and purified by gel filtration. Measurement of (A) antibody and (B) CB10 distribution 24 h after injection.

level of circulating mT84.66, as indicated by  $^{131}\text{I}$  activity, was markedly reduced in animals receiving the conjugate as compared to the control preparation (Figure 7A). Depressed levels of mT84.66 in normal tissues was also evident in animals injected with the conjugate. By contrast, animals injected with either the control or conjugate had similar elevated levels of CB10, as indicated by  $^{125}\text{I}$  activity, in the liver followed by spleen and large intestine (Figure 7B). Blood levels of CB10 were very low in both animal groups. Uptake of either mT84.66 or CB10 in other normal tissues such as heart, muscle, stomach, and small bowel was unremarkable and is not shown for clarity. An identical distribution pattern was observed at 48 h (data not shown). The elevated level of CB10 in the livers of mice injected with the conjugate suggests that the low level of circulating antibody observed in this group (Figure 7A) was due to the liver-mediated clearance of the conjugate. While it might be expected that the  $^{131}\text{I}$  labeled antibody in the conjugate should follow the  $^{125}\text{I}$ -labeled CB10 levels in the liver, this was not observed, and was probably due to dehalogenation of radioiodine from the antibody in the liver. Dehalogenation of  $^{125}\text{I}$  labeled CB10 did not occur in the liver, suggesting that radioiodine attached to CB10 is metabolically stable. Since CB10 was not covalently attached to mT84.66 in the control preparations, the liver uptake of CB10 in the control group did not affect the

**Table 4.** Tumor Localization of CB10 Following Injection of Whole CB10–mT84.66 Conjugate<sup>a</sup>

time (h)	group	% injected dose/g		
		mT84.66 ( $^{131}\text{I}$ )	CB10 ( $^{125}\text{I}$ )	tumor wt (g)
24	control	37.23 ± 3.86 <sup>b</sup>	1.16 ± 0.09	0.16 ± 0.03
	conjugate	5.32 ± 0.31	0.89 ± 0.06	0.22 ± 0.07
48	control	33.71 ± 3.47	0.83 ± 0.06	0.42 ± 0.07
	conjugate	6.61 ± 0.54	0.88 ± 0.06	0.23 ± 0.04

<sup>a</sup> Athymic nude mice bearing LS-174T colon carcinoma xenografts were injected iv with a mixture (control) of  $^{131}\text{I}$ -labeled antibody +  $^{125}\text{I}$ -labeled CB10 or the double labeled CB10–mT84.66 conjugate. <sup>b</sup> Mean ± SEM.

clearance of antibody from the blood. Mice injected with antibody alone had similar levels of circulating antibody as compared to the control group (data not shown).

The tumor localization of antibody and CB10 in the control and conjugate groups is depicted in Table 4. At both time points, accumulation of antibody in control group tumors was five to seven times higher than that in tumors from animals injected with conjugate. The reduced tumor targeting of the conjugate reflects its more rapid elimination from the blood (Figure 7A). Tumor uptake of CB10 was low and did not differ between the two groups at both time points.

## DISCUSSION

A method has been developed to rapidly synthesize oligomers of carboranyl phosphate diesters which mimic nucleotides and contain multiple *nido*-carborane cages (1–20 or more) (10). Starting with appropriately protected carboranyl monomers, the oligophosphate synthesis was performed on a standard automated DNA synthesis instrument with no modifications to the standard reagents or procedures. For convenience, the oligomers begin with a 3'-thymidine (which also contributes UV absorbance at 260nm), while the 5' terminal group is a hexylamine moiety to allow crosslinking to proteins. During deprotection with ammonium hydroxide the protecting groups are removed and each closo-CB cage is converted to the corresponding *nido*-structure. Thus, the CB oligomers are more negatively charged (two negative charges per CB) than their oligonucleotide counterparts (one negative charge per nucleotide). This property has made it difficult to analyze the CB oligomers by conventional positive ion mass spectrometry. However, we were able to confirm the mass of a CB20mer (10) and the CB10 used in this work by negative ion electrospray mass spectrometry and MALDI-TOF, respectively. Although the CB oligomers are very water soluble they exhibit some unusual properties, such as high binding to gel filtration media and anion exchangers (they are not bound to cation exchangers). In this work, attempts to purify CB10 by reversed phase HPLC in 0.1% TFA–acetonitrile were unsuccessful because the sample became hydrophobic after elution from the C18 column. We attribute this property to the expected increase in hydrophobicity of the fully protonated oligomer. Due to this problem, we decided to couple CB10 to antibody and then purify the conjugate by gel filtration.

Two cross-linking agents were studied, MBS for conjugation of the amino-CB10 to the sulfhydryl group of an F(ab') antibody fragment and DSS for conjugation of amino-CB10 to whole antibody (via the  $\epsilon$ -amino group of lysine). An organic extraction procedure was shown to successfully remove excess crosslinker from CB10 with no loss of the carborane oligomer. Conjugation of CB10 to either whole antibody or F(ab') fragment resulted in a product which was retarded relative to the protein on

polyacrylamide gel electrophoresis in the presence or absence of SDS. Free CB10 migrates near the dye front on gel electrophoresis, consistent with its highly negatively charged nature. Thus, it appears that the anionic nature of CB10 was not sufficient to increase the electrophoretic mobility of the protein but, in fact, actually retarded its migration. The conjugates were stained with a silver nitrate stain, specific for the carborane, and with Coomassie Blue, specific for the protein. The double staining pattern clearly revealed that the conjugate was retarded relative to the unmodified protein. The whole antibody conjugate could be purified by gel filtration with irreversible binding of free CB10 to the gel filtration media. In this case, the strong binding characteristic of the CB10 to gel filtration media was overcome by its conjugation to antibody. Analysis of the double-labeled purified conjugate by SDS gel electrophoresis revealed that the conjugate contains no free CB10. Analysis of the doubly labeled conjugate revealed a specific incorporation of 1–10 CB10mers per antibody molecule, corresponding to 90–900 boron atoms per antibody. In addition, the purified conjugate retained over 80% of its immunoreactivity as measured against a radiolabeled antibody control.

When the purified conjugate was injected into animals bearing a CEA positive tumor xenograft, a large portion of the conjugate (20–25% ID/g at 24 h) biodistributed to the liver. The tumor uptake was reduced from 30–40% ID/g in antibody controls to 5–7% ID/g in conjugate injected animals. These results are almost identical to those we obtained for carboranyl peptides attached to antibody (8). In those studies up to 600 boron atoms were attached per antibody, with retention of 80–90% immunoreactivity, and in biodistribution studies gave 15–25% ID/g in liver and 4–5% ID/g in tumor.

Recently, Barth et al. (12) conjugated highly boronated "starburst dendrimers" to the antimelanoma antibody IB16-6 using MBS and SPDP crosslinkers. Preparations with up to 2200 boron atoms per antibody molecule retained up to 82% immunoreactivity. However, in biodistribution studies, 11% ID/g was localized in the liver and only 0.4% ID/g in tumor xenografts. These results are similar to ours for liver uptake, but 10 times lower than ours for tumor accretion. Thus, three very different approaches to generate boron rich oligomers have been devised, as well as conjugation methods leading to antibodies which retain high immunoreactivities. In spite of this exciting progress, all of the boron rich oligomers have dramatically altered the antibody-targeting characteristics by increasing liver uptake at the expense of tumor targeting. It is possible that these compounds bind to an as yet unidentified receptor in the liver. Further studies are needed to understand the nature of the liver uptake so that a rational approach can be used to overcome this problem. We continue to be optimistic about this approach, since the formidable problems of chemical synthesis and antibody conjugation have been solved. It is reasonable to assume that further modifications of the carboranyl oligomers will reduce liver uptake.

## ACKNOWLEDGMENT

This research was supported by grants CA53870 and CA31753 from the NIH. R.R.K. was supported in part by a Tumor Cell Biology Fellowship (NIH NRSA CA09056). We gratefully acknowledge the technical assistance of Toby O'Neil.

## LITERATURE CITED

- (1) Hawthorne, M. F. (1993) The role of chemistry in the development of boron neutron capture therapy of cancer. *Angew. Chem., Int. Ed. Engl.* 32, 950–984.
- (2) Shively, J. E., and Beatty, J. D. (1985) CEA-related antigens: molecular biology and clinical significance. *Crit. Rev. Oncol. Hematol.* 2, 355–399.
- (3) Wagener, C., Yang, Y. H. J., Crawford, F. G., and Shively, J. E. (1983) Monoclonal antibodies for carcinoembryonic antigen and related antigens as a model system: a systematic approach for the determination of epitope specificities of monoclonal antibodies. *J. Immunol.* 130, 2308–2315.
- (4) Jakowatz, J. G., Beatty, B. G., Vlahos, W. G., Porduminski, D., Philben, V. J., Williams, L. E., Paxton, R. J., Shively, J. E., and Beatty, J. D. (1985) High specific activity indium-111-labeled anti-carcinoembryonic antigen monoclonal antibody: biodistribution and imaging in nude mice bearing human colon cancer xenografts. *Cancer Res.* 45, 5700–5706.
- (5) Beatty, J. D., Williams, L. E., Yamauchi, D., Morton, B. A., Hill, L. R., Beatty, B. G., Paxton, R. J., Merchant, B., and Shively, J. E. (1990) Presurgical imaging with indium-labeled anti-carcinoembryonic antigen for colon cancer staging. *Cancer Res.* 50S, 922s–926s.
- (6) Neumaier, M., Shively, L., Chen, F.-S., Gaida, F.-J., Ilgen, C., Paxton, J., Shively, J. E., and Riggs, A. D. (1990) Cloning of the genes for T84.66, an antibody that has a high specificity and affinity for carcinoembryonic, and expression of chimeric human/mouse T84.66 genes in myeloma and chinese hamster ovary cells. *Cancer Res.* 50, 2128–2134.
- (7) Hawthorne, M. F. (1991) Biochemical application of boron cluster chemistry. *Pure and Appl. Chem.* 24, 327–334.
- (8) Varadarajan, A., and Hawthorne, M. F. (1991) Novel carboranyl amino acids and peptides: reagents for antibody modification and subsequent neutron-capture studies. *Bioconjugate Chem.* 2, 242–253.
- (9) Paxton, R. J., Beatty, B. G., Varadarajan, A., and Hawthorne, M. F. (1992) Carboranyl peptide-antibody conjugates for neutron-capture therapy: preparation, characterization, and in vivo evaluation. *Bioconjugate Chem.* 3, 241–247.
- (10) Kane, R. R., Drechsel, K., and Hawthorne, M. F. (1993) Automated synthesis of carborane-derived homogeneous oligophosphates: reagents for use in the immunoprotein mediated boron neutron capture therapy of cancer. *J. Am. Chem. Soc.* 115, 8853–8854.
- (11) Wu, K. J., Steding, A., and Becker, C. H. (1993) Matrix-assisted laser desorption time of flight mass spectrometry of oligonucleotides using 3-hydroxypicolinic acid as an ultra-violet matrix. *Rapid Commun. Mass Spectrom.* 7, 142–146.
- (12) Barth, R. F., Adams, D. M., Soloway, A. H., Alam, F., and Darby, M. V. (1994) Boronated starburst dendrimer-mono-clonal antibody immunoconjugates: evaluation as a potential delivery system for neutron capture therapy. *Bioconjugate Chem.* 5, 58–66.

# A Facile, Water-Soluble Method for Modification of Proteins with DOTA. Use of Elevated Temperature and Optimized pH To Achieve High Specific Activity and High Chelate Stability in Radiolabeled Immunoconjugates

Michael R. Lewis,<sup>†</sup> Andrew Raubitschek,<sup>‡</sup> and John E. Shively<sup>\*,†</sup>

Division of Immunology, Beckman Research Institute of the City of Hope, Duarte, California 91010, and Department of Radioimmunotherapy, City of Hope National Medical Center, Duarte, California 91010. Received July 12, 1994 \*

We have developed a method for attachment of the macrocyclic chelating agent 1,4,7,10-tetraazacyclododecane *N,N',N'',N'''*-tetraacetic acid (DOTA) to proteins by activation of a single carboxyl group with *N*-hydroxysulfosuccinimide (sulfo-NHS). The sulfo-NHS active ester of DOTA was prepared in a single step using 1-ethyl-3-[3-(dimethylamino)propyl]carbodiimide (EDC), and DOTA conjugates of cytochrome c and the anti-carcinoembryonic antigen chimeric monoclonal antibody cT84.66 were prepared by adding the DOTA active ester reaction mixture to the proteins at pH 8.5–9.0. Mass spectrometry of the cytochrome c conjugates showed that as the molar ratio of DOTA active ester to protein in the reaction mixture was increased from 10:1 to 100:1, the average number of chelators attached to the protein molecule increased from 2.64 to 8.79. When DOTA active ester reacted with the antibody at a molar ratio of 100:1, the conjugate averaged 3.8 chelates per antibody. Immuno-reactivity of the antibody conjugate radiolabeled with <sup>111</sup>In(III) and <sup>90</sup>Y(III) remained quantitative. Variation of the DOTA:sulfo-NHS:EDC activation stoichiometry from 2:2:1 to 10:10:1 revealed that the kinetic stability of the radioconjugates increased as the molar ratio of carbodiimide, relative to DOTA and sulfo-NHS, was decreased. Radiolabeling of the protein conjugates with <sup>111</sup>In(III) and <sup>90</sup>Y(III) proved to be sensitive to pH, buffer, and temperature effects. The optimum pH for the labeling reaction was different for each protein and may be related to the isoelectric point of the protein. Radiometal incorporation at high specific activity was accomplished in acetate and Tris buffers, but the presence of citrate inhibited the labeling reaction. Increasing the temperature of the radiolabeling reaction from 25 to 43 °C greatly increased both the efficiency of radiometal incorporation and the kinetic stability of the radioconjugates. Stability studies of the conjugates in human serum and in the presence of a 5000- to 250 000-fold excess of diethylenetriaminepentaacetic acid (DTPA) demonstrated that the radiolabeled proteins are kinetically inert under physiological conditions. In serum, the <sup>111</sup>In(III)-labeled antibody showed a rate of radiometal loss of approximately 0.08% per day. In the presence of excess DTPA, both conjugates lost <sup>111</sup>In(III) at a rate of about 0.3% per day. No loss of <sup>90</sup>Y(III) from the conjugates was observed in serum, but in excess DTPA, both <sup>90</sup>Y(III) labeled proteins showed a rate of radiometal loss of approximately 0.2% per day. Therefore, kinetic analysis of metal loss from a radiolabeled immunoconjugate in the presence of a vast excess of DTPA may provide a better indication of the *in vivo* stability of that immunoconjugate than serum stability studies.

## INTRODUCTION

Labeling of monoclonal antibodies (mAbs) with radioactive metals for cancer diagnosis and therapy has usually been accomplished by the use of bifunctional chelating agents, which contain both a reactive functionality for covalent attachment to proteins and a strong metal-binding group capable of forming a physiologically stable complex with the radionuclide (1–3). Radiometals such as <sup>111</sup>In(III), <sup>67</sup>Ga(III), and <sup>99m</sup>Tc(VII) have physical properties which are well suited for tumor imaging with mAbs, while <sup>90</sup>Y(III), <sup>67</sup>Cu(II), <sup>186</sup>Re(VII), and <sup>177</sup>Lu(III) have cytotoxic properties which can be exploited for therapy by antibody-directed tumor targeting (2–6). Bifunctional chelating agents which form physiologically stable complexes with metal ions are desirable for radioimmunoscintigraphy and radioimmunotherapy in order to reduce radiation damage and toxicity to normal organs and tissues (7). One class of chelating agents that

has shown great promise for monoclonal antibody applications are the polyazamacrocyclic polycarboxylate ligands (8–23), and one of these compounds, 1,4,7,10-tetraazacyclododecane *N,N',N'',N'''*-tetraacetic acid (DOTA<sup>1</sup>), has become a subject of widespread interest because it forms extremely stable complexes with a wide variety of metals (24–29).

Conjugation of monoclonal antibodies to DOTA usually involves the use of a bifunctional derivative of the chelating agent that is the product of a nontrivial, multistep synthetic route (9, 12, 16–19). Considerable

<sup>1</sup> Abbreviations: DOTA, 1,4,7,10-tetraazacyclododecane *N,N',N'',N'''*-tetraacetic acid; DOTA-OSSu, *N*-hydroxysulfosuccinimide ester of DOTA; sulfo-NHS, *N*-hydroxysulfosuccinimide; EDC, 1-ethyl-3-[3-(dimethylamino)propyl]carbodiimide; DTPA, diethylenetriaminepentaacetic acid; EDTA, ethylenediaminetetraacetic acid; TFA, trifluoroacetic acid; PBS, phosphate-buffered saline; HSA, human serum albumin; CEA, carcinoembryonic antigen; cT84.66, human/murine chimeric anti-CEA mAb; cytochrome c-DOTA, cytochrome c conjugated to DOTA; cT84.66-DOTA, cT84.66 conjugated to DOTA; cT84.66-DTPA, cT84.66 conjugated to DTPA; MALDITOF MS, matrix assisted laser desorption ionization time of flight mass spectrometry; ESI MS, electrospray ionization mass spectrometry.

<sup>†</sup> Division of Immunology.

<sup>‡</sup> Department of Radioimmunotherapy.

\* Abstract published in *Advance ACS Abstracts*, October 15, 1994.



effort has been devoted to simplifying and scaling up these synthetic procedures (20, 21). Yet difficulties have been encountered in the radiolabeling of DOTA-conjugated mAbs because of the slow rate of formation of metal ion-DOTA complexes (30) and the presence of trace metals which can compete effectively for the ligand (27). Often the use of radiolabeling procedures which have been established for mAbs conjugated to other chelating agents results in low radiochemical yields when applied to mAb-DOTA conjugates (31). In order to utilize carrier-free radiometal solutions and minimize radiation damage to the protein, the formation of the radiolabeled immunoconjugate should be rapid and efficient.

This paper describes a facile and water-soluble method for the modification of proteins with DOTA using commercially available reagents. *In situ* formation of the *N*-hydroxysulfosuccinimide ester of DOTA allows a bifunctional chelating agent to be generated in one step and added immediately to a protein for rapid preparation of a DOTA conjugate. The reaction is expected to occur at the  $\epsilon$ -amino group of lysine residues, in the process converting one carboxyl group of DOTA to an amide functionality.

Cytochrome *c* was used as a model protein for this modification, and the conjugation chemistry was subsequently applied to the mAb cT84.66 (32), a human/murine chimeric anti-carcinoembryonic antigen antibody. Carcinoembryonic antigen is a well-characterized human tumor marker found in a variety of solid tumors including carcinomas of the colon, breast, and lung. Conditions utilizing elevated temperature, optimized pH, and appropriate buffers for the reactions of the protein-DOTA conjugates with the radiometals  $^{111}\text{In}(\text{III})$  and  $^{90}\text{Y}(\text{III})$  were explored in order to achieve rapid and efficient radiolabeling. The radioconjugates prepared with the DOTA active ester were incubated at physiological temperature in serum and in the presence of a large excess of DTPA to assess their kinetic stabilities under physiological conditions.

Derivatives of the acyclic chelating agent DTPA are among the most widely used compounds for the attachment of radiometals to monoclonal antibodies. The first mAb-DTPA conjugates were prepared with the bicyclic anhydride of DTPA (33, 34). Subsequently, DTPA was conjugated to antibodies using a mixed anhydride (35) or active ester (36, 37) of the chelating agent as the reactive species. The third generation of bifunctional DTPA compounds developed for antibody conjugation were the *p*-isothiocyanatobenzyl derivatives (38, 39). A conjugate of the mAb cT84.66 prepared with *p*-isothiocyanatobenzyl-DTPA (39) has been employed in human imaging and therapy trials with  $^{111}\text{In}$  and  $^{90}\text{Y}$ , respectively. The kinetic stabilities of the  $^{111}\text{In}$ -labeled and  $^{90}\text{Y}$ -labeled cT84.66-DOTA conjugate in human serum and in excess DTPA were compared to those of the cT84.66-DTPA conjugate labeled with the same radiometals.

## EXPERIMENTAL PROCEDURES

**General.** DOTA internal salt and trisodium salt were purchased from Parish Chemical Co. (Orem, UT). Sulfo-NHS, EDC, and triethylamine (Sequanal Grade) were purchased from Pierce. Horse heart cytochrome *c* was obtained from Sigma Chemical Co., and mAb cT84.66 was prepared as previously described (32). cT84.66-DTPA was prepared according to the method of Westerberg *et al.* (39). DTPA was purchased from Fluka, and EDTA was purchased from Aldrich. Human serum albumin (25% (w/v), USP) was obtained from Armour Pharmaceutical Co. Normal saline (0.9% sodium chloride, injection, USP) was purchased from American Regent Labo-

ratories, Inc., and Baxter Healthcare Corp. Sodium bicarbonate, dibasic potassium phosphate, sodium citrate, and citric acid were purchased from Mallinckrodt. Chel-ex 100 (Biotechnology Grade, 100–200 mesh, sodium form) was obtained from Bio-Rad. Sodium acetate trihydrate (99+%) and ammonium acetate (99.999%) were purchased from Aldrich, ultrapure Tris base was purchased from Boehringer Mannheim, and all buffers were passed over a Chelex 100 column (1  $\times$  15 cm) before use in radiolabeling reactions. Glacial acetic acid (Optima) was purchased from Fisher. Ultrapure water (18 M $\Omega$ -cm) was used for all procedures. Cobalt powder (99.995%) and yttrium chloride hexahydrate (99.999%) were purchased from Aldrich.  $^{111}\text{InCl}_3$ ,  $^{90}\text{YCl}_3$ , and  $^{57}\text{CoCl}_2$  were obtained from Amersham, Nordion, and ICN, respectively.

HPLC was performed at room temperature on a Beckman System Gold chromatograph or a Spectra-Physics system (SP8800 pump, SP4400 ChromJet integrator, WINner/386 data acquisition system). The columns, solvent systems, and gradients used are described below. UV detection was accomplished at 214 nm or 280 nm using a Shimadzu SPD-6A or Spectra-Physics Spectra 100 detector. Radioactivity detection was accomplished using a Technical Associates PRS-5 analyzing miniscaler/ratemeter. TLC was performed on EM Science plastic-backed silica gel plates (Kieselgel 60 F<sub>254</sub>, 0.2 mm layer thickness), using 10% (w/v) aqueous ammonium acetate (Fisher HPLC Grade):methanol (1:1) as the mobile phase. Radiation counting of TLC plates was performed with a Packard Cobra Auto-Gamma Model 5003 counting system or with a Beckman LS 6000IC liquid scintillation counter.

Laser desorption mass spectra were recorded on a Kratos Kompact MALDI III spectrometer, using  $\alpha$ -cyano-4-hydroxycinnamic acid as the matrix. Low mass MALDITOF mass spectra were recorded in reflectron mode and calibrated with an external standard containing DOTA internal salt and a synthetic peptide (TQLP-NEVDA,  $m/z = 1009.04$  ( $M + \text{Na}^+$ )). High mass MALDITOF mass spectra were recorded in linear mode and calibrated with an internal standard of soybean trypsin inhibitor. Electrospray mass spectra were recorded on a Finnigan MAT TSQ-700 triple quadrupole instrument equipped with an electrospray ion source and on-line microcapillary HPLC system (40, 41). The HPLC column, solvent system, and gradient employed are described below.

Concentrations of antibody were determined by UV spectrophotometry, measuring the absorbance at 280 nm ( $A_{280}$  at 1 mg/mL = 1.42, within 5% of the concentration determined by amino acid analysis). UV measurements were obtained on a Pharmacia LKB Ultraspec III spectrophotometer, using a 1-cm sample cell.

**Preparation of DOTA *N*-Hydroxysulfosuccinimide Ester.** To a solution of 60.0 mg (128  $\mu\text{mol}$ ) of trisodium DOTA and 27.7 mg (128  $\mu\text{mol}$ ) of sulfo-NHS in 960  $\mu\text{L}$  of  $\text{H}_2\text{O}$ , cooled to 4  $^\circ\text{C}$ , was added 49  $\mu\text{L}$  (2.45 mg, 12.8  $\mu\text{mol}$ ) of EDC, freshly prepared in  $\text{H}_2\text{O}$  (50 mg/mL) at 4  $^\circ\text{C}$ . The reaction mixture was stirred at 4  $^\circ\text{C}$  for 30 min, after which it was used immediately, without purification, to prepare the DOTA-conjugated proteins. The theoretical concentration of active ester in the reaction mixture was 12.7 mM.

**Preparation of Cytochrome *c*-DOTA Conjugate.** Cytochrome *c* was dissolved at 5 mg/mL in 20 mM DTPA, pH 5.0, and the resulting solution was allowed to stand at 4  $^\circ\text{C}$  for at least 18 h. The protein was purified by reversed phase HPLC using a Brownlee C<sub>4</sub> column (Aquapore Butyl (B03-GU) 7  $\mu\text{m}$ , 300  $\text{\AA}$ , 4.6  $\times$  30 mm)

**Table 1. Radiolabeling Conditions for Cytochrome c-DOTA<sup>a</sup>**

radiometal	labeling ratio (mCi/mg)	labeling buffer	T (°C)	time (min)	labeling efficiency (%)	specific activity (mCi/mg)
<sup>111</sup> In	11.0	0.25 M NH <sub>4</sub> OAc, pH 7.0	37	45	97.7	10.7
<sup>90</sup> Y <sup>b</sup>	20.1	0.25 M NH <sub>4</sub> OAc, pH 7.0	43	60	93.9	18.9
<sup>90</sup> Y <sup>b</sup>	18.6	0.25 M Tris-OAc, pH 7.0	43	60	90.1	16.8
<sup>90</sup> Y <sup>b</sup>	20.1	0.25 M Tris-HCl, pH 7.0	43	60	84.5	17.0

<sup>a</sup> Average number of chelators per protein = 2.57. <sup>b</sup> Radiometal solution was dried *in vacuo* and redissolved in labeling buffer before being added to the conjugate.

**Table 2. Radiolabeling Conditions for cT84.66-DOTA<sup>a</sup>**

radiometal	labeling ratio (mCi/mg)	labeling buffer	T (°C)	time (min)	labeling efficiency (%)	specific activity (mCi/mg)
<sup>111</sup> In	5.00	0.25 M NH <sub>4</sub> OAc, pH 6.0	43	45	84.4	4.22
<sup>90</sup> Y	5.00	0.25 M NH <sub>4</sub> OAc, pH 5.0	43	60	59.3	2.97

<sup>a</sup> Average number of chelates per mAb = 3.8.

and a linear gradient from 0% to 100% solvent B (solvent A, 0.1% TFA; solvent B, 0.1% TFA/90% CH<sub>3</sub>CN) in 30 min, beginning 10 min after injection. The cytochrome c peak, eluting with a retention time of 21 min, was collected, lyophilized, and dissolved in H<sub>2</sub>O. A solution containing 3.6 mg (0.29  $\mu$ mol) of cytochrome c in 720  $\mu$ L of H<sub>2</sub>O was cooled to 4 °C, and 231  $\mu$ L (2.91  $\mu$ mol theoretical) of the DOTA-OSSu reaction mixture was added. The pH of the reaction mixture was adjusted to 9.0 with 5% aqueous triethylamine, and the reaction mixture was incubated on a tube rotator for 18–24 h at 4 °C. The cytochrome c-DOTA conjugate was purified by reversed phase HPLC using a Vydac Protein C<sub>4</sub> column (5  $\mu$ m, 300 Å, 4.6  $\times$  250 mm) and a linear gradient from 2% to 100% solvent B in 60 min. The peak containing the cytochrome c-DOTA conjugate, eluting at 25.4 min, was collected, lyophilized, and dissolved in H<sub>2</sub>O at a concentration of 2 mg/mL for use in radiolabeling reactions.

**Preparation of cT84.66-DOTA Conjugate.** An aliquot of 0.5 mL of cT84.66, 10.76 mg/mL in PBS, pH 7.4, was diluted with normal saline to give a solution 5 mg/mL in antibody. This solution was dialyzed against 1 L of 0.25 M ammonium acetate/20 mM DTPA, pH 7.0, for 24 h at 4 °C, then against 1 L of 0.25 M ammonium acetate over Chelex 100 for 24 h at 4 °C, and finally against 1 L of 0.1 M NaHCO<sub>3</sub>/0.1 M K<sub>2</sub>HPO<sub>4</sub>, pH 8.5, over Chelex 100 for 18–24 h at 4 °C. To 4.47 mg (29.8 nmol) of cT84.66 in 0.75 mL of 0.1 M NaHCO<sub>3</sub>/0.1 M K<sub>2</sub>HPO<sub>4</sub>, pH 8.5, was added 235  $\mu$ L (2.98  $\mu$ mol theoretical) of the DOTA-OSSu reaction mixture at 4 °C, and the pH of the reaction mixture was adjusted to 8.5 with 1 M NaOH and 1 M HCl. The reaction mixture was incubated on a tube rotator for 18–24 h at 4 °C, after which it was dialyzed against 1 L of 0.25 M ammonium acetate/20 mM DTPA, pH 7.0, for 24 h at 4 °C. The conjugate was then dialyzed against 1 L of 0.25 M ammonium acetate over Chelex 100 for 143 h at 4 °C, with four buffer changes, and the final solution of cT84.66-DOTA was centrifuged at 16 000g to remove any aggregates or particulate matter.

**Radiolabeling of Cytochrome c-DOTA.** The cytochrome c-DOTA conjugate was labeled with the radiometals <sup>111</sup>In(III) and <sup>90</sup>Y(III). Labeling conditions are given in Table 1. In the <sup>111</sup>In labeling reaction, 2.2 mCi of <sup>111</sup>InCl<sub>3</sub> in 125  $\mu$ L of 0.04 N HCl was added to 200  $\mu$ L of the labeling buffer. Then 100  $\mu$ L (0.2 mg) of the cytochrome c-DOTA solution was added, and the reaction mixture was incubated as described in Table 1. The radiolabeled conjugate was challenged with the addition of 47.2  $\mu$ L of 10 mM EDTA, pH 6.5, and the reaction mixture was incubated at 37 °C for 15 min. The <sup>111</sup>In-labeled cytochrome c was purified by size exclusion HPLC

using a TosoHaas TSKgel G2000 SW column (10  $\mu$ m, 7.5  $\times$  300 mm) and an isocratic mobile phase of normal saline. The cytochrome c peak, eluting at 11.5 min retention time, was collected in 0.5-mL fractions containing 1 drop of 25% (w/v) HSA each.

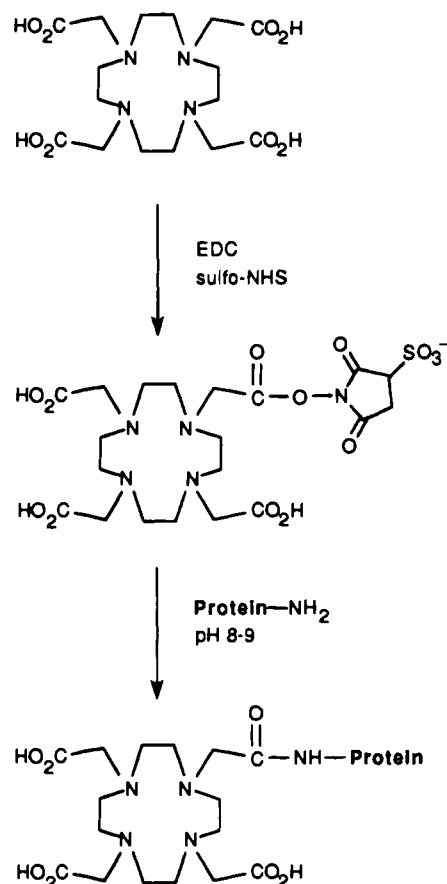
For labeling cytochrome c-DOTA with <sup>90</sup>Y, 1.49 mCi of <sup>90</sup>YCl<sub>3</sub> in 25  $\mu$ L of 0.05 N HCl was dried *in vacuo* at 37 °C for 1 h, after which it was dissolved in 128  $\mu$ L of labeling buffer. Then 40  $\mu$ L (80  $\mu$ g) of the cytochrome c-DOTA was added, and the resulting mixture was incubated as described in Table 1. The <sup>90</sup>Y-labeled protein was challenged with the addition of 18.7  $\mu$ L of 10 mM DTPA, pH 6.0, and the reaction mixture was incubated at 37 °C for 15 min. The radiolabeled conjugate was purified by size exclusion HPLC in the same manner as the <sup>111</sup>In-labeled cytochrome c.

**Radiolabeling of cT84.66-DOTA.** The cT84.66-DOTA conjugate was labeled with <sup>111</sup>In(III) and <sup>90</sup>Y(III) according to the conditions given in Table 2. For the <sup>111</sup>In(III) labeling reaction, 1 mCi of <sup>111</sup>InCl<sub>3</sub> in 54.6  $\mu$ L of 0.04 N HCl was added to 75  $\mu$ L of the labeling buffer, followed by 37.2  $\mu$ L (0.2 mg) of the cT84.66-DOTA solution. The reaction mixture was incubated as described in Table 2, after which the radiolabeled conjugate was challenged with the addition of 18.5  $\mu$ L of 10 mM EDTA, pH 6.5, and incubated at 37 °C for 15 min. The <sup>111</sup>In-labeled antibody was purified by size exclusion HPLC using a TosoHaas TSKgel G2000 SW column (10  $\mu$ m, 7.5  $\times$  300 mm) and an isocratic mobile phase of normal saline. The mAb peak, eluting at 8.3 min retention time, was collected in 0.5-mL fractions containing 1 drop of 25% (w/v) HSA each.

In the <sup>90</sup>Y labeling reaction, 1 mCi of <sup>90</sup>YCl<sub>3</sub> in 12.5  $\mu$ L of 0.05 N HCl was added to 75  $\mu$ L of the labeling buffer. Then 37.2  $\mu$ L (0.2 mg) of cT84.66-DOTA was added, and the reaction mixture was incubated as described in Table 2. The radiolabeled antibody was challenged with the addition of 13.9  $\mu$ L of 10 mM DTPA, pH 6.0, and the resulting mixture was incubated at 37 °C for 15 min. The <sup>90</sup>Y-labeled conjugate was purified by size exclusion HPLC in the same manner as the <sup>111</sup>In-labeled antibody.

**Immunoreactivity Determination.** Dilutions of the purified cT86.66-DOTA conjugate labeled with <sup>111</sup>In and <sup>90</sup>Y, containing approximately 100 000 cpm of radioactivity in 100  $\mu$ L, were applied to 2-mL CEA-Sepharose 4B spin columns preequilibrated with 1% HSA in PBS, pH 7.2. The spin columns were incubated at 37 °C for 15 min with continuous end-over-end mixing, after which the total amount of radioactivity in each column was measured by radiation counting. The columns were then drained by centrifugation at 3000 rpm for 1 min and washed three times with 1% HSA in PBS. The columns

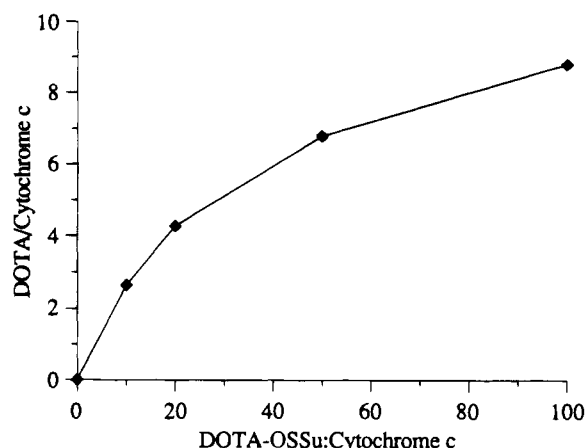
Scheme 1



were resuspended in 600  $\mu\text{L}$  of 1% HSA, and the amount of radioactivity remaining in each column was measured again by radiation counting. Immunoreactivity was calculated as the percentage of the total radioactivity bound to the CEA-Sepharose 4B column after elution.

**Serum Stability Studies.** An aliquot (10–50  $\mu\text{L}$ ) of the radiolabeled conjugate containing approximately  $8 \times 10^6$  cpm of  $^{111}\text{In}$  radioactivity or  $2 \times 10^7$  cpm of  $^{90}\text{Y}$  radioactivity was added to 1.1 mL of fresh human serum containing 10  $\mu\text{L}$  of 10%  $\text{NaN}_3$ . The mixture was incubated at 37  $^\circ\text{C}$  throughout the study, during which time 100- $\mu\text{L}$  samples of serum were analyzed by gel filtration HPLC on two Pharmacia Superose 12 HR 10/30 columns (1  $\times$  30 cm) in series, using an isocratic mobile phase of 0.05 M  $\text{Na}_2\text{SO}_4$ , 0.02 M  $\text{NaH}_2\text{PO}_4$ , 0.05%  $\text{NaN}_3$ , pH 6.8. Serum samples were analyzed at intervals ranging from 15 to 72 h for 10 days to determine conjugate stability.

**DTPA Stability Studies.** An aliquot (10–50  $\mu\text{L}$ ) of the radiolabeled conjugate having approximately  $8 \times 10^6$  cpm of  $^{111}\text{In}$  radioactivity or  $2 \times 10^7$  cpm of  $^{90}\text{Y}$  radioactivity was added to 1.1 mL of 1 mM DTPA in normal saline containing 1% HSA, pH 6.0. Under these conditions, the ratio of DTPA to protein-conjugated DOTA ranged from approximately 5000:1 to approximately 250 000:1. This solution was incubated at 37  $^\circ\text{C}$  throughout the study, during which time 100- $\mu\text{L}$  aliquots of the mixture were analyzed by size exclusion HPLC on a TosoHaas TSKgel G2000 SW column (10  $\mu\text{m}$ , 7.5  $\times$  300 mm) using an isocratic mobile phase of 0.05 M  $\text{Na}_2\text{SO}_4$ , 0.02 M  $\text{NaH}_2\text{PO}_4$ , 0.05%  $\text{NaN}_3$ , pH 6.8. Samples were analyzed at intervals ranging from 0.5 to 72 h during a 10-day period to determine conjugate stability.

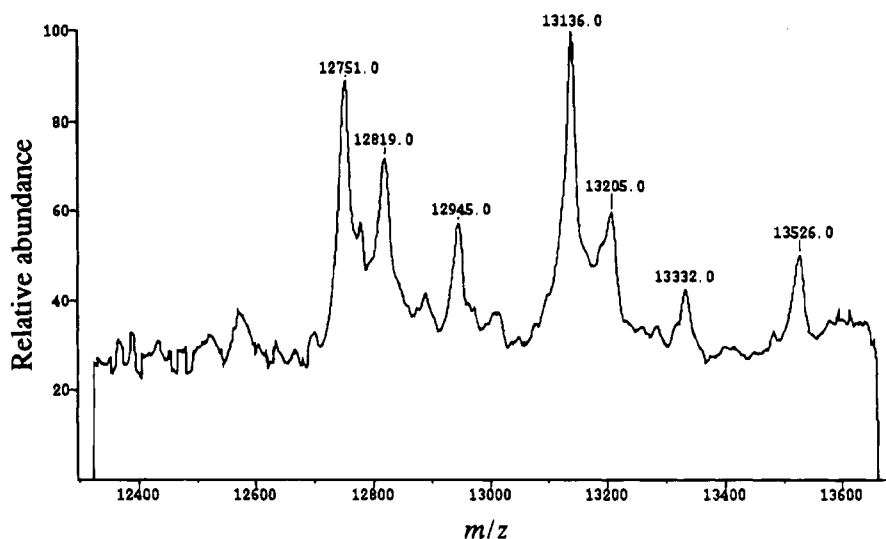


**Figure 1.** Average number of DOTA molecules conjugated per molecule of cytochrome c, determined by MALDITOF MS, as a function of DOTA-OSSu:cytochrome c reaction stoichiometry.

## RESULTS

**Preparation of DOTA *N*-Hydroxysulfosuccinimide Ester.** The preparation of the *N*-hydroxysulfosuccinimide ester of DOTA is shown in Scheme 1. DOTA-OSSu active ester was prepared by a method for water-soluble activation of carboxylic acids commonly used in peptide synthesis and protein modification (42–44). While the DOTA-OSSu active ester was not isolated prior to conjugation to proteins, the reaction was examined by mass spectrometry. An equimolar mixture of DOTA, sulfo-NHS, and EDC was incubated at 4  $^\circ\text{C}$  for 45 min, and subsequent analysis by MALDITOF MS identified the monofunctionalized active ester as the only product observed, at  $m/z = 582.26$  ( $M + H$ )<sup>+</sup> in positive ion mode (calcd for  $\text{C}_{20}\text{H}_{32}\text{N}_5\text{O}_{13}\text{S}$ , 582.56) and at  $m/z = 580.82$  ( $M - H$ )<sup>−</sup> in negative ion mode (calcd for  $\text{C}_{20}\text{H}_{30}\text{N}_5\text{O}_{13}\text{S}$ , 580.55). This result was consistent with experiments in which potentiometric titration of DOTA with 4 equiv of EDC resulted in the uptake of only 1 equiv of protons (data not shown).

**Conjugation of Cytochrome c and cT84.66 with DOTA-OSSu.** The reaction of DOTA-OSSu with proteins is expected to produce an amide bond between the activated carboxyl group of DOTA and the  $\epsilon$ -amino group of lysine residues (Scheme 1). Since the active ester of DOTA was not isolated, the theoretical concentration of the reagent, based on EDC as the limiting reactant, was used to define the DOTA-OSSu:protein reaction stoichiometry. To quantitate the degree of covalent modification as a function of the amount of activated DOTA added, cytochrome c was conjugated at DOTA-OSSu:protein molar ratios of 10:1, 20:1, 50:1, and 100:1, and the purified conjugates were analyzed by MALDITOF MS. The mass of each conjugate was determined from the average of two  $m/z$  values for the ( $M + 2H$ )<sup>2+</sup> ion, using soybean trypsin inhibitor as an internal standard. The mass of unconjugated cytochrome c, determined from the  $m/z$  ratio for the ( $M + 2H$ )<sup>2+</sup> ion, was then subtracted from the mass of each conjugate. To determine the average number of DOTA groups per cytochrome c molecule, the mass increase measured for each conjugate was divided by the calculated increase of 386 mass units afforded by the formation of an amide bond between DOTA and a lysine residue. Figure 1 shows that reaction of DOTA-OSSu with cytochrome c at a molar ratio of 10:1 produced a conjugate with an average of 2.64 chelating groups per protein molecule, while increasing the conjugation ratio to 20:1, 50:1, and 100:1 gave conjugates with 4.27, 6.78, and 8.79 chelators per cytochrome c,

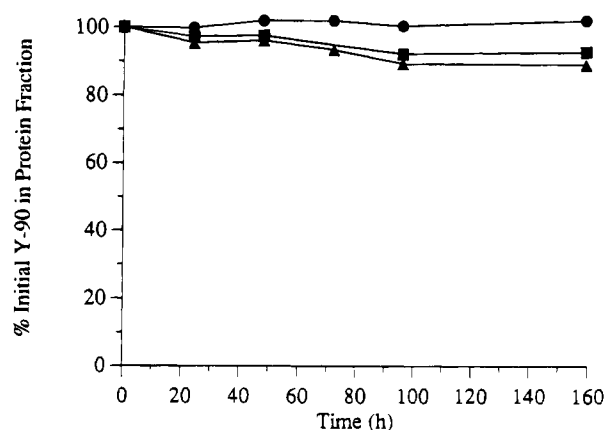


**Figure 2.** Electrospray ionization mass spectrum of cytochrome c-DOTA, conjugated at a DOTA-OSSu:protein molar ratio of 10:1. An aliquot of 16 pmol of the conjugate was injected onto a  $C_{18}$  microcapillary column ( $5\ \mu\text{m}$ ,  $300\ \text{\AA}$ ,  $0.25 \times 150\ \text{mm}$ ) and eluted with a linear gradient from 2% to 92% solvent B (solvent A, 0.1% TFA; solvent B, 0.07% TFA in 90%  $\text{CH}_3\text{CN}$ ) in 45 min at a flow rate of  $2\ \mu\text{L}/\text{min}$ . ESI MS scans were averaged over the entire cytochrome c-DOTA peak, eluting at 20 min retention time.

respectively. The cytochrome c-DOTA produced at a conjugation ratio of 10:1 was also analyzed by ESI MS (Figure 2). ESIMS revealed that the conjugate contained no detectable unmodified protein, but was a mixture of cytochrome c-DOTA species with one ( $m/z = 12\ 751.0$  ( $M + H$ ) $^+$ , calcd  $12\ 747$ ), two ( $m/z = 13\ 136.0$  ( $M + H$ ) $^+$ , calcd  $13\ 133$ ), and three ( $m/z = 13\ 526.0$  ( $M + H$ ) $^+$ , calcd  $13\ 519$ ) DOTA molecules covalently attached to the protein. The peaks in the electrospray mass spectrum of cytochrome c-DOTA at  $m/z = 12\ 819.0$  and  $13\ 205.0$  represent trisodium adducts of the conjugate species, while the peaks at  $m/z = 12\ 945.0$  and  $13\ 332.0$  correspond to species with one noncovalently associated anion of sulfo-NHS present.

The activation stoichiometry of DOTA:sulfo-NHS:EDC was varied from 2:2:1 to 4:4:1 to 10:10:1 prior to conjugation to cytochrome c at a DOTA-OSSu:protein molar ratio of 10:1. Analysis of these cytochrome c-DOTA conjugates by MALDITOF MS showed that in each case the cytochrome c was modified with an average of approximately 1.6 DOTA molecules per protein molecule. The purified conjugates were then labeled with  $^{90}\text{Y}(\text{III})$  at a ratio of 22.6 mCi/mg, and the kinetic stabilities of the radiolabeled cytochrome c preparations were evaluated in the presence of 1 mM DTPA at  $37\ ^\circ\text{C}$  (Figure 3). After 159 h in 1 mM DTPA at  $37\ ^\circ\text{C}$ , the cytochrome c conjugates prepared from DOTA activated at 2:2:1 and 4:4:1 stoichiometries had lost 11.0% and 7.3%, respectively, of the initial radiometal label, while the cytochrome c conjugate prepared from DOTA activated at a 10:10:1 stoichiometry showed essentially no loss of  $^{90}\text{Y}$ .

After activation of the chelating agent at a DOTA:sulfo-NHS:EDC ratio of 10:10:1, the anti-CEA mAb cT84.66 was conjugated with DOTA-OSSu at an active ester:protein ratio of 100:1. The average number of DOTA chelates attached to the antibody was determined by a modification of a  $^{57}\text{Co}(\text{II})$  binding assay (45). The cT84.66-DOTA conjugate was incubated at  $43\ ^\circ\text{C}$  in 0.25 M ammonium acetate with a 10-fold excess of a standardized  $^{57}\text{CoCl}_2$  solution for 24 h, after which the mixture was made 1 mM in DTPA and incubated at  $37\ ^\circ\text{C}$  for 15 min. TLC analysis showed the conjugate to be modified with an average of 3.8 chelates per mAb. An analogous assay using a standardized  $^{90}\text{YCl}_3$  solution gave a value of 3.1 chelates per mAb. Size exclusion HPLC of cT84.66-DOTA showed that no aggregates were formed in the

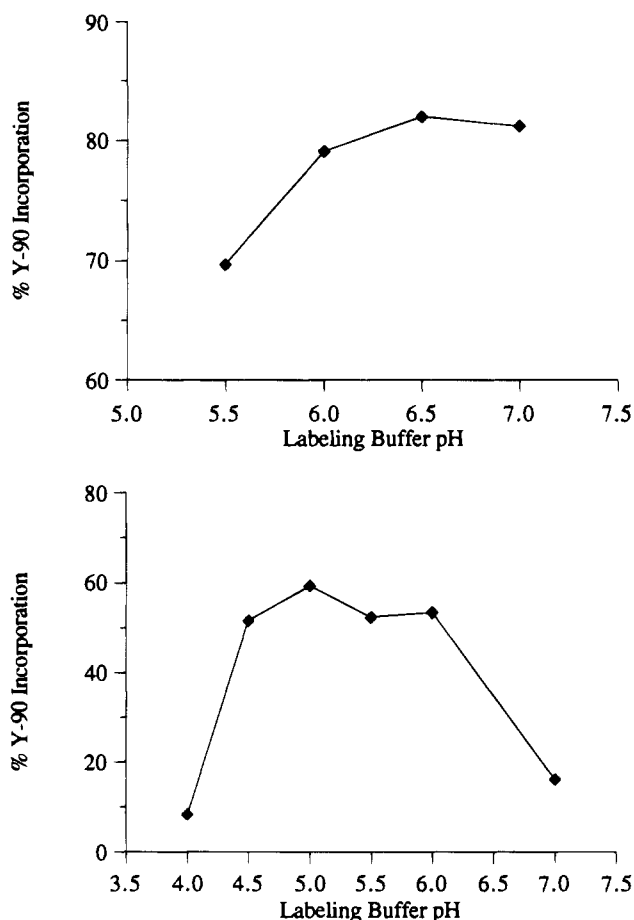


**Figure 3.** Percentage of  $^{90}\text{Y}$  bound to cytochrome c-DOTA as a function of time of incubation in 1 mM DTPA at  $37\ ^\circ\text{C}$ , determined by size exclusion HPLC. Cytochrome c was conjugated at a DOTA-OSSu:protein molar ratio of 10:1, after activation of DOTA at a DOTA:sulfo-NHS:EDC stoichiometry of 10:10:1 ( $\bullet$ ), 4:4:1 ( $\blacksquare$ ), and 2:2:1 ( $\blacktriangle$ ).

conjugation reaction, but approximately 6% antibody dimers were detected, which were removed from the preparation during purification of the radiolabeled mAb.

**Radiolabeling of Cytochrome c-DOTA and cT84.66-DOTA.** Cytochrome c-DOTA was labeled with  $^{111}\text{In}(\text{III})$  and  $^{90}\text{Y}(\text{III})$  under conditions in which the concentrations of radiometal and protein-conjugated DOTA approximated those anticipated for the corresponding antibody labeling reactions. Labeling conditions, radiometal incorporation, and specific activities for the cytochrome c-DOTA radioconjugates are given in Table 1.  $^{111}\text{InCl}_3$  in 0.04 N HCl and cytochrome c-DOTA in  $\text{H}_2\text{O}$  were added sequentially to 0.25 M ammonium acetate, and incorporation of  $^{111}\text{In}$  into the protein conjugate was 97.7% after 45 min at  $37\ ^\circ\text{C}$ .

The efficiency of labeling cytochrome c-DOTA with  $^{90}\text{YCl}_3$  in 0.05 N HCl was directly proportional to the pH of the labeling buffer over the range studied, as shown in Figure 4 (top). In 0.1 M sodium acetate, pH 5.5,  $^{90}\text{Y}$  incorporation into cytochrome c-DOTA was 69.7%, while in 0.1 M sodium acetate, pH 7.0,  $^{90}\text{Y}$  incorporation increased to 81.2%. The presence of citrate, a weakly chelating buffer, completely impeded the labeling of even highly modified cytochrome c-DOTA with  $^{90}\text{Y}$  (Table 3).



**Figure 4.** (Top) percentage of <sup>90</sup>Y incorporation into cytochrome c-DOTA, after 1 h incubation at 25 °C, as a function of pH of the sodium acetate labeling buffer. (Bottom) percentage of <sup>90</sup>Y incorporation into cT84.66-DOTA, after 1 h incubation at 43 °C, as a function of pH of the ammonium acetate labeling buffer.

**Table 3. Buffer Effects on the <sup>90</sup>Y Radiolabeling of Cytochrome c-DOTA<sup>a</sup>**

protein buffer	T (°C)	time (min)	labeling efficiency (%)
H <sub>2</sub> O	25	60	100
0.1 M sodium citrate, pH 6.0	25	60	0
0.1 M sodium acetate, pH 6.0	25	60	100

<sup>a</sup> Average number of chelators per protein = 6.7.

When cytochrome c-DOTA, conjugated with an average of 6.7 chelating groups per protein molecule, was dissolved in 0.1 M sodium citrate, pH 6.0, and incubated with <sup>90</sup>YCl<sub>3</sub> in 0.1 M sodium acetate, pH 6.0, no incorporation of the radiometal into the conjugate was observed. In contrast, quantitative labeling with <sup>90</sup>Y was obtained under the same conditions when this conjugate was dissolved in H<sub>2</sub>O or 0.1 M sodium acetate, pH 6.0.

<sup>90</sup>Y labeling of cytochrome c-DOTA was most efficient when the <sup>90</sup>YCl<sub>3</sub> solution was dried to remove HCl and reconstituted with the labeling buffer prior to being incubated with the protein conjugate for 1 h at 43 °C. Labeling of cytochrome c-DOTA with <sup>90</sup>Y was best in 0.25 M ammonium acetate (ambient pH 7.0), but the use of 0.25 M Tris acetate, pH 7.0, and 0.25 M Tris hydrochloride, pH 7.0, also gave high percentages of <sup>90</sup>Y incorporation (Table 1).

Labeling conditions, radiometal incorporation, and specific activities for the cT84.66-DOTA radioimmunoconjugates are given in Table 2. <sup>111</sup>InCl<sub>3</sub> in 0.04 N HCl and cT84.66-DOTA in 0.25 M ammonium acetate were

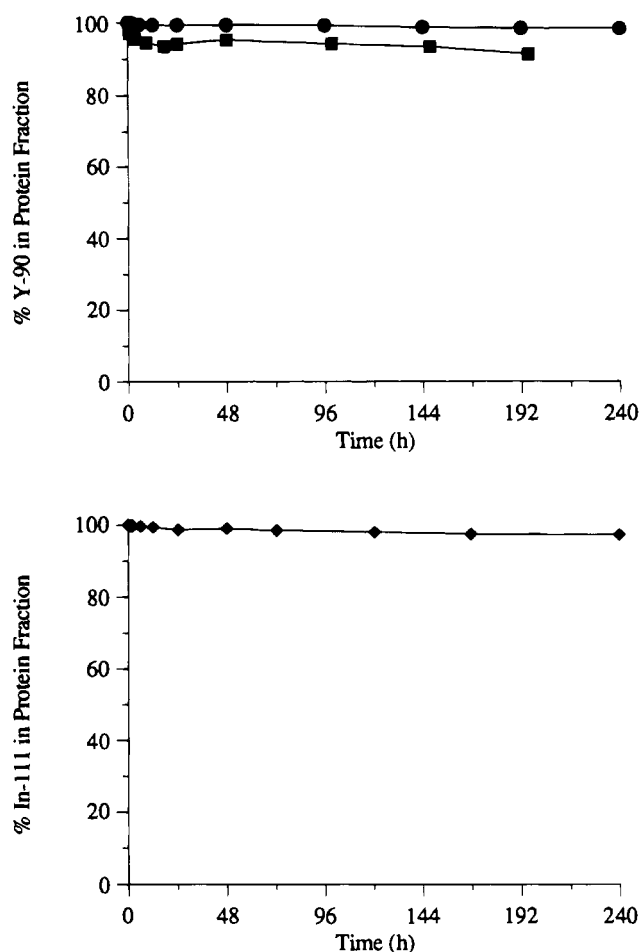
added sequentially to 0.25 M ammonium acetate, pH 6.0, and the reaction mixture was incubated at 43 °C for 45 min. <sup>111</sup>In incorporation into the antibody conjugate was determined to be 84.4%, resulting in a specific activity of 4.22 mCi/mg for the purified <sup>111</sup>In-labeled mAb.

Labeling of cT84.66-DOTA with <sup>90</sup>YCl<sub>3</sub> in 0.05 N HCl proved to be quite sensitive to pH. Unlike the <sup>90</sup>Y labeling of cytochrome c-DOTA, the most efficient incorporation of <sup>90</sup>Y occurred after 1 h at 43 °C in 0.25 M ammonium acetate, pH 4.5–6.0 (Figure 4 (bottom)). The highest efficiency of <sup>90</sup>Y labeling for cT84.66-DOTA was obtained in 0.25 M ammonium acetate, pH 5.0, affording a purified <sup>90</sup>Y-labeled mAb with a specific activity of 2.97 mCi/mg. At the extremes of the pH range studied, low efficiencies of <sup>90</sup>Y incorporation were obtained, 8.25% at pH 4.0 and 16.1% at pH 7.0. When the <sup>90</sup>YCl<sub>3</sub> solution was dried and redissolved in 0.25 M ammonium acetate, pH 7.0, the amount of <sup>90</sup>Y incorporation into the antibody conjugate dropped to approximately half that obtained under the same conditions when the HCl was not removed (data not shown).

**Immunoreactivity of Radiolabeled cT84.66-DOTA.** The immunoreactivity of <sup>111</sup>In-labeled and <sup>90</sup>Y-labeled cT84.66-DOTA was evaluated by a solid-phase assay using Sepharose 4B resin derivatized with CEA (46). The binding percentage for a 1:800 dilution of the purified <sup>111</sup>In-labeled mAb was 98.6%. Immunoreactivity of a 1:400 dilution of the purified <sup>90</sup>Y-labeled mAb was determined to be 102.1%. When the affinity of cT84.66-DOTA was compared to that of unconjugated cT84.66 using a Pharmacia BIAcore Biosensor, no difference in the association constant, dissociation constant, or affinity constant was observed between the DOTA-conjugated mAb and the unconjugated mAb (data not shown).

**Stability of Cytochrome c-DOTA and cT84.66-DOTA in Excess DTPA.** To assess the kinetic stabilities of the cytochrome c-DOTA and cT84.66-DOTA conjugates, the <sup>111</sup>In-labeled and <sup>90</sup>Y-labeled proteins were evaluated in the presence of a large excess of DTPA. In each DTPA stability study, the radiolabeled protein was incubated at 37 °C in 1% HSA/normal saline containing 1 mM DTPA. The molar ratio of DTPA to protein-conjugated DOTA ranged from 5000:1 to 250 000:1, depending on the concentration and specific activity of the radioconjugate. Each mixture was analyzed by size exclusion HPLC with radioactivity detection, and areas of the radioactive peaks corresponding to the proteins were divided by the total areas of the radioactive protein and DTPA peaks to determine the percentages of radiometal bound to the protein-DOTA conjugates. A comparison of the kinetic stability of <sup>90</sup>Y-labeled cytochrome c-DOTA in excess DTPA after otherwise identical radiolabeling reactions at 25 and 37 °C is shown in Figure 5 (top). Under the conditions employed in the radiolabeling reactions, the efficiency of <sup>90</sup>Y incorporation into cytochrome c-DOTA was 21.0% at 25 °C, but at 37 °C incorporation of <sup>90</sup>Y increased to 54.6%. When these conjugates were incubated in 1 mM DTPA for 240 h at 37 °C, the total loss of radiometal from the cytochrome c-DOTA labeled at room temperature was 8.80%, while the cytochrome c-DOTA labeled at 37 °C lost only 1.88% of its chelated <sup>90</sup>Y. Incubation of <sup>111</sup>In-labeled cytochrome c-DOTA in 1 mM DTPA at 37 °C (Figure 5 (bottom)) revealed that the protein-DOTA indium chelate is slightly less stable than the corresponding yttrium chelate, as the total loss of <sup>111</sup>In from the radioconjugate was 2.68% after 240 h.

The kinetic stabilities of <sup>111</sup>In-labeled and <sup>90</sup>Y-labeled cT84.66-DOTA in excess DTPA were compared to those of cT84.66 conjugated with *p*-isothiocyanatobenzyl-DTPA

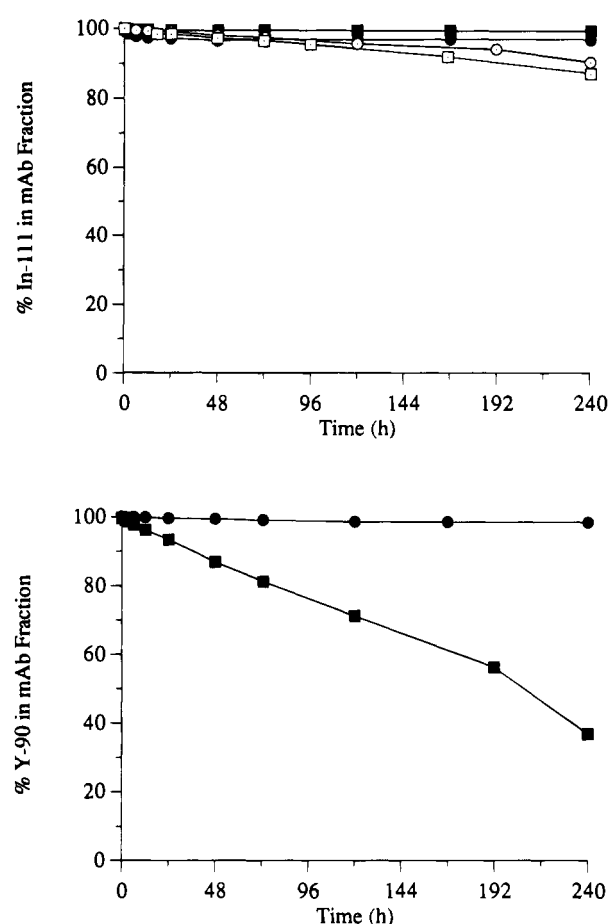


**Figure 5.** (Top) percentage of  $^{90}\text{Y}$  bound to cytochrome c-DOTA as a function of time of incubation in 1 mM DTPA at 37 °C, determined by size exclusion HPLC. Radiolabeling was performed at 25 °C (■) and at 37 °C (●). (Bottom) percentage of  $^{111}\text{In}$  bound to cytochrome c-DOTA as a function of time of incubation in 1 mM DTPA at 37 °C, determined by size exclusion HPLC. Radiolabeling was performed at 37 °C.

and labeled with the same radiometals. When the  $^{111}\text{In}$ -labeled antibody conjugates were incubated at 37 °C in 1 mM DTPA (Figure 6 (top)), cT84.66-DTPA lost 9.74% of its initial radiometal label after 240 h. Loss of  $^{111}\text{In}$  from cT84.66-DOTA was more rapid than from cT84.66-DTPA during the first 48 h of incubation in excess DTPA, but no further loss of radiometal occurred for the remainder of the incubation, and at 240 h the total amount of  $^{111}\text{In}$  lost from the mAb-DOTA chelate was 3.33%. The  $^{90}\text{Y}$ -labeled antibody conjugates were incubated in 1 mM DTPA at 37 °C for 240 h (Figure 6 (bottom)), during which the cumulative loss of radiometal from the mAb-DOTA chelate was 1.76%. In contrast, the mAb-DTPA chelate lost a total of 63.2% of the initial  $^{90}\text{Y}$  label over the same period of time.

**Serum Stability of Cytochrome c-DOTA and cT84.66-DOTA.** The kinetic stabilities of the  $^{111}\text{In}$ -labeled and  $^{90}\text{Y}$ -labeled protein-DOTA conjugates were also determined in fresh human serum at 37 °C. These mixtures were analyzed by gel filtration chromatography with radioactivity detection, and the areas of the radioactive peaks corresponding to the protein conjugates were divided by the total areas of all radioactive peaks to determine the percentages of radiometal bound to the DOTA-conjugated proteins.

The serum stabilities of cytochrome c-DOTA labeled with  $^{111}\text{In}$  and  $^{90}\text{Y}$  could not be evaluated conclusively because of the rapid formation of higher molecular weight



**Figure 6.** (Top) percentage of  $^{111}\text{In}$  bound to cT84.66-DOTA as a function of time of incubation in 1 mM DTPA (●) and in human serum (■) at 37 °C, compared to the percentage of  $^{111}\text{In}$  bound to cT84.66-DTPA as a function of time of incubation in 1 mM DTPA (○) and in human plasma (□) at 37 °C. (Bottom) percentage of  $^{90}\text{Y}$  bound to cT84.66-DOTA (●), compared to cT84.66-DTPA (■), as function of time of incubation in 1 mM DTPA at 37 °C.

complexes which obscured regions of the chromatogram where transferrin or albumin were expected to elute. The retention times of these serum complexes, however, did not correspond to that of either major serum protein. No low molecular weight radioactive species were observed when the  $^{111}\text{In}$ -labeled and  $^{90}\text{Y}$ -labeled cytochrome c-DOTA radioconjugates were incubated in serum.

The serum stability of  $^{111}\text{In}$ -labeled cT84.66-DOTA was compared to that of cT84.66-DTPA (Figure 6 (top)). After incubation in human serum for 240 h, the cT84.66-DOTA conjugate showed a cumulative loss of 0.824% of the initial  $^{111}\text{In}$  label. The  $^{111}\text{In}$ -labeled cT84.66-DTPA conjugate lost 13.0% of its initial radiolabel in plasma during the same period of time. The small fraction of  $^{111}\text{In}$  which was lost from cT84.66-DOTA was observed as a low molecular weight species, most likely generated by cleavage of the chelate from the antibody by hydrolysis (22, 47) or proteolysis. When the mAb-DOTA and mAb-DTPA conjugates were labeled with  $^{90}\text{Y}$  and incubated in human serum, no loss of radiometal was observed for either conjugate. The amount of  $^{90}\text{Y}$  bound to the antibody conjugates remained at 100% for 288 h at 37 °C (data not shown).

## DISCUSSION

Because DOTA forms extremely stable chelate complexes with a wide variety of metals (24–29), numerous derivatives of DOTA have been investigated for use in



magnetic resonance imaging, radioimmunoscinigraphy, and radioimmunotherapy. Several groups have reported the synthesis of backbone-substituted and side arm-substituted bifunctional polyazamacrocycles, including DOTA (9, 12, 16–19). Preparation of these derivatives, however, usually involves a nontrivial synthetic route comprised of at least 10 steps. Li and Meares reported the attachment of DOTA to a protein-reactive functionality via an amide bond to a carboxyl group of DOTA (22), using a less complicated eight-step synthetic route. To circumvent the need for lengthy organic synthesis in order to attach DOTA to monoclonal antibodies, we chose to develop a new method for facile modification of proteins with an active ester of DOTA. The process of converting one carboxyl group of DOTA to an amide group by this reaction has the potential to afford protein-DOTA conjugates that exhibit relatively rapid metal ion complexation rates while retaining high kinetic stability under physiological conditions. Furthermore, the direct attachment of DOTA to an amino acid side chain produces a minimal conjugate structure in close proximity to the peptide backbone of the protein, which could possibly minimize the chemical immunogenicity of the protein-DOTA conjugate.

Covalent attachment of DOTA to amines by acylation with the isobutyl formate mixed anhydride of the chelating agent has been employed to synthesize a variety of monofunctionalized DOTA amides. Wu *et al.* (48) conjugated DOTA to biotin in this manner and studied the serum stabilities of  $^{111}\text{In}$ -labeled and  $^{90}\text{Y}$ -labeled DOTA-biotin-avidin conjugates. Sherry *et al.* (49) used the same method to synthesize the Gd(III) complex of the monopropylamide of DOTA, a model for magnetic resonance imaging contrast agents consisting of monoconjugated DOTA macromolecules. Covalent modification of the  $\epsilon$ -amino groups of polylysine with DOTA isobutyl formate anhydride was reported by Sieving *et al.* (50) in the preparation of a protein conjugate containing a Gd(III)-DOTA polychelate manifold for magnetic resonance imaging.

While the isobutyl formate mixed anhydride could be used to prepare antibody conjugates of DOTA, preparation of the reactive intermediate is usually performed in DMSO or freezing acetonitrile. Because exposure to these organic solvents might result in denaturation, diminished recovery, or loss of biological activity of the conjugated protein, we decided to investigate the utility of water-soluble carbodiimide chemistry for direct modification of proteins with DOTA. Previously, a derivative of 1,4,8,11-tetraazacyclotetradecane bearing a carboxyl side chain had been activated with *N*-ethyl-*N'*-[3-(diethylamino)propyl]carbodiimide and *N*-hydroxysuccinimide (51), and subsequently with EDC and sulfo-NHS (52), prior to conjugation of the macrocycle to an anti-CEA mAb and radiolabeling with  $^{67}\text{Cu}$ (II). These methods afforded conjugates with up to 5.6 chelators per antibody at ligand:mAb reaction ratios as high as 408:1, while preserving the immunoreactivity of the modified antibody at >90%.

We examined the reaction between the tetracarboxylic acid DOTA and EDC in  $\text{H}_2\text{O}$  at room temperature and discovered that titration of DOTA with 4 equiv of EDC produced a pH increase consistent with the uptake of only 1 equiv of protons, suggesting that the monoactivated DOTA-EDC intermediate was formed preferentially. Mass spectrometric analysis of the reaction of DOTA, sulfo-NHS, and EDC in equimolar amounts and with 2 equiv of EDC showed that the monofunctionalized active ester of DOTA was the only detectable product. At room temperature and at 4 °C, no evidence for multiple

activation of DOTA or rearrangement of the DOTA-EDC intermediate to the *N*-acylurea was obtained by mass spectrometry.

However, it is possible that during the preparation of the DOTA-OSSu active ester, these side reactions might occur to a degree below the limits of detection by mass spectrometry or potentiometric methods. Potential reaction byproducts such as the *bis*-active ester of DOTA and the active ester of DOTA-EDC *N*-acylurea are likely to exhibit reduced chelate stability, and any multiply activated DOTA species could mediate protein cross-linking. In order to minimize the effect of attachment of DOTA byproducts on radioconjugate stability, the activation stoichiometry of DOTA:sulfo-NHS:EDC was varied in the conjugation of cytochrome *c*. An excess of DOTA over EDC should discourage multiple activation of the tetracarboxylic acid, and an excess of sulfo-NHS might allow the DOTA-EDC intermediate to be converted more efficiently to the active ester before rearrangement to the *N*-acylurea. As the amount of carbodiimide was decreased relative to the other two reactants, the kinetic stability of the cytochrome *c*-DOTA conjugate increased. This increase in kinetic stability may be attributable to a decrease in the presence of a minute amount of a side reaction product. Such a byproduct, even in quantities too small to be detected by analytical methods, could have a disproportionate destabilizing effect on the radiolabeled protein, since both the rates of metal complexation and loss of metal from a compromised DOTA species are expected to be greater than those of the desired monoamide of DOTA.

Additional evidence for a small amount of multiple activation of DOTA was observed in the conjugation of cT84.66 with DOTA-OSSu, as approximately 6% of the mAb was converted to dimers. These dimers were easily removed from the conjugate during purification of the radiolabeled mAb, and the immunoreactivity of cT84.66-DOTA remained quantitative. The kinetic stabilities of  $^{111}\text{In}$ -labeled and  $^{90}\text{Y}$ -labeled cT84.66-DOTA in serum and in excess DTPA were much higher than those of the corresponding DTPA-conjugated antibody, suggesting that the formation of undesirable DOTA byproducts had been minimized in the conjugation process. The initial loss of approximately 3% of the  $^{111}\text{In}$  label from the DOTA-conjugated mAb during the first 48 h of incubation in 1 mM DTPA might indicate the presence of a small population of less stable chelates, but the overall kinetic stability of  $^{111}\text{In}$ -labeled cT84.66-DOTA is still significantly better than that of cT84.66-DTPA.

In an effort to minimize the rate of hydrolysis of the *N*-hydroxysulfosuccinimide ester of DOTA, all protein conjugations with DOTA-OSSu were performed at 4 °C. However, the reaction is equally efficient at room temperature. Two experiments were performed in which the chelating agent was activated with a DOTA:sulfo-NHS:EDC ratio of 10:10:1 at 4 °C and at room temperature, and then the active ester was added to cytochrome *c* in a 10:1 molar ratio at 4 °C and room temperature, respectively. After purification, MALDITOF MS revealed that both cytochrome *c*-DOTA conjugates were modified with an average of 2.57 chelating groups per protein molecule.

Radiolabeling of antibodies conjugated to DOTA with  $^{111}\text{In}$ (III) and  $^{90}\text{Y}$ (III) has usually been accomplished by prolonged incubation of the conjugate with a radiometal solution at room temperature (22, 47, 53). Exposure of a mAb to a relatively concentrated solution of the high-energy  $\beta^-$  emitter  $^{90}\text{Y}$  for an extended period of time is likely to result in significant radiolysis of the protein. Therefore, rapid and efficient incorporation of  $^{90}\text{Y}$  into

DOTA-conjugated antibodies is desirable in order to afford a high yield and specific activity for the radiolabeled immunoconjugate. The chelation of metal ions by DOTA is often a two-step process in which a rapidly formed initial adduct slowly transforms to the final complex (54, 55). Kodama *et al.* reported that the pseudo-first-order rate for Y(III)-DOTA complex formation is nearly 1600 times slower than that for Y(III)-DTPA (30). Slow formation of Y(III)-DOTA complexes presents a challenge not only to achieving high radiolabeling yields in a short time, but also to obtaining a radioconjugate exhibiting high chelate stability. If postlabeling treatment with a large excess of free chelating agent fails to remove the radiometal rapidly from DOTA adducts which are not fully complexed, then subsequent loss of metal from these adducts could contribute to reduced radioconjugate stability.

By performing the radiolabeling reactions of the protein-DOTA conjugates at elevated temperatures, two important goals were achieved. First, increasing the temperature from 25 to 37 °C increased the efficiency of  $^{90}\text{Y}(\text{III})$  incorporation into cytochrome c-DOTA by a factor of 2.6 during a 1-h incubation. At 43 °C, the amount of  $^{90}\text{Y}(\text{III})$  incorporation was nearly 4-fold compared to the reaction performed at 25 °C. Second, the kinetic stability of the cytochrome c-DOTA labeled with  $^{90}\text{Y}$  at elevated temperatures was significantly greater than that of the radioconjugate labeled at room temperature. Desreux (56) postulated that the rigid conformational properties of lanthanide-DOTA complexes at low temperatures might account for the slow kinetics of formation of these compounds and concluded from NMR studies that the macrocyclic ligand is less rigid at higher temperatures, at which the kinetics of complexation are much faster. The use of higher temperatures in the radiolabeling of protein-DOTA conjugates is expected to impart higher ground-state energies to the reactants and a greater degree of conformational flexibility to the macrocyclic chelating agent, thereby accelerating not only the rate of formation of the initial, loosely associated metal ion-DOTA adduct, but also the considerably slower rate of formation of the final, fully coordinated chelate complex. Challenging the radiolabeled protein-DOTA conjugates with a high concentration of exogenous EDTA or DTPA at 37 °C further ensures that the radioconjugate will contain only stable, fully coordinated DOTA chelates. Thus, the use of elevated temperatures in the radiolabeling of cytochrome c-DOTA produced a conjugate with both higher specific activity and greater chelate stability than when the radiolabeling reaction was performed at room temperature.

The efficiency of  $^{90}\text{Y}(\text{III})$  incorporation into cytochrome c-DOTA was directly proportional to the pH of the labeling buffer over the pH range studied. The best  $^{90}\text{Y}$  labeling results for that conjugate were obtained when the HCl was removed by evaporation from the radiometal solution, which was reconstituted with pH 7.0 labeling buffer. However, when the mAb conjugate was mixed with  $^{90}\text{YCl}_3$  which had been dried and redissolved in the same labeling buffer, the amount of  $^{90}\text{Y}$  incorporation was only about 8% of the total. A study of the pH dependence of the  $^{90}\text{Y}$  labeling reaction of cT84.66-DOTA was undertaken, and it was discovered that efficient radiometal incorporation occurred in 1 h at 43 °C over a buffer pH range of 4.5–6.0, with a maximum at pH 5.0. At the extremes of the buffer pH range studied, pH 4.0 and 7.0, the efficiency of  $^{90}\text{Y}$  incorporation dropped precipitously. Such a pH profile for the  $^{90}\text{Y}$  labeling of the mAb conjugate may be related to the isoelectric point of the protein. The pI of cT84.66 (6.40–6.65) is consider-

ably lower than the pI of cytochrome c (10.4), and the optimum pH for labeling the DOTA conjugates of these proteins with  $^{90}\text{Y}$  follows the same trend. The pH dependence of the reaction of cT84.66-DOTA and  $^{90}\text{Y}(\text{III})$  may reflect a balance in the ionization states of negatively charged amino acid side chains, which could serve as nonspecific metal ion binding sites, and positively charged residues, which could possibly form ion pairs with the protein-conjugated DOTA sites and inhibit the chelation reaction. Efficient labeling of cT84.66-DOTA with  $^{111}\text{In}$  was accomplished under similar pH conditions, using a slightly higher pH buffer to offset the greater acid load presented by the less concentrated  $^{111}\text{InCl}_3$  solution.

Radiolabeling of cytochrome c-DOTA with  $^{90}\text{Y}$  proved to be efficient in ammonium acetate, Tris acetate, and Tris hydrochloride buffers at pH 7.0. On the other hand, when even heavily conjugated cytochrome c-DOTA was dissolved in citrate buffer, which has weak chelating properties, no  $^{90}\text{Y}$  incorporation was observed. Identical results were obtained with DOTA-conjugated mAb. These buffer effects suggest that the presence of citrate is detrimental to the  $^{90}\text{Y}$  labeling of protein-DOTA conjugates, yet the presence of acetate is not necessarily essential for an efficient reaction. Clearly, the scope of buffer conditions for the radiolabeling of antibody-DOTA conjugates needs to be explored further.

The conversion of one carboxylic acid of DOTA to an amide results in the introduction of a weaker metal coordination group and might be expected to reduce the stability of the chelate complex. Sherry *et al.* (49) measured the conditional stability constant for the Gd(III) complex of DOTA-propylamide to be 104.5 times lower at pH 7.4 than that for the DOTA complex. However, they observed that the conversion of a single carboxyl group to an amide did not increase the number of inner-sphere water molecules and suggested that the amide functionality occupies a metal coordination site. Further evidence for coordination of Gd(III) by the amide functionality of a DOTA monoamide derivative was obtained by Aime *et al.* (57), who determined from an X-ray structure that the Gd-O distance of the carboxamide group was very similar to the Gd-O distances of the three carboxylates. Y(III) has coordination properties which are in many ways similar to those of the trivalent lanthanide ions, and it is reasonable to expect that the amide group of a protein-conjugated DOTA monoamide species would participate in metal binding. Riesen *et al.* (58) determined from the X-ray structure of the In(III) complex with 1,4,7,10-tetraazacyclododecane *N,N',N''*-triacetic acid that the chelate has a relatively symmetrical, compact, heptadentate structure that is sufficient for coordinative saturation and stabilization of In(III). These investigators also found an insignificant difference in the serum stabilities of  $^{111}\text{In}$ -DOTA and the  $^{111}\text{In}$  compound lacking the fourth carboxyl group, concluding that this site can be used instead as a point of attachment for proteins.

Kinetic stabilities of radiometal chelates and conjugates under physiological conditions have traditionally been estimated by incubation in serum or plasma at 37 °C. The relatively high concentrations of metal-binding proteins such as transferrin and albumin, compared to the concentrations of the radiometal and chelating agent of interest, make it unlikely that any metal lost from the complex will be recaptured by the chelating agent. In this study, the kinetic stability of  $^{111}\text{In}$ -labeled cT84.66-DOTA in human serum was significantly better than that of the same antibody conjugated with *p*-isothiocyanatobenzyl-DTPA, and the minute amount of  $^{111}\text{In}$  lost from

the mAb-conjugated DOTA chelate was insufficient to produce detectable transchelation by transferrin. When the  $^{90}\text{Y}$ -labeled cT84.66 conjugates were incubated in serum, no loss of radiometal was observed for either cT84.66-DOTA or cT84.66-DTPA during a 12-day period.

Because serum studies did not reveal any differences in the kinetic stabilities of  $^{90}\text{Y}$ -labeled cT84.66-DOTA and cT84.66-DTPA, we decided to investigate the behavior of these radioimmunoconjugates in normal saline containing 1% human serum albumin and a vast excess of DTPA. Subramanian *et al.* (59) used a similar system to examine the kinetic stability of an  $^{111}\text{In}$ -labeled mAb conjugated to a bifunctional *bis*-DTPA compound. When free DTPA is present in concentrations  $10^3$ - to  $10^5$ -fold higher than the concentration of protein-conjugated chelating agent, any metal lost from the radiolabeled protein should be effectively scavenged by DTPA and unable to return to the conjugated chelator.

The kinetic stabilities of cytochrome c-DOTA and cT84.66-DOTA in the presence of excess DTPA were nearly identical for both  $^{111}\text{In}$  and  $^{90}\text{Y}$ . The stability of the  $^{111}\text{In}$ -labeled cT84.66-DTPA conjugate under these conditions was quantitatively similar to its stability in plasma. The  $^{111}\text{In}$ -labeled cT84.66-DOTA conjugate was slightly less stable in excess DTPA than in serum, suggesting that free DTPA captures metals lost from radiolabeled proteins more effectively than the metal-binding proteins in serum. Incubation of  $^{90}\text{Y}$ -labeled cT84.66-DOTA and cT84.66-DTPA in the presence of excess DTPA revealed a drastic difference in the kinetic stabilities of the two protein-conjugated chelates. In 10 days, the majority of  $^{90}\text{Y}$  bound to cT84.66-DTPA dissociated from the mAb conjugate and was trapped by the free DTPA. In contrast, cT84.66-DOTA lost only a very small percentage of its  $^{90}\text{Y}$  label during the same period of time in excess DTPA. Kinetic analysis of metal loss from a radioimmunoconjugate in the presence of a vast excess of DTPA may therefore give a better indication of the *in vivo* stability of that conjugate than its serum or plasma stability. Preliminary studies of the biodistribution of  $^{90}\text{Y}$ -labeled cT84.66-DOTA in non-tumor-bearing mice suggest that the deposition of  $^{90}\text{Y}$  in the liver, bone, and bone marrow is significantly less than that for the DTPA-conjugated mAb.

The labeling of cT84.66-DOTA with  $^{111}\text{In}$  and  $^{90}\text{Y}$  at 43 °C under optimum pH conditions affords kinetically inert radioimmunoconjugates with specific activities in a range sufficient for practical clinical use of a high affinity mAb. Since patient doses for radioimmuno-scintigraphy and radioimmunotherapy with this antibody are typically on the order of 5 mg, it is necessary to achieve high specific activity radiolabeling with both  $^{111}\text{In}$  and  $^{90}\text{Y}$ . The elevated temperature employed for radiometal incorporation into cT84.66-DOTA also enables the rapid preparation of radiolabeled antibody for immediate patient infusion.

A potential advantage of the use of an active ester of DOTA for direct attachment to the amino acid framework of an antibody may be a reduction in the immunogenicity of the macrocyclic chelate. Conjugation of DOTA to mAbs using 2-iminothiolane and a linker-substituted bifunctional chelating agent has resulted in the development of an immune response directed against the macrocyclic ring structure (60). Immune responses to benzyl-DTPA have also been observed in patients treated with intravenous  $^{111}\text{In}$ -labeled cT84.66-DTPA, and these responses appear to involve the aromatic thiourea linker and not

solely the chelate.<sup>2</sup> Use of the active ester for attaching DOTA to antibodies produces a minimal conjugate structure, containing no potentially immunogenic aromatic moiety, and ensures that the macrocyclic chelate will reside close to the peptide backbone of the protein, making it less likely to be presented effectively as a hapten on a carrier protein.

A simple water-soluble chemical procedure has been developed for conjugation of DOTA to proteins. The use of elevated temperature, optimum pH, and appropriate buffer conditions allows rapid and efficient labeling to high specific activity with both  $^{111}\text{In}(\text{III})$  and  $^{90}\text{Y}(\text{III})$  in the preparation of radioimmunoconjugates suitable for tumor imaging and therapy, respectively. The radiolabeled products show superior kinetic stabilities in serum and excess DTPA, compared to the corresponding mAb-DTPA conjugates. We are now testing the use of the radiolabeled cT84.66-DOTA conjugate in tumor-bearing animal models in preparation for human clinical trials.

#### ACKNOWLEDGMENT

We thank Randall Woo and Jim Kao for their excellent technical assistance, Jie Zhou and Kristine Swiderek for help in obtaining mass spectra, and Jim Primus and Karen Rickard-Dickson for providing the chimeric T84.66 antibody. This work was supported by Research Grant CA43904 from the National Cancer Institute, NIH.

#### LITERATURE CITED

- (1) Meares, C. F. (1986) Chelating Agents for the Binding of Metal Ions to Antibodies. *Int. J. Radiat. Appl. Instrum. Part B Nucl. Med. Biol.* 13, 311-318.
- (2) Gansow, O. A. (1991) Newer Approaches to the Radiolabeling of Monoclonal Antibodies by Use of Metal Chelates. *Int. J. Radiat. Appl. Instrum. Part B Nucl. Med. Biol.* 18, 369-381.
- (3) Liu, Y., and Wu, C. (1991) Radiolabeling of Monoclonal Antibodies with Metal Chelates. *Pure Appl. Chem.* 63, 427-463.
- (4) Wessels, B. W., and Rogus, R. D. (1984) Radionuclide selection and model absorbed dose calculations for radiolabeled tumor associated antibodies. *Med. Phys.* 11, 638-645.
- (5) Wolf, W., and Shani, J. (1986) Criteria for the Selection of the Most Desirable Radionuclide for Radiolabeling Monoclonal Antibodies. *Int. J. Radiat. Appl. Instrum. Part B Nucl. Med. Biol.* 13, 319-324.
- (6) Schlom, J., Siler, K., Milenic, D. E., Eggensperger, D., Colcher, D., Miller, L. S., Houchens, D., Cheng, R., Kaplan, D., and Goekeler, W. (1991) Monoclonal Antibody-based Therapy of a Human Tumor Xenograft with a  $^{177}\text{Lu}$ -labeled Immunoconjugate. *Cancer Res.* 51, 2889-2896.
- (7) Kozak, R. W., Raubitschek, A., Mirzadeh, S., Brechbiel, M. W., Junghaus, R., Gansow, O. A., and Waldmann, T. A. (1989) Nature of the Bifunctional Chelating Agent Used for Radioimmunotherapy with Yttrium-90 Monoclonal Antibodies: Critical Factors in Determining *In Vivo* Survival and Organ Toxicity. *Cancer Res.* 49, 2639-2644.
- (8) Moi, M. K., Meares, C. F., McCall, M. J., Cole, W. C., and DeNardo, S. J. (1985) Copper Chelates as Probes of Biological Systems: Stable Copper Complexes with a Macrocyclic Bifunctional Chelating Agent. *Anal. Biochem.* 148, 249-253.
- (9) Moi, M. K., Meares, C. F., and DeNardo, S. J. (1988) The Peptide Way to Macrocyclic Bifunctional Chelating Agents: Synthesis of 2-(*p*-Nitrobenzyl)-1,4,7,10-tetraazacyclododecane-*N,N',N'',N'''*-tetraacetic Acid and Study of Its Yttrium(III) Complex. *J. Am. Chem. Soc.* 110, 6266-6267.
- (10) Craig, A. S., Helps, I. M., Jankowski, K. J., Parker, D., Beeley, N. R. A., Boyce, B. A., Eaton, M. A. W., Millican, A. T., Millar, K., Phipps, A., Rhind, S. K., Harrison, A., and Walker, C. (1989) Towards Tumour Imaging with Indium-111 Labelled Macrocyclic-Antibody Conjugates. *J. Chem. Soc., Chem. Commun.* 794-796.

<sup>2</sup> Pant, K. D., and Raubitschek, A. (unpublished results).

- (11) Parker, D., Morphy, J. R., Jankowski, K., and Cox, J. (1989) Implementation of macrocycle conjugated antibodies for tumour-targeting. *Pure Appl. Chem.* 61, 1637–1641.
- (12) Cox, J. P. L., Jankowski, K. J., Katakay, R., Parker, D., Beeley, N. R. A., Boyce, B. A., Eaton, M. A. W., Millar, K., Millican, A. T., Harrison, A., and Walker, C. (1989) Synthesis of a Kinetically Stable Yttrium-90 Labelled Macrocycle-Antibody Conjugate. *J. Chem. Soc., Chem. Commun.* 797–798.
- (13) Moi, M. K., DeNardo, S. J., and Meares, C. F. (1990) Stable Bifunctional Chelates of Metals Used in Radiotherapy. *Cancer Res. (Suppl.)* 50, 789s–793s.
- (14) Meares, C. F., Moi, M. K., Diril, H., Kukis, D. L., McCall, M. J., Deshpande, S. V., DeNardo, S. J., Snook, D., and Epenetos, A. A. (1990) Macrocyclic chelates of radiometals for diagnosis and therapy. *Br. J. Cancer* 62, Suppl. X, 21–26.
- (15) Morphy, J. R., Parker, D., Katakay, R., Eaton, M. A. W., Millican, A. T., Alexander, R., Harrison, A., and Walker, C. (1990) Towards Tumour Targeting with Copper-radiolabelled Macrocycle-Antibody Conjugates: Synthesis, Antibody Linkage, and Complexation Behaviour. *J. Chem. Soc., Perkin Trans. 2* 573–585.
- (16) Cox, J. P. L., Craig, A. S., Helps, I. M., Jankowski, K. J., Parker, D., Eaton, M. A. W., Millican, A. T., Millar, K., Beeley, N. R. A., and Boyce, B. A. (1990) Synthesis of C- and N-Functionalised Derivatives of 1,4,7-Triazacyclononane-1,4,7-triyltriacetic acid (NOTA), 1,4,7,10-Tetra-azacyclododecane-1,4,7,10-tetrayltetra-acetic Acid (DOTA), and Diethylenetriaminepenta-acetic Acid (DTPA): Bifunctional Complexing Agents for the Derivatisation of Antibodies. *J. Chem. Soc., Perkins Trans. 1* 2567–2576.
- (17) Ruegg, C. L., Anderson-Berg, W. T., Brechbiel, M. W., Mirzadeh, S., Gansow, O. A., and Strand, M. (1990) Improved *In Vivo* Stability and Tumor Targeting of Bismuth-labeled Antibody. *Cancer Res.* 50, 4221–4226.
- (18) Kline, S. J., Betebenner, D. A., and Johnson, D. K. (1991) Carboxymethyl-Substituted Bifunctional Chelators: Preparation of Aryl Isothiocyanate Derivatives of 3-(Carboxymethyl)-3-azapentanedioic Acid, 3,12-Bis(carboxymethyl)-6,9-dioxo-3,12-diazatetradecanedioic Acid, and 1,4,7,10-Tetraazacyclododecane-*N,N',N'',N'''*-tetraacetic Acid for Use as Protein Labels. *Bioconjugate Chem.* 2, 26–31.
- (19) McMurry, T. J., Brechbiel, M., Kumar, K., and Gansow, O. A. (1992) Convenient Synthesis of Bifunctional Tetraaza Macrocycles. *Bioconjugate Chem.* 3, 108–117.
- (20) Renn, O., and Meares, C. F. (1992) Large-Scale Synthesis of the Bifunctional Chelating Agent 2-(*p*-Nitrobenzyl)-1,4,7,10-tetraazacyclododecane-*N,N',N'',N'''*-tetraacetic Acid, and the Determination of Its Enantiomeric Purity by Chiral Chromatography. *Bioconjugate Chem.* 3, 563–569.
- (21) Kruper, W. J., Jr., Rudolf, P. R., and Langhoff, C. A. (1993) Unexpected Selectivity in the Alkylation of Polyazamacrocycles. *J. Org. Chem.* 58, 3869–3876.
- (22) Li, M., and Meares, C. F. (1993) Synthesis, Metal Chelate Stability Studies, and Enzyme Digestion of a Peptide-Linked DOTA Derivative and Its Corresponding Radiolabeled Immunoconjugates. *Bioconjugate Chem.* 4, 275–283.
- (23) Li, M., Meares, C. F., Zhong, G.-R., Miers, L., Xiong, C.-Y., and DeNardo, S. J. (1994) Labeling of Monoclonal Antibodies with <sup>90</sup>Yttrium- and <sup>111</sup>Indium-DOTA Chelates: A Simple and Efficient Method. *Bioconjugate Chem.* 5, 101–104.
- (24) Loncin, M. F., Desreux, J. F., and Merciny, E. (1986) Coordination of Lanthanides by Two Polyamino Polycarboxylic Macrocycles: Formation of Highly Stable Lanthanide Complexes. *Inorg. Chem.* 25, 2646–2648.
- (25) Cacheris, W. P., Nickle, S. K., and Sherry, A. D. (1987) Thermodynamic Study of Lanthanide Complexes of 1,4,7-Triazacyclononane-*N,N',N'',N'''*-tri-acetic Acid and 1,4,7,10-Tetraazacyclododecane-*N,N',N'',N'''*-tetraacetic Acid. *Inorg. Chem.* 26, 958–960.
- (26) Kumar, K., Magerstädt, M., and Gansow, O. A. (1989) Lead(II) and Bismuth(III) Complexes of the Polyazacycloalkane-*N*-acetic Acids nota, dota, and tetra. *J. Chem. Soc., Chem. Commun.* 145–146.
- (27) Broan, C. J., Cox, J. P. L., Craig, A. S., Katakay, R., Parker, D., Harrison, A., Randall, A. M., and Ferguson, G. (1991) Structure and Solution Stability of Indium and Gallium Complexes of 1,4,7-Triazacyclononanetriacetic acid and of Yttrium Complexes of 1,4,7,10-Tetraazacyclododecanetriacetic acid and Related Ligands: Kinetically Stable Complexes for Use in Imaging and Radioimmunotherapy. X-Ray Molecular Structure of the Indium and Gallium Complexes of 1,4,7-Triazacyclononane-1,4,7-triacetic Acid. *J. Chem. Soc., Perkin Trans. 2* 87–99.
- (28) Clarke, E. T., and Martell, A. E. (1991) Stabilities of the alkaline earth and divalent transition metal complexes of the tetraazamacrocyclic tetraacetic acid ligands. *Inorg. Chim. Acta* 190, 27–36.
- (29) Clarke, E. T., and Martell, A. E. (1991) Stabilities of trivalent metal ion complexes of the tetraacetate derivatives of 12-, 13-, and 14-membered tetraazamacrocycles. *Inorg. Chim. Acta* 190, 37–46.
- (30) Kodama, M., Koike, T., Mahatma, A. B., and Kimura, E. (1991) Thermodynamic and Kinetic Studies of Lanthanide Complexes of 1,4,7,10,13-Pentaazacyclopentadecane-*N,N',N'',N'''*-pentaacetic Acid and 1,4,7,10,13,16-Hexaazacyclooctadecane-*N,N',N'',N'''*-hexaacetic Acid. *Inorg. Chem.* 30, 1270–1273.
- (31) Brechbiel, M. W., Pippin, C. G., McMurry, T. J., Milenic, D., Roselli, M., Colcher, D., and Gansow, O. A. (1991) An Effective Chelating Agent for Labelling of Monoclonal Antibody with <sup>212</sup>Bi for  $\alpha$ -Particle Mediated Radioimmunotherapy. *J. Chem. Soc., Chem. Commun.* 1169–1170.
- (32) Neumaier, M., Shively, L., Chen, F.-S., Gaida, F.-J., Ilgen, C., Paxton, R. J., Shively, J. E., and Riggs, A. D. (1990) Cloning of the Genes for T84.66, an Antibody That Has a High Specificity and Affinity for Carcinoembryonic Antigen, and Expression of Chimeric Human/Mouse T84.66 Genes in Myeloma and Chinese Hamster Ovary Cells. *Cancer Res.* 50, 2128–2134.
- (33) Hnatowich, D. J., Layne, W. W., Childs, R. L., Lanteigne, D., Davis, M. A., Griffin, T. W., and Doherty, P. W. (1983) Radioactive Labeling of Antibody: A Simple and Efficient Method. *Science (Washington, D.C.)* 220, 613–615.
- (34) Hnatowich, D. J., Childs, R. L., Lanteigne, D., and Najafi, A. (1983) The Preparation of DTPA-Coupled Antibodies Radiolabeled with Metallic Radionuclides: an Improved Method. *J. Immunol. Methods* 65, 147–157.
- (35) Halpern, S. E., Hagan, P. L., Garver, P. R., Koziol, J. A., Chen, A. W. N., Frincke, J. M., Bartholomew, R. M., David, G. S., and Adams, T. H. (1983) Stability, Characterization, and Kinetics of <sup>111</sup>In-labeled Monoclonal Antitumor Antibodies in Normal Animals and Nude Mouse-Human Tumor Models. *Cancer Res.* 43, 5347–5355.
- (36) Buckley, R. G., and Searle, F. (1984) An efficient method for labelling antibodies with <sup>111</sup>In. *FEBS Lett.* 166, 202–204.
- (37) Paxton, R. J., Jakowatz, J. G., Beatty, J. D., Beatty, B. G., Vlahos, W. G., Williams, L. E., Clark, B. R., and Shively, J. E. (1985) High-Specific-Activity <sup>111</sup>In-labeled Anticarcinoembryonic Antigen Monoclonal Antibody: Improved Method for the Synthesis of Diethylenetriaminepentaacetic Acid Conjugates. *Cancer Res.* 45, 5694–5699.
- (38) Brechbiel, M. W., Gansow, O. A., Atcher, R. W., Schlom, J., Esteban, J., Simpson, D. E., and Colcher, D. (1986) Synthesis of 1-(*p*-Isothiocyanatobenzyl) Derivatives of DTPA and EDTA. Antibody Labeling and Tumor-Imaging Studies. *Inorg. Chem.* 25, 2772–2781.
- (39) Westerberg, D. A., Carney, P. L., Rogers, P. E., Kline, S. J., and Johnson, D. K. (1989) Synthesis of Novel Bifunctional Chelators and Their Use in Preparing Monoclonal Antibody Conjugates for Tumor Targeting. *J. Med. Chem.* 32, 236–243.
- (40) Davis, M. T., and Lee, T. D. (1992) Analysis of peptide mixtures by capillary high performance liquid chromatography: A practical guide to small-scale separations. *Protein Sci.* 1, 935–944.
- (41) Swiderik, K. M., Deng, P. S. K., Lee, T. D., Shively, J. E., Hatefi, Y., and Chen, S. (1994) Electrospray Mass Spectral Analysis of the (N)-Arylazido- $\beta$ -Alanil NAD<sup>+</sup> Modified Bovine Heart Mitochondrial NADH Dehydrogenase. *Tech. Protein Chem.* 5, 49–57.

- (42) Yamada, H., Imoto, T., Fujita, K., Okazaki, K., and Motomura, M. (1981) Selective Modification of Aspartic Acid-101 in Lysozyme by Carbodiimide Reaction. *Biochemistry* 20, 4836–4842.
- (43) Staros, J. V., Wright, R. W., and Swingle, D. M. (1986) Enhancement by *N*-Hydroxysulfosuccinimide of Water-Soluble Carbodiimide-Mediated Coupling Reactions. *Anal. Biochem.* 156, 220–222.
- (44) Gilles, M. A., Hudson, A. Q., and Borders, C. L., Jr. (1990) Stability of Water-Soluble Carbodiimides in Aqueous Solution. *Anal. Biochem.* 184, 244–248.
- (45) Meares, C. F., McCall, M. J., Reardan, D. T., Goodwin, D. A., Diamanti, C. I., and McTigue, M. (1984) Conjugation of Antibodies with Bifunctional Chelating Agents: Isothiocyanate and Bromoacetamide Reagents, Methods of Analysis, and Subsequent Addition of Metal Ions. *Anal. Biochem.* 142, 68–78.
- (46) Sumerdon, G. A., Rogers, P. E., Lombardo, C. M., Schnobrich, K. E., Melvin, S. L., Hobart, E. D., Tribby, I. I. E., Stroupe, S. D., and Johnson, D. K. (1990) An Optimized Antibody-Chelator Conjugate for Imaging of Carcinoembryonic Antigen with Indium-111. *Int. J. Radiat. Appl. Instrum. Part B Nucl. Med. Biol.* 17, 247–254.
- (47) Deshpande, S. V., DeNardo, S. J., Kukis, D. L., Moi, M. K., McCall, M. J., DeNardo, G. L., and Meares, C. F. (1990) Yttrium-90-Labeled Monoclonal Antibody for Therapy: Labeling by a New Macrocyclic Bifunctional Chelating Agent. *J. Nucl. Med.* 31, 473–479.
- (48) Wu, C., Virzi, F., and Hnatowich, D. J. (1992) Investigations of N-linked Macrocycles for <sup>111</sup>In and <sup>90</sup>Y Labeling of Proteins. *Int. J. Radiat. Appl. Instrum. Part B Nucl. Med. Biol.* 19, 239–244.
- (49) Sherry, A. D., Brown, R. D., III, Gerald, C. F. G. C., Koenig, S. H., Kuan, K.-T., and Spiller, M. (1989) Synthesis and Characterization of the Gadolinium(3+) Complex of DOTA-Propylamide: A Model DOTA-Protein Conjugate. *Inorg. Chem.* 28, 620–622.
- (50) Sieving, P. F., Watson, A. D., and Rocklage, S. M. (1990) Preparation and Characterization of Paramagnetic Polychelates and Their Protein Conjugates. *Bioconjugate Chem.* 1, 65–71.
- (51) Smith-Jones, P. M., Fridrich, R., Kaden, T. A., Novak-Hofer, I., Siebold, K., Tschudin, D., and Maecke, H. R. (1991) Antibody Labeling with Copper-67 Using the Bifunctional Macrocyclic 4-[(1,4,8,11-Tetraazacyclotetradec-1-yl)methyl]benzoic Acid. *Bioconjugate Chem.* 2, 415–421.
- (52) Smith, A., Alberto, R., Blaeuenstein, P., Novak-Hofer, I., Maecke, H. R., and Schubiger, P. A. (1993) Preclinical Evaluation of <sup>67</sup>Cu-labeled Intact and Fragmented Anti-Colon Carcinoma Monoclonal Antibody MA35. *Cancer Res.* 53, 5727–5733.
- (53) Harrison, A., Walker, C. A., Parker, D., Jankowski, K. J., Cox, J. P. L., Craig, A. S., Sansom, J. M., Beeley, N. R. A., Boyce, R. A., Chaplin, L., Eaton, M. A. W., Farnsworth, A. P. H., Millar, K., Millican, A. T., Randall, A. M., Rhind, S. K., Secher, D. S., and Turner, A. (1991) The *In Vivo* Release of <sup>90</sup>Y from Cyclic and Acyclic Ligand-Antibody Conjugates. *Int. J. Radiat. Appl. Instrum. Part B Nucl. Med. Biol.* 18, 469–476.
- (54) Kasprzyk, S. P., and Wilkins, R. G. (1982) Kinetics of Interaction of Metal Ions with Two Tetraaza Tetraacetate Macrocycles. *Inorg. Chem.* 21, 3349–3352.
- (55) Wang, X., Jin, T., Comblin, V., Lopez-Mut, A., Merciny, E., and Desreux, J. F. (1992) A Kinetic Investigation of the Lanthanide DOTA Chelates. Stability and Rates of Formation and of Dissociation of a Macrocyclic Gadolinium(III) Polyaza Polycarboxylic MRI Contrast Agent. *Inorg. Chem.* 31, 1095–1099.
- (56) Desreux, J. F. (1980) Nuclear Magnetic Resonance Spectroscopy of Lanthanide Complexes with a Tetraacetic Tetraaza Macrocyclic. Unusual Conformation Properties. *Inorg. Chem.* 19, 1319–1324.
- (57) Aime, S., Anelli, P. L., Botta, M., Fedeli, F., Grandi, M., Paoli, P., and Uggeri, F. (1992) Synthesis, Characterization, and <sup>1</sup>T<sub>1</sub> NMRD Profiles of Gadolinium(III) Complexes of Monoamide Derivatives of DOTA-like Ligands. X-ray Structure of the 10-[2-[[2-Hydroxy-1-(hydroxymethyl)ethyl]amino]-1-[(phenylmethoxy)methyl]-2-oxo-ethyl]-1,4,7,10-tetraazacyclododecane-1,4,7-triacetic Acid-Gadolinium(III) Complex. *Inorg. Chem.* 31, 2422–2428.
- (58) Riesen, A., Kaden, T. A., Ritter, W., and Mäcke, H. R. (1989) Synthesis and X-Ray Structural Characterisation of Seven Co-ordinate Macrocyclic In<sup>3+</sup> Complexes with Relevance to Radiopharmaceutical Applications. *J. Chem. Soc., Chem. Commun.* 460–462.
- (59) Subramanian, R., Colony, J., Shaban, S., Sidrak, H., Haspel, M. V., Pomato, N., Hanna, M. G., Jr., and McCabe, R. P. (1992) New Chelating Agent for Attaching Indium-111 to Monoclonal Antibodies: In Vitro and In Vivo Evaluation. *Bioconjugate Chem.* 3, 248–255.
- (60) Kosmas, C., Snook, D., Gooden, C. S., Courtenay-Luck, N. S., McCall, M. J., Meares, C. F., and Epenetos, A. A. (1992) Development of Humoral Immune Responses against a Macrocyclic Chelating Agent (DOTA) in Cancer Patients Receiving Radioimmunoconjugates for Imaging and Therapy. *Cancer Res.* 52, 904–911.

# Temperature-Responsive Bioconjugates. 3. Antibody–Poly(*N*-isopropylacrylamide) Conjugates for Temperature-Modulated Precipitations and Affinity Bioseparations<sup>†</sup>

Yoshiyuki G. Takei, Miki Matsukata, Takashi Aoki, Kohei Sanui, Naoya Ogata, Akihiko Kikuchi,<sup>‡</sup> Yasuhisa Sakurai,<sup>‡</sup> and Teruo Okano<sup>\*,‡</sup>

Department of Chemistry, Faculty of Science and Technology, Sophia University, 7-1 Kioi-cho, Chiyoda, Tokyo 102, Japan, and Institute of Biomedical Engineering, Tokyo Women's Medical College, 8-1 Kawada-cho, Shinjuku, Tokyo 162, Japan. Received July 22, 1994<sup>\*</sup>

Immunoglobulin G (IgG) has been modified by poly(*N*-isopropylacrylamide) (PIPAAm) to create a novel bioconjugate which exhibits reversible phase transition behavior at 32 °C in aqueous media. A terminal carboxyl group introduced into PIPAAm molecule by polymerization of IPAAm with 3-mercaptopropionic acid was used for conjugation to IgG via coupling reaction of activated ester with protein amino group. These conjugates exhibited rapid response to changes in solution temperature and significant phase separation above a critical solution temperature corresponding to that for the original PIPAAm. These conjugates bound to antigen quantitatively in aqueous system, and antigen-bound complex also demonstrated phase separation and precipitation above a critical temperature. Precipitate was reversibly redissolved in cold buffer. Though particular conjugate which includes 12 molecules of PIPAAm with 6,100 molecular weight suppressed more than 95% of Fc-dependent binding with protein A, it retained approximately 60% of original specific antigen binding activity. It was manifested that polymer content of conjugate was 20–30 wt% for the case of 6,100 molecular weight of PIPAAm to demonstrate specific antigen binding activity most effectively and to reduce Fc-dependent binding with protein A. IgG-PIPAAm conjugates were soluble in water and formed antigen-bound complex in homogeneous solution system below a critical temperature. These conjugates were separated from solution and other solutes corresponding to PIPAAm nature and scarcely bound to antigen above a critical temperature. It is revealed that temperature-responsive PIPAAm conjugated to biomolecule operated as a switching molecule. These phenomena are attractive for not only reversible bioreactors and protein separations but also carrier substrate to localize biomolecules such as drugs, peptides and hormones in a living body.

## INTRODUCTION

In 1977, Abuchowski and coworkers demonstrated that covalent attachment of poly(ethylene glycol) (PEG) to a protein leads to minimal loss of activity and decreases protein immunogenicity and antigenicity entirely (1, 2). Since this time, many investigators have used PEG-modified biomolecules for chemical, biotechnological and biomedical applications, termed PEG-ylation (3). Bioactivity of PEG-modified proteins has been investigated and correlated to their structures. Bioactivities were strongly affected by the conjugated polymer chain mobility, corresponding to PEG polymer chain length (4–6). While PEG-ylation modifies biomolecule interface, it does not introduce any stimuli-response into these biomolecules to control the activity of biomolecules using external stimuli.

It is well-known that poly(*N*-isopropylacrylamide) (PIPAAm)<sup>1</sup> exhibits a remarkable phase transition in aqueous

media in response to changes in temperature, demonstrating a lower critical solution temperature (LCST) (7–9). The temperature-responsive phase transition behaviors of these networks have been investigated and utilized for drug delivery systems (10–13), cell culture substrates (14, 15), and immobilized enzymes (16, 17). Hoffman and co-workers have reported the synthesis and characterization of PIPAAm–biomolecule conjugates as devices for affinity immunoassay and bioseparation (18–22). In these biomolecule conjugates, *N*-(acryloxy)succinimide was used for conjugation of biomolecules to PIPAAm. Therefore, the characteristic of the conjugate is multipoint binding between biomolecule and the copolymer. It is sometimes difficult to control the solubility because of the formation of the crosslinking of the conjugate, and multipoint conjugation may also lead denaturalization of biomolecules.

We previously reported the synthesis of temperature-responsive PIPAAm with a carboxyl group at one end (semitelechelic PIPAAm) by polymerization of IPAAm using 3-mercaptopropionic acid as a telogen (23). We demonstrated that the number of conjugated PIPAAm per biomolecule affected the temperature-responsive behavior of the conjugate and the energy required to dehydrate the whole conjugate (24). PIPAAm–biomolecule conjugates using semitelechelic PIPAAm as a phase transition inducer achieved both rapid responses to changes in temperature and drastic phase separation. These conjugates were conveniently separated from reactive products and other solutes with small temperature

\* Author to whom correspondence should be addressed.

<sup>†</sup> Part 1: see ref 23. Part 2: ref 24.

<sup>‡</sup> Tokyo Women's Medical College.

<sup>\*</sup> Abstract published in *Advance ACS Abstracts*, November 1, 1994.

<sup>1</sup> Abbreviations used: IPAAm, *N*-isopropylacrylamide; PIPAAm, poly-IPAAm; DMF, *N,N*-dimethylformamide; IgG, immunoglobulin G; HSA, human serum albumin; FITC–HSA, fluorescein isothiocyanate-labeled HSA; G, goat IgG; AG, anti-human serum albumin goat IgG; G–X, G-PIPAAm conjugate; AG–X, AG-PIPAAm conjugate.



**Table 1. Preparation and Analysis of IgG-PIPAAm Conjugates**

code	IgG	activated PIPAAm <sup>a</sup> (mol/mol IgG)	molecular wt of conjugates ( $\times 10^3$ )		PIPAAm content		LCST (°C)
			HPSEC <sup>b</sup>	titration <sup>c</sup>	mol/mol IgG <sup>c</sup>	wt % <sup>d</sup>	
G-0	nonspecific	0	150	150	0		
G-3		10	167	170	3.2	10.7	34.4
G-13		25	220	223	13.1	31.6	33.8
G-21		50	264	276	20.6	43.2	33.6
AG-0	anti-HSA	0	150	150	0		
AG-4		10	169	177	4.4	11.2	34.2
AG-12		25	212	223	12.0	29.3	34.0
AG-20		50	245	273	20.1	38.8	33.6

<sup>a</sup> PIPAAm with  $M_w = 6100$  in ref 23. <sup>b</sup> Determined by HPSEC. <sup>c</sup> Estimated by consuming residual primary amino groups using fluorescamine. <sup>d</sup> (wt PIPAAm/wt conjugate) 100.

increases (23–25). It is reasoned therefore that conjugation of semitelechelic PIPAAm to IgG molecules would not only maintain high IgG–antigen binding activity associated with IgG conjugation to one reactive end group per polymer but also decrease protein immunogenicity with local and large steric hindrance due to the inherently high mobile nature of polymer free-end.

In this paper, the preparation of immunoglobulin G (IgG)–PIPAAm conjugates using semitelechelic PIPAAm with a carboxyl end group is described. Effect of the number of conjugated PIPAAm molecules on both temperature-responsive phase transition behavior and specific antigen binding activity of these conjugates is reported. In addition, the IgG Fc region demonstrates biological activity characteristic of immunoglobulins and their subclasses such as complement fixation. One of the major problems is that cellular Fc receptors exhibit undesirable entrapment of conjugate and interfere with binding specificity with particular antigens *in vivo*. Fluorescein isothiocyanate-labeled human serum albumin (FITC–HSA) was used as a model antigen, and specific antigen binding activity of the conjugate was estimated by measuring FITC fluorescence. Antigen binding activity was investigated by fluorescence spectroscopy, and the Fc-dependent binding activity was also estimated from the suppression of binding to protein A. The potential value of PIPAAm with a carboxyl end group as switching molecule for reversible bioreactors and temperature-modulated biochemotherapy is indicated.

## EXPERIMENTAL PROCEDURES

**Preparation of Polymers and Biochemicals.** Semitelechelic poly(*N*-isopropylacrylamide) (PIPAAm) with a carboxyl end group was synthesized by polymerization of IPAAm with 3-mercaptopropionic acid as a chain transfer agent in *N,N*-dimethylformamide (DMF) as described in our previous work (23). PIPAAm molecules of mol wt *ca.* 6100 ( $M_w/M_n = 1.22$ ), one carboxyl group per polymer chain, and exhibiting LCST near 32 °C were used for conjugation with IgG. Anti-human serum albumin goat IgG (AG) and fluorescein isothiocyanate-labeled human serum albumin (FITC–HSA) were purchased from Cappel Research Products, USA, and used as received. Goat IgG reagent grade (G) and fluorescamine were obtained from Sigma Chemical Co. Ultrapure water used for sample solutions was provided by a commercial water purification device (LV-10T, Toray, Japan). All other reagents were from Wako Pure Chemicals Co., Japan. Solvents were reagent grade and purified by conventional methods.

**Conjugation of PIPAAm to IgG.** PIPAAm with a carboxyl end group was activated by *N*-hydroxysuccinimide with dicyclohexylcarbodiimide in dry ethyl acetate

at 4 °C for 16 h in a molar ratio of 1:2:2, respectively. After filtration and concentration, the reactant was poured into diethyl ether to precipitate activated-PIPAAm. Activated PIPAAm was purified by reprecipitation with ethyl acetate/diethyl ether twice. Activated ester group was confirmed by infrared and ultraviolet spectroscopy (26). IgG–PIPAAm conjugates were synthesized following the protocol of Bückman *et al.* with a weight feed ratio of PIPAAm to IgG of 10–50 (27). The reaction solution was adjusted to and maintained at pH 8.5 during the course of the reaction, and all steps were carried out at 4 °C. The IgG was dissolved in 0.1 M carbonate–bicarbonate buffer (0.15 M NaCl, pH 8.5), and the IgG concentration of the solution was adjusted to 2 mg/mL. Activated-PIPAAm was dissolved in 4 mL of dry DMF and added to the IgG solution. This protocol was repeated four more times at 30 min intervals. Total reaction time was 8 h with gentle stirring at 4 °C. The solution was then dialyzed against phosphate buffer solution (PBS; 0.15 M NaCl, pH 7.4) using cellulose porous membrane tubing (50 000 molecular weight cutoff, Spectrum Medical Industries, USA) for 24 h at 4 °C and then lyophilized. The IgG–PIPAAm conjugates were stored at –20 °C in a biofreezer, and the IgG concentration was determined by the biuret method (28). Similar methods were also used to prepare the conjugates using anti-human serum albumin goat IgG for the antigen binding-activity measurement. The number of PIPAAm conjugated to IgG was estimated by measuring the amount of amino groups consumed during the conjugation process using fluorescamine-based assay as follows (29, 30). A series of conjugate solutions was prepared with PBS at the following concentrations: 0, 0.7, 1.2, 1.6, and 2.5  $\mu$ g/mL. Fluorescamine (0.3 mg/mL) in acetone (0.5 mL) was added to each 1.5 mL Eppendorf tube containing 1 mL of sample solution while vortexing, and then solutions were incubated for 10 min at 4 °C. The fluorescence of the solution was measured on a spectrofluorometer using a microvolume observation cell (0.8 mL maximum) with an excitation wavelength of 390 nm and emission at 475 nm. Preparation and analysis of IgG–PIPAAm conjugates are summarized in Table 1.

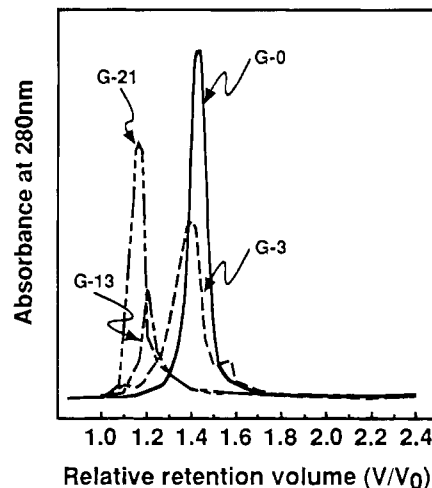
**Molecular Weight Measurement.** Molecular weights of the resulting IgG–PIPAAm conjugates were measured by high-performance size-exclusion chromatography (HPSEC; HLC-802, equipped with TSK-G-3000SW, Toso, Japan) using sodium azide-containing PBS (0.15 M NaCl, 3 mM NaN<sub>3</sub>, pH 7.4) as a mobile phase at 4 °C. A calibration curve for globular proteins was obtained by the retention of standard proteins, obtained from Boehringer Mannheim Biochemica, including  $\beta$ -galactosidase ( $M_r = 465\,000$ ), IgG ( $M_r = 150\,000$ ), IgG–Fab fragment ( $M_r = 50\,000$ ), myoglobin ( $M_r = 17\,000$ ), and Gly-Tyr ( $M_r = 238$ ).

**Transmittance Measurements.** Optical transmittance of IgG-PIPAAm conjugate aqueous solutions in PBS (pH 7.4, 1 mg/mL) at various temperatures was measured at 500 nm using a spectrophotometer (UV-240, Shimadzu, Japan). The observation cell was thermostated using a circular water jacket. AG-PIPAAm and HSA (used as antigen) mixture solutions were also measured. The procedure was performed as follows: AG-PIPAAm conjugate solution was prepared in PBS (pH 7.4) at the concentration of 1 mg/mL. FITC-HSA was dissolved in PBS to the concentration of 100  $\mu$ g/mL. FITC-HSA solution (500  $\mu$ L) was added to 500  $\mu$ L of AG-PIPAAm conjugate solution in a 1.5 mL Eppendorf tube and incubated for 1 h at 4  $^{\circ}$ C to allow specific complexation. Then optical transmittance of mixture was measured at various temperatures using a microvolume observation cell (0.8 mL maximum). Complexation of AG-PIPAAm conjugate with FITC-HSA was determined by the method described in the following section.

**Elutability Measurement of IgG-PIPAAm Conjugates.** Measurement of Fc-dependent binding activity of IgG-PIPAAm conjugates was performed by complexation with protein A. Five hundred  $\mu$ L of IgG-PIPAAm/PBS solution (10  $\mu$ g/mL) was applied to a protein A-immobilized prepacked column (approximately 2.5 mL bed volume, Protein A Sepharose CL-4B, Pharmacia LKB Biotechnology, Sweden). One hundred mL of PBS was then passed through the column to elute unbound conjugates. Bound conjugates were then eluted using 100 mL of PBS containing 8 M urea. UV absorbance of the elution at 280 nm was continuously recorded on a chart as a function of elution volume. All steps were carried out at 4  $^{\circ}$ C. Elutability was defined by the following equation:

$$\text{elutability (\%)} = \frac{\text{amount of unbound conjugates}}{\text{total amount of protein}} (100)$$

**Fluorescence Measurement for Antigen Binding Activity.** Fluorescence spectra were recorded on a spectrofluorometer (FP-770, JASCO, Japan). The temperature of the water-jacketed cell holder was controlled with a thermostated circulating bath to 20  $^{\circ}$ C. An excitation wavelength, 490 nm, and an emission wavelength, 520 nm, were used for the FITC emission measurement. Antigen binding activity was measured as follows: FITC-labeled HSA (FITC-HSA) was used as antigen to AGs. A series of FITC-HSA solutions was prepared with PBS at the following concentrations: 0, 4.1, 12.0, 20.2, 50.2, 100.0, and 480  $\mu$ g/mL. AG-PIPAAm conjugate was dissolved in PBS at a concentration of 1 mg/mL. Five hundred  $\mu$ L of FITC-HSA solution was added to 500  $\mu$ L of AG-PIPAAm conjugate solution in a 1.5 mL Eppendorf tube and incubated for 1 h at 4  $^{\circ}$ C to allow specific complexation. The mixture was then heated to 37  $^{\circ}$ C for 8 min to precipitate the polymer. The precipitate was collected by centrifugation at 4000g for 12 min at 37  $^{\circ}$ C. The supernatant was withdrawn, and the precipitate was redissolved in 1 mL of cold PBS. The temperature was heated to 37  $^{\circ}$ C again to precipitate the polymer, the precipitate was collected by centrifugation, the supernatant was withdrawn, and finally the precipitate was redissolved in 200  $\mu$ L of cold PBS. One hundred  $\mu$ L of the solution was diluted into 900  $\mu$ L of PBS, and the fluorescence was measured in a fluorophotometer. Fluorescence measurements were made on both supernatant and the precipitate for the assay of the conjugates. The complex formation of AG-0, i.e., native anti-human serum albumin goat IgG, with FITC-HSA was deter-



**Figure 1.** High-performance size exclusion chromatography elution patterns of IgG-PIPAAm conjugates.

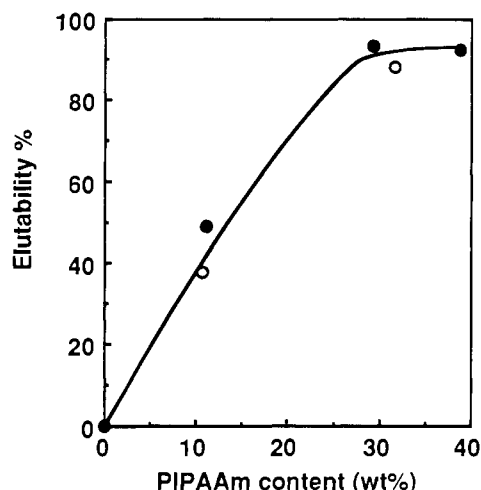
mined by high-performance liquid chromatography. AG-0 was incubated with FITC-HSA solution in a same manner with other AGs, and then the mixture solution was applied in HPLC equipped with TSK gel-G-3000-SW (Toso, Japan). PBS (pH 7.4, 0.15 M) was used as mobile phase at a flow rate of 1.0 mL/min. Fluorescence intensity of FITC-HSA was detected by fluorimeter (FS-8010, Toso, Japan) with excitation wavelength at 490 nm and emission wavelength at 520 nm. Percentage of immune complex formation was defined by the ratio of two areas corresponding to fluorescence from immune complex-formed HSA and free HSA.

All fluorescence measurements were performed at a concentration low enough so that the fluorescence intensity of the FITC was proportional to its concentration. Antigen binding activity of IgG-PIPAAm conjugate was expressed by the ratio of fluorescence intensity corresponding to IgG-PIPAAm/HSA complex and that of native IgG/HSA complex.

## RESULTS AND DISCUSSION

**Structure of IgG-PIPAAm Conjugates.** IgG-PIPAAm conjugates were prepared by coupling the activated ester of semitelechelic PIPAAm with amino group of IgG. Preparation and analysis of resulting bioconjugates are summarized in Table 1. The number of conjugated PIPAAm molecules was controlled by changing the molar ratio of IgG and semitelechelic PIPAAm in each preparation. IgG-PIPAAm conjugates are described by two sequential codes, such as AG-12, where AG refers to anti-HSA goat IgG and 12 to the number of PIPAAm molecules grafted per conjugate. The number of grafted PIPAAm molecules was estimated by measurement of primary amino group content using fluorescamine (29, 30). PIPAAm content was also determined by the data from HPSEC, which were in agreement with the results obtained by fluorescamine-based assay. All conjugates were soluble in water and saline solution (physiological pH and ionic strength) at room temperature. The results of molecular weight measurement by HPSEC are shown in Figure 1. As can be seen in Figure 1, IgG-PIPAAm conjugates were observed to elute earlier through the column than IgG (G-0). Elution time retarded with decreasing the amount of PIPAAm conjugated.

Fc-dependent binding of IgG-PIPAAm conjugates was estimated by elutability from the column corresponding to the complexation of the IgG Fc region with column-bound protein A at 4  $^{\circ}$ C. The result is shown in Figure

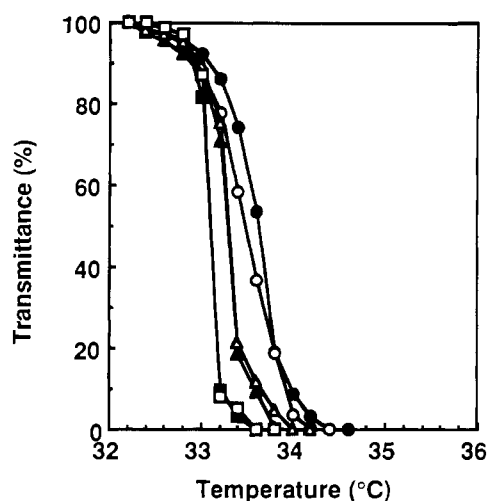


**Figure 2.** Elutability of IgG-PIPAAm from protein A-immobilized column as a function of PIPAAm content (○, G series; ●, AG series).

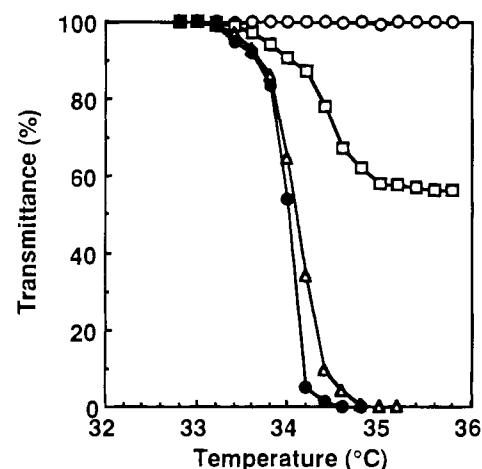
2. Fc-dependent complexation with protein A decreased significantly with increasing amounts of PIPAAm molecules conjugated with IgG, with the highest conjugate showing less than 10% of the binding which unconjugated IgG demonstrates. When PIPAAm content exceeds 30 wt % in the conjugate, free chain end mobility of the terminally grafted PIPAAm suggested prevention of Fc-dependent binding to protein A.

Many investigations have described the conjugation of polymers coupled with primary amines corresponding to lysine residue in biomolecules. Alterations in secondary and tertiary structures of biomolecule were often evaluated by circular dichroic spectra. Polymer-protein conjugation in mild conditions leads to no disruption of IgG native structure, and IgG molecules maintain their antigenic properties to some degree through the conjugation (5, 6, 31). These results and our own data support our contention that PIPAAm molecules are bound in the outer, exposed surface of globular IgG molecules and little disorganization of IgG structure occurred through conjugation. The Fc region of IgG strongly relates to the complement activation as well as the binding to Fc receptor on plasma membrane surface of leukocytes *in vivo*. The suppression of conjugate binding to protein A observed in Figure 2 suggests that Fc-dependent immunogenicity of conjugates decreases significantly when the conjugates are administered *in vivo*.

**Temperature-Responsive Polymers for Modulating Soluble-Insoluble Changes of the Protein Conjugates.** Transmittance changes in PBS solutions of IgG-PIPAAm conjugates are shown in Figure 3. Intact IgG in PBS solution is transparent at temperatures up to 50 °C (data not shown in Figure 3). IgG-PIPAAm conjugates exhibit reversible phase transitions; soluble at lower temperature and insoluble at higher temperature. Semitelechelic PIPAAm bound to outer surfaces of IgG molecules collapse with increasing solution temperature. It is thought that the biomolecules and PIPAAm molecules in the conjugate form an immiscible structure. Therefore, the segregated conformation of the conjugates provides rapid responses to changes in temperature and a corresponding, complete phase separation due to the highly mobile nature of polymer free-end. IgG-PIPAAm conjugates exhibit LCSTs ranging from 33.6 to 34.4 °C. It has already shown that conjugates constructed by water-soluble biomolecules and temperature-responsive polymers alter the PIPAAm dehydration mechanism and increase the energy required for precipitation (24). Con-



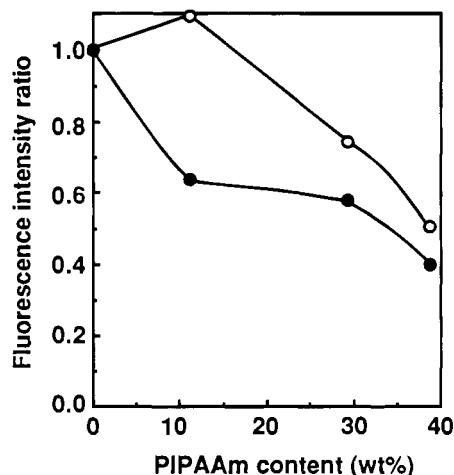
**Figure 3.** Temperature dependence of optical transmittance for IgG-PIPAAm aqueous solutions (●, G-3; ▲, G-13; ■, G-21; ○, AG-4; △, AG-12; □, AG-20;  $\lambda = 500$  nm).



**Figure 4.** Temperature dependence of optical transmittance for IgG-PIPAAm conjugate/HSA complex in PBS (○, AG-0; □, AG-4; △, AG-12; ●, AG-20).

jugate dehydration increases with an increase in the amount of PIPAAm molecules in the conjugate, and precipitated conjugates strongly aggregate with each other in aqueous media above the LCST. The amount of PIPAAm molecules is likely to produce slight shift in the LCST.

**Temperature-Modulated Precipitations and Affinity Separation.** Antigen binding activity of AG-PIPAAm conjugates using FITC-labeled HSA as a model antigen was studied. First, the ability of AG-PIPAAm conjugates to precipitate and to separate antigen-bioconjugate complexes from solution was investigated. Optical transmittance changes of PBS solution mixtures of AG-PIPAAm and HSA as a function of temperature are shown in Figure 4. Specific antigen-antibody complexation is confirmed by the data from HPSEC elution volume. While specific antigen-AG complexation still occurred, the sample AG-0 showed no transmittance changes in all temperatures examined because it lacks molecules of PIPAAm. AG-PIPAAm conjugates, however, reacted with antigen and showed transmittance changes. Sample AG-4 exhibited, however, only slight transmittance changes compared to AG-12 and AG-20 and was unable to collapse completely with temperature. As mentioned above, the amount of PIPAAm molecules in the conjugate dominates the aggregation behavior of the entire conjugates. AG-4 contained an average of 4

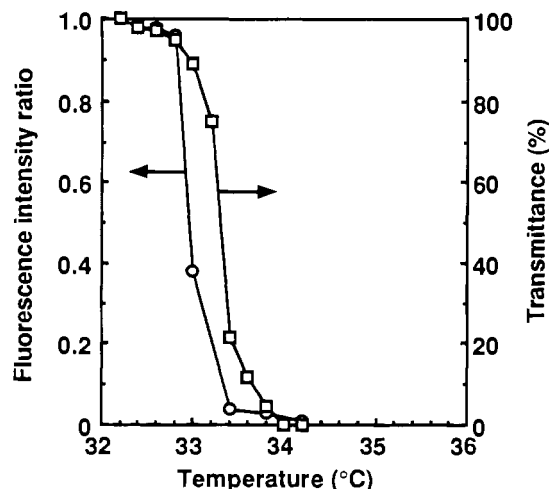


**Figure 5.** Relative antigen binding activity of IgG-PIPAAm conjugates as a function of PIPAAm content. (HSA concentration: ●, 1.52  $\mu\text{mol/L}$ ; ○, 7.29  $\mu\text{mol/L}$ ).

molecules of PIPAAm per IgG; the amount of PIPAAm molecules was 11.2 wt % of the conjugate as shown in Table 1. PIPAAm content of the resulting AG-4/HSA complex was calculated to be 8.1 wt %. Therefore, weak aggregation force of the AG-4/HSA complex produces insufficient precipitation. Complexes of antigen and AGs, AG-12 and AG-20, showed drastic changes in transmittance within a narrow temperature range. This result indicates that the transmittance change of the antigen-antibody complex can also be controlled by the amount of PIPAAm molecules conjugated.

Specific antigen binding activity of AG-PIPAAm conjugates against HSA as the model antigen was examined as a function of PIPAAm content. The results are shown in Figure 5. AG-PIPAAm conjugates in this experiment formed antigen-antibody complexes with FITC-HSA. At HSA concentration of 1.52  $\mu\text{mol/L}$ , and with increasing PIPAAm content, antigen binding activity of AG-PIPAAm conjugates decreases. A significant decrease in antigen binding activity was observed for over 30 wt % of PIPAAm conjugated. AG-PIPAAm conjugates with PIPAAm contents of about 4–12 molecules per IgG retained about 60% antigen binding activity at this concentration (recall that Fc-dependent binding activity was abolished at the same PIPAAm content). At higher HSA concentration (7.29  $\mu\text{mol/L}$ ), AG-4 retains almost same antigen binding activity and other AGs also keep relatively high antigen binding. Notable decreases in specific antigen binding activity observed in AG-20 might be due to the fact that excessive attachment of PIPAAm molecules yielded a steric hindrance of the IgG active binding site due to the free chain end mobility of the grafted polymers.

Increasing polymer chain length and degree of substitution are likely to enhance the solution temperature-response due to the increase in the temperature-responsive sequences of PIPAAm associated with the conjugates. Although there remains the possibility that long polymer chain mobility and high degree of substitution may denature biomolecule structure or destroy bioactivity due to steric hindrance, there should exist an optimum amount of polymer grafts for each biomolecule. We have collected data for temperature-responsive bioconjugates such as atelo collagen ( $M_r = 300\,000$ ) (23), bovine serum albumin ( $M_r = 66\,000$ ), bovine plasma fibrinogen ( $M_r = 340\,000$ ) (24) and *pseudomonas* lipase ( $M_r = 33\,000$ ) (25) using PIPAAm with a carboxyl end group as a modifier. These investigations suggest that temperature-responsive behavior of bioconjugates depends on the molecular size of the biomolecules and their



**Figure 6.** Relationship between antigen binding activity and phase transition of IgG-PIPAAm conjugate, AG-12.

respective hydration correlated to the substitution degree with polymer. Moreover, the mobility of the long polymer chains in aqueous medium may also elicit some effect on the bioactivity of the biomolecule conjugate. Chiu *et al.* reported substrate-size-dependent enzyme specificity corresponding to the ability of the polymer chains to exclude proteins and ligands from its surroundings using PEG-modified chymotrypsin (32). From these results, an optimal amount of PIPAAm grafts of approximately 6100 molecular weight is predicted to be 20–30 wt % for temperature-modulated precipitations and affinity bio-separations to reduce undesirable or conflicting biological reactions.

**Temperature-Responsive PIPAAm as Thermal Switching Sequences.** AG-12 was used to compare the antigen binding activity of AG-PIPAAm conjugates with HSA to the phase transition of AG-PIPAAm at each temperature. Figure 6 shows the relationship between relative fluorescence changes upon precipitation and optical transmittance changes for mixed aqueous solutions as a function of temperature. Transmittance changes for solution mixtures are observed at temperatures ranging from 32.8 to 34.0 °C. On the other hand, relative fluorescence changes upon precipitation are observed at temperatures ranging from 32.8 to 33.4 °C. Once phase transition of bioconjugate occurred in response to changes in solution temperature, specific antigen binding activity decreases drastically to less than 10% of that observed below the critical temperature. IgG-PIPAAm conjugates are soluble in aqueous milieu and readily form specific antigen-bound complexes in homogeneous solution below the critical temperature. These conjugates can be separated from solution and other solutes, depending on PIPAAm content and size, and remain unable to bind antigen above the critical temperature. It is proposed that grafted PIPAAm molecules contribute two features to the IgG bioconjugates: (1) as a thermally induced phase transition inducer and (2) as a switching molecule to control bioactivity and affinity in response to changes in temperature.

## CONCLUSIONS

IgG-PIPAAm conjugates were prepared by the coupling reaction of the activated ester of semitelechelic PIPAAm with the amino group of IgG. These conjugates exhibit a rapid response to changes in temperature and significant phase separation above the critical solution temperature. Amounts of PIPAAm in the conjugates determine the magnitude of bioconjugate aggregation and

precipitation in response to temperature changes. It is conceivable from the results presented in this paper that the conjugation of PIPAAm to IgG leads the reduced Fc-dependent immunogenicity in vivo, while conjugates retained specific antigen binding activity. Temperature-responsive behavior of PIPAAm imparts solubility changes to the conjugate in response to small temperature changes in aqueous media. Semitelechelic PIPAAm is highly efficient for temperature-modulated affinity bio-separations due to the highly intrinsic mobile nature of the polymer free-end.

#### ACKNOWLEDGMENT

The author is grateful to Prof. David W. Grainger, Colorado State University, for his valuable comments and discussion and Hideki Morikawa, M.D., School of Medicine, Keio University, for his cooperation in the research presented in this paper.

#### LITERATURE CITED

- (1) Abuchowski, A., van Es, T., Palczuk, N. C., and Davis, F. F. (1977) Alteration of immunological properties of bovine serum albumin by covalent attachment of polyethylene glycol. *J. Biol. Chem.* 252, 3578–3581.
- (2) Abuchowski, A., McCoy, J. R., Palczuk, N. C., van Es, T., and Davis, F. F. (1977) Effect of covalent attachment of polyethylene glycol on immunogenicity and circulating life of bovine liver catalase. *J. Biol. Chem.* 252, 3582–3586.
- (3) Harris, J. M. (1992) Introduction to biotechnological and biomedical applications of poly(ethylene glycol). *Poly(ethylene glycol) Chemistry: Biotechnical and Biomedical Applications* (J. M. Harris, Ed.) pp.1–14, Plenum Press, New York.
- (4) Suzuki, T., Ikeda, K., and Tomono, T. (1989) Physicochemical and biological properties of poly(ethylene glycol)-coupled immunoglobulin G. Part II. Effect of molecular weight of poly(ethylene glycol). *J. Biomater. Sci. Polym. Edn.* 1, 71–84.
- (5) Pasta, P., Riva, S., and Carrea, G. (1988) Circular dichroism and fluorescence of polyethylene glycol-subtilisin in organic solvents. *FEBS Lett.* 236, 329–332.
- (6) Caliceti, P., Schiavon, O., Veronese, F. M., and Chaiken, I. M. (1990) Effects of monomethoxypoly(ethylene glycol) modification of ribonuclease on antibody recognition, substrate accessibility and conformational stability. *J. Mol. Recognit.* 3, 89–93.
- (7) Heskins, M., Guillet, J. E., and James, E. (1968) Solution properties of poly(*N*-isopropylacrylamide). *J. Macromol. Sci. Chem.* A2, 1441–1445.
- (8) Bae, Y. H., Okano, T., Hsu, R., and Kim, S. W. (1987) Thermosensitive polymer as on-off switches for drug release. *Makromol. Chem. Rapid Commun.* 8, 481–485.
- (9) Okano, T., Bae, Y. H., Jacobs, H., and Kim, S. W. (1990) Thermally on-off switching polymers for drug permeation and release. *J. Controlled Release* 11, 255–265.
- (10) Bae, Y. H., Okano, T., and Kim, S. W. (1990) Temperature dependence of swelling of crosslinked poly(*N,N'*-alkyl substituted acrylamide) in water. *J. Polym. Sci. Polym. Phys. Edn.* 28, 923–936.
- (11) Yoshida, R., Sakai, K., Okano, T., Sakurai, Y., Bae, Y. H., and Kim, S. W. (1991) Surface-modulated skin layers of thermal responsive hydrogels as on-off switches; I. Drug release. *J. Biomater. Sci. Polym. Edn.* 3, 155–162.
- (12) Yoshida, R., Sakai, K., Okano, T., Sakurai, Y. (1991) Surface-modulated skin layers of thermal responsive hydrogels as on-off switches; II. Drug permeation. *J. Biomater. Sci. Polym. Edn.* 3, 243–252.
- (13) Okuyama, Y., Yoshida, R., Sakai, K., Okano, K., and Sakurai, Y. (1993) Swelling controlled zero order and sigmoidal drug release from thermo-responsive poly(*N*-isopropyl acrylamide-co-alkyl methacrylate) hydrogel. *J. Biomater. Sci. Polym. Edn.* 4, 545–556.
- (14) Yamada, N., Okano, T., Sakai, H., Karikura, F., Sawasaki, Y., and Sakurai, Y. (1990) Thermo-sensitive polymeric surfaces; control of attachment and detachment of cultured cells. *Makromol. Chem. Rapid Commun.* 11, 571–576.
- (15) Okano, T., Yamada, N., Sakai, H., and Sakurai, Y. (1993) A novel recovery system for cultured cells using plasma-treated polystyrene dishes grafted with poly(*N*-isopropylacrylamide). *J. Biomed. Mater. Res.* 27, 1243–1251.
- (16) Kokufuta, E. (1992) Functional immobilized biocatalysts. *Progress in Polymer Science* 17, pp 647–697, Pergamon Press, New York.
- (17) Dong, L. C., and Hoffman, A. S. (1986) Thermally reversible hydrogels: III. Immobilization of enzymes for feedback reaction control. *J. Controlled Release* 4, 223–227.
- (18) Chen, J. P., and Hoffman, A. S. (1990) Polymer–protein conjugates II. Affinity precipitation separation of human immunoglobulin by a poly(*N*-isopropylacrylamide). *Biomaterials* 11, 631–634.
- (19) Monji, N., and Hoffman, A. S. (1987) A novel immunoassay system and bioseparation process based on thermal phase separating polymers. *Appl. Biochem. Biotech.* 14, 107–120.
- (20) Monji, N., Cole, C.-A., Tam, M., Goldstein, L., Nowinski, R. C., and Hoffman, A. S. (1990) Application of a thermally-reversible polymer-antibody conjugate in a novel membrane-based immunoassay. *Biochem. Biophys. Res. Commun.* 172, 652–660.
- (21) Cole, C.-A., Schreiner, S. M., Priest, J. H., Monji, N., and Hoffman, A. S. (1987) *N*-isopropyl acrylamide and *N*-acryl succinimide copolymers: A thermally reversible water soluble activated polymer for protein conjugation. *ACS Symposium Series 350, Reversible Polymeric Gels and Related Systems* (P. Russo, Ed.) p 245, American Chemical Society, Washington DC.
- (22) Park, T. G., and Hoffman, A. S. (1993) Synthesis and characterization of a soluble, temperature-sensitive polymer-conjugated enzyme. *J. Biomater. Sci. Polym. Edn.* 4, 493–504.
- (23) Takei, Y. G., Aoki, Y. G., Sanui, K., Ogata, N., Okano, T., and Sakurai, Y. (1993) Temperature-responsive bioconjugates I. Synthesis of temperature-responsive oligomers with reactive end groups and their coupling to biomolecules. *Bioconjugate Chem.* 4, 42–46.
- (24) Takei, Y. G., Aoki, Y. G., Sanui, K., Ogata, N., Okano, T., and Sakurai, Y. (1993) Temperature-responsive bioconjugates II. Molecular design for temperature-modulated bio-separations. *Bioconjugate Chem.* 4, 341–346.
- (25) Matsukata, M., Takei, Y. G., Aoki, T., Sanui, K., Ogata, N., Sakurai, Y., and Okano, T. (1994) Temperature modulated solubility-activity alterations for poly(*N*-isopropylacrylamide)-lipase conjugates. *J. Biochem.: Biotechnol.* 116, 682–686.
- (26) Miron, T., and Wilchek, M. (1982) A spectrophotometric assay for soluble and immobilized *N*-hydroxysuccinimide esters. *Anal. Biochem.* 126, 433–435.
- (27) Bückman, A. F., and Morr, M. (1981) Functionalization of poly(ethylene glycol) and monomethoxy-poly(ethylene glycol). *Makromol. Chem.* 182, 1379–1384.
- (28) Gornall, A. G., Bardawill, C. S., and David, M. M. (1948) Determination of serum proteins by means of the biuret reaction. *J. Biol. Chem.* 177, 751–766.
- (29) Udenfrienel, S., Stein, S., Bohlen, P., Dairman, W., Leimgruber, W., and Weigle, M. (1972) Fluorescamine: A reagent for assay of amino acid, peptides, proteins, and primary amines in the picomole range. *Science* 178, 871–872.
- (30) Stocks, S. J., Jones, A. J. M., Ramey, C. W., and Brooks, D. E. (1986) A fluorometric assay of the degree of modification of protein primary amines with polyethylene glycol. *Anal. Biochem.* 154, 232–234.
- (31) Suzuki, T., Kanbara, N., Tomono, T., Hayashi, N., and Shinohara, I. (1984) Physicochemical and biological properties of poly(ethylene glycol)-coupled immunoglobulin G. *Biochim. Biophys. Acta* 788, 248–255.
- (32) Chiu, H.-C., Zalipsky, S., Kopecková, P., and Kopecek, J. (1993) Enzymatic activity of chymotrypsin and its poly(ethylene glycol) conjugates toward low and high molecular weight substrates. *Bioconjugate Chem.* 4, 290–295.

# Molecular Characterization of Surface Topology in Protein Tertiary Structures by Amino-Acylation and Mass Spectrometric Peptide Mapping

Michael O. Glocker, Christoph Borchers, Winfried Fiedler, Detlev Suckau,<sup>†</sup> and Michael Przybylski\*

Fakultät für Chemie, Universität Konstanz, P.O. Box 5560-M731, 78434 Konstanz, Germany. Received July 12, 1994<sup>®</sup>

Amino-acetylation and -succinylation reactions in combination with mass spectrometric peptide mapping of tryptic peptide mixtures have been employed for surface topology-probing of lysine residues in bovine ribonuclease A, lysozyme, and horse heart myoglobin as model proteins of different surface structures. Direct molecular weight determinations identifying the precise number of acyl groups in partially modified proteins were obtained by electrospray and <sup>252</sup>Cf-plasma desorption mass spectrometry. Electrospray mass spectra of multiply protonated molecular ions and deuterium exchange experiments provided a relative conformational characterization of protein derivatives and enabled the direct determinations of intact, partially acylated heme-myoglobin derivatives. Tryptic peptide mapping analysis, using plasma desorption and fast atom bombardment mass spectrometry, ascertained by mass spectrometric characterization of HPLC-separated modified peptides, yielded the exact identification of acylation sites. Relative reactivities of the amino acylation were derived from the peptide mapping data and from quantitative estimations of modified peptides upon acetylation/trideuteroacetylation and provided direct correlations with the relative surface accessibilities of lysine- $\epsilon$ -amino groups taken from X-ray crystallographic structure data of the proteins. The reactive lysine-41 residue in ribonuclease A which is part of the substrate binding site was directly identified from the mass spectrometric data. These results indicate tertiary structure-selective acylation combined with mass spectrometric peptide mapping as an efficient approach for the molecular characterization of surface topology and reactive fundamental lysine residues in proteins.

## INTRODUCTION

Despite the rapid development of powerful methods for determining protein tertiary structures and dynamics from crystals and in solution (1–5), there is a considerable need for experimental approaches that can provide molecular information on chemical reactivities in proteins, which are complementing X-ray crystallography and multidimensional NMR (6). Both methods have limitations, particularly in the characterization of chemical properties of specific amino acid residues. Protein-chemical modification reactions have long been employed in structure–function studies such as modifying enzymatic properties, immunological reactivity, and proteolytic digestion (7, 8). However, classical characterization methods generally require laborious analytical procedures (radioactive labeling) which in many cases do not provide an unambiguous identification of modification sites (9).

The development of efficient “soft” desorption–ionization methods of mass spectrometry (MS) has led to a recent breakthrough in the direct, molecular characterization of biopolymers, particularly polypeptides and proteins (10–12). Fast atom bombardment (FABMS) and <sup>252</sup>Cf-plasma desorption (PDMS) enable accurate molecu-

lar weight determinations of polypeptides and small proteins (approximately  $\leq 30$  kD) (10, 13), while electrospray (ESMS) and matrix-assisted laser desorption (LDMS) yield access to large ( $> 100$  kD) proteins (14, 15). Furthermore, the feasibility of mass spectrometry to the direct analysis of multicomponent proteolytic peptide mixtures (peptide mapping) has been demonstrated as a powerful method in several applications, such as the identification of covalent post-translational modifications (16, 17). Mass spectrometric peptide mapping (e.g., by FAB- or PDMS) has been shown to be well suited for the unequivocal characterization of multiple chemical modification sites in proteins (18, 19). The combination of limited, tertiary structure-selective chemical modification and mass spectrometric peptide mapping has been developed as a new approach, both for the molecular characterization of the selectivity and the determination of relative reactivities at specific modification sites (20). In the general analytical procedure (schematically depicted in Figure 1), the precise number of modifications introduced and their distribution in partially modified proteins are first determined by direct mass spectrometric molecular weight determinations. Assignments of the reactivities of modification sites are then derived from peptide mapping data using PDMS and/or FABMS (21). This method has been successfully employed in proteins, as well as in small peptides, with several specific modification reactions such as amino-acylation, tyrosine-iodination and -nitration, carboxylate-amidation, and the bifunctional cysteine-modification by phenyl arsin oxide (22, 23). In the present study, acetylation and succinylation of amino groups have been investigated in model proteins of different surface structures (hen egg-white lysozyme; bovine ribonuclease A; myoglobin). Mass spectrometric peptide mapping analyses of tryptic pro-

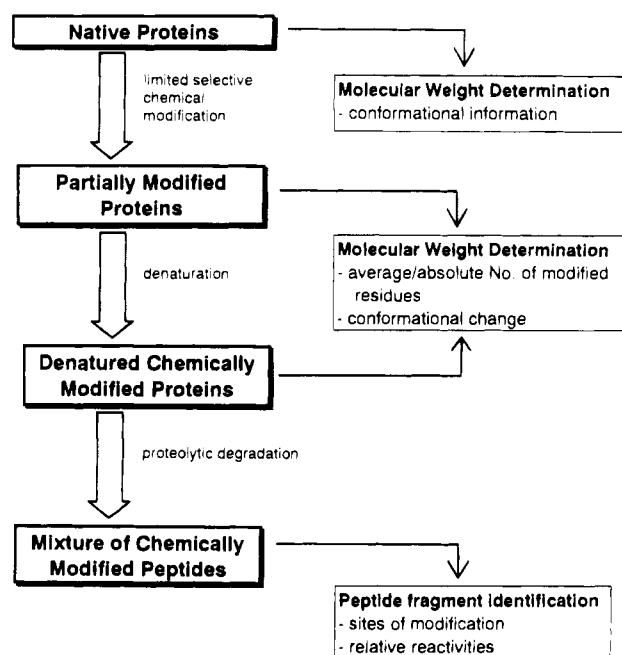
\* To whom correspondence should be addressed. Tel.: \*49-7531-88-2497. Fax: \*49-7531-88-3097. TelNet: chrprzyb@nyx.uni-konstanz.de.

<sup>†</sup> Present address: Bruker-Franzen Analytik GmbH, Fahrenheitstrasse 4, 28359 Bremen, Germany.

<sup>®</sup> Abstract published in *Advance ACS Abstracts*, October 1, 1994.

<sup>1</sup> Abbreviations: FAB, fast atom bombardment; PD, plasma desorption; ES, electrospray; HEL, hen egg white lysozyme; Myo, myoglobin; DTT, dithiothreitol; 4-VP, 4-vinylpyridine; SA, surface accessibility.





**Figure 1.** General analytical scheme of protein structure characterization by selective chemical modification combined with mass spectrometric peptide mapping.

teolytic mixtures provided direct information of specific reactivities which showed a clear correlation with the surface topology of lysine residues.

#### EXPERIMENTAL PROCEDURES

**Materials.** Henn egg-white lysozyme (HEL), bovine ribonuclease A (RNase A), and horse heart-myoglobin (Myo) were obtained from Sigma (St. Louis, MO/USA) and were analyzed for molecular homogeneity by SDS-polyacrylamide gel electrophoresis and by ESMS. The ES mass spectrum of Myo in 2 mM ammonium acetate (pH 6) yielded a single most abundant  $[M + 9H]^{9+}$  molecular ion of the intact heme-protein (24), while at the pH 3 employed for the ES mass spectrometric determination of acetylated myoglobin the molecular ions of the dissociated apoprotein forms are obtained (see below). Acetic anhydride (Riedel de Haen, Seelze, FRG), hexadeuterioacetic anhydride (Fluka, Buchs, Switzerland), and succinic anhydride (Fluka, Buchs, Switzerland) were of analytical grade. Bovine trypsin was obtained from Sigma. Dithiothreitol (DTT), 4-vinylpyridine (4-VP), and iodoacetamide were purchased from Merck (Darmstadt, FRG) and Sigma.

**Protein Amino-Acetylation, -Trideuteroacetylation, and -Succinylation.** Acetylation and succinylation of lysine- $\epsilon$ -amino and N-terminal amino groups were performed as previously described (20, 25, 26), with a 10–1000-fold molar excess of acyl anhydride/amino group added to 0.5 mL of protein solutions (10  $\mu$ g/ $\mu$ L) in 0.1 M  $\text{NH}_4\text{HCO}_3$ . Reactions were carried out for 30 min at 23 °C at pH 6.5, maintained by addition of 25%  $\text{NH}_3$  which is required to prevent the pH decrease due to the anhydride hydrolysis. A two-step acetylation/trideuteroacetylation was employed for the quantitative estimation of relative reactivities of aminoacetylation. First a 10–100-fold excess of acetic anhydride was used for partial modification at the reaction conditions described above. The reaction was stopped by dropping the pH to 5.5 and lyophilization. Complete modification was subsequently obtained by reaction of the redissolved protein with a 300-fold molar excess of hexadeuterioacetic an-

hydride. Acylated proteins were dialyzed against 0.1% trifluoroacetic acid (TFA) or 0.01 M ammonium acetate, lyophilized, and redissolved in 0.01 M ammonium acetate.

#### Disulfide Reduction and Alkylation of Proteins.

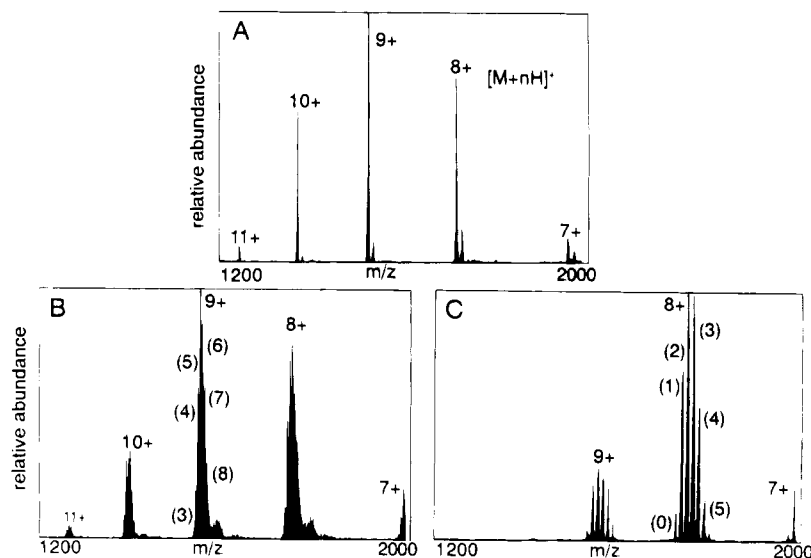
Reduction of disulfide bonds was carried out with solutions of protein derivatives (ca. 100  $\mu$ g) in 200  $\mu$ L of 0.1 M  $\text{NH}_4\text{HCO}_3$ , pH 8 (containing 6 M guanidine hydrochloride), to which a 10 mM solution of DTT (50-fold molar excess) in 0.1 M  $\text{NH}_4\text{HCO}_3$  was added. The reaction mixture was kept for 1 h at 57 °C and then was cooled to 20 °C, and a 10 mM solution of 4-VP (2.2-fold molar excess/DTT) in 0.1 M  $\text{NH}_4\text{HCO}_3$  was added. The alkylation was carried out for 20 min at 23 °C and stopped by acidification with glacial acetic acid to pH 3. Alkylated proteins were dialyzed against 0.1% TFA and lyophilized.

**Proteolytic Digestion.** Tryptic digestion in solution was carried out with 50  $\mu$ g of alkylated protein derivatives dissolved in 100  $\mu$ L of 0.1 M  $\text{NH}_4\text{HCO}_3$  (pH 8), to which a solution of trypsin (1  $\mu$ g/ $\mu$ L in 0.1 M  $\text{NH}_4\text{HCO}_3$ ; E:S ratio, 1:100) was added. The digestion was performed for 4 h at 37 °C and stopped by freeze-drying, and peptide mixtures were reconstituted in 0.1% TFA for mass spectrometric and HPLC analysis. In the case of myoglobin, tryptic digestion was carried out in the presence of 6 M urea. Urea was removed before HPLC separations of the tryptic peptides by filtration through Sep-Pak cartridges (Millipore Corp.) following the suppliers' instructions.

**In-Situ Tryptic Peptide Mapping Analysis.** Mass spectrometric peptide mapping analysis *in-situ* on the nitrocellulose (NC) target was performed as previously described (27). Protein derivatives (15  $\mu$ g) were adsorbed on the NC surface, and disulfide bridges were cleaved by addition of 5  $\mu$ L of 10 mM DTT solution in 0.1 M  $\text{NH}_4\text{HCO}_3$ . After 20 min reaction at 37 °C, the target was spin-dried and excess reagent removed by washing with 20  $\mu$ L of 0.1 M  $\text{NH}_4\text{HCO}_3$ . Proteolytic digestion was performed for 30 min at 37 °C by addition of 5  $\mu$ L of trypsin solution (1  $\mu$ g/ $\mu$ L in 0.1 M  $\text{NH}_4\text{HCO}_3$ ) under a microscope coverslip. The target was then prepared for PDMS analysis by spin-drying.

**Mass Spectrometry.** NC surfaces for sample adsorption in PDMS were prepared by electrospraying as described (28). Proteins (5–15  $\mu$ g) were allowed to adsorb for 2–3 min, followed by washing with 50  $\mu$ L of 0.1 M  $\text{NH}_4\text{HCO}_3$ . PDMS analyses were performed with a Bio-Ion 20 K (Bio-Ion, Uppsala/Sweden) time-of-flight mass spectrometer equipped with a 10  $\mu$ Ci  $^{252}\text{Cf}$  primary source (29), using an accelerating voltage of 16 kV. ESMS was performed on a Vestec-201A (Vestec, Houston, TX) quadrupole mass spectrometer equipped with a nozzle/skimmer electrospray interface (30). Solutions of protein samples (0.01–0.1  $\mu$ g/ $\mu$ L) in 2% acetic acid (pH 3) or 2 mM ammonium acetate (pH 6) containing 10% methanol were delivered to the ion source at 2–4  $\mu$ L/min with a Harvard Apparatus microinfusion pump by injection of 5  $\mu$ L solutions with a Rheodyne microloop injector, using a self-built 150  $\mu$ m fused silica insertion probe/sheath flow system (31). Spectra were obtained at a spray-desolvation temperature of 47 °C. FABMS analyses were performed on a Finnigan MAT-312/AMD-5000 modified double-focusing magnetic sector instrument, equipped with a 20 kV caesium primary ion source. Glycerol was used as matrix.

**HPLC.** Peptide separations were carried out on a Millipore/Waters M510/M45 system equipped with a 490-E variable absorbance detector. A 250  $\times$  4 mm, 7  $\mu$ m C18-nucleosil column (Macherey-Nagel, Düren/FRG)



**Figure 2.** Positive ion ES mass spectra of acetylated and succinylated bovine ribonuclease A derivatives. A: unmodified RNase A; molecular weight determined as 13682 Da. B: partially acetylated RNase A using a 10-fold molar excess of acetic anhydride/amino group. C: RNase A succinylated with 10-fold molar excess of anhydride/amino group. Positive charge numbers denote multiply protonated molecular ions; numbers in parentheses denote the number of acetyl and succinyl groups introduced. 2% acetic acid with 10% methanol (pH 3) was used as solvent.

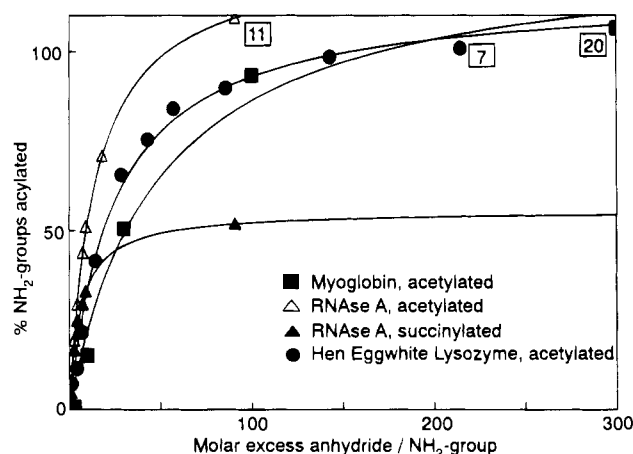
was used. The flow rate was adjusted to 1 mL/min. Linear gradient elution was performed with 0.04% aqueous TFA (solvent A) and 0.03% TFA in acetonitrile (solvent B), starting at 10% B and increasing to 60% B over 50 min. Peptide fractions for mass spectrometric analysis were collected with a Gilson CPR-45500 fraction collector.

**Protein Structure Examination.** The structures of HEL, bovine RNase A, and Myo were examined using the corresponding files of the Brookhaven Laboratory protein data bank on a Silicon Graphics workstation with the Biosym Insight II/Discover and Biopolymer software.

## RESULTS AND DISCUSSION

### Molecular Weight Determination and Structural Characterization of Acylated Protein Derivatives.

Acylation reactions of proteins were carried out in ammonium bicarbonate-buffered solution with the pH maintained at 6.5 (see Experimental Procedures) with up to  $10^4$ -fold molar excess of acyl anhydrides, and the extent of modifications were determined by direct PD and ES mass spectrometric molecular weight analyses of the protein derivatives (Figures 2 and 3). ES mass spectra of RNase A derivatives partially acetylated and succinylated with a 10-fold molar excess of acyl anhydride/amino group are shown in Figure 2, in comparison to the spectrum of unmodified native RNase A. For both protein derivatives, series of multiply protonated  $[M + nH]^{n+}$  molecular ions were obtained identifying the number of acyl groups introduced. The molecular ion series were partly resolved for the acetylated RNase A derivatives ( $\Delta m$ : 42 amu/acetyl group) but were completely resolved for the partially succinylated proteins ( $\Delta m$ : 100 amu/acetyl group). The charge distributions of  $[M + nH]^{n+}$  ions for the acetylated proteins were similar to those of unmodified RNase A with the most abundant  $[M + 9H]^{9+}$  ion, indicating that a sufficient number of protonable sites remains available upon modification. The reduced protonation (reduction of charge states) found in the succinylated proteins is well explained by the negatively charged succinyl carboxylate groups introduced. Conversion of the lysine-amino groups by succinylation results in a corresponding pI change of the protein, which showed in model experiments a good



**Figure 3.** Amino-acetylation and -succinylation of RNase A, HEL, and horse heart myoglobin as a function of molar excess acyl anhydride. The percentage of acylated amino groups (average numbers), relative to the total number of amino groups in the protein, was determined by ES and PD mass spectrometric molecular weight determinations of partially modified proteins. Boxed numbers denote the total numbers of amino groups of each protein.

correlation with the charge state reduction at the pH 3 employed (data not shown). However, no significant differences in the distributions of modifications were found for a given charge state, within the mass range (range of charge states) amenable to the quadrupole instrument employed ( $m/z$  2000); this might be different for lower charge state ions of succinylated protein derivatives.

ESMS analyses of acylated proteins after deuterium-exchange (32) showed a degree of deuterium incorporation similar to that of unmodified RNase A (47 vs 49%; 30 min). Furthermore, PD mass spectra of acylated proteins yielded molecular ion abundances and distributions comparable to the native proteins (data not shown), while strongly suppressed or undetectable molecular ion desorption has been demonstrated as a characteristic feature in PD spectra of denatured proteins (20). At the solvent conditions generally employed for molecular weight determinations of acylated protein derivatives (2%

**Table 1. Identification of Lysine-Succinylated Tryptic Peptides in Partially Modified RNase A Using a 40-fold Molar Excess of Succinic Anhydride by PDMS Peptide Mapping**

tryptic [acylated] peptide <sup>a</sup>	mol weight <sup>b</sup>	[M + H] <sup>+</sup>	lysine residue	
			modified	unmodified
[Suc-K <sup>1</sup> <sub>α,ε</sub> , Suc-K <sup>7</sup> ](1-10)	1150	1453	K1α, K1ε, K7	
(2-10)	1022	1025		K7
[Suc-K <sup>7</sup> ](2-10)	1022	1125	K7	
(11-31)	2412 <sup>d</sup>	2415		K31
(11-33)	2656 <sup>d</sup>	2658		K31
(11-33)	2678 <sup>d</sup>	2680 <sup>c</sup>		K31
(34-61)	3130	3133		K37, K41, K61
(34-61)	3152	3155 <sup>c</sup>		K37, K41, K61
[Suc-K <sup>41</sup> ](34-61)	3130	3234	K41	K37, K61
(38-66)	3188	3191		K41, K61, K66
(62-85)	3000 <sup>d</sup>	3003		K66
(62-85)	3022 <sup>d</sup>	3025 <sup>c</sup>		K66
[Suc-K <sup>91</sup> ](86-98)	1552 <sup>d</sup>	1654	K91	K98
(92-98)	962 <sup>d</sup>	965		K98
(99-104)	661	663		K104
(105-124)	2270	2272		
(105-124)	2292	2295 <sup>c</sup>		

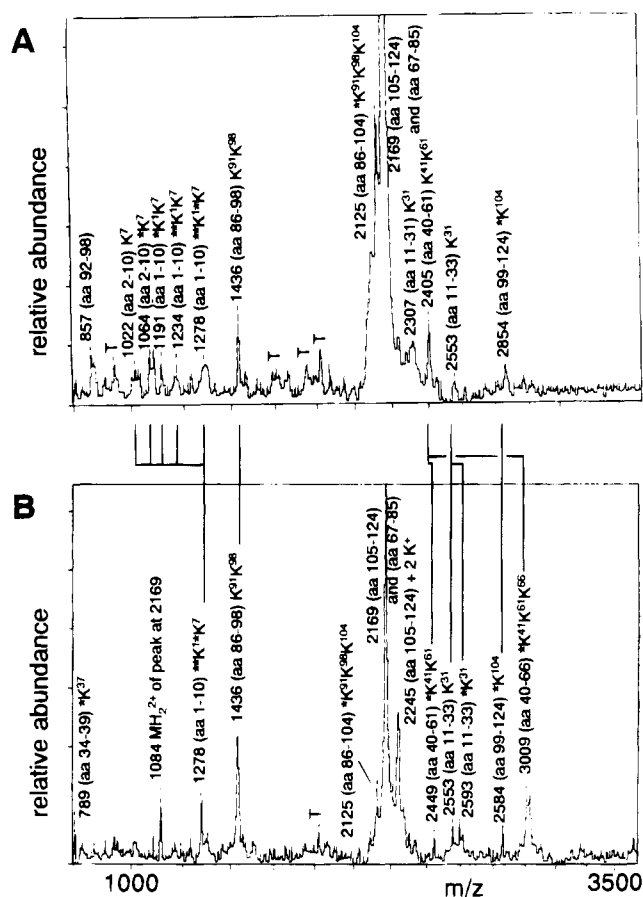
<sup>a</sup> Lysine-succinylated tryptic peptide. <sup>b</sup> Molecular weight of unmodified tryptic peptide. <sup>c</sup> Sodium adduct. <sup>d</sup> 4-VP alkylated.

acetic acid:methanol, 9:1; pH 3), the ES mass spectra of acylated myoglobin showed the  $[M + nH]^{n+}$  ions of the dissociated apoprotein forms. By contrast, at conditions that prevent dissociation (0.01 M ammonium acetate, pH 6)  $[M + nH]^{n+}$  ions of the intact heme-protein complex were obtained (32). Furthermore, myoglobin derivatives were found to retain full immunological reactivity toward a human anti-Myo monoclonal antibody up to a considerable extent of acetylation (14 of 21 amino groups) (22). These results, and previous studies showing no detectable structural changes by ORD/CD upon lysine-acetylation of HEL (33), are consistent with a native-like structure maintained in the acylated protein derivatives.

The average numbers of acyl groups introduced were determined from the molecular weight increase by both PD and ES mass spectrometry and yielded consistent results for the acylated protein derivatives. The number of acyl groups introduced as a function of molar excess of reagent is compared in Figure 3 for the three model proteins. A gradual increase of acetylation was found up to the total number of amino groups (lysine-ε-amino groups and N-terminus) in HEL, RNase A, and Myo (7, 11, and 20 amino groups, respectively). By comparison, considerably slower acylation rates were found for the modification by succinic anhydride, with approximately 50% succinylation of RNase A at a 100-fold molar excess of anhydride. However, at the reaction conditions used, selective N-acylation was ascertained in all cases by identification of the modification sites (see below), and additional O-acylation was only observed at >10 000-fold molar reagent excess. By contrast, a considerable extent of concomitant O-acylation at serine and tyrosine residues has been observed at strongly acidic reaction conditions (34).

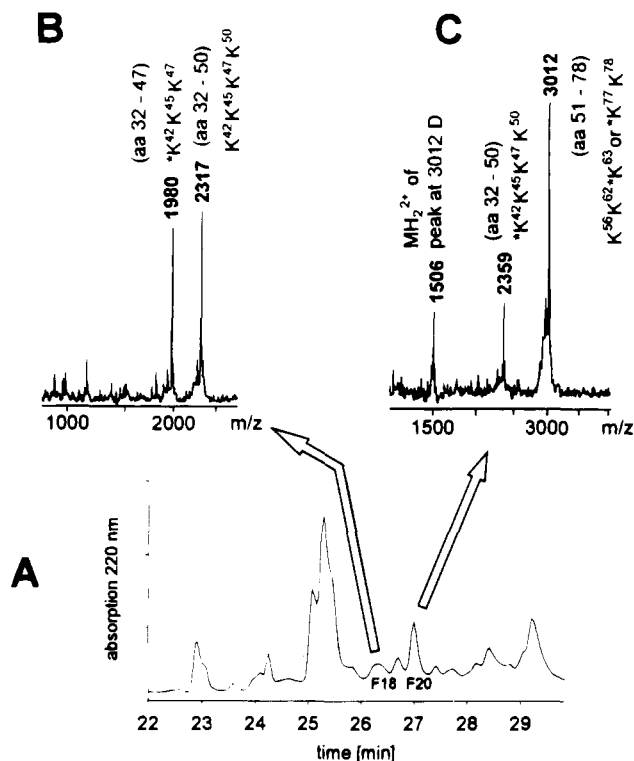
**Determination of Acylation Sites and Relative Reactivities.** The sites of N-acylations were identified by peptide mapping analyses of the reduced and alkylated protein derivatives by (i) *in-situ* trypsin digestion on the NC-sample target and PDMS and (ii) PDMS and FAB/MS analyses after tryptic digestion in solution (see Experimental Procedures). In addition, the modification sites were ascertained by HPLC isolation of acylated tryptic peptides and separate mass spectrometric identification.

The identification of acetylation sites by PDMS tryptic peptide mapping analysis is illustrated in Figure 4 (A, B) for two partially acetylated RNase A derivatives, and the complete identification of tryptic peptides and suc-



**Figure 4.** PD mass spectrometric peptide mapping analyses of peptide fragments after *in-situ* trypsin digestion of partially acetylated RNase A (see Experimental Procedures). A: RNase A acetylated with 10-fold excess anhydride/NH<sub>2</sub>-group (5.6-fold acetylated). B: RNase A acetylated with 40-fold excess anhydride (9.8-fold acetylated). Acetylated peptides are denoted by asterisks with the corresponding sequence positions of lysine residues.

cinylation sites is shown in Table 1. At low reagent excess, only the amino groups with the highest relative accessibilities (Lys-1, -7, and -104) were found to be initially acetylated (Figure 4A). The corresponding ions of modified peptides were found with increasing relative abundances at higher (40-fold) reagent excess (Figure 4B). However, a remarkably high reactivity was also



**Figure 5.** PD-mass spectrometric identification of amino-acetylated peptides in partially acetylated myoglobin after tryptic digestion. A: HPLC separation of tryptic peptides from myoglobin after limited acetylation with 60-fold molar excess of anhydride (see Experimental Procedures). B, C: PDMS analyses of isolated fractions F18 and F20. Acetylated peptides and sequence positions are denoted as in Figure 4.

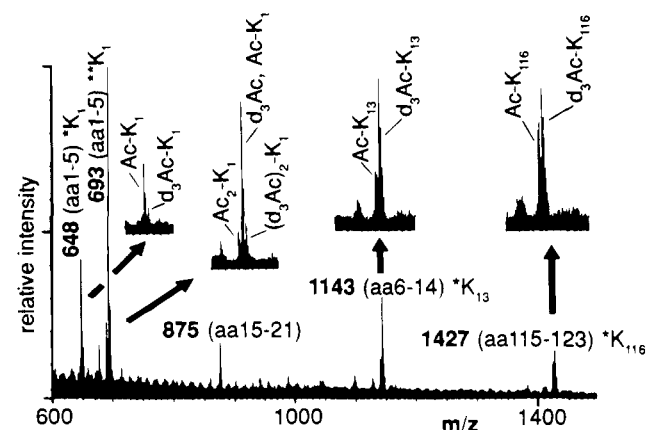
observed for the Lys-41 residue of low accessibility (see below) as is evident from the unmodified tryptic peptide (40–61) in Figure 4A, which is no longer observed and completely replaced in Figure 4B by the monoacetylated peptide ion at  $m/z$  2449 (40–61). No cleavage by trypsin was found at the Lys<sup>41</sup>-Pro<sup>42</sup> bond in the unmodified RNase A; hence the acetylation at Lys-41 was monitored by the peptide fragment (40–61) and, thus, is independent of the lack of tryptic cleavage at this bond. The molecular ions of the unmodified tryptic peptides 67–85 and 105–124 were only partially resolved by PD mass spectrometric peptide mapping. However, this does not affect the identification of acylation sites at Lys-91 and Lys-98 residues, within the peptide sequence (86–104). The monoacylation at Lys-91 and the nonacetylated site Lys-98 were clearly identified from the tryptic peptide (86–98) which was found throughout the course of the acylation (and hence showed unacetylated Lys-98), while the accessibility at Lys-91 was gradually reduced due to acylation at this site. A considerably higher reactivity at Lys-91 compared to Lys-98 was derived from this peptide, e.g., the monosuccinylated tryptic fragment (86–98) at  $m/z$  1654 (Table 1).

The partial acetylation and tryptic digestion of myoglobin yielded a complex mixture of modified peptide fragments, from which several partial sequences with closely spaced lysine residues could not be directly assigned from the mass spectrometric peptide mapping data. Therefore, HPLC separation and mass spectrometric analysis of isolated fractions were additionally used for peptide identification. The acetylation sites were assigned by comparison to the tryptic cleavage pattern as illustrated in Figure 5 by the partial sequence 32–50, in which only acetylation at Lys-42 was ascertained by the monoacetylated fragment at  $m/z$  2359, in contrast

**Table 2.** Relative Reactivities of Amino Groups in the Acetylation of RNase A (HEL and Myoglobin Determined by Plasma Desorption Mass Spectrometric Peptide Mapping)

relative reactivity NH <sub>2</sub> groups <sup>a</sup>	lysine residues, $\epsilon$ -amino groups		
	RNase A	HEL	myoglobin
	$\alpha$ -NH <sub>2</sub>		$\alpha$ -NH <sub>2</sub>
1	41, 104	97, 33 $\alpha$ -NH <sub>2</sub>	45, 63, 77, 79, 145, 147
2	1, 7, 37	1	16, 42, 87
3	31, 61, 91	13, 116	56, 50, 62, 78, 102
4	66, 98	96	96, 47, 87, 133, <sup>b</sup> 118 <sup>b</sup>

<sup>a</sup> Lysine residues are grouped by relative reactivities estimated from increasing abundances of acetylated peptide ions and decreasing abundances of ions of unmodified peptide fragments. <sup>b</sup> No or only very small abundances of modified peptide ions detected by mass spectrometric peptide mapping analysis.



**Figure 6.** Quantitative estimation by FAB-mass spectrometric tryptic peptide mapping of the extent of amino-acylation in partially acetylated HEL by acetylation (30-fold molar excess of anhydride) and subsequent complete trideuteroacetylation using 200-fold molar excess of hexadeuteroacetic anhydride (see Experimental Procedures). Acetylated peptides are denoted by asterisks with the corresponding sequence positions of lysine residues as in Figures 4 and 5.

to tryptic cleavage found at the Lys-47 and Lys-45 residues (fractions 18 and 20).

Sequences of the relative reactivities of the lysine- $\epsilon$ -amino groups toward acylation were derived from the increase in abundances of acylated peptide ions, as compared to the decrease in abundances of unmodified tryptic peptides (Table 2). The relative intensities of molecular ions generally are different in peptide mapping experiments of mixtures of unmodified and acetylated peptides, although large differences were found primarily between smaller oligopeptides but not for larger peptide fragments. Therefore, only a relative scaling of reactivity differences of acylation was derived by evaluation of abundance changes for modified vs unmodified peptides, as summarized in Table 2. Furthermore, quantitative estimations of the extent of acylation were obtained from FABMS analyses of protein derivatives which were (i) first partially acetylated and (ii) subsequently subjected to complete acetylation with hexadeuteroacetic anhydride (21). This procedure resulted in doublets of  $[M + H]^+$  ions of acetylated/trideuteroacetylated tryptic peptide fragments as illustrated in Figure 6 by the corresponding FAB mass spectrum of tryptic peptides of acetylated HEL. Each modification site is unequivocally assigned by this differential labeling procedure, e.g., yielding doublet and triplet molecular ions for mono- and diacetylated pep-

**Table 3. Comparison of Relative Reactivities of Amino Groups in the Acetylation of RNase A with Surface Accessibility and  $pK_{1/2}$  Values**

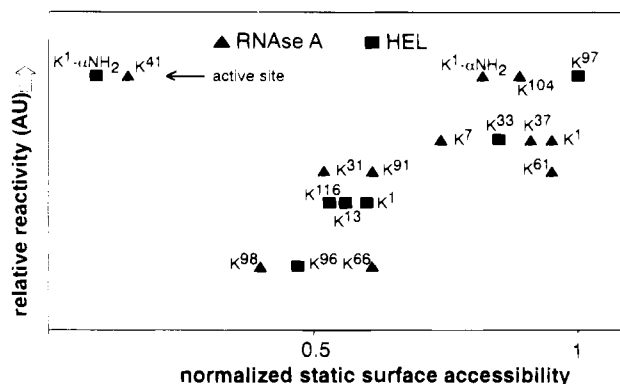
relative reactivity NH <sub>2</sub> groups	lysine residue	SA <sup>a</sup>	$pK_{1/2}$ <sup>a</sup>
	$\alpha$ -NH <sub>2</sub>	0.82	7.8
1	41	0.15	9.6
	104	0.89	10.6
2	1	0.95	10.5
	37	0.91	10.4
	7	0.74	10.3
3	61	0.95	10.5
	91	0.61	10.5
	31	0.52	10.6
4	66	0.61	11.0
	98	0.40	10.0

<sup>a</sup> SA values and  $pK_{1/2}$  values according to ref 37.

tides, respectively, but only single  $[M + H]^+$  ions for unmodified peptides. The results obtained were in good agreement with mass spectrometric peptide mapping data showing, e.g., the higher reactivity of Lys-116 compared to Lys-13 (Figure 6) which have comparable surface accessibilities (20).

The sequences of relative reactivities of Lys-residues derived for the three model proteins are summarized in Table 2. In contrast to these defined reactivity differences, tryptic peptide mapping analyses after acetylation of irreversibly denatured (DTT reduced and carboxymethylated) HEL and RNase A derivatives did not show characteristic reactivity differences and did not reveal any similarities to the reactivities of amino groups in Table 2 (data not shown). These results are also in accord with previous spectroscopic studies of acetylated HEL (33) and confirm that intact globular structures are required for the reactivity differences observed.

**Comparison of Relative Reactivities and Surface Accessibilities of Protein Amino Groups.** Possible structural parameters for correlation with the relative reactivities of amino-acylation are  $pK_{1/2}$  values of protein amino groups (35) and relative (static) surface accessibilities (SA values) defined at a 1.4 Å van der Waals sphere of solvent accessibility (36) which were obtained from the crystal structure data. SA values (relative to the tripeptide, Ala-Lys-Ala) and  $pK_{1/2}$  values of lysine- $\epsilon$ -amino groups are compared in Table 3 with the relative reactivities for the acetylation for RNase A. Ionic effects as derived from  $pK$  values did not indicate significant differences with the reactivities of lysine residues, in contrast to the most rapid N-terminal acylation which can be readily explained by the high nucleophilicity of the  $\alpha$ -amino group (37). An exception is the acetylation at the Lys-1 residue of HEL which has been previously shown to proceed in a rapid consecutive  $\alpha$ - and  $\epsilon$ -N-acetylation, due to the very low accessibility and shielding effect of the  $\alpha$ -amino group (20). The reaction sequence of the 2-fold acetylation was examined by HPLC separation of the Lys-1-monoacetylated N-terminal BrCN-fragment 1–12 of HEL (38, 39). Examination of this peptide by combined Edman degradation and PDMS analysis of the coupling and cleavage products revealed that approximately 90% of the peptide was blocked, thus demonstrating predominant  $\alpha$ -N-acetylation as the first step (data not shown). These results were corroborated by molecular modeling studies of the  $\alpha$ - or  $\epsilon$ -amino-monoacylated protein derivatives, using the corresponding structure file (7LYZ) of HEL in the Brookhaven protein data bank.



pattern, shown here with trypsin upon acylation of lysine residues, which become inaccessible to proteolytic digestion as a result of the modification, can be readily employed in other site-specific modifications. The same principle applies, e.g., to the digestion by the Glu-, Asp-specific *S. Aureus* V8-protease upon modification of carboxylate side chains (22). The unequivocal identification of modification sites by direct mass spectrometric peptide mapping may be limited in the case of partial sequences with closely spaced Lys-residues, which may require additional HPLC separation and separate mass spectrometric analysis. However, mass spectrometric peptide mapping generally appears to be a powerful tool for the molecular identification of initially, *partially modified* protein derivatives, which are most important for structure-reactivity correlations (41). The clear correlation of relative reactivities with surface accessibilities, obtained with model proteins of different surface structures, indicates the potential of mass spectrometric peptide mapping for probing the surface topology of amino groups in intact tertiary structures and enabled the direct detection of the unusually reactive active-site lysine-41 residue in RNase A.

Applications of this mass spectrometric approach to surface topology-probing by amino-acylation of  $\alpha$ -helical polypeptides, such as leucine zipper proteins (42) and corresponding complexes with oligonucleotides, are being carried out at present in our laboratory. A further, particular advantage is the possibility for direct determination of molecular weight and extent of modification of protein derivatives by electrospray mass spectrometry, due to the capability of the ES method of providing information about relative conformational differences for unmodified in comparison to partially modified proteins (32). Such information about a "native-like" conformation maintained upon selective, partial modification has been frequently missing or fraught with uncertainty in previous classical approaches of analyzing protein-chemical modifications (41). According to the general analytical scheme (Figure 1) it will be interesting to explore this feature of ESMS in the characterization of protein-chemical modifications.

#### ACKNOWLEDGMENT

We thank K. Hägele for valuable assistance with the FABMS analyses and C. Maier for help in the X-ray structure examination of HEL and the molecular modeling studies. This work was supported by the Deutsche Forschungsgemeinschaft (Bonn) and the Fonds der chemischen Industrie (Frankfurt, FRG).

#### LITERATURE CITED

- (1) McPherson, A. (1990) Current Approaches to Macromolecular Crystallization. *Eur. J. Biochem.* 189, 1–23.
- (2) Wüthrich, K. (1989) The Development of Nuclear Magnetic Resonance Spectroscopy as a Technique for Protein Structure Determination. *Acc. Chem. Res.* 22, 36–44.
- (3) Smith, L. J., Sutcliffe, M. J., Redfield, C., and Dobson, C. M. (1991) Analysis of Phi and Chi-1 Torsion Angles for Hen Lysozyme in Solution from H-1-NMR Spin Spin Coupling-Constants. *Biochemistry* 30, 986–996.
- (4) Miranker, A., Radford, S. E., Karplus, M., and Dobson, C. M. (1991) Demonstration by NMR of Folding Domains in Lysozyme. *Nature* 349, 633–636.
- (5) Artymiuk, P. J., Blake, C. C. F., Grace, D. E. P., Oatley, S. J., Phillips, D. C., and Sternberg, M. J. E. (1979) Crystallographic Studies of the Dynamic Properties of Lysozyme. *Nature* 280, 563–568.
- (6) Fasman, G. D. (1989) Protein Conformational Prediction. *Trends Biol. Sci.* 14, 295–299.
- (7) Glazer, A. N. (1976) The Chemical Modification of Proteins by Group-Specific and Site-Specific Reagents. In *The Proteins* (H. Neurath, and R.L. Hill, Eds.) 3rd ed., Vol. 2, pp 1–103, Academic Press, New York.
- (8) Burnens, A., Binz, H., Bosshard, H. R., Corradin, G., and Demetz, S. (1987) Epitope Mapping by Chemical Modification of Free and Antibody-Bound Protein Antigen. *Science* 235, 780–783.
- (9) Kaplan, H., Stevenson, K. J., and Hartleys, B. S. (1971) Competitive Labelling, a Method for Determining the Reactivity of Individual Groups in Proteins. *Biochem. J.* 124, 289–299.
- (10) Biemann, K., and Martin, S. A. (1987) Mass-Spectrometric Determination of the Amino-Acid Sequence of Peptides and Proteins. *Mass Spectrom. Rev.* 6, 1–75.
- (11) Fenn, J. B., Mann, M., Meng, C. K., Wong, S. F., and Whitehouse, C. M. (1989) Electrospray Ionization for Mass-Spectrometry of Large Biomolecules. *Science* 246, 64–71.
- (12) Karas, M., and Hillenkamp, F. (1988) Laser Desorption Ionization of Proteins with Molecular Masses Exceeding 10 000 Dalton. *Anal. Chem.* 60, 2299–2301.
- (13) Sundqvist, B., and Macfarlane, R. D. (1985) <sup>252</sup>Cf Plasma Desorption Mass Spectrometry. *Mass Spectrom. Rev.* 4, 421–460.
- (14) Karas, M., Bahr, U., Ingendoh, A., and Giessmann, U. (1991) Matrix-Assisted Laser Desorption Ionization Mass Spectrometry. *Mass Spectrom. Rev.* 10, 335–357.
- (15) Smith, R. D., Loo, J. A., Ogorzalek-Loo, R. R., Busman, M., and Udseth, H. (1991) Principles and Practice of Electrospray Ionization-Mass Spectrometry for Large Polypeptides and Proteins. *Mass Spectrom. Rev.* 10, 359–452.
- (16) Roepstorff, P., Nielsen, P. F., Klarskov, K., and Højrup, P. (1988) Application of Plasma Desorption Mass Spectrometry in Peptide and Protein Chemistry. *Biomed. Env. Mass Spectrom.* 16, 9–18.
- (17) Svoboda, M., Przybylski, M., Schreurs, J., Miyajima, A., Hogeland, K., and Deinzer, M. L. (1991) Mass Spectrometric Determination of Glycosylation Sites and Oligosaccharide Composition of Insect Expressed Mouse Interleukin-3. *J. Chromatogr.* 562, 403–411.
- (18) Glocker, M. O., Arbogast, B., Schreurs, J., and Deinzer, M. L. (1993) Assignment of the Inter- and Intramolecular Disulfide Linkages in Recombinant Human Macrophage Colony Stimulating Factor (rhM-CSF) Using Fast Atom Bombardment-Mass Spectrometry (FAB-MS). *Biochemistry* 32, 482–488.
- (19) Maier, C., Nave, R., Hägele, K., Hannappel, E., Bauer, E., Sturm, E., Krüger, U., Schäfer, K. P., and Przybylski, M. (1993) Primary Structure Elucidation, Microheterogeneity and Surfactant Function of Natural and Recombinant Fatty Acid-Acylated Lung Surfactant SP-C Lipopolypeptides. In *Peptides 1992*, (Proc. 22nd Eur. Peptide Sympos.) (C.H. Schneider, and A.N. Eberle, Eds.) pp 915–916, Escom Science Publ., Amsterdam.
- (20) Suckau, D., Mák, M., and Przybylski, M. (1992) Protein Surface Topology-Probing by Selective Chemical Modification and Mass Spectrometric Peptide Mapping. *Proc. Natl. Acad. Sci. U.S.A.* 89, 5630–5634.
- (21) Przybylski, M., Borchers, C., Suckau, D., Mák, M., and Jetschke, M. (1993) Selective Chemical Modification and Mass Spectrometric Peptide Mapping—A New Approach for the Molecular Characterization of Surface Topology and Microenvironment in Protein Tertiary Structures. In *Peptides 1992* (Proc. 22nd Eur. Peptide Sympos.) (C.H. Schneider, and A.N. Eberle, Eds.) pp 83–84, Escom Science Publ., Amsterdam.
- (22) Fiedler, W., Glocker, M. O., and Przybylski, M. (1994) Application of Mass Spectrometry in Molecular Immunology. *Mass Spectrom. Rev.* (in press).
- (23) Kussmann, M., and Przybylski, M. (1994) Tertiary Structure-Selective Characterization of Protein Dithiol Groups by Phenylarsinoxide Modification and Mass Spectrometric Peptide Mapping. *Methods Enzymol.* (in press).
- (24) Katta, V., and Chait, B. T. (1991) Observation of the Heme-Globin Complex in Native Myoglobin by Electrospray-Ionization Mass Spectrometry. *J. Am. Chem. Soc.* 113, 8534–8535.



- (25) Klotz, I. M. (1967) Succinylation. *Methods Enzymol.* **25**, 494–499.
- (26) Riordan, J. F., and Vallee, B. L. (1972) Acetylation. *Methods Enzymol.* **25**, 494–499.
- (27) Chait, B. T., and Field, F. H. (1986) A Rapid, Sensitive Mass-Spectrometric Method for Investigating Microscale Chemical-Reactions of Surface Adsorbed Peptides and Proteins. *Biochem. Biophys. Res. Commun.* **134**, 420–426.
- (28) Nielsen, P. F., Klarskov, K., Højrup, P., and Roepstorff, P. (1988) Optimization of Sample Preparation for Plasma Desorption Mass Spectrometry of Peptides Using a Nitrocellulose Matrix. *Biomed. Env. Mass Spectrom.* **17**, 355–362.
- (29) Jonsson, G. P., Hedin, A. B., Hakanson, P. L., Sundquist, B. U. R., Säve, B. G. S., Nielsen, P. F., Roepstorff, P., Johansson, K. E., Kamensky, I., and Lindberg, M. S. L. (1986) Plasma Desorption Mass Spectrometry of Peptides Adsorbed on Nitrocellulose. *Anal. Chem.* **58**, 1084–1087.
- (30) Allen, M. H., and Vestal, M. L. (1992) Design and Performance of a Novel Electrospray Interface. *J. Am. Soc. Mass Spectrom.* **3**, 18–26.
- (31) Weinmann, W., Maier, C., Baumeister, K., Przybylski, M., Tomer, C., and Tomer, K. B. (1994) Isolation of Hydrophobic Lipoproteins in Organic Solvents by Pressure Assisted Capillary Electrophoresis for Subsequent Mass Spectrometric Characterization. *J. Chromatogr. A* **664**, 271–275.
- (32) Przybylski, M., and Glocker, M. O. (1994) Electrospray Mass Spectrometry of Supramolecular Complexes of Biomacromolecules-New Analytical Perspectives for Supramolecular Chemistry and Molecular Recognition Processes. *Angew. Chem.* (in press).
- (33) Imoto, T., Johnson, L. N., North, A. C. T., Phillips, D. C., and Rupley, J. A. (1972) Vertebrate Lysozymes. In *The Enzymes* (P.D. Boyer, Ed.) Vol. 7, pp 666–868, Academic Press, New York.
- (34) Annan, R. S., and Biemann, K. (1993) Utility of N-Peracylation of Proteins for Their Structure Determination by Mass Spectrometry. *J. Am. Soc. Mass. Spectrom.* **4**, 87–96.
- (35) Spassov, V. Z., Karshikov, A. D., and Atanasov, B. P. (1989) Electrospray Interactions in Proteins. A Theoretical Analysis of Lysozyme Ionization. *Biochim. Biophys. Acta* **999**, 1–6.
- (36) Lee, B., and Richards, F. M. (1971) The Interpretation of Protein Structures: Estimation of Static Accessibilities. *J. Mol. Biol.* **55**, 379–400.
- (37) Matthew, J. B., and Richards, F. M. (1984) Anion Binding and pH-Dependent Electrostatic Effects in Ribonuclease. *Biochemistry* **21**, 4989–4999.
- (38) Borchers, C. (1992) Diplom Thesis, University of Konstanz.
- (39) Nielsen, P. F., Landis, B., Svoboda, M., Schneider, K., and Przybylski, M. (1990) N-Terminal Sequence Determination of Polypeptides and Peptide Mixtures by Edman Degradation Combined with 252-Cf Plasma Desorption Mass Spectrometry. *Anal. Biochem.* **191**, 302–311.
- (40) Wlodawer, A., Svensson, L. A., Sjölin, L., and Gilliland, G. L. (1988) Structure of Phosphate-free Ribonuclease A Refined at 1.26 Å. *Biochemistry* **27**, 2705–2717.
- (41) Bosshard, H. R. (1979) Mapping of Contact Areas in Protein-Nucleic Acid and Protein-Protein Complexes by Differential Chemical Modification. In *Methods of Biochemical Analysis* (D. Glick, Ed.) Vol. 25, pp 273–301, Interscience Publishers, J. Wiley & Sons.
- (42) Ellenberger, T. E., Brandl, C. J., Struhl, K., and Harrison, S. C. (1992) The GCN4 Basic Region Leucine Zipper Binds DNA as a Dimer of Uninterrupted-Helices: Crystal Structure of the Protein–DNA Complex. *Cell* **71**, 1223–1237.

# Multivalent Melanotropic Peptide and Fluorescent Macromolecular Conjugates: New Reagents for Characterization of Melanotropin Receptors<sup>†</sup>

Shubb D. Sharma,<sup>‡</sup> Michael E. Granberry,<sup>§</sup> Jinwen Jiang,<sup>⊥</sup> Stanley P. L. Leong,<sup>§</sup> Mac E. Hadley,<sup>⊥,||</sup> and Victor J. Hruby<sup>\*,‡</sup>

Departments of Chemistry, Surgery, Anatomy, and Molecular and Cellular Biology, University of Arizona, Tucson, Arizona 85721. Received April 8, 1994<sup>⊗</sup>

Radioreceptor binding studies have documented the presence of melanotropin receptors on some but not all of the various human melanoma cell lines that have been studied. Using a newly developed class of multivalent fluorescent melanotropin-macromolecular conjugates, we have demonstrated for the first time the presence of specific melanotropin receptors on all of the melanoma cell lines, both mouse and human, melanotic as well as amelanotic, that were investigated. The conjugates developed by us consisted of multiple copies of both a potent melanotropin analogue and a fluorophore, both arranged in a pendent fashion on a biologically inert macromolecule. While the multivalency of these conjugates may have established stronger binding with the melanotropin receptors on the cell surface (perhaps by establishing simultaneous multiple interactions), the presence of multiple copies of the fluorophore also greatly increased the level of detection in fluorescence labeling experiments. Membrane receptor-hormone-associated phenomena, such as capping and internalization of the receptor-ligand complex, also were observed. The details of these methods are described using B-16 mouse melanoma cells as a model system. The demonstration of MSH receptors as a *common marker for melanoma* suggests that this methodology might be employed for early clinical detection and anatomical localization of melanoma. These results also offer the possibility that substitution of the fluorophore in these conjugates by a chemical agent of (chemo-)therapeutic relevance may provide a powerful tool for site specific (tumor) targeting and cytotoxicity.

## INTRODUCTION

$\alpha$ -Melanocyte stimulating hormone (MSH,  $\alpha$ -melanotropin),<sup>1</sup> a tridecapeptide, Ac-Ser-Tyr-Ser-Met-Glu-His-Phe-Arg-Trp-Gly-Lys-Pro-Val-NH<sub>2</sub>, is the physiologically relevant hormone that controls skin pigmentation of the skin in most vertebrates (1). This systemic hormone is derived from the pars intermedia of the pituitary gland. Although adult humans do not possess a pars intermedia (1), there is ample evidence that a melanotropin [either  $\alpha$ -MSH or ACTH, (2)] increases melanin pigmentation of the skin under certain pathological conditions (3). Injections of  $\alpha$ -MSH and its potent analogues into humans increase melanin pigmentation of the skin (3-5). These observations suggest that human epidermal melanocytes possess melanotropin receptors.

It has long been speculated that, like mouse melanoma cells and human epidermal melanocytes, human mela-

noma cells may also possess receptors for melanotropic peptides. Radioreceptor binding assays and autoradiography techniques have been used to identify melanotropin receptors in mouse (6-12) and several human melanoma cell lines (13-16). These studies, however, revealed extremely varied results. Interestingly, the demonstration of the presence of MSH receptors was found to be dependent on the type of radiolabeled melanotropin analogue used in these studies. For example, Libert et al. (13) using radioiodinated  $\alpha$ -MSH showed that specific binding could be demonstrated only in four out of 10 human melanoma cell lines studied. The use of radioiodinated [Nle<sup>4</sup>-D-Phe<sup>7</sup>]- $\alpha$ -MSH, on the other hand, established the presence of MSH-receptors in six out of the same 10 cell lines (13). In spite of this dependence on the radioligand, investigations by various other workers also have substantiated the finding that not all human melanoma cell lines possesses melanotropin receptors (7, 13, 16). We have utilized [Nle<sup>4</sup>-D-Phe<sup>7</sup>]- $\alpha$ -MSH, a more stable, potent, and enzymatically resistant analogue of  $\alpha$ -MSH developed in our laboratory (17-20), to synthesize macromolecular conjugates (21). These conjugates consisted of a biocompatible carrier macromolecule to which multiple copies of this peptide as well as multiple copies of a reporter group (a fluorophore) were covalently attached. The fluorescent melanotropin macromolecular conjugate was used to visualize melanotropin receptors on mouse and human melanoma cells.

## EXPERIMENTAL PROCEDURES

Fluorescein isothiocyanate-isomer I (FITC), (*N,N*-dimethylamino)pyridine (DMAP), and poly(vinyl alcohol) (average molecular weight 110 000) were obtained from Aldrich Chemical Co. (St. Louis, MO). Dithiothreitol

<sup>†</sup> This work was supported by grants from the U.S. Public Health Service DK 17420 (V.J.H.) and the National Science Foundation (V.J.H.).

\* Author to whom correspondence should be addressed at the Department of Chemistry, University of Arizona, Tucson, AZ 85721.

<sup>‡</sup> Department of Chemistry.

<sup>§</sup> Department of Surgery.

<sup>⊥</sup> Department of Anatomy.

<sup>||</sup> Department of Molecular and Cellular Biology.

<sup>⊗</sup> Abstract published in *Advance ACS Abstracts*, September 1, 1994.

<sup>1</sup> Abbreviations:  $\alpha$ -MSH,  $\alpha$ -melanocyte stimulating hormone; [Nle<sup>4</sup>-D-Phe<sup>7</sup>]- $\alpha$ -MSH, [norleucine<sup>4</sup>, D-phenylalanine<sup>7</sup>]- $\alpha$ -melanocyte stimulating hormone; FITC, fluorescein isothiocyanate; PVA, poly(vinyl alcohol); DTT, dithiothreitol; 2-ME, 2-mercaptoethanol; DMF, *N,N*-dimethylformamide; DMAP, (*N,N*-dimethylamino)pyridine; HEPES, 4-(2-hydroxyethyl)-1-piperazineethanesulfonic acid.

(DTT), mercaptoethanol, 4-(*p*-maleimidophenyl)butyric acid *N*-hydroxysuccinimide ester, and 3-(2'-pyridyldithio)propionic acid *N*-hydroxysuccinimide ester were obtained from Sigma Chemical Co. (St. Louis, MO). Tissue culture media and fetal calf serum were obtained from GIBCO. Protected amino acid derivatives were obtained from Bachem California (Torrence, CA). The binding buffer for fluorescence labeling experiments was a low ionic strength (15 mM) buffer made isotonic by the addition of glucose and sucrose (22). The composition of this buffer was as follows: triethanolamine (0.015 M), glycine (0.24 M), sucrose (0.009 M), glucose (0.025 M), potassium acetate (0.004 M), and calcium chloride (0.0003 M). Acetic acid was used to adjust the pH of the buffer to 5, and if necessary the osmolality was adjusted to 0.310 osmol using sucrose. The concentrations of all the conjugates were calculated from their initial amounts and measurements of the volumes of the preparations after dialysis.

**Cell Cultures.** All cells were grown in Falcon 75-cm<sup>2</sup> tissue culture flasks at 37 °C in a humidified atmosphere of 5% CO<sub>2</sub> and 95% air.

**Mouse and Human Melanoma.** The B16/F10 mouse melanoma cell line was originally provided by Dr. A. Overjera of the Frederick Cancer Center, Frederick, MD. The human melanotic cell line A375P was obtained through the American Type Culture Collection (ATCC). The other human melanoma cells were obtained from Arizona Cancer Center Tissue Culture Core Facility, University of Arizona, Tucson, AZ. The cell lines were maintained in monolayer cultures and were grown in Ham's F-10 medium with NaHCO<sub>3</sub> (1.2 g/L) supplemented with 10% horse serum and 2% fetal calf serum (both heat-inactivated at 56 °C for 30 min) and 1% penicillin-streptomycin (100 units/mL, 100 µg/mL, respectively). Cells were subcultured weekly and were maintained in a monolayer culture for only 10 passages to avoid phenotypic drift that is often observed in long-term cultures.

**Other Cell Lines.** A human small cell lung cancer cell line (NCI-N592) was obtained from Dr. Tom Davis, Department of Pharmacology, University of Arizona. The NCI-N592 line grows as floating aggregates in Ham's F-10 medium supplemented with 10% heat-inactivated fetal calf serum and 1% penicillin-streptomycin. The human breast cancer MCF-7 cell line was obtained from Dr. D. Blask, Department of Anatomy, University of Arizona. The mammary cancer cells were maintained in monolayer culture and grown in Ham's F-10 medium supplemented with 10% heat-inactivated fetal calf serum and 1% penicillin-streptomycin.

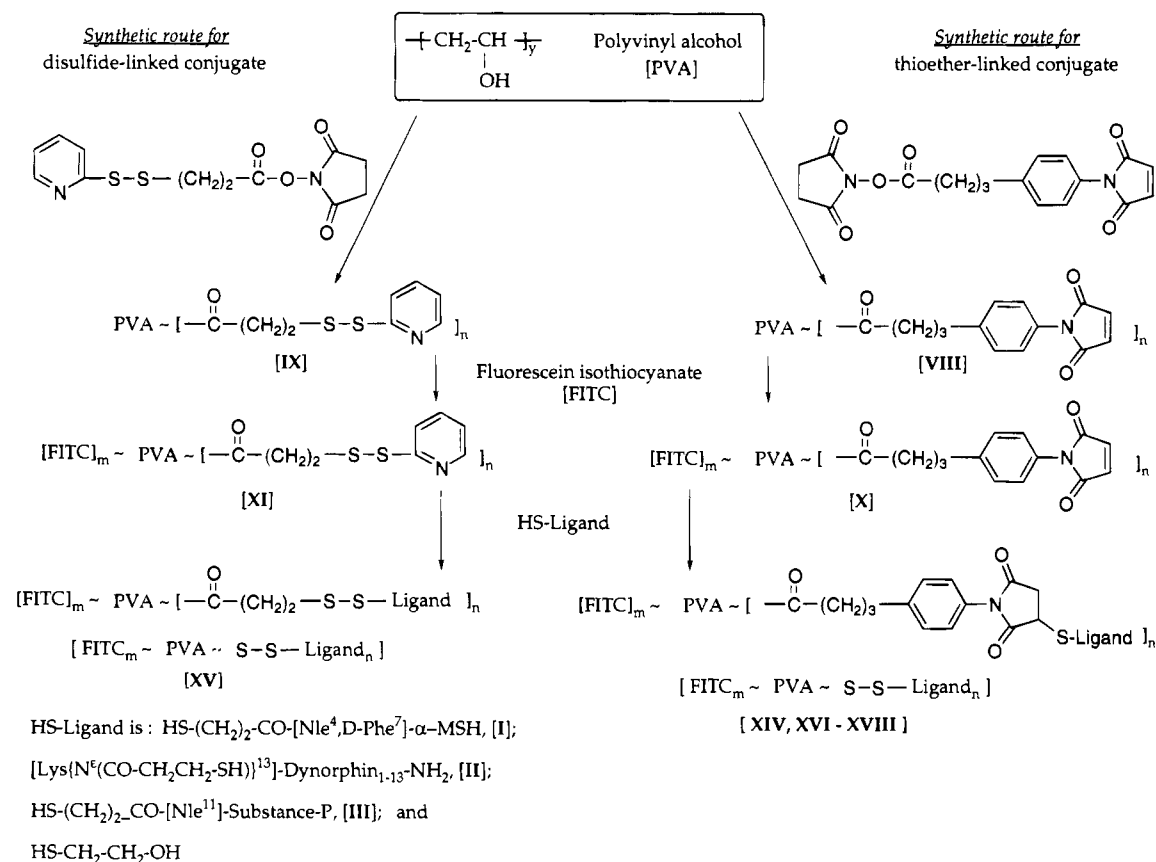
**Peptide Synthesis.** The three peptides used in this study, namely *N*<sup>α</sup>-desacetyl-*N*<sup>α</sup>-(3'-mercaptopropionyl)-[Nle<sup>4</sup>-D-Phe<sup>7</sup>]-α-MSH [I], [N<sup>ε</sup>-(3'-mercaptopropionyl)-Lys<sup>13</sup>]-dynorphin<sub>1-13</sub>-amide [II], and *N*<sup>α</sup>-(3'-mercaptopropionyl)-substance-P [III], were synthesized by solid-phase methods of peptide synthesis (23) on a *p*-methylbenzhydrylamine resin (substitution 0.51–0.72 mequiv of amine/g of resin) using a VEGA 250 semiautomated peptide synthesizer. A 4-fold excess of appropriate *N*<sup>α</sup>-Boc-protected amino acid was used at each coupling step. Couplings were performed by using diisopropylcarbodiimide-*N*-hydroxybenzotriazole (DIC-HOBt) as coupling reagent and were monitored by the Kaiser test (24) in all cases except when the incoming amino acid was coupled to the proline residue. In this instance the Chloranil test (25) was performed to ascertain the progress of the coupling. A mixture of trifluoroacetic acid-dichloromethane-anisole (TFA-DCM-anisole, 50:48:2) was used to deblock the Boc group after each coupling step. The following three

fully protected peptide-resins corresponding to peptides **I–III** were synthesized: *N*<sup>α</sup>-Boc-Ser(Bzl)-Tyr(BzlCl<sub>2</sub>)-Ser(Bzl)-Nle-Glu(OBzl)-His(Bom)-D-Phe-Arg(Tos)-Trp-Gly-Lys(ZCl)-Pro-Val-resin [IV], *N*<sup>α</sup>-Boc-Tyr(BzlCl<sub>2</sub>)-Gly-Gly-Phe-Leu-Arg(Tos)-Arg(Tos)-Ile-Arg(Tos)-Pro-Lys(ZCl)-Leu-Lys(*N*<sup>ε</sup>-Fmoc)-resin [V], and *N*<sup>α</sup>-Boc-Arg(Tos)-Pro-Lys(ZCl)-Pro-Gln-Gln-Phe-Phe-Gly-Leu-Met-resin [VI]. The *N*<sup>α</sup>-Boc groups from **IV** and **VI** and *N*<sup>ε</sup>-Fmoc group on the thirteenth amino acid residue in **V** were cleaved, respectively, by the treatment of **IV** and **V** with TFA-DCM-anisole (50:48:2) and **VI** with 20% piperidine in *N*-methylpyrrolidinone for 20 min. To each of the resulting peptide resins 3'-(*S*-(*p*-methylbenzylthio)propionic acid was individually coupled using DIC-HOBt. The dried peptide resins were individually treated with HF-thioanisole for 45 min at 0 °C and the resulting crude peptides purified by HPLC and characterized by fast atom bombardment mass spectrometry and amino acid analysis. Analytical HPLC was performed on a C<sub>18</sub> column (Vydac 218TP104, 25 cm × 4.6 mm). Thin layer chromatography (TLC) was performed on Baker 250-nm analytical silica gel glass plates in the following solvent systems: (A) 1-butanol/acetic acid/pyridine/water (5:5:1:4 v/v), (B) 2-propanol/25% aqueous ammonia/water (3:1:1 v/v), (C) ethyl acetate/pyridine/acetic acid/water (5:5:1:3 v/v), and (D) 1-butanol/acetic acid/water (4:1:5). The peptides were visualized by ninhydrin and iodine vapor. Analytical data for peptides: **I**: mass (M) = 1692.6 (calcd 1692.97); α<sup>23</sup><sub>D</sub> = −50.6° (c 0.41, 10% aqueous AcOH); HPLC *K'* = 7.02 (gradient of 10%–40% acetonitrile in 0.1% aqueous TFA completed in 30 min at 1.5 mL/min); TLC *R<sub>f</sub>* values = 0.33 (A), 0.61 (B), 0.0 (C), 0.02 (D). **II**: mass = 1691.5 (calcd 1691.13); α<sup>23</sup><sub>D</sub> = −28.1° (c 0.33, 10% aqueous AcOH); HPLC *K'* = 5.17 (gradient of 15%–45% acetonitrile in 0.1% aqueous TFA completed in 30 min at 1.5 mL/min); TLC *R<sub>f</sub>* values = 0.71 (A), 0.80 (B), 0.54 (C), 0.40 (D). **III**: mass = 1434.9 (calcd 1434.78); α<sup>23</sup><sub>D</sub> = −37.2° (c 0.41, 10% aqueous AcOH); HPLC *K'* = 5.6 (gradient of 10%–40% acetonitrile in 0.1% aqueous TFA completed in 30 min at 1.5 mL/min); TLC *R<sub>f</sub>* values = 0.53 (A), 0.75 (B), 0.64 (C), 0.36 (D).

**Synthesis of Fluorescent-Macromolecular-Peptide Conjugates.** Three types of macromolecular conjugates were synthesized: (A) conjugates containing multiple copies of fluorescein on the one hand and multiple copies of one of the three peptides synthesized above on the other (Scheme 1); (B) conjugates bound only to fluorescein; and (C) conjugates consisting only of the peptide component. The conjugates with only one of the two components present were synthesized for use in control experiments.

[Fluorescein]<sub>*m*</sub>-PVA [VII]. Ten mg (9.1 × 10<sup>−8</sup> mol) of poly(vinyl alcohol) (PVA, average MW 110 000) was dissolved in 4 mL of HEPES buffer (50 mM, pH 7.5). It was mixed with a mixture of fluorescein isothiocyanate (FITC, 1.77 mg, 4.55 × 10<sup>−6</sup> mol) and (*N,N*-dimethylamino)pyridine (DMAP, 0.5 mg, 4.55 × 10<sup>−6</sup> mol) dissolved in 1 mL of DMF. The resultant clear solution was mixed by shaking in the dark for 12–18 h. The reaction mixture was then placed in a dialysis bag (MW cutoff 10 000) and dialyzed extensively against 50 mM HEPES (pH 7.5) to remove the unconjugated FITC. The final volume of the resulting dialysate was measured. Spectrophotometric measurements at λ 492 for FITC (ε = 78 000) (26) indicated substitution of 12–18 FITC molecules per molecule of PVA in different preparations. This preparation was dialyzed extensively against the binding buffer for its use in the receptor binding experiments described below.

PVA-[(Maleimidophenyl)butyrate]<sub>*n*</sub> [VIII]. Twenty-

**Scheme 1. Synthetic Routes for the Fluorescent Macromolecular Conjugates in which the Ligand Is Either Linked to the Polymer through a Thioether [XIV, XVI, XVIII] or a Disulfide Bond [XV]**

five mg ( $2.27 \times 10^{-7}$  moles) of PVA (average MW 110 000) was dissolved in 9 mL of HEPES buffer (50 mM, pH 7.5). The solution was added to a mixture of 4-(*p*-maleimidophenyl)butyric acid *N*-hydroxysuccinimide ester (4.02 mg,  $1.13 \times 10^{-5}$  mol) and DMAP (1.38 mg,  $1.13 \times 10^{-5}$  mol) dissolved in 1 mL of DMF. The resultant clear solution was mixed by shaking for 12–18 h. The reaction mixture was then placed in a dialysis bag (MW cutoff 10 000) and dialyzed extensively against 50 mM HEPES (pH 7.5) to remove the unconjugated maleimide and the resulting volume of the dialysate measured. Spectrophotometric measurements at  $\lambda$  255 (measured  $\epsilon = 215$ ) (27) indicated a substitution of 10–16 maleimidophenyl moieties per molecule of PVA in various trials. Alternatively, the substitution was measured spectrophotometrically by reacting this product with thiophenol (5-fold molar excess) for 5 h, followed by extensive dialysis to remove unreacted thiophenol [ $\lambda$  269 ( $\epsilon = 700$ ) (28)], and the same substitution levels were obtained.

**PVA-[(Pyridyldithio)propionate]<sub>n</sub> [IX].** Twenty-five mg ( $2.27 \times 10^{-7}$  mol) of PVA (average molecular weight 110 000) was dissolved in 9 mL of HEPES buffer (50 mM, pH 7.5). It was mixed with a mixture of 3-(2'-pyridyldithio)propionic acid *N*-hydroxysuccinimide ester (3.53 mg,  $1.13 \times 10^{-5}$  mol) and DMAP (1.38 mg,  $1.13 \times 10^{-5}$  mol) dissolved in 1 mL of DMF. The resultant clear solution was mixed by shaking for 12–18 h. The reaction mixture was then placed in a dialysis bag (MW cutoff 10 000) and dialyzed extensively against 50 mM HEPES (pH 7.5) to remove the unconjugated reagent and the resultant volume of the dialysate measured. Spectrophotometric measurements done at  $\lambda$  255 (measured  $\epsilon = 215$ ) (29) indicated substitution of 10–16 pyridyl moieties per molecule of PVA in different trials. Alternatively, the substitution was also measured spectrophotometri-

cally by reacting this product with mercaptoethanol (5-fold molar excess) for 5 h, followed by direct measurements at  $\lambda$  343 ( $\epsilon = 8080$ ) for the 2-thiopyridine (30) that is released in this reaction. The same values for levels of substitution were obtained.

**[FITC]<sub>m</sub>-PVA-[(Maleimidophenyl)butyrate]<sub>n</sub> [X].** A sample of 10 mg ( $9.1 \times 10^{-8}$  mol) of VIII (ca. 4 mL in 50 mM HEPES buffer, pH 7.5) was added to a mixture of FITC (1.77 mg,  $4.55 \times 10^{-6}$  mol) and DMAP (0.5 mg,  $4.55 \times 10^{-6}$  moles) dissolved in 1 mL of DMF. The resultant clear solution was mixed in the dark by shaking for 12–18 h. The reaction mixture was then placed in a dialysis bag (MW cutoff 10 000) and dialyzed extensively against 50 mM HEPES (pH 7.5) to remove the unconjugated FITC. Spectrophotometric measurements done as above at  $\lambda$  492 ( $\epsilon = 78 000$ ) (26) indicated substitution 11–16 FITC moieties per molecule of PVA.

**[FITC]<sub>m</sub>-PVA-[(Pyridyldithio)propionate]<sub>n</sub> [XI].** A sample of 10 mg ( $9.1 \times 10^{-8}$  mol) of IX (ca. 4 mL in 50 mM HEPES buffer pH 7.5) was added to a mixture of FITC (1.77 mg,  $4.55 \times 10^{-6}$  mol) and DMAP (0.5 mg,  $4.55 \times 10^{-6}$  mol) dissolved in 1 mL of DMF. The resultant clear solution was treated in the same manner as described under the synthesis of X to give a similar substitution value.

**Synthesis of PVA-[S-MSH]<sub>n</sub> [XII] and PVA-[SS-MSH]<sub>n</sub> [XIII].** Treatment of 2 mg of the derivatized polymer VIII or IX in 1.5–2.0 mL of 50 mM HEPES (pH 7.5) with a 2–4-fold molar excess of I dissolved in DMF (0.3 mL) was accomplished at room temperature for 2–5 h. The conjugate was dialyzed extensively, and the degree of ligand substitution calculated spectrophotometrically at  $\lambda$  280 nm ( $\epsilon = 4840$ ) to be between 10 and 16 MSH molecules per molecule of the polymer. These

**Table 1. Results Demonstrating Specific Fluorescence Labeling of Melanotropin Receptors on Various Melanoma Cell Types by Fluorescent MSH-Macromolecular Composites**

conjugate	malignant cell types												
	mouse melanoma B-16 <sup>a</sup>	human								lung cancer NCI-N417	breast cancer MCF-7	normal cell types mouse Spleen Liver	
		melanoma											
		JH <sup>b</sup>	LH 1649 <sup>a</sup>	LR 1650 <sup>a</sup>	LR 1714 <sup>a</sup>	WC <sup>b</sup>	KE <sup>a</sup>	A375P <sup>a,c</sup>					
FITC-PVA [VII]	—	—	—	—	—	—	—	—	—	—	—	—	
FITC-PVA-S-MSH [XIV]	++	++	++	++	++	++	++	++	—	—	—	—	
FITC-PVA-SS-MSH [XV]	++		++	++	++								
FITC-PVA-SS-MSH [XV] + DTT	—		—	—	—								
FITC-PVA-S-MSH [XIV] + DTT	++		++	++	++								
FITC-PVA-ME [XVIII]	—	—	—	—	—					—			
FITC-PVA-S-DYN [XVI]	—		—	—	—								
FITC-PVA-S-SP [XVII]	—					—	—	—	—	—			

<sup>a</sup> Melanotic cell lines. <sup>b</sup> Amelanotic cell lines. <sup>c</sup> Similar positive responses were obtained with all other human melanoma cells that were assayed (>17 cell lines). ++, indicates strong fluorescence labeling. -, indicates no fluorescence labeling.

preparations were dialyzed against the binding buffer for their use in the binding experiments with the cultured cells.

**Synthesis of [FITC]<sub>m</sub>-PVA-[-S-MSH]<sub>n</sub> [XIV], [FITC]<sub>m</sub>-PVA-[-SS-MSH]<sub>n</sub> [XV], [FITC]<sub>m</sub>-PVA-[-S-dynorphin]<sub>n</sub> [XVI], [FITC]<sub>m</sub>-PVA-[-S-substance P]<sub>n</sub> [XVII], and [FITC]<sub>m</sub>-PVA-[-ME]<sub>n</sub> [XVIII].** Treatment of 2 mg of the derivatized polymer **X** or **XI** in 1.5–2.0 mL of 50 mM HEPES (pH 7.5) with a 2–4-fold molar excess of **I**, **II**, **III**, or mercaptoethanol (ME) dissolved in DMF (0.3 mL) was accomplished as described above under **XII** and **XIII**. The conjugate in each case was dialyzed extensively and the degree of ligand substitution calculated spectrophotometrically. The substitution in each case was found to range between 10 and 16 molecules of the ligand per molecule of the polymer. All these preparations were dialyzed against the binding buffer for this compatibility in the binding experiments with the cultured cells.

**Fluorescence Labeling of Melanotropin Receptors.** One million cells of each type (Table 1) per test tube were treated individually with conjugates **VII** and **XIV–XVIII** at various concentrations (0.5 mg/mL was the best concentration) for various lengths of time (15 min incubations were found to be best) at room temperature in the dark. The cells were then washed in the test tube with the binding buffer (3 × 1 mL). The final cell pellet was resuspended in 0.5 mL of buffer. About 30 μL of the resulting cell suspension was dropped onto a glass slide and mixed with the same volume of glycerin. Samples were examined under an fluorescence microscope for visualization of cellular fluorescence. The specimens were first photographed by phase contrast and then under fluorescence conditions.

## RESULTS

**Conjugate Synthesis.** PVA of average molecular weight 110 000 has 2500 hydroxy groups that could be derivatized for the synthesis of multivalent conjugates (Scheme 1). However, the limiting factor in these conjugation experiments turned out to be the water solubility of the resulting products at physiologically acceptable pH values. In general, all attempts to make more highly substituted conjugates, both in terms of the number of FITC and the number of ligand molecules per PVA monomer, were met with limited success. From a practical standpoint, introduction of 10–16 ligand molecules and almost the same number of the FITC molecules per polymer molecule yielded conjugates that were soluble in buffers of low ionic strength, pH 6. When transferred to buffers at physiological ionic strength, e.g., phosphate-buffered saline (150 mM), the conjugates

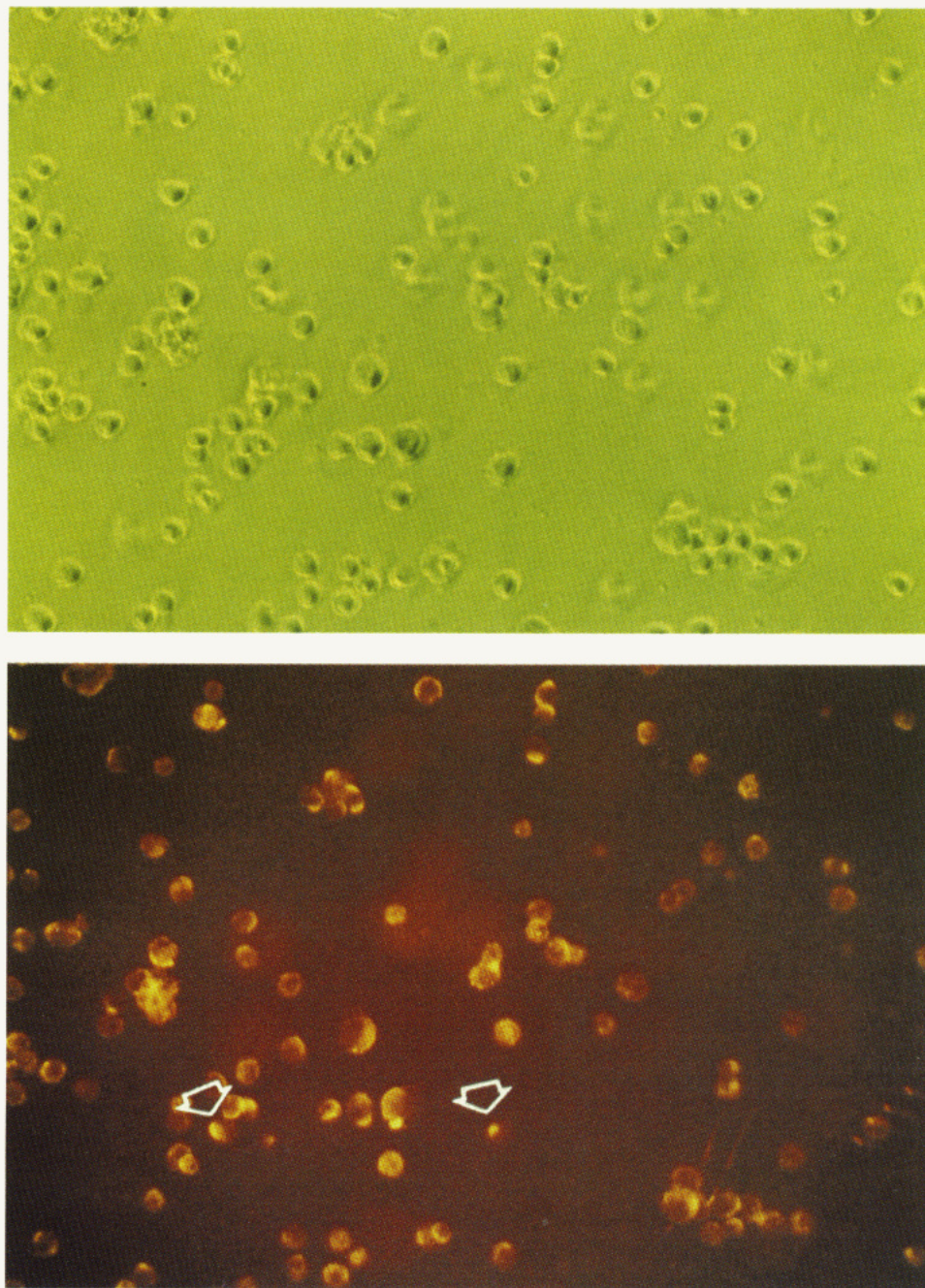
slowly precipitated. Once precipitated these conjugates would not go back into solution even in the binding buffer of low ionic strength. For these reasons all the intermediates as well as the final conjugates were stored as solutions. The preparations were observed to be stable for up to 2 months when stored at 4 °C.

**Conjugate Binding to Mouse and Human Melanoma Cells.** Binding of the conjugates with cell membrane receptors was established within 15 min (Figures 1–4). Binding was extremely strong so that all the incubations and washing protocols could be performed at room temperature. In addition, the binding buffer of pH 5 was utilized to remove any nonspecific binding. This pH had no effect on the specific binding that existed in all the positive controls. This strong binding probably resulted due to the fact that a single assembly of the conjugate is able to interact with more than one receptor on the cell membrane. This phenomenon of *cooperative affinity* that results in stronger binding properties associated with multivalent ligands has been documented previously in the literature (31, 32). Certain classes of polyvalent antibodies that also are capable of establishing multiple interactions also exhibit much higher binding affinities as the result of *cooperative affinity* (33).

**Specificity of Binding. Cleaving the Disulfide Linkage (by Treatment with 2-ME or DTT).** The disulfide-linked melanotropin conjugate offered the best possibility of a control experiment to establish the specificity of the fluorescence labeling by the MSH-containing conjugates. Agents such as dithiothreitol (DTT) are able to reduce the S–S bond and therefore release hormone. FITC-PVA-MSH (**XV**) was incubated with DTT (final concentration: 50 mM) for 1 h at room temperature with constant shaking. The DTT- or 2-ME-treated conjugate when incubated with B16/F10 mouse melanoma cells failed to label these cells (Table 1). This experiment indicates the specific labeling of melanotropin receptors by FITC-PVA-MSH. When a similar amount of DTT was included in the binding experiment using the thioether linked MSH macromolecule **XIV** (which is stable to DTT treatment) there was no effect on the fluorescence labeling (Table 1). This ruled out receptor inactivation by DTT during the labeling experiment in the earlier case.

**Preincubation in the Presence of Unconjugated Free Ligand ("Swamp Out").** It was interesting to note that the binding established between the MSH-containing macromolecules **XIV** or **XV** with the melanoma cells was so strong that the presence of even millimolar amounts of free ligand [Nle<sup>4</sup>-D-Phe<sup>7</sup>]-α-MSH as competitor for the receptors caused no effect on the fluorescence intensity. However, when the cells were pretreated with the free





**Figure 1.** Fluorescence labeling of mouse B16/F10 melanoma cells by fluorescent melanotropin macromolecular conjugate (FITC-PVA-S-MSH, **XIV**). Top: phase contrast micrograph. Bottom: fluorescent micrograph. Arrows illustrate the capping phenomena exhibited by cells.

ligand ( $1 \times 10^{-6}$  M) for 1 h before their exposure to the fluorescent macromolecular ligand **XIV**, a very dramatic loss of the fluorescence intensity was observed (data not shown). This suggests that either the receptor is blocked (occupied) or it is internalized. Though we do not have direct evidence for which is the case, the results do strongly indicate that the MSH conjugates are highly specific for the melanotropin receptors that interact with [Nle<sup>4</sup>-D-Phe<sup>7</sup>]- $\alpha$ -MSH.

**Binding Studies Using FITC-PVA [VII].** This conjugate that lacked any melanotropic ligand failed to bind to any type of cells used under all binding conditions (Table 1). This negative control established the biological inactivity of the fluorescent macromolecular carrier molecule (Figure 5).

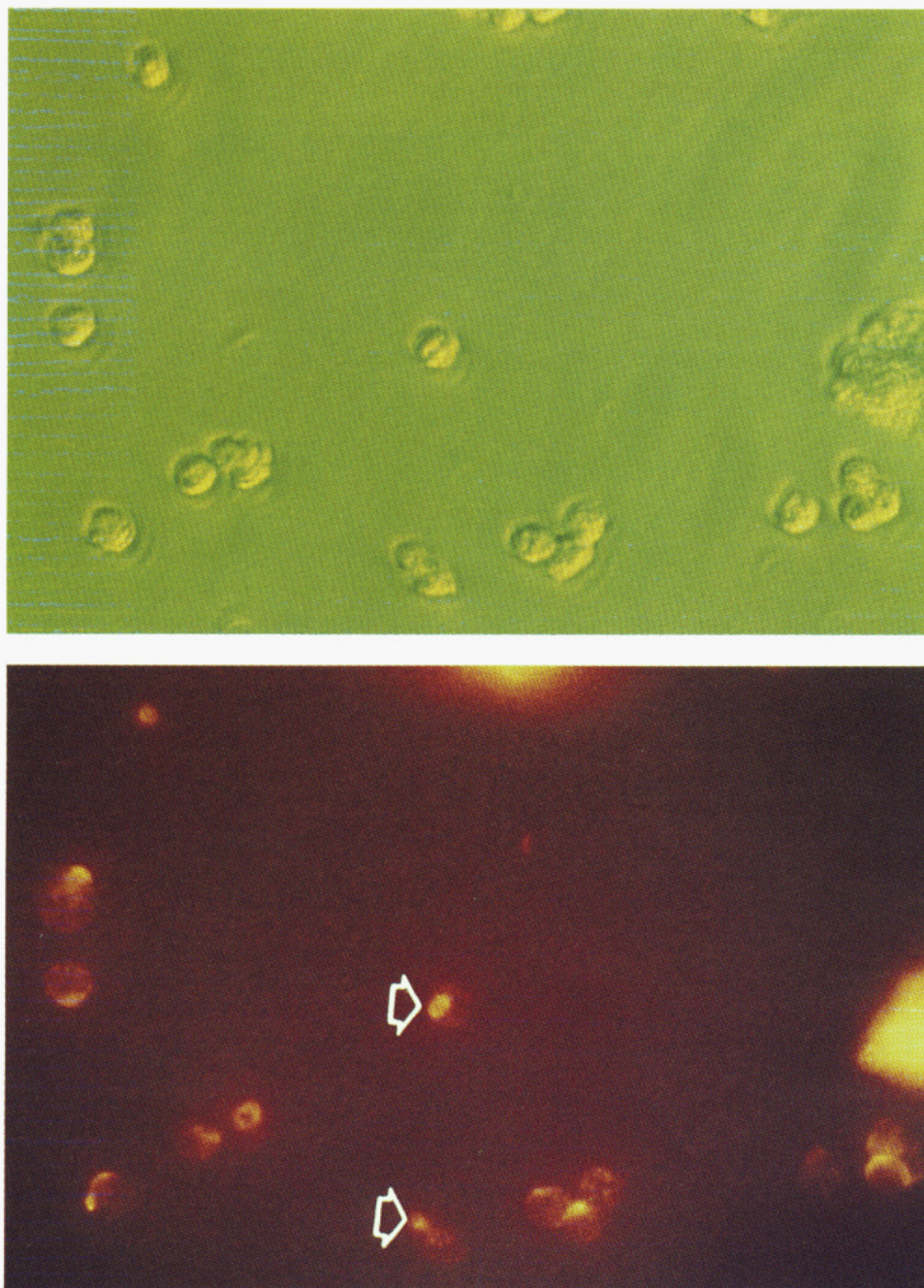
**Other Peptide Conjugates (e.g., Dynorphin, Substance P, and Mercaptoethanol).** These three ligands were chosen to act as negative controls to prove the point that

the binding seen with the MSH conjugate is specific for melanotropin receptors. All three of these nonmelanotropic ligands containing fluorescent conjugates (**XVI**, **XVII**, and **XVIII**) failed to label B-16 mouse melanoma cells (Table 1).

**Cellular Specificity (Other Cell Types).** A few cell types of nonmelanogenic origin (Table 1) were included in this study to act as negative controls for the demonstration of melanoma-specific melanotropin receptors. As is evident from the results, human small cell lung cancer (NCI-N592) and breast cancer cells (MCF-7) did not exhibit any fluorescent labeling after incubation with the fluorescent MSH conjugate (Table 1). Normal mouse liver, kidney, and spleen cells also failed to exhibit fluorescence following incubation with the conjugate.

**Homogeneity of Conjugate Binding to Melanoma Cells and Capping/Internalization of the Ligand.** During the fluorescence labeling experiments it was





**Figure 2.** B-16/F-10 mouse melanoma cells showing capping (or internalization) of MSH receptors visualized by specific binding of FITC-PVA-SS-MSH [XV]. Top: phase contrast micrograph. Bottom: fluorescent micrograph.

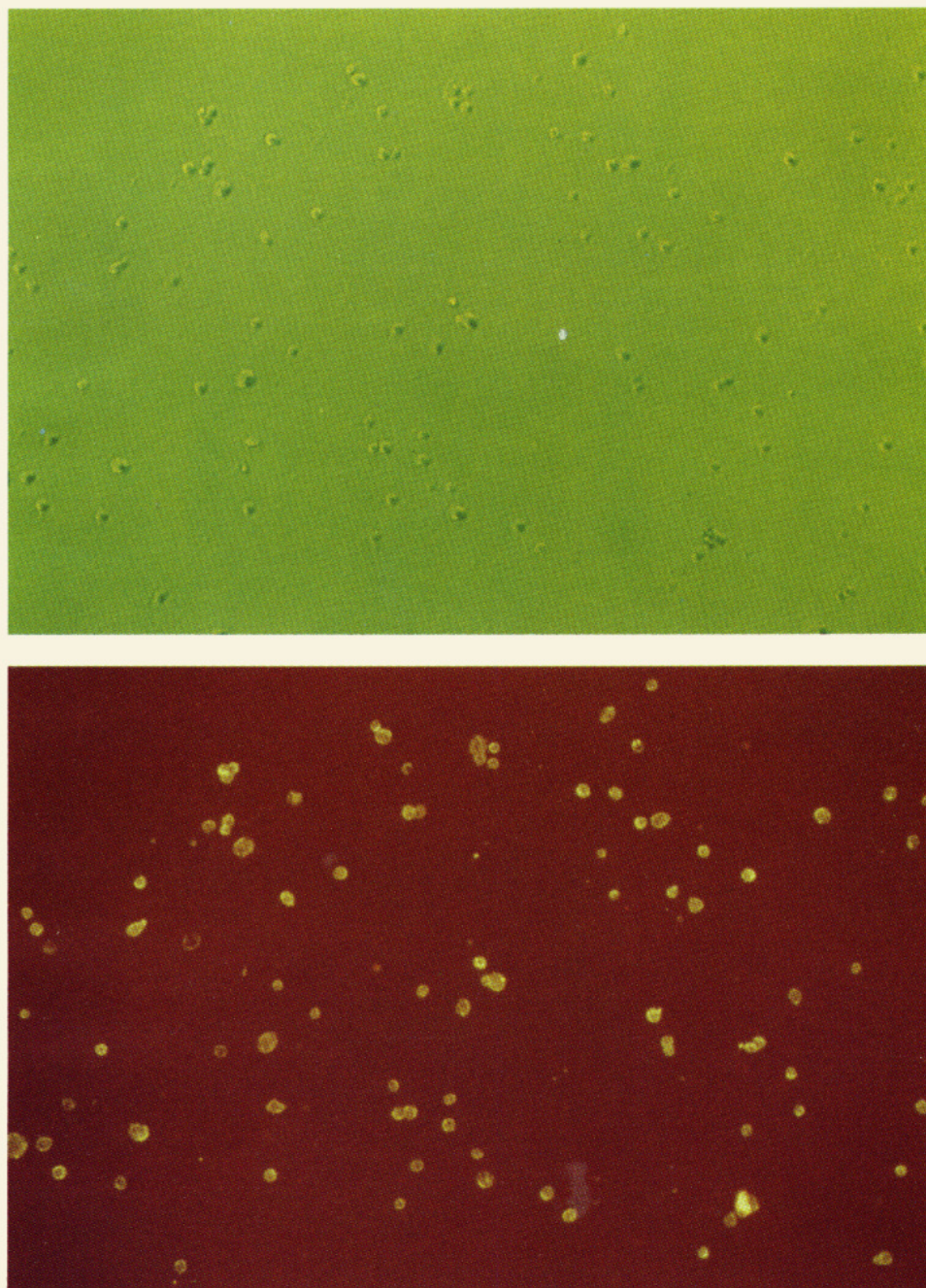
evident that *all* the cells in each and every melanoma cell line were uniformly labeled by the melanotropin conjugates **XII** or **XIII** (Figures 1–5). This suggests cellular homogeneity of all the melanoma cell lines with respect to melanotropin receptor expression. Some of the cells (in the case of both mouse and some human melanomas) that were oriented favorably (microscopically) to the observer exhibited capping of the receptors (Figures 1, 2, and 4). In certain instances the fluorescence appeared to be located intracellularly suggesting internalization of the receptor–ligand (macromolecule) complex (Figures 2 and 4). These observations are consistent with earlier experiments with fluorescence labeling of MSH-receptors using fluorescent tobacco mosaic virus–MSH peptide conjugates (32, 34). The capping and internalization phenomena were further examined using the disulfide-linked melanotropin macromolecular conjugate **XV**. In a fluorescence labeling experiment using this ligand a portion of the labeled cells

was incubated for 30 min in the binding buffer at pH 7.2 that also contained 50 mM DTT. As DTT cleaved the disulfide linkage, thereby removing the MSH molecules from the polymer, cell membranes were expected to lose the fluorescence. In the case of cells showing intracellular fluorescence, no loss of the fluorescence was observed. This clearly was indicative of the internalized receptor ligand complex.

#### DISCUSSION

The studies reported here using fluorescent microscopic visualization methods demonstrate specificity of the fluorescent melanotropin–PVA macromolecular conjugate (MSH–PVA–FITC) for melanotropin receptors associated with melanoma cells (Table 1). The specificity of receptor-mediated binding was demonstrated by the following observations: (1) The positive control, mouse B16/F10 melanoma cells (known to express MSH receptors), strongly bound the conjugate. (2) The negative





**Figure 3.** Binding of FITC-PVA-S-MSH [XIV] to an amelanotic human melanoma cell line (JH) showing cellular homogeneity of MSH receptors. Top: phase contrast micrograph. Bottom: fluorescent micrograph.

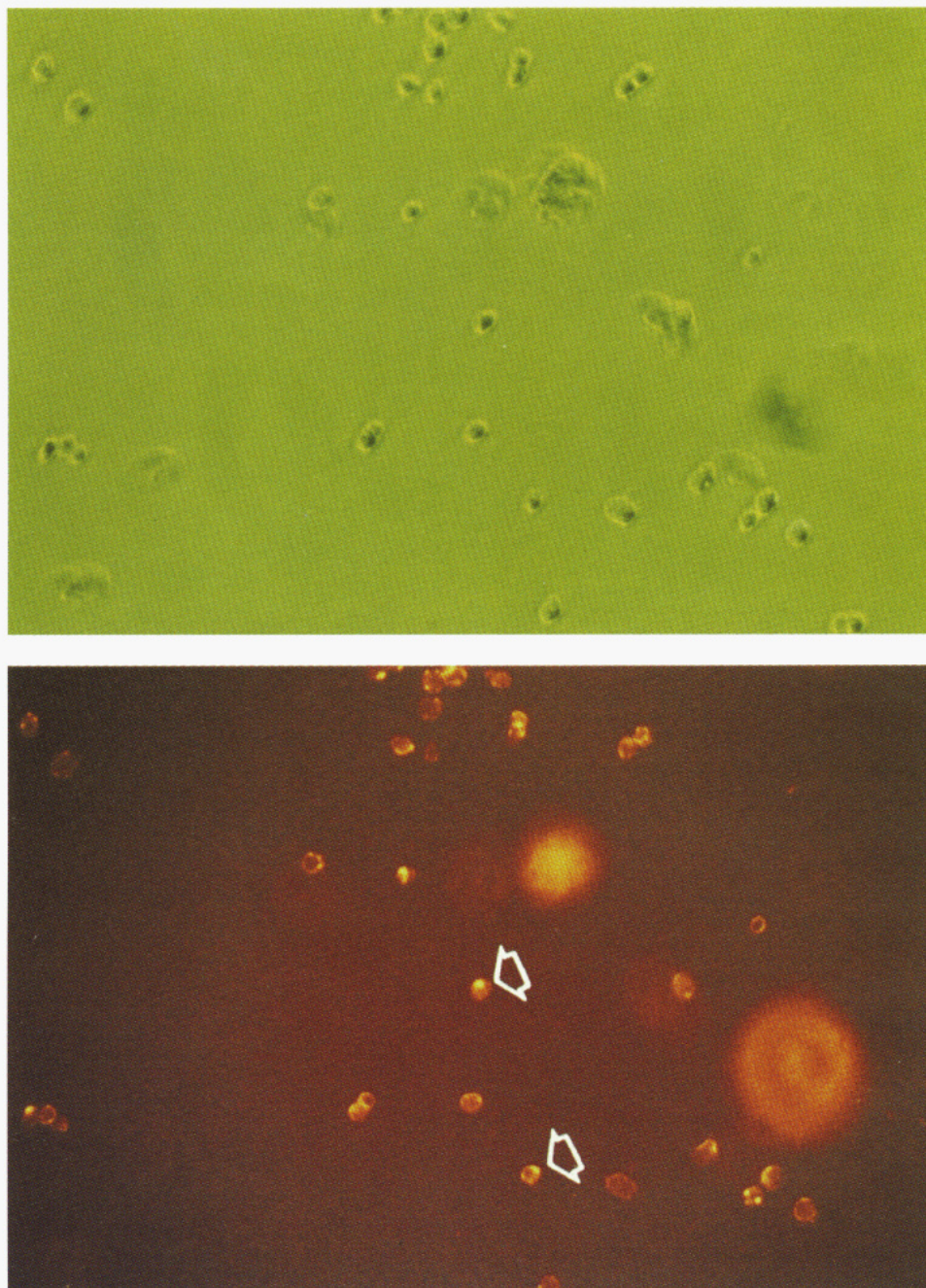
control, MCF-7 human breast cancer cells and NCI-N592 small cell lung cancer cells (both assumed not to express MSH receptors), failed to bind to the conjugate. In addition, a number of other cell lines of nonmelanocytic origin did not bind to the conjugate (data not shown). 3) Incubation of FITC-PVA alone (no hormone attached), or incubation of a fluorescent dynorphin or substance-P conjugate, did not result in binding of the conjugates to the cells (Table 1). (4) Pretreatment of **XV**, a disulfide linked melanotropin-conjugate (MSH-SS-PVA-FITC), with reducing agents (dithiothreitol or 2-mercaptoethanol), resulted in cleavage of the bond between the PVA backbone and the hormone, and this treatment resulted in a conjugate (now lacking ligand) that did not bind to receptors. (5) If binding is specific to melanotropin receptors, one would expect that the presence of the conjugated analog would compete with the unbound ligand ([Nle<sup>4</sup>-D-Phe<sup>7</sup>]- $\alpha$ -MSH) for receptor binding. In competition experiments preincubation of melanoma cells

with micromolar concentrations of [Nle<sup>4</sup>-D-Phe<sup>7</sup>]- $\alpha$ -MSH effectively blocked the binding of the fluorescent conjugate **XIV** to the binding sites on the melanoma cell membrane (data not shown).

Receptor internalization is one of the processes by which cells recycle (or degrade) receptors. Internalization has been observed for several different types of receptors (*e.g.*, 35–37). The “capping” phenomenon is believed to indicate receptor internalization (endocytosis). Similar receptor aggregation has been observed for some other polypeptide hormones (*e.g.*, 38–40). For example, Jarett and Smith (38) found insulin receptor aggregation on adipocyte plasma membranes by using a ferritin–insulin conjugate in conjunction with transmission electron microscopy. De Priester *et al.* (39) reported capping of concanavalin (Con A) receptors on *Dictyostelium* cell membranes after incubation of cells with fluorescent Con A.

This capping phenomenon was also observed using our





**Figure 4.** Capping of MSH receptors observed upon specific binding of FITC-PVA-S-MSH [XIV] with MSH receptors in a human melanoma cell line (LR 1649). Top: phase contrast micrograph. Bottom: fluorescent micrograph. Arrows illustrate the capping phenomena exhibited by cells.

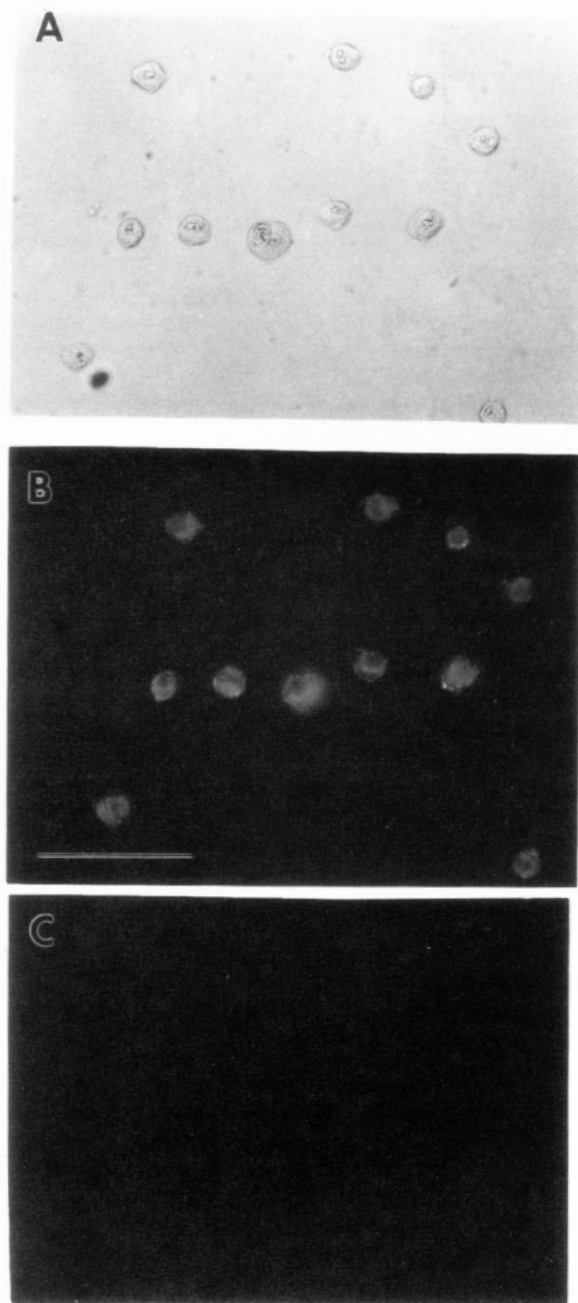
fluorescent conjugate (Figures 1, 3 and 4) and was observed on the surface of some cells of all human melanoma cell lines (Figure 4). The results suggest that capping may be a phenomenon involving one or more focal aggregates of receptors. These observations suggest that MSH receptors become internalized. These observations thus provide further evidence for the presence of melanotropin receptors on the cell surface of human melanoma cells. The observation of melanotropin-receptor internalization was first reported by Varga *et al.* (41). By using a fluorescent-labeled  $\beta$ -MSH, the authors found that the hormone was internalized at a physiological temperature in Cloudman (murine) melanoma cells. Later, Lerner *et al.* (42), using ferritin-labeled  $\beta$ -MSH, found that some of the internalized hormone may be further translocated to premelanosomes. Recently, Orlow *et al.* (43) demonstrated that receptor internalization resulted in translocation of the hormone

to internal binding sites within the cells. In these latter experiments the authors used  $^{125}\text{I}$ -labeled  $\beta$ -melanotropin ( $\beta$ -MSH) and sucrose density centrifugation techniques to determine the internal binding sites for MSH. Garcia-Borron *et al.* also have provided data that [ $^{125}\text{I}$ ]-[Nle<sup>4</sup>-D-Phe<sup>7</sup>]- $\alpha$ -MSH is internalized in B16/F10 mouse melanoma cells (10).

In our experiments, we did not investigate the time course for the formation and the duration of capping on the cell surface. This future study should provide more information as to the kinetics of the capping phenomenon and, therefore, may help us to better understand the metabolism or recycling of melanoma melanotropin receptors. Our unique and relatively simple methods for the visualization of ligand-receptor membrane capping may prove to be a useful tool for the study of other cell types and their specific hormone receptors.

Our results are consistent, in part, with previous work





**Figure 5.** FITC-PVA-S-MSH [XIV] binds to human melanotic melanoma cell line (A375P). A: Phase contrast micrograph. B: Fluorescent micrograph. C: FITC-PVA [VII], a conjugate that lacks [Nle<sup>4</sup>-D-Phe<sup>7</sup>]- $\alpha$ -MSH does not bind to A375P cells. Bar = 100  $\mu$ m.

reported by a number of other investigators. Ghanem *et al.* (15) found that three out of eight human melanoma cell lines displayed specific binding of [<sup>125</sup>I]- $\alpha$ -MSH to the cells. Siegrist *et al.* (7) reported that 10 out of 12 human melanoma cell lines showed specific binding sites for [<sup>125</sup>I]- $\alpha$ -MSH. Using an *in situ* binding technique to demonstrate melanotropin receptors in surgical specimens of human melanoma, Tatro *et al.* (16) reported that among the melanoma specimens from 11 patients, three of them showed a high level of specific binding, five a low level binding, and another three no detectable binding. Although the radioligand binding technique allows indirect estimation of binding sites for radiolabeled agents in target cells or tissues, the results generated from the binding assay are in general based upon the mass binding of the radioactive probe to a population of cells. This technique is unable to provide information about the receptor status of an individual single cell. In

addition, these previous radioligand technologies may not be sensitive enough for those cells with a low number of receptors or low numbers of cells actually expressing receptors at the time (cell cycle) of the experiment. Hence, it appears that our visualization methods may offer a unique advantage over other presently used methods to study the homogeneity or heterogeneity of melanotropin receptor distribution.

Several previous reports have indicated that melanotropin receptors may also exist in some tissues other than cutaneous tissue. Tatro and Reichlin (12) showed that MSH receptors were widely distributed *in vivo* in the tissues of rodents including glandular organs, adipose tissues, and bladder. However, in our experiments, the melanotropin-macromolecular conjugates failed to bind to a number of nonmelanotic cells, such as human small cell lung cancer cells, endometrial carcinoma (data not shown), breast cancer MCF-7 cells and some normal mouse cells, such as spleen cells as well as liver cells (Table 1). Similar results were reported by Siegrist *et al.* (7) where melanotropin receptors were found to be specifically present in human and mouse melanoma cells, but not in five other human neuroblastoma or glioma cell lines. The discrepancy between our results and others as to melanotropin receptor distribution in different tissues remains to be clarified.

It has been suggested by one research group that MSH receptors are predominantly expressed in the G<sub>2</sub> phase of the cell cycle (41, 44). Other investigations have been unable to confirm such G<sub>2</sub> restriction (45, 46). In the present studies we noted that our melanotropin conjugates were bound to every individual mouse or human melanoma cell. Since the cells were not synchronized, it is assumed that binding (30 min incubation) to the cells occurred during each phase of the cell cycle. It was also reported earlier that at least some of the responses to MSH (increased cyclic AMP production and tyrosinase activity) occur in the G<sub>2</sub> phase of the cell cycle (47), the reasons being that the receptors for MSH are most active at this time in the cycle. In fact, it is claimed that melanoma cells "regulate their response to MSH by the discontinuous appearance of receptors for the hormonal signal" (48). Although our results do not restrict the ability of cells to bind MSH to the G<sub>2</sub> phase of the cycle, the data provides no information on the functional ability (to transduce signals and effect second messenger formation) of melanotropin receptors throughout the cycle.

#### SUMMARY AND PERSPECTIVES

We have designed a new class of multivalent peptide hormone macromolecular composites which may serve as powerful diagnostic, imaging, and therapeutic tools. Composites have been synthesized in which multiple copies of a biospecific ligand (e.g., a hormone) were covalently attached to a biologically compatible but inert polyfunctional macromolecule. In addition, the conjugation of multiple copies of a fluorophore directly to the macromolecule provided an enhanced visual means of detection of ligand-macromolecular conjugates bound to target cells in *in vitro* binding assays. A fluorescent melanotropin macromolecular conjugate has been synthesized and used to demonstrate the presence of specific melanotropin receptors on various human melanoma cell lines.

Most importantly, every cell of every melanoma cell line possessed melanotropin receptors as visualized by fluorescence microscopy. Cells of nonmelanocyte origin did not exhibit such receptors. These cell specific melanotropin receptors may serve as cell surface markers for melanoma. Fluorescent melanotropin conjugates

should be useful in determining whether all (primary and metastatic) tumors possess such receptors. These receptors may provide targets for the identification, localization, and chemotherapy of melanoma (49). For example, a fluorescent melanotropin conjugate could be used to visually identify metastatic melanoma (particularly amelanotic melanoma) cells of lymph nodes following elective lymph node dissection.

## LITERATURE CITED

- (1) Hadley, M. E. (1992) *Endocrinology*, 3rd ed., Prentice-Hall, Inc., Englewood Cliffs, NJ.
- (2) Hadley, M. E. (1988) *The Melanotropic Peptides, Vol. I: Source, Synthesis, Chemistry, Secretion, and Metabolism* (M. E. Hadley, Ed.) CRC Press, Boca Raton, FL.
- (3) Lerner, A. B., and McGuire, J. S. (1961) Effect of alpha and beta melanocyte stimulating hormones on the skin colour of man. *Nature* 185, 176–179.
- (4) Lerner, A. B., and McGuire, J. S. (1964) Melanocyte-stimulating hormone and adrenocorticotrophic hormone: Their relation to pigmentation. *N. Engl. J. Med.* 270, 539–546.
- (5) Levine, N., Sheftel, S. N., Eytan, T., Dorr, R. T., Hadley, M. E., Weinrach, J. C., Ertl, G. A., Toth, K., McGee, D. L., and Hruby, V. J. (1991) Induction of skin tanning by the subcutaneous administration of a potent synthetic melanotropin. *J. Am. Med. Assoc.* 266, 2730–2736.
- (6) Panasci, L. C., McQuillan, A., and Kaufman, M. (1987) Biological activity, binding, and metabolic fate of Ac-[Nle<sup>4</sup>-D-Phe<sup>7</sup>]-MSH<sub>4-11</sub>-NH<sub>2</sub> with the F1 variant of B16 melanoma cells. *J. Cellular Physiol.* 132, 97–103.
- (7) Siegrist, W., Solca, F., Stutz, S., Giuffre, L., Carrel, S., Girard, J., and Eberle, A. N. (1989) Characterization of receptors for α-melanocyte stimulating hormone on human melanoma cells. *Cancer Res.* 49, 6352–6358.
- (8) Siegrist, W., Ostreicher, M., Stutz, S., Girard, J., and Eberle, A. (1988) Radioreceptor assay for α-MSH using mouse B16 melanoma cells. *J. Receptor Res.* 8, 323–343.
- (9) Solca, F., Siegrist, W., Drozd, R., Girard, J., and Eberle, A. N. (1989) The receptor for alpha-melanotropin of mouse and human melanoma cells: application of a potent photo-affinity label. *J. Biol. Chem.* 264, 14277–14281.
- (10) Garcia-Borron, J. C., Solano, F., Martinez-Liarte, J. H., Jara, J. R., Lozano, J. A., and Ghanem, G. (1993) Binding and subcellular distribution of [<sup>125</sup>I]-[Nle<sup>4</sup>-D-Phe<sup>7</sup>]α-MSH in B16/F10 mouse melanoma cells. (Private communication).
- (11) Tatro, J. B., Watson, M. L., Lester, B. R., and Reichlin, S. (1990) Melanotropin receptors of murine melanoma characterized in cultured cells and demonstrated in experimental tumors in situ. *Cancer Res.* 50, 1237–1242.
- (12) Tatro, J. B., and Reichlin, S. (1987) Specific receptors for α-melanocyte-stimulating hormone are widely distributed in tissues of rodents. *Endocrinology* 121, 1900–1907.
- (13) Libert, A., Ghanem, G., Arnould, R., and Lejeune, F. (1989) Use of an alpha-melanocyte-stimulating hormone analogue to improve alpha-melanocyte-stimulating hormone receptor binding assay in human melanoma. *Pigment Cell Res.* 2, 510–518.
- (14) Legros, F., Coel, J., Doyen, A., Hanson, P., Van Tieghem, N., Vercammen-Grandjean, A., Fruhling, J., and Lejeune, F. J. (1980) α-Melanocyte-stimulating hormone binding and biological activity in a human melanoma cell line. *Cancer Res.* 41, 1539–1544.
- (15) Ghanem, G. E., Comunale, A., Libert, A., Vercammen-Grandjean, A., and Lejeune, F. (1988) Evidence for alpha-melanocyte-stimulating hormone (α-MSH) receptors on human malignant melanoma cells. *Int. J. Cancer* 41, 248–255.
- (16) Tatro, J. B., Atkins, M., Mier, J. W., Hardarson, S., Wolfe, H., Smith, T., Entwistle, M. L., and Reichlin, S. (1990) Melanotropin receptors demonstrated in situ in human melanoma. *J. Clin. Invest.* 85, 1825–1832.
- (17) Sawyer, T. K., Sanfilippo, P. J., Hruby, V. J., Engel, M. H., Heward, C. B., Burnett, J. B., and Hadley, M. E. (1980) [Nle<sup>4</sup>-D-Phe<sup>7</sup>]α-melanocyte stimulating hormone: a highly potent α-melanotropin with ultralong biological activity. *Proc. Natl. Acad. Sci. U.S.A.* 77, 5754–5758.
- (18) Hadley, M. E., Abdel-Malek, Z., Marwan, M. M., and Kreutzfeld, K. L. (1985) [Nle<sup>4</sup>-D-Phe<sup>7</sup>]α-MSH: a superpotent melanotropin that “irreversibly” activates melanoma tyrosinase. *Endocr. Res.* 11, 157–170.
- (19) Abdel Malek, Z., Kreutzfeld, K. L., Marwan, M. M., Hadley, M. E., Hruby, V. J., and Wilkes, B. L. (1985) Prolonged stimulation of S91 melanoma tyrosinase by [Nle<sup>4</sup>-D-Phe<sup>7</sup>]α-MSH-substituted α-melanotropins. *Cancer Res.* 45, 4735–4740.
- (20) Hruby, V. J., Sharma, S. D., Toth, K., Jaw, J. W., Al-Obeidi, F., Sawyer, T. K., and Hadley, M. E. (1993) Design, synthesis, and conformation of superpotent and prolonged acting melanotropins. *Ann. N.Y. Acad. Sci.* 680, 51–63.
- (21) A previous preliminary account of some of this research has appeared. Sharma, S. D., Hruby, V. J., Hadley, M. E., Granberry, M. E., and Leong, S. P. (1992) Multivalent ligands for diagnosis and therapeutics. In *Peptides: Chemistry and Biology, Proceedings of the Twelfth American Peptide Symposium* (J. A. Smith and J. E. Rivier, Eds.) pp 599–600, ESCOM, Leiden, The Netherlands.
- (22) Zeiller, K., Pascher, G., and Hannig, K. (1972) Preparative electrophoretic separation of antibody forming cells. *Prepar. Biochem.* 2, 21–37.
- (23) Hruby, V. J., Wilkes, B. C., Hadley, M. E., Al-Obeidi, F., Sawyer, T. K., Staples, D. J., deVaux, A. E., Dym, O., Castrucci, A. M. L., Hintz, M. F., Riehm, J. R., and Rao, R. (1987) Alpha-Melanotropin: The minimum active sequence in the frog skin bioassay. *J. Med. Chem.* 30, 2126–2130.
- (24) Kaiser, E., Colescott, R. L., Bossinger, C. D., and Cook, P. I. (1970) Color test for detection of free terminal amino groups in the solid phase synthesis of peptides. *Anal. Biochem.* 34, 595–598.
- (25) Christensen, T. (1979) A chloranil color test for monitoring coupling completeness in solid phase peptide synthesis. In *Peptides, Structure and Biological Function* (E. Gross and J. Meienhofer, Eds.) pp 385–388, Pierce Chemical Co., Rockford, IL.
- (26) Haugland, R. P. (1991) Fluorescent labels. In *Biosensors with Fiber Optics* (D. L. Wise and L. B. Wingard, Eds.) pp 85–109, Humana Press.
- (27) Kitagawa, T., and Aikawa, T. (1976) Enzyme coupled immunoassay of insulin using a novel coupling reagent. *J. Biochem.* 79, 233–236.
- (28) Silverstein, R. M., Bassler, G. C., and Morrill, T. C. (1981) *Spectrometric Identification of Organic Compounds*, 4th ed., p 322, John Wiley and Sons, New York.
- (29) Carlsson, J., Drevin, H., and Axen, R. (1978) Protein thiolation and reversible protein–protein conjugation: N-succinimidyl 3-(2-pyridyldithio)propionate, a new heterobifunctional reagent. *Biochem. J.* 173, 723–737.
- (30) Stuchbury, T., Shipton, M., Norris, R., Malthouse, J. P. G., Brocklehurst, K., Herbert, J. A. L., and Suschitzky, H. (1975) A reporter group delivery system with absolute and selective specificity for thiol groups and an improved fluorescent probe containing the 7-nitrobenzo-2-oxa-1,3 diazole moiety. *Biochem. J.* 151, 417–432.
- (31) Schwyzer, R., and Kriwaczek, V. M. (1981) Tobacco mosaic virus as a carrier for small molecules: Artificial receptor antibodies and superhormones. *Biopolymers* 20, 2011–2020.
- (32) Wunderlin, R., Sharma, S. D., Minakakis, P., and Schwyzer, R. (1985) Melanotropin receptors II. Synthesis and biological activity of α-melanotropin/tobacco mosaic virus disulfide conjugates. *Helv. Chim. Acta* 68, 12–22.
- (33) Greenbury, C. L., Moore, D. H., and Nunn, L. A. C. (1965) The reaction with red cells of 7S rabbit antibody, its subunits and their recombinants. *Immunology* 8, 420–431.
- (34) Schwyzer, R., Kriwaczek, V. M., and Wunderlin, R. (1981) A method for mapping peptide receptors. *Naturwissenschaften* 68, 95–96.
- (35) White, J. G., and Escolar, G. (1990) Induction of receptor clustering, patching, and capping on surface-activated platelets. *Lab. Invest.* 63, 332–340.
- (36) Keller, G. A., Siegel, M. W., and Caras, I. W. (1992) Endocytosis of glycopospholipid-anchored and transmem-

- brane forms of CD4 by different endocytic pathways. *EMBO J.* 11, 863–874.
- (37) Weintraub, W. H., Negulescu, P. A., and Machen, T. E. (1992) Calcium signaling in endothelia: Cellular heterogeneity and receptor internalization. *Am. J. Physiol.* 263C, 1029–1039.
- (38) Jarrett, L., and Smith, R. M. (1974) Electron microscopic demonstration of insulin receptors on adipocyte plasma membranes utilizing a ferritin–insulin conjugate. *J. Biol. Chem.* 249, 7024–7031.
- (39) dePriester, W., Bakker, A., and Lamers, G. (1990) Capping of Con A receptors and actin distribution are influenced by disruption of microtubules in *Dictyostelium discoideum*. *Eur. J. Cell Biol.* 51, 23–32.
- (40) Orci, L., Rufener, C., Malaisse-Lagae, F., Blondel, B., Amherdt, M., Bataille, D., Freylet, P., and Perrelet, A. (1975) A morphological approach to surface receptors in islet and liver cells. *Isr. J. Med. Sci.* 11, 639–655.
- (41) Varga, J. B., Dipasquale, A., Pawelek, J., McGuire, J. S., and Lerner, A. B. (1974) Regulation of melanocyte stimulating hormone action at the receptor level: Discontinuous binding of hormone to synchronized mouse melanoma cell cycle. *Proc. Natl. Acad. Sci. U.S.A.* 71, 1590–1593.
- (42) Lerner, A. B., Moellmann, G., Varga, J. M., Halaban, R., and Pawelek, J. (1979) Action of melanocyte-stimulating hormone on pigment cells. In *Cold Spring Harbor Conference on Cell Proliferation* (G. H. Soto, A. B. Pardee, and D. A. Sirbascu, Eds.) Vol. 6, pp 187–197, Cold Spring Harbor Laboratory, Cold Spring Harbor, NY.
- (43) Orlow, S. J., Hotchkiss, S., and Pawelek, J. M. (1990) Internal binding sites for MSH: analyses in wild-type and variant Cloudman melanoma cells. *J. Cell. Physiol.* 142, 129–136.
- (44) McLane, J. A., and Pawelek, J. M. (1988) Receptors for  $\beta$ -melanocyte-stimulating hormone exhibit positive cooperativity in synchronized melanoma cells. *Biochem.* 27, 3743–3747.
- (45) Fuller, B. B., and Brooks, B. A. (1980) Application of percent labeled mitoses (PLM) analysis to the investigation of melanoma cell responsiveness to MSH stimulation throughout the cell cycle. *Exp. Cell Res.* 126, 183–190.
- (46) Shimizu, N., Shimizu, Y., and Fuller, B. B. (1981) Cell-cycle analysis of insulin binding and internalization on mouse melanoma cells. *J. Cell Biol.* 88, 241–244.
- (47) Wong, G., Pawelek, J., Sansone, M., and Morowitz, J. (1974) Response of mouse melanoma cells to melanocyte stimulating hormone. *Nature* 248, 351–354.
- (48) Pawelek, J. (1976) Factors regulating growth and pigmentation of melanoma cells. *J. Invest. Dermatol.* 66, 201–209.
- (49) Bard, D. R., Knight, C. G., and Page-Thomas, D. P. (1990) Targeting of a chelating derivative of a short-chain analog of  $\alpha$ -melanocyte stimulating hormone to Cloudman S91 melanomas. *Biochem. Soc. Trans.* 18, 882–883.



# Synthesis and Characterization of Carbohydrate-Linked Murine Monoclonal Antibody K20–Human Serum Albumin Conjugates

L. H. Kondejewski, J. A. Kralovec, A. H. Blair, and T. Ghose\*

Departments of Biochemistry and Pathology, Dalhousie University, Halifax, Nova Scotia, Canada B3H 4H7.  
Received April 22, 1994\*

Efficacy of antibody mediated targeting depends on retention of immunoreactivity in conjugates. Retention can be improved by site-specific linkage of drugs or drug-loaded carriers to residues that are located well away from the antigen-binding sites. In this study we describe the site-specific linkage of a potential drug carrier, human serum albumin (HSA), to the carbohydrate residues in Dal K20, a murine IgG<sub>1</sub> monoclonal antibody (mAb) against human renal cell carcinoma, using disulfide exchange between 3-(2-pyridyldithio)propionic acid succinimidyl ester (SPDP)-derivatized HSA and 11-[[3-(2-pyridyldithio)propionyl]amino]undecanoic acid hydrazide (AUPDP)-derivatized mAb Dal K 20. AUPDP gave a higher yield of the conjugate than a functionally analogous 3-(2-pyridyldithio)propionic acid hydrazide (HPDP), suggesting that the extra length of the former facilitated the linkage. The conjugates were found to be unstable without reduction of the hydrazone linkage using sodium cyanoborohydride. Stabilized 1:1 HSA:K20 carbohydrate-linked conjugates were isolated and compared with non-site-specific 1:1 conjugates in which HSA was conjugated to amino groups in mAb Dal K20. The yield and stability of the two conjugates were comparable, but the site-specific conjugate was found to retain three times more antibody activity than the non-site-specific conjugate.

## INTRODUCTION

Cancer chemotherapeutic agents have been conjugated to antibodies in an effort to make these agents more specific for cancer cells and to reduce their systemic toxicity (1–3). Both high drug loadings as well as the retention of immunoreactivity are important for the synthesis of potent and tumor-specific conjugates. A number of anticancer drugs have been conjugated directly to amino groups of immunoglobulins, but the general finding has been that in these conjugates immunoreactivity of the antibody is reduced, probably due to the direct modification of residues in the antigen binding site and/or changes in tertiary structure following derivatization of the antibody (3). In order to achieve higher drug loadings while retaining immunoreactivity, carriers have been loaded with drug molecules and then linked to antibodies (4–7). The linkage of drug-loaded carriers to a single or a very small number of sites in an antibody molecule may allow higher molar incorporation of the drug (e.g., >10) with retention of antibody activity, but linkage to residues such as amino groups that are present throughout the antibody molecule, including the antigen binding sites, has the inherent risk of interference with antibody activity. In recent years, the carbohydrate

residues of IgG<sup>1</sup> antibodies have become the preferred site for IgG modification because the majority of the carbohydrate residues in IgG are located in the hinge region of the molecule, well away from the antigen-binding site. Indeed, antibodies have been modified at their carbohydrate residues with low molecular weight drugs (2, 8–10), liposomes (11), toxin molecules (12), and radionuclides (13) with full retention of antibody activity in many cases. The specific modification of carbohydrate residues involves the oxidation of immunoglobulin carbohydrates with sodium periodate to generate aldehyde groups, followed by reaction with suitable hydrazides, resulting in the formation of a hydrazone bond.

We have used HSA as a model carrier protein and conjugated it to the carbohydrate moiety of a murine monoclonal antibody against a human renal cell carcinoma antigen, i.e., mAb Dal K20, using two different cross-linkers. HSA was selected primarily because of its well elucidated structure and anticipated lack of significant immunogenicity in patients. We also investigated the stability of the hydrazone bonds in these conjugates. In this study we report on the synthesis, stability, and immunoreactivity of carbohydrate-linked HSA–Dal K20 conjugates and compare them to a non-site-specific conjugate in which HSA was linked to amino groups in mAb Dal K20.

## MATERIALS AND METHODS

The antibody used in these studies was mAb Dal K20, a murine IgG<sub>1</sub> monoclonal antibody directed against a human renal cell carcinoma associated cell surface antigen (14). mAb Dal K20 was produced by standard hybridoma methods and purified from mouse ascites by protein A chromatography (Bio-Rad, Richmond, CA) following the instructions of the manufacturer. NRG was used to standardize some conjugation procedures and was isolated from rabbit serum using caprylic acid (15). HSA, 2,2'-dipyridyl disulfide, 3-mercaptopropionic acid, 5,5'-dithiobis(2-nitrobenzoic acid), Extravidin-peroxidase, biotin hydrazide, dicyclohexylcarbodiimide, and hydrazine were from Sigma (St. Louis, MO). 11-Aminoundecanoic

\* Abstract published in *Advance ACS Abstracts*, September 1, 1994.

<sup>1</sup> Abbreviations: AUPDP, 11-[[3-(2-pyridyldithio)propionyl]amino]undecanoic acid hydrazide; DMF, dimethylformamide; DNP-AU-hydrazide, 11-[(2,4-dinitrophenyl)amino]undecanoic acid hydrazide; DNP-AU-OMe, 11-[(2,4-dinitrophenyl)amino]undecanoic acid methyl ester; DNP-IgG, 11-[(2,4-dinitrophenyl)amino]undecanoic acid hydrazide-modified IgG; DTT, dithiothreitol; GMBS,  $\gamma$ -maleimidobutyric acid *N*-hydroxysuccinimide ester; HPDP, 3-(2-pyridyldithio)propionic acid hydrazide; HSA, human serum albumin; HSA–K20, conjugate consisting of HSA coupled to mAb Dal K20; IgG, immunoglobulin G; mAb, monoclonal antibody; MTX, methotrexate; NRG, normal rabbit globulin; PAGE, polyacrylamide gel electrophoresis; PBS, phosphate buffered saline (0.01 M phosphate in 0.15 M sodium chloride, pH 7.2); SPDP, 3-(2-pyridyldithio)propionic acid succinimidyl ester; SDS, sodium dodecyl sulfate.

acid and *N*-hydroxysuccinimide were from Aldrich Chemical Co. (Milwaukee, WI). PDG desalting columns, Bio-Gel P10, Bio-Gel P300, and goat anti-mouse IgG-peroxidase were from Bio-Rad (Richmond, CA). Sulfo-succinimidyl 6-(biotinamido)hexanoate was from Pierce (Rockford, IL).

Thin layer chromatography was performed on silica gel 60 F 254 plates (Merck, Darmstadt, FRG) using 9:1 chloroform/methanol (system A) or 19:1 chloroform/methanol (system B).  $^1\text{H}$  NMR spectra were recorded in  $\text{CDCl}_3$  on a Nicolet NT360NB spectrometer with shifts reported relative to tetramethylsilane. Melting points were determined with an Electrothermal 9100 melting point apparatus.

Buffer A, 0.1 M sodium acetate, pH 4.0; buffer B, 0.1 M sodium phosphate, pH 7.2, containing 1 mM ethylenediaminetetraacetic acid.

**3-(2-Pyridyldithio)propionic Acid Succinimidyl Ester (1a).** SPDP was synthesized by the method of Carlsson (16): yield 1.5 g, 56%;  $R_f$  0.84 (A);  $^1\text{H}$  NMR  $\delta$  2.83 (s, 4H), 3.13 (m, 4H), 7.13 (m, 1H), 7.69 (m, 2H), 8.50 (m, 1H).

**3-(2-Pyridyldithio)propionic Acid Hydrazide (1b).** To SPDP (1.0 g, 3.2 mmol) dissolved in 20 mL of methanol was added hydrazine (160  $\mu\text{L}$ , 4.8 mmol) in 5 mL of methanol. The solution was stirred at room temperature for 15 min, methanol removed under reduced pressure, the oil taken up in methylene chloride, washed with saturated sodium bicarbonate and then water, and dried with sodium sulfate, and the methylene chloride evaporated. The product was crystallized from diethyl ether to give a fine white powder: yield 0.63 g, 85%;  $R_f$  0.41 (A); mp 91.5–92.5  $^\circ\text{C}$ ;  $^1\text{H}$  NMR ( $\text{CDCl}_3$ )  $\delta$  2.62 (t, 2H), 3.10 (t, 2H), 3.98 (s, 2H), 7.14 (m, 1H), 7.62 (m, 2H), 8.24 (s, 1H), 8.52 (m, 1H).

**11-[[3-(2-Pyridyldithio)propionyl]amino]undecanoic Acid (2a).** To 11-aminoundecanoic acid (129 mg, 0.64 mmol) and sodium bicarbonate (108 mg, 1.28 mmol) dissolved in 2 mL of a water–ethanol mixture (2:1) was added SPDP (200 mg, 0.64 mmol) dissolved in 4 mL of ethanol. The solution was stirred at room temperature for 1 h, adjusted to pH 7.0 with 1.0 M HCl, and the solvent removed under reduced pressure. The residue was distributed between water and chloroform, extracted with water, and dried over sodium sulfate. Chloroform was evaporated to give a white powder: yield 232 mg, 91%;  $R_f$  0.46 (A).

**11-[[3-(2-Pyridyldithio)propionyl]amino]undecanoic Acid Hydrazide (2c).** To compound 2a (232 mg, 0.58 mmol) dissolved in 5 mL of methylene chloride was added *N*-hydroxysuccinimide (73 mg, 0.64 mmol) and dicyclohexylcarbodiimide (131 mg, 0.64 mmol). The mixture was stirred for 2 h at room temperature and cooled to  $-20\text{ }^\circ\text{C}$ , the dicyclohexylurea removed by filtration, and methylene chloride evaporated. The obtained 11-[[3-(2-pyridyldithio)propionyl]amino]undecanoic acid succinimidyl ester (2b),  $R_f$  0.64 (A) (284 mg, 0.58 mmol), was dissolved in 5 mL of methanol and treated with hydrazine (37  $\mu\text{L}$ , 1.16 mmol) dissolved in a small amount of methanol for 1 h at room temperature. Methanol was removed by evaporation, the residue taken up in methylene chloride, washed with saturated sodium bicarbonate and with saturated NaCl, dried over sodium sulfate, and evaporated, and the solid washed with ether to give a white powder: yield 160 mg, 61%; mp 105  $^\circ\text{C}$ ;  $R_f$  0.32 (A);  $^1\text{H}$  NMR  $\delta$  1.22 (s, 12H), 1.51 (p, 2H), 1.62 (p, 2H), 2.50 (t, 2H), 2.60 (t, 2H), 3.08 (t, 2H), 3.26 (q, 2H), 3.96 (bs, 2H), 6.50 (s, 1H), 7.13 (q, 1H), 7.20 (s, 1H), 7.66 (m, 2H), 8.45 (m, 1H).

**11-[(2,4-Dinitrophenyl)amino]undecanoic Acid**

**Methyl Ester (3a).** To 4 mL of methanol at  $-10\text{ }^\circ\text{C}$  was added thionyl chloride (1040  $\mu\text{L}$ , 14 mmol) followed by the slow addition of 11-aminoundecanoic acid (800 mg, 4 mmol) while stirring. The mixture was stirred at room temperature for 1 h, and then two volumes of diethyl ether were added and the precipitated 11-aminoundecanoic acid methyl ester hydrochloride was washed with ether and collected by filtration. To 11-aminoundecanoic acid methyl ester hydrochloride (150 mg, 600  $\mu\text{mol}$ ) and triethylamine (167  $\mu\text{L}$ , 1.2 mmol) in 10 mL of DMF was added 1-fluoro-2,4-dinitrobenzene (68  $\mu\text{L}$ , 540  $\mu\text{mol}$ ) and the solution stirred at room temperature for 1 h. DMF was removed by evaporation, the residue taken up in chloroform, extracted with 0.1 M HCl, washed with saturated NaCl, and dried with sodium sulfate, and the solvent evaporated. The product was azeotroped with ether to give a yellow powder: yield 155 mg, 75%;  $R_f$  0.96 (B);  $^1\text{H}$  NMR  $\delta$  1.29 (s, 12H), 1.46 (m, 2H), 1.78 (p, 2H), 2.33 (t, 2H), 3.44 (q, 1H), 3.68 (s, 3H), 6.94 (d, 1H), 8.28 (d, 1H), 8.58 (bs, 1H), 9.15 (t, 1H).

**11-[(2,4-Dinitrophenyl)amino]undecanoic Acid Hydrazide (3b).** To compound 3a (130 mg, 341  $\mu\text{mol}$ ) in 50 mL of methanol was added hydrazine (5.2 mL, 166 mmol) and the reaction mixture stirred for 16 h at room temperature. Methanol was removed by evaporation and the residue taken up in chloroform, extracted with saturated sodium bicarbonate, dried with sodium sulfate, and evaporated to give a yellow powder: yield 117 mg, 90%;  $R_f$  0.17 (B); mp 119–121  $^\circ\text{C}$ ;  $\nu_{\text{max}}$  = 360  $\text{cm}^{-1}$ ,  $\epsilon$  = 17 000  $\text{M}^{-1}\text{cm}^{-1}$ ;  $^1\text{H}$  NMR  $\delta$  1.29 (s, 10H), 1.46 (m, 2H), 1.60 (m, 2H), 1.78 (p, 2H), 2.33 (t, 2H), 3.44 (q, 2H), 3.68 (s, 3H), 6.94 (d, 1H), 8.28 (d, 1H), 8.58 (bs, 1H), 9.15 (t, 1H).

**Oxidation of IgG and Reaction with HPDP or AUPDP.** To mAb Dal K20 (10 mg/mL, 1.0 mL) in 0.1 M acetate buffer, pH 5.5, containing 0.15 M NaCl at 0  $^\circ\text{C}$  was added sodium periodate (23.4 mg in 0.1 mL) dropwise while stirring to give a final periodate concentration of 100 mM. After 20 min at 0  $^\circ\text{C}$  in the dark, the solution was desalted into 0.1 M sodium acetate, pH 4.0 (buffer A) and DMF added slowly while stirring to a concentration of 15% (v/v). HPDP or AUPDP dissolved in DMF was added to give a 100-fold molar excess of hydrazide spacer over mAb K20 and a final DMF concentration of 25% (v/v). After 2 h at room temperature the solutions were desalted into 0.1 M sodium phosphate, 1 mM EDTA, pH 7.2 (buffer B). The number of pyridyldithio groups incorporated into mAb Dal K20 was determined in the presence of 0.1 M DTT, using  $\epsilon$  = 8080  $\text{M}^{-1}\text{cm}^{-1}$  at 343 nm for released pyridine-2-thione (16). Protein concentration was determined by absorbance at 280 nm (1.0 mg/mL = 1.4) with correction for pyridyldithio contribution using the formula  $A_{280\text{ due to IgG}} = A_{280\text{ measured}} - (5100 [\text{PDT}])$ , where [PDT] is the molar concentration of pyridine-2-thione.

**Pilot Studies with NRG To Determine Conditions for Spacer Incorporation and Hydrazone Bond Stabilization.** (i) **Oxidation Conditions.** To NRG (8.7 mg/mL, 0.45 mL) in 0.1 M acetate buffer, pH 5.5, containing 0.15 M NaCl at 0  $^\circ\text{C}$  was added a 0.1%–1.0% aqueous solution of sodium periodate (0.55 mL) dropwise while stirring to give periodate concentrations in the range of 0.26–260 mM. After 20 min, reaction mixtures were desalted into buffer A and reacted with AUPDP, and the number of pyridyldithio groups incorporated was determined as described above. (ii) **Incorporation of DNP-AU-hydrazide.** To NRG (25 mg, 1.47 mL) at 0  $^\circ\text{C}$  in 0.1 M sodium acetate buffer, pH 5.5, containing 0.15 M NaCl, was added sodium periodate (100 mg in 0.8 mL  $\text{dH}_2\text{O}$ ) with stirring. After 20 min in the dark at

0 °C the solution was desalted into 3.2 mL of buffer A and 0.56 mL of DMF added followed by DNP-AU-hydrazide (6.4 mg in 0.63 mL of DMF). After 16 h at room temperature the solution was desalted into buffer A. The number of DNP-AU-hydrazide groups incorporated into the protein was determined using  $\epsilon = 17\,000\text{ M}^{-1}\text{ cm}^{-1}$  at 360 nm (18) and protein concentration was measured by the Lowry assay using NRG as the standard. Control reactions were carried out in which (i) a 100-fold molar excess of DNP-AU-OME was added to oxidized NRG in buffer A, and (ii) a 100-fold molar excess of DNP-AU-hydrazide was added to nonoxidized NRG in Buffer A. After 4 h at room temperature the mixtures were desalted into buffer A and the incorporation of DNP groups/NRG determined. (iii) **Stabilization of Hydrazone Bonds between IgG and DNP-AU-hydrazide with Sodium Cyanoborohydride.** NRG derivatized with DNP-AU-hydrazide in buffer A prepared as described above, at a concentration of 1.2 mg/mL, was incubated in the presence of 15 mM sodium cyanoborohydride or 15 mM sodium borohydride. After 48 h, the solutions were desalted into buffer A. A third sample was treated in the same way but received no reducing agent. After desalting, aliquots of cyanoborohydride-treated, borohydride-treated, and untreated protein were dialyzed against buffer A at 37 °C for 11 days. Periodic samples were taken, and the number of DNP groups per NRG was determined. A second group of aliquots of DNP-AU-hydrazide-derivatized NRG in buffer A were incubated with a 10 000-fold molar excess of propanal (80 mM), and after 48 h, the solutions were desalted into buffer A and the incorporation of DNP-AU-hydrazide in NRG was determined. To determine the effect of cyanoborohydride treatment prior to reaction with DNP-AU-hydrazide, oxidized NRG at a concentration of 4.1 mg/mL in buffer A was incubated with a molar excess of sodium cyanoborohydride ranging from 0 to 4000 (0–110 mM). The reaction mixtures were left at room temperature for 45 h after which time they were desalted into buffer A and reacted with DNP-AU-hydrazide, and the incorporation of DNP-AU-hydrazide into NRG was determined as described above.

**Coupling of SPDP and GMBS to IgG.** mAb Dal K20 was derivatized with SPDP or GMBS by reaction of mAb K20 at 10 mg/mL in PBS with a 5-fold molar excess of either SPDP or GMBS dissolved in a small volume of DMF for 30 min. The solutions were then desalted into buffer B. Incorporation of pyridyldithio groups was determined as described above, and incorporation of maleimide groups was determined using *N*-(2,4-dinitrophenyl)-L-cysteine (17). The latter compound was prepared from *N,N*-bis(2,4-dinitrophenyl)-L-cysteine by reduction with an excess of  $\beta$ -mercaptoethanol.

**Labeling of mAb Dal K20 with Biotin Hydrazide or Biotin Succinimidyl Ester.** mAb Dal K20 was labeled with either sulfosuccinimidyl 6-(biotinamido)hexanoate or biotin hydrazide. Non-site-specific mAb Dal K20–biotin was prepared by treating mAb Dal K20 (2.4 mg, 0.6 mL) in PBS with a 10-fold molar excess of sulfosuccinimidyl 6-(biotinamido)hexanoate (90  $\mu\text{g}$  in 25  $\mu\text{L}$  of DMF) and desalting the solution into PBS after 1 h. For the preparation of site-specifically modified mAb Dal K20–biotin, oxidized mAb K20 in buffer A was reacted with a 100-fold molar excess of biotin hydrazide dissolved in a small amount of DMF. The solution was left for 4 h at room temperature and then sodium cyanoborohydride added to a concentration of 13 mM and the solution desalted into PBS after 1 h.

**Digestion of Biotin-Labeled mAb Dal K20 with Pepsin.** To mAb K20 (10  $\mu\text{L}$ , 25  $\mu\text{g}$ ) in PBS modified

either site-specifically with biotin hydrazide or non-site-specifically with sulfosuccinimidyl 6-(biotinamido)hexanoate was added 30  $\mu\text{L}$  of 0.1 M sodium citrate buffer, pH 3.5, and 5  $\mu\text{L}$  of pepsin (0.25  $\mu\text{g}$ , 10  $\mu\text{g}/\text{mg}$  IgG) in citrate buffer. The digestion mixture was incubated at 37 °C for 30 min, at which time 4  $\mu\text{L}$  of 2.0 M Tris/HCl, pH 9.0, was added, and aliquots mixed with equal volumes of SDS–PAGE sample buffer and samples were analyzed by SDS–PAGE.

**Localization of Sites of Biotin Reactivity by Western Blotting.** Site-specific Dal K20–biotin, non-site-specific Dal K20–biotin, and their pepsin digests prepared as above were separated on SDS–PAGE in duplicate. Gels were transferred to nitrocellulose and either stained for total protein using India ink or probed for biotin using Extravidin-peroxidase. The composition of the transfer buffer was 50 mM Tris, 380 mM glycine, 0.1% SDS, and 20% methanol, and the transfer conditions were 85 V (constant) for 1.5 h at 4 °C. For total protein staining, blots were washed in PBS containing 0.4% Tween 20 (PBS/Tween) with two changes of 5 min each, stained with 0.1% (v/v) India ink in PBS/Tween for 30 min, and destained in PBS. For biotin-specific staining, blots were rinsed with PBS, blocked with 2% BSA in PBS (PBS/BSA) for 1 h, and incubated with Extravidin-peroxidase diluted to 1  $\mu\text{g}/\text{mL}$  in PBS/BSA for 1 h. Blots were washed with PBS/BSA and peroxidase detected with substrate solution consisting of 7 mg/mL of 4-chloro-1-naphthol in PBS containing 20% methanol and 0.03% (v/v)  $\text{H}_2\text{O}_2$ .

**Activation of HSA for Reaction with mAb Dal K20–Spacer.** 1. **HSA-SPDP-SH.** To HSA at 10 mg/mL in PBS was added a 5-fold molar excess of SPDP with stirring at room temperature. The SPDP had been dissolved in an amount of DMF that did not exceed 20% of the volume of the HSA solution. After 30 min, the solution was desalted into 0.1 M acetate buffer, pH 4.5, containing 0.1 M NaCl, and DTT added to give a concentration of 10 mM. After 20 min at room temperature, the DTT-treated mixture was desalted into buffer B. The number of pyridyldithio groups incorporated into HSA was determined as described for IgG above with the exception that protein was measured by the Lowry assay. 2. **HSA-SH.** HSA in PBS at a concentration of 10 mg/mL was reduced by the addition of a 20-fold molar excess of DTT (3 mM) for 20 min and desalted into buffer B. The number of thiol groups generated was determined with 5,5'-dithiobis(2-nitrobenzoic acid) (18).

**Conjugation of HSA to Spacer-Modified mAb Dal K20.** For the preparation of site-specific conjugates, mAb Dal K20 in buffer B (2.0 mg/mL, 1.0 mL) derivatized with HPDP (3.8 HPDP/mAb Dal K20) or AUPDP (4.6 AUPDP/mAb Dal K20) was mixed with HSA-SPDP-SH or HSA-SH in buffer B to give a 4:1 molar ratio of HSA over mAb Dal K20 in a final volume of 1.5 mL. For the preparation of non-site-specific conjugates, mAb Dal K20 (3.6 mg/mL, 3.0 mL) in buffer B derivatized with SPDP or GMBS (approximately 2.5 SPDP or GMBS/mAb Dal K20) was mixed with HSA-SPDP-SH in buffer B at a 4:1 molar ratio of HSA over mAb Dal K20 in a final volume of 6.2 mL. All reaction mixtures were stirred briefly and left at room temperature for 16 h at which time thiols were blocked by the addition of a 20-fold molar excess of *N*-ethylmaleimide over mAb Dal K20. Some site-specific conjugates were prepared on a 20 times larger scale, desalted into buffer A, and treated with 15 mM sodium cyanoborohydride for 90 min to reduce hydrazone bonds. The reactions were monitored by both SDS and native PAGE under nonreducing conditions (7% gels).

**Purification of Dal K20–HSA Conjugates.** Dal

K20–HSA conjugates were purified by gel filtration chromatography on Bio-Gel P 300 (2.5 cm × 90 cm) equilibrated with PBS using an upward flow system with a flow rate of 7.5 mL/h. Fractions containing purified 1:1 HSA–Dal K20 conjugates were pooled, concentrated by precipitation with ammonium sulfate (60% saturation), desalted into PBS, and stored at 4 °C.

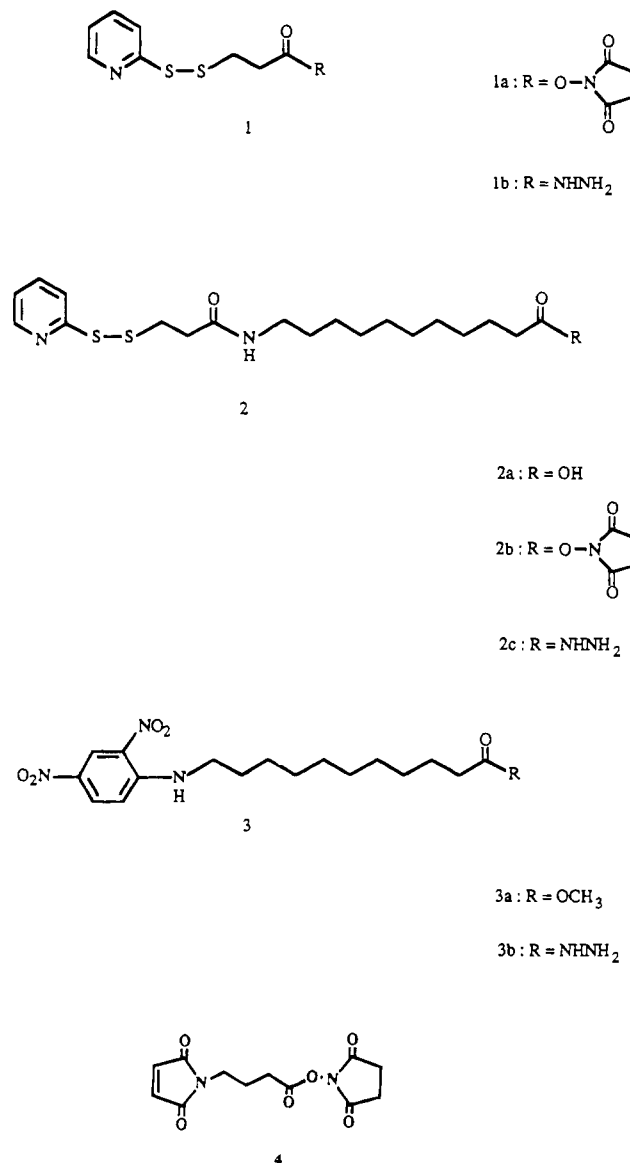
In certain experiments, Dal K20–HSA conjugates were isolated from native PAGE gels in which SDS was omitted. Conjugates were separated by native PAGE on 5% gels in a Bio Rad Mini-Protein II apparatus with gels of 0.75-mm thickness. Samples containing between 150 and 260 µg of mAb Dal K20 were mixed with an equal volume of sample buffer and loaded onto gels using a preparative comb. After electrophoresis, a narrow strip from the edge of the gel was cut out, stained, and used as a reference to cut out the remaining conjugate-containing band from the gel. The electroelution apparatus consisted of two reservoirs connected by dialysis bags in each reservoir and a bridge between the two bags. The reservoir, dialysis bags, and bridge were filled with 50 mM Tris/HCl, pH 8.6, with the gel-containing bag in the cathode compartment. Elution conditions were 100 V for 7 h, after which the collection bags were removed and eluted conjugates dialyzed against 50 mM NH<sub>4</sub>CO<sub>3</sub>, lyophilized, and analyzed by SDS–PAGE.

**Immunoreactivity of mAb Dal K20 and Its Conjugates.** <sup>125</sup>I-mAb K20 (3.38 µCi/µg, 0.52 µg) in PBS containing 0.1% (w/v) BSA (PBS/BSA) was mixed in duplicate with dilutions of either native mAb Dal K20 or conjugated mAb Dal K20 in a volume of 0.3 mL in PBS/BSA. Caki-1 cells (8) were removed from flasks by treatment with 0.02% (w/v) EDTA in Hank's buffered saline solution, washed with PBS, and resuspended in PBS/BSA and 5.0 × 10<sup>5</sup> cells in 0.1 mL added per tube. Cells were incubated at 4 °C with occasional shaking and after 2 h were washed three times with PBS/BSA and the tubes counted for radioactivity. The percent inhibition of <sup>125</sup>I-Dal K20 binding was determined using the formula [1 – (cpm bound in presence of noniodinated mAb Dal K20/cpm bound in absence of noniodinated mAb Dal K20)]100. Percent activity of mAb Dal K20 conjugates was determined using the formula (IC<sub>50</sub> native mAb Dal K20/IC<sub>50</sub> conjugated mAb Dal K20)100, where IC<sub>50</sub> is the concentration of noniodinated Dal K20 required to give 50% inhibition of iodinated Dal K20 binding.

**Other Methods.** Concentrations of unconjugated proteins were determined using the Lowry assay with HSA and NRG as protein standards (19) or by absorbance at 280 nm using A<sub>280</sub> = 1.4 for 1.0 mg/mL of IgG. For purified 1:1 HSA–Dal K20 conjugates, the protein concentration was determined by the Lowry assay using a 1:1 molar mixture of IgG and HSA as the standard. mAb Dal K20 was radiolabeled with <sup>125</sup>I using the chloramine-T method (20). SDS–PAGE was carried out according to the method of Laemmli (21). Samples were desalted using either disposable PDG columns or columns containing Bio-Gel P 10.

## RESULTS

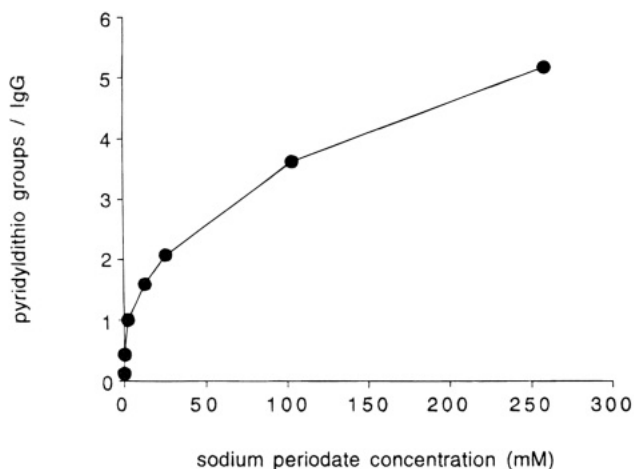
**Synthesis of HSA–Dal K20 Conjugates. Synthesis of Site-Specific Heterobifunctional Cross-Linkers.** The heterobifunctional spacer AUPDP was designed to contain an aldehyde-reactive hydrazide group and a thiol-reactive pyridyl disulfide group. In our first attempt to synthesize AUPDP **2c**, the methyl ester of 11-aminoundecanoic acid was reacted with SPDP **1a** (Figure 1). Treatment of the resulting methyl ester of **2a** with a 20-fold excess of hydrazine led to release of pyridine-2-thione. However, when SPDP was reacted with 11-



**Figure 1.** Structures of the cross-linkers 3-(2-pyridyldithio)propionic acid succinimidyl ester (SPDP, **1a**), 3-(2-pyridyldithio)propionic acid hydrazide (HPDP, **1b**), 11-[(3-(2-pyridyldithio)propionyl)amino]undecanoic acid hydrazide (AUPDP, **2c**), the hydrazone stability probe 11-[(2,4-dinitrophenyl)amino]undecanoic acid hydrazide (DNP-AU-hydrazide, **3b**), and  $\gamma$ -maleimido butyric acid succinimidyl ester (GMBS, **4**).

aminoundecanoic acid, the product **2a** was obtained which was then converted to the succinimidyl ester **2b**. Active ester **2b** was then treated with hydrazine to smoothly give the hydrazide derivative **2c**. A 1.5–2.0-fold excess of hydrazine over the succinimidyl ester was important in preventing the formation of side products. A similar sensitivity toward hydrazine was observed when defining optimal conditions for SPDP conversion to HPDP.

**Introduction of Pyridyldithio Spacers into mAb Dal K20.** mAb Dal K20 was oxidized with sodium periodate to render it reactive toward the hydrazide group of HPDP or AUPDP. IgG is typically oxidized with periodate using concentrations between 1 and 10 mM at pH 5.5 for 20 min at 0 °C for subsequent reaction with hydrazide-containing spacers (12, 22–24). However, we found that under these conditions few cross-linkers were incorporated into mAb Dal K20. We therefore investigated the effect of the NRG oxidation level on subsequent reactivity toward AUPDP. As shown in Figure 2, the use of 1 or

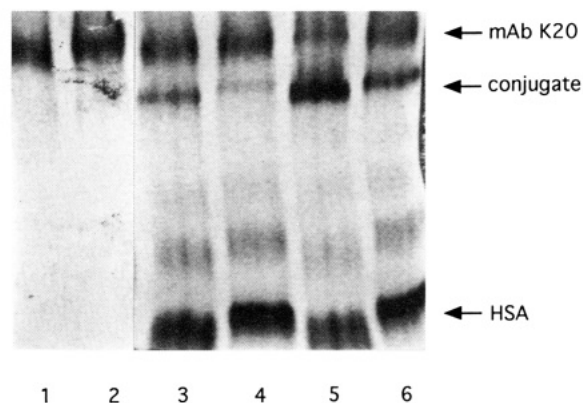


**Figure 2.** Effect of oxidation level on incorporation of AUPDP into NRG. NRG in 0.1 M sodium acetate, pH 5.5, 0.15 M NaCl, was oxidized with an excess of sodium periodate indicated. After 20 min at 0 °C, samples were desalted into 0.1 M sodium acetate, pH 4.0, DMF added to a concentration of 15%, and a 50-fold molar excess of AUPDP dissolved in DMF added to give a final DMF concentration of 25%. Samples were desalted into 0.1 M sodium acetate, pH 4.0, after 3 h and the incorporation of AUPDP into NRG determined as described in the Materials and Methods.

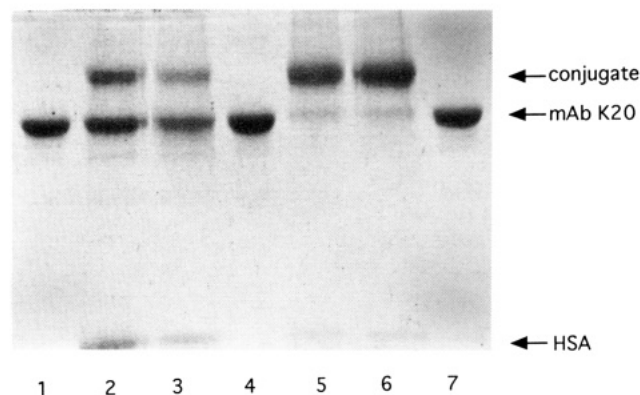
10 mM periodate resulted in the incorporation of 0.6 or 1.4 AUPDP/IgG, respectively. By increasing the excess of periodate over IgG, we were able to incorporate up to five spacers, i.e., when IgG was oxidized with 260 mM periodate. Approximately four pyridyldithio groups were routinely introduced into NRG or mAb Dal K20 using a periodate concentration of 100–150 mM. An average of three to four cross-linkers per IgG was found to be best for the subsequent reaction with thiol-containing HSA. It was also necessary to include DMF at a concentration of 25% during coupling to prevent cross-linker precipitation. Neither oxidation with periodate nor incubation in 25% DMF impaired antibody-binding activity. However, the incorporation of four AUPDP/mAb Dal K20 did result in a loss of 35% activity.

For the synthesis of non-site-specific conjugates, mAb Dal K20 was derivatized with the heterobifunctional cross-linkers SPDP (1a) or GMBS (4). Typically, a 5-fold molar excess of SPDP or GMBS over IgG resulted in the incorporation of 2.5 cross-linkers/IgG. mAb Dal K20 was found to be sensitive to amino group modification as the incorporation of 2.5 SPDP/mAb Dal K20 resulted in the loss of 60% binding activity. The incorporation of GMBS into DalK20 resulted in comparable loss of binding activity.

**Conjugation of HSA with mAb Dal K20.** In order to compare the two site-specific cross-linkers, we examined their ability to form conjugates between HSA and mAb Dal K20. mAb Dal K20 which had been derivatized with either HPDP (3.8 HPDP/Dal K20) or AUPDP (4.6 AUPDP/Dal K20) was reacted with either HSA-SH which was obtained by reduction of HSA directly with DTT (2 thiols/HSA) or with HSA-SPDP-SH, obtained from HSA which had been modified with SPDP and then reduced with DTT (2.5 thiols/HSA). The HSA-SPDP-SH gives an increase in the total spacer length between Dal K20 and HSA. Conjugate formation was monitored by native PAGE, and the yield of the conjugate with HSA-SH was found to be much greater with AUPDP-derivatized DalK20 than with HPDP-derivatized DalK20 (lanes 6 and 4, respectively, Figure 3). Irrespective of whether HSA-SPDP or DTT-reduced HSA was used for conjugation, Dal K20–AUPDP gave a higher yield of the conju-



**Figure 3.** Analysis of site-specific conjugation yields by native PAGE. HSA or SPDP-HSA were reduced with DTT and reacted with mAb K20 derivatized with AUPDP or HPDP as described in the text. Following conjugation, an aliquot of each reaction mixture was subjected to native PAGE; lane 1, HPDP–Dal K20; lane 2, AUPDP–Dal K20; lane 3, HPDP–Dal K20 + HSA-SPDP-SH; lane 4, HPDP–Dal K20 + HSA-SH; lane 5, AUPDP–Dal K20 + HSA-SPDP-SH; lane 6, AUPDP–Dal K20 + HSA-SH.



**Figure 4.** SDS-PAGE analysis of conjugates eluted from native PAGE gels. HSA–Dal K20 site-specific conjugates were prepared with either HPDP or AUPDP and non-site-specific conjugates with SPDP or GMBS as described in the Materials and Methods. Each conjugation mixture was subjected to preparative native PAGE, and conjugates were eluted from the gels and analyzed by SDS PAGE: lanes 1, 4, and 7, mAb Dal K20; lane 2, AUPDP conjugate; lane 3, HPDP conjugate; lane 5, SPDP conjugate; lane 6, GMBS conjugate.

gate than did Dal K20–HPDP (lanes 5 and 6 vs lanes 3 and 4). These results suggest that the ability to link HSA to the carbohydrate of mAb Dal K20 is dependent on the length of spacer or spacers between the two proteins (Figure 3).

Non-site-specific Dal K20–HSA conjugates synthesized using SPDP were isolated in pure form by gel filtration with no contamination by free HSA or mAb Dal K20. In contrast, gel filtration of site-specific conjugates synthesized using HPDP or AUPDP showed free HSA and mAb Dal K20 at the elution position for the conjugate, indicating partial breakdown of these conjugates. Figure 4 shows an experiment in which the site-specific conjugates were purified from reaction mixtures by native PAGE and bands corresponding to Dal K20–HSA conjugates eluted from the gels. When material from these bands was subjected to SDS–PAGE, there were substantial amounts of material that migrated to positions expected for free mAb Dal K20 and HSA (Figure 4, lanes 2 and 3), indicating instability of the hydrazone bond in the site-specific conjugate. In contrast, non-site-specific conjugates of HSA and Dal K20 prepared using SPDP or GMBS as the bifunctional linking reagent showed very little of the unbound components (lanes 5 and 6).



**Table 1. Reduction of IgG Aldehydes by Sodium Cyanoborohydride<sup>a</sup>**

molar excess of NaCNBH <sub>3</sub>	DNP groups (mol DNP/mol IgG)	molar excess of NaCNBH <sub>3</sub>	DNP groups (mol DNP/mol IgG)
0	6.2	2000	0.8
500	1.0	4000	1.2
1000	1.0		

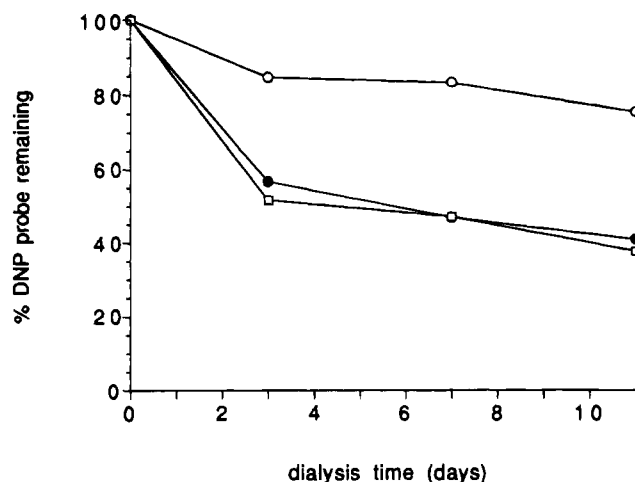
<sup>a</sup> NRG was oxidized with sodium periodate and treated with a molar excess of sodium cyanoborohydride (0–110 mM) for 48 h at pH 4.0. Samples were desalted into 0.1 M sodium acetate, pH 4.0, and reacted with a 100-fold molar excess of DNP-AU-hydrazide for 4 h. Unreacted DNP-AU-hydrazide was removed by gel filtration and the incorporation of DNP groups into IgG determined as described in the Materials and Methods.

**Stabilization and Isolation of Conjugates.** *Model Stabilization Studies with DNP-AU-hydrazide.* King et al. (25) demonstrated that hydrazone bonds in conjugates could be stabilized by cyanoborohydride reduction. To assist in defining conditions for stabilization, a chromophoric DNP-hydrazide was synthesized (**3b**, Figure 1). DNP-AU-hydrazide was expected to display similar reactivity toward oxidized IgG as AUPDP because both compounds possess an identical undecanoic acid hydrazide moiety. Retention of DNP groups in the protein was used to monitor stability of the hydrazone bonds instead of monitoring the pyridyldithio groups donated by AUPDP because the latter were susceptible to disulfide reduction by cyanoborohydride. DNP-AU-hydrazide was incorporated into NRG following the oxidation. Control reactions in which oxidized NRG was treated with DNP-AU-OME or where nonoxidized NRG was treated with DNP-AU-hydrazide showed no incorporation of DNP into NRG, indicating the specificity for reaction between oxidized NRG and hydrazide.

We first examined whether we could prevent incorporation of DNP-AU-hydrazide into oxidized IgG by reduction of IgG aldehydes with cyanoborohydride prior to reaction with the DNP-probe. Table 1 shows that IgG which had been oxidized and reacted with DNP-AU-hydrazide incorporated 6.2 DNP groups/IgG. IgG which was treated with an excess of cyanoborohydride prior to reaction with probe showed that approximately 1 DNP group/IgG was introduced, demonstrating that the majority of aldehydes generated by periodate oxidation of IgG carbohydrate were also sterically accessible to reduction by cyanoborohydride.

In order to evaluate the stability of the hydrazone bonds formed between IgG aldehydes and the hydrazide **3b**, DNP-IgG was dialyzed at 37 °C against 0.1 M acetate buffer, pH 4.0. Figure 5 shows that approximately 60% of probe in both untreated and borohydride-treated DNP-IgG was lost after 11 days. In contrast, DNP-IgG which had been treated with cyanoborohydride showed retention of 80% of the DNP moiety after the same period of time, indicating that a proportion of the hydrazone bonds had been stabilized by cyanoborohydride.

To further confirm the stabilization of hydrazone bonds by cyanoborohydride reduction, we treated DNP-IgG with an excess of propanal. As shown in Table 2, IgG which was initially derivatized with 7.9 DNP groups retained only 1.8 DNP/IgG after treatment with propanal for 48 h. DNP-IgG which had been treated with cyanoborohydride prior to aldehyde treatment retained substantially more DNP residues, i.e., 4.5 DNP/IgG. Data obtained from this competition system suggested that treatment of DNP-IgG with 15 mM cyanoborohydride at pH 4.0 for 1.5 h is sufficient to reduce the majority of hydrazone bonds.



**Figure 5.** Stabilization of hydrazone-linked DNP reporter groups by sodium cyanoborohydride. DNP–NRG was treated with 15 mM sodium cyanoborohydride (open circles), 15 mM sodium borohydride (open squares), or not treated (filled circles) as described in the Materials and Methods. Samples were dialyzed against 0.1 M sodium acetate, pH 4.0, at 37 °C, aliquots were taken at the times indicated, and the number of DNP groups bound to NRG was determined.

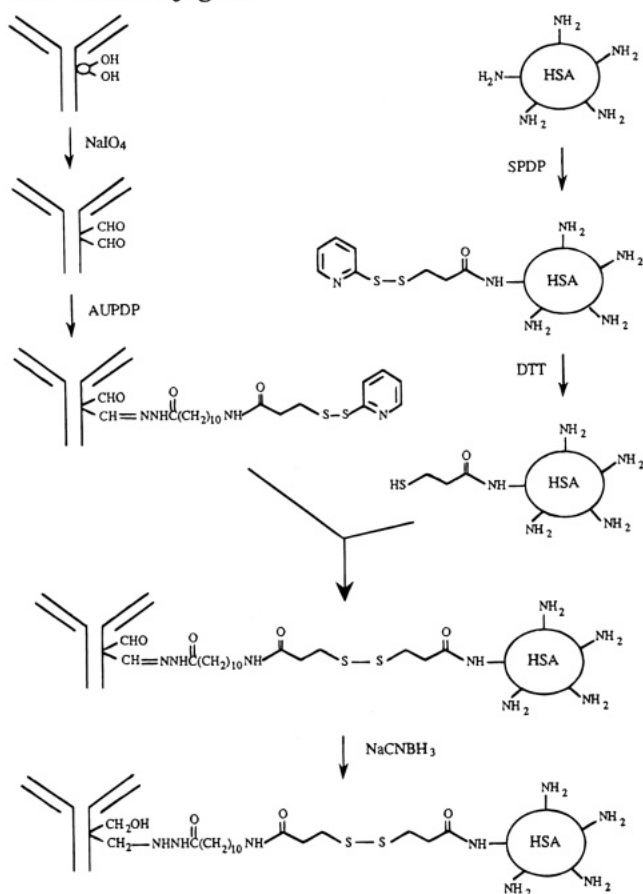
**Table 2. Competition of Hydrazone-Linked DNP Reporter Groups with an Excess of Propanal<sup>a</sup>**

treatment of DNP–IgG	DNP groups (mol DNP/mol IgG)	% DNP remaining
start	7.9	100
after NaCNBH <sub>3</sub>	5.1	65
control	7.0	89
NaCNBH <sub>3</sub> + aldehyde	4.5	57
control + aldehyde	1.8	23

<sup>a</sup> Periodate oxidized NRG in 0.1 M sodium acetate, pH 4.0, was reacted with a 100-fold molar excess of DNP-AU-hydrazide for 4 h and desalted into the same buffer. Samples were either treated with 15 mM sodium cyanoborohydride (NaCNBH<sub>3</sub>) or received no treatment (control). After 48 h, samples were desalted into 0.1 M sodium acetate, pH 4.0, and treated with a 10 000-fold molar excess of propanal (80 mM) for 48 h at room temperature, desalted, and the number of DNP reporter groups bound to NRG determined as described in the Materials and Methods.

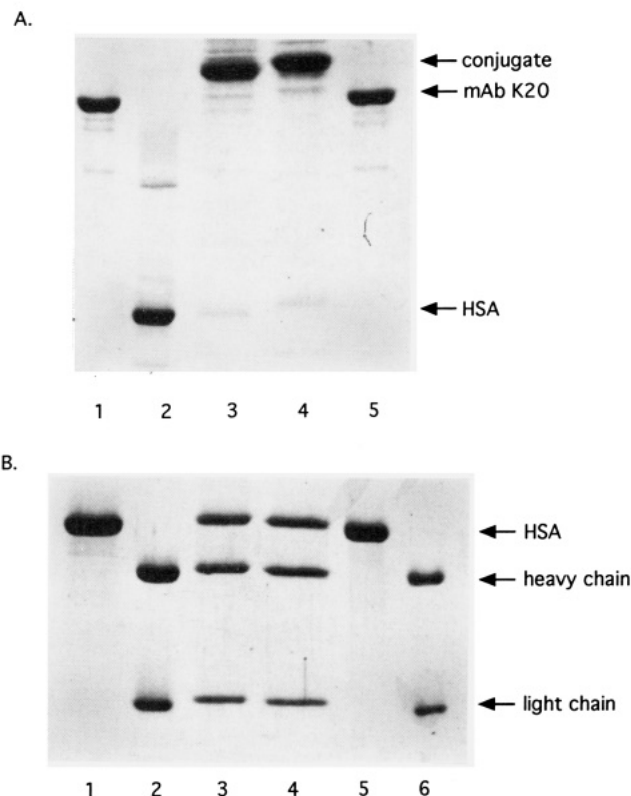
*Stabilization and Isolation of Carbohydrate-Linked HSA–Dal K20 Conjugates.* Conjugates between mAb Dal K20 and HSA were synthesized as shown in Scheme 1. AUPDP was incorporated into mAb Dal K20 by reaction with oxidized carbohydrate residues, and AUPDP-derivatized mAb K20 reacted with HSA-SPDP-SH. Following conjugation, reaction mixtures were treated with cyanoborohydride under the conditions determined with the DNP-probe in order to stabilize hydrazone bonds, and the conjugate was purified from the reaction mixture by gel filtration chromatography. As shown in Figure 6A (lane 4), the carbohydrate-linked conjugate could now be isolated without contamination by free HSA or mAb K20, indicating that the hydrazone bonds in the conjugate had also been reduced by cyanoborohydride. The yield of mAb K20 in conjugate form was on average 15%. A non-site-specific mAb K20–HSA conjugate prepared by reaction of SPDP-derivatized mAb K20 with HSA-SPDP-SH was also synthesized and purified for subsequent comparison with the site-specific conjugate (lane 3, Figure 6A). Recovery of mAb K20 in the non-site-specific conjugate was comparable to that of the site-specific conjugate, with 20% average recovery. These numbers represent yield of the two conjugates from the clean fractions only and do not include conjugates in unresolved fractions which were not rechromatographed. Rechromatography is likely to improve the yield.



**Scheme 1. Synthesis of Carbohydrate-Linked mAb K20-HSA Conjugates****Characterization of HSA-Dal K20 Conjugates.**

The conjugates shown in Figure 6A were analyzed by SDS-PAGE under reducing conditions. It can be seen that they were reduced to the components expected from disulfide-linked conjugates (Figure 6B, lanes 3 and 4), i.e., both contain IgG heavy and light chains as well as HSA. The migration position for 1:1 HSA-IgG conjugates was confirmed by a dual labeling experiment in which HSA was labeled with  $^{125}\text{I}$  and an NRG preparation with  $^{131}\text{I}$ . Conjugation was carried out by incorporating GMBS into the IgG followed by reaction with directly reduced HSA-MTX as described in the Materials and Methods. The conjugate preparation was subjected to SDS-PAGE and stained with Coomassie Blue. The band migrating directly above IgG itself contained  $^{125}\text{I}$  and  $^{131}\text{I}$  in a ratio of  $0.88 \pm 0.10$ .

To further investigate the site-specific nature of the linkage, we designed an experiment in which a low molecular weight probe, biotin hydrazide, was reacted with periodate-treated mAb Dal K20. We also reacted a sample of mAb Dal K20 non-site-specifically with a succinimidyl ester derivative of biotin, and each conjugate was digested with pepsin. Analysis under nonreducing conditions (Figure 7A) showed that the samples were completely digested and the labels were incorporated into both samples; however, only the non-site-specifically labeled mAb Dal K20 (lane 6) contained the biotin label in the  $\text{F}(\text{ab}')_2$  portion (lanes 5 and 6). The cleavage site for pepsin is below the interchain disulfide bonds joining the two heavy chains (26) and gives rise to  $\text{F}(\text{ab}')_2$  and a number of small fragments since the  $\text{Fc}$  portion is degraded by pepsin. The lack of staining of the site-specific  $\text{F}(\text{ab}')_2$  is consistent with labeling of the carbohydrate moiety, the location of which is known to be below the pepsin cleavage site (27). Analysis under



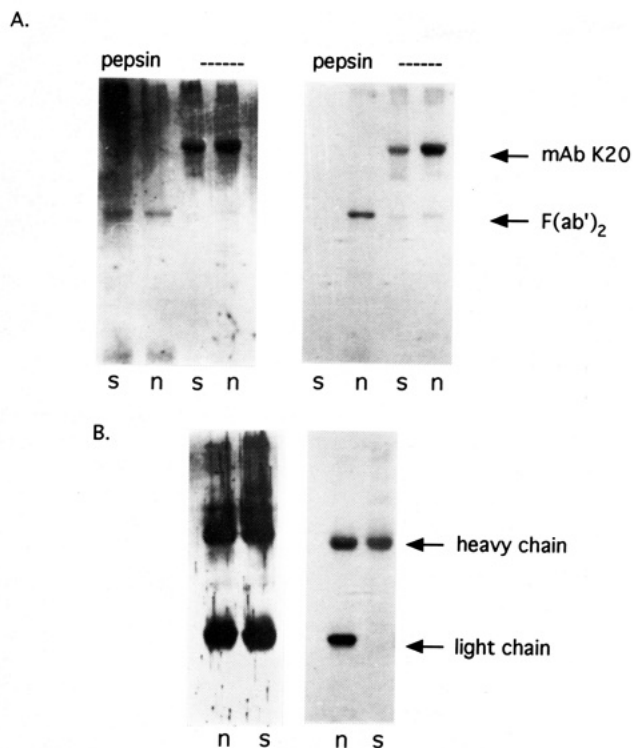
**Figure 6.** SDS-PAGE comparison of purified HSA-Dal K20 site-specific and non-site-specific conjugates. HSA-Dal K20 conjugates were synthesized using the non-site-specific cross-linker SPDP or with the site-specific cross-linker AUPDP as described in the Materials and Methods and the 1:1 HSA:mAb Dal K20 conjugates purified by gel filtration chromatography. Purified conjugates were analyzed by SDS-PAGE under non-reducing (A) or reducing (B) conditions. A: lanes 1 and 5, mAb Dal K20; lane 2, HSA; lane 3, purified non-site-specific HSA-Dal K20 conjugate; lane 4, purified site-specific HSA-Dal K20 conjugate. B: lanes 1 and 5, HSA; lanes 2 and 6, mAb Dal K20; lane 3, purified site-specific HSA-Dal K20 conjugate; lane 4, purified non-site-specific HSA-Dal K20 conjugate.

reducing conditions showed that the label was present on both heavy and light chains in the non-site-specifically modified sample, this being consistent with a random modification of amino groups by succinimidyl esters. Selective heavy chain reactivity was exhibited by biotin hydrazide, again indicating selective carbohydrate labeling by hydrazide compounds (Figure 7B).

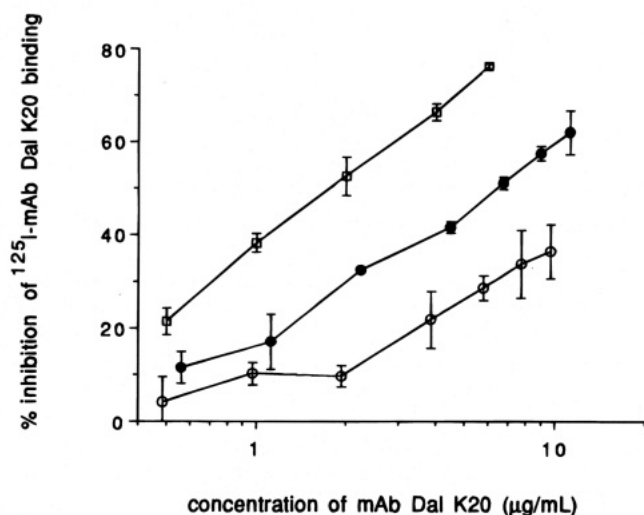
The retention of antigen-binding activity in the two types of HSA-Dal K20 conjugates was assayed as shown in Figure 8. The site-specific HSA-Dal K20 conjugate and the non-site-specific HSA-Dal K20 conjugate retained 30% and 10% activity, respectively, of the parent mAb.

**DISCUSSION**

Our results provide a method for the synthesis of structurally well-defined conjugates of antibodies with other macromolecules. We used HSA as a prototype multivalent carrier that may furnish the basis for production of active drug-HSA-mAb ternary conjugates. Although there are reports of site-specific conjugation of various unloaded (e.g., poly-g-glutamyl hydrazide (30)) or drug-loaded macromolecules (e.g., methotrexate-HSA (4), bleomycin-dextran (31), methotrexate-dextran (32)) to IgG, a successful site-specific linkage of HSA to IgG has not been reported. An advantage of HSA is that its discrete molecular weight helped significantly in the key purification step, i.e., fractionation of the reaction mix-



**Figure 7.** Localization of site-specific and non-site-specific biotin labels on mAb Dal K20. mAb Dal K20 was labeled site-specifically with biotin hydrazide (s) or non-site-specifically with sulfosuccinimidyl 6-(biotinamido)hexanoate (n), digested with pepsin, and separated by SDS PAGE under nonreducing (7% gels, A) or under reducing conditions (12% gels, B). Gels were run in duplicate, transferred to nitrocellulose, and either stained for total protein with India ink (left panels) or for biotin with Extravidin-peroxidase (right panels). For the lane number in the text the lanes are counted from left to right.



**Figure 8.** Retention of antigen binding activity in HSA–Dal K20 conjugates.  $^{125}\text{I}$ -mAb Dal K20 was mixed with native mAb Dal K20 (open squares), site-specific HSA–Dal K20 conjugate (filled circles), or non-site-specific HSA–Dal K20 conjugate (open circles) and the inhibition of  $^{125}\text{I}$ -mAb K20 binding to Caki-1 cells determined as described in the Materials and Methods. Each value is the mean and range from duplicate samples.

ture on Bio-Gel P-300, leading to the isolation of the 1:1 HSA–K20 conjugate.

Our method of conjugation is based on hydrazone bond formation between the oxidized carbohydrate moiety of IgG and HSA via a tandem of two heterobifunctional cross-linking spacers (AUPDP and SPDP). HPDP was selected originally as the site-specific linker bearing the hydrazide group, but the yield of conjugate was low. Our

perception was that insufficiency in the length of that spacer was responsible, and indeed, its replacement with AUPDP, carrying an extra 12 atoms of chain length, led to much better conversions. These findings can be attributed to steric restriction arising from the attachment of the carbohydrate at conserved Asn 297 residues of both heavy chains (28), lying between the two  $\text{C}_{\text{H}2}$  domains of IgG (33, 34). A similar dependence on chain length has been observed in conjugating toxins to IgM (12).

To prevent denaturation of IgG but at the same time promote the coupling reaction, it was important to restrict the incorporation ratio of AUPDP to a relatively narrow range, established in preliminary tests. Parallel considerations applied to introduction of the thiol into HSA. Defining these incorporation ratios served to favor the production of 1:1 conjugates over conjugates with multiple IgG or HSA units, thus making it possible to carry out purification by gel filtration.

Synthesizing 1:1 conjugates by these spacer-containing crosslinkers entailed limiting the number of hydrazone bonds between HSA and IgG. A potential consequence of this limitation is that the conjugate will be less stable than one linked by multiple hydrazones, and such instability was observed in our site-specific conjugates at the stage of hydrazone bond formation. However, cyanoborohydride reduction resulted in the stabilization of a significant proportion of hydrazone bonds, and this made it possible to isolate the conjugates. It is interesting that, in the stability evaluation experiment in which DNP-AU-hydrazide was used instead of AUPDP to act as a probe, we were unable to remove all DNP reporter groups either by dialysis or by competition with propanal. This indicates that a fraction of the hydrazone bonds formed between oxidized IgG and DNP-AU-hydrazide were stable without reduction. Formation of stable hydrazone bonds under comparable conditions has also been observed by others (2, 24) and could be attributed to the microenvironment of individual bonds.

The disulfide bond between HSA and mAb may not be adequately stable *in vivo* because disulfide bonds are subject to reduction by various serum and tissue components, e.g., glutathione. A thioether bond between HSA and mAb may be more appropriate for the construction of drug–HSA–mAb ternary conjugates. One of the ways to introduce a thioether linkage would be to replace SPDP, the agent modifying 11-aminoundecanoic acid, by a maleimido group-containing spacer, e.g., by succinimidyl  $\gamma$ -maleimidobutyrate. On the other hand a number of disulfide-linked immunotoxins have been found to be several times more potent than their thioether-linked counterparts (28) because dissociation of the toxin is essential for its translocation to intracytoplasmic target sites. If necessary, the disulfide bond in site-specific immunotoxins produced by our method can be rendered more stable by the introduction of “hindered disulfide bonds” using crosslinking agents such as 4-[(succinimidyl)oxy]carbonyl- $\alpha$ -methyl- $\alpha$ -(2-pyridyldithio)toluene (29) or derivatives of iminothiolane in which methyl groups are incorporated on the carbon atom adjacent to the disulfide bond (28).

The isolation of well-defined 1:1 HSA–K20 conjugates allowed comparison of the immunoreactivity of the site-specific and non-site-specific forms that were free of unreacted mAb and other high molecular weight conjugates. The site-specific HSA–K20 conjugate retained three times the antibody activity compared to corresponding non-site-specific conjugates, showing that the greater retention of activity was due to specific attachment of HSA to the carbohydrate of mAb K20. Non-site-

specific HSA-mAb conjugates obtained by others (4, 6) have been reported to retain 30% immunoreactivity but the preparations tested might have contained unreacted mAb which would be predicted to increase their apparent immunoreactivity.

In our study, site-specific derivatization of mAb Dal K20 with AUPDP led to 35% loss of its antibody activity. In synthesizing non-site-specific counterparts, incorporation of 2.5 thiol groups into mAb Dal K20 using SPDP led to 60% loss. The further losses in antibody activity in both the site-specific and non-site-specific forms were most likely due to steric factors imposed by the relatively large HSA molecule. The presence of HSA linked to the C<sub>H2</sub> domain of mAb K20 may sterically interfere with the flexibility of the antigen binding sites and antigen-binding capacity (35, 36).

Increasing the chain length in the linking spacer improved conjugation, but further studies will be required to define the optimal length. Also, other factors, e.g., lipophilicity, could have played a significant role, influencing steric orientation of the spacer and therefore its ability to react with thiols introduced into HSA with SPDP. A problem encountered with AUPDP was its limited solubility. This could have led to the tendency toward precipitation observed after the incorporation of AUPDP in IgG (Scheme 1) and therefore contribute to low yield of the conjugate. A more appropriate cross-linker of the required length may be one which is derived from an oligopeptide into which hydrophilic groups are introduced to confer increased solubility.

This study has shown that site-specific synthesis in conjugation with reductive stabilization can produce a stable, well-defined HSA-mAb conjugate with greater retention of antibody activity than that synthesized non-site-specifically. This site-specific approach utilizing carbohydrate residues in the immunoglobulin should be applicable to conjugation of other proteins including toxins and enzymes.

#### LITERATURE CITED

- (1) Kulkarni, P. N., Blair, A. H., and Ghose, T. (1981) Covalent binding of methotrexate to immunoglobulins and the effect of antibody-linked drug on tumor growth *in vivo*. *Cancer Res.* 41, 2700-2706.
- (2) Greenfield, R. S., Kaneko, T., Daues, A., Edson, M. A., Fitzgerald, D. A., Olech, L. J., Grattan, J. A., Spitalny, G. L., and Braslawsky, G. R. (1990) Evaluation *in vitro* of adriamycin immunoconjugates synthesized using an acid-sensitive hydrazone linker. *Cancer Res.* 50, 6600-6607.
- (3) Ghose, T., and Blair, A. H. (1987) The design of cytotoxic-agent-antibody conjugates. *CRC Crit. Rev. Ther. Drug Carrier Syst.* 3, 263-359.
- (4) Endo, N., Kato, Y., Takeda, Y., Saito, M., Umemoto, N., Kishida, K., and Hara, T. (1987) *In vitro* cytotoxicity of a human serum albumin-mediated conjugate of methotrexate with anti-MM46 monoclonal antibody. *Cancer Res.* 47, 1076-1080.
- (5) Garnett, M. C., Embleton, M. J., Jacobs, E., and Baldwin, R. W. (1983) Preparation and properties of a drug-carrier-antibody conjugate showing selective antibody-directed cytotoxicity *in vitro*. *Int. J. Cancer* 31, 661-670.
- (6) Garnett, M. C., and Baldwin, R. W. (1986) An improved synthesis of a methotrexate-albumin 79IT/36 monoclonal antibody conjugate cytotoxic to human osteogenic sarcoma cell lines. *Cancer Res.* 46, 2407-2421.
- (7) Arnon, R., and Sela, M. (1982) *In vitro* and *in vivo* efficacy of conjugates of daunomycin with anti-tumor antibodies. *Immunol. Rev.* 62, 5-27.
- (8) Kralovec, J., Singh, M., Mammen, M., Blair, A. H., and Ghose, T. (1989) Synthesis of site-specific methotrexate-IgG conjugates: comparison of stability and antitumor activity with active-ester based conjugates. *Cancer Immunol. Immunother.* 29, 293-302.
- (9) Starling, J. J., Maciak, R. S., Law, K. L., Hinson, A., Briggs, S. L., Laguzza, B. C., and Johnson, D. A. (1991) *In vitro* antitumor activity of a monoclonal antibody-vinca alkaloid immunoconjugate directed against a solid tumor membrane antigen characterized by heterogeneous expression and non-internalization of antibody-antigen complexes. (1991) *Cancer Res.* 51, 2965-2972.
- (10) Hinman, L. M., Hamann, P. R., Wallace, R., Menendez, A. T., Durr, F. E., and Upeslakis, J. (1993) Preparation and characterization of monoclonal antibody conjugates of the calicheamicins: a novel and potent family of antitumor antibiotics. *Cancer Res.* 53, 3336-3342.
- (11) Chau, W. M., Fan, S. T., and Karush, F. (1984) Attachment of immunoglobulin to liposomal membrane via protein carbohydrate. *Biochim. Biophys. Acta* 800, 291-300.
- (12) Zara, J. J., Wood, R. D., Boon, P., Kim, C. H., Pomato, N., Bredehorst, R., and Vogel, C.-W. (1991) A carbohydrate-directed heterobifunctional cross-linking reagent for the synthesis of immunoconjugates. *Anal. Biochem.* 194, 156-162.
- (13) Rodwell, J. D., Alvarez, V. L., Lee, C., Lopes, A. D., Goers, J. W. F., King, H. D., Powsner, H. J., and McKearn, T. J. (1986) Site-specific covalent modification of monoclonal antibodies: *in vitro* and *in vivo* evaluations. *Proc. Natl. Acad. Sci. U.S.A.* 83, 2632-2636.
- (14) Luner, S. J., Ghose, T., Chatterjee, S., Nolido-Cruz, H., and Belitsky, P. (1986) Monoclonal antibodies to kidney and tumor-associated surface antigens of human renal cell carcinoma. *Cancer Res.* 46, 5816-5820.
- (15) McKinney, M. M., and Parkinson, A. (1987) A simple, non-chromatographic procedure to purify immunoglobulins from serum and ascites fluid. *J. Immunol. Meth.* 96, 271-278.
- (16) Carlsson, J., Drevin, H., and Axen, R. (1978) Protein thiolation and reversible protein-protein conjugation: N-succinimidyl 3-(2-pyridyldithio)propionate, a new heterobifunctional reagent. *Biochem. J.* 173, 723-737.
- (17) Umemoto, N., Kato, Y., Takeda, Y., Saito, M., Hara, T., Seto, M., and Takahashi, T. (1984) Conjugates of mitomycin C with the immunoglobulin M monomer fragment of a monoclonal anti-MM46 immunoglobulin M antibody with or without serum albumin as intermediary. *J. Appl. Biochem.* 6, 297-307.
- (18) Ellman, G. L. (1959) Tissue sulfhydryl groups. *Arch. Biochem. Biophys.* 82, 70-77.
- (19) Lowry, O. H., Rosebrough, N. J., Farr, A. L., and Randall, R. J. (1951) Protein measurement with the Folin phenol reagent. *J. Biol. Chem.* 193, 265-275.
- (20) McConahey, P. J., and Dixon, F. J. (1980) Radioiodination of proteins by the use of the chloramine-T method. *Methods Enzymol.* 70, 210-247.
- (21) Laemmli, U. K. (1970) Cleavage of structural proteins during the assembly of the head of bacteriophage T4. *Nature* 227, 680-685.
- (22) Chamow, S. M., Kogan, T. P., Peers, D. H., Hastings, R. C., Byrn, R. A., and Ashkenazi, A. (1992) Conjugation of soluble CD4 without loss of biological activity via a novel carbohydrate-directed cross-linking reagent. *J. Biol. Chem.* 267, 15916-15922.
- (23) O'Shannessy, D. J., and Quarles, R. H. (1985) Specific conjugation reactions of the oligosaccharide moieties of immunoglobulins. *J. Appl. Biochem.* 7, 347-355.
- (24) O'Shannessy, D. J., and Quarles, R. H. (1987) Labeling of the oligosaccharide moieties of immunoglobulins. *J. Immunol. Meth.* 99, 153-161.
- (25) King, T. P., Zhao, S. W., and Lam, T. (1986) Preparation of protein conjugates via intermolecular hydrazone linkage. *Biochemistry* 25, 5774-5779.
- (26) Kabat, E. A., Wu, T. T., Perry, H. M., Gottesman, K. S.,

- and Foeller, C. (1991) *Sequences of proteins of immunological interest*, Public Health Services: Washington, D.C. NIH.
- (27) Parham, P. L. (1983) On the fragmentation of monoclonal IgG1, IgG2a, IgG2b from BALB/c mice. *J. Immunol.* **131**, 2895–2902.
- (28) Trown, P. W., Reardan, D. T., Carroll, S. F., Stoudemire, J. B., and Kawabata, R. T. (1991) Improved pharmacokinetics and tumor localization of immunotoxins constructed with the Mw 30,000 form of ricin A chain. *Cancer Res.* **51**, 4219–4225.
- (29) Thorpe, P. E., Wallace, P. M., Knowles, P. P., Relf, M. G., Brown, A. N. F., Watson, G. J., Blakey, D. C., and Newell, D. R. (1988) Improved antitumor effects of immunotoxins prepared with deglycosylated ricin A-chain and hindered disulfide linkages. *Cancer Res.* **48**, 6396–6403.
- (30) Hurwitz, E., Wilchek, M., and Pitha, J. (1980) Soluble macromolecules as carriers for daunorubicin. *J. Appl. Biochem.* **2**, 25–35.
- (31) Manabe, Y., Tsubota, T., Haruta, Y., Kataoka, K., Okazaki, M., Haisa, S., Nakamura, K. and Kimura, I. (1984) Production of a monoclonal antibody-methotrexate conjugate utilizing dextran T-40 and its biologic activity. *J. Lab. Clin. Med.* **104**, 445–454.
- (32) Shih, L. B., Sharkey, R. M., Primus, F. J. and Goldenberg, D. M. (1988) Site-specific linkage of methotrexate to monoclonal antibodies using an intermediate carrier. *Int. J. Cancer* **41**, 832–839.
- (33) Burton, D. R. (1985) Immunoglobulin G: functional sites. *Molec. Immunol.* **22**, 161–206.
- (34) Deisenhofer, J. (1981) Crystallographic refinement and atomic models of a human Fc fragment and its complex with fragment B of protein A from *Staphylococcus aureus* at 2.9- and 2.8-Å resolution. *Biochemistry* **20**, 2361–2370.
- (35) Sutton, B., and Phillips, D. (1983) The three-dimensional structure of the carbohydrate within the Fc fragment of immunoglobulin G. *Biochem. Soc. Trans.* **11**, 130–132.
- (36) Nezlin, R. (1990) Internal movements in immunoglobulin molecules. *Adv. Immunol.* **48**, 1–40.

## Targeted Delivery of DNA Using YEE(GalNAcAH)<sub>3</sub>, a Synthetic Glycopeptide Ligand for the Asialoglycoprotein Receptor

June Rae Merwin,\* G. Stephen Noell, Wendy L. Thomas, Henry C. Chiou, Mary E. DeRome, Timothy D. McKee, George L. Spitalny, and Mark A. Findeis

TargeTech, Inc., Meriden, Connecticut 06450. Received May 24, 1994\*

*In vivo* gene therapy shows promise as a treatment for both genetic and acquired disorders. The hepatic asialoglycoprotein receptor (ASGPr) binds asialoorosomucoid-polylysine-DNA (ASOR-PL-DNA) complexes and allows targeted delivery to hepatocytes. The tris(*N*-acetylgalactosamine aminohexyl glycoside) amide of tyrosyl(glutamyl) glutamate [YEE(GalNAcAH)<sub>3</sub>] has been previously reported to have subnanomolar affinity for the ASGPr. We have used an iodinated derivative of YEE-(GalNAcAH)<sub>3</sub> linked to polylysine and complexed to the luciferase gene (pCMV-Luc) in receptor-binding experiments to establish the feasibility of substituting ASOR with the synthetic glycopeptide for gene therapy. Scatchard analyses revealed similar *K*<sub>d</sub> values for both ASOR and the glycopeptide. Binding and internalization of <sup>125</sup>I-Suc-YEE(GalNAcAH)<sub>3</sub> were competitively inhibited with either unlabeled ASOR or glycopeptide. The reverse was also true; <sup>125</sup>I-ASOR binding was competed with unlabeled YEE(GalNAcAH)<sub>3</sub> suggesting specific binding to the ASGPr by both compounds. Examination of *in vivo* delivery revealed that the <sup>125</sup>I-labeled glycopeptide complex mimicked previous results observed with <sup>125</sup>I-ASOR-PL-DNA. CPM in the liver accounted for 96% of the radioactivity recovered from the five major organs (liver, spleen, kidney, heart, and lungs). Cryoautoradiography displayed iodinated glycopeptide complex bound preferentially to hepatocytes rather than nonparenchymal cells. *In vitro*, as well as *in vivo*, transfections using the glycopeptide-polylysine-pCMV-luciferase gene complex (YG3-PL-Luc) resulted in expression of the gene product. These data demonstrate that the YEE(GalNAcAH)<sub>3</sub> synthetic glycopeptide can be used as a ligand in targeted delivery of DNA to the liver-specific ASGPr.

### INTRODUCTION

The introduction of exogenous genes into cells is the basis for gene therapy. This expanding area of research encompasses widespread opportunities to treat both genetic and acquired disorders. Most of the gene therapy protocols currently in the clinic utilize an engineered viral vector and/or *ex vivo* manipulation of autologous cells followed by reintroduction into the donor (reviews, 1-5). The lack of cellular specificity and the impracticality of treating large populations with *ex vivo* protocols indicate the need for improved gene-transfer technologies. Targeted delivery of therapeutic genes via receptor-mediated endocytosis has the potential to address these concerns (6, 7).

Ehrlich conceptualized targeted delivery and coined the term "magic bullet" early in the 20th century as a result of his pioneering research in immunology and medicinal chemistry (8). However, it was not until the 1980's that this principle was extended to targeted delivery of DNA. Research in this area was initiated by Wu and Wu (9) using the asialoglycoprotein receptor (ASGPr)<sup>1</sup> which is

unique to hepatocytes and binds branched galactose-terminal glycoproteins, such as asialoorosomucoid (ASOR, 10). Ligand/receptor complexes have been shown to internalize via receptor-mediated endocytosis engaging the endosomal-lysosomal pathway (11). *In vitro* DNA delivery has been accomplished by targeting the more ubiquitous transferrin receptor (12, 13). Previous research has also included *in vitro* gene transfer using insulin-polylysine conjugates that are internalized by hepatocytes (14) and antibody conjugates specific to antigen-bearing cells (15). In general, the complex used for delivery consists of a covalently linked ligand-polycation conjugate which binds DNA in an electrostatic manner (16). To substantiate transcription and translation, the gene product of choice was measured. These gene products included membrane bound, intracellular, or secreted proteins (17-19).

Recently reported synthetic ligand-based conjugates for targeted delivery of DNA have demonstrated the viability of using galactose-containing ligands smaller than proteins to achieve receptor binding and internalization of the ligand-bound DNA (20, 21). The use of synthetic and semisynthetic ligands in DNA delivery is a relatively unexplored field. We show herein that the use of the synthetic peptide YEE(GalNAcAH)<sub>3</sub> parallels the biological activity of ASOR (a natural ligand for the ASGPr) in binding, uptake, and competition studies. We have also demonstrated *in vitro* and *in vivo* targeting and gene expression using a YEE(GalNAcAH)<sub>3</sub>-polylysine-DNA complex (YG3-PL-DNA).

### EXPERIMENTAL PROCEDURES

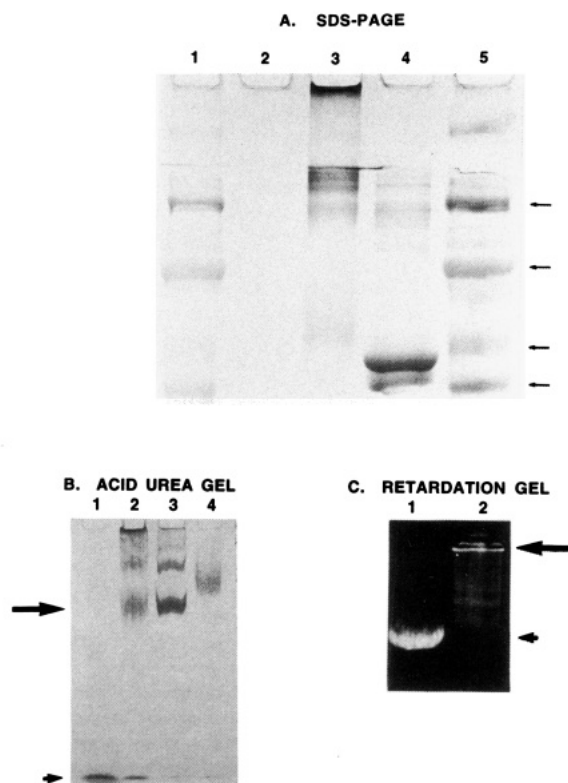
**Synthesis. General.** Poly-L-lysine and human serum albumin (HSA; ~97% pure) were purchased from Sigma, and 1-(3-(dimethylamino)propyl)-1'-ethylcarbodiimide (EDC) was purchased from Aldrich. *Synthetic Cluster*

\* Present address: Advanced Technologies-Cell Biology, The West Company, 101 Gordon Street, P.O. Box 645, Lionville, PA 19341-0645. Tel: 215-594-2900. Fax: 215-594-3000.

\* Abstract published in *Advance ACS Abstracts*, September 15, 1994.

<sup>1</sup> Abbreviations: ASGPr, asialoglycoprotein receptor; ASOR, asialoorosomucoid; ASOR-PL-DNA, asialoorosomucoid-polylysine-DNA complex; EDC, 1-(3-(dimethylamino)propyl)-1'-ethylcarbodiimide; Gal, Galactose; GalNAc, *N*-acetylgalactosamine; HSA, human serum albumin; O/N, overnight; PBS, phosphate buffered saline; rt, room temperature; YEE(GalNAcAH)<sub>3</sub>, tris(*N*-acetylgalactosamine aminohexyl glycoside) amide of tyrosyl(glutamyl)glutamate; YG3-PL-DNA, YEE-(GalNAcAH)<sub>3</sub>-polylysine-DNA complex; YG3-PL-Luc, YEE-(GalNAcAH)<sub>3</sub>-polylysine-luciferase DNA complex.





**Figure 1.** Electrophoresis of material. (A) 4–20% gradient SDS-PAGE: lanes 1 and 5, molecular weight markers 200, 97.4, 69, and 46 kD (small arrows); lane 2, YEE(GalNAcAH)<sub>3</sub>; lane 3, PL-HSA-Suc-YEE(GalNAcAH)<sub>3</sub>; lane 4, HSA. (B) Acid-urea gel: lane 1, 4 kD polylysine; lane 2, purified PL-HSA-Suc-YEE(GalNAcAH)<sub>3</sub> conjugate; lane 3, HSA; lane 4, ASOR. (C) Gel retardation assay: lane 1, DNA alone (arrowhead); lane 2, purified DNA fully retarded in the well due to complexation with conjugate (arrow).

**Ligands.** The synthesis (22) and an alternative stepwise synthesis of YEE(GalNAcAH)<sub>3</sub>, along with the synthesis of succinyl-YEE(GalNAcAH)<sub>3</sub> (23), have been described. **Polylysine-HSA-Suc-YEE(GalNAcAH)<sub>3</sub>.** Suc-YEE(GalNAcAH)<sub>3</sub> (25 mg, 17.3  $\mu$ mol) and HSA (50 mg) were dissolved in 10 mM MES Biological Buffer (EM Scientific Corp.), pH 5. EDC (33 mg, 172  $\mu$ mol) was added and the resulting mixture stirred for 2 h at room temperature (rt). Polylysine (4 kD average MW, 50 mg) and additional EDC (25 mg) were added to the reaction mixture which was stirred for an additional 2 h. The reaction mixture was dialyzed sequentially: two times against 1 M guanidine hydrochloride, one time against 1 M NaCl, two times against water, and then lyophilized. The final lyophilized yield was 53.6 mg (~43% of reactants). An amino acid analysis revealed an average of 6.9 mol of YEE(GalNAcAH)<sub>3</sub>/mol HSA and 0.7 mol of PL/mol of HSA. A 4–20% gradient SDS-PAGE was performed on Suc-YEE(GalNAcAH)<sub>3</sub>, purified PL-HSA-Suc-YEE(GalNAcAH)<sub>3</sub> conjugate, and HSA (Figure 1A). Suc-YEE(GalNAcAH)<sub>3</sub> ran through the gel due to its small MW (~1400 D; lane 2); while HSA alone displayed a prominent band at ~65 kD as well as higher molecular weight bands suggesting impurities in the HSA sample (lane 4). The PL-HSA-Suc-YEE(GalNAcAH)<sub>3</sub> conjugate, due to the high positive charge and possible aggregation, remains primarily at the top of the gel (lane 3). A small amount of conjugate entered the gel and is shown at ~70 kD which would be the expected MW when considering the addition of Suc-YEE(GalNAcAH)<sub>3</sub> and polylysine to HSA. Due to the difficulty in deciphering the conjugate on SDS-PAGE, it was necessary to perform acid urea gel electrophoresis on free polylysine, the purified con-

**Table 1. List of Compounds and Their Descriptions<sup>a</sup>**

compd	explanation
YEE(GalNAcAH) <sub>3</sub>	basic triantennary cluster ligand
Suc-YEE(GalNAcAH) <sub>3</sub>	cluster ligand plus succinyl group
HSA-Suc-YEE(GalNAcAH) <sub>3</sub>	cluster ligand plus human serum albumin linked via succinyl group
Luc-PL-HSA-Suc-YEE(GalNAcAH) <sub>3</sub> abbreviated as YG3-PL-Luc	cluster ligand plus human serum albumin linked via succinyl group, polylysine covalently linked to HSA, and complexed plasmid DNA (pCMV-Luc)
ASOR-PL-Luc	asialoorosomucoid plus polylysine and complexed plasmid DNA (pCMV-Luc) (positive control)

<sup>a</sup> The basic cluster ligand is used as the core molecule with additions of <sup>125</sup>I, a succinyl group, human serum albumin, polylysine, pCMV-Luc, or a combination thereof.

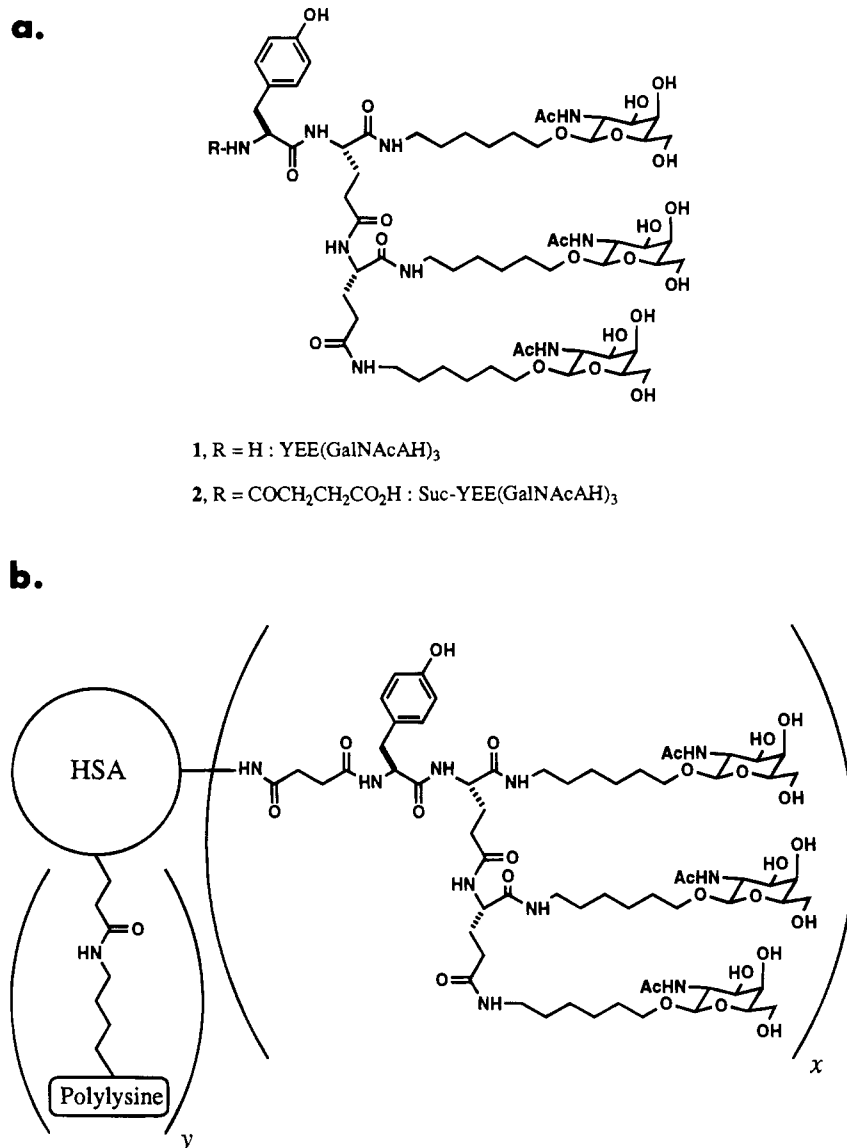
jugate, HSA, and ASOR (Figure 1B). This protocol, as described by McKee et al. (24), separates bands primarily on the basis of charge as well as size, due to the high concentration of urea and the acidic conditions. As a result, the ASOR molecule (lane 4), which is acidic in nature, does not migrate into the gel as far as HSA (lane 3). The rationale for this procedure was to determine the purity of the conjugate as far as the amount of free polylysine remaining in the conjugate sample. The arrow points out the prominent band for the purified conjugate (lane 2). A small amount of free polylysine within the sample appeared at the bottom of the gel (lane 1, arrowhead). The high MW banding pattern of the purified conjugate (lane 2) is similar to that of HSA alone (lane 3 and Figure 1A) which may be due to the impurities of the HSA sample as well as cross linking of the molecules. However, they do not appear to interfere with the ability of the conjugate to complex DNA. The asialoorosomucoid-polylysine conjugate was prepared as described previously using 5 kD MW polylysine (24).

**Plasmid Construct.** pCMV-Luc was a kind gift from Dr. James Economou (UCLA Medical Center, Los Angeles, CA). This plasmid contains the firefly luciferase gene derived from plasmid pXP1 (25) under the control of the cytomegalovirus immediate early promoter. The plasmid was maintained and propagated in *E. coli* strain DH5 $\alpha$ . Isolation of plasmid DNA was accomplished by standard alkaline/detergent lysis of saturated bacterial cultures grown in Terrific Broth (26). Supercoiled plasmids were then purified by double banding on cesium chloride gradients. All DNAs were EtOH precipitated and stored in 100 mM Tris pH 7.5, 10 mM EDTA at 4 °C.

**Complex Formation.** A YG3-PL-DNA complex was formed as described (24). Briefly, 3.0 mg of purified conjugate (as a 5 mg/mL aqueous solution) was slowly added to 1 mg of pCMV-Luc DNA resulting in 300  $\mu$ g of DNA/mL in 0.15 M NaCl. The complex was then filtered through a 0.45  $\mu$ m filter (Acrodisc, Gelman Sciences), and the final concentration was found to be 177  $\mu$ g/mL by UV absorbance. An aliquot of the complex was then run on a 1% agarose gel to confirm full retardation of the DNA (Figure 1C). Once the DNA is fully complexed with conjugate, the DNA will retard in the well and not enter the gel bed (lane 2, arrow). This sample retarded at a 3:1 conjugate:DNA weight:weight ratio. A complete list of compounds used in our experiments is shown in Table 1.

**Cell Surface Binding Analyses. Binding Studies.** HUH-7 human hepatoma cells (generous gift of Dr. T. J. Liang, Massachusetts General Hospital, Boston, MA) were plated at  $0.25 \times 10^6$  cells/well in 24 well plates and grown overnight (O/N) to ~75% confluence in MEM medium with 10% fetal calf serum. Suc-YEE(GalNAcAH)<sub>3</sub> was iodinated as described (27, 28). Half of the



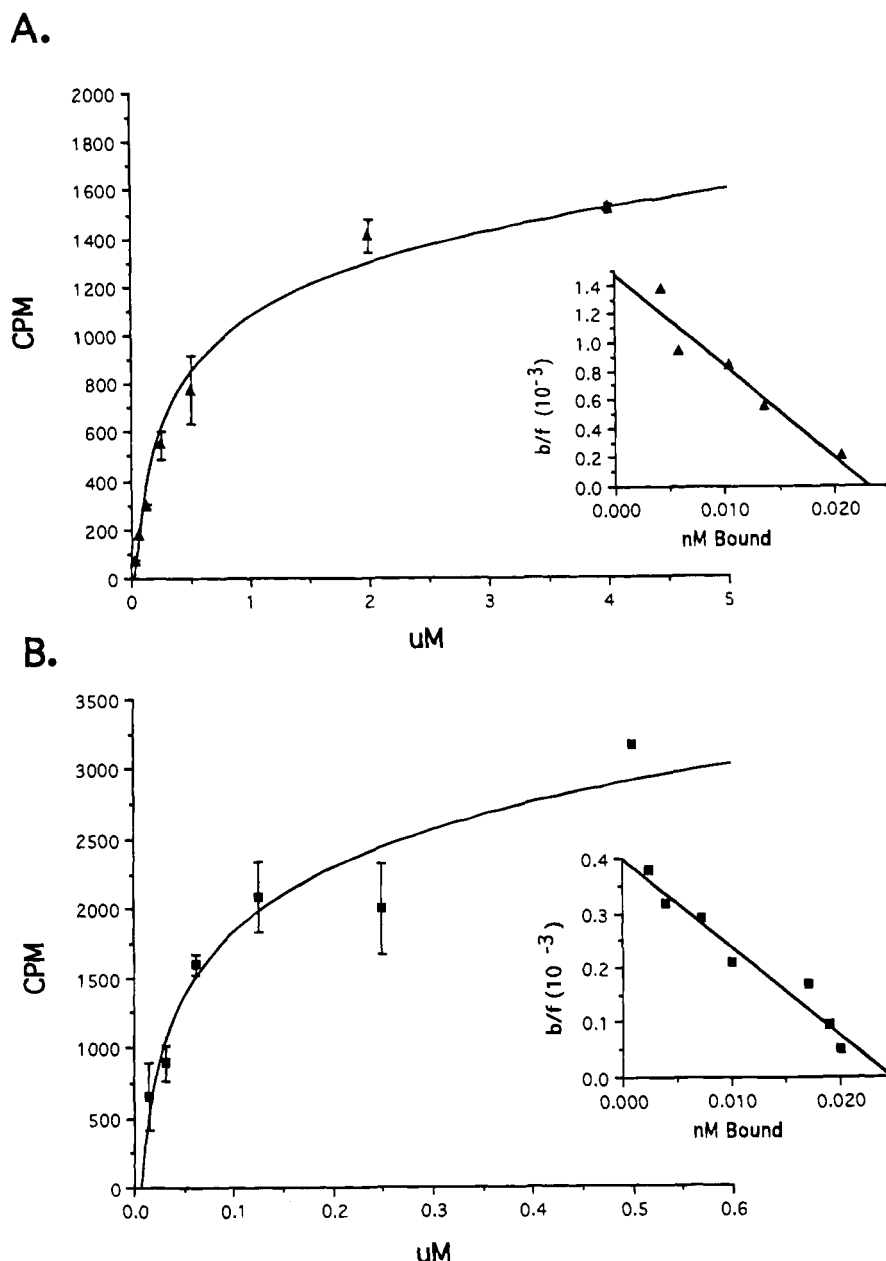


**Figure 2.** Chemical structures. (A) Structure of the trivalent cluster glycoside YEE(GalNAcAH)<sub>3</sub> (1) and its *N*-succinyl derivative (2). (B) Structure of polylysine-HSA-Suc-YEE(GalNAcAH)<sub>3</sub>. The number of equivalents of cluster ligand (*x*) and polylysine (*y*) bound to HSA will vary with the conditions under which the cross linking reactions are conducted.

samples were pretreated with 150-fold molar excess unlabeled Suc-YEE(GalNAcAH)<sub>3</sub> for 1 h at 4 °C enabling us to ascertain nonspecific binding. The cells were incubated with varying amounts of <sup>125</sup>I-Suc-YEE(GalNAcAH)<sub>3</sub> (specific activity = 1.5 × 10<sup>10</sup> CPM/μmol) in serum-free medium for 2 h at 4 °C. Free ligand was removed from the cells with three washes of phosphate buffered saline (PBS) and the cells lysed with 0.5 mL of 0.2 N NaOH. The lysate was measured for radioactivity in a γ counter. Similar analyses were performed on ASOR to compare the binding properties of both ASGPr ligands in our hands. **Internalization Studies.** To distinguish endocytosed from externally bound ligand, the cells were incubated with 0.1 μM radiolabeled YG3-PL-DNA complex (specific activity = 1.7 × 10<sup>6</sup> CPM/μg DNA) for up to 3 h in serum-free medium containing 3.8 mM Ca<sup>2+</sup> at 37 °C. The negative control was <sup>125</sup>I-orosomucoid which does not bind the ASGPr. The monolayers were rinsed three times with PBS and incubated with 10 mM EDTA/PBS, pH 2.5 for 5 min at rt to dissociate externally bound ligand (29, 30). Background binding was determined by preincubating cells with 0.1% sodium azide for 1 h at 4 °C to inhibit internalization and then treating

the cells with the experimental ligand for an additional hour at the same temperature. Samples were washed, and externally bound receptor/ligand complexes were dissociated as stated above. The remaining background counts were subtracted from the total radioactivity and the final value considered as ligand taken up by the cells. **Competition Studies.** To determine receptor specificity, HUH-7 cells were incubated simultaneously with 1 μM radiolabeled YEE(GalNAcAH)<sub>3</sub> plus varying concentrations of unlabeled glycopeptide or ASOR for 2 h at 4 °C. The reverse experiment was also performed using radiolabeled ASOR and increasing amounts of unlabeled YEE(GalNAcAH)<sub>3</sub>. Representative experiments are shown in the figures; however, binding, internalization, and competition studies were repeated using triplicate samples in three or more assays.

**In Vivo Targeting and Clearance.** Balb/C mice were tail vein injected with 10<sup>6</sup> CPM of <sup>125</sup>I-YG3-PL-Luc complex in 0.5 mL of PBS. Animals were sacrificed by cervical dislocation 5 min post-injection. Major organs were excised and, along with the remainder of the carcass, were counted in the γ counter to determine the amount of radioactivity distributed throughout the body.



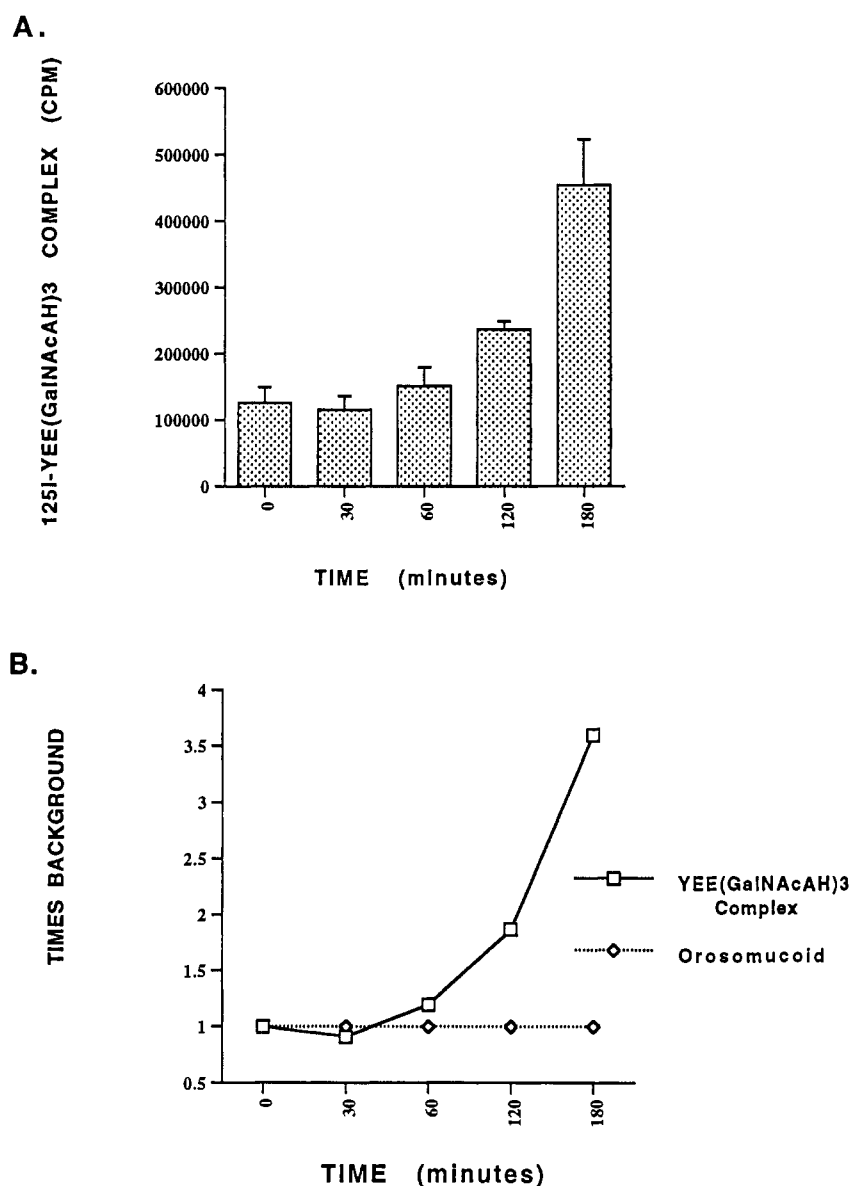
**Figure 3.** ASGPr/glycopeptide binding analyses. Binding studies were performed in which half of the samples were pretreated with 150-fold molar excess unlabeled ligand and then incubated with various concentrations of  $^{125}\text{I}$ -Suc-YEE(GalNAcAH)<sub>3</sub> (A) or  $^{125}\text{I}$ -ASOR (B) as described in the Experimental Procedures. Free ligand was removed, the cells lysed, and radioactivity counted. The data revealed dose-dependent binding curves which approached saturation of receptors. Scatchard plots are shown in the insets.

**Cryautoradiography. Frozen Section Preparation.**  $^{125}\text{I}$ -YG3-PL-Luc complex ( $4 \times 10^6$  CPM) in 0.5 mL of PBS was tail vein injected into Balb/C mice which were sacrificed 5 min post-injection. The liver was perfused with 3% paraformaldehyde, excised, cut into 2–3 mm pieces, and post fixed in the same fixative for 30 min at rt. The tissue was rinsed two times with PBS and infused with 0.5 M sucrose/PBS O/N at 4 °C for cryoprotection, after which it was infiltrated with two parts 20% sucrose/PBS to one part OCT embedding medium (Miles, Diagnostic Division, Elkhart, IN) in a cryomold for 30 min at rt. The tissue was rapidly submerged in liquid nitrogen cooled isopentane and stored at –80 °C until sectioned at 3  $\mu\text{m}$  on a cryostat, mounted onto chrom alum/gelatin subbed slides, air dried at rt, and stored at 4 °C until used.

**Authoradiography.** Under safelight conditions, the slides were dipped vertically into Kodak NTB-3 liquid emulsion film (International Biotechnologies, Inc., New

Haven, CT) at 43 °C, after which the backs of the slides were wiped clean. The slides were air dried for 1.5 h and placed into black slide boxes containing tissue-wrapped desiccant. The boxes were sealed with black electrical tape and stored on end with the emulsion facing upward at 4 °C for 3–7 days. After exposure, the slides were developed under red safelight conditions in Kodak Dektol (1:1 with distilled water) for 2 min, submerged in Kodak fix for 5 min, and rinsed with distilled water for 5 min (all at 14 °C). The slides were air dried in a dust free environment followed by staining with 0.5% toluidine blue in 1% benzoic acid for 1–2 min, rinsed three times in distilled water, and air dried. Coverslips were mounted onto slides with Cytoseal 60 (Stephens Scientific, Riverdale, NJ) and the slides viewed under a microscope. Negative controls consisted of livers excised from normal mice which were handled and treated in the same manner as experimental samples.

**In Vitro Transfections.** HUH-7 hepatocytes were



**Figure 4.** Internalization study. HUH-7 cells were incubated with  $0.1 \mu\text{M}$  iodinated Suc-YEE(GalNAcAH)<sub>3</sub> complex for increasing time periods. External receptor-bound ligand was dissociated and nonspecific background binding subtracted. (A) The assay revealed that YG3-PL-Luc complexes were taken up by the cell with the amount internalized increasing over time. (B) After 3 h of incubation, the amount of internalized YEE(GalNAcAH)<sub>3</sub> complex was  $>3.5$  times background.

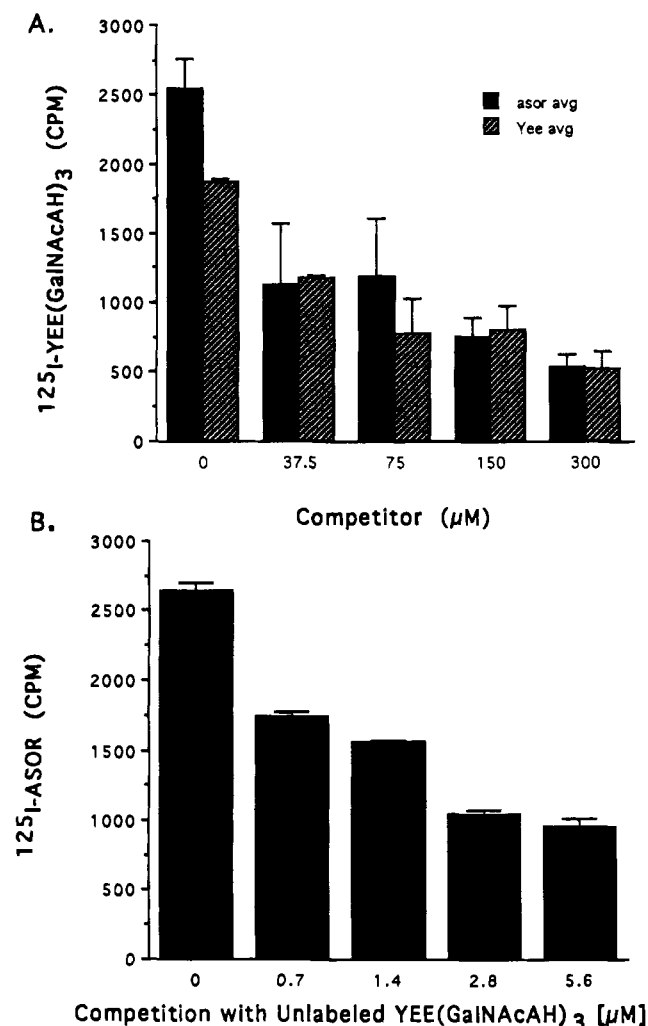
seeded at  $1.25 \times 10^6$  cells/100 mm tissue culture dish and grown O/N to 40–50% confluence in MEM medium with 10% fetal calf serum. The monolayers were rinsed three times with PBS and incubated in medium containing  $100 \mu\text{M}$  chloroquine for 1 h at  $37^\circ\text{C}$  and the rinse step repeated. Chloroquine is a lysosomotropic agent which has been shown to enhance the efficiency of receptor-mediated gene transfer *in vitro* (31). Fresh medium containing YG3-PL-Luc complex ( $12 \mu\text{g}$  of DNA) was added. The concentration of  $\text{CaCl}_2$  was increased to  $3.8 \text{ mM}$  as the transfections are mediated via receptor binding and endocytosis which is a calcium-dependent process. After 1.5–3 h, the cells were washed two times in PBS and the medium changed. At 48 hr the cells were harvested for quantitation of luciferase expression (32) using an AutoLumat Luminometer LB953 (EG & G Berthold, Pittsburgh, PA).

**In Vivo Gene Expression.** One h prior to IV injection of YG3-PL-Luc complex, Balb/C mice were treated with colchicine and chloroquine by ip injection ( $0.75$  and  $40 \text{ mg/kg}$ , respectively). Intravenous injection of YG3-PL-Luc complex was performed via the tail vein with a

standard dose of  $300 \mu\text{g}$  complexed DNA in  $1 \text{ mL}$  of saline containing  $0.15 \text{ M}$  NaCl. Three days post-injection, the mice were sacrificed. Approximately  $0.4 \text{ g}$  of liver was excised, homogenized, and processed, and the quantity of intracellular luciferase was determined as stated above (32).

## RESULTS AND DISCUSSION

**YEE(GalNAcAH)<sub>3</sub> Synthesis and Formation of the DNA Complex.** The cluster glycoside YEE(GalNAcAH)<sub>3</sub> (Figure 2A) is the highest affinity synthetic ligand of the ASGPr reported to date (22). In binding assays using rat hepatocytes, this compound was reported to effect a 50% inhibition at a concentration of  $0.2 \text{ nM}$  of ASOR binding (22). Lee and Lee obtained this high specificity through the use of *N*-acetylgalactosamine as the carbohydrate moiety which has higher affinity for the receptor in comparison with galactose. The use of a flexible branched peptide backbone provides a triantennary array of GalNAc groups to allow tight binding to the multivalent ASGPr. In light of the demonstrated affinity of this

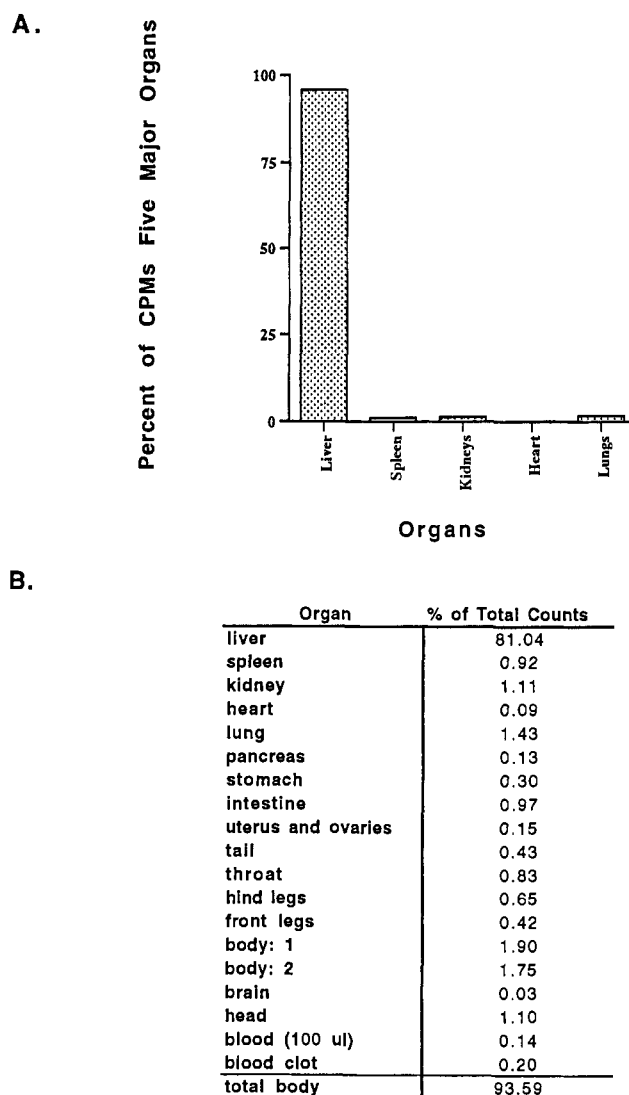


**Figure 5.** Competition studies. HUH-7 cells were incubated with 1  $\mu$ M iodinated Suc-YEE(GalNAcAH)<sub>3</sub> and varying concentrations of unlabeled glycopeptide or ASOR (A). The reverse competition study was also performed (B) using <sup>125</sup>I-ASOR competed with 300-fold molar excess unlabeled Suc-YEE(GalNAcAH)<sub>3</sub> which is the same maximum molar increase used in A.

compound for the ASGPr, we sought to evaluate it as a ligand for targeted delivery to liver cells.

To facilitate the formation of conjugates between YEE(GalNAcAH)<sub>3</sub> and amine-containing macromolecules, the *N*-succinyl derivative, Suc-YEE(GalNAcAH)<sub>3</sub>, was prepared by reaction of the tyrosyl *N*-terminal amino group with succinic anhydride. The free carboxyl group allows carbodiimide-mediated cross linking in aqueous solution between the fully deprotected cluster glycoside and polylysine or HSA. Polylysine-HSA-Suc-YEE(GalNAcAH)<sub>3</sub> was used directly to form a targetable electrostatic complex with DNA (Figure 2B).

**Binding Analysis.** To address whether YEE(GalNAcAH)<sub>3</sub> could replace ASOR as an ASGPr ligand, a series of binding studies were performed. <sup>125</sup>I-Suc-YEE(GalNAcAH)<sub>3</sub> was shown to bind to HUH-7 hepatocyte monolayers in a dose dependent manner approaching saturation of receptors at 2  $\mu$ M (Figure 3A). Non-specific background binding determined by incubation with 150-fold excess unlabeled peptide was subtracted from total binding. Duplicate experiments were performed using <sup>125</sup>I-ASOR (Figure 3B). Scatchard analyses of both <sup>125</sup>I-Suc-YEE(GalNAcAH)<sub>3</sub> and <sup>125</sup>I-ASOR binding revealed similar results; namely, *K<sub>d</sub>* values of  $6 \times 10^{-8}$  and  $2 \times 10^{-8}$  M, respectively (Figure 3A,B). Lee

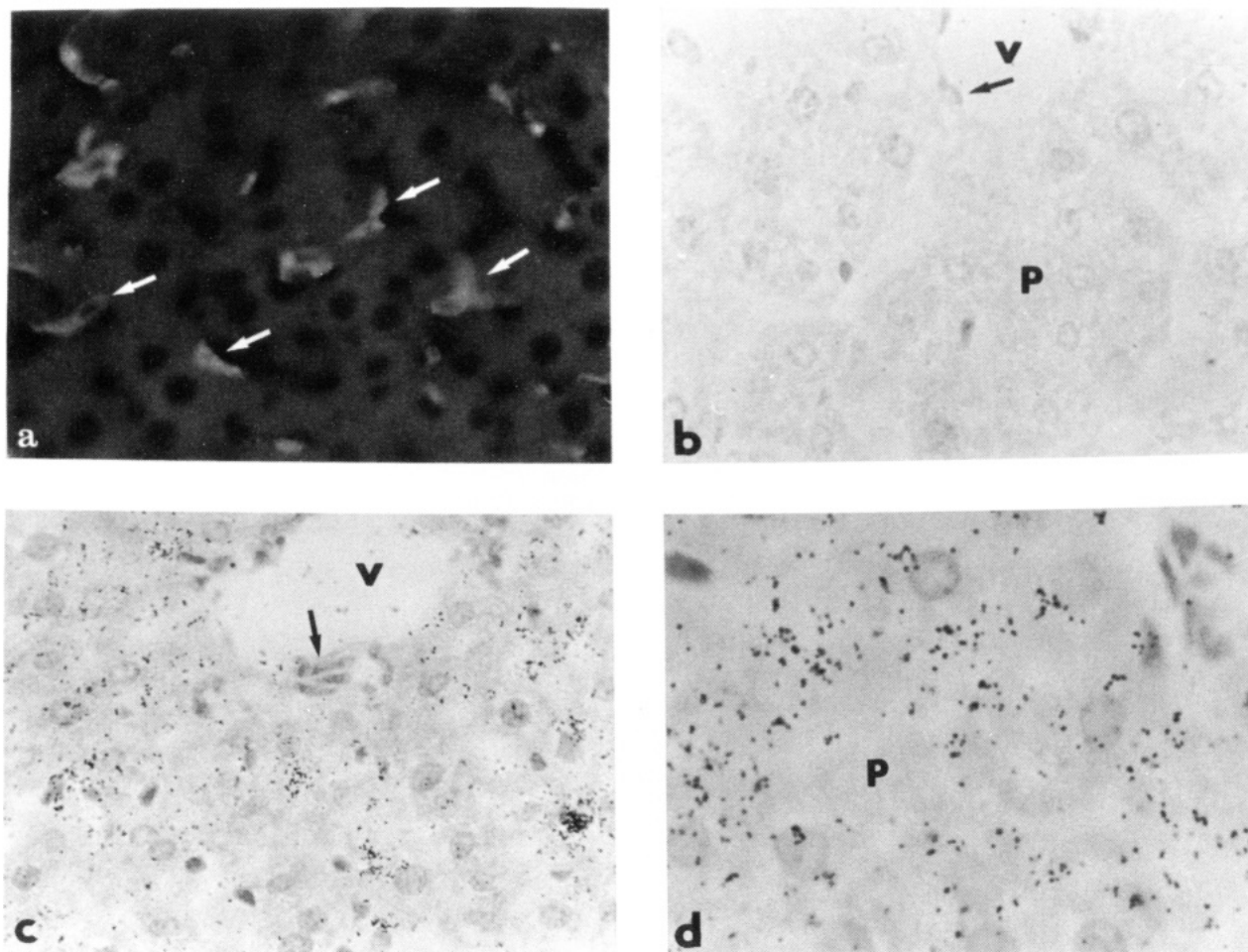


**Figure 6.** *In vivo* targeting and clearance analyses.  $10^6$  CPM of <sup>125</sup>I-Suc-YEE(GalNAcAH)<sub>3</sub> complex was tail vein injected into Balb/C mice. The major organs were removed at 5 min post-injection and radioactivity counted to determine percent of labeled complex targeted to the liver. The remaining carcass was dissected and counted to analyze total biodistribution.

and Lee (22) have shown that the glycopeptide without a succinyl group exhibited subnanomolar affinity for the ASGPr; however, we observed nanomolar range affinities for both ASOR and Suc-YEE(GalNAcAH)<sub>3</sub>. The differences in binding affinities may be attributed to the experimental protocol as well as the culture systems used (human hepatocyte cell line used in house versus freshly isolated hepatocytes or soluble ASGPr; 22). The object of this project was to compare Suc-YEE(GalNAcAH)<sub>3</sub> to ASOR using both *in vivo* and *in vitro* assays. While the affinity of Suc-YEE(GalNAcAH)<sub>3</sub> for ASGPr appears to be less than previously reported, our data affirm that Suc-YEE(GalNAcAH)<sub>3</sub> possesses similar ASGPr binding properties compared to ASOR in our hands.

Incubating the ASGPr-negative hepatocyte cell line, SK-Hep-1, with <sup>125</sup>I-Suc-YEE(GalNAcAH)<sub>3</sub> resulted in only minimal binding. In competition studies using 100-fold molar excess unlabeled Suc-YEE(GalNAcAH)<sub>3</sub>, no change was seen in the SK-Hep-1 binding results, suggesting nonspecific binding rather than ASGPr engagement (data not shown).

**Internalization Studies.** In order to validate YEE(GalNAcAH)<sub>3</sub> usage as a ligand for targeted delivery of



**Figure 7.** Hepatocyte localization of iodinated glycopeptide. Perfused livers were removed from Balb/C mice injected with  $4 \times 10^6$  counts of iodinated YG3-PL-Luc complex and processed for autoradiography as stated in the Experimental Procedures. Staining of negative control livers was negligible (B) while  $^{125}\text{I}$ -Suc-YEE(GalNAcAH)<sub>3</sub> complex injected livers exhibited positive silver grains located in the parenchymal hepatocytes (C, D). A section from the same liver was processed for immunofluorescence and stained with an antibody specific to Kupffer cells. Vascular cells gave no evidence of iodinated glycopeptide uptake (C). V = vasculature, P = parenchyma, arrows = endothelial cells. Original magnification (A, B, C) =  $600\times$ , (D) =  $1000\times$ .

DNA to the ASGPr, it was necessary to establish that the glycopeptide-PL-DNA complex was able to be taken up by hepatocytes. We established internalization by incubating HUH-7 cells with iodinated YG3-PL-Luc complex. Following incubation, half of the samples were treated to dissociate external ligand/receptor binding. As seen in Figure 4A, there was an escalating amount of internalization of complex over time. After 3 h of incubation, the amount of complex taken up by the cell was 3.5-fold (Figure 4B). Iodinated orosomucoid was used as a negative control and was not internalized by the hepatocytes. Our results verify that Suc-YEE-(GalNAcAH)<sub>3</sub> complexes were capable of binding the ASGPr and being endocytosed.

**Competition Studies.** To demonstrate receptor specificity, competition assays were performed using HUH-7 cells incubated with  $^{125}\text{I}$ -Suc-YEE(GalNAcAH)<sub>3</sub> and increasing concentrations of unlabeled Suc-YEE(GalNAcAH)<sub>3</sub> or ASOR (Figure 5A). As shown, both the unlabeled peptide and native ligand were able to compete for ASGPr binding with  $^{125}\text{I}$ -Suc-YEE(GalNAcAH)<sub>3</sub>. The reverse experiment, unlabeled peptide competing with iodinated ASOR, confirmed ASGPr specific binding (Figure 5B).

**In Vivo Targeting and Clearance.** *In vivo* studies demonstrated highly selective targeting and clearance of the  $^{125}\text{I}$ -YG3-PL-Luc complex to the liver. Within 5 min post-injection, ~96% of the radioactivity recovered

from the five major organs was located in the liver: lungs = 1.2%, heart = 0.3%, spleen = 1.7%, and kidneys = 0.7% (Figure 6A). The remainder of the carcass contained minimal amounts of the radioactivity recovered from the body (= ~94% of total radionucleotide injected; Figure 6B).

These *in vivo* data corroborate our *in vitro* results showing  $^{125}\text{I}$ -Suc-YEE(GalNAcAH)<sub>3</sub> complex uptake via the liver specific ASOR receptor. Cryoautoradiography was used to visualize labeled complex within the liver 5 min post-injection. Positive silver grains were observed located in and surrounding hepatocytes (Figure 7C,D) while nonparenchymal endothelial cells (arrows, Figure 7C) and control cultures (Figure 7B) exhibited only background amounts of radioactivity. In order to distinguish nonparenchymal Kupffer cells from hepatocytes, sections from the same liver were stained with antibodies specific for this macrophage. A representative photograph shown in Figure 7A revealed a pattern of staining markedly different from that of the silver grains which depicted localization of the YG3-PL-Luc complex in liver parenchyma.

**In Vitro Transfections.** In order to show that YEE-(GalNAcAH)<sub>3</sub> could be used for gene therapy, we transfected cells with a YG3-PL-Luc complex to demonstrate expression of the transfected gene. ASOR-PL-Luc transfections constituted the positive control while ASGPr-negative 3T3 fibroblasts from ATCC were used

**Table 2. In Vitro Transfections<sup>a</sup>**

cell type	YG3-PL-Luc	ASOR-PL-pCMV-Luc
HUH-7	197 319	667 077
	228 873	515 464
3T3	69	51
	91	63

<sup>a</sup> HUH-7 cells and ASGPr-negative 3T3 fibroblasts were transfected with both YG3-PL-Luc and ASOR-PL-Luc. Values from the 3T3 cells were at background levels (~50 RLU).

**Table 3. In Vivo Expression<sup>a</sup>**

animal	RLU
mouse 1	8836
mouse 2	12 097
mouse 3	1943
mouse 4	116 772

<sup>a</sup> Four mice were injected with YG3-PL-Luc complex and the livers excised 3 days later. Luciferase activity was measured from each animal with detection of gene expression in all cases (background ~50 RLU).

as the negative control. The results, presented in Table 2, revealed positive transfections by both YG3-PL-Luc and ASOR-PL-Luc complexes. Values equaling background were observed with the receptor-minus fibroblast cells. A 3T3 cell line stably transformed with the ASGPr (33) was also used for *in vitro* transfections and resulted in positive transfections by both ASOR and YEE(GalNAcAH)<sub>3</sub> complexes. However, the values for the transformed 3T3 fibroblasts were lower than the HUH-7 hepatocytes (data not shown). We have shown, herein, that YEE(GalNAcAH)<sub>3</sub> can substitute for ASOR in a ligand-PL-DNA complex for *in vitro* delivery of DNA to hepatocytes via the ASGPr.

**In Vivo Gene Expression.** To further illustrate the use of YEE(GalNAcAH)<sub>3</sub>, we injected the YG3-PL-Luc complex into mice. Two days later, the livers were removed and homogenized, followed by determination of luciferase activity. As shown in Table 3, all four mice were positive for luciferase activity. Mouse 4 expressed an unusually high value, while mice 1–3 are within a 6-fold difference in RLU.

**Summary.** We have demonstrated the use of the synthetic glycopeptide YEE(GalNAcAH)<sub>3</sub> as a ligand for targeted delivery of DNA via the ASGPr. Specific binding to this receptor has been validated by binding, competition, and internalization studies. Functional confirmation was provided by *in vitro* transfections as well as *in vivo* targeting, cryoautoradiography, and expression studies. YEE(GalNAcAH)<sub>3</sub> complexed to DNA was able to duplicate the results obtained in similar experiments using ASOR-PL-DNA. Taken together, these data demonstrate the use of the synthetic cluster ligand, YEE(GalNAcAH)<sub>3</sub>, for the delivery of DNA specifically to hepatocytes via the ASGPr.

#### ACKNOWLEDGMENTS

The authors would like to thank Mr. Thomas Ardito (Yale School of Medicine) for his assistance with microscopic techniques and Dr. T. J. Liang (Massachusetts General Hospital) and Dr. J. Economou (UCLA Medical Center) for their generous gifts of HUH-7 cells and pCMV-Luc, respectively.

#### LITERATURE CITED

- Anderson, W. F. (1992) Human gene therapy. *Science* 256, 808–813.
- Mulligan, R. C. (1993) The basic science of gene therapy. *Science* 260, 926–932.
- Mulligan, R. C. (1991) Gene transfer and gene therapy: Principles, prospects, and perspective. *Etiology of human disease at the DNA level*. (J. Lindsten, and U. Petterson, Eds.) pp 143–189, Raven Press, New York.
- Thompson, L. (1992) At age 2, gene therapy enters a growth phase. *Science* 258, 744–746.
- Miller, A. D. (1992) Human gene therapy comes of age. *Nature* 357, 455–460.
- Findeis, M. A., Merwin, J. R., Spitalny, G. L., and Chiou, H. C. (1993) Targeted delivery of DNA for gene therapy via receptors. *Trends Biotechnol.* 11, 202–205.
- Chiou, H. C., Spitalny, G. L., Merwin, J. R., and Findeis, M. A. (1994) *In vivo* gene therapy via receptor-mediated DNA delivery. *Gene Therapeutics: Methods and Applications and Direct Gene Transfer*. (J.A. Wolff, Ed.) pp 143–156, Birkhäuser Publishers, Boston.
- Bäumler, E. (1984) *Paul Ehrlich, Scientist for Life*, p 108, Holmes & Meier Publishers, New York.
- Wu, G. Y., and Wu, C. H. (1987) Receptor-mediated *in vitro* gene transformation by a soluble DNA carrier system. *J. Biol. Chem.* 262, 4429–4432.
- Ashwell, G., and Morell, A. G. (1974) The role of surface carbohydrates in the hepatic recognition and transport of circulating glycoproteins. *Adv. Enzymol. Relat. Areas Mol. Biol.* 41, 99–128.
- Wall, D. A., Wilson, G., and Hubbard, A. L. (1980) The galactose-specific recognition system of mammalian liver: the route of ligand internalization in rat hepatocytes. *Cell* 21, 79–83.
- Wagner, E., Zenke, M., Cotten, M., Beug, H., and Birnstiel, M. L. (1990) Transferrin-polycation conjugates as carriers for DNA uptake into cells. *Proc. Natl. Acad. Sci. U.S.A.* 87, 3410–3414.
- Wagner, E., Plank, C., Zatloukal, K., Cotten, M., and Birnstiel, M. (1992) Influenza virus hemagglutinin HA-2 N-terminal fusogenic peptides augment gene transfer by transferrin-polylysine/DNA complexes: Towards a synthetic virus-like gene transfer vehicle. *Proc. Natl. Acad. Sci. U.S.A.* 89, 7934–7938.
- Rosenkranz, A. A., Yachmenev, S. V., Jans, D. A., Serebryakova, N.V., Murav'ev, V. I., Peters, R., and Sobolev, A. S. (1992) Receptor-mediated endocytosis and nuclear transport of a transfecting DNA construct. *Exp. Cell Res.* 199, 323–329.
- Trubetskoy, V. S., Torchilin, V. P., Kennel, S. J., and Huang, L. (1992) Use of N-terminal modified poly(L-lysine)-antibody conjugate as a carrier for targeted gene delivery in mouse lung endothelial cells. *Bioconjugate Chem.* 3, 323–327.
- Wu, G. Y., and Wu, C. H. (1988) Receptor-mediated gene delivery and expression *in vivo*. *J. Biol. Chem.* 263, 14621–14624.
- Wilson, J. M., Grossman, M., Wu, C. H., Chowdhury, N. R., Wu, G. Y., and Chowdhury, J. R. (1992) Hepatocyte-directed gene transfer *in vivo* leads to transient improvement of hypercholesterolemia in low density lipoprotein receptor-deficient rabbits. *J. Biol. Chem.* 267, 963–967.
- Wu, G. Y., and Wu, C. H. (1988) Evidence for targeted gene delivery to Hep G2 hepatoma cells *in vitro*. *Biochemistry* 27, 887–892.
- Wu, G. Y., Wilson, J. M., Shalaby, F., Grossman, M., Shafritz, D. A., and Wu, C.H. (1991) Receptor-mediated gene delivery *in vivo*: Partial correction of genetic analbuminemia in Nagase rats. *J. Biol. Chem.* 266, 14338–14342.
- Plank, C., Zatloukal, K., Cotten, M., Mechtler, K., and Wagner, E. (1992) Gene transfer into hepatocytes using asialoglycoprotein receptor mediated endocytosis of DNA complexed with an artificial tetra-antennary galactose ligand. *Bioconjugate Chem.* 3, 533–539.
- Haensler, J., and Szoka, F. C., Jr. (1993) Synthesis and characterization of a trigalactosylated bisacridine compound to target DNA to hepatocytes. *Bioconjugate Chem.* 4(1), 85–93.
- Lee, R. T., and Lee, Y. C. (1987) Preparation of cluster glycosides of N-Acetylgalactosamine that have subnanomolar binding constants toward the mammalian hepatic Gal/GalNAc-specific receptor. *Glycoconjugate J.* 4, 317–328.



- (23) Findeis, M. A. (1994) Stepwise synthesis of a GalNAc-containing cluster glycoside ligand of the asialoglycoprotein receptor. *Intl. J. of Pept. Prot. Res.* **43**, 477–485.
- (24) McKee, T. D., DeRome, M. E., Wu, G. Y., and Findeis, M. A. (1994) Preparation of asialoorosomucoid-polylysine conjugates. *Bioconjugate Chem.* **5**, 306–311.
- (25) Nordeen, S. K. (1988) Luciferase reporter gene vectors for analysis of promoters and enhancers. *BioTechniques* **6**(5), 454–456.
- (26) Sambrook, J., Fritsch, E. F., and Maniatis, T. (1989) *Molecular cloning, A laboratory manual*, Appendix 2, Cold Spring Harbor Laboratory Press, New York.
- (27) Greenwood, F. C., and Hunter, W. M. (1963) The preparation of  $^{131}\text{I}$ -labeled human growth hormone of high specific radioactivity. *Biochem. J.* **89**, 114–123.
- (28) DeLarco, J. E., Preston, Y. A., and Todaro, G. J. (1981) Properties of a sarcoma-growth-factor-like peptide from cells transformed by a temperature-sensitive sarcoma virus. *J. Cell. Physiol.* **109**, 143–152.
- (29) Weigel, P. H., and Oka, J. A. (1982) Endocytosis and degradation mediated by the asialoglycoprotein receptor in isolated rat hepatocytes. *J. Biol. Chem.* **257**, 1201–1207.
- (30) Ghinea, N., Hai, M. T. V., Groyer-Picard, T.-T., Houllier, A., Schoëvaert, D., and Milgrom, E. (1992) Pathways of internalization of the hCG/LH receptor: Immunoelectron microscopic studies in Leydig cells and transfected L-cells. *J. Cell Biol.* **118**, 1347–1358.
- (31) Cotten, M., Längle-Rouault, F., Kirlappos, H., Wagner, E., Mechtler, K., Zenke, M., Beug, H., and Birnstiel, M. L. (1990) Transferrin-polycation-mediated introduction of DNA into human leukemic cells: Stimulation by agents that affect the survival of transfected DNA or modulate transferrin receptor levels. *Proc. Natl. Acad. Sci. U.S.A.* **87**, 4033–4037.
- (32) Brasier, A. R. (1993) Introduction of DNA into mammalian cells. *Current Protocols in Molecular Biology* (F.M. Ausubel et al., Eds.) pp 9.6.10–19.6.14, John Wiley & Sons, Inc., Boston.
- (33) Shia, M. A., and Lodish, H. F. (1989) The two subunits of the human asialoglycoprotein receptor have different fates when expressed alone in fibroblasts. *Proc. Natl. Acad. Sci. U.S.A.* **86**(4), 158–162.

# Conjugates of *cis*-4-Hydroxy-L-proline and Poly(PEG-Lys), a Water Soluble Poly(ether urethane): Synthesis and Evaluation of Antifibrotic Effects *in Vitro* and *in Vivo*

George J. Poiani,\* David J. Riley, and James D. Fox

Department of Medicine, University of Medicine and Dentistry of New Jersey—Robert Wood Johnson Medical School, Piscataway, New Jersey 08854-5635, and Lyons VA Medical Center, Lyons, New Jersey 07939-9998

John E. Kemnitzer, K. Fiorella Gean, and Joachim Kohn\*

Department of Chemistry, Rutgers, The State University of New Jersey, Piscataway, New Jersey 08855-0939. Received May 13, 1994\*

Synthetic approaches for the preparation of macromolecular conjugates of the antifibrotic agent *cis*-4-hydroxy-L-proline (cHyp) were explored, and the efficacy of the conjugates in inhibiting collagen accumulation was investigated *in vitro* and *in vivo*. In one approach, poly(PEG-Lys), an alternating copolymer of poly(ethylene glycol) (PEG) and lysine, was used as the carrier. To prepare pendent chain systems, cHyp was attached to poly(PEG-Lys) through an amide linkage [poly(PEG-Lys-cHyp amide)] or through an ester linkage [poly(PEG-Lys-cHyp ester)]. In an alternative approach, cHyp was incorporated into the backbone of a linear copolymer consisting of PEG, succinic acid, and cHyp units [poly(PEG-succinate-cHyp)]. Bioactivity *in vitro* was assessed by the ability of the cHyp conjugates to inhibit growth of cultured smooth muscle cells (SMC) and rat lung fibroblasts (RLF). Cell numbers were compared to control experiments in the presence of biologically inactive *trans*-4-hydroxy-L-proline (tHyp). After a 5 day period, the presence of 8  $\mu\text{g/mL}$  of cHyp delivered by poly(PEG-Lys-cHyp amide) resulted in a 47% reduction in the number of SMC ( $p < 0.05$ ), the presence of 36  $\mu\text{g/mL}$  of cHyp delivered by poly(PEG-Lys-cHyp ester) resulted in a 38% reduction in the number of SMC ( $p < 0.05$ ), while the presence of 118  $\mu\text{g/mL}$  of cHyp delivered by poly(PEG-succinate-cHyp) resulted in a 31% reduction in the number of cells ( $p < 0.05$ ). An identical trend was observed for the inhibition of RLF growth. In general, poly(PEG-Lys-cHyp amide) was most active, followed by poly(PEG-Lys-cHyp ester) and the backbone system, poly(PEG-succinate-cHyp). Specifically, poly(PEG-Lys-cHyp amide) was over 100-fold more active in inhibiting cell growth than free cHyp. Bioactivity *in vivo* was evaluated by measuring collagen accumulation in subcutaneously implanted poly(vinyl alcohol) sponges in rats. Among the tested conjugates, poly(PEG-Lys-cHyp amide) was most active, reducing collagen accumulation in the sponge by 33% after 14 days relative to controls ( $p < 0.05$ ). This result indicates that the covalent attachment of cHyp to poly(PEG-Lys) carriers may be a useful strategy for the local inhibition of collagen accumulation in tissues.

## INTRODUCTION

The use of water soluble polymers in drug delivery has been investigated in detail. Available evidence indicates that polymeric carriers can modify the body distribution of a therapeutic agent, the mode of cell uptake, drug permeability through physiological barriers, and the rate of excretion from the body (1-5). To achieve either a "targeting effect" or a "sustained release" effect, polymeric carriers have been suggested that contain drug moieties as terminal groups, as part of the backbone, or as pendent groups on the polymer chain (Figure 1).

Recently, the preparation and potential utility of the PEG-Lys copolymer system as a new, water-soluble polymeric carrier has been described (6, 7). In this system, low molecular weight chains of poly(ethylene glycol) (PEG)<sup>1</sup> are copolymerized with the natural amino acid L-lysine to form a water soluble poly(ether urethane) backbone which has free carboxylic acid pendent groups at each monomeric repeat unit (Figure 2). This polymeric carrier exhibits many of the advantageous properties of PEG (low toxicity, ready excretion, lack of nonspecific

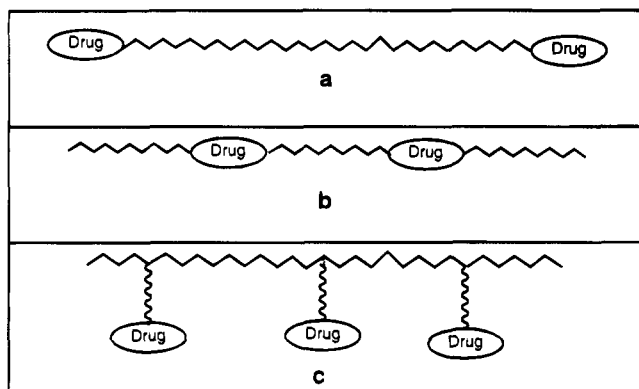
uptake by liver or elements of the reticuloendothelial system), while providing multiple attachment points for the covalent linkage of spacers and/or drugs. The covalent attachment of various antibiotics (7) and the anticancer agent doxorubicin (8) to the poly(PEG-Lys) backbone by biostable and biodegradable linkages has been described. Furthermore, the attachment of the naturally occurring amino acid *cis*-4-hydroxy-L-proline (cHyp) has been explored in a series of preliminary reports (9-11).

cHyp inhibits the biosynthesis of collagen and has been identified as a potential antifibrotic agent (12). Previ-

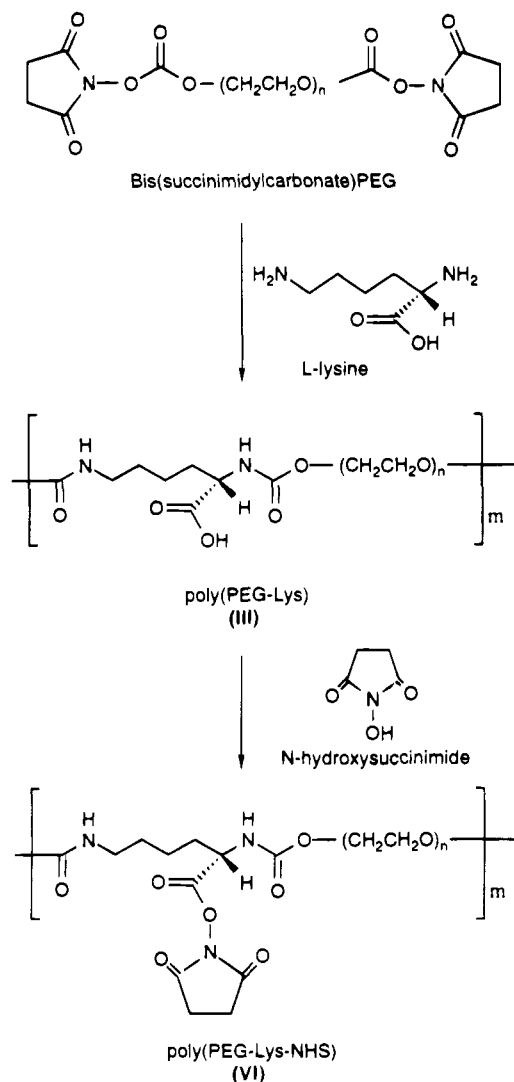
<sup>1</sup> Abbreviations: PEG, poly(ethylene glycol); Lys, L-lysine; cHyp, *cis*-4-hydroxy-L-proline; tHyp, *trans*-4-hydroxy-L-proline; Boc, *tert*-butoxycarbonyl; (Boc)<sub>2</sub>O, di-*tert*-butyl carbonate; DCC, 1,3-dicyclohexylcarbodiimide; DMAP, 4-(dimethylamino)pyridine; DIPC, 1,3-diisopropylcarbodiimide; DPTS, 4-(dimethylamino)pyridinium 4-toluenesulfonate; NHS, *N*-hydroxysuccinimide; DMF, dimethylformamide; EDTA, ethylenediaminetetraacetic acid; SMC, smooth muscle cell; RLF, rat lung fibroblast; MIC, minimum inhibitory concentration; FBS, fetal bovine serum; IU, international units; GPC, gel permeation chromatography;  $M_w$ , weight average molecular weight;  $M_n$ , number average molecular weight; ( $M_w/M_n$ ), polydispersity; rt, ambient temperature; NMR, nuclear magnetic resonance; ppm, parts per million; MHz, megahertz.

\* To whom correspondence should be addressed.

\* Abstract published in *Advance ACS Abstracts*, September 15, 1994.



**Figure 1.** Three different system configurations for the design of macromolecular drug conjugates: (a) drug molecules as terminal groups of a polymeric carrier; (b) drug molecules incorporated into a polymeric backbone; (c) drug molecules as pendent chains, attached to a polymeric backbone through linking groups and/or spacers. The symbol  $\sim$  represents a polymer backbone,  $\sim$  represents a linking group or spacer, and the encircled word drug represents a drug molecule.



**Figure 2.** Preparation of poly(PEG-Lys) (III) from bis(succinimidyl carbonate)-PEG of molecular weight 2000 and L-lysine, followed by the activation of the free carboxylic acid pendent chains as the *N*-hydroxysuccinimidyl active esters (VI). Detailed reaction schemes have been reported previously (23).

ously, administration of cHyp to rodents with experimental pulmonary fibrosis (13, 14) and pulmonary hy-

pertension (15, 16) has been shown to attenuate collagen accumulation in tissues. However, when injected in its free form, cHyp is too toxic to be considered as a potential clinical agent for the treatment of fibrotic disorders of the lung (16, 17) due primarily to its systemic effects on noncollagen proteins (18). To decrease the toxicity of free cHyp, liposomal delivery systems have been formulated and tested (17). As an alternative approach, cHyp has been attached in various configurations to the backbone of the poly(PEG-Lys) carrier (9–11). These delivery strategies have been developed to deliver cHyp to specific sites of active collagen formation, with the potential of maximizing the local concentration of cHyp relative to endogenous proline. In this context, the prevention of surgical adhesions, the reduction of scar formation during wound healing, and the treatment of fibrotic lung disorders are possible therapeutic applications.

This paper describes in detail the synthetic strategy utilized to obtain covalently bound conjugates of poly(PEG-Lys) and cHyp and reports on their biological activity. Results from *in vitro* studies on RLF and SMC as well as *in vivo* studies in a rat model indicated that high molecular weight conjugates of poly(PEG-Lys) and cHyp exhibit significantly improved and sustained anti-fibrotic effects as compared to monomeric cHyp.

## MATERIALS AND METHODS

**Materials.** *Reagents for Conjugate Synthesis.* PEG of high purity and narrow molecular weight distribution ( $M_w = 2000$  g/mol) was obtained from Fluka Chemical, Buchs, Switzerland. tHyp was from Sigma Chemical Co., St. Louis, MO. cHyp was obtained from Peptide International, Louisville, KY. All solvents were purified by distillation following standard methods, and all other reagents were synthesis grade.

*In Vivo and in Vitro Studies.* Six-week-old male Sprague-Dawley rats (CrI:CD[SD]BR), weighing 180–200 g, were obtained from Charles River Laboratories, Wilmington, MA. Penicillin G, streptomycin, gentamicin, ascorbic acid, and trypan blue were from Sigma Chemical Co., St. Louis, MO. Collagen (type I from rat tail) was from Collaborative Biomedical Products, Bedford, MA. Medium 199 with Earl's salts and fetal bovine serum (FBS) was purchased from ICN Biomedicals, Inc., Costa Mesa, CA. Trypsin-EDTA was from Gibco-BRL, Grand Island, NY. Poly(vinyl alcohol) (IVALON) was from Unipoint Industries, Inc., High Point, NC.

**Instrumental.** *Amino Acid Analyses.* Samples were hydrolyzed in sealed tubes at 110 °C for 48 h in 6 N HCl containing 0.1% phenol. Amino acid analyses were performed at the Rockefeller University Protein Sequence Facility, New York, NY.

*Nuclear Magnetic Resonance.* <sup>1</sup>H and <sup>13</sup>C NMR were recorded at 199.98 and 50.29 MHz, respectively, on a Varian Gemini 200 in 5 mm tubes using 7% wt/wt solutions in deuterated solvents. Chemical shifts were reported in ppm.

*Molecular Weight Analysis.* Molecular weights were determined by GPC using a Perkin-Elmer Model 410 pump, a Waters 410 differential refractometer detector, and the Perkin-Elmer 2600 chromatography software. Two TSK columns (G2000SW and G4000SW) were operated in series at a flow rate of 1 mL/min using sodium acetate buffer (0.1 M, pH 5.0) as the eluent. Molecular weights were calculated relative to poly(ethylene oxide) standards without further corrections.

**Synthesis.** Unless otherwise noted, all procedures are described for the *cis*-derivative. However, the procedures are generally applicable to both cHyp and tHyp. Roman numerals refer to the compounds shown in Figures 2–5.

**Preparation of Monomeric Derivatives of cHyp. Protection of the C- or N-Terminus.** cHyp-OMe (**I**) was prepared by reaction of cHyp with thionyl chloride in methanol (19). **I** was then Boc protected by reaction with di-*tert*-butyl dicarbonate using a common procedure (20). *N*-Boc-cHyp-OMe (**II**) was obtained in an overall yield of 84%; mp 82–83 °C; <sup>13</sup>C NMR (CDCl<sub>3</sub>, ppm) 28.2 [C(CH<sub>3</sub>)<sub>3</sub>], 37.2 (β-CH<sub>2</sub>), 54.9 (δ-CH<sub>2</sub>), 55.5 (CO<sub>2</sub>CH<sub>3</sub>), 57.9 (α-CH), 70.6 (γ-CH), 81.1 [C(CH<sub>3</sub>)<sub>3</sub>], 155.0 (NC=O), 176.2 (α-C=O). Likewise, cHyp was directly reacted with di-*tert*-butyl dicarbonate to yield *N*-Boc-cHyp (**VII**) in a yield of 90%, mp 140–141 °C.

**Preparation of 5-Aza-2-oxa-3-oxobicyclo[2.2.1]heptane (Hyp-lactone) (IX).** The procedure of Papaioannou was modified (21). In the first step, the Boc-protected lactone **VIII** was formed, followed by removal of the Boc group, to yield the free lactone HCl salt **IX**. This reaction scheme is applicable to the *cis*-derivative only.

To a 250 mL flask was added 2.0 g (8.7 mmol) of **VII**, 10.4 mg (0.87 mmol) of 4-(dimethylamino)pyridine, and 150 mL of acetonitrile. The resulting solution was cooled to –5 °C, followed by the addition of 2.1 g (10.4 mmol) of 1,3-dicyclohexylcarbodiimide. After 5 h at ambient temperature, the reaction mixture was filtered to remove the precipitate of 1,3-dicyclohexyl urea. The clear filtrate was evaporated to dryness. The crude *N*-Boc-Hyp-lactone (**VIII**) was redissolved in methylene chloride and extracted with water, saturated KHSO<sub>4</sub> solution, and saturated NaCl solution. The organic phase was dried over anhydrous Na<sub>2</sub>SO<sub>4</sub>, and **VIII** was isolated after filtration and evaporation of the filtrate. For final purification, flash chromatography on silica gel with methylene chloride as the eluent was employed. **VIII** was obtained as a white, crystalline solid: yield 0.65 g (35% theoretical), mp 112–113 °C (lit. mp 109–111 °C).

Next, the Boc group was removed by acidolysis under strictly anhydrous conditions. A 440 mg (2.1 mmol) portion of **VIII** was dissolved in 2 mL of 1,4-dioxane and treated for 30 min with 2 mL of 4 N HCl in 1,4-dioxane. **IX** was precipitated from diethyl ether. Three hundred mg (97%) of **IX** was obtained: mp 210–212 °C; <sup>13</sup>C NMR (CDCl<sub>3</sub>, ppm) 39.8 (CHCH<sub>2</sub>CH), 56.3 (CH<sub>2</sub>NH), 61.7 (CHC=O), 72.0 (OCH-CH<sub>2</sub>), 175.5 (C=O).

**Preparation of 4-Succinyl-*N*-(*tert*-butoxycarbonyl)pyrrolidinecarboxylic Acid (O-Suc-*N*-Boc-Hyp) (XI).** To a 50 mL flask was added 1.5 g (6.5 mmol) of *N*-Boc-Hyp, 0.85 g (8.5 mmol) of succinic anhydride, 0.80 g (6.5 mmol) of 4-(dimethylamino)pyridine, and 1.8 mL (13.1 mmol) of triethylamine in 25 mL of tetrahydrofuran. The reaction mixture was allowed to stir at room temperature for 15 h. The solvent was removed under reduced pressure and redissolved in water and the pH adjusted to 5 with 1 M KHSO<sub>4</sub>. **XI** was isolated by extraction with methylene chloride, followed by drying over anhydrous MgSO<sub>4</sub> and solvent removal under reduced pressure: <sup>13</sup>C NMR (CDCl<sub>3</sub>, ppm) 28.2 [C(CH<sub>3</sub>)<sub>3</sub>], 28.8 (CH<sub>2</sub>CO<sub>2</sub>H), 29.2 (CH<sub>2</sub>-CO<sub>2</sub>CH), 36.7 (β-CH<sub>2</sub> of Hyp), 51.6 (δ-CH<sub>2</sub> of Hyp), 57.3 (α-CH of Hyp), 72.5 (δ-CH of Hyp), 80.7 [C(CH<sub>3</sub>)<sub>3</sub>], 171.4 (NC=O), 177.4 (CO<sub>2</sub>CH), 178.7 (HO<sub>2</sub>CCH<sub>2</sub>), 179.2 (α-C=O of Hyp).

**Preparation of Poly(PEG-Lys).** Poly(PEG-Lys) (**III**) and the NHS active ester derivative poly(PEG-Lys-NHS) (**VI**) were prepared as previously described from PEG of molecular weight 2000 and L-lysine (7, 23). The molecular weight of poly(PEG-Lys) preparations differed slightly from batch to batch. For this study, batches were selected that had a weight average molecular weight of approximately 50 000 g/mol and a polydispersity of approximately 1.6 (Table 1).

**Preparation of "Ester-Linked" Conjugate, Poly(PEG-Lys-cHyp ester) (V).** To a solution of 5 g (2.3 mmol) of **III** in 350 mL of methylene chloride was added 1.13 g (4.6 mmol) of **II** and 0.61 g (2.3 mmol) of 4-(dimethylamino)pyridine. The solution was cooled to 4 °C, and 0.61 g (3.0 mmol) of 1,3-dicyclohexylcarbodiimide was added. Stirring was continued for 1 week at ambient temperature. The reaction mixture was concentrated to 100 mL by rotary evaporation, cooled to –25 °C to allow maximum precipitation of 1,3-dicyclohexylurea, and filtered. The clear filtrate was precipitated into cold (–5 °C) diethyl ether, isolated by suction filtration, rinsed with several portions of cold diethyl ether, and vacuum dried at room temperature. Yield of the Boc-protected conjugate (**IV**): 5.0 g (90% theoretical). The degree of cHyp attachment was determined by amino acid analysis.

Next, the Boc group was removed by acidolysis under strictly anhydrous conditions. A 2.0 g portion of **IV** in 6 mL of 1,4-dioxane was treated for 2 h with 3 mL of 4 N HCl in 1,4-dioxane. **V** was precipitated by the addition of diethyl ether, reprecipitated from 2-propanol, and vacuum dried, yield 1.77 g (90%). The degree of cHyp attachment was determined by amino acid analysis (see Table 1): <sup>13</sup>C NMR (D<sub>2</sub>O, ppm) 21.8 (γ-CH<sub>2</sub> of Lys), 28.9 (δ-CH<sub>2</sub> of Lys), 31.5 (β-CH<sub>2</sub> of Lys), 36.2 (β-CH<sub>2</sub> of Hyp), 40.0 (ε-CH<sub>2</sub> of Lys), 52.3 (δ-CH<sub>2</sub> of Hyp), 52.7 (–OCH<sub>3</sub> ester of Hyp), 53.5 (α-CH of Lys), 58.3 (α-CH of Hyp), 63.5–72.4 (PEG), 75.5 (γ-CH of Hyp), 155.7 (C=O of ε-NH urethane), 156.3 (C=O of α-NH urethane), 171.6 (α-C=O of Hyp), 174.6 (α-C=O of Lys).

**Preparation of the "Amide-Linked" Conjugate, Poly(PEG-Lys-cHyp amide) (X).** To a 500 mL flask was added 4.0 g (1.7 mmol) of **VI** and 300 mL of methylene chloride. A clear solution formed to which was added with stirring 520 mg (3.5 mmol) of **IX** and 0.70 mL (5.0 mmol) of triethylamine. The reaction mixture was stirred for 6 days at ambient temperature. A precipitate formed which was removed by filtration. The filtrate was evaporated to dryness. The crude product was redissolved in 50 mL of water, the pH was adjusted to 8.5 with solid NaHCO<sub>3</sub>, and the mixture was stirred for 3 h at ambient temperature to hydrolyze the lactone ring. Then, conjugate **X** was extracted into methylene chloride. The organic phase was dried over Na<sub>2</sub>SO<sub>4</sub> and concentrated to a final volume of 15 mL. **X** was precipitated from 2-propanol and vacuum dried, yield 2.3 g (60% theoretical). The degree of cHyp attachment was determined by amino acid analysis (see Table 1): <sup>13</sup>C NMR (D<sub>2</sub>O, ppm) 25.2 (γ-CH<sub>2</sub> of Lys), 31.5 (δ-CH<sub>2</sub> of Lys), 34.5 (β-CH<sub>2</sub> of Lys), 39.5 (β-CH<sub>2</sub> of Hyp), 43.2 (ε-CH<sub>2</sub> of Lys), 55.8 (α-CH of Lys), 57.6 (δ-CH<sub>2</sub> of Hyp), 59.6 (α-CH of Hyp), 63.4–72.6 (PEG), 74.8 (γ-CH of Hyp), 160.8 (ε-C=O of NH urethane), 161.4 (α-C=O of NH urethane), 175.7 (α-C=O of amide), 182.1 (C=O of Hyp).

**Preparation of "Backbone-Linked" Conjugate, Poly(PEG-succinate-cHyp) (XIII).** The procedure of Moore and Stupp was modified (24) as follows. To a 50 mL flask was added 2.4 g (1.2 mmol) of PEG (azeotropically dried with toluene) and 35 mL of methylene chloride. To this solution was added 397.2 mg (1.2 mmol) of **XI**, 141.3 mg (0.5 mmol) of 4-(dimethylamino)pyridinium 4-toluene-sulfonate, and 605.6 mg (4.8 mmol) of 1,3-diisopropylcarbodiimide. The solution was stirred at ambient temperature for 48 h. The precipitate of 1,3-diisopropylurea was removed by filtration. The filtrate was concentrated to 10 mL, and the product was precipitated into diethyl ether. Reprecipitation from 2-propanol, followed by filtration and vacuum drying, afforded poly(PEG-succinate-*N*-Boc-Hyp) (**XII**), yield: 2.1 g (76% theoretical).

**Table 1. Physical Data of the Polymeric Carriers Used**

compd	$M_w (\times 10^4)^a$ (g/mol)	$M_w/M_n$	loading (cHyp/Lys)
poly(PEG-Lys)	4.25	1.66	
poly(PEG-succinate-tHyp)	5.46	1.57	
poly(PEG-succinate-cHyp)	5.29	1.59	
poly(PEG-Lys-cHyp amide)	3.82	1.58	0.14 <sup>b</sup>
poly(PEG-Lys-cHyp ester)	7.77	1.83	0.63 <sup>b</sup>

<sup>a</sup> Weight average molecular weight as determined by GPC relative to poly(ethylene oxide) standards. <sup>b</sup> Loading was determined by amino acid analysis and is expressed as the ratio of cHyp to Lys. A ratio of 1 would indicate attachment of cHyp to all available pendent chains.

Next, the Boc group was removed by acidolysis under strictly anhydrous conditions. A 1.5 g portion of **XII** in 2 mL of 1,4-dioxane was treated for 4 h with 6 mL of 4 N HCl in 1,4-dioxane. **XIII** was precipitated into diethyl ether, filtered, rinsed with several portions of diethyl ether, and vacuum dried. The degree of cHyp incorporation was determined by amino acid analysis (see Table 1). For the *cis*-derivative: <sup>13</sup>C NMR (CDCl<sub>3</sub>) 28.5 (–O<sub>2</sub>CCH<sub>2</sub>CH<sub>2</sub>CO<sub>2</sub>–), 28.7 (–O<sub>2</sub>CCH<sub>2</sub>CH<sub>2</sub>CO<sub>2</sub>–), 34.9 (β-CH<sub>2</sub> of Hyp), 51.1 (δ-CH<sub>2</sub> of Hyp), 58.3 (α-CH of Hyp), 63.8–71.7 (PEG), 72.3 (γ-CH of Hyp), 168.4 (PEG-OC=O), 170.9 (CH<sub>2</sub>CH<sub>2</sub>CO<sub>2</sub>CH), 172.0 (NHCHC=O).

**Biological Studies. Cell Culture.** SMCs and RLFs (1 × 10<sup>6</sup> cells) from fetal rats (American Type Tissue Culture, Rockville, MD) were grown in medium 199 containing 10% FBS, 100 IU/mL of penicillin G, 100 μg/mL of streptomycin, 50 μg/mL of gentamicin, and 50 μg/mL of sodium ascorbate at pH 7.4 on 25 cm<sup>2</sup> plastic tissue culture flasks (Corning Glass Works, Corning, NY) at 37 °C. Cells were grown under 95% air, 5% CO<sub>2</sub>, harvested with trypsin–EDTA after the fourth passage, seeded (1 × 10<sup>5</sup> cells/dish) onto polystyrene dishes (35 mm diameter, 10 mm depth, Corning), and grown in the above medium with 0.5% FBS for 24 h. Cells were placed in fresh medium containing 10% FBS to stimulate growth, and the test substance was added. Cells were grown without changing the medium for 6 days. Cell number was counted with a hemocytometer at regular intervals. Cell viability was assayed by trypan blue exclusion.

**In Vitro Assay of the Antifibrotic Effect of Test Compounds.** Antifibrotic effects were tested by measuring inhibition of SMCs and RLFs grown on collagen-free plastic culture dishes in the presence of the test compounds. This assay is based on the principle that cells grown on plastic dishes must secrete a collagenous protein to attach and grow (25). Cell growth on collagen-free tissue culture dishes was compared to cell growth on plates precoated with type I rat tail collagen in the presence of the same test compound. This comparison made it possible to exclude cytotoxic effects and to check for specificity of inhibition of collagen secretion. The percent growth inhibition was determined relative to cell growth in the presence of biologically inactive tHyp using the following equation:

$$\text{growth inhibition (\%)} = \frac{[(\text{cells in presence of tHyp}) - (\text{cells in presence of test compound})]100}{(\text{cells in presence of tHyp})}$$

The “minimum inhibitory concentration” (MIC) was defined as that concentration of test compound which inhibited cell growth by 50 ± 10%.

In all assays, test or control compounds were added to the tissue culture medium at known concentrations at day 0 and cell numbers were monitored daily for up to 6

days. For macromolecular conjugates, the amount of cHyp contained per gram of conjugate was calculated based on the known chemical composition of the conjugate (Table 2).

**In Vivo Antifibrotic Effect of the Compounds.** The ability of the test substance to inhibit collagen accumulation in sponges implanted in rats was used as an index of the *in vivo* antifibrotic effect. Poly(vinyl alcohol) sponges, 1.6 cm<sup>3</sup> in size, were impregnated with the appropriate test compound dissolved in 1.0 mL of phosphate-buffered saline (0.1 M, pH 7.4) such that a cHyp content of 0.741 mg/sponge was achieved (Table 3). Each sponge was implanted subcutaneously in the dorsal thorax of rats anesthetized by intraperitoneal injection of 0.4 mL of ketamine solution (26). After 14 days, the rats were sacrificed, and the sponges were removed. After loose fibrinous material was removed from the surfaces of the sponge, the entire sponge was hydrolyzed in 6 N HCl for 48 h at 116 °C. The hydrolysate was evaporated, the residue suspended in water, and an aliquot assayed in triplicate for hydroxyproline using the method of Kiviriko *et al.* (27). Total protein content was determined in triplicate using the ninhydrin method (28) with leucine as the standard. The results were expressed as collagen content per gram of sponge and as total protein content per gram of sponge.

**Statistical Analysis.** Data were analyzed by two-way analysis of variance using a statistical software package ((1982) SAS User's Guide, Statistics, pp 119–137, SAS Institute: Carey, NC) followed by Duncan's post-hoc test (29). A *p* value < 0.05 was considered significant.

## RESULTS AND DISCUSSION

**Synthetic Aspects of Carrier Design.** It is well established that the biological activity of a drug carrier critically depends upon its molecular architecture. Therefore, two distinctly different synthetic strategies (Figure 1) were used in the design of cHyp conjugates. In one strategy, cHyp was attached as a pendent chain via covalent linkages to the poly(PEG-Lys) backbone. By varying the linking bond from ester (Figure 3) to amide (Figure 4), the effect of different rates of hydrolytic cleavage of the drug from the polymeric backbone could be explored. The corresponding conjugates were designated as poly(PEG-Lys-cHyp ester) (**V**) and poly(PEG-Lys-cHyp amide) (**X**), respectively. In a second approach, cHyp was incorporated via hydrolytically labile bonds into the polymeric backbone itself (Figure 5). Thus, free cHyp was expected to be liberated upon backbone degradation. The corresponding conjugate was designated as poly(PEG-succinate-cHyp) (**XIII**).

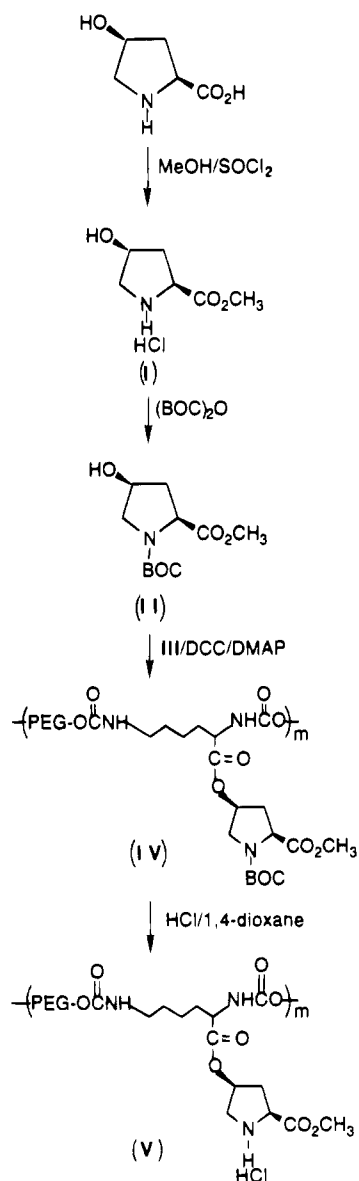
For the construction of the pendent chain systems, the previously described poly(PEG-Lys) was used as the backbone. As shown in Figure 2, this backbone can be regarded as a poly(ether urethane) which in previous studies (7) appeared to be nondegradable under physiological conditions. The poly(PEG-Lys) backbone was prepared by published procedures, and the molecular weight of all batches was characterized by GPC. Next, cHyp was attached to the polymeric backbone via ester or amide bonds, using the reactions outlined in Figures 3 and 4, respectively. Since different batches of poly(PEG-Lys) were used as starting materials in these reactions, some variations in the length of the backbone were unavoidable (Table 1). In general, the molecular weights were in the range of 50 000 g/mol, as determined by GPC relative to poly(ethylene oxide) standards.

The success of the attachment reactions was ascertained by amino acid analysis after total hydrolysis of the conjugate. Briefly, a ratio of 1:1 between Lys and

**Table 2. Molecular Conjugates Tested *in Vitro***

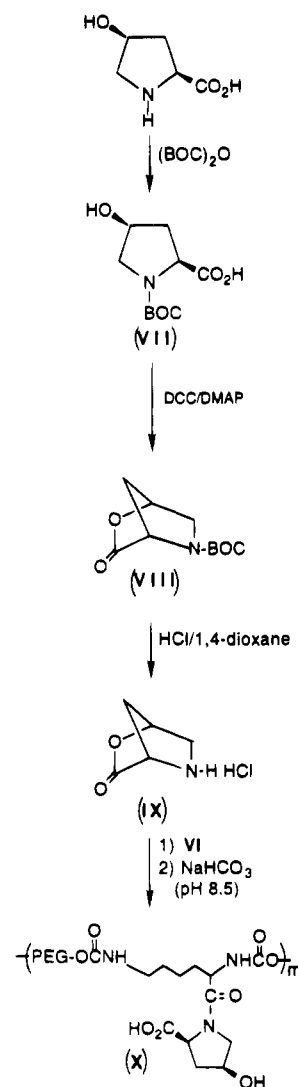
compd	conjugate concn <sup>a</sup> (μg/mL)	cHyp concn <sup>b</sup> (μg/mL)	growth inhibition after 5 days <sup>c</sup> (%)	
			SMC	RLF
poly(PEG-succinate-cHyp)	1000	59	13 <sup>d</sup>	<1 <sup>d</sup>
	2000	118	25 <sup>e</sup>	31 <sup>e</sup>
poly(PEG-Lys-cHyp amide)	1000	8	47 <sup>e</sup>	49 <sup>e</sup>
poly(PEG-Lys-cHyp ester)	1000	36	38 <sup>e</sup>	17 <sup>e</sup>
poly(PEG-Lys) + cHyp	943 + 57	57	4 <sup>d</sup>	3 <sup>d</sup>

<sup>a</sup> Concentration of the test compound added to the tissue culture medium. <sup>b</sup> Corresponding concentration of polymer-bound cHyp (μg/mL). <sup>c</sup> Growth inhibition (%) = [(cells in presence of tHyp) - (cells in presence of test compound)]100/(cells in presence of tHyp). <sup>d</sup> Difference in growth in presence of tHyp is not statistically significant ( $p > 0.05$ ). <sup>e</sup> Difference in growth in presence of tHyp is statistically significant ( $p < 0.05$ ).

**Figure 3.** Synthetic scheme for the preparation of poly(PEG-Lys-cHyp ester) (V).

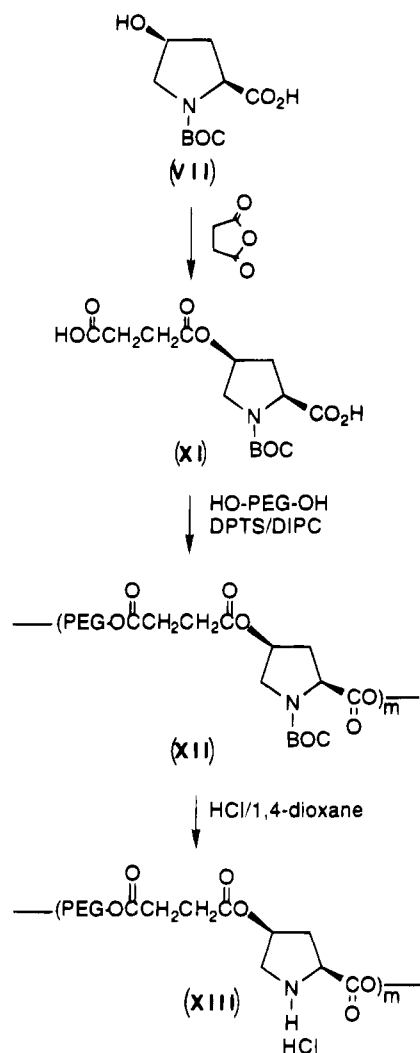
cHyp would indicate the quantitative attachment of cHyp to all available pendent chains. As shown in Table 1, this ideal situation was not achieved by the currently available reaction schemes. The differences in loading between individual conjugates were taken into account by calculating the amount of polymer-bound cHyp contained per gram of each conjugate (Table 2).

Crosslinking of two pendent carboxylic acid groups by DCC-mediated anhydride formation represented the most significant side reaction during the preparation of the conjugate V (Figure 3). The temporary formation of

**Figure 4.** Synthetic scheme for the preparation of poly(PEG-Lys-cHyp amide) (X).

anhydrides could be observed by <sup>13</sup>C NMR and by the gellation of the reaction product due to crosslinking. Fortunately, the anhydrides were readily hydrolyzed during the aqueous work up of the conjugate, thereby regenerating a freely soluble product with "unoccupied" carboxylic acid pendent groups. No loss of the covalently attached cHyp was observed during this step. In accordance with this mechanism, the degree of attachment of cHyp during preparation of the poly(PEG-Lys-cHyp ester) conjugate could be increased by increasing the molar excess of the protected cHyp derivative II in the coupling mixture. Striking a balance between the need to avoid unnecessary losses of cHyp and the need to achieve high loading, a 2-fold molar excess of II in the reaction mixture was selected. This resulted in an





**Figure 5.** Synthetic scheme for the preparation of poly(PEG-succinate-cHyp) (XIII).

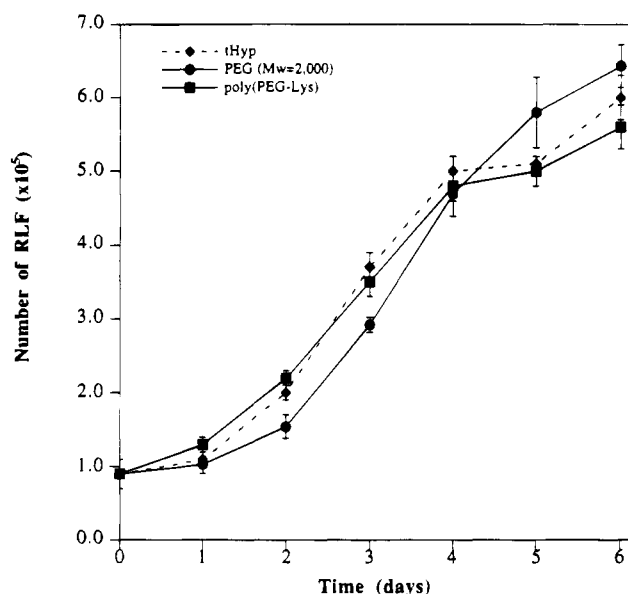
attachment yield of 63%; i.e., cHyp was linked to 63% of all available pendent chains.

The attachment of cHyp during the preparation of poly(PEG-Lys-cHyp amide) proceeded with an attachment yield of only about 14%; i.e., cHyp was linked to 14% of all available pendent chains. The low attachment yield was related to the surprisingly sluggish reaction of lactone **IX** with poly(PEG-Lys NHS) (**VI**), the activated succinimidyl ester of poly(PEG-Lys). In previous studies, **VI** reacted rapidly and at high yield with amine-containing ligands (7, 23). The low yield of the attachment reaction was likely due to the limited solubility of lactone **IX** in methylene chloride.

Treatment of poly(PEG-Lys-cHyp amide) during the final workup with aqueous base (pH 8.5) assured both the complete ring-opening of the attached lactone as well as the hydrolysis of any remaining succinimidyl pendent groups to free acid. One may therefore expect that any "unoccupied" pendent chains in the poly(PEG-Lys-cHyp amide) conjugate existed as free carboxylic acid groups.

In more recent studies, dimethylformamide (DMF) was used in place of methylene chloride. This change increased the cHyp attachment yield to 65%. However, this recently synthesized material was not available when the biological studies (see below) were performed.

**In Vitro Antifibrotic Activity.** As reported previously (25), the ability of RLFs and SMCs to produce a collagenous extracellular matrix is a requirement for cell

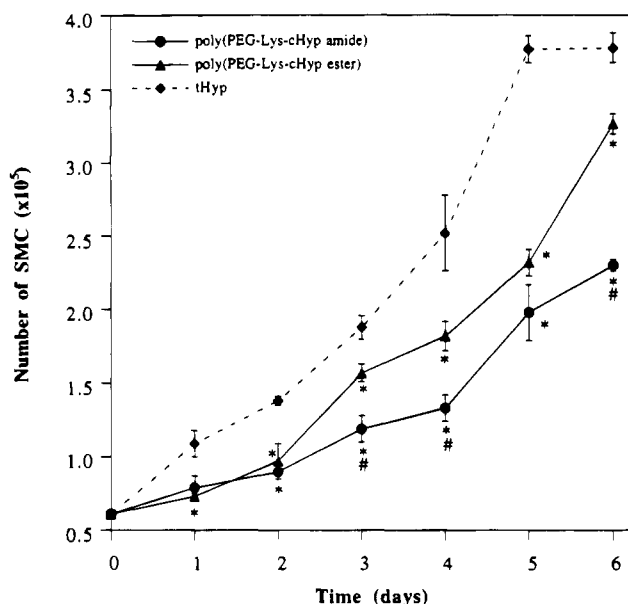


**Figure 6.** Control experiments ( $n = 5$ ) showing the absence of growth inhibition for tHyp, PEG ( $M_w = 2000$ ), and unloaded poly(PEG-Lys) at a concentration of 1 mg/mL in RLF cultures using uncoated (collagen-free) plates. The growth of quiescent cells was stimulated by addition of 10% FBS (day zero), and cells were counted daily. There were no statistically significant differences. Similar results were obtained in cultures of SMCs.

growth on tissue culture plates. Therefore, in collagen-free tissue culture plates, test substances that inhibit collagen synthesis also inhibit cell growth. This principle has been used for the development of an *in vitro* assay for collagen inhibition (17, 25). The assay can distinguish between a specific collagen synthesis inhibitory effect and nonspecific cytotoxicity. When tissue culture plates are precoated with collagen, cells do not have to synthesize their own collagen and will grow normally in the presence of a specific collagen synthesis inhibitor but will not grow in the presence of a cytotoxic agent. One limitation of the assay is that the test period is restricted to a maximum of 6 days due to the limited viability of RLF or SMC cultures. By defining the "minimum inhibitory concentration" (MIC) as that concentration resulting in  $50 \pm 10\%$  cell growth inhibition (see Materials and Methods), previous studies had established a MIC of 1 mg per mL of cell culture medium for free cHyp (17). On the basis of these prior observations, test compounds were usually dosed at 1 mg/mL and cell growth was monitored over a 6 day observation period in all assays.

A number of control experiments were conducted, using both uncoated and collagen-precoated tissue culture plates. At 1 mg/mL, tHyp, PEG ( $M_w = 2000$  g/mol), and "unloaded" poly(PEG-Lys) had no inhibitory or cytotoxic activity in either RLF or SMC cultures (Figure 6). Using collagen-precoated plates, the macromolecular conjugates [poly(PEG-Lys-cHyp amide) (**X**), poly(PEG-Lys-cHyp ester) (**V**), and poly(PEG-succinate-cHyp) (**XIII**)] were further tested for nonspecific cytotoxic effects in RLF and SMC cultures at an increased concentration of 2 mg/mL. Even at this higher dose, there was no growth inhibition (data not shown), indicating the absence of nonspecific cytotoxic effects.

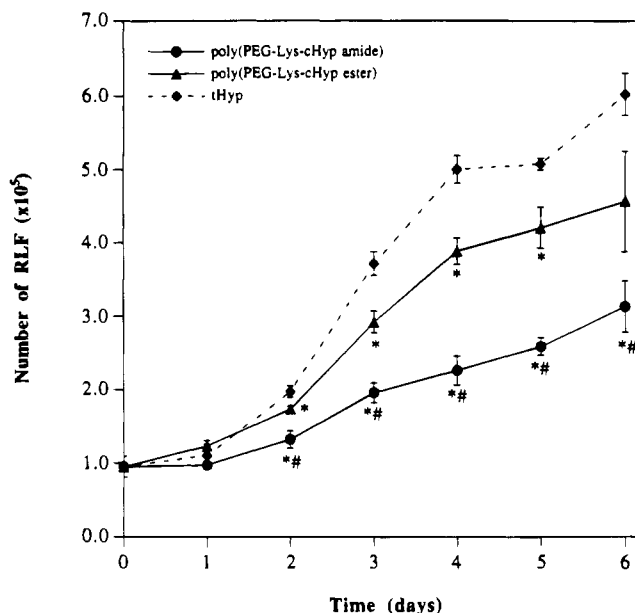
Then, the same macromolecular conjugates [poly(PEG-Lys-cHyp amide) (**X**), poly(PEG-Lys-cHyp ester) (**V**), and poly(PEG-succinate-cHyp) (**XIII**)] were tested in uncoated plates. Under these conditions, a statistically significant inhibition of cell growth (relative to cell growth in the presence of inactive tHyp) was observed.



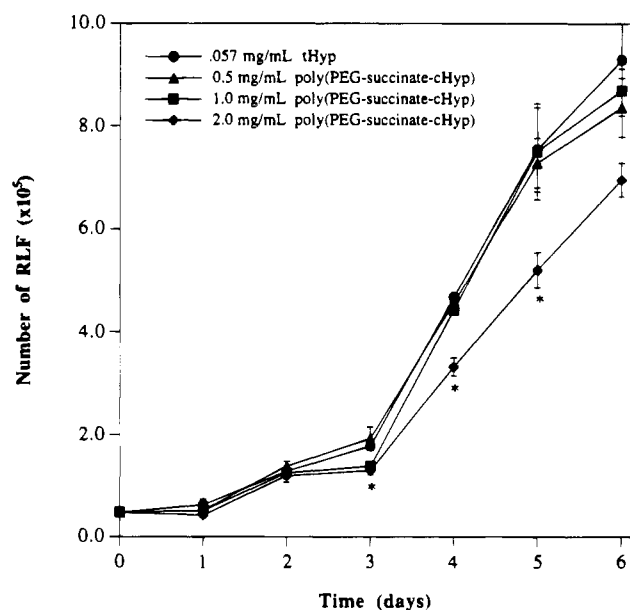
**Figure 7.** Inhibition of the growth of SMCs in uncoated plates by the macromolecular pendent chain systems poly(PEG-Lys-cHyp amide) (X) and poly(PEG-Lys-cHyp ester) (V), as compared to cell growth in the presence of biologically inactive tHyp (control). The growth of quiescent cells was stimulated by addition of 10% FBS (day zero), and cells were counted daily. The macromolecular conjugates were added at a concentration of 1 mg/mL. On the basis of their respective loading, the content of cHyp varied for each conjugate (see Table 2). Data points represent the mean of five repetitions. Error bars are the standard error of the mean. \* indicates that the data point is significantly different from the tHyp control, and # indicates a significant difference between the amide-linked (X) and ester-linked (V) conjugates ( $p < 0.05$ ).

In one set of experiments (Figure 7), the number of SMCs was significantly reduced in the presence of 1 mg/mL of the amide- and ester-linked pendent chain systems (X and V). Under identical experimental conditions, statistically significant growth inhibition was also observed in cultures of RLF (Figure 8). Since cHyp is bound to conjugates with different chemical structures, each type of polymeric conjugate contains a different quantity of bound cHyp per unit weight. In this situation, one could base the experimental design on keeping the amount of bound cHyp constant, which would require the use of varying quantities of cHyp-conjugates. Alternatively, one could keep the amount of drug conjugate constant, resulting in variations in the amount of bound cHyp. Since clinicians often think in terms of dosage, we chose to keep the amount of drug conjugate constant, using 1 mg/mL as the standard concentration in all comparative experiments (Table 2). On the basis of the experimentally determined loadings of the amide- and ester-linked pendent chain systems (X and V) the corresponding concentrations of polymer bound cHyp were 8 and 36  $\mu\text{g/mL}$  respectively (Table 2).

Initial experiments were conducted to develop dose-response correlations. For pendent chain systems X and V no inhibition of growth was observed for either SMC or RLF at 0.5 mg/mL, while significant inhibition of growth was observed at 1 mg/mL. On the basis of the data collected in Table 2, the MIC of poly(PEG-Lys-cHyp amide) (X) could be estimated to be about 8  $\mu\text{g}$  of bound cHyp per mL while the MIC of poly(PEG-Lys-cHyp ester) (V) was in the range of 36  $\mu\text{g}$  of bound cHyp per mL. Thus, for the amide-linked conjugate, polymer-bound cHyp had a MIC that was about 100-fold smaller than the MIC of free cHyp (1 mg/mL) (17), while for the ester-



**Figure 8.** Inhibition of the growth of RLFs in uncoated plates by the macromolecular pendent chain systems poly(PEG-Lys-cHyp amide) (X) and poly(PEG-Lys-cHyp ester) (V), as compared to cell growth in the presence of biologically inactive tHyp (control). For experimental details, see legend to Figure 7. \* indicates that the data point is significantly different from the tHyp control, and # indicates a significant difference between the amide-linked (X) and ester-linked (V) conjugates ( $p < 0.05$ ).



**Figure 9.** Dose-response studies for poly(PEG-succinate-cHyp) (XIII) in RLF cultures on untreated (collagen-free) plates. For experimental details, see legend to Figure 7. Data points representing statistically significant growth inhibition relative to the tHyp control ( $p < 0.05$ ) are marked by \*.

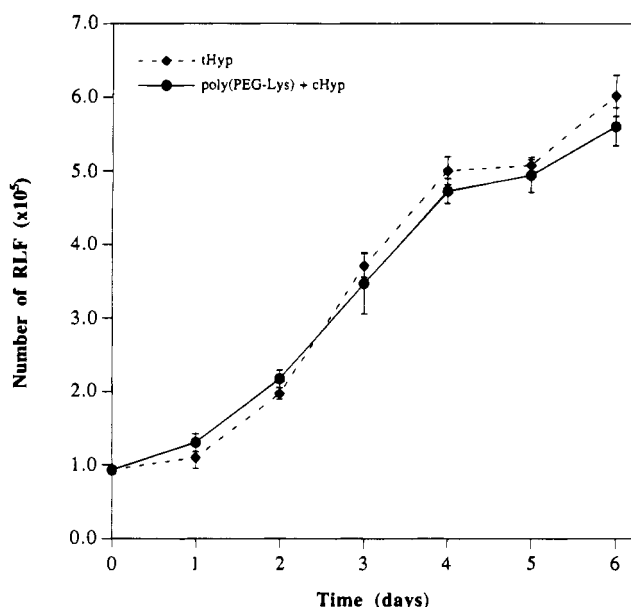
linked conjugate, polymer-bound cHyp had a MIC that was about 20-fold smaller than the MIC of free cHyp.

The backbone-linked system, poly(PEG-succinate-cHyp) (XIII), exhibited a reduced level of bioactivity relative to the pendent-linked systems. Dose-response studies showed that statistically significant growth inhibition required a dose of at least 2 mg/mL of conjugate, corresponding to 118  $\mu\text{g/mL}$  of polymer-bound cHyp. Experimental data for poly(PEG-succinate-cHyp) in cultures of RLF are summarized in Figure 9. Similar results were obtained for SMCs.

**Table 3. Results of Poly(vinyl alcohol) Sponge Studies *in Vivo***

compd	amount absorbed in sponge prior to implantation		sponge contents after explantation	
	test compd <sup>a</sup> (mg)	cHyp content <sup>b</sup> (mg)	total protein content <sup>c</sup> (mg/g of sponge)	collagen content <sup>d</sup> (mg/g of sponge)
controls				
phosphate buffered saline	N/A	N/A	56 ± 4	1.9 ± 0.1
poly(PEG-Lys) + cHyp	99.26 ± 0.74	0.741	58 ± 4	1.9 ± 0.1
poly(PEG-succinate-tHyp)	12.60	0	58 ± 5	2.0 ± 0.1
test compounds				
poly(PEG-succinate-cHyp)	12.56	0.741	55 ± 5	1.8 ± 0.1
poly(PEG-Lys-cHyp ester)	20.58	0.741		1.9 ± 0.1
poly(PEG-Lys-cHyp amide)	92.63	0.741	58 ± 1	1.3 ± 0.1 <sup>e</sup>

<sup>a</sup> Amount of macromolecular conjugate in 1.0 mL of phosphate-buffered saline (0.1 M, pH 7.4) used to saturate one poly(vinyl alcohol) sponge. <sup>b</sup> Calculated cHyp content of a single sponge. <sup>c</sup> Measured based on leucine after total hydrolysis of the sponge. <sup>d</sup> Measured as tHyp after total hydrolysis of the sponges. <sup>e</sup> Statistically significant ( $n = 5$ ,  $p < 0.05$ ) compared to all other groups.



**Figure 10.** Growth inhibition of RLF cultures in the presence of a physical mixture of 943  $\mu\text{g/mL}$  of poly(PEG-Lys) and 57  $\mu\text{g/mL}$  of cHyp. These proportions correspond to the theoretical composition of the pendent chain systems (V) and (X). For experimental details, see legend to Figure 7. There was no significant difference between growth in the presence of the mixture of poly(PEG-Lys) and cHyp and growth in the presence of tHyp.

In view of the lack of growth inhibition in collagen-coated plates, the results illustrated in Figures 7–9 indicate that the three tested macromolecular conjugates had a specific, inhibitory effect on the biosynthesis of collagen. Compared to free cHyp (MIC = 1 mg/mL), the bioactivity of polymer-bound cHyp was markedly increased. Furthermore, all macromolecular conjugates exhibited an inhibitory effect throughout the 6 day period of cell viability, while for free cHyp growth inhibition was observed for up to 4 days only (17).

To study the factors that led to the significant increase in the bioactivity of the macromolecular conjugates relative to free cHyp, the possibility of synergism between poly(PEG-Lys) and cHyp was explored. A synergistic effect could conceivably be caused by the "disruption" of the cell membrane by poly(PEG-Lys), resulting in enhanced cellular uptake of cHyp in a nonspecific manner (30). Therefore, a physical mixture of "unloaded" poly(PEG-Lys) and cHyp in proportions identical to the theoretical composition of the covalently linked pendent chain conjugates (V and X) was tested (Table 2 and Figure 10). The absence of any growth inhibitory effect in either RLF or SMC cultures excluded a synergistic effect between the unloaded carrier and cHyp. Thus, a

covalent linkage between the polymeric carrier and cHyp appeared to be a necessary requirement for the observed enhancement of the inhibitory activity.

***In Vivo* Antifibrotic Effect of the Test Compounds.** The antifibrotic effect of several cHyp conjugates *in vivo* was investigated using the subcutaneous implantation of porous poly(vinyl alcohol) sponges in rats as a model system (26). After implantation of these sponges, fibroblasts infiltrate into the sponge resulting in the accumulation of extracellular matrix proteins in the interior of the sponge.

In our preliminary screening experiments, sterile, dry sponges were impregnated with sterile PBS solutions containing known quantities of control and test compounds (Table 3). Two weeks postimplantation, the sponges were retrieved, freed of externally adhering fibrinous tissue, and hydrolyzed under conditions which led to the complete hydrolysis of all proteins contained within the sponge. Next, the amount of leucine (Leu), tHyp, and cHyp present in the hydrolysate was determined by amino acid analysis. Leu served as a marker for the total protein content of the sponge (28), while tHyp was taken as a marker for collagen content (27). cHyp served as an indicator for the presence of residual conjugates after 14 days of implantation. The ratio of "collagen content" to "total protein content" can be regarded as an approximate indicator of the level of collagen accumulation by cells residing within the poly(vinyl alcohol) sponge.

Three different control substances were used (Table 3): phosphate-buffered saline solution (pH 7.4), a physical mixture of unloaded poly(PEG-Lys) and cHyp in proportions corresponding to the theoretical composition of the pendent chain conjugates (V and X), and poly(PEG-succinate-tHyp), the backbone-linked conjugate containing biologically inactive tHyp instead of cHyp.

Fourteen days post implantation, these control sponges contained (per gram of sponge) about 58 mg of protein and about 1.9 mg of collagen (Table 3). Among sponges impregnated with the three macromolecular conjugates, poly(PEG-Lys-cHyp amide) (X), poly(PEG-Lys-cHyp ester) (V), and poly(PEG-succinate-cHyp) (XIII), only those treated with poly(PEG-Lys-cHyp amide) contained significantly less collagen ( $p < 0.05$ ). Compared to control sponges, poly(PEG-Lys-cHyp amide) suppressed the accumulation of collagen by 33%. Since there was no reduction in the total protein content of poly(PEG-Lys-cHyp amide)-treated sponges, the effect of poly(PEG-Lys-cHyp amide) seemed to be specific for inhibiting the biosynthesis of collagen.

It is noteworthy that cHyp could not be detected in the hydrolysates. This indicated that no detectable amounts of defective collagen (collagen containing cHyp) and no residual polymer-linked cHyp remained in the sponges.

## CONCLUSION

Among the different molecular architectures for macromolecular conjugates (Figure 1), the "pendent chain systems" had the most pronounced growth inhibitory effect. Both poly(PEG-Lys-cHyp ester) and poly(PEG-Lys-cHyp amide) showed prolonged inhibition of cell growth throughout the entire duration of the assays (6 days) at substantially lower doses than free cHyp. In comparison, the "backbone system", poly(PEG-succinate-cHyp), exhibited a less marked enhancement of bioactivity relative to free cHyp itself. The absence of cell growth inhibition on collagen-precoated tissue culture plates provided evidence that the observed growth inhibition was due to the specific inhibition of collagen synthesis.

Our results further indicated that a simple synergistic effect between poly(PEG-Lys), the "unloaded carrier", and cHyp can be excluded as a possible mechanism for the observed enhancement of the bioactivity of cHyp upon attachment to the polymeric carrier. The higher activity of the hydrolytically stable poly(PEG-Lys-cHyp amide) conjugate as compared to the less stable poly(PEG-Lys-cHyp ester) further strengthened the conclusion that a hydrolytically stable linkage between cHyp and the polymeric backbone is needed to maximize the antifibrotic activity of these conjugates. Since the biosynthesis of collagen occurs within the cytoplasm, the increased inhibitory effect of the macromolecular pendent chain systems could be an indication of the improved cellular uptake of the macromolecular conjugate as compared to free cHyp. This observation could have far-reaching implications since the efficacy of a wide range of drugs could be increased by improved cellular uptake.

A statistically significant antifibrotic effect of poly(PEG-Lys-cHyp amide) was also observed *in vivo*. Poly(vinyl alcohol) sponges impregnated with poly(PEG-Lys-cHyp amide) had a 33% decrease in collagen accumulation 14 days after subcutaneous implantation as compared to control sponges. These results are of a preliminary nature since the release kinetics of these conjugates from the sponge were not determined and no attempt was made to optimize the amount of test conjugate incorporated into the sponge. In spite of these shortcomings, the demonstration of an antifibrotic effect *in vivo* provided the first experimental evidence that "pendent chain-type" macromolecular conjugates of cHyp may be clinically useful as antifibrotic agents. By facilitating local, sustained release of cHyp, these conjugates may provide new treatment options in fibrotic disorders which produce scarring in humans.

The scope of this paper was limited to the synthesis of a new class of drug carriers and the evaluation of their *in vitro* and *in vivo* bioactivity. The observed bioactivity profiles pose a number of intriguing questions relating to the mode of action of the poly(PEG-Lys) system. To further study the mechanism of cellular uptake, radioactively labeled derivatives of all drug conjugates have been prepared. The results of these mechanistic studies will be reported in a future publication.

## ACKNOWLEDGMENT

This work was supported by the Research Service of the Department of Veterans Affairs, a Johnson & Johnson Focused Giving Award, and a Glaxo Cardiovascular Discovery Grant. We thank Dr. Holly Strong for assistance with the poly(vinyl alcohol) sponge studies and Mr. Samuel Kantor and Mr. Jeffrey Messinger for their assistance with the synthesis of some of the polymeric conjugates.

## LITERATURE CITED

- (1) Duncan, R., and Kopecek, J. (1984) Soluble synthetic polymers as potential drug carriers. *Adv. Polym. Sci.* 57, 53–101.
- (2) Drobnik, J. (1989) Biodegradable soluble macromolecules as drug carriers. *Adv. Drug Del. Rev.* 3, 229–245.
- (3) Li, X., Bennett, D. B., Adams, N. W., and Kim, S. W. (1991) Poly( $\alpha$ -amino acid)-drug conjugates. *Polymeric Drug and Drug Delivery Systems* (R. L. Dunn, and R. M. Ottenbrite, Eds.) pp 101–116, American Chemical Society, Washington, DC.
- (4) Yokoyama, M., Inoue, S., Kataoka, K., Yui, N., Okano, T., and Sakurai, Y. (1989) Molecular design for missile drug: Synthesis of adriamycin conjugated with immunoglobulin G using poly(ethylene glycol)-block-poly(aspartic acid) as intermediate carrier. *Macromol. Chem.* 190, 2041–2054.
- (5) Caliceti, P., Monfardini, C., Sartore, L., Schiavon, O., Baccichetti, F., Carlassare, F., and Veronese, F. M. (1993) Preparation and properties of monomethoxy poly(ethylene glycol) doxorubicin conjugates linked by an amino acid or a peptide as spacer. *Il Farmaco* 48, 919–932.
- (6) Nathan, A., Zalipsky, S., and Kohn, J. (1990) Polyethylene glycol-lysine copolymers: New biocompatible polymers for biomedical applications. *Am. Chem. Soc., Polym. Preprints* 31, 213–214.
- (7) Nathan, A., Zalipsky, S., Ertel, S. I., Agathos, S. N., Yarmush, M. L., and Kohn, J. (1993) Copolymers of lysine and polyethylene glycol: A new family of functionalized drug-carriers. *Bioconjugate Chem.* 4, 54–62.
- (8) Nathan, A., Zalipsky, S., and Kohn, J. (1994) Strategies for covalent attachment of doxorubicin to poly(PEG-Lys), a new water-soluble poly(ether urethane). *J. Bioact. Compat. Polym.* 9, 239–251.
- (9) Gean, K. F., Messinger, J. A., Poiani, G. G., Riley, D. J., and Kohn, J. (1992) New polymeric carriers of cis-hydroxy-L-proline: Potential agents for the inhibition of collagen synthesis. *Am. Chem. Soc., Polym. Preprints* 33, 51–52.
- (10) Gean, K. F., Kantor, S. A., Poiani, G. J., Riley, D. J., and Kohn, J. Polymeric carriers of cis-hydroxy-L-proline with improved antifibrotic activity. *20th International Symposium on Controlled Release of Bioactive Materials*, pp 152–153, Controlled Release Society, Washington, DC, 1993.
- (11) Kohn, J., Gean, K. F., Nathan, A., Poiani, G. J., Riley, D. J., and Zalipsky, S. (1993) New drug conjugates: Attachment of small molecules to poly(PEG-Lys). *Proc. Am. Chem. Soc., Div. Polym. Mat. Sci. Eng.* pp 515–516, American Chemical Society, Washington, DC.
- (12) Uitto, J., and Prockop, D. J. (1975) Inhibition of collagen accumulation by proline analogues: the mechanism of their action. *Collagen metabolism in the liver* (M. P. K. Becker, Ed.) pp 139–148, Stratton Intercontinental Medical Book Corp., New York.
- (13) Riley, D. J., Kerr, J. S., and Berg, R. A. (1981) Prevention of bleomycin-induced pulmonary fibrosis in the hamster by cis-4-hydroxy-L-proline. *Am. Rev. Respir. Dis.* 123, 388–393.
- (14) Riley, D. J., Berg, R. A., Edelman, N. H., and Prockop, D. J. (1980) Prevention of collagen deposition following pulmonary oxygen toxicity in the rat by cis-4-hydroxy-L-proline. *J. Clin. Invest.* 65, 643–651.
- (15) Kerr, J. S., Ruppert, C. L., Tozzi, C. A., Neubauer, J. A., Frankel, H. M., Yu, S. Y., and Riley, D. J. (1987) Reduction of chronic hypoxic pulmonary hypertension in the rat by an inhibitor of collagen production. *Am. Rev. Respir. Dis.* 135, 300–306.
- (16) Poiani, G. J., Tozzi, C. A., Choe, J. K., Yohn, S. E., and Riley, D. J. (1990) An antifibrotic agent reduces blood pressure in established pulmonary hypertension. *J. Appl. Physiol.* 68, 1542–1547.
- (17) Poiani, G. J., Gean, K. F., Fox, J. D., Kohn, J., and Riley, D. J. (1993) Antifibrotic effect of a proline analogue delivered in liposomes to cells in culture. *Amino Acids* 4, 237–248.
- (18) Eldridge, C. F., Bunge, R. P., and Bunge, M. E. (1988) Effects of cis-4-hydroxy-L-proline, an inhibitor of Schwann cell differentiation, on the secretion of collagenous and noncollagenous proteins by Schwann cells. *Exp. Cell. Res.* 174, 491–501.

- (19) Greenstein, J. P., and Winitz, M. (1961) *Chemistry of the Amino Acids*, pp Illustrative procedure 10–51, 927, John Wiley and Sons, New York.
- (20) Perseo, D. G., Piani, S., and Castiglione, R. (1983) Preparation and analytical data of some unusual t-butoxycarbonyl-amino acids. *Int. J. Peptide Protein Res.* 21, 227–230.
- (21) Papaioannou, D., Stavropoulos, G., Karagiannis, K., Francis, G., Brekke, T., and Aksnes, D. (1990) Simple synthesis of cis-4-hydroxy-L-proline and derivatives for use as intermediates in peptide synthesis. *Acta. Chem. Scand.* 44, 243–251.
- (22) Bowers-Nemia, M. M., and Joullie, M. (1983) A short improved synthesis of N-substituted 5-aza-2-oxa-3-oxo-bicyclo[2.2.1] heptanes. *Heterocycles* 20, 817–828.
- (23) Nathan, A., Bolikal, D., Vyavahare, N., Zalipsky, S., and Kohn, J. (1992) Hydrogels based on water-soluble poly(ether urethanes) derived from L-lysine and poly(ethylene glycol). *Macromolecules* 25, 4476–4484.
- (24) Moore, J. S., and Stupp, S. I. (1990) Room temperature polyesterification. *Macromolecules* 23, 65–70.
- (25) Kao, W. W.-Y., and Prockop, D. J. (1977) Proline analogue removes fibroblasts from cultured mixed cell populations. *Nature* 266, 63–64.
- (26) Dayan, D., and Shosban, S. (1982) The effect of cis-hydroxyproline on de-novo synthesized collagen in subcutaneously implanted polyvinyl sponges in rats. *Cell. Molec. Biol.* 28, 217–219.
- (27) Kiviriko, K. I., Laitinen, O., and Prockop, D. J. (1967) Modifications of a specific assay for hydroxyproline in urine. *Anal. Biochem.* 19, 249–255.
- (28) Moore, S., and Stein, W. H. (1948) Photometric ninhydrin method for use in the chromatography of amino-acids. *J. Biol. Chem.* 176, 367–388.
- (29) Duncan, D. B. (1975) t-Tests and intervals for comparisons suggested by the data. *Biometrics* 31, 339–359.
- (30) Jayasuriya, N., Bosak, S., and Regen, S. (1990) Design, synthesis, and activity of membrane-disrupting bolaphiles. *J. Am. Chem. Soc.* 112, 5844–5850.

# Characterization of Protein–Hapten Conjugates. 1. Matrix-Assisted Laser Desorption Ionization Mass Spectrometry of Immuno BSA–Hapten Conjugates and Comparison with Other Characterization Methods<sup>1</sup>

Maciej Adamczyk,\* Alex Buko,<sup>†</sup> Yon-Yih Chen, Jeffrey R. Fishpugh, John C. Gebler, and Donald D. Johnson

Division Organic Chemistry Research (D-9NM), Abbott Diagnostics Division, Abbott Laboratories, Abbott Park, Illinois 60064, and Structural Chemistry (D-418), Pharmaceutical Products Division, Abbott Laboratories, Abbott Park, Illinois 60064. Received April 5, 1994<sup>®</sup>

Several different low molecular weight haptens were conjugated to BSA to produce immunogens useful for antibody development. The extent of BSA modification due to covalent attachment of hapten was estimated by matrix-assisted laser desorption ionization mass spectrometry. The average number of hapten incorporated to immunogen was determined from the difference in the measured molecular weights of the conjugate from nonmodified BSA. The results from mass spectrometry were compared with results obtained from other more traditional methods of immunogen characterization (UV analysis, trinitrobenzenesulfonic acid titrations, and gel electrophoresis). In each case we were able to calculate the average number of hapten covalently bound to BSA for each synthetically prepared immunogen using matrix-assisted laser desorption ionization mass spectrometry. The other methods presented limitations in certain cases.

## INTRODUCTION

Immunogens are structurally complex high molecular weight materials which evoke an immune response in host animals leading to antibody production. Small molecules (haptens < 1000 Da) generally do not, as such, trigger an immune response since their low molecular weight and simplicity is not sufficient to trigger a recipient's immune system. However, it is possible to elicit antibodies with affinity to such haptens by conjugating to a carrier protein forming an immunogen (1). Two very common carrier proteins employed are bovine serum albumin (BSA) and keyhole limpet hemocyanin (KLH) (2). BSA is well suited as a carrier protein due to its high solubility in various aqueous buffers, moderate molecular weight (~66 kDa), and high content of available primary amines (59 lysines plus the terminal amine) which facilitate easy attachment of hapten. The popularity of BSA is further enhanced by its availability from several different manufacturers in large quantities, reasonable cost, and high purity. Resulting immunogens are generally easy to reproduce and characterize using a variety of methods. Immunogens based on KLH have been frequently used; however, they are difficult to characterize due to poor solubility, variable mass ( $4.5 \times 10^5$ – $1.3 \times 10^7$ ) of the starting protein, and inconsistencies in the purity of the KLH between manufacturers and manufacturing lots. Chemistries used for covalent attachment of haptens to the carrier protein have been well established for many functional groups available on

polypeptides. This process may be accomplished either by direct conjugation between an existing functional group on the hapten and the protein carrier (3) or by more complex methods involving modification of the hapten and/or insertion of linker arms to present a certain molecular feature (4, 5).

A fundamental characteristic of an immunogen is the number of hapten covalently attached to the carrier protein which can be determined from the new molecular weight of the modified protein. The optimal number of hapten attached to the carrier protein has been debated concerning relevance to immunogenicity directed to the newly created epitope (6–8). Several methods have been used to determine the extent of hapten incorporation. The UV absorbance spectrum of the synthesized conjugate is commonly used when the hapten or linker has a strong chromophore which differs from the carrier protein (9). If the hapten/linker's chromophore is similar, a differential UV spectrum obtained by subtraction of the nonconjugated protein spectra from conjugated protein spectra has been employed (10). When immunogens are obtained by modification of the reactive free amines (lysine) of the polypeptide, the degree of incorporation can be estimated as a difference between the number of reactive groups before and after conjugation by titration with TNBS (11, 12). When available, employment of radiolabeled haptens can permit determination of hapten associated with protein (13). Gel electrophoresis has also been found to have some utility. SDS–PAGE, which separates proteins on the basis of molecular size, has been useful when small proteins ( $\leq 20\,000$  Da) are conjugated with larger haptens ( $> 800$  Da) (14). More recently reported is the use of isoelectric focusing electrophoresis of protein–ligand conjugates where the separation method is based on charge (pI) which will change when amines or carboxylic acids of the polypeptide are modified by conjugation with hapten (9, 15).

Matrix-assisted laser desorption ionization mass spectrometry (MALDI) has been effectively utilized in the molecular weight determination of various proteins with

<sup>®</sup> Abstract published in *Advance ACS Abstracts*, October 1, 1994.

<sup>1</sup> Abbreviations: BSA, bovine serum albumin; DMF, dimethylformamide; equiv, molar equivalent; GMP, good manufacturing practice; ISO, International Organization for Standardization; kV, kilovolts; MALDI, matrix-assisted laser desorption ionization mass spectrometry; SDS, sodium dodecyl sulfate; SDS–PAGE, sodium dodecyl sulfate polyacrylamide gel electrophoresis; TFA, trifluoroacetic acid; TNBS, trinitrobenzenesulfonic acid.



a claimed limit of 500 000 Da (16). The practical limit for routine analysis of proteins is approximately 300 000 Da with a sensitivity in the low pmol range and an accuracy of up to  $\pm 0.1\%$  (17). There are a few published reports employing MALDI for the characterization of protein-hapten conjugates (18–22). Wengatz *et al.* analyzed various conjugates by MALDI and compared the results to UV analysis which revealed discrepancy between the two methods (17). Siegel *et al.* measured the amount of attached anticancer drugs and sugars conjugated to human serum albumin and found these values to be in close agreement, in some cases, with data obtained by UV spectrometry (22). In light of these findings we were interested in investigating MALDI characterization of immunogens and comparing the results against commonly used methods: colorimetric titration with trinitrobenzenesulfonic acid (TNBS), UV analysis, and gel electrophoresis.

## MATERIALS AND METHODS

Haptens for desipramine, doxepin, and nortriptyline (1–5) were prepared using previously described methods (4, 5, 9, 23, 24). The remaining haptens, 6–9, were purchased: 6, 3-methoxy-4-hydroxyphenylglycol, and 8, 17 $\beta$ -estradiol 6-(*O*-carboxymethyl) oxime (Sigma Chemical Co., St. Louis, MO); 7, homovanillic acid (Aldrich, Milwaukee WI); and 9, 3 $\alpha$ -hydroxy-5-androsten-17-one hemisuccinate (Steraloids, Wilton, NH). All other chemicals were of the purest grades commercially available. All solutions were prepared using water from a Millipore water system (Millipore, Marlborough, MA). Dialysis tubing (MW cutoff 15 000 Da) was obtained from Spectrum Medical Industries, Inc. (Los Angeles, CA).

Hapten was conjugated to BSA by activation of the carboxylic group of the hapten to a reactive ester using the following general procedure (4, 5, 25). Each hapten was dissolved in DMF (1.0 mg/mL), 1.1 equiv of *N*-hydroxysuccinimide and 1.1 equiv of 1,3-dicyclohexylcarbodiimide were added, and the solution was stirred for 24 h. The reaction mixture was filtered through a glass pipette equipped with a cotton plug, and the resulting filtrate was combined with 0.026 equiv of a BSA solution (46 mg/mL in 4:1 pH 7.8, 100 mM phosphate buffer:DMF) and stirred overnight. The protein solution was placed into cellulose dialysis tubing and dialyzed against 2 L of 0.1 M sodium phosphate (pH 7.8) for 4 h and then against water (2 L) with changes every 2 h for a total of seven changes. The resulting dialyzate from the dialysis tubing was lyophilized and the conjugate was sealed in amber vials under argon and stored at  $-20^\circ\text{C}$  (conjugation of hapten 3 required additional protection/deprotection steps which are described in detail in ref 5).

TNBS titrations were carried out by adding to 0.5 mL of a BSA or conjugate solution (1.0 mg/mL) in a glass vial, 1.0 mL of 4% sodium bicarbonate, and 1.0 mL of a 0.1% TNBS solution. The vials were incubated for 2 h at  $37^\circ\text{C}$  in a water bath, and then 1.0 mL of a 10% SDS solution was added followed by 0.5 mL of 1 M HCl. UV absorbance were measured at 342 nm (a sample which contained 0.5 mL water instead of protein was used as a blank). Each sample was tested in triplicate, and the results were averaged. The calculated percent of hapten bound to BSA was derived from the extent of BSA free amine modification (11).

Gel electrophoresis employed a Pharmacia Phast-System (Piscataway, NJ) utilizing 12.5% polyacrylamide SDS-PAGE precast gels (PhastGel). Conjugates were dissolved in SDS-PAGE sample buffer (10 mM Tris/HCl,

1 mM EDTA, 2.5% SDS, and 5.0%  $\beta$ -mercaptoethanol, pH 8.0) to 1 mg/mL and heated to  $100^\circ\text{C}$  for 5 min. Gels were loaded with 2–3  $\mu\text{L}$  of sample and run under denaturing conditions using the manufacturer's protocol. Upon completion, the gels were stained with Coomassie Blue using a standard developing routine from the manufacturer.

UV absorption spectra were recorded on a Beckman 640 UV spectrophotometer. Conjugates and nonmodified BSA (0.1–0.5 mg/mL in deionized water) were scanned from 200 to 500 nm. The number of hapten attached to BSA was calculated from the intensity of a difference spectra obtained by subtracting nonmodified BSA from the conjugates (10). Molar extinction coefficients for hapten were taken from the literature for 1–6 (26) and were determined for homovanillic acid (7), estradiol carboxymethyl oxime (8), and 3 $\alpha$ -hydroxy-5-androsten-17-one hemisuccinate (9) by UV titration of the hapten in water.

Analysis by matrix-assisted laser desorption ionization mass spectrometry employed a Bruker Reflex (Bruker Instruments, Billerica, MA) time-of-flight mass spectrometer equipped with a nitrogen laser (337 nm). The crystal matrix, sinapinic acid (Aldrich Chemical Co., Milwaukee, WI), was prepared at a concentration of 15 mg/mL in acetonitrile. Protein samples were typically 10–50 pmol/ $\mu\text{L}$  in 2:1 water:acetonitrile solution. Sample and matrix solutions were mixed in equal volumes (typically 1.5  $\mu\text{L}$  each) directly on the stainless steel probe tip (target) and allowed to dry ( $\sim 10$  min) in a fume hood at room temperature. The crystallized analyte-matrix sample was then rinsed with 0.1% TFA solution by placing approximately 2  $\mu\text{L}$  of the solution on the probe sample at room temperature, allowing it to stand for about 5 s, and then gently drying the crystals with a stream of nitrogen. Spectra were recorded at a threshold laser irradiance for 50–150 shots in the linear mode at 30 kV. The resulting data were analyzed using XMASS, ver. 2.0.0, the post acquisition software supplied with the spectrometer.

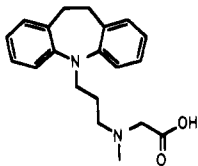
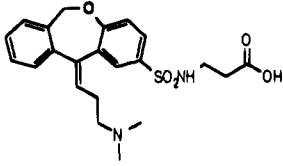
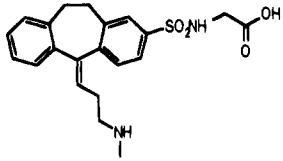
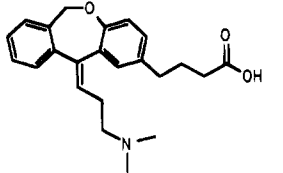
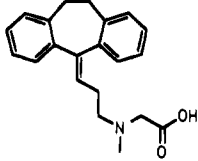
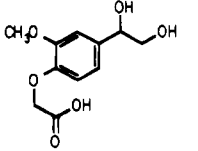
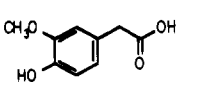
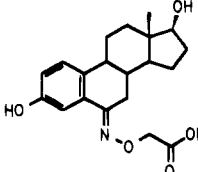
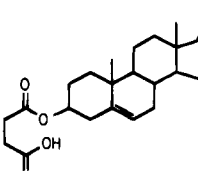
## RESULTS AND DISCUSSION

Immunogens were prepared by covalent attachment of haptens 1–9, containing a terminal carboxylic group, to the free-amino groups (lysine residues and *N*-terminal amine) of BSA. In each case the carboxylic group of the hapten was activated by formation of the *N*-hydroxysuccinimide ester using 1,3-dicyclohexylcarbodiimide (see Materials and Methods). Resulting conjugates were freed of unbound hapten by extensive dialysis in aqueous buffer and then lyophilized. Conjugates in this study were characterized by the following four methods: MALDI, differential UV analysis, titration with TNBS, and gel electrophoresis. In addition, the immunogens prepared were used for the immunization of animals and, in each case, resulted in the production of antibodies with affinity to the specific hapten.

Table 1 lists the results of conjugate characterization by MALDI, UV, and TNBS. All of the results are reported as percent modified free amines (60 total, 59 lysines plus *N*-terminal amine) in BSA by the hapten.

Molecular weight determination of proteins by MALDI is becoming a routine procedure. Typically, 10–50 pmol of a sample is cocrystallized with sinapinic acid and then irradiated with a high intensity pulsed laser beam to generate, intact, gas-phase molecular ions of the intact protein. A molecular weight of 66 521 Da was observed for nonmodified BSA which is within 0.2% of the molecular mass (66 430 Da) based on the complete amino acid sequence (27). The observed value for BSA was used

Table 1

	Hapten	Hapten Mol. Wt. <sup>1</sup>	Hapten Incorporation <sup>2</sup>		
			MS	UV	TNBS
1		324.42	28% (71,808)	21%	31%
2		430.51	9% (68,704)	4%	32%
3		400.49	19% (70,999)	21%	13%
4		365.47	45% (76,038) 100% (89,893)	25%	64%
5		321.41	42% (74,365)	22%	40%
6		242.22	16% (68,646) 100% (81,995)	ND	20%
7		182.17	18% (68,923)	ND	37%
8		359.42	13% (69,305)	34%	11%
9		388.50	38% (75,048)	>100%	48%

1. Hapten mol wt. decreases by 17 mass units upon conjugation to BSA.

2. All substitution values are based on the number of primary amines (lysine and N-terminus) which have been modified.

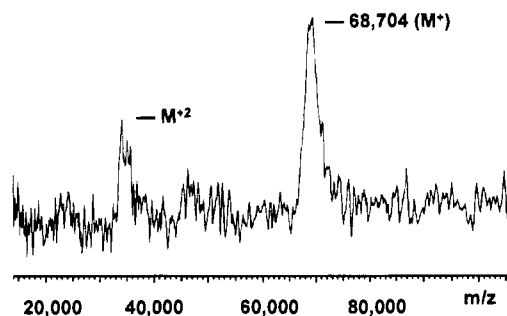


Figure 1. Mass spectrum of immunogen 2.

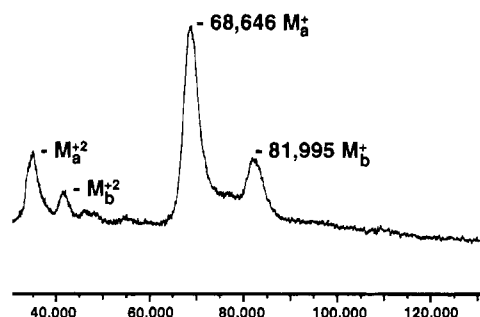


Figure 2. Mass spectrum of immunogen 6.

in the following equation to determine the percent of modified BSA free amino groups.

$$\% \text{ modification} = \frac{(100) \times (\text{conjugate mol wt}) - (\text{BSA mol wt})}{(\text{hapten mol wt}) (\text{total BSA free amines})}$$

We successfully obtained spectra for all immunogens discussed in this paper (Figure 1 illustrates an representative example). Each spectrum contained at least two peaks which represent singly ( $M^+$ ) and doubly ( $M^{+2}$ ) charged states. The molecular weight of each conjugate was calculated from the peak centroid using the software supplied with the instrument. Experimentation with different concentrations of the conjugate were found to be an important factor for successful generation of a MS spectrum (see Materials and Methods). In addition, an enhancement of the ion generated signal was observed by washing the sample-matrix crystals with a weak solution of TFA just prior to analysis. It is presumed that washing removes residual salts from the sample which had precipitated out during crystallization of the matrix. It was very interesting to observe additional peaks of low ion abundance for conjugates 4 and 6 (Figure 2) which represent the maximum number of hapten that could be introduced onto the free amines of BSA. These peaks represent different populations of hapten incorporation. Circumstances behind distinct populations could be a phenomenon of folding/unfolding of BSA during conjugation, hapten type and size, conjugation conditions, and/or coupling reagents used. Distinct populations of hapten within immunogens would effect immunological response. It has been reported that immunogens containing high incorporation of hapten generally result in poor immunogenicity or antibodies of the IgM type with low binding affinity to the antigen (7, 8). On the other hand, some evidence has been provided that low incorporation of hapten triggers a thymus dependent immuno response giving rise to high affinity antibodies of the IgG type (7).

UV analysis was limited to those conjugates which were water soluble and possessed a usable chromophore.

Conjugates of tricyclic antidepressant drugs 1–5 were soluble, yet 4 and 5 produced slightly turbid appearance in water, the solvent used for analysis. Evaluation was not performed on the conjugates 7 and 9 which lacked solubility in water. The remaining conjugates 6 and 8 exhibited good solubility. Analysis was performed using conjugate/water solutions (0.5 mg/mL) by measuring the absorbance at a known chromophore and subtracting out the contribution from BSA. The ratio of hapten to free amines in BSA was determined from the ratio of calculated hapten molarity to the molar concentration of lysine amines in nonmodified BSA (0.46 mM, at 0.5 mg/mL). The range of estimated hapten incorporation was 4% for 2 to 100% for 9 with only three conjugates (1–3) having values similar to the MALDI analysis. Wengatz *et al.* observed higher values from UV analysis when compared with MALDI (18). They proposed that noncovalently bound hapten was associated with their conjugates resulting in the higher values. We observed higher UV values for immunogens 8 and 9, and it is possible that these conjugates have noncovalently bound hapten which was not completely removed by dialysis. On the other hand, we observed low UV values (when compared with MALDI) for immunogens 4 and 5 and attribute the results to limited solubility of these conjugates.

Analysis of immunogens by UV has a number of routinely applied assumptions such as the following: all noncovalently bound hapten (including salts and buffers) are removed, the immunogen is completely soluble in the matrix used for analysis, and the chromophores of BSA and hapten do not change upon conjugation. In reality these assumptions outline the deficiencies and difficulties associated with UV analysis of immunogens since the perfect situation is virtually impossible to achieve.

Titration of immunogens using TNBS is a popular colorimetric method used to determine the number of free amino groups in proteins and peptides (11). This method is specific for primary amines producing trinitrophenyl derivatives which are easily quantified using a UV-vis spectrophotometer (28). As with the UV analysis, solubility of the conjugates is critical for obtaining useful results. Conjugates 1–9 were all solubilized at room temperature (1 mg/mL) by the addition of 10% SDS (11). TNBS results were in close agreement with MALDI estimates except for conjugates 2 and 7 where the titration greatly overestimated the number of hapten. As with UV analysis, similar problems are associated with this method which are difficult to control. It is presupposed that the TNBS reagent reacts with all non-modified free amines of a given protein. However, folding/unfolding and aggregation between proteins could hinder some nonmodified amines from reacting with the reagent and result in overestimation of amine modification.

Gel electrophoresis of our immunogens yielded limited information about their molecular weight. We encountered difficulties of immunogen solubility in the SDS-PAGE buffer gel along with precipitation of the conjugate on the gel during electrophoresis. In addition, bands on the gel associated to the immunogens were often smeared, which suggested heterogeneous distribution of hapten but prevented accurate assessment of the immunogen molecular weight. The accuracy of SDS-PAGE is poor (>5%) when compared with MS techniques (29).

We needed valid methods for characterization of hapten-protein conjugates prepared in our labs to meet the high demands of quality policies (GMP and ISO) being implemented by governments worldwide (30, 31). Each procedure presented here has its own advantages. We found analysis using MALDI to be very useful, it being the only method which directly measures the conjugate's

molecular weight. Unlike the other methods assessed, MALDI is not limited by rigid solubility constraints, has a high tolerance for impurities such as salt/buffers used in immunogen preparation, and is not dependent on the physical/chemical composition of the hapten. TNBS titrations were surprisingly close to the MALDI estimates. UV analysis had the most limitations in our hands giving results which did not correlate well with the other methods. Electrophoresis was found to have limited utility in this study.

MALDI is also not without its own demands. Our initial attempts to obtain spectra of the immunogens were challenging. We found it necessary to test different conditions of sample concentration and sample preparation. An improvement of the ion generated signal was obtained by treating the sample-matrix crystals with a TFA solution. Such optimization might be necessary with any immunogen. Our work was limited to small haptens conjugated to BSA under very similar conditions. It may be necessary to investigate other variables such as crystal matrixes to obtain useful spectra for other hapten-protein conjugates. Further work is needed to determine the scope and limitations of MALDI in this area.

In summary, we have demonstrated that MALDI can be very useful for the analyses of synthetically prepared immunogens to determine the number of covalently bound hapten. This tool is particularly useful due to the discovery of multiple populations of hapten incorporation observed for some immunogens. Such information is advantageous in determining the possible impact an immunogen may have on antibody development. Furthermore, the results of this work illustrate the power of physical/chemical methods of characterization of organic compounds which for many years was reserved only for small molecular weight haptens.

#### LITERATURE CITED

- (1) Benjamini, E., and Leskowitz, S. (1991) *Immunology: A short course*, 2nd ed., Chapter 3, Wiley-Liss, New York.
- (2) Liddell, J. E., and Cryer, A. (1991) *A practical guide to monoclonal antibodies*, Chapter 3, John Wiley & Sons, Ltd., New York.
- (3) Erlanger, B. F. (1980) The preparation of antigenic hapten-carrier conjugates: A survey. *Methods Enzymol.* 70, 85.
- (4) Adamczyk, M., Fishpaugh, J., Harrington, C., Hartter, D., Johnson, D., and Vanderbilt, A. (1993) Immunoassay reagents for psychoactive drugs I. The method for the development of antibodies specific to amitriptyline and nortriptyline. *J. Immunol. Methods* 162, 47.
- (5) Adamczyk, M., Fishpaugh, J., Harrington, C., Johnson, D., and Vanderbilt, A. (1993) Immunoassay reagents for psychoactive drugs II. The method for the development of antibodies specific to imipramine and desipramine. *J. Immunol. Methods* 163, 187.
- (6) Niswender, G. D., and Midgley A. R., Jr. (1970) *Immunological methods in steroid determination*, Chapter 8, Appleton, New York.
- (7) Klaus, G. G. B., and Cross, H. M. (1974) The influence of epitope density on the immunological properties of hapten-protein conjugates. *Cell. Immunol.* 14, 226.
- (8) Malaitsev, V. V., and Azhipa, O. Y. (1993) Influence of Epitope Density on Immunogenic Properties of Hapten-Protein Conjugates. *Bull. Exp. Biol. Med.* 115, 726.
- (9) Barbarakis, M. S., and Bachas, L. G. (1991) Isoelectric focusing electrophoresis of protein-ligand conjugates: Effect of the degree of substitution. *Clin. Chem.* 37, 87.
- (10) Metelitz, D. I., Eryomin, A. N., Karasyova, E. I., and Markina, V. L. (1991) Catalytic activity and thermostability of dehydrogenase conjugates with cortisol and progesterone. *Bioconjugate Chem.* 2, 309.
- (11) Shinoda, T., and Tsuzukida, Y. (1974) Identification of rapidly trinitrophenylating amino groups of human Bence-Jones proteins modified by incubating for 45 min at 37 °C before measuring UV absorbance. *J. Biochem.* 75, 23.
- (12) Habeeb, A. F. S. A. (1966) Determination of free amino groups in proteins by trinitrobenzenesulfonic acid. *Anal. Biochem.* 14, 328.
- (13) Feng, P. C. C., Horton, S. R., and Sharp, C. R. (1992) A general method for developing immunoassays to chloroacetanilide herbicides. *J. Agric. Food Chem.* 40, 211.
- (14) Wetzel, R., Halualani, R., Stults, J. T., and Quan, C. (1990) A general method for highly selective cross-linking of unprotected polypeptides via pH-controlled modification of N-terminal  $\alpha$ -amino groups. *Bioconjugate Chem.* 1, 114.
- (15) Kamps-Holtzapfel, C., Carlin, R. J., Sheffield, C., Kubena, L., Stanker, L., and DeLoach, J. F. (1993) Analysis of hapten-carrier protein conjugates by nondenaturing gel electrophoresis. *J. Immunol. Methods* 164, 245.
- (16) Hillenkamp, F., Karas, M., Beavis, R. C., and Chait, B. T. (1991) Matrix-assisted laser desorption/ionization mass spectrometry of biopolymers. *Anal. Chem.* 63, 1193A.
- (17) Burlingame, A. L., Boyd, R. K., and Gaskell, S. J. (1994) Mass Spectrometry. *Anal. Chem.* 66, 634R, and references therein.
- (18) Wengatz, I., Schmid, R. D., Kreissig, S., Wittmann, C., Hock, B., Ingendoh, A., and Hillenkamp, F. (1992) Determination of the hapten density of immuno-conjugates by matrix-assisted UV laser desorption/ionization mass spectrometry. *Anal. Lett.* 25, 1983.
- (19) Shoyama, Y., Sakata, R., Isobe, R., and Murakami, H. (1993) Direct determination of forskolin-bovine serum albumin conjugate by matrix-assisted laser desorption ionization mass spectrometry. *OMS Lett.* 28, 987.
- (20) Shoyama, Y., Fukada, T., Tanaka, T., Kusai, A., and Nojima, K. (1993) Direct determination of opium alkaloid-bovine serum albumin conjugate by matrix-assisted laser desorption/ionization mass spectrometry. *Biol. Pharm. Bull.* 16, 1051.
- (21) Siegel, M. M., Hollander, I. J., Hamann, P. R., James, J. P., Hinman, L., Smith, B. J., Farnsworth, P. H., Phipps, A., King, D. J., Karas, M., Ingendoh, A., and Hillenkamp, F. (1991) Matrix-Assisted UV-Laser Desorption/Ionization Mass Spectrometric Analysis of Monoclonal Antibodies for the Determination of Carbohydrate, Conjugated Chelator, and Conjugated Drug Content. *Anal. Chem.* 63, 2470.
- (22) Siegel, M. M., Tsou, H.-R., Lin, B., Hollander, I. J., Wissner, A., Karas, M., Ingendoh, A., and Hillenkamp, F. (1993) Determination of the Loading Values for High Levels of Drugs and Sugars Conjugated to Proteins by Matrix-assisted Ultraviolet Laser Desorption/Ionization Mass Spectrometry. *Bio. Mass Spec.* 22, 369.
- (23) Hu, M. W. (1980) Amitriptyline conjugates to antigenic proteins and enzymes. United States Patent 4,223,013.
- (24) Keenan, C. L., and Koopowitz, H. (1981) Limitations in Identifying Neurotransmitters Within Neurons by Fluorescent Histochemistry Techniques. *Science* 214, 1151.
- (25) Samokhin, G. P., and Filimonov, I. N. (1985) Coupling of peptides to protein carriers by mixed anhydride procedure. *Anal. Biochem.* 145, 311.
- (26) (1989) The Merck Index (S. Budavari, ed.) 11th ed., Merck & Co., Inc., Rahway.
- (27) Hirayama, K., Akashi, S., Furuya, M., and Fukuhara K. (1990) Rapid confirmation and revision of the primary structure of bovine serum albumin by ESIMS and FRIT-FAB LC/MS. *Biochem. Biophys. Res. Commun.* 173, 639.
- (28) Sashidhar, R. B., Capoor, A. K., and Ramana, D. (1994) Quantitation of  $\epsilon$ -amino group using amino acids as reference standards by trinitrobenzene sulfonic acid. *J. Immunol. Methods* 167, 121.
- (29) Barinaga, M. (1989) Protein Chemists Gain a New Analytical Tool *Science* 246, 32.
- (30) ISO 9000 Standard-international organization for standardization, ANSI/ASQC Q90 ISO 9000 Guidelines, ASQC Quality Press, Milwaukee, WI, 1992.
- (31) GMP (Good Manufacturing Practice), Part 820, Code of federal regulations, United States Government, Washington, DC, 1992.

## High Yield, Site-Specific Coupling of N-Terminally Modified $\beta$ -Lactamase to a Proteolytically Derived Single-Sulfhydryl Murine Fab'

Stephen D. Mikolajczyk,<sup>\*,†</sup> Damon L. Meyer,<sup>†</sup> James J. Starling,<sup>‡</sup> Kevin L. Law,<sup>‡</sup> Keith Rose,<sup>§</sup> Brigitte Dufour,<sup>§</sup> and Robin E. Offord<sup>§</sup>

Hybritech Incorporated, P.O. Box 269006, San Diego, California 92196-9006, Lilly Research Laboratories, Eli Lilly and Company, Indianapolis, Indiana 46285, and Département de Biochimie Médicale, Centre Médical Universitaire, 1 rue Michel-Servet, 1211 Geneva 4, Switzerland. Received June 21, 1994<sup>®</sup>

The preparation of bispecific protein conjugates capable of performing diverse biological functions is an area of active investigation. Such conjugates are routinely prepared using techniques which employ random derivatization of lysine residues, but the overall utility of these methods is limited due to poor yields and heterogeneous conjugates. In this report we describe the development of site-specific linkage methodology for the chemical synthesis of a homogeneous enzyme–antibody Fab' conjugate with coupling efficiencies of at least 72%. The N-terminal threonine residue of  $\beta$ -lactamase from the P99 strain of *Enterobacter cloacae* was oxidized to an aldehyde functional group under mild conditions with a 5-fold molar excess of sodium periodate. The murine Fab' with a single sulfhydryl at the hinge region was generated by further digestion of the peptic Fab' fragment with lysyl endopeptidase to remove a decapeptide containing two of the three cysteine residues. Coupling of the two modified proteins was accomplished through a bifunctional coupling reagent containing maleimide and aminooxy functional groups. Synthesis of the linker is described. Yields of 1:1 enzyme–Fab' were at least three times higher than for comparable random derivatization methods. Immunoreactivity and enzymatic activity were unaffected. Biodistribution studies showed a more favorable tumor to blood ratio with the site-specifically linked conjugate.

### INTRODUCTION

Most schemes to synthesize enzyme–antibody conjugates for therapeutic applications begin with the random derivatization of lysine  $\epsilon$ -amino groups with bifunctional reagents designed to impart new functionality to the protein. Reagents such as SMCC<sup>1</sup> contain an *N*-hydroxy-succinimidyl ester to react with lysine  $\epsilon$ -amino groups and a maleimide functional group for subsequent reaction with thiols (1). When not naturally present (2), free thiols on the second protein can be created either by partial reduction of endogenous disulfide bonds (3, 4) or by derivatization of lysines with reagents such as SPDP or 2-iminothiolane (Traut's reagent) (5–8).

In our laboratories and others, Fab' fragments of monoclonal antibodies have been substituted for intact

antibodies to reduce the overall size of the conjugate for better biodistribution (9) as well as improved blood clearance for better tumor/blood ratio (10, 11). Fab' fragments have the added advantage of a specific coupling site at the hinge region sulfhydryl groups. For this reason the enzyme portion of the conjugate has been the primary focus for site-specific modification.

In previous work sulfo-SMCC was used to couple the enzyme  $\beta$ -lactamase to the free Fab' sulfhydryl groups of anti-CEA, anti-TAG-72, and antihapten antibodies (12, 13). Problems common to this mode of conjugation include heterogeneous derivatization of lysines by SMCC which results in limited control of the subsequent coupling reaction and yields typically 20% or less (5, 7, 8, 12). For any sample with an average of 1 SMCC per protein molecule there exists 0, 1, 2, or more SMCC molecules attached to any single protein molecule in the population. While the average distribution range of SMCC per protein in the reaction mixture *e.g.*, 0–2, 2–4, *etc.*, can be influenced by controlling reaction conditions such as time of incubation, pH, and reagent concentration, the presence of multiple lysine residues on the surface of proteins precludes the possibility of selectively modifying any single lysine under normal circumstances.

An added complication of working with Fab's is that, while coupling is *generally* site-specific, murine Fab's contain three closely spaced cysteine residues in the hinge region (14), giving rise to the potential for the attachment of three maleimide-modified enzyme molecules per Fab'. This problem is minimized by maintaining an excess of Fab' over enzyme (12), but this approach wastes material in the coupling step and still requires the removal of unacceptable levels of 2:1 conjugate formed during the reaction, *i.e.*, conjugate composed of two  $\beta$ -lactamases attached to a single Fab'. The overall effect of the above limitations is to reduce formation of

\* Author to whom correspondence should be addressed. Phone: (619) 535-8754. Fax: (619) 457-5308.

<sup>†</sup> Hybritech Incorporated.

<sup>‡</sup> Lilly Research Laboratories.

<sup>§</sup> Centre Médical Universitaire.

<sup>®</sup> Abstract published in *Advance ACS Abstracts*, October 15, 1994.

<sup>1</sup> Abbreviations: SMCC, *N*-succinimidyl-*N*-(4-carboxycyclohexyl)methylmaleimide; SPDP, *N*-succinimidyl 3-(pyridyldithiol)propionate; sulfo-SMCC, *N*-sulfosuccinimidyl-*N*-(4-carboxycyclohexyl)methylmaleimide;  $\beta$ L,  $\beta$ -lactamase; MES, 2-(morpholino)ethanesulfonic acid; DTT, dithiothreitol; EDTA, ethylenediaminetetraacetic acid; anti-CEA, anti-carcinoembryonic antigen; anti-TAG-72, antitumor-associated glycoprotein-72; MBTH, 3-methyl-2-benzothiazolinone hydrazone; BPM, *N*-[p-(2-benzoxazolyl)phenyl] maleimide; TFA, trifluoroacetic acid;  $\beta$ L-MBTH, MBTH covalently attached to  $\beta$ L; Fab'-3SH, Fab' with three cysteines in hinge region; Fab'-1SH, Fab' with single cysteine in hinge region; NEM, *N*-ethylmaleimide; DMSO, dimethyl sulfoxide; HIC, hydrophobic interaction chromatography; SDS-PAGE, sodium dodecyl sulfate–polyacrylamide gel electrophoresis; rt, room temperature.

the desired 1:1 conjugate in favor of either conjugate ratios greater than 1:1 or unreacted monomer.

In the present work a single site for coupling was created on each of the proteins investigated. In the case of  $\beta$ -lactamase, advantage was taken of an N-terminal threonine which was converted to an aldehyde by mild treatment with sodium periodate. The conversion of amino alcohols to aldehydes has been well studied (15–18, and references cited therein). The particular difficulty of quantitatively assessing the degree of protein aldehyde formation in the current study was addressed by development of an HPLC method capable of resolving oxidized and unoxidized  $\beta$ L after treatment with a commercially available aldehyde-selective reagent. The ability to quantitatively measure protein aldehyde formation as a function of reactivity toward a model hydrazide proved to be the most effective method of optimizing the procedure. In addition, we have found that further digestion of the pepsin-derived Fab' with the lysyl endopeptidase from *Achromobacter lyticus* removes a decapeptide from the C-terminus of the truncated heavy chain, leaving only one of the three hinge region cysteine residues on the Fab'. Conversion to the single-sulfhydryl Fab' was monitored by HPLC after reaction with a fluorescent thiol reagent.

The ease of use and high coupling efficiencies achieved by development of this site-specific methodology should prove useful for both small and large scale construction of protein conjugates.

#### EXPERIMENTAL PROCEDURES

**Preparation of  $\beta$ -Lactamase.** Purified  $\beta$ L was obtained by passage of a crude extract of *Enterobacter cloacae* strain P99 over an agarose affinity column derivatized with aminophenylboronic acid prepared according to the method of Cartwright (19). The bacterial cell paste was mixed thoroughly with an equal volume of buffer consisting of 20 mM MES, 0.5 M NaCl pH 6.5 and then frozen in an acetone/dry ice bath, thawed in a warm water bath, and centrifuged at 12000g for 25 min. The supernatant solution was removed, an additional volume of MES buffer was added, and the process repeated four more times for a total of five extractions. The supernatant solutions were combined and applied directly to a 2 cm  $\times$  15 cm bed volume of the affinity resin at a flow rate of 1 mL/min at 4 °C. The column was then washed with approximately 400 mL of the above buffer until the 280 nm absorbance eluting from the column leveled off at a minimum.  $\beta$ L was then eluted with the above MES buffer with added 0.5 M borate, pH 6.5. The  $\beta$ L was concentrated by ultrafiltration to 5–10 mg/mL and dialyzed against 50 mM borate, 100 mM NaCl pH 8.0 for storage. The yield was 1–2 mg of  $\beta$ L per gram of cell paste starting material.

**Periodate Oxidation of  $\beta$ L and HPLC Detection.** The optimum procedure for producing  $\beta$ L aldehyde is described below. The results of variations on this procedure are given in the Results and Table 1.  $\beta$ L at a concentration of 10 mg/mL was dialyzed against 40 mM sodium phosphate pH 6.5. Sodium periodate was freshly prepared in water and added with mixing at a 5-fold molar excess over  $\beta$ L. The extinction coefficient at 280 nm determined in this laboratory for a 1 mg/mL solution of  $\beta$ L was 2.2, and the molecular weight of  $\beta$ L was 39.2 kDa (see Results). The  $\beta$ L and periodate were allowed to react at room temperature for 8 min, and then the reaction was quenched with a 7-fold excess of DTT over periodate (one mole of periodate was found to oxidize approximately 5 mol of DTT).  $\beta$ L contains no cysteine residues (20). Quenching agents such as 1,3-diamino-

propan-2-ol or ethylene glycol can be substituted if DTT is undesirable for any reason.

In order to determine the percentage of N-terminal aldehyde formed during this step an aliquot of the  $\beta$ L mixture was removed and mixed with an equal volume of 100 mM sodium acetate pH 4.5. A freshly prepared solution of 100 mM MBTH (Aldrich Chem Co., Milwaukee, WI), prepared in the same buffer, was added at 100-fold molar excess over  $\beta$ L and allowed to react for at least 15 min before dilution in elution buffer A for injection on the HPLC. A Bio-Rad HPLC Model 800 with dual gradient pumps, a scanning UV-vis Bio-Dimension detector, and a refrigerated Model AS100 autosampler was employed. Resolution of the  $\beta$ L from  $\beta$ L-MBTH was achieved by hydrophobic interaction chromatography on a PolyLC 4.6  $\times$  250 mm, 1000 Å pore size polypropyl aspartamide column (distributed by Western Analytical, Temecula, CA). Buffer A was 1.2 M sodium sulfate, 20 mM sodium phosphate pH 6.3, and buffer B was 50 mM sodium phosphate, 5% 2-propanol pH 7.3. The flow rate was 1 mL/min. Sample was injected at 100% buffer A, and peaks were eluted with a gradient of 0–20% B over 5 min and 20–40% B from 5–15 min. Approximately 20  $\mu$ g of  $\beta$ L was injected per run, and the eluent was monitored simultaneously at 280 nm and 350 nm.

**Digestion of Fab'-3SH to Single-Sulfhydryl Fab'.** F(ab')<sub>2</sub> fragments of the murine IgG1 anti-CEA antibody, ZCE025 (11), were prepared by pepsin digestion of intact antibody for 2 h at 37 °C in 100 mM sodium citrate pH 3.5 with 3% pepsin (w/w) (14). F(ab')<sub>2</sub> was reduced to Fab' by incubation with 20 mM cysteine for 10 min at 37 °C at pH 8. Excess cysteine was removed by gel filtration over a small Bio-Rad P-6 sizing column equilibrated with a buffer containing 20 mM MES, 100 mM sodium chloride, 1 mM EDTA, pH 6.3 which is referred to as MBS buffer below. The optimum procedure for producing single-sulfhydryl Fab' is described here. The effect of altering these parameters is described in the Results. The extinction coefficient at 280 nm used for a 1 mg/mL solution of F(ab')<sub>2</sub> and Fab' was 1.8. Fab' at 5–10 mg/mL in MBS buffer was incubated with 3% (w/w) lysyl endopeptidase (Wako Chemicals USA, Richmond, VA) at 37 °C for 16–20 h. The lysyl endopeptidase used in this work had an activity of 2 AU/mg as specified by the manufacturer. Solutions of the fluorescent thiol reagent BPM (Kodak Laboratory Chemicals, Rochester, NY) were prepared in DMSO. A typical sample for HPLC analysis was prepared as follows: 2  $\mu$ L of 10 mM BPM in DMSO was added to 5  $\mu$ L of Fab' and incubated for 10 min prior to addition of 100  $\mu$ L of HPLC buffer A. The HPLC system was the same as described above except that a Varian Model 9070 fluorescence detector was added in series after the UV-vis detector so that absorbance at 280 nm and fluorescence at 300 nm excitation and 360 nm emission could be monitored for each sample injection.

**Synthesis of the (Aminoxy)maleimide Bifunctional Linker, N<sup>α</sup>-[(aminooxy)acetyl]-N<sup>ε</sup>-(maleoyl- $\beta$ -alanyl)-L-lysine.** Reactants and products I–VII are shown in Scheme 2. (a) N<sup>α</sup>-[[[(tert-Butyloxycarbonyl)-amino]oxy]acetyl]-N<sup>ε</sup>-(trifluoroacetyl)lysine (III). To 371 mg of N<sup>ε</sup>-(trifluoroacetyl)lysine (I) (NovaBiochem, 4448 Laefelfingen, Switzerland) suspended in 3 mL of DMSO was added, in suspension in 1 mL of DMSO, 576 mg of the N-hydroxysuccinimido ester of [[[(tert-butyloxycarbonyl)amino]oxy]acetic acid (II), prepared as described previously (21), modified as described (22). N-Ethylmorpholine was then added to the suspension, with mixing, until the apparent pH as indicated externally on moist narrow-range pH paper was about 8. The suspension



clarified almost immediately upon adjustment to pH 8, and the resulting solution was left overnight at room temperature. Subsequent thin-layer chromatography (22) of a small sample showed that little or no ninhydrin-positive material remained. Residual hydroxysuccinimide ester in the reaction mixture was destroyed by dilution with an equal volume of water and incubation at 37 °C for 1 h. The mixture was then further diluted with 32 mL of water, cooled to 0 °C, and brought to an apparent pH of 3.0 (glass electrode) with acetic acid. The solution was then divided in two and each half placed on a Chromabond 1000 mg (Machery-Nagel, Dürren, 52348, Germany) equilibrated with 0.1% aqueous TFA. Each Chromabond was then washed with 20 mL of the same solution and eluted with 4 mL of a mixture of 0.1% TFA:acetonitrile, 4:6 (v/v). Acetonitrile was removed from the eluates in a current of filtered air and the remaining liquid removed by vacuum centrifugation. Analytical reversed-phase HPLC of this material using the system previously described (22) showed that it was substantially homogeneous and could be used satisfactorily for the subsequent steps without further purification.

(b)  $N^\alpha$ -[[[(*tert*-Butyloxycarbonyl)amino]oxy]acetyl]lysine (IV). The trifluoroacetyl group was removed from the  $\epsilon$ -amine of the lysine by adding 3 mL of water to each of the dried down eluates, cooling to 0 °C, then adding 330  $\mu$ L of piperidine. The mixture was maintained in an ice bath with occasional agitation for 3 h. The reaction was stopped by the careful addition of 500  $\mu$ L of glacial acetic acid, and solutions could be stored frozen at this point. To continue the procedure, each mixture was diluted to 10 mL with water and the pH adjusted with acetic acid to pH 3.0 (glass electrode) if necessary. The mixtures were applied to two Chromabonds as before, except that (a) elution of the wanted fraction was carried out with 4 mL of a mixture of 0.1% TFA:acetonitrile, 7:3 (v/v), and (b) for each Chromabond the material passing through unchecked was pooled with the subsequent 20 mL wash fraction and passed a second time over the same Chromabond after re-equilibration. For each Chromabond, the two eluates were pooled and dried down to give approximately 40 mg each of the desired product. Analytical reversed-phase HPLC of this material using the system previously described (22) showed that it was substantially homogeneous. Positive fast-atom bombardment mass spectrometry (23) gave as base  $m/z$  320.26 (calcd  $M + H^+$  320.18) together with signals corresponding to  $M + Na^+$  ( $m/z$  342) and to losses from  $M + H^+$  of  $CO_2$ ,  $C_4H_8$ ,  $C_4H_8 + CO_2$ , and  $CO_2 + C_4H_8 + CO_2$  (at  $m/z$  276, 264, 220, and 176 respectively).

(c)  $N^\alpha$ -[[[(*tert*-Butyloxycarbonyl)amino]oxy]acetyl]- $N^\epsilon$ -maleoyl- $\beta$ -alanyllysine (VI). To 40 mg of IV was added 1242  $\mu$ L of DMSO, and the resulting solution was adjusted with *N*-ethylmorpholine to an apparent pH of 7.0–7.5, indicated with pH paper as above. This solution was added slowly over 10 min with careful mixing to 66 mg of the hydroxysuccinimido ester of maleoyl- $\beta$ -alanine (V) (biochemical grade, Fluka, 9470 Buchs, Switzerland) dissolved in 1242  $\mu$ L of DMSO. The order and timing of the addition is important so as to minimize reaction of the maleoyl group with excess amine. Thin-layer chromatography of an aliquot, carried out as above, showed complete disappearance of the Boc-[(aminooxy)acetyl]-lysine after 1 h. The reaction mixture was diluted with 2.23 mL of 0.1% TFA and acidified with 223  $\mu$ L of acetic acid. The wanted product was isolated by preparative HPLC on a C-8 column with a gradient from 20% to 50% solvent B over 100 min as described previously (22) except that a flow rate of 5 mL/min was used. Sample

aliquots of 800  $\mu$ L were diluted with 100  $\mu$ L of 0.1% TFA prior to injection on the HPLC. The wanted product was the last major peak in the run, eluting approximately at the midpoint of the gradient. After removal of the acetonitrile in a current of filtered air and drying down in a vacuum centrifuge, the yield of product was found to be 5.0 mg for each 800  $\mu$ L aliquot injected which corresponds to 36% of the theoretical yield. The compound was characterized by electrospray ionization mass spectrometry (22) through signals at  $m/z$  493 ( $M + Na^+$ ) and 471.1 ( $M + H^+$ , calcd 471.49). The pooled product was stored in 2 mg aliquots at –20 °C in this more stable Boc-protected form.

(d)  $N^\alpha$ -[(Aminooxy)acetyl]- $N^\epsilon$ -(maleoyl- $\beta$ -alanyl)-*L*-lysine (VII). Each 2 mg aliquot was deprotected by incubation with 300  $\mu$ L of anhydrous TFA for 45 min at room temperature. This solution was then dried down and redissolved in 174  $\mu$ L of water to give a nominal concentration of 31 mM. Solutions could be stored frozen for some weeks with several cycles of freezing and thawing without apparent loss of reactivity. The product (VII) was characterized by electrospray ionization mass spectrometry (22) through signals at  $m/z$  371.1 (base peak,  $M + H^+$  calcd 371.37) and 393.1 (relative intensity 45%,  $M + Na^+$  calcd 393.35). A test reaction of this material with 2,4-dihydroxybenzaldehyde, followed by isolation of the adduct by HPLC (data not shown), gave a substance having a single peak in the electrospray ionization mass spectrum at  $m/z$  491.4 ( $M + H^+$  calcd for the expected oxime 491.48).

**Preparation of  $\beta$ -Lactamase-Fab' Conjugate.** After oxidation of  $\beta$ L and quenching of the excess periodate as described above, the mixture was applied to a small Bio-Rad P-6 column equilibrated with 100 mM sodium acetate pH 4.5 buffer to remove the low molecular weight components and to lower the pH. Storage of oxidized  $\beta$ L under these conditions for several days showed no apparent loss of coupling efficiency or aggregation/precipitation. The maleimide-aminooxy bifunctional linker was prepared at 31 mM in water and added in 50-fold molar excess over  $\beta$ L. After incubation for 90 min the excess linker was removed by gel filtration over a P-6 column equilibrated in MBS buffer. After digestion of the Fab'-3SH to the single-sulfhydryl Fab' described above, the lysyl endopeptidase and the decapeptide cleaved from the heavy chain were removed from the single-sulfhydryl Fab' by size exclusion chromatography on a 1  $\times$  30 cm Pharmacia Superose 12A FPLC column attached to the HPLC described above. Approximately 10 mg of Fab' mixture could be applied per run. The elution buffer was 100 mM phosphate pH 7.0 with a flow rate of 0.7 mL/min.

Samples of oxidized  $\beta$ L and single-sulfhydryl Fab' were concentrated to approximately 5 mg/mL by ultrafiltration, if necessary, and then mixed and allowed to incubate for 60–90 min at room temperature. NEM was then added at 10 mM to quench the reaction and prevent oxidation of unreacted Fab' to F(ab')<sub>2</sub>. The 1:1 conjugate was purified by size exclusion chromatography: the mixture was concentrated to about 20 mg/mL whereupon samples of at least 5 mg could be applied to the Superose 12A column described above with good resolution between the  $\beta$ L-Fab' conjugate and unreacted monomers. SDS-PAGE of proteins was performed with a Pharmacia Phast System using 4–15% gradient gels under nonreducing conditions. The gel in Figure 3 was electronically scanned using a densitometer scanner.

**Mass Spectrometry of  $\beta$ L-MBTH.** A 4 mg sample of periodate-oxidized  $\beta$ L reacted with MBTH was applied to the HIC column as described above, and the peak

containing the  $\beta$ L-MBTH adduct was collected. To eliminate traces of salts which can interfere with analysis by electrospray mass spectrometry, the sample was dialyzed against 5 L of ultra pure water (MilliQ system). After 2 days the water was replaced and dialysis was continued for a further 2 days. Mass spectrometric analysis was then performed on a VG-Trio 2000 instrument (22).

**Immunoreactivity and Biodistribution of the  $\beta$ L-Fab' Conjugates.** Fab'- $\beta$ L conjugates were iodinated by the solid state Iodobead (Pierce) procedure according to the method of Markwell (24). A specific activity of  $7.8 \times 10^6$  cpm/ $\mu$ g was obtained for both SMCC and site-specifically linked conjugates. The immunoreactivity was tested by solid-phase RIA against antigen(+) LS174T and antigen(-) M14 tumor cells.  $^{125}$ I-Labeled conjugate was diluted in PBS plus 10%  $\gamma$  globulin-free horse serum (AHS) (Gibco) and added to duplicate wells at serial dilutions from  $10^6$  to  $3.125 \times 10^4$  cpm in 23  $\mu$ L aliquots. After incubation for 60 min at room temperature the cells were washed with PBS plus 10% AHS, and bound cpm in the wells was determined by  $\gamma$  counting.

Immunoreactivity of unlabeled conjugates was also measured in a two-step assay using iodinated anti-mouse antibody (25). LS174T cells (ATCC) were harvested from culture flasks using 0.05% trypsin/EDTA and washed with PBS, and 150 000 cells were aliquoted into flexible 96 well microtiter plates. Cells were air dried and then rehydrated with PBS plus 10% AHS.  $\beta$ L conjugates were diluted in PBS plus 10% AHS and incubated for 1 h on target cells at room temperature. Wells were washed, and 100 000 cpm of  $^{125}$ I-labeled anti-mouse IgG (light chain specific, Jackson ImmunoResearch Laboratories, Avondale, PA) were incubated 1 h at rt. Wells were washed and counted as above.

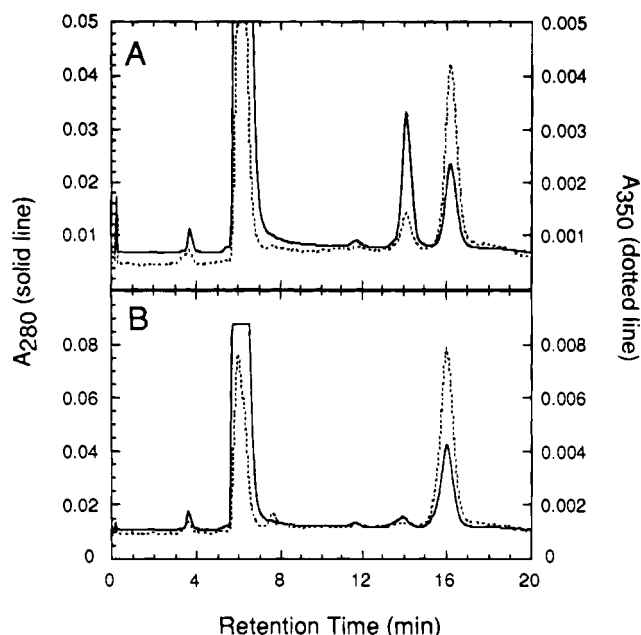
For biodistribution experiments the iodinated conjugates prepared and tested above were injected into female nude mice bearing LS174T tumors. Mice received either randomly linked (SMCC) or site-specifically linked  $\beta$ L-Fab' conjugate containing  $2.4 \times 10^7$  and  $2.8 \times 10^7$  cpm, respectively. At specific time intervals, described in Results, the mice were sacrificed, organs were removed and weighed, and the remaining radioactivity was assessed by  $\gamma$  counting.

## RESULTS

### Periodate Oxidation of N-Terminal Threonine.

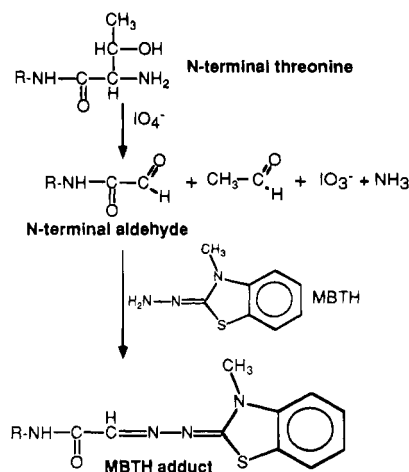
Quantitative measurement of the percentage of protein aldehyde formed after treatment of  $\beta$ L with sodium periodate was achieved by high-performance hydrophobic interaction chromatography (HIC-HPLC) after reaction with MBTH (Figure 1). Scheme 1 shows the reaction of N-terminal threonine with periodate and the structure of the subsequent adduct formed after reaction with MBTH. The spectrum of unreacted MBTH showed negligible absorbance above 300 nm, while reaction with acetone gave a major new absorbance peak at 306 nm, and reaction with the  $\beta$ -lactamase aldehyde produced a broad absorbance from 300 to 400 nm with a maximum at 340–350 nm (spectra not shown). The  $\beta$ L-MBTH adduct was monitored simultaneously at 350 nm and 280 nm during the HPLC runs. The ratio of 350 to 280 nm absorbance of the  $\beta$ L adduct was approximately 0.2 as shown in Figure 1.

Electrospray mass spectrometry gave a molecular weight of  $39\,235.6 \pm 4.2$  for native  $\beta$ -lactamase and  $39\,353.2 \pm 5.6$  for the  $\beta$ -lactamase-MBTH adduct purified by HIC-HPLC. This gave a measured net mass increase of  $118 \pm 9.8$  Da compared to the predicted value



**Figure 1.** HPLC profile of  $\beta$ L and  $\beta$ L-MBTH separated by hydrophobic interaction chromatography. Native  $\beta$ L elutes at 14 min and the  $\beta$ L-MBTH adduct at 16 min. The  $A_{280}$  and  $A_{350}$  were monitored simultaneously during the run. Panel A: periodate oxidation with a 2:1 molar excess of periodate over  $\beta$ L at pH 8 shows about 40% of the  $A_{280}$  eluting at 16 min, indicating the percentage of reactive aldehyde that was formed. Panel B: periodate oxidation of  $\beta$ L at pH 6.5 with 4:1 excess periodate over  $\beta$ L shows approximately 90% of the  $\beta$ L reacted with MBTH. These were injections of the complete reaction mixture (see the Experimental Procedures) which included the excess DTT, MBTH, acetaldehyde (see Scheme 1) presumably present as an MBTH adduct, and buffer components, all of which elute in the peaks prior to 10 min. Unreacted MBTH, when injected alone, eluted at 6 min with high  $A_{280}$  and minor  $A_{350}$  (chromatogram not shown).

### Scheme 1. Periodate Oxidation of Protein N-Terminal Threonine to Aldehyde and Reaction with MBTH



R = the remainder of the protein from the second amino acid residue to the carboxyl terminus

of 116 Da, consistent with an adduct containing a single MBTH per  $\beta$ -lactamase.

Table 1 shows the percentage of the  $\beta$ L-MBTH adduct formed under different periodate oxidation conditions. Variables including time of periodate incubation, the concentration of periodate, the buffer, and pH were all found to significantly influence formation of reactive aldehyde. The most important factor for maximum

Table 1

periodate oxidation buffer <sup>a</sup>	% MBTH adduct <sup>b</sup> molar ratio of periodate: $\beta$ L		
	2:1	4:1	6:1
40 mM phosphate, pH 6.5	76	89	90
40 mM phosphate, pH 7.0	72	77	78
40 mM phosphate, pH 8.0	43	50	53
100 mM Na acetate, pH 4.5	0		
20 mM MES, pH 6.3	49		
1% ammonium bicarbonate, pH 8.0	29		
50 mM borate, pH 8.0	35		
40 mM phosphate, pH 7.0 at 90 min	18		

<sup>a</sup> All incubations for 8 min at room temperature except where noted otherwise. <sup>b</sup> Integrated HPLC peak area of 16 min peak divided by 16 + 14 peaks. Typical chromatograms seen in Figure 1.

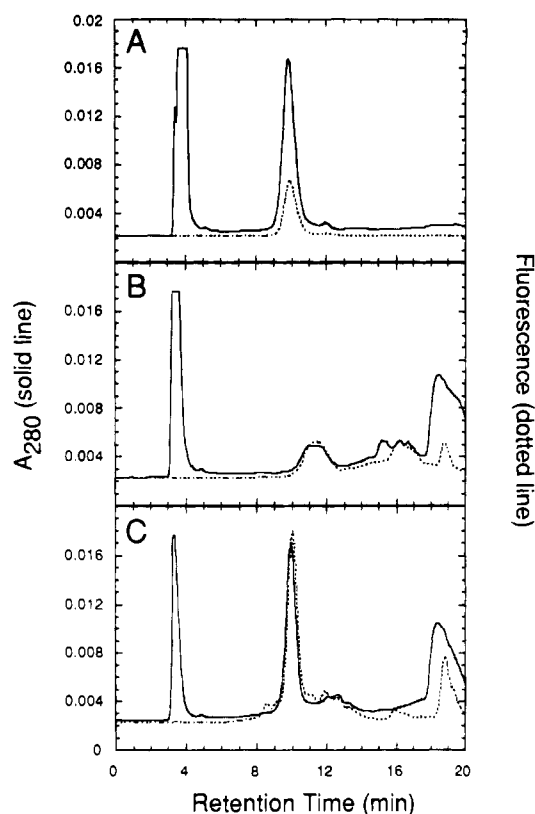
aldehyde formation was found to be periodate treatment at a pH less than 7. Also, oxidation in phosphate buffer showed better subsequent MBTH reactivities than those obtained with borate or MES at similar pH's. However, periodate treatment at a pH below 5 in 100 mM acetate buffer resulted in no subsequent MBTH reaction.

The second major factor influencing aldehyde formation was the time oxidation was allowed to proceed before being quenched. In general, incubation times from 5 to 15 min showed no significant differences in MBTH reactivities (data not shown) while incubation for 90 min dramatically decreased the subsequent yield of  $\beta$ L-MBTH to 25% of the control value (Table 1), due possibly to overoxidation. The protein carbonyl groups adjacent to the aldehyde as shown in Scheme 1 are capable of further reaction with periodate, although at much slower rates. It was not determined what percentage of the material eluting at the position of native  $\beta$ L after treatment with periodate under the various conditions in Table 1 was unoxidized native  $\beta$ L or this degraded, unreactive form of  $\beta$ L.

Higher periodate levels also had detrimental effects. MBTH reaction was comparable after  $\beta$ L oxidation with a molar excess of periodate from 2- to 6-fold over  $\beta$ L (Table 1) while incubation with a 16-fold excess of periodate gave rise to a major uncharacterized third peak at 11 min with an altered 350/280 ratio (data not shown).

A control variant of  $\beta$ L shown by amino acid sequence analysis in our laboratory to have an alanine at the N-terminus, when treated with 16-fold excess of periodate for 10 min at pH 6.5 and then reacted with MBTH gave only one peak which had a retention time and 350/280 ratio identical to the untreated starting protein. Thus, no specific or nonspecific MBTH-reactive sites were formed in a  $\beta$ L which did not contain threonine as the N-terminal residue.

The mechanism by which  $\beta$ L-MBTH interacted with the HIC column matrix appeared to be specific to the presence of the MBTH residue on the protein and not due primarily to increase in hydrophobicity of the protein as a whole. Reaction with reagents such as dansyl hydrazide, *o*-(4-nitrobenzyl)hydroxylamine, and 2,4-dinitrophenylhydrazine all showed negligible shifts in the HIC-HPLC retention time compared to unreacted  $\beta$ L (data not shown). Injection of the sample onto an alternate HIC column, a TSK phenyl 5PW column, also gave resolution of the  $\beta$ L-BTH from native  $\beta$ L though both eluted at a much higher %B buffer concentration due, presumably, to the more hydrophobic matrix. Attempts to effect separations by reversed phase 300 Å C-4



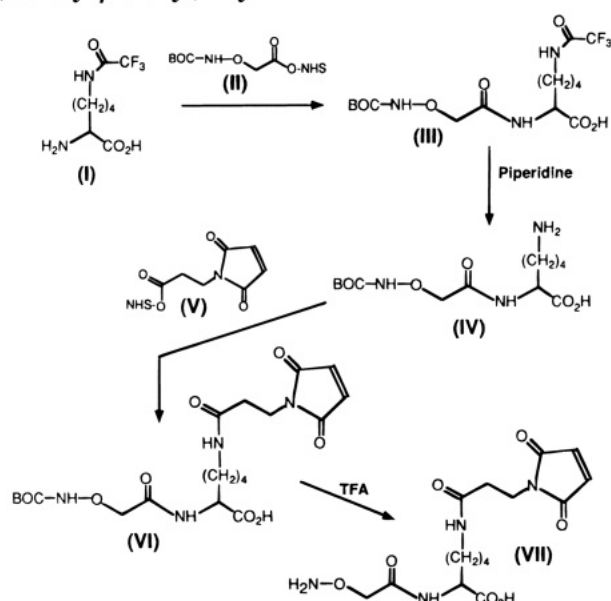
**Figure 2.** HPLC profile of Fab' reacted with BPM and separated by hydrophobic interaction chromatography. Unreacted BPM elutes at 3–4 min. Solid line is  $A_{280}$  with the scale indicated on the y-axis and the dotted line is fluorescence (300 nm ex/360 nm em) at a scale of 5 fluorescence units full scale. Panel A: elution profile of Fab'-3SH treated with NEM prior to addition of BPM showed no Fab' reaction with BPM as indicated by low level of fluorescence. Panel B: reaction of Fab'-3SH with BPM resulted in degradation of the peak profile. Panel C: reaction of Fab'-1SH (Fab'-3SH digested with lysyl endopeptidase) showed elution profile comparable to panel A except for increased fluorescence. The slight retention time offset in the fluorescence profile is due to placement of the fluorescence detector in series after  $A_{280}$  detector.

and C-8 columns using standard acetonitrile/water gradients were unsuccessful with all reagents tested, including MBTH.

**Proteolytic Cleavage of Fab' by Lysyl Endopeptidase.** The hinge region amino acid sequence of the last 16 residues (221–236) of the truncated heavy chain of pepsin-derived Fab' is RDCGCKPCICTVPEVS. This shows a lysine-proline linkage (residues 226–227) between the second and third cysteine as counted from the C-terminus. Lysyl endopeptidase can cleave lysine-proline bonds unlike proteases such as trypsin (26). While the linkage 226–227 was found to be available for cleavage by this protease after reduction of the  $F(ab')_2$  to a Fab', it was found to be poorly available in the  $(Fab')_2$  form, presumably due to steric factors. No differences were observed whether or not the cysteines had been capped with NEM. The mixture obtained after digestion with lysyl endopeptidase would therefore include a Fab' with a C-terminal lysine and decapeptide containing two cysteines.

Because the Fab' with 10 fewer amino acid residues was not distinguishable from peptic Fab' by size exclusion chromatography a method was developed employing HIC-HPLC, as with the MBTH adduct with  $\beta$ L described above. All samples in Figure 2 were treated with BPM, a hydrophobic thiol reagent which becomes fluorescent upon reaction with thiols. In Figure 2A the elution

**Scheme 2. Synthesis of  $N^{\alpha}$ -[(Aminoxy)acetyl]- $N^{\epsilon}$ -(maleoyl- $\beta$ -alanyl)-L-lysine<sup>a</sup>**

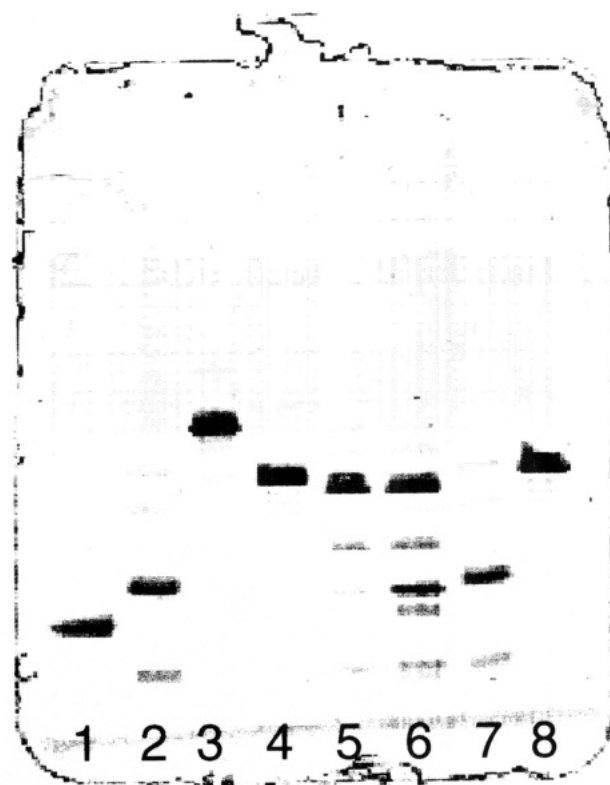


<sup>a</sup> Structures I–VII described in the Experimental Procedures.

profile of peptic Fab' is shown. The small peak at 12 min was residual unreduced F(ab')<sub>2</sub>. In this control experiment the cysteines in the Fab' were blocked with NEM prior to treatment with BPM. The chromatogram of Fab'-NEM without BPM treatment gave an identical retention time for the Fab' (not shown). If, however, the peptic Fab' with three cysteines (Fab'-3SH) was treated directly with BPM the single peak deteriorated into a series of broad poorly defined peaks (Figure 2B). After incubation with lysyl endopeptidase, reaction of the Fab' with BPM gave a peak eluting only about 0.5 min later than the NEM adduct in panel A, but, as would be expected for the wanted product, this peak was about five times more fluorescent (Figure 2C). Thus, the fluorescent peak in Figure 2C was used to monitor removal of the decapeptide from Fab' by lysyl endopeptidase.

Once this simple method for detecting single-sulfhydryl Fab' was in place, conditions for digestion by lysyl endopeptidase were investigated. Parameters tested were as follows: time of incubation, 4, 8, 16 h; percentage (w/w) of protease to Fab', 1, 2, 3%; temperature, rt, 37 °C; and pH, 8, 7, 6.3. Because cleavage of the lysine-proline bond was not especially fast the stronger test conditions were determined to be the most suitable: 3% lysyl endopeptidase at pH 6.3 in MES for 16–20 h at 37 °C. Although digestion rates followed the order pH 8 > 7 > 6.3, digestion at pH 8 was avoided because of difficulties in designing convenient reaction conditions which did not also result in degradation of the protein as determined by loss of integrated peak area by HPLC. The action of the lysyl endopeptidase on the Fab' was completely inhibited by the addition of an equal mass (5-fold molar excess) of the protease inhibitor, aprotinin (Sigma Chemical Co., St. Louis, MO) over lysyl endopeptidase. Quenching of the digestion mixture with aprotinin was, however, not necessary prior to reaction with BPM or direct application to the HPLC.

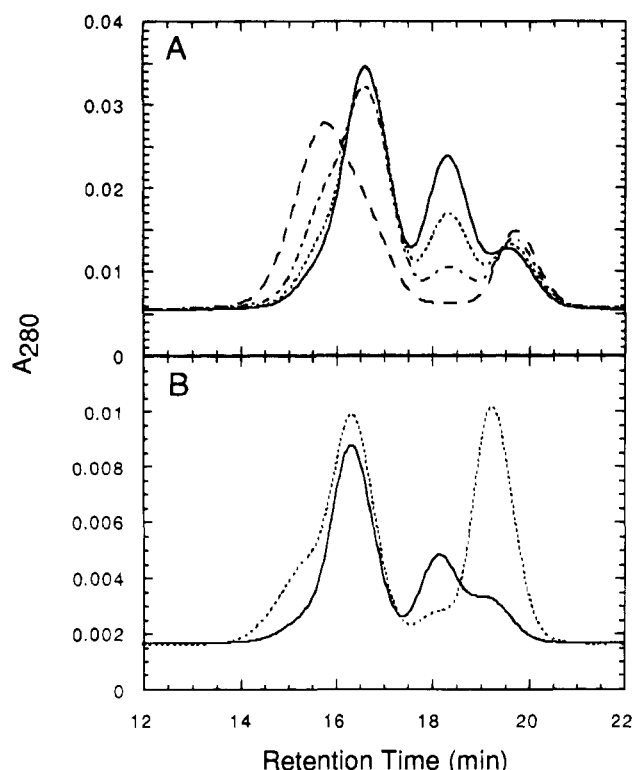
**Coupling of Single-Sulfhydryl Fab' to Oxidized  $\beta$ -Lactamase.** In order to couple Fab' to  $\beta$ -lactamase it was necessary to synthesize a bifunctional linker reactive with both thiols and aldehydes. Scheme 2 shows the synthetic scheme for the linker containing maleimide and aminoxy functional groups. The conjugation was performed by first reacting the linker with the aldehyde on



**Figure 3.** SDS-PAGE of conjugation components on 4–15% gradient Pharmacia Phast gel under nonreducing conditions. Gels stained with Coomassie R 350. Lanes slightly overloaded to better visualize minor bands: lane 1,  $\beta$ L; lanes 2 and 7, Fab' used in the conjugation reactions; minor bands near dye front are free Fab' heavy and light chain (~25 kDa) from cysteine reduction of F(ab')<sub>2</sub>; lane 3, intact antibody; lanes 4 and 8, F(ab')<sub>2</sub>; lane 5, purified 1:1  $\beta$ L–Fab' conjugate; lane 6, reaction mixture (Fab' added in 25% excess over  $\beta$ L) prior to purification of conjugate by size exclusion chromatography. The nominal molecular weights of the proteins are 40, 50, 90, 100, and 150 kDa for  $\beta$ L, Fab', 1:1 conjugate, F(ab')<sub>2</sub>, and intact antibody, respectively.

the  $\beta$ L N-terminus followed by removal of the excess linker by passage over a small P-6 column (see the Experimental Procedures). The derivatized  $\beta$ L was then mixed with purified single-sulfhydryl Fab'. The 1:1 conjugate (molecular weight ~90 kDa) was purified from the unreacted monomers (Fab', ~50 kDa, and  $\beta$ L, ~40 kDa) by size exclusion chromatography. The profile of conjugation mixture used to generate the 1:1 conjugate for subsequent biodistribution studies is shown in Figure 4B, solid line. Figure 3 shows the SDS-PAGE pattern of the different components in the reaction mixture including the final purified conjugate. Since recovery of the modified  $\beta$ L and Fab'-1SH precursors was essentially quantitative from the gel filtration columns, and because no higher order conjugates were formed (see below), the overall yield of 1:1 conjugate was effectively determined by the area of the peaks in the final chromatographic profile. In the case of Figure 4B, solid line, the 1:1 conjugate was well separated from the monomers and contained approximately 65% of the starting material. Incubation of Fab'-1SH at equimolar ratios with MBTH-reactive  $\beta$ L would be expected to result in the maximum percentage yields.

Figure 4 also shows size exclusion chromatograms of the conjugates formed with different ratios of  $\beta$ L to Fab'. Panel A shows the gradual increase in 2:1 conjugate as the ratio of linker-modified  $\beta$ L over Fab'-3SH is increased. Incubation at a ratio of 2  $\beta$ L per Fab' resulted in almost 80% of the peak area eluting at greater than



**Figure 4.** Size exclusion chromatography on Pharmacia Superose 12A. Peak eluting at 16.5 min was 1:1 conjugate; 18 min, Fab' and 19.5 min,  $\beta$ L. Panel A: conjugate formation with decreasing ratios of Fab'-3SH to  $\beta$ L. Solid line, 2:1; dotted line, 1.5:1; dot-dash, 1:1; dashed line 0.5:1. Absorbance eluting as a front shoulder on the 16 min peak indicated the presence of Fab' with more than one  $\beta$ L attached. With  $\beta$ L in 2-fold excess over Fab' (dashed line) 80% of the peak area corresponding to molecules greater in size than the 1:1 conjugate peak which eluted at about 15–16 min. Panel B: conjugate formation with Fab'-1SH. Solid line: the profile of the reaction mixture of Fab'/ $\beta$ L at a ratio of 1.25:1. The peak area of the conjugate is 65% of the total A<sub>280</sub>. Reinjection of purified conjugate showed a single peak at the same position (not shown). Dotted line: in the same experiment when an aliquot of  $\beta$ L was added in 3-fold excess over Fab'-1SH only 16% of the conjugate peak area corresponds to molecules greater in size than the 1:1 conjugate (integrated area of the front shoulder at ~15 min).

1:1 conjugate retention time. This was also confirmed by SDS-PAGE which, in addition, showed 10–20% of 3:1 conjugate in this sample (gel not shown). At a Fab'-3SH/ $\beta$ L ratio of 1:1 about 25% of the conjugate formed was 2:1, as estimated from integration of the HPLC peak areas, and even with Fab'-3SH at twice the  $\beta$ L concentration about 5–10% 2:1 conjugate was estimated from the chromatograms. These results demonstrated that close spacing of the hinge region cysteines did not appreciably hinder multiple protein attachments.

In contrast to Fab'-3SH, coupling reactions using Fab'-1SH showed minimal higher order conjugation. Incubation of Fab'-1SH/ $\beta$ L at a ratio of 1.25:1 formed negligible quantities of material behaving as 2:1 conjugate (Figure 4, solid line; Figure 3, lane 5). Even when Fab'-1SH was incubated with a 3-fold excess of maleimide-modified  $\beta$ L only about 16% of the conjugate formed was 2:1. This may have been due to a few percent residual Fab'-3SH but the majority was likely due to reaction with the sulfhydryls produced by the 10–20% of free light and heavy chains formed upon treatment of the F(ab')<sub>2</sub> with cysteine (see Figure 3, lanes 2 and 7). This light-heavy chain reduction can also be seen in the purified conjugate, lane 5. The only significant band in lane 5, aside from the 1:1 conjugate, ran between the

**Table 2**

ratio of Fab' to $\beta$ L	peak area <sup>a</sup>		% reactive $\beta$ L	
	conjugate	$\beta$ L	w/MBTH <sup>b</sup>	w/Fab' <sup>c</sup>
Fab'-3SH <sup>d</sup>				
2:1	92	17	90	72
1.5:1	100	20	90	71
1:1	106	22	90	71
0.5:1	97	21	90	70
Fab'-1SH <sup>d</sup>				
1.25:1	65	11	90	75
Fab'-3SH <sup>e</sup>				
1.5:1	20	40	35	20

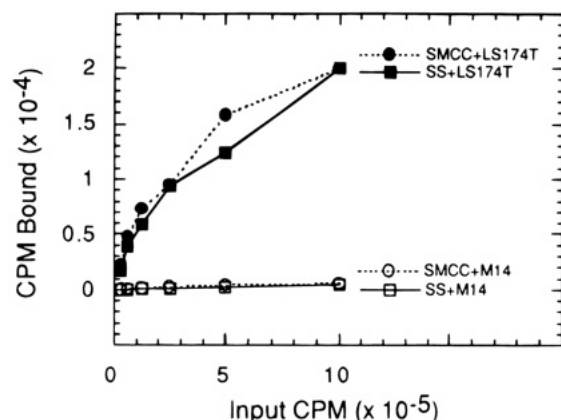
<sup>a</sup> Arbitrary HPLC integrator units from chromatograms in Figure 5, rounded off to nearest integer. <sup>b</sup> Percentage of  $\beta$ L-MBTH adduct as determined from relative A<sub>280</sub> of HPLC peak areas as seen in Figure 1. <sup>c</sup> Percentage of total  $\beta$ L found as conjugate with Fab', based on relative peak areas. Extinction coefficients used in calculation: A<sub>280</sub> of 2.2 and 2.0 equals 1 mg/mL for  $\beta$ L and  $\beta$ L-Fab' conjugate, respectively. Also  $\beta$ L comprises 45% of the conjugate mass. <sup>d</sup>  $\beta$ L oxidized at pH 6.5 in phosphate as shown in Table 1. <sup>e</sup>  $\beta$ L oxidized at pH 8 in borate buffer as shown in Table 1. This is the simple average of four determinations with less than 10% variation between values. Chromatograms not shown.

position of free Fab' and the conjugate and represented a similar percentage (10–20%) of 1:1 conjugate minus the light chain, which can be seen running near the dye front. Noncovalently bound light-heavy chains can only be separated under denaturing conditions such as SDS gels since strong hydrogen bonding keeps the molecules together under native conditions including size exclusion chromatography. Immunoreactivity is not noticeably affected by reduction of the light-heavy chain disulfide bond (unpublished observation).

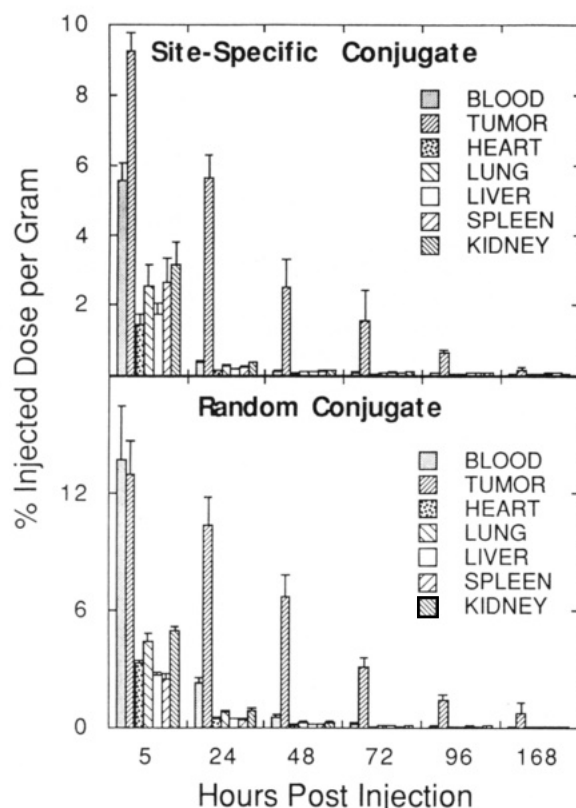
The protein coupling efficiency was highly correlated to the percentage reaction of oxidized  $\beta$ L with MBTH shown in Table 1. By integrating the peaks of Figure 4 the percentage of nonreactive oxidized  $\beta$ L could be calculated for each set of conditions. In all chromatograms except Figure 4B, dotted line, the concentration of available Fab' thiols was equal to or greater than that of the reactive  $\beta$ L. The last column in Table 2 shows that under a wide variety of ratios of Fab' to  $\beta$ L the reactive  $\beta$ L maintained a nearly constant coupling efficiency with Fab' from 70–75%, with a simple average of 72%. The coupling efficiency was not significantly impaired even when two or more molecules of  $\beta$ L were attached to Fab'-3SH. By contrast, under conditions where only 35% of the  $\beta$ L reacted with MBTH (Table 2, bottom line) the coupling efficiency with Fab' dropped to 20%.

**Characterization of the  $\beta$ L-Fab' Conjugate.** All procedures used in the preparation and modification of  $\beta$ L and Fab' had no measurable effect on their individual activities. For  $\beta$ L, assay of its activity using PADAC substrate (12) showed identical hydrolysis rates for native  $\beta$ L and the  $\beta$ L conjugate on a molar basis. Immunoreactivity of the two conjugates was shown to be comparable by direct binding of <sup>125</sup>I-labeled conjugate to LS174T-(antigen+) and M14(antigen-) tumor cells (Figure 5). In addition unlabeled conjugate was also tested in a two-step method employing labeled sheep anti-mouse antibody (see the Experimental Procedures) to detect conjugate bound to antigen. This result also demonstrated identical immunoreactivity for the two conjugates (data not shown). The labeled conjugates shown in Figure 5 were injected into tumor-bearing nude mice to study the biodistribution (Figure 6). The major difference between the conjugates is seen in the blood pool where the site-specifically linked conjugate is cleared more rapidly. At 5 h the tumor/blood ratio was 1.65 for the site-specific





**Figure 5.** Comparison of the immunoreactivity of  $^{125}\text{I}$ -labeled randomly conjugated (SMCC) versus site-specifically linked (SS)  $\beta\text{L}$ -Fab' conjugates towards antigen positive (LS174T) and antigen negative (M14) tumor cells. See the Experimental Procedures for details.



**Figure 6.** Biodistribution of  $^{125}\text{I}$ -labeled  $\beta\text{L}$ -Fab' conjugates in nude mice bearing LS174T tumors. Corrected for isotopic decay.

conjugate compared to 0.95 for the randomly linked conjugate. At 24 h this ratio increased to 15 and 4.2, respectively. The site-specific linked  $\beta\text{L}$ -Fab' conjugate would therefore be expected to give better therapeutic index upon administration of a  $\beta\text{L}$ -cleavable prodrug.

## DISCUSSION

The current study demonstrates the efficiency of site-specific coupling methodology over random derivatization methods in the conjugation of proteins. Overall coupling efficiencies were at least 3-fold greater than those achieved by random methods. Schemes for site-specific modification of proteins have focused primarily on the N- and C-terminal amino acid residues since, in principle, there will be only one of each per polypeptide chain. For instance, we have found reverse proteolysis to be an

effective method of introducing carbohydrazide to C-terminal lysines on antibodies (27, 28). This procedure can be applied to the naturally occurring C-terminal lysine on intact antibody or to C-terminal lysine produced artificially by the action of proteases such as lysyl endopeptidase or trypsin. The C-terminal carbohydrazide on the protein reacts to form a stable hydrazone bond with a second, aldehyde-containing molecule such as a synthetic chelate, drug, linker or modified protein. While applicable in theory to most proteins, this method can give wide variability in the coupling efficiency from one protein to another.

Efforts to take advantage of the  $\text{pK}$  differential between the N-terminal  $\alpha$ -amine ( $\text{pK} \sim 8$ ) and the  $\epsilon$ -amino group on lysine ( $\text{pK} \sim 10$ ) have not proved sufficiently selective for general use on proteins. For smaller peptides with only a single competing lysine group the reagent iodoacetic anhydride can acylate the N-terminal  $\alpha$ -amine with selectivities greater than 90% at pH 6 (29). The attached iodoacetyl functional group is then available for reaction with thiols. However, even a low percentage nonselective reaction with lysine  $\epsilon$ -amines becomes unacceptable when working with larger peptides and proteins where available lysines are in molar excess over the single N-terminal by a factor of 20 or more.

In the present work the N-terminal threonine of P99 strain of  $\beta$ -lactamase was converted to an aldehyde by mild treatment with sodium periodate. This mechanism of action requires either a threonine or serine at the N-terminus (16–18). The mechanism of oxidation for a threonine-containing protein is shown in Scheme 1. The vicinal diols present in carbohydrates attached to some proteins are also subject to oxidation to aldehydes by periodate (30–32) but at rates 100–1000 times slower than for vicinal amino alcohols (15). Hence, this method can be applied to glycoproteins without appreciable degradation of the carbohydrate regions or formation of more than one aldehyde site for coupling. The N-terminal threonine of  $\beta\text{L}$  was found to be highly susceptible to periodate oxidation. The failure to see any MBTH reactivity toward a control  $\beta\text{L}$  terminating with alanine after periodate treatment emphasizes the specificity of vicinal amino alcohols in the formation of aldehydes under these mild conditions. This was in agreement with other work suggesting that periodate uptake by N-terminal threonine/serine is 1000 times faster than other protein reactions (15).

These results, together with the substantial loss in MBTH reactivity after 90 min exposure of the P99 strain of  $\beta\text{L}$  to periodate (Table 1), suggest that the threonine is quickly and easily oxidized to aldehyde and that overoxidation or degradation of the initially formed aldehyde is the primary cause of reduced reactivity toward hydrazine/aminooxy reagents.

It should be noted that the P99 strain of  $\beta\text{L}$  contains no cysteine residues which would be expected to compete effectively as a periodate scavenger (16). Proteins containing free cysteines may require additional periodate and should be tested for adverse effects due to periodate oxidation of those cysteines. In addition, the DTT used in the current work for quenching excess periodate should be avoided if disulfide bonds are present in the protein. Agents such as 1,3-diaminopropan-2-ol or ethylene glycol have also been used successfully in the current work to quench excess periodate though ethylene glycol must be added in large molar excess.  $\beta\text{L}$ -Fab' coupling percentages were shown to be proportional to the degree of the  $\beta\text{L}$ -linker formation as predicted by the reactivity of the oxidized  $\beta\text{L}$  with MBTH. However,  $\beta\text{L}$ -MBTH formation suggested that 90% of the  $\beta\text{L}$  contained reactive aldehyde



while the percentage of  $\beta$ L coupled to Fab' actually observed in Figure 4 ranged from 70 to 75% (Table 2). Possible reasons for differences include incomplete linker reaction with  $\beta$ L or partial hydrolysis of the maleimide functional group on the linker.

In theory the reactive carbonyl group liberated at the N-terminus of the chain could form inter- or intrachain Schiff bases with side-chain amino groups on the protein. In practice, however, as extensive previous work has shown (16–18), this is not a problem: any Schiff base structures that do form are most probably unstable at the mild acid pH of the oximation reaction and decompose in favor of the wanted oxime product.  $\beta$ L showed no tendency toward precipitation or loss of aldehyde reactivity even after many days storage in the oxidized form.

In the absence of chromatographic separation of reactive and nonreactive components in a mixture the extent of oxidation based solely on predicted chromogenic coefficients becomes even more difficult to assess. For example, in the current study the hydrazone formed by the MBTH reaction with acetone gave a new peak at 306 nm and had negligible absorbance above 340 nm. In contrast the maximum >300 nm absorbance for purified  $\beta$ L–MBTH was 340 nm. Thus, the environment and nature of the chemical bond formed affected the extinction coefficient of the MBTH adduct. Similarly, the fluorescence yield for BPM was observed to be highly solvent dependent. While attempts to separate Fab'–BPM adducts from unreacted Fab' by reversed-phase chromatography using acetonitrile/water solvents were unsuccessful (data not shown), it was noted, not surprisingly, that the Fab'–BPM peak had 5–10 times higher ratio of fluorescence to 280 nm absorbance than in the high salt buffers required for HIC. Hence, chromatographic separation of the reactive component obviated the need for the far more difficult task of determining precise extinction coefficients for each set of conditions. Along this same line, while it may be possible to resolve species of  $\beta$ L  $\pm$  the  $\alpha$ -amine directly by careful application of cation exchange chromatography, Table 1 suggests this alone would not be sufficient to predict subsequent hydrazide reactivity. It is the quantitative determination of hydrazide-reactive species which is essential for designing optimized conjugation reaction conditions.

It is not clear why the  $\beta$ L–MBTH adduct was resolved from  $\beta$ L, while similar hydrophobic adducts with dansyl hydrazide, 2,4-dinitrophenylhydrazine, and *o*-(nitrobenzyl)hydroxylamine were not. The thiazolinone carbon–nitrogen double bond (see Scheme 1) together with the resonance from both nitrogen lone-pair electrons might confer a favorable rigid, planar conformation to the entire adduct up to the point of the first protein carbonyl group, which would not be true for adducts with the other reagents described. It may be that the more rigid conformation of the MBTH adduct imparts increased selectivity upon interaction with a hydrophobic matrix.

The biodistribution studies of the conjugates demonstrated that no undesirable properties were introduced into the conjugate because of the linker (33) or site of conjugation. In fact, a more favorable tumor to blood ratio was achieved due to the more rapid clearance of the site-specifically linked conjugate from the blood at the early time points. The decreased percent injected dose per gram at the tumor may reflect this more rapid clearance from the blood, but any reduction in tumor uptake is offset by the more favorable tumor to blood ratio. Since the tumor to blood ratio is frequently the limiting factor in the efficiency of therapeutic applications (34) it may be that a more homogeneous conjugate confers an additional advantage in this area.

The current methodology may find wide applicability in combination with genetic engineering. Expression of a threonine or serine N-terminal on a protein not normally terminating in these amino acids creates an entirely new and effective site for conjugation with minimal impact on the protein. With regard to antibodies, many examples already exist of various Fv and Fab' fragments being expressed as chimeric or humanized forms (9, 35–38) which could, in theory, be expressed with only a single cysteine at the C-terminal region.

The expression of fusion proteins of enzymes attached to Fab's or Fv fragments does not necessarily preclude the need for chemical synthetic methods. In recombinant technology the separate antigen-binding and enzymatic domains are expressed as a single molecule, each half of which must fold properly in the presence of the other. Improper folding can lead to inactive or unstable constructs. In contrast, the individual domains in chemical constructs remain intact throughout. In addition, therapeutic conjugates generally require repeated injections, and while the technology for expression of humanized antibody fragments already exists, there is not yet a proven means of humanizing a bacterial protein such as  $\beta$ -lactamase. Expression of an active  $\beta$ L–Fv fusion protein has been achieved (39) but this construct would still be expected to be immunogenic. For this reason it is desirable to maintain individual control over the component halves when working with  $\beta$ L conjugates. One method which has been shown to decrease immunogenicity of proteins is dextranation (40). While  $\beta$ L activity was found to be unaffected by this process the immunoreactivity of anti-CEA and anti-TAG-72 Fab's were both severely compromised (data not shown). A method to modulate the degree of dextranation has, however, allowed construction of a conjugate with modified dextranation which maintains good immunoreactivity (manuscript in preparation). In this case, the addition of an effective conjugation strategy promises high yields of a bacterial protein in a conjugate with reduced immunogenicity.

The above considerations have been avoided entirely by expression of a human enzyme,  $\beta$ -glucuronidase, with a humanized Fab', a fusion protein which would be expected to elicit minimal immunogenic response in humans (41). Even in such cases, however, the availability of an otherwise inert but readily activatable threonine/serine residue offers additional advantages. One application might be as a site for the easy introduction of chelates in a defined manner for controlled radiolabeling and biodistribution experiments. Other options include combined drug (generated by the enzyme moiety of the fusion protein)–radioisotope (on the chelate) therapy, or even the introduction of a third protein (enzyme or antibody) for model trifunctional studies.

Thus, the presence of an N-terminal threonine/serine, used as described in this paper, can greatly increase the flexibility available in the construction and study of bioconjugates.

#### ACKNOWLEDGMENT

We thank Mr. P.-O. Regamey for mass spectrometric analysis. The Fonds National Suisse pour la Recherche Scientifique provided valuable background facility to the Geneva laboratory.

#### LITERATURE CITED

- (1) Yoshitake, S., Yamada, Y., Ishikawa, E., and Masseyeff, R. (1979) Conjugation of Glucose Oxidase from *Aspergillus niger* and Rabbit Antibodies Using N-Hydroxysuccinimide Ester of

- N-(4-Carboxycyclohexylmethyl)-Maleimide *Eur. J. Biochem.* 101, 395-9.
- (2) Wang, S.-M., Chern, J.-W., Yeh, M.-Y., Ng, J. C., Tung, E., and Roffler, S. R. (1992) Specific Activation of Glucuronide Prodrugs by Antibody-targeted Enzyme Conjugates for Cancer Therapy *Cancer Res.* 52, 4484-4491.
- (3) Kerr, D. E., Garrigues, U. S., Wallace, P. M., Hellstrom, K. E., Hellstrom, I., and Senter, P. D. (1993) Application of Monoclonal Antibodies against Cytosine Deaminase for the in Vivo Clearance of a Cytosine Deaminase Immunoconjugate *Bioconjugate Chem.* 4, 353-357.
- (4) Heindel, N. D., Zhao, H., Egolf, R. A., Chang, C.-H., Schray, K. J., Emrich, J. G., McLaughlin, J. P., and Woo, D. V. (1991) A novel Heterobifunctional Linker for Formyl to Thiol Coupling *Bioconjugate Chem.* 2, 427-430.
- (5) Kerr, D. E., Senter, P. D., Burnett, W. V., Hirshberg, D. L., Hellstrom, I., and Hellstrom, K. E. (1990) Antibody-penicillin-V-amidase conjugates kill antigen-positive tumor cells when combined with doxorubicin phenoxacetamide. *Cancer Immunol. Immunother.* 31, 202-206.
- (6) Haisma, H. J., Boven, E., Muijen, M. v., Jong, J. d., Vijgh, W. J. F. v. d., and Pinedo, H. M. (1992) A Monoclonal Antibody-beta-Glucuronidase Conjugate of the Prodrug Epirubicin-Glucuronide for Specific Treatment of Cancer. *Br. J. Cancer* 66, 474-8.
- (7) Haisma, H. J., Boven, E., Muijen, M. v., Vries, R. D., and Pinedo, H. M. (1992) Analysis of a Conjugate Between Anti-Carcinoembryonic Antigen Monoclonal Antibody and Alkaline Phosphatase for Specific Activation of the Prodrug Etoposide Phosphate. *Cancer Immunol. Immunother.* 34, 343-8.
- (8) Vruthula, V. M., Svensson, H. P., Kennedy, K. A., Senter, P. D., and Wallace, P. M. (1993) Antitumor Activities of a Cephalosporin Prodrug in Combination with Monoclonal Antibody-beta-Lactamase Conjugates. *Bioconjugate Chem.* 4, 334-340.
- (9) Yokota, T., Milenic, D. E., Whitlow, M., and Schlom, J. (1992) Rapid Tumor Penetration of a Single-Chain Fv and Comparison with Other Immunoglobulin Forms. *Cancer Res.* 52, 3402-3408.
- (10) Mather, S. J., Durbin, H., and Taylor-Papadimitriou, J. (1987) Identification of Immunoreactive Monoclonal Antibody Fragments for Improved Immunoscintigraphy. *J. Immunol. Meth.* 96, 255-64.
- (11) Buchegger, F., Haskell, C. M., Schreyer, M., Scazziga, B. R., Randin, S., Carrel, S., and Mach, J.-P. (1983) Radiolabeled Fragments of Monoclonal Antibodies Against Carcinoembryonic Antigen for Localization of Human Colon Carcinoma Grafted into Nude Mice. *J. Exp. Med.* 158, 413-427.
- (12) Meyer, D. L., Jungheim, L. N., Mikolajczyk, S. D., Shepherd, T. A., Starling, J. J., and Ahlem, C. N. (1992) Preparation and Characterization of beta-Lactamase-Fab' Conjugates for the Site Specific Activation of Oncolytic Agents. *Bioconjugate Chem.* 3, 42-8.
- (13) Meyer, D. L., Jungheim, L. N., Law, K. L., Mikolajczyk, S. D., Shepherd, T. A., Mackensen, D. G., Briggs, S. L., and Starling, J. J. (1993) Site-Specific Prodrug Activation by Antibody-beta-Lactamase Conjugates: Regression and Long-Term Growth Inhibition of Human Colon Carcinoma Xenograft Models. *Cancer Res.* 53, 3956-63.
- (14) Parham, P. (1983) On the Fragmentation of Monoclonal IgG1, IgG2a, and IgG2b from Balb/c Mice. *J. Immunol.* 131, 2895-2902.
- (15) Fields, R., and Dixon, H. B. F. (1968) A Spectrophotometric Method for the Microdetermination of Periodate. *Biochem. J.* 108, 883-887.
- (16) Dixon, H. B. F., and Fields, R. (1972) Specific Modifications of NH<sub>2</sub>-Terminal Residues by Transamination. *Meth. Enzymol.* 25, 409-419.
- (17) Gaertner, H. F., Rose, K., Cotton, R., Timms, D., Camble, R., and Offord, R. E. (1992) Construction of protein analogues by site-specific condensation of unprotected fragments. *Bioconjugate Chem.* 3, 262-268.
- (18) Geoghegan, K. F., and Strohm, J. G. (1992) Site-directed conjugation of nonpeptide groups to peptides and proteins via periodate oxidation of a 2-amino alcohol *Bioconjugate Chem.* 3, 138-146.
- (19) Cartwright, S. J., and Waley, S. G. (1984) Purification of beta-Lactamases by Affinity Chromatography on Phenylboronic Acid-Agarose. *Biochem. J.* 221, 505-12.
- (20) Galleni, M., Lindberg, F., Normark, S., Cole, S., Honore, N., Joris, B., and Frere, J.-M. (1988) Sequence and Comparative Analysis of Three *Enterobacter cloacae* ampC beta-Lactamase Genes and their Products. *Biochem. J.* 250, 753-760.
- (21) Pochon, S., Buchegger, F., Plegrin, A., Mach, J.-P., Offord, R. E., Ryser, J. E., and Rose, K. (1989) A novel derivative of the cheon desferrioxamine for site-specific conjugation to antibodies *Int. J. Cancer* 43, 1188-1194.
- (22) Vilaseca, L. A., Rose, K., Werlen, R., Meunier, A., Offord, R. E., Nichols, C. L., and Scott, W. L. (1993) Protein conjugates of defined structure: synthesis and use of a new carrier molecule. *Bioconjugate Chem.* 4, 515-520.
- (23) Savoy, L.-A., Jones, R. M. L., Pochon, S., Davies, J. G., Muir, A. V., Offord, R. E., and Rose, K. (1988) Identification by fast atom bombardment mass spectrometry of insulin fragments produced by insulin proteinase. *Biochem. J.* 249, 215-222.
- (24) Markwell, M. A. K. (1982) A new solid-state reagent to iodinate proteins. *Anal. Biochem.* 125, 427-432.
- (25) Starling, J. J., Mariak, R. S., Henson, N. A., Nichols, C. L., Briggs, S. L., and Laguzza, B. C. (1989) In Vivo efficacy of monoclonal antibody-drug conjugates of three different subtypes which bind the human tumor-associated antigen defined by the KS1/4 monoclonal antibody. *Cancer Immunother.* 28, 171-178.
- (26) Masaki, T., Fujihashi, T., Nakamura, K., and Soejima, M. (1981) Studies on a new proteolytic enzyme from *Achromobacter lyticus* M497-1: (II) Specificity and inhibition studies on *Achromobacter* protease 1. *Biochim. Biophys. Acta* 660, 51-55.
- (27) Fisch, I., Kunzi, G., Rose, K., and Offord, R. E. (1992) Site-Specific Modification of a Fragment of a Chimeric Monoclonal Antibody Using Reverse Proteolysis. *Bioconjugate Chem.* 3, 147-153.
- (28) Fisch, I. (1993) Ph. D Thesis, University of Geneva.
- (29) Wetzel, R., Halualani, R., Stults, J. T., and Quan, C. (1990) A General Method for Highly Selective Cross-Linking of Unprotected Polypeptides via pH-Controlled Modification of N-Terminal alpha-Amino Groups. *Bioconjugate Chem.* 1, 114-122.
- (30) Shih, L. B., Goldenberg, D. M., Xuan, H., Lu, H., Sharkey, R. M., and Hall, T. C. (1991) Anthracycline Immunoconjugates Prepared by a Site-Specific Linkage via an Amino-Dextran Intermediate Carrier. *Cancer Res.* 51, 4192-4198.
- (31) O'Shannessy, D. J. (1988) Hydrazides as specific reagents for the labeling of glycoproteins. *ISBT Commun.* 3, 4-6.
- (32) Wilchek, M., and Bayer, E. A. (1987) Labeling glycoconjugates with hydrazide reagents. *Methods Enzymol.* 138, 429.
- (33) Johnson, D. A., Barton, R. L., Fix, D. V., Scott, W. L., and Gutowski, M. C. (1991) Induction of Immunogenicity of Monoclonal Antibodies by Conjugation with Drugs. *Cancer Res.* 51, 5774-5776.
- (34) Jain, R. K. (1989) Delivery of Novel Therapeutic Agents in Tumors: Physiological Barriers and Strategies. *J. Natl. Cancer Inst.* 81, 570-6.
- (35) Milenic, D. E., Yokota, T., Filpula, D. R., Finkelman, M. A. J., Dodd, S. W., Wood, J. F., Whitlow, M., Snoy, P., and Schlom, J. (1991) Construction, binding properties, metabolism and tumor targeting of a single-chain Fv derived from the pancreatic carcinoma monoclonal antibody CC49. *Cancer Res.* 51, 6363-6371.
- (36) Khazaeli, M. B., Saleh, M. N., Liu, T. P., Meredith, R. F., Wheeler, R. H., Baker, T. S., King, D., Secher, D., Allen, L., Rogers, K., Colcher, D., Schlom, J., Shochat, D., and LoBuglio, A. F. (1991) Pharmacokinetics and Immune Response of 131I-Chimeric Mouse/Human B72.3 (Human g4) Monoclonal Antibody in Humans. *Cancer Res.* 51, 5461-5466.
- (37) Chaudhary, V. K., Balra, J. K., Gallo, M. K., Willingham, M. C., FitzGerald, D. J., and Pastan, I. (1990) A rapid method of cloning functional variable-region antibody genes in

- Escherichia coli*. as single-chain immunotoxins *Proc. Natl. Acad. Sci. U.S.A.* 87, 1066–1070.
- (38) Colcher, D., Bird, R., Roselli, M., Hardman, K. D., Johnson, S., Pope, S., Dodd, S. W., Pantoliano, M. W., Milenic, D. E., and Schlom, J. (1990) In vivo tumor targeting of a recombinant single-chain antigen binding protein. *J. Natl. Cancer Inst.* 82, 1191–1197.
- (39) Gashorn, S. C., Svensson, H. P., Kerr, D. E., Somerville, J. E., Senter, P. D., and Fell, H. P. (1993) Genetic Construction Expression, and Characterization of a Single Chain Anti-Carcinoma Antibody Fused to  $\beta$ -Lactamase. *Cancer Res.* 53, 2123–2127.
- (40) Fagnani, R., Hogan, M. S., and Bartholomew, R. (1990) Reduction of Immunogenicity by Covalent Modification of Murine and Rabbit Immunoglobulins with Oxidized Dextran of Low Molecular Weight. *Cancer Res.* 50, 3638–3645.
- (41) Bosslet, K., Czech, J., Lorenz, P., Sedlacek, H. H., Schuermann, M., and Seemann, G. (1992) Molecular and Functional Characterisation of a Fusion Protein Suited for Tumour Specific Prodrug Activation. *Br. J. Cancer* 65, 234–8.

# Gene Transfer with a Series of Lipophilic DNA-Binding Molecules

Jean-Serge Remy, Claude Sirlin, Pierre Vierling,<sup>†</sup> and Jean-Paul Behr\*

Laboratoire de Chimie génétique (CNRS URA 1386), Faculté de Pharmacie de Strasbourg, F-67401-Illkirch Cedex, France, and Unité de Chimie moléculaire (URA 426), Faculté des Sciences, F-06108-Nice, France. Received July 1, 1994\*

Synthetic gene transfer vectors could be an attractive alternative to biological vehicles for gene therapy. In an effort to improve the previously developed lipopolyamine-mediated transfection technique, various amphiphilic DNA-binding molecules have been synthesized. Besides Transfectam, several lipospermines display very high gene delivery levels. The structure–activity relationship obtained points to the central role played by the polyamine headgroup in condensing the plasmid and binding it to the cell surface, provided the hydrophobic moiety is capable to generate nonmicellar mesomorphic structures. It also highlights other favorable (albeit more speculative) properties shared by protonable lipospermines as compared to quaternary ammonium-bearing lipids, such as their ability to act as a buffer and their strong affinity for chromatin. The former property may prevent the pH decrease along the degradative lysosomal pathway. The ability to bind to chromatin even in the presence of endogenous polyamines should have two consequences: a nuclear tropism of the transfecting particles and plasmid uncoating in the nucleus by competitive dilution of the lipopolyamine into an ocean of DNA.

## INTRODUCTION

The design of artificial systems able to carry genes into eukaryotic cells has become a field of considerable interest. Although most ongoing gene therapy protocols rely on very efficient recombinant viral vectors, the large scale or repetitive use of biological carriers in humans indeed is expected to raise several problems which are not shared by inert vectors. The latter ones are far less efficient, however. Several types of cationic molecules able to bind DNA and to carry it into cells have been described (reviewed in Felgner (1990), Behr (1993), and Cotten and Wagner (1993)), essentially including chimeric polypeptides and synthetic lipids.

Within the latter context (Felgner et al., 1987; Leventis and Silviu, 1990; Gao and Huang, 1991), we have synthesized lipopolyamines (Behr et al., 1989) and developed them in vitro into one of the most efficient nonviral gene transfer techniques (Loeffler and Behr, 1993; Barthel et al., 1993; Behr, 1994). These vectors, however, remain orders of magnitude behind the biological ones, and in an effort to reduce this gap we have designed various other lipophilic DNA-binding structures. Here we describe the syntheses and transfection properties of these new molecules. Although no real breakthrough was made, several compounds display efficiencies comparable to that of the originally described lipopolyamines. Furthermore, the structure–activity relationship obtained allows us to circumvent some of the structural elements required for efficient gene transfer and, most significantly, gives an experimental support to the mechanism of transfer of lipopolyamine-coated DNA into the cell.

## EXPERIMENTAL PROCEDURES

The syntheses of  $(C_{18})_2\text{GlySper}^{3+}$  and  $\text{DPPEsper}^{2+}$  have been described previously (Behr et al., 1989; Loeffler & Behr, 1993).  $(C_{18})_2\text{GlySper}^{3+}$  (Transfectam) is available

from Promega and DOTMA was a gift from Dr R. Debs (San Francisco).

**Preparation of the Fluorinated Amine Precursors.** A solution of nonafluorotetradecylcarbonyl chloride (Santaella et al., 1991) (1.20 g, 2.4 mmol) in 10 mL of  $\text{CHCl}_3$  was added dropwise under argon to a solution of heptadecafluorodecylamine hydrochloride (Nivet et al., 1992) (1.16 g, 2.4 mmol) and triethylamine (1 mL, 7.3 mmol) in 10 mL of  $\text{CHCl}_3$ . After 12 h, the solution was concentrated and chromatographed (silica,  $\text{CHCl}_3$ ) to afford 1.80 g of the amide as a white powder (90% yield). This compound was added to 0.32 g of  $\text{LiAlH}_4$  in 20 mL of diethyl ether, and the suspension was heated under reflux for 12 h. After usual workup and chromatography (silica,  $\text{CHCl}_3$ ), 1.6 g of *N*-(heptadecafluorodecyl)-*N*-nonafluoropentadecylamine was obtained (90% yield).

**Preparation of *N*-(Benzyloxycarbonyl)glycinamides.** *N',N'*-Dioctyl-*N*-(benzyloxycarbonyl)glycinamide: A solution of dioctylamine (1g, 4.14 mmol), *N*-(benzyloxycarbonyl)glycine *p*-nitrophenyl ester (1.37g, 4.14 mmol), and triethylamine (1.37g, 4.14 mmol) in 5 mL of  $\text{CH}_2\text{Cl}_2$  was refluxed during 24 h. The reaction mixture was diluted with 20 mL of  $\text{Et}_2\text{O}$  and extracted with 0.5 M  $\text{Na}_2\text{CO}_3$  until hydrolysis of the unreacted ester was completed. The organic phase was washed with  $\text{H}_2\text{O}$  and 1 M HCl, dried with  $\text{MgSO}_4$ , and evaporated. Yield: 810 mg (45%).

*N'*-(Heptadecafluorodecyl)-*N'*-(nonafluoropentadecyl)-*N*-(benzyloxy)glycinamide: A solution of *N*-(heptadecafluorodecyl)-*N*-(nonafluoropentadecyl)amine (505 mg, 0.6 mmol), *N*-(benzyloxycarbonyl)glycine *p*-nitrophenyl ester (240 mg, 0.73 mmol), and triethylamine (100  $\mu\text{L}$ , 0.73 mmol) in 1.5 mL of THF was refluxed during 48 h. The reaction mixture was diluted with 20 mL of  $\text{CH}_2\text{Cl}_2$  and successively washed with a saturated solution of  $\text{NaHCO}_3$ , with  $\text{H}_2\text{O}$ , and with a 5% citric acid solution. The crude product was chromatographed (silica,  $\text{CH}_2\text{Cl}_2$ , 0–2% MeOH). Yield: 440 mg (70%).

**Preparation of Glycinamides.** A solution of 1 mmol of *N*-(benzyloxycarbonyl)glycinamide in 10 mL of  $\text{CH}_2\text{Cl}_2/\text{EtOH}$  (1:1) containing 120 mg of 10% Pd/C was hydrogenated during 48 h at atmospheric pressure. The

\* To whom correspondence should be addressed.

<sup>†</sup> Unité de Chimie moléculaire.

\* Abstract published in *Advance ACS Abstracts*, October 15, 1994.

reaction mixture was filtered through Celite which was further washed with  $\text{CH}_2\text{Cl}_2/\text{EtOH}$  1/1.

The  $N',N'$ -dioctylglycinamide filtrate was evaporated, redissolved in  $\text{CH}_2\text{Cl}_2$ , and washed with 0.1 M NaOH. The organic phase was dried with  $\text{MgSO}_4$  and evaporated. Yield: 85%.

The  $N'$ -(heptadecafluorodecyl)- $N'$ -(nonafluoropentadecyl)glycinamide filtrate was evaporated and successively washed with  $\text{CHCl}_3$  and MeOH. The desired compound was recovered after evaporation of the MeOH solution. Yield: 40%.

**Direct Coupling with Dicyclohexylcarbodiimide (DCC).**  $N',N'$ -Diocetyl(butoxycarbonyl)ornithylglycinamide;  $N'$ -(nonafluoropentadecyl)tetrakis(butoxycarbonyl)spermincarboxamide;  $N'$ -(heptadecafluorodecyl)- $N'$ -(nonafluoropentadecyl)[(tetrabutoxycarbonyl)spermincarbonyl]glycinamide;  $N'$ -[3,6,9-trioxa-7-(2'-oxaeicos-11'-enyl)heptaicos-18-enyl][tetrakis(butoxycarbonyl)spermincarbonyl]glycinamide.

DCC (1 mmol) was added to a solution of 1 mmol of (tetrabutoxycarbonyl)spermincarboxylic acid (Behr, 1993) and 1 mmol of amine in 2 mL of  $\text{CH}_2\text{Cl}_2$ . After 24 h, the reaction mixture was filtered, diluted, and successively washed with a saturated solution of  $\text{NaHCO}_3$ , with  $\text{H}_2\text{O}$ , and with a 5% citric acid solution. The crude product was chromatographed (silica,  $\text{CH}_2\text{Cl}_2$ , 0–4% MeOH). Yield: 55–70%.

Reaction of the  $N'$ -(heptadecafluorodecyl)- $N'$ -(nonafluoropentadecyl) derivative was performed in THF with 1 equiv of triethylamine. The reaction medium was diluted with  $\text{CCl}_4$ , filtered, and chromatographed (silica,  $\text{CH}_2\text{Cl}_2$ , 0–2% MeOH).

**Indirect Coupling via an Activated Ester.**  $N'$ -Octadecyltetrakis(butoxycarbonyl)spermincarboxamide;  $N',N'$ -dioctadecyltetrakis(butoxycarbonyl)spermincarboxamide;  $N',N'$ -dioctyl[tetrakis(butoxycarbonyl)spermincarbonyl]glycinamide;  $N'$ -(1,2-dioleoyl-*sn*-glycero-3-phosphoethanolyl)tetrakis(butoxycarbonyl)spermincarboxamide.

Tetrakis(butoxycarbonyl)spermincarboxylic acid was activated with  $N$ -hydroxysuccinimide (1 mmol of acid, 1 mmol of  $N$ -hydroxysuccinimide, and 1 mmol of DCC in 4 mL of  $\text{CH}_2\text{Cl}_2$ ; reaction time 0.5 h). The resulting ester was reacted with 1 mmol of amine in the presence of 1 mmol of triethylamine. After being stirred for 24 h, the reaction mixture was filtered, diluted, and washed with 0.5 M  $\text{Na}_2\text{CO}_3$ , with  $\text{H}_2\text{O}$ , and with a 5% citric acid solution. When present (TLC), the unreacted ester was hydrolyzed at once with 0.5 M KOH in order to facilitate the purification step. The crude product was chromatographed (silica,  $\text{CH}_2\text{Cl}_2$ , 0–2% MeOH). Yield: 55–75%.

In the case of the 1,2-dioleoyl-*sn*-glycero-3-phosphoethanolamine derivative, the reaction mixture was refluxed, diluted, and washed with a 5% citric acid solution. The crude product was chromatographed (silica,  $\text{CH}_2\text{Cl}_2$ , 0–15% MeOH).

**Final Deprotection of the Amino Groups.** The butoxycarbonyl protective groups were quantitatively removed by dissolving the protected compound (100 mg) into trifluoroacetic acid (1 mL) and removing the solvent in vacuo; this procedure was repeated three times to ensure complete removal of the four butoxycarbonyl groups.

$^1\text{H-NMR}$  (200 MHz) spectra were run in  $\text{CD}_3\text{OD}$ , except when indicated. Chemical shifts are expressed in ppm and coupling constants in Hz.

$N',N'$ -Diocetylornithylglycinamide, hydrotrifluoroacetate ( $\text{C}_{18}$ )<sub>2</sub>GlyOrn<sup>2+</sup>:  $^1\text{H-NMR}$  4.24; 4.00 (dd,  $J_{AB} = 16$ , 2H,  $\text{CH}_2\text{CO}$ ), 3.96 (t,  $J = 7$ , 1H,  $\text{CHN}^+$ ), 3.2–3.4 (m, 4H,  $\text{CH}_2\text{N}$ ), 2.97 (t,  $J = 7$ , 2H,  $\text{CH}_2\text{N}^+$ ), 1.55–1.95 (m, 12H,

$\text{CH}_2\text{CH}_2\text{N}^+$ ,  $\text{CH}_2\text{CH}_2\text{N}$ ,  $\text{CH}_2\text{CH}_2\text{CH}_2\text{N}$ ), 1.27 (bs, 56H,  $(\text{CH}_2)_{14}$ ), 0.88 (t,  $J = 6$ , 6H,  $\text{CH}_3$ ).

$N'$ -Octadecylspermincarboxamide, hydrotrifluoroacetate  $\text{C}_{18}\text{Sper}^{3+}$ :  $^1\text{H-NMR}$  3.90 (t,  $J = 6$ , 1H,  $\text{CHN}^+$ ), 3.25 (t,  $J = 7.5$ , 2H,  $\text{CH}_2\text{N}$ ), 3.0–3.2 (m, 10H,  $\text{CH}_2\text{N}^+$ ), 1.75–2.15 (m, 10H,  $\text{CH}_2\text{CH}_2\text{N}^+$ ,  $\text{CH}_2\text{CH}_2\text{N}$ ), 1.5–1.75 (m, 2H,  $\text{CH}_2\text{CH}_2\text{CH}_2\text{N}$ ), 1.28 (bs, 28H,  $(\text{CH}_2)_{14}$ ), 0.89 (t,  $J = 6.5$ , 3H,  $\text{CH}_3$ ).

$N',N'$ -Diocetylpermincarboxamide, hydrotrifluoroacetate ( $\text{C}_{18}$ )<sub>2</sub>Sper<sup>3+</sup>:  $^1\text{H-NMR}$  4.45 (t, 1H,  $\text{CHN}^+$ ), 3.0–3.2 (m, 14H,  $\text{CH}_2\text{N}^+$ ,  $\text{CH}_2\text{N}$ ), 1.75–2.15 (m, 12H,  $\text{CH}_2\text{CH}_2\text{N}^+$ ,  $\text{CH}_2\text{CH}_2\text{N}$ ), 1.5–1.75 (m, 4H,  $\text{CH}_2\text{CH}_2\text{CH}_2\text{N}$ ), 1.27 (bs, 56H,  $(\text{CH}_2)_{14}$ ), 0.88 (t,  $J = 6.5$ , 6H,  $\text{CH}_3$ ).

$N'$ -Nonafluoropentadecylspermincarboxamide, hydrotrifluoroacetate FCSper<sup>3+</sup>:  $^1\text{H-NMR}$  3.89 (t,  $J = 6$ , 1H,  $\text{CHN}^+$ ), 3.23 (t,  $J = 7.5$ , 2H,  $\text{CH}_2\text{N}$ ), 3.0–3.2 (m, 10H,  $\text{CH}_2\text{N}^+$ ), 1.8–2.2 (m, 10H,  $\text{CH}_2\text{CH}_2\text{N}^+$ ,  $\text{CH}_2\text{CH}_2\text{N}$ ), 1.4–1.6 (m, 2H,  $\text{CH}_2\text{CH}_2\text{CH}_2\text{N}$ ), 1.31 (bs, 16H,  $(\text{CH}_2)_8$ ).

$N',N'$ -Diocetyl(spermincarbonyl)glycinamide, hydrotrifluoroacetate ( $\text{C}_8$ )<sub>2</sub>GlySper<sup>3+</sup>:  $^1\text{H-NMR}$  4.14 (s, 2H,  $\text{CH}_2\text{CO}$ ), 4.00 (t,  $J = 6$ , 1H,  $\text{CHN}^+$ ), 3.0–3.2 (m, 14H,  $\text{CH}_2\text{N}^+$ ,  $\text{CH}_2\text{N}$ ), 1.8–2.15 (m, 8H,  $\text{CH}_2\text{CH}_2\text{N}^+$ ), 1.45–1.7 (m, 4H,  $\text{CH}_2\text{CH}_2\text{N}$ ), 1.25 (bs, 20H,  $(\text{CH}_2)_8$ ), 0.88 (t,  $J = 6.5$ , 6H,  $\text{CH}_3$ ).

$N'$ -(Heptadecafluorodecyl)- $N'$ -(nonafluoropentadecyl)spermincarbonyl]glycinamide, hydrotrifluoroacetate (FC)<sub>2</sub>GlySper<sup>3+</sup>:  $^1\text{H-NMR}$  4.18 (s, 2H,  $\text{CH}_2\text{CO}$ ), 4.02 (t, 1H,  $\text{CHN}^+$ ), 3.55–3.75 (m, 2H,  $\text{CH}_2\text{N}$ ), 2.95–3.1 (m, 12H,  $\text{CH}_2\text{N}^+$ ,  $\text{CH}_2\text{N}$ ), 1.45–2.1 (m, 16H,  $\text{CH}_2\text{CH}_2\text{N}^+$ ,  $\text{CH}_2\text{CH}_2\text{N}$ ,  $\text{CH}_2\text{CF}_2$ ,  $\text{CH}_2\text{CH}_2\text{CF}_2$ ), 1.35 (bs, 14H,  $(\text{CH}_2)_7$ ).

$N'$ -[3,6,9-Trioxa-7-(2'-oxaeicos-11'-enyl)heptaicos-18-enyl]spermincarboxamide, hydrotrifluoroacetate DO-Sper<sup>3+</sup>:  $^1\text{H-NMR}$  5.34; 5.09 (2t,  $J = 7$ , 4H,  $\text{CH}=\text{CH}$ ), 3.92 (t,  $J = 7.5$ , 1H,  $\text{CHN}^+$ ), 3.7–3.75 (m, 2H,  $\text{OCH}_2\text{CH}_2\text{O}$ ), 3.55–3.65 (m, 5H,  $\text{CHCH}_2\text{O}$ ,  $\text{OCH}_2\text{CH}_2\text{O}$ ,  $\text{OCH}_2\text{CH}_2\text{N}$ ), 3.4–3.5 (m, 10H,  $\text{CH}_2\text{N}$ ,  $\text{CHCH}_2\text{OCH}_2$ ), 3.0–3.2 (m, 10H,  $\text{CH}_2\text{N}^+$ ), 1.5–2.1 (m, 20H,  $\text{CH}_2\text{CH}_2\text{N}^+$ ,  $\text{CH}_2\text{CH}_2\text{O}$ ,  $\text{CH}_2\text{C}=\text{CCH}_2$ ), 1.30 (bs, 44H,  $\text{CH}_2$ ), 0.90 (t,  $J = 6$ , 6H,  $\text{CH}_3$ ).

$N'$ -(1,2-Dioleoyl-*sn*-glycero-3-phosphoethanolyl)spermincarboxamide, hydrotrifluoroacetate DOPE-Sper<sup>3+</sup>:  $^1\text{H-NMR}$  5.33; 5.08 (2t,  $J = 6$ , 4H,  $\text{CH}=\text{CH}$ ), 5.23 (m, 1H,  $\text{CHO}_2\text{C}$ ), 4.43; 4.16 (dd,  $J_{AB}=12$ , 2H,  $\text{CH}_2\text{O}_2\text{C}$ ), 3.75–4.05 (m, 5H,  $\text{CHN}^+$ ,  $\text{CH}_2\text{OP}$ ), 3.18 (t,  $J = 7$ ,  $\text{CH}_2\text{N}$ ), 2.85–3.1 (m, 10H,  $\text{CH}_2\text{N}^+$ ), 2.33; 2.31 (2t,  $J = 7$ , 4H,  $\text{CH}_2\text{CO}$ ), 1.5–2.2 (m, 20H,  $\text{CH}_2\text{CH}_2\text{N}^+$ ,  $\text{CH}_2\text{CH}_2\text{CO}$ ,  $\text{CH}_2\text{C}=\text{CCH}_2$ ), 1.23 (bs, 44H,  $\text{CH}_2$ ), 0.89 (t,  $J = 6.5$ , 6H,  $\text{CH}_3$ ).

**Synthesis of ( $\text{C}_{18}$ )<sub>2</sub>Acr.**  $N',N'$ -Diocetylglycinamide (460 mg, 0.79 mmol), 9-chloroacridine (Albert and Ritchie, 1955) (180 mg, 0.79 mmol) and phenol (1.7 g) were heated at 80 °C for 15 h. After addition of  $\text{CH}_2\text{Cl}_2$ , the solution was washed with 2 M KOH and dried over  $\text{MgSO}_4$ . The crude product was chromatographed (silica,  $\text{CH}_2\text{Cl}_2$ , 2% EtOH), yield 480 mg (80%),  $R_f$  (MeOH 2%  $\text{NEt}_3$ ) = 0.53. 9-( $N',N'$ -Diocetylglycinamido)acridine ( $\text{C}_{18}$ )<sub>2</sub>Acr ( $\text{CDCl}_3$ ):  $^1\text{H-NMR}$  8.23 (d,  $J = 8.7$ , 2H), 8.07 (d,  $J = 8.7$ , 2H), 7.66 (t,  $J = 7.4$ , 2H), 7.36 (t,  $J = 7.4$ , 2H), 7.22 (bs, 1H, NH), 4.47 (s, 2H,  $\text{NCOCH}_2$ ), 3.31 (t,  $J = 7.5$ , 2H,  $\text{CH}_2\text{N}$ ), 3.15 (t,  $J = 7.7$ , 2H,  $\text{CH}_2\text{N}$ ), 1.52 (bs, 4H,  $\text{CH}_2\text{CH}_2\text{N}$ ), 1.26 (bs, 30H,  $\text{CH}_2$ ), 0.88 (t,  $J = 6.5$ , 6H,  $\text{CH}_3$ ).

**Synthesis of ( $\text{C}_{18}$ )<sub>2</sub>Netr.** Ethyl 4-aminopyrrole-2-carboxylate ( $\text{NH}_2\text{-Pyr-CO}_2\text{Et}$ ): Ethyl 4-nitropyrrole-2-carboxylate (Morgan & Morrey, 1966; Lee et al., 1988) (184 mg, 1 mmol) was hydrogenated in the presence of 50 mg of 10% Pd/C in 5 mL of MeOH/ $\text{H}_2\text{O}$  (9:1) for 3.5 h. After filtration, the solvent was removed to give an oil, which was coevaporated twice with  $\text{CH}_2\text{Cl}_2$ .  $\text{NH}_2\text{-Pyr-CO}_2\text{Et}$  was used immediately for the next step without further purification,  $R_f$  (MeOH/hexane/AcOEt (5:45:55)) = 0.30.

Ethyl 4-[(*tert*-Butyloxycarbonyl)amino]pyrrole-2-carboxylate (BocNH-Pyr-CO<sub>2</sub>Et). NH<sub>2</sub>-Pyr-CO<sub>2</sub>Et (155 mg, 1 mmol) was dissolved in 1.2 mL of H<sub>2</sub>O/dioxane (1:1). NEt<sub>3</sub> (0.2 mL, 1.5 mmol) and BOC-ON (247 mg, 1 mmol) were added. After 1 day, the solvent was evaporated, 20 mL of CH<sub>2</sub>Cl<sub>2</sub> was added, and the solution was washed twice with 100 mL of 0.15 M K<sub>2</sub>CO<sub>3</sub>. The crude product was chromatographed (silica, CH<sub>2</sub>Cl<sub>2</sub>), yield 161 mg (63%), *R<sub>f</sub>* (CH<sub>2</sub>Cl<sub>2</sub>/MeOH/AcOH (90:9:1)) = 0.70.

4-[(*tert*-Butyloxycarbonyl)amino]pyrrole-2-carboxylic Acid (BocNH-Pyr-CO<sub>2</sub>H). BocNH-Pyr-CO<sub>2</sub>Et (100 mg, 0.393 mmol) was saponified in the presence of 15% (w/w) KOH (2.24 mL, 6 mmol) in 3 mL of MeOH for 16 h. The solvent was replaced by 2 mL of water, the solution was cooled to 3 °C, and HCl 1 M was added until precipitation of the desired product occurred. The solution was extracted twice with 175 mL of ether, yield 89 mg (100%), *R<sub>f</sub>* (CH<sub>2</sub>Cl<sub>2</sub>/MeOH/AcOH (90:9:1)) = 0.33.

Ethyl [[4-[(*tert*-Butyloxycarbonyl)amino]pyrrolyl]-2-carboxamido]-4-pyrrole-2-carboxylate (BocNH-Pyr<sub>2</sub>-CO<sub>2</sub>Et). BocNH-Pyr-CO<sub>2</sub>H (30 mg, 0.133 mmol) and NH<sub>2</sub>-Pyr-CO<sub>2</sub>Et (25 mg, 0.160 mmol) were coupled in the presence of DCC (30 mg, 0.143 mmol) and NEt<sub>3</sub> (21 μL, 0.143 mmol) in THF/CHCl<sub>3</sub> (1:1) for 2 days. The crude product was chromatographed (silica, CH<sub>2</sub>Cl<sub>2</sub>), yield 28 mg (58%); *R<sub>f</sub>* (CH<sub>2</sub>Cl<sub>2</sub>/MeOH/AcOH (90:9:1)) = 0.63.

Ethyl *N*-[3-Bis(octadecylcarbonyl)-2-oxapropylcarbonyl]glycinate. Glycine ethyl ester hydrochloride (1.228 g, 8.8 mmol) and 3-bis(octadecylcarbonyl)-2-oxapropylcarboxylic acid (5.104 g, 8 mmol) were coupled for 4 h in the presence of NEt<sub>3</sub> (1.226 mL, 8.8 mmol) and DCC (1.816 g, 8.8 mmol) in 75 mL of CHCl<sub>3</sub>. The solution was washed four times with a 2% (w/w) citric acid solution. The organic layer was dried over MgSO<sub>4</sub>, filtered, and chromatographed (silica, hexane/AcOEt (4:1); CHCl<sub>3</sub>; CHCl<sub>3</sub>/MeOH (9:1): yield 4.3 g (67%), *R<sub>f</sub>* (CH<sub>2</sub>Cl<sub>2</sub>/MeOH/AcOH (90:9:1)) = 0.72.

*N*-[3-Bis(octadecylcarbonyl)-2-oxapropylcarbonyl]glycine. The previous compound (4.3 g, 5.93 mmol) was saponified by 5 M NaOH (1.35 mL, 6.82 mmol) in 25 mL of MeOH for 1 day. The solvent was evaporated, CHCl<sub>3</sub> was added, and the solution was washed with 0.1 N HCl, dried over MgSO<sub>4</sub>, and evaporated: yield 4.05 g (98%), *R<sub>f</sub>* (CH<sub>2</sub>Cl<sub>2</sub>/MeOH/AcOH (90:9:1)) = 0.51.

Ethyl 4-[[*N*-[3-Bis(octadecylcarbonyl)-2-oxapropylcarbonyl]glycinamido]pyrrole-2-carboxamido]-4-pyrrole-2-carboxylate (C<sub>18</sub>)<sub>2</sub>Netr. BocNH-Pyr<sub>2</sub>-CO<sub>2</sub>Et (13 mg, 36 μmol) was deprotected in CF<sub>3</sub>CO<sub>2</sub>H (1 mL) for 2.5 h to give ethyl 4-(aminopyrrole-2-carboxamido)-4-pyrrole-2-carboxylate (NH<sub>2</sub>-Pyr<sub>2</sub>-CO<sub>2</sub>Et), *R<sub>f</sub>* (CH<sub>2</sub>Cl<sub>2</sub>/MeOH 9/1, 1% AcOH) = 0.07, which was used immediately. NH<sub>2</sub>-Pyr<sub>2</sub>-CO<sub>2</sub>Et (36 μmol) was coupled to the lipid (27.5 mg, 40 μmol) in the presence of DCC (8.2 mg, 40 μmol) and DMAP (4.8 mg, 40 μmol) in 360 μL of dry THF for 3 days. The crude product was chromatographed (silica, CH<sub>2</sub>Cl<sub>2</sub>, 2–10% MeOH): yield 8 mg (24%); *R<sub>f</sub>* (CH<sub>2</sub>Cl<sub>2</sub>/MeOH/AcOH (90:9:1)) = 0.5; <sup>1</sup>H-NMR 7.38 (s, 1H), 7.25 (s, 1H), 6.94 (s, 1H), 6.89 (s, 1H), 4.40 (s, 2H, CH<sub>2</sub>O), 4.28 (q, 2H, OCH<sub>2</sub>CH<sub>3</sub>), 4.14 (s, 2H, CH<sub>2</sub>O), 4.05 (s, 2H, NHCH<sub>2</sub>CO), 3.16–3.37 (m, 4H, CH<sub>2</sub>N), 1.54 (b, 4H, CH<sub>2</sub>CH<sub>2</sub>N), 1.34 (t, 3H, CH<sub>2</sub>CH<sub>3</sub>), 1.26 (bs, 30H, CH<sub>2</sub>), 0.89 (t, *J* = 6.4, 6H, CH<sub>3</sub>).

**Cell Culture.** 3T3 murine fibroblasts were cultured in 80 mL flasks (NUNC) in Dulbecco's modified Eagle medium (DMEM, GIBCO) supplemented with 10% calf serum (GIBCO), 100 UG/mL streptomycin (GIBCO), 100 UI/mL penicillin (GIBCO), 0.1 mg/mL kanamycin (INTERMED), 0.286 g/L glutamine (LANCASTER), and 2 g/L glucose (JANSSEN) at 37 °C in a humidified atmosphere containing 5% CO<sub>2</sub>. At confluence, the cells

were trypsinized and seeded at approximately 25–30% confluence in six- or 24-well dishes (Falcon) in 2 mL culture medium. After 12 h, the cells were rinsed with serum-free medium, and the transfection mixture was added.

**Plasmid.** The bacterial chloramphenicol acetyl transferase (CAT) reporter gene was used throughout this study. This enzyme is easily detectable by a sensitive assay, and the results have been quantified.

The plasmid used in this study is the 4xTRE-tk-CAT with four collagenase gene TPA responsive elements (TGACTCA) inserted 5' to the Herpes Simplex virus thymidine kinase (tk) gene minimal promoter (Behr et al., 1989). It was propagated and purified by standard techniques.

**Transfection Procedure.** Plasmid coating with the lipid was performed in isotonic sodium chloride (Barthel et al., 1993). Two μg of plasmid and the desired amount of a 2 mM lipid solution in ethanol were each diluted into 50 μL of 150 mM NaCl and vortexed. If more than one lipid was used, ethanolic lipid solutions were mixed prior to the dilution step. After ca. 10 min, the two solutions were mixed and vortexed. After another 10 min, 900 μL of serum-free culture medium was added and the solution was vortexed. This transfection medium was added to the cells 10 min later.

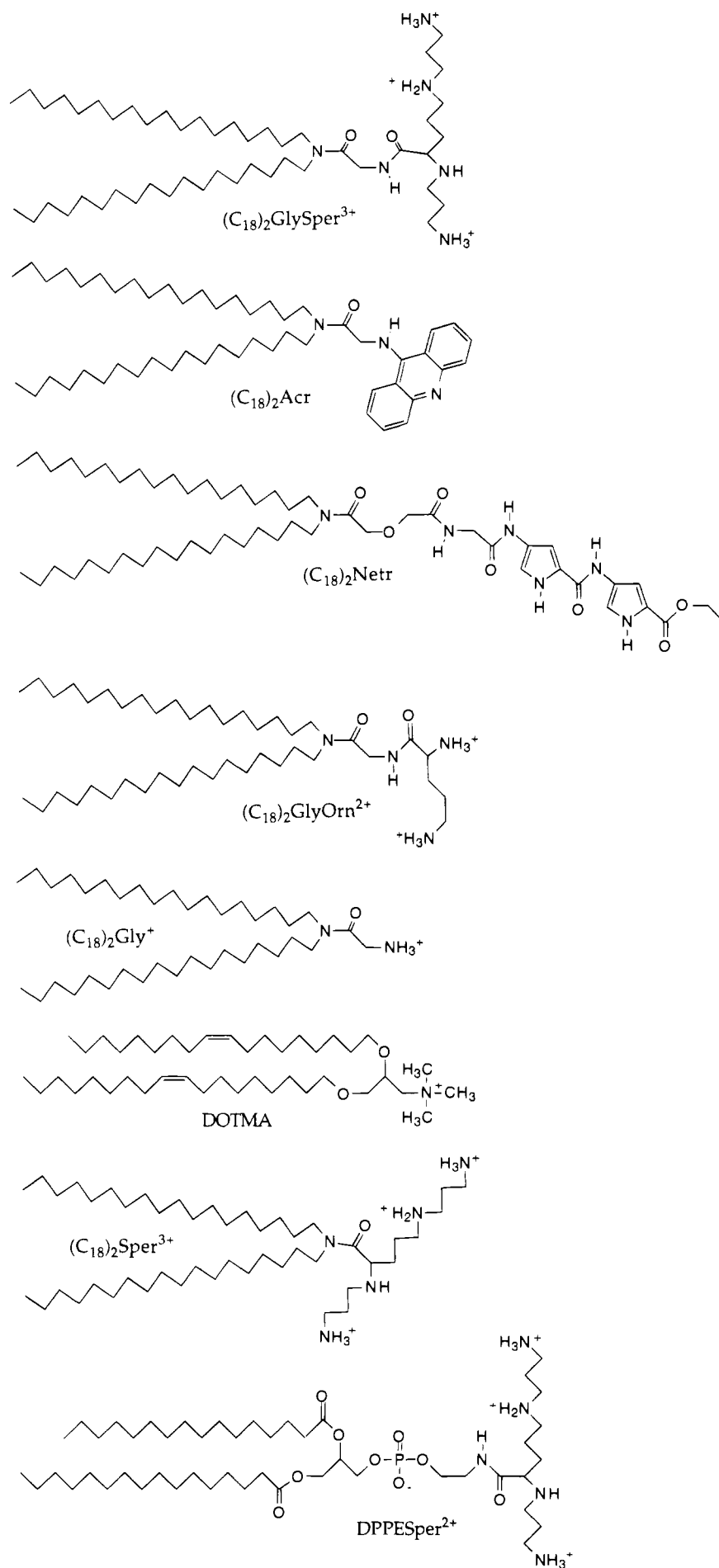
After 8 h, the transfection medium was replaced by 1.5 mL of DMEM supplemented with 10% FCS. After 24 h, the medium was removed and the cells were frozen.

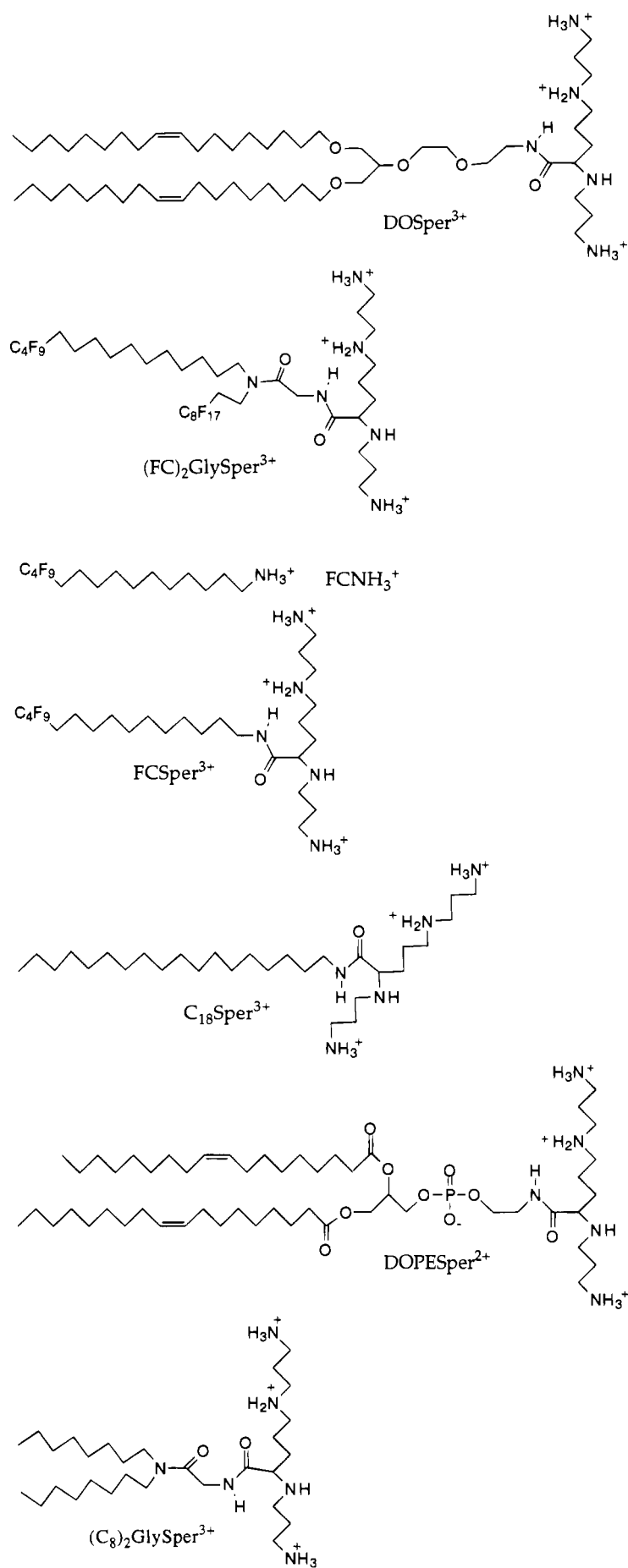
**CAT-ELISA Test.** Immunological quantification of CAT was performed with a commercial ELISA test (Boehringer), according to the manufacturer's instructions. Cells were thawed and lysed with 200 μL of lysis buffer. After centrifugation, 80 μL (more or less if outside the calibration curve) were used for the CAT-ELISA test. The volume of cell extract was completed to 200 μL with sample buffer, added to rehydrated precoated wells, and incubated for 1 h at 37 °C. The cell extracts were discarded, and the wells were washed three times with washing buffer. Two hundred μL of anti-CAT-DIG (2 μg/mL) was added into each well, and the plate was incubated for 1 h at 37 °C. The anti-CAT-DIG was discarded, and the wells were washed again as described above. Two hundred μL of anti-DIG-POD (150 mU/mL) was added into each well, and the plate was incubated for 1 h at 37 °C. After another washing cycle, 200 μL of POD substrate was added, and the plate was incubated for 1 h at room temperature. The OD<sub>405 nm</sub> of the samples was converted to picograms CAT per well with a calibration curve of the native enzyme (typically linear from 20 pg up to 500 pg per cell extract).

## RESULTS AND DISCUSSION

Lipopolyamines such as Transfectam ((C<sub>18</sub>)<sub>2</sub>GlySper<sup>3+</sup>, Figure 1) were originally designed to bind DNA and to condense it into particles coated with a cationic lipid layer, which in turn binds to anionic residues present on the cell surface (Behr et al., 1989). Various other lipophilic DNA-binding molecules were synthesized and their transfection properties were compared to this reference compound. The chemical structures were chosen to explore other types of DNA-binding headgroups ((C<sub>18</sub>)<sub>2</sub>Acr, (C<sub>18</sub>)<sub>2</sub>Netr), to vary the cationic charge density ((C<sub>18</sub>)<sub>2</sub>GlyOrn<sup>2+</sup>, (C<sub>18</sub>)<sub>2</sub>Gly<sup>+</sup>), to prevent miscibility with endogenous cellular lipids (FCSper<sup>3+</sup>, (FC)<sub>2</sub>GlySper<sup>3+</sup>), and to assess the importance of a spacer ((C<sub>18</sub>)<sub>2</sub>Sper<sup>3+</sup>), of the lipid fluidity (DPESper<sup>2+</sup>, DOESper<sup>2+</sup>, DOSper<sup>3+</sup>) and of the hydrophilic/lipophilic balance ((C<sub>8</sub>)<sub>2</sub>GlySper<sup>3+</sup>, C<sub>18</sub>Sper<sup>3+</sup>). Calcium phosphate coprecipitation and a commercially available gene transfer agent (DOTMA)







**Figure 1.** Structures of the amphiphiles used in this study.

**Table 1. Transfection Efficiencies of Various Amphiphilic Compounds,<sup>a</sup> Relative to That of (C<sub>18</sub>)<sub>2</sub>GlySper<sup>3+</sup>**

compd <sup>b</sup>	efficiency <sup>c</sup>	cation/anion ratio <sup>d,e</sup>	cyto-toxicity <sup>e,f</sup>	particle <sup>g</sup> formation
CaPhosphate	<0.01		+	+++
(C <sub>18</sub> ) <sub>2</sub> GlySper <sup>3+</sup>	1	0.5–10 (4)	–	++
(C <sub>18</sub> ) <sub>2</sub> Ac	UD <sup>h</sup>	0.7–6.7	–	–
(C <sub>18</sub> ) <sub>2</sub> Netr	UD	0.66–6.6	–	++
	2	(C <sub>18</sub> ) <sub>2</sub> GlySper <sup>3+</sup> (6)	–	++
		+(C <sub>18</sub> ) <sub>2</sub> Netr (0.2)		
	2	(C <sub>18</sub> ) <sub>2</sub> GlySper <sup>3+</sup> (6)	–	++
		+(C <sub>18</sub> ) <sub>2</sub> Netr (0.8)		
(C <sub>18</sub> ) <sub>2</sub> GlyOrn <sup>2+</sup>	0.05	1–10 (4)	± (10)	–
(C <sub>18</sub> ) <sub>2</sub> Gly <sup>+</sup>	UD	1–10	± (10)	–
DOTMA	0.12	2–4 (2)	–	+
(C <sub>18</sub> ) <sub>2</sub> Sper <sup>3+</sup>	UD	0.75–10.7	–	–
DPPEsper <sup>2+</sup>	1.3	1.3–5.3 (2.6)	–	++
DOPEsper <sup>2+</sup>	1	0.5–10 (2)	–	++
DOSper <sup>3+</sup>	1	2–20 (10)	+	++
(C <sub>8</sub> ) <sub>2</sub> GlySper <sup>3+</sup>	UD	0.5–10	+	–
(FC) <sub>2</sub> GlySper <sup>3+</sup>	1	2–20 (20)	+	++
	2	(C <sub>18</sub> ) <sub>2</sub> GlySper <sup>3+</sup> (6)	–	++
		+(FC) <sub>2</sub> GlySper <sup>3+</sup> (0.3)		
FCNH <sub>3</sub> <sup>+</sup>	UD	1–10	+++ (4)	–
FCSper <sup>3+</sup>	UD	0.75–7.5	–	–
C <sub>18</sub> Sper <sup>3+</sup>	UD	0.75–6.8	++ (4)	–

<sup>a</sup> See Experimental Procedures. <sup>b</sup> Structures are shown in Figure 1. <sup>c</sup> Mean value of a triplicate with a 30% sd. <sup>d</sup> Range of cationic lipid charges to anionic DNA phosphates which was explored (or moles of lipid per mole DNA base in the case of neutral lipids). <sup>e</sup> Values in parentheses are cation/anion ratio corresponding to the highest efficiency (row 3) or to the onset of toxicity (row 4). <sup>f</sup> The apparent onset of cytotoxicity was assessed by the morphological change of the fibroblasts, from their typical extended shape with thick pseudopods (–) to a reversible spherical shape with thin pseudopods (+), to an irreversible detachment of most cells (+++). <sup>g</sup> Tiny particles (Figure 2) may appear over the cells during transfection (+ several/cell, ++ tens/cell). <sup>h</sup> UD: undetectable (<0.01).

were included for scaling purposes and for comparison of protonated ammonium cations with a quaternary ammonium salt, respectively.

Transfection experiments were performed in standard conditions (Barthel et al., 1993), on a single chloramphenicol–acetyltransferase reporter plasmid/cell line combination (TRE-tk/CAT with NIH-3T3 murine fibroblasts). This narrow experimental window, however, allowed us to explore a wide range of lipid-to-DNA ratios. Thus, various amounts of each lipid were mixed with the same amount of DNA (2 µg), and transfection levels were directly compared to that of (C<sub>18</sub>)<sub>2</sub>GlySper<sup>3+</sup> taken as the reference compound. The highest efficiencies obtained are given in Table 1 together with the range of vector/DNA ratios which was explored. Since we showed earlier that for cationic lipids the most important parameter is the net electric charge of the complexes, this range was expressed as lipid cation/phosphate anion ratio (and as the molar lipid per nucleic base ratio for neutral lipids). Some relevant direct microscopical observations have been included as well, such as the apparent cytotoxicity and the eventual appearance of tiny particles covering the cells during transfection.

#### Comparison of Various DNA Binding Modes.

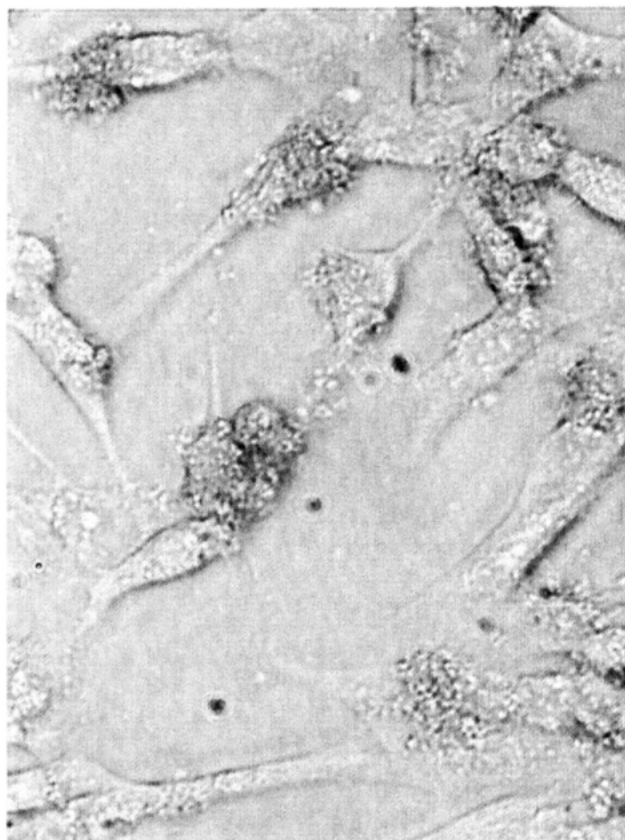
Polyamines have been shown to hydrogen bond to the floor of the DNA minor groove (Schmid and Behr, 1991), 9-aminoacridine derivatives to intercalate between base pairs (Georgiou, 1977), and netropsin derivatives to fill the minor groove (Zimmer and Wahnert, 1986), all with affinities for DNA within the range of 10<sup>4</sup>–10<sup>6</sup> M<sup>–1</sup>. In addition, earlier work had shown that lipointercalators and lipopolyamines form stable and discrete complexes with DNA (Behr, 1986). In order to see whether noncationic modes of DNA-binding could lead to gene transfer

agents as well, (C<sub>18</sub>)<sub>2</sub>Ac and (C<sub>18</sub>)<sub>2</sub>Netr were synthesized and compared to (C<sub>18</sub>)<sub>2</sub>GlySper<sup>3+</sup>. The glycine and glycolyl-glycine spacers between the lipid and nucleic acid binding moieties were chosen after CPK molecular model examination so as to leave the headgroups interact freely with DNA. This was indeed the case, as shown by a 50% hypochromism and a 5 nm bathochromic shift for the acridine chromophore ((C<sub>18</sub>)<sub>2</sub>Ac), and by a turbidity increase ((C<sub>18</sub>)<sub>2</sub>Netr) after complex formation of the corresponding lipid with DNA. However, when mixed with the CAT plasmid in the concentration ranges and ratios where the lipopolyamine was active, none of these molecules showed any detectable transfection property on 3T3 cells (some preliminary positive results obtained for (C<sub>18</sub>)<sub>2</sub>Ac were in fact due to its decomposition to acridone and *N,N*-dioctadecylglycinamide which has weak transfection properties). The pK<sub>a</sub> of acridine in aqueous solutions of (C<sub>18</sub>)<sub>2</sub>Ac was found to be 8.4 by absorption spectroscopy, which leaves a positive charge on the molecule at physiological pH. However, even with a net cationic balance of charges for the complex with DNA, no CAT enzyme activity could be detected. Non-lipidic gene delivery systems exploiting receptor binding on the cell surface have been synthesized with an intercalator in place of a polycation for DNA binding (Wagner et al., 1991; Haensler and Szoka, 1993). These compounds are inefficient as well when compared to their polylysine counterparts, highlighting the importance of DNA compaction to reach efficient gene transfer. Indeed, cationic polyamines and polybasic peptides induce nucleic acid condensation into toroids and rods in diluted aqueous solutions (Bloomfield, 1991). Acridine intercalation is rather expected to rigidify the DNA backbone and does not compact it even when linked to a lipid tail. Netropsine, like polyamines, may induce DNA bending and (C<sub>18</sub>)<sub>2</sub>Netr forms very tiny and apparently monodisperse nucleolipidic particles. We took advantage of this property in (C<sub>18</sub>)<sub>2</sub>GlySper<sup>3+</sup>/(C<sub>18</sub>)<sub>2</sub>Netr admixtures which increased slightly transfection efficiency (Table 1).

**The number, nature, and location of charges dramatically change the transfection properties of the cationic lipid.** The strength of polyamine binding to nucleic acids is a function of the number of charges, with a ca. 1 order of magnitude increment per ammonium group (Braunlin et al., 1982). Three lipids, (C<sub>18</sub>)<sub>2</sub>GlySper<sup>3+</sup>, (C<sub>18</sub>)<sub>2</sub>GlyOrn<sup>2+</sup>, and (C<sub>18</sub>)<sub>2</sub>Gly<sup>+</sup>, with identical backbones bearing, respectively, three, two, and one ammonium residue, were compared to each other as transfection agents (their protonation states at neutral pH rest on pK measurements). Varying the charge per molecule had a surprisingly profound effect on efficiency, which cannot be understood only on the basis of reduced plasmid binding of the (C<sub>18</sub>)<sub>2</sub>GlyOrn<sup>2+</sup> and (C<sub>18</sub>)<sub>2</sub>Gly<sup>+</sup> head groups. Indeed, DOTMA (Table 1) and dioctadecyldimethylammonium bromide (Behr et al., 1989) bear quaternary ammonium heads which are known to bind even weaker to DNA and still transfect 3T3 cells (although less efficiently than (C<sub>18</sub>)<sub>2</sub>GlySper<sup>3+</sup>). However, lipospermene-coated particles will bind to chromatin even in the presence of millimolar concentrations of endogenous spermine. Consequently, nuclear accumulation of the particles as well as plasmid uncoating through cationic lipid dilution into an ocean of DNA may be favored, hence, their better performance. When the glycine spacer is absent ((C<sub>18</sub>)<sub>2</sub>Sper<sup>3+</sup>), the lipospermene leads to an abundant flocculent precipitate in aqueous solution, which hampers proper complex formation with DNA and transfection. Yet DPPEsper<sup>2+</sup>, DOPEsper<sup>2+</sup>, and DOSper<sup>3+</sup> are very active, suggesting that although a spacer is required, its precise structure is not impor-

tant. Altogether these results highlight the key role played by spermine, but also show that many properties besides DNA binding strength and compaction are of importance for efficient gene transfer (see below). Indeed, once bound to the cell surface, the cationic nucleolipid particles enter the cell either by membrane fusion or spontaneous endocytosis (for a more detailed discussion, see Behr (1994)). The latter pathway eventually directs the particle to the degradative lysosomal compartment. The relative importance of the fusion/endocytosis routes of DNA entry into the cell may be assessed by buffering the acidic lysosome interior with a diffusing weak base such as chloroquine. DOTMA-mediated transfection is improved in the presence of chloroquine (Legendre and Szoka, 1993), whereas  $(C_{18})_2\text{GlySper}^{3+}$  transfection increases only 1.5-fold. The latter observation may have two explanations: either most particles enter the cell (and possibly the nucleus) by direct membrane fusion or DNA escapes from the degradative lysosomal route owing to the unique buffering property of the spermine headgroup. Indeed, titration of an aqueous dispersion of  $(C_{18})_2\text{GlySper}^{3+}$  leads to basicity constants,  $pK_{1-4} = 10.5, 9.5, 8.4, 5.5$ , among which the lowest incidentally equals the internal pH of lysosomes.<sup>1</sup> Ornithine and glycine headgroups are unable to play this role since their  $pK$ 's are above 8; nonprotonable quaternary ammonium lipids such as DOTMA and dioctadecyldimethylammonium bromide lack any buffering property.

**The hydrocarbon moiety of the lipospermine can be changed without loss of the transfection efficiency.** The spermine headgroup being essential for activity, several lipospermines were synthesized in order to explore the influence of the hydrocarbon moiety on transfection. DPPEsper<sup>3+</sup> has a natural phosphatidylethanolamine backbone as opposed to the synthetic glycinedioctadecylamide of  $(C_{18})_2\text{GlySper}^{3+}$ ; it was somewhat more efficient than the latter, and most importantly it showed no noticeable cytotoxicity (Behr et al., 1989). This interesting property may be due to its degradation into endogenous compounds, dipalmitoylphosphatidylethanolamine, and spermine (intermediate spermine-6-carboxylic acid is a substrate of ornithine decarboxylase; M. Laduron, personal communication). As a result, DPPEsper<sup>2+</sup> can be used to transfect routinely 20–30% of fragile primary human keratinocyte populations (Staedel et al., 1994).  $(C_{18})_2\text{GlySper}^{3+}$  and DPPEsper<sup>2+</sup> bear saturated octadecyl and hexadecanoyl hydrocarbon chains, respectively, and therefore, they are expected to have melting temperatures above 37 °C. On the contrary, DOPEsper<sup>2+</sup> possesses oleoyl chains with a cis-double bond and DOSper<sup>3+</sup> further has a flexible ethylene glycol spacer (Figure 1); these lipids probably melt below room temperature. Yet the four compounds have similar transfection properties, suggesting that the physical state of the lipid during DNA compaction and along the cell entry pathway may be of little importance. In order to check if cationic lipid mixing with cellular lipids is part of the gene transfer process, a partially fluorinated analog of  $(C_{18})_2\text{GlySper}^{3+}$  was synthesized  $((\text{FC})_2\text{GlySper}^{3+}$ , Figure 1). Indeed, perfluorinated hydrocarbon chains are both hydrophobic and lipophobic. Although the best



**Figure 2.** Phase contrast microscopic view of transfected 3T3 fibroblasts. Numerous submicrometric particles appear as clear dots on the cells several hours after transfection ( $2\ \mu\text{g}$  of plasmid mixed with 6 equiv of cationic charges of  $(C_{18})_2\text{-Gly-Sper}^{3+}$ ), giving a rough aspect to the cell surface.

activity for this compound was reached at a somewhat higher lipid/DNA ratio, its properties are similar to that of  $(C_{18})_2\text{GlySper}^{3+}$ , highlighting again the diversity of lipid backbones leading to comparable transfection efficiencies.

**Micelle-forming cationic amphiphiles alone are unable to deliver DNA into cells.** Finally, a short double chain  $((C_8)_2\text{GlySper}^{3+})$  and several single tailed  $(C_{18}\text{Sper}^{3+}, \text{FCNH}_3^+, \text{FCSper}^{3+})$  cationic amphiphiles were synthesized, which are expected to form micellar structures instead of the more organized phases formed by the other cationic lipids. When mixed with calf thymus DNA in standard transfection conditions, quasielastic light scattering measurements showed that particles of size 100–300 nm ( $C_{18}\text{Sper}^{3+}$ ) and 600 nm ( $\text{FCSper}^{3+}$ ) were formed (90–150 nm for  $(C_{18})_2\text{GlySper}^{3+}$ ). However, these particles were unable to transfect cells, and the amphiphiles had a pronounced effect on the cell morphology (Table 1). Both observations may be attributed to the micellar properties of these molecules: When added in charge excess to DNA, they condense it but are unable to coat the resulting particles with an excess cationic layer, hence the inability to deliver the nucleic acid to the cells; rather, the excess of amphiphile remains as separate micelles having deleterious detergent effects on the cells.

## CONCLUSION

The dozen of amphiphiles which were synthesized allowed us to explore a palette of structural elements and to determine those required for the design of efficient gene transfer vehicles. These elements are a cationic polyamine and a pendent mesomorphogenic moiety capable of forming long-lived structures other than micelles.

<sup>1</sup> A rough calculation shows that the buffering capacity of a 1000 Å radius transfecting particle included in a 1 micron lysosome lies in the millimolar range, which is higher than the concentration of chloroquine required to buffer lysosomes: Assuming the particle at 6 equ. charge to be essentially constituted by the lipospermine of molecular volume  $70\ \text{\AA}^3 \times 30\ \text{\AA}$ , the particle contains  $2.10^6$  protonable molecules in a  $4.10^{-15}\ \text{dm}^3$  lysosome, i.e. a concentration of  $2.10^6/(6.10^{23} \times 4.10^{-15}) = 0.8 \cdot 10^{-3}\ \text{M}$ .

The polyamine interacts with DNA, condenses it, binds the nucleolipidic particle to the cell surface, buffers the endosomal compartment, and eventually drives nuclear accumulation and uncoating of the particle through interaction with chromatin. Covalent linking of the polyamine to a hydrophobic self-aggregating moiety allows to coat the particle with excess cationic lipid which protects the nucleic acid and provides a means to destabilize membranes. Along these lines, it is remarkable that particle formation, as seen by the appearance of tiny spots on the cell surface during transfection (Figure 2), seems to be a necessary, although not sufficient, condition for transfection (Table 1). Such particles are seldom seen in between the cells and seem to result from the fusion of smaller, submicroscopic nucleolipidic particles bound to the fluid cell surface.

Although the in vitro results obtained here with various structures lead to a rather modest improvement over the first compounds described 5 years ago, this conclusion does not prejudice their behavior in vivo. Indeed, gene transfer into cells belonging to a tissue is a much harder task to achieve, and many additional variables, such as the mode of delivery, the cell type, and environment, may induce at first sight equivalent vectors to behave quite differently (Behr, 1994). Recently, several positive reports of gene therapy protocols using cationic amphiphiles have appeared. These encouraging results however should not obscure the real need for much more efficient molecules to achieve successful gene therapy of diseases requiring delivery of DNA in vivo.

#### ACKNOWLEDGMENT

We thank Professor B. Spiess for  $pK_a$  measurements of the lipopolyamine. This work was supported by grants from the Centre National de la Recherche Scientifique, Association Francaise contre les Myopathies, Association Francaise de Lutte contre la Mucoviscidose, and Association pour la Recherche contre le Cancer.

#### LITERATURE CITED

- Albert, A., and Ritchie, B. (1995) 9-Aminoacridine. *Organic Syntheses, Collect. Vol. III*, pp 53–56, Wiley, New York.
- Barthel, F., Remy, J. S., Loeffler, J. P., and Behr, J. P. (1993) Gene transfer optimization with Lipospermine-coated DNA. *DNA Cell Biol.* 12, 553–560.
- Behr, J. P. (1986) DNA strongly binds to micelles and vesicles containing lipopolyamines or lipointercalants. *Tetrahedron Lett.* 27, 5861–5864.
- Behr, J. P. (1993) Synthetic gene transfer vectors. *Acc. Chem. Res.* 26, 274–278.
- Behr, J. P. (1994) Gene Transfer with Synthetic Cationic Amphiphiles; prospects for gene therapy. *Bioconjugate Chem.* 5, 382–389.
- Behr, J. P., Demeneix, B., Loeffler, J. P., and Perez-Mutul, J. (1989) Efficient gene transfer into mammalian primary endocrine cells with lipopolyamine coated DNA. *Proc. Natl. Acad. Sci. U.S.A.* 86, 6982–6986.
- Bloomfield, V. A. (1991) *Biopolymers* 31, 1471–1481.
- Braunlin, W. H., Strick, T. J., and Record, M. T., Jr. (1982) *Biopolymers* 21, 1301–1314.
- Cotten, M., and Wagner, E. (1993) Non-viral approaches to gene therapy. *Current Op. Biotech.* 4, 705–710.
- Felgner, P. L. (1990) Particulate systems and polymers for in vitro and in vivo delivery of polynucleotides. *Adv. Drug Deliv. Rev.* 5, 163–187.
- Felgner, P. L., Gadek, T. R., Holm, M., Roman, R., Chan, H. W., Wenz, M., Northrop, J. P., Ringold, G. M., and Danielsen, M. (1987) Lipofection: a highly efficient, lipid-mediated DNA-transfection procedure. *Proc. Natl. Acad. Sci. U.S.A.* 84, 7413–7417.
- Gao, X., and Huang, L. (1991) A novel cationic liposome reagent for efficient transfection of mammalian cells. *Biochem. Biophys. Res. Commun.* 179, 280–285.
- Georgiou, S. (1977) Interaction of acridine drugs with DNA and nucleotides. *Photochem. Photobiol.* 26, 59–68.
- Haensler, J., and Szoka, F. C., Jr. (1993) Synthesis and characterization of trigalactosylated bisacridine compound to target DNA to hepatocytes. *Bioconjugate Chem.* 4, 85–93.
- Lee, M., Coulter, D. M., and Lown, J. W. (1988) Total Synthesis and Absolute Configuration of the Antibiotic Oligopeptide (4S)-(+)-Anthelvincin A and Its (4R)-(-) Enantiomer. *J. Org. Chem.* 53, 1855–1859.
- Legendre, J. Y., and Szoka, F. C. (1992) Delivery of plasmid DNA into mammalian cell lines using pH-sensitive liposomes: comparison with cationic liposomes. *Pharm. Res.* 9, 1235–1242.
- Leventis, R., and Silvius, J. R. (1990) Interactions of mammalian cells with lipid dispersions containing novel metabolizable cationic amphiphiles. *Biochim. Biophys. Acta* 1023, 124–132.
- Loeffler, J. P., and Behr, J. P. (1993) Gene transfer into primary and established mammalian cell lines with lipopolyamine-coated DNA. In *Methods in Enzymology Recombinant DNA* (Wu, R., Ed.) Vol. 217, pp 599–618, Academic Press, New York.
- Morgan, K. J., and Morrey, D. P. (1966) The preparation and properties of 2- and 3-nitropyrrole. *Tetrahedron* 22, 57–62.
- Nivet, J. B., Bernelin, R., Le Blanc, M., and Riess, J. G. (1992) Synthesis and bioacceptability of fluorinated surfactants derived from F-alkylated tertiary amines. *Eur. J. Med. Chem.* 27, 891–898.
- Santaella, C., Vierling, P., and Riess, J. G. (1991) New perfluoroalkylated phospholipids as injectable surfactants: Synthesis, preliminary physicochemical and biocompatibility data. *New J. Chem.* 15, 685–692.
- Schmid, N., and Behr, J. P. (1991) Location of spermine and other polyamines on DNA as revealed by photoaffinity cleavage with polyaminobenzenediazonium salts. *Biochemistry* 30, 4357–4361.
- Staedel, Remy, J. S., C., Hua, Z., Broker, T. R., Chow, L. T., and Behr, J. P. (1994) High efficiency transfection of primary human keratinocytes with positively charged lipopolyamine: DNA complexes. *J. Invest. Dermatol.* 102, 768–772.
- Wagner, E., Cotten, M., Mechtler, K., Kirlappos, H., and Birnstiel, M. L. (1991) DNA-binding transferrin conjugates as functional gene-delivery agents: synthesis by linkage of polylysine or ethidium homodimer to the transferrin carbohydrate moiety. *Bioconjugate Chem.* 2, 226–231.
- Zimmer, C., and Wahnert, U. (1986) *Prog. Biophys. Molec. Biol.* 47, 31–112.

# **[ $\eta^5$ -Cyclopentadienyl]metal Tricarbonyl Pyrylium Salts: Novel Reagents for the Specific Conjugation of Proteins with Transition Organometallic Labels**

Michèle Salmain,<sup>†</sup> Krisztina L. Malisza,<sup>†</sup> Siden Top,<sup>†</sup> Gérard Jaouen,<sup>\*,†</sup> Marie-Claude Sénéchal-Tocquer,<sup>‡</sup> Denis Sénéchal,<sup>‡</sup> and Bertrand Caro<sup>‡</sup>

Ecole Nationale Supérieure de Chimie de Paris, URA CNRS 403, 11 rue Pierre et Marie Curie, F-75231 Paris Cedex 05, France, and Institut Universitaire de Technologie, F-22303 Lannion Cedex, France. Received April 28, 1994<sup>§</sup>

New specific reagents for the conjugation of organo transition metal species to proteins are described. These reagents are pyrylium salts bearing a ( $\eta^5$ -C<sub>5</sub>H<sub>4</sub>)M(CO)<sub>3</sub> (M = Mn and Re) at position 4. They couple with simple amines (*n*-butylamine and *tert*-butylamine) and to lysine side chains of proteins (bovine serum albumin and lysozyme) with varying yields. In almost all cases, the final conjugated species is a pyridinium salt, with the exception of lysozyme, for which the reaction ends at the divinyllogous amide form. Differences in reactivity for bovine serum albumin and lysozyme can be explained in terms of differences of isoelectric point and steric local environment around the reactive lysine residue.

## **INTRODUCTION**

Pyrylium salts of general formula **I** have been thoroughly investigated by several authors (Balaban et al., 1982). Specifically, they react with primary amines leading to pyridinium salts, **III**. Interestingly, they are also able to react with proteins (O'Leary and Sanberg, 1971). However, the few examples concerning the reaction of pyrylium salts with proteins have dealt with the introduction of novel functionalities under mild conditions, taking advantage of the reactivity of pyridinium salts with nucleophiles, rather than for labeling purposes (Katritzky et al., 1984a).

In the past few years, we have developed reagents for the introduction of organometallic entities into biologically active molecules with different objectives in mind. First, we demonstrated that metal-carbonyl groups can act as sensitive analytical probes when detected by IR spectroscopy (Salmain et al., 1991). This property forms the basis of a new immunological test for haptens (Salmain et al., 1992) and antigens (Varenne et al., 1992). Second, when the transition metal belongs to the 5d row (like tungsten), we described a new class of reagents designed to aid in the solution of three-dimensional X-ray crystal structures of proteins (Gorfti et al., 1994). So far, we have successfully designed *N*-succinimidyl organometallic reagents which lead to the formation of a strong amide bond between the lysine side chains of proteins and the organometallic probe. There are, however, several drawbacks to the use of *N*-succinimidyl esters as labeling agents of proteins. As they are neutral, they are often insoluble in water, necessitating the use of an amount of organic cosolvent for solubilization. This can cause damage to some proteins and can induce denaturation. This problem has been solved by using *N*-sulfo-succinimidyl esters which are hydrophilic compounds (Staros, 1982). Furthermore, the modification of proteins

by *N*-succinimidyl esters involves a change in the global charge of the protein which in turn changes its solubility properties.

In the preceding work, the syntheses of several pyrylium salts bearing an organometallic moiety at the 4-position, such as [ $\eta^5$ -C<sub>6</sub>H<sub>5</sub>]Cr(CO)<sub>3</sub> (Caro et al., 1993), [ $\eta^5$ -C<sub>5</sub>H<sub>4</sub>]Fe[ $\eta^5$ -C<sub>5</sub>H<sub>5</sub>], [ $\eta^5$ -C<sub>5</sub>H<sub>4</sub>]Mn(CO)<sub>3</sub>, and [ $\eta^5$ -C<sub>5</sub>H<sub>4</sub>]Re(CO)<sub>3</sub> (Dorofeenko and Krasnikov, 1972), have been described. Briefly, cyclopentadienylmanganese (rhenium) tricarbonyl was lithiated with *n*-BuLi at -78 °C in THF and then added to (2,6-diphenylpyrylium)<sup>+</sup>PF<sub>6</sub><sup>-</sup>. This was followed by exchange of counteranion with (Ph<sub>3</sub>C)<sup>+</sup>BF<sub>4</sub><sup>-</sup> and precipitation of red (green) crystals upon addition of ethyl ether. Their reactivities toward simple amines like  $\beta$ -alanine and benzylamine have been investigated (K. L. Malisza, S. Top, M. J. McGlinchey, and G. Jaouen, unpublished results). Furthermore, we have studied the reactions of manganese and rhenium pyrylium salts (Figure 1) with proteins such as bovine serum albumin (BSA) and hen egg-white lysozyme. Reactions were followed by UV-vis spectroscopy and compared to that observed with *n*-butylamine in organic medium. In the case of BSA, we clearly observed the quantitative formation of an organometallic pyridinium derivative. As for lysozyme, the reaction was not quantitative, and average coupling ratios measured were low. Furthermore, no pyridinium salt was observed; instead, we believe that the coupling reaction is stopped at the divinyllogous amide form.

## **EXPERIMENTAL PART**

**Materials.** 4-( $\eta^5$ -Cyclopentadienyl)tricarbonylmanganese-2,6-diphenylpyrylium tetrafluoroborate (**Ia**) and 4-( $\eta^5$ -cyclopentadienyl)tricarbonylrhenium-2,6-diphenylpyrylium tetrafluoroborate (**Ib**) (Figure 1) were synthesized according to the literature method (Dorofeenko and Krasnikov, 1972). *n*-Butylamine and *tert*-butylamine were purchased from Aldrich. Bovine serum albumin fraction V and hen egg-white lysozyme (three times crystallized) were obtained from Sigma. Borate buffer (0.1 M, pH 9.0) was prepared from demineralized water. Acetonitrile was of HPLC grade. Gel filtration chromatography was performed on Econo-Pac 10DG columns

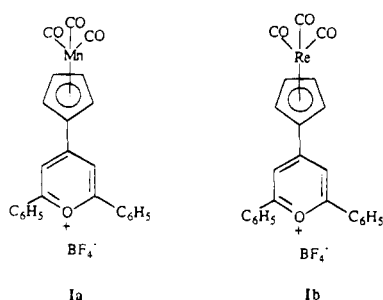
\* To whom correspondence should be sent.

<sup>†</sup> Ecole Nationale Supérieure de Chimie de Paris.

<sup>‡</sup> Institut Universitaire de Technologie.

<sup>§</sup> Abstract published in *Advance ACS Abstracts*, October 15, 1994.





**Figure 1.** Organometallic pyrylium salts.

(Biorad). UV-vis measurements were performed on a Uvikon 860 spectrophotometer (Kontron).

**Methods.** *Reaction of *n*-Butylamine with Ia* (Scheme 1). A stock solution of **Ia** in acetonitrile ( $1 \times 10^{-3}$  M) was prepared; this solution has not shown any signs of decomposition after several months at 4 °C. A stock solution of the amine ( $2 \times 10^{-2}$  M) in acetonitrile was prepared. To 1 mL of the pyrylium salt solution was added 100  $\mu$ L of the amine solution. After 10 min, the solution was diluted to one-tenth, and its UV-visible spectrum was recorded. Subsequently, a solution of acetic acid (100  $\mu$ L,  $2 \times 10^{-2}$  M) was added, the solution diluted to one-tenth, and the reaction followed by UV-vis spectroscopy (scan speed 250 nm/min).

*Reaction of *n*-Butylamine and *tert*-Butylamine with Ib* (Scheme 1). To 1 mL of **Ib** in acetonitrile ( $1 \times 10^{-3}$  M) was added a solution of *n*-butylamine or *tert*-butylamine in acetonitrile (100  $\mu$ L,  $2 \times 10^{-2}$  M). The solution was immediately diluted to one-tenth, and UV-visible spectra were recorded every 5 min (scan speed 250 nm/min).

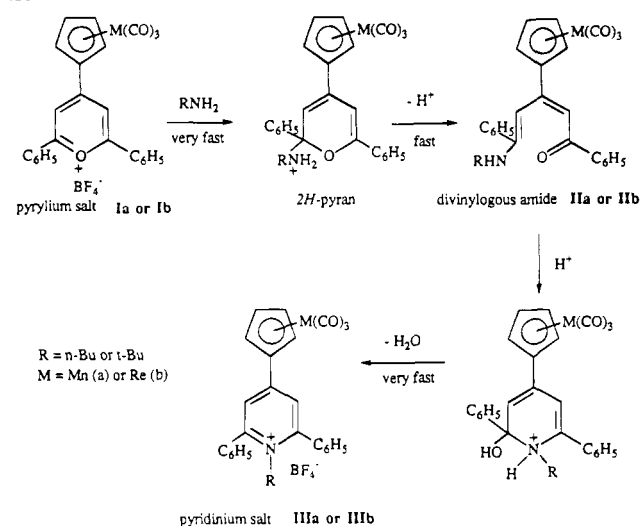
*Labeling of BSA with Ia and Ib* (Scheme 2). A solution of BSA (1 mg/mL,  $1.5 \times 10^{-5}$  M) was prepared in borate buffer. Nine parts of the protein solution were mixed with one part of the pyrylium salt stock solution (6 equiv, 10% of acetonitrile). The reaction was followed by UV-visible spectroscopy in a 1 cm cuvette. After 24 h at room temperature, the solution was centrifuged and chromatographed in a gel filtration column (eluent: demineralized water). Ten fractions of 1 mL were collected and analyzed for protein concentration (Bradford method) and label, taking compounds **IIIa** and **IIIb** as references ( $\epsilon$  (440 nm) = 10 300 for **IIIa**;  $\epsilon$  (410 nm) = 9030 for **IIIb**). Coupling ratios [bound label]/[protein] were calculated from the UV-vis data for each fraction collected.

*Labeling of Lysozyme with Ib* (Scheme 3). Lysozyme (12.3 mg, 842 nmol) was dissolved in borate buffer (2.7 mL, 0.01 M, pH = 9.0), and **Ib** in acetonitrile (300  $\mu$ L,  $5 \times 10^{-3}$  M, 1500 nmol) was added. The mixture was incubated for 24 h at room temperature, and the resulting suspension was centrifuged (15 min at 4000 rpm) to yield a bright yellow supernatant which was stored at 4 °C pending further analysis.

## RESULTS AND DISCUSSION

**Reaction of *n*-Butylamine with Ia in Acetonitrile** (Scheme 1). The reaction of 1 equiv of **Ia** (red) with 2 equiv of *n*-butylamine rapidly gives a yellow compound, **IIa**, which is sufficiently stable to be characterized by UV-vis spectroscopy. This intermediate is referred to as a divinylogous amide, **IIa**; the second equivalent of base catalyzes its formation (Katritzky et al., 1984b). The divinylogous amide shows an absorbance band at 390 nm ( $\epsilon$  = 6300). After addition of acetic acid, this open ring intermediate slowly closes (2 h) to give the expected pyridinium salt absorbing at 441 nm ( $\epsilon$  = 10 300) (Figure 2A). This assertion has been proven by comparing the

**Scheme 1.** Reaction of the Organometallic Pyrylium Salts with Amines in Acetonitrile

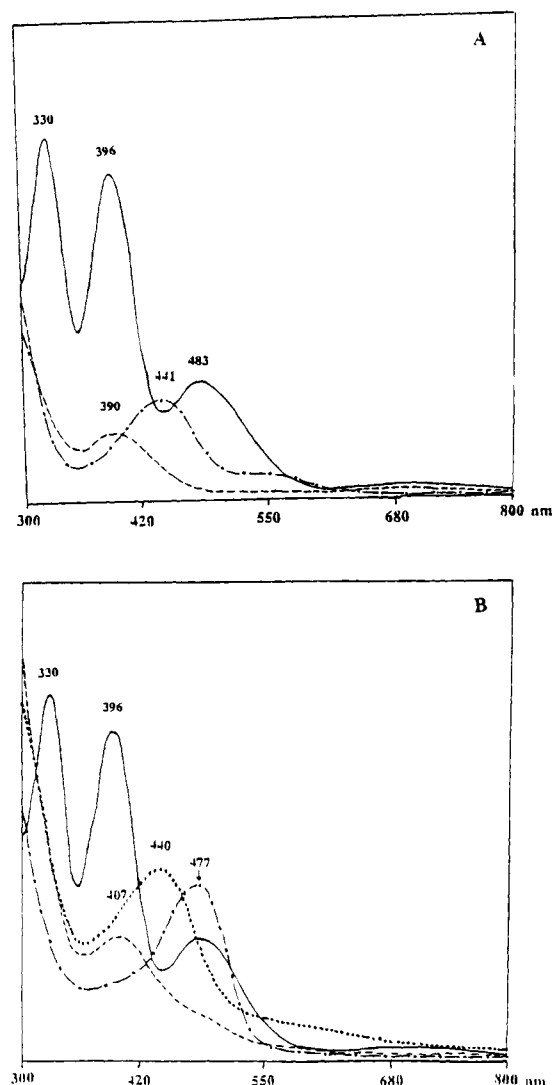


UV-vis spectrum of *N*-butylpyridinium Mn(CO)<sub>3</sub>, **IIIa**, which was synthesized independently.

**Reaction of BSA with Ia in Borate Buffer (Scheme 2).** The reaction of 6 equiv of **Ia** with BSA in borate buffer pH 9.0 has been performed at room temperature. This time, the mechanism proceeds quite differently as observed by UV-vis spectroscopy. Immediately after a solution of **Ia** is mixed in acetonitrile with BSA, the solution becomes strongly orange corresponding to a species absorbing at 477 nm ( $\epsilon$  = 8800). This species slowly transforms (30–40 min) into a second yellow intermediate absorbing at 407 nm and then finally into a compound absorbing at 440 nm (Figure 2B). If we compare these results to that of *n*-butylamine, we can reasonably assign the second intermediate to the divinylogous amide form as the first one is more likely a "pseudobase" form **II'a**, resulting from the reaction of **Ia** with H<sub>2</sub>O. In the experimental conditions described, this hydrolysis reaction is predominant and the pseudobase form appears as the reactive species toward the lysine residues of BSA. **II'a** then reacts slowly with the protein to give **IIa** which slowly (20 h) closes into **IIIa**. This last step is much slower than in the *n*-butylamine case because no acid was added in this case. This result is different from what has been previously reported (Katritzky et al., 1984a). Indeed, Katritzky et al. did not observe any reaction between the pseudobase and the protein when the latter was present in large excess.

After 24 h, the mixture was chromatographed by gel filtration and the elution was followed by colorimetry at 440 nm for the label. Furthermore, the protein content of each fraction was measured by the Bradford test at 595 nm (Figure 3A). Elution profiles are exactly superimposable, indicating that all the label was bound to the protein. Quantitative characterization of fractions 2 to 4 was performed by calculating an average coupling rate based on UV-vis data. These coupling ratios were found in the range 5.5–6.1, which is a coupling yield of nearly 90% (Table 1).

**Reaction of *n*-Butylamine with Ib in Acetonitrile** (Scheme 1). A similar experiment was performed by mixing 2 equiv of *n*-butylamine with **Ib** in acetonitrile. This time, however, the reaction takes place more rapidly, and even in the absence of acetic acid it proved impossible to characterize correctly the divinylogous form intermediate which rapidly transforms into the final pyridinium salt. By UV-vis spectroscopy, a bathochrome shift from 401 nm (pyrylium) to 428 nm was observed



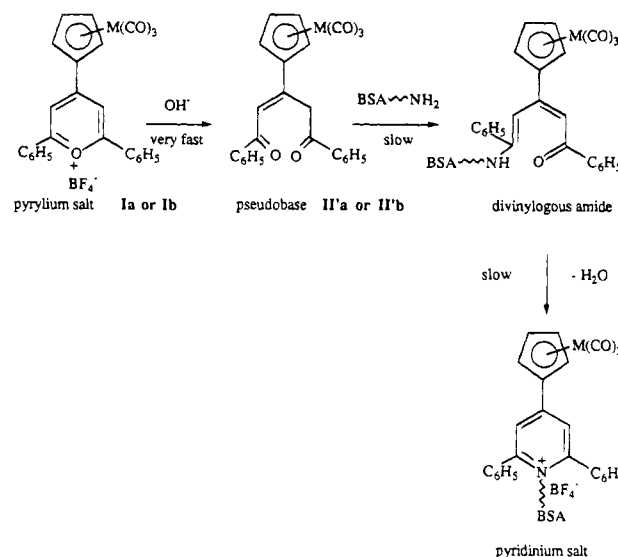
**Figure 2.** A. UV-vis spectra of the reaction of **Ia** with *n*-butylamine in acetonitrile: (—) **Ia**; (---) divinylogous amide **IIa**; (- · -) *N*-butylpyridinium salt **IIIa**. B. UV-vis spectra of the reaction of **Ia** with BSA in borate buffer pH 9.0/acetonitrile 9/1: (—) **Ia**; (---) pseudobase **II'a**; (- · -) divinylogous amide form; (- · ·) pyridinium salt.

within 2 min and then an isochromic shift to about 380 nm, as a shoulder, within 15 more min. We conclude that the rhenium divinylogous amide intermediate is much more reactive than the manganese derivative. Moreover, band shifts are weak, making assignments more difficult than in the manganese case.

**Reaction of BSA with **Ib** in Borate Buffer (Scheme 2).** The protocol followed for **Ia** was applied to **Ib**. After 24 h at room temperature, the mixture was chromatographed and elution profiles in protein (595 nm) and label (410 nm) were plotted (Figure 3B). Once again, a perfect superposition of both plots is observed, indicating that all the label is bound to the protein. The average coupling rate is calculated from UV-vis data of *N*-butylpyridinium  $\text{Re}(\text{CO})_3$  ( $\epsilon(410 \text{ nm}) = 4300$ ). It was found in the range 4.3–5.3, which is less than with the manganese derivative but can possibly be explained by the presence of impurities in the starting reagent **Ib**.

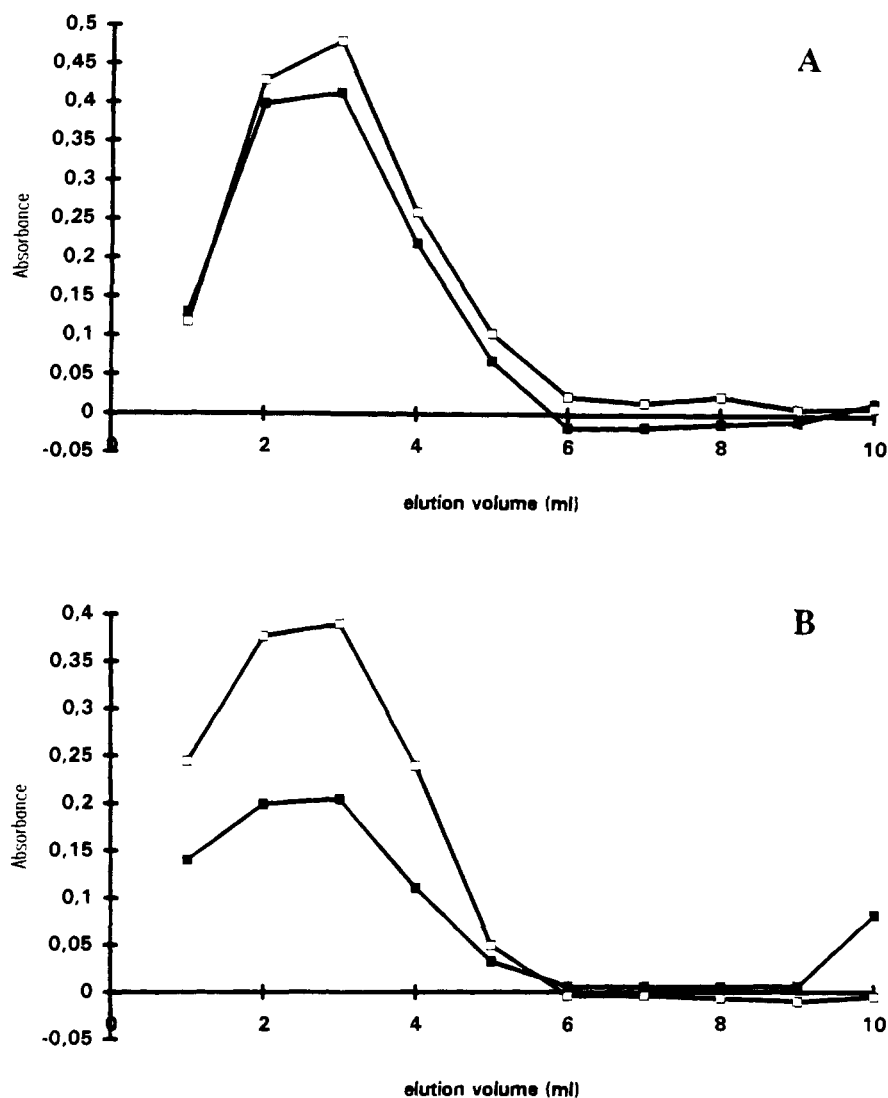
**Reaction of Lysozyme with **Ib** in Borate Buffer (Scheme 3).** Hen egg-white lysozyme is a 129 amino acid protein of 14.3 kDa and of isoelectric point 11. It possesses six lysine residues plus one amino terminal residue, which is seven theoretically modifiable functions. We tried to label lysozyme by adding 1.8 equiv of **Ib** to

**Scheme 2.** Reaction of Bovine Serum Albumin with the Pyrylium Salts in Borate Buffer pH 9.0/Acetonitrile 9/1 (**M** = Mn (**a**) or Re (**b**))



protein at pH 9.0. After 24 h, a significant amount of a light-brown precipitate appeared which was readily separated by centrifugation. A blank assay was performed in which the same amount of **Ib** was incubated in borate buffer alone. After one night incubation, the same kind of precipitate is also formed resulting from the hydrolysis of **Ib** into **II'b** then its decomposition. We conclude that the reaction of lysozyme with **Ib** is incomplete so that most of the reagent suffers degradation.

The UV-vis spectrum of the yellow supernatant was measured and compared to that of *N*-butylpyridinium  $\text{Re}(\text{CO})_3$  and the BSA adduct (Figure 4). While the last two do not present any separate band, the first presents a well-resolved band at 453 nm. The structure of the species conjugated to the protein is not a pyridinium salt. One reasonable hypothesis arising from this finding is that the reaction stopped at the divinylogous amide step. Unfortunately, we have just seen that it was very difficult to characterize **IIb** with *n*-butylamine as the reagent. Previous examples showed that the ring closure step was greatly slowed if the primary amine is bulky (like *tert*-butylamine or cyclohexylamine) (Katritzky, 1980). In order to characterize the divinylogous amide intermediate, **Ib** was allowed to react with *tert*-butylamine and the reaction course was followed by UV-vis spectroscopy. After 3 min, an intermediate with a separate band at 438 nm ( $\epsilon = 5500$ ) was observed (Figure 5). Within a few hours, in the absence of acetic acid, this intermediate transforms into the pyridinium salt ( $\lambda = 410 \text{ nm}$ ;  $\epsilon = 4300$ ). Indeed, with a bulky amine like *tert*-butylamine, the first step (ring opening) is as fast as with *n*-butylamine but the second step (ring closure) is greatly slowed but not completely hindered. The UV-vis spectrum of the divinylogous amide is similar to that of the lysozyme adduct. Thus, unlike BSA, ring closure is not observed with lysozyme. This hypothesis is confirmed by repeating the reaction with **Ia**. If the pyridinium species is formed, we should measure a band at 440 nm; if not, there should be a band or a shoulder near 390 nm (open ring form). Immediately **Ia** and lysozyme were mixed in borate buffer, a well-separated band appeared at 484 nm corresponding to the pseudobase species. This band slowly disappears (16 h) giving rise to a very weak shoulder around 400 nm. No band was observed at 440 nm corresponding to a pyridinium salt. This experiment clearly confirms that in the case of lysozyme, no pyri-



**Figure 3.** A. Elution profile of BSA labeled with **Ia**: (■) protein at 595 nm; (□) label at 440 nm. B. Elution profile of BSA labeled with **Ib**: (□) protein at 595 nm; (■) label at 410 nm.

**Table 1.** Reaction of **Ia** and **Ib** with *n*-Butylamine, *tert*-Butylamine, BSA, and Lysozyme

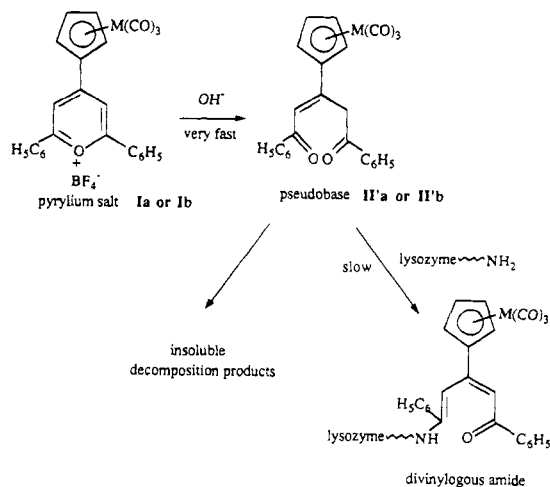
reagent	<i>n</i> -butylamine $\lambda_{\max}$ , nm ( $\epsilon$ )	<i>tert</i> -butylamine $\lambda_{\max}$ , nm ( $\epsilon$ )	BSA		lysozyme	
			$\lambda_{\max}$ , nm	CR <sup>a</sup>	$\lambda_{\max}$ , nm	CR
<b>Ia</b>	390 (6300) <sup>b</sup>	nd			390 (sh) <sup>b</sup>	0.23
	440 (10300)		440	6		
<b>Ib</b>		438 (5500) <sup>b</sup>			453 <sup>b</sup>	0.23
	380 (9030, sh)	409 (4300)	390 (sh)	5		

<sup>a</sup> Coupling ratio: [bound label]/[protein]. <sup>b</sup> Divinyllogous amide intermediate.

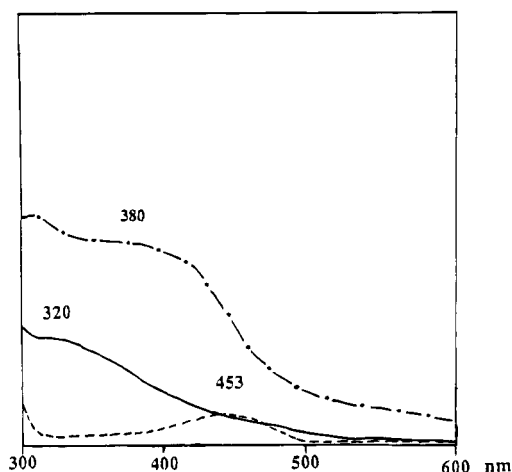
dinium salt is formed, as the coupling reaction stops at the divinyllogous amide. The coupling ratios for both complexes were found around 0.25 when taking as references the  $\epsilon$  measured for divinyllogous amide forms observed previously (reaction of *n*-butylamine with **Ia** and reaction of *tert*-butylamine with **Ib**).

Clearly, results differ considerably for the two proteins studied. For BSA, coupling yields are almost quantitative and the final conjugated species is a pyridinium form. For lysozyme, coupling yields are low and the species conjugated is a divinyllogous amide. Lysine residues, because of their hydrophilic character, are usually located at the surface of globular proteins (Metzler, 1977). This property makes them useful targets for chemical modification of proteins. However, previous examples related

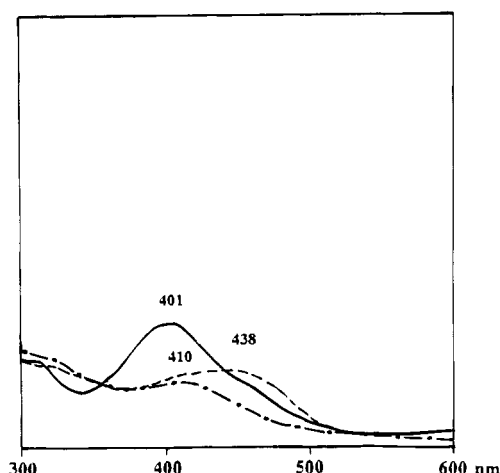
**Scheme 3.** Reaction of the Organometallic Pyrylium Salts with Lysozyme in Borate Buffer pH 9.0/Acetonitrile 9/1 (M = Mn (a) or Re (b))



to the reactivity of lysine side-chains of lysozyme showed that three residues out of seven are chemically modified by iodoacetic acid (Kravchenko et al., 1965). Furthermore, we have shown that when the *N*-succinimidyl ester of tungsten was used, only 1.2 residues were modified at



**Figure 4.** UV-vis spectra of **IIIb** (---); BSA labeled with **Ib** (—) and lysozyme labeled with **Ib** (- · -).



**Figure 5.** UV-vis spectra of the reaction of **Ib** with *tert*-butylamine in acetonitrile: (—) **Ib**; (---) after 3 min; (- · -) after a few days.

pH 9.0 (Gorfti et al., 1994). The use of pyrylium salts in the place of *N*-succinimidyl esters gives evidence that local environment around the reactive lysine side chain may prevent the ring closure reaction. As for the low yield, it must be remembered that lysozyme is a very basic protein. At pH 9.0, the protein is still positively charged, and protonated lysine side chains are relatively unreactive toward the pyrylium salts (or their derivated pseudobases). Consequently, the main reaction in the case of lysozyme is hydrolysis of the pyrylium salts.

## CONCLUSION

We have described here a new strategy of protein labeling by organometallic complexes. This strategy is based on the specificity of the reaction of primary amines with pyrylium salts to give pyridinium salts. Reaction courses were followed by UV-vis spectrophotometry, and different reaction intermediates were characterized. With an acidic protein like BSA, we showed that coupling reactions were almost quantitative at pH 9.0 and that the final species conjugated was the expected pyridinium derivative. Conversely, with a small and highly basic protein like lysozyme, the coupling reaction did not lead to a pyridinium salt but the label was in the form of a divinyllogous amide, with low coupling ratios. Pyrylium

salts, therefore, appear as very useful reagents for the specific chemical modification of proteins at the exception of highly basic ones. Organometallic pyrylium salts are interesting alternatives to organometallic *N*-succinimidyl esters as labeling agents of proteins.

## ACKNOWLEDGMENT

The Centre National de la Recherche Scientifique (CNRS) is acknowledged for financial support. K.L.M. thanks the French government for a Chateaubriant postdoctoral fellowship.

## LITERATURE CITED

- Balaban, A. T., Fischer, G. W., Dinulescu, A., Koblik, A. V., Dorofeenko, G. N., Mezheritski, V. V., and Schroth, W. (1982) Pyrylium salts: Synthesis, reactions and physical properties. *Advances in heterocyclic chemistry, Suppl. II* (A. R. Katritzky, Ed.) Academic Press, New York.
- Caro, B., Sénéchal-Tocquer, M.-C., Sénéchal, D., Marrec, P., Saillard, J.-Y., Triuki, C. and Kahlal, S. (1993). Diacetylation of ethylenics of benzene chrometricarbonyl. Access to  $\gamma$ -benchrotrenic pyrylium salts. X-ray structural analysis and unusual electronic influence of the Cr(CO)<sub>3</sub> moiety. *Tetrahedron Lett.* 34, 7259–7262.
- Dorofeenko, G. N., and Krasnikov, V. V. (1972) Synthesis of pyrylium and pyridinium derivatives of ferrocene. *Zh. Org. Khim.* 8, 2120.
- Gorfti, A., Salmmain, M., and Jaouen, G. (1994) Novel *N*-succinimidyl and *N*-sulfosuccinimidyl organotungsten reagents for the labelling of biological systems. *J. Chem. Soc., Chem. Commun.* (in press).
- Katritzky, A. R. (1980) Conversions of primary amino groups into other functionality mediated by pyrylium cations *Tetrahedron* 36, 679–699.
- Katritzky, A. R., Mokrosz, J. L. and Lopez-Rodriguez, M. L. (1984a) Pyrylium-mediated transformations of natural products. Part 5. Reactions of gelatin and chymotrypsin with 4-(4-methoxy-3-sulphophenyl) 2,6-bis-(4-sulphophenyl)pyrylium perchlorate. *J. Chem. Soc., Perkin Trans.* 2 875–878.
- Katritzky, A. R., Mokrosz, J. L., and De Rosa, M. (1984b) Pyrylium-mediated transformations of natural products. Part 2. Reaction of 4-(4-methoxy-3-sulphophenyl)-2,6-bis-(4-sulphophenyl)pyrylium perchlorate with primary amines. *J. Chem. Soc., Perkin Trans.* 2 849–855.
- Kravchenko, N. A., Kleopina, G. V., and Kaverzneva, E. D. (1964) Investigation of the active sites of lysozyme. Carboxymethylation of the imidazole group of histidine and of the  $\epsilon$ -amino group of lysine. *Biochim. Biophys. Acta* 92, 412–414.
- Metzler, D. E. (1977) *Biochemistry*, Academic Press, New York.
- O'Leary, M. H., and Sanberg, G. A. (1971) Chemical modification of proteins by pyrylium salts *J. Am. Chem. Soc.* 93, 3530–3532.
- Salmmain, M., Vessièrès, A., Jaouen, G., and Butler, I. S. (1991) Fourier transform infrared spectroscopic technique for the quantitative analysis of transition metal carbonyl-labeled bioligands. *Anal. Chem.* 63, 2323–2329.
- Salmmain, M., Vessièrès, A., Brossier, P., Butler, I. S., and Jaouen, G. (1992) Carbonyl-metalloimmunoassay (CMIA), a new type of non-radioisotopic immunoassay. I. Principles and application to phenobarbital assay. *J. Immunol. Methods* 148, 65–75.
- Staros, J. V. (1982) *N*-hydroxysulfosuccinimide active esters: bis(*N*-hydroxysulfosuccinimide) esters of two carboxylic acids are hydrophilic, membrane-impermeant, protein cross-linkers. *Biochemistry* 21, 3950–3955.
- Varenne, A., Salmmain, M., Brisson, C., and Jaouen, G. (1992) Transition metal carbonyl labeling of proteins. A novel approach to a solid phase two-site immunoassay using Fourier transform infrared spectroscopy. *Bioconjugate Chem.* 3, 471–476.

## Preparation and Characterization of a Bifunctional Fusion Enzyme Composed of UDP-galactose 4-Epimerase and Galactose-1-P Uridyltransferase

Yasushi Tamada,<sup>\*,‡</sup> Barbara A. Swanson,<sup>†</sup> Abolfazl Arabshahi,<sup>†</sup> and Perry A. Frey<sup>\*,‡</sup>

Institute for Enzyme Research, The Graduate School, and Department of Biochemistry, College of Agricultural and Life Sciences, University of Wisconsin—Madison, Madison, Wisconsin, and Tsukuba Research Laboratory, Japan Synthetic Rubber, 25 Miyukigaoka Tsukuba, Ibaraki 305, Japan. Received March 8, 1994<sup>§</sup>

A fusion enzyme consisting of UDP-galactose 4-epimerase and galactose-1-P uridyltransferase with an intervening Ala<sub>3</sub> linker was constructed by in-frame fusion of *E. coli* gene *galT* to the 3'-terminus of the *E. coli* gene *galE* that had been extended with the coding sequence for three alanine residues, all contained within a high-expression plasmid. The fusion enzyme was expressed in *E. coli* and purified 24-fold to about 98% homogeneity by chromatography on hydroxylapatite and Q-Sepharose. On the basis of the comparison of the elution profile for enzyme activities upon gel permeation chromatography (Sephacryl S-400) with the molecular weight of 80 000 determined by sodium dodecyl sulfate polyacrylamide gel electrophoresis, the fusion enzyme appears to exist in monomeric, dimeric, and tetrameric forms, all of which exhibit both enzymatic activities. The  $K_m$  values of the fusion enzyme for substrates were similar to those for the corresponding native enzymes, except for UDP-glucose, but the  $k_{cat}$  values were smaller than those for the native enzymes. The fusion enzyme shows kinetic advantages in that the initial velocity to produce glucose-1-P from UDP-galactose and galactose-1-P is about 20% faster than that for a mixture of equal activities of the separate enzymes.

Commercial and medical applications of enzymes are often enhanced by immobilization to a solid support (1–3). In some applications, two or more enzymes acting sequentially in a process may be coimmobilized. In cases such as the latter, there may be advantages to using fusion proteins formed from enzymes acting in sequence. A potential advantage includes the recycling of an expensive cofactor, which may be covalently attached to the fusion protein through a flexible spacer. Another is that the product of one enzyme, being a substrate for the next, might be captured by the second enzyme because of its proximity and gives a kinetic advantage.

Techniques have been reported for obtaining these benefits in enzymatic production systems (4). In the most typical method, the enzymes are chemically crosslinked. However, crosslinking can be difficult to control and produces a multiplicity of species. Fusion enzymes resulting from in-frame fusion of the genes specifying the respective enzymes, as originally described by Bulow et al. (5), lead to specific products, the structures and composition of which can be controlled through manipulation of the structures of the fusion genes.

UDP-galactose 4-epimerase and galactose-1-P uridyltransferase, hereafter referred to as epimerase and transferase, are key enzymes in the Leloir pathway for galactose metabolism (6). Galactose in the cell is initially phosphorylated by ATP to galactose-1-P by the action of galactokinase. This is followed by the reaction of UDP-glucose<sup>1</sup> and galactose-1-P to give UDP-galactose and glucose-1-P, catalyzed by galactose-1-P uridyltrans-

ferase. In subsequent steps, phosphoglucosyltransferase catalyzes the isomerization of glucose-1-P to glucose-6-P, and UDP-galactose 4-epimerase catalyzes the isomerization of UDP-galactose to UDP-glucose.

UDP-galactose 4-epimerase, from *E. coli*, is a dimer of identical subunits with an overall molecular weight of 79 000 (7). It contains one tightly but noncovalently bound NAD<sup>+</sup> or NADH per subunit. The crystal structure was determined by Bauer et al. (8). The catalytic mechanism includes the reversible oxidation of UDP-galactose or UDP-glucose to UDP-4-ketoglucose and concomitant reduction of NAD<sup>+</sup> to NADH at the active site. Galactose-1-P uridyltransferase from *E. coli* consists of two identical subunits and has an overall molecular weight of 80 000 (9). The enzymatic mechanism is a double-displacement of the uridylyl group that obeys ping-pong kinetics and requires the formation of a covalent uridylyl-enzyme as the intermediate (10). In the intermediate, the uridylyl group is bonded to histidine 166 (11).

We have begun a study of fused enzymes by creating a bifunctional fusion protein composed of UDP-galactose 4-epimerase and galactose-1-P uridyltransferase. These two enzymes were chosen because they have been cloned, expressed, and characterized, and the product of one enzyme is a substrate for the other. This relationship could allow a fusion enzyme composed of them to catalyze the interconversion of galactose-1-P and glucose-1-P without the addition or intermediate formation of free nucleotide sugars, which are expensive and labile, provided that the nucleotide sugars can be covalently attached. In Scheme 1, the nucleotide sugars are shown

\* Address for correspondence: Institute for Enzyme Research, University of Wisconsin—Madison, 1710 University Ave., Madison, WI 53705.

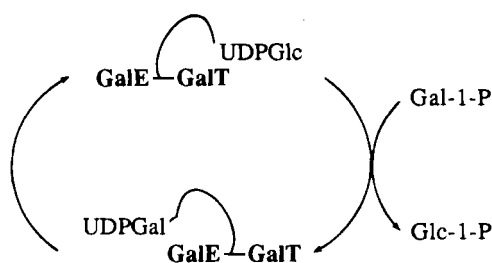
<sup>†</sup> Institute for Enzyme Research, University of Wisconsin—Madison.

<sup>‡</sup> Tsukuba Research Laboratory, Japan Synthetic Rubber, 25 Miyukigaoka Tsukuba, Ibaraki 305, Japan.

<sup>§</sup> Abstract published in *Advance ACS Abstracts*, September 15, 1994.

<sup>1</sup> Abbreviations: UDP-glucose, uridine 5'-diphosphoglucose; UDP-galactose, uridine 5'-diphosphogalactose; NAD<sup>+</sup>, nicotinamide adenine dinucleotide; NADP<sup>+</sup>, nicotinamide adenine dinucleotide phosphate; NADH, reduced NAD<sup>+</sup>; NADPH, reduced NADP<sup>+</sup>; PMSF, phenylmethanesulfonyl fluoride; EDTA, ethylenediaminetetraacetic acid; SDS—PAGE, sodium dodecyl sulfate polyacrylamide gel electrophoresis.

Scheme 1



attached through a long spacer to the fusion linkage between the enzymatic components, but in practice the spacer could be attached to either component, provided it is long enough. The spacer must be long, flexible, and inert under the conditions of the enzymatic reaction.

In this paper, we describe the construction of a fusion gene between *galE* and *galT*. We also describe the expression, purification, characterization, and some of the properties of this fusion protein.

#### EXPERIMENTAL PROCEDURES

**Chemicals and Reagents.** All restriction enzymes and polynucleotide kinase were purchased from New England Biolabs, and T4 DNA ligase and alkaline phosphatase were purchased from Boehringer Mannheim. UDP-glucose, UDP-galactose, UDP-glucose dehydrogenase, galactose-6-P dehydrogenase, phosphoglucomutase, NAD<sup>+</sup>, NADP<sup>+</sup>, ampicillin, streptomycin sulfate, and PMSF were purchased from Sigma. Ammonium sulfate (enzyme grade) was purchased from Schwarz/Mann Biotech. Bacto tryptone and bacto yeast extract were purchased from Difco Labs. The reagents and enzymes for DNA sequencing were from the Sequenase version 2.0 kit (United States Biochemical), and [ $\alpha$ -<sup>35</sup>S]dATP (600 Ci/mmol) was purchased from Amersham. Hydroxylapatite (Bio-Gel HTP) was the product of BioRad, and Q-Sepharose (fast flow) was purchased from Sigma. Sephacryl S-400 high resolution was the product of Pharmacia. The reagents for oligonucleotide synthesis were obtained from Glen Research Co. All other chemicals were obtained in reagent grade from commercial suppliers.

**Bacterial Strains and Plasmids.** *E. coli* JM110 (dam, dcm, sup E44hsdR17phi leu rpsL lacY galK galT ara tonA thr tsx D(lac-proAB)F[traD36 proAB<sup>+</sup> lacI<sup>a</sup> lacZ DM15]) was purchased from Strategy Gene, DH5 $\alpha$  (supE44 DlacU169 (f80 lacZ DM15) hsdR17 recA1 endA1 gyrA96 thi<sup>-1</sup> relA1) from Gibco BRL Life Technology, and BL21(DE3) (hsdS gal (xllts857 ind1 sam7 nin5 lacUV-T7 gene1)) pLysS was from Novagen, Inc. Because the BL21 cell strain does not contain the *gal* operon, it does not produce any endogenous epimerase or transferase. The LysS plasmid encode for a small lysozyme and the presence of this enzyme tends to decrease the loss of construct plasmid during cell growth (11).

Plasmid pT7E2 containing the *galE* gene was constructed as described by Swanson and Frey (12), and the plasmid pKfT containing the *galT* gene was described by Kim et al. (13).

**Construction of Plasmid.** Restriction enzyme digestion and other enzymatic reactions for DNA manipulations were performed as directed by the manufacturers. Oligonucleotides to make the linker and a primer for DNA sequencing were synthesized using a Biosearch Model 8600 DNA synthesizer and purified according the procedure as described (14). The purification of DNA was performed using QIAGEN columns according to the specified procedure. DNA sequencing was performed by

the chain-termination method using Sequenase version 2.0 according to the protocol. A detailed description of the construction of the fusion gene, pT7ET, is given in the Results and Discussion.

#### Expression and Purification of Fusion Enzyme.

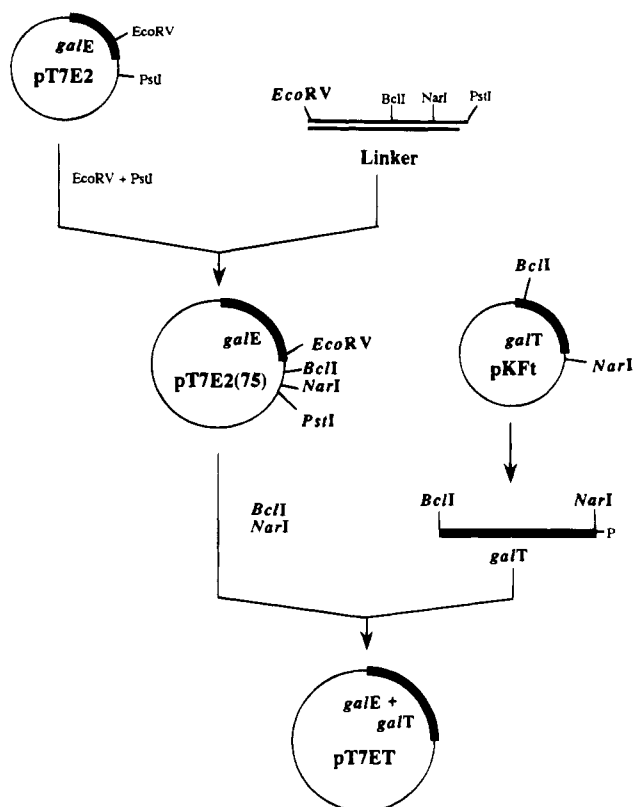
*E. coli* BL21(DE3), pLysS, pT7ET cells were streaked out on LB plates and grown at 37 °C overnight. A single colony was used to inoculate 5 mL of 2xYT medium with ampicillin (0.1 mg/mL) and chloramphenicol (0.1 mg/mL), which was shaken at 37 °C for 16 h. This starter culture was used to inoculate 1 L of 2xYT medium containing ampicillin (0.1 mg/mL). The growth medium was shaken at 37 °C for 9 h with the addition of ampicillin (0.1 mg/mL) every 3 h. The cells were harvested by centrifugation, quick-frozen in liquid nitrogen, and stored at -70 °C.

The purification scheme for the fusion enzyme is similar to that for the purification of epimerase (15). All procedures were carried out at 0–5 °C, and all buffers contained 1 mM EDTA, 10 mM 2-mercaptoethanol, and 1 mM PMSF. All centrifugations were at 14000g. The cells from a 1 L growth were thawed and suspended in 5 mL of 20 mM potassium phosphate buffer (KP<sub>i</sub> buffer) at pH 7.4. The pLysS plasmid encodes a lysozyme which effectively served to lyse the cells within 40 min. Trace amounts of deoxyribonuclease (DNase) and CaCl<sub>2</sub> were added to the solution. After cell debris was removed by centrifugation, streptomycin sulfate (10%) was slowly added to the supernatant to a concentration of 25.4 mg/mL. The solution was stirred for an additional 20 min and centrifuged to remove the precipitate. Finely ground ammonium sulfate was slowly added to the supernatant fluid with stirring to 45% of saturation. The suspension was stirred for an additional 30 min and then centrifuged. The pellet was resuspended in a minimum of 20 mM KP<sub>i</sub> buffer at pH 7.4 and dialyzed against the same buffer overnight.

This crude protein solution (ca. 5 mL) was loaded onto a 20 mL column of hydroxylapatite that had been equilibrated with 20 mM KP<sub>i</sub> buffer at pH 7.4. The column was eluted with the same buffer, and fractions containing both epimerase and transferase activities were pooled and carefully titrated to pH 8.5 with KOH. This protein solution was then loaded onto a 20 mL Q-Sepharose column that had been equilibrated with 20 mM KP<sub>i</sub> buffer at pH 8.5. The protein was eluted by a linear gradient of KP<sub>i</sub> buffer 200 mL in total volume and increasing from 20 mM to 300 mM at pH 8.5. Fractions containing both enzyme activities were pooled and concentrated to 1 mL in a Centriprep-30 concentrator (Amicon). This protein solution was subjected to gel filtration on a Sephacryl S-400 high resolution column (1  $\times$  90 cm) that had been equilibrated with 20 mM KP<sub>i</sub> buffer containing 100 mM KCl at pH 7.4. Fractions from the main peak showing both enzyme activities were pooled and concentrated by a Microcon 10 concentrator (Amicon).

**Enzyme Assay.** Galactose-1-P uridylyltransferase activity was assayed in a coupled assay (16) in which the formation of glucose-1-P is coupled to NADPH production. The reaction mixture consisted of 0.2 mM galactose-1-P, 0.051 mM UDP-glucose, 0.326 mM NADP<sup>+</sup>, 3.3  $\mu$ M glucose-1-6-P<sub>2</sub>, and excess phosphoglucomutase and glucose-6-P dehydrogenase in 0.1 M sodium bicinate at pH 8.5 at 27 °C. The reaction was started by adding the test enzyme and monitoring NADPH formation at 340 nm. The activity unit was defined to be the production of 1  $\mu$ mol of glucose-1-P per hour. Epimerase activity was measured using the coupled assay described by Wilson and Hogness (17), in which the formation of UDP-glucose





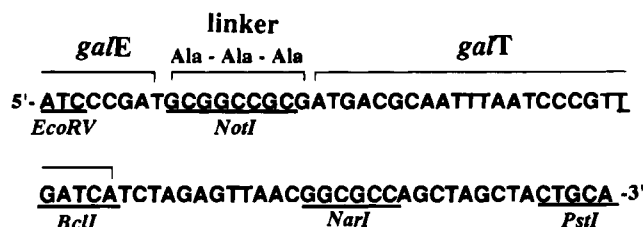
**Figure 1.** Construction of the plasmid pT7ET encoding an in-frame fusion gene between *galE* and *galT*.

is coupled to NADH formation by UDP-glucose dehydrogenase. The enzyme was added to UDP-galactose (0.05 mM),  $\text{NAD}^+$  (0.25 mM), UDP-glucose dehydrogenase (200 units), and 0.125 M potassium bicarbonate buffer at pH 8.5 at 27 °C; NADH formation was monitored at 340 nm. One unit of enzyme is defined as the amount catalyzing the formation of 1  $\mu\text{mol}$  of UDP-glucose per hour. To determine the catalytic activity of the fusion enzyme, the initial rate was measured by a modification of standard assay for the transferase, in which UDP-galactose was substituted for UDP-glucose. The fusion enzyme was added to UDP-galactose (0.051 mM),  $\text{NADP}^+$  (0.326 mM), glucose-1,6- $\text{P}_2$  (3.3  $\mu\text{M}$ ), and excess phosphoglucosmutase and glucose-6-P dehydrogenase in 0.1 M sodium bicarbonate buffer at pH 8.5 and varying amounts of galactose-1-P at 27 °C; NADPH formation was monitored at 340 nm.

**Electrophoresis.** SDS-PAGE was performed using a Phast Gel System (Pharmacia) on a 8–25% linear gradient polyacrylamide gel. The protein bands were visualized by staining with Coomassie brilliant blue G250. The molecular weight of the enzyme subunits was determined by comparing their relative mobilities with those of proteins in a molecular weight standard kit (Pharmacia).

## RESULTS AND DISCUSSION

**Construction of pT7ET.** The strategy used for the construction of a plasmid (pT7ET) containing a fusion gene composed of *galE* and *galT* separated by an in-frame linker coding for Ala<sub>3</sub> is illustrated in Figure 1. A 75 bp DNA fragment, whose sequence in the coding strand is shown in Figure 2, was prepared by synthesis of the complementary single strands and hybridization. It contains a coding sequence for the 3'-end of *galE* that eliminates the stop codon and then encodes a linker of three alanine residues. The last part of the oligomer is the 5'-end of the *galT* start codon and the *Bcl*I site. The



**Figure 2.** DNA sequence of the linker used to fuse the genes *galE* and *galT*. Shown is the coding strand for the synthetic double-stranded linker used in the fusion of the genes for UDP-galactose 4-epimerase and galactose-1-P uridylyltransferase in Figure 1.

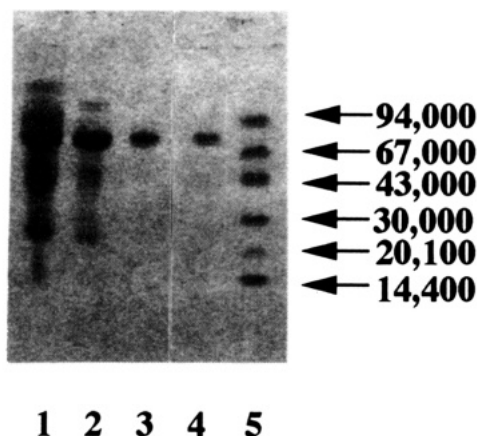
unique *Not*I restriction site was designed into the linker region of the fragment sequence in order to facilitate a check of the construction of the fusion gene after cloning and to allow for future addition of linkers into this site. This oligomer sequence contains *Bcl*I and *Nar*I restriction sites to facilitate insertion of the *galT* gene. As shown in Figure 1, the linker fragment was ligated into the *Pst*I and *Eco*RV sites of pT7E2. The plasmid obtained, pT7E(75), was transformed into DH5 $\alpha$  cells. Purified plasmid was linearized by cleavage with *Nar*I, dephosphorylated, and then digested with *Bcl*I. This procedure efficiently prevented self-ligation. The *galT* gene was prepared by digesting pKFt, grown in JM110 cells to prevent dam methylation, with *Nar*I and *Bcl*I. Because pKFt has five *Nar*I sites and two *Bcl*I sites, eight fragments were obtained from pKFt. The 1095 bp fragment, containing most of the *galT* gene, was isolated and purified, using low melting temperature agarose gel electrophoresis, and then ligated into the linearized pT7E(75). The plasmid obtained, pT7ET, encoding for a fusion enzyme, was checked by restriction analysis and by sequencing the linker region in the fusion gene. The pT7ET plasmid confers ampicillin resistance and contains the T7 promoter just ahead of the fusion gene.

The fusion gene in pT7ET was efficiently expressed, as determined by transformation into *E. coli* BL21 and SDS-PAGE analysis of cell extracts. The fusion protein appeared as a prominent band corresponding to a molecular weight of 80 000, which was absent in untransformed cells (see, for example, lane 1 of Figure 3).

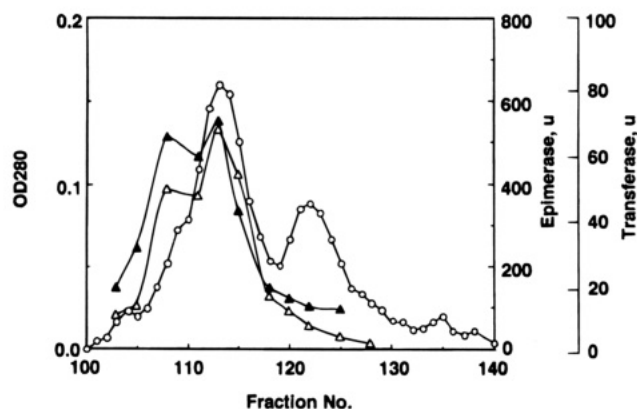
**Purification of Fusion Enzyme.** Purification of the fusion enzyme was initially attempted according to protocols developed for the epimerase and transferase. The fusion enzyme did not bind to the Affi-Gel Blue column used in the transferase procedure; however, application of the procedure for purifying the epimerase led to the purified fusion protein in a high degree of homogeneity. The results are summarized in Table 1, and in each step the purity of the fusion enzyme was confirmed by SDS-PAGE as shown in Figure 3. On the basis of the results of SDS-PAGE, the purified fusion enzyme was estimated to be approximately 95% homogeneous. In addition to the original epimerase protocol, gel filtration on Sephacryl S-400 high resolution was employed as the final step of the purification. The elution profile after gel filtration shown in Figure 4 shows that the two enzyme activities are copurified. Selected fractions corresponding to the major protein peak in Figure 4 were pooled as the main form of the fusion protein. The purified fusion enzyme exhibits 2460 units of epimerase activity per mg of protein and a transferase specific activity of 1000 U/mg. These specific activities are less than those of the corresponding native enzymes, which are normally 8000–10 000 U/mg for epimerase and 10 000–11 000 U/mg for the transferase in our laboratory. Therefore, the fusion protein exhibited about 25%

**Table 1. Purification of Fusion Protein**

	protein (mg)	yield (%)	epimerase activity		transferase activity	
			total (units)	specific (units/mg)	total (units)	specific (units/mg)
ammonium sulfate	320	100	34 600	108	37 400	117
hydroxylapatite	27	8.4	27 200	1011	14 600	543
Q-Sepharose	4.8	1.6	8500	1720	3930	795
Sephacryl S400	2.7	0.84	6470	2460	2910	1080



**Figure 3.** SDS-PAGE of the fusion enzyme. Shown are 8%–25% electrophoretic gels of the fusion enzyme at various points in its purification. The bands were stained with Coomassie Brilliant Blue G250. Lanes: 1, after ammonium sulfate precipitation; 2, after hydroxylapatite chromatography; 3, after Q-Sepharose chromatography; 4, after Sephacryl S-400 HR chromatography; 5, standards phosphorylase b (94 000), bovine serum albumin (67 000), ovalbumin (43 000), carbonic anhydrase (30 000), soybean trypsin inhibitor (20 100),  $\alpha$ -lactalbumin (14 400).



**Figure 4.** Gel filtration chromatography of the fusion enzyme on Sephacryl S-400. The fusion enzyme was chromatographed through a 1  $\times$  90 cm column of Sephacryl S-400 high resolution equilibrated and eluted with 20 mM  $\text{KPi}$ , 1 mM EDTA, 10 mM 2-mercaptoethanol, 100 mM KCl, pH 7.4 at 4  $^{\circ}\text{C}$ : (O) OD 280, ( $\Delta$ ) UDP-galactose 4-epimerase activity, ( $\blacktriangle$ ) galactose-1-P uridylyltransferase activity.

and 10%, respectively, of the activities of the individual enzymes. Part of the reason for the lower activities is that the molecular weight of the fusion protein is twice that of either enzyme, so that the measured specific activity for each enzyme would be half that for the separate enzyme. On this basis the specific activities of the fusion enzyme are 50% and 20% of the activities of epimerase and transferase, respectively.

On the basis of the activity of the crude extract from cells carrying the overexpression vector, the epimerase activity was purified 24-fold, and the transferase activity was purified 9-fold. Galactose-1-P uridylyltransferase is reported to be labile to proteolysis and oxidation (16). Because the transferase moiety in the fusion enzyme may

**Table 2. Kinetics parameters of Fusion protein<sup>a</sup>**

	$K_m$ (mM)			$k_{cat}$ ( $\text{s}^{-1}$ )
	UDP-galactose	galactose-1-P	UDP-glucose	
epimerase <sup>b</sup>	0.16			500
transferase <sup>c</sup>		0.30 $\pm$ 0.03	0.20 $\pm$ 0.02	960
fusion protein				
epimerase	0.14 $\pm$ 0.02			160 $\pm$ 20
transferase		0.29 $\pm$ 0.01	0.08 $\pm$ 0.01	24 $\pm$ 3

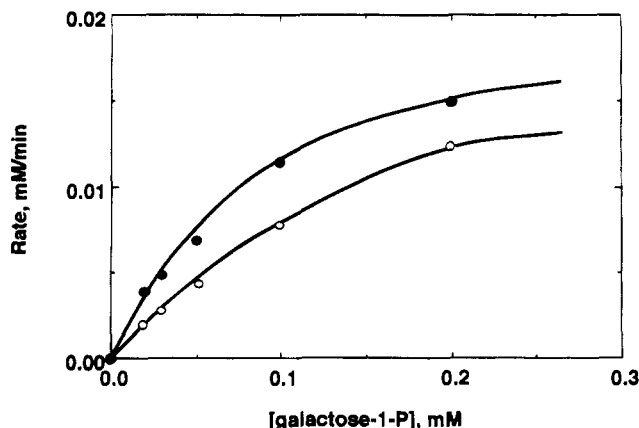
<sup>a</sup>  $K_m$  and  $k_{cat}$  values were determined by the initial rate measurements at six different concentrations according to the method described under enzyme assay. <sup>b</sup> Wilson, D. B., and Hogness, D. S. (1964) *J. Biol. Chem.* 230, 2469. <sup>c</sup> Wong, L. J., and Frey, P. A. (1974) *Biochemistry* 13, 3889.

also be unstable, its activity may have declined in the course of purification despite the addition of PMSF, EDTA, and 2-mercaptoethanol to the buffers.

**Molecular Weight of Fusion Enzyme.** The molecular weight of the fusion enzyme was determined by gel filtration and SDS-PAGE. As shown in Figure 3, the subunit molecular weight of the fusion enzyme is estimated to be about 80 000 based on the results of SDS-PAGE. This value is in good agreement with the expected size. Because UDP-galactose 4-epimerase and galactose-1-P uridylyltransferase are dimeric enzymes with total molecular weights of 79 000 and 80 000, respectively, the molecular weight of a subunit of the fusion enzyme should be about 80 000.

Gel permeation chromatography of the fusion enzyme purified through the Sepharose Q step and comparison of the elution volumes with protein standards showed the fusion enzyme to be heterogeneous with respect to molecular weight. As shown in Figure 4, three peaks for the fusion enzyme were observed in the gel filtration profile. The peak at fractions 120–125 corresponds to a molecular weight of 60 000–80 000, the peak at fractions 112–117 corresponds to a molecular weight of 140 000–160 000, and the third peak at fractions 107–110 is approximately 320 000–380 000 in molecular weight. These results indicate that the fusion enzyme exists in three forms, which appear to be monomeric (E–T), dimeric (E–T)<sub>2</sub>, and tetrameric (E–T)<sub>4</sub>. The monomeric fusion enzyme exhibits very low epimerase and significant transferase activity. The dimeric fusion enzyme exhibits both activities at high levels, and this is the peak containing the major total activity. The specific activities of both epimerase and transferase are higher in the apparent tetrameric form of the enzyme but could not be accurately estimated from the elution profile in Figure 4. Only a small percentage of the fusion enzyme exists in the tetrameric form, as indicated by the amount of protein associated with this form in the elution profile of Figure 4.

**Kinetic Parameters for the Fusion Enzyme.** Kinetic parameters for the fusion enzyme are summarized in Table 2, together with the corresponding values for the native epimerase and transferase determined under the same experimental conditions. The  $K_m$  values of the fusion enzyme for galactose-1-P and UDP-galactose are similar to those of the corresponding native enzymes, but the  $K_m$  value for UDP-glucose is much smaller than that

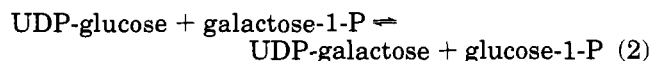


**Figure 5.** Initial rates of the coupled actions of fused epimerase-transferase and of the separate enzymes. Initial rates of the coupled actions of epimerase and transferase in the transformation of galactose-1-P into glucose-1-P at various concentrations of galactose-1-P are plotted. The rates glucose-1-P formation were measured in assay for galactose-1-P uridylyltransferase assay method, except that UDP-galactose was substituted for UDP-glucose. The epimerase and transferase activities associated with a sample of the fusion enzyme (16.8 units and 1.0 unit, respectively) were matched by mixing the same amounts of the separate enzymes assayed at the same time. Symbols: (●) fusion enzyme, (○) mixed native epimerase and transferase.

of the transferase. During the kinetic determinations, UDP-galactose can be converted by the epimerase moiety into UDP-glucose, effectively increasing the concentration of this compound from what was initially added. This effect would result in an apparently smaller  $K_m$  value of the fusion protein for UDP-glucose. The  $k_{cat}$  values of each moiety in the fusion enzyme are somewhat smaller than those of the corresponding native enzymes.

The wild type transferase is more labile than the epimerase, owing to its greater susceptibility to oxidation and cleavage by adventitious proteases. This is also true of the fusion enzyme. The activity of the transferase component decreases with time more rapidly than that of the epimerase component. The wild type transferase is stabilized by cysteine or dithiothreitol, the absence of dioxygen, and the presence of proteolytic inhibitors; it seems likely that the transferase component of the fusion enzyme can be similarly stabilized.

**Proximity Effect.** The fusion enzyme contains both epimerase and transferase activities and so will catalyze the transformation of galactose-1-P into glucose-1-P in the presence of a catalytic amount of UDP-galactose (or UDP-glucose) according to eq 3. This results from the coupled actions of the epimerase (eq 1) and transferase (eq 2). The rate of the conversion of galactose-1-P into



glucose-1-P in the presence of UDP-galactose was measured in a modification of the transferase assay. The results are shown in Figure 5, together with the results obtained from a matched mixture of the two native enzymes. The epimerase and transferase activities of the fusion enzyme used in Figure 5 were 16.8 units and 1 unit, respectively. In comparing the rates produced by the fusion enzyme with those produced by the mixed native enzymes, the same amounts of each native en-

zyme, 1 unit of transferase and 16.8 units of epimerase, were used. As shown in Figure 5, the initial rates generated by the fusion enzyme are faster than those from the mixed native enzymes at all substrate concentrations used in this experiment. This result suggests that a proximity effect is operating in the fusion enzyme to increase the catalytic activity for the overall reaction. Inasmuch as the distance between the UDP-galactose 4-epimerase moiety and the galactose-1-P uridylyltransferase moiety in the fusion enzyme could be much less than that between the two unfused enzymes, UDP-glucose produced by the epimerase might be captured by the transferase faster in the fusion enzyme than between the two separate enzymes. This form of substrate channeling effect improves the overall performance of the fusion enzyme (18). While the channeling in Figure 5 is significant, it is not a great or important effect.

**The Enzyme Linker.** The trialanyl linker connecting the epimerase and transferase in the fusion enzyme may influence its physical conformation and enzymatic activities. In this study a short linker, three alanine residues, was chosen because it had been reported that longer linkers are susceptible to proteolytic degradation during expression, resulting in a low yield of the fusion enzyme (19). However, three alanyl residues may not provide sufficient flexibility to allow for optimal folding and subunit-subunit association of both enzymes in the fusion enzyme. This could explain why the catalytic activities for each moiety of the fusion enzyme were only 50% and 20% of those of the native epimerase and transferase, respectively. It is also possible that reversing the sequence of the two genes in the construct could affect channeling efficiency. In the future, other linkers will be introduced into the fusion enzyme in order to investigate the role of the linker region and perhaps to prepare a new fusion enzyme exhibiting higher, more stable, or more efficiently coupled enzymatic activities. The linker region in the fusion gene is designed to allow extensions of the linker region in the fusion protein through the introduction of synthetic double-stranded oligodeoxynucleotides into the unique *NotI* site.

#### ACKNOWLEDGMENT

This research was supported by Grant No. GM 30480 from the National Institute of General Medical Sciences of the U.S. Public Health Service.

#### LITERATURE CITED

- (1) Chibata, I., Tosa, T., and Sato, T. (1991) Industrial applications of immobilized proteins. *Protein Immobilization: Fundamentals and Applications* (R. F. Taylor, Ed.) pp 339–362, Marcel Dekker, Inc., New York.
- (2) Chang, T. M. S. (1991) Therapeutic applications of immobilized proteins and cells. *Protein Immobilization: Fundamentals and Applications* (R. F. Taylor, Ed.) pp 305–318, Marcel Dekker, Inc., New York.
- (3) Scouten, W. H. (1981) *Affinity Chromatography: Bioselective Adsorption on Inert Matrices*, pp 305–337, John Wiley & Sons, New York.
- (4) Cabral, J. M. S., and Kennedy, J. F. (1991) Covalent and coordination immobilization of proteins. *Protein Immobilization: Fundamentals and Applications* (R. F. Taylor, Ed.) pp 73–138, Marcel Dekker, Inc., New York.
- (5) Bulow, L. (1987) Characterization of an artificial bifunctional enzyme,  $\beta$ -galactosidase/galactokinase, prepared by gene fusion. *Eur. J. Biochem.* 163, 443–448.
- (6) Caputto, R., Leloir, L. F., Trucco, R. E., Cardini, C. E., and Paladini, A. C. (1949) The enzymatic transformation of

- galactose into glucose derivatives. *J. Biol. Chem.* 179, 497–498.
- (7) Frey, P. A. (1987) Complex pyridine nucleotide-dependent transformations. *Pyridine Nucleotide Coenzymes: Chemical, Biochemical, and Medical Aspects* (D. Dolphin, R. Poulson, and O. Avramovic, Eds.) pp 461–511, Wiley, New York.
- (8) Bauer, A. J., Rayment, I., Frey, P. A., and Holden, H. M. (1992) The molecular structure of UDP-galactose 4-epimerase from *Escherichia coli* determined at 2.5 Å resolution. *Proteins* 12, 372–381.
- (9) Saito, S., Ozutsumi, M., and Kurahashi, K. (1967) Galactose 1-phosphate uridylyltransferase of *Escherichia coli*: II Further Purification and characterization. *J. Biol. Chem.* 243, 2362–2368.
- (10) Frey, P. A., Wong, L. J., Sheu, K. F., and Yang, S. L. (1982) Galactose-1-phosphate uridylyltransferase: detection, isolation, and characterization of uridylyl enzyme. *Methods Enzymol.* 87, 20–36.
- (11) Moffat, B. A., and Studier, F. W. (1987) Use of T7 lysozyme to improve the T7 gene expression system. *Cell* 49, 221–227.
- (12) Swanson, B. A., and Frey, P. A. (1993) Identification of Lys 153 as a functionally important residue on UDP-galactose 4-epimerase from *Escherichia coli*. *Biochemistry* 32, 13231–13236.
- (13) Kim, J., Ruzicka, F., and Frey, P. A. (1990) Remodeling hexose-1-phosphate uridylyltransferase: Mechanism-inspired mutation into a new enzyme, UDP-hexose synthase. *Biochemistry* 29, 10590–10593.
- (14) Sambrook, J., Fritsch, E. F., and Maniatis, T. (1989) *Molecular Cloning: A laboratory manual*, Vol. 2, Cold Spring Harbor Laboratory Press, New York.
- (15) Bauer, A. J., Rayment, I., Frey, P. A., and Holden, H. M. (1991) The isolation, purification, and preliminary crystallographic characterization of UDP-galactose 4-epimerase from *Escherichia coli*. *Proteins* 9, 135–142.
- (16) Wong, L. J., and Frey, P. A. (1974) Galactose-1-phosphate uridylyltransferase: Rate studies confirming a uridylyl-enzyme intermediate on the catalytic pathway. *Biochemistry* 13, 3889–3894.
- (17) Wilson, D. B., and Hogness, D. S. (1964) The enzymes of the galactose operon in *Escherichia coli*: I. Purification and characterization of uridine diphosphogalactose 4-epimerase. *J. Biol. Chem.* 239, 2469–2481.
- (18) Ljungcrantz, P., Carlsson, H., Mansson, M. O., Buckel, P., Moshach, K., and Bulow, L. (1989) Construction of an artificial enzyme,  $\beta$ -galactosidase/galactose dehydrogenase, exhibiting efficient galactose channeling. *Biochemistry* 28, 8786–8792.
- (19) Bulow, L., and Moshach, K. (1991) Multienzyme systems obtained by gene fusion. *Trends Biotechnol.* 9, 226–231.

# TECHNICAL NOTES

## Synthesis and Properties of Cholesteryl-Modified Triple-Helix Forming Oligonucleotides Containing a Triglycyl Linker

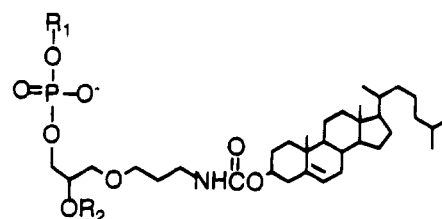
Huynh Vu,\* Theresa Schmaltz Hill, and Krishna Jayaraman

Triplex Pharmaceutical Corporation, 9391 Grogans Mill Road,  
The Woodlands, Texas 77380. Received June 2, 1994\*

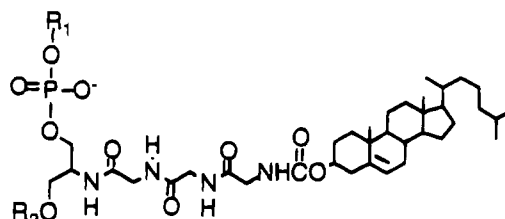
In order to enhance the nuclear uptake of triple-helix forming oligonucleotides (TFOs), a triglycyl-cholesterol group was attached to the 3' end. The peptide unit was introduced as a "labile" linker with the aim of releasing the oligonucleotide from the endosomes by the action of peptidases after crossing the cell membrane. Cholesteryl-CPG (**8**) and -TentaGel (**9**) supports containing 2-[N-(glycylglycylglycyl)amino]propane-1,3-diol (GAP-3) linker were prepared and used for automated oligonucleotide synthesis. The synthesis, characterization, and stability of these compounds are described.

The permeability of the oligonucleotides across the cell membrane and into the nucleus plays a critical role in determining the cellular efficacy of antisense or antigene oligonucleotide (**1**, **2**). Lipophilic end modifications of oligonucleotides have been shown to enhance the uptake and cellular efficacy (**2-7**). We have shown that cholesteryl-conjugated TFOs containing 3-aminopropyl glycerol (APG) linker (Figure 1) are taken up more efficiently than the unmodified or 3'-amine modified TFOs (**8**). Fluorescence microscopy studies with these cholesterol-modified TFOs show that a major portion of them is still retained in the endosomes resulting in only a small enhancement in nuclear uptake (N. Chaudhary et al., unpublished results).

The isolated yields in the preparation of these cholesteryl-modified TFOs containing APG linker were low, the first coupling being only ~50%. The solubility of G-rich TFOs containing this end modification was also low. In order to increase the nuclear uptake and overcome the synthesis and solubility problems, we have designed and synthesized a 2-[N-(glycylglycylglycyl)amino]propane-1,3-diol (GAP-3) linker (Figure 2) for the attachment of cholesterol at the 3' end. Another function of this group is to serve as a "labile" linker that will help in the release of the oligonucleotide from endosomes into the nucleus. The "labile" linker approach is well known in the pro-drug strategy for the delivery of therapeutic molecules (**9**). An essential requirement of such a "labile" linker is that its linkage to cholesterol should be stable enough to enhance uptake into the cell and subsequently help in the release of the oligonucleotide from the endosomes by the action of peptidases. The hydrophobic cholesterol moiety is expected to be embedded in the endosomal membrane anchoring the oligonucleotide on the luminal surface. We postulated that the tethered oligonucleotide along with the triglycyl moiety may then be flipped or transported into the cytosol by as yet an undescribed mechanism. The peptidases which are abundant in the cytosol could cleave the oligonucleotide from the chole-



**Figure 1.** Cholesteryl-conjugated TFOs containing 3-aminopropyl glycerol (APG) linker. R<sub>1</sub>: oligonucleotide, R<sub>2</sub>: -OH or -CPG, TentaGel support.



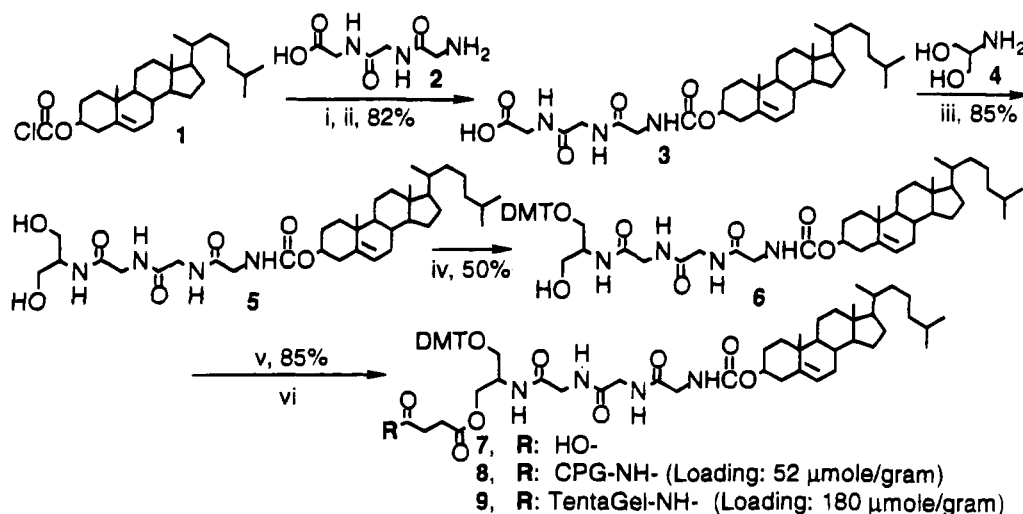
**Figure 2.** Cholesteryl-conjugated TFOs containing 2-[N-(glycylglycylglycyl)amino]propane-1,3-diol (GAP-3) linker. R<sub>1</sub>: oligonucleotide, R<sub>2</sub>: -OH or -CPG, TentaGel support.

terol moiety using the triglycyl group as a substrate. To test our hypothesis, a triglycyl linker (GAP-3 linker) was designed as a model compound. The GAP-3 linker was also designed to overcome the steric problems that resulted in low yield in the first coupling step of the APG linker containing oligonucleotides (**8**). The synthesis of the GAP-3 linker and the linked-oligonucleotides and preliminary data on their properties are described in this paper.

The GAP-3 linker-cholesterol was introduced at the 3' end by using solid supports **8** and **9** (Figure 3) for the synthesis of TFOs. Cholesteryl chloroformate (**1**) was reacted with the silylated glycylglycylglycine, followed by desilylation with 2% HCl to give N-[(cholesteryloxy)carbonyl]glycylglycylglycine (**3**, 82%) (**10**). Compound **3** was coupled with 2-aminopropane-1,3-diol (**4**) by using 1-[3-(dimethylamino)propyl]-3-ethylcarbodiimide hydrochloride (EDC) to give 2-[N-[N-(cholesteryloxy)carbonyl]glycylglycylglycyl]amino]propane-1,3-diol (**5**, 85%) (**11**). Compound **5** was tritylated by 4,4'-dimethoxytrityl chlo-

\* To whom correspondence should be addressed. Tel: 713-363-8761. Fax: 713-363-1168

\* Abstract published in *Advance ACS Abstracts*, September 15, 1994.



**Figure 3.** (i) (a) 2, bis(trimethylsilyl)acetamide, DMF; (b)  $-20^{\circ}\text{C}$ , 1; (ii) 2% HCl; (iii) EDC, pyridine; (iv) pyridine,  $\text{Et}_3\text{N}$ , 4,4'-dimethoxytrityl chloride; (v) succinic anhydride, DMAP, pyridine; (vi) (a) TBTU, HOBT, DMF, N-ethylmorpholine,  $\text{NH}_2$ -support; (b) acetic anhydride, DMAP.

ride in the presence of 4-(dimethylamino)pyridine and triethylamine to provide 1-O-(4,4'-dimethoxytrityl)-2-[N-[N-[(cholesteryl)oxycarbonyl]glycylglycylglycyl]amino]propane-1,3-diol (**6**, 50%) (**12**). The supports CPG (**8**, loading:  $52\ \mu\text{mol/g}$ , 64% loaded) and TentaGel (**9**, loading:  $180\ \mu\text{mol/g}$ , 86% loaded) were prepared by succinylation of compound **6**, followed by coupling of the succinate (**7**) (**13**) to the free amino group.

The stability of the GAP-3 linker-cholesterol conjugate was determined before oligonucleotide synthesis was initiated. DMT-cholesteryl supports (**8**, **9**) were treated with various deprotection solutions: (hydrazine/MeOH; 1:3 v/v, 0.4 M NaOH in 75% MeOH/water, at room temperature, overnight, or concd  $\text{NH}_4\text{OH}$ , 0.1 M NaOH aqueous solution,  $56^{\circ}\text{C}$ , overnight) as well as the buffer conditions (1.5 M NaCl containing 15 mM NaOH, at room temperature, overnight) used in the purification. The support was then filtered and washed thoroughly with dichloromethane, dichloromethane:methanol 1:1 (v/v), and methanol to extract the hydrolyzed products from the support completely. The crude material was analyzed by thin layer chromatography (dichloromethane:methanol 1:9, v/v). The product bands were isolated by preparative TLC and characterized by  $^1\text{H-NMR}$ . The compound, 1-O-(4,4'-dimethoxytrityl)-2-[N-[N-[(cholesteryl)oxycarbonyl]glycylglycylglycyl]amino]propane-1,3-diol (**6**) was shown to be fairly stable under the standard deprotection conditions (concentrated  $\text{NH}_4\text{OH}$ ,  $56^{\circ}\text{C}$  overnight). Only minor amounts of degraded products were detected. TLC analysis showed that treatment with 0.4 N NaOH overnight in methanol:water (3:1, v/v) solution at room temperature yielded cholesterol and unidentified products. The yield of cholesterol as judged by visual inspection of the TLC was  $\sim 90\%$ .

On the basis of these stability studies, several 3' end cholesteryl-modified TFO sequences were synthesized on a 0.2–300  $\mu\text{mol}$  scale using cholesteryl supports **8** and **9** on Applied Biosystems Models 380B, 392/4, and/or MilliGen Models 8700 and 8800 with a coupling efficiency of  $\geq 97\%$ , including the first step. Several sequences of G-rich TFOs were synthesized using these supports. Cleavage and deprotection were carried out under standard conditions (concentrated  $\text{NH}_4\text{OH}$ ,  $56^{\circ}\text{C}$ , overnight). Crude oligonucleotides were purified on a Pharmacia FPLC system by anion exchange chromatography on a Q-Sepharose column (1 cm  $\times$  10 cm) (**14**). Enzymatic digestion of the cholesteryl oligonucleotides by P1 nu-

lease/bacterial alkaline phosphatase gave the expected deoxynucleoside composition. Gel electrophoresis analysis of purified oligonucleotides after end labeling with  $^{32}\text{P}$ -ATP and using polynucleotide kinase showed two bands in the ratio of 7:3. The slower band (one unit slower than the oligonucleotides containing 3' end free amino group) contained cholesterol. Electrospray mass spectroscopy analysis of the slower band (on the gel) of a G-rich oligonucleotide, 21 mer, containing GAP-3-linker and cholesterol had an observed mass of 7097.14 while the calculated mass was 7096.55. The faster moving band does not appear to contain cholesterol suggesting that some cholesterol is cleaved during the deblocking procedure. It is not clear why the linker-cholesterol is unstable during deblocking of the oligonucleotide while it appears to be stable by itself before the oligonucleotide is attached. A possible explanation could be that on cleavage of the oligonucleotide-linker-cholesterol from the support, an hydroxyl group is liberated that is in position to attack the neighboring phosphate group via the formation of a six-membered ring intermediate. However, on deblocking, the support containing linker cholesterol (compound **8** or **9**) generated compound **6** which lacks the phosphate group. The above-mentioned pathway is, therefore, not possible. There was no loss of linker-cholesterol when the oligonucleotide was deblocked at room temperature for 48 h. Under these conditions, the isobutyryl protecting group on the bases was also completely deprotected from the oligonucleotide. There was essentially only one band on purification by gel. Electrospray mass spectroscopy analysis of this band confirmed the presence of cholesterol on oligonucleotide.

A comparison of binding affinities for TFOs containing 3'-propanolamine and 3'-cholesteryl GAP-3 linker modifications showed that cholesteryl attachment to the TFOs did not affect the binding significantly. A 3'-propanolamine TFO, 5'-GTGGTGGTGGTGGTGGTGGTGGTTTGGGGGTGGGG-propanolamine-3', had a  $K_d$  of  $5 \times 10^{-10}$  M while the same sequence with 3' GAP-3 linker-cholesteryl group 5'-GTGGTGGTGGTGGTGGTGGTGGTTTGGGGGTGGGG-cholesterol-3' had also a  $K_d$  of  $5 \times 10^{-10}$  M. Triplex formation was assessed using the gel shift assay, essentially as described (**15**).

Preliminary uptake studies of TFOs containing GAP-3 linker and cholesterol showed a 2–5-fold enhancement in nuclear uptake and is in agreement with the expected enhancement in uptake using this approach.



The "labile" linker approach presented in this paper appears to be promising and may serve as a general and powerful tool for enhancing the nuclear uptake of oligonucleotides.

#### ACKNOWLEDGMENT

The authors would like to thank the National Cancer Institute, SBIR Grant (No. 1 R43 CA 61649-01, PI-K.J.) for supporting this work. We wish to thank Dr. Uhlmann, Hoechst AG, Germany, for carrying out the electrospray mass spectroscopy of the cholesterol containing oligonucleotides and N. Chaudhary for helpful discussions.

#### LITERATURE CITED

- (1) Uhlmann, E., and Peyman, A. (1990) Antisense oligonucleotides: a new therapeutic principle. *Chemical Rev.* 90, 543-584.
- (2) Jaroszewski, J. W., and Cohen, J. S. (1991) Cellular uptake of antisense oligonucleotides *Adv. Drug Design Res.* 6, 235-250.
- (3) de Smidt, P. C., Doan, T. L., deFalco, S., and Van Berkel, T. J. C. (1991) Association of antisense oligonucleotides with lipoproteins prolongs the plasma half-life and modifies the tissue distribution. *Nucl. Acids Res.* 19, 4695-4700.
- (4) Letsinger, R. L., Zhang, G., Sun, D. K., Ikeuchi, T., and Sarin, P. S. (1989) Cholesteryl-conjugated oligonucleotides: synthesis, properties, and activity as inhibitors of replication of human immunodeficiency virus in cell culture. *Proc. Natl. Acad. Sci. U.S.A.* 86, 6553-6556.
- (5) Shea, R. G., Marsters, J. C., and Bischofberger, N. (1990) Synthesis, hybridization properties and antiviral activity of lipid-oligonucleotide conjugates *Nucl. Acids Res.* 18, 3777-3783.
- (6) Will, D. W., and Brown, T. (1992) Attachment of vitamin E derivatives to oligonucleotides during solid-phase synthesis. *Tetrahedron Lett.* 33, 2729-2732.
- (7) Ing, N. H., Beekman, J. M., Kessler, D. J., Murphy, M., Jayaraman, K., Zendegui, J. G., Hogan, M. E., O'Malley, B. W., and Tsai, M. (1993) *In vivo* transcription of a progesterone-responsive gene is specifically inhibited by a triplex-forming oligonucleotide. *Nucl. Acids Res.* 21, 2789-2796.
- (8) Vu, H., Singh, P., Lewis, L., Zendegui, G. J., and Jayaraman, K. (1993) Synthesis of cholesteryl supports and phosphoramidite for automated DNA synthesis of triple-helix forming oligonucleotides (TFOs). *Nucleosides Nucleotides* 12, 853-864.
- (9) H. Bundgaard, Ed. (1985) *Design of Pro-Drugs*, Elsevier, New York.
- (10) Compound 3: a white solid; mp 194-198 °C dec; <sup>1</sup>H-NMR (DMSO-*d*<sub>6</sub>) δ 0.67 (s, 3H, -CH<sub>3</sub>, chol), 0.84 (s, 3H, -CH<sub>3</sub>, chol), 0.85 (s, 3H, -CH<sub>3</sub>, chol), 0.91 (d, *J* = 6.4 Hz, 3H, -CH<sub>3</sub>, chol), 0.98 (s, 3H, -CH<sub>3</sub>, chol), 2.59-0.95 (m, 29H, chol), 3.66 (d, *J* = 5.8 Hz, 2H, -CO-CH<sub>2</sub>NH-, linker), 3.77 (d, *J* = 5.8 Hz, 4H, 2(-COCH<sub>2</sub>NH-), linker), 4.34 (m, 1H, -CH<sub>2</sub>CHCH<sub>2</sub>-, chol), 5.33 (b, s, 1H, C=CH-, chol), 7.04, 7.98, and 8.03 (3 b, s, 3H, 3 (NH), linker), 12.30 (b, s, 1H, -COOH, linker). Anal. Calcd for C<sub>34</sub>H<sub>56</sub>N<sub>3</sub>O<sub>6</sub> (601.82): C, 67.86; H, 9.21; N, 6.98. Found: C, 67.97; H, 9.23; N, 6.91.
- (11) Compound 5: a white solid; mp 205-206 °C. <sup>1</sup>H-NMR (DMSO-*d*<sub>6</sub>) δ 0.65 (s, 3H, -CH<sub>3</sub>, chol), 0.84 (s, 3H, -CH<sub>3</sub>, chol), 0.85 (s, 3H, -CH<sub>3</sub>, chol), 0.89 (d, *J* = 6.3 Hz, 3H, -CH<sub>3</sub>, chol), 0.97 (s, 3H, -CH<sub>3</sub>, chol), 2.59-0.95 (m, 29H, chol), 3.40 (t, *J* = 5.32 and 5.36 Hz, 4H, -CH<sub>2</sub>OH, linker), 3.63 (d, *J* = 5.28 Hz, 2H, -COCH<sub>2</sub>NH-, linker), 3.7 (t, *J* = 5.8 and 5.52 Hz, 4H, 2(-COCH<sub>2</sub>NH-), linker), 3.75 (b, s, 1H, -CH<sub>2</sub>CHNH-, linker), 4.34 (m, 1H, -CH<sub>2</sub>CHCH<sub>2</sub>-, chol), 4.59 (t, *J* = 5.52 and 5.48 Hz, 2H, 2 (-OH)), 5.33 (b, s, 1H, C=CH-, chol), 7.22, 8.03, and 8.12 (3 b, s, 3H, 3 (NH), linker), 7.47 (d, *J* = 7.9 Hz, 1H, (NH), linker). Anal. Calcd for C<sub>37</sub>H<sub>62</sub>N<sub>4</sub>O<sub>7</sub> (674.918): C, 65.85; H, 9.26; N, 8.30. Found: C, 66.09; H, 9.23; N, 8.16.
- (12) Compound 6: a white solid; mp 172-173 °C. <sup>1</sup>H-NMR (DMSO-*d*<sub>6</sub>) δ 0.65 (s, 3H, -CH<sub>3</sub>, chol), 0.84 (s, 3H, -CH<sub>3</sub>, chol), 0.85 (s, 3H, -CH<sub>3</sub>, chol), 0.89 (d, *J* = 6.3 Hz, 3H, -CH<sub>3</sub>, chol), 0.97 (s, 3H, -CH<sub>3</sub>, chol), 2.59-0.95 (m, 29H, chol), 2.98 (m, 2H, CH<sub>2</sub>ODMT), 3.51 (t, *J* = 5.4 and 5.36 Hz, 2H, -CH<sub>2</sub>-OH, linker), 3.63 (d, *J* = 5.32 Hz, 2H, -COCH<sub>2</sub>NH-, linker), 3.74 (s, 6H, 2(CH<sub>3</sub>O-)), 3.74 (m, 4H, 2(-COCH<sub>2</sub>NH-), linker), 4.0 (m, 1H, -CH<sub>2</sub>CHNH-, linker), 4.34 (m, 1H, -CH<sub>2</sub>CHCH<sub>2</sub>-, chol), 4.59 (t, *J* = 5.52 and 5.48 Hz, 1H, -OH), 5.33 (b, s, 1H, C=CH-, chol), 6.60-7.30 (m, 13H, DMT), 7.22, 8.03, and 8.11 (3 b, s, 3H, 3 (NH), linker), 7.63 (d, *J* = 8.2 Hz, 1H, (NH), linker). Anal. Calcd for C<sub>58</sub>H<sub>80</sub>N<sub>4</sub>O<sub>9</sub> (977.297): C, 71.28; H, 8.25; N, 5.73. Found: C, 71.27; H, 8.39; N, 5.73.
- (13) Compound 7: a white solid; mp 110-112 °C. <sup>1</sup>H-NMR (DMSO-*d*<sub>6</sub>) δ 0.65 (s, 3H, -CH<sub>3</sub>, chol), 0.83 (s, 3H, -CH<sub>3</sub>, chol), 0.84 (s, 3H, -CH<sub>3</sub>, chol), 0.89 (d, *J* = 6.3 Hz, 3H, -CH<sub>3</sub>, chol), 0.96 (s, 3H, -CH<sub>3</sub>, chol), 2.34 and 2.40 (m, m, 4H, -CH<sub>2</sub>CH<sub>2</sub>-, succinyl), 2.59-0.95 (m, 29H, chol), 3.0 (m, 2H, CH<sub>2</sub>ODMT), 3.62 (m, 2H, -COCH<sub>2</sub>NH-, linker), 3.73 (s, 6H, 2(CH<sub>3</sub>O-)), 3.76 (m, 4H, 2(-COCH<sub>2</sub>NH-), linker), 4.08 (t, *J* = 4.68, 5.60 Hz, 1H, -CH<sub>2</sub>CHNH-, linker), 4.20 (m, 2H, -CH<sub>2</sub>OH, linker), 4.31 (m, 1H, -CH<sub>2</sub>CHCH<sub>2</sub>-, Chol), 5.32 (b, s, 1H, C=CH-, chol), 6.88-7.38 (m, 13H, DMT), 7.38, 7.87, 8.31, and 8.49 (4 b, s, 4H, 4 (NH), linker). Anal. Calcd for C<sub>62</sub>H<sub>84</sub>N<sub>4</sub>O<sub>12</sub>+H<sub>2</sub>O (1095.38): C, 67.97; H, 7.91; N, 5.11. Found: C, 68.36; H, 7.84; N, 5.12.
- (14) Murphy, M., Rieger, M., and Jayaraman, K. (1993) Large-scale synthesis of triple-helix forming oligonucleotides using a controlled-pore glass support. *Biotechniques* 15, 1004-1010.
- (15) Durland, R. H., Kessler, D. J., Gunnell, S., Duvic, M., Pettitt, B. M., and Hogan, M. E. (1991) Binding of triple helix forming oligonucleotides to site in gene promoters. *Biochemistry* 30, 9246-9255.